Cover Picture



Rodrigue Lescouëzec, Jacqueline Vaissermann, Catalina Ruiz-Pérez, Francesc Lloret, Rosa Carrasco, Miguel Julve,* Michel Verdaguer,* Yves Dromzee, Dante Gatteschi, and Wolfgang Wernsdorfer

Magnetic nanowires are among new objects that chemists can design with a view to magnetic information storage. The cover picture shows views of an ordered bimetallic double chain of iron(III) and cobalt(II) ions, bridged by cyanide groups. Each chain has remarkable anisotropic magnetic properties (axes of easy magnetization are shown) and shows slow relaxation of the magnetization. Find out more about these nanowires in the Communication by M. Julve, M. Verdaguer et al. on page 1483 ff.

Contents

Obituary

D. John Faulkner (1942–2002) — 1438–1439 — Marine Natural Products Chemistry and Marine Chemical Ecology — *William Fenical*

Books

Topics in Stereochemistry — 1440–1442 — Scott E. Denmark — *reviewed by H. Hopf*

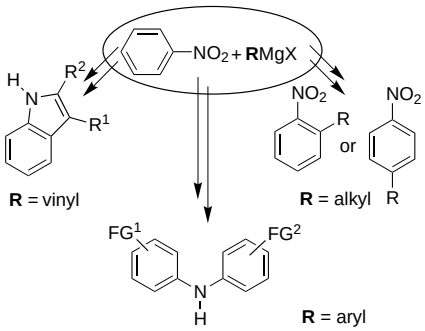
L'Architecture du Vivant — 1442–1443 — Pierre Laszlo — *reviewed by R. Neier*

Highlights

Grignard Reactions with Nitroarenes

A. Ricci,* M. Fochi — 1444–1446

Reactions between Organomagnesium Reagents and Nitroarenes: Past, Present, and Future



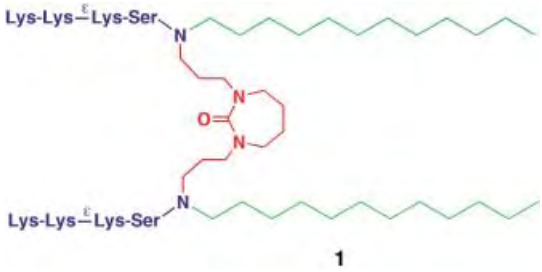
Grignard reagents display useful diversity in their reactions with nitroarenes. Depending on the organomagnesium species used, these reactions, the results of which can be predicted from mechanistic studies, may lead to significantly diverse products (see scheme), and can be tailored towards the synthesis of substituted nitroarenes, indoles, and diarylamines. FG = functional group.

Minireviews

Gene Transfection Agents

A. J. Kirby,* P. Camilleri, J. B. F. N. Engberts, M. C. Feiters, R. J. M. Nolte, O. Söderman, M. Bergsma, P. C. Bell, M. L. Fielden, C. L. García Rodríguez, P. Guédat, A. Kremer, C. McGregor, C. Perrin, G. Ronsin, M. C. P. van Eijk — 1448–1457

Gemini Surfactants: New Synthetic Vectors for Gene Transfection



1

The powerful combination of the superior surfactant properties of gemini surfactants with the cationic character necessary for binding and compacting DNA has led to a new class of gene transfection agents (e.g. **1**). The compounds are derived from natural metabolites and combine high transfection activity with low cell toxicity.

Reviews

Anion-Directed Processes

R. Vilar* — 1460–1477

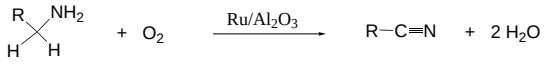
Anion-Templated Synthesis

Anion templates in vogue: In contrast to the well-studied templating properties of cationic and neutral species until very recently only a handful of anion-templated syntheses had been reported. That this is beginning to change is evident from the number of anion-templated assemblies—such as macrocycles (see scheme), cages, helicates, rotaxanes, and extended structures—that have emerged over the past few years. Such systems are summarized in this review.



© 2003 Wiley-VCH Verlag GmbH & Co. KGaA, Weinheim

Communications

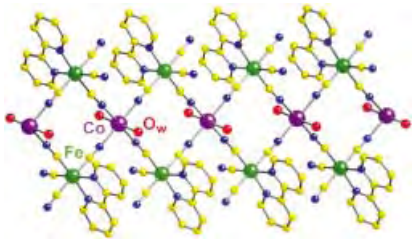


Supported Ru Catalysis of Amines

K. Yamaguchi, N. Mizuno* . 1480 – 1483

Efficient Heterogeneous Aerobic Oxidation of Amines by a Supported Ruthenium Catalyst

An inexpensive supported ruthenium catalyst (Ru/Al_2O_3) can be used to convert a broad range of primary (see scheme) and secondary amines into the corresponding nitriles and imines in high yields using either dioxygen or air as oxidants. The catalyst can be recycled and reused with no detectable loss of ruthenium and without an observed reduction in catalytic activity.

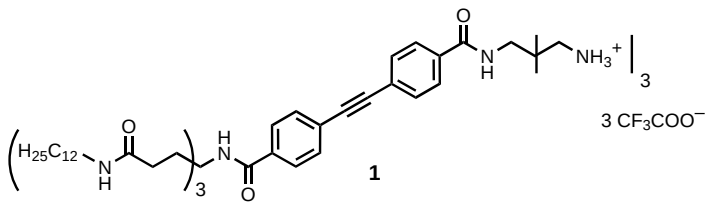


Magnetic Nanowires

R. Lescouëzec, J. Vaissermann, C. Ruiz-Pérez, F. Lloret, R. Carrasco, M. Julve,* M. Verdaguer,* Y. Dromzee, D. Gatteschi, W. Wernsdorfer _____ 1483 – 1486

Cyanide-Bridged Iron(III)–Cobalt(II) Double Zigzag Ferromagnetic Chains: Two New Molecular Magnetic Nanowires

The Ising on the cake: The cyanide-bridged low-spin Fe^{III}–high-spin Co^{II} compounds of formula $[\{FeL(CN)_4\}_2Co(H_2O)_2]\cdot 4H_2O$ with L = 2,2′-bipyridine (bpy; see picture; O_w = water O-atom) or 1,10-phenanthroline are 1D Ising systems and the first examples of ferromagnetically coupled bimetallic chains which show slow magnetic relaxation and hysteresis effects. The compounds, therefore, behave as magnetic nanowires.



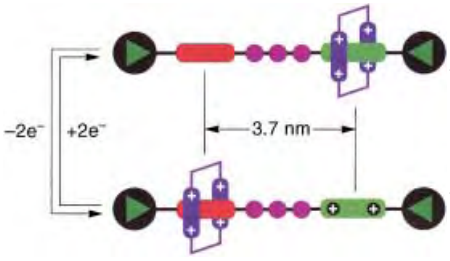
1

Transfection Agents

D. Joester, M. Losson, R. Pugin, H. Heinzelmann, E. Walter, H. P. Merkle, F. Diederich* _____ 1486 – 1490

Amphiphilic Dendrimers: Novel Self-Assembling Vectors for Efficient Gene Delivery

A sharp maximum in the structure–activity relationship, a surprisingly strong influence of the hydrophobic part on DNA binding and transport, and an unusual serum effect on relative transfection activities were found in preliminary biological data on a series of four amphiphilic dendrimers designed as transfection agents. The lowest generation dendrimer **1** was found to be the most active.



Redox-Controllable [2]Rotaxane

H.-R. Tseng, S. A. Vignon, J. F. Stoddart* _____ 1491 – 1495

Toward Chemically Controlled Nanoscale Molecular Machinery

Mechanical displacement of the ring by around 40% along the approximately 9-nm long dumbbell-shaped component has been seen in a bistable redox-controllable [2]rotaxane. Chemical oxidation of the tetrathiafulvalene recognition station (green, see scheme) in the dumbbell-shaped component, which also contains a 1,5-dioxynaphthalene recognition station (red), results in the cyclobis(paraquat-*p*-phenylene) tetracation (blue) undergoing translation from the much preferred green station to the second-choice, red station.

For the USA and Canada:
ANGEWANDTE CHEMIE International Edition (ISSN 1433-7851) is published weekly by Wiley-VCH PO Box 191161, D 69451 Weinheim, Germany. Air freight and mailing in the USA by Publications Expediting Inc. 200 Meacham Ave., Elmont, NY 11003. Periodicals postage paid at Jamaica NY 11431. US POSTMASTER: send address changes to *Angewandte Chemie*, Wiley-VCH, 111 River Street, Hoboken, NJ 07030. Annual institutional subscription price for institutions: Europe € 2998.00/3148.00. Outside Europe US$ 3718.00/3904.00 (valid for print or electronic/print and electronic delivery); for individuals who are personal members of a national chemical society, or whose institution already subscribes, or who are retired or self-employed consultants, print only (including postage and handling charges): Europe € 248.00/Outside Europe US$ 348.00.

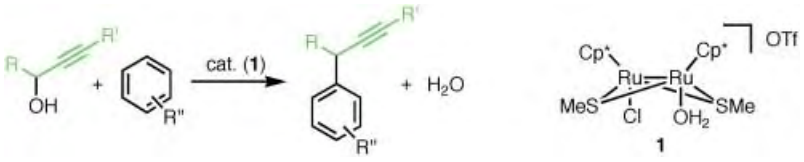
 © 2003 Wiley-VCH Verlag GmbH & Co. KGaA, Weinheim

Contents

C-H Activation with Ru

Y. Nishibayashi, Y. Inada, M. Yoshikawa, M. Hidai,* S. Uemura* ____ **1495 – 1498**

Propargylation of Aromatic Compounds with Propargylic Alcohols Catalyzed by a Cationic Diruthenium Complex



Two metals are better than one: The cationic methanethiolate-bridged diruthenium complex **1** ($Cp^* = C_5Me_5$, $OTf = CF_3SO_3$) promotes the catalytic propargylation of aromatic compounds with propargylic alcohols bearing not only *terminal* alkyne but also *internal* alkyne units, reactions that can not be carried out with some mononuclear catalysts. This reaction provides a general and environmentally friendly (atom economical, only H_2O as byproduct) method for the synthesis of a variety of propargylated aromatic compounds.

Diels-Alder Reactions

K. Juhl, K. A. Jørgensen* ____ **1498 – 1501**

The First Organocatalytic Enantioselective Inverse-Electron-Demand Hetero-Diels–Alder Reaction

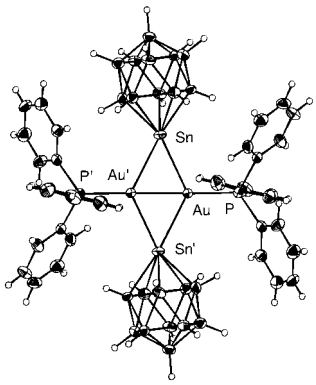


Catalyzed by chiral amines, aldehydes undergo diastereo- and enantioselective inverse-electron-demand hetero-Diels–Alder reactions with enones (see scheme; PCC = pyridine chlorochromate). The reaction has been optimized with respect to different pyrrolidine catalysts, and tested with various aldehydes and enones.

Sn-Bridged Au–Au Interactions

S. Hagen, I. Pantenburg, F. Weigend, C. Wickleder, L. Wesemann* ____ **1501 – 1505**

Gold–Gold Interaction—Stannaborate $[SnB_{11}H_{11}]^{2-}$ Coordination Chemistry

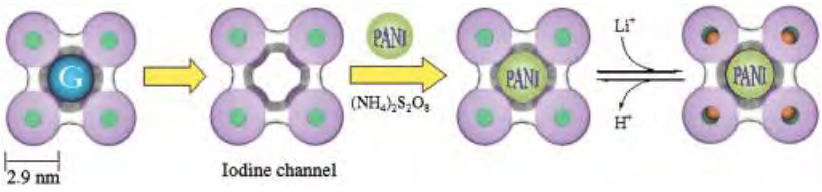


A stannaborate bridge supports the gold–gold interaction in the product (see picture) of the reaction of $[SnB_{11}H_{11}]^{2-}$ with $[(Ph_3P)AuCl]$. A significant preference for the dimer $[(Me_3P)Au(SnB_{11}H_{11})]_2^{2-}$ over the two monomers $[(Me_3P)Au(SnB_{11}H_{11})]^-$ ($\Delta E = 160\ kJ\,mol^{-1}$) was demonstrated on the basis of MP2 calculations.

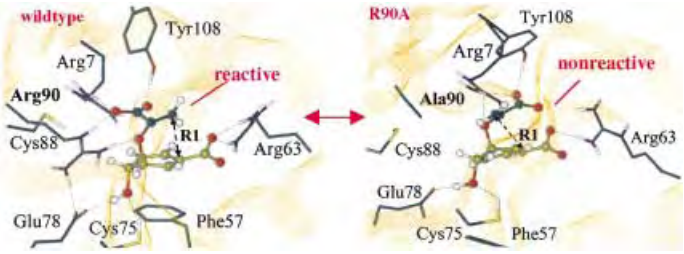
Electron/Ion-Conducting Materials

L.-L. Li, C.-J. Yang, W.-H. Chen, K.-J. Lin* ____ **1505 – 1508**

Towards the Development of Electrical Conduction and Lithium-Ion Transport in a Tetragonal Porphyrin Wire



One-dimensional porphyrin wires were self-assembled by solvothermal methods. The porous framework, sustained by van der Waals and electrostatic interactions, is thermally stable up to 350 °C. Encapsulation of polyaniline (PANI) filaments in the host matrix provides a pathway for electron conduction (see picture). Moreover, it exhibits a highly reversible lithium-ion cycle in a C/Li·PANI @porphyrin cell. These features make this material very attractive for secondary battery solid-electrolyte applications.

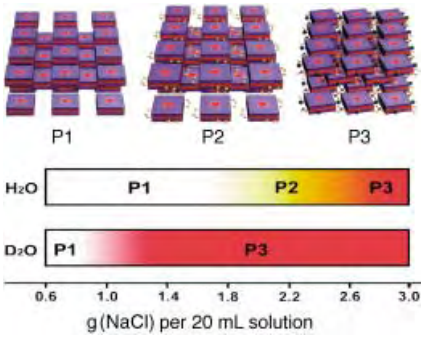


The removal of a key residue (Arg 90) from the chorismate mutase enzyme destroys the balance of the interactions in the active site required for stabilizing the conformation of the transition state in the Claisen rearrangement of chorismate to prephenate (see picture).

Molecular Modeling of Enzymes

H. Guo, Q. Cui, W. N. Lipscomb, M. Karplus* ——— 1508 – 1511

Understanding the Role of Active-Site Residues in Chorismate Mutase Catalysis from Molecular-Dynamics Simulations

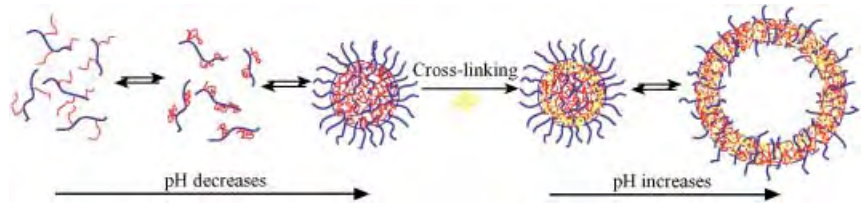


The independent variation of two seemingly unrelated parameters, namely NaCl concentration and water hydrogen isotopologues, can tune the formation of both similar (P1 and P2) and dissimilar (P3) supramolecular Mn_{16} aggregates in aqueous solutions. Surprisingly, a structurally intermediate phase P2, however, forms in H_2O, but not in D_2O.

Isotope-Induced Structural Effects

J. Lee, S. M. Gorun* ——— 1512 – 1515

Compositional and Isotopologue-Induced Phase Differentiation in Supramolecular Aggregates

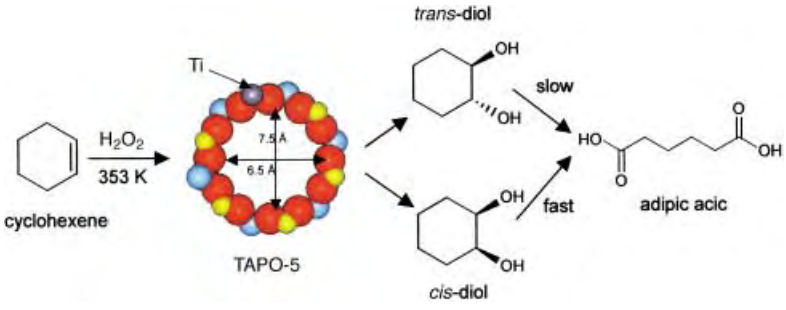


Simply by decreasing the pH of the medium, hydroxyethyl cellulose-*graft*-polyacrylic acid (HEC-*g*-PAA) can form micelles in water. Cross-linking the PAA chains at the periphery of the micellar core can efficiently lock the integrality of the micelles (see scheme). The resultant micelles transform into hollow spheres as the pH value increases. Both the micellization and the transition from micelles to hollow spheres are reversible. The hollow spheres show "on-off" character at a pH value of about 3.

Polymeric Hollow Spheres

H. Dou, M. Jiang,* H. Peng, D. Chen, Y. Hong ——— 1516 – 1519

pH-Dependent Self-Assembly: Micellization and Micelle–Hollow-Sphere Transition of Cellulose-Based Copolymers



The stereochemistry of the 1,2-cyclohexanediol intermediate plays an important role with regard to both the rate and selectivity of the production of adipic acid from cyclohexene in the absence of an organic solvent. A titanium-containing aluminophosphate molecular sieve (TAPO-5) is shown to serve as a good heterogeneous catalyst for this reaction.

Solvent-Free Route to Adipic Acid

S.-O. Lee, R. Raja, K. D. M. Harris, J. M. Thomas,* B. F. G. Johnson, G. Sankar ——— 1520 – 1523

Mechanistic Insights into the Conversion of Cyclohexene to Adipic Acid by H_2O_2 in the Presence of a TAPO-5 Catalyst

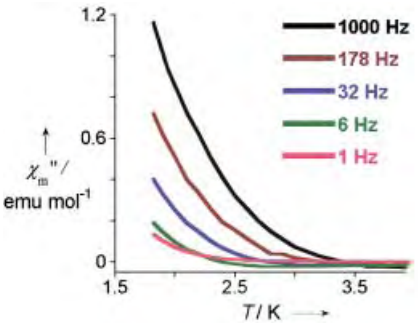
 © 2003 Wiley-VCH Verlag GmbH & Co. KGaA, Weinheim

Contents

Single-Molecule Magnets

C. P. Berlinguette, D. Vaughn, C. Cañada-Vilalta, J. R. Galán-Mascarós, K. R. Dunbar* ——— **1523 – 1526**

A Trigonal-Bipyramidal Cyanide Cluster with Single-Molecule-Magnet Behavior: Synthesis, Structure, and Magnetic Properties of $\{[Mn^{II}(tmphen)_2]_3[Mn^{III}(CN)_6]_2\}$

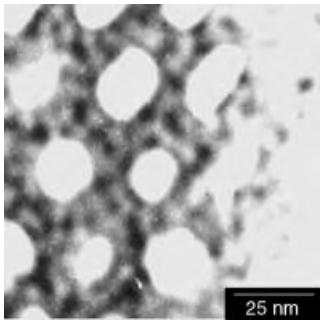


Slow paramagnetic relaxation was observed at low temperatures from ac susceptibility measurements in the form of a frequency-dependent out-of-phase (χ''_m) signal for the title complex (see picture). This provides compelling evidence that this cluster is a rare example of a cyanide-bridged single-molecule magnet.

Superparamagnetic Aluminosilicates

C. Garcia, Y. Zhang, F. DiSalvo, U. Wiesner* ——— **1526 – 1530**

Mesoporous Aluminosilicate Materials with Superparamagnetic γ-Fe_2O_3 Particles Embedded in the Walls

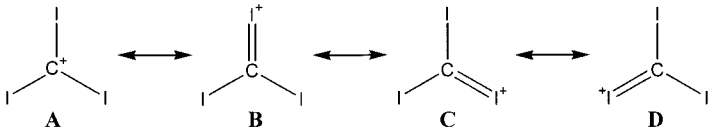


An iron constitution: Dark superparamagnetic iron oxide nanoparticles are present within the walls of a hexagonal mesoporous aluminosilicate (as shown by the associated bright-field TEM image). The simple block-copolymer-based "one-pot" self-assembly approach enables potential applications in magnetic separation and catalyst technologies.

Trihalogencarbenium Ions

I. Krossing,* A. Bihlmeier, I. Raabe, N. Trapp ——— **1531 – 1534**

Structure and Characterization of $CI_3^+[Al\{OC(CF_3)_3\}_4]^-$; Lewis Acidities of CX_3^+ and BX_3



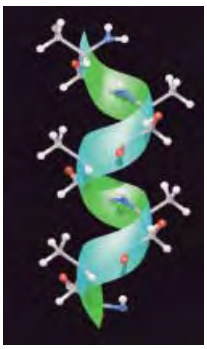
Lewis acidity versus F^- in CH_2Cl_2: $CF_3^+ > CCl_3^+ > CBr_3^+ > CI_3^+ = BI_3 = BBr_3 > BCl_3 > BF_3$

Where is the charge? The positive charge of the CI_3^+ ion in $CI_3^+[Al\{OC(CF_3)_3\}_4]^-$ is located exclusively on the I atoms (see resonance structures **B**–**D**), and not on the formal carbenium center **A**. According to calculations and experimental findings, the Lewis acidity of the CX_3^+ homologues (X = F–I) versus fluoride is reversed in comparison to that of the isoelectronic boron halides BX_3, and decreases from CF_3^+ to CI_3^+.

Helical Peptide Secondary Structure

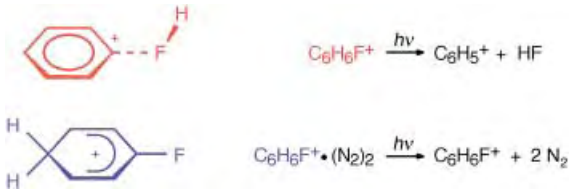
K. Gademann, A. Häne, M. Rueping, B. Jaun, D. Seebach* ——— **1534 – 1537**

The Fourth Helical Secondary Structure of β-Peptides: The (*P*)-2_8-Helix of a β-Hexapeptide Consisting of (2*R*,3*S*)-3-Amino-2-hydroxy Acid Residues



Small change with great effect! An oligomer of α-hydroxy-β-amino acids folds into a right-handed helical structure (see picture) in MeOH; in contrast, the methyl analogue has a pleated sheet structure. Including this new helix, four different helical secondary structures of β-peptides have been discovered—a structural diversity that should allow the generation of elaborate proteomimetics.

© 2003 Wiley-VCH Verlag GmbH & Co. KGaA, Weinheim



Simply a question of the technique! Carbenium and fluoronium isomers of protonated fluorobenzene are unambiguously identified for the first time in the gas phase by spectroscopy (see scheme; blue: *C*-$C_6H_6F^+$, red: *F*-$C_6H_6F^+$). The *C*-$C_6H_6F^+$ ions are detected by IR photodissociation (IRPD) spectra of weakly bound $C_6H_6F^+ \cdot (N_2)_2$ complexes, whereas the *F*-$C_6H_6F^+$ ions are selectively observed by IRPD of bare $C_6H_6F^+$.

Protonated Fluorobenzene Isomers

N. Solcà, O. Dopfer* ——— **1537 – 1540**

Separate Spectroscopic Detection of Carbenium and Fluoronium Isomers of Protonated Fluorobenzene

$$N_{2(g)} + 3\,FeS + 3\,H_2S_{(aq)} \longrightarrow 3\,FeS_{2(s)} + 2\,NH_{3(g)}$$

Teaching an old dog a new fix: Nitrogen fixation under mild conditions is still one of the most challenging tasks in chemistry. A method for the synthesis of ammonia from molecular nitrogen using hydrogen sulfide as a reductant and freshly precipitated iron sulfide as a mediator is described. The reaction (see scheme) may be a primordial inorganic ancestor of the enzyme nitrogenase.

Prebiotic Fixation of Ammonia

M. Dörr, J. Käßbohrer, R. Grunert, G. Kreisel,* W. A. Brand, R. A. Werner, H. Geilmann, C. Apfel, C. Robl, W. Weigand* ——— **1540 – 1543**

A Possible Prebiotic Formation of Ammonia from Dinitrogen on Iron Sulfide Surfaces

VIP Communications labeled with this symbol have been judged by two referees as being "very important papers".

The publication of Communications labeled with this symbol has been accelerated because of their topical or highly competitive nature.

Supporting information for articles labeled with this symbol can be found at www.angewandte.org or www.interscience.wiley.com.

The issues for March 2003 appeared online on the following dates
Issue 9: February 26. · Issue 10: March 10. · Issue 11: March 13. · Issue 12: March 26

DOI: The fastest way to find an article online is the *Digital Object Identifier* (DOI). Starting in this issue, DOIs will be printed in the footer of the first page of every article. For example, an article with a DOI of 10.1002/anie.200390049 can be found on the WWW at http://dx.doi.org/10.1002/anie.200390049. Please use the DOI of your article to link from your home page to the articles in Wiley InterScience. The DOI is a result of a cross-publisher initiative to create a system for the permanent identification of documents on digital networks. More information is available from www.doi.org.

Service

Events ——— *1447, 1550*

Keywords ——— *1544*

Authors ——— *1545*

Sources ——— *A19*

Preview ——— *1549*

 © 2003 Wiley-VCH Verlag GmbH & Co. KGaA, Weinheim

Grignard Reactions with Nitroarenes

Reactions between Organomagnesium Reagents and Nitroarenes: Past, Present, and Future

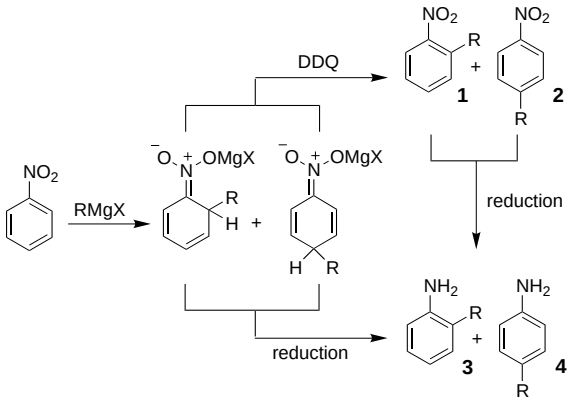
Alfredo Ricci and Mariafrancesca Fochi*

Keywords:
Grignard reagents · indoles · magnesium · N ligands · nitroarenes

The direct synthesis of organomagnesium halides from magnesium and alkyl halides a hundred years ago[1] led to the vast development of organometallic chemistry. Since then, Grignard reagents have been shown to be widely applicable in the formation of C–C bonds by reactions with carbonyl electrophiles, which are some of the most investigated reactions in organic chemistry. Coupling and addition processes can be involved, in which the outcome of the reaction is generally not influenced, even with profound structural variations in the organomagnesium partners.

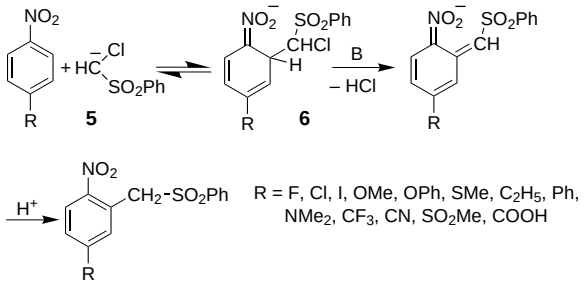
In contrast with classical reactions that are aimed at the formation of C–C bonds through the coupling of a Grignard reagent with an electrophilic carbon atom, the course of the reaction between nitroarenes and Grignard reagents depends strongly upon the nature of the carbanionic moiety in the organometallic species. Nowadays, these routes have been exploited to achieve important synthetic targets, thus devising new synthetic protocols that are highly competitive with those previously reported.

In a series of mechanistic investigations carried out some years ago,[2] Bartoli and co-workers were able to transform once poorly known or misinterpreted procedures into a series of rational reaction pathways. It could be determined from their studies that the reaction between a generic nitroarene and an alkyl magnesium halide proceeded through 1,4 and/or 1,6 conjugate addition, to yield nitronate compounds.[2] Decomposition of these adducts leads to ring-alkylated aromatic nitro compounds **1** and **2** (Scheme 1) or to alkylanilines **3** and **4**, thus devising a route of remarkable synthetic interest, in view of the fact that the few available methods for the preparation of these compounds all have serious limitations.



Scheme 1. Alkylated nitroarenes **1** and **2,** and alkylanilines **3** and **4** formed by the reaction between alkyl Grignard reagents and nitroarenes.[2] DDQ = 2,3-dichloro-5,6-dicyano-1,4-benzoquinone.

The orientation of alkylation depends mainly on the structure of the aromatic substrates, and also on the presence of substituents in reactive positions. This route to alkylated nitroarenes compares favorably with the well-known protocol of Mąkosza et al., [3] which is based on the vicarious nucleophilic substitution (VNS) of hydrogen in electrophilic arenes by stable carbanions **5** (Scheme 2), and is exploited in a number of important synthetic applications. In contrast with the previous mechanism in Scheme 1, no direct interaction between the carbanionic species and the nitro group takes place in this reaction. Furthermore, whereas the addition of unstabilized Grignard reagents was shown by Bartoli to proceed, at least partially,[2] through single-electron transfer (SET) and radical–anion coupling, polar effects play a major role in VNS (Scheme 2), since solvation has profound influence on the orientation. Carbanions, not free radicals, add to the ring and, therefore, direct nucleophilic addition accounts for the formation of the σ adduct **6**.

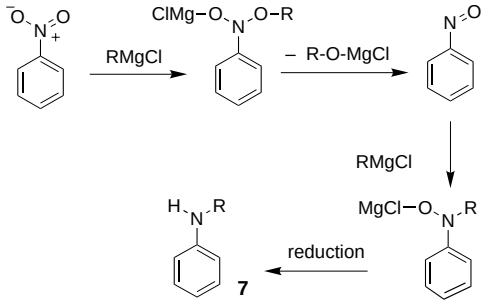


Scheme 2. Vicarious nucleophilic substitution of hydrogen in nitroarenes, according to Mąkosza et al.[3] The reaction is aided by the electron-withdrawing property of the SO_2Ph group.

[*] Prof. Dr. A. Ricci, Dr. M. Fochi
Dipartimento di Chimica Organica
"A. Mangini"
Facoltà di Chimica Industriale
Università di Bologna
Via Risorgimento N°4
40136 Bologna (Italy)
Fax: (+39) 051-209-3635
E-mail: ricci@ms.fci.unibo.it

 © 2003 Wiley-VCH Verlag GmbH & Co. KGaA, Weinheim DOI: 10.1002/anie.200201618

Other investigations based on the use of Grignard reagents have led to reactions with different results, brought about by changing the carbanionic moiety from unstabilized alkyl carbanions to their stabilized aryl counterparts. In fact, PhMgX and related compounds[4] predominantly give hydroxylamines through a 1,2-addition process. These products can be subsequently reduced to the corresponding secondary amines **7** (Scheme 3). However, no firm mechanistic conclusions have been made regarding the reactions of PhMgX.



Scheme 3. Mechanism of the reaction between aryl Grignard reagents and nitroarenes.[4] R = aryl.

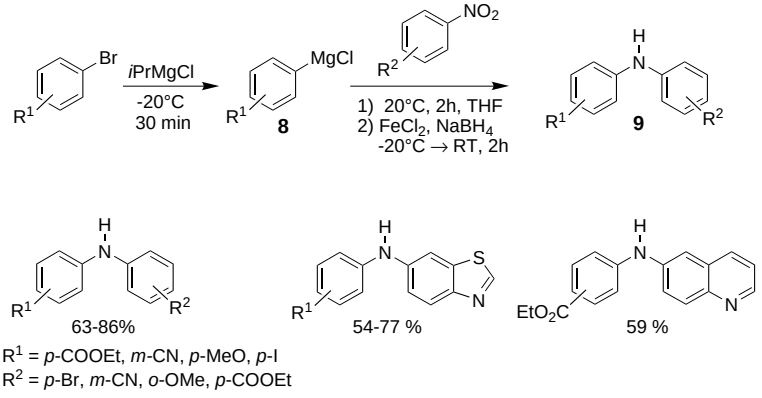
Such reactions have been extensively investigated in the past, but a preparative synthesis of diarylamines **9** has not resulted from these studies, and the possibility of performing a reaction between aromatic nitrogen compounds with N in a higher oxidation state and organometallic reagents, aimed at the formation of a C–N bond, has remained an unanswered question for a long time. Very recently however, a major breakthrough has been made[5] as a result of the chemistry of Knochel et al., which has focused on highly functionalized Grignard reagents.[6] This reaction (Scheme 4) could be applied to many functionalized aryl magnesium reagents **8**, and to nitroarenes that bear reactive functional groups. It relies on previous mechanistic studies[4] that indicate the necessity of a reductive work-up of the poorly stable intermediate hydroxylamino derivative.

The importance of this reaction stems from the fact that amination is among the most investigated reactions in organic chemistry, and in the past few years, significant advances have occurred in the development of cross-coupling methodologies.[7] This is at least partly because of the importance and practicality of amination reactions as a tool for obtaining target compounds. The prominence of aryl and diarylamines in medicinal, agricultural, and natural product chemistry, as well as in the pharmaceutical industry, is now fully acknowledged. The use of organometallic complexes, either as catalysts or reagents, is common to much of the novel and highly efficient amination methods that have been developed over the last ten years. Among such processes, C–N bond-forming reactions that involve the cross-coupling of amines with aryl halides, and that are catalyzed by palladium, copper, or nickel, have proved to be particularly challenging.[8] Oxidative coupling procedures between boronic acids and amines, mediated by Cu^{II} salts[9] or involving preformed copper amides[10] are also effective. In all of these approaches, however, amines are always used as precursors.

On first inspection, the route devised in Scheme 4 appears both simple and promising, and nicely complements the catalytic approaches used by the research groups of Hartwig[7a] and Buchwald[8] for the generation of diarylamines. However, as is often the case in the rather subtle science of organic synthesis, both systems present, besides obvious advantages and wide applicability, some obstacles. In the Hartwig–Buchwald system, the choice of the ligand and of the base is crucial and their effect is not always predictable, while for Knochel's novel arylation of functionalized aromatic or heterocyclic nitro derivatives to yield amines, the excess of organometallic reagents involved in the process makes this reaction a poor atom-economical process.[11]

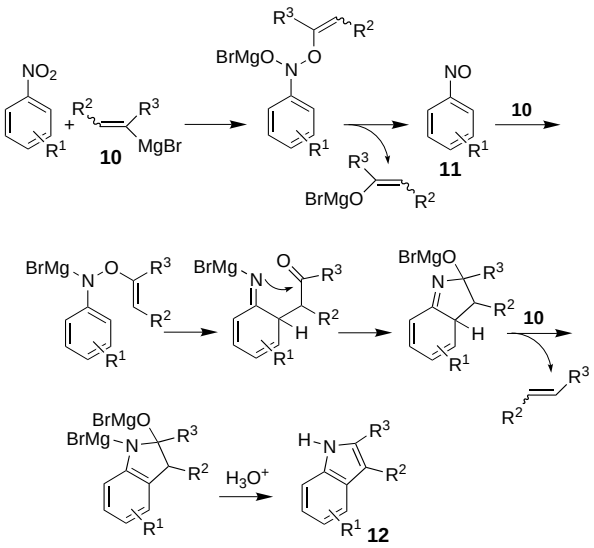
Another diverse outcome in these reactions can be observed when vinyl magnesium reagents are used. In 1989,[12] Bartoli et al. described the reaction of vinylmagnesium bromide with nitroarenes (3:1 molar ratio), which led to the formation of indoles in satisfactory yields, after an aqueous work-up of the reaction mixture. Further work[13] allowed for the elucidation of the mechanism of this reaction (Scheme 5). First, a molecule of Grignard reagent adds to the oxygen atoms of the nitro group, followed by decomposition of the unstable O-alkylated product to give nitrosoarene **11**. This compound reacts with vinyl reagents much more rapidly than the parent nitroarene, and undergoes both normal and inverse addition to form *N*-aryl-*N*-vinylhydroxylamino and *N*-aryl-*O*-vinylhydroxylamino magnesium salts, respectively. The latter compound ultimately affords indoles **12** by a [3,3] sigmatropic rearrangement, analogous to the venerable Fischer indolization.[14]

Interest in this reaction, frequently reported as the "Bartoli reaction" and which has rapidly become the shortest and most flexible synthesis for 7-substituted indoles, is raised by the fact that the indole ring system is present in many natural products, in pharmaceuticals, and in agrochemicals. Thus, there is a



Scheme 4. Preparation of polyfunctional diarylamines **9** by the addition of functionalized aryl magnesium compounds **8** to nitroarenes, according to Knochel et al.[5]

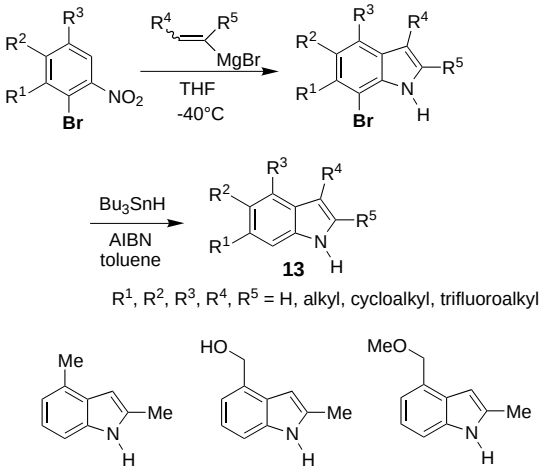
 © 2003 Wiley-VCH Verlag GmbH & Co. KGaA, Weinheim



Scheme 5. Mechanism of the formation of indoles **12** in the Bartoli reaction.[12]

This short overview reminds us that the traditional synthetic chemist can often be relied on to call on his or her untapped potential for discovering hidden treasures. So far, the combined chemistry of nitroarenes and Grignard reagents can be exploited as a flexible tool for facing synthetic challenges of great applied importance. The search for new targets and, to a greater extent, the use of these methods in preparative organic chemistry, will be closely related in the near future to the novel options that revisited organomagnesium chemistry will be able to offer.

continuous quest for efficient synthetic methods towards indole derivatives.[15] However, as a synthetically useful procedure, the Bartoli method is restricted to aromatic nitro compounds that bear an *ortho* substituent. Perhaps the most attractive variant of this approach, which suggests that it may not be limited exclusively to the synthesis of 7-substituted indoles, lies in the combination of the Bartoli protocol and a heteroaryl radical pathway (Scheme 6).[16] Accordingly the bromine atom in the 7-position acts as a transient group that enforces selectivity in the [3,3] sigmatropic rearrangement, and can be easily removed with tributyltin hydride to give the 7-unsubstituted indoles **13**.



Scheme 6. Utilization of bromine as a transient group in the selective preparation of 7-unsubstituted indole alkaloids **13**, according to Dobbs.[16]

[1] V. Grignard, *Ann. Chim.* **1901**, *24*, 433–490.

[2] G. Bartoli, *Acc. Chem. Res.* **1984**, *17*, 109–115.

[3] M. Mąkosza, J. Winiarski, *Acc. Chem. Res.* **1987**, *20*, 282–289.

[4] a) Y. Yost, H. R. Gutmann, C. C. Muscoplat, *J. Chem. Soc. C* **1971**, 2119–2122; b) G. Bartoli, M. Bosco, G. Cantagalli, R. Dalpozzo, *J. Chem. Soc. Perkin Trans. 2* **1985**, 773–779.

[5] I. Sapountzis, P. Knochel, *J. Am. Chem. Soc.* **2002**, *124*, 9390–9391.

[6] For reviews, see: a) M. Röttlander, L. Boymond, L. Berillon, A. Lepretre, G. Varchi, S. Avolio, H. Laaziri, G. Queguiner, A. Ricci, G. Cahiez, P. Knochel, *Chem. Eur. J.* **2000**, *6*, 767–770; b) G. Varchi, A. E. Jensen, W. Dohle, A. Ricci, G. Cahiez, P. Knochel, *Synlett* **2001**, 477–480; c) A. E. Jensen, W. Dohle, I. Sapountzis, D. M. Linsday, V. A. Vu, P. Knochel, *Synthesis* **2002**, 565–569.

[7] a) *Modern Amination Methods* (Ed.: A. Ricci), Wiley-VCH, Weinheim, **2000**; b) P. Dembech, G. Seconi, A. Ricci, *Chem. Eur. J.* **2000**, *6*, 1281–1286.

[8] a) A. Klapars, J. C. Antilla, X. Huang, S. L. Buchwald, *J. Am. Chem. Soc.* **2001**, *123*, 7727–7729; b) J. P. Wolfe, S. Wagan, J.-F. Marcoux, S. L. Buchwald, *Acc. Chem. Res.* **1998**, *31*, 805–818.

[9] a) J. C. Antilla, S. L. Buchwald, *Org. Lett.* **2001**, *3*, 2077–2079; b) P. Y. S. Lam, S. Deudon, K. M. Averill, R. Li, M. Y. He, P. DeShong, C. G. Clark, *J. Am. Chem. Soc.* **2000**, *122*, 7600–7601.

[10] A. Alberti, F. Canè, P. Dembech, D. Lazzari, A. Ricci, G. Seconi, *J. Org. Chem.* **1996**, *61*, 1677–1681.

[11] B. M. Trost, *Angew. Chem.* **1995**, *107*, 285–307; *Angew. Chem. Int. Ed. Engl.* **1995**, *34*, 259–281.

[12] G. Bartoli, G. Palmieri, M. Bosco, R. Dalpozzo, *Tetrahedron Lett.* **1989**, *30*, 2129–2132.

[13] a) M. Bosco, R. Dalpozzo, G. Bartoli, G. Palmieri, M. Petrini, *J. Chem. Soc. Perkin Trans. 2* **1991**, 657–663;b) G. Bartoli, M. Bosco, R. Dalpozzo, G. Palmieri, E. Marcantoni, *J. Chem. Soc. Perkin Trans. 1* **1991**, 2757–2761.

[14] B. Robinson, *The Fischer Indole Synthesis*, Wiley-Interscience, New-York, **1982**.

[15] a) R. J. Sundberg, *Indoles*, Academic Press, San Diego, **1996**;b) G. W. Gribble, *J. Chem. Soc. Perkin Trans. 1* **2000**, 1045–1075.

[16] A. Dobbs, *J. Org. Chem.* **2001**, *66*, 638–641.

 © 2003 Wiley-VCH Verlag GmbH & Co. KGaA, Weinheim

Gene Transfection Agents

Gemini Surfactants: New Synthetic Vectors for Gene Transfection

Anthony J. Kirby, Patrick Camilleri, Jan B. F. N. Engberts, Martin C. Feiters, Roeland J. M. Nolte, Olle Söderman, Mark Bergsma, Paul C. Bell, Matthew L. Fielden, Cristina L. García Rodríguez, Philippe Guédat, Andreas Kremer, Caroline McGregor, Christele Perrin, Gaël Ronsin, and Marcel C. P. van Eijk*

Keywords:
DNA · drug delivery · gene therapy · surfactants · transfection

The superior surfactant properties of cationic gemini surfactants are applied to the complex problem of introducing genes into cells. Of almost 250 new compounds tested, of some 20 different structural types, a majority showed very good transfection activity in vitro. The surfactant is shown to bind and compact DNA efficiently, and structural studies and calculations provide a working picture of the "lipoplex" formed. The lipoplex can penetrate the outer membranes of many cell types, to appear in the cytoplasm encapsulated within endosomes. Escape from the endosome—a key step for transfection—may be controlled by changes in the aggregation behavior of the lipoplex as the pH falls. The evidence suggests that DNA may be released from the lipoplex before entry into the nucleus, where the new gene can be expressed with high efficiency.

[*] Prof. A. J. Kirby, Dr. P. Guédat, Dr. C. McGregor, Dr. G. Ronsin
University Chemical Laboratory
Cambridge CB2 1EW (UK)
Fax: (+44) 1223-336-362
E-mail: ajk1@cam.ac.uk

Dr. P. Camilleri, Dr. A. Kremer, Dr. C. Perrin
Glaxo-SmithKline Pharmaceuticals
Science Complex 1, New Frontiers Science Park North
Third Avenue, Harlow, Essex CM19 5AW (UK)

Prof. J. B. F. N. Engberts, M. Bergsma, Dr. P. C. Bell, Dr. M. L. Fielden
Department of Chemistry, University of Groningen
Nijenborgh 4, 9747 AG Groningen (The Netherlands)

Dr. M. C. Feiters, Prof. Dr. R. J. M. Nolte, Dr. C. L. García Rodríguez
Department of Organic Chemistry, University of Nijmegen
Toernooiveld 1, 6525 ED Nijmegen (The Netherlands)

Prof. O. Söderman, Dr. M. C. P. van Eijk
Division of Physical Chemistry 1
Chemical Center, University of Lund
P.O.B. 124, 22100 Lund (Sweden)

1. Introduction

This Minireview describes an extensive interdisciplinary investigation of gemini surfactants as vectors for gene transfection in vitro. It reflects a highly successful collaboration involving five independent groups from three European countries.[1] The long-term objective is the development of synthetic vectors for gene therapy, which in its simplest form requires the introduction of a missing or defective gene into the cell nucleus. It is known that some cationic surfactants can support transfection, and that gemini surfactants possess superior surfactant properties. We find that geminis are also—in many cases—superior transfection agents.

1.1. Gemini Surfactants

Gemini surfactants[2] are a relatively new class of amphiphilic molecules containing two head groups and two aliphatic chains, linked by a rigid[3] or flexible[4] spacer, as illustrated in Figure 1. They typically show greatly enhanced surfactant properties relative to the corresponding monovalent (single chain, single head group) compounds—surface activity can be increased 1000-fold. This makes them of special interest for biological and especially biomedical applications, where it is

 © 2003 Wiley-VCH Verlag GmbH & Co. KGaA, Weinheim DOI: 10.1002/anie.200201597

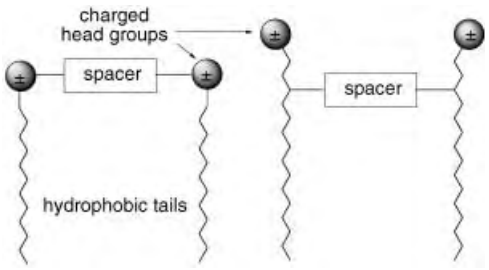


Figure 1. The basic structure of gemini (twinned) surfactants.

essential to optimize the safety profile of any foreign compound: the first and simplest step is to minimize its concentration in vivo. Since using less compound to achieve the same effect also has clear economic advantages, recent years have seen a rapidly growing number of patents describing a whole range of applications of gemini surfactants.

1.2. Gene Therapy and Transfection

The simplest form of gene therapy involves the introduction of a missing or defective gene into the cell nucleus. Once in place it can be expressed, using the natural machinery of the cell, to produce proteins needed to correct a specific pathological condition. A major problem for the routine use of gene therapy in the treatment of disease is the efficient introduction of DNA into the cell nucleus (transfection). The research effort in this field is correspondingly intense.[5–8]

There is broad agreement[9] that the most significant barriers to efficient transfection are the cell and nuclear membranes, and there is intense interest in the development of practical techniques that will allow DNA to cross these membranes. Potentially the most promising approach involves chemical or biological modification, or packaging, of the genetic material. Currently the most efficient method is the incorporation of therapeutic DNA into engineered viruses,[10–12] which have the inherent advantage of specific biological "keys" that allow them passage across the various membranes and into the nucleus. However, their DNA carrying-capacity is limited, and a cloud hangs over their therapeutic use, because of their unpredictable immune response and concerns about safety.[13,14] As a result the search for alternative vectors has intensified.



Tony Kirby studied chemistry at the University of Cambridge, where he obtained his PhD in 1962. He then spent a postdoctoral year with William P. Jencks at Brandeis University. He has been coordinator of three European networks on catalytic antibodies (1993–1996), gemini surfactants (1997–2001), and artificial nucleases (2000–2004). He retired in October 2002 as Professor of Bioorganic Chemistry at the University of Cambridge, and he is now free to concentrate on research and on some exciting new collaborations, most recently in Brazil.

2. The Delivery Problem

Gene transfection can be regarded as a special problem in drug delivery. It is typically dependent on such factors as solubility (which will be pH-dependent for ionizable compounds), how the drug is transported through the system, how long it survives before it is metabolized, and how easily it can penetrate various physical barriers. It is special in that the "drug" to be delivered is a specific piece of DNA, with success depending absolutely on effective penetration of the cell and nuclear membranes. The problems are illustrated schematically in Figure 2.

2.1. Steps Leading to Transfection and Protein Expression

The essential first step is the complexation and consequent compaction (Section 4.2) of the nucleic acid polyanion by the cationic surfactant (Figure 2, step 1). In the absence of a suitable vector no significant level of transfection is observed. This step is discussed in detail in Section 4.3 in the light of our new results, which show that lipoplexes are readily formed from gemini surfactants with various forms of DNA (and RNA), at lower than critical aggregation concentrations of surfactant.

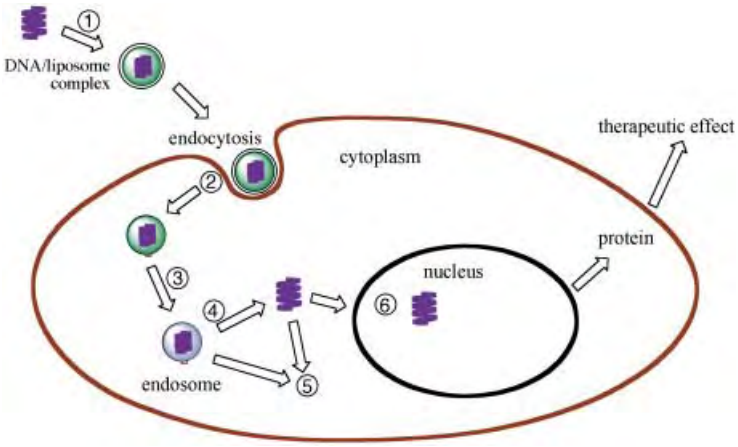


Figure 2. Simplified summary of the key steps involved in liposome-mediated transfection, leading to the expression of a new protein. (Steps 1–6: see text for details.)

The initial passage through the cell membrane mediated by synthetic surfactants is presumed to occur by endocytosis (Figure 2), as demonstrated by Zabner et al. using electron microscopy.[15] Endocytosis involves a controlled invagination of the cell membrane, allowing the DNA/liposome complex to be enveloped by the cell membrane. The membrane then "buds off" (step 2) to form a new vesicle inside the cell. Such vesicles can combine to form endosomes (step 3), which develop increasingly powerful hydrolytic capabilities, with the internal pH falling sharply, until they eventually merge with lysosomes. Only a fraction of the complexed DNA escapes from the endosome: the rest is eventually digested either in the late endosome or after fusion with a lysosome. (Lyso-

 © 2003 Wiley-VCH Verlag GmbH & Co. KGaA, Weinheim

somes deploy powerful acid hydrolases—nucleases, peptidases, glycohydrolases, etc.—to provide an efficient recycling capability.) DNA within the liposome complex is protected from nuclease action, but will inevitably be degraded unless it is released from the endosome, perhaps still complexed to the vector. This key step (4) is discussed in detail in Section 4.4. Release of the DNA from the DNA/liposome complex presumably occurs at or before this stage because passage through the nuclear membrane (step 6) appears—at least from the circumstantial evidence from our systems—to involve uncomplexed DNA (see Section 3.2). Passage through the nuclear membrane has to compete with the rapid degradation of uncomplexed DNA by cytoplasmic nucleases (step 5).

Thus the strategic points at which vector design can be expected to have significant effects on the efficiency of gene delivery are the formation of the lipoplex (Figure 2, step 1), its passage through the cell membrane (step 2), and the release of the lipoplex from the endosome and its subsequent dissociation (step 4). These processes are discussed in Section 4.

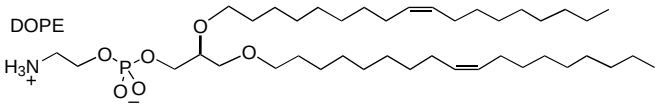
2.2. Principles of Vector Design

Essential requirements for a vector are thus that it should bind DNA sufficiently strongly and rapidly, readily penetrate the target cell and perhaps its nucleus, and eventually release DNA from the lipoplex inside the target cell at the right time and in the correct place. It should also be nontoxic, nonimmunogenic, and biodegradable, though it must be reasonably stable in biological fluids to survive long enough to carry out its functions. The first, key step in the whole process (Figure 2, step 1) is the compaction of the extended, high-molecular-mass, negatively charged DNA into a dense, positively charged (possibly neutral) particle small enough to be taken up by the cell. This generally requires a chemical species bearing multiple positive charges to replace the monovalent counterions of DNA. (Something as simple as calcium phosphate has been used,[16] but gives very low transfection efficiency.)

Many macromolecular and supramolecular systems have been developed to carry the positive charge. These include cationic polyelectrolytes such as DEAE-dextran,[17] polylysine,[18,19] polyethyleneimine,[20] polynorbornane,[21] and polyamine dendrimers.[22,23] The supramolecular systems of particular interest are those that form amphiphile aggregates, most commonly liposomes (or vesicles).[8] Synthetic cationic surfactants are involved in 18% of current clinical trials based on gene therapy, and this proportion increases year by year.[24]

Cationic amphiphiles can compact and stabilize DNA by a combination of attractive electrostatic interactions and hydrophobic interactions between the apolar hydrocarbon tails.[25] The DNA in the aggregate (lipoplex) is protected from endogenous nucleases, while the hydrophobic elements of the aggregate may also promote escape from the endosome by fusion or aggregation with the endosomal membrane.

This step—escape from the endosome—appears to be a major obstacle to efficient transfection using these multivalent cationic vectors, since generally only a small fraction of the compacted DNA escapes (the rest being digested in the lysosome). Various methods have been devised to promote endosomal escape, in particular the use of additional "helper lipids" such as DOPE that are capable of changing the



morphology of the lipoplex from vesicular to inverted hexagonal in the endosome, and thus the interaction with the endosomal membrane. The similarities between these structures and some of the amphiphilic transfection agents discussed below suggest that suitable compounds could play both roles, dispensing with the need for additional helper lipids.

3. Application of Gemini Surfactants

We have developed a new class of transfection agents, designed to combine the cationic character necessary for binding and compacting DNA, with the superior surface activities of gemini surfactants.[26,27] In the basic design (Figure 1) the central "spacer" bears pairs of identical long-chain hydrophobic tails and cationic head groups derived from positively charged α-amino acids and/or amine-linked carbohydrates. All three components are based on natural metabolites, to minimize potential problems with toxicity. The design allows an enormous range of structural variation.

This basic structure offers several opportunities to take advantage of the "chelate effect",[28] by which multiple binding interactions can deliver binding constants and derived effects much greater than the sum of individual binding interactions. (The general principle operates in many different systems, ranging from metal-ion binding and intramolecular reactions to antibiotic activity.[28,29]) Our basic design proved to be remarkably successful: of some 250 new compounds with the basic structure shown in Figure 1 the majority (Figure 3) showed good to very good activity in standard in vitro transfection assays. Thus it is of great interest to identify the structural, physicochemical, and pharmacological factors that are responsible for this activity.

3.1. Structures

The basic gemini design (Figure 1) lends itself to an almost unlimited range of potential structures (we have made and tested only some 20 different structural types), allowing extensive structure–activity studies aimed at identifying features necessary for optimum transfection activity. The central spacer can be derived from any available system with twofold symmetry, or can be custom-made by linking together two molecules of interest. To minimize potential problems

 © 2003 Wiley-VCH Verlag GmbH & Co. KGaA, Weinheim

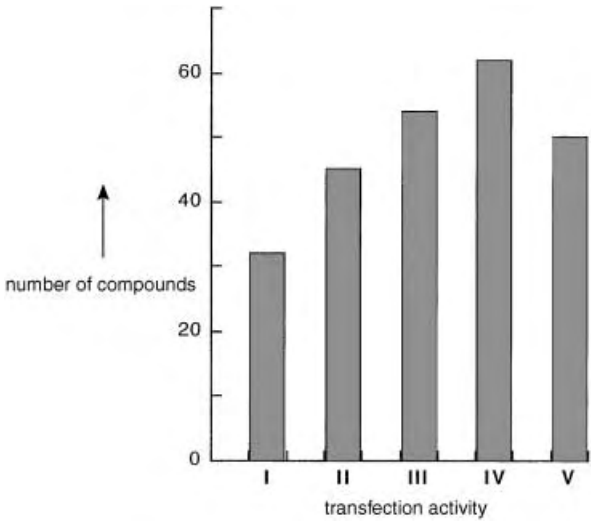


Figure 3. *In vitro* transfection activities of all gemini surfactants produced in this investigation. Activities are defined in broad ranges, from I (low) to V (very high). See text for details.

with toxicity our structures are based on naturally occurring subunits—fatty acids, α-amino acids, lipids, and carbohydrates—to make them generally readily biodegradable. Carbohydrate-based systems are of special interest for potential cell targeting.

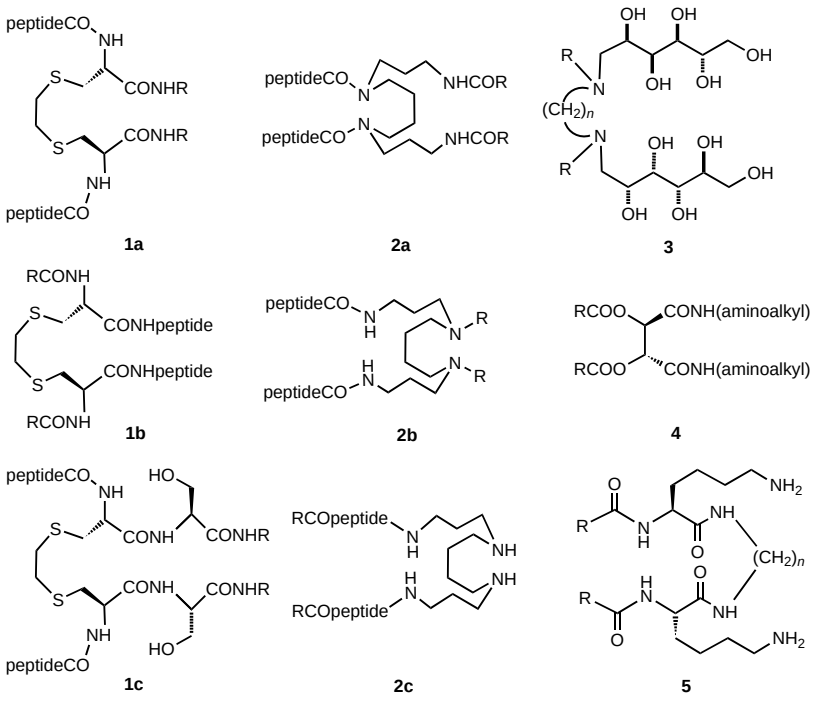
Of the twenty different systems, five were investigated in more depth (Scheme 1): gemini vectors **1** (based on a synthetic cysteine dimer),[30] **2** (based on spermine), **3** and **5** (based on simple symmetrical diamines), and **4** (derived from symmetrical dicarboxylic acids). The polar head groups are in most cases oligopeptides based on naturally occurring α-amino acids, though some of the most effective transfectants are those with amine-linked carbohydrate-based head groups. The hydrophobic tails are derived from naturally occurring fatty acids. Simple changes of connectivity allow two or more series of structures based on each spacer, and these can be multiplied by including branching points based, for example, on α-amino acids such as lysine, with functionality in the side chain. Potential future developments include the use of head groups or spacers designed to bind selectively to cell-surface receptors, and of structural features introduced to control the release of gemini–DNA complexes from the endosome following endocytosis.

3.2. Structure–Activity Correlations

The assisted path of a gene from outside an organism to the nucleus of a particular cell depends on so many variables that simple relationships between transfection efficiency and vector structure are not to be expected. Experimental investigations typically use relatively simple systems, working in vitro with cell lines known to be easy to transfect, and genes coding for proteins that are not native and thus readily detected. The most effective vectors at this level can then be challenged with more testing systems: those that show most promise will make the much bigger jump to in vivo trials. The most effective vectors in vitro of the many gemini structures summarized in Scheme 1 are now reaching the in vivo stage.

For an efficient primary measure of transfection efficiency we developed a 96-well-plate assay, using a luciferase reporter gene.[31] This assay is both convenient and sensitive, with no background in normal animal cells. Levels of transfection were classified into five broad groups, ranging from I (no activity) to V (most active). (Activities are based on a minimum of eight parallel runs for each compound. These biological systems do not give the high reproducibility familiar to most physical scientists, and our comparisons of activity in plasmid DNA delivery by our gemini surfactants are deliberately based on this broad classification scheme.) To allow informed comparisons with results obtained in other laboratories with other types of vectors, we routinely ran parallel "control" experiments with the commercial nonviral transfection agent lipofectamine 2000/+. (These agents fall in the middle of class V of active transfectants in our experiments.)

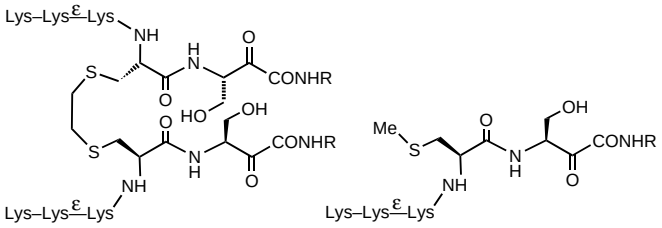
The most striking effect is the greatly enhanced activity afforded by the complete gemini surfactant structure. Systems such as **6** with oligolysine head groups including one or



Scheme 1. Structural features of the main classes of gemini surfactants showing excellent gene transfection efficiencies. The R groups are generally long hydrocarbon chains (C_{12}–C_{18}), though in a few cases also steroidal. Structure **3** contains a reduced glucose head group: variants with two of the methylene groups in the spacer replaced by oxygen atoms show particularly high gene-transfer efficacy.

 © 2003 Wiley-VCH Verlag GmbH & Co. KGaA, Weinheim

more ε linkages (as opposed to the natural peptide α linkages) are among the most active transfection agents of their type (Scheme 2, R = oleyl). Activity disappears almost completely for the surfactant monomer **7**, and similarly for the compound **6** (R = methyl), which lacks the long aliphatic



6 **7**

Scheme 2. Structure of compounds **6** and **7**. R is defined under Scheme 1.

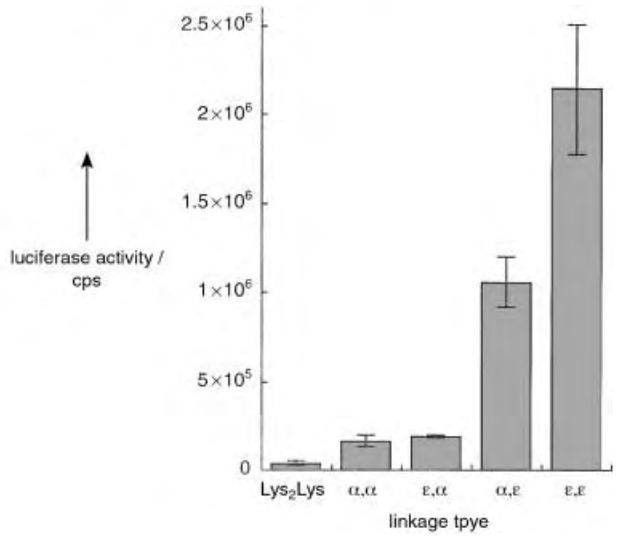


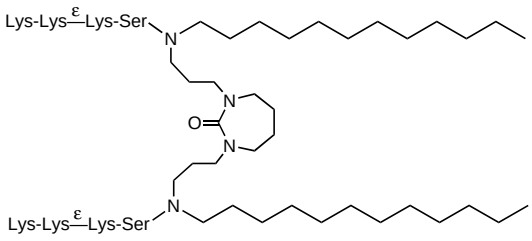
Figure 4. Effect of varying trilysine linkage; data are shown for compounds (e.g. **6**) with an oleyl (C18) side chain.

chain that makes it amphiphilic. All three compounds have the hydrophobic chain linked through a serine residue. This effective extension of the spacer was found empirically to improve transfection activity. Similarly, in most, but not all, series of geminis the oleyl chain R gives the highest activity.[32]

The widest scope for structural variation lies in the polar head group (Scheme 1). Of special interest are oligopeptide sequences corresponding to nuclear localization signals (NLS), which offer a key to allow much larger molecules to be transported through nuclear membranes. We find that typical NLS sequences offer no advantage over the best, shorter peptide sequences in our systems **2** based on spermine and conclude that—at least in the systems tested—the lipoplexes involved in the initial stages of the delivery process (Figure 2) have dissociated before the (presumably unassisted) passage of the DNA through the nuclear membrane.

We found another clear-cut correlation in the cysteine-based series **1a** when the hydrophobic chain R is the preferred oleyl group and the peptide head group is varied. As a general rule lysine is the preferred basic α-amino acid when compared with histidine and arginine; we found no advantage in using units longer than a tetrapeptide. Three lysine units can be attached to an amino group in five different ways, and we found a strong dependence on the connectivity, and thus the spacing, of the positive charges along the trilysine chain (Figure 4).

It should be emphasized that such well-defined correlations are the exception rather than the rule, even when closely similar structures are compared. Selected examples of all the main classes of gemini surfactant structures shown in Scheme 1 support highly efficient transfection, but a wide range of activities is found in all series (Figure 3). Apparently minor changes in structure can have major effects on biological activity. Thus compound **8**, based on cyclospermine with the head group Lys-Lys-ε-Lys-Ser (that is, with one ε linkage between the inner two lysine units), is one of the most active gemini transfectants, whereas the corresponding structure with *both* lysine units ε-linked (the optimal combination in systems **1a**, as indicated in Figure 4) is one of the



8

least active. Similarly, compound **5** (RCO = oleyl, $n = 6$) based on a hexamethylenediamine spacer is highly active in transfection, whereas the same structure with a saturated 18-membered chain is inactive. The generally (but not invariably) superior properties of the oleyl tails confer good (class IV) activity on the otherwise inactive system with $n = 4$. Notably, the oleyl chains in the natural, commercially available amine and alcohol are a mixture of geometrical isomers, *cis*/*trans* ≈ 80:20. We made the compounds **1a** (R = oleyl, peptide = ε-linked trilysyl), based on one of the most effective transfection agents, with exclusively *cis* and *trans* double bonds, and found no significant difference in activity compared with various mixtures of isomers.

The unsurprising but unhelpful conclusion is that the complex series of processes involved in transfection involve multiple interactions, which depend on the unique, combined effects of the head group, spacer, and hydrophobic tail of a particular vector. Clear-cut structure–activity relationships are thus not generally to be expected, except perhaps in series involving minor changes in a single structural parameter. Of the various classes of gemini surfactant summarized in Scheme 1, structures **3** with the carbohydrate-based head groups showed the highest activity: the majority of these compounds showed very high activity and all showed at least some activity (Figure 5). However, high activity was observed in at least some cases in almost all the series tested.

 © 2003 Wiley-VCH Verlag GmbH & Co. KGaA, Weinheim

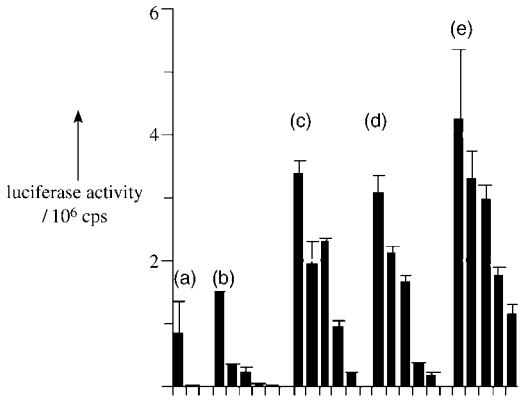


Figure 5. Transfection efficiencies (for luciferase expression in CHO cells) of a series of cationic gemini surfactant vectors, compared with lipofectamine 2000 (a). The surfactants tested were glucosyl derivatives **3** with $n = 6$ (b) and with a -$(CH_2)_2O(CH_2)_2O(CH_2)_2$- spacer (c). The results for the corresponding two mannosyl derivatives are shown in (d) and (e). (Gemini surfactant concentrations: 4, 8, 10, 20, and 30 μM).

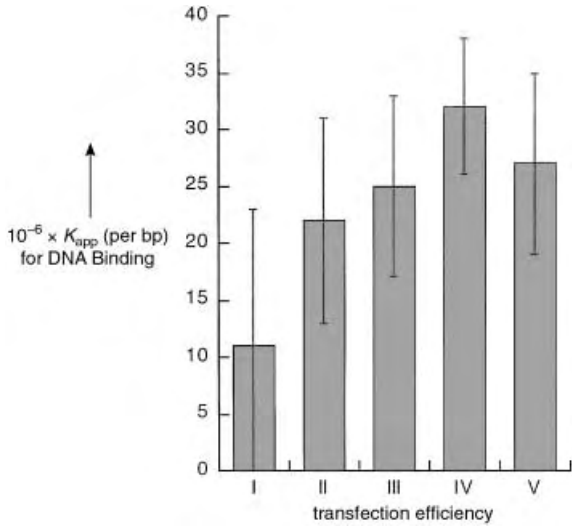
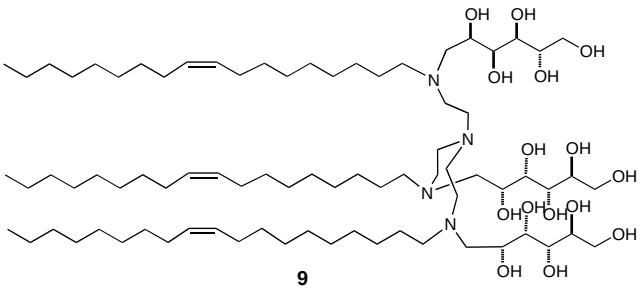


Figure 6. Relationship between transfection efficiency and the strength of DNA binding for 46 gemini surfactants with the general structure **1**.[34]

Since gemini surfactants are generally much more efficient transfection agents than the corresponding monomeric structures, a key basic question is whether the effectiveness of the gemini structure can be improved further by increasing the multiplicity of the structural elements. We have no comprehensive answer to this question, but tests on two compounds based on the most reliable carbohydrate-based structure **3** proved decisively negative. Thus both compound **9** and the corresponding system with saturated C_{16} chains showed no significant transfection activity.



9

4. Structure of the Lipoplex

Of the complex series of noncovalent interactions involved in transfection only the first, the formation of the lipoplex, can be readily studied in isolation. We can measure the strength of the binding of DNA and examine the structures of the aggregates formed by the surfactant in the presence and in the absence of DNA. Subsequently, we attempt to relate this information to the transfection process and thus to apply it to the design of improved vectors.

4.1. DNA Binding and Transfection Activity

We know that the efficiency of transfection is not likely to show a simple dependence on the strength of DNA binding by the amphiphile. The initial binding process must be strong enough for the lipoplex to form rapidly and to survive the subsequent passage through various solutions and membranes. Yet it must also eventually dissociate efficiently, presumably at or after the point of release from the endosome, thus the binding must not be too strong. A series of measurements on 46 compounds with general structure **1** (Scheme 1) gave results consistent with this picture (Figure 6). The binding constants, in the order of 10^7 per base pair, are clearly lower for less efficient vectors, but this trend of efficiency increasing with the binding constant is not maintained for the most efficient transfectants, consistent with the idea that there is an optimal level of binding.[34]

4.2. Aggregation States

To complement the synthetic and transfection studies, the aggregation behavior of selected surfactants was investigated by physical and calculation methods. Although gemini surfactants are active in transfection at well below typical aggregation concentrations, their aggregation behavior must be at least indirectly relevant to lipoplex formation. In practice aggregation behavior observed by transmission electron microscopy (TEM) generally shows no clear correlation with transfection efficiency. An interesting exception is a series of compounds with the general structure **1c** (Scheme 1), with saturated tails (R = dodecyl) linked to the cysteine-based spacer through a serine residue, and short head groups made up of 1–3 basic α-amino acids. Five compounds with this structure all bound DNA well, but the two with single α-amino acids as head groups were poor transfectants. These two formed characteristic fibrillar aggre-

 © 2003 Wiley-VCH Verlag GmbH & Co. KGaA, Weinheim

gates when absorbed from water onto carbon/Formvar-coated grids, whereas the three highly active compounds with di- or tripeptide head groups did not.[35] More typically, the series of tartaric acid based gemini transfectants **4**, compounds of moderate transfection efficiency studied by TEM, formed variously short ribbons, ribbons with a tendency to twist, or no aggregates at all.[27]

For the same series of compounds **4**, a circular dichroism titration with λ-phage DNA showed that the gemini surfactant:DNA stoichiometry in the lipoplex is dictated by charge complementarity.[31] A more detailed CD study suggests that the immediate hydration shell in the region of the backbone phosphate groups is not significantly changed on complexation.[27] Conductivity studies showed that some of these compounds have very low critical aggregation concentrations ($\leq 0.24\ mol\,m^{-3}$).[36] The compaction of DNA by cationic gemini surfactants (or any other cationic surfactant) presumably involves an initial interaction of a small cluster of surfactant molecules with DNA (especially for compounds with singly charged head groups). Further interactions, strengthened by the combined (chelate) effect of electrostatic and hydrophobic attraction, enhance compaction even more. This process will depend on some of the same factors as self-association and should thus be favored by a low critical aggregation concentration.

The interaction of a range of cationic gemini surfactants with bacteriophage T4 DNA was studied by means of fluorescence microscopy.[36] Upon addition of surfactant, the DNA undergoes a transition from a random coil to a globule with an intermediate coexistence region. The state behavior of a DNA–gemini surfactant system depends on spacer length, valency, head group size, and tail length. A series of simple alkanediyl-α,ω-bis(dimethylalkylammonium bromide) gemini surfactants ($Me_2N(CH_2)_{12}NH(CH_2)_s$-$(CH_2)_{12}NMe_2$, [12-*s*-12]), with fixed tail length and variable spacer lengths, showed a minimum in compaction efficiency at $s = 6$, as a result of the competition between entropy loss and enthalpy gain. This occurs at roughly the same spacer length as a maximum (at $s = 5$) in the critical aggregation concentration. In comparison with a single-tailed divalent surfactant [12-3-1] it was shown that the gemini equivalent [12-3-12] was more efficient in compacting DNA. A series of gemini surfactants **5** based on cationic peptides with α,ω-diamino alkyl spacers showed similar behavior with changing spacer length. Additionally, two surfactants **4**, based on diastereomers of tartaric acid, with hexadecanoic acid tails and α,ω-diaminopropyl and spermidine head groups, respectively, showed effects of head group size that depended strongly on entropy effects.[36]

The most detailed studies concentrated on gemini surfactant **3** (R = oleyl, $n = 6$) because of its relatively simple molecular structure and because it is one of the most active transfection agents discovered in this study. This compound undergoes a proton-induced vesicle-to-micelle transition as the pH value is decreased to below 7. This behavior was investigated in more detail by using self-consistent-field theory and was explained in terms of significant protonation of the two amine centers in combination with the flexible sugar head groups.[37] A high-level molecular-dynamics simulation for the neutral surfactant shows a 46-Å thick bilayer with significant interdigitation of the alkyl chains (Figure 7). The dimensions of the bilayer, and the degree of interdigitation, closely match those obtained from small-angle X-ray-scattering (SAXS) experiments (Section 4.3).[37]

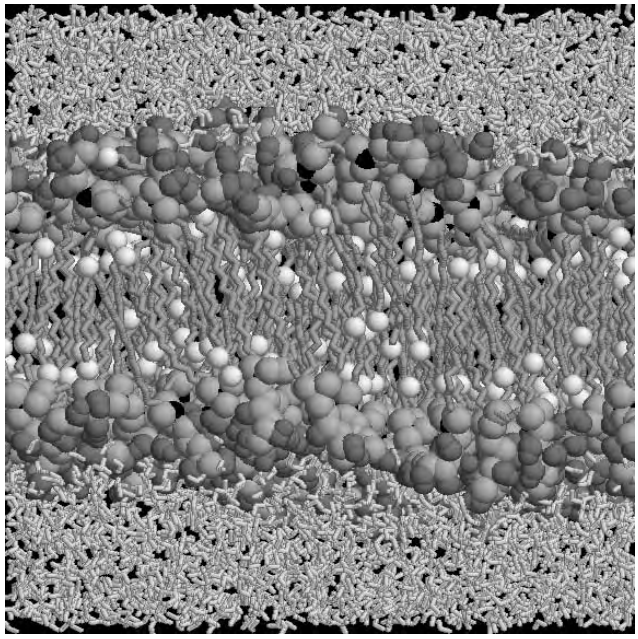


Figure 7. Molecular dynamics simulation for the neutral gemini surfactant **3** (R = oleyl, $n = 6$) in water.[36]

The morphology of the aggregates formed by compounds with the general structure **5** and of their complexes with λ-phage DNA, were also investigated by means of transmission and cryo-scanning electron microscopy (TEM and cryo-SEM).

4.3. SAXS Studies of Selected Gemini Surfactants and Lipoplexes

Selected gemini surfactants were studied as concentrated dispersions and as lipoplexes formed with salmon-sperm DNA[*].[38] All dispersions studied showed at least some long-range order, which changed on addition of DNA, although the diffraction peaks were often broad. Higher-order diffraction peaks were observed in some cases. Assignments of packing were made by using these higher-order diffraction peaks and/or correlation with the dimensions of the extended molecular structures, obtained from molecular modeling by Quanta/Charm or estimated from Corey–Pauling–Koltun (CPK) models. Selected results are shown in Table 1.

The results for most tartaric acid and lysine-based surfactants are consistent with lamellar packing, which is expanded upon binding of DNA. When the most active

[*] These experiments were carried out at the Small Angle X-ray Scattering station of the Dutch-Belgian beamline (DUBBLE) at the ESRF in Grenoble, France, with financial support from the NWO.

 © 2003 Wiley-VCH Verlag GmbH & Co. KGaA, Weinheim

Table 1: Molecular Dimensions and Packings Derived from SAXS experiments.

Compound (RCO, headgroup)	Activity	Estimated length [Å][a]	Obs. spacing/ Free surfactant	Obs. spacing/ Lipoplex
4 ($C_{15}H_{31}$, 3-aminopropyl)	I	*24*: 29 Å	lam., $d = 53$ Å	lam., $d = 64$–65 Å
4 ($C_{15}H_{31}$, lysine amide)	III	*26*: 31 Å	lam., $d = 57$ Å	?, $d = 61$ Å
5 (dodecyl, $n = 2$)	I	*19*: 23 Å	lam., $d = 36$ Å	lam., $d = 45$ Å
5 (oleyl, $n = 4$)	IV	*25*: 30 Å	lam., $d = 46$ Å	lam., $d = 52$–55 Å
5 (oleyl, $n = 6$)	V	*25*: 30 Å	lam., $d = 45$ Å	lam., $d = 52$ Å
5 (dodecyl, $n = 8$)	III	*25*: 30 Å	lam., $d = 44$ Å	lam., $d = 51$–54 Å
3 (R = oleyl, $n = 6$)	IV/V	*26*: 31 Å	lam., $d = 49$ Å	ext. lam., $d = 59$ Å
pH 7.0				cd. lam., $d = 57$ Å
pH 6.5				cd. lam., $d = 55$ Å
pH 5.5				hex., $a = 58$ Å

[a] *No. of atoms* and estimated maximum length of the molecule in its extended conformation. *lam. = lamellar; ext. = extended; cd. = condensed; hex. = hexagonal; d = lamellar spacing; a = hexagonal or columnar spacing.*

compound of this structural type **5** (RCO = oleyl, $n = 6$) was studied in more detail, it was found to exhibit temperature-dependent transitions between expanded and condensed lamellar phases.

The structure of the lipoplex formed from DNA and the sugar-based cationic gemini surfactant **3** (R = oleyl, $n = 6$), which exhibits excellent transfection efficiency, was investigated over the pH range 8.8–3.0 by both SAXS and cryo-TEM. Uniquely, three well-defined morphologies of the lipoplex were observed as the pH was reduced (Figure 8): a lamellar phase (between pH 8.80–7.97), with dimensions consistent with the molecular dynamics simulation results described above,[37] a condensed lamellar phase (from pH 7.49–6.00), and an inverted hexagonal (H_{II}) columnar phase (from pH 5.75–3.81). Molecular modeling suggested a correlation between the observed lipoplex morphologies and physical behavior, and specific structural features in the surfactant.

These results suggest that key factors for future surfactant design are: a spacer of six methylene groups, the presence of two nitrogen atoms that can be protonated in the physiological pH range, two unsaturated alkyl tails, and hydrophilic sugar head groups. Assuming that the mechanism of transfection by synthetic cationic surfactants involves endocytosis, we suggest that the efficacy of gemini surfactant **3** (R = oleyl, $n = 6$) as a gene delivery vehicle can be explained by this unprecedented observation of a pH-induced formation of the inverted hexagonal phase of the lipoplex in the endosomal pH range. This change in morphology could lead to destabilization of the endosome through fusion of the lipoplex with the endosomal wall, resulting in release of DNA into the cytoplasm.

We suppose that the acid-induced change in morphology of the lipoplex formed from **3** (R = oleyl, $n = 6$) and salmon-sperm DNA from condensed lamellar to hexagonal is driven by the close association of mostly doubly protonated surfactant molecules with the phosphate groups of the DNA. The increase in pH observed to accompany this event can be explained by the exposure and subsequent protonation of unprotonated amine groups that were initially internalized in the condensed bilayers. In earlier studies on these gemini surfactants[31,39] a proton-induced vesicle-to-micelle transition was observed and explained in terms of significant protonation of the second amine center. This would result in a greater extent of counterion association and increased hydration, leading to an increase in the head group size. Thus the formation of micelles is favored over that of bilayers, in line with the shape-structure concept.[40]

The change from a lamellar to an inverted hexagonal phase observed here for the lipoplex formed from **3** (R = oleyl, $n = 6$) requires a decrease in head-group size, and can be rationalized by a strong association between the doubly charged head group of **3** and phosphate moieties of the DNA, leading to 1) local charge neutralization and 2) dehydration of both phosphate and head groups, which results in an effective reduction in head group size. The occurrence of the morphological change at pH 5.45 is consistent with a vesicular pK_a value for **3** (R = oleyl, $n = 6$) at around this pH value. Thus we suggest that DNA is a template for the H_{II} columnar phase, a result of "specific" association of pairs of phosphate groups with the doubly charged gemini surfactant, as opposed to the "atmospheric" DNA association with the singly charged species observed in the lamellar phases. The lipoplex of **3** ($R = C_{18}H_{37}$, $n = 6$) the saturated analogue of **3** (R = oleyl, $n = 6$) does not undergo pH-induced morphological changes: it shows a lower but still good activity in transfection (class IV).

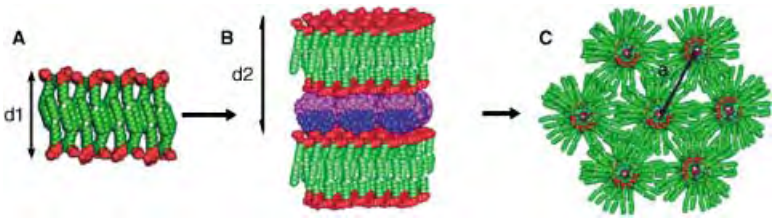


Figure 8. Space-filling molecular models of aggregates of **3** and DNA based on morphology and geometry obtained by SAXS/EM studies: a) free vesicles, d1 = 48.7 Å; b) initial lamellar phase of lipoplex, d2 = 59.8 Å; c) columnar H_{II} structure of lipoplex, $a = 57.8$ Å. Green: alkyl tails; red: sugar head groups; blue and lilac: complementary DNA strands.

© 2003 Wiley-VCH Verlag GmbH & Co. KGaA, Weinheim

4.4. Escape from the Endosome

It has been suggested that the escape of DNA from the endosome mediated by synthetic surfactants depends, in some cases at least, on the formation of a fusogenic inverted hexagonal phase.[41] This phase can be induced by the shape of the cationic surfactant molecule[42] or of a "helper" lipid,[43] or by the interaction of the lipoplex with anionic lipids.[44] The pH-induced formation of an inverted hexagonal (H_{II}) phase for the lipoplex of **3** (R = oleyl, $n = 6$) and DNA in the endosomal pH range, as evidenced by the SAXS and cryo-SEM results described, may facilitate its fusion with the endosomal membrane, an important step toward release of the DNA into the cytoplasm.

This observation of the pH-induced and DNA-templated formation of the hexagonal phase of the lipoplex led us to propose the detailed mechanism for the transfection by **3** (R = oleyl, $n = 6$) outlined in Figure 9. The initial passage through the cell membrane is presumed to be by endocytosis (Figure 2).[44a]

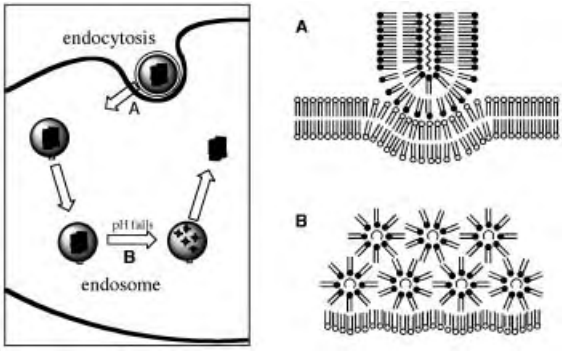


Figure 9. Proposed mechanism for transfection mediated by **3** (R = oleyl, $n = 6$) adapted from Xu and Szoka.[44a] White and black head groups represent zwitterionic/anionic membrane components and cationic gemini surfactants, respectively. **A**: onset of endocytosis of the lipoplex at the cell membrane; **B**: formation of a DNA-templated fusogenic hexagonal phase at low pH value, allowing escape from the endosome. (The Box is a section from Figure 2.)

Although it is highly significant for the mechanism of transfection that such a fundamental change in the morphology of the lipoplex can occur simply on encounter with anionic membranes, the question arises as to why it does not occur when the lipoplex interacts with either the cell or, initially, the endosomal membrane. We propose that the factor that triggers the escape of the DNA from the endosome is the gradual decrease in pH that this organelle undergoes after formation.[45] Our finding that the inverted hexagonal phase can be formed from unadulterated cationic lipids, simply by lowering the pH, is significant for the mechanism of transfection since it provides a reasonable explanation for why escape occurs from the endosome under these circumstances.

5. Summary and Outlook

1. The gemini surfactant structure, as realized in a wide range of systems based on cationic head groups, gives rise to a high proportion of compounds that show excellent activity in the transfection of a wide variety of cell types. Recent (unpublished) work has extended the scope of the process to transfection with oligoribonuceotides and to a number of cell lines that are normally difficult to transfect. These gemini surfactants generally show very low toxicity, and transfection efficiencies can be as high as 90%.
2. These compounds bind strongly to DNA, and there is evidence to support the logical conclusion that the strength of binding goes through an optimum.
3. Binding to DNA can be assumed to involve an important electrostatic contribution. The spacing between the two NH^+ centers in the most efficient transfectants (**3** (R = oleyl, $n = 6$) and **1a** (R = oleyl, peptide = ε-linked trilysyl)) of two of the most interesting series of gemini surfactants, is closely similar, at about 10 Å. This spacing of the NH^+ groups complements the spacing of the anionic phosphodiester groups on either side of the minor groove of DNA.
4. The α NH^+ groups of **1a** (R = oleyl, peptide = ε-linked trilysyl) and **3** (R = oleyl, $n = 6$) have low pK_a values (about 7.5 versus 5.8 and 8.3 in free solution), much lower than those of ε NH^+ groups, which will be fully protonated at all pH values of interest.
5. It is proposed that the key to the exceptional efficacy of **3** (R = oleyl, $n = 6$) in gene transfection is its ability to form a lamellar lipoplex, which changes to the fusogenic inverted hexagonal phase at a critical (endosomal) pH value. a) The spacing of the ammonium centers allows the DNA to template the morphology of the complex into the fusogenic inverted H_{II} columnar phase. b) The second of the two amine nitrogen atoms in the head group has a vesicular pK_a value in the endosomal pH region; its protonation causes a morphological change at a critical pH value. c) Its unsaturated alkyl chains reduce T_c (the gel to liquid crystal main phase transition temperature) to below physiological temperatures, thus increasing the susceptibility of the aggregate to morphological change. d) The hydrophilic sugar head groups increase aqueous solubility but do not obstruct localized ammonium phosphate interactions.
6. Finally, gemini surfactants can confidently be expected to show other sorts of biological activity. For example, many cationic surfactants are active bactericidal agents, and a group of gemini surfactants **2a** (Scheme 2) based on spermine with cholic acid as the hydrophobic tail turn out to be very effective against a broad range of bacteria.[46]

The insight arising from this work offers potential guidelines for surfactant and polymer design, and underlines the need to concentrate attention not just on DNA release from a lipoplex (for example, by using surfactants with chemically labile moieties), but also on the possibility of engineering morphological transformations to take place under critical cellular conditions such as pH change. Of course these are

 © 2003 Wiley-VCH Verlag GmbH & Co. KGaA, Weinheim

complex systems, but eventually rules will emerge—most likely from work with simple systems in vitro. This belief is widely held, as witnessed by the hundreds of patents appearing annually that describe the applications of cationic lysosomes to gene transfection. Much of this work tells only the beginning of the story, because structure–activity relationships in vivo and in vitro are not necessarily the same.[41c]

This work is a contribution from the European Network on Gemini Surfactants, and was supported by the European Commission as part of its Training and Mobility of Researchers (TMR) Programme.

Received: September 18, 2002 [M1597]

[1] ENGEMS—the European Network on Gemini Surfactants (1997–2001, web site www.ch.cam.ac.uk/misc/ENGEMS/)—brought together groups from the UK, the Netherlands, and Sweden under the aegis of the Framework 4 Training and Mobility of Researchers (TMR) Program of the European Commission. The compounds discussed have been patented.

[2] The name gemini was coined in 1991 by Menger, who has recently reviewed the chemistry of these remarkable compounds: F. M. Menger, J. S. Keiper, *Angew. Chem.* **2000**, *112*, 1980 – 1996; *Angew. Chem. Int. Ed.* **2000**, *39*, 1906 – 1920.

[3] F. M. Menger, C. A. Littau, *J. Am. Chem. Soc.* **1993**, *115*, 10083 – 10090; R. Zana, M. Bennraou, R. Rueff, *Langmuir* **1991**, *7*, 1072 – 1075; R. Zana, *Adv. Colloid Interface Sci.* **2002**, *97*, 205 – 253; R. Zana, *J. Colloid Interface Sci.* **2002**, *248*, 203 – 220.

[4] R. Zana, Y. Talmon, *Nature* **1993**, *362*, 228 – 230; S. Karaborni, K. Esselink, P. A. J. Hilbers, B. Smit, J. Karthauser, N. M. van Os, R. Zana, *Science* **1994**, *266*, 254 – 256.

[5] L. Felgner, T. R. Gadek, M. Holm, R. Roman, H. W. Chan, M. Wenz, J. P. Northrop, G. M. Ringold, M. Danielsen, *Proc. Natl. Acad. Sci. USA* **1987**, *84*, 7413 – 7417; D. D. Lasic, N. S. Templeton, *Adv. Drug Delivery Rev.* **1996**, *20*, 221 – 266.

[6] J.-P. Behr, *Bioconjugate Chem.* **1994**, *5*, 382 – 389.

[7] J.-Y. Legendre, F. C. J. Szoka, *Pharm. Res.* **1992**, *9*, 1235 – 1242.

[8] A. D. Miller, *Angew. Chem.* **1998**, *110*, 1862 – 1880; *Angew. Chem. Int. Ed.* **1998**, *37*, 1768 – 1785.

[9] F. Labat-Moleur, A.-M. Steffan, C. Brisson, H. Perron, O. Feugeas, P. Furstenberger, F. Oberling, E. Brambilla, J.-P. Behr, *Gene Ther.* **1996**, *3*, 1010 – 1017.

[10] A. D. Miller, *Nature* **1992**, *357*, 455 – 460.

[11] E. Marshall, *Science* **1995**, *270*, 1751.

[12] B. Abdallah, L. Sachs, B. A. Demeneix, *Biol. Cell* **1995**, *85*, 1 – 7.

[13] S. Lehrman, *Nature* **1999**, *401*, 517 – 518.

[14] H. Pearson, *Nature* **2000**, *403*, 9.

[15] J. Zabner, A. J. Fasbender, T. Moninger, K. A. Poellinger, M. J. Welsh, *J. Biol. Chem.* **1995**, *270*, 18997 – 19007.

[16] F. L. Graham, A. J. Van der Eb, *Virology* **1973**, *54*, 536 – 539.

[17] K. Ohtani, M. Nakamura, S. Saito, K. Nagata, K. Sugamura, Y. Hinuma, *Nucleic Acids Res.* **1989**, *17*, 1589.

[18] J. P. Lemaitre, B. Bayard, B. Lebleu, *Proc. Natl. Acad. Sci. USA* **1987**, *84*, 648 – 652.

[19] P. L. Felgner, *Adv. Drug Delivery Rev.* **1990**, *5*, 163 – 187.

[20] O. Boussif, F. Lezoualc'h, M. A. Zanta, M. D. Mergny, D. Scherman, B. Demeneix, J. P. Behr, *Proc. Natl. Acad. Sci. USA* **1995**, *92*, 7297 – 7301.

[21] E. Serres, P. Vicendo, E. Perez, T. Noel, I. Rico-Lattes, *Langmuir* **1999**, *15*, 6956 – 6960.

[22] J. Haensler, F. C. Szoka, *Bioconjugate Chem.* **1993**, *4*, 372 – 379.

[23] J. F. Kukowska-Latallo, A. U. Bielinska, C. Chen, M. Rymaszewski, D. A. Tomalia, J. R. Baker, Jr, in *Self-Assembling Complexes for Gene Delivery: from Laboratory to Clinical Trial* (Eds.: A. V. Kabanov, P. L. Felgner, L. W. Seymour), Wiley, New York, **1998**, pp. 241 – 253.

[24] Y. Barenholz, *Curr. Opin. Colloid Interface Sci.* **2001**, *6*, 66 – 77.

[25] D. Matulis, I. Rouzina, V. Bloomfield, *J. Am. Chem. Soc.* **2002**, *124*, 7331 – 7342.

[26] a) K. Jennings, I. Marshall, H. Birrell, A. Edwards, N. Haskins, O. Södermann, A. J. Kirby, P. Camilleri, *Chem. Commun.* **1998**, 1951 – 1952; b) G. Ronsin, C. Perrin, P. Guedat, A. Kremer, P. Camilleri, A. J. Kirby, *J. Chem. Soc. Chem. Commun.* **2001**, 2234 – 2235.

[27] P. J. J. A. Buynsters, C. L. García Rodríguez, E. L. Willighagen, N. A. J. M. Sommerdijk, A. Kremer, P. Camilleri, M. C. Feiters, R. J. M. Nolte, B. Zwanenburg, *Eur. J. Org. Chem.* **2002**, 1397 – 1406.

[28] R. Breslow, *Recl. Trav. Chim. Pays-Bas* **1994**, *113*, 493 – 498; M. Mammen, S.-K. Choi, G. M. Whitesides, *Angew. Chem.* **1998**, *110*, 2908 – 2953; *Angew. Chem. Int. Ed.* **1998**, *37*, 2754 – 2794.

[29] K. C. Nicolaou, R. Hughes, S. Y. Cho, N. Winssinger, H. Labischinski, R. Endermann, *Chem. Eur. J.* **2001**, *7*, 3824 – 3843.

[30] Gemini surfactants structurally related to **1**, derived from the oxidative dimerization of cysteine-based monomers, have been reported by the Strasbourg group to show interesting transfection capabilities; see: E. Dauty, J.-S. Remy, T. Blessing, J.-P. Behr, *J. Am. Chem. Soc.* **2001**, *123*, 9227 – 9234.

[31] M. L. Fielden, C. Perrin, A. Kremer, M. Bergsma, M. C. Stuart, P. Camilleri, J. B. F. N. Engberts, *Eur. J. Biochem.* **2001**, *268*, 1269 – 1279.

[32] C. McGregor, C. Perrin, M. Monck, P. Camilleri, A. J. Kirby, *J. Am. Chem. Soc.* **2001**, *123*, 6215 – 6220.

[33] M. A. Zanta, P. BelguiseValladier, J. P. Behr, *Proc. Natl. Acad. Sci. USA* **1999**, *96*, 91 – 96.

[34] C. McGregor, Ph.D. Thesis, University of Cambridge, **2001**.

[35] K. H. Jennings, I. C. B. Marshall, M. J. Wilkinson, A. Kremer, A. J. Kirby, P. Camilleri, *Langmuir* **2002**, *18*, 2426 – 2429.

[36] L. Karlsson, M. C. P. van Eijk, O. Söderman, *J. Colloid Interface Sci.* **2002**, *252*, 290 – 296.

[37] M. Johnsson, A. Wagenaar, J. B. F. N. Engberts, *J. Am. Chem. Soc.* **2003**, *125*, 757 – 760; M. C. P. van Eijk, M. Bergsma, S.-J. Marrink, *Eur. Phys. J. E* **2002**, *7*, 317 – 324.

[38] P. C. Bell, M. Bergsma, I. P. Dolbnya, W. Bras, M. C. Stuart, A. E. Rowan, M. C. Feiters, J. B. F. N. Engberts, *J. Am. Chem. Soc.* **2003**, *125*, 1551 – 1558.

[39] M. Bergsma, M. L. Fielden, J. B. F. N. Engberts, *J. Colloid Interface Sci.* **2001**, *243*, 491 – 495.

[40] J. N. Israelachvili, S. Marcelja, R. G. Horn, *Q. Rev. Biophys.* **1980**, *13*, 121 – 200.

[41] a) H. H. Ellens, D. P. Siegel, D. Alford, P. L. Yeagle, L. Boni, L. J. Lis, P. J. Quinn, J. Bentz, *Biochemistry* **1989**, *28*, 3692 – 3703; b) D. P. Siegel, R. M. Epand, *Biophys. J.* **1997**, *73*, 3089 – 3111; c) S. Audouy, D. Hoekstra, *Mol. Membr. Biol.* **2001**, *18*, 129 – 143; d) V. Oberle, I. Zuhorn, S. Audouy, U. Bakowsky, J. Smisterová, J. B. F. N. Engberts, D. Hoekstra in *Targeting of Drugs* (Eds.: G. Gregoriades, B. McCormack), IOS Press, **2000**, pp. 146 – 155.

[42] J. Smisterová, A. Wagenaar, M. C. A. Stuart, E. Polushkin, G. Ten Brinke, R. Hulst, J. B. F. N. Engberts, D. Hoekstra, *J. Biol. Chem.* **2001**, *276*, 47615 – 47622.

[43] I. Koltover, T. Salditt, J. O. Rädler, C. R. Safinya, *Science* **1998**, *281*, 78 – 81.

[44] a) Y. Xu, F. C. Szoka, Jr., *Biochemistry* **1996**, *35*, 5616 – 5623; b) I. M. Hafez, P. R. Cullis, *Adv. Drug Delivery Rev.* **2001**, *47*, 139 – 148; c) I. M. Hafez, N. Maurer, P. R. Cullis, *Gene Ther.* **2001**, *8*, 1188 – 1196.

[45] B. Tycko, F. R. Maxfield, *Cell* **1982**, *28*, 643 – 651.

[46] G. Ronsin, A. J. Kirby, S. Rittenhouse, G. Woodnutt, P. Camilleri, *J. Chem. Soc. Perkin Trans. 2* **2002**, 1302 – 1306.

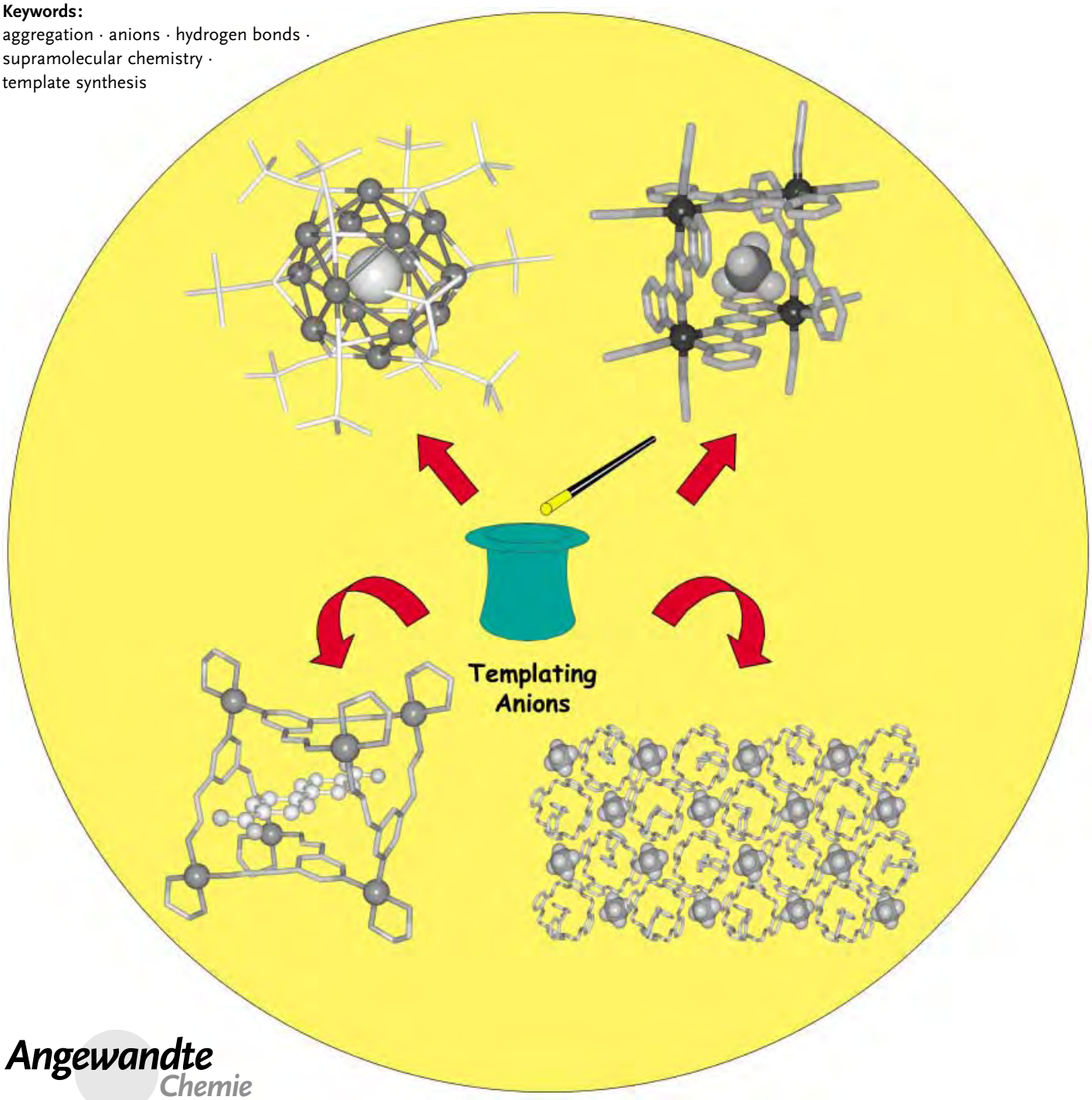
 © 2003 Wiley-VCH Verlag GmbH & Co. KGaA, Weinheim

Anion-Directed Processes

Anion-Templated Synthesis

*Ramón Vilar**

Keywords:
aggregation · anions · hydrogen bonds · supramolecular chemistry · template synthesis



 © 2003 Wiley-VCH Verlag GmbH & Co. KGaA, Weinheim DOI: 10.1002/anie.200200551

Angewandte Chemie

In contrast to the well-studied templating properties of cationic and neutral species there are relatively few examples of anion-templated syntheses. This is attributed to some of the intrinsic properties of anions such as their diffuse nature, pH sensitivity, and their relative high solvation free energies. However, the increasing number of anion-templated assemblies reported over the past few years demonstrates that these limitations are not as critical as first thought. This review summarizes the most important results on the use of anions as directing agents for the syntheses of a wide range of inorganic and organic assemblies (such as macrocycles, cages, helicates, rotaxanes, and extended structures). It is hoped that this will stimulate a closer look into this emerging area of supramolecular chemistry.

From the Contents

1. Introduction	1461
2. Anion-Directed Synthesis of Finite Assemblies	1461
3. Anion-Templated Synthesis of Polymers and Networks	1471
4. Conclusions and Outlook	1475

1. Introduction

During the past two decades supramolecular chemistry has provided important advances in developing strategies for the synthesis of complex molecular architectures such as molecular cages, helicates, rotaxanes and catenanes. One of the approaches used to prepare such complex assemblies involves chemical templates. As defined by Busch *"A chemical template organizes an assembly of atoms, with respect to one or more geometric loci, in order to achieve a particular linking of atoms"*.[1] When there are several potential ways of linking a group of molecular components, the template provides the instructions for the formation of a single product. In the presence of another template a different assembly is expected leading to the formation of a different product. In general, after the template has directed the formation of the assembly, it can be removed to yield the template-free product. However, this is not possible if the templating agent is an integral part of the final product. In this review, a template (or directing agent) will be considered any species that organizes an assembly of atoms or molecules (using noncovalent interactions) for specific linking and is either removed from the final product or kept as an integral part of it by supramolecular interactions.

As has been discussed elsewhere,[2] there are two types of templates: thermodynamic and kinetic. In the first case, the templating agent binds to one of the products present in a specific equilibrium (i.e. under thermodynamic control); by doing so, it shifts the equilibrium towards this product, which as a consequence is obtained in high yields. On the other hand, kinetic templates operate under irreversible conditions and hence they need to stabilize all the transition states leading to the desired product. The template can be temporary, in which case it can even act catalytically, or permanent (if it is an integral part of the final product). In many of the kinetically controlled reactions, the template ends up strongly bound to the final product and hence it acts, not only as a kinetic template but also as a thermodynamic one. In practice it is not easy to determine precisely if a templated reaction is kinetically or thermodynamically controlled.

In contrast to the well-studied templating properties of cationic and neutral species,[3,4] anion templates have been very little exploited in synthetic chemistry. Although the first examples were reported in the late 1980s, it was not until the second half of the 1990s that the area started to grow. This relative lack of anion-templated processes is partially attributed to some of the intrinsic properties of anions such as their diffuse nature, pH sensitivity, and their relative high solvation free energies.[5] However, as has been demonstrated by the increasing number of anion-directed assemblies reported in the last few years, these *limitations* are not as critical as first thought. Besides their templating role in synthetic chemistry, anions have also been found to act as templates in some biological processes such as in protein folding.[6]

The aim of this review is to highlight the great potential that anions have as templates in synthetic chemistry. It is hoped that this will stimulate the design and synthesis of novel assemblies by using anionic templates. Previously, Beer and Gale have reviewed some of the work here presented as part of their recent reviews on the supramolecular chemistry of anions.[7–9]

2. Anion-Directed Synthesis of Finite Assemblies

In a given templated reaction the size and shape of the directing anions are the main factors that determine the geometry and connectivity of the final structures. In the following sections, it is intended to draw similarities between different assemblies templated by the same anions. The discussion will focus on finite species such as macrocycles, cages, helicates, and rotaxanes (while extended structures will be dealt with in Section 3 of this review).

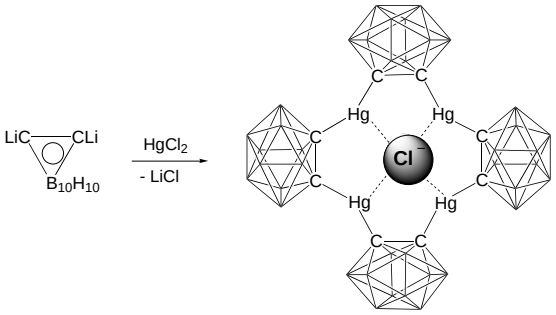
[*] Dr. R. Vilar
Department of Chemistry
Imperial College of Science, Technology and Medicine
South Kensington, London SW7 2AY (UK)
Fax: (+44) 20-7594-5804
E-mail: r.vilar@ic.ac.uk

 © 2003 Wiley-VCH Verlag GmbH & Co. KGaA, Weinheim

2.1. Halides

The spherical anionic halides have been shown to direct the formation of a wide range of organic and metal-organic assemblies. Their monoatomic nature, simple spherical symmetry, and variable size (from 1.33 Å for fluoride to 2.20 Å for iodide[5]) make these anions very versatile templating agents.

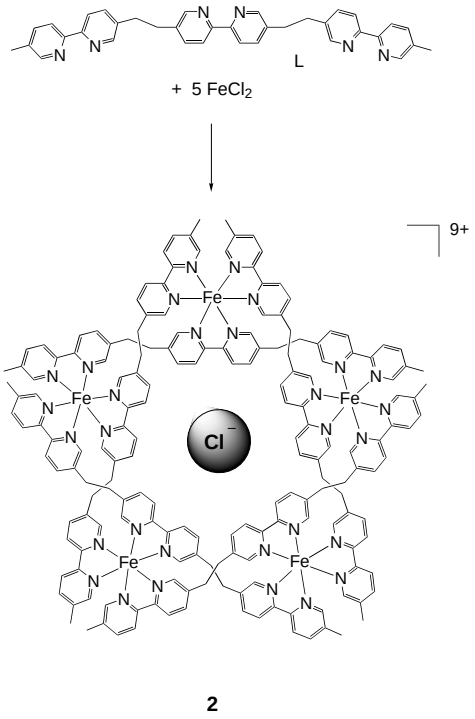
Halides have proven to effectively direct the synthesis of several metallamacrocycles. Hawthorne et al. reported the first example of such halide-templated species in 1991 with the tetranuclear [12]mercuracarborand-4 (**1**; Scheme 1).[10] Compound **1** was prepared by reacting 1,2-dilithiocarborane with mercury(II) in the presence of chloride ions. In the presence of other anions such as acetate, it was demonstrated that the formation of acyclic compounds was favored. A bigger spherical anion such as iodide led to the formation of a compound analogous to **1** (although in this complex the anion was not perfectly encapsulated at the center of the macrocycle but at 1.25 Å above the square formed by the mercury atoms). Since these results were first presented, halides have been utilized for the synthesis of several other metallamacrocycles, which, in spite of their chemical differences, have important structural similarities.



1

Scheme 1. Chloride-templated synthesis of the tetranuclear [12]mercuracarborand-4 (**1**).[10]

Other examples of metal-containing cycles prepared by halide-templated process are the penta- and hexanuclear circular helicates reported by Lehn et al. (Scheme 2).[11] In this work it was demonstrated that the assembly of iron(II) salts and a tris(bipyridine) ligand (L) is highly dependent on the presence of specific anions. With $FeCl_2$, the pentanuclear circular helicate $[Fe_5L_5Cl]^{9+}$ (**2**) was formed in high yields, while a mixture of the penta- and hexanuclear helicates was obtained in the presence of bromide (and only the hexanuclear helicate $[Fe_6L_6(SO_4)]^{10+}$ (**3**) was formed with sulfate).



2

Scheme 2. Synthesis of the circular helicate **2** by chloride-templated assembly of five tris(bipyridine) strands and five equivalents of $FeCl_2$.[11]

Further studies by Lehn and co-workers[11c] have demonstrated that in the reaction with $FeCl_2$ (and also in the analogous one with $NiCl_2$) a linear helicate is formed first (i.e., the kinetic product), which progressively converts into the thermodynamic circular helicate product $[Fe_5L_5Cl]^{9+}$ (**2**). The structural characterization of **2** confirmed it to be a circular double helix with an inner cavity radius of 1.75 Å. The chloride ion, which has an ionic radius of 1.80 Å, fits well within the cavity of this macrocyclic assembly. Interestingly, the internal radius of this structure is very similar to the one found in mercuracarborane **1** (i.e., 1.73 Å) prepared by Hawthorne et al., exemplifying the importance of the template's structural parameters in determining the size and geometry of the final assembly.

Zheng et al. has recently reported the halide-templated syntheses of a series of metallamacrocycles based on polynuclear lanthanide complexes.[12] These polynuclear hydroxolanthanide compounds were synthesized by the tyrosine-controlled hydrolysis of lanthanide perchlorates in the presence of specific halides. The pentadecanuclear complexes with a core formula $[Ln_{15}(\mu_3\text{-}OH)_{20}(\mu_5\text{-}X)]^{24+}$ (X = Cl, Br; Ln = Eu, Nd, Gd, Pr, Eu) were formed when the added halide was either chloride or bromide (Figure 1). These species can be described as pentagons formed by the assembly of five units of the cubane-type structure $[Ln_4(\mu_3\text{-}OH)_4]^{8+}$ (templated

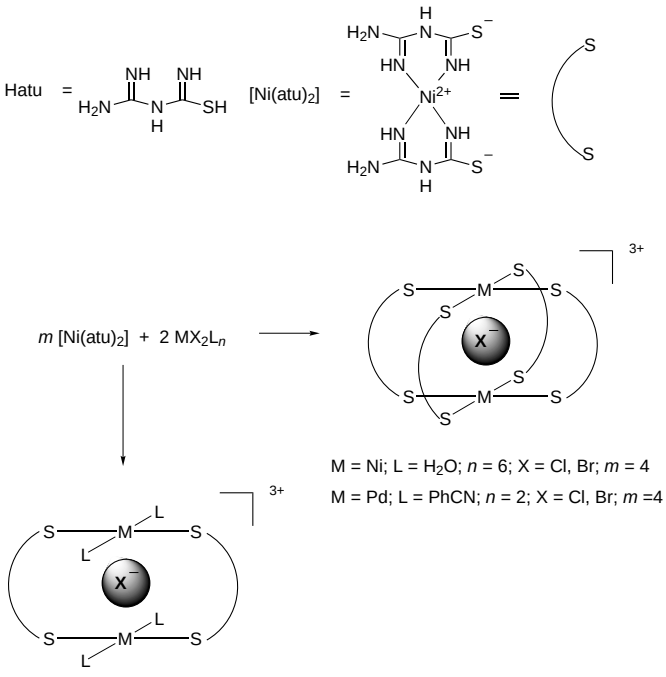


Ramón Vilar, born in Mexico City in 1969, studied chemistry at the Universidad Nacional Autónoma de México (UNAM). In 1993, he joined the group of Prof. D. M. P. Mingos at Imperial College London, where, since completing his doctoral research on palladium cluster compounds, he has been a postdoctoral associate and, since 1999, a lecturer in chemistry. His current research interests include various aspects of supramolecular chemistry (with particular focus on developing metallareceptors for anionic species) and the development of metal-containing species for biomedical research.

 © 2003 Wiley-VCH Verlag GmbH & Co. KGaA, Weinheim



Figure 1. Schematic representation of the core component of the metallapentagon formed by the chloride-templated assembly of five units of the cubane-type structure $[Eu_4(\mu_3\text{-}OH)_4]^{8+}$. An encapsulated chloride ion is located at the center of the polygon.[12]



Scheme 3. Halide-templated assembly of atu and Ni^{II} or Pd^{II} complexes to give different metallacages and metaalmacrocycles.[13c]

by the corresponding halide). The distances between the encapsulated halides and the metal centers are longer than the addition of the van der Waals radii of the anion and the metals, which reflects primarily an electrostatic interaction. In contrast, when iodide was used as templating agent the dodecanuclear lanthanide assemblies with core formula $[Ln_{12}(\mu_3\text{-}OH)_{16}(I)_2]^{18+}$ (Ln = Dy, Er) were obtained. These dodecanuclear complexes are based on square cyclic structures with one iodide ion located on each side of the plane of the squares (which is analogous to the behavior observed in the iodide-templated mercuracarborands reported by Hawthorne et al.[10b]).

In the previous examples the templating halides interact with the building blocks through electrostactic and Lewis acid–base interactions. However, hydrogen-bonding interactions can also be used to direct the assembly process. Examples of this are the halide-templated syntheses of the metallamacrocycles $[Pd_2Ni_2(atu)_4(PPh_3)_4X]^{3+}$ (X = Cl (**4a**), Br (**4b**), I (**4c**); atu = amidinothiourea) and metallacages $[M_2Ni_4(atu)_8X]^{3+}$ (M = Ni (**5a**,**b**), Pd (**6a**,**b**); X = Cl, Br) (Scheme 3).[13] These species were obtained by reacting the $[Ni(atu)_2]$ complex with $[PdX_2(PPh_3)_2]$ (to form the metallamacrocycles), and NiX_2 or $[PdX_2(PhCN)_2]$ (to obtain the molecular cages). Such assemblies only formed in the presence of the appropriate halides; with other anions such as triflate, nitrate, or acetate the formation of the macrocycles and cages was not observed and instead monometallic species were formed (which, upon addition of stoichiometric amounts of halide yielded the corresponding metalla-assembly confirming the templating role of the halides). The crystallographic characterization of these compounds demonstrated the halides to be encapsulated tightly at the center of the cages interacting through hydrogen bonds with the NH groups from the surrounding atu ligands. There is also an important attractive interaction between the corresponding $MS_2(PPh_3)_2$ and MS_4 (M = Ni, Pd) units located at the *poles* of the cages and the encapsulated halides (Figure 2).

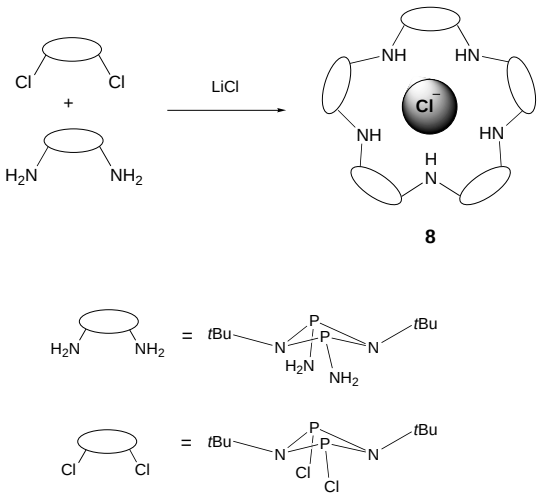


Figure 2. Molecular structure of the nickel cage $[Ni_6(atu)_8Cl]^{3+}$ with the encapsulated halide ion at the center of the assembly. The anion is tightly held inside this metallacage by multiple hydrogen-bonding interactions with the NH groups of the atu ligands and by Lewis acid–base interactions with the nickel atoms at the top and bottom of the cage.[13a]

Hydrogen-bonding interactions also play an important role in the halide-templated synthesis of a series of macrocycles containing $[\{P(\mu\text{-}NtBu)_2\}(\mu\text{-}NH)]_n$ frameworks recently reported by Wright et al.[14] These macrocyclic species can be prepared by reacting $[ClP(\mu\text{-}NtBu)]_2$ with $[NH_2P(\mu\text{-}NtBu)]_2$ in the presence of a base. When the reaction is carried out in THF/NEt_3 the major product is the tetrameric species $[\{P(\mu\text{-}NtBu)_2\}(\mu\text{-}NH)]_4$ (**7**). However, investigation of the same reaction in the presence of an excess of LiCl revealed that tetramer formation is suppressed and the formation of the pentamer $[\{P(\mu\text{-}NtBu)_2\}(\mu\text{-}NH)]_5(HCl)$ (**8**) is amplified (Scheme 4). Structural characterization of this pentamer has demonstrated that the chloride ion is positioned at the center of the macrocycle (structurally analogous to the lanthanide pentagons synthesized by Zheng et al.), and forms five hydrogen bonds with the NH groups of the ring.

Halides have also been demonstrated to play an important role in the formation of a series of organometallic silver–

 © 2003 Wiley-VCH Verlag GmbH & Co. KGaA, Weinheim



Scheme 4. Reaction of $[ClP(\mu\text{-}NtBu)]_2$ with $[NH_2P(\mu\text{-}NtBu)]_2$, which in the presence of chloride (and other halides) yields the larger pentamer **8** as the major product. In the absence of the halide template the cyclic tetramer is formed preferentially.[14]

alkynyl cages.[15] The 1:1 reaction between coinage metals (Cu, Ag, Au) and alkynes leads to the formation of insoluble materials that have been usually formulated as linear organometallic polymers. Accordingly, when *tert*-butyl alkyne and $AgBF_4$ were allowed to react in the presence of a base the expected organometallic polymer $[Ag(C{\equiv}CtBu)]_n$ was formed. However, this practically insoluble material can be converted (in high yields) into the cages $[Ag_{14}(C{\equiv}CtBu)_{12}X]^+$ (X = F (**9a**), Cl (**9b**), Br (**9c**)) upon addition of fluoride, chloride, or bromide salts, respectively (but not when other anions such as triflate or tosylate are used). These novel cages have been characterized by X-ray crystallography, which has shown them to have rhombohedral geometries with the corresponding halide encapsulated at their center (Figure 3).

Interestingly, structural dimensions of these three silver cages are very similar to those of the Ni/Pd hexanuclear cages **5** and **6** (**5a**: Ni···Cl 3.123(1)–3.140(1) Å, **6a**: Pd···Cl 3.169(2)–3.190(2) Å). The Ag···Cl distances in the silver cage **9b** range between 3.116(2) and 3.297(1) Å. These dimensional similarities in two very different systems clearly demonstrate the importance of the geometrical constrains imposed by the templating anions on the structure of the final product.

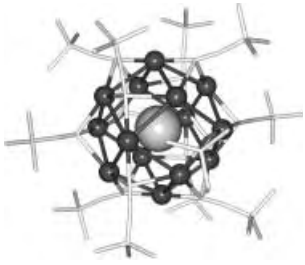


Figure 3. The products resulting from the reactions between silver salts and *tert*-butyl alkyne are highly dependent on the nature of the anionic counterions. In the presence of fluoride, chloride, or bromide ions, rhombohedral cages are formed. The molecular structure of one the cages with an encapsulated chloride ion is depicted (silver atoms dark).[15a]

Another example of fluoride-templated assembly of silver cages was recently provided by Steel and Sumby.[16] The reaction of $AgBF_4$ with the hexa(2-pyridyl)[3]radialene (L) ligand led to the formation of the hexanuclear cage $[Ag_6L_2F][BF_4]_5$ (**10**) with a fluoride ion at the center, (Figure 4) which stems from the BF_4^- ion. Interestingly, when the reaction was carried out using alternative silver salts such as $AgNO_3$ or $AgPF_6$ (which do not act as good fluoride sources), the formation of polymeric materials, and not the cage, was observed. These results demonstrate the ability of anionic species to dramatically change the preferred way of assembling a group of molecular building blocks; in this case a metallacage versus a coordination polymer.

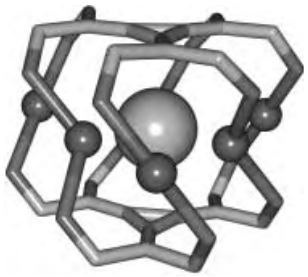
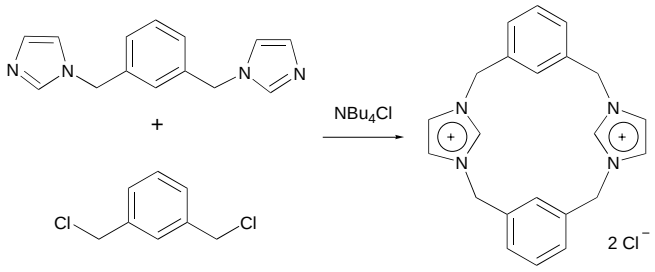


Figure 4. Simplified representation of the molecular structure of hexanuclear silver cage **10**, which results from the assembly of Ag^I and hexa(2-pyridyl)[3]radialene in the presence of a templating fluoride ion (located at the center of the cage).[16a]

The use of halide templates to prepare cyclic structures is not exclusive to metal-containing assemblies (which due to the positive charge on the metal are particularly prone to interact with negatively charged species), but it is also found in organic systems. Alcalde et al., for example, have reported the halide-directed synthesis of a series of $[1_4]$imidazoliophanes,[17] which is based on a [3+1] convergent macrocyclization reaction (Scheme 5). The yields of the resulting macrocycles are highly dependent on the presence of specific anions (e.g. from 42% yield when no anion is present to 83% in the presence of chloride ions and 88% with bromide ions). The templating role of the halides is attributed to the formation of an intermediate, which, because of C–H···Cl^-

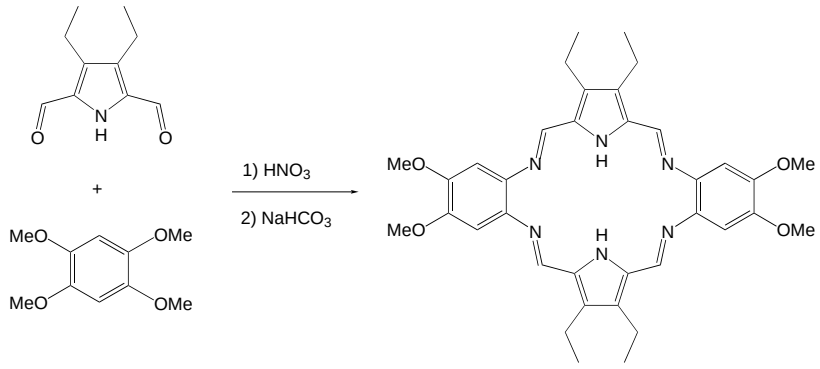


Scheme 5. The convergent macrocyclization of dicationic $[1_4]$imidazoliophanes is driven by chloride and bromide ions.[17]

 © 2003 Wiley-VCH Verlag GmbH & Co. KGaA, Weinheim

hydrogen bonds, adopts the optimal conformation for the cyclization step.

Halides have also been employed as templates for the synthesis of interlocking species such as pseudorotaxanes. Although the first examples of anion-directed syntheses of rotaxanes and pseudorotaxanes were reported by Stoddart et al.[18] and Vögtle et al.[19] (using larger anions as discussed in Sections 2.3 and 2.4), Beer et al. have recently reported the chloride-directed assembly of the [2]pseudorotaxane **11** (Figure 5).[20] In this structure, the chloride ion plays a directing role by organizing the two ligands (that is, the macrocycle and the linear species) in an orthogonal fashion by means of hydrogen bonding. In contrast to the good templating role played by the chloride, other anions such as Br^-, I^-, and PF_6^- proved to be poor templates.



12

Scheme 6. Assembly of macrocycle **12**; the presence of NO_3^- seems to play an important templating role in this reaction.[21]

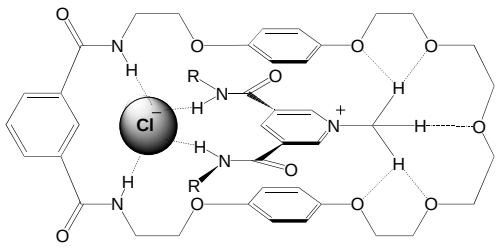


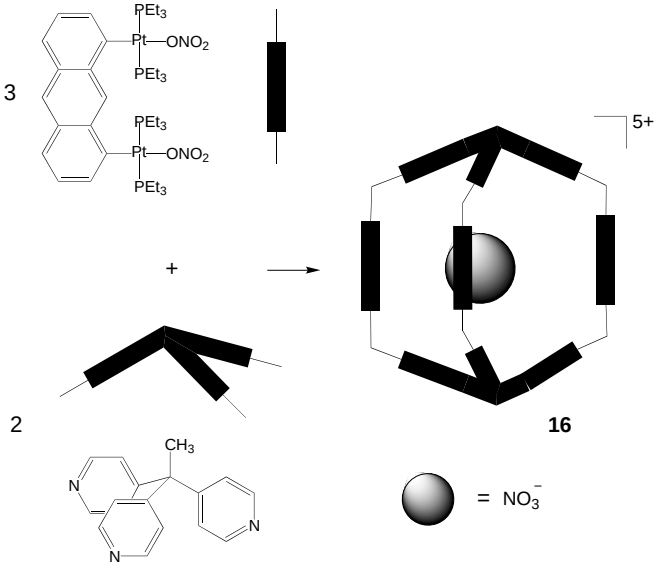
Figure 5. Pseudorotaxane **11**, which is assembled from three components: the templating chloride ion, the macrocycle, and the rod-shaped cation (based on a pyridinium nicotinamide). $R = (CH_2)_5CH_3$.[20]

2.2. Linear and Trigonal-Planar Anions

Although a good number of the known anion-directed processes make use of the spherical halides, polynuclear anions with different geometries and sizes (such as the trigonal-planar nitrate) have also been employed as templates. An early example of the use of nitrate as a directing agent is the macrocyclization reaction reported by Sessler et al.[21] In this work, it was demonstrated that the acid-catalyzed synthesis of the oligopyrrolic macrocycle **12** (see Scheme 6) requires HNO_3, rather than other acids such as HCl, to take place in high yields. Under these conditions the nitrate salt of the protonated macrocycle precipitated out of the reaction mixture, leading the authors to suggest a templating effect exerted by the anionic nitrate.

As reported by Müller et al., nitrate ions (as well as halides and linear SCN^- ions) direct the formation of a series of polyoxometallates cages.[22] In these reactions anions control the aggregation of $V^{n+}O_x$ polyhedra into cage-type structures such as $[HV_{18}O_{44}(NO_3)]^{10+}$ (**13**), $[H_4V_{18}O_{42}Br]^{9+}$ (**14**), and $[HV_{22}O_{54}(SCN)]^{6+}$ (**15**), in which the anions are encapsulated inside the cavity of these spherical clusters. With other anions such as acetate, V–O aggregates are formed in which the anions are located on the outer surface of the shell. The size of the anion dictates the structure and geometry of the products obtained (this work is thoroughly reviewed in reference [22a]).

Stang et al. have recently reported the formation of the nanoscale-sized supramolecular cage **16** (Scheme 7), which appears to be templated by nitrate ions.[23] The trigonal-prismatic cage results from the assembly of a platinum-based molecular "clip" and a pyridyl-based tripodal ligand. Structural characterization of **16** has demonstrated that a nitrate ion is incarcerated inside the metallacage which is the ideal size-match for this anion. The authors have pointed out that the formation of analogous cages with larger tripodal ligands can also be accomplished but in their structure no encapsulation of the anion is observed. Interestingly, the synthesis of the "empty" cages occurs an order of magnitude slower than that of **16** suggesting that when the size-match is appropriate for the templating nitrate to direct the assembly, it does so.



16

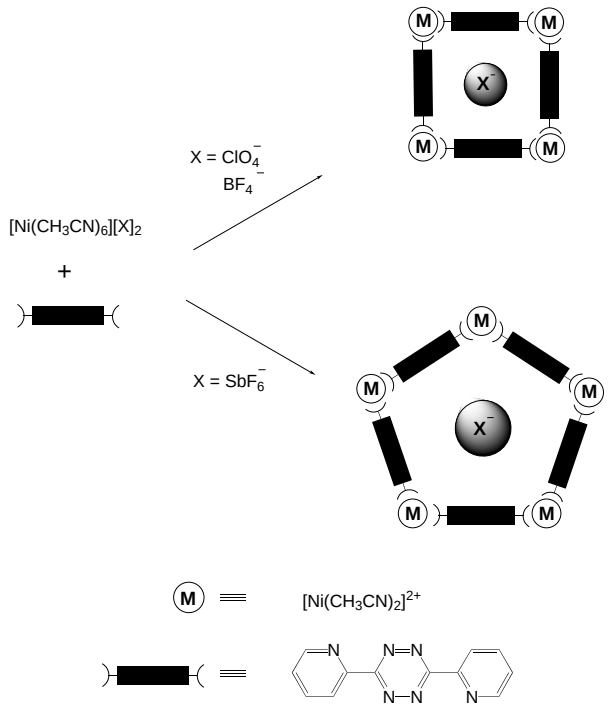
Scheme 7. Schematic reresentation of the assembly of nanocage **16** by the nitrate-templated reaction between a platinum-based "clip" and a tripodal ligand.[23]

 © 2003 Wiley-VCH Verlag GmbH & Co. KGaA, Weinheim

2.3. Tetrahedral and Octahedral Anions

Increasing the complexity (and size) of the templating anions can potentially lead to the formation of higher order assemblies. For example, tetrahedral anions, in contrast to the spherical halides, have potentially templating groups pointing in four different directions (and in six different directions in octahedral anions). This restricts the number of possible assemblies that can be formed; hence, it can then be suggested that tetrahedral and octahedral anions contain a larger amount of "templating information" than the simpler spherical and trigonal-planar species.

Dunbar et al. have recently reported some elegant examples in which the geometrical constrains imposed by the templating anions (with tetrahedral or octahedral geometry) play a crucial role in determining the geometry of the final assemblies.[24] Specifically, the structure of the species resulting from the reaction between nickel (or zinc) salts with the bischelating ligand 3,6-bis(2-pyridyl)1,2,4,5-tetrazine (bptz) has proven to be anion-dependent (as demonstrated by X-ray crystallography and ES mass spectrometry). In the presence of the tetrahedral anions BF_4^- or ClO_4^-, the molecular squares $[M_4(bptz)_4(CH_3CN)_8][X]_8$ (M = Ni, X = BF_4^- (**17a**), ClO_4^- (**17b**), M = Zn, X = BF_4^- (**18a**), ClO_4^- (**18b**)) were formed in high yields (Scheme 8). In contrast, when the reaction between $[Ni(MeCN)_6][SbF_6]_2$ and bptz was carried out the pentanuclear compound $[Ni_5(bptz)_5(CH_3CN)_{10}][SbF_6]_{10}$ (**15**) was obtained as the main product of the reaction.



Scheme 8. The assembly of 3,6-bis(2-pyridyl)-1,2,4,5-tetrazine and nickel salts yields metallasquares in the presence of BF_4^- or ClO_4^- ions. In the presence of the larger SbF_6^- ion a metallapentagon is formed, which indicates the important templating role of the anions in the assembly of these structures.[24]

X-ray crystallography demonstrated that **17a** is a molecular square with the tetrahedral ClO_4^- ion positioned at its center (Figure 6). A structural comparison between these tetra- and pentanuclear assemblies demonstrates the important relation between the size of the polygon's cavity and the anion used for templating. The molecular squares have an approximate diameter of 4.6 Å, which is ideal to accommodate the BF_4^- or ClO_4^- ions (with volumes[25] of 38 and 47 Å^3 and ionic radii[4] of 2.32 and 2.40 Å, respectively). The larger octahedral anion SbF_6^- (with a volume of 63 Å^3) is too big to fit in such a cavity and, hence, given the opportunity, it templates the formation of larger pentagonal species.



Figure 6. Molecular structure of the nickel-based square **17b** showing the encapsulated ClO_4^- ion (nickel centers black).[24a]

Tetrahedral anions have also been used as directing agents for the synthesis of the metallacages $[Co_4L_6(X)][X]_7$ (L = bidentate pyrazolyl–pyridine ligands; X = BF_4^- (**18a**), ClO_4^- (**18b**)).[26] The structural characterization of of **18a** revealed that it was a tetrahedron with a metal ion on each vertex and that the ligands bridge the metal ions (Figure 7). One of the BF_4^- ions is located at the center of the cage with the fluoride groups pointing to the center of the triangular faces of the structure (in an analogous cage, the BF_4^- forms F···H–C hydrogen bonds with the methylene protons of the bridging ligands). NMR spectroscopic measurements in solution indicated that in the absence of either BF_4^- or ClO_4^- ions, a mixture of Co^{II} and the corresponding ligand do not give rise

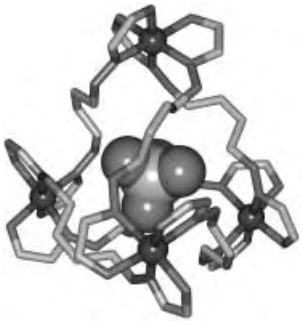


Figure 7. Molecular structure of cage **18a**; Co^{II} ions form a tetrahedron in the center of which is located the templating BF_4^- ion. The bridging ligands are simplified for clarity.[26a]

 © 2003 Wiley-VCH Verlag GmbH & Co. KGaA, Weinheim

to the formation of the cage. Addition of the appropriate anion to this mixture leads to the quantitative assembly of the tetranuclear cages.

In most of the examples discussed so far, the templating anion acts by preorganizing the building blocks *around* itself. However, there are systems in which anions act as "external" templates, that is, instead of organizing the building blocks around a central template they do it be interacting with the surface of the assembly. An example of such external anion-directed assembly is the super-adamatoid silver cage $[Ag_6(triphos)_4X_4]^{2+}$ (triphos = $(PPh_2CH_2)_3CMe$; $X = O_3SCF_3^-$ (**19a**), ClO_4^- (**19b**), NO_3^- (**19c**)) reported by James, Mingos, et al. (Figure 8).[27] The silver cage only forms in the presence of the above-mentioned oxo anions and not with other anionic



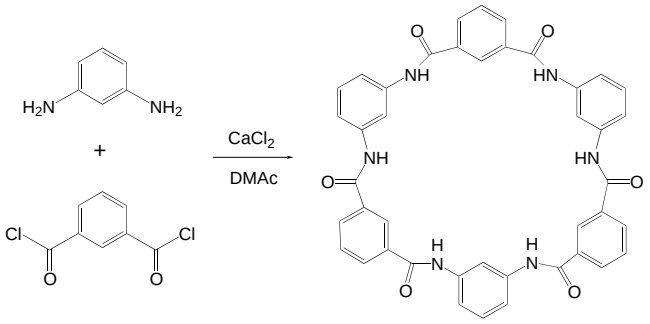
Figure 8. The central core of the super-adamatoid silver cage **19a** (silver centers dark). The templating anions (in this case triflate ions) are located in the surface of the cage and not inside the assembly.[27]

species such as SbF_6^-. It has been suggested that the anion-specific behavior observed in these reactions may be related to the μ_3-face-capping coordination mode of the anion in the final structure (which is satisfied by the templating oxo anions but not by other species such as SbF_6^-). Recently, this anion-templated reaction was further exploited to prepare metallodendrimers.[28]

Polynuclear anions (with tetrahedral and octahedral geometries) have also been used for the synthesis of organic macrocycles, helicates, and rotaxanes. Kim et al. have reported the directing role of the pseudo-octahedral anion $[CaCl_3(DMAc)_3]^-$ (DMA*c* = dimethyl acetamide) in the synthesis of cyclic aromatic amides such as **20** (Scheme 9).[29] The $[CaCl_3(DMAc)_3]^-$ ion, which is formed in situ from $CaCl_2$ and free chloride, has an influence on the size of the macrocycle formed in the reaction of isophthalic acid chloride with *m*-phenylenediamine, and leads to the formation of a cyclic hexamer. In the absence of $[CaCl_3(DMAc)_3]^-$, the [3+3] macrocycle is not the major product and the formation of oligomers and macrocycles of different sizes is observed.

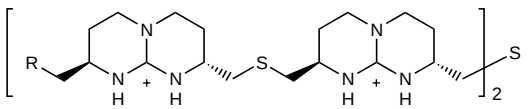
In contrast to the well-documented cation-directed assembly of helicates only few examples of anion-templated assembly of helical structures have been reported. de Mendoza et al. reported the first example in 1996,[30a] in which it was shown that the tetraguanidinium strand **21** self-assembles around a sulfate anion to produce a double helical structure (Scheme 10). The formation of the double helix and its anion-dependence was proposed on the basis of NMR and CD spectroscopic studies. A related system was recently published by Král et al. in which porphyrins substituted with bicyclic guanidines (such as the tetrasubstituted species **22** shown is Scheme 10) form highly ordered chiral assemblies in aqueous solution.[30b] The aggregation and chirality of the supramolecular aggregates is controlled by anionic species such as dicarboxylates.

Using a different set of hydrogen-bonding fragments Kruger, Martin, et al. have reported the formation (and structural characterization) of the double helicate **23**, which

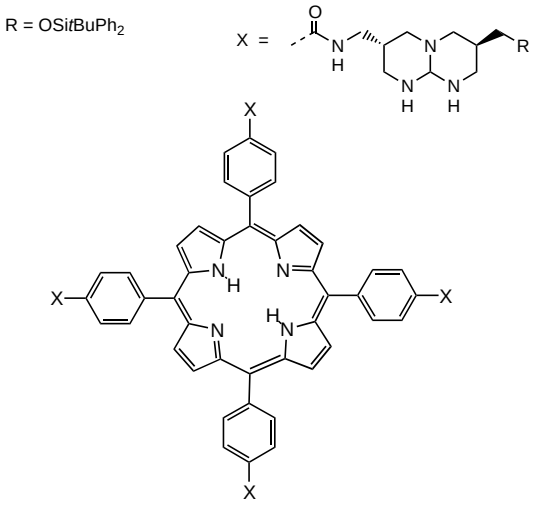


20

Scheme 9. The reaction between isophthalic acid chloride and *m*-phenylendiamine in dimethyl acetamide (DMAc) is influenced by the presence of anionic species. In particular, the presence of $[CaCl_3(DMAc)_3]^-$ ions (generated in situ from $CaCl_2$) favors the formation of the six-membered macrocycle **20**.[29]



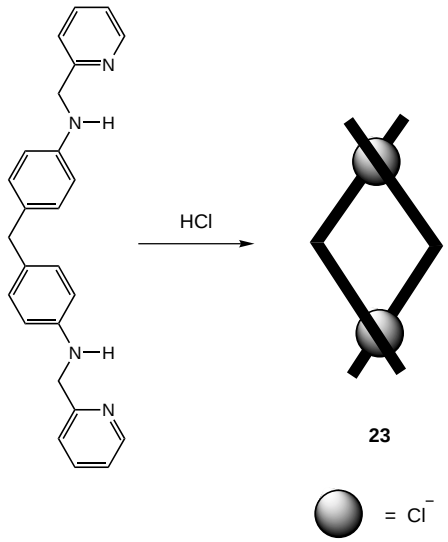
21



22

Scheme 10. Two strands of the tetraguanidinium compound **21** can assemble into double-helical structures in the presence of sulfate; [30a] similarly, **22** in the presence of dicarboxylates forms helical structures.[30b]

 © 2003 Wiley-VCH Verlag GmbH & Co. KGaA, Weinheim



Scheme 11. Chloride ions direct the assembly of hydrogen-bonding fragments into helicate **23**.[31]

was prepared by assembling two strands of a diammonium bispyridinium salt around two chloride ions (Scheme 11).[31] Steel and McMorran have reported the anion-templated assembly of a quadruply stranded metallahelicate.[32] The 1:2 reaction between $[PdCl_2L_2]$ ($L = PPh_3$, pyridine) and 1,4-bis(3-pyridyloxy)benzene (N–N) in the presence of PF_6^- leads to the formation of the helicate $[Pd_2(N{-}N)_4(PF_6)][PF_6]_3$ (**24**). The X-ray crystal structure of **24** shows that the PF_6^- ion is located at the center of this metalla-assembly and that it interacts with the two palladium ions through Lewis acid–base interactions (Figure 9). If the specific anions (PF_6^-, ClO_4^-, or BF_4^-) are not present in the reaction mixture, the formation of the corresponding quadruply stranded helicate is not observed.[32b]

The octahedral geometry of the PF_6^- ion has also been used for the anion-assisted self-assembly of pseudorotaxanes. Stoddart, Williams, et al. reported that by mixing four equivalents of $[NH_2(CH_2Ph)_2][PF_6]$ with one equivalent of

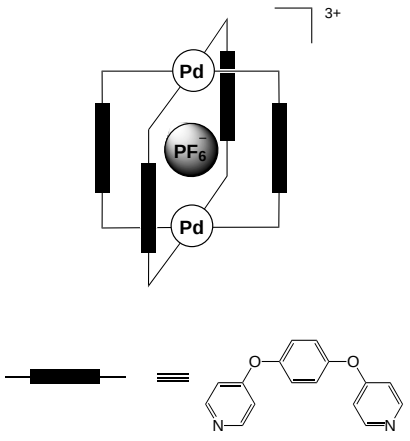
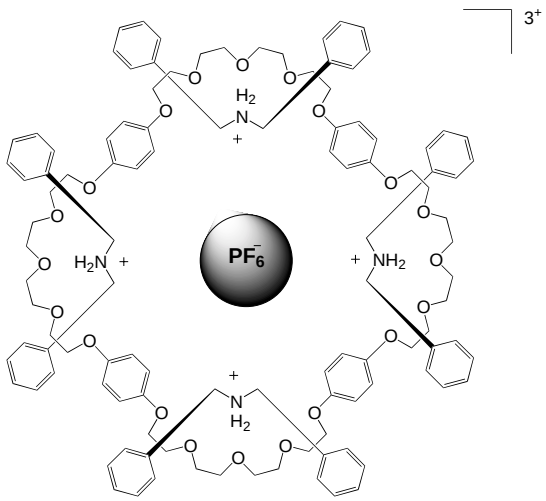


Figure 9. Schematic representation of the quadruply stranded palladium helicate **23** with an encapsulated PF_6^- ion that plays an important templating role.[32a]

the large macrocycle tetrakis-*p*-phenylene[68]crown-20, a quadruply stranded pseudorotaxane (**25**) can be prepared (Scheme 12).[18a] The structural characterization of **25** revealed the presence of a PF_6^- ion at the center of this supramolecular assembly, which formed multiple C–H···F hydrogen bonds with the hydroquinone methine and the benzylic methylene hydrogen atoms. As the authors suggest,



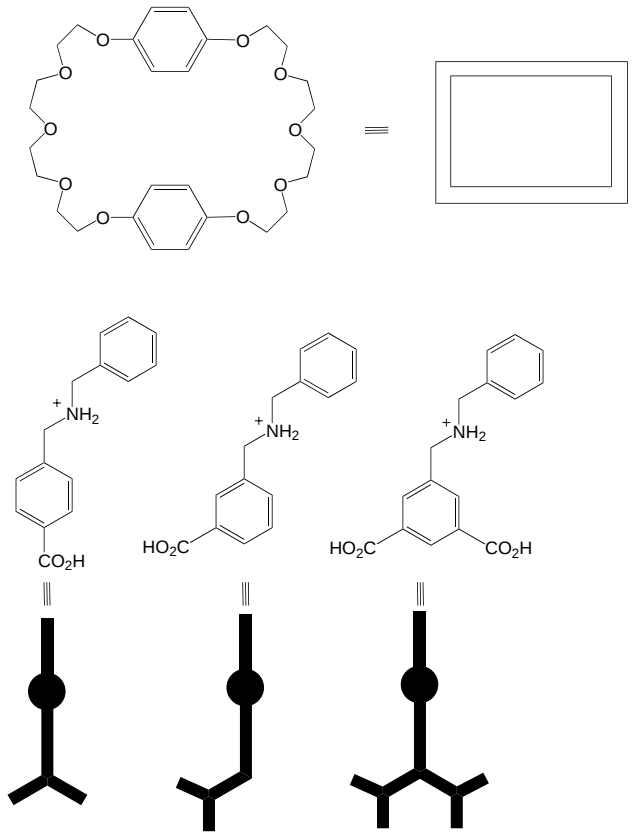
25

Scheme 12. PF_6^- ions assist in the assembly of the macrocycle tetrakis-*p*-phenylene[68]crown-20 and the ammonium salt $[NH_2(CH_2Ph)_2][PF_6]$ into the pseudorotaxane **25**.[18a]

it is not unreasonable to conclude that the geometry of this superstructure is programmed by the negatively charged PF_6^- ion. Further studies by the same authors have demonstrated that PF_6^- ions play a directing role in the self-assembly of other interwoven structures.[18b] In an extensive study aimed at using a combination of hydrogen-bonding motifs to self-assemble pseudorotaxanes into more complex structures it was discovered that PF_6^- ions assist the organization of the components that yield the final superstructure. In particular, it was found that the PF_6^- ion dictates the orientation of the two carboxylic acid groups of the [3]pseudorotaxanes **26a** and **26b** (Scheme 13 and 14a,b); when these groups are co-directional with respect to each other the formation of discrete hydrogen-bonded dimers is observed. The crystals structures of **26a** and **26b** demonstrate that the PF_6^- ion is indeed located in the cleft between the two dialkylammonium ions and forms hydrogen bonds with the benzylic hydrogen atoms of one of the cations and with one of the hydrogen atoms of a hydroquinone ring (Figure 10).

When the analogous isophthalic acid substituted cation (Scheme 13) is used, the [3]pseudorotaxane **27** is formed, the resulting hydrogen-bonded superstructure of which is not dimeric but polymeric (Scheme 14c). The X-ray diffraction analysis demonstrated that the solid-state structure of **27** consists of an interwoven hydrogen-bonded cross-linked polymer. The formation of an extended structure (instead of

 © 2003 Wiley-VCH Verlag GmbH & Co. KGaA, Weinheim



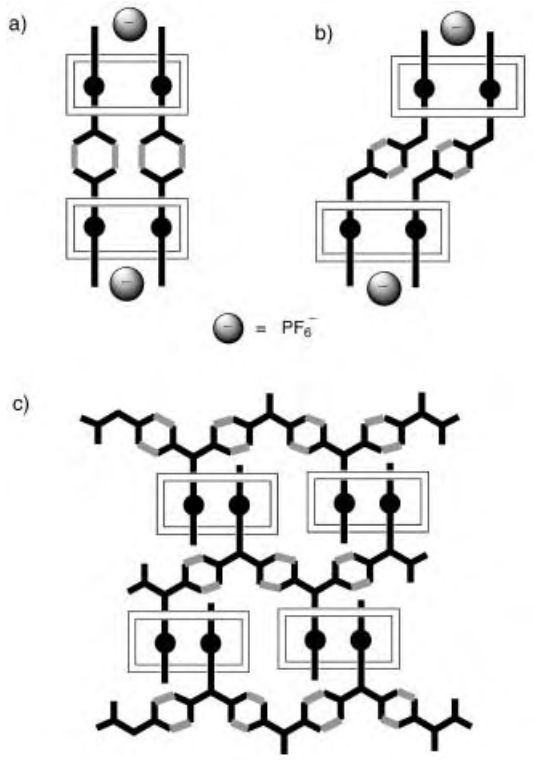
Scheme 13. Schematic representation of the components that form pseudorotaxanes **26a, 26b**, and **27** (see Scheme 14).[18b]

dimeric assemblies) is attributed to the opposite orientation of the carboxylic acid groups. Interestingly, in **27** the PF_6^- ions do not seem to play an important role in orienting the components to yield specific solid-state structures.

An elegant application of the anion-directed construction of [3]pseudorotaxane assemblies is the solid-state photodimerization of olefins.[18c] Similarly to the dimeric species **26a** and **26b**, a combination of supramolecular interactions (one of them being hydrogen bonding to PF_6^-) has been used to preorganize bis(dialkylammonium) salts containing *trans*-stilbenoid units into the [3]pseudorotaxane assembly **28** (Scheme 15). When a powdered crystalline sample of this supramolecular assembly is irradiated with UV light, the formation of the corresponding cyclobutane with *syn-anti-syn* stereochemistry is observed. The photodimerization of the *trans*-stilbenoid units does not take place in the absence of the macrocycle, indicating the importance of preorganizing the stilbenoid units for this solid-state reaction to occur.

2.4. Organic Anions

Templating anions and the building blocks that they preorganize, usually interact by a combination of electrostatic and hydrogen-bonding forces. Polynuclear anionic species, on the other hand, have a wider range of potential supramolecular interactions (such as π–π and hydrophobic interactions), which can provide better specificity in the templating process. Fujita et al., for example, have reported a series of reactions where organic anions are used as templates for the formation of metallacages and coordination channels. One example of such a templated process is the reaction between $[Pd(en)_2(NO_3)_2]$ and 1,3,5-tris(4-pyridylmethyl)benzene, which, in the presence of anionic species having a hydrophobic moiety (such as 4-methoxyphenylacetate), leads to the



Scheme 14. Schematic representation of the hydrogen-bonded assemblies formed from two [3]pseudorotaxanes **26a** (a) and **26b** (b) (see Scheme 13); the PF_6^- ion determines the direction of the axles. c) Schematic representation of the hydrogen-bonded cross-linked polymer formed from **27**.[18b]

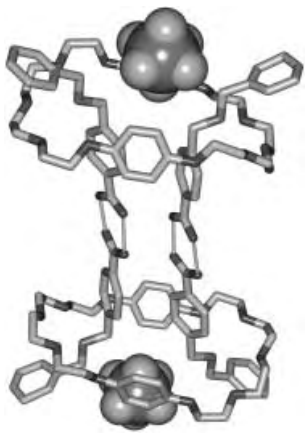
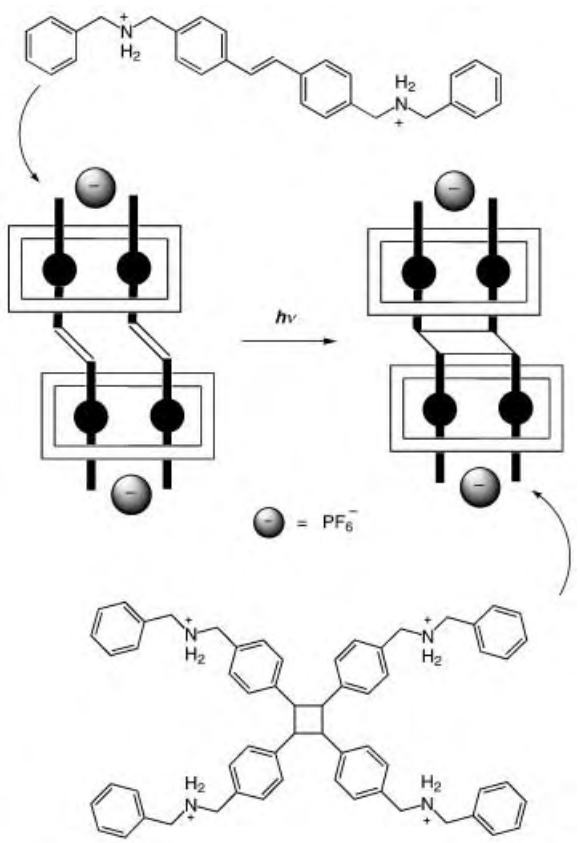


Figure 10. Molecular structure of the supermolecule formed from two [3]pseudorotaxane units **26a** and the PF_6^- ions. The thin lines denote the hydrogen bonds between the carboxylate groups of the four axles.[18b]

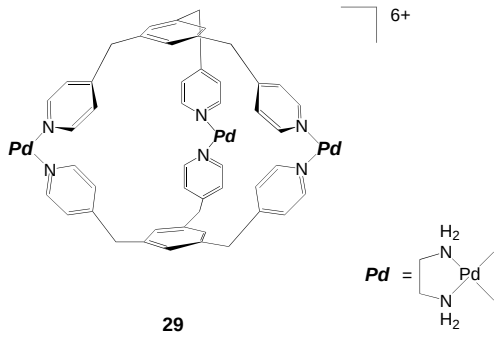
 © 2003 Wiley-VCH Verlag GmbH & Co. KGaA, Weinheim



Scheme 15. Reaction scheme showing the important role played by the PF_6^- ion in preorganizing the *trans*-stilbene bis(dialkylammonium) salts for their photodimerization.[18c]

nearly quantitative formation of the cage structure **29** (Scheme 16).[33] However, if such hydrophobic anions are not present oligomeric products are formed.

Similarly, the quantitative formation of "coordination channels" was observed in the reaction of $[Pd(en)_2(NO_3)_2]$ with oligo(3,5-pyridine)s in the presence of rodlike anionic species such as 4,4′-biphenylenedicarboxylate (Figure 11).[34] In these examples the anionic template displays a richer supramolecular chemistry than simpler anions directing the assembly process, not only through electrostatic interactions, but also through π–π stacking and hydrophobic effects.



Scheme 16. The palladium cage **29** assembles in high yields only in the presence of specific guest molecules such as anionic species containing a hydrophobic moiety (e.g. 4-methoxyphenylacetate).[33]

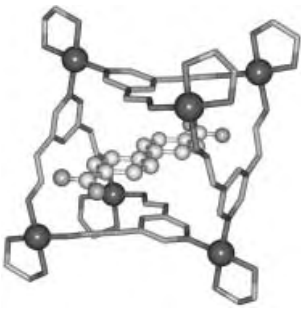
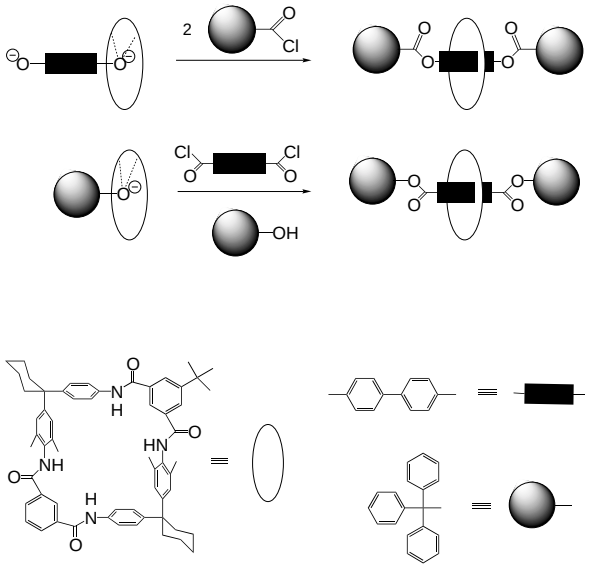


Figure 11. Molecular structure of a coordination channel formed by the anion-directed assembly of $[Pd(en)(NO_3)_2]$ and oligo(3,5-bispyridine). The biphenyldicarboxylate ion, which functions both as guest and as template, is found inside the channel (palladium centers black).[34]

As an extension of the anion-directed assembly of the above-mentioned cage and channels, Kubota and Fujita et al. have reported that anionic organic guests can induce the formation of an optimal receptor (for that specific guest) from a dynamic receptor library.[35] In this approach, the complex $[Pd(en)(NO_3)_2]$ is mixed with several *exo*-bidentate and *exo*-tridentate ligands to yield an equilibrium mixture of several metal-linked receptors (referred to as a dynamic receptor library). Upon addition of a specific guest (e.g. CCl_3COO^-) the mixture shifts the equilibrium to the formation of the metal-linked receptor that can accommodate the guest in the best way (i.e. the guest is templating the formation of the receptor from the dynamic library). This concept promises to be a very active field of research within the area of anion-templated synthesis.[36]

Vögtle et al. have utilized organic anions to induce the formation of rotaxanes.[19] In such processes, a strong host–guest complex between a tetralactam macrocycle and a phenolate ion is initially formed (Scheme 17). In such a



Scheme 17. Schematic representation of the principle of the anion-directed synthesis of rotaxanes by formation of a host–guest complex between a tetralactam macrocycle and a phenolate ion, and subsequent reaction with an alkyl bromide or acyl chloride.[19]

 © 2003 Wiley-VCH Verlag GmbH & Co. KGaA, Weinheim

supramolecular complex the anion is properly positioned at the center of the ring to further react with a second component (e.g. an alkyl bromide or acyl chloride) and subsequently yields a rotaxane. The negatively charged phenolic functionality can be located either at the stopper component or at the axle precursor. This provides variability to the type of products that can be formed.

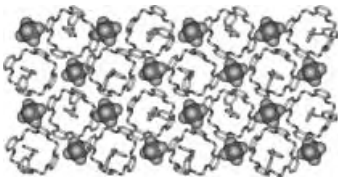


Figure 12. The solid-state structure of the assembly resulting from mixing tetrabenzo[24]crown-8 and dibenzylamonium hexafluorophosphate;[37a] the PF_6^- ions are located in between the pseudorotaxanes and generate a two-dimensional grid.

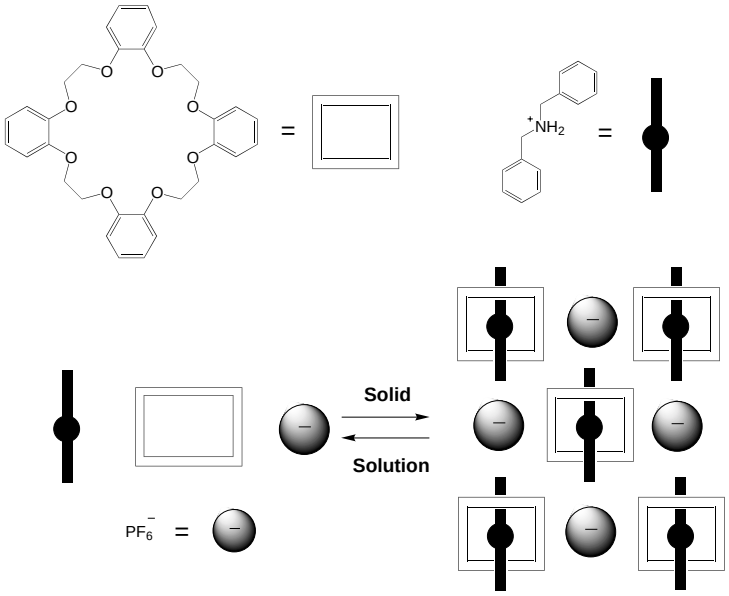
3. Anion-Templated Synthesis of Polymers and Networks

The discussion in Section 2 concentrated on finite (or molecular) assemblies in which anions template the formation of cages, macrocycles, helicates, or rotaxanes. Anions can also be very powerful templating agents for the synthesis of extended (infinite) structures such as polymers and networks. However, it is not always easy to unambiguously identify anion-templated processes that lead to the formation of polymeric (or extended) structures due to the inherent difficulties associated with the characterization and monitoring of the reaction pathways that lead to such extended assemblies. Furthermore, in the specific case of coordination polymers the anions present in the reaction mixture (which could potentially act as templates) very often end up coordinated to the metal centers in the final polymer or network. Consequently, in many cases it is difficult to establish if their influence is as templating agents or simply due to their different coordination modes. In spite of these difficulties, there are already several systems in which anions have been clearly identified as templates for the formation of extended structures. Some of these examples are presented in the following sections.

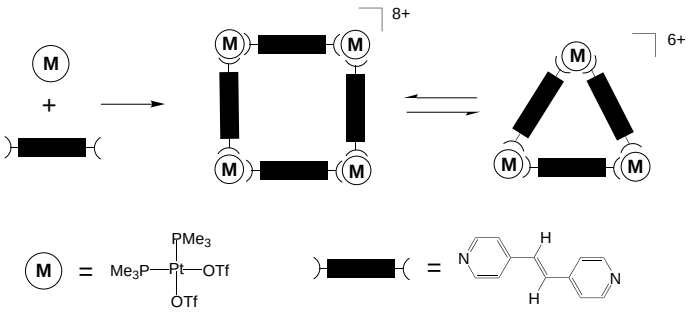
3.1. Anion-Directed Crystallization of Supramolecular Assemblies

The presence of anions in a reaction mixture can induce the crystallization of a specific supramolecular assembly in favor of other supramolecular aggregates (or induce the assembly in the solid state of components found "free" in solution). Although this behavior is probably a very widely spread phenomenon in chemistry, there are only a few reports in which it has been identified and systematically studied. Stoddart et al., for example, have reported the anion-orchestrated assembly of an extended [2]pseudorotaxane array in the crystalline state.[37] In general, the affinity that a ring and a thread have for each other is highly dependant on their electronic and structural properties. This can be exemplified by the different binding ability of dibenzo[24]crown-8 in comparison to tetrabenzo[24]crown-8. While the dibenzo compound interacts strongly with dibenzylammonium hexafluorophosphate to form a 1:1 threaded complex, the tetrabenzo compound shows negligible binding to dialkylammonium salts in solution. However, upon crystallization of an equimolar mixture of tetrabenzo[24]crown-8 and dibenzylammonium hexafluorophosphate an infinite array of [2]pseudorotaxanes is obtained (Figure 12). The stability of this extended assembly is based on the strong C–H···F hydrogen bonds between the PF_6^- ions and the the pseudorotaxane units (Scheme 18).

Another example of anion-induced crystallization was recently reported by Stang et al.[38] While studying the triangle–square equilibrium shown in Scheme 19, it was found that the selective crystallization of each one of the two metallapolygons can be selectively achieved by the appropriate choice of solvents and ratio of anions. In acetonitrile a mixture of the square **30** (11 %) and the triangle



Scheme 18. Schematic representation of the anion-orchestrated assembly of an extended [2]pseudorotaxane assembly in the solid state.[37]



Scheme 19. Formation and equilibrium of the metallasquare **30** and metallatriangle **31**; the crystallization of these assemblies is anion-dependent.[38]

 © 2003 Wiley-VCH Verlag GmbH & Co. KGaA, Weinheim

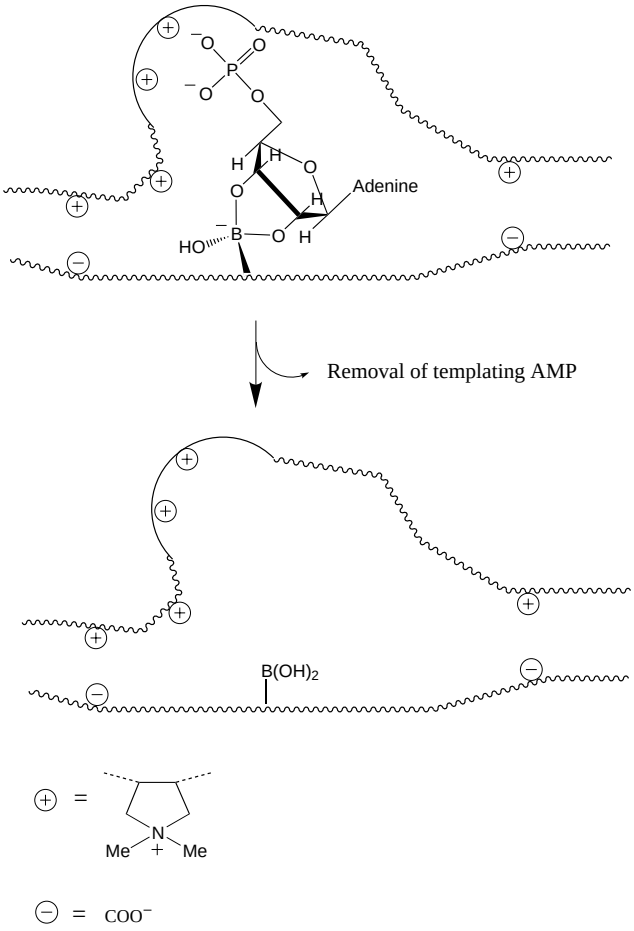
31 (89%) was formed. However, the crystals obtained from this reaction mixture were found to be exclusively the square compound **30**. Interestingly, when the crystallized solid was redissolved in acetonitrile and immediately analyzed by ^{1}H NMR spectroscopy the square–triangle ratio was 54:46. The importance of the anion was further demonstrated by the selective crystallization of **31** (from nitromethane/diethyl ether) in the presence of an excess of the large $[CoB_{18}C_4H_{22}]^-$ ion. The crystal structure analysis showed that two of the six triflate ions of **31** were exchanged for the larger anion. When a sample of the crystallized triangle was redissolved in nitromethane and immediately analyzed by NMR spectroscopy, the triangle was found exclusively. After approximately 45 min an equilibrium between the triangle and square structures of 95:5 was reached.

These two systems described by Stoddart et al.[37] and by Stang et al. [38] demonstrate the importance of anions in inducing selective crystallization of a specific supramolecular assembly. They also point out that the solid-state structure of a thermodynamically controlled system does not necessarily have to be the same than that one present in solution. Consequently, one needs to be very cautions when assigning the nature of an assembly both in solution and in the solid state. In these systems, once again, the very fine control exercised by anions in determining the structure of supramolecular assemblies is demonstrated.

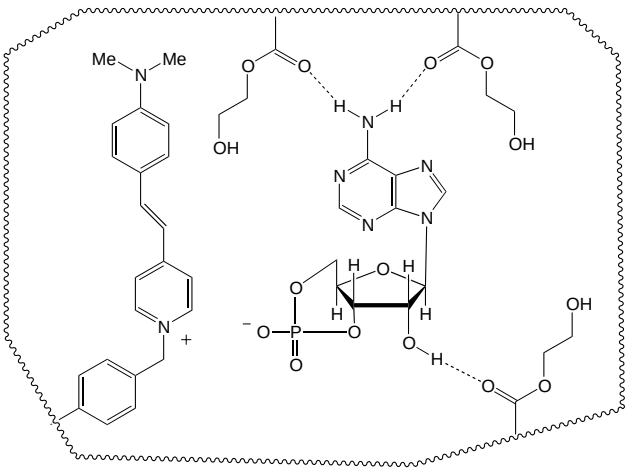
3.2. Molecularly Imprinted Polymers

Molecularly imprinted polymers (MIP) are materials with substrate recognition properties that can be prepared by polymerizing monomers in the presence of a templating agent.[39] This process generates cavities of specific size and shape (defined by the template) in the polymer that act as selective hosts for specific guests. Although MIPs have been studied for several years and imprinted materials for a wide range of substrates have been obtained, only a few examples have been reported where the templating agent is an anionic species. Examples of anion-templated MIPs are the AMP (adenosine monophoshate)-imprinted polymers reported by Shinkai et al.[40] The imprinted material was obtained by mixing the cationic polymer poly(diallyldimethylammonium chloride) with an anionic polymer functionalized with boronic acid groups in the presence of the templating anion AMP. The boronic groups of the polyanion are capable of binding to the *cis*-diol group of the ribose moiety of AMP, while the cationic polymer interacts electrostatically with the negatively charged phosphate group of AMP. When the templating anion is removed from this 1:1 polycation–polyanion complex, a polymeric material with clefts for selective binding of AMP is obtained (Scheme 20).

Another example of anion-templated MIP is the polymer-based fluorescent chemosensor for cyclic adenosine 3′:5′-monophosphate (cAMP) reported by Powell et al.[41] In this case the molecular imprints were prepared by using cAMP as a template and incorporating a fluorescent dye as an integral part of the recognition cavity (Scheme 21). In this way, the templated cavities not only recognize the cAMP guest, but



Scheme 20. Schematic representation of the AMP-templated synthesis of a molecularly imprinted polymer. The anionic AMP template organizes the monomers so that, after polymerization, a cavity is formed with the appropriate size and geometry to bind AMP selectively.[40]



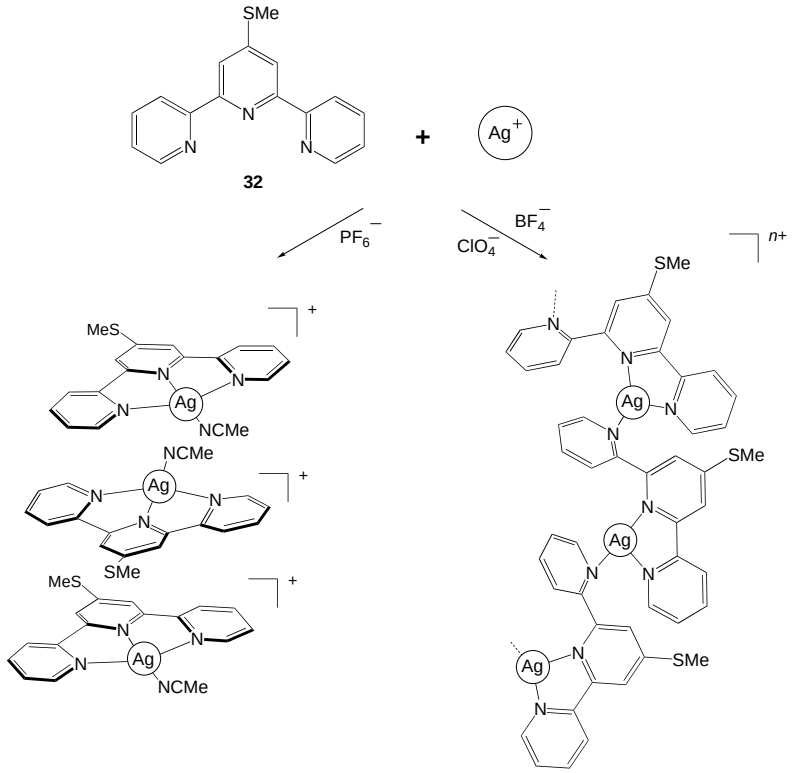
Scheme 21. Schematic representation of a cAMP-templated MIP with a luminescent fragment incorporated in the polymer. The anionic cAMP template organizes the monomers (one of which has optical properties associated) so that, after polymerization, a cavity is formed with the appropriate size and geometry to bind cAMP selectively.[41]

 © 2003 Wiley-VCH Verlag GmbH & Co. KGaA, Weinheim

also signal its presence by changes in luminescence (more specifically by quenching the luminescence in the presence of cAMP). The MIP synthesized in this way has good selectivity for the cAMP guest, but little affinity for the structurally similar cyclic guanosine 3′:5′-monophosphate (cGMP).

3.3. Coordination Networks and Polymers

The synthesis of metal-organic polymers and networks is an area that has received a great deal of attention within supramolecular chemistry during the past 10 to 15 years. In these systems the geometry, bulkiness, and flexibility of the ligands around the metal centers play a very important role in determining the structure of the final (thermodynamic) infinite assembly. However, several other factors can have an enormous influence on the outcome of these reactions, for example the nature of the anionic counterions present in the reaction mixture. Although it is tempting to propose that they should then be considered templating agents, on most occasions the anions act as ligands (and not true templating agents). The following discussion (with selected examples of anion-directed coordination networks and polymers) is not intended to be an exhaustive review of the topic and is limited to identifying some representative examples in which the role of anions as directing agents has been established. Moreover, only those systems in which the anions act as directing species *without* forming strong coordination bonds to the metal centers will be discussed. In those cases where there is coordination to the metal, although the anion clearly has an important effect on the final structure, it cannot be really considered a templating agent. For reviews on the area of metal-organic extended assemblies see reference [42].



Scheme 22. Silver(I) assemblies that are obtained in the presence of different anions. With PF_6^-, aggregates of monomers are obtained, while with smaller anions such as ClO_4^- and BF_4^-, a polymeric spiral structure is formed.[43]

Most of the reported anion-directed coordination polymers and networks are based on Ag^I and Cu^I centers. To prepare these extended structures, a metal salt is usually allowed to react with multipodal ligands in the appropriate stoichiometry. There are then several potential ways in which the components can assemble together; the choice of assembly will be influenced by the experimental conditions and by the nature of the anionic counterions. A systematic study of the role of different anions in the self-assembly of Ag^I and the terpyridine ligand **32** was recently published by Hannon et al.[43] When different silver salts were treated with **32** under the same experimental conditions, a range of assemblies was obtained. For example, the reaction of $AgBF_4$ or $AgClO_4$ in acetonitrile with **32** yields a polymeric spiral, while the analogous reaction with $AgPF_6$ leads to aggregates of monomers (Scheme 22). For the former assembly, the polymeric chains are packed in a grid surrounded by anions and solvents; in the second case, π–π stacks of silver complexes are obtained, which are separated by the PF_6^- ions.

Interestingly, when the same reactions are carried our in nitromethane, different products are formed: with $AgPF_6$ a polymeric spiral is assembled, while with $AgBF_4$ a pentanuclear spiral complex is obtained. These differences indicate the fine balance existing between the different supramolecular forces involved in the self-assembly process (i.e. not only do the anions play an important role but also the experimental conditions, such as the solvents used).

Suh and Min have reported another interesting example of anion-directed assembly of Ag^I extended structures by using the multipodal ligand ethylendiamine–tetrapropionitrile (**33**).[44] This ligand possess several potential coordination sites that can be used to form the one-dimensional chain $[Ag(L)(NO_3)]$ (**34**), the two-dimensional layer $[Ag(L)][OTf]$ (**35**), or the two-dimensional network $[Ag(L)][ClO_4]$ (**36**), when allowed to react with $AgNO_3$, AgOTf, or $AgClO_4$, respectively. In **34**, the nitrate anions are directly coordinated to the silver atoms, and hence it is not considered as a true anion-directed assembly. However, in **35** and **36** the anions are not coordinated to the silver center but encapsulated by the metal-organic assembly (Figures 13 and 14), suggesting that a combination of weak supramolecular interactions determines the final structure of the assemblies.

An interesting aspect of these systems is that they display anion-induced interconversion in the crystalline state. For example, when an insoluble crystalline sample of **35** was immersed in an aqueous solution of $NaNO_3$ (for 1 to 10 h depending on the concentration of the solution), the triflate anions in **35** were quantitatively exchanged by nitrate ions. The crystallinity of the sample was retained and the X-ray powder diffraction pattern was fully coincident with that of **34** (prepared directly from $AgNO_3$). This process was found to

 © 2003 Wiley-VCH Verlag GmbH & Co. KGaA, Weinheim

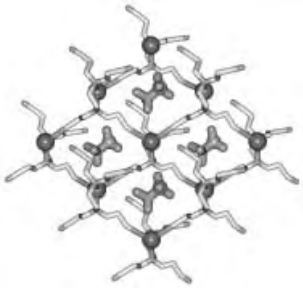


Figure 13. The two-dimensional layer structure of **35**, comprising a silver complex framework with encapsulated $CF_3SO_3^-$ ions.[44]

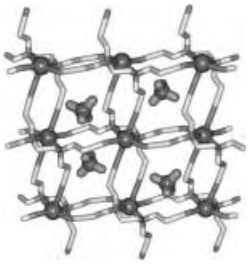


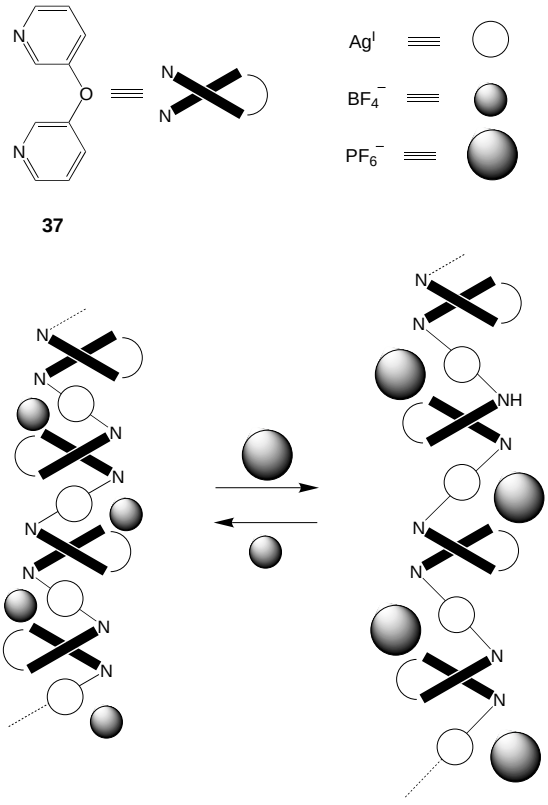
Figure 14. The two-dimensional layer structure of **36**, comprising a silver complex framework with encapsulated ClO_4^- ions.[44]

be reversible since the immersion of **34** into an aqueous solution of LiOTf led to the complete conversion of **34** to **35**. Similarly, when either **34** or **35** were immersed in an aqueous solution of $NaClO_4$ their conversion to **36** was observed. Interestingly, in this case the conversion was not reversible since **36** did not exchange the perchlorate anions for nitrate or triflate ions to yield **34** or **35**, respectively.

Jung et al. have reported the use of anions to fine-tune the conformation of silver-based helical polymers.[45] The reaction between ligand **37** and AgX ($X = NO_3^-$, BF_4^-, ClO_4^-, PF_6^-) yields the infinite helices [Ag(L)][X] (Scheme 23). The structural characterization of these polymers reveals that they have a helical conformation with the anions located in the columns between/inside the helical pitch. Depending on the counterion the helical pitch can be stretched from 7.430(2) ($X = NO_3^-$) to 9.621(2) Å ($X = PF_6^-$). An interesting aspect of these helices is that, once formed, the anions in each one of the four different helices can be exchanged in aqueous solution without destruction of the helical structure (although the corresponding change in the pitch of the helix is observed).

Although only a selected group of anion-directed silver-based polymers and networks has been discussed here, other relevant examples are those reported by the groups of Schröder,[46] Duan,[47] Champness,[48] Ciani,[49] Kang,[50] Sun,[51] Moore,[52] and Hong.[53] A thorough discussion of the role of anions in the assembly of each of these systems is out of the scope of this review and hence the reader is directed to the relevant references.

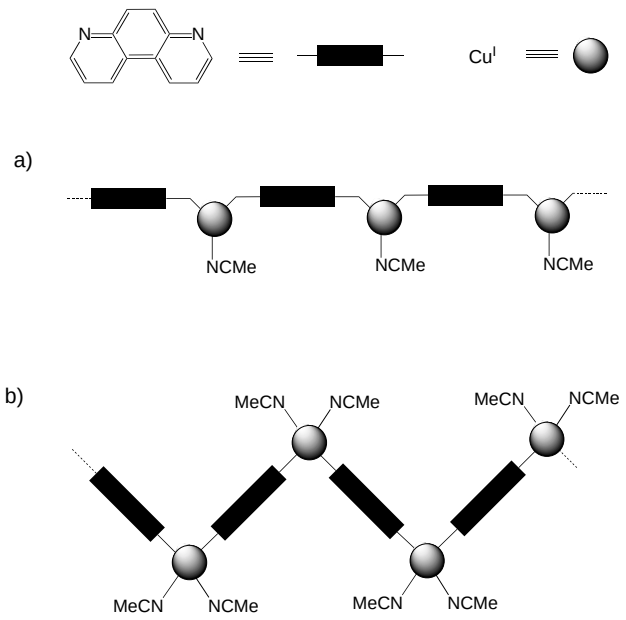
Likewise, there are many examples of coordination networks and polymers based on Cu^I (and Cu^{II}). In several of these metal-organic systems, anions have been identified to play important directing roles in the formation of the assemblies. As with the silver systems, it is not the intention here to discuss in detail all the reported examples where anions have been claimed to have a directing role. Hence, only a representative group of copper-based systems will be discussed (for other examples see the review by Munakata et al. where several examples of silver(I) and copper(I) polymers are discussed[54]). Keller and Lopez have studied systematically the influence of different anions on the formation of extended structures based on copper(I).[55] The structure of the linear polymeric assemblies formed when Cu^I



Scheme 23. Schematic representation of the silver-based polymers formed from ligand **37** and silver(I) salts. The helical pitch of the polymers is tuned by the anions.[45]

salts are treated with the 4,7-phenanthroline ligand (**38**) (Scheme 24), depends on the solvent—which coordinates to the metal center—and on the noncoordinating anions. In the presence of BF_4^- ions the formation of a polymer with the formula [Cu(L)(MeCN)][BF_4] (**39**) is observed, whereas with PF_6^- ions the polymeric assembly [Cu(L)$(MeCN)_2$][PF_6] (**40**) is formed. To accommodate the additional acetonitrile in **40**, a different arrangement of the polymeric chain (in comparison to **39**) is observed. As the authors of this system point out "*the question remains as to why the different anions preferentially form the two structures*". Although it is likely that a fine balance between several supramolecular interactions is responsible for these differences, the structural parameters of **39** and **40** indicate that, in **40**, there are four H···F contacts

 © 2003 Wiley-VCH Verlag GmbH & Co. KGaA, Weinheim



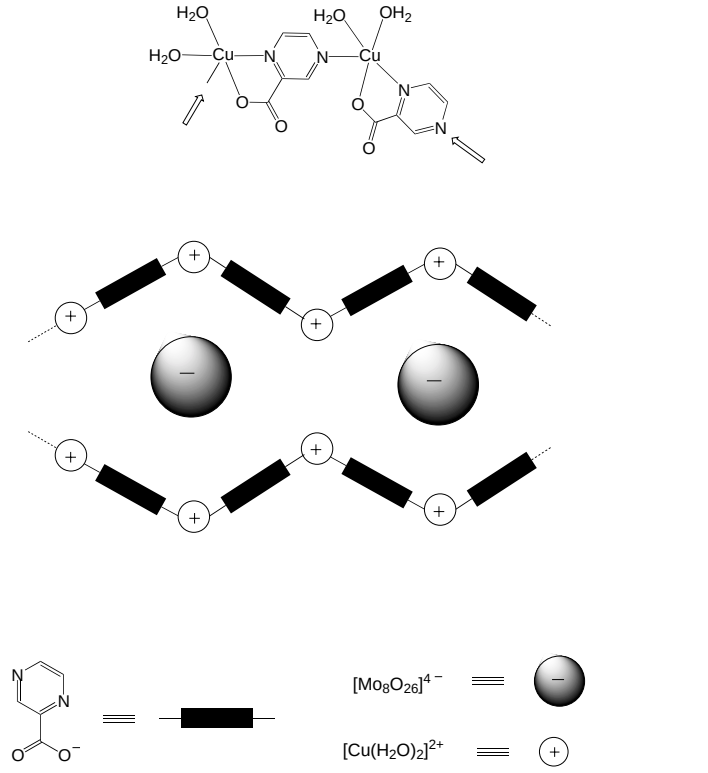
Scheme 24. Schematic representation of the copper-based polymers formed from 4,7-phenanthroline and copper(I) salts in the presence of BF_4^- (a) or PF_6^- (b).[55]

shorter than 2.6 Å (ranging from 2.42 to 2.60 Å). In contrast, there are seven H···F contacts shorter than 2.6 Å in **39** (ranging from 2.36 to 2.53 Å). The shorter average distances in **39** have been attributed to the better C–H···F accepting ability of the BF_4^- ion compared to the PF_6^- ion.

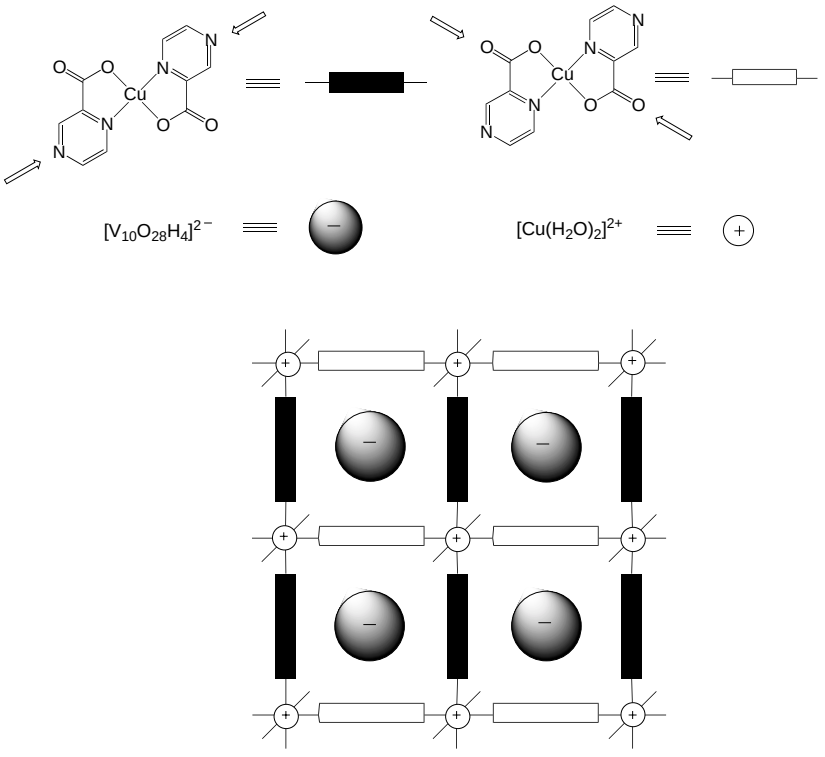
Jacobson et al. have recently reported the use of the large $[Mo_8O_{26}]^{4-}$ and $[V_{10}O_{28}H_4]^{2-}$ ions as directing species in the formation of copper(II) coordination polymers.[56] The reaction between $Cu(NO_3)_2$ and 2-pyrazinecarboxylate (L) led to the formation of the mononuclear compound $[Cu(L)_2(H_2O)_2]$ (**41**). However, when the reaction was carried out in the presence of $[Mo_8O_{26}]^{4-}$ and $[V_{10}O_{28}H_4]^{2-}$ (which are generated in situ in the course of the reaction) a one-dimensional chain and a two-dimensional layer were obtained, respectively (see Schemes 25 and 26). It is likely that the differences in shape, size, and charge between the two anions are the factors responsible for the formation of two very different assemblies. Other examples of copper-based polymers and networks in which anions play a role in their structures can be found in the review by Munakata et al.[54] and in the papers listed in reference [57].

4. Conclusions and Outlook

The recent developments in the supramolecular chemistry of anions have allowed us to uncover the *hidden* templating role of anionic species. The examples presented in this review demonstrate the wide range of different assemblies that can be prepared by using the directing properties of anions.



Scheme 25. Schematic representation of the one-dimensional polymer formed between 2-pyrazinecarboxylate and copper(II) salts in the presence of the polyoxo anion $[Mo_8O_{26}]^{-}$. The arrows indicate the coordination sites used to generate the polymer.[56]



Scheme 26. Schematic representation of the two-dimensional layer formed between 2-pyrazinecarboxylate and copper(II) salts in the presence of the polyoxo anion $[V_{10}O_{28}H_4]^{2-}$. The arrows indicate the coordination sites used to generate the network.[56]

 © 2003 Wiley-VCH Verlag GmbH & Co. KGaA, Weinheim

Although most of the anion-templated processes reported to date have been the results of serendipitous discoveries, they have provided an important body of results to allow a more rational approach to this area. There is now a pressing need to understand the thermodynamic and kinetic parameters that control such templated reactions so that reliable predictions and rational designs can be made. A better understanding of the templating properties of these species will have an important impact on several areas of chemical research. For example, the synthesis of selective anion receptors by using dynamic combinatorial libraries will greatly benefit from the use of anion-templated processes (as has been already shown by Fujita et al.[35]). The anion-templated synthesis of MIPs demonstrates that cavities for the selective binding of anionic species can be prepared. Such polymeric materials have important implications in the development of sensing and separation materials. In summary, a wide range of novel organic and inorganic assemblies can be selectively obtained by using anion templates. These examples are, without any doubt, only the "tip of the iceberg" of the many fascinating assemblies that will be prepared in the years to come by anion-templated processes.

I thank Prof. Kim Dunbar for useful discussions and for encouraging me to write this review; Dr. Joachim Steinke, Prof. Fraser Stoddart, and Prof. David Williams for their valuable comments; Dr. Andrew White for his enormous help with the figures presented in this review. The Engineering and Physical Sciences Research Council (EPSRC) is acknowledged for financial support.

Received: July 1, 2002 [A551]

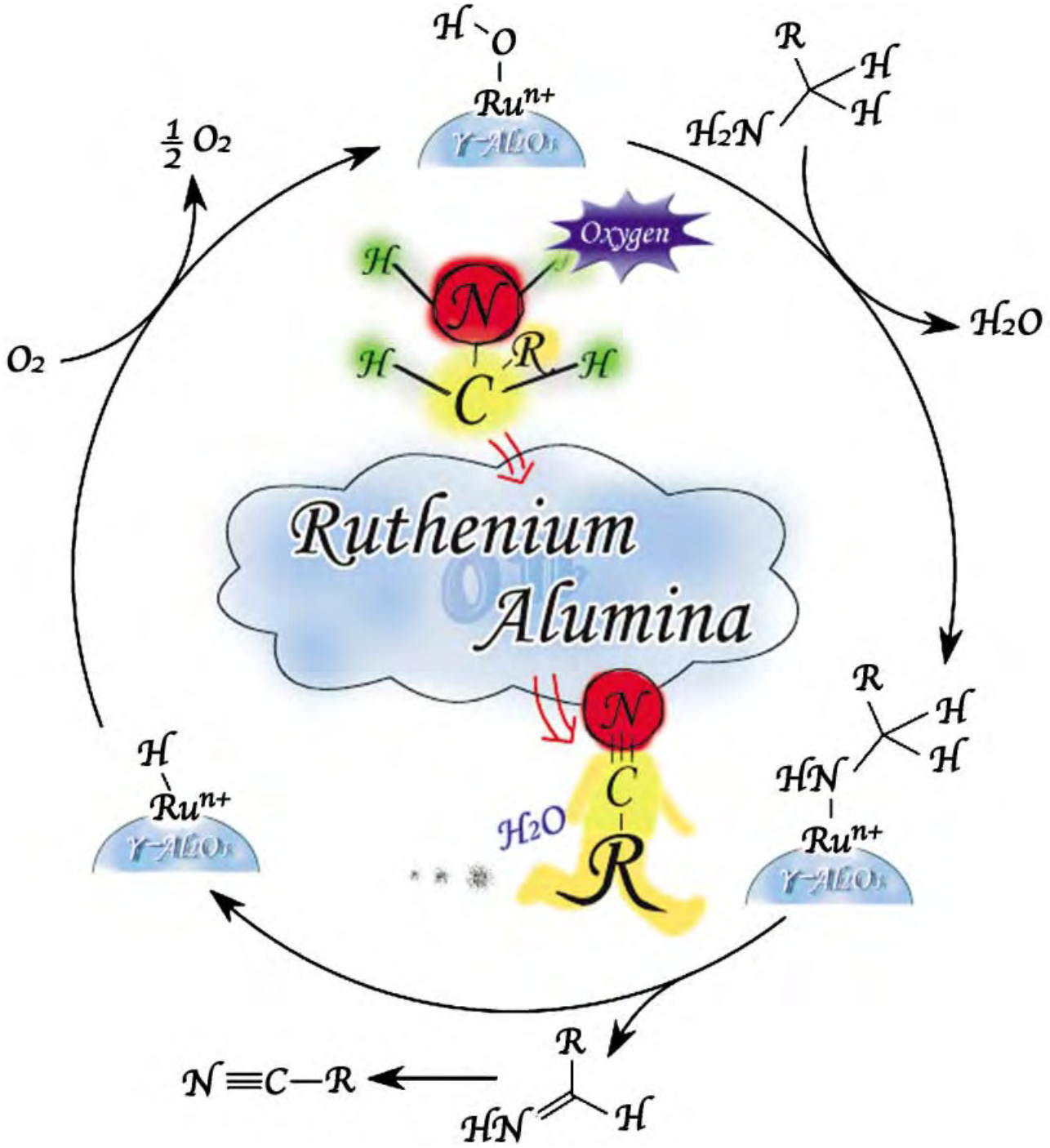
[1] D. H. Busch, *J. Inclusion Phenom. Mol. Recognit. Chem.* **1992**, *12*, 389 – 395.
[2] S. Anderson, H. L. Anderson, J. K. M. Sanders, *Acc. Chem. Res.* **1993**, *26*, 469 – 475.
[3] R. Hoss, F. Vögtle, *Angew. Chem.* **1994**, *106*, 389 – 398; *Angew. Chem. Int. Ed. Engl.* **1994**, *33*, 375 – 384.
[4] *Templated Organic Synthesis* (Ed.: F. Diederich, P. J. Stang), Wiley-VCH, Weinheim, **2000**.
[5] B. A. Moyer, P. V. Bonnesen in *Supramolecular Chemistry of Anions* (Eds.: A. Bianchi, K. Bowman-James, E. García-España), Wiley-VCH, Weinheim, **1997**, pp. 1 – 41.
[6] C. H. Henkels, J. C. Kurz, C. A. Fierke, T. G. Oas, *Biochemistry* **2001**, *40*, 2777 – 2789.
[7] P. A. Gale, *Coord. Chem. Rev.* **2001**, *213*, 79 – 128.
[8] P. A. Gale, *Coord. Chem. Rev.* **2000**, *199*, 181 – 233.
[9] P. D. Beer, P. A. Gale, *Angew. Chem.* **2001**, *113*, 502 – 532; *Angew. Chem. Int. Ed.* **2001**, *40*, 487 – 516.
[10] a) X. Yang, C. B. Knobler, M. F. Hawthorne, *Angew. Chem.* **1991**, *103*, 1519 – 1520; *Angew. Chem. Int. Ed. Engl.* **1991**, *30*, 1507 – 1508; b) Z. Zheng, C. B. Knobler, M. F. Hawthorne, *J. Am. Chem. Soc.* **1995**, *117*, 5105 – 5113.
[11] a) B. Hasenknopf, J.-M. Lehn, B. O. Kneisel, G. Baum, D. Fenske, *Angew. Chem.* **1996**, *108*, 1987 – 1989; *Angew. Chem. Int. Ed. Engl.* **1996**, *35*, 1838 – 1840; b) B. Hasenknopf, J.-M. Lehn, N. Boumediene, A. Dupont-Gervais, A. Van Dorsselaer, B. O. Kneisel, D. Fenske, *J. Am. Chem. Soc.* **1997**, *119*, 10956 – 10962; c) B. Hasenknopf, J.-M. Lehn, N. Boumediene, E. Leize, A. Van Dorsselaer, *Angew. Chem.* **1998**, *110*, 3458 – 3460; *Angew. Chem. Int. Ed.* **1998**, *37*, 3265 – 3268.
[12] a) R. Wang, H. D. Selby, H. Liu, M. D. Carducci, T. Jin, Z. Zheng, J. W. Anthis, R. J. Staples, *Inorg. Chem.* **2002**, *41*, 278 – 286; b) R. Wang, Z. Zheng, R. J. Staples, *Angew. Chem.* **1999**, *111*, 1927 – 1930; *Angew. Chem. Int. Ed.* **1999**, *38*, 1813 – 1815.
[13] a) R. Vilar, D. M. P. Mingos, A. J. P. White, D. J. Williams, *Angew. Chem.* **1998**, *110*, 1323 – 1326; *Angew. Chem. Int. Ed.* **1998**, *37*, 1258 – 1261; b) R. Vilar, D. M. P. Mingos, A. J. P. White, D. J. Williams, *Chem. Commun.* **1999**, 229 – 230; c) S.-T. Cheng E. Doxiadi, R. Vilar, A. J. P. White, D. J. Williams, *J. Chem. Soc. Dalton Trans.* **2001**, 2239 – 2244.
[14] A. Bashall, A. D. Bond, E. L. Doyle, F. García, S. Kidd, G. T. Lawson, M. C. Parry, M. McPartlin, A. D. Woods, D. S. Wright, *Chem. Eur. J.* **2002**, *8*, 3377 – 3385.
[15] a) D. Rais, J. Yau, D. M. P. Mingos, R. Vilar, A. J. P. White, D. J. Williams, *Angew. Chem.* **2001**, *113*, 3572 – 3575; *Angew. Chem. Int. Ed.* **2001**, *40*, 3464 – 3467; b) D. Rais, D. M. P. Mingos, R. Vilar, A. J. P. White, D. J. Williams, *J. Organomet. Chem.* **2002**, *652*, 87 – 93.
[16] a) P. J. Steel, C. J. Sumby, *Chem. Commun.* **2002**, 322 – 323; b) P. J. Steel, C. J. Sumby, *Inorg. Chem. Commun.* **2002**, *5*, 323 – 327.
[17] a) E. Alcalde, S. Ramos, L. Pérez-García, *Org. Lett.* **1999**, *1*, 1035 – 1038; b) E. Alcalde, C. Alvarez-Rúa, S. García-Granda, E. García-Rodriguez, N. Mesquida, L. Pérez-García, *Chem. Commun.* **1999**, 295 – 296.
[18] a) M. C. T. Fyfe, P. T. Glink, S. Menzer, J. F. Stoddart, A. J. P. White, D. J. Williams, *Angew. Chem.* **1999**, *111*, 2158 – 2160; *Angew. Chem. Int. Ed. Engl.* **1997**, *36*, 2068 – 2070; b) P. R. Ashton, M. C. T. Fyfe, S. K. Hickingbottom, S. Menzer, J. F. Stoddart, A. J. P. White, D. J. Williams, *Chem. Eur. J.* **1998**, *4*, 577 – 589; c) D. G. Amirsakis, M. A. García-Garibay, S. J. Rowan, J. F. Stoddart, A. J. P. White, D. J. Williams, *Angew. Chem.* **2001**, *113*, 4386 – 4391; *Angew. Chem. Int. Ed.* **2001**, *40*, 4256 – 4261; d) S. J. Cantrill, A. R. Pease, J. F. Stoddart, *J. Chem. Soc. Dalton Trans.* **2000**, 3715 – 3734.
[19] a) G. M. Hübner, J. Gläser, C. Seel, F. Vögtle, *Angew. Chem.* **1999**, *111*, 395 – 398; *Angew. Chem. Int. Ed.* **1999**, *38*, 383 – 386; b) C. Reuter, W. Wienand, G. M. Hübner, C. Seel, F. Vögtle, *Chem. Eur. J.* **1999**, *5*, 2692 – 2697; c) C. Seel, F. Vögtle, *Chem. Eur. J.* **2000**, *6*, 21 – 24.
[20] a) J. A. Wisner, P. D. Beer, M. G. B. Drew, *Angew. Chem.* **2001**, *113*, 3718 – 3721; *Angew. Chem. Int. Ed.* **2001**, *40*, 3606 – 3609; b) J. A. Wisner, P. D. Beer, N. G. Berry, B. Tomapatanget, *Proc. Natl. Acad. Sci. USA* **2002**, *99*, 4983 – 4986.
[21] J. L. Sessler, T. D. Mody, V. Lynch, *Inorg. Chem.* **1992**, *31*, 529 – 531.
[22] a) A. Müller, H. Reuter, S. Dillinger, *Angew. Chem.* **1995**, *107*, 2540 – 2558; *Angew. Chem. Int. Ed. Engl.* **1995**, *34*, 2328 – 2361; b) A. Müller, M. Penk, R. Rohlfing, E. Krickemeyer, J. Döring, *Angew. Chem.* **1990**, *102*, 927 – 928; *Angew. Chem. Int. Ed. Engl.* **1990**, *29*, 926 – 927; c) A. Müller, R. Rohlfing, E. Krickemeyer, H. Bögge, *Angew. Chem.* **1993**, *105*, 916 – 919; *Angew. Chem. Int. Ed. Engl.* **1993**, *32*, 909 – 912.
[23] C. J. Kuehl, Y. K. Kryschenko, U. Radhakrishnan, S. R. Seidel, S. D. Huang, P. J. Stang, *Proc. Natl. Acad. Sci. USA* **2002**, *99*, 4932 – 4936.
[24] a) C. S. Campos-Fernández, R. Clérac, K. R. Dunbar, *Angew. Chem.* **1999**, *111*, 3685 – 3688; *Angew. Chem. Int. Ed.* **1999**, *38*, 3477 – 3479; b) C. S. Campos-Fernández, R. Clérac, J. M. Koomen, D. H. Rusell, K. R. Dunbar, *J. Am. Chem. Soc.* **2001**, *123*, 773 – 774.
[25] D. M. P. Mingos, A. L. Rohl, *Inorg. Chem.* **1991**, *30*, 3769 – 3771.
[26] a) J. S. Fleming, K. L. V. Mann, C-A. Carraz, E. Psillakis, J. C. Jeffery, J. A. McCleverty, M. D. Ward, *Angew. Chem.* **1998**, *110*, 1315 – 1318; *Angew. Chem. Int. Ed.* **1998**, *37*, 1279; b) R. L. Paul, Z. R. Bell, J. C. Jeffery, J. A. McCleverty, M. D. Ward, *Proc. Natl. Acad. Sci. USA* **2002**, *99*, 4883 – 4888.

 © 2003 Wiley-VCH Verlag GmbH & Co. KGaA, Weinheim

[27] S. L. James, D. M. P. Mingos, A. J. P. White, D. J. Williams, *Chem. Commun.* **1998**, 2323 – 2324.
[28] X. Xu, E. J. MacLean, S. J. Teat, M. Nieuwenhuyzen, M. Chambers, S. L. James, *Chem. Commun.* **2002**, 78 – 79.
[29] Y. H. Kim, J. Calabrese, C. McEwen, *J. Am. Chem. Soc.* **1996**, *118*, 1545 – 1546.
[30] a) J. Sánchez-Quesada, C. Seel, P. Prados, J. de Mendoza, *J. Am. Chem. Soc.* **1996**, *118*, 277 – 278; b) V. Král, F. P. Schmidtchen, K. Lang, M. Berger, *Org. Lett.* **2002**, *4*, 51 – 54.
[31] J. Keegan, P. E. Kruger, M. Nieuwenhuyzen, J. O'Brien, N. Martin, *Chem. Commun.* **2001**, 2192 – 2193.
[32] a) D. A. McMorran, P. J. Steel, *Angew. Chem.* **1998**, *110*, 3483 – 3485; *Angew. Chem. Int. Ed.* **1998**, *37*, 3295 – 3297; b) P. J. Steel, personal communication.
[33] M. Fujita, S. Nagao, K. Ogura, *J. Am. Chem. Soc.* **1995**, *117*, 1649 – 1650.
[34] M. Aoyagi, K. Biradha, M. Fujita, *J. Am. Chem. Soc.* **1999**, *121*, 7457 – 7458.
[35] Y. Kubota, S. Sakamoto, K. Yamaguchi, M. Fujita, *Proc. Natl. Acad. Sci. USA* **2002**, *99*, 4854 – 4856.
[36] For references on dynamic libraries see: a) J. M. Lehn, *Chem. Eur. J.* **1999**, *5*, 2455 – 2463; b) R. L. E. Furlan, Y. F. Ng, S. Otto, J. K. M. Sanders, *J. Am. Chem. Soc.* **2001**, *123*, 8876 – 8877; c) S. J. Rowan, S. J. Cantrill, G. R. L. Cousins, J. K. M. Sanders, J. F. Stoddart, *Angew. Chem.* **2002**, *114*, 938 – 993; *Angew. Chem. Int. Ed.* **2002**, *41*, 898 – 952, and references therein.
[37] a) P. R. Ashton, S. J. Cantrill, J. A. Preece, J. F. Stoddart, Z.-H. Wang, A. J. P. White, D. J. Williams, *Org. Lett.* **1999**, *1*, 1917 – 1920; b) S. J. Cantrill, J. A. Preece, J. F. Stoddart, Z.-H. Wang, A. J. P. White, D. J. Williams, *Tetrahedron* **2000**, *56*, 6675 – 6681.
[38] M. Schweiger, S. R. Seidel, A. M. Arif, P. J. Stang, *Inorg. Chem.* **2002**, *41*, 2556 – 2559.
[39] a) J. H. G. Steinke, D. C. Sherrington, I. R. Dunkin, *Adv. Polym. Sci.* **1995**, *123*, 81 – 125; b) M. J. Whitcombe, E. N. Vulfson, *Adv. Mater.* **2001**, *13*, 467 – 491.
[40] Y. Kanekiyo, Y. Ono, K. Inoue, M. Sano, S. Shinkai, *J. Chem. Soc. Perkin Trans. 2* **1999**, 557 – 561.
[41] P. Turkewitsch, B. Wandelt, G. D. Darling, W. S. Powell, *Anal. Chem.* **1998**, *70*, 2025 – 2030.
[42] a) B. Moulton, M. J. Zaworotko, *Chem. Rev.* **2001**, *101*, 1629 – 1658; b) S. R. Batten, R. Robson, *Angew. Chem.* **1998**, *110*, 1558 – 1595; *Angew. Chem. Int. Ed.* **1998**, *37*, 1460 – 1494; c) P. J. Hagrman, D. Hagrman, J. Zubieta, *Angew. Chem.* **1999**, *111*, 2798 – 2848; *Angew. Chem. Int. Ed.* **1999**, *38*, 2638 – 2684.
[43] M. J. Hannon, C. L. Painting, E. A. Plummer, L. J. Childs, N. W. Alcock, *Chem. Eur. J.* **2002**, *8*, 2225 – 2238, and references therein.
[44] K. S. Min, M. P. Suh, *J. Am. Chem. Soc.* **2000**, *122*, 6834 – 6840.
[45] O.-S. Jung, Y. J. Kim, Y.-A. Lee, J. K. Park, H. K. Chae, *J. Am. Chem. Soc.* **2000**, *122*, 9921.
[46] a) M. A. Withersby, A. J. Blake, N. R. Champness, P. Hubberstey, W.-S. Li, M. Schröder, *Angew. Chem.* **1997**, *109*, 2421 – 2423; *Angew. Chem. Int. Ed. Engl.* **1997**, *36*, 2327 – 2329; b) A. J. Blake, G. Baum, N. R. Champness, S. S. M. Chung, P. A. Cooke, D. Fenske, A. N. Khlobystov, D. A. Lemenovskii, W.-S. Li, M. Schröder, *J. Chem. Soc. Dalton Trans.* **2000**, 4285 – 4291.
[47] C. He, B.-G. Zhang, C.-Y. Duan, J.-H. Li, Q.-J. Meng, *Eur. J. Inorg. Chem.* **2000**, 2549 – 2554.
[48] a) N. S. Oxtoby, A. J. Blake, N. R. Champness, C. Wilson, *Proc. Natl. Acad. Sci. USA* **2002**, *99*, 4905 – 4910; b) A. J. Blake, N. R. Champness, P. A. Cooke, J. E. B. Nicolson, C. Wilson, *J. Chem. Soc. Dalton Trans.* **2000**, 3811 – 3819.
[49] L. Carlucci, G. Ciani, D. M. Proserpio, A. Sironi, *Inorg. Chem.* **1998**, *37*, 5941 – 5943.
[50] Y. Kang, S. S. Lee, K.-M. Park, S. H. Lee, S. O. Kang, J. Ko, *Inorg. Chem.* **2001**, *40*, 7027 – 7031.
[51] B.-L. Fei, W.-Y. Sun, K.-B. Yu, W.-X. Tang, *J. Chem. Soc. Dalton Trans.* **2000**, 805 – 811.
[52] K. A. Hirsch, S. R. Wilson, J. S. Moore, *Inorg. Chem.* **1997**, *36*, 2960 – 2968.
[53] M. Hong, W. Su, R. Cao, M. Fujita, J. Lu, *Chem. Eur. J.* **2000**, *6*, 427 – 431.
[54] a) M. Munakata, L. P. Wu, T. Kuroda-Sowa, *Adv. Inorg. Chem.* **1999**, *46*, 173 – 303, and references therein; b) A. N. Khlobystov, A. J. Blake, N. R. Champness, D. A. Lemenovskii, A. G. Majouga, N. V. Zyk, M. Schröder, *Coord. Chem. Rev.* **2001**, *222*, 155 – 192.
[55] S. Lopez, S. W. Keller, *Inorg. Chem.* **1999**, *38*, 1883.
[56] L.-M. Zheng, Y. Wang, X. Wang, J. D. Korp, A. J. Jacobson, *Inorg. Chem.* **2001**, *40*, 1380 – 1385.
[57] a) M. Maekawa, H. Konaka, Y. Suenaga, T. Kuroda-Sowa, M. Munakata, *J. Chem. Soc. Dalton Trans.* **2000**, 4160 – 4166, and references therein; b) T. Kuroda-Sowa, T. Horino, M. Yamamoto, Y. Ohno, M. Maekawa, M. Munakata, *Inorg. Chem.* **1997**, *36*, 6382 – 6389; c) M.-L. Tong, B.-H. Ye, J.-W. Cai, X.-M. Chen, S. W. Ng, *Inorg. Chem.* **1998**, *37*, 2645 – 2650; d) C. Inman, J. M. Knaust, S. W. Keller, *Chem. Commun.* **2002**, 156 – 157.

 © 2003 Wiley-VCH Verlag GmbH & Co. KGaA, Weinheim

Communications



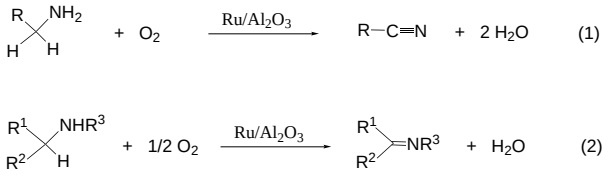
A heterogeneous alumina-supported ruthenium catalyst, which is easy to prepare, inexpensive to use, and capable of being recycled, has been shown to successfully promote the oxidation of a number of primary and secondary amines to the corresponding nitriles and imines in good yield. For more information see the Communication by N. Mizuno and K. Yamaguchi on the following pages.

DOI: 10.1002/anie.200250779
© 2003 Wiley-VCH Verlag GmbH & Co. KGaA, Weinheim

Supported Ru Catalysis of Amines

Efficient Heterogeneous Aerobic Oxidation of Amines by a Supported Ruthenium Catalyst**

*Kazuya Yamaguchi and Noritaka Mizuno**



Oxidative functional transformations of organic compounds are important in industry and synthetic chemistry.[1–3] Stoichiometric amounts of metal oxidants such as dichromate ions, permanganate ions, manganese dioxide, silver oxide, and lead tetraacetate are often still used for the transformations.[1–3] The stoichiometric use and disposal of such oxidants is undesirable from both economical and environmental points of view. Therefore, much attention has been paid to the use of transition-metal catalysts to achieve effective oxidation, with dioxygen and hydrogen peroxide as oxidants.[4,5]

Nitriles and imines are used as versatile synthetic intermediates. Although several oxidation procedures that use stoichiometric reagents for the synthesis of nitriles and imines from amines are known,[6–9] only a few catalytic procedures have been reported.[10–16] A number of ruthenium complexes have been used for the oxidation of amines with dioxygen,[11–14] iodosylbenzene,[15] and persulfate ions[16] as oxidants. However, these systems are not generally useful because of their low turnover numbers and frequencies, the formation of significant amounts of by-products, severe deactivation of the catalysts, and narrow applicability to a limited number of amines.[10–16]

Very recently we reported the effective aerobic heterogeneous oxidation of both activated and nonactivated alcohols containing sulfur, nitrogen, and carbon–carbon double bonds with dioxygen or in air, catalyzed by ruthenium supported on alumina (Ru/Al_2O_3).[17] During the course of our investigation of Ru/Al_2O_3-catalyzed aerobic alcohol oxidation we found that this system could be effective for the oxidation of various amines to the corresponding nitriles or imines [Eqs. (1) and (2)]. To the best of our knowledge, the procedure reported in this paper is an efficient and widely applicable method for the aerobic oxidation of various amines.

The catalytic activity and selectivity for the oxidation of 4-methylbenzylamine with O_2 (1 atm) at 373 K were compared for a variety of ruthenium catalysts; the results are shown in Table 1. Oxidation did not occur in the absence of the catalyst or in the presence of γ-Al_2O_3. Among the various ruthenium catalysts tested, Ru/Al_2O_3 showed the highest catalytic activity (93% yield after 1 h) for the oxidation of 4-methylbenzylamine to 4-methylbenzonitrile under the experimental conditions. The reaction rate for the oxidation of 4-methylbenzylamine was 6.25×10^{-3} M min^{-1}, approximately 40 times higher than that for the active heterogeneous catalyst $[(RuCl)_2Ca_8(PO_4)_6(OH)_2]$ (1.60×10^{-4} M min^{-1}; Table 1, entry 2),[11] and higher than for homogeneous ruthenium catalysts, such as $[n\mathrm{Pr}_4\mathrm{NRuO}_4]$, $RuCl_3$, $[RuCl_2(PPh_3)_3]$, $[RuCl_2(dmso)_4]$, $[\{RuCl_2(p\text{-cymene})\}_2]$, and $[RuCl_2(bpy)_2]$ (bpy = 2,2′-bipyridyl).

Table 1: The oxidation of 4-methylbenzylamine with dioxygen using various catalysts.[a]

Entry	Catalyst	Rate $\times 10^3$ [M^{-1} min^{-1}]	Conversion of amine [%]	Selectivity to nitrile [%]
1	Ru/Al_2O_3	6.25	>99	93
2[b]	$[(RuCl)_2Ca_8(PO_4)_6(OH)_2]$	0.16	5	97
3	$Ru(OH)_3 \cdot n\,H_2O$	0.07	2	95
4	RuO_2	–	no reaction	–
5	$[n\mathrm{Pr}_4\mathrm{NRuO}_4]$	2.24	46	88
6	$RuCl_3 \cdot n\,H_2O$	0.94	24	81
7	$[Ru(acac)_3]$	–	no reaction	–
8	$[RuCl_2(PPh_3)_3]$	0.98	25	94
9	$[RuCl_2(DMSO)_4]$	0.72	22	75
10	$[\{RuCl_2(p\text{-cymene})\}_2]$	0.19	6	96
11	$[RuCl_2(bpy)_2]$	0.09	3	97
12[c]	Al_2O_3	–	no reaction	–
13	no catalyst	–	no reaction	–

[a] Reaction conditions: 4-Methylbenzylamine (1 mmol), Ru catalyst (Ru: 2.8 mol%), $PhCF_3$ (5 mL), 373 K, O_2 (1 atm), 1 h. Conversion and selectivity were determined by GC using diphenyl as an internal standard. The main by-product was *N*-(4-methylbenzylidene)-4-methylbenzylamine. [b] Prepared according to the literature procedure.[11] [c] Al_2O_3 (0.2 g).

After oxidation, the Ru/Al_2O_3 catalyst could be easily separated by filtration; induced coupled plasma (ICP) analysis confirmed that no Ru was present in the filtrate. In addition, the oxidation process was terminated by the removal of Ru/Al_2O_3 from the reaction solution. These results indicate that any Ru species that had leached into the reaction solution were not catalytically active and that the observed catalysis is truly heterogeneous.[18] The Ru/Al_2O_3 catalyst could be reused, and both the catalytic activity and selectivity towards oxidation reactions were retained (entry 11 in Table 2).

[*] Prof. Dr. N. Mizuno, Dr. K. Yamaguchi
Department of Applied Chemistry, School of Engineering
The University of Tokyo
7-3-1 Hongo, Bunkyo-ku, Tokyo 113-8656 (Japan)
Fax: (+81) 3-5841-7220
E-mail: tmizuno@mail.ecc.u-tokyo.ac.jp

[**] This work was supported in part by a Grant-in-Aid for Scientific Research from the Ministry of Education, Culture, Sports, Science, and Technology of Japan.

Supporting information for this article is available on the WWW under http://www.angewandte.org or from the author.

 © 2003 Wiley-VCH Verlag GmbH & Co. KGaA, Weinheim DOI: 10.1002/anie.200250779

Table 2: The oxidation of various amines with dioxygen, catalyzed by Ru/Al_2O_3.[a]

Entry	Substrate	Time [h]	Conversion [%]	Product	Selectivity [%]
1	benzylamine	1	>99	benzonitrile	82
2	2-methoxybenzylamine	1	>99	2-methoxybenzonitrile	97
3	3-methoxybenzylamine	1	94	3-methoxybenzonitrile	93
4	4-methylbenzylamine	1	>99	4-methylbenzonitrile	93
5	geranylamine	10	98	geranylnitrile	90
6	*n*-octylamine	2	>99	*n*-octanenitrile	96
7	*n*-dodecylamine	3	84	*n*-dodecanenitrile	90
8	*N*-benzylaniline	15	85	*N*-benzylideneaniline	94
9[b]	dibenzylamine	16	85	*N*-benzylidenebenzylamine	84[c]
10	indoline	2	>99	indole	>99
11[d]	indoline	2	>99	indole	>99
12	1,2,3,4-tetrahydroquinoline	7	95	quinoline	>99

[a] Reaction conditions: Amine (1 mmol), Ru/Al_2O_3 (Ru: 2.8 mol%), $PhCF_3$ (5 mL), 373 K, O_2 (1 atm). Conversion and selectivity were determined by GC using naphthalene or diphenyl as an internal standard. The main by-products were *N*-alkylimines. [b] *p*-Xylene (5 mL) was used as a solvent, and the reaction was carried out at 403 K. [c] Benzonitrile (7% selectivity) and benzaldehyde (6% selectivity) were formed as by-products. [d] This experiment used a recycled catalyst; the reaction conditions were the same as those in entry 10, except that the recovered Ru/Al_2O_3 catalyst was used.

The Ru/Al_2O_3 catalyst showed high activity for the oxidation of activated and non-activated amines with dioxygen; the results are summarized in Table 2. All primary benzylic amines with $-CH_2NH_2$ functional groups were converted into the corresponding benzonitriles in high yields (Table 2; entries 1–4). The olefinic carbon–carbon double bond did not affect oxidation under the chosen reaction conditions, and only the amino function was dehydrogenated to a nitrile, without isomerization of the double bond and intramolecular hydrogen transfer (Table 2; entry 5). Primary aliphatic amines such as *n*-octylamine and *n*-dodecylamine were effectively oxidized to the corresponding nitriles (Table 2; entries 6 and 7). Secondary and heterocyclic amines, as well as primary amines, were also selectively oxidized. In the case of the secondary amine *N*-benzylaniline, *N*-benzylideneaniline was obtained in a high yield (Table 2; entry 8). Dibenzylamine also afforded the corresponding *N*-benzylidenebenzylamine as the main product, together with benzaldehyde and benzonitrile (Table 2; entry 9). Heterocyclic amines of indoline and 1,2,3,4-tetrahydroquinoline gave indole and quinoline in greater than 99 and 95% yields, respectively (Table 2; entries 10 and 12). The oxidation of tertiary amines, such as pyridine and quinoline did not proceed at all under the chosen reaction conditions.

Small quantities of *N*-alkylimine products were observed in the oxidation of primary amines, which are formed as condensation products of the starting amines and aldehydes through imine hydrolysis. Such findings show that imines are formed as intermediate products which are rapidly dehydrogenated to nitriles. The conversion and selectivity of the oxidation of 1,2,3,4-tetrahydroquinoline was not affected by the addition of the radical scavenger 2,6-di-*tert*-butyl-4-methylphenol. In accordance with ref. [17], the skeletal isomerization of a cyclopropyl ring does not take place. This evidence shows that a radical is not involved in the present oxidation reaction. The amount of dioxygen consumed was equivalent to the quantity of 4-methylbenzylamine produced; this 1:1 relationship suggests that simple dehydrogenation does not occur. A good linear correlation between values of $\log(k_X/k_H)$ and the Brown–Okamoto constant σ^+[19] ($R^2 = 0.99$; Figure 1) was observed for the competitive oxidation of substituted benzylamines (X = *p*-Cl, *p*-H, *p*-Me, *m*-OMe, and *p*-OMe). The resulting Hammett parameter ρ was -0.154, which indicates that a carbocation-type intermediate is involved in the oxidation process.[20] When *N*-(4-methylbenzylidene)aniline (1 mmol) was treated with benzylamine (2 mL) under an argon atmosphere, *N*-phenyl-4-methylbenzylamine was obtained together with a small quantity of benzonitrile [Eq. (3)].

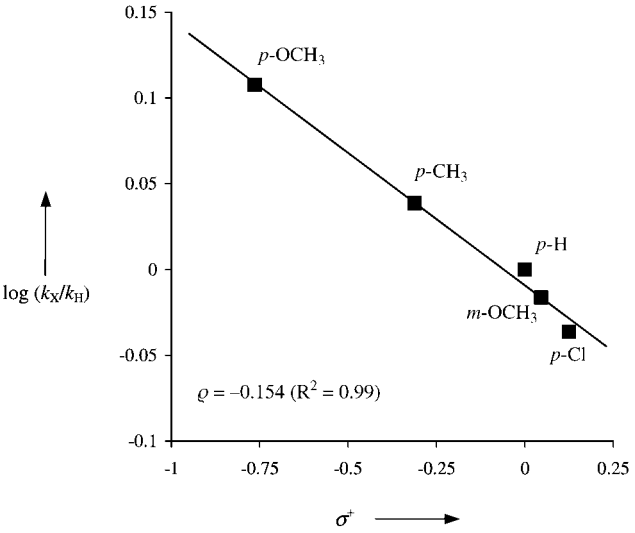
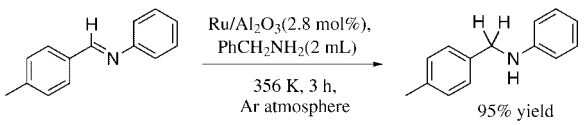


Figure 1. Hammett plots for the oxidation of substituted benzylamines with dioxygen using a Ru/Al_2O_3 catalyst; the reaction conditions are given in Table 2.

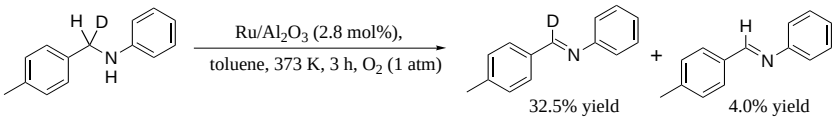
This fact illustrates that transfer hydrogenation from benzylamine to *N*-(4-methylbenzylidene)aniline takes place, which suggests that a ruthenium hydride species is formed.[21–24]



(3)

On the basis of the experimental results, a possible reaction mechanism (Figure 2) is proposed. Initially, ligand exchange between ruthenium hydroxide species and an amine takes place to form a ruthenium amide species. The ruthe-

 © 2003 Wiley-VCH Verlag GmbH & Co. KGaA, Weinheim



(4)

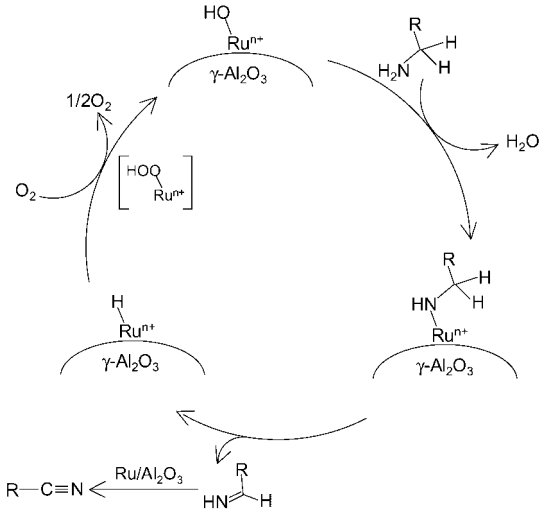


Figure 2. A possible reaction mechanism for the catalytic formation of imines and nitriles from amines.

nium amide then undergoes β-hydrogen elimination to form the corresponding imine and ruthenium hydride species, a process that has been discussed elsewhere.[25] The hydride species was then reoxidized by dioxygen,[26] and the dehydrogenation of the imine to the nitrile rapidly takes place in the same way as for the oxidation of primary amines with $-CH_2NH_2$ functions. Kinetic studies show a zero-order dependence for the reaction rate on both the partial pressure of dioxygen (P_{O2}: 0.2–2.0 atm) and the amine concentration (0.099–0.471M), and a first-order relationship with the amount of Ru/Al_2O_3 catalyst employed (Ru: 1.4–5.6 mol%). Furthermore, the value for the kinetic isotope effect (k_H/k_D) was 8.1 ± 0.3 for the intramolecular competitive oxidation of *N*-phenyl-α-deutero-4-methylbenzylamine at 373 K [Eq. (4)]. Based on these facts, it is probable that β-hydrogen elimination of the ruthenium amide species is the rate-determining step.

In conclusion, Ru/Al_2O_3 can act as an efficient heterogeneous catalyst for the oxidation of non-activated, as well as activated amines to the corresponding nitriles or imines with 1 atm of dioxygen or air.

Experimental Section

The Ru/Al_2O_3 catalyst (1.4 wt% Ru) was prepared by a previously reported method.[17] Solvents were carefully dried and purified according to a literature procedure,[27] and substrates were also purified before use.[27] *N*-Phenyl-α-deutero-4-methylbenzylamine was synthesized by the reduction of *N*-(4-methylbenzylidene)aniline with lithium aluminum deuteride, in a modification of the procedure reported for the synthesis of deuterium-labeled toluene.[28]

The oxidation of amines was typically carried out as follows: A suspension of Ru/Al_2O_3 (Ru: 2.8 mol%) in trifluorotoluene (5 mL) was stirred for 5 min at room temperature. 4-Methylbenzylamine (1 mmol) was added and dioxygen was passed through the suspension. The resulting mixture was then heated at 373 K and water was removed azeotropically under an O_2 flow. After 1 h, 4-methylbenzonitrile was obtained in a 93% yield (by gas chromatography). The catalyst was separated by filtration, washed with acetone, and dried in vacuo prior to being recycled.

Received: December 16, 2002 [Z50779]

Keywords: amines · heterogeneous catalysis · oxidation · oxygen · ruthenium

[1] R. A. Sheldon, J. K. Kochi, *Metal Catalyzed Oxidations of Organic Compounds,* Academic Press, New York, **1981**.
[2] C. L. Hill in *Advances in Oxygenated Processes, Vol. 1* (Eds.: A. L. Baumstark), JAI, London, **1988**, p. 1.
[3] M. Hudlucky, *Oxidations in Organic Chemistry*, American Chemical Society, Washington, DC, **1990** (ACS Monograph Series).
[4] R. A. Sheldon, *Green Chem.* **2000**, *2*, G1.
[5] P. T. Anastas, L. B. Bartlett, M. M. Kirchhoff, T. C. Williamson, *Catal. Today* **2000**, *55*, 11.
[6] P. Capdevielle, A. Lavigne, M. Maumy, *Synthesis* **1989**, 453.
[7] M. V. George, K. S. Balachandran, *Chem. Rev.* **1975**, *75*, 491.
[8] J. B. Lee, C. Parkin, M. J. Shaw, N. A. Hampson, K. I. MacDonald, *Tetrahedron*, **1973**, *29*, 751.
[9] J. S. Belew, C. Garza, J. W. Mathieson, *J. Chem. Soc.* **1970**, 634.
[10] S. Yamazaki, Y. Yamazaki, *Bull. Chem. Soc. Jpn.* **1990**, *63*, 301.
[11] K. Mori, K. Yamaguchi, T. Mizugaki, K. Ebitani, K. Kaneda, *Chem. Commun.* **2001**, 461.
[12] A. J. Bailey, B. R. James, *Chem. Commun.* **1996**, 2343.
[13] S. Cenini, F. Porta, M. Pizzottio, *J. Mol. Catal.* **1982**, *15*, 297.
[14] R. Tang, S. E. Diamond, N. Neary, F. Mares, *J. Chem. Soc. Chem. Commun.* **1978**, 562.
[15] F. Porta, C. Crotti, S. Cenini, *J. Mol. Catal.* **1989**, *50*, 333.
[16] G. Green, W. P. Griffith, D. M. Hollinshead, S. V. Ley, M. Schröder, *J. Chem. Soc. Perkin Trans. 1* **1984**, 681.
[17] K. Yamaguchi, N. Mizuno, *Angew. Chem.* **2002**, *114*, 4720; *Angew. Chem. Int. Ed.* **2002**, *41*, 4538.
[18] R. A. Sheldon, M. Wallau, I. W. C. E. Arends, U. Schuchardt, *Acc. Chem. Res.* **1998**, *31*, 485.
[19] H. C. Brown, Y. Okamoto, *J. Am. Chem. Soc.* **1958**, *80*, 4979.
[20] K. A. Connors, *Chemical Kinetics, The Study of Reaction Rates in Solution*, VCH Publishers, New York, **1990**.
[21] R. Noyori, M. Yamakawa, S. Hashiguchi, *J. Org. Chem.* **2001**, *66*, 7932.
[22] E. Mizushima, M. Yamaguchi, T. Yamagishi, *Chem. Lett.* **1997**, 237.
[23] R. L. Chowdhury, J.-E. Bäckvall, *J. Chem. Soc. Chem. Commun.* **1991**, 1063.
[24] S.-I. Murahashi, T. Naota, K. Ito, Y. Maeda, H. Taki, *J. Org. Chem.* **1987**, *52*, 4319.
[25] S. E. Diamond, F. Mares, *J. Organomet. Chem.* **1977**, *142*, C55.
[26] While the reoxidation of ruthenium hydride species may proceed through the formation of hydrogen peroxide, the filtrate for the oxidation of 4-methylbenzylamine with dioxygen gave a negative result in a peroxide test (Quantofix test stick; detection limit = 1 mg L^{-1} H_2O_2). The catalytic oxidation of 4-methylbenzylamine with hydrogen peroxide was only moderately success-

 © 2003 Wiley-VCH Verlag GmbH & Co. KGaA, Weinheim

ful as a result of the rapid decomposition of hydrogen peroxide, which is in agreement with the rapid decomposition of the Ru^{n+}–OOH species that do not contribute to the oxidation of the amines described in Figure 2.

[27] *Purification of Laboratory Chemicals*, 3rd ed. (Eds.: D. D. Perrin, W. L. F. Armarego), Pergamon, Oxford, UK, **1988**.

[28] H. L. Holland, F. M. Brown, M. Conn, *J. Chem. Soc. Perkin Trans. 2* **1990**, 1651.

 © 2003 Wiley-VCH Verlag GmbH & Co. KGaA, Weinheim

Magnetic Nanowires

Cyanide-Bridged Iron(III)–Cobalt(II) Double Zigzag Ferromagnetic Chains: Two New Molecular Magnetic Nanowires**

Rodrigue Lescouëzec, Jacqueline Vaissermann, Catalina Ruiz-Pérez, Francesc Lloret, Rosa Carrasco, Miguel Julve, Michel Verdaguer,* Yves Dromzee, Dante Gatteschi, and Wolfgang Wernsdorfer*

The occurrence of a slow relaxation of the magnetization in a one-dimensional (1D) system was recently reported by one of us.[1] The system was claimed to illustrate, for the first time, a theoretical model designed by Glauber in 1963 for anisotropic Ising systems[2] and opened the perspective of a potential use of 1D magnetic molecular nanowires for information storage. Even though 1D magnetism is a very active area of research, such dynamic behavior was never detected before since it is not clear how to fulfill experimentally the requirements of a perfect 1D Ising-type chain. This finding prompted us to look carefully at 1D systems containing anisotropic elements, such as cobalt(II) and low-spin iron(III) centers that we synthesized recently,[3] to investigate their anisotropic magnetic properties and to study the dynamics of their magnetization.

The stable low-spin cyanide-containing iron(III) precursors $[Fe^{III}(L)(CN)_4]^-$ (L = bidentate nitrogen donor) react with hydrated metal ions in aqueous solution[4,5] and afford single crystals of the bimetallic double zigzag chains $[\{Fe^{III}(L)(CN)_4\}_2Co^{II}(H_2O)_2]\cdot 4H_2O$ (**1** with L = 2,2′-bipyridine (bpy) and **2** with L = 1,10-phenanthroline (phen)). We found that **1** and **2** show intrachain ferromagnetic coupling, 1D Ising-type behavior, slow relaxation of the magnetization, and hysteresis effects and thus are the second examples of anisotropic molecular magnetic nanowires and the first with an intrachain ferromagnetic coupling. Their preparation, X-ray crystal structure,[6] and preliminary static and dynamic magnetism are reported herein.

Compounds **1** and **2** are isostructural (monoclinic system, space group $P2_1/n$). They are made up of neutral cyanide-bridged Co^{II}–Fe^{III} double zigzag chains and uncoordinated water molecules which are linked through van der Waals forces and hydrogen bonds. Within each chain, the $[FeL(CN)_4]^-$ entity acts as a bismonodentate ligand towards two *trans*-diaquacobalt(II) units through two of its four cyanide groups in *cis* positions (Figure 1) affording bimetallic double chains which run parallel to the *a* axis (Figure 2). They show two orientations of their mean planes (Fe_2Co_2), forming an angle of $\pm 70°$ with the *b* axis. The metal atoms in **1** and **2** are six-coordinate: two nitrogen atoms from bpy (**1**) or phen (**2**) and four cyanide carbon atoms around the Fe centers, two water molecules in *trans* position and four cyanide nitrogen atoms around the Co centers build distorted octahedral geometries. Bond lengths and angles around the Fe atom in **1** and **2** are close to those observed in the low-spin iron(III) unit $[FeL(CN)_4]^-$ (L = bpy and phen) in mononuclear,[4,5] heterotrinuclear,[5] and bimetallic chain[4,5] compounds. The values of the Fe-C-N angles for both terminal (176.3(3) and 176.7(2)° in **1** and 177.4(1) and 176.1(1)° in **2**) and bridging cyanides (174.6(2) and 178.7(2)° in **1** and 175.0(1) and 174.7(1)° in **2**) depart somewhat from strict linearity. The $Co–O_{water}$ bond (2.103(2) in **1** and 2.0886(4) Å in **2**) is similar to those observed in aqua complexes of high-spin cobalt(II).[7] The values of the $Co–N_{cyanide}$ bond lengths in **1** (2.125(2) and 2.104(2) Å) and **2** (2.147(2) and 2.113(2) Å) are significantly longer than those observed in the Co^{III}-N≡C-Fe^{III} unit (diamagnetic Co^{III} and low-spin Fe^{III}) of the single cyanide-bridged complexes $[L^1Co^{III}NCFe^{III}(CN)_5]\cdot 4H_2O$ (L^1 = 6-methyl-1,4,8,11-tetraazacyclotetra-decan-6-amine; 1.941(8) Å) and $[L^2Co^{III}NCFe^{III}(CN)_5]\cdot 4H_2O$ (L^2 = 10-methyl-1,4,8,12-tetraazacyclopentadecan-10-amine; 1.897(14) Å),[8] which is in agreement with the presence of high-spin cobalt(II) ions. The Co-N≡C entities in **1** (165.8(2) and 169.4(2)°) and **2** (164.77(2)

[*] Prof. Dr. M. Julve, Dr. R. Lescouëzec, Prof. Dr. F. Lloret, Dr. R. Carrasco
Departament de Química Inorgànica/Instituto de Ciencia Molecular
Facultat de Química de la Universitat de València
Dr. Moliner 50, 46100 Burjassot, València (Spain)
Fax: (+34) 96-386-4322
E-mail: miguel.julve@uv.es
Prof. Dr. M. Verdaguer, Dr. J. Vaissermann, Dr. Y. Dromzee
Laboratoire de Chimie Inorganique et Matériaux Moléculaires
Unité CNRS 7071, Université Pierre et Marie Curie
4 Place Jussieu, Case 42, 75252 Paris Cedex 05 (France)
Fax: (+33) 1-4427-3841
E-mail: miv@ccr.jussieu.fr
Prof. Dr. C. Ruiz-Pérez
Laboratorio de Rayos X y Materiales Moleculares
Departamento de Física Fundamental II
Facultad de Física de la Universidad de La Laguna
Avda. Astrofísico Francisco Sánchez s/n, 38204 La Laguna, Tenerife (Spain)
Prof. Dr. D. Gatteschi
Dipartimento di Chimica
Università degli Studi di Firenze
Via della Lastruccia, 3, 50019 Sesto Fiorentino (FI) (Italy)
Dr. W. Wernsdorfer
Laboratoire Louis Néel, C.N.R.S.
BP 166, 25 Avenue des Martyrs, 38042 Grenoble Cedex 9 (France)

[**] This work was supported by the TMR Programme from the European Union (contract ERBFM-RXCT98-0181), the Spanish Ministry of Science and Technology (project BQU2001-2928), the French Ministry of National Education and the European Science Foundation through the Molecular Magnets Programme.

Supporting information for this article is available on the WWW under http://www.angewandte.org or from the author.

 DOI: 10.1002/anie.200250243 © 2003 Wiley-VCH Verlag GmbH & Co. KGaA, Weinheim

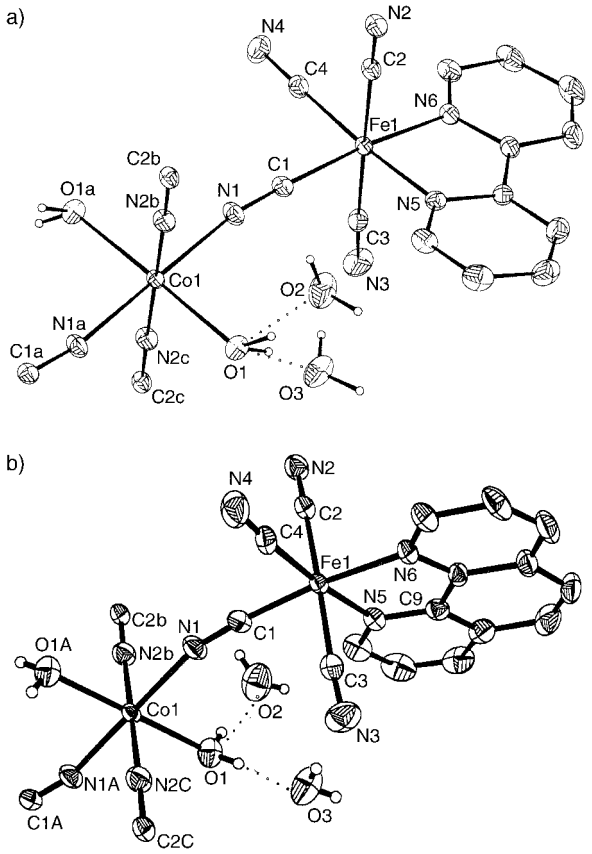


Figure 1. Perspective view of the crystallographically independent unit of **1** (a) and **2** (b), thermal ellipsoids set at 30% probability and hydrogen atoms of bpy omitted for clarity. The hydrogen bonds involving the water molecules are illustrated by broken lines. Selected bond lengths [Å] and angles [°] for compounds **1**/**2**: Fe1-C1 1.923(3)/1.925(3), Fe1-C2 1.951(2)/1.950(2), Fe1-C3 1.949(3)/1.954(2), Fe1-C4 1.909(3)/1.912(3), Fe1-N5 1.980(2)/1.999(2), Fe1-N6 1.991(2)/1.999(2), Co1-N1 2.125(2)/2.147(2), Co1-N2b 2.104(2)/2.113(2), Co1-O1 2.103(2)/2.089(2); N5-Fe1-N6 81.23(9)/81.86(8), N1-Co1-N2b 88.00(9)/90.55(8). See text for further details.

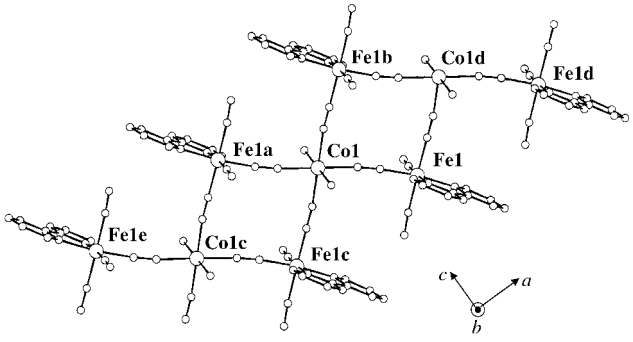


Figure 2. Perspective view of a fragment of the double zigzag chain of **1** running parallel to the *a* axis. The uncoordinated water molecules have been omitted for clarity. Symmetry codes: (a) $-x$, $1-y$, $-z$; (b) $1-x$, $1-y$, $-z$; (c) $-1+x$, y, z; (d) $1+x$, y, z; (e) $-1-x$, $1-y$, $-z$.

and 165.37(1)°) are significantly bent. The shortest interchain metal–metal distances are 7.595(1) (**1**) and 7.656(1) Å (**2**) [Fe(1)···Co(1f); (f) = $1/2-x$, $1/2+y$, $-1/2-z$] and 8.372(1) (**1**) and 9.856(2) Å (**2**) [Fe(1)···Fe(1f)].

At room temperature, the $\chi_M T$ product for powder samples of **1** and **2** (χ_M is the magnetic susceptibility per Fe_2Co unit) is 4.4 and 3.9 $cm^3 mol^{-1} K$, respectively (Figure S1 and S2 in the Supporting Information), and corresponds to the presence of one high-spin Co^{II} ($S_{Co} = 3/2$) and two low-spin Fe^{III} ($S_{Fe} = 1/2$) ions, with significant orbital contributions. Upon cooling under an applied magnetic field of 100 Oe, $\chi_M T$ increases linearly, in line with an intrachain ferromagnetic coupling between Fe^{III} and Co^{II} centers. The increase is smooth in the high-temperature range and sharp at $T < 50$ K. $\chi_M T$ reaches a maximum value of about 460 $cm^3 mol^{-1} K$ (**1** and **2**) at 7.5 K and further decreases linearly with T (as the magnetization becomes field dependent). Below 8 K, hysteresis loops as well as maxima of the in-phase and out-of-phase signals which are strongly frequency dependent are observed for both compounds. In this temperature range, a thermally activated mechanism appears to be involved. Such a behavior has been observed in superparamagnets,[9] spin glasses,[10] molecular anisotropic high-spin clusters,[11] and in the anisotropic chain reported in ref. [1]. To characterize the anisotropy of **1** and **2**, we performed magnetization measurements on single crystals. For complex **1** the main results are summarized in Figures 3, 5, and 6 (similar behavior is observed for **2**). The static magnetization was measured under an applied magnetic field (Figure 3). The magnetization along the *b* axis ($\alpha = 90$ or 270°) is greater than that along the *c* axis ($\alpha = 0$ or 180°). Minima of the magnetization are observed at $\pm 59°$ with respect to the *b* axis ($\alpha = 31$ or 149°). These features indicate that each chain within the crystal presents an easy magnetization axis along the Co–O_{water} bond. These compounds have two chains, the Co–O_{water} bonds of which make an angle of $\pm 31°$ with the *b* axis, and this bond defines the direction of the easy magnetization axis for each chain (see Figure 4). So, the magnetization along any direction ($M\alpha$) in the *bc* plane would correspond to the sum of these vectors (noted m_1 and m_2 in Figure 4) through Equation (1).

$$M\alpha = m_1 \cos\alpha + m_2 \cos(\alpha + 62) \quad (1)$$

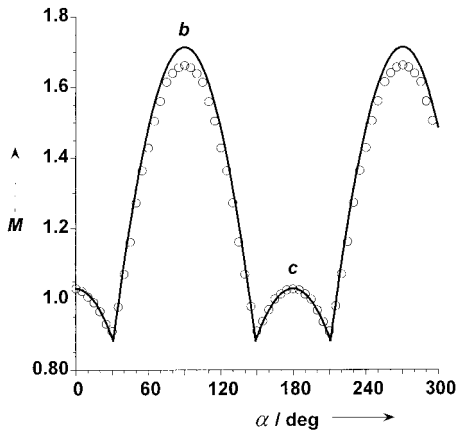


Figure 3. Dependence of the magnetization *M* (arbitrary units) of a single crystal of **1** versus the rotation angle α in the *bc* plane and under an applied magnetic field *H* of 5000 Oe at 5 K. The 0 and 90° angles correspond to $H \parallel c$ and $H \parallel b$, respectively: (○) experimental data; (——) theoretical data obtained from Equation (1) (see text).

 © 2003 Wiley-VCH Verlag GmbH & Co. KGaA, Weinheim

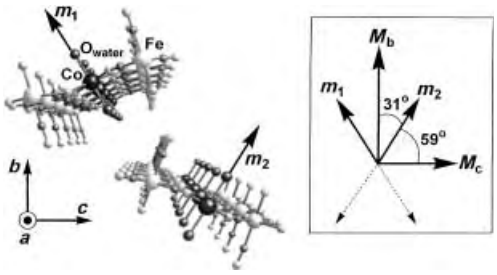


Figure 4. Orientation of the vectors of the double-chain structure.

This equation reproduces the experimental data in Figure 3. The magnetization is greater along the *b* axis than along the *c* axis because the m_1 and m_2 vectors make a smaller angle with the *b* axis than the *c* axis (31° at *b* versus 59° at *c*). The magnetization minima are observed when the magnetic field is perpendicular to one of the two vectors (that is $\pm 59°$ with respect to *b*).

The magnetization along the *a* axis is very weak (Figure 5). This can be understood taking into account that the chains run parallel to the *a* axis, and consequently, the m_1 and m_2 vectors are practically perpendicular to this axis (they form an angle of 89°). All these features demonstrate the anisotropic, Ising-type behavior of each of the two chains.

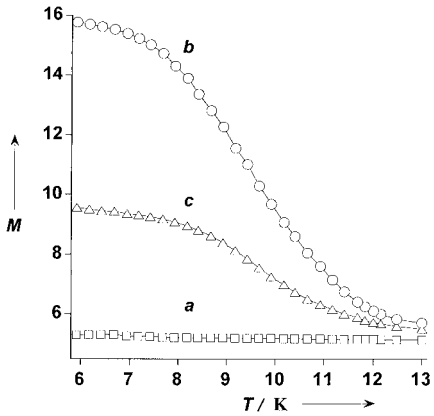


Figure 5. Field-cooled magnetization (FCM) of a single crystal of **1** along the *a*, *b*, and *c* axes, with an external field of 1000 Oe.

They are in agreement with the results obtained on a micro SQUID (superconducting quantum-interference device) applying a transversal magnetic field.

The value of the coercive field (H_c) of the hysteresis loop for a single crystal of **1** is strongly dependent on the temperature and the sweep rate. So, for $H \parallel b$, H_c increases from 1000 to 12000 Oe when going from 2 to 1.1 K at 0.002 T s^{-1} whereas it decreases when increasing the sweep rate (5000 and 750 Oe when going from 0.07 to 0.001 T s^{-1} at $T = 2$ K) (Figure S4 and S5, Supporting Information).

The ac measurements along the *b* axis show a frequency dependence (Figure 6), and the relaxation time of the magnetization (τ, not shown) presents an exponential behavior [$\tau = \tau_0 \exp(E_a/kT)$] in the frequency range explored (0.1–1000 Hz). The best-fit parameters for **1** are $\tau_0 = 9.4 \times 10^{-12}$ s; $E_a/k_B = 142$ K.

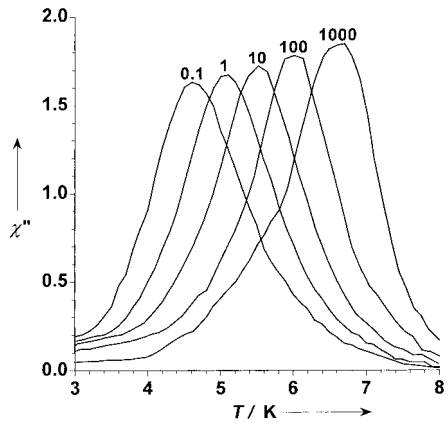


Figure 6. Temperature dependence of the out-of-phase (χ'') component of the ac susceptibility on a single crystal of **1** in zero applied static field and with the oscillating field (1 Oe) applied along the *b* axis. The values of the frequency of the oscillating field are 1000, 100, 10, 1, and 0.1 Hz.

All these magnetic data clearly do not correspond to a 3D-ordered system. In fact, heat-capacity measurements on single crystals of **1** (Figure S3, Supporting Information) do not show any λ peak down to 1.8 K. A spin-glass system would have presented similar ac behavior but the hypothesis can be discarded since the measurements were carried out on well organized single crystals. We are left with the presence of a slow relaxation of the magnetization in these two new 1D compounds. These compounds are reminiscent of the mixed radical cobalt(II) chain in ref. [1]. The chains **1** and **2** are 1D Ising systems, and fulfill the conditions required to observe slow relaxation of the magnetization. In summary, the double-chain topology, the bimetallic character with two anisotropic spin bearers, and the ferromagnetic coupling in **1** and **2** lead to the observation of a slow relaxation of the magnetization and to original properties which deserve more theoretical and experimental studies on pure and doped systems.

The lack of an appropriate analytical expression of the magnetic susceptibility impedes the evaluation of the ferromagnetic *J* constant. Nevertheless, it is possible to understand qualitatively the ferromagnetic nature of the coupling between low-spin Fe^{III} and high-spin Co^{II} centers in **1** and **2** thanks to DFT calculations. They show that in a local octahedral symmetry, the three unpaired electrons on the cobalt center are in d_{z^2}, $d_{x^2-y^2}$, and d_{xy} orbitals (*z* axis along the $Co{-}O_{water}$ bonds and *x* and *y* axes along the Co-N≡C(cyanide) bonds) whereas that of the iron atom is in a mixture of d_{xy} and d_{xz} orbitals (keeping the same reference axes). The situation corresponds to a predominant orthogonality between the two sets of orbitals on the cobalt and iron centers and accounts for the observed ferromagnetic coupling.

Experimental Section

1: Red rodlike single crystals of **1** were obtained by slow diffusion of aqueous solutions of $Li[Fe(bpy)(CN)_4]$ (isolated by metathetic reaction of $PPh_4[Fe(bpy)(CN)_4]{\cdot}H_2O$ and $LiClO_4$ in a 1:1 molar ratio in acetonitrile) and $[Co(H_2O)_6](NO_3)_2$ in an H-shaped tube in

 © 2003 Wiley-VCH Verlag GmbH & Co. KGaA, Weinheim

the dark. In a typical experiment, aqueous solutions of the iron salt (0.2 mmol) in one arm and of the cobalt salt (0.1 mmol) in the other one were allowed to diffuse in the dark. X-ray quality single crystals of **1** were formed in the iron-containing arm after a few weeks, the yield being practically quantitative. When the experiment was carried out in day light, the yield was very low because of the precipitation of an insoluble green solid $[\{Fe^{II}(bpy)(CN)_4\}_3Co_2^{III}]$ as the main product. Elemental analysis (C, H, N) and the Fe:Co molar ratio (electron microscopy) on crystals of **1** agree well with its formulation as a tetrahydrate. IR (KBr disk) of **1**: $\tilde{\nu} = \nu_{CN}$ 2167w and 2156m (bridging cyanide) and 2124s cm^{-1} (terminal cyanide).

2: Purple-red platelike single crystals of **2** were obtained by following the procedure described for **1** but using the $PPh_4[Fe(phen)(CN)_4]\cdot 2H_2O$ complex as the iron precursor. The yield was also quantitative when working in the dark. Elemental analysis (C, H, N) and the Fe:Co molar ratio (electron microscopy) on crystals of **2** agree well with its formulation as a tetrahydrate. IR (KBr disk) of **2**: $\tilde{\nu} = \nu_{CN}$ 2165w and 2155m (bridging cyanide) and 2123s cm^{-1} (terminal cyanide).

Received: September 25, 2002 [Z50243]

Keywords: chain structures · cobalt · cyanide ligands · ferromagnetism · iron

[1] A. Caneschi, D. Gatteschi, N. Lalioti, C. Sangregorio, R. Sessoli, G. Venturi, A. Vindigni, A. Rettori, M. G. Pini, M. A. Novak, *Angew. Chem.* **2001**, *113*, 1810; *Angew. Chem. Int. Ed.* **2001**, *40*, 1760.

[2] R. J. Glauber, *J. Math. Phys.* **1963**, *4*, 294.

[3] R. Lescouëzec, PhD Thesis, Valencia and Paris, **2002**.

[4] R. Lescouëzec, F. Lloret, M. Julve, J. Vaissermann, M. Verdaguer, R. Llusar, S. Uriel, *Inorg. Chem.* **2001**, *40*, 2065.

[5] R. Lescouëzec, F. Lloret, M. Julve, J. Vaissermann, M. Verdaguer, *Inorg. Chem.* **2002**, *41*, 818.

[6] Crystal data: compound **1**: $C_{28}H_{28}CoFe_2N_{12}O_6$, $M_r = 799.2$, monoclinic, space group $P2_1/n$, $a = 7.592(1)$, $b = 15.190(7)$, $c = 14.714(3)$ Å, $\beta = 92.92(1)°$, $V = 1694.6(9)$ Å^3, $Z = 2$, $\rho_{calcd} = 1.57$ g cm^{-3}, $\lambda = 0.71069$ Å, $\mu(Mo_{K\alpha}) = 13.8$ cm^{-1}, $F(000) = 816$, GoF = 1.04. A total of 3354 reflections were collected and 2972 are unique ($R_{int} = 0.02$). $R1$ and $wR2$ are 0.0342 and 0.0401, respectively, for 224 parameters and 2546 reflections [$I > 3\sigma(I)$]. Compound **2**: $C_{32}H_{28}CoFe_2N_{12}O_6$, $M_r = 847.29$, monoclinic, space group $P2_1/n$, $a = 7.4315(18)$, $b = 15.614(4)$, $c = 15.344(4)$ Å, $\beta = 93.444(6)°$, $V = 1777.3(7)$ Å^3, $Z = 2$, $\rho_{calcd} = 1.583$ g cm^{-3}, $\lambda = 0.71073$ Å, $\mu(Mo_{K\alpha}) = 13.29$ cm^{-1}, $F(000) = 862$, GoF = 0.890. A total of 14566 reflections were collected and 5316 are unique ($R_{int} = 0.054$). $R1$ and $wR2$ are 0.0396 and 0.0823, respectively, for 298 parameters and 3318 reflections [$I > 2\sigma(I)$]. The data were collected on Enraf-Nonius MACH-3 (**1**) and Bruker Smart CCD (**2**) diffractometers with $Mo_{K\alpha}$ radiation at 295 K. The structures were solved by direct methods through the SHELX-86 (**1**) and SHELX-97 (**2**) programs and refined with full-matrix least-squares technique on F (**1**) and F^2 (**2**) through the PC version of CRYSTALS (**1**) and the SHELXL-97 (**2**) program. All non-hydrogen atoms were refined anisotropically. CCDC-191049 (**1**) and CCDC-191050 (**2**) contain the supplementary crystallographic data for this paper. These data can be obtained free of charge via www.ccdc.cam.ac.uk/conts/retrieving.html (or from the Cambridge Crystallographic Data Centre, 12, Union Road, Cambridge CB21EZ, UK; fax: (+44) 1223-336-033; or deposit@ccdc.cam.ac.uk).

[7] G. De Munno, M. Julve, F. Lloret, J. Faus, A. Caneschi, *J. Chem. Soc. Dalton Trans.* **1994**, 1175; J. Brunzelle, A. Fitch, Y. Wang, S. F. Pavkovic, *Acta Crystallogr. Sect. C* **1996**, *52*, 2984.

[8] P. V. Bernhardt, B. P. Macpherson, M. Martínez, *Inorg. Chem.* **2000**, *39*, 5203.

[9] A. H. Morrish, *The Physical Principles of Magnetism*, Wiley, New York, **1966**.

[10] J. A. Mydosh, *Spin Glasses: An Experimental Introduction*, Taylor&Francis, London, **1993**.

[11] a) R. Sessoli, D. Gatteschi, A. Caneschi, M. A. Novak, *Nature* **1993**, *365*, 141; b) L. Thomas, F. Lionti, R. Ballou, D. Gatteschi, R. Sessoli, B. Barbara, *Nature* **1996**, *383*, 145; c) W. Wernsdorfer, R. Sessoli, *Science* **1999**, *284*, 133.

 © 2003 Wiley-VCH Verlag GmbH & Co. KGaA, Weinheim



Transfection Agents

Amphiphilic Dendrimers: Novel Self-Assembling Vectors for Efficient Gene Delivery**

*Derk Joester, Myriam Losson, Raphaël Pugin, Harry Heinzelmann, Elke Walter, Hans P. Merkle, and François Diederich**

Nonviral gene delivery remains an outstanding challenge to the scientific community.[1] Fifteen years of interdisciplinary effort since the introduction of cationic amphiphiles for DNA and RNA transfection by Felgner et al.[2] compare to millions of years of evolutionary optimization of the competing viral vectors. While actual progress has been moderate, some key issues for efficient delivery have been identified.[3] Biocompatibility, charge/receptor-mediated uptake, tissue-specific targeting, endosomal escape, nuclear tropism, and vector unpacking all contribute to the canon of requirements. The hunt for a "magic bullet" has led to a stunning multitude of synthetic vector systems, including small molecule amphiphiles,[4] linear, branched, and more sophisticated block copolymers,[5] as well as dendrimers.[6,7] As a recent development, polymeric controlled-release drug-delivery systems

[*] Prof. Dr. F. Diederich, D. Joester
Laboratorium für Organische Chemie
ETH-Hönggerberg, HCI
8093 Zürich (Switzerland)
Fax: (+41) 1-632-1109
E-mail: diederich@org.chem.ethz.ch
M. Losson, Dr. R. Pugin, Dr. H. Heinzelmann
CSEM SA
Rue Jaquet-Droz 1, 2007 Neuchâtel (Switzerland)
Dr. E. Walter, Prof. Dr. H. P. Merkle
Institut für Pharmazeutische Wissenschaften
ETH Zürich
Winterthurerstrasse 190, 8057 Zürich (Switzerland)

[**] Financial support by the NCCR "Nanoscale Science" is gratefully acknowledged.

Supporting information for this article is available on the WWW under http://www.angewandte.org or from the author.

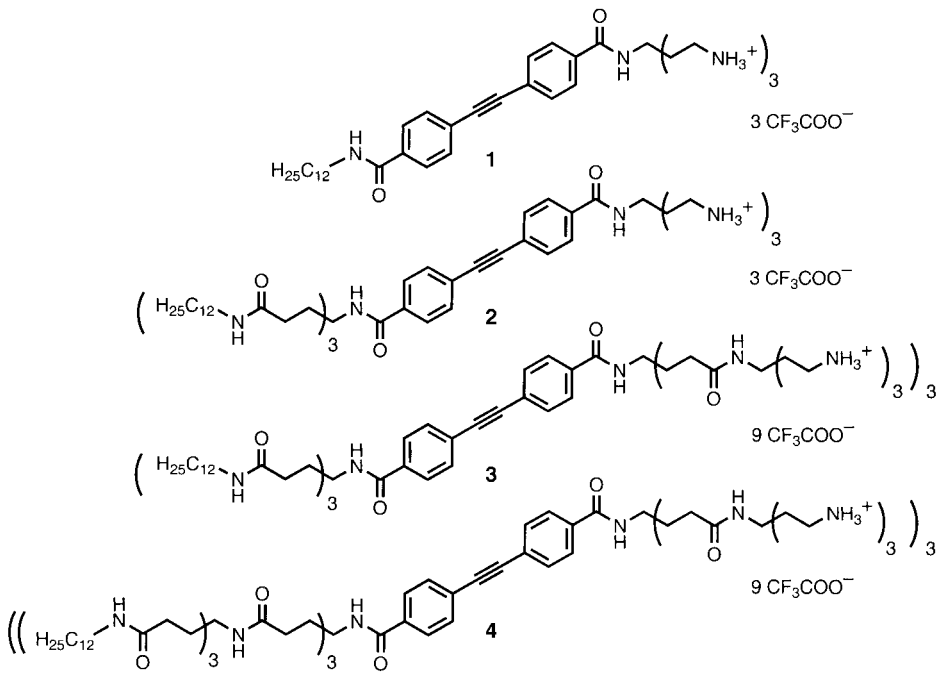
 © 2003 Wiley-VCH Verlag GmbH & Co. KGaA, Weinheim DOI: 10.1002/anie.200250284

have also shown promising features.[8] While members of all classes have been commercialized, and some structure–activity relationship (SAR) data compiled, no breakthrough has yet been achieved. It seems that "magic potions" rather than "magic bullets"[9] will provide the three orders of magnitude of efficiency that the nonviral systems are still lacking.

However, classic architectures can still be optimized in surprising ways.[10] Nevertheless, the above observations have induced a search for new modular self-assembling platforms that try to combine features of the first-generation vectors.[11]

With the aim of producing programmable supramolecular architectures of defined and controllable composition in space, it seems advantageous to introduce a rigid scaffold. Drawing on the low toxicity, geometric tunability, and ease of multiple functionalization of cationic dendrimers on the one hand and the classic self-assembly of amphiphilic molecules on the other, we have developed a set of molecular building blocks to prepare amphiphilic dendrimers with rigid cores which feature a variety of geometries and substitution patterns. Self-assembly is of central importance, as it permits remaining at relatively low molecular weight, which has been shown to be advantageous in other systems.[12] High cationic charge density at the dendrimer surface should favor both DNA binding and endosomal escape once internalized. Here we describe the series of amphiphilic dendrimers **1**–**4** (for the synthesis, see the Supporting Information), based on a rigid tolane (diphenylethyne) core and describe their remarkable activity as transfection agents with a surprising structure–activity relationship.

Preliminary DNA-binding experiments were carried out by a dye-exclusion assay (see Experimental Section).[13] As a measure for binding affinity, c_{50} and CE_{50}, the concentration and charge excess ratio,[14] respectively, at which 50% of the dye complexed to DNA was displaced by added compounds **1**–**4**, were determined (Table 1). Ranking compounds based on their CE_{50} values gives an idea of the per-charge affinities, that is, the affinities based on the c_{50} value divided by the nominal charge of the molecule in question. In this way, a binding affinity ranking based on c_{50} was found to be **3** > **2** > **1** > **4** (based on CE_{50}: **2**≅**3** > **1** ⩾ **4**). These data suggest that the number of C_{12} chains in the lipophilic dendron has an important influence on binding affinity. The 2.5-fold increase in the c_{50} value from **3** to **2** is easily explained by the concomitant threefold decrease in nominal charge. As expected, the difference disappears when the ranking is based on the CE_{50} value. In contrast, going from three lipophilic side chains in **2** to one in **1** results in a twofold higher c_{50} value, and changing from three chains in **3** to nine in



1 **2** **3** **4**

Table 1: Dye-exclusion assay.[13][a]

	Number of C_{12} chains	Nominal charge	M_W [g M^{-1}][b]	c_{50} [μM][c]	CE_{50}[d]
1	1	3+	917.9	5.4	5.4
2	3	3+	1481.8	2.5	2.5
3	3	9+	2679.7	1.0	3.0
4	9	9+	4371.4	9.0	26.9

[a] GFP reporter plasmid (1 μg mL^{-1}) and Picogreen dye[18] concentrations were kept constant. The PicoGreen–DNA complex fluorescence intensity was monitored at λ_{em} = 530 nm (λ_{exc} = 485 nm) and was plotted against the concentration (*c*) or charge excess ratio[14] (*CE*) of compounds **1**–**4**. [b] Molecular weight including trifluoroacetate counteranions. [c] Concentration at which the fluorescence intensity was reduced to 50%. [d] *CE* value at which the fluorescence intensity was reduced to 50%.

 © 2003 Wiley-VCH Verlag GmbH & Co. KGaA, Weinheim

4 even gives a ninefold increase. Clearly, a structure with three lipophilic chains is strongly favored. However, **4** can still almost completely displace the dye, that is, compete for all the binding sites on the DNA. This result gives rise to the assumption that **4**, with its large lipophilic segment, may form stable aggregates that interact with DNA on a small part of their surface only. Clearly, the self-assembly[15] properties play a much more important role on binding than anticipated.

In a study of the transfection efficiency (TE), systematic variation of the *CE*[14] gave clear and strong maxima for **2** (CE_{max} = 8–12, c_{max} = 20–30 μM) and **3** (CE_{max} = 12–16, c_{max} = 10–14 μM; Figure 1). Dendrimers **1** and **4** did not show

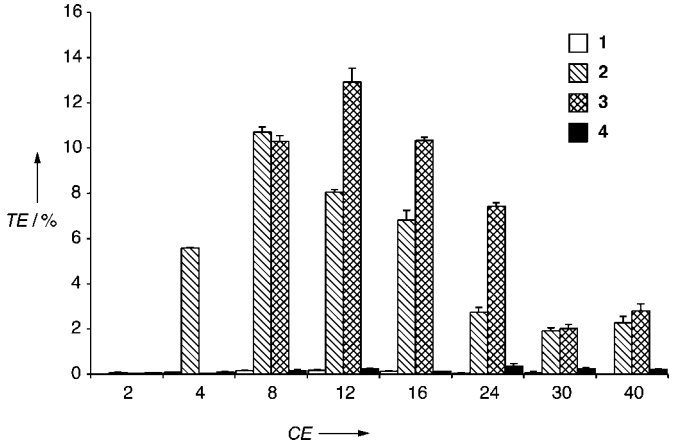


Figure 1. Transfection efficiency (TE) of **1**–**4** is given as a function of the charge excess ratio *CE*. Standard deviation (SD, n = 2) within an experiment was less than 10%. The SD (n = 3) became much larger (up to 30%) between experiments, primarily because of the fact that the absolute position of the maxima varied (CE_{max} = 8–12 for **2**, CE_{max} = 12–16 for **3**). However, the separation between the maxima of **2** and **3** was always $\Delta CE_{max} = 4$. The data shown are from one experiment carried out in duplicate.

significant transfection activity. Again the geometry and thus the aggregation properties determined by the lipophilic dendron in the molecule dominate the activity, as indicated by the comparison between dendrimers with identical hydrophilic dendrons (**2** versus **1** and **3** versus **4**, respectively). While the size and nominal charge of the hydrophilic part affects the optimum concentration (c_{max} of **3** is one half that of **2**), the absolute TE is not significantly affected by it. The small difference that was observed could be attributed to the fact that the surface charge density of **3** is higher, thus the pK_a values of some of the terminal ammonium centers should drop and some buffer capacity be gained. This effect is consistent with the proton sponge endosomal escape hypothesis.[16]

To assess the overall quality of our vectors we used commercially available compounds as a reference. A clear ranking could be determined from the maximum TE values observed (Figure 2): **3**≅**2** > DOTAP > PEI≅SuperFect > **4** > **1**. Only very basic optimization has been carried out so far, and even at this unrefined state the activities of our low generation amphiphilic dendrimers **2** and **3** surpass those of traditional medium-sized poly(amidoamine) (PAMAM) dendrimers (SuperFect) by a factor of 3 to 5.

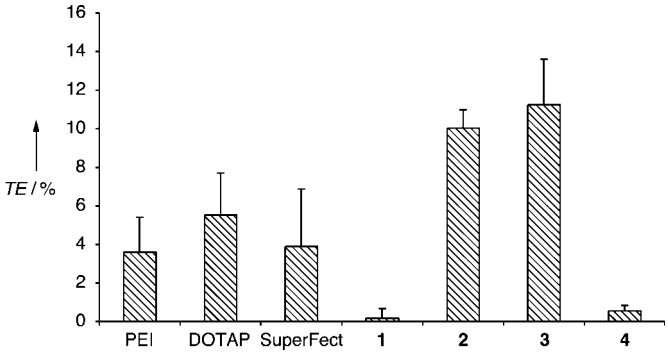


Figure 2. Maximum TE of **1**–**4** at optimum conditions are compared to reference compounds PEI, DOTAP, and SuperFect. Error bars represent SD (n = 3) between different experiments, each carried out in duplicate.

All the compounds in the optimum *CE* range (8–16) were found to have low cytotoxicity (Figure 3). Performance was similar to the reference compounds, the ratio of dead cells (R_{dead}, see Experimental Section) being less than 20%. Toxicity increased at a disproportionate rate for $CE > 16$ ($CE > 30$ for **4**). This trend coincides with the drop in

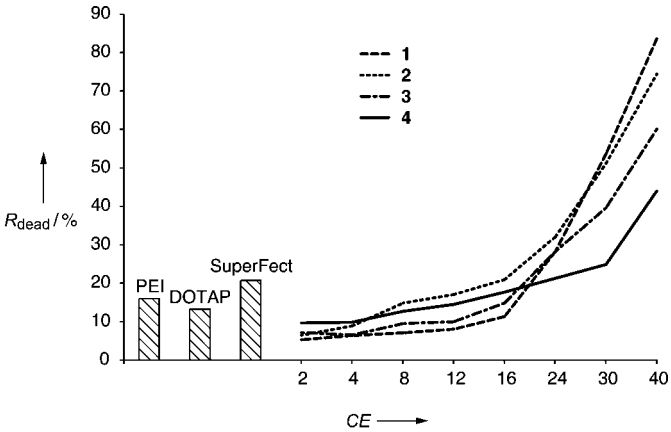


Figure 3. The ratio of dead cells (R_{dead}) after exposure of the cells to the vector–DNA constructs of **1**–**4** (lines) is given as a function of *CE*. R_{dead} is also given for the reference compounds DOTAP and SuperFect under the conditions according to the manufacturer's instructions (columns).

transfection activity at the same *CE* values. Lethal concentrations that would kill 50% of the exposed cells (LC_{50}) were estimated (**1**: 75, **2**: 75, **3**: 30, and **4**: 35 μM). These values are at least three times higher than the optimal concentration range for transfection with the respective compound. It is clear that the tripling in nominal charge from **2** to **3** is responsible for a 50% decrease in the LC_{50} value. The effect of the lipophilic part of the molecules seems to be of less importance. Toxicities at optimum concentrations for transfection do not show a recognizable correlation with structural features.

The presence of serum is known to impede transfection in the case of small molecular amphiphiles. Thus, exposure of the cells to vector–DNA constructs is usually carried out in a medium with reduced serum, or completely without serum.

 © 2003 Wiley-VCH Verlag GmbH & Co. KGaA, Weinheim

To assess the effect of serum on the TE we carried out a *CE* series in the presence of fetal bovine serum (FBS) during the transfection step (see Experimental Section).

To our surprise, compounds **2** and **3** that performed so similarly in all other experiments did exhibit a significant difference in this regard (Figure 4). While **3** lost almost all of its transfection activity, **2** was much less affected, and

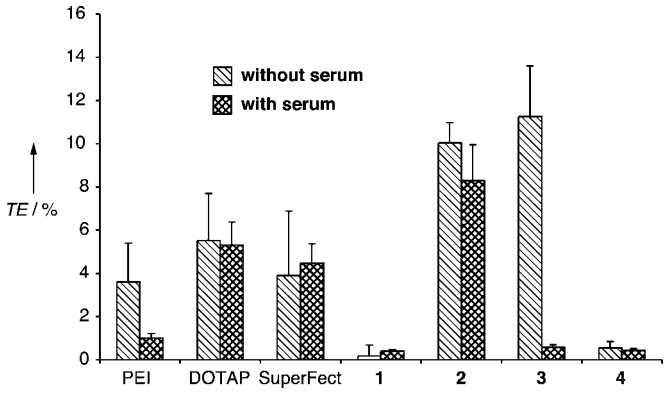


Figure 4. TE of **1**–**4** as well as the reference compounds PEI, DOTAP, and SuperFect are contrasted for the absence (hatched columns) and presence (crosshatched columns) of fetal bovine serum (FBS) during the incubation of the vector–DNA construct with cells. Error bars represent SD ($n = 3$) between different experiments, each carried out in duplicate.

maintained an activity comparable to DOTAP. The *CE* series for **2** (as in Figure 1) revealed a lower, broad maximum (data not shown) centered around $CE = 8$. The strongly reduced activity of **3** in the presence of serum probably results from the presence of anionic serum proteins. These could significantly alter the structure of the DNA complex of **3** with its high nominal charge (9+) in its hydrophilic part. This result warrants a detailed study on the aggregation states in aqueous buffers, which is currently underway.[15]

Assembly of DNA–dendrimer complexes was studied by tapping mode atomic force microscopy (AFM). Single adsorbed plasmids became clearly visible (Figure 5A) when pure DNA was deposited by drop casting on freshly cleaved mica in the absence of **2** (see Experimental Section). Deposition of **2** without DNA gave homogenous thin layers

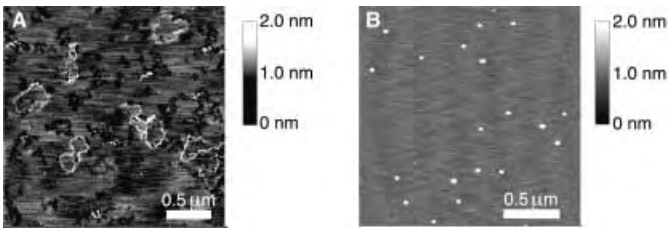


Figure 5. A) AFM image of pGFP on mica in the absence of dendrimer. No divalent cations were added, such that only a small amount of DNA is adsorbed on the surface. Individual plasmids are visible as white loops. B) AFM image of pGFP and **2** mixed as described in the Experimental Section and deposited on freshly cleaved mica. The structures observed resembled flattened spheres (height: 5–10 nm, diameter: 60–80 nm). No free plasmid was found. This is a clear indication of efficient condensation of DNA by compound **2**.

of about 1.5 nm thickness (not shown). However, a large number of flattened spheroidal or slightly oblong complexes were observed when DNA and **2** were mixed at $CE = 5.6$ prior to deposition (Figure 5B). No free plasmid could be detected. This result clearly indicates that **2** not only binds to DNA, as demonstrated by the dye-exclusion assay, but also very efficiently condenses DNA into well-defined structures.

To conclude, a series of amphiphilic dendrimers featuring extended rigid cores has been prepared, which not only showed high transfection activity, but also brought a couple of surprises. A sharp maximum in SARs, a much stronger influence of the hydrophobic part on DNA binding and transport than anticipated, low toxicity, and an unusual serum effect warrant more detailed analysis of the factors at hand. In contrast to classical cationic dendrimers, where there is a minimum size for transfection, our dendrimers do not show that limitation. However, while an optimum M_W value greater than 116000 was found for PAMAM dendrimers,[7] we determined an optimum activity with rather small dendrimers ($M_W = 1500$–2700). A similar effect has been noted for lysine oligopeptides, which reached maximum efficiency at $M_W = 2800$.[17] While the biological characterization is far from complete, we are confident that the synthetic building blocks and the modular vector assembly strategy will enable us to explore this new class of amphiphilic dendrimers in breadth and depth.

Experimental Section

Green fluorescent protein reporter plasmid (pGFP) was generated by cloning the green fluorescent protein (GFP) gene into the VR1012 vector. Plasmid DNA was prepared with Qiagen (Basel, Switzerland) endotoxin-free buffers according to the manufacturer's instructions and resuspended in sterile Millipore 18.2 MΩ water at 1 mg mL^{-1}. The bacterial β-galactosidase (LacZ) containing plasmid (placZ) was generated accordingly.

DNA binding study: Binding affinity was monitored by a dye-exclusion assay.[14] GFP reporter plasmid (pGFP) was used for all experiments. The pGFP (1 µg mL^{-1}) and dye concentration where kept constant in the presence of increasing amounts (1–20 µM) of compounds **1**–**4**. Expulsion of the PicoGreen dye[18] from the complex with pGFP was followed by the reduction of its fluorescence intensity I_{530} ($\lambda_{exc} = 485$, $\lambda_{em} = 530$ nm). The change in fluorescence intensity (ΔI_{530}) was plotted against the concentration (or *CE*). The concentrations (or *CE*) at which 50% of the dye are displaced from the complex with pGFP (c_{50} and CE_{50}) were determined from the titration curves.

Transfection efficiency study: For transfection experiments, the human embryonic kidney HEK293 model cell line (ATCC CRL-1573) was cultured as previously described.[19] Cells were transferred into 96-well plates to give approximately 2×10^5 cells per well at 90% confluency. pGFP was mixed with different volumes of thoroughly sonicated solutions of dendrimers **1**–**4** (1.0 mg mL^{-1} in 20 mM HEPES[20] buffer at pH 7.4). Equilibration of the samples was allowed for at least 30 min before vortexing and adding Dulbecco's modified Eagle medium (DMEM[21]) growth medium containing penicillin (100 U mL^{-1}) and streptomycin (100 µg mL^{-1}). The growth medium was removed from the cells before aliquots of 0.5 µg pGFP per well were added in a total volume of 200 µL. Cells were then incubated (37 °C, 5% CO_2) for 2 h. The plasmid-containing medium was then replaced by DMEM (penicillin (100 U mL^{-1}), streptomycin (100 µg mL^{-1}), 10% FBS) and the cells incubated (37 °C, 5% CO_2) for another 24 h. Transfection efficiency[22] (TE) was determined by

 © 2003 Wiley-VCH Verlag GmbH & Co. KGaA, Weinheim

manual counting of green-fluorescent cells under a fluorescence microscope. The commercially available transfection agents DOTAP[23] and SuperFect[24] were used as reference compounds according to the manufacturer's instructions (scaled to 0.5 μg pGFP per well). For two wells, 24 μL of a solution (42 $\mu g\,mL^{-1}$) of poly(ethyleneimine) (PEI)[25] were mixed with 1 μL of pGFP stock solution and incubated for 30 min before diluting to 400 μL with DMEM. All experiments were carried out in duplicate or triplicate and repeated at least once.

Cell viability study: Cells were transfected with placZ according to the experimental details given for the transfection study at *CE* values between 2 and 40. The ratio of dead (R_{dead}) cells was determined after application of a "Live/Dead" kit[26] according to the manufacturer's instructions. Readout of the data was performed with a fluorescence plate reader (transfection with pGFP would have given false high readings for live cells). LC_{50} values were estimated by linear interpolation of the R_{dead} values (extrapolation in the case of **4**).

Serum effect study: Exactly the same conditions as for the transfection study were used, with the sole difference that, after equilibration of vector and DNA, DMEM containing 10% FBS was added and incubation of cell with vector and DNA was thus carried out in the presence of serum.

AFM: Studies were performed with a Nanoscope 3100 (Digital Instruments, Santa Barbara, CA) operated in noncontact (tapping) mode using NSG01 probes (NT-MDT, Moscow) with a spring constant of 2.5–5.5 $N\,m^{-1}$ and a resonance frequency of 120–150 kHz. Measurements were done under ambient conditions (20 °C). Image analysis was performed with the Nanoscope III Control (Digital Instruments, Santa Barbara, CA) software package. Unless otherwise stated, data processing was limited to first- or second-order plane fitting and zeroth or first-order flattening.

Drop casting: 10 μL of a solution of pGFP (0.2 $ng\,\mu L^{-1}$) were mixed with 2 μL of a solution of **2** in Millipore water (8 $ng\,\mu L^{-1}$). After equilibration (30 min), 2 μL of this mixture were deposited on freshly cleaved mica. The water was then allowed to evaporate (1 h at 20 °C, ambient pressure). Imaging was performed immediately afterwards.

Received: October 2, 2002 [Z50284]

Keywords: amphiphiles · cross-coupling · dendrimers · DNA recognition · gene transfection

[1] J. A. Wolff, *Nat. Biotechnol.* **2002**, *20*, 768–769.
[2] a) P. L. Felgner, T. R. Gadek, M. Holm, R. Roman, H. W. Chan, M. Wenz, J. P. Northrop, G. M. Ringold, M. Danielsen, *Proc. Natl. Acad. Sci. USA* **1987**, *84*, 7413–7417; b) R. W. Malone, P. L. Felgner, I. M. Verma, *Proc. Natl. Acad. Sci. USA* **1989**, *86*, 6077–6081.
[3] a) M. E. Davis, *Curr. Opin. Biotechnol.* **2002**, *13*, 128–131; b) C. W. Pouton, L. W. Seymour, *Adv. Drug Delivery Rev.* **2001**, *46*, 187–203.
[4] a) A. D. Miller, *Angew. Chem.* **1998**, *110*, 1862–1880; *Angew. Chem. Int. Ed.* **1998**, *37*, 1769–1785; b) M. C. P. de Lima, S. Simoes, P. Pires, H. Faneca, N. Duzgunes, *Adv. Drug Delivery Rev.* **2001**, *47*, 277–294.
[5] a) Y. Kakizawa, K. Kataoka, *Adv. Drug Delivery Rev.* **2002**, *54*, 203–222; b) T. Merdan, J. Kopecek, T. Kissel, *Adv. Drug Delivery Rev.* **2002**, *54*, 715–758.
[6] a) F. W. Zeng, S. C. Zimmerman, *Chem. Rev.* **1997**, *97*, 1681–1712; b) M. X. Tang, C. T. Redemann, F. C. Szoka, *Bioconjugate Chem.* **1996**, *7*, 703–714; c) S. E. Stiriba, H. Frey, R. Haag, *Angew. Chem.* **2002**, *114*, 1385–1390; *Angew. Chem. Int. Ed.* **2002**, *41*, 1329–1334; d) J. Haensler, F. C. Szoka, *Bioconjugate Chem.* **1993**, *4*, 372–379; e) A. W. Bosman, H. M. Janssen, E. W. Meijer, *Chem. Rev.* **1999**, *99*, 1665–1688.
[7] a) J. F. Kukowska-Latallo, A. U. Bielinska, J. Johnson, R. Spindler, D. A. Tomalia, J. R. Baker, *Proc. Natl. Acad. Sci. USA* **1996**, *93*, 4897–4902; b) J. Dennig, E. Duncan, *Rev. Mol. Biotechnol.* **2002**, *90*, 339–347.
[8] a) C. Erni, C. Suard, S. Freitas, D. Dreher, H. P. Merkle, E. Walter, *Biomaterials* **2002**, in press; b) T. Segura, L. D. Shea, *Annu. Rev. Mater. Res.* **2001**, *31*, 25–46.
[9] G. Zuber, E. Dauty, M. Nothisen, P. Belguise, J. P. Behr, *Adv. Drug Delivery Rev.* **2001**, *52*, 245–253.
[10] a) E. Guènin, A. C. Herve, V. Floch, S. Loisel, J. J. Yaouanc, J. C. Clement, C. Ferec, H. des Abbayes, *Angew. Chem.* **2000**, *112*, 643–645; *Angew. Chem. Int. Ed.* **2000**, *39*, 629–631.
[11] M. A. W. Eaton, T. S. Baker, C. F. Catterall, K. Crook, G. S. Macaulay, B. Mason, T. J. Norman, D. Parker, J. J. B. Perry, R. J. Taylor, A. Turner, A. N. Weir, *Angew. Chem.* **2000**, *112*, 4229–4233; *Angew. Chem. Int. Ed.* **2000**, *39*, 4063–4067.
[12] a) D. Fischer, T. Bieber, Y. X. Li, H. P. Elsasser, T. Kissel, *Pharm. Res.* **1999**, *16*, 1273–1279; b) S. C. W. Richardson, H. J. V. Kolbe, R. Duncan, *Int. J. Pharm.* **1999**, *178*, 231–243; c) S. J. Hwang, N. C. Bellocq, M. E. Davis, *Bioconjugate Chem.* **2001**, *12*, 280–290.
[13] M. E. Ferrari, C. M. Nguyen, O. Zelphati, Y. L. Tsai, P. L. Felgner, *Hum. Gene Ther.* **1998**, *9*, 341–351.
[14] The charge excess ratio (*CE*) is defined as the nominal "number of positive charges" of the material added (namely, the amount of substance times its formula charge) divided by the "number of negative charges" present on the amount of DNA in solution. Based on an average molecular weight of 660 $g\,mol^{-1}$ per base pair (bp), 1 μg of DNA is assumed to carry 3 nmol negative charges. The *CE* has no unit.
[15] Self-assembly of **1**–**3** was observed by dynamic light scattering measurements in aqueous HEPES buffer after sonication. Preliminary data show a particle size distribution with a maximum centered around 100 nm for all compounds. Both **1** and **3** exhibit one additional maximum centered around 5 nm; D. Joester, S. Bufali, P. Walde, P. L. Luisi, F. Diederich, unpublished results.
[16] O. Boussif, F. Lezoualch, M. A. Zanta, M. D. Mergny, D. Scherman, B. Demeneix, J. P. Behr, *Proc. Natl. Acad. Sci. USA* **1995**, *92*, 7297–7301.
[17] D. L. McKenzie, W. T. Collard, K. G. Rice, *J. Pept. Res.* **1999**, *54*, 311–318.
[18] PicoGreen is a proprietary cyanine dye of Molecular Probes (Lucerne, Switzerland). It exhibits a 1000-fold increase in fluorescence upon binding to DNA. For more information, see http://www.probes.com/handbook/sections/0803.html.
[19] E. Walter, K. Moelling, J. Pavlovic, H. P. Merkle, *J. Controlled Release* **1999**, *61*, 361–374.
[20] HEPES: *N*-2-hydroxyethylpiperazine-*N*′-2-ethanesulfonic acid.
[21] GIBCO high-glucose DMEM (4.5 $g\,L^{-1}$ glucose) from Invitrogen life technologies (Basel, Switzerland).
[22] TE is defined as the number of transfected cells divided by the total number of cells.
[23] DOTAP is an aqueous dispersion of *N*-[1-(2,3-dioleoyl-oxy)-propyl]-*N,N,N*-trimethylammonium methyl-sulfate from Roche Diagnostics. It carries one permanent charge and is a classic small-molecule amphiphile.
[24] SuperFect is an activated (that is, fractured) PAMAM dendrimer formulation from Qiagen (Basel, Switzerland).
[25] PEI $M_W = 600\,000$–$1\,000\,000$ from FLUKA (Buchs, Switzerland) is a randomly branched cationic polymer.
[26] Live/Dead Kit from Molecular Probes (Lucerne, Switzerland).

 © 2003 Wiley-VCH Verlag GmbH & Co. KGaA, Weinheim

Redox-Controllable [2]Rotaxane

Toward Chemically Controlled Nanoscale Molecular Machinery**

*Hsian-Rong Tseng, Scott A. Vignon, and J. Fraser Stoddart**

Richard Feynman, in his famous address[1] entitled "There is Plenty of Room at the Bottom" to the American Physical Society in December 1959, raised the fascinating question: "what are the possibilities of small but movable machines?" The rapid growth in supramolecular chemistry[2] provides a convincing answer to Feynman's question—namely, mechanically interlocked molecules, such as certain nondegenerate catenanes and rotaxanes,[3] which can be induced to switch between different ground-state geometries, thus creating substantial relative movement between their, at least, partially "asymmetrical" components and allowing these molecules to behave as nanoscale machines.[4,5] The ability to control the movement of components within these molecular machines, in response to either physical (light[6] or electrical[7]) or chemical (redox[8] or pH[9] changes) stimuli, is critical, because it relates directly to the performance of solid-state devices incorporating them.[7]

A [2]rotaxane consists of two components: a ring and a dumbbell-shaped one.[3] The ring component encircles the linear rodlike portion of the dumbbell and is trapped mechanically by two bulky stoppers at each end of the rod. When two constitutionally different recognition sites[10] are incorporated into the rodlike portion of the dumbbell, the [2]rotaxane can exist in two nondegenerate co-conformations[11] as translational isomers whose relative populations reflect the free energy difference for binding at these two sites. Thus, [2]rotaxanes of this ilk can be likened to a linear motor, since they possess two states between which the ring component can undergo translational motion along part of the rodlike portion of the dumbbell component. There are two fundamental requirements of a switchable [2]rotaxane for achieving the most efficient possible conversion of chemical, electrical, or optical energy into mechanical energy: one is the "complete" occupation of one of the two sites on the dumbbell by the ring component, and the other is the complete reversal of this occupation when the external stimulus is applied.

[*] Prof. J. F. Stoddart, Dr. H.-R. Tseng, S. A. Vignon
Department of Chemistry and Biochemistry
University of California, Los Angeles
405 Hilgard Avenue, Los Angeles, CA 90095-1569 (USA)
Fax: (+1) 310-206-1843
E-mail: stoddart@chem.ucla.edu

[**] This work was supported by the Defense Advanced Research Projects Agency (DARPA). Some of the compound characterizations were supported by the National Science Foundation under equipment grant no. CHE-9974928.

Supporting information for this article is available on the WWW under http://www.angewandte.org or from the author.

Recently, we reported[12] the template-directed syntheses of an amphiphilic bistable [2]rotaxane composed of a ring component, cyclobis(paraquat-*p*-phenylene)[13] ($CBPQT^{4+}$), and a dumbbell-shaped component with two π-electron-rich aromatic sites, namely, a 1,5-dioxynaphthalene (DNP) one and a monopyrrolotetrathiafulvalene (MPTTF) one. Ideally, the π···π stacking interactions[14] between the π-electron-deficient $CBPQT^{4+}$ ring and the more π-electron-donating MPTTF site would result in this [2]rotaxane existing as a single co-conformation wherein the $CBPQT^{4+}$ ring encircles only the MPTTF site ($K_a = 1300\,M^{-1}$ in MeCN).[15] However, both UV/Vis and ^1H NMR spectroscopies have indicated[12] the presence, in Me_2CO (CD_3COCD_3) solution, of two stable translational isomers[16] in a 1:1 ratio at room temperature. Since the MPTTF site fails to entice the $CBPQT^{4+}$ ring to reside exclusively on it, its subsequent oxidation, and removal of its stabilizing interactions with the $CBPQT^{4+}$ ring, produces a switch that works no more than 50% of the time. This inherent lack of precise mechanical control compromises the utility of this [2]rotaxane when it comes to fabricating molecular electronic devices and construction of artificial motor-molecules. In an effort to produce a [2]rotaxane that will function as a prototypical linear molecular motor with 100% positional efficiency, we elected to employ a disubstituted TTF site in competition with the DNP site. After all, we know that TTF forms a strong, green 1:1 complex ($K_a = 8000\,M^{-1}$ in MeCN)[17] with $CBPQT^{4+}$ whereas 1,5-dihydroxy naphthalene forms a much weaker, red 1:1 complex with $CBPQT^{4+}$ ($K_a = 768\,M^{-1}$ in MeCN).[18] Moreover, a closely related nondegenerate [2]catenane based on the same TTF and DNP recognition sites has been demonstrated to behave as a "clean" switch, both in solution[19] and in a solid-state device.[19c,d] Here we describe 1) a [2]rotaxane ($\mathbf{1}\cdot 4PF_6$) incorporating TTF and DNP recognition sites in its dumbbell component which is encircled exclusively on the TTF site by $CBPQT^{4+}$ and 2) the characterization by UV/Vis and ^1H NMR spectroscopies of its "clean" redox-switching action in solution, wherein the $CBPQT^{4+}$ component moves an estimated[20] 3.7 nm between the TTF and DNP recognition sites (Figure 1).

The UV/Vis spectrum (Figure 2, curve a) of $\mathbf{1}\cdot 4PF_6$ reveals a charge-transfer (CT) absorption band, centered on 846 nm, which is characteristic[19a,b] of the translational isomer in which the TTF site is encircled by the $CBPQT^{4+}$ moiety. No absorption band is observed in the 500–600 nm region for a CT interaction which would result from the other translational isomer in which the DNP site is encircled by the $CBPQT^{4+}$ unit. Switching of $\mathbf{1}^{4+}$ was observed in an 8×10^{-4} M solution of the $4PF_6^-$ salt in MeCN when $Fe(ClO_4)_3$ was added. Addition of the oxidant (1.0 equiv) led (Figure 2, curve b) to a decrease in the intensity of the CT band at 846 nm and the appearances of absorption bands centered on 450 and 600 nm that are characteristic[19a,b] of the $TTF^{+\bullet}$ radical cation. A new CT band was also observed at 515 nm as a hump between these two larger bands. The hump indicates[19a,b] the presence of a CT interaction between the DNP site and the $CBPQT^{4+}$ unit which now encircles it. Further addition (up to 2.0 equiv) of the oxidant caused the absorption bands for the $TTF^{+\bullet}$ radical cation to disappear and a new

 DOI: 10.1002/anie.200250453 © 2003 Wiley-VCH Verlag GmbH & Co. KGaA, Weinheim

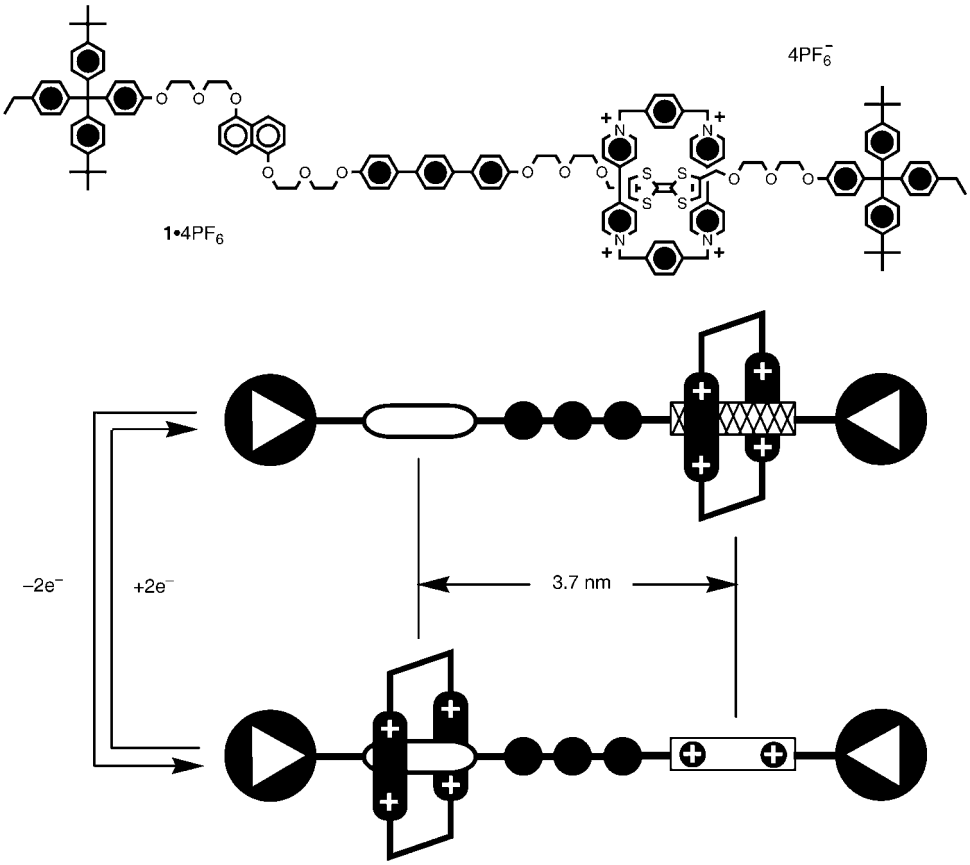


Figure 1. A [2]rotaxane with the TTF (hatched) and DNP (open) recognition units separated by a rigid terphenylene spacer (black circles) demonstrates a relative mechanical movement between the macrocyclic and dumbbell-shaped components of about 3.7 nm.

band to appear at 375 nm, which corresponds to the TTF^{2+} ion.[19a,b] The new CT band was now evident (Figure 2, curve c) at 530 nm. Addition of 2.0 equivalents of the reductant, ascorbic acid, led to the original spectrum being restored (Figure 2, curve d).

^{1}H NMR spectroscopy has established (Figure 3) the precise and quantitative nature[21] of the redox-controlled switching process undergone by the [2]rotaxane $\mathbf{1}^{4+}$. The

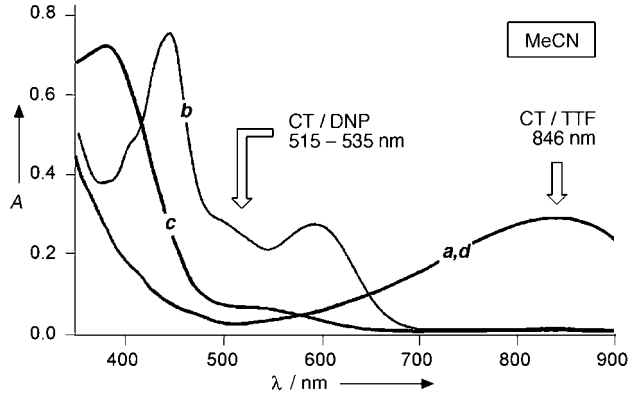


Figure 2. Absorption spectra (MeCN, 298 K) of a 8×10^{-4} M solution of [2]rotaxane $\mathbf{1}\cdot4\,PF_6$ (curve a) and of the same solution after addition of 1.0 and 2.0 equivalents of $Fe(ClO_4)_3$ (curves b and c). Addition of ascorbic acid (2 equiv) regenerates the original spectrum (curve d).

^{1}H NMR spectrum (Figure 3a) of $\mathbf{1}\cdot4\,PF_6$ was recorded in CD_3CN. The oxidant, tris(*p*-bromophenyl)aminium hexachloroantimonate,[22] was added (2.2 equiv) to the sample, the temperature was lowered[23] to 243 K, and the spectrum (Figure 3b) was recorded again. Prior to oxidation of the [2]rotaxane, two pairs of peaks of unequal intensities (47:53) at $\delta = 6.02$ and 6.12 ppm, and $\delta = 6.22$ and 6.28 ppm, respectively, can be assigned to the constitutionally heterotopic TTF methine protons in the *cis* and *trans* isomers (it is not clear from the data which peaks belong to which isomer) associated with the TTF unit in $\mathbf{1}^{4+}$. On oxidation, the signals for the constitutionally heterotopic methine protons on the TTF^{2+} ion resonate[24] at $\delta = 9.15$ and 9.25 ppm, while those for the methylene protons on the adjacent CH_2 groups resonate[25] at $\delta = 5.00$ and 5.16 ppm. In the case of the oxidized [2]rotaxane containing the TTF^{2+} ion, the presence of two isomers is no longer evident, presumably on account of the nonplanar geometry of the TTF^{2+} ion removing the possibility for *cis–trans* isomerism. Evidence for movement of the $CBPQT^{4+}$ ring from the TTF to the DNP site upon oxidation of the [2]rotaxane is apparent from observation of upfield shifts of the peaks corresponding to the protons of the DNP site. The H-2/6 and H-3/7 protons resonate at $\delta = 6.28$ and 5.99 ppm, respectively (although H-2 and H-6 are nonequivalent protons, their signals in the ^{1}H NMR spectrum overlap and likewise for H-3/7), in the spectrum (Figure 3b)

 © 2003 Wiley-VCH Verlag GmbH & Co. KGaA, Weinheim

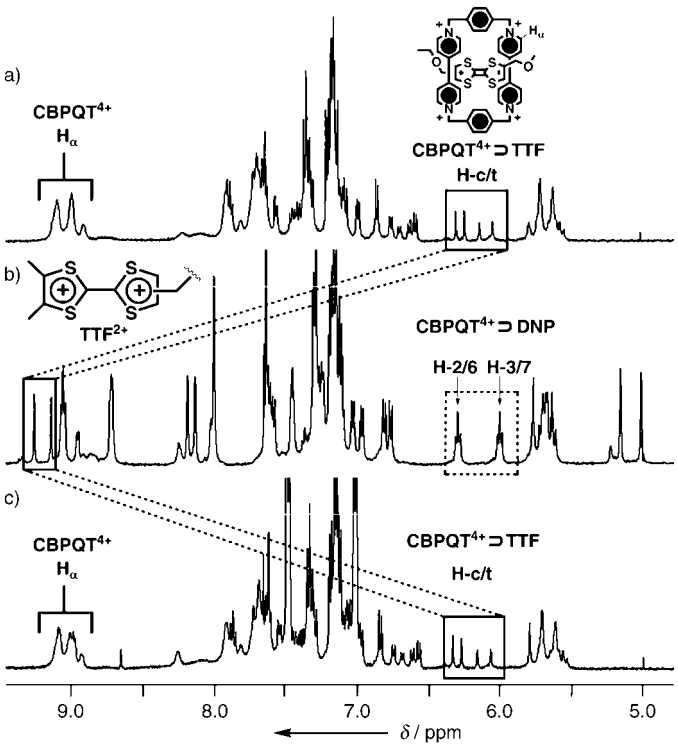


Figure 3. a) ^{1}H NMR spectrum of **1**·4 PF_6 in CD_3CN recorded at 500 MHz at room temperature. The solid box highlights the peaks for the H-c/t (*cis*/*trans*) protons in the neutral TTF unit. b) ^{1}H NMR spectrum of bis-oxidized **1**·4 PF_6 in CD_3CN recorded at 500 MHz at 243 K. The solid box highlights the peaks for the TTF^{2+} dicationic residues and the dotted box indicates the peaks for H-2/6 and H-3/7 of the "inside" DNP unit. (The peaks corresponding to H-4/8 appear at $\delta = 2.34$ and 2.32 ppm and are not shown here.) c) ^{1}H NMR spectrum of reduced **1**·4 PF_6 in CD_3CN recorded at 500 MHz at room temperature. The solid box highlights the peaks for the neutral TTF unit.

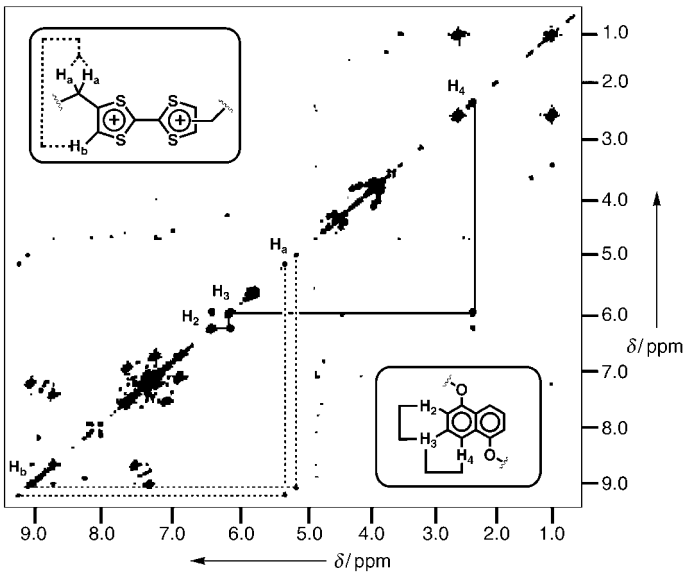


Figure 4. ^{1}H DQF-COSY spectrum at 500 MHz of the bis-oxidized form of **1**·4 PF_6 in CD_3CN at 243 K. The solid lines indicate coupling between peaks corresponding to the protons of the DNP site encircled by a $CBPQT^{4+}$ unit. Dotted lines show the weak long-range coupling between the protons on the TTF^{2+} unit and the adjacent CH_2 groups.

of oxidized $\mathbf{1}^{4+}$. The upfield shifts of about 1.5 ppm result from anisotropic shielding of the protons on the DNP site by the aromatic rings present in the encircling $CBPQT^{4+}$ ring. Additionally, the H-4/8 protons of the encircled DNP site participate in C–H···π interactions with the paraphenylene bridges in the $CBPQT^{4+}$ ring, which results in large upfield shifts of approximately 4.5 ppm to $\delta = 2.34$ and 2.32 ppm. Examination of the ^{1}H DQF-COSY (double quantum filtered correlation spectroscopy) spectrum (Figure 4) for the oxidized [2]rotaxane shows clearly the scalar coupling between the protons of the DNP site. No observation of signals corresponding to the uncomplexed DNP site or the complexed TTF^{2+} ion are observed in the ^{1}H NMR spectrum of oxidized $\mathbf{1}^{4+}$, which indicates that all of the [2]rotaxane molecules have been switched within the limits of detection by ^{1}H NMR spectroscopy. Addition of Zn powder to the sample and vigorous shaking of the mixture led to reduction of the TTF^{2+} ion to its neutral form and movement of the $CBPQT^{4+}$ ring away from the DNP site and back to the much stronger π-electron-donating TTF unit. The original ^{1}H NMR spectrum (Figure 3c) was restored.

While UV/Vis spectroscopy indicates the general nature of the redox-controlled switching process undergone by the [2]rotaxane, ^{1}H NMR spectroscopy provides a precise and quantitative probe of the process, and yields fine, as well as gross, structural information. However, a further issue remains to be addressed in the near future. It relates to the incoherence associated with motor-molecules operating in solution, a deficiency which results in the dissipation of their mechanical energy during the switching process. Only by the mounting[26] of working motor-molecules at interfaces and on surfaces can we hope to harness their mechanical energy. In the wake of being able to monitor the redox-controlled switching of $\mathbf{1}^{4+}$ in solution, we are now exploring the potential of using nanoparticles as platforms for the self-assembly of motor-molecules, prior to their characterization by NMR spectroscopy. A link between solution-state molecular signatures, where incoherence is rife, and characterization of solid-state devices, where coherence occurs, is essential if further progress is to be made in the realization of small but movable machines.[1]

Received: October 29, 2002 [Z50453]

Keywords: chemical switching · molecular devices · rotaxanes · self-assembly · supramolecular chemistry

[1] R. P. Feynman, *Eng. Sci.* **1960**, *23*, 22–36.
[2] a) J.-M. Lehn, *Supramolecular Chemistry: Concepts and Perspectives*, VCH, Weinheim, **1995**; b) viewpoint on supramolecular chemistry and self-assembly: *Science* **2002**, *295*, 2400–2421.
[3] a) G. Schill, *Catenanes, Rotaxanes and Knots*, Academic Press, New York, **1971**; b) D. M. Walba, *Tetrahedron* **1985**, *41*, 3161–3212; c) C. O. Dietrich-Buchecker, J.-P. Sauvage, *Chem. Rev.* **1987**, *87*, 795–810; d) H. W. Gibson, H. Marand, *Adv. Mater.* **1993**, *5*, 11–21; e) D. B. Amabilino, J. F. Stoddart, *Chem. Rev.*

 © 2003 Wiley-VCH Verlag GmbH & Co. KGaA, Weinheim

1995, *95*, 2725 – 2828; f) R. Jäger, F. Vögtle, *Angew. Chem.* **1997**, *109*, 966 – 980; *Angew. Chem. Int. Ed. Engl.* **1997**, *36*, 930 – 944; g) G. A. Breault, C. A. Hunter, P. C. Mayers, *Tetrahedron* **1999**, *55*, 5265 – 5293; h) *Molecular Catenanes, Rotaxanes, and Knots* (Eds.: J.-P. Sauvage, C. O. Dietrich-Buchecker), Wiley-VCH, Weinheim, **1999**; i) J. F. Stoddart, H.-R. Tseng, *Proc. Natl. Acad. Sci. USA* **2002**, *99*, 4797 – 4800; j) L. Raehm, D. G. Hamilton, J. K. M. Sanders, *Synlett* **2002**, 1743 – 1761.

[4] a) J. F. Stoddart, *Chem. Aust.* **1992**, *59*, 576 – 577; J. F. Stoddart, *Chem. Aust.* **1992**, *59*, 581; b) M. Gómez-López, J. A. Preece, J. F. Stoddart, *Nanotechnology* **1996**, *7*, 183 – 192; c) V. Balzani, M. Gómez-López, J. F. Stoddart, *Acc. Chem. Res.* **1998**, *31*, 405 – 414; d) V. Balzani, A. Credi, F. M. Raymo, J. F. Stoddart, *Angew. Chem.* **2000**, *112*, 3484 – 3530; *Angew. Chem. Int. Ed.* **2000**, *39*, 3348 – 3391; e) R. Ballardini, V. Balzani, A. Credi, M. T. Gandolfi, M. Venturi, *Struct. Bonding (Berlin)* **2001**, *99*, 163 – 188; f) L. Raehm, J.-P. Sauvage, *Struct. Bonding (Berlin)* **2001**, *99*, 55 – 78; g) C. A. Stanier, S. J. Alderman, T. D. W. Claridge, H. L. Anderson, *Angew. Chem.* **2002**, *114*, 1847 – 1850; *Angew. Chem. Int. Ed.* **2002**, *41*, 1769 – 1772; h) V. Balzani, A. Credi, M. Venturi, *Chem. Eur. J.* **2002**, *8*, 5525 – 5532.

[5] a) Y. Yokoyama, *Chem. Rev.* **2000**, *100*, 1717 – 1740; b) G. Berkovic, V. Krongauz, V. Weiss, *Chem. Rev.* **2000**, *100*, 1741 – 1754; c) B. L. Feringa, R. A. van Delden, N. Koumura, E. M. Geertsema, *Chem. Rev.* **2000**, *100*, 1789 – 1816; d) T. R. Kelly, *Acc. Chem. Res.* **2001**, *34*, 514 – 522; e) R. Ballardini, V. Balzani, A. Credi, M. T. Gandolfi, M. Venturi, *Acc. Chem. Res.* **2001**, *34*, 445 – 455; f) A. Harada, *Acc. Chem. Res.* **2001**, *34*, 456 – 464; g) C. A. Schalley, K. Beizai, F. Vögtle, *Acc. Chem. Res.* **2001**, *34*, 465 – 476; h) J.-P. Collin, C. Dietrich-Buchecker, P. Gaviña, M. C. Jimenez-Molero, J.-P. Sauvage, *Acc. Chem. Res.* **2001**, *34*, 477 – 487; i) V. Amendola, L. Fabbrizzi, C. Mangano, P. Pallavicini, *Acc. Chem. Res.* **2001**, *34*, 488 – 493; j) S. Shinkai, M. Ikeda, A. Sugasaki, M. Takeuchi, *Acc. Chem. Res.* **2001**, *34*, 494 – 503; k) N. Koumura, E. M. Geertsema, M. B. van Gelder, A. Meetsma, B. L. Feringa, *J. Am. Chem. Soc.* **2002**, *124,* 5037 – 5051.

[6] a) P. R. Ashton, R. Ballardini, V. Balzani, A. Credi, R. Dress, E. Ishow, O. Kocian, J. A. Preece, N. Spencer, J. F. Stoddart, M. Venturi, S. Wenger, *Chem. Eur. J.* **2000**, *6*, 3558 – 3574; b) A. M. Brouwer, C. Frochot, F. G. Gatti, D. A. Leigh, L. Mottier, F. Paolucci, S. Roffia, G. W. H. Wurpel, *Science* **2001**, *291*, 2124 – 2128; c) F. G. Gatti, S. León, J. K. Y. Wong, G. Bottari, A. Allieri, M. A. F. Morales, S. J. Teat, C. Frochot, D. A. Leigh, A. M. Brouwer, F. Zerbetto, *Proc. Natl. Acad. Sci. USA* **2003**, *100*, 10 – 14.

[7] a) C. P. Collier, G. Mattersteig, E. W. Wong, Y. Luo, K. Beverly, J. Sampaio, F. M. Raymo, J. F. Stoddart, J. R. Heath, *Science* **2000**, *289*, 1172 – 1175; b) A. R. Pease, J. O. Jeppesen, J. F. Stoddart, Y. Luo, C. P. Collier, J. R. Heath, *Acc. Chem. Res.* **2001**, *34*, 433 – 444; c) C. P. Collier, J. O. Jeppesen, Y. Luo, J. Perkins, E. W. Wong, J. R. Heath, J. F. Stoddart, *J. Am. Chem. Soc.* **2001**, *123*, 12632 – 12641; d) Y. Luo, C. P. Collier, J. O. Jeppesen, K. A. Nielsen, E. DeIonno, G. Ho, J. Perkins, H.-R. Tseng, T. Yamamoto, J. F. Stoddart, J. R. Heath, *ChemPhysChem* **2002**, *3*, 519 – 525.

[8] a) R. A. Bissell, E. Córdova, A. E. Kaifer, J. F. Stoddart, *Nature* **1994**, *369*, 133 – 137; b) L. Raehm, J.-M. Kern, J.-M. Sauvage, *Chem. Eur. J.* **1999**, *5*, 3310 – 3317.

[9] a) P. R. Ashton, R. Ballardini, V. Balzani, M. Gómez-López, S. E. Lawrence, M.-V. Martínez-Díaz, M. Montali, A. Piersanti, L. Prodi, J. F. Stoddart, D. J. Williams, *J. Am. Chem. Soc.* **1997**, *119*, 10641 – 10651; b) P. R. Ashton, R. Ballardini, V. Balzani, I. Baxter, A. Credi, M. C. T. Fyfe, M. T. Gandolfi, M. Gómez-López, M.-V. Martínez-Díaz, A. Piersanti, N. Spencer, J. F. Stoddart, M. Venturi, A. J. P. White, D. J. Williams *J. Am. Chem. Soc.* **1998**, *120*, 11932 – 11942; c) A. M. Elizarov, T. Chang, H.-S. Chiu, J. F. Stoddart, *J. Org. Chem.* **2002**, *67*, 9175 – 9181.

[10] When two recognition sites on the dumbbell component of a [2]rotaxane are identical, the ring component shuttles back and forth between the sites: we refer to this kind of [2]rotaxane as a molecular shuttle, see P.-L. Anelli, N. Spencer, J. F. Stoddart, *J. Am. Chem. Soc.* **1991**, *113*, 5131 – 5133.

[11] M. C. T. Fyfe, J. F. Stoddart, *Acc. Chem. Res.* **1997**, *30*, 393 – 401.

[12] J. O. Jeppesen, J. Perkins, J. Becher, J. F. Stoddart, *Angew. Chem.* **2001**, *113*, 1256 – 1261; *Angew. Chem. Int. Ed.* **2001**, *40*, 1216 – 1121.

[13] M. Asakawa, W. Dehaen, G. L'abbé, S. Menzer, J. Nouwen, F. M. Raymo, J. F. Stoddart, D. J. Williams, *J. Org. Chem.* **1996**, *61*, 9591 – 9595.

[14] For accounts and reviews on π···π stacking interactions, see a) C. A. Hunter, J. K. M. Sanders, *J. Am. Chem. Soc.* **1990**, *112*, 5525 – 5534; b) M. H. Schwartz, *J. Inclusion Phenom. Macrocyclic Chem.* **1990**, *9*, 1 – 35; c) J. H. Williams, *Acc. Chem. Res.* **1993**, *26*, 539 – 598; d) C. A. Hunter, *Angew. Chem.* **1993**, *105*, 1653 – 1655; *Angew. Chem. Int. Ed. Engl.* **1993**, *32*, 1584 – 1586; e) C. A. Hunter, *J. Mol. Biol.* **1993**, *230*, 1025 – 1054; f) T. Dahl, *Acta. Chem. Scand.* **1994**, *48*, 95 – 116; g) F. Cozzi, J. S. Siegel, *Pure Appl. Chem.* **1995**, *67*, 683 – 689; h) C. G. Claessens, J. F. Stoddart, *J. Phys. Org. Chem.* **1997**, *10*, 254 – 272; i) G. Chessari, C. A. Hunter, C. M. R. Low, M. J. Packer, J. G. Vinter, C. Zonta, *Chem. Eur. J.* **2002**, *8*, 2860 – 2867.

[15] J. O. Jeppesen, S. A. Vignon, J. F. Stoddart *Chem. Eur. J.*, submitted.

[16] J. O. Jeppesen, K. A. Nielsen, J. Perkins, S. A. Vignon, A. D. Fabio, R. Ballardini, M. T. Gandolfi, M. Venturi, V. Balzani, J. Becher, J. F. Stoddart, *Chem. Eur. J.*, in press.

[17] P.-L. Anelli, M. Asakawa, P. R. Ashton, R. A. Bissell, G. Clavier, R. Górski, A. E. Kaifer, S. J. Langford, G. Mattersteig, S. Menzer, D. Philp, A. M. Z. Slawin, N. Spencer, J. F. Stoddart, M. S. Tolley, D. J. Williams, *Chem. Eur. J.* **1997**, *3*, 1113 – 1135.

[18] R. Castro, K. R. Nixon, J. D. Evanseck, A. K. Kaifer, *J. Org. Chem.* **1996**, *61*, 7298 – 7303.

[19] a) M. Asakawa, P. R. Ashton, V. Balzani, A. Credi, C. Hamers, G. Mattersteig, M. Montalti, A. N. Shipway, N. Spencer, J. F. Stoddart, M. S. Tolley, M. Venturi, A. J. P. White, D. J. Williams, *Angew. Chem.* **1998**, *110*, 357 – 361; *Angew. Chem. Int. Ed.* **1998**, *37*, 333 – 337; b) V. Balzani, A. Credi, G. Mattersteig, O. A. Matthews, F. M. Raymo, J. F. Stoddart, M. Venturi, A. J. P. White, D. J. Williams, *J. Org. Chem.* **2000**, *65*, 1924 – 1936; c) C. L. Brown, U. Jonas, J. A. Preece, H. Ringsdorf, M. Seitz, J. F. Stoddart, *Langmuir* **2000**, *16*, 1924 – 1930; d) M. Asakawa, M. Higuchi, G. Mattersteig, T. Nakamura, A. R. Pease, F. M. Raymo, T. Shimizu, J. F. Stoddart, *Adv. Mater.* **2000**, *12*, 1099 – 1102.

[20] Molecular modeling studies were performed using the MM2 force-field as implemented in Chem3D version 7.0. The molecule was "stretched" and then minimized to give the most linear conformation possible. The distance of 3.7 nm was measured from the center of the TTF unit to the center of the DNP ring system and can be compared to an overall length of approximately 9 nm for the rotaxane.

[21] A variable temperature ^{1}H NMR spectroscopic investigation (H.-R. Tseng, S. Kang, S. A. Vignon, J. F. Stoddart, unpublished results) of a degenerate model [2]rotaxane, in which the DNP ring system is replaced by a TTF unit, reveals that shuttling of the CBPQT^{4+} ring between the two TTF units is slow at room temperature on the ^{1}H NMR timescale. An energy barrier in excess of 16 kcal mol^{-1} can be associated with this shuttling process. It follows that the ^{1}H NMR spectrum shown in Figure 3a is not an averaged one but a discrete one which indicates that the CBPQT^{4+} ring encircles the TTF unit exclusively.

[22] This oxidant was chosen for three reasons: 1) it has a high enough oxidative potential (0.7 V versus ferrocene) to oxidize

the TTF unit completely to TTF^{2+}, 2) the reduced form will give only two signals in the ^1H NMR spectrum and will not interfere with interpretation of the data, and 3) the solubilities of both the oxidant and its reduced form are good in the same solvents as the rotaxanes of interest. For details, see a) N. G. Connelly, W. E. Geiger, *Chem. Rev.* **1996**, *96*, 877 – 910; b) E. Steckhan, *Top. Curr. Chem.* **1987**, *142*, 1 – 69.

[23] It was necessary to lower the temperature to avoid decomposition of the oxidized [2]rotaxane during the accumulation of data for the ^1H DQF-COSY spectrum reproduced in Figure 4.

[24] An ^1H NMR spectrum showing the signals corresponding to TTF^{2+} has been reported previously, see P. R. Ashton, V. Balzani, J. Becher, A. Credi, M. C. T. Fyfe, G. Mattersteig, S. Menzer, M. B. Nielsen, F. M. Raymo, J. F. Stoddart, M. Venturi, D. J. Williams, *J. Am. Chem. Soc.* **1999**, *121*, 3951 – 3957.

[25] Peak assignments for the TTF^{2+} and adjacent CH_2 groups were made on the basis of an observed long-range coupling between the two, which led to the TTF^{2+} and TTF signals being triplets with a small splitting (ca. 1 Hz). This coupling can also be observed in the ^1H DQF-COSY spectrum (Figure 4) for the oxidized [2]rotaxane. Additional evidence to support the assignments was obtained by peak integrations, as well as by monitoring the peaks during titration with the oxidant. Similar dramatic chemical shift changes have been observed in our laboratory for other TTF-containing compounds upon oxidation.

[26] S. Chia, J. Cao, J. F. Stoddart, J. I. Zink, *Angew. Chem.* **2001**, *113*, 2513 – 2517; *Angew. Chem. Int. Ed.* **2001**, *40*, 2447 – 2451.

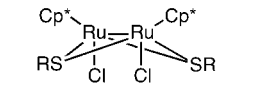
 © 2003 Wiley-VCH Verlag GmbH & Co. KGaA, Weinheim

C-H Activation with Ru

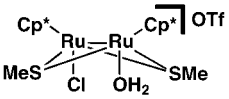
Propargylation of Aromatic Compounds with Propargylic Alcohols Catalyzed by a Cationic Diruthenium Complex**

Yoshiaki Nishibayashi, Youichi Inada, Masato Yoshikawa, Masanobu Hidai, and Sakae Uemura**

We have recently disclosed that the ruthenium-catalyzed propargylation of aromatic compounds with propargylic alcohols affords the corresponding propargylated aromatic compounds in good yields with a complete regioselectivity.[1] The reactions are only catalyzed by thiolate-bridged diruthenium complexes, such as [Cp*RuCl(μ_2-SR)$_2$RuCp*Cl][2] (Cp* = η^5-C$_5$Me$_5$; R = Me (**1a**), *i*Pr (**1b**), *n*Pr (**1c**)). In this catalytic reaction, usable propargylic reagents were unfortunately strictly limited to the propargylic alcohols bearing *terminal* acetylene groups, because the reactions proceeded by an electrophilic aromatic-substitution reaction at the γ-carbon of the allenylidene intermediates, which can only be produced from this type of propargylic alcohol.[3a–c] During our study of the catalytic propargylation of aromatic compounds, we have now found that a cationic methanethiolate-bridged diruthenium complex [Cp*RuCl(μ_2-SMe)$_2$RuCp*(OH$_2$)]OTf (**1d**; OTf = CF$_3$SO$_3$)[3d] promotes the catalytic propargylation of aromatic compounds with propargylic alcohols bearing not only *terminal* acetylene but also *internal* acetylene units. The reaction described herein provides a general preparative synthetic method for a variety of propargylated aromatic compounds. The most characteristic features of this reaction are its high atom economy and environmental friendliness, the only stoichiometric by-product being water (H$_2$O).



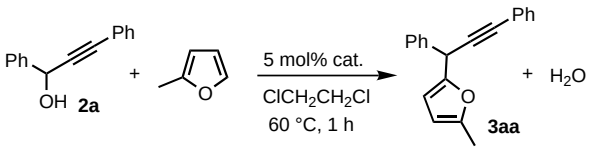
R = Me (**1a**), *i*Pr (**1b**), *n*Pr (**1c**)



R = Me (**1d**), *i*Pr (**1e**)

We investigated the propargylation of 2-methylfuran with propargylic alcohols, such as 1,3-diphenyl-2-propyn-1-ol (**2a**), with internal acetylene units. Treatment of 2-methylfuran with **2a** in 1,2-dichloroethane in the presence of **1d** (5 mol%) at 60°C for 1 h afforded 5-methyl-2-(1,3-diphenyl-2-propynyl)furan (**3aa**) in 88% isolated yield (Table 1; entry 1).

Table 1: Propargylation of 2-methylfuran with 1,3-diphenyl-2-propyn-1-ol (**2a**).[a]



Entry	Catalyst	Yield [%][b]
1	[Cp*RuCl(μ-SMe)$_2$Cp*Ru(OH$_2$)]OTf (**1d**)	88
2[c]	[Cp*RuCl(μ-SMe)$_2$Cp*Ru(OH$_2$)]OTf (**1d**)	50
3	[Cp*RuCl(μ-S*i*Pr)$_2$Cp*Ru(OH$_2$)]OTf (**1e**)	81
4	[Cp*RuCl(μ-SMe)$_2$Cp*RuCl] (**1a**)[d]	0
5	[Cp*RuCl(μ-S*i*Pr)$_2$Cp*RuCl] (**1b**)[d]	0
6	[CpRuCl(PPh$_3$)$_2$]	0
7	[RuCl$_2$(PPh$_3$)$_3$]	0
8	[{RuCl$_2$(*p*-cymene)}$_2$]	0
9	[(indenyl)RuCl(PPh$_3$)$_2$]	0
10	[Cp*RuCl(μ_2-Cl)$_2$RuCp*Cl]	0

[a] All of the reactions of 2-methylfuran (1.500 mmol) with **2a** (0.300 mmol) were carried out in the presence of catalyst (0.015 mmol) in ClCH$_2$CH$_2$Cl (8 mL) at 60°C for 1 h. [b] Isolated yield. [c] At room temperature for 5 h. [d] No reaction even in the presence of NH$_4$BF$_4$.

[*] Prof. Dr. S. Uemura, Dr. Y. Nishibayashi, Y. Inada, M. Yoshikawa
Department of Energy and Hydrocarbon Chemistry
Graduate School of Engineering
Kyoto University, Yoshida, Sakyo-ku, Kyoto 606-8501 (Japan)
Fax: (+81) 75-753-3573
E-mail: uemura@scl.kyoto-u.ac.jp
Prof. Dr. M. Hidai
Department of Materials Science and Technology
Faculty of Industrial Science and Technology
Tokyo University of Science, Noda, Chiba 278-8510 (Japan)
Fax: (+81) 471-23-9362
E-mail: hidai@rs.noda.sut.ac.jp

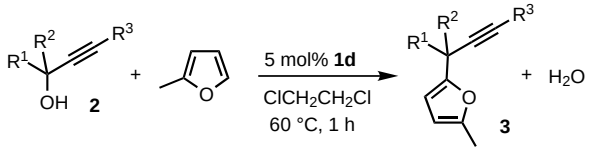
[**] This work was supported by a Grant-in-Aid for Scientific Research (No. 13305062) from the Ministry of Education, Science, Sports, and Culture of Japan.

 DOI: 10.1002/anie.200250532 © 2003 Wiley-VCH Verlag GmbH & Co. KGaA, Weinheim

Neither other products nor regioisomers of **3aa** were detected by GLC and ^{1}H NMR. The reaction proceeded even at room temperature, but a longer reaction time was required to obtain **3aa** even in 50% isolated yield (Table 1; entry 2). The complex with the sterically demanding S*i*Pr group (**1e**) exhibited a slightly lower catalytic activity (Table 1; entry 3). It is noteworthy that neutral thiolate-bridged diruthenium complexes (**1a** and **1b**), which are known to promote the propargylation of aromatic compounds with propargylic alcohols bearing *terminal* acetylene groups,[1] did not work at all (Table 1; entries 4 and 5). Other di- and monoruthenium complexes such as $[CpRuCl(PPh_3)_2]$ ($Cp = \eta^5$-C_5H_5), $[RuCl_2(PPh_3)_3]$, $[\{RuCl_2(p\text{-cymene})\}_2]$, [(indenyl)-$RuCl(PPh_3)_2$], and $[Cp^*RuCl(\mu_2\text{-}Cl)_2RuCp^*Cl]$ were ineffective for this catalytic propargylation (Table 1; entries 6–10).

Reactions of 2-methylfuran with other propargylic alcohols bearing internal acetylene units have been similarly carried out. Typical results are shown in Table 2. The

Table 2: Propargylation of 2-methylfuran with propargylic alcohols (**2**).[a]

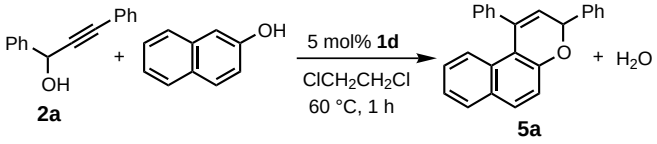


Entry		Propargylic alcohol			Yield of **3** [%][b]
		R^1	R^2	R^3	
1	**2b**	Ph	H	*n*Bu	**3ab**, 91
2	**2c**	Ph	H	*t*Bu	**3ac**, 80
3	**2d**	Ph	H	*n*-hexyl	**3ad**, 83
4	**2e**	*p*-MeC_6H_4	H	Ph	**3ae**, 91
5	**2f**	$Ph_2C{=}CH$	H	Ph	**3af**, 60
6	**2g**	Ph	Me	Ph	**3ag**, 49[c]
7[d]	**2h**	Me	Me	Ph	**3ah**, 20[e]
8[d]	**2i**	Et	H	Ph	**3ai**, 0[f]

[a] All of the reactions of 2-methylfuran (1.500 mmol) with **2** (0.300 mmol) were carried out in the presence of **1d** (0.015 mmol) in $ClCH_2CH_2Cl$ (8 mL) at 60°C for 1 h. [b] Isolated yield. [c] 2,4-Diphenyl-1-buten-3-yne (20%) was formed. [d] For 3 h. [e] 2-Methyl-4-phenyl-1-buten-3-yne (40%) was formed. [f] No reaction.

corresponding 2-propargylic furans (**3ab**–**3ae**) were obtained from various alkyl and aryl substituted propargylic alcohols (**2b**–**2e**) in excellent yields with a complete regioselectivity (Table 2; entries 1–4). The reaction with 1-alkenyl substituted propargylic alcohol (**2f**) gave the corresponding propargylic furan (**3af**) in 60% isolated yield (Table 2; entry 5). The propargylation of 2-methylfuran with 1,1-disubstituted propargylic alcohol such as 2,4-diphenyl-3-butyn-2-ol (**2g**) afforded the expected propargylic furan (**3ag**) in slightly lower yield, but together with the formation of 2,4-diphenyl-1-buten-3-yne in 20% yield (Table 2; entry 6). Similarly, the reaction with 1,1-dialkyl substituted propargylic alcohol gave both the corresponding propargylated furan (**3ah**) in only 20% yield and the conjugated enyne in 40% yield (Table 2; entry 7). On the other hand, no propargylation proceeded when 1-alkyl substituted propargylic alcohol such as **2i** was used (Table 2; entry 8).

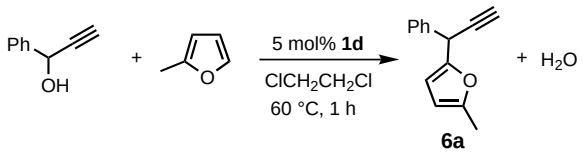
Next, the propargylation of various aromatic compounds with **2a** was examined in the presence of **1d** (5 mol%) at 60°C. Typical results are summarized in Table 3. The corresponding propargylic compounds (**4aa**–**4ad**) were obtained from a variety of heterocyclic compounds such as furan, 2,3-dimethylfuran, pyrrole, and 2-methylthiophene in good yields with a complete regioselectivity (Table 3; entries 1–4). In all cases, propargylation occurred selectively at the α position of heterocyclic rings. These results indicate that the reaction proceeds electrophilically. In the cases of electron-rich arenes such as 1,3-dimethoxybenzene, 1,3,5-trimethoxybenzene, an acetanilide derivative, and phenol, the corresponding propargylated benzene derivatives (**4ae**–**4ah**) were obtained in 91%, 73%, 41%, and 80% isolated yields, respectively (Table 3; entries 5–8). Although the reaction of 2-methoxynaphthalene with **2a** gave 1-propargylic naphthalene (**4ai**) in 94% yield (Table 3; entry 9), that of 2-naphthol afforded the unexpected 3*H*-naphtho[2,1-b]pyrane (**5a**) in 21% yield with the formation of unidentified compounds (Scheme 1).[4] The



Scheme 1. Reaction of 1,3-diphenyl-2-propyn-1-ol with 2-naphthol.

high yield formation of 1-propargylated azulene (**4aj**) was observed in the reaction of azulene with **2a** (Table 3; entry 10). No propargylation occurred under these reaction conditions, however, when naphthalene, anisole, 1,4-dimethoxybenzene, *p*-xylene, toluene, and *N,N*-dimethylaniline were used as aromatic compounds.

The complex **1d** also catalyzed the propargylation of aromatic compounds with propargylic alcohols bearing terminal acetylene groups.[1] In fact, the treatment of 2-methylfuran with 1-phenyl-2-propyn-1-ol in the presence of **1d** (5 mol%) at 60°C for 1 h afforded 2-methyl-5-(1-phenyl-2-propynyl)furan (**6a**) in quantitative yield (Scheme 2), showing that the cationic complex exhibited almost the same catalytic activity as the neutral diruthenium complex **1a**.[1] Thus, the novel cationic methanethiolate-bridged diruthenium complex **1d** promotes the catalytic propargylation of a variety of aromatic compounds with propargylic alcohols bearing not only terminal acetylene but also internal acetylene groups.

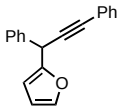
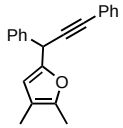
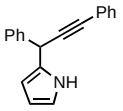
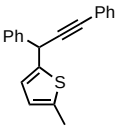
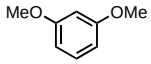
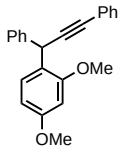
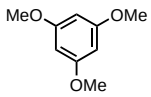
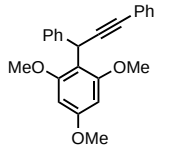
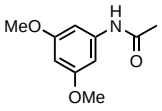
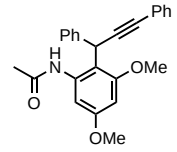
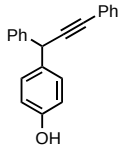
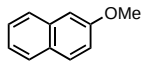
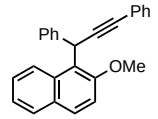
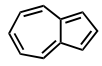
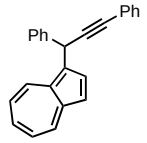


Scheme 2. Propargylation of 2-methylfuran with 1-phenyl-2-propyn-1-ol.

A ^{1}H NMR spectroscopy investigation was carried out by mixing a stoichiometric amount of **1d** and **2a** at room temperature in CD_2Cl_2, but no formation of intermediates

 © 2003 Wiley-VCH Verlag GmbH & Co. KGaA, Weinheim

Table 3: Propargylation of aromatic compounds with **2a**.[a]

Entry	Aromatic compound	*t* [h]	Product		Yield [%][b]
1		2		**4aa**	71
2		2		**4ab**	41
3		17		**4ac**	60
4		1		**4ad**	88
5		3		**4ae**	91
6		1		**4af**	73
7		20		**4ag**	41
8		20		**4ah**	80
9		1		**4ai**	94
10		25		**4aj**	91

[a] All of the reactions of aromatic compound (1.500 mmol) with **2a** (0.300 mmol) were carried out in the presence of **1d** (0.015 mmol) in $ClCH_2CH_2Cl$ (8 mL) at 60 °C. [b] Isolated yield.

was observed. The addition of an excess amount of 2-methylfuran to this reaction mixture, however, led to the high-yield formation of **3aa** together with an almost complete recovery of **1d**. These results may indicate that the intermediates of this catalytic reaction are too labile to be identified. Although direct evidence of the reactive intermediates has not yet been obtained, we believe that the catalytic reaction with propargylic alcohols with internal acetylene units may proceed via (η-propargyl)ruthenium species.[5,6] An electrophilic attack of the (η-propargyl)ruthenium complexes on aromatic compounds should afford the corresponding propargylated aromatic products. On the other hand, the propargylation of aromatic compounds with propargylic alcohols bearing terminal acetylene groups is considered to proceed by electrophilic attack of the cationic Cγ atom in the allenylidene intermediate, as shown previously.[1]

In summary, we have now found that the cationic diruthenium complex **1d** promotes the catalytic propargylation of aromatic compounds with propargylic alcohols bearing not only terminal acetylene but also internal acetylene units. The catalytic reaction described here provides a general and environmentally friendly preparative synthetic method (atom economical, only H_2O as byproduct) for a variety of propargylated aromatic compounds. The electrophilic aromatic-substitution reaction by free propargylic cations has been reported, but the products are either propargylated or allenylated aromatic products and/or a mixture of them, depending on the substituents of the propargylic cations.[7,8] Also, the well known Nicholas reaction requires several steps and uses a stoichiometric amount of $[Co_2(CO)_8]$ for the preparation of these compounds.[9,10] Some propargylated aromatic compounds are useful monomers in the field of material science. Further investigations for the elucidation of the detailed reaction mechanism and broadening the scope of this catalytic propargylation are currently in progress.

Experimental Section

1d: **1a** (965 mg, 1.52 mmol)[3a,b] was placed in a 50-mL flask under N_2. Anhydrous THF (20 mL) was added, and then the mixture was stirred with a magnetic stirrer at room temperature for 5 min. After the addition of AgOTf (398 mg, 1.52 mmol), the reaction flask was kept

 © 2003 Wiley-VCH Verlag GmbH & Co. KGaA, Weinheim

at room temperature for 20 h. Then, the solvent was removed under reduced pressure, and the residue was recrystallized from CH_2Cl_2/*n*-hexane to give black crystals of **1d** (1.02 g, 1.26 mmol, 82%); ^{1}H NMR (270 MHz, $CDCl_3$): $\delta = 1.63$ (s, 30H), 2.51 (s, 6H), 3.30 ppm (brs, 2H); ^{13}C NMR (67.5 Hz, $CDCl_3$) $\delta = 1.1$, 10.5, 96.5 ppm; elemental analysis calcd (%) for $C_{23}H_{38}ClF_3O_4Ru_2S_3$: C 35.91, H 4.98; found: C 35.78, H 4.71.

A typical reaction of 2-methylfuran with 1,3-diphenyl-2-propyn-1-ol (**2a**) catalyzed by **1d**: **1d** was placed in a 20-mL flask (12.2 mg, 0.015 mmol) under N_2. Anhydrous $ClCH_2CH_2Cl$ (8 mL) was added, and then the mixture was magnetically stirred at room temperature for 5 min. After the addition of **2a** (62.6 mg, 0.300 mmol) and 2-methylfuran (123.2 mg, 1.500 mmol), the reaction flask was kept at 60 °C for 1 h. The solvent was concentrated under reduced pressure (aspirator), and then the residue was purified by column chromatography on SiO_2 with EtOAc/hexane (1/9) as eluent to give 5-methyl-2-(1,3-diphenyl-2-propynyl)furan (**3aa**) as a pale yellow oil (71.8 mg, 0.264 mmol, 88% yield); ^{1}H NMR (270 MHz, $CDCl_3$): $\delta = 2.23$ (s, 3H), 5.20 (s, 1H), 5.88 (d, $J = 3.0$ Hz, 1H), 6.12 (d, $J = 3.0$ Hz, 1H,) 7.27–7.47 ppm (m, 10H); ^{13}C NMR (67.5 Hz, $CDCl_3$): $\delta = 13.7$, 37.9, 83.7, 87.7, 106.1, 107.2, 123.2, 127.1, 127.7, 127.9, 128.1, 128.4, 131.6, 139.0, 151.6, 151.7 ppm; elemental analysis calcd (%) for $C_{20}H_{16}O$: C 88.20, H 5.92; found: C 88.38, H 6.09.

Received: November 12, 2002 [Z50532]

Keywords: alkynes · aromatic substitution · C–H activation · ruthenium · S ligands

[1] Y. Nishibayashi, M. Yoshikawa, Y. Inada, M. Hidai, S. Uemura, *J. Am. Chem. Soc.* **2002**, *124*, 11846.

[2] The thiolate-bridged diruthenium complexes have been found to provide unique bimetallic reaction sites for activation and transformation of various terminal alkynes, see: Y. Nishibayashi, M. Yamanashi, I. Wakiji, M. Hidai, *Angew. Chem.* **2000**, *112*, 3031; *Angew. Chem. Int. Ed.* **2000**, *39*, 2909, and references therein.

[3] a) Y. Nishibayashi, I. Wakiji, M. Hidai, *J. Am. Chem. Soc.* **2000**, *122*, 11019; b) Y. Nishibayashi, I. Wakiji, Y. Ishii, S. Uemura, M. Hidai, *J. Am. Chem. Soc.* **2001**, *123*, 3393; c) Y. Nishibayashi, Y. Inada, M. Hidai, S. Uemura, *J. Am. Chem. Soc.* **2002**, *124*, 7900; d) Y. Inada, Y. Nishibayashi, M. Hidai, S. Uemura, *J. Am. Chem. Soc.* **2002**, *124*, 15172.

[4] K. Tanaka, H. Aoki, H. Hosomi, S. Ohba, *Org. Lett.* **2000**, *2*, 2133.

[5] For recent reviews, see a) C.-T. Chen, *Coord. Chem. Rev.* **1999**, *190–192*, 1143; b) A. Wojcicki, *Inorg. Chem. Commun.* **2002**, *5*, 82.

[6] For recent examples, see a) S. Ogoshi, T. Nishida, Y. Fukunishi, K. Tatsumi, H. Kurosawa, *J. Organomet. Chem.* **2001**, *620*, 190; b) C. P. Casey, T. M. Boller, S. Kraft, I. A. Guzei, *J. Am. Chem. Soc.* **2002**, *124*, 13215.

[7] G. A. Olah, *Friedel-Crafts and Related Reactions*, Interscience, New York, **1964**.

[8] a) T. Ishikawa, M. Okano, T. Aikawa, S. Saito, *J. Org. Chem.* **2001**, *66*, 4635; b) T. J. J. Müller, *Eur. J. Org. Chem.* **2001**, 2021, and references therein.

[9] For recent reviews, see a) K. M. Nicholas, *Acc. Chem. Res.* **1987**, *20*, 207; b) A. J. M. Caffyn, K. M. Nicholas in *Comprehensive Organometallic Chemistry II, Vol. 12* (Eds.: E. W. Abel, G. A. Stone, G. Wilkinson,) Pergamon, New York, **1995**, chap. 7.1; c) J. R. Green, *Curr. Org. Chem.* **2001**, *5*, 811; d) B. J. Teobald, *Tetrahedron* **2002**, *58*, 4133.

[10] For recent examples, see a) K.-D. Roth, *Synlett* **1993**, 529; b) A. V. Muehldorf, A. Guzman-Perez, A. F. Klug, *Tetrahedron Lett.* **1994**, *35*, 8755; c) D. D. Grove, J. R. Corte, R. P. Spencer, M. E. Pauly, N. P. Rath, *J. Chem. Soc. Chem. Commun.* **1994**, 49; d) J.-Y. LeBrazidec, P. J. Kocienski, J. D. Connolly, K. W. Muir, *J. Chem. Soc. Perkin Trans. 1* **1998**, 2475; e) R. Guo, J. R. Green, *Chem. Commun.* **1999**, 2503.

 © 2003 Wiley-VCH Verlag GmbH & Co. KGaA, Weinheim

Diels-Alder Reactions

The First Organocatalytic Enantioselective Inverse-Electron-Demand Hetero-Diels–Alder Reaction**

*Karsten Juhl and Karl Anker Jørgensen**

The use of chiral amines as catalysts for organic reactions has emerged as a new and important field in chemistry and several new reactions have been developed.[1] Among the amines studied, L-proline and (*S*)-2-(1-pyrrolidinylmethyl)-pyrrolidine have been successfully applied as chiral catalysts for reactions of aldehydes or ketones in aldol,[2] Mannich,[3] Michael,[4] and α-amination reactions.[5] The mechanisms for these reactions are presumed to go via the enamine intermediate, that is, the aldehyde or ketone reacts with the amine to form an enamine, which then adds as a nucleophile to the C=O-, C=N-, C=C-, or N=N-moiety, respectively. Simultaneously, MacMillan and co-workers have developed organocatalytic cycloaddition reactions of electron-poor alkenes with dienes[6] or 1,3 dipoles[7] and 1,4-addition of aromatic compounds.[8]

Herein we present the development of a new organocatalytic reaction. We envisioned that chiral enamines, generated from aldehydes and chiral pyrrolidines, could act as electron-rich alkenes and undergo an enantioselective hetero-Diels–Alder (HDA) reaction with enones via the catalytic cycle outlined in Scheme 1:[9,10] In situ generation of a chiral enamine **2** from a chiral pyrrolidine **1** and an aldehyde **3** followed by a stereoselective HDA reaction with enone **4** would give the aminal **5**. Hydrolysis of aminal **5** would then give hemiacetal **6** and release the chiral catalyst **1** to complete the catalytic cycle.

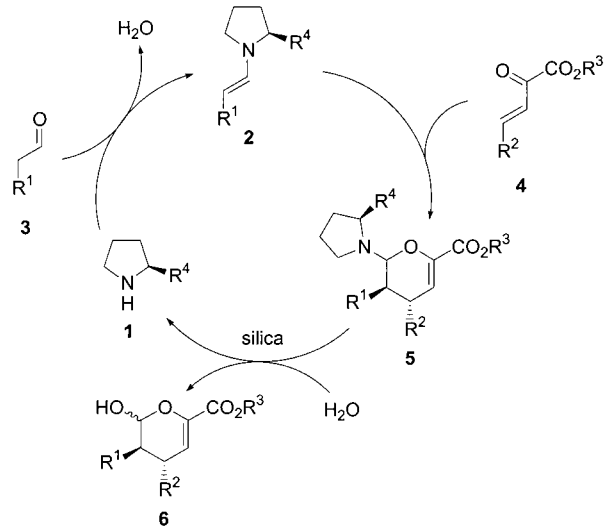
A key step in the catalytic cycle is the hydrolysis of the aminal **5**. We have found that the reaction of a stoichiometric

[*] Prof. Dr. K. A. Jørgensen, Dr. K. Juhl
The Danish National Research Foundation: Center for Catalysis
Department of Chemistry, Aarhus University
8000 Aarhus C (Denmark)
Fax: (+45) 8619-6199
E-mail: kaj@chem.au.dk

[**] This work was made possible by a grant from The Danish National Research Foundation. Thanks are expressed to Dr. R. G. Hazell for solving the X-ray crystal structure of **8bb**.

Supporting information for this article is available on the WWW under http://www.angewandte.org or from the author.

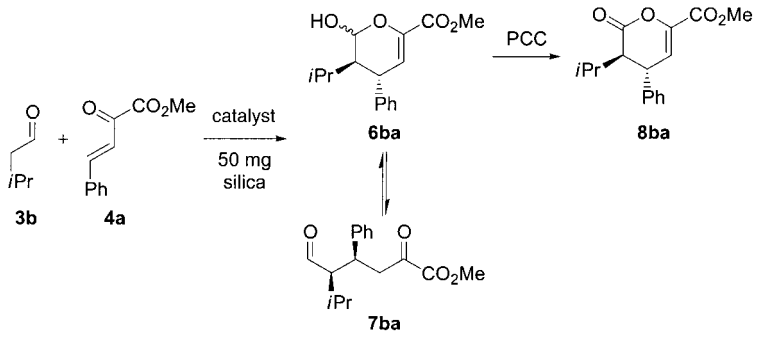
 © 2003 Wiley-VCH Verlag GmbH & Co. KGaA, Weinheim DOI: 10.1002/anie.200250652



Scheme 1. Catalytic cycle for the organocatalytic hetero-Diels–Alder reaction.

amount of a chiral enamine **2** with enone **4** gives only one diastereomer of **5** and in attempts to purify **5** we found that the cycloaddition adduct was easily hydrolyzed by silica gel to give a mixture of the two anomers of hemiacetal **6** and aldehyde **7** (e.g. see Scheme 2).[11] Thus, the presence of silica would facilitate the hydrolysis step in the catalytic cycle.

Indeed, the enamine of isovaleraldehyde **3b** generated in situ reacted with the electron-poor enone **4a** in a HDA reaction eventually yielding a mixture of the two anomers of hemiacetal **6ba** and aldehyde **7ba** (Scheme 2). Oxidation of this mixture with pyridine chlorochromate (PCC) yielded lactone **8ba** as a single diastereomer.

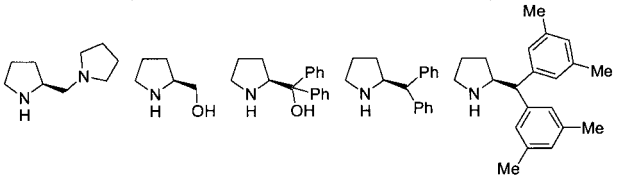


Scheme 2. The HDA reaction of aldehyde **3b** and enones **4a** in the presence of a chiral pyrrolidine catalyst yields the two anomers of hemiacetal **6ba** and aldehyde **7ba**.

Catalytic turnover was accomplished by the addition of silica (50 mg on a 0.5 mmol scale) to the reaction mixture. Table 1 shows representative results from the optimization of this reaction using different substituted (2*S*)-pyrrolidines **1a–e** as catalysts.

(*S*)-2-(1-Pyrrolidinylmethyl)pyrrolidine (**1a**) worked well as a catalyst yielding the HDA adduct in 69% with 51% *ee*

Table 1: Optimization of the organocatalytic hetero-Diels–Alder reaction of isovaleraldehyde **3b** with enone **4a** with various catalysts **1**.



1a **1b** **1c** **1d** **1e**

Entry	Catalyst (mol%)	Enone [equiv]	Solvent[a]	T[b]	Yield[c] [%]	*ee*[d] [%]
1	**1a** (20)	1.1	CH_2Cl_2	RT	69	51
2	**1b** (20)	1.1	CH_2Cl_2	RT	54	56
3	**1c** (20)	1.1	CH_2Cl_2	RT	6	97
4	**1d** (20)	1.1	CH_2Cl_2	RT	46	88
5	**1e** (10)	2	CH_2Cl_2	RT	71	87
6	**1e** (10)	1.5	CH_2Cl_2	−15 °C→RT	70	91
7	**1e** (10)	2	CH_2Cl_2	−15 °C→RT	93	89
8	**1e** (10)	2	toluene	−15 °C→RT	77	90
9	**1e** (10)	2	$CDCl_3$	−15 °C→RT	69	92
10	**1e** (10)	2	$ClCH_2CH_2Cl$	−15 °C→RT	74	90
11	**1e** (10)	2	MeCN	−15 °C→RT	59	90

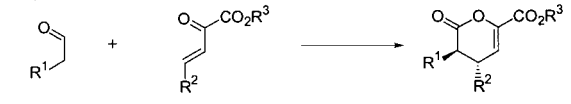
[a] Solvent (0.5 mL). [b] RT = room temperature. [c] Combined yield of **6ba** and **7ba**. [d] The *ee* values were determined by HPLC.

(Table 1, entry 1). Use of the chiral prolinol (**1b**) resulted in a similar yield and selectivity (Table 1, entry 2), whereas the diphenylprolinol (**1c**) promoted a highly enantioselective HDA reaction, providing **8ba** with 97% *ee* (Table 1, entry 3). Unfortunately, the increased steric bulk of the substituent at C2 led to a low yield. However, the two phenyl groups of **1c** were required to obtain the high enantioselectivity. We therefore anticipated that the dehydroxylated catalyst **1d** would maintain high enantioinduction, whereas the smaller size of the substituent at C2 would lead to higher yield. Application of catalyst **1d** did, indeed, lead to a higher yield but also to a slight decrease in enantioselectivity (Table 1, entry 4). Catalyst **1e** was also applied and similar enantioselectivity was observed. The catalytic turnover was even more efficient, and the catalyst loading could be decreased to 10 mol% (Table 1, entry 5). Mixing the reagents and the catalyst at −15 °C and allowing the reaction mixture to warm to room temperature resulted in a cleaner reaction and higher yield. Under these reaction conditions, different solvents were tested (Table 1, entries 7–11). The highest yield (93%) was obtained with CH_2Cl_2 as solvent, and up to 92% *ee* could be reached in $CHCl_3$.

The scope of the enantioselective organocatalytic HDA reaction was demonstrated by the reaction of various aldehydes (**3a–c**) and enones **4a–c** and the results are presented in Table 2. The β,γ-unsaturated-α-ketoesters with aromatic substituents in the γ-position, **4a,b**, and the β,γ-unsaturated-α-ketoesters with an aliphatic substituent such as methyl in the γ-position, **4c**, all underwent the HDA reaction smoothly with both very high diastereo-[12] and enantioselectivity. The aliphatic aldehydes were also varied and different substitution patterns were

 © 2003 Wiley-VCH Verlag GmbH & Co. KGaA, Weinheim

Table 2: Scope of the organocatalytic hetero-Diels–Alder reaction catalyzed by **1e**.[a]



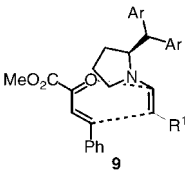
3a R^1 = Et **3b** R^1 = *i*Pr **3c** R^1 = Bn
4a R^2 = Ph, R^3 = Me **4b** R^2 = 4-ClC_6H_4, R^3 = Me **4c** R^2 = Me, R^3 = Et
8

Entry	3	4	8	Yield [%][b]	*ee* [%][c]
1	**a**	**a**	**aa**	69	84
2	**b**	**a**	**ba**	93	89
3[d]	**b**	**a**	**ba**	69	92
4[e]	**c**	**a**	**ca**	65	86
5[f]	**a**	**b**	**ab**	79	85
6[f]	**b**	**b**	**bb**	70	90
7[e,f]	**c**	**b**	**cb**	62	80
8	**a**	**c**	**ac**	81	86
9	**b**	**c**	**bc**	75	94
10[e]	**c**	**c**	**cc**	72	89

[a] Reaction conditions (0.5 mmol scale): 1) **1e** (10 mol%), silica (50 mg), −15 →RT, CH_2Cl_2 (0.5 mL), 17 h; 2) PCC, CH_2Cl_2. [b] Combined yield of **6** and **7**. [c] The *ee* values were determined by HPLC or GC (entries 8 and 9) of **8**. [d] $CDCl_3$ used as solvent. [e] Reaction time = 40 h. [f] Solvent (2 mL).

allowed. In general, good yields were observed (62–93%) and the enantioselectivities were as high as 94% *ee*.

The absolute and relative stereochemistry of the outcome of the organocatalytic HDA reaction was determined on the basis of the X-ray crystal structure of the HDA adduct **8bb**.[13] The configuration of the HDA adduct was assigned to be 4*S*,5*R*. The observed absolute and relative stereochemistry is consistent with the proposed transition state model **9**. The electronic properties of the enamine govern the regioselectivity, while the 2,2-diarylmethyl substituent on the pyrrolidine ring shields the *Si* face of the enamine. Thus, the 2,2-diarylmethyl substituent of the enamine intermediate controls the addition of the enone to the *Re* face of the alkene fragment in an *endo*-selective fashion. At the present stage of investigations we have no direct evidence for a concerted versus a stepwise cycloaddition reaction; the latter reaction path would take place by an initial Michael addition followed by a ring-closure reaction.



9

In conclusion, we have developed a new concept in organocatalysis—the use of a chiral enamine intermediate as an alkene in catalytic asymmetric cycloaddition reactions. The present work presents the catalytic asymmetric hetero-Diels–Alder reaction of aldehydes with enones to give highly functionalized, optically active molecules with excellent diastereo- and enantioselectivity.

Received: November 28, 2002 [Z50652]

Keywords: aldehydes · amines · asymmetric catalysis · cycloaddition · enones

[1] a) H. Gröger, J. Wilken, *Angew. Chem.* **2001**, *113*, 545; *Angew. Chem. Int. Ed.* **2001**, *40*, 529; b) P. I. Dalko, L. Moisan, *Angew. Chem.* **2001**, *113*, 3840; *Angew. Chem. Int. Ed.* **2001**, *40*, 3709; c) B. List, *Tetrahedron* **2002**, *58*, 5573.

[2] For example, see: a) B. List, R. A. Lerner, C. F. Barbas III, *J. Am. Chem. Soc.* **2000**, *122*, 2395; b) K. Sakthivel, W. Notz, T. Bui, C. F. Barbas III, *J. Am. Chem. Soc.* **2001**, *123*, 5260; c) A. Córdova, W. Notz, C. F. Barbas III, *J. Org. Chem.* **2002**, *67*, 301; d) A. Bøgevig, N. Kumaragurubaran, K. A. Jørgensen, *Chem. Commun.* **2002**, 620; e) W. Notz, B. List, *J. Am. Chem. Soc.* **2000**, *122*, 7386; f) L. Hoang, S. Bahmanyar, K. N. Houk, B. List, *J. Am. Chem. Soc.* **2003**, *125*, 16; g) B. List, P. Polarjiev, H. J. Martin, *Org. Lett.* **2001**, *3*, 2423; h) A. Northrup, D. W. C. MacMillan, *J. Am. Chem. Soc.* **2002**, *124*, 6798.

[3] For example, see: a) B. List, *J. Am. Chem. Soc.* **2000**, *122*, 9336; b) B. List, P. Polarjiev, W. T. Biller, H. J. Martin, *J. Am. Chem. Soc.* **2002**, *124*, 827; c) A. Córdova, S.-i. Watanabe, F. Tanaka, W. Notz, C. F. Barbas III, *J. Am. Chem. Soc.* **2002**, *124*, 1842; d) A. Córdova, W. Notz, G. Zhong, J. M. Betancort, C. F. Barbas III, *J. Am. Chem. Soc.* **2002**, *124*, 1866; e) S.-I Watanabe, A. Córdova, F. Tanaka, C. F. Barbas III, *Org. Lett.* **2002**, *4*, 4519.

[4] For example, see: a) J. M. Betancort, C. F. Barbas III, *Org. Lett.* **2001**, *3*, 3737; b) D. Enders, A. Seki, *Synlett*, **2002**, 26; see also: c) S. Hanessian, V. Pham, *Org. Lett.* **2000**, *2*, 2975; d) A. Alexakis, O. Andrey, *Org. Lett.* **2002**, *4*, 3611; e) N. Halland, R. G. Hazell, K. A. Jørgensen, *J. Org. Chem.* **2002**, *67*, 8331; f) N. Halland, P. S. Aburel, K. A. Jørgensen, *Angew. Chem.* **2003**, *115*, 685; *Angew. Chem. Int. Ed.* **2003**, *42*, 661; g) B. List, P. Polarjiev, H. J. Martin, *Org. Lett.* **2001**, *3*, 2423; h) A. G. Wenzel, E. N. Jacobsen, *J. Am. Chem. Soc.* **2002**, *124*, 12964; i) M. Yamaguchi, T. Shiraishi, M. Hirami, *J. Org. Chem.* **1996**, *61*, 3520; j) D. J. Gurin, S. J. Miller, *J. Am. Chem. Soc.* **2002**, *124*, 2134.

[5] a) A. Bøgevig, K. Juhl, N. Kumaragurubaran, W. Zhuang, K. A. Jørgensen, *Angew. Chem.* **2002**, *114*, 1868; *Angew. Chem. Int. Ed.* **2002**, *41*, 1790; b) B. List, *J. Am. Chem. Soc.* **2002**, *124*, 5656; c) N. Kumaragurubaran, K. Juhl, W. Zhuang, A. Bøgevig, K. A. Jørgensen, *J. Am. Chem. Soc.* **2002**, *124*, 6254.

[6] a) K. A. Ahrendt, C. J. Borths, D. W. C. MacMillan, *J. Am. Chem. Soc.* **2000**, *122*, 4243; b) A. B. Northrup, D. W. C. MacMillan, *J. Am. Chem. Soc.* **2002**, *124*, 2458.

[7] a) W. S. Jen, J. J. M. Wiener, D. W. C. MacMillan, *J. Am. Chem. Soc.* **2000**, *122*, 9874; see also: b) S. Karlsson, H.-E. Högberg, *Tetrahedron: Asymmetry* **2002**, *13*, 923.

[8] a) J. F. Austin, D. W. C. MacMillan, *J. Am. Chem. Soc.* **2002**, *124*, 1172; b) N. A. Paras, D. W. C. MacMillan, *J. Am. Chem. Soc.* **2001**, *123*, 4370; c) N. A. Paras, D. W. C. MacMillan, *J. Am. Chem. Soc.* **2001**, *123*, 7894.

[9] The Lewis acid catalyzed enantioselective hetero-Diels–Alder reaction of electron-rich alkenes with electron-poor enones has been developed: a) K. A. Jørgensen, *Angew. Chem.* **2000**, *112*, 3702; *Angew. Chem. Int. Ed.* **2000**, *39*, 3559; b) J. S. Johnson, D. A. Evans, *Acc. Chem. Res.* **2000**, *33*, 325; c) K. A. Jørgensen, M. Johannsen, S. Yao, H. Audrain, J. Thorhauge, *Acc. Chem. Res.* **1999**, *32*, 605; see also: d) K. Gademann, D. E. Chavez, E. N. Jacobsen, *Angew. Chem.* **2002**, *114*, 3185; *Angew. Chem. Int. Ed.* **2002**, *41*, 3059.

[10] The stoichiometric HDA reaction of achiral enamines with β,γ-unsaturated-α-ketoesters has been reported earlier: F. Eiden, W. Winkler, *Arch. Pharm.* **1986**, *319*, 704. Schreiber et al. have used a stoichiometric asymmetric enamine–enal cycloaddition for the synthesis of a series of brefeldin isomers: S. L. Schreiber, H. V. Meyers, *J. Am. Chem. Soc.* **1988**, *110*, 5198.

[11] B. B. Snider, *Tetrahedron Lett.* **1980**, *21*, 1133.

[12] In all cases, only one diastereomer of **8** was detected, with the exception of **8ac** (d.r. = 45:1).

 © 2003 Wiley-VCH Verlag GmbH & Co. KGaA, Weinheim

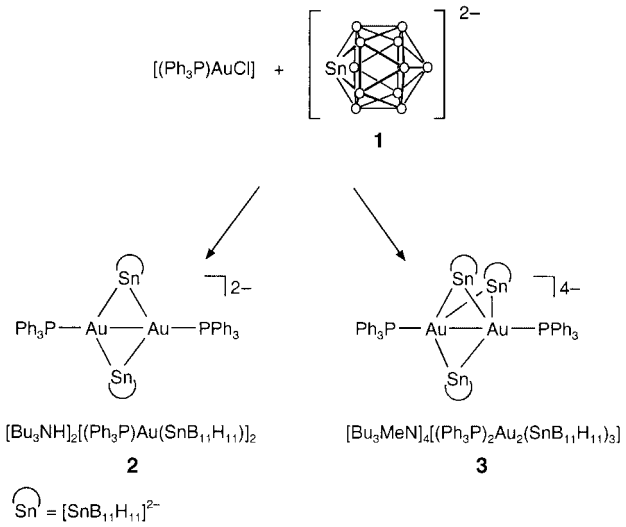
[13] CCDC-198535 contains the supplementary crystallographic data for this paper. These data can be obtained free of charge via www.ccdc.cam.ac.uk/conts/retrieving.html (or from the Cambridge Crystallographic Data Centre, 12, Union Road, Cambridge CB21EZ, UK; fax: (+44) 1223-336-033; or deposit@ccdc.cam.ac.uk).

 © 2003 Wiley-VCH Verlag GmbH & Co. KGaA, Weinheim

Sn-Bridged Au–Au Interactions

Gold–Gold Interaction—Stannaborate $[SnB_{11}H_{11}]^{2-}$ Coordination Chemistry**

*Siegbert Hagen, Ingo Pantenburg, Florian Weigend, Claudia Wickleder, and Lars Wesemann**



Scheme 1. Reaction of stanna-*closo*-dodecaborate $[SnB_{11}H_{11}]^{2-}$ (**1**) with the gold complex $[(Ph_3P)AuCl]$.

We are currently investigating the coordination chemistry and ligand properties of the dianionic stanna-*closo*-dodecaborate cluster $[SnB_{11}H_{11}]^{2-}$ (**1**). So far, in a variety of transition-metal complexes, the ligand was found to coordinate exclusively as a terminal ligand with the formation of a tin–metal bond.[1]

Here we present the surprising results of preliminary investigations on the stannaborate chemistry with gold electrophiles. Two different gold–tin clusters $[Bu_3NH]_2[(Ph_3P)Au(SnB_{11}H_{11})]_2$ (**2**) and $[Bu_3MeN]_4[(Ph_3P)_2Au_2(SnB_{11}H_{11})_3]$ (**3**) (Scheme 1), which were characterized by NMR spectroscopy, elemental analysis, and X-ray crystal structure analysis, were isolated from equimolar mixtures of **1** and the gold complex $[(Ph_3P)AuCl]$ depending on the counterion of the stannaborate.

^{31}P NMR spectra (recorded at 213 K) reveal that the different countercations $[Bu_3NH]^+$ or $[Bu_3MeN]^+$ have no influence on the composition of the 1:1 reaction mixture ($[SnB_{11}H_{11}]^{2-}$:$[(Ph_3P)AuCl]$). Interestingly, 50% of the starting material $[(Ph_3P)AuCl]$ is still present in the mixture. The other signals in the ^{31}P NMR spectrum exhibit tin satellites, which provides direct spectroscopic evidence for the formation of a covalent Au–Sn bond. In this solution the anion of **3** is the major Au–Sn component (35%) and exhibits a characteristic signal in the ^{31}P NMR spectrum at $\delta =$ 54.4 ppm with a $^2J(Sn,P)$ coupling constant of 109.4 Hz. The anion of **2** was identified in solution by a small signal (3%) at $\delta = 62.9$ ppm ($^2J(Sn,P) = 186.9$ Hz). A bis(triphenylphosphane) substitution product ($[(Ph_3P)_2Au(SnB_{11}H_{11})]^-$) is also present in solution (5%) and displays a signal in the ^{31}P NMR spectrum at $\delta = 44.5$ ppm ($^2J(P,^{117}Sn) = 984.2$ Hz, $^2J(P,^{119}Sn) =$ 1027.5 Hz). This compound was synthesized in a separate experiment from nucleophile **1**, PPh_3, and $[(Ph_3P)AuCl]$ in reasonable yield and details will be published later. Treatment of the $[(Ph_3P)AuCl]$ with 1.5 equivalents of heteroborate **1**, led to an increase in the amount of Au_2Sn_3 cluster **3** formed (68.6% yield).

The geometry of the metal core in the anions of **2** (Figure 1) and **3** (Figure 2) shows a surprising correspondence with the respective arrangements in $[Au_2Pt_2(PPh_3)_4(CN\text{-}xylyl)_4]^{2+}$ [2] and the trigonal bipyramid in $[(Ph_3P)_2Pt_2\{Sn(acac)_2\}_3]$ (acac = acetylacetonate).[3]

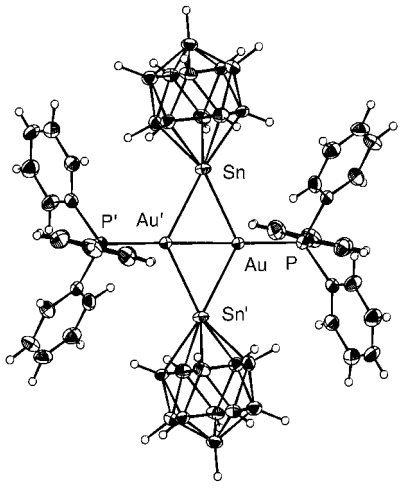


Figure 1. Molecular structure of the anion of **2** in the solid state; the dianion lies on the center of symmetry. Interatomic distances [pm] and angles [°]: Au-Sn 273.7(1), Au′-Sn 276.1(1), Au-Au′ 262.5(1), Au-P 233.2(1); P-Au-Au′ 178.78(4), P-Au-Sn 116.86(3), P-Au-Sn′ 120.17(3), Au-Sn-Au′ 57.03(1), Au-Au′-Sn 61.95(2).

[*] Prof. Dr. L. Wesemann, S. Hagen, Dr. I. Pantenburg, Dr. C. Wickleder
Institut für Anorganische Chemie
Universität zu Köln
Greinstrasse 6, 50939 Köln (Germany)
Fax: (+49) 221-470-4899
E-mail: lars.wesemann@uni-koeln.de
Dr. F. Weigend
Institut für Nanotechnologie
Forschungszentrum Karlsruhe
Postfach 3640, 76021 Karlsruhe (Germany)

[**] This work was supported by the Deutsche Forschungsgemeinschaft (DFG-Schwerpunktprogramm "Polyeder").

 DOI: 10.1002/anie.200250698 © 2003 Wiley-VCH Verlag GmbH & Co. KGaA, Weinheim

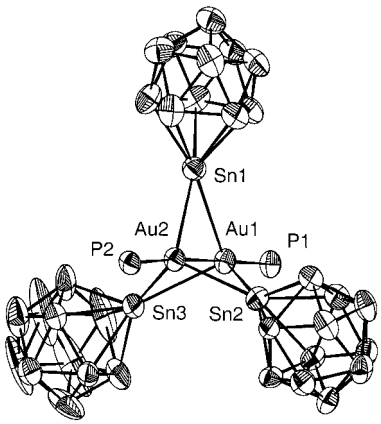


Figure 2. Molecular structure of the anion of **3** in the solid state. Hydrogen atoms and phenyl substituents have been omitted for clarity. Interatomic distances [pm] and angles [°]: Au1-Au2 259.0(1), Au1-Sn1 272.7(1), Au1-Sn2 271.1(1), Au1-Sn3 271.8(1), Au1-P1 231.5(2), Au2-Sn1 294.7(1), Au2-Sn2 303.2(1), Au2-Sn3 298.0(1), Au2-P2 230.1(2); P1-Au1-Au2 176.56(6), P2-Au2-Au1 179.05(6), P1-Au1-Sn1 111.22(6), P1-Au1-Sn2 108.45(6), P1-Au1-Sn3 115.31(6), P2-Au2-Sn1 121.57(6), P2-Au2-Sn2 122.24(6), P2-Au2-Sn3 122.72(6), Au1-Sn1-Au2 54.23(2), Au1-Sn2-Au2 53.26(2), Au1-Sn3-Au2 53.76(2), Sn1-Au1-Sn2 111.71(2), Sn1-Au1-Sn3 105.79(2), Sn2-Au1-Sn3 104.19(2), Sn1-Au2-Sn2 97.44(2), Sn1-Au2-Sn3 94.24(2), Sn2-Au2-Sn3 91.08(2).

The most striking features in the gold–tin clusters **2** and **3** are the novel bridging mode of the stannaborate ligand and the short Au–Au interatomic distance. Tin ligands bridging two transition metal centers are well known;[4] for example, the tetrahedral gold cluster $[Au_4(PPh_3)_4(\mu_2\text{-}SnCl_3)_2]$, in which two of the Au–Au edges are bridged by the $SnCl_3$ groups, was presented by Mingos et al. as the first example of μ_2-$SnCl_3$ coordination.[5] In **2** we find a nearly symmetrically μ_2-coordinated heteroborate; the Au–Sn distances are 276.1(1) and 273.7(1) pm. Owing to steric crowding in the tetraanion of **3**, the three heteroborates are unsymmetrically bonded to the Au–Au edge with three shorter distances to Au1 (271.1(1)–272.7(1) pm) and three very long contacts to Au2 (294.7(1)–303.2(1) pm). The short Au–Sn distances in **2** and **3** are in the middle of the range of known Au–Sn bond lengths (256.5(1)–297.3(8) pm),[5–10] whereas the longer Au–Sn distances in **3** can be compared with the respective bond lengths in $[Au_4(PPh_3)_4(\mu_2\text{-}SnCl_3)_2]$ (281.5(7), 297.3(8) pm) and are indicative of weak interactions between the ligand and the Au2 atom in the solid state.[10] Although gold chemistry is one of the most active fields of research, very few compounds bearing Au–Sn bonds are known.[11]

Au–Au bond formation has been studied extensively and the short Au–Au distances (262.5(1) and 259.0(1) pm) in **2** and **3** suggest strong metal–metal interactions.[12] Formally, we find Au^I in clusters **2** and **3**, but the Au–Au bond lengths are shorter than the discussed values for Au^I–Au^I interactions (275–325 pm).[12] In both **2** and **3** the P-Au-Au-P axis is linear, and this geometry together with the short Au–Au bonds can be compared with those in the heteroatomic gold clusters $[(dppe)_2Au_3In_3Cl_6(thf)_3]$ (dppe = 1,2-bis(diphenylphosphanyl)ethane),[13] $[(dppe)_2Au][(dppe)_2Au_3In_3Br_7(thf)]$,[14] $[Au_4(PPh_3)_4(\mu_2\text{-}SnCl_3)_2]$,[5] $[Au_2Pt_2(PPh_3)_4(CN\text{-}xylyl)_4]$,[2] and $[Au_4(PPh_3)_4(\mu_2\text{-}I)_2]$.[15] On the basis of these findings and in agreement with the situation in Au_3In_3 clusters, an oxidation state of zero can be considered for the gold atoms in **2** and **3**.[13,14]

Quantum-chemical calculations[16] have been carried out for the anion of **2**. This dianion might be regarded as a dimer consisting of two $[(Ph_3P)Au(SnB_{11}H_{11})]^-$ units. Such a monomer could be expected to be quite stable, since the Au atom in this case would be linearly coordinated by the ligands, which often is preferred by Au due to relativistic effects.[17] We initially calculated the stability of the dimer to fragmentation into monomers, that is, the energy difference between the dimer and two monomers in optimized geometries, and then we investigated the interactions that are responsible for the stability of the dimer.

Results obtained with DFT[18] (B-P functional[19,20]), HF, and HF + MP2 calculations[21] were compared; to keep computational effort moderate, Ph_3P was replaced by Me_3P throughout, and in the MP2 calculations orbitals with energies below −100 eV were neglected (frozen core). The description of anionic species requires the use of flexible basis sets; we used TZVP-quality basis sets for the DFT calculations, whereas we used TZVPP-type basis sets for Au, Sn, P, and S and SV(P)-type basis sets for B, C, and H for the HF and the MP2 calculations,[22] in case of Au (Sn) the inner 60 (46) electrons were represented by effective core potentials, which also include scalar relativistic effects.[23] With these basis sets we obtained negative values for the HOMO at the HF level: −3.2 eV for the dimer, −4.6 eV for the monomer (smaller basis sets might lead to positive values corresponding to unbound states). Moreover one might suspect, that due to its higher charge, the dimer is not described as well as the monomer. To estimate this effect single-point DFT calculations were performed for compounds in which both anions were embedded in a metallic environment;[24] in this way the negative charges are compensated by positive image charges.

A significant preference of the dimer over the two monomers is observed only at the HF + MP2 level (ΔE = 160 kJ mol^{-1}). This is not observed for the DFT calculations (+4 kJ mol^{-1}), even if the anion is embedded in a metallic environment (+23 kJ mol^{-1}). At the HF level the dimer is even disadvantaged (−50 kJ mol^{-1}); moreover, at this level it is not a minimum structure, since calculation of the vibration spectrum yields two imaginary modes. These large differences can be attributed to the different treatment of dynamical electron correlation at each level. In the case of HF it is neglected, at the DFT level it is modeled by an exchange-correlation functional of the electronic density, and MP2 accounts for it by means of perturbation theory applied to the HF wave function; only the latter method explicitly includes the description of dispersive interactions, which are clearly relevant for the stability of the dimer. This is also evident from the Au–Au and Au–Sn distances, which are accurately described only at the HF + MP2 level (denoted "full" MP2 in Table 1); differences to the experimental values are negligible, −1 pm to +2 pm. At the DFT (HF) level errors are much larger; Sn–Au distances are overestimated by about 13 (17) pm, for the Au–Au distance the difference is less pronounced, +3 (+9) pm.

 © 2003 Wiley-VCH Verlag GmbH & Co. KGaA, Weinheim

Table 1: Distances obtained at different levels of theory. In the case of MP2, the groups of orbitals that were included in the treatment are given in the second column (see also Figure 3).

	Correlated electrons	Au–Au [ppm]	Sn–Au [ppm]
experiment		263	274–276
DFT	(all)	266	287–288
HF	(none)	272	292–293
"full" MP2	I–V + 4p(Au) ($\varepsilon > -100$ eV)	262	274
MP2	III	262	285–286
MP2	V	272	293
MP2	III + V	262	276

As in previous work,[25] the following procedure was used to determine whether particular electrons are in any way responsible for the binding correlation effects. Figure 3 shows the density of states (DOS), which results from the HF wave function[26] in the MP2 geometry. Contributions of different parts of the molecule to the DOS were calculated by a Mulliken population analysis for each orbital and are also

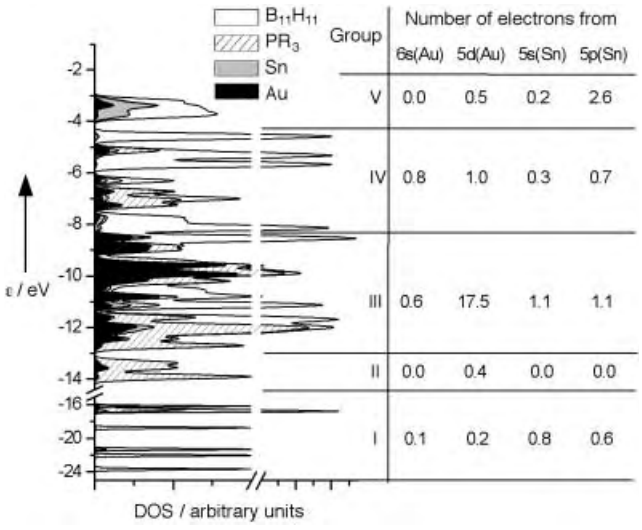


Figure 3. Density of states resulting from a Mulliken population analysis of the HF wave function in the MP2 geometry for $[(Ph_3P)Au(SnB_{11}H_{11})]_2^{2-}$. Orbital energies are superimposed by Gauss functions of width = 0.1 eV to help the eye. Contributions from different parts of the system are indicated; at the right-hand side contributions of the valence electrons of Sn and Au are listed separately.

displayed in Figure 3. Orbitals thus may be partitioned into groups. Groups I, II, and V are energetically separated from groups III and IV, group III was regarded as separated from group IV, because group III contains the main contribution from the 5d(Au) electrons, whereas their contribution to group IV is very small; 5p(Sn) electrons are mainly found in group V.

In the next step geometry optimizations at the HF + MP2 level were performed in which only electrons from some of the groups in the MP2 treatment were included; the resulting bond lengths are displayed in Table 1. Mulliken population analyses were also carried out for the optimized geometries, and the results were very similar to that shown in Figure 3, which indicates that changes in orbital characteristics are rather small.

Including only electrons of group III (5d(Au)) is sufficient to obtain an Au–Au distance very similar to that from the full MP2 treatment; the Sn–Au distances are 6 pm shorter than those calculated at the HF level (probably because there are also small contributions from the Sn atoms in group III), but still 10 pm longer than the value determined from the full MP2 treatment. Including only electrons from group V (p(Sn)) in the MP2 treatment yields results very similar to those from the HF calculation; but when electrons from group III and V are included, the Sn–Au and Au–Au distances are nearly the same as those determined in the full MP2 calculation. This indicates that the stability of the dimer over two monomers is predominantly due to dispersive interactions between the valence electrons of both Sn and Au.

Finally we confirmed the assignment of an oxidation state of 0 for the gold atom. Mulliken population analyses of the HF and the (HF + MP2) density yield charges of 0.15 (0.028) electrons for the Au atom; values in Au^I compounds are significantly larger (e.g. Au_2S: 0.41 (0.23)).

The luminescence of many polynuclear gold complexes has attracted considerable attention.[27,28] The Au_2Sn_3 cluster **3** luminesces in the solid state and displays an intense red emission at low temperatures upon excitation in the UV range (Figure 4).

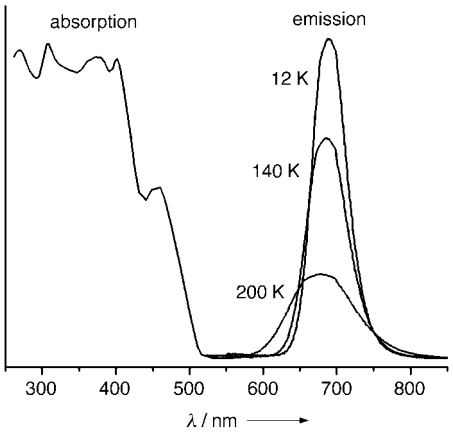


Figure 4. Temperature-dependent emission spectra of **3**. The absorption spectra was recorded at 12 K.

At 12 K the maximum of the emission is located at 690 nm (14490 cm^{-1}) with $\Delta_{1/2} = 1150$ cm^{-1}. Thermal excitation of the vibrational levels of the electronic excited state causes a blue shift of the maximum, and an increase of the band width occurs on increasing the temperature (200 K: $\lambda_{max} = 679$ nm, $\nu_{max} = 14732$ cm^{-1}, $\Delta_{1/2} = 2328$ cm^{-1}). Temperature-dependent lifetime measurements were performed on the excitation at 355 nm (8 ns pulse) and on the emission at 690 nm: $\tau =$ 138.4 μs at 12 K; $\tau = 10.2$ μs at 240 K (single exponential decay).

In conclusion, coordination of the tin nucleophile at Au^I centers results in signifcant gold–gold interaction and reduction of the oxidation state to Au^0.[29]

 © 2003 Wiley-VCH Verlag GmbH & Co. KGaA, Weinheim

Experimental Section

2: Treatment of [(Ph_3P)AuCl] (151 mg, 0.31 mmol) in CH_2Cl_2 (15 mL) at room temperature with a solution of $[Bu_3NH]_2[SnB_{11}H_{11}]$ (185 mg, 0.3 mmol) in CH_2Cl_2 (15 mL) led to an orange solution. After the mixture had been stirred for 1 h, volatiles were removed in vacuum and the residue was washed with water. Crystallization by slow diffusion of hexane into a solution of the crude product in CH_2Cl_2 afforded **2** (166 mg, 31% yield) as colorless crystals. ^{11}B {^1H} NMR: $\delta = -14.5$ ppm; ^{31}P {^1H} NMR: $\delta = 62.9$ ppm ($^2J(Sn,P) = 186.9$ Hz); elemental analysis (%) calcd: C 40.29, H 6.09, N 1.57; found: C 39.15, H 5.54, N 1.61.

3: Treatment of [(Ph_3P)AuCl] (148 mg, 0.3 mmol) in CH_2Cl_2 (15 mL) at room temperature with a solution of $[Bu_3MeN]_2[SnB_{11}H_{11}]$ (292 mg, 0.45 mmol) in CH_2Cl_2 (20 mL) led to an orange solution. After the mixture had been stirred for 1 h, volatiles were removed in vacuum and the residue was washed with water. Crystallization of the crude product from a mixture of CH_2Cl_2/hexane at room temperature afforded **3** (218 mg, 59% yield with respect to tin ligand) as pale yellow crystals. ^{11}B {^1H} NMR: $\delta = -14.1$ ppm; ^{31}P {^1H} NMR: $\delta =$ 54.4 ppm ($^2J(Sn,P) = 109.4$ Hz); ^{119}Sn {^1H} NMR: $\delta = -332$ ppm; elemental analysis (%) calcd: C 42.86, H 7.48, N 2.27; found: C 42.68, H 7.74, N 2.31.

Single-crystal structure determination: The intensity data were collected on an imaging-plate diffractometer (IPDSII, Stoe & Cie) with $Mo_{K\alpha}$ radiation ($\lambda = 71.073$ pm, graphite monochromator) at 170 K. Several C atoms of the cations in **3** show large thermal displacement factors. Therefore, these atoms were refined isotropically by using a split model without consideration of the H atoms.[30–33] All of the other non-hydrogen atoms were refined with anisotropic temperature factors. The hydrogen-atom positions for **2** were taken from the difference Fourier map at the end of the refinement. The hydrogen atoms for **3** are in calculated positions.

Crystal data for **2**: $C_{60}H_{108}B_{22}N_2P_2Sn_2Au_2$, triclinic space group $P\bar{1}$, $a = 1075.0(1)$, $b = 1181.8(2)$, $c = 1623.6(2)$ pm, $\alpha = 74.45(1)$, $\beta =$ 85.80(1), $\gamma = 68.97(1)°$, $Z = 1$, $\mu = 4.691$ mm^{-1}; $F(000) = 880$, $R_{int} =$ 0.0493, no. collected/unique/$I_0 > 2\sigma I_0$ data = 21 407/9869/6623, $R1/wR2$ (all data) = 0.0672/0.0618, $R1/wR2$ ($I_0 > 2\sigma I_0$) = 0.0348/0.0552, max./min. electron density = 1.42/−2.11 × 10^{-6} e pm^{-3}.

Crystal data for **3**: $C_{88}H_{183}B_{33}N_4P_2Sn_3Au_2$, monoclinic space group $P2_1/c$, $a = 2607.5(1)$, $b = 1699.0(1)$, $c = 2806.5(1)$ pm, $\beta = 106.47(1)°$, $Z = 4$, $\mu = 3.139$ mm^{-1}; $F(000) = 4968$, $R_{int} = 0.1062$, no. of collected/unique/$I_0 > 2\sigma I_0$ data = 109 394/20 724/14 474, $R1/wR2$ (all data) = 0.0863/0.1359, $R1/wR2$ ($I_0 > 2\sigma I_0$) = 0.0589/0.1299, max./min. electron density = 2.09/−1.12 × 10^{-6} e pm^{-3}.

CCDC-198734 (**2**) and CCDC-198733 (**3**) contain the supplementary crystallographic data for this paper. These data can be obtained free of charge via www.ccdc.cam.ac.uk/conts/retrieving.html (or from the Cambridge Crystallographic Data Centre, 12, Union Road, Cambridge CB21EZ, UK; fax: (+44) 1223-336-033; or deposit@ccdc.cam.ac.uk).

Received: December 4, 2002 [Z50698]

Keywords: ab initio calculations · boranes · cluster compounds · gold · tin

[1] a) L. Wesemann, S. Hagen, T. Marx, I. Pantenburg, M. Nobis, B. Drießen-Hölscher, *Eur. J. Inorg. Chem.* **2002**, 2261 – 2265; b) T. Marx, L. Wesemann, S. Dehnen, I. Pantenburg, *Chem. Eur. J.* **2001**, *7*, 3025 – 3032.

[2] C. E. Briant, D. I. Gilmour, D. M. Mingos, *J. Organomet. Chem.* **1984**, *267*, C52 – C55.

[3] G. W. Bushnell, D. T. Eadie, A. Pidcock, A. R. Sam, R. D. Holmes-Smith, S. R. Stobart, E. T. Brennan, T. S. Cameron, *J. Am. Chem. Soc.* **1982**, *104*, 5837 – 5839.

[4] a) W. Petz, *Chem. Rev.* **1986**, *86*, 1019 – 1047; b) M. S. Holt, W. L. Wilson, J. H. Nelson, *Chem. Rev.* **1989**, *89*, 11 – 49; c) D. J. Cardin in *Metal Clusters in Chemistry* (Eds.: P. Braunstein, L. A. Oro, P. R. Raithby), Wiley-VCH, Weinheim, **1999**, p. 48 – 72; d) M. Veith in *Metal Clusters in Chemistry* (Eds.: P. Braunstein, L. A. Oro, P. R. Raithby), Wiley-VCH, Weinheim, **1999**, p. 73 – 90.

[5] D. M. Mingos, H. R. Powell, T. L. Stolberg, *Transition Met. Chem.* **1992**, *17*, 334 – 337.

[6] Z. Demidowicz, R. L. Johnston, J. C. Machell, D. M. P. Mingos, I. D. Williams, *J. Chem. Soc. Dalton Trans.* **1988**, 1751 – 1756.

[7] W. Clegg, *Acta Crystallogr. Sect. B* **1978**, *34*, 278 – 281.

[8] L. H. Gade, *Eur. J. Inorg. Chem.* **2002**, 1257 – 1268.

[9] M. Contel, K. W. Hellmann, L. H. Gade, I. Scowen, M. McPartlin, *Inorg. Chem.* **1996**, *35*, 3713 – 3715.

[10] B. Findeis, M. Contel, L. H. Gade, M. Laguna, M. C. Gimeno, I. J. Scowen, M. McPartlin, *Inorg. Chem.* **1997**, *36*, 2386 – 2390.

[11] a) *Gold: Progress in Chemistry and Biochemistry and Technology* (Ed.: H. Schmidbaur), Wiley, Chichester, UK, **1999**; b) H. Schmidbaur, *Chem. Soc. Rev.* **1995**, *24*, 391 – 400; c) D. M. Mingos, *J. Chem. Soc. Dalton Trans.* **1996**, 561 – 566.

[12] a) H. Schmidbaur, *Gold. Bull.* **1990**, *23*, 11 – 21; b) P. Pyykkö, *Chem. Rev.* **1997**, *97*, 597 – 636, and references therein.

[13] F. Gabbaï, A. Schier, J. Riede, H. Schmidbaur, *Inorg. Chem.* **1995**, *34*, 3855 – 3856.

[14] F. Gabbaï, S.-C. Chung. A. Schier, S. Krüger, N. Rösch, H. Schmidbaur, *Inorg. Chem.* **1997**, *36*, 5699 – 5705.

[15] F. Demartin, M. Manassero, L. Naldini, R. Ruggeri, M. Sansoni, *J. Chem. Soc. Chem. Commun.* **1981**, 222 – 223.

[16] R. Ahlrichs, M. Bär, M. Häser, H. Horn, C. Kölmel, *Chem. Phys. Lett.* **1989**, *162*, 165 – 169.

[17] P. Pyykkö, *Chem. Rev.* **1988**, *88*, 563 – 594.

[18] O. Treutler, R. Ahlrichs, *J. Chem. Phys.* **1995**, *102*, 346 – 352.

[19] A. D. Becke, *J. Chem. Phys.* **1993**, *98*, 5648 – 5652.

[20] J. P. Perdew, *Phys. Rev. B* **1986**, *33*, 8822 – 8824.

[21] F. Weigend, M. Häser, *Theor. Chim. Acc.* **1997**, *97*, 331 – 340.

[22] TURBOMOLE (auxiliary) basis sets can be retrieved from http://www.turbomole.dea) as cited in A. Schäfer, H. Horn, R. Ahlrichs, *J. Chem. Phys.* **1992**, *97*, 2571 – 2577; b) A. Schäfer, C. Huber, R. Ahlrichs, *J. Chem. Phys.* **1994**, *100*, 5829 – 5835; c) K. Eichkorn, O. Treutler, H. Öhm, M. Häser, R. Ahlrichs, *Chem. Phys. Lett.* **1995**, *240*, 283 – 290; d) K. Eichkorn, F. Weigend, O. Treutler, R. Ahlrichs, *Theor. Chim. Acc.* **1997**, *97*, 119 – 124; e) F. Weigend, H. Patzelt, R. Ahlrichs, *Chem. Phys. Lett.* **1998**, *294*, 143 – 152.

[23] D. Andrae, U. Häußermann, H. Stoll, H. Preuß, *Theor. Chim. Acta* **1990**, *77*, 123 – 141.

[24] A. Schäfer, A. Klamt, D. Sattel, J. C. W. Lohrenz, F. Eckert, *Phys. Chem. Chem. Phys.* **2000**, *2*, 2187 – 2193.

[25] P. Reiß, F. Weigend, R. Ahlrichs, D. Fenske, *Angew. Chem.* **2000**, *112*, 4085 – 4089; *Angew. Chem. Int. Ed.* **2000**, *39*, 3925 – 3929.

[26] The HF wave function was used because it represents the reference wave function for the MP2 calculations.

[27] a) T. McClesky, H. B. Gray, *Inorg. Chem.* **1992**, *31*, 1733 – 1734; b) C. King, J.-C. Wang, M. N. I. Khan, J. P. Fackler Jr. , *Inorg. Chem.* **1989**, *28*, 2145 – 2149; c) C. King, M. N. I. Khan, R. J. Staples, J. P. Fackler Jr. , *Inorg. Chem.* **1992**, *31*, 3236 – 3238; d) V. W.-W. Yam, W.-K. Lee, *J. Chem. Soc. Dalton Trans.* **1993**, 2097 – 2103; e) V. W.-W. Yam, E. C.-C. Cheng, Z.-Y. Zhou, *Angew. Chem.* **2000**, *112*, 1749- 1751; *Angew. Chem. Int. Ed.* **2000**, *39*, 1683 – 1685; f) D. V. Toronto, B. Weissbart, D. S. Tinti, A. J. Balch, *Inorg. Chem.* **1996**, *35*, 2484 – 2489.

[28] Z. Assefa, B. G. McBrunett, R. J. Staples, J. P. Fackler Jr. , B. Assmann, K. Angermaier, H. Schmidbaur, *Inorg. Chem.* **1995**, *34*, 75 – 83.

[29] P. Schwerdtfeger, P. D. W. Boyd, *Inorg. Chem.* **1992**, *31*, 327 – 329.

 © 2003 Wiley-VCH Verlag GmbH & Co. KGaA, Weinheim

[30] G. M. Sheldrick, SHELXS-97, Program for Crystal Structure Analysis, University of Göttingen, Göttingen (Germany), **1998**.
[31] G. M. Sheldrick, SHELXL-93, Program for the Refinement of Crystal Structures, University of Göttingen, Göttingen (Germany), **1993**.
[32] X-RED 1.22, STOE Data Reduction Program, Darmstadt, **2001**.
[33] X-SHAPE 1.06, Crystal Optimisation for Numerical Absorption Correction, Darmstadt, **1999**.

 © 2003 Wiley-VCH Verlag GmbH & Co. KGaA, Weinheim

Electron/Ion-Conducting Materials

Towards the Development of Electrical Conduction and Lithium-Ion Transport in a Tetragonal Porphyrin Wire**

*Lu-Lin Li, Chia-Jung Yang, Wei-Hung Chen, and Kuan-Jiuh Lin**

Dedicated to Professor Yu Wang on the occasion of her 60th birthday

The development of porous organic solids that can simultaneously support the transport of both electrons and lithium ions is of considerable technological importance for several fields of research, such as solid-state lithium batteries, nanoelectronics, and nanotechnologies.[1–6] Towards this goal, the following requirements should be satisfied: 1) construction of a robust open framework, 2) introduction of good conductivity, and 3) use of lithium motion channels. One can learn by studying naturally occurring membranes, such as the thylakoid membrane in a chloroplast envelope,[7] in which channels or pores control ion flow, charge transport, and signal transduction. Hence, self-assembly of π-conjugating supramolecules may be a powerful tool in the production of suitable functional materials.[8–10] Metallophthalocyanine stacks have been intensively studied as organic conductors,[11] but related porphyrins have attracted less attention. Although a large number of porphyrin-based supramolecules have been synthesized,[12–14] the discotic phase self-assembly of porphyrins is difficult to perform in a controlled manner. Herein, we report the design of a hybrid electronic/ionic conduction material based on a self-assembled porphyrin architecture in which tetragonal packing gives rise to square iodine-channels and prophyrin wires.

During the exploration of new classes of π-functional coordination zeolites under hydrothermal techniques,[15] one-step $C{-}N^{+}(sp^2)$ bond formation was found serendipitously, thereby opening the way to the rational design and synthesis of 1D porphyrin wires. Solvothermal reactions of H_2TPyP (H_2TPyP = 5,10,15,20-tetra(4-pyridyl)-21*H*,23*H*-porphine), CdI_2, I_2, CH_3CH_2OH, and CH_3COOH in the molar ratio 1:2:10:680:700 at 180 °C for 72 h produced purple crystals. The solvothermal synthesis is reproducible and gives the product in high yield (87 %). The X-ray structural analysis of these purple crystals (Figure 1) reveals an infinite wirelike

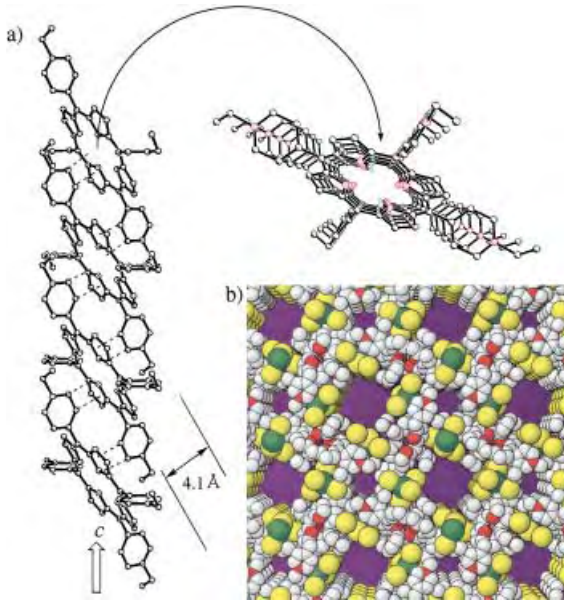


Figure 1. Molecular structure of **1**. a) Ball-and-stick representation of self-assembling prophyrin wires from porphyrins through CH···π interactions (-----). b) Space-filling view of the open-framework structure of **1** along the crystallographic *c* axis. If the van der Waals radius of an iodine ion (2.1 Å) is taken into account, the square iodine channels have the dimension of 6 × 6 Å^2. Hydrogen and solvent molecules are omitted for clarity. (C: white; N: red; Cd: green; I: yellow).

chain, $[H_2TPyPR_4]_n^{4+}$. (**1**; R = CH_2CH_3), in which the porphyrin molecules assemble into columnar aggregates sustained by cooperative π-facial hydrogen bonds. The dihedral angle formed between the plane of the pyridine ring and that of the porphyrin is around 96°. The interatomic CH···π and H···π distances of 2.99 Å and 2.33 Å, respectively, are indicative of π-facial hydrogen bonding (i.e., less than 2.6 Å). As polycationic backbones are created, the charge-compensating tetrahedral CdI_4^{2-} ions are self-included, which stabilizes the prophyrin wires through CH···I hydrogen bonds, aromatic π···I, and N^{+}···I (4.0 Å) electrostatic interactions. The cylindrical prophyrin wires are further glued together by a combination of efficient van der Waals (vdW) and electrostatic interactions, thus yielding tetragonal packing rather than hexagonal topologies (Figure 1b). Therefore, the secon-

[*] Prof. K.-J. Lin, L.-L. Li, C.-J. Yang, W.-H. Chen
Department of Chemistry
Nanocenter, National Chung-Hsing University
Taichung 402, Taiwan (Republic of China)
Fax: (+886) 4-2286-2547
E-mail: kjlin@dragon.nchu.edu.tw

[**] We thank Professor J.-H. Liao at Chung-Cheng University for solid-state UV/Vis measurements, and Dr. C. T. Chen at Academia Sinica for constructive discussions. This work was supported by the National Science Council of the Republic of China (NSC 89-2113-M-005-021), the Chinese Petroleum Corporation (NSC 89-CPC-7-005-002), and the Academia Sinica. Professor Yu Wang is a member of the academic staff at the National Taiwan University.

 DOI: 10.1002/anie.200219523 © 2003 Wiley-VCH Verlag GmbH & Co. KGaA, Weinheim

dary building unit was identified with the general formula $[(H_2TPyPR_4)(CdI_4)_2]_4 \cdot G$ (G = guest molecules, determined to be $8\,H_2O$ and $4\,CH_3COOH$ per unit cell).

The benefits of the presence of two types of functional channel, namely the iodine channels and prophyrin wires in **1,** have prompted us to study the development of the hybrid transport of electrons and lithium ions, the strategy of which is given in Figure 2. The most intriguing feature of **1** is the presence of the highly disordered guest molecules trapped in the square pores. The stability of the framework was assessed by thermogravimeteric analysis (TGA) and powder X-ray-diffraction (XRD) studies. TGA reveals that the guest molecules were released below 100 °C, whereas no weight loss was observed between 100 and 350 °C. When the sample was heated at 250 °C for 8 h, the powder XRD patterns remained unchanged relative to the unheated sample of **1**, which indicates that the porous framework was retained even after the loss of some solvent molecules. Therefore, the structure is robust enough to sustain such open spaces in the crystal caused by the loss of guest molecules. Given the thermal and structural stability of the open framework, we aspired to create nanostructures that are electrical conductors by intercalation methods. With a bottom-up nanoelectronic approach in mind, we examined the encapsulation of conducting polyaniline (PANI) molecules in the 1D iodine channels (Figure 2, I). The adsorption–desorption behavior of aniline molecules was studied between 40–150 °C; the TGA traces for cooling and heating scans are given in Figure 3a. These traces reveal a reversible aniline sorption in the pores of **1**. Furthermore, the electronic reflectance spectrum of PANI@**1** reveals an additional peak at 468 nm, which is attributed to emeraldine polyaniline (Figure 3b).[16] Consequently, the conductivity of PANI@**1** is approximately $10^{-3}\,S\,cm^{-1}$, which is an increase of six orders of magnitude compared to that of **1** ($10^{-9}\,S\,cm^{-1}$; Figure 3c). This result demonstrates that the conjugated polymers can be encapsulated in the nanoscale channels and still support mobile charge carriers.

Another unusual feature of **1** is that the porphyrin wires may function as a transport matrix for lithium ions by ion-exchange processes (Figure 2, II). The feasibility of the lithium-ion insertion was investigated by using a C/Li·PANI@**1** cell, which involves simultaneous intercalation–deintercalation of lithium ions in two-electrode host materials. Some preliminary reversible cycling data are presented in Figure 4. The cyclability of the cell was determined to be over 100 cycles between 0 and 2 V, which indicates that lithium

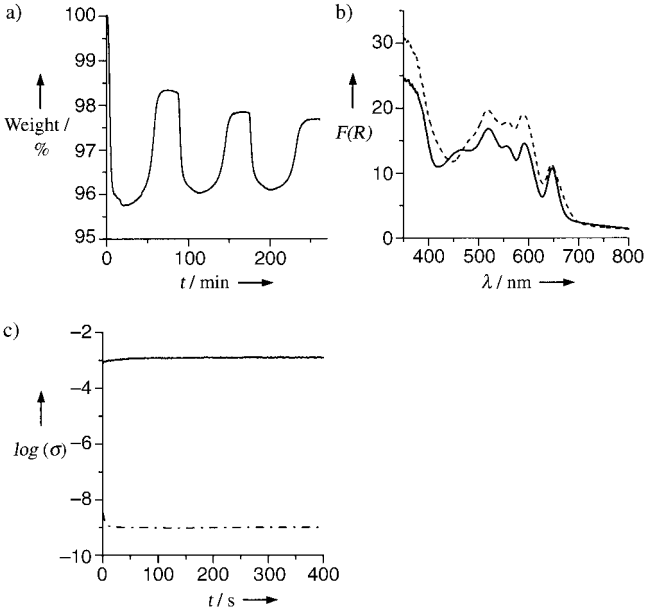


Figure 3. a) TGA profile of the reversible adsorption-desorption of aniline on **1**. Repeated heating and cooling cycles were conducted between 40–150 °C. b) Diffuse reflectance spectra of **1** (-----) and PANI@**1** (——), showing one envelope of the feature at about 468 nm, which is attributed to PANI in addition to four visible Q bands from the porphyrin at 517, 558, 589, and 646 nm. The relative reflectance for a powder, $F(R)$, is given by $F(R) = (1\text{-}R)^2/2R$, where R is the ratio of reflected intensity of the sample to that of a nonabsorbing standard. c) Electrical conductivity (σ/S cm^{-1}) of **1** (–•–•) and PANI@**1** (——).

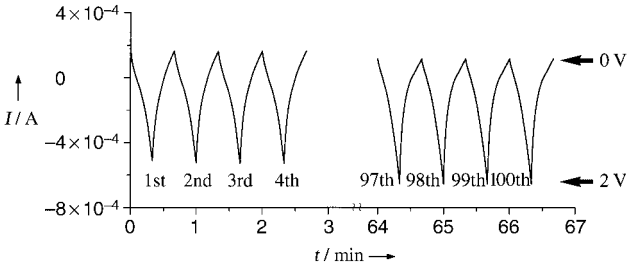


Figure 4. Cyclic voltammogram of a C/Li·PANI@**1** cell. A 1 M solution of $LiClO_4$ in EC–DMC–MF was used as the electrolyte (T = 30 °C, scan rate 100 mV s^{-1}). Measurements between 0 and 2 V revealed the cyclability of Li·PANI@**1** by intercalating/de-intercalating lithium ions. I = current.

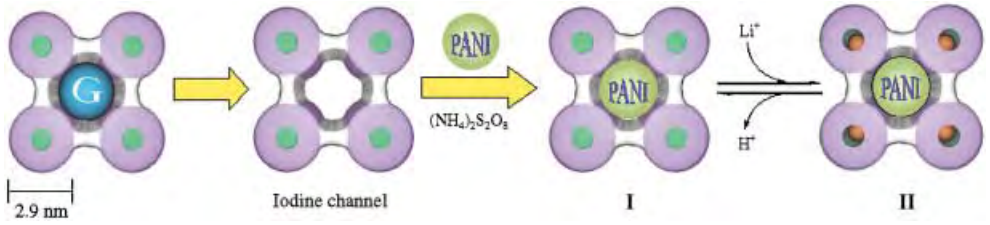


Figure 2. Scheme showing two routes to the development of electrical conductivity for **1**: I: the encapsulation of conducting polyaniline (PANI) into iodine cavities; II: the insertion of a lithium ion into the prophyrin wires through proton–lithium ion-exchange processes.

 © 2003 Wiley-VCH Verlag GmbH & Co. KGaA, Weinheim

ions and electrons can be removed and reinserted in **1**; such cyclability is a key aspect of lithium batteries.[17] An intriguing question is whether lithium ions intercalate in porphyrin wires. Using electron reflectance spectroscopy as the diagnostic technique, we found that the chromophore of the porphyrin was perturbed with significant changes in the visible Q band (i.e. a red shift of 27 nm),[18] because metal-ion insertion leads to an increase in the electron density of the porphyrin wire. This result has encouraged us to focus on optimizing the intercalation and obtaining a precise understanding of the lithium-ion-insertion mechanism.

In summary, we have demonstrated the first porous organic solids capable of mediating hybrid electronic/ionic conduction. This work may lead to the development of lithium-battery materials and a new lithium-sensitive electrode for the determination of the concentration of lithium ions in body fluids.

Experimental Section

Synthesis of **1**: A mixture of H_2TPyP (0.0732 g), CdI_2 (0.0619 g), I_2 (0.3 g), CsOH (0.3 mL), CH_3COOH (4 mL), and ethanol (4 mL) was sealed in a 23 mL Telflon-lined stainless-steel autoclave and heated to 180 °C for 48 h, then cooled to 70 °C at a rate of 6 K h^{-1}. Purple needles (0.1847 g, 87 % based on H_2TpyP) were isolated by filtration from the reaction mixture, and washed with ethanol. This synthesis was highly reproducible. X-ray data: tetragonal, space group $P4_2/n$, $a = b = 29.078(3)$, $c = 8.134(1)$ Å, $V = 6872(1)$ Å^3, $R_1 = 0.065$, $wR_2(F^2) = 0.173$, GOF = 0.943. The pore solvent molecules could not be completely located in the structure analysis. Furthermore, a preliminary N_2 adsorption/desorption isothermal study indicated that the pore size is around 5.6 Å. CCDC-158530 contains the supplementary crystallographic data for this paper. These data can be obtained free of charge via www.ccdc.cam.ac.uk/conts/retrieving.html (or from the Cambridge Crystallographic Data Centre, 12 Union Road, Cambridge CB2 1EZ, UK; fax: (+44) 1223-336-033; or deposit@ccdc.cam.ac.uk). Fitting the formula composition with the elemental analysis, and thermogravimetric analysis (weight loss of 4.3 %), we found a composition that contains four acetic acid molecules and eight water molecules per unit cell in these channels. (Elemental analysis (%): calcd: C 29.00, N 5.41, O 3.09, H 2.63; found: C 28.21, N 5.42, O 3.40, H 2.92).

Inclusion of polyaniline filaments in **1**: The structure of **1** has an open pore size of about 0.6 nm in diameter. The molecule-size channels of these hosts limit the thickness of polymer filaments to molecular dimensions. Aniline vapor was diffused into the desolvated **1** at 60 °C for 24 h. The resulting product was isolated by filtration and washed thoroughly with $CHCl_3$ to remove aniline molecules on the solid surface of **1**. The presence of aniline in **1** was determined by ^{1}H NMR spectroscopy (600 MHz, $\delta = 7.002$, 7.088, and 7.173 ppm). The aniline@**1** product was suspended in ethanol (25 mL), and a solution of peroxydisulfate was added. The suspension was stirred at 0 °C for 4 h and the purple-green solid was isolated by filtration, washed with ethanol and dried at 60 °C.

Cyclic voltammogram of a C/Li·PANI@**1** cell: Owing to the robust nature of the host of **1**, the prophyrin wires have a strong affinity for lithium insertion or ion-exchange. Li·PANI@**1** solids were obtained after immersion of the PANI@**1** solids in a solution containing Lithium ions. The presence of Li^+ in PANI@**1** was determined by ^{7}Li NMR spectroscopy, as a signal was observed at $\delta = -1.735$ ppm relative to that of free $LiNO_3$. Furthermore, the cathode was fabricated by compressing powdered Li·PANI@**1** (85 %), black carbon (10 %), and PTFE (5 %) on to an aluminum disk. The pellet was then dried at 120 °C in air. The electrolyte was prepared by dissolving $LiClO_4$ in a mixture of ethylene carbonate (EC), dimethyl carbonate (DMC), and methyl formate (MF) (volume ratio 50:45:5) to give a 1 M solution. Some properties of the cathode and of the electrolyte were reported.[19]

Received: June 12, 2002
Revised: December 16, 2002 [Z19523]

Keywords: conducting materials · electron transport · microporous materials · porphyrinoids · self-assembly

[1] J.-M. Tarascon, M. Armand, *Nature* **2001**, *414*, 359 – 367.
[2] Z. Gadjourova, Y. G. Andreev, D. P. Tunstall, P. G. Bruce, *Nature* **2001**, *412*, 520 – 523.
[3] T. Nakamura, T. Akutagawa, K. Honda, A. E. Underhill, A. T. Coomber, R. H. Friend, *Nature* **1998**, *394*, 159 – 162.
[4] R. F. Service, *Science* **2002**, *295*, 2398 – 2399.
[5] L. W. Huang, C. J. Yang, K. J. Lin, *Chem. Eur. J.* **2002**, *8*, 396 – 400.
[6] J. R. Dahn, T. Zheng, Y. Liu, J. S. Xue, *Science* **1995**, *270*, 590 – 593.
[7] D. O. Hall, K. F. Rao, *Photosynthesis, 4th ed*, Cambridge University, Cambridge, **1988**, p. 98.
[8] M. R. Ghadiri, J. R. Granja, L. K. Buehler, *Nature* **1994**, *369*, 301 – 304.
[9] O. Ikkala, G. T. Brinke, *Science* **2002**, *295*, 2407 – 2409.
[10] L. Schmidt-Mende, A. Fechtenkotter, K. Mullen, E. Moons, R. H. Friend, J. D. MacKenzie, *Science* **2001**, *293*, 1119 – 1122.
[11] a) T. Inabe, J. G. Gaudiello, M. K. Moguel, J. W. Lyding, R. L. Burton, W. J. McCarthy, C. R. Kannewurf, T. J. Marks, *J. Am. Chem. Soc.* **1986**, *108*, 7595 – 7608, and references therein; b) J. Ern, A. Bock, L. Oddos-Marcel, H. Rengel, G. Wegner, H. P. Trommsdorf, C. Kryschi, *J. Phys. Chem. A* **1999**, *103*, 2446 – 2450; c) R. Silerva(Back), L. Kalvoda, D. Neher, A. Ferencz, J. Wu, G. Wegner, *Chem. Mater.* **1998**, *10*, 2284 – 2292; d) C. W. Dirk, T. Inabe, K. F. Schoch, Jr., T. J. Marks, *J. Am. Chem. Soc.* **1983**, *105*, 1539 – 1550; e) H. L. Anderson, *Inorg. Chem.* **1994**, *33*, 972 – 981.
[12] a) Y. Diskin-Posner, S. Dahal, I. Goldberg, *Angew. Chem.* **2000**, *112*, 1344 – 1348; *Angew. Chem. Int. Ed.* **2000**, *39*, 1288 – 1292, and reference therein; b) B. F. Abrahams, B. F. Hoskins, D. M. Michail, R. Robson, *Nature* **1994**, *369*, 727 – 729; c) S. Belanger, J. T. Hupp, *Angew. Chem.* **1999**, *111*, 2360 – 2362; *Angew. Chem. Int. Ed.* **1999**, *38*, 2222 – 2224; d) C. M. Drain, F. Nifiatis, A. Vasenko, J. D. Batteas, *Angew. Chem.* **1998**, *110*, 2478 – 2481; *Angew. Chem. Int. Ed.* **1998**, *37*, 2344 – 2347; e) T. Schareina, R. Kempe, *Z. Anorg. Allg. Chem.* **2000**, *626*, 1279 – 1281; f) K.-J. Lin, *Angew. Chem.* **1999**, *111*, 2894 – 2897; *Angew. Chem. Int. Ed.* **1999**, *38*, 2730 – 2732; g) M. E. Kosal, J. H. Chou, S. Wilson, K. S Suslick, *Nature Mater.* **2002**, *1*, 118 – 121.
[13] M. P. Byrn, C. J. Curtis, I. Goldberg, Y. Hsiou, S. I. Khan, P. A. Sawin, S. K. Tendick, C. E. Strouse, *J. Am. Chem. Soc.* **1991**, *113*, 6549 – 6557.
[14] C. V. K. Sharma, G. A. Broker, J. G. Huddleston, J. W. Baldwin, R. M. Metzger, R. D. Rogers, *J. Am. Chem. Soc.* **1999**, *121*, 1137 – 1144.
[15] S. F. Lia, C. Y. Cheng, K. J. Lin, *Chem. Commun.* **2001**, 1082 – 1083.
[16] a) P. Enzel, T. Bein, *J. Phys. Chem.* **1989**, *93*, 6270 – 6272; b) C. G. Wu, T. Bein, *Science* **1994**, *264*, 1757 – 1759.
[17] The current density of PANI dramatically decreased as the cycling number increased because of the lack of Li^+ storage ability in PANI, while the redox electroactivity of Li·PANI@**1** was over 200 cycles. Thus, a new approach to the development of a composite organic lithium-battery material was achieved in the presence of PANI in **1**. This result will be reported later.

 © 2003 Wiley-VCH Verlag GmbH & Co. KGaA, Weinheim

[18] It reveals a red shift of the Q band by 9 nm for Fe^{2+}, but no influence for Na^+ and K^+. This result illustrates that the ion exchange takes place when the diameters of metal ions (Li^+ 1.48 Å; Na^+ 2.04 Å) are smaller than that of the porphyrin core (1.56 Å).

[19] a) A. R. Armstrong, P. G. Bruce, *Nature* **1996**, *381*, 499 – 500; b) S. R. S. P. Prabaharan, M. S. Michael, S. Radhakrishna, C. Julien, *J. Mater. Chem.* **1997**, *7*, 1791 – 1796.

 © 2003 Wiley-VCH Verlag GmbH & Co. KGaA, Weinheim

Molecular Modeling of Enzymes

Understanding the Role of Active-Site Residues in Chorismate Mutase Catalysis from Molecular-Dynamics Simulations**

*Hong Guo, Qiang Cui, William N. Lipscomb, and Martin Karplus**

Understanding the role of active-site residues in enzymatic catalysis is of fundamental importance for a microscopic description of the catalytic mechanism, but also for the design of effective enzyme mimics or improvement of existing enzymes (or abzymes) for catalyzing chemical reactions. Site-directed mutagenesis and kinetic studies are able to identify key residues involved in the catalysis, but determination of their exact role from experimental information alone can be difficult. This is the case for the chorismate mutase of *Bacillus subtilis* (BsCM), which catalyzes the Claisen rearrangement of chorismate to prephenate (Figure 1 a and b) in the biosynthetic pathway that forms Tyr and Phe.[1] Mutation experiments[1–5] have identified several residues that are important for the catalysis. For instance, it was shown that replacement of Arg 90 by Gly or Ala leads to a significant reduction in k_{cat} by a factor of more than 10^5, while k_{cat}/K_m is decreased by a factor of 10^5–10^7. Interestingly, the double mutants Cys 88 Lys/Arg 90 Ser and Cys 88 Ser/Arg 90 Lys restore a factor of more than 10^3 in k_{cat}.[5] Arg 90 interacts with the ether oxygen atom of the transition-state analogue (TSA) in the X-ray structure of the wildtype BsCM complex,[6–7] and this observation led to the suggestion that Arg 90 stabilizes developing negative charge on the enolic oxygen atom in the transition state[1–3,6] as well as the transition-state conformation.[2,6] Nevertheless, the exact role of Arg 90 and other active-site residues is not clear.

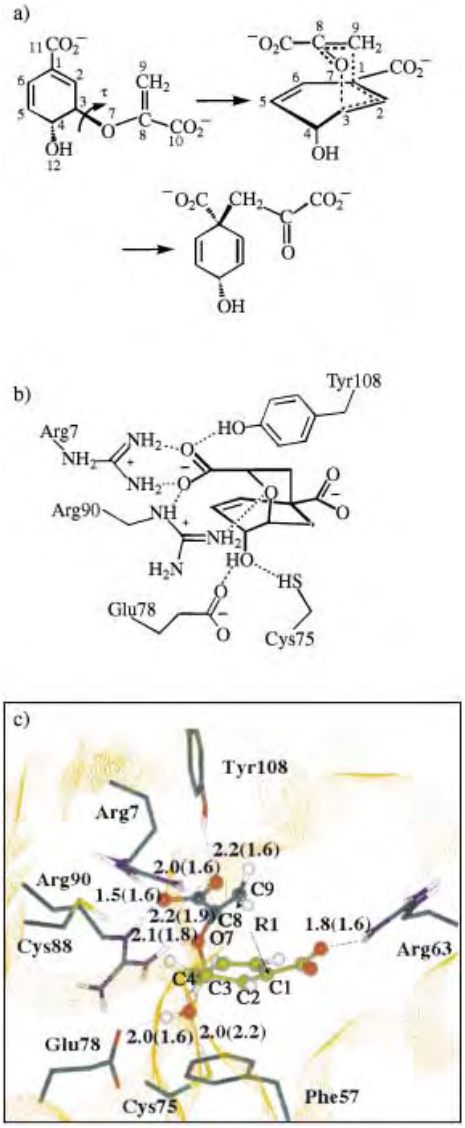


Figure 1. a) Claisen rearrangement of chorismate to prephenate via the chair-like transition state. b) Interactions between the TSA and important active site residues in BsCM.[6] c) The initial docking configuration of CHAIR in the wild-type BsCM as well as certain structural data after energy minimization (in parentheses). Distances are in Å. R_1(C1···C9) and τ(C2–C3-O7–C8) are used in monitoring the motion of the substrate during dynamics. Insight II of Molecular Modeling System from Accelrys, San Diego, was used to make the figure.

Herein we apply quantum-mechanical/molecular-mechanical (QM/MM) molecular-dynamics simulations to study the role of Arg 90 in the BsCM catalysis. It is demonstrated that the existence of this residue is essential for stabilizing the reactive-substrate conformation (CHAIR) in the active site, as both the Arg 90→Ala and Arg 90→Gly mutations destroy the ability of the wildtype enzyme to stabilize CHAIR.[8] Free-energy simulations suggest that the loss of this ability may contribute significantly to the reduction of k_{cat} for Arg 90 Ala and Arg 90 Gly observed

[*] Prof. M. Karplus, Dr. H. Guo, Dr. Q. Cui, Prof. W. N. Lipscomb
Department of Chemistry and Chemical Biology, Harvard University
12 Oxford Street, Cambridge, MA 02138 (USA)
Fax: (+1) 617-496-3204
E-mail: marci@tammy.harvard.edu
Prof. M. Karplus
Laboratoire de Chimie Biophysique, ISIS
Université Louis Pasteur, 67 000 Strasbourg (France)

[**] Helpful discussions with Dr. Wei Yang are gratefully acknowledged. This work was supported by grants GM06920 (W.N.L.) and GM030804 (M.K.) from the National Institutes of Health.

Supporting information for this article is available on the WWW under http://www.angewandte.org or from the author.

 © 2003 Wiley-VCH Verlag GmbH & Co. KGaA, Weinheim DOI: 10.1002/anie.200219878

experimentally.[2–5] The restoration of the catalytic efficiency by the double mutant Cys88Lys/Arg90Ser can be explained by a corresponding argument; that is, the CHAIR conformer is found to be more stable in this double mutant than in Arg90Ala. Thus, the simulations suggest that the removal of the single key residue Arg90 destroys the balance of the interactions in the active site required for stabilizing the reactive conformation of the substrate,[8] leading to a dramatic reduction in the catalytic efficiency of BsCM.

The reactive conformation (CHAIR) obtained from gas-phase ab initio calculations[8] was manually docked into the active sites of the wildtype enzyme, Arg90Ala, Arg90Gly, and Cys88Lys/Arg90Ser based on the BsCM TSA structures.[5–6] The initial docking and minimized configurations in the wildtype enzyme are given in Figure 1c, and those of the Arg90Ala, Arg90Gly, and Cys88Lys/Arg90Ser complexes are given in the Supporting Information. Figure 1c shows that CHAIR has interactions with the active-site residues that are similar to those of TSA (Figure 1b). The motion of CHAIR in BsCM and in different mutants during the QM/MM molecular-dynamics simulations is monitored by τ(C2–C3-O7–C8) and R_1(C1···C9) (See Figure 1c for definition) in Figure 2a and Figure 2b, respectively. The substrate remains in CHAIR in the wildtype enzyme ($\tau = 60$–$70°$ and $R_1 = 3$–3.5 Å), but it undergoes a conformational transition to a nonreactive conformation in Arg90Gly and Arg90Ala in 50–100 ps, as indicated by the decrease in τ (to about $\sim -40°$) and the increase of R_1 (to 4.5–5 Å). Strikingly, for Cys88Lys/Arg90Ser, the substrate remains in the neighborhood of the reactive conformation, although it is distorted and there are large fluctuations of R_1 (i.e., $\tau \sim 40°$ and $R_1 = 3.5$–5 Å). Figure 3 shows active-site structures for the wildtype enzyme and the mutants from the MD simulations. Figure 3a shows the substrate in the reactive CHAIR conformation at 1 ns with essentially the same interactions as those in the minimized structure (Figure 1c) and in the BsCM TSA complex structure (Figure 1b). For instance, Arg90 interacts with both the side-chain carboxylate group and the oxygen atom of the ether function, whereas Arg7 interacts with the side-chain carboxylate group only. Detailed discussions of the different interactions and a comparison with the available X-ray structures[5–7] will be given in a full paper. In the Arg90Gly and Arg90Ala complex structures (Figure 3b and c, respectively) the substrate has moved away from CHAIR, consistent with Figure 2, and it is now in an inactive (DIAX) conformation in which the side-chain carboxylate group, rather than the side-chain methylene group, is over C1. The DIAX conformer was identified earlier[8] as a stable conformation in solution simulations. In the DIAX conformation, it is Arg7 that interacts with the ether oxygen atom and the side-chain carboxylate group; these interactions replace those involving Arg90 in the wildtype enzyme complex (see Figure 3a). Figure 3d shows that the substrate is near the reactive CHAIR conformation in the double mutant Cys88Lys/Arg90Ser: the side chain is rotated toward DIAX by about 20°. The substrate is stabilized by a hydrogen-bonding network (side-chain carboxylate···S90···Lys88···Glu78···C4 hydroxy), which along with Arg7, appears to play a similar role in stabilizing CHAIR to that of the Arg90,

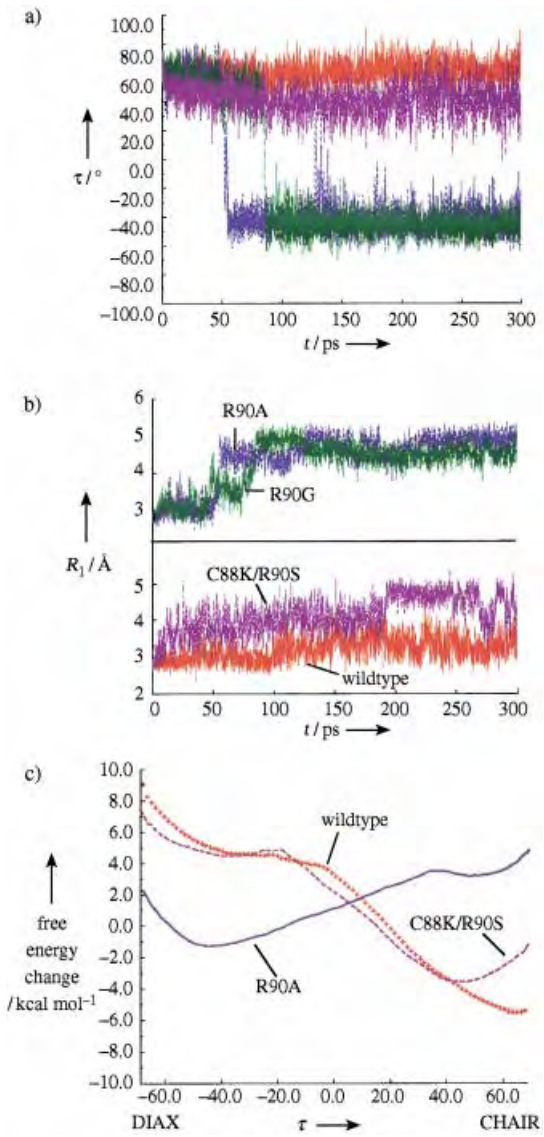


Figure 2. The motion of the substrate during the QM/MM MD simulations and the free energy (potential of mean force) changes. a) τ; b) R_1; c) free-energy changes. The initial substrate conformation is CHAIR. Red: wildtype; blue: Arg90Ala; green: Arg90Gly; purple: Cys88Lys/Arg90Ser.

Glu78 diad in the wildtype (see above). Consistent with the X-ray structure of Cys88Lys/Arg90Ser without TSA,[5] Lys88 forms a salt bridge with Glu78. No hydrogen bond is observed between Lys88 and the ether oxygen atom during the MD simulations; this hydrogen bond formed in the initial docking configuration, but broke during energy minimization and was absent during the dynamics simulations (see Supporting Information).

The removal of the Arg90 side chain through the Arg90→Ala or Arg90→Gly mutation leads to a reduction in k_{cat} by at least 5 orders of magnitude,[2–5] corresponding to an increase in the activation barrier by more than 8 kcal mol^{-1}. The X-ray crystal structure[5] shows that the integrity of the three-dimensional structure is well-maintained after the mutations. One widely accepted role for

 © 2003 Wiley-VCH Verlag GmbH & Co. KGaA, Weinheim

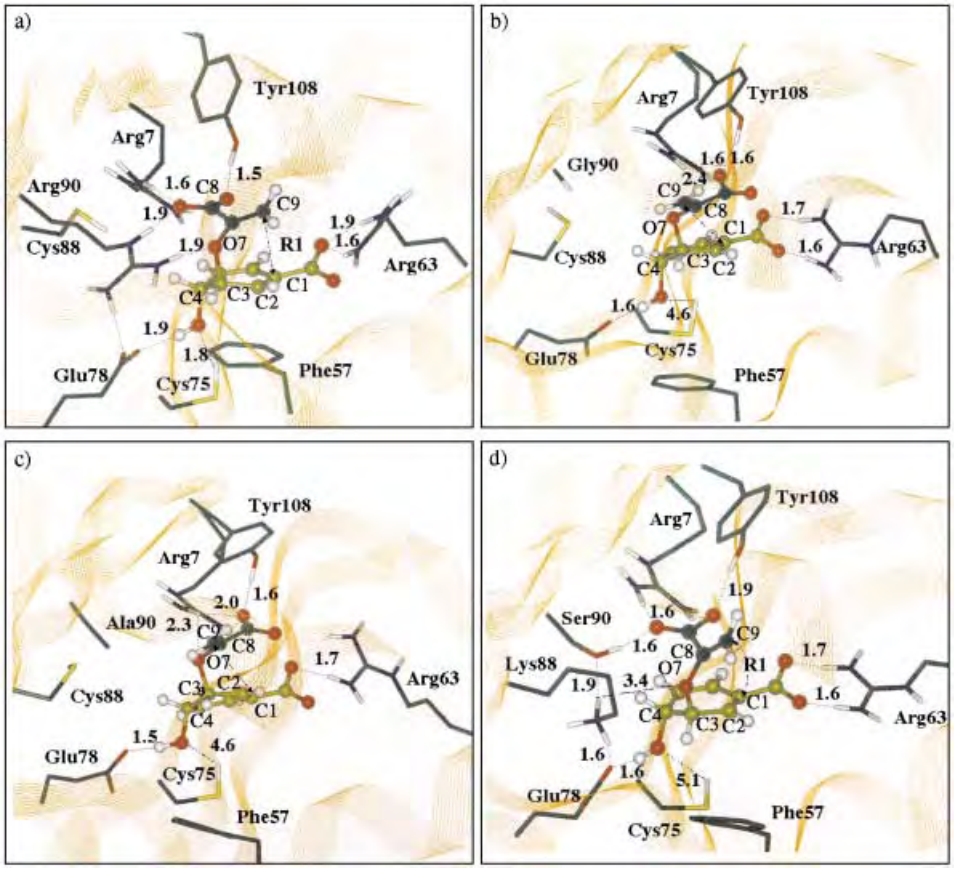


Figure 3. Typical active-site structures observed during the MD simulations; a single structure is shown. a) Wildtype at 1 ns: $R_1 = 3.0$ Å and $\tau = 53°$; b) Arg90Gly at 400 ps: $R_1 = 4.9$ Å and $\tau = -49°$; c) Arg90Ala at 400 ps: $R_1 = 4.9$ Å and $\tau = -45°$; d) Cys88Lys/Arg90Ser at 400 ps: $R_1 = 4.0$ Å and $\tau = 37°$.

Arg90 in the catalysis is to stabilize developing negative charge on the enolic oxygen atom in the transition state.[1–6] This suggestion is supported by a QM/MM study[10] of the BsCM catalysis by using a perturbation approach[11] based on fixed BsCM CHAIR and BsCM transition-state (TS) structures, in which it was shown that the deletion of Arg90 increases the activation barrier by 5 kcal mol^{-1} in going from CHAIR to TS. This increase is significantly smaller than the effect observed experimentally (> 8 kcal mol^{-1}).

To examine the free energy involved in the stabilization of the CHAIR form in the active site, umbrella sampling simulations[9] were performed for the wildtype and mutant enzymes. Figure 2c shows that whereas CHAIR is about 10 kcal mol^{-1} more stable than DIAX in the wildtype BsCM, it becomes 5 kcal mol^{-1} less stable in Arg90Ala. CHAIR is also found to be considerably less stable than DIAX in solution; the calculated free-energy difference is about 10 kcal mol^{-1}. CHAIR is stable in the mutant Cys88Lys/Arg90Ser, but the free-energy minimum is shifted somewhat ($\tau = 40°$). Thus, the results of the MD simulations point to an additional role for Arg90. Its existence appears to be essential for stabilizing the reactive substrate conformation (CHAIR) in the active site. The extra energy cost ~5 kcal mol^{-1} necessary for generating CHAIR in Arg90Ala and Arg90Gly would contribute to the loss of activity of the mutants; presumably, this would appear in the observed reduction in k_{cat}.[5] Correspondingly, the activity of the double mutant Cys88Lys/Arg90Ser (i.e., k_{cat} is 10^3-fold greater than that of Arg90Ala and Arg90Gly) involves its ability to stabilize a substrate conformation close to CHAIR. In this mutant, the substrate is distorted, and additional energy (~2 kcal mol^{-1}, see Figure 2c) is necessary to generate the optimal reactive CHAIR conformation (i.e., from $\tau = 40°$ to 60°). This factor, as well as the lack of a stable hydrogen-bonding interaction with the ether oxygen atom, would make the double mutant less efficient than the wildtype enzyme (k_{cat} is 10^2-fold less than that of the wildtype).

BsCM has been the subject of a large number of experimental[1–7,12–13] and theoretical investigations.[10,15–17] It has been shown experimentally that the transformation of chorismate into prephenate in solution has a free energy of activation of 24.5 kcal mol^{-1}[12] and that the activation barrier is reduced to 15–16 kcal mol^{-1} in the BsCM-catalyzed reaction.[13] Our earlier study of yeast CM[8] suggested that the catalysis may arise from the ability of the enzyme to lower the free energy of the transition state by stabilizing the reactive CHAIR conformation, in addition to the lowering of the chemical reaction barrier once the CHAIR conformation is present; the latter had been analyzed in many QM/MM studies.[10,15,17] The role of the stabilization of the CHAIR

 © 2003 Wiley-VCH Verlag GmbH & Co. KGaA, Weinheim

conformation is supported by the present free-energy simulations for BsCM, which demonstrate that Arg90 stabilizes the reactive conformation relative to the solution conformation.[18] Free-energy calculations for the much less active Arg90Ala and Arg90Gly mutants show that they destroy the ability of the enzyme to stabilize the CHAIR conformation. Moreover, the Cys88Lys/Arg90Ser mutant, which increases k_{cat} by a factor of more than 10^3 relative to Arg90Ala is found to be able to stabilize the CHAIR conformation in the active site. The present results provide strong evidence for the hypothesis that chorismate mutase uses conformational optimization of the substrate to lower the transition-state barrier. Efforts to design enzyme mimics or to improve existing enzymes (or abzymes) for transforming chorismate into prephenate should thus consider the conformational change required to achieve the transition-state geometry.

Received: August 2, 2002
Revised: December 27, 2002 [Z19878]

Keywords: enzyme catalysis · molecular dynamics · pericyclic reaction · reaction mechanisms · transition states

[1] B. Ganem, *Angew. Chem.* **1996**, *108*, 1014 – 1023; *Angew. Chem. Int. Ed. Engl.* **1996**, *35*, 936 – 945.
[2] S. T. Cload, D. R. Liu, R. M. Pastor, P. G. Schultz, *J. Am. Chem. Soc.* **1996**, *118*, 1787 – 1788.
[3] P. Kast, J. D. Hartgerink, M. Asif-Ullah, D. Hilvert, *J. Am. Chem. Soc.* **1996**, *118*, 3069 – 3070.
[4] P. Kast, J. D. Hartgerink, M. Asif-Ullah, N. Jiang, D. Hilvert, *Proc. Natl. Acad. Sci. USA* **1996**, *93*, 5043 – 5048.
[5] P. Kast, C. Grisostomi, I. A. Chen, S. Li, U. Krengel, Y. Xue, D. Hilvert, *J. Biol. Chem.* **2000**, *275*, 36832 – 36838.
[6] Y. M. Chook, J. V. Gray, H. Ke, W. N. Lipscomb, *J. Mol. Biol.* **1994**, *240*, 476 – 500.
[7] J. E. Ladner, P. Reddy, A. Davis, M. Tordova, A. J. Howard, G. L. Gilliland, *Acta Crystallogr. Sect. D* **2000**, *56*, 673 – 683.
[8] H. Guo, Q. Cui, W. N. Lipscomb, M. Karplus, *Proc. Natl. Acad. Sci. USA* **2001**, *98*, 9032 – 9037.
[9] A fast semi-empirical density-functional approach (SCC-DFTB) (M. Elstner, D. Porezag, G. Jungnickel, J. Elsner, M. Haugk, T. Frauenheim, S. Suhai, G. Seigert, *Phys. Rev. B* **2001**, *58*, 7260 – 7268; Q. Cui, M. Elstner, E. Kaxiras, T. Frauenheim, M. Karplus, *J. Phys. Chem. B* **2001**, *105*, 569 – 585), recently implemented in the CHARMM program (B. R. Brooks, *J. Comput. Chem.* **1983**, *4*, 187), was used for QM/MM molecular-dynamics simulations. The chorismate substrate was treated by QM and the rest of the system by MM. The all-hydrogen potential function (PARAM22) (A. D. MacKerell, Jr., D. Bashford, M. Bellott, R. L. Dunbrack, Jr., J. Evanseck, M. J. Field, S. Fischer, J. Gao, H. Guo, S. Ha, D. Joseph-McCarthy, L. Kuchnir, K. Kuczera, F. T. K. Lau, C. Mattos, S. Michnick, T. Ngo, D. T. Nguyen, B. Prodhom, W. E. Reiher III, B. Roux, M. Schlenkrich, J. C. Smith, R. Stote, J. Straub, M. Watanabe, J. Wiřkiewicz-Kuczera, D. Yin, M. Karplus, *J. Phys. Chem. B* **1998**, *102*, 3586-3616) was used for MM atoms. A modified TIP3P water model (W. L. Jorgensen, *J. Am. Chem. Soc.* **1981**, *103*, 335; E. Neria, S. Fischer, M. Karplus, *J. Chem. Phys.* **1996**, *105*, 1902 – 1921) was employed for the solvent. The stochastic boundary molecular-dynamics method (C. L. Brooks III, A. T. Brunger, M. Karplus, *Biopolymers* **1985**, *24*, 843 – 865) was used for the QM/MM MD simulations. The initial coordinates for the simulations were obtained from the crystal structure of BsCM,[6] which has the TSA bound to the active site. For Cys88Lys/Arg90Ser, the side-chain conformations of Lys88 and Ser90 were taken from the X-ray crystal structure of Cys88Lys/Arg90Ser without TSA.[5] The umbrella sampling method (G. M. Torrie, J. P. Valleau, *Chem. Phys. Lett.* **1974**, *28*, 578) implemented in the CHARMM program along with the Weighted Histogram Analysis Method (WHAM) (M. Kumar, D. Bouzida, R. H. Swendsen, P. A. Kollman, J. M. Rosenberg, *J. Comput. Chem.* **1992**, *13*, 1011 – 1021; Q. Cui, unpublished results) was applied to determine the change of the free energy (potential of mean force) from the reactive CHAIR to the nonreactive DIAX conformation in the wildtype BsCM, Arg90Ala, and Cys88Lys/Arg90Ser; harmonic umbrella potentials with a force constant of 50 kcal(mole)$^{-1}$(radian)$^{-2}$ were used and τ(C2–C3-O7–C8) was chosen as the reaction coordinate. Nine windows were used to go from $\tau = 60°$ (CHAIR) to $\tau = -60$ (DIAX). See the Supporting Information for more details of the methods.
[10] P. D. Lyne, A. J. Mulholland, W. G. Richards, *J. Am. Chem. Soc.* **1995**, *117*, 11345 – 11350.
[11] P. A. Bash, M. J. Field, R. C. Davenport, G. A. Petsko, D. Ringe, M. Karplus, *Biochemistry* **1991**, *30*, 5826.
[12] P. R. Andrews, G. D. Smith, I. G. Young, *Biochemistry* **1973**, *12*, 3492 – 3498.
[13] P. Kast, M. Asif-Ullah, D. Hilvert, *Tetrahedron Lett.* **1996**, *37*, 2691 – 2694.
[14] J. V. Gray, D. Eren, J. R. Knowles, *Biochemistry* **1990**, *29*, 8872 – 8878.
[15] M. M. Davidson, I. R. Gould, I. H. Hillier, *J. Chem. Soc. Perkin Trans. 2* **1996**, 525 – 532.
[16] S. E. Worthington, A. E. Roitberg, M. Krauss, **2001**, *J. Phys. Chem. B* **105**, 7087 – 7095.
[17] S. Martí, J. Andrés, V. Moliner, E. Silla, I. Tuñón, J. Bertrán, M. J. Field, *J. Am. Chem. Soc.* **2001**, *123*, 1709 – 1712.
[18] We would like to emphasize that stabilizing the active conformation, which is very different from the stable conformation in solution, could contribute to lowering the free energy of the transition state, which is the essential factor in enzyme catalysis (see, for example, reference [19]). This should not be confused with the proposal by Bruice concerning the role of NACs (near attack conformations) in enzymatic catalysis.[20]
[19] R. L. Schowen in *Transition States of Biochemical Processes* (Eds.: R. D. Gandour, R. L. Schowen), Plenum, New York, **1976**, pp. 77 – 113.
[20] T. C. Bruice, *Acc. Chem. Res.* **2002**, *35*, 139 – 148; see also S. Hur, T. C. Bruice, *Proc. Natl. Acad. Sci. USA* **2001**, *99*, 1176 – 1181 for a related study of the chorismate mutase from *E. coli*.

 © 2003 Wiley-VCH Verlag GmbH & Co. KGaA, Weinheim

Isotope-Induced Structural Effects

Compositional and Isotopologue-Induced Phase Differentiation in Supramolecular Aggregates**

*Jaeho Lee and Sergiu M. Gorun**

To date there have been few experimental studies that have probed deuterium effects upon aggregations. In biology, a 1975 report links deuterium effects with the K^+-, Cs^+-, and NH_4^+-induced assembly of tetrameric *Clostridium cylindrosporum* formyltetrahydrofolate synthetase (FTHFS) from monomeric units.[1] Monomer association is enhanced 50-fold in D_2O due, at least in part, to the 2.8-fold increase in the FTHFS monomer–alkaline cation association constant in D_2O. The hydrated cations are coordinated by the carboxylato and carbonyl oxygen atoms of amino acids, as revealed recently.[2] The assembly of inorganic aggregates that exhibit controlled topologies and nuclearities, remains a challenge for the synthetic chemist.

We have recently reported the discovery of a novel structural (thermodynamic) hydrogen isotope effect, and provided examples of isotope-dependent formation of Mn and Fe aggregates in inorganic and bioinorganic chemistry.[3] In the Mn case, repeated preparations in H_2O and D_2O have revealed the formation of similar Mn_{16} units, aggregated further in supramolecular assemblies by additional Cl^- and hydrated Na^+ and Ba^{2+} ions. Four peripheral Ba^{2+} ions, present in the Mn_{16} aggregates obtained from both H_2O and D_2O, are coordinated by water and carbonyl oxygen atoms. In the D_2O case, but not in the H_2O case, Cl^- ions are hydrogen-bonded to deuteroxo groups that bridge two Mn centers, while water molecules of hydration coordinate additional Ba^{2+} ions, which, in turn, are linked to Na^+ ions by extra water molecules (Figure 1).

Despite identical Na/Cl/Ba solution concentrations, the Mn_{16} phases obtained from D_2O, P3 (L = the pentaanion of 1,3-diamino-2-hydroxypropane-*N,N,N′,N′*-tetraacetic acid), contain two extra Na^+, Cl^-, and Ba^{2+} ions relative to the Mn_{16} phases obtained from H_2O, P1.[3] The extra four charges in P3 require four fewer deuterons and/or lower average Mn oxidation states (maximum four units) for overall charge neutrality. The high, 4/*m* symmetry of the aggregates, however, precludes a precise determination of these differences by X-ray diffraction.[4]

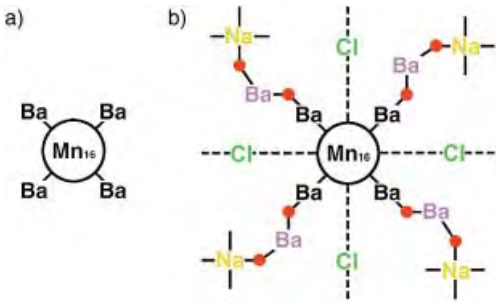


Figure 1. Schematic representation of a) the peripheral Ba^{2+} ions linked directly to the Mn_{16} aggregate from H_2O, phase P1, and b) the additional Ba^{2+} and Na^+ ions linked to the first set through bridging D_2O molecules (shown as dots), phase P3.

$$[Mn_{16}O_4(OD)_4(CO_3)_4L_8Ba_{10\pm0.5}Na_{4\pm1}Cl_3]\cdot 80\pm3\,D_2O \quad P3$$

$$[Mn_{16}O_4(OH)_4(CO_3)_4L_8Ba_8Na_2Cl]\cdot 54\pm8\,H_2O \quad P1$$

The reasons for isotopologue-dependent formation of different aggregates, starting with solutions of otherwise identical compositions, are not fully understood.

We report here the discovery of correlations between the variable *concentration* of NaCl in H_2O and D_2O solutions and the type *and number* of solid-state phases derived from them, correlations that are dependent on the hydrogen isotopologue. Surprisingly, a new, structurally intermediate phase is observed in H_2O, but not in D_2O, a phenomenon reminiscent of the formation of the ice IV structure for D_2O, but not for H_2O.[5]

All Mn_{16} phases were prepared following the procedure in reference [3]. Considering the higher NaCl content of the D_2O phase P3, we wondered if this aggregate could also be produced in H_2O by increasing the NaCl concentration. To this end, the concentration of NaCl in H_2O was varied from about 0.5 to about 5.0 g per 20 mL solution, while maintaining the concentrations of all other reagents, as well as the reaction conditions, constant (see Experimental Section). This procedure amounts to a NaCl "titration". The solids were characterized by X-ray diffraction studies (several single crystals per batch), and the unit cells of the bulk materials were verified by powder X-ray diffraction.

The results, summarized schematically in Figure 2, incorporate the single-point concentration of 1.0 g NaCl per 20 mL solution.[3] As seen in Figure 2 (upper trace), phase P3 is indeed obtained in H_2O, but only when the NaCl concen-

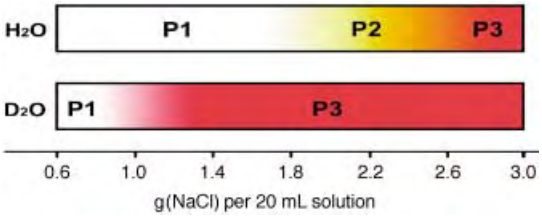


Figure 2. Chart of solid-state Mn_{16} phases versus the concentration of NaCl in solution. The phase boundaries, as expected, are not clearly defined. Crystalline materials do not form outside the chart NaCl limits.

[*] Prof. Dr. S. M. Gorun, J. Lee
Department of Chemistry
Brown University
Providence, RI 02912 (USA)
Fax: (+1) 401-863-9046
E-mail: sergiu_gorun@brown.edu

[**] The partial financial assistance of the National Science Foundation (DMR-0233811), use of MIT SQUID facility, and contributions of Dr. N. R. Brooks and Dr. V. G. Young, Jr. to the X-ray work, are acknowledged.

Supporting information for this article is available on the WWW under http://www.angewandte.org or from the author.

 © 2003 Wiley-VCH Verlag GmbH & Co. KGaA, Weinheim DOI: 10.1002/anie.200250200

tration approaches 2.6 g per 20 mL solution.[6a] However, the crystallization becomes more difficult as the concentration of NaCl increases. Phase P3 forms after weeks, as opposed to days in D_2O. In H_2O, phase P1 also crystallizes faster (days).

The simulation of the "D_2O effect" by an enhanced NaCl concentration, prompted us to seek, following the same logic, the reverse "H_2O effect", that is, the formation of the H_2O phase P1 in D_2O. The lower trace of Figure 2 shows that this phase forms in D_2O when the NaCl concentration is *lowered*, approximately below 0.9 g per 20 mL solution.[6b] The phases P1 from H_2O and D_2O are quasi-isomorphous. The phases P3 behave similarly. There are, however, small differences.[7]

Interestingly, these phases contain different amounts of Ba^{2+}, despite the fact that the Ba^{2+} concentration in solution was kept constant. This observation suggests that the variation in the concentration of NaCl suffices for phase selectivity *at constant isotope composition*.

Taken together, the above data indicate that the variation in NaCl concentration simulates the effect of the other, seemingly independent parameter, namely the variation of the hydrogen isotopologue in the aqueous solvent. This parallel, however, is not complete. A new phase, P2, is obtained in H_2O at NaCl concentrations between those required for P1 and P3. The structure comprises two crystallographically distinct Mn_{16} aggregates, both of which exhibit 4/*m* symmetry.[7] The first one, labeled Unit 1, is actually P1. The second one, Unit 2, is also P1, but with an additional 8 Na^+ ions, consistent with the increased NaCl concentration in the solution from which P2 is obtained. However, Cl^- ions, found in P3, are not present in Unit 2. The P2 formula is $\{[Mn_{16}O_4(OH)_4(CO_3)_4L_8Ba_8Na_2Cl]\}\{[Mn_{16}O_4(OH)_4(CO_3)_4L_8Ba_8Na_{10}Cl]\}$, written as {Unit 1}{Unit 2} (Figure 3; see also Figure S2 and S3 in the Supporting Information):

The two unique Mn centers have different average oxidation states and coordination geometries. One Mn center is roughly pentagonally bipyramidal coordinated, with a chelating carbonate ion (one Mn–O bond is drawn in Figure 3 with dashed lines) in the equatorial plane. Bond lengths of about 2.13–2.30 Å, and equatorial angles of about 71–76°, are common for both Unit 2 and Unit 1. Both the coordination type and metal–ligand distances indicate a predominance of Mn^{II} at this site. The μ-alkoxo oxygen atom (Figure 3a) is in the apical position of the coordination polyhedra of both Mn centers, but the second Mn atom is only six-coordinate. For this site, the average equatorial bond length of both Unit 1 and Unit 2 (2.080(3) Å) is shorter than those for the Mn^{II} site, and an axial compression is noted: 1.951(3) and 1.956(3) Å for Unit 1 and Unit 2, respectively. The above parameters characterize a site with a predominant, Jahn–Teller compressed, high-spin Mn^{III} occupancy, while excluding higher oxidation levels. A similar, rare Jahn–Teller distortion, was noted for the same ligand in Mn_4 complexes,[8] as well as P1 and P3 phases.[3] Similar to the case of the latter complexes, the high, 4/*m* symmetry of both Unit 1 and Unit 2, precludes the precise determination of the Mn^{II}/Mn^{III} ratios. Iodometric titrations, however, indicate similar ratios of the oxidation states: 8.0(2)/8.0(2) and 7.8(2)/8.2(2) for P2 and P3, respectively, consistent with the presence in Unit 2 of eight additional Na^+ ions. Thus, there are four average charges per Mn_{16} unit of P2. In P3, these extra charges (relative to P1) are due to two Ba^{2+} ions.

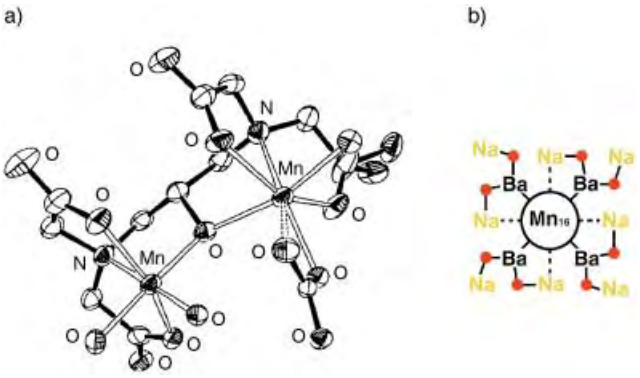


Figure 3. Structures of the Mn_{16} aggregate of Unit 2 of P2. a) The alkoxo-bridged dinuclear Mn center, common to both Unit 2 and Unit 1 and P1 phases (thermal ellipsoids are at 40% probability level; hydrogen atoms and carbon atom labels are omitted for clarity). b) Schematic view down the fourfold axis of the assembly of Unit 2 from phase P1 (Figure 1a) and Na^+ ions. Each dot represents H_2O bridges; the dashed lines represent ligand coordination.

The solid-state packing diagrams of P1, P2, and P3 phases exhibit significant differences (Figure 4). The supramolecular architectures of Mn_{16} building blocks of the three phases are related. Phase P1, which consists only of "pure" building blocks, provides the basic scaffold. In phase P2, every other P1 layer of blocks (see the *ac* plane view) acquires Na^+ ions, but the topology of the blocks remains the same. In phase P3, more interstitial ions are incorporated, resulting in a twist of the building blocks around axes parallel to the *c* direction, and a simultaneous increase and decrease of their spatial density in the *ab* plane and *c* directions, respectively (Figure 4d). As more ions are incorporated, the unit cell volumes *decrease*: P2 and P3 have volumes 95 and 89% of that of P1, respectively. The similarities and differences between the structures of P1 and P2 or P3 are reflected in their magnetic signatures. Variable-temperature magnetic susceptibility measurements of P2 and P3 reveal an overall antiferromagnetic coupling of the Mn ions, characterized by an initial increase of the molar susceptibility (normalized per Mn_{16} unit) as the temperature decreases, and the appearance of soft Néel-type maxima at 10.0 K and 15.6 K for P2 and P3, respectively (see Supporting Information). In both cases, the total spin state values tend toward $S_T = 0$ below 6 K. In contrast, a Néel-type maximum is not observed above 4 K for P1.[3] This data suggests that P2, like P3, is qualitatively different from P1, with manifestations of extended solidlike magnetic behavior, consistent with either different *intra* Mn_{16} aggregate *J* values, or *inter* Mn_{16} aggregate couplings mediated by the peripheral main-group elements. The latter possibility is supported by the above-mentioned enhanced compactness of P2 and P3 relative to P1.

Considering that P1 can also be obtained from D_2O by lowering the NaCl concentration characteristic for P3, it was expected that a P2 phase, like in the case of H_2O, could be obtained from D_2O at intermediate NaCl concentrations. However, we have failed to observe any intermediate phases despite numerous attempts, which suggests that, at least when

 © 2003 Wiley-VCH Verlag GmbH & Co. KGaA, Weinheim

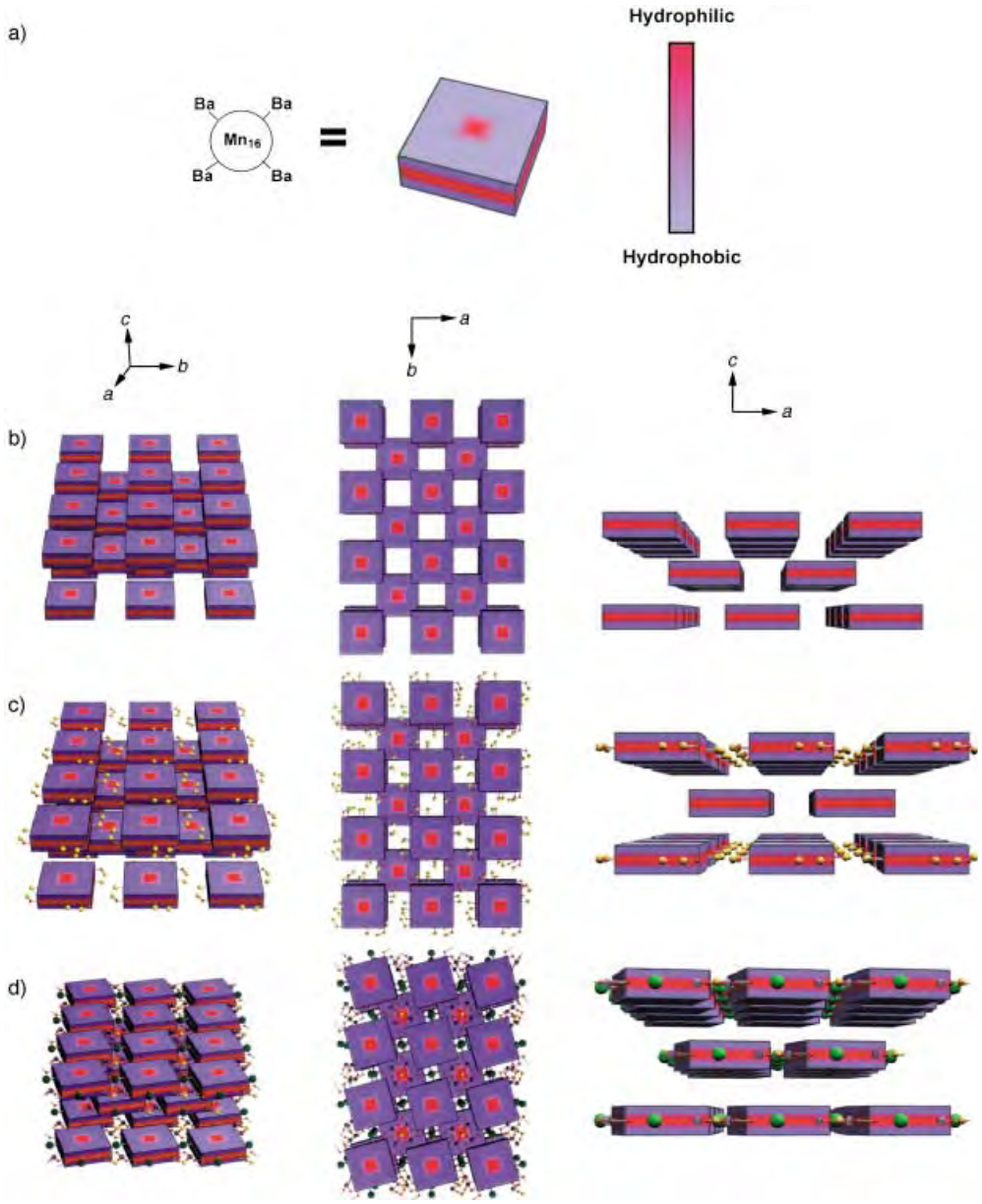


Figure 4. Comparative packing diagrams of P1, P2, and P3 phases. Peripheral Ba^{2+} and Na^{+} ions are shown as spheres, colored as in Figure 1. a) Representation of P1 as a block with 4/*m* symmetry, and hydrophobic (ligand L backbone) and hydrophilic (H_2O and carbonyl oxygen atoms) regions. b) The P1 phase. c) The P2 phase. P1 layers alternate with Unit 2 layers that contain additional Na^{+} ions. d) The P3 phase, including the peripheral Ba^{2+} and Na^{+} ions.

only one compositional degree of freedom (NaCl concentration) is varied, phase P2 is specific to H_2O.

The relationship between the isotope type and NaCl concentration is not entirely clear. However, as shown in Figure 2, the heavy isotopologue appears to compensate to a certain extent for a diminished NaCl concentration. The formation of phase P3 at higher NaCl concentrations in H_2O, and of phase P1 at lower NaCl concentrations in D_2O, is consistent with this notion. This effect could be due to differences in solvation numbers and osmotic and activity coefficients observed for NaCl solutions in D_2O and H_2O.[9] The composition (NaCl concentration)–isotopologue equivalency, however, cannot explain the formation of P2 only in H_2O, or the differences in crystallization times. Other factors, such as hydrogen bonding and the more organized "structure" of liquid D_2O[10] may also play a role.

Differences in hydrogen bonding is an interesting possibility considering that formation of a solid-state phase in only one type of water is known for ice, namely the high-pressure ice IV phase being identified only for D_2O.[5] Hydrogen bonding, if important in this case, is expected to manifest itself ultimately in the structure of the ordered water molecules within the Mn_{16} crystalline lattices. However, the degree of association (or even existence) of the Mn_{16} phases in solution is not known, while a variable degree of disordered water molecules are present in the solid-state within the same, well-

 © 2003 Wiley-VCH Verlag GmbH & Co. KGaA, Weinheim

defined molecular architectures. Alternatively, hydrophobic effects, attributed to the organic ligand backbone, may play a role. Thus, it is known that the self-association of both α-chymotrypsin[11] and some antibodies[12] is enhanced as the solution ionic strength is increased by the addition of NaCl. This enhancement, which is not due to specific ion interactions, is entropically driven, and was ascribed to hydrophobic effects.[12] Similar to the case of the Mn_{16} aggregates, a change from H_2O to D_2O has the same effect as an increase in NaCl concentration, namely a higher degree of self-association, an observation consistent with the notion that hydrophobic effects are stronger in D_2O.[13] Whether the hydrophobic effect is the common denominator for the above biological effect and the parallel relationship between deuterium content and ionic strength we observe for inorganic associations, remains to be determined. If the answer is affirmative, then the hydrophobic effect may have synthetic value in the rational design of mixed organic–inorganic aggregates.

In summary, isotope-induced structural effects manifest themselves primarily in the assembly of two supramolecular architectures through the incorporation, or lack of incorporation, of additional ions, an effect that is mimicked by increases, or decreases in ionic concentrations, respectively. A third, structurally intermediate solid-state material forms in H_2O, but not in D_2O. The topologies and nuclearities of polynuclear metal oxo/hydroxo aggregates, that can seldom be predicted, let alone controlled, might be tuned, perhaps even in a rational way, with the help of isotope effects. Unique, isotopologue-specific aggregates may also be obtained.

Experimental Section

The synthesis of Mn_{16} clusters was performed as previously reported,[3] in both H_2O and D_2O, except that amounts of NaCl, ranging from 0.300 g to 5.00 g, were dissolved in each solution. Crystalline materials were dried briefly and subjected to multiple, standard iodometric titrations for the determination of average Mn oxidation states. The results are reported with standard errors that incorporate a possible 10% uncertainty in the amount of water of hydration. Single-crystal X-ray studies were performed at low temperature by using standard procedures. The number of disordered water molecules was estimated from the total electron density present in the structural voids. Magnetic susceptibility measurements of microcrystalline samples were performed in a constant field of 10000 G using a Quantum Design SQUID MPMS 5L magnetometer. The samples were briefly dried in air, sealed in plastic containers and inserted into the SQUID magnetometer, which was prestabilized at 5 K. Several data sets, which were collected between 5 and 300 K in both temperature ascending and descending modes, gave identical results. No difference was observed even after storing the sealed samples for 4 h at room temperature. Diamagnetic corrections were calculated using Pascal's constants.

For the complete crystallographic data for P2, see the Supporting Information. CCDC-199051 (P1), CCDC-192461 (P2), and CCDC-199050 (P3) contain the supplementary crystallographic data for this paper. These data can be obtained free of charge via www.ccdc.cam.ac.uk/conts/retrieving.html (or from the Cambridge Crystallographic Data Centre, 12, Union Road, Cambridge CB21EZ, UK; fax: (+44) 1223-336-033; or deposit@ccdc.cam.ac.uk).

Received: September 19, 2002
Revised: January 27, 2003 [Z50200]

Keywords: aggregation · isotope effects · manganese · supramolecular chemistry

[1] J. A. K. Harmony, R. H. Himes, R. L. Schowen, *Biochemistry* **1975**, *14*, 5379.
[2] R. Radfar, A. Leaphart, J. M. Brewer, W. Minor, J. D. Odom, R. B. Dunlap, C. R. Lovell, L. Lebioda, *Biochemistry* **2000**, *39*, 14481.
[3] J. Lee, N. D. Chasteen, G. Zhao, G. C. Papaefthymiou, S. M. Gorun, *J. Am. Chem. Soc.* **2002**, *124*, 3042.
[4] The Mn oxidation states are better determined by X-ray absorption spectroscopy. See: M. M. Grush, J. Chan, T. L. Stemmler, S. J. George, C. Y. Ralston, R. T. Stibrany, A. Gelasco, G. Christou, S. M. Gorun, J. E. Penner-Hahn, S. P. Cramer, *J. Am. Chem. Soc.* **1996**, *118*, 65. Such measurements are planned in collaboration with Dr. Serena DeBeer George.
[5] "The Hydrogen Bond in Ice": E. Whalley in *The Hydrogen Bond* (Eds.: P. Schuster, G. Zundel, C. Sandorfy) North-Holland, Amsterdam, **1976**.
[6] a) X-ray data for P3 from H_2O. The unit cell parameters of P3 from H_2O are similar.[3] Tetragonal, *I*4/*m*. Unit cell dimensions at $T = 173(2)$ K: $a = 20.9287(10)$, $c = 26.788(3)$ Å; $V = 11733.4(15)$ Å^3; $Z = 2$. Data/restraints/parameters: 6854/0/344. R indices, $[I > 2\sigma(I)]$: $R1 = 0.0450$, $wR2 = 0.0981$; b) X-ray data for P1 from D_2O. The unit cell parameters of P1 from H_2O are similar.[3] Tetragonal, *I*4/*m*. Unit cell dimensions at $T = 173(2)$ K: $a = 25.296(4)$, $c = 20.565(4)$ Å; $V = 13159(4)$ Å^3; $Z = 2$. Data/restraints/parameters: 6008/0/293. R indices, $[I > 2\sigma(I)]$: $R1 = 0.0725$, $wR2 = 0.1629$.
[7] X-ray data for P2. Tetragonal, *P*4/*m*. Unit cell dimensions at $T = 173(2)$ K: $a = 23.583(2)$, $c = 22.539(3)$ Å; $V = 12535(2)$ Å^3; $Z = 8$. Data/restraints/parameters: 11356/0/788. R indices, $[I > 2\sigma(I)]$: $R1 = 0.0532$, $wR2 = 0.1449$.
[8] a) R. T. Stibrany, S. M. Gorun, *Angew. Chem.* **1990**, *102*, 1195; *Angew. Chem. Int. Ed. Engl.* **1990**, *29*, 1156; b) S. M. Gorun, R. T. Stibrany, A. Lillo, *Inorg. Chem.* **1998**, *37*, 836.
[9] a) O. D. Bonner, G. B. Woolsey, *J. Phys. Chem.* **1968**, *72*, 899; b) O. D. Bonner, *J. Am. Chem. Soc.* **1970**, *92*, 4197.
[10] P. Mukerjee, P. Kapauan, H. G. Meyer, *J. Phys. Chem.* **1966**, *70*, 783.
[11] K. C. Aune, L. C. Goldsmith, S. N. Timasheff, *Biochemistry* **1971**, *10*, 1617.
[12] J. M. R. Moore, T. W. Patapoff, M. E. M. Cromwell, *Biochemistry* **1999**, *38*, 13960.
[13] G. C. Kresheck, H. Schneider, H. A. Scheraga, *J. Phys. Chem.* **1965**, *69*, 3132.

 © 2003 Wiley-VCH Verlag GmbH & Co. KGaA, Weinheim

Polymeric Hollow Spheres

pH-Dependent Self-Assembly: Micellization and Micelle–Hollow-Sphere Transition of Cellulose-Based Copolymers**

Hongjing Dou, Ming Jiang, Huisheng Peng, Daoyong Chen, and Yan Hong*

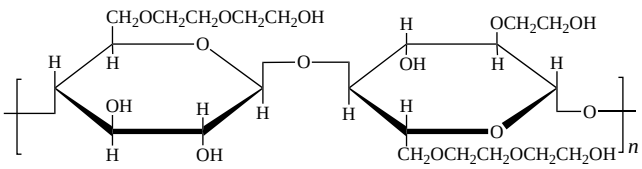
pH-Sensitive micelles are usually made from double-hydrophilic block copolymers which can dissolve molecularly in water in a certain pH range and aggregate spontaneously upon an appropriate change in the pH value. Significant advances in this field have been achieved in recent years.[1]

Polymeric hollow spheres have great potential for the encapsulation of large quantities of guest molecules. Different approaches, such as by the use of block copolymers as precursors,[2] as well as colloidal particles[3a,b] or liposomes[3c,d] as templates, have been developed to obtain such nanocapsules. Our research group has produced micelles in which no chemical bonds connect the core and the shell,[4] thus enabling hollow spheres to be obtained by simple dissolution of the inner component of the micelles.[4a–c] However, these approaches are mostly irreversible, that is, once the hollow structure forms, the core–shell micelles cannot be reformed.

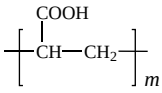
Hydroxyethylcellulose (HEC) has been extensively studied as a nonionic and water-soluble cellulose ether (Scheme 1).[5] However, studies on the self-assembly of HEC are limited, despite its biocompatibility and biodegradability. Here we report the self-assembly of HEC-*graft*-poly(acrylic acid) (HEC-*g*-PAA) in water, which was prepared by free-radical graft polymerization of acrylic acid from HEC backbones (Table 1). The results demonstrate its micellization and the transition between micelles and hollow spheres; both processes were found to be pH-dependent and reversible.

Figure 1 shows the relative scattering intensity I/I_0 of the solutions of two HEC-*g*-PAA copolymers, CAA-1 and CAA-2, as a function of the pH value (I_0 is the intensity of the starting solution at pH 13.5). The two solutions exhibit a similar behavior, namely, I/I_0 shows almost no change as the pH value decreases from about 13.5 to 4. However, as the pH value decreases further, the value of I/I_0 abruptly increases by about a factor of 50 over a small pH range (from pH 3 to 1.8), which indicates the formation of aggregates with high molar mass. Figure 1b shows the variation of the average hydrodynamic diameter $\langle D_h \rangle$ of the copolymers as the pH value decreases. The diameter of about 50–70 nm does not change between pH 13.5 and 4.[6] As the

HEC backbone



PAA graft



Scheme 1. Chemical structures of HEC and PAA.

Table 1: Characteristic data of HEC-*g*-PAA copolymers.

Sample no.	AA:AGU[a] (molar radio)	$M\eta \times 10^{-5}$ (HEC backbone)	$M\eta \times 10^{-5}$ [b] (PAA grafts)	Average graft point	$Mw \times 10^{-5}$ [c] (HEC-*g*-PAA)	$\langle D_h \rangle$ [nm] [d]
CAA-1	1.28:1	0.9	0.175	1.58	1.67	53.8
CAA-2	2.54:1	0.9	0.210	2.61	3.33	75.6

[a] The molar ratio of acrylic acid units to anhydroglucose units (AGU) was determined by enzymatic degradation. [b] Calculated from viscosity measurements. [c] Determined by SLS in 0.1 M NaOH, the *M*w data were obtained using standard Zimm plot analysis. [d] Determined by DLS at the same condition as for SLS.

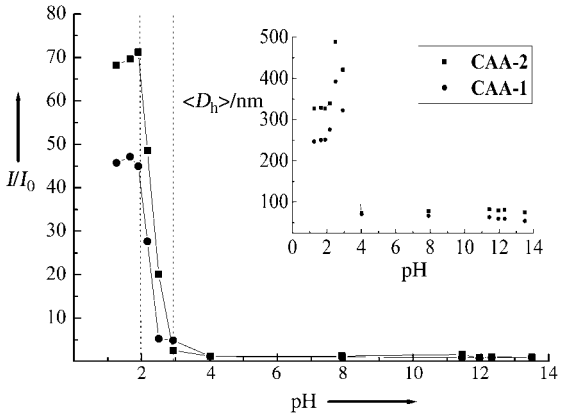


Figure 1. $\langle I/I_0 \rangle$ and $\langle D_h \rangle$ of HEC-*g*-PAA copolymers as a function of pH. The concentration was 1 mg mL^{-1}. I and I_0 are the scattering intensity at various pH values and at pH 13.5, respectively. The solution at pH 2–3 was unstable: the apparent $\langle D_h \rangle$ value increased with time. The $\langle D_h \rangle$ values measured 20 min after the solution preparation were used. However, the $\langle D_h \rangle$ values at pH < 2 and pH > 3 ranges did not change for several months.

[*] Prof. M. Jiang, H. Dou, H. Peng, Prof. D. Chen, Y. Hong
Department of Macromolecular Science and
the Key Laboratory of Molecular Engineering of Polymers
Fudan University
Shanghai, 200433 (China)
Fax: (+86) 21-6564-0293
E-mail: mjiang@fudan.edu.cn

[**] The National Natural Science Foundation of China (NNSFC, Project Nos. 29992590 and 50173006) is acknowledged for supporting this research. Part of the light-scattering studies was performed in Prof. Chi Wu's laboratory, Department of Chemical Physics, University of Science and Technology of China.

 © 2003 Wiley-VCH Verlag GmbH & Co. KGaA, Weinheim DOI: 10.1002/anie.200250254

pH value decreases to less than 4, the value of $\langle D_h \rangle$ jumps to 250 and 330 nm for CAA-1 and CAA-2, respectively. This abrupt increase in the $\langle D_h \rangle$ value between pH 2 and 4 reflects the transition from individual molecules to aggregates. In addition, the transition was found to be reversible: the aggregates dissociated into individual molecules when the pH value of the solution was increased to about 4.

It is well known that polyacrylic acid chains undergo dramatic conformational changes, from an extended chain to a hypercoil, as the pH value decreases.[8,9a] Such a change occurs gradually over a large pH range. We also found that the viscosity of the PAA solutions continuously diminishes as the pH value decreases. However, as shown in Figure 1, the jump in the relative scattering intensity and the $\langle D_h \rangle$ value takes place over a narrow pH range. Therefore, it cannot be attributed to the conformational variation of the PAA chains.

Polyacrylic acid can be considered as a proton-donating polymer, and thus could form complexes with many proton-accepting polymers.[9b] Recently, Nikolaeva et al. reported the interpolymer complexation between HEC and PAA in water resulting from the formation of hydrogen bonds when the PAA chains are sufficiently protonated.[10] Therefore, the aggregation of CAA in the low pH region can be attributed, in our opinion, to interpolymer complexation between HEC and PAA. As no macroscopic precipitation took place in this process, we suggest that the HEC chains which have less complexed segments may still remain solvated and thus stabilize the complex aggregates.

Figure 2a shows the morphologies of CAA-1 micelles in an acidic medium. All the micelles have a perfect spherical shape with a distinct boundary between the core and the shell. The micrograph of CAA-1 at a high magnification clearly shows the details of the micellar structure (Figure 2b). The difference in rigidity between the HEC and PAA chains means that the core composed of the complex shows a much higher packing density than the shell composed mainly of semi-rigid HEC. Such a clear core–shell structure of the micelles is seldom seen in micelles composed of either coil–coil block copolymers[1d–f] or homopolymer pairs.[4a,b] The CAA-2 micelles show a much larger proportion of the core and a less distinct core–shell boundary than CAA-1; this effect is a consequence of it containing a higher percentage of PAA (Figure 2c).

The PAA chains of the micelles were cross-linked simply by treating them with a desired amount of a cross-linker, 2,2′-(ethylenedioxy)bis(ethylamine), at room temperature[11] (see Experimental Section). Dialysis against water was then performed to remove all the impurities, which was accompanied by an increase in the pH value to 7. The bluish tinge characteristic of nanosized micelles was maintained in the resulting neutral medium, thus indicating that the cross-linking has successfully locked the integral structure.

Dynamic light scattering (DLS) studies showed the micelles had expanded after the cross-linking and dialysis. The size of the expansion depends on the composition of the parent copolymers and degree of cross-linking (Table 2). The most remarkable feature of the cross-linked micelles after dialysis, as found by TEM, is that the core–shell structure of the micelles is transformed into hollow spheres. A typical microimage of such hollow spheres of CAA-2 (Figure 2d) displays a clear contrast between the center and the shell that indicates the presence of a cavity. It is noteworthy that this cavitation was caused by neither degradation[2,4d] nor dissolution of the core;[4a–c] a change in the pH value is exclusively responsible for the transition in morphology. DLS and static light scattering (SLS) measurements were made to estimate the parameter $\langle R_g \rangle / \langle R_h \rangle$, which is sensitive to particle morphologies, and so confirm the presence of a hollow structure. Both CAA-1 and CAA-2 have $\langle R_g \rangle / \langle R_h \rangle$ values in the range from 0.83 to 0.89 (Table 2), which are in accordance

Table 2: Light-scattering characterization data of the cross-linked CAA-1 and CAA-2 after dialysis against water.[a]

Sample no.	Cross-linker [%][b]	$\langle R_h \rangle$ [nm]	$\langle R_g \rangle$ [nm]	$\langle R_g \rangle / \langle R_h \rangle$	PDI
CAA-1	50	182	162	0.89	0.21
CAA-1	100	169	140	0.83	0.14
CAA-2	50	386	339	0.88	0.08
CAA-2	100	322	270	0.85	0.08

[a] The concentration of the measured solution here was very low (0.9×10^{-2} mg mL^{-1}) as required for the SLS apparatus. The original solution of $c = 0.9$ mg mL^{-1} was used for other DLS measurements and TEM observations. [b] This refers to the molar ratio of amine groups in the cross-linker to carboxylic acid groups of the PAA grafts. It reflects only the maximum possible degree of cross-linking.

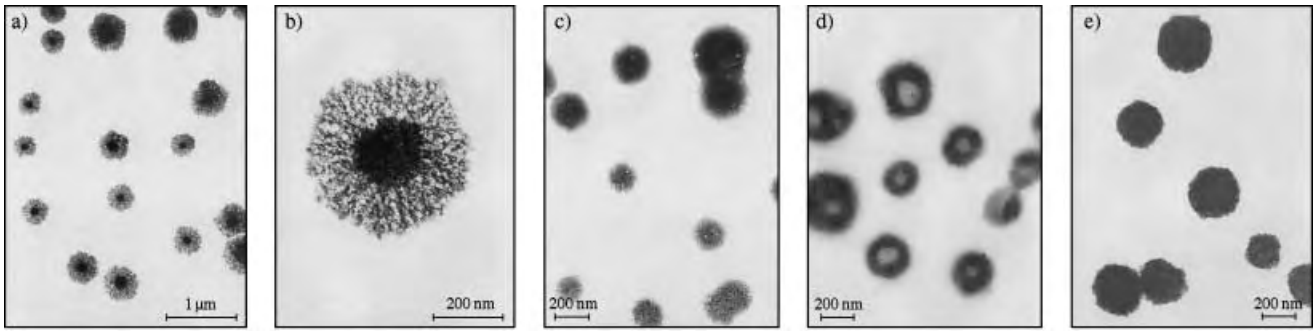


Figure 2. TEM image for a) the micelles of CAA-1 formed at pH 1.3 and b) that at a high magnification; c) the micelles of CAA-2 formed at pH 1.3; d) the hollow spheres of CAA-2 after cross-linking and dialysis, and e) the micelles of CAA-2 obtained by adjusting the acidity of the cross-linked and dialyzed CAA-2 solution to pH 1.3.

 © 2003 Wiley-VCH Verlag GmbH & Co. KGaA, Weinheim

with the values derived from a model consisting of thick-layer hollow spheres.[12]

This transition between the micelle and hollow sphere can be rationalized as follows. Under the given conditions of cross-linking, the reaction proceeds mainly at the periphery of the micellar core. An increase in the pH value partially deprotonates the carboxylic acid in the PAA, which leads to de-complexation between the PAA and HEC, and hence a disintegration of the center part of the core.[14] As both the HEC and cross-linked PAA chains are highly hydrophilic, the cross-linked shell swells and forms hollow spheres. This swollen nanocage is expected to be very soft. Therefore, deformation and collapse of the network during the preparation of the TEM sample, led to a much smaller size (Figure 2d) than measured by DLS studies.

The pH-dependent cavitation of the micelles was also found to be reversible. Figure 3 shows the variation in the

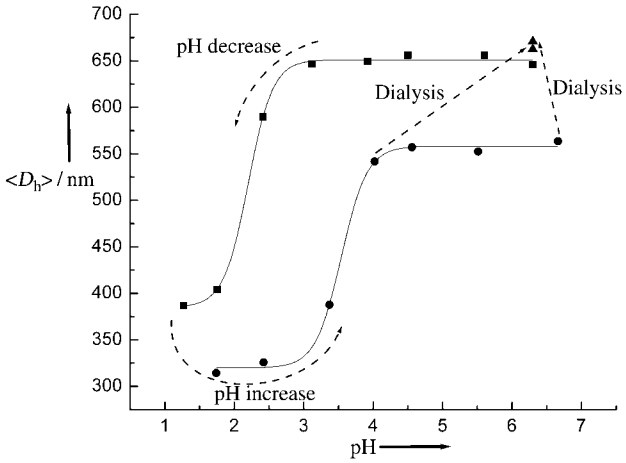


Figure 3. Average hydrodynamic diameter $\langle D_h \rangle$ of CAA-2 aggregates as a function of pH during the transition from micelle to hollow sphere (one reversible cycle). The concentration was 0.9 mg mL^{-1}.

$\langle D_h \rangle$ value of CAA-2 during pH cycling. The starting point corresponds to the cross-linked micelles in neutral solution. The $\langle D_h \rangle$ value does not change until the pH decreases to around 3. A sudden decrease in the $\langle D_h \rangle$ value occurs between pH 3 and 1.5, which is the same range where complexation and micellization occurs. Therefore, it is clear that complexation between the HEC and PAA is resumed as the pH value decreases to this range and, consequently, the hollow spheres revert to core–shell micelles. As shown in Figure 2e for the micelles at pH 1.3, the cavity has disappeared and the morphology clearly resembles the original micelles prior to cross-linking (Figure 2c).

The second half of the $\langle D_h \rangle$ versus pH cycle in Figure 3 shows the reverse process, that is, the micelles revert to hollow spheres as indicated by a jump in the size at a higher pH range (pH 3–4). The $\langle D_h \rangle$ value of 550 nm at the plateau of the second half is somewhat smaller than its value in the first half, 644 nm. This discrepancy could be caused by a difference in the ionic strength between the solutions. This argument is confirmed by the following fact: The micelle solutions at pH 4.0 and pH 6.7 in the second half of the cycle were dialyzed against water. After dialysis, the $\langle D_h \rangle$ values in both cases jumped to approximately 650 nm, a value very close to the plateau value of $\langle D_h \rangle$ in the first half of the cycle (Figure 3).

Our findings can be summarized as follows (Figure 4): The PAA chains are sufficiently protonated at pH 3 to be able to form a complex with HEC and form small aggregates which are stablized by the free HEC; thus micellization takes place. Cross-linking of the PAA chains in the micelles can efficiently lock the integrality of the micelles. Decomplexation occurs in neutral medium, which causes disintegration of the micellar core; thus pH-induced cavitation takes place. This morphological transition from core–shell micelles to hollow spheres was found to be reversible by DLS studies and TEM. The resultant spheres are characterized by large hydrophilic cavities and have an on-off character: open at pH > 3 but closed at pH < 3. Such a unique micelle is expected to be useful in broad application fields.

Experimental Section

HEC-*g*-PAA was synthesized by cerium(IV)-initiated free-radical graft polymerization of acrylic acid from HEC.[15] The HEC backbones were degraded in the presence of cellulase for 3 days to enable characterization of the grafts.[16] The molecular weight of the PAA grafts was calculated from viscosity measurements: $[\eta] = 42.2 \times 10^{-3}\,M^{0.64}$ (in 2 M NaOH at 25 °C).[17]

Micellization: A 5 mg mL^{-1} stock solution of HEC-*g*-PAA in 0.1 M NaOH was further diluted to 1 mg mL^{-1} and the required pH value. The core cross-linking reaction of the micelles prepared at pH 1.26 was performed by adding the desired amount of 2,2′-(ethylenedioxy)-bis(ethylamine) as cross-linker in the presence of 1-(3-dimethylaminopropyl)-3-ethylcarbodiimide methiodide at room temperature for 10 h.[11] The cross-linked product was dialyzed against distilled water for 3 days to remove the by-products.

Malvern Autosizer 4700 and ALV/SP-125 laser light scattering (LLS) spectrometers were used. DLS measurements were performed at a fixed scattering angle (θ) of 15°. Static LLS studies were

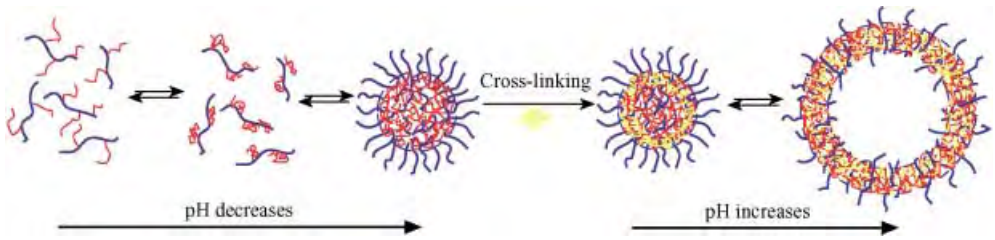


Figure 4. A proposed scheme of the pH-dependent micellization and transition of HEC-*g*-PAA from micelle to hollow sphere.

 © 2003 Wiley-VCH Verlag GmbH & Co. KGaA, Weinheim

conducted at a low scattering angle range of 15 to 40°. The $\langle D_h \rangle$ and polydispersity index (PDI, that is, $(\langle \mu_2 \rangle / \Gamma^2)$ were obtained by a cumulant analysis. The respective d*n*/d*c* data of CAA-1 and CAA-2 were determined to be 0.124 and 0.150 in 0.1 M NaOH aqueous solution by using an Optilab DSP differential refractometer. TEM observations were performed on a Philips CM 120 electron microscope at an acceleration voltage of 80 KV. For all TEM observations, carbon-coated copper grids were dipped in the solutions of micelles followed by drying in a desiccator for at least 72 h.

Received: September 27, 2002
Revised: January 7, 2003 [Z50254]

Keywords: cellulose · micelles · pH dependence · polymerization · self-assembly

[1] a) T. J. Martin, K. Prochakza, P. Munk, S. E. Webber, *Macromolecules* **1996**, *29*, 6071; b) J.-F. Gohy, S. K. Varshney, S. Antoun, R. Jérôme, *Macromolecules* **2000**, *33*, 9298; c) J.-F. Gohy, S. K. Varshney, R. Jérôme, *Macromolecules* **2001**, *34*, 3361; d) J.-F. Gohy, S. Greutz, M. Garcia, B. Mahltig, M. Stamm, R. Jérôme, *Macromolecules* **2000**, *33*, 6378; e) J.-F. Gohy, S. K. Varshney, R. Jérôme, *Macromolecules* **2001**, *34*, 7435; f) S. Y. Liu, S. P. Armes, *Angew. Chem.* **2002**, *114*, 1471; *Angew. Chem. Int. Ed.* **2002**, *41*, 1413; g) V. Bütün, A. B. Lowe, N. C. Billingham, S. P. Armes, *J. Am. Chem. Soc.* **1999**, *121*, 4288; h) A. S. Lee, A. P. Gast, V. Bütün, S. P. Armes, *Macromolecules* **1999**, *32*, 4302.

[2] a) H. Huang, E. E. Remsen, T. Kowalewski, K. L. Wooley, *J. Am. Chem. Soc.* **1999**, *121*, 3805; b) S. Stewart, G. J. Liu, *Chem. Mater.* **1999**, *11*, 1048; c) T. Sanji, Y. Nakatsuka, S. Ohnishi, H. Sakurai, *Macromolecules* **2000**, *33*, 8524.

[3] a) E. Donath, G. B. Sukhorukov, F. Caruso, S. A. Davis, H. Möhwald, *Angew. Chem.* **1998**, *110*, 2323; *Angew. Chem. Int. Ed.* **1998**, *37*, 2202; b) G. Ibarz, L. Dähne, E. Donath, H. Möhwald, *Adv. Mater.* **2001**, *13*, 1324; c) M. Sauer, W. Meier, *Chem. Commun.* **2001**, 55; d) M. Sauer, D. Streich, W. Meier, *Adv. Mater.* **2001**, *13*, 1649.

[4] a) M. Wang, G. Z. Zhang, D. Y. Chen, M. Jiang, S. Y. Liu, *Macromolecules* **2001**, *34*, 7172; b) M. Wang, M. Jiang, F. L. Ning, D. Y. Chen, S. Y. Liu, H. W. Duan, *Macromolecules* **2002**, *35*, 5980; c) X. F. Yuan, M. Jiang, H. Y. Zhao, M. Wang, Y. Zhao, C. Wu, *Langmuir* **2001**, *20*, 6122; d) X. Y. Liu, M. Jiang, S. L. Yang, M. Q. Chen, D. Y. Chen, C. Yang, K. Wu, *Angew. Chem.* **2002**, *114*, 3074; *Angew. Chem. Int. Ed.* **2002**, *41*, 2950; e) H. W. Duan, D. Y. Chen, M. Jiang, W. J. Gan, S. J. Li, M. Wang, J. Gong, *J. Am. Chem. Soc.* **2001**, *123*, 12097.

[5] a) I. S. Chronakis, M. Egermayer, L. Piculell, *Macromolecules* **2002**, *35*, 4113; b) L. M. Zhang, L. Q. Chen, *J. Appl. Polym. Sci.* **2002**, *83*, 2755; c) P. E. Luner, E. Oh, *Colloids Surf. A* **2001**, *181*, 31.

[6] The $\langle D_h \rangle$ values of the copolymers at pH > 4 are clearly larger than those of ordinary flexible chains with similar molecular weights but comparable to the values reported previously for single molecule of cellulose ether in aqueous solution, see reference [7].

[7] a) J. Gao, G. Haidar, X. H. Lu, Z. B. Hu, *Macromolecules* **2001**, *34*, 2242; b) B. Porsch, S. Nilsson, L.-O. Sundelöf, *Macromolecules* **1997**, *30*, 4626.

[8] a) A. F. Olea, J. K. Thomas, *Macromolecules* **1989**, *22*, 1165; b) T. S. Chen, T. K. Thomas, *J. Polym. Sci. Polym. Chem. Ed.* **1979**, *17*, 1103.

[9] a) J. Chen, M. Jiang, *Macromolecules* **1999**, *32*, 4861; b) M. Jiang, M. Li, M. L. Xiang, H. Zhou, *Adv. Polym. Sci.* **1999**, *146*, 121.

[10] a) O. Nikolaeva, T. Budtova, V. Alexeev, S. Frenkel, *J. Polym. Sci. Part B Polym. Phys.* **2000**, *38*, 1323; b) O. Nikolaeva, T. Budtova, N. Bobrova, S. Bronnikov, *J. Macromol. Sci. Phys.* **2001**, *B40*, 539.

[11] Q. Zhang, E. E. Remsen, K. L. Wooley, *J. Am. Chem. Soc.* **2000**, *122*, 3642.

[12] The $\langle R_g \rangle / \langle R_h \rangle$ values for polymer coils, uniform spheres, and thin-layer hollow spheres are 1.50, 0.77, and 1.0, respectively, see reference [13]. For a hollow sphere with an outer radius *R* and wall thickness *R*/3, the $\langle R_g \rangle / R$ value is 0.86 according to a simple calculation. The $\langle R_g \rangle / \langle R_h \rangle$ values of CAA-1 and CAA-2 molecules in water at pH 13.5 are 1.48 and 1.58, respectively. The $\langle R_g \rangle / \langle R_h \rangle$ results support the hollow-sphere structure of CAA-2 shown in Figure 2d. However, as a major change in the particles may take place during the TEM sample preparation, for example, drying and subsequent shrinking of the swollen micelles, the image in Figure 2d can not be attributed to the hollow spheres exclusively.

[13] a) C. Wu, S. Q. Zhou, *Phys. Rev. Lett.* **1996**, *77*, 3053; b) W. Burchard, *Adv. Polym. Sci.* **1983**, *48*, 1.

[14] Prolonging the cross-linking time to 24 h and increasing the amount of cross-linker to 200% led to different results, namely, homogeneous microspheres without a central cavity were observed by TEM. The $\langle R_g \rangle / \langle R_h \rangle$ values of the heavily cross-linked CAA-1 and CAA-2 particles after dialysis are 0.74 and 0.76, respectively. In our opinion, strengthening the cross-linking reaction enabled the reaction to occur in the center as well as the periphery of the core. Thus, swollen microgel instead of hollow spheres was obtained when the pH value of the solutions increases.

[15] a) W. M. Doane, *Polym. Prepr. Am. Chem. Soc. Div. Polym. Chem.* **1987**, *28*, 103; b) G. Mino, S. Kaizerman, *J. Polym. Sci.* **1958**, *31*, 122; c) V. D. Athawale, V. Lele, *Carbohydr. Polym.* **2000**, *41*, 407.

[16] a) A. Martínez-Richa, *Polymer* **1998**, *39*, 14, 3115; b) X. Ni, Y. Hu, B. Liu, X. Xu, *Eur. Polym. J.* **2001**, *37*, 201; c) *The Chemistry and Technology of Cellulosic Copolymers* (Eds.: A. Hebeish, J. T. Guthrie), Springer, Berlin, **1981**, pp. 251–257.

[17] *Polymer Handbook* (Eds.: J. Brandrup, E. H. Immergut), 3rd ed., Wiley, New York, **1989**, p. VII/8.

 © 2003 Wiley-VCH Verlag GmbH & Co. KGaA, Weinheim

Solvent-Free Route to Adipic Acid

Mechanistic Insights into the Conversion of Cyclohexene to Adipic Acid by H_2O_2 in the Presence of a TAPO-5 Catalyst**

Sang-Ok Lee, Robert Raja, Kenneth D. M. Harris, John Meurig Thomas, Brian F. G. Johnson, and Gopinathan Sankar*

The current, widely used and environmentally harmful industrial method of producing adipic acid (**2**) first entails the oxidation of cyclohexane by nitric acid (with extensive liberation of the greenhouse gas N_2O) to a mixture of cyclohexanol and cyclohexanone.[1,2] This mixture is then rather inefficiently converted to adipic acid (and some other products) by using a homogeneous cobalt-containing catalyst. Research into alternative, more benign methods of producing **2** is therefore called for; and we have previously reported how appropriately designed Co^{III}- or Mn^{III}-containing microporous aluminophosphate catalysts offer a means of yielding **2** in air, in a solvent-free fashion either from cyclohexane[3] or from *n*-hexane.[4] Since cyclohexene (**1**) is nowadays readily produced by catalytic partial hydrogenation of benzene,[5,6] there is interest in using aqueous H_2O_2 as an oxidant[7–10] to produce **2** and **4** with the aid of a suitable catalyst. Sato et al.[11] used a peroxytungstate (Na_2WO_4) in the presence of a phase-transfer catalyst ($CH_3(n\text{-}C_8H_{17})HSO_4$) to convert **1** to **2**; and Deng et al.,[12] employing a similar overall approach, replaced the harmful phase-transfer catalyst with a peroxytungstate–organic complex prepared in situ (such as $[W(O)(O_2)L_2]^{2-}$, where L_2 is an organic acid with multifunctional groups).

[*] Prof. Sir J. M. Thomas, G. Sankar
The Royal Institution of Great Britain
Davy Faraday Research Laboratory
21 Albemarle Street, London W1S 4BS (UK)
and
Department of Materials Science and Metallurgy
New Museums Site
Pembroke Street, Cambridge CB2 3QZ (UK)
Fax: (+44) 1223-334-567
E-mail: jmt@ri.ac.uk
Dr. S.-O. Lee, Dr. R. Raja, Prof. B. F. G. Johnson
Department of Chemistry
University of Cambridge
Lensfield Road, Cambridge CB2 1EW (UK)
Fax: (+44) 1223-336-017
Prof. K. D. M. Harris
School of Chemical Sciences
University of Birmingham
Edgbaston, Birmingham B15 2TT (UK)

[**] We thank the EPSRC (UK) for a rolling grant to Prof. Sir John Meurig Thomas and awards to Professors B.F.G. Johnson and K.D.M. Harris. We also thank Bayer AG, Leverkusen (Germany) for their support to Dr. Robert Raja, the Leverhulme Centre (UK), for supporting Dr. G. Sankar, Dr. M. Sanchez for helpful discussions, and Mr. G. Burns for technical assistance.

We here report another direct, environmentally benign method involving aqueous H_2O_2 and a molecular sieve catalyst based on TAPO-5 (Figure 1; titanium framework-substituted aluminophosphate number 5 in the IZA classification, see Experimental Section), which greatly facilitates

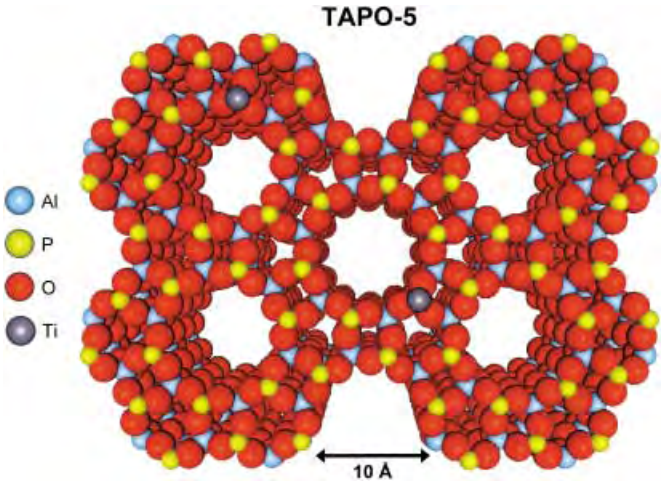


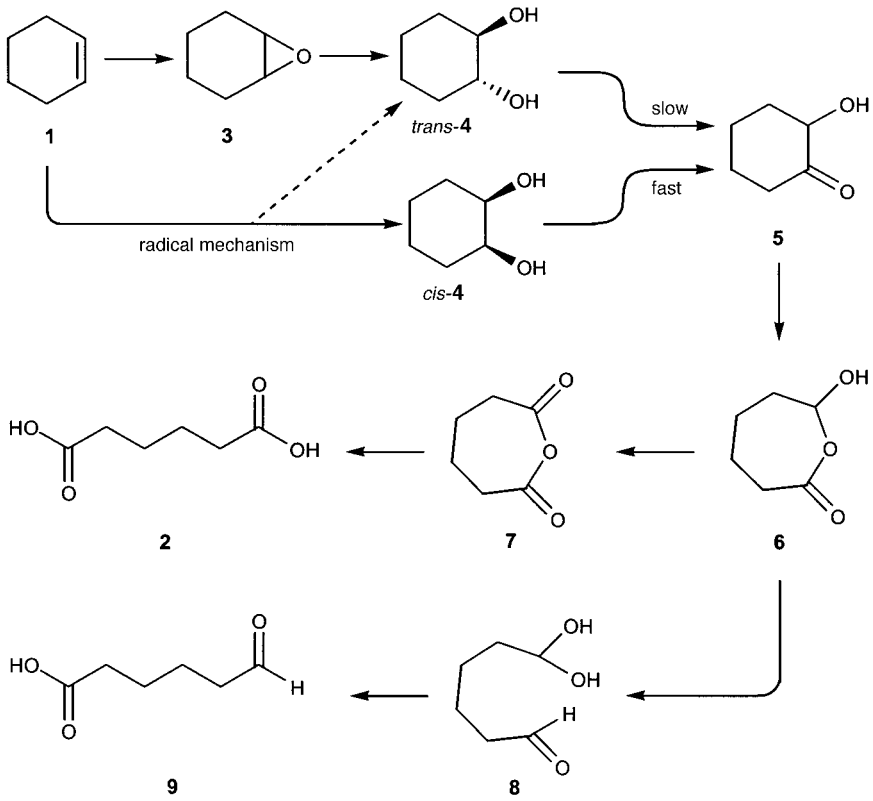
Figure 1. The structure of TAPO-5.

recycling and the separation of products, and which requires no organic solvent.[13] Our TAPO-5 catalyst is bifunctional in that it possesses both Brønsted acidity (signified by its ability to catalyze the dehydration of methanol to dimethyl ether) and the ability to release nascent oxygen from H_2O_2. (Whilst the conversion of cyclohexene to adipic acid by H_2O_2 is a step in the right direction, it does suffer from the disadvantage of requiring four molecules of H_2O_2 per molecule of alkene converted. Ideally, it would be better if O_2 were used, as an oxidant with the right catalyst, and it is our belief that discovering such a catalyst will be facilitated by mechanistic studies of the kind we describe below).

From the results of our parallel ^{13}C and ^{1}H NMR and GC-MS analyses conducted during the course of the catalytic conversion of **1** to **2** in the presence of TAPO-5, and from additional analytical measurements starting with certain intermediates (notably **3** and **4**) we conclude that the mechanistic pathway from **1** to **2** is as shown in Scheme 1. This conclusion is further confirmed by the fact that there is essentially no change in the concentration of the diols and of the other products when the catalyst is filtered off after 24 h. This further proves that there is no significant leaching of the Ti center during catalysis, as otherwise there would be appreciable changes with time in the concentration of the diols and other products as a result of a homogeneously catalyzed reaction made possible by the leached titanium. When, however, the filtered TAPO-5 catalyst is reused, its activity is seen to be significantly diminished. (There could well be ways, which we shall explore, for reactivating the filtered catalyst).

Importantly, we found that the *cis*-diol (*cis*-**4**), but not the *trans*-diol (*trans*-**4**), is formed by a free radical mechanism. The *cis*-diol is also seen to react significantly more readily than its *trans* analogue.

 © 2003 Wiley-VCH Verlag GmbH & Co. KGaA, Weinheim DOI: 10.1002/anie.200250351



Scheme 1. Mechanistic pathway for the oxidation of cyclohexene (**1**) to adipic acid (**2**).

The performance, including turnover numbers (TONs), of TAPO-5 in the conversion of **1** to **2** is shown in Figure 2 and Table 1. Note that the conversion of **1** reaches essentially 100% at 72 h, and that the selectivity towards adipic acid increases steadily throughout the course of reaction, attaining about 30% at 72 h. GC-MS provided unambiguous evidence for the production of relatively small amounts of cyclohexene oxide (**3**), which are detectable at the early stages (ca. 10 min) of the reaction.

Table 1: Conversion and selectivity, determined from GC-MS analysis, for the reaction of cyclohexene and aqueous H_2O_2 in TAPO-5 (see Experimental Section for reaction conditions and Scheme 1 for identity of products).

Time	Conversion	TON	Selectivity [%]							
[h]	[%]		**4**	**5**	**6**	**7**	**8**	**9**	others	**2**
5	6.1	18.9	53.1	21.5	16.4	4.7	0	0	4.3	0
12	17.3	53.6	58.2	15.7	9.4	6.8	2.3	0	5.3	3
24	49.5	153.5	66.4	3.7	2.8	2.9	3.1	1.3	6.7	13.1
48	99.1	307.2	55.2	3.2	3.4	3.5	3.3	2.5	7.8	21.1
72	100	310	30	2.9	3.4	3.2	9.2	7.5	13.5	30.3

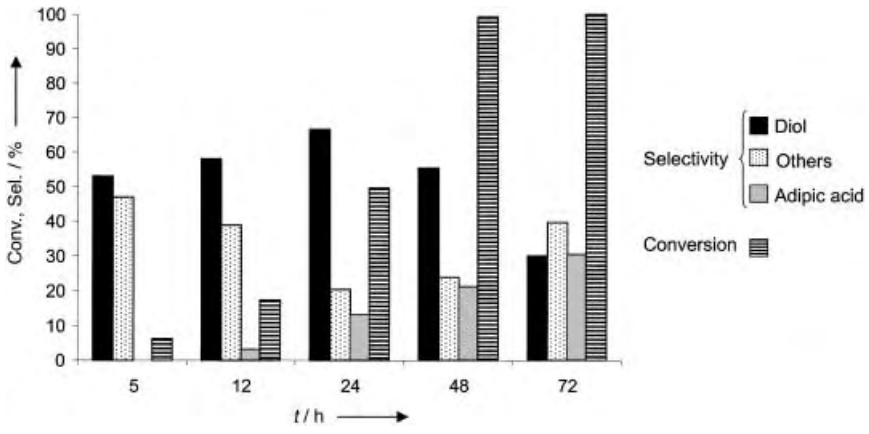


Figure 2. Conversion and selectivity for the reaction of cyclohexene (**1**) and aqueous H_2O_2 in TAPO-5 (see also Table 1).

^{13}C NMR measurements showed that the concentration of **4** reaches a maximum at about 24 h and that the concentrations of **5, 6**, and **7** reach maxima at about 48 h, whereas those of **2, 8**, and **9** continue to increase even at 72 h. A separate experiment (Table 2), discussed below, involving **3** as a starting reagent (in place of **1**), confirmed the rapidity of its catalytic conversion under our (mild) reaction conditions.

1,2-Cyclohexanediol (**4**) has two stereoisomers (*trans* and *cis*), and our recorded ^{13}C NMR spectra yield a ratio of *cis*/*trans* of 0.4 at 5 h, which subsequently decreases to 0.1 (at 12 h), then to 0.05 (48 h), and zero at 72 h. The fact that both stereoisomers are formed prompts two questions: 1) are they each produced by the same mechanism, and 2) what are their relative reactivities insofar as producing **2** is concerned?

The second of these questions is readily answered by using authentic (pure) samples of either the *cis*-diol or the *trans*-diol as starting reagents (Table 3); it is evident that, in each case, reaction proceeds smoothly to **2** by the same sequence (shown in Scheme 1). The faster reaction of the *cis*-diol compared with the *trans*-diol can provide an explanation for the fact that, in the reaction starting from **1**, the relative amount of *cis*-diol is lower throughout the course of reaction. (It is difficult to ascertain whether the *cis*- and *trans*-diols are produced in comparable amounts from **1** given that their subsequent rates of reaction are substantially different). The reasons for the faster reaction of the *cis*-diol are not yet clear. But it could devolve upon the subtleties of conformation. Thus, the *cis*-diol has two energetically equivalent conformations (axial–equatorial and equatorial–axial).

 © 2003 Wiley-VCH Verlag GmbH & Co. KGaA, Weinheim

Table 2: Conversion and selectivity, determined from GC-MS analysis, for the reaction using **3** as the starting reagent (see Experimental Section for reaction conditions and Scheme 1 for identity of products).

Time	Conversion [%]	TON	Selectivity [%]							
			4	**5**	**6**	**7**	**8**	**9**	others	**2**
10 min	99.9	309.7	82.9	5.6	3.7	2.3	0	0	5.5	0
24 h	100	310	36.7	2.9	3.3	3.1	2.3	4.3	7.6	39.8
48 h	100	310	8.2	3.2	3.4	3.4	11.4	13.7	17.9	38.8

Table 3: Conversion and selectivity, determined from GC-MS analysis, for the separate reactions using *trans*-1,2-cyclohexanediol and *cis*-1,2-cyclohexanediol as the starting reagent (see Experimental Section for reaction conditions and Scheme 1 for identity of products).

Reagent	Time [h]	Conversion [%]	TON	Selectivity [%]						
				5	**6**	**7**	**8**	**9**	others	**2**
trans-diol	6	10.2	31.6	9.4	4.7	4.1	2.3	4.1	4.1	71.3
	12	31.2	96.7	3.8	3.2	3.7	5.6	7.9	8.3	67.5
	24	71.5	221.7	3.2	3.4	3.4	8.7	10.3	12.8	58.2
cis-diol	6	30.8	95.5	4.3	3.6	3.2	3.8	6.4	8.7	70
	12	73.2	226.9	3.7	3.3	3.6	6.4	8.3	9.1	65.7
	24	100	310	0	1.8	3.4	11.6	17.1	21.3	44.8

The two conformations of the *trans*-diol (axial–axial and equatorial–equatorial), on the other hand, are of different energy, and for the isolated molecule it is the equatorial–equatorial conformation that is of lower energy. If this conformation of the *trans*-diol also predominates inside the pores of the TAPO-5 catalyst, the faster reaction of the *cis*-diol may be related to the presence of an axial substituent, which is more readily displaced than an equatorial substituent in a reaction that proceeds by nucleophilic substitution.

In answering the first question raised above, we note that in the reaction carried out using the epoxide **3** as a starting reactant only the *trans*-diol is produced. This is indeed the expected product from the acid-catalyzed ring opening of the epoxide by nucleophilic substitution—in this case one of the OH groups of the *trans*-diol would derive from the nucleophile. Clearly, the *cis*-diol must be generated by a different mechanism, one that does not proceed via cyclohexene oxide (**3**). To explore the possibility that this reaction is radical based, we took cyclohexene as the starting reagent but in the presence of a free radical scavenger (hydroquinone).[14,15] In this reaction only the *trans*-diol is formed. The radical scavenger evidently suppresses all production of the *cis*-diol, the production of which from **1** under normal conditions therefore occurs by a free-radical mechanism. With the epoxide **3** as the starting reagent, both in the presence or in the absence of hydroquinone scavenger, the products were the same in each case, showing that the conversion of **3** to the *trans*-diol does not proceed by a radical mechanism.

To assess whether subsequent stages of the overall reaction of cyclohexene (from **4** onwards, Scheme 1) also involve participation of free radicals, separate experiments were carried out using either the *cis*-diol or the *trans*-diol as starting reagents in the presence of the radical scavenger. The fact that reaction proceeds in the same manner as in the absence of the scavenger proves that the formation of **2** from both the *cis* and *trans* diols (**4**) does not involve a radical mechanism.

Finally, a control experiment was carried out in which **1** and aqueous H_2O_2, but with no TAPO-5 catalyst, were allowed to react under conditions identical to those of the catalytic reaction. Very small amounts of the *cis*-diol and *trans*-diol were produced, but no further reaction ensued even after 24 h. The TAPO-5 catalyst is clearly implicated in all the stages shown in Scheme 1.

In summary, we have shown that a TAPO-5 molecular sieve catalyst is effective in the production of adipic acid from cyclohexene in the absence of an organic solvent, and have gained insights into the intermediates and the mechanism of the overall reaction by means of NMR and GC-MS analyses. Although the yield of adipic acid is not as high as in other, recently evolved[3,4,11,12,16] methods of synthesis, we have uncovered mechanistic details not hitherto detected, and, in particular, established the key importance of the stereochemistry of the 1,2-cyclohexanediol in the progress of the reaction. The task now is first, to pursue methods, especially those that promote radical participation, which increase the proportion of the *cis*-diol in the initial stages of the reaction, and, second, to design other transition-metal-ion-substituted aluminophosphate catalysts that will convert cyclohexene (**1**) in air to adipic acid (**2**). There is at least one open-structure catalyst that we have already identified that effects such a conversion at low temperatures, in a solvent-free fashion.

Experimental Section

The reagents for TAPO-5 synthesis were 85% H_3PO_4 (Aldrich), aluminium hydroxide hydrate (Aldrich), titanium(diisopropoxide)-bis(2,4-pentanedionate) (75%, Aldrich), and tetraethylammonium hydroxide (TEAOH 35%, Aldrich). The reactant gel was prepared according to the following procedure. Aluminum hydroxide hydrate and a solution of titanium(diisopropoxide)bis(2,4-pentanedionate) in 2-propanol were added to a solution of phosphoric acid in water, and the mixture was stirred until homogeneous. A solution of TEAOH was then added slowly with vigorous stirring to obtain a gel with empirical composition 1.0 Al:1.48 P:0.02 Ti:0.8 TEAOH:40 H_2O. The gel was sealed in a teflon-lined stainless steel autoclave and heated at 175 °C under autogeneous pressure for 2 h. The solid product was isolated by filtration, washed with deionized water and dried in air (90 °C). The as-prepared product was calcined at 550 °C, first in nitrogen for 1 h and then in dry oxygen for 10 h. The material was characterized by powder X-ray diffraction to confirm the AFI structure. Prior to use in the catalytic reaction, the material was dehydrated at 110 °C under vacuum for 1 h.

The catalytic reactions were carried out in the batch mode using a glass vessel fitted with a condenser circulating chilled water. The vessel was heated in an oil bath to 80 °C. The substrate (cyclohexene, cyclohexene oxide, *cis*-1,2-cyclohexanediol or *trans*-1,2-cyclohexanediol, ca. 0.062 mol), H_2O_2 (30 g, 0.22 mol; 25% in aqueous solution) and catalyst (0.5 g of TAPO-5) were introduced into the glass vessel and the contents were stirred using a magnetic stirrer. Small aliquots of reaction medium (both aqueous and organic) were removed periodically, and subsequently analyzed by gas chromatography

 © 2003 Wiley-VCH Verlag GmbH & Co. KGaA, Weinheim

(Varian model 3400 CX) employing a HP-1 capillary column (25 m × 0.32 mm) and a flame ionization detector. The identity of the products was further confirmed by using GC-MS (VG Prospec mass spectrometer equipped with a Fisons 8000 series gas chromatograph employing a 25 m DB5 capillary column). Solution-state ^{1}H and ^{13}C NMR recorded at 400.14 MHz and 100.61 MHz, respectively, on a Bruker AMX 400 spectrometer.

Received: October 11, 2002
Revised: January 15, 2003 [Z50351]

Keywords: adipic acid · aluminophosphates · green chemistry · heterogeneous catalysis · oxidation

[1] D. D. Davis, D. R. Kemp, Kirk-othmer Encyclopedia of Chemical Technology, *Vol. 1* (Eds.: J. I. Kroschwitz, M. Howe-Grant), 4th ed., Wiley, New York, **1991**, p. 466.
[2] M. T. Musser in *Ullmanns Encyclopedia of Industrial Chemistry, Vol. A8*, VCH, Weinheim, **1985**, p. 217.
[3] M. Dugal, G. Sankar, R. Raja, J. M. Thomas, *Angew. Chem.* **2000**, *112*, 2399; *Angew. Chem. Int. Ed.* **2000**, *39*, 2310.
[4] R. Raja, G. Sankar, J. M. Thomas, *Angew. Chem.* **2000**, *112*, 2403; *Angew. Chem. Int. Ed.* **2000**, *39*, 2313.
[5] H. Nagahara, M. Ono, M. Konishi, Y. Fukuoka, *Appl. Surf. Sci.* **1997**, *121*, 448.
[6] F. Döbert, J. Gaube, *Catal. Lett.* **1995**, *31*, 431.
[7] E. Jorda, A. Tuel, R. Teissier, J. Kervennal, *J. Catal.* **1998**, *175*, 93.
[8] A. Bhaumik, S. Inagaki, *J. Am. Chem. Soc.* **2001**, *123*, 691.
[9] M. Salavati-Niasari, F. Farzaneh, M. Ghandi, *J. Mol. Catal. A* **2002**, *186*, 101.
[10] J. M. Fraile, J. I. Garcia, J. A. Mayoral, E. Vispe, *J. Catal.* **2000**, *189*, 40.
[11] K. Sato, M. Aoki, R. Noyori, *Science* **1998**, *281*, 1646.
[12] Y. Q. Deng, Z. F. Ma, K. Wang, J. Chen, *Green Chem.* **1999**, *1*, 275.
[13] J. M. Thomas, R. Raja, G. Sankar, B. F. G. Johnson, D. W. Lewis, *Chem. Eur. J.* **2001**, *7*, 2973.
[14] R. Raja, G. Sankar, J. M. Thomas, *J. Am. Chem. Soc.* **1999**, *121*, 11926.
[15] J. M. Thomas, R. Raja, G. Sankar, R. G. Bell, *Nature* **1999**, *398*, 227.
[16] J. M. Thomas, R. Raja, G. Sankar, R. G. Bell, *Acc. Chem. Res.* **2001**, *34*, 191.

 © 2003 Wiley-VCH Verlag GmbH & Co. KGaA, Weinheim

Single-Molecule Magnets

A Trigonal-Bipyramidal Cyanide Cluster with Single-Molecule-Magnet Behavior: Synthesis, Structure, and Magnetic Properties of $\{[Mn^{II}(tmphen)_2]_3[Mn^{III}(CN)_6]_2\}$**

*Curtis P. Berlinguette, Derek Vaughn, Cristina Cañada-Vilalta, José Ramón Galán-Mascarós, and Kim R. Dunbar**

Molecules that exhibit magnetic bistability, commonly referred to as single-molecule magnets (SMMs), are of high interest because of their unusual physical properties and potential applications in quantum computing.[1] In contrast to traditional magnets, which are characterized by the bulk ordering of spins within a 3D solid, SMM behavior arises from the intrinsic magnetic properties of the individual molecules. The signature of an SMM is a slow paramagnetic relaxation of the magnetization evidenced by a frequency-dependent out-of-phase (χ_m'') ac susceptibility signal and hysteretic behavior. The presence of an appreciable thermal barrier for reversing the magnetization is related to the combination of a large total spin ground state (S) and negative uniaxial anisotropy (D). The existence of the phenomenon of single-molecule magnetism was first noted a decade ago in the compound $[Mn_{12}O_{12}(O_2CCH_3)_{16}(OH_2)_4]$, which displays a ground state of $S = 10$.[2] Since this discovery, a number of oxo-bridged clusters containing V,[3] Mn,[4–6] Fe,[7] Co,[8] and Ni[9] have also been shown to display SMM behavior. In all cases, the molecules that have longer paramagnetic relaxation times have values of $S > 3$ or higher and a negative D value.

In considering the prospects for preparing non-oxide SMMs, we turned our attention to chemistry inspired by the face-centered Prussian-blue solids. The recognition that bimetallic Prussian-blue solids exhibit spontaneous magnetization at temperatures as high as 376 K[10] prompted an extrapolation of this chemistry to the realm of magnetic

[*] Prof. K. R. Dunbar, C. P. Berlinguette, D. Vaughn
Department of Chemistry, Texas A&M University
PO Box 30012, College Station, TX 77842-3012 (USA)
Fax: (+1) 979-845-7177
E-mail: dunbar@mail.chem.tamu.edu
C. Cañada-Vilalta
Department of Chemistry, Indiana University
Bloomington, IN 47405 (USA)
Dr. J. R. Galán-Mascarós
Instituto de Ciencia Molecular, Universidad de Valencia
Dr. Moliner, 50, 46100 Burjasot (Spain)

[**] The authors thank Prof. Ernest R. Davidson for the program used for the reduced magnetization fitting. K.R.D. gratefully acknowledges the National Science Foundation for a Nanoscale Science and Engineering (NIRT) Grant (DMR-0103455), the Telecommunication&Informatics Task Force (TITF 2001-3), and for equipment grants to purchase the CCD X-ray equipment (CHE-9807975) and the SQUID magnetometer (NSF-9974899).

Supporting information for this article is available on the WWW under http://www.angewandte.org or from the author.

 DOI: 10.1002/anie.200250479 © 2003 Wiley-VCH Verlag GmbH & Co. KGaA, Weinheim

molecules. This goal can be accomplished by introducing capping ligands to circumvent the formation of the face-centered cubic structure. Among the metal cyanide clusters prepared by this general strategy are molecular squares, cubes, and other more complex architectures.[11] Despite the large ground-state spin values detected for several molecules (e.g., $S = 27/2$, 39/2, 51/2),[12] SMM behavior has not been confirmed in any of these cases, a fact that is generally attributed to the lack of sufficient single-ion and/or shape anisotropy. A recent report of a trigonal-prismatic cluster, however, has provided evidence that magnetic bistability can indeed exist in a cyanide-bridged molecule.[13]

One of the goals of our research program in cyanide chemistry is to introduce magnetically anisotropic metal ions into clusters, the symmetry of which allows the existence of an easy axis of magnetization. Herein we describe the first results of these efforts, namely the synthesis, X-ray structure analysis, and magnetic behavior of $\{[Mn^{II}(tmphen)_2]_3[Mn^{III}(CN)_6]_2\}$ (**1**; tmphen = 3,4,7,8-tetramethyl-1,10-phenanthroline) whose unique axis of symmetry is a C_3 axis on which the Mn^{III} ions reside.

Slow diffusion of solutions of $[K([18]crown-6)]_3[Mn(CN)_6]$ and $Mn^{II}(tmphen)_2(NO_3)_2$ in acetonitrile led to the formation of X-ray quality yellow needles of compound **1**.[14] The molecular geometry of **1** is that of a trigonal bipyramid in which low-spin Mn^{III} ($S = 1$) ions occupy the apical positions and high-spin Mn^{II} ($S = 5/2$) ions reside in the equatorial plane (Figure 1).[15] Each Mn^{III} ion is linked by three nearly linear cyanide bridges to Mn^{II} centers and is capped by three terminal cyanide ligands. The Mn^{II} ions are coordinated to *cis*-tmphen ligands as well as to the N ends of two cyanide bridges. The Mn^{II} centers in each molecule have a homochiral coordination geometry, but the crystal is racemic, as evidenced by the fact that the compound crystallizes in a centrosymmetric space group ($P2_1/c$). The presence of the methylated phenanthroline ligands prevents the clusters from packing with close intermolecular metal distances (the closest intermolecular Mn···Mn distance is 8.77 Å).

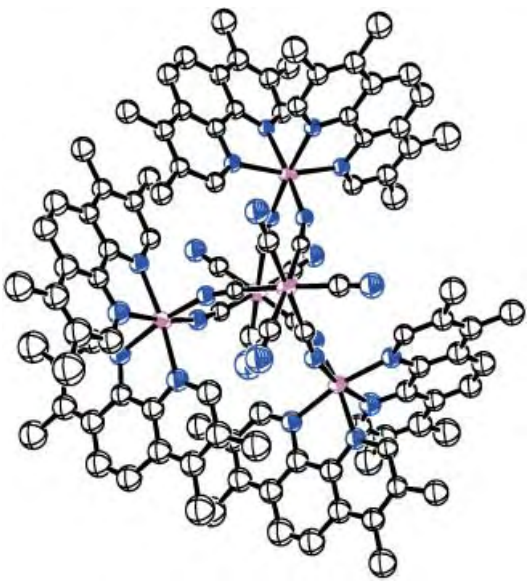


Figure 1. Molecular structure of **1** (thermal ellipsoids set at the 50% probability level, H atoms are omitted for clarity); Mn: purple; N: blue.

Magnetic susceptibility measurements were performed on crushed single crystals of **1** at 1000 G in the temperature range 1.8–300 K (Figure 2). The room temperature $\chi_m T$ value of ~13.70 emu K mol^{-1} is slightly lower than the expected spin-only value of 15.125 emu K mol^{-1}, which can be attributed to a value of $g < 2$. The $\chi_m T$ value decreases as the temperature is lowered to 10.41 emu K mol^{-1} at 45 K, after which point $\chi_m T$ increases to a maximum of 15.69 emu K mol^{-1} at 4.0 K. The magnetic behavior below 45 K is indicative of a strong antiferromagnetic interaction between the paramagnetic centers, which stabilizes a high-spin ground state. The least-squares fit of the reduced magnetization data (Figure 3) indicates an $S = 11/2$ ground state with $g = 1.784(2)$ and $D = -0.348(3)$ cm^{-1}.[16] The calculated D parameter supports the conclusion that compound **1** is an SMM with a thermal barrier for magnetization reversal of $U = (S^2 - 1/4)\,|D| = 10$ cm^{-1}.

One of the characteristics of an SMM is the observation of an out-of-phase (χ_m'') ac susceptibility signal. To probe the dynamics of the magnetization relaxation of compound **1**, ac susceptibility measurements were performed in a 3 G ac field

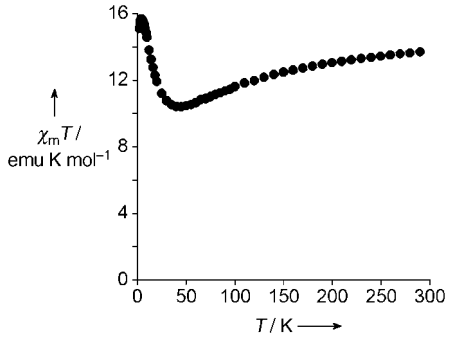


Figure 2. Temperature dependence of $\chi_m T$ versus T for a crushed crystalline sample of **1** in a 1000 G applied DC field.

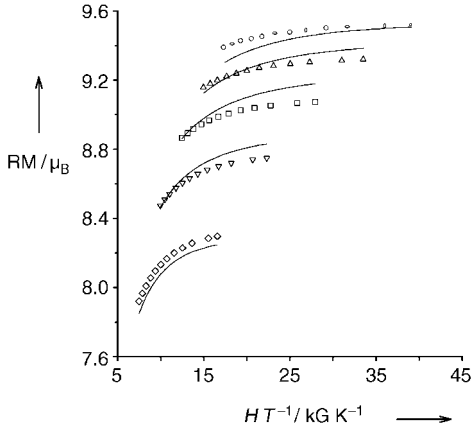


Figure 3. Reduced magnetization (RM) versus the ratio of the external field and temperature (HT^{-1}) for **1**. The solid lines are the best fit of the data to an $S = 11/2$ ground state with $g = 1.784(2)$ and $D = -0.348$ cm^{-1}. Data were measured at 30 (◇), 40 (▽), 50 (□), 60 (△), and 70 kG (○).

 © 2003 Wiley-VCH Verlag GmbH & Co. KGaA, Weinheim

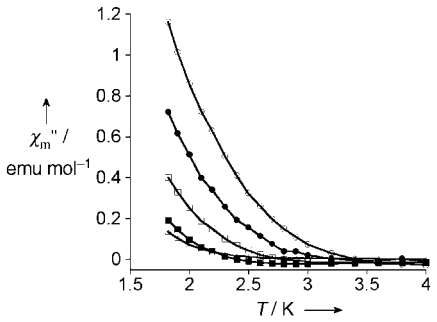


Figure 4. Frequency dependence of the out-of-phase (χ_m'') ac magnetic susceptibility versus T for **1**. Data were measured at 1 (△), 6 (■), 32 (□), 178 (●), and 1000 Hz (○).

oscillating at 1–1500 Hz in the temperature range of 1.8–8.0 K (Figure 4) on the same sample of crystals that was used for the dc studies. The in-phase magnetic susceptibility signal (χ_m') follows the expected behavior for a paramagnetic system. In addition to the χ_m' signal, the compound exhibits an out-of-phase (χ_m'') signal below 4 K (Figure 4). Although no maximum was observed down to 1.8 K, there is an obvious frequency dependence of the χ_m'' signal consistent with SMM behavior. Noteworthy, the magnitude of the χ_m'' signal relative to the χ_m' signal is comparable to that of the Mn_{12} SMM family, a good sign that the χ_m'' response is not an artifact. Lower temperature measurements (<1.8 K) are in progress to confirm whether the frequency dependence is in accord with Arrhenius behavior, and to check for hysteresis.

The title compound is important to the field of SMMs, as it is a rare example of a cyanide-based molecule that exhibits this behavior. The role of the anisotropic Mn^{III} ions in the trigonal-bipyramidal (tbp) molecular geometry appears to be crucial for dictating this magnetic phenomenon. Previous studies have demonstrated that isostructural clusters of the type $\{[Fe(CN)_6]_2[Ni(\widehat{NN})_2]_3\}$ do not exhibit SMM behavior.[15] This observation lends further credence to the idea that incorporating anisotropic ions into these clusters is fundamentally important for observing slow relaxation, and must be considered along with S in the design of new SMMs. Plans are in progress to investigate systematically the role of the metal ion in the two different positions of the tbp cluster (apical versus equatorial) in determining the sign and magnitude of the D parameter of these clusters. The main targets are anisotropic metal ions such as Co^{II} and Re^{III}. Armed with comprehensive magnetic data for a homologous series of paramagnetic clusters, we hope to gain more insight into how different parameters affect the ability of a molecule to act as a single-molecule magnet.

Experimental Section

A solution of $[Mn(tmphen)_2(NO_3)_2]$ was prepared by combining $Mn(NO_3)_2{\cdot}6H_2O$ (75 mg, 0.3 mmol) with two equivalents of tmphen (140 mg, 0.6 mmol) in acetonitrile (50 mL). A solution of $[K([18]crown\text{-}6)]_3[Mn(CN)_6]$ was prepared in situ by stirring an excess of $K_3[Mn(CN)_6]$ (200 mg, 0.7 mmol) in a solution of [18]crown-6 (240 mg, 0.9 mmol) in acetonitrile (50 mL). The two solutions were slowly combined and the reaction mixture was left to stand undisturbed for one week. Yellow X-ray quality crystals of **1** were obtained: Yield = 45 mg (~15%). IR (Nujol): $\tilde{\nu} = 2138$, 2131, 2113, 2068 cm^{-1}; ν(C≡N).

Received: November 5, 2002 [Z50479]

Keywords: cluster compounds · cyanides · magnetic properties · manganese · single-molecule studies

[1] a) G. Christou, D. Gatteschi, D. N. Hendrickson, R. Sessoli, *MRS Bull.* **2000**, *25*, 66–71; b) D. D. Awschalom, D. P. DiVencenzo, *Phys. Today* **1995**, *48*, 43–48.

[2] a) R. Sessoli, H.-L. Tsai, A. R. Schake, S. Wang, J. B. Vincent, K. Folting, D. Gatteschi, G. Christou, D. N. Hendrickson, *J. Am. Chem. Soc.* **1993**, *115*, 1804–1816; b) R. Sessoli, D. Gatteschi, A. Caneschi, M. A. Novak, *Nature* **1993**, *365*, 141–143.

[3] S. L. Castro, Z. Sun, C. M. Grant, J. C. Bollinger, D. N. Hendrickson, G. Christou, *J. Am. Chem. Soc.* **1998**, *120*, 2365–2375.

[4] a) H. J. Eppley, H.-L. Tsai, N. de Vries, K. Folting, G. Christou, D. N. Hendrickson, *J. Am. Chem. Soc.* **1995**, *117*, 301–317; b) S. M. J. Aubin, Z. Sun, L. Pardi, J. Krzystek, K. Folting, L.-C. Brunel, A. L. Rheingold, G. Christou, D. N. Hendrickson, *Inorg. Chem.* **1999**, *38*, 5329–5340.

[5] a) W. Wernsdorfer, N. Aliaga-Alcalde, D. N. Hendrickson, G. Christou, *Nature*, **2002**, *416*, 406–409; b) S. M. J. Aubin, M. W. Wemple, D. M. Adams, H.-L. Tsai, G. Christou, D. N. Hendrickson, *J. Am. Chem. Soc.* **1996**, *118*, 7746–7754.

[6] a) C. Boskovic, W. Wernsdorfer, K. Folting, J. C. Huffman, D. N. Hendrickson, G. Christou, *Inorg. Chem.* **2002**, *41*, 5107–5118; b) E. K. Brechin, C. Boskovic, W. Wernsdorfer, J. Yoo, A. Yamaguchi, E. C. Sanudo, T. R. Concolino, A. L. Rheingold, H. Ishimoto, D. N. Hendrickson, G. Christou, *J. Am. Chem. Soc.* **2002**, *124*, 9710–9711.

[7] A. L. Barra, P. DeBrunner, D. Gatteschi, C. E. Schultz, R. Sessoli, *Europhys. Lett.* **1996**, *35*, 133–138.

[8] E. C. Yang, D. N. Hendrickson, W. Wernsdorfer, M. Nakano, L. N. Zakharov, R. D. Sommer, A. L. Rheingold, M. Ledezma-Gairaud, G. Christou, *J. Appl. Phys.* **2002**, *91*, 7382–7384.

[9] S. T. Ochsenbein, M. Murrie, E. Rusanov, H. Stoeckli-Evans, C. Sekine, H. U. Güdel, *Inorg. Chem.* **2002**, *41*, 5133–5140.

[10] S. D. Holmes, G. S. Girolami, *J. Am. Chem. Soc.* **1999**, *121*, 5593–5594.

[11] a) J. J. Sokol, M. P. Shores, J. R. Long, *Angew. Chem.* **2001**, *113*, 242–245; *Angew. Chem. Int. Ed.* **2001**, *40*, 236–239; b) K. K. Klausmeyer, S. R. Wilson, T. B. Rauchfuss, *J. Am. Chem. Soc.* **1999**, *121*, 2705–2711; c) J. A. Smith, J. R. Galán-Mascarós, R. Clerac, J. S. Sun, O. Y. Xiang, K. R. Dunbar, *Polyhedron* **2001**, *20*, 1727–1734.

[12] a) A. Scuiller, T. Mallah, M. Verdaguer, A. Nivorozkhin, J. L. Tholence, P. Veillet, *New J. Chem.* **1996**, *20*, 1–3; b) Z. J. Zhong, H. Seino, Y. Mizobe, M. Hidai, A. Fujishima, S. Ohkoshi, K. Hashimoto, *J. Am. Chem. Soc.* **2000**, *122*, 2952–2953; c) J. Larionova, G. Mathias, M. Pilkington, H. Andres, H. Stoeckli-Evans, H. U. Gudel, S. Decurtins, *Angew. Chem.* **2000**, *112*, 1667–1672; *Angew. Chem. Int. Ed.* **2000**, *39*, 1605–1609.

[13] A frequency-dependent out-of-phase (χ_m'') signal was observed for the $S = 13/2$ ground state cluster $[(Me_3tacn)_6Mn^{II}\text{-}Mo_6^{III}(CN)_{18}]^{2+}$ ($Me_3tacn = N,N',N''$-trimethyl-1,4,7-triazacyclonane): J. J. Sokol, A. G. Hee, J. R. Long, *J. Am. Chem. Soc.* **2002**, *124*, 7656–7657.

[14] **1**·7 H_2O ($C_{112}H_{110}Mn_5N_{26}O_7$), $M_w = 2209$, monoclinic, $P2_1/c$, $a = 19.724(5)$, $b = 25.379(6)$, $c = 24.411(5)$ Å, $\beta = 99.251(6)°$, $V = 12061(5)$ Å^3, $Z = 4$, $T = 110(2)$ K, $\rho_{calcd} = 1.222$ g cm^{-3}, $\mu = 6.69$ cm^{-1}, $F(000) = 4604$, 69503 measured reflections, 17418 unique reflections, collected on a SMART 1K area detector diffractometer equipped with graphite monochromated $Mo_{K\alpha}$ radiation ($\lambda = 0.71073$ Å). Refinement (G. M. Sheldrick,

 © 2003 Wiley-VCH Verlag GmbH & Co. KGaA, Weinheim

SHELXL-97, University of Göttingen, Göttingen (Germany), **1997**) of 1368 parameters for 8974 independent reflections with $I > 4\sigma(I)$ gave $R1 = 0.0883$, $wR2 = 0.2185$. CCDC-196445 contains the supplementary crystallographic data for this paper. These data can be obtained free of charge via www.ccdc.cam.ac.uk/conts/retrieving.html (or from the Cambridge Crystallographic Data Centre, 12 Union Road, Cambridge CB2 1EZ, UK; fax: (+44) 1223-336-033; or deposit@ccdc.cam.ac.uk).

[15] This cluster shape has been observed for other combinations of metals of general formula $\{[Fe(CN)_6]_2[Ni(\widehat{NN})_2]_3\}$ ($\widehat{NN}$ = 2-pyridylimino nitroxide, bis(1-pyrazolyl)methane, 1,10-phenanthroline): a) K. E. Vostrikova, D. Luneau, W. Wernsdorfer, P. Rey, M. Verdaguer, *J. Am. Chem. Soc.* **2000**, *122*, 718–719; b) K. Van Langenberg, S. R. Batten, K. J. Berry, D. C. R. Hockless, B. Moubaraki, K. S. Murray, *Inorg. Chem.* **1997**, *36*, 5006–5015; c) C. P. Berlinguette, J. R. Galán-Mascarós, K. R. Dunbar, *Inorg. Chem.*, in press.

[16] The least squares fitting of the reduced magnetization curves with a "$+D$" value was optimized to the parameters: $S = 11/2$, $g = 1.83(2)$, $D = 0.68(7)$ cm^{-1}, $error = 0.1$. Error contour plots (D versus g) for the reduced magnetization data confirm the minimum arising from the "$-D$" value leads to the global minimum (error = 0.05). For details of these fittings see Supporting Information.

 © 2003 Wiley-VCH Verlag GmbH & Co. KGaA, Weinheim

Superparamagnetic Aluminosilicates

Mesoporous Aluminosilicate Materials with Superparamagnetic γ-Fe_2O_3 Particles Embedded in the Walls**

*Carlos Garcia, Yuanming Zhang, Francis DiSalvo, and Ulrich Wiesner**

Silica-based mesostructured and mesoporous materials have sparked much interest among researchers over the last decade[1–5] expanding their functionality by the incorporation of functional organic compounds,[6–8] substitution or addition of other inorganic materials,[9] or templating into carbon-based materials.[10] Here we will focus on magnetic mesoporous materials. Although research has been performed on surfactant-based templating and sonochemical approaches to layered iron oxide/oxyhydroxide mesophases,[11,12] polymer-derived magnetic bulk ceramics,[13] and bulk iron oxide silicates prepared through sol–gel techniques,[14–17] research on mesostructured iron-containing silicates is scarce and limited to surfactant-based systems where the iron compound was loaded after synthesis.[18,19] Backfilling the pores is a common technique to functionalize mesoporous materials,[20] but it requires more synthesis and characterization steps and, more importantly, risks clogging the pore structure. We present a simple block-copolymer-based "one-pot" self-assembly approach to multifunctional γ-iron oxide aluminosilicates that are mesoporous and exhibit superparamagnetic behavior. Nanoscopic iron oxide particles are incorporated in the walls of the aluminosilicate matrix. Therefore, the blocking of the pores, as observed in earlier studies on backfilled materials, is overcome, even for high iron loadings.[19] We anticipate that this simple and versatile block-copolymer-directed approach to large-pore structures will lead to new techniques for the separation of magnetically labeled biological macromolecules that combine size exclusion as well as magnetic interactions. Also, the robust matrix has thick walls (>10 nm) which give the material good thermal stability (as high as 800 °C) allowing for catalytic applications at elevated temperatures.

The synthesis is unique in allowing for precise control over the structure and composition of the final materials. Although only the inverse-hexagonal cylinder morphology is described (cylindrical pores in a aluminosilicate matrix), several morphologies were observed in our laboratories, similar to those seen for diblock copolymers and their mixtures with homopolymers.[21,22] These morphologies include the hexagonal cylinder (inorganic cylinders in a polymer matrix) and the lamellar phases. The approach can also be extended to other transition-metal oxide systems. Iron oxide was used in our study for its potential magnetic properties, but also serves as an example of what should be possible from a wide range of commercially available metal alkoxides. The actual composition of the resulting materials can be tailored according to the application, which becomes particularly important in catalyst technology.

The amphiphilic diblock copolymer, poly(isoprene-*block*-ethylene oxide) (PI-*b*-PEO), served as a structure-directing agent. Two polymers of different molecular weight and PEO fraction were used (P5: $M_W = 22\,400$, 15 wt % PEO; P7: $M_W = 38\,600$, 32 wt % PEO). The polymers had a low molecular-weight distribution with a polydispersity index of less than 1.05. A sol was prepared using (3-glycidoxypropyl)trimethoxysilane (Sigma–Aldrich) and aluminum-*sec*-butoxide (Sigma–Aldrich), which was mixed with a solution of the polymer and iron(III) ethoxide powder (Gelest, Inc.) to prepare polymer–inorganic composites with 25 mol % Fe, based on the cation. The ratio of inorganic material to polymer was 2.37 for the composite made with P5 (designated as C5) and 2.25 for the composite made with P7 (designated

[*] Prof. Dr. U. Wiesner, C. Garcia, Y. Zhang
Department of Materials Science and Engineering
Cornell University
329 Bard Hall, Ithaca, NY 14853 (USA)
Fax: (+1) 607-255-2365
E-mail: ubw1@cornell.edu
Prof. Dr. F. DiSalvo
Department of Chemistry and Chemical Biology
Cornell University
Baker Laboratory, Ithaca, NY 14853-2501 (USA)

[**] This work was supported by the National Science Foundation (DMR-0072009), Philip Morris, and the Cornell Center for Materials Research (CCMR), a Materials Research Science and Engineering Center of the National Science Foundation (DMR-0079992). In particular, we thank Malcolm Thomas in the CCMR UHV-STEM laboratory for support as well as the CCMR X-Ray Diffraction Facility, the CCMR Hudson Mesoscale Processing Facility, and the Electron and Optical Microscopy Facility. We thank Yuri Suzuki and Bruce Van Dover for the use of the SQUID magnetometer and fruitful discussions of the magnetic data.

 © 2003 Wiley-VCH Verlag GmbH & Co. KGaA, Weinheim DOI: 10.1002/anie.200250618

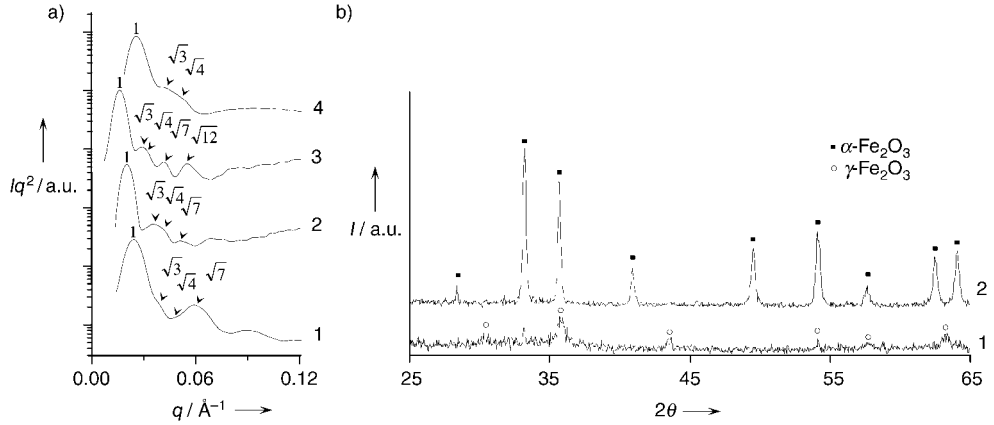


Figure 1. a) SAXS analysis of the pure block-copolymer P7 (trace 1), the as-prepared 25 mol% Fe-containing polymer–inorganic composites C5 and C7 (traces 2 and 3, respectively), and C7 calcined to 750 °C (trace 4). Positions of the higher order peaks suggest a hexagonal structure in all cases; b) XRD analysis of the bulk ceramics (prepared without block copolymer) calcined to 550 °C. Pure $Fe(OH)_3$ and 50 mol% Fe-containing aluminosilicate (diffractograms 1 and 2, respectively) prepared using the same sol–gel synthesis procedure as for the composites. Symbols indicate expected peaks from α-Fe_2O_3 (■) and γ-Fe_2O_3 (○), respectively. SAXS experiments were performed on a Bruker-AXS Nanostar diffractometer ($Cu_{K\alpha}$, 1.54 Å) operated at 40 kV, 40 mA in transmission. Data were recorded using a 2D Hi-Star aerial detector with a sample to detector distance of 62.5 cm. Integration of the images was performed over all azimuthal angles and resulting profiles smoothed using an FFT filter. XRD data was obtained from powdered samples using a Scintag Inc. θ–θ diffractometer ($Cu_{K\alpha}$, 1.54 Å).

as C7). This ratio was based on the amount of inorganic material remaining after evaporation of all the volatile components (experimentally found to be 55% of initial weight of the sol).

Figure 1a shows small-angle X-ray scattering (SAXS) data for the pure diblock copolymer P7 and the two as-prepared polymer–inorganic composites C5 and C7 (traces 1–3, respectively). The scattering data exhibit higher order peaks for both the polymer and the composites, indicative of cylinders in a hexagonal array. Transmission electron microscopy (TEM) corroborates these assignments. Figure 2 depicts representative TEM micrographs of the as-prepared composite C5 (Figure 2a,b) showing a well-defined inverse-hexagonal morphology. The absence of large-angle X-ray diffraction (XRD) peaks (data not shown) demonstrates that the inorganic and polymer components of the composites are amorphous.

For the production of a crystalline magnetic iron oxide phase, the as-prepared composites were calcined at elevated temperatures in air. To elucidate the effect of our aluminosilicate matrix on the iron oxide formation, XRD experiments were performed on two test samples made from only the inorganic precursors (that is, without block copolymer) and heated to 550 °C in air. The results of these measurements are shown in Figure 1b. The first sample was made by heating fully hydrolyzed iron ethoxide, and was shown to be crystalline non-magnetic α-Fe_2O_3 (Figure 1b, upper diffractogram). The second sample was made from an iron-containing aluminosilicate (50 mol% Fe) and showed a poorly crystalline γ-Fe_2O_3 phase (Figure 1b, lower diffractogram). These results on model materials suggest that in a bulk aluminosilicate matrix, γ-Fe_2O_3 is the only detected crystalline phase after heat treatment at elevated temperatures (550 °C). It should be noted that comparable results, that is, the formation of only γ-Fe_2O_3 in iron-containing silicate materials prepared by similar means, were also obtained by other groups.[14–17,23] Although pure γ-Fe_2O_3 usually decomposes to nonmagnetic α-Fe_2O_3 at approximately 350 °C, the remaining amorphous aluminosilicate matrix apparently hinders the transformation, thus stabilizing the γ-phase, even when heated to 750 °C.[17] This is fortunate since one can now exploit the magnetic behavior of γ-Fe_2O_3.

Small-angle X-ray data for composite C7 after calcination at 750 °C is shown in Figure 1a (trace 4). Compared to the as-prepared material (Figure 1a, trace 3) the diffractogram is shifted to significantly higher q values, as expected from the considerable weight loss (approximately 70%, as given by thermogravimetric analysis) during heat treatment.[21,24] This weight loss results from the oxidation of all organic constituents to volatile products. The diffractogram clearly shows higher order reflections suggesting that the mesoscopic order has been preserved. Assuming retention of the hexagonal structure, the (10) interplane distance after calcination at 750 °C was reduced by 36% from the as-prepared composite owing to the shrinkage of the matrix. XRD experiments on this material did not generate any identifiable diffraction peaks from iron oxide particles. This is most likely because of the small size of the iron oxide crystallite domains (see below).

The magnetic properties of C7 before and after calcination at different temperatures were investigated using a SQUID magnetometer (Figure 3). As expected, the magnetization of the as-prepared composite exhibits paramagnetic behavior. However, after calcination at 550 °C, the onset of an inflection point and the absence of residual magnetization at zero applied field in the field (H) versus magnetization (M) plot indicates superparamagnetic behavior. As the calcination temperatures were increased above 550 °C, the measured magnetization also increased. At the same time, the sigmoidal nature of the superparamagnetic response became more

 © 2003 Wiley-VCH Verlag GmbH & Co. KGaA, Weinheim

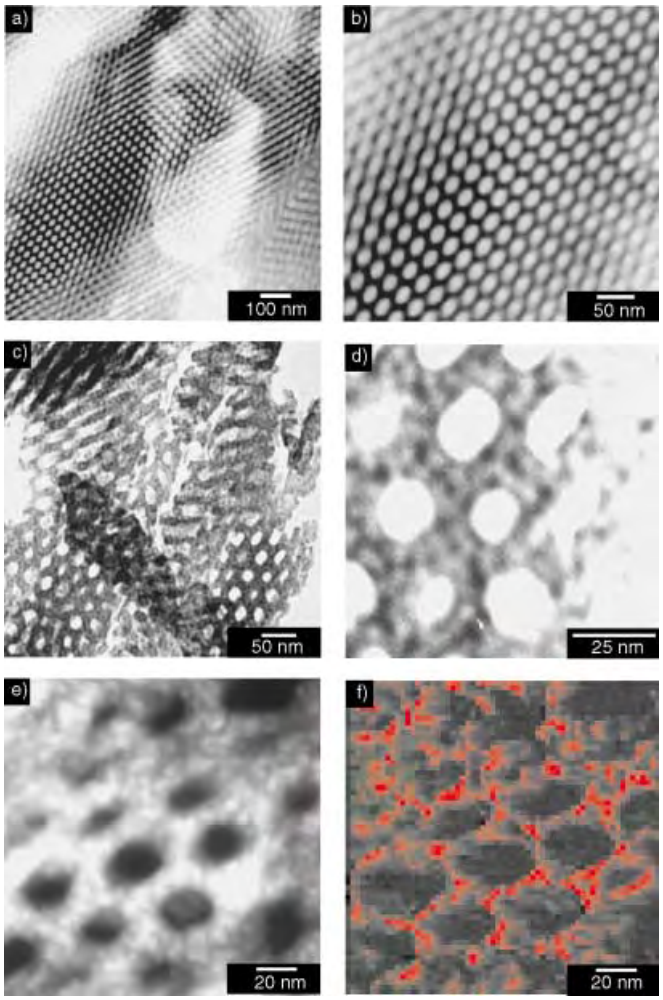


Figure 2. a,b) Bright-field TEM images of the as-made C5 sample at two different magnifications revealing the inverse-hexagonal morphology; c,d) bright-field TEM images of C7 after calcination to 750 °C at two different magnifications. Hexagonal order is shown (c) to be preserved after calcination, while at higher magnification (d), the iron oxide precipitates show up as dark spots within the matrix of the inverse-hexagonal morphology; e,f) annular dark-field STEM images of C7 calcined to 750 °C (e), together with the corresponding energy-filtered iron distribution map (f). Samples were cut into ultrathin sections with a Leica Ultracut UCT microtome at 300 K. Bright-field TEM micrographs were taken on a Jeol 1200EX operating at 120 kV. A VG HB-501UX dedicated STEM was used to acquire images e) and f) operating at 100 keV with a cold field emission source to produce high-resolution bright-field (resolution ~0.3 nm) and annular dark-field (resolution ~0.2 nm) images. A single-crystal YAP scintillator/PMT combination was used for serial EELS and energy-filtered imaging with resolution of less than 1 eV obtained in the 0–2 keV range.

apparent, and was most developed for the composite calcined at 750 °C. The magnetic response of the ceramic material suggests the nucleation and growth of small γ-Fe_2O_3 particles.

To quantitatively determine the iron oxide precipitate size, zero-field-cooling (ZFC) and field-cooling (FC) experiments were performed on C7 calcined to 750 °C. The data in the inset of Figure 3 indicates a blocking temperature of 25 K and a collapse temperature (the temperature where the two curves deviate from each other) of 35 K. Both the narrowness of the ZFC curve around the maximum and the low collapse temperature are strong indications of a narrow size distribution of the particles within the matrix.[25] According to superparamagnetic theory,[26] the particle volume can be determined from the blocking temperature based on the Arrhenius relationship:

$$\tau_m = \tau_0 \exp\left(\frac{K V}{k_B T_B}\right) \quad (1)$$

where τ_m is the experimental measurement time (100 s for the SQUID magnetometer), τ_0 is a time constant characteristic to the material, K is the anisotropy constant, V is the volume of the magnetic particle, k_B is the Boltzmann constant, and T_B is the blocking temperature. Detailed analysis of the magnetic properties of small magnetic domains based on γ-Fe_2O_3 have been performed by several research groups.[15,25,27] From these studies, the anisotropy constant K was estimated to be $1 \times 10^5\ J\,m^{-3}$ and τ_0 to be 10^{-10} s, which results in a calculated average γ-Fe_2O_3 particle size of 5.6 nm. Fitting the magnetization curve (M versus H) of sample C7 (750 °C calcination) at 60 K, that is, 35 K above T_B, to the Langevin function from the classical theory of paramagnetism indicates approximately 350 spins per particle.[28]

To corroborate the scattering and SQUID results, TEM was performed on C7 calcined to 750 °C. The TEM micrograph in Figure 2c demonstrates that upon calcination the inverse-hexagonal morphology of the material is preserved, as suggested by the SAXS data in Figure 1. From the TEM micrograph the (10) interplane distance was measured to be 25 nm, which is in good agreement with the value of 24.5 nm calculated from SAXS. Furthermore, the higher resolution image in Figure 2d shows homogeneously distributed dark spots within the matrix. A histogram of the size distribution of these precipitates reveals an average particle diameter of approximately 5 nm. Considering that TEM is a local technique, this number is in excellent agreement with the calculated γ-Fe_2O_3 particle size of 5.6 nm determined by the SQUID data, which represents measurements integrated over macroscopic sample dimensions. This remarkable result indicates that the particle-size distribution reflected from the TEM micrograph in Figure 2d is representative of the entire sample, and suggests the amazing structural control of the present approach. To directly show that these precipitates contain iron, we performed elemental mapping on a scanning transmission electron microscope (STEM) using electron energy loss spectroscopy (EELS).[29] The dark-field image of C7 calcined to 750 °C and the corresponding elemental iron map are shown in Figure 2e and f, respectively. Iron is clearly abundant and clustered together, which is consistent with iron oxide precipitates.

These data demonstrate that, first, a ceramic with ordered mesoscale pores is obtained upon calcination to temperatures as high as 750 °C and, secondly, that nucleation and growth of γ-Fe_2O_3 precipitates occurs inside the amorphous aluminosilicate matrix walls. This latter result is consistent with the phase separation of Fe_2O_3 and SiO_2 observed in their bulk phase diagram.[30] The result is a mesoporous material with open and accessible pores and superparamagnetic properties.

 © 2003 Wiley-VCH Verlag GmbH & Co. KGaA, Weinheim

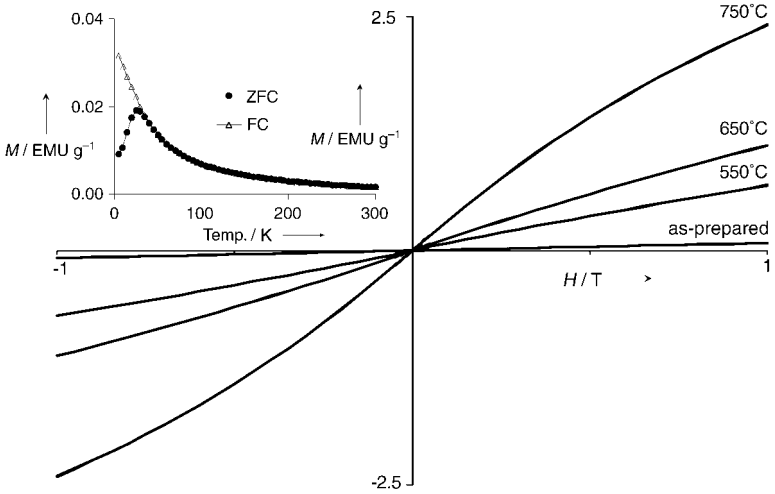


Figure 3. Field dependence of the magnetic properties of C7, both as-prepared and calcined to different temperatures, as indicated in the figure. Inset: zero-field cooling (ZFC) and field cooling (FC) curves for sample P7-C25 calcined to 750 °C. Data were collected on a Quantum Design MPMS SQUID magnetometer at 300 K for the *H* versus *M* curves and a 200 Oe field was used for the ZFC/FC experiments.

Indeed, the calcined materials exhibit a nitrogen sorption isotherm of type IV according to BDDT classification, with a specific surface area of 310 m^2g^{-1} according to the Brunnauer–Emmett–Teller (BET) method, and a pore-size distribution with an average pore diameter according to Barrett–Joyner–Halenda (BJH) of 8.3 nm (data not shown).[31,32] These values are in excellent agreement with measurements on similar PI-*b*-PEO block-copolymer-derived mesoporous aluminosilicate materials prepared without the addition of iron and show that the present self-assembly approach does not lead to clogging of the pore structure,[21] even for significant iron loadings. In contrast, previous studies on mesoporous materials backfilled with iron oxide in a post-synthesis step showed significant pore clogging with as little as 6 wt % iron incorporation.[19] It is interesting to note from the TEM micrograph in Figure 2 d that the iron oxide precipitates extend to the surface of the pores in the mesoporous aluminosilicate matrix. For applications in catalysis this is a particularly important feature and originates from the present one-pot synthesis without additional synthesis steps. Furthermore, with the wall thickness easily exceeding 10 nm, the materials are unusually stable to high temperatures.

Completely novel applications can also be envisioned for such multifunctional materials, for example, the separation of magnetically labeled biomolecules. In the presence of an external magnetic field, diffusion of these labeled molecules through the pores would be retarded through multiple interactions with the fringe magnetic fields of the γ-Fe_2O_3 at the pore surfaces. After unlabeled material passes through, the magnetic field could be switched off to release the labeled molecules from the medium, thus leading to efficient separation of labeled and unlabeled species. The present materials have not been optimized for any of these applications, but clearly engineering the pore and precipitate sizes, as well as particle distribution towards these goals, is now possible.

In this paper we have presented a simple block-copolymer-based one-pot self-assembly approach to superparamagnetic mesoporous materials with large pores, thick walls, and well-defined magnetic iron oxide particles within the walls of the matrix. Blocking of the pores as observed in earlier studies on backfilled materials is thus overcome, even for high iron loadings. The multifunctional nanostructured materials open up access to novel biopolymer separation technologies combining size-exclusion principles with separation of magnetically labeled materials. Furthermore, they should enable potential catalytic applications at elevated temperatures.

Experimental Section

Each polymer was dissolved in a dry THF/chloroform mixture (1:1 w/w) to form a 5 wt % solution. Iron(III) ethoxide powder (Gelest, Inc.) was added to this solution in the desired amounts. A separate solution of (3-glycidoxypropyl)trimethoxysilane (GLYMO) and aluminum-*sec*-butoxide (9:1 molar ratio) was prepared following a two-step acid-catalyzed hydrolysis procedure described previously.[4] Potassium chloride was added (0.3 wt %) to shield surface charges for improved cross-linking of the sol. This sol was then added in varying amounts to the polymer–iron(III) ethoxide solution and stirred for one hour. It is important to note that the iron ethoxide was not added to the aluminosilicate sol–gel precursor solution since the rapid hydrolysis and condensation kinetics of this compound in the presence of water and an acid catalyst leads to premature precipitation of an iron oxide phase. Films were cast by evaporation of the solvents and byproducts on a hotplate at 50 °C and then at 130 °C in a vacuum oven for one hour.

Heat treatment was performed in a tube furnace under aerobic conditions by ramping up the temperature in 1 °C min^{-1} increments to the final calcination temperatures. Each ramp was held at 350 °C for three hours and then for another six hours at the final calcination temperature.

Received: November 25, 2002 [Z50618]

Keywords: block copolymers · iron · magnetic properties · mesoporous materials · oxides

[1] C. T. Kresge, M. E. Leonowicz, W. J. Roth, J. C. Vartuli, J. S. Beck, *Nature* **1992**, *359*, 710.
[2] G. S. Attard, J. C. Glyde, C. G. Göltner, *Nature* **1995**, *378*, 366.
[3] S. A. Bagshaw, E. Prouzet, T. J. Pinnavaia, *Science* **1995**, *269*, 1242.
[4] M. Templin, A. Franck, A. Du Chesne, H. Leist, Y. Zhang, R. Ulrich, V. Schädler, U. Wiesner, *Science* **1997**, *278*, 1795.
[5] D. Zhao, J. Feng, Q. Huo, N. Melosh, G. H. Fredrickson, B. F. Chmelka, G. D. Stucky, *Science* **1998**, *279*, 548.
[6] Y. Lu, Y. Yang, A. Sellinger, M. Lu, J. Huang, H. Fan, R. Haddad, G. Lopez, A. R. Burns, D. Y. Sasaki, J. Shelnutt, C. J. Brinker, *Nature* **2001**, *410*, 913.
[7] T. Asefa, M. J. MacLachlan, N. Coombs, G. A. Ozin, *Nature* **1999**, *402*, 867.
[8] S. Inagaki, S. Guan, T. Ohsuna, O. Terasaki, *Nature* **2002**, *416*, 304.

 © 2003 Wiley-VCH Verlag GmbH & Co. KGaA, Weinheim

[9] P. Yang, D. Zhao, D. I. Margolese, B. F. Chmelka, G. D. Stucky, *Nature* **1998**, *396*, 152.
[10] S. H. Joo, S. J. Choi, I. Oh, J. Kwak, Z. Liu, O. Terasaki, R. Ryoo, *Nature* **2001**, *412*, 169.
[11] G. Wirnsberger, K. Gatterer, H. P. Fritzer, W. Grogger, P. Behrens, M. F. Hansen, C. B. Koch, *Chem. Mater.* **2001**, *13*, 1153.
[12] Y. Wang, L. Yin, A. Gedanken, *Ultrason. Sonochem.* **2002**, *9*, 285.
[13] M. J. MacLachlan, G. Madlen, N. Coombs, T. W. Coyle, N. P. Raju, J. E. Greedan, G. A. Ozin, I. Manners, *Science* **2000**, *287*, 1460.
[14] F. del Monte, M. P. Morales, D. Levy, A. Fernandez, M. Ocana, A. Roig, E. Molins, K. O'Grady, C. J. Serna, *Langmuir* **1997**, *13*, 3627.
[15] G. Ennas, A. Musinu, G. Piccaluga, D. Zedda, D. Gatteschi, C. Sangregorio, J. L. Stanger, G. Concas, G. Spano, *Chem. Mater.* **1998**, *10*, 495.
[16] C. Cannas, M. F. Casula, G. Concas, A. Corrias, D. Gatteschi, A. Falqui, A. Musinu, C. Sangregorioc, G. Spanob, *J. Mater. Chem.* **2001**, *11*, 3180.
[17] M. F. Casula, A. Corrias, G. Paschina, *J. Non-Cryst. Solids* **2001**, *293–295*, 25.
[18] M. Fröba, R. Köhn, G. Bouffaud, O. Richard, G. van Tendeloo, *Chem. Mater.* **1999**, *11*, 2858.
[19] L. Zhang, G. C. Papaefthymiou, J. Y. Ying, *J. Phys. Chem. B* **2001**, *105*, 7414.
[20] X. He, D. Antonelli, *Angew. Chem.* **2002**, *114*, 222; *Angew. Chem. Int. Ed.* **2002**, *41*, 214.
[21] P. F. W. Simon, R. Ulrich, H. W. Spiess, U. Wiesner, *Chem. Mater.* **2001**, *13*, 3464.
[22] I. W. Hamley, *The Physics of Block Copolymers*, Oxford University Press. Oxford, **1998**.
[23] D. Niznansky, N. Viart, J. L. Rehspringer, *J. Sol-Gel Sci. Technol.* **1997**, *8*, 615.
[24] A. C. Finnefrock, R. Ulrich, A. Du Chesne, C. C. Honeker, K. Schumacher, K. K. Unger, S. M. Gruner, U. Wiesner, *Angew. Chem.* **2001**, *113*, 1247; *Angew. Chem. Int. Ed.* **2001**, *40*, 1208.
[25] B. H. Sohn, R. E. Cohen, G. C. Papaefthymiou, *J. Magn. Magn. Mater.* **1998**, *182*, 216.
[26] A. Aharoni, *Relaxation Processes in Small Particles*, North Holland, Amsterdam, **1992**.
[27] C. Djega-Mariadassou, J. L. Dormann, M. Nogués, G. Villers, S. Sayouri, *IEEE Trans. Magn.* **1990**, *26*, 1819.
[28] B. D. Cullity, *Introduction to Magnetic Materials*, Addison-Wesley, Reading, MA, **1972**.
[29] M. M. Disko, *Transmission Electron Energy Loss Spectroscopy in Materials Science, Vol. 2*, The Minerals, Metals and Materials Society, Pennsylvania, **1992**.
[30] *Phase Diagrams for Ceramists, Vol. 1*, American Ceramic Society, Columbus, OH, **1985**.
[31] E. P. Barrett, L. G. Joyner, P. P. Halenda, *J. Am. Chem. Soc.* **1951**, *73*, 373.
[32] S. Brunauer, L. S. Deming, W. S. Deming, E. Teller, *J. Am. Chem. Soc.* **1940**, *62*, 1723.

 © 2003 Wiley-VCH Verlag GmbH & Co. KGaA, Weinheim

Trihalogencarbenium Ions

Structure and Characterization of $CI_3^+[Al\{OC(CF_3)_3\}_4]^-$; Lewis Acidities of CX_3^+ and BX_3**

Ingo Krossing, Angela Bihlmeier, Ines Raabe, and Nils Trapp*

There has been continuing interest in the elicidation of the properties of reactive small carbon-containing cations[1] such as CX_3^+[2–4] or OCX^+[5–8] (X = F–I), which are frequently observed in fragmentation reactions of gaseous ions in the mass spectrometer[9] and are thought to be reactive intermediates in organic synthesis. The solid-state structures of several salts of related cations such as Me_2CF^+,[10] $C(OH)_3^+$, and $(H_3CO)C(H)X^+$ (X = F, Cl) have been structurally characterized.[11] The CX_3^+ ions of the heavier homologues (X = Cl–I) were characterized by ^{13}C NMR spectroscopy[2a,e,12] as long-lived intermediates at −78 °C in SO_2ClF solution [Eq. (1)].

$$CX_4 + SbF_5(\text{excess}) \xrightarrow[-78\,^\circ C]{SO_2ClF} CX_3^+[Sb_nF_{5n+1}]^- + \ldots \quad (1)$$

Recent computational work[3,4,12] revealed that, in contrast to earlier[2a] conclusions, cations bearing the heavier halogens should be thermodynamically more stable and less electrophilic than the F and Cl homologues. However, despite the strong σ-acceptor effect of the electronegative fluorine atoms there is sufficient π donation to stabilize the CF_3^+ ion over the parent methenium ion CH_3^+.[3] By contrast, the heavier halogens Cl, Br, and I in CX_3^+ ions were shown to be σ and π donors towards the C atom.[3] For gaseous CX_3^+ it was suggested[3] that the partial C=X$^+$ double-bond character also remained for X = I. To test the influence of π bonding on the solid-state structure of the CX_3^+ ions it was therefore desirable to prepare a stable salt of these species, in particular for the CI_3^+ ion which would include an unusual partial 2p–5p double bond.[13]

Recently we reported on nonoxidizing weakly coordinating anions of the type $Al(OR)_4^-$ ($R = C(CF_3)_3$)[14,15] and their ability to stabilize gas-phase cations such as $Ag(\eta^2\text{-}P_4)_2^+$[16] and $Ag(\eta^4\text{-}S_8)_2^+$[17] as well as the highly electrophilic binary P–X cations PX_4^+, $P_2X_5^+$, $P_3I_6^+$, and $P_5X_2^+$, which arose through halide-ion abstraction from $Ag[Al(OR)_4]$ and PX_3 (X = Br, I).[18] A similar halide-abstraction approach was used for the successful preparation of $CI_3^+[Al(OR)_4]^-$ from CI_4 and $Ag[Al(OR)_4]$ [Eq. (2)].[19]

$$CI_4 + Ag[Al(OR)_4] \xrightarrow[\text{RT, exclusion of light}]{CH_2Cl_2} CI_3^+[Al(OR)_4]^- + AgI \quad (2)$$

From computational and experimental work it was clear that the solvent CH_2Cl_2 should be stable against H^- and Cl^- abstractions by CI_3^+ because the then formed cations CH_2Cl^+ or $CHCl_2^+$ are much less stable than CI_3^+.[2–4] Preparations according to Equation (2)[19] had to be performed with the complete exclusion of light and with carefully purified diiodine-free CI_4, since CI_4 decomposes within minutes in solution in light with formation of I_2 and other carbon iodides, and $Ag[Al(OR)_4]$ reacts immediately with I_2 to give yet unidentified decomposition products.[20] With these precautions $CI_3^+[Al(OR)_4]^-$ (**1**) was prepared in quantitative yield.[19] According to calculations at the MP2/TZVPP level and estimation of the sublimation and lattice enthalpies in a suitable cycle, we estimate that Equation (2) is exothermic by −33 kJ mol^{-1} in the gas phase and by −127 kJ mol^{-1} in the solid state.[21–24] In CH_2Cl_2 solution, **1** is dark blood red and in situ NMR reactions show only resonance signals for the CI_3^+ ion ($\delta(^{13}C) = 97$ ppm; in SO_2ClF: $\delta(^{13}C) = 95$ ppm;[2a,e] calculated value: $\delta(^{13}C) = 106$ ppm[12]) and the anion ($\delta(^{13}C) = 121.5$ ppm (q); $\delta(^{27}Al) = 38.0$ ppm). A CH_2Cl_2 solution of **1** is stable for about 8 to 12 h at ambient temperature and much longer if stored at −30 or −78 °C. Single crystals that appeared yellow as thin plates but black when thicker were grown at −78 °C from cooled concentrated CH_2Cl_2 solutions of **1**. The crystal structure determination[25] of a dark orthorhombic block of **1** showed that it contained isolated trigonal-planar CI_3^+ ions with a sum of I-C-I bond angles of 360.0° (range: 118.8–122.1°) and $Al(OR)_4^-$ ions (Figure 1).

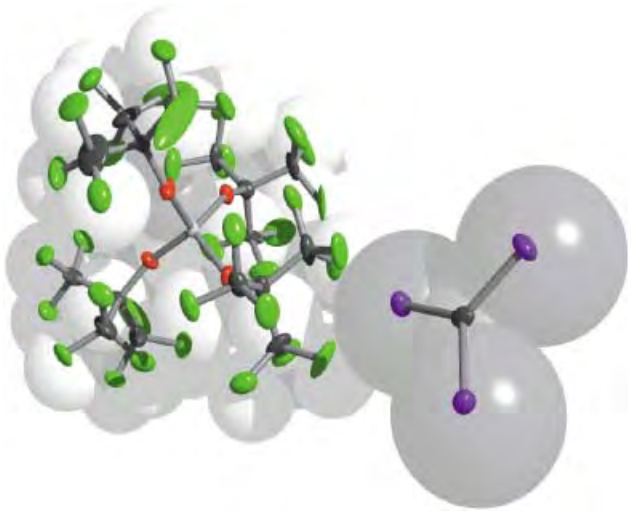


Figure 1. Solid-state structure of **1**. Superposition of a space-filling (faint in gray scale) and a 25% probability ellipsoid model.

[*] Priv.-Doz. Dr. I. Krossing, A. Bihlmeier, Dipl.-Chem. I. Raabe, N. Trapp
Universität Karlsruhe
Institut für Anorganische Chemie
Engesserstrasse Geb. 30.45, 76128 Karlsruhe (Germany)
Fax: (+49) 721-608-48-54
E-mail: krossing@chemie.uni-karlsruhe.de

[**] This work was supported by the Deutsche Forschungsgemeinschaft and the Fonds der Chemischen Industrie. We thank Prof. H. Schnöckel and Dr. H.-J. Himmel for valuable discussions. X = H, F–I.

 DOI: 10.1002/anie.200250172 © 2003 Wiley-VCH Verlag GmbH & Co. KGaA, Weinheim

The average C–I bond length of 201.3(9) pm in **1** (range 199.3 to 203.9 pm) is 15 pm shorter than that of solid or gaseous CI_4 (215.9 pm),[26] and 11 pm shorter than the B–I bond length of the isoelectronic BI_3 molecule (211.8 pm).[22] All three iodine atoms in **1** exhibit three to five I–F contacts to the CF_3 groups of the anion at d(I–F) = 328.9 to 358.2 pm, and the average distance of the 13 I–F contacts is 344.5 pm (sum of van der Waals radii I + F: 360 pm). In contrast, the shortest C–F contact (326.4 pm) is longer than the sum of the C and F van der Waals radii (320 pm). This indicates an accumulation of a high positive charge on the three iodine atoms, but no positive charge on the carbon atom. In the related Me_2CF^+ ion the carbon atom exhibits two strong C–F contacts to the AsF_6^- counterion (d(C–F) = 266 and 278 pm),[10] which indicates that in this case at least part of the positive charge remains at the C^+ carbenium center. Vibrational spectra of **1**[27] also confirm the presence of strong C–I bonds: The C–I stretching frequency (e′ symmetry) is 739 cm^{-1}, the comparable mode in $^{11}BI_3$ appears at lower energy at 693 cm^{-1}. Experimental and computed data on CI_3^+ and BI_3 are compared in Table 1, and the CI_3^+ molecular orbitals of π symmetry are shown in Figure 2.

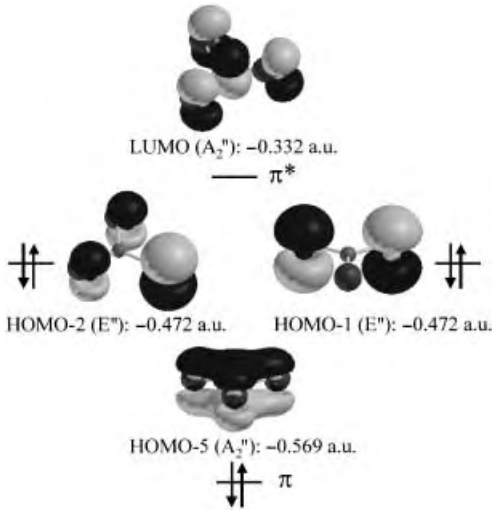


Figure 2. CI_3^+ molecular orbitals of π symmetry.

From the available experimental and computational data it is evident that a CI_3^+ resonance structure in which the C atom bears the positive charge is not important and that only the three resonance structures with partial C=I$^+$ double bonds carry weight. This leads to an expected C–I bond order of 1.33 which is in good agreement with the high AIM[29] bond order (C–I) of 1.616 and the molecular orbitals shown in Figure 2. The four p_z atomic orbitals of the C and I atoms combine to give a totally bonding π MO, two nonbonding MOs, and an empty π* MO (the LUMO). It is noteworthy that the sizes of the 2p and 5p orbitals in the bonding π orbital in Figure 2 fit nicely although both sets of atomic orbitals are separated by three principal quantum numbers! A comparison of the E–I (E = B, C) bond orders, bond lengths, stretching frequencies, electron densities ρ residing on the bond critical point and bond ellipticities ε in the bond critical point suggests that the partial π bond in BI_3 is considerably weaker than in CI_3^+. For a complete analysis of the Laplacians of CX_3^+ (X = F–I) see reference [4]. Since π bonding in CI_3^+ is stronger than in CF_3^+,[3] a reverse of the Lewis acidities of CX_3^+ compared to BX_3 (X = F–I) should occur (see ammonia affinities in reference [3,4]). The Lewis acidity of BX_3 increases according to $BF_3 < BCl_3 < BBr_3 \approx BI_3$. To test this proposal, that is, whether CF_3^+ is a stronger Lewis acid than CI_3^+, we calculated the fluoride ion affinity (FIA) of all BX_3 and CX_3^+ (X = H,F–I) species according to an isodesmic reaction.[31] The FIA is a well-established measure for the strengths of a Lewis acid and corresponds to the negative reaction enthalpy of a reaction of the gaseous Lewis acid A with the gaseous F^- ion to give gaseous AF^-.[31–33] We determined the FIA values of all $EX_3^{0/+}$ species in the gas phase by ab initio MP2/TZVPP calculations[34–37] as well as in CH_2Cl_2 solution (COSMO model[38]).

Table 2: Calculated FIA values of all $EX_3^{0/+}$ species in the gas phase and in CH_2Cl_2 solution.

	FIA(CX_3^+) [kJ mol^{-1}]		FIA(BX_3) [kJ mol^{-1}]	
X	gaseous	in CH_2Cl_2	gaseous	in CH_2Cl_2
H	1112	501	290	164
F	1099	497	351	225
Cl	904	359	405	279
Br	871	343	433	307
I	813	302	448	322

Table 1: Comparison of experimental and computed data of CI_3^+ (in **1**) and BI_3.

	CI_3^+		BI_3	
Parameter	exptl.	calcd[a]	exptl.	calcd[a]
d(E–I) [pm]	201.3(9)	202.0	211.8[b]	211.4
			210(4)[c]	
ν_3(e′) [km mol^{-1}]	739 (vs)	792 (296)	693 (^{11}B)[d]	745 (266)
ν_2(a_2'') [km mol^{-1}]	339 (w)	378 (10)	305 (^{11}B)[d]	337 (1)
ν_1(a_1') [km mol^{-1}]	–	236 (0)	189 (^{11}B)[d]	202 (0)
ν_4(e′) [km mol^{-1}]	–	127 (0)	101 (^{11}B)[d]	107 (0)
b.o. (E–I)[e]	–	1.616	–	1.198
q(I)[e]	–	+0.555	–	−0.185
q(E)[e]	–	−0.666	–	+0.551
ρ(b.c.p.)[e] [e Å^{-3}]	–	0.123	–	0.112
ε(b.c.p.)[e]	–	0.0853	–	0.0808

[a] MP2/TZVPP. [b] Electron diffraction. [c] X-ray. [d] from ref. [28]. [e] Atoms in molecules (AIM) calculations at the MPW1PW91/3-21G* level.[29,30] b.o. = bond order; b.c.p. = bond critical point.

The FIA values in CH_2Cl_2 given in Table 2 allow a unifying approach, since the approximate inclusion of solvation energies reduces the large differences in the gas phase, which are due to the loss of charge and the formation of a neutral species ($CX_3^+ + F^- \rightarrow FCX_3$), to chemically meaningful values. With this procedure the Lewis acid strengths of CX_3^+ and BX_3 towards F^- can be compared directly in solution.

In agreement with the experimental results the calculations show that the Lewis acidity of boron

 © 2003 Wiley-VCH Verlag GmbH & Co. KGaA, Weinheim

halides versus fluoride ions increases in the gas phase as well as in CH_2Cl_2 solution from BF_3 to BI_3. The order of the Lewis acidity of CX_3^+ versus fluoride ions is reversed: CF_3^+ (and CH_3^+) are the strongest Lewis acids in this series. The FIA of CI_3^+ in CH_2Cl_2 is similar to those of BI_3 and BBr_3, whereas all other CX_3^+ ions are stronger Lewis acids versus F^- than the BX_3 molecules. This is ascribed to the better π- and σ-donor ability of the heavier halogens in combination with the unipositive charge in CX_3^+ which efficiently enforces the delocalization of the positive charge onto the halogen atoms (see the mesomeric structures). The delocalization of positive charge as the driving force for effective π-bond formation is missing for the boron halides and, therefore, appears to be less favorable in BX_3. Consequently, BI_3, which presumably has the weakest π bond, is the strongest Lewis acid of the boron halides and CI_3^+, which has a strong π bond, is the weakest Lewis acid of the homologous CX_3^+ series.[39]

Experimental Section

All manipulations were performed by using grease-free Schlenk or dry box techniques and a dinitrogen or argon atmosphere. The solvents were rigorously dried over P_2O_5, degassed prior to use, and stored under N_2 on molecular sieves (4 Å). Solvents were added by condensation techniques. Commercial CI_4 (Aldrich) was handled in the dark; smaller amounts of I_2 were removed by prolonged (several days) evacuation at room temperature in the dark. $Ag[Al(OR)_4]$ was prepared as previously described.[14] All manipulations involving CI_4 were performed in the dark, that is, in a dark room with additional aluminum foil wrapped around the entire vessel.

Received: September 16, 2002
Revised: December 5, 2002 [Z50172]

Keywords: acidity · boron · cations · halogens · Lewis acids

[1] a) G. A. Olah, *Fredel-Crafts Chemistry*, Wiley, New York, **1973**; b) G. A. Olah, *Carbocations and Elektrophilic Reactions*, Wiley, New York, **1973**; c) *Stable Carbocation Chemistry* (Eds.: P. von R. Schleyer, G. K. S. Prakash), Wiley, New York, **1997**.

[2] a) G. A. Olah, G. Rasul, L. Heiliger, G. K. S. Prakash, *J. Am. Chem. Soc.* **1996**, *118*, 3580; b) G. A. Olah, L. Heiliger, G. K. S. Prakash, *J. Am. Chem. Soc.* **1989**, *111*, 8020; c) H. Vancik, K. Percac, D. E. Sunko, *J. Am. Chem. Soc.* **1990**, *112*, 7418; d) J. W. Hudgens, R. D. Johnson III, B. P. Tsai, S. A. Kafafi, *J. Am. Chem. Soc.* **1990**, *112*, 5763; e) G. A. Olah, Y. K. Mo, E. G. Melby, H. C. Lin, *J. Org. Chem.* **1973**, *38*, 367; f) G. A. Olah, G. Rasul, A. K. Yudin, A. Burrichter, G. K. S. Prakash, A. L. Chistyakov, A. V. Stankevich, I. S. Akhrem, N. P. Gambaryan, M. E. Vol'pin, *J. Am. Chem. Soc.* **1996**, *118*, 1446.

[3] a) G. Frenking, S. Fau, C. M. Marchand, H. Grützmacher, *J. Am. Chem. Soc.* **1997**, *119*, 6648; b) C. H. Reynolds, *J. Chem. Soc. Chem. Commun.* **1991**, 975; c) H. Basch, T. Hoz, S. Hoz, *J. Phys. Chem. A* **1999**, *103*, 6458.

[4] H. Grützmacher, C. M. Marchand, *Coord. Chem. Rev.* **1997**, *163*, 287.

[5] G. K. S. Prakash, J. W. Bausch, G. A. Olah, *J. Am. Chem. Soc.* **1991**, *113*, 3203.

[6] K. O. Christe, B. Hoge, J. A. Hoatz, G. K. S. Prakash, G. A. Olah, J. A. Sheehy, *Inorg. Chem.* **1999**, *38*, 3132.

[7] E. Bernhardt, H. Willner, F. Aubke, *Angew. Chem.* **1999**, *111*, 830; *Angew. Chem. Int. Ed.* **1999**, *38*, 823.

[8] a) G. A. Olah, A. Burrichter, T. Mathew, Y. D. Yankar, G. Rasul, G. K. S. Prakash, *Angew. Chem.* **1997**, *109*, 1958; *Angew. Chem. Int. Ed. Engl.* **1997**, *36*, 1875; b) T. S. Sorensen, *Angew. Chem.* **1998**, *110*, 623; *Angew. Chem. Int. Ed.* **1998**, *37*, 603.

[9] a) R. H. Martin, F. W. Lampe, R. W. Taft, *J. Am. Chem. Soc.* **1965**, *87*, 2490; b) R. H. Martin, F. W. Lampe, R. W. Taft, *J. Am. Chem. Soc.* **1966**, *88*, 1353.

[10] K. O. Christe, X. Zhang, R. Bau, J. Hegge, G. A. Olah, G. K. S. Prakash, J. A. Sheehy, *J. Am. Chem. Soc.* **2000**, *122*, 481.

[11] a) R. Minkwitz, S. Schneider, *Angew. Chem.* **1999**, *111*, 749; *Angew. Chem. Int. Ed.* **1999**, *38*, 714; b) R. Minkwitz, S. Reinemann, O. Becher, H. Hartl, I. Brüdgam, *Inorg. Chem.* **1999**, *38*, 844.

[12] M. Kaupp, O. L. Malkina, V. G. Malkin, *Chem. Phys. Lett.* **1997**, *265*, 55.

[13] Compare with $2p_\pi$-$5p_\pi$-bonded $[C(TeR)_3]^+$, see: D. Ohlmann, C. M. Marchand, H. Grützmacher, G. S. Chen, D. Farmer, R. Glaser, A. Currao, R. Nesper, H. Pritzkow, *Angew. Chem.* **1996**, *108*, 317; *Angew. Chem. Int. Ed. Engl.* **1996**, *35*, 300.

[14] I. Krossing, *Chem. Eur. J.* **2001**, *7*, 490.

[15] S. M. Ivanova, B. G. Nolan, Y. Kobayashi, S. M. Miller, O. P. Anderson, S. H. Strauss, *Chem. Eur. J.* **2001**, *7*, 503.

[16] a) I. Krossing, *J. Am. Chem. Soc.* **2001**, *123*, 4603; b) I. Krossing, L. van Wüllen, *Chem. Eur. J.* **2002**, *8*, 700.

[17] T. S. Cameron, A. Decken, I. Dionne, M. Fang, I. Krossing, J. Passmore, *Chem. Eur. J.* **2002**, *8*, 3386.

[18] a) I. Krossing, *J. Chem. Soc. Dalton Trans.* **2002**, 500; b) I. Krossing, I. Raabe, *Angew. Chem.* **2001**, *113*, 4544; *Angew. Chem. Int. Ed.* **2001**, *40*, 4406; c) M. Gonsior, I. Krossing, L. Müller, I. Raabe, M. Jansen, L. van Wüllen, *Chem. Eur. J.* **2002**, *8*, 4475.

[19] Synthesis of **1**: $Ag[Al(OR)_4]$ (1.05 g, 0.977 mmol) and CI_4 (0.52 g, 1.001 mmol) were weighed into a two-bulb frit plate vessel equipped with two J. Young valves. CH_2Cl_2 (10 mL) was condensed onto the solid mixture at −78 °C and the resulting dark red solution above the yellow precipitate (AgI) was stirred overnight at 0 °C. The suspension was filtered, and all volatiles were removed in vaccuo to leave 1.575 g nonvolatile material in the flask (theoretically expected **1** + AgI: 1.570 g). Dark red, soluble **1** was isolated (1.247 g, 94 %) and characterized by IR and NMR spectroscopy (see text). Crystals suitable for X-ray crystallography were obtained by recrystallizing some of the dark red material in very little CH_2Cl_2 (ca. 1 mL) at −80 °C.

[20] I. Krossing, I. Raabe, unpublished results.

[21] The unknown sublimation enthalpy of CI_4 ($M_r = 519$ a.u.) was estimated by linear extrapolation of the sublimation enthalpies[22] of CBr_4 (54.5 kJ mol^{-1}, $M_r = 332$ a.u.), $SnBr_4$ (62.8 kJ mol^{-1}, $M_r = 438$ a.u.), and TiI_4 (97.7 kJ mol^{-1}, $M_r = 556$ a.u.) as 88.3 kJ mol^{-1}. The lattice potential enthalpies of $Ag[Al(OR)_4]$ were estimated from the published thermochemical volumes[24] of $Al(OR)_4^-$ (0.758 nm^3)[23] and Ag^+ (0.004 nm^3),[24] and that of **1** from the unit cell volume divided by Z (0.867 nm^3) as 364 ($Ag[Al(OR)_4]$) and 350 kJ mol^{-1} (**1**). The sublimation enthalpy of AgI of 197.7 kJ mol^{-1} was taken from reference [22].

[22] D. R. Lide, *Handbook of Chemistry and Physics*, 76th ed., CRC, Boca Raton, FL, **1998**.

[23] I. Krossing, H. Brands, R. Feuerhake, S. Koenig, *J. Fluorine Chem.* **2001**, *112*, 83.

[24] H. D. B. Jenkins, H. K. Roobottom, J. Passmore, L. Glasser, *Inorg. Chem.* **1999**, *38*, 3609.

[25] Crystal structure determination of **1**: IPDS (Stoe), graphite-monochromated $Mo_{K\alpha}$ radiation, $T = 150(2)$ K, unit cell determination: 5000 reflections; Lorentz, polarization, and numerical absorption correction, $\mu = 2.95$ cm^{-1}; solution: direct methods with SHELXS-97, refinement against F^2 with SHELXL-97. Orthorhombic space group: $Pna2_1$, $Z = 4$, $a = 19.698(4)$, $b =$

 © 2003 Wiley-VCH Verlag GmbH & Co. KGaA, Weinheim

9.554(2), $c = 18.435(4)$ Å, $V = 3469.4(12)$ Å^3, $\rho_{calcd} = 2.603\ g\,cm^{-1}$, $2\theta_{max} = 52°$; reflections: 18432 collected, 6006 unique ($R_{int.} = 0.1321$), 4839 observed ($4\,\sigma$); 607 parameters, 103 SADI restraints (to fix the $C(CF_3)_3$ groups of the anion), $R_1 = 0.0671$, wR_2 (all data) $= 0.1550$, GooF $= 0.987$. CCDC-193387 contains the supplementary crystallographic data for this paper. These data can be obtained free of charge via www.ccdc.cam.ac.uk/conts/retrieving.html (or from the Cambridge Crystallographic Data Centre, 12, Union Road, Cambridge CB21EZ, UK; fax: (+44) 1223-336-033; or deposit@ccdc.cam.ac.uk).

[26] M. Hargittai, G. Schultz, P. Schwerdtfeger, M. Seth, *Struct. Chem.* **2001**, *12*, 377.

[27] Vibrational spectra of **1** were obtained in Nujol mull between AgBr plates on a Bruker IFS 66v spectrometer (CsI plates reacted with the CI_3^+ ion giving CI_4 and the Cs^+ aluminate). Full details of the vibrational spectra including Raman, resonance Raman as well as electronic spectra are subject to ongoing research and will be published later.

[28] a) A. Finch, I. J. Hyams, D. Steele, *Trans. Faraday Soc.* **1965**, *61*, 398; b) T. Wentink, V. H. Tiensuu, *J. Chem. Phys.* **1958**, *28*, 826.

[29] R. F. W. Bader, *Atoms in Molecules: A Quantum Theory*, Oxford University Press, Oxford, **1990**.

[30] Gaussian 98 (Revision A.7), M. J. Frisch, G. W. Trucks, H. B. Schlegel, G. E. Scuseria, M. A. Robb, J. R. Cheeseman, V. G. Zakrzewski, J. A. Montgomery, R. E. Stratmann, J. C. Burant, S. Dapprich, J. M. Millam, A. D. Daniels, K. N. Kudin, M. C. Strain, O. Farkas, J. Tomasi, V. Barone, M. Cossi, R. Cammi, B. Mennucci, C. Pomelli, C. Adamo, S. Clifford, J. Ochterski, G. A. Petersson, P. Y. Ayala, Q. Cui, K. Morokuma, D. K. Malick, A. D. Rabuck, K. Raghavachari, J. B. Foresman, J. Cioslowski, J. V. Ortiz, B. B. Stefanov, G. Liu, A. Liashenko, P. Piskorz, I. Komaromi, R. Gomperts, R. L. Martin, D. J. Fox, T. Keith, M. A. Al-Laham, C. Y. Peng, A. Nanayakkara, C. Gonzalez, M. Challacombe, P. M. W. Gill, B. G. Johnson, W. Chen, M. W. Wong, J. L. Andres, M. Head-Gordon, E. S. Replogle, J. A. Pople, Gaussian, Inc., Pittsburgh, PA, **1998**.

[31] The FIA values of several Lewis acids A were determined with experimental[32] and computational[33] methods; for the latter approach it was shown[33] that the isodesmic reaction (3) is best suited to obtain thermochemically reliable results:

$$A + OCF_3^- \rightarrow AF^- + OCF_2 \qquad (3).$$

The desired FIA value can then be assessed based on the experimental FIA value of OCF_2 (209 kJ mol^{-1}).[33a] We therefore used the isodesmic reaction (3) to establish the FIA values of all the $EX_3^{0/+}$ species.

[32] a) T. E. Mallouk, G. L. Rosenthal, G. Muller, R. Brusasco, N. Bartlett, *Inorg. Chem.* **1984**, *23*, 3167; b) S. Brownridge, I. Krossing, J. Passmore, H. D. B. Jenkins, H. K. Roobottom, *Coord. Chem. Rev.* **2000**, *197*, 397.

[33] a) K. O. Christe, D. A. Dixon, D. McLemore, W. W. Wilson, J. Sheehy, J. A. Bootz, *J. Fluorine Chem.* **2000**, *101*, 151; b) I.-C. Wang, K. Seppelt, *Angew. Chem.* **2001**, *113*, 3803; *Angew. Chem. Int. Ed.* **2001**, *40*, 3803; c) T. S. Cameron, R. J. Deeth, I. Dionne, H. D. B. Jenkins, I. Krossing, J. Passmore, H. Roobottom, *Inorg. Chem.* **2000**, *39*, 5614.

[34] Performed with the program TURBOMOLE.[35]

[35] TURBOMOLE, version 5: a) R. Ahlrichs, M. Bär, M. Häser, H. Horn, C. Kölmel, *Chem. Phys. Lett.* **1989**, *162*, 165; b) M. v. Arnim, R. Ahlrichs, *J. Chem. Phys.* **1999**, *111*, 9183.

[36] F. Weigend, M. Häser, *Theor. Chim. Acta* **1997**, *97*, 331.

[37] a) A. Schäfer, H. Horn, R. Ahlrichs, *J. Chem. Phys.* **1992**, *97*, 2571; b) A. Schäfer, C. Huber, R. Ahlrichs, *J. Chem. Phys.* **1994**, *100*, 5829.

[38] A. Klamt, G. Schürmann, *J. Chem. Soc. Perkin Trans. 1* **1993**, *2*, 799.

[39] This is in line with the earlier observation that cationic nonmetal main-group iodides maximize nonclassical π-bonding contributions in their structures; compare the structures of the isoelectronic P_2I_4 and $S_2I_4^{2+}$ species: As classically expected P_2I_4 is an all-σ-bonded C_{2h}-symmetric molecule, whereas the isoelectronic C_{2v}-symmetric $S_2I_4^{2+}$ ion maximizes π bonding and is best described as consisting of a $S_2^{0.67+}$ unit of bond order 2.33(!) that coordinates to two $I_2^{0.67+}$ units of bond order 1.33 through two four-center, π*–π* interactions, see: M. P. Murchie, J. P. Johnson, J. Passmore, G. W. Sutherland, M. Tajik, T. K. Whidden, F. Grein, *Inorg. Chem.* **1992**, *31*, 273.

 © 2003 Wiley-VCH Verlag GmbH & Co. KGaA, Weinheim



Helical Peptide Secondary Structure

The Fourth Helical Secondary Structure of β-Peptides: The (*P*)-2_8-Helix of a β-Hexapeptide Consisting of (2*R*,3*S*)-3-Amino-2-hydroxy Acid Residues**

*Karl Gademann, Andreas Häne, Magnus Rueping, Bernhard Jaun, and Dieter Seebach**

The proteomics era calls for synthetic mimics of protein architecture, as these structural analogues could fulfill protein-like molecular function.[1] Oligomers of β-amino acids (β-peptides) have recently emerged as the most prominent class of such proteomimetics.[2] Many different types of secondary structural elements such as helices, turns, and pleated sheets of β-peptides have been discovered, both in the solid state and in solution.[2] Exploiting these features has allowed the generation of compounds with new properties such as interesting biological activity.[3]

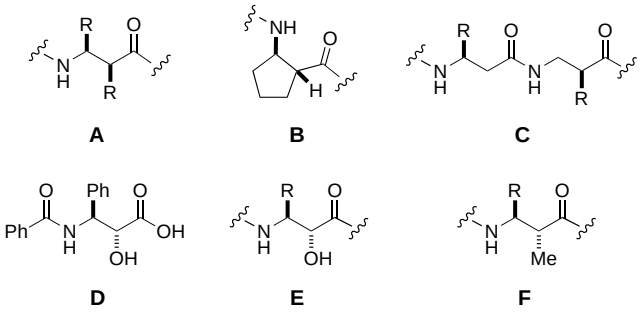
Up to now, three different types of helical structures based on different substitution patterns of the constituent β-amino acids have been identified. A 3_{14}-helix[4] was identified as the secondary structure of β-peptides composed of type **A** residues. In contrast, a 2.6_{12}-helical conformation is adopted by β-peptides, which are composed of *trans*-2-aminocyclopentanecarboxylic acid residues **B**.[5] An interesting case of helicity, unprecedented in α-proteins, was found for mixed β-peptides **C**: the helix comprises alternating 10- and 12-membered hydrogen-bonded rings.[6] Herein, we report compelling evidence for the formation of a fourth type of helical secondary structure of β-peptides (in MeOH solution),

[*] Prof. Dr. D. Seebach, Dr. K. Gademann, Dipl.-Chem. A. Häne, Dr. M. Rueping, Prof. Dr. B. Jaun
Laboratorium für Organische Chemie der
Eidgenössischen Technischen Hochschule Zürich
Hönggerberg, 8093 Zürich (Switzerland)
Fax: (+41) 1-632-11-44
E-mail: seebach@org.chem.ethz.ch

[**] K.G. thanks the ETH for a Nachwuchsförderungsstipendium and Prof. Dr. E. M. Carreira for financial support. Continuous support by Novartis Pharma (Basel) is gratefully acknowledged.

Supporting information for this article is available on the WWW under http://www.angewandte.org or from the author.

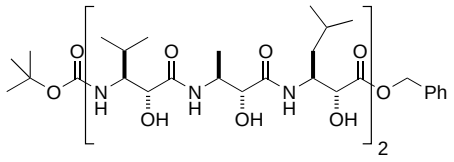
 © 2003 Wiley-VCH Verlag GmbH & Co. KGaA, Weinheim DOI: 10.1002/anie.200250290



which occurs if each amino acid residue has a hydroxy group in the 2-position (**E**).

β-Amino acids of this type have been extensively studied in the past two decades due to the presence of a 2-hydroxy-3-amino acid (as benzoyl derivative **D**) in the side chain of taxol. Two groups reported conformational analyses of oligomers of type **E** with 3-amino-2-hydroxy acid residues: Grierson and co-workers examined an α-silyloxy oligomer and used NMR spectroscopy and theoretical computations to assign an extended chainlike conformation.[7] Tromp et al. prepared an oligomer containing residues, which are diastereoisomers of **E,** but did not report conclusive evidence for its conformation.[8]

We became interested in synthesizing the β-hexapeptide **1** to study the conformational consequences of the attachment



1

of heteroatoms directly to the peptidic backbone.[9,10] The relative configuration *unlike* was chosen which should prevent folding to the 3_{14}-helix: Notably, the analogous compound (cf. **F**) with α-methyl substituents instead of α-hydroxy substituents has been shown to attain a pleated-sheet structure and to be extremely insoluble.[11] Surprisingly, the terminally protected β-peptide **1** was very soluble in CH_3OH. Moreover, the ^1H NMR spectrum in CD_3OH showed good dispersion of the signals from the backbone protons—an indication for the presence of a preferred conformation. Encouraged by these observations, we performed several 2D NMR experiments in CD_3OH to gather structural information on **1**.

All signals in the ^1H and ^{13}C NMR spectra were assigned by a combination of COSY, TOCSY, HSQC, and HMBC experiments,[12] and the coupling constants $J(NH,C_\beta H)$ and $J(C_\beta H,C_\alpha H)$ were extracted from the ^1H NMR spectrum. Upon inspection of these values, two conformational variables could be determined. We measured large values for $J(NH,C_\beta\text{-}H)$ of 9.0 to 10.6 Hz, in agreement with an *antiperiplanar* orientation of the NH and $C_\beta H$ atoms. In contrast, the observed small coupling constants $J(C_\beta H,C_\alpha H)$ of 2.3 to 3.9 Hz are in agreement with a preferential *synclinal* (*sc*) arrangement around the C_β–C_α bond. The differentiation between the (+)- and (−)-*sc* conformation was established by long-range C–H correlation experiments: No cross-peaks between the carbonyl-C and the C_β-H atom could be detected, corroborating a (+)-*sc* conformation around the central bond. All these experimental findings are consistent with a well-defined secondary structure in solution.

A series of ROESY spectra were acquired and 40 NOE cross-peaks were extracted and assigned.[12] The presence of weak NH_i to $NH_{(i+1)}$ cross-peaks and NOEs from NH_i to $C_{\beta(i-1)}$-H and to $C_{\alpha(i-1)}$-H atoms suggests a compact secondary structure. The cross-peaks were then integrated and transformed to distance restraints calibrated with known distances. The structure was calculated by employing the simulated annealing protocol of X-PLOR with 40 distance restraints, together with 12 dihedral angle restraints derived from the *J* values determined by using modified Karplus equations.[12] The calculation converged well and out of 50 structures the 20 lowest in energy with no NOE violations >0.2 Å were selected as representative for the secondary structure in solution (Figure 1).

Both terminal amino acid residues, in particular the protecting groups, as well as the side chains display fraying (Figure 1, left). The backbone, however, especially for residues 2–5 is well-defined (Figure 1, right; root mean square deviation (RMSD) of the backbone atoms = 0.82). The structure can be characterized as a right-handed helix with approximately two residues per turn and a pitch of 4.7–4.9 Å. The amide groups are aligned in a sequential up/down

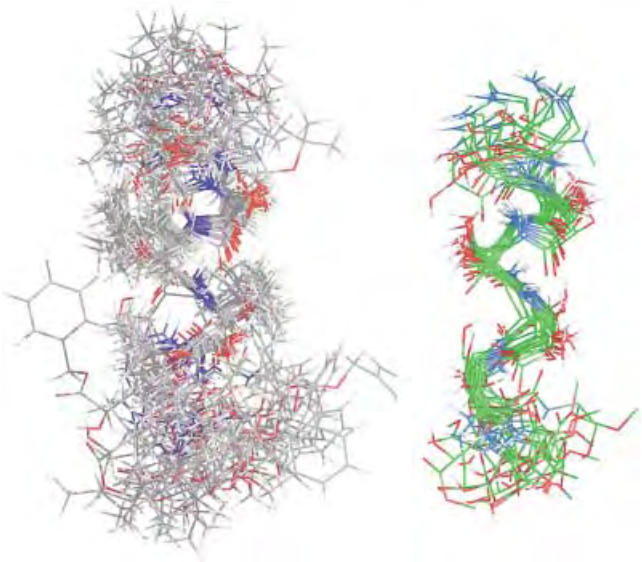


Figure 1. Structure of β-peptide **1** derived from NMR data. Left: Bundle of the 20 lowest-energy conformations with no violation of NOE restraints >0.2 Å and of dihedral restraints $>5°$, the structures are superimposed on the backbone atoms of residues 2–5 (color code: C: gray; H: white; N: blue; O: red). Right: View of the same bundle, with protecting groups, side chains, and hydrogen atoms omitted for clarity (color code: C: green; H: white; N: blue; O: red). Graphics program: MOLMOL.[16]

 © 2003 Wiley-VCH Verlag GmbH & Co. KGaA, Weinheim

arrangement twisted out from the helix axis. Moreover, the NMR structure calculation suggests a preferred arrangement around the CO–C_α dihedral angle with the carbonyl group and the α-hydroxy group in a *synperiplanar* arrangement. It was not possible by our NMR experiments to directly observe hydrogen bonds and hence no restraints for hydrogen bonds were introduced in the structure determination process. However, by simple inspection of the structural bundle, hydrogen bonds from α-hydroxy protons to the adjacent carbonyl groups appear reasonable. In addition, the formation of eight-membered hydrogen-bonded rings between the NH group of the amino acid *i* and the C=O group of the amino acid *i*−2 might be another contribution to the driving force for the formation of the secondary structure (Figure 2, left).

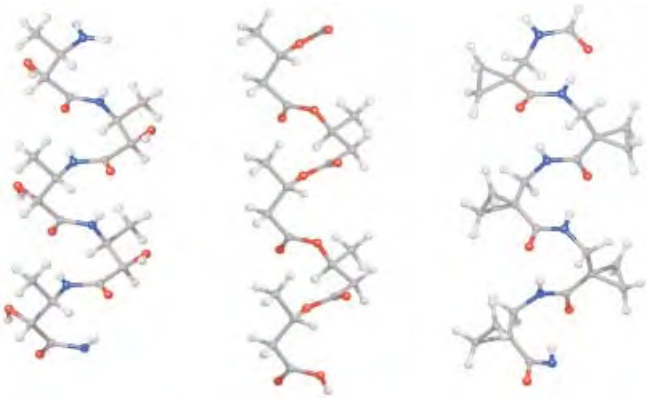


Figure 2. Comparison of the model structure of β-peptide **1** (left) with the fiber structure of poly((*S*)-3-hydroxybutanoate) determined by X-ray crystallography (center),[13] and the model derived from the crystal structure of the dimer, trimer, and tetramer of 1-aminomethylcyclopropanecarboxylic acid (right).[14]

A comparison of the torsion angles of the new helix with those of other secondary structures reveals a fascinating correlation. The structure type of β-peptide **1** (Figure 2, left) is reminiscent of the so-called 2_1-helix found for the polymer of β-hydroxybutanoic acid (PHB) (Figure 2, center).[13] The major difference in the structures is that the C=O bonds of the oligoester are almost perpendicular to the helix axis, whereas the amide planes in **1** form a smaller angle with the helix axis, making hydrogen bonding possible. Another related structure was modeled (from X-ray structural data of dimers, trimers, and tetramers) for an oligomer of 1-aminomethylcyclopropanecarboxylic acid (Figure 2, right). This structure contains folded eight-membered hydrogen-bonded rings, but differs only slightly from our new structure with regard to the torsion angle C_β-C_α-CO-N.[14] Finally, oligomers of β-aminoxymethanecarboxylic acids have been shown to adopt a similar structure (1.8_8-helix) with comparable backbone torsion angles.[15]

A search in the Cambridge Crystallographic Database revealed many similarities between the backbone torsion angles of our new helix and those of taxol derivatives. For example, ten out of eleven crystal structures display a *synperiplanar* arrangement of the C=O and the hydroxy groups. It might thus be concluded that the structural information for helix formation is "encoded" in the monomers.

Finally, it is remarkable that the replacement of methyl (**F**) by hydroxy (**E**) induces a dramatic change in secondary structure from pleated sheet to helix! Our investigation of the β-hexapeptide **1** extends the fascinating wealth of helical structures found in β-peptides. Moreover, different structures can be accessed by subtle changes of the building blocks used. We are confident that the structural arsenal of β-peptides will be used to generate protein-like architecture, and, ultimately, protein-like function.

Received: October 4, 2002 [Z50290]

Keywords: amino acids · beta-peptides · conformational analysis · peptidomimetics · secondary structure

[1] Reviews: D. J. Hill, M. J. Mio, R. B. Prince, T. S. Hughes, J. S. Moore, *Chem. Rev.* **2001**, *101*, 3893–4011; J. Venkatraman, S. C. Shankaramma, P. Balaram, *Chem. Rev.* **2001**, *101*, 3131–3152; S. H. Gellman, *Acc. Chem. Res.* **1998**, *31*, 173–180.

[2] Reviews: R. P. Cheng, S. H. Gellman, W. F. DeGrado, *Chem. Rev.* **2001**, *101*, 3219–3232; K. Gademann, T. Hintermann, J. V. Schreiber, *Curr. Med. Chem.* **1999**, *6*, 905–925; D. Seebach, J. L. Matthews, *Chem. Commun.* **1997**, *21*, 2015–2022. For β-carbopeptoids (carbohydrate amino acids), see: T. D. W. Claridge, J. M. Goodman, A. Moreno, D. Angus, S. F. Barker, C. Taillefumier, M. P. Watterson, G. W. J. Fleet, *Tetrahedron Lett.* **2001**, *42*, 4251–4255, and references therein.

[3] Selected examples: K. Gademann, M. Ernst, D. Hoyer, D. Seebach, *Angew. Chem.* **1999**, *111*, 1302–2304; *Angew. Chem. Int. Ed.* **1999**, *38*, 1223–1336; M. Werder, H. Hauser, S. Abele, D. Seebach, *Helv. Chim. Acta* **1999**, *82*, 1774–1783; E. A. Porter, X. F. Wang, H. S. Lee, B. Weisblum, S. H. Gellman, *Nature* **2000**, *404*, 565–566, Erratum: E. A. Porter, X. F. Wang, H. S. Lee, B. Weisblum, S. H. Gellman, *Nature* **2000**, *405*, 298–298; Y. Hamuro, J. P. Schneider, W. F. DeGrado, *J. Am. Chem. Soc.* **1999**, *121*, 12200–12201.

[4] D. Seebach, M. Overhand, F. N. M. Kühnle, B. Martinoni, L. Oberer, U. Hommel, H. Widmer, *Helv. Chim. Acta* **1996**, *79*, 913–941; D. H. Appella, L. A. Christianson, I. L. Karle, D. R. Powell, S. H. Gellman, *J. Am. Chem. Soc.* **1996**, *118*, 13071–13072.

[5] D. H. Appella, L. A. Christianson, D. A. Klein, D. R. Powell, X. L. Huang, J. J. Barchi, S. H. Gellman, *Nature* **1997**, *387*, 381–384.

[6] D. Seebach, K. Gademann, J. V. Schreiber, J. L. Matthews, T. Hintermann, B. Jaun, L. Oberer, U. Hommel, H. Widmer, *Helv. Chim. Acta* **1997**, *80*, 2033–2039; D. Seebach, S. Abele, K. Gademann, G. Guichard, T. Hintermann, B. Jaun, J. L. Matthews, J. V. Schreiber, *Helv. Chim. Acta* **1998**, *81*, 932–982.

[7] I. A. Motorina, C. Huel, E. Quiniou, J. Mispelter, E. Adjadj, D. S. Grierson, *J. Am. Chem. Soc.* **2001**, *123*, 8–17.

[8] R. A. Tromp, M. van der Hoeven, A. Amore, J. Brussee, M. Overhand, G. A. van der Marel, A. van der Gen, *Tetrahedron: Asymmetry* **2001**, *12*, 1109–1112; R. A. Tromp, Ph.D. thesis, Leiden University, The Netherlands, **2002**.

[9] For hydroxylated γ-peptides and a general discussion, see: M. Brenner, D. Seebach, *Helv. Chim. Acta* **2001**, *84*, 1181–1189.

[10] The aminohydroxy acids and the β-peptide **1** were prepared by established methods, see reference [9] and: M. T. Reetz, M. W. Drewes, K. Harms, W. Reif, *Tetrahedron Lett.* **1988**, *29*, 3295–3298.

 © 2003 Wiley-VCH Verlag GmbH & Co. KGaA, Weinheim

[11] D. Seebach, S. Abele, K. Gademann, B. Jaun, *Angew. Chem.* **1999**, *111*, 1700 – 1703; *Angew. Chem. Int. Ed.* **1999**, *38*, 1595 – 1597.
[12] Tables of ^{1}H and ^{13}C chemical shifts, *J* values, and NOE values, as well as spectra and full details of the structure determination process are included as Supporting Information. See http://www.angewandte.org for retrieval.
[13] Reviews: H. M. Müller, D. Seebach, *Angew. Chem.* **1993**, *105*, 483 – 509; *Angew. Chem. Int. Ed. Engl.* **1993**, *32*, 477 – 502; D. Seebach, M. G. Fritz, *Int. J. Biol. Macromol.* **1999**, *25*, 217 – 236; R. H. Marchessault, G.-E. Yu in *Biopolymers* (Ed.: A. Steinbrüchel), Wiley-VCH, Weinheim, **2002**, pp. 157 – 202.
[14] S. Abele, K. Vögtli, D. Seebach, *Helv. Chim. Acta* **1999**, *82*, 1539 – 1558.
[15] D. Yang, J. Qu, B. Li, F.-F. Ng, X.-C. Wang, K.-K. Cheung, D.-P. Wang, Y.-D. Wu, *J. Am. Chem. Soc.* **1999**, *121*, 589 – 590; Y.-D. Wu, D.-P. Wang, K. W. K. Chan, D. Yang, *J. Am. Chem. Soc.* **1999**, *121*, 11189 – 11196.
[16] R. Koradi, M. Billeter, K. Wüthrich, *J. Mol. Graphics* **1996**, *14*, 51 – 54.

 © 2003 Wiley-VCH Verlag GmbH & Co. KGaA, Weinheim

Protonated Fluorobenzene Isomers

Separate Spectroscopic Detection of Carbenium and Fluoronium Isomers of Protonated Fluorobenzene**

*Nicola Solcà and Otto Dopfer**

Protonation of aromatic molecules is of importance in many areas of chemistry and biology. Protonated aromatic molecules (AH^+) occur, for example, as intermediates in electrophilic aromatic substitution reactions, a typical reaction mechanism for aromatic molecules.[1] Solution studies established that central properties of such ion–molecule reactions depend sensitively on the environment.[1,2] Accordingly, a large number of mass spectrometric experiments have been carried out to analyze the intrinsic molecular electronic properties of AH^+ ions without the interference of solvation effects.[3] However, the results obtained provide only indirect and often disputable structural information (e.g., about the protonation site).[3] Spectral data for the direct and conclusive structural characterization of isolated AH^+ ions have become available only very recently,[4–6] as the usually low ion concentrations require the application of highly sensitive spectroscopic techniques.[7] In the past two years, IR photodissociation (IRPD) of either AH^+ ions or their weakly bound complexes ($AH^+{\cdot}L_n$) provided the first spectral determination of AH^+ geometries under controlled solvation conditions.[4–6] In $AH^+{\cdot}L_n$, the inert ligands L (e.g., L = Ar or N_2) act barely as a messenger and their weak intermolecular interaction with AH^+ has essentially no influence on the AH^+ properties. IRPD spectra of $C_6H_7^+{\cdot}L_n$ reveal that the σ complex of protonated benzene is more stable than the π complex.[5] Corresponding spectra of $C_6H_7O^+{\cdot}Ar_n$ demonstrate that protonation of phenol occurs preferentially at *para* and *ortho* position of the ring as well as at oxygen.[4] We report herein on IRPD spectra of $C_6H_6F^+{\cdot}(N_2)_2$, with the aim of characterizing carbenium isomers of protonated fluorobenzene. This work complements a recent IRPD study of bare $C_6H_6F^+$, in which selectively only the less stable fluoronium isomer was detected.[6]

Figure 1 shows the calculated structures and relative energies of the minima on the $C_6H_6F^+$ potential surface.[6,8,9] Protonation of C_6H_5F may occur at the aromatic ring to form carbenium (*C*-$C_6H_6F^+$, **1**–**4**) or at the F atom to form fluoronium ions (*F*-$C_6H_6F^+$, **5**). Their relative energies increase within the series: *p*-$C_6H_6F^+$ (**1**) < *o*-$C_6H_6F^+$ (**2**) ≪ *m*-$C_6H_6F^+$ (**3**) ≪ *i*-$C_6H_6F^+$ (**4**) ≪ *F*-$C_6H_6F^+$ (**5**). A large energy barrier separates **5** from the *C*-$C_6H_6F^+$ isomers **1**–**4**, whereas **1**–**4** are separated by smaller energy barriers. All *C*-$C_6H_6F^+$ minima are σ complexes and no stable π complex has been predicted from calculations. Early NMR studies on $C_6H_6F^+$ in solution are consistent with static **1** at low temperature.[10] All protons become equivalent at high temperature due to a rapid intramolecular 1,2-H-shift.[10] Only the σ complexes **1**–**3** were detected in solution; that is, **4**, **5**, and π complexes of $C_6H_6F^+$ were not observed.[10] Nearly all experiments on $C_6H_6F^+$ in the gas phase are based on mass spectrometric methods, and the

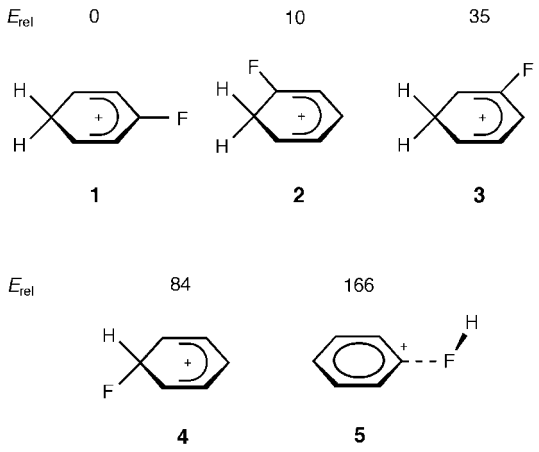


Figure 1. Structures and relative energies (E_{rel} in kJ mol^{-1}) of isomers of protonated fluorobenzene calculated at the B3LYP/6-311G(2df,2pd) level.[6] **1**: *p*-$C_6H_6F^+$ (C_{2v}); **2**: *o*-$C_6H_6F^+$ (C_s); **3**: *m*-$C_6H_6F^+$ (C_s); **4**: *i*-$C_6H_6F^+$ (C_s); **5**: *F*-$C_6H_6F^+$ (C_s).

[*] Priv.-Doz. Dr. O. Dopfer, Dipl.-Chem. N. Solcà
Chemistry Department
University of Basel
Klingelbergstrasse 80, 4056 Basel (Switzerland)
Fax: (+41) 61-267-3855
E-mail: otto.dopfer@unibas.ch

[**] This study was supported by the Swiss National Science Foundation (project No. 20-63459.00). O.D. is supported by a Heisenberg Fellowship from the Deutsche Forschungsgemeinschaft (DO 729/1-1). We thank Prof. Dr. H. Schwarz and Dr. D. Schröder (TU Berlin) for stimulating discussions.

 DOI: 10.1002/anie.200250730 © 2003 Wiley-VCH Verlag GmbH & Co. KGaA, Weinheim

two isomers observed are interpreted as *C*-$C_6H_6F^+$ (usually not further specified) and *F*-$C_6H_6F^+$ (**5**), with site-specific proton affinities (PAs) of 756 and 577 ± 24 kJ mol^{-1}, respectively.[6,9,11,12] The ratio of both isomers strongly depends on the experimental conditions (e.g., pressure, temperature, protonating agent). For example, **5** is produced in significant abundance using CH_5^+ for protonation, because of the similar PAs of CH_4 (544 kJ mol^{-1})[12] and C_6H_5F for F-protonation (577 ± 24 kJ mol^{-1}).[11a] In contrast, the production of **5** is suppressed when Brønsted acids with much smaller or larger PAs are used for protonation, leading to the selective preparation of *C*-$C_6H_6F^+$ isomers only.[9,11]

Recently, isolated *F*-$C_6H_6F^+$ (**5**) was characterized in detail by quantum-chemical calculations and IRPD spectroscopy (Figure 2).[6] F-protonation of C_6H_5F activates the

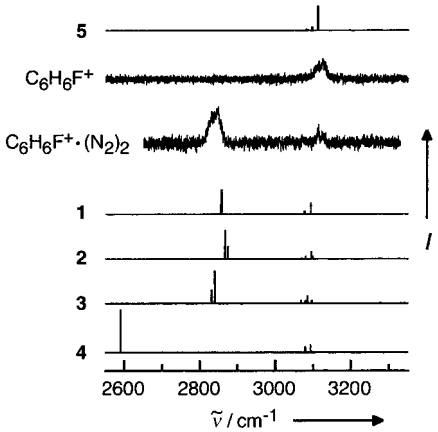


Figure 2. Experimental IRPD spectra of $C_6H_6F^+$ (recorded in the $C_6H_5^+$ channel)[6] and $C_6H_6F^+\cdot(N_2)_2$ (recorded in the $C_6H_6F^+$ channel) in the range of the C–H stretching modes are compared to calculated stick spectra of the five isomers of $C_6H_6F^+$.[6] The $C_6H_6F^+$ spectrum shows only absorptions of *F*-$C_6H_6F^+$, whereas the $C_6H_6F^+\cdot(N_2)_2$ spectrum is dominated by transitions of *p*-$C_6H_6F^+$ and *o*-$C_6H_6F^+$ (Table 1).

usually strong C–F bond, so that **5** is best described as a weakly bound ion–dipole complex between the phenyl cation and HF ($C_6H_5^+\cdot$FH; Figure 1). The low dissociation threshold of **5** with respect to dehydrofluorination (ca. 50 kJ mol^{-1}) can be exploited to record selectively the IRPD spectrum of this specific $C_6H_6F^+$ isomer in the $C_6H_5^+$ fragment channel (see Equation (1a) in the Experimental Section).[6] The absorptions in the ranges of the C–H and F–H stretching modes provide unambiguous spectroscopic confirmation of the $C_6H_5^+\cdot$FH notation of **5**. For example, the aromatic C–H stretch of **5** ($\sigma_{CH}(sp^2)$, ca. 3125 cm^{-1}, Table 1) is nearly unshifted from the corresponding $C_6H_5^+$ transition.[13] Moreover, Figure 2 shows excellent agreement between the experimental IRPD spectrum of $C_6H_6F^+$ and the IR spectrum calculated for **5**. Significantly, the IRPD spectrum of $C_6H_6F^+$ completely lacks absorptions of the more stable carbenium isomers **1**–**4**, although at least some of them are clearly produced in large abundance in the ion source using CH_5^+ for protonation.[6,9,11] IR spectra calculated for **1**–**4** demonstrate that the aliphatic C–H stretches of the (substituted) methylene group ($\sigma_{CH}(sp^3)$, ca. 2850 (**1**–**3**) and ca. 2600 cm^{-1} (**4**)) are

Table 1: Positions, widths (full-width half maximum), and assignments of the transitions ($\tilde{\nu}$ in cm^{-1}) observed in the IRPD spectra of $C_6H_6F^+$ and $C_6H_6F^+\cdot(N_2)_2$.

Species	Position (Width)	Assignment
$C_6H_6F^+$[a]	3125 (30)	σ_{CH} (sp^2) of *F*-$C_6H_6F^+$
$C_6H_6F^+\cdot(N_2)_2$[b]	3125 (8)	σ_{CH} (sp^2) of *C*-$C_6H_6F^+$
	3113 (5)	σ_{CH} (sp^2) of *C*-$C_6H_6F^+$
	2840 (36)	σ_{CH} (sp^3) of *C*-$C_6H_6F^+$
		$2\sigma_{CC}$ (sp^2) of *C*-$C_6H_6F^+$ (?)

[a] Reference [6]. [b] The observed clusters are probably composed of only the *C*-$C_6H_6F^+$ isomers **1** and **2**.

characteristic spectroscopic fingerprints of the *C*-$C_6H_6F^+$ isomers (Figure 2). The absence of these transitions in the IRPD spectrum of $C_6H_6F^+$ is rationalized by the large energy required for HF elimination for all *C*-$C_6H_6F^+$ isomers (> 160 kJ mol^{-1}), which is well above the IR photon energy (ca. 30–40 kJ mol^{-1}).[6,14,15]

In an effort to spectroscopically detect selectively only *C*-$C_6H_6F^+$ isomers, the IRPD spectrum of $C_6H_6F^+\cdot(N_2)_2$ was recorded in the $C_6H_6F^+$ fragment channel (see Equation (1b) in the Experimental Section). According to IRPD spectra and calculations for the related $C_6H_7^+\cdot(N_2)_2$ complex,[5] both N_2 ligands in *C*-$C_6H_6F^+\cdot(N_2)_2$ form weak intermolecular π bonds to the *C*-$C_6H_6F^+$ ring (with dissociation energies of the order of 800 cm^{-1} (ca. 10 kJ mol^{-1})). In contrast, in *F*-$C_6H_6F^+\cdot(N_2)_2$ one N_2 ligand is relatively strongly hydrogen-bonded to the acidic FH group of **5** (with a calculated dissociation energy of about 57 kJ mol^{-1}),[16] whereas the second ligand is probably π-bonded (ca. 10 kJ mol^{-1}). Hence, whereas the IR photon energy (ca. 30–40 kJ mol^{-1}) is sufficient to separate both N_2 ligands of *C*-$C_6H_6F^+\cdot(N_2)_2$, it is not enough to cleave both intermolecular bonds in *F*-$C_6H_6F^+\cdot(N_2)_2$. Consequently, the IRPD spectrum of $C_6H_6F^+\cdot(N_2)_2$ should selectively show absorptions of only the *C*-$C_6H_6F^+\cdot(N_2)_2$ isomers. Moreover, as both N_2 ligands are only weakly π-bonded to *C*-$C_6H_6F^+$, the IRPD spectra of *C*-$C_6H_6F^+\cdot(N_2)_2$ are expected to be very similar to that of the bare *C*-$C_6H_6F^+$ ions. For example, the corresponding complexation shifts in $C_6H_7^+\cdot(N_2)_2$ are less than 10 cm^{-1} (0.3%) in the range of C–H stretching modes.[5] The IRPD spectrum of $C_6H_6F^+\cdot(N_2)_2$ is indeed in close agreement with those calculated for the *C*-$C_6H_6F^+$ isomers **1**–**3**, confirming the small perturbation by the ligands. The spectrum is dominated by the symmetric and antisymmetric C–H stretching modes of the aliphatic CH_2 group ($\sigma_{CH}(sp^3)$, ca. 2840 cm^{-1}). Weaker absorptions at about 3125 and 3113 cm^{-1} ($\sigma_{CH}(sp^2)$) arise from aromatic C–H stretching modes (Table 1). Comparison with $C_6H_7^+\cdot(N_2)_2$ suggests that the band at 2840 cm^{-1} is possibly contaminated by a C–C stretch overtone ($2\sigma_{CC}(sp^2)$).[5] The widths of the transitions in the $C_6H_6F^+$ spectrum (≥ 30 cm^{-1})[6] are much larger than those of individual bands in the $C_6H_6F^+\cdot(N_2)_2$ spectrum (< 10 cm^{-1}) because of better effective cooling in the latter case.[15,17]

In the following, several plasma-chemical, thermochemical, theoretical, and spectroscopic arguments are presented that strongly suggest that the observed $C_6H_6F^+\cdot(N_2)_2$ spectrum arises mainly from complexes of **1** and **2**. First, $C_6H_6F^+$ is

 © 2003 Wiley-VCH Verlag GmbH & Co. KGaA, Weinheim

produced by protonation of C_6H_5F using acids XH^+ in which X has a PA very different from that of C_6H_5F for F-protonation (X (PA in kJ mol^{-1}) = He (178), H_2 (422) and N_2 (494)),[12] leading to nearly exclusive production of *C*-$C_6H_6F^+$ isomers.[9,11] Even if *F*-$C_6H_6F^+\cdot(N_2)_2$ were produced in significant abundance, the large total dissociation energy for both ligands (ca. 67 kJ mol^{-1}) prevents the observation of the IRPD process described in Equation (1b) (see Experimental Section). Previous experience with the generation of related AH^+ ions in the employed ion source[4,18] suggests that the production of **3** and **4** is probably very inefficient due to low isomerization barriers (35 and 15 kJ mol^{-1}, respectively) toward the significantly more stable *C*-$C_6H_6F^+$ isomers **1** or **2**.[6] Furthermore, the observed relative intensity ratios of the $\sigma_{CH}(sp^3)$ and $\sigma_{CH}(sp^2)$ transitions are in good agreement with those calculated for **1–3,** indicating that the $C_6H_6F^+\cdot(N_2)_2$ spectrum lacks large contributions from complexes of both **4** and **5**. Moreover, the calculated $\sigma_{CH}(sp^3)$ frequencies of **3** are significantly lower than those for **1** and **2** (by ≥ 20 cm^{-1}, Table 2). Hence, as (scaled) calculated frequencies tend to underestimate $\sigma_{CH}(sp^2)$ but overestimate $\sigma_{CH}(sp^3)$,[5] comparison with the spectra calculated for **1–3** implies only minor contributions of **3** to the $C_6H_6F^+\cdot(N_2)_2$ spectrum. In summary, although on the basis of the calculated and experimental spectra in Figure 2 alone a small contamination of clusters of **3–5** to the aromatic C–H stretching bands in the $C_6H_6F^+\cdot(N_2)_2$ spectrum cannot be completely ruled out, all arguments strongly suggest clusters of **1** and **2** to be by far the predominant carrier of the observed spectrum.

Table 2: Averaged bond lengths (r_{CH} in Å) and stretching frequencies (σ_{CH}: $\tilde{\nu}$ in cm^{-1}) of the aliphatic and aromatic C–H groups of the $C_6H_6F^+$ isomers.[a]

$C_6H_6F^+$	$r_{CH}(sp^2)$	$r_{CH}(sp^3)$	$\sigma_{CH}(sp^2)$	$\sigma_{CH}(sp^3)$
1	1.0818	1.1038	3085	2856
2	1.0816	1.1026	3086	2871
3	1.0824	1.1063	3082	2836
4	1.0822	1.1350	3084	2591
5[b]	1.0801		3097	

[a] Calculated at the B3LYP/6-311G(2df,2pd) level; harmonic vibrational frequencies are scaled by a factor of 0.96406. [b] Reference [6].

Table 2 compares the averaged lengths r_{CH} and stretching frequencies $\tilde{\nu}$ for σ_{CH} of the aromatic and aliphatic C–H bonds in all $C_6H_6F^+$ isomers **1–5**. As expected, $r_{CH}(sp^3)$ and $\sigma_{CH}(sp^3)$ are much more sensitive to the protonation site than $r_{CH}(sp^2)$ and $\sigma_{CH}(sp^2)$. Comparison with the corresponding data of $C_6H_7^+$[19] reveals that F substitution has a smaller effect on the aromatic C–H bonds, whereas the aliphatic C–H bonds in $C_6H_7^+$ are significantly weaker and longer than in **1** and **2**. These trends are in agreement with the experimental frequencies of $C_6H_7^+$ and *C*-$C_6H_6F^+$ ($\sigma_{CH}(sp^3)$, ca. 2800 and 2840 cm^{-1}, respectively), under the assumption that only complexes of **1** and **2** contribute to the $C_6H_6F^+\cdot(N_2)_2$ spectrum. On the other hand, the corresponding properties of $C_6H_7^+$ and **3** are very similar. Hence, the significant observed blue shift in the $\sigma_{CH}(sp^3)$ frequencies upon fluorination provides further spectroscopic support for the absence of complexes of **3** in the $C_6H_6F^+\cdot(N_2)_2$ spectrum, in agreement with the *ortho*/*para*-directing nature of the F substituent.

In conclusion, the carbenium and fluoronium isomers of protonated fluorobenzene (*C*-$C_6H_6F^+$ and *F*-$C_6H_6F^+$) have separately been detected and identified by means of IRPD spectroscopy of $C_6H_6F^+\cdot(N_2)_2$ and $C_6H_6F^+$, respectively. The spectroscopic approach complements previous mass spectrometric efforts to separate different $C_6H_6F^+$ isomers on the basis of their stability and reactivity.[9,11] In contrast to mass spectrometric studies, the IR spectra provide for the first time direct structural information of the observed isomers. The potential of the spectroscopic tools should allow the characterization of the protonation process of related (substituted) aromatic molecules and its dependence on the nature of the solvent, the degree of solvation, and the substitution of functional groups. The demonstrated spectroscopic preparation of **1** and **2** by reaction (1b) opens the possibility to further investigate gas-phase processes of these (and other) isomer selected arenium ions.

Experimental Section

IRPD spectra of $C_6H_6F^+$ and $C_6H_6F^+\cdot(N_2)_2$ were recorded in a tandem mass spectrometer coupled to an ion source and octopole ion trap.[6] The (cluster) ions were produced in a supersonic plasma expansion generated by electron ionization of a molecular beam. The expansion gas was produced by passing a suitable carrier gas at about 296 K and about 8 bar through a reservoir filled with liquid fluorobenzene. The gas mixture employed for the IR spectrum of $C_6H_6F^+$ was composed of CH_4 and Ar in the ratio 1:1. Chemical ionization of this mixture produced a significant amount of **5**.[6] The gas mixture used for the generation of $C_6H_6F^+\cdot(N_2)_2$ was H_2/He/N_2 in the ratio 1:1:20. Chemical ionization of this mixture suppressed the production of **5** and generated mainly *C*-$C_6H_6F^+$ isomers of $C_6H_6F^+$. Clusters with N_2 ligands were created by subsequent three-body association reactions. $C_6H_6F^+$ or $C_6H_6F^+\cdot(N_2)_2$ ions were selected by a quadrupole mass spectrometer and interacted in an adjacent octopole with a tunable IR laser pulse. Resonant vibrational excitation of $C_6H_6F^+$ or $C_6H_6F^+\cdot(N_2)_2$ parent ions induced vibrational predissociation according to Equations (1a) and (1b), respectively.

$$C_6H_6F^+ \xrightarrow{h\nu} C_6H_5^+ + HF \quad (1a)$$

$$C_6H_6F^+\cdot(N_2)_2 \xrightarrow{h\nu} C_6H_6F^+ + 2N_2 \quad (1b)$$

The produced fragment ions ($C_6H_5^+$ or $C_6H_6F^+$) were selected by a second quadrupole mass filter and monitored as a function of the IR wavenumber to obtain the IRPD spectra of the parent ions.

Received: December 10, 2002 [Z50730]

Keywords: arenium ions · aromatic substitution · carbocations · IR spectroscopy · reactive intermediates

[1] a) J. March, *Advanced Organic Chemistry: Reactions, Mechanisms, and Structure*, Wiley, New York, **1992**; b) G. A. Olah, *Acc. Chem. Res.* **1971**, *4*, 240.

[2] a) V. A. Koptyug, *Top. Curr. Chem.* **1984**, *122*, 1; b) D. M. Brouwer, E. L. Mackor, C. MacLean, in *Carbonium Ions, Vol. 2* (Eds.: G. A. Olah, P. von R. Schleyer), Wiley, New York, **1970**, p. 837.

[3] a) D. Kuck, *Mass Spectrom. Rev.* **1990**, *9*, 583; b) S. Fornarini, *Mass Spectrom. Rev.* **1996**, *15*, 365; c) S. Fornarini, M. E.

 © 2003 Wiley-VCH Verlag GmbH & Co. KGaA, Weinheim

Crestoni, *Acc. Chem. Res.* **1998**, *31*, 827; d) M. Speranza, *Mass Spectrom. Rev.* **1992**, *11*, 573; e) R. S. Mason, C. M. Williams, P. D. J. Anderson, *J. Chem. Soc. Chem. Commun.* **1995**, 1027.
[4] N. Solcà, O. Dopfer, *Chem. Phys. Lett.* **2001**, *342*, 191.
[5] a) N. Solcà, O. Dopfer, *Angew. Chem.* **2002**, *114*, 3781; *Angew. Chem. Int. Ed.* **2002**, *41*, 3628; b) N. Solcà, O. Dopfer, *Chem. Eur. J.* **2003**, in press.
[6] N. Solcà, O. Dopfer, *J. Am. Chem. Soc.* **2003**, *125*, 1421.
[7] E. J. Bieske, O. Dopfer, *Chem. Rev.* **2000**, *100*, 3963.
[8] a) R. F. W. Bader, C. Chang, *J. Phys. Chem.* **1989**, *93*, 5095; b) T. B. Maksic, B. Kovacevic, D. Kovacek, *J. Phys. Chem. A* **1997**, *101*, 7446; c) R. S. Mason, P. D. J. Anderson, C. M. Williams, *J. Chem. Soc. Faraday Trans.* **1998**, 2549.
[9] a) J. Hrusak, D. Schröder, T. Weiske, H. Schwarz, *J. Am. Chem. Soc.* **1993**, *115*, 2015; b) D. Schröder, I. Oref, J. Hrusak, T. Weiske, E. E. Nikitin, W. Zummack, H. Schwarz, *J. Phys. Chem. A* **1999**, *103*, 4609.
[10] G. A. Olah, Y. K. Mo, *J. Org. Chem.* **1973**, *38*, 3212.
[11] a) R. Mason, D. Milton, F. Harris, *J. Chem. Soc. Chem. Commun.* **1987**, 1453; b) R. S. Mason, A. J. Parry, D. M. P. Milton, *J. Chem. Soc. Faraday Trans.* **1994**, *90*, 1373; c) M. Tkaczyk, A. G. Harrison, *Int. J. Mass Spectrom. Ion Processes* **1994**, *132*, 73; d) F. Cacace, M. Speranza, *J. Am. Chem. Soc.* **1976**, *98*, 7299.
[12] E. P. L. Hunter, S. G. Lias, *J. Phys. Chem. Ref. Data* **1998**, *27*, 413.
[13] M. Winkler, W. Sander, *Angew. Chem.* **2000**, *112*, 2091; *Angew. Chem. Int. Ed.* **2000**, *39*, 2014.
[14] Multiphoton processes do not occur for the employed laser intensities of $< 200\ \mathrm{kW\,cm^{-2}}$.[15]
[15] N. Solcà, O. Dopfer, *Chem. Phys. Lett.* **2001**, *347*, 59.
[16] Calculations are carried out at the MP2/6-311G(2df,2pd) level. Further details are available from references [5,6].
[17] The effective rovibrational temperature of a cluster in a molecular beam is (partly) determined by the dissociation energy of the most weakly bound ligand. The stronger the intermolecular bond to this ligand, the more internal energy can be stored in the complex (before cooling through evaporation processes will become effective).
[18] N. Solcà, PhD thesis, University of Basel, **2003**.
[19] $r_{CH}(sp^3) = 1.1054$, $r_{CH}(sp^2) = 1.0819$ Å, $\sigma_{CH}(sp^3)$: 2845, $\sigma_{CH}(sp^2)$: 3085 $\mathrm{cm^{-1}}$.

 © 2003 Wiley-VCH Verlag GmbH & Co. KGaA, Weinheim

Prebiotic Fixation of Ammonia

A Possible Prebiotic Formation of Ammonia from Dinitrogen on Iron Sulfide Surfaces**

Mark Dörr, Johannes Käßbohrer, Renate Grunert, Günter Kreisel, Willi A. Brand, Roland A. Werner, Heike Geilmann, Christina Apfel, Christian Robl, and Wolfgang Weigand**

Dedicated to Professor Wolfgang Beck and Professor Wolfgang Seidel

How the formation of ammonia from dinitrogen occurs within the theory of the chemautotrophic origin of life under reducing conditions is a hitherto unanswered question. It has been argued that the biochemical process of ammonia formation, from dinitrogen, by iron–sulfur enzymes may be traced back to a prebiotic "pyrite-pulled" nitrogen fixation.[1]

Nitrogen-fixing bacteria convert molecular nitrogen (N_2) into ammonia (NH_3) at a rate of about 1.7×10^8 tons per year.[2] This reaction is catalyzed by nitrogenase enzymes, which operate under rather mild conditions at atmospheric pressure (10^5 Pa) and ambient temperature (273–323 K). The details of this reaction are largely unknown and are currently being discussed.[3] Recently an improved high-resolution X-ray structure analysis of the nitrogenase FeMo protein from *Azotobacter vinelandii* was reported.[4] The FeMo protein contains the FeMo cofactor, which comprises two cubanelike building blocks [4Fe:3S] and [Mo:3Fe:3S] linked by sulfide ligands and clearly accommodating a light atom, possibly nitrogen, in an interstitial void. Thus, the ubiquitous and abundant elements Fe and S play an important role in nitrogen fixation. They also form the central components of the much-discussed theory of a chemoautotrophic origin of life in a primordial iron–sulfur world.[1,5]

[*] Prof. Dr. W. Weigand, Dipl.-Chem. M. Dörr, Dipl.-Ing. (FH) C. Apfel, Prof. Dr. C. Robl
Institut für Anorganische und Analytische Chemie
Universität Jena
August-Bebel Strasse 2, 07743 Jena (Germany)
Fax: (+49) 3641-948102
E-mail: c8wewo@uni-jena.de

Prof. Dr. G. Kreisel, Dr. J. Käßbohrer, Dipl.-Ing. (FH) R. Grunert
Institut für Technische und Umweltchemie
Universität Jena
Lessingstrasse 11, 07743 Jena (Germany)
Fax: (+49) 3641-948402
E-mail: guenter.kreisel@uni-jena.de

Dr. W. A. Brand, Dr. R. A. Werner, H. Geilmann
Max Planck Institut für Biogeochemie
Winzerlaer Strasse 10, 07745 Jena (Germany)

[**] We would like to thank Prof. H. Schnöckel, Prof. D. Sellmann, Prof. K. O. Stetter, Prof. G. Wächtershäuser for helpful discussion, Dr. Rolf Russow (UFZ Halle) for nitrogen analysis and Dipl.-Ing. Marina Sammler for serving the pilot plant apparatus. We gratefully acknowledge financial support by the Deutsche Forschungsgemeinschaft (SFB 436/A8) and the Fonds der Chemischen Industrie.

 © 2003 Wiley-VCH Verlag GmbH & Co. KGaA, Weinheim DOI: 10.1002/anie.200250371

Herein we describe a method for the synthesis of NH_3 from N_2 using H_2S as a reductant and freshly precipitated iron sulfide as a mediator, which could have served as a primordial inorganic substitute for the enzyme nitrogenase. The reductant as well as the reaction conditions (atmospheric nitrogen pressure and temperatures of the order of 70–80 °C) are rather mild and comparable to biological processes. The driving forces of the overall reaction are the oxidation of iron sulfide to iron disulfide and the formation of hydrogen from H_2S.[6]

Hazen et al. reported a nitrogen reduction at temperatures between 300 and 800 °C and pressures of 0.1 to 0.4 GPa.[7] The molecular hydrogen necessary for this reduction was obtained from H_2O by using the magnetite/formic acid/metallic iron system as a reductant. Hazen et al. consider this a typical reaction, which could have taken place under conditions prevailing on the primordial earth.

In addition to the remarkable work done by biological scientists,[8] several models have been developed to study and understand how nitrogenase could work. These models are often based on low-molecular-weight compounds, such as metal complexes and metal hydroxide compounds. Important studies on the fixation of N_2 have been carried out by Shilov and Bazhenova:[9] Aqueous suspensions of Mo^{III}, Ti^{II}, V^{II}, Mn^{II}, and Ta^{III} hydroxides have been reported to reduce N_2 at pressures of approximately 10^7 Pa. Significant yields could be obtained from mixtures of V^{II} and Mg^{II} hydroxides. However, iron hydroxides did not reduce N_2 under the conditions chosen. The highest reaction rates were reported by Folkesson and Larsson for a catecholate V^{II} complex in methanol under a pressure of 1.5×10^6 Pa.[10]

Numerous experiments to reduce N_2 in nonaqueous environments have been made[11] since the pioneering work of Chatt et al.[12] A stepwise reduction of an end-on coordinated dinitrogen molecule via diazenido and hydrazido intermediates has been described.[13] Sellmann et al. synthesized a diiron diazene complex containing two pentadentate NS_4 ligands and characterized it by X-ray structure determination.[14–17] Diazene is considered to be an intermediate in the nitrogen-fixation process. This compound enabled Sellmann et al. to develop an alternative ammonia-formation model from N_2 and H_2 in the coordination sphere of metal–sulfur complexes.[15] Coucouvanis et al. reported structural analogues for the $MoFe_3S_3$ subunit in the nitrogenase cofactor and they discuss the accommodation and activation of N_2 by insertion into an Fe–Fe bond.[18]

Our approach uses the moderate reduction potential according to reaction (1) in the synthesis of ammonia by the following overall reaction (2; Scheme 1).[19] Thermodynamic calculations show that the redox system $FeS–H_2S/FeS_2$ is able to reduce dissolved molecular nitrogen to ammonia.[20]

$$FeS_{(s)} + H_2S_{(aq)} \longrightarrow FeS_{2(s)} + H_{2(g)} \quad (1)$$

$\Delta G^\circ = -38.6$ kJ/mol, $E^\circ = -600$ mV, pH = 6.5

$$N_{2(g)} + 3\,FeS + 3\,H_2S_{(aq)} \longrightarrow 3\,FeS_{2(s)} + 2\,NH_{3(g)} \quad (2)$$

Scheme 1. Synthesis of ammonia using iron sulfide and hydrogen sulfide.

To our knowledge, no successful attempts for the reduction of molecular nitrogen to ammonia in aqueous solutions at ambient pressure, with temperatures below 90 °C, and in the presence of iron sulfide have been reported.[20]

The activation energy of molecular nitrogen is high. The activation barrier can be reduced if N_2 is bound on a catalytically active surface. Thus, specific surface features of fresh iron sulfide are crucial for the N_2-fixing behavior. Commercially purchased or aged iron sulfide did not show any N_2-fixing activity. The surface of freshly precipitated iron sulfide can be regarded as a library of different Fe–S clusters, some of which are seemingly well tailored for the fixation and reduction of N_2. It may be assumed that molecular nitrogen is chemisorbed at the surface and subsequently protonated in a stepwise manner under acidic conditions. To obtain a sufficient amount of ammonia for quantification the reaction was carried out on a large-scale (Figure 1).

An iron sulfide suspension was prepared by the reaction of $FeSO_4$ with Na_2S in water at room temperature under argon. Under the scanning electron microscope the iron sulfide obtained revealed a highly rugged surface. The pH value was lowered to 3–4 by adding diluted H_2SO_4, which resulted in production of H_2S. Subsequently, highly purified N_2 was bubbled through the suspension for a period of two weeks using a flow rate of 0.5 L h^{-1}.

To retain or decompose all the nitrogen-containing contaminations (e.g. NO, NO_2, N_2O, NH_3), the N_2 used was purified in a four-step procedure (Figure 1): 1) N_2-gaspurifier, 2) $KMnO_4/H_2SO_4$, 3) 10 M KOH-solution, and 4) 0.1 N H_2SO_4 solution. The ammonia formed was released by adding NaOH and then transferred to a diluted high-purity H_2SO_4 solution using a flow of argon (5 L h^{-1}). The argon was purified prior to use by the same four-step procedure used for nitrogen. Ammonia was detected using a commercially available quantitative color test (MERCK). Ammonia formation proved to be reliably reproducible. The oxidation of sulfide to disulfide led to the formation of iron disulfide (pyrite) which was detected in the X-ray powder diffraction pattern.

Blank tests revealed that there was no appreciable ammonia formation without the presence of iron sulfide. Very low amounts of ammonia could be detected when using iron sulfide in an argon gas flow instead of a nitrogen gas flow. These amounts were significantly smaller ($< 10\,\%$) than in the reaction with N_2.

Final proof for ammonia formation from dinitrogen was obtained by carrying out the ammonia synthesis with ^{15}N labeled N_2, ($\delta^{15}N = 138$ ‰).[21] Isotope ratio mass spectrometry (IRMS) showed significant enrichment of ^{15}N in the synthesized $(NH_4)_2SO_4$.[22–24] An enrichment of up to 61 ‰ over the natural $^{15}N/^{14}N$ isotope ratio was detected. This result exceeds by a factor of 10 any possible enrichment from variation in the natural $^{15}N/^{14}N$ isotope distribution.

An ammonia yield of the order of 0.1 % (3 mmol), based on 3 mol of iron sulfide, was found to be typical. To estimate the yield of ammonia relative to dinitrogen appears to be without merit, since for experimental reasons, the reaction with dinitrogen could not be carried out in a closed system. Studies upon reactivity changes of the system as a function of time are in progress. Considering the long reaction times, as

 © 2003 Wiley-VCH Verlag GmbH & Co. KGaA, Weinheim

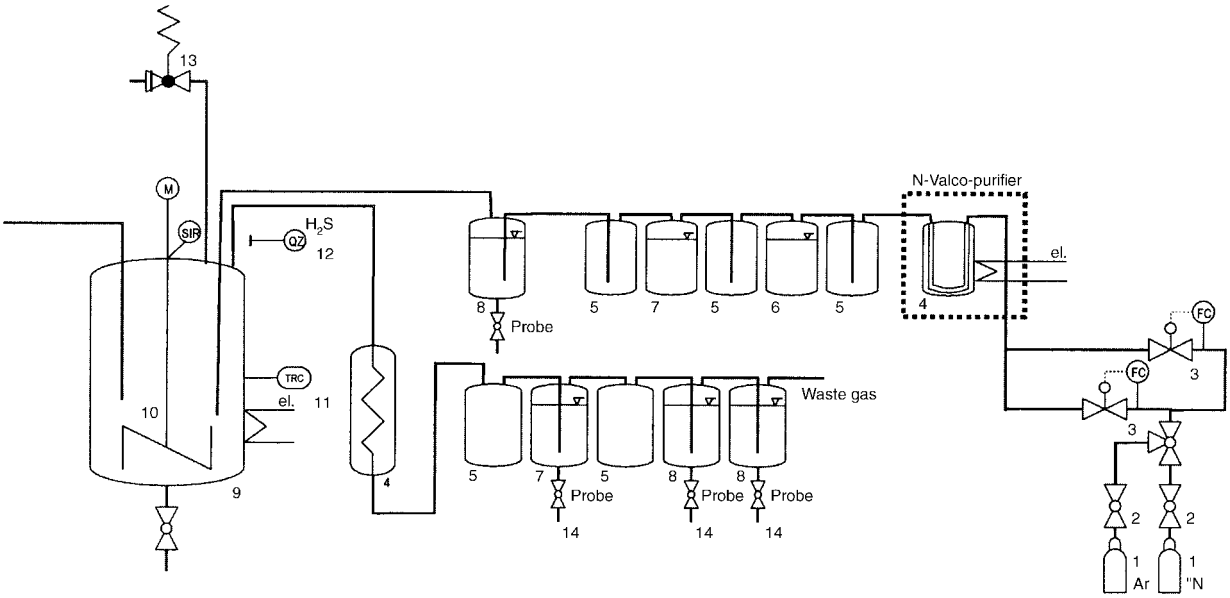


Figure 1. Flow scheme of pilot-plant size ammonia apparatus. 1) gas cylinders, 2) pressure control, 3) mass-flow controller, 4) N_2 gaspurifier (Valco Instr. Inc.), 5) security bottles, 6) oxidizing wash: acidic $KMnO_4$ solution, 7) alkaline wash: KOH, 8) acidic wash:0.001 N H_2SO_4, 9) 15-L reactor, 10) stirrer, 11) temperature control, 12) H_2S sensor, 13) safety valve, 14) NH_4^+ ion test.

well as the large amounts of iron sulfide and H_2S available on the primordial earth, a synthesis of ammonia similar to the one we describe herein could have contributed significantly to the ammonia budget on the early Earth. Hence, our synthesis of ammonia may serve as a model for a primordial nitrogen-fixing system and it conforms well with theories of chemoautotrophic origin of life.

Experimental Section

Iron(II) sulfate heptahydrate (834.1 g, 3 mol) and sodium sulfide nonahydrate (720.6 g, 3 mol) each were dissolved in 3 L of O_2-free water at room temperature. O_2-free water was obtained by heating water to 80 °C for 24 h while bubbling through high-purity argon. Both solutions were mixed at room temperature, followed by heating to 80 °C. To remove all nitrogen-containing compounds, the pH of the black iron sulfide suspension was raised to 13 using NaOH (10 M) and then heated for eight days to 80 °C while bubbling highly purified argon (5 $L\,h^{-1}$) through the suspension. Subsequently, the pH value was lowered to 4 by mixing the suspension with diluted H_2SO_4. Highly purified molecular nitrogen was then bubbled through the suspension (0.5 $L\,h^{-1}$) for seven days. The possible loss of H_2S was prevented by the steady formation of H_2S from FeS in the acidic solution, the pH of which was maintained between 3 and 4 over the entire reaction time. Finally, the pH value was raised to 13 with a solution of NaOH in water. Ammonia was released by passing argon through the suspension, and the ammonia was then captured in a solution of H_2SO_4 (0.001 N). The water was removed by evaporation. The resulting ammonium sulfate was directly suitable for the IRMS experiments, which were carried out on a Delta plus (XL) mass spectrometer (Finnigan MAT, Bremen). The powder-diffraction patterns were recorded using $Fe_{K\alpha}$ radiation to minimize the effects of X-ray fluorescence.

Received: October 16, 2002
Revised: January 31, 2003 [Z50371]

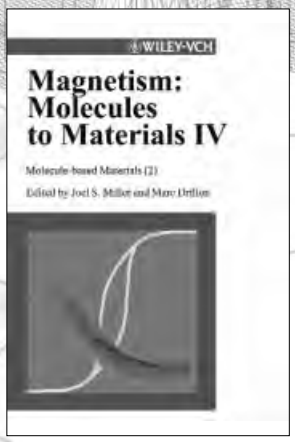
Keywords: iron · isotope labeling · nitrogen fixation · nitrogen · sulfur

[1] G. Wächtershäuser, *Prog. Biophys. Mol. Biol.* **1992**, *58*, 85–201.
[2] M. Appl, *Ammionia: Principles and Industrial Practice*, 1st ed, Weinheim, New York, **1999**.
[3] B. E. Smith, *Science* **2002**, *297*, 1654–1655.
[4] O. Einsle, F. A. Tezcan, S. L. A. Andrade, B. Schmid, M. Yoshida, J. B. Howard, D. C. Rees, *Science* **2002**, *297*, 1696–1700.
[5] G. Wächtershäuser, *Microbiol. Rev.* **1988**, *52*, 452–484.
[6] E. Drobner, H. Huber, G. Wächtershäuser, D. Rose, K. O. Stetter, *Nature* **1990**, *346*,742–744.
[7] J. A. Brandes, N. Z. Boctor, G. D. Cody, B. A. Cooper, R. M. Hazen, H. S. Yoder, Jr., *Nature* **1998**, *395* 365–367.
[8] B. K. Burgess, D. J. Lowe, *Chem. Rev.* **1996**, *96*, 2983–3011.
[9] T. A. Bazhenova, A. E. Shilov, *Coord. Chem. Rev.* **1995**, *144*, 69–145.
[10] B. Folkesson, R. Larsson, *Acta Chem. Scand. Ser. A* **1979**, *33*, 347–357.
[11] M. D. Fryzuk, S. A. Johnson, *Coord. Chem. Rev.* **2000**, *200*, 379–409, and references therein.
[12] J. Chatt, A. J. Pearman, R. L. Richards, *J. Chem. Soc. Dalton Trans.* **1977**, 1852–1860; J. Chatt, J. R. Dilworth, R. L. Richards, *Chem. Rev.* **1978**, *78*, 589–625.
[13] R. L. Richards, *Coord. Chem. Rev.* **1996**, *154*, 83–97, and references therein.
[14] D. Sellmann, A. Hennige, *Angew. Chem.* **1997**, *109,* 270–271; *Angew. Chem. Int. Ed. Engl.* **1997**, *36*, 276–278.
[15] D. Sellmann, J. Sutter, *Acc. Chem. Res.* **1997**, *30*, 460–469.
[16] D. Sellmann, J. Utz, N. Blum, F. W. Heinemann, *Coord. Chem. Rev.* **1999**, *192*, 607–627.
[17] D. Sellmann, A. Fürsattel, *Angew. Chem.* **1999**, *111,* 2142–2145; *Angew. Chem. Int. Ed.* **1999**, *38*, 2023–2026.
[18] D. Coucouvanis, J. Han, N. Moon, *J. Am. Chem. Soc.* **2002**, *124*, 216–224.

 © 2003 Wiley-VCH Verlag GmbH & Co. KGaA, Weinheim

[19] W. Weigand, G. Kreisel, J. Kässbohrer, M. Sammler, R. Grunert. Procedure for the production of ammonia, DE 98-19846242, 1998 [*Chem. Abstr.* **1998**, *132*, 239002].
[20] M. A. A. Schoonen, Y. Xu, *Astrobiology* **2001**, *1*, 133 – 142.
[21] Isotope ratios are reported in the delta notation, which is a relative deviation of a sample (sa) from a reference (ref), expressed in per mil "units": $\delta[‰] = (R_{sa}/R_{ref} - 1)\,1000$. For nitrogen, the $^{15}N/^{14}N$ ratio ($= R_{ref}$) in air dinitrogen defines the origin of the scale.
[22] W. A. Brand, *J. Mass Spectrom.* **1996**, *31*, 225 – 235.
[23] R. A. Werner, B. A. Bruch, W. A. Brand, *Rapid Commun. Mass Spectrom.* **1999**, *13*, 1237 – 1241.
[24] R. A. Werner, W. A. Brand, *Rapid Commun. Mass Spectrom.* **2001**, *15*, 501 – 519.

Magnetism: Molecules to Materials



J.S. MILLER, University of Utah, Salt Lake City, USA; **M. DRILLON**, Inst. de Physique et Chimie des Materiaux de Strasbourg, France (Eds)

As a depository of contemporary knowledge on key topics related to magnetism, this open series of volumes provides a much-needed comprehensive overview of this growing interdisciplinary field. In topical reviews written by foremost scientists trends and recent advances focusing on the correlations between electronic structure and magnetic properties are explained in a clear and detailed way. The balance between theory and experiment within this series will guide advanced students and specialists alike to this research area. It will help evaluate own experimental observations and serve as a base for the design of new magnetic materials. A unique reference work, indispensable for everyone concerned with the phenomena of magnetism!

Reviews for Volume II:
"... presents a good ... current overview of an active and diverse research area."
Journal of the American Chemical Society

NEW: Magnetism: Molecules to Materials IV
Molecule-based Materials (2)
2002. XI, 492 pp. 300 fig. HC
€ 159.-/£ 95.-/US$ 125.-
3-527-30429-0

Magnetism: Molecules to Materials III
Nanosized Magnetic Materials
2001. XV, 388 pp. 209 fig. 14 tab. HC
€ 139.-/£ 80.-/US$ 125.-
3-527-30302-2

Magnetism: Molecules to Materials II
Molecule-Based Materials
2001. XIV, 489 pp. 323 fig. 43 tab. HC
€ 159.-/£ 95.-/US$ 125.-
3-527-30301-4

Magnetism: Molecules to Materials I
Models and Experiments
2001. XVI, 437 pp. 270 fig. 33 tab. HC
€ 139.-/£ 80.-/US$ 125.-
3-527-29772-3

John Wiley & Sons, Ltd.
Baffins Lane Chichester, West Sussex, PO 19 1UD, UK
Fax: +44 (0)1243-775878

WILEY-VCH · P.O. Box 10 11 61 · 69451 Weinheim, Germany · Fax: +49 (0) 62 01-60 61 84 · e-mail: service@wiley-vch.de · http://www.wiley-vch.de

WILEY

WILEY-VCH

14602094_vi

 © 2003 Wiley-VCH Verlag GmbH & Co. KGaA, Weinheim

Cover Picture



Satoshi Yamamoto, Kenji Matsuda, and Masahiro Irie*

Absolute Asymmetric Photochromism in chiral crystals has enormous potential. The cover picture shows this phenomenon for 1,2-bis(2-methyl-5-(3-formylphenyl)-3-thienyl)perfluorocyclopentene, which has no chiral resources, but forms chiral crystals. Upon UV irradiation the diarylethene unit undergoes the photochromic reaction both in the single crystals and in solution, and each chiral crystal gives one enantiomer. The photocyclization/cycloreversion cycle can be repeated by using UV and visible light alternately. Details of the study are reported by M. Irie et al. on page 1636 ff.

Contents

News

Polymerization Catalysis: S. Mecking honored ——— 1562

Gas-phase Chemistry: H. Schwarz recognized ——— 1562

Polymers: Staudinger Prize to W. Kaminsky ——— 1562

Books

Naturally Dangerous ——— 1563 — James P. Collman — *reviewed by D. Lenoir*

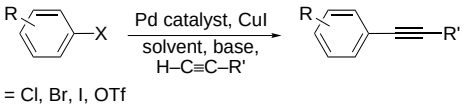
Guidelines for Achieving High Accuracy in Isotope Dilution Mass Spectrometry ——— 1564 — Mike Sargent, Chris Harrington, Rita Harte — *reviewed by K. G. Heumann*

Highlights

Advances in Sonogashira Reactions

R. R. Tykwinski* ——— 1566 – 1568

Evolution in the Palladium-Catalyzed Cross-Coupling of sp- and sp^2-Hybridized Carbon Atoms

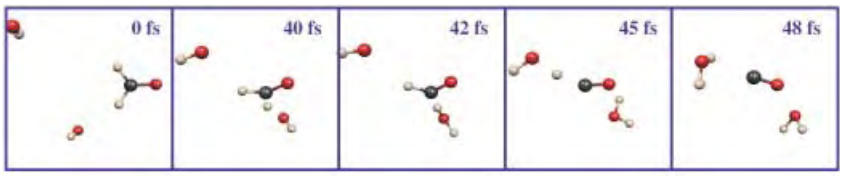


Palladium-catalyzed bond-formation between alkynes and aryl halides and triflates is as fascinating today as it was nearly 30 years ago when such reactions were introduced by Sonogashira (see scheme; OTf = CF_3SO_3). More facile procedures, new acetylide coupling partners, and more efficient catalysts and ligand systems all combine to expand the limits of this versatile reaction.

Molecular Dynamics Simulations

I. Frank* ——— 1569 – 1571

Chemical Reactions "On the Fly"



Molecular dynamics "on-the-fly" gives new insights in chemical reactivity on very short time scales. The pictures resulting from the simulations offer a precise and comprehensive view of chemical reactions in three-dimensional space. Processes such as the reaction between formaldehyde and two hydroxyl radicals shown here, as well as very complex reaction pathways, can be determined in this way.

Correspondence

Macrolamellar Structure?

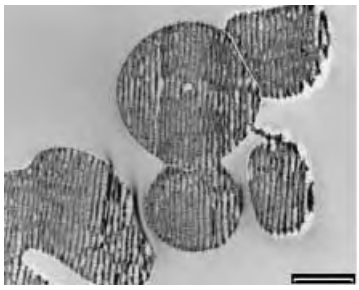
Z.-Y. Yuan, M.-F. Six-Boulanger, B.-L. Su* ——— 1572 – 1573

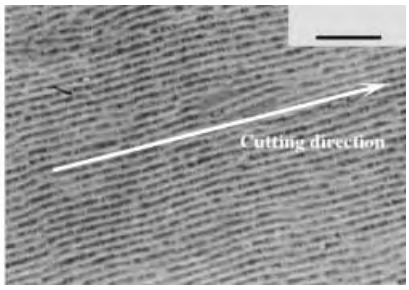
Do Mesostructured Materials Have an Unusual Macrolamellar Structure?

Microlamellar Structure?

A.-W. Xu* ——— 1574 – 1575

Additional Proof for the Existence of Microlamellar Structured ZSU-L Templated from Silicone Surfactants



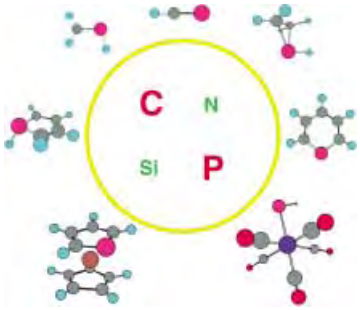


The macrolamellar structure observed in some highly ordered mesoporous materials (see left image: scale bar = 2 μm) has been suggested by Professor Su et al. to occur as a result of the ultramicrotoming process. Further evidence is now put forward by Professor Xu that attempts to show that such structural characteristics are, in fact, inherent to the ZSU-L material (see right image: scale bar = 1.5 μm).

© 2003 Wiley-VCH Verlag GmbH & Co. KGaA, Weinheim

Reviews

The great pretender: Phosphorus mimics quite closely the chemistry of carbon in its low coordination states (that is, one and two). The picture illustrates some of the molecules which highlight this analogy: clockwise from the top: phosphaacetylene, phosphirane, phosphinine, the transient phosphinidene complex [HP-$W(CO)_5$], phosphaferrocene, phosphole, and phosphaethene.

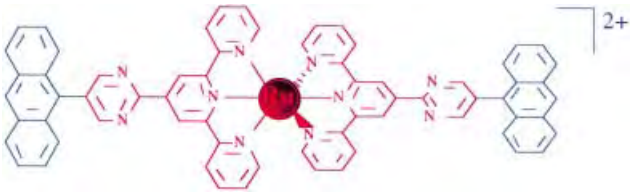


Organophosphorus Compounds

F. Mathey* ____ **1578 – 1604**

Phospha-Organic Chemistry: Panorama and Perspectives

Communications

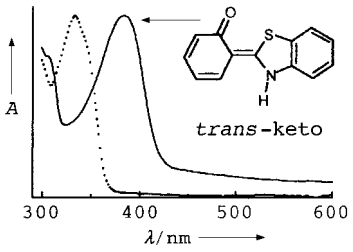


Time trials: A ruthenium(II) complex based on tridentate polypyridine ligands (see picture) featuring the longest luminescence lifetime (1.8 μs) ever reported is described. This new species has been obtained by applying the multichromophore approach, in which the various metal- and organic-based chromophores are only weakly interacting, so that their individual properties are essentially maintained.

Long-Lived Luminescence

R. Passalacqua, F. Loiseau, S. Campagna,* Y.-Q. Fang, G. S. Hanan* ____ **1608 – 1611**

In Search of Ruthenium(II) Complexes Based on Tridentate Polypyridine Ligands that Feature Long-lived Room-Temperature Luminescence: The Multichromophore Approach



Inside knowledge: UV/Vis (absorption spectrum depicted) and Raman data reveal the stabilization of the *trans*-keto tautomer of 2-(2-hydroxyphenyl)benzothiazole (HBT) inside the nanosized FAU zeolite. The *trans*-keto tautomer exhibits highly intensive fluorescence in the zeolite, as compared to the *cis*-keto tautomer, which is formed in solution during the excited-state intramolecular proton-transfer (ESIPT) process.

Nanostructured Functional Materials

S. Mintova,* V. De Waele, U. Schmidhammer, E. Riedle,* T. Bein* ____ **1611 – 1614**

In Situ Incorporation of 2-(2-Hydroxyphenyl)benzothiazole within FAU Colloidal Crystals

For the USA and Canada:
ANGEWANDTE CHEMIE International Edition (ISSN 1433-7851) is published weekly by Wiley-VCH PO Box 191161, D 69451 Weinheim, Germany. Air freight and mailing in the USA by Publications Expediting Inc. 200 Meacham Ave., Elmont, NY 11003. Periodicals postage paid at Jamaica NY 11431. US POSTMASTER: send address changes to *Angewandte Chemie*, Wiley-VCH, 111 River Street, Hoboken, NJ 07030. Annual institutional subscription price for institutions: Europe € 2998.00/3148.00. Outside Europe US$ 3718.00/3904.00 (valid for print or electronic/print and electronic delivery); for individuals who are personal members of a national chemical society, or whose institution already subscribes, or who are retired or self-employed consultants, print only (including postage and handling charges): Europe € 248.00/Outside Europe US$ 348.00.

 © 2003 Wiley-VCH Verlag GmbH & Co. KGaA, Weinheim

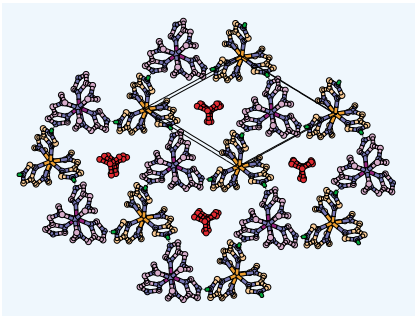
Contents

Mixed-Valent Spin-Crossover System

Y. Sunatsuki, Y. Ikuta, N. Matsumoto,* H. Ohta, M. Kojima, S. Iijima, S. Hayami, Y. Maeda, S. Kaizaki, F. Dahan, J.-P. Tuchagues — **1614 – 1618**

An Unprecedented Homochiral Mixed-Valence Spin-Crossover Compound

Spin doctoring: $[Fe^{II}H_3L][Fe^{III}L](NO_3)_2$, where H_3L is a hexadentate tripod ligand bearing three imidazole groups, is formed in a one-pot assembly reaction, and is shown to be a homochiral mixed-valence spin-crossover compound. The structure consists of a 2D assembled sheet that is held together by imidazole–imidazolate hydrogen bonds between $[Fe^{II}H_3L]^{2+}$ and $[Fe^{III}L]$ units (see picture). At least three electronic states can be accessed by temperature effects and photoirradiation.



Nanoparticle-Coated Electrodes

J. Cho,* Y.-W. Kim, B. Kim, J.-G. Lee, B. Park* — **1618 – 1621**

A Breakthrough in the Safety of Lithium Secondary Batteries by Coating the Cathode Material with $AlPO_4$ Nanoparticles



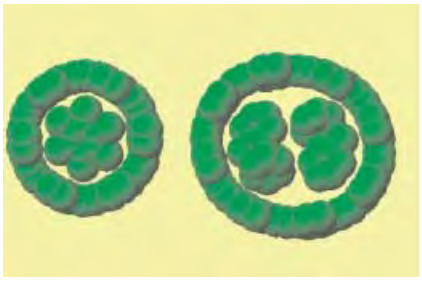
The hard cell! There have been numerous reports highlighting the questionable safety of lithium secondary batteries, an example of which is shown here, where exothermic reactions of $LiCoO_2$ electrodes have considerable fire and explosion potential. The coating of such electrodes with a layer of $AlPO_4$ nanoparticles is shown to reduce these risks significantly, even where a short circuit of the cell was observed.

Carbon Nanorings

T. Kawase,* Y. Seirai, H. R. Darabi, M. Oda,* Y. Sarakai, K. Tashiro* — **1621 – 1624**

All-Hydrocarbon Inclusion Complexes of Carbon Nanorings: Cyclic [6]- and [8]Paraphenyleneacetylenes

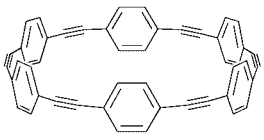
Ringing the changes: The belt-shaped π-conjugated [6]- and [8]paraphenylene-acetylenes exhibit nanosized cavities (see picture), and act as host molecules in crystalline inclusion complexes with hexamethylbenzene and toluene, respectively. The concave side of the cavities appears to possess a negative electronic potential.



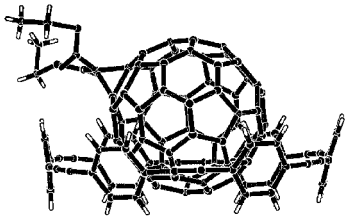
Nanoring–Fullerene Complexes

T. Kawase,* K. Tanaka, N. Fujiwara, H. R. Darabi, M. Oda* — **1624 – 1628**

Complexation of a Carbon Nanoring with Fullerenes

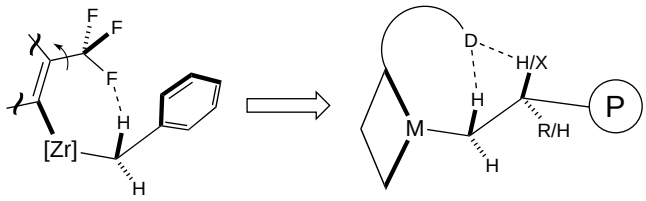


[6]CPPA



Unusually stable complexes are formed between [6]paraphenyleneacetylene ([6]CPPA, see picture) and fullerenes (either C_{60} or bis(ethoxycarbonyl)methanofullerene). Crystallographic analysis reveals that a major driving force for the formation of such complexes is the existence of a novel concave–convex π–π interaction (see structure).

© 2003 Wiley-VCH Verlag GmbH & Co. KGaA, Weinheim

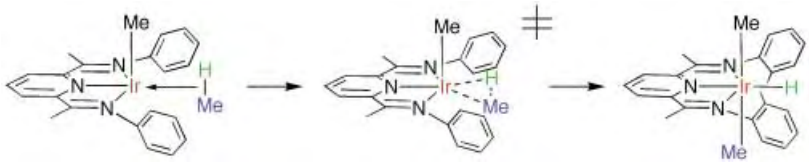


Attracting attention! The existence of *attractive* interactions between a functionalized ancillary ligand and a growing alkyl chain is a highly novel concept in olefin polymerization reactions (see scheme). Such interactions must be very weak so that the chain-propagation process is not perturbed, and "controversial" hydrogen bonds with strong dispersive character, such as CH···FC, are therefore ideal in this role (see scheme).

Weak Interactions in Polymerization

S. C. F. Kui, N. Zhu, M. C. W. Chan* ——— 1628 – 1632

Observation of Intramolecular C–H···F–C Contacts in Non-Metallocene Polyolefin Catalysts: Model for Weak Attractive Interactions between Polymer Chain and Noninnocent Ligand

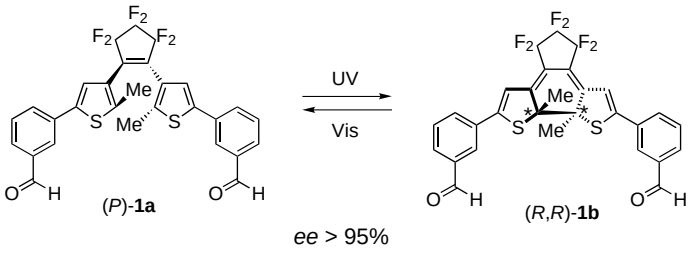


Teaching an old dog a new trick: A novel square-planar iridium(I) system undergoes facile thermal intermolecular C–H activation process at ambient temperature (see scheme). The observed unusual low activation barrier is analyzed and traced by DFT methods which provide guidelines for the design of novel systems, which would allow the activation of methane under mild conditions.

C-H Bond Activation

S. Nückel, P. Burger* ——— 1632 – 1636

Transition-Metal Complexes with Sterically Demanding Ligands: Facile Thermal Intermolecular C–H Bond Activation in a Square-Planar Ir^{I} Complex

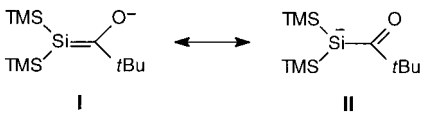


Chirality from the crystal lattice: The achiral diarylethene **1a** crystallizes in a monoclinic chiral space group, that is, two different kinds of crystals, (*M*)-**1a** and (*P*)-**1a**, are obtained. Photoirradiation of (*P*)-**1a** furnished optically pure closed-ring isomer (*R*,*R*)-**1b** in the single crystal (see scheme). The photochemical cycles can be repeated by alternating UV and visible photoirradiation.

Photochemistry of Chiral Crystals

S. Yamamoto, K. Matsuda, M. Irie* ——— 1636 – 1639

Absolute Asymmetric Photocyclization of a Photochromic Diarylethene Derivative in Single Crystals



Reversed Si=C bond polarity is displayed by the first isolable 2-silenolate. $[(TMS)_2SiC(O)tBu]^-K^+$, which is thermally stable at room temperature and structurally characterized by X-ray crystallography, contains a C=O double bond and a Si–C single bond with a strongly pyramidal Si center. These results in combination with NMR spectroscopic and atomic-charge data indicate that resonance structure **II** domincates the electronic structure. TMS = trimethylsilyl.

Stable Silenolates

T. Guliashvili, I. El-Sayed, A. Fischer, H. Ottosson* ——— 1640 – 1642

The First Isolable 2-Silenolate

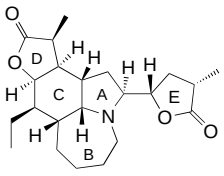
 © 2003 Wiley-VCH Verlag GmbH & Co. KGaA, Weinheim

Contents

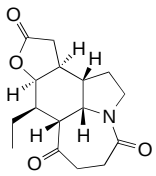
Natural-Product Synthesis

K. I. Booker-Milburn,* P. Hirst, J. P. H. Charmant, L. H. J. Taylor _____ **1642 – 1644**

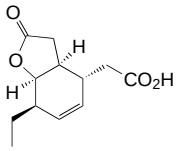
A Rapid Stereocontrolled Entry to the ABCD Tetracyclic Core of Neotuberostemonine



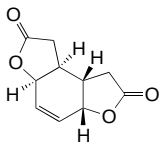
1



2



3



4

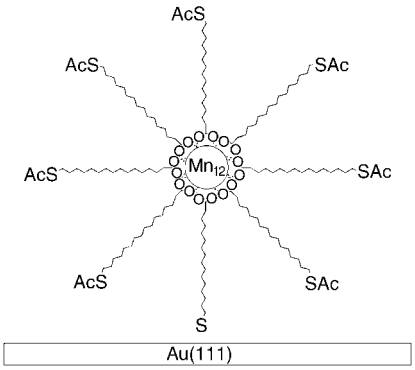
Four out of the five rings of the alkaloid neotuberostemonine (**1**) are present in the advanced precursor **2**. The tetracyclic compound **2** has now been prepared in a short, linear route via lactone acid **3**. A key step in the synthesis was the cuprate-mediated S_N2' ring-opening desymmetrization of the C_2-symmetric bislactone **4**.

Single-Molecule Magnets on Gold

A. Cornia,* A. C. Fabretti, M. Pacchioni, L. Zobbi, D. Bonacchi, A. Caneschi, D. Gatteschi, R. Biagi, U. Del Pennino, V. De Renzi, L. Gurevich, H. S. J. Van der Zant _____ **1645 – 1648**

Direct Observation of Single-Molecule Magnets Organized on Gold Surfaces

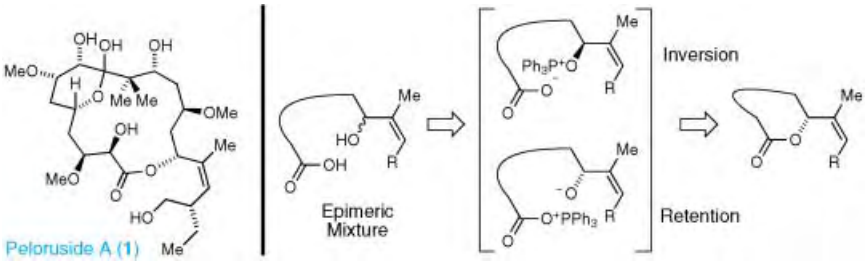
Scanning tunneling microscopy can be utilized to individually probe single-molecule magnets that have been deposited on gold substrates (see schematic). Dilute solutions (in $THF/H_2O/NH_4OH$) of a dodecamanganese(III,IV) cluster surrounded by acetyl-protected thiol groups, $[Mn_{12}O_{12}(L)_{16}(H_2O)_4]$, have been used to prepare Au(111) adsorbates that are a first step towards ultra-high-density information storage using single-molecule magnets.



Macrolide Total Synthesis

X. Liao, Y. Wu, J. K. De Brabander* _____ **1648 – 1652**

Total Synthesis and Absolute Configuration of the Novel Microtubule-Stabilizing Agent Peloruside A

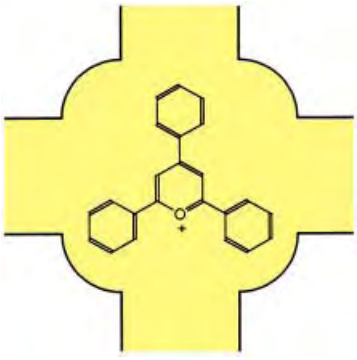


A unique configuration-dependent mechanistic switch, observed when epimeric seco-acids are subjected to typical Mitsunobu lactonization conditions, is just one of the many unexpected, yet insightful surprises of a synthetic adventure culminating in the first enantioselective total synthesis of the novel microtubule-stabilizing natural product peloruside A (**1**).

Cation-Containing Zeolites

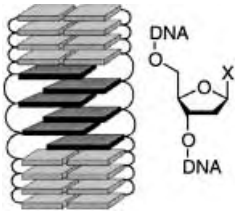
A. M. Amat,* A. Arques, S. H. Bossmann, A. M. Braun,* S. Göb, M. A. Miranda* _____ **1653 – 1655**

A "Camel through the Eye of a Needle": Direct Introduction of the TPP^+ Ion inside Y-Zeolites by Formal Ion Exchange in Aqueous Medium



Photocatalytic fillings for cavities: A very simple, yet highly efficient method to introduce triphenylpyrylium (TPP) ions into Y-zeolite cavities has been found (see picture). It consists of simply stirring the non-activated NaY-zeolite with an aqueous solution of triphenylpyrylium hydrogen sulfate at 40 °C, before drying the doped support. The FTIR and elemental analyses of the product (TPP-Y), as well as the repeated and reproducible photocatalytic reactivity of the TPP-Y confirm the presence of the TPP^+ electron acceptor inside the cavities of the support.

© 2003 Wiley-VCH Verlag GmbH & Co. KGaA, Weinheim



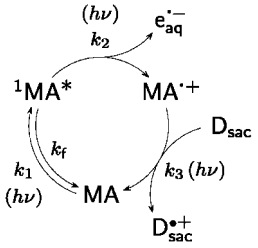
Back to basis: Short DNA duplexes can be packed with at least four hydrophobic, not-hydrogen-bonding biphenyl base pairs in the center of the sequence without compromising stability. Recognition of Bph occurrs by interstrand-stacking interactions as illustrated (X = biphenyl or bipyridyl). This new zipperlike recognition motif opens exciting possibilities for the introduction of new function into double-helical recognition systems based on the DNA backbone.

DNA Recognition

C. Brotschi, C. J. Leumann* **1655 – 1658**

DNA with Hydrophobic Base Substitutes: A Stable, Zipperlike Recognition Motif Based On Interstrand-Stacking Interactions

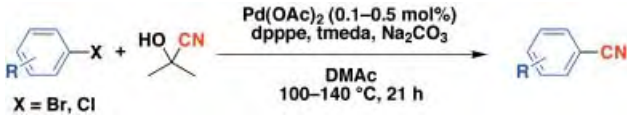
Sacrificial offerings: *N*-Methylacridon (MA) is a catalyst for the production of hydrated electrons $e^{\bullet-}_{aq}$ by a three-photon process, with the surfactant sodium dodecylsulfate acting as sacrificial donor (D_{sac}; see scheme).



Kinetics of Photoionization

M. Goez,*
B. H. M. Hussein **1659 – 1661**

Generation of Hydrated Electrons by an Acridone-Sensitized Three-Photon Cycle



A useful source of cyanide for the palladium-catalyzed cyanation of aryl halides is acetone cyanohydrin (see scheme; dppe = 1,5-bis(diphenylphosphanyl)pentane, tmeda = *N*,*N*,*N*′,*N*′-tetramethylethylenediamine). The key to the success of the reaction is the slow dosage of the cyanation reagent to the reaction mixture to prevent the deactivation of the palladium catalyst caused by excess cyanide ions in solution.

Synthesis of Benzonitriles

M. Sundermeier, A. Zapf, M. Beller* **1661 – 1664**

A Convenient Procedure for the Palladium-Catalyzed Cyanation of Aryl Halides

Communications labeled with this symbol have been judged by two referees as being "very important papers".

The publication of Communications labeled with this symbol has been accelerated because of their topical or highly competitive nature.

Supporting information for articles labeled with this symbol can be found at www.angewandte.org or www.interscience.wiley.com.

Deadline for recruitment adverts

16/2003	April 4	Publication date: April 29
17/2003	April 15	Publication date: May 9

Angewandte Chemie International Edition
Advertising Sales Department:
Marion Schulz
Phone: 0 62 01 – 60 65 65
Fax: 0 62 01 – 60 65 50
E-Mail: MSchulz@wiley-vch.de

Place an advert in the printed version and have it made available online for 1 month, free of charge!

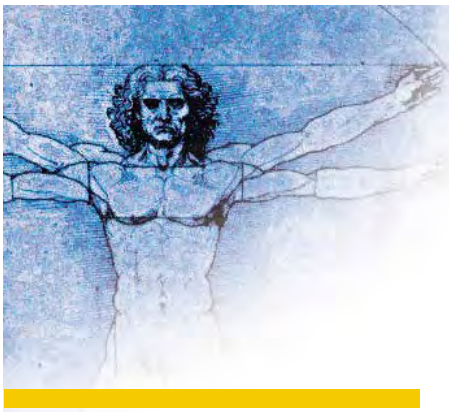
Service

Keywords **1666**

Authors **1667**

Preview **1669**

 © 2003 Wiley-VCH Verlag GmbH & Co. KGaA, Weinheim



Polymer Chemist Mecking to Receive Catalysis Award

Good news for Stefan Mecking, the Materials Research Center and Institute of Macromolecular Chemistry of the University of Freiburg (Germany): As an outstanding young researcher, he will receive the BASF Catalysis Award 2003 worth 10000 € during the "Heidelberg Forum of Molecular Catalysis" (June 27, 2003). The prize lecture is entitled "Catalysis and Polymerization with Nanoscale Multiphase Properties."



Stefan Mecking

Mecking earned his doctorate in 1994 from the Technical University of Aachen (Germany) under the guidance of Wilhelm Keim for a thesis entitled "Cooligomerization of ethylene with carbon monoxide by palladium complexes with hemilabile P,O-ligands." After a postdoc time with Maurice Brookhart in Chapel Hill, NC (USA), he joined Hoechst Corporate Research and Technology in Frankfurt (Main, Germany). He has worked at the University of Freiburg since 1998 to earn a habilitation in 2002. The research of his group is devoted to catalytic polymerization in water as a reaction medium and polymer-based functional colloids in catalysis. Recently, he published a Review on "Aqueous Catalytic Polymerization of Olefins" in *Angewandte*.[1]

Otto Hahn Award for Helmut Schwarz

The list of awards Helmut Schwarz has received during his career is certainly not a short one. A very prestigious one will now be added: the Otto Hahn Award for Chemistry and Physics. It commemorates the discovery of nuclear fission and has been given jointly by the German Chemical and Physical Societies at irregular intervals since 1955. The list of awardees includes renowned researchers such as Lise Meitner, Manfred Eigen, and Friedrich Hund.



Helmut Schwarz

After training as a chemical technician, Helmut Schwarz has resisted all temptation to leave the Technical University of Berlin for good despite numerous visiting appointments in Great Britain, Switzerland, Israel, France, Japan, and Australia: He earned his doctorate and habilitation under the guidance of the late natural-products chemist Ferdinand Bohlmann (1921–1991) and has been a professor of Organic Chemistry since 1983. Schwarz is a member of several academies in Germany, Great Britain, the Czech Republic, and Estonia and holds honorary doctorates of the universities of Jerusalem and Haifa.

Schwarz's research is undissociably linked to mass spectrometry and gas-phase chemistry. As a physical organic chemist, he is interested in the activation of C–C and C–H bonds and the role of metals in catalysis.[2] He is recognized for his achievements in chemistry, especially the fundamentally important processes on the molecular level in the gas phase, as well as physics through the continuous development of mass spectrometry. His Review on "Relativistic Effects in Gas-Phase Ion Chemistry: An Experimentalist's View" will appear in *Angewandte Chemie* soon.

Hermann Staudinger Prize to Walter Kaminsky

In memory of the pioneer of polymer chemistry who received the Nobel Prize 50 years ago, the German Chemical Society awards the Hermann Staudinger Prize every two years. This year, Walter Kaminsky (University of Hamburg, Germany) was awarded the prize in honor of his outstanding scientific achievements at the frontiers of industrial and polymer chemistry. The prize was given during the Macromolecular Colloquium in Freiburg (Germany) in February.



Walter Kaminsky

His pioneering advances in the field of catalytic olefin polymerization have stimulated the development of single-site catalysts which can be tailored to fine-tune property profiles of modern polymeric materials based upon 1-olefin and cycloolefin feedstocks. He is one of the leading scientists in the field of methylaluminoxane activators, homogeneous stereospecific metallocene catalysts,[3a] and cycloolefin homo- and copolymers.

Walter Kaminsky has been a most valuable member of the joint International Advisory Board of *Macromolecular Chemistry and Physics* and *Macromolecular Rapid Communications* since 1995.

Also see his recent contributions "Tuning the ligand structure in metallocene polymerization catalysts" and "New Pathways in Plastics Recycling."[3b,c]

[1] S. Mecking, A. Held, F. M. Bauers, *Angew. Chem.* **2002**, *114*, 564; *Angew. Chem. Int. Ed.* **2002**, *41*, 544.

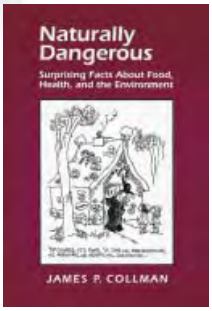
[2] D. Schröder, H. Schwarz, *Angew. Chem.* **1995**, *107*, 2126; *Angew. Chem. Int. Ed. Engl.* **1995**, *34*, 1973.

[3] a) W. Kaminsky, K. Külper, H. H. Brintzinger, F. R. W. P. Wild, *Angew. Chem.* **1985**, *97*, 507; *Angew. Chem. Int. Ed. Engl.* **1985**, *24*, 507; b) W. Kaminsky, F. Freidanck, *Macromol. Symp.* **2002**, *183*, 89; c) W. Kaminsky, F. Hartmann, *Angew. Chem.* **2000**, *112*, 339; *Angew. Chem. Int. Ed.* **2000**, *39*, 331.

 © 2003 Wiley-VCH Verlag GmbH & Co. KGaA, Weinheim



Naturally Dangerous



Surprising Facts about Food, Health, and the Environment. By *James P. Collman*. University Science Books, Sausalito, California 2001. 270 pp., hardcover £21.00.—ISBN 1-891389-09-2

Which substances and processes are potentially dangerous to people and to the environment? This book of ten chapters describes the benefits and dangers of everyday foodstuffs, delicacies, and medicines, and the effects of disease-causing agents, radioactive emissions, and metals. The author who has taken on the task of writing a clearly understandable book on this subject is not a scientific journalist, as one might assume, but a well-known chemist. He has avoided giving chemical formulas or equations, and has presented the facts and issues in a conversational style that can be understood by everyone. Thus, for example, a table listing amino acids gives only their names and whether they are essential or nonessential. Chirality is explained clearly and graphically by means of examples such as the human hand and snail shells. Most of the information is presented in the form of 27 figures (ten of which are in color) and nine tables. There are also many cartoons to maintain the reader's interest and prevent boredom. The book makes easy and relaxed reading, and non-chemists too will probably like it.

The first chapter is concerned with food products, and explains the constitution of carbohydrates, proteins, and fats, and their different roles. The author expresses the opinion that isomerization during the hydrogenation of unsaturated fats can result in the formation of "*trans* fats", which are therefore present in margarine and are a danger to health because of their carcinogenic potential. On another topic, it is now known that excessive consumption of chocolate can lead to addiction because it contains the alkaloid theobromine and exophins (peptides that stimulate pleasure centers in the brain). The brief history of chocolate which follows is full of interesting information. The average US citizen eats 10 kg of fat per year in the form of snacks, and as consumers try to correct that, sales of fat alternatives such as "Crisco" are booming. However, it has now been found that such "low calorie" fats have damaging side-effects. A table shows which foods are most likely to cause kidney stones consisting of calcium oxalate. The same chapter also explains in detail why eating the meat of wild animals such as deer can lead to trichinosis and other parasitic diseases.

In the chapters on pharmaceutical products and "natural" medicines, including homeopathic remedies, the reader learns about the uses and dangers of the various substances. The effects of using marihuana, opium, and heroin are described in detail. Many homeopathic remedies are not subject to regulation by the American Food and Drug Administration (FDA), and the book describes the damaging effects of some of these substances, and discusses, for example, the *Echinacae* extracts that are widely used in common cold remedies. The consumption and history of various types of alcoholic drinks is also treated at length here.

A chapter on the uses and/or dangers of microorganisms such as bacteria, molds, and viruses comes next, and is then followed by a discussion of the causes of cancers. The author states that contact with and ingestion of harmful man-made chemicals as residues in food is only responsible for about 2% of cancers. He claims that the average US citizen takes in about 1 g of "natural" pesticides daily, which is considerably more than is taken in as industrially produced pesticide residues in food. However, the nature and identity of the "natural" pesticides is not clearly explained. The author expresses the view that it is only since the development of modern techniques of trace and ultratrace analysis that residues of man-made chemicals have come to be seen as the main problem. He believes that excessive smoking and drinking and unhealthy eating habits are the main causes of cancer in humans.

The chapter on "Natural and Unnatural Molecules" begins by describing various natural toxins derived from animals and plants, then discusses aphrodisiacs and pheromones. Only three pages are devoted to man-made chemicals. We learn that the use of DDT is estimated to have saved the lives of about 300 million people who would have died of malaria, but the negative effects are not discussed. The following chapter, "Is the Sky Falling", contains a mainly open and factual discussion of the problems of acid rain, global warming caused by the increase in the concentration of greenhouse gases, and the effects of the hole in the ozone layer. On reading that "burning fossil fuels regenerates energy and turns the former plant products back into carbon dioxide" (p. 188), one is curious to know what is the author's view on why the USA has still not signed the 1997 Kyoto protocol about limiting carbon dioxide emissions; we find that he believes the main reasons are political. In the chapter on dust, magnetism, and sports such as scuba diving, one learns much about the associated risks, especially from the inhalation of asbestos and carbon particles. Aspects discussed here include the dangers that arise during the removal of asbestos from public buildings, and measures for reducing the emission of carbon particles from diesel engines. The chapter titled "We are all Radioactive" describes the sources and occurrence of "natural" radioactivity, but the risks arising from industrial activities such as disposing of spent nuclear fuel are only mentioned in passing.

Unfortunately the book belongs to the category of "educational" literature, in the sense that it has a message. The information about historical aspects is interesting and well presented. For example, we learn that before the invention of aspirin an extract from

 © 2003 Wiley-VCH Verlag GmbH & Co. KGaA, Weinheim

willow bark was used as an antipyretic agent. American readers will certainly find much useful information in the book and will be stimulated to join in the environmental debate. But the author's message to the public that comes out clearly from the book is this: the environmental pollutants and other dangers generally regarded as the main risks are comparatively harmless, and the dangers caused by consuming certain foods and delicacies are greater than those from man-made toxins. Based on a risk assessment procedure, Table 10 claims to list in order the 30 most important potentially fatal dangers to humans. Pesticide residues come well down the list, ranked 28th. This crude and undifferentiated analysis distorts and drastically oversimplifies the environmental debate. Following that theme the author contrasts scientists with "environmentalists" (also called "environmental advocates"). A curious idiosyncrasy is that instead of referring to anthropogenic (man-made) substances and activities, the author describes these as "anthropologic", a word that the referee could not find in any of the usual dictionaries.

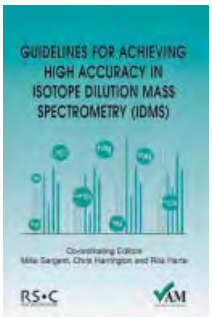
Perhaps the position taken by the author in this book is intended to rehabilitate the standing of the chemist in society. The author believes that the bad reputation of chemistry in the eyes of the public is largely caused by misinformation in newspapers and television, which he now hopes to counteract.

The book has a good subject index, but the choice of literature references is not balanced. A fundamental weakness of the book is that it tries to include too much information, attempting a scope that is too wide-ranging at the cost of neglecting depth and accuracy. The chapter on fats provides some examples of that. The general statement on page 17 that "lipids are water-insoluble biomolecules …" is incorrect, since many emulsifying agents are lipids that are partly soluble. Also not all lipids are "biomolecules", as is shown by the "fat substitutes" described in the same chapter. By the term "*trans* fats" the author presumably means *trans* fatty acids. Although *cis* fatty acids occur less frequently than the corresponding *trans* isomers, they are not "unnatural" as implied, since they are formed during the breakdown of *trans* fatty acids by metabolization in humans and animals. The author uncritically cites the alleged influence of the consumption of *trans* fatty acids on the incidence of breast cancer, whereas it is a matter of scientific controversy, and publications to the contrary should have been mentioned. Weaknesses such as these come to light on careful looking through the book. The description of the aromatic hydrocarbons present in gasoline as "mild carcinogens" (p. 166) is an incorrect generalization. Also the book completely fails to mention the effects of endocrine disruptors that have recently been discovered.

In this book the author has tried to cover in a brief form the whole field of environmental dangers. It should be read with a critical attitude, and can only be recommended with reservations.

Dieter Lenoir
GSF Forschungszentrum
Neuherberg/München (Germany)

Guidelines for Achieving High Accuracy in Isotope Dilution Mass Spectrometry (IDMS)



Edited by *Mike Sargent, Chris Harrington* and *Rita Harte*. Royal Society of Chemistry, Cambridge 2002. 50 pp., paperback £ 29.95.––ISBN 0-85404-418-3

The aim of this little paperback book, as stated at the beginning, is to describe procedures in isotope dilution mass spectrometry (IDMS) that will enable laboratories to obtain reliable analytical data for specific applications, without themselves having to undertake the considerable work of developing suitable protocols. It is mainly based on the findings of a sub-committee that forms part of a Valid Analytical Measurement (VAM) program set up by the UK Department of Trade and Industry, aimed at defining accurate and reliable analytical procedures. Although the book has not achieved its ambitious aims completely in every detail, it can be said at once that it will be useful to every analytical laboratory which, in view of the increasing importance of validating analytical data, wishes to begin using the highly reliable method of IDMS.

The principle of the isotope dilution method is that one adds to the analytical sample a precisely known amount (the "spike") of the element that is to be determined, in isotopically enriched form, or, in the case of molecular analysis, of an isotopically labeled form of the compound in question. After allowing time for equilibration between the original sample and the spike, whereby the spike becomes diluted, one measures the resulting isotope ratio, usually by mass spectrometry (hence IDMS). Since its introduction, IDMS has already proved to be very successful for some specific applications, especially for the determination of uranium and the transuranium elements in nuclear technology, and of radioactive nuclides in the dating of geological specimens. Other fields in which the method has become very important are the analysis of clinical specimens, some special types of environmental problems (e.g., determination of dioxins), and in connection with the certification of concentrations of elements in reference materials. In all these cases the reason for using IDMS is the necessity to achieve a high level of accuracy in the analytical data. Until recently the main obstacle preventing wider use of the method in the areas of elemental trace and element species analysis was the need for laborious sample preparation, to enable the measurements to be carried out by thermal ionization mass spectrometry (TIMS). However, in recent years the level of interest in applying IDMS in those areas has risen sharply because of the enormous growth in the use of inductively coupled plasma mass spectrometry (ICP-MS), with the advantages of easier sample preparation in most cases, multi-element capability, and—for the identification of element species—the ease of on-line coupling to chromatographic methods.

The book begins by listing and discussing the advantages and disadvan-

 © 2003 Wiley-VCH Verlag GmbH & Co. KGaA, Weinheim

tages of IDMS. The main advantage is that, subject to certain preconditions, it can yield accurate and reliable analytical data, so that it is now widely regarded internationally as a definitive method. Provided that complete equilibration between the spike and the sample has occurred, one can be confident that the analytical result is not affected by any loss of material, as the only quantity measured is the isotope *ratio*, rather than an amount of material that must be isolated from the analyte. However, the book's discussion of the advantages and disadvantages contains some statements that might result in a misleading evaluation of IDMS. For example, it is wrongly stated that the *accuracy* of an IDMS analysis is determined by the *precision* with which the isotope ratio can be measured. Since the determination of the isotope ratio requires the measurement of the MS peaks of two isotopes (or of two different mass numbers in the case of molecular analysis) free from spectroscopic interferences, the possibility of such interferences is a significant source of error in IDMS analysis. Also the mention of the (supposedly high) cost of the isotopically enriched spike as a disadvantage is only justified in some circumstances. Apart from a few exceptions, the IDMS method is still used almost exclusively for trace analysis. In these applications the optimal amount of the spike to be added is of the same order as the amount of the element present in the sample. For trace analysis that typically requires one to use a few micrograms of the spike or even less. Since 1 μg of an isotopically enriched material is likely to cost only between $ 0.001 and $ 1, that is not of much practical importance for elemental trace analysis. On the other hand, for organic molecular analysis or element species analysis, where one has to take into account the time needed to synthesize an isotopically enriched compound in one's own laboratory (because very few isotopically labeled compounds are yet commercially available), the IDMS analysis can be relatively expensive.

The book has a number of defects. For example, some of the literature citations mentioned in the text are missing from the list of "Keynote References", the diagrams for determining the optimum quantities of spike to be added are very badly drawn, and are only valid for a spike with an arbitrarily assumed level of isotopic enrichment, and the book neglects the use of IDMS for element species analysis, an application that is becoming increasingly important. But for the reader who is not too disturbed by these shortcomings, this little book at least offers a compact and useful introduction to the fundamentals of IDMS. However, laboratories intending to begin using IDMS should not regard the book as a substitute for reading some important review articles and original papers on the subject.

Klaus G. Heumann
Institut für Anorganische Chemie
und Analytische Chemie
Universität Mainz (Germany)

 © 2003 Wiley-VCH Verlag GmbH & Co. KGaA, Weinheim

Advances in Sonogashira Reactions

Evolution in the Palladium-Catalyzed Cross-Coupling of sp- and sp²-Hybridized Carbon Atoms

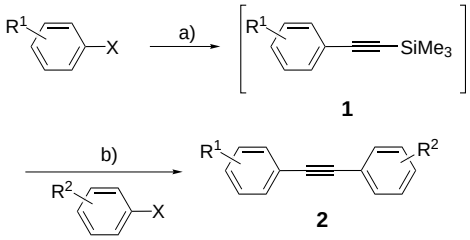
*Rik R. Tykwinski**

Keywords:
alkynes · C–C coupling · cross-coupling · heterogeneous catalysis · Sonogashira reactions

The carbon–carbon triple bond is a ubiquitous structural feature of organic molecules.[1] Alkynes, for example, are outstanding building blocks for unsaturated molecular scaffolds because of their rigid structure and conjugating π system(s). They are a surprisingly common feature of natural products that have been isolated from plants and marine organisms, and they are also a common motif in drugs, for example, in enediyne antibiotics and the contraceptive pill. Furthermore, their unsaturated, high-energy structure makes alkynes an attractive functional group for further derivatization in many synthetic transformations.

In the arena of alkyne chemistry, one of the most significant developments over the past 30 years is the Sonogashira reaction: the palladium-catalyzed cross-coupling between vinyl/aryl halides and terminal acetylenes in the presence of CuI.[2] Since its introduction in 1975, numerous modifications to Sonogashira's original protocol have been reported, and improvements for many aspects of sp–sp² carbon-bond formation under palladium catalysis have been achieved.[3] The past few years have been no exception, as extensive research continues to push the limits of this methodology through the discovery and development of more facile procedures, improved metal acetylide coupling partners, as well as more active palladium catalysts for cross-coupling with unactivated arenes.

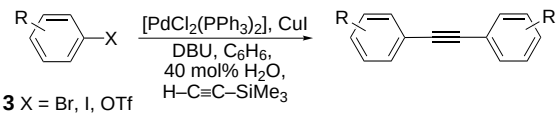
A single Sonogashira cross-coupling reaction is straightforward. The iterative assembly of extended molecules, however, quite often employs an alkynyl trialkylsilyl group in a rather tedious step-wise sequence consisting of: 1) cross-coupling of the alkynyl silane, 2) protiodesilylation, and 3) a second cross-coupling step to afford the desired product. The efficiency of this process can be substantially improved using the "sila"-Sonogashira coupling, introduced by Mori, Nishahara, and co-workers.[4,5] In this case, the trimethylsilyl protecting group is removed in situ to afford the terminal acetylene, which is coupled directly to afford the desired diaryl acetylene (Scheme 1).[6] This one-pot coupling protocol still incorporates two distinct steps. First, cross-coupling of an aryl triflate with (trimethylsilyl)acetylene under copper-free conditions gives intermediate **1**. This is followed by the addition of a copper salt that promotes both in situ desilylation and the second coupling event to an electron-deficient aryl triflate (Scheme 1).



Scheme 1. One-pot synthesis of unsymmetrical bisaryl ethynes, by the sila-Sonogashira reaction. For X = OTf (Mori/Nishihara): a) $[Pd(PPh_3)_4]$, NEt_3/DMF, $HC{\equiv}CSiMe_3$, 60 °C, 6 h; b) CuCl, 80 °C, 12 h. For X = I (Brisbois/Grieco): a) $[PdCl_2(PPh_3)_2]$, CuI, NEt_3, C_6H_6, $HC{\equiv}CSiMe_3$, RT, 18 h; b) DBU, H_2O, RT, 18 h.

The scope of the sila-Sonogashira reaction has been substantially broadened recently by Brisbois, Grieco, and co-workers (Scheme 1).[7] Their procedure utilizes traditional Sonogashira conditions for the first coupling step of a terminal alkyne to an aryl iodide. This is followed by addition of a sub-stoichiometric amount of water and 1,8-diazabicyclo[5.4.0]undec-7-ene (DBU, 6 equiv), which effects desilylation and cross-coupling to the second aryl iodide, to give **2**. Using a similar catalytic system, symmetrically substituted diaryl ethynes are easily produced from a variety of electrophilic aryl precursors **3** in a single step (Scheme 2). It is noteworthy that the presence of DBU is essential to the success of the second cross-coupling event.

Whereas the traditional Sonogashira coupling is believed to involve a copper acetylide intermediate, numerous other metal acetylides can also be utilized.[8] Blum and co-workers[9] have shown that tetraalkynyl aluminate salts **4**, which are easily prepared in situ from $NaAlH_4$ and a terminal acetylene, are quite effective in palladium-catalyzed cross-coupling

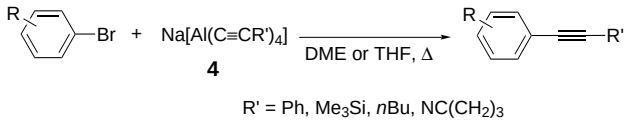


3 X = Br, I, OTf

Scheme 2. One-pot synthesis of symmetrical bisaryl ethynes, by the sila-Sonogashira reaction.

[*] Prof. R. R. Tykwinski
Department of Chemistry
University of Alberta
Edmonton, AB T6G 2G2 (Canada)
Fax: (+1) 780-492-8231
E-mail: rik.tykwinski@ualberta.ca

 © 2003 Wiley-VCH Verlag GmbH & Co. KGaA, Weinheim DOI: 10.1002/anie.200201617

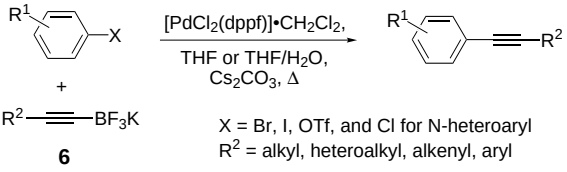


Scheme 3. Palladium-catalyzed cross-coupling with tetraalkynyl aluminates according to Blum and co-workers.[9]

reactions with aryl or heteroaryl bromides (Scheme 3).[10] Although requiring rather rigorous conditions (THF or DME at reflux), the transformations are gratifyingly free from the oxidative homocoupling byproduct that normally plagues typical Sonogashira conditions. Excellent chemoselectivity is observed, with reaction occurring solely with the aryl bromide moiety, while potentially vulnerable substituents such as chloro, cyano, trifluoromethanesulfonyl, carboxy, and olefinic groups are left untouched. The reaction is also economical; all four of the alkynyl moieties can be utilized for cross-coupling, although using a slight excess of the aluminate provides the best results. Di-, tri-, and tetraethynyl arenes are also afforded in high yields from the corresponding bromides, and initial evidence suggests that the use of tetraalkynyl aluminates can also be extended to the alkynylation of vinyl bromides.

The use of organoboron acetylides for effecting sp–sp^2 carbon-bond formation by Suzuki–Miyaura coupling was introduced several years ago by both Fürstner and Seidel[11] and Soderquist et al.[12] using borate complexes that were generated in situ. Increasing the stability of the borate nucleophile has allowed for the scope of this reaction to be substantially improved by using alkynyl trialkoxyborate complexes **5** (Scheme 4), as reported by Colobert et al.[13] and Oh and Jung[14]. Whereas moderate to good yields have been achieved using alkyl- or phenylacetylenes as coupling partners in these systems, the presence of a silyl moiety ($R^2 = Me_3Si$ or tBuMe$_2$SiOCH$_2$) generally results in lower yields.

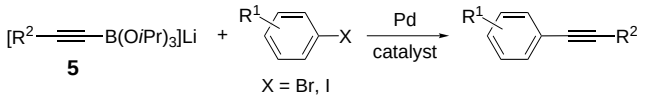
Molander et al. have recently shown that potassium alkynyl trifluoroborates **6** are suitable for cross-coupling with aryl halides and triflates (Scheme 5).[15]



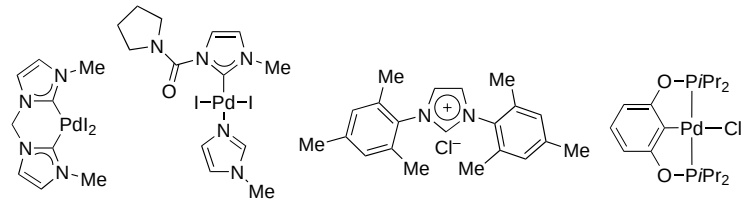
Scheme 5. Palladium-catalyzed cross-coupling with alkynyl trifluoroborates according to Molander et al.[15]

The primary advantage of these boron acetylide complexes is their remarkably robust nature. They are isolated as air- and water-stable crystalline solids that can be stored indefinitely, attributes that make them particularly well-adapted for potential use in combinatorial chemistry. Using a catalyst/base system of [PdCl$_2$(dppf)]·CH$_2$Cl$_2$/Cs$_2$CO$_3$ (dppf = 1,1′-bis(diphenylphosphanyl)ferrocene), two distinct solvent combinations are applicable, dependent on substitution; one using a mixture of THF/H$_2$O, the other anhydrous THF. The order of reactivity for aryl electrophiles under anhydrous THF conditions is surprising: OTf > Br > I ~ Cl. Extensive functional-group compatibility has been demonstrated, which includes the use of aryl halides containing hydroxy and carboxylic acid moieties that might, a priori, be expected to promote protiodeboration. Furthermore, silyl functionality is also tolerated ($R^2 = Me_3Si$ or tBuMe$_2$SiOCH$_2$CH$_2$) despite the presence of a fluoride source.

Palladium catalysts with enhanced reactivity that are suitable for cross-coupling reactions with electron-rich aryl bromides and aryl chlorides continue to be attractive targets.[16] Some success in this area has been achieved using bulky, electron-rich phosphane ligands such as PtBu$_3$, reported by the groups of Buchwald and Fu,[17] as well as Böhm and Herrmann.[18] These systems show unusually high activity in cross-coupling reactions with aryl bromides at room temperature. More recently, considerable attention has been directed toward N-heterocyclic carbene (NHC) ligands as "phosphane mimics" for use as alternatives to sterically hindered phosphanes. Herrmann's group initiated these efforts by demonstrating proof-of-principle by using the chelating ligand complex **7** (Scheme 6) in Sonogashira reactions, although these reactions required elevated temperatures and activated aryl bromides.[19,20]



Scheme 4. Palladium-catalyzed cross-coupling with alkynyl trialkoxyborates.



Scheme 6. Improved catalyst/ligand systems for Sonogashira cross-coupling reactions: **7** (1 mol%), Et$_3$N, △;[19] **8** (1 mol%), PPh$_3$ (1 mol%), CuI (2 mol%), Et$_3$N (1.2 equiv), DMF, RT or 80°C;[21] **9** (6 mol%), Pd(OAc)$_2$ (3 mol%), CuI (2 mol%), Cs$_2$CO$_3$, *N,N*-dimethylacetamide, 80°C;[22] **10** (5 mol%), ZnCl$_2$ (10 or 100 mol%), Cs$_2$CO$_3$, dioxane, 160°C.[23]

 © 2003 Wiley-VCH Verlag GmbH & Co. KGaA, Weinheim

The two most promising NHC approaches to date come from the research groups of Batey and Nolan. Batey et al. have shown that the carbamoyl-substituted NHC complex **8** (Scheme 6) is thermally and hydrolytically stable, and it efficiently promotes cross-coupling with electron-rich aryl iodides and bromides.[21] These reactions proceed in excellent yield, albeit only at elevated temperature (80 °C) in the case of aryl bromides. In combination with $Pd(OAc)_2$, the imidazolium system **9** of Nolan and co-workers. also demonstrates the effectiveness of NHC ligands for palladium in cross-coupling reactions with deactivated aryl bromides and chlorobenzene.[22] Excellent yields have been obtained for a variety of substrates in coupling reactions with $Me_3Si{-}C{\equiv}C{-}Ph$. As with Batey's system, however, an elevated temperature (80 °C) is required.

An interesting approach toward the Holy Grail of the Sonogashira reaction, effective cross-coupling of alkynes with aryl chlorides, has been reported by Eberhard et al.[23] Using the phosphinito palladium pincer complex **10** (Scheme 6), a wide array of aryl chloride substrates could be effectively cross-coupled with phenyl acetylene in a one-pot procedure. While these reactions require quite high temperatures and a fivefold excess of the aryl chloride, reasonable yields have been achieved in a number of cases.

Clearly, our ability to effect bond formation between sp- and sp^2-hybridized carbon atoms continues to evolve, and new catalysts, substrates, and conditions have all enhanced the effectiveness of these reactions. Somewhat surprising, however, is that a quick survey of the literature suggests that the most popular protocol in use today still consists of a mixture of an aryl iodide or bromide, a terminal alkyne, $[PdCl_2(PPh_3)_2]$, an amine, and CuI: the same protocol as introduced many years ago by Sonogashira and Hagihara.

[1] *Modern Acetylene Chemistry* (Eds.: P. J. Stang, F. Diederich), VCH, Weinheim, **1995**.

[2] K. Sonogashira, Y. Tohda, N. Hagihara, *Tetrahedron Lett.* **1975**, 4467; K. Sonogashira, *J. Organomet. Chem.* **2002**, *653*, 46.

[3] *Metal-Catalyzed Cross-Coupling Reactions* (Eds.: P. J. Stang, F. Diederich), Wiley-VCH, Weinheim, **1997**.

[4] Y. Nishihara, K. Ikegashira, K. Hirabayashi, J. Ando, A. Mori, T. Hiyama, *J. Org. Chem.* **2000**, *65*, 1780; Y. Nishihara, K. Ikegashira, A. Mori, T. Hiyama, *Chem. Lett.* **1997**, 1233.

[5] See also: D. A. Shultz, K. P. Gwaltney, H. Lee, *J. Org. Chem.* **1998**, *63*, 4034.

[6] This concept of the one-pot formation of diaryl alkynes by in situ deprotection of an alkyne can be traced back to Rossi, see: A. Carpita, A. Lessi, R. Rossi, *Synthesis* **1984**, 571.

[7] M. J. Mio, L. C. Kopel, J. B. Braun, T. L. Gadzikwa, K. L. Hull, R. G. Brisbois, C. J. Markworth, P. A. Grieco, *Org. Lett.* **2002**, *4*, 3199.

[8] For a recent summary of some of the Sonogashira couplings with other metal acetylides, see: E. Negishi, *J. Organomet. Chem.* **2002**, *653*, 34.

[9] D. Gelman, D. Tsvelikhovsky, G. A. Molander, J. Blum, *J. Org. Chem.* **2002**, *67*, 6287.

[10] Alkynylation of *o*-iodotoluene using $[n\text{-}C_5H_{11}{-}C{\equiv}CAlBu_3Li]$ had been demonstrated early on by Negishi, albeit affording low yields; see E. Negishi, *Acc. Chem. Res.* **1982**, *15*, 340, and references therein.

[11] A. Fürstner, G. Seidel, *Tetrahedron* **1995**, *51*, 11165.

[12] J. A. Soderquist, K. Matos, A. Rane, J. Ramos, *Tetrahedron Lett.* **1995**, *36*, 2401.

[13] A.-S. Castanet, F. Colobert, T. Schlama, *Org. Lett.* **2000**, *2*, 3559.

[14] C. H. Oh, S. H. Jung, *Tetrahedron Lett.* **2000**, *41*, 8513.

[15] G. A. Molander, B. W. Katona, F. Machrouhi, *J. Org. Chem.* **2002**, *67*, 8416.

[16] In addition to new catalyst systems, the effects of numerous additives have also been probed. See, for example: A. Mori, M. S. M. Ahmed, A. Sekiguchi, K. Masui, T. Koike, *Chem. Lett.* **2002**, 756; A. Mori, T. Shimada, T. Kondo, A. Sekiguchi, *Synlett* **2001**, 649.

[17] A. F. Littke, G. C. Fu, *Angew. Chem.* **2002**, *114*, 4350; *Angew. Chem. Int. Ed.* **2002**, *41*, 4176; T. Hundertmark, A. F. Littke, S. L. Buchwald, G. C. Fu, *Org. Lett.* **2000**, *2*, 1729.

[18] V. P. W. Böhm, W. A. Herrmann, *Eur. J. Org. Chem.* **2000**, 3679.

[19] W. A. Herrmann, C.-P. Reisinger, M. Spiegler, *J. Organomet. Chem.* **1998**, *557*, 93.

[20] Cavell has also reported a catalyst system based on an NHC, but only one $sp{-}sp^2$ cross-coupling has be demonstrated, see: D. S. McGuinness, K. J. Cavell, *Organometallics* **2000**, *19*, 741.

[21] R. A. Batey, M. Shen, A. J. Lough, *Org. Lett.* **2002**, *4*, 1411.

[22] A. C. Hillier, G. A. Grasa, M. S. Viciu, H. M. Lee, C. Yang, S. P. Nolan, *J. Organomet. Chem.* **2002**, *653*, 69.

[23] M. R. Eberhard, Z. Wang, C. M. Jensen, *Chem. Commun.* **2002**, 818.

 © 2003 Wiley-VCH Verlag GmbH & Co. KGaA, Weinheim

Molecular Dynamics Simulations

Chemical Reactions "On the Fly"

*Irmgard Frank**

Keywords:
density functional calculations · femtochemistry · molecular dynamics · quantum chemistry · reaction mechanisms

The enormous advances in the field of quantum chemistry have encouraged the pursuit of understanding more and more complicated molecular systems on an atomic basis. While quantum-chemical investigations have traditionally concentrated on studying previously defined reaction pathways with static calculations, several studies that employ quantum-chemical methods to *determine* complex reaction pathways have appeared in recent years. For complex chemical systems, it is sometimes not possible to obtain sufficient experimental knowledge of the reaction mechanism to study the reaction with conventional static calculations. Clearly the complete potential surface of the system contains the relevant information. However, if the reaction pathway is not a priori restrictable to a few internal degrees of freedom, the determination of the corresponding multidimensional surface becomes prohibitive, no matter what quantum-chemical method is used. This situation may emerge if, for example, several molecules react with each other or if solvent molecules are involved in the reaction. In addition, it may be difficult even in relatively small molecular systems to assess the real motion of the system on the basis of the potential surface.[1] In such cases, quantum-chemical molecular dynamics approaches that treat the problem "on the fly" represent the method of choice to investigate the full molecular motion in three-dimensional space.

[*] Dr. I. Frank
Department Chemie
Butenandtstrasse 5–13, Haus E
81377 München (Germany)
E-mail: frank@cup.uni-muenchen.de

Pioneering work in this field was done by Car and Parrinello in 1985.[2,3] The basic concept is simple: Instead of trying to compute the potential surface of the system in as many dimensions as possible and performing dynamics on this surface in a second step, on-the-fly methods consider only those points that are reached during a molecular dynamics run. Only for these structures is the energy and the gradient of the energy determined by a quantum-chemical method during the simulation. It is apparent that this approach has the advantage that very complex systems can be treated without prior knowledge of the possible reaction pathways. A disadvantage is that relatively high demands have to be made concerning the quantum-chemical method used. It is not possible to improve potential surfaces by applying, for example, different levels of accuracy for geometry optimization and energy calculation when using on-the-fly methods. A single method must be able to yield both good geometies and reliable energies at moderate computational costs. Furthermore, the quantum-chemical method employed must be a robust black-box method with good convergence properties, since it is not practical to take care individually of the many thousand points that are computed during an on-the-fly run. The most successful on-the-fly concept is still the one originally described by Car and Parrinello (Car–Parrinello molecular dynamics, CPMD), which is based on the following:[4]

- Description of the valence electrons by density functional theory[5,6] using a plane-wave basis set;
- Description of the inner electrons by pseudopotentials;
- Simultaneous motion of electrons and nuclei according to the Car–Parrinello equations.[2]

The development of modern density functionals[7] gave a large boost to this approach in recent years. These functionals are sufficiently accurate to describe most types of chemical systems, not only in the gas phase, but also in the condensed phase. Since the inner electrons are not usually relevant for the description of chemical reactions, they can be represented by fixed potentials. The Car–Parrinello equations describe the classical motion of the nuclei in the potential generated by the electrons according to the Newton equations. The electronic motion is also treated with a classical formalism, instead of solving the time-dependent Schrödinger equation. In this way it is possible to move electrons and nuclei simultaneously in an efficient way during a molecular dynamics run.

The use of a plane–wave basis to describe the wavefunction encompasses several advantages in dynamics runs compared to the more common description of the wavefunction from Gaussian basis sets: Since the basis functions fill the whole space, there is no distortion of the potential surfaces resulting from pulling basis functions through space (so-called basis-set superposition error, BSSE) and no artificial forces result during the dynamics. In addition, it is simple to switch to the condensed phase and thus to describe liquids and solids on the same footing as isolated molecules.

The most important alternative to CPMD is Born–Oppenheimer molecular dynamics (BOMD). In this approach the wavefunction is converged to the potential surface (Born–Oppenheimer

DOI: 10.1002/anie.2002605
© 2003 Wiley-VCH Verlag GmbH & Co. KGaA, Weinheim

surface) in every step. An advantage of BOMD over CPMD is that it is not restricted to self-consistent methods but can also be applied in combination with, for example, perturbation theory or configuration interaction. Experience has shown that to keep the total energy (the sum of kinetic and potential energy) constant during a BOMD run, it is necessary to converge the wavefunctions precisely for every step, which renders CPMD more efficient.[4]

Probably the most fascinating field of application of on-the-fly methodologies is the simulation of chemical reactions. In principle, it is possible to set up an arbitrary arrangement of atoms and simply "let it go". In this way it is possible to observe any kind of chemical reaction that would occur in the system on the timescale of the simulation. However, it should be emphasized that the computational cost of on-the-fly simulations is still very high, thus restricting typical simulations to the picosecond timescale. Nevertheless, many interesting chemical phenomena can be observed in this time regime (femtoseconds to picoseconds).

Several approaches can be chosen depending on the nature of the problem: If the reaction is expected to be completed within a few picoseconds, it is possible to simply run unconstrained dynamics at a certain temperature. Several reactions have been elucidated with this elegant approach by using density functional theory or other quantum-chemical methods.[8–15] It has the advantage that the reaction time (and with it ΔG) is obtained directly from the simulation. The reaction pathway is not specified in advance, but is a result of this simulation. Even very complex reaction pathways can be simulated in this way.

However, the energy barriers to most chemical reactions are too high to be accessible by an unconstrained on-the-fly simulation. While it usually takes just some ten femtoseconds to cross the barrier, a system may oscillate for a very long time in the starting material state before a sufficient amount of energy is accidentally accumulated in the relevant mode to make the transition. Several research groups are currently working on the problem of how to avoid observing this vibrational motion in full detail.[16] Fundamental work on the problem of accelerating processes in molecular systems without predefining a certain pathway has been done by Grubmüller,[17] and the applicability of the methodology to chemical reactions has been demonstrated recently.[18]

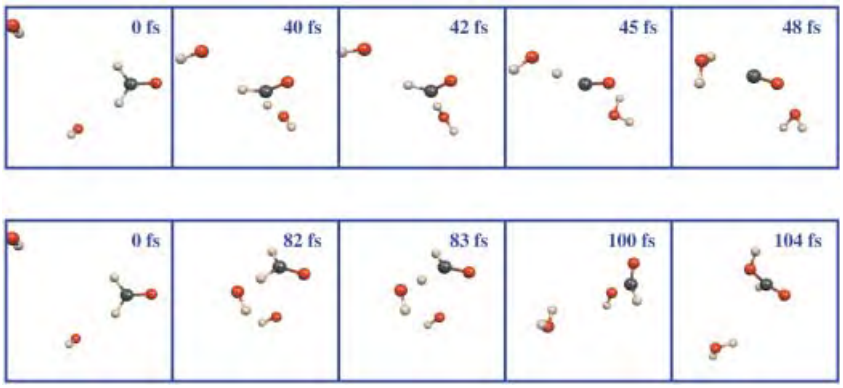


Figure 1. The reaction of formaldehyde with two OH radicals. Snapshots from two molecular dynamics runs are presented. The system reacts more slowly at lower kinetic energy (bottom row) and HCOOH is formed instead of CO.

Only one conceptually simple approach that can be applied if the reaction is adequately described by the motion across a transition state will be outlined here.[1] In this case, it is possible to start the simulation at this transition state and to integrate forwards and backwards in time, that is, to simulate the way down to both starting material and product. This type of calculation has been shown by Sun et al.[1] to yield significantly more information than the minimum energy path of the reaction. A different behavior of the molecules was observed in separate molecular dynamics runs; the system either got trapped in a local minimum or directly formed the product, depending on the initial conditions.

A simple radical reaction, namely the reaction of formaldehyde with OH radicals, is considered to illustrate the critical influence of changes in the reaction conditions. Two initial reactions may proceed in this system without an enthalpic barrier: hydrogen abstraction or OH addition. While both reactions seem equally possible on the basis of static calculations, dynamic simulations show that the abstraction clearly dominates. This is a consequence of the fact that the conservation law for energy and impetus is easier to fulfill in the abstraction reaction. The product of hydrogen abstraction, the CHO radical, reacts with a second OH radical to form either HCOOH or CO and water. Figure 1 shows snapshots from two simulation runs at different kinetic energies starting from the same initial geometry. The change of selected internal coordinates during the formation of CO is presented in Figure 2.

To conclude, the on-the-fly simulation of chemical reactions represents a quickly growing field of research that extends the experimental knowledge on chemical reactivity to scales that are not

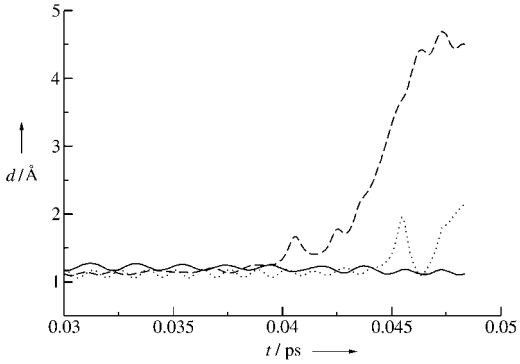
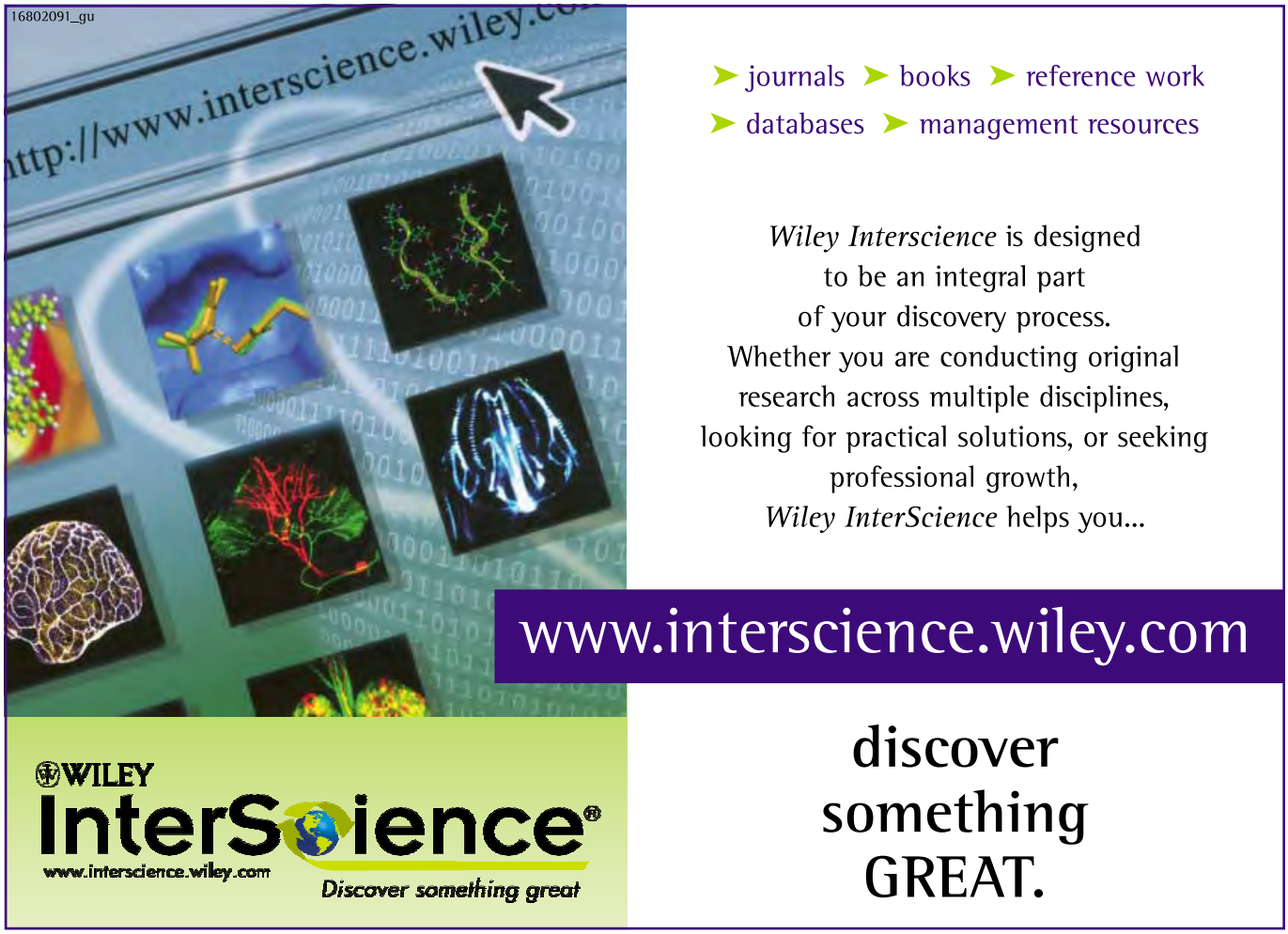


Figure 2. The variation of single internal coordinates during the reaction $CH_2O + 2\,OH^{\bullet} \rightarrow CO + 2\,H_2O$. Solid line: C···O distance of the carbonyl group, dashed and dotted lines: C···H distances. The C···O distance gets shorter upon abstraction of the hydrogen atoms. Immediately after the breaking of the C—H bonds, very short lived hydrogen bonds are formed, as indicated by an oscillatory motion of the C···H distance at about 1.7–1.8 Å.

 © 2003 Wiley-VCH Verlag GmbH & Co. KGaA, Weinheim

easily accessible by experiments. The resulting pictures of the molecular motion give a realistic view of chemical reactions in three dimensions. Future developments will extend the methodology to larger systems and longer time scales, thus enlarging the overlap with spectroscopic and microscopic experiments. Of special interest is their combination with classical molecular mechanics for the description of the unreactive part of a system (QM/MM)[19,20] that in the future will greatly enlarge our knowledge of chemical reactions in biomolecules.

[1] L. Sun, K. Song, W. L. Hase, *Science* **2000**, *296*, 875.
[2] R. Car, M. Parrinello, *Phys. Rev. Lett.* **1985**, *55*, 2471.
[3] M. Parrinello, *Solid State Commun.* **1997**, *102*, 107.
[4] "Ab Initio Molecular Dynamics: Theory and Implementation": D. Marx, J. Hutter in *Modern Methods and Algorithms of Quantum Chemistry, NIC Series, Vol. 1* (Ed.: J. Grotendorst), John von Neumann Institute for Computing, Jülich, **2000**, p. 301.
[5] P. Hohenberg, W. Kohn, *Phys. Rev. B* **1964**, *136*, 864.
[6] W. Kohn, L. J. Sham, *Phys. Rev. A* **1965**, *140*, 1133.
[7] A. D. Becke, *Phys. Rev. A* **1988**, *38*, 3098.
[8] A. Curioni, M. Sprik, W. Andreoni, H. Schiffer, J. Hutter, M. Parrinello, *J. Am. Chem. Soc.* **1997**, *119*, 7218.
[9] E. J. Meijer, M. Sprik, *J. Phys. Chem. A* **1998**, *102*, 2893.
[10] E. J. Meijer, M. Sprik, *J. Am. Chem. Soc.* **1998**, *120*, 6345.
[11] I. Frank, M. Parrinello, A. Klamt, *J. Phys. Chem. A* **1998**, *102*, 3614.
[12] S. Reinhardt, C. Marian, I. Frank, *Angew. Chem.* **2001**, *113*, 3795; *Angew. Chem. Int. Ed.* **2001**, *40*, 3683.
[13] M. Ben-Nun, T. J. Martinez, *Chem. Phys. Lett.* **1998**, *298*, 57.
[14] J. Quenneville, M. Ben-Nun, T. J. Martinez, *J. Photochem. Photobiol. A* **2001**, *144*, 229.
[15] R. L. Hayes, E. Fattal, N. Govind, E. A. Carter, *J. Am. Chem. Soc.* **2001**, *123*, 641.
[16] "Finding Transition Pathways: Throwing Ropes Over Rough Mountain Passes, in the Dark": D. Chandler in *Computer Simulation of Rare Events and Dynamics of Classical and Quantum Condensed-Phase Systems—Classical and Quantum Dynamics in Condensed Phase Simulations* (Eds.: B. J. Berne, G. Ciccotti, D. F. Coker), World Scientific, Singapore, **1998**, p. 51.
[17] H. Grubmüller, *Phys. Rev. E* **1995**, *52*, 2793.
[18] E. M. Müller, A. de Meijere, H. Grubmüller, *J. Chem. Phys.* **2002**, *116*, 897.
[19] M. Eichinger, P. Tavan, J. Hutter, M. Parrinello, *J. Chem. Phys.* **1999**, *110*, 10452.
[20] A. Laio, J. VandeVondele, U. Röthlisberger, *J. Chem. Phys.* **2002**, *116*, 6941.



 © 2003 Wiley-VCH Verlag GmbH & Co. KGaA, Weinheim

Macrolamellar Structure?

Do Mesostructured Materials Have an Unusual Macrolamellar Structure?**

*Zhong-Yong Yuan, Marie-France Six-Boulanger, and Bao-Lian Su**

Keywords:
lamellar structures · mesophases · oxides · silicon · surfactants

The synthesis of inorganic mesoporous materials by using organic molecules as structure-directing agents or templates is an area of rapid growth with diverse applications that include separation technology and catalysis. Surfactant templating techniques based on electrostatic, hydrogen-bonding, covalent, and van der Waals interactions between amphiphilic and ceramic species have been developed for the synthesis of these materials with a narrow mesopore size distribution and controlled pore structure.[1,2] Despite considerable successes, it remains a challenge for chemists and materials scientists to mimic the natural pathways that would aid the development of simple and efficient routes to advanced functional materials. Recently Xu and co-workers[3–11] have published a series of papers reporting the synthesis of a highly ordered long-range lamellar structure (designated ZSU-L) and hierarchically ordered silica mesostructures (designated ZSU-4, -5, -38). An amphiphilic silicone surfactant was used to direct highly ordered lamellar oxides with large interlayer spacings (160–240 nm).[3–11] The mixture of a silicone surfactant and conventional surfactants (for example, P123, TX-100, C_{16}TAB) was claimed to be able to direct the formation of the unusual hierarchical mesostructures.[3,9–11] The macrolamellar structures reported by Xu and co-workers were investigated by transmission electron microscopy (TEM), and the specimens for TEM observation were prepared by embedding samples in epoxy resin and then ultramicrotoming them. In this communication, we would like to comment on the highly ordered macrolamellar structure presented in the studies of Xu and co-workers, on the basis of our previous work and on work that was carried out after the appearance of Xu's papers.

In our laboratory we have synthesized various mesoporous materials with different pore structures and compositions by using surfactant-templating techniques. CMI-1[12] is a mesoporous silica material with an ordered hexagonal-pore array synthesized by using polyoxyethylene oxide surfactant under weakly acidic conditions. The specimens for TEM observation were prepared by embedding in epoxy resin and ultramicrotoming. Figure 1 presents several TEM images of CMI-1. Clear striped patterns are observed in low-magnification images and the repeat distance of the striped patterns was approximately 160–200 nm (Figure 1 a–c). Both the striped patterns and the "interlayer distance" are quite similar to those in the images in Xu's papers.[3–11] Moreover, these striped patterns have almost the same directionality in all particle slices (Figure 1 b and d). Figure 1 e and f are typical high-magnification TEM images showing an ordered hexagonal array of 4-nm mesopores between the more widely spaced stripes. Under electron-beam irradiation, the particle slices could become split up or constricted (see Figure 1 c). Such wide striped patterns can also be seen in all the ultrathin sections of other mesostructured materials synthesized in our laboratory, whatever their mesostructures or compositions.

Have all mesostructured materials such a macrolamellar structure? For the sake of comparison, we also prepared specimens by dispersing the particles in alcohol by ultrasonic treatment, and dropping them onto a holey carbon film supported on a copper grid. In the analysis of these samples by TEM, we continued to see the ordered mesopore array, but the large stripes were now absent. No macrolamellar structure was seen in any of our mesostructured materials. This is a strong indication that the macrolamellar structure observed by Xu and co-workers is artificial.

In order to further confirm the artificialness of the so-called macrolamellar structure, samples of amorphous silica, titania, and zirconia were prepared by the simple hydrolysis of Si, Ti, and Zr alkoxides in water without the addition of any organic surfactant species, followed by preparation of the TEM specimen by ultrathin sectioning. The same striped patterns are present in low-magnification images of these ultrathin sections. We can even modify the "interlayer distance" of the "macro-

[*] Prof. B.-L. Su, Dr. Z.-Y. Yuan
Laboratory of Inorganic Materials Chemistry (CMI)
Institute for Studies in Interface Sciences (ISIS)
The University of Namur (FUNDP)
61 rue de Bruxelles, 5000 Namur (Belgium)
Fax: (+32) 81-725414
E-mail: bao-lian.su@fundp.ac.be
M.-F. Six-Boulanger
Interfaculty Unit of Electron Microscopy
The University of Namur (FUNDP)
61 rue de Bruxelles, 5000 Namur (Belgium)

[**] The authors have chosen to use the term "macrolamellar" to describe the features observed in the materials presented herein. This choice is based on the IUPAC definition of macroporosity (larger than 50 nm in diameter) and microporosity (smaller than 2 nm in diameter).

 © 2003 Wiley-VCH Verlag GmbH & Co. KGaA, Weinheim DOI: 10.1002/anie.200320060

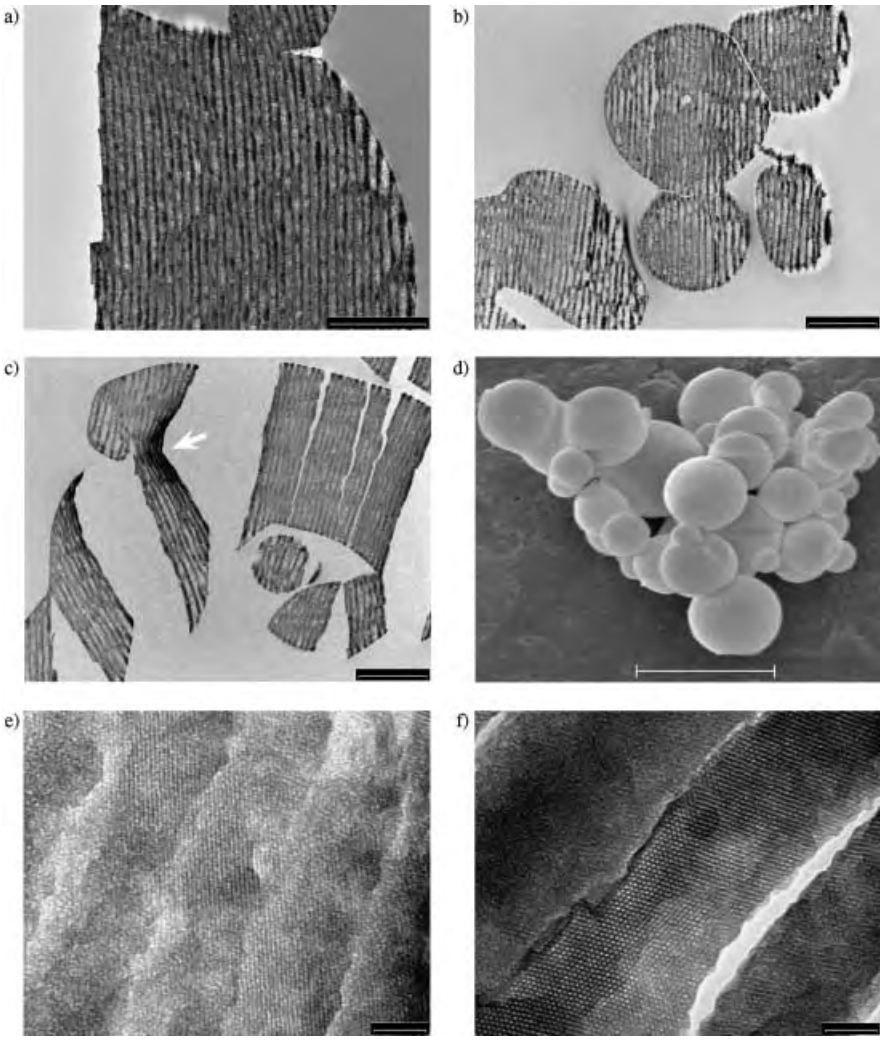


Figure 1. a,b) Low-magnification TEM images of ultrathin sections of mesoporous CMI-1 silica showing striped patterns with a wide interlayer distance (scale bar = 2 μm); c) low-magnification image showing that the particle slices are split up and constricted (marked with a white arrow) after electron-beam irradiation (scale bar = 2 μm); d) scanning electron micrograph of spherical CMI-1 particles (scale bar = 5 μm); e,f) high-magnification TEM images showing an ordered mesopore array when viewed perpendicular and parallel to the pore directions, respectively (scale bar = 50 nm).

lamellar structure" by changing the velocity of cutting during microtoming and altering the size of the blade of the diamond knife. In addition, wide striped patterns with the same orientation can be clearly observed even in the resin region of the ultramicrotomed specimens.

It is thus clear that the highly ordered macrolamellar structure described in the papers of Xu and co-workers is an artifact arising from the ultramicrotoming. Additional evidence to this effect can also be found in the TEM images within these papers. For example, in Figure 2 of ref. [4] and Figure 1 of ref. [6], the striped patterns in all of the randomly dispersed particle slices have the same directionality. It is impossible that the direction of the lamellar structure in such randomly dispersed particles can be the same (Figure 1 b and d) even if these materials had a true macrolamellar structure. Therefore, the so-called "hierarchically ordered silica mesophases" described in the papers of Xu and co-workers cannot be real, and the claimed "macrolamellar structure" is only an artifact.[3–11]. It is not surprising to see the same artifact on the amorphous samples prepared either by sol–gel or simple precipitation methods if the same sample preparation for TEM measurement is applied, that is, by ultramicrotoming.

[1] A. Sayari, P. Liu, *Microporous Mater.* **1997**, *12*, 149.
[2] J. Y. Ying, C. P. Mehnert, M. S. Wong, *Angew. Chem.* **1999**, *111*, 58; *Angew. Chem. Int. Ed.* **1999**, *38*, 56.
[3] A. W. Xu, Y. P. Cai, H. X. Zhang, L. Z. Zhang, J. C. Yu, *Angew. Chem.* **2002**, *114*, 4000; *Angew. Chem. Int. Ed.* **2002**, *41*, 3844.
[4] A. W. Xu, *J. Phys. Chem. B* **2002**, *106*, 13161.
[5] A. W. Xu, J. C. Yu, Y. P. Cai, H. X. Zhang, L. Z. Zhang, *Chem. Commun.* **2002**, 1614.
[6] A. W. Xu, *Chem. Mater.* **2002**, *14*, 3625.
[7] A. W. Xu, Y. P. Cai, L. Z. Zhang, J. C. Yu, *Adv. Mater.* **2002**, *14*, 1064.
[8] A. W. Xu, *Chem. Lett.* **2002**, 878.
[9] A. W. Xu, *J. Phys. Chem. B* **2002**, *106*, 11713.
[10] A. W. Xu, J. C. Yu, H. X. Zhang, L. Z. Zhang, D. B. Kuang, Y. P. Fang, *Langmuir* **2002**, *18*, 9570.
[11] A. W. Xu, *Chem. Lett.* **2002**, 982.
[12] J. L. Blin, A. Léonard, B. L. Su, *Chem. Mater.* **2001**, *13*, 3542.

 © 2003 Wiley-VCH Verlag GmbH & Co. KGaA, Weinheim

Microlamellar Structure?

Additional Proof for the Existence for Microlamellar Structured ZSU-L Templated from Silicone Surfactants

*An-Wu Xu**

Keywords:
lamellar structures · mesophases · oxides · silicon · surfactants

According to mass conservation, if we use tetraethylorthosilicate (TEOS, 0.02 mol) and silicone surfactant (1 g) to prepare a sample of ZSU-L, 1.9–2.1 g of the product can always be obtained (after being thoroughly washed with water and ethanol and then dried). A maximum of 1.2 g of SiO_2 is obtained when completely converting 0.02 mol of TEOS into SiO_2. It can be shown that almost all of the silicone surfactant molecules enter the SiO_2 matrix. TEOS is stable in neutral aqueous solutions, and no precipitate is obtained. However, in the presence of silicone surfactant, TEOS can hydrolyze to form silica/surfactant composites in neutral water. The formation of such composites in neutral aqueous solution has been shown to proceed by the co-assembly of the TEOS hydrolysis product and neutral silicone surfactants, coupled with inorganic polymerization through hydrogen-bonding interactions. Low-angle X-ray diffraction (XRD) patterns show no peaks for ZSU-L. Therefore, one may wish to discover which structure ZSU-L has adopted. A large number of experiments in our laboratory have demonstrated that ZSU-L has a lamellar structure, as confirmed by some evident proof including TEM images of an ultrathin section of the material.[1–5] Su et al. have commented that the microlamellar structure in ZSU-L is created by ultramicrotoming. Here we present some additional proof that confirms the nature of the microlamellar structure of ZSU-L.

It is well-known from TEM textbooks that the striped patterns, similar to those mentioned by Su et al., can be produced by ultramicrotoming. To rule out the possibility that the lamellar structure of ZSU-L is caused by ultrathin sectioning, a large number of experiments were performed. For example, amorphous SiO_2, TiO_2, and ZrO_2, M41S,[6] SBA-15,[7] MSU-X,[8] and ZSU-L samples were sent to three different laboratories for ultramicrotoming; each sample was ultramicrotomed 10 times. TEM analysis shows that the striped patterns caused by ultramicrotoming can be occasionally observed in amorphous samples of the above-listed materials. However, these striped patterns only take up an extremely small portion on an ultrathin section, and show poorly ordered structure. In our ZSU-L samples, however, highly ordered microlamellar structure was always observed. Moreover, an ultrathin section of ZSU-L consists almost entirely of the highly ordered microlamellar structure. Therefore, we confirm that our ZSU-L samples have true microlamellar structures, as demonstrated in our previously published papers. According to our experience, if the blade of a diamond knife is not sharp or the microtoming process is not optimal, the striped patterns can be often be observed for an ultrathin section of an amorphous sample.

The mixture of ZSU-L (TiO_2) and CMI-1 (SiO_2) with different mass ratios was ultramicrotomed for TEM observation. We found that the number of particles containing microlamellar structure decrease with an increase in the mass ratio of CMI-1 to ZSU-L. Electron dispersive spectroscopy (EDS) analysis performed on lamellar structured particles shows that both Ti and O were detected, as well as a small amount of Si, which comes from the silicone surfactant. But on nonlamellar structured particles, only Si and O were detected (Figure 1). All TiO_2 particles have a lamellar structure, while almost all of the CMI-1 particles do not display the striped pattern. The results supply strong evidence that ZSU-L has microlamellar structure in nature, which is not created by ultramicrotoming. Mixtures of ZSU-L (SiO_2, ZrO_2) and CMI-1 were also ultramicrotomed for TEM analysis, in which we also found that the number of particles having microlamellar structure decreased with an increase in the mass ratio of CMI-1 to ZSU-L (SiO_2, ZrO_2).

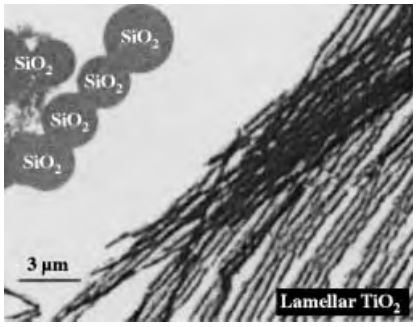


Figure 1. TEM image of an ultrathin section of the mixture of ZSU-L (TiO_2) and CMI-1 (SiO_2). The lamellar structure belongs to ZSU-L (TiO_2), and the black spherical particles are of SiO_2, as determined by EDS analysis.

In general, ultrathin sections are normally ultramicrotomed into a trape-

[*] Prof. A.-W. Xu
School of Chemistry and Chemical Engineering
Zhongshan University, Guangzhou 510275 (China)
Fax: (+86) 20-84111088
E-mail: cedc17@zsu.edu.cn

 © 2003 Wiley-VCH Verlag GmbH & Co. KGaA, Weinheim DOI: 10.1002/anie.200320064

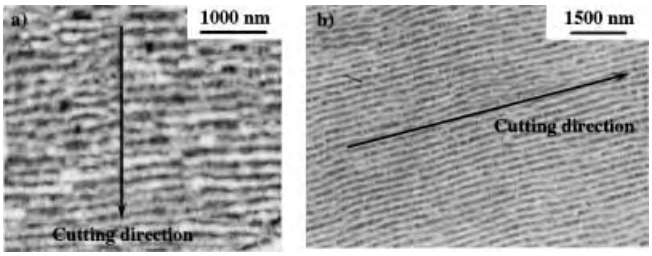


Figure 2. a) TEM image of an ultrathin section of an amorphous silica sample. The striped patterns were created by ultramicrotoming. The cutting direction (arrow) of a diamond knife is perpendicular to the stripes; b) TEM image of an ultrathin section of microlamellar structured ZSU-L. The cutting direction (arrow) of the knife is parallel to the direction of the lamellar structure, which indicates that the lamellar structure was not produced by ultramicrotoming.

zoidal shape; one can always know the cutting direction of a diamond knife on an ultrathin section. Therefore, the stripes produced by ultramicrotoming should be perpendicular to the cutting direction of the knife. Figure 2a shows the striped patterns created by ultramicrotoming. However, in our ZSU-L samples, we found that the direction of the lamellar structure in many slices is not perpendicular to the cutting direction of the knife; some aligned silica wall lines are even parallel to the cutting direction of the knife. Figure 2b shows the cutting direction of the knife and the direction of the lamellar structure of ZSU-L. Moreover, the different directions of lamellar structure in ZSU-L can be always observed. TEM observation was performed under a low electron-energy beam (100 kV) to make sure that the slices did not move.

N_2 sorption analyses show that the as-prepared ZSU-L has a BET surface area of only approximately 2 $m^2 g^{-1}$, but the calcined ZSU-L exhibits a type I isotherm with a hysteresis loop of type H_4 that is typical of lamellar materials (Figure 3),[4,9] and a surface area of 288 $m^2 g^{-1}$. It demonstrates that the co-assembly of a silicone surfactant silicate forms a lamellar structure.

To study the location of the silicone surfactant between the walls (stripes), high-resolution electron energy loss spectroscopy (HREELS) analysis was performed on an ultrathin section of microlamellar-structured TiO_2. HREELS line scans were performed across aligned TiO_2 walls (Figure 4) which indicated that the walls only contain Ti and O; no Si was detected. However, in the area within the walls, Si can be always found, which originates from the silicone surfactant bilayers. These results clearly show that silicone surfactant bilayers were sandwiched by titania walls to form a highly ordered microlamellar structure. The ZSU-L products are constructed of silicone surfactant layers that are sandwiched by thick titania walls that are arranged parallel to each other. It indicates that microlamellar structured TiO_2 was templated from the silicone surfactant. It supplies strong evidence that the lamellar structure in TiO_2 is not produced by ultramicrotoming. Recently, Saravanamuttu et al. has also reported the formation of an ordered microlamellar structure, similar to that of ZSU-L.[10]

In conclusion, the results presented here further demonstrate that ZSU-L has an inherently microlamellar structure, which is not created by ultramicrotoming. We will report our new results in the near future. Finally, we thank Professor Su and co-workers for their comments, which encouraged us to supply additional evidence that confirms the microlamellar nature of the ZSU-L structure.

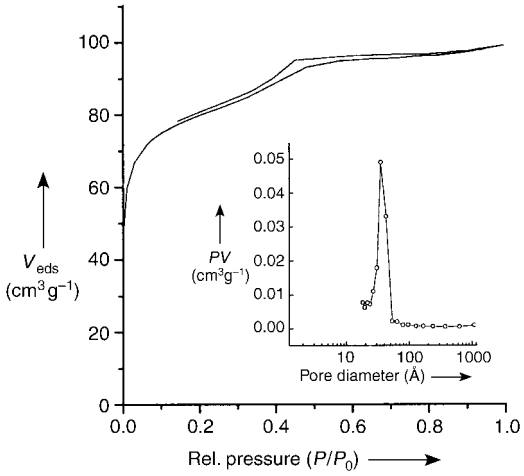


Figure 3. N_2 adsorption–desorption isotherms for the calcined ZSU-L sample (V_{ads} = gas volume adsorbed at standard temperature and pressure). Inset: The corresponding Barret–Joyner–Halenda (BJH) pore-size-distribution curve (PV = pore volume).

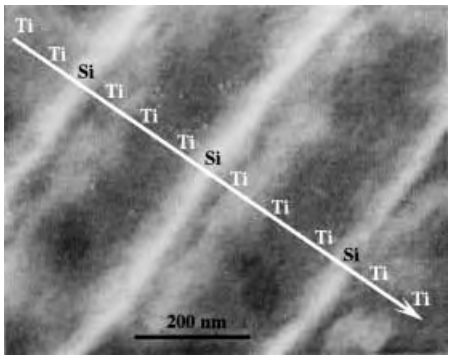


Figure 4. HREELS line scans across the lamellae of microlamellar-structured TiO_2/silicone surfactant composites, which indicate that the silicone surfactant is sandwiched by TiO_2 walls. Si originates from the silicone surfactant, and Ti from TiO_2.

[1] A. W. Xu, Y. P. Cai, H. X. Zhang, L. Z. Zhang, J. C. Yu, *Angew. Chem.* **2002**, *114*, 4000; *Angew. Chem. Int. Ed.* **2002**, *41*, 3844.
[2] A. W. Xu, Y. P. Cai, L. Z. Zhang, J. C. Yu, *Adv. Mater.* **2002**, *14*, 1064.
[3] A. W. Xu, J. C. Yu, Y. P. Cai, H. X. Zhang, L. Z. Zhang, *Chem. Commun.* **2002**, 1614.
[4] A. W. Xu, *Chem. Mater.* **2002**, *14*, 3625.
[5] A. W. Xu, *J. Phys. Chem. B* **2002**, *106*, 13161.
[6] C. T. Kresge, M. E. Leonowicz, W. J. Roth, J. C. Vartuli, J. S. Beck, *Nature* **1992**, *359*, 710.
[7] D. Zhao, J. Feng, Q. Huo, N. Melosh, G. H. Fredrickson, B. F. Chmelka, G. D. Stucky, *Science* **1998**, *279*, 548.
[8] S. A. Bagshaw, E. Prouzet, T. J. Pinnavaia, *Science* **1995**, *269*, 1242.
[9] P. T. Tanev, T. J. Pinnavaia, *Science* **1996**, *271*, 1267; P. T. Tanev, Y. Liang, T. J. Pinnavaia, *J. Am. Chem. Soc.* **1997**, *119*, 8616; S. S. Kim, W. Zhang, T. J. Pinnavaia, *Science* **1998**, *282*, 1302; K. S. W. Sing, *Pure Appl. Chem.* **1985**, *57*, 603.
[10] K. Saravanamuttu, M. P. Andrews, *Chem. Mater.* **2003**, *15*, 14.

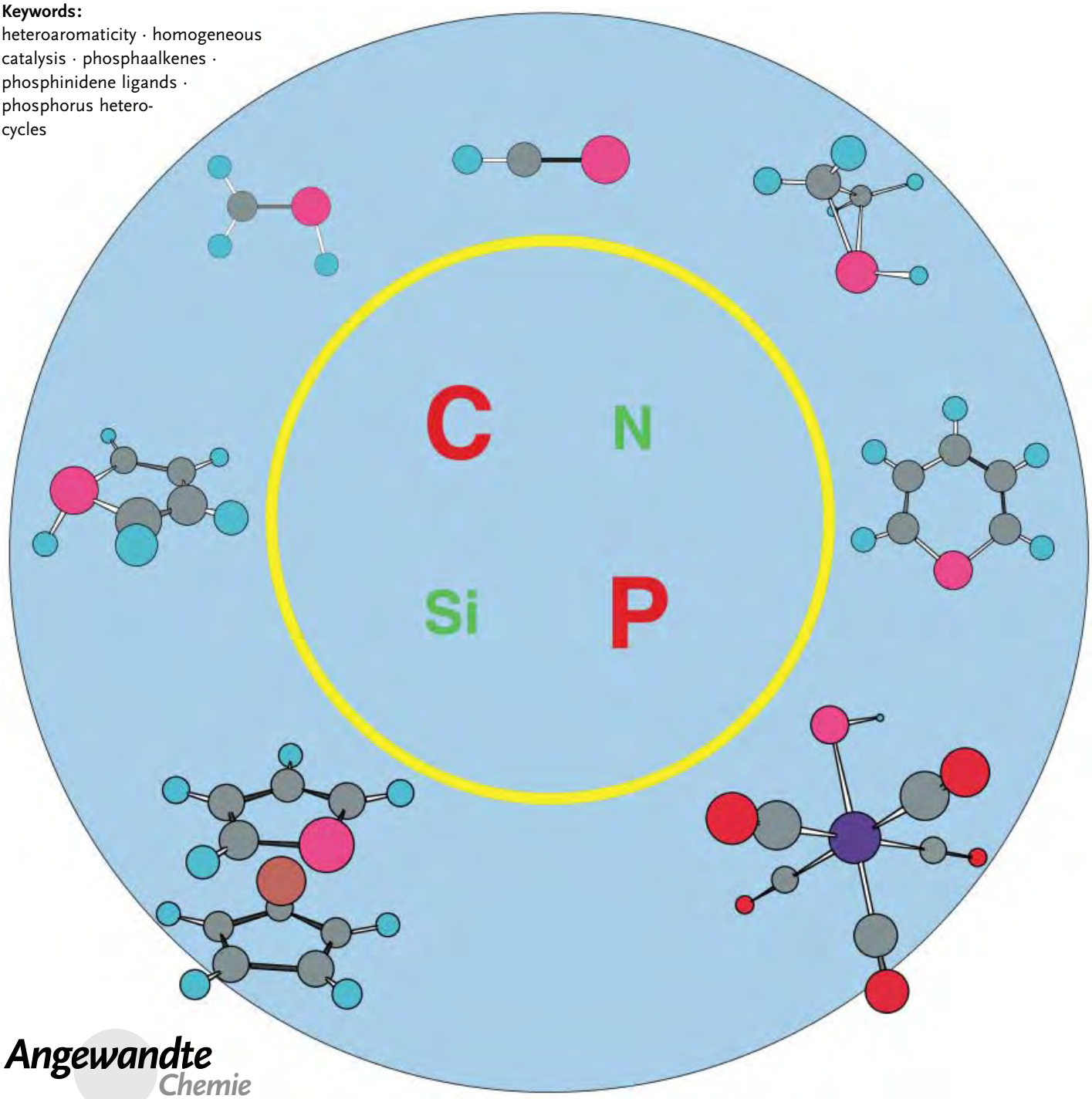
 © 2003 Wiley-VCH Verlag GmbH & Co. KGaA, Weinheim

Organophosphorus Compounds

Phospha-Organic Chemistry: Panorama and Perspectives

*François Mathey**

Keywords:
heteroaromaticity · homogeneous catalysis · phosphaalkenes · phosphinidene ligands · phosphorus heterocycles



© 2003 Wiley-VCH Verlag GmbH & Co. KGaA, Weinheim
DOI: 10.1002/anie.200200557

Since the beginning of the seventies, organophosphorus chemistry has been completely rejuvenated by the discovery of stable derivatives in which phosphorus has the coordination numbers one or two. The chemistry of these compounds mimics the chemistry of their all-carbon analogues. In this Review article this analogy is discussed for the phosphorus counterparts of alkenes, alkynes, and carbenes. In each case, the synthesis, reactivity, and coordination modes are briefly examined. Some special electronic configurations are also discussed, which include one-electron P–P bonds, strained bonds, and aromatic systems. To conclude, some potential applications of this chemistry in the areas of molecular materials and homogeneous catalysis are presented.

From the Contents

1. Introduction 1579
2. The Phosphorus–Carbon Analogy 1579
3. Phosphaalkenes 1579
4. Phosphaalkynes 1583
5. Terminal Phosphinidene Complexes 1586
6. Special Electronic Configurations 1588
7. Applications 1594
8. Conclusion and Outlook 1597

1. Introduction

For over a century, organophosphorus chemistry was built around the interplay between tervalent $\lambda^3\sigma^3$ tricoordinate and pentavalent $\lambda^5\sigma^4$ tetracoordinate configurations. In this classical chemistry, reactions at phosphorus centers were often driven by the formation of highly stable P–O single or double bonds. This simple Scheme is still prevalent in the minds of most of the users of organophosphorus compounds, both in organic and inorganic chemistry. Indeed, many organic chemists still merely consider organophosphorus chemistry as a source of reagents for performing deoxygenation reactions, oxygen–halogen exchange reactions, or Wittig-type alkene syntheses. On the other hand, coordination chemists and specialists in homogeneous catalysis mainly consider organophosphorus chemistry as an almost endless source of easily tunable $\lambda^3\sigma^3$ ligands, which are basically viewed as softer and somewhat π-accepting versions of the corresponding nitrogen ligands. The reality is far more complex. With the decisive help of ^{31}P NMR spectroscopy, organophosphorus chemistry specialists have conducted a complete reinvestigation of their field since the beginning of the sixties. The outcome of all this work has been the emergence of a whole range of well-characterized σ^1, σ^2, σ^5, and σ^6 species. In turn, the development of the chemistry of these low- and high-coordinate species has led those in the field to realize that phosphorus is a multi-faceted element which mimics silicon for high-,[1] nitrogen for medium-, and carbon for low-coordination states.[2] In fact, the analogy between the chemistry of low-coordinate carbon and phosphorus species is so deep, specific, and fertile that, with Keith Dillon and John Nixon, we have felt the need to coin the new term "phospha-organic chemistry"[2] to differentiate this domain from more classical organophosphorus chemistry. The aim of this Review is to summarize for non-specialists the most striking and potentially useful aspects of this new chemistry. The topics reflect my personal viewpoint and are neither encyclopedic nor perfectly representative. I have not tried to achieve a comprehensive coverage of the selected topics but prefer to extract some of the most informative publications to highlight the new concepts and trends underlying this new field.

2. The Phosphorus–Carbon Analogy

The phosphorus–carbon analogy basically reflects that the ability of phosphorus to accept or release electrons is similar to that of carbon. This ability of course depends on the electronic structures of the compounds under consideration. Whereas the σ electronegativity of phosphorus is somewhat lower than that of carbon (2.1 versus 2.5), the effective π electronegativity of phosphorus is very similar to, or even higher than, that of carbon as was shown by Michl et al. in a UV absorption and magnetic circular dichroism study of phosphinines.[3] In line with this finding, the π component of the double bond in phosphaethene ($HP{=}CH_2$) is almost apolar, whereas the σ component is highly polarized ($P^{\delta-}$–$C^{\delta-}$).[4] This situation induces some fascinating analogies between the reactivity of low-coordinate derivatives of carbon and phosphorus. Within the limited space available for this review, we shall focus our attention on the most fundamental low-coordinate units, the phosphorus analogues of alkenes, alkynes, and carbenes.

3. Phosphaalkenes

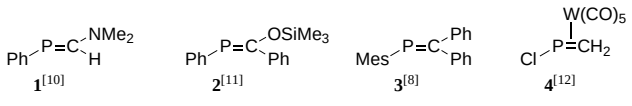
3.1. General Considerations

UV Photoelectron spectroscopy indicates that the HOMO of $HP{=}CH_2$ at −10.3 eV is the π bond and that the lone pair is at −10.7 eV.[5] For comparison, the π ionization

[*] F. Mathey
Laboratoire Hétéroéléments et Coordination
UMR CNRS 7653, DCPH, Ecole Polytechnique
91128 Palaiseau Cedex (France)
Fax: (+33) 1-69-33-39-90
E-mail: francois.mathey@polytechnique.fr

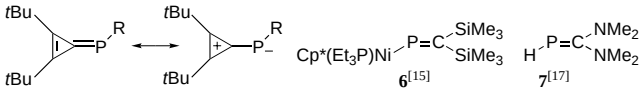
 © 2003 Wiley-VCH Verlag GmbH & Co. KGaA, Weinheim

energy of ethene is 10.51 eV. The P=C π-bond strength is calculated to be 43 kcal mol^{-1} as opposed to 65 kcal mol^{-1} for the C=C π bond of ethene.[6] The conjugative properties are similar for P=C and C=C bonds,[7] and that the P=C π bond is apolar has already been mentioned.[4] A typical phosphaalkene has a P=C bond length in the range 1.60–1.70 Å. For example in $MesP{=}CPh_2$, (Mes = mesityl) the P=C bond length is 1.69 Å.[8] In some cases, *E*/*Z* photoisomerization has been successfully carried out.[9] As might be expected from the theoretical data, the P=C bond is generally highly reactive and phosphaalkenes cannot be observed under ordinary conditions unless some kind of stabilization is provided, by conjugation, steric hindrance, or complexation. The compounds **1**–**4** are representative examples of these types of stabilization.



1[10] **2**[11] **3**[8] **4**[12]

When no stabilization is provided, phosphaalkenes tend to oligomerize. In some cases, clean [2+2] head-to-head or head-to tail dimerizations are observed.[13a] As already stated, normal phosphaalkenes have a positive charge at the phosphorus center which results mainly from the polarization of the σ bond. However, a series of phosphaalkenes exists in which an inverse electron distribution is observed. They have been the subject of a recent review.[13b] Their inversion of polarity generally results from the presence of an amino substituent at the carbon center (e.g. **1**). Cyclopropylidene derivatives, such as **5**, also belong to this category.[14]



5[14] **6**[15] **7**[17]

^{31}P NMR spectroscopy provides an easy means of discriminating between the two categories. Normal phosphaalkenes display ^{31}P resonances at low field, generally around $\delta = +200$ ppm (e.g., **3**, $\delta^{31}P = +233$ ppm),[8] although much lower-field chemical shifts have been recorded (e.g., **6**, $\delta^{31}P = +740$ ppm).[15] These low-field chemical shifts reflect the positive charge at the phosphorus center and the small HOMO–LUMO gap.[16] Inverse-polarized phosphaalkenes resonate at much higher fields (e.g., **7**, $\delta^{31}P = -62.6$ ppm).[17]

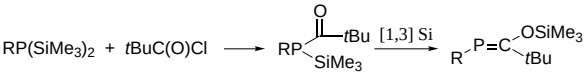


François Mathey, born in 1941 in Paris (France), studied chemistry at Paris VI University. He received his doctorate from this university in 1971 and worked in industry until 1988. Then, he was appointed Professor at Ecole Polytechnique in Palaiseau and Research Director at the CNRS. He has published around 500 papers and has received several awards from the Société Française de Chimie, the CNRS, and the Académie des Sciences. He has also been awarded a research prize from the Humboldt Foundation, the Main Group Chemistry Award, and the Arbuzov Prize. He is currently President of the French Chemical Society.

3.2. Synthesis

Since many earlier reviews describe the synthesis and properties of phosphaalkenes,[13b,18–21] this section will concentrate on the most practical routes or on those which highlight the phosphorus–carbon analogy.

Both from historical and practical standpoints, Becker's synthesis of the first stable phosphaalkenes is a landmark [Eq. (1)].[22]

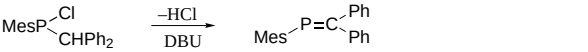


(1)

R = Me, Ph

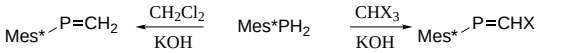
The [1,3] shift is driven by the oxophilicity of the silicon atom. Stability is conferred upon the P=C bond by the bulky siloxy and *tert*-butyl groups. A series of related syntheses relying on the reaction of bis(trimethylsilyl)phosphanes with phosgene,[23] CO_2,[24] imino chlorides and dichlorides,[25] carbodiimides,[26] and CS_2[267] are also based on the oxo-, aza-, and thiophilicity of silicon.

Another approach involves the classical 1,2-elimination of HX from the appropriate precursors. The synthesis of **3** illustrates this route [Eq. (2); DBU = 1,8-diazabicyclo[5.4.0]undec-7-ene].[8]



(2)

Two other examples are depicted in Equation (3) (Mes* = 2,4,6-$tBu_3C_6H_2$),[28] in which carbene insertion initiates both reactions.

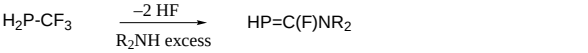


(3)

X = Cl, Br

In other cases, the halogen substituent can be located on the α-carbon as shown in Equation (4).[29]

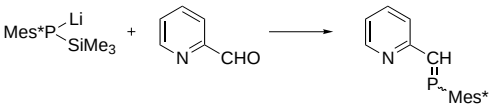
The "phospha-Peterson" reaction constitutes a third reliable route. An example is given in Equation (5).[30] For other examples, see ref. [31]. The synthesis of **5** follows the



(4)

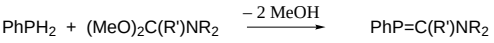
R = Me, Et...

 © 2003 Wiley-VCH Verlag GmbH & Co. KGaA, Weinheim

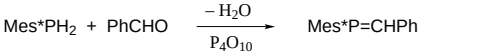


(5)

same scheme. This silicon–lithium activation of the phosphane is not necessary in all cases and the synthesis of highly stabilized phosphaalkenes can be performed by condensation of primary phosphanes with the appropriate carbonyl derivatives [Eqs. (6), (7)].[10a,32]

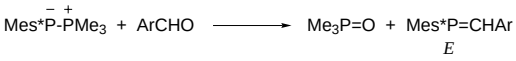


(6)



(7)

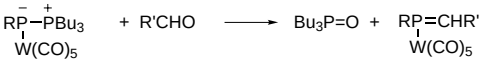
The "phospha-Wittig" reaction is another illustration of the phosphorus–carbon analogy. It exists in three versions.[33] Phospha-Wittig ylids are reasonably stable whenever bulky groups are found at the two-coordinate phosphorus atom. They are readily obtained from the appropriate dichlorophosphanes, trialkylphosphanes and zinc in THF. They react with aldehydes to produce the corresponding phosphaalkenes [Eq. (8)].[34]



(8)

Ar = Ph, *p*-X-C_6H_4 (X = Cl, NO_2, OMe, NMe_2); 78–94% yield

The severe limitation put on this process by the low stability of phospha-Wittig reagents bearing non-sterically demanding substituents can be circumvented by complexation of the phosphinidene group, for which, pentacarbonyltungsten is the species of choice. It stabilizes both the starting phospha-ylid and the final phosphaalkene [Eq. (9)].[35]



(9)

The final method involves nucleophilic phosphinidene complexes derived from Ta^{V}[36] or Zr^{IV} species [Eq. (10); Fc = ferrocenyl].[37]

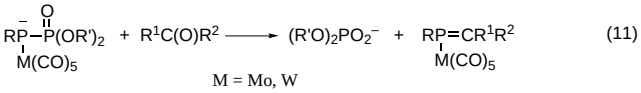


(10)

$N_3N = N[CH_2CH_2N(SiMe_3)]_3$; R = *t*Bu, Fc

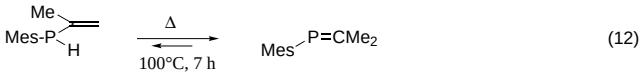
Except when these rather exotic transition-metal reagents are used, the phospha-Wittig reaction does not work with ketones. This limitation can be removed by using anionic phosphorylphosphane complexes which mimic the Horner–Wittig reaction [Eq. (11)].[38]

An intramolecular version of these metal-assisted phospha-Wittig reactions which generates cyclic phosphaalkene complexes[39] has been investigated with some success. Several 1-phosphadiene complexes have also been prepared by this route.[40]



(11)

Before leaving this section, we wish to stress a striking observation. Appropriately substituted secondary vinylphosphanes tend to equilibrate with the corresponding phosphaalkenes [Eq. (12)].[41]

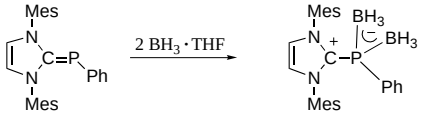


(12)

This thermal isomerization has been studied from a theoretical standpoint.[42] Unlike the corresponding all-carbon systems, a concerted suprafacial [1,3] sigmatropic shift of the hydrogen atom seems to be possible.

3.3. Reactivity

The small energy gap between the phosphaalkene π and n_P (phosphorus lone pair) orbitals means that an electrophilic reagent will often not discriminate between the C=P bond and the phosphorus lone pair. This is the case for oxidation[43a] and sulfurization.[44] Phosphaalkene oxides are normally unstable and can be isolated only if high steric protection is provided about the phosphorus atom.[43b] In general, quaternization at phosphorus centers is slow and difficult.[45] Naturally, this chemistry is much easier to perform with inversely polarized phosphaalkenes.[13b] When the inversion of polarity C^{+}–P^{-} is very strong, as for **8**, it becomes possible to coordinate two borane units at the phosphorus center [Eq. (13)].[45b] The bis-adduct (**8**-2BH_3) has a P^{-}–C^{+} bond length of 1.856(2) Å in agreement with its single bond character.



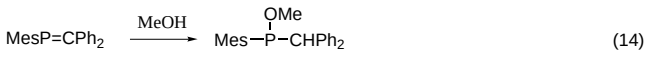
8

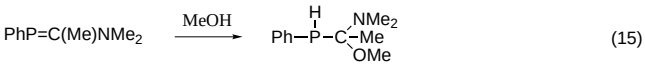
(13)

But the most significant reactions of phosphaalkenes are, of course, those of the P–C double bond. Reactions with protic reagents can either lead to C–H (normal) or P–H (inverse) products depending upon the polarity of the bond [Eqs. (14), (15)].[8,46]

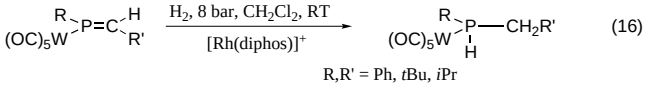
Classical reactions of olefins, such as catalytic hydrogenation[47] and epoxidation[48] can only be achieved after

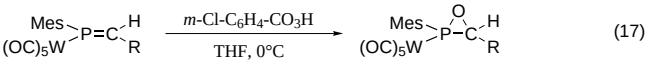
 © 2003 Wiley-VCH Verlag GmbH & Co. KGaA, Weinheim

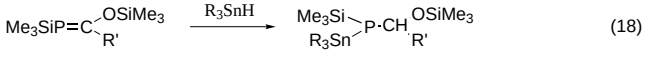

(14)

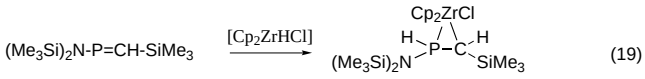

(15)

protection of the phosphorus lone pair by complexation [Eqs. (16), (17); diphos = $Ph_2PCH_2CH_2PPh_2$]. Hydrostannylation gives the P–Sn product[49] whereas hydrozirconation[50] leads to the P–H products [Eqs. (18), (19)].

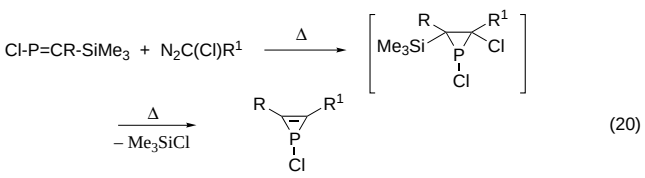

(16)


(17)


(18)

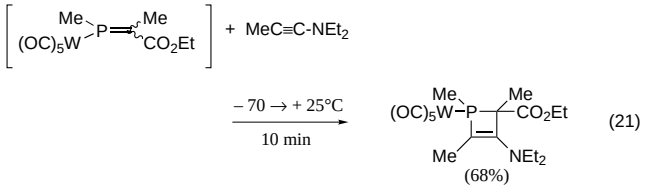

(19)

A large variety of [2+1], [2+2], [2+3], [2+4], and even [2+8] cycloaddition reactions have been reported. In general, the concerted reactions follow the Woodward–Hoffmann rules.[2] Only some of the most significant cases will be treated here. The[2+1] cycloaddition of phosphaalkenes to chlorocarbenes under neutral conditions provides an access to 1-chlorophosphirenes [Eq. (20)].[51]


(20)

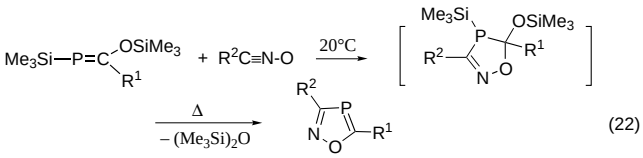
Electron-poor phosphaalkenes, generated at low temperature by a phospha-Wittig reaction [Eq. (11)], readily cycloadd to electron-rich alkenes or alkynes [Eq. (21)].[52]

A wide variety of [2+3] cycloadditions of phosphaalkenes with 1,3-dipole compounds has been studied.[53,54] In many

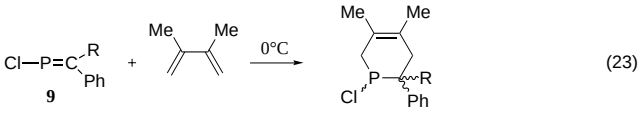

(21)

cases, the final products are aromatic heterophospholes. One typical example is given in Equation (22).[54]

Diels–Alder [4+2] cycloadditions have also been studied in some detail.[55] In most cases, the Woodward–Hoffmann

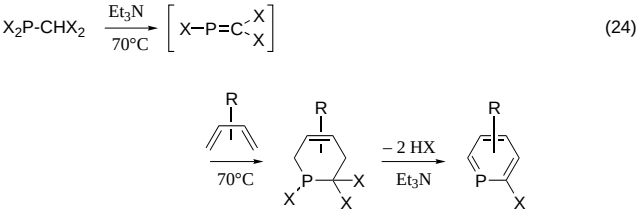

(22)

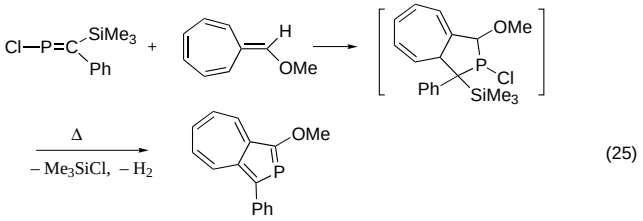
rules are respected, although some exceptions have been recorded. For example, all four possible isomers have been obtained in the reaction of a pure isomer of **9** with 2,3-dimethyl-1,3-butadiene [Eq. (23)].[56] An efficient one-pot


(23)

synthesis of 2-halophosphinines is based on this type of Diels–Alder chemistry [Eq. (24)].[57]

Numerous heterodienes have also been shown to participate to such [2+4] cycloaddition reactions.[58] Finally, one example of a [2+8] cycloaddition has been reported to date [Eq. (25)].[59]


(24)

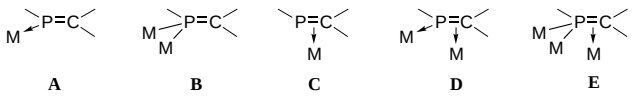

(25)

The analogy between C=C and P=C bonds is completed by the participation of P=C bonds in ene reactions,[60] [1,5],[61] and [3,3] sigmatropic shifts,[62] as well as 4π[63] and 6π electrocyclizations.[64] Finally, numerous conjugated or cumulated phosphapolyenes and phosphaketenes show chemistry which quite nicely parallels that of their all-carbon analogues.[2]

3.4. Coordination Chemistry

Phosphaalkenes are able to give five different types of complexes (**A**–**E**). In complexes of type **A**, the P=C bond is

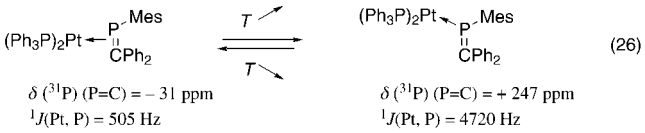
 © 2003 Wiley-VCH Verlag GmbH & Co. KGaA, Weinheim



A **B** **C** **D** **E**

still available for reactions and the structure of the phosphaalkene is practically unaffected by the σ complexation.[65] Whenever a protection of the phosphorus lone pair is required in reactivity studies, this type of complex can be used advantageously, see Equations (16) and (17). As P ligands, phosphaalkenes are relatively poor σ donors and good π acceptors. Complexes of type **B** reflect the tendency of phosphorus to increase its coordination number from three to four.[66] In complexes of type **C**, the P=C bond is elongated as a result of the ligand-to-metal electron donation from the occupied π orbital and metal-to-ligand backdonation adding electronic density into the π* orbital.

An equilibrium sometimes occurs between complexes of type **A** and **C**, as shown by Bickelhaupt et al. [Eq. (26)].[67]



δ (^{31}P) (P=C) = − 31 ppm
^1J(Pt, P) = 505 Hz

δ (^{31}P) (P=C) = + 247 ppm
^1J(Pt, P) = 4720 Hz

(26)

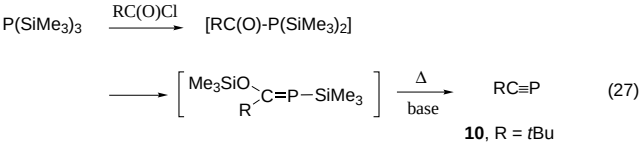
The shift to high field seen in the ^{31}P NMR spectrum upon π complexation is very characteristic, although some recent examples seem to question its generality.[68] The sharp decrease in the ^1J(P,M) (M = metal center) coupling when moving from σ to π complexation seems to be systematic. Four-electron complexes, such as **D** or **E** are also known.[69,70] Similar subunits are incorporated in unusual η^4-1- and 2-phosphabutadiene complexes.[63,71] All this coordination chemistry now has more than just academic interest since the first applications of phosphaalkene complexes in homogeneous catalysis have recently been unveiled.[72]

4. Phosphaalkynes

4.1. General Considerations

A very extensive series of reviews on the chemistry of phosphaalkynes is available,[73] so only the most significant aspects of the field will be treated here. The UV photoelectron spectrum of *t*BuC≡P shows a first ionization at −9.61 eV corresponding to the π bonds and a much lower second ionization at −11.44 eV corresponding to the lone pair.[74] Consequently, the lone pair of phosphaalkynes is much less reactive than the lone pair of phosphaalkenes and the large gap between the π and n_P ionization energies suggests that the overlap between the chemistry of the π bonds and the chemistry of the lone pair will be minimal. As expected the P≡C bond of *t*BuC≡P is very short at 1.548(1) Å.[75]

When Gier discovered phosphaacetylene HC≡P in 1961,[76] the long-term impact of this discovery was not fully realized by the chemical community. The compound was mostly considered as a curiosity. Its instability and nonconventional synthesis through the decomposition of PH_3 in an electric arc between graphite electrodes precluded any development of its chemistry. Subsequent work of Nixon and Kroto et al. on the double dehydrohalogenation of RCH_2PCl_2 by flash pyrolysis[77] provided support for the pioneering work of Gier, but it was only in 1981 with the work of Becker et al. that the chemistry of phosphaalkynes was firmly established [Eq. (27)].[78]



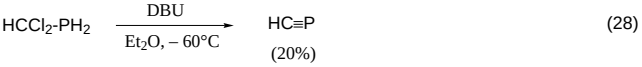
10, R = *t*Bu

(27)

tert-Butylphosphaacetylene (**10**), an easily handled colorless liquid with a boiling point of +61 °C, is surprisingly stable, and this compound proved to be the starting point for the rapid development of the chemistry of the P≡C bond. It soon became clear that phosphaalkynes can be stabilized in a variety of ways. For example, the anions in P≡C-O$^-$ Li$^+$ (**11**) and P≡C-S$^-$ Li$^+$ (**12**) are stable at room temperature.[79,80] The P≡C bond is usually polarized: $P^{\delta+}$–$C^{\delta-}$. As with phosphaalkenes, amino groups at the carbon center stabilize the multiple bond and modify its polarization.[29,81] From a spectroscopic standpoint, the ^{31}P resonance signals of RC≡P are found in a large range from −384 (R = OLi) to +96 ppm (R = $SiMe_3$). In most cases, the ^{31}P chemical shifts are at high fields relative to the standard reference H_3PO_4: $\delta = -32$ (R = H), −60 (R = Me), −69 ppm (R = *t*Bu). Recent work analyzing the spectroscopic data of phosphaalkynes from a theoretical standpoint suggests a δ^{31}P value of $\delta = -350$ ppm for R = F.[82]

4.2. Synthesis

The only reliable low-temperature preparation of phosphaacetylene [Eq. (28)], can be generalized for the synthesis of other phosphaalkynes.[83] This method can be transposed to prepare MeC≡P in 75 % yield.



(28)

Another well-described procedure for HC≡P relies on the thermolysis of triallylphosphane.[84] In this case, the multistep reaction pathway is not fully understood. Among the other syntheses of phosphaalkynes, the base-promoted rearrangement of primary alkynylphosphanes is especially noteworthy [Eq. (29)].[85]



(29)

© 2003 Wiley-VCH Verlag GmbH & Co. KGaA, Weinheim

More classical approaches include the thermal or base-induced 1,2-eliminations of HX or $XSiMe_3$ from the appropriate precursors. Two typical examples are depicted in Equation (30)[86] and (31).[87] A less general and less predictable approach involves the rearrangement of vinylphosphinidene into phosphapropyne [Eq. (32)].[88] The mechanism of this rearrangement has been studied in some detail from a theoretical standpoint.[89] However, the only routinely used approach is still that of Becker [Eq. (27)] which has been optimized and generalized by Regitz et al.[90]



(30)



(31)

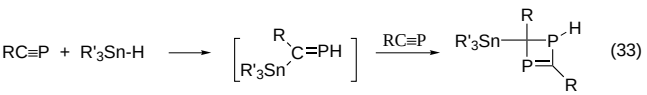


(32)

Steric bulk is not essential for the stability of phosphaalkynes, HC≡P itself can be kept for months in diethyl ether below −20 °C. Alkyl-substituted phosphaalkynes are stable at room temperature when rigorously pure. On the contrary, PhC≡P and $Me_3SiC{\equiv}P$ have limited lifetimes under similar conditions.

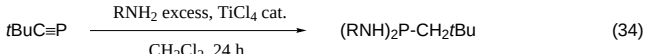
4.3. Reactivity

As expected, the phosphorus lone pair of phosphaalkynes displays very low reactivity. Protonation by superacids takes place exclusively at the carbon center.[91] The resulting phosphavinyl cation is then trapped by the superacid counterion to give a phosphaalkene. The reaction with Lewis acids, such as BCl_3 or $AlCl_3$[92] initially follows the same pathway. 1,2-Additions are observed to Sn–H[93] and Zr–H bonds [Eq. (33)].[94]

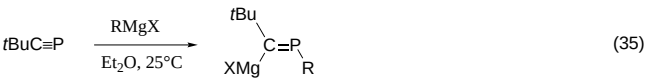


(33)

Titanium(IV) ions have been shown to catalyze the dihydroamination of the P≡C bond [Eq. (34)].[95] Organomagnesium compounds give stable phosphavinylmagnesium halides [Eq. (35)].[96] The reaction with organolithium reagents is more complex.[97]

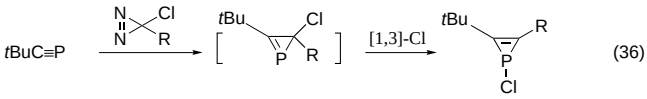


(34)



(35)

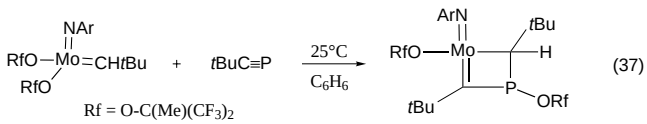
As with phosphaalkenes, the cycloaddition chemistry of phosphaalkynes is extremely well developed. Again, we shall only point out a few representative examples. [2+1] Cycloadditions have been reported with carbenes,[98] silylenes,[99] germylenes,[100] phosphinidenes,[101] and terminal phosphinidene complexes.[102] Cycloadditions with chlorocarbenes[98a,b] have served as a route to 1-chlorophosphirenes [Eq. (36)].



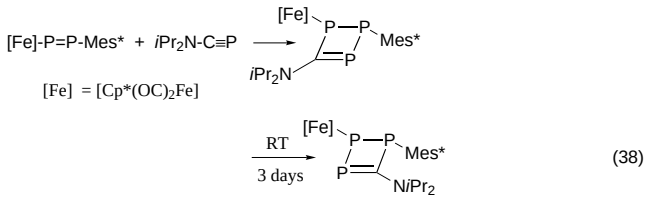
(36)

The reaction of RC≡P (R = iPr$_2$N or tBu) with a stable benzimidazolinylidene carbene follows a more complex pathway and yields either a 1,2,3-triphosphetene when R = iPr$_2$N or a 1,2,4-triphosphole when R = tBu.[98c]

[2+2] Cycloadditions are relatively rare for phosphaalkynes and their precise mechanisms (stepwise or concerted) have not been generally established. A first interesting experiment was carried out with a Schrock carbene complex [Eq. (37)].[103] The initial [2+2] cycloaddition, which shows the expected regiochemistry ($P^{\delta+}$–$C^{\delta-}$), is followed by the [1,3] migration of an alkoxy group from the molybdenum to the phosphorus center. The groups of Grobe and Weber have also shown that a [2+2] cycloaddition can be performed between a diphosphene and a phosphaalkyne [Eq. (38)].[104] The initial adduct isomerizes slowly at room temperature.



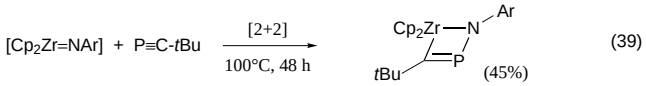
(37)



(38)

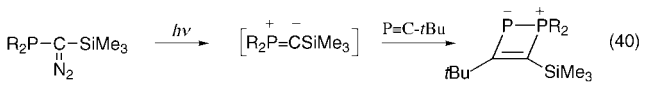
Following on the work of Regitz et al. on an efficient synthesis of 1,3,5-triphosphinines by trimerization of phosphaalkynes in the presence of vanadium(v) imido catalysts, the [2+2] cycloaddition of phosphaalkynes was exemplified with V^{V},[105] Ti^{IV}, and Zr^{IV} imido complexes [Eq. (39)].[106]

Another interesting case concerns a formal [2+2] cycloaddition between λ^3- and λ^5-phosphaalkynes [Eq. (40)],[107] in which an intermediate phosphinophosphirene has been



(39)

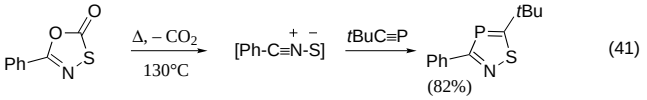
 © 2003 Wiley-VCH Verlag GmbH & Co. KGaA, Weinheim



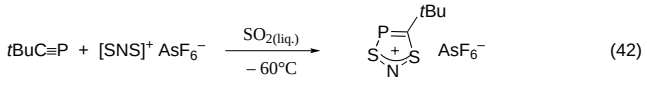
(40)

characterized. The antiaromaticity is switched off in the resulting λ^3,λ^5-diphosphete.[108] Finally, distannenes also give [2+2] cycloadducts with phosphaalkynes.[109]

[2+3] Cycloadditions of phosphaalkynes with 1,3-dipole compounds, such as diazoalkanes, azides, nitrile ylids, nitrilimines, nitrile oxides, nitrile sulfides, nitrones, selenadiazoles (selenoxocarbenes) have been studied in depth. This class of reactions is a gold mine for the synthesis of heterophospholes.[110] Here, only two examples are presented, one typical [Eq. (41)],[111] the other quite unusual [Eq. (42)].[112]

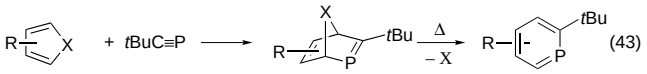


(41)



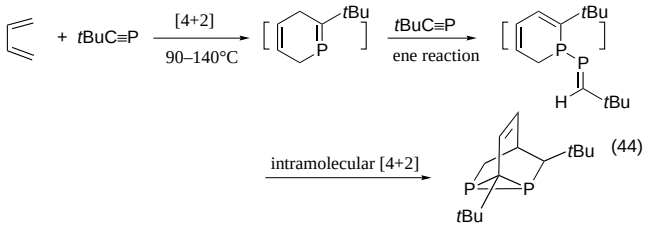
(42)

[2+4] Cycloadditions of phosphaalkynes have also been studied in some depth. The initial [2+4] cycloadduct is normally unstable and evolves, either to give an aromatic phosphinine [Eq. (43)][113] or through an ene-reaction with an additional molecule of phosphaalkyne [Eq. (44)].[114]



(43)

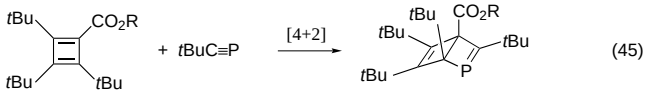
X = CO, CO_2, P(S)Ph, C_2H_4, $SnMe_2$



(44)

Several other variations are possible. [4+2] Cycloadditions have also served to prepare the first Dewar-phosphinine [Eq. (45)][115] and a $\lambda^3,\lambda^5,\lambda^5$-1,3,5-triphosphinine [Eq. (46)].[116]

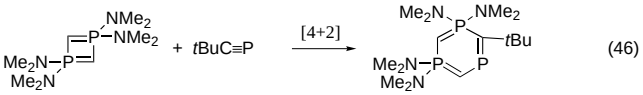
As already shown in Equation (44), phosphaalkynes readily take part in ene reactions. These have been studied



(45)

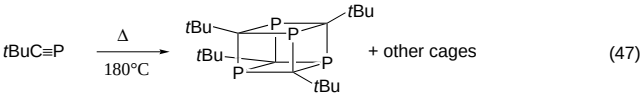
in some depth.[117] Homo-Diels–Alder reactions and [8+2] cycloadditions have been also reported.

Perhaps the most curious facet of phosphaalkyne chemistry is the great variety of oligomerization reactions. These reactions generally lead to complicated cage compounds.[118]

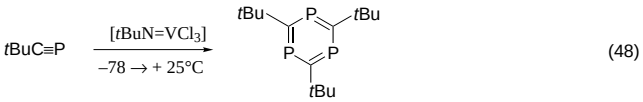


(46)

However, in some cases, more classical alkyne-like behavior is observed. Two representative examples are presented in Equation (47)[119] and (48).[120]



(47)

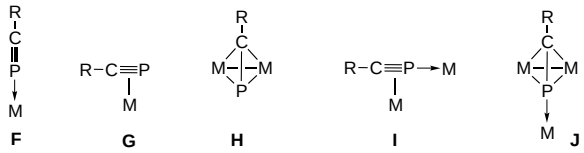


(48)

A more efficient synthesis of the tetraphosphacubane compound in Equation (47) is now available.[121] It must be stressed here that all these oligomerization studies have been carried out on sterically protected phosphaalkynes and that oligomerization and polymerization of classical alkenes and alkynes are known to be extremely dependent on the steric bulk of the substituents. Thus, the knowledge available at present is of questionable use in predicting the outcome of the polymerization studies of nonstabilized phosphaalkynes, such as MeC≡P.

4.4. Coordination Chemistry

Phosphaalkynes can give five different types of complexes (**F**—**J**). Complexes **G** and **H** are analogous to the classical alkyne two- and four-electron π complexes. This side-on



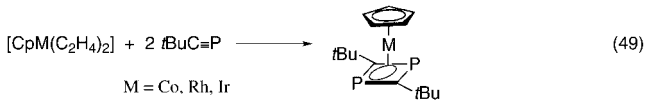
coordination appears to be much more favorable than the coordination at the phosphorus lone pair, in agreement with the very high ionization energy of the phosphorus lone pair. In fact, only a few complexes of type **F** are known.[122] In these cases, the P≡C bond is not elongated (unlike the case of side-on complexes) and its reactivity is enhanced.[123]

The favored η^2-coordination mode underlies a chemistry which is often similar to that of alkynes. A first illustration is provided by the cyclodimerization of phosphaalkynes in the coordination spheres of metal centers including Fe, Co, Ni,

 © 2003 Wiley-VCH Verlag GmbH & Co. KGaA, Weinheim

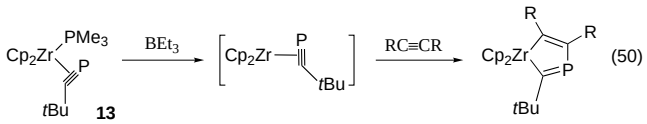
Rh, Ir. This dimerization generally gives the head-to-tail 1,3-cycloadducts [Eq. (49)].[124]

In some cases however, the head-to-head 1,2-isomer has been isolated.[125] Surprisingly, DFT calculations indicate that

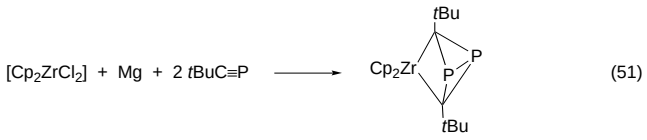


(49)

these 1,2-isomers are systematically more stable than their 1,3-counterparts.[126] The chemistry in the coordination sphere of zirconium is more diverse. From the η^2-complex **13**, a normal alkyne-like chemistry can be developed [Eq. (50)].[127] However, under different experimental conditions, a new type of dimeric derivative is obtained [Eq. (51)].[121]

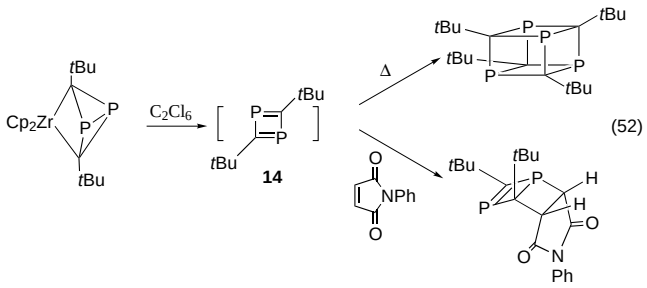


(50)



(51)

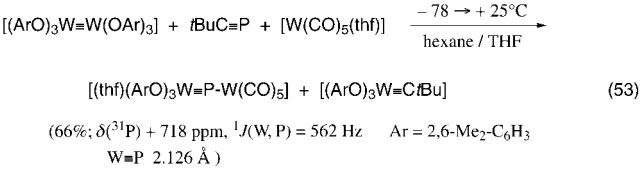
This dimer is the starting point for some very useful chemistry. Upon chlorination under mild conditions using C_2Cl_6, it yields the free 1,3-diphosphacyclobutadiene (**14**) which dimerizes to give the corresponding tetraphosphacubane [see Eq. (47)].[121] Alternatively, **14** can be trapped by various dienophiles [Eq. (52)].[128]



(52)

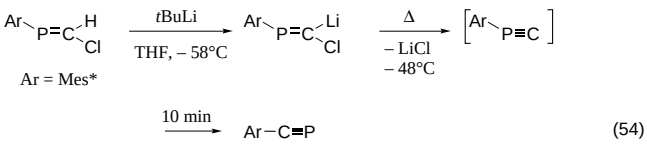
The fascinating analogy which exists between the chemistry of alkynes and phosphaalkynes inevitably led several research groups to wonder whether it would be possible to duplicate the metathesis of alkynes with phosphaalkynes. A significant result has been obtained by Scheer's group [Eq. (53)].[129]

Another question was the potential existence of the isophosphaalkynes RP≡C. Whilst both the isoelectronic isonitriles (RN≡C) and carbon monoxide are metastable,



(53)

both of the heavier congeners, the isoelectronic RP≡C and carbon monosulfide are highly unstable. When generated from the appropriate carbenoids, an isophosphaalkyne immediately rearranges to the isomeric phosphaalkyne [Eq. (54)].[130]



(54)

Theoretical calculations indicate that HP≡C is 85 kcal mol^{-1} higher in energy than HC≡P.[131] The situation changes in the coordination spheres of transition metals. Several complexes of RP≡C and the so-called cyaphide ion $[C{\equiv}P]^-$ have been structurally characterized.[132]

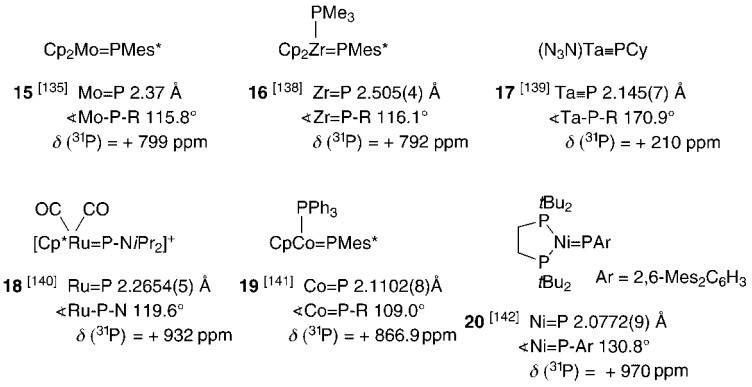
5. Terminal Phosphinidene Complexes

5.1. General Considerations

Over quite a long period, phosphorus chemists explored the possibility of replicating the chemistry of carbenes by using phosphorus-based species. To fulfill this objective, it was not sufficient only to mimic the reactions of carbenes. It was also desirable to provide a chemistry which would eliminate any restriction on the nature of the phosphorus substituents and, if possible, to avoid working in highly acidic or basic media to allow a compatibility with reactive functional groups. An attractive first solution relied on the analogy between carbenes, silylenes, and the isoelectronic phosphenium cations.[133] These species are easily obtained by reaction of $AlCl_3$ with R_2PCl and satisfactorily reproduce the main reactions of carbenes, but there are severe limitations on the nature of the substituents. In practice, one or two dialkylamino groups are almost always necessary. Furthermore, the phosphonium salts resulting from the reactions of $[R_2P]^+$ ions with organic substrates are generally difficult to purify and to work with. A second approach relied on the generation and trapping of transient phosphinidenes (RP). These unstable triplet species can be generated by photolysis of phosphiranes.[134] Unfortunately, for practical reasons, this approach is limited to compounds having bulky aryl substituents at the phosphorus center. At this point, it became clear that it might be quite useful to stabilize the singlet state of phosphinidenes and to control their reactivity by coordination to a transition-metal atom. The resulting terminal phosphinidene complexes exist in two types, as bent two-electron complexes[135] and as linear four-electron complexes.[136] Their reactivity can be

 © 2003 Wiley-VCH Verlag GmbH & Co. KGaA, Weinheim

tuned from nucleophilic to electrophilic by changing the ligands supporting the metal center from σ donors to π acceptors (see, for example, the compounds **15**–**20**). This effect has been studied in some depth in a recent DFT analysis.[137] As expected, the four-electron complexes show a shorter phosphorus–metal bond than their two-electron counterparts with the same metal; they also display a ^{31}P resonance signal significantly further up-field.

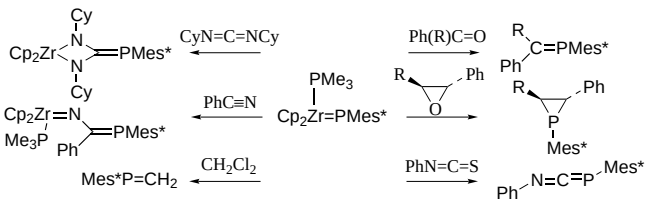


5.2. The Nucleophilic Complexes

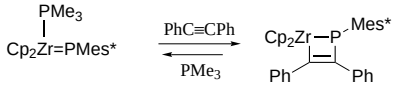
Since the ground state of phosphinidene (PH) is a triplet and the lowest energy singlet state lies about 22 kcal mol^{-1} higher in energy,[143] it is clear that phosphinidene should bind easily to triplet-ground-state metallic moieties to give terminal complexes having a genuine P–M double bond. This bond is very similar to that found in Schrock carbene complexes. Phosphorus is substantially more electronegative than transition metal atoms, so the P=M bond is normally polarized in the sense $P^{\delta-}$–$M^{\delta+}$. With highly electropositive metals such as Zr and Ta, this double bond participates in the phospha-Wittig chemistry mentioned in Section 3.2 [Eq. (10)]. Other examples are depicted in Scheme 1.[144]

The reversible [2+2] cycloaddition reaction with alkynes is also quite significant. It mimics the first step of the metathesis of alkynes [Eq. (55)].[145]

As with any polarizable double bond, it is possible to change the charge distribution about the P=M bond by having electron-accepting ligands at the metal center. (Some results from a DFT study[137] are given in Table 1.) Thus, the



Scheme 1. Reactivity of terminal zirconium phosphinidene complex.



(55)

Table 1: Calculated charges at the phosphorus atom in various phosphinidene complexes.[137]

Complex	Charge at P atom
[Cp$_2$Ti=PH]	−0.270
[Cp$_2$Zr=PH]	−0.295
[Cp(OC)Co=PH]	−0.118
[(OC)$_4$Fe=PH]	−0.060

electrophilic behavior of the phosphinidene in [*i*Pr$_2$NP=Fe(CO)$_4$][146] can be understood through the polarization induced within the P=Fe bond by the π-donating amino substituent on the phosphorus center. The electrophilic complexes prepared by Carty et al. (e.g. **18**)[140] are characterized by the presence of a positive charge which is delocalized between the metal and the phosphorus atoms. The amino substituent provides additional stabilization for the electrophilic phosphorus atom.[147] The reaction of these complexes with alkynes gives phosphirene complexes.[148]

5.3. The Electrophilic Complexes

In practice, by far the most useful terminal phosphinidene complexes are the unstable species derived from [M(CO)$_5$] (M = Cr, Mo, W). They have been the subject of two recent reviews.[149] They perfectly mimic the chemistry of singlet carbenes and there is practically no limit to the nature of the substituents which can be tolerated at the phosphorus center.[149a] Furthermore, several techniques are available for the release of the final products from the metal coordination spheres.[149a] From an electronic standpoint, these [RP–M(CO)$_5$] complexes are quite different from the nucleophilic phosphinidenes described in Section 5.2. The ground states of [M(CO)$_5$] are singlets,[150] with singlet–triplet separation being approximately 33.7 kcal mol^{-1} for [Cr(CO)$_5$][150a] and approximately 40 kcal mol^{-1} for [Mo(CO)$_5$].[150b] Thus, combining the triplet ground states of phosphinidenes with the triplet excited states of [M(CO)$_5$] costs more in energy than combining the singlet excited states of phosphinidenes with the singlet ground states of [M(CO)$_5$], especially for amino-phosphinidenes. The calculated triplet–singlet separations for RP,[151] the P–W bond lengths in the corresponding [RP–W(CO)$_5$] complexes, and the charges at phosphorus in these complexes[152,153] are given in Table 2.

When the calculated P–W bond lengths are compared with the experimental values found for P=W (2.349(5) Å[135]) and P≡W bonds (2.169(1) Å[136]), it is quite clear that [RP–

Table 2: Calculated parameters of [RP–W(CO)$_5$].

R	$\Delta E_{S\text{-}T}$ [kcal mol^{-1}] (RP)	P–W bond length[152,153] [Å]	Charge at P atom[152]
H	28[a]	2.423–2.417	+0.282
Me	26	2.430	
NH_2	1.2	2.466–2.448	+0.725

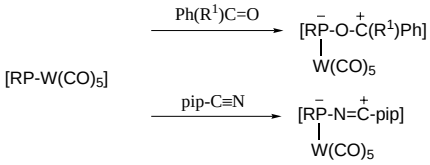
[a] Experimental value: 22 kcal mol^{-1}.

 © 2003 Wiley-VCH Verlag GmbH & Co. KGaA, Weinheim

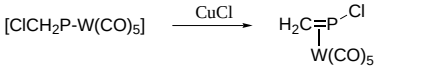
$W(CO)_5$] has single bond character. A similar conclusion has been drawn for [RP–$Cr(CO)_5$].[151] An extensive comparison between [Cp_2Ti=PH] and [$(OC)_5Cr$=PH] using an electron localizing function (ELF) analysis led to the same conclusions: a Ti=P double bond and negative charge at the phosphorus center in the former, a Cr–P single bond and positive charge at phosphorus in the latter.[154] Hence, [RP–$M(CO)_5$] species are best represented as Fischer-type phosphinidene complexes having a dative P→M single bond and a small contribution from π backdonation.

Some chemistry of [RP–$W(CO)_5$] is summarized in Scheme 2. This chemistry is highly reminiscent of the reactivity of singlet carbene compounds. Thus, the retention of stereochemistry in the reaction with alkenes is quite significant.[155] The reaction with alkynes gives the corresponding phosphirene complexes[156] rather than the [2+2] cycloadducts observed with Schrock's phosphinidene complexes [Eq. (55)]. With ketones and nitriles, zwitterionic 1,3-dipolar adducts, the evolution of which depends on the nature of the substituents, are formed [Eq. (56); pip = piperidyl].[157]

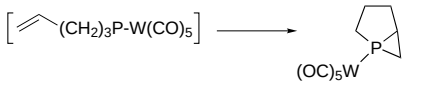
It is possible to characterize stable adducts prepared from the reactions of electrophilic terminal phosphinidene complexes with trialkylphosphanes. These species undergo phospha-Wittig chemistry [see Eq. (9)].[35] The almost limitless choice of substituents is illustrated by some striking intramolecular reactions [Eq. (57), (58)].[12,163] As these examples show, the carbene-like chemistry of [RP–$W(CO)_5$] complexes provides a very versatile and significant advance in synthetic organophosphorus chemistry.



(56)



(57)



(58)

6. Special Electronic Configurations

6.1. P–P One-Electron Bonds and Stable Biradicals

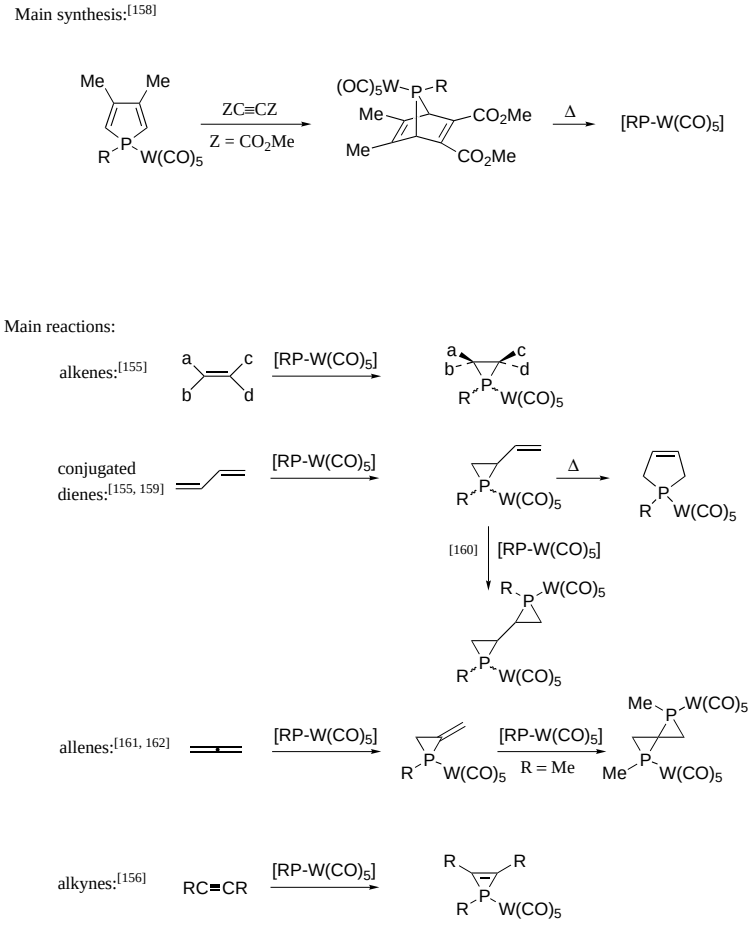
As with any element of the third period, phosphorus is characterized by having rather diffuse frontier orbitals which favor long-range interactions. This property is certainly one of the reasons underlying the successful identification of one-electron P–P bonds.

Upon cleavage of the P–N bond of 1,2-diphosphirene **21**, a transient diphosphirenyl radical is produced. It dimerizes spontaneously to give **22** [Eq. (59)].[164]

Compound **22** is a red, diamagnetic compound ($\delta^{31}P = -164.5$ ppm) with very long P–P bridges of 2.634(3) Å. From a theoretical standpoint, it can be viewed as a π*π* dimer of two [P=P] units, the low-lying π* orbitals correspond to the SOMOs of the monomers. The two electrons are delocalized over the four phosphorus centers. Using a mesomeric formulation, the electronic configuration corresponds to a bond–no-bond resonance with an average bond order of 0.5 for the P–P bridges. In the same vein, a localized one-electron P–P bond is formed upon the one-electron reduction of a flexible macrocycle containing two phosphinine units [Eq. (60)].[165]

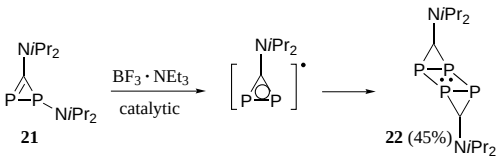
The P···P separation is reduced from 3.256 Å in the starting macrocycle (X-ray data) to 2.763 Å (DFT calculation) in the one-electron-reduction product. The calculated structure shows two parallel head-to-tail phosphinine units with a perpendicular P–P bond which indicates partial occupation of two overlapping π* orbitals.

Another singlet biradical based upon a four-membered P_2C_2 ring (**23**) has been prepared by the

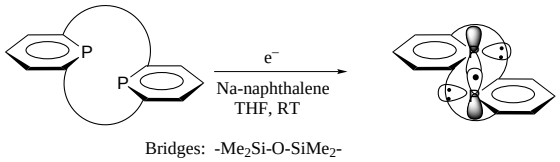


Scheme 2. Main reactions of [RP–$W(CO)_5$].

 © 2003 Wiley-VCH Verlag GmbH & Co. KGaA, Weinheim

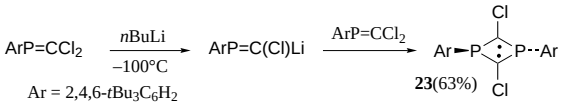


(59)



(60)

group of Niecke [Eq. (61)].[166] Compound **23** is a deep red, diamagnetic solid ($\delta^{31}P = +26.5$ ppm) of high stability (m.p. 155–157 °C, dec.). The X-ray crystal-structure analysis shows a planar and approximately square P_2C_2 ring with two pyrami-

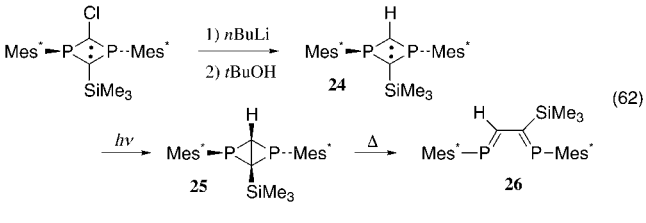


(61)

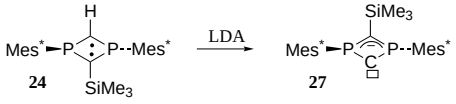
dal phosphorus atoms (sum of the C-P-C angles 337.9°), and two almost planar carbon atoms (sum of the P-C-P angles 347.3°). The P–C ring bonds are short at 1.75 Å. The pyramidalization of both phosphorus atoms prevents a significant participation of the lone pairs in a 6-π delocalization over the ring. Hyperconjugative interactions involving the σ orbitals of the exocyclic P–C bonds probably play some role in the stabilization of this system. The planarization of one phosphorus induces the pyramidalization of the other. These various questions are discussed in a recent theoretical paper.[167]

Some chemistry has already been developed with compounds similar to **23**. The biradical structure **24** evolves under irradiation to give the bicyclic product **25** which then rearranges to the 1,4-diphosphadiene **26** [Eq. (62)].[168]

With amino substituents at phosphorus, another thermal rearrangement leads to the isomeric 1,2-dihydro-1,2-diphosphete.[169] Still another transformation is observed upon metalation of **24** which yields a stable anionic cyclic carbene **27** [Eq. (63); LDA = iPr_2NLi].[170]

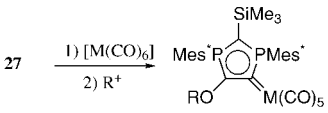


(62)



(63)

The nucleophilic carbene **27** gives a stable adduct with $AlMe_3$.[170] Carbene **27** also reacts with $[M(CO)_6]$ (M = Cr, W) to give a CO insertion product [Eq. (64)].[171]

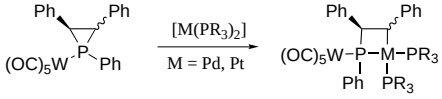


(64)

Although somewhat outside the scope of this account, it seems appropriate to mention that another type of stable singlet biradical based on the four-membered P_2B_2 unit has recently been reported.[172] Quite clearly, phosphorus allows interesting variations from classical closed-shell electronic configurations.

6.2. Bent Bonds and Strained Rings

In organic chemistry, bent C–C bonds are typically found in cyclopropanes and are conveniently described by Walsh molecular orbitals. A similar bonding situation is found in organophosphorus chemistry with phosphiranes and phosphirenes. A recent review extensively describes the chemistry of both ring systems.[173] Thus, this section focuses on the nature and reactivity of the phosphirane P–C ring bonds. Both from theoretical and synthetic standpoints, phosphiranes can be viewed as combinations of alkenes and phosphinidenes. The electronic structure of parent phosphirane is characterized by a lone-pair orbital lying at relatively low energy (−9.75 compared with −9.10 eV for the n_P orbital of Me_2PH).[174] The next ionization at 10.21 eV corresponds to the antisymmetric Walsh-type orbital essentially localized on the P–C ring bonds.[174] As can be seen, the gap between the lone pair and P–C bond ionization energies is small (−0.46 eV) when compared to the corresponding data for aziridine (−1.96 eV).[174] In fact, the situation is rather similar to that found in phosphaalkenes. An electrophilic reagent will "hesitate" between the lone pair and the P–C ring bonds. If the phosphorus lone pair is blocked by complexation, a clean reaction at the P–C ring bonds will be observed. A striking illustration is provided by the reactivity of 14-electron transition-metal fragments $[ML_2]$ (M = Pd, Pt) towards phosphirane complexes [Eq. (65)].[175]



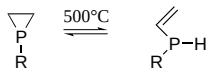
(65)

The transition state leading to the insertion product can be viewed as an η^2 complex of the P–C ring bond, thus explaining the retention of stereochemistry at the ring carbons. An interconversion can be envisaged between the insertion product and the η^1-phopshorus complex when the lone pair is available. As a consequence of their high reactivity, these P–C ring bonds participate in a variety of concerted reactions. An equilibrium occurs at high temperature between phos-

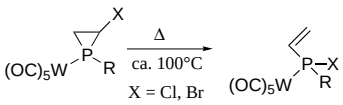
 © 2003 Wiley-VCH Verlag GmbH & Co. KGaA, Weinheim

phiranes and secondary vinylphosphanes through a concerted [1,3] hydrogen migration [Eq. (66)].[176,177]

A related [1,3] halogen shift has been described for 2-halophosphirane complexes [Eq. (67)].[178] The stereochemistry of the C–C unit is preserved during the ring-opening step.

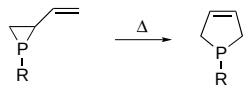


(66)



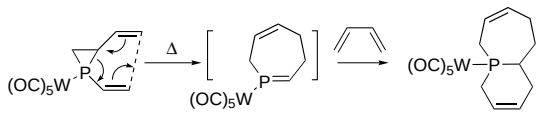
(67)

When catalyzed by Pd^0 species the reaction takes place under mild conditions and might have some practical applications. The rearrangement of 2-vinylphosphiranes into phospholenes[179] is reminiscent of the thermal transformation of vinylcyclopropenes into cyclopentenes [Eq. (68)]. It proceeds through a two-step biradical mechanism.[180]



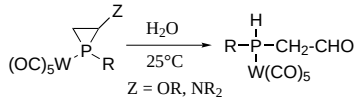
(68)

Similar rearrangements are known for 2-vinylphosphirane complexes [155] where both biradical and [1,3] concerted mechanisms are possible.[159,181] A related [3,3]-phospha-Cope rearrangement has been described for 1,2-divinylphosphirane complexes [Eq. (69)].[182]



(69)

Finally, as with any bond lying at high energy, the P–C ring bonds of phosphiranes are easily polarized. The normal charge distribution $P^{\delta+}$–$C^{\delta-}$ can be inverted by electron-releasing substituents at the C2 atom [Eq. (70)].[155,183]



(70)

Another way of looking at phosphiranes is to consider them as being analogous to alkene–transition-metal π complexes. If the π-accepting capacity of the phosphinidene unit increases, then the donor–acceptor complex becomes stronger. The comparison between the structures of the PR- and PCl-substituted phosphiranes demonstrates this assertion. 1-Chlorophosphiranes have shorter P–C ring bonds and a higher positive charge at phosphorus than the corresponding PH phosphiranes.[184] They also display higher thermal stability (e.g. the parent 1-chlorophosphirane[185] is reasonably stable at room temperature unlike the parent phosphirane). Thus, it is also easy to rationalize why the inversion of configuration at phosphorus in 1-halophosphiranes occurs by turnstile rotation rather than the classical pyramidal-inversion mechanism.[186] Schematically, the PX unit rotates around the symmetry axis of the three-membered ring. This inversion pathway is 10 to 20 kcal mol^{-1} lower in energy than the pyramidal inversion and reminiscent of rotation in alkene–transition-metal π complexes.

Finally, the dissociation of phosphirane derivatives into alkenes and low-coordinate phosphorus units is well documented for terrvalent phosphiranes,[134] phosphirane oxides,[187] phosphiranium salts,[188] and phosphirane complexes.[189] It has also been studied from a theoretical standpoint.[177a] Quite clearly, phosphiranes lie half-way between cyclopropanes and alkene–transition-metal π complexes.

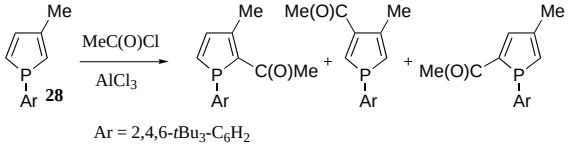
6.3. Aromatic Systems

The aromaticity in phosphorus heterocycles is the subject of a recent review.[190] The definition of heteroaromaticity remains somewhat vague, but the notion reflects a group of well-correlated thermodynamic, magnetic, structural, and chemical properties.[191a] To date, this property has been unambiguously detected in several phosphorus-containing 6-π systems.

Recent reviews extensively describe the chemistry of phospholes,[192] polyphospholes,[110] and the corresponding anions. Thus the following will focus on the aromaticity of these rings and the various attempts to modulate it. Phospholes display a pyramidal ground state which was first demonstrated in the case of 1-benzylphosphole (sum of C-P-C angles 302°).[193] This pyramidality is sensitive to the nature of the substituents. Conjugating substituents at the ring α-positions tend to increase the pyramidality of phosphorus, as exemplified in the structure of a 2,5-bis(alkynyl)phosphole (sum of the C-P-C angles 292.4°).[194] Apparently, the conjugation between the diene and the phosphorus lone pair is switched off and replaced by conjugation with the alkynyl substituents. The substituents at the phosphorus atom also modulate the pyramidality, but in a rather unpredictable way: for a 1-alkoxyphosphole: sum of the C-P-C angles 309.5°; for a 1-cyanophosphole: sum of the C-P-C angles 290.3°.[195] The pyramidality about phosphorus influences two different diene–phosphinidene interactions which confer stability upon the ring: classical 6-π delocalization involving the phosphorus lone pair and hyperconjugation involving the P–R exocyclic bond. When the pyramidality at phosphorus falls the delocalization increases and the hyperconjugation decreases. In the parent phosphole, the aromatic stabilization energy (ASE), which includes both interactions,[191b] is, according to the most recent calculations, low: 3.20[191a] or 5.87 kcal mol^{-1},[196]. Experimentalists have tried, on the one hand, to increase the conjugation to develop an "aromatic" chemistry at the phosphole ring and, on the other, to diminish

 © 2003 Wiley-VCH Verlag GmbH & Co. KGaA, Weinheim

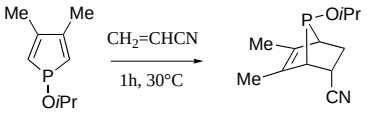
conjugation and hyperconjugation to promote Diels–Alder reactivity in the diene. At present, the most impressive increases in aromatic reactivity have been obtained with the very bulky 2,4,6-tris(*tert*-butylphenyl) substituent at the phosphorus center.[197] The corresponding phosphole **28** is almost planar: sum of the C-P-C angles 331.7°. The out-of-plane angle of the P–R bond is reduced from 66.9 in 1-benzylphosphole to 45.0°, and the P–C intracyclic bonds from 1.786 (mean) to 1.743 Å. The combination of this enhanced delocalization and steric protection of the phosphorus center allows this phosphole to undergo Friedel–Crafts acylation at the ring carbon atoms [Eq. (71)].[197]



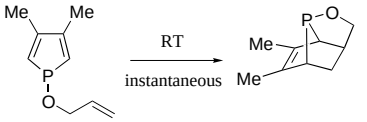
(71)

Dibromophosphination at a ring carbon atom is also possible by using phosphorus tribromide.[198] In the same vein, C-acylation can also be performed on phosphole–$Mo(CO)_5$ complexes.[199]

The best means to switch off both the 6-π delocalization and the hyperconjugation in phospholes is to install an electronegative substituent at the phosphorus center. Both the n_P and the σ(P–R) orbital energies are lowered and their interaction with the appropriate diene π orbitals (mainly the $\pi(b_1)$ and the $\pi^*(b_1)$) becomes less effective. As a result, the ASE of 1-methoxyphosphole falls to −0.97 kcal mol^{-1}.[196] The dienic unit of these 1-alkoxyphospholes is extremely reactive, as shown by the examples in Equations (72) and (73).[195,200]



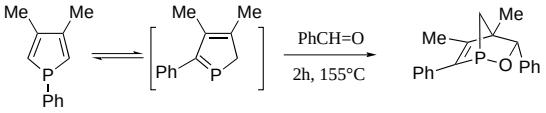
(72)



(73)

When substituted at the phosphorus center by simple sp-[201] or sp^2-carbon-containing substituents[202] or hydrogen,[203] the reactivity of phospholes is governed by the hyperconjugative interaction favoring the shift of the substituent from phosphorus to the α-carbon atoms of the ring. These concerted [1,5]-sigmatropic shifts leading to 2*H*-phospholes have been studied from a theoretical standpoint.[204] The conversion of the parent 1*H*- into 2*H*-phosphole requires a very low activation enthalpy of approximately 16 kcal mol^{-1}. The 2*H*-phosphole products can be trapped by alkynes,[202] alkenes,[205] dienes,[202] and aldehydes [Eq. (74)].[206]

2*H*-phospholes can also be deprotonated in situ to give the corresponding fully aromatic phospholide ions. Numerous phospholides functionalized in the 2-position have been



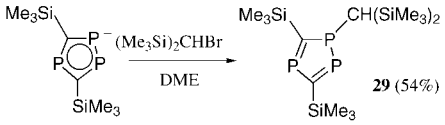
(74)

prepared by this method.[207] The parallel between the chemistry of phospholes and cyclopentadienes in this area is quite striking.

Since polyphospholes contain sp^2-phosphorus centers, they tend to display some instability. However, the following computed data quite clearly show that the pyramidal-inversion barrier decreases as the number of phosphorus atoms in the ring increases:[208]

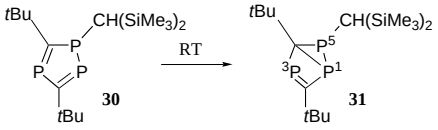
1,2-P_2 8.17; 1, 3-P_2 10.56; 1,2,3-P_3 (1*H*) 4.43; 1,2,3-P_3 (2*H*) 2.69; 1,2,4-P_3 (1*H*) 3.79; 1,2,4-P_3 (4*H*) 4.35 kcal mol^{-1}. These values may be compared with 17.19 kcal mol^{-1} for parent 1*H*-phosphole. Conversely, the ASE increases with the number of ring phosphorus atoms:[191a]

1,2-P_2 4.97; 1, 3-P_2 3.03; 1,2,3-P_3 (1*H*) 4.25; 1,2,3-P_3 (2*H*) 7.97; 1,2,4-P_3 (1*H*) 6.18; 1,2,4-P_3 (4*H*) 4.11; 1,2,3,4-P_4 (1*H*) 7.22; 1,2,3,4,5-P_5 11.24 kcal mol^{-1}, which may be compared with 3.20 kcal mol^{-1} for the parent 1*H*-phosphole and 14.77 kcal mol^{-1} for furan. Thus, the successful isolation and structural characterization of the planar aromatic 1,2,4-triphosphole **29** is not a complete surprise and fully confirms these calculated trends [Eq. (75)].[209]



(75)

The ^{31}P NMR spectrum of **29** displays an ABX pattern: $\delta_A = 179$, $\delta_B = 180$, $\delta_X = 288.3$ ppm (C_6D_6). As expected, the $^1J_{PA,PB}$ coupling is huge at 571 Hz. The strong deshielding of the sp^3-phosphorus nucleus is noteworthy. The X-ray crystal-structure analysis of **29** reveals a planar sp^3-phosphorus atom (sum of the angles 358.7°) with short bonds between the ring atoms (P–C 1.684(7) and P–P 2.056(3) Å). The slightly pyramidal triphosphole **30** (sum of the angles at the sp^3 phosphorus center 342.3°)[210] has a sp^3-phosphorus-atom resonance signal at higher field (112.0 ppm) and longer P–C and P–P ring bonds (1.734(4) and 2.098(1) Å). It slowly electrocyclizes at room temperature [Eq. (76)].[211]



(76)

In compound **31**, the phosphorus atoms P^1 and P^3 are equivalent at room temperature on the NMR time scale. Under these conditions, a rapid [1,3] sigmatropic shift of P^5 takes place along the P^1, P^3 diphosphaallyl unit. It is also

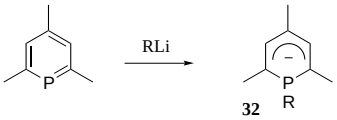
 © 2003 Wiley-VCH Verlag GmbH & Co. KGaA, Weinheim

significant that a triphosphole, such as **30**, gives stable η^5 complexes with $[M(CO)_3]$ (M = Cr, Mo, W).[212]

With polyphospholide ions, the situation is much simpler: every member of the series $[C_nR_nP_{5-n}]^-$ ($n = 1$–4) is known and each of these species is stable and aromatic. The discovery of $[P_5]^-$ by Baudler and her group is a landmark in phosphorus chemistry.[213] The following indexes of aromaticity were calculated for the parent ions in an early study:[214] $[C_5H_5]^-$ 100, $[C_4H_4P]^-$ 90.7, 1,3-$[C_3H_3P_2]^-$ 88.4, 1,2-$[C_3H_3P_2]^-$ 86.0, 1,2,3-$[C_2H_2P_3]^-$ 86.0, 1,2,4-$[C_2H_2P_3]^-$ 95.9, $[CHP_4]^-$ 94.8, $[P_5]^-$ 100.6. Subsequent work has not altered this general picture. X-ray crystal-structure analyses are available for $[C_4Me_4P]^-$ (Li^+ salt),[215] 1,3-$[C_3tBu_3P_2]^-$ (K^+ salt),[216] and 1,2,4-$[C_2tBu_2P_3]^-$ (Li^+ salt).[217] In all of these species, short P–C bonds of between 1.69 and 1.75 Å, and equalized C–C bonds of between 1.396 and 1.424 Å are found. In the $[C_2P_3]$ ion, the P–P bond length is 2.078(6) Å.[217] The alkali-metal counterions are η^5 bonded to the rings in all cases. The ^{31}P resonance signals are, in general, found at low fields. This trend has been explained in terms of a coupling between the phosphorus lone pair(s) and the ring π electrons.[218] The low-field shift increases with the number of phosphorus atoms. For $[P_5]^-$, the ^{31}P resonance signal is found at +470.8 ppm (K^+ salt in DMF).[219] These chemical shifts are also quite sensitive to substituent effects. The phosphorus atom of the parent phospholide ion $[C_4H_4P]^-$ resonates at +77.2 ppm (Li^+ salt in THF),[220] whereas that of a 3,4-dimethyl-2,5-dibenzoyl derivative resonates at +209.6 ppm (Li^+ salt in THF).[207c] All of the chemistry of these ions known at present takes place at the phosphorus center. The parent ion $[C_4H_4P]^-$ has a much lower gas-phase proton affinity than the corresponding pyrrolide ion, that is, 338 ± 3 versus 359 ± 3 kcal mol^{-1}.[221]

Several recent reviews describe the chemistry of phosphinines and polyphosphinines extensively.[222] Thus, only selected aspects will be covered here. The discovery of 2,4,6-triphenylphosphinine by Märkl in 1966[223] ignited intense research on two-coordinate phosphorus derivatives. It was supplemented in 1971 by the synthesis of the parent phosphinine by Ashe.[224] As expected, these species are characterized by a ^{31}P resonance at low field, for example, C_5H_5P, $\delta^{31}P = +211$ ppm.[224] The extent of aromaticity in phosphinine was initially evaluated as being 88% of that of benzene[225] but more recent calculations (employing bond separation and homodesmic reaction energies) suggest it to be about 97%.[226] λ^5 Phosphinines, whilst behaving like delocalized cyclic ylids, have similar degrees of aromatic stabilization.[226] From a structural standpoint, it seems that the most reliable structural data come from theoretical studies[226,227] which give bond lengths of P–C 1.739, C_α–C_β 1.393, C_β–C_γ 1.396 Å. As can be seen, the bond-length equalization within the carbon framework is almost perfect.

In phosphinine, the lone-pair orbital n_P is only the HOMO–2. The HOMO itself, $\pi(b_1)$, is a symmetric orbital which is highly localized at the P and C_γ atoms. The HOMO–1 $\pi(a_2)$ orbital is an antisymmetric orbital with no localization at the P and C_γ atoms. This order is inverted in pyridine, the HOMO of which is the lone pair. The charge distribution in phosphinine is:[226] P = +0.32, C_α = −0.43, C_β = −0.15, C_γ = −0.19. Pyridine is basic and nucleophilic, in complete contrast to phosphinine which shows no basicity (the gas-phase proton affinity of C_5H_5P is 195.8 kcal mol^{-1} which is 23.6 kcal mol^{-1} lower than that of C_5H_5N[228]) and its phosphorus center readily reacts with strong nucleophiles, organolithium derivatives, for example, to give phosphacyclohexadienyl anions **32** [Eq. (77)].[229]



32 (77)

The reactivity of **32** towards electrophiles is complicated; R′X reacts at the phosphorus center to give a λ^5 phosphinine, H^+ reacts at the C_α atom to give a 1,2-dihydrophosphinine, and ArC(O)Cl reacts at the C_γ atom to give a 1,4-dihydrophosphinine. The development of chemistry at the ring carbon atoms has proven to be difficult. One of the few preparative reaction involves 2-halo-phosphinines [Eq. (24)] which insert $[PdL_2]$[230] and $[ZrCp_2]$[231] into their C–X bonds to give organometallic derivatives which allow the synthesis of a wide-range of 2-functional and 2,6-difunctional phosphinines.

The coordination chemistry of phosphinine ligands is dominated by σ complexes at the phosphorus center, in which they display strong π-acceptor properties. A series of homoleptic complexes containing the parent phosphinine (L) includes $[NiL_4]$, $[CrL_6]$, and $[FeL_5]$.[232] η^6 Complexes, such as the sandwich $[V(\eta^6\text{-}L)_2]$ are also known.[233] 2,2′-Biphosphinines (BP), easily obtained by C–C homocoupling of the 2-zirconium derivatives,[234] also give a wide range of very stable homoleptic chelates: $[Ni(BP)_2]$, $[M(BP)_3]$ (M = Cr, Mo, W), $[M(BP)_3]^{2-}$ (M = Ti, Zr), $[M(BP)_2]^-$ (M = Co, Rh), $[M(BP)_2]^{2-}$ (M = Fe, Ru).[235] Apparently, biphosphinines stabilize highly reduced metallic centers by delocalization of the negative charge over the ligands.[236] Biphosphinine dianions have been structurally characterized. Their C–C bridge shows some double bond character.[237] Noteworthy is also the synthesis of several polyphosphinine macrocycles.[238] The coordination chemistry of phosphinines has been extensively reviewed.[239]

Among diphosphinines, only the 1,3-isomers are stable, the first example being prepared by Zenneck et al.[240] Only one 1,4-diphosphinine is known:[241] this is an unstable $(CF_3)_4$-substituted molecule which behaves as a very reactive 1,4-diphosphadiene.[242] No 1,2-diphosphinine is known to date and a recent synthetic study has cast some doubt upon their existence.[243] This experimental picture is rather surprising in the light of recent theoretical studies which indicate that all of the diphosphinine isomers show extensive cyclic delocalization, with the lowest energy form being the unknown 1,2-diphosphinine.[244,245] The much-sought-after 1,3,5-triphosphinine was first prepared by Binger et al.[246] The best method for its preparation relies on the trimerization of phosphaalkynes in the presence of a vanadium(v) imido complex [see Eq. (48)].[120] The X-ray crystal-structure analysis of 2,4,6-

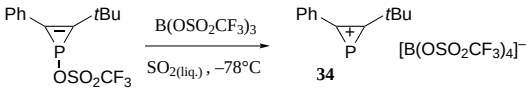
 © 2003 Wiley-VCH Verlag GmbH & Co. KGaA, Weinheim

tris(*tert*-butyl)-1,3,5-triphosphinine (**33**) shows a planar ring with P–C separations of 1.727(8) Å.[247] An evaluation of the ASE of 1,3,5-triphosphinine indicates a slightly higher value than for benzene, with the 1,2,3 isomer being less stable than the 1,3,5 isomer by 5.7 kcal mol^{-1}. Calculated NICS (nucleus-independent chemical shifts) indicate the same overall trends.[245]

Heteroaromaticity is not restricted to phosphole and phosphinine derivatives. An extensive series of heterophospholes incorporating O, S, Se, and N heteroatoms is known[110] and all these cyclic compounds display substantial ASE.[190] A few 2-π and 10-π aromatic systems have also been described.

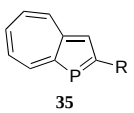
The phosphirenylium cation **34** was first obtained by Laali, Regitz et al. [Eq. (78)].[248] Cation **34** is a highly reactive species with a ^{31}P resonance in the ^{31}P NMR spectrum at 309.7 ppm. A close relative has been stabilized as a η^3-nickel complex.[249]

In spite of a theoretical study indicating substantial aromatic character,[250] the free cation is unstable and its

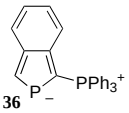


(78)

chemistry has not been developed. A few 10-π systems, such as **35**[251] and **36**[252] have been described but their chemistry remains poorly explored.



35



36

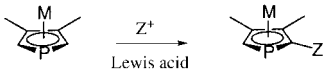
6.4. Phosphametallocenes

Under this heading, we include all η^5 complexes containing mono- and polyphospholyl ligands. Several recent reviews have treated this topic, either in part,[253] or comprehensively.[254] For convenience, we shall discuss the monophospholyl and polyphospholyl complexes separately.

The first η^5 monophospholyl complexes were discovered in 1976 [$LMn(CO)_3$][255] and 1977 [LFeCp].[256] A review from 1998[254b] records η^5-phospholyl complexes of Ti, Mn, Fe, Co, Ni, Zr, Mo, Ru, Rh, W, Re, Y, Sm, Yb, Lu, and U. Recent additions include Ga,[257] Tl,[258] Hf,[259] Ge,[260] Sn,[260] Pb,[260] Cr,[261] Ir,[262] Nd,[263] and Tm.[264] In addition, several η^5 complexes of Group 1 and 2 metals have been structurally characterized, including Na,[265] K,[265] Cs,[266] Ca,[267] and Ba.[268]

The chemistry of phosphaferrocenes and phosphacymantrenes has been studied in some detail. They are still the only phosphorus heterocycles displaying an extensive aromatic chemistry. Electrophilic acylation, formylation, and carboxylation reactions are possible with these compounds [Eq. (79)].[255,256,269,270]

In the case of phosphacymantrenes, it is necessary to replace [$Mn(CO)_3$] by the more electron-rich [$Mn(CO)_2(PPh_3)$] to perform the Vilsmeier formylation.[271] The direct carboxylation of phosphaferrocenes by $CO_2/AlCl_3$ has also been described recently.[272] The resulting derivatives

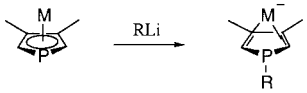


(79)

M = FeCp, Fe(η^5-phospholyl), $Mn(CO)_3$
Z = C(O)R, CHO, C(O)OR

have been subjected to numerous classical chemical transformations. Among the recent results, a careful study of the formation, stability, and reactivity of α-phosphaferrocenylmethyl carbocations[273] and two studies on the McMurry coupling of 2-acylphosphacymantrenes[274] and 2-formylphosphaferrocenes[275] are noteworthy. This chemistry is possible because the in-plane lone pair of phosphaferrocenes and phosphacymantrenes lies very low in energy, it is the HOMO–3 in phosphaferrocenes,[276] and because the diffuse nature of the phosphorus orbitals allows extensive overlap with the metal d-orbitals, thus providing a very stable system. Both of these characteristics are absent in the much less stable aza analogues.[277]

Strong nucleophiles such as organolithium compounds attack these phosphametallocenes at the phosphorus atom from the *exo* side [Eq. (80)].[278,279]



(80)

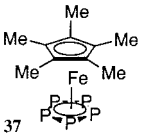
The phosphorus centers in the resulting anionic, η^4-phosphole complexes are quaternized by alkyl or acyl halides. Electrochemical studies of phosphaferrocenes show that the switching a CH group for a phosphorus atom in ferrocenes favors reduction and disfavors oxidation.[280] The first structurally characterized phosphaferricinium salt has only recently been described.[281]

The replacement of a Cp unit by a phospholyl ligand in any η^5 complex confers electronic stabilization upon the reduced species. One of the best recent illustrations of this phenomenon is provided by the isolation of a stable thulium(II) derivative.[264] Other consequences are the relative electrochemical stability of phosphacobaltocenes[282] and phosphanickelocenes.[283] When appropriately substituted, these compounds are stable as 19- and 20-electron sandwiches species, even though it has been demonstrated elsewhere that η^5–η^1 fluctuation is easy even in 16-electron phospholyl complexes.[284]

As phosphorus ligands, phosphametallocenes generally behave as poor σ donors and rather good π acceptors. It is clear that the phosphametallocene P–M bond can participate in the bonding to the second metal center, which explains why

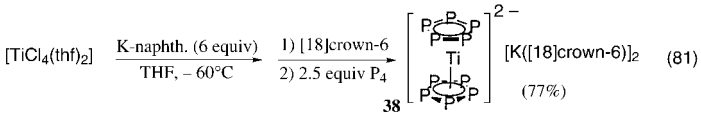
 © 2003 Wiley-VCH Verlag GmbH & Co. KGaA, Weinheim

a 1,1′-diphosphaferrocene can chelate to some transition-metal centers without geometrical distortion even though the two phosphorus lone pairs are lying in parallel planes. Structurally characterized chelates have been isolated with Ag^+[285] and Pd^0.[286] This bonding potential also explains why the insertion of a metal center into the phosphametallocene P–M bond, as observed with Pd centers in phosphacymantrenes[287] and phosphaferrocenes,[288] is a relatively easy process.


37

Albeit more complicated, the chemistry of η^5-polyphospholyl complexes reflects the same basic trends. In this field, the breakthrough came with the discovery of the first 1,2,3,4,5-pentaphosphaferrocene **37** by Scherer and Brück.[289] This product is now more conveniently prepared from the $[P_5]^-$ ion.[290] An extensive theoretical treatment of penta- and decaaza-, penta- and decaphospha-, penta- and decaarsa-, and penta- and decastibaferrocenes recently concluded that the most stable species is the pentaphospha derivative.[291]

Very recently, a very stable decaphosphatitanocene dianion **38** has also been described [Eq. (81)].[292] Compound **38** has a genuine sandwich structure (angle between the planes ca. 1.5°, Ti—centroid separation 1.797(1) Å, P–P separation (mean) 2.154(9) Å) and is diamagnetic ($\delta^{31}P = +60$ ppm). Its existence—it must be emphasized that the $[Cp_2Ti]^{2-}$ ion is


(81)

unknown—once again demonstrates that mono- and polyphospholyl ligands have a great potential for the stabilization of metal centers in low oxidation states.

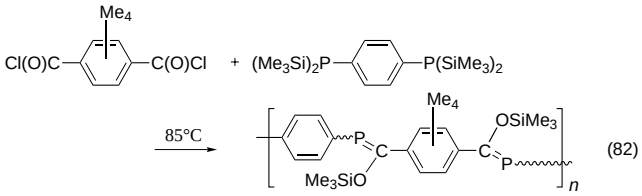
Numerous η^5 complexes of 1,2-di-, 1,3-di-, and 1,2,4-triphospholyl ligands are also known. Most of them feature 1,3-$P_2C_3tBu_3$ (P_2C_3) and 1,2,4-$P_3C_2tBu_2$ (P_3C_2) ligands, and many have been synthesized by cocondensation of metal vapors with *t*BuC≡P (**10**). Among the most noteworthy structures are the slightly bent (angle between the planes 16°), neutral, and diamagnetic hexaphosphatitanocene $[Ti(\eta^5\text{-}P_3C_2)_2]$,[293] the paramagnetic pentaphosphavadanocene $[V(\eta^5\text{-}P_2C_3)(\eta^5\text{-}P_3C_2)]$,[294] the hexaphosphachromocene $[Cr(\eta^5\text{-}P_3C_2)_2]$,[295] the hexaphosphamanganocene $[Mn(\eta^5\text{-}P_3C_2)_2]$[296] which shows an unprecedented ^2A ground state, and the extraordinary 22-valence-electron triple decker $[(\eta^5\text{-}P_3C_2)Sc(\mu\text{-}\mathbf{33})Sc(\eta^5\text{-}P_3C_2)]$.[297] Other recent work includes the synthesis of Ga, In, and Tl derivatives[298,299] and several $(\eta^5\text{-}P_3C_2)$ metal carbonyl complexes.[300] Several theoretical studies of such complexes are available,[296,299,301,302] one of which explains the diamagnetism of the hexaphosphatitanocene in terms of significant backdonation from the Ti center to the LUMO of the P_3C_2 ring to form a δ bond.[301]

7. Applications

In spite of its extraordinary potential for generating new structures and reactions, phospha-organic chemistry will be doomed to failure if practical applications cannot be envisaged. Fortunately, such applications are emerging in two areas, molecular materials and homogeneous catalysis. It must be admitted that only very preliminary results are available in the first case but, in the second, exciting data suggest that real applications do not lie far ahead.

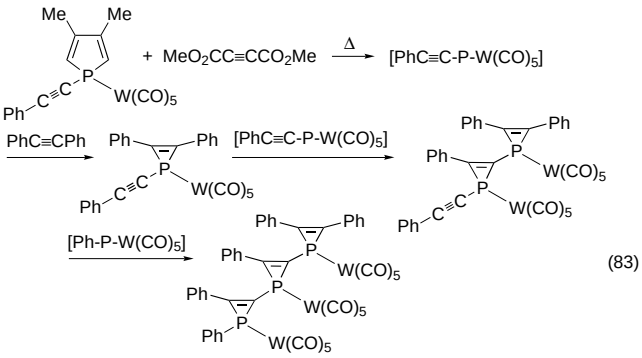
7.1. Molecular Materials

The first polyphosphaalkene was described very recently.[303] The authors have employed a polycondensation approach based on Becker chemistry [see Eq. (1)], as depicted in Equation (82). Molecular weights up to 10500


(82)

(corresponding to 21 monomeric units) have been obtained. A UV/Vis study of the yellow soluble polymer suggests some degree of electronic communication through the π-conjugated backbone.

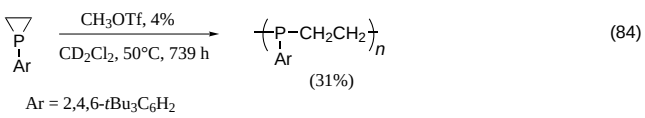
In a different vein, the chemistry of terminal phosphinidene complexes (see Scheme 2) has provided access to a phosphirene oligomer. The iterative approach is depicted in Equation (83).[304] The trimer has been characterized by X-ray


(83)

crystal-structure analysis. Higher oligomers can be detected in the crude reaction mixtures by ^{31}P NMR spectroscopy.

Strained phosphorus–carbon rings, such as phosphiranes, have provided an access to polyphosphanes through cationic ring-opening polymerization (ROP) [Eq. (84)].[305] The initiator (CH_3OTf ($OTf = CF_3SO_3$) or CH_3I) initially gives a phosphiranium salt which is then attacked by the phosphorus

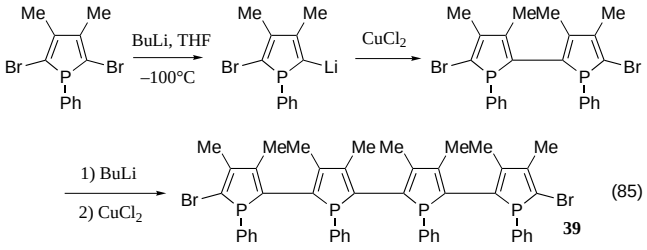
 © 2003 Wiley-VCH Verlag GmbH & Co. KGaA, Weinheim



(84)

lone pair of another trivalent phosphirane. Molecular weights up to 7800 have been obtained. These polymers are waxy yellow solids which are soluble in organic solvents. Related phosphane polymers have very recently been obtained by radical polymerization of phosphaalkene **3**.[351]

By analogy with the thoroughly investigated polypyrroles and polythiophenes which provide very interesting n- or p-doped electroconducting organic materials, it is tempting to investigate the synthesis of polyphospholes. Several recent DFT studies[306–308] have demonstrated that α-connected polyphospholes should be good substrates for making efficient organic conductors. Their band gap is predicted to be much lower than in polypyrroles or polythiophenes, for example 1.49 eV for polyphosphole[306] versus 2.0 eV for polythiophene in the first study. Even lower values (1.2[307] and 1.08 eV[308]) have been computed in the other studies. The relative lack of aromaticity in phospholes means that their π electrons are not confined within the rings, thus allowing a better delocalization along the polymer backbone than in the case of polypyrroles and polythiophenes. To date, the only experimental attempt to make a polyphosphole has yielded the tetraphosphole **39** [Eq. (85)].[309]

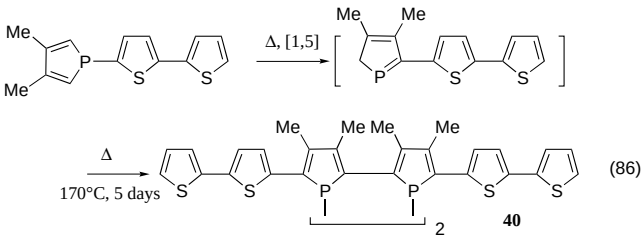


(85)

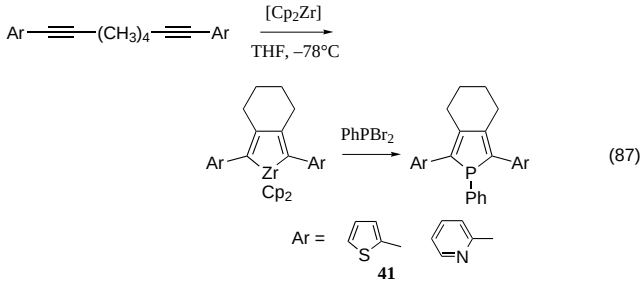
The deep red THF-soluble tetraphosphole **39** has been characterized by X-ray crystal-structure analysis, it has C-C inter-ring separations (1.43 and 1.45 Å) compatible with some delocalization along the chain. Unfortunately, the attempted synthesis of the octaphosphole by the same iterative process has failed; the chain appears to break down under the conditions required. The replacement of bromine by hydrogen also destabilizes the structure. No attempt to elaborate a material from this tetraphosphole has been made to date.

More stable and accessible structures have been obtained by linking thiophene and phosphole units. The chemistry of 2*H*-phospholes provides an easy access to an α-linked bithiophene-biphosphole-bithiophene hexameric system **40** [Eq. (86)].[310] A combined X-ray and electrochemical study clearly demonstrated that extended π conjugation is present in the P(S)R derivatives of **40**.[311] Shorter chains have been obtained by the more conventional route employing zirconacycles [Eq. (87)].[312,313]

UV/Vis spectra indicate extended π conjugation in **41** and its phosphorus oxide. Through electropolymerization of the P=O, P=S, and P=Se derivatives of **41** on platinum electrodes electroactive films were produced. A theoretical study confirmed that 2-thienyl is better adapted to enter into extended π conjugation with the phosphole ring than Ph or 2-pyridyl

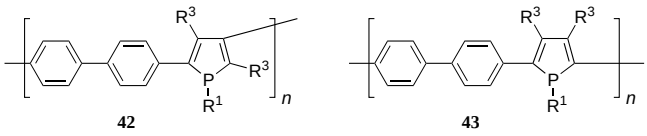


(86)

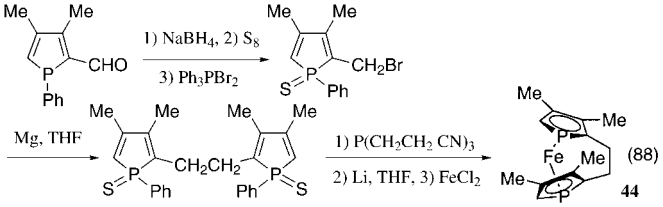


(87)

units. The zirconocene route has also been used for making polymers such as **42** or **43**,[314] which are efficient emitters of blue light.



Finally, a 1,1′-diphospha[2]ferrocenophane **44** has recently been synthesized [Eq. (88)].[315] The inter-ring angle of 20° in **44** is identical to that found in its all-carbon analogues which are known to polymerize by ROP at 300 °C.[316,317] A diphosphaferrocene oligomer is thus probably accessible by thermolysis of **44**.



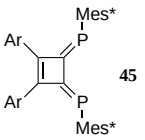
(88)

7.2. Homogeneous Catalysis

Low-coordinate-phosphorus chemistry can contribute to the development of homogeneous catalysis in two ways. In the first, the low-coordinate organophosphorus species can be used as ligands in catalytically active transition-metal complexes. In this case, sufficient stability must be conferred upon

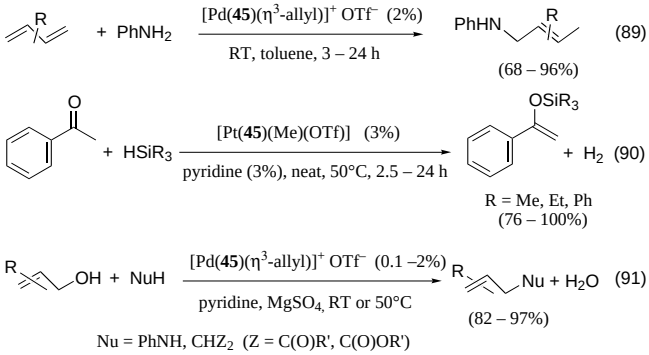
 © 2003 Wiley-VCH Verlag GmbH & Co. KGaA, Weinheim

the ligands, either by steric protection or by electronic delocalization, to prevent their decomposition. This approach has been reviewed recently.[72] Alternatively, the unusual reactivity of low-coordinate phosphorus species can be used to prepare otherwise inaccessible ligands containing sp^3-hybridized phosphorus atoms. A brief survey of both approaches will be made here.

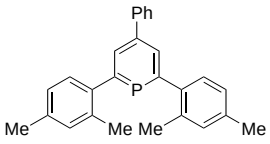


45

The potential of a series of diphosphinidenecyclobutenes **45** as chelating ligands in catalytically active Pd and Pt complexes[318–321] has been investigated by Ozawa and Yoshifuji et al. Striking results have been obtained in the hydroamination of 1,3-dienes [Eq. (89)],[319] the dehydrogenative silylation of ketones [Eq. (90)],[320] and the allylation of aniline and active methylene compounds by allylic alcohols [Eq. (91)].[321]

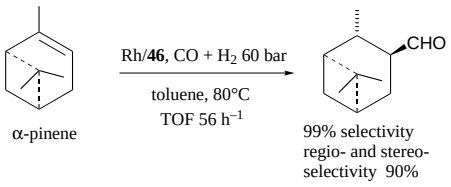


In collaboration with BASF, Breit and his group have studied the use of phosphinines as ligands in the rhodium-catalyzed hydroformylation of alkenes in some depth.[322–324] Detailed comparisons led to the selection of **46** as the ligand



46

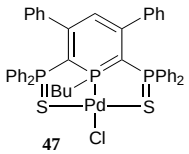
of choice. In the classical hydroformylation of 1-octene (130 °C under a CO/H_2 pressure of 40 bar), turnover frequencies (TOFs) as high as 45370 h^{-1} have been measured. This catalyst efficiently hydroformylates polysubstituted alkenes. A striking example is shown in Equation (92).[324] Classical



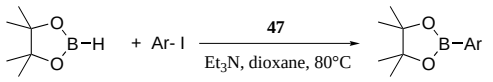
(92)

Rh/PPh_3 catalysts are unable to perform this conversion. The low-lying LUMOs and associated π-acceptor capacity of phosphinines favor the reductive-elimination steps. This rationalizes their efficiency in the rhodium-catalyzed hydroformylation of alkenes.

The use of phosphinines in the nickel-catalyzed carbocyclization of a dieneyne has also been reported.[325] In a different vein, some η^6-phosphinine–iron complexes display a low activity in the co-cyclotrimerization of alkynes and nitriles to give pyridines, and in the dimerization of butadiene to 1,5-cyclooctadiene.[326] The very robust λ^5-phosphinine complex **47** has been applied to the Pd-catalyzed coupling of pinacolborane with some iodoaryls [Eq. (93)].[327] The reaction is slow, but



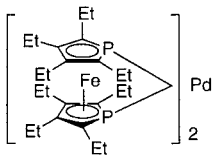
47



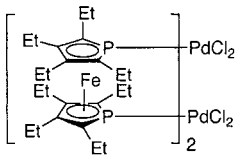
(93)

turnover numbers (TONs) as high as 76500 have been observed with iodobenzene.

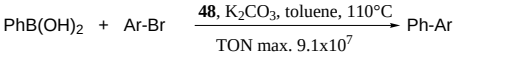
Phosphaferrocenes are another class of promising ligands for catalytic applications. The palladium(0) chelate **48** has been shown to efficiently catalyze the Suzuki coupling reaction [Eq. (94)].[228]



48



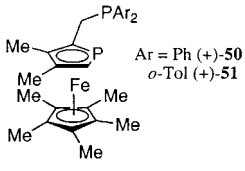
49



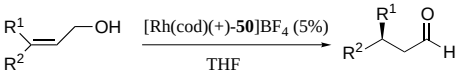
(94)

Although less efficient than **47**, complex **49** also displays some activity in the Miyaura coupling reaction (TON max. 2966, see Equation (93)).[328]

But the most spectacular applications of phosphaferrocenes are found in enantioselective catalysis. Rhodium complexes of **50** not only catalyze the hydrogenation of dehydroaminoacid methyl esters with high *ee* values (up to 96%),[329] but also, in a major advance, catalyze the asymmetric isomerization of allylic alcohols [Eq. (95); cod = cyclooctadiene].[330] Even better *ee* values (up to 93%) are obtained with **51**.[331]

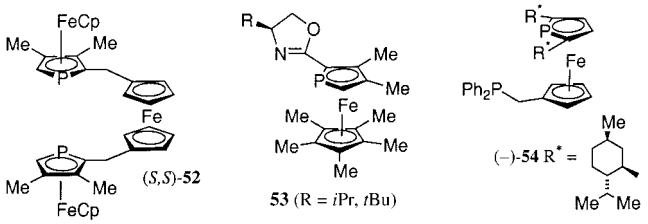


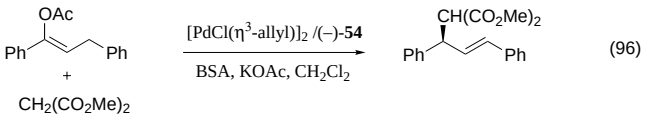
 © 2003 Wiley-VCH Verlag GmbH & Co. KGaA, Weinheim



(95)

Several phosphaferrocene derivatives, that is, **52**,[332] **53**,[333] and **54**,[334] have been tested in the palladium-catalyzed asymmetric allylic alkylation of 1,3-diphenyl-2-propenyl acetate. The most impressive results have been obtained with **54** [Eq. (96); BSA = *N,O*-bis(trimethylsilyl)acetamide].[334] At

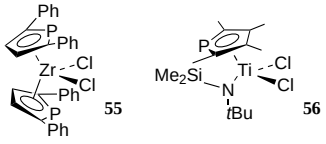




(96)

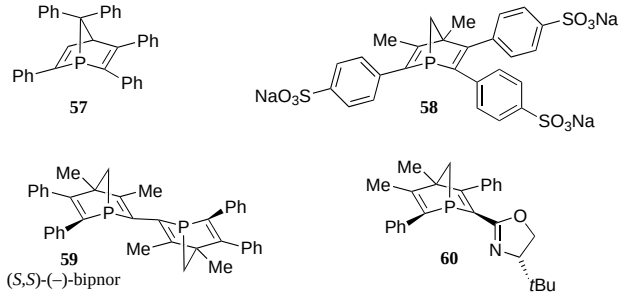
−20 °C, with a ligand:Pd ratio of 0.75:1, a 99 % yield with 99 % *ee* was obtained in 96 h. From another standpoint, the work with **53** has demonstrated that the chirality of the phosphaferrocene (rather than the chirality of oxazoline) dominates the stereochemical outcome of the reaction.[333]

The prototypical catalyst for alkene polymerization results from the reaction of $[Cp_2ZrCl_2]$ with $(MeAlO)_n$ (MAO). The active species is the $[Cp_2ZrMe]^+$ ion. Replacing the Cp ligand by an η^5-phospholyl unit in this cation probably increases the electrophilicity of zirconium as a result of the slightly reduced σ-donor capacity of the phosphorus ring. Higher electrophilicity of Zr is supposed to induce higher catalytic activity. This is the reason why several groups have started to investigate the catalytic activity of η^5-phospholyl titanium and zirconium complexes in the polymerization of alkenes.[259,335–340] When using a huge excess of MAO, the phosphorus lone pairs can be complexed by the acidic aluminum centers, which hinders the catalytic center and lowers its activity. Substituents on the α-positions of the heterocyclic ring prevent this complexation. The two most interesting phospholyl-based precatalysts described to date are **55**[337] and **56**.[338] In both cases, the activity and the properties of the resulting polymers are rather similar to those observed with the analogous all-carbon catalysts. With its structure related to that of the Pd-diimine catalysts, the



cationic $[Pd(\mathbf{45})(Me)]^+$ complex is also a good ethene polymerization catalyst.[341]

As mentioned at the beginning of this section, low-coordinate-phosphorus chemistry can also provide otherwise inaccessible sp^3-hydridized phosphorus derivatives which are potentially interesting for homogeneous catalysis. The best illustration of this approach is provided by the synthesis of 1-phosphanorbornadienes from transient 2*H*-phospholes [see Eq. (74)] and alkynes.[202] An extensive investigation of this class of bicyclic phosphanes has been carried out. Compound **57** is a very efficient ligand for the rhodium-catalyzed hydroformylation of alkenes.[342] A TOF of 402 h^{-1} has been observed in the hydroformylation of 1-hexene at 80 °C under a CO/H_2 pressure of 20 bar, and compound **57** has also been used in the hydroformylation of ethyl acrylate.[343] Water-soluble **58** is the best monophosphane ligand for the rhodium-catalyzed biphasic hydroformylation of propene.[344] The phosphorus at the bridgehead of 1-phosphanorbornadienes cannot epimerize, so these compounds are, in terms of optical stability, ideal ligands for enantioselective catalysis. The bisphosphane bipnor **59** is comparable to binap and DuPhos in the rhodium-catalyzed asymmetric hydrogenation of



dehydroaminoacids.[345] In some cases, it appears to be superior to the binap ligand, as shown by comparative experiments on the rhodium-catalyzed asymmetric isomerization of a cyclic diene.[346] Phosphanorbornadiene oxazolines, such as **60**, are also efficient ligands for the palladium-catalyzed asymmetric Heck reaction and allylic coupling [see Eq. (96)], with *ee* values as high as 93 % being reported.[347]

8. Conclusion and Outlook

This selective survey of low-coordinate-phosphorus chemistry clearly shows that the phosphorus–carbon analogy is a useful guiding principle for predicting the outcome of a reaction, conceiving new reactions, or synthesizing new products. However, even in its low-coordination states, phosphorus is not just a copy of carbon. This is mainly because of the presence of a lone pair. In many instances, it is necessary to mask this lone pair, usually by complexation, to take full advantage of the analogy with carbon. In spite of this restriction, the richness and potential of the chemistry of low-coordinate-phosphorus species is quite impressive. This situation is all the more true given that we have only covered the chemistry of phosphorus–carbon bonds and excluded

 © 2003 Wiley-VCH Verlag GmbH & Co. KGaA, Weinheim

highly significant results, such as the discoveries of the P=N,[348] P≡N,[349] and P=P bonds[350] and their associated chemistry. Even with such constraints, it is clear that phospha-organic chemistry has already produced an array of efficient new synthetic tools for building organophosphorus compounds, these tools include well-developed cycloaddition chemistry, several variants of the phospha-Wittig reaction, and some versatile analogues of singlet carbenes. To fully realize what this chemistry means, it is only necessary to imagine what would be left of organic chemistry if alkenes, alkynes, and carbenes did not exist. As we have seen, this new chemistry translates directly into new structures having significant potential as ligands in coordination chemistry and homogeneous catalysis, new molecular and polymeric phosphorus-containing materials, to name but a few. These areas are now wide open for investigation. I hope that this brief survey will promote their exploration.

The author thanks Dr. Duncan Carmichael for reading and language polishing this manuscript, and CNRS and Ecole Polytechnique for financial support.

Received: September 13, 2002 [A557]

[1] a) R. J. P. Corriu, J.-P. Dutheil, G. F. Lanneau, *J. Am. Chem. Soc.* **1984**, *106*, 1060; b) G. F. Lanneau, *Phosphorus Sulfur Relat. Elem.* **1986**, *27*, 43; c) R. J. P. Corriu, G. F. Lanneau, D. Leclercq, *Tetrahedron* **1989**, *45*, 1959.
[2] K. B. Dillon, F. Mathey, J. F. Nixon, *Phosphorus: The Carbon Copy*, Wiley, Chichester, **1998**.
[3] J. Waluk, H.-P. Klein, A. J. Ashe III, J. Michl, *Organometallics* **1989**, *8*, 2804.
[4] W. W. Schoeller, *J. Chem. Soc. Chem. Commun.* **1985**, 334.
[5] S. Lacombe, D. Gonbeau, J.-L. Cabioch, B. Pellerin, J.-M. Denis, G. Pfister-Guillouzo, *J. Am. Chem. Soc.* **1988**, *110*, 6964.
[6] a) M. W. Schmidt, P. N. Truong, M. S. Gordon, *J. Am. Chem. Soc.* **1987**, *109*, 5217; b) P. von R. Schleyer, D. Kost, *J. Am. Chem. Soc.* **1988**, *110*, 2105.
[7] L. Nyulaszi, T. Veszprémi, J. Réffy, *J. Phys. Chem.* **1993**, *97*, 4011.
[8] T. C. Klebach, R. Lourens, F. Bickelhaupt, *J. Am. Chem. Soc.* **1978**, *100*, 4886.
[9] M. Yoshifuji, K. Toyota, N. Inamoto, *Tetrahedron Lett.* **1985**, *26*, 1727.
[10] a) H. Oehme, E. Leissring, H. Meyer, *Tetrahedron Lett.* **1980**, *21*, 1141; b) G. Becker, O. Mundt, *Z. Anorg. Allg. Chem.* **1980**, *462*, 130.
[11] G. Becker, *Z. Anorg. Allg. Chem.* **1976**, *423*, 242.
[12] a) B. Deschamps, F. Mathey, *J. Chem. Soc. Chem. Commun.* **1985**, 1010; b) B. Deschamps, F. Mathey, *J. Organomet. Chem.* **1988**, *354*, 83.
[13] a) R. Appel, C. Casser, F. Knoch, *Chem. Ber.* **1984**, *117*, 269; b) L. Weber, *Eur. J. Inorg. Chem.* **2000**, 2425.
[14] E. P. O. Fuchs, H. Heydt, M. Regitz, W. W. Schoeller, T. Busch, *Tetrahedron Lett.* **1989**, *30*, 5111.
[15] E. Niecke, H.-J. Metternich, M. Nieger, D. Gudat, P. Wenderoth, W. Malisch, C. Hahner, W. Reich, *Chem. Ber.* **1993**, *126*, 1299.
[16] A. B. Rozhenko, W. W. Schoeller, M. I. Povolotskii, *Magn. Reson. Chem.* **1999**, *37*, 551.
[17] K. Issleib, E. Leissring, M. Riemer, *Z. Chem.* **1983**, *23*, 99.
[18] L. N. Markovski, V. D. Romanenko, *Tetrahedron* **1989**, *45*, 6019.
[19] R. Appel in *Multiple Bonds and Low Coordination in Phosphorus Chemistry* (Eds.: M. Regitz, O. J. Scherer), Thieme, Stuttgart, **1990**, pp. 157–269.
[20] Ref. [2], pp. 88–163.
[21] F. Mathey, *Acc. Chem. Res.* **1992**, *25*, 90.
[22] a) G. Becker, *Z. Anorg. Allg. Chem.* **1976**, *423*, 242; b) G. Becker, O. Mundt, *Z. Anorg. Allg. Chem.* **1978**, *443*, 53; c) G. Becker, M. Rössler, W. Uhl, *Z. Anorg. Allg. Chem.* **1981**, *473*, 7.
[23] a) R. Appel, V. Barth, *Angew. Chem.* **1979**, *91*, 497; *Angew. Chem. Int. Ed. Engl.* **1979**, *18*, 469; b) R. Appel, V. Barth, M. Halstenberg, G. Huttner, J. von Seyerl, *Angew. Chem.* **1979**, *91*, 935; *Angew. Chem. Int. Ed. Engl.* **1979**, *18*, 872.
[24] R. Appel, B. Laubach, M. Siray, *Tetrahedron Lett.* **1984**, *25*, 4447.
[25] a) K. Issleib, H. Schmidt, H. Meyer, *J. Organomet. Chem.* **1978**, *160*, 47; b) R. Appel, B. Laubach, *Tetrahedron Lett.* **1980**, *21*, 2497.
[26] K. Issleib, H. Schmidt, H. Meyer, *J. Organomet. Chem.* **1980**, *192*, 33.
[27] a) G. Becker, G. Gresser, W. Uhl, *Z. Anorg. Allg. Chem.* **1980**, *463*, 144; b) R. Appel, P. Fölling, L. Krieger, M. Siray, F. Knoch, *Angew. Chem.* **1984**, *96*, 981; *Angew. Chem. Int. Ed. Engl.* **1984**, *23*, 970.
[28] R. Appel, C. Casser, M. Immenkeppel, F. Knoch, *Angew. Chem.* **1984**, *96*, 905; *Angew. Chem. Int. Ed. Engl.* **1984**, *23*, 895.
[29] a) J. Grobe, D. Le Van, B. Lüth, M. Hegemann, *Chem. Ber.* **1990**, *123*, 2317; b) A.-C. Gaumont, B. Pellerin, J.-L. Cabioch, X. Morise, M. Lesvier, P. Savignac, P. Guenot, J.-M. Denis, *Inorg. Chem.* **1996**, *35*, 6667.
[30] A. Jouaiti, M. Geoffroy, G. Bernardinelli, *Tetrahedron Lett.* **1992**, *33*, 5071.
[31] a) A. Jouaiti, M. Geoffroy, G. Bernardinelli, *Tetrahedron Lett.* **1993**, *34*, 3413; b) A. Jouaiti, M. Geoffroy, G. Bernardinelli, *Chem. Commun.* **1996**, 437; c) H. Kawanami, K. Toyota, M. Yoshifuji, *J. Organomet. Chem.* **1997**, *535*, 1; d) G. Becker, W. Uhl, H.-J. Wessely, *Z. Anorg. Allg. Chem.* **1981**, *479*, 41.
[32] V. D. Romanenko, A. V. Ruban, M. I. Povolotskii, L. K. Polyachenko, L. N. Markovskii, *J. Gen. Chem. USSR* **1986**, *56*, 1044.
[33] S. Shah, J. D. Protasiewicz, *Coord. Chem. Rev.* **2000**, *210*, 181.
[34] a) S. Shah, J. D. Protasiewicz, *Chem. Commun.* **1998**, 1585; b) S. Shah, T. Concolino, A. L. Rheingold, J. D. Protasiewicz, *Inorg. Chem.* **2000**, *39*, 3860.
[35] a) P. Le Floch, A. Marinetti, L. Ricard, F. Mathey, *J. Am. Chem. Soc.* **1990**, *112*, 2407; b) P. Le Floch, F. Mathey, *Synlett* **1990**, 171.
[36] C. C. Cummins, R. R. Schrock, W. M. Davis, *Angew. Chem.* **1993**, *105*, 758; *Angew. Chem. Int. Ed. Engl.* **1993**, *32*, 756.
[37] T. L. Breen, D. W. Stephan, *J. Am. Chem. Soc.* **1995**, *117*, 11914.
[38] a) A. Marinetti, F. Mathey, *Angew. Chem.* **1988**, *100*, 1435; *Angew. Chem. Int. Ed. Engl.* **1988**, *27*, 1382; b) A. Marinetti, S. Bauer, L. Ricard, F. Mathey, *Organometallics* **1990**, *9*, 793.
[39] A. Marinetti, P. Le Floch, F. Mathey, *Organometallics* **1991**, *10*, 1190.
[40] A. Marinetti, L. Ricard, F. Mathey, *Organometallics* **1990**, *9*, 788.
[41] a) F. Mercier, C. Hugel-Le Goff, F. Mathey, *Tetrahedron Lett.* **1989**, *30*, 2397; b) Y. A. Veits, N. B. Karlstadt, I. P. Beletskaya, *Tetrahedron Lett.* **1995**, *36*, 4121.
[42] M. T. Nguyen, L. Landuyt, L. G. Vanquickenborne, *Chem. Phys. Lett.* **1993**, *212*, 543.
[43] a) T. A. van der Knaap, T. C. Klebach, R. Lourens, M. Vos, F. Bickelhaupt, *J. Am. Chem. Soc.* **1983**, *105*, 4026; b) R. Appel, C. Casser, *Tetrahedron Lett.* **1984**, *25*, 4019.
[44] E. Niecke, D.-A. Wildbredt, *J. Chem. Soc. Chem. Commun.* **1981**, 72.
[45] a) T. A. van der Knaap, F. Bickelhaupt, *Tetrahedron Lett.* **1982**, *23*, 2037; b) A. J. Arduengo III, C. J. Carmalt, J. A. C. Clyburne, A. H. Cowley, R. Pyati, *Chem. Commun.* **1997**, 981.

 © 2003 Wiley-VCH Verlag GmbH & Co. KGaA, Weinheim

[46] A. Meriem, J.-P. Majoral, M. Revel, J. Navech, *Tetrahedron Lett.* **1983**, *24*, 1975.
[47] R. de Vaumas, A. Marinetti, F. Mathey, *J. Organomet. Chem.* **1991**, *413*, 411.
[48] S. Bauer, A. Marinetti, L. Ricard, F. Mathey, *Angew. Chem.* **1990**, *102*, 1188; *Angew. Chem. Int. Ed. Engl.* **1990**, *29*, 1166.
[49] a) M. Schmitz, R. Göller, M. Regitz, *Synthesis* **1997**, 455; b) M. Schmitz, S. Leininger, U. Bergträsser, M. Regitz, *Heteroat. Chem.* **1998**, *9*, 453.
[50] a) J.-P. Majoral, N. Dufour, F. Meyer, A.-M. Caminade, R. Choukroun, D. Gervais, *J. Chem. Soc. Chem. Commun.* **1990**, 507; b) N. Dufour, A.-M. Caminade, M. Basso-Bert, A. Igau, J.-P. Majoral, *Organometallics* **1992**, *11*, 1131.
[51] W. Schnurr, M. Regitz, *Tetrahedron Lett.* **1989**, *30*, 3951.
[52] A. Marinetti, F. Mathey, *J. Chem. Soc. Chem. Commun.* **1990**, 153.
[53] T. A. van der Knaap, T. C. Klebach, F. Visser, R. Lourens, F. Bickelhaupt, *Tetrahedron* **1984**, *40*, 991.
[54] T. Allspach, M. Regitz, G. Becker, W. Becker, *Synthesis* **1986**, 31.
[55] M. Abbari, P. Cosquer, F. Tonnard, Y. Y. C. Yeung Lam Ko, R. Carrié, *Tetrahedron* **1991**, *47*, 71, and references therein.
[56] Ref. [19], pp. 164–165.
[57] a) P. Le Floch, F. Mathey, *Tetrahedron Lett.* **1989**, *30*, 817; b) P. Le Floch, L. Ricard, F. Mathey, *Polyhedron* **1990**, *9*, 991.
[58] T. A. van der Knaap, F. Bickelhaupt, *Tetrahedron* **1983**, *39*, 3189.
[59] G. Märkl, E. Seidl, I. Trötsch, *Angew. Chem.* **1983**, *95*, 891; *Angew. Chem. Int. Ed. Engl.* **1983**, *22*, 879.
[60] T. W. Mackewitz, C. Peters, U. Bergträsser, S. Leininger, M. Regitz, *J. Org. Chem.* **1997**, *62*, 7605.
[61] S. M. Bachrach, *J. Org. Chem.* **1993**, *58*, 5414, and references therein.
[62] R. Appel, V. Barth, M. Halstenberg, *Chem. Ber.* **1982**, *115*, 1617.
[63] A. Marinetti, L. Ricard, F. Mathey, *Organometallics* **1990**, *9*, 788.
[64] P. Le Floch, F. Mathey, *J. Chem. Soc. Chem. Commun.* **1993**, 1295.
[65] T. C. Klebach, R. Lourens, F. Bickelhaupt, C. H. Stam, A. Van Herk, *J. Organomet. Chem.* **1981**, *210*, 211.
[66] J.-P. Lorenz, W. Pohl, H. Nöth, M. Schmidt, *J. Organomet. Chem.* **1994**, *475*, 211.
[67] T. A. van der Knaap, F. Bickelhaupt, J. G. Kraaykamp, G. van Koten, J. P. C. Bernards, H. T. Edzes, W. S. Veeman, E. de Boer, E. J. Baerends, *Organometallics* **1984**, *3*, 1804.
[68] D. Gudat, M. Nieger, K. Schmitz, L. Szarvas, *Chem. Commun.* **2002**, 1820.
[69] R. Appel, C. Casser, F. Knoch, *J. Organomet. Chem.* **1985**, *293*, 213.
[70] K. Knoll, G. Huttner, M. Wasiucionek, L. Zsolnai, *Angew. Chem.* **1984**, *96*, 708; *Angew. Chem. Int. Ed. Engl.* **1984**, *23*, 739.
[71] a) N. H. Tran Huy, J. Fischer, F. Mathey, *J. Am. Chem. Soc.* **1987**, *109*, 3475; b) A. Marinetti, S. Bauer, L. Ricard, F. Mathey, *J. Chem. Soc. Dalton Trans.* **1991**, 597.
[72] L. Weber, *Angew. Chem.* **2002**, *114*, 583; *Angew. Chem. Int. Ed.* **2002**, *41*, 563.
[73] Eselected reviews: a) M. Regitz, *Chem. Rev.* **1990**, *90*, 191; b) M. J. Maah, J. F. Nixon in *The Chemistry of Organophosphorus Compounds, Vol. 1* (Ed.: F. R. Hartley), Wiley, New York, **1990**, pp. 255–294; c) M. Regitz, P. Binger in ref. [19], pp. 58–111; d) A. C. Gaumont, J. M. Denis, *Chem. Rev.* **1994**, *94*, 1413; e) J. F. Nixon, *Coord. Chem. Rev.* **1995**, *145*, 201; f) ref. [2], pp. 40–87.
[74] J. C. T. R. Burckett St. -Laurent, M. A. King, H. W. Kroto, J. F. Nixon, R. J. Suffolk, *J. Chem. Soc. Dalton Trans.* **1983**, 755.
[75] M. Y. Antipin, A. N. Chernega, K. A. Lysenko, Y. T. Struchkov, J. F. Nixon, *J. Chem. Soc. Chem. Commun.* **1995**, 505.
[76] T. E. Gier, *J. Am. Chem. Soc.* **1961**, *83*, 1769.
[77] H. J. Hopkinson, H. W. Kroto, J. F. Nixon, N. P. C. Simmons, *J. Chem. Soc. Chem. Commun.* **1976**, 513.
[78] G. Becker, G. Gresser, W. Uhl, *Z. Naturforsch. B* **1981**, *36*, 16.
[79] G. Becker, W. Schwarz, N. Seidler, M. Westerhausen, *Z. Anorg. Allg. Chem.* **1992**, *612*, 72.
[80] G. Becker, K. Hübler, *Z. Anorg. Allg. Chem.* **1994**, *620*, 405.
[81] R. Appel, M. Poppe, *Angew. Chem.* **1989**, *101*, 70; *Angew. Chem. Int. Ed. Engl.* **1989**, *28*, 53.
[82] K. Hübler, P. Schwerdtfeger, *Inorg. Chem.* **1999**, *38*, 157.
[83] J.-C. Guillemin, T. Janati, J.-M. Denis, *J. Org. Chem.* **2001**, *66*, 7864.
[84] P. Le Floch, F. Mathey in *Synthetic Methods of Organometallic and Inorganic Chemistry, Vol. 3* (Ed.: H. H. Karsch), Thieme, Stuttgart, **1996**, pp. 8–11.
[85] J. C. Guillemin, T. Janati, J.-M. Denis, *J. Chem. Soc. Chem. Commun.* **1992**, 415.
[86] H. W. Kroto, J. F. Nixon, N. P. C. Simmons, N. P. C. Westwood, *J. Am. Chem. Soc.* **1978**, *100*, 446.
[87] R. Appel, A. Westerhaus, *Tetrahedron Lett.* **1981**, *22*, 2159.
[88] S. Haber, P. Le Floch, F. Mathey, *J. Chem. Soc. Chem. Commun.* **1992**, 1799.
[89] a) D. J. Berger, P. P. Gaspar, R. S. Grev, F. Mathey, *Organometallics* **1994**, *13*, 640; b) D. J. Berger, P. P. Gaspar, P. Le Floch, F. Mathey, R. S. Grev, *Organometallics* **1996**, *15*, 4904.
[90] W. Rösch, T. Allspach, U. Bergträsser, M. Regitz in ref. [19], pp. 11–16.
[91] K. K. Laali, B. Geissler, M. Regitz, J. J. Houser, *J. Org. Chem.* **1995**, *60*, 6362.
[92] B. Breit, U. Bergträsser, G. Maas, M. Regitz, *Angew. Chem.* **1992**, *104*, 1043; *Angew. Chem. Int. Ed. Engl.* **1992**, *31*, 1055.
[93] M. Schmitz, R. Göller, U. Bergträsser, S. Leininger, M. Regitz, *Eur. J. Inorg. Chem.* **1998**, 227.
[94] M. H. A. Benvenutti, N. Cenac, J. F. Nixon, *Chem. Commun.* **1997**, 1327.
[95] F. G. N. Cloke, P. B. Hitchcock, J. F. Nixon, D. J. Wilson, *Chem. Commun.* **2000**, 2387.
[96] a) D. E. Hibbs, C. Jones, A. F. Richards, *J. Chem. Soc. Dalton Trans.* **1999**, 3531; b) J. Renner, U. Bergträsser, P. Binger, M. Regitz, *Eur. J. Inorg. Chem.* **2000**, 2337.
[97] a) A. M. Arif, A. R. Barron, A. H. Cowley, S. W. Hall, *J. Chem. Soc. Chem. Commun.* **1988**, 171; b) S. Ito, H. Sugiyama, M. Yoshifuji, *Chem. Commun.* **2002**, 1744.
[98] a) O. Wagner, M. Ehle, M. Regitz, *Angew. Chem.* **1989**, *101*, 227; *Angew. Chem. Int. Ed. Engl.* **1989**, *28*, 225; b) O. Wagner, M. Ehle, M. Birkel, J. Hoffmann, M. Regitz, *Chem. Ber.* **1991**, *124*, 1207; c) F. E. Hahn, L. Wittenbecher, D. Le Van, R. Fröhlich, B. Wibbeling, *Angew. Chem.* **2000**, *112,* 2393; *Angew. Chem. Int. Ed.* **2000**, *39,* 2307.
[99] a) A. Schäfer, M. Weidenbruch, W. Saak, S. Pohl, *Angew. Chem.* **1987**, *99*, 806; *Angew. Chem. Int. Ed. Engl.* **1987**, *26*, 776; b) M. Weidenbruch, S. Olthoff, K. Peters, H. G. von Schnering, *Chem. Commun.* **1997**, 1433.
[100] a) A. H. Cowley, S. W. Hall, C. M. Nunn, J. M. Power, *J. Chem. Soc. Chem. Commun.* **1988**, 753; b) F. Meiners, W. Saak, M. Weidenbruch, *Chem. Commun.* **2001**, 215.
[101] E. Niecke, R. Streubel, M. Nieger, D. Stalke, *Angew. Chem.* **1989**, *101*, 1708; *Angew. Chem. Int. Ed. Engl.* **1989**, *28*, 1673.
[102] a) F. Mercier, L. Ricard, F. Mathey, M. Regitz, *J. Chem. Soc. Chem. Commun.* **1991**, 1305; b) R. Streubel, L. Ernst, J. Jeske, P. G. Jones, *J. Chem. Soc. Chem. Commun.* **1995**, 2113.
[103] J. M. Jamison, R. S. Saunders, D. R. Wheeler, M. D. McClain, D. A. Loy, J. W. Ziller, *Organometallics* **1996**, *15*, 16.
[104] J. Grobe, D. Le Van, T. Pohlmeyer, B. Krebs, O. Conrad, E. Dobbert, L. Weber, *Organometallics* **1998**, *17*, 3383.

 © 2003 Wiley-VCH Verlag GmbH & Co. KGaA, Weinheim

[105] F. Tabellion, C. Peters, U. Fischbeck, M. Regitz, F. Preuss, *Chem. Eur. J.* **2000**, *6*, 4558.
[106] F. G. N. Cloke, P. B. Hitchcock, J. F. Nixon, D. J. Wilson, P. Mountford, *Chem. Commun.* **1999**, 661.
[107] a) R. Armbrust, M. Sanchez, R. Réau, U. Bergsträsser, M. Regitz, G. Bertrand, *J. Am. Chem. Soc.* **1995**, *117*, 10785; b) see also: M. Sanchez, R. Réau, C. J. Marsden, M. Regitz, G. Bertrand, *Chem. Eur. J.* **1999**, *5*, 274.
[108] G. Bertrand, *Angew. Chem.* **1998**, *110*, 282; *Angew. Chem. Int. Ed.* **1998**, *37*, 270.
[109] A. H. Cowley, S. W. Hall, C. M. Nunn, J. M. Power, *Angew. Chem.* **1988**, *100*, 874; *Angew. Chem. Int. Ed. Engl.* **1988**, *27*, 838.
[110] A. Schmidpeter in *Phosphorus-Carbon Heterocyclic Chemistry: The Rise of a New Domain* (Ed.: F. Mathey), Pergamon, Oxford, **2001**, pp. 363–461.
[111] W. Rösch, M. Regitz, *Synthesis* **1987**, 689.
[112] S. Parsons, J. Passmore, X. Sun, M. Regitz, *Can. J. Chem.* **1995**, *73*, 1312.
[113] a) W. Rösch, M. Regitz, *Z. Naturforsch. B* **1986**, *41*, 931; b) G. Märkl, A. Kallmünzer, *Tetrahedron Lett.* **1989**, *30*, 5245; c) B. Wrackmeyer, U. Klaus, *J. Organomet. Chem.* **1996**, *520*, 211.
[114] a) E. P. O. Fuchs, W. Rösch, M. Regitz, *Angew. Chem.* **1987**, *99*, 1058; *Angew. Chem. Int. Ed. Engl.* **1987**, *26*, 1011; b) H. Heydt, U. Bergsträsser, R. Fässler, E. Fuchs, N. Kamel, T. Mackewitz, G. Michels, W. Rösch, M. Regitz, P. Mazerolles, C. Laurent, A. Faucher, *Bull. Soc. Chim. Fr.* **1995**, *132*, 652.
[115] J. Fink, W. Rösch, U.-J. Vogelbacher, M. Regitz, *Angew. Chem.* **1986**, *98*, 265; *Angew. Chem. Int. Ed. Engl.* **1986**, *25*, 280.
[116] E. Fluck, G. Becker, B. Neumüller, R. Knebl, G. Heckmann, H. Riffel, *Angew. Chem.* **1986**, *98*, 1018; *Angew. Chem. Int. Ed. Engl.* **1986**, *25*, 1002.
[117] T. W. Mackewitz, M. Regitz, *Synthesis* **1996**, 100.
[118] a) Ref. [2], pp. 63–74; b) R. Streubel, *Angew. Chem.* **1995**, *107*, 478; *Angew. Chem. Int. Ed. Engl.* **1995**, *34*, 436.
[119] T. Wettling, J. Schneider, O. Wagner, C. G. Kreiter, M. Regitz, *Angew. Chem.* **1989**, *101*, 1035; *Angew. Chem. Int. Ed. Engl.* **1989**, *28*, 1013.
[120] F. Tabellion, A. Nachbauer, S. Leininger, C. Peters, F. Preuss, M. Regitz, *Angew. Chem.* **1998**, *110*, 1318; *Angew. Chem. Int. Ed.* **1998**, *37*, 1233.
[121] T. Wettling, B. Geissler, R. Schneider, S. Barth, P. Binger, M. Regitz, *Angew. Chem.* **1992**, *104*, 761; *Angew. Chem. Int. Ed. Engl.* **1992**, *31*, 758.
[122] a) P. B. Hitchcock, M. J. Maah, J. F. Nixon, J. A. Zora, G. J. Leigh, M. A. Bakar, *Angew. Chem.* **1987**, *99*, 497; *Angew. Chem. Int. Ed. Engl.* **1987**, *26*, 474; b) R. B. Bedford, A. F. Hill, J. D. E. T. Wiltar-Ely, M. D. Francis, C. Jones, *Inorg. Chem.* **1997**, *36*, 5142.
[123] a) P. B. Hitchcock, J. A. Johnson, M. A. N. D. A. Lemos, M. F. Meidine, J. F. Nixon, A. J. L. Pombeiro, *J. Chem. Soc. Chem. Commun.* **1992**, 645; b) M. F. Meidine, M. A. N. D. A. Lemos, A. J. L. Pombeiro, J. F. Nixon, P. B. Hitchcock, *J. Chem. Soc. Dalton Trans.* **1998**, 3319.
[124] a) P. B. Hitchcock, M. J. Maah, J. F. Nixon, *J. Chem. Soc. Chem. Commun.* **1986**, 737; b) P. Binger, R. Milczarek, R. Mynott, M. Regitz, W. Rösch, *Angew. Chem.* **1986**, *98*, 645; *Angew. Chem. Int. Ed. Engl.* **1986**, *25*, 644.
[125] P. Binger, G. Glaser, S. Albus, C. Krüger, *Chem. Ber.* **1995**, *128*, 1261.
[126] S. Creve, M. T. Nguyen, L. G. Vanquickenborne, *Eur. J. Inorg. Chem.* **1999**, 1281.
[127] P. Binger, B. Biedenbach, A. T. Herrmann, F. Langhauser, P. Betz, R. Goddard, C. Krüger, *Chem. Ber.* **1990**, *123*, 1617.
[128] A. Mack, S. Danner, U. Bergsträsser, H. Heydt, M. Regitz, *J. Organomet. Chem.* **2002**, *643–644*, 409.
[129] P. Kramkowski, G. Baum, U. Radius, M. Kaupp, M. Scheer, *Chem. Eur. J.* **1999**, *5*, 2890.
[130] M. Yoshifuji, H. Kawanami, Y. Kawai, K. Toyota, M. Yasunami, T. Niitsu, N. Inamoto, *Chem. Lett.* **1992**, 1053.
[131] M. T. Nguyen, T. K. Ha, *J. Mol. Struct.* **1986**, *139*, 145.
[132] a) H. Jun, V. G. Young, Jr., R. J. Angelici, *J. Am. Chem. Soc.* **1991**, *113*, 9379; b) H. Jun, R. J. Angelici, *Organometallics* **1994**, *13*, 2454; c) L. Weber, I. Schumann, T. Schmidt, H.-G. Stammler, B. Neumann, *Z. Anorg. Allg. Chem.* **1993**, *619*, 1759; d) L. Weber, I. Schumann, H.-G. Stammler, B. Neumann, *Chem. Ber.* **1994**, *127*, 1349; e) W. V. Konze, V. G. Young, Jr., R. J. Angelici, *Organometallics* **1999**, *18*, 258; f) T. Agapie, P. L. Diaconescu, C. C. Cummins, *J. Am. Chem. Soc.* **2002**, *124*, 2412.
[133] M. Sanchez, M.-R. Mazières, L. Lamandé, R. Wolf in ref. [19], pp. 129–148.
[134] a) X. Li, D. Lei, M. Y. Chiang, P. P. Gaspar, *J. Am. Chem. Soc.* **1992**, *114*, 8526; b) X. Li, S. I. Weissman, T.-S. Lin, P. P. Gaspar, A. H. Cowley, A. I. Smirnov, *J. Am. Chem. Soc.* **1994**, *116*, 7899.
[135] a) P. B. Hitchcock, M. F. Lappert, W.-P. Leung, *J. Chem. Soc. Chem. Commun.* **1987**, 1282; b) R. Bohra, P. B. Hitchcock, M. F. Lappert, W.-P. Leung, *Polyhedron* **1989**, *8*, 1884.
[136] A. H. Cowley, B. Pellerin, J. L. Atwood, S. G. Bott, *J. Am. Chem. Soc.* **1990**, *112*, 6734.
[137] A. W. Ehlers, E. J. Baerends, K. Lammertsma, *J. Am. Chem. Soc.* **2002**, *124*, 2831.
[138] Z. Hou, T. L. Breen, D. W. Stephan, *Organometallics* **1993**, *12*, 3158.
[139] Ref. [36].
[140] B. T. Sterenberg, K. A. Udachin, A. J. Carty, *Organometallics* **2001**, *20*, 2657.
[141] A. T. Termaten, H. Aktas, M. Schakel, M. Lutz, A. L. Spek, K. Lammertsma, personal communication.
[142] R. Melenkivitz, D. J. Mindiola, G. L. Hillhouse, *J. Am. Chem. Soc.* **2002**, *124*, 3846.
[143] P. F. Zittel, W. C. Lineberger, *J. Chem. Phys.* **1976**, *65*, 1236.
[144] T. L. Breen, D. W. Stephan, *J. Am. Chem. Soc.* **1995**, *117*, 11914.
[145] T. L. Breen, D. W. Stephan, *J. Am. Chem. Soc.* **1996**, *118*, 4204.
[146] J. B. M. Wit, G. T. van Eijkel, F. J. J. de Kanter, M. Schakel, A. W. Ehlers, M. Lutz, A. L. Spek, K. Lammertsma, *Angew. Chem.* **1999**, *111*, 2716; *Angew. Chem. Int. Ed.* **1999**, *38*, 2596.
[147] a) B. T. Sterenberg, K. A. Udachin, A. J. Carty, *Organometallics* **2001**, *20*, 4463; b) B. T. Sterenberg, A. J. Carty, *J. Organomet. Chem.* **2001**, *617–618*, 696.
[148] J. Sánchez-Nieves, B. T. Sterenberg, K. A. Udachin, A. J. Carty, *J. Am. Chem. Soc.*, in press.
[149] a) F. Mathey, N. H. Tran Huy, A. Marinetti, *Helv. Chim. Acta* **2001**, *84*, 2938; b) K. Lammertsma, M. J. M. Vlaar, *Eur. J. Org. Chem.* **2002**, 1127.
[150] a) H. Jacobsen, T. Ziegler, *Inorg. Chem.* **1996**, *35*, 775; b) T. E. Taylor, M. B. Hall, *J. Am. Chem. Soc.* **1984**, *106*, 1576.
[151] S. Creve, K. Pierloot, M. T. Nguyen, L. G. Vanquickenborne, *Eur. J. Inorg. Chem.* **1999**, 107.
[152] S. Grigoleit, A. Alijah, A. B. Rozhenko, R. Streubel, W. W. Schoeller, *J. Organomet. Chem.* **2002**, *643–644*, 223.
[153] A. W. Ehlers, K. Lammertsma, E. J. Baerends, *Organometallics* **1998**, *17*, 2738.
[154] G. Frison, F. Mathey, A. Sevin, *J. Organomet. Chem.* **1998**, *570*, 225.
[155] A. Marinetti, F. Mathey, *Organometallics* **1984**, *3*, 456.
[156] A. Marinetti, F. Mathey, J. Fischer, A. Mitschler, *J. Am. Chem. Soc.* **1982**, *104*, 4484.
[157] a) Y. Inubuchi, N. H. Tran Huy, L. Ricard, F. Mathey, *J. Organomet. Chem.* **1997**, *533*, 83; b) R. Streubel, A. Ostrowski, H. Wilkens, F. Ruthe, J. Jeske, P. G. Jones, *Angew. Chem.* **1997**, *109*, 409; *Angew. Chem. Int. Ed. Engl.* **1997**, *36*, 378; c) R. Streubel, U. Schiemann, P. G. Jones, N. H. Tran Huy, F. Mathey,

Angew. Chem. **2000**, *112*, 3845; *Angew. Chem. Int. Ed.* **2000**, *39*, 3686.
[158] A. Marinetti, F. Mathey, J. Fischer, A. Mitschler, *J. Chem. Soc. Chem. Commun.* **1982**, 667.
[159] a) K. Lammertsma, J.-T. Hung, P. Chand, G. M. Gray, *J. Org. Chem.* **1992**, *57*, 6557; b) M. J. van Eis, T. Nijbacker, F. J. J. de Kanter, W. H. de Wolf, K. Lammertsma, F. Bickelhaupt, *J. Am. Chem. Soc.* **2000**, *122*, 3033.
[160] M. J. M. Vlaar, A. W. Ehlers, F. J. J. de Kanter, M. Schakel, A. L. Spek, K. Lammertsma, *Angew. Chem.* **2000**, *112*, 3071; *Angew. Chem. Int. Ed.* **2000**, *39*, 2943.
[161] S. Krill, B. Wang, J.-T. Hung, C. J. Horan, G. M. Gray, K. Lammertsma, *J. Am. Chem. Soc.* **1997**, *119*, 8432.
[162] N. H. Tran Huy, R. Salemkour, N. Bartes, L. Ricard, F. Mathey, *Tetrahedron* **2002**, *58*, 7191.
[163] J. Svara, A. Marinetti, F. Mathey, *Organometallics* **1986**, *5*, 1161.
[164] Y. Canac, D. Bourissou, A. Baceiredo, H. Gornitzka, W. W. Schoeller, G. Bertrand, *Science* **1998**, *279*, 2080.
[165] L. Cataldo, S. Choua, T. Berclaz, M. Geoffroy, N. Mézailles, L. Ricard, F. Mathey, P. Le Floch, *J. Am. Chem. Soc.* **2001**, *123*, 6654.
[166] E. Niecke, A. Fuchs, F. Baumeister, M. Nieger, W. W. Schoeller, *Angew. Chem.* **1995**, *107*, 640; *Angew. Chem. Int. Ed. Engl.* **1995**, *34*, 555.
[167] W. W. Schoeller, C. Begemann, E. Niecke, D. Gudat, *J. Phys. Chem. A* **2001**, *105*, 10731.
[168] E. Niecke, A. Fuchs, M. Nieger, *Angew. Chem.* **1999**, *111*, 3213; *Angew. Chem. Int. Ed.* **1999**, *38*, 3028.
[169] O. Schmidt, A. Fuchs, D. Gudat, M. Nieger, W. Hoffbauer, E. Niecke, W. W. Schoeller, *Angew. Chem.* **1998**, *110*, 995; *Angew. Chem. Int. Ed.* **1998**, *37*, 949.
[170] E. Niecke, A. Fuchs, M. Nieger, O. Schmidt, W. W. Schoeller, *Angew. Chem.* **1999**, *111*, 3216; *Angew. Chem. Int. Ed.* **1999**, *38*, 3031.
[171] A. Fuchs, D. Gudat, M. Nieger, O. Schmidt, M. Sebastian, L. Nyulaszi, E. Niecke, *Chem. Eur. J.* **2002**, *8*, 2188.
[172] D. Scheschkewitz, H. Amii, H. Gornitzka, W. W. Schoeller, D. Bourissou, G. Bertrand, *Science* **2002**, *295*, 1880.
[173] F. Mathey, M. Regitz in ref. [110], pp. 17–55.
[174] D. H. Aue, H. M. Webb, W. R. Davidson, M. Vidal, M. T. Bowers, H. Goldwhite, L. E. Vertal, J. E. Douglas, D. A. Kollman, G. L. Kenyon, *J. Am. Chem. Soc.* **1980**, *102*, 5151.
[175] a) D. Carmichael, P. B. Hitchcock, J. F. Nixon, F. Mathey, L. Ricard, *J. Chem. Soc. Chem. Commun.* **1989**, 1389; b) D. Carmichael, P. B. Hitchcock, J. F. Nixon, F. Mathey, L. Ricard, *J. Chem. Soc. Dalton Trans.* **1993**, 1811.
[176] S. Haber, P. Le Floch, F. Mathey, *J. Chem. Soc. Chem. Commun.* **1992**, 1799.
[177] a) M. T. Nguyen, L. Landuyt, L. G. Vanquickenborne, *J. Chem. Soc. Faraday Trans.* **1994**, *90*, 1771; b) N.-N. Pham-Tran, H. M. T. Nguyen, T. Veszprémi, M. T. Nguyen, *J. Chem. Soc. Perkin Trans. 2* **2001**, 766.
[178] a) N. H. Tran Huy, F. Mathey, *Synlett* **1995**, 353; b) N. H. Tran Huy, F. Mathey, *J. Org. Chem.* **2000**, *65*, 652.
[179] W. J. Richter, *Chem. Ber.* **1985**, *118*, 1575.
[180] W. J. Richter, *Chem. Ber.* **1983**, *116*, 3293.
[181] a) B. Wang, C. H. Lake, K. Lammertsma, *J. Am. Chem. Soc.* **1996**, *118*, 1690; b) M. J. van Eis, T. Nijbacker, F. J. J. de Kanter, W. H. de Wolf, K. Lammertsma, F. Bickelhaupt, *J. Am. Chem. Soc.* **2000**, *122*, 3033.
[182] N. H. Tran Huy, A. Marinetti, L. Ricard, F. Mathey, *Organometallics* **1992**, *11*, 1438.
[183] A. Marinetti, F. Mathey, *Organometallics* **1984**, *3*, 1492.
[184] K. D. Dobbs, J. E. Boggs, A. R. Barron, A. H. Cowley, *J. Phys. Chem.* **1988**, *92*, 4886.
[185] P. Le Floch, F. Mathey, *Synlett* **1991**, 743.
[186] A. Göller, T. Clark, *Chem. Commun.* **1997**, 1033.
[187] H. Quast, M. Heuschmann, *Chem. Ber.* **1982**, *115*, 901.
[188] a) D. C. R. Hockless, M. A. McDonald, M. Pabel, S. B. Wild, *J. Chem. Soc. Chem. Commun.* **1995**, 257; b) D. C. R. Hockless, M. A. McDonald, M. Pabel, S. B. Wild, *J. Organomet. Chem.* **1997**, *529*, 189.
[189] a) F. Mercier, B. Deschamps, F. Mathey, *J. Am. Chem. Soc.* **1989**, *111*, 9098; b) A. Marinetti, L. Ricard, F. Mathey, *Synthesis* **1992**, 157.
[190] L. Nyulaszi, *Chem. Rev.* **2001**, *101*, 1299.
[191] a) M. K. Cyranski, T. M. Krygowski, A. R. Katritzky, P. von R. Schleyer, *J. Org. Chem.* **2002**, *67*, 1333; b) L. Nyulazsi, P. von R. Schleyer, *J. Am. Chem. Soc.* **1999**, *121*, 6872.
[192] a) L. D. Quin in ref. [110], pp. 219–305; b) L. D. Quin, G. S. Quin in ref. [110], pp. 307–362.
[193] P. Coggon, A. T. McPhail, *J. Chem. Soc. Dalton Trans.* **1973**, 1888.
[194] S. Holand, F. Gandolfo, L. Ricard, F. Mathey, *Bull. Soc. Chim. Fr.* **1996**, *133*, 33.
[195] E. Mattmann, D. Simonutti, L. Ricard, F. Mercier, F. Mathey, *J. Org. Chem.* **2001**, *66*, 755.
[196] E. Mattmann, F. Mathey, A. Sevin, G. Frison, *J. Org. Chem.* **2002**, *67*, 1208.
[197] G. Keglevich, Z. Böcskei, G. M. Keserü, K. Ujszaszy, L. D. Quin, *J. Am. Chem. Soc.* **1997**, *119*, 5095.
[198] G. Keglevich, T. Chuluunbaatar, A. Dobo, L. Toke, *J. Chem. Soc. Perkin Trans. 1* **2000**, 1495.
[199] C. C. Santini, F. Mathey, *J. Org. Chem.* **1985**, *50*, 467.
[200] E. Mattmann, F. Mercier, L. Ricard, F. Mathey, *J. Org. Chem.* **2002**, *67*, 5422.
[201] F. Laporte, F. Mercier, L. Ricard, F. Mathey, *Bull. Soc. Chim. Fr.* **1993**, *130*, 843.
[202] F. Mathey, F. Mercier, C. Charrier, J. Fischer, A. Mitschler, *J. Am. Chem. Soc.* **1981**, *103*, 4595.
[203] C. Charrier, H. Bonnard, G. de Lauzon, F. Mathey, *J. Am. Chem. Soc.* **1983**, *105*, 6871.
[204] S. M. Bachrach, *J. Org. Chem.* **1993**, *58*, 5414.
[205] P. Le Goff, F. Mathey, L. Ricard, *J. Org. Chem.* **1989**, *54*, 4754.
[206] P. Toullec, L. Ricard, F. Mathey, unpublished results.
[207] a) S. Holand, M. Jeanjean, F. Mathey, *Angew. Chem.* **1997**, *109*, 117; *Angew. Chem. Int. Ed. Engl.* **1997**, *36*, 98; b) S. Holand, N. Maigrot, C. Charrier, F. Mathey, *Organometallics* **1998**, *17*, 2996; c) P. Toullec, F. Mathey, *Synlett* **2001**, 1977; d) G. Frison, L. Ricard, F. Mathey, *Organometallics* **2001**, *20*, 5513; e) M. Melaimi, L. Ricard, F. Mathey, P. Le Floch, *Org. Lett.* **2002**, *4*, 1245.
[208] L. Nyulaszi, *J. Phys. Chem.* **1996**, *100*, 6194.
[209] F. G. N. Cloke, P. B. Hitchcock, P. Hunnable, J. F. Nixon, L. Nyulaszi, E. Niecke, V. Thelen, *Angew. Chem.* **1998**, *110*, 1139; *Angew. Chem. Int. Ed.* **1998**, *37*, 1083.
[210] V. Caliman, P. B. Hitchcock, J. F. Nixon, *J. Chem. Soc. Chem. Commun.* **1995**, 1661.
[211] S. M. Bachrach, V. Caliman, J. F. Nixon, *J. Chem. Soc. Chem. Commun.* **1995**, 2395.
[212] V. Caliman, P. B. Hitchcock, J. F. Nixon, L. Nyulaszi, N. Sakarya, *Chem. Commun.* **1997**, 1305.
[213] M. Baudler, D. Düster, D. Ouzounis, *Z. Anorg. Allg. Chem.* **1987**, *544*, 87.
[214] E. J. Padma Malar, *J. Org. Chem.* **1992**, *57*, 3694.
[215] T. Douglas, K. H. Theopold, *Angew. Chem.* **1989**, *101*, 1394; *Angew. Chem. Int. Ed. Engl.* **1989**, *28*, 1367.
[216] F. G. N. Cloke, P. B. Hitchcock, J. F. Nixon, D. J. Wilson, *Organometallics* **2000**, *19*, 219.
[217] V. Caliman, C. Jones, P. B. Hitchcock, J. F. Nixon, unpublished results; see ref. [213].
[218] D. B. Chesnut, L. D. Quin, *J. Am. Chem. Soc.* **1994**, *116*, 9638.
[219] M. Baudler, T. Etzbach, *Chem. Ber.* **1991**, *124*, 1159.
[220] C. Charrier, F. Mathey, *Tetrahedron Lett.* **1987**, *28*, 5025.

 © 2003 Wiley-VCH Verlag GmbH & Co. KGaA, Weinheim

[221] L. S. Sunderlin, D. Panu, D. B. Puranik, A. J. Ashe III, R. R. Squires, *Organometallics* **1994**, *13*, 4732.
[222] P. Le Floch in ref. [110], pp. 485–533; G. Märkl, P. Kreitmeier in ref. [110], pp. 535–630.
[223] G. Märkl, *Angew. Chem.* **1966**, *78*, 907; *Angew. Chem. Int. Ed. Engl.* **1966**, *5*, 846.
[224] A. J. Ashe III, *J. Am. Chem. Soc.* **1971**, *93*, 3293.
[225] K. K. Baldridge, M. S. Gordon, *J. Am. Chem. Soc.* **1988**, *110*, 4204.
[226] L. Nyulaszi, T. Veszprémi, *J. Phys. Chem.* **1996**, *100*, 6456.
[227] V. Jonas, G. Frenking, *Chem. Phys. Lett.* **1993**, *210*, 211.
[228] R. V. Hodges, J. L. Beauchamp, A. J. Ashe III, W.-T. Chan, *Organometallics* **1985**, *4*, 457.
[229] a) G. Märkl, F. Lieb, A. Merz, *Angew. Chem.* **1967**, *79*, 59; *Angew. Chem. Int. Ed. Engl.* **1967**, *6*, 87; b) G. Märkl, A. Merz, *Tetrahedron Lett.* **1968**, 3611.
[230] a) P. Le Floch, D. Carmichael, L. Ricard, F. Mathey, *J. Am. Chem. Soc.* **1993**, *115*, 10665; b) H.-G. Trauner, P. Le Floch, J.-M. Lefour, L. Ricard, F. Mathey, *Synthesis* **1995**, 717.
[231] a) P. Le Floch, L. Ricard, F. Mathey, *J. Chem. Soc. Chem. Commun.* **1993**, 789; b) P. Le Floch, A. Kolb, F. Mathey, *J. Chem. Soc. Chem. Commun.* **1994**, 2065; P. Rosa, P. Le Floch, L. Ricard, F. Mathey, *J. Am. Chem. Soc.* **1997**, *119*, 9417.
[232] a) C. Elschenbroich, M. Nowotny, A. Behrendt, W. Massa, S. Wocadlo, *Angew. Chem.* **1992**, *104*, 1388; *Angew. Chem. Int. Ed. Engl.* **1992**, *31*, 1343; b) C. Elschenbroich, M. Nowotny, J. Kroker, A. Behrendt, W. Massa, S. Wocadlo, *J. Organomet. Chem.* **1993**, *459*, 157; c) C. Elschenbroich, M. Nowotny, A. Behrendt, K. Harms, S. Wocadlo, J. Pebler, *J. Am. Chem. Soc.* **1994**, *116*, 6217.
[233] C. Elschenbroich, M. Nowotny, B. Metz, W. Massa, J. Graulich, K. Biehler, W. Sauer, *Angew. Chem.* **1991**, *103*, 601; *Angew. Chem. Int. Ed. Engl.* **1991**, *30*, 547.
[234] P. Rosa, N. Mézailles, F. Mathey, P. Le Floch, *J. Org. Chem.* **1998**, *63*, 4826.
[235] a) P. Le Floch, L. Ricard, F. Mathey, A. Jutand, C. Amatore, *Inorg. Chem.* **1995**, *34*, 11; b) P. Rosa, L. Ricard, P. Le Floch, F. Mathey, G. Sini, O. Eisenstein, *Inorg. Chem.* **1998**, *37*, 3154; c) P. Rosa, N. Mézailles, L. Ricard, F. Mathey, P. Le Floch, *Angew. Chem.* **2000**, *112*, 1893; *Angew. Chem. Int. Ed.* **2000**, *39*, 1823; d) N. Mézailles, P. Rosa, L. Ricard, F. Mathey, P. Le Floch, *Organometallics* **2000**, *19*, 2941; e) P. Rosa, N. Mézailles, L. Ricard, F. Mathey, P. Le Floch, Y. Jean, *Angew. Chem.* **2001**, *113*, 1291; *Angew. Chem. Int. Ed.* **2001**, *40*, 1251.
[236] S. Choua, H. Sidorenkova, T. Berclaz, M. Geoffroy, P. Rosa, N. Mézailles, L. Ricard, F. Mathey, P. Le Floch, *J. Am. Chem. Soc.* **2000**, *122*, 12227.
[237] P. Rosa, N. Mézailles, L. Ricard, F. Mathey, P. Le Floch, *Angew. Chem.* **2001**, *113*, 4608; *Angew. Chem. Int. Ed.* **2001**, *40*, 4476.
[238] a) N. Avarvari, N. Mézailles, L. Ricard, P. Le Floch, F. Mathey, *Science* **1998**, *280*, 1587; b) N. Avarvari, N. Maigrot, L. Ricard, F. Mathey, P. Le Floch, *Chem. Eur. J.* **1999**, *5*, 2109; c) N. Mézailles, N. Avarvari, N. Maigrot, L. Ricard, F. Mathey, P. Le Floch, L. Cataldo, T. Berclaz, M. Geoffroy, *Angew. Chem.* **1999**, *111*, 3390; *Angew. Chem. Int. Ed.* **1999**, *38*, 3194.
[239] N. Mézailles, F. Mathey, P. Le Floch, *Prog. Inorg. Chem.* **2001**, *49*, 455.
[240] D. Böhm, F. Knoch, S. Kummer, U. Schmidt, U. Zenneck, *Angew. Chem.* **1995**, *107*, 251; *Angew. Chem. Int. Ed. Engl.* **1995**, *34*, 198.
[241] Y. Kobayashi, I. Kumadaki, A. Ohsawa, H. Hamana, *Tetrahedron Lett.* **1976**, 3715.
[242] Y. Kobayashi, S. Fujino, I. Kumadaki, *J. Am. Chem. Soc.* **1981**, *103*, 2465.
[243] N. H. Tran Huy, H. Vong, F. Mathey, *Organometallics* **2002**, *21*, 336.
[244] L. Colombet, F. Volatron, P. Maître, P. C. Hiberty, *J. Am. Chem. Soc.* **1999**, *121*, 4215.
[245] M. Hofmann, P. von R. Schleyer, M. Regitz, *Eur. J. Org. Chem.* **1999**, 3291.
[246] P. Binger, S. Leininger, J. Stannek, B. Gabor, R. Mynott, J. Bruckmann, C. Krüger, *Angew. Chem.* **1995**, *107*, 2411; *Angew. Chem. Int. Ed. Engl.* **1995**, *34*, 2227.
[247] R. Gleiter, H. Lange, P. Binger, J. Stannek, C. Krüger, J. Bruckmann, U. Zenneck, S. Kummer, *Eur. J. Inorg. Chem.* **1998**, 1619.
[248] K. K. Laali, B. Geissler, O. Wagner, J. Hoffmann, R. Armbrust, W. Eisfeld, M. Regitz, *J. Am. Chem. Soc.* **1994**, *116*, 9407.
[249] A. G. Avent, F. G. N. Cloke, K. R. Flower, P. B. Hitchcock, J. F. Nixon, D. M. Vickers, *Angew. Chem.* **1994**, *106*, 2406; *Angew. Chem. Int. Ed. Engl.* **1994**, *33*, 2330.
[250] W. Eisfeld, M. Regitz, *J. Org. Chem.* **1998**, *63*, 2814.
[251] a) G. Märkl, E. Seidel, *Angew. Chem.* **1983**, *95*, 58; *Angew. Chem. Int. Ed. Engl.* **1983**, *22*, 57; b) G. Märkl, J. Reindel, *Tetrahedron Lett.* **1992**, *33*, 5495.
[252] a) D. Gudat, V. Bajorat, S. Häp, M. Nieger, G. Schröder, *Eur. J. Inorg. Chem.* **1999**, 1169; D. Gudat, S. Häp, L. Szarvas, M. Nieger, *Chem. Commun.* **2000**, 1637.
[253] a) F. Mathey in *Science of Synthesis, Vol. 9* (Ed.: G. Maas), Thieme, Stuttgart, **2001**, pp. 585–600; b) F. Nief, *Eur. J. Inorg. Chem.* **2001**, 891; c) F. Mathey, *J. Organomet. Chem.* **2002**, *646*, 15; d) D. Carmichael, F. Mathey, *Top. Curr. Chem.* **2002**, *220*, 27.
[254] a) F. Mathey, *Coord. Chem. Rev.* **1994**, *137*, 1; b) ref. [2], pp. 294–342.
[255] F. Mathey, *Tetrahedron Lett.* **1976**, 4155.
[256] F. Mathey, A. Mitschler, R. Weiss, *J. Am. Chem. Soc.* **1977**, *99*, 3537.
[257] a) A. Schnepf, G. Stösser, D. Carmichael, F. Mathey, H. Schnöckel, *Angew. Chem.* **1999**, *111*, 1757; *Angew. Chem. Int. Ed.* **1999**, *38*, 1646; b) J. Chojnacki, E. Baum, I. Krossing, D. Carmichael, F. Mathey, H. Schnöckel, *Z. Anorg. Allg. Chem.* **2001**, *627*, 1209.
[258] F. Nief, L. Ricard, *Organometallics* **2001**, *20*, 3884.
[259] S. Bellemin-Laponnaz, M. M.-C. Lo, T. H. Peterson, J. M. Allen, G. C. Fu, *Organometallics* **2001**, *20*, 3453.
[260] K. Forissier, L. Ricard, D. Carmichael, F. Mathey, *Chem. Commun.* **1999**, 1273.
[261] R. Feher, F. H. Köhler, F. Nief, L. Ricard, S. Rossmayer, *Organometallics* **1997**, *16*, 4606.
[262] K. Forissier, L. Ricard, D. Carmichael, F. Mathey, *Organometallics* **2000**, *19*, 954.
[263] F. Nief, P. Riant, L. Ricard, P. Desmurs, D. Baudry-Barbier, *Eur. J. Inorg. Chem.* **1999**, 1041.
[264] F. Nief, D. Turcitu, L. Ricard, *Chem. Commun.* **2002**, 1646.
[265] F. Paul, D. Carmichael, L. Ricard, F. Mathey, *Angew. Chem.* **1996**, *108*, 1204; *Angew. Chem. Int. Ed. Engl.* **1996**, *35*, 1125.
[266] F. Nief, L. Ricard, *J. Organomet. Chem.* **2002**, *642*, 208.
[267] M. Westerhausen, M. H. Digeser, C. Gückel, H. Nöth, J. Knizek, W. Ponikwar, *Organometallics* **1999**, *18*, 2491.
[268] M. Westerhausen, M. H. Digeser, H. Nöth, T. Seifert, A. Pfitzner, *J. Am. Chem. Soc.* **1998**, *120*, 6722.
[269] G. de Lauzon, B. Deschamps, J. Fischer, F. Mathey, A. Mitschler, *J. Am. Chem. Soc.* **1980**, *102*, 994.
[270] G. de Lauzon, B. Deschamps, F. Mathey, *Nouv. J. Chim.* **1980**, *4*, 683.
[271] B. Deschamps, L. Ricard, F. Mathey, *Organometallics* **1999**, *18*, 5688.
[272] A. Klys, J. Zakrzewski, *J. Organomet. Chem.* **2002**, *642*, 143.
[273] L. Brassat, B. Ganter, C. Ganter, *Chem. Eur. J.* **1998**, *4*, 2148.
[274] P. Toullec, L. Ricard, F. Mathey, *Organometallics* **2002**, *21*, 2635.
[275] S. O. Agustsson, C. Hu, U. Englert, T. Marx, L. Wesemann, C. Ganter, *Organometallics* **2002**, *21*, 2993.

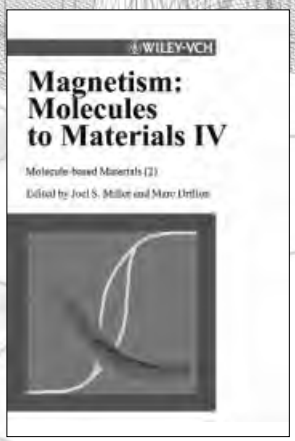
 © 2003 Wiley-VCH Verlag GmbH & Co. KGaA, Weinheim

[276] N. M. Kostic, R. F. Fenske, *Organometallics* **1983**, *2*, 1008.
[277] G. Frison, F. Mathey, A. Sevin, *J. Phys. Chem. A* **2002**, *106*, 5653.
[278] a) B. Deschamps, J. Fischer, F. Mathey, A. Mitschler, *Inorg. Chem.* **1981**, *20*, 3252; b) B. Deschamps, J. Fischer, F. Mathey, A. Mitschler, L. Ricard, *Organometallics* **1982**, *1*, 312.
[279] B. Deschamps, P. Toullec, L. Ricard, F. Mathey, *J. Organomet. Chem.* **2001**, *634*, 131.
[280] P. Lemoine, M. Gross, P. Braunstein, F. Mathey, B. Deschamps, J. H. Nelson, *Organometallics* **1984**, *3*, 1303.
[281] X. Sava, L. Ricard, F. Mathey, P. Le Floch, *Inorg. Chim. Acta*, in press.
[282] a) C. Burney, D. Carmichael, K. Forissier, J. C. Green, F. Mathey, L. Ricard, unpublished results; b) pp. 42–43 in ref. [253 d].
[283] pp. 44–45 in ref. [253 d].
[284] T. K. Hollis, L.-S. Wang, F. Tham, *J. Am. Chem. Soc.* **2000**, *122*, 11 737.
[285] D. A. Atwood, A. H. Cowley, S. M. Dennis, *Inorg. Chem.* **1993**, *32*, 1527.
[286] X. Sava, L. Ricard, F. Mathey, P. Le Floch, *Organometallics* **2000**, *19*, 4899.
[287] L. Brunet, F. Mercier, L. Ricard, F. Mathey, *Angew. Chem.* **1994**, *106*, 812; *Angew. Chem. Int. Ed. Engl.* **1994**, *33*, 742.
[288] X. Sava, L. Ricard, F. Mathey, P. Le Floch, *Chem. Eur. J.* **2001**, *7*, 3159.
[289] O. J. Scherer, T. Brück, *Angew. Chem.* **1987**, *99*, 59; *Angew. Chem. Int. Ed. Engl.* **1987**, *26*, 59.
[290] V. A. Myliukov, O. G. Sinyashin, O. Scherer, E. Hey-Hawkins, *Mendeleev Commun.* **2002**, 1.
[291] J. Frunzke, M. Lein, G. Frenking, *Organometallics* **2002**, *21*, 3351.
[292] E. Urnezius, W. W. Brennessel, C. J. Cramer, J. E. Ellis, P. von R. Schleyer, *Science* **2002**, *295*, 832.
[293] F. G. N. Cloke, J. R. Hanks, P. B. Hitchcock, J. F. Nixon, *Chem. Commun.* **1999**, 1731.
[294] F. G. N. Cloke, K. R. Flower, P. B. Hitchcock, J. F. Nixon, *J. Chem. Soc. Chem. Commun.* **1995**, 1659.
[295] R. Bartsch, P. B. Hitchcock, J. F. Nixon, *J. Organomet. Chem.* **1988**, *356*, C1.
[296] T. Clark, A. Elvers, F. W. Heinemann, M. Hennemann, M. Zeller, U. Zenneck, *Angew. Chem.* **2000**, *112*, 2174; *Angew. Chem. Int. Ed.* **2000**, *39*, 2087.
[297] P. L. Arnold, F. G. N. Cloke, P. B. Hitchcock, J. F. Nixon, *J. Am. Chem. Soc.* **1996**, *118*, 7630.
[298] M. D. Francis, P. B. Hitchcock, J. F. Nixon, H. Schnöckel, J. Steiner, *J. Organomet. Chem.* **2002**, *646*, 191.
[299] G. K. B. Clentsmith, F. G. N. Cloke, M. D. Francis, J. C. Green, P. B. Hitchcock, J. F. Nixon, J. L. Suter, D. M. Vickers, *J. Chem. Soc. Dalton Trans.* **2000**, 1715.
[300] F. W. Heinemann, H. Pritzkow, M. Zeller, U. Zenneck, *Organometallics* **2001**, *20*, 2905.
[301] F. G. N. Cloke, J. C. Green, J. R. Hanks, J. F. Nixon, J. L. Suter, *J. Chem. Soc. Dalton Trans.* **2000**, 3534.
[302] M. Al-Ktaifani, J. C. Green, P. B. Hitchcock, J. F. Nixon, *J. Chem. Soc. Dalton Trans.* **2001**, 1726.
[303] V. A. Wright, D. P. Gates, *Angew. Chem.* **2002**, *114*, 2495; *Angew. Chem. Int. Ed.* **2002**, *41*, 2389.
[304] N. H. Tran Huy, L. Ricard, F. Mathey, *Angew. Chem.* **2001**, *113*, 1293; *Angew. Chem. Int. Ed.* **2001**, *40*, 1253.
[305] S. Kobayashi, J.-I. Kadokawa, *Macromol. Rapid Commun.* **1994**, *15*, 567.
[306] U. Salzner, J. B. Lagowski, P. G. Pickup, R. A. Poirier, *Synth. Met.* **1998**, *96*, 177.
[307] D. Delaere, M. T. Nguyen, L. G. Vanquickenborne, *Phys. Chem. Chem. Phys.* **2002**, *4*, 1522.
[308] J. Ma, S. Li, Y. Jiang, *Macromolecules* **2002**, *35*, 1109.
[309] E. Deschamps, L. Ricard, F. Mathey, *Angew. Chem.* **1994**, *106*, 1214; *Angew. Chem. Int. Ed. Engl.* **1994**, *33*, 1158.
[310] M.-O. Bévierre, F. Mercier, L. Ricard, F. Mathey, *Angew. Chem.* **1990**, *102*, 672; *Angew. Chem. Int. Ed. Engl.* **1990**, *29*, 655.
[311] M.-O. Bévierre, F. Mercier, F. Mathey, A. Jutand, C. Amatore, *New J. Chem.* **1991**, *15*, 545.
[312] C. Hay, C. Fischmeister, M. Hissler, L. Toupet, R. Réau, *Angew. Chem.* **2000**, *112*, 1882; *Angew. Chem. Int. Ed.* **2000**, *39*, 1812.
[313] C. Hay, M. Hissler, C. Fischmeister, J. Rault-Berthelot, L. Toupet, L. Nyulaszi, R. Réau, *Chem. Eur. J.* **2001**, *7*, 4222.
[314] S. S. H. Mao, T. D. Tilley, *Macromolecules* **1997**, *30*, 5566.
[315] E. Deschamps, L. Ricard, F. Mathey, *Organometallics* **2001**, *20*, 1499.
[316] J. M. Nelson, H. Rengel, I. Manners, *J. Am. Chem. Soc.* **1993**, *115*, 7035.
[317] I. Manners, *Angew. Chem.* **1996**, *108*, 1712; *Angew. Chem. Int. Ed. Engl.* **1996**, *35*, 1602.
[318] K. Toyota, K. Masaki, T. Abe, M. Yoshifuji, *Chem. Lett.* **1995**, 221.
[319] T. Minami, H. Okamoto, S. Ikeda, R. Tanaka, F. Ozawa, M. Yoshifuji, *Angew. Chem.* **2001**, *113*, 4633; *Angew. Chem. Int. Ed.* **2001**, *40*, 4501.
[320] F. Ozawa, S. Yamamoto, S. Kawagishi, M. Hiraoka, S. Ikeda, T. Minami, S. Ito, M. Yoshifuji, *Chem. Lett.* **2001**, 972.
[321] F. Ozawa, H. Okamoto, S. Kawagishi, S. Yamamoto, T. Minami, M. Yoshifuji, *J. Am. Chem. Soc.* **2002**, *124*, 10 968.
[322] a) B. Breit, *Chem. Commun.* **1996**, 2071; b) B. Breit, *J. Mol. Catal. A* **1999**, *143*, 143.
[323] B. Breit, R. Winde, K. Harms, *J. Chem. Soc. Perkin Trans. 1* **1997**, 2681.
[324] B. Breit, R. Winde, T. Mackewitz, R. Paciello, K. Harms, *Chem. Eur. J.* **2001**, *7*, 3106.
[325] E. F. DiMauro, M. C. Kozlowski, *J. Chem. Soc. Perkin Trans. 1* **2002**, 439.
[326] a) F. Knoch, F. Kremer, U Schmidt, U. Zenneck, P. Le Floch, F. Mathey, *Organometallics* **1996**, *15*, 2713; b) P. Le Floch, F. Knoch, F. Kremer, F. Mathey, J. Scholz, W. Scholz, K.-H. Thiele, U. Zenneck, *Eur. J. Inorg. Chem.* **1998**, 119.
[327] M. Doux, N. Mézailles, M. Melaimi, L. Ricard, P. Le Floch, *Chem. Commun.* **2002**, 1566.
[328] M. Melaimi, F. Mathey, P. Le Floch, *J. Organomet. Chem.* **2001**, *640*, 197.
[329] S. Qiao, G. C. Fu, *J. Org. Chem.* **1998**, *63*, 4168.
[330] K. Tanaka, S. Qiao, M. Tobisu, M. M.-C. Lo, G. C. Fu, *J. Am. Chem. Soc.* **2000**, *122*, 9870.
[331] K. Tanaka, M. M.-C. Lo, G. C. Fu, mentioned as unpublished results in ref. [72].
[332] C. Ganter, C. Kaulen, U. Englert, *Organometallics* **1999**, *18*, 5444.
[333] R. Shintani, M. M.-C. Lo, G. C. Fu, *Org. Lett.* **2000**, *2*, 3695.
[334] M. Ogasawara, K. Yoshida, T. Hayashi, *Organometallics* **2001**, *20*, 3913.
[335] C. Janiak, U. Versteeg, K. C. H. Lange, R. Weimann, E. Hahn, *J. Organomet. Chem.* **1995**, *501*, 219.
[336] C. Janiak, K. C. H. Lange, U. Versteeg, D. Lentz, P. H. M. Budzelaar, *Chem. Ber.* **1996**, *129*, 1517.
[337] E. J. M. de Boer, I. J. Gilmore, F. M. Korndorffer, A. D. Horton, A. van der Linden, B. W. Royan, B. J. Ruisch, L. Schoon, R. W. Shaw, *J. Mol. Catal. A* **1998**, *128*, 155.
[338] S. J. Brown, X. Gao, D. G. Harrison, L. Koch, R. E. v. H. Spence, G. P. A. Yap, *Organometallics* **1998**, *17*, 5445.
[339] M. Sone in *Metallocene-Based Polyolefins* (Eds.: J. Scheirs, W. Kaminsky), Wiley, New York, **2000**, pp. 219–232.
[340] C. Janiak, K. C. H. Lange, P. Marquardt, *J. Mol. Catal. A* **2002**, *180*, 43.
[341] S. Ikeda, F. Ohhata, M. Miyoshi, R. Tanaka, T. Minami, F. Ozawa, M. Yoshifuji, *Angew. Chem.* **2000**, *112*, 4686; *Angew. Chem. Int. Ed.* **2000**, *39*, 4512.

 © 2003 Wiley-VCH Verlag GmbH & Co. KGaA, Weinheim

[342] D. Neibecker, R. Réau, *Angew. Chem.* **1989**, *101*, 579; *Angew. Chem. Int. Ed. Engl.* **1989**, *28*, 500.
[343] D. Neibecker, R. Réau, *New J. Chem.* **1991**, *15*, 279.
[344] W. A. Herrmann, C. W. Kohlpaintner, R. B. Manetsberger, H. Bahrmann, H. Kottmann, *J. Mol. Catal. A* **1995**, *97*, 65.
[345] F. Robin, F. Mercier, L. Ricard, F. Mathey, M. Spagnol, *Chem. Eur. J.* **1997**, *3*, 1365.
[346] T. Faitg, J. Soulié, J.-Y. Lallemand, F. Mercier, F. Mathey, *Tetrahedron* **2000**, *56*, 101.
[347] S. R. Gilbertson, D. G. Genov, A. L. Rheingold, *Org. Lett.* **2000**, *2*, 2885.
[348] E. Niecke, W. Flick, *Angew. Chem.* **1973**, *85*, 586; *Angew. Chem. Int. Ed. Engl.* **1973**, *12*, 585.
[349] E. Niecke, M. Nieger, F. Reichert, *Angew. Chem.* **1988**, *100*, 1781; *Angew. Chem. Int. Ed. Engl.* **1988**, *27*, 1715.
[350] M. Yoshifuji, I. Shima, N. Inamoto, K. Hirotsu, T. Higuchi, *J. Am. Chem. Soc.* **1981**, *103*, 4587.
[351] C.-W. Tsang, M. Yam, D. P. Gates, *J. Am. Chem. Soc.* **2003**, *125*, 1480.

Magnetism: Molecules to Materials



J.S. MILLER, University of Utah, Salt Lake City, USA; **M. DRILLON**, Inst. de Physique et Chimie des Materiaux de Strasbourg, France (Eds)

As a depository of contemporary knowledge on key topics related to magnetism, this open series of volumes provides a much-needed comprehensive overview of this growing interdisciplinary field. In topical reviews written by foremost scientists trends and recent advances focusing on the correlations between electronic structure and magnetic properties are explained in a clear and detailed way. The balance between theory and experiment within this series will guide advanced students and specialists alike to this research area. It will help evaluate own experimental observations and serve as a base for the design of new magnetic materials. A unique reference work, indispensable for everyone concerned with the phenomena of magnetism!

Reviews for Volume II:
"... presents a good ... current overview of an active and diverse research area."
Journal of the American Chemical Society

NEW: Magnetism: Molecules to Materials IV
Molecule-based Materials (2)
2002. XI, 492 pp. 300 fig. HC
€ 159.-/£ 95.-/US$ 125.-
3-527-30429-0

Magnetism: Molecules to Materials III
Nanosized Magnetic Materials
2001. XV, 388 pp. 209 fig. 14 tab. HC
€ 139.-/£ 80.-/US$ 125.-
3-527-30302-2

Magnetism: Molecules to Materials II
Molecule-Based Materials
2001. XIV, 489 pp. 323 fig. 43 tab. HC
€ 159.-/£ 95.-/US$ 125.-
3-527-30301-4

Magnetism: Molecules to Materials I
Models and Experiments
2001. XVI, 437 pp. 270 fig. 33 tab. HC
€ 139.-/£ 80.-/US$ 125.-
3-527-29772-3

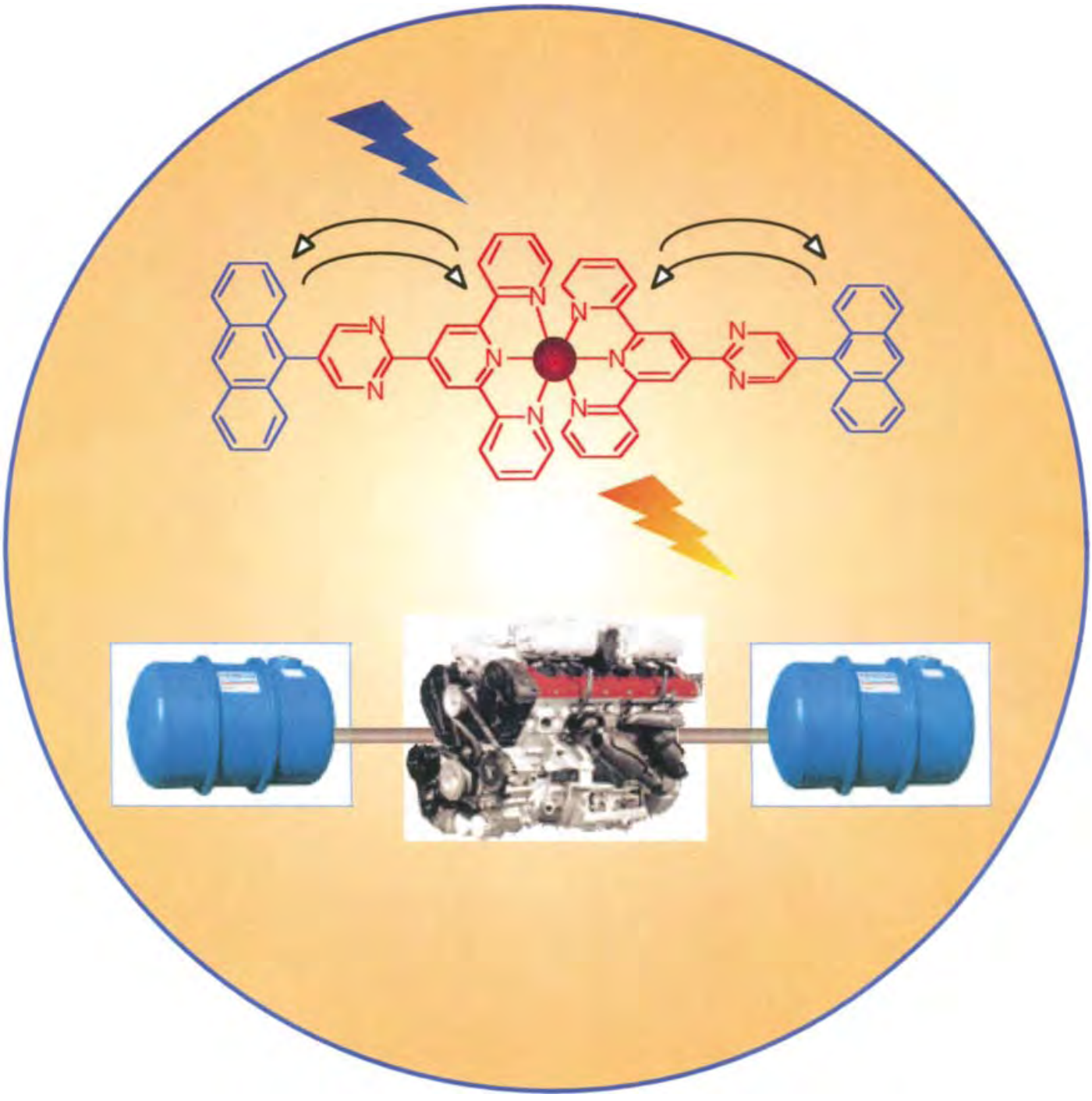
John Wiley & Sons, Ltd.
Baffins Lane Chichester, West Sussex, PO 19 1UD, UK
Fax: +44 (0)1243-775878

WILEY-VCH · P.O. Box 10 11 61 · 69451 Weinheim, Germany · Fax: +49 (0) 62 01-60 61 84 · e-mail: service@wiley-vch.de · http://www.wiley-vch.de

14602094_vi

WILEY WILEY-VCH

Communications



In the multichromophoric ruthenium(II) species with anthracene subunits, the subunits play the role of excited-state reservoir elements for the luminescence of the metal chromophore (the "engine"). The overall effect is metal-to-ligand charge transfer (MLCT) emission with prolonged lifetimes. For more information see the following article by Campagna, Hanan, and co-workers.

DOI: 10.1002/anie.200250613
© 2003 Wiley-VCH Verlag GmbH & Co. KGaA, Weinheim

Long-Lived Luminescence

In Search of Ruthenium(II) Complexes Based on Tridentate Polypyridine Ligands that Feature Long-lived Room-Temperature Luminescence: The Multichromophore Approach**

Rosalba Passalacqua, Frédérique Loiseau, Sebastiano Campagna, Yuan-Qing Fang, and Garry S. Hanan**

Dedicated to Professor Manfred T. Reetz on the occasion of his 60th birthday

Within the field of inorganic photochemistry, there is considerable interest in the design of ruthenium(II) complexes based on tridentate ligands that exhibit long-lived metal-to-ligand charge-transfer (MLCT) excited states.[1] Indeed, ruthenium(II) polypyridyl complexes play outstanding roles in fields connected to solar-energy conversion and the storage of light and/or electronic information at the molecular level.[2] The prototype of this class of compounds, $[Ru(bpy)_3]^{2+}$ (bpy = 2,2′-bipyridine), has been one of the most studied metal-containing species in the last two decades.[2a,3] However, its homologous compound $[Ru(tpy)_2]^{2+}$, based on the tridentate polypyridine ligand 2,2′:6′,2″-terpyridine (tpy), is structurally more appealing than $[Ru(bpy)_3]^{2+}$ for several reasons: 1) $[Ru(bpy)_3]^{2+}$ is a mixture of Δ and Λ enantiomers; 2) monosubstitution of bpy ligands introduces *fac* and *mer* isomerism, so that polynuclear arrays based on the $[Ru(bpy)_3]^{2+}$ motif are rarely pure species; 3) a linear arrangement of such $[Ru(bpy)_3]^{2+}$ chromophores, useful for the design of molecular wires and consequently vectorial energy and electron migration, is difficult to obtain. These problems can indeed be overcome by the use of tridentate, tpy-type polypyridine ligands. However, the photophysical properties of the $[Ru(tpy)_2]^{2+}$ ion and its derivatives are much less useful than those of the $[Ru(bpy)_3]^{2+}$ ion, essentially because the $[Ru(tpy)_2]^{2+}$ ion has a short excited-state lifetime at room temperature.[4]

Several strategies have been employed to prolong the room-temperature excited-state lifetime of ruthenium complexes with tridentate polypyridine ligands, these include the use of 1) cyclometalating ligands,[1e] 2) electron withdrawing and/or donor substituents,[1d] and 3) ligands with extended π^* orbitals, to increase delocalization in the acceptor ligand of the MLCT state.[1c,5] The aim of the first two strategies is to increase the energy gap between the MLCT and the MC excited state, thereby minimizing the thermally activated surface crossing which dominates the MLCT deactivation processes,[4] while the third strategy is based on modification of the Frank–Condon factors for nonradiative decay.

Another approach has emerged as a very efficient tool to increase the excited-state lifetime of metal polypyridine complexes: the combination of metal complexes and organic chromophores which have triplet excited states (very long-lived, since their deactivation processes are strongly forbidden ones) at energies close to the triplet MLCT state of the metal chromophore.[6] This requires the synthesis of multichromophoric species (therefore this approach can be termed as "the multichromophore approach"), in which the various metal- and organic-based chromophores are only weakly interacting, so that their individual properties are essentially maintained.[7] However, if the electronic interaction is large enough, equilibration between the ^{3}MLCT and the lowest-lying organic triplet can occur, and the organic triplet may play the role of an energy-storage site, with the overall effect of extending the MLCT luminescence lifetime.[6]

Herein, we present a new strategy based on the fusion of two approaches: the coupling of ligands with extended π^* orbitals and organic chromophores with suitable triplet states (the multichromophore approach). For the ligands containing extended π^* orbitals, we chose pyrimidine-substituted tpy ligands, which recently have proved to be effective in achieving this aim,[5d] whereas anthracene derivatives have been selected to act as the suitable energy storage site(s). By applying this strategy, two novel, multichromophoric species have been prepared: $[(an\text{-}pym\text{-}tpy)Ru(tpy)](PF_6)_2$ (**1**, an-pym-tpy = 2‴-(2,2′:6′,2″-terpyrid-4′-yl)-5‴-(9-anthryl)pyrimidine) and $[(an\text{-}pym\text{-}tpy)Ru(tpy\text{-}pym\text{-}an)](PF_6)_2$ (**2**). The results are extraordinary: compound **2** exhibits a MLCT luminescence lifetime of 1.8 μs at room temperature which, to our knowledge, is the longest-lived room-temperature emission reported for a ruthenium polypyridyl species based on tridentate ligands.

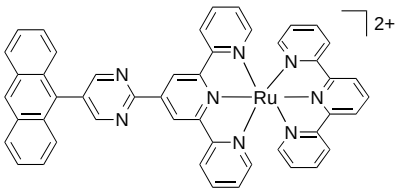
Complexes **1** and **2** were synthesized using the "chemistry-on-the-complex" methodology,[8] in which the an-pym-tpy ligands were synthesized while directly attached to the metal ions. Thus, ruthenium complexes **5** and **6** were allowed to react with 9-anthrylboronic acid under Suzuki coupling conditions to afford complexes **1** (83% yield) and **2** (60% yield), respectively (full details are given in the Supporting Information).[9] Although previous work has shown that a chloro substituent in the 5-position of a pyrimidine group is relatively inert to heterocoupling reactions, the ruthenium cation effectively activates the 5-chloro group by an inductive effect.[10,11]

[*] Prof. S. Campagna, R. Passalacqua, Dr. F. Loiseau
Dipartimento di Chimica Inorganica
Chimica Analitica e Chimica Fisica
Università di Messina, 98166 Messina (Italy)
Fax: (39) 090-393756
E-mail: photochem@chem.unime.it
Prof. G. S. Hanan,[+] Y.-Q. Fang
Department of Chemistry, University of Waterloo (Canada)
E-mail: garry.hanan@umontreal.ca
[+] Present address:
Département de chimie, Université de Montréal
2900 Edouard-Montpetit, Montréal, QC, H3T 1J4 (Canada)
Fax: (+1) 514-343-7586

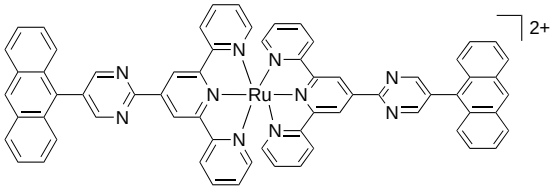
[**] Financial support by the MIUR, CNR (Agenzia 2000), NSERC (Canada), and EU-TMR Research Network on Nanometer Size Metal Complexes is gratefully acknowledged. F.L. also thanks the Marie Curie fellowships program.

Supporting information (synthetic methods) for this article is available on the WWW under http://www.angewandte.org or from the author.

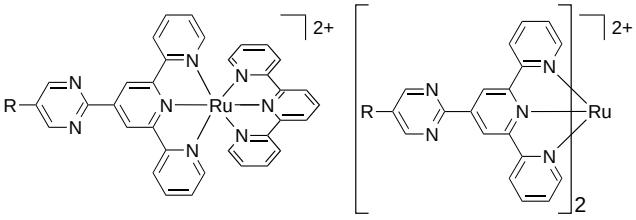
 © 2003 Wiley-VCH Verlag GmbH & Co. KGaA, Weinheim DOI: 10.1002/anie.200250613



1



2



3; R = phenyl
5; R = Cl

4; R = phenyl
6; R = Cl

The absorption spectra of the new species (Figure 1) are dominated by spin-allowed MLCT bands in the visible and by spin-allowed polypyridine ligand-centered (LC) bands in the UV region. Moreover, typical anthracene absorption signatures appear in the 350–400 nm region (because of population of the ^1L_a state) and at about 254 nm (because of population of the ^1B_a state). As expected, the molar absorptivities of the anthracene-based absorption bands are larger in **2** than **1**. The absorption features indicate that in **1** and **2** the metal-based and organic chromophores are at best weakly interacting with one another.

The luminescence data of **1** and **2** and of the reference compounds $[(tpy)Ru(tpy\text{-}pym\text{-}ph)]^{2+}$ (**3**, tpy-pym-ph = 2‴-(2,2′:6′,2″-terpyrid-4′-yl)-5‴-(phenyl)pyrimidine) and $[Ru(tpy\text{-}pym\text{-}ph)_2]^{2+}$ (**4**), are collected in Table 1, while the emission spectra of **2** are shown in Figure 1, inset. The experimental results at 77 K (in particular, lifetimes and emission spectra) clearly allow the low temperature emission to be attributed to the anthracene triplet.[12] At room temperature, the emission spectra of **1** and **2** are typical of MLCT emitters.[3] However, their luminescence decays are biexponential (Table 1, Figure 2), and in both cases one of the decay components is long-lived when compared to the emission lifetimes of similar species,[1,2,5] including **3** and **4**. Indeed, compounds **3** and **4** have emission spectra which are practically coincident with those of **1** and **2**, respectively. As the effect of the extended π* orbital(s) in **3** and **4** is already present in **1** and **2**,[13] the additional increase in the luminescence lifetimes of the anthracene-containing species is related to the presence of the anthracene triplet. It can be assumed that the ^{3}MLCT state(s) initially formed in **1** and **2** deactivate by energy transfer to the anthracene-based triplet states, which are lower in energy.[14] The fastest component of the luminescence decays of **1** and **2** can be assigned to decay of the initially formed ^{3}MLCT state, shortened in comparison with the luminescence lifetimes of the model species **3** and **4** (Table 1) because of the occurrence of the above mentioned energy-transfer to the anthracene-based triplet states. Equi-

Table 1: Luminescence data.

Compound	298 K[a] λ_{max} [nm]	τ [ns]	Φ	77 K[b] λ_{max} [nm]	τ
1	680	5.5; 402	1.3×10^{-4}	692	3.5 ms
2	675	5.8; 1806	1.8×10^{-4}	694	3.5 ms
3	680	15	1.8×10^{-4}	654	15.0 μs
4	675	21	4.4×10^{-4}	651	13.8 μs

[a] In deaerated CH_3CN. [b] In butyronitrile.

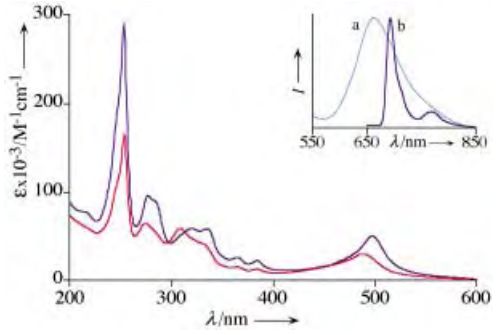


Figure 1. Absorption spectra of **1** (red) and **2** (blue) in acetonitrile solution and inset: uncorrected emission spectra of **2** in acetonitrile solution at room temperature (a) and in butyronitrile at 77 K (b). Corrected values for emission maxima are given in Table 1.

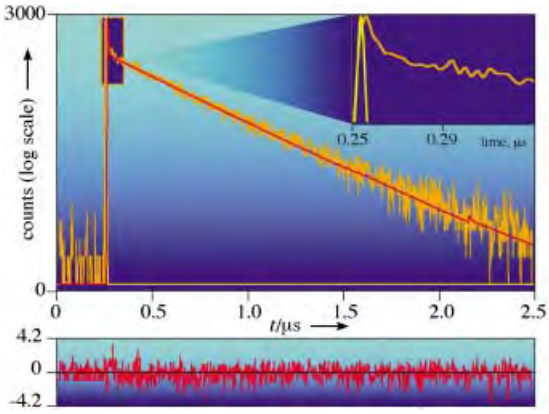


Figure 2. Luminescence decay (orange), lamp profile (yellow), and fitting (red) of the emission of **2** at room temperature in degassed acetonitrile.

 © 2003 Wiley-VCH Verlag GmbH & Co. KGaA, Weinheim

libration between ^{3}MLCT and the triplet anthracene states is established by the Boltzmann distribution,[6] which results in a significant increase of the ^{3}MLCT luminescence lifetime. The extension of the ^{3}MLCT luminescence lifetime is particularly noticeable in **2**, as the slower component of its luminescence decay lasts up to 1.8 μs.

To further confirm our interpretation, we performed transient absorption spectroscopy experiments on **1**–**4** at room temperature. Whereas no transient spectrum was obtained for **3** and **4** 100 ns after the laser flash, transient spectra with typical features of anthracene triplet absorption[6e,12] were obtained for **1** and **2**, with decays in very good agreement with their respective long-lived luminescence lifetimes.

It has been reported that there is a linear dependence between the extension of lifetime of Ru^{II} polypyridine chromophores and the number of identical organic chromophores added.[6e] On looking at Table 1, it appears that the data for **1** and **2** do not agree with this statement: it should be considered that their ^{3}MLCT levels are slightly different to one another (as well as those of their respective model compounds **3** and **4**), since an-pym-tpy is a better electron-withdrawing ligand than tpy and is expected to leave less electron density on the metal center, thus increasing the energy of the MLCT state(s). This argument also agrees with emission maxima of **1**–**4** at room temperature (Table 1). As a consequence, the partitioning of the population between the MLCT and anthracene triplet levels changes on passing from **1** to **2** not only because of the change in the number of the organic chromophores, but also because of the difference in the energy gap between the relevant states. As such, **1** and **2** are not totally homologous, which translates into an extension of the luminescence lifetime in **2** by much more than twice that of **1**.

In conclusion, the fusion of two design strategies affords long-lived luminescence at room temperature in Ru^{II} complexes based on tridentate ligands. In particular, the multichromophore approach proved to be very efficient and allowed us to obtain novel species (**1** and **2**) which displayed impressive long-lived MLCT luminescence. Coupling of the novel chromophores with suitable acceptor/donor subunits to prepare multicomponent species for vectorial-energy and electron-transfer studies is under way.

Received: November 22, 2002 [Z50613]

Keywords: chromophores · luminescence · N ligands · photochemistry · ruthenium

[1] a) S. Encinas, L. Flamigni, F. Barigelletti, E. C. Constable, C. E. Housecroft, E. R. Schofield, E. Figgemeier, D. Fenske, M. Neuburger, J. G. Vos, M. Zehnder, *Chem. Eur. J.* **2002**, *8*, 137; b) F. Barigelletti, L. Flamigni, *Chem. Soc. Rev.* **2000**, *29*, 1; c) A. El-ghayoury, A. Harriman, A. Khatyr, R. Ziessel, *Angew. Chem.* **2000**, *112*, 191; *Angew. Chem. Int. Ed.* **2000**, *39*, 185; d) M. Maestri, N. Armaroli, V. Balzani, E. C. Constable, A. M. W. Cargill Thompson, *Inorg. Chem.* **1995**, *34*, 2759; e) J.-P. Sauvage, J.-P. Collin, J.-C. Chambron, S. Guillerez, C. Coudret, V. Balzani, F. Barigelletti, L. De Cola, L. Flamigni, *Chem. Rev.* **1994**, *94*, 993.

[2] a) V. Balzani, A. Juris, M. Venturi, S. Campagna, S. Serroni, *Chem. Rev.* **1996**, *96*, 956, and references therein; b) A. Hagfeldt, M. Graetzel, *Acc. Chem. Res.* **2000**,*33*, 269; c) L. Sun, L. Hammarström, B. Akermark, S. Styring, *Chem. Soc. Rev.* **2001**, *30*, 36; d) R. Ballardini, V. Balzani, A. Credi, M. T. Gandolfi, M. Venturi, *Acc. Chem. Res.* **2001**, *34*, 445; e) D. Pomeranc, V. Heitz, J.-C. Chambron, J.-P. Sauvage, *J. Am. Chem. Soc.* **2001**, *123*, 12215; f) C. J. Kleverlaan, M. T. Indelli, C. A. Bignozzi, L. Pavanin, F. Scandola, G. M. Hasselman, T. J. Meyer, *J. Am. Chem. Soc.* **2000**, *122*, 2840; g) G. Benkö, J. Kallioinen, J. E. I. Korppi-Tommola, A. P. Yartsev, V. Sundström, *J. Am. Chem. Soc.* **2002**, *124*, 489.

[3] a) T. J. Meyer, *Pure Appl. Chem.* **1986**, *58*, 1193; b) A. Juris, V. Balzani, F. Barigelletti, S. Campagna, P. Belser, A. von Zelewsky, *Coord. Chem. Rev.* **1988**, *84*, 85, and references therein.

[4] These unfavorable photophysical properties result from the proximity (in energy) of the lowest-lying MLCT and metal-centered (MC) states, with the latter governing the excited-state decay dynamics by thermally activated surface crossing. This topic has been clarified and is reported in detail in several reviews.[1e,2a,3a,b]

[5] a) A. Harriman, R. Ziessel, *Chem. Commun.* **1996**, 1707; b) A. C. Benniston, A. Harriman, V. Grosshenny, R. Ziessel, *New J. Chem.* **1997**, *21*, 405; c) A. El-ghayoury, A. Harriman, A. Khatyr, R. Ziessel, *J. Phys. Chem. A* **2000**, *104*, 1512; d) Y.-Q. Fang, N. J. Taylor, G. S. Hanan, F. Loiseau, R. Passalacqua, S. Campagna, H. Nierengarten, A. Van Dorsselaer, *J. Am. Chem. Soc.*, **2002**, *124*, 7912.

[6] See for example: a) W. E. Ford, M. A. J. Rodgers, *J. Phys. Chem.* **1992**, *96*, 2917; b) G. J. Wilson, A. Launikonis, W. H. F. Sasse, A. W.-H. Mau, *J. Phys. Chem. A* **1997**, *101*, 4860; c) J. A. Simon, S. L. Curry, R. H. Schmehl, T. R. Schatz, P. Piotrowiak, X. Jin, R. P. Thummel, *J. Am. Chem. Soc.* **1997**, *119*, 11012; d) D. S. Tyson, C. R. Luman, X. Zhou, F. N. Castellano, *Inorg. Chem.* **2001**, *40*, 4063; e) B. Maubert, N. D. McClenaghan, M. T. Indelli, S. Campagna, *J. Phys. Chem. A*, in press.

[7] The electronic interaction between the chromophores has to be weak, otherwise a single (delocalized) excited state is populated and equilibration between states, the key point of the strategy (see later), is meaningless.

[8] a) Y.-Q. Fang, M. I. J. Polson, G. S. Hanan, *Inorg. Chem.* **2003**, *42*, 5; b) F. Loiseau, R. Passalacqua, S. Campagna, Y.-Q. Fang, M. I. J. Polson, G. S. Hanan, *Photochem. Photobiol. Sci.* **2002**, *1*, 982; c) C. J. Aspley, J. A. G. Williams, *New J. Chem.*, **2001**, *25*, 1136; d) S. Fanni, C. Di Pietro, S. Serroni, S. Campagna, J. G. Vos, *Inorg. Chem. Commun.* **2000**, *3*, 42; f) K. O. Johansson, J. A. Lotoski, C. C. Tong, G. S. Hanan, *Chem. Commun.* **2000**, 819; g) G. R. Pabst, O. C. Pfuller, J. Sauer, *Tetrahedron* **1999**, *55*, 8045; h) S. J. Dunne, E. C. Constable, *Inorg. Chem. Commun.* **1998**, *1*, 167; i) C. Patoux, J.-P. Launay, M. Beley, S. Chodorowski-Kimmes, J.-P. Collin, S. James, J.-P. Sauvage, *J. Am. Chem. Soc.* **1998**, *120*, 3717; j) E. C. Constable, A. M. W. Cargill Thompson, S. Greulich, *J. Chem. Soc. Chem. Commun.* **1993**, 1444; k) M. Beley, J.-P. Collin, R. Louis, B. Metz, J.-P. Sauvage, *J. Am. Chem. Soc.* **1991**, *113*, 8521.

[9] The reactions to form **1** and **2** were catalyzed by $[Pd(PPh_3)_2Cl_2]$ in DMF at 110°C and 140°C, respectively: A. Suzuki, *J. Organomet. Chem.* **1999**, *576*, 147.

[10] The 5-chloro group is deactivated as it is *meta* to both nitrogens of the pyrimidine; V. Farina, V. Krishnamurthy, W. J. Scott, *The Stille Reaction*, Wiley, New York, **1998**.

[11] A boronic acid group on a ruthenium complex has been coupled with 9-bromoanthracene although the newly formed complex was not isolated in pure form: see ref [8c].

[12] M. Klessinger, J. Michl, *Excited States and Photochemistry of Organic Molecules*, Wiley, New York, **1995**.

 © 2003 Wiley-VCH Verlag GmbH & Co. KGaA, Weinheim

[13] Compounds **3** and **4** have extended lifetimes compared to that of the prototype $[Ru(tpy)_2]^{2+}$ ion, which under the same experimental conditions has a lifetime of 250 ps. This increase is partly because of the use of the extended π^* orbital, as described in ref. [5d].

[14] The energy of the triplet anthracene can be inferred by the highest-energy emission maximum of **1** and **2** at 77 K, and the energy of the ^{3}MLCT states can be approximatly equal to the highest-energy emission maximum of **3** and **4** at 77 K (Table 1). Based on these data, driving forces for the energy-transfer process are 840 and 960 cm^{-1} in **1** and **2**, respectively.

 © 2003 Wiley-VCH Verlag GmbH & Co. KGaA, Weinheim

Nanostructured Functional Materials

In Situ Incorporation of 2-(2-Hydroxyphenyl)benzothiazole within FAU Colloidal Crystals**

Svetlana Mintova, Vincent De Waele, Uli Schmidhammer, Eberhard Riedle,* and Thomas Bein**

Novel nanostructured functional materials can be constructed by encapsulation of optically active guests in microporous hosts. Incorporation of organic molecules inside the cages of zeolites permits the control of both their molecular and optical properties. To achieve this goal, it is essential to accommodate specific molecules within the voids of the zeolite structures and to create nanosized assemblies such as thin films, layers, or monolith structures for specific applications. Generally, the microporous materials used for the preparation of nanostructured assemblies are synthesized in colloidal form from clear aluminosilicate or aluminophosphate solutions, which results in a mean particle size in the range of about 20–600 nm.[1–5] Nanoscale organosilicate clusters in the precursor solutions used for the synthesis of colloidal zeolites have been observed with different techniques.[6–10] Nanoscale amorphous gel particles (with a size of 5–50 nm) are formed in the precursor solutions before long-range crystalline order is established.[3,4] Based on these insights, the encapsulation of additional organic molecules in the crystalline internal voids of zeolite structures should be possible by direct incorporation from the precursor colloidal solutions. Moreover, colloidal molecular sieves with particle sizes in the nanometer range can have high colloidal stability in different solvents with respect to further agglomeration and sedimentation. These features make the encapsulation of functional optical molecules in nanoscale zeolite suspensions an attractive synthetic goal. Such suspensions are 1) promising systems for optical investigations of host–guest interactions, and 2) interesting precursors for the construction of nanostructured assemblies such as optical coatings and selective chemical sensors. The application of nanosized zeolites opens up possibilities for the preparation of homogeneous zeolite films on many different supports, as well as inert substrates, by efficient spin-coating of stable colloidal solutions. The generation of defined porous nanocrystals with encapsulated, optically active guests provides a route to two-dimensional functional constructs for further applications, for example, in the area of optical sensors.

Molecules with excited-state intramolecular proton-transfer (ESIPT) properties constitute a promising family of potential guests in functionalized zeolite materials for applications in the area of UV filtering,[11] sensing,[12] or even molecular switching. Among the different ESIPT systems, the HBX dyes (X = S,O or NH for 2-(2-hydroxyphenyl)benzothiazole (HBT), -benzooxazole, or -benzimidazole systems, respectively) have received particular attention, and their properties are being extensively studied regarding their steady-state[13–18] and time-dependent behavior.[19] The photophysical properties of these compounds are strongly dependent on the polar and protic character of the solvent that influences the relative stability of different tautomers. In addition to their potential as molecular devices, the high sensitivity of HBX dyes to their surroundings renders them interesting probes for the specific microenvironment of the zeolite host.

Herein, we report on the in situ incorporation of HBT inside the supercages of nanosized FAU zeolites as a co-template from a precursor colloidal solution.

Nanosized FAU crystals were prepared from colloidal solutions with (HBT–FAU) and without HBT (FAU) under hydrothermal conditions (see Experimental Section). According to X-ray powder diffraction analysis, both samples correspond to the FAU zeolite-type structure (Figure 1).[4] Dynamic light scattering (DLS) studies reveal that the FAU and HBT–FAU zeolite suspensions contain only monodisperse particles with a mean hydrodynamic radius r of 60 nm and 80 nm, respectively. Figure 2 shows the distribution function analysis (DFA) data of these two colloidal suspensions. The crystalline nature and the morphology of these particles were confirmed with transmission electron microscopy (TEM). The TEM image in the inset in Figure 2 shows well-defined octahedral crystals (ca. 60 nm in size) and crystalline fringes corresponding to the FAU structure. The HBT–FAU crystals show a slight increase in the particle size from 60 to 80 nm (not shown).

[*] Dr. S. Mintova, Prof. Dr. T. Bein
Department of Chemistry
University of Munich
Butenandtstrasse 5–11, 81377 Munich (Germany)
Fax: (+49) 89-2180-77622
E-mail: svetlana.mintova@cup.uni-muenchen.de
tbein@cup.uni-muenchen.de
Prof. Dr. E. Riedle, Dr. V. De Waele, U. Schmidhammer
Lehrstuhl für BioMolekulare Optik
University of Munich
Oettingenstrasse 67, 80538 Munich (Germany)
Fax: (+49) 89-2180-9202
E-mail: eberhard.riedle@physik.uni-muenchen.de

[**] This research was supported by a Marie Curie Fellowship of the European Community program (contract no. HPMFCT-2000-00684).

 DOI: 10.1002/anie.200219900 © 2003 Wiley-VCH Verlag GmbH & Co. KGaA, Weinheim

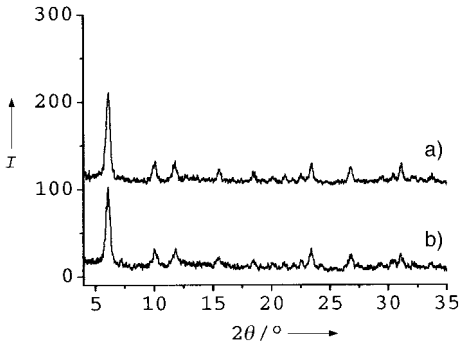


Figure 1. X-ray powder diffraction patterns of a) pure FAU and b) HBT–FAU nanocrystals.

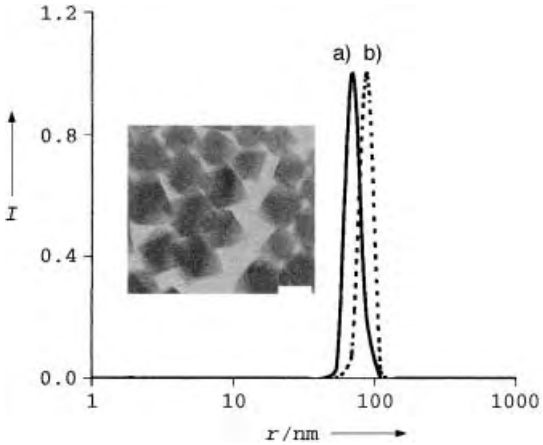


Figure 2. Distribution function analysis data based on DLS of a) pure FAU and b) HBT-FAU nanocrystals. Inset: TEM image of FAU nanocrystals; bar = 20 nm.

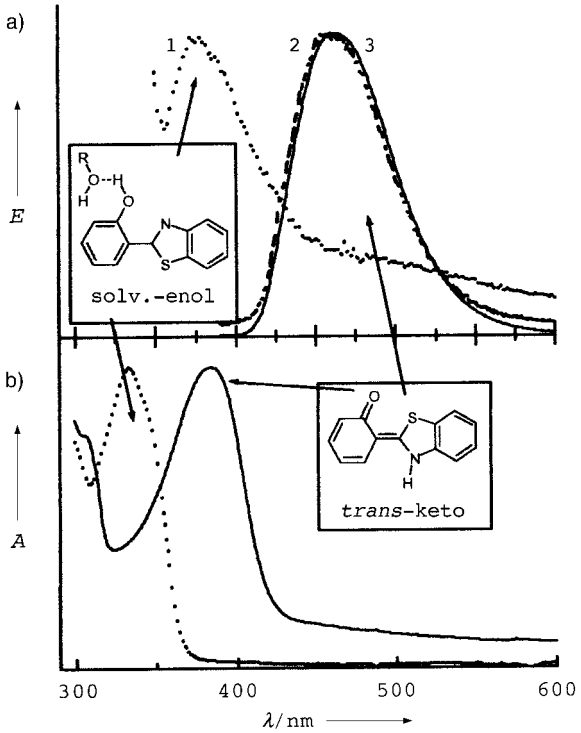


Figure 3. a) Normalized emission spectra of HBT in ethanol excited at 340 nm (trace 1) and at 380 nm (trace 2), and in the HBT–FAU sample (trace 3) excited at 380 nm. b) Absorption spectra of HBT in ethanol (•••••) and in the HBT–FAU sample (——). Insets: the solv-enol and *trans*-keto HBT conformations assigned to the observed absorption and emission spectra.

The absorption and emission spectra of the HBT–FAU and pure HBT in ethanol are depicted in Figure 3. The spectroscopic properties of HBT incorporated in FAU crystals change significantly with respect to those of HBT dissolved in pure ethanol. In ethanol HBT absorbs at 335 nm (Figure 3b), while its emission spectrum (excited at 340 nm; Figure 3a, trace 1) exhibits a maximum at 370 nm. In the HBT–FAU sample, the absorption band is at 380 nm (Figure 3b), while the emission (excited at 380 nm; Figure 3a, trace 3) exhibits a strong band centered at 465 nm. In ethanol, the strong absorption band of HBT was assigned to the solvated enol (solv-enol) tautomer, and the keto tautomer is present in trace quantities.[13–15] The keto tautomer absorbs at 380 nm and its emission is centered at 460 nm (Figure 3a, trace 2). From the comparison of the spectra shown in Figure 3a, it is evident that the solv-enol tautomer is not present in the HBT–FAU sample. Instead, in HBT-FAU we observe an absorption band at 380 nm that is characteristic of the keto tautomer. Moreover, since the emission excited at 380 nm is virtually identical for both the HBT–FAU sample and the keto trace species in ethanol (see Figure 3a, trace 2 and 3), we attribute the spectroscopic properties of HBT–FAU to the presence of the keto tautomer. Owing to the excellent match of the above spectral signatures, the alternative interpretation based on the formation of the HBT anion is excluded. Notably, the UV/Vis spectra clearly indicate that after preparation of HBT–FAU, the HBT molecules are only located in the zeolite, and not in the ethanolic solution.

As mentioned above, the properties of HBT are very sensitive to the surroundings of the molecule. This sensitivity derives from the competition between intra- and intermolecular hydrogen bonding, as well as from polarity effects that influence the relative stability of the different conformations and tautomers. The UV/Vis data clearly shows that no ESIPT process, which would require the enol ground state, occurs in the voids of zeolite Y. As mentioned above, the HBT–FAU absorbs at longer wavelength than the enol (380 nm for HBT–FAU versus 335 nm for HBT in ethanol). In addition, the usual strong red shift of the emission, which is the typical signature of the ESIPT process, was not observed. For example, in cyclohexane, the maximum of the ESIPT emission is observed at 540 nm.[19a] Thus the intramolecular hyrogen bond of HBT is broken in the zeolite, and HBT in the inner space of the FAU zeolite interacts with its microenvironment (zeolite framework or other guest molecules).

To characterize the surroundings of HBT and to provide experimental evidence for the incorporation of HBT within the FAU nanosized crystals, Raman spectra of pure FAU and HBT–FAU samples were recorded (Figure 4). Both spectra are dominated by the Raman lines assigned to the presence of tetramethylammonium (TMA) ions.[20] Moreover, numerous

 © 2003 Wiley-VCH Verlag GmbH & Co. KGaA, Weinheim

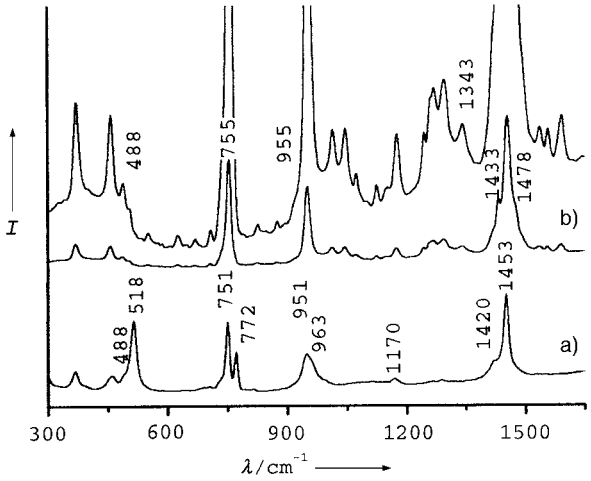


Figure 4. Raman spectra of a) FAU and b) HBT–FAU samples.

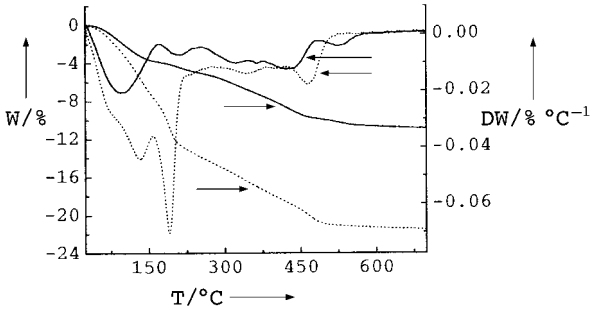


Figure 5. Thermogravimetric (W = weight loss)/differential thermogravimetric data (DW = differential weight loss) of pure FAU (——) and HBT–FAU nanocrystals (•••••) (heating rate 10 K min^{-1}, in air).

new lines due to the presence of HBT in the zeolite are observed in the Raman spectrum of the HBT–FAU sample. For example, the three Raman lines of HBT incorporated within the FAU nanocrystals at 1343, 1433, and 1478 cm^{-1} are associated with the enol–HBT lines in ethanol at 1320, 1440, and 1464 cm^{-1},[21] respectively. These three bands involve C–C stretching modes and notably the biaryl central C–C bond.[21] The displacement of the above Raman lines is attributed to the electronic reorganization of the molecule, as expected to occur during the tautomerization.

The Raman data confirm the presence of HBT in the HBT–FAU sample and also reveal a modification of the TMA ion surroundings when the faujasite is synthesized in presence of HBT. The Raman spectrum of the FAU sample displays several strong lines between 500 and 1000 cm^{-1}, whereas only two strong lines are present in the same region in the corresponding spectrum of the HBT–FAU sample. The presence of double lines around 750 and 950 cm^{-1} reflects the existence of two different conformations of the TMA ion in the FAU structure, while only two single lines at 755 and 955 cm^{-1} are observed in the Raman spectrum of HBT–FAU. This observation suggests that only one conformation or local environment of the TMA ion is present in HBT–FAU.

To probe the association of HBT and TMA molecules with the pure FAU and HBT–FAU samples, we performed thermogravimetric analysis (TGA) of washed and freeze-dried samples (Figure 5). The weight loss of the FAU sample in the temperature range 200–600 °C is 6 wt %, which is attributed to combustion of TMA (weight loss below 200 °C is attributed to the removal of zeolite-type water molecules). The TMA template in pure FAU decomposes in at least two steps, that is, at 420 and 510 °C, which may suggest different local environments of the TMA template in the FAU structure. In contrast to the thermal degradation of the pure FAU sample, that of the TMA and HBT occurs predominantly at 450 °C (9 wt %). These results point to the different local environments of the organic molecules in the two samples.

In conclusion, the dye 2-(2-hydroxyphenyl)benzothiazole (HBT) was successfully incorporated into the voids of nanoscale FAU zeolites. The mechanism of inclusion appears to involve a complex interaction between the TMA ion and HBT that occurs during the templating phase of the synthesis. UV/Vis and Raman spectroscopic data reveal that the *trans*-keto tautomer of HBT is stabilized inside this large-pore molecular sieve. The *trans*-keto tautomer exhibits highly intensive fluorescence in the zeolite, as compared to the *cis*-keto tautomer formed in solution during the ESIPT process. This indicates a profound modification of the excited-state properties, and especially the internal conversion mechanism associated with the ESIPT process. Further studies are in progress to elucidate the time-resolved photophysics of these and related functional host–guest systems.

Experimental Section

Nanosized HBT–FAU and pure FAU crystals were prepared from clear precursor solutions with the following molar compositions: FAU: 5.5 $(TMA)_2O$:2.3 Al_2O_3:10 SiO_2:570 H_2O; HBT-FAU: 0.05 HBT:2.7 $(TMA)_2O$:2.3 Al_2O_3:10 SiO_2:100 H_2O:400 EtOH.

Precursor solution for FAU: Tetramethylammonium hydroxide pentahydrate ($TMAOH{\cdot}5H_2O$) (5.18 g) was added to an aqueous solution (26.68 g water) of aluminum isopropoxide (2.44 g) to give a clear solution. Then a second solution (5.1 g) containing silica sol (30 wt %, particle size ~5 nm) was added under stirring.

Precursor solution for HBT–FAU: Tetramethylammonium hydroxide pentahydrate ($TMAOH{\cdot}5H_2O$) (2.54 g) was added to an aqueous solution (4.68 g water) of aluminum isopropoxide (2.44 g) to give a clear solution. Commercially available HBT was purified by recrystallization, dissolved in ethanol (0.030 g in 47.9 g EtOH), and then was mixed with the silica sol (5.1 g).

Synthesis of FAU[4] and HBT–FAU: The above precursor solutions were further stirred for about 60 min at room temperature. The final precursor solutions were aged on an orbital shaker (180 rpm) at room temperature for 24 h prior to further crystallization at 90 °C for 28 h. The nanosized FAU crystals resulting from this hydrothermal treatment were purified by separation from the mother liquid by three steps of centrifugation (20000 rpm, 60 min). After each step the nanoparticles were redispersed in ethanol (98 %, Aldrich) by using an ultrasonic bath for 3 h; the concentration of the solid nanocrystals in the final suspensions was about 1.5 wt %. The X-ray diffraction data were collected on a Scintag XDS 2000 diffractometer using $Cu_{K\alpha}$ radiation. The TG measurements were performed with a Setaram TG-ATD LABSYS thermal analyzer. In situ dynamic light scattering was used (ALV-NIBS/HPPS) to investigate the particle size distributions at room temperature and upon hydrothermal treatment at 90 °C. The distribution function analysis data and high-resolution transmission electron microscopy (HR-TEM)

 © 2003 Wiley-VCH Verlag GmbH & Co. KGaA, Weinheim

data provided information about the size and crystalline nature of the nanosized particles. Raman spectra of the purified and freeze-dried HBT–FAU and FAU samples were recorded on a Bruker Equinox 55 FT-Raman spectrometer (500 mW at 1064 nm; collection time 180 min). The steady-state absorption of the ethanolic solutions of HBT–FAU and FAU were measured with a Specord S100 spectrometer from Analytik Jena, while the steady-state emission spectra were recorded with a fluorescence spectrometer type Spex-Fluorolog-2.

Received: August 6, 2002
Revised: January 15, 2003 [Z19900]

Keywords: fluorescence · inclusion chemistry · microporous materials · zeolites

[1] a) B. J. Schoeman, *Zeolites* **1997**, *18*, 97; b) B. J. Schoeman, *Microporous Mesoporous Mater.* **1998**, *22*, 9,
[2] C. E. A. Kirschhock, R. Ravishankar, F. Verspeurt, P. J. Grobet, P. A. Jacobs, J. A. Martens, *J. Phys. Chem. B* **1999**, *103*, 4965.
[3] S. Mintova, N. Olson, V. Valtchev, T. Bein, *Science* **1999**, *283*, 958.
[4] S. Mintova, N. Olson, T. Bein, *Angew. Chem.* **1999**, *111*, 3400; *Angew. Chem. Int. Ed.* **1999**, *38*, 3201.
[5] S. Mintova, N. H. Olson, J. Senker, T. Bein, *Angew. Chem.* **2002**, *114*, 2670; *Angew. Chem. Int. Ed.* **2002**, *41*, 2558.
[6] C. E. A. Kirschhock, R. Ravishankar, P. A. Jacobs, J. A. Martens, *J. Phys. Chem. B* **1999**, *103,* 11 021.
[7] P. P. E. A. de Moor, T. P. M. Beelen, R. A. van Santen, *J. Phys. Chem. B* **1999**, *103*, 1639.
[8] Q. Li, B. Mihailova, D. Creaser, J. Sterte, *Microporous Mesoporous Mater.* **2001**, *43,* 51.
[9] C. E. A. Kirschhock, V. Buschmann, S. Kremer, R. Ravishankar, C. J. Y. Houssin, B. L. Mojet, R. A. van Santen, P. J. Grobet, P. A. Jacobs, J. A. Martens, *Angew. Chem.* **2001**, *113,* 2707; *Angew. Chem. Int. Ed.* **2001**, *40*, 2637.
[10] O. Regev, Y. Cohen, E. Kehat, Y. Talmon, *Zeolites* **1994**, *14*, 314.
[11] a) P. T. Chou, M. L. Martinez, S. L. Studer, *Appl. Spectrosc.* **1991**, *45*, 918; b) J. Keck, H. E. A. Kramer, H. Port, T. Hirsch, P. Fischer, G. Rytz, *J. Phys. Chem.* **1996**, *100*, 144 468; c) M. Stein, J. Keck, F. Waiblinger, H. E. A. Kramer, A. Hartschuh, H. Port, D. Leppard, G. Rytz, *J. Phys. Chem. A* **2002**, *106*, 2055.
[12] Y. Kubo, S. Maeda, S. Tokita, M. Kubo, *Nature* **1996**, *382*, 522.
[13] G. J. Woolfe, M. Melzig, S. Schneider, F. Dörr, *Chem. Phys.* **1983**, *77*, 213.
[14] M. Mosquera, J. C. Penedo, M. C. Rios Rodriguez, F. R. Rodriguez-Prieto, *J. Phys. Chem.* **1996**, *100*, 5398.
[15] E. L. Robert, J. Dey, I. M. Warner, *J. Phys. Chem. A* **1997**, *101*, 5296.
[16] T. Elsaesser, B. Schmetzer, *Chem. Phys. Lett.* **1987**, *140*, 293.
[17] C. S. Potter, R. G. Brown, *Chem. Phys. Lett.* **1988**, *153*, 7.
[18] M. M. Henary, C. J. Fahrni, *J. Phys. Chem. A* **2002**, *106*, 5210.
[19] a) W. Frey, F. Laermer, T. Elsaesser, *J. Phys. Chem.* **1991**, *95*, 10 391; b) C. Chudoba, E. Riedle, M. Pfeiffer, T. Elsaesser, *Chem. Phys. Lett.* **1996**, *263*, 622; c) S. Lochbrunner, A. J. Wurzer, E. Riedle, *J. Chem. Phys.* **2000**, *112*, 10 699; d) S. Lochbrunner, K. Stock, V. De Waele, E. Riedle, *Femtochemistry and Femtobiology: Ultrafast Dynamics in Molecular Science* (Eds.: A. Douhal, J. Santamaria), World Scientific Publishing House, Singapore, **2002**, p. 202.
[20] a) P. K. Dutta, B. Del Barco, D. C. Shieh, *Chem. Phys. Lett.* **1986**, *127*, 200; b) B. D. McNicol, G. T. Pott, K. R. Loos, *J. Phys. Chem.* **1972**, *76*, 3388; c) S. B. Hong, *Microporous Mater.* **1995**, *4*, 309.
[21] M. Pfeiffer, K. Lenz, A. Lau, T. Elsaesser, *J. Raman Spectrosc.* **1995**, *26*, 607.
[22] J. Gao, L. W. Chou, A. Auerbach, *Biophys. J.* **1993**, *65*, 43.

 © 2003 Wiley-VCH Verlag GmbH & Co. KGaA, Weinheim

Mixed-Valent Spin-Crossover System

An Unprecedented Homochiral Mixed-Valence Spin-Crossover Compound**

Yukinari Sunatsuki, Yuichi Ikuta, Naohide Matsumoto, Hiromi Ohta, Masaaki Kojima, Seiichiro Iijima, Shinya Hayami, Yonezo Maeda, Sumio Kaizaki, Françoise Dahan, and Jean-Pierre Tuchagues*

The phenomenon of spin-crossover between the low-spin (LS) and high-spin (HS) states,[1] which is observed in some octahedral $3d^n$ ($4 \leq n \leq 7$) metal complexes and is induced by an external perturbation, such as temperature, pressure, or light irradiation, is one of the most spectacular examples of molecular bistability.[2,3] Such phenomena can be utilized in new electronic devices, such as molecular memories and switches that are controlled by many different physical channels.[4,5] It is now established that cooperative spin-crossover, the interaction between spin-crossover sites, is the predominant factor governing bistability.[6,7] We now report the first homochiral mixed-valence spin-crossover compound, in which three independent properties are united, namely, mixed valence states of iron metal centers, spin-crossover of the Fe^{II} and Fe^{III} electronic structures, and homochiral assembly of the chiral $[Fe^{II}H_3L]^{2+}$ and $[Fe^{III}L]$ building blocks into a conglomerate structure (H_3L = tris{[2-{(imidazole-4-yl)methylidene}amino]ethyl}amine). Mixed valence states can allow access to several electronic states as a result of spin-crossover in both the Fe^{II} and Fe^{III} centers, and supramolecular assembly can produce a cooperative effect between the spin-crossover sites. Furthermore, optical activity can be used to observe the switching of spin states (reading process).

[*] Prof. Dr. N. Matsumoto, Y. Ikuta
Department of Chemistry, Faculty of Science, Kumamoto University, Kurokami 2-39-1, Kumamoto 860-8555 (Japan)
Fax: (+81) 96-342-3390
E-mail: naohide@aster.sci.kumamoto-u.ac.jp
Dr. Y. Sunatsuki, H. Ohta, Prof. Dr. M. Kojima
Department of Chemistry, Faculty of Science, Okayama University, Tsushima-naka 3-1-1, Okayama 700-8530 (Japan)
Dr. S. Iijima
National Institute of Advanced Industrial Science and Technology, Tsukuba 305-8566 (Japan)
Dr. S. Hayami, Prof. Dr. Y. Maeda
Division of Chemistry, Faculty of Sciences, Kyushu University, Hakozaki, Fukuoka 812-8581 (Japan)
Prof. Dr. S. Kaizaki
Department of Chemistry, Graduate School of Science, Osaka University, Machikaneyama Cho 1-1, Toyonaka 560-0043 (Japan)
Dr. F. Dahan, Prof. Dr. J.-P. Tuchagues
Laboratoire de Chimie de Coordination du CNRS, UP 8241, 205 Route de Narbonne, 31077 Toulouse cedex (France)

[**] This work was supported by a Grant-in-Aid for Science Research (No. 14340209) from the Ministry of Education, Science, Sports, and Culture, Japan, the Fund for Project Research from the Venture Business Laboratory, Graduate School of Okayama University, and the JSPS Research Fellowship for Young Scientists (Y.S.).

 © 2003 Wiley-VCH Verlag GmbH & Co. KGaA, Weinheim DOI: 10.1002/anie.200250399

Yellow-orange crystals of $[Fe^{II}H_3L](NO_3)_2{\cdot}3H_2O$ were prepared by the reaction of the tripod ligand H_3L and $Fe^{III}(NO_3)_3{\cdot}9H_2O$ in MeOH under acidic conditions, where it should be noted that with this ligand, the Fe^{II} complex is obtained from the Fe^{III} salt. When three equivalents of NaOH solution were added to a solution of $[Fe^{II}H_3L](NO_3)_2{\cdot}3H_2O$ in methanol under aerobic conditions, the color of the solution changed from yellow-orange to blue; the fully deprotonated $[Fe^{III}L]{\cdot}2.5H_2O$ was obtained as blue-black crystals. However, when only 1.5 equivalents of NaOH was added under similar conditions, the color of the solution became green, and the mixed-valence compound, $[Fe^{II}H_3L][Fe^{III}L](NO_3)_2$ (**1**) was obtained. The IR spectrum of **1** showed two intense bands at 1635 and 1603 cm^{-1} that were assigned to the C = N stretching vibration of the Schiff base ligand at room temperature, and are ascribed to the $[Fe^{II}H_3L]^{2+}$ and $[Fe^{III}L]$ species, respectively; the bands are sensitive to the oxidation and spin states of iron in both building units.

The synthetic procedure is schematically drawn in Figure 1. In accordance with what has already been observed for the analogous Co^{III} complex with the tripod ligand,[8] this synthetic procedure gives an example of the evolution of chirality.[9] The coordination of an achiral tripod ligand to a transition-metal ion yields Δ (clockwise) and Λ (anticlockwise) chiral molecules, as a result of a screw coordination arrangement of the ligand. In the iron system, deprotonation and oxidation of the $[Fe^{II}H_3L]^{2+}$ species occurred to generate the fully-deprotonated $[Fe^{III}L]$ species, which functions as a constituent component of the mixed-valence compound. Deprotonation at the imidazole moiety initiates a self-organization process that is associated with intermolecular homochiral discrimination arising from the formation of an imidazole–imidazolate hydrogen bond between the $[Fe^{II}H_3L]^{2+}$ and $[Fe^{III}L]$ species. This process results in the formation of an extended homochiral two-dimensional (2D) sheet, which, in turn, leads to a conglomerate structure, constructed through the homochiral stacking of the 2D sheets.

The crystal structure of **1** was determined at both 295 and 100 K.[10] The structure consists of two pairs of protonated $[Fe^{II}H_3L]^{2+}$ (Fe2 and Fe4) and deprotonated $[Fe^{III}L]$ (Fe1 and Fe3) species, and four nitrate counterions (Figure 2). The $[Fe^{II}H_3L]^{2+}$ and $[Fe^{III}L]$ components with octahedral N_6 coordination environments are chiral species with either the Δ or *Λ* configuration. These components act as chiral complementary building units that assemble together to form a 2D extended sheet arising from the network of imidazole–imidazolate hydrogen bonds. In this 2D supramolecular structure, the capped tripodlike $[Fe^{II}H_3L]^{2+}$ and $[Fe^{III}L]$ components form an alternate "up-and-down" array that yields a homochiral extended 2D puckered sheet based on a hexanuclear unit centered on a trigonal void. In addition, sheets with the same chirality are arranged parallel to each

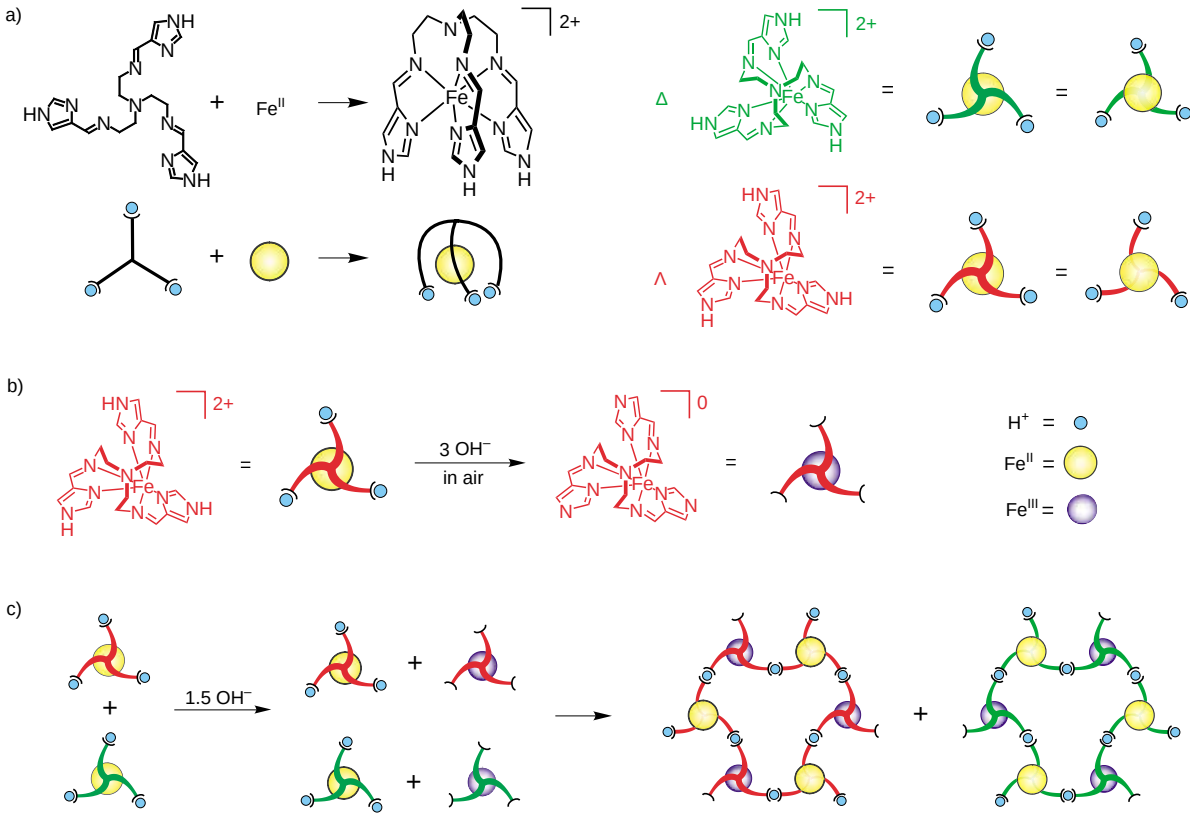


Figure 1. a) Formation of the isolated chiral molecule $[Fe^{II}H_3L]^{2+}$ (Δ and Λ) from the achiral H_3L ligand and an Fe^{II} ion. Schematic drawings are viewed along the molecular C_3 axis; b) deprotonation at the imidazole moieties of $[Fe^{II}H_3L]^{2+}$ in air generates $[Fe^{III}L]$; c) formation of a homochiral assembled hexamer which constitutes a unit of a 2D sheet. The organization process is accompanied by intermolecular homochiral discrimination between $[Fe^{II}H_3L]^{2+}$ and $[Fe^{III}L]$ units to produce an extended homochiral 2D sheet held together by imidazole–imidazolate hydrogen bonds.

 © 2003 Wiley-VCH Verlag GmbH & Co. KGaA, Weinheim

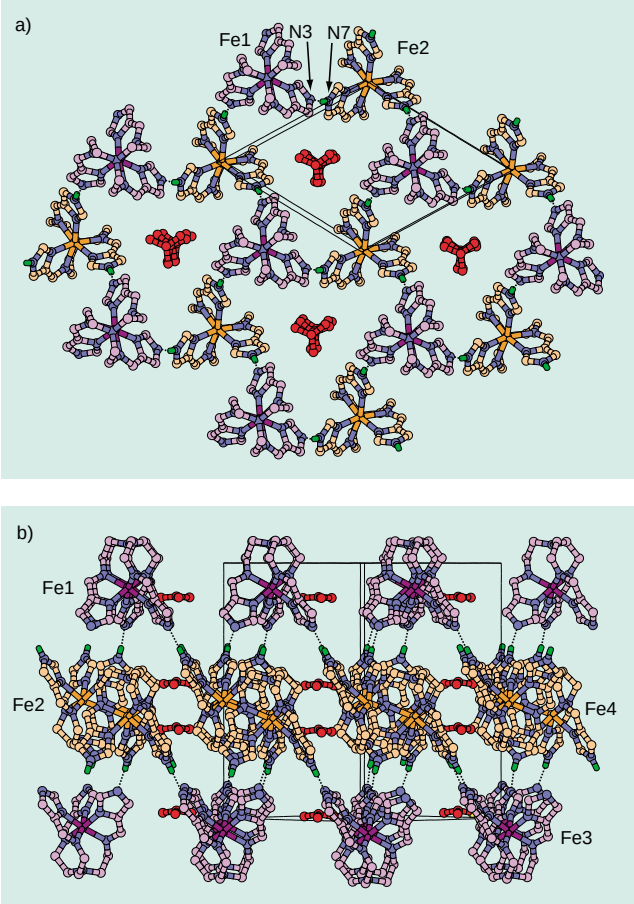


Figure 2. X-ray crystal structure of **1**. a) A view showing the homochiral 2D sheet with trigonal voids. The two complementary molecular building units having the same chirality, that is, the protonated species $[Fe^{II}H_3L]^{2+}$ (Λ enantiomer, orange) and the deprotonated species $[Fe^{III}L]^{0}$ (Λ enantiomer, purple), which are linked by hydrogen bonds and arranged alternately in an up-and-down fashion; b) a side view showing the stacking arrangement of adjacent sheets having the same chirality. Their up-and-down formation favors the stacking of adjacent sheets that have the same chirality along the *c* axis. The nitrate counterions are located in the cavities and between the sheets.

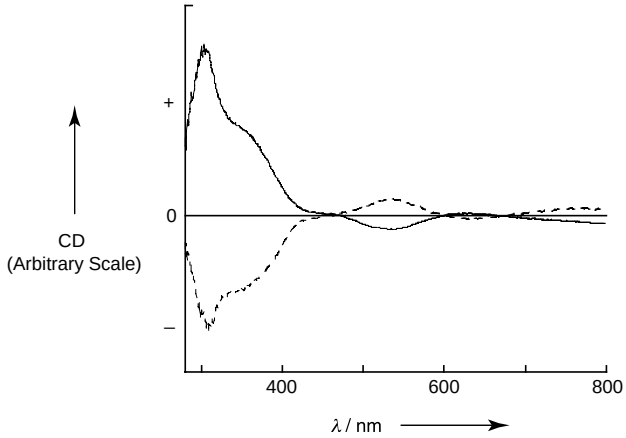


Figure 3. CD spectra of crystallites of **1** in KBr pellets. The two pellets were prepared using selected crystals, and showed enantiomeric CD patterns that provide definitive evidence that spontaneous resolution had occurred.

other, which results in a chiral (conglomerate) crystal. Enantiomeric circular dichroism (CD) spectra obtained from selected crystals provide definitive evidence that spontaneous resolution has occurred (Figure 3).

The Fe–N bond lengths for the protonated $[Fe^{II}H_3L]^{2+}$ species (Fe2 and Fe4) at 295 K range from 2.146(2) to 2.210(2) Å, which are typical values for HS Fe^{II} centers, while those at 100 K range from 2.019(2) to 2.044(2) Å, more typical for LS Fe^{II} ions. In the deprotonated $[Fe^{III}L]$ species (Fe1 and Fe3), the Fe–N bond lengths are in the range 1.974(2) to 2.023(2) Å at 295 K, and 1.926(2) to 1.996(2) Å at 100 K, both suggestive of LS Fe^{III} species. Figure 2b illustrates that there are two types of flat layers: One layer contains only $[Fe^{II}H_3L]^{2+}$ species (Fe2 and Fe4), the other layer contains only $[Fe^{III}L]$ species (Fe1 and Fe3), with both layers stacked alternately along the *c* axis.

Magnetic susceptibility measurements, Mössbauer spectra, and X-band ESR spectra provide evidence of spin-crossover in both the Fe^{II} and Fe^{III} centers. The magnetic properties are shown in Figure 4a in the form of $\chi_M T$ versus T plots, in which χ_M is the molar magnetic susceptibility and T is the absolute temperature. When the sample was warmed or cooled slowly without prior quenching at low temperature, the $\chi_M T$ value is constant at 0.4 $cm^3 K mol^{-1}$ at temperatures of 2–120 K, which is the expected spin-only value (0.38 $cm^3 K mol^{-1}$) for LS Fe^{II} ($S=0$) and LS Fe^{III} ($S=1/2$) of both the Fe^{II} ($S=0$) and Fe^{III} ($S=1/2$) sites. The $\chi_M T$ value increases rapidly in the 140 to 180 K region, which corresponds with a spin-transition at the Fe^{II} site from the LS Fe^{II} ($S=0$) to the HS Fe^{II} ($S=2$) state. The $\chi_M T$ value at 200 K was 3.6 $cm^3 K mol^{-1}$, which is in the expected range for HS Fe^{II} ($S=2$) and LS Fe^{III} ($S=1/2$) states. Above 200 K, the $\chi_M T$ value increased gradually owing to the spin transition from the LS Fe^{III} ($S=1/2$) to the HS Fe^{III} ($S=5/2$) state. X-band EPR spectroscopy indicates that the onset of the LS-to-HS transition at the Fe^{III} site occurs at around 200 K. The above data demonstrates that there are at least three accessible electronic states: LS Fe^{II}–LS Fe^{III}, HS Fe^{II}–LS Fe^{III}, and HS Fe^{II}–HS Fe^{III}. The temperature dependence of the Mössbauer spectra agreed with the magnetic susceptibility results. At 78 K, the Mössbauer spectrum consisted of two doublets exhibiting quadrupolar splitting (LS Fe^{III}: $\delta=0.20$, $\Delta E_Q=1.83$; LS Fe^{II}: $\delta=0.43$, $\Delta E_Q=0.32$ $mm s^{-1}$), which demonstrates that both the Fe^{II} and the Fe^{III} sites are in the LS state. At 140–170 K, three doublets coexist because of the existence of LS and HS Fe^{II} sites, and the LS Fe^{II} doublet disappears at 200 K. Deconvolution of the Mössbauer spectrum was performed at each temperature, and the molar fraction of the HS Fe^{II} species, measured as a function of temperature, was consistent with the magnetic susceptibility results (Figure 4b).

Considering the LS–HS switching ability of the electronic structure in the separate $[Fe^{II}H_3L]^{2+}$ and $[Fe^{III}L]$ constituents, it is clear that their supramolecular association in this mixed-valence homochiral complex not only modifies the spin-crossover of the $[Fe^{II}H_3L]^{2+}$ unit, but also triggers the spin-crossover of the otherwise low-spin $[Fe^{III}L]$ unit. Indeed,

 © 2003 Wiley-VCH Verlag GmbH & Co. KGaA, Weinheim

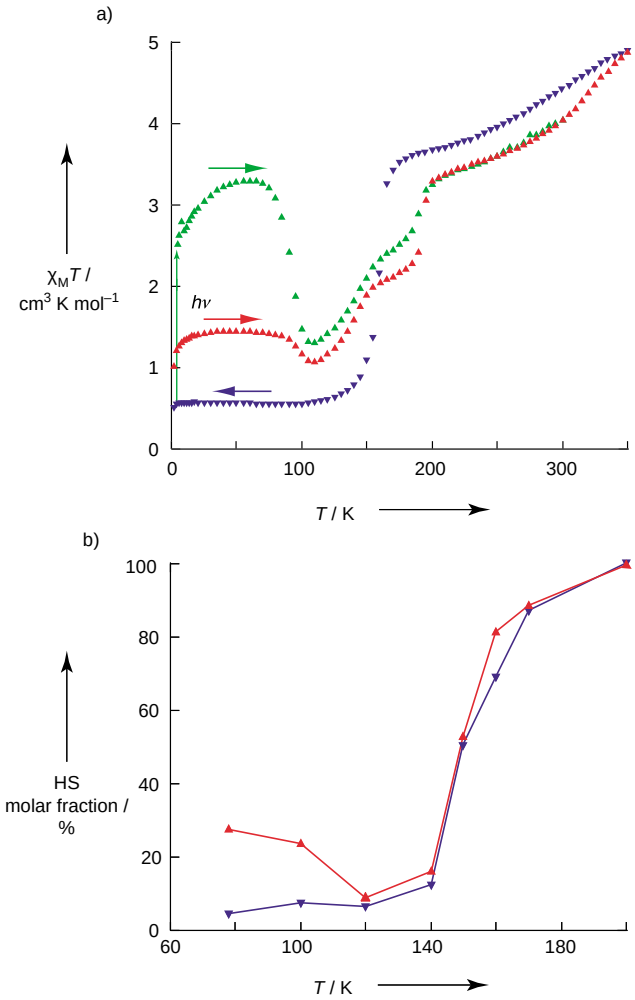


Figure 4. a) Thermal variation of $\chi_M T$ for **1** under cooling (▼) and warming (▲) modes. After quenching to 2 K, the sample was warmed (▲) and both a frozen-in effect and a two-step spin-crossover on the Fe^{II} site were observed. The ▲ symbols represent the $\chi_M T$ versus T plot that highlights the LIESST effect at 5 K and the subsequent thermal relaxation; b) the molar fraction of HS Fe^{II} versus T during cooling (▼) and warming (▲) as calculated by Mössbauer spectroscopy. When the sample was warmed after quenching to 78 K (▲), a frozen-in effect was observed.

$[Fe^{II}H_3L](NO_3)_2$ is in the HS state in its unsolvated form, and exhibits gradual spin-crossover (at 100–250 K) in its hydrated form. However, $[Fe^{III}L]\cdot 2.5\,H_2O$ is in the LS state over the entire temperature range. There must be interdependence in the LS–HS switching ability of the Fe^{II} and Fe^{III} sites. When the sample of **1** was warmed after quenching to 2 K, a "frozen-in" effect and a two-step spin-crossover at the Fe^{II} site were observed from magnetic susceptibility measurements.

Compound **1** exhibits the light-induced excited-spin-state trapping (LIESST) effect.[3] Irradiation with green light ($\lambda \approx$ 500 nm) at 5 K affords an increase in the $\chi_M T$ value, which is attributed to the spin-transition from the LS to the HS state at the Fe^{II} site. After the light is switched off, the HS Fe^{II} state is maintained at 5 K, and on warming, the thermal relaxation is complete above 100 K (Figure 4). Variable-temperature laser Raman spectroscopy[11] using an argon-ion laser ($\lambda =$ 514.5 nm) has also confirmed the LIESST effect.

Herein, we have demonstrated that a compound with bulk optical activity, spin-crossover, and mixed valency was obtained by a one-pot assembly reaction of a programmed single molecule. The conditions necessary to achieve a chiral and magnetochiral switch are thus present in this material.[12] This unprecedented combination of optical, spin-crossover, and mixed-valence properties opens up new prospects for the effective use of spin-crossover materials. For example, this chiral photochromic compound may be used in high-density optical data storage media with a nondestructive readout property. With conventional achiral optical recording media based on photochromic compounds, the data that is stored can be erased when it is exposed to the light used to read the data by UV/Vis spectroscopy (destructive readout). Our chiral material, however, provides a solution to such a problem by using an optical rotation measurement. Since the optical rotation originates from the difference in refractive indices, it can be detected at much longer wavelengths than the absorption band, and thus, we can avoid photoinduced data destruction while reading the data.

Experimental Section

1: The reaction mixture of the H_3L ligand and $Fe^{III}(NO_3)_3\cdot 9\,H_2O$ (1:1 molar ratio) in methanol was acidified with HCl and the resulting solution was allowed to stand for several days. During this time, yellow-orange crystals of $[Fe^{II}H_3L](NO_3)_2\cdot 3\,H_2O$ were obtained. An aqueous solution of NaOH was added to a warmed solution of $[Fe^{II}H_3L](NO_3)_2\cdot 3\,H_2O$ in MeOH (1.5:1 ratio). The solution was allowed to stand for several days, from which, $[Fe^{II}H_3L][Fe^{II}L](NO_3)_2$ (**1**) was obtained.

Physical measurements: Magnetic susceptibilities were measured using an MPMS5 SQUID susceptometer (Quantum Design) in the 2–350 K temperature range at a 1 K min^{-1} sweeping rate under an applied magnetic field of 1 T. For the LIESST experiment, a xenon arc lamp (Hamamatsu L7810) was used as the light source. The Mössbauer spectra were recorded by using a Wissel 1200 spectrometer and a proportional counter. A $^{57}Co(Rh)$ radioactive source was used in a constant acceleration mode. The isomer shifts are reported relative to metallic iron foil. The diffraction data were collected using an IPDS-Stoe diffractometer at 295 and 100 K. The structures were solved by direct methods and refined with full-matrix least-squares procedures using SHELXS-97. CCDC-196219 and CCDC-196220 contain the supplementary crystallographic data for this paper. These data can be obtained free of charge via www.ccdc.cam.ac.uk/conts/retrieving.html (or from the Cambridge Crystallographic Data Centre, 12 Union Road, Cambridge CB2 1EZ, UK; fax: (+44) 1223-336-033; or deposit@ccdc.cam.ac.uk).

Received: October 21, 2002 [Z50399]

Keywords: bistability · chirality · hydrogen bonds · mixed-valent compounds · spin-crossover

[1] a) L. Cambi, L. Szego, A. Cassaro, *Accad. Naz. Lincei Atti Mem. Cl. Sci. Fis. Mat. Nat. Sez. 3* **1931**, *13*, 809; b) E. König, *Prog. Inorg. Chem.* **1987**, *35*, 527; c) O. Kahn, *Molecular Magnetism*, VCH, Weinheim, **1993**.

 © 2003 Wiley-VCH Verlag GmbH & Co. KGaA, Weinheim

[2] a) O. Kahn, J. C. Martinez, *Science* **1998**, *279*, 44; b) M. Irie, *Chem. Rev.* **2000**, *100*, 1685; c) M. E. Itkis, X. Chi, A. W. Cordes, R. C. Haddon, *Science* **2002**, *296*, 1443.
[3] a) S. Decurtins, P. Gütlich, C. P. Kohler, H. Spiering, A. Hauser, *Chem. Phys. Lett.* **1984**, *105*, 1; b) P. Gütlich, A. Hauser, H. Spiering, *Angew. Chem.* **1994**, *106*, 2109; *Angew. Chem. Int. Ed. Engl.* **1994**, *33*, 2024.
[4] A. Hauser, J. Jeftic, H. Romstedt, R. Hinek, H. Spiering, *Coord. Chem. Rev.* **1999**, *190–192*, 471.
[5] a) J. A. Real, E. Andres, M. C. Munoz, M. Julve, T. Granier, A. Bousseksou, F. Varret, *Science* **1995**, *268*, 265; b) P. J. van Koningsbruggen, Y. Garcia, O. Kahn, L. Fournes, H. Kooijman, A. L. Spek, J. G. Haasnoot, J. Moscovici, K. Provost, A. Michalowicz, F. Renz, P. Gütlich, *Inorg. Chem.* **2000**, *39*, 1891; c) E. Breuning, M. Ruben, J.-M. Lehn, F. Renz, Y. Garcia, V. Ksenofontov, P. Gütlich, E. Wegelius, K. Rissanen, *Angew. Chem.* **2000**, *112*, 2563; *Angew. Chem. Int. Ed.* **2000**, *39*, 2504.
[6] a) D. Boinnard, A. Bousseksou, A. Dworkin, J.-M. Savariault, F. Varret, J. P. Tuchagues, *Inorg. Chem.* **1994**, *33*, 271; b) J.-F. Letard, J. A. Real, N. Moliner, A. B. Gaspar, L. Capes, O. Cador, O. Kahn, *J. Am. Chem. Soc.* **1999**, *121*, 10630.
[7] a) S. Hayami, Z. Gu, M. Shiro, Y. Einaga, A. Fujishima, O. Sato, *J. Am. Chem. Soc.* **2000**, *122*, 7126; b) S. Hayami, Z. Gu, H. Yoshiki, A. Fujishima, O. Sato, *J. Am. Chem. Soc.* **2001**, *123*, 11644.
[8] a) I. Katsuki, Y. Motoda, Y. Sunatsuki, N. Matsumoto, T. Nakashima, M. Kojima, *J. Am. Chem. Soc.* **2002**, *124*, 629; b) Y. Sunatsuki, Y. Motoda, N. Matsumoto, *Coord. Chem. Rev.* **2002**, *226*, 199.
[9] J. Jacques, A. Collet, S. H. Wilen, *Enantiomers, racemates and resolutions*, Wiley, New York, **1981**.
[10] Crystal data at $T = 295$ K: $Mo_{K\alpha}$ ($\lambda = 0.71073$ Å), $C_{36}H_{45}N_{22}O_6Fe_2$, $M_r = 993.64$, dimensions $0.35 \times 0.35 \times 0.25$ mm, trigonal, space group $P\bar{3}$, $a = b = 11.9138(9)$, $c = 18.9783(15)$ Å, $V = 2332.9(3)$ Å^3, $Z = 2$, $\rho_{calcd} = 1.415$ g cm^{-3}, $\mu = 0.690$ mm^{-1}, 18316 reflections collected, 5959 independent reflections, wR(all) = 0.0864, R(all) = 0.0435; Fe1-N1 2.023(2), Fe1-N2 1.985(2), Fe2-N5 2.146(2), Fe2-N6 2.210(2), Fe3-N9 2.021(2), Fe3-N10 1.974(2), Fe4-N13 2.172(3), Fe4-N14 2.196(2) Å. Crystal data at $T = 100$ K, trigonal, space group $P\bar{3}$, $a = b = 11.6475(9)$, $c = 18.7992(16)$ Å, $V = 2208.7(3)$ Å^3, $Z = 2$, $\rho_{calcd} = 1.494$ g cm^{-3}, $\mu = 0.729$ mm^{-1}, 17219 reflections collected, 5603 independent reflections, wR(all) = 0.0679, R(all) = 0.0361, Fe1-N1 1.9963(15), Fe1-N2 1.9268(16), Fe2-N5 2.0279(19), Fe2-N6 2.0263(16), Fe3-N9 1.9908(15), Fe3-N10 1.9262(15), Fe4-N13 2.0439(18), Fe4-N14 2.0192(16) Å.
[11] N. Suemura, M. Ohama, S. Kaizaki, *Chem. Commun.* **2001**, 1538.
[12] P. Gütlich, Y. Garcia, T. Woike, *Coord. Chem. Rev.* **2001**, *219–221*, 839.

 © 2003 Wiley-VCH Verlag GmbH & Co. KGaA, Weinheim

Nanoparticle-Coated Electrodes

A Breakthrough in the Safety of Lithium Secondary Batteries by Coating the Cathode Material with $AlPO_4$ Nanoparticles **

Jaephil Cho, Young-Woon Kim, Byoungsoo Kim, Joon-Gon Lee, and Byungwoo Park**

The production of lithium secondary batteries (Li-ion and Li-polymer cells) has rapidly expanded because of their applicability to mobile electronics, such as cellular phones, camcorders, personal digital assistants (PDAs), and notebook personal computers. Sales of Li secondary batteries were expected to increase to more than 1 billion cells in 2002. Even though most Li secondary batteries use $LiCoO_2$ as a cathode material, because of its high volumetric energy density and excellent high-temperature performance (such as the cycle life at 60 °C and swelling characteristics at 90 °C), their safety is still a major concern, and are less safe as the capacity of the battery increases.[1,2] In particular, one of the unsolved problems that can occur during operation, abrupt overcharge to the voltage-supply limit (12 V) owing to a defect or a malfunction in the protective devices[+] of the cell, has not been prevented. Moreover, numerous battery accidents with accompanying fires and explosions have been reported.[3] The main cause of such disasters is that $LiCoO_2$ cathodes can undergo a violent exothermic reaction with the electrolyte during overcharge, which may result in the cell short-circuiting. In addition, lithium deposited on the graphite anode accelerates the reaction, and results in a sharp rise in temperature.[4–6] Furthermore, this process converts $LiCoO_2$ into the strong oxidizing agent Co_2O_3, which releases oxygen during overcharging. A combination of the temperature increase and the internal short circuit of the cell eventually results in an explosion of the cell. In spite of this, no fundamental solution has been found. In particular, Li-ion batteries using a laminated film case are more susceptible to these hazards during an overcharge than those using an

[*] Prof. Dr. J. Cho
Department of Applied Chemistry
Kumoh National Institute of Technology
Gumi 730-701 (Korea)
Fax: (+82) 54-467-4477
E-mail: jpcho@kumoh.ac.kr

Prof. Dr. B. Park, Prof. Dr. Y.-W. Kim, B. Kim, J.-G. Lee
School of Materials Science and Engineering
Research Center for Energy Conversion and Storage
Seoul National University, Seoul 151-744 (Korea)
Fax: (+82) 2-885-9671
E-mail: byungwoo@snu.ac.kr

[**] This work was supported by the Kumoh National Institute of Technology and KOSEF through the Research Center for Energy Conversion and Storage at Seoul National University.

[+] Protective devices consist of a positive temperature coefficient (PTC) material and protective circuits that block the overcharging above 4.2 V, the overdischarging below 3 V, and the overcurrent above 1 C.

 © 2003 Wiley-VCH Verlag GmbH & Co. KGaA, Weinheim DOI: 10.1002/anie.200250452

aluminum case, because the former is not able to withstand the severe deformation of the electrodes.

There have been many reports of the surface modification of nanoparticles with a functional monolayer or a polymer shell that tailors their surface properties.[7–12] In contrast, a nanoparticle coating on oxides or other inorganic compounds has remained a technical challenge, and has not been reported in the literature. In this communication, we report a drastic improvement in both the safety and the electrochemical properties of $LiCoO_2$ cathodes by applying a direct coating of $AlPO_4$ nanoparticles from an aqueous solution.

The overcharge safety tests were conducted following guidelines set out for the safety evaluation of secondary lithium cells. The guidelines require that although the casing of the cells may become swollen, the cells should not explode or catch fire.[13,14] Figure 1 shows the voltage and temperature profiles of the cell with both bare $LiCoO_2$ cathodes and cathodes coated with $AlPO_4$ nanoparticles, in addition to the cell morphologies after the overcharge test. The cells used for the 12 V overcharge safety test were initially charged to 4.2 V, and subsequently charged to 12 V at a rate of 1 C (equivalent to 140 mA g^{-1} = 1.6 A). The cells were then maintained at that voltage for 2 h.

Figure 2 shows transmission electron microscopy (TEM) images of the $AlPO_4$ nanoparticle-coated $LiCoO_2$. As shown in Figure 2a, a nanoscalar $AlPO_4$ layer (approximately 15 nm) was coated homogeneously over the $LiCoO_2$ surface, and energy-dispersive spectroscopy (EDS) confirms the Al and P components of the coating layer. Figure 2b displays a high-resolution TEM image showing $AlPO_4$ nanoparticles embedded in the nanoscalar coating layer. The layer consisted of randomly oriented $AlPO_4$ nanoparticles with an average

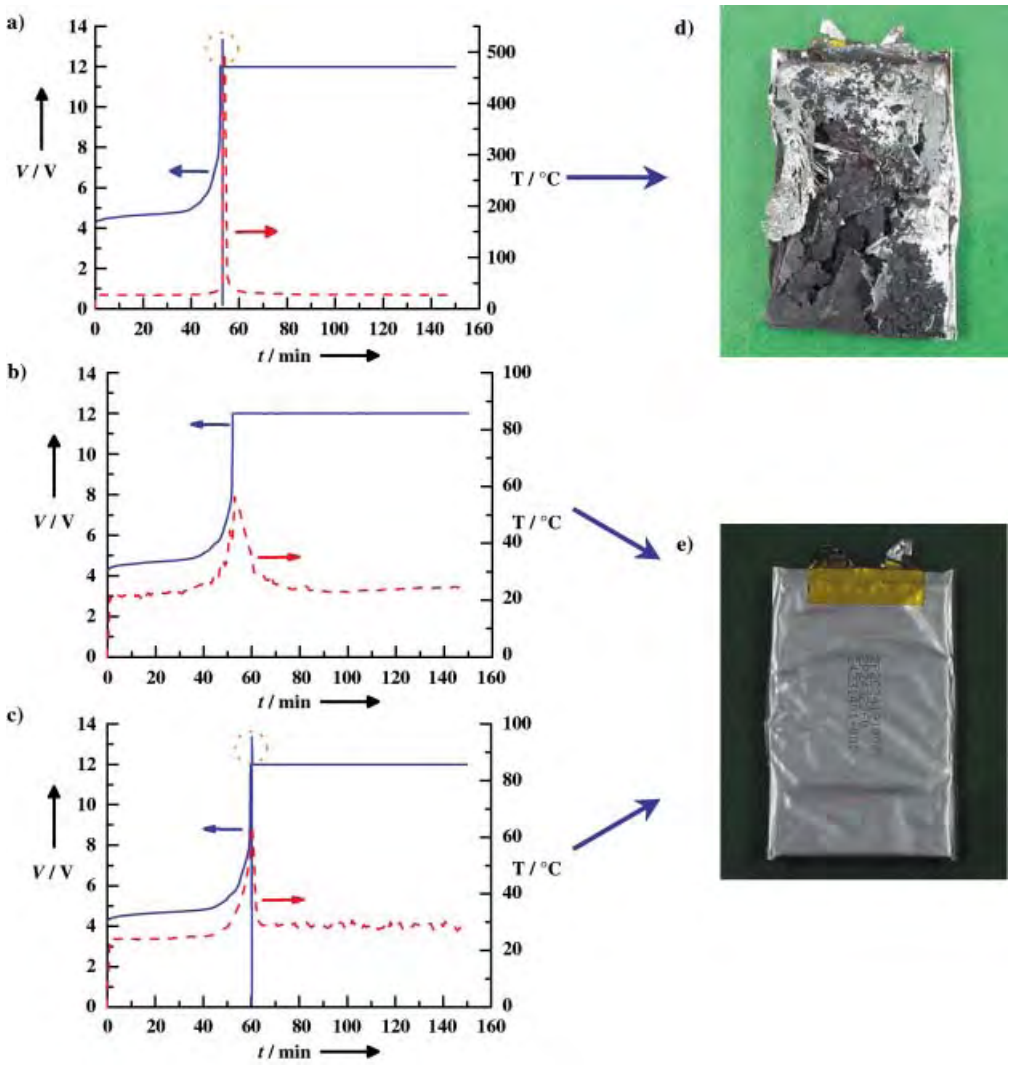


Figure 1. a) Voltage and temperature profiles of a cell with a bare $LiCoO_2$ cathode, as a function of time. All the cells were initially charged to 4.2 V, then charged to 12 V at a rate of 1 C (equivalent to 140 mA g^{-1} = 1.6 A), and then maintained at that voltage for 2 h. Cells with bare cathodes exhibit an abrupt voltage drop to 0 V resulting from a short circuit and a rapid temperature increase to approximately 500 °C; b, c) temperature and voltage profiles of a cell with an $AlPO_4$ nanoparticle-coated $LiCoO_2$ cathode. Even though the cell had a short circuit (Figure 1c), the temperature only increased to approximately 60 °C without burning; d) a picture of a cell containing a bare $LiCoO_2$ cathode after the 12 V overcharge test; the cell burned and exploded at that voltage. e) a picture of a cell containg the $AlPO_4$ nanoparticle-coated $LiCoO_2$ after the 12 V overcharge test.

 © 2003 Wiley-VCH Verlag GmbH & Co. KGaA, Weinheim

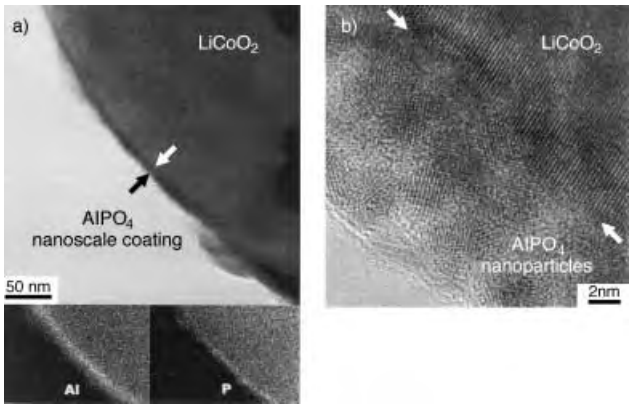


Figure 2. a) TEM bright-field image of the $AlPO_4$ nanoparticle-coated $LiCoO_2$; EDS confirms the Al and P components in the coating layer. b) High-resolution TEM image showing the $AlPO_4$ nanoparticles (≈3 nm in diameter) in the nanoscale coating layer; the arrows indicate the interface between the $AlPO_4$ layer and $LiCoO_2$.

diameter of approximately 3 nm, with a regular distribution of Al and P components throughout the layer. X-ray diffraction patterns of the $LiCoO_2$ powders, before and after coating, and after annealing, were identical even though it was not possible to rule out the formation of other phases or interdiffusion. While Figure 2b shows $AlPO_4$ nanoparticles embedded in the amorphous phase, the exact stoichiometry and phases of both the nanoparticle and the matrix need to be identified, which will aid the understanding of any reaction between $LiCoO_2$ and the $AlPO_4$ nanoparticle layer at 700 °C.

Figure 1 shows the voltage and cell-surface temperature profiles during the 12 V overcharge test. Overcharging to this voltage increases the electrolyte decomposition rate, and the internal cell resistance (joule heat) increases because of electrolyte decomposition. At 12 V, a separator melts down and shrinks when the temperature inside the cell increases to approximately 120 °C. Therefore, any direct contact of the anode and cathode electrodes induces a short circuit. This has been the problem in cells with a bare $LiCoO_2$ cathode, as shown in Figure 1a. Electrolyte decomposition occurs at a plateau of approximately 5 V, followed by a rapid increase in the cell voltage to 12 V. Immediately after the cell voltage reaches 12 V, an internal short circuit occurs (note the abrupt voltage drop to 0 V), and the surface temperature increases to almost 500 °C, which results in a fire and an explosion of the cell (Figure 1d). All 15 cells without a nanoparticle coating exhibited the same failure pattern. This result shows that thermal runaway from cathode decomposition during accidental overcharging must be avoided. Nanoscalar metal oxides (Al_2O_3 or ZrO_2) as a coating layer on $LiCoO_2$ powders have been tried as they are less reactive against the electrolyte.[15,16] Even though the metal-oxide coatings are able to enhance the electrochemical properties, they failed to improve the thermal stability during overcharging. Aluminum phosphates have been reported to have a good chemical stability. Therefore, a surface coating of such materials is a potential candidate for improving the corrosion resistance.[17–19] When the $AlPO_4$ nanoparticles were coated uniformly on the cathode, the cells did not exhibit any short-circuiting problems after being maintained at 12 V for up to 2 h (Figure 1b). However, the cell case, with a surface temperature of approximately 60 °C, was swollen because of electrolyte decomposition. Furthermore, even with an instant short circuit, the voltage recovered to 12 V instantly and the surface temperature did not exceed 60 °C (Figure 1c), with the result that no explosion was observed (Figure 1e). These findings show that the nanosized $AlPO_4$ coating layer remains stable, with a double layer (Helmholtz and diffuse layers) exhibiting a steep voltage drop within a few nm.[20] The reason that the $AlPO_4$ nanoparticle-coated $LiCoO_2$ is superior to bare $LiCoO_2$ or other metal-oxide coated cathodes, may be attributed to the strong P=O bond (bond energy = 5.64 eV), which is very resistant to chemical attack.[17–19] High thermal stability of the $AlPO_4$ nanoparticle layer can be attributed to the strong covalency of the PO_4 polyanions with the Al^{3+} ions in $AlPO_4$.[19] Differential scanning calorimetry (DSC) analysis of the $AlPO_4$-coated $LiCoO_2$ (charged to 4.3 V) exhibited an increased onset temperature of exothermic reaction by approximately 50 °C, with a drastic decrease of heat generation by approximately one order of magnitude, when compared to bare $LiCoO_2$. The effect of $AlPO_4$ concentration on the thermal stability is currently being evaluated.

Furthermore, the electrochemical properties of the $AlPO_4$ nanoparticle-coated $LiCoO_2$ are superior to bare $LiCoO_2$ or to Al_2O_3-coated cathodes, prepared using sol–gel techniques.[15,16] As shown in Figure 3, the $AlPO_4$ nanoparticle-coated $LiCoO_2$ shows approximately 99% retention of capacity at 1 C (equivalent to 140 mA g^{-1}), even after 20 cycles, whereas the bare $LiCoO_2$ gives only 88% retention. This result is also better than that reported for Al_2O_3-coated $LiCoO_2$ at a charging rate of 0.5 C (~94%).[16] In contrast to Al_2O_3- and ZrO_2-coated $LiCoO_2$, the $AlPO_4$ nanoparticle coating did not suppress *c*-axis expansion (approximately

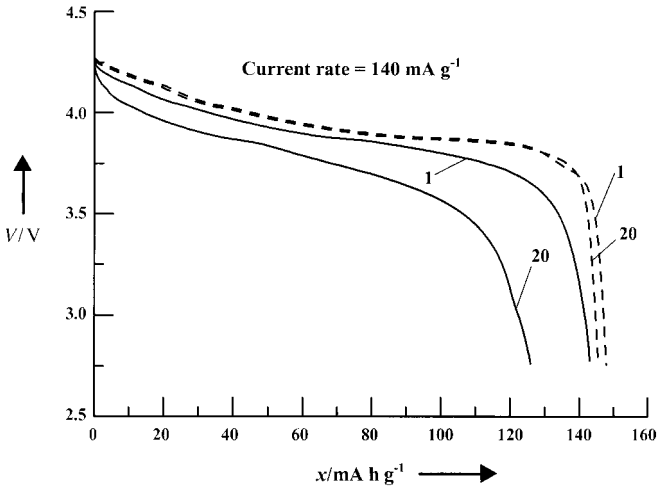


Figure 3. Voltage profiles of coin-type half cells with bare (——) and $AlPO_4$ nanoparticle-coated $LiCoO_2$ (----) cathodes between 4.3 V and 2.75 V, after the first and twentieth charge cycles; the anode of the half cell was Li metal. After 0.1 C charging and discharging rates for the first two cycles, the charge and discharge current rates were 1 C (equivalent to 140 mA g^{-1}).

 © 2003 Wiley-VCH Verlag GmbH & Co. KGaA, Weinheim

2.6%). More detailed experiments regarding lattice constants are currently under way.

The remarkable improvements described herein can provide more tolerable cell design to battery manufacturers and hazard-free portable electronics to users. The simple process of using a water-based nanoparticle solution to prepare a nanoscalar coating on the cathode material can be easily extended to mass production.

Experimental Section

$Al(NO_3)_3 \cdot 9H_2O$ (3 g) and $(NH_4)_2HPO_4$ (1 g) were dissolved in distilled water until a white suspension (of $AlPO_4$ nanoparticles) was obtained. $LiCoO_2$ powders (with an average particle size of $\approx$ 10 μm) were then slowly added to the coating solution and were mixed until the final viscosity of the slurry reached approximately 100 poise. The weight ratio of $AlPO_4$ and $LiCoO_2$ was 3:97. The $LiCoO_2$ powders were obtained from Nippon Chemicals, and inductively coupled plasma (ICP) analysis showed that the Li content in Li_xCoO_2 was 1.0. Subsequently, the slurry was poured into a tray, dried in an oven for 6 h at 130 °C, and annealed at 700 °C for 5 h in a furnace. Several-hundred Li-ion batteries with bare and $AlPO_4$ nanoparticle-coated $LiCoO_2$ cathodes were assembled using an automated pilot production line in a clean room. The cell standard capacity was set at 1600 mA h (cell size: $3.2 \times 85 \times 53$ mm^3). $AlPO_4$ nanoparticle-coated $LiCoO_2$ or bare $LiCoO_2$ was used as the cathode, and the anode material was synthetic graphite. The electrolyte used was 1.03 M $LiPF_6$ in ethylene carbonate/diethylene carbonate/ethyl methyl carbonate (EC/DEC/EMC; 3:3:4 v/v/v).

Received: October 29, 2002 [Z50452]

Keywords: coatings · electrochemistry · electrodes · lithium · safety

[1] J.-M. Tarascon, M. Armand, *Nature* **2001**, *414*, 359 – 367.
[2] a) *Advanced Rechargeable Battery Industry 2001/02*, Nomura Research Institute Ltd., **2002**; b) *Annual Report on Sales of Li Secondary Battery in 2002*, Samsung SDI Co. Ltd., **2001**.
[3] a) "Laptop Batteries Are Linked to Fire Risk": New York Times, March 15, **2001**; b) US Consumer Product Safety Commission (http://www.cpsc.gov/cpscpub).
[4] R. A. Leising, M. J. Palazzo, E. S. Takeuchi, K. J. Takeuchi, *J. Electrochem. Soc.* **2001**, *148*, A838-A844.
[5] H. Maleki, S. A. Hallaj, J. R. Selman, R. B. Dinwiddie, H. Wang, *J. Electrochem. Soc.* **1999**, *146*, 947 – 954.
[6] Ph. Biensan, B. Simon, J. P. Pérès, A. de Guibert, M. Broussely, J. M. Bodet, F. Perton, *J. Power Sources* **1999**, *81–82*, 906 – 912.
[7] R. P. Andres, T. Bein, M. Dorogi, S. Feng, J. I. Henderson, C. P. Kubiak, W. Mahoney, R. G. Osifchin, R. Reifenberger, *Science* **1996**, *272*, 1323 – 1325.
[8] C. B. Murray, C. R. Kagan, M. G. Bawendi, *Science* **1995**, *270*, 1335 – 1338.
[9] L. N. Lewis, *Chem. Rev.* **1993**, *93*, 2693 – 2730.
[10] X. Peng, T. E. Wilson, A. P. Alivisatos, P. G. Schultz, *Angew. Chem.* **1997**, *109*, 113 – 115; *Angew. Chem. Int. Ed. Engl.* **1997**, *36*, 145 – 147.
[11] A. P. Alivisatos, K. P. Johnsson, X. Peng, T. E. Wilson, C. J. Loweth, M. P. Bruchez, Jr., P. G. Schultz, *Nature* **1996**, *382*, 609 – 611.
[12] T. Cassagneau, F. Caruso, *Adv. Mater.* **2002**, *14*, 732 – 736.
[13] *Guideline for the Safety Evaluation of Secondary Lithium Cells*, Japan Battery Association, **1997**.
[14] *A Safety Standard for Lithium Batteries, UL1642*, 3rd ed., Underwriters Laboratories, **1995**.
[15] J. Cho, Y. J. Kim, T.-J. Kim, B. Park, *Angew. Chem.* **2001**, *113*, 3471 – 3473; *Angew. Chem. Int. Ed.* **2001**, *40*, 3367 – 3369.
[16] J. Cho, Y. J. Kim, B. Park, *Chem. Mater.* **2000**, *12*, 3788 – 3791.
[17] P. K. Rastogi, Y.-W. Kim, *J. Appl. Phys.* **1985**, *57*, 4223 – 4225.
[18] S. W. Martin, Ph.D. Thesis, Purdue University, **1986**.
[19] *Encyclopedia of Inorganic Chemistry, Vol. 1* (Ed.: R. B. King), Wiley, New York, **1994**, pp. 302 – 305.
[20] A. J. Bard, L. R. Faulkner, *Electrochemical Methods: Fundamentals and Applications*, 2nd ed., Wiley, New York, **2001**, pp. 544 – 554.

 © 2003 Wiley-VCH Verlag GmbH & Co. KGaA, Weinheim

Carbon Nanorings

All-Hydrocarbon Inclusion Complexes of Carbon Nanorings: Cyclic [6]- and [8]Paraphenyleneacetylenes**

Takeshi Kawase, Yohko Seirai, Hossein R. Darabi, Masaji Oda,* Yasuyuki Sarakai, and Kohji Tashiro**

The discovery and large-scale synthesis of fullerenes[1] has aroused renewed interest in π-conjugated systems on curved surfaces. The subsequent discovery of layered carbon nanotubes,[2,3] bucky onions,[4] and the "fullerene peapod"[5] has raised questions about the nature of the attractive force involved in the layering of curved π-conjugated systems. However, the poor solubility of these substances has prohibited detailed studies that might answer such questions. Suitable model compounds would be needed—in this context, fullerenes, corannulene,[6] and related compounds,[7,8] as well as belt-shaped molecules[9] have been studied both experimentally and theoretically—however, the question has remained to be answered clearly. We have recently reported the synthesis and spectroscopic characterization of cyclic paraphenyleneacetylenes, [6]CPPA (**1**) and [8]CPPA (**2**), as strained but isolable compounds.[10] Semi-empirical calcula-

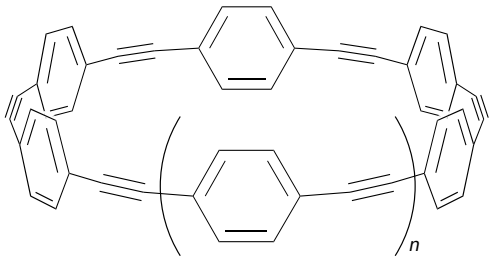
[*] Prof. Dr. T. Kawase, Prof. Dr. M. Oda, Y. Seirai, Dr. H. R. Darabi
Department of Chemistry
Graduate School of Science, Osaka University
Toyonaka, Osaka 560-0043 (Japan)
Fax: (+81) 6-6850-5387
E-mail: tkawase@chem.sci.osaka-u.ac.jp
moda@chem.sci.osaka-u.ac.jp

Prof. Dr. K. Tashiro, Y. Sarakai
Department of Macromolecular Science
Graduate School of Science, Osaka University
Toyonaka, Osaka 560-0043 (Japan)
Fax: (+81) 6-6850-5453
E-mail: ktashiro@chem.sci.osaka-u.ac.jp

[**] This work was supported by a Grant-in-Aid for Scientific Research (No. 10146102 and 14340197) and from the Ministry of Education, Science, Sports, and Culture, Japan.

 DOI: 10.1002/anie.200250727 © 2003 Wiley-VCH Verlag GmbH & Co. KGaA, Weinheim

tions (AM1 and PM3) predict that they have cylindrical structures with diameters of 1.31 and 1.74 nm, respectively, and thus may be termed "carbon nanorings", which would serve as good model compounds for carbon nanotubes. Here we report the X-ray crystallographic characterization of inclusion complexes of **1** with hexamethylbenzene (HMB) and **2** with four toluene (Tol) molecules, which are the first all-hydrocarbon inclusion complexes of cylindrical conjugated systems.



1 (n = 1); **2** (n = 3)

Crystallization from a solution of [6]CPPA (**1**) in dichloromethane/hexane containing a stoichiometric excess of HMB (approximately 5 equiv) afforded the 1:1 inclusion complex **1**·HMB as distorted hexagonal prisms (decomp. 156 °C).[11] Similarly, a solution of [8]CPPA (**2**) in toluene furnished the 1:4 inclusion complex **2**·4 Tol as prismatic single crystals.[12] In contrast to HMB, hexachlorobenzene, the molecular size of which (van der Waals diameter, $D = 9.7$ Å) is almost the same as that of HMB ($D = 9.8$ Å), failed to yield a crystalline complex with **1**. While the fine needlelike crystals of **1** obtained from benzene or carbon tetrachloride are sensitive to air (oxygen) even at low temperatures,[10] it is notable that the crystals of **1**·HMB are fairly stable in air at room temperature. On the other hand, crystals of **2**·4 Tol tend to effloresce with the loss of the toluene molecules at around room temperature. Crystals were, therefore, loaded in sealed capillaries for X-ray analysis.

Figure 1 shows the structures of the inclusion complexes. There are a number of notable features in the results: First, the host molecules **1** and **2** have fairly smooth cylindrical structures, as predicted by theoretical calculations, with bent triple bonds and shallow benzene rings in a boat conformation (Table 1). The average bond angle of the sp carbon atoms of **1** (164.3°) and **2** (168.6°) are similar to those found in the strained but fairly stable cyclooctyne (165°)[13] and [2.2.2.2]metacyclophanetetrayne (168.8°);[14] the high stability of the **1**·HMB complex seems reasonable from the above results. Second, while the cyclic paraphenyleneacetylene moiety of **1**·HMB is almost circular when viewed from above and slightly oblique from a side-on view, its counterpart in **2**·4 Tol is rather elliptical, with a more upright geometry. Since the ring sizes of **1** and **2** are very large relative to their constituent carbon–carbon bonds, the carbon nanorings would be expected to be considerably flexible and, hence, susceptible to deformation by the packing forces within the crystals. Therefore, the relatively high reactivity of **1** and **2** after efflorescence would result from the flexibility as well as the ring strain of these compounds. Third, the cavity size of **1**

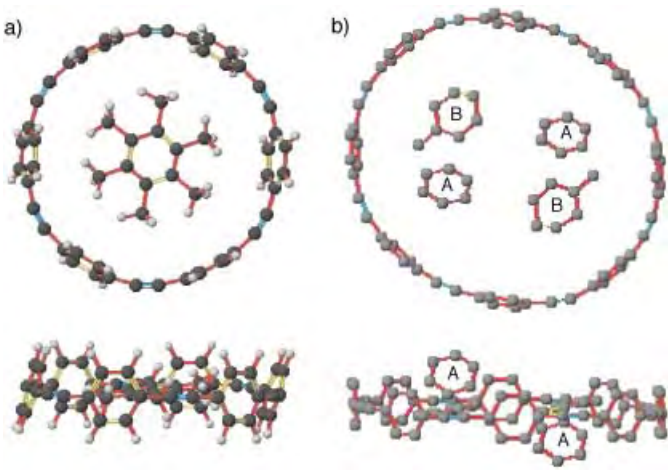


Figure 1. Molecular structures of: a) **1**·HMB and b) **2**·4 Tol. The protons as well as the methyl carbon atoms of toluene molecules A in the **2**·4 Tol complex have been removed for clarity. A and B indicate toluene molecules with different spatial geometries.

Table 1: Structural parameters of host molecules of the reported inclusion complexes.

	1	**2**
long axis [Å]	13.3	18.4
short axis [Å]	13.0	16.3
average bond angles of sp carbon atoms [°]	162.5, ≈165.6 (164.4)	164.3, ≈171.4 (168.6)
twist angles of benzene rings [°][a]	1, −9, 17	1, 2, 2, 5
bend angles of benzene rings [°][b]	151.9, 149.2, 149.5	160.5, 157.6, 156.6, 154.0

[a] Evaluated from dihedral angles between least-square planes. [b] The angles between the two *para*-benzyl bonds of each boat-form benzene ring.

is comparable to that of (10,10) carbon nanotubes (13.8 Å),[15] and that of **2** is larger than that of well-known tubular host molecules, such as [8]calixarenes,[16] cyclic oligosaccharides (cyclodextrins),[17] and cyclic peptides.[18] Fourth, the crystal structures (Figure 2) can be classified as possessing a γ structure, similar to those of coronene and kekulene,[19] in which the host molecules overlap each other in a parallel-displaced manner. In both complexes, diphenyleneacetylene units

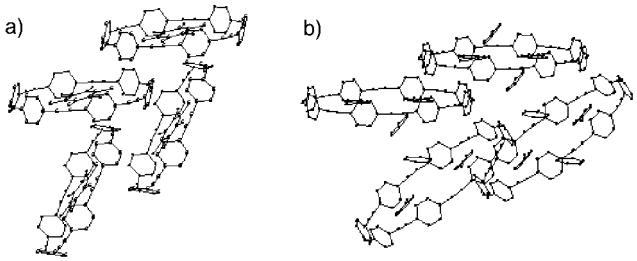


Figure 2. Crystal packing of: a) **1**·HMB and b) **2**·4 Tol. The protons of both complexes have been omitted for clarity as have the methyl carbon atoms of the toluene molecules A in the **2**·4 Tol compound.

 © 2003 Wiley-VCH Verlag GmbH & Co. KGaA, Weinheim

interlock each other, rather like gear wheels. Therefore, these crystals do not possess any open channels that result from the arrangement of the host molecules.

In complex **1**·HMB, the guest HMB molecule is situated at the center of the cavity of **1**, tilted at 9° from the horizontal plane of the host ring. Although no particularly short contacts are seen, there are contacts close to the van der Waals distance between the carbon framework of **1** and the methyl groups of the HMB moiety (3.7–3.8 Å).

In contrast, there are two pairs of toluene molecules with differing spatial geometry in complex **2**·4Tol: One pair of toluene molecules (A; see Figure 1) is situated at the severely bent sites of the elliptical cylinder and the molecules are only moderately tilted (12°), while those of the other pair (B) are somewhat disordered and are tilted to a greater extent. The A-type toluene molecules appear to act as an adhesive between the neighboring host molecules through multiple edge-to-face interactions (Figure 3); the π face of a guest

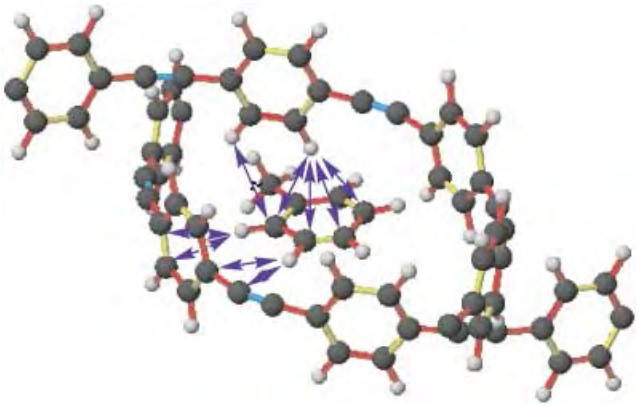


Figure 3. A partial molecular structure of **2**·4Tol. Short contacts (less than 3.2 Å) between **2** and the toluene molecule A are indicated with blue arrows.

molecule is in contact with the edge of an aromatic ring of a neighboring host molecule (the closest C···H contact is 3.0 Å), and the edge of the guest is also in contact with the inner surface of the host (the closest C···H contact of this variety is 2.9 Å). The rapid efflorescence of the crystal may be a result of the higher mobility of the disordered B-type toluene molecules.

It is noteworthy that although CPPAs **1** and **2** form the complexes **1**·HMB and **2**·4Tol as crystalline substances, spectroscopic studies (electronic absorption and ^{1}H NMR) have provided little evidence for the complexation between the host and guest molecules in nonpolar solvents such as benzene and chloroform. Therefore the attractive force between the host and guest molecules or their association constants must be weak or small, respectively. Nevertheless, the formation of such crystalline complexes indicates the existence of an attractive force between the hosts and guests.

Theoretical studies predict that curved aromatic hydrocarbons would be polarized owing to the unsymmetrical nature of their π orbitals.[7c,20–22] It has been reported, however, that a semi-empirical calculation (AM1) and a density functional calculation (BP/DN**) gave inconsistent predictions for the electrostatic potential on the inside surface of corannulene.[7c]

In view of the higher electronegativity of an sp^2 carbon atom, as compared to its sp^3 counterpart, and the hyperconjugative property of a methyl group, the methyl protons of HMB and toluene and the aromatic protons of toluene should be positively charged, though only very slightly.[23] On the contrary, hexachlorobenzene, which failed to form a crystalline complex, should take on partial negative charge on the outer chlorine atoms. Thus, the attractive force in the complexes **1**·HMB and **2**·4Tol, although weak, would be best understood when assuming that the concave surfaces of the carbon nanorings **1** and **2** have an electrostatically negative potential. Polarization of the π-conjugated systems of **1** and **2** is further supported by the formation of significantly stable complexes between **1** and fullerenes, which are reported in the accompanying paper.[24]

Received: December 9, 2002 [Z50727]

Keywords: cyclophanes · host–guest systems · inclusion compounds · noncovalent interactions

[1] H. W. Kroto, J. R. Heath, S. C. O'Brien, R. F. Curl, R. E. Smalley, *Nature* **1985**, *318*, 162–164; W. Krätschmer, L. D. Lamb, K. Fostiropoulos, D. R. Huffman, *Nature* **1990**, *347*, 354–358.

[2] S. Iijima, *Nature* **1991**, *354*, 56–58; S. Iijima, T. Ichibashi, Y. Ando, *Nature* **1992**, *356*, 776–778; P. M. Ajayan, S. Iijima, *Nature* **1993**, *361*, 333–334.

[3] J. Sloan, M. L. H. Green in *Fullerenes* (Eds.: K. M. Kadish, R. S. Ruoff), Wiley, New York, **2000**, pp. 795–838.

[4] H. W. Kroto, *Science* **1988**, *242,* 1139–1145; D. Ugarte, *Nature* **1992**, *359*, 707–709.

[5] B. W. Smith, M. Monthioux, D. E. Luzzi, *Nature* **1998**, *396*, 323–324; J. Sloan, A. I. Kirkland, J. L. Hutchison, M. L. H. Green, *Chem. Commun.* **2002**, 1319–1332.

[6] A. Ayalon, A. Sygula, P.-C. Cheng, M. Rabinovitz, P. W. Rabideau, L. T. Scott, *Science* **1994**, *265*, 1065–1067.

[7] a) L. T. Scott, *Pure Appl. Chem.* **1996**, *68,* 291–300; b) L. T. Scott, H. B. Bronstein, D. V. Preda, R. B. M. Ansems, M. S. Bratcher, S. Hagen, *Pure Appl. Chem.* **1999**, *71*, 209–219; c) R. B. M. Ansems, L. T. Scott, *J. Am. Chem. Soc.* **2000**, *122*, 2719–2724.

[8] P. R. Ashton, N. S. Isaacs, F. H. Kohnke, A. M. Z. Slawin, C. M. Spencer, J. F. Stoddart, D. J. Williams, *Angew. Chem.* **1988**, *100,* 981–983; *Angew. Chem. Int. Ed. Engl.* **1988**, *27*, 966–969.

[9] S. Kammermeier, R. Herges, *Angew. Chem.* **1996**, *108*, 470–472; *Angew. Chem. Int. Ed. Engl.* **1996**, *35*, 417–419; S. Kammermeier, P. G. Jones, R. Herges, *Angew. Chem.* **1996**, *108*, 2834–2836; *Angew. Chem. Int. Ed. Engl.* **1996**, *35*, 2669–2671; S. Kammermeier, P. G. Jones, R. Herges, *Angew. Chem.* **1997**, *109*, 2317–2319; *Angew. Chem. Int. Ed. Engl.* **1997**, *36*, 2200–2202; M. Ohkita, K. Ando, T. Tsuji, *Chem. Commun.* **2001**, 2570–2571.

[10] T. Kawase, H. R. Darabi, M. Oda, *Angew. Chem.* **1996**, *108*, 2803–2805; *Angew. Chem. Int. Ed. Engl.* **1996**, *35*, 2664–2666; T. Kawase, N. Ueda, K. Tanaka, Y. Seirai, M. Oda, *Tetrahedron Lett.* **2001**, *42*, 5509–5511.

[11] Crystal data for **1**·HMB ($C_{60}H_{42}$): yellow prism, crystal dimensions $0.3\times0.1\times0.1$ mm, $M_r = 762.97$: monoclinic, space group $P2_1/a$ (No. 14), $a = 14.343(2)$, $b = 10.227(1)$, $c = 15.487(2)$ Å, $\beta = 106.76(2)°$, $V = 2277.6(51)$ Å^3, $Z = 2$, $\rho_{calcd} = 1.164$ g cm^{-3}, $Mo_{K\alpha}$ ($\lambda = 0.71069$ Å), $2\theta_{max} = 55°$. Intensity data were collected on a

 © 2003 Wiley-VCH Verlag GmbH & Co. KGaA, Weinheim

Rigaku RAXIS-RAPID Imaging Plate diffractometer at 296 K. The structure was solved with direct methods on F^2 with SHELXS-86. A total of 8006 reflections were collected, 4892 unique reflections were measured and used in the refinement, 271 parameters, $R1 = 0.082$, w$R2$ (Rw) = 0.165 (0.168) for 853 reflections with $I > 2\sigma(I)$, GOF = 0.67, max. peak in final difference map = 0.78 e Å^{-3}. All non-hydrogen atoms were refined anisotropically. Hydrogen atoms were placed geometrically and refined by using a rigid model. The high $R1$ value is a result of the disorder of an included molecule.

[12] a) Crystal data for **2**·4 Tol ($C_{92}H_{64}$): Crystal dimensions 0.2 × 0.2 × 0.3 mm, $M_r = 1159.49$, monoclinic, space group $C2/c$ (No. 15), $a = 20.320(9)$, $b = 12.892(5)$, $c = 29.131(2)$ Å, $\beta = 105.02(2)°$, $V = 7370.6(1)$ Å^3, $Z = 4$, $\rho_{calcd} = 1.263$ g cm^{-3}, $Mo_{K\alpha}$ ($\lambda = 0.71069$ Å), $\theta_{max} = 23.86°$. Intensity data were collected on a KappaCCD diffractometer at 298 K. A total of 6643 reflections were collected, 6639 independent reflections were measured and used in the refinement, 431 parameters, $R1 = 0.062$, $wR2 = 0.093$ for 2217 reflections, GOF = 2.61, max. peak in final difference map = 0.78 e Å^{-3}. The structure was solved with direct methods on $F > 3\sigma$ with maXus (MacScience Japan). All non-hydrogen atoms, except for the methyl carbon atoms of the disordered toluene molecules, were refined anisotropically. Hydrogen atoms associated with **2** and the fixed toluene molecules were refined isotropically, and the other hydrogen atoms were placed geometrically and refined by using a rigid model. The high GOF value results from the disordered toluene molecules. b) CCDC-153427 (**1**·HMB) and CCDC-153428 (**2**·4 Tol) contain the supplementary crystallographic data for this paper. These data can be obtained free of charge via www.ccdc.cam.ac.uk/conts/retrieving.html (or from the Cambridge Crystallographic Data Centre, 12 Union Road, Cambridge CB2 1EZ, UK; fax: (+44) 1223-336-033; or deposit@ccdccam.ac.uk).

[13] H. Meier in *Advances in Strain in Organic Chemistry, Vol. 1* (Ed.: B. Halton), JAI, London, **1991**, pp. 215 – 273.

[14] T. Kawase, N. Ueda, H. R. Darabi, M. Oda, *Angew. Chem.* **1996**, *108*, 1658 – 1660; *Angew. Chem. Int. Ed. Engl.* **1996**, *35*, 1556 – 1558.

[15] A. Thess, R. Lee, P. Nikolaev, H. Dai, P. Petit, J. Robert, C. Xu, Y. H. Lee, S. G. Kim, A. G. Rinzler, D. T. Colbert, G. E. Scuseria, D. Tomanek, J. E. Fischer, R. E. Smalley, *Science* **1996**, *273*, 483 – 487.

[16] D. C. Gutsche, *Calixarenes*, Royal Society of Chemistry, Cambridge, **1989**.

[17] G. Gattuso, S. Menzer, S. A. Nepogodiev, J. F. Stoddart, D. J. Williams, *Angew. Chem.* **1997**, *109*, 1615 – 1617; *Angew. Chem. Int. Ed. Engl.* **1997**, *36*, 1451 – 1454.

[18] T. D. Clark, J. M. Buriak, J. R. Granja, K. Kobayashi, M. P. Isler, D. E. McRee, M. R. Ghadiri, *J. Am. Chem. Soc.* **1998**, *120*, 8949 – 8962.

[19] G. R. Desiraju, A. Gavezzotti, *Acta Crystallogr. Sect. B* **1989**, *45*, 482 – 486.

[20] R. C. Haddon, *Science* **1993**, *261*, 1545 – 1550.

[21] M. Kamieth, F.-G. Klärner, F. Diederich, *Angew. Chem.* **1998**, *110,* 3497 – 3500; *Angew. Chem. Int. Ed.* **1998**, *37*, 3303 – 3306.

[22] K. K. Baldridge, J. S. Siegel, *J. Am. Chem. Soc.* **1999**, *121*, 5332 – 5333.

[23] a) M. Nishio, M. Hirota, Y. Umezawa, *The CH/π Interaction. Evidence, Nature and Consequences*, Wiley-VCH, Weinheim, **1998**; b) C. A. Hunter, K. R. Lawson, J. Perkins, C. J. Urch, *J. Chem. Soc. Perkin Trans. 2* **2001**, 651 – 669; c) M. O. Sinnokrot, E. F. Valeev, C. D. Sherrill, *J. Am. Chem. Soc.* **2002**, *124*, 10887 – 10893.

[24] T. Kawase, K. Tanaka, N. Fujiwara, H. R. Darabi, M. Oda, *Angew. Chem.* **2003**, *115*, 1662; *Angew. Chem. Int. Ed.* **2003**, *42*, 1624.

 © 2003 Wiley-VCH Verlag GmbH & Co. KGaA, Weinheim

Nanoring–Fullerene Complexes

Complexation of a Carbon Nanoring with Fullerenes**

Takeshi Kawase, Kenji Tanaka, Naoki Fujiwara, Hossein R. Darabi, and Masaji Oda**

Dedicated to Emeritus Professor Soichi Misumi on the occasion of his 77th birthday

Recently, a variety of layered carbon networks with closed, curved structures, such as carbon nanotubes,[1] bucky onions,[2] and "fullerene peapods"[3] have been discovered and have attracted much attention. Although the nature of the concave–convex interactions between the curved graphene sheets should be important in the formation and properties of these materials, they are yet to be well understood because of the absence of good model compounds. There have been considerable efforts towards the synthesis of belt-shaped conjugated systems.[4,5] In the accompanying paper,[6] we reported that the carbon nanorings [6]- and [8]paraphenyleneacetylene (**1** and **2**) have cavities with diameters of 13.2 and 17.3 Å, respectively (average values determined by X-ray diffraction), and form rather weak inclusion complexes with hexamethylbenzene and toluene, respectively. The size of the cavity in **1** appears to be suitable for the inclusion of C_{60} (7.1 Å in diameter), although it is actually slightly too small when the depth of p orbitals (3.4 Å for benzene) is considered (Figure 1). Therefore, the host–guest chemistry of **1** with fullerenes would give an insight into the concave–convex π-π interactions that are associated with the bucky onion and fullerene peapod. Here, we report on the formation of unusually stable complexes of the carbon nanoring **1** with C_{60} and bis(ethoxycarbonyl)methanofullerene (**3**),[7] and X-ray crystallographic analysis of the crystalline 1:1 complex **1**·**3**.

Despite being only sparingly soluble in $CHCl_3$,[8] C_{60} was found to be much more soluble (approximately 5 mg per mL) in the presence of **1**, to give the 1:1 complex **1**·C_{60} as a reddish brown solution, or a dark red-brown solid which precipitated out at higher concentrations. The solid complex could be redissolved completely in $CHCl_3$, which is in sharp contrast to the behavior of the solid calix[8]arene–C_{60} complex,[9,10] where C_{60} remained undissolved when added to $CHCl_3$;

[*] Prof. Dr. T. Kawase, Prof. Dr. M. Oda, K. Tanaka, N. Fujiwara, Dr. H. R. Darabi
Department of Chemistry
Graduate School of Science, Osaka University
Toyonaka, Osaka 560-0043 (Japan)
Fax: (+81) 6-6850-5387
E-mail: tkawase@chem.sci.osaka-u.ac.jp
moda@chem.sci.osaka-u.ac.jp

[**] This work was supported by a Grant-in-Aid for Scientific Research (No. 10146102 and 14340197) and from the Ministry of Education, Science, Sports, and Culture, Japan. We thank Dr. Hirose (Osaka University) for helpful discussion.

Supporting information for this article is available on the WWW under http://www.angewandte.org or from the author.

 © 2003 Wiley-VCH Verlag GmbH & Co. KGaA, Weinheim DOI: 10.1002/anie.200250728

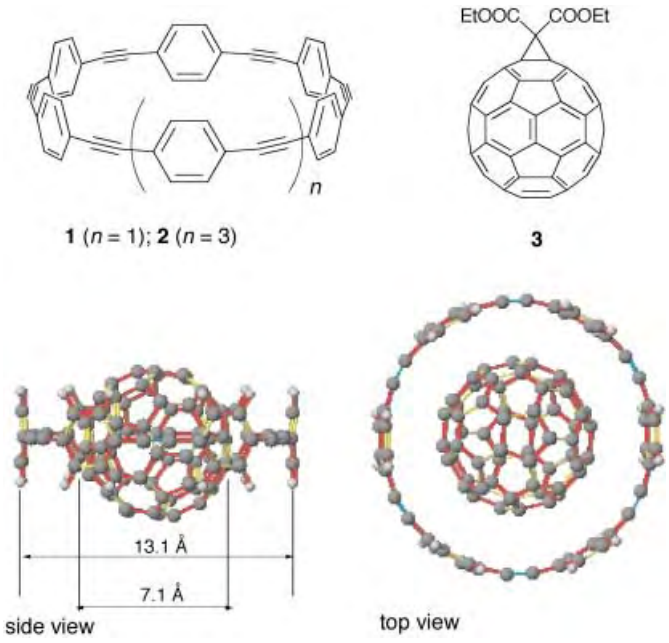


Figure 1. Paraphenyleneacetylenes **1** and **2**, fullerene derivative **3**, and a possible molecular structure of **1**·C_{60}.

these results suggest that a much higher association constant exists between **1** and C_{60} in $CHCl_3$. A similar procedure also afforded the 1:1 complex **1**·**3**. In contrast, the larger carbon nanoring **2** did not show any degree of complexation with either type of fullerene.

The interactions between **1** and C_{60} in solution were examined by absorption spectroscopy. Gradual addition of **1** to a solution of C_{60} in benzene causes a gradual change in the absorption spectrum. The isosbestic point at 583 nm, as well as a continuous-variation (Job's) plot, [11] provides evidence for a 1:1 complex in solution. The association constant (K_a) of the **1**·C_{60} complex, as determined by Hirose's method,[12] is $(1.6 \pm 0.3) \times 10^4$ dm^3 mol^{-1}. The absorption spectra of **1**·**3** also showed some variation, but the changes were too small for the measurement of a reliable association constant.

^{1}H NMR spectroscopy at low temperature afforded further important information (Figure 2). The spectrum of a solution of C_{60} and **1** (1:2.5) in CD_2Cl_2 exhibits a sharp singlet at 7.36 ppm for the aromatic protons at 30 °C. However, the signal broadens as the temperature is lowered and splits into two singlets which can be assigned to the protons of complex **1**·C_{60} (7.37 ppm), and the free host **1** (7.35 ppm) at −100 °C (Figure 2b). This dynamic behavior was not observed in [D_8]toluene. In-and-out motion of C_{60} against the cavity of **1** in CD_2Cl_2 is thus fast at room temperature and becomes slow enough for the NMR timescale at lower temperatures. Importantly, the ^{1}H NMR spectrum of the isolated **1**·C_{60} complex, thus an exact 1:1 ratio of two components, exhibits only the signal of the complex at −100 °C (Figure 2a). Taking the concentration of **1**·C_{60} (2.2×10^{-4} mol dm^{-3}) and possible detection of the free host **1** (down to 2%) into account, the value for K_a between **1** and C_{60} is estimated to be very large (exceeding 10^7 dm^3 mol^{-1}).[13] Variable-temperature NMR experiments also reveal that the Gibbs activation energy ($\Delta G^{\neq}$) for dissociation of **1**·C_{60} is (9.9 ± 0.3) kcal mol^{-1} (T_c = (-80 ± 5) °C) in CD_2Cl_2. The appearance of all the protons as a singlet points to near standstill or fast vibration of the C_{60} molecule around the center of the cavity and also its fast rotation inside the cavity, even at −100 °C. Moreover, a 1:1 mixture of **1** and **3** in CD_2Cl_2 showed a sharp singlet at 7.38 ppm for the aromatic protons of **1** at room temperature, a broadened singlet as the temperature was lowered, and finally two singlets (7.26 and 7.42 ppm) of equal intensity at −100 °C (Figure 2c). The appearance of two singlets is consistent with a lowering in the symmetry of **3**. The value of $\Delta G^{\neq}$ for dissociation was calculated to be (9.4 ± 0.2) kcal mol^{-1} (T_c = -78 ± 3 °C) which is a little lower than that of **1**·C_{60}. Thus, the **1**·**3** complex is slightly less stable than its **1**·C_{60} counterpart.

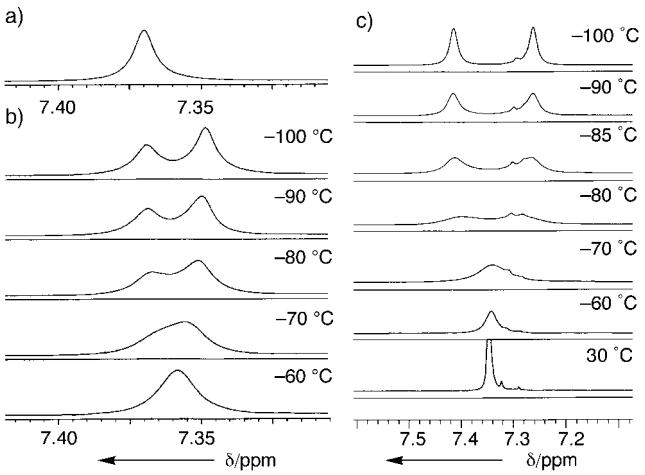


Figure 2. ^{1}H NMR spectra of a) **1**·C_{60} (0.22 mmol dm^{-3}; isolated as a solid) at −100 °C; b) a 1:2.5 mixture of **1** and C_{60}; c) a 1:1 mixture of **1** and **3**.

X-ray crystallographic analysis of these crystalline complexes should provide definitive information on their structures. However, attempted X-ray analyses of the **1**·C_{60} complex have so far failed to give adequate diffraction data, probably because of rotation of the guest molecules. Actually, a CP-MAS-NMR spectrum of the **1**·C_{60} complex at 30 °C shows a singlet peak (143.2 ppm) for C_{60} in the solid state. On the other hand, good single crystals of the **1**·**3** complex, suitable for X-ray analysis, were obtained from a toluene solution by slow evaporation of the solvent.[14] The molecular structure obtained reveals that each molecule of the complex is associated with two toluene molecules (Figure 3), and that the C_{60} cage of **3** is not deeply embedded in the cavity of **1** but situated at a floating position away from the center of the cavity, which takes on a bowl-shaped conformation. Even in this "ball-on-bowl" structure, all of the benzene rings of **1** are facing the C_{60} cage of **3**. The ester groups of **3** lean on the aromatic rings of **1**, and therefore the aromatic protons of nanoring **1** act like a gear wheel hindering easy rotation of the guest.

Table 1 lists the structural parameters of **1** in the complex **1**·**3** compared with those of the complex with hexamethylbenzene (**1**·HMB).[6] These data are almost identical except for the twist angles of the aromatic rings. The bond lengths and angles of **3** in this complex are also almost identical to those of the known structural data of **3**.[7c] There are

 © 2003 Wiley-VCH Verlag GmbH & Co. KGaA, Weinheim

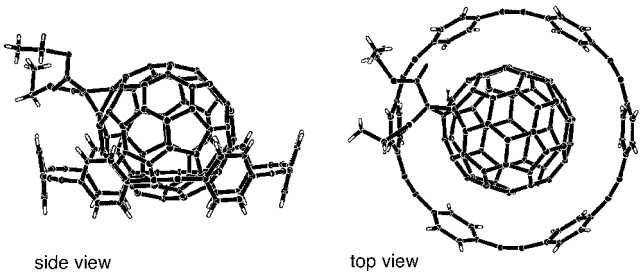


Figure 3. Molecular structure of **1**·**3**. Toluene molecules are omitted for clarity.

Table 1: Structural parameters of **1** in inclusion complexes.

	1·HMB	**1**·**3**
long axis [Å]	13.3	13.3
short axis [Å]	13.0	13.0
average bond angles of sp carbon atoms [°]	162.5 ≈165.6 (164.4)	162.2 ≈166.2 (164.5)
twist angles of benzene rings [°][a]	−9, 1, 17	20.3, 14.8, 16.9, 19.6, 16.5, 5.1
bend angles of benzene rings [°][b]	151.9, 149.2, 149.5	153.0, 151.6, 150.9, 149.0, 148.4, 148.1

[a] Evaluated from dihedral angles between least-square planes. [b] The angles between the two *para*-benzyl bonds of each boat-form benzene ring.

altogether 41 short interatomic distances (< 3.6 Å) and eight particularly short contacts (< 3.4 Å) between the host and guest (Figure 4). There are, however, no short contacts between the C_{60} cage and the outer surface of **1**. Most of the carbon atoms of **1** (37 out of 48) are in close contact with the C_{60} cage of **3**. The average distance between the host and guest is roughly estimated to be 3.4 Å, which is almost equal to the interlayer distance of multiwall carbon nanotubes. Taking into account the van der Waals distance between sp^2 carbon atoms (3.4 Å), the diameter of **1** (13.2 Å) seems a little too small to allow C_{60} to be fully embedded, and therefore the floating position of **3** would be a consequence of energetic favoring. Therefore, the singlet signal of **1**·C_{60} and the two singlets of **1**·**3** in their NMR spectra at −100 °C suggest that fast vibrational motion of the C_{60} molecule around the center of the cavity is evident, even at such a low temperature.

The short contacts seem to bear little correlation with the molecular orbital interaction between the HOMO of **1** and the LUMO of **3**.[7b] For example, although the C(103)···C(19) separation is the shortest contact of its type (3.26 Å), C(103) has no coefficient in the LUMO orbital. It is noteworthy that all the benzene rings of **1** lie over the [5:6] ring fusions of the C_{60} cage, which represent centers of positive charge on the C_{60} surface.[15,16]

According to many studies,[17–20] noncovalent interactions between aromatic rings have been explained in terms of van der Waals (dispersion force) and polar electrostatic (PE) interactions rather than as charge-transfer interactions. The high affinity between **1** and C_{60} cannot be explained in terms of dispersion forces alone because the complex of **1** and hexamethylbenzene described before,[6] where the dispersion force would be expected to play a greater role, is almost dissociated in nonpolar solvents. Charge-transfer effects would also be negligible because **1** has poor electron-donating properties (the first electrochemical oxidation potential is over +1.0 V in CH_2Cl_2), and only a slight change is observed in the charge-transfer absorption band (450–650 nm) in every case. In contrast, the complex of C_{60} with *N*,*N*-dimethylaniline exhibits a rather intense charge-transfer absorption band.[21] Thus, the PE interaction remains the most probable driving force for complexation.

Theoretical studies have predicted that curved aromatic hydrocarbons should be polarized with regard to their convex and concave faces because π systems on a curved surface suffer an anisotropic distribution of π electrons, which results in the segregation of electrostatic charge.[22] However, the results of theoretical calculations have been controversial as to the direction of polarization.[22c] The significantly strong complexation found here between **1** and fullerenes, as well as the good face-to-face solvating ability of benzene and

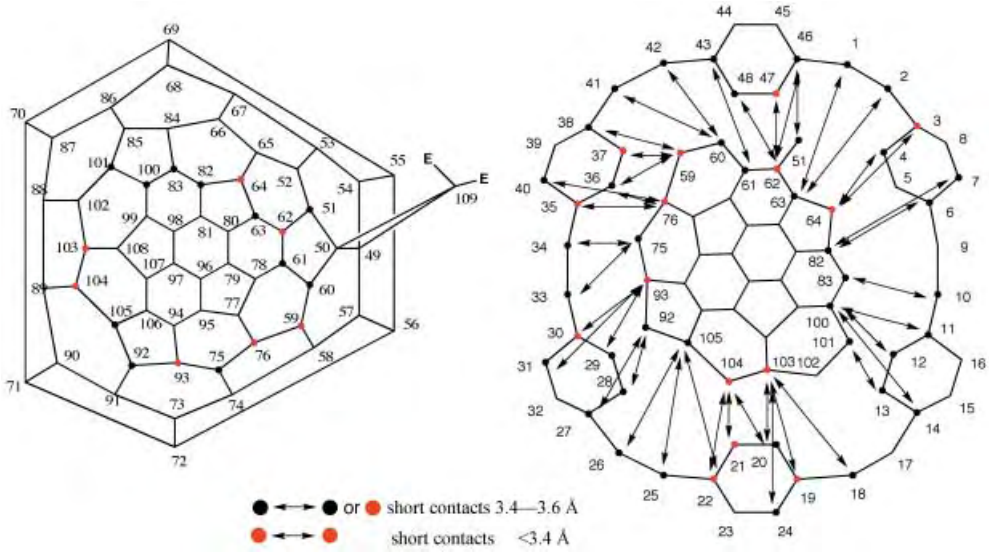


Figure 4. The short contacts between the host and guest in the **1**·**3** complex.

 © 2003 Wiley-VCH Verlag GmbH & Co. KGaA, Weinheim

alkylbenzenes, may be understood by assuming the electronic potential of the convex surface of the fullerenes to be positive.[16a] An electrostatic attractive force, namely, a quadrupolar–quadrupolar interaction between the electrostatically opposite concave and convex surfaces, as well as the dispersion force, would play an important role in the formation of complexes between **1** and fullerenes,[23] and hence the spontaneous formation of layered carbon nanotubes, bucky onions, and fullerene peapods.

Received: December 9, 2002 [Z50728]

Keywords: cyclophanes · fullerenes · host–guest systems · inclusion compounds · noncovalent interactions

[1] a) S. Iijima, *Nature* **1991**, *354*, 56–58; b) S. Iijima, T. Ichibashi, Y. Ando, *Nature* **1992**, *356*, 776–778; c) P. M. Ajayan, S. Iijima, *Nature* **1993**, *361*, 333–334; d) A. Thess, R. Lee, P. Nikolaev, H. Dai, P. Petit, J. Robert, C. Xu, Y. H. Lee, S. G. Kim, A. G. Rinzler, D. T. Colbert, G. E. Scuseria, D. Tomanek, J. E. Fischer, R. E. Smalley, *Science* **1996**, *273*, 483–487.

[2] a) H. W. Kroto, *Science* **1988**, *242*, 1139–1145; b) D. Ugarte, *Nature* **1992**, *359*, 707–709.

[3] B. W. Smith, M. Monthioux, D. E. Luzzi, *Nature* **1998**, *396*, 323–324.

[4] The synthetic challenges for belt-shaped conjugated systems: a) F. Vögtle, *Top. Curr. Chem.* **1983**, *115*, 157–159; b) P. R. Ashton, N. S. Isaacs, F. H. Kohnke, A. M. Z. Slawin, C. M. Spencer, J. F. Stoddart, D. J. Williams, *Angew. Chem.* **1988**, *100*, 981–983; *Angew. Chem. Int. Ed. Engl.* **1988**, *27*, 966–969; c) F. Diederich, Y. Rubin, C. B. Knobler, R. L. Whetten, K. E. Schriver, K. N. Houk, Y. Li, *Science* **1989**, *245*, 1088–1090; d) Y. Rubin, C. B. Knobler, F. Diederich, *J. Am. Chem. Soc.* **1990**, *112*, 1607–1617; e) Y. Tobe, T. Fujii, H. Matsumoto, K. Naemura, Y. Achiba, T. Wakabayashi, *J. Am. Chem. Soc.* **1996**, *118*, 2758–2759; f) R. Friederich, M. Neiger, F. Vögtle, *Chem. Ber.* **1993**, *126*, 1723–1732; g) R. M. Cory, C. L. McPhail, A. J. Dikmans, J. J. Vittal, *Tetrahedron Lett.* **1996**, *37*, 1983–1986; h) R. M. Cory, C. L. McPhail, *Tetrahedron Lett.* **1996**, *37*, 1987–1990.

[5] Some belt-shaped conjugated systems have been reported since the first synthesis by Herges and co-workers, however, the host properties have not been reported so far: a) S. Kammermeier, R. Herges, *Angew. Chem.* **1996**, *108*, 470–472; *Angew. Chem. Int. Ed. Engl.* **1996**, *35*, 417–419; b) T. Kawase, H. R. Darabi, M. Oda, *Angew. Chem.* **1996**, *108*, 2803–2805; *Angew. Chem. Int. Ed. Engl.* **1996**, *35*, 2664–2666; c) S. Kammermeier, P. G. Jones, R. Herges, *Angew. Chem.* **1996**, *108*, 2834–2836; *Angew. Chem. Int. Ed. Engl.* **1996**, *35*, 2669–2671; d) S. Kammermeier, P. G. Jones, R. Herges, *Angew. Chem.* **1997**, *109*, 2317–2319; *Angew. Chem. Int. Ed. Engl.* **1997**, *36*, 2200–2202; e) T. Kawase, N. Ueda, K. Tanaka, Y. Seirai, M. Oda, *Tetrahedron Lett.* **2001**, *42*, 5509–5511; f) M. Ohkita, K. Ando, T. Tsuji, *Chem. Commun.* **2001**, 2570–2571.

[6] T. Kawase, Y. Seirai, H. R. Darabi, M. Oda, Y. Sarakai, K. Tashiro, *Angew. Chem.* **2003**, *115*, 1659; *Angew. Chem. Int. Ed.* **2003**, *42*, 1621.

[7] a) C. Bingel, *Chem. Ber.* **1993**, *126*, 1957–1959; b) A. Hirsch, I. Lamparth, T. Grösser, H. R. Karfunkel, *J. Am. Chem. Soc.* **1994**, *116*, 9385–9386; c) E. F. Paulus, C. Bingel, *Acta Crystallogr. Sect. C* **1995**, *51*, 143–146.

[8] Detailed reviews on fullerenes: *Fullerenes: Chemistry, Physics, and Technology* (Eds.: K. M. Kadish, R. S. Ruoff), Wiley, New York, **2000**.

[9] J. L. Atwood, G. A. Koutsantonis, C. L. Raston, *Nature* **1994**, *368*, 229–231.

[10] T. Suzuki, K. Nakashima, S. Shinkai, *Chem. Lett.* **1994**, 699–702.

[11] J.-M. Lehn, J. L. Atwood, J. E. D. Davies, D. D. MacNicol, *Supramolecular Chemistry, Vol. 8*, Pergamon, Oxford, **1996**.

[12] K. Hirose, *J. Inclusion Phenom. Macrocycl. Chem.* **2001**, *39*, 193–209.

[13] Recently, some fullerene complexes with extremely high association constants ($>10^6$ in benzene) have been reported. These hosts involve transition-metal ions as well as heteroatoms. In contrast, CPPAs are composed of only carbon and hydrogen atoms: a) K. Tashiro, T. Aida, J.-Y. Zheng, K. Kinbara, K. Saigo, S. Sakamoto, K. Yamaguchi, *J. Am. Chem. Soc.* **1999**, *121*, 9477–9478; b) O. D. Fox, M. G. B. Drew, E. J. S. Wilkinson, P. D. Beer, *Chem. Commun.* **2000**, 391–392; c) P. D. W. Boyd, M. C. Hodgson, L. Chaker, C. E. F. Rickard, A. G. Oliver, P. J. Brothers, R. Bolskar, F. S. Tham, C. A. Reed, *J. Am. Chem. Soc.* **1999**, *121*, 10487–10489; d) D. Sun, F. S. Tham, C. A. Reed, L. Chaker, M. Burgess, P. D. W. Boyd, *J. Am. Chem. Soc.* **2000**, *122*, 10704–10705; e) J.-Y. Zheng, K. Tashiro, Y. Hirabayashi, K. Kinbara, K. Saigo, T. Aida, S. Sakamoto, K. Yamaguchi, *Angew. Chem.* **2001**, *113,* 1909–1913; *Angew. Chem. Int. Ed.* **2001**, *40*, 1857–1861.

[14] a) Crystal data for **1**·**3** ($C_{129}H_{34}O_4$): black prism, crystal dimension $0.4\times0.2\times0.2$ mm, $M_r=1647.69$; triclinic, space group $P\bar{1}$ (No. 2), $a=16.5892(3)$, $b=18.6608(4)$, $c=15.5599(2)$ Å, $\alpha=105.317(4)$, $\beta=107.893(2)$, $\gamma=107.128(2)°$, $V=4033.7(2)$ Å^3, $Z=2$, $\rho_{calcd}=1.356$ g cm^{-3}, $Mo_{K\alpha}$ ($\lambda=0.71069$ Å), $2\theta_{max}=55°$. Intensity data were collected on a Rigaku RAXIS-RAPID Imaging Plate diffractometer at 296 K. The structure was solved with direct methods on F^2 with SHELXS-86. A total of 37335 reflections were collected, 18026 unique reflections were measured and used in the refinement, 1107 parameters, $R1=0.101$, w$R2$ (Rw) $=0.143$ (0.178) for 5883 reflections with $I>2\sigma(I)$, GOF $=1.67$, max. peak in final difference map $=0.77$ e Å^{-3}. All non-hydrogen atoms were refined anisotropically. Hydrogen atoms were placed geometrically and refined by using a rigid model. The high $R1$ value results from the disorder of included toluene molecules; b) CCDC-199147 contains the supplementary crystallographic data for this paper. These data can be obtained free of charge via www.ccdc.cam.ac.uk/conts/retrieving.html (or from the Cambridge Crystallographic Data Centre, 12 Union Road, Cambridge CB21EZ, UK; fax: (+44) 1223-336-033; or deposit@ccdc.cam.ac.uk).

[15] a) M. F. Meidine, P. B. Hitchcock, H. W. Kroto, R. Taylor, D. R. M. Walton, *J. Chem. Soc. Chem. Commun.* **1992**, 1534–1537; b) A. L. Balch, J. W. Lee, B. C. Noll, M. M. Olmstead, *J. Chem. Soc. Chem. Commun.* **1993**, 56–58; c) M. M. Olmstead, A. S. Ginwalla, B. C. Noll, D. S. Tinti, A. L. Balch, *J. Am. Chem. Soc.* **1996**, *118*, 7737–7751; d) L. J. Barbour, G. W. Orr, J. L. Atwood, *Chem. Commun.* **1998**, 1439–1440; e) M. Fedurco, M. M. Olmstead, W. R. Fawcett, *Inorg. Chem.* **1995**, *34*, 388–392; f) D. M. Forkey, S. Attar, B. C. Noll, R. Koerner, M. M. Olmstead, A. L. Balch, *J. Am. Chem. Soc.* **1997**, *119*, 5766–5767.

[16] a) F. Diederich, M. Gomez-Lopez, *Chem. Soc. Rev.* **1999**, *28*, 263–277; b) M. J. Hardie, C. L. Raston, *Chem. Commun.* **1999**, 1153–1163, and references therein.

[17] F. Diederich, *Angew. Chem.* **1988**, *100*, 372–396; *Angew. Chem. Int. Ed. Engl.* **1988**, *27*, 362–386.

[18] C. A. Hunter, J. K. M. Sanders, *J. Am. Chem. Soc.* **1990**, *112*, 5525–5534; C. A. Hunter, *Angew. Chem.* **1993**, *105*, 1653–1655; *Angew. Chem. Int. Ed. Engl.* **1993**, *32*, 1584–1586; C. A. Hunter, *Chem. Soc. Rev.* **1994**, *101*–109; C. A. Hunter, K. R. Lawson, J. Perkins, C. J. Urch, *J. Chem. Soc. Perkin Trans. 2* **2001**, 651–669.

[19] a) F. Cozzi, M. Cinquini, R. Annuziata, T. Dwyer, J. S. Siegel, *J. Am. Chem. Soc.* **1992**, *114*, 5729–5733; b) F. Cozzi, M. Cinquini, R. Annuziata, J. S. Siegel, *J. Am. Chem. Soc.* **1993**, *115*, 5330–

 © 2003 Wiley-VCH Verlag GmbH & Co. KGaA, Weinheim

5331; c) F. Cozzi, J. S. Siegel, *Pure Appl. Chem.* **1995**, *67*, 683 – 689.
[20] A. S. Shetty, J. Zhang, J. S. Moore, *J. Am. Chem. Soc.* **1996**, *118*, 1019 – 1027.
[21] Y.-P. Sun, C. E. Bunker, B. Ma, *J. Am. Chem. Soc.* **1994**, *116*, 9692 – 9699.
[22] a) R. C. Haddon, *Science* **1993**, *261*, 1545 – 1550; b) M. Kamieth, F.-G. Klärner, F. Diederich, *Angew. Chem.* **1998**, *110,* 3497 – 3500; *Angew. Chem. Int. Ed.* **1998**, *37*, 3303 – 3306; c) L. T. Scott, H. B. Bronstein, D. V. Preda, R. B. M. Ansems, M. S. Bratcher, S. Hagen, *Pure Appl. Chem.* **1999**, *71*, 209 – 219; d) K. K. Baldridge, J. S. Siegel, *J. Am. Chem. Soc.* **1999**, *121*, 5332 – 5333.
[23] The driving force for fullerene complexation was referred to in the following publications: Z. Yoshida, H. Takekuma, S. Takekuma, Y. Matsubara, *Angew. Chem.* **1994**, *106*, 1658 – 1670; *Angew. Chem. Int. Ed. Engl.* **1994**, *33*, 1597 – 1599; E. C. Constable, *Angew. Chem.* **1994**, *106*, 2359 – 2361; *Angew. Chem. Int. Ed. Engl.* **1994**, *33*, 2269 – 2271; A. Ikeda, Y. Suzuki, M. Yoshimura, S. Shinkai, *Tetrahedron* **1998**, *54*, 2497 – 2508; T. Haino, M. Yanase, Y. Fukazawa, *Angew. Chem.* **1998**, *110*, 1044 – 1046; *Angew. Chem. Int. Ed.* **1998**, *37*, 997 – 998; M. Yamase, M. Matsuoka, Y. Tatsumi, M. Suzuki, H. Iwamoto, T. Haino, Y. Fukazawa, *Tetrahedron Lett.* **2000**, *41*, 493 – 497; S. Mizyed, M. Ashram, D. O. Miller, P. E. Georghiou, *J. Chem. Soc. Perkin Trans. 2* **2001**, 1916 – 1919; Y. Yamaguchi, S. Kobayashi, N. Amita, T. Wakamiya, Y. Matsubara, K. Sugimoto, Z. Yoshida, *Tetrahedron Lett.* **2002**, *43*, 3277 – 3280.

 © 2003 Wiley-VCH Verlag GmbH & Co. KGaA, Weinheim

Weak Interactions in Polymerization

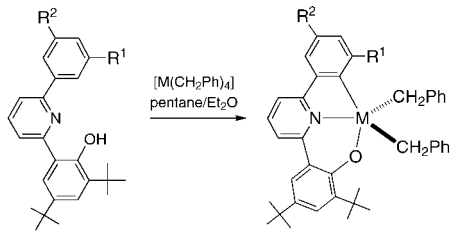
Observation of Intramolecular C–H···F–C Contacts in Non-Metallocene Polyolefin Catalysts: Model for Weak Attractive Interactions between Polymer Chain and Noninnocent Ligand**

*Steven C. F. Kui, Nianyong Zhu, and Michael C. W. Chan**

The mechanisms of stereoselectivity for the polymerization of prochiral α-olefins by Group 4 metallocene catalysts are well understood and are principally derived from steric effects (i.e. repulsive nonbonded interactions).[1] By comparison, the study of attractive interactions between the ancillary ligand and the polymer chain remains uncharted. In this context, multidentate ligands with mixed functionalities ("hemilabile" ligands) in which the labile moiety is employed to stabilize the metal center have been extensively utilized in late transition-metal catalysts[2] and more recently in metallocene-type derivatives.[3,4]

The application of attractive interactions between the ligand and growing alkyl chain to manipulate the reactivity of polyolefin catalysts becomes viable only if such interactions are weak and reversible, so that the intrinsic polymerization process is not disrupted. Significantly, the Fujita and Coates groups have recently described a novel class of fluorinated phenoxyimine titanium polyolefin catalysts. Fujita et al. reported that these catalysts can mediate living polyethylene formation at remarkably elevated temperatures[5] as well as highly syndiotactic living polymerization of propylene,[6a] and elucidated that propylene insertions occur with predominant 2,1 regiochemistry,[6b] which is exceedingly rare for Group 4 catalysts. Coates and co-workers observed virtually exclusive 2,1 regiochemistry for these Ti^{IV} fluorine-rich catalysts in ethylene/propylene copolymerization and cyclopolymerization processes.[7] Based on DFT calculations,[5b] Fujita and co-workers proposed that a fluorine atom adjacent to the imine nitrogen atom, which interacts with the polymer chain to curtail β-hydrogen-transfer pathways, is required for a living process. We now report the first direct observation of weak intramolecular C–H···F–C contacts in neutral and cationic Group 4 polyolefin procatalysts. The CH···FC interaction is amongst the weakest hydrogen bond to be proposed and apparent consensus regarding its validity has only just been reached.[8] Herein, the potential importance of such weak attractive interactions between the ligand and polymer chain in olefin polymerization processes will be emphasized.

We have targeted unsymmetric tridentate ligand sets that can support active olefin polymerization catalysts. In particular, we are evaluating the suitability of aromatic σ-carbanions, because the resultant metal–carbon bond should be more inert than aliphatic analogues and its relative covalency is expected to yield a highly electrophilic catalytic center. Metalation of 2-(2′-phenol)-6-arylpyridine substrates containing acidic protons ensues upon reaction with the basic metal precursors $[M(CH_2Ph)_4]$ (M = Zr, Ti) and is accompanied by elimination of toluene to afford complexes **1–3** as orange to red crystalline solids (Scheme 1). The cyclometalation process



M = Zr, $R^1 = R^2 = CF_3$ (**1**)
R^1 = H, $R^2 = CF_3$ (**2**)
M = Ti, $R^1 = R^2 = CF_3$ (**3**)

Scheme 1. Synthesis of **1–3**.

[*] Dr. M. C. W. Chan, S. C. F. Kui, Dr. N. Zhu
Department of Chemistry and
HKU-CAS Joint Laboratory on New Materials
The University of Hong Kong
Pokfulam Road, Hong Kong SAR (China)
Fax: (+852) 2857-1586
E-mail: mcwchan@hku.hk

[**] We acknowledge financial support from the Research Grants Council of the Hong Kong SAR, China (HKU 7095/00P) and The University of Hong Kong (URC-administered Seed Funding Grant). We are grateful to Prof. Chi-Ming Che for supporting this work and for his invaluable suggestions.

Supporting information for this article is available on the WWW under http://www.angewandte.org or from the author.

 © 2003 Wiley-VCH Verlag GmbH & Co. KGaA, Weinheim DOI: 10.1002/anie.200219832

readily proceeds at room temperature and appears highly regioselective; for complex **2**, in which two cyclometalation sites are available, only the pictured compound (where R^1 is less bulky) has been isolated or detected. We note that endeavors to synthesize Zr derivatives where $R^1 = R^2 =$ *tert*-butyl groups yielded intractable mixtures, characterization of which (by ^{1}H NMR spectroscopy) signified non-cyclometalation.

Characterization of complexes **1** and **3** by NMR spectroscopy was highly informative (also see Supporting Information). The ^{1}H NMR spectrum (C_6D_6) of **1** is typical for η^2-coordinated benzyl groups,[9] except that one of the two expected doublets for the diastereotopic methylene hydrogen atoms, at $\delta = 3.09$ ppm, appears as an overlapping doublet of quartets (Figure 1). Furthermore, the ^{13}C{^{1}H} NMR spectrum displays a quartet signal at $\delta = 70.50$ ppm ($J = 5.9$ Hz) for the methylene groups. The magnitudes of the coupling constants are clearly not consistent with formal six- or five-bond coupling. Subsequent ^{19}F decoupling of the ^{1}H NMR spectrum demonstrates coupling between one of the two CH_2 protons and three equivalent ^{19}F nuclei. Similarly, while the coupling in the ^{19}F[^{1}H] NMR spectrum is not clearly resolved, the ^{19}F{^{1}H} NMR spectrum undergoes significant narrowing for the downfield signal at $\delta = -58.09$ ppm only (Figure 1). A ^{19}F–^{1}H 2D correlation experiment (see Supporting Information) also revealed a cross-peak between the upfield ^{1}H multiplet and the downfield ^{19}F signal only. These observations thus strongly implicate the existence of intramolecular "through-space" coupling through C–H···F–C hydrogen bonds.[10] The effects of solvent polarity upon this coupling have been probed, and $^{1h}J_{H,F}$ values of 3.3 and 3.1 Hz in C_6D_6 and CD_2Cl_2, respectively, have been obtained, whereas in [D_8]THF this coupling is unresolved yet still apparent (Figure 1). The decreases in the $^{1h}J_{H,F}$ value correspond to the increasing hydrogen-bonding capabilities of the solvents. The persistence of CH···FC coupling in [D_8]THF is surprising and can be attributed to the "locked" conformation of the rigid molecular framework.

The proposed hydrogen-bonding interaction and the environment around the CF_3 moieties in complex **1** were further investigated by ^{1}H/^{19}F NOE difference experiments (see Supporting Information). When the signal for the proximal CF_3 group was selectively irradiated, strong enhancement was apparent for the multiplet exhibiting ^{19}F coupling at $\delta = 3.09$ ppm only, and no response was perceived for the doublet at $\delta = 3.26$ ppm. Intriguingly, we also observed moderate enhancement for the *ortho*-benzyl protons. Irradiation of the distal CF_3 substituent resulted in enrichment for the two adjacent aromatic proton signals only as anticipated. An illustration of the weak hydrogen bonding involving one of the methylene hydrogen atoms and the rapidly rotating trifluoromethyl unit is depicted in Figure 1. A virtually identical intramolecular CH···FC interaction in complex **3** is indicated by analogous NMR experiments, although the

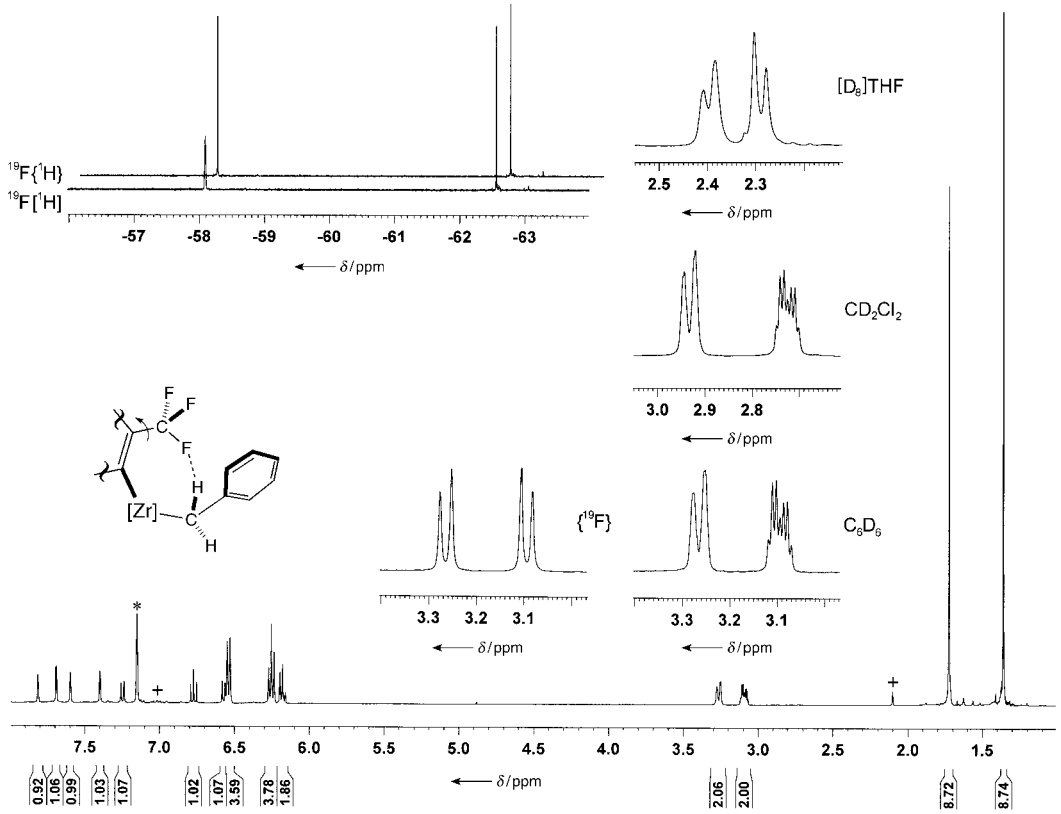


Figure 1. ^{1}H (400 MHz) and ^{19}F (376 MHz, CF_3 region) NMR spectra (C_6D_6, 300 K) of **1**, demonstrating the effects of ^{19}F and ^{1}H decoupling (ppm axis displaced for clarity), respectively, and of solvent polarity upon the diastereotopic methylene hydrogen atoms (* = C_6D_6, + = residual toluene).

 © 2003 Wiley-VCH Verlag GmbH & Co. KGaA, Weinheim

through-space coupling is slightly weaker (in C_6D_6: $^{1h}J_{H,F} \approx 2$ Hz, $^{2h}J_{C,F} = 5.3$ Hz).

We have also attempted to characterize the corresponding benzyl cationic species. The reaction of complex **1** with $B(C_6F_5)_3$ in CD_2Cl_2 yielded a complicated mixture of products. However, in the presence of a few drops of [D_8]THF, the transformation resulted in the clean generation of an η^2-CH_2Ph cation that is presumably stabilized by the OC_4D_8 ligand (Figure 2; see Supporting Information for ^1H–^1H COSY spectrum). Saliently, the broad upfield ^1H doublet peak for one of the methylene protons and the downfield ^{19}F signal for the proximal CF_3 group are both partially sharpened upon decoupling of the ^{19}F and ^1H nuclei, respectively. Moreover, the $^{13}C\{^1H\}$ NMR spectrum reveals a rather broad but partially resolved quartet signal at $\delta = 76.9$ ppm ($^{2h}J_{C,F} \approx 4$ Hz) for the $ZrCH_2$ group. These observations imply the presence of weak C–H···F–C contacts between the ancillary ligand and an alkyl fragment in a Group 4 metal cation.

The molecular structures of complexes **1** (Figure 3) and **2** have been determined by X-ray crystallography.[11] The zirconium center in both structures is chelated by a phenolate–pyridine–carbanion [O,N,C] ligand in a distorted trigonal-bipyramidal geometry, with axial O,C atoms and equatorial N and C(benzyl) groups. The most striking difference between **1** and **2** is the orientation of the benzyl moieties, which exist in the "*anti,anti*" and "*syn,anti*" configurations, respectively (see below). Nevertheless, like in their solution structures, the benzyl units can participate in η^2 coordination to the electrophilic metal core,[12] although this interaction appears fractionally weaker in **1**. While there are no close Zr···F contacts[4] (shortest Zr···F distance 2.940(2) Å) in the crystal lattice of **1**, the structural parameters concerning the C–H···F–C fragment are consistent with a weak hydrogen bond[8] (e.g. H···F 2.47 and 2.59 Å, C–H···F 114°). The unusual *anti,anti* benzyl arrangement in **1** may be attributed to a combination of the stabilizing effect from the CH···FC interactions and the congested environment around the equatorial central cleft (see space-filling diagram in Supporting Information), although crystal packing effects cannot be disregarded. Interestingly, the N-Zr-C-C_{ipso} dihedral angles for the *anti* benzyl ligands (which wrap around the pyridyl ring) are 8.4 and 26.5° (the corresponding angle in **2** is 2.8°), hence the CH_2Ph units appear to incline *towards* the more crowded surroundings of the CF_3 moiety (Figure 3b). We note the position of the *ortho*-phenyl hydrogen atoms H34 and H41 relative to the CF_3 group.

The intramolecular CH···FC contacts depicted in this work, demonstrated in the solution state and supported by X-ray structural determinations, represent unique models of weak attractive interactions between a functionalized ligand and a polymer chain at an active catalytic center.[13] Our results provide substantiating evidence for the proposition derived by Fujita et al. from DFT calculations regarding ligand–polymer interactions originating from (sp^2)C–F moieties.[5b]

In conclusion, this study highlights the potential of weak attractive interactions between the ligand and polymer chain as a new paradigm in olefin polymerization reactions. Fragile

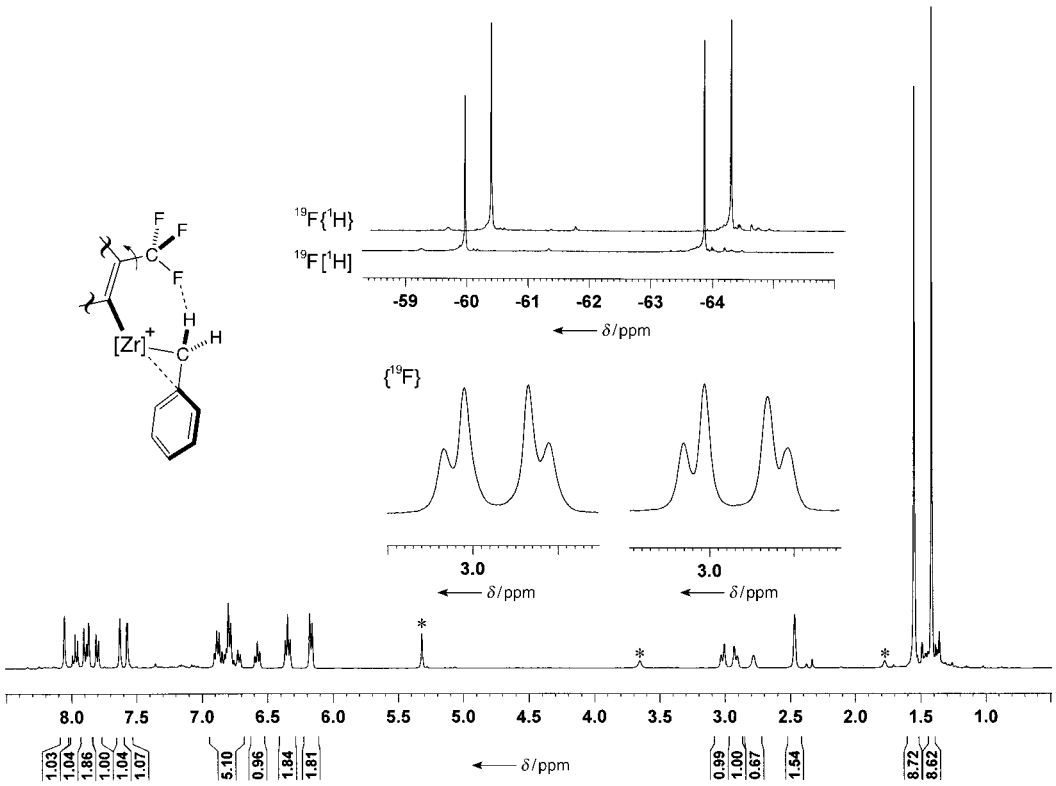


Figure 2. ^1H (400 MHz) and ^{19}F (376 MHz, CF_3 region) NMR spectra (CD_2Cl_2 + [D_8]THF, 300 K) for the η^2-CH_2Ph cation derived from the reaction of **1** with $B(C_6F_5)_3$, demonstrating the effects of ^{19}F and ^1H decoupling (ppm axis displaced for clarity), respectively (* = deuterated solvents).

 © 2003 Wiley-VCH Verlag GmbH & Co. KGaA, Weinheim

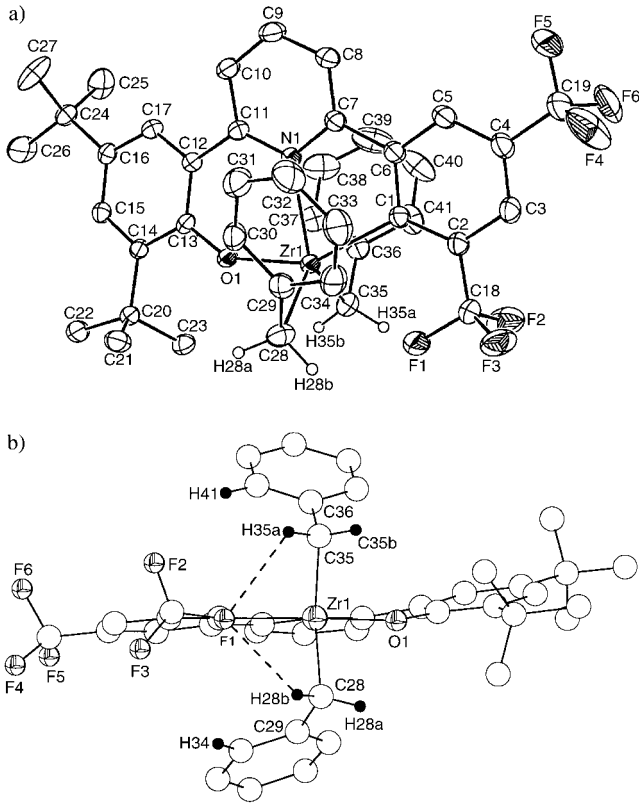


Figure 3. a) Structure of **1** (30% probability ellipsoids, only methylene hydrogen atoms are shown for clarity). Selected bond lengths [Å] and angles [°]: Zr1-C1 2.330(3), Zr1-N1 2.391(2), Zr1-O1 1.952(2), Zr1-C28 2.276(3), Zr1···C29 2.729(3), Zr1-C35 2.267(3), Zr1···C36 2.765(3); C13-O1-Zr1 147.3(2), C29-C28-Zr1 90.7(2), C36-C35-Zr1 92.8(2). b) View along the Zr1–N1 vector in **1**, depicting the short CH···FC contacts (F1···H28b 2.471, F1···C28 2.996(3), F1···H35a 2.592, F1···C35 3.115(3) Å; F1···H28b-C28 113.8, F1···H35a-C35 114.0°) and the apparent "tilt" of the CH_2Ph planes towards the CF_3 moiety.

noncovalent contacts such as hydrogen bonds are ideal for this role, and their diverse nature paves the way for molecular recognition possibilities. These weak interactions may potentially be exploited for the stabilization of hitherto unstable intermediates and new polymer architectures.

Experimental Section

Synthetic procedure: The 2-(2′-phenol)-6-arylpyridine substrate in pentane/diethyl ether (5:1) was slowly added to a stirred solution of $[M(CH_2Ph)_4]$ in pentane/diethyl ether (5:1) at −78 °C. The reaction mixture was allowed to warm up to room temperature and stirred for 12 h. The resultant solution was filtered, concentrated to about 10 mL and stored at −15 °C to afford a crystalline solid. Analytically pure products were obtained by recrystallization from pentane (see Supporting Information for detailed characterization data and labeling schemes).

1: red crystals; yield: 0.19 g, 62%; elemental analysis calcd (%) for $C_{41}H_{39}F_6NOZr$ (766.98): C 64.21, H 5.13, N 1.83; found: C 63.99, H 5.57, N 1.89; selected NMR data (C_6D_6, 300 K): ^{1}H NMR (400 MHz): $\delta = 1.36$ (s, 9H; 5-*t*Bu), 1.72 (s, 9H; 3-*t*Bu), 3.09 (dq, $J = 9.6$ Hz, $^{1h}J_{H,F} = 3.3$ Hz, 2H; $ZrCH_2$), 3.26 (d, $J = 9.4$ Hz, 2H; $ZrCH_2$), 6.18 (t, $J = 7.3$ Hz, 2H; *p*-Ph), 6.25 (t, $J = 7.7$ Hz, 4H; *m*-Ph), 6.54 (d, $J = 7.4$ Hz, 4H; *o*-Ph), 6.57 (d, $J = 7.9$ Hz, 1H; H^{10}), 6.77 (t, $J = 8.0$ Hz, 1H; H^9), 7.25 (d, $J = 8.0$ Hz, 1H; H^8), 7.40 (d, $J = 2.3$ Hz, 1H; H^6), 7.60 (s, 1H; H^{13}), 7.69 (d, $J = 2.4$ Hz, 1H; H^4), 7.81 ppm (s, 1H; H^{15}); ^{19}F NMR (376 MHz): $\delta = -58.09$ (CF_3 at R^1), −62.56 ppm (CF_3 at R^2); ^{13}C NMR (126 MHz): $\delta = 70.50$ ppm (q, $^{2h}J_{C,F} = 5.9$ Hz ($J_{CH} = 133.3$ Hz); $ZrCH_2$).

2: orange-red crystals; yield: 0.23 g, 60%; elemental analysis calcd (%) for $C_{40}H_{40}F_3NOZr$ (698.98): C 68.73, H 5.77, N 2.00; found: C 68.21, H 5.68, N 2.02; selected NMR data (C_6D_6, 300 K): ^{1}H NMR (500 MHz): $\delta = 1.36$ (s, 9H; 5-*t*Bu), 1.58 (s, 9H; 3-*t*Bu), 2.27 (d, $J = 9.3$ Hz, 2H; $ZrCH_2$), 2.49 (d, $J = 9.3$ Hz, 2H; $ZrCH_2$), 6.64 (t, $J = 7.3$ Hz, 2H; *p*-Ph), 6.71 (d, $J = 7.2$, 4H; *o*-Ph), 6.80 (m, 5H; *m*-Ph and H^{10}), 6.86 (t, $J = 7.9$ Hz, 1H; H^9), 7.20 (d, $J = 7.4$ Hz, 1H; H^8), 7.39 (d, $J = 2.3$ Hz, 1H; H^6), 7.41 (d, $J = 7.3$ Hz, 1H; H^{15}), 7.63 (d, $J = 2.4$ Hz, 1H; H^4), 7.70 (s, 1H; H^{13}), 7.79 ppm (d, $J = 7.3$ Hz, 1H; H^{16}); ^{19}F NMR (376 MHz): $\delta = -62.27$ ppm; ^{13}C NMR (126 MHz): $\delta = 66.33$ ppm ($J_{C,H} = 135.0$ Hz; $ZrCH_2$).

3: dark red crystals; yield: 0.18 g, 57%; elemental analysis calcd (%) for $C_{41}H_{39}F_6NOTi$ (723.66): C 68.05, H 5.43, N 1.93; found: C 68.08, H 5.58, N 2.09; selected NMR data (C_6D_6, 300 K): ^{1}H NMR (500 MHz): $\delta = 1.34$ (s, 9H; 5-*t*Bu), 1.77 (s, 9H; 3-*t*Bu), 4.00 (dq, $J = 8.4$ Hz, $^{1h}J_{H,F} = 1.2$ Hz, 2H; $TiCH_2$), 4.04 (d, $J = 8.3$ Hz, 2H; $TiCH_2$), 6.25 (t, $J = 7.2$ Hz, 2H; *p*-Ph), 6.32 (t, $J = 7.1$ Hz, 4H; *m*-Ph), 6.42 (d, $J = 8.3$ Hz, 1H; H^{10}), 6.44 (d, $J = 7.3$ Hz, 4H; *o*-Ph), 6.66 (t, $J = 8.0$ Hz, 1H; H^9), 7.21 (d, $J = 8.0$ Hz, 1H; H^8), 7.40 (d, $J = 2.1$ Hz, 1H; H^6), 7.60 (s, 1H; H^{13}), 7.70 (d, $J = 2.3$ Hz, 1H; H^4), 8.12 ppm (s, 1H; H^{15}); ^{19}F (376 MHz): $\delta = -56.45$ (CF_3 at R^1), −62.60 ppm (CF_3 at R^2); ^{13}C (126 MHz): $\delta = 96.19$ ppm (q, $^{2h}J_{C,F} = 5.3$ Hz ($J_{CH} = 138.9$ Hz); $TiCH_2$).

Received: July 26, 2002
Revised: January 13, 2003 [Z19832]

Keywords: fluorine · hydrogen bonds · polymerization · through-space interactions · zirconium

[1] a) H. H. Brintzinger, D. Fischer, R. Mülhaupt, B. Rieger, R. M. Waymouth, *Angew. Chem.* **1995**, *107*, 1255 – 1283; *Angew. Chem. Int. Ed. Engl.* **1995**, *34*, 1143 – 1170; b) L. Resconi, L. Cavallo, A. Fait, F. Piemontes, *Chem. Rev.* **2000**, *100*, 1253 – 1345.

[2] a) A. Bader, E. Lindner, *Coord. Chem. Rev.* **1991**, *108*, 27 – 110; b) C. S. Slone, D. A. Weinberger, C. A. Mirkin, *Prog. Inorg. Chem.* **1999**, *48*, 233 – 350.

[3] a) J. Ruwwe, G. Erker, R. Fröhlich, *Angew. Chem.* **1996**, *108*, 108 – 110; *Angew. Chem. Int. Ed. Engl.* **1996**, *35*, 80 – 82; b) Y. Sun, R. E. von H. Spence, W. E. Piers, M. Parvez, G. P. A. Yap, *J. Am. Chem. Soc.* **1997**, *119*, 5132 – 5143; c) U. Siemeling, *Chem. Rev.* **2000**, *100*, 1495 – 1526; for agostic interactions between metal and polymer chain, see: d) W. E. Piers, J. E. Bercaw, *J. Am. Chem. Soc.* **1990**, *112*, 9406 – 9407; e) M. Brookhart, M. L. H. Green, L. L. Wong, *Prog. Inorg. Chem.* **1998**, *36*, 1 – 124.

[4] Related examples of weak Zr···F interactions: a) A. R. Siedle, R. A. Newmark, W. M. Lamanna, J. C. Huffman, *Organometallics* **1993**, *12*, 1491 – 1492; b) X. Yang, C. L. Stern, T. J. Marks, *J. Am. Chem. Soc.* **1994**, *116*, 10015 – 10031; c) J. Karl, G. Erker, R. Fröhlich, *J. Am. Chem. Soc.* **1997**, *119*, 11165 – 11173; d) L. H. Gade, *Chem. Commun.* **2000**, 173 – 181.

[5] a) J. Saito, M. Mitani, J. Mohri, Y. Yoshida, S. Matsui, S. Ishii, S. Kojoh, N. Kashiwa, T. Fujita, *Angew. Chem.* **2001**, *113*, 3002 – 3004; *Angew. Chem. Int. Ed.* **2001**, *40*, 2918 – 2920; b) M. Mitani, J. Mohri, Y. Yoshida, J. Saito, S. Ishii, K. Tsuru, S. Matsui, R. Furuyama, T. Nakano, H. Tanaka, S. Kojoh, T. Matsugi, N. Kashiwa, T. Fujita, *J. Am. Chem. Soc.* **2002**, *124*, 3327 – 3336; c) S. Ishii, J. Saito, M. Mitani, J. Mohri, N. Matsukawa, Y. Tohi, S. Matsui, N. Kashiwa, T. Fujita, *J. Mol. Catal. A* **2002**, *179*, 11 – 16.

[6] a) M. Mitani, R. Furuyama, J. Mohri, J. Saito, S. Ishii, H. Terao, N. Kashiwa, T. Fujita, *J. Am. Chem. Soc.* **2002**, *124*, 7888 – 7889;

 © 2003 Wiley-VCH Verlag GmbH & Co. KGaA, Weinheim

b) J. Saito, M. Mitani, M. Onda, J. Mohri, S. Ishii, Y. Toshida, T. Nakano, H. Tanaka, T. Matsugi, S. Kojoh, N. Kashiwa, T. Fujita, *Macromol. Rapid Commun.* **2001**, *22*, 1071 – 1075.

[7] a) J. Tian, P. D. Hustad, G. W. Coates, *J. Am. Chem. Soc.* **2001**, *123*, 5134 – 5135; b) P. D. Hustad, J. Tian, G. W. Coates, *J. Am. Chem. Soc.* **2002**, *124*, 3614 – 3621.

[8] a) G. R. Desiraju, *Acc. Chem. Res.* **2002**, *35*, 565 – 573; b) J. Parsch, J. W. Engels, *J. Am. Chem. Soc.* **2002**, *124*, 5664 – 5672; c) W. Caminati, S. Melandri, P. Moreschini, P. G. Favero, *Angew. Chem.* **1999**, *111*, 3105 – 3107; *Angew. Chem. Int. Ed.* **1999**, *38*, 2924 – 2925.

[9] M. Bochmann, S. J. Lancaster, *Organometallics* **1993**, *12*, 633 – 640.

[10] The fact that only one of the two methylene hydrogen atoms exhibits ^{19}F coupling eliminates the possibility of the involvement of Zr···F interactions (and more generally of the coupling occurring "through-bond" through the methylene carbon atom).

[11] For **1**: $C_{41}H_{39}F_6NOZr$, $M_r = 766.98$, triclinic, $P\bar{1}$ (no. 2), $a = 9.613(2)$, $b = 11.860(2)$, $c = 16.928(3)$ Å, $\alpha = 109.37(3)$, $\beta = 90.88(3)$, $\gamma = 97.88(3)°$, $V = 1799.7(6)$ Å^3, $Z = 2$, $\rho_{calcd} = 1.415$ g cm^{-3}, $\mu(Mo_{K\alpha}) = 0.370$ mm^{-1}, $F(000) = 788$, $T = 253(2)$ K, $2\theta_{max} = 50.9°$, 5448 independent reflections ($R_{int} = 0.0252$), 479 variable parameters, $R_1 = 0.032$ ($I > 2\sigma(I)$), $wR_2 = 0.081$, GOF(F^2) = 0.976, largest diff. peak/hole = 0.41/−0.39 e Å^{-3}. For **2**: $C_{43}H_{47}F_3NOZr$, $M_w = 742.07$, triclinic, $P\bar{1}$ (no. 2), $a = 10.948(2)$, $b = 13.354(3)$, $c = 13.922(3)$ Å, $\alpha = 73.36(3)$, $\beta = 82.38(3)$, $\gamma = 82.56(3)°$, $V = 1923.9(7)$ Å^3, $Z = 2$, $\rho_{calcd} = 1.281$ g cm^{-3}, $\mu(Mo_{K\alpha}) = 0.333$ mm^{-1}, $F(000) = 774$, $T = 301(2)$ K, $2\theta_{max} = 50.7°$, 6262 independent reflections ($R_{int} = 0.0273$), 436 variable parameters, $R_1 = 0.045$ ($I > 2\sigma(I)$), $wR_2 = 0.118$, GOF(F^2) = 1.007, largest diff. peak/hole = 0.63/−0.60 e Å^{-3}. CCDC-190342 (**1**) and CCDC-190343 (**2**) contain the supplementary crystallographic data for this paper. These data can be obtained free of charge via www.ccdc.cam.ac.uk/conts/retrieving.html (or from the Cambridge Crystallographic Data Centre, 12 Union Road, Cambridge CB2 1EZ, UK; fax: (+44) 1223-336-033; or deposit@ccdc.cam.ac.uk).

[12] E. Y. Tshuva, I. Goldberg, M. Kol, Z. Goldschmidt, *Organometallics* **2001**, *20*, 3017 – 3028.

[13] Preliminary ethylene polymerization data revealed that complex **1** is an efficient catalyst (ca. 800 g(PE) (mmol catalyst)$^{-1}$ h^{-1} atm^{-1}; 2000 equiv MAO) at 25 °C, while the activity of **2** under identical conditions is low (< 10 g mmol^{-1} h^{-1} atm^{-1}). We note that this difference in activity may also be attributed to other factors, such as the electron-withdrawing effect of multiple CF_3 groups (see ref. [5c]). We thank the reviewers for helpful comments, and we are indebted to Dr. Wa-Hung Leung (HKUST) for assistance in variable-temperature NMR experiments.

 © 2003 Wiley-VCH Verlag GmbH & Co. KGaA, Weinheim

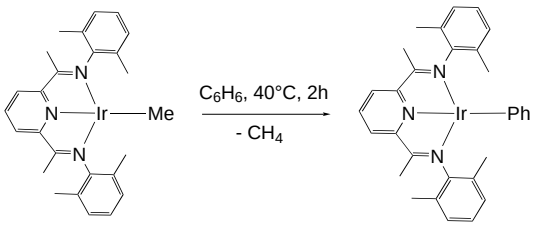
C-H Bond Activation

Transition-Metal Complexes with Sterically Demanding Ligands: Facile Thermal Intermolecular C–H Bond Activation in a Square-Planar Ir^{I} Complex**

*Stefan Nückel and Peter Burger**

Dedicated to Professor Robert G. Bergman on the occasion of his 60th birthday

The intermolecular activation of C–H bonds is a highly desirable process[1–8] and is part of many catalytic systems,[9–11] for example, the dehydrogenation of alkanes to alkenes.[12–14] Detailed studies by various groups clearly established that the C–H activation process is under kinetic rather than thermodynamic control in most cases.[12,13] Thus, highly reactive species, such as photochemically generated short-lived transients, for example, [Cp*Ir(PMe_3)] (Cp* = C_5Me_5), are often required,[3,15] while thermally initiated C–H activation processes under mild conditions are less common.[2,4,16] Herein, we describe a novel square-planar iridium(I) system **1**, which undergoes facile thermal *intermolecular* C–H activation in benzene at ambient temperature [Eq. (1)]. The observed



1 **2**

quantitative (1)

unusual low barrier is analyzed and traced by DFT methods providing guidelines for the design of novel systems, which would allow the activation of methane under mild conditions.

We have recently reported the synthesis of the iridium complex **1** and its rhodium analogue.[1] In the course of this study, we noticed facile intermolecular C–H activation in benzene leading quantitatively to the phenyl complex **2** and methane [Eq. (1)]. In the analogous reaction of **1** with C_6D_6 formation of [D_5]phenyl analogue of **2** and [D_1]methyl was observed. Both **1** and **2** could be characterized unambiguously

[*] Dr. P. Burger, Dr. S. Nückel
Anorg.-chem. Institut
Universität Zürich
Winterthurerstrasse 190, 8057 Zürich (Switzerland)
Fax: (+41) 1-635-6802
E-mail: chburger@aci.unizh.ch

[**] Part IV. We would like to thank the Swiss National Science Foundation for financial support. We are indebted to Prof. Heinz Berke for his generous support. For Part III see ref. [1].

 © 2003 Wiley-VCH Verlag GmbH & Co. KGaA, Weinheim DOI: 10.1002/anie.200219908

as square-planar complexes by their X-ray crystal structures (Figure 1).[17] Compound **2** was also obtained by independent synthesis from the corresponding methoxy complex[1] and phenylmagnesium chloride in 38% yield.

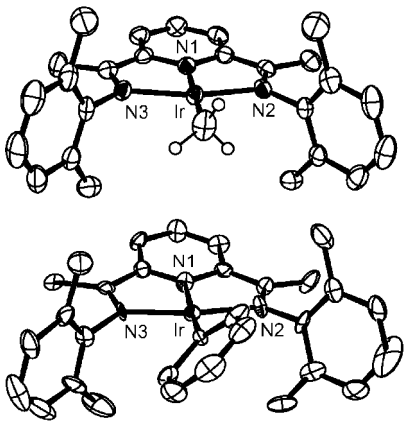


Figure 1. ORTEP plots (thermal elipsoids set at 50% probability) of complexes **1** (top) and **2** (bottom).

Monitoring the C–H activation process shown in Equation (1) by ^{1}H NMR spectroscopy indicated a clean conversion from **1**→**2** without detectable traces of intermediates. In neat [D_6]benzene under pseudo first-order conditions, a first-order decay of the starting material **1** with a free enthalpy of activation, $\Delta G_{313} = 23$ kcal mol^{-1} was measured.

Overall, the outcome of the C–H activation reaction resembles a σ-bond metathesis process, which is the anticipated mechanism for d^0 early-transition-metal and lanthanide row complexes.[8,18,19] For d^n-configured complexes with $n \geq 2$ there are other mechanistic alternatives, for example, a C–H oxidative-addition step, followed by C–H reductive elimination.[4,20,21] Investigations of late-transition-metal systems of which the cationic Ir^{III} compounds [Cp*Ir(PMe_3)Me]$^+X^-$ are prominent examples,[16,22] indicate that the two-step pathway is followed for these systems. However, it is extraordinary difficult to distinguish between these two mechanistic scenarios in the absence of experimental evidence for a C–H oxidative intermediate.[2,4,20,21,23] In the aforementioned Ir^{III} system, support for the two-step pathway was provided by DFT calculations prior to the recent isolation of a related Ir^V Si–H and C–H oxidative-addition product.[20,21]

To elucidate mechanistic details of the C–H activation system in the square-planar complex **1**, we also resorted to DFT methods. Since steric factors were deemed to play a crucial role in the C–H activation process, DFT calculations were performed on the full system. The efficient parallel RI-DFT implementation[24,25] (BP-86 functional; basis: TZVP, ECP-60-MWB (Ir), SVP (C,H,N)) of the Turbomole program package[26] allowed the use of a pure quantum-mechanical approach rather than the potentially less reliable quantum mechanical/molecular modeling methods,[27,28] which have been applied by other groups for systems of related size.

Although we did not intend to prejudge the mechanism, after considering the d^8-configuration of **1** we preferred the notion of the two-step mechanism. Preliminary experimental evidence for an Ir^{III} intermediate was provided by the reaction of **1** with H_2, which led to a tentatively assigned, trihydride Ir^{III} complex and methane.[29] The two-step view was partially supported by the absence of a transition state for the σ-bond metathesis pathway in our DFT calculations. Furthermore, we considered C–H bond activation at a three-coordinate metal center, with C–H activation in benzene by [Ir($P i Pr_3$)$_2$Cl] being a well-established example.[30] Related results were recently reported for an iridium cycloalkane-dehydrogenation catalyst bearing a terdentate cyclometalated bisphosphane donor (PCP pincer ligand).[13] Considering the rigid chelating ligand in **1**, the cleavage of one of the nitrogen donor arms from the metal center was deemed to be inconsistent with the observed low activation energy. This idea was supported by the DFT calculations, which revealed an Ir–$N_{diimine}$ bond-dissociation enthalpy of 35 kcal mol^{-1}.

These results suggested that an alternative mechanistic scenario was operative; we have therefore studied the two-step mechanism starting from the square-planar complex **1**. For this pathway, we were able to identify the required transition states TS_{OA} and TS_{RE} and the C–H oxidative Ir^{III} intermediate I_{OA} (OA = oxidative addition, RE = reductive elimination) as stationary points[31] (Figure 2).

The calculated barrier of 22 kcal mol^{-1} leading from **1** via the square-pyramidal transition state TS_{OA} to the octahedral H_5C_6–H (with benzene) oxidative-addition product I_{OA} is in excellent agreement with the observed experimental value. It is noteworthy that the Ir^{III} intermediate, I_{OA}, is energetically "uphill" (+10 kcal mol^{-1}) from **1** and benzene. This readily explains the calculated low barrier of 12 kcal mol^{-1} for the reductive elimination of CH_4 passing over TS_{RE} to give the energetically favored final products **2** and methane (−4 kcal mol^{-1}). For the corresponding Rh system, $\mathbf{1_{Rh}}$, we calculated a significantly higher barrier of 27 kcal mol^{-1}, which is consistent with the observed reluctance of $\mathbf{1_{Rh}}$ to undergo C–H activation in benzene even at elevated temperatures.

The results of the DFT calculations for C–H activation in methane by complex **1** are also included in Figure 2. In accordance with previous studies,[2,3] the barrier is higher (by +6 kcal mol^{-1}) than for the C–H activation process in benzene. For the analogous less crowded, $\mathbf{1_{H4}}$ (Figure 2) however, we derived a substantially smaller barrier of just 19 kcal mol^{-1} for the C–H oxidative-addition step in methane (Figure 2). Using a value of 9 kcal mol^{-1} for the $T\Delta S^{\neq}$ term ($\Delta S^{\neq} = +30$ cal mol^{-1} K^{-1}) at RT, a free enthalpy of activation of $\Delta G^{\neq} \approx 28$ kcal mol^{-1} is estimated. This result suggested that methane could be activated under relatively mild thermal conditions in the $\mathbf{1_{H4}}$ system.

To understand the unprecedented low barriers for the C–H oxidative-addition process in the square-planar systems **1** and $\mathbf{1_{H4}}$,[32] we performed an intrinsic reaction coordinate (IRC) calculation [33] starting from the square-pyramidal (Figure 2) transition state TS_{OA} for the methane oxidative-addition step in $\mathbf{1_{H4}}$. In the forward direction, this led to the anticipated octahedral Ir^{III} product $\mathbf{I_{H4,CH4}}$. Following the backward reaction mode, the anticipated lengthening of the Ir–H and Ir–C and shortening of the C–H bond was

 © 2003 Wiley-VCH Verlag GmbH & Co. KGaA, Weinheim

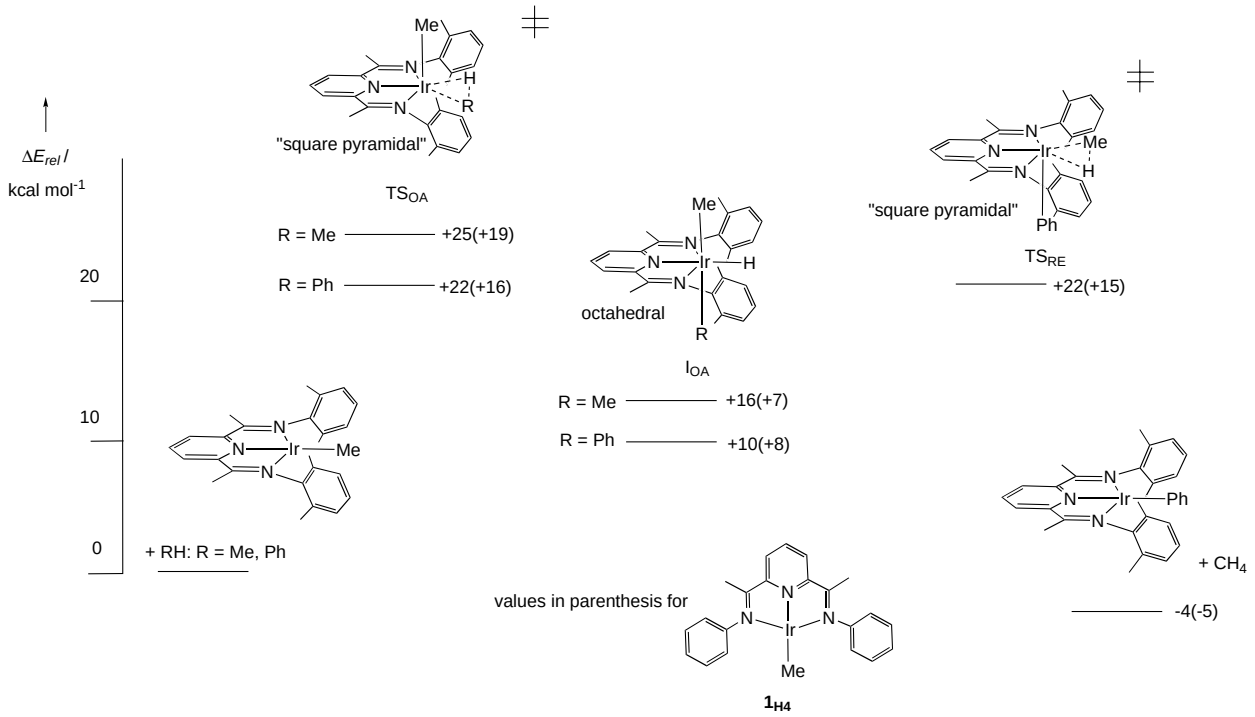


Figure 2. Energy diagram and proposed intermediates and transition states for the C–H activation process shown in Equation (1) based on DFT theory.

observed. More importantly, substantial opening of the $N_{pyridyl}$-Ir-Me angle from approximately 90° in the transition state was noticeable, and significant bending was still observed after methane was essentially fully released ($d(\mathrm{Ir}\cdots\mathrm{H}-\mathrm{CH_3}) = 2.5$ Å). This result clearly indicated bending of the methyl group away from the chelating-ligand–metal plane in the Ir complex as a crucial part of the C–H activation process and prompted us to calculate a Walsh diagram for this out-of-plane bending in complex **1** (Figure 3).

The small energy required for out-of-plane bending of the methyl group in complex **1** is noteworthy, approximately 12 kcal mol^{-1} for $\alpha = 70°$. For the unsubstituted model compound [{2,6-[C(CH$_3$)=NH]$_2$pyridine}IrMe] (**1$_{model}$**) we noticed an even more shallow potential for the bending process, with the Walsh diagrams of **1$_{model}$** and **1$_{H4}$** being essentially superimposable (Figure 3). Since identical kinetic and thermodynamic data for the methane C–H oxidative activation process were also derived for **1$_{model}$** and **1$_{H4}$**, we anticipate that the lower barriers in the N-phenyl substituted complex **1$_{H4}$** (compared to **1**) can be attributed to the more shallow potential of the bending process, which is a consequence of the reduced steric crowding. This situation is in contrast to the Walsh diagram obtained for this process in the tridentate phosphorus donor complex, [{κ^3-MePCH$_2$CH$_2$PMe$_2$)$_2$}IrMe]. For the latter, a significantly steeper potential for the bending process is observed and therefore a substantially larger contribution to the activation energy is anticipated. Before the origin of the difference between the N and P ligands will be addressed, the electronic structure of the bent species will be discussed.

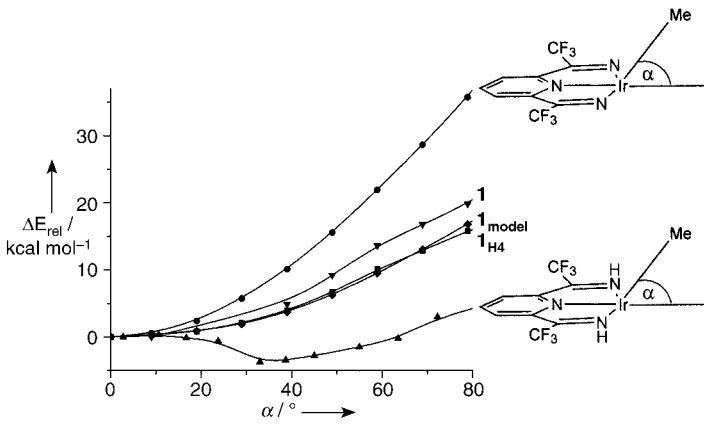


Figure 3. Walsh diagram for out-of-plane bending of [{κ^3-MeP(CH$_2$CH$_2$PMe$_2$)$_2$}IrMe] (●), complex **1** (▼), **1$_{model}$** (◆), **1$_{H4}$** (■), and [{2,6-[C(CF$_3$)=NH]$_2$-pyridine}IrMe] (▲).

As previously analyzed in EHT and DFT studies, an out-of-plane bending distortion of one ligand in a d^8-configured square-planar ML$_4$ complex leads to a C_{2v}-symmetrical ML$_4$ species which is isolobal to the methylene carbene unit, CH$_2$.[34,35] The [Fe(CO)$_4$] singlet state is a prominent representative of this type of compound. In the bent complex **1**, this is also nicely reflected in the frontier orbitals ($\alpha = 90°$) which have the required π(HOMO) and σ(LUMO) symmetry (Figure 4). Small C–H activation barriers would therefore be expected for this type of species. It should be noted that for angles $\alpha < 90°$, a residual two-orbital four-electron repulsive term between a filled metal d orbital and the occupied σ CH orbital raises the barrier.[35] This term vanishes when a bending angle of 90° is attained, as observed in the transition state TS$_{OA}$ of complex **1**.

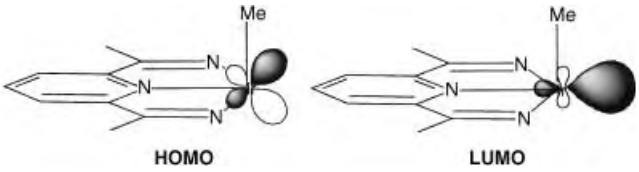


Figure 4. Frontier orbitals of complex **1**.

Out-of-plane bending potentials in d^8-configured square-planar ML_4 complexes have been discussed in the context of oxidative addition of H_2.[36,37] The major contribution to this unfavorable process arises from a two-orbital-four-electron repulsive interaction between the occupied metal-based d_{xz} orbital and the methyl σ orbitals upon bending, which is nonbonding in the undistorted square-planar ML_4 complex. As shown in Figure 5 this repulsive interaction is significantly lowered by mixing of a diimine, pyridine-ligand-based π-acceptor orbital in the iridium methyl complex **1**.

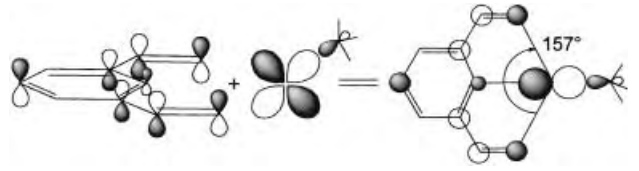


Figure 5. Lowering of the repulsive interaction between the metal d_{xz} and the methyl σ orbitals by mixing of a π-acceptor orbital in complex **1**.

The major stabilizing contribution stems from back donation into the -C=$N_{diimine}$ unit. It has to be emphasized that this interaction is nonbonding if the ligands are located in the nodal plane of the d_{xz} orbital. As can be readily seen from the $N_{diimine}$-Ir-$N_{diimine}$ angle of 157° in the X-ray crystal structure of **1,** the diimine N_{donor} atoms are significantly "bent back" from the Ir-Me unit. This arrangement is a consequence of the ligand constraints, that is, the "too-short" C–N bonds, which enable strong back donation. Further evidence for this view was provided by the Walsh diagram of the CF_3 substituted diimine model compound, [{2,6-[$C(CF_3)$=$NH]_2$pyridine}IrMe] (Figure 3) bearing a stronger π-acceptor ligand. This situatiuon leads to a preference for the bent over the square-planar structure with a calculated minimum at $\alpha =$ 154°. Finally, this rationale also serves to explain the larger barrier for the bending process in the aforementioned triphosphorus donor complex. Inspection of the DFT optimized structure revealed that the σ* phosphorus π-acceptor orbitals are located in close proximity to the d_{xz} nodal plane and thus, significantly less stabilization through back donation can be achieved.

We have presented a novel thermal C–H activation system and have traced the low activation energies by DFT methods, sterically less crowded complexes are predicted to display even lower C–H activation barriers.

Received: August 8, 2002
Revised: December 30, 2002 [Z19908]

Keywords: C–H bond activation · density functional theory · iridium · N ligands

[1] S. Nückel, P. Burger, *Organometallics* **2001**, *20*, 4345 – 4359.
[2] B. A. Arndtsen, R. G. Bergman, T. A. Mobley, T. H. Peterson, *Acc. Chem. Res.* **1995**, *28*, 154 – 162, and references therein.
[3] R. G. Bergman, *J. Organomet. Chem.* **1990**, *400*, 273 – 282, and references therein.
[4] R. H. Crabtree, *J. Chem. Soc. Dalton Trans.* **2001**, 2437 – 2450.
[5] C. L. Hill, *Activation and Functionalization of Alkanes*, Wiley-Interscience, New York, **1989**, and references therein.
[6] A. E. Shilov, G. B. Shul'pin, *Chem. Rev.* **1997**, *97*, 2879 – 2932, and references therein.
[7] G. A. Luinstra, J. A. Labinger, J. E. Bercaw, *J. Am. Chem. Soc.* **1993**, *115*, 3004 – 3005.
[8] P. L. Watson, *J. Am. Chem. Soc.* **1983**, *105*, 6491 – 6493.
[9] A. Sen, *Acc. Chem. Res.* **1998**, *31*, 550 – 557.
[10] R. A. Periana, D. J. Taube, S. Gamble, H. Taube, T. Satoh, H. Fujii, *Science* **1998**, *280*, 560 – 564.
[11] R. A. Periana, D. J. Taube, E. R. Evitt, D. G. Loffler, P. R. Wentrcek, G. Voss, T. Masuda, *Science* **1993**, *259*, 340 – 343.
[12] W. W. Xu, G. P. Rosini, M. Gupta, C. M. Jensen, W. C. Kaska, K. Krogh-Jespersen, A. S. Goldman, *Chem. Commun.* **1997**, 2273 – 2274.
[13] M. Kanzelberger, B. Singh, M. Czerw, K. Krogh-Jespersen, A. S. Goldman, *J. Am. Chem. Soc.* **2000**, *122*, 11017 – 11018.
[14] R. H. Crabtree, *The Organometallic Chemistry of the Transition Metals*, Wiley-Interscience, New York, **2001**.
[15] S. E. Bromberg, H. Yang, M. C. Asplund, T. Lian, B. K. McNamara, K. T. Kotz, J. S. Yeston, M. Wilkens, H. Frei, R. G. Bergman, C. B. Harris, *Science* **1997**, *278*, 260 – 263.
[16] B. A. Arndtsen, R. G. Bergman, *Science* **1995**, *270*, 1970 – 1973.
[17] Data collection: Stoe IPDS Image Plate System, absorption corrections were carried out numerically. Structure solution: Direct methods using the SHELXS-97 program package; refinement against F^2 with SHELXL-97.[38] All non-hydrogen atoms were refined anisotropically; the position of the hydrogen atoms were calculated in idealized positions and refined using a riding model. Complex **1**: Green needle ($0.37 \times 0.11 \times 0.09$ mm). Orthorhombic cell, space group $P2_12_12_1$ (No. 19), $Z = 4$, $a = 12.914(1)$, $b = 13.021(1)$, $c = 14.0217(8)$ Å, $V = 2357.8(3)$ Å^3, $\rho_{calcd} = 1.625$ g cm^{-3}. 18190 reflections collected, thereof 4360 independent; 4360 reflections used for structure solution and refinement. The refinement converged at final R values $R(I > 2\sigma(I))$: $R1 = 0.0150$ and $wR2 = 0.0301$ for 278 parameters; GOF 1.01, residual electron density: 0.51, −0.5 e Å^{-3} (Flack X-Parameter −0.030(6) and 1.05(2) for the inverted structure). Complex **2**: The crystals were of low quality (presumably twinned); repeated attempts under varied conditions did not provide better single crystals. Brown rectangular parallelepiped ($0.3 \times 0.3 \times 0.2$ mm); triclinic cell, space group $P\bar{1}$ (No. 2), $Z = 2$ with two independent molecules per unit cell. $a = 10.020(1)$, $b = 14.688(1)$, $c = 18.741(2)$ Å, $\alpha = 85.13(1)°$, $\beta = 89.65(1)°$, $\gamma = 72.31(1)°$. $V = 2617.8(2)$ Å^3, $\rho_{calcd} = 1.628$ g cm^{-3}. 9272 independent reflections used for structure solution and refinement. Final R-values (635 parameters) $R(I > 2\sigma(I))$: $R1 = 0.1156$ and $wR2 = 0.3235$. CCDC-191048 (**1**) CCDC-203880 (**2**) contains the supplementary crystallographic data for this paper. These data can be obtained free of charge via www.ccdc.cam.ac.uk/conts/retrieving.html (or from the Cambridge Crystallographic Data Centre, 12 Union Road, Cambridge CB2 1EZ, UK; fax: (+44) 1223-336-033; or deposit@ccdc.cam.ac.uk).
[18] P. L. Watson, G. W. Parshall, *Acc. Chem. Res.* **1985**, *18*, 51 – 56.
[19] P. L. Watson, *J. Chem. Soc. Chem. Commun.* **1983**, 276 – 277.
[20] S. R. Klei, T. D. Tilley, R. G. Bergman, *J. Am. Chem. Soc.* **2000**, *122*, 1816 – 1817.

 © 2003 Wiley-VCH Verlag GmbH & Co. KGaA, Weinheim

[21] S. Q. Niu, M. B. Hall, *J. Am. Chem. Soc.* **1998**, *120*, 6169 – 6170.
[22] P. Burger, R. G. Bergman, *J. Am. Chem. Soc.* **1993**, *115*, 10462 – 10463.
[23] T. M. Gilbert, I. Hristov, T. Ziegler, *Organometallics* **2001**, *20*, 1183 – 1189.
[24] K. Eichkorn, O. Treutler, H. Öhm, M. Häser, R. Ahlrichs, *Chem. Phys. Lett.* **1995**, *242*, 652 – 660.
[25] K. Eichkorn, O. Treutler, H. Öhm, M. Häser, R. Ahlrichs, *Chem. Phys. Lett.* **1995**, *240*, 283 – 289.
[26] R. Ahlrichs, M. Bär, M. Häser, H. Horn, C. Kölmel, *Chem. Phys. Lett.* **1989**, *162*, 165 – 169.
[27] S. Dapprich, I. Komaromi, K. S. Byun, K. Morokuma, M. J. Frisch, *J. Mol. Struct.* **1999**, *462*, 1 – 21.
[28] J. Gao in *Reviews in Computational Chemistry, Vol. 7* (Eds.: D. B. Boyd, K. B. Lipkowitz), Wiley, New York, **1996**.
[29] S. Nückel, Dissertation, Universität Zürich **2002**.
[30] H. Werner, A. Höhn, M. Dziallas, *Angew. Chem.* **1986**, *98*, 1112 – 1114; *Angew. Chem. Int. Ed. Engl.* **1986**, *25*, 1090 – 1092.
[31] All stationary points were characterized by the calculation of second derivatives through the absence (minima) or one imaginary frequency (transition states). Transition-state optimizations were performed with John Baker's OPTIMIZE program, available from Parallel Quantum Solutions, Fayetteville, AR, USA, interfaced with Turbomole.
[32] R. T. Price, R. A. Andersen, E. L. Muetterties, *J. Organomet. Chem.* **1989**, *376*, 407 – 417.
[33] M. Sierka, J. Sauer, *J. Chem. Phys.* **2000**, *112*, 6983 – 6996.
[34] J. Y. Saillard, R. Hoffmann, *J. Am. Chem. Soc.* **1984**, *106*, 2006 – 2026.
[35] T. Ziegler, V. Tschinke, L. Y. Fan, A. D. Becke, *J. Am. Chem. Soc.* **1989**, *111*, 9177 – 9185.
[36] A. Dedieu, A. Strich, *Inorg. Chem.* **1979**, *18*, 2940 – 2943.
[37] S. A. Macgregor, O. Eisenstein, M. K. Whittlesey, R. N. Perutz, *J. Chem. Soc. Dalton Trans.* **1998**, 291 – 300.
[38] G. M. Sheldrick, SHELXL-97, Programs for Crystal Structure Solution and Refinement, Universität Göttingen (Germany) **1997**.

 © 2003 Wiley-VCH Verlag GmbH & Co. KGaA, Weinheim

Photochemistry of Chiral Crystals

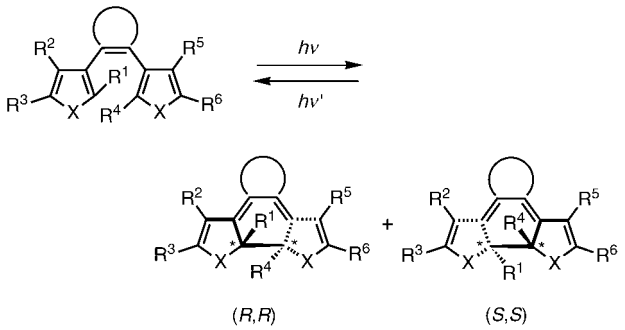
Absolute Asymmetric Photocyclization of a Photochromic Diarylethene Derivative in Single Crystals**

*Satoshi Yamamoto, Kenji Matsuda, and Masahiro Irie**

In recent years there has been considerable scientific interest in the photochemistry of compounds in crystals.[1] The topics range widely from chemiluminescence in silicon nanocrystals[2] to chemical reactivity in crystals.[3] One unique aspect of crystal-phase reactions is topochemical reactivity. The crystal lattice provides a matrix for reactions with stereo-, regio-, and enantiospecificity. Enantiospecific reactions can take place in chiral crystals containing chiral auxiliaries such as chiral host molecules[4] and covalently bonded chiral substituents.[5] Moreover, an ensemble of achiral molecules can be transformed by reactions into chiral molecules on crystallization in a chiral space group. Such an asymmetric reaction in the absence of any outside chiral influence is referred to as absolute asymmetric synthesis.

The first example of absolute asymmetric synthesis, a gas/solid-phase reaction was carried out by Penzien and Schmidt.[6] Absolute asymmetric synthesis in a photochemical intramolecular reaction was first reported by Scheffer and coworkers.[7] The photochemical absolute asymmetric syntheses of 1,4-disubstituted phenylenediacrylate derivatives[8] and ethyl 4-[2-(4-pyridyl)ethenyl]cinnamate[9] are other typical examples of topochemical reactions.

Photochromic compounds characteristically exhibit two different chemical forms that are reversibly transformed from one to the other upon irradiation with light of appropriate wavelengths. Although numerous photochromic compounds have been reported, compounds that undergo reaction in the crystal phase are relatively rare.[10] Some diarylethene derivatives undergo thermally irreversible and fatigue-resistant photochromic reactions even in single crystals. The photochemical conrotatory cyclization produces two enantiomeric closed-ring isomers (*R,R* and *S,S*), in which the chirality originates from asymmetric carbon atoms (Scheme 1).



Scheme 1. Photochromism of diarylethene. The photogenerated closed-ring form has two enantiomers, (*R,R*) and (*S,S*).

The photocyclization of diarylethene derivatives in solution, in general, results in the formation of two enantiomers in equal amounts. Even when a chiral substituent is introduced into the diarylethene, enrichment of one of the diastereomers hardly takes place.[11] Enrichment of one of the enantiomers or diastereomers in photochemical reactions requires a chiral environment like that formed on complexation to a copper(I) center having chiral ligands[12] or chiral crystal packing induced by a chiral substituent.[13] If the open isomers would crystallize with chiral packing, absolute asymmetric photochromism, in which achiral compounds produce chiral products in the absence of any external chiral

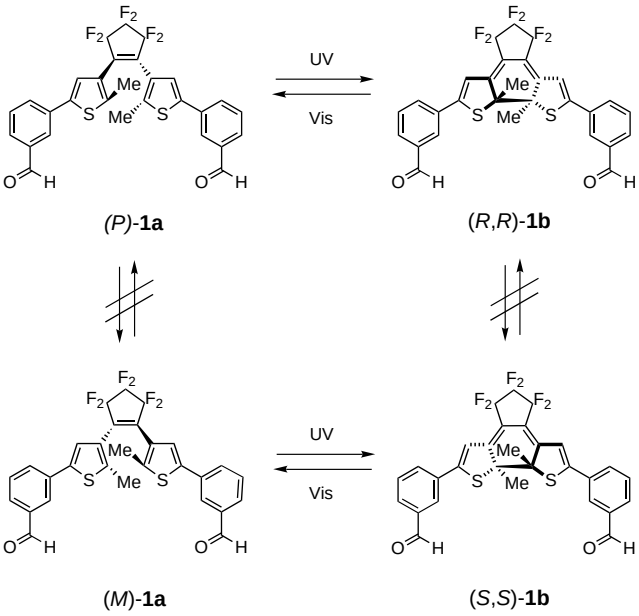
[*] Prof. M. Irie, S. Yamamoto, Dr. K. Matsuda
Department of Chemistry and Biochemistry
Graduate School of Engineering, Kyushu University
Hakozaki 6-10-1, Higashi-ku, Fukuoka 812-8581 (Japan)
Fax: (+81) 92-642-3568
E-mail: irie@cstf.kyushu-u.ac.jp

[**] This work was supported by CREST (Core Research for Evolutional Science and Technology) of Japan Science and Technology Corporation (JST).

Supporting information for this article is available on the WWW under http://www.angewandte.org or from the author.

 © 2003 Wiley-VCH Verlag GmbH & Co. KGaA, Weinheim DOI: 10.1002/anie.200250417

agent, would be possible. Herein we report on the absolute asymmetric photocyclization of achiral 1,2-bis(5-*m*-formylphenyl-2-methyl-3-thienyl)perfluorocyclopentene (**1a**) in chiral crystals (Scheme 2).



Scheme 2. Enantioselective photochromic reaction of (*M*)-**1a** and (*P*)-**1a** in single crystals.

The achiral diarylethene **1a** was synthesized from 2,4-dibromo-5-methylthiophene in four steps according to previously reported methods (see Supporting Information). The formyl substituents were introduced at the *meta* positions of the two phenyl groups. The structure of **1a** was confirmed by mass spectrometry, ^{1}H NMR and UV/Vis spectroscopy, and elemental analysis.[14]

Figure 1 shows the absorption spectrum of **1a** and racemic **1b** in ethyl acetate solution. Upon irradiation with 313-nm light **1a** underwent a photochromic reaction. The colorless solution of **1a** ($\lambda_{max} = 255$ nm, $\varepsilon_{max} = 45\,000\,M^{-1}cm^{-1}$) became blue, and the absorption maximum was observed at 588 nm ($\varepsilon_{max} = 15\,000\,M^{-1}cm^{-1}$). The color change is due to the generation of the closed-ring isomer **1b**. The conversion

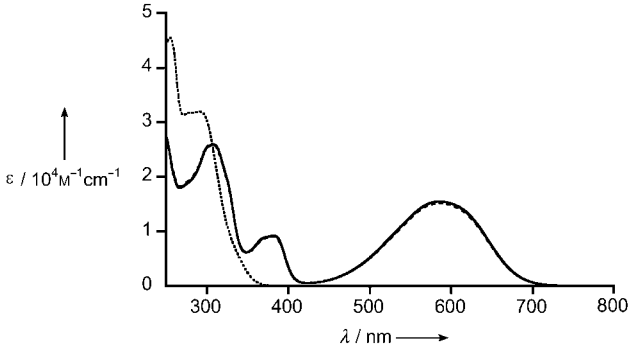


Figure 1. Absorption spectra in ethyl acetate for the open-ring isomer **1a** (•••••), closed-ring isomer **1b** (——), and the photostationary state under irradiation with 313-nm light (-----).

ratio on photoirradiation with 313-nm light from the open- to the closed-ring isomer was 98%. Upon irradiation with 578-nm light the blue solution once again became colorless, and the open-ring isomer formed.

Colorless needles of **1a** were obtained from solution in acetonitrile. The absolute crystal structure was determined by X-ray crystallographic analysis. Two different kinds of crystals, (*M*)-**1a** and (*P*)-**1a** (Scheme 2), which are mirror images of each other, were obtained in the same sample tube.[15] Figure 2a shows the packing diagram of (*P*)-**1a**. Single crystals of (*P*)-**1a** adopt the monoclinic chiral space group $P2_1$, although no optically active unit is incorporated in the diarylethene unit. In the crystal the open-ring isomer was restricted to only one conformation in which the hexatriene unit adopted a *P* helix. The distance between the reactive carbon atoms is 3.54 Å, which is short enough for the reaction to take place in the crystal phase. The molecular configuration and packing of crystal (*M*)-**1a** is the mirror image of that of (*P*)-**1a**.

Both (*M*)-**1a** and (*P*)-**1a** underwent photochromic reaction in single crystals. Upon irradiation with 366-nm light the single crystals turned blue, and the blue color disappeared upon irradiation with visible light ($\lambda > 500$ nm). The coloration/decoloration cycles could be repeated more than 100 times without change in the crystal shape. The color of the crystal was observed under polarized light at the (001) face. Figure 2b shows the plot of absorption versus the angle of the incident polarized light at the (001) face of the chiral crystal,

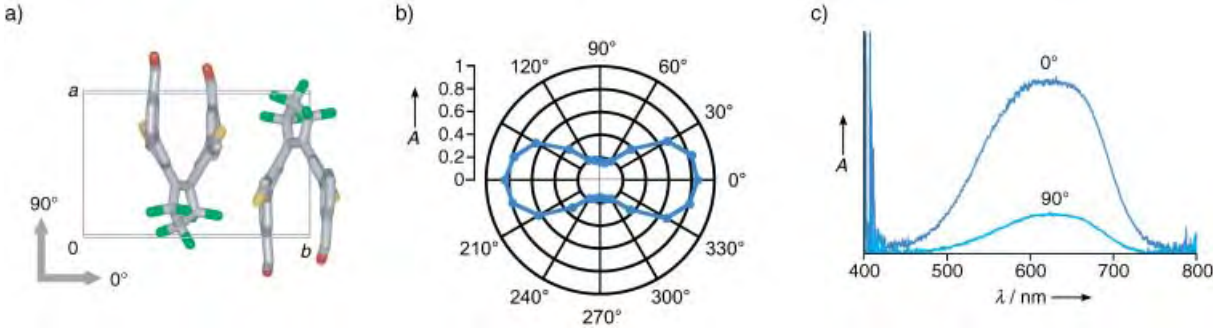


Figure 2. a) Packing diagram of (*P*)-**1a** in the chiral crystal projected to the (001) face (S: yellow; O: red; F: green). b) Plot of absorption versus angle of indicent polarized light ($\lambda = 620$ nm). c) Polarized absorption spectra of the (001) face. *A* = absorbance.

 © 2003 Wiley-VCH Verlag GmbH & Co. KGaA, Weinheim

and Figure 2c shows the absorption anisotropy. At a certain angle the crystal has a deep color (0°). When the crystal is rotated by as much as 90°, the intensity of the color decreases. The changes of color intensity on rotating the crystal sample indicate that the closed-ring isomers are regularly oriented in the crystal and that the photochromic reaction takes place in the crystal lattice. Upon irradiation with visible light ($\lambda >$ 500 nm), the crystal returns to the colorless original state.

The enantioselectivity of the cyclization process in solution as well as in single crystals of (*M*)-**1a** and (*P*)-**1a** was examined by HPLC analysis of the products with a chiral column.[16] A monitoring wavelength of 588 nm was used, because only the closed-ring isomers have absorption in the visible region. After a solution of achiral **1a** in hexane, ethyl acetate, or ethanol had been irradiated ($\lambda = 313$ nm), a racemic mixture of the two enantiomeric products **1b** was observed; enantioselective cyclization was not observed (Figure 3a).

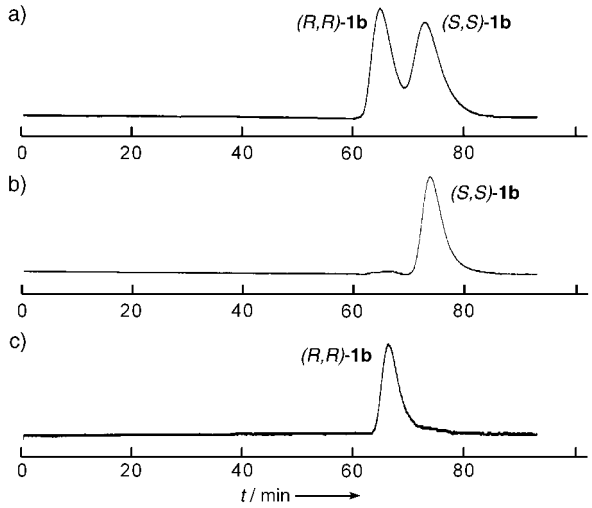


Figure 3. HPLC traces (monitored at $\lambda = 588$ nm) for the products obtained from a) the photocyclization reaction of **1a** in hexane solution, b) the photocyclization reaction in single crystals of (*M*)-**1a**, and c) the photocyclization reaction in single crystals of (*P*)-**1a**.

In the single crystals the selectivity of the photogenerated enantiomers was dramatically changed, as shown in Figure 3b and 3c. The irradiation wavelength was 400 nm. The chiral crystal (*P*)-**1a** gave optically pure (*R,R*)-**1b,** and (*M*)-**1a** gave pure (*S,S*)-**1b** by topochemical photocyclization. Table 1 shows the relationship between conversion and enantiomeric excess (*ee*). The reaction was still quite enantioselective up to a conversion of around 10% and decreased slightly at higher conversions. The decrease of selectivity is attributable to distortion of the crystal lattice as the reaction proceeds.

Direct observation of the photocyclization process by using an in situ X-ray crystallographic method[17] would be very helpful to understand the details of the enantioselective reaction along with topochemical photocyclization in the crystal phase. To study the reaction process by X-ray crystallography, we required a conversion higher than 5%. At $\lambda = 400$ nm the chiral crystals (*M*)-**1a** and (*P*)-**1a** have an

Table 1: Asymmetric induction in the photochromism of crystals of (*P*)-**1a** and (*M*)-**1a**.

Conversion [%][a]	*ee* [%][b,c]	Chirality
12.0	94	(*R,R*)
10.8	96	(*S,S*)
7.9	97	(*R,R*)
7.3	95	(*R,R*)
4.3	93	(*S,S*)
1.8	96	(*R,R*)
1.7	98	(*S,S*)
0.6	99	(*R,R*)

[a] Determined by HPLC (monitored at $\lambda = 310$ nm) with a Wakosil 5SIL column and eluting with dichloromethane. [b] Determined by HPLC (monitored at 588 nm) with a Chiralpack AD-H column and eluting with hexane/2-propanol/ethanol (99/0.9/0.1 volume ratio). [c] The error of the *ee* values was less than ±2%.

absorption tail, and the absorption of the closed-ring isomer is minimum. Thus, we irradiated the (100) face selectively with polarized light ($\lambda = 400$ nm) for 80 h.[17f,g]

The final molecular structure of the closed-ring isomer (*R,R*)-**1b** and the structure of the open-ring isomer (*P*)-**1a** are shown in Figure 4. The positions of the sulfur atoms S1B and

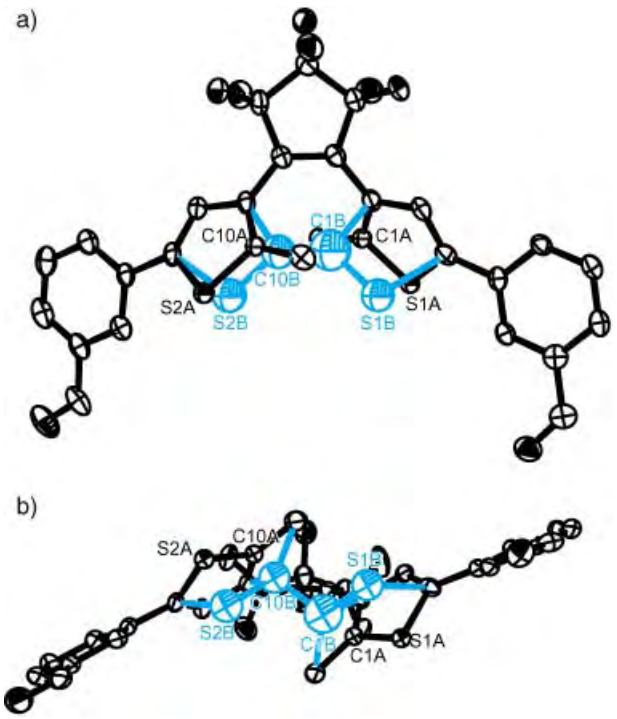


Figure 4. X-ray crystal structure of (*P*)-**1a** after irradiation with 400-nm light: a) top and b) side views (ORTEP drawings). Blue atoms and bonds represent the photogenerated closed-ring moieties of (*R,R*)-**1b** whose occupancy was estimated to be roughly 9%. Hydrogen atoms are omitted for clarity.

S2B and carbon atoms C1B and C10B, which are affected by irradiation, were found (see Supporting Information). The structure change indicates that the topochemically controlled cyclization reaction proceeds in the crystal lattice of open-ring

 © 2003 Wiley-VCH Verlag GmbH & Co. KGaA, Weinheim

isomer (*P*)-**1a**. The yield of the photogenerated (*R,R*)-**1b** was estimated from the occupancy factors to be approximately 9%.

In conclusion, chiral crystals of (*M*)-**1a** and (*P*)-**1a** were obtained by recrystallization of the achiral molecule **1a** from acetonitrile. The crystals underwent highly enantioselective photocyclization, while racemic mixtures were obtained for the reaction in solution. This is the first report on absolute reversible photocyclization reactions in chiral crystals. The asymmetric photochromic material has potential application in nonlinear optics, for example, in switchable second-harmonic generation devices.

Received: October 23, 2002
Revised: December 16, 2002 [Z50417]

Keywords: asymmetric synthesis · chirality · enantioselectivity · photochemistry · photochromism

[1] a) *Photochemistry in Organized and Constrained Media* (Ed.: V. Ramamurthy), VCH, Weinheim, **1991**; b) V. Ramamurthy, K. Venkatesan, *Chem. Rev.* **1987**, *87*, 433–481; c) F. Toda, *Acc. Chem. Res.* **1995**, *28*, 480–486; d) J. N. Gamlin, R. Jones, M. Leibovitch, B. Patrick, J. R. Scheffer, J. Trotter, *Acc. Chem. Res.* **1996**, *29*, 203–209; e) K. Tanaka, F. Toda, *Chem. Rev.* **2000**, *100*, 1025–1074.

[2] a) J. Hu, L.-S. Li, W. Yang, L. Manna, L.-W. Wang, A. P. Alivisatos, *Science* **2001**, *292*, 2060–2063; b) L. Pavesi, L. Dal Negro, C. Mazzoleni, G. Franzò, F. Priolo, *Nature* **2000**, *408*, 440–444; c) Z. Ding, B. M. Quinn, S. K. Haram, L. E. Pell, B. A. Korgel, A. J. Bard, *Science* **2002**, *296*, 1293–1297.

[3] a) V. R. Pedireddi, A. R. P. Sarma, G. R. Desiraju, *J. Chem. Soc. Perkin Trans. 2* **1992**, 311–320; b) Y. Ito, B. Borecka, G. Olovsson, J. Trotter, J. R. Scheffer, *Tetrahedron Lett.* **1995**, *36*, 6087–6090; c) S. H. Shin, A. E. Keating, M. A. Garcia-Garibay, *J. Am. Chem. Soc.* **1996**, *118*, 7626–7627; d) D. G. Amirsakis, M. A. Garcia-Garibay, S. J. Rowan, J. F. Stoddart, A. J. P. White, D. J. Williams, *Angew. Chem.* **2001**, *113*, 4386–4391; *Angew. Chem. Int. Ed.* **2001**, *40*, 4256–4261.

[4] a) H. Aoyama, T. Hasegawa, Y. Omote, *J. Am. Chem. Soc.* **1979**, *101*, 5343–5347; b) F. Toda, K. Tanaka, *Tetrahedron Lett.* **1986**, *29*, 4299–4302; c) F. Toda, K. Tanaka, O. Kakinoki, T. Kawakami, *J. Org. Soc.* **1993**, *58*, 3783–3784; d) K. Tanaka, F. Toda, E. Mochizuki, N. Yasui, Y. Kai, I. Miyahara, K. Hirotsu, *Angew. Chem.* **1999**, *111*, 3733–3736; *Angew. Chem. Int. Ed.* **1999**, *38*, 3523–3525; e) H. Hosomi, S. Ohba, K. Tanaka, F. Toda, *J. Am. Chem. Soc.* **2000**, *122*, 1818–1819.

[5] a) A. G. Schultz, A. G. Taveras, R. E. Taylor, F. S. Tham, R. K. Kulling, *J. Am. Chem. Soc.* **1992**, *114*, 8725–8727; b) M. Sakamoto, M. Takahashi, N. Hokari, T. Fujita, S. Watanabe, *J. Org. Chem.* **1994**, *59*, 3131–3134; c) Y. Ito, G. Kano, N. Nakamura, *J. Org. Chem.* **1998**, *63*, 5643–5647.

[6] K. Penzien, G. M. J. Schmidt, *Angew. Chem.* **1969**, *81*, 628–629; *Angew. Chem. Int. Ed. Engl.* **1969**, *8*, 608–609.

[7] S. V. Evans, M. Garcia-Garibay, N. Omkaram, J. R. Scheffer, J. Trotter, F. Wireko, *J. Am. Chem. Soc.* **1986**, *108*, 5648–5650.

[8] L. Addadi, J. van Mil, M. Lahav, *J. Am. Chem. Soc.* **1982**, *104*, 3422–3429.

[9] C. M. Chung, M. Hasegawa, *J. Am. Chem. Soc.* **1991**, *113*, 7311–7316.

[10] a) M. Irie, *Chem. Rev.* **2000**, *100*, 1685–1716; b) K. Matsuda, K. Takayama, M. Irie, *Chem. Commun.* **2001**, 363–364; c) K. Shibata, K. Muto, S. Kobatake, M. Irie, *J. Phys. Chem. A* **2002**, *106*, 209–214; d) K. Higashiguchi, K. Matsuda, M. Matsuo, T. Yamada, M. Irie, *J. Photochem. Photobiol. A* **2002**, *152*, 141–146; e) M. Morimoto, S. Kobatake, M. Irie. *Adv. Mater.* **2002**, *14*, 1027–1029; f) T. Yamada, S. Kobatake, M. Irie, *Bull. Chem. Soc. Jpn.* **2002**, *75*, 167–173.

[11] T. Yamaguchi, K. Uchida, M. Irie, *J. Am. Chem. Soc.* **1997**, *119*, 6066–6071.

[12] E. Murguly, T. B. Norsten, N. R. Branda, *Angew. Chem.* **2001**, *113*, 1802–1805; *Angew. Chem. Int. Ed.* **2001**, *40*, 1752–1755.

[13] a) T. Kodani, K. Matsuda, T. Yamada, M. Irie, *Chem. Lett.* **1999**, 1003–1004; b) T. Kodani, K. Matsuda, T. Yamada, S. Kobatake, M. Irie, *J. Am. Chem. Soc.* **2000**, *122*, 9631–9637; c) K. Matsuda, S. Yamamoto, M. Irie, *Tetrahedron Lett.* **2001**, *42*, 7291–7293.

[14] Physical properties of **1a**: m. p. 137–138°C; ^{1}H NMR (200 MHz, $CDCl_3$, 25°C, TMS): $\delta = 2.01$ (s, 6H), 7.38 (s, 2H), 7.57 (t, $J = 8$ Hz, 2H), 7.78–7.83 (m, 4H), 8.04 (s, 2H), 10.06 ppm (s, 2H); UV/Vis (ethyl acetate): λ_{max} (ε): 255 (45000), 292 (32000); MS: *m/z*: 576 [M^+]; elemental analysis calcd (%) for $C_{29}H_{18}F_6O_2S_2$: C 60.41, H 3.15; found: C 60.28, H 3.16.

[15] Crystallographic data for (*P*)-**1a,** (*P*)-**1a′,** which is the (*P*)-**1a** after photoirradiation for 80 h, and (*M*)-**1a**: Recorded at 123 K with $Mo_{K\alpha}$ radiation: (*P*)-**1a**: $a = 8.3543(18)$, $b = 13.106(3)$, $c = 11.347(3)$ Å, $\beta = 93.389(4)°$, monoclinic, space group $P2_1$, $Z = 2$, 5592 measured reflections, 3477 unique ($R_{int} = 0.0306$), 354 parameters, $R_1 = 0.0432$ [$I > 2\sigma(I)$] and $wR_2 = 0.1029$ (for all data), Flack parameter $\chi = -0.10(9)$; (*P*)-**1a′**: $a = 8.374(2)$, $b = 13.050(4)$, $c = 11.314(3)$ Å, $\beta = 93.637(5)°$, monoclinic, space group $P2_1$, $Z = 2$, 8310 measured reflections, 4894 unique ($R_{int} = 0.0283$), 369 parameters, $R_1 = 0.0442$ [$I > 2\sigma(I)$] and $wR_2 = 0.0948$ (for all data), Flack parameter $\chi = -0.09(8)$; (*M*)-**1a**: $a = 8.3543(18)$, $b = 13.106(3)$, $c = 11.347(3)$ Å, $\beta = 93.389(4)°$, monoclinic, space group $P2_1$, $Z = 2$, 5693 measured reflections, 3536 unique ($R_{int} = 0.0247$), 354 parameters, $R_1 = 0.0488$ [$I > 2\sigma(I)$] and $wR_2 = 0.1290$ (for all data), Flack parameter $\chi = -0.02(12)$. CCDC-194695 ((*P*)-**1a**), CCDC-194696 ((*P*)-**1a′**), and CCDC-194694 ((*M*)-**1a**) contain the supplementary crystallographic data for this paper. These data can be obtained free of charge via www.ccdc.cam.ac.uk/conts/retrieving.html (or from the Cambridge Crystallographic Data Centre, 12 Union Road, Cambridge CB2 1EZ, UK; fax: (+44) 1223-336-033; or deposit@ccdc.cam.ac.uk).

[16] The photoirradiated sample was separated with a chiral column (Daicel Chiralpak AD-H, hexane/2-propanol/ethanol = 99/0.9/0.1 volume ratio, 0.6 mL min^{-1}).

[17] a) J. Harada, H. Uekusa, Y. Ohashi, *J. Am. Chem. Soc.* **1999**, *121*, 5809–5810; b) M. Kawano, T. Sano, J. Abe, Y. Ohashi, *J. Am. Chem. Soc.* **1999**, *121*, 8106–8107; c) M. Kawano, T. Sano, J. Abe, Y. Ohashi, *Chem. Lett.* **2000**, 1372–1373; d) S. Kobatake, K. Shibata, K. Uchida, M. Irie, *J. Am. Chem. Soc.* **2000**, *122*, 12135–12141; e) T. Yamada, K. Muto, S. Kobatake, M. Irie, *J. Org. Chem.* **2001**, *66*, 6164–6168; f) T. Yamada, S. Kobatake, K. Muto, M. Irie, *J. Am. Chem. Soc.* **2000**, *122*, 1589–1592; g) T. Yamada, S. Kobatake, M. Irie, *Bull. Chem. Soc. Jpn.* **2000**, *73*, 2179–2184.

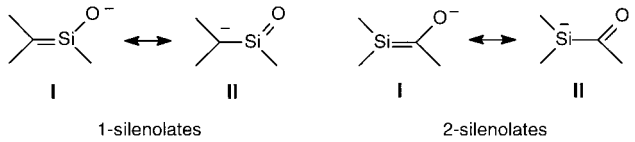
 © 2003 Wiley-VCH Verlag GmbH & Co. KGaA, Weinheim

Stable Silenolates

The First Isolable 2-Silenolate**

*Tamaz Guliashvili, Ibrahim El-Sayed, Andreas Fischer, and Henrik Ottosson**

Enolates hold a central position in organic chemistry.[1] However, there has been much less focus on silenolates, that is, Si analogues of enolates (Scheme 1). So far 1-silenolates have not been made, and even computational



Scheme 1. The resonance structures of silenolates.

studies of these species are absent. With regard to 2-silenolates, there are only a handful of reports from the groups of Bravo-Zhivotovskii and Apeloig[2,3] and Ishikawa and Ohshita.[4] It was found that 2-silenolates with bulky alkyl or aryl substituents on the carbonyl carbon atom are moderately stable at low temperatures, thus allowing their characterization by NMR spectroscopy. At room temperature these compounds undergo degradation within a few hours, presumably preceded by dimerization.[4]

Our interest lies in silenes that display reversed Si=C bond polarity ($Si^{\delta-}=C^{\delta+}$),[5] which is enabled by delocalization of the negative charge from π-electron-donating substituents in the 2-position to the silene Si atom.[6] These reverse-polarized silenes are less reactive towards moisture and alcohols than naturally polarized silenes ($Si^{\delta+}=C^{\delta-}$), and addition of alcohol proceeds by an unexpected regiochemistry because C–O instead of Si–O bonds are formed.[5,7,8] The reverse-polarized silenes also react selectively with dienes to yield only [4+2] adducts.[4,5,7] This is in contrast to the naturally polarized silenes, which give [2+2] and ene adducts as well.[9]

[*] Dr. H. Ottosson, T. Guliashvili, Dr. I. El-Sayed
Department of Organic Chemistry
Institute of Chemistry, Box 599
Uppsala University
751 24 Uppsala (Sweden)
Fax: (+46) 18-417-3818
E-mail: henrik.ottosson@kemi.uu.se
Dr. A. Fischer
Department of Chemistry (Inorganic Chemistry)
Royal Institute of Technology
100 44 Stockholm (Sweden)

[**] This work was supported by the Swedish Research Council (Vetenskapsrådet) and the Wenner–Gren Foundations. We thank the National Supercomputer Center in Linköping, Sweden, for generous allotment of computer time.

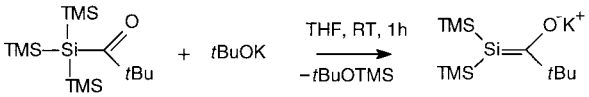
Supporting information for this article is available on the WWW under http://www.angewandte.org or from the author.

The negative charge in 2-silenolates resides on the O and/or Si atom (Scheme 1). If resonance structure **II** dominates, then the electronic structure resembles that of a reverse-polarized silene. Such 2-silenolates should contain Si–C single bonds (≈1.87 Å),[10] and the Si atoms will be similar to those of silyl anions, that is, strongly pyramidal.[11] On the other hand, if 2-silenolates are dominated by structure **I** the SiC bond lengths will be close to that of a Si=C double bond (1.704 Å in $H_2Si{=}CH_2$),[12] and the Si atoms will be planar.

There is very little structural information available on 2-silenolates. According to HF/6-31G(d) calculations, $[(H_3Si)_2SiC(O)Me]^-$ has a SiC bond of 1.926 Å, corresponding to a Si–C single bond.[4b] However, can Hartree–Fock correctly describe 2-silenolates, and how does the result obtained for the gas phase transfer to condensed phases? Indeed, variable temperature ^{1}H NMR spectroscopy suggests a partial Si=C double bond with an activation energy for bond rotation of 14.3 kcal mol^{-1}.[4b]

As part of our study on how reversed polarization affects Si=C-bonded compounds, we have now generated a crystallizable 2-silenolate. This is also the first experimentally determined crystal structure of a heavy Group 14 enolate.

We started from tris(trimethylsilyl)acylsilane (**1**, Scheme 2), but instead of applying a silyllithium reagent for abstraction of a trimethylsilyl group we used *t*BuOK.[13] This



Scheme 2. Synthesis of the 2-silenolate **2**. TMS = trimethylsilyl.

procedure leads to facile and quantitative formation of 2-silenolates at room temperature, in contrast to the more difficult preparation of lithium 2-silenolates using silyllithium. The products prepared by our method are resistent to decomposition. For instance, $[(TMS)_2SiC(O)tBu]^-K^+$ (**2**) formed by application of *t*BuOK in THF can be kept under inert atmosphere at room temperature for three months, whereas the corresponding lithium 2-silenolate decomposes within a few hours. Nonetheless, the potassium 2-silenolates degrade instantaneously when exposed to air. Further reaction with [18]crown-6, which enhances the crystallization of silyl anions,[14,15] leads to an orange compound. Crystals suitable for a structure determination can then be grown from solutions in toluene.

The X-ray structure of **2** is shown in Figure 1.[16] This compound is described by resonance form **II** (see Scheme 1) since it has a SiC bond that is even longer than a normal Si–C single bond (1.926 versus 1.87 Å for reference Si–C bonds[10]), a C=O double bond (1.245 versus ≈1.20 Å for reference C=O bonds[17]), and a pyramidal Si atom (sum of valence angles $\Sigma Si = 317.8°$). Thus, **2** is strongly influenced by reversed polarization. The coordination to K^+ is distant, with the O atom showing a closer contact than the Si atom. In the B3LYP/6-31+G(d)-optimized structure[18–20] of the smaller $[(H_3Si)_2SiC(O)Me]^-K^+(OMe_2)_3$ complex (**3**, Figure 2), the K^+

 © 2003 Wiley-VCH Verlag GmbH & Co. KGaA, Weinheim DOI: 10.1002/anie.200250400

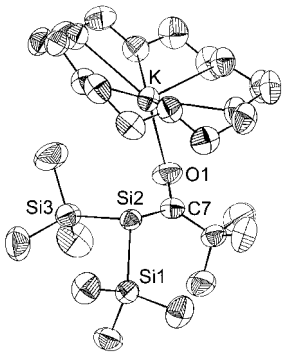


Figure 1. Structure of **2** (ORTEP drawing). The hydrogen atoms have been omitted for clarity, and the thermal ellipsoids are set at the 50% probability level. Selected bond lengths [Å], bond angles [°], and dihedral angles [°]: Si1-Si2 2.350(1), Si2-Si3 2.333(1), Si2-C7 1.926(3), C7-O1 1.245(3), K1-O1 2.846(2), K1-Si2 3.714(1); Si1-Si2-Si3 103.21(3), Si1-Si2-C7 117.95(8), Si3-Si2-C7 96.61(8), C7-O1-K1 113.2(2), Si2-C7-O1 116.6(2), C8-C7-O1 117.2(2), C8-C7-Si2 125.9(2); O1-C7-Si2-Si1 15.1(3), O1-C7-Si2-Si3 56.7(2).

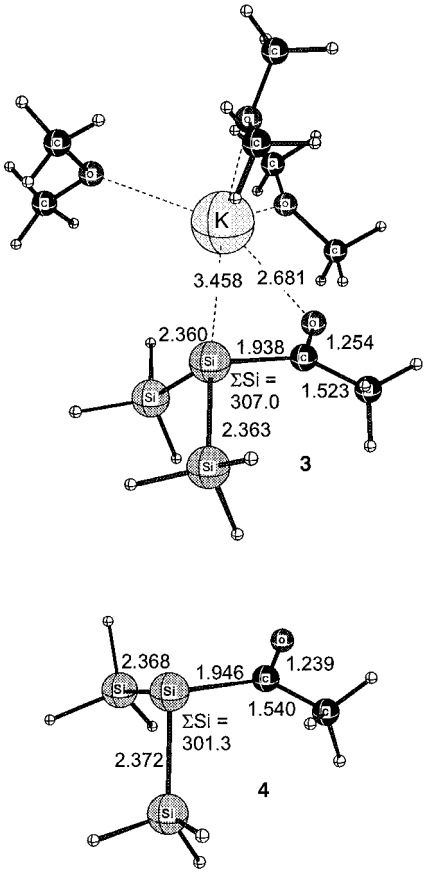


Figure 2. The optimized geometries of **3** and **4** calculated at the B3LYP/6-31+G(d) level, with selected bond lengths [Å] and angles [°].

ion is also closer to O than to Si. However, computations of the corresponding bare 2-silenolate **4** reveal that the presence of the solvated K^+ ion only alters the structure of the 2-silenolate a little. Potassium 2-silenolates should essentially correspond to unperturbed 2-silenolates, even in absence of crown ethers. The smaller degree of pyramidalization of the Si atom in **2** than in **3** is most likely due to the larger steric repulsion between the TMS groups in **2** than between the SiH_3 groups in **3**.

The ^{29}Si and ^{13}C NMR chemical shifts of the Si and C atoms of the Si–C bond of **2** are $\delta = -78.7$ and 274.1 ppm in THF and $\delta = -93.8$ and 268.7 ppm when [18]crown-6 is present. The ^{29}Si NMR shift for the central Si atom of **2** is within the range measured for silyl anions,[11] indicating that resonance structure **II** dominates the electronic structure. Furthermore, the NPA charge calculated at the B3LYP/6-31+G(d) level for the silenolate Si atom of **4** (−0.120 e) resembles that of the $(H_3Si)_2SiMe^-$ silyl anion (−0.108 e), even though this comparison neglects the fact that methyl and acyl groups show different degrees of inductive electron-withdrawing ability. In complex **3** the negative charge at Si increases to −0.198 e. Trapping of **2** by MeI yields the Si-methylated product, in agreement with previous findings by Ishikawa, Ohshita, and co-workers.[4] In analogy with other reverse-polarized silenes, only the [4+2] adduct is found upon the reaction of **2** with 2,3-dimethyl-1,3-butadiene.

To conclude, the X-ray structural, NMR spectroscopic, and atomic charge data reveal that 2-silenolates are dominated by resonance structure **II**. They have pyramidal Si atoms, Si–C single bonds, and C=O double bonds. The much stronger C=O than Si=C double bond favors resonance structure **II** over **I**. Our results reveal that silenes that are strongly affected by reversed polarization ($Si^{\delta-}=C^{\delta+}$) have structures that are unconventional for Si=C double-bonded compounds. This also shows that 2-silenolates are structurally dissimilar to enolates.

Received: October 21, 2002
Revised: December 13, 2002 [Z50400]

Keywords: electronic structure · silenes · silenolates · silicon

[1] D. Caine, *Comprehensive Organic Synthesis, Vol. 3*, Pergamon, Oxford, **1991**, chap. 1.1.
[2] I. S. Biltueva, D. A. Bravo-Zhivotovskii, I. D. Kalikhman, V. Yu. Vitkovskii, S. G. Shevchenko, N. S. Vyazankin, M. G. Voronkov, *J. Organomet. Chem.* **1989**, *368*, 163.
[3] D. Bravo-Zhivotovskii, Y. Apeloig, Y. Ovchinnikov, V. Igonin, Y. T. Struchkov, *J. Organomet. Chem.* **1993**, *446*, 123.
[4] a) J. Ohshita, Y. Masaoka, S. Masaoka, M. Ishikawa, A. Tachibana, T. Yano, T. Yamabe, *J. Organomet. Chem.* **1994**, *473*, 15; b) J. Ohshita, S. Masaoka, Y. Masaoka, H. Hasebe, M. Ishikawa, A. Tachibana, T. Yano, T. Yamabe, *Organometallics* **1996**, *15*, 3136; c) J. Ohshita, S. Masaoka, M. Ishikawa, *Organometallics* **1996**, *15*, 2198; d) J. Ohshita, S. Masaoka, Y. Morimoto, M. Sano, M. Ishikawa, *Organometallics* **1997**, *16*, 1123; e) J. Ohshita, H. Sakurai, Y. Tokunaga, A. Kunai, *Organometallics* **1999**, *18*, 4545; f) J. Ohshita, H. Sakurai, S. Masaoka, M. Tamai, A. Kunai, M. Ishikawa, *J. Organomet. Chem.* **2001**, *633*, 131; g) J. Ohshita, M. Tamai, H. Sakurai, A. Kunai, *Organometallics* **2001**, *20*, 1065.
[5] I. El-Sayed, T. Guliashvili, R. Hazell, A. Gogoll, H. Ottosson, *Org. Lett.* **2002**, *4*, 1915.
[6] Y. Apeloig, M. Karni, *J. Am. Chem. Soc.* **1984**, *106*, 6676.
[7] a) K. Sakamoto, J. Ogasawara, H. Sakurai, M. Kira, *J. Am. Chem. Soc.* **1997**, *119*, 3405; b) T. Veszprémi, M. Takahashi, J. Ogasawara, K. Sakamoto, M. Kira, *J. Am. Chem. Soc.* **1998**, *120*,

 © 2003 Wiley-VCH Verlag GmbH & Co. KGaA, Weinheim

2408; c) T. Veszprémi, M. Takahashi, B. Hajgató, J. Ogasawara, K. Sakamoto, M. Kira, *J. Phys. Chem. A* **1998**, *102*, 10530; d) M. Takahashi, K. Sakamoto, M. Kira, *Int. J. Quantum Chem.* **2001**, *84*, 198; e) K. Sakamoto, J. Ogasawara, Y. Kon, T. Sunagawa, C. Kabuto, M. Kira, *Angew. Chem.* **2002**, *114*, 1460; *Angew. Chem. Int. Ed.* **2002**, *41*, 1402.
[8] M. Ichinohe, T. Tanaka, A. Sekiguchi, *Chem. Lett.* **2001**, 1074.
[9] A. G. Brook, M. Brook, *Adv. Organomet. Chem.* **1996**, *39*, 71.
[10] M. Kaftory, M. Kapon, M. Botoshansky, *The Chemistry of Organic Silicon Compounds, Vol. 2* (Eds.: Z. Rappoport, Y. Apeloig), Wiley, Chichester, **1998**, p. 181.
[11] K. Tamao, A. Kawashi, *Adv. Organomet. Chem.* **1995**, *38*, 1, and references therein.
[12] S. Bailleux, M. Bogey, J. Demaison, H. Bürger, M. Senzlober, J. Breidung, W. Thiel, R. Fajgar, J. Pola, *J. Chem. Phys.* **1997**, *106*, 10016.
[13] C. Marchner, *Eur. J. Inorg. Chem.* **1998**, 221.
[14] J. R. Blanton, J. B. Diminnie, T. Chen, A. M. Wiltz, Z. Xue, *Organometallics* **2001**, *20*, 5542.
[15] C. Kayser, R. Fischer, J. Baumgartner, C. Marschner, *Organometallics* **2002**, *21*, 1023.
[16] Crystal structure determination of **2**: orthorhombic, space group $Pna2_1$, $a = 1981.1(1)$, $b = 1063.2(2)$, $c = 1574.4(3)$ pm. $V = 3319.49(7) \times 10^6$ pm^3. $\rho_{calcd} = 1.127$ g cm^{-3}; $2\theta_{max} = 52.74°$, $Mo_{K\alpha}$ radiation, $\lambda = 71.073$ pm, $T = 297$ K. The diffraction data were collected on a Bruker-Nonius Kappa CCD diffractometer. All non-hydrogen atoms were refined with anisotropic temperature parameters. The structure was solved with SHELXS97 and refined against F^2 using SHELXL97. Final R values: $R_1 = 0.0475$, $wR_2 = 0.0932$; GOF = 1.043 for 6668 unique reflections and 307 parameters; Flack parameter $x = 0.00(4)$; min./max. residual electron density 0.18/−0.14. CCDC-191717 contains the supplementary crystallographic data for this paper. These data can be obtained free of charge via www.ccdc.cam.ac.uk/conts/retrieving.html (or from the Cambridge Crystallographic Data Centre, 12 Union Road, Cambridge CB2 1EZ, UK; fax: (+44) 1223-336-033; or deposit@ccdc.cam.ac.uk).
[17] G. Berthier, J. Serre, *The Chemistry of the Carbonyl Group, Vol. 1* (Ed.: S. Patai), Wiley, London, **1966**, p. 1.
[18] Gaussian 98 (Revision A.7), M. J. Frisch, G. W. Trucks, H. B. Schlegel, G. E. Scuseria, M. A. Robb, J. R. Cheeseman, V. G. Zakrzewski, J. A. Montgomery, R. E. Stratmann, J. C. Burant, S. Dapprich, J. M. Millam, A. D. Daniels, K. N. Kudin, M. C. Strain, O. Farkas, J. Tomasi, V. Barone, M. Cossi, R. Cammi, B. Mennucci, C. Pomelli, C. Adamo, S. Clifford, J. Ochterski, G. A. Petersson, P. Y. Ayala, Q. Cui, K. Morokuma, D. K. Malick, A. D. Rabuck, K. Raghavachari, J. B. Foresman, J. Cioslowski, J. V. Ortiz, B. B. Stefanov, G. Liu, A. Liashenko, P. Piskorz, I. Komaromi, R. Gomperts, R. L. Martin, D. J. Fox, T. Keith, M. A. Al-Laham, C. Y. Peng, A. Nanayakkara, C. Gonzalez, M. Challacombe, P. M. W. Gill, B. G. Johnson, W. Chen, M. W. Wong, J. L. Andres, M. Head-Gordon, E. S. Replogle, J. A. Pople, Gaussian, Inc., Pittsburgh, PA, **1998**.
[19] A. D. Becke, *J. Chem. Phys.* **1993**, *98*, 5648.
[20] P. S. Hariharan, J. A. Pople, *Theor. Chim. Acta* **1973**, *28*, 213.

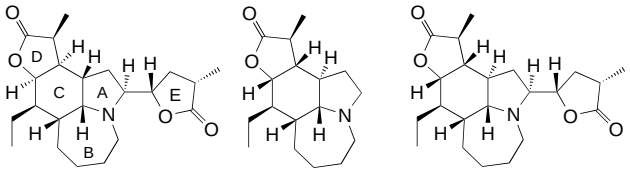
 © 2003 Wiley-VCH Verlag GmbH & Co. KGaA, Weinheim

Natural-Product Synthesis

A Rapid Stereocontrolled Entry to the ABCD Tetracyclic Core of Neotuberostemonine**

Kevin I. Booker-Milburn, Paul Hirst, Jonathan P. H. Charmant, and Luke H. J. Taylor*

Neotuberostemonine (**1**), stenine (**2**), and tuberostemonine (**3**) are three of a number of complex polycyclic alkaloids isolated from the roots of stemonaceous plants. Extracts of these plants have long been used in China and Japan as



human cough remedies and antihelminthics in domestic animals.[1] X-ray crystallography and 2D NMR spectroscopic studies have confirmed that neotuberostemonine differs from **2** and **3** at three of the contiguous stereocentres on the ACD ring junctures.[2] A number of syntheses of **2** have now been reported reported since the first successful total synthesis by Hart and Chen,[3] and include contributions from the groups of Wipf,[4] Morimoto,[5] and Padwa.[6] Morimoto et al.[7] have described a full account of their total synthesis of **2**, from which they aim to develop a strategy towards **3**. Very recently, Wipf et al.[8] described the first total synthesis of **3**. To date no synthesis of **1** has been reported.

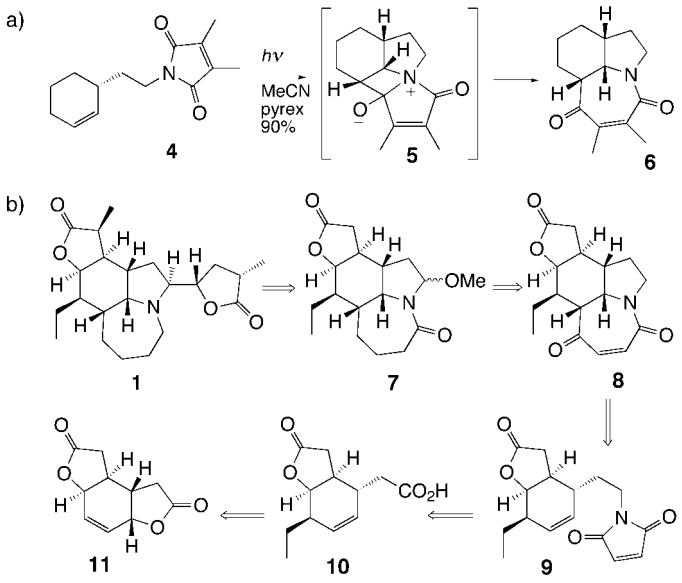
Previously we demonstrated that *N*-alkenyl maleimide derivatives undergo a very powerful [5+2] photocycloaddition reaction to yield the hexahydroazaazulene ring system common to all the *Stemona* alkaloids. For example, irradiation of the maleimide **4** gave the tricyclic azepine **6** in excellent yield. The reaction is thought to proceed through the fragmentation of the zwitterionic [2+2] cycloadduct **5** formed initially (Scheme 1 a).[9] Recently, we showed that this reaction can be used to construct the tricyclic core of the

[*] Dr. K. I. Booker-Milburn, Dr. P. Hirst
School of Chemistry, University of Bristol
Cantock's Close, Bristol, BS8 1TS (UK)
Fax: (+44) 117-929-8611
E-mail: k.booker-milburn@bristol.ac.uk
Dr. J. P. H. Charmant, L. H. J. Taylor
Structural Chemistry Laboratory
School of Chemistry, University of Bristol
Cantock's Close, Bristol, BS8 1TS (UK)

[**] This work was supported by a grant (GR/R02382/01) from the Engineering and Physical Sciences Research Council (EPSRC).

Supporting information for this article (NMR data and experimental details) is available on the WWW under http://www.angewandte.org or from the author.

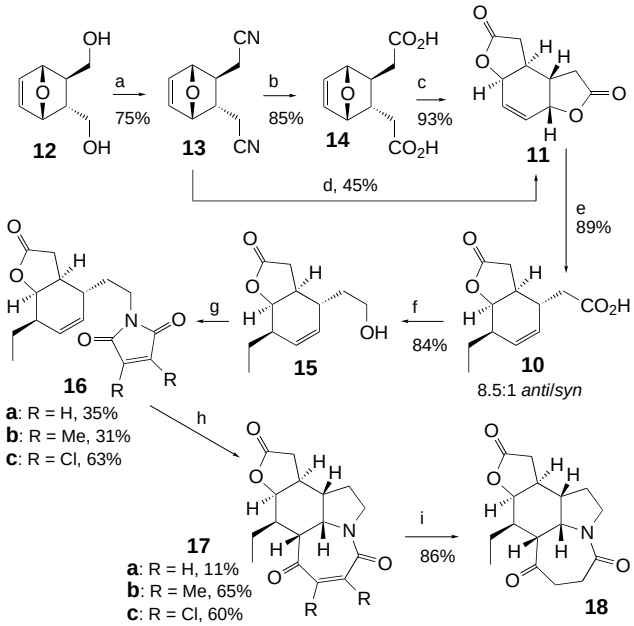
 © 2003 Wiley-VCH Verlag GmbH & Co. KGaA, Weinheim DOI: 10.1002/anie.50507



Scheme 1. a) The formation of the tricyclic azepine **6** in excellent yield by irradiation of maleimide **4** is thought to proceed via zwitterionic cycloadduct **5**. b) Retrosynthetic analysis of neotuberostemonine (**1**).

antileukemia alkaloid cephalotaxine.[10] As the azepine **6** contains three of the five rings of neotuberostemonine (**1**) we undertook a total synthesis program with the aim of synthesizing **1**, using our [5+2] photocycloaddition as the key step. The retrosynthetic analysis outlined in Scheme 1b illustrates our overall strategy. It was envisaged that the E ring could be installed in **7** by using elements of the elegant iminium ion chemistry developed both by Martin et al.[11] and by Morimoto et al.[12] in their independent studies on the synthesis of *Stemona* alkaloids. It is anticipated that the pyrrolidine ring of reduced derivatives of **8** will undergo selective alkoxylation by use of the Mn^{III} salen chemistry developed by Katsuki and Punniyamurthy.[13] The tetracycle **8** could, in turn, be assembled in a key step from the maleimide lactone **9** by using our [5+2] photocycloaddition. It was envisaged that the key cycloaddition precursor could be derived from the lactone acid **10** after chemoselective reduction and Mitsunobu coupling with maleimide. In one of a number of strategies it was conceived that **10** could derived from the C_2-symmetric bislactone **11** by way of an appealing cuprate-mediated S_N2' ring-opening desymmetrization sequence. *Anti*-selective ring-opening reactions of a monolactone related to **11** were recently reported by Helmchen and Bergner.[14]

Multigram quantities of the racemic diol **12** were easily prepared from furan and fumaryl chloride according to the Diels–Alder/reduction sequence described by Paquette et al.[15] Mesylation of **12** followed by treatment of the labile bismesylate with KCN gave the dinitrile **13** in 75% overall yield (Scheme 2). Compound **13** was easily converted into the diacid **14** by hydrolysis under basic conditions. Diacid **14** was then cyclized to the C_2-symmetric bislactone **11** by an acid-catalyzed tandem furan-ring-opening–lactonization sequence. This same sequence was also possible in a single hydrolytic step from **13**, albeit at the expense of overall yield. To our knowledge this acid-catalyzed bislactonization procedure is novel and may well prove to have application in the synthesis of other C_2-symmetric bislactones. Helmchen and Bergner described the successful S_N2' ring-opening of cyclohexene-fused lactones using an organocopper species derived from Grignard reagents and $CuBr{\cdot}Me_2S$.[14] Unfortunately, the bislactone **11** proved to be remarkably insoluble in most organic solvents and as a result the initial cuprate-mediated S_N2' ring-opening experiments based on the literature conditions met with failure. Eventually it was found that the use of *10 equivalents* of the organocopper reagent derived from $EtMgBr–CuBr{\cdot}Me_2S$ in a THF/Me_2S solvent mixture (2:1) led to the ring-opened lactone acid **10** in 89% yield as a separable mixture of isomers (*anti*/*syn* = 8.5:1). Use of less organocopper reagent led to very slow and incomplete conversion into product. Interestingly, ring opening of **11** with the less stereochemically demanding MeMgBr led to better *anti*/*syn* ratios (11:1). Selective reduction of the acid with the $NaBH_4$/mixed anhydride technique described by Zoutani et al.[16] gave the alcohol **15** in good yield. Mitsunobu coupling with maleimide, dimethylmaleimide, and dichloromaleimide then gave three photocyclization precursors **16** in low to moderate yields. Very pleasingly, irradiation of the dimethyl derivative **16b** was found to proceed without event and gave the key tetracycle **17b**[17] in 65% yield as a single diastereoomer (Scheme 2). The correct relative stereochemistry of **17b** was confirmed by X-ray crystallographic analysis (Figure 1). In



Scheme 2. Synthesis of the ABCD core of **1**: a) MsCl, Et_3N, Et_2O, 2 h, then KCN, DMSO, 100 °C, 5 h; b) KOH, EtOH, H_2O; c) *p*TSA, toluene, reflux; d) H_2SO_4 (6 M), heat, 2 h; e) EtMgBr (10 equiv), $CuBr{\cdot}Me_2S$ (10 equiv), THF/Me_2S (2:1), −20 °C; f) EtOCOCl, Et_3N, then $NaBH_4$; g) maleimide/dimethylmaleimide/dichloromaleimide, DIAD, PPh_3, THF, −78 °C→RT, 24 h; h) *hν*, pyrex, MeCN, 30–120 min; i) Zn, AcOH, room temperature, 1.5 h. Ms = methanesulfonyl, DMSO = dimethyl sulfoxide, *p*TSA = *para*-toluenesulfonic acid, DIAD = diisopropylazodicarboxylate.

 © 2003 Wiley-VCH Verlag GmbH & Co. KGaA, Weinheim

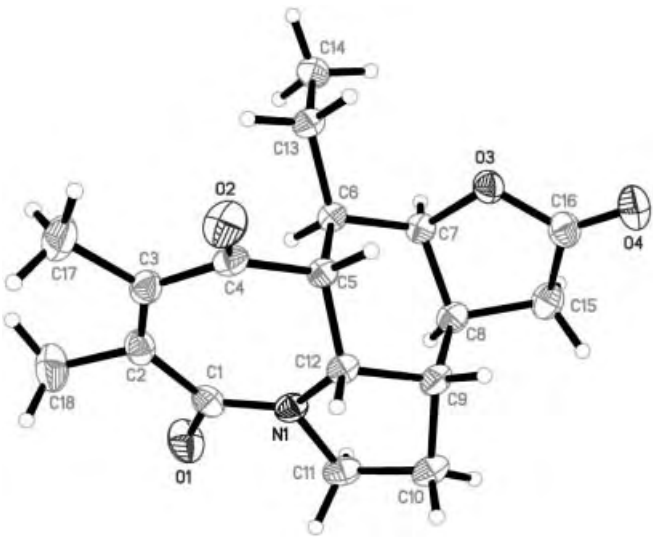


Figure 1. Molecular structure of the tetracyclic [5+2] photocycloadduct **17b** (R = Me). Ellipsoids set at the 50% probability level.

light of our previous experience with substrates derived from the parent maleimide, [9] it was perhaps not too surprising to find that **16a** (R = H) gave only a low yield (11%) of the corresponding photoadduct **17a**; the majority of the product underwent further photoreactions as it was formed. Fortunately the dichloro derivative **16c** underwent photolysis to give the [5+2] cycloadduct **17c** in 60% yield. Finally, reduction of the alkene, with concomitant dehalogenation, yielded the ketoamide **18** in excellent yield upon treatment of **17c** with zinc in acetic acid under our previously developed conditions.[9] This ketoamide has all the functionality necessary for completion of the synthesis of **1**. After reduction of the ketone and deoxygenation, we will investigate the installation of the methyl group of the lactone either by direct methylation or by a methylenation–hydrogenation sequence. Alkoxylation and lactone formation will be attempted as described in Scheme 1, after which thioamide formation and reduction with Raney nickel[3] should complete the synthesis of **1**.

In summary, an original route to the tetracyclic core of neotuberostemonine (**1**) has been described which highlights the application of the maleimide [5+2] photocycloaddition in natural-product synthesis. This linear route is notable for its brevity, partly a result of the fact that *no protecting groups* are used anywhere in the sequence—six steps to **17** from **12** by the shortest sequence. Also of note is a novel cuprate-mediated ring-opening desymmetrization of a C_2-symmetric bislactone, which may prove useful for the synthesis of other highly functionalized cyclohexene-fused butyrolactones. Present work is concerned with exploring the reactivity of **18** and ultimate implementation of this as an advanced intermediate for the total synthesis of **1**.

Received: November 8, 2002 [Z50507]

Keywords: asymmetric synthesis · cuprates · lactones · natural products · photocyclization · total synthesis

[1] For a comprehensive review on the *Stemona* alkaloids, see: R. A. Pilli, M. C. Ferreira de Oliveira, *Nat. Prod. Rep.* **2000**, *17*, 117–127.
[2] C. N. Dao, P. Luger, P. T. Ky, V. N. Kim, N. X. Dung, *Acta. Crystallogr. Sect. C* **1994**, *50*, 1612–1615.
[3] C. Y. Chen, D. J. Hart, *J. Org. Chem.* **1990**, *55*, 6236; C. Y. Chen, D. J. Hart, *J. Org. Chem.* **1993**, *58*, 3840–3849.
[4] P. Wipf, Y. Kim, D. M. Goldstein, *J. Am. Chem. Soc.* **1995**, *117*, 11106–11112.
[5] Y. Morimoto, M. Iwahashi, K. Nishida, Y. Hayashi, H. Shirahama, *Angew. Chem.* **1996**, *108*, 968–970; *Angew. Chem. Int. Ed. Engl.* **1996**, *35*, 904–906.
[6] J. D. Ginn, A. Padwa, *Org. Lett.* **2002**, *4*, 1515–1517.
[7] Y. Morimoto, M. Iwahashi, T. Kinoshita, K. Nishida, *Chem. Eur. J.* **2001**, *7*, 4107–4116.
[8] P. Wipf, S. R. Rector, H. Takahashi, *J. Am. Chem. Soc.* **2002**, *124*, 14848–14849.
[9] K. I. Booker-Milburn, C. E. Anson, C. Clissold, N. J. Costin, R. F. Dainty, M. Murray, D. Patel, A. Sharp, *Eur. J. Org. Chem.* **2001**, 1473–1482.
[10] K. I. Booker-Milburn, L. F. Dudin, C. E. Anson, S. D. Guile, *Org. Lett.* **2001**, *3*, 3005–3008.
[11] S. F. Martin, K. J. Barr, *J. Am. Chem. Soc.* **1996**, *118*, 3299–3300.
[12] Y. Morimoto, K. Nishida, Y. Hayashi, *Tetrahedron Lett.* **1993**, *34*, 5773–5776.
[13] T. Punniyamurthy, T. Katsuki, *Tetrahedron* **1999**, *55*, 9439–9454.
[14] E. J. Bergner, G. Helmchen, *Eur. J. Org. Chem.* **2000**, 419–423.
[15] L. A. Paquette, T. M. Kravetz, P. Charumilind, *Tetrahedron* **1986**, *42*, 1789–1795.
[16] M. A. N. Zoutani, A. Pancrazi, J. Ardisson, *Synlett* **2001**, 769–772.
[17] Crystal dimensions: $0.75 \times 0.60 \times 0.10$ mm^3, orthorhombic, space group *Pbca*, $a = 11.7444(16)$, $b = 7.6959(10)$, $c = 34.758(6)$ Å, $V = 3141.5(8)$ Å^3, $\rho_{calcd} = 1.342$, $2\theta_{max} = 55.0°$, $Mo_{K\alpha}$ radiation (0.71073 Å). Data were collected at 100 K as a series of frames, each covering 0.3° in ω, and integrated software (SAINT, Bruker 2001) to give a Lorentz polarization corrected data set of 18721 measured and 3579 independent reflections. An absorption correction (SADABS, Sheldrick 2001) was applied ($\mu = 0.094$, $T_{min} = 0.772$, $T_{max} = 1.000$). Solution and refinement (SHELXTL, Bruker-AXS 2001) against $|F^2|$ used 211 parameters with all hydrogen atoms constrained to ideal geometries and refined with isotropic displacement parameters equal to 1.5× (methyl) or 1.2× (all other hydrogen atoms) the equivalent isotropic displacement parameter of their parent atom. Final residuals: R_1 [2715 data with $I > 2\sigma(I)$] = 4.4%, wR_2 (all data) = 12.5%. Max/min residual electron density: +0.310, −0.265 e Å^{-3}. CCDC 196931 contains the supplementary crystallographic data for this paper. These data can be obtained free of charge via www.ccdc.cam.ac.uk/conts/retrieving.html (or from the Cambridge Crystallographic Data Centre, 12 Union Road, Cambridge CB2 1EZ, UK; fax: (+44) 1223-336-033; or deposit@ccdc.cam.ac.uk).



Single-Molecule Magnets on Gold

Direct Observation of Single-Molecule Magnets Organized on Gold Surfaces**

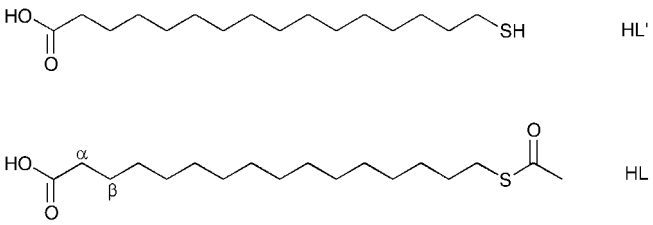
Andrea Cornia, Antonio C. Fabretti, Mirko Pacchioni, Laura Zobbi, Daniele Bonacchi, Andrea Caneschi, Dante Gatteschi, Roberto Biagi, Umberto Del Pennino, Valentina De Renzi, Leonid Gurevich, and Herre S. J. Van der Zant*

An aim of molecular electronics is to use single (or a few) molecules as active components of electronic devices, based on the idea that a small number of molecules, or even a single molecule, can perform basic electronic functions, that is, rectification, amplification, and storage.[1,2]

In the last decade, it was discovered that single molecules can, in principle, be used to store magnetic information. The research in this field started from the observation that a dodecamanganese(III,IV) cluster, $[Mn_{12}O_{12}(OAc)_{16}(H_2O)_4]\cdot 4H_2O\cdot 2AcOH$ (**1**·4 H_2O·2 AcOH),[3] exhibits a hysteresis cycle under cryogenic conditions.[4] This compound is considered to be the prototype of a class of materials referred to as single-molecule magnets (SMMs), so-called because their magnetic behavior is strongly reminiscent of bulk magnets.[4b] Magnetic hysteresis in SMMs arises from a purely molecular mechanism rather than from bulk magnetic interactions, a fact firmly established by magnetic dilution experiments.[5] Practical applications of SMMs as molecular-scale units for information storage or "qubits" for quantum computation[6] require the addressing of individual molecules, that is, imaging, probing, and eventually manipulating individual molecules. This goal can be realized most easily by depositing target molecules on a suitable substrate with monolayer[7a,b] or submonolayer[7c] coverage, and by addressing them individually using scanning probe microscopy techniques, such as scanning tunneling microscopy (STM), atomic force microscopy (AFM), and magnetic force microscopy (MFM). The first technique is particularly attractive for the study of the interplay between charge transport and the magnetic properties of the clusters. Partially ordered Langmuir–Blodgett films of Mn_{12} clusters have been prepared,[8] but no successful attempt to deposit SMMs on conducting substrates (for example, on gold) has been reported to date.

We present herein a method to deposit suitably derivatized Mn_{12}-type clusters on a gold film, and to observe them directly at the single-molecule level using STM. This result, which has been achieved for the first time, opens exciting perspectives for the storage of magnetic information in an individual cluster.

Since the clusters **1** do not adhere to gold surfaces in a stable fashion, suitable variants need to be designed that contain surface-binding functionalities, such as thiol or thioether groups. In particular, we have attempted to introduce 16-sulfanylhexadecanoate ligands (L′) around the Mn_{12} core by exploiting a well-known ligand-exchange reaction.[5b] However, treatment of **1**·4 H_2O·2 AcOH with HL′ in toluene or CH_2Cl_2 affords intractable solids, presumably as a result of the oxidative instability of free thiols in the presence of Mn_{12} centers.[9] In contrast, the use of the corresponding acetyl-protected acid HL yields a fully-substituted derivative $[Mn_{12}O_{12}(L)_{16}(H_2O)_4]$ (**2**) which is highly soluble in organic solvents (See Experimental Section).



The composition of **2** has been established by elemental analysis, FT-IR and ^{1}H NMR spectroscopy, and MALDI-TOF mass spectrometry. Mass spectrometry is emerging as a powerful new tool for the characterization of molecular clusters in a noncrystalline form.[11] Mass spectra collected in positive and negative mode show isolated molecular peaks at $m/z = 6125$ and 6123, which correspond to $[M+H]^+$ and $[M-H]^-$, respectively, for the species $[Mn_{12}O_{12}(L)_{16}]$ ($M = 6124$). Neither the positive nor the negative mode spectra exhibit peaks that correspond to a cluster with H_2O ligands; these ligands are presumably lost under the experimental conditions used.[11b] Satellite peaks for the partially substituted species $[Mn_{12}O_{12}(OAc)_n(L)_{16-n}]$ with molecular weight $M' = M - 270n$ are not observed (Figure 1). Infrared spectra are dominated by a very strong band at 1695 cm^{-1}, which arises from the stretching vibration of the acetyl C=O group.

The magnetization dynamics studied by variable-frequency ac susceptibility measurements on a polycrystalline sample exhibits the distinctive features of Mn_{12} derivatives.

[*] Dr. A. Cornia, Prof. Dr. A. C. Fabretti, M. Pacchioni, L. Zobbi
Dipartimento di Chimica
INSTM and Università di Modena e Reggio Emilia
via G. Campi 183, 41100 Modena (Italy)
Fax: (+39) 059-373543
E-mail: acornia@unimo.it
D. Bonacchi, Dr. A. Caneschi, Prof. Dr. D. Gatteschi
Dipartimento di Chimica
INSTM and Università di Firenze
via della Lastruccia 3, 50019 Sesto Fiorentino (Italy)
Dr. R. Biagi, Prof. Dr. U. Del Pennino, Dr. V. De Renzi
INFM National Center on nanoStructures and bioSystems at Surfaces (S3) and Dipartimento di Fisica
Università di Modena e Reggio Emilia
via G. Campi 213/A, 41100 Modena (Italy)
Dr. L. Gurevich, H. S. J. Van der Zant
Department of Nanoscience
Delft University of Technology
Lorentzweg 1, 2628 CJ Delft (The Netherlands)

[**] Work financed in part by ERATO, Italian MIUR and CNR, and the MOLNANOMAG network. H.S.J.VdZ. is supported by the Dutch Royal Academy of Arts and Sciences (KNAW). MALDI-TOF data were kindly provided by Dr. Ing. Roel H. Fokkens, Laboratory of Supramolecular Chemistry and Technology MESA+ Research Institute, University of Twente (The Netherlands).

 DOI: 10.1002/anie.200350981 © 2003 Wiley-VCH Verlag GmbH & Co. KGaA, Weinheim

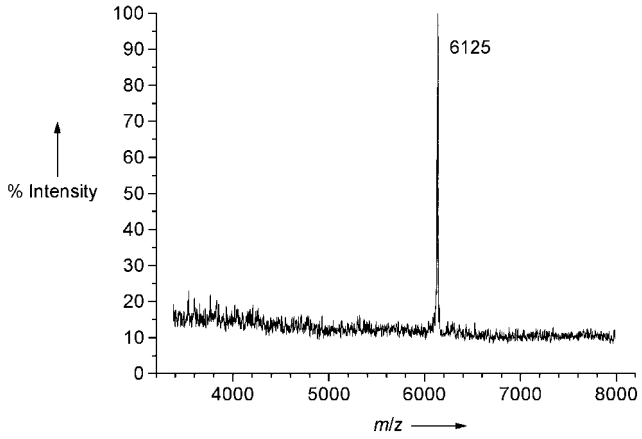


Figure 1. Positive-mode MALDI-TOF spectrum of **2**.

The relaxation time of the magnetization (τ) is plotted in Figure 2 as a function of the inverse blocking temperature $1/T_{max}$ (that is, the temperature at which the out-of-phase susceptibility reaches a maximum at each frequency). An Arrhenius-type behavior is observed [Eq (1)] with $\tau_0 = 2.4 \pm 0.4 \times 10^{-8}$ s and $\Delta/k_B = 55.1 \pm 0.8$ K, which suggests a thermally activated mechanism for magnetization reversal. The energy barrier (Δ/k_B) is close to that found for **1**·4 H_2O·2 AcOH (61 K),[4a] which confirms that the Mn_{12} core remains intact during the ligand-exchange reaction.

$$\tau = \tau_0 \exp(\Delta/k_B T) \quad (1)$$

Deposition of the nanoclusters on a Au(111) surface was carried out by incubating gold substrates[12a] in diluted solutions of **2** in THF, together with aqueous NH_4OH to facilitate deprotection of the thiol groups and to promote robust anchoring to the gold surface through Au–thiolate bonds. This technique has proved to be very effective in circumventing the oxidative instability of organic thiols in the deposition of self-assembled monolayers.[12b]

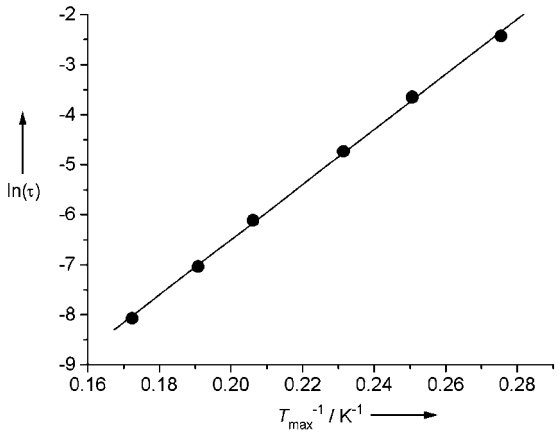


Figure 2. Relaxation time of the magnetization of **2** plotted as a function of inverse blocking temperature.

X-ray photoelectron spectroscopy (XPS) measurements reveal the presence of all the elements expected from the molecular structure of **2** and atomic proportions in excellent agreement with the calculated composition (Table 1). In particular, two different oxygen signals, labeled as O(1s)′ and O(1s)″ in Table 1, can be resolved at binding energies (BEs) of approximately 530 and 532 eV, respectively. The two peaks have been assigned to the 12 oxygen atoms of the $\{Mn_{12}O_{12}\}$ core, and to the remaining 52 oxygen atoms from carboxylate and water ligands, respectively. This interpretation is in agreement with that suggested in a recent XPS investigation of **1**·4 H_2O·2 AcOH[13a] and is supported by a comparison with the BEs found in Mn_2O_3 and MnO_2 (529–530 eV).[13b]

Table 1: Experimental XPS data and expected composition of the layers of **2**.

	Binding energy [eV][a]		Atom % (exp)		Atom % (calcd)[b]
	$Mg_{K\alpha}$	$Al_{K\alpha}$	$Mg_{K\alpha}$	$Al_{K\alpha}$	
Mn(3p)	48.8	48.8	3.1	2.6	3.2
S(2p)	162.6	162.6	4.0	4.2	4.2
C(1s)	285.1	285.0	75.2	76.1	75.8
O(1s)′	530.3	530.2	3.2	3.1	3.2
O(1s)″	532.3	532.3	14.5	14.1	13.6

[a] Relative to Au($4f_{7/2}$) = 84.0 eV. [b] Values for a mono-deprotected cluster are within 0.1 % of those reported for all of the elements.

Decomposition of the O(1s) spectra yields a 1:4.5 intensity ratio for the two oxygen types, which is in good agreement with the expected ratio in **2** (1:4.3).

It is well-known that the BE of S(2p) electrons can be used to discriminate between free (163.4 eV) and Au-bound (161.9 eV) sulfur atoms in simple thiols.[13c] The width of the S(2p) signal at 162.6 eV is indeed larger than the experimental resolution, and decomposition of the peak suggests that the free and the Au-bound sulfur atoms exist in a 1:2 ratio with BEs of 163.3 and 161.8 eV, respectively, for the S($2p_{3/2}$) electrons. Considering the conformational flexibility of the alkyl chains, such a large fraction of Au-bound sulfur atoms is not surprising. Although further studies are needed to clarify the details of the interaction, it is likely that thioacetyl end-groups may contribute significantly to cluster adsorption.[13d]

STM analysis of the sample (Figure 3) shows complete coverage of the gold substrate by a disordered layer of round particles with an apparent lateral size of approximately 5.8 nm, which is in reasonable agreement with the size of **2** obtained from molecular-modeling studies (5.0–5.6 nm). Disorder may originate from the specific arrangement of the alkyl chains of the deposited molecules, which prevents pairing for steric reasons and an epitaxial growth of the layer.[7b] In addition, the conformational flexibility of the chains may prevent the formation of the hexagonal or cubic arrangements that have been previously reported, for instance, for gold clusters.[14] Prolonged scanning of the surface under the adopted experimental conditions (0.8–1.3 V, 5–10 pA) causes extensive motion of the mole-

 © 2003 Wiley-VCH Verlag GmbH & Co. KGaA, Weinheim

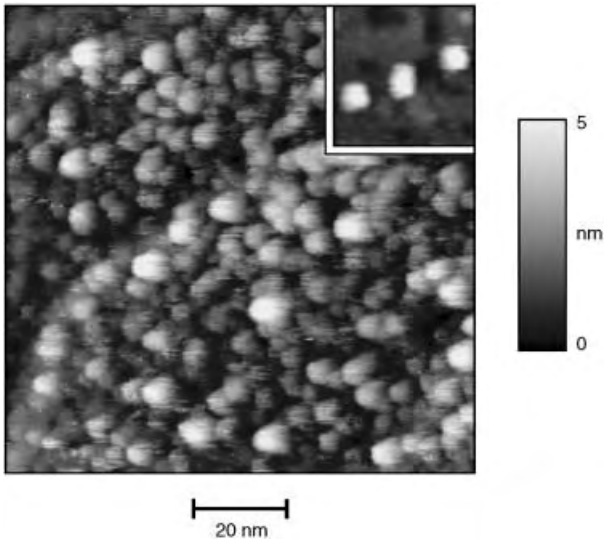


Figure 3. Constant-current STM image of Au-bound Mn_{12} clusters (setpoint = 5 pA, bias = 1.3 V, scan size = 100 nm, scan rate = 3 Hz). The inset shows three isolated molecules (setpoint = 10 pA, bias = 0.8 V, scan size = 30 nm, scan rate = 3 Hz).

cules at the surface and progressive disruption of the layer. Well-isolated molecules can then be imaged, as shown in the inset of Figure 3.

Given the small quantities of available material, a magnetic proof of the existence of SMMs on the surface cannot be obtained from bulk measurements,[8] and requires techniques such as the surface magneto-optical Kerr effect,[15a] spin-polarized STM,[15b] or MFM.[15c] Our experiments, however, show that it is indeed possible to address single molecules of Mn_{12}, and that the idea of storing information in one molecule has considerable credibility.

Experimental Section

16-(acetylthio)hexadecanoic acid was obtained by reacting 16-sulfanylhexadecanoic acid with acetyl chloride, as described elsewhere.[16] Compound **2** was synthesized by a modified ligand-exchange method.[5b] A slurry of freshly-prepared **1**·4 H_2O·2 AcOH[3] (304 mg, 0.147 mmol) in anhydrous toluene (10 mL) was treated with 16-(acetylthio)hexadecanoic acid (819 mg, 2.478 mmol) and the solvent was distilled off under reduced pressure (50 mmHg). Additional azeotropic distillations were performed with toluene (10 mL, 80 mmHg; 2 × 10 mL, 100 mmHg). The residue was dissolved in CH_2Cl_2, the solution was centrifuged, and the solvent was evaporated to give **2** as a black lustrous solid (765 mg, yield 84 %).

Elemental analysis (%) calcd for $C_{288}H_{536}Mn_{12}O_{64}S_{16}$: C 55.83, H 8.72, S 8.28; found: C 55.72, H 8.72, S 7.98; FT-IR (KBr pellet): $\tilde{\nu}$ = 2920 (CH), 2852 (CH), 1695 (C=O), 1588 (OCO), 1422 (OCO), 1112, 953, 720, 629 cm^{-1}; ^1H NMR (200 MHz, [D_8]toluene, 25 °C, TMS): δ = 47.5 (8H; CH_2 (α, axial, $Mn^{III}Mn^{III}$)), 46.2 (8H; CH_2 (α, equitorial, $Mn^{III}Mn^{III}$)), 43.1 (8H; CH_2 (α, equitorial, $Mn^{III}Mn^{III}$)), 13.9 (8H; CH_2 (α, axial, $Mn^{III}Mn^{IV}$)), 8.8 (8H; CH_2 (β, axial, $Mn^{III}Mn^{III}$)), 5.1 (8H; CH_2 (β, axial, $Mn^{III}Mn^{IV}$)), 2.8 (32H; CH_2S), 2.0 (48H; CH_3), 1.3 (384H; CH_2), −3.9 (8H; CH_2 (β, equitorial, $Mn^{III}Mn^{III}$)), −4.7 ppm (8H; CH_2 (β, equitorial, $Mn^{III}Mn^{III}$)). For the assignment of ^1H NMR signals, see ref. [5b].

Mass spectra were collected using a Voyager-DE-RP MALDI-TOF mass spectrometer (Applied Biosystems/PerSeptive Biosystems, Inc., Framingham, MA, USA) equipped with delayed extraction.[17] A 337-nm UV nitrogen laser was used and the mass spectra were obtained in both linear and reflection modes. Samples were prepared by mixing a solution of the sample in CH_2Cl_2 (10 μL) with a solution of the matrix (dihydroxybenzoic acid in CH_2Cl_2, 30 μL, 1 mg L^{-1}). 1 μL of the solution was loaded on to a gold-sample plate, the solvent was removed in warm air, and the sample transferred to the mass spectrometer for analysis.

A Cryogenic S600 SQUID magnetometer was used to perform ac magnetic measurements. Gold films (150-nm thick) on freshly cleaved muscovite mica were prepared using standard procedures;[12a] the films exhibited a preferred orientation in the (111) direction. The substrates were immersed for at least 5 min in a solution of **2** (0.3 mM) in THF that contained a catalytic amount of aqueous NH_4OH, then rinsed thoroughly with THF and dried in a nitrogen stream.

XPS measurements were carried out in an ultra-high vacuum (UHV) chamber with a base pressure of 7×10^{-9} Pa. Photoemission spectra were excited by a non-monochromated X-ray source equipped with two anodes (K_α lines; Al = 1486.6 eV and Mg = 1256.6 eV) and measured by means of a hemispherical electron-energy analyzer with a multichannel detection system and an angular acceptance of ± 8°. Electrons were collected at a take-off angle of 55° with respect to the surface normal of the samples, to enhance the sensitivity to the surface; the overall energy resolution was 1.7 eV. The Au($4f_{7/2}$) signal was used as a reference for the XPS energy scale, and was set at 84 eV of BE. The integrated intensities were corrected for the angular asymmetry of electronic levels and for the analyzer transmittivity, and directly used to evaluate the atomic percentages from tabulated photoionization cross-sections. Since the electron attenuation length (approximately 0.5–0.7 nm) is shorter than the cluster dimensions (5–6 nm), the XPS intensities should also reflect the electron signal attenuation, which depends, in turn, on the location of the emitting atoms and on the adsorption geometry. Nevertheless, given the low electronic density of the ligand shell the corrections to the measured intensities are expected to be small.

Constant-current STM images were recorded in air at room temperature using a Digital Instruments Nanoscope III equipped with mechanically sharpened Pt/Ir tips.

Received: January 21, 2003 [Z50981]

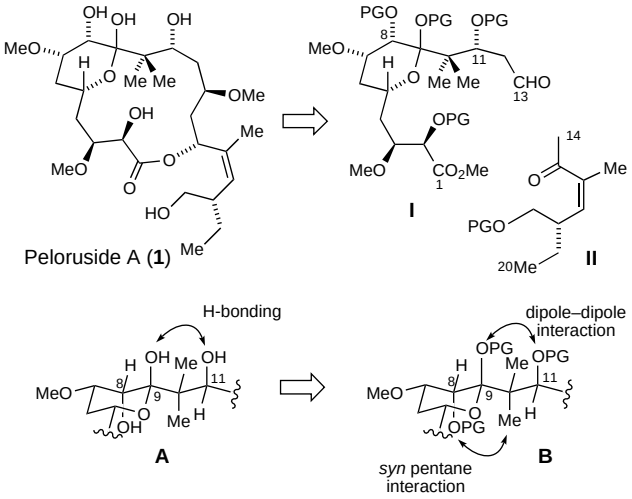
Keywords: cluster compounds · magnetic properties · manganese · single-molecule magnets · thin films

[1] a) C. Joachim, J. K. Gimzewski, A. Aviram, *Nature* **2000**, *408*, 541; b) R. M. Metzger, *Acc. Chem. Res.* **1999**, *32*, 950.
[2] a) J. Park, A. N. Pasupathy, J. I. Goldsmith, C. Chang, Y. Yaish, J. R. Petta, M. Rinkoski, J. P. Sethna, H. D. Abruña, P. L. McEuen, D. C. Ralph, *Nature* **2002**, *417*, 722; b) W. Liang, M. P. Shores, M. Bockrath, J. R. Long, H. Park, *Nature* **2002**, *417*, 725.
[3] T. Lis, *Acta Crystallogr. Sect. B* **1980**, *36*, 2042.
[4] a) R. Sessoli, D. Gatteschi, A. Caneschi, M. A. Novak, *Nature* **1993**, *365*, 141; b) G. Christou, D. Gatteschi, D. N. Hendrickson, R. Sessoli, *MRS Bull.* **2000**, *25*, 66.
[5] a) M. R. Cheesman, V. S. Oganesyan, R. Sessoli, D. Gatteschi, A. J. Thomson, *Chem. Commun.* **1997**, *17*, 1677; b) H. J. Eppley, H.-L. Tsai, N. de Vries, K. Folting, G. Christou, D. N. Hendrickson, *J. Am. Chem. Soc.* **1995**, *117*, 301.
[6] a) W. Wernsdorfer, N. Aliaga-Alcalde, D. N. Hendrickson, G. Christou, *Nature* **2002**, *416*, 406; b) M. N. Leuenberger, D. Loss, *Nature* **2001**, *410*, 789.
[7] a) A. Ulman, *Chem. Rev.* **1996**, *96*, 1533; b) G. E. Poirier, *Chem. Rev.* **1997**, *97*, 1117; c) S. A. Levi, P. Guatteri, F. C. J. M. van Veggel, G. J. Vancso, E. Dalcanale, D. N. Reinhoudt, *Angew. Chem.* **2001**, *113*, 1945; *Angew. Chem. Int. Ed.* **2001**, *40*, 1892.

 © 2003 Wiley-VCH Verlag GmbH & Co. KGaA, Weinheim

[8] M. Clemente-León, H. Soyer, E. Coronado, C. Mingotaud, C. J. Gómez-García, P. Delhaès, *Angew. Chem.* **1998**, *110*, 3053; *Angew. Chem. Int. Ed.* **1998**, *37*, 2842.
[9] Iodides are efficient reducing agents toward Mn_{12} complexes (see ref. [10]). Since elemental iodine readily oxidizes free thiols to disulfides, Mn_{12} complexes are expected to undergo spontaneous reduction in the presence of thiols.
[10] M. Soler, S. K. Chandra, D. Ruiz, J. C. Huffman, D. N. Hendrickson, G. Christou, *Polyhedron* **2001**, *20*, 1279.
[11] a) E. Coronado, M. Feliz, A. Forment-Aliaga, C. J. Gómez-García, R. Llusar, F. M. Romero, *Inorg. Chem.* **2001**, *40*, 6084; b) D. Ruiz-Molina, P. Gerbier, E. Rumberger, D. B. Amabilino, I. A. Guzei, K. Folting, J. C. Huffman, A. Rheingold, G. Christou, J. Veciana, D. N. Hendrickson, *J. Mater. Chem.* **2002**, *12*, 1152.
[12] a) H. Ron, S. Matlis, I. Rubinstein, *Langmuir* **1998**, *14*, 1116; b) J. M. Tour, L. Jones II, D. L. Pearson, J. J. S. Lamba, T. P. Burgin, G. M. Whitesides, D. L. Allara, A. N. Parikh, S. V. Atre, *J. Am. Chem. Soc.* **1995**, *117*, 9529.
[13] a) J.-S. Kang, J. H. Kim, Y. J. Kim, W. S. Jeon, D.-Y. Jung, S. W. Han, K. H. Kim, K. J. Kim, B. S. Kim, *J. Korean Phys. Soc.* **2002**, *40*, L402; b) B. R. Strohmeier, D. M. Hercules, *J. Phys. Chem.* **1984**, *88*, 4922; c) D. G. Castner, K. Hinds, D. W. Grainger, *Langmuir* **1996**, *12*, 5083; d) M. M. Yu Chen, A. Katz, *Langmuir* **2002**, *18*, 2413.
[14] G. Schmid, M. Bäumle, N. Beyer, *Angew. Chem.* **2000**, *112*, 187; *Angew. Chem. Int. Ed.* **2000**, *39*, 181.
[15] a) W. J. Geerts, B. Donehew, V. Williams, T. Schmiedel, *Rev. Sci. Instrum.* **2002**, *73*, 2086; b) S. Heinze, M. Bode, A. Kubetzka, O. Pietzsch, X. Nie, S. Blügel, R. Wiesendanger, *Science* **2000**, *288*, 1805; c) S. P. Li, W. S. Lew, J. A. C. Bland, L. Lopez-Diaz, M. Natali, C. A. F. Vaz, Y. Chen, *Nature* **2002**, *415*, 600.
[16] S. Svedhem, C.-A. Hollander, J. Shi, P. Konradsson, B. Liedberg, S. C. T. Svensson, *J. Org. Chem.* **2001**, *66*, 4494.
[17] M. L. Vestal, P. Juhasz, S. A. Martin, *Rapid Commun. Mass Spectrom.* **1995**, *9*, 1044.

 © 2003 Wiley-VCH Verlag GmbH & Co. KGaA, Weinheim



Scheme 1. Peloruside A (**1**): Structure and Strategy. PG = protecting group.

Macrolide Total Synthesis

Total Synthesis and Absolute Configuration of the Novel Microtubule-Stabilizing Agent Peloruside A**

*Xibin Liao, Yusheng Wu, and Jef K. De Brabander**

Recently, we became interested in peloruside A (**1**, Scheme 1), a marine metabolite isolated from sponge specimens of the species *Mycale* by Northcote and co-workers.[1] Peloruside A (**1**) is a potent cytotoxin and induces apoptosis in cultured mammalian cells.[2] Of potential clinical relevance is the recent observation that **1** affects microtubule dynamics in a manner similar to paclitaxel (Taxol).[2b] The relative stereochemistry of **1** was assigned based on extensive data gathered from a variety of high-field NMR experiments, although the absolute configuration remained to be solved. In addition to the presence of an array of ten stereogenic centers and a *Z*-configured trisubstituted olefin, we anticipated that one of the main challenges of a peloruside synthetic venture would be to find an efficient solution to the sterically crowded C8–C11 unit. In the solution-phase structure of **1**, this region adopts a conformation determined by optimal minimization of *syn* and *gauche* pentane interactions with potential intramolecular hydrogen bonding between the C9 and C11 hydroxy groups (**A**, Scheme 1). On a synthetic pathway, the introduction of the C8, C9, and C11 hydroxy functionality will by necessity introduce additional *syn* pentane and dipole–dipole interactions depending on the protection scheme used (**B**, Scheme 1). Herein, we communicate a solution to these synthetic challenges that culminates in the first total synthesis of (−)-peloruside A (**1**), and in doing so, document the absolute configuration of the natural isolate (opposite to the one shown in Scheme 1).[3]

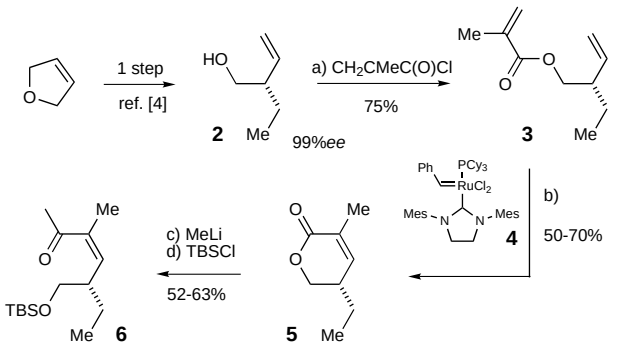
Strategically, we opted for a late-stage aldol coupling between a fully functionalized aldehyde **I** with methyl ketone **II**. This approach is driven by the perception that access to diastereomeric seco-acids, through reduction of a common C15 ketone, will increase the odds for a successful macrocyclization by accessing two mechanistically distinct pathways, namely acylative or invertive macrolactonization. A concise, enantioselective synthesis of fragment **II** is outlined in Scheme 2. The known homoallylic alcohol **2**, prepared in enantiopure form according to an elegant procedure described by Hoveyda et al.,[4] was acylated with methacryloyl chloride followed by ring-closing olefin metathesis with Grubb's second generation catalyst **4**.[5] The resulting lactone **5** then provides a valuable entry to the *Z*-trisubstituted enone

[*] Prof. Dr. J. K. De Brabander, Dr. X. Liao, Dr. Y. Wu
Department of Biochemistry
University of Texas Southwestern Medical Center at Dallas
5323 Harry Hines Blvd, Dallas, TX 75390-9038 (USA)
Fax: (+1) 214-648-6455
E-mail: jdebra@biochem.swmed.edu

[**] Financial support provided by the Advanced Research Program of the Texas Higher Education Coordinating Board, the Robert A. Welch Foundation, and the Howard Hughes Medical Institute (junior faculty support). J.K.D.B. is a fellow of the Alfred P. Sloan Foundation.

Supporting information for this article is available on the WWW under http://www.angewandte.org or from the author.

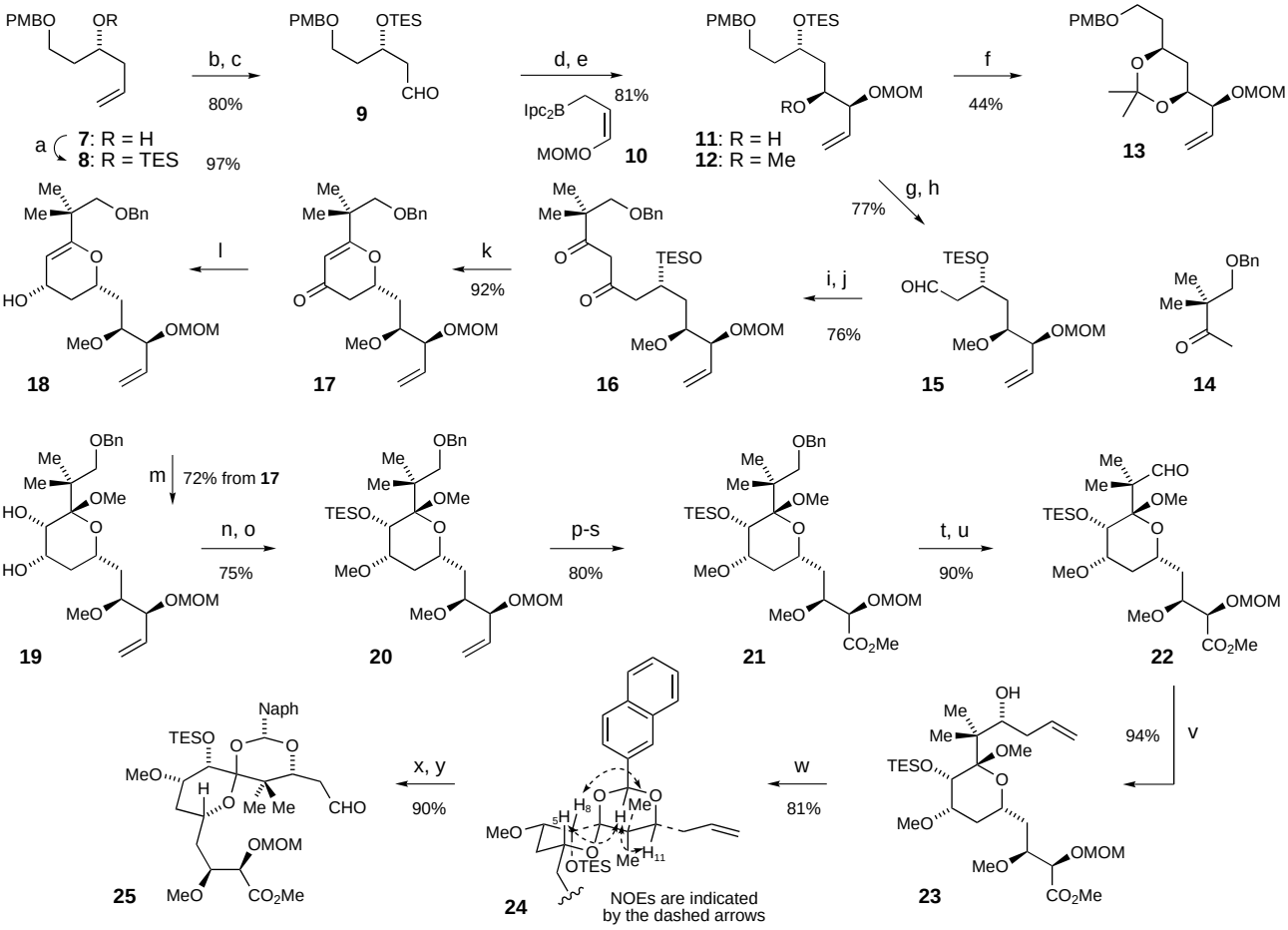
 © 2003 Wiley-VCH Verlag GmbH & Co. KGaA, Weinheim DOI: 10.1002/anie.200351145



Scheme 2. a) $CH_2CMeC(O)Cl$, iPr_2NEt, DMAP, CH_2Cl_2 (75%); b) 10 mol% **4**, CH_2Cl_2 (0.0025 M), reflux, 17 h (50–70% + 20% dimer derived from **3**); c) MeLi, THF, −78 °C; or Me_3SiCH_2Li, pentane, −78 °C; d) TBSCl, imidazole, DMAP, DMF (52–63% from **5**). DMAP = 4-dimethylaminopyridine, TBS = *tert*-butyldimethylsilyl.

6 by treatment with methyllithium and silylation of the primary alcohol.

Our approach towards the densely functionalized tetrahydropyranyl fragment is shown in Scheme 3. Addition of aldehyde **9** (derived from **7**[6] as shown) to (*Z*)-alkoxyallylborane **10** at low temperature produced the desired homoallylic alcohol diastereomer **11** (> 10:1).[7] The relative 1,3-*syn* stereochemical relationship was demonstrated by ^{13}C NMR analysis of the acetonide derivative **13** (resonances for the isopropylidene carbon atoms at $\delta = 20.0$, 30.3, and 98.8 ppm).[8] Compound **11** was advanced to aldehyde **15** by methylation (→**12**), oxidative debenzylation (DDQ), and oxidation of the resulting primary alcohol. Addition of aldehyde **15** to a cold solution of the lithium enolate derived from **14** and Dess–Martin oxidation[9] of the resulting aldol product fashioned β-diketone **16**. Transformation to dihydropyranone **17** ensued by stirring **16** in an acidic toluene



Scheme 3. a) TESOTf, 2,6-lutidine, CH_2Cl_2 (97%); b) cat. OsO_4, NMO, acetone/H_2O; c) $Pb(OAc)_4$, pyridine, CH_2Cl_2 (80% from **8**); d) **10**, *s*BuLi, THF, −78 °C, 15 min, then (+)-Ipc_2BOMe, −78 °C, 1 h, −78→0 °C, 1.5 h, then **9**, −95 °C, 3 h, slowly warm to RT; 30% H_2O_2, NaOH, 16 h (91%); e) NaH, MeI, DMF, −5 °C (89%); f) PTSA, MeOH, 20 min, remove solvent, then $Me_2C(OMe)_2$ (44%); g) DDQ, CH_2Cl_2/H_2O, 0 °C (88%); h) py·SO_3, Et_3N, DMSO, CH_2Cl_2, 0 °C (87%); i) **14**, LDA, THF, −78 °C, then **15**, −78 °C (94%); j) Dess–Martin periodinane, CH_2Cl_2, −10 °C (81% based on recovered starting material); k) PTSA, PhMe, RT (92%); l) $NaBH_4$, $CeCl_3 \cdot 7H_2O$, MeOH, −30 °C; m) *m*CPBA, $NaHCO_3$, CH_2Cl_2/MeOH, 0 °C (72%, two steps); n) *t*BuOK, MeI, THF, 0 °C; o) TESOTf, 2,6-lutidine, CH_2Cl_2 (75% from **19**); p) cat. OsO_4, NMO, acetone/H_2O; q) $Pb(OAc)_4$, pyridine, CH_2Cl_2; r) $NaClO_2$, NaH_2PO_4, 2-Me-2-butene, *t*BuOH/H_2O; s) CH_2N_2, Et_2O, 0 °C (80% from **20**); t) H_2, Pd/C (10%), MeOH (quant.); u) py·SO_3, Et_3N, DMSO, CH_2Cl_2, 0 °C (90%); v) allylBEt_2, Et_2O, −10 °C (94%); w) TESOTf, 2-naphthaldehyde, −78 °C, then 2,6-lutidine, TESOTf, 0 °C (81%); x) cat. OsO_4, NMO, acetone/H_2O; y) $NaIO_4$ on silicagel, CH_2Cl_2 (90% from **24**). PMB = *p*-methoxybenzyl, TES = triethylsilyl, Tf = trifluoromethane sulfonate, NMO = 4-methylmorpholine-*N*-oxide, MOM = methoxymethyl, Ipc = isopinocampheyl, DDQ = 2,3-dichloro-5,6-dicyano-1,4-benzoquinone, LDA = lithium diisopropylamide, PTSA = *p*-toluenesulfonic acid, *m*CPBA = *m*-chloroperbenzoic acid.

 © 2003 Wiley-VCH Verlag GmbH & Co. KGaA, Weinheim

solution. It proved critical to perform the subsequent Luche[10] reduction (→**18**) at −30 °C to prevent decomposition. Most satisfactorily, hydroxy-directed epoxidation of crude **18** followed by in situ methanolysis of the incipient glycal–epoxide produced one single glycoside, **19**, in high yield (72 % from **17**).[11] Sequential methylation (equatorial OH)/silylation (axial OH) of the α-diol (→**20**), oxidative transformation of the double bond to a C1 carboxylic acid, and diazomethane treatment furnished methyl ester **21**. Access to the aldehyde **22** by hydrogenolytic removal of the benzyl ether and oxidation set the stage for progression through C11–C12 bond formation. Concerns related to the feasibility of this critical event[12] seemed justified when various attempts to add carbon nucleophiles to the sterically demanding aldehyde **22** failed.[13] Ultimately, a highly efficient allyl transfer was achieved with allyldiethylborane. Remarkably, a single alcohol diastereomer, **23**, was produced with C11 configuration ascertained by NOE analysis of spirocyclic ketal **24** and advancement of **23** to peloruside A (see below).[14]

With fragments **6** and **25** (derived from **24** as shown) at hand, their union and completion of the peloruside macrocycle seemed an attainable goal, yet unexpected surprises lay ahead (Scheme 4). Mukaiyama-type aldol reaction of aldehyde **25** with the enol silane derived from methyl ketone **6** afforded almost exclusively (14:1) the compound that was assumed to be the expected 1,3-*anti* aldol product based on extensive literature precedent.[15] Evidence provided below, however, indicates that aldehyde **25** entered this reaction with an unprecedented bias for the formation of the 1,3-*syn* β-hydroxy ketone **26** instead (80 % yield). Initially unaware of this stereochemical outcome, we continued with methyl ether formation (→**27**), CBS reduction,[16] and ester hydrolysis to reach seco-acid **28**. Slow addition of this compound to a premixed solution of PPh_3 and diisopropylazodicarboxylate instigated formation of macrolactone **29** in 40–50 % yield.[17] We were able to deduce the stereochemistry of **29** based on a series of NOE correlations that locate H11, H13, and H15 on the same upper side of the macrolactone ring in agreement with the assigned C13(*S*) configuration (Figure 1). At this point, we were left with the obvious challenge of correcting the stereochemistry at C13. Various attempts to remove the (2-naphthyl)methylidene acetal failed.[18] Undeterred, we embraced the opportunity to explore a more attractive avenue that would eliminate this protecting group problem altogether, that is, we decided to advance materials with a free C11 alcohol through the remainder of the synthesis.

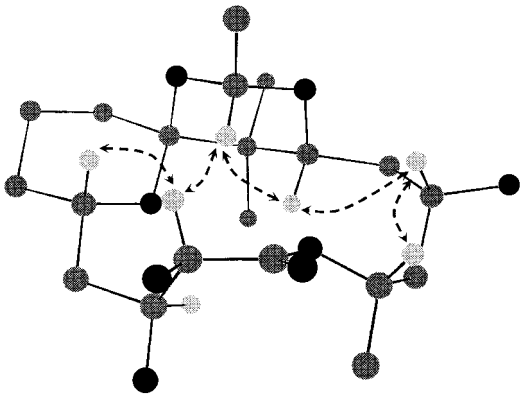
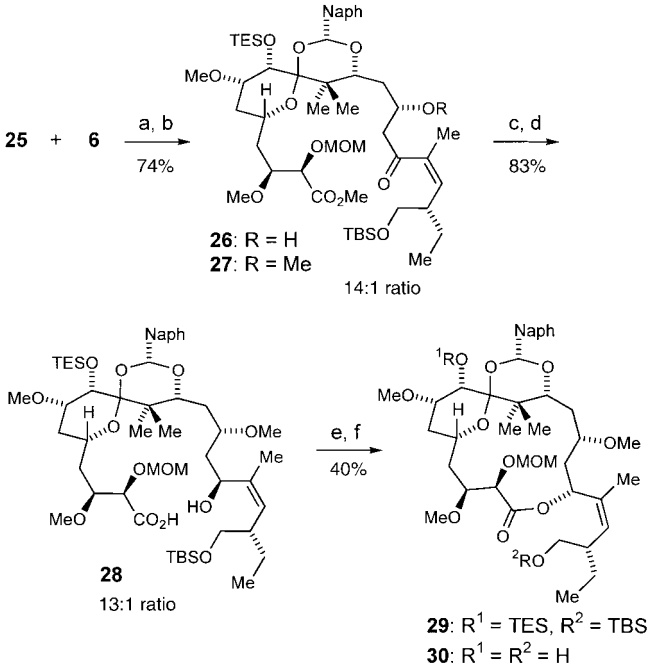


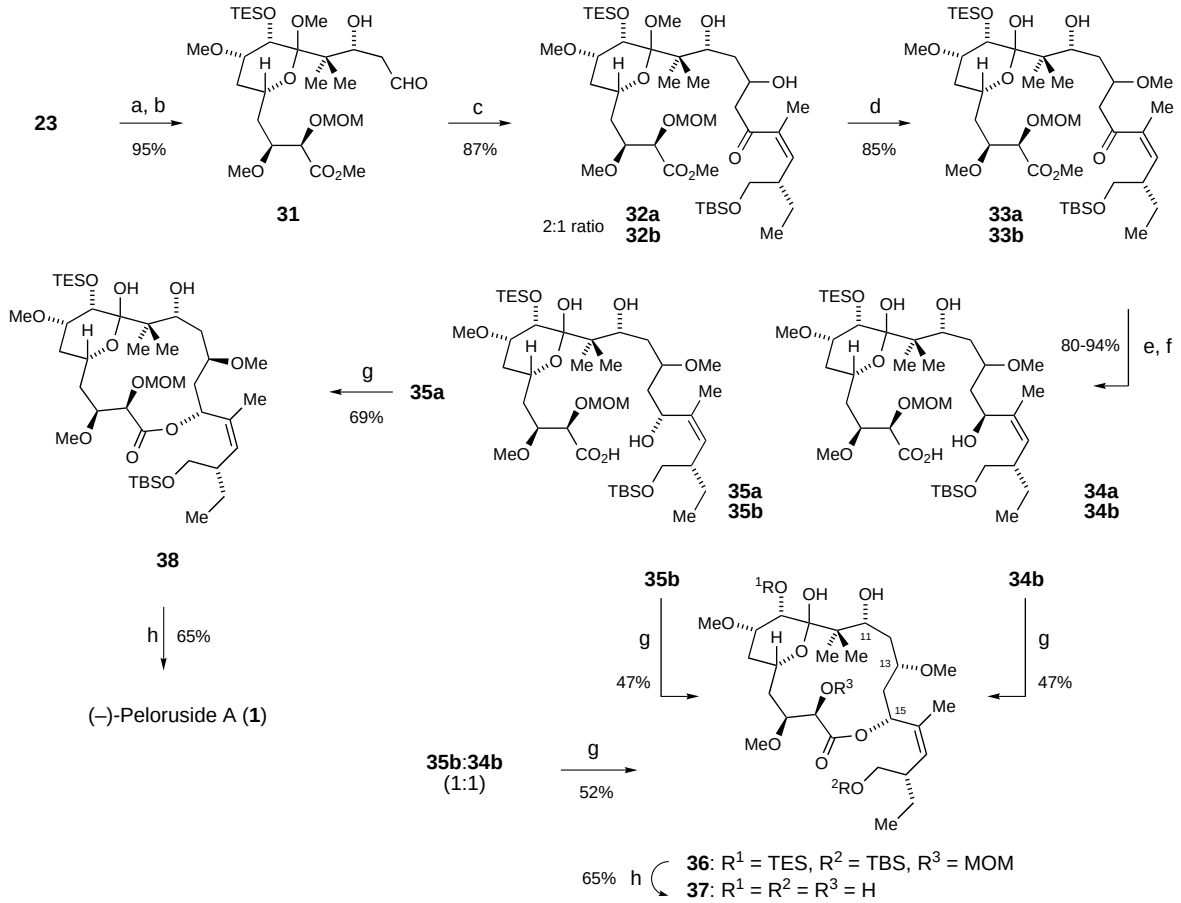
Figure 1. Chem3D representation of **29** (C in dark gray, H in light gray, and O in black). Important NOEs are illustrated with dashed arrows.



Scheme 4. a) Enolsilane derived from **6** (TMSOTf, Et_3N, CH_2Cl_2, −10 °C, 25 min, aqueous extraction), **25**, CH_2Cl_2, −78 °C, add $BF_3{\cdot}Et_2O$, 2 h (80 %, 14:1 ratio); b) Me_3OBF_4, 1,8-bis(dimethylamino)naphthalene, CH_2Cl_2, RT (92 %); c) (*S*)-*B*-Me-CBS (20 equiv), $BH_3{\cdot}SMe_2$ (7 equiv), CH_2Cl_2, −30 °C, 1 h, →RT (4 h), add MeOH (83 %, 13:1 ratio); d) 0.3 N aq. LiOH, THF, RT (quant.); e) PPh_3, DIAD, THF (0.05 M), RT, 15 min, add **28** (0.003 M in THF) through syringe pump over 2 h, 1 h at RT (40–50 %); f) 48 % aq. HF, MeCN/H_2O, RT, 20 h (88 %). TMS = trimethylsilyl, CBS = catalyst named after Corey, Bakshi, and Shibata, DIAD = diisopropylazodicarboxylate.

As illustrated in Scheme 5, β-hydroxy aldehyde **31** (derived from **23** as shown) was a viable partner for coupling with the enolborinate derived from **6**. Most gratifyingly, a separable 2:1 mixture of C13 epimers (**32a**/**32b**) was generated in 87 % yield. This rather unselective reaction was welcomed when contrasted with the situation described above (cf. **25** + **6** → **26**). At this stage, we left the stereochemical assignment unresolved, and advanced both isomers **32a**/**32b** individually. Surprisingly, methylation of these compounds occurred with concomitant hydrolysis to the C9 hemiketals **33a**/**33b**. We did not reprotect these materials but instead positioned ourselves to explore, in line with our original conception, two mechanistically distinct macrocyclization pathways. Intramolecular acylation through an active ester intermediate required access to the C15(*R*)-configured seco-acids **35a**/**35b**, while Mitsunobu-type lactonization would initiate from the C15-epimeric relatives **34a**/**34b**. These requirements were best fulfilled by asymmetric reduction of enones **33a**/**33b** by using (*S*)- or (*R*)-*B*-Me-CBS-oxazabor-

 © 2003 Wiley-VCH Verlag GmbH & Co. KGaA, Weinheim



Scheme 5. a) Cat. OsO_4, NMO, acetone/H_2O; b) $Pb(OAc)_4$, pyridine, CH_2Cl_2 (95% from **23**); c) **6**, iPr_2NEt, Et_2BOTf, CH_2Cl_2, −78°C, 15 min, −30°C, 45 min, −78°C, add **31**, −78°C, 2 h (87%, 2:1 ratio); d) Me_3OBF_4 (20 equiv), 2,6-di-*tert*-butyl-4-methylpyridine, CH_2Cl_2, RT (85%); e) **33a** or **33b**, (*R*)- or (*S*)-*B*-Me-CBS (20 equiv), $BH_3{\cdot}SMe_2$ (7 equiv), CH_2Cl_2, −30°C, 1 h, →RT (4 h), add MeOH (**34a**: 80%, **34b**: 80%, **35a**: 94%, **35b**: 80%); f) 0.3 N aq. LiOH, THF, RT (quant.); g) PPh_3, DIAD, THF (0.05 M), RT, 15 min, add seco-acid (0.003 M in THF) through syringe pump over 2 h, then 1 h at 0°C (**36**: 47% from **34b** or **35b**, 52% from ≈1:1 mixture of **34b**:**35b**, **38**: 69% from **35a**); h) 4 N HCl, THF, RT, 3 h (**37**: 65%, **1**: 65%).

olidine and $H_3B{\cdot}SMe_2$ (80–94% yield, ratios $>12:1$).[16] Note that no concomitant reduction of the C9 hemiketal was observed under these conditions! The corresponding carboxylic acids **34a**,**b**/**35a**,**b** were liberated by saponification.[19]

Since the C15 configuration could not be unambiguously inferred from the Corey model,[16] we explored both epimers **34b** and **35b** as substrates for a Mitsunobu-type macrolactonization, Remarkably, the same lactone **36** was produced from either **34b**, **35b**, or an equimolar mixture of both.[20] This lactone was later shown to have a C13 epimeric relationship to peloruside A (see below).[21] To the best of our knowledge, this represents the first documented case of a configuration-dependent mechanistic switch for a Mitsunobu lactonization.[22] We speculate that geometrical/conformational constraints preclude the formation of C15 epimeric lactones[23] and enforce the cyclization of substrate **35b** via an acyloxyphosphonium intermediate (retention) and **34b** via the familiar alkoxyphosphonium intermediate (inversion).[24,25]

The structure of **36** was assigned retrospectively,[21] that is, after the completion of peloruside A (**1**) from precursor **35a**. Initial evidence for a C13 epimeric configuration surfaced, however, when the ^1H NMR data of the deprotected lactone **37** (aq. HCl/THF) did not match those reported for the natural product. By inference, we realized peloruside A would fortuitously derive from the major aldol diastereomer **32a**. In the event, Mitsunobu lactonization of **35a** (69%) followed by simultaneous cleavage of the MOM and silyl protecting groups in lactone **38** (65%), did produce a pure compound (**1**) with spectroscopic properties (^1H and ^{13}C NMR, IR, HRMS) identical to those of the natural isolate.[1] However, the optical rotation of synthetic peloruside A (**1**) was of opposite sign ($[\alpha]_D^{23} = -16$; $c = 0.12$ in CH_2Cl_2) to the one reported for the natural product ($[\alpha]_D^{20} = +16$; $c = 0.30$ in CH_2Cl_2).[1] Also, synthetic **1** (up to 10 μM) had no effect on the growth of cultured human tumor cell lines (SK-MEL-5, HeLa).[26] Based on these results, we assign the absolute configuration of natural (+)-peloruside A as 2*S*, 3*R*, 5*R*, 7*R*, 8*R*, 9*R*, 11*S*, 13*S*, 15*S*, 18*R*.

In summary, we accomplished the first total synthesis of (−)-peloruside A and documented the absolute configuration of the dextrorotatory natural product. The advancement of minimally protected intermediates merits recapitulation, and was key to a successful endgame. A particularly noteworthy configuration-dependent mechanistic switch was observed

 © 2003 Wiley-VCH Verlag GmbH & Co. KGaA, Weinheim

when epimeric seco-acids **34b**/**35b** were subjected to typical Mitsunobu lactonization conditions. Current efforts focus on gaining additional insights into the mechanistic aspects of this reaction, and the synthesis of naturally configured peloruside and tailored derivatives for structure–function studies.

Received: February 10, 2003 [Z51145]

Keywords: antitumor agents · configuration determination · cyclization · natural products · total synthesis

[1] L. M. West, P. T. Northcote, C. N. Battershill, *J. Org. Chem.* **2000**, *65*, 445 – 449.
[2] a) K. A. Hood, B. T. Bäckström, L. M. West, P. T. Northcote, M. V. Berridge, J. H. Miller, *Anti-Cancer Drug Des.* **2001**, *16*, 155 – 166; b) K. A. Hood, L. M. West, B. Rouwé, P. T. Northcote, M. V. Berridge, S. J. Wakefield, J. H. Miller, *Cancer Res.* **2002**, *62*, 3356 – 3360.
[3] For the synthesis of peloruside fragments, see: I. Paterson, M. E. Di Francesco, T. Kühn, *Org. Lett.* **2003**, 5, 599 – 602.
[4] Z. Xu, C. W. Johannes, A. F. Houri, D. S. La, D. A. Cogan, G. E. Hofilena, A. H. Hoveyda, *J. Am. Chem. Soc.* **1997**, *119*, 10302 – 10316.
[5] a) A. K. Chatterjee, J. P. Morgan, M. Scholl, R. H. Grubbs, *J. Am. Chem. Soc.* **2000**, *122*, 3783 – 3784; b) A. Bhattacharjee, O. Soltani, J. K. De Brabander, *Org. Lett.* **2002**, *4*, 481 – 484.
[6] a) A. B. Smith III, K. P. Minbiole, P. R. Verhoest, M. Schelhaas, *J. Am. Chem. Soc.* **2001**, *123*, 10942 – 10953; b) Y. Wu, X. Liao, R. Wang, X.-S. Xie, J. K. De Brabander, *J. Am. Chem. Soc.* **2002**, *124*, 3245 – 3253.
[7] a) H. C. Brown, P. K. Jadhav, K. S. Bhat, *J. Am. Chem. Soc.* **1988**, *110*, 1535 – 1538; b) A. L. Smith, E. N. Pitsinos, C.-K. Hwang, Y. Mizuno, H. Saimoto, G. R. Scarlato, T. Suzuki, K. C. Nicolaou, *J. Am. Chem. Soc.* **1993**, *115*, 7612 – 7624.
[8] S. D. Rychnovsky, B. Rogers, G. Yang, *J. Org. Chem.* **1993**, *58*, 3511 – 3515.
[9] D. B. Dess, J. C. Martin, *J. Am. Chem. Soc.* **1991**, *113*, 7277 – 7287.
[10] J. L. Luche, L. Rodriguez-Hahn, P. Crabbé, *J. Chem. Soc. Chem. Commun.* **1978**, 601 – 602.
[11] For related examples, see: a) P. A. Wender, J. De Brabander, P. G. Harran, J.-M. Jimenez, M. F. T. Koehler, B. Lippa, C.-M. Park, M. Shiozaki *J. Am. Chem. Soc.* **1998**, *120*, 4534 – 4535; b) D. A. Evans, P. H. Carter, E. M. Carreira, A. B. Charette, J. A. Prunet, M. Lautens, *J. Am. Chem. Soc.* **1999**, *121*, 7540 – 7552.
[12] Problematic carbon–carbon bond formation adjacent to related α *gem*-dimethyl substituted C-glycoside units has been documented. For pertinent examples, see ref. [11] and M. Kageyama, T. Tamura, M. H. Nantz, J. C. Roberts, P. Somfai, D. C. Whritenour, S. Masamune, *J. Am. Chem. Soc.* **1990**, *112*, 7407 – 7408.
[13] Allylmagnesium bromide reacted competitively with the methyl ester. Lewis-acid catalyzed allyl transfer (allylSiMe$_3$, TiCl$_4$ or $BF_3{\cdot}Et_2O$) or acetate aldol reactions (lithium or boron enolates) resulted in recovery of starting material.
[14] This fortunate stereochemical outcome was not predicted a priori, nor are we able to offer a plausible rationale for it. For a related, nonselective allylation, see ref. [11a].
[15] D. A. Evans, M. J. Dart, J. L. Duffy, M. G. Yang, *J. Am. Chem. Soc.* **1996**, *118*, 4322 – 4343, and references therein.
[16] For an excellent review, see: E. J. Corey, C. J. Helal, *Angew. Chem.* **1998**, *110*, 2092 – 2118; *Angew. Chem. Int. Ed.* **1998**, *37*, 1986 – 2012.
[17] O. Mitsunobu, *Synthesis* **1981**, 1 – 28.
[18] We have explored a variety of solvolytic (protic or Lewis acid mediated), oxidative, and reductive pathways. Other protecting group schemes (cyclic and acyclic) were briefly investigated with no indication for success. Details will be included in a later disclosure.
[19] Reesterification with CH_2N_2 demonstrated that no epimerization had occurred. The *Z* configuration of the double bond was maintained throughout the synthesis and verified by NOE interactions.
[20] No diastereomeric or transposed (allylic) macrolactones were detected by NMR analysis of the nonpurified mixture.
[21] Clues about the stereochemistry of **36** were provided at this point by virtue of mutual NOE enhancements between the H11–H13 and H13–H15 proton pairs (cf. **29**).
[22] For selected examples of Mitsunobu esterifications leading to retention of configuration when hindered alcohols are involved, see: a) C. Ahn, P. DeShong, *J. Org. Chem.* **2002**, *67*, 1754 – 1759; b) A. B. Smith III, I. G. Safonov, R. M. Corbett, *J. Am. Chem. Soc.* **2002**, *124*, 11102 – 11113.
[23] At a superficial level, molecular models of C15 epimeric lactones appear to be highly strained. More comprehensive computational studies are currently pursued.
[24] Acyloxyphosphonium salts have been implicated as intermediates in Mitsunobu esterifications. For examples and mechanistic studies, see: ref. [22] and a) D. Camp, I. D. Jenkins, *J. Org. Chem.* **1989**, *54*, 3049 – 3054; b) C. Ahn, R. Correia, P. DeShong, *J. Org. Chem.* **2002**, *67*, 1751 – 1753; c) J. McNulty, A. Capretta, V. Laritchev, J. Dyck, A. J. Robertson, *J. Org. Chem.* **2003**, *68*, 1597 – 1600.
[25] A referee rightfully pointed out that our observations could also be explained by invoking a diastereoselective S_N1 reaction mechanism for the Mitsunobu lactonization with allylic alcohols. We had tentatively ruled out this possibility because we have not been able to detect[20] any products expected to derive to some extent from allylic carbocation intermediates (allylic transposition, double bond isomerization, elimination). For a reference pertinent to this issue, see: B. K. Shull, T. Sakai, J. B. Nichols, M. Koreeda, *J. Org. Chem.* **1997**, *62*, 8294 – 8303, and references therein.
[26] We are grateful to Dr. Michael G. Roth and Maria G. Kosfiszer (UT Southwestern Medical Center) for assistance with the cell-based assays.

 © 2003 Wiley-VCH Verlag GmbH & Co. KGaA, Weinheim

Cation-Containing Zeolites

A "Camel through the Eye of a Needle": Direct Introduction of the TPP^+ Ion inside Y-Zeolites by Formal Ion Exchange in Aqueous Medium**

A. M. Amat, A. Arques, S. H. Bossmann, A. M. Braun,* S. Göb, and M. A. Miranda**

Triarylpyrylium salts are well established electron-transfer photosensitizers.[1] They can mediate the photochemically induced oxidative degradation of a number of contaminants present in waste water. As triarylpyrylium salts exhibit absorption maxima in the UV-A and visible spectral ranges, they can be used in conjunction with solar light and inexpensive and environmentally friendly irradiation sources.[2]

In the last few years, considerable effort has been devoted to the preparation of zeolites containing 2,4,6-triphenylpyrylium cations (TPP^+) in their cavities and consequently of potential use as heterogeneous photosensitizers. As a result of the kinetic control of the electron-transfer process in the cavities, such photosensitizer systems would show enhanced electron-transfer reactions because of the retardation of back electron transfer after formation of the primary radical ion pairs inside the cavities. In addition, the stability of TPP^+ within the zeolite cavities is improved, and the heterogeneous photosensitizer can be easily separated and recycled after filtration.

A very elegant strategy to prepare TPP^+ inside the cavities of the Y-zeolite (TPP-Y) has been the "ship-in-a-bottle" synthesis of the cation from acetophenone and benzaldehyde using the internal (Lewis) acidic sites of the zeolite as catalyst.[3] The supercages of Y-zeolites (diameter: 1.3 nm) are large enough to host the triphenylpyrylium ion; however, the channels connecting the supercages are too small (diameter: 0.74 nm) to allow a free diffusion of TPP^+ ions.

Although the ship-in-a-bottle synthesis of TPP-Y was a real breakthrough,[4] it is not devoid of disadvantages: the preparation is quite slow (typically the mixture is heated under reflux for a week), the loading of the support is poor (because of the increasingly restricted diffusion of the reactants), and the removal of the byproducts and excess starting material is not complete, even after prolonged Soxhlet extraction.[3]

Herein we report a very simple, yet highly efficient method to introduce TPP^+ ions into Y-zeolite. At first sight, this new method appears to contradict two currently accepted principles concerning the adsorption of organic compounds inside zeolites: a) the zeolites have to be activated at high temperatures to remove the water molecules that fill the cavities, and b) organic compounds can only diffuse into the supercages, if the molecular dimensions of the compound permit its passage through the zeolite channel system. The TPP-Y material reported herein is prepared by simply stirring the non-activated NaY zeolite with an aqueous solution of triphenylpyrylium hydrogensulfate at 40 °C. After filtration, the solid is dried at 100 °C. Thus, instead of activating the zeolite before loading to remove water, the reaction is performed in aqueous medium, and the TPP^+ ions are fixed inside the supercages by a formal ion-exchange mechanism (TPP^+ vs. Na^+) in spite of the bulk of the TPP^+ ion. For this reason, we associate this approach with the parable of the "a camel passing through the eye of a needle".

Among the data supporting the presence of the TPP^+ ion inside the supercages of the zeolite are the results of elemental analyses that show, after repeated washing procedures, almost constant carbon values between 9 to 10 % of the total weight of the samples. Such high carbon values cannot be explained by adsorption of the TPP^+ ion onto the external surface of the zeolite. In addition, the total absence of sulfur registered for the same samples indicates that sulfate counterion of the TPP^+ ion has been replaced by the negatively charged sites of the zeolite lattice. Consistent with the proposed ion exchange, sodium is found in the water employed as a solvent in the preparative procedure. The infrared spectrum of the TPP-Y matches that of the TPP^+ ion (Figure 1a and b).

We explain the result of our novel TPP-Y synthesis by a sequence of three steps: 1) hydrolysis and ring opening of TPP^+ ion which can be catalyzed by the zeolite surface to yield the diketone 1,3,5-triphenylpent-2-en-1,5-dione, then 2) diffusion of the product into the Y-zeolite, and 3) thermal dehydration of the diketone inside the zeolite (during the drying at 100 °C) which leads to TPP-Y by recyclization (Figure 2). The occurrence and mechanism of such ring-opening/recyclization processes have been reported for TPP^+ ions in homogeneous solution.[5] Our hypothesis is supported by the IR spectra shown in Figure 1. When the doped zeolite is heated for a relatively short time (2 h, 70 °C; Figure 1c), absorption bands corresponding to the pyrylium cation (1625 cm^{-1}) and the diketone (1650 and 1682 cm^{-1}; Fig-

[*] Prof. Dr. A. M. Amat, Dr. A. Arques
Departamento de Ingeniería Textil y Papelera
Escuela Politécnica Superior de Alcoy
Universidad Politécnica de Valencia
Paseo Viaducto 1, 03801 Alcoy (Spain)
Fax: (+34) 96-652-8471
E-mail: aamat@txp.upv.es
Prof. Dr. A. M. Braun, Priv.-Doz. Dr. S. H. Bossmann, Dr. S. Göb
Lehrstuhl für Umweltmesstechnik
Engler-Bunte-Institut
Universität Karlsruhe, 76128 Karlsruhe (Germany)
Fax: (+49) 721-608-6240
E-mail: andre.braun@ciw.uni-karlsruhe.de
Prof. Dr. M. A. Miranda
Departamento de Química
Instituto de Tecnología Química UPV-CSIC
Universidad Politécnica de Valencia
46071 Valencia (Spain)
Fax: (+34) 96-38777809
E-mail: mmiranda@qim.upv.es

[**] Financial support by the Spanish MCYT (Grant BQ2001-2725) is gratefully acknowledged. Generalitat Valenciana (GV00-114-2), Universidad Politécnica de Valencia, and BMBF (PWT-A94194-02WA9625/0) are also acknowledged for their financial support of the cooperative research of the Spanish and German groups.
TPP^+ = 2,4,6-Triphenylpyrylium.

 DOI: 10.1002/anie.200219624 © 2003 Wiley-VCH Verlag GmbH & Co. KGaA, Weinheim

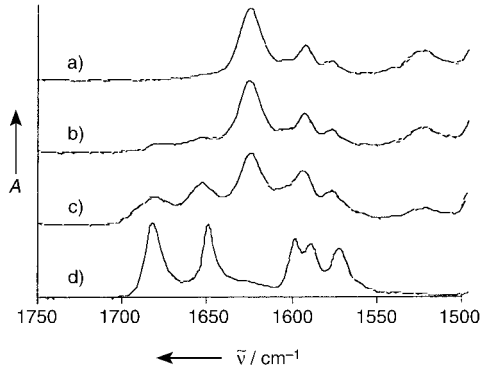


Figure 1. IR spectra (KBr) of a) 2,4,6-triphenylpyrylium hydrogen sulfate, b) TPP^+ ion (ca. 10% w/w) hosted in Y-zeolite (dry product), c) TPP^+ ion hosted in Y-zeolite (wet product), d) 1,3,5-triphenylpent-2-en-1,5-dione. A = absorbance.

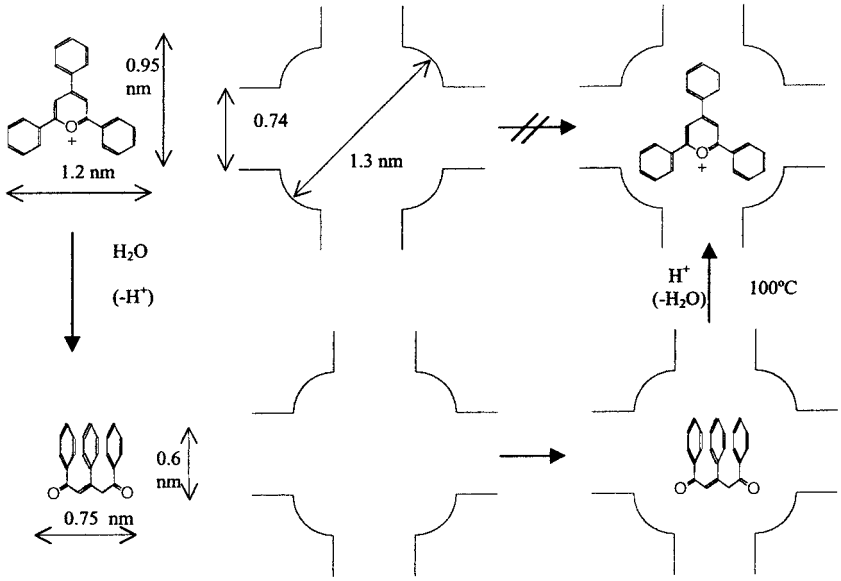


Figure 2. Mechanism of the formal ion exchange to introduce TPP^+ ions inside the Y-zeolite: hydrolytic ring opening leading to the corresponding linear diketone, diffusion through the channel, and recyclization inside the supercage.

ure 1d) are observed. However, when the sample is dehydrated (100 °C, 2 days), the IR spectrum closely matches that of the TPP^+ ion.

In a control experiment, the aqueous TPP^+ solution was treated at 40 °C in the absence of Y-zeolite, under otherwise identical reaction conditions. This also led to hydrolysis of the TPP^+ ion, although at a much slower rate (as monitored by UV/Vis spectrophotometry). Hence, the zeolite actually plays a catalytic role in ring opening. The only product observed upon extraction with CH_2Cl_2 of the two aqueous reaction mixtures (obtained in the presence and in the absence of zeolite) was the diketone. Furthermore, when the independently synthesized diketone was adsorbed onto Y-zeolite and the filtered solid dried at 100 °C, recyclization to the TPP^+ ion and formation of TTP-Y was detected (infrared spectrum identical to those shown in Figure 1a or b).

This new synthetic method, based on the migration of a neutral species through the channels of the Y-zeolite, does not block the outer pores, hence, it allows improved diffusion and leads to higher degrees of loading. In fact, depending on the experimental conditions chosen, TPP^+ loading could be varied between 3 and 18%. In addition, as no supercage-filling byproducts are formed, diffusion of the substrates (to be oxidized) through the channel system should be enhanced. This feature should results in improved efficiency of TPP-Y as a photocatalyst.

Our mechanistic working hypothesis is based, however, on the assumption that the regular structure of the zeolite would not be altered during the preparation of the catalyst material. Full diffractograms before and after the preparative step are identical, and a crystallinity of more than 99% has been calculated in both cases.

As a convenient test to check the performance of this photocatalyst, the oxidation of 2,4-xylidine (2,4-dimethylaniline) was chosen.[6] A continuously air-saturated suspension of TPP-Y in an aqueous solution of 2,4-xylidine was irradiated with a mercury lamp at wavelengths >300 nm. The total oxidation of the substrate was complete within 6 h (Figure 3a).

In a parallel experiment, a similar reaction system was irradiated for 2 h under the same conditions. Subsequently, an amount of 2,4-xylidine equal to the one already oxidized was added to re-establish the initial concentration, and the system was irradiated for another 2 h, before repeating this procedure a second time. Pseudo-first-order kinetic

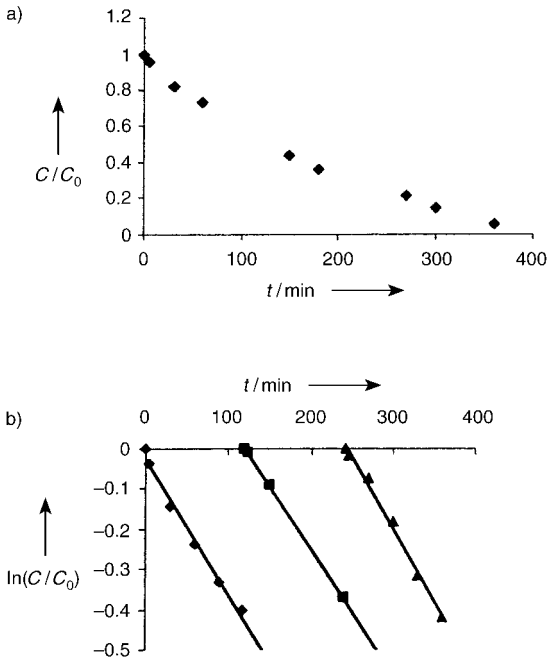


Figure 3. TPP-Y (0.6 g/500 mL) photocatalyzed oxidation of 2,4-xylidine a) total oxidation of 2,4-xylidine (100 ppm), b) procedure with further addition of 2,4-xylidine after 2 and 4 h of irradiation time. C_0 = initial concentration of 2,4-xylidine, C = concentration of 2,4-xylidine at irradiation time t.

 © 2003 Wiley-VCH Verlag GmbH & Co. KGaA, Weinheim

constants were obtained for all three cycles (Figure 3b), with very similar k values (3.3×10^{-3}, 3.1×10^{-3}, 3.5×10^{-3} min^{-1}). The result indicates that the catalyst may be recycled and hence has potential for further development.

A careful investigation on the products of the TPP-Y photocatalyzed oxidation of 2,4-xylidine reveals the absence of hydroxylated intermediate products, which are typical of hydroxyl-radical-initiated oxidations.[7] The oxidation of 2,4-xylidine by means of an electron-transfer mechanism with excited TPP-Y as acceptor yields 2,4-dimethyl-phenol[8] which under the given experimental conditions will be oxidatively degraded to CO_2 and H_2O (dissolved organic carbon (DOC) analyses were not made). This working hypothesis is also in agreement with quenching experiments in aqueous solutions, where the fluorescence of TPP^+ ions was found to decrease in the presence of 2,4-xylidine. The rate constant of the quenching electron-transfer process in aqueous solution (k_q), calculated from the K value obtained from the slope of the Stern–Volmer plot ($12\,M^{-1}$), and from the singlet lifetime of TPP^+ ion in aqueous solutions (3.9 ns),[2] was found to be $3.1\times10^{9}\,M^{-1}\,s^{-1}$.

Experimental Section

Y-zeolite (10 g) was suspended in an aqueous solution (adjusted to pH 2 with HCl) of 2,4,6-triphenylpyrylium hydrogensulfate (40 mL, 1.62 g). The suspension was stirred in the dark for 24 h at 40 °C and then filtered. The solid was collected and washed with water (50 mL, acidified to pH 2 with HCl) and dried at 100 °C for one day.

Continuously aerated suspensions of TPP-Y (0.6 g) in aqueous solutions (500 mL) of 2,4-xylidine (50 or 100 ppm) were irradiated in an immersion reactor (pyrex) with an Hg medium-pressure light source (Philips, HPK 125). Samples of the irradiated solutions were analyzed by HPLC.

Received: June 27, 2002
Revised: January 28, 2003 [Z19624]

Keywords: heterogeneous catalysis · photochemistry · photooxidation · synthetic methods · zeolites

[1] M. A. Miranda, H. García, *Chem. Rev.* **1994**, *94*, 1063–1089.
[2] a) A. M. Amat, A. Arques, M. A. Miranda, *Appl. Catal. B* **1999**, *23*, 205–214; b) M. A. Miranda, F. Galindo, A. M. Amat, A. Arques, *Appl. Catal. B* **2000**, *28,* 127–133.
[3] A. Corma, V. Fornés, H. García, M. A. Miranda, J. Primo, M. J. Sabater, *J. Am. Chem. Soc.* **1994**, *116*, 2276–2280.
[4] For interesting applications see: a) A. Sanjuán, M. Alvaro, G. Aguirre, H. García, J. C. Scaiano, *J. Am. Chem. Soc.* **1998**, *120*, 7351–7352; b) A. Sanjuán, G. Aguirre, M. Alvaro, H. García, *Appl. Catal. B* **1998**, *15*, 247–257; c) W. Adam, A. Corma, M. A. Miranda, M. J. Sabater, C. Sahin, *J. Am. Chem. Soc.* **1996**, *118,* 2380; d) M. L. Cano, F. L. Cozens, H. García, V. Martí, J. C. Scaiano, *J. Phys. Chem*, **1996**, *100*, 18152–18157; e) A. Doménech, M. T. Doménech-Carbó, H. García, M. S. Galletero. *Chem. Commun.* **1999**, 2173–2174; f) A. Sanjuán, G. Aguirre, M. Alvaro, H. García, J. C. Scaiano, *Appl. Catal. B* **2000**, *25*, 257–265; g) A. Sanjuán, M. Alvaro, A. Corma, H. García, *Chem. Commun.* **1999**, 1641–1642; h) A. Sanjuán, A. Guillermo, M. Alvaro, H. García, *Water Res.* **2000**, *34*, 320–326.
[5] A. Williams, *J. Am. Chem. Soc.* **1971**, *93*, 2733–2737.
[6] a) S. H. Bossmann, D. Herrmann, A. M. Braun, C. Turro, *J. Inf. Rec.* **1998**, *24*, 271–275; b) S. Göb, E. Oliveros, S. H. Bossmann, A. M. Braun, R. Guardani, C. A. Oller do Nascimento, *Chem. Eng. Process.* **1999**, *38*, 373–382; c) S. Göb, E. Oliveros, S. H. Bossmann, A. M. Braun, R. Guardani, C. A. Oller do Nascimento, *J. Inf. Rec.* **2000**, *25*, 447–454; d) E. Oliveros, S. Göb, S. H. Bossmann, A. M. Braun, C. A. Oller do Nascimento, R. Guardani, 3rd Asia Pacific Conference on Sustainable Energy and Environmental Technology (Hong Kong), 3–6 December, 2000, Proceedings (Eds.: X. Hu, P. L. Yue), World Scientific Singapore, **2001**, pp. 577–581).
[7] O. Legrini, E. Oliveros, A. M. Braun, *Chem. Rev.* **1993**, *93*, 671–698.
[8] S. H. Bossmann, E. Oliveros, S. Göb, S. Siegwart, E. P. Dahlen, L. Payawan, Jr., M. Straub, M. Wörner, A. M. Braun, *J. Phys. Chem. A* **1998**, *102*, 5542–5550.

 © 2003 Wiley-VCH Verlag GmbH & Co. KGaA, Weinheim

DNA Recognition

DNA with Hydrophobic Base Substitutes: A Stable, Zipperlike Recognition Motif Based On Interstrand-Stacking Interactions

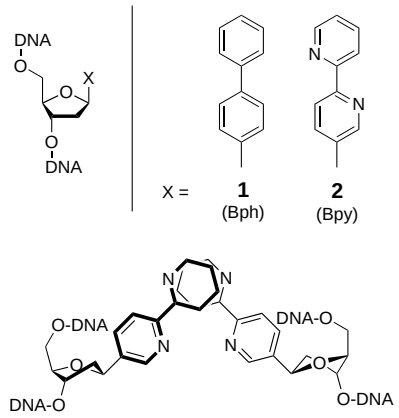
*Christine Brotschi and Christian J. Leumann**

Hydrogen-bonding and stacking interactions between nucleobases are the major noncovalent forces that stabilize the DNA and RNA double helix.[1,2] The relative contributions of each to stability has been a matter of debate since the discovery of the structure of the double helix. New insight into the importance of stacking and hydrogen bonding for DNA structure and function recently came from the investigation of shape mimics of complementary natural bases, devoid of the possibility of hydrogen-bond formation.[3–8] It was shown that such isosteres, although destabilizing a DNA duplex, can code for each other with high precision in DNA-polymerase-based primer-template-extension reactions. These findings triggered an extensive search for non-natural, stable, hydrophobic base pairs that are orthogonal to the natural base pairs in their recognition properties, and that could be of potential use in expanding the genetic alphabet.[9–14] Along similar lines, DNA duplexes containing transition-metal-mediated base-pair interactions,[15–18] or electronically complementary aromatic units that preferentially recognize each other by their quadrupolar interactions were reported.[19]

Recently we found that two bipyridyl (Bpy) C-nucleoside residues **2** (Scheme 1) can recognize each other within a DNA duplex with an affinity equal to a G-C base pair even in the

[*] Prof. C. J. Leumann, Dipl.-Chem. C. Brotschi
Departement für Chemie und Biochemie
Universität Bern
Freiestrasse 3, 3012 Bern (Switzerland)
Fax: (+41) 31-631-4355
E-mail: leumann@ioc.unibe.ch

 DOI: 10.1002/anie.200250516 © 2003 Wiley-VCH Verlag GmbH & Co. KGaA, Weinheim



Scheme 1. Top: the hydrophobic base substitutes investigated; bottom: interstrand-stacking pattern of two opposite, partially intercalated Bpy residues as determined by molecular modeling (double bonds in the distal pyridine rings are omitted for clarity).[20]

absence of transition-metal ions.[20] Based on molecular modeling of a corresponding duplex we proposed interstrand stacking of the distal rings of the Bpy residues as the duplex-stabilizing force. Herein we provide further evidence for the interstrand-stacking model and show that up to eight Bph C-nucleosides **1**, which lack any heteroatoms, can be accommodated in the center of a DNA duplex to form a stable, zipperlike recognition motif.

The synthesis of the C-nucleosides and the corresponding phosphoramidite building blocks of **1** and **2** as well as the synthesis of the corresponding oligodeoxynucleotides followed standard routes in C-nucleoside- and DNA-chemistry and will be described elsewhere.[21] We like to note here that, independently from our work and in a different context, the Bph-nucleoside **1** was recently synthesized and incorporated into DNA by Seitz et al.[22]

In initial pairing experiments we focused on non-self-complementary oligonucleotide duplex 12-mers containing one unit of **1** or **2** in opposing positions in the center of the sequence (Table 1). The thermal stabilities of the corresponding duplexes were determined by UV-melting curve analysis, and the corresponding T_m-data are summarized in Table 1.

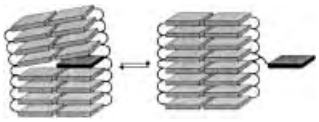
From the T_m data it is clear that within the given sequence, the arrangement of the Bpy–Bpy units (**2**–**2**) is more stable than a T–A and almost as stable as a C–G base pair. This is in agreement with our earlier observations on longer DNA duplexes.[20] Two opposing Bph residues (**1**–**1**) show a reduced T_m by 5.4 K and 9.4 K, relative to a T–A and a C–G base pair, respectively. The T_m of duplexes with mixed arrangements of Bph and Bpy residues (**1**–**2** or **2**–**1**) lie in between. The thermodynamic data of duplex formation (Table 1), as obtained from fits to the experimental, normalized melting curves according to known procedures,[23] show distinct differences in the enthalpy terms (ΔH_{fit}). Association of two Bph residues seems to cause a larger enthalpy change than the association of two Bpy residues. Hydrophobic pairs with **1** and **2**, however, show less enthalpic stabilization than a T–A or C–G base pair. The thermodynamic stability of the duplexes (ΔG_{fit}) is in line with the thermal stabilities deduced from the T_m data.

The results conform with the proposed interstrand-stacking model. The origin of the advantage in thermal stability of a Bpy relative to a Bph residue is not yet clear. We exclude differences in the polarizability (α_m) of the two aromatic systems as the major factor, as calculations revealed very similar α_m values (18.64 Å^3 for Bpy, both *syn* and *anti* isomer, 20.15 Å^3 for Bph). More likely, differences in solvation of the edges of the aromatic units in the major or minor groove in the duplex state, or structural differences around the biphenylic axis (intrinsically planar in the case of Bpy and intrinsically nonplanar in the case of Bph) are responsible for the stability differences.

To evaluate the effect of a Bph or Bpy residue in a bulge position, we performed a series of melting experiments with the 18-mer duplexes indicated in Table 2, in which the two aromatic residues are compared with any of the four natural bases in a typical single-nucleotide bulge arrangement.

As can be seen from the T_m data in Table 2, insertion of either a Bph or a Bpy residue into the bulge surprisingly does not lead to a decrease in T_m relative to the regular duplex while the natural nucleoside units in this position decrease duplex stability by 5.6–7.6 K. To probe the state of the equilibrium between the intrahelically

Table 2: Effect on T_m of Bph and Bpy in bulge positions, relative to a natural base (right). Base-sequence information as well as a graphical representation of the equilibrium between the looped out and the intrahelically stacked base (left).

5′-GATGAC-X-GCTAGCTAGGAC CTACTG – CGATCGATCCTG-5′	X	T_m[a] [°C]
	-	64.0
	1	64.0
	2	64.3
	A	57.6
	G	58.4
	T	56.4
	C	57.7

[a] $c = 1.2$ μM in 10 mM NaH_2PO_4, 0.15 M NaCl, pH 7.0. Estimated error in $T_m = \pm 0.5$ °C.

Table 1: Sequence information and schematic representation of the arrangement of the aromatic units in the duplex, as well as the corresponding T_m and thermodynamic data from UV spectroscopy determined melting curves (260 nm) for all the possible arrangements of units **1** and **2**.

5′-GATGAC-X-GCTAG CTACTG-Y-CGATC-5′	X–Y	T_m [a] [°C]	$-\Delta H_{fit}$[b] [kcal mol^{-1}]	$-\Delta S_{fit}$[b] [cal K^{-1} mol^{-1}]	$-\Delta G_{fit}^{25\,°C}$[b] [kcal mol^{-1}]
	**1**–**1**	42.5	78.8	220.0	13.2
	2–**2**	50.4	68.6	183.3	14.0
	1–**2**	46.2	72.7	199.2	13.3
	2–**1**	45.7	71.3	194.1	13.4
	T–A	47.9	81.4	224.5	14.4
	C–G	51.9	82.4	224.0	15.6

[a] c = 1.2 μM in 10 mM NaH_2PO_4, 0.15 M NaCl, pH 7.0. Estimated error in $T_m = \pm 0.5$ °C. [b] Determined by curve fitting to the experimental melting curve; estimated error ±5%.

 © 2003 Wiley-VCH Verlag GmbH & Co. KGaA, Weinheim

stacked and the looped-out state of the hydrophobic residues we collected the T_m data of the corresponding duplex in H_2O/EtOH solvent mixtures (Figure 1). This indirect procedure was necessary as a direct evaluation based on fluorescence quenching of Bph was unsuccessful because of extensive band overlap.

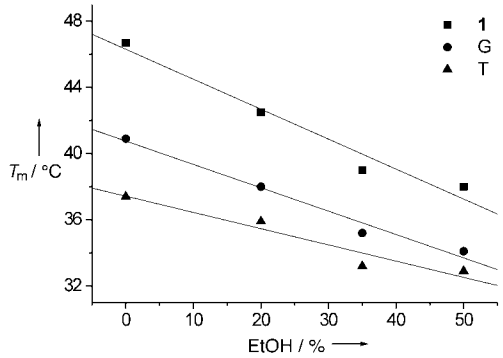


Figure 1. Relative stabilities of selected duplexes with X = **1**, G, T (from Table 2) as a function of the concentration of EtOH. $c = 1.2$ μM in 10 mM NaH_2PO_4, pH 7.0. Estimated error in $T_m = \pm 0.5$ °C.

We observed a linear decrease of the T_m with increasing concentration of EtOH, with a steeper, negative slope in the case of the Bph bulge than the thymine control bulge. This result is in agreement with a greater preference of the hydrophobic base to be in the looped-out state in a less polar medium than thymine, and points to a preferential stacked state of Bph and Bpy residues under typical physiological conditions. That there is essentially no difference in T_m between the Bpy and Bph bulge indicates an equal extent of intrahelical stacking which implies that Bph and Bpy adopt a planar arrangement of the two rings within the base-stack. This arrangement seems plausible as the rotational barrier of Bph in the gas phase is only approximately 2 kcal mol^{-1} at room temperature.[24] Furthermore Bph is planar in the crystalline state.

Consequently we investigated the effect of multiple Bph substitutions in the center of an oligodeoxynucleotide on duplex stability. We prepared the sequences depicted in Table 3, containing 1–4 Bph residues opposing each other in the duplex. The corresponding T_m data are summarized in Table 3 and selected UV spectroscopy determined melting curves are depicted in Figure 2. Again, to our surprise, the T_m values increase by 3.0–4.4 K per each additional Bph pair. The melting profiles showed in all cases only one single, highly cooperative transition. Also in these cases we determined the thermodynamic parameters of duplex formation by a curve-fitting procedure. We observed a tendency for a gradual reduction of the enthalpy term (ΔH_{fit}) with a parallel increase in the free enthalpy of duplex formation (ΔG_{fit}) as a function of the increasing number of Bph base pairs. Thus, the double helices containing Bph base pairs seem to be entropically stabilized relative to the single strands, which is again in agreement with the nonpolar, nonfunctionalized Bph residues escaping extensive solvation upon duplex formation. We would like to stress here that the thermodynamic data strongly rely on a true two-state melting behavior and a heat capacity change $\Delta C_p^\circ = 0$ between the unpaired and paired state, and therefore may not be completely accurate.

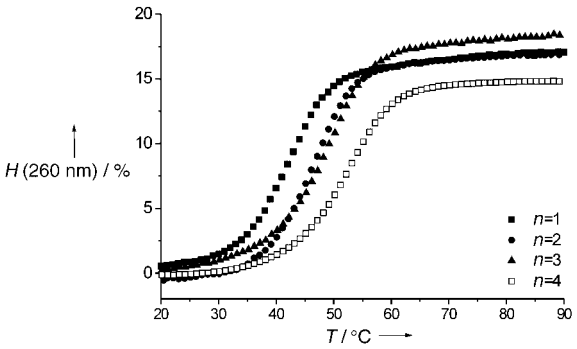


Figure 2. T_m curves (260 nm) of the duplexes represented in Table 3 ($n = 1$–4). $c = 1.2$ μM in 10 mM NaH_2PO_4, 0.15 M NaCl, pH 7.0.

A preliminary investigation on the structure of singularly and multiply Bph-substituted duplexes (Table 3, $n = 1$, 3) by circular dichroism (CD) spectroscopy was performed and the spectra compared to that of the unmodified duplex (Table 3, $n = 0$). The CD traces are overlaid in Figure 3. Comparison of the CD spectra reveals no major difference to the B-DNA conformation as a function of the number of Bph base pairs. The spectra are thus in agreement with the Bph residues adopting a highly ordered, stacked arrangement within the double helix.

Table 3: Duplex sequence information and a schematic representation of the interstrand-stacking zipper model, and corresponding T_m and thermodynamic data.

5′-GATGAC(**1**)$_n$GCTAG CTACTG(**1**)$_n$CGATC-5′	n	T_m[a] [°C]	$-\Delta H_{fit}$[b] [kcal mol^{-1}]	$-\Delta S_{fit}$[b] [cal K^{-1} mol^{-1}]	$-\Delta G_{fit}^{25\,°C}$[b] [kcal mol^{-1}]
	0	45.0	71.8	196.1	13.3
	1	42.5	78.8	220.0	13.2
	2	46.9	77.9	213.9	14.1
	3	49.9	69.0	184.5	14.0
	4	53.2	67.6	178.5	14.4

[a] $c = 1.2$ μM in 10 mM NaH_2PO_4, 0.15 M NaCl, pH 7.0. Estimated error in $T_m = \pm 0.5$ °C. [b] Determined by curve fitting to the experimental melting curve; estimated error ±5%.

There now exists ample data on the energetics of π-stacking interactions of natural bases and non-natural base substitutes as the dangling ends of oligonucleotide duplexes. The relative contributions of the various physicochemical factors, hydrophobicity, polarizability, surface area, and dipole moment, to duplex stability have been discussed in detail.[25–28] Our results demonstrate for the first time the existence of stable oligonucleotide duplexes with uninterrupted stretches of up to four hydrophobic, not hydrogen-

 © 2003 Wiley-VCH Verlag GmbH & Co. KGaA, Weinheim

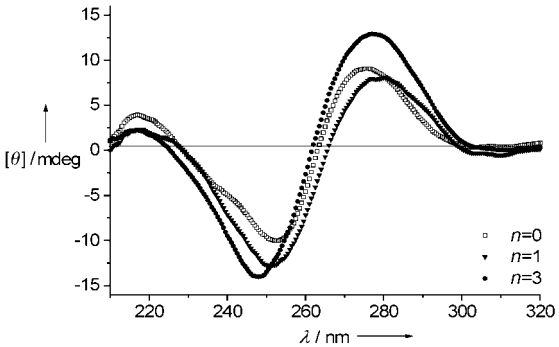


Figure 3. CD spectra of selected duplexes from Table 3 ($n=0$, 1, 3). $c=3.6$ μM, in 10 mM NaH_2PO_4, 0.15 M NaCl, pH 7.0, $T=20$ °C.

bonding, aromatic base pairs in the center of their sequence.[29] Recognition most likely occurs via a zipperlike interstrand-stacking motif of the Bph and Bpy residues. This result highlights the importance of stacking interactions for nucleic acid duplex stability as well as the relative ease with which the DNA backbone can compensate for structural elongation along the helical axis, through alternate intercalation of aromatic units. Further support for the zipper model comes from recent NMR spectroscopy structural investigations on unusual 5′-(GXA)/(AYG)-5′ sequence motifs (X/Y = T/A, A/T, C/G, G/C, and G/G) in oligodeoxynucleotides, in which the X and Y bases were found not to be hydrogen bonded, but intercalated, forming a similar zipperlike arrangement.[30]

The herein described recognition motif opens possibilities for the introduction of new functions into double-helical recognition systems based on the DNA backbone. Experiments towards making fully modified, artificial duplexes containing only hydrophobic bases of the biphenyl type, as well as investigations towards a binary recognition code based entirely on differential stacking energies is currently underway.

Received: November 11, 2002 [Z50516]

Keywords: biaryls · bioorganic chemistry · DNA recognition · hydrophobic effect · nucleosides

[1] C. R. Cantor, P. R. Schimmel in *Biophysical Chemistry Part III: The Behavior of Biological Macromolecules, Vol. 2* (Ed.: P. C. Vapnek), W. H. Freeman & Co., New York, **1980**, pp. 1109 – 1181.
[2] W. Saenger, *Principles of Nucleic Acid Structure*, Springer, New York, **1984**.
[3] K. M. Guckian, J. C. Morales, E. T. Kool, *J. Org. Chem.* **1998**, *63*, 9652 – 9656.
[4] T. J. Matray, E. T. Kool, *J. Am. Chem. Soc.* **1998**, *120*, 6191 – 6192.
[5] J. C. Morales, E. T. Kool, *Nat. Struct. Biol.* **1998**, *5*, 950 – 954.
[6] S. Moran, R. X.-F. Ren, E. T. Kool, *Proc. Natl. Acad. Sci. USA* **1997**, *94*, 10506 – 10511.
[7] B. M. O'Neill, J. E. Ratto, K. L. Good, D. C. Tahmassebi, S. A. Helquist, J. C. Morales, E. T. Kool, *J. Org. Chem.* **2002**, *67*, 5869 – 5875.
[8] B. A. Schweitzer, E. T. Kool, *J. Am. Chem. Soc.* **1995**, *117*, 1863 – 1872.
[9] M. Berger, A. K. Ogawa, D. L. McMinn, Y. Q. Wu, P. G. Schultz, F. E. Romesberg, *Angew. Chem.* **2000**, *112*, 3069 – 3071; *Angew. Chem. Int. Ed.* **2000**, *39*, 2940 – 2942.
[10] M. Berger, S. D. Luzzi, A. A. Henry, F. E. Romesberg, *J. Am. Chem. Soc.* **2002**, *124*, 1222 – 1226.
[11] D. L. McMinn, A. K. Ogawa, Y. Wu, J. Liu, P. G. Schultz, F. E. Romesberg, *J. Am. Chem. Soc.* **1999**, *121*, 11585 – 11586.
[12] A. K. Ogawa, Y. Q. Wu, D. L. McMinn, J. Liu, P. G. Schultz, F. E. Romesberg, *J. Am. Chem. Soc.* **2000**, *122*, 3274 – 3287.
[13] E. L. Tae, Y. Wu, G. Xia, P. G. Schultz, F. E. Romesberg, *J. Am. Chem. Soc.* **2001**, *123*, 7439 – 7440.
[14] C. Yu, A. A. Henry, F. E. Romesberg, P. G. Schultz, *Angew. Chem.* **2002**, *114*, 3997 – 4000; *Angew. Chem. Int. Ed.* **2002**, *41*, 3841 – 3844.
[15] S. Atwell, E. Meggers, G. Spraggon, P. G. Schultz, *J. Am. Chem. Soc.* **2001**, *123*, 12364 – 12367.
[16] E. Meggers, P. L. Holland, W. B. Tolman, F. E. Romesberg, P. G. Schultz, *J. Am. Chem. Soc.* **2000**, *122*, 10714 – 10715.
[17] K. Tanaka, M. Shionoya, *J. Org. Chem.* **1999**, *64*, 5002 – 5003.
[18] K. Tanaka, Y. Yamada, M. Shionoya, *J. Am. Chem. Soc.* **2002**, *124*, 8802 – 8803.
[19] G. Mathis, J. Hunziker, *Angew. Chem.* **2002**, *114*, 3335 – 3338; *Angew. Chem. Int. Ed.* **2002**, *41*, 3203 – 3205.
[20] C. Brotschi, A. Häberli, C. J. Leumann, *Angew. Chem.* **2001**, *113*, 3101 – 3103; *Angew. Chem. Int. Ed.* **2001**, *40*, 3012 – 3014.
[21] All modified oligodeoxynucleotides were synthesized on a commercial DNA synthesizer, they were detached from solid support and deproteced using standard procedures. Oligonucleotides were purified by ion exchange (DEAE) and reversed-phase HPLC and routinely analyzed by ESI mass spectrometry (negative mode). All oligonucleotides were within ± 1 m/z of the expected molecular mass $[M-H]^-$.
[22] I. Singh, W. Hecker, A. K. Prasad, V. S. Parmar, O. Seitz, *Chem. Commun.* **2002**, 500 – 501.
[23] M. Petersheim, D. H. Turner, *Biochemistry* **1983**, *22*, 256 – 263.
[24] F. Grein, *J. Phys. Chem. A* **2002**, *106*, 3823 – 3827.
[25] K. M. Guckian, B. A. Schweitzer, R. X.-F. Ren, C. J. Sheils, P. L. Paris, D. C. Tahmassebi, E. T. Kool, *J. Am. Chem. Soc.* **1996**, *118*, 8182 – 8183.
[26] K. M. Guckian, B. A. Schweitzer, R. X.-F. Ren, C. J. Sheils, D. C. Tahmassebi, E. T. Kool, *J. Am. Chem. Soc.* **2000**, *122*, 2213 – 2222.
[27] H. Rosemeyer, F. Seela, *J. Chem. Soc. Perkin Trans. 2* **2002**, 746 – 750.
[28] S. Bommarito, N. Peyret, J. SantaLucia, Jr., *Nucleic Acids Res.* **2000**, *28*, 1929 – 1934.
[29] For a very recent report on stable duplexes containing non-nucleosidic phenanthrene units see: S. M. Langenegger, R. Häner, *Helv. Chim. Acta* **2002**, *85*, 3414 – 3421.
[30] S.-H. Chou, K.-H. Chin, *J. Mol. Biol.* **2001**, *312*, 753 – 768.

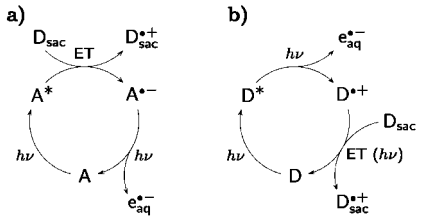
 © 2003 Wiley-VCH Verlag GmbH & Co. KGaA, Weinheim

Kinetics of Photoionization

Generation of Hydrated Electrons by an Acridone-Sensitized Three-Photon Cycle**

Martin Goez and Belal Hussein Mohammed Hussein*

The photochemistry of organic systems at high light levels is intriguing because the successive absorption of more than one photon opens up new reaction routes. As we have recently shown,[1] illumination of an electron acceptor A in the presence of a sacrificial electron donor D_{sac} can produce hydrated electrons e^-_{aq} by the catalytic cycle displayed in Scheme 1a. A related cycle (Scheme 1b) is conceivable with



Scheme 1. Cyclic photoionization mechanisms for an electron acceptor (a) and for an electron donor (b).

an electron donor D as the substrate. Herein, we present examples of this mechanism, using *N*-methyl acridone and its parent compound as donors. Their photoionization in solution has not been reported to date. Our experimental method is laser flash photolysis with detection of absorption and/or luminescence; the experimental setup has been described in ref. [1b].

For *N*-methyl acridone (MA), radiationless deactivation of the first excited singlet state is negligible,[2] and triplet formation can be disregarded (quantum yield $\Phi_{trip} \leq 0.05$)[3] in our reaction media, micellar solutions of sodium dodecylsulfate (SDS) with $0.01\,\text{M} \leq [\text{SDS}] \leq 0.2\,\text{M}$. We found that ^{1}MA* is the only emitting species in this system, and is not quenched by SDS under our conditions, in accordance with the literature.[3] The fluorescence intensity I_{fl} was, therefore, used to monitor the concentration of ^{1}MA*.

The dependence of I_{fl} on the excitation intensity I_{ex} can be seen in Figure 1. [^{1}MA*] clearly passes through a maximum, so the excited state is not only formed by a photoreaction but also destroyed by one. It is natural to assume that the latter process is the photoionization of ^{1}MA* because hydrated electrons e^-_{aq} are observed under these conditions. Absolute electron concentrations were obtained by absorption measurements ($\lambda_{max} = 720$ nm, $\varepsilon_{max} = 18\,500\,\text{M}^{-1}\,\text{cm}^{-1}$).[4] To eliminate the absorbances arising from concomitantly formed species, difference experiments on solutions free from, and saturated with, N_2O, an efficient scavenger of e^-_{aq}, were performed. It was ascertained that N_2O does not influence the reaction in any other way.

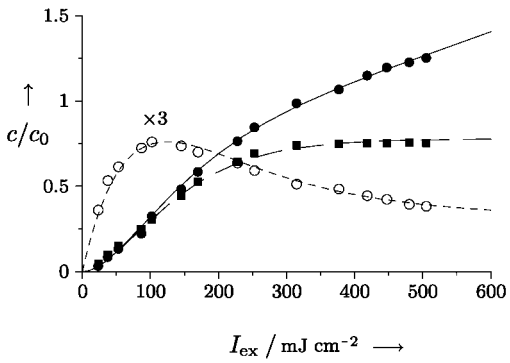


Figure 1. Photoreaction of 5.33×10^{-5} M *N*-methyl acridone MA in 0.1 M aqueous SDS solution, excitation wavelength 355 nm. Shown are the concentrations c relative to the starting concentration of the substrate c_0 as functions of the laser intensity I_{ex}. Filled circles and solid line: e^-_{aq}; open circles and short-dashed line: ^{1}MA* after convolution with the response function of the detection system; filled squares and long-dashed line: $MA^{\bullet+}$. The curves are simultaneous fits of Equations (2), (5), and (3) to the data. Constant parameters, $\kappa_1 = 1.17 \times 10^{-2}\,\text{cm}^2\,\text{mJ}^{-1}$, $k_f\tau = 0.6$, $\chi\tau = 2.5$; best-fit kinetic parameters, $\kappa_2 = 1.37 \times 10^{-2}\,\text{cm}^2\,\text{mJ}^{-1}$, $\kappa_3 = 1.75 \times 10^{-3}\,\text{cm}^2\,\text{mJ}^{-1}$.

Strikingly, at very high excitation intensities the fluorescence does not fall back to zero but to a constant level. This behavior is apparent in Figure 1, and is unambiguously seen when the pulse of a second laser (308 nm) is superimposed on the 355-nm pulse to increase the maximum available intensity to about 800 mJ cm^{-2}. With any sequential mechanism, the concentration of the excited state must approach zero for $I_{ex} \to \infty$ owing to the consumption of the substrate. The observation of a steady state for this intermediate is only compatible with a *cyclic* mechanism comprising as an additional step the regeneration of ^{1}MA* (most likely via the starting material, which is then reexcited) from the ionized substrate in yet another photoreaction. Such a cyclic mechanism is also able to account for the observed dependence of the e^-_{aq} concentration on I_{ex}, specifically that $[e^-_{aq}]$ becomes larger than the substrate concentration c_0 (compare Figure 1); at the highest intensity obtainable with two superimposed laser pulses, the electron concentration exceeds c_0 by almost 60 %.

Absorption spectra recorded in N_2O saturated solutions reveal that the photoreaction essentially involves only one additional intermediate: apart from a small contribution of ^{3}MA* (below 330 nm and in the range from 500 to 630 nm, with a maximum at 580 nm), which is noticeable at low I_{ex} only[5] and can be removed by saturating the solutions with oxygen, spectra taken at different excitation intensities can be made to coincide simply by multiplication with a scaling factor. We ascribe this absorption (maxima at 320 and 790 nm) to the radical cation $MA^{\bullet+}$ because photoionization of ^{1}MA* must lead to this species. As long as I_{ex} is small, the concentration of $MA^{\bullet+}$ displays an intensity dependence

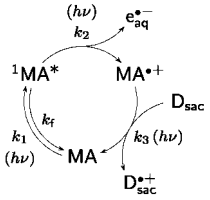
[*] Prof. Dr. M. Goez, B. H. M. Hussein
Fachbereich Chemie
Martin–Luther-Universität Halle–Wittenberg
Kurt–Mothes-Strasse 2, 06120 Halle/Saale (Germany)
Fax: (+49) 345-55-27345

[**] This work was supported by the Volkswagenstiftung.

 DOI: 10.1002/anie.200250731 © 2003 Wiley-VCH Verlag GmbH & Co. KGaA, Weinheim

identical to that of $e^{\bullet-}_{aq}$, but at high I_{ex} it levels off to a steady state while that of $e^{\bullet-}_{aq}$ increases linearly under these conditions (Figure 1). This result provides further evidence for a cyclic photoionization mechanism.

Scheme 2 shows the mechanism inferred from the evidence presented. Fluorescence of ^{1}MA*(rate constant k_f) was included in the kinetic scheme because it occurs on a time scale comparable to the duration of the laser pulse which drives the three photoreactions. For thermodynamic reasons, the photoreaction of the radical cation was assumed to regenerate the substrate in its ground state, not in its excited state. This step must involve an electron donor D_{sac} (see below).



Scheme 2. Photoionization mechanism of MA with the rate constants used for the kinetic description.

Because optically thin solutions were used throughout, a linearization of the Lambert–Beer law is permissible, and the three intensity-dependent reactions can be described as first-order steps. During the laser pulse, their rate "constants" k_1, k_2, and k_3 vary with the envelope of the pulse. However, the assumption of a rectangular pulse causes a negligible error only, so we can write k_i $(i=1\ldots3)$ as $\kappa_i I_{ex}/\tau$, where τ is the duration of the pulse and the constant κ_i has the dimension of a reciprocal intensity. Solving the corresponding system of differential equations and taking the values of the resulting functions at the end of the laser pulse, one gets the Equations (1)—(3).

$$\frac{[^1\mathrm{MA}^*]}{c_0}=\frac{\kappa_1\kappa_3}{\kappa_a\kappa_b}\left(1-\frac{\kappa_b(\kappa_a-\kappa_3)}{\kappa_3(\kappa_a-\kappa_b)}\exp(-\kappa_a I_{ex})+\frac{\kappa_a(\kappa_b-\kappa_3)}{\kappa_3(\kappa_a-\kappa_b)}\exp(-\kappa_b I_{ex})\right) \quad (1)$$

$$\frac{[e^{\bullet-}_{aq}]}{c_0}=\frac{\kappa_1\kappa_2}{\kappa_a\kappa_b}\left(1+\frac{\kappa_b(\kappa_a-\kappa_3)}{\kappa_a(\kappa_a-\kappa_b)}\exp(-\kappa_a I_{ex})-\frac{\kappa_a(\kappa_b-\kappa_3)}{\kappa_b(\kappa_a-\kappa_b)}\exp(-\kappa_b I_{ex})-\frac{\kappa_3(\kappa_a+\kappa_b)}{\kappa_a\kappa_b}+\kappa_3 I_{ex}\right) \quad (2)$$

$$\frac{[\mathrm{MA}^{\bullet+}]}{c_0}=\frac{\kappa_1\kappa_2}{\kappa_a\kappa_b}\left(1+\frac{\kappa_b}{\kappa_a-\kappa_b}\exp(-\kappa_a I_{ex})-\frac{\kappa_a}{\kappa_a-\kappa_b}\exp(-\kappa_b I_{ex})\right) \quad (3)$$

$\kappa_{a,b}$ is given by Equation (4).

$$\kappa_{a,b}=\frac{\left(\kappa_1+\kappa_2+\kappa_3+k_f\frac{\tau}{I_{ex}}\right)}{2}\pm\sqrt{\frac{\left(\kappa_1+\kappa_2+\kappa_3+k_f\frac{\tau}{I_{ex}}\right)^2}{4}-\left(\kappa_1\kappa_2+\kappa_1\kappa_3+\kappa_2\kappa_3+\kappa_3 k_f\frac{\tau}{I_{ex}}\right)} \quad (4)$$

As an additional complication, the observed fluorescence signal is the convolution of the true signal with the delta-function response of our detection system, $\exp(-\chi t)$. This convolution transforms Equation (1) into Equation (5).

$$I_{fl}\propto\frac{\kappa_1\kappa_3}{\kappa_a\kappa_b}\left(1-\frac{\kappa_b(\kappa_a-\kappa_3)\chi\tau/I_{ex}}{\kappa_3(\kappa_a-\kappa_b)(\chi\tau/I_{ex}-\kappa_a)}\exp(-\kappa_a I_{ex})+\frac{\kappa_a(\kappa_b-\kappa_3)\chi\tau/I_{ex}}{\kappa_3(\kappa_a-\kappa_b)(\chi\tau/I_{ex}-\kappa_b)}\exp(-\kappa_b I_{ex})-\frac{\kappa_a\kappa_b(\chi\tau/I_{ex}-\kappa_3)}{\kappa_3(\chi\tau/I_{ex}-\kappa_a)(\chi\tau/I_{ex}-\kappa_b)}\exp(-\chi\tau)\right) \quad (5)$$

By fitting Equations (2), (5), and (3) to the data, the kinetic constants can be extracted. Besides $k_f\tau$ and the κ_i value a scaling factor for the fluorescence curve and one for the absorbance of the radical cation are needed because neither the luminescence collection efficiency nor the extinction coefficient of $MA^{\bullet+}$ are known. As many variables as possible were determined independently: κ_1 can be calculated[1d] from the extinction coefficient of the ground state, k_f was taken from the literature,[3] and τ and χ were measured. Because this leaves only four parameters (κ_2 and κ_3 as well as the two scaling factors) for a *simultaneous* fit of three curves totally differing in shape, we consider the fit results to be quite reliable, not only as far as parameter values are concerned but also with respect to the mechanism: we regard the excellent fit (see Figure 1) obtained in this way as strong evidence that the proposed cyclic reaction is correct.

With the limiting concentration given by Equation (3), the extinction coefficient ε_{355} of $MA^{\bullet+}$ at the excitation wavelength was determined to be $3900\,\mathrm{M^{-1}cm^{-1}}$ from spectra recorded in N_2O saturated solution at high I_{ex}. These spectra were recorded with delayed acquisition to allow ^{1}MA* to decay completely to the ground state, and correcting for the remaining ground-state depletion. From ε_{355} and the best-fit parameter κ_3, the quantum yield of ground-state regeneration is calculated (see ref. [1d]) to be 0.065. Unfortunately, measuring the extinction coefficient of the $S_1\rightarrow S_n$ absorption was not feasible owing to the short life of ^{1}MA*, so the absolute quantum yield of photoionization cannot be specified.

To occur on the time scale of our laser pulse, about 6 ns, regeneration of the substrate must involve a reactant present in high concentration or in close proximity. The only presumable candidates for this in our systems are water or SDS. To distinguish between these alternatives, we carried out experiments in water/alcohol mixtures. For this reaction medium, the intensity dependencies of the concentrations can be fitted well with κ_3 set to zero, that is, without a regeneration of the substrate; as a corollary, $[e^{\bullet-}_{aq}]/c_0$ does not exceed 1 even in the two-laser experiment. Hence, in the original system SDS is indeed the sacrificial donor D_{sac}.

The second striking feature in the absence of SDS is a considerably lower electron yield at given I_{ex} that can be traced to a reduction of the parameter κ_2 by a factor of about 2.7. This result indicates that the influence of SDS on the reaction is twofold: in addition to enhancing the efficiency by enabling a catalytic cycle it also directly increases the ionization quantum yield. The latter effect was also observed for the photoionization of the tris(bipyridyl)ruthenium ion.[8]

With the parent compound acridone, quantitative detection of the radical cation was not feasible because of its

 © 2003 Wiley-VCH Verlag GmbH & Co. KGaA, Weinheim

unfavorably low extinction coefficient. For the electron and the excited singlet, a three-parameter fit (κ_2, κ_3, and a scaling factor for the fluorescence) of Equations (2) and (5) to the data gave an equally good fit as with the *N*-methyl derivative; the best-fit parameters were quite similar.

The described reaction scheme is expected to be relevant to other systems, and we have already obtained preliminary evidence for it in several other cases (e.g., xanthone, proflavine). Two features of the mechanism might make it attractive as a light-driven electron source: First, the amount of $e^{\cdot-}_{aq}$ formed is not limited by depletion of the substrate but rather by that of the sacrificial donor SDS, which is necessarily present in large excess. Second, the micellar environment efficiently suppresses recombination of the electron and the radical cation; while the latter remains in the micelle, $e^{\cdot-}_{aq}$ rapidly escapes owing to its high mobility, and is then available for reactions with other substances in the aqueous phase outside the micelle.

Received: December 10, 2002 [Z50731]

Keywords: kinetics · laser chemistry · photochemistry · photoionization

[1] a) M. Goez, V. Zubarev, *Angew. Chem.* **1997**, *109*, 2779 – 2781; *Angew. Chem. Int. Ed. Engl.* **1997**, *36*, 2664 – 2666; b) M. Goez, V. Zubarev, G. Eckert, *J. Am. Chem. Soc.* **1998**, *120*, 5347 – 5348; c) M. Goez, V. Zubarev, *J. Phys. Chem. A* **1999**, *103*, 9605 – 9613; d) M. Goez, V. Zubarev, *Chem. Phys.* **2000**, *256*, 107 – 116.

[2] a) M. Siegmund, J. Bendig, *Ber. Bunsen-Ges.* **1978**, *82*, 1061 – 1068; b) M. Siegmund, J. Bendig, *Z. Naturforsch. A* **1980**, *35*, 1076 – 1086.

[3] W. L. Hinze, T. E. Riehl, H. N. Singh, Y. Baba, *Anal. Chem.* **1984**, *56*, 2180 – 2191.

[4] E. M. Fielden, E. J. Hart, *Trans. Faraday Soc.* **1967**, *63*, 2975 – 2982.

[5] For *N*-ethyl acridone, a similar absorption at 580 nm was observed at low excitation intensity[6] but not at high excitation intensity;[7] this discrepancy remained inexplicable at that time. ^{3}MA* cannot be photoionized in our experiments because it does not absorb at the laser wavelength, as is evident from the transient spectra. Its intensity dependence can be explained quantitatively by intersystem crossing (isc) of ^{1}MA*. Calculations show that the curves of Figure 1 are uninfluenced by isc as long as the sum of k_{fl} and k_{isc} remains constant.

[6] S. N. Ščerbo, G. A. Valkova, D. N. Šigorin, *Z. Fiz. Chim.* **1981**, *55*, 795 – 797.

[7] S. Mory, H.-J. Weigmann, A. Rosenfeld, M. Siegmund, R. Mitzner, J. Bendig, *Chem. Phys. Lett.* **1985**, *115*, 201 – 204.

[8] a) D. B. Naik, W. Schnabel, *Chem. Phys. Lett.* **1994**, *228*, 616 – 620; b) D. B. Naik, W. Schnabel, *Chem. Phys. Lett.* **1999**, *315*, 416 – 420.

 © 2003 Wiley-VCH Verlag GmbH & Co. KGaA, Weinheim

Synthesis of Benzonitriles

A Convenient Procedure for the Palladium-Catalyzed Cyanation of Aryl Halides**

*Mark Sundermeier, Alexander Zapf, and Matthias Beller**

Benzonitriles are of substantial interest in organic chemistry as integral ingredients of dyes, herbicides, natural products, agrochemicals, and pharmaceuticals.[1] In addition, they represent versatile intermediates for further transformations in synthetic organic chemistry. An elegant method for the preparation of benzonitriles is the transition-metal-catalyzed cyanation of aryl halides.[2,3] Recently, we reported a new, generally applicable palladium catalyst system for the cyanation of aryl and heteroaryl chlorides to the desired nitriles in good yields using potassium cyanide as the source of cyanide.[4] The main problem of this and other reported palladium- or nickel-catalyzed cyanation protocols is catalyst deactivation by an excess of dissolved cyanide ions in the reaction mixture (Scheme 1).[3b,4b] Therefore, catalyst productivity is comparably low in cyanation reactions (TON typically 10–50) compared to other palladium-catalyzed coupling reactions (TON 10000 to 100000).[5]

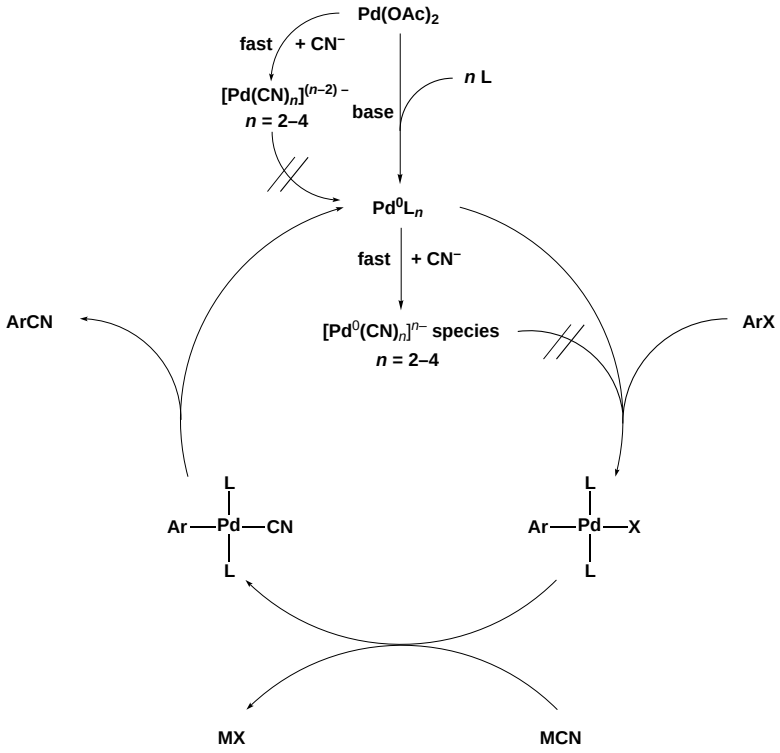
We thought that a continuous addition of cyanide could provide a general solution to the problem of inhibition of the catalyst by cyanide ions. Surprisingly, the constant dosage of cyanide has, to the best of our knowledge, never been described for the palladium-catalyzed cyanation of aryl halides. This might be explained because of the difficulties associated with the dosage of solid cyanide salts. A liquid cyanation reagent would be clearly favorable. One of the simplest soluble cyanide sources for this reaction is acetone cyanohydrin, which is cheap and commercially available on a large scale (Scheme 2).[6] To date, the use of acetone cyanohydrin as a cyanide source has been described only for nickel-catalyzed cyanation reactions[7] and other transition-metal-catalyzed reactions of epoxides, aldehydes, and dienes.[8]

A slow and reproducible dosage of acetone cyanohydrin is a prerequisite for successful coupling reactions, as a result of the sensitivity of the palladium catalyst to cyanide ions. Clearly, the dosage of the cyanide should not be significantly

[*] Prof. Dr. M. Beller, Dr. M. Sundermeier, Dr. A. Zapf
Leibniz-Institut für Organische Katalyse an der
Universität Rostock e.V.
Buchbinderstr. 5–6, 18055 Rostock (Germany)
Fax: (+49) 381-4669324
E-mail: matthias.beller@ifok.uni-rostock.de

[**] The authors thank Mrs. H. Baudisch (IfOK) for analytical support (GC–MS). Dr. S. Weiss, Dr. J. Sans, Dr. H.-P. Krimmer, and Dr. M. Gómez Andreu (Degussa AG) are thanked for general discussions. Generous support for this project from the state Mecklenburg-Western Pomerania, the Fonds der Chemischen Industrie, and the Bundesministerium für Bildung und Forschung (BMBF) is gratefully acknowledged. We thank OMG for providing us with palladium compounds.

 DOI: 10.1002/anie.200250778 © 2003 Wiley-VCH Verlag GmbH & Co. KGaA, Weinheim



Scheme 1. Proposed reaction mechanism of the palladium-catalyzed cyanation of aryl halides.

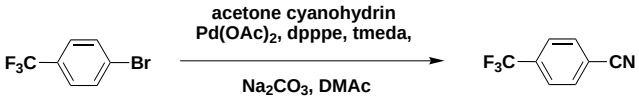


Scheme 2. Acetone cyanohydrin, a useful HCN equivalent.

faster than its consumption in order to prevent an increase in the cyanide concentration. By using a syringe pump, which guarantees a continuous addition of small volumes, this is easily possible. As shown in Table 1, entry 1, the cyanation of 4-bromobenzotrifluoride with acetone cyanohydrin proceeds smoothly using our previously optimized catalyst system at 120 °C (Scheme 3). The corresponding nitrile is obtained in quantitative yield without any by-product being observed! This is the first example of a palladium-catalyzed cyanation of aryl halides using acetone cyanohydrin as the cyanide source.

Table 1, entries 2 and 3 show that a reduction of the reaction temperature is possible to some extent without any loss of catalytic productivity. Even at 80 °C 4-cyanobenzotrifluoride is formed almost quantitatively. However, at 60 °C (Table 1, entry 4) the catalytic activity breaks down, probably because the oxidative addition becomes more difficult (Scheme 1).

Regarding the feasibility of a larger-scale application of this protocol, the most important point is the reduction of the catalyst/substrate ratio. As shown in Table 1, entries 5 and 6, a decrease in the catalyst concentration to 0.5 mol % is possible without any loss of yield. However, at a concentration of 0.1 mol % of Pd, a higher phosphane/palladium ratio and a slower addition of acetone cyanohydrin are required to keep the catalyst active. The corresponding nitrile is formed in 80 % yield, which corresponds to a TON of 800 (Table 1, entry 8). A further improvement of the catalyst activity is shown in entry 10. The cyanation proceeds efficiently with only 0.05 mol % palladium(II)



Scheme 3. Palladium-catalyzed cyanation of 4-bromobenzotrifluoride with acetone cyanohydrin.

acetate by increasing the phosphane/palladium ratio up to 16. Under these conditions, 4-trifluoromethylbenzonitrile is obtained in excellent yield (95 %; TON 1900) and selectivity (98 %). This corresponds to the highest TON reported for a palladium-catalyzed cyanation of aryl bromides.[9]

With these encouraging results in hand we were interested in the scope and limitation of our new protocol. Table 2 shows a variety of different aryl halides tested in the palladium-catalyzed cyanation with acetone cyanohydrin using a relatively low catalyst loading (0.5 mol % Pd) (Scheme 4).

Activated aryl bromides such as 4-bromobenzotrifluoride, 4′-bromoacetophenone, and methyl 4-bromobenzoate were converted into the desired nitriles at 100 °C with excellent yields (> 95 %; Table 2, entries 1–3). No side products were observed under these conditions. 4-Bromofluorobenzene requires a slightly higher reaction temperature for excellent conversion and selectivity (120 °C; Table 2, entry 4). Unactivated and deactivated (electron-rich) aryl

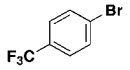
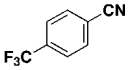
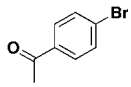
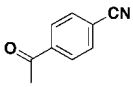
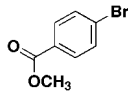
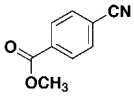
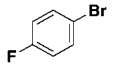
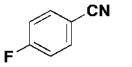
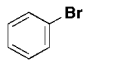
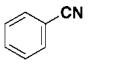
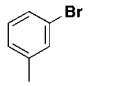
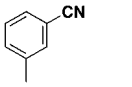
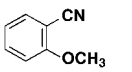
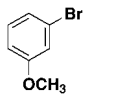
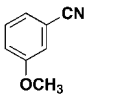
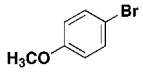
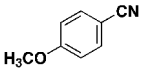
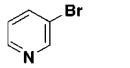
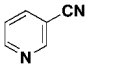
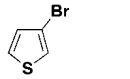
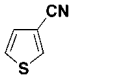
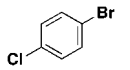
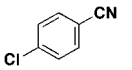
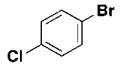
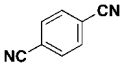
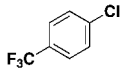
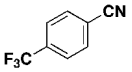
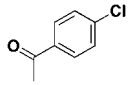
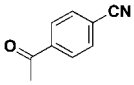
Table 1: Palladium-catalyzed cyanation of 4-bromobenzotrifluoride using acetone cyanohydrin.[a]

Entry	$Pd(OAc)_2$ [mol %]	Pd/P	tmeda [mol %][b]	Dosage rate [mmol h^{-1}]	*t* [h]	*T* [°C]	Conversion [%][c]	Yield [%][c]
1	2	1:4	20	0.1	21	120	100	≥ 99
2	2	1:4	20	0.1	21	100	100	≥ 99
3	2	1:4	20	0.1	21	80	100	≥ 99
4	2	1:4	20	0.1	21	60	1	1
5	1	1:4	20	0.1	21	100	100	≥ 99
6	**0.5**	**1:4**	**10**	**0.1**	**21**	**100**	**100**	**≥ 99**
7	0.1	1:4	10	0.1	21	120	0	0
8	0.1	1:8	10	0.05	42	120	81	80
9	0.1	1:8	–	0.05	42	120	8	0
10	**0.05**	**1:16**	**10**	**0.05**	**42**	**140**	**97**	**95**

[a] General conditions: 4-bromobenzotrifluoride (2 mmol), acetone cyanohydrin solution (1 M, 2.1 mmol), 1,5-bis(diphenylphosphanyl)pentane (dpppe), sodium carbonate (2.1 mmol), *N*,*N*-dimethylacetamide (DMAc, 2 mL). [b] *N*,*N*,*N*′,*N*′-Tetramethylethylenediamine (tmeda). [c] Conversions and yields were determined by GC using an internal standard (diethyleneglycol di-*n*-butyl ether).

 © 2003 Wiley-VCH Verlag GmbH & Co. KGaA, Weinheim

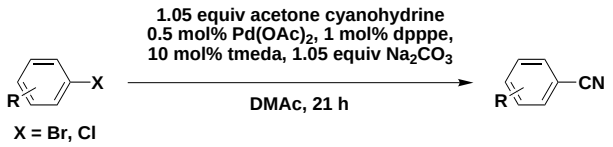
Table 2: Scope of the palladium-catalyzed cyanation using acetone cyanohydrin.[a]

Entry	Substrate	Product	*T* [°C]	Conversion [%][b]	Yield [%][b]
1			100	100	≥99
2			100	100	≥99
3			100	100	95
4			120	98	96
5			120	96	96
6			120	100	≥99
7			140	27	21
8			120	99	99
9			120	98	98
10			100	82	82
11			140	46	46
12			100	82	82
13[c]			120	100	≥99
14[d]			140	78	77
15[d]			140	90	89

[a] General conditions: aryl or heteroaryl halide (2 mmol), acetone cyanohydrin solution (1 M, 2.1 mmol, dosage rate: 0.1 mL h^{-1}), palladium(II) acetate (0.01 mmol), dpppe (0.02 mmol), tmeda (0.2 mmol), sodium carbonate (2.1 mmol), DMAc (2 mL), 21 h. [b] Conversions and yields were determined by GC using an internal standard (diethyleneglycol di-*n*-butyl ether). [c] Acetone cyanohydrin solution (1 M, 4.2 mL, dosage rate: 0.1 mL h^{-1}), sodium carbonate (4.2 mmol), 42 h. [d] Palladium(II) acetate (0.02 mmol), dpppe (0.04 mmol).

bromides require higher temperatures, too. For example, at 100 °C bromobenzene gives benzonitrile in just 59% yield, but at 120 °C an excellent yield of 96% is observed (Table 2, entry 5). A slightly deactivated aryl bromide, 3-bromotoluene, leads to 3-cyanotoluene in more than 99% yield (Table 2, entry 6). Entries 7–9 show the reaction of even more deactivated bromoanisoles. Both *meta*- and *para*-bromoanisole give the corresponding methoxybenzonitriles in almost quantitative yields (>98%). In contrast, the sterically more congested *ortho* isomer undergoes cyanation in only 21% yield, even at higher temperatures (140 °C).

The cyanation of *N*-heteroaryl bromides is also possible. 3-Bromopyridine gave the corresponding nitrile in 82% yield at 100 °C (Table 2, entry 10). 3-Bromothiophene is a more difficult substrate: the corresponding 3-cyanothiophene was obtained in only 46% yield at 140 °C (Table 2, entry 11). An interesting substrate is 4-bromochlorobenzene. In this case both halogen substituents can be replaced by cyanide. Nevertheless, the reaction was highly chemoselective: At 100 °C only substitution of the bromine atom (82% yield for 4-chlorobenzonitrile) is observed in the presence of 1.05 equivalents of acetone cyanohydrin (Table 2, entry 12). The addition of 2.1 equivalents of the cyanide precursor at 120 °C and double the amount of base (sodium carbonate) leads to 1,4-dicyanobenzene in 99% yield (Table 2, entry 13). This demonstrates that a cyanation of aryl *chlorides* is also possible. Other examples are shown in Table 2, entries 14 and 15. 4-Chlorobenzotrifluoride gave the corresponding 4-trifluoromethylbenzonitrile under standard reaction conditions in moderate yield (45%), whereas an increase in the amount of catalyst to 1 mol% led to the product in 77% yield. In the case of 4′-chloroacetophenone, the desired product was obtained in good yield (89%). Notably, the concentrations of catalyst used for the cyanation of aryl chlorides are thus far the lowest reported in literature.



Scheme 4. Palladium-catalyzed cyanation of different aryl halides with acetone cyanohydrin.

The presented results demonstrate that the palladium-catalyzed cyanation of a wide variety of aryl halides with acetone cyanohydrin as the cyanide source is possible in a very efficient manner. Substituted benzonitriles are obtained in excellent yield and selectivity (in general >99%) from the corresponding aryl bromides. Also activated aryl chlorides can be transformed into the desired products in moderate to very good yield. The new method is more advantageous than other known cyanation protocols with respect to catalyst amount, reproducibility, and the absence of stoichiometric amounts of zinc salts, which are often required for successful cyanation reactions.

 © 2003 Wiley-VCH Verlag GmbH & Co. KGaA, Weinheim

With our protocol, we have shown that the deactivation of the palladium catalyst can be prevented by slow addition of cyanide to the reaction mixture. The presented method also opens up new possibilities for other transition metal-catalyzed cyanation reactions.

Experimental Section

General: All chemicals are commercially available and were used without further purification. Acetone cyanohydrin was used as a 1M solution in *N,N*-dimethyl acetamide. Products were fully characterized after isolation (NMR, IR, MS, EA) or in the case of commercially available products by comparison of GC–MS data.

General procedure: A two-necked round-bottomed reaction flask (25 mL) with condenser was charged with sodium carbonate (223 mg, 2.1 mmol) and purged with argon. The aryl bromide (2 mmol), tmeda (30 μL; 0.2 mmol), catalyst solution[10] (1 mL), and DMAc (1 mL) were added. The reaction mixture was heated to 100 °C and while magnetically stirring a 1M acetone cyanohydrin solution (2.1 mL, 2.1 mmol) was dosed through a syringe pump with a dosage rate of 0.1 mL h^{-1} (0.1 mmol h^{-1}). After 21 h, the reaction was cooled to room temperature, the internal standard diethyleneglycol di-*n*-butyl ether (400 μL) was added, and the reaction mixture was diluted with dichloromethane. Conversions and yields were determined by GC analysis.

Received: December 16, 2002 [Z50778]

Keywords: acetone cyanohydrin · aryl halides · benzonitriles · cyanation · palladium

[1] A. Kleemann, J. Engel, B. Kutscher, D. Reichert, *Pharmaceutical substances: syntheses, patents, applications*, 4th ed., Georg Thieme, Stuttgart, **2001**.

[2] For the nickel-catalyzed cyanation of aryl halides, see: a) L. Cassar, *J. Organomet. Chem.* **1973**, *54*, C57-C58; b) L. Cassar, M. Foà, F. Montanari, G. P. Marinelli, *J. Organomet. Chem.* **1979**, *173*, 335–339; c) Y. Sakakibara, F. Okuda, A. Shimoyabashi, K. Kirino, M. Sakai, N. Uchino, K. Takagi, *Bull. Chem. Soc. Jpn.* **1988**, *61*, 1985–1990; d) Y. Sakakibara, Y. Ido, K. Sasaki, M. Sakai, N. Uchino, *Bull. Chem. Soc. Jpn.* **1993**, *66*, 2776–2778; e) M.-H. Rock, A. Merhold (Bayer AG), WO 98/37058 **1998**.

[3] For the palladium-catalyzed cyanation of aryl halides, see: a) K. Takagi, T. Okamoto, Y. Sakakibara, S. Oka, *Chem. Lett.* **1973**, 471–473; b) A. Sekiya, N. Ishikawa, *Chem. Lett.* **1975**, 277–278; c) K. Takagi, T. Okamoto, Y. Sakakibara, A. Ohno, S. Oka, N. Hayama, *Bull. Chem. Soc. Jpn.* **1975**, *48*, 3298–3301; d) K. Takagi, T. Okamoto, Y. Sakakibara, A. Ohno, S. Oka, N. Hayama, *Bull. Chem. Soc. Jpn.* **1976**, *49*, 3177–3180; e) J. R. Dalton, S. L. Regen, *J. Org. Chem.* **1979**, *44*, 4443–4444; f) Y. Akita, M. Shimazaki, A. Ohta, *Synthesis* **1981**, 974–975; g) N. Chatani, T. Hanafusa, *J. Org. Chem.* **1986**, *51*, 4714–4716; h) K. Takagi, K. Sasaki, Y. Sakakibara, *Bull. Chem. Soc. Jpn.* **1991**, *64*, 1118–1121; i) Y. Anderson, B. Långström, *J. Chem. Soc. Perkin Trans. 1* **1994**, 1395–1400; j) T. Okano, J. Kiji, Y. Toyooka, *Chem. Lett.* **1998**, 425–426; k) B. A. Anderson, E. C. Bell, F. O. Ginah, N. K. Harn, L. M. Pagh, J. P. Wepsiec, *J. Org. Chem.* **1998**, *63*, 8224–8228; l) P. E. Maligres, M. S. Waters, F. Fleitz, D. Askin, *Tetrahedron Lett.* **1999**, *40*, 8193–8195; m) F. Jin, P. N. Confalone, *Tetrahedron Lett.* **2000**, *41*, 3271–3273.

[4] a) M. Sundermeier, A. Zapf, M. Beller, J. Sans, *Tetrahedron Lett.* **2001**, *42*, 6707–6710; b) M. Sundermeier, A. Zapf, S. Mutyala, W. Baumann, J. Sans, S. Weiss, M. Beller, *Chem. Eur. J.*, in press.

[5] a) R. B. Bedford, C. S. J. Cazin, S. L. Hazelwood (née Welch), *Angew. Chem.* **2002**, *114*, 4294–4296; *Angew. Chem. Int. Ed.* **2002**, *41*, 4120–4122; b) R. Jackstell, M. Gómez Andreu, A. Frisch, H. Klein, K. Selvakumar, A. Zapf, A. Spannenberg, D. Röttger, O. Briel, R. Karch, M. Beller, *Angew. Chem.* **2002**, *114*, 1028–1031; *Angew. Chem. Int. Ed.* **2002**, *41*, 986–989; c) J. A. Loch, M. Albrecht, E. Peris, J. Mata, J. W. Faller, R. H. Crabtree, *Organometallics* **2002**, *21*, 700–706; d) M. Feuerstein, H. Doucet, M. Santelli, *Tetrahedron Lett.* **2001**, *42*, 6667–6670; e) A. Zapf, A. Ehrentraut, M. Beller, *Angew. Chem.* **2000**, *112*, 4315–4317; *Angew. Chem. Int. Ed.* **2000**, *39*, 4153–4155; f) A. Zapf, M. Beller, *Chem. Eur. J.* **2000**, *6*, 1830–1833; g) A. F. Littke, C. Dai, G. C. Fu, *J. Am. Chem. Soc.* **2000**, *122*, 4020–4028; h) R. B. Bedford, S. M. Draper, P. N. Scully, S. L. Welch, *New J. Chem.* **2000**, *24*, 745–747; i) V. P. W. Böhm, W. A. Herrmann, *Chem. Eur. J.* **2000**, *6*, 1017–1025; j) J. M. Fox, X. Huang, A. Chieffi, S. L. Buchwald, *J. Am. Chem. Soc.* **2000**, *122*, 1360–1370; k) M. Kawatsura, J. F. Hartwig, *J. Am. Chem. Soc.* **1999**, *121*, 1473–1478; l) J. P. Wolfe, S. L. Buchwald, *Angew. Chem.* **1999**, *111*, 2570–2573; *Angew. Chem. Int. Ed.* **1999**, *38*, 2413–2416; m) J. P. Wolfe, R. A. Singer, B. H. Yang, S. L. Buchwald, *J. Am. Chem. Soc.* **1999**, *121*, 9550–9561; n) M. Ohff, A. Ohff, M. E. van der Boom, D. Milstein, *J. Am. Chem. Soc.* **1997**, *119*, 11687–11688; o) W. A. Herrmann, C. Broßmer, C.-P. Reisinger, T. H. Riermeier, K. Öfele, M. Beller, *Chem. Eur. J.* **1997**, *3*, 1357–1364; p) W. A. Herrmann, C. Broßmer, K. Öfele, C.-P. Reisinger, T. Priermeier, M. Beller, H. Fischer, *Angew. Chem.* **1995**, *107*, 1989–1992; *Angew. Chem. Int. Ed. Engl.* **1995**, *34*, 1844–1848; q) M. Beller, H. Fischer, W. A. Herrmann, K. Öfele, C. Broßmer, *Angew. Chem.* **1995**, *107*, 1992–1993; *Angew. Chem. Int. Ed. Engl.* **1995**, *34*, 1848–1849; r) W. A. Herrmann, M. Elison, J. Fischer, C. Köcher, G. R. J. Artus, *Angew. Chem.* **1995**, *107*, 2602–2605; *Angew. Chem. Int. Ed. Engl.* **1995**, *34*, 2371–2374.

[6] a) G. Tennant in *Comprehensive Organic Chemistry, Vol. 2* (Eds.: D. Barton, W. D. Ollis, E. Haslam, D. Neville Jones, P. G. Sammes, J. F. Stoddart, I. O. Sutherland, C. J. Drayton), Pergamon Press, Oxford, **1979**, pp. 528–539; b) A. Mori, S. Inoue in *Comprehensive Asymmetric Catalysis, Vol. 2* (Eds.: E. N. Jacobsen, A. Pfaltz, H. Yamamoto), Springer, Berlin, **1999**, pp. 983–994; c) R. J. H. Gregory, *Chem. Rev.* **1999**, *99*, 3649–3682.

[7] L. Cassar, S. Ferrara, M. Foá, *Adv. Chem. Ser.* **1974**, *132*, 252–273.

[8] For example, see: a) Y. Kobayashi, H. Hayashi, K. Miyaji, S. Inoue, *Chem. Lett.* **1986**, 931–934; b) H. Ohno, A. Mori, S. Inoue, *Chem. Lett.* **1993**, 375–378; c) H. Ohno, A. Mori, S. Inoue, *Chem. Lett.* **1993**, 975–978; d) E. M. Campi, E. S. Elmes, W. R. Jackson, C. G. Lovel, M. K. S. Probert, *Aust. J. Chem.* **1987**, *40*, 1053–1061; e) W. C. Drinkhard (DuPont), US 3655723 **1972**; f) W. Goertz, P. C. J. Kamer, P. W. N. M. van Leeuwen, D. Vogt, *Chem. Eur. J.* **2001**, *7*, 1614–1618; g) W. Goertz, W. Keim, D. Vogt, U. Englert, M. D. K. Boele, L. A. van der Veen, P. C. J. Kamer, P. W. N. M. van Leeuwen, *J. Chem. Soc. Dalton Trans.* **1998**, 2981–2988; h) W. Goertz, P. C. J. Kamer, P. W. N. M. van Leeuwen, D. Vogt, *Chem. Commun.* **1997**, 1521–1522; i) T. V. RajanBabu, *Chim. Oggi* **2000**, *18*, 26–31.

[9] Previously, the highest TON was described in: P. E. Maligres, M. S. Waters, F. Fleitz, D. Askin, *Tetrahedron Lett.* **1999**, *40*, 8193–8195 (Pd (0.1 mol%); dppf (1,1′-bis(diphenylphosphanyl)ferrocene, $Zn(CN)_2$, *N,N*-dimethylformamide, 120 °C, 20 h, 95% yield for bromobenzene).

[10] Palladium(II) acetate (0.01M) and dpppe (0.02M) freshly prepared from palladium(II) acetate (11.2 mg) and dpppe (44.1 mg) in DMAc (5 mL).

 © 2003 Wiley-VCH Verlag GmbH & Co. KGaA, Weinheim

Cover Picture

P. Andrew Evans,* Jian Cui, and Gerald P. Buffone

Taking control of stereochemistry should lead to an enhanced understanding of the conformational aspects that affect diastereoselectivity in medium-sized ring systems. The temporary silicon-tethered ring-closing-metathesis reactions described by P. A. Evans et al. on page 1734 ff. represent a new strategy for long-range asymmetric induction that provides a useful approach to 1,4-, 1,5-, and 1,6-stereocontrol.



Contents

Web Sites

Superconductors ——— 1682 The Link of the Least Resistance *W. Grochala*

Books

Oils and Fats Authentication ——— 1683 Michael Jee *reviewed by J. O. Metzger*

Handbook of Porous Solids ——— 1684 Ferdi Schüth, Kenneth S. W. Sing, Jens Weitkamp *reviewed by P. Yang*

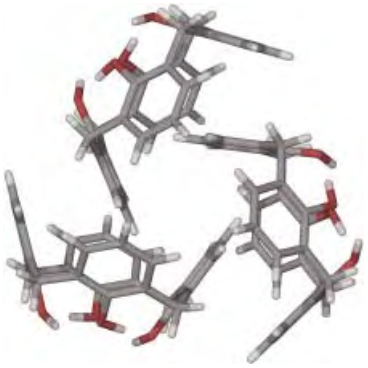
Highlights

Crystal Lattice Complexes

B. C. Gibb* ——— 1686 – 1687

A Solid-State Supramolecular Sweet Spot

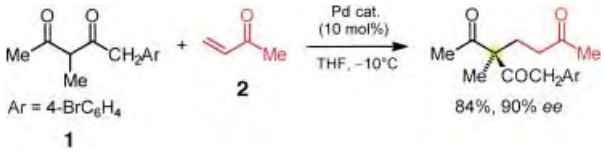
The beauty of crystals: A bridge between crystals that degrade when their guests are removed and crystalline solids that refuse to release their guests has been provided by Atwood et al. with the report of a calix[4]arene that forms an approximate hexagonal close-packed array of quasi-spherical trimers in the presence and absence of guest molecules (see X-ray crystal structure).



Enantioselective Michael Addition

J. Christoffers,* A. Baro ——— 1688 – 1690

Construction of Quaternary Stereocenters: New Perspectives through Enantioselective Michael Reactions



Pd^{II}-catalyzed Michael reactions of β-dicarbonyl compounds **1** and enones **2** can generate quaternary stereocenters (shown in yellow) with selectivities of 90% *ee* at relatively high temperatures (−10°C). This method represents a breakthrough in enantioselective synthesis.

Reviews

Soft Nanomaterials

I. W. Hamley* ——— 1692 – 1712

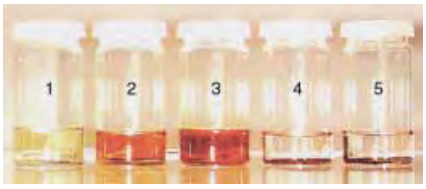
Nanotechnology with Soft Materials



It pays to be organized: The intricate structures that can be formed by self-organizing molecules are amazing (see picture). In the next few decades, the creation of a wealth of new materials and devices using soft nanotechnology will be witnessed. This review covers developments to date in fabricating nanostructures and devices using self-organizing polymers, colloids, surfactants, and biomolecules.

© 2003 Wiley-VCH Verlag GmbH & Co. KGaA, Weinheim

Communications

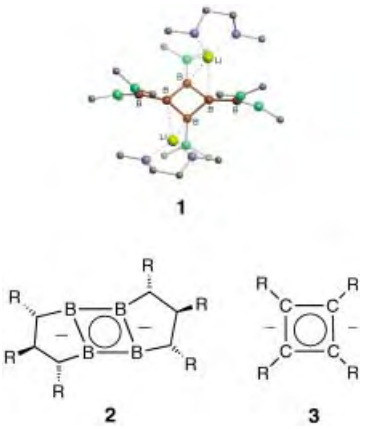


Up to 50% dye relative to the dead weight may be loaded into poly(organosiloxane) nanoparticles that contain quaternary ammonium groups (vessels 1–3 with hydrophilic thymol blue as a model substance), whereas nanoparticles without quaternary ammonium groups take up no dye (vessels 4, 5). The loading depends inter alia on the construction of the nanoparticles (core–shell, hollow spheres), on the amphiphilicity, which is adjustable by synthesis, and on the method of the phase transfer.

Dye Incorporation in Polymers

N. Jungmann, M. Schmidt, J. Ebenhoch, J. Weis, M. Maskos* ——— **1714 – 1717**

Dye Loading of Amphiphilic Poly(organosiloxane) Nanoparticles

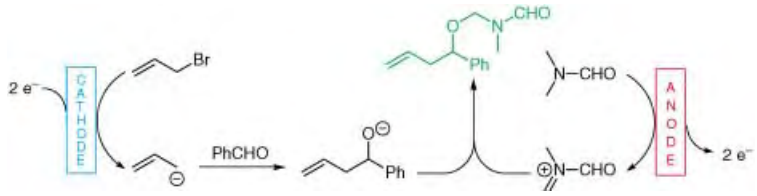


Aromatic with boron: Two-electron heteroaromatic compounds **1** and **2** undergo oxidations and reactions with electrophiles (reducing the number of framework electrons by two and four, respectively) under conservation of aromaticity. In contrast, corresponding reactions of the known dianion **3**, a six-electron aromatic four-membered ring, lead to loss of aromaticity (R = $SiMe_3$).

Boron Aromatics

W. Mesbah, C. Präsang, M. Hofmann, G. Geiseler, W. Massa, A. Berndt* ——— **1717 – 1719**

Dianions of Tetraboranes(4): Puckered Aromatic Four-Membered Rings and Their Reactions with Conservation of Aromaticity



The holy grail of electrochemistry, a convergent paired electrolysis, is a step closer in the metal-free electrochemical allylation of aromatic aldehydes in DMF. A three-component coupling product is obtained in a one-pot procedure when anodically generated electrophiles and cathodically generated nucleophiles react in solution to give a single product.

Organic Electrosynthesis

G. Hilt* ——— **1720 – 1721**

Convergent Paired Electrolysis for the Three-Component Synthesis of Protected Homoallylic Alcohols

For the USA and Canada:
ANGEWANDTE CHEMIE International Edition (ISSN 1433-7851) is published weekly by Wiley-VCH PO Box 191161, D 69451 Weinheim, Germany. Air freight and mailing in the USA by Publications Expediting Inc. 200 Meacham Ave., Elmont, NY 11003. Periodicals postage paid at Jamaica NY 11431. US POSTMASTER: send address changes to *Angewandte Chemie*, Wiley-VCH, 111 River Street, Hoboken, NJ 07030. Annual institutional subscription price for institutions: Europe € 2998.00/3148.00. Outside Europe US$ 3718.00/3904.00 (valid for print or electronic/print and electronic delivery); for individuals who are personal members of a national chemical society, or whose institution already subscribes, or who are retired or self-employed consultants, print only (including postage and handling charges): Europe € 248.00/Outside Europe US$ 348.00.

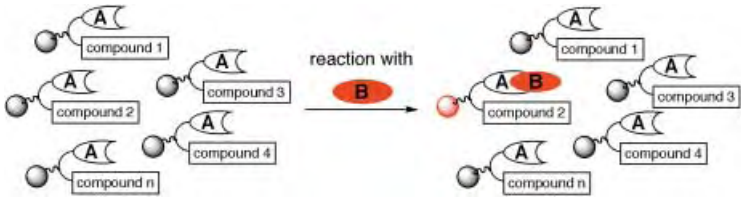
 © 2003 Wiley-VCH Verlag GmbH & Co. KGaA, Weinheim

Contents

Catalyst Screening

P. Krattiger, C. McCarthy, A. Pfaltz, H. Wennemers* ——— **1722 – 1724**

Catalyst–Substrate Coimmobilization: A Strategy for Catalysts Discovery in Split-and-Mix Libraries



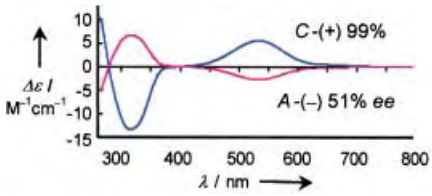
Potentially applicable to any bimolecular reaction: A new method for the discovery of catalysts among the members of split-and-mix libraries is described. A reaction partner (**A**) is immobilized along with each library member (the potential catalyst) on the same bead. The reaction partner **B** is labeled with a dye, thus a reaction between **A** and **B** is easily visualized through the attachment of the marker to the beads that carry the active catalyst.

Spontaneous Resolution

W. K. Rybak,* A. Skarżyńska, T. Głowiak ——— **1725 – 1727**

Efficient Asymmetry Generation in the Synthesis of Oxo-Rhenium(v) Complex *cis*-[$ReOCl_2${$OCMe_2CMe_2OP(OCMe_2CMe_2O)$}py]

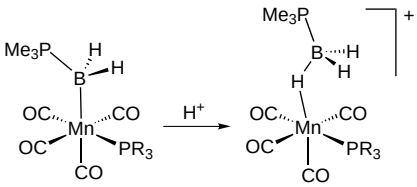
Its all done without mirrors: A simple procedure that randomly produces enantiomers of an oxo-rhenium(v) complex with a large enantiomeric excess (99% *ee*) from optically inactive precursors is presented. The chirally autocatalytic synthesis is achieved by the spontaneous resolution of the conglomerate in a stirred crystallization following the formation of the complex in the reaction system. The results are supported by circular dichroism spectroscopy (see picture).



Coordination Modes of Boron

T. Yasue, Y. Kawano,* M. Shimoi* ——— **1727 – 1730**

Proton-Induced Change of the Coordination Mode of a Boron Group: Boryl Complexes [$Mn(CO)_4(PR_3)(BH_2{\cdot}PMe_3)$] and Cationic Borane σ Complexes [$Mn(CO)_4(PR_3)(\eta^1\text{-}BH_3{\cdot}PMe_3)$]$^+$



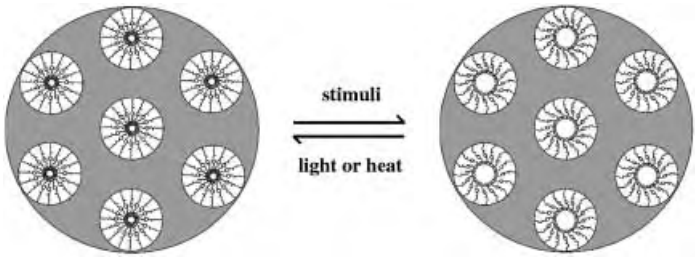
1 **2**

Mode change on protonation: New borylmanganese complexes **1** undergo protonation to give cationic borane σ complexes **2**. Heterolytic cleavage of the metal-coordinated B–H bond was observed in the decomposition process of **2**.

Photoresponsive Nanocomposites

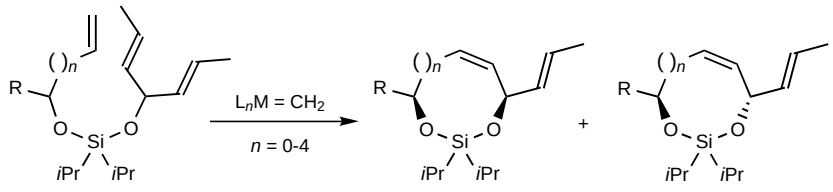
N. Liu, Z. Chen, D. R. Dunphy, Y.-B. Jiang, R. A. Assink, C. J. Brinker* ——— **1731 – 1734**

Photoresponsive Nanocomposite Formed by Self-Assembly of an Azobenzene-Modified Silane



Organization of photoresponsive azobenzene ligands within a 3D porous framework imparts new molecular-level functionality. The *trans* ⇌ *cis* conformation change of azobenzene ligands triggered by photoirradiation transduces photo energy into mechanical work, which can be used for opening and closing valves (see picture).

 © 2003 Wiley-VCH Verlag GmbH & Co. KGaA, Weinheim



R = alkyl, aryl etc.

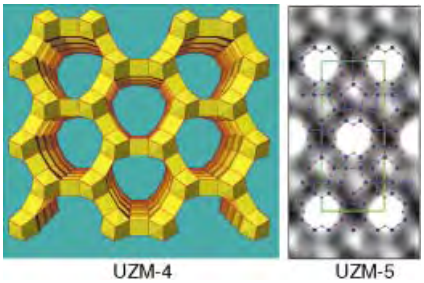
d.r. ≥ 1:27 to ≥ 99 : 1

Si-Tethered Asymmetric Induction

P. A. Evans,* J. Cui, G. P. Buffone ——— 1734 – 1737

Diastereoselective Temporary Silicon-Tethered Ring-Closing-Metathesis Reactions with Prochiral Alcohols: A New Approach to Long-Range Asymmetric Induction

A useful approach to 1,4-, 1,5-, and 1,6-stereocontrol, diastereoselective ring-closing-metathesis reactions that utilize temporary silicon tethers represent a new strategy for long-range asymmetric induction. This method facilitates the construction of *cis*-1,4-silaketals ($n = 0$, d.r. = 20:1; see scheme), whereas the extension of this concept to higher alkenyl alcohols ($n = 1$–4) results in a reversal of diastereoselectivity that favors formation of the *trans* isomer.

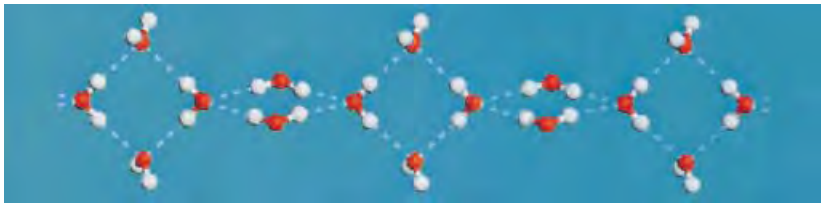


Low Si/Al Ratio Zeolites

C. S. Blackwell, R. W. Broach, M. G. Gatter, J. S. Holmgren, D.-Y. Jan, G. J. Lewis,* B. J. Mezza, T. M. Mezza, M. A. Miller, J. G. Moscoso, R. L. Patton, L. M. Rohde, M. W. Schoonover, W. Sinkler, B. A. Wilson, S. T. Wilson ——— 1737 – 1740

Open-Framework Materials Synthesized in the TMA^+/TEA^+ Mixed-Template System: The New Low Si/Al Ratio Zeolites UZM-4 and UZM-5

The right mix! Combinations of two of the most studied templates in zeolite synthesis, the tetramethylammonium (TMA^+) and tetraethylammonium (TEA^+) ions, are employed to synthesize the new species UZM-4, a stable large-pore zeolite with the BPH toplogy, and UZM-5, which has a new framework topology related to zeolite A in two dimensions and large surface cups capable of catalysis of aromatic compounds.

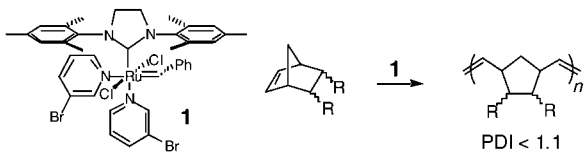


H Bonds in Chains of Water Molecules

S. Pal, N. B. Sankaran, A. Samanta* ——— 1741 – 1743

Structure of a Self-Assembled Chain of Water Molecules in a Crystal Host

The role of hydrogen bonding in water is important in determining the structure, stability, and function of biological assemblies. The supramolecular structure of 1,4,7,10-tetraazacyclododecane, a molecule that has secondary N–H bonds similar to those found in biological systems, contains an infinite chain of tetrameric water clusters (depicted, oxygen: red; hydrogen: white). This motif, until now, has not even been speculated upon.



Ultrafast-Initiating ROMP Catalyst

T.-L. Choi, R. H. Grubbs* ——— 1743 – 1746

Controlled Living Ring-Opening-Metathesis Polymerization by a Fast-Initiating Ruthenium Catalyst

Highly active with ultrafast initiation, the catalyst **1** promotes the controlled, living, ring-opening polymerization of various norbornene and 7-oxonorbornene derivatives (see scheme). The high k_i/k_p ratio associated with the polymerization reactions results in better molecular-weight control and narrower polydispersity indexes (PDIs, k_i = rate constant for initiation, k_p = rate constant for polymerization).

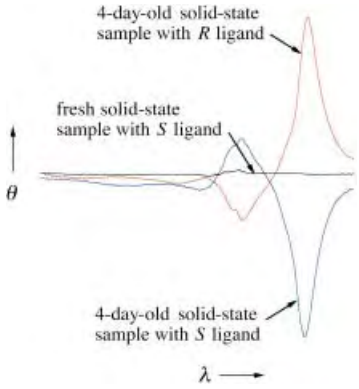
 © 2003 Wiley-VCH Verlag GmbH & Co. KGaA, Weinheim

Contents

Supramolecular Chirogenesis

V. V. Borovkov,* T. Harada, G. A. Hembury, Y. Inoue,* R. Kuroda* ——— **1746 – 1749**

Solid-State Supramolecular Chirogenesis: High Optical Activity and Gradual Development of Zinc Octaethylporphyrin Aggregates

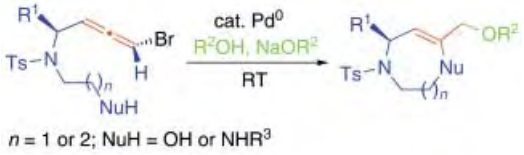


Slow formation of J-type helical aggregates occurs when the simple achiral zinc octaethylporphyrin interacts with enantiopure 1-cyclohexylethylamines in the solid state. These chiral solid-state aggregates exhibit a high degree of optical activity and are remarkably stable, as evidenced in the circular dichroism spectra (see picture).

Medium-Sized Heterocycles

H. Ohno, H. Hamaguchi, M. Ohata, T. Tanaka* ——— **1749 – 1753**

Bromoallenes as Synthetic Equivalents of Allyl Dications: Synthesis of Medium-Sized Nitrogen Heterocycles through the Cyclization of Bromoallenes in the Presence of a Palladium(0) Catalyst and an Alcohol

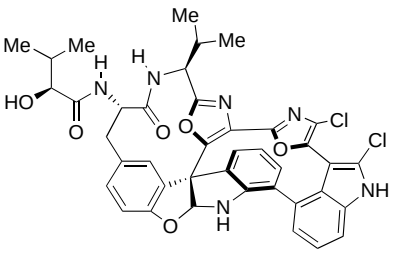


A highly regio- and stereoselective synthesis of medium-sized nitrogen heterocycles has been developed (see scheme), based on the discovery that bromoallenes can act as an allyl dication equivalent in the presence of a palladium(0) catalyst and an alcohol. The intramolecular nucleophilic attack takes place exclusively at the central carbon atom of the allene moiety.

Total Synthesis of Diazonamide A

K. C. Nicolaou,* P. Bheema Rao, J. Hao, M. V. Reddy, G. Rassias, X. Huang, D. Y.-K. Chen, S. A. Snyder ——— **1753 – 1758**

The Second Total Synthesis of Diazonamide A



1

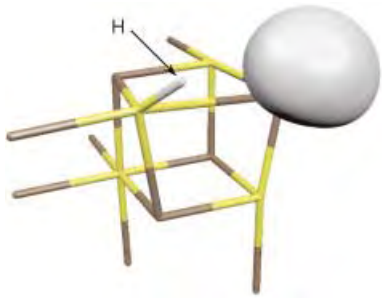
The uniquely woven, highly strained molecular architecture and the potent antitumor activity of diazonamide A (**1**) make this natural product an attractive synthetic target. The key steps in this total synthesis of **1** include a novel SmI_2-induced ring-closing cascade sequence and an unusual oxidation of an indoline to an oxindole in the presence of $Pd(OH)_2/C$.

Single-Ion Electron Traps

M. Chiesa, M. C. Paganini, E. Giamello,* C. Di Valentin, G. Pacchioni **1759 – 1761**

First Evidence of a Single-Ion Electron Trap at the Surface of an Ionic Oxide

A single electron can be trapped by a triply coordinated single cation at a magnesium oxide surface (see picture). The resulting center, denoted $MgO_{corner}(H^+/e^-)$, is a member of a new family of surface color centers and represents a significant advance for the concept of electron-trapping sites in solids.



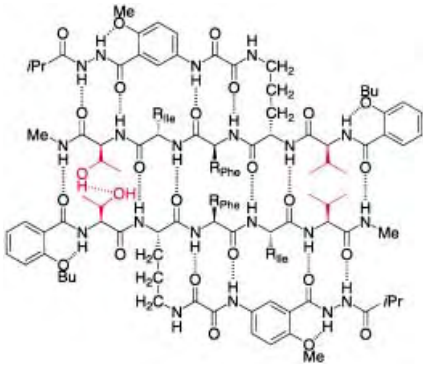
 © 2003 Wiley-VCH Verlag GmbH & Co. KGaA, Weinheim

Transition-State Models

D. A. Evans,* S. J. Siska, V. J. Cee ——— 1761 – 1765

Resurrecting the Cornforth Model for Carbonyl Addition: Studies on the Origin of 1,2-Asymmetric Induction in Enolate Additions to Heteroatom-Substituted Aldehydes

Further experimental support for the Cornforth model is obtained from a systematic study of aldol reactions between methyl-substituted *E* and *Z* enolates and α-oxygen-substituted aldehydes. The observed dependence of diastereofacial selectivity on enolate configuration in this case is more consistent with the Cornforth model than with the the polar Felkin–Anh model (see scheme; X = OR, NR_2, Cl).



Molecular recognition between peptide β sheets is sequence selective! By simply controlling the placement of two threonine (Thr) or valine (Val) residues, peptides that preferentially form either homodimers or heterodimers with about tenfold selectivity can be generated. The picture shows the structure of a Thr–Val·Val–Thr heterodimer.

Sequence-Selective Recognition

J. S. Nowick,* D. M. Chung . 1765 – 1768

Sequence-Selective Molecular Recognition between β Sheets



Communications labeled with this symbol have been judged by two referees as being "very important papers".



The publication of Communications labeled with this symbol has been accelerated because of their topical or highly competitive nature.



Supporting information for articles labeled with this symbol can be found at www.angewandte.org or www.interscience.wiley.com.

DOI: The fastest way to find an article online is the *Digital Object Identifier* (DOI). DOIs will be printed in the footer of the first page of every article. For example, an article with a DOI of 10.1002/anie.200390049 can be found on the WWW at http://dx.doi.org/10.1002/anie.200390049. Please use the DOI of your article to link from your home page to the articles in Wiley InterScience. The DOI is a result of a cross-publisher initiative to create a system for the permanent identification of documents on digital networks. More information is available from www.doi.org.

Service

Keywords ——— *1770*

Authors ——— *1771*

Vacancies ——— *1681*

Preview ——— *1773*

 © 2003 Wiley-VCH Verlag GmbH & Co. KGaA, Weinheim

Statement

The following statement was received by the Editorial Office:

We are writing as co-authors on the following manuscript published in this journal:

T. Siegrist, C. Kloc, J. H. Schön, B. Batlogg, R. C. Haddon, S. Berg, G. A. Thomas, *Angew. Chem.* **2001**, *113*, 1782; *Angew. Chem. Int. Ed.* **2001**, *40*, 1732.

We wish to apprise the readers of the independent investigation conducted at the behest of the Bell Laboratories division of Lucent Technologies Inc. The independent committee reviewed concerns related to the validity of data associated with device measurements described in a number of papers that have appeared in the literature. The committee's full report can be accessed at http://www.lucent.com/news_events/researchreview/.

As a result of the Committee's findings related to the manuscripts they examined, we are concerned about aspects of the data associated with device measurements presented in the above mentioned Communication. The current–voltage data (SCLC spectroscopy) should be viewed with caution, as should conclusions that rely on those data. We do not have access to the original data and are not in a position to independently confirm the results.

We stand by the X-ray, crystal structure, and morphological results in this Communication; we are confident that they are valid and correct. Conclusions drawn from these results and from our earlier work on these and related compounds remain standing.

Bertram Batlogg, Steffen Berg, Christian Kloc, Gordon A. Thomas, Robert C. Haddon, Theo Siegrist

A similar statement was received concerning *ChemPhysChem* **2001**, *3*, 167.



 © 2003 Wiley-VCH Verlag GmbH & Co. KGaA, Weinheim

Crystal Lattice Complexes

A Solid-State Supramolecular Sweet Spot**

*Bruce C. Gibb**

Keywords:
calixarenes · crystal engineering · host–guest chemistry · inclusion compounds · supramolecular chemistry

Crystals possess an allure that is hard to pin down. The luster of a diamond can take the breath away, but even humble crystals of table salt have a certain something related to their symmetry, clean lines, or "purity". Beyond aesthetics, another reason for wanting a crystal is when it performs a function. Ignoring for the moment any healing powers that a soothsayer may claim, the advent of X-ray crystallography greatly added to the overall desirability of crystals by turning them into (structural) information-storage devices. Slowly but surely, almost every chemist or biochemist wanted crystals. Arguably, however, the group of chemists that desire crystals the most is that special breed of supramolecular chemists, the crystal engineers.[1–5] Beyond both structural information and aesthetics, they desire crystals that are capable of performing complex functions.

Two common themes in crystal engineering are the synthesis of polar solids with nonlinear optical or piezoelectric properties, and the formation of crystals possessing porous networks for tasks such as purification and storage. These complex functions necessarily require complex structures, and hence the dominion of the crystal engineers often relies on that versatile of versatile elements, carbon. Regrettably, the complexity of molecular structure, combined with the complexities of the crystallization process, see to it that there is nothing routine about forecasting which crystal structure(s) will arise from a particular subunit, or "tecton".[6] Nevertheless, some remarkable breakthroughs have been made over the last few years; for example, in regards to the synthesis of polar crystals, where one of the main problems is persuading molecular dipoles to align, new general design principles for forming polar solid-state host frameworks have been determined.[7] Recent advances have also been made in regard to the use of crystals as storage devices.[8] For example, organozinc frameworks exhibiting a high capacity for methane storage[9] has whetted the appetite of the automobile industry. Likewise, research into organoplatinum crystals that reversibly take up sulfur dioxide, and signify so with a color change from colorless to orange,[10] represents a step forward for those interested in new detection systems. These advances have necessarily surmounted two ubiquitous problems that arise through nature's dislike of vacuums. First, tectons that have been designed to form a series of adjoining cavities may instead interpenetrate and create a structure devoid of any channels. Second, the solvent or guest that fills cavities in a crystal frequently plays an important supporting role in the overall architecture. In these cases, the integrity of the crystal lattice is often lost when the solvent or guest is removed. How many of us have delicately removed that one particular crystal from the mother liquor, only to watch it turn to dust? Just to add insult to injury, after your crystal turns to dust it often transpires that getting rid of all the solvent is virtually impossible. No matter how high the remnants are heated or how hard a vacuum is applied to them, the solvent remains. This is why supramolecular chemists, who so often form molecules possessing interesting cavities, nooks, and crannies, are more forgiving than other organic chemists when it comes to obtaining elemental analyses.

So what are the rules governing the synthesis of porous solids? What laws do we need to learn to not only avoid the aforementioned pitfalls, but to be able to control the thermodynamics and kinetics of guest storage and exchange? The field is some way from fully answering these questions. However, a recent paper from the Atwood research group[11] has gone part of the way there by demonstrating that it is possible to form crystals that hold onto their guests so well that even prolonged heating at temperatures well above the boiling point of the guest is not sufficient to release the guest and degrade the crystal. In effect, this study bridges the gap between crystals that degrade when their guests are removed and crystalline solids that refuse to release their guests.

The crystal lattice at the center of our story is built from calix[4]arene **1**. Bowl-shaped calixarenes are no strangers to supramolecular chemistry,[12] and in the case of **1** this bowl shape is reinforced by a cyclic array of hydrogen bonds between adjacent OH groups. Atwood et al. determined that the solid-state structure of **1** in the absence of any guest is an approximate hexagonal close-packed (hcp) array of quasi-spherical shaped trimers (Figure 1). No intermolecular hydrogen bonds are present; the two levels of structure are held together only by van der Waals forces.

[*] Prof. B. C. Gibb
Department of Chemistry
University of New Orleans
New Orleans LA 70148 (USA)
Fax: (+1) 504-280-6860
E-mail: bgibb@uno.edu

[**] Partial support by the National Science Foundation (CHE-0111133) and The Petroleum Research Fund, administered by the American Chemical Society, is acknowledged. Special thanks are also due to Leonard J. Barbour for providing Figure 1.

 © 2003 Wiley-VCH Verlag GmbH & Co. KGaA, Weinheim DOI: 10.1002/anie.20021547

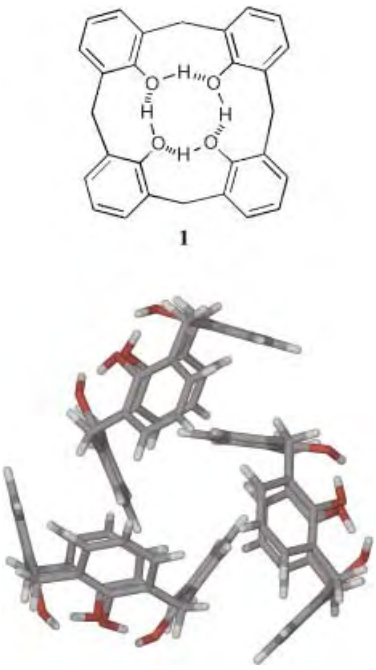


Figure 1. The solid-state trimer of calixarene **1**.

This structure deviates from ideality in two important ways: first, the continuous channels normally present in the ideal hcp array are constricted such that the lattice is nonporous and, second, the deviation results in the dilation of one of the noncontiguous channels present in the idealized form. That said, the most remarkable feature of this lattice is not found within this one crystal structure. Rather, it is the observation that this same architecture is repeatedly found when a number of different guest molecules occupy the aforementioned noncontiguous voids. As the authors point out, only a handful of compounds have demonstrated the phenomenon whereby guest-free and guest-included host lattices are essentially identical. A corollary of these results is that the lattice is a very stable structure, and that guests that perfectly fit the voids should produce highly stable crystals. To test this hypothesis a number of guests were included in the hcp structure of **1**, and the differences between the temperature of the onset of guest release (T_{on}) and the boiling point (T_b) were determined. Normally these values are low, or even negative. For example, structurally unrelated crystals of **1** grown by the slow evaporation of an acetone solution possess a $T_{on}-T_b$ value of $-8\,^{\circ}C$.[11] Hence, this 1:1 solvate readily loses two thirds of its acetone and the crystals disintegrate upon removal from the mother liquor. Things are very different for the guests CCl_4, BrF_3C, CF_4, and CH_4 within the hcp lattice. For these crystals, remarkable $T_{on}-T_b$ values of 120, 260, 370, and 320 °C were recorded, respectively. Guest methane molecules could only be persuaded to vacate the crystal lattice by heating it to approximately 150 °C! An analysis of these and other structures suggests rules for forming stable crystals that possess an hcp array. More generally, they also demonstrate that remarkable levels of guest stabilization can be obtained if the packing within a crystal is optimal.

We now have examples of systems where the guests can be removed and inserted without disrupting the periodicity of the crystal, as well as crystal lattice/guest systems that are so stable that guests are tightly wrapped within the lattice.[11] These define two extremes of stable guest@crystal lattice complexes. The secret now is to fill in the "in between", and learn how to tailor the thermodynamic and/or kinetic stability of such complexes. By doing so, it should be possible to make a range of functional crystals capable of storing and then releasing guests on demand. What are the limits of these accomplishments? Maybe the soothsayers will ultimately be proven correct. Maybe one day, crystals will cure cancer.

[1] G. R. Desiraju, *Nature* **2001**, *412*, 397–400.

[2] See *Comprehensive Supramolecular Chemistry, Vol. 6* (Eds.: J.-M. Lehn, J. L. Atwood, J. E. D. Davies, D. D. MacNicol, F. Vögtle), Pergamon, New York, **1996**.

[3] M. D. Hollingsworth, *Science* **2002**, *295*, 2410–2413.

[4] "Design of Organic Solids": *Top. Curr. Chem.* **1999**, *198*.

[5] G. R. Desiraju, *Acc. Chem. Res.* **2002**, *35*, 565–573.

[6] G. R. Desiraju, *Nat. Mater.* **2002**, *1*, 77–79.

[7] a) K. T. Holman, A. M. Pivovar, M. D. Ward, *Science* **2001**, *294*, 1907–1911; b) J. Hulliger, *Chem. Eur. J.* **2002**, *8*, 4578–4586.

[8] D. V. Soldatov, E. V. Grachev, J. A. Ripmeester, *Cryst. Growth Des.* **2002**, *2*, 401–408.

[9] M. Eddaoudi, J. Kim, N. Rosi, D. Vodak, J. Wachter, M. O'Keeffe, O. M. Yaghi, *Science* **2002**, *295*, 469–472.

[10] M. Albrecht, M. Lutz, A. Spek, G. van Koten, *Nature* **2000**, *406*, 970–974.

[11] J. L. Atwood, L. J. Barbour, A. Jerga, *Science* **2002**, *296*, 2367–2369.

[12] C. D. Gutsche, *Calixarenes Revisited*, Royal Society of Chemistry, London, **2000**.

 © 2003 Wiley-VCH Verlag GmbH & Co. KGaA, Weinheim

Enantioselective Michael Addition

Construction of Quaternary Stereocenters: New Perspectives through Enantioselective Michael Reactions

Jens Christoffers and Angelika Baro*

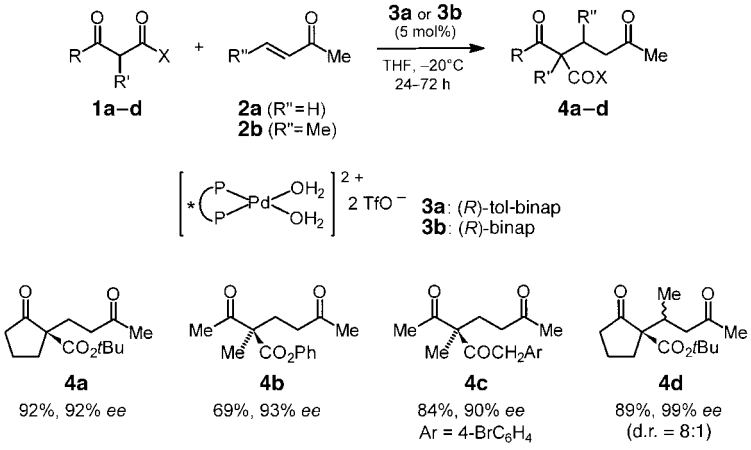
Keywords:
asymmetric catalysis · C–C coupling · enantioselectivity · Michael addition · transition metals

Stereoselective C–C bond-forming reactions are of particular importance for the preparation of enantiopure natural compounds and pharmaceuticals. The wide variety of available chiral auxiliaries, reagents, and catalysts nowadays enables the generation of tertiary stereocenters in most cases without any difficulty. However, the approach to complex compounds with quaternary stereocenters is still a challenge for synthetic organic chemists, and every enantioselective procedure in which a fully substituted carbon center is constructed is of value.[1]

The Michael reaction, the conjugated or 1,4-addition of enolates to acceptor-substituted olefins, is a fundamental C–C-coupling reaction, which is catalyzed not only by Brønsted bases,[2] but also by a number of metal compounds.[3] An important breakthrough in the field of extensively investigated metal-catalyzed, enantioselective Michael reactions[4] was recently reported by Sodeoka and co-workers.[5] For the first time, quaternary stereocenters could be generated with >90% *ee* at a relatively high temperature of −20 °C in a Michael reaction of β-dicarbonyl compounds **1** with enones **2** using palladium(II) as the catalytically active transition metal. The Pd^{II}–diaquadiphosphane complexes **3a** and **3b** are formed with chiral ligands (*R*)-tol-binap and (*R*)-binap, respectively. Scheme 1 shows four typical reaction products **4a–d** as examples.

Both cyclic (**1a**) and acyclic (**1b**) β-ketoesters react with methyl vinyl ketone (**2a**) at −20 °C in a Michael reaction promoted by **3a** to give the corresponding products **4a** and **4b** in moderate to good yields with >90% *ee*. Noteworthy is the use of the sterically demanding *tert*-butyl and phenyl β-ketoesters. The conversion of β-diketone **1c** (X = CH_2Ar) in the presence of catalyst **3b** (10 mol%) at −10 °C is an outstanding example of an asymmetric Michael addition to acyclic triketones such as **4c** with very high stereoselectivity, an achievement thus far not reported in the literature. Furthermore, the reaction of **1d** with substituted enone **2b** catalyzed by **3b** at −20 °C affords a mixture of two diastereoisomers (d.r. = 8:1), and an enantiomeric excess of 99% for the major diastereomer of **4d**.

The high efficiency of the method developed by Sodeoka and co-workers is clearly demonstrated in view of the work published so far: In 1975 Wynberg and co-workers applied cinchona alkaloids in base-catalyzed, enantioselective Michael reactions.[6] About 10 years later, the first of these reactions catalyzed by a transition metal, cobalt, was published by Brunner and Hammer.[7] Both methods result in quaternary stereocenters with up to 68% *ee*, which was improved in the following years by Desimoni et al. to 75% *ee*.[8] The introduction of rhodium catalysts in 1992 by Ito and co-workers in Michael reactions of α-methyl-substituted cyanoacetates and vinyl ketones or acrolein represented an important breakthrough in this field. The catalyst was generated in situ from the chiral ligand 2,2′′-bis[1-(diphenylphosphanyl)ethyl]-1,1′′-biferrocene [(*R*,*R*)-(*S*,*S*)-Phtrap] (**5**) and

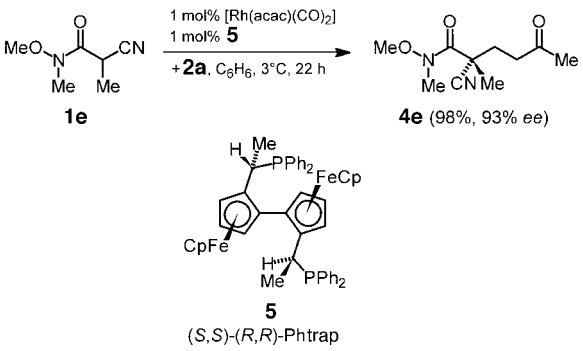


Scheme 1. Enantioselective Pd catalysis according to Sodeoka and co-workers. **4c, d**: conversion at −10 °C. The *ee* value of the major diastereoisomer of **4d** is given. tol-binap = 2,2′-bis(di-*p*-tolylphosphanyl)-1,1′-binaphthyl, binap = 2,2′-bis(diphenylphosphanyl)-1,1′-binaphthyl.

[*] Prof. Dr. J. Christoffers, Dr. A. Baro
Institut für Organische Chemie
Universität Stuttgart
Pfaffenwaldring 55
70569 Stuttgart (Germany)
Fax: (+49) 711-685-4269
E-mail: jchr@po.uni-stuttgart.de

 © 2003 Wiley-VCH Verlag GmbH & Co. KGaA, Weinheim DOI: 10.1002/anie.200201614

$[RhH(CO)(PPh_3)_3]$.[9] The diphosphane ligand with both planar and central chiral elements forms a *trans*-chelate complex with rhodium. Under the same conditions, cyanoacetic acid amides such as **1e** can be alkylated in the α position with vinyl ketones or acrolein (Scheme 2),[9d] using a catalyst formed



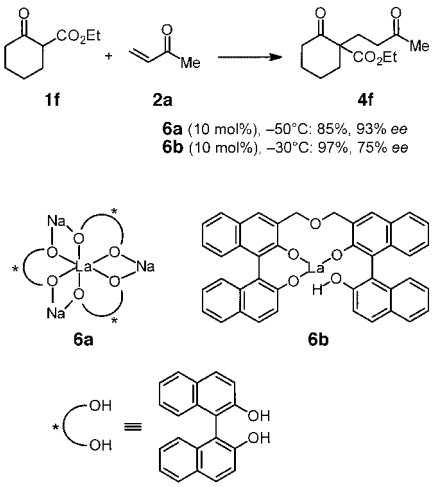
Scheme 2. Rhodium-catalyzed asymmetric Michael reaction according to Ito and co-workers. Cp = cyclopentadienyl, Phtrap = 2,2′-bis[1-(diphenylphosphanyl)ethyl]-1,1′-biferrocene, acac = acetylacetonato.

in situ from the phosphane-free $[Rh(acac)(CO)_2]$. The resulting Weinreb amide **4e**, which is obtained in good yield and selectivity, can be utilized as a precursor for further carbonyl derivatives. A very similar reaction was recently published by Motoyama et al.:[10] In the presence of the catalyst, prepared in situ from $[\{RhCl(coe)_2\}_2]$ and [(Phebox)$SnMe_3$], the reaction of α-cyanopropionates with acrolein proceeds with up to 86% *ee* (coe = cyclooctene, phebox = 2,6-bis(oxazolinyl)).

The decisive breakthrough in the field of metal-catalyzed, asymmetric Michael reactions, however, came in 1994 with the class of widely applicable heterobimetallic catalysts developed by Shibasaki and co-workers.[11] These catalysts currently define the state-of-the-art for the formation of tertiary stereocenters at 0 °C in high yields and with excellent selectivities (up to 99% *ee*).[12] The generation of quaternary stereocenters, however, requires low temperatures (Scheme 3).[13] Furthermore, relatively high amounts of the catalyst **6a** (lanthanum–sodium binaphtholate). The rare-earth metal lanthanum in **6a** is octahedrally coordinated to three chiral binaphtholate ligands, which are bridged in pairs by alkali-metal ions (Scheme 3).

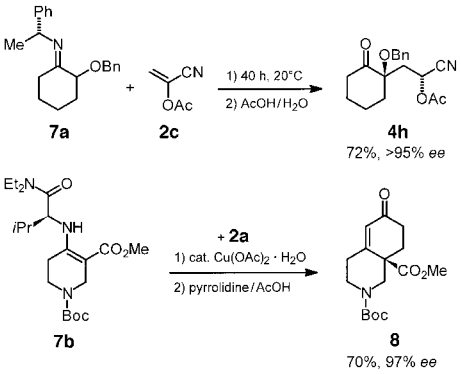
In the past years, Shibasaki's group has attempted to develop a La–binol catalyst (binol = 2,2′-dihydroxy-1,1′-binaphthyl) that is air-stable, storable, and reusable. These efforts resulted in the so-called linked-binol system **6b** (Scheme 3), which combines all the desired attributes.[14,15] For the synthesis of tertiary stereocenters, this type of catalyst is almost optimal with regard to stereoselectivity, handling, and reuse. However, as exemplified in Scheme 3 for the preparation of **4f**, these expectations cannot be extended to quaternary stereocenters (75% *ee* at −30 °C). The replacement of lanthanum by zinc as the central metal, however, improves the selectivities for this linked-binol ligand in the conversion of α-hydroxyketone donors such as **1g**. For example, tertiary alcohols **4g** were obtained at −20 °C with up to 96% *ee* (Scheme 4).[16] Hence, from this point of view, the above-mentioned latest Pd-catalyzed reaction developed by Sodeoka and co-workers appears to be a milestone in generating quaternary stereocenters by Michael reactions.

Apart from catalytic procedures, auxiliary-mediated asymmetric Michael reactions are of great practical relevance, as a wide range of substrates are tolerated under relatively mild and neutral reaction conditions. In 1985 Pfau et al. reported the use of 1-phenylethylamine, which is now established as an easily accessible and universal auxiliary.[17] The C–C coupling proceeds as an enamine-Michael reaction via a cyclic transition state related to that of an azaene reaction. In some cases, elevated temperatures and (especially for simple

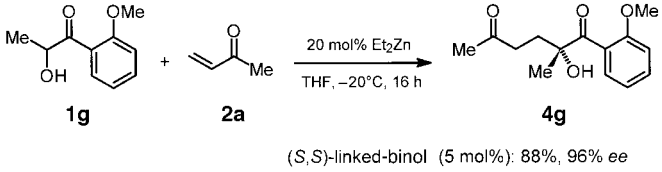


Scheme 3. La-catalyzed enantioselective Michael reaction following the method of Shibasaki and co-workers.

vinyl ketones as Michael acceptors) stoichiometric amounts of a Lewis acid or high-pressure conditions are necessary. Following the method of d'Angelo and co-workers,[18] the reaction of α-alkoxyimine **7a** and acrylonitrile derivative **2c**, which may be regarded as a synthetic equivalent of acetaldehyde (polarity reversal), affords the product in good yield with excellent diastereo- and enantioselectivity (Scheme 5).



Scheme 5. Auxiliary-assisted Michael reaction of **7a** according to d'Angelo and co-workers and of piperidone derivative **7b** according to Christoffers and co-workers. Boc = *tert*-butoxycarbonyl, Bn = benzyl.



Scheme 4. Zn-catalyzed enantioselective Michael reaction with the linked-binol ligand according to Shibasaki and co-workers. binol = 2,2′-dihydroxy-1,1′-binaphthyl.

 © 2003 Wiley-VCH Verlag GmbH & Co. KGaA, Weinheim

α-Amino acid amides were introduced recently as efficient auxiliaries for copper-catalyzed Michael reactions. In the presence of a catalytic amount of $Cu(OAc)_2 \cdot H_2O$, enamines such as **7b** react with simple vinyl ketones **2a** at ambient temperature in acetone as the solvent, yielding the product with selectivities of up to 99% *ee* after acidic hydrolysis.[19] The auxiliaries, readily available from natural α-amino acids, can be recovered almost quantitatively after workup. As proved in the synthesis of bicyclic compound **8** starting from piperidone derivative **7b** (Scheme 5), the copper-catalyzed Michael reaction is compatible with substrates bearing donor functions, for example, a carbamate moiety, and is therefore superior to the lanthanide-catalyzed procedure of Shibasaki and co-workers.[20]

[1] For reviews, see: a) J. Christoffers, A. Mann, *Angew. Chem.* **2001**, *113*, 4725 – 4732; *Angew. Chem. Int. Ed.* **2001**, *40*, 4591 – 4597; b) E. J. Corey, A. Guzman-Perez, *Angew. Chem.* **1998**, *110*, 402 – 415; *Angew. Chem. Int. Ed.* **1998**, *37*, 388 – 401; c) K. Fuji, *Chem. Rev.* **1993**, *93*, 2037 – 2066; d) S. F. Martin, *Tetrahedron* **1980**, *36*, 419 – 460.

[2] For reviews, see: a) E. D. Bergmann, D. Ginsburg, R. Pappo, *Org. React.* **1959**, *10*, 179 – 555; b) D. A. Oare, C. H. Heathcock in *Topics in Stereochemistry, Vol. 19* (Eds.: E. L. Eliel, S. H. Wilen), Wiley-Interscience, New York, **1989**, pp. 227 – 407; c) Tetrahedron Organic Chemistry Series, *Vol. 9*: P. Perlmutter, *Conjugate Addition Reactions in Organic Synthesis*, Pergamon, Oxford, **1992**; d) For intramolecular Michael reactions, see: R. D. Little, M. R. Masjedizadeh, O. Wallquist, J. I. McLoughlin, *Org. React.* **1995**, *47*, 315 – 552.

[3] For a review, see: J. Christoffers, *Eur. J. Org. Chem.* **1998**, 1259 – 1266.

[4] For reviews, see: a) N. Krause, A. Hoffmann-Röder, *Synthesis* **2001**, 171 – 196; b) M. P. Sibi, S. Manyem, *Tetrahedron* **2000**, *56*, 8033 – 8061; c) J. Leonard, E. Díez-Barra, S. Merino, *Eur. J. Org. Chem.* **1998**, 2051 – 2061; d) Y. Yamamoto, S. G. Pyne, D. Schinzer, B. L. Feringa, J. F. G. A. Jansen, *Methoden Org. Chem. (Houben-Weyl), 4th ed. 1952–, Vol. E21b*, **1995**, pp. 2011 – 2155; e) B. E. Rossiter, N. M. Swingle, *Chem. Rev.* **1992**, *92*, 771 – 806.

[5] Y. Hamashima, D. Hotta, M. Sodeoka, *J. Am. Chem. Soc.* **2002**, *124*, 11240 – 11241.

[6] a) H. Wynberg, R. Helder, *Tetrahedron Lett.* **1975**, 4057 – 4060; b) K. Hermann, H. Wynberg, *Helv. Chim. Acta* **1977**, *60*, 2208 – 2212.

[7] H. Brunner, B. Hammer, *Angew. Chem.* **1984**, *96*, 305 – 306; *Angew. Chem. Int. Ed. Engl.* **1984**, *23*, 312 – 313.

[8] a) G. Desimoni, P. Quadrelli, P. P. Righetti, *Tetrahedron* **1990**, *46*, 2927 – 2934; b) G. Desimoni, G. Dusi, G. Faita, P. Quadrelli, P. P. Righetti, *Tetrahedron* **1995**, *51*, 4131 – 4144; c) G. Desimoni, G. Faita, S. Filippone, M. Mella, M. G. Zampori, M. Zema, *Tetrahedron* **2001**, *57*, 10203 – 10212.

[9] a) M. Sawamura, H. Hamashima, Y. Ito, *Tetrahedron: Asymmetry* **1991**, *2*, 593 – 596; b) M. Sawamura, H. Hamashima, Y. Ito, *J. Am. Chem. Soc.* **1992**, *114*, 8295 – 8296; c) M. Sawamura, H. Hamashima, Y. Ito, *Tetrahedron* **1994**, *50*, 4439 – 4454; d) M. Sawamura, H. Hamashima, H. Shinoto, Y. Ito, *Tetrahedron Lett.* **1995**, *36*, 6479 – 6482; e) M. Sawamura, H. Hamashima, Y. Ito, *Bull. Chem. Soc. Jpn.* **2000**, *73*, 2559 – 2562.

[10] Y. Motoyama, Y. Koga, K. Kobayashi, K. Aoki, H. Nishiyama, *Chem. Eur. J.* **2002**, *8*, 2968 – 2975.

[11] For reviews, see: a) M. Shibasaki, N. Yoshikawa, *Chem. Rev.* **2002**, *102*, 2187 – 2209; b) M. Kanai, M. Shibasaki in *Catalytic Asymmetric Synthesis*, 2nd ed. (Ed.: I. Ojima), Wiley-VCH, Weinheim, **2000**, pp. 569 – 592.

[12] Y. Xu, K. Ohori, T. Ohshima, M. Shibasaki, *Tetrahedron* **2002**, *58*, 2585 – 2588.

[13] H. Sasai, E. Emori, T. Arai, M. Shibasaki, *Tetrahedron Lett.* **1996**, *37*, 5561 – 5564.

[14] Y. S. Kim, S. Matsunaga, J. Das, A. Sekine, T. Ohshima, M. Shibasaki, *J. Am. Chem. Soc.* **2000**, *122*, 6506 – 6507.

[15] a) S. Matsunaga, T. Ohshima, M. Shibasaki, *Tetrahedron Lett.* **2000**, *41*, 8473 – 8478; b) N. Kumagai, S. Matsunaga, M. Shibasaki, *Org. Lett.* **2001**, *3*, 4251 – 4254; c) R. Takita, T. Ohshima, M. Shibasaki, *Tetrahedron Lett.* **2002**, *43*, 4661 – 4665; For reviews, see: d) S. Matsunaga, T. Ohshima, M. Shibasaki, *Adv. Synth. Catal.* **2002**, *344*, 3 – 15; e) M. Shibasaki, M. Kanai, K. Funabashi, *Chem. Commun.* **2002**, 1989 – 1999.

[16] S. Harada, N. Kumagai, T. Kinoshita, S. Matsunaga, M. Shibasaki, *J. Am. Chem. Soc.* **2003**, *125*, 2582 – 2590.

[17] a) M. Pfau, G. Revial, A. Guingant, J. d'Angelo, *J. Am. Chem. Soc.* **1985**, *107*, 273 – 274; b) I. Jabin, G. Revial, M. Pfau, P. Netchitaïlo, *Tetrahedron: Asymmetry* **2002**, *13*, 563 – 567; c) C. Camara, D. Joseph, F. Dumas, J. d'Angelo, A. Chiaroni, *Tetrahedron Lett.* **2002**, *43*, 1445 – 1448; For a review, see: d) J. d'Angelo, D. Desmaële, F. Dumas, A. Guingant, *Tetrahedron: Asymmetry* **1992**, *3*, 459 – 505.

[18] L. Keller, C. Camara, A. Pinheiro, F. Dumas, J. D'Angelo, *Tetrahedron Lett.* **2001**, *42*, 381 – 383.

[19] a) J. Christoffers, A. Mann, *Angew. Chem.* **2000**, *112*, 2871 – 2874; *Angew. Chem. Int. Ed.* **2000**, *39*, 2752 – 2754; b) J. Christoffers, A. Mann, *Chem. Eur. J.* **2001**, *7*, 1014 – 1027.

[20] J. Christoffers, H. Scharl, *Eur. J. Org. Chem.* **2002**, 1505 – 1508.

 © 2003 Wiley-VCH Verlag GmbH & Co. KGaA, Weinheim

Soft Nanomaterials

Nanotechnology with Soft Materials

*I. W. Hamley**

Keywords:
amphiphiles · colloids · nanostructures · polymers · self-assembly



Angewandte Chemie

 © 2003 Wiley-VCH Verlag GmbH & Co. KGaA, Weinheim DOI: 10.1002/ange.200200546

Nature exploits self-organization of soft materials in many ways, to produce cell membranes, biopolymer fibers and viruses, to name just three. Mankind is now able to design materials at the nanoscale, whether through atom-by-atom or molecule-by-molecule methods (top-down) or through self-organization (bottom-up). The latter method encompasses soft nanotechnology. Self-organization of soft materials can be exploited to create a panoply of nanostructures for diverse applications. The richness of structures results from the weak ordering because of noncovalent interactions. Thus, thermal energy is important as it enables transitions between phases with differing degrees of order. The power of self-organization may be harnessed most usefully in a number of nanotechnology applications, which include the preparation of nanoparticles, the templating of nanostructures, nanomotor design, the exploitation of biomineralization, and the development of functionalized delivery vectors.

From the Contents

1. Introduction	1693
2. Principles of Self-Assembly	1694
3. Self-Assembly Methods to Prepare and to Pattern Nanoparticles	1697
4. Templated Nanostructures	1702
5. Liquid-Crystal Mesophases	1705
6. Summary and Outlook	1708

1. Introduction

The last few decades have seen a huge growth in research on "soft materials". The buzzword "nanotechnology" is now around us everywhere. Together these two terms herald the forthcoming era of "soft nanotechnology". Just as the bronze and iron ages followed the stone age (when wood and other bio-derived materials were also vital) then surely the most recent materials age was one in which mankind learned to exploit the secrets of silicon and to design synthetic materials like polymers. A new era is upon us—many argue it is the bio-age, where the secrets of genetic codes and protein structures are unraveled, to bring in a new range of treatments, and possibly lifestyles. At the same time we are starting to be able to manipulate materials at the nanoscale. One way to do this is to move atoms or molecules around one by one. This procedure is required to make nonperiodic structures. However, an efficient route when a patterned nanostructure is needed, is to exploit self-assembly in soft matter. We are learning more every year about the huge number of nanostructures that can be formed through self-assembly and are beginning to learn how to exploit these to create materials with new mechanical, optical, or electronic properties as well as specific functionality. Devices can also be fabricated using an appropriate combination of self-organized elements, together with a suitable power source.

Soft nanotechnology encompasses the use of soft materials to pattern inorganic ("hard") materials, a technique already used by nature to make bone, teeth, and shells. Inorganic nanoparticles can be created within self-assembled nanoreactors, such as micelles or vesicles, and then patterned into superstructures through an additional self-organization step. Or naturally occurring nanoparticles can be arranged using polymer or colloid self-assembly. The particles can be functionalized for nanotechnology applications, such as tagging or recognition. A recurring theme in this article is the templating of inorganic structures. Apart from making nanoparticles and hollow nanoparticles the templating of silica into regular arrays using crystals of colloidal sol particles is an important example. Similarly, lyotropic liquid-crystal phases formed by surfactants and block copolymers can be used to template lamellar, hexagonal, and cubic (bicontinuous or micellar) structures in silica and other inorganic materials, which have attracted attention for application in catalysis as they are nanoporous materials, analogous to zeolites but with a nanometer (rather than Ångström) pore size.

A key challenge in nanotechnology is to design nanomotors and actuators. A number of strategies for this are described in Section 2.4. Some take inspiration from biological motors or muscle (powered by ATP synthesis) whilst others use concepts from physical chemistry, for example harnessing oscillating chemical reactions in polymer gels.

The self-organization of block copolymers is particularly interesting from the viewpoint of fabricating nanostructures where one block is, for example, a conductive or electroluminescent polymer. A number of rod–coil copolymers of this type have been synthesized, although not yet exploited in nanotechnology applications. All-polymer ferroelectric and waveguide materials are also possible using block copolymers. Self-organizing nanolaminates with unique barrier properties can also be envisaged. Nanotechnology applications involving thin films are particularly wide-ranging, and are discussed in Section 4.3; nanolithography and patterning of nanoparticles or holes (for membranes or filters) are among the possibilities.

In this review the principles of self-assembly underpinning nanoscale structure formation in soft materials are elucidated. Examples of the application of nanoscale self-assembly are provided. The topics selected reflect the preferences of the author. In such a broad subject there are inevitably omissions. Nanotube systems are not self-assembling systems in the

[*] Dr. I. W. Hamley
Department of Chemistry
University of Leeds
Leeds LS2 9 JT (UK)
Fax: (+44) 113-343-6430
E-mail: i.w.hamley@chem.leeds.ac.uk

 © 2003 Wiley-VCH Verlag GmbH & Co. KGaA, Weinheim

sense intended here (see Section 2) and so are not discussed. In addition, nanotechnology applications of self-assembled monolayer structures are not considered. There is only a brief discussion of some aspects of bionanotechnology, since in the main the purpose of this review is to emphasize synthetic nanomaterials. Supramolecular chemistry is also not considered, although it is a powerful tool for the programmed self-organization of molecules,[1] and has been proposed as a means to create nanomachines.[2,3]

There have been few reviews of soft nanotechnology. Introductory textbooks on soft matter, primarily covering synthetic systems (colloids, polymers, surfactants and liquid crystals), have appeared recently.[4,5] Niemeyer has reviewed DNA-based bionanotechnology.[6] A brief review discussing some examples of molecular nanotechnology touches on some aspects of self-assembly for nanostructure fabrication.[7] Brief accounts of selected applications of polymers in soft nanotechnology can also be found.[8,9] A good review of colloidal routes to nanoparticle synthesis and ordering is available.[10] There is little on the nanotechnology of self-assembling systems in the nanotechnology book by Timp,[11] though the chapter by Deming et al.[12] covers some aspects of the synthesis of proteins and peptides capable of forming tailored nanostructures. Similarly, the main thrust of the text edited by Edelstein and Cammarata[13] is inorganic materials. One chapter does cover a limited subset of biological nanomaterials, in particular magnetic proteins,[14] and the use of colloidal sols in sol–gel processing methodologies is encountered in chapter 7.[15]

This review is organized as follows. In Section 2, the principles of self-assembly are outlined. In Section 3, self-assembly routes to the preparation of nanoparticles are considered, as well as applications in nanotechnology. Nanoobjects are also briefly discussed. In Section 4, templating methods for the fabrication of inorganic nanostructures are summarized. Section 5 covers the nanotechnology applications of liquid-crystal phases, both lyotropic and thermotropic. Section 6 contains a summary and outlook.

2. Principles of Self-Assembly

The term "self-assembly" does not have a precise definition, and indeed has often been abused.[16] It does not refer to the formation of any assembly of atoms or molecules, rather the reversible and cooperative assembly of predefined components into an ordered superstructure. Two types of self-assembly have been identified by Whitesides.[16] Static self-assembly involves systems at equilibrium that do not dissipate energy. The formation of a structure may require energy, but once formed it is stable. In dynamic self-assembly on the other hand the formation of structures or patterns occurs when the system dissipates energy. Examples are patterns formed by reaction and diffusion processes in oscillating chemical reactions. The focus of this section is on materials that form static self-assembled structures, although a brief summary of possible routes to the fabrication of nanomotors involving dynamic self-assembly is given.

Self-assembly in soft materials relies on the fact that the energy dissipated by fluctuations in the position and the orientation of the molecules or particles, which are the result of Brownian motion, is comparable to the thermal energy. Thermal energy has a dramatic influence on soft materials at the nanoscale as weak noncovalent bonds are broken and sometimes re-formed. This process enables the system to reach thermodynamic equilibrium, which is often a non-uniform state. Because of the relatively weak interactions between molecules, transitions between different structures can readily be driven by changes in conditions, for example, temperature or pH value. Such external triggers that induce phase transitions could lead to a host of responsive materials, or coupled with an appropriate source of energy to nanomechanical systems. There is a diversity of phase transitions between different structures in soft materials, examples of which are considered in subsequent sections.



Ian Hamley, born in 1965, received his BSc degree from the University of Reading in 1987 and PhD in 1991 from the University of Southampton. He was then Royal Society Leverhulme William and Mary postdoctoral fellow at the FOM-Institute for Atomic and Molecular Physics, Amsterdam. In 1992, he took up a postdoc position at the University of Minnesota. He returned to a lectureship in the Department of Physics at the University of Durham in 1993, leaving to take up an appointment as lecturer in Physical Chemistry at the University of Leeds in 1996, where he was promoted to Senior Lecturer in 2000 and to Reader in 2001.

2.1. Noncovalent interactions

For self-assembly to be possible in soft materials, it is evident that the forces between molecules must be much weaker than the covalent bonds between the atoms of a molecule. The weak intermolecular interactions responsible for molecular ordering in soft materials include hydrogen bonds, coordination bonds in ligands and complexes, ionic interactions, dipolar interactions, van der Waals forces, and hydrophobic interactions:

The hydrophobic effect arises when a nonpolar solute is inserted into water. The hydrophobic effect can be distinguished from hydrophobic interactions, which result from the association of two nonpolar moieties in water.[17] The hydrophobic effect is conventionally ascribed to the ordering of water molecules around an unassociated hydrophobic molecule. This effect leads to a reduction in entropy. This entropy loss can be offset when the association of hydrophobic molecules into micelles occurs because this leads to an increase in entropy as the "structured water" structure is broken up. An enthalpy penalty for demixing of water and solute should also be outweighed by the entropy increase so that the Gibbs free-energy change for micellization is negative. The "structured-water" model is based on ordering of water molecules around the solute molecule. An alternative to the structured-water model proposes that the high

 © 2003 Wiley-VCH Verlag GmbH & Co. KGaA, Weinheim

free-energy cost of inserting a nonpolar solute into water is because it is difficult to find a suitable cavity between the small water molecules. However, Dill et al. have argued that the hydrophobic effect is more subtle, and depends on solute size and shape as well.[17]

Hydrogen bonding is particularly important in biological systems, where many protein structures in water are held together by hydrogen bonds. Of course, the existence of life as we know it depends on hydrogen bonds, which stabilize H_2O in the liquid form. In proteins, intramolecular hydrogen bonds between N–H groups and C=O groups that are four residues apart underpin the formation of the α helix structure. On the other hand, hydrogen bonds between neighboring peptide chains lead to β sheet formation. Similarly, collagen fibers contain triple-helical proteins held together by hydrogen bonding. The folding pattern of proteins is also based on internal hydrogen bonding. The smaller the number of hydrogen bonds in the folded protein, the higher its free energy and the lower the stability. The reason that nature exploits hydrogen bonds in this way is because of the strength of this bond. Hydrogen bonds are weaker than covalent bonds (ca. 20 kJ mol^{-1} for the former compared to ca. 500 kJ mol^{-1} for the latter), so that superstructures can self-assemble without the need for chemical reactions to occur, but nevertheless the bonds are strong enough to hold the structures together once formed.

Molecular recognition between artificial receptors and their guests can be combined with self-organization to program the self-assembly of nanostructures.[18] Many types of noncovalent interaction can be exploited in supramolecular chemistry, these include hydrogen bonding, donor–acceptor binding, and metal complexation. Diverse methods have been employed to create receptors for ionic and molecular guests. The use of cyclodextrins as hosts for the delivery of drugs or pesticides, for example. Details are outside the scope of this section, although further information is available elsewhere.[1,19]

Stabilizing colloidal dispersions against aggregation (termed coagulation if irreversible, flocculation if reversible) is important in every-day applications, such as, food or personal-care products. Often the system is an oil-in-water dispersion that can be stabilized by adding interfacially active components, such as amphiphiles or proteins. These segregate to the oil–water interface and stabilize emulsions by reducing interfacial tension, the enhanced rigidity and elasticity of the membrane formed also help to prevent coalescence. Colloidal sols as found in paints and pastes also need to be stabilized to ensure a long shelf-life. This stabilization can be achieved in a number of ways. First, for charged colloidal particles in an electrolyte medium, the balance between the repulsive electrostatic and attractive van der Waals contributions to the total potential energy can be adjusted, so that a barrier to aggregation is created. A second method to prevent aggregation is steric stabilization. Long-chain molecules are attached to colloidal particles, and when the particles approach one another a repulsive force is created as the chains interpenetrate. The attached long-chain molecule may be chemisorbed (for example a long-chain fatty acid) or more commonly an adsorbed polymer. In contrast to charge stabilization, steric stabilization works in nonaqueous media and over a wide range of particle concentrations. The choice and concentration of polymer is critical in steric stabilization, since at low concentration, polymer chains can attach themselves to two (or more) particles, which leads to so-called bridging flocculation. On the other hand, at higher polymer concentrations, if the polymer is nonadsorbing it can lead to depletion flocculation, the mechanism for which was first recognized by Asakura and Oosawa.[20] The polymers cannot penetrate the particles, and are excluded from a depletion zone around them. When the particles are close together the depletion zones overlap, and the dispersal of polymers into the bulk solution is favored entropically. An osmotic pressure of solvent from the gaps between particles leads to an effective attraction between particles, and hence flocculation. When the colloidal particle concentration is such that they are on average further apart than a polymer coil radius, and the polymer concentration is high, depletion stabilization is possible.[21] Forcing the particles together would require the "demixing" of polymer from bulk solution. This process increases the free energy so that the effective interaction between particles is repulsive.

2.2. Intermolecular Packing

At high concentration, the packing of block copolymer or low-molar-mass amphiphilic molecules in solution leads to the formation of lyotropic liquid-crystal phases, such as cubic-packed spherical micelles, hexagonal-packed cylindrical micelles, lamellae, or bicontinuous cubic phases. The phase formed depends on the curvature of the surfactant–water interface. In one approach to the understanding of lyotropic phase behavior, the free energy associated with curved interfaces is computed. The curvature is analyzed using differential geometry,[22] neglecting details of molecular organization. In the second main model the interfacial curvature is described by a molecular packing parameter.[23] These two approaches will be described in turn.[4]

In the model for interfacial curvature of a continuous surfactant film, we use results from the differential geometry of surfaces. A surface can be described by two fundamental types of curvature at each point P on it: mean curvature and Gaussian curvature. Both can be defined in terms of the principal curvatures $c_1 = 1/R_1$ and $c_2 = 1/R_2$, where R_1 and R_2 are the radii of curvature. The mean curvature is $H = (c_1 + c_2)/2$ and the Gaussian curvature is defined as $K = c_1 c_2$.

Radii of curvature for a portion of a so-called saddle surface (a portion of a surfactant film in a bicontinuous cubic structure) are shown in Figure 1, although they can equally

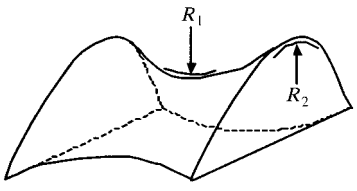


Figure 1. Principal radii of curvature of a saddle surface.

 © 2003 Wiley-VCH Verlag GmbH & Co. KGaA, Weinheim

well be defined for other types of surface, such as convex or concave surfaces found in micellar phases. To define the signs of the radii of curvature, the normal direction to the surface at a given point P must be specified. The curvature is conventionally defined to be positive if the surface points outwards at point P. In Figure 1, c_1 is negative and c_2 is positive.

It should be noted that "end effects" in elongated micelles, a result of capping by surfactant molecules which lead to an ellipsoidal or spherocylindrical structure, are neglected. Such end effects will, however, change both mean and Gaussian curvatures, to an extent which depends on the relative surface area of the "cap" and "tubular" parts. The elastic free-energy density associated with the curvature of a surface contains, for small deformations, the sum of the contributions from mean and Gaussian curvature. The interfacial curvature model is thus useful because it defines the elastic moduli κ and $\overline{\kappa}$ for mean and Gaussian curvature, respectively. These parameters can be measured (by light scattering, for example) and characterize the flexibility of surfactant films. Uncharged surfactant films typically have elastic energies $F_{el} \leq k_B T$, that is, they are quite flexible ($k_B =$ Boltzmann's constant)

An alternative approach to the description of lyotropic mesophases in concentrated solution is based on the packing of molecules. The effective area of the headgroup, a, with respect to the length of the hydrophobic tail for a given molecular volume controls the interfacial curvature. The effective area of the headgroup (an effective molecular cross-sectional area) is governed by a balance between the hydrophobic force between surfactant tails which drives the association of molecules (and hence reduces a) and the tendency of the headgroups to maximize their contact with water (and thus increase a). The balance between these opposing forces leads to the optimal area per headgroup, a, for which the interaction energy is minimum.

Simple geometrical arguments can be used to define a packing parameter, the magnitude of which controls the preferred aggregate shape. For a spherical micelle, it can be shown[4] that the following condition holds: $V/la \leq 1/3$, where V is the volume of a molecule and l is the length of an extended hydrophobic chain (which can easily be calculated). The term $N_s = V/la$ is called the surfactant packing parameter,[24] or critical packing parameter. The surfactant packing parameter can be used to estimate the effective headgroup area a, or vice versa. The surfactant parameter is concentration dependent, and reflects changes primarily in a (but to a lesser extent in V) upon varying the amount of solvent.

Just as spherical micelles can be considered to be built from the packing of cones, which correspond to effective molecular volumes, other aggregate shapes can be considered to result from packing of truncated cones, or cylinders.

The surfactant packing model and the interfacial curvature description are related. A decrease in the surfactant packing parameter corresponds to an increase in mean curvature. The packing-parameter approach has also been used to account for the packing stabilities of more complex structures, such as the bicontinuous cubic phases. Here, the packing unit is a wedge, which is an approximation to an element of a surface with saddle-type curvature (Figure 1). Then it is possible to allow for differences in Gaussian curvature between different structures, as well as mean curvature.

2.3. Biological Self-Assembly

Understanding the folding of proteins is one of the outstanding challenges of science, let alone biophysics and biochemistry. Although much progress has been made in modeling protein folding (for reviews see refs. [25–27]), there is no consensus on the best method. Most methods consider a protein folding energy landscape. The problem is that this is a rough surface, with many local minima, and it can often be hard to model the guiding forces that stabilize the native structure, and cause the free energy to adopt a "funnel" landscape. Many minimalist models are based on computer simulations of particles on a lattice, these are always based on coarse-grained approaches.[26,28] Fully atomistic models seem some way off. Analytical methods have modeled the free-energy landscape based on random energy models, the most recent of which analyze the conformational transition in a random heteropolymer by using spin-glass methods.[29–31] Mean-field methods based on replica techniques will also be developed further. Some structural insights into protein conformational dynamics have emerged from steered molecular-dynamics simulations in which Monte Carlo moves are used as well as molecular-dynamics trajectories.[32]

DNA will be an important component of many structures and devices in nanobiotechnology. DNA computing is an application currently attracting considerable attention.[33] In one approach[34] single DNA strands are attached to a silicon chip. Computational operations can then be performed in which certain DNA strands couple to added DNA molecules. Multistep computational problems can also be solved.[34] In these systems the DNA strands encode all possible values of the variables. Complementary DNA strands are then added, and attach themselves to any strand that represents a solution to one step of the computation. The remaining single strands are removed. This process is repeated sequentially for each step, and the DNA that is left is read out (via PCR amplification) to provide the solution (represented in binary form, a given binary number corresponding to an eight-nucleotide sequence).

The DNA-directed assembly of proteins, by using oligonucleotides capped with streptavidin, is another exciting realm of applications.[35] The method can be used to fabricate laterally patterned arrays of many types of biotinylated macromolecules.[35,36]

The charged nature of DNA has been exploited to bind metal ions, for example, silver, which aggregate into nanoparticles, these are then used as seeds for the further deposition of silver to produce nanowires.[37] Positively charged C_{60} fullerene derivatives have also been condensed onto DNA.[38] Similarly, CdS nanoparticles have been templated on the charged DNA backbone.[39] Arrays of DNA-functionalized CdS nanoparticles have been assembled layer-by-layer on a gold electrode by using a set of two populations of DNA-capped CdS nanoparticles and a soluble DNA

 © 2003 Wiley-VCH Verlag GmbH & Co. KGaA, Weinheim

analyte. The two oligonucleotides bound to CdS nanoparticles are complementary to the ends of the target DNA.[40] The construction of nanoscale geometric objects[41] and frameworks[42] by using three-and four-arm synthetic DNA molecules has also been reported. The use of nanoparticle-tagged DNA solutions in gene-sequence detection is discussed in Section 3.2. Several reviews on the use of DNA in nanotechnology have appeared recently.[35,43]

Vesicles formed by lipids (termed liposomes) are model systems for the cell membrane. The incorporation of channel-forming proteins (porins) into lipid bilayers has been studied for many years,[44–48] and synthetic structural and functional mimics have been devised.[49,50] It is straightforward to form vesicles from the lipid bilayers.[4] Block copolymers form vesicles that can be polymerized,[51] which is clearly advantageous in encapsulation applications. The incorporation of channel-forming proteins into planar polymerized triblock copolymer membranes has been reported.[52,53] This result extends further the delivery/nanoreactor capabilities of the biomimetic structures. Recently, porous core-shell latexes with pH-dependent swelling properties have been developed.[54,55] These are analogous to the pH-controlled pore opening of the protein shell of cowpea chlorotic mosaic virus.[56] By appropriate surface functionalization, the recognition properties of bilayers can be enhanced, as required for many drug-delivery applications. A model recognition system is the biotin–streptavidin complex, for which the free energy of binding is comparable to that of a covalent bond.[57,58]

2.4. Nanomotors

A key element of any nanomachine is a nanomotor. A variety of approaches to the manufacture of nanomotors is being followed. The crudest is to make miniature versions of motors from the macroscopic world, however, the ability to scale such structures downwards is limited by energy dissipation from friction.[2,59] Alternative strategies include attempts to mimic motors in biological systems, and the simpler "motors" driven by chemical potential or concentration gradients, for example, in oscillating gels. Here, nanomotors based on soft matter are briefly discussed. Surveys of the vast literature on molecular nanomotors can be found elsewhere.[60,61]

By considering biological motors as models for artificial motors we can define two classes. In the first, proteins, such as kinesin, dynein, and myosin behave as linear slides. Among rotary motors, well-studied systems include the ATP-synthesis complex, and bacterial flagellar motors. The proton gradient across the mitochondrion drives the synthesis of ATP by ATPase which is a multisubunit transmembrane protein with a complex structure consisting of a spindle to which six alternating (α, β-type) globular proteins are attached. The spindle attachment rotates in a sleeve formed by six copies of a binding protein. The rotation of the spindle drives binding changes of ADP such that the synthesis of ATP is catalyzed.[62]

Flagella in eukaryotes (for example sperm-cell tails) and cilia move by the sliding of subfibers formed from microtubule arrays past one another.[62] Linear sliding motions are also responsible for the action of muscles. In all cases, the motion is driven by an ATPase that acts as a transducer, which converts the energy from ATP-to-ADP hydrolysis into mechanical energy.

Artificial motors exploit out-of-equilibrium chemical phenomena, for example, a concentration gradient, as in ATP synthesis. Using this knowledge, simpler systems than those operating in nature can be designed. A minimal system can be constructed based on osmotic pumping by using lipid vesicles in a solute concentration gradient.[63] The lipid bilayers act as osmotic membranes, which allow the passage of water molecules but not of solute molecules. Thus, when placed in a high osmotic pressure environment, the vesicles shrink and in a uniform solution do not move. However, in a solute concentration gradient, a directional motion is imposed.[63] Unidirectional motion can also be imparted to liquids confined in capillaries by a temperature gradient. A novel concept to drive fluid motion in microcapillaries uses optical trapping of colloid particles, which can be manipulated to create pumps and valves.[64] Although the scale of the particles is on the order of micrometers, it would be exciting if this could be extended to the nanoscale using smaller particles and shorter-wavelength radiation. Other systems rely on the Marangoni effect.[4] As a result of dynamic surface-tension fluctuations, surface-active molecules flow into higher surface-tension regions (or away from low surface-tension regions), to restore the original surface tension.[65] This effect is the origin of the motion of camphor "boats" which move freely on the surface of water. The origin of this motion was explained over a century ago,[66] but the system has been revisited recently as a simple analogue of artificial motors.[67,68]

A particularly attractive artificial motor system relies on oscillating chemical reactions to drive volume changes in polymer gels. Yoshida et al. used the Belousov–Zhabotinsky (BZ) reaction to create an oscillating redox potential.[69,70] This reaction was coupled to the most familiar polymer–gel system exhibiting a volume phase transition—poly(*N*-isopropylacrylamide) (PNIPAM) in water. The PNIPAM was modified by attachment through covalent bonds of ruthenium tris(2,2′-bipyridine) units which act as catalysts for the BZ reaction. Thus, the oscillations in the BZ reaction were translated into periodic swelling and deswelling of the gel as a result of changes in the charge on the ruthenium complex. Using the same concept, pH oscillations in a Landolt reaction have been used to drive volume changes in poly(methacrylic acid) gels in water.[71]

3. Self-Assembly Methods to Prepare and to Pattern Nanoparticles

3.1. Nanoparticles from Micellar and Vesicular Polymerization Routes

The fabrication of nanoparticles of controlled size, shape, and functionality is a key challenge in nanotechnology.[72–74] There are several established routes to nanoparticle preparation. Roughly spherical nanoparticles can be prepared by

 © 2003 Wiley-VCH Verlag GmbH & Co. KGaA, Weinheim

very fine milling[75]—this route is used, for example, to prepare iron oxide nanoparticles in ferrofluid dispersions[76] or zinc oxide nanoparticles for use in sunscreens.[73] So-called colloidal methods[10,15,77] produce nanoparticles with much more uniform size and shape distribution than milling. Metal and metal oxide nanoparticles have been prepared using micellar "nanoreactors" where, for example, salts are selectively sequestered in the micellar core, and then reduced or oxidized.[78–90] Such nanoparticles can be used in catalysis, separation media, biopolymer tagging, and light-emitting semiconductor (e.g. CdS) "quantum dots". A good review of nanoparticles prepared within block copolymer micelles discusses several of these applications.[91]

Recent work has shown that metal nanoparticles on surfaces can be patterned by using the self-organization of block copolymers. Two main routes have been exploited—nanoparticle formation within micelles in solution[89,91,92] which may subsequently be deposited on a solid substrate,[93] or direct patterning at the surface by using selective wetting. Examples of nanoparticle patterning at the surface of a diblock copolymer by the latter route are shown in Figure 2.[94,95]

Nanocapsules, that is, shell particles with a hollow interior, can be prepared by a number of routes, which include the cross-linking of the shell of block-copolymer vesicles.[51] The Möhwald group has recently developed an alternative approach using polyelectrolyte multilayers assembled around a colloidal core which is subsequently dissolved.[96–98] Biological particles, such as apoferritin and cowpea chlorotic mosaic virus, with hollow fillable interiors are described in Sections 3.6 and 2.3, respectively.

3.2. Functionalized Nanoparticles

Functionalized nanoparticles will find numerous applications, for example, in catalysis and as biolabels. Gold nanoparticles functionalized with proteins have been used as markers for the detection of biological molecules for some time. They may also be used to deliver DNA in a so-called "gene-gun". Further details on functionalized nanoparticles with applications in the biological sciences can be found in the review by Niemeyer.[6]

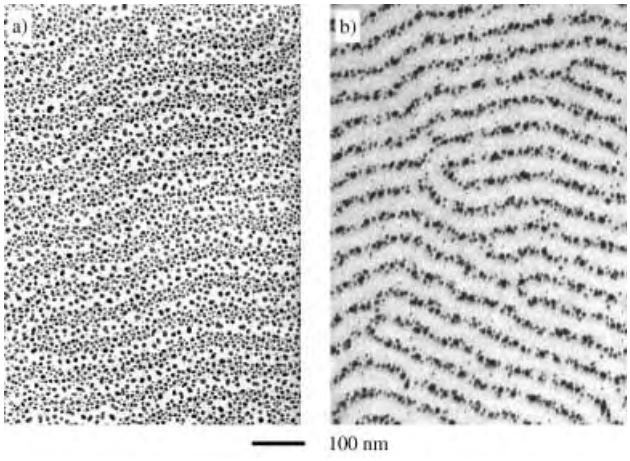


Figure 2. Examples of a) nanoparticle and b) nanowire arrays templated by a stripe pattern formed at the surface of a polystyrene-poly(methyl methacrylate) diblock copolymer by vapor deposition of gold. The gold selectively wets polystyrene domains.[94,95] Reproduced with permission from W. A. Lopes and Nature.

Arrays of nanoparticles, can be prepared by "dip pen nanolithography". For example, magnetic nanoparticles can be patterned into arrays, a process with potential applications in magnetic storage devices.[99] In dip pen nanolithography,[100] nanodroplets of an "ink" (e.g. 16-mercaptohexadecanoic acid) are chemisorbed with nm-scale resolution onto a substrate that is an atomic-force-microscope (AFM) tip (see Figure 3). Subsequently, "surfacted" (i.e. charged surfactant coated) Fe_3O_4 nanoparticles can be deposited from solution onto the charged ink patches on the surface in defined arrays of dots and stripes.[99] Dip pen nanolithography can be extended from serial printing to parallel printing by using multiple pens (i.e. AFM tips).[101] Clearly the method can be extended to pattern other materials that can be adsorbed onto the ink monolayers, for example proteins.[102] Such protein arrays are expected to find applications in panel screening, for example, in immunoassays or proteomics.

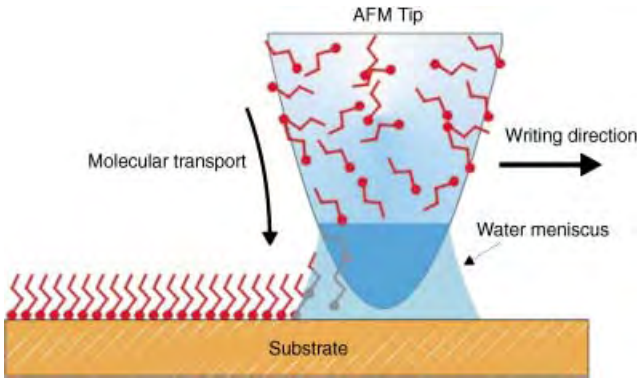


Figure 3. Schematic of dip pen nanolithography.[100] Reprinted with permission from Science. Copyright ©1999 AAAS.

Functionalized nanoparticles are required for many biotechnological applications. A technique for detecting specific gene sequences that could be used in genetic screening has been developed,[103,104] as illustrated in Figure 4. First, the sequence of bases in the target DNA is identified. Then two sets of gold particles are prepared—one has DNA attached that binds to one end of the target DNA, and the second set carries DNA that binds to the other end. The nanoparticles are dispersed in water. When the target DNA is added, it binds both types of nanoparticle together, linking them together to form an aggregate. The formation of this aggregate causes a shift in the light-scattering spectrum from the solution, that is, a color change in the solution that can easily be detected. Recently, this technique has been developed to allow the electrical detection of DNA.[105] The principle is similar to that of the color-change-based detection system, except one end of the target DNA binds to a short "capture" oligonucleotide attached to the surface of a micro-

 © 2003 Wiley-VCH Verlag GmbH & Co. KGaA, Weinheim

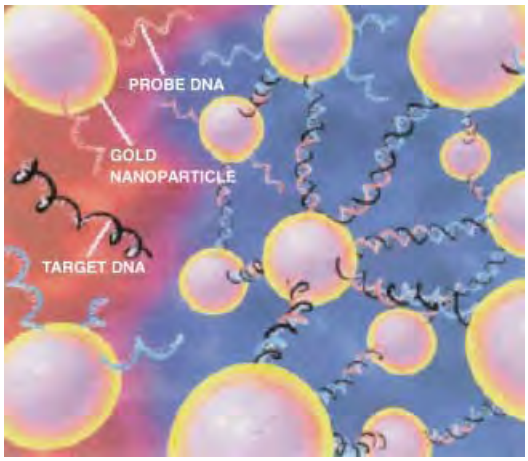


Figure 4. DNA-functionalized gold nanoparticle gene sequence detection system (Figure reproduced with permission from Scientific American, Sept 2001, p. 63).

electrode, and the other end binds to an oligonucleotide attached to gold nanoparticles. Binding of the target DNA causes gold nanoparticles to fill the gap between a pair of electrodes, an event that can be detected from capacitance or conductivity measurements. In practice, the sensitivity of the device was enhanced by silver deposition on the nanoparticles. Arrays of electrode pairs were assembled to form "DNA chip arrays" in which each pair contained a different oligonucleotide capture strand.

3.3. Colloidal Nanoparticle Crystals

There is an immense interest in photonic bandgap crystals because they can be used to confine photons, modulate or control stimulated light emission, or to construct lossless waveguides. A photonic bandgap crystal, also called a photonic crystal, is a structure with a periodic variation in its dielectric properties. The propagation of electromagnetic waves in such a crystal is analogous to that of electrons in semiconductors, in particular there are bandgaps that exclude the photon propagation modes in certain frequency intervals. In principle, 3D crystals could have a complete bandgap, that is, one for which photon propagation is prevented in all spatial directions, that is, throughout the Brillouin zone to adopt nomenclature from solid-state physics. The main focus on 3D structures has been the face-centered cubic (fcc) structure because the Brillouin zone of this lattice is most closely spherical, which might favor the formation of a complete photonic bandgap. However, for an fcc crystal formed by colloidal spheres (opal structure), it has been shown that, independent of the dielectric contrast, there is never a complete bandgap.[106,107] The inverse structure (spheres of air in a continuous solid medium), however, is promising because calculations indicate the possibility of a complete 3D bandgap.[107] By coating the air pores with nematic liquid crystal, a switchable photonic bandgap material can be formed.[108] Here, the tunable localization of light or of waveguiding results from the electrooptic properties of the liquid crystal, where an electric field can be used to orient molecules in a particular direction with respect to the lattice.

To create a 3D photonic bandgap, two conditions must be fulfilled. First, the colloidal particles must have low polydispersity, this favors formation of a cubic crystal. Second, the number of defects in the cubic crystal must be minimized. A number of strategies have been adopted to create macroscopic colloidal crystals. A common technique relies on sedimentation of particles under gravity. However, the resulting samples generally contain polycrystalline domains.[109] Other approaches rely on surfaces to act as templates to induce order. For example, spin coating onto planar substrates can provide well-ordered monolayers.[110] Flow-induced ordering has also been exploited.[111] A method that relies on so-called convective self-assembly has been used to create ordered crystals upon rapid evaporation of solvent.[112] A related technique is the controlled withdrawal of a substrate from a colloidal solution (similar to Langmuir–Blodgett film deposition), where lateral capillary forces at the meniscus induce crystallization of spheres. If the meniscus is slowly swept across the substrate, well-ordered crystal films can be deposited.[113,114] Convective flow acts to prevent sedimentation and to continuously supply particles to the moving meniscus. Actually, the controlled evaporation process alone is sufficient to produce films of controlled thickness that are well ordered up to the centimeter size scale.[109] Van Blaaderen et al. have employed an epitaxial mechanism, which uses a lithographically patterned polymer substrate to template crystal growth.[115] Holes just large enough to hold one colloidal particle were created in a rectangular array. Controlled layer-by-layer growth on this template was then achieved by slow sedimentation of the silica spheres used. The formation of well-ordered crystal-monolayer "rafts" of charged colloid particles on the surface of oppositely charged surfactant vesicles has also been demonstrated.[116]

As mentioned above, inverse opal structures offer the greatest potential for photonic crystals. The most promising materials for the matrix seem to be certain wide-bandgap semiconductors, such as CdS and CdSe, because they have a high refractive index and are optically transparent in the visible and near-IR region.[117] The preparation of porous metallic (gold) nanostructures within the interstices of a latex colloidal crystal has been demonstrated. Here a solution of gold nanoparticles fills the pores between colloidal particles, and the latex is subsequently removed by calcination.[118] A similar method has been used to fabricate inverse opal structures of titanium dioxide.[119,120] The same idea has been applied to form a nanoporous polycrystalline silica (deposited by low-pressure chemical vapor deposition (CVD), see Figure 5.[114] In a related approach, silica spheres are coated with gold (to reinforce the colloidal crystal) and then immersed in electroless deposition baths to deposit metal films within the porous template, the silica then being removed in a HF rinse.[121] These types of approach have been extended to a "lost wax approach" to prepare high-quality arrays of hollow colloidal particles (or filled particles) of various ceramic and polymer materials.[122] Here, a well-ordered silica colloidal crystal is taken and used as a template for polymerization in the interstices.[123] If the pores are

 © 2003 Wiley-VCH Verlag GmbH & Co. KGaA, Weinheim

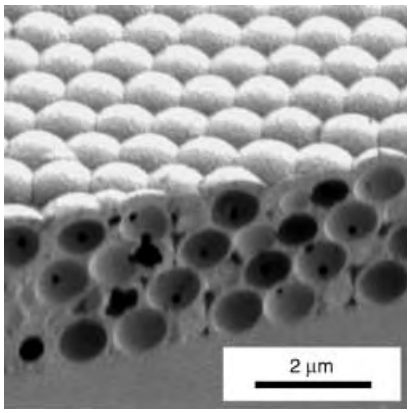


Figure 5. Cross-sectional scanning electron micrograph image of thin film inverse opal structure of polycrystalline silicon templated by 855 nm silica spheres.[114] Reproduced with permission from D. J. Norris and Nature.

interconnected, the polymer forms a continuous porous matrix. By appropriate choice of polymer, either hollow or solid nanoparticles can be grown in it (the former grow from the polymer matrix inwards, the latter form within the voids).[122] In this way it was possible to prepare colloidal crystals of solid or hollow TiO_2 particles, as well as conducting polymer nanoparticles. An extension of colloidal polymerization techniques can be used to prepare defined waveguides. Crossed laser beams were used to polymerize polymer precursors within particular pores. By scanning the laser beams, a waveguide with a chosen path and shape can be fabricated.[124]

The use of microgel particles of PNIPAM to form colloidal crystal arrays that selectively diffract light has been reported.[125] Poly(*N*-isopropylacrylamide) in aqueous solution has a volume phase transition at 32 °C, below which temperature gels are hydrated and swollen but above which the gel dehydrates and collapses. This transition has been used to vary the dimensions of PNIPAM microgel particles from 100 nm at 40 °C to 300 nm at 10 °C, a 27-fold volume change. This property can be exploited to prepare a switchable, selective diffraction array. Below the transition, the particles are swollen and only diffract light weakly, however, in the compact state the diffracted intensity increases dramatically because of the enhanced contrast between particles and medium (the Bragg diffraction wavelength is unaffected). Wavelength-tunable arrays were fabricated by polymerizing PNIPAM in the presence of 99-nm polystyrene spheres.[125] The embedded polystyrene spheres follow the swelling or shrinking of the PNIPAM hydrogel so that the wavelength of the Bragg diffraction can be tuned across the visible range of the spectrum.

3.4. Self-Organizing Inorganic Nanoparticles

Within the last few years, there has been a surge of interest in composite materials consisting of a polymer filled with platelike particles, such as clay particles. Such fillers are extremely effective in modifying the properties of polymers, and orders-of-magnitude improvements in transport, mechanical, and thermal properties have been reported. Examples of applications include low-permeability packaging for food and electronics, toughened automotive components, and heat and flame resistant materials.[126,127] Polymer–clay nanocomposites have several unique features:[128–134] First, they are lighter in weight than conventional filled polymers with the same mechanical performance. Second, their mechanical properties are potentially superior to fiber reinforced polymers because reinforcement from the inorganic layers occurs in two rather than one dimension. Third, they exhibit outstanding diffusional-barrier properties without requiring a multipolymer layered design, and thus can be recycled.

Clays are colloidal suspensions of platelike mineral particles, with a large aspect ratio. Typically the particles are formed from silicate layers combined with layers of octahedrally coordinate aluminum or magnesium atoms.[21] The layer structure leads to a lamellar phase for the clay in water. The aim in applications is to retain this structure in the polymer–clay nanocomposite, possible structures for which are illustrated schematically in Figure 6. Exfoliation and phase separation should be avoided and there is an immense literature (especially patent literature) on how to achieve this by chemical treatment of the clay particles (in particular adsorption of organic molecules). The intercalated structure leads to enhanced barrier properties, which result from the tortuous path for gas diffusion around the clay platelets.

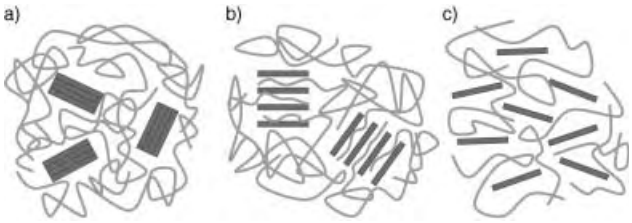


Figure 6. Possible structures for polymer–clay nanocomposites. a) Phase separated, b) intercalated, c) exfoliated. Reproduced with permission from ref. [130]. Copyright Springer Verlag, Heidelberg.

Liquid-crystal phases formed by mineral moieties have been known for almost as long as organic liquid crystals. Renewed interest in them has arisen because of the ability to combine the properties of liquid crystals, in particular anisotropy and fluidity, with the electronic and structural properties of minerals. They may also be cheaper to produce than conventional liquid crystals, which require organic synthesis. Rodlike mineral systems that form nematic phases have been well studied. Sheet-forming mineral compounds that form smectic (layered) structures in solution are also known.

The colloidal behavior of vanadium pentoxide (V_2O_5) has been investigated since the 1920s. Under appropriate conditions of pH, ribbonlike chains can be obtained by the condensation of V–OH bonds in a plane.[135] A scanning electron micrograph of dried ribbons is shown in Figure 7. A

 © 2003 Wiley-VCH Verlag GmbH & Co. KGaA, Weinheim

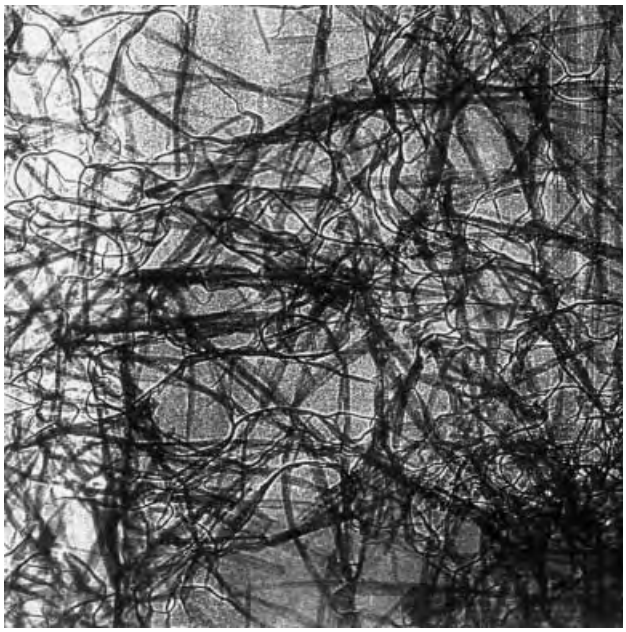


Figure 7. Scanning electron micrograph of a dried V_2O_5 suspension. Reproduced with permission from J. Livage.[136]

nematic liquid crystal forms in aqueous suspensions if the particle volume fraction, ϕ, exceeds 0.7%. A sol–gel transition occurs at $\phi = 1.2\%$, which divides the nematic domain into a nematic sol and a nematic gel. For $\phi > 5\%$, a biaxial nematic gel phase is formed.[135] Suspensions of V_2O_5 can be aligned in electric and magnetic fields, similar to the organic nematogens used in liquid-crystal displays.[137] Laponite and bentonite montmorillonite clay particles also form nematic gels.

The formation of layered structures in intercalated clay suspensions has been discussed in the preceding section. It can be argued that these are not lamellar or smectic phases since long-range order is not preserved upon swelling, where exfoliation occurs.[138] Colloidal smectic phases have been observed for β-FeOOH, which forms "Schiller layers" (from the German for iridescent). The rodlike β-FeOOH particles form layers at the bottom of the flask. The spacing between the layers is comparable to the wavelength of light, hence the iridescence.[139] A swollen liquid-crystalline lamellar phase based on extended solidlike sheets (rather than rodlike particles) has been rationally prepared using a solid acid $H_3Sb_3P_2O_{14}$.[138] In contrast, platelike $Ni(OH)_2$ nanoparticles (91 nm radius, 12 nm thick)[140,141] and $Al(OH)_3$ nanodiscs (radius 200 nm, thickness 14 nm)[142] self-assemble into columnar mesophases. A nematic phase has also been observed for the latter material. The formation of a smectic phase rather than a columnar phase is expected if the polydispersity in particle radius is large enough to prevent the efficient packing of columns.[142,143] In fact, at very high volume fractions in the $Al(OH)_3$ suspensions, evidence was obtained for a smectic phase, which can accommodate the polydispersity in radius (although a low polydispersity of particle thickness is required).[142]

3.5. Liquid-Crystal Nanodroplets

Figure 8 shows an array of block-copolymer micelles containing liquid crystals solubilized in the micellar core.[144] The self-assembly of the block-copolymer micelles into a hexagonal close-packed arrangement is apparent. The long-range ordering of the structures could be improved as in other soft materials by the use of an alignment substrate or by annealing. The ability to pattern liquid-crystal nanodroplets at the nanoscale is not required for conventional display applications (which do not require a resolution beyond that of visible light) but may find applications in phased array optics. Phased array optics is a method to reconstruct a 3D image on a 2D surface.[145] This can be done if the phase and amplitude of the light waves from the virtual image are controlled. An array of switchable light sources 200 nm apart is sufficient to reconstruct any desired light wave pattern.[145] It has been proposed that liquid crystals can be used as switchable birefringent phase shifters. However, as yet the means to arrange the liquid crystal in nm-scale arrays has been lacking. Patterning of liquid crystals in micelles or microemulsions is a promising way to achieve this.

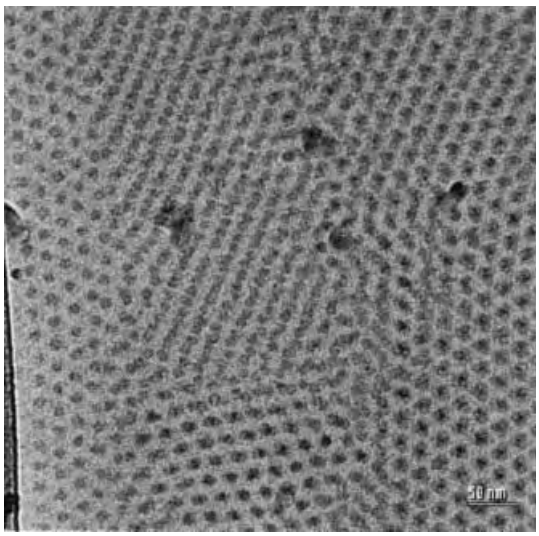


Figure 8. Transmission electron micrograph of a quench–cooled block-copolymer-micelle film of poly(styrene oxide)-*b*-poly(ethylene oxide) containing liquid crystal solubilized in the poly(styrene oxide) core.[144]

3.6. Bionanoparticles

Viruses are natural nanoparticles, which have evolved into a variety of shapes. A number of nanotechnology applications of viruses are now considered. First, they may be used as responsive delivery agents. Recent work has focused on the use of modified cowpea chlorotic mottle virus nanoparticles as biocompatible responsive delivery agents. At pH < 6.5, the virus adopts a compact spherical structure, however, at pH > 6.5, the structure becomes porous allowing the pH-controlled release of encapsulated drug molecules, for example.[146,147] In nonresponsive mode, viruses may be used as "trojan horses" for the delivery of genes in transfection applications. Gene

 © 2003 Wiley-VCH Verlag GmbH & Co. KGaA, Weinheim

therapy is attracting immense attention as a means to treat diseases by modifying the expression of genetic material.[148–150] Its premise is that disease can be prevented at the level of DNA molecules, thus compensating for the effects of abnormal genes. With an eleven-year history of clinical trials, and many more in progress, recent evidence that gene therapy may be efficacious in the treatment of medical conditions arising from the deficiency of single genes has attracted worldwide media attention.[148]

Both viral and non-viral approaches have been used in clinical trials to treat illnesses, such as cystic fibrosis and several forms of cancer. Viruses have evolved efficient ways of targeting cells, delivering genetic material, and expressing it. However, inflammatory and immunology responses induced by viruses may limit their utility for repeated administration. Numerous systems have been studied for non-viral gene delivery, which include synthetic polymers, such as polylysine[151–153] and poly(oxyethylene)-based block and graft copolymers,[154,155] biologically derived liposomes,[156] cationic lipids,[152,157] and the cationic polyelectrolyte poly(ethyleneimine) (PEI). PEI has a very high cationic charge density, which makes it useful for binding anionic DNA within the physiological pH range[158] and forcing the DNA to form condensates small enough to be effectively endocytozed, which is the primary mode of delivery of the PEI–DNA complex into the cell. Furthermore, it has been shown that PEI enhances transgene expression when DNA–-polymer complexes are injected into the cytoplasm.[159–161]

Magnetotactic bacteria exploit magnetic nanoparticles to navigate from regions of oxygen-rich water (toxic to them) to nutrient-rich sediment.[14,162] The bacteria contain grains of magnetite aligned in chains, as shown in Figure 9. The chain of crystals (and hence the bacterium) aligns along a magnetic field, which contains vertical and horizontal components (except at the poles). In the Northern hemisphere, the bacteria move downwards by moving towards the north pole. In the Southern hemisphere, the bacteria are south-seeking. Nanotechnologists can take inspiration from nature's use of chains of magnetic particles as navigational aids.

The use of chemically modified versions of the iron-storage protein ferritin in high-density magnetic data storage devices is the focus of current commercialization efforts.[163,164]

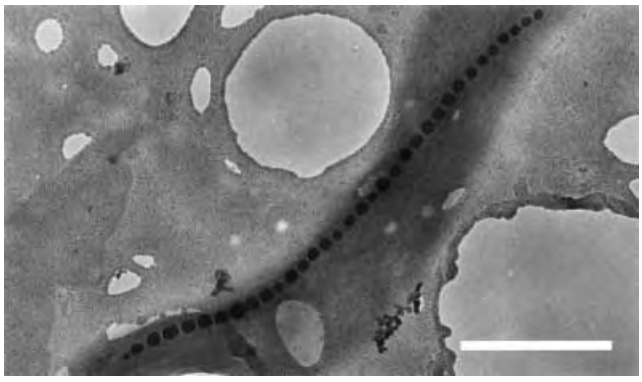


Figure 9. Chain of magnetite nanoparticles in a magnetotactic bacterium. Scalebar = 500 nm. Reproduced from ref. [162] with permission from S. Mann and Oxford University Press.

Ferritin is a nearly spherical protein with a 8-nm diameter core of ferrihydrite ($5Fe_2O_3{\cdot}9H_2O$).[14,162] The core can be removed by reductive dissolution to produce the shell protein "apoferritin". The core can then be "refilled" by incubation with metal salts, and subsequent oxidation. In this way, the core can be filled with magnetite (Fe_3O_4),[165,167] which unlike the native ferrihydrite is ferrimagnetic at room temperature, thus the resulting ferritin is termed magnetoferritin.[162]

3.7. Nanoobjects

Nanoparticles with shapes other than simple spheres, shells, or tubes have been prepared by soft-material-mediated methods. The photoinduced conversion of silver nanospheres into silver nanoprisms has been reported.[168] Photoinduced fragmentation of silver nanoparticles is believed to produce the single-crystal prism-shaped particles (the faces of which correspond to planes of the crystal lattice). The growth habit of (nano)crystals can be controlled by using organic agents, such as surfactants (as well as through the degree of supersaturation or ionic strength), to produce polyhedra with faces controlled by the growth rate of certain planes in the crystal unit cell.[162,169] Nanoparticles of CdSe with rod, arrow, teardrop, and tetrapod shapes may be fabricated[170] by using surfactants to selectively control the growth of certain crystal faces. String and other superstructures of spherical nanoparticles may be prepared in the same way.[171] Nature exploits soft materials to template the synthesis of hard nanostructures, this is discussed further in Section 4.2, which includes examples of the intricate structures made by certain organisms. Self-assembled nanostructures may also be used to template the formation of helical nanoparticles (using peptides in solution) or of string, necklace, or vesicular structures formed by block-copolymers in solution.[172–174] The self-assembly of rod–coil block copolymers can, for example, be used to make mushroom-shaped nanoobjects that assemble into lamellar stacks which have polar ordering.[175,176]

4. Templated Nanostructures

4.1. Mesoporous Silica

The self-assembly of surfactants can be exploited to template inorganic minerals, such as silica, alumina, and titania (titanium dioxide). The resulting structures resemble those of zeolites, except that the pore size is larger for the surfactant-templated materials than those in classical zeolite structures. In conventional zeolites, the pore size is typically up to 0.1 nm, whereas using amphiphile solutions it is possible to prepare an inorganic material with pores up to several tens of nanometers in diameter. Such materials are thus said to be mesoporous. They are of immense interest because of their potential applications as catalysts and molecular sieves. Just as the channels in conventional zeolites have the correct size for the catalytic conversion of methanol into petroleum, the pore size in surfactant-templated materials could catalyze reactions involving larger molecules. An excellent review of

 © 2003 Wiley-VCH Verlag GmbH & Co. KGaA, Weinheim

the templating of mesoporous materials using lyotropic liquid crystals is available.[177]

It was initially believed that the templating process simply consisted of the formation of an inorganic "cast" of a lyotropic liquid-crystal phase.[177] In other words, pre-formed surfactant aggregates were envisaged to act as nucleation and growth sites for the inorganic material. However, it now appears that the inorganic material plays an important role, and that the structuring occurs through a cooperative organization of inorganic and organic material.[177] Considering, for example, the templating of silica, a common method is to mix a tetraalkoxy silane and surfactant in an aqueous solution. Both ionic[178–181] and nonionic[182,183] surfactants have been used to template structures, as have amphiphilic block copolymers[184,185] (these behave as giant surfactants, and enable larger pore sizes). The cooperative self-assembly process leads to a structure in which the silica forms a shell around amphiphilic aggregates, the latter being removed by calcination.

Figure 10 shows a hexagonal honeycomb pattern where the silica has been templated from the hexagonal-packed cylinder (H_I) phase. Layered or bicontinuous structures have been prepared in a similar manner, by templating lamellar (L_α) or bicontinuous phases, respectively. Similarly, highly monodisperse silica beads have been made by templating spherical micelles.

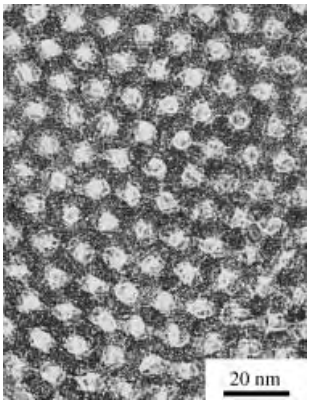


Figure 10. Hexagonal structure of calcined mesoporous silica, templated using an amphiphilic triblock copolymer.[184] Reproduced with permission from G. D. Stucky and Science. Copyright ©1998 AAAS.

4.2. Biomineralization

Biomineralization involves the uptake and controlled deposition of inorganic moieties from the environment in biological systems. A recent textbook[162] and several reviews[169,186,187] cover the subject in greater depth (that the subject deserves), than can be done here. In this section, the focus is on nanoscale structures formed by biomineralization.

The main types of biominerals are the various forms of calcium carbonate (e.g. calcite and aragonite) and calcium phosphate. Calcium carbonate is the principal component of shells, which consist of an outer layer of large calcite crystals, and an inner region of layers of aragonite several-100 nm thick. Other marine organisms live within intricate exoskeletons formed by calcium carbonate. Examples include the so-called coccospheres (see Figure 11). Calcium phosphate is the building material for bone and teeth, in the form of hydroxyapatite, which can be represented as $Ca_{10}(PO_4)_6(OH)_2$. Bone is formed by the organized mineralization of hydroxyapatite in a matrix of collagen fibrils and other proteins to form a porous structure. The mineral content controls the rigidity or elasticity of the bone. Tooth enamel also contains hydroxyapatite (more than in bone), and its ability to withstand abrasion results from a complex structure where ribbonlike crystals are interwoven into an inorganic fabric.[162] A great deal of research activity is currently focussed on the construction of artificial bone for replacement joints, and as scaffolds for tissue engineering.[188] However, the porous macrostructure of bone is outside the nanodomain, and so this fascinating subject is not considered further here.

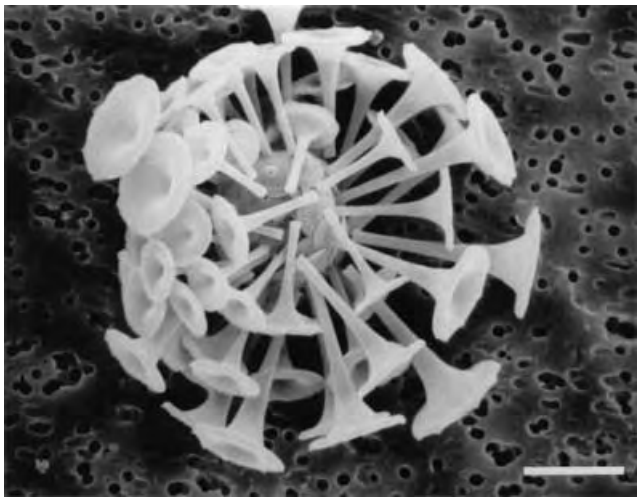


Figure 11. Example of a coccosphere.[162] Scale bar = 3 μm. Reproduced from ref. [162] with permission from S. Mann and Oxford University Press.

Radiolarians and diatoms produce their beautiful microskeletons (Figure 12) from amorphous silica.[162,187] Lamellar aluminophosphates can also be templated to create patterns that mimic diatom and radiolarian microskeletons.[189,190] The nanoscale features of these microskeletons are formed by the self-assembly of minerals which is templated by biological structures. In particular, the lacelike structures are formed from vesicles, packed together at the cell wall. The vesicles are arranged in a thin foamlike film, and biomineralization occurs in the continuous matrix.

4.3. Nanostructures Templated by Block-Copolymer Self-Assembly

Masks made from block-copolymer films in which one component has selectively been removed have been used to pattern semiconductors.[191–193] This is a novel technique for

 © 2003 Wiley-VCH Verlag GmbH & Co. KGaA, Weinheim

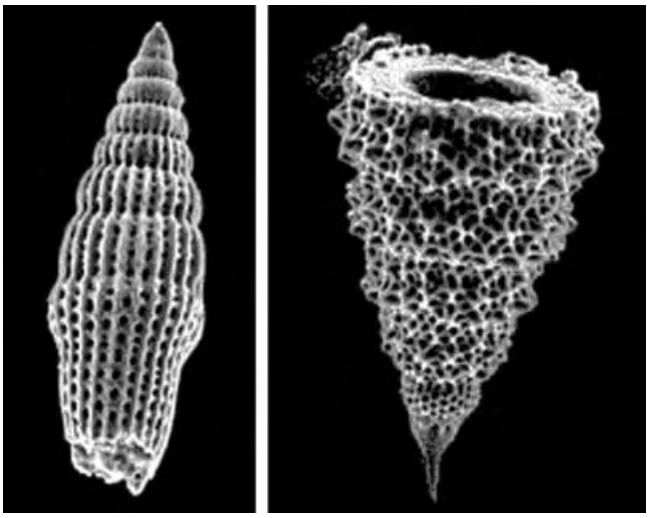


Figure 12. Examples of radiolarian microskeletons (reprinted with permission from http://www.ucmp.berkeley.edu/protista/radiolaria/radmm.html).

lithography at the nanoscale, which may be an attractive alternative to photolithography using hard (UV or X-ray) radiation. The feature density achieved is approximately 10^{11} holes cm^{-2},[191] such a high capacity being of clear interest in regard to Moore's law for the density of components in integrated circuits. The block copolymer lithography method relies on the selective ozonation of polyisoprene or polybutadiene in block copolymers containing polystyrene as the other component. Ozone cleaves the double bonds in the unsaturated polymers, so that they can be etched away. This process leaves holes or stripes in a polystyrene matrix. This pattern can be transferred from the block-copolymer mask into silicon by reactive ion etching (Figure 13).

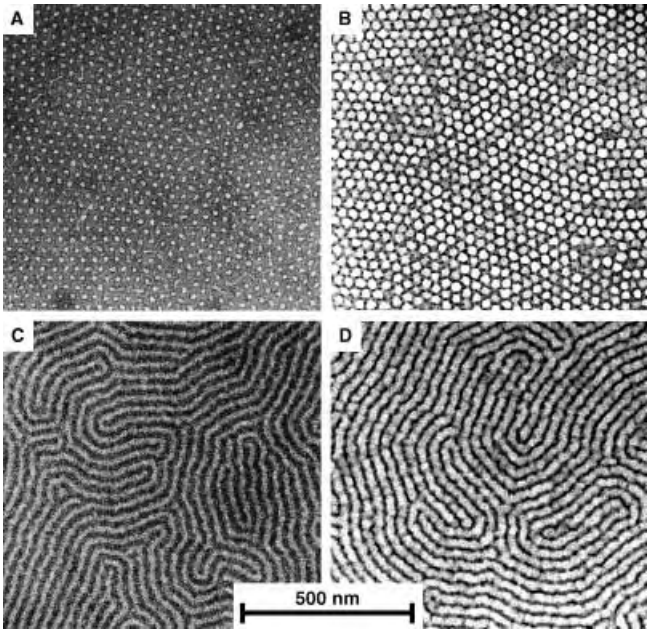


Figure 13. TEM micrographs of polystyrene–polybutadiene diblock copolymer film masks (a,c) and lithographically patterned silicon nitride (b,d).[191] Reproduced with permission from C. Harrison and Science. Copyright ©1997 AAAS

Magnetic nanostructures have also been templated using block copolymer self-assembly. Several strategies have been pursued. One method is to prepare vertically oriented hexagonal-packed cylinders from an asymmetric copolymer and then remove the minority cylinder-forming component (Figure 14).[194] Thurn-Albrecht et al. employed this method using polystyrene-poly(methyl methacrylate) (PS-PMMA) diblocks, the minority PMMA component being removed by short wavelength ultraviolet radiation (which also cross-links the PS domains ensuring that the glassy matrix is retained).[194] The resulting nanopores were then filled with Co or Cu atoms by electrodeposition. The result is a magnetic nanowire array, with potential use as ultrahigh-density recording media.

An alternative lithographic method has also been demonstrated. Minority domains in a diblock film deposited on a metallic multilayer structure are selectively etched by reactive-ion etching (RIE) forming a mask (Figure 15).[195] The diblock used was a polystyrene-polyferrocenyldimethylsiloxane (PS-PFS), in which the PS matrix can be selectively etched away in an O_2 plasma, leaving PFS spheres. An SEM image of the structure at this stage is shown in Figure 16. The mask pattern is transferred into silica (which improves pattern transfer) then into tungsten by RIE. The multilayer structure is necessary because magnetic materials, such as cobalt, nickel, and iron are not amenable to RIE. In the next step, the polymer and silica are removed. Finally, the pattern is transferred from the tungsten hard mask into the magnetic cobalt layer using ion-beam etching.

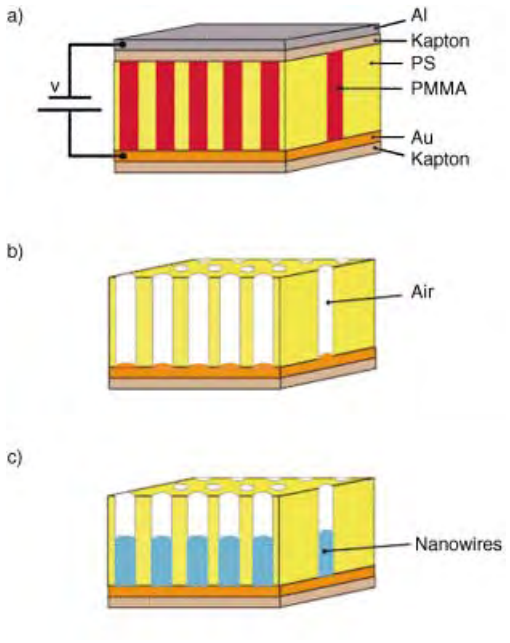


Figure 14. Schematic of high-density nanowire-array formation.[194] a) An asymmetric diblock copolymer is annealed above the glass transition temperature of the copolymer between two electrodes under an applied electric field. b) After removal of the minor component, a nanoporous film is formed. c) Nanowires formed by electrodeposition in the pores. Reproduced with permission from M. T. Tuominen and Science. Copyright ©2000 AAAS

 © 2003 Wiley-VCH Verlag GmbH & Co. KGaA, Weinheim

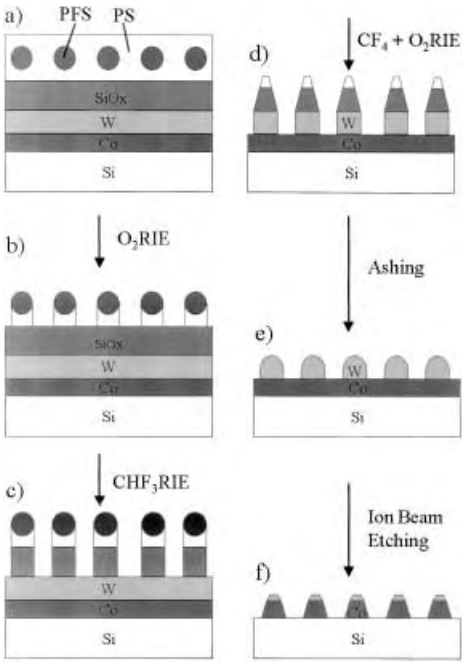


Figure 15. Fabrication of a magnetic cobalt dot array using block-copolymer nanolithography. a) The block-copolymer film is spin coated onto a multilayer. b) A mask is formed by selective etching of the PS domains by O_2 RIE, c), d) the silica and then tungsten layers are etched using different ion beams. e) The silica and polymer are removed by CHF_3 RIE. f) The cobalt dot array is formed using ion-beam etching. Reproduced with permission from ref. [195].

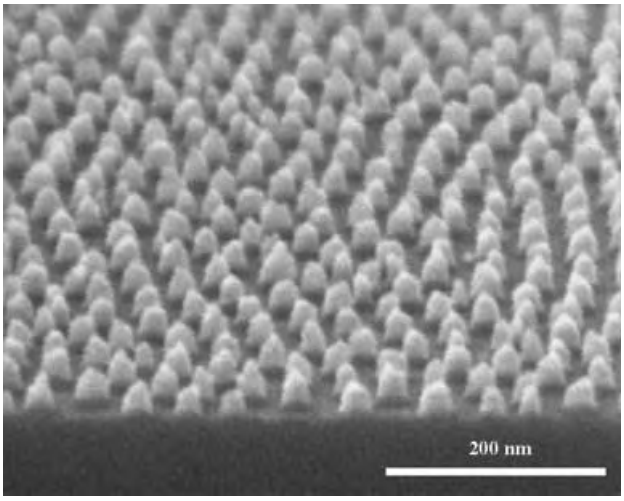


Figure 16. SEM image of PS–PFS mask, after the PS has been removed by O_2 RIE. Reproduced with permission from ref. [195]

The patterning of inorganic nanoparticles using block copolymer micelles adsorbed onto solid substrates is another exciting application of block-copolymer self-assembly, as discussed in Section 3.1.

5. Liquid-Crystal Mesophases

5.1. Micelles and Vesicles

Micelles and vesicles formed by surfactants and block copolymers are widely used in systems as diverse as personal-care products, agrochemicals, and pharmaceuticals to solubilize fragrances, pesticides/herbicides, or drugs. Usually the aim is to solubilize organic compounds in the core of micelles in aqueous media.

The primary nanotechnology applications of micelles and vesicles result from their use as templates to synthesize nanoparticles with a multitude of structures and functionalities. The use of core cross-linking reactions to form organic nanoparticles containing functionalized coatings (tailored through the choice of corona block) has also been reported.[196–198] In particular, cross-linking of the nontoxic, biodegradable polylactide core of micelles with an end-functionalized poly(ethylene glycol) corona lead to sterically stabilized and biocompatible nanoparticles for drug-delivery applications.[196,197] Another approach is to cross-link the shell and remove the core by, for example, ozonolysis.[199] Similarly, cross-linking the shell of a vesicle leads to hollow nanoparticles that can be used to encapsulate compounds.[51,53,200,201] Alternative methods to deliver drugs using molecular complexes, inclusion compounds, and microemulsions, are discussed elsewhere.[202]

As mentioned in Section 3.1, micelles can also be used as media for the production of inorganic nanoparticles. The synthesis of metal nanoparticles in aqueous block-copolymer micelles has recently attracted a great deal of attention.[78–91] Metal ions or complexes that are insoluble in water are sequestered in the micellar core. The block-copolymer micelles containing the metal compounds then act as nanoreactors where, upon reduction, the nucleation and growth of metal nanoparticles occurs. Applications of such metal nanoparticles are extensive, and include catalysis, electrooptical materials (quantum dots), and the patterning of semiconductors.[90] Using block-copolymer micelles it is possible to control the size of the particles by changing the copolymer composition and molecular weight. This feature is very important for the synthesis of magnetic nanoparticles, to ensure that the nanoparticles are large enough to exceed the superparamagnetic limit but small enough to comprise a single domain (see Section 3.6).

5.2. Lamellar Phases

The lamellar phase (known as the smectic phase for low-molar-mass liquid crystals) is found in diverse systems, ranging from surfactants in solution to clays to block copolymers. The layered structures in clays and polymer–clay nanocomposites were discussed in Section 3.4. In this section the focus is on recent examples of high-tech applications for lamellar phases in block copolymers.

Noncentrosymmetric structures can have a macroscopic electric polarization, and hence piezo- and pyroelectricity as well as second-order nonlinear optical (NLO) activity. The

 © 2003 Wiley-VCH Verlag GmbH & Co. KGaA, Weinheim

fabrication of noncentrosymmetric stacks of block-copolymer lamellae has been demonstrated in blends of ABC triblock and ac diblock copolymers (the letters refer to the different blocks in the polymers).[203] The resulting structure is illustrated schematically in Figure 17. It is favored over others (macrophase separated, random lamellar, centrosymmetric lamellar stack) if the difference in the aA and cC contact energies is large enough.

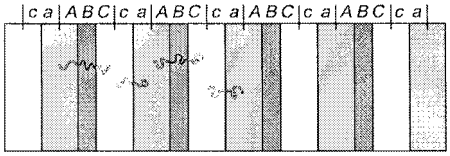


Figure 17. Schematic of a noncentrosymmetric lamellar structure observed in a blend of ABC triblock and ac diblock copolymers.[203] Reproduced with permission from L. Leibler and Nature.

It has been proposed to exploit lamellar block-copolymer structures to self-assemble all-polymer solid-state batteries, by using a triblock copolymer where the three blocks correspond to the anode, electrolyte, and cathode.[204] This approach has the advantage that possible leakage of a toxic liquid electrolyte is avoided, and furthermore the processing is straightforward (e.g. spin coating of thin films). Similar applications of lamellar block-copolymers in nanocapacitors[91] and nanotransistors have also been envisaged.

Lamellar block-copolymer nanostructures can be used as selective 1D dielectric reflectors if the layer thickness is large enough (close to the wavelength of light) and the difference in refractive index between blocks is large enough. Polystyrene–polyisoprene diblocks swollen with the corresponding homopolymers was shown to have a limited angular range stop band at visible frequencies with potential applications in photonics,[205,206] for example, in waveguiding.[207,208]

Rod–coil diblocks can form a range of lamellar structures, as demonstrated by the work of Chen et al.[209] on polystyrene–poly(hexylisocyanate) diblocks, which form wavelike lamellar, zigzag, and arrowhead morphologies. Distinct structures result because the rod block can tilt with respect to the layers, and the tilt can alternate between domains. The coupling of liquid-crystal ordering to that of block copolymers extends considerably the range of nanostructures available to the nanotechnologist.

Inspired by a similar concept, Ruokolainen et al. have shown that ordering as multiple lengthscales can be achieved using complexes of diblock copolymers and the amphiphilic, long-chain alcohol, pentadecylphenol (PDP).[210,211] Hydrogen bonding of the alcohol to the −NH group in poly(4-vinylpyridine) (P4VP) produced a comblike block, whereas no hydrogen bonding occurred to the coil-like polystyrene block. The usual ordered structures were observed which result from microphase separation in the melt of the diblock, however, in addition, mesogenic ordering was observed within the P4VP-PDP phase as a result of formation of a lamellar structure below the liquid–crystal–isotropic phase transition for the PDP. Since the lamellar–isotropic phase transition for the PDP/P4VP lamellae occurs below that for the PS-P4VP block copolymer, it is possible to switch off the lamellar ordering on one lengthscale independent of the other. It was shown that this transition was accompanied by a large change in the electrical conductivity (P4VP is a semiconducting side-chain conjugated polymer). The potential to create switchable nanoscale structures with ordering in two- and three-dimensions has implications for other applications, such as alignment layers in liquid-crystal displays, nanoscale sensors, and optical waveguides.

5.3. ABC Triblock Structures

The phase behavior of ABC triblock polymers is much richer than that of AB diblock polymers[212–214] because in triblock polymers there are two independent compositional order parameters and three Flory–Huggins interaction parameters, the subtle interplay of which gives a varied morphospace. Examples of the intricate morphologies observed are shown in Figure 18 and Figure 19. A remarkable structure consisting of helices of a minority polybutadiene domain wrapped around polystyrene cylinders in a PMMA matrix has even been reported.[215] These observations of complex phases formed by midblock segregation at the AC interface have been accounted for theoretically by Stadler et al.,[216] the theory being in good agreement with experiments for several morphologies. However, it has to be emphasized that achieving thermodynamic equilibrium (e.g through annealing) in ABC triblock copolymer melts is even more challenging than for diblock copolymers[217] since they are usually more strongly segregated, so that great caution is required in assigning equilibrium phase behavior.

State-of-the-art self-consistent mean field (SCMF) theory calculations have been used to predict a number of intricate nanostructures at the surface of ABC triblock copolymers (Figure 20). It should be noted that the patterns in Figure 20 are simulated in a 2D system. As a result of confinement and surface-energy effects, such morphologies may not be realizable at the surface of a bulk sample,[220,221] however, they could be accessed by sectioning of a glassy bulk sample. Potential exploitation of the surface structures formed by ABC triblock copolymers can be envisaged if domains are selectively doped with metal atoms or semiconductors (see Figure 2 for an example corresponding to the diblock copolymer case). Applications include nanowire arrays for addressing nanoscale electronic devices or three-color arrays for high-resolution displays.

5.4. Smectic and Nematic Materials

Conventional methods of fabricating liquid-crystal displays are not usually regarded as nanotechnology. Present-day displays are based on nematics sandwiched in thin films between electrode-coated glass substrates.

The fabrication of a liquid-crystal display on a single substrate, which could ultimately lead to flexible or paintable

 © 2003 Wiley-VCH Verlag GmbH & Co. KGaA, Weinheim

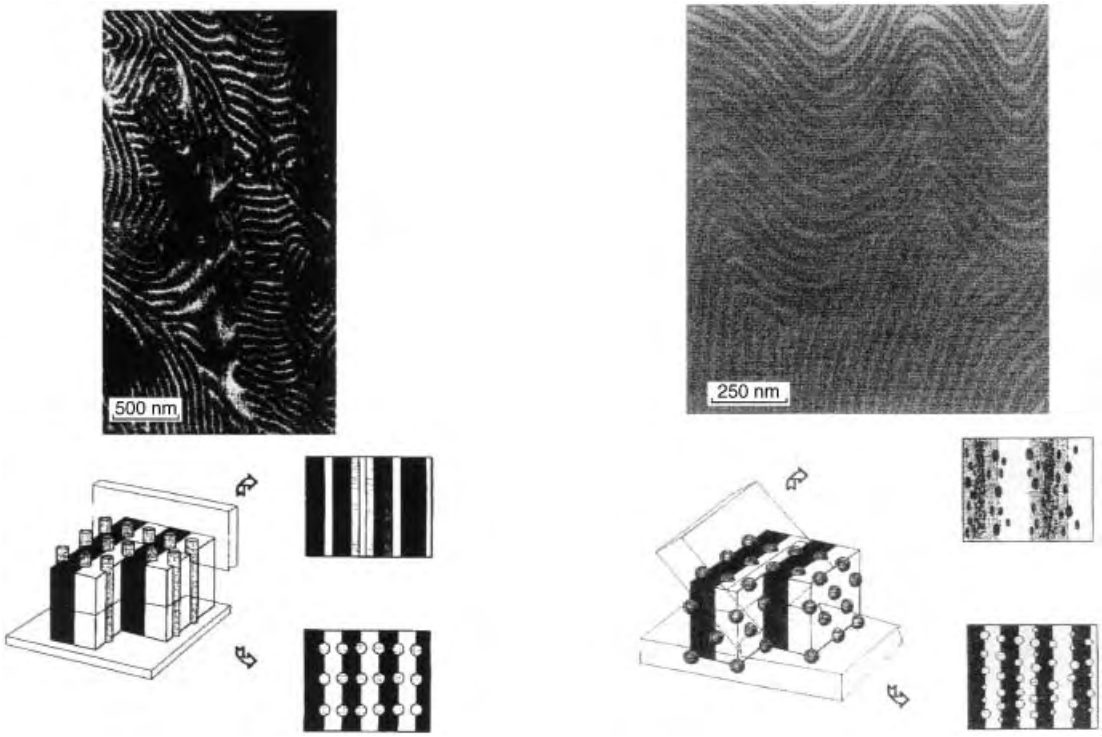


Figure 18. Examples of morphologies observed for polystyrene—polybutadiene–poly(methyl methacrylate) triblock copolymers with a minority midblock component.[216] Left: cylinders at a lamellar interface, right: Spheres at a lamellar interface ("ball at the wall" morphology). The upper images are transmission electron micrographs. The lower figures are schematics. Reproduced with permission from ref. [216].

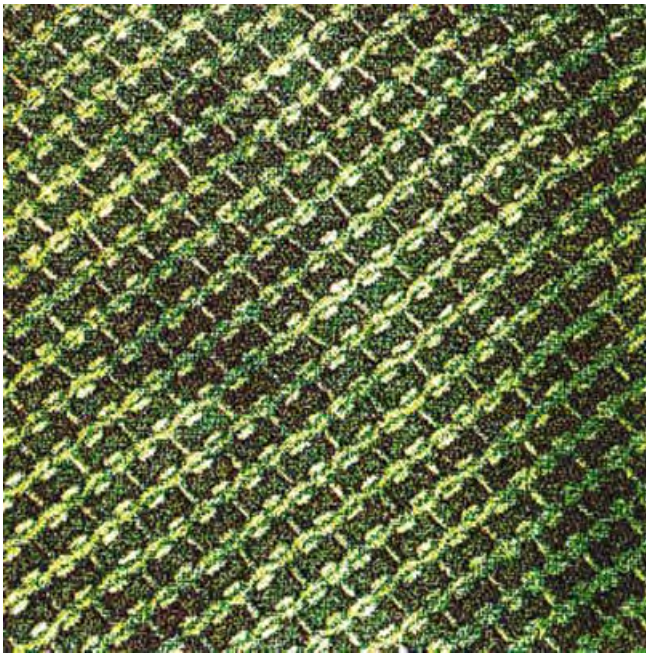


Figure 19. "Knitting pattern" morphology observed by TEM on a polystyrene–poly(ethylene-co-butylene)–poly(methyl methacrylate) triblock copolymer (stained with RuO_4). Reproduced with permission from ref. [218].

displays has recently been demonstrated based on an array of encapsulated liquid-crystal cells.[222] Stratified polymer structures self-assemble through phase separation of a photopolymerizable prepolymer and a nematic liquid crystal.

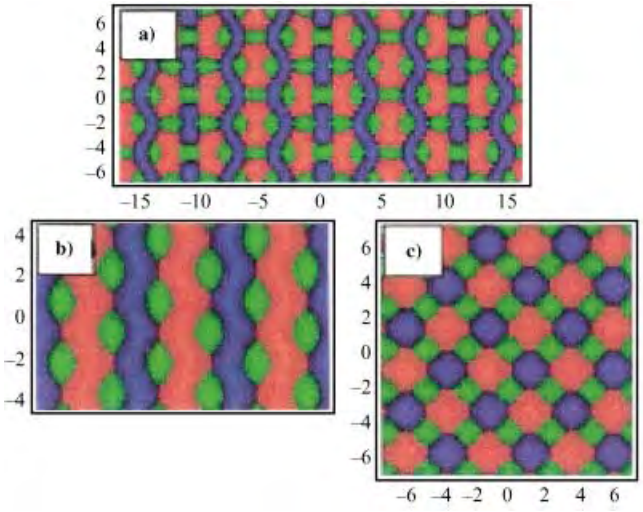


Figure 20. Examples of predicted morphologies for linear ABC triblock copolymers, from self-consistent mean field calculations. Reproduced with permission from ref. [219].

Horizontal stratification creates the walls of the cells and vertical stratification (using a different UV wavelength) produces lids. To date, the technique has been used to fabricate micron-size polymer cells, although extension to the nanoscale using harder radiation should be feasible.

Usually a nematic phase is cloudy because of light scattering from fluctuating micron-size domains with different orientations (creating refractive-index variations, since the refractive index of liquid-crystal phases is anisotropic).

 © 2003 Wiley-VCH Verlag GmbH & Co. KGaA, Weinheim

The presence of nanometer-scale phase-separated structures in an inverse lyotropic structure of surfactant micelles in a liquid-crystal matrix has been shown to lead to a transparent nematic phase.[223] In the "nanoemulsion" the droplets of surfactant disrupt the long-range orientational order of the nematic phase, which leads to optical isotropy and transparency, although the local nematic ordering is retained. Mixing spherical colloidal particles with liquid crystals likewise produces a phase-separated structure as colloidal particles are expelled from nematic droplets below the isotropic–nematic phase-transition temperature.[224] The particles are expelled because the trapping of defects in the nematic phase by colloidal particles has too high an energy penalty. The colloid particles therefore separate into an interconnected network (the struts of which are several nanometers thick). The result is a waxy soft solid with a high storage modulus.

5.5. Discotic Liquid Crystals

Columnar phases formed by discotic liquid crystals, such as those based on triphenylene compounds, form 1D conductors, because of the overlap of π^* orbitals of the aromatic moieties which are surrounded by a hydrocarbon insulator coating.[225,226] Each column thus acts as a nanowire, and applications in molecular electronics have resulted, in particular in gas sensors.[227] They could also be used in molecular electronic devices, for example, in electroluminescent displays or in 3D integrated circuits.

6. Summary and Outlook

Self-assembly is responsible for nanostructure formation in colloidal, amphiphilic, polymeric, and biomolecular materials. In this review, the principles of self-assembly in synthetic and biological systems were considered. Then selected examples of self-assembly routes to the production of nanostructures and nanodevices were presented. A key theme is that self-assembly in soft materials (synthetic and biological) can be used to template nanostructures in inorganic matter, either in bulk or at a surface. The range of structures that can be fabricated in equilibrium depends (following the Gibbs phase rule) on the number of components in the system. In the case, for example, of ABC triblock copolymers this leads to a large number of possible nanostructures with different symmetries. An additional complexity in phase behavior results from the coupling of distinct types of order, for example, orientational order of liquid crystals with translationally ordered block-copolymer nanostructures.

Out-of-equilibrium processes can also be exploited, for example, in nanoscale motors or actuators. Out-of-equilibrium structures may also be useful, since they could be captured when templating a hard material. It has to be kept in mind that the rich structural diversity and access to out-of-equilibrium structures are both different aspects of the weak ordering resulting from noncovalent interactions that characterizes soft materials.

Many developments are underway to exploit self-assembling soft materials in nanotechnology. Considering nanostructures, the first commercial products are likely to be nanoparticles fabricated in micellar or vesicular nanoreactors, and mesoporous templated materials for catalysis and separation media. Uses of more intricate structures, such as those formed by ABC triblock copolymers are still some way off. Downstream applications of biomineralization (in prostheses, artificial bone and teeth) are less distant. The development of drug-delivery systems using functionalized nanoparticles is also the subject of intense research activity at present. Only a sample of the many different approaches being investigated has been covered here. The use of block-copolymer films in nanolithography and to pattern nanoparticles into regular arrays are the focus of much attention.

Arguably the most important nanodevice is the nanomotor, and self-assembly routes to the production of simple oscillating "motors" have already been developed. To fabricate directional motors with a renewable energy source, inspiration is being taken from nature, where ATP synthesis underpins distinct linear and rotory motors. Supramolecular chemistry has much to offer here, although this is outside the scope of this review. Other nanodevices will contain passive nanostructures which can be built by using self-assembly, examples include waveguides and optical filters. Nanowires and ferroelectric piezo- and pyroelectric structures can also be produced. Self-assembled nanocapacitors and nanotransistors can also be envisaged, although as yet there has been little research in this area. Using a combination of self-assembled nanostructure elements from the broad palette available, together with a suitable power source (e.g. a nanostructured-polymer solid-state battery) a customized nanodevice could readily be put together. The prime limitation is that certain nonperiodic structures require atomic or molecular manipulation, outside the realm of self-assembly.

The time is now ripe to harvest the benefits of research in the last few decades on soft materials, and to take advantage of self-assembly to prepare tailored nanostructures. The diversity of possible nanostructures and the techniques to make use of them constitute a rich smorgasboard. Only a taste has been provided here, hopefully enough to capture the flavor.

The AFM images of block-copolymer films for the collage on the frontispiece were obtained by Dr. T. Mykhaylyk, University of Leeds, UK.

Received: July 24, 2002 [A546]

[1] J.-M. Lehn, *Supramolecular Chemistry: Concepts and Perspectives*, VCH, Weinheim, **1995**.
[2] K. E. Drexler, *Engines of Creation*, Fourth Estate, London, **1990**.
[3] V. Balzani, A. Credi, F. M. Raymo, J. F. Stoddart, *Angew. Chem.* **2000**, *112*, 3484; *Angew. Chem. Int. Ed.* **2000**, *39*, 3349.
[4] I. W. Hamley, *Introduction to Soft Matter*, Wiley, Chichester, **2000**.
[5] R. A. L. Jones, *Soft Condensed Matter*, Oxford University Press, Oxford, **2002**.

 © 2003 Wiley-VCH Verlag GmbH & Co. KGaA, Weinheim

[6] C. M. Niemeyer, *Angew. Chem.* **2001**, *113*, 4254; *Angew. Chem. Int. Ed.* **2001**, *40*, 4128.
[7] S. L. Gillett, *Nanotechnology* **1996**, *7*, 168.
[8] R. A. L. Jones in *Emerging Themes in Polymer Science* (Ed.: A. J. Ryan), Royal Society of Chemistry, Cambridge, **2001**.
[9] M. Shimomura, T. Sawadaishi, *Curr. Opin. Colloid Interface Sci.* **2001**, *6*, 11.
[10] J. H. Fendler, *Korean J. Chem. Eng.* **2001**, *18*, 1.
[11] *Nanotechnology* (Ed.: G. Timp), Springer, New York, **1999**.
[12] T. J. Deming, V. P. Conticello, D. A. Tirrell in *Nanotechnology* (Ed.: G. Timp), Springer, New York, **1999**, p. 371.
[13] *Nanomaterials: Synthesis, Properties and Applications* (Ed.: A. S. Edelstein, R. C. Cammarata), Institute of Physics, Bristol, **1996**.
[14] D. P. E. Dickson in *Nanomaterials: Synthesis, Properties and Applications* (Eds.: A. S. Edelstein, R. C. Cammarata), Institute of Physics, Bristol, **1996**, p. 495.
[15] L. C. Klein in *Nanomaterials: Synthesis, Properties and Applications* (Eds.: A. S. Edelstein, R. C. Cammarata), Institute of Physics, Bristol, **1996**, p. 147.
[16] G. M. Whitesides, B. Grzybowski, *Science* **2002**, *295*, 2418.
[17] N. T. Southall, K. A. Dill, A. D. J. Haymet, *J. Phys. Chem. B* **2002**, *106*, 521.
[18] J.-M. Lehn, *Science* **2002**, *295*, 2400.
[19] *Comprehensive Supramolecular Chemistry* (Eds.: J. L. Attwood, J. E. D. Davies, D. D. MacNicol, F. Vögtle), Pergamon, Oxford, **1996**.
[20] S. Asakura, F. Oosawa, *J. Chem. Phys.* **1954**, *22*, 1255.
[21] R. J. Hunter, *Foundations of Colloid Science*, 2nd ed., Oxford University Press, Oxford, **2001**.
[22] J. M. Seddon, *Biochim. Biophys. Acta* **1990**, *1031*, 1.
[23] J. N. Israelachvili, D. J. Mitchell, B. W. Ninham, *J. Chem. Soc. Faraday Trans. 2* **1976**, *72*, 1525.
[24] D. F. Evans, H. Wennerström, *The Colloidal Domain. Where Physics, Chemistry, Biology and Technology Meet*, Wiley, New York, **1999**.
[25] J. N. Onuchic, Z. Schulten-Luthey, P. G. Wolynes, *Annu. Rev. Phys. Chem.* **1997**, *48*, 545.
[26] C. M. Dobson, A. Sali, M. Karplus, *Angew. Chem.* **1998**, *110*, 908; *Angew. Chem. Int. Ed.* **1998**, *37*, 868.
[27] K. A. Dill, *Protein Sci.* **1999**, *8*, 1166.
[28] M. Karplus, D. L. Weaver, *Protein Sci.* **1994**, *3*, 650.
[29] S. S. Plotkin, J. Wang, P. G. Wolynes, *J. Chem. Phys.* **1997**, *106*, 2932.
[30] V. S. Pande, A. Y. Grosberg, T. Tanaka, D. S. Rokhsar, *Curr. Opin. Struct. Biol.* **1998**, *8*, 68.
[31] V. S. Pande, A. Y. Grosberg, T. Tanaka, *Biophys. J.* **1997**, *73*, 3192.
[32] S. Izraielev, S. Stepaniants, M. Balsera, Y. Oono, K. Schulten, *Biophys. J.* **1997**, *72*, 1568.
[33] C. Lieber, *Sci. Am.* **2001**, *285*(3), 51.
[34] Q. Lu, L. Wang, A. G. Frutos, A. E. Condon, R. M. Corn, L. M. Smith, *Nature* **2000**, *403*, 175.
[35] C. M. Niemeyer, *Curr. Opin. Chem. Biol.* **2000**, *4*, 609.
[36] C. M. Niemeyer, L. Boldt, B. Ceyhan, D. Blohm, *Anal. Biochem.* **1999**, *268*, 54.
[37] E. Braun, Y. Eichen, U. Sivan, G. Ben-Yoseph, *Nature* **1998**, *391*, 775.
[38] A. M. Cassel, W. A. Scrivens, J. M. Tour, *Angew. Chem.* **1998**, *110*, 1528; *Angew. Chem. Int. Ed.* **1998**, *37*, 1670.
[39] J. L. Coffer, S. R. Bigham, R. F. Pinizzotto, H. Yang, *Nanotechnology* **1992**, *3*, 69.
[40] I. Willner, F. Patolsky, J. Wasserman, *Angew. Chem.* **2001**, *113*, 1913; *Angew. Chem. Int. Ed.* **2001**, *40*, 1861.
[41] J.-H. Chen, N. R. Kallenbach, N. C. Seeman, *J. Am. Chem. Soc.* **1989**, *111*, 6402.
[42] E. Winfree, F. Liu, L. A. Wenzler, N. C. Seeman, *Nature* **1998**, *394*, 539.
[43] C. M. Niemeyer, *Appl. Phys. A* **1999**, *68*, 119.
[44] M. C. Goodall, *Arch. Biochem. Biophys.* **1971**, *147*, 129.
[45] *Molecular Biology of Ionic Channels, Vol. 33* (Eds.: W. S. Agnew, T. Claudio, F. J. Sigworth), Academic Press, San Diego, **1988**.
[46] *Membrane Permeability, Current Topics in Membranes, Vol. 48* (Eds.: D. W. Deamer, A. Kleinzeller, D. M. Fambrough), Academic Press, San Diego, **1999**.
[47] D. S. Cafiso, *Membrane Permeability, Current Topics in Membranes, Vol. 48,* Academic Press, San Diego, **1999**.
[48] Y. Cheng, R. J. Bushby, S. D. Evans, P. F. Knowles, R. E. Miles, S. D. Ogier, *Langmuir* **2001**, *17*, 1240.
[49] T. M. Fyles, W. F. van Straaten-Nijenhuis in *Comprehensive Supramolecular Chemistry, Vol. 10* (Ed.: D. N. Reinhoudt), Pergamon, Oxford, **1996**, p. 53.
[50] K. S. Åkerfeldt, P. K. Kienker, J. D. Lear, W. F. Degrado in *Comprehensive Supramolecular Chemistry, Vol. 10* (Ed.: D. N. Reinhoudt), Pergamon, Oxford, **1996**, p. 659.
[51] C. Nardin, T. Hirt, J. Leukel, W. Meier, *Langmuir* **2000**, *16*, 1035.
[52] W. Meier, C. Nardin, M. Winterhalter, *Angew. Chem.* **2000**, *112*, 4747; *Angew. Chem. Int. Ed.* **2000**, *39*, 4599.
[53] C. Nardin, J. Widmer, M. Winterhalter, W. Meier, *Eur. Phys. J. E* **2001**, *4*, 403.
[54] M. Sauer, W. Meier, *Chem. Commun.* **2001**, 55.
[55] M. Sauer, D. Streich, W. Meier, *Adv. Mater.* **2001**, *13*, 1649.
[56] J. A. Speir, S. Munski, G. Wang, T. S. Baker, J. E. Johnson, *Structure* **1995**, *3*, 63.
[57] N. M. Green, *Adv. Protein Chem.* **1975**, *29*, 85.
[58] C. Booth, R. J. Bushby, Y. Cheng, S. D. Evans, Q. Liu, H. Zhang, *Tetrahedron* **2001**, *57*, 9859.
[59] E. Regis, *Nano. The Emerging Science of Nanotechnology: Remaking the World—Molecule by Molecule*, Little, Brown, Boston, **1995**.
[60] M. Gómez-López, J. F. Stoddart in *Handbook of Nanostructured Materials, Vol. 5* (Ed.: H. S. Nalwa), Academic, San Diego, **2000**, p. 225.
[61] *Molecular Machines and Motors, Vol. 99* (Ed.: J. P. Sauvage), Springer, Heidelberg, **2001**.
[62] D. Voet, J. G. Voet, *Biochemistry*, Wiley, New York, **1995**.
[63] J. Nardi, R. Bruinsma, E. Sackmann, *Phys. Rev. Lett.* **1999**, *82*, 5168.
[64] A. Terray, J. Oakey, D. W. M. Marr, *Science* **2002**, *296*, 1841.
[65] D. E. Bennett, B. S. Gallardo, N. L. Abbott, *J. Am. Chem. Soc.* **1996**, *118*, 6499.
[66] L. Rayleigh, *Proc. R. Soc. London* **1890**, *47*, 364.
[67] M. I. Kohira, Y. Hayashima, M. Nagayama, S. Nakata, *Langmuir* **2001**, *17*, 7124.
[68] Y. Hayashima, M. Nagayama, Y. Doi, S. Nakata, M. Kimura, M. Iida, *Phys. Chem. Chem. Phys.* **2002**, *4*, 1386.
[69] R. Yoshida, K. Uchida, Y. Kaneko, K. Sakai, A. Kikuchi, Y. Sakurai, T. Okano, *Nature* **1995**, *374*, 240.
[70] R. Yoshida, T. Takahashi, T. Yamaguchi, H. Ichijo, *J. Am. Chem. Soc.* **1996**, *118*, 5134.
[71] C. J. Crook, A. Smith, R. A. L. Jones, A. J. Ryan, *Phys. Chem. Chem. Phys.* **2002**, *4*, 1367.
[72] E. Cartlidge, *Phys. World* **2001**, *14*(4), 42.
[73] *Technology Alert: Nanotechnology. The Huge Opportunity that comes from Thinking Small*, Report, Institute of Nanotechnology, London, **2001**.
[74] G. Stix, *Sci. Am.* **2001**, *285*(9), 26.
[75] H. J. Fecht in *Nanomaterials: Synthesis, Properties and Applications* (Eds.: A. S. Edelstein, R. C. Cammarata), Institute of Physics, Bristol, **1996** p. 89.

 © 2003 Wiley-VCH Verlag GmbH & Co. KGaA, Weinheim

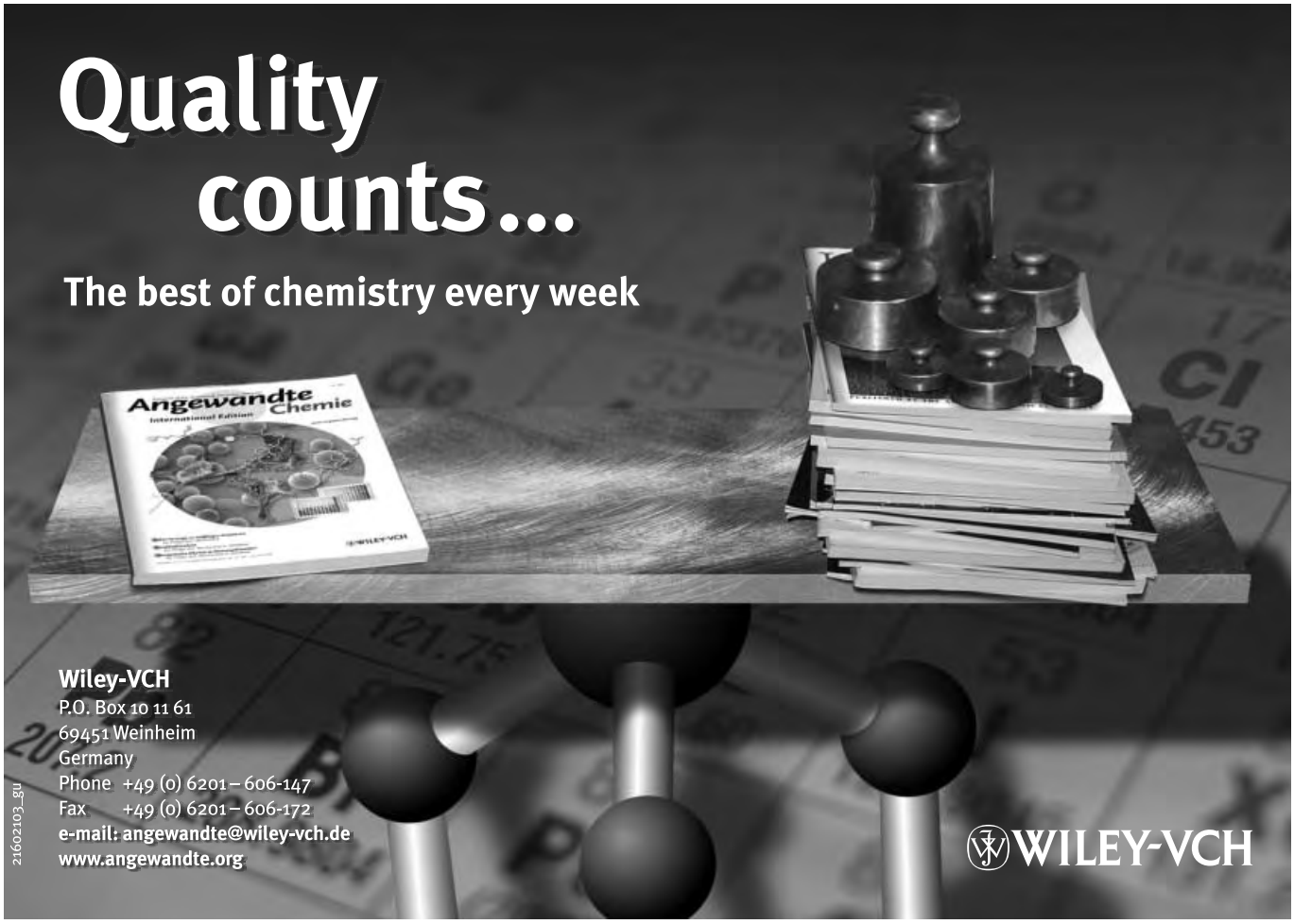
[76] R. E. Rosensweig (Ferrofluidics Corporation), US 3917538 **1975**.
[77] G. M. Chow, K. E. Gonsalves in *Nanomaterials: Synthesis, Properties and Applications* (Eds.: A. S. Edelstein, R. C. Cammarata), Institute of Physics, Bristol, **1996**.
[78] Y. N. C. Chan, R. R. Schrock, R. E. Cohen, *Chem. Mater.* **1992**, *4*, 24.
[79] R. T. Clay, R. E. Cohen, *Supramol. Sci.* **1995**, *2*, 183.
[80] B. H. Sohn, R. E. Cohen, *Acta Polym.* **1996**, *47*, 340.
[81] L. Bronstein, M. Seregina, P. Valetsky, U. Breiner, V. Abetz, R. Stadler, *Polym. Bull.* **1997**, *39*, 361.
[82] L. Bronstein, D. Chernyshov, P. Valetsky, *Langmuir* **1999**, *15*, 83.
[83] L. M. Bronstein, S. N. Sidorov, P. M. Valetsky, J. Hartmann, H. Cölfen, M. Antonietti, *Langmuir* **1999**, *15*, 6256.
[84] L. M. Bronstein, D. M. Chernyshov, G. I. Timofeeva, L. V. Dubrovina, P. M. Valetsky, E. S. Obolonkova, A. R. Khokhlov, *Langmuir* **2000**, *16*, 3626.
[85] L. M. Bronstein, D. M. Chernyshov, G. I. Timofeeva, L. V. Dubrovina, P. M. Valetsky, A. R. Khokhlov, *J. Colloid Interface Sci.* **2000**, *230*, 140.
[86] M. Moffitt, L. McMahon, V. Pessel, A. Eisenberg, *Chem. Mater.* **1995**, *7*, 1185.
[87] M. Antonietti, E. Wenz, L. Bronstein, M. Seregina, *Adv. Mater.* **1995**, *7*, 1000.
[88] J. P. Spatz, A. Roescher, M. Möller, *Adv. Mater.* **1996**, *8*, 337.
[89] J. Spatz, S. Mössmer, M. Möller, M. Kocher, D. Neher, G. Wegner, *Adv. Mater.* **1998**, *10*, 473.
[90] B. Koslowski, S. Strobel, T. Herzog, B. Heinz, H. G. Boyen, R. Notz, P. Ziemann, J. P. Spatz, M. Möller, *J. Appl. Phys.* **2000**, *87*, 7533.
[91] S. Förster, M. Antonietti, *Adv. Mater.* **1998**, *10*, 195.
[92] L. M. Bronstein, D. M. Chernyshov, G. I. Timofeeva, L. V. Dubrovina, P. M. Valetsky, *Langmuir* **1999**, *15*, 6195.
[93] J. P. Spatz, S. Mössmer, C. Hartmann, M. Möller, T. Herzog, M. Krieger, H.-G. Boyen, P. Ziemann, B. Kabius, *Langmuir* **2000**, *16*, 407.
[94] W. A. Lopes, H. M. Jaeger, *Nature* **2001**, *414*, 735.
[95] W. A. Lopes, *Phys. Rev. E* **2002**, *65*, 031606.
[96] A. A. Antipov, G. B. Sukhorukov, S. Leporatti, I. L. Radtchenko, E. Donath, H. Möhwald, *Colloids Surf. A* **2002**, *198*–200, 535.
[97] G. B. Sukhorukov, A. S. Susha, S. Davis, S. Leporatti, E. Donath, J. Hartmann, H. Möhwald, *J. Colloid Interface Sci.* **2002**, *247*, 251.
[98] I. L. Radtchenko, G. B. Sukhorukov, H. Möhwald, *Colloids Surf. A* **2002**, *202*, 127.
[99] X. Liu, L. Fu, S. Hong, V. P. Dravid, C. A. Mirkin, *Adv. Mater.* **2002**, *14*, 231.
[100] R. D. Piner, J. Zhu, F. Xu, S. Hong, C. A. Mirkin, *Science* **1999**, *283*, 661.
[101] S. Hong, C. A. Mirkin, *Science* **2000**, *288*, 1808.
[102] K.-B. Lee, S.-J. Park, C. A. Mirkin, J. C. Smith, M. Mrksich, *Science* **2002**, *295*, 1702.
[103] C. A. Mirkin, R. L. Letsinger, R. C. Mucic, J. J. Storhoff, *Nature* **1996**, *382*, 607.
[104] C. A. Mirkin, *Inorg. Chem.* **2000**, *39*, 2258.
[105] S.-J. Park, T. A. Taton, C. A. Mirkin, *Science* **2002**, *295*, 1503.
[106] J. Haus, *J. Mod. Opt.* **1994**, *41*.
[107] K. Busch, S. John, *Phys. Rev. E* **1998**, *58*, 3896.
[108] K. Busch, S. John, *Phys. Rev. Lett.* **1999**, *83*, 967.
[109] P. Jiang, J. F. Bertone, K. S. Hwang, V. L. Colvin, *Chem. Mater.* **1999**, *11*, 2132.
[110] H. W. Deckmann, J. H. Dunsmuir, *Appl. Phys. Lett.* **1982**, *41*, 377.
[111] S. H. Park, Y. Xia, *Adv. Mater.* **1998**, *10*, 1045.
[112] P. C. Ohara, D. V. Leff, J. R. Heath, W. M. Gelbart, *Phys. Rev. Lett.* **1995**, *75*, 3466.
[113] A. S. Dimitrov, K. Nagayama, *Langmuir* **1996**, *12*, 1303.
[114] Y. A. Vlasov, X.-Z. Bo, J. C. Sturm, D. J. Norris, *Nature* **2001**, *414*, 289.
[115] A. van Blaaderen, R. Ruel, P. Wiltzius, *Nature* **1997**, *385*, 321.
[116] L. Ramos, T. C. Lubensky, N. Dan, P. Nelson, D. A. Weitz, *Science* **1999**, *286*, 2325.
[117] Y. Xia, B. Gates, Y. Yin, Y. Lu, *Adv. Mater.* **2000**, *12*, 693.
[118] O. D. Velev, P. M. Tessier, A. M. Lenhoff, E. W. Kaler, *Nature* **1999**, *401*, 548.
[119] J. E. G. J. Wijnhoven, W. L. Vos, *Science* **1998**, *281*, 802.
[120] G. Subramania, K. Constant, R. Biswas, M. M. Sigalas, K.-M. Ho, *Appl. Phys. Lett.* **1999**, *74*, 3933.
[121] P. Jiang, J. Cizeron, J. F. Bertone, V. L. Colvin, *J. Am. Chem. Soc.* **1999**, *121*, 7957.
[122] P. Jiang, J. F. Bertone, V. L. Colvin, *Science* **2001**, *291*, 453.
[123] S. A. Johnson, P. J. Ollivier, T. E. Mallouk, *Science* **1999**, *283*, 963.
[124] W. Lee, S. A. Pruzinsky, P. V. Braun, *Adv. Mater.* **2002**, *14*, 271.
[125] J. M. Weissman, H. B. Sunkara, A. S. Tse, S. A. Asher, *Science* **1996**, *274*, 959.
[126] Y. Kojima, A. Usuki, M. Kawasumi, A. Okada, T. Kurachi, O. Kamigaito, K. Kaji, *J. Polym. Sci. Polym. Phys. Ed.* **1994**, *32*, 625.
[127] Y. Kojima, A. Usuki, M. Kawasumi, A. Okada, T. Kurachi, O. Kamigaito, K. Kaji, *J. Polym. Sci. Polym. Phys. Ed.* **1995**, *33*, 1039.
[128] E. P. Giannelis, *Adv. Mater.* **1996**, *8*, 29.
[129] A. C. Balazs, C. Singh, E. Zhulina, Y. Lyatskaya, *Acc. Chem. Res.* **1999**, *32*, 651.
[130] E. P. Giannelis, R. Krishnamoorti, E. Manias, *Adv. Polym. Sci.* **1999**, *138*, 108.
[131] P. C. LeBaron, Z. Wang, T. J. Pinnavaia, *Appl. Clay Sci.* **1999**, *15*, 11.
[132] *Polymer-Clay Nanocomposites* (Eds.: T. J. Pinnavaia, G. W. Beall), Wiley, Chichester, **2000**.
[133] *Polymer Nanocomposites: Synthesis, Characterization and Modeling* (Eds.: R. Krishnamoorti, R. A. Vaia), American Chemical Society, Washington, DC, **2001**.
[134] "High IV Polyester Compositions Containing Platelet Particles": J. C. Matayabas, S. C. Turner, B. J. Sublett, G. W. Connell, J. W. Gilmer, R. B. Barbee, US Patent 6,084,019 **2000**.
[135] J.-C. P. Gabriel, P. Davidson, *Adv. Mater.* **2000**, *12*, 9.
[136] O. Pelletier, C. Bourgaux, O. Diat, P. Davidson, J. Livage, *Eur. Phys. J. E* **2000**, *2*, 191.
[137] S. Lamarque-Forget, O. Pelletier, I. Dozov, P. Davidson, P. Martinot-Lagarde, J. Livage, *Adv. Mater.* **2000**, *12*, 1267.
[138] J.-C. P. Gabriel, F. Camerel, B. Lemaire, H. Desvaux, P. Davidson, P. Batail, *Nature* **2001**, *413*, 504.
[139] Y. Maeda, S. Hachisu, *Colloids Surf.* **1983**, *6*, 1.
[140] A. B. D. Brown, S. M. Clarke, A. R. Rennie, *Langmuir* **1998**, *14*, 3129.
[141] A. B. D. Brown, C. Ferrero, T. Narayanan, A. R. Rennie, *Eur. Phys. J. B* **1999**, *11*, 481.
[142] F. M. van der Kooij, K. Kassapidou, H. N. W. Lekkerkerker, *Nature* **2000**, *406*, 868.
[143] M. Bates, D. Frenkel, *J. Chem. Phys.* **1998**, *109*, 6193.
[144] I. W. Hamley, V. Castelletto, J. Fundin, M. Crothers, D. Attwood, I. Talmon, **2002**, unpublished results.
[145] B. Wowk in *Nanotechnology* (Ed.: B. C. Crandall), MIT Press, Cambridge, MA, **1996**.
[146] T. Douglas, M. Young, *Nature* **1998**, *393*, 152.
[147] T. Douglas, M. Young, *Adv. Mater.* **1999**, *11*, 679.
[148] D. Ferber, *Science* **2001**, *294*, 1638.
[149] T. Segura, L. D. Shea, *Annu. Rev. Mater. Res.* **2001**, *31*, 25.
[150] S. Afione, R. Kotin, *Chem. Ind.* **2002**, *4*, 16.

 © 2003 Wiley-VCH Verlag GmbH & Co. KGaA, Weinheim

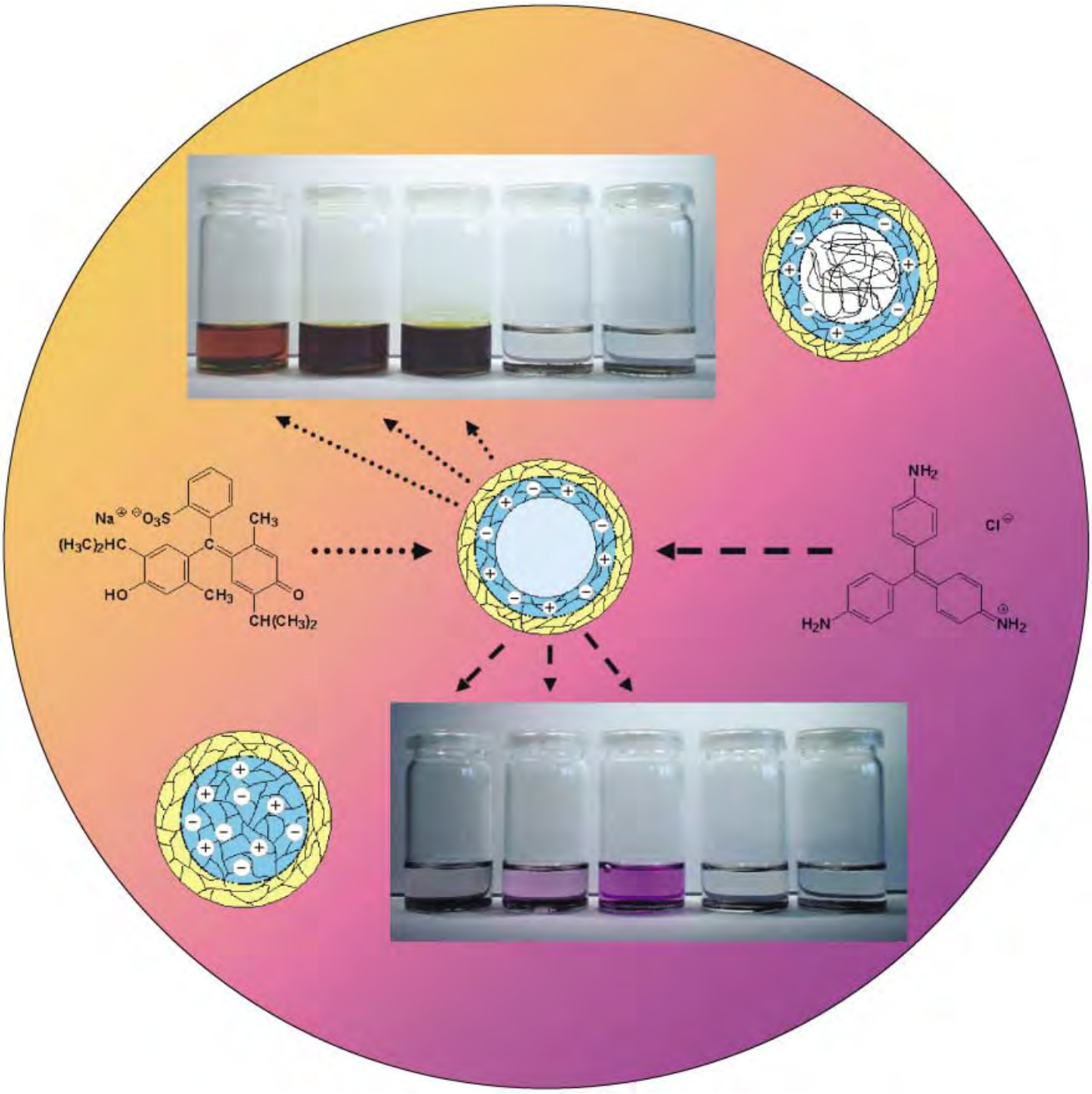
[151] M. A. Woolfert, V. Schacht, V. Toncheva, K. Ulbrich, O. Nazarova, L. W. Seymour, *Hum. Gene Ther.* **1996**, *7*, 2123.
[152] C. W. Pouton, P. Lucas, B. J. Thomas, A. N. Uduchi, D. A. Milroy, S. H. Moss, *J. Controlled Release* **1998**, *53*, 289.
[153] H. Pollard, J.-S. Remy, G. Loussouarn, S. Demolombe, J.-P. Behr, D. Escande, *J. Biol. Chem.* **1998**, *273*, 7507.
[154] H.-K. Nguyen, P. Lemieux, S. V. Vinogradov, C. L. Gebhart, N. Guérin, G. Paradis, T. K. Bronich, V. Y. Alakhov, A. V. Kabanov, *Gene Ther.* **2000**, *7*, 126.
[155] C. L. Gebhart, A. V. Kabanov, *J. Controlled Release* **2001**, *73*, 401.
[156] P. Badnyopadhyay, X. Ma, C. Linehan-Stieers, B. T. Kren, C. J. Steer, *J. Biol. Chem.* **1999**, *274*, 10163.
[157] E. Dodds, T. A. Piper, S. J. Murphy, G. Dickson, *J. Neurochem.* **1999**, *72*, 2105.
[158] O. Boussif, F. Lezoualc'h, M. A. Zanta, M. D. Mergny, D. Scherman, B. Demeneix, J. P. Behr, *Proc. Natl. Acad. Sci. USA* **1995**, *92*, 7297.
[159] A. R. Klemm, D. Young, J. B. Lloyd, *Biochem. Pharmacol.* **1998**, *56*, 41.
[160] W. T. Godbey, K. K. Wu, A. G. Mikos, *Proc. Natl. Acad. Sci. USA* **1999**, *96*, 5177.
[161] C. Horbinski, M. K. Stachowiak, D. Higgins, S. G. Finnegan, *BMC Neurosci.* **2001**, *2*, 2.
[162] S. Mann, *Biomineralization. Principles and Concepts in Bioinorganic Materials Chemistry*, Oxford University Press, Oxford, **2001**.
[163] "Magnetizable Device": E. L. Mayes, M. V. Tyler, International Patent Application WO 98/22942 **1998**.
[164] www.nanomagnetics.com, **2002**.
[165] F. C. Meldrum, B. R. Heywood, S. Mann, *Science* **1992**, *257*, 522.
[166] "Protein Magnetics": S. Mann, US patent 5,941,219 **1996**.
[167] K. K. W. Wong, T. Douglas, S. Gider, D. D. Awschalom, S. Mann, *Chem. Mater.* **1998**, *10*, 279.
[168] R. Jin, Y. Cao, C. A. Mirkin, K. L. Kelly, G. C. Schatz, J. G. Zheng, *Science* **2001**, *294*, 1901.
[169] S. Mann, *Angew. Chem.* **2000**, *112*, 3532; *Angew. Chem. Int. Ed.* **2000**, *39*, 3392.
[170] L. Manna, E. C. Scher, A. P. Alivisatos, *J. Am. Chem. Soc.* **2000**, *122*, 12700.
[171] V. F. Puntes, K. M. Krishnan, A. P. Alivisatos, *Science* **2001**, *291*, 2115.
[172] L. Zhang, A. Eisenberg, *Science* **1995**, *268*, 1728.
[173] L. Zhang, A. Eisenberg, *J. Am. Chem. Soc.* **1996**, *118*, 3168.
[174] L. Zhang, K. Yu, A. Eisenberg, *Science* **1996**, *272*, 1777.
[175] S. I. Stupp, V. LeBonheur, K. Walker, L. S. Li, K. E. Huggins, M. Keser, A. Amstutz, *Science* **1997**, *276*, 384.
[176] H.-A. Klok, S. Lecommandoux, *Adv. Mater.* **2001**, *13*, 1217.
[177] M. E. Raimondi, J. M. Seddon, *Liq. Cryst.* **1999**, *26*, 305.
[178] C. T. Kresge, M. E. Leonowicz, W. J. Roth, J. C. Vartuli, J. S. Beck, *Nature* **1992**, *359*, 710.
[179] J. S. Beck, J. C. Vartuli, W. J. Roth, M. E. Leonowicz, C. T. Kresge, K. D. Schmitt, C. T. Chu, D. H. Olson, E. W. Sheppard, S. B. McCullen, J. B. Higgins, J. L. Schlenker, *J. Am. Chem. Soc.* **1992**, *114*, 10834.
[180] Q. S. Huo, D. I. Margolese, U. Ciesla, P. Y. Feng, T. E. Gier, P. Sieger, R. Leon, P. M. Petroff, F. Schuth, G. D. Stucky, *Nature* **1994**, *368*, 317.
[181] A. Firouzi, D. Kumar, L. M. Bull, T. Besier, P. Sieger, Q. Huo, S. A. Walker, J. A. Zasadzinski, C. Glinka, J. Nicol, D. Margolese, G. D. Stucky, B. F. Chmelka, *Science* **1995**, *267*, 1138.
[182] S. A. Bagshaw, E. Prouzet, T. J. Pinnavaia, *Science* **1995**, *269*, 1242.
[183] G. S. Attard, P. N. Bartlett, N. R. B. Coleman, J. M. Elliott, J. R. Owen, J. H. Wang, *Science* **1997**, *278*, 838.
[184] D. Zhao, J. Feng, Q. Huo, N. Melosh, G. H. Fredrickson, B. F. Chmelka, G. D. Stucky, *Science* **1998**, *279*, 548.
[185] K. M. Ryan, N. R. B. Coleman, D. M. Lyons, J. P. Hanrahan, T. R. Spalding, M. A. Morris, D. C. Steytler, R. K. Heenan, J. D. Holmes, *Langmuir* **2002**, *18*, 4996.
[186] S. Mann in *Comprehensive Supramolecular Chemistry, Vol. 9* (Eds.: J.-P. Sauvage, M. W. Hosseini), Pergamon, Oxford, **1996**, p. 529.
[187] E. Dujardin, S. Mann, *Adv. Mater.* **2002**, *14*, 775.
[188] S. Rimmer in *Emerging Themes in Polymer Science* (Ed.: A. J. Ryan), Royal Society of Chemistry, Cambridge, **2001**.
[189] S. Oliver, A. Kuperman, N. Coombs, A. Lough, G. A. Ozin, *Nature* **1995**, *378*, 47.
[190] S. Oliver, G. A. Ozin, L. A. Ozin, *Adv. Mater.* **1995**, *7*, 948.
[191] M. Park, C. Harrison, P. M. Chaikin, R. A. Register, D. H. Adamson, *Science* **1997**, *276*, 1401.
[192] C. Harrison, M. Park, P. M. Chaikin, R. A. Register, D. H. Adamson, *J. Vac. Sci. Technol. B* **1998**, *16*, 544.
[193] R. R. Li, P. D. Dapkus, M. E. Thompson, W. G. Jeong, C. Harrison, P. M. Chaikin, R. A. Register, D. H. Adamson, *Appl. Phys. Lett.* **2000**, *76*, 1689.
[194] T. Thurn-Albrecht, J. Schotter, G. A. Kästle, N. Emley, T. Shibauchi, L. Krusin-Elbaum, K. Guarini, C. T. Black, M. T. Tuominen, T. P. Russell, *Science* **2000**, *290*, 2126.
[195] J. Y. Cheng, C. A. Ross, V. Z.-H. Chan, E. L. Thomas, R. G. H. Lammertink, G. J. Vancso, *Adv. Mater.* **2001**, *13*, 1174.
[196] M. Iijima, Y. Nagasaki, T. Okano, M. Kato, K. Kataoka, *Macromolecules* **1999**, *32*, 1140.
[197] K. Emoto, Y. Nagasaki, K. Kataoka, *Langmuir* **1999**, *15*, 5212.
[198] H. Otsuka, Y. Nagasaki, K. Kataoka, *Curr. Opin. Colloid Interface Sci.* **2001**, *6*, 3.
[199] S. Stewart, G. Liu, *Chem. Mater.* **1999**, *11*, 1048.
[200] H. Aranda-Espinoza, H. Bermudez, F. S. Bates, D. E. Discher, *Phys. Rev. Lett.* **2001**, *87*, 208301.
[201] R. Dimova, U. Seifert, B. Pouligny, S. Förster, H.-G. Döbereiner, *Eur. Phys. J. E* **2002**, *7*, 241.
[202] K.-H. Frömming in *Comprehensive Supramolecular Chemistry, Vol. 10* (Ed.: D. N. Reinhoudt), Pergamon, Oxford, **1996**, p. 445.
[203] T. Goldacker, V. Abetz, R. Stadler, I. Erukhimovich, L. Leibler, *Nature* **1999**, *398*, 137.
[204] P. Kofinas, University of Maryland, **2002**, personal communication.
[205] A. Urbas, Y. Fink, E. L. Thomas, *Macromolecules* **1999**, *32*, 4748.
[206] Y. Fink, A. M. Urbas, M. G. Bawendi, J. D. Joannopoulos, E. L. Thomas, *J. Lightwave Technol.* **1999**, *17*, 1963.
[207] J. T. Chen, E. L. Thomas, C. G. Zimba, J. F. Rabolt, *Macromolecules* **1995**, *28*, 5811.
[208] A. C. Edrington, A. M. Urbas, P. DeRege, C. X. Chen, T. M. Swager, N. Hadjichristidis, M. Xenidou, L. J. Fetters, J. D. Joannopoulos, Y. Fink, E. L. Thomas, *Adv. Mater.* **2001**, *13*, 421.
[209] J. T. Chen, E. L. Thomas, C. K. Ober, G.-P. Mao, *Science* **1996**, *273*, 343.
[210] J. Ruokolainen, R. Mäkinen, M. Torkkeli, T. Mäkelä, R. Serimaa, G. ten Brinke, O. Ikkala, *Science* **1998**, *280*, 557.
[211] J. Ruokolainen, M. Saariaho, O. Ikkala, G. ten Brinke, E. L. Thomas, M. Torkkeli, R. Serimaa, *Macromolecules* **1999**, *32*, 1151.
[212] I. W. Hamley, *The Physics of Block Copolymers*, Oxford University Press, Oxford, **1998**.
[213] V. Abetz in *Encyclopedia of Polymer Science and Technology* (Ed.: J. E. Mark), Wiley, New York, **2002**.
[214] F. S. Bates, G. H. Fredrickson, *Phys. Today* **1999**, *52*(2), 32.
[215] U. Breiner, U. Krappe, V. Abetz, R. Stadler, *Macromol. Chem. Phys.* **1997**, *198*, 1051.

 © 2003 Wiley-VCH Verlag GmbH & Co. KGaA, Weinheim

[216] R. Stadler, C. Auschra, J. Beckmann, U. Krappe, I. Voigt-Martin, L. Leibler, *Macromolecules* **1995**, *28*, 3080.
[217] P. M. Lipic, F. S. Bates, M. W. Matsen, *J. Polym. Sci. Part B* **2001**, *37*, 2229.
[218] U. Breiner, U. Krappe, E. L. Thomas, R. Stadler, *Macromolecules* **1998**, *31*, 135.
[219] Y. Bohbot-Raviv, Z.-G. Wang, *Phys. Rev. Lett.* **2000**, *85*, 3428.
[220] A. Böker, A. H. E. Müller, G. Krausch, *Macromolecules* **2001**, *34*, 7477.
[221] N. Rehse, A. Knoll, M. Konrad, R. Magerle, G. Krausch, *Phys. Rev. Lett.* **2001**, *87*, 035505.
[222] R. Penterman, S. I. Klink, H. de Koning, G. Nisato, D. J. Broer, *Nature* **2002**, *417*, 55.
[223] J. Yamamoto, H. Tanaka, *Nature* **2001**, *409*, 321.
[224] S. P. Meeker, W. C. K. Poon, J. Crain, E. M. Terentjev, *Phys. Rev. E* **2000**, *61*, 6083.
[225] N. Boden, R. J. Bushby, J. Clements, B. Movaghar, K. J. Donovan, T. Kreouzis, *Phys. Rev. B* **1995**, *52*, 13274.
[226] N. Boden, R. J. Bushby, J. Clements, K. J. Donovan, B. Movaghar, *Phys. Rev. B* **1998**, *58*, 3063.
[227] N. Boden, R. J. Bushby, J. Clements, B. Movaghar, *J. Mater. Chem.* **1999**, *9*, 2081.



Communications



The loading of amphiphilic poly(organosiloxane) nanoparticles with hydrophilic dyes in organic solvents depends inter alia on the construction of the nanoparticles (core–shell, hollow spheres), on the amphiphilicity, is adjustable by synthesis, and on the method of the phase transfer. For more information see the Communication by M. Maskos et al. on the following pages.

DOI: 10.1002/anie.200250288
© 2003 Wiley-VCH Verlag GmbH & Co. KGaA, Weinheim

Dye Incorporation in Polymers

Dye Loading of Amphiphilic Poly(organosiloxane) Nanoparticles**

*Nadja Jungmann, Manfred Schmidt, Jochen Ebenhoch, Johann Weis, and Michael Maskos**

Interest in amphiphilic core–shell nanoparticles is increasing continually and their use for possible applications in which, for example, they are loaded with small molecules or even proteins is under discussion.[1–4] Typical examples are dendrimers,[5] cyclodextrins,[6] star-shaped block copolymers,[7] and cross-linked block copolymer micelles.[8] The covalent construction of these macromolecular-based systems inhibits the structural self-disintegration of the nanoparticles. However, the synthesis of these structures is usually time-consuming, and, in the case of dendrimers and cyclodextrins, their size is limited to a few nanometers. Non-cross-linked block copolymer micelles,[9] polyelectrolyte capsules,[10] and liposomes[11] are potential and partially evaluated capsule systems, which form from their constituent subunits as a result of specific interactions. Unlike the covalent systems they have the undesirable tendency to break down under certain circumstances through changes in the external conditions. These structures are usually of 50–100 nm up to micrometers in size. In the case of liposomes, in particular, the amphiphilicity of the structures created is determined by the starting components used and normally cannot be varied, or only to a limited extent.

Unlike the described nanoparticles the novel amphiphilic poly(organosiloxane) nanoparticles are very versatile with respect to the variation of the many parameters that affect loading, and thus allow systematic investigation. In particular, it was possible to prepare different core–shell arrangements. Figure 1 illustrates this schematically for the spherical nanoparticles we have investigated.

The nanoparticles were prepared by the hydrolysis and condensation of dialkoxydialkyl- and trialkoxyalkylsilanes in aqueous dispersion. After surface modification they may be re-dispersed in organic solvents such as toluene.[12] Core–shell arrangements are formed through sequential monomer addition. Quaternary ammonium groups in the siloxane network provide the hydrophilic character of the core (QC*x*-S) or the inner shell (QC-S*x*-S, QS*x*-S). In the sample categorization, *x* correlates with the number of quaternary ammonium groups in the network. The outer hydrophobic shell ensures the solubility in organic solvents. In addition to the comparatively simply constructed core–shell nanoparticles more complex spherical arrangements can also be built up by the synthesis used. On the one hand, it is possible in this way to prepare a flexible core of siloxane chains (QC-S*x*-S), in which the chains are bonded chemically to the surrounding shell. On the other hand, nonbonded chains can be removed from the core, to leave hollow spheres (QS*x*-S). A prerequisite for this is an adequate pore size in the surrounding shell network, which can also be adjusted during synthesis.[13] These chemically similar but differently constructed amphiphilic nanoparticles are used to investigate the loading with hydrophilic dyes as low-molecular-weight model compounds. The difference in construction permits the investigation of the dependency of dye uptake on the respective arrangement. Furthermore, as previously described, the amphiphilicity of the nanoparticles can also be adjusted during synthesis by altering the number of quaternary ammonium groups, which allows the investigation of the nature of the interaction between substrate and nanoparticle.

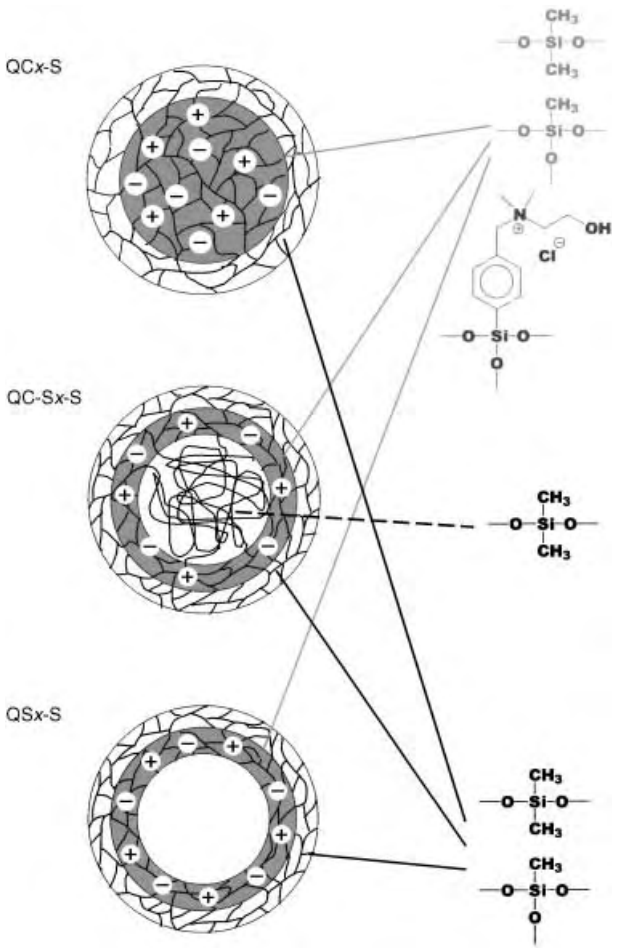


Figure 1. Schematic representation of the amphiphilic poly(organosiloxane) nanoparticles (see text for details). Also shown are the basic building blocks of the core and the shells.

Dye loading of the amphiphilic poly(organosiloxane) nanoparticles is carried out by solid/liquid or liquid/liquid

[*] Dr. M. Maskos, Dipl.-Chem. N. Jungmann, Prof. Dr. M. Schmidt
Institut für Physikalische Chemie
Universität Mainz
Welder-Weg 11, 55099 Mainz (Germany)
Fax: (+49) 6131/392-2970
E-mail: maskos@mail.uni-mainz.de
Dr. J. Ebenhoch, Dr. J. Weis
Wacker-Chemie GmbH
84480 Burghausen (Germany)

[**] This work was supported by the BMBF (FKZ 03C0288A8), the Fonds der Chemischen Industrie, and Wacker-Chemie GmbH (Germany).

 © 2003 Wiley-VCH Verlag GmbH & Co. KGaA, Weinheim DOI: 10.1002/anie.200250288

phase transfer. In the solid/liquid phase transfer the dye is added as a solid to the dispersion of the nanoparticles in toluene. In liquid/liquid phase transfer an aqueous solution of the dye is covered with a layer of the nanoparticle dispersion. Diffusion of the dye into the nanoparticle then takes place. The first visual indication of successful loading is the coloration of the toluene phase. The schematic representations of the respective phase transfer and photographs of a number of experiments are illustrated in Figure 2.

It can be readily seen with the naked eye that the loading with both basic parafuchsin, a cationic dye, and thymol blue, an anionic dye, is dependent on the number of quaternary ammonium groups, and grows with increasing number. In contrast, the control experiments with nanoparticles that contain no quaternary ammonium groups and with pure toluene show no coloration. Encapsulation occurs primarily independently of the choice of phase transfer. In a comparable manner both the anionic dyes calmagite and brilliant sulfaflavin as well as the anionically and cationically charged dye sulforhodamine B and the pyrene dye pyrene-1-sulfonic acid are also taken up into the nanoparticles successfully.

Dye uptake is also evident in the UV/Vis spectrum. A number of representative spectra of the toluene phases after loading with dye are illustrated in Figure 3. The spectra were measured two weeks after dye addition since prolongation of the experiments led to no change in dye uptake, regardless of the method of phase transfer.



Figure 2. Solid/liquid (A) and liquid/liquid phase transfer (B) for loading the amphiphilic poly(organosiloxane) nanoparticles (Q spheres) with the respective dye. The identical experiments carried out with poly(organosiloxane) nanoparticles which contain no quaternary ammonium groups in the interior (C12-S) and with pure toluene are shown in the photographs for comparison. Both show no coloration.

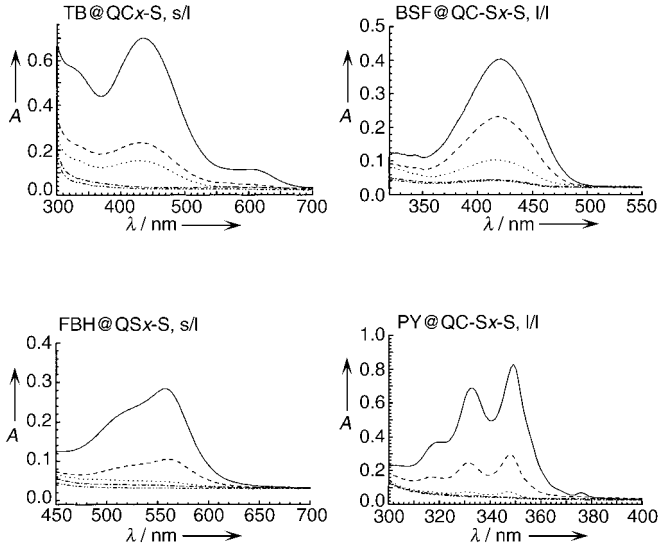


Figure 3. UV/Vis absorption spectra of the respective toluene phase after loading with dye. —— $x=12$; -----: $x=8$; •••••: $x=4$; —•—•: C12-S; —··—: toluene. s/l = solid/liquid phase transfer, l/l = liquid/liquid phase transfer. dyes: BSF = brilliant sulfaflavin, FBH = basic parafuchsin, PY = pyrene-1-sulfonic acid, TB = thymol blue.

For all the dyes and nanoparticles used loading of the nanoparticles with the respective dye by both solid/liquid and liquid/liquid phase transfer increases with the number of quaternary ammonium groups in the nanoparticle. The corresponding comparison of the two methods of phase transfer shows, however, that lower intensities are observed by UV/Vis spectroscopy for solid/liquid phase transfer. In contrast, the control experiments show almost no absorption in the range of the respective coloration in all cases.

It may be noted at this juncture that ionic interactions between the positively charged ammonium groups in the nanoparticles and the negatively charged groups of the dye are not solely critical for the loading of nanoparticles since the cationic, basic parafuchsin is taken up in addition to the anionic dyes.

Quantitative analyses of the UV/Vis absorption spectra were employed to draw more detailed conclusions. However, because of the poor solubility of the dyes in toluene this is not possible in the organic solvent since no calibration can be carried out. Instead, the loading of the nanoparticles with the respective dye was determined indirectly by the reduction in the absorption of the aqueous phase after liquid/liquid phase transfer. The results are collated in Table 1.

 © 2003 Wiley-VCH Verlag GmbH & Co. KGaA, Weinheim

Table 1: Quantification of the dye uptake by liquid/liquid phase transfer into the amphiphilic poly(organosiloxane) nanoparticles by UV/Vis spectroscopy of the aqueous phase.[a]

Sample	n_N[b]	BSF		CM		FBH		SRB		TB	
		n_{dye}[c]	n_{dye}/n_N	n_{dye}	n_{dye}/n_N	n_{dye}	n_{dye}/n_N	n_{dye}	n_{dye}/n_N	n_{dye}	n_{dye}/n_N
QC4-S	0.7	1.4	2.0	6.4	9.1	0.8	1.1	0.3	0.4	6.3	9.0
QC8-S	1.1	2.9	2.6	7.3	6.6	1.1	1.0	0.3	0.3	8.8	8.0
QC12-S	4.4	9.0	2.0	8.1	1.8	3.8	0.9	4.3	1.0	9.6	2.2
QC-S4-S	1.1	–	–	6.7	6.1	–	–	–	–	4.7	4.3
QC-S8-S	1.9	1.4	0.7	8.4	4.4	–	–	–	–	6.3	3.3
QC-S12-S	5.9	6.4	1.1	10.9	1.8	2.5	0.4	4.3	0.7	9.4	1.6
QS4-S	2.2	2.2	1.0	5.9	2.7	-	-	0.5	0.2	4.9	2.2
QS8-S	4.8	5.3	1.1	–	–	1.0	0.2	–	–	2.5	0.5
QS12-S	6.1	5.5	0.9	13.7	2.2	1.6	0.3	2.9	0.5	6.5	1.1

[a] Concentration of the nanoparticle in toluene (5 mL): $c = 2.0\ g\,L^{-1}$, concentration of the dye solutions (in each case 5 mL): $c_{BSF} = 2.26\ g\,L^{-1}$, $c_{CM} = 4.92\ g\,L^{-1}$, $c_{FBH} = 1.30\ g\,L^{-1}$, $c_{SRB} = 3.60\ g\,L^{-1}$, $c_{TB} = 5.58\ g\,L^{-1}$. BSF = brilliant sulfaflavin, CM = calmagite, FBH = basic parafuchsin, SRB = sulforhodamine B, TB = thymol blue, sodium salt. [b] n_N = amount of quaternary ammonium ions in μmol per 10 mg of nanoparticle.[12] [c] n_{dye} = amount of dye in μmol per 10 mg of nanoparticle. No data: nanoparticles partially precipitated at the interface.

To achieve a high as possible loading in these experiments the aqueous phase contained significantly more dye than could be taken up into the nanoparticles in total. The loading of the amphiphilic nanoparticles with pyrene-1-sulfonic acid could not be determined quantitatively by UV/Vis spectroscopy of the aqueous phase, however, since the reduction in absorption compared with the starting concentration was too small and consequently the changes lay within the range of measurement error. The amount of the respective dye taken up was determined by prior calibration.

If the different dyes are compared it emerges that the two anionic dyes calgamite and thymol blue have the highest uptake values, followed by brilliant sulfaflavin. In contrast, much lower values are obtained for basic parafuchsin and sulforhodamine B. Especially remarkable is the loading of QS12-S with calgamite. In this case it is possible to incorporate 50% of the dye into the spheres relative to the weight of nanoparticles used. If merely the aforementioned specific ionic interactions were responsible for the loading this should be directly reflected in the relationship between the number of dyes incorporated (n_{dye}) and the ammonium groups present in the nanoparticles (n_N). The respective quotient n_{dye}/n_N, for which a theoretical ratio of $n_{dye}/n_N = 1$ would be expected, is also given for the corresponding experiments in Table 1. For calmagite and thymol blue the quotient lies significantly above the theoretical value. In contrast, the corresponding quotients n_{dye}/n_N for the dye brilliant sulfaflavin lie close to the expected theoretical value. For sulforhodamine B lower values are obtained, and for basic parafuchsin unexpectedly high values since it is a cationic dye which should actually exhibit no attractive ionic interactions. The loading of the nanoparticles with further cationic dyes is currently under investigation.

It may be concluded from these results that in addition to ionic interactions the local polarity within the nanoparticles is of pivotal importance for loading. The hollow sphere systems QS*x*-S are especially suitable for loading with calmagite, whereas the other dyes prefer QC*x*-S nanoparticles with their more homogeneous construction. The loading into QC-Sx-S, which contain the poly(dimethylsiloxane) chains in their core occupies a middle position in all cases.

The size of the dye relative to the mesh width of the siloxane network of the nanoparticles is also of considerable importance for loading since the dye must diffuse through the outer shell in every case.[13] The dyes used do not differ significantly from each other in respect of their size. Only for sulforhodamine B, the most sterically demanding of the dyes investigated, is the mesh width of the nanonetwork presumably not large enough to achieve a high degree of loading. Control experiments with sterically demanding dyes such as reactive red 120, with which no coloration of the dispersed nanoparticles in toluene occurs, confirm this observation.

If the loading values at identical particle architecture are compared, an increase in the loading with increasing number of quaternary ammonium groups is revealed for all dyes. At the same time the quotient n_{dye}/n_N usually falls. The increase in the number of quaternary ammonium groups effects a suppression of the influence of the local network polarity in favor of the ionic interaction. Unfortunately, the expected loading saturation as a function of the number of quaternary ammonium groups could not be achieved since the increase in the proportion of quaternary ammonium groups leads to irreversible aggregation of the growing nanoparticles during synthesis.

That specific interactions are vital for loading can be inferred from two further observations. On the one hand, during loading of the nanoparticles with brilliant sulfaflavin, calmagite, and thymol blue by liquid/liquid phase transfer a deficiency of dye (relative to the maximum amount which can be incorporated) leads to complete decoloration of the aqueous phase. On the other hand, a comparison of the methods of phase transfer reveals that less dye is normally taken up by solid/liquid phase transfer than by liquid/liquid phase transfer. This suggests an effect of the water present on the local polarity in the nanoparticles. The interactions of, for example, calmagite incorporated into QS12-S are so strong that the dye could not be removed from the nanoparicle even by repeated ultrafiltration in THF, a good solvent for calmagite. This behavior and the pronounced solvatochromic shift in the absorption spectrum of a number of dyes after encapsulation are the subject matter of on-going research.

In summary, it can be demonstrated that it is possible to incorporate hydrophilic dyes in the interior of amphiphilic poly(organosiloxane) nanoparticles. In addition to ionic interactions the local polarity of the siloxane network, the size of the dye in relation to the mesh width of the network, and the method of phase transfer are critical for the extent of loading. By variation of these parameters up to 50% dye relative to the dead weight of the nanoparticles can be encapsulated in the siloxane network.

 © 2003 Wiley-VCH Verlag GmbH & Co. KGaA, Weinheim

Experimental Section

The synthesis of amphiphilic nanoparticles is described in detail in reference [12]. The preparation is based on the hydrolysis and cocondensation of dialkoxydialkylsilane (D) and trialkoxyalkylsilane (T) in aqueous dispersion by sequential addition of monomer mixtures in the presence of a surfactant. Saturation of reactive silanol or silanolate groups prevents the aggregation of the particles and permits the transfer into toluene as re-dispersable nanoparticles. The use of chloromethylphenyltrimethoxysilane (ClBz-T) in the core (C) or in the inner shell (S) leads after polymer-analoguous quaternization (Q) with dimethylaminoethanol to the amphiphilic poly(organosiloxane) nanoparticles. The mass fraction of ClBz-T relative to the total amount of monomer is designated by an *x* in the sample code. Thus QC4-S, for example, is a nanoparticle with a fraction of 4% ClBz-T in the core, with QC-S8-S the nanoparticles have a fraction of 8% ClBz-T in the inner shell. With QC-S*x*-S and QS*x*-S the D units are first condensed to chains, which in the case of QS*x*-S are prevented from reacting with subsequently added monomer by the addition of monoalkoxysilanes. By the use of mixtures of D and T in the construction of the shells these chains can diffuse out of the interior after transfer into toluene and are removed by ultrafiltration. In QC-S*x*-S the chains remain in the interior since they are bonded covalently to the surrounding shell.

Solid/liquid phase transfer: The dye (10 mg) was added to a dispersion of the amphiphilic poly(organosiloxane) nanoparticles (10 mg) in toluene (5 mL). After two weeks the UV/Vis spectra were recorded with a Lambda 17 spectrophotometer (Perkin Elmer). Liquid/liquid phase transfer: The solution of the respective dye in water (5 mL; concentration see Table 1) was carefully covered with a dispersion of the amphiphilic nanoparticles (10 mg) in toluene (5 mL). After two weeks the UV/Vis spectra of the toluene and aqueous phases were recorded. The reduction in the absorption of the aqueous phase was determined quantitatively by comparison with a calibration curve of the dye in water.

Received: October 2, 2002 [Z50288]

Keywords: chromophores · colloids · materials science · nanostructures · polymers

[1] D. Horn, J. Rieger, *Angew. Chem.* **2001**, *113*, 4460; *Angew. Chem. Int. Ed.* **2001**, *40*, 4330.
[2] S. J. Risch, *ACS Symp. Ser.* **1995**, *590*, 2.
[3] P. Couvreur, C. Dubernet, F. Puisieux, *Eur. J. Pharm. Biopharm.* **1995**, *41*, 2.
[4] J. G. Weers, *Curr. Opin. Colloid Interface Sci.* **1998**, *3*, 540.
[5] A. Manna, T. Imae, K. Aoi, M. Okada, T. Yogo, *Chem. Mater.* **2001**, *13*, 1674.
[6] E. Lemos-Senna, D. Wouessidjewe, D. Duchene, S. Lesieur, *Colloids Surf. B* **1998**, *10*, 291.
[7] K. F. Pistel, B. Bittner, H. Koll, G. Winter, T. Kissel, *J. Controlled Release* **1999**, *59*, 309.
[8] a) G. J. Liu, Z. Lu, F. Liu, *Polym. Prepr. Am. Chem. Soc. Div. Polym. Chem.* **2001**, *42*, 103; b) M. Maskos, J. R. Harris, *Macromol. Rapid Commun.* **2001**, *22*, 271; c) S. V. Solomatin, T. K. Bronich, V. A. Kabanov, A. Eisenberg, A. V. Kabanov, *Polym. Prepr. Am. Chem. Soc. Div. Polym. Chem.* **2001**, *42*, 107; d) W. Meier, *Chem. Soc. Rev.* **2000**, *29*, 295; e) H. M. Kao, R. D. O'Connor, A. K. Mehta, H. Y. Huang, B. Poliks, K. L. Wooley, J. Schaefer, *Macromolecules* **2001**, *34*, 544; f) T. Sanji, Y. Nakatsuka, S. Ohnishi, H. Sakurai, *Macromolecules* **2000**, *33*, 8524.
[9] C. Allen, A. Eisenberg, J. Mrsic, D. Maysinger, *Drug Delivery* **2000**, *7*, 139.
[10] a) X. Y. Shi, F. Caruso, *Langmuir* **2001**, *17*, 2036; b) O. P. Tiourina, A. A. Antipov, G. B. Sukhorukov, N. L. Larinova, H. Möhwald, *Macromol. Biosci.* **2001**, *1*, 209.
[11] C. Leonetti, A. Biroccio, B. Benassi, A. Stringaro, A. Stoppacciaro, S. C. Semple, G. Zupi, *Cancer Gene Ther.* **2001**, *8*, 459.
[12] N. Jungmann, M. Schmidt, M. Maskos, J. Weis, J. Ebenhoch, *Macromolecules* **2002**, *35*, 6851.
[13] a) C. Roos, M. Schmidt, J. Ebenhoch, F. Baumann, B. Deubzer, J. Weis, *Adv. Mater.* **1999**, *11*, 761; b) O. Emmerich, N. Hugenberg, M. Schmidt, S. Sheiko, F. Baumann, B. Deubzer, J. Weis, J. Ebenhoch, *Adv. Mater.* **1999**, *11*, 1299.

 © 2003 Wiley-VCH Verlag GmbH & Co. KGaA, Weinheim

Boron Aromatics

Dianions of Tetraboranes(4): Puckered Aromatic Four-Membered Rings and Their Reactions with Conservation of Aromaticity **

*Wahid Mesbah, Carsten Präsang, Matthias Hofmann, Gertraud Geiseler, Werner Massa, and Armin Berndt**

Dedicated to Professor Gernot Boche on the occasion of his 65th birthday

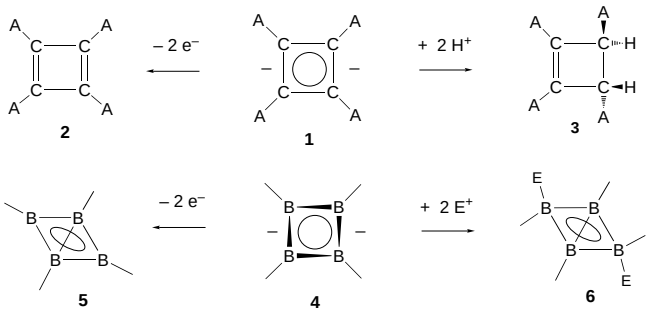
Sekiguchi et al. recently described the planar dianion **1**, a six-electron aromatic four-membered ring (Scheme 1).[1a] Upon two-electron oxidation, **1** is transformed into the *anti*aromatic compound **2**,[1b] and double protonation, which requires four electrons for bonding the two protons, produces the *non*-aromatic compound **3**.[1a] Thus, both reactions proceed with loss of aromaticity. Here we present the puckered dianions **4a** and **4b** (Scheme 2), aromatic two-electron four-membered rings of type **4**, the corresponding reactions of which result in compounds of types **5** and **6**, conserving the aromaticity.

Dianion **4a** is obtained by treating **5a**[2,3] with lithium in DME at 25 °C. Treatment with hexachloroethane quantitatively reoxidizes **4a** to **5a**, whereas the reaction of **4a** with Et_2NBCl_2 results in the formation of amino(triboryl)tetraborane(4) **5c**. Compound **4b**, which is obtained by the reaction of **5b**[4] with lithium in THF at −78 °C, is stable in solution below −30 °C; at higher temperatures a recently described[5] double aromatic B_3 ring is formed by migration of a trimethylsilyl

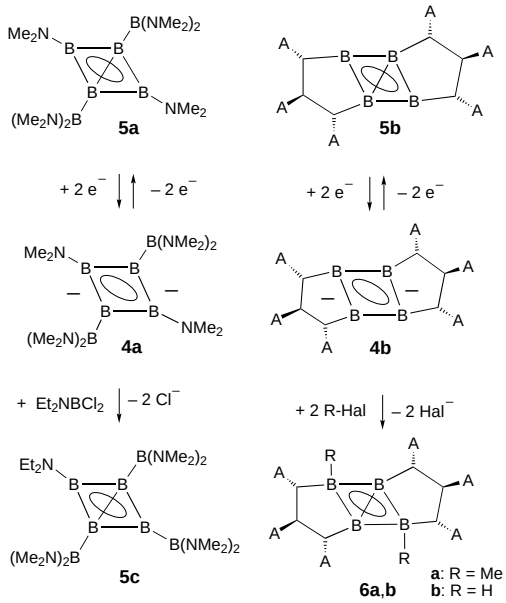
[*] Prof. Dr. A. Berndt, W. Mesbah, Dr. C. Präsang, G. Geiseler, Prof. Dr. W. Massa
Fachbereich Chemie
Universität Marburg
35032 Marburg (Germany)
Fax: (+49) 6421-282-8917
E-mail: berndt@chemie.uni-marburg.de
Dr. M. Hofmann
Anorganisch-Chemisches Institut
Universität Heidelberg
Im Neuenheimer Feld 270, 69120 Heidelberg (Germany)

[**] This work was supported by the Deutsche Forschungsgemeinschaft and the Fonds der Chemischen Industrie.

 DOI: 10.1002/anie.200250700 © 2003 Wiley-VCH Verlag GmbH & Co. KGaA, Weinheim



Scheme 1. Reactions of the four-membered aromatic dianions **1** and **4** with loss (**1**→**2** and **3**) and conservation (**4**→**5** and **6**) of aromaticity. Circles and ellipses symbolize the delocalized electrons in the aromatic compounds: six in **1**, two in **4**–**6**. Lines between the boron atoms of **5** and **6** represent connectivities; only six and four electrons, respectively, are available for the σ frameworks of **5** and **6** (A = $SiMe_3$).



Scheme 2. Syntheses and reactivities of the four-membered, two-electron aromatic compounds **4a** and **4b**. All the reactions maintain the two-electron aromaticity (A = $SiMe_3$).

group. Traces of oxygen or hexachloroethane reoxidize **4b** to **5b**. Compound **4b** reacts with two equivalents of methyl iodide to form tetraborane(6) **6a** and with two equivalents of HCl to form the analogous product **6b**, a stereoisomer of the known tetraborane(6) with an inversion center.[3]

The constitutions of the new compounds were deduced from their NMR data (Table 1) and, with the exception of **4b** and **6b**, were confirmed by X-ray structure analyses. Figure 1 shows the structures of **4a**·$Li_2(DME)_2$ and **5c** in the crystal.[6]

Dianion **4a** forms a contact-ion triple with two lithium ions, which are coordinated side-on to opposite B–B bonds as well as to one amino group and to one molecule of DME each. According to computations,[7] the side-one coordination of lithium ions to B–B σ bonds in **4c**·Li_2 (Scheme 3) is 7.1 kcal mol^{-1} lower in energy than the π coordination in **4d**·Li_2.[8] In contrast, the lithium counterions of the cyclobutadiene dianion **1** described by Sekiguchi et al. are located

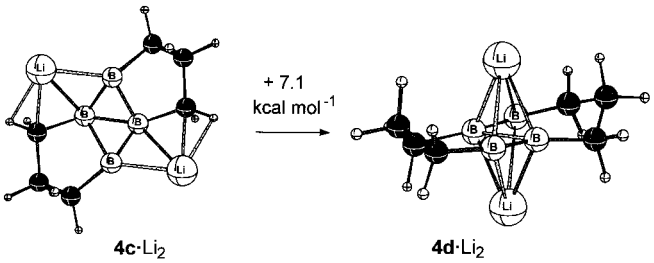
Table 1: Selected physical and spectroscopic properties of **4a**·$Li_2(DME)_2$, **4b**·$Li_2(THF)_n$, **5c**, and **6a**.

4a·$Li_2(DME)_2$: Colorless crystals, m.p. >200 °C, yield 85 %; ^{1}H NMR (300 MHz, [D_8]THF, 27 °C): δ = 3.44, 3.28 (each s, 8 H and 12 H, DME), 2.62 (s, 24 H, NMe_2), 2.49 ppm (s, 12 H, NMe_2); ^{13}C NMR (75 MHz, [D_8]THF, 27 °C): δ = 72.6, 58.9 (DME), 48.4 (q, 4 C, NMe_2), 43.7 ppm (q, 8 C, NMe_2); ^{11}B NMR (96 MHz, [D_8]THF, 27 °C): δ = 48 (2 B), 37 ppm (4 B); ^{11}B NMR (96 MHz, DME, 27 °C): δ = 48 (2 B), 38 (2 B), 31 ppm (2 B).

4b·$Li_2(THF)_n$: Red solid, yield 90 % (determined by NMR spectroscopy); ^{1}H NMR (500 MHz, [D_8]THF, −20 °C): δ = 2.25 (pseudo t, 2 H, C_2CHSi), 1.44, 0.39 (each d, each 2 H, BCHSi), 0.17, 0.08, −0.02 ppm (each s, each 18 H, $SiMe_3$); ^{13}C NMR (125 MHz, [D_8]THF, −30 °C): δ = 43.3 (d, C_2CHSi), 29.1, 26.0 (each br d, BCHSi), 2.5, 1.8, 1.0 ppm (each q, $SiMe_3$); ^{11}B NMR (160 MHz, [D_8]THF, 0 °C): δ = 50, 35 ppm.

5c: Colorless solid, m.p. 80–82 °C, yield 95 %; ^{1}H NMR (300 MHz, C_6D_6, 27 °C): δ = 3.33 (q, 4 H, CH_2), 2.80 (s, 12 H, NMe_2), 2.75 (s, 24 H, NMe_2), 1.17 ppm (t, 6 H, CH_2CH_3); ^{13}C NMR (75 MHz, C_6D_6, 27 °C): δ = 48.4 (t, 2 C, CH_2), 42.0 (q, 4 C, NMe_2), 41.9 (q, 8 C, NMe_2), 15.9 ppm (q, 2 C, CH_2CH_3); ^{11}B NMR (96 MHz, C_6D_6, 27 °C): δ = 87 (1 B), 76 (1 B), 41 (2 B), 37 (1 B), 15 ppm (2 B).

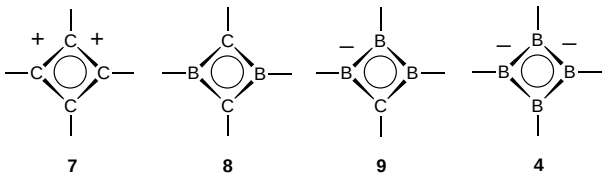
6a: Yellow solid, m.p. 125 °C (decomp), yield 80 %; ^{1}H NMR (300 MHz, C_6D_6, 27 °C): δ = 2.18, 1.87 (each d, each 2 H, BCHSi), 1.71 (pseudo t, 2 H, C_2CHSi), 1.30 (s, 6 H, BMe), 0.28, 0.25, 0.10 ppm (each s, each 18 H, $SiMe_3$); ^{13}C NMR (75 MHz, C_6D_6, 27 °C): δ = 47.7 (br d, MeBCHSi), 28.6 (d, C_2CHSi), 26.8 (br d, B_3BCHSi), 12.7 (br q, BMe), 2.4, 0.4, −3.0 ppm (each q, $SiMe_3$); ^{11}B NMR (96 MHz, C_6D_6, 27 °C): δ = 62, 29 ppm.



Scheme 3. Computed[7] structures of **4c**·Li_2 and **4d**·Li_2 and their difference in energy: Coordination of the lithium ions to B–B σ bonds is preferred over π coordination. In contrast, the lithium ions in **1**·Li_2 are π-coordinated.

above and below the four-membered ring.[1a] Whereas **1** is planar, the B_4 ring of **4a** is puckered (121°),[9–11] as expected for a four-membered, two-electron aromatic compound (Scheme 4). Computations[7] on the dianion **4c** provide a folding angle of 131°.

The ^{11}B NMR chemical shifts of dianions **4a** (δ = 35 and 46 ppm) and **4b** (δ = 35 and 50 ppm) correspond well with the



Scheme 4. Puckered frameworks of four-membered, two-electron aromatic compounds.

 © 2003 Wiley-VCH Verlag GmbH & Co. KGaA, Weinheim

computed shifts[7] of **4c**·Li_2 ($\delta = 31.3$ and 48.4 ppm): Apparently dianion **4b** also contains a puckered four-membered ring. The distorted tetrahedral dianion of tetramethyltetraborane(4) is computed to have $\delta(^{11}B) = 6.8$ ppm,[12] whereas $\delta(^{11}B) = 51.4$ ppm is obtained at the same level of theory for the puckered four-membered ring. Computations also show that for the dianion of tetramethyltetraborane(4) a four-membered ring structure is 4.9 kcal mol^{-1} lower in energy than a distorted tetrahedral geometry.[12]

Dianions **4a** and **4b** supplement the known four-membered, two-electron aromatic compounds **7** (C_4),[9] **8** (C_2B_2),[10] and **9** (CB_3)[11] by the long sought-after[13] first examples with four boron atoms. Such compounds have so far only been known from computations.[14]

The reaction **4b**→**6b** is the first experimental "corner protonation"[15] of a two-electron aromatic compound. Here, the four electrons required for the bonding of two protons are taken from the reservoir of σ framework electrons, and aromaticity is conserved. Four π electrons are employed when the cyclobutadiene dianion **1** is protonated to **3**,[1a] and its aromaticity is lost. In the case of the oxidations **4a,b**→**5a,b** two σ framework electrons are removed preserving the two-electron aromaticity. In contrast, π electrons are lost in the oxidation of **1** leading to antiaromatic **2**.[1b] The main cause of the differences in reactivity between the four-membered dianions **1** and **4** is the considerably larger aromatic stabilization energy of two-electron aromatic compounds with respect to six-electron aromatic compounds, which has been pointed out by Schleyer repeatedly.[16] An equivalent explanation is as follows: The HOMOs of **4** and **5** are σ orbitals,[17] whereas those of **1** are π orbitals.

Received: December 5, 2002 [Z50700]

Keywords: anions · aromaticity · boron · density functional calculations

[1] a) A. Sekiguchi, T. Matsuo, H. Watanabe, *J. Am. Chem. Soc.* **2000**, *122*, 5652; b) A. Sekiguchi, M. Tanaka, T. Matsuo, H. Watanabe, *Angew. Chem.* **2001**, *113*, 1721; *Angew. Chem. Int. Ed.* **2001**, *40*, 1675.

[2] A. Maier, M. Hofmann, H. Pritzkow, W. Siebert, *Angew. Chem.* **2002**, *114*, 1600; *Angew. Chem. Int. Ed.* **2002**, *41*, 1529.

[3] C. Präsang, M. Hofmann, G. Geiseler, W. Massa, A. Berndt, *Angew. Chem.* **2002**, *114*, 1597; *Angew. Chem. Int. Ed.* **2002**, *41*, 1526.

[4] C. Präsang, M. Hofmann, G. Geiseler, W. Massa, A. Berndt, *Angew. Chem.* **2003**, *115,* 1079; *Angew. Chem. Int. Ed.* **2003**, *42*, 1049.

[5] C. Präsang, A. Mlodzianowska, M. Hofmann, G. Geiseler, W. Massa, A. Berndt, *Angew. Chem.* **2002**, *114*, 3529; *Angew. Chem. Int. Ed.* **2002**, *41*, 3380.

[6] Crystal structure analysis: **4a**·Li_2(DME)$_2$: Measurements were made on a colorless crystal ($0.45 \times 0.20 \times 0.10$ mm) at 193 K with an IPDS area detector system (Stoe) with $Mo_{K\alpha}$ radiation. $C_{20}H_{56}B_6Li_2N_6O_4$, monoclinic, space group $P2_1$, $Z = 4$, $a =$ 1808.5(1), $b = 1217.7(1)$, $c = 1525.0(1)$ pm, $\beta = 91.78(1)°$, $V =$ $3356.8(4) \times 10^{-30}$ m^3, $\rho_{calcd} = 1.036$ Mg m^{-3}. Of 25510 reflections up to $\theta = 25.91°$, 6493 were independent ($R_{int} = 0.1173$) and 2179 with $I > 2\sigma(I)$. The structure was solved with direct methods and refined with full matrix against all F^2 data. Hydrogen atoms were calculated in "riding" positions, $wR_2 = 0.0969$ for all reflections, $R = 0.0431$ for the observed reflections. **5c**: Colorless crystal ($0.55 \times 0.30 \times 0.20$ mm) $C_{16}H_{46}B_7N_7$, triclinic, space group $P\bar{1}$, $Z =$ 2, $a = 887.2(1)$, $b = 1018.8(1)$, $c = 1703.6(1)$ pm, $\alpha = 98.08(1)$, $\beta =$ 91.02(1), $\gamma = 114.73(1)°$, $V = 1379.7(2) \times 10^{-30}$ m^3, $\rho_{calcd} =$ 0.992 Mg m^{-3}. Of 13684 reflections up to $\theta = 25.93°$, 5022 were independent ($R_{int} = 0.0898$), and 2805 with $I > 2\sigma(I)$. The structure was solved and refined in an analogous manner to **4a**·Li_2(DME)$_2$ with $wR_2 = 0.1340$ for all reflections and $R =$ 0.0503 for the observed reflections. CCDC-198895 (**4a**·Li_2(DME)$_2$) and CCDC-198896 (**5c**) contain the supplementary crystallographic data for this paper. These data can be obtained free of charge via www.ccdc.cam.ac.uk/conts/retrieving.html (or from the Cambridge Crystallographic Data Centre, 12, Union Road, Cambridge CB21EZ, UK; fax: (+44) 1223-336-033; or deposit@ccdc.cam.ac.uk).

[7] All geometries were optimized by employing the B3LYP hybrid functional together with the 6-31G(d) basis set. Relative energies are based on energy computations with 6-311+ G(d,p) and are corrected for zero-point vibrational energies. a) Gaussian 98 (Revision A.7), M. J. Frisch, G. W. Trucks, H. B. Schlegel, G. E. Scuseria, M. A. Robb, J. R. Cheeseman, V. G. Zakrzewski, J. A. Montgomery, R. E. Stratmann, J. C. Burant, S. Dapprich, J. M. Millam, A. D. Daniels, K. N. Kudin, M. C. Strain, O. Farkas, J. Tomasi, V. Barone, M. Cossi, R. Cammi, B. Mennucci, C. Pomelli, C. Adamo, S. Clifford, J. Ochterski, G. A. Petersson, P. Y. Ayala, Q. Cui, K. Morokuma, D. K. Malick, A. D. Rabuck, K. Raghavachari, J. B. Foresman, J. Cioslowski, J. V. Ortiz, A. G. Baboul, B. B. Stefanov, G. Liu, A. Liashenko, P. Piskorz, I. Komaromi, R. Gomperts, R. L. Martin, D. J. Fox, T. Keith, M. A. Al-Laham, C. Y. Peng, A. Nanayakkara, C. Gonzalez, M. Challacombe, P. M. W. Gill, B. G. Johnson, W. Chen, M. W. Wong, J. L. Andres, M. Head-Gordon, E. S. Replogle, J. A. Pople, Gaussian, Inc., Pittsburgh, PA, **1998**; b) A. D. Becke, *J. Chem. Phys.* **1993**, *98*, 1372; A. D. Becke, *J. Chem. Phys.* **1993**, *98*, 5648; c) C. Lee, W. Yang, R. G. Parr, *Phys. Rev. B* **1988**, *37*, 785.

[8] According to computations on $Li_2B_3H_3$, side-on coordination of the lithium ions to B–B σ bonds is 17.0 kcal mol^{-1} lower in energy than π coordination: A. A. Korkin, P. von R. Schleyer, M. McKee, *Inorg. Chem.* **1995**, *34*, 961.

[9] M. Bremer, P. von R. Schleyer, U. Fleischer, *J. Am. Chem. Soc.* **1989**, *111*, 1147, and references therein.

[10] M. Hildenbrand, H. Pritzkow, W. Siebert, *Angew. Chem.* **1985**, *97*, 769; *Angew. Chem. Int. Ed. Engl.* **1985**, *24*, 759, and references therein; P. H. M. Budzelaar, K. Krogh-Jespersen, T. Clark, P. von R. Schleyer, *J. Am. Chem. Soc.* **1985**, *107*, 2723; M. McKee, *Inorg. Chem.* **2000**, *39,* 4206, and references therein.

[11] Y. Sahin, C. Präsang, P. Amseis, M. Hofmann, G. Geiseler, W. Massa, A. Berndt, *Angew. Chem.* **2003**, *115*, 693; *Angew. Chem. Int. Ed.* **2003**, *42*, 669.

[12] A. Neu, T. Mennekes, U. Englert, P. Paetzold, M. Hofmann, P. von R. Schleyer, *Angew. Chem.* **1997**, *109*, 2211; *Angew. Chem. Int. Ed. Engl.* **1997**, *36*, 2117. The distorted tetrahedral dianions of the type $B_4R_4^{2-}$ presented do not represent local minima.

[13] H. Klusik, A. Berndt, *J. Organomet. Chem.* **1982**, *234*, C17.

[14] M. J. S. Dewar, M. L. McKee, *Inorg. Chem.* **1978**, *17,* 1569; A. Dreuw, N. Zint, L. S. Cederbaum, *J. Am. Chem. Soc.*, **2002**, *124*, 10903.

[15] T. Clark, R. Weiss, *J. Org. Chem.* **1980**, *45*, 1790; M. W. Wong, L. Radom, *J. Mol. Struct.* **1989**, *198*, 391; K. Lammertsma, P. von R. Schleyer, *J. Am. Chem.* Soc. **1990**, *112*, 7935.

[16] P. H. M. Budzelaar, P. von R. Schleyer, *J. Am. Chem.* Soc. **1986**, *112*, 3967, and references therein.

[17] See the computed orbital scheme for the diamond-shaped B_4H_4 in ref. [2].

 © 2003 Wiley-VCH Verlag GmbH & Co. KGaA, Weinheim

Organic Electrosynthesis

Convergent Paired Electrolysis for the Three-Component Synthesis of Protected Homoallylic Alcohols

*Gerhard Hilt**

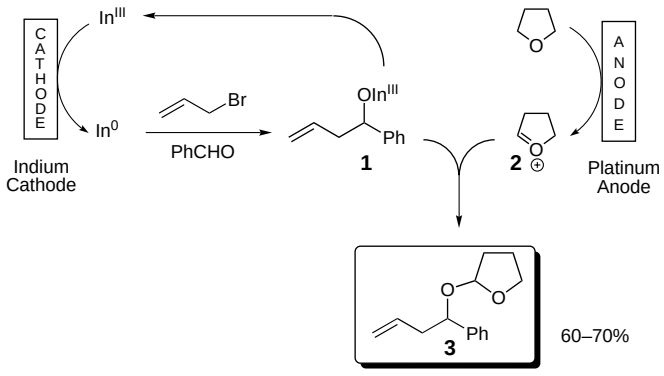
The fundamental advantage of electrochemical methods over conventional redox reagents in organic synthesis is the mass-free charge transfer between the electrode and the starting material; the waste treatment of the spent redox reagents is not necessary after the reaction has been completed.[1] The problems associated with the use of stoichiometric ammounts of expensive and/or toxic reagents, can be diminished by electrochemical regeneration of the spent reagent, which is used in catalytic amounts.[2] In addition, there are tendencies towards a direct electrochemical transformation of the starting materials so that the expensive and/or toxic reagents are completely substituted.[2a,3]

In paired electrolysis the electrochemical power is used both on the working electrode and the counter electrode to generate synthetically useful products.[4] In principle three types of paired electrolysis can be differentiated:

- divergent (one starting material is oxidized as well as reduced⇒two products),
- linear (one starting material is reduced, while another starting material is oxidized⇒two products), and
- convergent paired electrolysis (see Scheme 1).

Although divergent and linear electrolysis can contain interesting reaction pathways, such reactions often require the tedious separation of the two products,[5] while in principle such problems will not occur for convergent electrolysis.

In previous investigations on the electrochemical regeneration of low-valent indium(I) reagents,[6] we observed that the direct electrochemical reduction of indium(III) salts is associated with high overpotentials on platinum and glassy carbon electrodes.[7] This disadvantage was circumvented when indium metal cathodes were used (see Scheme 1). In the reaction of allyl bromide with benzaldehyde in THF in a quasi-divided cell[8] (In cathode 6.25 cm^2; Pt wire anode) the desired homoallylic alcohol was not obtained as the main product. Instead, the tetrahydrofuranyl-protected derivative **3** was isolated as a three-component product of a convergent paired electrolysis.



Scheme 1. Convergent indium-mediated paired electrosynthesis of protected homoallylic alcohols.

[*] Prof. Dr. G. Hilt
Fachbereich Chemie, Philipps-Universität Marburg
Hans-Meerwein-Strasse, 35043 Marburg (Germany)
Fax: (+49) 6421-2825677
E-mail: Hilt@chemie.uni-marburg.de

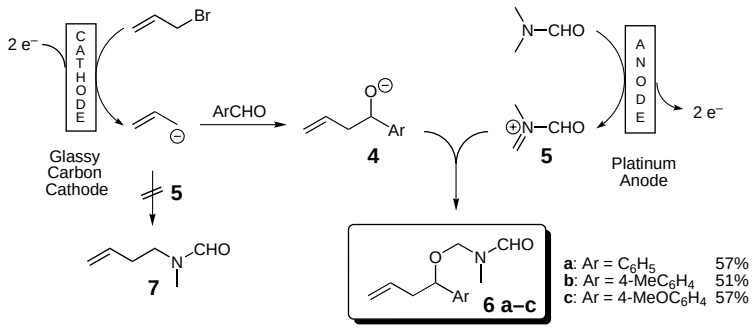
However, this paired electrosynthesis for the formation of the three-component coupling products is impaired by the fact that (over-)stoichiometric amounts of indium (massive indium electrode) are used. The fast reaction of the allyl bromide with the indium metal of the electrode generates the allylindium sesquibromide, which is responsible for the allylation of the benzaldehyde to form the homoallylic alcoholate **1**. Over the course of the electrochemical reaction the indium salts are reduced on the cathode, while the solvent is oxidized on the anode[9] and the oxonium ion **2** thereby generated reacts with the alcoholate **1** to give the final product **3**. Whereas the formation of the homoallylic alcoholate (**1**) was complete (GC control), the yields for the three-component product **3** after consumption of 3.0 $F\,mol^{-1}$ of current were typically between 60 and 70%, and the product was formed with good selectivity with only traces of by-products. Further electrolysis under galvanostatic conditions (typically 100–150 mA) led to an increased number and amount of by-products, which resulted in more difficult separation problems in column chromatography and the yield of isolated **3** could not be increased.

The allylation of the aldehyde in a convergent paired electrolysis under indium-free conditions was performed in DMF, and the formation of the corresponding three-component product was observed.[10] The reaction, which is shown in Scheme 2, affords the desired products **6a–c** in a quasi-divided cell through the reaction of the anodically generated electrophile **5**[11] with an homoallylic alcoholate (**4**), which was generated by metal-free allylation of the benzaldehyde.

The best results for the paired electrolysis for the formation of such formamide-protected homoallylic alcohols were obtained when the allyl bromide/aldehyde ratio was 2:1. The electrolyses were conducted in DMF (0.1M $LiClO_4$) at constant current (150 mA) and under external cooling, and a platinum wire anode and a glassy carbon cathode were used to prevent the generation of an allyl metal agents.[12] At higher current densities (> 25–30 mA cm^{-2} at the cathode) a fast darkening of the solution from almost colorless over yellow to brown was detected accompanied with the formation of several by-products. In contrast, at lower current densities around 10–15 mA cm^{-2}, the solution stayed light yellow for a long period of time and the amount of by-products was minimal. After consumption of 3.0 $F\,mol^{-1}$ of current under these conditions, the aldehydes were completely consumed (control by thin-layer chromatography and GC analysis) and around 50–60% of the homoallylic alcohols were converted into the three-component coupling products **6a–c** with good purities (> 90%).

To our surprise the coupling product *N*-but-3-enyl-*N*-methylformamide (**7**), which should be obtained by the

 © 2003 Wiley-VCH Verlag GmbH & Co. KGaA, Weinheim DOI: 10.1002/anie.200350892



Scheme 2. Convergent paired electrosynthesis of formamide-protected homoallylic alcohols.

reaction of the cathodically generated allylic anion with the anodically generated formyl iminium ion **5** could not be detected in reasonable amounts (GC: $<5\%$) even in the absence of the aldehydes. Therefore, the electrochemically generated species could be adsorbed on the electrodes (e.g. the allylic anion) so that a reaction between the electrogenerated species is minimized or the stability of these reactive species in solution is too low.[13] The reason why an excess of allyl bromide needs to be applied is presumably that the protons produced in the anodic oxidation of the DMF react with the allylic anion to give propene. Surprisingly, the addition of bases such as pyridine, triethylamine, K_2CO_3, KO*t*Bu, NaOMe, or K_3PO_4 to quench the anodically generated protons was contraproductive and did not lead to better yields or higher product selectivities. Nevertheless, the secondary nucleophile, the homoallylic alcoholate **4**, reacts even under acidic conditions with the formyl iminium ion. This could be shown in the electrolysis of a preformed homoallylic alcohol in DMF (0.05 M toluene-4-sulfonic acid (TosOH)), which also led to the three-component product **6a**.

As can be expected, the conversion of aldehydes containing electrochemically sensitive functional groups such as a cyano, nitro, dimethylamino group or a halide functionality, led to side reactions and to several by-products. Other functionalities, which are "electrochemically inert" under these conditions, such as an alkyl (**6b**, 51%) or an alkoxy functionality (**6c**, 57%), are well tolerated.

Experimental Section

6a (general procedure): In a 35-mL beaker-type cell with external water cooling, benzaldehyde (1.18 mL, 1.23 g, 11.6 mmol), allyl bromide (2.0 mL, 2.80 g, 23.1 mmol), and $LiClO_4$ (212 mg, 2.0 mmol, 0.1 M) were dissolved in DMF (20 mL) under a nitrogen atmosphere. The solution was electrolyzed on a platinum-wire anode and a glassy-carbon cathode (10 cm^2) under galvanostatic conditions at a constant current of 150 mA until 2.5 F mol^{-1} of current were consumed. After the electrolysis, the pale yellow solution was stirred for another 15 min, water was added, and sample was extracted with diethyl ether (4×50 mL). The combined organic phases were washed with brine, dried over Na_2SO_4, filtered, and the volatiles were removed. The crude product was purified on silica gel (pentane/diethyl ether 1:1 to 1:3), and the product was obtained as a light yellow oil (1.45 g, 6.61 mmol, 57% yield).

^{1}H NMR (300 MHz, $CDCl_3$): $\delta=2.27$–2.40 (m, 1H; CH_2), 2.43–2.55 (m, 1H; CH_2), 2.83 (s, 3H; CH_3N), 4.18–4.23 (m, 1H; CH_2OCH), 4.42 (d, $J=10.7$ Hz; CH_2N), 4.53 (d, $J=10,7$ Hz; CH_2N), 4.94–5.03 (m, 2H; $=CH_2$), 5.59–5.75 (m, 1H; $=CH$), 7.17–7.33 (m, 5H; H_{ar}), 7.85 ppm (s, 1H; NCH=O); ^{13}C NMR (75 MHz, $CDCl_3$): $\delta=28.9$, 42.3, 77.6, 117.5, 126.7, 128.2, 128.3, 128.8, 134.1, 140.3, 162.9 ppm; IR: $\tilde{\nu}=704$, 761, 1049, 1404, 1689, 2935 cm^{-1}; MS: *m*/*z* (%): 220 $[M+1]^+$ (1), 178 (1), 147 (4), 131 (19), 105 (16), 72 (100); ESI-MS calcd and found for $[M+Na]^+$: $C_{13}H_{17}NO_2Na$: *m*/*z*: 242; HRMS: calcd for $[M-H]^+$ $C_{13}H_{16}NO_2$: *m*/*z*: 218.1181, found: 218.1184.

Received: January 7, 2003 [Z50892]

Keywords: aldehydes · allylation · electrochemistry · electrolysis · homoallylic alcohols

[1] E. Steckhan, T. Arns, W. R. Heineman, G. Hilt, D. Hoormann, J. Jörissen, L. Kröner, B. Lewall, H. Pütter, *Chemosphere* **2001**, *43*, 63.
[2] Leading references for electrochemical sustainable processes: a) T. Siu, A. K. Yudin, *J. Am. Chem. Soc.* **2002**, *124*, 530; b) S. Torii, *Electrochem. Soc. Interface* **1997**, *6*, 46; c) A. R. Amundsen, E. N. Balko, *J. Appl. Electrochem.* **1992**, *22*, 810.
[3] The concept of a paired electrochemical generation of reagents (e.g. Br_2) in a 200% cell could be realized and current yields of up to 190% were obtained; T. Arns, E. Steckhan, Diplomarbeit, Bonn, **1998** and reference [1].
[4] M. M. Baizer in *Organic Electrochemistry* (Eds.: M. M. Baizer, H. Lund), Marcel Dekker, **1991**, chap. 35, pp. 1421–1430; and selected examples: Y. Takahashi, M. Tokuda, M. Itoh, A. Suzuki, *Synthesis* **1976**, 616; X. D. Wei, B. Speiser, *Electrochim. Acta* **1995**, *40*, 2477; M. Ishifune, H. Yamashita, M. Matsuda, H. Ishida, N. Yamashita, Y. Kera, S. Kashimura, H. Masuda, H. Murase, *Electrochim. Acta* **2001**, *46*, 3259; S. Kim, R. Uchiyama, Y. Kitano, M. Tada, K. Chiba, *J. Electroanal. Chem.* **2001**, *507*, 152.
[5] For an elegant procedure for the workup of an industrial-scale paired electrolysis see: H. Pütter, H. Hannebaum, *Proc. Electrochem. Soc.* **2000**, *15*, 25.
[6] G. Hilt, K. I. Smolko, *Angew. Chem.* **2001**, *113*, 3514; *Angew. Chem. Int. Ed.* **2001**, *40*, 3399; G. Hilt, K. I. Smolko, C. Waloch, *Tetrahedron Lett.* **2002**, *43*, 1437.
[7] Electroanalytical investigations showed that the reduction of the $InCl_3$ salts proceeds at very negative potentials (≈ -2.2 V versus Ag/AgCl) accompanied with a "trace crossing" in the back sweep of the cyclic voltammogram.
[8] K. Danielmeier, K. Schierle, E. Steckhan, *Tetrahedron* **1996**, *52*, 9743.
[9] T. Shono, Y. Matsumura, *J. Am. Chem. Soc.* **1969**, *91*, 2803; M. Ishifune, H. Yamashita, M. Matsuda, H. Ishida, N. Yamashita, Y. Kera, S. Kashimura, H. Masuda, H. Murase, *Electrochim. Acta* **2001**, *46*, 3259.
[10] M. Tokuda, S. Satoh, H. Suginome, *J. Org. Chem.* **1989**, *54*, 5608.
[11] M. Genies, *Bull. Soc. Chim. Fr.* **1975**, 389; S. D. Ross, M. Finkelstein, R. C. Petersen, *J. Org. Chem.* **1966**, *31*, 128.
[12] The electrochemically generated allylic anion might be absorbed on the electrode surface and the concentration of an allyllithium species seems to be low in solution.
[13] J.-i. Yoshida, S. Suga, *Chem. Eur. J.* **2002**, *8*, 2650.

 © 2003 Wiley-VCH Verlag GmbH & Co. KGaA, Weinheim

Catalyst Screening

Catalyst–Substrate Coimmobilization: A Strategy for Catalysts Discovery in Split-and-Mix Libraries**

*Philipp Krattiger, Catherine McCarthy, Andreas Pfaltz, and Helma Wennemers**

The discovery of highly active and specific catalysts is one of the most fundamental goals of chemistry. Since rational design is usually an enormous challenge, the discovery process often involves the separate syntheses of many potential catalysts and testing their catalytic properties in individual reaction containers.[1] More efficient is the simultaneous screening of the members of one-bead-one-compound libraries.[1–5] However, because of the difficulty of visualizing a reaction mediated by a catalyst on a single bead, examples of such screening methods are still rare. Successful methods rely on: IR thermography,[2] the generation of an insoluble colored reaction product,[3] fluorescent pH indicators,[4] or the use of gels that prevent the free diffusion of reaction products.[5] Except for the use of IR thermography, most methods have been established for specific reactions and rely either on a change of the pH value or on the generation of colored or fluorescent products. Herein we disclose a method for the screening of the members of split-and-mix libraries that is applicable to the search for catalysts for most bimolecular reactions.

Our concept for the visualization of catalysts among the members of a one-bead-one-compound library is based on the immobilization of one reaction partner along with each library member, the potential catalyst, on the same bead. This setup can be easily accomplished with a bifunctional linker that carries the reactant **A** on one end and the library member on the other end (Figure 1). If the reaction partner **B** is labeled with, for example, a dye, a fluorophor, or radioactivity, a reaction between **A** and **B** leads to the covalent attachment of the marker to those beads that carry catalytically active library members. These beads can then easily be detected with a microscope.

The concept relies on the assumption that reactions between the immobilized reactant **A** and the labeled reaction partner **B** can only occur on beads that carry active catalysts; cross-catalysis between different beads must not occur. Herein, we demonstrate the feasibility of the method by using the acylation of an alcohol (reactant **A**) with a dye-marked pentafluorophenyl (Pfp) ester (reactant **B**) as a simple test reaction.

Initially we evaluated the hypothesis that reactions are only mediated by catalytically active compounds that are immobilized on the same bead as the reactant **A**. For this purpose, we prepared poly(ethylene glycol)polystyrene (TentaGel)[6] with a bifunctional linker based on lysine functionalized on one end with an alcohol derived from serine and on the other end with a derivative of the acylation catalyst 4-dimethylaminopyridine DMAP (resin **1**).[7,8] Negative control beads (resin **2**) were acetylated in place of the DMAP derivative. Both kinds of resins were encoded to allow the identification of single beads (Scheme 1).[9]

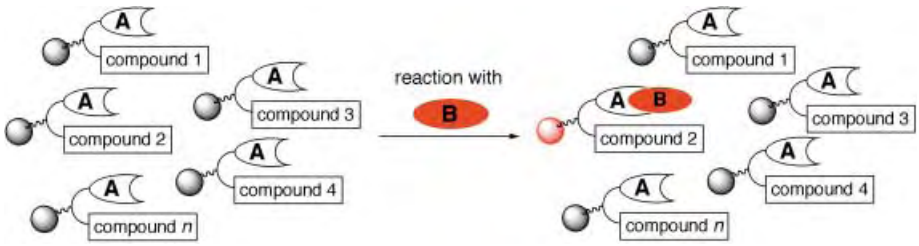


Figure 1. General concept for the discovery of catalysts in one-bead-one-compound libraries. In this example only compound **2** is an active catalyst.

Upon addition of the red Pfp-ester **3**[10] to the beads carrying the DMAP derivative (resin 1) in CH_2Cl_2 at a concentration of ≥ 2 mM the beads became dark red within 30 seconds.[11] The color remained even after extensive washings[12] which indicates that the dye was covalently bound to the resin beads.[13] In contrast, the beads that were acetylated (resin **2**) stayed colorless under identical reaction conditions. When a mixture of the two kinds of resins **1** and **2** was treated with the Pfp-ester **3**, only half of the beads turned red, the other half remained colorless. Isolation of approximately 20 red beads and analysis of the encoding tag molecules revealed only beads with DMAP; none of the acetylated beads had turned red. Thus, a reaction is only mediated on the same bead, cross-reactions between two beads do not occur.

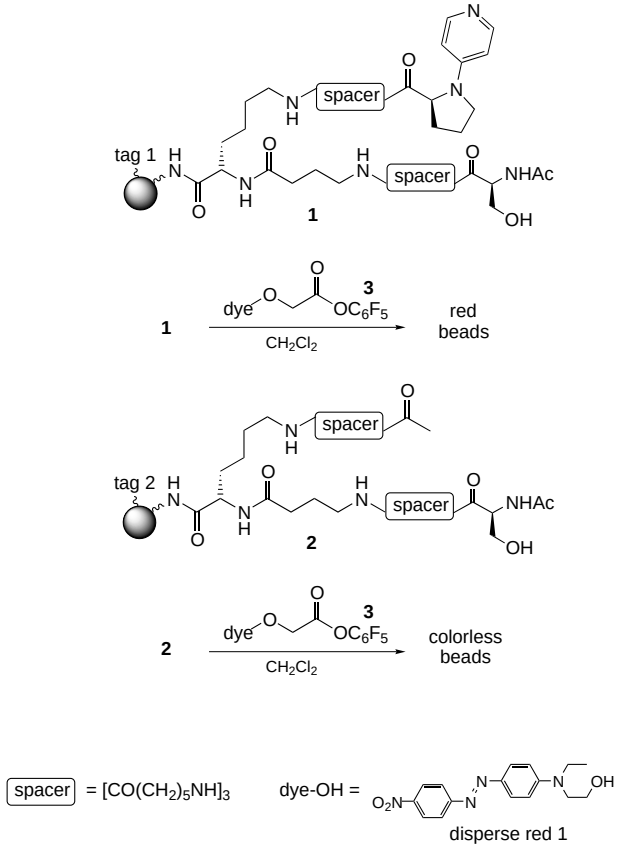
We then extended the method to the testing of a combinatorial tripeptide library. The library was prepared by encoded[9] split-and-mix synthesis[14] on one end of the bifunctional linker. The other end of the linker was functionalized as before with a primary alcohol derived from serine (Figure 2). Since 15 different amino acids were used in each position, the library consists of up to 15^3 (=3375) different tripeptides.[15] The library was designed to contain no amino acids that could be acylated themselves. Thus, Ser, Thr, Cys,

[*] Dr. H. Wennemers, Dipl.-Chem. P. Krattiger, Dr. C. McCarthy, Prof. Dr. A. Pfaltz
Departement Chemie
Universität Basel
St. Johanns-Ring 19, 4056 Basel (Switzerland)
Fax: (+41) 61-267-1105
E-mail: Helma.Wennemers@unibas.ch

[**] This work was supported by the BACHEM company and the Swiss National Science Foundation. H.W. is grateful to the Fonds der Chemischen Industrie for a Liebig Fellowship and an assistant professorship sponsored by the BACHEM company.

Supporting information for this article is available on the WWW under http://www.angewandte.org or from the author.

 © 2003 Wiley-VCH Verlag GmbH & Co. KGaA, Weinheim DOI: 10.1002/anie.200250422



Scheme 1. Reaction of resins **1** and **2** with the dye-marked Pfp-ester **3**.

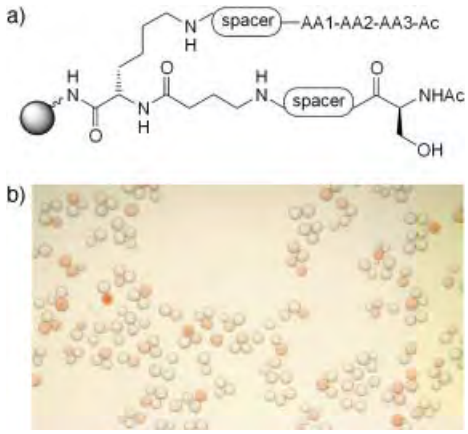


Figure 2. a) Tripeptide library, b) microscope view after reaction of the library with **3**.

and Lys were not employed. His was incorporated as a known weak acylation catalyst. Upon mixing the library with the dye-marked Pfp-ester **3** at a concentration of 200 μM in CH_2Cl_2 for 75 min at 20 °C followed by extensive washings,[12] several beads picked up the red color (Figure 2).[16]

Higher concentrations or longer reaction times led to more red beads and a poorer contrast between colored and colorless beads. Isolation of 17 of the red beads and analysis of the encoding tag molecules revealed the active peptides (Table 1).

Table 1: Peptides found in the combinatorial assay

AA3	AA2	AA1
L-Leu	L-Phe	L-His
L-Tyr	L-Val	L-His
D-Pro	L-Pro	L-His
L-Pro	D-Pro	D-His
D-Pro	D-His	D-His
D-Pro	L-His	L-His
L-Leu	D-His	L-His
L-Pro	L-His	L-Tyr
D-Pro	L-His	L-Tyr
L-His	D-His	D-Val
D-His	D-His	D-Val
D-His	L-Asn	D-Asp
D-His	L-Asn	L-Tyr
L-His	L-Asp	D-Asn
D-His	L-Phe	L-Leu
L-His	D-His	D-His
D-His	L-His	L-His

All the active peptides contained, as expected, at least one His residue: Two of the 17 analyzed tripeptides consist of three His residues, five sequences include two, and the remaining ten sequences contain only a single His residue. Unexpectedly, the selected sequences are not random combinations of any amino acids with His, but clear preferences are detected. In approximately half of the sequences with either one or two His residues Pro is flanking His at the N-terminal site. This distribution is a significantly higher percentage than expected statistically and suggests that peptides containing the dipeptide Pro-His have a higher activity than His alone.

To ascertain that the detected peptides are catalytically active when they and the substrate alcohol are in free solution and not bound to a solid support we resynthesized the His-containing peptides **4**–**9** and determined their relative catalytic activities by kinetic NMR spectroscopy studies. The peptide Ac-Pro-Phe-NHPr **10** (Pr = propyl) was tested as a negative control.

4: Ac-L-His-NHPr
5: Ac-L-Pro-L-His-NHPr
6: Ac-L-His-L-His-NHPr
7: Ac-D-His-L-His-NHPr
8: Ac-L-Pro-L-His-L-His-NHPr
9: Ac-L-His-L-His-L-His-NHPr
10: Ac-L-Pro-L-Phe-NHPr

The kinetic NMR spectroscopy studies were performed with a mixture of benzylalcohol, triethylamine (1 equiv each), *p*-nitrophenylacetate (2 equiv), and 10 mol% of the peptide in a mixture of CD_2Cl_2:DMF 4:1 at a concentration of 25 mM (peptide). These conditions allow the monitoring of catalytic activity in a reasonable time frame. However, under these conditions a background reaction without any catalyst is observed, the rate of which is equal to the rate observed with the negative control peptide **10** (Figure 3).

The other peptides **4**–**9** accelerate the reaction to extents that are comparable to the activity of imidazole. His (**4**) is the weakest acylation catalyst, the histidylhistidine dipeptide **6** is approximately twice as active.[17] The activity of the diastereomeric dipeptide **7** is equal to **6** indicating that the relative configuration has no effect on the reactivity (data for **7** not shown in Figure 3). The addition of Pro at the N-terminal site (from His) leads to a significant rate acceleration especially in

 © 2003 Wiley-VCH Verlag GmbH & Co. KGaA, Weinheim

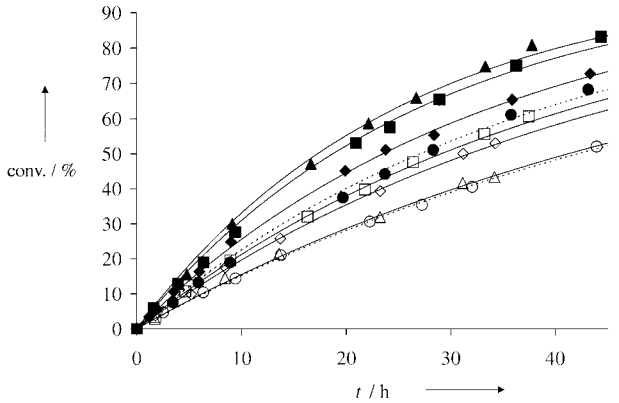


Figure 3. Kinetic NMR spectroscopy studies with 10 mol% of the peptides **4**—**6**, **8**—**10**, and imidazole ($k[10^{-3}\ h^{-1}]$): **9** (▲, $k=40$), **8** (■, $k=37$), **6** (◆, $k=30$), imidazole (●, dotted line, $k=26$), **5** (□, $k=24$), **4** (◇, $k=22$), **10** (△, $k=17$), background (○, dotted line, $k=17$); error 5%.

the comparison of the tripeptide **8** with the dipeptide **6** and the tripeptide **9**. Although **8** contains only two imidazole moieties, it is approximately as active as **9** which has three imidazole moieties, a result that correlates well with the combinatorial assay where both peptides were found equally often.

Thus, the immobilization of a library of potential catalysts, along with a reaction partner **A**, on either end of a bifunctional linker, and reaction of these beads with a marked reaction partner **B** is a feasible tool for identifying catalytically active members in split-and-mix libraries. While the present study was designed as a proof-of-principle experiment and not to yield highly active acylation catalysts that are comparable to DMAP[7] or the small peptides established by Miller et al.[4,5b,18] it yielded the dipeptide motif Pro-His as a promising starting point for a second library generation.

In conclusion, we have established a general methodology for testing the members of combinatorial split-and-mix libraries for catalytic activity in bimolecular reactions. Recent work demonstrated not only the value of small peptides as catalysts in various reactions but also the difficulty in rationally designing catalytically active peptides.[18] Our combinatorial method is ideally suited for the testing of peptides—as well as libraries of other small molecules—and should accelerate the discovery of peptides that are able to catalyze synthetically important reactions.

Received: October 23, 2002
Revised: February 3, 2003 [Z50422]

Keywords: acylation · combinatorial chemistry · immobilization · peptides

[1] For reviews see: a) H. Wennemers, *Comb. Chem. High Throughput Screening* **2001**, *4*, 273–285; b) M. T. Reetz, *Angew. Chem.* **2001**, *113*, 292–320; *Angew. Chem. Int. Ed.* **2001**, *40*, 312–329; c) S. Dahmen, S. Bräse, *Synthesis* **2001**, 1431–1449; d) B. Jandeleit, D. J. Schaefer, T. S. Powers, H. W. Turner, W. H. Weinberg, *Angew. Chem.* **1999**, *111*, 2648–2689; *Angew. Chem. Int. Ed.* **1999**, *38*, 2494–2532; e) R. H. Crabtree, *Chem. Commun.* **1999**, 1611–1616; f) K. D. Shimizu, M. L. Snapper, A. H. Hoveyda, *Chem. Eur. J.* **1998**, *4*, 1885–1889.

[2] S. J. Taylor, J. P. Morken, *Science* **1998**, *280*, 267–270.

[3] A. Berkessel, D. A. Hérault, *Angew. Chem.* **1999**, *111*, 99–102; *Angew. Chem. Int. Ed.* **1999**, *38*, 102–105.

[4] a) G. T. Copeland, S. J. Miller, *J. Am. Chem. Soc.* **2001**, *123*, 6496–6502; b) G. T. Copeland, S. J. Miller, *J. Am. Chem. Soc.* **1999**, *121*, 4306–4307.

[5] a) M. Müller, T. W. Mathers, A. P. Davis, *Angew. Chem.* **2001**, *113*, 3929–3931; *Angew. Chem. Int. Ed.* **2001**, *40*, 3813–3815; b) R. F. Harris, A. J. Nation, G. T. Copeland, S. J. Miller, *J. Am. Chem. Soc.* **2000**, *122*, 11270–11271.

[6] TentaGel S NH_2 from Rapp Polymere. E. Bayer, *Angew. Chem.* **1991**, *103*, 117–133; *Angew. Chem. Int. Ed. Engl.* **1991**, *30*, 113–129.

[7] a) E. J. Delaney, L. E. Woods, I. M. Klotz, *J. Am. Chem. Soc.* **1982**, *104*, 799–807; b) G. Höfle, W. Steglich, H. Vorbrüggen, *Angew. Chem.* **1978** *90*, 602–615; *Angew. Chem. Int. Ed. Engl.* **1978**, *17*, 569–583.

[8] a) In place of serine, glycolic acid was also used with the same results. b) Long spacers (27 atoms/arm) were utilized to ascertain conformational freedom between the catalyst and the hydroxy group. However, shorter or longer spacers on either arm also gave the same results (see Supporting Information).

[9] a) M. H. J. Ohlmeyer, R. N. Swanson, L. W. Dillard, J. C. Reader, G. Asouline, R. Kobayashi, M. H. Wigler, W. C. Still, *Proc. Natl. Acad. Sci. USA* **1993**, *90*, 10922–10926; b) H. P. Nestler, P. Bartlett, W. C. Still, *J. Org. Chem.* **1994**, *59*, 4723–4724.

[10] H. De Muynck, A. Madder, N. Farcy, P. J. De Clercq, M. N. Pérez-Payán, L. M. Öhberg, A. P. Davis, *Angew. Chem.* **2000**, *112*, 149–152; *Angew. Chem. Int. Ed.* **2000**, *39*, 145–148.

[11] A small portion ($\leq 0.1\%$) of the beads stayed almost colorless indicating that the beads are not entirely homogeneous. Catalysts on these beads would be missed.

[12] Typical washing method: CH_2Cl_2 (6×), DMF (3×) CH_2Cl_2 (3×), CH_2Cl_2:TFA (3:1) (3×), CH_2Cl_2 (3×), *i*PrOH:NEt_3 (3:1) (3×), *i*PrOH (3×); 3 ml each for 1–2 min.

[13] Control beads functionalized with DMAP but without the hydroxy group remained colorless.

[14] a) Á. Furka, F. Sebestyén, M. Asgedom, G. Dibô, *Int. J. Pept. Protein Res.* **1991**, *37*, 487–493; b) K. S. Lam, S. E. Salmon, E. M. Hersh, V. J. Hruby, W. M. Kazmierski, R. J. Knapp, *Nature* **1991**, *354*, 82–84.

[15] AA1 and AA3 = Gly, D-Val, L-Ala, L-Leu, D-Pro, L-Pro, D-Phe, L-Tyr, D-His, L-His, D-Arg, D-Asp, L-Glu, D-Asn, L-Gln; AA2 = Gly, L-Val, D-Ala, D-Leu, D-Pro, L-Pro, L-Phe, D-Tyr, D-His, L-His, L-Arg, L-Asp, D-Glu, L-Asn, D-Gln.

[16] A total of at least three theoretical copies of the library was used per screening to ensure the presence of each library member: a) K. Burgess, A. I. Liaw, N. Y. Wang, *J. Med. Chem.* **1994**, *37*, 2985–2987; b) P.-L. Zhao, R. Zambias, J. A. Bolognese, D. Boulton, K. T. Chapman, *Proc. Natl. Acad. Sci. USA* **1995**, *92*, 10212–10216.

[17] This result cannot be compared to the activity of 20 mol% of **4** since **4** is not soluble enough to allow the experiment.

[18] For reviews see: a) E. J. Jarvo, S. J. Miller, *Tetrahedron* **2002**, *58*, 2481–2495; b) H. Gröger, J. Wilken, *Angew. Chem.* **2001**, *113*, 545–548; *Angew. Chem. Int. Ed.* **2001**, *40*, 529–532.

 © 2003 Wiley-VCH Verlag GmbH & Co. KGaA, Weinheim

Spontaneous Resolution

Efficient Asymmetry Generation in the Synthesis of Oxo-Rhenium(V) Complex *cis*-[$ReOCl_2\{OCMe_2CMe_2OP(OCMe_2CMe_2O)\}py$]**

Witold K. Rybak, Anna Skarżyńska, and Tadeusz Głowiak*

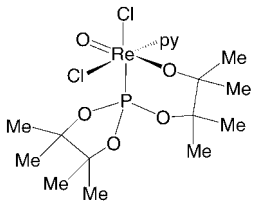
One of the most intriguing challenges of stereochemistry is deracemization and the preparation of homochiral compounds.[1] Despite the great progress in asymmetric organic synthesis, there are only several instances of genuine "absolute" asymmetric preparation of inorganic compounds,[2] these include spontaneous resolution processes too.[3] Thus, a partial photoresolution either in circularly polarized light[4a,b] or a parallel magnetic field[4c] has been observed for the $[Cr(ox)_3]^{3-}$ ion and its derivatives. Gillard and his associates have described the synthesis of the chiral polysulphide $(NH_4)_2[Pt(S_5)(S_6)_2]\cdot 2H_2O$.[5] The complex crystallizes spontaneously with one enantiomer in excess. It was obtained from a well-stirred water reaction mixture of K_2PtCl_6 and an excess of $(NH_4)_2S_n$, maintained at pH 9.4. Kondepudi and coworkers have shown that, whereas the crystallization of $NaClO_3$ from unstirred solutions yields a racemic conglomerate of (+)- and (−)-$NaClO_3$ (cubic space group $P2_13$), vigorous stirring triggers spontaneous symmetry breaking and produces almost exclusively crystals of single handedness.[6] Asakura et al. have demonstrated the generation of optically active *cis*-$[CoBr(NH_3)(en)_2]Br_2$ (en = 1,2-ethanediamine) from optically inactive substrates in a stirred suspension by a chiral autocatalysis mechanism.[7] More recently, it has been reported that the crystallization of $NaClO_3$ from a solution irradiated by antiparallel-spin electrons results in dextrorotatory crystals in excess, whereas irradiation by parallel-spin positrons yields crystals with the opposite handedness.[8] Keszthelyi and Szabó-Nagy have described a small enantiomeric excess found in polycrystalline material upon crystallization from racemic solutions of (+)- and (−)-tartrate(2−) with either (+)- and (−)-$[Co(en)_3]^{3+}$ or $[Ir(en)_3]^{3+}$ ions.[9] The authors of the latter two works have claimed that the observed partial deracemization is because of electroweak forces. Clearly, these preparations could only be successful under nonequilibrium conditions involving physical fields and/or autocatalytic chirality-amplification mechanisms. Nevertheless, in the preparation of transition-metal complexes, the generation of chiral asymmetry with substantial optical yields still remains rather rare.

[*] Dr. W. K. Rybak, Dr. A. Skarżyńska, Prof. Dr. T. Głowiak
Faculty of Chemistry
University of Wrocław
14 F. Joliot-Curie, 50-383 Wrocław (Poland)
Fax: (+48) 71-3757-356
E-mail: rybak@wchuwr.chem.uni.wroc.pl

[**] py = Pyridine.

Supporting information for this article is available on the WWW under http://www.angewandte.org or from the author.

In the course of our research on the coordination capability of the spirophosphorane $HP(OCMe_2CMe_2O)_2$,[10] we synthesized a chiral complex *cis*-$[ReOCl_2\{OCMe_2CMe_2OP(OCMe_2CMe_2O)\}py]$ (*cis*-**1**, py = pyridine) as a racemate.[10a] In addition to monodentate ligands, the six-coordinate complex also contains a chelating phosphite diolato(1−) ligand, a deprotonated tautomeric form of the spirophosphorane $(OCMe_2CMe_2O)POCMe_2CMe_2OH$. The complex appeared to be rigid on the NMR time scale.



cis-**1**
[*OC*-6-52-*C*]

Subsequently, we discovered that, depending on the reaction conditions, some built-in right or left handedness could be obtained, particularly if the synthesis was carried out under vigorous stirring conditions. Thus, the toluene suspension of *trans*-$[ReOCl_2(OEt)py_2]$[11] and a twofold excess of $HP(OCMe_2CMe_2O)_2$,[10a,12] boiled and vigorously stirred, affords the polycrystalline title compound in yields of approximately 70% with a large excess of one optical isomer. Figure 1 shows the circular dichroism (CD) spectra of the representative samples of the compound prepared with and without stirring and boiling.

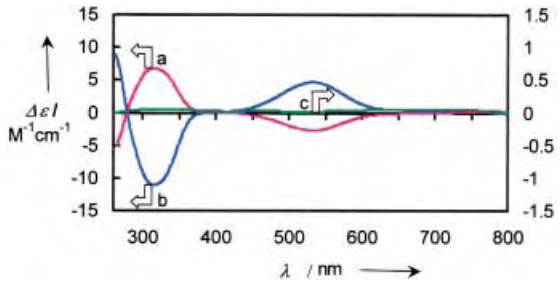


Figure 1. CD spectra for samples of *cis*-**1** in MeCN solution ($c = 1\times10^{-3}$ M, 20 °C, 1 cm cell): a) sample made with excess levorotatory $(-)_{535}$ enantiomer (red), b) sample made with excess dextrorotatory $(+)_{535}$ enantiomer, obtained with stirring (blue), and c) racemic sample obtained without stirring (green).

While the absence of absorption indicates formation of a racemate, certain differences in $\Delta\varepsilon$ intensity at 535 nm and 310 nm, observed for the two congeners, suggest a disparate distribution of enantiomers in these samples.

Figure 2 shows the optical yields (*ee* evaluation, see below) of the product obtained for a number of syntheses under different reaction conditions. The syntheses conducted with stirring and boiling (Figure 2a) afford products with randomly distributed optical yields. But the residual optical activity or lack of such activity in the CD spectra observed for the samples with no boiling, no stirring (Figure 2b) implies

 DOI: 10.1002/anie.200219501 © 2003 Wiley-VCH Verlag GmbH & Co. KGaA, Weinheim

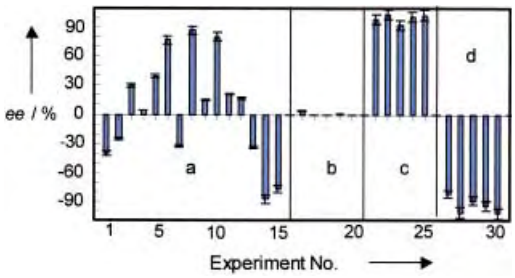


Figure 2. Chiral-symmetry-breaking syntheses of *cis*-**1**. The optical yields *ee* (± max. absolute error) for samples obtained from: a) stirred and boiled reaction mixture, b) neither stirred nor boiled reaction mixture (but at the same reaction temperature as in (a)), c) stirred and boiled reaction mixture seeded with 2 mol% of dextrorotatory $(+)_{535}$ solid sample, d) stirred and boiled reaction mixture seeded with 2 mol% of levorotatory $(-)_{535}$ solid sample.

racemate formation and equilibrium reaction conditions. Furthermore, when the preparations were performed with seeding with a small amount (2 mol%) of the dextrorotatory $(+)_{535}$ or levorotatory $(-)_{535}$ solid sample (from exp. No. 8 and 14, Figure 2a) with sustained stirring and boiling, products related to the *ee* value of the seeds (exp. No. 21, Figure 2c exp. No. 26, Figure 2d) were obtained. Repeated seeding with samples of either handedness from previous preparations (exp. Nos. 22–25, Figure 2c, and exp. Nos. 27–30, Figure 2d) resulted in products of similar, fairly high optical purity (*ee*).

Fortunately, X-ray diffraction studies along with CD studies of different single crystals made it possible to assign the absolute configuration and pertinent CD spectra. The complex *cis*-**1** crystallizes at ambient temperature from acetonitrile solution in an enantiomorphic space group as a conglomerate of either *A* or *C* enantiomers.[13,14] CD studies of the single crystals[15] allowed us to assign CD spectra inherent to the enantiomer *C* ($\Delta\varepsilon_{535} = 5.45(\pm 0.07)$ and $\Delta\varepsilon_{310} = -12.1$ (± 0.2 std error) and consequently to evaluate the enantiomeric excess values for all the described preparations (Figure 2). In seeded syntheses the *ee* values appeared to be particularly high, up to 99% (±3% max. absolute error).

Thus, depending on the reaction conditions, the chiral-symmetry-breaking synthesis of *cis*-**1** produces a disparate distribution of *C* $(+)_{535}$ and *A* $(-)_{535}$ enantiomers and the system clearly exhibits chirally autocatalytic behavior (random *ee* distribution, strong chiral seeding effect). This synthesis may involve two processes currently under investigation, both exhibiting autocatalytic phenomena. The first is a spontaneous resolution of conglomerates in stirred crystallization owing to a secondary nucleation mechanism.[16] The second is asymmetric autocatalytic reaction[17] driven by kinetic nonlinear effects[18] and/or agglomerate formation.[19]

Our preliminary studies on racemization allowed us to elucidate some mechanistic aspects of this synthesis. Starting either with a highly enriched dextrorotatory sample (*ee* +99%) or a racemate and similar conditions to those applied for the synthesis, the readily soluble (1.6 g per 100 cm^3 at RT and approximately 8 g per 100 cm^3 at 100°C in toluene) achiral *trans* complex can be obtained in low yield.[20]. The only species left is the starting, hardly soluble, *cis* complex (*cis–rac* 0.0018 g per 100 cm^3 at 110°C in toluene) with its optical (*ee*) purity retained.

Furthermore, the *trans*-**1** complex reacts under similar conditions affording *cis*-**1**, either the *rac* complex in 73% yield (it the reaction was not seeded) or the *C* complex with *ee* +48% in 81% yield if seeded with 2% of the *C* complex (Supporting Information). These findings strongly suggest that in solution, the soluble *trans* complex participates as an intermediate in the equilibrium (Figure 3) between the two hardly soluble enantiomers.

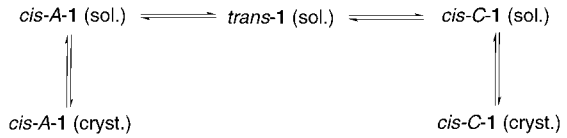


Figure 3. The role of the soluble *trans* complex as an intermediate between the two enantiomers.

Owing to this *cis–trans* isomerization reaction, the equilibrium between the two enantiomers is readily shifted by growth of the available crystals (either formed or added) and the spontaneous resolution is achieved by an autocatalytic secondary nucleation process.

Thus, it appears that the chirally autocatalytic synthesis presented is an example of a highly efficient, spontaneous resolution of the conglomerate during a stirred crystallization while the complex forms, a process rarely observed for coordination compounds.

Experimental Section

Typical procedure for syntheses with stirring: *trans*-[$ReO_2Cl_2(OEt)py_2$] (0.150 g, 0.315 mmol) was added to a toluene (25 cm^3) solution of $HP(OCMe_2CMe_2O)_2$ (0.167 g, 0.633 mmol) in a 50-cm^3 Schlenk flask under nitrogen. The flask, equipped with a teflon stirbar (16×7 mm), condenser, and oil bubbler, was placed in an oil bath heated to 120°C. The reaction mixture was boiled and vigorously stirred (ca. 1100 rpm) for 5 h to afford the pink-violet precipitate. After cooling to room temperature, the product was collected by filtration, washed with methanol and ethyl ether and dried under vacuum; yield 0.146 g (0.237 mmol, 75%). The seeded experiments were conducted under the same reaction conditions save for the addition of the seeds (finely ground, 2% (mol Re/mol Re)) from previously obtained samples before the start of the synthesis. For unstirred experiments, similar reaction conditions were applied except for the glassware. A thick-walled round-bottom flask (50 cm^3) equipped with a teflon pressure-release valve was charged with the reagents and toluene, sealed, and immersed entirely in preheated (120°C) oil bath. After one minute the overpressure was partially reduced, yet reaction-mixture boiling was avoided.

The experiments for mechanistic studies were performed under similar conditions (reactant amounts, stirring, boiling toluene) to those used for syntheses except that previously obtained products were used as substrates (Supporting Information).

CD measurements of the single-crystal samples in solution (six solutions and five crystals in each), together with concentration determination (by means of the UV spectra calibration curve), gave six values of $\Delta\varepsilon_{535} = 5.64, 5.54, 5.54, 5.46, 5.36, 5.16$ (± 0.10); and $\Delta\varepsilon_{310} = -13.0, -12.2, -12.1, -11.9, -11.7, -11.7(\pm 0.16$ max. absolute error), respectively. Hence, the mean values: $\Delta\varepsilon_{535} = 5.45(\pm 0.07)$ and $\Delta\varepsilon_{310} = -12.1(\pm 0.2$ std error) for the pure enantiomer *C*-$(+)_{535}$. The

 © 2003 Wiley-VCH Verlag GmbH & Co. KGaA, Weinheim

CD spectra of the products were recorded for acetonitrile solutions in a 1 cm cell at 20 °C with a Jasco J 715 instrument.

Received: June 7, 2002
Revised: December 9, 2002 [Z19501]

Keywords: asymmetric amplification · autocatalysis · chiral resolution · configuration determination · rhenium

[1] a) E. L. Eliel, S. H. Wilen, L. N. Mander, *Stereochemistry of Organic Compounds*, Wiley, New York, **1994**; b) A. von Zelewsky, *Stereochemistry of Coordination Compounds*, Wiley, New York, **1996**; c) *Comprehensive Asymmetric Catalysis* (Eds.: E. Njacobsen, A. Pfaltz, H. Yamamoto), Springer, Berlin, **1999**.

[2] a) M. Avalos, P. Babiano, P. Cintas, J. L. Jimenez, J. C. Palacios, L. D. Barron, *Chem. Rev.* **1998**, *98*, 2391 – 2404; b) B. L. Feringa, R. A. van Delden, *Angew. Chem.* **1999**, *111*, 3624 – 3645; *Angew. Chem. Int. Ed.* **1999**, *38*, 3418 – 3438; c) M. Avalos, P. Babiano, P. Cintas, J. L. Jimenez, J. C. Palacios, *Tetrahedron: Asymmetry* **2000**, *11*, 2845 – 2874.

[3] a) I. Bernal, G. B. Kauffman, *J. Chem. Educ.* **1987**, *64*, 604 – 610; b) J. Jacques, A. Collet, S. H. Wilen, *Enantiomers, Racemates and Resolutions*, W. Krieger Publishing, Malabar Florida, **1994**.

[4] a) K. L. Stevenson, J. F. Verdieck, *J. Am. Chem. Soc.* **1968**, *90*, 2974 – 2975; b) B. Norden, *Acta Chem. Scand.* **1970**, *24*, 23 – 25; c) G. L. J. A. Rikken, E. Raupach, *Nature* **2000**, *405*, 932 – 935.

[5] a) R. D. Gillard, F. L. Wimmer, J. P. G. Richards, *J. Chem. Soc. Dalton Trans.* **1985**, 253 – 258; b) E. H. M. Evans, J. P. G. Richards, R. D. Gillard, F. L. Wimmer, *Nouv. J. Chim.* **1986**, *10*, 783 – 791.

[6] a) D. K. Kondepudi, R. Kaufman, N. Singh, *Science* **1990**, *250*, 975 – 976; b) D. K. Kondepudi, K. L. Bullock, J. A. Digits, J. K. Hall, J. M. Miller, *J. Am. Chem. Soc.* **1993**, *115*, 10211 – 10216.

[7] a) K. Asakura, K. Kobayshi, Y. Mizusawa, T. Ozawa, S. Osanai, S. Yoshikawa, *Phys. D* **1995**, *84*, 72 – 78; b) K. Asakura, D. K. Kondepudi, R. Martin, *Chirality* **1998**, *10*, 343 – 348; c) K. Asakura, A. Ikumo, K. Kurihara, S. Osanai, D. K. Kondepudi, *J. Phys. Chem.* **2000**, *104*, 2689 – 2694.

[8] S. Mahurin, M. McGinnis, J. S. Bogard, L. D. Hulett, R. M. Pagni, R. N. Compton, *Chirality* **2001**, *13*, 636 – 640.

[9] A. Szabó-Nagy, L. Keszthelyi, *Proc. Natl. Acad. Sci. USA* **1999**, *96*, 4252 – 4255.

[10] a) T. Głowiak, W. K. Rybak, A. Skarżyńska, *Polyhedron* **2000**, *19*, 2667 – 2672; b) A. Skarżyńska, W. K. Rybak, T. Głowiak, *Polyhedron* **2001**, *20*, 2667 – 2674.

[11] a) N. P. Johnson, F. J. M. Taha, G. W. Wilkinson, *J. Chem. Soc.* **1964**, 2614 – 2618; b) M. Freni, D. Giusto, P. Romiti, G. Minghetti, *Gazz. Chim. Ital.* **1969**, *99*, 286 – 299; c) A. Guest, C. J. L. Lock. *Can. J. Chem.* **1971**, *49*, 603 – 610.

[12] a) R. R. Holmes, *J. Am. Chem. Soc.* **1974**, *26*, 4143 – 4149; b) R. Burgada, *Bull. Soc. Chim. Fr.* **1975**, 407 – 424.

[13] Crystal structure determination of *cis-C*-$(+)_{535}$-[$ReOCl_2${$OCMe_2CMe_2OP(OCMe_2CMe_2O)$}py], $C_{17}H_{29}Cl_2NO_5PRe$, orthorhombic, space group $P2_12_12_1$, $a = 9.988(2)$, $b = 11.655(2)$, $c = 18.301(4)$ Å, $V = 2130.4(7)$ Å^3, $Z = 4$, $\rho_{calcd} = 1.919$ Mg m^{-3}, $\mu = 6.057$ mm^{-1}, $F(000) = 1208$, $\lambda(Mo_{K\alpha}) = 0.71073$ Å, $T = 90(1)$ K, crystal dimensions $0.1 \times 0.1 \times 0.15$ mm, $2\theta_{max} = 57.28°$, 14435 reflections collected, 5031 unique; *R* indices $R_1 = 0.0199$, $wR_2 = 0.0515$ (all data) and Flack parameter 0.024(5). For the opposite absolute configuration *A*: $R_1 = 0.0501$, $wR_2 = 0.1268$ and Flack parameter 0.973(6). The data collected on KM4CCD camera diffractometer were corrected for Lorentz and polarization effects. Data reduction and analysis were carried out using the Kuma Diffraction (Wrocław) programs. The structure was solved by means of heavy atom methods using SHELXS-97 and refined by the full-matrix least-squares method on all F^2 using SHELXL-97 procedures (G. M. Sheldrick, Universität Göttingen, **1997**). Non-hydrogen atoms were refined with anisotropic thermal parameters. Hydrogen atoms were included from the $\Delta\rho$ maps and refined with isotropic thermal parameters. CCDC-167174 (**1**) contains the supplementary crystallographic data for this paper. These data can be obtained free of charge via www.ccdc.cam.ac.uk/conts/retrieving.html (or from the Cambridge Crystallographic Data Centre, 12 Union Road, Cambridge CB21EZ, UK; fax: (+44) 1223-336-033; or deposit@ccdc.cam.ac.uk).

[14] Five different individual crystals grown from highly enriched dextrorotatory $(+)_{535}$, polycrystalline products (set c in Figure 2) consistently revealed similar Flack parameters and the same *C* stereochemistry in X-ray analyses, which indicates that there was no racemic twinning of the single crystals and the high optical purity of these polycrystalline products.

[15] The six dextrorotatory-originated crystalline samples, each containing five single crystals, yielded six very similar CD spectra in acetonitrile solution (Experimental Section), corroborating the homochirality of the single crystals and the optical purity of the obtained six crystalline samples.

[16] a) D. K. Kondepudi, J. Laudadio, K. Asakura, *J. Am. Chem. Soc.* **1999**, *121*, 1448 – 1451; b) D. K. Kondepudi, K. Asakura, *Acc. Chem. Res.* **2001**, *34*, 946 – 954.

[17] a) I. Sato, K. Kadowaki, K. Soai, *Angew. Chem.* **2000**, *112*, 1570 – 1572; *Angew. Chem. Int. Ed.* **2000**, *39*, 1510 – 1512; b) K. Soai, T. Shibata, I. Sato, *Acc. Chem. Res.* **2000**, *33*, 382 – 390.

[18] a) C. Girard, H. Kagan, *Can. J. Chem.* **2000**, *78*, 816 – 828; b) D. G. Blackmond, *Acc. Chem. Res.* **2000**, *33*, 402 – 411.

[19] D. G. Blackmond, Ch. R. McMilan, S. Ramdechul, A. Schorm, J. M. Brown, *J. Am. Chem. Soc.* **2001**, *123*, 10103 – 10104.

[20] The *cis* complex, *C* or *rac*, stirred and boiled in toluene for 5 h, affords the *trans* complex in 10.5 % or 17.5 % yields, respectively, and the corresponding *cis* complex with *ee* +99 % (*C*) or *ee* 0 % (*rac*). After another 15 h reaction time, no further conversion was observed within the experimental error (Supporting Information).

 © 2003 Wiley-VCH Verlag GmbH & Co. KGaA, Weinheim

Coordination Modes of Boron

Proton-Induced Change of the Coordination Mode of a Boron Group: Boryl Complexes $[Mn(CO)_4(PR_3)(BH_2{\cdot}PMe_3)]$ and Cationic Borane σ Complexes $[Mn(CO)_4(PR_3)(\eta^1\text{-}BH_3{\cdot}PMe_3)]^+$**

Takahiro Yasue, Yasuro Kawano, and Mamoru Shimoi**

Protonation of hydrido complexes is one of the important synthetic methods in the chemistry of these interesting systems.[1–5] However, this methodology has been applied

[*] Dr. Y. Kawano, Prof. M. Shimoi, Dr. T. Yasue
Department of Basic Science
Graduate School of Arts and Sciences
University of Tokyo, Meguro-ku, Tokyo 153-8902 (Japan)
Fax: (+81) 3-5454-6567
E-mail: ykawano@jcom.home.ne.jp
cshimoi@mail.ecc.u-tokyo.ac.jp

[**] ($PR_3 = PMe_2Ph$, PEt_3).

 DOI: 10.1002/anie.200219992 © 2003 Wiley-VCH Verlag GmbH & Co. KGaA, Weinheim

sparsely in the preparation of other types of mononuclear σ complexes.[6] We have explored the coordination chemistry of $BH_3{\cdot}PMe_3$ and reported base-stabilized boryl complexes (e.g., $[Cp^*M(CO)_3(BH_2{\cdot}PMe_3)]$ (M = Mo, W[7]) and $[Cp^*M(CO)_2(BH_2{\cdot}PMe_3)]$ (M = Fe, Ru[8])) and borane σ complexes (e.g., $[M(CO)_5(\eta^1\text{-}BH_3{\cdot}PMe_3)]$ (M = Cr, Mo, W[9]) and $[CpMn(CO)_2(\eta^1\text{-}BH_3{\cdot}PMe_3)]$[10]). Herein, we report new manganese–boryl complexes, $[Mn(CO)_4(PR_3)(BH_2{\cdot}PMe_3)]$ (**1**) and their protonation to produce cationic borane σ complexes, $[Mn(CO)_4(PR_3)(\eta^1\text{-}BH_3{\cdot}PMe_3)]^+$ (**2**). Heterolytic cleavage of the metal-coordinated B–H bond of **2** is also described here.

Photolysis of $[MnMe(CO)_4(PR_3)]$ with $BH_3{\cdot}PMe_3$ resulted in the evolution of methane and gave an orange solution, from which boryl complexes $[Mn(CO)_4(PR_3)(BH_2{\cdot}PMe_3)]$ (**1a**: $PR_3 = PMe_2Ph$; **1b**: $PR_3 = PEt_3$) were isolated as pale yellow crystals in moderate yields (Scheme 1). The ^{11}B NMR spectra of complexes **1a** and **1b** display a boryl signal at lower field ($\delta = -29.4$ and -29.6 ppm, respectively) than that of $BH_3{\cdot}PMe_3$ ($\delta = -37.0$ ppm). The IR spectra of **1** show carbonyl bands shifted to lower energy in comparison to those of the precursor $[MnMe(CO)_4(PR_3)]$. These observations indicate polarization of the Mn–B bond in a Mn(−)–B(+) fashion and a resultant increase of electron density on the metal center. Similar polarization of the M–B bond has been found in phosphane-coordinated primary boryl complexes of Group 6 and 8 metals.[7,8] The solid-state structure of **1a** (Figure 1)[11] shows that this molecule adopts a highly distorted octahedral geometry. The phosphane ligand is located *cis* to the boryl group. The manganese–boron bond length (2.314(2) Å) is substantially longer than that in the catecholboryl complex $[Mn(CO)_5\{B(1,2\text{-}O_2C_6H_4)\}]$ (2.108(6) Å)[12] because of the absence of a vacant p orbital on the boron center that can be utilized for π interaction with the metal center. Two of the *cis*-carbonyl groups significantly tilt toward the boryl group. The C(2)-Mn-C(3) bond angle is 154.62(6)°. Owing to the pronounced Mn(−)–B(+) polarization mentioned above, the nature of compounds **1** closely resembles a contact ion pair composed of $[Mn(CO)_4(PR_3)]^-$ and $[BH_2{\cdot}PMe_3]^+$; the anion-like manganese moiety is isoelectronic with $Fe(CO)_5$. Consequently, the geometry of the $[Mn(CO)_4(PR_3)]$ moiety approaches a trigonal bipyramid,

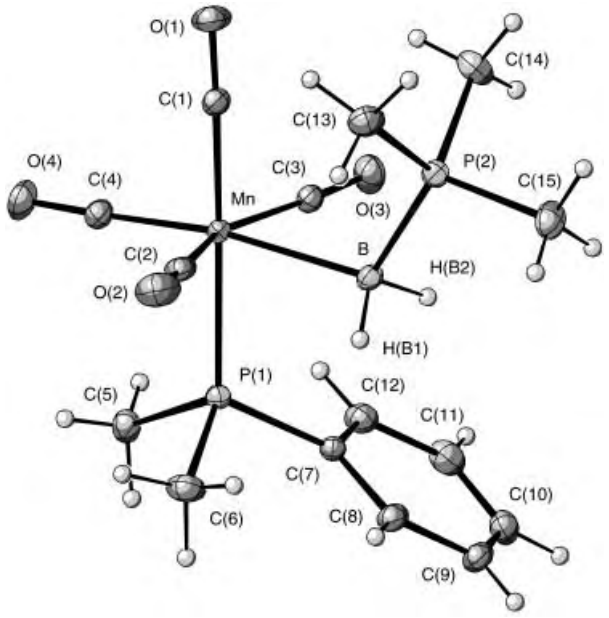
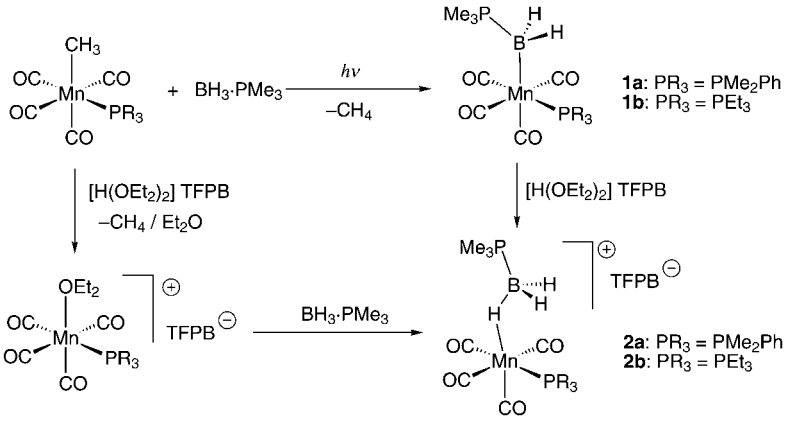


Figure 1. Structure of **1a** (ORTEP diagram; thermal ellipsoids at the 30% probability level). Selected interatomic distances [Å] and angles [°]: Mn-B 2.314(2), Mn-P(1) 2.302(1), B-P(2) 1.901(2), B-H(B1) 1.08(2), B-H(B2) 1.12(2), Mn-C(1) 1.792(2), Mn-C(2) 1.811(1), Mn-C(3) 1.814(1), Mn-C(4) 1.801(1); C(2)-Mn-C(3) 154.62(6), C(4)-Mn-B 171.76(6), Mn-B-P(2) 114.99(9).

and the Mn–B bond becomes longer. Note that more π-acidic ligands prefer to be located at equatorial positions in trigonal-bipyramidal complexes. In the $[Mn(CO)_4(PR_3)]$ fragment, π-acidic carbonyl ligands occupy the equatorial positions, and a less π-acidic phosphane ligand is situated at an apical position, which is *cis* to the boryl group in **1**.

The boryl complexes were protonated by treating **1** in $[D_2]$dichloromethane with the Brønsted acid $[H(OEt_2)_2](TFPB)$ ($TFPB = [B\{3,5\text{-}C_6H_3(CF_3)_2\}_4]$), which has a weakly coordinating anion.[13] The resulting pale yellow solutions showed a broad BH resonance signal around $\delta = -4.5$ ppm in the ^1H NMR spectra. The ^{11}B NMR spectrum of the product displayed a doublet of quartets at higher field ($\delta = -40.3$ to -40.4 ppm) than that of free $BH_3{\cdot}PMe_3$. The appearance of these signals clearly shows the formation of borane σ complexes $[Mn(CO)_4(PR_3)(\eta^1\text{-}BH_3{\cdot}PMe_3)](TFPB)$ (**2**, see Scheme 1). The value of the chemical shift of the ^{11}B NMR signal falls in the range of those for σ complexes of $BH_3{\cdot}PMe_3$.[9,10] The ^1H NMR signal around $\delta = -4.5$ ppm is assigned to the BH resonance; the ^1H NMR signals of the metal-coordinated and terminal BH protons are averaged through fast site-exchange. This process was not frozen out even at −80 °C. Similar fluxional behavior has been found in other complexes of phosphaneboranes.[9,10,14,15] Complexes **2** were also generated by methyl abstraction from $[MnMe(CO)_4(PR_3)]$ using $[H(OEt_2)_2](TFPB)$, followed by addition of $BH_3{\cdot}PMe_3$. These complexes have a lifetime of a few days, and can be observed by spectroscopy; however, they could not be isolated in pure forms.



Scheme 1. Syntheses of complexes **1** and **2**.

 © 2003 Wiley-VCH Verlag GmbH & Co. KGaA, Weinheim

Figure 2 shows the DFT-optimized structure of the model compound $[Mn(CO)_4(PH_3)(\eta^1\text{-}BH_3{\cdot}PMe_3)]^+$ (**2c**).[16,17] It resembles the structure of $[M(CO)_5(\eta^1\text{-}BH_3{\cdot}PMe_3)]$ (M = Cr, W) except for the metal-coordinated phosphane ligand. The Mn···B interatomic distance (2.780 Å) is far longer than that of **1a**, and the Mn-H-B bond angle is 133.44°. Thus, the mode of coordination for the borane ligand is essentially end-on. The B–H(1) bond length is 1.270 Å, and the B–H σ bond is elongated by about 6% on coordination.

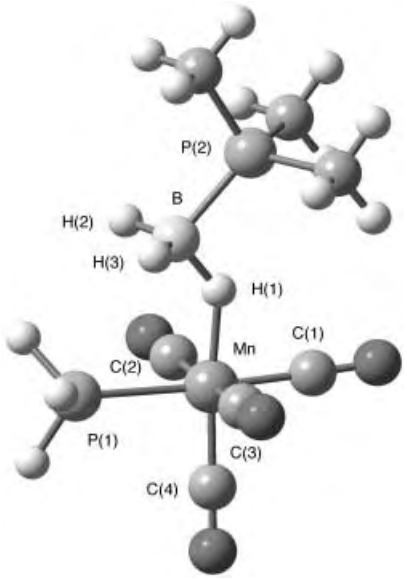
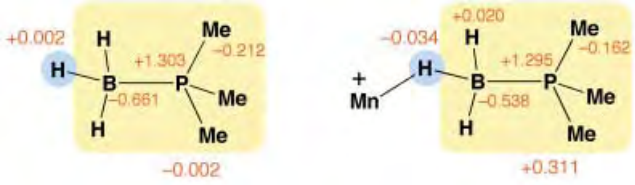


Figure 2. DFT-optimized structure of **2c**. Selected interatomic distances [Å] and angles [°]: Mn···B 2.780, Mn-H(1) 1.753, B-H(1) 1.270, B-H(2) 1.200, B-H(3) 1.200, B-P(2) 1.950, Mn-P(1) 2.380, Mn-C(1) 1.840, Mn-C(2) 1.880, Mn-C(3) 1.880, Mn-C(4) 1.840; Mn-H(1)-B 133.44, P(1)-Mn-C(1) 176.80.

Borane σ complexes **2** are formally the conjugate acids of **1**. However, deprotonation from **2** did not occur even when they were treated with bases such as NaH and diazabicycloundecene. On the other hand, a solution of **2** decomposed in a few days at room temperature to give a mixture containing $[MnH(CO)_4(PR_3)]$ and $[BH_2{\cdot}2PMe_3]^+$, although the decomposition process was not very clean. This suggests the coordinated B–H σ bond of complexes **2** cleaves heterolytically into H^- and "$[BH_2{\cdot}PMe_3]^+$".[18] Recently, Kubas and co-workers reported similar heterolytic cleavage of H_2 and silanes on the cationic manganese or rhenium fragments $[M(CO)_{5-n}(PR_3)_n]^+$ (M = Mn, Re, n = 1, 2).[19] The electron-deficient metal centers undergo strong σ donation from the H–H, Si–H, as well as B–H σ orbitals, but backdonation into the corresponding σ* orbitals hardly occurs. Therefore, the electron density of these σ ligands is significantly reduced and the metal-coordinated σ bond is activated heterolytically. The natural bond orbital (NBO) analysis based on the aforementioned DFT calculations on **2c** shows that the bridging hydrogen atom of the borane ligand becomes more hydridic on coordination to the cationic manganese center.[20] Its natural charge is −0.034, whereas that of the B–H hydrogen atom of free $BH_3{\cdot}PMe_3$ is +0.002. At the same time, that of the "$BH_2{\cdot}PMe_3$" group increases from −0.002 to +0.311 (Scheme 2). The electron density of the $BH_3{\cdot}PMe_3$ ligand is thus withdrawn toward the bridging hydrogen by the highly electrophilic $[Mn(CO)_4(PR_3)]^+$ ion in the cationic borane complexes.



Scheme 2. NBO charge distribution in free $BH_3{\cdot}PMe_3$ (left) and **2c** (right).

Experimental Section

1a: A mixture of $[MnMe(CO)_4(PMe_2Ph)]$ (247 mg, 0.75 mmol) and $BH_3{\cdot}PMe_3$ (203 mg, 2.28 mmol) in hexane (10 mL) was photolyzed at 3 °C for 90 min using a 450 W medium-pressure Hg arc lamp. The resulting solution was evaporated and evacuated for 1 h to remove excess $BH_3{\cdot}PMe_3$. Recrystallization of the solid residue from hexane at −80 °C provided pale yellow crystals of **1a** (90 mg, 31%). Compound **1b** was obtained in an analogous manner in 15% yield.

Data for **1a**: ^{1}H NMR (500 MHz, [D$_6$]benzene, 23 °C, TMS): δ = 0.88 (d, ^2J(P,H) = 10.0 Hz, 9H; PMe_3), 1.49 (d, ^2J(P,H) = 8.5 Hz, 6H; P*Me*$_2$Ph), 7.02, 7.09, 7.36 ppm (m, 5H; PMe_2*Ph*), the BH proton signals were too broad to be observed; ^{11}B NMR (160.4 MHz, [D$_6$]benzene, 23 °C, $BF_3{\cdot}OEt_2$): δ = −29.4 ppm (dt, ^1J(B,H) = 105.3 Hz, ^1J(B,P) = 73.5 Hz); ^{31}P NMR (202.4 MHz, [D$_6$]benzene, 23 °C, 85% H_3PO_4): δ = 27.3 (br; PMe_2Ph), 0.9 ppm (br; PMe_3); ^{13}C NMR (125.7 MHz, [D$_6$]benzene, 23 °C, TMS): δ = 13.0 (d, ^1J(C,P) = 36.7 Hz; PMe_3), 16.6 (d, ^1J(C,P) = 29.3 Hz; P*Me*$_2$Ph), 129.0, 129.4 (d, ^1J(C,P) = 7.3 Hz), 140.7 (d, ^1J(C,P) = 38.1 Hz) (Ph), 219.9, 226.8, 227.9 ppm (CO); IR (KBr): $\tilde{\nu}$ = 1893.8 (vs), 1906.3 (vs), 1925.6 (vs), 2008.5 (s) (C≡O), 2357 (w) (BH) cm^{-1}; MS (EI, 70 eV): *m*/*z* (%): 394 (12) [*M*$^+$], 366 (89) [*M*$^+$−CO], 338 (24) [*M*$^+$−2CO], 320 (60) [*M*$^+$−PMe_3], 310 (30) [*M*$^+$−3CO], 282 (100) [*M*$^+$−4CO]; elemental analysis (%) calcd for $C_{15}H_{22}BMnO_4P_2$: C 45.72, H 5.63; found: C 45.64; H, 5.57.

Data for **1b**: ^{1}H NMR (500 MHz, [D$_6$]benzene, 23 °C, TMS): δ = 0.91 (dt, ^3J(H,H) = 7.5 Hz, ^3J(P,H) = 15.5 Hz, 9H; $P(CH_2CH_3)_3$), 0.92 (d, ^2J(P,H) = 10.5 Hz, 9H; PMe_3), 1.59 ppm (dq, ^3J(H,H) ≈ ^2J(P,H) = 7.5 Hz, 6H; $P(CH_2CH_3)_3$), the BH proton signals were too broad to be observed; ^{11}B NMR (160.4 MHz, [D$_6$]benzene, 23 °C, $BF_3{\cdot}OEt_2$): δ = −29.6 ppm (dt, ^1J(B,H) = 106.3 Hz, ^1J(B,P) = 71.2 Hz); ^{31}P NMR (202.4 MHz, [D$_6$]benzene, 23 °C, 85% H_3PO_4): δ = 43.0 (br; PEt_3), 0.7 ppm (br; PMe_3); ^{13}C NMR (125.7 MHz, [D$_6$]benzene, 23 °C, TMS): δ = 7.5 ($P(CH_2CH_3)_3$), 12.9 (d, ^1J(C,P) = 37.1 Hz; PMe_3), 19.0 (d, ^1J(C,P) = 24.6 Hz; $P(CH_2CH_3)_3$), 129.0, 129.4 (d, ^1J(C,P) = 7.3 Hz), 140.7 (d, ^1J(C,P) = 38.1 Hz) (Ph), 220.5, 227.8, 228.0 ppm (br; CO); IR (KBr): $\tilde{\nu}$ = 1889 (vs), 1910 (vs), 2004 (vs) (C≡O), 2357 (w) (BH) cm^{-1}; MS (EI, 70 eV): *m*/*z* (%): 374 (5) [*M*$^+$], 346 (24) [*M*$^+$−CO], 318 (5) [*M*$^+$−2CO], 290 (3) [*M*$^+$−3CO], 262 (100) [*M*$^+$−4CO], 173 (27) [$Mn(PEt_3)^+$], 144 (60) [$Mn(BH_2{\cdot}PMe_3)^+$]; elemental analysis (%) calcd for $C_{13}H_{26}BMnO_4P_2$: C 41.74, H 7.01; found: C 41.57, H 6.85.

2a: Compound **1a** (41 mg, 0.10 mmol) and $[H(OEt_2)_2](TFPB)$ (362 mg, 0.36 mmol) were combined in dichloromethane (10 mL) under vacuum. After the mixture had been stirred for 3 h, volatiles were evaporated to dryness. The ^{1}H, ^{11}B, and ^{31}P NMR spectra of the resulting yellow residue indicated complete consumption of **1a** and

 © 2003 Wiley-VCH Verlag GmbH & Co. KGaA, Weinheim

displayed new signals assignable to **2a**. Alternatively, **2a** was cleanly generated by addition of $BH_3{\cdot}PMe_3$ to a solution of $[Mn(CO)_4(PMe_2Ph)(OEt_2)]^+$, which was produced by the reaction of $[MnMe(CO)_4(PMe_2Ph)]$ with $[H(OEt_2)_2](TFPB)$ in diethyl ether. The PEt_3 derivative **2b** was prepared by similar methods.

Data for **2a**: ^{1}H NMR (500 MHz, $[D_2]$dichloromethane, 23 °C, TMS): $\delta = -4.48$ (br, 3H; BH), 1.32 (d, $^2J(P,H) = 11.5$ Hz, 9H; PMe_3), 1.98 (d, $^2J(P,H) = 9.0$ Hz, 6H; PMe_2Ph), 7.57, 7.72 ppm (s, 1H, 2H; $[B\{C_6H_3(CF_3)_2\}_4]$); ^{11}B NMR (160.4 MHz, $[D_2]$dichloromethane, 23 °C, $BF_3{\cdot}OEt_2$): $\delta = -40.4$ (dq, $^1J(B,H) = 81$ Hz, $^1J(B,P) = 70$ Hz; $BH_2{\cdot}PMe_3$), −6.7 ppm (s; TFPB); ^{31}P NMR (202.4 MHz, $[D_2]$dichloromethane, 23 °C, 85% H_3PO_4): $\delta = -4.0$ (br; PMe_3), 15.0 ppm (br; PMe_2Ph); MS (FAB, sulfolane): *m/z* (%): 367 (10) $[M^+-CO]$, 193 (100) $[Mn(PMe_2Ph)^+]$, 139 (43) $[PHMe_2Ph^+]$.

Data for **2b**: ^{1}H NMR (500 MHz, $[D_2]$dichloromethane, 23 °C, TMS): $\delta = -4.43$ (br, 3H; BH), 1.10–1.22 (m, 9H; $P(CH_2CH_3)_3$), 1.35 (d, $^2J(P,H) = 11.5$ Hz, 9H; PMe_3), 1.72–1.80 (m, 6H; $P(CH_2CH_3)_3$), 7.57, 7.72 ppm (s, 1H, 2H; $[B\{C_6H_3(CF_3)_2\}_4]$); ^{11}B NMR (160.4 MHz, $[D_2]$dichloromethane, 23 °C, $BF_3{\cdot}OEt_2$): $\delta = -40.3$ (br), −6.7 ppm (s; TFPB); ^{31}P NMR (202.4 MHz, $[D_2]$dichloromethane, 23 °C, 85% H_3PO_4): $\delta = -5.3$ (br; PMe_3), 48.7 ppm (br; PEt_3); MS (FAB, sulfolane): *m/z* (%): 173 (100) $[Mn(PEt_3)^+]$, 120 (28) $[PHEt_3^+]$.

Received: August 19, 2002
Revised: December 3, 2002 [Z19992]

Keywords: boranes · boron · coordination modes · manganese · protonation

[1] R. H. Crabtree, *Acc. Chem. Res.* **1990**, *23*, 95.
[2] R. H. Morris, P. G. Jessop, *Coord. Chem. Rev.* **1992**, *121*, 155.
[3] D. M. Heinkey, W. J. Oldham, Jr., *Chem. Rev.* **1993**, *93*, 913.
[4] R. H. Crabtree, *Angew. Chem.* **1993**, *105*, 823; *Angew. Chem. Int. Ed. Engl.* **1993**, *32*, 789.
[5] G. J. Kubas, *Metal Dihydrogen and σ-Bond Complexes*, Kluwer Academic/Plenum Publishers, New York, **2001**.
[6] a) Protonation of a silyl complex $[CpRu(PMe_3)_2SiCl_3]$: F. R. Lemke, *J. Am. Chem. Soc.* **1994**, *116*, 11183; S. T. N. Freeman, F. R. Lemke, L. Brammer, *Organometallics* **2002**, *21*, 2030; b) protonation of $[CpFe(CO)(PEt_3)SiEt_3]$: E. Scharrer, S. Chang, M. Brookhart, *Organometallics* **1995**, *14*, 5686.
[7] Y. Kawano, T. Yasue, M. Shimoi, *J. Am. Chem. Soc.* **1999**, *121*, 11744.
[8] T. Yasue, Y. Kawano, M. Shimoi, *Chem. Lett.* **2000**, 58.
[9] M. Shimoi, S. Nagai, M. Ichikawa, Y. Kawano, K. Katoh, M. Uruichi, H. Ogino, *J. Am. Chem. Soc.* **1999**, *121*, 11704.
[10] T. Kakizawa, Y. Kawano, M. Shimoi, *Organometallics* **2001**, *20*, 3211.
[11] Crystal data for **1a**: pale yellow crystals, triclinic, space group $P\bar{1}$ (no. 2); $T = 150$ K; $a = 10.5746(8)$, $b = 10.6779(9)$, $c = 9.0029(7)$ Å; $\alpha = 109.026(2)$, $\beta = 96.043(3)$, $\gamma = 88.092(2)°$; $V = 955.69(13)$ Å^3; $Z = 2$, $R = 0.024$, $wR2 = 0.060$ for 4070 reflections with $|F_o| > 3\sigma(F_o)$, 296 parameters, GoF = 1.110. The boron-attached hydrogen atoms were found by the difference Fourier syntheses and their positions were refined. CCDC-190001 contains the supplementary crystallographic data for this paper. These data can be obtained free of charge via www.ccdc.cam.ac.uk/conts/retrieving.html (or from the Cambridge Crystallographic Data Centre, 12, Union Road, Cambridge CB21EZ, UK; fax: (+44) 1223-336-033; or deposit@ccdc.cam.ac.uk).
[12] K. M. Waltz, H. He, C. N. Muhoro, J. F. Hartwig, *J. Am. Chem. Soc.* **1995**, *117*, 11357.
[13] M. Brookhart, B. Grant, A. F. Vople, Jr., *Organometallics* **1992**, *11*, 3920.
[14] R. Macías, N. P. Rath, L. Barton, *Angew. Chem.* **1999**, *111*, 203; *Angew. Chem. Int. Ed.* **1999**, *38*, 162.
[15] M. Ingleson, N. J. Patmore, G. D. Ruggiero, C. G. Frost, M. F. Mahon, M. C. Willis, A. S. Weller, *Organometallics* **2001**, *20*, 4434.
[16] The stationary point was located at the B3LYP level of theory, by using density functional theory calculations based on hybrid functionals. A double ζ plus polarization valence basis set, 6-31G(d) was employed for all the atoms except manganese. For Mn, a basis set with an approximation of effective core potentials, LANL2DZ was applied. The NBO analysis was carried out on the resulting structure at the B3LYP level using a 6–311 + G(2d,p) basis set.[20] All calculations were performed with the Gaussian 98W package of programs.[17]
[17] Gaussian 98 (Revision A.11), M. J. Frisch, G. W. Trucks, H. B. Schlegel, G. E. Scuseria, M. A. Robb, J. R. Cheeseman, V. G. Zakrzewski, J. A. Montgomery, R. E. Stratmann, J. C. Burant, S. Dapprich, J. M. Millam, A. D. Daniels, K. N. Kudin, M. C. Strain, O. Farkas, J. Tomasi, V. Barone, M. Cossi, R. Cammi, B. Mennucci, C. Pomelli, C. Adamo, S. Clifford, J. Ochterski, G. A. Petersson, P. Y. Ayala, Q. Cui, K. Morokuma, D. K. Malick, A. D. Rabuck, K. Raghavachari, J. B. Foresman, J. Cioslowski, J. V. Ortiz, B. B. Stefanov, G. Liu, A. Liashenko, P. Piskorz, I. Komaromi, R. Gomperts, R. L. Martin, D. J. Fox, T. Keith, M. A. Al-Laham, C. Y. Peng, A. Nanayakkara, C. Gonzalez, M. Challacombe, P. M. W. Gill, B. G. Johnson, W. Chen, M. W. Wong, J. L. Andres, M. Head-Gordon, E. S. Replogle, J. A. Pople, Gaussian, Inc., Pittsburgh, PA, **2001**.
[18] Several boryl cations with the formula $[BX_2{\cdot}L]^+$ (L = neutral Lewis base) have been reported: P. Kölle, H. Nöth, *Chem. Rev.* **1985**, *85*, 399.
[19] a) J. Huhmann-Vincent, B. L. Scott, G. J. Kubas, *Inorg. Chim. Acta* **1999**, *294*, 240; b) J. Huhmann-Vincent, B. L. Scott, G. J. Kubas, *J. Am. Chem. Soc.* **1998**, *120*, 6808; c) X. Fang, J. Huhmann-Vincent, B. L. Scott, G. J. Kubas, *J. Organomet. Chem.* **2000**, *609*, 95; d) J. Huhmann-Vincent, B. L. Scott, G. J. Kubas, *Inorg. Chem.* **1999**, *38*, 115; e) X. Fang, B. L. Scott, K. D. John, G. J. Kubas, *Organometallics* **2000**, *19*, 4141.
[20] E. D. Glendening, A. E. Reed, J. E. Carpenter, F. Weinhold, NBO version 3.1.

Photoresponsive Nanocomposites

Photoresponsive Nanocomposite Formed by Self-Assembly of an Azobenzene-Modified Silane**

*Nanguo Liu, Zhu Chen, Darren R. Dunphy, Ying-Bing Jiang, Roger A. Assink, and C. Jeffrey Brinker**

Mesoporous materials made by surfactant-directed self-assembly (SDSA) have been of great interest in the past decade because of their potential applications in catalysis, membrane separations, adsorption, and chemical sensing.[1–6] In SDSA, inorganic moieties formed by alkoxide hydrolysis interfacially coorganize with hydrophilic surfactant headgroups to form periodically ordered hybrid mesophases. After condensation and removal of surfactant molecules by heat or solvent extraction, a periodic mesoporous inorganic matrix is created. To expand the range of applications as well as create new properties, various organic functional groups have been covalently incorporated onto the pore surfaces of mesoporous materials, including phenyl, octyl, aminoalkyl, cyanoalkyl, thioloalkyl, epoxyl, and vinyl groups.[6–10] However, to date, these modifications have provided mainly "passive" functionality, such as controlled wetting properties, reduced dielectric constants, or enhanced adsorption of metal ions. By comparison, materials with "active" functionality would enable properties to be dynamically controlled by external stimuli, such as pH, temperature, or light. In an effort to make such active hybrid materials, Ogawa et al. intercalated azobenzene moieties within a clay (magadiite), which resulted in a hybrid layered composite in which restricted photoisomerization caused the *d* spacing to change reversibly by 0.6 Å upon exposure to UV and visible light.[11] Several groups have reported[12 13] or suggested the formation of photoactive hybrids through SDSA of azobenzene of pyridylethylene bridged silsesquioxanes. For a lamellar mesostructure, Brinker and co-workers. showed the *d* spacing to be optically controllable through photoisomerization of the azobenzene moiety before or after self-assembly. Alvaro et al.[13] doped 1,2-bis(4-pyridyl)ethylene in the wall of a hexagonal mesoporous silica and provided preliminary evidence of photo-induced changes in the surface area and pore volume.

As shown in Figure 1, the incorporation of covalently bonded "switchable" ligands as pendant groups (as opposed to bridging groups[12–14]) within a porous (rather than a layered[11 12]) framework is expected to result in nanocomposites, in which the pore size, surface area, and adsorptive properties are externally controllable. In such synergistic nanocomposites, the 3D organization of the responsive ligands allows the transduction of photo, chemical, or thermal energy into a useful mechanical response of interest for molecular valves or gates, with potential applications in smart gas masks, membranes, controlled release systems, and new types of externally controlled micro/nanofluidic-channel systems. In addition, the rigid framework could serve to enhance the mechanical, chemical, and thermal stability of the responsive moieties, thus fostering their integration into devices.

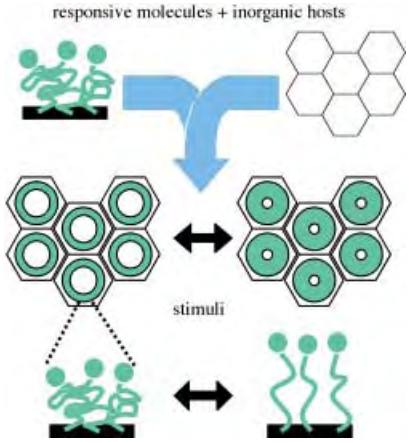


Figure 1. Concept of responsive nanocomposites: Organization of stimuli responsive ligands within a 3D porous framework imparts new molecular-level functionality, which is useful for opening and closing a nanoscale valve. (Adapted from Bruce Bunker, unpublished work).

Herein we report the SDSA of a novel photoresponsive azobenzene-containing organosilane, 4-(3-triethoxysilylpropylureido)azobenzene (TSUA) into an ordered, periodic silica framework to make photoresponsive nanocomposites. Azobenzene derivatives were selected because of their well-studied response to light.[15–18] UV irradiation of the *trans* isomer causes transformation to the *cis* isomer. Removal of the UV radiation, heating, or irradiation with a longer wavelength switches the system back to the *trans* form.

Photoresponsive thin-film nanocomposites were fabricated by an evaporation-induced self-assembly (EISA) procedure by using the nonionic surfactant, Brij56 ($C_{16}H_{33}(OCH_2CH_2)_nOH$, $n \sim 10$), as a structure-directing agent.[19] TSUA was mixed with tetraethyl orthosilicate (TEOS) in a homogeneous ethanol/water solution with an initial surfactant concentration less than the critical micelle concentration (cmc) and an acid concentration designed to minimize the siloxane condensation rate, thereby avoiding

[*] Prof. Dr. C. J. Brinker, Dr. D. R. Dunphy, Dr. R. A. Assink
Sandia National Laboratories, MS 1349
Albuquerque, NM 87106 (USA)
Fax: (+1) 505-272-7336
E-mail: cjbrink@sandia.gov
Prof. Dr. C. J. Brinker, N. Liu, Z. Chen, Y.-B. Jiang
Chemical and Nuclear Engineering Department and
Center for Micro-Engineered Materials
The University of New Mexico
Albuquerque, NM 87131 (USA)

[**] This work was supported by the Air Force Office of Scientific Research Award Number F49620-01-1-0168, the DOD MURI Program Contract 318651, the DOE Office of Basic Energy Sciences, and SNL Lab Directed Research and Development Program. Sandia National Laboratories (SNL) is a Lockheed Martin Company, operated by the U.S. Department of Energy under Contract DE-AC04–94AL85000.

Supporting information for this article is available on the WWW under http://www.angewandte.org or from the author.

 DOI: 10.1002/anie.200250189 © 2003 Wiley-VCH Verlag GmbH & Co. KGaA, Weinheim

premature gelation, which would frustrate the self-assembly process. In EISA, ethanol evaporation accompanying spin or dip coating enriches the depositing film in water, surfactant, and silica constituents, which results in the self-assembly of silica-surfactant micelles and their further organization into liquid-crystalline mesophases.[2,19] For TSUA-containing sols, we suspect that the amphiphilic nature of the hydrolyzed TSUA molecule will position the hydrophobic propylureidoazobenzene groups in the hydrophobic micellar cores and that the silicic acid groups will be coorganized with hydrolyzed TEOS moieties at the hydrophilic micellar exteriors. In this fashion, TSUA is ultimately incorporated onto the pore surfaces with the azobenzene ligands disposed towards the pore interiors. A subsequent solvent extraction[7,8] results in a mesoporous silica framework derivatized with azobenzene ligands, which are isomerizable by light and thermal stimuli (Figure 2). The dimensional change of the propylureidoazobenzene ligand associated with this isomerization mechanism is estimated to be 3.4 Å based on molecular modeling with Chem3D Pro 5.5 software (Figure 2).

Figure 3 shows a representative X-ray diffraction (XRD) pattern and cross-sectional transmission electron microscopy (TEM) image of a prepared nanocomposite film. The XRD pattern shows a strong reflection at 2.8 nm and a weaker reflection at 1.4 nm. The TEM cross-sectional image and electron diffraction pattern (Figure 3, inset) are consistent with a cubic mesostructure with an average center-to-center pore spacing of 5.6 nm (measured directly from the TEM image and calculated from the electron diffraction pattern) in the direction perpendicular to the substrate. A TEM plan-view image shows a similar pattern. Based on these results, we suggest that the (100) plane of the body-centered cubic (BCC, $Im\bar{3}m$ space group) mesophase is oriented parallel to the substrate, consistent with previous reports,[20,21] which allows the two XRD peaks to be assigned to the d_{200} and d_{400} reflections, respectively. The BCC mesophase is distorted slightly because of greater shrinkage in the direction perpendicular to the substrate than parallel to the substrate resulting from siloxane condensation.

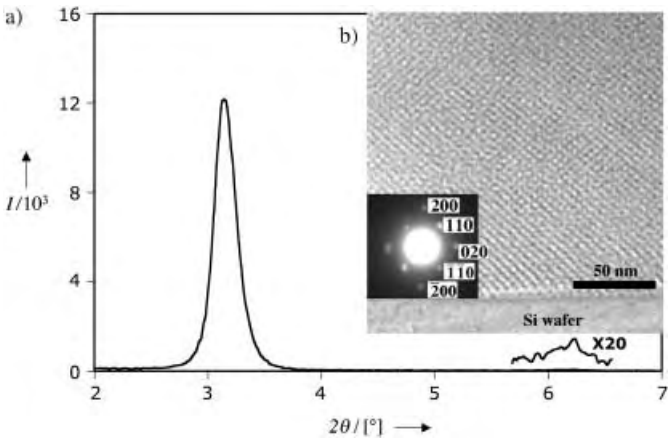


Figure 3. a) XRD and b) TEM cross-section image of a photoresponsive nanocomposite. The inset is an electron diffraction pattern corresponding to the [001] zone axis.

UV/Vis spectroscopy was used to characterize the photo and thermal responsiveness of the incorporated azobenzene ligands. Figure 4 shows the UV/Vis spectra of thin films after exposure to varying conditions of UV irradiation (8 W, $\lambda =$ 302 nm), room light, or heat. The absorption band at 350 nm is attributed to the $\pi \rightarrow \pi^*$ transition of the *trans* isomer and the band at 460 nm to the $n \rightarrow \pi^*$ transition of the *cis* isomer. UV irradiation causes a progressive *trans* to *cis* isomerization as noted by the decrease of the 350 nm band and increase of the 460 nm band, with a photostationary state reached after 30 minutes (Figure 4 spectrum b). Exposure to room light or heat caused the reverse isomerization (*cis*→*trans*). For example, from the photostationary state (Figure 4 spectrum b), a room-light exposure resulted in a progressive increase in the intensity of the 350 nm absorption band and a progressive decrease in the 460 nm absorption band (Figure 4 spectra c–f). A lengthy (12 hour) room-light exposure resulted in an increase in the intensity of the 350 nm absorption band close to that of the prepared film. Alternatively heat treatment (100 °C, for 5 minutes in the dark) caused the intensity of the 350 nm absorption band to exceed

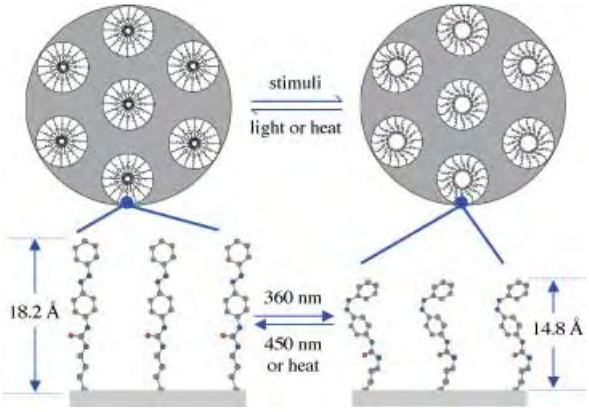


Figure 2. Photoresponsive nanocomposites prepared by EISA. The *trans* or *cis* conformation of azobenzene unit was calculated using Chem3D Pro 5.5 molecular modeling analysis software. Atom labels: C: grey, O: red, N: dark blue, Si: blue, H atoms are omitted.

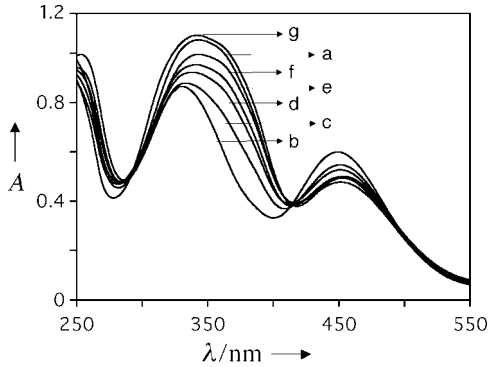


Figure 4. Photo and thermal isomerization of azobenzene ligands in the nanocomposite films prepared with Brij56 template. a) Prepared; b) after UV irradiation for 30 minutes; c, d, e, f) after room-light exposure of the sample (b) for 3, 15, 35, and 60 minutes, respectively; g) after heating the sample (b) to 100 °C for 5 minutes.

 © 2003 Wiley-VCH Verlag GmbH & Co. KGaA, Weinheim

that of the prepared nanocomposite film (Figure 4 spectrum g), which indicates that a certain amount of azobenzene ligands were in the *cis* conformation in the prepared films. These results, which are completely reversible, demonstrate the facile photoisomerization characteristics of the pendant azobenzene ligands in the ordered porous nanocomposite. As a control experiment, we prepared films with the same sol in the absence of Brij56. In this case, the azobenzene ligands were randomly incorporated into a microporous silica matrix and exhibited no detectable photoisomerization. Similarly we observed no photoisomerization for the ordered self-assembled films prior to solvent extraction of the surfactant templates. Only upon surfactant removal did we create the pore volume required (estimated as 127 $Å^3$ [22]) for photoisomerization. These results unambiguously locate the photosensitive azobenzene ligands along with surfactant within the uniform nanopores of the self-assembled films, and emphasize the need to accommodate the steric demands of the photoisomerization process by engineering the pore size (as noted previously for adsorbed azobenzene dyes[18]) and by positioning the photoactive species on the pore surface. Correspondingly, nanocomposite films prepared by using a triblock copolymer surfactant $EO_{20}PO_{70}EO_{20}$ (P123), which had larger pores (about 6.5 nm in diameter), exhibited a faster and more complete *trans* to *cis* isomerization, close to that of TSUA in EtOH, presumably because the azobenzene ligands were less sterically constrained (see Supporting Information).

Studies of the photoresponsive mesoporous films by ^{29}Si MAS NMR spectroscopy (MAS = magic-angle spinning) showed T^2, T^3, Q^2, Q^3, and Q^4 resonances at $\delta = -52.81$, -62.11, -93.18, -99.69, and -107.12 ppm, respectively. The total amount of T ($T^2 + T^3$) is 11%, consistent with the molar ratio of TSUA/TEOS added in the starting sol. The extents of condensation of the T and Q species are 93% and 82%, respectively, thus proving covalent attachment of the azobenzene ligands to the pore surface and demonstrating the stability of the Si–C bonds throughout the self-assembly and extraction processes.

Thermogravimetric analysis (TGA) of photoresponsive mesoporous materials in air showed about 16% weight loss from 194 to 288 °C and about 18% weight loss from 288 to 620 °C, the latter arising from the decomposition of the azobenzene ligands. Analysis of the N_2 sorption isotherms[23] by SAW techniques (SAW = surface acoustic wave) after calcination at 450 °C, to remove the azobenzene ligands, indicated a pore diameter of 2.5 nm and surface area of 619 $m^2 g^{-1}$. Taking into account film shrinkage during calcination (~30 vol%) versus solvent extraction (~10 vol%), we estimate pore diameters to be about 3.6 nm and 3.2 nm before and after surfactant removal, respectively, thus requiring the *trans* isomers to be at least slightly tilted from the surface normal in of the extracted films. Based on surface area and weight loss, the surface coverage is estimated to be about 1.2 azobenzene ligands nm^{-2}, which corresponds to an average ligand-to-ligand spacing of $(1/1.2\ nm^2)^{1/2} = 0.9$ nm. By using a molar absorption coefficient of $2.59 \times 10^4\ M^{-1} cm^{-1}$ for the *trans* isomer (determined from UV/Vis spectra of TSUA solutions in ethanol), we calculated the *trans* isomer concentration in the films to be 1.55, 1.52, and 1.12 M, respectively, for samples g, a, and b in Figure 4. Both the surface coverage and the molar concentrations of azobenzene ligands in the self-assembled films greatly exceed those attainable by dye adsorption in mesoporous films.[18]

As illustrated in Figure 2, the positioning of photoisomerizable ligands on the surface of uniformly sized pores should enable photo control of the pore size.[*] Ideally, with radially oriented azobenzene ligands, we can expect to change the pore size by about 6.8 Å. This optomechanical actuation could serve to open or close a nanopore or change the transport-limiting pore size in a membrane. Additionally, there is a significant dipole moment change associated with *trans–cis* isomerization (0–3 D),[24] which could strongly influence ion transport. Optical control of both pore size and dipole moment in a uniform silica nanopore could lead to robust, synthetic ion channels needed for practical stochastic sensing devices.[25] In this regard it is noteworthy that the modification of a gramicidin A channel with a single azobenzene moiety enabled optical switching of ion fluxes.[24]

Experimental Section

TSUA was prepared by an isocyanato–amino coupling reaction between triethoxysilylpropyl isocyanate and 4-phenylazoaniline, then purified by recrystallization. In a typical synthesis of a photoresponsive nanocomposte thin film, Brij56 (0.27 g) and TSUA (0.26 g, 0.58 mmoles) were dissolved in EtOH (6 mL) which contained TEOS (1.0 g, 4.8 mmol; Aldrich, 99.99%). After addition of HCl (0.5 mL, 0.1 M), the solution was sonicated for 3 minutes. The final molar ratio of TSUA, TEOS, EtOH, Brij56, H_2O, and HCl was 1.0:8.2:177:0.68:47.5:0.085. The mixed sol was aged for 30 minutes at room temperature and then deposited on silicon substrates by dip coating, spin coating, or casting. The surfactant molecules in the mesostructured film were extracted by refluxing the condensed thin films in an acidic ethanol solution according to previously reported procedures.[7,8]

Received: September 18, 2002
Revised: November 18, 2002 [Z50189]

Keywords: azo compounds · molecular devices · nanotechnology · photosensors · self-assembly

[1] C. T. Kresge, M. E. Leonowicz, W. J. Roth, J. C. Vartuli, J. S. Beck, *Nature* **1992**, *359*, 710–712.

[*] As noted by one reviewer it would be of interest to measure the accessible nanocomposite pore volume for the *trans* and *cis* forms of the azobenzene. We have attempted this using SAW-based nitrogen sorption. However, to get meaningful data we need to degas the coated SAW device for several hours. By using UV/Vis spectroscopy we have determined that in the dark the *cis* isomer converts into the *trans* form over a period of several hours. Thus, we are unable to acquire and legitimately compare nitrogen sorption isotherms of the *trans* and *cis* forms. However, in a preliminary experiment we modified the electrode of a photochemical cell with our photoresponsive film and, by using ferrocene as a molecular probe, performed a chronoamperometry experiment with and without UV exposure. We observed a reversible optically mediated response, which indicates the reversible photoregulation of mass transport.

 © 2003 Wiley-VCH Verlag GmbH & Co. KGaA, Weinheim

[2] Y. Lu, R. Ganguli, C. A. Drewien, M. T. Anderson, C. J. Brinker, W. L. Gong, Y. X. Guo, H. Soyez, B. Dunn, M. H. Huang, J. I. Zink, *Nature* **1997**, *389*, 364 – 368.
[3] G. Wirnsberger, B. J. Scott, G. D. Stucky, *Chem. Commun.* **2001**, 119 – 120.
[4] N. A. Melosh, P. Lipic, F. S. Bates, F. Wudl, G. D. Stucky, G. H. Fredrickson, B. F. Chmelka, *Macromolecules* **1999**, *32*, 4332 – 4342.
[5] D. Grosso, A. R. Balkenende, P. A. Albouy, A. Ayral, H. Amenitsch, F. Babonneau, *Chem. Mater.* **2001**, *13*, 1848 – 1856.
[6] X. Feng, G. E. Fryxell, L.-Q. Wang, A. Y. Kim, J. Liu, K. M. Kemner, *Science* **1997**, *276*, 923 – 926.
[7] S. L. Burkett, S. D. Sims, S. Mann, *Chem. Commun.* **1996**, *11*, 1367 – 1368.
[8] C. E. Fowler, S. L. Burkett, S. Mann, *Chem. Commun.* **1997**, 1769 – 1770.
[9] C. E. Fowler, B. Lebeau, S. Mann, *Chem. Commun.* **1998**, 1825 – 1826.
[10] S. R. Hall, C. E. Fowler, B. Lebeau, S. Mann, *Chem. Commun.* **1999**, 201 – 202.
[11] M. Ogawa, T. Ishii, N. Miyamoto, K. Kuroda, *Adv. Mater.* **2001**, *13*, 1107 – 1109.
[12] N. Liu, K. Yu, B. Smarsly, D. R. Dunphy, Y.-B. Jiang, C. J. Brinker, *J. Am. Chem. Soc.* **2002**, *124*, 14540 – 14541.
[13] M. Alvaro, B. Ferrer, H. Garcia, F. Rey, *Chem. Commun.* **2002**, 2012 – 2013.
[14] M. J. MacLachlan, T. Asefa, G. A. Ozin, *Chem. Eur. J.* **2002**, *6*, 2507 – 2511.
[15] G. S. Kumar, D. C. Neckers, *Chem. Rev.* **1989**, *89*, 1915 – 1925.
[16] M. Ueda, H.-B. Kim, T. Ikeda, K. Ichimura, *Chem. Mater.* **1992**, *4*, 1229 – 1233.
[17] L. M. Siewierski, W. J. Brittain, S. Petrash, M. D. Foster, *Langmuir* **1996**, *12*, 5838 – 5844.
[18] M. Ogawa, K. Kurodacd, J.-i. Moric, *Chem. Commun.* **2000**, 2441 – 2442.
[19] C. J. Brinker, Y. Lu, A. Sellinger, H. Fan, *Adv. Mater.* **1999**, *11*, 579 – 565.
[20] P. C. A. Alberius, K. L. Frindell, R. C. Hayward, E. J. Kramer, G. D. Stucky, B. F. Chmelka, *Chem. Mater.* **2002**, *14*, 3284 – 3294.
[21] Y. Sakamoto, M. Kaneda, O. Terasaki, D. Y. Zhao, J. M. Kim, G. Stucky, H. J. Shin, R. Ryoo, *Nature* **2000**, *408*, 449 – 453.
[22] J. G. Victor, J. M. Torkelson, *Macromolecules* **1987**, *20*, 2241 – 2250.
[23] G. C. Frye, A. J. Ricco, S. J. Martin, C. J. Brinker, *Mater. Res. Soc. Symp. Proc.* **1988**, *121*, 349 – 354.
[24] V. Borisenko, D. C. Burns, Z. Zhang, G. A. Woolley, *J. Am. Chem. Soc.* **2000**, *122*, 6364 – 6370.
[25] H. Bayley, P. S. Cremer, *Nature* **2001**, *413*, 226 – 230.

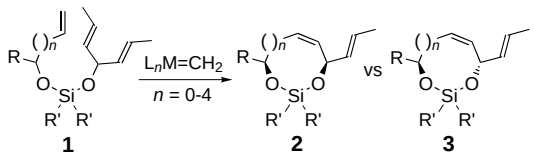
 © 2003 Wiley-VCH Verlag GmbH & Co. KGaA, Weinheim

Si-Tethered Asymmetric Induction

Diastereoselective Temporary Silicon-Tethered Ring-Closing-Metathesis Reactions with Prochiral Alcohols: A New Approach to Long-Range Asymmetric Induction**

P. Andrew Evans, Jian Cui, and Gerald P. Buffone*

The ability to control stereochemistry in substrates where the reactive elements are distal represents a fundamentally important area of investigation that is commonly referred to as long-range asymmetric induction.[1,2] Although there are numerous examples of this phenomenon, a significant limitation with this type of process is the ability to predict the manner in which the chiral group attains proximity to the reactive site in order to translate stereochemical information. The inherent challenge associated with this requirement provided the incentive for the development of a new process where the elements of stereocontrol could be conserved in a predictable manner.[1,2] Herein, we describe a new approach to long-range asymmetric induction using the diastereoselective temporary silicon-tethered (TST) ring-closing-metathesis (RCM) reaction of mixed bisalkoxy silanes **1**, derived from an allylic and prochiral alcohol, for the construction of *cis*-1,4-silaketals **2** (Scheme 1; $n = 0$). This methodology was also extended to higher homologues (where $n = 1$–4), which resulted in the formation of the opposite *trans* diastereoisomer.[3–8]



Scheme 1. General approach to the diastereoselective TST-RCM reactions with alkenyl and prochiral alcohols.

[*] Dr. P. A. Evans, Dr. J. Cui
Department of Chemistry
Indiana University
Bloomington, IN 47405 (USA)
Fax: (+1) 812-855-8300
E-mail: paevans@indiana.edu
G. P. Buffone
Department of Chemistry and Biochemistry
University of Delaware
Newark, DE 19716 (USA)

[**] We sincerely thank the National Institutes of Health (GM54623) for generous financial support. We also thank Johnson and Johnson for a Focused Giving Award, Pfizer Pharmaceuticals for the Creativity in Organic Chemistry Award, and Novartis Pharmaceuticals for an Academic Achievement Award. The Camille and Henry Dreyfus Foundation is thanked for a Camille Dreyfus Teacher-Scholar Award (P.A.E.).

Supporting information for this article is available on the WWW under http://www.angewandte.org or from the author.

 © 2003 Wiley-VCH Verlag GmbH & Co. KGaA, Weinheim DOI: 10.1002/anie.200250486

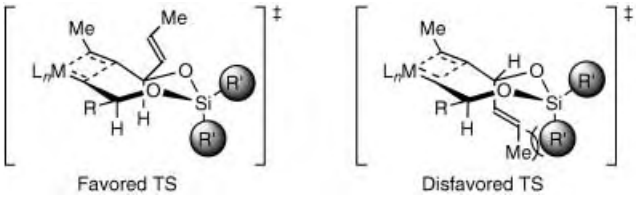
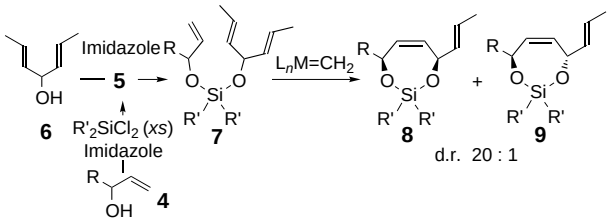


Figure 1. Proposed transition states for 1,4-stereocontrol in the TST-RCM reaction of an allylic alcohol.

We envisioned that the TST-RCM of the mixed bisalkoxy silane **1** (Scheme 1; $n = 0$) should proceed through the favored transition state illustrated in Figure 1. The basis for this hypothesis was the assumption that the substituents (R′) on silicon would result in nonbonding interactions with the pseudoaxial propenyl moiety in the disfavored transition state, and thereby prefer the formation of the *cis*-1,4-silaketal **2**. The potential advantage of this approach is that the reactive elements involved in diastereoselection are conserved irrespective of ring size, which should translate into a convenient stereochemical relay, provided the relative orientation of the substituents is maintained in the medium rings. Moreover, the ability for ring-closing metathesis to facilitate the formation of medium and large rings should allow the application of this concept to higher homologues.

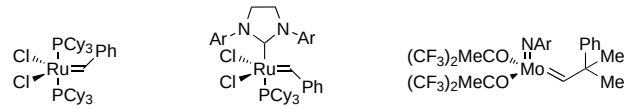
Preliminary studies examined the feasibility of this hypothesis for 1,4-stereocontrol (Scheme 2) through the examination of various substituents on silicon[9,10] and metal



Scheme 2. Preparation of bisalkoxy silanes **7** and the resulting diastereoselective TST-RCM reaction to form the *cis*-1,4-silaketals.

alkylidene catalysts,[11] as outlined in Table 1. Initial studies determined that the steric nature of the substituents on the silicon tether were indeed crucial in terms of silaketal construction, overall efficiency, and the level of diastereoselection, in which the diisopropylsilane proved optimal (Table 1; entry 3 versus 1 and 2). Treatment of the triene **7a** (R = 2-naphthyl (Np), R′ = *i*Pr) with Grubbs' catalyst **10** at reflux in dichloromethane furnished the silaketals **8a** and **9a** in 75% yield, with ≥99:1 diastereoselectivity favoring **8a** (Table 1; entry 3).[12] Additional studies explored the effects of more reactive metal alkylidene catalysts, in which the second-generation Grubbs catalyst **11** and the molybdenum-based Schrock catalyst **12** proved significantly inferior for this particular transformation (Table 1; entries 4 and 5).[11]

Table 2 summarizes the scope of the TST-RCM, under the optimized reaction conditions (Table 1, entry 3). The construction of the mixed bisalkoxy silane **7** was achieved from



Cy = Cyclohexyl — **10** — Grubbs' Catalyst

Ar = 2,4,6-Trimethylbenzene — **11** — Carbene Catalyst

Ar = 2,6-Diisopropylbenzene — **12** — Schrock's Catalyst

Table 1: Optimization of the diastereoselective TST-RCM reaction with silicon tether **7a** (R = Np).

Entry	**7a**; R′ =	Catalyst[a]	**8a**:**9a**[b,c]	Yield of **8a**+**9a** [%]
1	Me	**10**	23:1	41
2	Ph	**10**	15:1	70
3	*i*Pr	**10**	≥99:1	75
4	*i*Pr	**11**	6:1	31[d]
5	*i*Pr	**12**	14:1	23[e]

[a] All reactions (0.1 mmol) were carried out using 10 mol% of the catalyst in dichloromethane (0.05 M) at 40°C except for entry 5. [b] Ratios of diastereoisomers were determined by capillary GLC on aliquots of the crude reaction mixture. [c] Authentic standards were prepared independently from the corresponding 1,4-diols. [d] The more reactive second-generation catalyst proved less selective in furnishing significant amounts of polymeric and recovered starting material (30%). [e] This reaction was carried out using 10 mol% catalyst in benzene (0.04 M) at room temperature.

Table 2: Scope of the diastereoselective TST-RCM reaction (Scheme 2; R′ = *i*Pr).

Entry	**4**; R =	Yield of **7** [%][a]	**8**:**9**[b,c,d]	Yield of **8**+**9** [%]
1	Np (**1a**)	88	≥99:1	75
2	Ph (**1b**)	76	≥99:1	90
3	*n*Pr (**1c**)	71	29:1	66
4	*c*-Hex (**1d**)	85	22:1	54
5	*i*Bu (**1e**)	77	34:1	73
6	$PhCH_2$ (**1f**)	86	20:1	82
7	$Ph(CH_2)_2$ (**1g**)	85	32:1	66
8	$BnOCH_2$ (**1h**)	72	41:1	61
9	BnO_2CCH_2 (**1i**)	72	40:1	73

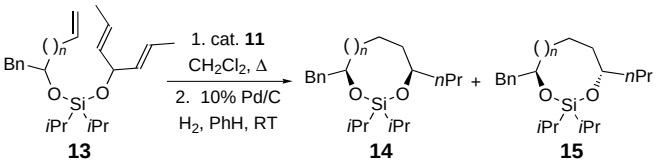
[a] The bisalkoxy silanes were prepared on a 0.5 mmol reaction scale using diisopropyldichlorosilane (10 equiv) and imidazole. [b] The metathesis reactions were carried out on a 0.05–0.1 mmol reaction scale (0.05 M) using 10–15 mol% of Grubbs' catalyst **10** in dichloromethane at 40°C. [c] Ratios of diastereoisomers were determined by capillary GLC on aliquots of the crude reaction mixture. [d] The major stereoisomer was confirmed by nOe experiments in each case.[12]

the requisite allylic alcohol **4**, through treatment with excess diisopropyldichlorosilane, to afford the monoalkoxychlorosilane **5**, followed by the removal of the excess silylating agent and addition of the prochiral alcohol **6** (Scheme 2). The diastereoselective TST-RCM proved remarkably tolerant to a range of aryl, linear, and branched alkyl substituents (Table 2; entries 1–7), albeit with lower conversion for the α-branched allylic alcohol derivatives (Table 2; entry 4). Moreover, in nearly all cases the bisalkoxy silanes **7a–i** were recovered and could be resubmitted to the reaction conditions. This transformation is also tolerant of both benzyloxymethyl and carboalkoxy substituents (Table 2; entries 8–9).[13]

 © 2003 Wiley-VCH Verlag GmbH & Co. KGaA, Weinheim

We envisioned that the application of diastereoselective TST-RCM to higher homologues would extend this concept, and provide a general method for long-range asymmetric induction. Table 3 summarizes the results of this study. Treatment of the trienes **13a–d** with the second-generation Grubbs catalyst **11** in refluxing dichloromethane furnished, after hydrogenation, the saturated silaketal intermediates **14**/**15a–d**, with the *trans* isomers **15a–d** favored (Table 3; entries 1–4).[14] The unsaturated silaketals were reduced in this particular case to remove the *E* and *Z* isomers and simplify the stereochemical analysis. The origin of diastereoselectivity is consistent with the previous model, albeit with the caveat that the pseudoaxial/equatorial positions are reversed in the medium rings (Figure 2). Hence, the preferred transition state in the medium rings also places both substituents in pseudoequatorial positions, thus avoiding the steric interaction derived from the axial isopropyl group on the silicon tether.

Table 3: Diastereoselective TST-RCM reactions with homologated alkenyl alcohols.



Entry	Ring size *n* =	Yield of **13** [%][a]	**14**:**15**[b–d]	Yield of **14**+**15** [%]
1	1 (**13a**)	92	1:11	90
2	2 (**13b**)	68	1:27	92
3	3 (**13c**)	75	1:3	75
4	4 (**13d**)	87	1:3	73

[a] The bisalkoxy silanes were prepared on an analogous reaction scale to those in Table 2. [b] The RCM reactions (0.1 mmol) were carried out using new Grubbs catalyst **11** (6 mol%) in dichloromethane (0.003 M) at 40 °C.[14] [c] Ratios of diastereoisomers were determined by capillary GLC on the saturated silaketals **14** and **15** after hydrogenation. [d] The major isomer was assigned by analogy to an independently prepared authentic sample.

Additional studies demonstrated that the RCM is consistent with a kinetic reaction that affords the more thermodynamically stable product. Although there is evidence for reversibility in the formation of **15a** and **15b**, the *trans* isomer appears to be the major product throughout the course of the reaction, as outlined in Figure 3. Periodic analysis of the reaction revealed that the diastereoselectivity for **15a** and **15b** decreases and increases respectively with time at 95% conversion.[15] Hence, the level of stereocontrol in these reactions may be optimized accordingly. For example, the diastereoselectivity for the formation of **15a** can be improved to approximately 18:1, provided the reaction is quenched after about 10 min at room temperature.

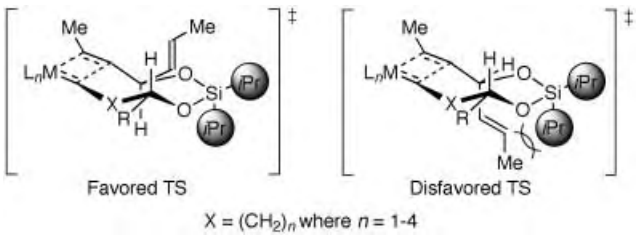


Figure 2. Proposed transition states for 1,*n*-stereocontrol in the TST-RCM reaction of homologated alkenyl alcohols (where *n* = 1–4).

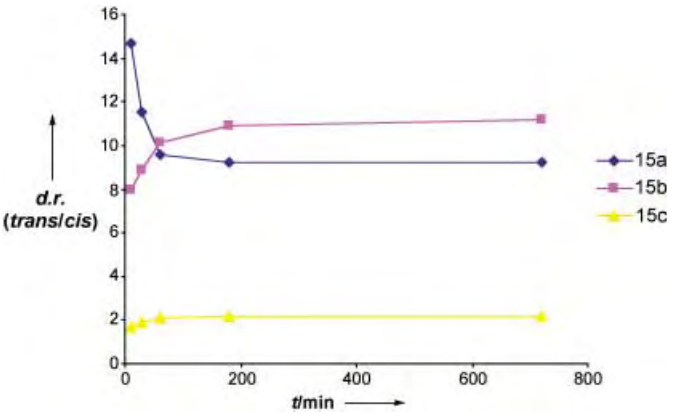


Figure 3. Plot of diastereoselectivity with time for the TST-RCM reactions of **15a–c** at min. 95% conversion. All aliquots were quenched with DMSO and directly hydrogenated prior to GLC analysis.

In conclusion, diastereoselective TST-RCM provides a useful approach to 1,4-, 1,5-, and 1,6-stereocontrol, and thus represents a new strategy for long-range asymmetric induction. This method facilitates the construction of *cis*-1,4-silaketals **8a–i** (Scheme 1; d.r. $\geq$ 20:1), whereas the extension of this concept to homologated alkenyl alcohols (Table 3; *n* = 1–4), results in reversal in diastereoselectivity favoring the *trans* isomers **15a–d**. The ability to systematically examine medium-ring stereocontrol in this manner should provide a greater understanding of the conformational factors that control diastereoselection in these systems.

Received: November 6, 2002 [Z50486]

Keywords: cyclization · diastereoselectivity · medium-sized rings · metathesis · silicon

[1] For recent reviews on long-range asymmetric induction, see: a) H. Sailes, A. Whiting, *J. Chem. Soc. Perkin Trans. 1* **2000**, 1785–1805; b) K. Mikami, M. Shimizu, H.-C. Zhang, B. E. Maryanoff, *Tetrahedron* **2001**, *57*, 2917–2951, and references therein.

[2] For recent examples of long-range asymmetric induction, see: a) M. Date, Y. Tamai, T. Hattori, H. Takayama, Y. Kamikubo, S. Miyano, *J. Chem. Soc. Perkin Trans. 1* **2001**, 645–653; b) R. D. A. Hudson, C. E. Anson, M. F. Mahon, G. R. Stephenson, *J. Organomet. Chem.* **2001**, *630*, 88–103; c) S. J. O'Malley, J. L. Leighton, *Angew. Chem.* **2001**, *113*, 2999–3001; *Angew. Chem. Int. Ed.* **2001**, *40*, 2915–2917; d) M. W. Carson, G. Kim, S. J. Danishefsky, *Angew. Chem.* **2001**, *113*, 4585–4588; *Angew. Chem. Int. Ed.* **2001**, *40*, 4453–4456; d) E. M. Flamme, W. R. Roush, *J. Am. Chem. Soc.* **2002**, *124*, 13644–13645, and references therein.

[3] For recent reviews on ring-closing metathesis, see: a) R. H. Grubbs, S. Chang, *Tetrahedron* **1998**, *54*, 4413–4450; b) U. K.

 © 2003 Wiley-VCH Verlag GmbH & Co. KGaA, Weinheim

Pandit, H. S. Overkleeft, B. C. Borer, H. Bieräugel, *Eur. J. Org. Chem.* **1999**, 959 – 968; c) A. Fürstner, *Angew. Chem.* **2000**, *112*, 3140 – 3172; *Angew. Chem. Int. Ed.* **2000**, *39*, 3012 – 3043, and references therein.

[4] G. C. Fu, R. H. Grubbs, *J. Am. Chem. Soc.* **1992**, *114*, 5426 – 5427.

[5] For a stereospecific approach to C_2-symmetrical 1,4-diols, see: a) P. A. Evans, V. S. Murthy, *J. Org. Chem.* **1998**, *63*, 6768 – 6769; b) M. Lobbel, P. Köll, *Tetrahedron: Asymmetry* **2000**, *11*, 393 – 396.

[6] For examples of silicon-tethered ring-closing-metathesis cross-coupling reactions, see: a) T. R. Hoye, M. A. Promo, *Tetrahedron Lett.* **1999**, *40*, 1429 – 1432; b) J.-G. Boiteau, P. Van de-Weghe, J. Eustache, *Tetrahedron Lett.* **2001**, *42*, 239 – 242; c) B. A. Harrison, G. L. Verdine, *Org. Lett.* **2001**, *3*, 2157 – 2159.

[7] For a related example of an enantioselective RCM using a prochiral alcohol, see: A. F. Kiely, J. A. Jernelius, R. R. Schrock, A. H. Hoveyda, *J. Am. Chem. Soc.* **2002**, *124*, 2868 – 2869.

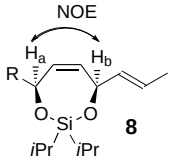
[8] For examples of diastereoselective ring-closing-metathesis reactions, see: a) C. M. Huwe, J. Velder, S. Blechert, *Angew. Chem.* **1996**, *108*, 2542 – 2544; *Angew. Chem. Int. Ed. Engl.* **1996**, *35*, 2376 – 2378; b) S. D. Burke, M. Müller, C. M. Beaudry, *Org. Lett.* **1999**, *1*, 1827 – 1829; c) H. Oguri, S.-Y. Sasaki, T. Oishi, M. Hirama, *Tetrahedron Lett.* **1999**, *40*, 5405 – 5408; d) M. Lautens, G. Hughes, *Angew. Chem.* **1999**, *111*, 160 – 162; *Angew. Chem. Int. Ed.* **1999**, *38*, 129 – 131; e) G. C. Lloyd-Jones, M. Murray, R. A. Stentiford, P. A. Worthington, *Eur. J. Org. Chem.* **2000**, 975 – 985; f) D. J. Wallace, C. J. Cowden, D. J. Kennedy, M. S. Ashwood, I. F. Cottrell, U.-H. Dolling, *Tetrahedron Lett.* **2000**, *41*, 2027 – 2029; g) B. Schmidt, M. Westhus, *Tetrahedron* **2000**, *56*, 2421 – 2426; h) D. S. Stoianova, P. R. Hanson, *Org. Lett.* **2000**, *2*, 1769 – 1772; i) Y. Fukuda, H. Sasaki, M. Shindo, K. Shishido, *Tetrahedron Lett.* **2002**, *43*, 2047 – 2049; j) M. Ogasawara, T. Nagano, T. Hayashi, *J. Am. Chem. Soc.* **2002**, *124*, 9068 – 9069.

[9] For reviews on temporary silicon-tethered strategies, see: a) L. Fensterbank, M. Malacria, S. M. Sieburth, *Synthesis* **1997**, 813 – 854; b) D. R. Gauthier, Jr., K. S. Zandi, K. J. Shea, *Tetrahedron* **1998**, *54*, 2289 – 2338.

[10] S. M. Sieburth, L. Fensterbank, *J. Org. Chem.* **1992**, *57*, 5279 – 5281.

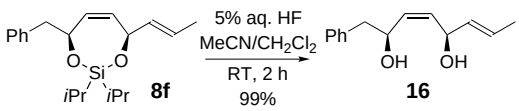
[11] a) R. R. Schrock, J. S. Murdzek, G. C. Bazan, J. Robbins, M. DiMare, M. O'Regan, *J. Am. Chem. Soc.* **1990**, *112*, 3875 – 3886; b) P. Schwab, R. H. Grubbs, J. W. Ziller, *J. Am. Chem. Soc.* **1996**, *118*, 100 – 110; c) M. Scholl, S. Ding, C. W. Lee, R. H. Grubbs, *Org. Lett.* **1999**, *1*, 953 – 956.

[12] The major stereoisomer was confirmed from nOe experiments in each case (**8a–i**). Details are available in the Supporting Information.



8

[13] The silyl tether can be readily removed in each case to afford the corresponding diol. For example, treatment of **8f** with 5% aqueous HF at room temperature furnished the bisallylic 1,4-diol **16** in 99% yield.



8f **16**

[14] Although Grubbs' catalyst **10** was not optimal for the larger rings, it also furnished **15** as the major diastereoisomer, which confirmed that the catalyst was not responsible for the reversal in selectivity.

[15] The diastereoselectivities in Figure 3, refer to crude product ratios, whereas the selectivities in Table 3 are for the purified silaketals **14a–d** and **15a–d**.

 © 2003 Wiley-VCH Verlag GmbH & Co. KGaA, Weinheim

Low Si/Al Ratio Zeolites

Open-Framework Materials Synthesized in the TMA^+/TEA^+ Mixed-Template System: The New Low Si/Al Ratio Zeolites UZM-4 and UZM-5**

C. Scott Blackwell, Robert W. Broach, Michael G. Gatter, Jennifer S. Holmgren, Deng-Yang Jan, Gregory J. Lewis, Beckay J. Mezza, Thomas M. Mezza, Mark A. Miller, Jaime G. Moscoso, R. Lyle Patton, Lisa M. Rohde, Michael W. Schoonover, Wharton Sinkler, Ben A. Wilson, and Stephen T. Wilson*

For over half a century, zeolites have played a major role in the development of modern processes in the chemical and petroleum industries.[1] Their unique combination of physical and chemical properties are ideal for catalysis and separations for a broad range of molecules. Recent advances in zeolite synthesis have centered on high silica zeolite systems or have employed exotic templates.[2] However, low Si/Al ratio zeolites are particularly attractive because they can offer high acid site density for catalytic applications and greater ion-exchange capacity and compositional diversity for separation processes. We report here our discovery of two new zeolite materials, UZM-4 and UZM-5, synthesized at low Si/Al ratios ($Si/Al < 10$) by using combinations of two of the most common organic templating agents, the tetramethylammonium (TMA^+) and tetraethylammonium (TEA^+) ions.[3] UZM-4 is a large pore 12-ring zeolite with the BPH framework type[4,5] and a sufficiently high Si/Al ratio (1.5–2.5) to enable thermal stability. UZM-5 has an unprecedented framework type that contains an 8-ring pore system similar

[*] Dr. G. J. Lewis, Dr. C. S. Blackwell, Dr. R. W. Broach, Dr. M. G. Gatter, Dr. J. S. Holmgren, Dr. D.-Y. Jan, B. J. Mezza, Dr. T. M. Mezza, M. A. Miller, J. G. Moscoso, Dr. R. L. Patton, L. M. Rohde, Dr. M. W. Schoonover, Dr. W. Sinkler, B. A. Wilson, Dr. S. T. Wilson
UOP LLC
50 E. Algonquin Rd.
Des Plaines, IL 60017 (USA)
Fax: (+1) 847-391-3719
E-mail: gregory.lewis@uop.com

[**] TMA^+ = tetramethylammonium ion, TEA^+ = tetraethylammonium ion.

Supporting information for this article is available on the WWW under http://www.angewandte.org or from the author.

 DOI: 10.1002/anie.200250076 © 2003 Wiley-VCH Verlag GmbH & Co. KGaA, Weinheim

to that of zeolite A in two dimensions, and a catalytically active surface that contains 16-ring cups.

UZM-4 is a thermally stable zeolite synthesized with the BPH framework type, which exhibits appropriate stability (600 °C) for use in catalytic and adsorbent applications.

The BPH framework type, first described for the beryllophosphate $K_7Na_7Be_{14}P_{14}O_{56}$,[6] has hexagonal symmetry and consists of one-dimensional 12-ring pores linked by intersecting 8-ring pores. Zeolite Q,[7] the first zeolite discovered with this framework type, was unstable and not shown to be a large-pore zeolite until 30 years later by Andries et al.[8] Whereas zeolite Q is crystallized in the K^+-Al-Si-O system with an Si/Al ratio of 1, UZM-4 has been prepared with an Si/Al ratio of 1.5:1–2.5:1 in the Li^+, TMA^+, TEA^+ template system. A typical reaction mixture formulation is $4.0\,TEAOH:2.5\,SiO_2:Al(OH)_3:1\,TMACl:0.5\,LiCl:100\,H_2O$, which yields a product of unit cell formulation $Li_{6.1}TMA_{3.3}TEA_{0.1}Al_{10}Si_{18}O_{56}$.

The higher Si/Al ratio is evident in the X-ray diffraction pattern and IR spectrum of UZM-4, in which diffraction lines were shifted to higher 2Θ values and asymmetric T-O-T stretches to higher frequencies, respectively.[9] The resultant shrinkage of the unit cell from $a = 13.50$ and $c = 13.40$ Å for zeolite Q (Si/Al = 1) to $a = 13.3069(6)$ and $c = 13.2510(8)$ Å for UZM-4 (Si/Al = 1.78) is consistent with the substitution of the smaller Si^{4+} ion for the Al^{3+} ion. As is well known for many zeolites, the higher Si/Al ratio in UZM-4 increases its thermal stability. Variable-temperature X-ray diffraction studies show as-synthesized UZM-4 is stable to 600 °C under dry conditions.[10] By comparison, the structure of zeolite Q collapses at 200 °C.[11]

An unusual aspect of UZM-4 is that most or all (typically > 95 %) of the organic template can be removed from the pores directly by ion exchange. This is facilitated by the 12-ring pore with a free diameter of 7 Å that periodically opens up to a cavity with a diameter of 12.5 Å. These exchange properties may be enhanced by the fact that UZM-4 crystallizes as hexagonal plates 10–40 nm thick, and the 12-ring pores run perpendicular to the plate surface. The ability to remove the organic template from the pores without calcining circumvents the need to deal with potentially unstable acidic forms that would result from template decomposition. Thus, ion-exchanged UZM-4 compositions are directly accessible for adsorbent applications. In addition, the higher Si/Al ratio of UZM-4 affords enough stability to withstand the modifications necessary to develop acidic catalysts.[12] Therefore, UZM-4 is a novel, large-pore zeolite with sufficient stability for both adsorbent and catalytic applications.

The second zeolite presented here, UZM-5, is a completely new framework type. It can be synthesized from the TMA^+/TEA^+ mixed-template system and has a Si/Al ratio of 5:1–12:1 and a framework density of 14.8 T atoms per 1000 Å^3. A typical synthesis composition (molar ratios) of $8\,TEAOH:8\,SiO_2:Al(OH)_3:1\,TMACl:240\,H_2O$ is crystallized by digestion at 150 °C for 96 h to yield a material with an approximate unit cell composition $TMA_4TEA_4Al_8Si_{56}O_{128}$.

UZM-5 typically crystallizes as thin plates (2–20 nm) in the TMA^+/TEA^+ system but forms rosette-shaped platelike aggregates in the $Na^+/TMA^+/TEA^+$ system. The UZM-5 materials are characterized by two peaks in the X-ray diffraction pattern at $d \sim 8.7$ and 3.9 Å, which were indexed as the (110) and (310) peaks, respectively. These peaks are apparent after 12 h and remain major features of the diffraction pattern until the final stages of crystallization. The lack of a *c*-axis component in these peaks indicates that the initial crystal growth is primarily in the *a* and *b* axis directions. As a consequence of the very small crystallite size and anisotropic morphology, X-ray diffraction patterns for UZM-5 samples were not of sufficient quality to solve the structure by ab initio methods, although indexing the patterns did provide the crystal system (tetragonal) and approximate lattice parameters ($a = 12.3$ Å, $c = 28.5$ Å). The structure of UZM-5 was solved by model building, incorporating information from a broad range of analytical techniques. Adsorption measurements showed a diminished uptake of *i*-C_4H_{10} versus *n*-C_4H_{10}, suggesting an 8-ring or small 10-ring channel system.[13] Also, peaks in the IR absorption spectrum at 1216 and 545 cm^{-1} implied the presence of 5-rings, while a band at 569 cm^{-1} suggested the possibility of double 4- or double 6-rings in the structure.[14] Electron diffraction was used to confirm the unit cell from X-ray diffraction data and to narrow the range of possible space groups to five body-centered groups. The information from high-resolution transmission electron microscopy (HRTEM; Figure 1 a) was key to the model building, as it pinpointed the locations of the channels and double 4-rings. The light areas in Figure 1 indicate positions of low atomic density (e.g., the main pore system), and dark areas indicate positions of high projected atomic density (e.g., the double 4-rings). A trial model of the structure consistent with the TEM images and the analytical data mentioned above was built in the space group *I4/mmm*. The atomic coordinates were optimized by distance least-squares (DLS) refinement.[15] The constraints used, the atomic coordinates, and the residuals are given in Table 1. The DLS refinement technique is commonly used particularly

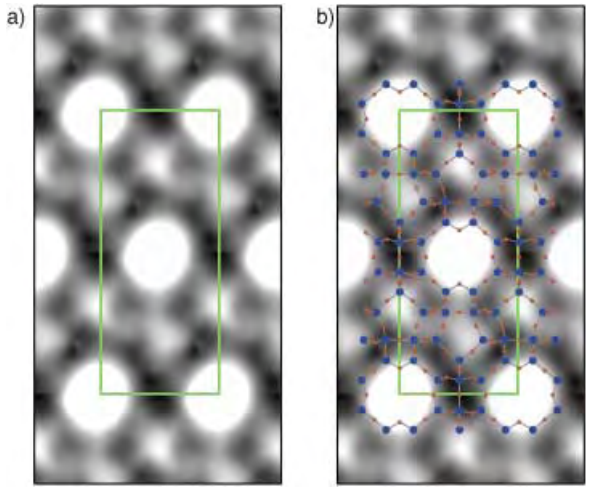


Figure 1. a) HRTEM image along [100], after averaging the contrast from several adjacent unit cells. Unit cell outline is shown. b) As (a), but with structure model overlain. The image clearly shows the body-centered arrangement of 8-ring pores, as well as the arrangement of the smaller 5-ring channels.

 © 2003 Wiley-VCH Verlag GmbH & Co. KGaA, Weinheim

Table 1: Distance least-squares optimized atomic coordinates for UZM-5.[a]

Atom label	Wyckoff notation	*x*	*y*	*z*
Si1	16n	0.1776	0.0000	0.0556
Si2	32o	0.3784	0.1909	0.2013
Si3	16n	0.3727	0.0000	0.1281
O1	16n	0.2941	0.0000	0.0827
O2	8i	0.1993	0.0000	0.0000
O3	16m	0.1085	0.1085	0.0698
O4	16k	0.3757	0.1243	0.2500
O5	32o	0.3483	0.1085	0.1590
O6	16n	0.5000	0.2410	0.1931
O7	16m	0.2899	0.2899	0.2030
O8	8g	0.5000	0.0000	0.1119

[a] Space group *I*4/*mmm*; optimized cell constants $a = 12.332$, $c = 29.096$ Å. Reference constants: ⟨T–O⟩ 1.639, ⟨O–O⟩ 2.676, ⟨T–T⟩ 3.126 Å (assuming Si:Al 7.0; Si–O 1.623, Al–O 1.748 Å; ⟨O-T-O⟩ 109.5, ⟨T-O-T⟩ 145°). Final convergence gave $R_{DLS} = 0.0017$, $\sigma = 0.008$, $R_{DLS} = (\Sigma(w(D_o - D))^2/\Sigma(w D_o)^2)^{1/2}$, $\sigma_{DLS} = (\Sigma(w(D_o - D))^2/(M - NV))^{1/2}$.

in the zeolite community for the evaluation and preliminary refinement of hypothetical structures. The calculated diffraction pattern based on the DLS coordinates agrees well with the experimental diffraction pattern as shown in Figure 2. The UZM-5 framework is confirmed by agreement between the model and HRTEM images along several crystallographic directions (see for example Figure 1b). Rietveld refinement of the X-ray powder data also confirms the structure, but because of peak broadening and asymmetry the resulting atomic coordinates are considered preliminary.[16]

The structure of the fully connected three-dimensional end member of the UZM-5 family consists of alternating layers along the *c* axis of two different composite building units or polyhedra, designated *cub* and *cle* (Figure 3).[17] Alternatively, the structure can be visualized as being built from two larger composite building units, designated *grc* and

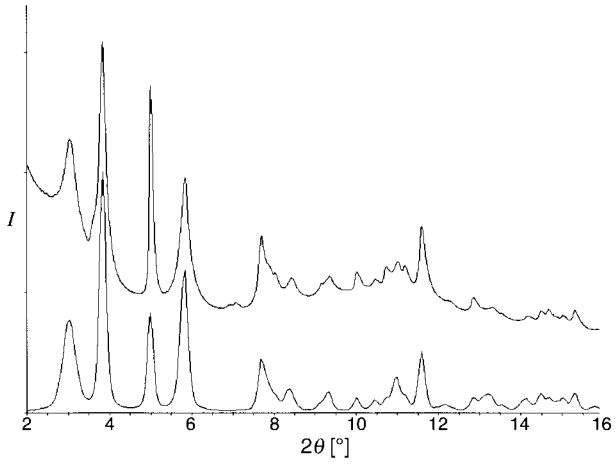


Figure 2. Comparison of the experimental diffraction pattern for a calcined never rehydrated UZM-5 (top) with a simulation using DLS coordinates (bottom). For the observed pattern, synchrotron wavelength = 0.7527 Å, space group *I*4/*mmm*, $a = 12.193(3)$ Å, $c = 28.403(17)$ Å. The simulation was done using Accelrys Materials Studio Version 2.1.5 and pseudo-voigt profiles with anisotropic crystallite size broadening (coherence lengths: $L_a = L_b = 125$ Å, $L_c = 50$ Å).

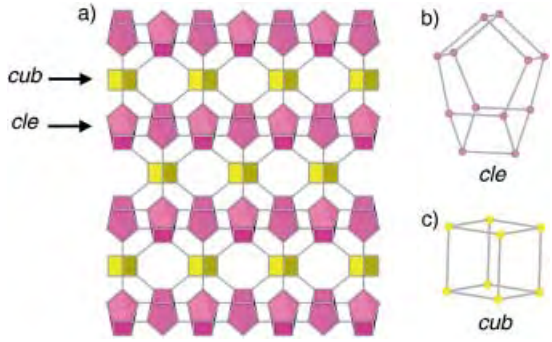


Figure 3. a) (100) projection of the UZM-5 structure showing *cle* (pink) and *cub* (yellow) polyhedra. b) *cle* polyhedron c) *cub* polyhedron (double 4-ring).

wbc (Figure 4a). The *grc* polyhedron, found in several other zeolites such as LTA, has usually been called an alpha cage but according to recent IUPAC recommendations is more properly called an alpha cavity.[18] The *wbc* polyhedron has not previously been found in any zeolite to our knowledge. Both of these cavities are accessible for adsorption of molecules larger than water through 8-ring windows. In UZM-5, the alpha cavities are fused through 8-rings along the *a* and *b* axis directions to form a two-dimensional 8-ring channel system. In the *c* direction *wbc* cavities are fused with the 8-rings above and below each alpha cavity (Figure 4a). The three-dimensional structure is formed by linking the bicapped alpha cavities in the *c* direction, which creates a *cub* cage at the apices. The UZM-5 framework is projected on a HRTEM image along the ⟨100⟩ direction in Figure 1b. The body-centered 8-ring pore system and the 5-ring channels in the model fit the features of the high-resolution image.

The layers of fused alpha cavities in UZM-5 are similar to those found in zeolites of framework type LTA; both structures have the same 12.3 Å lattice repeat distance along *a* and *b*. In LTA-type zeolites successive layers of alpha cavities are connected through 8-ring windows, which allows three-dimensional diffusion. However, in UZM-5 successive alpha cavity layers are separated by intervening

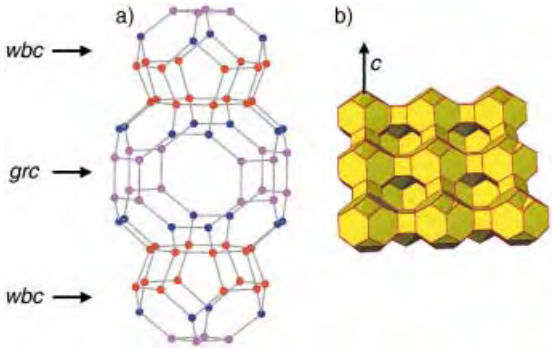


Figure 4. a) View of the alpha *(grc)* cavity bicapped in the *c*-axis direction by *wbc* cavities that form pockets accessible though 8-rings on opposite sides of each alpha cavity. The three unique T-atoms in the structure are color-coded. b) The predominant (001) surface contains 16-ring cups with an 8-ring bottom. These cups are essentially the bottom halves of alpha cavities sitting over *wbc* cavities.

 © 2003 Wiley-VCH Verlag GmbH & Co. KGaA, Weinheim

layers of *wbc* cavities which block diffusion along the *c*-axis direction. The resulting 8-ring pore system is consistent with the observed adsorption of *n*-C_4H_{10} and the relative exclusion of *i*-C_4H_{10}.[13] In addition, the greatly favored crystal growth of UZM-5 in the *a* and *b* directions provides many sites on the (001) surface. This surface formed by the layer of the *wbc* cavities consists of 16-ring cups that are essentially the bottom halves of alpha cavities (Figure 4b). These cups are likely the sites where important catalytic reactions such as xylene isomerization and benzene alkylation occur, both of which involve molecules too large to fit in the 8-ring pores.[19] The presence of these surface cups is reminiscent of the MWW structure.[20]

The isolation of the new zeolite materials UZM-4 and UZM-5 by using combinations of simple well-studied organic templates such as TMA^+ and TEA^+ suggests the applicability of the mixed-template approach. In fact, we have discovered a number of other novel zeolites using this synthesis strategy that will be published at a future date. Moreover, these types of templates have the advantage of low cost and availability, which facilitates scale-up and applications testing. In addition, the mixed-template approach is compatible with modern exploratory screening capabilities such as combinatorial chemistry, which should accelerate invention in this field.

Experimental Section

UZM-4 synthesis: Aluminum hydroxide (27.2% Al, 75.6 g) was dissolved in TEAOH (35%; 1305.62 g) with vigorous stirring. To this mixture, de-ionized water (331.22 g) and then colloidal silica (287.56 g; Ludox AS-40, 40% SiO_2) were added. After homogenization, followed by aging for 24 h at 95 °C, the resulting reaction mixture contained 2.65% Si. To a 1600 g portion of this aluminosilicate mixture, a solution containing TMACl (97%; 67.95 g) and LiCl (13.30 g) dissolved in de-ionized water (80 g) was added slowly with vigorous stirring. After homogenization for 2 h, the reaction mixture was placed in a static 2-liter Parr autoclave and digested for 72 h at 125 °C. The solid products were isolated by centrifugation, washed with de-ionized water, and dried at room temperature. Analysis: Si/Al = 1.78:1, Li/Al = 0.61:1, N/Al = 0.34:1, C/N = 4.1:1. The experimental X-ray diffraction patterns for UZM-4 and zeolite Q, along with the calculated diffraction pattern from a DLS simulation of UZM-4 are included in the Supporting Information.

UZM-5 synthesis: Aluminum *sec*-butoxide (95 + %; 58.75 g), was added to TEAOH (35%; 836.34 g) with vigorous stirring. To this mixture, colloidal silica (294.73 g; Ludox AS-40, 40% SiO_2) and then distilled water (10.18 g) were added. After homogenization for 1 h, followed by aging for 18 h at 95 °C, the resulting reaction mixture contained 4.67% Si. To a 500 g portion of this aluminosilicate reaction mixture, a solution containing TMACl (97%; 11.77 g) dissolved in deionized water (23.0 g) was added with vigorous mixing. After homogenization for 30 min, the reaction mixture was distributed among eight teflon-lined autoclaves and digested at 150 °C for four days. The solid products were recovered by centrifugation, washed, and dried at 95 °C. Analysis: Si/Al = 6.88, N/Al = 0.83, C/N = 6.05.

Received: August 30, 2002
Revised: February 20, 2003 [Z50076]

Keywords: hydrothermal synthesis · microporous materials · structure elucidation · templates · zeolites

[1] E. M. Flanigen, *Stud. Surf. Sci. Catal.* **2001**, *137*, 11–35; J. D. Sherman, *Proc. Natl. Acad. Sci. USA* **1999**, *96*, 3471–3478.
[2] S. A. Elomari, S. I. Zones, *Stud. Surf. Sci. Catal.* **2001**, *135*, 479–486; P. Wagner, M. Yoshikawa, M. Lovallo, K. Tsuji, M. Taspatsis, M. E. Davis, *Chem. Commun.* **1997**, 2179–2180; K. J. Balkus, Jr., A. G. Gabrielov, US patent 5489424 **1996**.
[3] Structure code: UZM = *U*OP *Z*eolitic *M*aterial.
[4] The uppercase three-letter codes in this article refer to zeolite framework types. Lowercase three-letter codes refer to composite building units or polyhedra (see reference [17]).
[5] *Atlas of Zeolite Framework Types*, 5th rev. ed. (Eds.: C. Baerlocher, W. M. Meier, D. H. Olson), Elsevier, New York, **2001**; see also http://www.iza-structure.org/databases/.
[6] G. Harvey, C. Baerlocher, T. Wroblewski, *Z. Kristallogr.* **1992**, *201*, 113–123.
[7] D. W. Breck, N. A. Acara, US Patent 2991151 **1961**.
[8] K. J. Andries, H. J. Bosmans, P. J. Grobet, *Zeolites* **1991**, *11*, 124–131.
[9] The asymmetric T-O-T stretch shifts from 961 cm^{-1} in zeolite Q to 1007 cm^{-1} in UZM-4.
[10] Hot-stage X-ray diffraction patterns were collected on samples bathed in a stream of dry air; measurements were taken at room temperature and then at multiples of 100 °C to 600 °C.
[11] Zeolite Q with improved stability had been attained by rare-earth exchange, D. E. W. Vaughan, US Patent 5382420 **1995**.
[12] D. W. Breck, *Zeolite Molecular Sieves*, Wiley, New York, **1974**, p. 441.
[13] A McBain–Bakr gravimetric apparatus was used to determine adsorption capacities. At room temperature and $P/P_0 = 0.3$, UZM-5 adsorbed 0.22 mL *n*-C_4H_{10} per gram and 0.050 mL *i*-C_4H_{10} per gram. The kinetic diameters of *n*-C_4H_{10} and *i*-C_4H_{10} are 4.3 Å and 5.0 Å, respectively.
[14] E. M. Flanigen, *Zeolite Chemistry and Catalysis* (Ed.: J. A. Rabo), American Chemical Society, New York, **1976**, pp. 80–117 (ACS Monograph 171); J. C. Jansen, F. J. van der Gaag, H. van Bekkum, *Zeolites* **1984**, *4*, 369–372.
[15] C. Baerlocher, A. Hepp, W. M. Meier, DLS-76, A Program for the Simulation of Crystal Structures by Geometric Refinement, Institute of Crystallography and Petrography, ETH, Zurich (Switzerland) **1977**.
[16] The Rietveld refinement is problematic because of the nature of the UZM-5 crystals. Various ways of modeling the peak shapes have not been entirely successful. Although fits are in general very good and give convincing evidence of the correctness of the UZM-5 framework, there are misfits that lead to high uncertainties in some atomic parameters. This may be the result of diffraction features such as faulting, intergrowths, and small crystallite size that cannot be modeled with current Rietveld software. Recent progress in the Rietveld refinement is included in the Supporting Information.
[17] Landolt Börnstein, New Ser. IV/14, subvolume A: "Tetrahedral Frameworks of Zeolites, Clathrates, and Related Materials":J. V. Smith in *Microporous and other Framework Materials with Zeolite-Type Structures*, Springer, Berlin, **2000**.
[18] L. B. McCusker, F. Liebau, G. Engelhardt, *Pure Appl. Chem.* **2001**, *73*, 381.
[19] D.-Y. Jan, G. J. Lewis, J. G. Moscoso, M. A. Miller, US Patent 6388157 **2002**; D.-Y. Jan, G. J. Lewis, J. G. Moscoso, M. A. Miller, US Patent 6388159 **2002**.
[20] M. E. Leonowicz, J. A. Lawton, S. L. Lawton, M. K. Rubin, *Science* **1994**, *264*, 1910–1913.

 © 2003 Wiley-VCH Verlag GmbH & Co. KGaA, Weinheim

H Bonds in Chains of Water Molecules

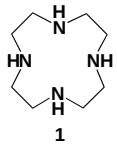
Structure of a Self-Assembled Chain of Water Molecules in a Crystal Host**

*Satyanarayan Pal, N. B. Sankaran, and Anunay Samanta**

Some of the properties of water are considered "anomalous".[1–3] Although hydrogen-bonding interactions and their fluctuations are known to determine the properties of water, the major obstacle to fully comprehend its behavior has been the complexity of correctly describing the interactions between water molecules.[1–4] The diversity of the cooperative association of the water molecules is attested by a large number of polymorphic forms of ice.[5–7] The key to understanding the behavior of water is precise structural data of various hydrogen-bonded water networks in diverse environments. It is this realization that has prompted extensive investigations of water structures in recent years.[1–18]

As it is possible to obtain precise information on the nature of cooperative association of a small collection of water molecules, various water clusters have been studied theoretically and experimentally.[2–4,8–11] These studies have revealed a quasiplanar cyclic structure for the trimer, tetramer and pentamer. Although 3D structures have been theoretically predicted and experimentally observed for the hexamer and higher water clusters, a quasiplanar hexamer has also been reported.[11] Recent studies have led to the characterization of several water clusters in various crystal hosts at room temperature.[12–18] Notable among these are hexamers,[14–16] octamers[12,17] and a decamer.[13] While these studies have significantly advanced our understanding of the structure of several "discrete" water clusters, very little is known of how these clusters link themselves to form a larger network of water molecules. Herein, we report the structure of a highly ordered infinite chain of water molecules found in a crystal host at room temperature. It is shown that the chain consists of cyclic water tetramers linked by two bridging water molecules. We believe that the water structure demonstrated herein brings to light yet another novel mode of the cooperative association of water molecules. This discovery is helpful in improving the modeling of some of the unexplained properties of water, and understanding better the structure and behavior of water molecules in biological systems.

Organic compounds with functional moieties that are present in biological molecules can help stabilize various water topologies in environments resembling those in living systems.[19] Taking this fact into consideration, we have examined the crystal structure of the supramolecular assembly of 1,4,7,10-tetraazacyclododecane **1** and the water molecules within.[19] The X-ray crystallographic study[20] reveals that the supramolecular assembly is the result of cooperative hydrogen-bonding interactions between water molecules, and between water molecules and organic molecules. The crystal-packing diagram (Figure 1a) shows that the organic molecules in the crystal are stacked one on top of the other along the crystallographic *c* axis, and are associated with



1

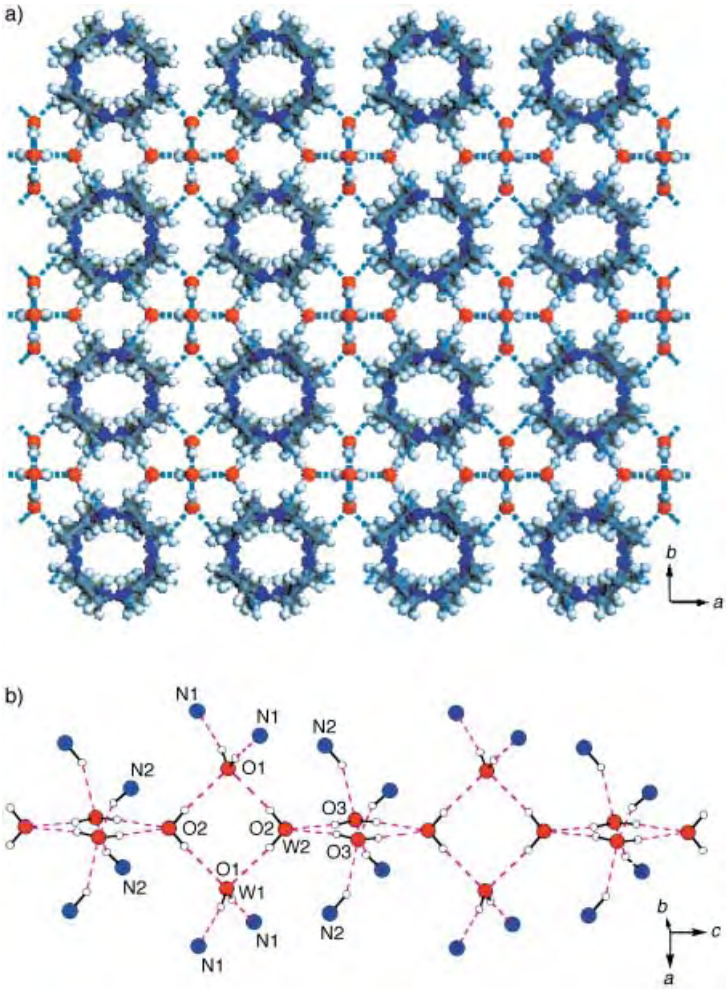


Figure 1. a) Packing diagram of the supramolecular system viewed along the crystallographic *c* axis. Carbon: gray; oxygen: red; nitrogen: blue; hydrogen: white; H bonds: dashed blue lines. The water clusters that are seen in the center of the organic molecules are not connected to each other along the crystallographic *a* or *b* axis but are H bonded to the NH groups of the adjacent organic moieties and the infinite water chain is formed only along the *c* axis. b) Hydrogen-bonding motif of the self-assembled chain of water molecules. Nitrogen: blue; H bonds: dashed purple lines. Selected bond lengths and angles are provided in Table 1.

[*] Prof. Dr. A. Samanta, S. Pal, N. B. Sankaran
School of Chemistry
University of Hyderabad
Hyderabad 500 046 (India)
Fax: (+91) 40-2301-2460
E-mail: assc@uohyd.ernet.in

[**] The authors thank the Department of Science and Technology (DST) and the Council of Scientific and Industrial Research (CSIR) for financial support. The authors acknowledge the National Single Crystal Diffractometer Facility at the School of Chemistry, University of Hyderabad for the crystal structure analysis. We also thank Drs S. Pal and S.K. Das for useful discussion.

Supporting information for this article is available on the WWW under http://www.angewandte.org or from the author.

 DOI: 10.1002/anie.200250444 © 2003 Wiley-VCH Verlag GmbH & Co. KGaA, Weinheim

neighboring water molecules through N–H···O and O–H···N hydrogen-bonding interactions.

The hydrogen-bonding association leads to the formation of an infinite chain of water molecules along the *c* axis (Figure 1b). The chain consists of cyclic water tetramers formed by two types of water molecules, W1 and W2, the corresponding oxygen atoms of which are represented by O1 and O2. The individual tetrameric clusters are bridged along the *c* axis by two water molecules of type W3[21] that lie in a plane perpendicular to that containing the four water molecules forming the tetramer. Each water molecule involved in the formation of the infinite chain is hydrogen bonded to four neighboring molecules in an almost-tetrahedral arrangement. While W2 is hydrogen bonded to four other water molecules, W1 and W3 are involved in forming two O–H···N and N–H···O hydrogen bonds, respectively, with the neighboring organic moiety in addition to forming two hydrogen bonds with W2 water molecules. The oxygen atoms involved in the formation of the cyclic tetramer lie in a plane. It may appear from Figure 1b that the chain is formed by "corner-sharing tetramers", where the successive tetrameric units lie in two perpendicular planes. However, we consider "bridged tetramers" is a more appropriate description of the chain than the former description, because of the following observations: The distance between two O2 atoms forming the tetramer is 3.968(2) Å, while that separating the O2 atoms of the successive tetramers is significantly larger, 4.923(2) Å along the *c* axis. The O···O hydrogen-bonding distance is measured to be 2.896(2) Å in the tetramer while that involved in the bridging is 3.004(2) Å. The data presented in Table 1 also suggest that the hydrogen-bonding interaction of W1 with the surrounding amino moieties, O1–H···N, is significantly stronger than the interaction of W3, N–H···O3. These structural parameters imply that one of the three types of water molecules, W3, is held less tightly in the lattice compared to the other two.

Table 1: Selected bond lengths and bond angles associated with the chain of water molecules.

D–H···A	D–H [Å]	H···A [Å]	D···A [Å]	D-H-A [°]
O2–H···O1	0.83(2)	2.07(2)	2.896(2)	172(3)
O3–H···O2	0.93(2)	2.08(3)	3.004(2)	172(2)
O1–H···N1	0.87(2)	1.97(2)	2.8383(17)	170(2)
N2–H···O3	0.897(18)	2.401(18)	3.1871(19)	146.4(14)

D = donor atom, A = acceptor atom.

Tetrameric clusters of water molecules were investigated theoretically and experimentally.[22,23] Both theoretical calculations and vibration rotation tunneling spectroscopy of the water tetramer in the gas phase indicated a quasiplanar cyclic structure, in which each water molecule forms two hydrogen bonds; one as a donor and the other as an acceptor. The free hydrogen available with each water molecule alternates above and below the plane. Assuming an S_4 symmetry for the tetramer, the average O–H···O bond length in this tetramer was estimated to be 2.79 Å.[23] Interestingly, the hydrogen-bonding motif of the water tetramer in the self-assembled system presented herein, in which each water molecule is involved in the formation of four hydrogen bonds, is very different from that theoretically predicted or experimentally observed in the gas phase. This difference is because of the influence of the surrounding organic moieties and nearby water molecules. What is even more interesting is the manner in which tetrameric water clusters are self-assembled in the form of an infinite chain. We believe that this motif of association of the water molecules has not even been speculated previously.

In summary, we have characterized a novel water structure in an organic molecular host. The structure reported herein demonstrates that tetrameric water clusters can be important constituents of a water chain. As water molecules play a crucial role in contributing to the stability and function of the biological assemblies, and because the details of the water structures in channels, in energy-transducing proteins, and in enzymes are largely unknown,[24–26] the present finding may provide insight into the hydrogen-bonding motif of the aqueous environments in living systems and help unravel the mechanism of proton conduction in living systems.

Received: October 28, 2002
Revised: December 10, 2002 [Z50444]

Keywords: hydrogen bonds · self-assembly · supramolecular chemistry · water chemistry · X-ray diffraction

[1] D. Eisenberg, W. Kauzmann, *The Structure and Properties of Water*, Oxford University Press, New York, **1969**.
[2] R. Ludwig, *Angew. Chem.* **2001**, *113*, 1856; *Angew. Chem. Int. Ed.* **2001**, *40*, 1808.
[3] F. N. Keutsch, R. J. Saykally, *Proc. Natl. Acad. Sci. USA* **2001**, *98*, 10533.
[4] K. Liu, J. D. Cruzan, R. J. Saykally, *Science* **1996**, *271*, 929.
[5] N. H. Fletcher, *The Chemical Physics of Ice*, Cambridge University Press, Cambridge, **1970**.
[6] M. Koza, H. Schober, A. Tölle, J. Fujara, T. Hansen, *Nature* **1999**, *397*, 660.
[7] C. Lobban, J. L. Finney, W. F. Kuhs, *Nature* **1998**, *391*, 268.
[8] R. Ludwig, *ChemPhysChem* **2000**, *1*, 53.
[9] M. Matsumoto, S. Saito, I. Ohmine, *Nature* **2002**, *416*, 409.
[10] J. M. Ugalde, I. Alkorta, J. Elguero, *Angew. Chem.* **2000**, *112*, 733; *Angew. Chem. Int. Ed.* **2000**, *39*, 717.
[11] K. Nauta, R. E. Miller, *Science* **2000**, *287*, 293.
[12] J. L. Atwood, L. J. Barbour, T. J. Ness, C. L. Raston, P. L. Raston, *J. Am. Chem. Soc.* **2001**, *123*, 7192.
[13] L. J. Barbour, G. W. Orr, J. L. Atwood, *Nature* **1998**, *393*, 671.
[14] R. Custelcean, C. Afloroaei, M. Vlassa, M. Polverejan, *Angew. Chem.* **2000**, *112*, 3224; *Angew. Chem. Int. Ed.* **2000**, *39*, 3094.
[15] K. M. Park, R. Kuroda, T. Iwamoto, *Angew. Chem.* **1993**, *105*, 939; *Angew. Chem. Int. Ed. Engl.* **1993**, *32*, 884.
[16] J. N. Moorthy, R. Natarajan, P. Venugopalan, *Angew. Chem.* **2002**, *114*, 3567; *Angew. Chem. Int. Ed.* **2002**, *41*, 3417.
[17] W. B. Blanton, S. W. Gordon-Wylie, G. R. Clark, K. D. Jordan, J. T. Wood, U. Geiser, T. J. Collins, *J. Am. Chem. Soc.* **1999**, *121*, 3551.
[18] L. Infantes, S. Motherwell, *CrystEngComm* **2002**, *4*, 454.
[19] The chosen molecule contains several secondary NH groups that mimic those present in biological systems (see for example, *Water and Biological Macromolecules* (Ed.: E. Westhoff), CRC Press, Boca Raton, FL, **1993**.

 © 2003 Wiley-VCH Verlag GmbH & Co. KGaA, Weinheim

[20] Crystal data for **1**·3 H_2O: Single crystals were grown from a toluene solution of **1**. The X-ray data were collected on an Enraf-Nonius Mach 3 single-crystal diffractometer that uses graphite monochromated Mo Kα radiation ($\lambda = 0.71073$ Å) by ω-scan method. Unit cell parameters were determined by least squares fit of 25 reflections having 2θ values in the range 18–21°.The structure was solved by direct methods and refined by least squares procedures on F^2 using SHELX-97 (G. M. Sheldrick, Program for the solution and refinement of crystal structures, University of Göttingen, Germany, **1997**) package. The non-hydrogen atoms were refined anisotropically. The hydrogen atoms of the methylene groups were included in the structure factor calculation at idealized positions by using a riding model, but not refined. The hydrogen atoms of the water molecules and the amino moieties were located from the difference Fourier transform and refined isotropically. Crystal dimension: 0.68 × 0.48 × 0.40 mm; $T = 298(2)$ K; orthorhombic, *Ccca;* $a = 16.658(2)$, $b = 16.908(5)$ and $c = 8.891(4)$ Å, $V = 2504.3(12)$ Å^3, $Z = 8$, $\rho_{calc} = 1.201$ g cm^{-3}, $2\theta_{max} = 27.95°$; 1713 reflections collected of which 1514 were unique; $R_1 = 0.0404$, $wR_2 = 0.0900$ for $I > 2\sigma(I)$; residual electron density: 0.155 and −0.175 e Å^{-3}. Even though a crystal structure of **1** was previously reported (J. H. Reibenspies, *Acta Crystallogr. Sect. C* **1992**, *48*, 1717), the arrangement of the water molecules in the crystal lattice was never examined. Moreover, the present crystallographic data show that ours is an improved structure that allows determination of the location of the water-hydrogen atoms more precisely. CCDC-195982 contains the supplementary crystallographic data for this paper. These data can be obtained free of charge via www.ccdc.cam.ac.uk/conts/retrieving.html (or from the Cambridge Crystallographic Data Centre, 12 Union Road, Cambridge CB2 1EZ, UK; fax: (+44) 1223-336-033; or deposit@ccdc.cam.ac.uk).

[21] The corresponding oxygen atoms are representated as O3 in Figure 1b.

[22] S. X. Xantheas, T. H. Dunning, Jr., *J. Chem. Phys.* **1993**, *99*, 8774.

[23] J. D. Cruzan, L. B. Braly, K. Liu, M. G. Brown, J. G. Loeser, R. J. Saykally, *Science* **1996**, *271*, 59.

[24] M. Wikström, *Curr. Opin. Struct. Biol.* **1998**, *8*, 480.

[25] M. Y. Okamura, M. L. Paddock, M. S. Graige, G. Feher, *Biochim. Biophys. Acta* **2000**, *1458*, 148.

[26] D. Zaslavsky, R. B. Gennis, *Biochim. Biophys. Acta* **2000**, *1458*, 164.

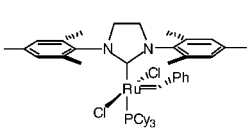
 © 2003 Wiley-VCH Verlag GmbH & Co. KGaA, Weinheim

Ultrafast-Initiating ROMP Catalyst

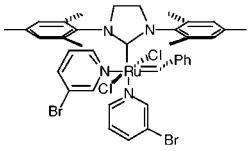
Controlled Living Ring-Opening-Metathesis Polymerization by a Fast-Initiating Ruthenium Catalyst**

*Tae-Lim Choi and Robert H. Grubbs**

Ring-opening-metathesis polymerization (ROMP) has expanded the realm of polymer synthesis, and has provided access to many structurally unique polymers.[1] With the developments of well-defined olefin-metathesis catalysts, such as $[(t\text{BuO})_2(\text{ArN})\text{Mo}{=}\text{CH}(t\text{Bu})]$ (**1**)[2] and $[(\text{PCy}_3)_2(\text{Cl})_2\text{Ru}{=}\text{CHPh}]$ (**2**; Cy = cyclohexyl),[3] controlled living polymerization became possible, making ROMP a novel method to synthesize polymers with various architectures. However, these catalysts suffer from either a lack of functional-group tolerance (**1**) or decreased activity and produces polymer with a moderate polydispersity index (PDI) around 1.2 (**2**). The recent development of N-heterocyclic carbene ruthenium catalysts[4] led to catalyst **3**, which exhibited activity comparable to or higher than **1**, while retaining the functional group tolerance of **2**.[5] Catalyst **3** was



3



4

found to be extremely useful in organic transformations such as cross and ring-closing metathesis.[6] Nevertheless, **3** generally gives polymers with uncontrolled molecular weights and broad PDIs, owing to high propagation rates and slow initiation rates (low k_i/k_p; k_i = the rate constant for initiation, k_p = the rate constant for propagation)[7] and competing chain-transfer reactions.[8]

From the previous study on ring-opening-insertion-metathesis polymerization,[9] we found that norbornene derivatives were not viable comonomers as the steric hindrance around the olefin in the polymers prevented the required insertion into catalyst **3**. This observation suggested that chain transfer or "back-biting" was minimal even with the active catalyst **3** at 40 °C.[10] Previously, a new member of the family of catalysts, **4**, was found to initiate more rapidly than **3**.[11,12] Therefore an increased k_i/k_p ratio should promote the

[*] Prof. R. H. Grubbs, T.-L. Choi
Arnold and Mabel Laboratories of Chemical Synthesis
California Institute of Technology
Division of Chemistry and Chemical Engineering
MC 164-30 Pasadena, CA 91125 (USA)
Fax: (+1) 626-564-9297
E-mail: rhg@its.caltech.edu

[**] The authors would like to thank the National Science Foundation for generous support of this research, and D. Benitez, D. P. Sanders, J. P. Morgan, and O. A. Scherman for helpful discussions, and A. Hejl for the generous supply of catalyst **4**.

 DOI: 10.1002/anie.200250632 © 2003 Wiley-VCH Verlag GmbH & Co. KGaA, Weinheim

controlled living polymerization if chain transfer and chain termination are absent. Herein, we report the controlled living ROMP of norbornene and 7-oxonorbornene derivatives by the highly active and rapidly initiating Ru-based catalyst **4** to make monodisperse homopolymers and block copolymers.

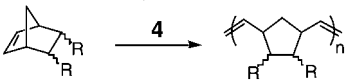
When a solution of monomer was added to a solution of catalyst **4** in dichloromethane (to give a monomer concentration 0.2–0.4 M), the color instantaneously changed from green to yellow, which implies the immediate initiation of catalyst **4**. After 30 minutes, the reactions were complete (monitored by TLC and ^{1}H NMR) and were quenched by adding ethyl vinyl ether, and the polymers were precipitated by pouring the reaction mixture into methanol. The polymers were obtained in high yields with very narrow PDIs, as low as 1.04 (Table 1), which is indicative of controlled living polymerization. All the PDI values are much lower than typical controlled living ROMP products obtained from catalyst **2** (PDI $\approx$ 1.2).[13] Additionally, *endo*-monomers **5** and **8** (Table 1), which are polymerized slowly if at all with catalyst **2**, undergo ROMP readily with the highly active catalyst, **4**.[3a,13]

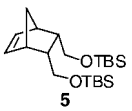
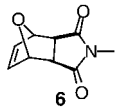
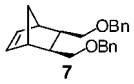
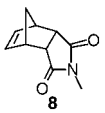
Norbornene (**10**) is a unique monomer, since only catalyst **1** and [$(PPh_3)_2(Cl)_2Ru$=CHPh] (**11**),[3b] promote its controlled living polymerization. Catalysts **2**, and **3** give poor PDIs because of chain-transfer reactions.[3b,8b] Not surprisingly, **4** also produced polynorbornene (PNB) with a broad PDI (1.65) at room temperature. However, PNB with a narrower PDI (1.28) was obtained when the polymerization was carried out at 0 °C, and furthermore, the PDI was lowered to 1.08 at −20 °C (Table 1), which demonstrates that **4** initiates rapidly even at −20 °C and chain-transfer reactions on PNB are suppressed at low temperatures.[14]

The effects of changing the polymerization conditions were studied using 100 equivalents of monomer **6** to catalyst **4**. When the monomer concentration was lowered to 0.05 M in dichloromethane or the temperature was lowered to 0 °C, there were no effects on the product yields, molecular weights, or PDI values. Furthermore, the reaction of the isolated polymer with 20 mol % of a chain-transfer agent, 1,4-bis(acetoxy)-*cis*-2-butene, and 1 mol % of **4** for 10 hours at room temperature resulted in no change of the polymer structure. A change in the solvent of the reaction had no marked effects, but increasing the starting temperature from 23 °C to 55 °C in 1,2-dichloroethane gave a polymer with a similar $\bar{M}_n$ but a much broader PDI of 1.25. These results suggest that chain transfer or backbiting does occur at higher temperatures.[8a]

Encouraged by the narrow PDI, we examined the relationship between the molecular weight and M/C. Representative graphs of $\bar{M}_n$ versus M/C for monomers **6** and **7** are in Figure 1, which clearly shows a linear relationship between $\bar{M}_n$ and M/C. Importantly, the linear relationship holds for both low- (as low as DP = 10; DP = degree of polymerization) and high-molecular-weight polymers with narrow PDIs (< 1.1). Other monomers give similar linear relationships. The control of the molecular weight through the M/C ratio, and the low PDI values suggest that for **4**, k_i/k_p is high enough that all the chains initiate and grow at a similar rate.[15] The high k_i/k_p ratio is attributed to the fact that although the k_p value of catalyst **4** is much larger than that of catalyst **2**, the extremely high k_i value (more than ten thousands times higher that that of **2**)[7,11] overrides the effect of the increase in k_p relative to that of catalyst **2**, which results in a narrower PDI and good molecular-weight

Table 1: ROMP of various monomers with catalyst **4**.[a]



Monomer	M/C	Yield[b] [%]	Obs. $\bar{M}_n$ [c] [$\times 10^3$]	Theo. $\bar{M}_n$ [$\times 10^3$][d]	PDI[c]
 **5**	50	–[e]	14.0	19.2	1.08
	100	84	24.5	38.3	1.06
	200	84	50.0	76.6	1.05
	400	83	114.0	153.1	1.04
 **6**	100	84	29.1	18.0	1.05
	150	–[e]	41.7	26.8	1.05
	200	86	53.1	35.9	1.06
	400	97	106.0	71.7	1.04
 **7**	100	–[e]	30.4	33.5	1.05
	200	92	60.9	67.0	1.04
	400	90	131.5	133.9	1.06
 **8**	50	–[e]	11.5	8.9	1.08
	100	87	22.9	17.8	1.08
	200	73	40.2	35.5	1.09
 **9**	100	–[e]	28.7	19.9	1.10
	200	81	50.6	39.7	1.09
	400	87	91.1	79.4	1.10
 **10**	100	87	9.0[f]	9.5	1.09
	150	–[e]	15.1[f]	14.2	1.06
	200	93	22.0[f]	18.9	1.10

[a] 0.2 M in CH_2Cl_2 at 23 °C (or −20 °C for **10**) for 30 min. [b] Isolated by precipating into methanol. [c] Determined by CH_2Cl_2 GPC relative to polystyrene standards. [d] Assuming quantitative conversion. [e] Samples prepared by quenching and removing the solvent without precipitation. [f] The correction factor of 0.5 applied to PNB.[8a] GPC = gel-permeation chromatography, TBS = *tert*-butyldimethylsilyl, Bn = Benzyl, Bz = Benzoyl, M/C = monomer to catalyst ratio, $\bar{M}_n$ = number-average molar mass.

 © 2003 Wiley-VCH Verlag GmbH & Co. KGaA, Weinheim

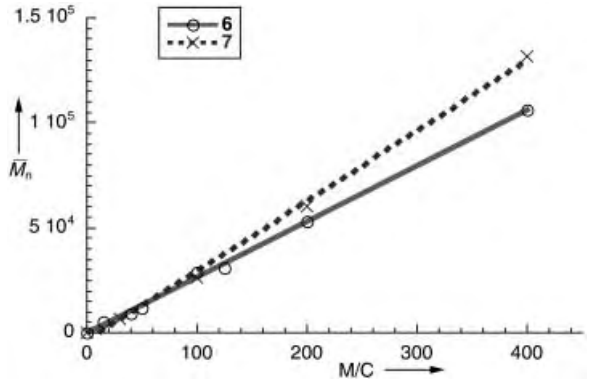


Figure 1. $\bar{M}_n$ versus M/C for the polymers produced from momomers **6** and **7** by using catalyst **4**.

control. Thus, catalyst **4** promotes living ROMP with both higher activity and better control.

If **4** indeed promotes the controlled living polymerization for norbornenes and 7-oxonorbornene derivatives, it should produce block copolymers from sequential additions of monomers. Monomer **7** (M/C = 200) was treated with catalyst **4**, followed by the addition of monomer **5** (M/C = 200) after 30 minutes (Table 2, entry 1). The resulting polymer had almost twice the $\bar{M}_n$ of the initial homopolymer **7**, and the PDI of 1.10. The ^{1}H NMR spectrum of this product shows only two sets of overlaying signals identical to those of the two homopolymers. To confirm that **4** produces diblock copolymers, another block copolymer was synthesized by treating monomer **6** (M/C = 50) with catalyst **4**, followed by monomer **7** (M/C = 200). The well-resolved GPC traces for the diblock copolymer of entry 2 (Table 2) show the complete shift to higher molecular weights (Figure 2a).

The $\bar{M}_n$ value of the final copolymer (73000) agrees with the value obtained by adding the $\bar{M}_n$ of individually synthesized homopolymers of **6** and **7** (10000 + 60000 = 70000). One can also make ABC-triblock copolymers by the sequential addition of three different monomers (entry 3). Figure 2b displays well-resolved GPC traces of monodisperse triblock copolymer. No fractions are observed in the low-molecular-weight regions, which indicates that no termination processes occurred during the course of the two sequential additions of monomers. In all cases, the ratios of the monomers, obtained by ^{1}H NMR studies of the final block copolymers, are in good agreement with the added feed ratios.

In conclusion, we have demonstrated that catalyst **4** bearing an N-heterocyclic carbene, which greatly enhances the activity, and a 3-bromopyridine[16] ligand, which significantly increases the initiation process, effects controlled living polymerization of norbornene and oxo-norbornene derivatives, even those derivatives that do not undergo living polymerization with other catalysts.

Table 2: Synthesis of block copolymers.[a]

Entry	First Monomer	M/C	$\bar{M}_n$[b] [×10^3]	Second monomer	M/C	$\bar{M}_n$[b] [×10^3]	Yield[c] [%]	PDI[b]
1	**7**	200	60.6	**5**	200	115.1 (143.5)	90	1.10
2	**6**	50	10.0	**7**	200	72.7 (75.9)	86	1.07
3	**6**	15	5.1	**7**	75	37.4 (27.9)		1.06
		third	monomer	**5**	370	154.8 (169.5)	90	1.05

[a] 0.2 M in CH_2Cl_2 at 23 °C for 30 min for each monomer. [b] Determined by GPC with CH_2Cl_2 relative to polystyrene standards. [c] Yield of product isolated by precipating into methanol.

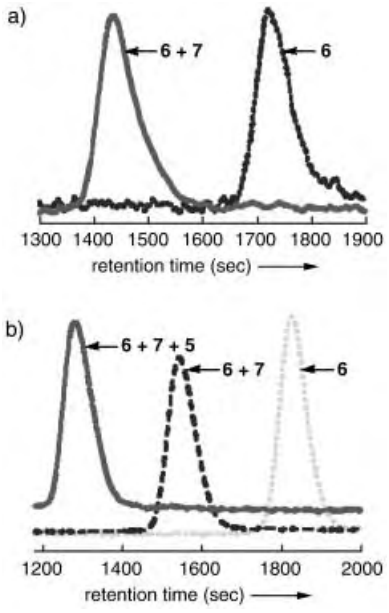


Figure 2. GPC traces for diblock (a) and triblock (b) copolymers.

Experimental Section

Representative procedure for the ROMP of monomer **7**: A solution of **7** (150 mg, 0.45 mmol) in CH_2Cl_2 (0.5 mL) was added rapidly by syringe to a vial charged with **4** (1.0 mg, 1.1 μmol) in CH_2Cl_2 (1 mL) under an argon atmosphere at room temperature. After 30 minutes excess ethyl vinyl ether was added and the polymer was precipitated by pouring the reaction mixture into methanol. Yield 135 mg (90%, 59% *cis* olefin). ^{1}H NMR (300 MHz, $CDCl_3$): δ = 7.25 (brs, 10H), 5.25 (brm, 2H), 4.30 (brm, 4H), 3.45 (brs, 4H), 2.76 (brs, 1.2H for *cis*), 2.38 (brs, 0.8H for *trans*), 2.03 (3H, brm), 1.12 ppm (brs, 1H). ^{13}C NMR (75 MHz, $CDCl_3$): δ = 138.9 (brm), 134.0 (brm), 128.5, 127.7, 127.6, 73.2, 70.7, 70.4, 48.0, 47.7, 45.4 (brm), 41.3 (brm), 40.3 ppm. Other homopolymers referred to herein are known and characterized.

Received: November 26, 2002
Revised: March 17, 2003 [Z50632]

Keywords: copolymerization · metathesis · N ligands · ring-opening polymerization · ruthenium

[1] For recent reviews on ROMP, see: a) B. M. Novak, W. Risse, R. H. Grubbs, *Adv. Polym. Sci.* **1992**, *102*, 47; b) K. J. Ivin, J. C. Mol, *Olefin Metathesis and Metathesis Polymerization*, Academic Press, San Diego, CA, **1997**; c) R. H. Grubbs, E. Khosravi, *Mater. Sci. Technol.* **1999**, *20*, 65; d) M. R. Buchmeiser, *Chem. Rev.* **2000**, *100*, 1565; e) U. Frenzel, O. Nuyken, *J. Polym. Sci. Part A* **2002**, *40*, 2895.

[2] a) R. R. Schrock, *Acc. Chem. Res.* **1990**, *23*, 158; b) G. C. Bazan,

 © 2003 Wiley-VCH Verlag GmbH & Co. KGaA, Weinheim

R. R. Schrock, H. N. Cho, V. C. Gibson, *Macromolecules* **1991**, *24*, 4495.

[3] a) S. Kanaoka, R. H. Grubbs, *Macromolecules* **1995**, *28*, 4707; b) P. Schwab, R. H. Grubbs, J. W. Ziller, *J. Am. Chem. Soc.* **1996**, *118*, 100; c) M. Weck, P. Schwab, R. H. Grubbs, R. H. *Macromolecules* **1996**, *29*, 1789.

[4] a) T. Weskamp, W. C. Schattenmann, M. Spiegler, W. A. Herrman, *Angew. Chem.* **1998**, *110,* 2631; *Angew. Chem. Int. Ed.* **1998**, *37*, 2490; b) T. Weskamp, F. J. Kohl, W. Hieringer, D. Gleich, W. A. Herrman, *Angew. Chem.* **1999**, *111,* 2573; *Angew. Chem. Int. Ed.* **1999**, *38*, 2416; c) J. Huang, E. D. Stevnes, S. P. Nolan, J. L. Petersen, *J. Am. Chem. Soc.* **1999**, *121*, 2675.

[5] M. Scholl, S. Ding, C. W. Lee, R. H. Grubbs, *Org. Lett.* **1999**, *1*, 953.

[6] a) A. K. Chatterjee, R. H. Grubbs, *Org. Lett.* **1999**, *1*, 1751; b) A. K. Chatterjee, J. P. Morgan, M. Scholl, R. H. Grubbs, *J. Am. Chem. Soc.* **2000**, *122*, 3783; c) T.-L. Choi, A. K. Chatterjee, R. H. Grubbs, *Angew. Chem.* **2001**, *113*, 1317; *Angew. Chem. Int. Ed.* **2001**, *40*, 1277; d) A. K. Chatterjee, T.-L. Choi, R. H. Grubbs, *Synlett* **2001**, 1034; e) T.-L. Choi, C. W. Lee, A. K. Chatterjee, R. H. Grubbs, *J. Am. Chem. Soc.* **2001**, *123*, 10417; f) T.-L. Choi, R. H. Grubbs, *Chem. Commun.* **2001**, 2648; g) C. W. Lee, T.-L. Choi, R. H. Grubbs, *J. Am. Chem. Soc.* **2002**, *124*, 3224.

[7] a) M. S. Sanford, M. Ulman, R. H. Grubbs, *J. Am. Chem. Soc.* **2001**, *123*, 749; b) M. S. Sanford, J. A. Love, R. H. Grubbs, *J. Am. Chem. Soc.* **2001**, *123*, 6543.

[8] a) C. W. Bielawski, R. H. Grubbs, *Angew. Chem.* **2000**, *112,* 3025; *Angew. Chem. Int. Ed.* **2000**, *39*, 2903; b) C. W. Bielawski, D. Benitez, R. H. Grubbs, *Macromolecules* **2001**, *34*, 8610; c) O. A. Scherman, H. M. Kim, R. H. Grubbs, *Macromolecules* **2002**, *35*, 5366.

[9] T.-L. Choi, I. M. Rutenberg, R. H. Grubbs, *Angew. Chem.* **2002**, *114*, 3995; *Angew. Chem. Int. Ed.* **2002**, *41*, 3839.

[10] ROMP with catalyst **3** gives extremely high-molecular-weight polymers that are often insoluble, but low PDIs have been observed in some special cases, see: H. D. Maynard, S. Y. Okada, R. H. Grubbs, *Macromolecules* **2000**, *33*, 6239.

[11] J. A. Love, J. P. Morgan, T. M. Trnka, R. H. Grubbs, *Angew. Chem.* **2002**, *114*, 4207; *Angew. Chem. Int. Ed.* **2002**, *41*, 4035.

[12] For ROMP with other fast-initiating catalysts (but slower than **4**), see: a) U. Frenzel, T. Weskamp, F. J. Kohl, W. C. Schattenmann, O. Nuyken, W. A. Herrmann, *J. Organomet. Chem.* **1999**, *586*, 263; b) C. Slugovc, S. Demel, F. Stelzer, *Chem. Commun.* **2002**, 2572.

[13] ROMP of *endo-n*-alkyl norbornene dicarboxyimides with catalyst **1** gave polymers with PDI of 1.3, see: E. Khosravi, W. J. Feast, A. A. Al-Hajaji, T. Leejarkpai, *J. Mol. Catal. A* **2000**, *160*, 1. Crude solutions of polymers (i.e. without precipitation) were subjected to GPC analysis resulting in clean traces that displayed low PDIs. These traces show that the low PDIs are not a consequence of fractionation of polymers of low molecular weight by precipitation.

[14] This PNB contained 61% of the *cis*-olefin isomer and is much higher than PNB produced with **3** (35% *cis*), which undergoes chain-transfer reactions.[8b]

[15] Ten equivalents of **8** were mixed with **4** at −10°C resulting in complete initiation (the only propagating carbene signal in the corresponding ^{13}C NMR spectrum was observed at $\delta =$ 18.2 ppm) and 13% product conversion. Based on the assumption of at least 99% initiation, a minimum value of $k_i/k_p = 19$ is calculated by using the Gold equation. See reference [1b] page 232.

[16] Complexes with other substituted-pyridine ligands can show similar rapid initiation rates A. Hejl, R. Grubbs, unpublished results.

 © 2003 Wiley-VCH Verlag GmbH & Co. KGaA, Weinheim

Supramolecular Chirogenesis

Solid-State Supramolecular Chirogenesis: High Optical Activity and Gradual Development of Zinc Octaethylporphyrin Aggregates

Victor V. Borovkov, Takunori Harada, Guy A. Hembury, Yoshihisa Inoue,* and Reiko Kuroda**

Aggregation processes leading to chirality transfer or induction or amplification phenomena are currently one of the "hot topics" of modern chemical science. The investigation of such processes has influenced research in many areas including studies on the origin of the homochirality of life, various biomimetic systems, materials and polymer science, nonlinear optics, molecular devices, molecular recognition, and the determination of absolute configuration.[1] In the course of our investigations on supramolecular chirogenesis phenomena in porphyrin chromophores,[2] we recently discovered a new type of highly optically active aggregates based on bis(zinc porphyrin) upon interaction with chiral amines in the solid state.[2a] Extension of this research revealed that not only more structurally complex bisporphyrins form chiral aggregated species in the solid state, but that even a conventional and simple monomeric zinc porphyrin may generate chiral aggregates under certain conditions. Here we describe the time-dependent formation of chiral aggregates of zinc octaethylporphyrin (ZnOEP, Figure 1) upon interaction with enantiopure chiral amines in the solid state. This results in the highest optical activity ever reported for a supramolecular chirogenic system based on porphyrin chromophores.

Recently it was shown that ZnOEP exhibits either no or only negligible optical activity in the porphyrin absorption region upon interaction with chiral amines in solution[2d] and in the solid state.[3] However, and exclusively for the case of enantiopure 1-cyclohexylethylamines (CHEAs), further analysis of the solid-state mixture with ZnOEP revealed the gradual development of a supramolecular chirogenic process. The solid-state samples were prepared according to the standard procedure for obtaining a glassy KBr matrix.[4] Then the process of supramolecular chirogenesis was monitored by UV/Vis and circular dichroism (CD) spectroscopy over time.

In the beginning the UV/Vis spectrum of freshly prepared ZnOEP·L (L = (*S*)-CHEA) in a KBr matrix closely resembles that in CH_2Cl_2 (Figure 2b, see also ref. [2d] and the Support-

[*] Dr. V. V. Borovkov, Prof. Dr. Y. Inoue, Dr. G. A. Hembury
Entropy Control Project, ICORP, JST, 4-6-3 Kamishinden
Toyonaka-shi, Osaka 560-0085 (Japan)
Fax: (+81) 6-6836-1636
E-mail: victrb@inoue.jst.go.jp
inoue@chem.eng.osaka-u.ac.jp
Prof. Dr. R. Kuroda, Dr. T. Harada
Kuroda Chiromorphology Project, ERATO, JST
Park bldg., 4-7-6 Komaba, Meguro-ku, Tokyo 153-0041 (Japan)
Fax: (+81) 3-5452-0599
E-mail: ckuroda@mail.ecc.u-tokyo.ac.jp

Supporting information for this article is available on the WWW under http://www.angewandte.org or from the author.

 © 2003 Wiley-VCH Verlag GmbH & Co. KGaA, Weinheim DOI: 10.1002/anie.200250524

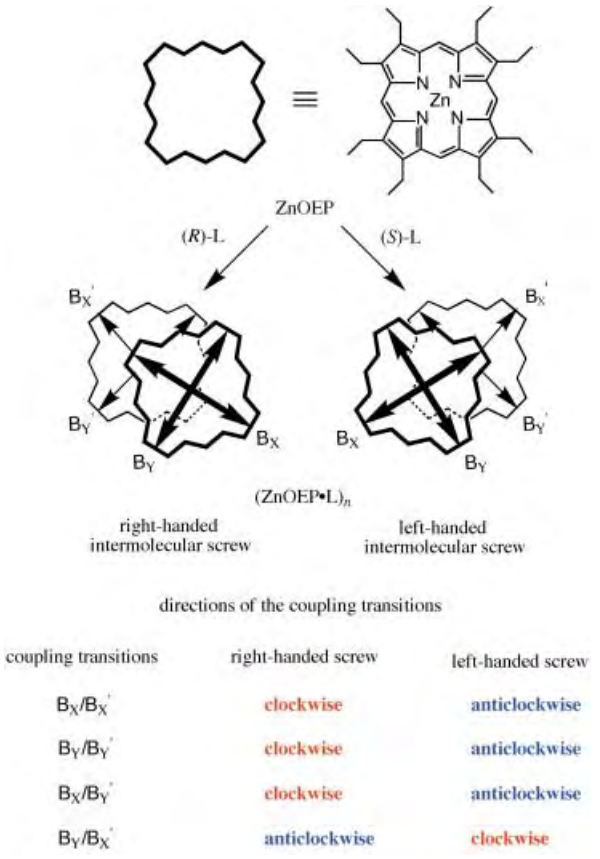


Figure 1. Schematic representation of the formation of chiral aggregates $(ZnOEP{\cdot}L)_n$ upon interaction of ZnOEP with chiral ligands L in the solid state and the directions of the corresponding coupling transitions. The structures of $(ZnOEP{\cdot}L)_n$ are drawn schematically to show the opposite orientation of the transition coupling directions (other stacked orientations are possible as a result of rotations of the ZnOEP·L monomers against each other).

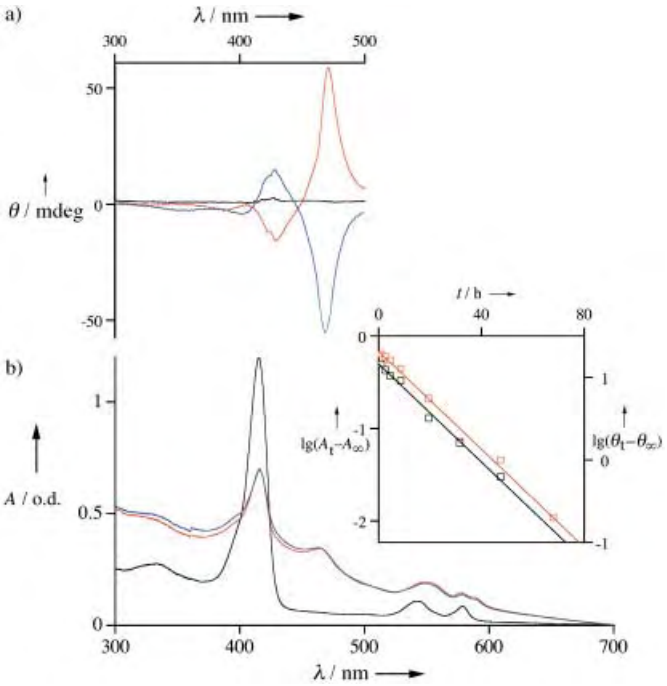


Figure 2. The CD (a) and UV/Vis spectra (b) of ZnOEP in a KBr matrix in the presence of (*S*)-CHEA recorded immediately after preparation (black lines) and after four days (red lines), and (*R*)-CHEA recorded after 4 days (blue lines). The spectra of (*S*)- and (*R*)-CHEA are normalized to the same optical density. Inset: Kinetics data of the UV/Vis (black) and CD (red) spectral changes of ZnOEP in the presence of (*S*)-CHEA in a KBr matrix monitored at the maximum of the B transition ($\lambda = 415$ nm) and the position of the first Cotton effect ($\lambda = 469$ nm). The solid lines represent the best linear fit of the experimental data.

ing Information) and the CD spectrum (Figure 2a) indicates there is only minor optical activity. This indicates clearly that the initial structure and aggregation state of ZnOEP·L in the solid state is very similar to that in solution.

Subsequent measurements of the same sample after four days[5] revealed extensive changes in the UV/Vis and CD spectra. In the UV/Vis spectrum the amplitude of the initial B band was considerably diminished, with a new bathochromically shifted transition appearing at $\lambda = 464$ nm; similar but smaller changes were also clearly observed in the Q absorption region. These observations suggest an intermolecular J-type association of the ZnOEP·L molecules to form a stacked $(ZnOEP{\cdot}L)_n$ species, as they are in good agreement with exciton coupling theory[6] and other literature data on various J aggregates.[1a,f,k,7] Simultaneous CD monitoring of the same solid-state sample showed induction of extraordinarily high optical activity in the aggregated species.[8] Specifically, this includes an intense CD couplet in the region of the new low-energy B band (Figure 2a) and conspicuous monosignate Cotton effects corresponding to the porphyrin Q transitions (see the Supporting Information).

Although the spectral profile of this CD signal somewhat resembles that observed for the bis(zinc porphyrin)/(*S*)-CHEA system under solid-state conditions[2a] and the induced chirality sign is also the same, thus indicating similarity in the structural organization and helical orientation between the chiral aggregates, there are two crucially important differences. These are a considerable low-energy shift of the first Cotton effect ($\lambda^{CD} = 469$ nm) and a remarkable enhancement of the anisotropy (g) factor at the wavelength corresponding to the first Cotton effect ($g = -0.015$), which is 10–100 times greater than the g factors reported for typical allowed π–π transitions. This is apparently a result of the formation of larger J aggregates of $(ZnOEP{\cdot}L)_n$ and the amplification of chirality by intermolecular excitonic coupling within the aggregates. In the case of bisporphyrin chromophores the formation of larger aggregates is less probable because of the larger molecular size in comparison to the monomeric porphyrin. Furthermore, the intermolecularly induced chirality is considerably reduced in the bisporphyrin case by intramolecular coupling of opposite orientation.[2a,b] However, all other chiral amines studied to date do not generate any supramolecular chirogenic processes upon interaction with ZnOEP in the solid state.[3]

Although the precise origin of the selectivity of CHEA is not yet well understood, it is likely that the exceptionally high binding ability of these ligands among the amines used[2c] may contribute greatly to the formation of chiral aggregates in the

 © 2003 Wiley-VCH Verlag GmbH & Co. KGaA, Weinheim

solid state. The strong binding of CHEA may compete successfully with the achiral H-type interporphyrin stacking, thus causing the chiral J-type interporphyrin association. In particular, the approach of the second ZnOEP·L complex to the first ZnOEP·L from the same side as the CHEA ligand forces the former to adopt a screw offset spatial orientation in relation to the latter. The direction of the twist is governed by the relative bulkiness of the substituents at the asymmetric center, which depends upon the absolute configuration of the chiral ligand. For example, in the case of (*S*)-CHEA the screw orientation is left-handed, based on examination of Corey—Pauling–Koltun molecular models, while in the case of (*R*)-CHEA the screw direction is right-handed. Importantly, these spatial arrangements correspond to the negative and positive chirality,[9] which was observed experimentally. Further replication of this process results in formation of the helically twisted J aggregates of $(ZnOEP{\cdot}L)_n$ inducing the high optical activity.

The plausible mechanism of chirality induction in $(ZnOEP{\cdot}L)_n$ can be rationalized on the basis of a simple dimeric subunit (where $n=2$) of the whole chiral aggregate, the schematic structure of which is shown in Figure 1. Interaction of ZnOEP with (*S*)-CHEA produces negative chirality that corresponds to the left-handed interporphyrin screw structure in the solid state as described above and has also been observed for the bis(zinc porphyrin) systems.[2a] In this twisted conformation the coupled porphyrin electronic transitions become optically active. In particular, the two degenerate transitions (B_X and B_Y) of the first ZnOEP·L molecule couple with the $B_{X'}$ and $B_{Y'}$ transitions of the second porphyrin complex in a stereospecific manner. Thus, the $B_X/B_{X'}$, $B_Y/B_{Y'}$, and $B_X/B_{Y'}$ pairs adopt an anticlockwise orientation, and the $B_Y/B_{X'}$ pair forms a clockwise orientation, which correspond to negative and positive chirality, respectively, according to the exciton chirality method.[9] As a result of the three negative and one positive couplets in the same B band region, the overall sum of these should be a complex CD signal with a first Cotton effect of negative sign, which is exactly what is observed experimentally (Figure 2a). In the case of the *R* enantiomer the coupling directions of the dipoles are exactly opposite, resulting in the mirror-image CD spectrum of positive chirality.

As noted above, this supramolecular chirogenesis proceeds slowly in the solid state. The course of the aggregation process was monitored at the most intense porphyrin absorption region of the Soret band by UV/Vis and CD spectroscopy (see the Supporting Information). In the UV/Vis spectra the intensity of the Soret band of ZnOEP·L gradually decreases with time, while a new spectral band associated with $(ZnOEP{\cdot}L)_n$ simultaneously appears. In the CD spectra there is a stepwise transformation of the initial small signal into the bisignate CD couplet induced by the aggregation process as described above. Although the intermolecular porphyrin association is apparently a complex and multistep process, there is a clear pseudo-isosbestic point in the UV/Vis spectrum at $\lambda = 425$ nm which is due to the similarity of the absorption profiles of the porphyrin aggregates and intermediate species. However, in contrast to the UV/Vis spectra the CD spectra do not show an isodichroic point because of the different chiroptical properties of the various chiral species. In the case of UV/Vis spectroscopy the monitoring parameter was the absorbance at the wavelength corresponding to the maximum of the initial B transition ($\lambda =$ 415 nm) as this is most affected by the aggregation process. For CD spectroscopy the intensity of the newly developed Cotton effect ($\lambda = 469$ nm) was selected to monitor the corresponding spectral changes. The bathochromically shifted CD transition was chosen to minimize the contribution of the intermediate chiral species, which appear to absorb at higher energies in comparison to the larger chiral aggregates.

Both the UV/Vis and CD kinetic experimental data fit well to a theoretical equation for a first-order processes [Eq. (1)], where A_0, A_t, and A_∞ are UV/Vis absorbances (in

$$A_t = A_\infty + (A_0 - A_\infty)(-k_{obs}\, t) \qquad (1)$$

the case of CD the ellipticities θ were used) at the initial, intermediate, and final stages of the aggregation process, respectively. This allows determination of the pseudo-first-order rate constants k_{obs} by a nonlinear least-square fitting procedure (inset of Figure 2). The k_{obs} values obtained from both spectroscopic techniques are almost identical ($k_{obs}^{UV} =$ 0.026 h^{-1} and $k_{obs}^{CD} = 0.030$ h^{-1}), indicating that the supramolecular chirogenesis is simultaneously generated by slow interporphyrin aggregation.

To prove the absence of any chemical reactions in the solid state that might yield new chiral compounds rather than an aggregated species, the four-day-old KBr sample of $(ZnOEP{\cdot}L)_n$ was destroyed by treatment with water and then extracted into CH_2Cl_2. The UV/Vis spectra of the resulting extract is essentially identical to that of ZnOEP in the same solvent, and the CD spectrum does not show any optical activity (see the Supporting Information). This result clearly demonstrates that the aggregation process is the sole reason for the supramolecular chirality induction in the solid state.

Finally, these $(ZnOEP{\cdot}L)_n$ solid-state aggregates are remarkably stable over time. Even after storage for over six months in a dark, dry environment, reexamination of the chiroptical properties by CD spectroscopy showed that the integrity of the developed chiral structure was retained.

In summary, this work provides a unique example of a time-dependent, solid-state chirogenesis phenomenon in supramolecular systems based on a simple monomeric porphyrin chromophore by the formation of helical intermolecular aggregates possessing a high degree of optical activity.

Received: November 11, 2002 [Z50524]

Keywords: chirality · circular dichroism · porphyrinoids · solid-state structures · supramolecular chemistry

[1] a) J. M. Ribó, J. Crusats, F. Sagués, J. Claret, R. Rubires, *Science* **2001**, *292*, 2063–2066; b) H. Nakashima, J. R. Koe, K. Torimitsu, M. Fujiki, *J. Am. Chem. Soc.* **2001**, *123*, 4847–4849; c) J. M. Fox, T. J. Katz, S. Van Elshocht, T. Verbiest, M. Kauranen, A. Persoons, T. Thongpanchang, T. Kraus, L. Brus, *J. Am. Chem. Soc.* **1999**, *121*, 3453–3459; d) R. Purrello, A. Raudino, L. M.

 © 2003 Wiley-VCH Verlag GmbH & Co. KGaA, Weinheim

Scolaro, A. Loisi, E. Bellacchio, R. Lauceri, *J. Phys. Chem. B* **2000**, *104*, 10900 – 10908; e) D. B. Steensgaard, H. Wackerbarth, P. Hildebrandt, A. R. Holzwarth, *J. Phys. Chem. B* **2000**, *104*, 10379 – 10386; f) D. Iarossi, A. Mucci, F. Parenti, L. Schenetti, R. Seeber, C. Zanardi, A. Forni, M. Tonelli, *Chem. Eur. J.* **2001**, *7*, 676 – 685; g) M. de Loos, J. van Esch, R. M. Kellogg, B. L. Feringa, *Angew. Chem.* **2001**, *113*, 633 – 636; *Angew. Chem. Int. Ed.* **2001**, *40*, 613 – 616; h) W. Steffen, B. Kohler, M. Altmann, U. Scherf, K. Stitzer, H.-C. zur Loye, U. H. F. Bunz, *Chem. Eur. J.* **2001**, *7*, 117 – 126; i) J. H. Jung, H. Kobayashi, M. Masuda, T. Shimizu, S. Shinkai, *J. Am. Chem. Soc.* **2001**, *123*, 8785 – 8789; j) L. Brunsveld, E. W. Meijer, R. B. Prince, J. S. Moore, *J. Am. Chem. Soc.* **2001**, *123*, 7978 – 7984; k) M. Wang, G. L. Silva, B. A. Armitage, *J. Am. Chem. Soc.* **2000**, *122*, 9977 – 9986; l) P. Wittung, P. Nielsen, O. Buchart, M. Egholm, B. Norden, *Nature* **1994**, *368*, 561 – 563.

[2] a) V. V. Borovkov, T. Harada, Y. Inoue, R. Kuroda, *Angew. Chem.* **2002**, *114*, 1436 – 1439; *Angew. Chem. Int. Ed.* **2002**, *41*, 1378 – 1381; b) V. V. Borovkov, J. M. Lintuluoto, M. Sugiura, Y. Inoue, R. Kuroda, *J. Am. Chem. Soc.* **2002**, *124*, 11282 – 11283; c) V. V. Borovkov, J. M. Lintuluoto, H. Sugeta, M. Fujiki, R. Arakawa, Y. Inoue, *J. Am. Chem. Soc.* **2002**, *124*, 2993 – 3006; d) V. V. Borovkov, J. M. Lintuluoto, Y. Inoue, *J. Am. Chem. Soc.* **2001**, *123*, 2979 – 2989; e) V. V. Borovkov, J. M. Lintuluoto, Y. Inoue, *Org. Lett.* **2002**, *4*, 169 – 171; f) V. V. Borovkov, J. M. Lintuluoto, Y. Inoue, *Org. Lett.* **2000**, *2*, 1565 – 1568; g) V. V. Borovkov, J. M. Lintuluoto, M. Fujiki, Y. Inoue, *J. Am. Chem. Soc.* **2000**, *122*, 4403 – 4407; h) V. V. Borovkov, J. M. Lintuluoto, Y. Inoue, *J. Phys. Chem. A* **2000**, *104*, 9213 – 9219.

[3] The interaction of ZnOEP with other chiral amines in the solid state will be reported elsewhere.

[4] R. Kuroda, Y. Saito, *Bull. Chem. Soc. Jpn.* **1976**, *49*, 433 – 436.

[5] All solid-state samples have been kept in a desiccator under dark conditions.

[6] M. Kasha, H. R. Rawls, M. A. El-Bayoumi, *Pure Appl. Chem.* **1965**, *11*, 371 – 392.

[7] a) R. Rubires, J.-A. Farrera, J. M. Ribó, *Chem. Eur. J.* **2001**, *7*, 436 – 446; b) Z. Bikádi, F. Zsila, J. Deli, G. Mády, M. Simonyi, *Enantiomer* **2002**, *7*, 67 – 76; c) H. von Berlepsch, C. Böttcher, A. Ouart, C. Burger, S. Dähne, S. Kirstein, *J. Phys. Chem. B* **2000**, *104*, 5255 – 5262; d) W. Xu, H. Guo, D. L. Akins, *J. Phys. Chem. B* **2001**, *105*, 1543 – 1546; e) I. Struganova, *J. Phys. Chem. A* **2000**, *104*, 9670 – 9674.

[8] Using a solid-state specialized universal chiroptical spectrophotometer UCS: J-800KCM (R. Kuroda, T. Harada, Y. Shindo, *Rev. Sci. Instrum.* **2001**, *72*, 3802 – 3810) it was shown that optical anisotropies of the solid-state samples are negligibly small (see the Supporting Information). For example, linear dichroism, which is the major source of the artifacts observed in the CD signal of solid-state samples, contributes less than 1% to the total observed amplitude.

[9] N. Harada, K. Nakanishi, *Circular Dichroic Spectroscopy. Exciton Coupling in Organic Stereochemistry*, University Science Books, Mill Valley, CA, **1983**.

 © 2003 Wiley-VCH Verlag GmbH & Co. KGaA, Weinheim

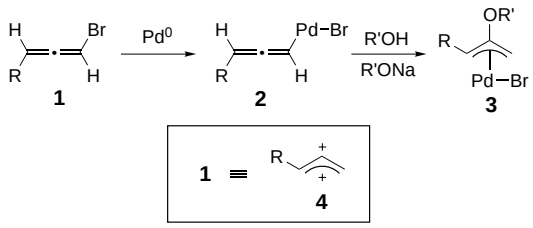
Medium-Sized Heterocycles

Bromoallenes as Synthetic Equivalents of Allyl Dications: Synthesis of Medium-Sized Nitrogen Heterocycles through the Cyclization of Bromoallenes in the Presence of a Palladium(0) Catalyst and an Alcohol**

*Hiroaki Ohno, Hisao Hamaguchi, Miyo Ohata, and Tetsuaki Tanaka**

Medium-sized nitrogen heterocycles (7- to 12-membered rings) are an extremely important class of compounds, which occur in a wide range of natural and non-natural products.[1] In particular, seven- and eight-membered nitrogen heterocycles are constituents of a number of compounds with interesting pharmacological properties.[2,3] Cyclization to medium-sized heterocycles is often slow and is hampered by the unfavorable enthalpies (strain in medium rings) and entropies (probability of the chain ends meeting) of the reaction. Accordingly, the construction of medium-sized heterocycles is a popular challenge for synthetic chemists.[4,5]

Currently, the reactivity of bromoallenes is attracting much interest as a result of their interesting chemical properties associated with their cumulated double bonds and bromine substituent.[6–8] In contrast, as far as we are aware, ring-forming reactions of bromoallenes have scarcely been studied.[9] This Communication is based on a new finding that the bromoallene **1** can act as allyl dication equivalent **4** when treated with palladium(0) in an alcohol solvent, presumably by the mechanism shown in Scheme 1.[10] Although similar types of reaction are often observed with propargylic carbonates in the presence of a palladium catalyst and a soft nucleophile such as active methylene, aryl alcohols,



Scheme 1. Bromoallenes as allyl dication equivalents.

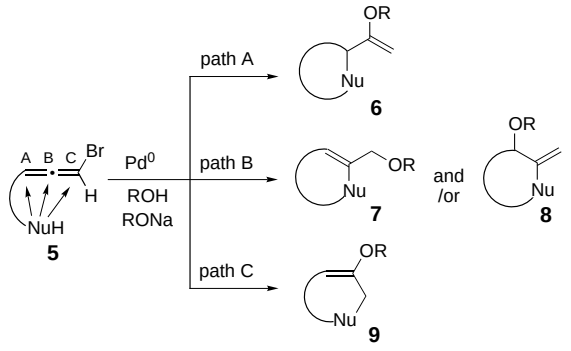
[*] Prof. Dr. T. Tanaka, Dr. H. Ohno, H. Hamaguchi, M. Ohata
Graduate School of Pharmaceutical Sciences, Osaka University
1-6 Yamadaoka, Suita, Osaka 565-0871 (Japan)
Fax: (+81) 6-6879-8214
E-mail: t-tanaka@phs.osaka-u.ac.jp

[**] We thank Prof. Dr. M. Mori, Hokkaido University, for useful information regarding the mechanism of the reaction. This work was supported by a Grant-in-Aid for Encouragement of Young Scientists from the Ministry of Education, Science, Sports, and Culture of Japan. H.H. is grateful for a Research Fellowship for Young Scientists from the Japan Society for the Promotion of Science (JSPS).

 DOI: 10.1002/anie.200250589 © 2003 Wiley-VCH Verlag GmbH & Co. KGaA, Weinheim

or amides,[10,11] the reaction of allenic substrates and the synthesis of eight-membered rings are unprecedented.

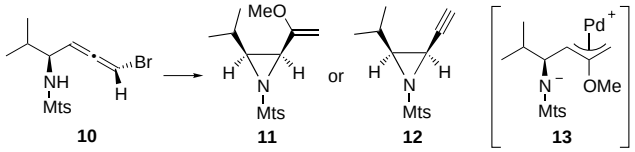
Utilizing this chemistry, we expected that various heterocyclic medium-sized rings could be formed through the intramolecular attack of an appropriate nucleophilic functionality such as an oxygen or nitrogen nucleophile. This sequence can lead to different products depending on whether the intramolecular nucleophilic attack takes place at the proximal (path A), central (path B), or distal (path C) position of the allenyl moiety (Scheme 2). Furthermore, in path B, the regioselectivity of the attack of an external nucleophile would make prediction of the product complicated. Herein we describe a highly regioselective method for the synthesis of heterocyclic medium-sized rings containing nitrogen atoms, through the palladium(0)-catalyzed cyclization of bromoallenes.[12]



Scheme 2. Synthesis of medium-sized rings by palladium(0)-catalyzed cyclization of bromoallenes.

In an initial experiment, we found that the reaction of bromoallene **10**, which bears a protected amino group at the α position, with $[Pd(PPh_3)_4]$ and NaOMe in MeOH provided 2,3-*cis*-2-(1-methoxy)vinylaziridine **11** stereoselectively (Table 1, entry 1). Considering that an N-activated 3-alkyl-2-vinylaziridine can be easily equilibrated with a palladium(0) catalyst via a π-allyl palladium complex to give predominantly the more stable 2,3-*cis* isomer,[13] this result strongly suggests the formation in the reaction of an intermediate π-allyl palladium complex **13**, which bears a methoxy group on the central carbon atom. This cyclization did not proceed in the absence of a palladium catalyst (Table 1, entry 2). When the reaction was carried out in THF in the presence or absence of palladium (Table 1, entries 3 and 4), *cis*-2-ethynylaziridine **12** was obtained as a single isomer, consistent with the results of our previous study.[9]

Table 1: Aziridination of bromoallene **10** in the presence of a palladium catalyst.[a]



Entry	$[Pd(PPh_3)_4]$ [mol %]	Solvent	*t* [h]	Product[b]	Yield [%][c]
1	10	MeOH	6	**11** (96:4)	81
2	–	MeOH	6	–	–
3	10	THF	5.5	**12** (>99:1)	82
4	–	THF	6	**12** (>99:1)	69[d]

[a] Reactions were carried out at 25 °C in THF or MeOH with diastereomerically pure bromoallene **10** and NaOMe (1.2 equiv) in the presence or absence of $[Pd(PPh_3)_4]$. [b] Ratios were determined by ^{1}H NMR (300 MHz). [c] Yields of isolated products. [d] 30% of **10** was recovered. Mts = 2,4,6-trimethylphenylsulfonyl.

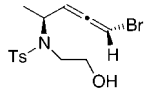
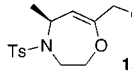
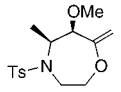
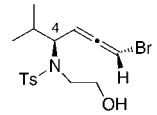
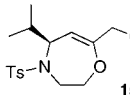
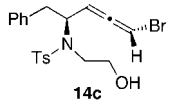
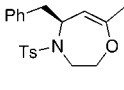
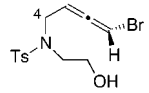
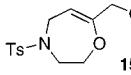
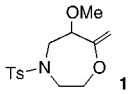
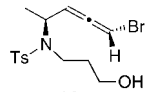
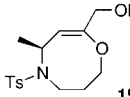
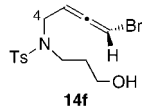
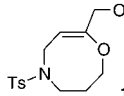
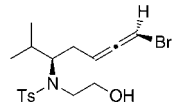
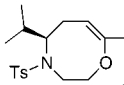
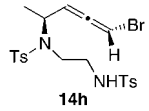
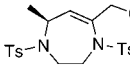
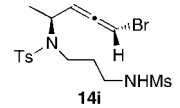
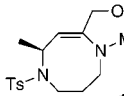
Next, according to the working hypothesis depicted in Scheme 2, we investigated the synthesis of medium-sized heterocycles through the cyclization of bromoallenes in the presence of a palladium catalyst. To investigate the effect of axial chirality on the cyclization reaction, diastereomerically pure (*S*,a*S*)-bromoallenes **14a–i** were prepared from known intermediates.[9] The results of the cyclization reactions are summarized in Table 2. Bromoallene **14a**, which bears an oxygen functionality, was treated with NaOMe (1.5 equiv) in MeOH in the presence of $[Pd(PPh_3)_4]$ (5 mol %) to afford the seven-membered ring **15a** (73%) and a small amount of its regioisomer **16a** (9%; Table 2, entry 1). In contrast, bromoallenes **14b** and **14c** with a bulkier substituent at C4 gave the seven-membered rings **15b** and **15c**, respectively, as the only isolable isomers. When bromoallene **14d**, which lacks a substituent at C4, was used, a considerable amount of regioisomer **16d** was isolated (28%; Table 2, entry 4). These results clearly demonstrate that the regioselectivity of the second nucleophilic attack is controlled by the steric size of the substituent at C4 of the bromoallenes. Next, similar reactions were conducted with bromoallenes **14e–g** (Table 2, entries 5–7), which bear a five-atom tether between the allenyl and hydroxy groups. In contrast to what was observed for the formation of seven-membered rings by this method, reaction of bromoallenes **14e–g** gave the eight-membered rings **15e–g** as the only isolable isomers, irrespective of the substituent at C4. Furthermore, bromoallenes **14h** and **14i**, which bear nitrogen functionalities, also gave the corresponding seven-membered ring **15h** and eight-membered ring **15i**, respectively, as a single isomer (Table 2, entries 8 and 9). These results show that the intramolecular nucleophilic attack takes place at the central position of the allenyl moiety (path B in Scheme 2) and, in most cases, the regioselectivity of the attack of methoxide is extremely high.

As shown in Scheme 3, the reaction of bromoallene (*S*,a*R*)-**17** also gave 1,4-oxazepine derivative **15a** (67%) along with **16a** (10%), a comparable result to the reaction of bromoallene (*S*,a*S*)-**14a** (Table 1, entry 1). Similarly, (*S*,a*R*)-**18** was cyclized into 1,4-diazepine derivative **15h** under identical reaction conditions in 50% yield (compare Table 1, entry 8). Based on these results, as both the *S*,a*S* and *S*,a*R* bromoallenes undergo the described transformation to provide the same products, a diastereomeric mixture of bromoallenes can be used directly in these reactions.

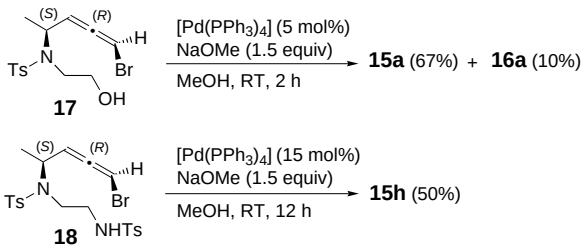
In analogy to this work, other alcohols can be used instead of MeOH in the cyclization reaction (Scheme 4). For example, bromoallene **14c** was treated with a preformed mixture of NaH (1.5 equiv) and EtOH/THF (1:1) in the presence of $[Pd(PPh_3)_4]$ (10 mol %) to afford the seven-membered ring **19** (60%). Similarly, the reaction of bromoallene **14a** with

 © 2003 Wiley-VCH Verlag GmbH & Co. KGaA, Weinheim

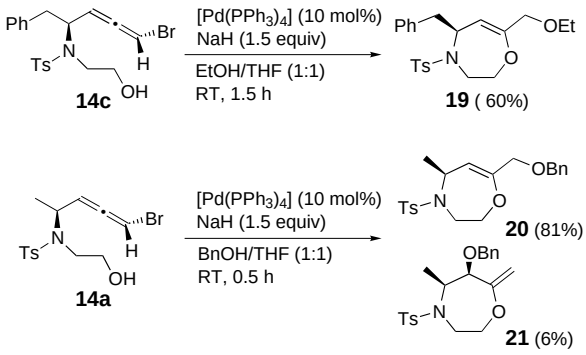
Table 2: Synthesis of medium-sized nitrogen heterocycles by cyclization of bromoallenes.[a]

Entry	Substrate	$[Pd(PPh_3)_4]$ [mol%]	*t* [h]	Product (Yield [%])[c]
1	 **14a**	5	3	 **15a** (73%)  **16a** (9%)
2	 **14b**	5	6	 **15b** (62%)
3	 **14c**	10	3.5	 **15c** (73%)
4	 **14d**	10	6	 **15d** (61%)  **16d** (28%)
5	 **14e**	5	6	 **15e** (84%)
6	 **14f**	10	11	 **15f** (67%)
7	 **14g**	10	3[b]	 **15g** (73%)
8	 **14h**	10	10	 **15h** (48%)
9	 **14i**	10	12	 **15i** (63%)

[a] Reactions were carried out at 25 °C in MeOH with diastereomerically pure bromoallenes, $[Pd(PPh_3)_4]$ (5–10 mol%), and NaOMe (1.5 equiv). [b] The reaction was conducted at 50 °C. [c] Yields of isolated products.



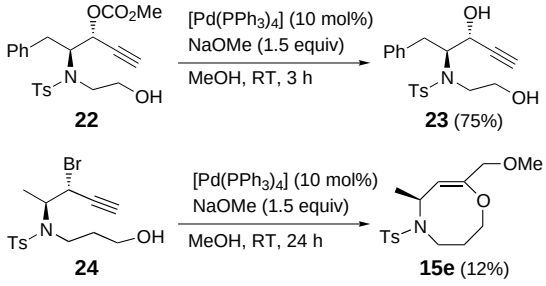
Scheme 3. Reaction of *S*,a*R* bromoallenes.



Scheme 4. Cyclizations with other alcohols as the second nucleophile.

BnOH gave the seven-membered rings **20** (81%) and **21** (6%).

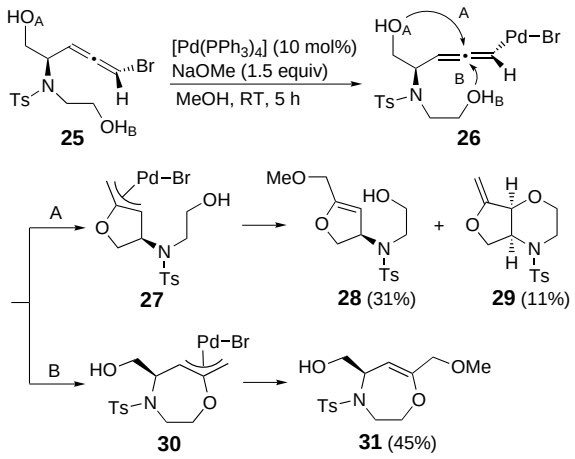
Propargylic carbonates are well-known to undergo a similar type of palladium-catalyzed transformation.[10,11] To investigate the possibility of using propargylic substrates as medium-sized-ring precursors, propargylic carbonate **22** was exposed to identical reaction conditions to those employed above (Scheme 5). However, only solvolysis of the carbonate **22** occurred and the diol **23** was obtained. Similarly, treatment of propargyl bromide **24**, which was found to be relatively unstable, with NaOMe in MeOH in the presence of $[Pd(PPh_3)_4]$ yielded only a small amount of the desired cyclized product **15e** (12% yield).[14] These results suggest that the efficient palladium(0)-catalyzed cyclization to form medium-sized rings is a reaction characteristic of bromoallenes.



Scheme 5. Reaction of a propargylic carbonate and of a propargylic bromide under identical reaction conditions.

Finally, we investigated the reaction of bromoallene **25**, which bears two oxygen functionalities and has two possible reaction pathways open to it (Scheme 6). If the hydroxy group A (OH_A) attacks the central position of the allene in allenyl palladium(II) bromide **26** (path A), **28** and/or **29** will be produced via the intermediate **27**. In contrast, reaction of OH_B in **26** (path B) would lead to the seven-membered ring **31**. Interestingly, exposure of **25** to the palladium-catalyzed cyclization conditions gave a mixture of **28** (31% yield), **29** (11%), and **31** (45%). This result clearly shows that the bromoallenes cyclize into seven-membered heterocycles as easily as they do into five-membered rings, even in cases in

 © 2003 Wiley-VCH Verlag GmbH & Co. KGaA, Weinheim



Scheme 6. Cyclization of bromoallene **25** bearing two oxygen functionalities.

which the resulting seven-membered heterocycle (such as **31**) contains two heteroatoms.

In conclusion, we have developed a novel synthesis of medium-sized heterocycles through the cyclization of bromoallenes that bear an oxygen or nitrogen functionality in the presence of a palladium(0) catalyst and an alcohol. In many cases, this reaction proceeds with high regioselectivity and affords the products in good to high yields. This is the first example that demonstrates the synthesis of medium-sized rings through the cyclization of haloallenes, and is a reaction that provides a very useful method for the synthesis of seven- or eight-membered heterocycles.

Experimental Section

General procedure: A solution of bromoallene **14a** (54 mg, 0.15 mmol) in MeOH (1 mL) was added to a stirred mixture of NaOMe (12.2 mg, 0.225 mmol) and $[Pd(PPh_3)_4]$ (8.7 mg, 7.5 μmol) in MeOH (1 mL) under a nitrogen atmosphere at room temperature, and the mixture was stirred for 3 h at this temperature. Concentration under reduced pressure gave an oily residue, which was purified by column chromatography over silica gel with *n*-hexane/EtOAc (3:1) to give, in order of elution, **16a** (4.4 mg, 9%) and **15a** (34.1 mg, 73%) as colorless oils. **15a**: $[\alpha]_D^{25} = +24.7$ ($c = 1.00$, $CHCl_3$); IR (KBr): $\tilde{\nu} =$ 1674 (C=C–O), 1331 cm^{-1} (NSO_2); ^1H NMR (500 MHz, $CDCl_3$): $\delta =$ 1.28 (d, $J = 7.0$ Hz, 3H; CCH_3), 2.41 (s, 3H; $PhCH_3$), 3.24 (s, 3H; OCH_3), 3.48 (ddd, $J = 14.5$, 6.0, 2.5 Hz, 1H; CH_aH_b), 3.56 (d, $J =$ 12.5 Hz, 1H; $MeOCH_aH_b$), 3.60 (d, $J = 12.5$ Hz, 1H; $MeOCH_aH_b$), 3.91 (ddd, $J = 12.5$, 6.0, 3.0 Hz, 1H; CH_aH_b), 4.04 (ddd, $J = 14.5$, 7.0, 3.0 Hz, 1H; CH_aH_b), 4.14 (ddd, $J = 12.5$, 7.0, 2.5 Hz, 1H; CH_aH_b), 4.68 (qd, $J = 7.0$, 6.5 Hz, 1H; CHMe), 4.86 (d, $J = 6.5$ Hz, 1H; C=CH), 7.26–7.27 (m, 2H; Ph), 7.68–7.70 ppm (m, 2H; Ph); ^{13}C NMR (75 MHz, $CDCl_3$): $\delta = 20.3$, 21.4, 45.0, 50.2, 58.0, 71.0, 73.0, 108.0, 127.1 (2C), 129.5 (2C), 137.7, 143.1, 154.5 ppm; MS (FAB): *m*/*z* (%): 312 [MH^+] (71), 296 (100); HRMS (FAB): calcd for $C_{15}H_{22}NO_4S$ (MH^+): 312.1270; found: 312.1274. **16a**: $[\alpha]_D^{28} = +46.8$ ($c = 0.49$, $CHCl_3$); IR (KBr): $\tilde{\nu} = 1635$ (C=C), 1346 cm^{-1} (NSO_2); ^1H NMR (500 MHz, $CDCl_3$): $\delta = 1.22$ (d, $J = 6.5$ Hz, 3H; CCH_3), 2.43 (s, 3H; $PhCH_3$), 3.18 (ddd, $J = 13.0$, 5.0, 3.5 Hz, 1H; CH_aH_b), 3.46 (ddd, $J =$ 13.0, 8.5, 3.0 Hz, 1H; CH_aH_b), 3.53 (s, 3H; OCH_3), 3.67 (ddd, $J = 11.5$, 5.0, 3.0 Hz, 1H; CH_aH_b), 3.83–3.88 (m, 2H; CHMe and CHOMe), 3.90 (ddd, $J = 11.5$, 8.5, 3.5 Hz, 1H; CH_aH_b), 4.22 (d, $J = 2.5$ Hz, 1H; C=CH_aH_b), 4.40 (d, $J = 2.5$ Hz, 1H; C=CH_aH_b), 7.30–7.32 (m, 2H; Ph), 7.67–7.69 ppm (m, 2H; Ph); ^{13}C NMR (75 MHz, $CDCl_3$): $\delta =$ 15.6, 21.5, 42.5, 50.9, 55.0, 62.8, 79.1, 85.4, 127.4 (2C), 129.7 (2C), 136.4, 143.4, 158.6 ppm; MS (FAB): *m*/*z* (%): 312 [MH^+] (24), 136 (100); HRMS (FAB): calcd for $C_{15}H_{22}NO_4S$ (MH^+): 312.1270; found: 312.1286.

Received: November 20, 2002 [Z50589]

Keywords: allenes · cyclization · heterocycles · palladium

[1] For a recent review, see: P. A. Evans, A. B. Holmes, *Tetrahedron* **1991**, *47*, 9131–9166.

[2] For selected examples of seven-membered nitrogen heterocycles, see: a) T. Duong, R. H. Prager, J. M. Tippett, A. D. Ward, D. I. Kerr, *Aust. J. Chem.* **1976**, *29*, 2667–2682; b) C. Boros, S. M. Hamilton, B. Katz, P. Kulanthaivel, *J. Antibiot.* **1994**, *47*, 1010–1016; c) Y. Ishihara, K. Hirai, M. Miyamoto, G. Goto, *J. Med. Chem.* **1994**, *37*, 2292–2299; d) F. Morís-Varas, X.-H. Qian, C.-H. Wong, *J. Am. Chem. Soc.* **1996**, *118*, 7647–7652; e) G. L. Grunewald, V. H. Dahanukar, P. Ching, K. R. Criscione, *J. Med. Chem.* **1996**, *39*, 3539–3546.

[3] For selected examples of eight-membered nitrogen heterocycles, see: a) B. Basil, E. C. J. Coffee, D. L. Gell, D. R. Maxwell, D. J. Sheffield, K. R. H. Wooldridge, *J. Med. Chem.* **1970**, *13*, 403–406; b) D. L. Klayman, J. P. Scovill, J. F. Bartosevich, C. J. Mason, *J. Med. Chem.* **1979**, *22*, 1367–1373; c) E. Vedejs, R. J. Galante, P. G. Goekjian, *J. Am. Chem. Soc.* **1998**, *120*, 3613–3622, and references therein.

[4] Most recent precedents for the synthesis of medium-sized nitrogen heterocycles are based on ring-closing metathesis. For a recent review, see: a) M. E. Maier, *Angew. Chem.* **2000**, *112*, 2153–2157; *Angew. Chem. Int. Ed.* **2000**, *39*, 2073–2077; for selected examples, see: b) G. C. Fu, R. H. Grubbs, *J. Am. Chem. Soc.* **1992**, *114*, 7324–7325; c) S. J. Miller, S.-H. Kim, Z.-R. Chen, R. H. Grubbs, *J. Am. Chem. Soc.* **1995**, *117*, 2108–2109; d) M. S. Visser, N. M. Heron, M. T. Didiuk, J. F. Sagal, A. H. Hoveyda, *J. Am. Chem. Soc.* **1996**, *118*, 4291–4298; e) L. A. Paquette, S. M. Leit, *J. Am. Chem. Soc.* **1999**, *121*, 8126–8127; f) M. Mori, T. Kitamura, N. Sakakibara, Y. Sato, *Org. Lett.* **2000**, *2*, 543–545.

[5] For other recent syntheses of medium-sized nitrogen heterocycles, see: a) X. Ouyang, A. S. Kiselyov, *Tetrahedron* **1999**, *55*, 8295–8302; b) J. Zhang, A. Jacobson, J. R. Rusche, W. Herlihy, *J. Org. Chem.* **1999**, *64*, 1074–1076; c) R. Räcker, K. Döring, O. Reiser, *J. Org. Chem.* **2000**, *65*, 6932–6939; d) A. I. Meyers, S. V. Downing, M. J. Weiser, *J. Org. Chem.* **2001**, *66*, 1413–1419; e) T. J. Donohoe, A. Raoof, I. D. Linney, M. Helliwell, *Org. Lett.* **2001**, *3*, 861–864; f) F. Iradier, R. G. Arrayás, J. C. Carretero, *Org. Lett.* **2001**, *3*, 2957–2960; g) P. Tempest, V. Ma, M. G. Kelly, W. Jones, C. Hulme, *Tetrahedron Lett.* **2001**, *42*, 4963–4968; see also: ref. [3c].

[6] For organocopper-mediated substitutions, see: a) E. J. Corey, N. W. Boaz, *Tetrahedron Lett.* **1984**, *25*, 3059–3062; b) A. M. Caporusso, C. Polizzi, L. Lardicci, *Tetrahedron Lett.* **1987**, *28*, 6073–6076; c) F. D'Aniello, A. Mann, M. Taddei, *J. Org. Chem.* **1996**, *61*, 4870–4871; d) F. Chemla, N. Bernard, J. Normant, *Eur. J. Org. Chem.* **1999**, 2067–2078; e) A. M. Caporusso, S. Filippi, F. Barontini, P. Salvadori, *Tetrahedron Lett.* **2000**, *41*, 1227–1230; f) J. J. Conde, W. Mendelson, *Tetrahedron Lett.* **2000**, *41*, 811–814.

[7] For palladium-catalyzed cross-coupling reactions, see: a) G. Märkl, P. Attenberger, J. Kellner, *Tetrahedron Lett.* **1988**, *29*, 3651–3654; b) T. Gillmann, T. Hülsen, W. Massa, S. Wocadlo, *Synlett* **1995**, 1257–1259; c) R. W. Saalfrank, M. Haubner, C. Deutscher, W. Bauer, T. Clark, *J. Org. Chem.* **1999**, *64*, 6166–6168.

 © 2003 Wiley-VCH Verlag GmbH & Co. KGaA, Weinheim

[8] For the formation of nucleophilic allenyl metal reagents, see: J. A. Marshall, N. D. Adams, *J. Org. Chem.* **1997**, *62*, 8976 – 8977.
[9] a) H. Ohno, H. Hamaguchi, T. Tanaka, *Org. Lett.* **2001**, *3*, 2269 – 2271; b) H. Ohno, K. Ando, H. Hamaguchi, Y. Takeoka, T. Tanaka, *J. Am. Chem. Soc.* **2002**, *124*, 15255 – 15266.
[10] It has been proposed that in the palladium-catalyzed reaction of propargyl carbonates, the protonation of a palladium carbene complex, generated by the reaction of an η^1-allenyl palladium intermediate with an appropriate nucleophile, would produce the π-allyl palladium intermediate: a) J. Tsuji, H. Watanabe, I. Minami, I. Shimizu, *J. Am. Chem. Soc.* **1985**, *107*, 2196 – 2198; for an excellent review, see: b) J. Tsuji, T. Mandai, *Angew. Chem.* **1995**, *107*, 2830 – 2854; *Angew. Chem. Int. Ed. Engl.* **1995**, *34*, 2589 – 2612. More recently, an alternative mechanism was proposed, in which the protonation of a palladacyclobutene generates the same allyl palladium intermediate: c) C. P. Casey, J. R. Nash, C. S. Yi, A. D. Selmeczy, S. Chung, D. R. Powell, R. K. Hayashi, *J. Am. Chem. Soc.* **1998**, *120*, 722 – 733. The reaction of a cationic η^3-propargyl palladium species with a nucleophile to afford the allyl palladium complex has also been described: d) K. Tsutsumi, S. Ogoshi, S. Nishiguchi, H. Kurosawa, *J. Am. Chem. Soc.* **1998**, *120*, 1938 – 1939; e) K. Tsutsumi, T. Kawase, K. Kakiuchi, S. Ogoshi, Y. Okada, H. Kurosawa, *Bull. Chem. Soc. Jpn.* **1999**, *72*, 2687 – 2692.
[11] For recent examples, see: a) N. Monteiro, A. Arnold, G. Balme, *Synlett* **1998**, 1111 – 1113; b) M. Yoshida, M. Ihara, *Angew. Chem.* **2001**, *113*, 636 – 639; *Angew. Chem. Int. Ed.* **2001**, *40*, 616 – 619; c) Y. Kozawa, M. Mori, *Tetrahedron Lett.* **2001**, *42*, 4869 – 4873; d) J.-R. Labrosse, P. Lhoste, D. Sinou, *J. Org. Chem.* **2001**, *66*, 6634 – 6642; e) Y. Kozawa, M. Mori, *Tetrahedron Lett.* **2002**, *43*, 1499 – 1502.
[12] For other syntheses of medium-sized heterocycles from allenes, see: a) R. W. Shaw, T. Gallagher, *J. Chem. Soc. Perkin Trans. 1* **1994**, 3549 – 3555; b) T. Okawara, S. Ehara, A. Takenaka, T. Hiwatashi, M. Furukawa, *Heterocycles* **1995**, *41*, 1709 – 1714; c) R. Grigg, J. M. Sansano, *Tetrahedron* **1996**, *52*, 13441 – 13454; d) B. M. Trost, P.-Y. Michellys, V. J. Gerusz, *Angew. Chem.* **1997**, *109*, 1837 – 1839; *Angew. Chem. Int. Ed. Engl.* **1997**, *36*, 1750 – 1753; e) R. C. Larock, C. Tu, P. Pace, *J. Org. Chem.* **1998**, *63*, 6859 – 6866.
[13] a) T. Ibuka, N. Mimura, H. Aoyama, M. Akaji, H. Ohno, Y. Miwa, T. Taga, K. Nakai, H. Tamamura, N. Fujii, Y. Yamamoto, *J. Org. Chem.* **1997**, *62*, 999; b) T. Ibuka, N. Mimura, H. Ohno, K. Nakai, M. Akaji, H. Habashita, H. Tamamura, Y. Miwa, T. Taga, N. Fujii, Y. Yamamoto, *J. Org. Chem.* **1997**, *62*, 2982; c) H. Ohno, K. Ishii, A. Honda, H. Tamamura, N. Fujii, Y. Takemoto, T. Ibuka, *J. Chem. Soc. Perkin Trans. 1* **1998**, 3703; d) H. Ohno, A. Toda, N. Fujii, Y. Miwa, T. Taga, Y. Yamaoka, E. Osawa, T. Ibuka, *Tetrahedron Lett.* **1999**, *40*, 1331; e) N. Mimura, Y. Miwa, T. Ibuka, Y. Yamamoto, *J. Org. Chem.* **2002**, *67*, 5796 – 5801.
[14] The undesired methyl ether, produced by the S_N2 substitution reaction of methoxide, was also detected in the product mixture.

 © 2003 Wiley-VCH Verlag GmbH & Co. KGaA, Weinheim



The Second Total Synthesis of Diazonamide A**

K. C. Nicolaou, Paraselli Bheema Rao, Junliang Hao, Mali Venkat Reddy, Gerasimos Rassias, Xianhai Huang, David Y.-K. Chen, and Scott A. Snyder*

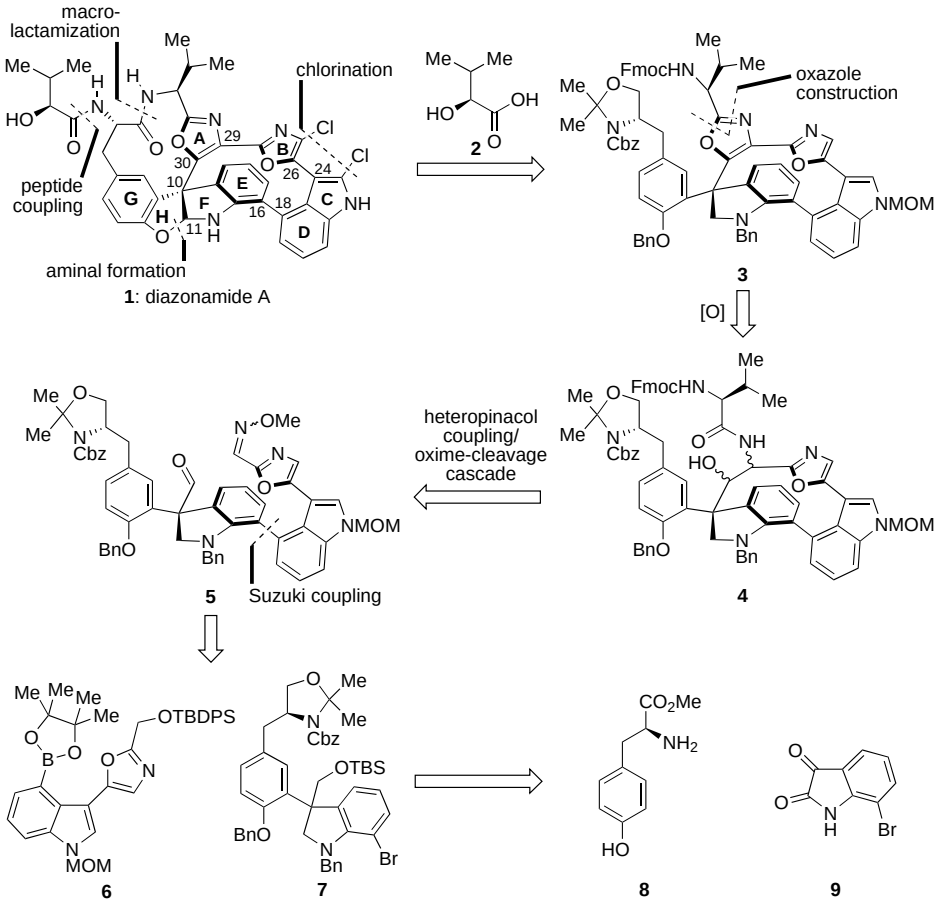
Unique and challenging molecular motifs within secondary metabolites have long presented synthetic chemists with golden opportunities for discovery, whether simply as a source of inspiration for creative strategies and tactics, or as a stringent testing ground that reveals weaknesses in the power of existing methods.[1] Among recent isolates, the natural product diazonamide A (**1**, Scheme 1)[2] perhaps constitutes one of the best affirmations of this statement as its unprecedented molecular architecture has stimulated the development of numerous inventive synthetic approaches.[3–13] Last year, these efforts provided dividends in the form of the first laboratory synthesis of diazonamide A.[14] Herein, we report the second total synthesis of this formidable target by our group through an entirely distinct route.

The retrosynthetic blueprint that guided this new campaign is defined in Scheme 1. The critical difference from our previous strategy[14] is a reversed order for the construction of the daunting macrocyclic domains of the target, that is, forming the heterocyclic core first, and then generating the 12-membered AG macrolactam system. Accordingly, we initially set intermediate **3** as the crucial subgoal structure of the program, for which we assumed that application of a route based on C_{16}–C_{18} biaryl coupling of advanced building blocks **6** and **7** to access an intermediate such as **5**, followed by macrocyclization through a heteropinacol coupling/oxime-cleavage cascade reaction, could provide a functionalized platform (**4**) for eventual conversion into this advanced compound through a Robinson–Gabriel cyclodehydration reaction. The constrained AG macrolactam could then be formed from an amino acid derivative obtained from **4**. Subsequent chlorination, aminal formation, several func-

[*] Prof. Dr. K. C. Nicolaou, Dr. P. Bheema Rao, Dr. J. Hao, Dr. M. V. Reddy, Dr. G. Rassias, Dr. X. Huang, Dr. D. Y.-K. Chen, S. A. Snyder
Department of Chemistry and
The Skaggs Institute for Chemical Biology
The Scripps Research Institute
10550 North Torrey Pines Road, La Jolla, CA 92037 (USA)
Fax: (+1) 858-784-2469
E-mail: kcn@scripps.edu
and
Department of Chemistry and Biochemistry
University of California, San Diego
9500 Gilman Drive, La Jolla, CA 92093 (USA)

[**] We thank Dr. D. H. Huang and Dr. G. Siuzdak for NMR spectroscopic and mass spectrometric assistance, respectively. Financial support for this work was provided by The Skaggs Institute for Chemical Biology, American Biosciences, the National Institutes of Health (USA), predoctoral fellowships from the National Science Foundation and Pfizer (S.A.S.), and a postdoctoral fellowship from The Skaggs Institute for Chemical Biology (X.H.).

 DOI: 10.1002/anie.200351112 © 2003 Wiley-VCH Verlag GmbH & Co. KGaA, Weinheim



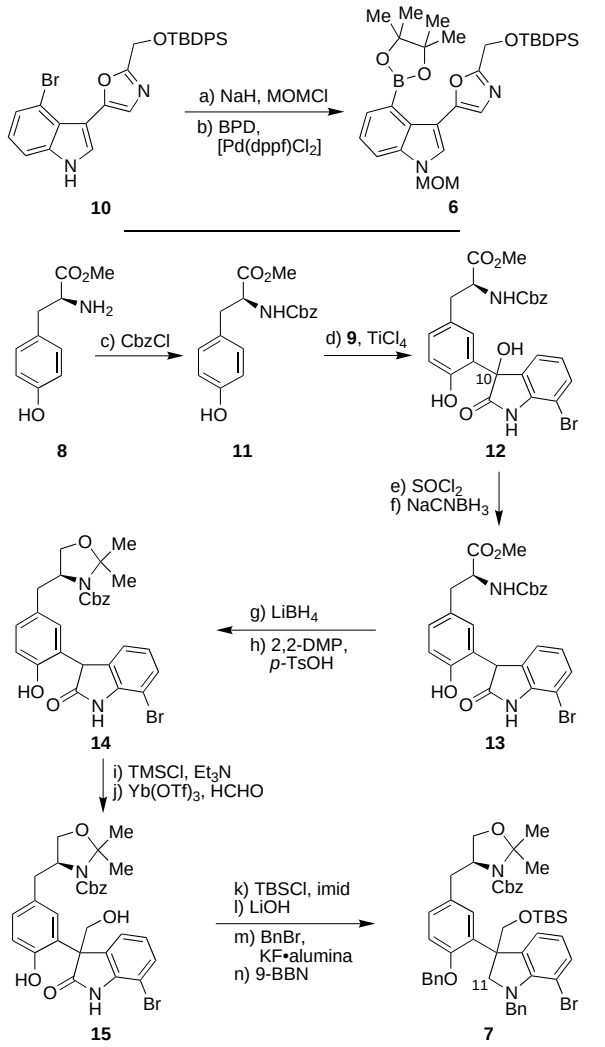
Scheme 1. Structure of diazonamide A (**1**) and general retrosynthetic analysis.

tional-group manipulations, and a final chain extension with (*S*)-hydroxyisovaleric acid (**2**) would complete the total synthesis of diazonamide A (**1**). Although an ambitious plan, we had faith that the operations expected to afford intermediate **3** could be reduced to practice based on a series of model studies that demonstrated their viability in the context of the originally proposed, but incorrect, structure of diazonamide A.[15]

We first needed to prepare indole–oxazole **6** and functionalized EFG-ring system **7**. As shown in Scheme 2, the first of these targets was quite easily accessed from the previously reported **10**[15a] (available in six steps from 4-bromoindole) through initial protection of its indole nitrogen atom with a MOM ether followed by subsequent reaction with BPD and $[Pd(dppf)Cl_2]\cdot CH_2Cl_2$[16] to afford boronate ester **6**. With these two steps proceeding in a combined yield of 80%, effort was then directed towards the assembly of **7**, starting with the protection of commercially available tyrosine methyl ester (**8**) as a benzyl carbamate (Cbz) to afford **11** in 94% yield. Although a conventional beginning, this operation served an important purpose as it set the stage for a subsequent $TiCl_4$-promoted merger with 7-bromoisatin (**9**), an event which gave rise to **12** bearing most of the desired functionality of the targeted EFG fragment **7** in 58% yield.[17] Indeed, the only major structural element that separated **12** from **7** was appropriate functionalization of its C10 quaternary center. Thus, to fix this deficiency, the newly generated tertiary alcohol was exchanged for a hydrogen atom to form **13** via an intermediate chloride in 76% yield. The upper tyrosine portion was converted into an acetonide (see **14**) in nearly quantitative yield through reduction of the methyl ester ($LiBH_4$, THF) followed by *p*-TsOH-catalyzed reaction with 2,2-dimethoxypropane. The required hydroxymethyl group at C10 was then installed onto this lactam intermediate **14** through a two-step protocol developed by Padwa et al. for the addition of such groups to carbon atoms adjacent to lactones,[18] affording **15** as an equimolar mixture of both C10 stereoisomers in 70% yield. Since these diastereomeric compounds could not be separated at this juncture, they were carried forward as a mixture in the hope that eventually the incorporation of a suitable functional group would confer sufficient differences in their physical properties to allow their separation.

With the architectural skeleton **15** of the EFG fragment now completed, only protecting- and functional-group manipulations remained before we could attempt Suzuki coupling with **6**. These alterations were accomplished over four steps (see Scheme 2) starting with silylation of the free primary alcohol group of **15** with TBSCl and imidazole in CH_2Cl_2, conditions that also led to protection of the free A-ring phenol (84% yield). Since the latter event was unintended, subsequent treatment with LiOH served to excise this

 © 2003 Wiley-VCH Verlag GmbH & Co. KGaA, Weinheim



Scheme 2. Synthesis of indole–oxazole **6** and advanced EFG fragment **7**: a) NaH (2.0 equiv), THF, 0 °C, 5 min, then MOMCl (2.0 equiv), 0 °C, 10 min, 94%; b) BPD (2.5 equiv), $[Pd(dppf)Cl_2]\cdot CH_2Cl_2$ (0.1 equiv), KOAc (5.0 equiv), 1,4-dioxane, 95 °C, 6 h, 85%; c) CbzCl (1.1 equiv), aqueous $NaHCO_3$, $CHCl_3$, 25 °C, 3 h, 94%; d) **9** (1.1 equiv), $TiCl_4$ (1.0 M in CH_2Cl_2, 1.0 equiv), CH_2Cl_2, 25 °C, 10 h, 58% (70% based on recovered **11**); e) $SOCl_2$, 25 °C, 10 h, 90%; f) $NaCNBH_3$ (3.0 equiv), MeCN, 0→25 °C, 5 h, 84%; g) $LiBH_4$ (3.0 equiv), 0→25 °C, THF, 2 h, 95%; h) 2,2-DMP (10 equiv), *p*-TsOH (0.1 equiv), acetone, 25 °C, 2 h, 98%; i) TMSCl (4.0 equiv), Et_3N (6.0 equiv), CH_2Cl_2, 0 °C, 1.5 h; j) HCHO (37% in H_2O, 5.0 equiv), $Yb(OTf)_3$ (0.1 equiv), THF, 25 °C, 24 h, 70% over two steps; k) TBSCl (3.0 equiv), imid (6.0 equiv), CH_2Cl_2, 25 °C, 6 h, 84%; l) LiOH (3.0 equiv), DMF, 25 °C, 5 h; m) BnBr (4.0 equiv), KF·alumina (8.0 equiv), DME, 25 °C, 12 h, 95% over two steps; n) 9-BBN (0.5 M in THF, 5.0 equiv), THF, 65 °C, 36 h, 72%. BPD = bis(pinacolato)diboron, MOM = methoxymethyl, dppf = 1,1′-bis(diphenylphosphanyl)ferrocene, Cbz = benzyloxycarbonyl, TBDPS = *tert*-butyldiphenylsilyl, 2,2-DMP = 2,2-dimethoxypropane, *p*-TsOH = *p*-toluenesulfonic acid, TMS = trimethylsilyl, Tf = trifluoromethylsulfonyl, TBS = *tert*-butyldimethylsilyl, imid = imidazole, 9-BBN = 9-borabicyclo[3.3.1]nonane.

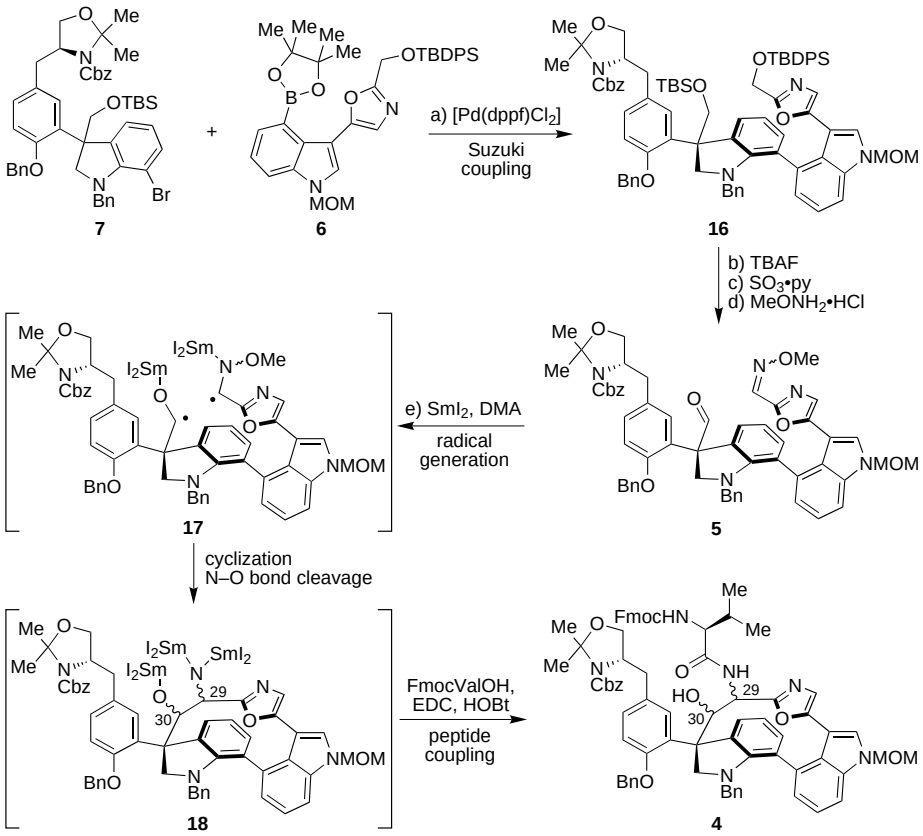
superfluous group. Finally, both the lactam nitrogen atom and the free phenol group were protected with a benzyl group upon reaction with BnBr and KF·alumina in DME (95% overall for two steps), and the carbonyl group of the lactam was then fully reduced with excess 9-BBN in refluxing THF to afford **7** in 72% yield. Although the excision of the oxygen atom of the lactam in this final operation might seem wasteful, as we have already demonstrated that a carbonyl group at C11 can enable the construction of the FH aminal system of diazonamide A, it was forced upon us by the fact that this functionality did not prove compatible with the next series of steps.[19] Therefore, although removing this group facilitated our objectives in the short term, it would have to be reintroduced to complete the target molecule.

Pressing forward nonetheless, initial Suzuki coupling between aryl halide **7** and boronate **6** proceeded without incident in the presence of $[Pd(dppf)Cl_2]\cdot CH_2Cl_2$ and K_2CO_3 in DME at reflux as shown in Scheme 3, affording **16** in 78% yield after 12 h. From this intermediate, aldehyde–oxime **5** was then formed in 78% overall yield through a tandem deprotection/oxidation sequence using TBAF and $SO_3\cdot$py, followed by selective capture of the more reactive aldehyde with $MeONH_2\cdot HCl$ upon stirring in DMSO at ambient temperature. As such, the stage was now set to examine the crucial heteropinacol cyclization cascade sequence anticipated for macrocycle formation with concomitant installation of a suitable precursor functionality for the requisite second oxazole. Most gratifyingly, a modified form of our previously reported protocol[15b] for this reaction proceeded smoothly as treatment of **5** with a premixed complex of SmI_2 (9.0 equiv) and DMA (36 equiv)[20] in THF at ambient temperature, followed by quenching with aqueous NH_4Cl, extraction, solvent removal, and subsequent peptide coupling with a solution of Fmoc-protected L-valine, EDC, and HOBt in DMF, gave rise to **4** in a reproducible yield of 45–50%.[21] Overall, this outcome accounts for an average efficiency of 79% per step based on the three distinct operations of pinacol cyclization, N–O bond scission, and peptide-bond formation effected during this one-pot conversion.

Having established a functionalized C_{29}–C_{30} bridge through this powerful cascade, the A-ring oxazole in **3** (Scheme 4) was then generated in an overall yield of 33% through initial oxidation of the relatively hindered alcohol group of **4** with TPAP and subsequent Robinson–Gabriel cyclodehydration of the resultant ketoamide with a mixture of $POCl_3$ and pyridine (1:2) at 70 °C.[22] Although the material throughput for this sequence is modest, it accurately reflects the severely strained and highly hindered nature of the diazonamide heteroaromatic system. In fact, experimentation with numerous oxazole-forming protocols revealed that only the indicated reagent combination could accomplish this task in any measurable yield.[23] As such, this finding suggests that this cyclodehydration protocol may prove to be useful when more conventional techniques fail.

With the complete heteroaromatic core of diazonamide A finally in place, the next step toward diazonamide A (**1**) was the formation of the second macrocyclic subunit through lactamization, a transformation for which we anticipated few difficulties based on the literature precedent for such ring closures.[24] Indeed, our initial forays along these lines were encouraging, as **3** (see Scheme 4) was readily converted into **19** in 83% overall yield through HF-mediated cleavage of the acetonide, generation of a free acid from the resultant alcohol

 © 2003 Wiley-VCH Verlag GmbH & Co. KGaA, Weinheim



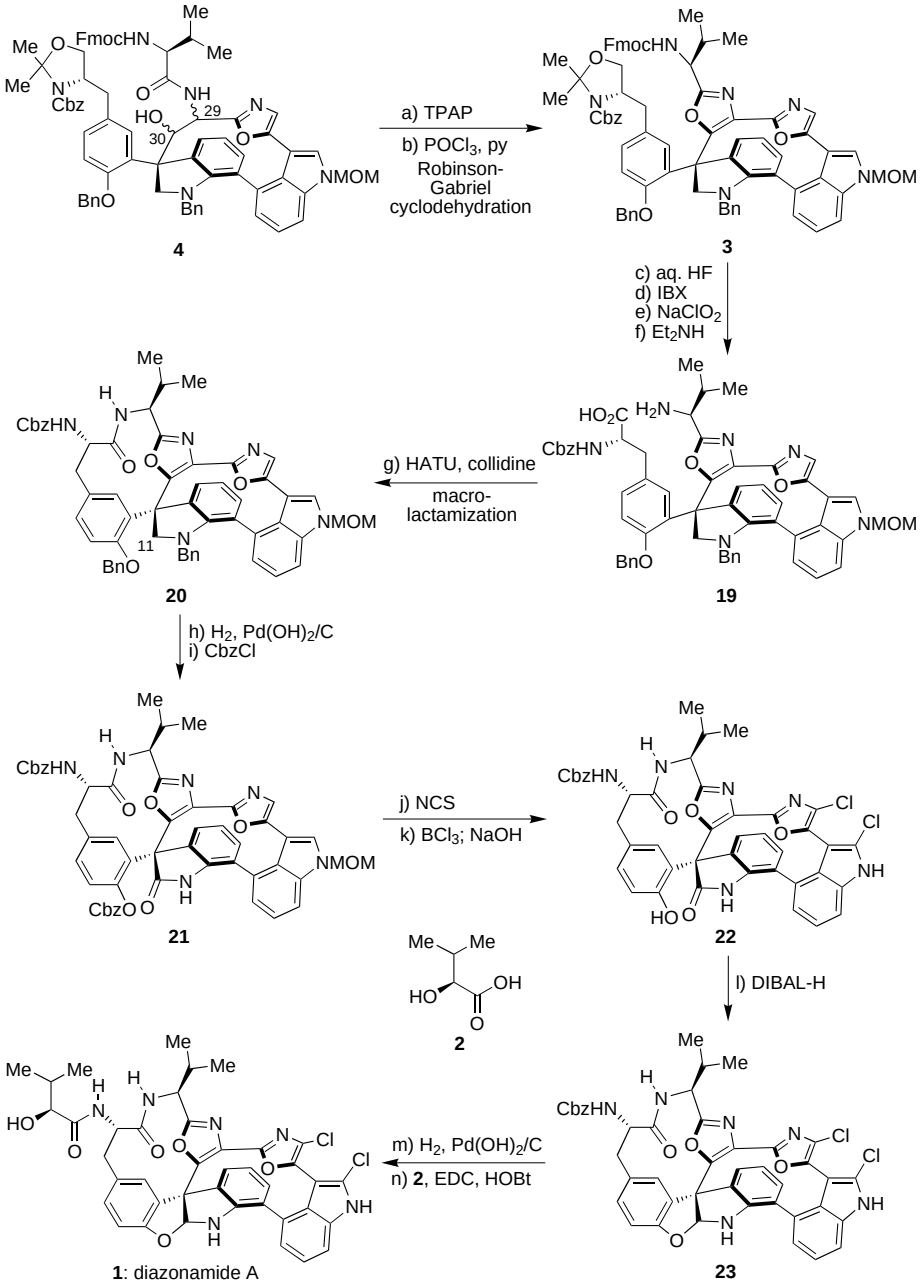
Scheme 3. Construction of the fully functionalized heterocyclic core **4** of diazonamide A through Suzuki and heteropinacol coupling reactions: a) **6** (1.0 equiv), **7** (1.2 equiv), $[Pd(dppf)Cl_2]\cdot CH_2Cl_2$ (0.2 equiv), K_2CO_3 (5.0 equiv), DME, 85 °C, 12 h, 78%; b) TBAF (6.0 equiv), THF, 45 °C, 2.5 h, 94%; c) Et_3N (10 equiv), SO_3·py (8.0 equiv), DMSO/CH_2Cl_2 (1:1), 0 °C, 2 h, 91%; d) $MeONH_2$·HCl (5.0 equiv), DMSO, 25 °C, 20 min, 91%; e) SmI_2 (0.1 M in THF, 9.0 equiv), DMA (36 equiv), THF, 25 °C, 1 h, then saturated aqueous NH_4Cl, 25 °C, 10 min; solvent removal, then FmocValOH (3.0 equiv), EDC (3.0 equiv), HOBt (3.0 equiv), DMF, 25 °C, 10 h, 45–50% overall, ca. 79% per synthetic operation in the cascade sequence. DME = ethylene glycol dimethyl ether, TBAF = tetra-*n*-butylammonium fluoride, DMSO = dimethyl sulfoxide, DMA = *N,N*-dimethylacetamide, Fmoc = 9-fluorenylmethoxycarbonyl, EDC = 3-(3-dimethylaminopropyl)-1-ethylcarbodiimide, HOBt = 1-hydroxy-1*H*-benzotriazole, DMF = *N,N*-dimethylformamide.

through a two-stage oxidation protocol, and finally Et_2NH-induced lysis of the Fmoc protecting group.[25] Unfortunately, initial attempts to form the macrolactam from this advanced compound **19** met with significant resistance despite an almost exhaustive screening of peptide-forming reagents, leading in all cases either to decomposition or dimerization (even when the reaction was run at low concentration).[26] Eventually, we found that **20** could be obtained in yields of 10–15% when **17** was treated with HATU and collidine for several days at ambient temperature in DMF/CH_2Cl_2 (1:2) at a final concentration of 1.0×10^{-4} M.[27] Significantly, apart from completing the second highly strained macrocyclic domain, this step also served to resolve the previously formed mixture of C10 epimers, as only material with the stereochemical disposition of **20** resulted (which matched the absolute configuration of diazonamide A).[28]

Having constructed both macrocycles of the target molecule, we then faced the challenge of completing the structure by introducing the final aminal ring system. Thus, in advance of oxidation at C11 to enable the synthesis of this motif, we attempted to remove the two benzyl ethers attached to **20** through a standard hydrogenation reaction facilitated by an excess of $Pd(OH)_2$/C (Pearlman catalyst). Amazingly, however, following subsequent reaction of the intermediate product with benzyl chloroformate, all spectral data indicated that although the debenzylations had occurred as intended, the indoline ring had been oxidized to an oxindole as expressed in **21**! As such, the conditions employed for the hydrogenation reaction had served both to formally reduce as well as oxidize the substrate **20**.[29] We are currently investigating the mechanism behind this puzzling transformation. Although a complete picture has not yet been painted, initial studies have revealed that this reaction requires an excess of $Pd(OH)_2$/C and that it is probably substrate-specific, as application of the same conditions to **7** (cf. Scheme 2) served only to excise its benzyl ethers. It is, therefore, conceivable that both the rigidity of the substrate and the neighboring phenolic group play a crucial role in this process.

After this fortuitous conversion, the completion of diazonamide A (**1**) required only a few finishing touches, starting with the installation of the two chlorine substituents. This goal was smoothly accomplished through an electrophilic aromatic substitution reaction using NCS as the chlorine source at 60 °C in a mixture of THF and CCl_4 (1:1), a reaction that proceeded with complete atropselectivity as a result of the constraints of the macrocyclic system. Next, the long resilient MOM protecting group was excised from the C-ring indole through a one-pot, two-step protocol involving initial reaction with BCl_3 to selectively cleave its methyl group, followed by exposure to NaOH to expel the residual hydroxymethyl group as a molecule of formaldehyde. These conditions also served to selectively cleave the Cbz group residing on the phenol, thereby generating **22** in 75% overall yield from **21** and providing an intermediate which intersected our early total synthesis.[14] Gratifyingly, the spectral data of **21** perfectly matched those of the previously obtained compound.[30] As such, application of the same three steps which we had already developed to complete diazonamide A (**1**) from this advanced intermediate served to finish the second

 © 2003 Wiley-VCH Verlag GmbH & Co. KGaA, Weinheim



Scheme 4. Final stages and completion of the second total synthesis of diazonamide A (**1**): a) TPAP (1.0 equiv), NMO (5.0 equiv), molecular sieves (4 Å), CH_2Cl_2, 25 °C, 4 h, 62%; b) $POCl_3$/pyridine (1:2), 70 °C, 6 h, 35% (53% based on recovered starting material); c) aqueous HF (48%, 3.0 equiv), MeCN, 0 °C, 2 h, 95%; d) IBX (5.0 equiv), DMSO, 25 °C, 4 h; e) $NaClO_2$ (5.0 equiv), NaH_2PO_4 (5.0 equiv), resorcinol (5.0 equiv), DMSO/H_2O (10:1), 25 °C, 1 h, 89% over two steps; f) Et_2NH/THF (1:5), 25 °C, 4 h, 98%; g) HATU (2.0 equiv), collidine (6.0 equiv), DMF/CH_2Cl_2 (1:2, 1.0×10^{-4} M), 25 °C, 7 d, 10–15%; h) H_2 (1.0 atm), $Pd(OH)_2$/C (20 wt%, excess), EtOH, 25 °C, 10 h; i) CbzCl (5.0 equiv), aqueous $NaHCO_3$/1,4-dioxane (1:2), 25 °C, 12 h, 35% over two steps; j) NCS (4.0 equiv), CCl_4/THF (1:1), 60 °C, 2 h; k) BCl_3 (1.0 M in CH_2Cl_2, 5.0 equiv), CH_2Cl_2, −78 °C, 10 min, then aqueous NaOH (15%, excess), THF, 25 °C, 12 h, 75% over two steps; l) DIBAL-H (1.0 M in toluene, 10 equiv, added portionwise), THF, −78→25 °C, 3 h, 56%; m) H_2 (2.0 atm), $Pd(OH)_2$/C (20 wt%, catalytic), EtOH, 25 °C, 2 h; n) **2** (5.0 equiv), EDC (5.0 equiv), HOBt (5.0 equiv), $NaHCO_3$ (15 equiv), DMF, 25 °C, 12 h, 79% over two steps. TPAP = tetra-*n*-propylammonium perruthenate, NMO = 4-methylmorpholine *N*-oxide, py = pyridine, IBX = 1-hydroxy-1,2-benziodoxol-3(1*H*)-one 1-oxide, HATU = 2-(1*H*-9-azabenzotriazole-1-yl)-1,1,3,3-tetramethyluronium hexafluorophosphate, NCS = *N*-chlorosuccinimide, DIBAL-H = diisobutylaluminum hydride.

total synthesis of this intricate molecule in comparable yields to those of the first.

In summary, our group has chartered a second path to the marine-derived antitumor agent diazonamide A (**1**) through an approach that featured a SmI_2-induced heteropinacol coupling cascade to fashion the 12-membered heterocyclic core of the target and an unprecedented oxidation of an indoline to an oxindole using $Pd(OH)_2$/C. Equally significant as the gathered knowledge from this particular campaign, the complementary nature of our two total syntheses now affords routes capable of delivering simplified structural analogues of either macrocyclic domain. We expect that examination of such compounds will reveal clear structure–activity relationships for the diazonamide class that could potentially instigate new pathways of investigation in the field of cancer chemotherapy. Explorations along these lines, as well as a full account of our synthetic studies in the diazonamide A area, will be reported in due course.

Received: February 5, 2003 [Z51112]

Keywords: domino reactions · macrocycles · natural products · samarium · total synthesis

[1] For discussions of this topic in the context of total synthesis, see examples in the following: a) K. C. Nicolaou, D. Vourloumis, N. Winssinger, P. S. Baran, *Angew. Chem.* **2000**, *112*, 46–126; *Angew. Chem. Int. Ed.* **2000**, *39*, 44–122; b) K. C. Nicolaou, S. A. Snyder, T. Montagnon, G. A. Vassilikogiannakis, *Angew. Chem.* **2002**, *114*, 1742–1773; *Angew. Chem. Int. Ed.* **2002**, *41*, 1668–1698; c) K. C. Nicolaou, P. S. Baran, *Angew. Chem.* **2002**, *114*, 2800–2843; *Angew. Chem. Int. Ed.* **2002**, *41*, 2678–2720.

[2] For the isolation and original structural assignments, see: a) N. Lindquist, W. Fenical, G. D. Van Duyne, J. Clardy, *J. Am. Chem.*

 © 2003 Wiley-VCH Verlag GmbH & Co. KGaA, Weinheim

Soc. **1991**, *113*, 2303 – 2304; for the synthesis of the originally proposed structure and revision of the structure of diazonamide A, see: b) J. Li, S. Jeong, L. Esser, P. G. Harran, *Angew. Chem.* **2001**, *113*, 4901 – 4906; *Angew. Chem. Int. Ed.* **2001**, *40*, 4765 – 4770; c) J. Li, A. W. G. Burgett, L. Esser, C. Amezcua, P. G. Harran, *Angew. Chem.* **2001**, *113*, 4906 – 4909; *Angew. Chem. Int. Ed.* **2001**, *40*, 4770 – 4773.

[3] For highlights of previous synthetic studies towards the diazonamides, see: a) V. Wittmann, *Nachr. Chem.* **2002**, *50*, 477 – 482; b) T. Ritter, E. M. Carreira, *Angew. Chem.* **2002**, *114*, 2601 – 2606; *Angew. Chem. Int. Ed.* **2002**, *41*, 2489 – 2495.

[4] a) J. Li, X. Chen, A. W. G. Burgett, P. G. Harran, *Angew. Chem.* **2001**, *113*, 2754 – 2757; *Angew. Chem. Int. Ed.* **2001**, *40*, 2682 – 2685; b) X. Chen, L. Esser, P. G. Harran, *Angew. Chem.* **2000**, *112*, 967 – 970; *Angew. Chem. Int. Ed.* **2000**, *39*, 937 – 940; c) S. Jeong, X. Chen, P. G. Harran, *J. Org. Chem.* **1998**, *63*, 8640 – 8641.

[5] a) E. Vedejs, M. A. Zajac, *Org. Lett.* **2001**, *3*, 2451 – 2454; b) E. Vedejs, J. Wang, *Org. Lett.* **2000**, *2*, 1031 – 1032; c) E. Vedejs, D. A. Barba, *Org. Lett.* **2000**, *2*, 1033 – 1035.

[6] a) P. Wipf, J.-L. Methot, *Org. Lett.* **2001**, *3*, 1261 – 1264; b) P. Wipf, F. Yokokawa, *Tetrahedron Lett.* **1998**, *39*, 2223 – 2226.

[7] a) J. D. Kreisberg, P. Magnus, E. G. McIver, *Tetrahedron Lett.* **2001**, *42*, 627 – 629; b) P. Magnus, E. G. McIver, *Tetrahedron Lett.* **2000**, *41*, 831 – 834; c) F. Chan, P. Magnus, E. G. McIver, *Tetrahedron Lett.* **2000**, *41*, 835 – 838; d) P. Magnus, J. D. Kreisberg, *Tetrahedron Lett.* **1999**, *40*, 451 – 454.

[8] D. E. Fuerst, B. M. Stoltz, J. L. Wood, *Org. Lett.* **2000**, *2*, 3521 – 3523.

[9] a) S. Schley, A. Radspieler, G. Christoph, J. Liebscher, *Eur. J. Org. Chem.* **2002**, 369 – 374; b) A. Radspieler, J. Liebscher, *Synthesis* **2001**, 745 – 750.

[10] a) F. Lach, C. J. Moody, *Tetrahedron Lett.* **2000**, *41*, 6893 – 6896; b) M. C. Bagley, S. L. Hind, C. J. Moody, *Tetrahedron Lett.* **2000**, *41*, 6897 – 6900; c) M. C. Bagley, C. J. Moody, A. G. Pepper, *Tetrahedron Lett.* **2000**, *41*, 6901 – 6904; d) C. J. Moody, K. J. Doyle, M. C. Elliott, T. J. Mowlem, *J. Chem. Soc. Perkin Trans. 1* **1997**, 2413 – 2419; e) C. J. Moody, K. J. Doyle, M. C. Elliott, T. J. Mowlem, *Pure Appl. Chem.* **1994**, *66*, 2107 – 2110.

[11] K. S. Feldman, K. J. Eastman, G. Lessene, *Org. Lett.* **2002**, *4*, 3524 – 3528.

[12] a) H. C. Hang, E. Drotleff, G. I. Elliott, T. A. Ritsema, J. P. Konopelski, *Synthesis* **1999**, 398 – 400; b) J. P. Konopelski, J. M. Hottenroth, H. M. Oltra, E. A. Veliz, Z. C. Yang, *Synlett* **1996**, 609 – 611.

[13] A. Boto, M. Ling, G. Meek, G. Pattenden, *Tetrahedron Lett.* **1998**, *39*, 8167 – 8170.

[14] K. C. Nicolaou, M. Bella, D. Y.-K. Chen, X. Huang, T. Ling, S. A. Snyder, *Angew. Chem.* **2002**, *114*, 3645 – 3649; *Angew. Chem. Int. Ed.* **2002**, *41*, 3495 – 3499.

[15] a) K. C. Nicolaou, S. A. Snyder, K. B. Simonsen, A. E. Koumbis, *Angew. Chem.* **2000**, *112*, 3615 – 3620; *Angew. Chem. Int. Ed.* **2000**, *39*, 3473 – 3478; b) K. C. Nicolaou, X. Huang, N. Giuseppone, P. Bheema Rao, M. Bella, M. V. Reddy, S. A. Snyder, *Angew. Chem.* **2001**, *113,* 4841 – 4845; *Angew. Chem. Int. Ed.* **2001**, *40*, 4705 – 4709.

[16] T. Ishiyama, M. Murata, N. Miyaura, *J. Org. Chem.* **1995**, *60*, 7508 – 7510.

[17] This step was inspired by related work: D. A. Klumpp, K. Y. Yeung, G. K. Surya Prakash, G. A. Olah, *J. Org. Chem.* **1998**, *63*, 4481 – 4484, and references therein.

[18] A. Padwa, D. Dehm, T. Oine, G. A. Lee, *J. Am. Chem. Soc.* **1975**, *97*, 1837 – 1845.

[19] The presence of the C11 carbonyl group retarded Suzuki coupling with **6** and led to the loss of the hydroxymethyl function on several intermediates as a result of the same type of fragmentation discussed in reference [15a] that afforded benzofuran products; for a productive use of this pathway, see: K. C. Nicolaou, S. A. Snyder, A. Bigot, J. A. Pfefferkorn, *Angew. Chem.* **2000**, *112*, 1135 – 1138; *Angew. Chem. Int. Ed.* **2000**, *39*, 1093 – 1096.

[20] M. Nishiura, K. Katagiri, T. Imamoto, *Bull. Chem. Soc. Jpn.* **2001**, *74*, 1417 – 1424.

[21] Examination of other activating ligands for SmI_2, such as our previously reported choice of HMPA (see reference [15b]), did lead to the desired product, albeit in a lower yield.

[22] To the best of our knowledge, this particular reagent combination for oxazole synthesis from ketoamides has not been reported previously except by us (see reference [15b]); however, there are examples with neat $POCl_3$: R. L. Dow, *J. Org. Chem.* **1990**, *55*, 386 – 388.

[23] For examples of other conditions attempted to engender a Gabriel–Robinson dehydration, see: a) P. Wipf, C. P. Miller, *J. Org. Chem.* **1993**, *58*, 3604 – 3606; b) C. T. Brain, J. M. Paul, *Synlett* **1999**, 1642 – 1644.

[24] For numerous examples of challenging macrolactamizations, see: D. L. Boger, S. H. Kim, Y. Mori, J.-H. Weng, O. Rogel, S. L. Castle, J. J. McAtee, *J. Am. Chem. Soc.* **2001**, *123*, 1862 – 1871.

[25] For another example of this set of conditions to remove an Fmoc group in the final step of a total synthesis (calicheamicin γ_1^I), see: K. C. Nicolaou, C. W. Hummel, M. Nakada, K. Shibayama, E. N. Pitsinos, H. Saimoto, Y. Mizuno, K.-U. Baldenius, A. L. Smith, *J. Am. Chem. Soc.* **1993**, *115*, 7625 – 7635.

[26] Although molecular models suggested the proximity of the reactive units, the steric hindrance within the system, in combination with the entropic penalties associated with the formation of a 12-membered ring with multiple elements of unsaturation from a far more flexible precursor, were the likely culprits that led to such recalcitrance.

[27] For other syntheses that benefited from this reagent combination, see: a) K. C. Nicolaou, A. E. Koumbis, M. Takayanagi, S. Natarajan, N. F. Jain, T. Bando, H. Li, R. Hughes, *Chem. Eur. J.* **1999**, *5*, 2622 – 2647; b) T. Hu, J. S. Panek, *J. Org. Chem.* **1999**, *64*, 3000 – 3001; c) D. A. Evans, M. R. Wood, B. W. Trotter, T. I. Richardson, J. C. Barrow, J. L. Katz, *Angew. Chem.* **1998**, *110*, 2864 – 2868; *Angew. Chem. Int. Ed.* **1998**, *37*, 2700 – 2704.

[28] This result, combined with the yields obtained for the macrocyclization steps in our first total synthesis, indicates that the presence of either macrocyclic unit does not favor the formation of the second, once again revealing the truly constrained and compact nature of diazonamide A.

[29] Oxidative cleavage of benzyl ethers has been reported, although none of the substrates possessed nitrogen atoms; for an example, see: J. D. Prugh, C. S. Rooney, A. A. Deana, H. G. Ramjit, *Tetrahedron Lett.* **1985**, *26*, 2947.

[30] Selected data for compound **22**: $R_f = 0.35$ (EtOAc/hexanes = 5:1); $[\alpha]_D^{20}$ (CH_3OH, $c = 0.69$) = −277.25; IR (film): $\tilde{\nu}_{max} = 3260$, 2919, 1713, 1660, 1602, 1496, 1443, 1401, 1302, 1261, 1214, 1155, 1055, 750 cm^{-1}; ^1H NMR (600 MHz, CD_3CN): $\delta = 10.38$ (s, 1H), 8.42 (s, 1H), 7.54 (d, $J = 7.9$ Hz, 1H), 7.42–7.33 (m, 7H), 7.27 (br m, 1H), 7.22 (d, $J = 7.0$ Hz, 1H), 7.10 (d, $J = 7.4$ Hz, 1H), 6.89–6.87 (m, 2H), 6.82 (t, $J = 7.9$ Hz, 1H), 6.77 (d, $J = 7.9$ Hz, 1H), 6.73 (s, 1H), 6.15 (d, $J = 7.9$ Hz, 1H), 5.08 (AB quart, $J = 12.7$ Hz, $\tilde{\nu}_{AB} = 17.1$ Hz, 2H), 4.55 (t, $J = 7.4$ Hz, 1H), 4.24 (ddd, $J = 11.4$, 8.8, 3.1 Hz, 1H), 3.23 (t, $J = 12.7$ Hz, 1H), 2.68 (d, $J = 11.4$ Hz, 1H), 2.00 (m, 1H), 1.01 (d, $J = 6.1$ Hz, 3H), 0.91 ppm (d, $J = 6.1$ Hz, 3H); ^{13}C NMR (150 MHz, $CDCl_3$): $\delta = 174.9$, 173.8, 164.3, 156.3, 154.6, 152.9, 152.8, 143.2, 140.6, 138.0, 135.9, 134.5, 131.6, 130.6, 130.0, 129.4, 129.3, 128.8, 128.6, 128.2, 127.2, 126.9, 124.8, 124.5, 123.2, 122.7, 116.6, 112.4, 98.3, 67.0, 57.8, 57.0, 56.4, 37.8, 31.0, 19.6, 19.0 ppm; HRMS (MALDI): calcd for $C_{43}H_{32}Cl_2N_6O_7^+$: 815.1782 [$M+H^+$], found: 815.1778.

 © 2003 Wiley-VCH Verlag GmbH & Co. KGaA, Weinheim

Single-Ion Electron Traps

First Evidence of a Single-Ion Electron Trap at the Surface of an Ionic Oxide**

Mario Chiesa, Maria Cristina Paganini, Elio Giamello, Cristiana Di Valentin, and Gianfranco Pacchioni*

Electron trapping and the stabilization of charge-separated states in solid systems is an exciting area of research in various branches of chemistry including the synthesis of new materials (for example, electrides),[1] surface science and heterogeneous catalysis,[2] and solar energy storage and conversion.[3] Microporous aluminosilicates (zeolites), for example, have been used to stabilize the products of spontaneous ionization (positive ions and electrons) of various atoms[4] and molecules.[5] Moissette et al indicated that for H-ZSM-5 zeolites,[5] the most probable electron-trapping site is an Al^{3+} Lewis acid center that is located close to an OH group. This implicitly advances the concept that a single, nonreducible surface ion of a solid can stabilize and trap an electron.

In the present communication we report experimental evidence, corroborated by ab initio calculations, of a surface electron trap that consists of a single metal ion at a magnesium oxide surface. Trapped electron centers on MgO are intrinsically important for the general problem of charge-carrier stabilization, as mentioned above, but are also of further interest:

1) They are excellent probes of the local environment of defective sites, which act as electron-trapping centers (topological spectroscopy);[6]
2) They are strong reducing agents (stable up to 320–370 K), which results in remarkable chemical reactivity;[7,8]
3) They play a role in the technological applications of MgO, for example, in catalysis[9] or as protecting layer in plasma displays.[10]

Despite their importance, the nature and location of the surface sites capable of trapping electrons are still elusive. While excess localized electrons (color centers) in the bulk of ionic solids are generally well understood, based on the classical model of de Boer (an electron trapped in an anion vacancy),[11,12] a totally different scenario is observed at the surface. The natural extension of de Boer's model[12] to the surface of a face-centered cubic (fcc) oxide, such as MgO, is a five-coordinated vacancy located on the dominant (100) faces. Many years ago, Tench[13] proposed this model to account for the formation of surface paramagnetic centers created by electron transfer from a dopant to a bare oxygen vacancy,

$$F_S^{2+} + e^- \rightarrow F_S^+ \quad (1)$$

where F_S^{2+} is the diamagnetic precursor of the paramagnetic center and formally derives from the removal of a surface O^{2-} ion. This model suffers from several drawbacks, such as the high formation energy of the oxygen vacancy and the need to compensate negative charge to maintain electroneutrality. In recent years several alternative models have been proposed, which range from low-coordinated vacancies at steps and corners,[14] to neutral divacancies,[15] or morphological defects,[16] all of which involve an array of cations that act as an electron trap. However, recent theoretical calculations[17] surprisingly predicted that single low-coordinate cations on MgO can act as potential electron-trapping sites.

Herein we report the first experimental evidence of the interaction of a trapped electron with a single Mg ion using continuous-wave electron paramagnetic resonance (CW-EPR) spectroscopy, and we present a detailed structural model for this site derived from density functional theory (DFT) calculations.

High-surface-area MgO ($300\ m^2 g^{-1}$) was obtained from samples prepared by chemical vapor deposition (CVD). The sample was placed into a vacuum manifold that contained the EPR cell and then activated "in situ" at 1173 K. Excess surface electrons were generated by irradiation with a laser beam ($\lambda = 244$ nm) under an H_2 atmosphere. The same EPR signal, although less sharp, has been obtained with a polychromatic UV lamp. In both cases, the sample changes color from white to deep blue. H_2 is believed to dissociate heterolytically at specific sites to form an H^+/H^- pair.[18] Under UV irradiation, neutral H atoms are desorbed leaving a trapped electron at the surface, close to an adsorbed proton (H^+/e^-). Under these circumstances, a proton is always present near the trapped electron, as shown by a small hyperfine coupling with the ^1H nucleus; the term $F_S^+(H)$ has been coined to indicate this small but important feature.[13] The new centers are formed in small amounts along with the above-mentioned $F_S^+(H)$ centers (7–8% of the paramagnetic color centers). The EPR spectrum obtained upon irradiation is shown in Figure 1a. The signal results from excess electrons localized at the surface; in fact, the blue color is bleached instantaneously by adsorption of a reactive gas, such as O_2. The g values, as well as the ^1H and ^{25}Mg hyperfine coupling constants (see Figure 1a) are the same as those previously reported.[14] Some line broadening is observed in the present study, which results from a higher concentration of defects. These results allow an observation of new features which can be discussed in terms of the ^{25}Mg hyperfine interaction. The dominant ^{25}Mg hyperfine sextet has a relatively small separation (11 G, Figure 1a). This value indicates a small interaction of the unpaired electron with the array of Mg^{2+} ions at the surface, and its preferential localization within the electron trap. By recording the spectrum in conditions of overamplification and overmodulation, two

[*] Prof. E. Giamello, Dr. M. Chiesa, Dr. M. C. Paganini
Dipartimento di Chimica IFM, Università di Torino
Istituto Nazionale per la Fisica della Materia
via P. Giuria 7, 10125 Torino (Italy)
Fax: (+39) 011-6707855
E-mail: elio.giamello@unito.it
Dr. C. Di Valentin, Prof. G. Pacchioni
Dipartimento di Scienza dei Materiali, Università di Milano-Bicocca
Istituto Nazionale per la Fisica della Materia
via R. Cozzi, 53-20125, Milano (Italy)

[**] This work is supported in part by the Italian INFM through the PRA-ISADORA project. We thank Prof. A. Zecchina for making the LASER source available. MgO samples were kindly supplied by Prof. E. Knotzinger (T. U. Wien).

 DOI: 10.1002/anie.200250811 © 2003 Wiley-VCH Verlag GmbH & Co. KGaA, Weinheim

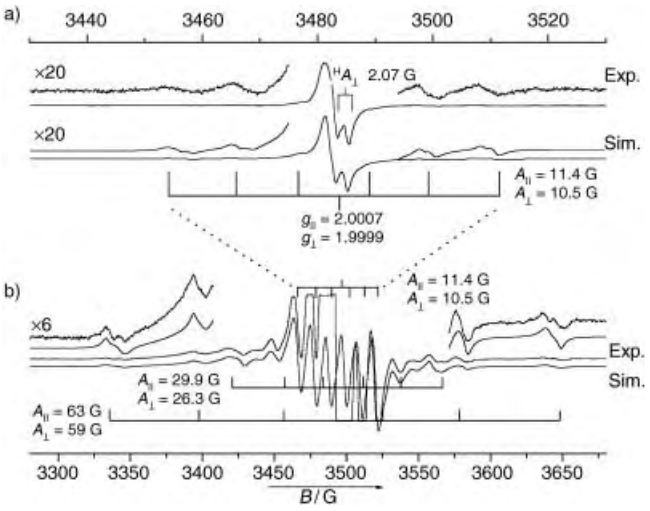


Figure 1. Experimental (upper trace) and simulated CW-EPR spectra of F_s^+(H) centers on MgO. a) 100 G scan-range spectrum recorded with a modulation amplitude of 0.5 G. The ^{1}H hf coupling (2.07 G) and the main ^{25}Mg sextet (average value: 11 G) are both highlighted with the lines shown below the traces. b) 400 G scan-range spectrum (lower scale) of the same sample recorded with a modulation amplitude of 3.5 G. The spectrum is the result of 20 accumulated scans; two new hyperfine structures are observed. Both spectra were recorded at room temperature with a microwave power of 1 mW.

new additional and less intense hyperfine features are observed (Figure 1b). The two new hyperfine structures have axial symmetry ($A_\perp \neq A_\parallel$) and much higher coupling constants than the main sextet. The first structure has $A_\perp = 27.6$ and $A_\parallel = 30.4$ G ($a_{iso} = 28.5$, $B = 0.9$ G). For the second structure, $A_\perp = 59$ and $A_\parallel = 63$ G ($a_{iso} = 60.3$, $B = 1.5$ G). The A values were obtained by computer simulation of the spectral profile (Figure 1b). The first hyperfine structure ($a_{iso} = 28.5$ G) can be ascribed to a "classical" center of the F_s^+(H) family, with an electron trapped by a group of Mg^{2+} ions. In fact, theoretical calculations have shown that the presence of a proton near an F_S^+ center polarizes the trapped electron towards one particular Mg^{2+} ion, which results in a_{iso} values of 20–30 G.[14] In contrast, hyperfine constants as high as 60 G have never been found in theoretical calculations for a model of F_S^+, F_S^+(H), or any other surface paramagnetic centers. Thus, the second sextet must be attributed to an unprecedented trapping site, the high hyperfine constant of which is not compatible with a site that contains several Mg^{2+} ions.

The theoretical study by Shluger and co-workers,[17] shows that a low-coordinate Mg^{2+} ion at the corner site of the MgO surface (Mg_{3c}^{2+}, Figure 2a), is a shallow trap that binds one electron by 0.6 eV. Mg_{3c}^{2+} sites are present, in low concentrations, on the surface of polycrystalline MgO, as shown by the vibrational shifts of adsorbed CO molecules.[19] In principle, these sites are candidates for the new features described above, but it can be shown that this is not the case. In fact, by means of embedded-cluster DFT calculations[20,21] we can confirm that an Mg_{3c}^{2+} ion is a shallow trap with an electron affinity of 0.65 eV, but the calculated hyperfine coupling constant of this center ($a_{iso} = -35.3$ G) is inconsistent with the experiment, being about one half of the measured constant. Thus, a bare Mg_{3c}^{2+} ion can be ruled out as a possible candidate for the observed features.

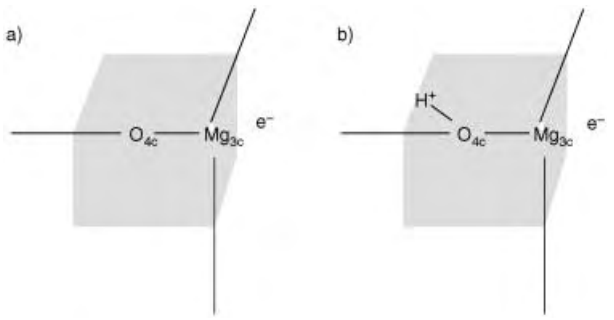


Figure 2. Schematic representation of electron-trapping sites. a) $MgO_{corner}(e^-)$; b) $MgO_{corner}(H^+/e^-)$.

Paramagnetic centers on MgO are, as has been already mentioned, created by the reaction of the oxide surface with H_2 under UV irradiation. This process has been considered here for the special case of a Mg_{3c}^{2+} corner site (Figure 2b) using the same theoretical approach described above.[21] The reaction proceeds in two steps: First, the H_2 molecule is adsorbed with concomitant dissociation to form a proton and an hydride, O_{4c}^{2-}/H^+ and Mg_{3c}^{2+}/H^-, as shown by the Mulliken populations, $H^+ = 0.5$, $H^- = 1.8$. The reaction is exothermic, and the computed value for ΔE (−0.66 eV) is close to that measured using microcalorimetry (−0.5 eV).[16] The Mg−H stretching frequency is found at $\tilde{\nu} = 1446$ cm^{-1} and a bending motion at $\tilde{\nu} = 852$ cm^{-1}; both values are typical for hydride species.[18] The O−H group vibrates at $\tilde{\nu} = 3624$ cm^{-1}. If a H atom is removed from the hydride site (the energy cost, 3.34 eV, is consistent with the use of UV light) one electron is left with the Mg_{3c}^{2+} ion while the proton is still bound to the O_{4c} nearest neighbor. In the resulting $MgO_{corner}(H^+/e^-)$ system (Figure 2b), the electron density is localized on the corner cation, which can be schematically classified as Mg_{3c}^+ (see Figure 3). It is noteworthy that the same result is obtained by adding a neutral H atom to the corner site. The

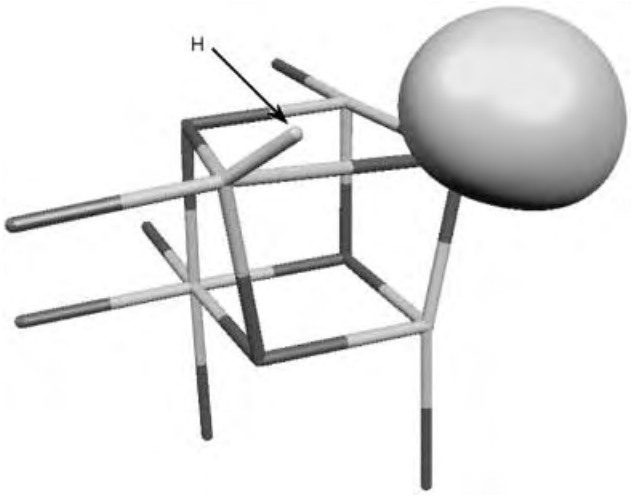


Figure 3. Spin-density plot representing the unpaired electron trapped at the $MgO_{corner}(H^+/e^-)$ site.

 © 2003 Wiley-VCH Verlag GmbH & Co. KGaA, Weinheim

hyperfine splitting in $MgO_{corner}(H^+/e^-)$, $a_{iso}(^{25}Mg) = -61.3$ G, is in quantitative agreement with the observed experimental value ($a_{iso} = 60.3$ G; the sign cannot be determined in the experiment). Moreover, the calculations show that the $MgO_{corner}(H^+/e^-)$ center is a deep trap for the electron, which is bound by 3.71 eV, and gives rise to two intense electronic transitions in the visible range at 2.07 ($f = 0.16$) and 2.39 eV ($f = 0.03$).[21] On the basis of these results, the new centers are therefore predicted to be "true" color centers. This is also in agreement with the thermal stability of the new centers. In fact, the hyperfine sextet disappears upon annealing between 320 and 370 K, as do the majority of the $F_s^+(H)$ centers. Because of the absence of experimental data for ^{25}Mg A_0 (the Fermi contact term for an electron in a Mg 3s orbital) and B_0 (the dipolar term for a 3p electron) values, the spin density on the Mg ion has been evaluated on the basis of Mulliken population analysis. The result shows that the unpaired electron is located mainly on the Mg 3s (56%) and Mg 3p orbitals (29%), with the remainder delocalized over a neighboring Mg center.

In conclusion, we have presented experimental and theoretical evidence for a new type of surface paramagnetic defect on MgO. These defects consist of electrons and protons bound at morphological sites, such as at a corner position. The main characteristic of these new centers is the large interaction of the unpaired electron with a Mg ion, a feature which can be schematically related to the formation of Mg^+ ions. Moreover, these findings provide a new scenario in the concept of electron trapping, which shows that morphological features that are naturally present on surfaces can act as potential wells that go beyond the classical de Boer model of an electron trapped in an oxygen vacancy. These findings may also be an interesting aid to understanding the case where electrons are trapped at the Lewis acid sites of H-ZSM-5 zeolites.[5]

Received: December 20, 2002 [Z50811]

Keywords: ab initio calculations · electron traps · EPR spectroscopy · paramagnetism · surface chemistry

[1] A. S. Ichimura, J. L. Dye, M. A. Camblor, L. A. Villaescusa, *J. Am. Chem. Soc.* **2002**, *124*, 1170.
[2] a) G. Pacchioni in *The Chemical Physics of Solid Surfaces-Oxide Surfaces, Vol. 9* (Ed.: P. Woodruff), Elsevier, Amsterdam **2000**, pp. 94–135; b) I. Kiricisi, H. Förster, G. Tasi, J. B. Nagy, *Chem. Rev.* **1999**, *99*, 2085.
[3] M. Grätzel, *Acc. Chem. Res.* **1981**, *14*, 376.
[4] P. P. Edwards, P. A. Anderson, J. M. Thomas, *Acc. Chem. Res.* **1996**, *29*, 23.
[5] A. Moissette, H. Verzin, I. Gener, J. Patarin, C. Bremard, *Angew. Chem.* **2002**, *114*, 1289; *Angew. Chem. Int. Ed.* **2002**, *41*, 1241.
[6] a) M. C. Paganini, M. Chiesa, E. Giamello, D. M. Murphy, G. Martra, S. Coluccia, G. Pacchioni, *Surf. Sci.* **1999**, 421, 246; b) M. Sterrer, O. Diwald, E. Knözinger, *J. Phys. Chem. B* **2000**, *104*, 3601.
[7] a) M. Chiesa, M. C. Paganini, E. Giamello, D. M. Murphy, Z. Sojka, *J. Chem. Phys.* **2002**, *116*, 4266; b) M. Chiesa, M. C. Paganini, E. Giamello, R. Soave, G. Pacchioni, D. M. Murphy, Z. Sojka, *J. Phys. Chem. B* **2001**, *105*, 2001.
[8] T. Risse, J. Schmidt , H. Hamann, H. J. Freund, *Angew. Chem.* **2002**, *114*, 1587; *Angew. Chem. Int. Ed.* **2002**, *41*, 1518.
[9] J. H. Lunsford, *Catal. Today* **1990**, *6*, 235.
[10] Y. T. Matulevich, T. J. Vink, P. A. Zeijlmans van Emmichoven, *Phys. Rev. Lett.* **2002**, *89*, 167601.
[11] G. Feher, *Phys. Rev.* **1957**, 105, 1122.
[12] J. H. de Boer, *Recl. Trav. Chim. Pays-Bas* **1937**, 56, 301.
[13] A. J. Tench, R. L. Nelson, *J. Colloid Interface Sci.* **1968**, *26*, 364.
[14] E. Giamello, M. C. Paganini, D. M. Murphy, A. M. Ferrari, G. Pacchioni *J. Phys. Chem. B* **1997**, 101, 971.
[15] A. D'Ercole, C. Pisani, *J. Chem. Phys.* **1999**, *111*, 9743.
[16] D. Ricci, C. Di Valentin, G. Pacchioni, P. V. Sushko, A. L. Shluger, E. Giamello, *J. Am. Chem. Soc.*, **2003**, *125*, 738.
[17] P. V. Sushko, J. L. Gavartin, A. Shluger, *J. Phys. Chem. B* **2002**, *106*, 2269.
[18] O. Diwald, P. Hofmann, E. Knözinger, *Phys. Chem. Chem. Phys.* **1999**, *1*, 713.
[19] L. Marchese, S. Coluccia, . G. Martra, A. Zecchina, *Surf. Sci.* **1992**, 269/270, 135.
[20] P. V. Sushko, A. L. Shluger, C. R. A. Catlow, *Surf. Sci.* **2000**, *450*, 153.
[21] DFT calculations were carried out using the B3LYP exchange-correlation functional (A. D. Becke, *J. Chem. Phys.* **1993**, *98*, 5648; C. Lee, W. Yang, R. G. Parr, *Phys. Rev. B* **1988**, *37*, 785). The MgO surface is represented as a large cluster, divided into regions I and II. Region I is centered on a corner site and includes an Mg_4O_4 quantum-mechanical unit that is surrounded by six interface ions and 932 polarizable classical shell-model ions. Region II is represented by 7054 point charges. All centers in region I are allowed to relax during the geometry optimization. A 6-311+G** basis set has been used on all atoms. Excitation energies have been determined using the time-dependent DFT approach (TD-DFT).

 © 2003 Wiley-VCH Verlag GmbH & Co. KGaA, Weinheim

Transition-State Models

Resurrecting the Cornforth Model for Carbonyl Addition: Studies on the Origin of 1,2-Asymmetric Induction in Enolate Additions to Heteroatom-Substituted Aldehydes**

David A. Evans, Sarah J. Siska, and Victor J. Cee*

Transition-state models that reliably predict the stereochemical outcome of pivotal organic reactions are essential to synthesis design. This statement is true even if the proposed model is purely empirical. Historically, such has been the case for models that predict the stereochemical course of nucleophilic additions to chiral α-substituted aldehydes and

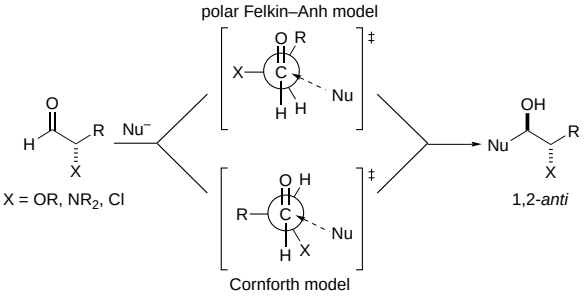
[*] Prof. D. A. Evans, S. J. Siska, V. J. Cee
Department of Chemistry and Chemical Biology
Harvard University
Cambridge, MA 02138 (USA)
Fax: (+1) 617-495-1460
E-mail: evans@chemistry.harvard.edu

[**] Financial support was provided by the National Institutes of Health (GM33327-16) and by Merck Research Laboratories.

 DOI: 10.1002/anie.200350979 © 2003 Wiley-VCH Verlag GmbH & Co. KGaA, Weinheim

ketones.[1] The first stereoinduction model for this process was introduced by Cram and Elhafez in 1952.[2] More realistic models have subsequently evolved over the last five decades on the basis of new insights into stabilizing transition-state geometries and interactions.[3]

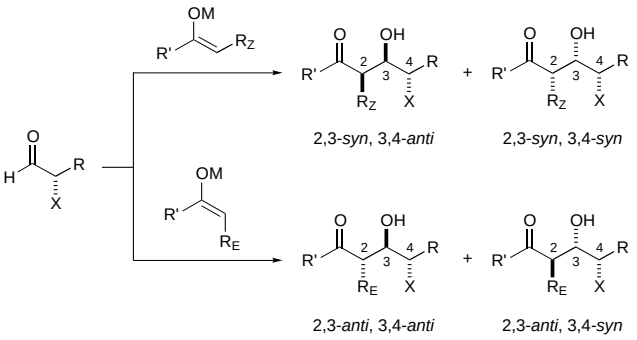
The present study is concerned with the design of experiments that might differentiate between the polar Felkin–Anh (PFA)[3d,4,5] and modified[6] Cornforth[3a,7] models for α-heteroatom-substituted aldehydes (Scheme 1). In the absence of chelate organization, both models predict the observed 1,2-*anti* product stereochemistry through differ-



Scheme 1. Stereochemical models for 1,2-induction in α-heteroatom-substituted aldehydes.

ent rotamers of the α-stereocenter. The PFA model[3d,4,5] is based on transition-state stabilization through hyperconjugative interaction of the forming bond (HOMO) with the best vicinal acceptor, the C–X bond (LUMO); in contrast, the Cornforth model[3a,6,7] is based on dipole minimization between the C–X bond and the adjacent carbonyl group. Since Anh and Eisenstein's pioneering theoretical investigation,[4] however, the PFA model has been commonly accepted as the preferred explanation for 1,2-asymmetric induction in α-heteroatom-substituted aldehydes. Subsequent theoretical studies have generally supported the PFA model,[5] although there are some exceptions.[7] Experimentally, these two transition-state models can be distinguished for carbonyl addition reactions in which the nucleophile imposes a transition-state conformational constraint on the orientation of the α-stereocenter of the electrophile. Substituted enolate nucleophiles meet this criterion (see below). Accordingly, we report a systematic study of aldol reactions between methyl-substituted *Z* and *E* enolates and α-oxygen-substituted aldehydes. In this study, the observed dependence of diastereofacial selectivity on enolate configuration is more consistent with the Cornforth model. This conclusion has also been drawn by both Hoffmann et al. and Roush et al. in their comparable studies on aldehyde crotylboration.[8]

Boron-mediated aldol reactions[9] between *Z*- and *E*-substituted enolates and a chiral aldehyde provide two principal diastereomers for each reaction (Scheme 2) since boron enolate configuration strongly correlates with the product stereochemistry (2,3-relationship).[9a] The enolate configuration can also greatly affect the aldehyde diastereofacial selectivity (3,4-relationship) as a result of potential destabilizing *syn*-pentane interactions between the enolate



Scheme 2. Aldol reactions of an α-heteroatom-substituted aldehyde with substituted enolates.

substituent and the α stereocenter of the aldehyde in the transition state.[10] In this study, we have included the data for the analogous lithium enolates for reference purposes and acknowledge the fact that these nucleophiles are inherently less diastereoselective (2,3-relationship). Mechanistic projections from lithium enolates, while less reliable, are nonetheless important for the purpose of generalization.

The cyclic transition states for the aldol reaction between substituted enolates and an α-heteroatom-substituted aldehyde are shown in Figure 1. Structures **I** and **II** incorporate

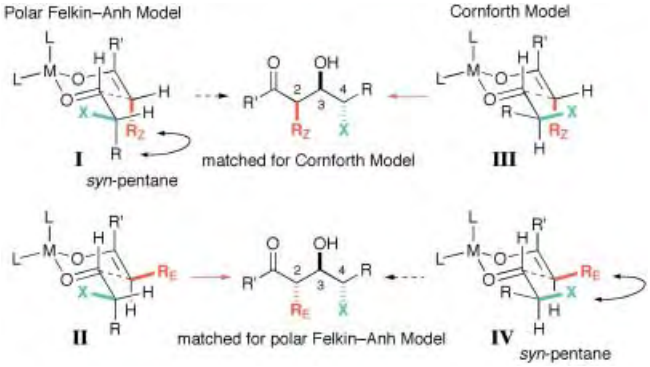


Figure 1. Comparative transition state analysis using the polar Felkin–Anh and Cornforth models.

the rotamer of the α stereocenter advanced by the PFA model, while structures **III** and **IV** incorporate the rotamer of the Cornforth model. The enolate substituent imposes an additional conformational constraint on the aldehyde rotamer due to the possibility of destabilizing *syn*-pentane interactions. It is through analysis of these interactions that the following predictions can be made regarding the relationship between enolate configuration and aldehyde diastereofacial selectivity.

PFA model prediction: The *Z* enolate substituent causes a destabilizing *syn*-pentane interaction (**I**), while the *E* enolate substituent experiences no such interaction (**II**). *Therefore,* E *enolates are predicted to give superior 3,4-*anti *selectivity relative to* Z *enolates.*

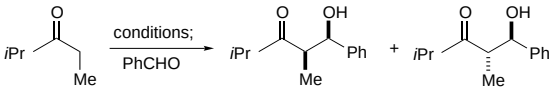
Cornforth model prediction: The *E* enolate substituent causes a destabilizing *syn*-pentane interaction (**IV**), while the

 © 2003 Wiley-VCH Verlag GmbH & Co. KGaA, Weinheim

Z enolate substituent experiences no such interaction (**III**). *Therefore, Z enolates are predicted to give superior 3,4-*anti *selectivity relative to* E *enolates.* As a consequence of this dichotomy, the experimentally determined relationship between enolate configuration and aldehyde diastereofacial selectivity should validate a single model for asymmetric induction.

Boron and lithium enolates of both *Z* and *E* configurations are readily available from 2-methyl-3-pentanone (Table 1).[11] The configurational purity of *Z* and *E* boron enolates correlates well with the *syn*/*anti* ratio of the aldol adducts. While *Z* and *E* lithium enolates are also formed with good configurational purity, the characteristic decline in *syn*/*anti* selectivity is observed, particularly with the *E* enolate.[9]

Table 1: Enolization and aldol addition of 2-methyl-3-pentanone.

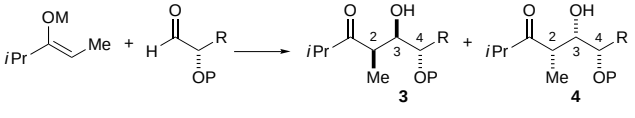


Conditions[a]	Solvent	Configuration (*Z*:*E*)[d]	**1**:**2**[d]	Yield [%][e]
9-BBNOTf, DIPEA	Et_2O	95:05[b]	94:06	82
(c-Hex)$_2$BCl, TEA	Et_2O	07:93[b]	04:96	79
LiHMDS	THF	95:05[c]	90:10	66
LiNTMS(*t*Bu)	THF	09:91[c]	48:52	86

[a] For reaction conditions, see Experimental Section. [b] Boron enolates were treated with *n*BuLi, then silylated with trimethylsilyl chloride. [c] Lithium enolates were silylated directly with trimethylsilyl chloride. [d] Ratios were determined by integration of the ^{1}H NMR spectrum of the unpurified reaction mixture. [e] Yields are reported for the mixture of diastereomeric adducts.

The *Z* boron and *Z* lithium enolates of 2-methyl-3-pentanone were allowed to react with a representative set of α-oxygen-substituted aldehydes (Table 2). As anticipated for *Z* enolates, the 2,3-*syn* aldol adducts **3** and **4** predominate.[9] The diastereofacial selectivity is uniformly high, with the 3,4-*anti* diastereomer **3** being greatly favored. This observation alone is inconsistent with the PFA model, which predicts a destabilizing *syn*-pentane interaction in the transition state (Figure 1, **I**) leading to the observed products.

Table 2: Aldol reactions of *Z* enolates.[a]

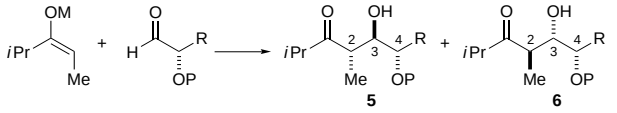


M	P	R	2,3-*syn*:2,3-*anti*	**3**:**4**	Yield [%][c]
9-BBN	Bn	Me	95:05[b]	89:11[b]	95
9-BBN	Bn	*i*Pr	95:05	98:02	73
9-BBN	TBS	Me	93:07	98:02	77
9-BBN	TBS	*i*Pr	94:06	98:02	72
Li	Bn	Me	93:07[b]	89:11[b]	67
Li	Bn	*i*Pr	98:02	98:02	77
Li	TBS	Me	96:04	95:05	65
Li	TBS	*i*Pr	98:02	99:01	71

[a] For reaction conditions, see Experimental Section. All products were unambiguously characterized. Ratios were determined by GC analysis after silylation (TMS-imidazole) or acetylation (Ac_2O/pyr) of the unpurified reaction mixtures, unless noted. [b] Ratios were determined by HPLC analysis of the unpurified reaction mixtures. [c] Yields are reported for the mixture of diastereomeric adducts.

The analogous reactions of the *E* boron enolate provide predominantly 2,3-*anti* aldol adducts **5** and **6** (Table 3). In striking contrast to the reactions of *Z* boron enolates, the diastereofacial selectivity is uniformly poor and often favors the 3,4-*syn* diastereomer **6**. As anticipated, the *E* lithium enolate affords poor 2,3-*anti*/2,3-*syn* selectivity, but exhibits moderate diastereofacial selectivity within the 3,4-*anti* diastereomer manifold. Overall, relative to *Z* enolates, the *E* enolates result in greatly diminished levels of 3,4-*anti* diastereoselection.[12] This finding is inconsistent with the PFA model, which contains reinforcing steric and stereoelectronic effects for *E* enolates (Figure 1, **II**). In the Cornforth model for *E* enolates, the *syn*-pentane and C–X dipole control elements are not reinforcing (Figure 1, **IV**), a circumstance that would be expected to lead to diminished aldehyde face selectivity.

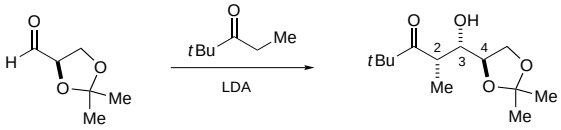
Table 3: Aldol reactions of *E* enolates.[a]



M	P	R	2,3-*anti*:2,3-*syn*	**5**:**6**	Yield [%]
(c-Hex)$_2$B	Bn	Me	>99:01[b]	33:67[b]	59
(c-Hex)$_2$B	Bn	*i*Pr	>99:01	67:33	77
(c-Hex)$_2$B	TBS	Me	>99:01	21:79	77
(c-Hex)$_2$B	TBS	*i*Pr	>99:01	43:57	85
Li	Bn	Me	45:55[b]	93:07[b]	92
Li	Bn	*i*Pr	46:54	80:20	78
Li	TBS	Me	62:38	85:15	78
Li	TBS	*i*Pr	67:33	88:12	80

[a] For reaction conditions, see Experimental Section. All products were unambiguously characterized. Ratios were determined by GC analysis after silylation (TMS-imidazole) or acetylation (Ac_2O/pyr) of the unpurified reaction mixtures, unless noted. [b] Ratios were determined by HPLC analysis of the unpurified reaction mixtures. [c] Yields are reported for the mixture of diastereomeric adducts.

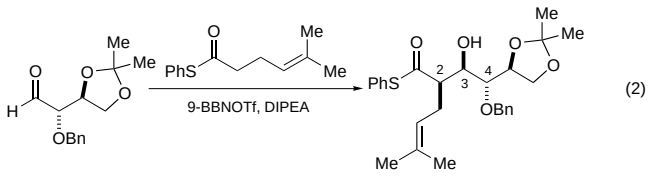
Other reactions between achiral, substituted sp^2 nucleophiles and α-oxygen-substituted aldehydes have been reported.[8,13,14] Lithium, boron, and titanium enolates have been shown to provide *syn* aldol adducts with high levels of selectivity for the 3,4-*anti* diastereomer [Eqs. (1)–(3)].[13a,c,e] While Urpí and co-workers have noted the inconsistency of



(1)

3,4-*anti* : 3,4-*syn* 85 : 15

 © 2003 Wiley-VCH Verlag GmbH & Co. KGaA, Weinheim



(2)

3,4-*anti* : 3,4-*syn* >95 : 05



(3)

3,4-*anti* : 3,4-*syn* >99 : 01

these results [Eq. (3)] with the PFA model,[13e] a satisfactory explanation was not presented. In light of the preceding analysis, the high 2,3-*syn*, 3,4-*anti* diastereoselectivity in these cases is consistent with a *Z* enolate reacting via a Cornforth transition state (Figure 1, **III**). The mechanistically related crotylboration of chiral oxygen-substituted aldehydes has provided further corroboration of the Cornforth model.[8,14,15]

The modified[6] Cornforth model[3a] (Scheme 1) is receiving increasing support from the growing body of experimental data on nucleophilic additions to α-heteroatom-substituted aldehydes. The success of this model might be because of a concurrence of optimal positions for the aldehyde heteroatom and alkyl substituents in the transition state of nucleophilic addition reactions. The experimental evidence applies directly only to differentially substituted sp^2 nucleophiles reacting with aldehydes via pericyclic chair transition states. However, it is plausible that the factors stabilizing the Cornforth transition states in these specific cases are operating in all nucleophilic additions to α-heteroatom-substituted carbonyl groups. Further experimental and theoretical work will be necessary to substantiate this hypothesis.[16]

Experimental Section

General procedure for the aldol reactions of 9-borabicyclo[3.3.1]-nonyl (9-BBN) enolates: To a 0.2 M solution of ketone (1.0 equiv) in Et_2O at 0 °C was added 1.2 equivalents of diisopropylethylamine and 1.1 equivalents of 9-borabicyclo[3.3.1]nonyl trifluoromethanesulfonate. The resulting light yellow suspension was warmed to ambient temperature and stirred for 1 h, then cooled to −78 °C. A solution of aldehyde (1.0 equiv) in Et_2O was added. The mixture was stirred at −78 °C for 2 h, then warmed to 0 °C and stirred for 10 min. The reaction was quenched at 0 °C by the sequential addition of equal quantities of 0.05 M pH 7 buffer, MeOH, and 30 % aqueous H_2O_2. The mixture was stirred vigorously at ambient temperature for 30 min, and was then diluted with pH 7 buffer and CH_2Cl_2, and extracted twice with CH_2Cl_2. The combined organic layers were washed with 1:1 saturated aqueous $NaHCO_3$:0.1N aqueous $Na_2S_2O_3$, dried over Na_2SO_4, filtered, concentrated in vacuo, and purified by silica gel chromatography.

General procedure for the aldol reactions of dicyclohexylboryl enolates: To a 0.2 M solution of ketone (1.0 equiv) in Et_2O at 0 °C was added 1.05 equivalents of dicyclohexylboron chloride and 1.1 equivalents of triethylamine. The resulting white suspension was stirred at 0 °C for 1 h, then cooled to −78 °C. A solution of aldehyde (1.0 equiv) in Et_2O was added. The reaction mixture was stirred at −78 °C for 2 h, then warmed to 0 °C and stirred for 10 min. The reaction was quenched and isolated as described for 9-BBN enolates.

General procedure for the aldol reactions of Z lithium enolates: To a 0.1 M solution of hexamethyldisilazane (1.1 equiv) in THF at 0 °C was added 1.1 equivalents of *n*-butyllithium (2.95 M in hexanes). The solution was stirred for 10 min at 0 °C, then cooled to −78 °C. Ketone (1.0 equiv) was added slowly, and the resulting solution was stirred at −78 °C for 1 h. A solution of aldehyde (1.0 equiv) in THF was added. The reaction mixture was stirred at −78 °C for 10 min, then the reaction was quenched by adding 1:1 (v:v) saturated aqueous NH_4Cl. The mixture was allowed to warm to ambient temperature with vigorous stirring, then diluted with Et_2O. The organic layer was washed with saturated aqueous NH_4Cl and brine. The aqueous washings were extracted with an additional portion of Et_2O. The combined organic layers were dried over $MgSO_4$, filtered, concentrated in vacuo, and purified by silica gel chromatography.

General procedure for the aldol reactions of *E* lithium enolates**:** To a 0.1 M solution of *tert*-butyl(trimethylsilyl)amine (1.2 equiv) in THF at 0 °C was added 1.1 equivalents of *n*-butyllithium (2.95 M in hexanes) rapidly dropwise. The solution was warmed to ambient temperature and stirred for 15 min. Ketone (1.0 equiv) was added rapidly dropwise, and the solution was stirred for 30 s at ambient temperature, then cooled to −78 °C. A solution of aldehyde (1.0 equiv) in THF was added. The reaction mixture was stirred at −78 °C for 10 min, then the reaction was quenched and isolated as described for the *Z* lithium enolate reaction.

Received: January 21, 2003 [Z50979]

Keywords: aldol reaction · reaction mechanisms · stereoselectivity · transition states

[1] A. Mengel, O. Reiser, *Chem. Rev.* **1999**, *99*, 1191 – 1223, and references therein.

[2] D. J. Cram, F. A. B. Elhafez, *J. Am. Chem. Soc.* **1952**, *74*, 5828 – 5835.

[3] a) J. W. Cornforth, R. H. Cornforth, K. K. Mathew, *J. Chem. Soc.* **1959**, 112 – 127; b) D. J. Cram, D. R. Wilson, *J. Am. Chem. Soc.* **1963**, *85*, 1245 – 1249; c) G. J. Karabatsos, *J. Am. Chem. Soc.* **1967**, *89*, 1367 – 1371; d) M. Chérest, H. Felkin, N. Prudent, *Tetrahedron Lett.* **1968**, 2199 – 2204. For additional discussion of some of these models, see: e) E. L. Eliel in *Asymmetric Synthesis, Vol. 2* (Ed.: J. D. Morrison), Academic Press, New York, **1983**, pp. 125 – 155. For a discussion of electrostatic versus frontier molecular orbital (FMO) effects in carbonyl additions, see: f) B. W. Gung, *Tetrahedron* **1996**, *52*, 5263 – 5301.

[4] a) N. T. Anh, O. Eisenstein, *Nouv. J. Chim.* **1977**, *1*, 61 – 70; b) N. T. Anh, *Top. Curr. Chem.* **1980**, *88*, 145 – 162.

[5] For theoretical studies which support the polar Felkin–Anh model, see: a) Y.-D. Wu, K. N. Houk, *J. Am. Chem. Soc.* **1987**, *109*, 908 – 910; b) S. S. Wong, M. N. Paddon-Row, *J. Chem. Soc. Chem. Commun.* **1990**, 456 – 458; c) Y.-D. Wu, J. A. Tucker, K. N. Houk, *J. Am. Chem. Soc.* **1991**, *113*, 5018 – 5027; d) S. S. Wong, M. N. Paddon-Row, *J. Chem. Soc. Chem. Commun.* **1991**, 327 – 330; e) S. S. Wong, M. N. Paddon-Row, *Aust. J. Chem.* **1991**, *44*, 765 – 770; f) G. Frenking, K. F. Köhler, M. T. Reetz, *Tetrahedron* **1991**, *47*, 9005 – 9018; g) G. Frenking, K. F. Köhler, M. T. Reetz, *Tetrahedron* **1993**, *49*, 3983 – 3994; h) N. T. Anh, F. Maurel, J.-M. Lefour, *New J. Chem.* **1995**, *19*, 353 – 364.

[6] The Cornforth model has been modified from its original form to incorporate torsional effects and the Bürgi–Dunitz trajectory. For a discussion of torsional effects in transition states, see: M. N. Paddon-Row, N. G. Rondan, K. N. Houk, *J. Am. Chem. Soc.* **1982**, *104*, 7162 – 7166.

 © 2003 Wiley-VCH Verlag GmbH & Co. KGaA, Weinheim

[7] Addition of cyanide anion to fluoroacetaldehyde in solution: a) A. S. Cieplak, K. B. Wiberg, *J. Am. Chem. Soc.* **1992**, *114*, 9226 – 9227. Addition of cyanide anion to chlorofluoroacetaldehyde in the gas phase: b) G. Frenking, K. F. Köhler, M. T. Reetz, *Tetrahedron* **1994**, *50*, 11197 – 11204. Allylboration of α-methoxypropanal in the gas phase: c) B. W. Gung, X. Xue, *Tetrahedron: Asymmetry* **2001**, *12*, 2955 – 2959.

[8] a) R. W. Hoffmann, *Chem. Scr.* **1985**, *25*, 53 – 60 (Sp. Iss.); b) W. R. Roush, M. A. Adam, A. E. Walts, D. J. Harris, *J. Am. Chem. Soc.* **1986**, *108*, 3422 – 3434; c) R. W. Hoffmann, R. Metternich, J. W. Lanz, *Liebigs Ann. Chem.* **1987**, 881 – 887; d) H. Brinkmann, R. W. Hoffmann, *Chem. Ber.* **1990**, *123*, 2395 – 2401.

[9] a) D. A. Evans, J. V. Nelson, E. Vogel, T. R. Taber, *J. Am. Chem. Soc.* **1981**, *103*, 3099 – 3111. For an extensive review of boron enolate based aldol additions see: b) C. J. Cowden, I. Paterson, *Org. React.* **1997**, *51*, 1 – 200.

[10] This effect is well known for α-methyl chiral aldehydes. See: a) D. A. Evans, J. V. Nelson, T. R. Taber, *Top. Stereochem.* **1982**, *13*, 1 – 115; b) W. R. Roush, *J. Org. Chem.* **1991**, *56*, 4151 – 4157.

[11] Boron enolates: a) H. C. Brown, K. Ganesan, R. K. Dhar, *J. Org. Chem.* **1993**, *58*, 147 – 153; *Z* lithium enolate: b) C. H. Heathcock, C. T. Buse, W. A. Kleschick, M. C. Pirrung, J. E. Sohn, J. Lampe, *J. Org. Chem.* **1980**, *45*, 1066 – 1081; *E* lithium enolate: c) L. Xie, K. M. Isenberger, G. Held, L. M. Dahl, *J. Org. Chem.* **1997**, *62*, 7516 – 7519.

[12] In the case of the boron aldol reactions, it is possible that the difference in aldehyde diastereofacial selectivity between *E* and *Z* enolates is simply due to differences in the nature of the boron ligands that are necessary for the control of enolate configuration. However, both 9-BBN and $(c\text{-Hex})_2$B enolates of cyclohexanone give similar results, indicating that enolate configuration is primarily responsible for the selectivity difference.

[13] Lithium enolates: a) C. H. Heathcock, S. D. Young, J. P. Hagen, M. C. Pirrung, C. T. White, D. VanDerveer, *J. Org. Chem.* **1980**, *45*, 3846 – 3856. Boron enolates: b) C. Gennari, A. Bernardi, S. Cardani, C. Scolastico, *Tetrahedron* **1984**, *40*, 4059 – 4065; c) D. R. Williams, J. L. Moore, M. Yamada, *J. Org. Chem.* **1986**, *51*, 3916 – 3918. Titanium enolates: d) R. Annunziata, M. Cinquini, F. Cozzi, P. G. Cozzi, E. Consolandi, *Tetrahedron* **1991**, *47*, 7897 – 7910; e) C. Esteve, M. Ferreró, P. Romea, F. Urpí, J. Vilarrasa, *Tetrahedron Lett.* **1999**, *40*, 5079 – 5082. Samarium enolates: f) L. Lu, H.-Y. Chang, J.-M. Fang, *J. Org. Chem.* **1999**, *64*, 843 – 853.

[14] In contrast, crotylation of α-chiral oxygen-substituted aldehydes with crotyl bromide and $CrCl_2$ is reported to proceed with good to excellent selectivity for the 2,3-*anti*, 3,4-*anti* diastereomer. See: a) S. F. Martin, W. Li, *J. Org. Chem.* **1989**, *54*, 6129 – 6133; b) J. Mulzer, L. Kattner, A. R. Strecker, C. Schröder, J. Buschmann, C. Lehmann, P. Luger, *J. Am. Chem. Soc.* **1991**, *113*, 4218 – 4229.

[15] The matched/mismatched relationship between *Z* and *E* chiral γ-chloroallylborane reagents and α-chiral oxygen-substituted aldehydes is also consistent with Cornforth transition states (Figure 1, **III** and **IV**). See: S. Hu, S. Jayaraman, A. C. Oehlschlager, *J. Org. Chem.* **1998**, *63*, 8843 – 8849.

[16] Abbreviations: PFA = polar Felkin–Anh; DIPEA = diisopropylethylamine; 9-BBNOTf = 9-borabicyclo[3.3.1]nonyl trifluoromethanesulfonate; TEA = triethylamine; LiHMDS = lithium hexamethyldisilazide; TMS = trimethylsilyl; THF = tetrahydrofuran; Bn = benzyl; TBS = *tert*-butyldimethylsilyl; pyr = pyridine; LDA = lithium diisopropylamide; TBDPS = *tert*-butyldiphenylsilyl.

 © 2003 Wiley-VCH Verlag GmbH & Co. KGaA, Weinheim

Sequence-Selective Recognition

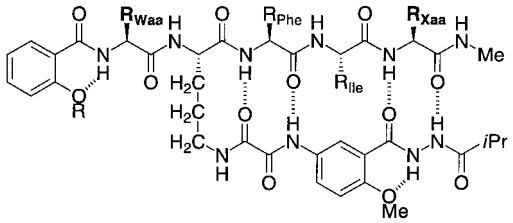
Sequence-Selective Molecular Recognition between β Sheets**

James S. Nowick and De Michael Chung*

Dedicated to Professor Larry Overman on the occasion of his 60th birthday

Interactions between the hydrogen-bonding edges of β sheets occur widely in protein quaternary structure, protein–protein interactions, and protein aggregation and are involved in both healthy biological processes and in diseases ranging from cancer and AIDS to anthrax and Alzheimer's.[1,2] These protein–protein interactions constitute a form of molecular recognition that deserves more attention, both because of its importance in biological processes and because of its fundamental nature. This paper asks whether interactions between β-sheet-forming peptides can be sequence selective and finds that patterning valine and threonine residues across the non-hydrogen-bonded rings formed at the interface between antiparallel β sheets can impart dramatic sequence selectivity.[3]

We had previously reported that peptides such as **1a**, which contain the amino acid Orn(*i*PrCO-Hao), fold into β-



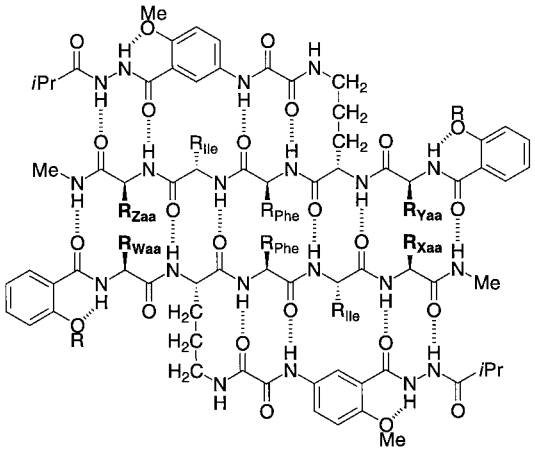
o-MeO-C_6H_4CO-Val-Orn(*i*PrCO-Hao)-Phe-Ile-Leu-NHMe (**1a**)
o-BuO-C_6H_4CO-**Thr**-Orn(*i*PrCO-Hao)-Phe-Ile-**Val**-NHMe (**1b**, **Thr-Val**)
o-BuO-C_6H_4CO-**Val**-Orn(*i*PrCO-Hao)-Phe-Ile-**Thr**-NHMe (**1c**, **Val-Thr**)
o-BuO-C_6H_4CO-**Thr**-Orn(*i*PrCO-Hao)-Phe-Ile-**Thr**-NHMe (**1d**, **Thr-Thr**)
o-BuO-C_6H_4CO-**Val**-Orn(*i*PrCO-Hao)-Phe-Ile-**Val**-NHMe (**1e**, **Val-Val**)

sheetlike structures that dimerize through β-sheet interactions in organic solvents (Scheme 1).[4] In the present study, we chose to replace the valine and leucine residues of **1a** with threonine and valine in all possible orders: Thr–Val (**1b**), Val–Thr (**1c**), Thr–Thr (**1d**), and Val–Val (**1e**). We selected these residues with the expectation that Val would pair preferentially with Val, and that Thr would pair preferentially with Thr, through self-complementary noncovalent interactions

[*] Prof. J. S. Nowick, D. M. Chung
Department of Chemistry
University of California, Irvine
Irvine, CA 92697-2025 (USA)
Fax: (+1) 949-824-9920
E-mail: jsnowick@uci.edu

[**] We thank the NIH for grant support (GM-49076). D.M.C. thanks the Bill and Melinda Gates Foundation and the UCI Institute for Brain Aging and Dementia for a fellowship and training grant support (NIA-5T32AG000096).

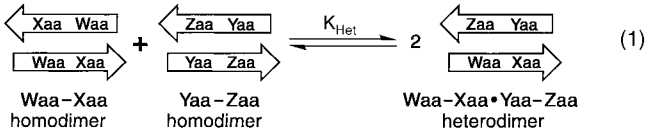
 DOI: 10.1002/anie.200250750 © 2003 Wiley-VCH Verlag GmbH & Co. KGaA, Weinheim



Scheme 1. The β-sheet dimer of peptides **1**.

and with the knowledge that these pairings frequently occur in the non-hydrogen-bonded rings of antiparallel β sheets.[5]

To evaluate the sequence selectivity of molecular recognition between threonine- and valine-containing β-sheet peptides **1b–e**, we measured the propensity of these peptides to form heterodimers. Mixing solutions of (homodimeric) peptides ArCO-**Waa**-Orn(*i*PrCO-Hao)-Phe-Ile-**Xaa**-NHMe (**Waa–Xaa**) and ArCO-**Yaa**-Orn(*i*PrCO-Hao)-Phe-Ile-**Zaa**-NHMe (**Yaa–Zaa**) gives an equilibrium mixture of homodimers [(**Waa–Xaa**)$_2$ and (**Yaa–Zaa**)$_2$] and heterodimer [(**Waa–Xaa**)·(**Yaa–Zaa**)] [Eq. (1)]. A heterodimeric equilibrium constant K_{Het} can be defined as [(**Waa–Xaa**)·(**Yaa–Zaa**)]^2/[(**Waa–Xaa**)$_2$][(**Yaa–Zaa**)$_2$]. If the equilibrium is statistical, $K_{Het} = 4$; if the heterodimer forms preferentially, $K_{Het} > 4$; if the homodimers are preferred, $K_{Het} < 4$. The quantity $K_{Het}/4$ provides a convenient gauge of the dimerization preference, with a value of 1.0 indicating no preference.



(1)

^{1}H NMR spectroscopic studies readily permit the direct measurement of K_{Het}. Chemical exchange between the homo- and heterodimers occurs slowly on the NMR time scale at ambient and subambient temperatures in $CDCl_3$ or in [D_6]DMSO/$CDCl_3$. The hydrazide and anilide NH resonance signals of the Orn(*i*PrCO-Hao) group are well dispersed and allow the various species present to be quantified accurately. Each homodimer presents two doublets associated with the hydrazide NH resonance signals in the $\delta = 11$–12 ppm region of the spectrum and a singlet near $\delta = 10$ ppm associated with the anilide NH resonance signal; the heterodimer presents four doublets and two singlets. Integration of these peaks allows the determination of the ratios of the species; deconvolution of the spectra by fitting the peaks with Lorentzian functions provides even greater accuracy. The spectra shown in Figure 1 and 2 are representative of these studies.

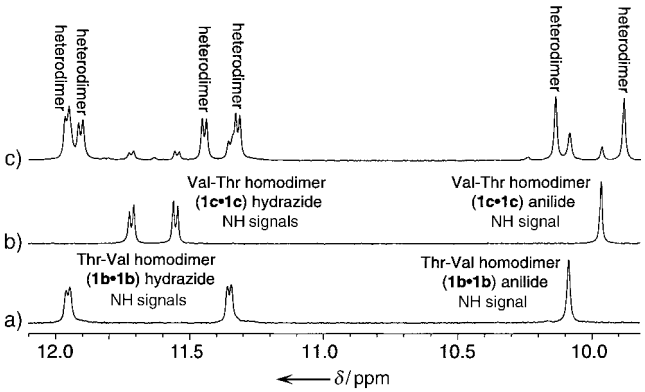


Figure 1. ^{1}H NMR spectra of the hydrazide and anilide NH groups of Thr–Val peptide **1b** (a), Val–Thr peptide **1c** (b), and a mixture of the two peptides (c). The *heterodimer* predominates in the mixture. Spectra were recorded at 500 MHz and 253 K in 10% [D_6]DMSO in $CDCl_3$ at a) 2.0 mM **1b**, b) 2.0 mM **1c** , and c) 2.1 mM **1b** and 1.5 mM **1c**.

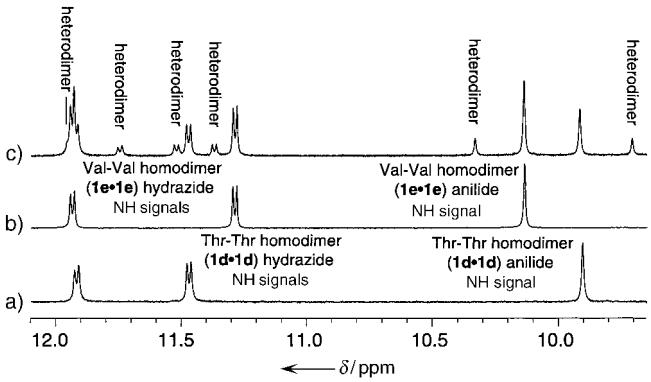


Figure 2. ^{1}H NMR spectra of the hydrazide and anilide NH groups of Thr–Thr peptide **1d** (a), Val–Val peptide **1e** (b), and a mixture of the two peptides (c). The *homodimers* predominate in the mixture. Spectra were recorded at 500 MHz and 253 K in 10% [D_6]DMSO in $CDCl_3$ at a) 2.0 mM **1d**, b) 2.0 mM **1e**, and c) 1.5 mM **1d** and 1.7 mM **1e**.

Analysis of spectra collected in 10% [D_6]DMSO in $CDCl_3$ (Figure 1 and 2) reveals a strong preference for Thr–Val (**1b**) and Val–Thr (**1c**) to form a heterodimer ($K_{Het}/4 = 8.9$) and for Thr–Thr (**1d**) and Val–Val (**1e**) to remain as homodimers ($K_{Het}/4 = 0.083$).[6] In contrast with these results, controls involving all four other possible combinations of peptides **1b–e** show little or no preferences for forming either homo- or heterodimers ($K_{Het}/4 = 0.8$–1.0; Table 1). These results confirm the hypothesis that pairing of like residues is preferred, Thr with Thr, and Val with Val. Calculation of free energies based on these K_{Het} values reveals that a Thr–Thr pair and a Val–Val pair collectively are 0.6 kcal mol^{-1} more stable than two Thr–Val pairs, under the conditions of these experiments.

The [D_6]DMSO cosolvent is essential for sequence selectivity. When pure $CDCl_3$ is used for these studies, no

Table 1: Propensities of peptides **1b–e** to form heterodimers.

	1b&1c	**1d&1e**	**1b&1d**	**1b&1e**	**1c&1d**	**1c&1e**
$K_{Het}/4$	8.9	0.083	0.87	0.80	1.0	1.0

 © 2003 Wiley-VCH Verlag GmbH & Co. KGaA, Weinheim

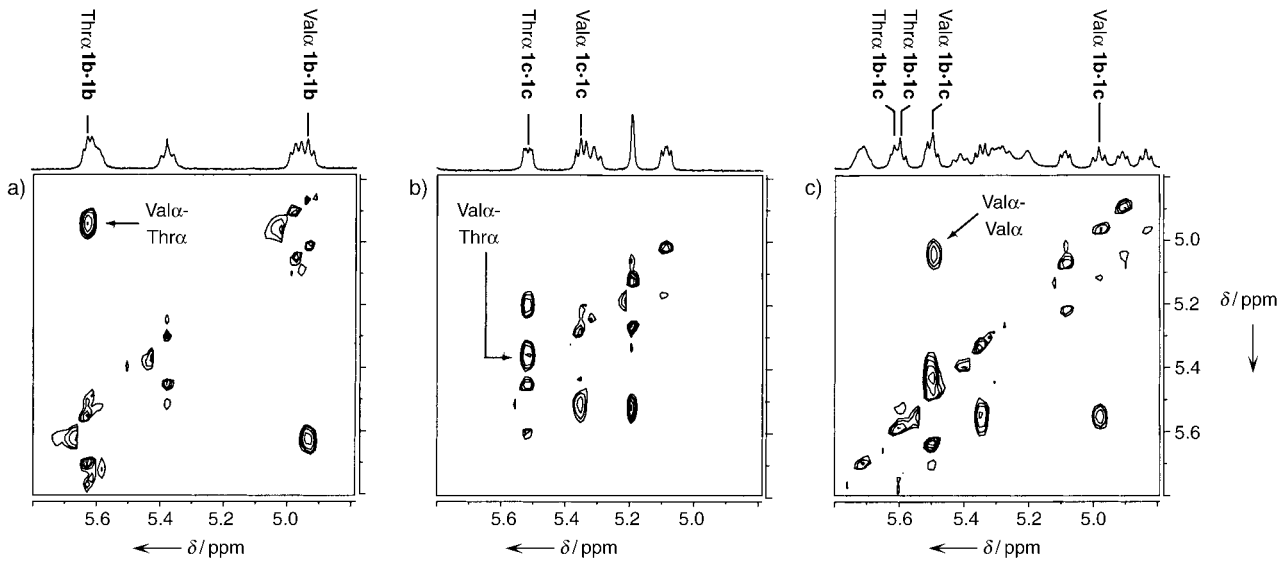


Figure 3. ^{1}H NMR Tr-ROESY spectra of the α-proton region of Thr–Val peptide **1b** (a), Val–Thr peptide **1c** (b), and a mixture of the two peptides (c), illustrating intermolecular NOEs associated with the respective homodimers and the heterodimer. Spectra were recorded at 500 MHz and 253 K with a 250 ms mixing time in 10% [D_6]DMSO in $CDCl_3$ at a) 2.0 mM **1b**, b) 2.0 mM **1c**, and c) 1.4 mM **1b** and 2.6 mM **1c**.

significant selectivity is observed. Selectivity emerges and increases as [D_6]DMSO is added. At 3.9% [D_6]DMSO, for example, $K_{Het}/4 = 2.7$ for Thr–Val (**1b**) and Val–Thr (**1c**) and 0.28 for Thr–Thr (**1d**) and Val–Val (**1e**).[7] The DMSO cosolvent may effect selectivity by promoting interaction between Val side chains (e.g., through solvophobic interactions), destabilizing interactions between Val and Thr side chains, or enhancing hydrogen-bonding interactions between the Thr side chains. In light of the known interactions between DMSO and water dimers, the latter explanation appears to be most likely.[8]

^{1}H NMR transverse-ROESY (Tr-ROESY)[9] studies (Figure 3) corroborate that the peptides form well-defined homo- and heterodimers. Strong NOEs between the Thr and Val α protons in the Tr-ROESY spectra of unmixed **1b** and **1c**, similar to those we reported previously for peptide **1a**,[4] help establish the formation of homodimers. A strong NOE between the two different Val α protons of the new species formed upon mixing **1b** and **1c** confirms the formation of the heterodimer.[10]

The experiments described above establish that sequence-selective molecular recognition of β sheets may be achieved through side chain interactions. The measurement of equilibrium constants by these experiments is appealing, because it provides the same information about side chain interaction energies as a double-mutant cycle experiment, but does so directly in a single measurement.[11,12] The peptide model system developed here is arguably simpler and better defined than other related model systems.[13,14] We envision modifying this system to generate peptides that recognize protein β sheets in a sequence-selective fashion.

Received: December 11, 2002 [Z50750]

Keywords: β sheets · molecular recognition · peptides · proteins · supramolecular chemistry

[1] S. Maitra, J. S. Nowick in *The Amide Linkage: Structural Significance in Chemistry, Biochemistry, and Materials Science* (Eds.: A. Greenberg, C. M. Breneman, J. F. Liebman), Wiley, New York, **2000**, pp. 495–518.

[2] C. Petosa, R. J. Collier, K. R. Klimpel, S. H. Leppla, R. C. Liddington, *Nature* **1997**, *385*, 833–838.

[3] For related observations in proteins associated with genetic diseases, see: a) P. Hammarström, F. Schneider, J. W. Kelly, *Science* **2001**, *293*, 2459–2462; b) E. G. Huizinga, S. Tsuji, R. A. P. Romijn, M. E. Schiphorst, P. G. de Groot, J. J. Sixma, P. Gros, *Science* **2002**, *297*, 1176–1179.

[4] J. S. Nowick, K. S. Lam, T. V. Khasanova, W. E. Kemnitzer, S. Maitra, H. T. Mee, R. Liu, *J. Am. Chem. Soc.* **2002**, *124*, 4972–4973.

[5] a) S. Lifson, C. Sander, *J. Mol. Biol.* **1980**, *139*, 627–639; b) M. A. Wouters, P. M. G. Curmi, *Proteins Struct. Funct. Genet.* **1995**, *22*, 119–131; c) E. G. Hutchinson, R. B. Sessions, J. M. Thornton, D. N. Woolfson, *Protein Sci.* **1998**, *7*, 2287–2300; d) Y. Mandel-Gutfreund, S. M. Zaremba, L. M. Gregoret, *J. Mol. Biol.* **2001**, *305*, 1145–1159.

[6] Studies were performed at 253 K. Although the resonance signals are resolved in the 500 MHz ^{1}H NMR spectrum at 298 K, they are sharper at lower temperatures. Measurement of the relative concentrations of the homo- and heterodimers at varying ratios of peptides verifies that K_{Het} is invariant and supports its use to gauge the preferences of amino acid pairings.

[7] Further addition of [D_6]DMSO beyond 10% results in additional increases in selectivity, however shimming of the NMR instrument becomes difficult at higher [D_6]DMSO concentrations. In pure [D_6]DMSO, dimers do not form.

[8] B. Kirchner, M. Reiher, *J. Am. Chem. Soc.* **2002**, *124*, 6206–6215, and references therein.

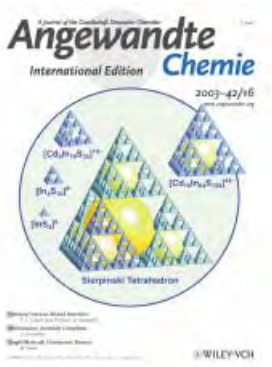
[9] a) T.-L. Hwang, A. J. Shaka, *J. Am. Chem. Soc.* **1992**, *114*, 3157–3159; b) T.-L. Hwang, A. J. Shaka, *J. Magn. Reson. Ser. B* **1993**, *102*, 155–165.

 © 2003 Wiley-VCH Verlag GmbH & Co. KGaA, Weinheim

[10] NOEs between the Thr α-protons of the heterodimer could not be observed because the resonance signals of these protons are nearly coincident.
[11] a) C. K. Smith, L. Regan, *Science* **1995**, *270*, 980 – 982; b) C. A. Blasie, J. M. Berg, *Biochemistry* **1997**, *36*, 6218 – 6222.
[12] A. Horovitz, *Folding Des.* **1996**, *1*, R121-R126.
[13] M. W. Peczuh, A. D. Hamilton, *Chem. Rev.* **2000**, *100*, 2479 – 2494.
[14] For some leading examples of related work involving peptide recognition, see: a) S. R. LaBrenz, J. W. Kelly, *J. Am. Chem. Soc.* **1995**, *117*, 1655 – 1656; b) Y. Cheng, T. Suenaga, W. C. Still, *J. Am. Chem. Soc.* **1996**, *118*, 1813 – 1814; c) X. Cha, K. Ariga, T. Kunitake, *J. Am. Chem. Soc.* **1996**, *118*, 9545 – 9551; d) R. Zutshi, J. Franciskovich, M. Shultz, B. Schweitzer, P. Bishop, M. Wilson, J. Chmielewski, *J. Am. Chem. Soc.* **1997**, *119*, 4841 – 4845; e) C. N. Kirsten, T. H. Schrader, *J. Am. Chem. Soc.* **1997**, *119*, 12061 – 12068; f) T. D. Clark, J. M. Buriak, K. Kobayashi, M. P. Isler, D. E. McRee, M. R. Ghadiri, *J. Am. Chem. Soc.* **1998**, *120*, 8949 – 8962; g) M. A. Hossain, H.-J. Schneider, *J. Am. Chem. Soc.* **1998**, *120*, 11208 – 11209; h) B. Baumeister, S. Matile, *Chem. Eur. J.* **2000**, *6*, 1739 – 1749; i) Y. Takahashi, A. Ueno, H. Mihara, *ChemBioChem* **2001**, *2*, 75 – 79; j) G. Xu, W. Wang, J. T. Groves, M. H. Hecht, *Proc. Natl. Acad. Sci. USA* **2001**, *98*, 3652 – 3657; k) A. Cox, M. M. Arroyo, K. H. Mayo, *Biochem. J.* **2001**, *357*, 739 – 747; l) Y. Hamuro, A. D. Hamilton, *Bioorg. Med. Chem.* **2001**, *9*, 2355 – 2363; m) H. Wennemers, M. Conza, M. Nold, P. Krattiger, *Chem. Eur. J.* **2001**, *7*, 3342 – 3347; n) S. T. Phillips, M. Rezac, U. Abel, M. Kossenjans, P. A. Bartlett, *J. Am. Chem. Soc.* **2002**, *124*, 58 – 66; o) H. Zeng, X. Yang, R. A. Flowers, B. Gong, *J. Am. Chem. Soc.* **2002**, *124*, 2903 – 2910; p) K. B. Jensen, T. M. Braxmeier, M. Demarcus, J. G. Frey, J. D. Kilburn, *Chem. Eur. J.* **2002**, *8*, 1300 – 1309.

 © 2003 Wiley-VCH Verlag GmbH & Co. KGaA, Weinheim

Cover Picture



Hailian Li, Jaheon Kim, Michael O'Keeffe, and Omar M. Yaghi*

It begins with a single InS_4 tetrahedron (blue), then, in the hierarchical structure of the $[Cd_{16}In_{64}S_{134}]^{44-}$ ion, comes a supertetrahedron of these tetrahedra, a supertetrahedron of supertetrahedra (a super-supertetrahedron, extra Cd atoms in white), and finally a supertetrahedron of super-supertetrahedra. The yellow sphere marks a huge cavity and the Sierpinski tetrahedron the next level of the hierarchy. For more details see the Communication by O. M. Yaghi et al. on page 1819 ff.

Contents

News

Catalysis: P. Schultz and R. Lerner recognized ——— 1786

Books

Surfactants and Polymers in Drug Delivery ——— 1787 — Martin Malmsten — *reviewed by W. von Rybinski*

Spin Dynamics ——— 1787 — Malcolm H. Levitt — *reviewed by S. Berger*

The Amide Linkage ——— 1788 — Arthur Greenberg, Curt M. Breneman, Joel F. Liebman — *reviewed by J. Clayden*

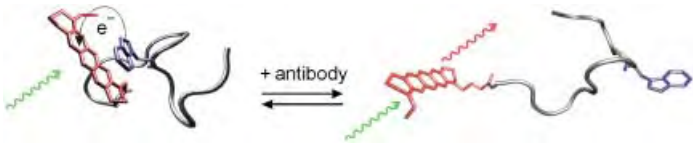
From Classical to Modern Chemistry ——— 1789 — Peter J. T. Morris — *reviewed by G. W. H. Potter*

Highlights

Single-Molecule Sensors

M. Sauer* ——— 1790 – 1793

Single-Molecule-Sensitive Fluorescent Sensors Based on Photoinduced Intramolecular Charge Transfer



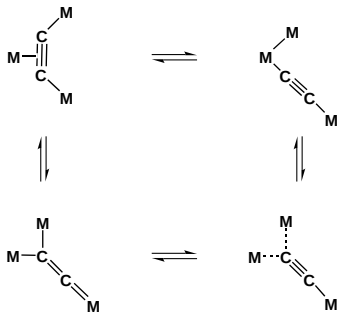
Triggered by ions and antibodies: Fluorescent sensors based on intramolecular photoinduced electron transfer (PET) enable the monitoring of individual recognition and binding events at the single-molecule level with high optical and temporal resolution. The fluorophore can be directly involved in the binding process or act as reporter sensitive to binding-induced conformational changes, for example, conformational changes within a peptide induced by antibody binding (see scheme).

Multinuclear Acetylide Complexes

U. Rosenthal* ——— 1794 – 1798

To "Dress" the "Naked" Acetylide with Metal Complexes: How and Why?

The high mobility of the C_2^{2-} ligand in trinuclear complexes of the type $[M]_3C_2$ (shown schematically) and alkynyl-bridged $[M]_2C_2R$ complexes provides information for attaining a better understanding of the topomerization processes of alkyne complexes and alkynes via vinylidene complexes $[M]{=}C{=}CR_2$ and vinylidenes $:C{=}CR_2$, respectively, in which the carbon atoms exchange their positions.



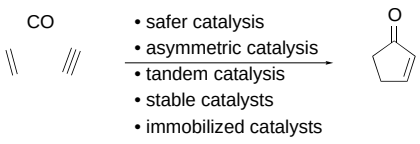
Reviews

Catalytic Pauson-Khand Reaction

S. E. Gibson (née Thomas),*
A. Stevenazzi* ——— 1800 – 1810

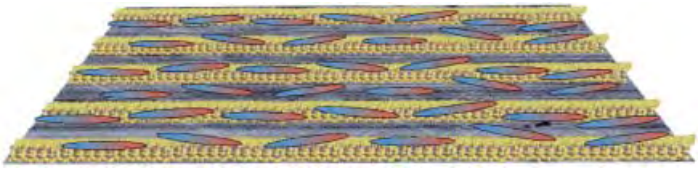
The Pauson–Khand Reaction: The Catalytic Age Is Here!

La catalisi è ormai una realtà! Recent exciting developments in the catalytic Pauson–Khand reaction (PKR) have resulted from its systematic optimization (see scheme). In a comprehensive and critical review of the catalytic PKR, the authors argue the need for even more economic and environmentally friendly processes. Thus, high priority should now be given to the catalytic PKR rather than to its stoichiometric version.



 © 2003 Wiley-VCH Verlag GmbH & Co. KGaA, Weinheim

Communications

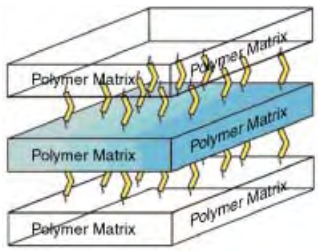


Groovy surfaces: The small increase in π-electronic character that results from the change from a phenyl- to a naphthalene-functionalized optical switch can have significant consequences. The latter creates a well-defined, grooved surface (see picture), which has been prepared by utilizing a method of noncontact alignment-layer construction. Such a process for liquid-crystal alignment, which is based on a hierarchical process, does not necessitate the use of a clean room.

Liquid-Crystal Alignment

J. Hoogboom, M. Behdani, J. A. A. W. Elemans, M. A. C. Devillers, R. de Gelder, A. E. Rowan, T. Rasing, R. J. M. Nolte* _____ **1812 – 1815**

Noncontact Liquid-Crystal Alignment by Supramolecular Amplification of Nanogrooves



Robust noncentrosymmetric polymer networks with a net polarization and bulk pyroelectric properties are achieved by aligning a polymerizable bent-core mesogen in the liquid-crystalline state and cross-linking under a static electric field (see schematic representation).

Polymerizable Bent-Core Mesogen

A. C. Sentman, D. L. Gin* _____ **1815 – 1819**

Polymerizable Bent-Core Mesogens: Switchable Precursors to Ordered, Polar Polymer Materials



The hole story? A super-supertetrahedral anionic cluster of 214 atoms and 80 tetrahedral units is prepared. The crystal structure has finite tetrahedral units of $[Cd_{16}In_{64}S_{134}]^{44-}$ ions composed of four T4 supertetrahedra (see picture). Each cluster is nearly a regular tetrahedron with edge lengths of 31.06 and 31.07 Å, and has large octahedral cavity (yellow sphere).

Super-Supertetrahedral Cluster VIP

H. Li, J. Kim, M. O'Keeffe, O. M. Yaghi* _____ **1819 – 1821**

$[Cd_{16}In_{64}S_{134}]^{44-}$: 31-Å Tetrahedron with a Large Cavity

For the USA and Canada:
ANGEWANDTE CHEMIE International Edition (ISSN 1433-7851) is published weekly by Wiley-VCH PO Box 191161, D 69451 Weinheim, Germany. Air freight and mailing in the USA by Publications Expediting Inc. 200 Meacham Ave., Elmont, NY 11003. Periodicals postage paid at Jamaica NY 11431. US POSTMASTER: send address changes to *Angewandte Chemie*, Wiley-VCH, 111 River Street, Hoboken, NJ 07030. Annual institutional subscription price for institutions: Europe € 2998.00/3148.00. Outside Europe US$ 3718.00/3904.00 (valid for print or electronic/print and electronic delivery); for individuals who are personal members of a national chemical society, or whose institution already subscribes, or who are retired or self-employed consultants, print only (including postage and handling charges): Europe € 248.00/Outside Europe US$ 348.00.

 © 2003 Wiley-VCH Verlag GmbH & Co. KGaA, Weinheim

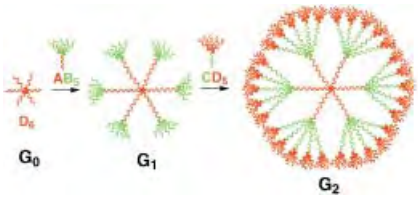
Contents

Divergent Dendrimer Synthesis

V. Maraval, A.-M. Caminade,* J.-P. Majoral,* J.-C. Blais — **1822 – 1826**

Dendrimer Design: How to Circumvent the Dilemma of a Reduction of Steps or an Increase of Function Multiplicity?

Bridging the generation gap: Building up molecules of considerable molecular weight in a step-by-step manner from small units generally consumes energy and produces a lot of waste. This is not the case here since only three steps are necessary to built a dendrimer of generation 3 (M_w around 265 000), bearing 750 phosphanyl end groups, with the production of environmentally friendly byproducts: water and dinitrogen. The

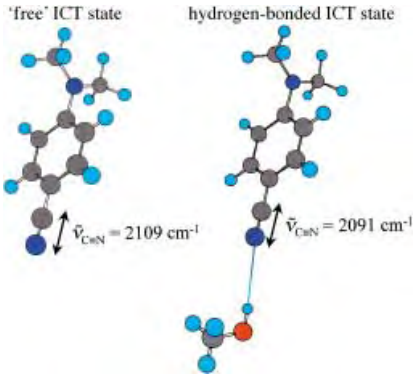


scheme shows the two-step formation of a generation 2 (G_2) dendrimer from components AB_5 and CD_5.

Time-Resolved IR Spectroscopy

W.-M. Kwok, M. W. George, D. C. Grills, C. Ma,* P. Matousek, A. W. Parker, D. Phillips, W. T. Toner, M. Towrie — **1826 – 1830**

Direct Observation of a Hydrogen-Bonded Charge-Transfer State of 4-Dimethylaminobenzonitrile in Methanol by Time-Resolved IR Spectroscopy

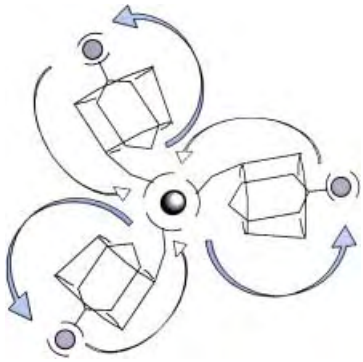


Anomalies in the fluorescence spectra of dual fluorescence molecules explained? A comparison of the time-resolved IR absorption of the C≡N band of photoexcited 4-dimethylaminobenzonitrile in MeCN and MeOH provides the first direct observation of the formation of a hydrogen-bonded intramolecular charge-transfer (ICT) state in MeOH and its coexistence with a "free" ICT state (see picture). The so-called dual fluorescence will be triple, not dual.

Two-Way Energy Transfer

J. M. Haider, R. M. Williams, L. De Cola,* Z. Pikramenou* — **1830 – 1833**

Vectorial Control of Energy-Transfer Processes in Metallocyclodextrin Heterometallic Assemblies

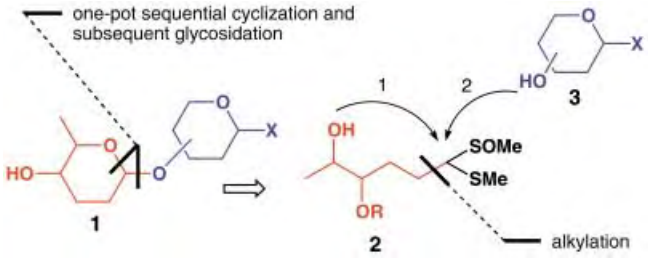


Shedding light on water wheels: Photoinduced energy transfer is demonstrated between metal centers by a Ru^{II}) cyclodextrin "wheel" assembled in water. Os- and Ir-complex guests with hydrophobic tails can be bound noncovalently in the cyclodextrin cavities. In such systems two-way communication is possible as energy transfer can occur from the Ru core to the outer metal centers (purple arrows) or from the outer metal units to the Ru core (white arrow).

Deoxyglycoside Synthesis

T. Amaya, D. Takahashi, H. Tanaka, T. Takahashi* — **1833 – 1836**

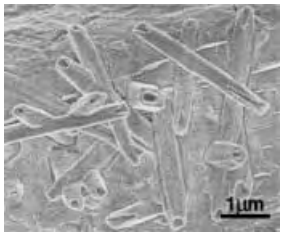
Synthesis of 2,3,6-Trideoxysugar-Containing Disaccharides by Cyclization and Glycosidation through the Sequential Activation of Sulfoxide and Methylsulfanyl Groups in a One-Pot Procedure



A one-pot procedure for the synthesis of 2,3,6-trideoxyglycosides 1 has been developed, based on the sequential activation of a sulfoxide group and a methylsulfanyl group in **2**, cyclization, and subsequent glycosidation with a glycosyl acceptor **3**.

© 2003 Wiley-VCH Verlag GmbH & Co. KGaA, Weinheim

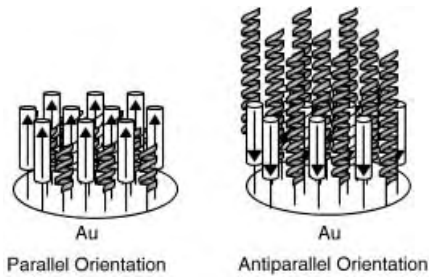
IR irradiation of a boron thin film coated on a Si(001) wafer in the presence of Mg vapor in an Ar/O_2 atmosphere results in the formation of magnesium borate nanotubes (see picture). The structural characterizations demonstrated that the nanotubes are single crystalline orthorhombic $Mg_3B_2O_6$ ($3\,MgO{\cdot}B_2O_3$). The formation mechanism of this particular tubular morphology is discussed.



Magnesium Borate Nanotubes

R. Ma,* Y. Bando, D. Golberg, T. Sato ——— **1836 – 1838**

Nanotubes of Magnesium Borate



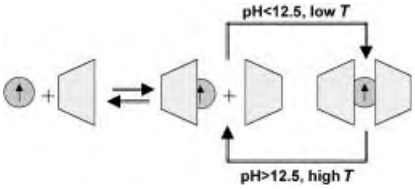
The right moment for polymerization: Preformed helical rods on gold surfaces are shown to control N-carboxyanhydride polymerization through the helix-macrodipole interaction (see picture; polymer length depends on the direction of the dipole), and have allowed the successful preparation of densely, perpendicularly bound helical brushes on gold surfaces.

Graft Polymerization on Gold

M. Niwa,* Y. Kuwagaki, S. Yamaguchi, N. Higashi* ——— **1839 – 1841**

Effect of the Helix Macrodipole on Surface-Initiated N-Carboxyanhydride Polymerization on Gold

---



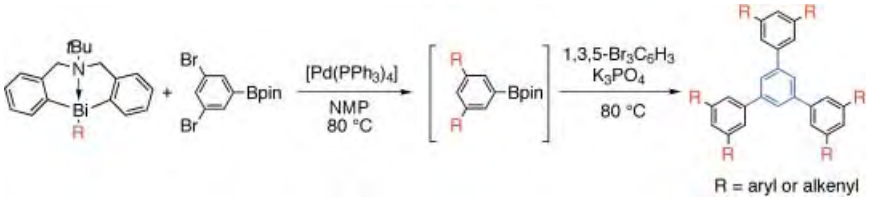
Three's company: The construction of a three-component organic free radical has been obtained with symmetric nitroxides and β-cyclodextrin. Its formation can be reversibly controlled by changing pH or temperature (see scheme).

pH-Dependent Inclusion Complexes

P. Franchi, M. Lucarini,* G. F. Pedulli ——— **1842 – 1845**

Detection of Paramagnetic pH-Dependent Inclusion Complexes between β-Cyclodextrin Dimers and Nitroxide Radicals

---



Hypervalent organobismuth compounds efficiently couple with aryl bromides in the presence of $[Pd(PPh_3)_4]$ catalyst. Application of this protocol to a one-pot multicoupling reaction with bromophenylboronic esters leads to the formation of up to nine bonds in good yields (see scheme).

Bi Reagents for C-C Cross-Coupling

S. Shimada,* O. Yamazaki, T. Tanaka, M. L. N. Rao, Y. Suzuki, M. Tanaka* ——— **1845 – 1848**

5,6,7,12-Tetrahydrodibenz[*c*,*f*][1,5]azabismocines: Highly Reactive and Recoverable Organobismuth Reagents for Cross-Coupling Reactions with Aryl Bromides

 © 2003 Wiley-VCH Verlag GmbH & Co. KGaA, Weinheim

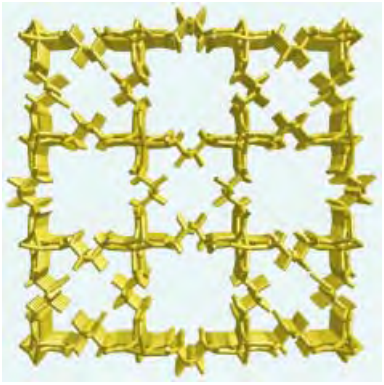
Contents

A Zinc-Saccharate 3D Network

B. F. Abrahams, M. Moylan, S. D. Orchard, R. Robson* _____ **1848 – 1851**

Zinc Saccharate: A Robust, 3D Coordination Network with Two Types of Isolated, Parallel Channels, One Hydrophilic and the Other Hydrophobic

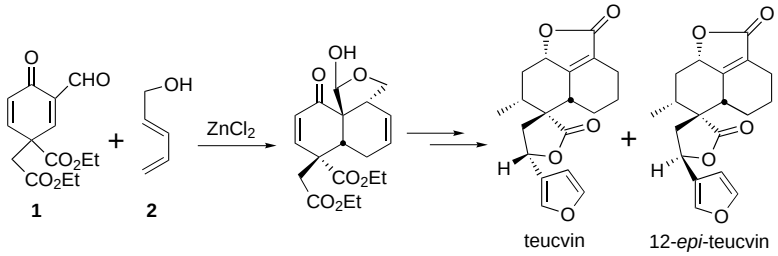
A chessboard pattern: Saccharic acid, which could become a cheap chiral feedstock for possible "green" heterogeneous catalysts and sieves of the future, gives a robust crystalline zinc derivative, which is unusual in having within the same crystal structure two types of channels with very different characteristics: one hydrophilic, the other hydrophobic. These channels are isolated from each other by seemingly impenetrable walls, which produces, in projection, the pattern shown.



19-Norclerodane Diterpenoids

H.-J. Liu,* J.-L. Zhu, I.-C. Chen, R. Jankowska, Y. Han, K.-S. Shia _____ **1851 – 1853**

The Total Synthesis of Racemic Teucvin and 12-*epi*-Teucvin

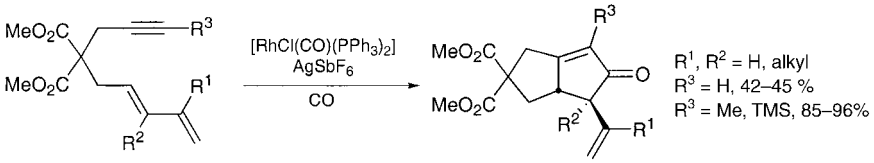


Complete face-, stereo-, and regioselectivity in the Diels–Alder reaction of compounds **1** and **2** was the key to the first total synthesis, in racemic form, of the 19-norclerodane diterpenoids teucvin and 12-*epi*-teucvin.

Pauson–Khand Reaction of Dienynes

P. A. Wender,* N. M. Deschamps, G. G. Gamber _____ **1853 – 1857**

The Dienyl Pauson–Khand Reaction



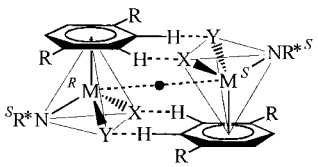
The diene plays a key role in the Pauson–Khand [2+2+1] reaction of tethered dienynes (see scheme). These reactions are accelerated by the diene (relative to an alkene) and proceed in good to excellent yields, often at room temperature, in the presence of carbon monoxide, $[RhCl(CO)(PPh_3)_2]$, and $AgSbF_6$.

Diastereomers in Single Crystals

H. Brunner,* M. Weber, M. Zabel, T. Zwack _____ **1859 – 1862**

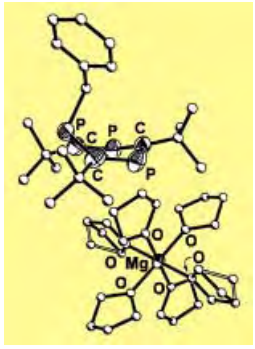
Inverted Piano Stools: A Molecular Recognition Motif That Enforces 1:1 Cocrystallization of Two Diastereomers in the Same Single Crystal

Half-sandwich complexes of the type [(Ar)MXY(NR*)] (see structure; X, Y = electronegative substituents; M = Ru, Os, Rh, Ir) tend to form inversion pairs in the solid state, which are characterized by short M···M separations and C–H···X/Y hydrogen bonds between the pairs of molecules. As a consequence, two diastereomers with a given chirality in the Z substituent, usually an NR* substituent, and different metal configurations



approach each other with their "racemic sides" resulting in an unusually preferred 1:1 diastereomer cocrystallization in the same single crystal.

 © 2003 Wiley-VCH Verlag GmbH & Co. KGaA, Weinheim

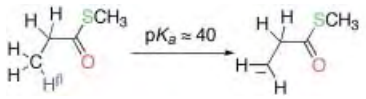


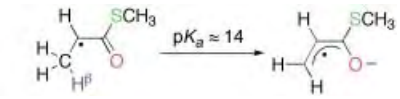
Salts of diorganomagnesium compounds are obtained by 1,4-addition of Grignard reagents to 1,3,5-triphosphabenzene (see picture; for clarity, only one of the two ligands are shown). Upon hydrolysis, these salts furnish 1,4-triphosphacyclohexadienes or a dihydrotriphospha Dewar benzene derivative, depending on the size of the substituent.

Diorganomagnesium Compounds

J. Renner, U. Bergsträßer, P. Binger,* M. Regitz* ——— **1863 – 1866**

1,4-Addition of Grignard Reagents to 2,4,6-Tri-*tert*-butyl-1,3,5-triphosphabenzene





The enhanced acidity at the β position of enoxy radicals may allow enzymes to abstract an aliphatic proton from an unactivated thioester. Although this phenomenon was proposed half a century ago, validation has now been found by combining high-level ab initio calculations with both implicit and explicit representations of aqueous solvation, and a pK_a value of 14 for the β-H atom of a model enoxy radical was predicted. Relative to the unactivated β-H atom of the closed-shell thioester, this corresponds to an acidity enhancement of over 25 orders of magnitude (see scheme).

Mechanisms of Enzyme Catalysis

D. M. Smith, W. Buckel, H. Zipse* ——— **1867 – 1870**

Deprotonation of Enoxy Radicals: Theoretical Validation of a 50-Year-Old Mechanistic Proposal

Communications labeled with this symbol have been judged by two referees as being "very important papers".

The publication of Communications labeled with this symbol has been accelerated because of their topical or highly competitive nature.

DOI: The fastest way to find an article online is the *Digital Object Identifier* (DOI). DOIs will be printed in the footer of the first page of every article. For example, an article with a DOI of 10.1002/anie.200390049 can be found on the WWW at http://dx.doi.org/10.1002/anie.200390049. Please use the DOI of your article to link from your home page to the articles in Wiley InterScience. The DOI is a result of a cross-publisher initiative to create a system for the permanent identification of documents on digital networks. More information is available from www.doi.org.

Service

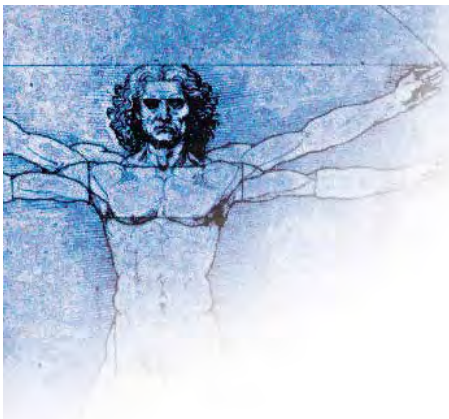
Keywords ——— **1872**

Authors ——— **1873**

Vacancies ——— **1785**

Preview ——— **1875**

 © 2003 Wiley-VCH Verlag GmbH & Co. KGaA, Weinheim



Peter Schultz and Richard Lerner Receive Paul Ehrlich Prize

Paul Ehrlich (1854–1915) was a pioneer of chemotherapy. His work on the staining of tissue, immunization, and the combating of pathogens through the use of substances that bind to them specifically formed the foundation of modern medicine. He was awarded the Nobel Prize in 1908, together with Ilya Mechnikov, "in recognition of their work on immunity." We now know how right he was when he proclaimed in his acceptance speech the end of the era of the microscope and beginning of that of cell chemistry. The companies Hoechst and Cassella established a fund to help support Ehrlich's research. This fund was converted into the Paul Ehrlich Foundation by his wife Hedwig Ehrlich after his death. Today, it is financed equally through the German Ministry of Health and donations from companies. It has its headquarters at the University of Frankfurt am Main. Every year on March 14, Ehrlich's birthday, the Paul Ehrlich and Ludwig Darmstaedter Prize is given for outstanding achievements in biomedical research. Darmstaedter (1846–1927) was a scientist and a friend of Ehrlich's. The Foundation's Scientific Council has 14 members from five countries, including the Nobel Prize winners Manfred Eigen and Hartmut Michel. There are 13 Nobel Laureates among the recipients of the Paul Ehrlich and Ludwig Darmstaedter Prize.



Peter Schultz



Richard Lerner

This year, the chemist Peter G. Schultz and the chemist and medical researcher Richard A. Lerner (both at The Scripps Research Institute, La Jolla, CA) received the Prize worth 60000 € in the presence of the President of the Federal Republic of Germany in St. Paul's Church in Frankfurt. The laudation was delivered by Manfred Eigen, who had himself received the prize in 1992.

Schultz and Lerner are recognized for their independent discoveries of catalytic antibodies, which were first published in the same issue of *Science* in 1986.[1,2] Schultz was an assistant professor in Berkeley at the time, having received his doctorate from the California Institute of Technology and undertaken a period of postdoctoral research at the Massachusetts Institute of Technology. He joined the Faculty at Scripps in 1999. Between 1995 and 2001, Schultz founded three biotechnology enterprises, which he still directs. Lerner read chemistry in Chicago and attended medical school in Stanford, where he also received his doctorate. In 1991, he became President of The Scripps Research Institute, where he has worked since 1969. Lerner is a member of the International Advisory Board of *Angewandte Chemie*; Schultz is member of the Editorial Board of *ChemBioChem*.

Antibodies are proteins used by the body to fight bacteria and viruses by specifically binding to them. Binding capacity and memory play a decisive role in this process. These findings have been gathered over a period of 100 years with significant early contributions by Paul Ehrlich. Schultz's and Lerner's idea was based on the concept that antibodies, which are able to bind in a highly specific way to any number of target compounds, have something essential in common with enzymes. Enzymes force a specifically bound substrate to adopt a transition state, thereby initiating product formation. Schultz and Lerner independently found substances that sufficiently resembled the structure of transition states of enzymatic reactions. Such substances can be used to induce the production of antibodies in animals, such as rabbits, and these antibodies can be studied subsequently in vitro. Catalysts with properties and efficiencies similar to those of enzymes are thus obtained, which can even catalyze reactions that do not occur in nature. These findings reopened the discussion on enzyme evolution: Evidently, the evolution of chemical mechanisms does not require millions of years, as antibodies are generated within days.

Schultz's research has allowed us to gain a deeper insight into this process. At an initial stage, antibodies with moderate specificity are formed, which recognize a large spectrum of substances. Ripening and mutation help to narrow this spectrum down to the specific substance used for immunization and the binding stability is increased by a factor of 1000 within just a few days. Lerner demonstrated that all naturally occurring antibodies exhibit two catalytic centers close to one another in a conserved region, which can bind oxygen and produce ozone as an intermediate. This result shows that catalytic antibody reactions are also found in nature. Antibodies can take part in the decomposition of antigens and actually create holes in cell walls, which may have been the initial step in the evolution of the immune system. Paul Wentworth and Albert Eschenmoser contributed significantly to these findings. More on "The Chemistry of the Antibody Molecule" can be found in a Minireview by the two Prize winners in Issue 23/2002.[3]

[1] A. Tramontano, K. D. Janda, R. A. Lerner, *Science* **1986**, *234*, 1566.

[2] S. J. Pollack, J. W. Jacobs, P. G. Schultz, *Science* **1986**, *234*, 1570.

[3] P. G. Schultz, J. Y. Lin, R. A. Lerner, *Angew. Chem.* **2002**, *114*, 4607; *Angew. Chem. Int. Ed.* **2002**, *41*, 4427.

 © 2003 Wiley-VCH Verlag GmbH & Co. KGaA, Weinheim

Single-Molecule Sensors

Single-Molecule-Sensitive Fluorescent Sensors Based on Photoinduced Intramolecular Charge Transfer

*Markus Sauer**

Keywords:
electron transfer · fluorescence probes · fluorescence spectroscopy · sensors · time-resolved spectroscopy

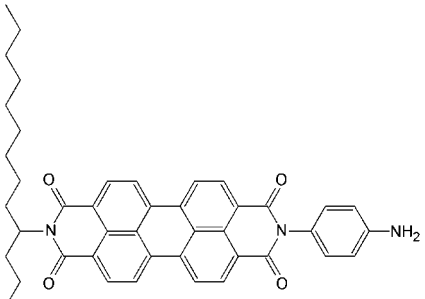
The development and investigation of molecular systems and methods that enable the monitoring of specific recognition and binding events is crucial for a better understanding of molecular signaling and information transfer in biological systems.[1] In the ideal case, the molecular system should signal selective recognition or binding events by a change in a characteristic property, for example, fluorescence or luminescence intensity, that can be conveniently transmitted into an electronic signal by the appropriate detector. Besides signaling, sensors have potential for information processing if measurable characteristic properties can be switched between two distinguishable states by environmental stimuli.

In general, photoinduced electron transfer (PET) or electronic energy transfer (EET) reactions can be used to transfer discrete and stoichiometric recognition events into an altered fluorescence signal of a fluorophore. Molecular systems in which the excited state of a fluorophore is controlled by the redox properties of a receptor module, covalently attached to the fluorophore, form an important class of chemosensory materials.[1]

To date, chemosensor have been used in homogeneous solution to detect target molecules present in micromolar to nanomolar concentration.[1–3] Optical probing of individual binding events represents the ultimate degree of sensitivity for sensing and imaging.

Recent advances in optical spectroscopy and microscopy have made it possible not only to detect and identify freely diffusing or immobilized molecules, but to make spectroscopic measurements and monitor dynamic processes of single molecules as well. Although very young, single-molecule spectroscopy (SMS) has evolved as an important tool to study the behavior of single molecules under ambient temperature.[4,5] However, there have been only a few SMS studies of potential chemo- or biosensors, that is, fluorophores that respond to binding events through changes in their spectroscopic properties. This is mainly because most fluorophores used in sensors to date, for example, anthracene or coumarin derivatives, have to be excited in the UV range and have a low photostability.[6] Besides the absorption cross section, the fluorescence, and triplet quantum yield, the photostability of fluorophores used for SMS is of fundamental importance because of the irreversible loss of fluorescence. To detect single molecules, relatively high excitation intensities must be applied. Usually, this results in the excitation of chromophores to not only the first electronic excited singlet and triplet states, S_1 and T_1, but also to higher electronic states, S_N and T_N, by absorption of a second photon. Unfortunately, the population of higher electronic states opens additional bleaching channels, such as the formation of dye radical ions and solvated electrons.[6] This so-called two-step photolysis is of particular importance at higher excitation intensities in the UV region. Optimally, new fluorescence sensors should be excitable in the visible range and exhibit a fluorescence quantum yield and photostability sufficient enough to ensure their detection at the single-molecule level.

Recently, Adams and co-workers investigated a new class of extremely sensitive fluorescent single-molecule sensors to probe local structure, reversible chemical reactions, and interfacial processes, such as electron transfer.[7] The perylene 3,4,9,10-tetracarboxyl bisimide (**1**) used in their SMS study can be excited in the green wavelength range using, for example, an argon ion laser at 488 nm. In addition, it exhibits a high photostability and fluorescence quantum yield (> 99 %). To make a chemical sensor, they attached a *p*-aminophenyl group conjugated to the perylene bisimide that efficiently quenches the fluorescence of the fluorophore in the unbound state by intramolecular PET. Benzylic amino moieties covalently linked to a fluorophore have been used widely to detect the presence of metal ions or protons.[1] Here, the high-energy



1

[*] Priv.-Doz. Dr. M. Sauer
Physikalisch-Chemisches Institut
Universität Heidelberg
Im Neuenheimer Feld 253
69120 Heidelberg (Germany)
Fax: (+49) 6221-544-255
E-mail: sauer@urz.uni-heidelberg.de

 © 2003 Wiley-VCH Verlag GmbH & Co. KGaA, Weinheim DOI: 10.1002/anie.200201611

nonbonding electron pair of the nitrogen atom efficiently quenches the excited state of the fluorophore by PET (Figure 1). Thermally induced back electron transfer of the from the LUMO of the fluorophore follows as a self-repair mechanism to regenerate the potentially damaged PET sensor. Protonation of the nonbonding electron pair of the amino group or titration with solutions of $ZnCl_2$ in THF, $[Pt(SEt_2)_2Cl_2]$ in $CHCl_3$, TiO_2 nanoparticles in THF, or aldehydes in $CHCl_3$ lower the energy of the electron pair. Thus, PET is thermodynamically no longer possible and fluorescence is restored.

To investigate whether this sensor system can be used to locally probe nanoscale surface structure, the perylene bisimide derivative NDAPP (*N*-(1-nonyldecyl)-*N*′-(*p*-aminophenyl)perylene-3,4,9,10-tetracarboxyl bisimide) was spin-coated onto glass and quartz cover slips. Scanning confocal fluorescence images show bright fluorescent spots of single NDAPP molecules only on glass (Figure 2a). This result demonstrates that the free amine of NDAPP binds to metal and metal-oxide impurities, such as TiO_2, ZnO, or Al_2O_3 centers, in the glass. No significant fluorescence is observed from NDAPP molecules dispersed on freshly cleaned quartz since there are no such binding sites available (Figure 2b). Molecules of NDAPP dispersed in a thin film of polyvinyl butylaldehyde (PVB) also fluoresce brightly as a result of reactions of the amine with the butylaldehyde on the polymer backbone. Exposure of the NDAPP molecules on quartz to dioxane/HCl vapor causes fluorescence as a result of protonation of the amine group (Figure 2c). Moreover, exposure of the NDAPP molecules on the quartz slide to air for several days also generates bright fluorescence spots (Figure 2d). Since the slides are prepared by acid cleaning prior to spin-casting, fluorescence spots seem to arise from molecular diffusion of the amine to protonated sites on the surface.

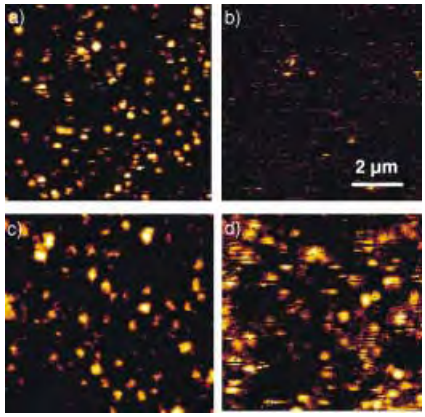


Figure 2. Single-molecule fluorescence scanning confocal images of NDAPP on glass and quartz cover slides. Imaging was performed under argon using an excitation wavelength of 488 nm (~50 Wcm^{-2}), and an integration time of 20 ms/bin. a) NDAPP on glass (0–316 counts/20 ms), b) NDAPP on quartz (0–104 counts/20 ms), c) NDAPP on quartz after exposure to dioxane/HCl vapor (0–203 counts/20 ms), d) NDAPP on quartz after 4–5 days in air (0–114 counts/20 ms). Reproduced with permission from Ref. [7], Copyright 2002 American Chemical Society.

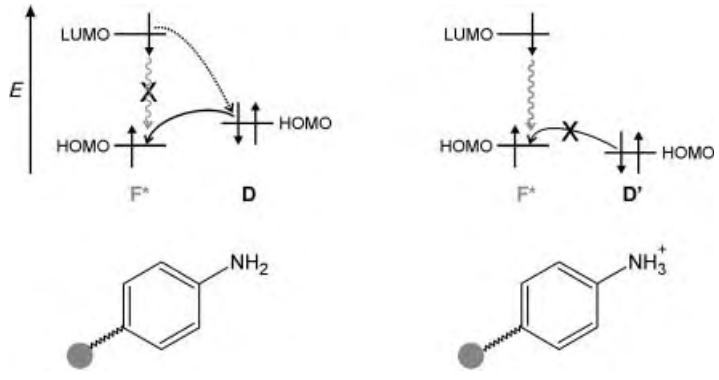


Figure 1. Simplified frontier-orbital energy diagrams illustrating the thermodynamics of intramolecular PET for a fluorophore that is quenched by a benzylic amino moiety covalently attached to the fluorophore. Upon excitation, fluorescence is quenched efficiently by a PET reaction from the electron donor to the first excited singlet state of the fluorophore. Thermally induced back electron transfer occurs to regenerate the ground state of the fluorophore. Protonation of the nitrogen group or reactions with metal atoms lower the energy of the HOMO and prevent PET and fluorescence of the fluorophore is restored.

To obtain detailed information about the binding processes, fluorescence time trajectories of single NDAPP molecules can be measured. That is, single NDAPP molecules are positioned in the laser focus and the fluorescence intensity is recorded continuously until irreversible photobleaching occurs (Figure 3). While single NDAPP molecules in a thin PVB film, or adsorbed on quartz slides following exposure to dioxane/HCl vapor show nearly constant fluorescence intensity with infrequent off-times which are caused by triplet-state formation (Figure 3a), molecules adsorbed on untreated glass surfaces show longer off-times of up to 100 s (Figure 3b, Figure 3c). As proposed for other fluorophores, these off-times can be attributed to nonfluorescent charge-separated states, that is, radical cations or anions generated by an electron transfer reaction with the metal center. The fluorescence that appears on quartz slides after several-days exposed to air shows frequent blinking between an off- and the on-state on the millisecond time scale (Figure 3e, Figure 3f), which indicates dynamic binding of the amine. This rather classical method of transducing a metal-binding event into a fluorescent signal relies on metal-binding-induced alterations of the redox potential of a receptor molecule covalently attached to a fluorophore. In contrast, the design presented recently by Walkup and Imperiali consists of a synthetic polypeptide template (zinc-finger domain) and a covalently attached fluorescent reporter that is sensitive to metal-induced conformational changes of the supporting polypeptide framework, yet remote from the metal-binding site.[8] These sensors rely on site-specific labeling with appropriate fluorophores and conformationally induced alterations in EET efficiency upon binding.

Although fluorescence resonance energy transfer (FRET) has been successfully transposed to the single-molecule level to study, for example, conformational fluctuations of individual biomolecules,[5] few potential biosensors based on EET have been investigated.

 © 2003 Wiley-VCH Verlag GmbH & Co. KGaA, Weinheim

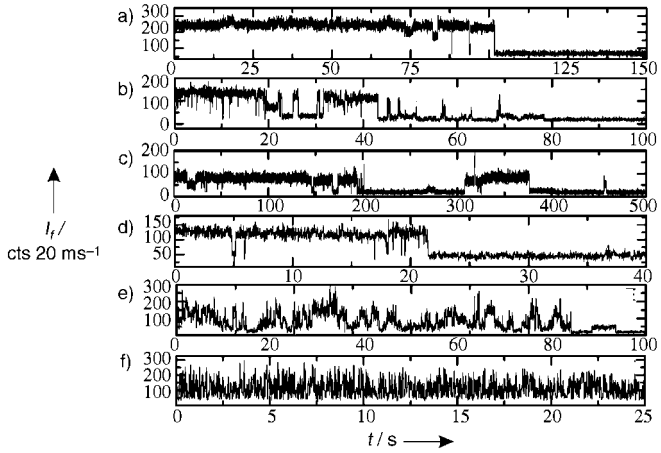


Figure 3. Fluorescence trajectories of single NDAPP molecules (fluorescence intensity, I_f, in photon counts, 20 ms^{-1} versus time, t, in seconds). a) In a PVB film, b) and c) on glass, d) on quartz following exposure to dioxane/HCl vapor, e) and f) on quartz after 4–5 days in air. Reproduced with permission from Ref. [7], Copyright 2002 American Chemical Society.

On the other hand, new PET biosensors have been developed that use conformationally induced alterations in PET efficiency upon binding for the specific detection of DNA or RNA sequences and antibodies at the single-molecule level.[9,10] These biosensors take advantage of specific properties of naturally occurring DNA nucleotides and amino acids. In particular, the low oxidation potential of the DNA base guanosine and the amino acid tryptophan, and the tendency of many fluorophores to aggregate in aqueous environment is used. In contrast to EET-based systems where long-range dipole–dipole interactions occur, these PET biosensors require contact formation (van der Waals contact) between the fluorophore and the guanosine or tryptophan residue for efficient PET. Depending on the reduction potential of the fluorophore used, efficient fluorescence quenching by PET occurs (Figure 4).

With careful design of these conformationally flexible sensors and the use of appropriate fluorophores (rhodamine and oxazine dyes are well suited) efficient single-molecule sensitive PET sensors can be produced. If quenching interactions between the fluorophore and the guanosine or tryptophan residue deteriorate upon specific binding to the target, for example, because of binding of a complementary DNA sequence or antibody, or through cleavage by an endonuclease or protease enzyme, fluorescence of the sensor is restored. In addition to detecting the presence of a target, the contact-induced quenching process can also be used to monitor the rate of intramolecular-contact forma-

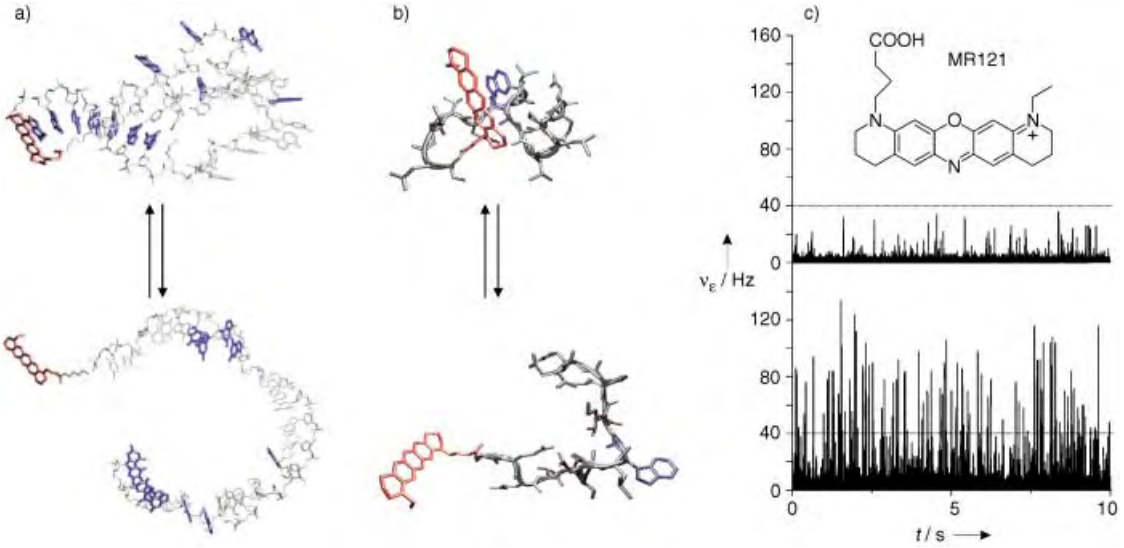


Figure 4. Principle of operation of PET-based biosensors using the red-absorbing oxazine derivative MR121 ($\lambda_{abs} = 661$ nm, $\lambda_{em} = 673$ nm). a) DNA hairpins based on selective fluorescence quenching of MR121 (red) by the DNA base guanosine (blue). The fluorophore is attached at the 5′-end of the cytosine-containing stem and quenched through PET by the complementary guanosine residues. Upon hybridization of the loop to the complementary target sequence, the fluorophore and the guanosine residues are forced apart and fluorescence is restored.[9] b) Fluorescently labeled peptide epitopes derived from the immunodominant region of human p53 protein can be used as PET biosensors to detect single p53 autoantibodies. Driven by hydrophobic effects the peptide adopts a conformation where the dye MR121 (red) undergoes PET quenching interactions with the tryptophan residue (blue). Upon specific binding to an p53 autoantibody and subsequent conformational rearrangement the fluorescence intensity increases.[10] c) Single-molecule fluorescence signals (count rate, ν_c, in kHz versus time, t, in seconds) observed from a 5×10^{-11} M solution of a PET-based DNA hairpin sensor (using a 635 nm laser diode for excitation) in the absence (top) and presence (bottom) of an excess of complementary target sequence. In the absence of target sequence the fluorescence intensity of the oxazine derivative is efficiently quenched through PET by the guanosine residues in the complementary stem. Upon addition of a target sequence, the number of fluorescence bursts counted above a certain threshold level can be easily used to quantify the concentration of target molecules.[9]

 © 2003 Wiley-VCH Verlag GmbH & Co. KGaA, Weinheim

tion in peptides or the opening or closure dynamics of DNA hairpins at the single-molecule level. Therefore, they are ideally suited for single-molecule studies (Figure 4c) and offer an elegant alternative to conventional biosensors based on EET processes.[9,10]

This Highlight hopefully demonstrates that intramolecular PET chemo- and biosensors can be used as single-molecule sensitive probes to specifically detect individual binding events in solution as well as on surfaces or in polymers. Detailed information about the interactions of these sensors with their environment can be obtained from fluorescence time trajectories of single molecules. Further improvement of selectivity in combination with new single-molecule-sensitive detection methods, such as polarization or spectrally resolved fluorescence lifetime spectroscopy, will enable the detection of specific target molecules in the sub-picomolar range and allow one to follow their molecular binding dynamics with temporal resolutions comparable to those within reach with the new techniques of molecular dynamic simulations.

[1] A. P. de Silva, H. Q. N. Gunaratne, T. Gunnlaugsson, A. J. M. Huxley, C. P. McCoy, J. T. Rademacher, T. E. Rice, *Chem. Rev.* **1997**, *97*, 1515 – 1566.

[2] S. C. Burdette, G. K. Walkup, B. Spingler, R. Y. Tsien, S. J. Lippard, *J. Am. Chem. Soc.* **2001**, *123*, 7831 – 7841.

[3] R. E. Gawley, S. Pinet, C. M. Cardona, P. K. Datta, T. Ren, W. C. Guida, J. Nydick, R. M. Leblanc, *J. Am. Chem. Soc.* **2002**, *124*, 13448 – 13453.

[4] X. S. Xie, J. K. Trautman, *Annu. Rev. Phys. Chem.* **1998**, *49*, 441 – 480.

[5] S. Weiss, *Science* **1999**, *283*, 1676 – 1683.

[6] C. Eggeling, L. Brand, C. A. M. Seidel, *Bioimaging* **1997**, *5*, 105 – 115.

[7] L. Zang, R. Liu, M. W. Holman, K. T. Nguyen, D. M. Adams, *J. Am. Chem. Soc.* **2002**, *124*, 10640 – 10641.

[8] G. K. Walkup, B. Imperiali, *J. Am. Chem. Soc.* **1998**, *118*, 3053 – 3054.

[9] J. P. Knemeyer, N. Marmé, M. Sauer, *Anal. Chem.* **2000**, *72*, 3717 – 3724.

[10] H. Neuweiler, A. Schulz, A. C. Vaiana, J. C. Smith, S. Kaul, J. Wolfrum, M. Sauer, *Angew. Chem.* **2002**, *114*, 4964 – 4968; *Angew. Chem. Int. Ed.* **2002**, *41*, 4769 – 4773.

 © 2003 Wiley-VCH Verlag GmbH & Co. KGaA, Weinheim

Multinuclear Acetylide Complexes

To "Dress" the "Naked" Acetylide with Metal Complexes: How and Why?**

*Uwe Rosenthal**

Keywords:
alkyne ligands · alkynes · carbides · cluster compounds · coordination modes

> *"I see C_2 in the carbon arc and in the tail of Halley's Comet. I see it in acetylene, ethylene, and ethane. I see it in the lovely molecular complexes of P. Wolczanski, M. I. Bruce, G. Longoni and their co-workers...I see it in CaC_2 and in W. Jeitschko, A. Simon, and their co-worker's rare-earth carbides. It's staggering!"*
> Roald Hoffmann[1a]

Introduction

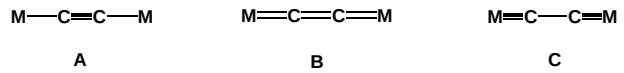
The simplest molecular unit of carbon, C_2, existing as a small part of the linear polyynes $[-(C{\equiv}C)_n-]$ (also named "carbynes" or "chaoite"), is extremely reactive and has only been characterized by spectroscopic methods. Its chemistry has been limited to its generation in a carbon arc and condensation of its vapor at low temperatures.[1c]

One method of stabilizing the C_2 unit is by end-capping through the derivatization of both ends under the formation of organic acetylenes RC_2R, acetylide complexes $[M]C_2R$, or acetylide bridges between two metal centers $[M]C_2[M]$ ([M] = any metal complex fragment). Three types of $[M]_2C_2$ complexes, **A**, **B**, and **C**, are known (Scheme 1), the formation of which depends on the metal complexes involved.[2]

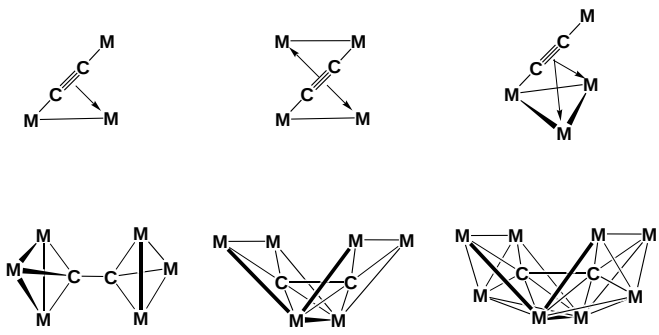
There are now many examples of $[M](C_2)_n[M]$ complexes, both of the smallest possible type ($n = 1$), and also the higher homologues with an even-numbered C_{2n} ($n = 1, 2, 3,\ldots$) "naked" carbon bridge between two metal centers, which have been obtained by Beck, Bruce, Gladysz, Lang, Lapinte, and many others, as described in many reviews.[2] The importance of such compounds for putative applications in materials synthesis, as well as for basic research, has been outlined in three Highlights in *Angewandte Chemie* by Bunz, Chisholm, and Lang.[3]

The interaction of $[M]_2C_2$ compounds with metal centers leading to the formation of polymetallic systems $[M]_m(\mu_n\text{-}C_2)$[4a] has been systematically summarized in the excellent review by Akita and Moro-oka.[4b] The $[M]_2C_2$ complexes react with up to six metal species to yield clusters in which the C_2 unit is complexed by up to eight metal centers (i.e., $m = 8$ in $[M]_m(\mu_n\text{-}C_2)$), and which formally contains permetalated ethyne, ethene, or ethane moieties as subunits (Scheme 2).[2–4]

Our interest in this chemistry originates from the investigations into the complexes of the 1,3-butadiynes $RC{\equiv}C{-}C{\equiv}CR$, as the organic analogues of the organometallic complexes $[M]{\equiv}C{-}C{\equiv}[M]$ (**C**).[5] A very recent paper by Koutsantonis and co-workers[6] on trimetallic complexes $[\{Ru(CO)_2(\eta\text{-}C_5H_4R)\}_3(\mu\text{-}C{\equiv}C)][BF_4]$ (**1**, R = H or Me) of the type $[Ru]_3C_2$, prompted us to consider here the complexation of $[M]_2C_2$ with a further metal fragment



Scheme 1. Bonding modes in $[M_2]C_2$ complexes.



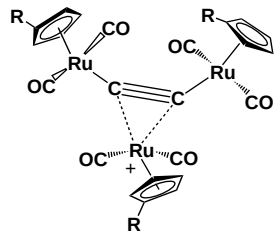
Scheme 2. Coordination of the acetylide unit in complexes of the type $[M]_m(\mu_n\text{-}C_2)$.

[*] Prof. Dr. U. Rosenthal
Leibniz-Institut für Organische Katalyse
Universität Rostock e.V.
Buchbinderstrasse 5–6, 18055 Rostock
(Germany)
Fax: (+49) 381-46693-76
E-mail: uwe.rosenthal@ifok.uni-rostock.de

[**] To the best of our knowledge, the term "naked" was first used in chemistry by Professor Günther Wilke, former Director of the Max-Planck-Institut für Kohlenforschung in Mülheim an der Ruhr, for nickel complexes without "supporting ligands", otherwise known as "naked nickel". An American once called him "a man who brought sex into chemistry".[1b] Later, the unsaturated and noncoordinated carbon bridges between metals were also called "naked units".

 © 2003 Wiley-VCH Verlag GmbH & Co. KGaA, Weinheim DOI: 10.1002/anie.20021619

[M]. Based on this simple interaction, an enhanced understanding of the more complex polymetallic species, as well as compounds that contain even-numbered C_{2n} ($n = 1, 2, 3\ldots$) "naked" carbon bridges between two metal centers can be developed.

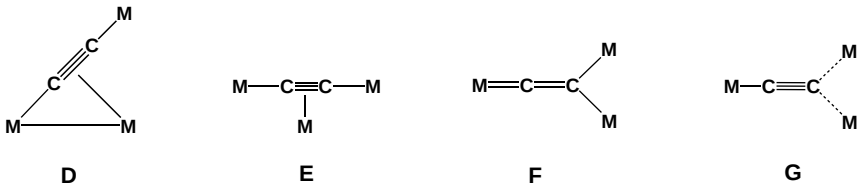


1a: R = H; **b:** R = Me

The C_2 ligand in **1** is surrounded by three ruthenium atoms; there are no metal–metal bonds. The relatively short bond of the acetylide ligand $\{C{\equiv}C\}^{2-}$ (1.222(9) Å) and the C-C-η^1-[M] angles (152.5(4) and 155.2(5)°) indicate only a small contribution of the metallacyclopropene structure to the canonical structure. The solid-state structure is not retained in solution, but according to NMR spectroscopic studies is found to be fluxional on the NMR timescale, with respect to the coordination of the acetylide ligands between the metal centers. These novel complexes were described by the authors as the first known example of an $[M]_nC_2$ complex ($n = 3$) with no metal–metal bonding.[6]

Complexes of the Type $[M]_3C_2$

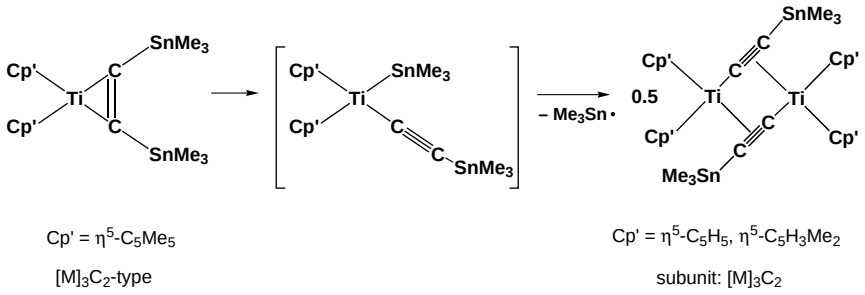
Complexes of the type $[M]_2C_2$ have been frequently reported,[2] but their complexation with another fragment [M] to give discrete $[M]_3C_2$ complexes is very rare. Cluster compounds with more than three metal centers often contain the $[M]_3C_2$ subunit. In principle, one can distinguish between four of the most important interactions (Scheme 3): A σ,π-bridging mode with a metal–metal interaction (**D**), an analogous mode without metal–metal bonding (**E**), and two modes (**F** and **G**) in which one metal center is coordinated to one carbon atom, and two other metal centers are coordinated to the second carbon atom.



Scheme 3. Types of interactions in $[M]_3C_2$ complexes.

Mach et al. described the reactions of the titanocene–bis(trimethylsilyl)-acetylene complex $[Cp_2Ti(\eta^2\text{-}Me_3SiC_2SiMe_3)]$ ($Cp = \eta^5\text{-}C_5H_5$) as a titanocene source[5] or alternatively the reduction of titanocene dichlorides $[Cp'_2TiCl_2]$ with magnesium in the presence of bis(trimethylstannyl)acetylene ($Me_3SnC{\equiv}CSnMe_3$; Scheme 4).[7] Complexes of type **E** were obtained only for complexes with the pentamethylcyclopentadienyl ($Cp^* = \eta^5\text{-}C_5Me_5$) ligand, whereas with unsubstituted Cp ligands (probably through oxidative addition and the release of tin radicals, $Me_3Sn^{\bullet}$) $[M]_4C_4$ complexes with σ,π-bridging groups were formed that contained the $[M]_3C_2$ (**E**) subunit, but did not show any significant Ti···Ti interactions (3.752–3.631 Å).

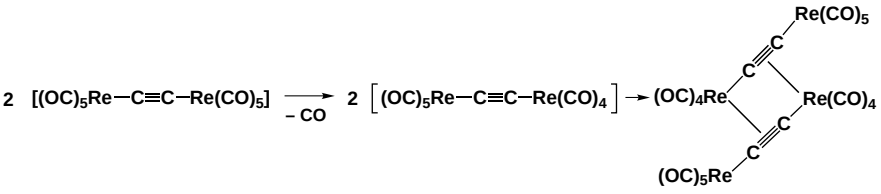
A similar $[Re]_4C_4$ complex, which likewise exhibits σ,π-bridging groups and a $[Re]_3C_2$ subunit (**E**) lacking short Re···Re interactions (3.732–3.752 Å), was obtained by Beck et al., by CO elimination from $[(OC)_5ReC{\equiv}CRe(CO)_5]$ (Scheme 5).[8a,c] Prior to that, only the acetylide-bridged complexes



Cp' = η^5-C_5Me_5 — $[M]_3C_2$-type

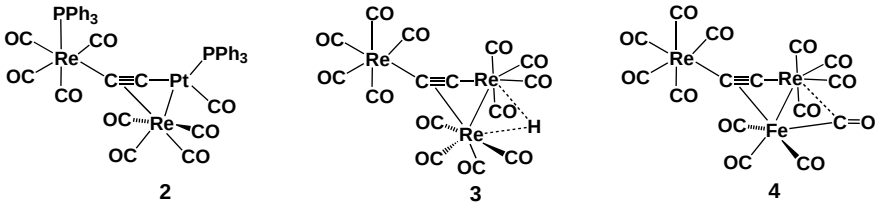
Cp' = η^5-C_5H_5, η^5-$C_5H_3Me_2$ — subunit: $[M]_3C_2$

Scheme 4. Structure and reactivity of the acetylene complexes described by Mach et al.[7]



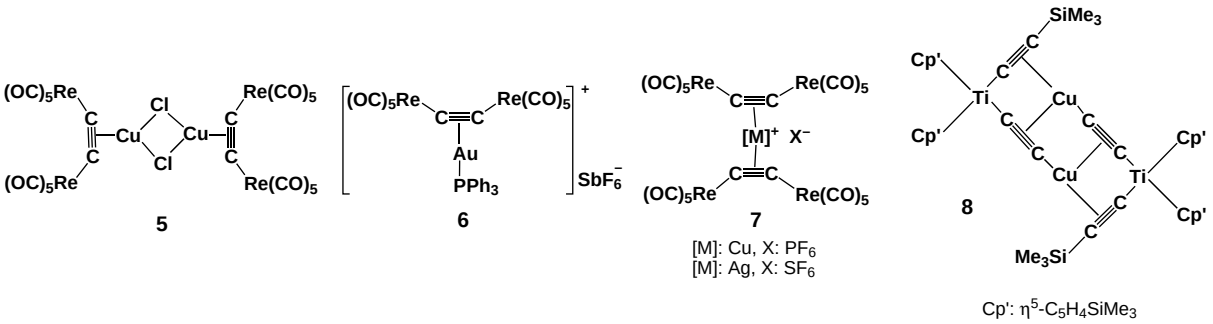
Scheme 5. Formation of the $[Re]_4C_4$ complex by CO elimination, according to Beck et al.[8]

containing $[PtRe_2]C_2$ (**2**) or $[FeRe_2]C_2$ units (**4**) with metal–metal bonds (Pt–Re 2.731 and Fe–Re 2.847 Å) had been obtained in the reactions of



2 **3** **4**

 © 2003 Wiley-VCH Verlag GmbH & Co. KGaA, Weinheim

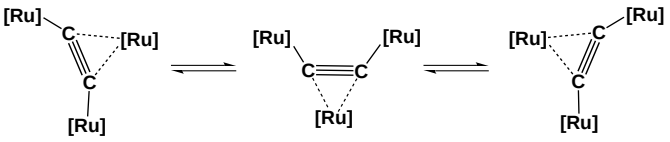


$[(OC)_5ReC{\equiv}CRe(OC)_5]$ with $[(Ph_3P)_2Pt(C_2H_4)]$ or $[Fe_2(CO)_9]$, respectively.[8b] In addition, complex **3**, which has a Re–Re bond of 3.099 Å, shows that complexes with metal–metal interactions predominate for the $[M]_3C_2$ complexes.[8c] Additional examples of related complexes of the type **E** encompass Cu^I, Ag^I, and Au^I derivatives (**5**–**7**).[8d] Another interesting $[M]_4C_8$ complex, which contains two $[TiCu_2]C_2$ subunits, was reported by Lang et al. (**8**; Cu–Cu 2.998 Å).[9] The above examples illustrate that there is a whole series $[M]_3C_2$ compounds that do not exhibit metal–metal interactions.

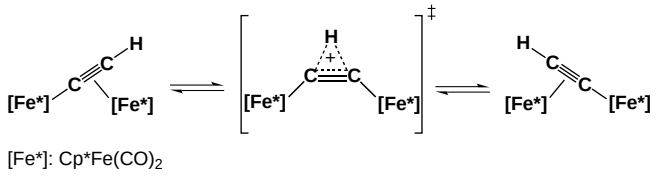
Molecular Dynamics

The most interesting feature of the trimetallic complexes **1** is the dynamic nature of the C_2 ligand, which was described by Koutsantonis et al. as being "bearing-like" (Scheme 6).[6] A similar fluxional motion of acetylide fragments was also reported by Akita et al. for the binuclear cationic complexes $[\{Cp(CO)_2Fe\}_2(\mu\text{-}C{\equiv}CH)]^+$.[4c] Results of solution NMR measurements suggested a 1,2-shift of the hydrogen atom along the carbide bridge, via the intermediate shown in Scheme 7. The dynamic behavior of **1** could be based on an analogous process.

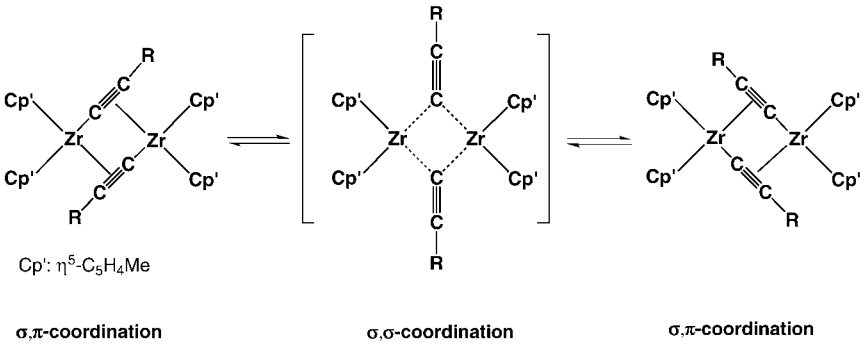
σ,π-Alkynyl-bridged complexes of the type $[M](\mu\text{-}C{\equiv}CR)_2[M]$ (Scheme 8), described by Erker et al., also display nonrigid behavior.[10] There are some experimental data as well as theoretical calculations[5a,11] concerning intermediates formed in such transformations, which are important in respect to the C–C coupling reactions of alkynyl groups, but the question remains whether complexes of the form $[M](\mu\text{-}C{\equiv}C[R])_2[M]$, with [R] = [Sn] or [Re] ($[M]_4C_4$-type complex with an $[M]_3C_2$ subunit), behave in an analogous manner (Scheme 9).



Scheme 6. Dynamic behavior of trinuclear Ru complexes **1a** and **1b**, according to Koutsantonis et al.[6]



Scheme 7. Fluctuation of acetylide units resulting from a 1,2-hydrogen-atom shift.



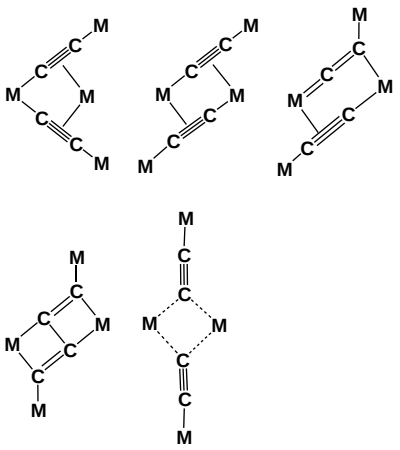
Scheme 8. Molecular dynamics in zirconium complexes, according to Erker et al.[10]

Conclusions and Outlook

In addition to the isolobal concept discussed for $[M]_2C_2$ complexes and alkynes of the form RC_2R,[8] the C_2 ligand is also an extremely mobile group in compounds such as $[M]_3C_2$, $[M]_2C_2R$, and $[M]_2C_2$.[6,10] This could have some more general consequences for the chemistry of alkynes (C_2R_2), and their metal complexes ($[M]C_2R_2$). It is noteworthy that the topomerization of disubstituted alkynes, which involves the transposition of a carbon atom, has been observed. This thermal interconversion of alkynes via vinylidenes at higher temperature is known as the "Roger Brown rearrangement" (Scheme 10).[12a]

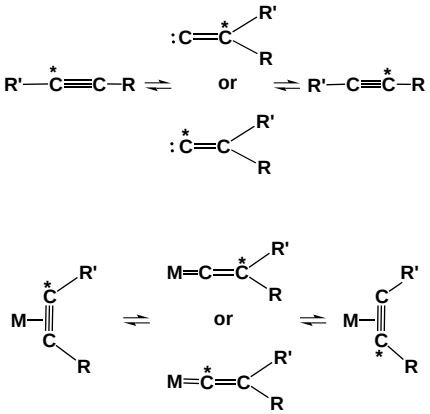
As reported by Werner, metal complexes with disubstituted alkynes

 © 2003 Wiley-VCH Verlag GmbH & Co. KGaA, Weinheim

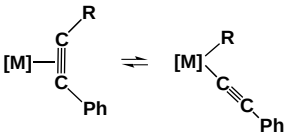


Scheme 9. Types of interactions in $[M]_4C_4$ complexes.

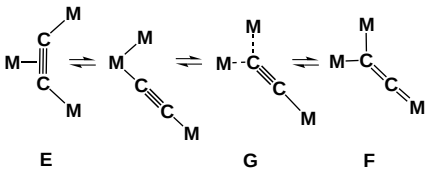
[M](RC$_2$R) can produce vinylidene complexes.[13a] Calculations for acetylene and 1-alkynes given therein were explained more accurately as a "concerted" metal shift with 1,2-H-migration,[13b–d] rather than as a stepwise oxidative addition via {[M](H)(alkynyl)} intermediates.[13e] If this process is also reversible[13f] for disubstituted alkynes, the catalytic influence of metals on the above-mentioned topomerization effect is conceivable. Two very recent reports describe the reversible cleavage of C–C or C–Si bonds in RC≡CPh (R = Ph, Me_3Si) leading to the formation of the platinum(II) compounds [Pt](σ-R)(σ-C_2Ph) (Scheme 11).[14] It is not known whether the formation of vinylidene complexes such as [Rh]=C=C(Si-Me_3)(Ph),[13g] with a 1,2-shift of the Me_3Si groups (Scheme 10), proceeds via a similar intermediate. Interestingly, the same type of reaction shown in Scheme 4[7] was also assumed for an $[M]_3C_2$ compound (Scheme 11). Accordingly, it is conceivable that the carbon-atom transposition (Scheme 6) of compound **1**,[6] proceeds via the **F** and **G** structural types (Scheme 11).



Scheme 10. The "Roger Brown" rearrangement of alkynes.



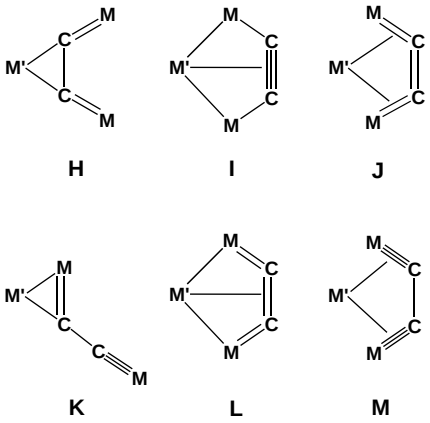
[M]: (iPr$_2$PCH$_2$CH$_2$NMe$_2$)Pt, R: Ph, SiMe$_3$



Scheme 11. Reversible transformation of η^2- and η^1-alkyneplatinum(II) complexes.

Finally, an answer to the question "*Why?*" that was alluded to in the title is provided: The structure and reactivity principles that have been discussed here for the relatively simple C_2 unit can be extended to more complicated compounds with longer C_{2n} ($n = 1, 2, 3\ldots$) "naked" carbon bridges between two or more metal centers, even though the increased number of triple bonds in these molecules allows other reactions to occur. For example, for the 1,3-butadiynes ($n = 2$) topomerization,[12b] formation of butatrienylidene complexes,[2c] and many other different modes of complexation by metal complexes were observed.[2c,5] Additionally, the metal centers can "walk" along the backbone of the polyyne as, for example, described for the 1,3,5-hexatriynes.[15] Similar reactivity is expected for dimetallic $[M]_2C_{2n}$ ($n = 2, 3\ldots$) compounds.

Using the isolobal concept and results from the complex chemistry of 1,3,5-butatrienes and 1,3-butadiynes (using **B** and **C** from Scheme 1) one could envisage additional interactions in $[M]_3C_2$ complexes. (Scheme 12). Relevant examples are the metalla[3]radialenes **H** (M′ = Ti; M = CR_2) described by Maercker and Groos,[16a] metallacyclopentynes **I** or bis-π-complexes **J** (M′ = Zr; M = CR_2) by Suzuki et al.,[16b] metallacyclopropenes **K** or metallacyclocumulenes **L** (M′ = Ti, Zr; M = RC) from our research group,[5] and the bis-π-complexes **M** (M′ = Zr; M = RC) by Erker et al.[16c] There is no reason to assume that $[M'M_2]C_2$ compounds with three metal centers, like those presented in Scheme 12, cannot be prepared.



Scheme 12. Types of interactions in $[M]_3C_2$ complexes.

I thank Profs. M. Akita, W. Beck, R. Beckhaus, B. Bildstein, M. I. Bruce, H. Lang, K. Pörschke, K. P. C. Vollhardt, and H. Werner for some important information and comments. In particular, I am grateful to my group members Drs. P. Arndt, W. Baumann, and A. Spannenberg, as well our guest Dr. V. V. Burlakov for many fruitful discussions.

[1] a) R. Hoffmann, *Angew. Chem.* **1988**, *100*, 1653; *Angew. Chem. Int. Ed. Engl.* **1988**, *27*, 1593; b) A. Yamamoto, *Organotransition Metal Chemistry, Fundamental Concepts and Applications*, Wiley, New York, **1986**, p. 99; c) F. Diederich, Y. Rubin, *Angew. Chem.* **1992**, *104*, 1123; *Angew. Chem. Int. Ed. Engl.* **1992**, *31*, 1101.

[2] Examples: a) W. Beck, B. Niemer, M. Wieser, *Angew. Chem.* **1993**, *105*, 969; *Angew. Chem. Int. Ed. Engl.* **1993**, *32*, 923; b) M. I. Bruce, *Coord. Chem. Rev.* **1997**, *166*, 91; c) P. J. Low, M. I. Bruce, *Adv. Organomet. Chem.* **2002**, *48*, 71; d) M. Brady, W. Wenig, Y. Zhou, J. W. Seyler, A. J. Amoroso, A. M. Arif, M. Böhme, G. Frenking, J. A. Gladysz, *J. Am. Chem. Soc.* **1997**, *119*, 775; e) H. Lang, D. S. A. George, G. Rheinwald, *Coord. Chem. Rev.* **2000**, *206/207*, 101; f) F. Paul, C. Lapinte, *Coord. Chem. Rev.* **1998**, *178–180*, 431.

[3] a) M. H. Chisholm, *Angew. Chem.* **1991**, *103*, 690; *Angew. Chem. Int. Ed. Engl.* **1991**, *30*, 673; b) H. Lang, *Angew. Chem.* **1994**, *106*, 569; *Angew. Chem. Int. Ed. Engl.* **1994**, *33*, 547; c) U. H. F. Bunz,

 © 2003 Wiley-VCH Verlag GmbH & Co. KGaA, Weinheim

Angew. Chem. **1996**, *108*, 1047; *Angew. Chem. Int. Ed. Engl.* **1996**, *35*, 968.
[4] a) P. J. Low, M. I. Bruce, *Adv. Organomet. Chem.* **2003**, *50*, in press; b) M. Akita, Y. Moro-oka, *Bull. Chem. Soc. Jpn.* **1995**, *68*, 420; c) M. Akita, M. Terada, S. Oyama, Y. Moro-oka, *Organometallics* **1990**, *9*, 816; d) M. Akita, S. Sugimoto, H. Hirikawa, S. Kato, M. Terada, M. Tanaka, Y. Moro-oka, *Organometallics* **2001**, *20*, 1555; e) M. Tarada, M. Akita, *Organometallics* **2002**, *22*, 355.
[5] a) U. Rosenthal, P.-M. Pellny, F. G. Kirchbauer, V. V. Burlakov, *Acc. Chem. Res.* **2000**, *33*, 119; b) U. Rosenthal, V. V. Burlakov in *Titanium and Zirconium in Organic Synthesis* (Ed.: I. Marek), Wiley-VCH, **2002**, p. 355.
[6] C. G. Griffith, G. A. Koutsantonis, B. W. Skelton, A. H. White, *Chem. Commun.* **2002**, 2174.
[7] V. Varga, K. Mach, J. Hiller, U. Thewalt, P. Sedmera, M. Polasek, *Organometallics* **1995**, *14*, 1410.
[8] a) J. Heidrich, M. Steimann, M. Appel, W. Beck, J. R. Phillips, W. C. Trogler, *Organometallics* **1990**, *9*, 1269; b) T. Weidmann, V. Weinrich, B. Wagner, C. Robl, W. Beck, *Chem. Ber.* **1991**, *124*, 1363; c) S. Mihan, T. Weidmann, V. Weinrich, D. Fenske, W. Beck, *J. Organomet. Chem.* **1997**, *541*, 423; d) S. Mihan, K. Sünkel, W. Beck, *Chem. Eur. J.* **1999**, *5*, 745.
[9] M. D. Janssen, M. Herres, L. Zsolnai, D. M. Grove, A. L. Spek, H. Lang, G. van Koten, *Organometallics* **1995**, *14*, 1098.
[10] G. Erker, W. Frömberg, R. Benn, R. Mynott, K. Angermund, C. Krüger, *Organometallics* **1989**, *8*, 911.
[11] a) P. N. V. Pavankumar, E. D. Jemmis, *J. Am. Chem. Soc.* **1988**, *110*, 125; b) E. D. Jemmis, K. T. Giju, *Angew. Chem.* **1997**, *109*, 633; *Angew. Chem. Int. Ed. Engl.* **1997**, *36*, 606; c) E. D. Jemmis, K. T. Giju, *J. Am. Chem. Soc.* **1998**, *120*, 6952; d) E. D. Jemmis, A. K. Phukan, K. T. Giju, *Organometallics* **2002**, *21*, 2254; e) G. Aullon, S. Alvarez, *Organometallics* **2002**, *21*, 2627.
[12] a) R. F. C. Brown, *Eur. J. Org. Chem.* **1999**, 3211; b) J. Mabry, R. P. Johnson, *J. Am. Chem. Soc.* **2002**, *124*, 6497.
[13] Examples: a) H. Werner, *Nachr. Chem. Tech. Lab.* **1992**, *40*, 435; b) J. Silvestre, R. Hoffmann, *Helv. Chim. Acta* **1985**, *68*, 1461; c) R. Stegmann, G. Frenking, *Organometallics* **1998**, *17*, 2089; d) F. D. Angelis, A. Sgamellotti, *Organometallics* **2002**, *21*, 2715; e) A. B. Antonova, N. E. Kolobova, P. V. Petrovsky, B. V. Lokshin, N. S. Obezyuk, *J. Organomet. Chem.* **1977**, *137*, 69; f) R. S. Bly, Z. Zhong, C. Kane, R. K. Bly, *Organometallics* **1994**, *13*, 899; g) D. Schneider, H. Werner, *Angew. Chem.* **1991**, *103*, 710; *Angew. Chem. Int. Ed. Engl.* **1991**, *30*, 700.
[14] a) C. Müller, C. N. Iverson, R. J. Lachicotte, W. D. Jones, *J. Am. Chem. Soc.* **1997**, *119*, 775; b) C. Müller, R. J. Lachicotte, W. D. Jones, *Organometallics* **2002**, *21*, 1190.
[15] P.-M. Pellny, V. V. Burlakov, P. Arndt, W. Baumann, A. Spannenberg, U. Rosenthal, *J. Am. Chem. Soc.* **2000**, *122*, 6317.
[16] a) A. Maercker, A. Groos, *Angew. Chem.* **1996**, *108*, 216; *Angew. Chem. Int. Ed. Engl.* **1996**, *35*, 210; b) N. Suzuki, M. Nishiura, Y. Wakatsuki, *Science* **2002**, *295*, 660; c) B. Temme, G. Erker, R. Fröhlich, M. Grehl, *Angew. Chem.* **1994**, *106*, 1570; *Angew. Chem. Int. Ed. Engl.* **1994**, *33*, 1480.

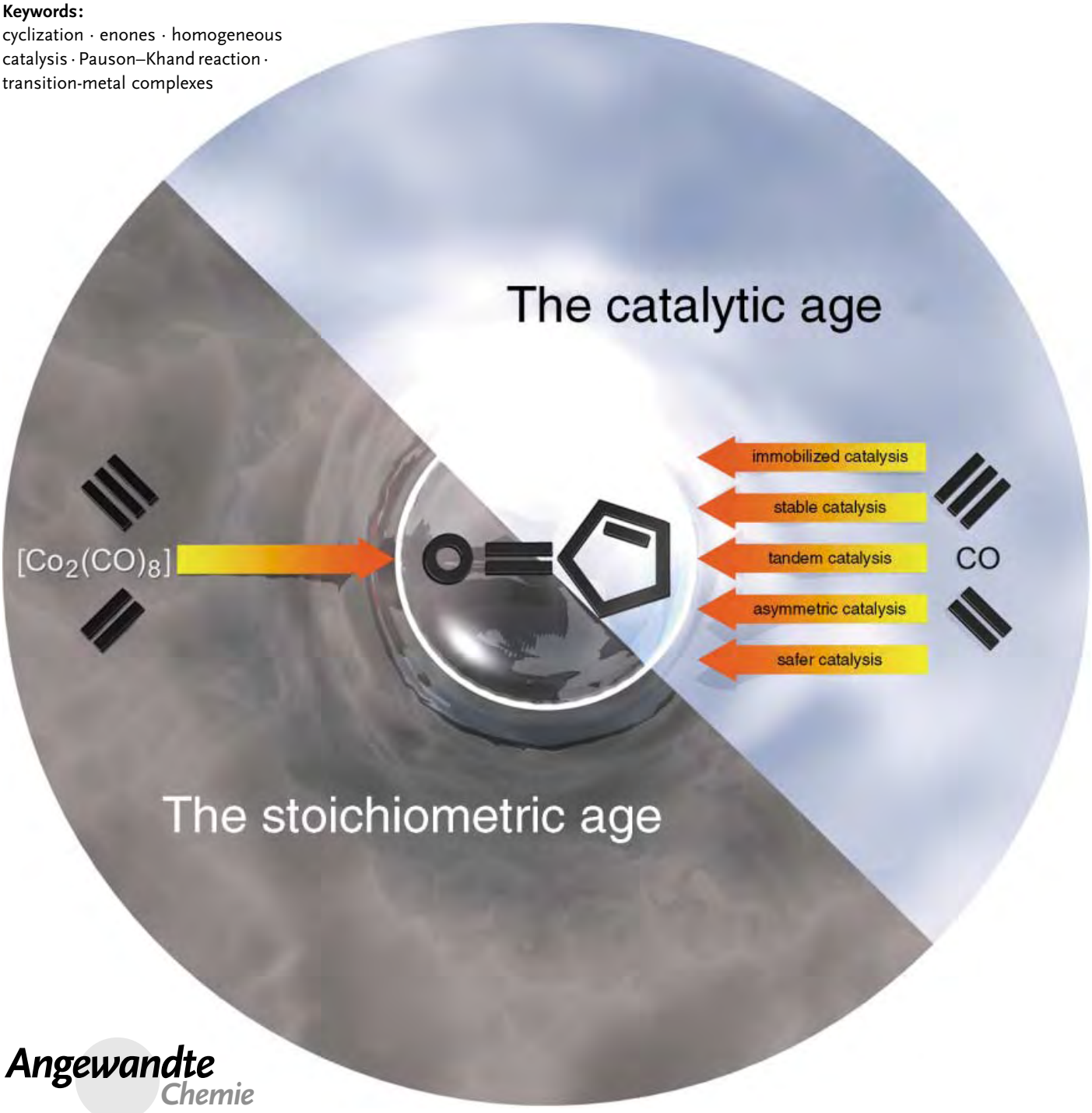
 © 2003 Wiley-VCH Verlag GmbH & Co. KGaA, Weinheim

Catalytic Pauson-Khand Reaction

The Pauson–Khand Reaction: the Catalytic Age Is Here!

Susan E. Gibson (née Thomas) and Andrea Stevenazzi**

Keywords:
cyclization · enones · homogeneous catalysis · Pauson–Khand reaction · transition-metal complexes



© 2003 Wiley-VCH Verlag GmbH & Co. KGaA, Weinheim
DOI: 10.1002/anie.200200547

As a consequence of growing environmental awareness, it is now inappropriate to design a synthetic metal-mediated transformation that involves a noncatalytic use of toxic and expensive transition-metal species. One of the earliest examples of such a metal-mediated transformation is the Pauson–Khand reaction, a [2+2+1] cyclocarbonylation that generates a cyclopentenone. Despite the early descriptions by Pauson and co-workers of catalytic versions of the reaction with octacarbonyldicobalt(0), applications of the Pauson–Khand reaction have to date almost exclusively used approaches that involve stoichiometric quantities of cobalt–carbonyl complexes. In the last decade, and, most markedly, in the last two to three years, however, there have been many exciting and novel developments in the catalytic Pauson–Khand reaction. Furthermore, asymmetric catalysis of the Pauson–Khand reaction has been shown to be a viable process. In view of the impressive developments in Pauson–Khand catalysis in the last two to three years, we present a comprehensive and critical coverage of the catalytic Pauson–Khand reaction that is designed to facilitate its application and to point to exciting future developments.

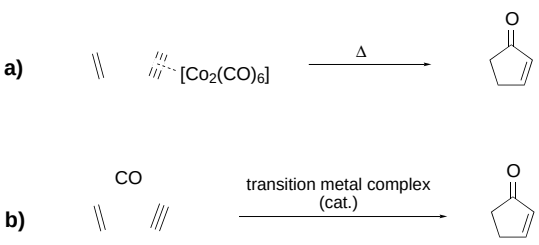
From the Contents

1. Introduction	1801
2. Towards More Practical Catalysis	1802
3. Towards Different Metals	1805
4. Towards Asymmetric Catalysis	1807
5. Summary and Outlook	1808

1. Introduction

The chemical industry is under increasing pressure to develop novel methodologies that reduce both the consumption of raw materials and the generation of toxic waste, as environmental issues acquire increasing relevance within the scientific community and amongst the general public. To fulfill the issue of atom economy raised by Trost, "an ideal chemical reaction must be not only selective, but also a simple addition in which the other reactants are required only in catalytic amounts".[1] Metal-mediated transformations and catalysis play an important role in addressing the atom-economy issue. One of the earliest examples of a metal-mediated transformation is the Pauson–Khand reaction (PKR), first reported in 1971.[2] This is a [2+2+1] cycloaddition that results in the formation of a cyclopentenone from hexacarbonyldicobalt(0) complexes of alkynes, heated in the presence of an alkene (Scheme 1a).

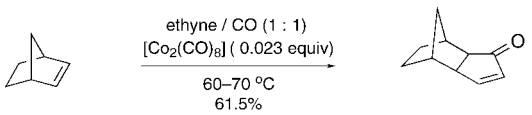
In view of the considerations expressed above it is unthinkable, in terms of cost and waste, to conceive a process that involves a stoichiometric use of a toxic and expensive transition-metal species. A superior approach would be to use catalytic amounts of transition-metal complexes to combine an alkyne, an alkene, and carbon monoxide (Scheme 1b). Indeed, in 1973, Pauson and co-workers reported the first examples of the catalytic cycloaddition with octacarbonyldicobalt(0).[3] These early examples involved only constrained reactive alkenes such as norbornene and were carried out with a continuous supply of ethyne (Scheme 2). All the reactions were conducted within a narrow thermal window (60–70 °C), and a range of pressures of carbon monoxide were employed.



Scheme 1. The PKR: a) the stoichiometric approach; b) the catalytic version.

Despite early documentation of the catalytic PKR (CPKR) by Pauson and co-workers, applications of the PKR have to date almost exclusively exploited the stoichiometric approach (Scheme 1a).[4] In the last decade, and most markedly in the last two to three years, however, there have been many exciting and novel developments in the CPKR. More practical alternatives to the original catalyst, $[Co_2(CO)_8]$, have been designed, and investigations of other transition-metal complexes based on titanium, rhodium, ruthenium, and iridium have been rewarded with the discovery of impressive catalytic activity. Asymmetric variants of the catalytic cycloaddition are now available,[5] while safer and more environmentally friendly procedures that avoid the use of toxic carbon monoxide are starting to appear.

We believe that the developments of the last two to three years mean that we are now entering the catalytic age of the PKR, rendering the stoichiometric use of toxic metal



Scheme 2. One of the first examples of the CPKR employing a continuous supply of ethyne (Pauson and co-workers).

[*] Prof. S. E. Gibson (née Thomas), A. Stevenazzi
Department of Chemistry, King's College London
Strand, London, WC2 R2LS (UK)
Fax: (+44) 207-848-2810

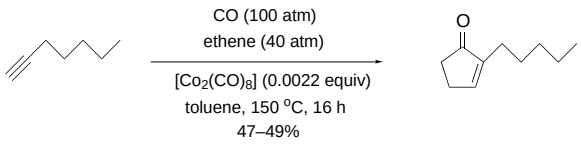
 © 2003 Wiley-VCH Verlag GmbH & Co. KGaA, Weinheim

complexes more and more difficult to justify. We have thus provided in this Review a comprehensive and critical coverage of the catalytic PKR that is designed to a) facilitate the matching of synthetic problems with catalyst systems, b) highlight areas in need of further development, and c) point to the potential of the CPKR in one-pot multicomponent catalysis.

2. Towards More Practical Catalysis

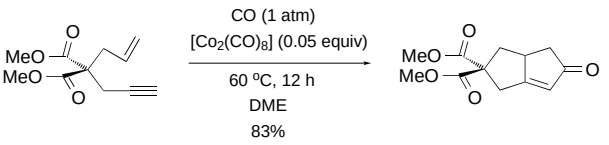
2.1. Tuning the Reaction Conditions

Following the work of Pauson and co-workers described in Section 1,[3] it was not until 1990 that the next truly CPKR was reported.[6] Rautenstrauch et al. used nonconstrained alkenes, and in one of their best experiments a TON (turnover number)[7] of 110 was obtained employing 0.0022 equivalents of the catalyst $[Co_2(CO)_8]$, under very high partial pressures of carbon monoxide and ethene (Scheme 3). However, as reported by the author, the results were not always reproducible.



Scheme 3. CPKR under high pressures of carbon monoxide end ethene (Rautenstrauch et al.).[6]

More than 20 years after the initial results of Pauson and co-workers, Livinghouse and Pagenkopf drew our attention again to a catalytic approach of the PKR with a partial pressure of carbon monoxide of just 1 atm. In 1996 he reported a procedure in which photoactivation of $[Co_2(CO)_8]$ was required,[8] but a subsequent report from the same group related that careful control of the temperature to within the same narrow window employed earlier by Pauson and co-workers[3] dispenses with the need for photolytic promotion (Scheme 4).[9] For both the thermal and photochemical variations of the CPKR, Livinghouse and Pagenkopf stressed the importance of using high purity $[Co_2(CO)_8]$ to ensure reproducible results. One approach to overcoming this problem, as shown in Section 2.2, is the introduction of additives with the aim of stabilizing intermediates in the CPKR.



Scheme 4. Thermal CPKR employing just one atmosphere pressure of carbon monoxide (Livinghouse and Pagenkopf).[9]

2.2. Use of Additives

Since the discovery of the PKR in the early 1970s, new procedures have been developed to improve the performances of the stoichiometric variants of the reaction. A wide range of compounds have been employed as promoters or additives, and the scope and limitations of the use of tertiary amine *N*-oxides, phosphanes, phosphane oxides, dimethyl sulfoxide (DMSO), hard Lewis bases, and sulfides have been well documented.[4] However, the employment of promoters such as tertiary amine *N*-oxides or DMSO in the CPKR produced only trace amounts of the desired products.[10] Presumably, the regeneration of Co^0 species within the catalytic process is not permitted under these oxidizing conditions.

It has been suggested that the formation of cobalt clusters is an impediment to catalysis in the thermal PKR. At 50 °C, $[Co_2(CO)_8]$ is converted into $[Co_4(CO)_{12}]$, which was believed to be inert towards alkyne substrates.[11] In an attempt to overcome the formation of inactive clusters, Pauson, Billington, and co-workers studied the influence of phosphanes and phosphites as coligands for the stoichiometric variants of the PKR.[12] Subsequently, a catalytic conversion of enynes into cyclopentenones employing phosphites as coligands was reported by Jeong, Chung, and co-workers (Table 1, entry 3).[10] Remarkably, under 1 atm of CO the use of phosphites as coligands did not show any positive effect on the PKR conversions (they were either ineffective or detrimental); the advantages of this procedure were only apparent at pressures of 3 atm.



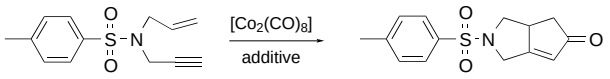
Sue E. Gibson obtained her BSc in Cambridge and her D. Phil. in Oxford under the supervision of Prof. S. Davies. She was then awarded a Royal Society European Fellowship to study at the ETH, Zürich, with Prof. A. Eschenmoser. In 1985 she returned to the UK as a lecturer in organic chemistry at the University of Warwick. In 1990 she was appointed as a lecturer at Imperial College, London, and in 1999 she took up the Daniell Chair of Chemistry at King's College London. Her research interests revolve around the application of transition metals in organic synthesis.



Andrea Stevenazzi completed a degree in chemistry at the Università degli Studi, Milan, in 1999. Under the supervision of Prof. S. Gibson at King's College London and Dr. C. Johnstone of AstraZeneca, his PhD has focused on the development of novel cobalt(0)–carbonyl complexes as catalysts of the Pauson–Khand reaction. In particular, he has been investigating the catalytic properties of phosphane-substituted cobalt–carbonyl complexes, both in homogeneous protocols and immobilized on a solid support.

 © 2003 Wiley-VCH Verlag GmbH & Co. KGaA, Weinheim

Table 1: The influence of different additives on the cobalt-catalyzed Pauson–Khand reaction.



Entry	$[Co_2(CO)_8]$ [mol%]	Additive (mol%)	T [°C]	p(CO) [atm]	Yield [%]
1[a]	7.5	none	60	1	86
2[b]	10	none	70	1	63
3[c]	5	$P(OPh)_3$ (20)	120	3	94
4[d]	3	DME (12)	120	7	84
5[e]	10	$CyNH_2$ (20)	70	1	89
6[f]	5	Bu_3PS (30)	70	1	87

Solvents and reaction times: [a] DME (12 h).[9a] [b] DME (10.5 h).[16] [c] DME (24 h).[10] [d] Toluene (10 h).[14] [e] DME (14 h).[16] [f] Benzene (4 h).[17]

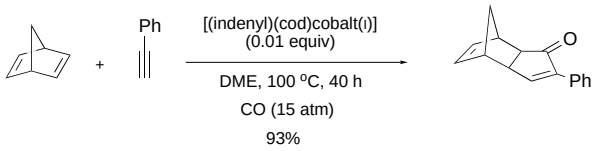
Based on their own previous work on the stoichiometric version of the reaction,[13] Sugihara and Yamaguchi used hard Lewis bases to effect both the inter- and the intramolecular CPKR, employing 0.01–0.03 equivalents of octacarbonyldicobalt(0).[14] Hard Lewis bases are known to make the ligands of low-valent organotransition metal complexes more labile. 1,2-Dimethoxyethane (DME) was found to be the best promoter, giving cycloaddition products in very good yields (Table 1, entry 4). Water was found to be less efficient under the same conditions, but comparable yields were obtained at higher concentrations. It should be noted that under the conditions developed by Sugihara and co-workers the use of DME as solvent was detrimental to catalysis.[15] Interestingly, although cyclohexylamine was the best promoter in the stoichiometric version of the reaction,[13] it had no effect on the progress of the CPKR under 7 atm of CO.[14] On the other hand, Krafft et al. used cyclohexylamine as an additive for the thermal CPKR (Table 1, entry 5)[16] when they developed a set of conditions that removed the need for the "rigorous purification" of $[Co_2(CO)_8]$ reported by Livinghouse and purification.[8,9a]

Hashimoto and co-workers has proved that the addition of phosphane sulfides to the CPKR results in higher yields and faster conversions under 1 atm of CO (Table 1, entry 6).[17] The TONs were high and they was even able to catalyze an intermolecular PKR under these mild conditions.

Although some success has been achieved by the use of additives, it has clearly emerged that in most cases the advantages observed are restricted to the particular conditions employed. The examples of $CyNH_2$ and phosphites reported earlier in this section show how the same additive can be either effective or ineffective depending on the reaction conditions utilized, which suggests that the use of additives cannot be considered as a universal approach to the CPKR.

2.3. Generation of Cobalt(0) In Situ

Problems associated with the very labile $[Co_2(CO)_8]$ have led to the development of catalytic variants of the reaction that generate the active catalyst in situ from Co^I or Co^{II} precursors. One of the first systems studied employed [(indenyl)(cod)cobalt(I)] (cod = cycloocta-1,5-diene) as the precatalyst, presumably reduced in situ to cobalt(0) by carbon monoxide.[18] Under high pressures of CO, very good conversions were obtained for both intramolecular cyclizations and intermolecular reactions between constrained alkenes and terminal alkynes (Scheme 5); TONs up to 97 in 40 h). Experiments with nonconstrained alkenes, however, were unsuccessful.



Scheme 5. The use of [(indenyl)(cod)cobalt(I)] as a precatalyst for the PKR (Chung and co-workers).[18]

Inspired by work of Lautens and co-workers,[19] Lee and Chung reported that a catalytic combination of $[Co(acac)_2]$ and $NaBH_4$ can effectively promote both inter- and intramolecular versions of the PKR under high pressures of CO.[20] Despite the fact that the use of a strong reducing agent may limit the range of compatible functional groups, this system gave high TONs. It was presumed by the author that $NaBH_4$ prevented the formation of inactive cobalt species.

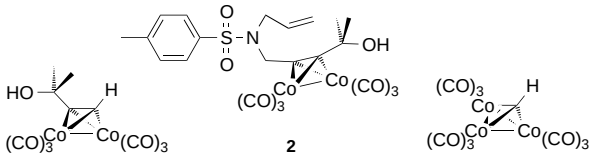
Rajesh and Periasamy developed a system in whih the cobalt catalyst was obtained in situ by reducing $CoBr_2$ with Zn under 1 atm of CO.[21] Under these mild conditions a demanding substrate such as cyclopentene was cyclized. This system gave very low TONs, however, and can hardly be termed catalytic.

2.4. More Stable Sources of Cobalt(0)–Carbonyl Complexes

As reported by several research groups, the cobalt species $[Co_2(CO)_8]$ is not very easy to handle: it is highly toxic and it ignites spontaneously upon contact with air. The development of more practical catalyst precursors that can either retain or improve the performance of $[Co_2(CO)_8]$, without requiring reducing steps in situ, would bring substantial advantages to the catalytic versions of the PKR.

It has been known since the earliest investigations of the PKR that complexation of $[Co_2(CO)_8]$ with the alkyne to form a more stable alkyne–$[Co_2(CO)_6]$ species, is the first step of the cyclization.[3,22] Early attempts by Billington to use preformed ethyne–$[Co_2(CO)_6]$ in a catalytic protocol, employing demanding alkenes such as 2,5-dihydrofuran under an ethyne/CO atmosphere, however, resulted in very low TONs.[23] Subsequently, Livinghouse and Belanger tried a similar protocol employing complex **1** for the cyclization of simpler intramolecular substrates (Scheme 6). Unfortunately, this species did not prove to be very active towards the enynes and Et_3SiH was required to get good conversions.[24] This

 © 2003 Wiley-VCH Verlag GmbH & Co. KGaA, Weinheim



1 2 3

Scheme 6. Examples of more stable sources of cobalt(0)–carbonyl complexes.

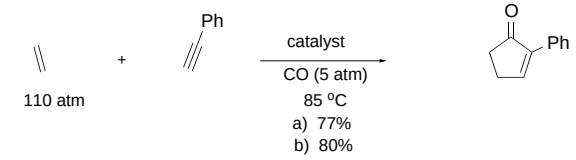
additive can be avoided, as Krafft reported, by using hexacarbonyldicobalt(0) complexes of enynes (**2**, Scheme 6).[25]

The use of cobalt(0)–carbonyl clusters as a more stable source of catalytically active species has been investigated by independent research groups.[26–29] Sugihara and Yamaguchi reported that air-stable alkylidyne nonacarbonyltricobalt clusters mediated the PKR under catalytic conditions.[26] Methylidynenonacarbonyltricobalt (**3**, Scheme 6), easily prepared from octacarbonyldicobalt(0) and trihalomethanes,[30] catalyzed both inter- and intramolecular cycloadditions under 7 atm of CO, with TONs of up to 17.

The cobalt cluster compound $[Co_4(CO)_{12}]$ has always been believed to be catalytically inactive towards the PKR. Exploiting the equilibrium established under high pressures of CO between $[Co_4(CO)_{12}]$ and $[Co_2(CO)_8]$, Chung and Kim utilized $[Co_4(CO)_{12}]$ (which is commercially available and more air-stable than $[Co_2(CO)_8]$) as a source of cobalt for both inter- and intramolecular cyclocarbonylations.[27] Under 10 atm of CO, $[Co_4(CO)_{12}]$ proved to be a more active catalyst than $[Co_2(CO)_8]$.

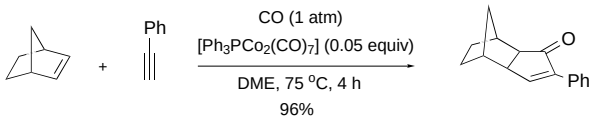
Jeong et al. have demonstrated that supercritical fluids promote the CPKR.[28,31] Advantages of this technique, as reported by the author, include high solubility of gaseous reactants, rapid diffusion of solutes, and weakening of the solvation around the reacting species. In a recent communication, they described the intermolecular versions of the CPKR in supercritical ethene, employing $[Co_2(CO)_8]$ and the two cobalt clusters $[Co_4(CO)_{12}]$ and $[Co_4(CO)_{11}\{P(OPh)_3\}]$ as catalysts under 5 atm of carbon monoxide (Scheme 7).[28] Although the TONs were generally not impressive, it noteworthy that the phosphite-substituted cobalt species was remarkably easier to handle than the unsubstituted complexes.

Evidence that $[Co_4(CO)_{12}]$ cannot be considered inactive towards the CPKR, even under atmospheric pressures of carbon monoxide, has recently been provided by Krafft and Boñaga.[29] In early experiments from this group, the observed activity of $[Co_4(CO)_{12}]$ was associated with the use of $CyNH_2$ as an additive, but it was shown in the same study that the cobalt cluster $[Co_4(CO)_{12}]$ was active even in the absence of the amine. Indeed, a test conducted employing different solvents revealed that under certain conditions $[Co_4(CO)_{12}]$ can give higher TONs than the less-stable cobalt species $[Co_2(CO)_8]$.[29]



Scheme 7. CPKR in supercritical ethene according to Jeong et al.:[28] a) $[Co_4(CO)_{12}]$ (0.03 equiv), 24 h; b) more practical $[Co_4(CO)_{11}\{P(OPh)_3\}]$ (0.03 equiv) was used, 46 h.

Despite the significant use of phosphane- and phosphite-substituted alkyne complexes in the stoichiometric PKR, in which coordination leads to a decrease in the rate and overall efficiency of the reaction,[12,22] and despite the fact that triphenylphosphite additive in the $[Co_2(CO)_8]$-mediated catalytic PKR leads to an improved reaction efficiency,[10] only recently was it shown that preformed complexes of phosphanes and phosphites can catalyze the PKR under atmospheric pressures of carbon monoxide.[32,33] The TONs observed in work by our own group with these stable complexes were comparable with those of other similar mild systems (Scheme 8). The triphenylphosphane derivative, $[Ph_3PCo_2(CO)_7]$, in particular,[33] proved to be amongst the most robust species examined so far for the CPKR. Like other phosphite-substituted cobalt complexes examined earlier,[28] $[Ph_3PCo_2(CO)_7]$ does not ignite spontaneously upon contact with air. Moreover, this species retains its catalytic activity even after being stored at 4 °C for many months exposed to air.

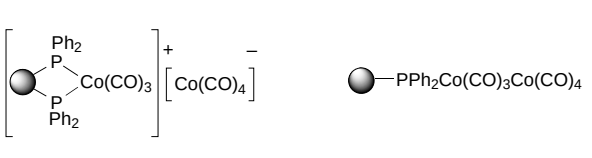


Scheme 8. PKR catalyzed by the robust complex $[Ph_3PCo_2(CO)_7]$ carried out by our group.

2.5. Heterogeneous Catalysts

The increasing awareness of the environmental and handling advantages conferred by solid-phase methodologies has recently spurred different research groups to develop new heterogeneous catalysts for the PKR.

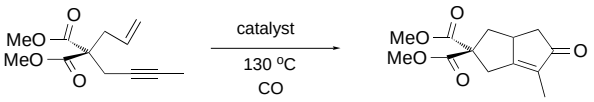
The first example of a polymer-supported catalyst for the PKR, the resin-bound mixture of phosphane-substituted cobalt–carbonyl complexes **4** and **5**, was reported by our group in 2000 and proved to be an effective and practical catalyst of the PKR under mild conditions (Scheme 9).[34] Despite relatively low TONs, this system so far remains the only example of an effective heterogeneous catalyst for the PKR under only 1 atm of carbon monoxide.



4 5

Scheme 9. The polymer-supported cobalt(0)–carbonyl complexes employed by our group.

Table 2: Heterogeneous catalysts for the PKR developed by Jeong, Chung, and co-workers.[35–38]



Entry	Catalyst	Co loading [mol%]	Solvent	*p*(CO) [atm]	Yield [mol%]	Reuse[a]
1[b]	Co/silica	13	DCM	20	92	3
2[c]	Co/charcoal	16	THF	20	98	9
3[d]	colloidal Co	45	THF	5	97	4
4[e]	colloidal Co	67	H_2O	20	96	4

[a] Number of times that the catalyst was reused without any loss in activity. Reaction times: [b] 18 h.[35] [c] 18 h.[36] [d] 12 h.[37] [e] 12 h.[38]

Chung and co-workers recently showed clearly how the dream of "more practical heterogeneous catalysts" for the PKR may be realized. They developed catalytic systems that require harsh conditions (high CO pressures and high catalyst loading), but are reusable and clean (Table 2).[35–38] The first system documented employs a 13 mol% loading of metallic cobalt supported on mesoporous silica as the catalyst precursor of the PKR.[35] This material proved to be active towards different intramolecular substrates under 20 atm of CO and could be recovered and reused three times without any loss of catalytic activity (Table 2, entry 1). Intermolecular substrates failed to cyclize in good yields under these conditions.

The next heterogeneous catalyst precursor reported by Chung and co-workers was cobalt on charcoal.[36] In this system a 16 mol% loading of cobalt was required for the cyclizations, but this time the catalyst could be recovered and reused nine times without losing any catalytic activity (Table 2, entry 2). Moreover, several intermolecular substrates could be cyclized in very good yields.

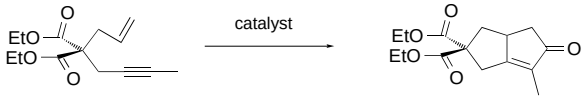
Colloidal cobalt nanoparticles were also observed to act as a reusable catalyst for the PKR.[37] Milder pressures of CO were used (5 atm), but a 45 mol% loading of cobalt was necessary for the cycloadditions. Colloidal cobalt gave good results for both inter- and intramolecular variants of the reaction and could be recovered and reused four times without showing any loss of activity (Table 2, entry 3). More recently, they were able to apply this technique in an aqueous environment.[38] Although this reaction can hardly be considered catalytic (loading = 67 mol%), this colloidal cobalt system proved to be active under highly oxidizing conditions for cobalt(0), and it could be recovered and reused four times without any loss of activity (Table 2, entry 4).

3. Towards Different Metals

3.1. Optimization of Titanium Catalysts

Following the work of Negishi et al. on the zirconocene-mediated cyclization of enynes,[39] Buchwald and co-workers showed that the cyclocarbonylation of enynes could be mediated[40] and even catalyzed by titanocene complexes (Table 3).[41–43] The first protocol involved the use of the complex $[Cp_2Ti(PMe_3)_2]$, which proved to be extremely air-sensitive and failed to cyclize common enynes under 1 atm of carbon monoxide.[41] To overcome this problem, trialkylsilyl cyanides were used to generate isocyanides in situ. The resulting bicyclic iminocyclopentenes were hydrolyzed to the classical cycloadducts of the PKR (Table 3, entry 1). A slightly more practical procedure was subsequently developed by the same group: The extremely unstable complex $[Cp_2Ti(PMe_3)_2]$ was replaced by the commercially available and stable catalyst precursor $[Cp_2TiCl_2]$.[42] In the presence of *n*BuLi and triethylsilyl cyanides, this system showed the same activity as the previous one. The overall yields were still generally poor, however, because of the hydrolysis step.

Table 3: PKR catalyzed by titanocene complexes (Buchwald and co-workers).[41–43]



Entry	Catalyst (mol%)	R_3SiCN (equiv)	*p*(CO) [atm]	Yield [%]
1[a]	$[Cp_2Ti(PMe_3)_2]$ (10)	Et_3SiCN (1.3)	–	71
2[b]	$[Cp_2Ti(CO)_2]$ (5)	–	1.22	91

[a] Ar, benzene, 45 °C, 16–24 h, then $CuSO_4$ (sat. aq.), room temperature, 3–5 h.[41] [b] Toluene, 90 °C, 12–48 h.[43]

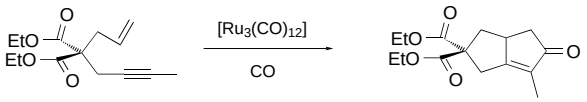
Remarkable improvements were achieved by Buchwald and co-workers when the commercially available species $[Cp_2Ti(CO)_2]$ was employed as a catalyst for the cyclocarbonylation.[43] This complex cyclized a range of enynes under low pressures of carbon monoxide (1.22 atm), thus avoiding the use of isocyanides and the unwanted hydrolysis step (Table 3, entry 2). Moreover, the TONs were substantially higher and the system displayed an increased level of functional-group compatibility. Notably, in the cases of some 1,2-disubstituted alkene substrates, lower pressures of CO (0.34 atm) were required for complete consumption of the starting materials. Another protocol developed by the same group uses a nickel(0) complex as a catalyst for a Pauson–Khand-type reaction.[44] Despite its higher tolerance of different functional groups, this system showed only slight advantages over previous ones, and the TONs were very low.

3.2. Ruthenium-Catalyzed Variants

In 1997 two research groups independently showed that $[Ru_3(CO)_{12}]$ can catalyze the PKR (Table 4).[45,46] Murai and co-workers reported that catalytic quantities of $[Ru_3(CO)_{12}]$ (0.02 equiv) cyclized a range of enynes with a disubstituted alkyne group under 10 atm of carbon monoxide (Table 4,

 © 2003 Wiley-VCH Verlag GmbH & Co. KGaA, Weinheim

Table 4: The $[Ru_3(CO)_{12}]$-catalyzed PKR (Murai and co-workers[45] and Mitsudo and co-workers[46]).



Entry	$[Ru_3(CO)_{12}]$ [mol%]	*T* [°C]	*t* [h]	*p*(CO) [atm]	Yield [mol%]
1[a]	2	160	20	10	86
2[b]	2	140	8	15	78

[a] In dioxane.[45] [b] In *N,N*-dimethylacetamide (DMAc).[46]

entry 1).[45] On the other hand, enynes with a terminal alkyne group proved to be poor substrates for the cycloaddition. One month later, Mitsudo and co-workers reported that $[Ru_3(CO)_{12}]$ in DMAc (*N,N*-dimethylacetamide), under 15 atm of CO, catalyzed the cyclocarbonylation of several enynes with disubstituted alkyne groups (Table 4, entry 2); examples of enynes with terminal alkyne groups were not included.[46]

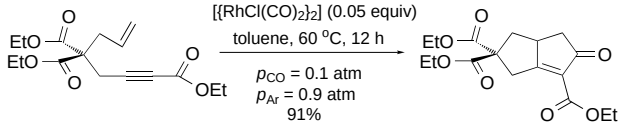
3.3. The Rhodium Approach

Rhodium catalyzed PKRs have recently attracted much attention.[47] Early studies by Narasaka and co-workers revealed that 0.02 equivalents of $[\{RhCl(CO)_2\}_2]$ catalyzed the reaction under 1 atm of CO.[47a] Later, the performance of the catalyst was optimized with respect to the solvent (xylene was replaced by toluene) and the catalyst loading (decreased to 0.05 equivalents).[47b] This system is excellent for substrates containing electron-deficient alkenes and alkynes (Scheme 10). Notably, the catalytic cycle for these particularly demanding substrates was accelerated by decreasing the partial pressure of CO down to 0.1 atm. Moreover, this rhodium-based catalyst has proven to be good even in the cyclizations of the allenyne **6** (Scheme 11). Under these catalytic conditions, the reaction is regioselective and involves exclusively the external double bond of the allene, yielding cyclopentenone **7**. This result in the rhodium-catalyzed PKR of allenes was subsequently confirmed by Mukai et al.[47d] and Brummond et al.[47e]

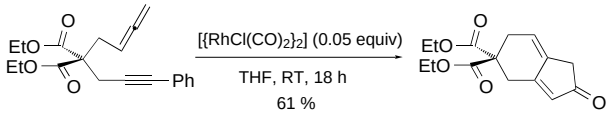
3.4. A Safety Note

As described above, the catalytic PKR has improved remarkably in terms of reaction conditions, TONs, and practicability over the last decade. The use of highly toxic carbon monoxide, however, still represents a major drawback to this procedure. A cyclocarbonylation reaction that did not use carbon monoxide would be a safer reaction and would be an important breakthrough in this area.

Based on one example reported earlier by Schore,[48] Krafft and Boñaga reported that cyclocarbonylation of a range of enynes can be achieved under an atmosphere of N_2 employing 35–50% of $[Co_2(CO)_8]$.[49] This procedure removes



Scheme 10. Rhodium-catalyzed PKR (Narasaka and co-workers).[47b] Note that this example employs an electron-deficient alkyne.



6 **7**

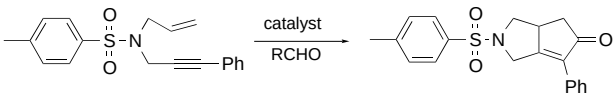
Scheme 11. $[\{RhCl(CO)_2\}_2]$-catalyzed cyclization of the allene **6**.

the need to use highly toxic carbon monoxide by increasing the amount of a toxic cobalt species and, therefore, cannot be considered the ideal approach to solve the toxicity problem.

More recently two astonishing communications from two independent research groups have reported the use of aldehydes as a CO source for the PKR (Table 5).[50,51] In the search for CO-transfer catalysts, Morimoto et al. tested different aromatic aldehydes with Rh, Ir, and Ru species. The most active system was a combination of the complex $[\{RhCl(cod)\}_2]$ (0.05 equiv) with C_6F_5CHO (2 equiv), and several enynes could be cyclized under a nitrogen atmosphere (Table 5, entry 1).[50]

Shibata et al. tested different aldehydes in a solvent-free system, employing the rhodium species $[Rh(dppp)_2Cl]$ (dppp = 1,3-bis(diphenylphosphanyl)propane) as the catalyst.[51] In this case, cinnamaldehyde was the most efficient aldehyde of those tested. The reactions were carried out employing 0.05 equivalents of the catalyst under 1 atm of argon (Table 5, entry 2). In a preliminary experiment, Shibata et al. tested this protocol under asymmetric conditions using tolbinap (0.1 equiv) as a chiral ligand and $[\{Rh(cod)Cl\}_2]$ as the catalyst (0.05 equiv). Only one commonly used enyne was employed under these conditions, but a very encouraging result was obtained (89% yield, 83% *ee*).[51]

Table 5: The CPKR using aldehydes as CO source (Morimoto et al.[50] and Shibata et al.[51]).



Entry	Catalyst (mol%)	Additive (mol%)	RCHO	Solvent	Yield [mol%]
1[a]	$[\{RhCl(cod)\}_2]$ (5)	dppp (11)	C_6F_5CHO	xylene	95
2[b]	$[Rh(dppp)_2Cl]$ (5)	–	cinnamaldehyde	–	98

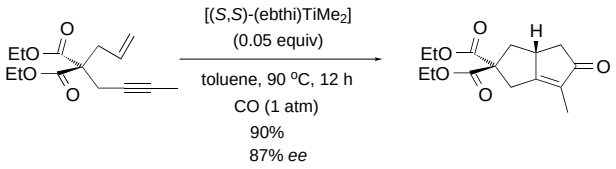
[a] N_2, 130°C, 4 h.[50] [b] Ar, 120°C, 2 h, cinnamaldehyde (20 equiv).[51]

 © 2003 Wiley-VCH Verlag GmbH & Co. KGaA, Weinheim

4. Towards Asymmetric Catalysis

Until a few years ago, asymmetric protocols for the PKR were restricted to stoichiometric approaches to the reaction.[4,5] At that time, catalytic systems that could induce asymmetry were only speculative, presumably because in most of the cases they required very harsh conditions (high temperatures and very high pressures of carbon monoxide).[6,10,18,20]

In 1996, however, Buchwald and Hicks reported the first example of an asymmetric PKR involving a catalytic amount of a chiral titanocene complex (Scheme 12).[52] Following their own work on the use of the highly active species $[Cp_2Ti(CO)_2]$

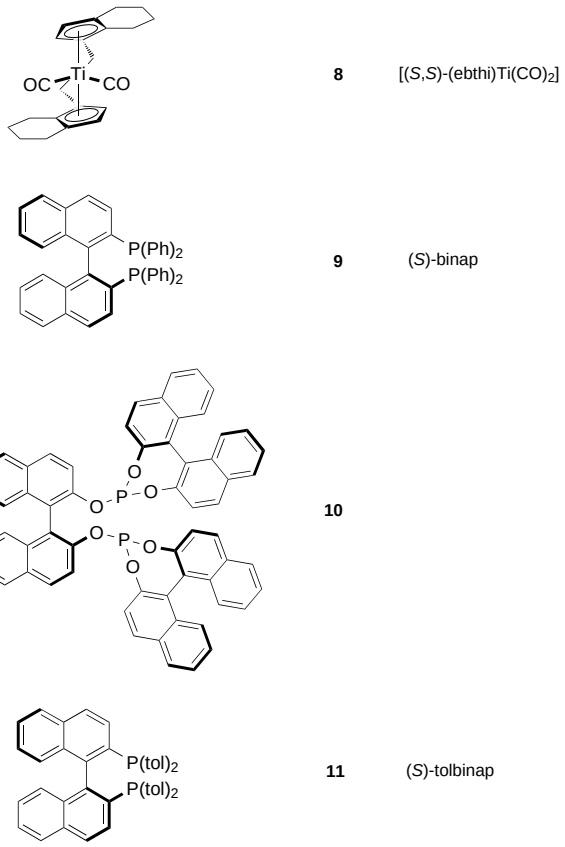


Scheme 12. Asymmetric CPKR employing the chiral titanocene complex **8** (Buchwald and Hicks).

as a catalyst for the cyclization of enynes under mild conditions, they succeeded in inducing asymmetry by employing the enantiomerically pure analogue (*S,S*)-$[(ebthi)Ti(CO)_2]$ (**8**)—generated in situ from (*S,S*)-$[(ebthi)Ti(Me)_2]$ (Scheme 13, ebthi = ethylene-1,2-bis(η^5-4,5,6,7-tetrahydro-1-indenyl)). This methodology showed some limitations in terms of substrate scope as a result of the sterically hindered nature of the ebthi ligand; otherwise good yields and *ee* values were obtained employing 0.05–0.2 equivalents of the catalyst. Subsequently the same group undertook a systematic study to develop an asymmetric protocol for nitrogen-containing enynes.[53] In the presence of (*S,S*)-$[(ebthi)Ti(Me)_2]$ precatalyst, high levels of enantioselectivity could be achieved for the cyclization of substrates bearing an electron-rich, sterically undemanding nitrogen substituent.

The first example of an asymmetric cobalt-catalyzed PKR was reported by Hiroi et al.,[54] who employed chiral phosphanes as ligands. The chelating diphosphane (*S*)-binap (**9**; Scheme 13) induced the highest enantioselectivity. Unfortunately, high catalyst loadings were required for this system and consequently the TONs were quite low. More recently, Buchwald and Sturla studied the influence of a chiral phosphite on the cobalt-catalyzed PKR.[55] The reaction conditions were optimized with respect to solvent, temperature, partial pressure of carbon monoxide, and ligand/metal ratio. Good *ee* values (64–75%) were obtained for just two substrates in the presence of $[Co_2(CO)_8]$ (0.06 equiv) and the chiral biaryl phosphite **10** (0.1 equiv; Scheme 13).

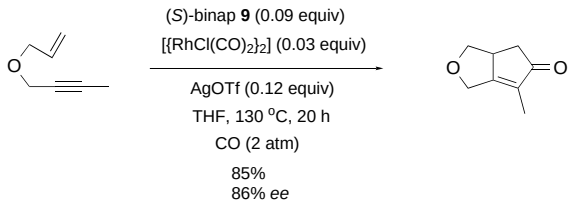
Following on the good results in their own work on a rhodium(I)-containing catalyst for the PKR,[47c] Jeong and coworkers recently reported an asymmetric rhodium-based system.[56] The conditions were optimized with respect to partial pressure of carbon monoxide, reaction temperature, and time. Good to very good *ee* values were found for a small



Scheme 13. Asymmetric ligands and catalysts employed in the CPKR.

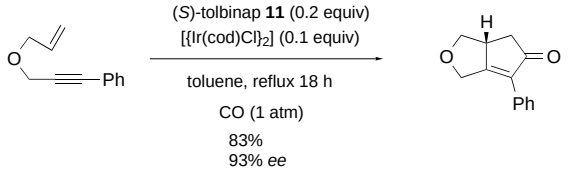
range of intramolecular substrates treated with $[\{RhCl(CO)_2\}_2]$ (0.03 equiv), (*S*)-binap (**9**) (0.09 equiv, Scheme 13), and AgOTf (0.12 equiv), as shown in Scheme 14.

In view of the interest in cobalt(0) and rhodium(I) catalysts, it was natural that attention would turn to iridium complexes at some point.[57] In preliminary studies by Shibata and Tagaki with a catalytic amount of $[\{Ir(cod)Cl\}_2]$ for the cyclization of a commonly used enyne, only relatively low conversions were achieved. After observing that the addition of phosphanes as coligands improved the yields of the reaction, Shibata and Tagaki decided to move directly to chiral phosphanes and examine the enantioselectivity of this protocol. Impressively, the use of (*S*)-tolbinap (**11**, Scheme 13) as an additive resulted in both excellent yields and enantiomeric excesses (Scheme 15). A small range of enynes were cyclized and the first catalytic example of an asymmetric intermolecular cyclization was reported.



Scheme 14. Rhodium-catalyzed asymmetric PKR under optimized conditions (Jeong et al.).[56]

 © 2003 Wiley-VCH Verlag GmbH & Co. KGaA, Weinheim



Scheme 15. Iridium-catalyzed asymmetric PKR employing the chiral diphosphane **11** (Shibata and Tagaki).[57]

5. Summary and Outlook

To rationalize all the results obtained thus far in the CPKR, we have analyzed all the catalytic systems reported and made a number of observations with respect to catalyst–substrate compatibility and to catalyst activity and practicability.

5.1. Substrate Compatibility

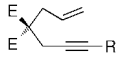
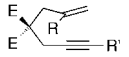
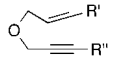
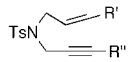
Before discussing our general observations on catalyst–substrate compatibility, it should be noted that different metals have been studied and documented to different degrees. Cobalt complexes are the most thoroughly investigated system,[58] followed by titanium[59] and rhodium[60] systems; only two reports on ruthenium complexes[45,46] and one on an iridium species[57] are available. As the nature of the catalytic species is unknown in most cases and to provide a simple comparison of catalyst activity, TONs have been calculated with respect to the number of moles of Co_1, Ti_1, Rh_1, Ru_1, and Ir_1 in the catalysts. Based on an analysis of all the results reported to date, the following observations can be tentatively made:

a) The PKR of enynes with terminal alkyne groups is more favorable under Co or Rh catalysis than under Ti catalysis (Table 6, entry 1).
b) Enynes with disubstituted alkyne groups are annelated better by Ti and Rh systems than by Co, Ru, and Ir systems (Table 6, entry 2).
c) Enynes with a disubstituted alkyne group and a substituted alkene function react well with Ti-based catalysts, but give poorer results with Co, Rh, and Ru catalysts (Table 6, entry 3).
d) Oxygen-containing enynes cyclize well in the presence of Ti-, Rh-, and Ru-based systems, but not with Co catalysts (Table 6 entry 4).[61]
e) Nitrogen-containing enynes react well under Rh and Ru catalysis, but not under Ti and Ir catalysis (Table 6, entry 5).
f) As a general trend, polar functionalities are tolerated better by late-transition-metal complexes (cobalt and rhodium) than by titanium complexes.
g) Enynes containing electron-withdrawing groups, either on the alkyne or on the alkene moiety, have been successfully cyclized only by Rh complexes under a particular set of conditions.[47b]
h) Intermolecular substrates have only really been examined with Co systems; in these cases, they show greater limitations than intramolecular substrates.

5.2. Catalyst Activity and Practicability

To identify the most attractive approaches to the CPKR, we have analyzed all the systems reported to date with respect to cost, sensitivity, and activity, as defined by TON.[7] The 16 systems that gave the best results are listed in Table 7. Given that TONs can be highly sensitive to the pressure of carbon monoxide employed, and that CO pressure may be a key concern for a potential user of the PKR, the systems have been divided into four groups: 1) systems that do not employ CO (Table 7, entries 1 and 2), 2) systems that employ 1 atm of CO (Table 7, entries 3–8), 3) systems that employ 5–7 atm CO (Table 7, entries 9–12), and 4) systems that employ 10–40 atm CO (Table 7, entries 13–16). Within these groups the systems are ranked with respect to TONs. The details in Table 7 should not be overinterpreted as the different catalysts reported have been employed under different reaction conditions (different temperatures, reaction times, and solvents).

Table 6: Average TONs observed with different metal-based complexes.

Entry	Substrates	TON Co[a]	TON Ti[b]	TON Rh[c]	TON Ru[d]	TON Ir[e]
1		12±4	4	14±10	8	–
2		10±5	18	20±10	13±2	4
3		10±5	19	7	12	–
4		2±2	18	14±7	12	4
5		10±4	6	16±6	15	4

[a] Average value according to references [8, 9a, 10, 16, 17, 26, 33]. [b] Average value according to references [43, 53]. [c] Average value according to references [47b,c, 50, 51]. [d] Average value according to references [45, 46]. [e] The generally low values observed herein may be a function of the high catalyst loading employed to obtain good enantioselectivity.[57]

 © 2003 Wiley-VCH Verlag GmbH & Co. KGaA, Weinheim

Table 7: Catalyst activity and practicability.

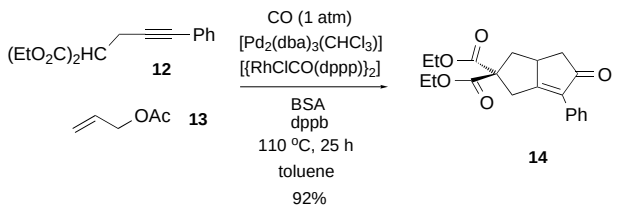
Entry	Catalyst system	p(CO) [atm]	TON[a]	Cost	Sensitivity grade[b]
1[51]	$[Rh(dppp)_2Cl]$	0	20–11	–	–
2[50]	$[\{RhCl(cod)\}_2]$	0	10–7	high	1
3[47b]	$[\{RhCl(CO)_2\}_2]$	1	82–7	high	3
4[43]	$[Cp_2Ti(CO)_2]$	1.22	19–9	high	4
5[17]	$[Co_2(CO)_8]+R_3PS$	1	16–4	low	3
6[33]	$[Ph_3PCo_2(CO)_7]$	1.05	11–5	–	1
7[8]	$[Co_2(CO)_8]+h\nu$	1	10–7	low	3
8[16]	$[Co_2(CO)_8]+CyNH_2$	1	10–4	low	3
9[14]	$[Co_2(CO)_8]+DME$	7	50–36	low	3
10[26]	$[Co_3(CO)_9(\mu^3\text{-}CH)]$	7	17–4	–	2
11[28]	$[Co_4(CO)_{12}]$[c]	5	7–2	medium	2
12[28]	$[Co_4(CO)_{11}P(OPh)_3]$[c]	5	7–2	–	1
13[20]	$[Co(acac)_2]+NaBH_4$	30–40	100–7	low	0
14[18]	indenyl cobalt(I)	15	97–10	–	0
15[27]	$[Co_4(CO)_{12}]$	10	50–38	medium	2
16[45,46]	$[Ru_3(CO)_{12}]$	10–15	16–7	medium	1

[a] TONs calculated with respect to the number of moles of Co_1, Ti_1, Rh_1, and Ru_1 in the catalysts. [b] 0 = stable, 4 = highly sensitive. [c] Reaction run in supercritical ethene.

5.3. Tandem Reactions—The Shape of Things to Come

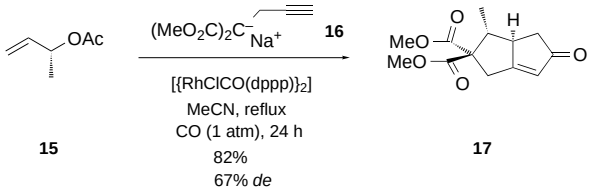
Before ending this report on the CPKR we would like to highlight one of its most promising areas of application. It is common knowledge that in living organisms most of the required metabolites are synthesized by a programmed sequence of enzymes that show high specificity towards the different intermediates involved. Consequently, as an extension of the principle of atom economy,[1] a whole sequence of organic reactions should ideally be carried out in one pot, employing a range of catalysts that likewise show high specificity towards the different substrates. Tandem reactions, in which one or more catalysts are employed in one pot, can be considered as an approach to this ideal situation. Demonstrations of this strategy employing some of the most recently developed catalysts for the PKR are starting to appear in the literature.[62]

In one of the first examples, Jeong et al. reported that the catalytic combination of $[Pd_2(dba)_3(CHCl_3)]$ with $[\{RhCl(CO)(dppp)\}_2]$ converts the malonate derivative **12** and allyl acetate **13** into the bicyclic cyclopentenone **14** in high yield (Scheme 16) through a palladium-catalyzed allylic substitution and a rhodium-catalyzed PKR.[62a,b]



Scheme 16. Tandem palladium and rhodium catalysis (Jeong et al.):[62a,b] **12** (1 equiv), **13** (2 equiv), $[Pd_2(dba)_3(CHCl_3)]$ (0.015 equiv), $[\{RhClCO(dppp)\}_2]$ (0.07 equiv), dppb (0.03 equiv), and BSA (1.2 equiv). BSA = bis(trimethylsilyl)acetamide.

A different approach was subsequently reported by Evans and Robinson. Cyclopentenone **17** was synthesized from allylic acetate **15** and the nucleophile **16** (prepared in situ by deprotonation of the malonate with a strong base) in the presence of catalytic rhodium-based complex $[\{RhClCO(dppp)\}_2]$ according to Scheme 17.[62c]



Scheme 17. The rhodium-catalyzed tandem reactions (Evans and Robinson):[62c] **16** (1.2 equiv) and $[\{RhClCO(dppp)\}_2]$ (0.06 equiv).

5.4. Final Comments

The catalytic protocols available in the literature represent excellent alternatives to the stoichiometric reaction types studied to date. And so, in view of the need for even more economic and environmentally friendly processes, high priority should now be given to the application and development of the catalytic PKR rather than to the stoichiometric version. In particular, the substrate scope needs to be broadened, especially to include more-demanding intermolecular systems, while convincing catalytic applications of the PKR in the synthesis of more-sophisticated molecules would strengthen this approach even further.

Asymmetric catalysis of the PKR is now a viable process and we are confident that developments in coming years will produce an efficient approach to chiral cyclopentenones, effectively replacing the currently favored noncatalytic chiral-auxiliary approach. From a personal perspective, the authors believe that recent developments in the areas of CO-free catalysis[50,51] and one-pot multicomponent catalysis[62] are very exciting and we look forward to seeing these areas develop in the near future.

Received: July 25, 2002 [A547]

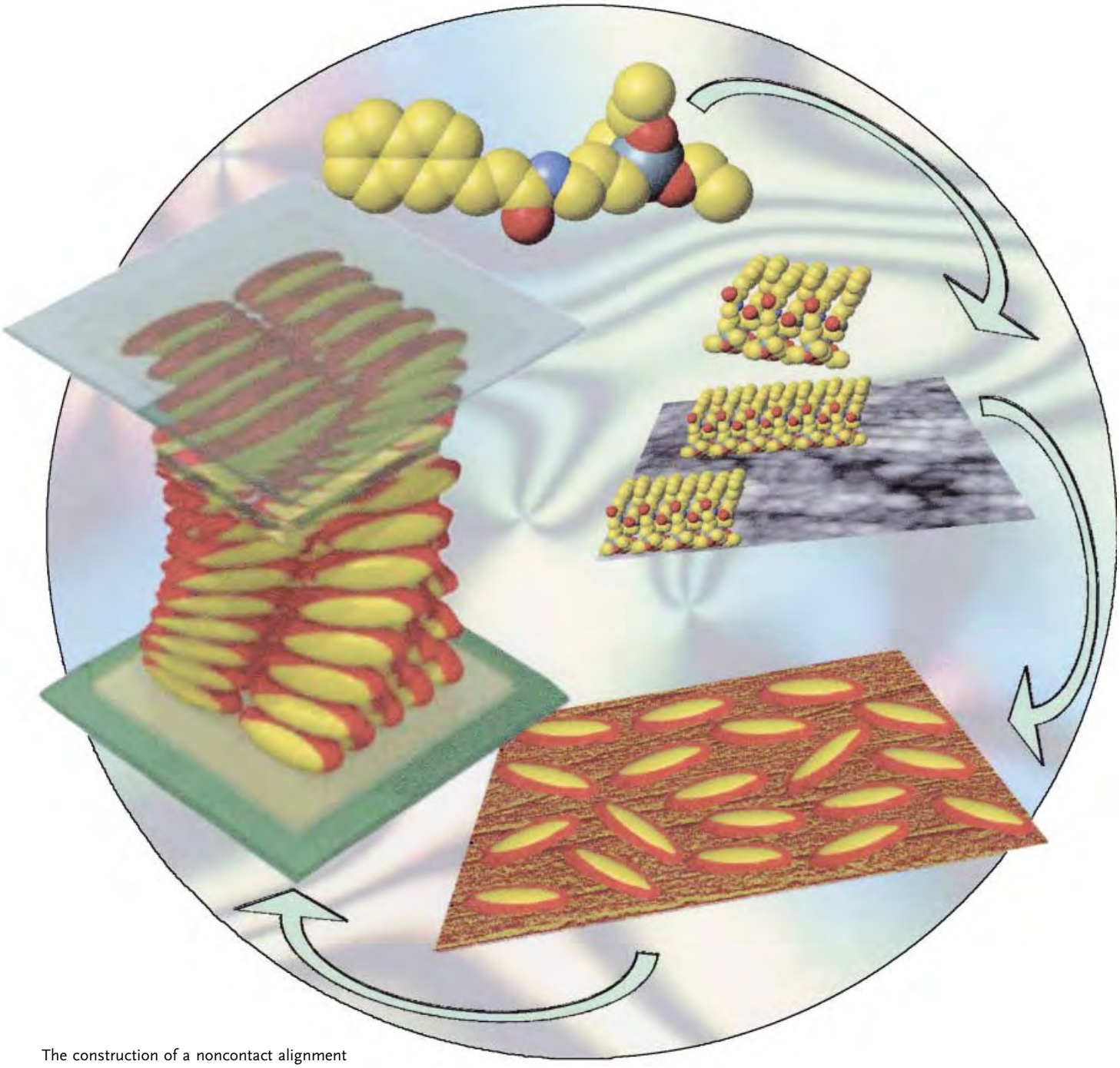
[1] B. M. Trost, *Angew. Chem.* **1995**, *107*, 285; *Angew. Chem. Int. Ed. Engl.* **1995**, *34*, 259.
[2] I. U. Khand, G. R. Knox, P. L. Pauson, W. E. Watts, *J. Chem. Soc. D* **1971**, 36.
[3] I. U. Khand, G. R. Knox, P. L. Pauson, W. E. Watts, M. I. Foreman, *J. Chem. Soc. Perkin Trans. 1* **1973**, 977.
[4] For recent reviews of the PKR, see: a) H.-W. Frühauf, *Chem. Rev.* **1997**, *97*,523; b) O. Geis, H.-G. Schmalz, *Angew. Chem.* **1998**, *110*, 955; *Angew. Chem. Int. Ed.* **1998**, *37*, 911; c) K. M. Brummond, J. L. Kent, *Tetrahedron* **2000**, *56*, 3263; d) A. J. Fletcher, S. D. R. Christie, *J. Chem. Soc. Perkin Trans. 1* **2000**, 1657; e) B. E. Hanson, *Comments Inorg. Chem.* **2002**, *23*, 289.
[5] a) S. T. Ingate, J. M. -Contelles, *Org. Prep. Proced. Int.* **1998**, *30*, 121; b) S. L. Buchwald, F. A. Hicks in *Comprehensive Asym-*

 © 2003 Wiley-VCH Verlag GmbH & Co. KGaA, Weinheim

metric Catalysis I-III, Vol. 2 (Eds.: E. N. Jacobsen, A. Pfaltz, H. Yamamoto), Springer, **1999**, p. 491.
[6] V. Rautenstrauch, P. Mégard, J. Conesa, W. Küster, *Angew. Chem.* **1990**, *102*, 1441; *Angew. Chem. Int. Ed. Engl.* **1990**, *29*, 1413.
[7] TONs have always been calculated with respect to the number of moles of Co_1, Ti_1, Rh_1, Ru_1, and Ir_1 in the catalysts (see Section 5.1).
[8] B. L. Pagenkopf, T. Livinghouse, *J. Am. Chem. Soc.* **1996**, *118*, 2285.
[9] a) D. B. Belanger, D. J. R. O. 'Mahony, T. Livinghouse, *Tetrahedron Lett.* **1998**, *39*, 7637; b) it was shown recently that the selectivity of the CPKR can be improved by substrate modification through alkyne sulfenylation; see: B. L. Pagenkopf, D. B. Belanger, D. J. R. O'Mahony, T. Livinghouse, *Synthesis* **2000**, *7*, 1009.
[10] N. Jeong, S. H. Hwang, Y. Lee, Y. K. Chung, *J. Am. Chem. Soc.* **1994**, *116*, 3159.
[11] a) P. Magnus, L. M. Principe, M. J. Slater, *J. Org. Chem.* **1987**, *52*, 1483; b) I. U. Khand, G. R. Knox, P. L. Pauson, W. E. Watts, *J. Chem. Soc. Perkin Trans. 1* **1973**, 975, and references therein.
[12] D. C. Billington, I. M. Helps, P. L. Pauson, W. Thomson, D. Willison, *J. Organomet. Chem.* **1988**, *354*, 233.
[13] T. Sugihara, M. Yamada, H. Ban, M. Yamaguchi, C. Kaneko, *Angew. Chem.* **1997**, *109*, 2884; *Angew. Chem. Int. Ed. Engl.* **1997**, *36*, 2801.
[14] T. Sugihara, M. Yamaguchi, *Synlett* **1998**, 1384.
[15] DME is the most common solvent employed in the CPKR. See, for example, references [8–10, 16, 18, 24, 25, 33].
[16] M. E. Krafft, L. V. R. Bonaga, C. Hirosawa, *Tetrahedron Lett.* **1999**, *40*, 9171.
[17] M. Hayashi, Y. Hashimoto, Y. Yamamoto, J. Usuki, K. Saigo, *Angew. Chem.* **2000**, *112*, 645; *Angew. Chem. Int. Ed.* **2000**, *39*, 631.
[18] B. Y. Lee, Y. K. Chung, N. Jeong, Y. Lee, S. H. Hwang, *J. Am. Chem. Soc.* **1994**, *116*, 8793.
[19] a) M. Lautens, W. Tam, C. Sood, *J. Org. Chem.* **1993**, *58*, 4513; b) M. Lautens, W. Tam, J. C. Lautens, L. G. Edwards, C. M. Crudden, A. C. Smith, *J. Am. Chem. Soc.* **1995**, *117*, 6863.
[20] N. Y. Lee, Y. K. Chung, *Tetrahedron Lett.* **1996**, *37*, 3145.
[21] T. Rajesh, M. Periasamy, *Tetrahedron Lett.* **1999**, *40*, 817.
[22] P. L. Pauson, *Tetrahedron* **1985**, *41*, 5855.
[23] D. C. Billington, *Tetrahedron Lett.* **1983**, *24*, 2905.
[24] D. B. Belanger, T. Livinghouse, *Tetrahedron Lett.* **1998**, *39*, 7641.
[25] M. E. Krafft, C. Hirosawa, L. V. R. Bonaga, *Tetrahedron Lett.* **1999**, *40*, 9177.
[26] a) T. Sugihara, M. Yamaguchi, *J. Am. Chem. Soc.* **1998**, *120*, 10782; b) T. Sugihara, M. Yamaguchi, M. Nishizawa, *Chem. Eur. J.* **2001**, *7*, 1589.
[27] J. W. Kim, Y. K. Chung, *Synthesis* **1998**, 142.
[28] N. Jeong, S. H. Hwang, *Angew. Chem.* **2000**, *112*, 650; *Angew. Chem. Int. Ed.* **2000**, *39*, 636.
[29] a) M. E. Krafft, L. V. R. Boñaga, *Angew. Chem.* **2000**, *112*, 3822; *Angew. Chem. Int. Ed.* **2000**, *39*, 3676; b) M. E. Krafft, L. V. R. Boñaga, C. Hirosawa, *J. Org. Chem.* **2001**, *66*, 3004.
[30] See reference [26a] and references therein.
[31] N. Jeong, S. H. Hwang, Y. W. Lee, J. S. Lim, *J. Am. Chem. Soc.* **1997**, *119*, 10549.
[32] A. C. Comely, S. E. Gibson, A. Stevenazzi, N. J. Hales, *Tetrahedron Lett.* **2001**, *42*, 1183.
[33] S. E. Gibson, C. Johnstone, A. Stevenazzi, *Tetrahedron* **2002**, *58*, 4937.
[34] a) A. C. Comely, S. E. Gibson, N. J. Hales, *Chem. Commun.* **2000**, 305; b) A. C. Comely, S. E. Gibson, N. J. Hales, *Chem. Commun.* **1999**, 2075.
[35] S. -W. Kim, S. U. Son, S. I. Lee, T. Hyeon, Y. K. Chung, *J. Am. Chem. Soc.* **2000**, *122*, 1550.
[36] S. U. Son, S. I. Lee, Y. K. Chung, *Angew. Chem.* **2000**, *112*, 4318; *Angew. Chem. Int. Ed.* **2000**, *39*, 4158.
[37] S. -W. Kim, S. U. Son, S. S. Lee, T. Hyeon, Y. K. Chung, *Chem. Commun.* **2001**, 2212.
[38] S. U. Son, S. I. Lee, Y. K. Chung, S. -W. Kim, T. Hyeon, *Org. Lett.* **2002**, *4*, 277.
[39] E. -i. Negishi, S. J. Holmes, J. M. Tour, J. A. Miller, *J. Am. Chem. Soc.* **1985**, *107*, 2568.
[40] R. B. Grossman, S. L. Buchwald, *J. Org. Chem.* **1992**, *57*, 5803.
[41] a) S. C. Berk, R. B. Grossman, S. L. Buchwald, *J. Am. Chem. Soc.* **1993**, *115*, 4912; b) S. C. Berk, R. B. Grossman, S. L. Buchwald, *J. Am. Chem. Soc.* **1994**, *116*, 8593.
[42] F. A. Hicks, S. C. Berk, S. L. Buchwald, *J. Org. Chem.* **1996**, *61*, 2713.
[43] a) F. A. Hicks, N. M. Kablaoui, S. L. Buchwald, *J. Am. Chem. Soc.* **1996**, *118*, 9450; b) F. A. Hicks, N. M. Kablaoui, S. L. Buchwald, *J. Am. Chem. Soc.* **1999**, *121*, 5881.
[44] M. Zhang, S. L. Buchwald, *J. Org. Chem.* **1996**, *61*, 4498.
[45] T. Morimoto, N. Chatani, Y. Fukumoto, S. Murai, *J. Org. Chem.* **1997**, *62*, 3762.
[46] T. Kondo, N. Suzuki, T. Okada, T. -A. Mitsudo, *J. Am. Chem. Soc.* **1997**, *119*, 6187.
[47] a) Y. Koga, T. Kobayashi, K. Narasaka, *Chem. Lett.* **1998**, 249; b) T. Kobayashi, Y. Koga, K. Narasaka, *J. Organomet. Chem.* **2001**, *624*, 73; c) N. Jeong, S. Lee, B. K. Sung, *Organometallics* **1998**, *17*, 3642; d) C. Mukai, I. Nomura, K. Yamanishi, M. Hanaoka, *Org. Lett.* **2002**, *4*, 1755; e) K. M. Brummond, H. Chen, K. D. Fisher, A. D. Kerekes, B. Rickards, P. C. Sill, S. J. Geib, *Org. Lett.* **2002**, *4*, 1931.
[48] N. E. Shore, *Synth. Commun.* **1979**, *9*, 41.
[49] M. E. Krafft, L. V. R. Boñaga, *Synlett* **2000**, *7*, 959.
[50] T. Morimoto, K. Fuji, K. Tsutsumi, K. Kakiuchi, *J. Am. Chem. Soc.* **2002**, *124*, 3806.
[51] T. Shibata, N. Toshida, K. Takagi, *Org. Lett.* **2002**, *4*, 1619.
[52] a) F. A. Hicks, S. L. Buchwald, *J. Am. Chem. Soc.* **1996**, *118*, 11688; b) F. A. Hicks, S. L. Buchwald, *J. Am. Chem. Soc.* **1999**, *121*, 7026.
[53] S. J. Sturla, S. L. Buchwald, *J. Org. Chem.* **1999**, *64*, 5547.
[54] a) K. Hiroi, T. Watanabe, R. Kawagishi, I. Abe, *Tetrahedron Lett.* **2000**, *41*, 891; b) K. Hiroi, T. Watanabe, R. Kawagishi, I. Abe, *Tetrahedron: Asymmetry* **2000**, *11*, 797.
[55] S. J. Sturla, S. L. Buchwald, *J. Org. Chem.* **2002**, *67*, 3398.
[56] N. Jeong, B. K. Sung, Y. K. Choi, *J. Am. Chem. Soc.* **2000**, *122*, 6771.
[57] T. Shibata, K. Takagi, *J. Am. Chem. Soc.* **2000**, *122*, 9852.
[58] See, for example, references [8, 9a, 10, 16, 17, 26, 33].
[59] See, for example, references [43, 53].
[60] See, for example, references [47b,c, 50, 51].
[61] As reported by Jeong et al., propargyl allyl ether–dicobalt–carbonyl complexes are quite sensitive to acids.[10]
[62] a) N. Jeong, S. D. Seo, J. Y. Shin, *J. Am. Chem. Soc.* **2000**, *122*, 10220; b) N. Jeong, B. K. Sung, J. S. Kim, S. B. Park, S. D. Seo, J. Y. Shin, K. Y. In, Y. K. Choi, *Pure Appl. Chem.* **2002**, *74*, 85; c) P. A. Evans, J. E. Robinson, *J. Am. Chem. Soc.* **2001**, *123*, 4609; d) S. U. Son, K. H. Park, H. Seo, Y. K. Chung, S. -G. Lee, *Chem. Commun.* **2001**, 2440.

 © 2003 Wiley-VCH Verlag GmbH & Co. KGaA, Weinheim

Communications



The construction of a noncontact alignment layer for the preparation of a liquid-crystal display is shown. Supramolecular interactions underpin a hierarchical process, in which molecular recognition in solution leads to the production of rigid oligomers that graft onto nanosized alignment seeds at an ITO surface. The resulting grooved surface, and its properties and applications, are described by Nolte and co-workers on the following pages...

DOI: 10.1002/anie.200250394
© 2003 Wiley-VCH Verlag GmbH & Co. KGaA, Weinheim

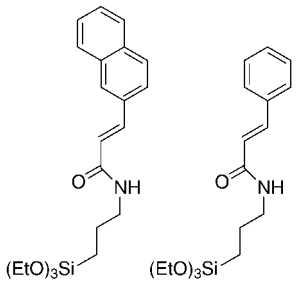
Liquid-Crystal Alignment

Noncontact Liquid-Crystal Alignment by Supramolecular Amplification of Nanogrooves**

*Johan Hoogboom, Mohammad Behdani, Johannes A. A. W. Elemans, Marijn A. C. Devillers, René de Gelder, Alan E. Rowan, Theo Rasing, and Roeland J. M. Nolte**

The construction of surfaces that control the orientation of liquid crystals (LCs) is of key importance in liquid-crystal display (LCD) technology. Current industrial manufacture of such surfaces involves the mechanical rubbing of polymers, which have been spin-coated onto an indium-tin oxide (ITO) surface, with a velvet cloth. This creates microscopic grooves on the surface, which form an alignment layer that causes the LCs to align in the direction of rubbing.[1] The invasive nature of this process causes the surface to be prone to the generation of electrostatic charges and to contamination from, for example, dust particles, which can lead to faulty pixels in the final product. Therefore, the development of less contact-intensive techniques to achieve LC alignment is a prerequisite for the production of cheap, large LCD screens.[2] In this report, we describe a very simple, robust, and completely non-contact method for creating an alignment layer, which eliminates the need for clean rooms, and is based on a hierarchical process involving supramolecular interactions and surface grafting that results in a more than 1000-fold amplification of the initial ITO surface ordering.

One widely investigated alternative to mechanical rubbing is photoinduced alignment, in which a cinnamic acid derivative is deposited onto a surface and irradiated with linearly polarized (UV) light.[2b,3] Although this procedure induces enough surface ordering for LC alignment, in most cases there is little control over the orientation of the photoswitches on the surface and the interaction with the LC is poor, compared to conventionally manufactured alignment layers. To have more control over the surface orientation, we designed and synthesized compound **1**, which can be covalently linked to the ITO surface. It contains a photoswitch with a large aromatic surface and an amide group, both of which can be expected to increase intermolecular interaction by π stacking and hydrogen bonding, possibly resulting in a surface which is better preorganized for LC alignment.



1 **2**

A twisted nematic LCD (TN-LCD) was constructed by using one plate covered with **1** (from immersion in a 2 wt % toluene solution), without any conventional treatment to form an alignment layer (for example, irradiation with UV light or rubbing), and a conventionally rubbed polyimide (PI) counterplate (Figure 1 a). To our surprise, optical microscopy showed that about 80 % of this cell was capable of liquid-crystal alignment. Scanning electron microscopy (SEM) and tapping-mode atomic force microscopy (TM-AFM) studies on the plates containing **1** revealed that the surface contained large domains of groove-like structures, which resemble those present in conventionally rubbed polymer alignment layers.[1b] The inherent ITO topography can alone serve as a template on which the grooves develop (see below). The grooves were 0.5–8.0 nm deep and hundreds of micrometers long (Figure 2 a and c). TM-AFM also showed that the width of the grooves are mainly found in two sizes; the largest have a width of 150–200 nm, while the smallest have an average width of 50 nm, the latter being the most predominant. The direction of the grooves could not be attributed to any dipping effect or flow effect; they were found to be independent even of intentionally induced flow or dipping. Furthermore, the grooves were not formed during the baking process (for example, by film cracking), as on unbaked plates the same structures were also formed.

The azimuthal anchoring energy (W_ϕ), which is an indication of the interaction energy between the alignment layer and the LC, was measured to be 1.8×10^{-5} J m^{-2} by using the cell-rotation method.[1b] This value is of the same order of magnitude as found for conventionally rubbed polymer alignment layers[1b] and about 20 times higher than observed for cinnamic acid-based systems in the literature,[2b,3a–3c,4] which suggests that increasing the π-electronic character of the molecules in the alignment layer improves the interaction with the LC molecules. Furthermore, attempts to change the alignment direction induced by the surface by irradiating the photoswitches with (polarized) light did not succeed, which is an indication that the LC-alignment capability of the surface is quite strong.

To investigate the origin of the formation of the alignment layer in more detail, a series of experiments was carried out. Ellipsometry measurements showed that the surface features

[*] Prof. Dr. R. J. M. Nolte, J. Hoogboom, Dr. J. A. A. W. Elemans, Dr. M. A. C. Devillers, Dr. R. de Gelder, Dr. A. E. Rowan, Prof. Dr. T. Rasing
NSRIM
University of Nijmegen
Toernooiveld 1, NL-6525ED Nijmegen (The Netherlands)
Fax: (+31) 24-3652929
E-mail: nolte@sci.kun.nl
Dr. M. Behdani
Department of Physics
University of Birjand, Birjand (Iran)

[**] We thank Huub P. M. Geurts and Dr. Pall Thordarson for experimental assistance and Dr. Abbas Rastegar for useful discussions. These studies were supported by the Dutch Technology Foundation (STW), project number NNS4857.

Supporting information for this article is available on the WWW under http://www.angewandte.org or from the author.

 © 2003 Wiley-VCH Verlag GmbH & Co. KGaA, Weinheim DOI: 10.1002/anie.200250394

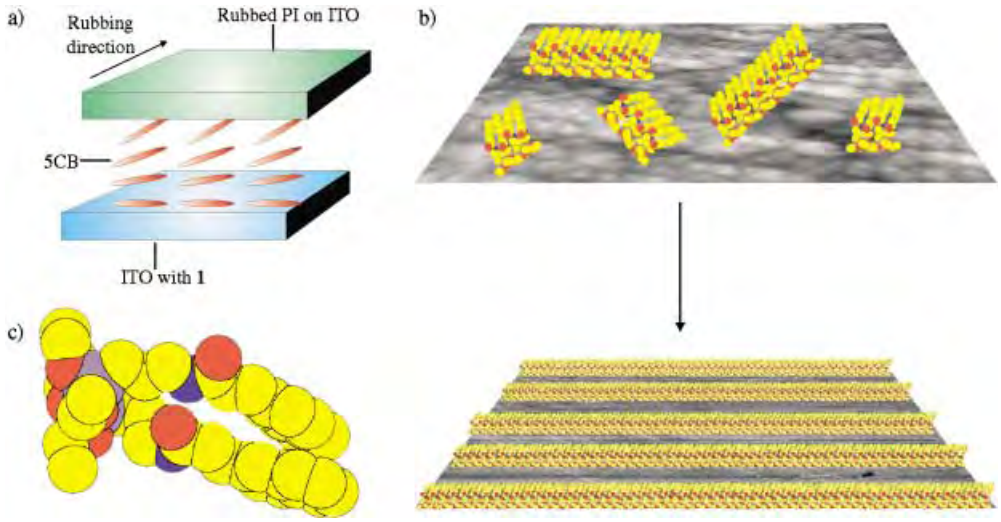


Figure 1. a) Schematic drawing of a twisted nematic LCD; 4-*n*-pentyl-4′-cyanobiphenyl (5CB) was used as the LC; b) proposed alignment of covalently linked oligomers of **1** on the surface of ITO resulting in a more than 1000-fold amplification of the initial ordering; c) lowest-energy structure (PM3) of the dimer of **1**.

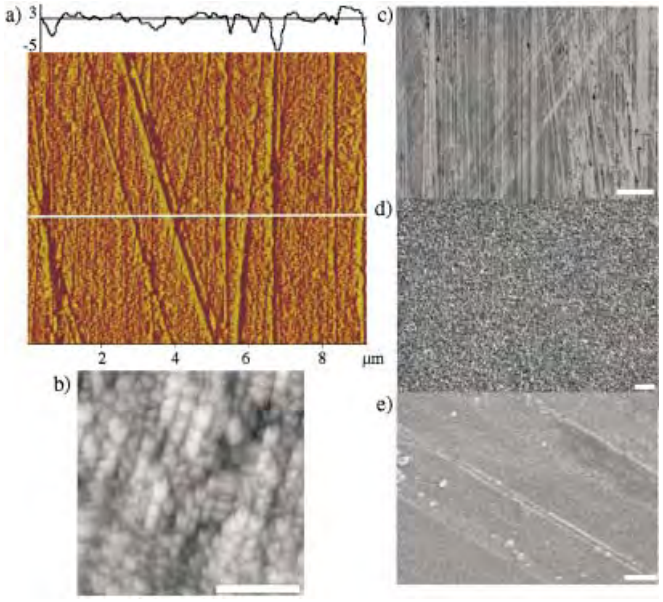


Figure 2. a) TM-AFM image of an ITO plate covered with **1**, above: the height profile along the displayed white line (nm); b) STM image of a blank ITO surface (bar = 100 nm); SEM images of ITO plates covered with: c) **1** from a 2 wt% solution at room temperature (bar = 10 µm); d) **2** from a 2 wt% solution at room temperature (bar = 1 µm); e) **1** from a 2 wt% solution at 90 °C (bar = 1 µm).

were formed within 6 min of the immersion of the plates into a monomer solution. From the ellipsometry data, a layer thickness of 8.0 ± 2.0 nm was calculated, which is in excellent agreement with the TM-AFM results. Since the length of a fully elongated molecule of **1** is only 1.6 nm, it can be assumed that the surface is partly covered by multilayers of **1**.

To determine the role π–π interactions and hydrogen bonding play in the formation of the alignment layer, reference compound **2** was synthesized. Although its crystal structure clearly showed the presence of a hydrogen-bonded array (Figure 3),[5] with the aromatic groups preorganized for LC alignment, ITO plates covered with **2** did not exhibit any grooves (Figure 2d), nor did they show LC-alignment capability. To explain this remarkable difference to **1**, we studied molecular recognition interactions for both molecules, in particular their self-association in solution and hydrogen-bond strength. Although the interactions are weak at the concentrations studied (0.2–20 wt% in toluene), it was clear that compound **1** formed stronger intermolecular hydrogen bonds than **2**. For instance, in 2 wt% solutions, the NH signals for **1** and **2** in their ^{1}H NMR spectra appeared at a $\delta = 5.45$ and 4.91 ppm, respectively. This difference was retained in the solid state, as highlighted by the frequency shifts between the

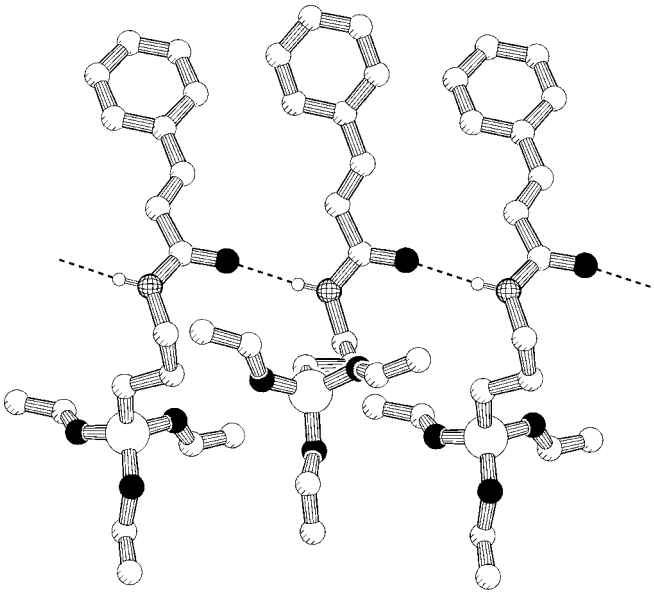


Figure 3. Representation of the unit cell of **2**, as determined by X-ray diffraction. Hydrogen atoms, except amide protons, are omitted for clarity. Hydrogen bonds are indicated by a dotted line.

 © 2003 Wiley-VCH Verlag GmbH & Co. KGaA, Weinheim

two amide stretching vibrations ($\Delta\tilde{\nu}$) in their IR spectra, which were 97 and 105 cm^{-1} for **1** and **2**, respectively. Although we were not able to obtain crystals of **1** that were suitable for X-ray diffraction, the NMR and IR measurements suggest that hydrogen bonding occurs in the same geometry as between the molecules of **2**.

In solutions of **1** in toluene, covalently linked oligomers were shown to precipitate. Of these oligomers, only the dimer could be studied in solution; higher oligomers could not be redissolved. In a concentration range of 1–10 wt % in toluene, no oligomerization was observed for **2**. The dimer of **1** appeared to have a very strong intramolecular hydrogen bond; ^{1}H NMR spectroscopy showed an amide signal in THF at $\delta = 7.02$ ppm. In addition, 2D-NOESY measurements indicated that the dimer has a very well defined preferential geometry (Figure 1c). Solid-state IR spectroscopy displayed a very sharp NH stretching vibration at 3304 cm^{-1}, which indicates that the direction of the intramolecular hydrogen bond in the dimer is very well defined. With MALDI-TOF spectrometry, linear oligomers up to a heptamer and cyclic oligomers up to a decamer were observed. Solid-state IR spectroscopy showed two sharp NH stretching vibrations at 3421 and 3286 cm^{-1} for the mixture of oligomers, which also indicates strong, well defined, directional hydrogen bonding. The above data indicates that intramolecular hydrogen bonding is required for forming structurally well-defined oligomers.[6]

To investigate the role of the surface in the formation of the grooves, **1** was deposited onto isotropic quartz from 1–5 wt % solutions in toluene. The resulting surfaces displayed no grooves and did not show LC alignment, an indication that the ITO surface fulfils a crucial role in the formation of the alignment layer. Furthermore, scanning tunneling microscopy (STM) showed that the blank ITO surfaces used in these experiments intrinsically contain alignment seeds, so-called "nanogrooves". These ordered regions have dimensions of approximately 100×100 nm, are all aligned parallel to each other (see below), and are surrounded by isotropic ITO (Figure 2b). It is known that the morphology of the blank ITO surface can be strongly dependent on deposition conditions (for example, pressure, temperature, and ITO composition), and the occurrence of similar structures has been observed before.[7] To determine whether the surface controls the groove direction, an ITO plate was cut in half and the pieces were positioned at 90° with respect to each other in a 2 wt % solution of **1**. After the formation of the alignment layer, the direction of the grooves was found to be dependent on the initial rotation of the ITO plate in the solution, which shows that the underlying ITO dictates their general direction. Apparently, the chemisorption of **1** on to the ITO plate causes the small degree of surface-ordering to be amplified more than a thousand times.

The combined experimental results suggest that the deposition of structurally well-defined linear and cyclic oligomers of **1** amplifies the small groove-like surface features which are initially present on the ITO surface, and results in the formation of long parallel grooves (Figure 1b). Under layer-forming conditions, there are two (competing) processes: oligomerization in solution and surface grafting. Although the rate of the grafting reaction is not easily altered, the oligomerization can be influenced by changing the reaction conditions. When the concentration of **1** was lowered to 1 wt % or increased to 4 or 5 wt %, which respectively slows down and increases the oligomerization rate, the surface contained no discernable features. An increase in temperature to 90 °C, which accelerates the oligomerization reaction, resulted in a surface with approximately 85 % less grooves (Figure 2e). None of these samples were capable of LC alignment. In the latter case, this is probably a result of the fact that the distance between the grooves is larger than the correlation length of the LC.[8] These experiments indicate that the fine balance between the rate of grafting and the formation of oligomers is a key factor in the formation of the grooves, which, in turn, is essential for successful LC alignment.

In summary, we have presented an easy and robust, noncontact procedure for constructing an alignment layer for LC alignment, based on a hierarchical process involving a combination of supramolecular interactions and surface grafting. The initial surface-ordering is amplified over a thousand times, going from small 100 nm-sized parallel domains already present on the underlying ITO surface, to spontaneously formed 100-μm long, aligned grooves that resemble those observed for conventionally rubbed polymer alignment layers. The present system displays an anchoring energy which is 20 times higher than that measured for comparable systems in the literature, and is in the same order of magnitude as observed for conventionally rubbed polymer alignment layers. Present research is focused on the effect of larger aromatic head groups on the surface morphology, and their influence on the LC alignment.

Experimental Section

TN-LCD cells with a thickness of 6 μm (Mylar spacer) were prepared according to the literature.[1b] The ITO used in these experiments was purchased from the Applied Film Corporation (6797 Winchester Circle, Boulder, CO 80301, USA); the exact manufacturing process is unknown to the authors. Ellipsometry measurements indicated that the ITO plates consisted of 20-nm thick ITO layer, coated by rf sputtering, over a polycrystalline SiO_2 layer (20 nm) on a 1.1-mm soda lime glass substrate (BK7). The ITO layer was polished by the manufacturer to obtain optical quality for LCD application. Sample plates were prepared by immersing an ozone-cleaned ITO or quartz plate in a solution of **1** or **2** in toluene, with a drop of acetic acid which serves to activate the surface. After one hour, the plates were washed with dry acetonitrile and baked at 120 °C for 10 min. The PI counterplate was prepared by spin-coating with a 2 wt % solution of Pyralin PI2555 (HD Microsystems) in 1-methyl-2-pyrrolidinone, after which it was baked at 180 °C for 60 min. The plate was rubbed with a home-built rubbing machine. LP-UV irradiation was achieved with a 150 W Xe lamp, $180 < \lambda < 350$ nm, at an intensity of 0.15 mW cm^{-2} for 20 min. The cells were filled with 4-*n*-pentyl-4′-cyanobiphenyl (5CB; $T_{NI} = 35.3$ °C), heated to 40 °C, and then cooled to room temperature. In all experiments, at least five plates were examined. Seven working TN-cells were made of ITO with **1** and rubbed PI.

Received: October 21, 2002 [Z50394]

Keywords: hydrogen bonds · liquid crystals · pi interactions · self-assembly · supramolecular chemistry

[1] a) D. W. Berreman, *Phys. Rev. Lett.* **1972**, *28*, 1683; b) A. Rastegar, M. Škarabot, B. Blij, T. Rasing, *J. Appl. Phys.* **2001**, *89*, 960; c) N. Ito, K. Sakamoto, R. Arafune, S. Ushioda, *J. Appl. Phys.* **2000**, *88*, 3235; d) C. L. H. Devlin, S. D. Glab, S. Chiang, T. P. Russell, *J. Appl. Polym. Sci.* **2001**, *80*, 1470.

[2] a) J. van Haaren, *Nature* **2001**, *411*, 29; b) M. Schadt, K. Schmitt, V. Kozinkov, V. Chigrinov, *Jpn. J. Appl. Phys.* **1992**, *31*, 2155; c) M. Schadt, H. Seiberle, A. Schuster, *Nature* **1996**, *381*, 212; d) W. M. Gibbons, P. J. Shannon, S.-T. Sun, B. J. Swetlin, *Nature* **1991**, *351*, 49; e) R. Penterman, S. I. Klink, H. de Koning, G. Nisato, D. J. Broer, *Nature* **2002**, *417*, 55.

[3] a) G. P. Ryan-Brown, I. C. Sage, *Liq. Cryst.* **1996**, *20*, 825; b) J. Liu, X. Liang, H. Gao, *Jpn. J. Appl. Phys.* **2000**, *39*, 1221; c) J. L. Lenhart, J. H. van Zanten, J. P. Dunkers, R. S. Parnas, *Langmuir* **2000**, *16*, 8145; d) K. Ichimura, Y. Akita, H. Akiyama, K. Kudo, Y. Hayashi, *Macromolecules* **1997**, *30*, 903; e) J. Naciri, J. Y. Fang, M. Moore, D. Shenoy, C. S. Dulcey, R. Shashidhar, *Chem. Mater.* **2000**, *12*, 3288; f) J. Y. Fang, M.-S. Chen, R. Shashidhar, *Langmuir* **2001**, *17*, 1549.

[4] N. Klopcar, I. Drevensik-Olenik, M. Copic, M.-W. Kim, A. Rastegar, T. Rasing, *Mol. Cryst. Liq. Cryst.* **2001**, *368*, 4163.

[5] X-ray crystal data for **2** at 293 K ($C_{18}H_{29}NO_4Si$, $M_r = 351.51$): monoclinic, space group $P2_1/a$, $\rho_{calcd} = 1.143\ g\,cm^{-3}$, $Z = 4$, $a = 9.7056(10)$, $b = 17.8378(17)$, $c = 12.599(2)$ Å, $\beta = 110.578(16)°$, $V = 2042.0(4)$ Å^3. Enraf-Nonius CAD4 diffractometer, $Mo_{K\alpha}$ radiation, $\lambda = 0.71073$ Å. A single crystal with linear dimensions of $0.40 \times 0.33 \times 0.22$ mm was grown from a hexane solution at 295 K. A semi-empirical absorption correction, based on ψ scans, was applied to the data ($T_{max} = 1.051$, $T_{min} = 0.928$). The structure was solved by Patterson and direct methods (DIRDIF-96) and refined by full-matrix least-squares (SHELXL-97), using $w = 1/[\sigma^2(F_o^2) + (0.0987P)^2 + 2.0737P]$, where $P = (F_o^2 + 2F_c^2)/3$. All non-hydrogen atoms were refined anisotropically and hydrogen atoms isotropically. H-atom positions are based on stereochemical considerations. Final $R(F) = 0.0904$, $wR(F^2) = 0.2081$ for 217 parameters and 1235 reflections with $I > 2\sigma(I)$ and $2.86 < \theta < 22.98°$ (corresponding R values based on all 3021 reflections are 0.2036 and 0.2662, respectively). CCDC-192583 contains the supplementary crystallographic data for this paper. These data can be obtained free of charge via www.ccdc.cam.ac.uk/conts/retrieving.html (or from the Cambridge Crystallographic Data Centre, 12 Union Road, Cambridge CB2 1EZ, UK; fax: (+44) 1223-336-033; or deposit@ccdc.cam.ac.uk).

[6] a) C. Elsenbroich, A. Salzer, *Organometallics, a Concise Introduction*, VCH, Weinheim, **1992**, pp. 102–103; b) I. Yilgör, J. E. McGrath, *Adv. Polym. Sci.* **1988**, *86*, 1.

[7] a) S. Kasiviswanathan, P. S. Asoka Kumar, B. K. Mathur, K. L. Chopra, *Bull. Mater. Sci.* **1996**, *19*, 411; b) W. Deng, T. Oghi, H. Nejo, D. Fujita, *Jpn. J. Appl. Phys.* **2001**, *40*, 3364; c) Y.-H. Liau, K. Rhodes, N. F. Scherer, *J. Phys. Chem. B* **2001**, *105*, 3282; d) S. Kasiviswanathan, V. Srinivas, A. K. Kar, B. K. Mathur, K. L. Chopra, *Solid State Commun.* **1997**, *101*, 831; e) W. Deng, T. Oghi, H. Nejo, D. Fujita, *Appl. Phys. A* **2001**, *75*, 595; f) T. Asikainen, M. Ritala, M. Leskelä, T. Prohaska, G. Friedbacher, M. Grasserbauer, *Appl. Surf. Sci.* **1996**, *99*, 91.

[8] M. Behdani, A. Rastegar, S. H. Keshmiri, S. I. Missat, E. Vlieg, T. Rasing, *Appl. Phys. Lett.* **2002**, *80*, 4635.

 © 2003 Wiley-VCH Verlag GmbH & Co. KGaA, Weinheim

Polymerizable Bent-Core Mesogen

Polymerizable Bent-Core Mesogens: Switchable Precursors to Ordered, Polar Polymer Materials**

*Alan C. Sentman and Douglas L. Gin**

Bent-core (that is, banana-shaped) liquid crystals (LCs) have recently emerged as one of the most significant discoveries in the area of ferroelectric LCs.[1–3] These polar, chevron-shaped molecules have the ability to form switchable ferro- and antiferroelectric liquid-crystalline phases, even though the molecules are achiral.[1–3] Prior to the discovery of these materials, ferroelectric and antiferroelectric liquid-crystalline phases had only been possible with chiral, rodlike mesogens that adopt tilted layered phases (that is, smectic C (SmC) phases).[4] There is currently a great deal of interest in bent-core mesogens because they exhibit complex phase behavior not seen in other liquid-crystalline molecular architectures. They also offer certain advantages over traditional rodlike chiral SmC mesogens as switching materials in ferroelectric LC displays[5] and as building blocks for ordered, noncentrosymmetric polar polymer materials (for example, for nonlinear optical (NLO), piezoelectric, and pyroelectric applications).[2,6–8] For example, bent-core LCs can be more readily designed, synthesized, and modified since enantiomerically pure or enriched starting materials are not required. Unfortunately, bent-core mesogens generally form liquid-crystalline phases at relatively high temperatures (greater than ca. 140 °C).[1,2] This not only limits their usefulness in device applications, but also makes detailed analysis of their mesophases more difficult. It has also not yet been possible to synthesize a polymerizable derivative of a bent-core mesogen that retains the desired liquid-crystalline properties. Polymerizable or cross-linkable bent-core LCs would afford the ability to stabilize/trap the switchable liquid-crystalline mesophases. This situation would not only aid in their structural characterization, but the resulting polar polymers could also be used for

[*] Prof. D. L. Gin
Department of Chemistry & Biochemistry, and
Department of Chemical Engineering
University of Colorado
Boulder, CO 80309 (USA)
Fax: (+1) 303-492-8595
E-mail: gin@spot.colorado.edu

A. C. Sentman
Department of Chemistry
University of California
Berkeley, CA 94720 (USA)

[**] Financial support for this work was provided by the National Science Foundation (DMR-0111193) and the NSF Ferroelectric Liquid Crystal Materials Research Center at the University of Colorado, Boulder (DMR-0213918). The authors also thank Dr. E. Körblova, Dr. R. Zhao, Mr. A. Klittnick, and Profs. D. M. Walba and N. A. Clark for their assistance in the analysis of the bent-core liquid-crystalline phases.

Supporting information for this article is available on the WWW under http://www.angewandte.org or from the author.

 DOI: 10.1002/anie.200250680 © 2003 Wiley-VCH Verlag GmbH & Co. KGaA, Weinheim

NLO and transducer applications if aligned.[2,9] Ikeda and coworkers recently made a diacrylate derivative of a bent-core mesogen for this purpose; however, this compound was found to be completely nonmesogenic, which suggests that there is a certain sensitivity or incompatibility of this bent-core platform to polymerizable groups in the tails.[9] Blending with a large fraction of a conventional bent-core mesogen was required to obtain a switchable liquid-crystalline mixture that could be gelled.

Herein, we report the first example of a family of intrinsically polymerizable and cross-linkable bent-core mesogens (**1**, see scheme 1). These bent-core LC monomers are based on the 1,3-phenylenebis[4-(4-alkoxyphenyliminomethyl)benzoate] structure,[1] but contain a pair of reactive 1,3-dienoxy tails.[10,11] These tails more closely resemble *n*-alkyl and *n*-alkoxy tails than most other polymerizable tail systems and thereby allow retention of the desired liquid-crystalline properties. Some of the bent-core homologues exhibit a switchable smectic (Sm) phase which appears to be ferroelectric SmC in nature. They can also be thermally or photochemically cross-linked with retention of the phase microstructure. Ordered polymer films with pyroelectric properties have been obtained by aligning and cross-linking these mesogens under an electric field. This result demonstrates the viability of these monomers as precursors to ordered, polar polymer materials.

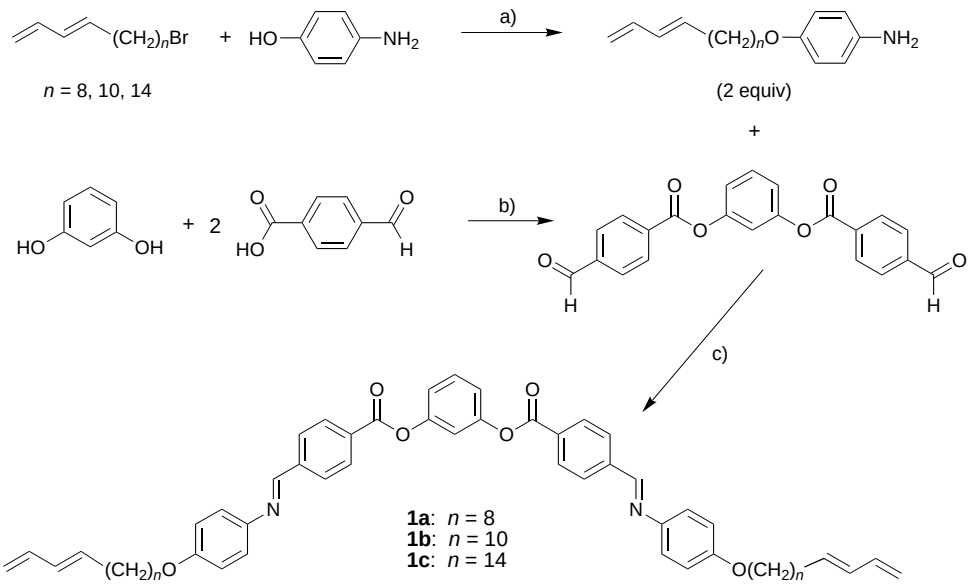
Three homologues (**1a–c**) containing an even number of methylene units in the tails were initially synthesized to investigate the properties of a system comprised of a bent-core and 1,3-diene tails. These diene tail units were originally developed by our group as a means of making polymerizable analogues of LCs which were sensitive to or incompatible with conventional polar or bulky polymerizable moieties in the tails.[10,11] Compounds **1a–c** were synthesized as shown in Scheme 1, using ω-bromoalkan-1,3-dienes as modular polymerizable tail units.[10,11] The detailed procedures for the synthesis, characterization, and property testing of these compounds are provided in the Supporting Information. The one drawback with the 1,3-diene tail system is that it tends to undergo spontaneous thermal polymerization at about 90 °C when coupled to a rodlike mesogenic core.[10] However, the effect of tail unsaturation on thermotropic liquid-crystalline behavior is a complex function of both the nature of the mesogenic core and the olefin units in the tails.[12] It was hoped that the unprecedented combination of diene tails with a bent core might afford lower phase-transition temperatures and reduced susceptibility to thermal cross-linking.

The thermotropic liquid-crystalline behavior of compounds **1a–c** was studied by polarized light microscopy (PLM), differential scanning calorimetry (DSC), and powder X-ray diffraction (XRD; Table 1). Upon heating, **1a** ($n = 8$) begins to change from a crystalline solid to a liquid-

Table 1: Thermotropic liquid-crystalline phases and transition temperatures of compounds **1a–c**.[a]

Compound	*n*	Transition	*T* [°C]
1a	8	K→LC[b]	90–95
1b	10	K→B_4	107
		B_4→SmC	141
		SmC→I	145
		I→SmC	143
		SmC→B_4	128
		B_4→K	101
1c	14	G→SmC	119
		SmC→I	135
		I→SmC	136
		SmC→G	125

[a] K = crystalline phase, LC = unknown liquid-crystalline phase, G = ordered glassy phase, I = isotropic melt. [b] Cross-links upon entering the liquid-crystalline phase.



Scheme 1. Synthesis of cross-linkable bent-core mesogens **1a–c** containing 1,3-diene tails. a) K_2CO_3, methyl ethyl ketone, Δ, b) 4-dimethylaminopyridine (DMAP), *N,N'*-dicyclohexylcarbodiimide (DCC), CH_2Cl_2, c) molecular sieves, CH_2Cl_2.

 © 2003 Wiley-VCH Verlag GmbH & Co. KGaA, Weinheim

crystalline phase at about 90–95 °C. However, the monomer spontaneously cross-links in a matter of seconds as it begins to enter the liquid-crystalline phase, which makes phase identification difficult. In contrast, **1b** ($n = 10$) exhibits well-defined enantiotropic liquid-crystalline behavior without premature diene polymerization. Thermally induced polymerization of **1b** only occurs if samples are held at temperatures above 90 °C for several hours. Upon cooling from the isotropic melt at 5 °C min^{-1}, **1b** initially enters a stable liquid-crystalline phase with a fan-type optical texture at 143 °C, which persists down to 128 °C (see Supporting Information). XRD analysis of this mesophase revealed a single diffraction peak at 49.6 Å, consistent with a lamellar phase with a layer spacing of that magnitude (Figure 1a). Based on the calculated length of **1b** of 54 Å[13] and assuming there is little or no tail interdigitation, the observed layer spacing is consistent with a SmC phase with a tilt angle of 23°. Upon cooling below 128 °C, **1b** forms an anisotropic phase with a blue fan-type texture that does not respond to applied pressure, which is consistent with the so-called solid B_4 phase.[1] Below 101 °C, **1b** forms a solid crystalline phase which has the same optical texture as the "B_4 phase" but lacking the blue color. The longest homologue **1c** ($n = 14$) is a glassy solid at ambient temperature and also forms a reversible SmC phase upon heating, but the phase transitions are weaker and much harder to observe. In addition, **1c** partially thermally polymerizes upon initial heating. These diene mesogens exhibit very different trends with respect to their initial melting and final clearing temperatures as a function of tail length compared to *n*-alkoxy and *n*-alkenoxy analogues with the same bent core.[1,14] As a consequence of the susceptibility of **1a** and **1c** to thermal polymerization in the liquid-crystalline state, all subsequent studies were performed with **1b** since it has the most stable and most well-defined liquid-crystalline behavior.

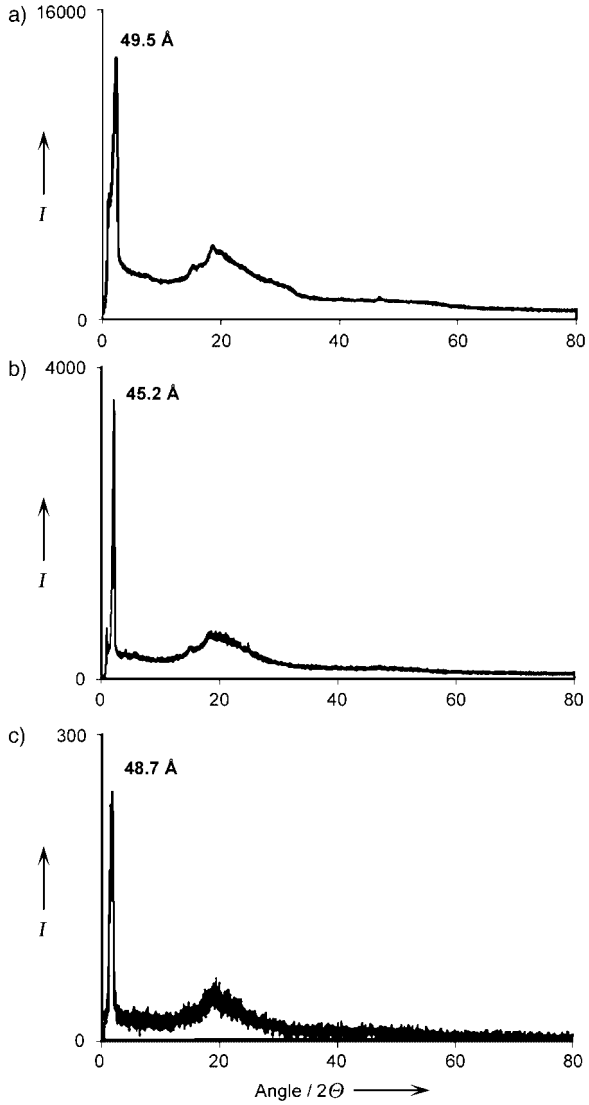


Figure 1. XRD profiles of **1b** taken at a) 133 °C in the SmC phase before polymerization; b) 180 °C after thermal polymerization; and c) 160 °C after photopolymerization.

Bent-core mesogens can adopt four general SmC packing configurations (not including enantiomeric forms), depending on the nature of the layer interface (namely, synclinic ($_S$) or anticlinic ($_A$)), and whether the mesogens are parallel or antiparallel in adjacent layers (that is, ferroelectric (P_F) or antiferroelectric (P_A)).[3] Only two of these four possible geometries (the SmC_SP_F and SmC_AP_F phases) are ferroelectric (Figure 2).[3] To help identify the SmC phase observed in our bent-core monomers, the electro-optic switching behavior of **1b** at 135 °C was examined in a 4-μm thick ferroelectric test cell using the triangular wave method.[2,3,11] The resulting current versus applied voltage curve (Figure 3) exhibits a single peak during voltage ramp-up and ramp-down, with a maximum polarization of 210 ± 30 nC cm^{-2} and a rise-time of 190 μs (averaged from five runs). This single-peak response is characteristic of ferroelectric behavior.[3,12,15] No signs of a double peak response indicative of antiferroelectric switching were observed, even when the frequency was varied from 10 to 1000 Hz,[3,12] so there is a high degree of confidence that the phase is ferroelectric in nature. Unfortunately, the magnitude of the observed polarization and the switching behavior steadily decrease over several minutes until a nonswitching sample with a fixed optical texture is formed. This behavior is

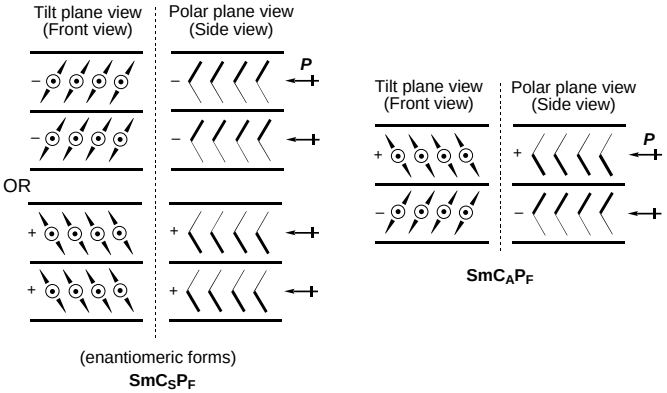


Figure 2. Schematic representations of the ferroelectric SmC_AP_F and SmC_SP_F bent-core phases. The symbols + and − indicate the enantiomeric layer configurations, and *P* is the layer polarization.

 © 2003 Wiley-VCH Verlag GmbH & Co. KGaA, Weinheim

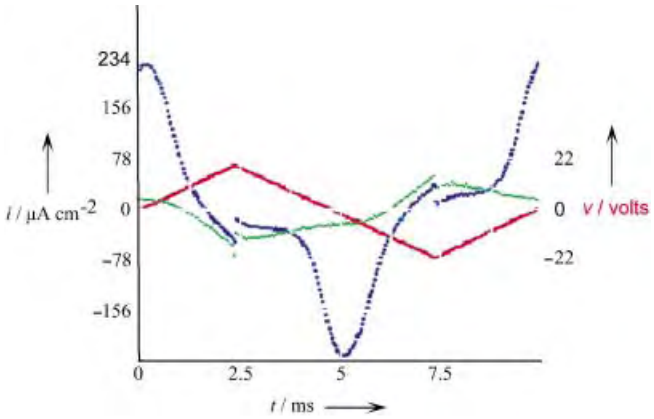


Figure 3. Triangular wave switching curve for **1b** in the SmC phase at 135 °C. The blue curve is the initial switching response, and the green curve is the switching response after 15 min.

consistent with accelerated thermal cross-linking under the oscillating electric field. It also accounts for the unusual broadness of the switching curve (which complicates phase identification), since the sample is polymerizing and becoming more viscous as switching proceeds. It should also be noted that the current response appears to lead the applied voltage by a small amount. This phenomenon is a characteristic artifact of an electro-optic switching system with little or no hysteresis, which has been observed before in surface-stabilized ferroelectric LC cells.[16] Only small changes in optical texture were observed upon switching,[17] so it was not possible to unequivocally determine whether the observed phase has a SmC_SP_F or SmC_AP_F configuration. Nevertheless, **1b** does form a switchable Sm phase that can be aligned for subsequent polymerization.

Compound **1b** was subjected to both thermal and radical photopolymerization experiments to investigate the polymerization behavior of the bent-core dienes and whether they can be cross-linked with retention of the liquid-crystalline microstructure. Samples of **1b** were thermally cross-linked by maintaining the samples in the SmC phase at 135 °C for 16 h, which resulted in completely insoluble samples that no longer responded to pressure. XRD analysis of the resulting material shows retention of the phase order even at temperatures well above the clearing point of the original monomer (Figure 1b), and even down to room temperature. Only a slight decrease in the primary XRD peak occurs upon cross-linking. The optical textures of the materials before and after thermal polymerization were essentially unchanged. Similar results were observed for samples of **1b** that were mixed with 2 wt % of a radical photoinitiator and irradiated with 365-nm UV light for 30 min (Figure 1c). The extent of 1,3-diene conversion in both polymerization cases was estimated to be approximately 50 % using FTIR analysis as previously described.[10,11]

To demonstrate that the bent-core monomer can be aligned and cross-linked to form an ordered, polar noncentrosymmetric network, a sample of **1b** was placed in a 4-μm thick ITO cell and thermally cross-linked in the SmC phase for 3 h under a static 10 V electric field. Retention of order in the polymerized sample was confirmed by observation of the optical texture of the LC even down to room temperature. Pyroelectric measurements were performed on the sample to confirm the presence of a permanent net polarization.[18] As can be seen in Figure 4, the polymer exhibits a well-defined electrical response to changes in temperature, indicative of an aligned material with a permanent net polarization.[18] In contrast, a sample of **1b** similarly cross-linked in the absence of an applied field yields no pyroelectric response. The calculated pyroelectric coefficient for the material is 4.8 $\mu C m^{-2} K^{-1}$, which is similar to values observed for noncentrosymmetric Langmuir–Blodgett films (10–20 $\mu C m^{-2} K^{-1}$) and poled polymers (30–40 $\mu C m^{-2} K^{-1}$).[18,19] The optical texture of **1b** aligned and cross-linked in the field shows that it is still a polydomain sample (see Supporting Information). Samples with more uniform alignment under applied field and better bulk noncentrosymmetric properties might be possible if methods can be developed for aligning bent-core mesogens at the surface.

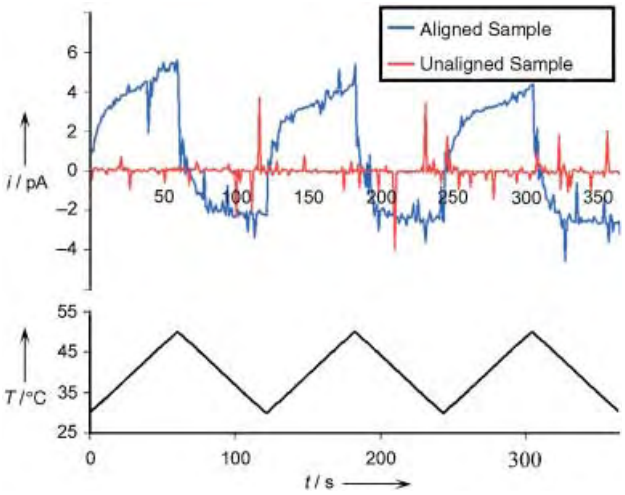


Figure 4. Pyroelectric response curve for **1b** thermally cross-linked in the SmC phase under a 10 V electric field.

In conclusion, we have designed and synthesized the first example of a cross-linkable bent-core mesogen. This achiral mesogen adopts a SmC phase with switching behavior consistent with a ferroelectric phase. When aligned and cross-linked in the liquid-crystalline state under a static electric field, ordered polymer networks with a net polarization are generated that exhibit pyroelectric properties. Studies are currently underway to identify the exact structure of the liquid-crystalline phase formed and to examine the noncentrosymmetric properties of the resulting networks in more detail.

Received: December 2, 2002 [Z50680]

Keywords: liquid crystals · mesogens · nanostructures · polymerization · polymers

 © 2003 Wiley-VCH Verlag GmbH & Co. KGaA, Weinheim

[1] G. Pelzl, S. Diele, W. Weissflog, *Adv. Mater.* **1999**, *11*, 707, and references therein.
[2] D. Shen, A. Pegenau, S. Diele, I. Wirth, C. Tschierske, *J. Am. Chem. Soc.* **2000**, *122*, 1593.
[3] "Anisotropic Organic Materials—Approaches to Polar Order": D. M. Walba, E. Körblova, R. Shao, J. E. Maclennan, D. E. Link, M. A. Glaser, N. A. Clark, *ACS Symp. Ser.* **2001**, *789*, 281.
[4] J. W. Goodby, *J. Mater. Chem.* **1991**, *1*, 307.
[5] A. W. Hall, J. Hollingshurst, J. W. Goodby in *Handbook of Liquid Crystal Research* (Eds.: P. J. Collings, J. S. Patel), Oxford University Press, New York, **1997**, p. 17.
[6] R. A. M. Hikmet, *Macromolecules* **1992**, *25*, 5759.
[7] M. Trollsås, C. Orrenius, F. Sahlen, U. W. Gedde, T. Norin, A. Hult, D. Hermann, R. Rudquist, L. Komitov, S. T. Lagerwall, J. Lindström, *J. Am. Chem. Soc.* **1996**, *118*, 8542.
[8] J. Oertegren, G. Andersson, P. Busson, A. Hult, U. W. Gedde, A. Eriksson, M. Lindgren, *J. Phys. Chem. B*, **2001**, *105*, 10223.
[9] C. Keum, A. Kanazawa, T. Ikeda, *Adv. Mater.* **2001**, *13*, 321.
[10] B. P. Hoag, D. L. Gin, *Macromolecules* **2000**, *33*, 8549.
[11] B. A. Pindzola, B. P. Hoag, D. L. Gin, *J. Am. Chem. Soc.* **2001**, *123*, 4617.
[12] S. M. Kelly, *Liq. Cryst.* **1996**, *20*, 493.
[13] The extended length of **1b** was calculated by molecular modeling using CS Chem3D Ultra software and employing MM2 force field parameters.
[14] C.-K. Lee, S.-S. Kwon, S.-T. Shin, E.-J. Choi, S. Lee, L.-C. Chien, *Liq. Cryst.* **2002**, *29*, 1007. The bis(*n*-alkenoxy) bent-core LCs contain unactivated terminal olefins which are difficult to polymerize without transition-metal catalysts or ionizing radiation.
[15] To our knowledge, ferroelectric, nontilted Sm phases of bent-core mesogens have not been observed before, so the ferroelectric response observed also adds support to a SmC phase.
[16] L. M. Blinov, E. P. Pozhidaev, F. V. Podgornov, S. A. Pikin, S. P. Palto, A. Sinha, A. Yasuda, S. Hashimoto, W. Haase, *Phys. Rev. E* **2002**, *66*, 021701.
[17] The small optical changes observed upon switching can be attributed to partial polymerization of the sample, or an unusual domain alignment in the LC cell.
[18] T. Kamata, J. Umemura, T. Takenaka, N. Koizumi, K. Takehara, K. Isomura, H. Taniguchi, *Jpn. J. Appl. Phys. Part 1* **1994**, *33*, 1074.
[19] R. W. Whatmore, R. Watton, in *Infrared Detectors and Emitters: Materials and Devices, Electronic Materials 8* (Eds.: P. Capper, C. T. Elliott), Kluwer Academic, Boston, **2001**, chap. 5, p. 118.

 © 2003 Wiley-VCH Verlag GmbH & Co. KGaA, Weinheim

Super-Supertetrahedral Cluster

$[Cd_{16}In_{64}S_{134}]^{44-}$: 31-Å Tetrahedron with a Large Cavity**

*Hailian Li, Jaheon Kim, Michael O'Keeffe, and Omar M. Yaghi**

Dedicated to Professor Gérard Férey on the occasion of his 60th birthday

Structures constructed from supertetrahedral clusters of TX_4 tetrahedra may have giant pores representing more than 80% of their crystal volume and cation-exchange properties.[1] As well as creating porous materials we note that larger clusters are comparable in size with the individual nanocrystallites of tetrahedral sulfide (e.g. CdS) "quantum dots" which show great promise and are currently being investigated as quantum-dot lasers and other optical devices.[2] Similarly, interesting optical properties might be expected in supertetrahedral crystals of semiconducting sulfides.[2h] Clusters labeled T*n* have *n* tetrahedra along each edge.[1] Isolated T2 units are very familiar in chemistry, in molecules such as P_4O_{10}, $Ge_4S_6Br_4$, anions such as $[Ge_4S_{10}]^{4-}$, and condensed (corner-sharing) in framework crystals particularly of halides,[3] but also of sulfides[4] and of nitrides.[5] A number of extended tetrahedral frameworks based on T3 sulfides, mostly of B[6] or In,[1,7] with a variety of frameworks have been prepared.

To prepare the T4 generation of the indium sulfide clusters, we and others have recently shown that in addition to In^{3+}, it is necessary to have divalent metal ions, such as Cd^{2+}.[8,9] The likely distribution of different valence cations in larger T*n* clusters was also delineated.[8] A number of compounds with frameworks of alternating T1 and T2 units[10] and recently containing T3 and T5 units[11] have also been described. Other even larger (not supertetrahedral) chalcogenide clusters are known.[12]

Herein we report the preparation of the first compound representing the next stage of a structural hierarchy, that is, supertetrahedra of supertetrahedra; specifically a T2 supertetrahedron of T4, a discrete anionic cluster of 214 atoms and 80 tetrahedral centers.

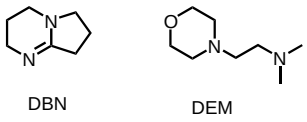
This material was synthesized by combining an aqueous mixture (2.2 mL) of In (50.0 mg, 0.44 mmol), S (70.0 mg, 2.18 mmol), $Cd(CH_3CO_2)_2{\cdot}2H_2O$ (200 mg, 0.75 mmol), DBN

[*] Prof. O. M. Yaghi, Dr. H. Li, Dr. J. Kim
Department of Chemistry
University of Michigan
Ann Arbor, MI 48103 (USA)
Fax: (+1) 734-615-9751
E-mail: oyaghi@umich.edu
M. O'Keeffe
Department of Chemistry, Arizona State University
Tempe, AZ 85287 (USA)

[**] The National Science Foundation support to MO'K (DMR-0103036) and OMY (DMR-0097938) is gratefully acknowledged.

 DOI: 10.1002/anie.200250748 © 2003 Wiley-VCH Verlag GmbH & Co. KGaA, Weinheim

(1,5-diazabicyclo[4,3,0]-non-5-ene) (0.40 mL, 3.24 mmol), and DEM (4-[2-(dimethylamino)ethyl]morpholine) (0.75 mL, 4.38 mmol), which was heated at 138 °C in a 23-mL teflon-lined vessel for 5 days.



The resulting yellow octahedral crystals (12.8 % yield based on In) were isolated by density-difference separation and washed with several aliquots of water, ethanol, and acetone, and formulated as $Cd_{16}In_{64}S_{134}\cdot(DBNH_2)_{11}(DEMH_2)_{11}(H_2O)_{50}$ (hereafter CdInS-420) from elemental microanalysis and single-crystal X-ray diffraction results.[13,14]

The crystal structure revealed the presence of finite tetrahedral anionic units of $[Cd_{16}In_{64}S_{134}]^{44-}$ that have an underlying T2 type of structure in which the individual tetrahedra have each been replaced by a T4 supertetrahedron (Figure 1) forming a super-supertetrahedron. Since In^{3+} and Cd^{2+} centers are isoelectronic they cannot be distinguished directly by X-ray diffraction. However, the Cd/In ratio was determined by elemental microanalysis[13] and verified by analysis of the bond lengths. The bonds to S atoms from the four inner metal sites in each T4 unit range from 2.502(11)–2.532(11) Å (average 2.516(11) Å). This value can be compared with the Cd–S separation of 2.525 Å in the sphalerite structure of CdS and the 2.55 Å expected from bond valence parameters.[15] For the remaining sites, the T–S bond lengths are significantly shorter: 2.382(10)–2.520(11) Å (average 2.453(11) Å), a value that is typical for a tetrahedral In–S bond length (expected[15] 2.47 Å).

The clusters (with S_4 symmetry) are nearly regular tetrahedra with edge lengths (S···S separations) of 31.06 and 31.07 Å, and with an overall volume of 3531 Å^3. Each has a large octahedral cavity of diameter of 22.3 Å (S···S distance between opposing vertices), which can be accessed through open triangular faces of edge 15.8 Å.

Although the positions of Cd, In, and S of the cluster were determined accurately, the guest molecules and organic ammonium counterions filling the pores and residing between the anions in the crystal were not all located because of the disorder problems usually encountered in this kind of structure. Nevertheless, ^{13}C cross-polarization magic-angle spining (CPMAS) NMR spectroscopy measurements showed resonance signals for all the anticipated types of C atoms, which appeared in their respective chemical shift regions.[16] Furthermore, elemental microanalysis and FTIR[17] confirmed the presence of 50 water molecules plus 11 $DBNH_2^{2+}$ and 11 $DEMH_2^{2+}$ ions. There are four clusters per unit cell, packed around 4_1 and 4_3 axes (Figure 1). The unit cell also contains 200 water molecules, and 88 organic ammonium dications. These guests fill an otherwise void space calculated to be 55 % of the crystal volume.

Thermogravimetric measurements on CdInS-420 showed two major weight-loss steps in two temperature ranges indicating the removal of water guests and decomposition of the cations: a) 5.16 % between 25 °C and 150 °C associated with the removal of 50 water molecules per formula unit (calcd: 5.14 %), and b) 20.73 % between 170 °C and 440 °C attributed to the decomposition of 11 $DBNH_2^{2+}$ and 11 $DEMH_2^{2+}$ counterions (calcd: 18.1 %) and the loss of 2.72 % of the S atoms. Preliminary attempts to exchange the organic counterions with small inorganic cations by exposing solids of CdInS-420 to concentrated solutions of simple inorganic salts showed no exchange, which points to the strong ionic forces existing between the ions in the crystal.

The structure of this anion is intriguing since it represents a new level of complexity in the structures of tetrahedra. At the outset of this study all tetrahedral units of TX_4 tetrahedra have been limited to the simple Tn (n = 1–5) series in which the resulting units are composed entirely of condensed tetrahedra. The present compound shows how open tetrahedra can be prepared using those T4 condensed clusters as building blocks. Thus, we propose to extend the notation for supertetrahedra[1] to include this first member of what we believe will be an extensive series. Specifically, Tp,q will be used to describe a Tq supertetrahedron of Tp supertetrahedra. The number of tetrahedra (T atoms) in a Tp supertetrahedron is the pth tetrahedral number, $t_p = p(p+1)(p+2)/6$, and the number of X atoms is t_{p+1}. In a Tp,q super-supertetrahedron the number of T atoms is $t_q t_p$ and the number of X atoms is $t_q(t_{p+1}-2)+2$. In this notation the cluster in CdInS-420 is T4,2.

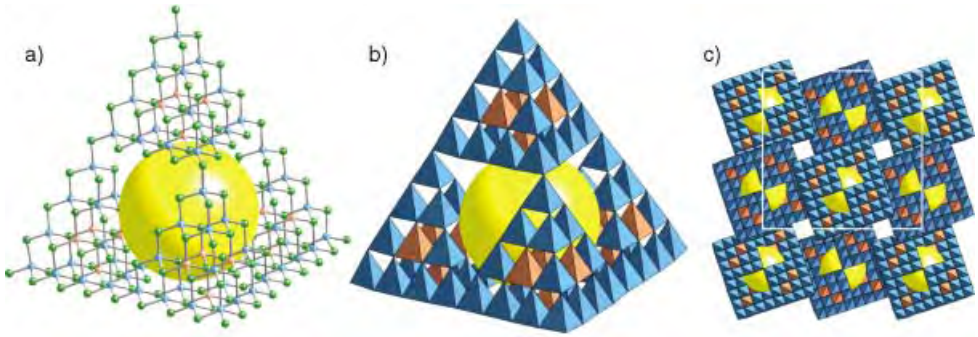


Figure 1. a) The CdInS-420 cluster as a ball and stick model. In blue; Cd orange; S green. The large yellow sphere indicates the central cavity. b) The same view as (a) shown as metal-centered tetrahedra. c) Crystal packing of the clusters illustrated as metal-centered tetrahedra, view down the *c* axis with the unit cell outlined in white.

 © 2003 Wiley-VCH Verlag GmbH & Co. KGaA, Weinheim

An obvious extension of the notation is to structures T*p,q,r* which are T*r* supertetrahedra of T*p,q* super-supertetrahedra. We note (Figure 1) that the In-S structure of CdInS-420 alone is a T2,2,2 structure which we may also write $T2^3$. The infinite sequence $T2^\infty$ describes the structure of the famous self-similar fractal structure known as the Sierpinski tetrahedron.[18] In condensed frameworks (e.g. diamond-like) of $T2^n$ units the overall composition is always TX_2, and their realization in a compound such as GeS_2 (already known as $n=0$ and 1 structures[4a]) is an interesting synthetic challenge.[19]

Received: December 11, 2002 [Z50748]

Keywords: clusters · indium · microporous materials · sulfides · supertetrahedra

[1] H. Li, A. Laine, M. O'Keeffe, O. M. Yaghi, *Science* **1999**, *283*, 1145 – 1147.

[2] Some recent papers which give references to earlier work are: a) S. Empedocles, M. Bawendi, *Acc. Chem. Res.* **1999**, *32*, 389 – 396; b) U. Banin, Y. Cao, D. Katz, O. Milo, *Nature* **1999**, *400*, 542 – 544; c) V. I. Klimov, A. A. Mikhailovsky, S. Xu, A. Malko, J. A. Hollingsworth, C. A. Leatherdale, H.-J. Eisler, M. Bawendi, *Science* **2000**, *290*, 314 – 317; d) F. W. Wise, *Acc. Chem. Res.* **2000**, *33*, 773 – 780; e) X. Peng, I. Manna, W. Yang, J. Wickham, E. Scher, A. Kadavanich, A. P. Alivistos, *Nature* **2000**, *404*, 59 – 61; f) X. Huang, J. Li, *J. Am. Chem. Soc.* **2000**, *122*, 8789 – 8790; g) V. N. Soloviev, A. Eichhöfer, D. Fenske, U. Banin, *J. Am. Chem. Soc.* **2001**, *123*, 2354 – 2364; h) M. Fuentes-Cabrera, H. Wang, B. Daniels, O. F. Sankey, *Phys. Rev. B* **2002**, *66*, 045109; i) P. N. Trikalitis, K. K. Rangan, T. Bakas, M. G. Kanatzidis, *Nature* **2001**, *410*, 671 – 675.

[3] a) ZnI_2: P. H. Fourcroy, D. Carre, J. Rivet, *Acta Crystallogr. Sect. B* **1978**, *34*, 3160 – 3162; b) $ZnBr_2$: C. Chieh, M. A. White, *Z. Kristallogr.* **1984**, *166*, 189 – 197; c) $BeCl_2$: E. Spundflasche, H. Fink, H. J. Siefert, *Z. Anorg. Allg. Chem.* **1995**, *621*, 1723 – 1726; d) HgI_2: D. Schwarzenbach, *Z. Kristallogr. Kristallgeom. Kristallphys. Kristallchem.* **1969**, *128*, 97 – 114.

[4] GeS_2: a) N. Wang, E. Horn, *Neues Jahrb. Mineral. Abh.* **1973**, *9*, 413 – 416; b) $(C_7H_{13}N)Mn_{0.25}Ge_{1.75}S_2{\cdot}H_2O$: C. L. Cahill, Y. Ko, J. C. Hanson, K. Tan, J. B. Parise, *Chem. Mater.* **1998**, *10*, 1453 – 1458.

[5] a) $Mg(NH_2)_2$: H. Jacobs, *Z. Anorg. Allg. Chem.* **1971**, *382*, 97 – 109; b) $Be(NH_2)_2$: H. Jacobs, *Z. Anorg. Allg. Chem.* **1976**, *427*, 1 – 8; c) $Ca_3Ga_2N_4$: S. J. Clark, F. J. DiSalvo, *J. Alloys Compd.* **1998**, *274*, 118 – 121.

[6] a) B. Krebs, *Angew. Chem.* **1983**, *95*, 113 – 134; *Angew. Chem. Int. Ed. Engl.* **1983**, *22*, 113 – 134; b) A. Hammerschmidt, P. zum Hebel, F. Hiltmann, B. Krebs, *Z. Anorg. Allg. Chem.* **1996**, *622*, 76 – 84.

[7] a) C. L. Cahill. Y. Ko, J. B. Parise, *Chem. Mater.* **1998**, *10*, 10 – 19; b) C. L. Cahill, J. B. Parise, *J. Chem. Soc. Dalton Trans.* **2000**, 1475 – 1482, and references therein; c) H. Li, M. Eddaoudi, A. Laine, M. O'Keeffe, O. M. Yaghi, *J. Am. Chem. Soc.* **1999**, *121*, 6096 – 6097.

[8] H. Li, J. Kim, T. L. Groy, M. O'Keeffe, O. M. Yaghi, *J. Am. Chem. Soc.* **2001**, *123*, 4867 – 4868.

[9] C. Wang, Y. Li, X. Bu, N. Zheng, O. Zivkovic, C.-S. Yang, P. Feng, *J. Am. Chem. Soc.* **2001**, *123*, 11506 – 11507.

[10] a) O. M. Yaghi, Z. Sun, D. A. Richardson, T. L. Groy, *J. Am. Chem. Soc.* **1994**, *116*, 807 – 808; b) C. L. Bowes, A. J. Lough, A. Malek, G. A. Ozin, S. Petrov, D. Young, *Chem. Ber.* **1996**, *129*, 283 – 287; c) C. L. Cahill, J. B. Parise, *Chem. Mater.* **1997**, *9*, 807 – 811.

[11] a) W. Su, X. Huang, J. Li, H. Fu, *J. Am. Chem. Soc.* **2002**, *124*, 12944 – 12945; b) C. Wang, X. Bu, N. Zheng, P. Feng, *J. Am. Chem. Soc.* **2002**, *124*, 10268 – 10269.

[12] a) I. G. Dance, K. G. Fisher, *Prog. Inorg. Chem.* **1994**, *41*, 637 – 803; b) D. Fenske, N. Zhu, T. Langetepe, *Angew. Chem.* **1998**, *110*, 2784 – 2788; *Angew. Chem. Int. Ed.* **1998**, *37*, 2640 – 2644; c) S. Dehnen, A. Eichhöfer, D. Fenske, *Eur. J. Inorg. Chem.* **2002**, *2*, 279 – 317; d) C. Wang, X. Bu, N. Zheng, P. Feng, *Angew. Chem.* **2002**, *114*, 2039 – 2041; *Angew. Chem. Int. Ed.* **2002**, *41*, 1959 – 1961.

[13] Elemental microanalysis calcd (%) for $C_{165}H_{474}N_{44}O_{61}S_{134}Cd_{16}In_{64} = Cd_{16}In_{64}S_{134}{\cdot}(DBNH_2)_{11}(DEMH_2)_{11}(H_2O)_{50}$: C 11.33, H 2.73, N 3.52, S 24.56, Cd 10.28, In 42.00; found C 11.28, H 2.35, N 3.61, S 22.94, Cd 10.56, In 41.82.

[14] Crystal data for CdInS-420: A yellow octahedral crystal ($0.16\times0.16\times0.16$ mm^3) of CdInS-420 was analyzed: Siemens SMART CCD diffractometer, ω scans, graphite-monochromated $Mo_{K\alpha}$ radiation, $T=158(2)$ K, tetragonal, space group $I4_1/a$ (No. 88) with $a=43.297$ (2), $c=27.7067$ (14) Å, $V=51940$ (4) Å^3, $Z=4$, $\rho_{calcd}=2.237$ g cm^{-3}, and $\mu(Mo_{K\alpha})=40.01$ cm^{-1}. Total 184910 reflections were collected within $2\theta_{max}=41.36°$ with a ω scan width of 0.3°; 18710 independent reflections, 7385 with $I>2\sigma(I)$. Absorption correction with SADABS $T_{min}=0.2799$, $T_{max}=0.8369$. All Cd, In, and S atoms were located on the general positions except for the S(21) atom that sits on the twofold crystallographic axis with occupancy a half. Because of the severe disorder of the guest molecules, it was difficult to locate the counterions; only two DBN units were found in the asymmetric unit and fifty randomly distributed peaks were considered and included as part of guest molecules in the refinement process. All the atoms in the cluster were refined anisotropically, but the disordered guest molecules were treated isotropically. Final full-matrix least-squares refinement on F^2 converged to $R1=0.1247$ ($I>2\sigma(I)$) and $wR2=0.2959$ (all data) with GOF = 1.082. The maximum and minimum peaks on the final difference Fourier map corresponded to 1.48 and -1.92 e Å^{-3}, respectively. CCDC-197754 contains the supplementary crystallographic data for this paper. These data can be obtained free of charge via www.ccdc.cam.ac.uk/conts/retrieving.html (or from the Cambridge Crystallographic Data Centre, 12 Union Road, Cambridge CB2 1EZ, UK; fax: (+44) 1223-336-033; or deposit@ccdc.cam.ac.uk).

[15] N. E. Brese, M. O'Keeffe, *Acta Crystallogr. Sect. B* **1991**, *47*, 192 – 197.

[16] ^{13}C CPMAS NMR: $\delta=166$, 33 ppm (DBN), $\delta=56$, 20 ppm (DEM).

[17] FTIR for DBN and DEM (KBr, 1500—700 cm^{-1}): $\tilde{\nu}=1454.0$ (w), 1423.5 (w), 1387.8 (w), 1311.5 (s), 1209.6 (m), 1133.2 (w), 1107.8 (m), 1067.0 (m), 970.3 (w), 909.2 (w), 878.6 cm^{-1} (w).

[18] See for example, M. Schroeder, *Fractals, Chaos, Power Laws*, Freeman, New York, **1991**. Figure 13 in this book is an illustration of a $T2^5$ super-supertetrahedron.

[19] The process of replacing a tetrahedral vertex by a tetrahedron of vertices has been termed "augmentation". M. O'Keeffe, M. Eddaoudi, H. Li, T. Reineke, O. M. Yaghi, *J. Solid State Chem.* **2000**, *152*, 3 – 20. For a discussion of some topological properties of $T2^n$ diamond nets see M. O'Keeffe, S. T. Hyde, *Z. Kristallogr.* **1996**, *211*, 73 – 78.

 © 2003 Wiley-VCH Verlag GmbH & Co. KGaA, Weinheim

Divergent Dendrimer Synthesis

Dendrimer Design: How to Circumvent the Dilemma of a Reduction of Steps or an Increase of Function Multiplicity?

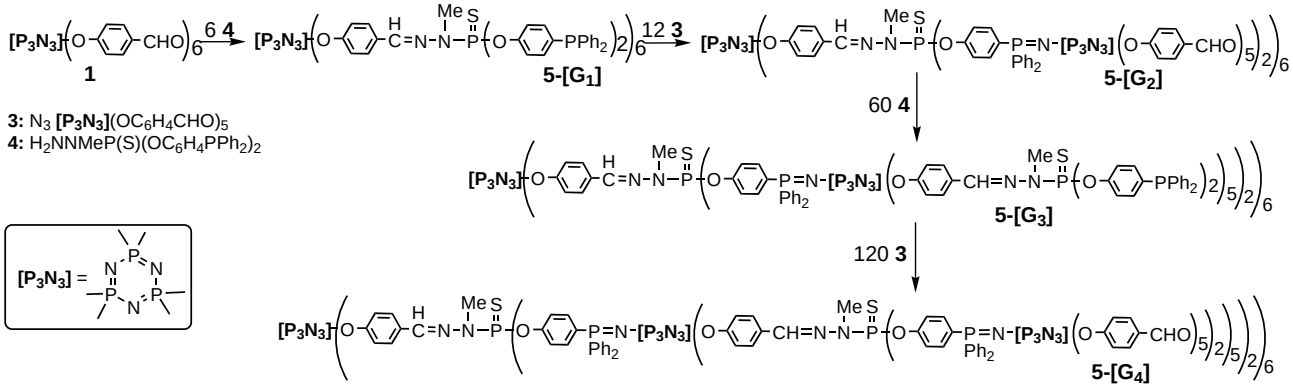
Valérie Maraval, Anne-Marie Caminade, Jean-Pierre Majoral,* and Jean-Claude Blais*

The development of dendrimer chemistry is due, without any doubt, to the extraordinary pallet of very unique properties of these monodisperse polymers which have applications in numerous fields which include biology, material sciences, catalysis, surface modification, electronics, electrooptics, chemical or biological sensors, and coatings.[1] It is clear that further growth depends crucially on the availability of new or more efficient synthetic methods which offer precise atom-by-atom control but remain as close as possible to the conditions required for a green and cheap chemistry.[2–7]

One of the most important and promising class of dendrimers, phosphorus dendrimers,[8] has also to fulfill this last point even though convenient syntheses have already been proposed. Up to the end of the 1990s the most convenient method of preparation of phosphorus-containing dendrimers was the reiteration of a sequence of two reactions dealing with an AX_2 system (mono(methylhydrazino)dichlorothiophosphane) and a YD one (sodium salt of the hydroxybenzaldehyde).[9,10] Then in 2001 the first divergent strategy using AB_2 ($H_2NN(CH_3)P(S)(OC_6H_4PPh_2)_2$, $B = PPh_2$) and CD_2 ($N_3P(S)(OC_6H_4CHO)_2$) unprotected monomers for the rapid synthesis of phosphorus-containing dendrimers was proposed.[7] Four steps were necessary to prepare a dendrimer of generation 4 (G_4) decorated on the surface with 48 aldehyde groups. This approach was attractive but does not allow a significant increase in the number of terminal groups for a given generation. This last point appears to be highly desirable since it is well demonstrated that the properties, and therefore the applications of dendrimers strongly depend on the nature and the density of functional groups grafted onto the surface.[1,11] These problems can be addressed in large part by designing highly functionalized cores of the form D_6 and new monomers AB_5 and CD_5.

To apply such a concept, we prepared monomers offering more possibilities for the design of targeted phosphorus dendrimers. Monomers **2** (AB_5 type) and **3** (CD_5 type, for preparation of **2** and **3** see the Supporting Information) were prepared from hexachlorocyclotriphosphazene, a commercially available reagent. Remarkably, they can react spontaneously without any activating agent by two reactions known to be quantitative (the condensation reaction between phosphorhydrazides and aldehydes, and the reaction between phosphanes and azides) and give only environmentally friendly byproducts: water and dinitrogen.

We choose the hexaaldehyde **1** as a core, and to react in an alternate fashion an AB_2 monomer, namely the hydrazinodiphosphane **4** and the CD_5 monomer **3** (Scheme 1). Such a strategy allows a generation per reaction to be created, and



Scheme 1. Divergent synthesis of the dendrimer **5-[G_4]** through the alternate use of the AB_2 monomer **4** and the CD_5 monomer **3**.

also allows the number of end groups of the dendrimer at each generation to be multiplied by two when **4** is involved or by five when **3** is used. This divergent synthesis of dendrimers was conducted up to generation 4 and was monitored by NMR spectroscopy (^1H, ^{13}C, ^{31}P) as well as by IR spectroscopy and by MALDI-TOF mass spectrometry in some cases. As far as the condensation of aldehyde groups with hydrazino groups is concerned, the reaction can be monitored by ^1H NMR (disappearance of the signal of the aldehyde protons), and by ^{13}C NMR (disappearance of the signal of the carbonyl group, and appearance of the signal of the hydrazino carbon atom CH=N–N) spectroscopy. In the case of the Staudinger reaction between phosphanyl end groups

[*] Dr. A.-M. Caminade, Dr. J.-P. Majoral, Dr. V. Maraval
Laboratoire de Chimie de Coordination, CNRS
205 route de Narbonne
31077 Toulouse cedex 4 (France)
Fax: (+33) 5-61-55-30-03
E-mail: caminade@lcc-toulouse.fr
majoral@lcc-toulouse.fr
Dr. J.-C. Blais
Laboratoire de Chimie Structurale Organique et Biologique Université Pierre et Marie Curie, CNRS, UMR 7613
75252 Paris cedex 05 (France)

Supporting information (experimental details) for this article is available on the WWW under http://www.angewandte.org or from the author.

 © 2003 Wiley-VCH Verlag GmbH & Co. KGaA, Weinheim DOI: 10.1002/anie.200250827

and azido groups the disappearance of the N_3 groups is monitored by IR spectroscopy and the formation of P=N–P units through the incorporation of the P_3N_3 unit by ^{31}P NMR spectroscopy. MALDI TOF experiments (PerSeptive Biosystems Voyager Elite TOFMS-Framingham, USA; dithranol matrix with addition of LiI) conducted on some of these dendrimers confirm their structure. The molecular peak was observed for the dendrimer of generation 2 **5-[G_2]** ([*M*Li]$^+$ 13791.8) and for the dendrimer of generation 3 **5′-[G_3]** prepared after sulfuration of the terminal phosphanyl groups of **5-[G_3]** ([*M*li]$^+$ 56315.3). Some fragmentation patterns were also detected which result from two types of bond breaking: cleavage of the exocyclic nitrogen–phosphorus bond in N-[P_3N_3] linkages and cleavage of nitrogen–nitrogen bond in HC=N–N–P moieties. None of these fragmentation patterns comes from incomplete coupling (Figure 1). The molecular peak for the dendrimer **5-[G_4]**

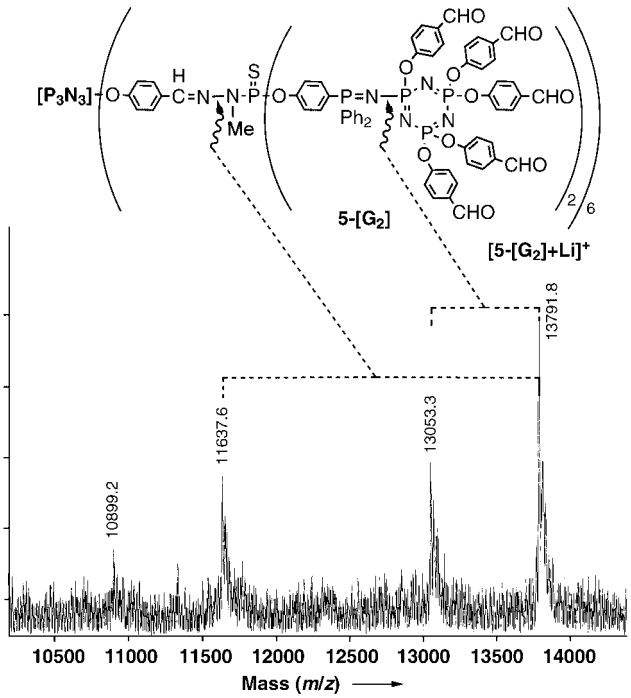


Figure 1. MALDI TOF analysis for **5-[G_2]** showing the molecular peak [*M*Li]$^+$ and the two types of fragmentation.

was not observed because of numerous fragmentation patterns (N–N and =N–P bond cleavages as in the G_2 and G_3 dendrimers).Thus the new dendrimers **5-[G_1], 5-[G_2], 5-[G_3]**, and **5-[G_4]**, were obtained cleanly and in good yields. (92–95%, Figure 2)

This process allows the preparation of a dendrimer of generation 4 bearing 600 aldehyde end groups in just 4 steps! This can be compared to the classical way (use of AX_2 and YD monomers) which gives rise, using 4 steps, to a dendrimer of generation 2 bearing only 24 terminal groups and also to our previous accelerated method using AB_2 and CD_2 monomers which affords after 4 steps generation 4 dendrimer having only 96 end groups! (Figure 3)

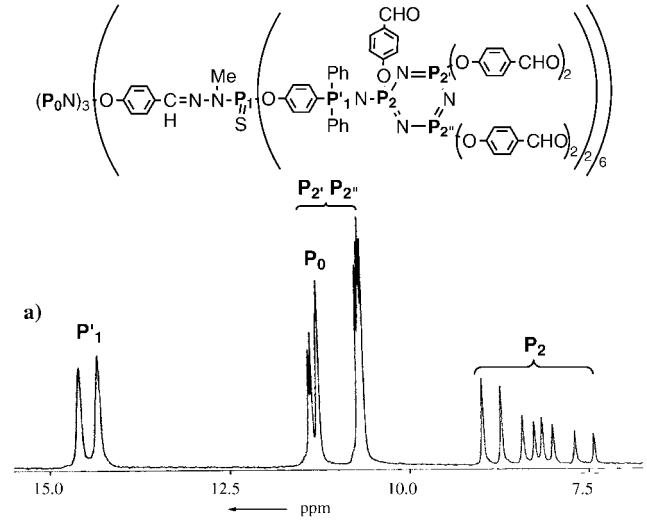


Figure 2. a) ^{31}P NMR spectrum of **5-[G_2]** in THF (the singlet at $\delta = 64.4$ ppm corresponding to the P_1=S unit is not shown). b) Theoretical ^{31}P NMR spectrum of **5-[G_2]** without the singlet at $\delta = 64.4$ ppm.

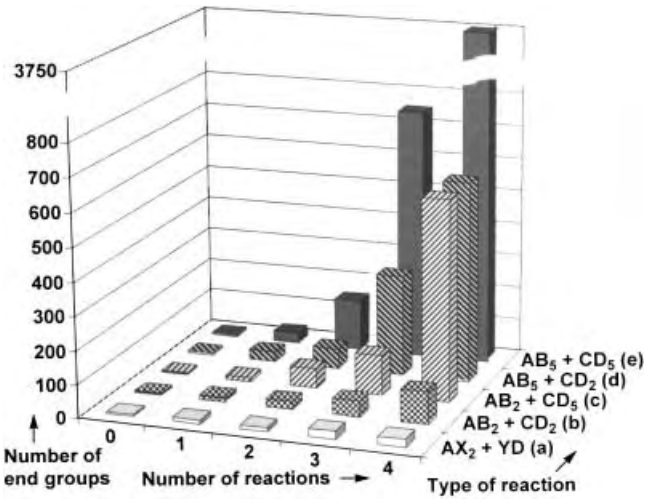
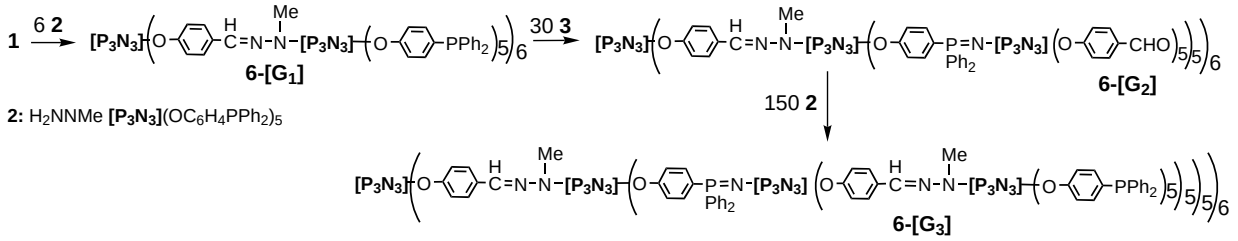


Figure 3. Comparison of the variation of the number of end groups at each generation a) use of AX_2 and YD monomers, b) use of AB_2 and CD_2 monomers, c) use of AB_2 and CD_5 monomers, d) use of AB_5 and CD_2 monomers, e) use of AB_5 and CD_5 monomers.

To have an idea of the scope and limitations of this method, we tried to perform similar reactions starting from the hexaaldehyde **1** which was treated with the AB_5 monomer **2** and not with the AB_2 monomer **4** as reported above. As a result the number of functions, here phosphanyl groups, is multiplied by five, which gives a dendrimer of generation 1, **6-[G_1]**, decorated with 30 phosphanyl groups (Scheme 2).

 © 2003 Wiley-VCH Verlag GmbH & Co. KGaA, Weinheim



Scheme 2. Divergent synthesis of the dendrimer **6-[G$_3$]** by the alternate use of the AB$_5$ monomer **2** and the CD$_5$ monomer **3**.

These functional groups remain accessible to further transformation since the addition of the CD$_5$ monomer **3** allows the formation of the dendrimer of generation 2, **6-[G$_2$]**, bearing 150 aldehyde groups on the outer shell to go to completion. Lastly treatment of this dendrimer with the monomer **2** leads to the dendrimer of generation 3, **6-[G$_3$]** (Scheme 2). Indeed this methodology permits the preparation of a dendrimer of generation 3 bearing 750 phosphanyl end groups in only 3 steps (Figure 3)! The reaction leading to generation 4 was not attempted because of the expected steric hindrance of the third generation outer shell.

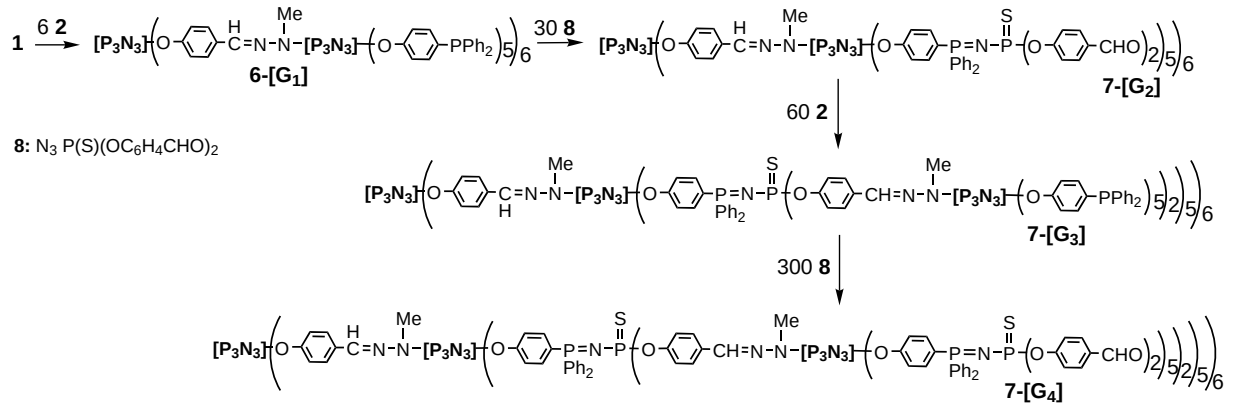
Therefore this method can be considered as the most convenient reported to date, offering several advantages 1) a strict minimum of steps is needed to build a generation: one step per generation, 2) a maximum number of functional groups is anchored to the surface of a dendrimer of a given generation, 3) purification of the resulting dendrimers is easy (simple washings), 4) reactions are easily monitored (^{1}H and ^{31}P NMR spectroscopy) 5) a minimum of solvent is used and the byproducts, water and dinitrogen are compatible with a green chemistry, 6) the degree of freedom for the construction of dendrimers is very high: depending of the sequence of monomer additions, dendrimers with different backbones but with the same number of identical functional groups on the surface can be obtained. This is illustrated in Scheme 1 and Scheme 3 and in Figure 4 where it is shown that by changing the order of addition of the reagents to **1** (AB$_2$, CD$_5$, AB$_2$, CD$_5$, Scheme 1 and, AB$_5$, CD$_2$, AB$_5$, CD$_2$, Scheme 3) it is possible to obtain different dendrimers of generation 2 (**5-[G$_2$], 7-[G$_2$]**,[12] (Figure 4) or generation 4 (**5-[G$_4$], 7-[G$_4$]**) bearing the same number of aldehyde end groups, 60 or 600, respectively, 7). This concept could be applied to other multifunctionalized cores (A$_6$, C$_6$, and the corresponding octafunctionalized monomers built from P$_4$N$_4$Cl$_8$), and to other unsymmetrical systems bearing, like AB$_5$ or CD$_5$, two different functions or to other easily accessible multifunctionalized starting reagents (A$_2$B$_4$…).

Experimental Section

General procedure for the reaction of phosphane-terminated dendrimers **5-[G$_1$], 5-[G$_3$], 6-[G$_1$], 7-[G$_3$]**, with CD$_2$ or CD$_5$ monomers: A 2% excess of the CD$_2$ or CD$_5$ monomer dissolved in THF (5 mL) was added to a solution of the dendrimer (0.200 g) in distilled and degassed THF (5 mL). The resulting solution was stirred at room temperature (in the case of CD$_2$) or at 45 °C (in the case of CD$_5$) for 2 days, then the solvent was removed under vacuum. The residue was washed three times with a mixture THF/pentane (1/5) for the reaction performed with CD$_2$, or with a mixture ethylacetate/diethyl ether/pentane (1/1/2) for the reaction performed with CD$_5$, to remove the small excess of monomer. Products **5-[G$_2$], 5-[G$_4$], 6-[G$_2$], 7-[G$_2$]**, and **7-[G$_4$]** were obtained as white powders.

General procedure for the reaction of aldehyde terminated dendrimers **5-[G$_2$], 6-[G$_2$]**, and **7-[G$_2$]** with AB$_2$ or AB$_5$ monomers. A 2% excess of the AB$_2$ or AB$_5$ monomer dissolved in THF (5 mL) was added to a solution of the dendrimer (0.200 g) in distilled and degassed THF (5 mL). The resulting solution was stirred in a sealed flask for 2 days (for AB$_2$) or 4 days (for AB$_5$) at 100 °C. After cooling at room temperature, the solvent was removed under vacuum and the residue was washed three times with diethyl ether (for AB$_2$) or with a mixture THF/pentane (1/5) (for AB$_5$) to give **5-[G$_3$], 6-[G$_3$]**, and **7-[G$_3$]** as white powders.

Received: December 23, 2002 [Z50827]



Scheme 3. Divergent synthesis of the dendrimer of generation 4, **7-[G$_4$]**, by the alternate use of the AB$_5$ monomer **2** and the CD$_2$ monomer **8**.

 © 2003 Wiley-VCH Verlag GmbH & Co. KGaA, Weinheim

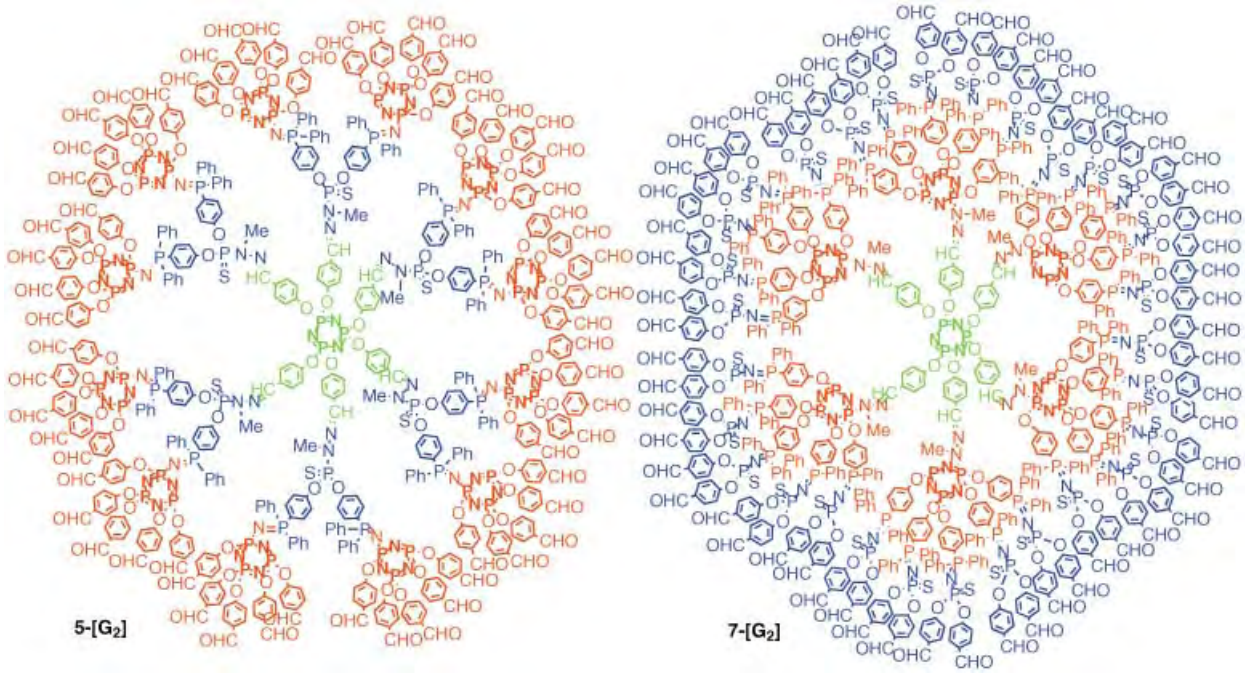


Figure 4. Representation of dendrimers **5-[G$_2$]**, and **7-[G$_2$]** bearing 60 aldehyde end groups.

Keywords: dendrimers · divergent synthesis · green chemistry · phosphorus · synthetic methods

[1] Some recent reviews: a) G. R. Newkome, F. Vögtle, C. N. Moorefield, *Dendrimers and dendrons*, Wiley, New York, **2001**; b) J. M. J. Fréchet, D. A. Tomalia, *Dendrimers and other dendritic polymers*, Wiley, New York, **2001**; c) D. C. Tully, J. M. J. Fréchet, *Chem. Commun.* **2001**, 1229; d) S. M. Grayson, J. M. J. Fréchet, *Chem. Rev.* **2001**, *101*, 3819; e) J. P. Majoral, A. M. Caminade, *Chem. Rev.* **1999**, *99*, 84.

[2] A number of new methods have been proposed for the fast synthesis of organic dendrimers ("double stage",[3] "double exponential growth",[4] use of hypermonomer,[5] orthogonal-coupling strategy[6]) but most of them still suffer numerous drawbacks: the number of steps often is not significantly decreased, byproducts are not easy to remove, the use of an activating agent is frequently necessary.

[3] a) K. L. Wooley, C. J. Hawker, J. M. J. Fréchet, *J. Am. Chem. Soc.* **1991**, *113*, 4252; b) T. M. Miller, T. X. Neenan, R. Zayas, H. Bair, *J. Am. Chem. Soc.* **1992**, *114*, 1018; c) Z. F. Xu, M. Kahr, K. L. Walker, C. L. Wilkins, J. S. Moore, *J. Am. Chem. Soc.* **1994**, *116*, 4537; d) H. Ihre, A. Hult, J. M. J. Fréchet, I. Gitsov, *Macromolecules* **1998**, *31*, 4061; e) B. Forier, W. Dehaen, *Tetrahedron* **1999**, *55*, 9829; f) V. Maraval, R. Laurent, B. Donnadieu, M. Mauzac, A. M. Caminade, J. P. Majoral, *J. Am. Chem. Soc.* **2000**, *122*, 2499.

[4] a) T. Kawaguchi, K. L. Walker, C. L. Wilkins, J. S. Moore, *J. Am. Chem. Soc.* **1995**, *117*, 2159; b) H. T. Chang, C. T. Chen, T. Kondo, G. Siuzdak, K. B. Sharpless, *Angew. Chem.* **1995**, *107*, 202; *Angew. Chem. Int. Ed. Engl.* **1996**, *35*, 182; c) R. Klopsch, P. Franke, A. D. Schlüter, *Chem. Eur. J.* **1996**, *2*, 1330; d) P. R. Ashton, D. W. Anderson, C. L. Brown, A. N. Shipway, J. F. Stoddart, M. S. Tolley, *Chem. Eur. J.* **1998**, *4*, 781.

[5] a) K. L. Wooley, C. J. Hawker, J. M. J. Fréchet, *Angew. Chem.* **1994**, *106*, 123; *Angew. Chem. Int. Ed. Engl.* **1994**, *33*, 82; b) L. J. Twyman, A. E. Beezer, J. C. Mitchell, *J. Chem. Soc. Perkin Trans. 1* **1994**, 407; c) G. L'abbé, B. Forier, W. Dehaen, *Chem. Commun.* **1996**, 2143; d) M. Ohta, J. M. J. Fréchet, *J. Macromol. Sci. Pure Appl. Chem.* **1997**, *A34*, 2025; e) Z. S. Bo, X. Zhang, C. M. Zhang, Z. Q. Wang, M. L. Yang, J. C. Shen, Y. P. Ji, *J. Chem. Soc. Perkin Trans. 1* **1997**, 2931; f) F. Morgenroth, A. J. Berresheim, M. Wagner, K. Müllen, *Chem. Commun.* **1998**, 1139; g) U. M. Wiesler, K. Müllen, *Chem. Commun.* **1999**, 2293; h) S. L. Gilat, A. Adronov, J. M. J. Fréchet, *J. Org. Chem.* **1999**, *64*, 7474; i) D. A. Scott, T. M. Krülle, M. Finn, G. W. J. Fleet, *Tetrahedron Lett.* **2000**, *41*, 3959.

[6] a) R. Spindler, J. M. J. Fréchet, *J. Chem. Soc. Perkin Trans. 1* **1993**, 913; b) Z. Xu, J. S. Moore, *Angew. Chem.* **1993**, *105*, 1394; *Angew. Chem. Int. Ed. Engl.* **1993**, *32*, 1354; c) F. W. Zeng, S. C. Zimmerman, *J. Am. Chem. Soc.* **1996**, *118*, 5326; d) S. K. Deb, T. M. Maddux, L. P. Yu, *J. Am. Chem. Soc.* **1997**, *119*, 9079; e) S. K. Deb, T. M. Maddux, L. P. Yu, *Polym. Mater. Sci. Eng.* **1997**, *77*, 163; f) R. Klopsch, S. Koch, A. D. Schlüter, *Eur. J. Org. Chem.* **1998**, 1275; g) A. Ingerl, I. Neubert, R. Klopsch, A. D. Schlüter, *Eur. J. Org. Chem.* **1998**, 2551; h) A. W. Freeman, J. M. J. Fréchet, *Org. Lett.* **1999**, *1*, 685; i) Y. Ishida, M. Jikei, M. Kakimoto, *Macromolecules* **2000**, *33*, 3202.

[7] L. Brauge, G. Magro, A.-M. Caminade, J.-P. Majoral, *J. Am. Chem. Soc.* **2001**, *123*, 6698; corrected L. Brauge, G. Magro, A.-M. Caminade, J.-P. Majoral, *J. Am. Chem. Soc.* **2001**, *123*, 8486.

[8] For applications of phosphorus dendrimers, see for example: a) C. Loup, M.-A. Zanta, A.-M. Caminade, J.-P. Majoral, B. Meunier, *Chem. Eur. J.* **1999**, *5*, 3644; b) M. K. Boggiano, G. J. A. A. Soler-Illia, L. Rozes, C.-O. Turrin, A.-M. Caminade, J.-P. Majoral, *Angew. Chem.* **2000**, *112*, 4419; *Angew. Chem. Int. Ed.* **2000**, *39*, 4249; c) C.-O. Turrin, V. Maraval, A.-M. Caminade, J.-P. Majoral, A. Mehdi, C. Reyé, *Chem. Mater.* **2000**, *12*, 3848; d) V. Maraval, R. Laurent, A.-M. Caminade, J.-P. Majoral, *Organometallics* **2000**, *19*, 4025; e) F. Le Derf, E. Levillain, A. Gorgues, M. Sallé, R.-M. Sebastian, A.-M. Caminade, J.-P. Majoral, *Angew. Chem.* **2001**, *113*, 230; *Angew. Chem. Int. Ed.* **2001**, *40*, 224; f) C. Marmillon, F. Gauffre, T. Gulik-Krzywicki, C. Loup, A.-M. Caminade, J.-P. Majoral, J.-P. Vors, E. Rumps, *Angew. Chem.* **2001**, *113*, 2699; *Angew. Chem. Int. Ed.* **2001**, *40*, 2626; g) E. Trevisiol, J. Leclaire, G. Pratviel, A.-M. Caminade, J.-

 © 2003 Wiley-VCH Verlag GmbH & Co. KGaA, Weinheim

M. François, J.-P. Majoral, B. Meunier, , French Patent 0205049 **2002**; h) J.-P. Majoral, A.-M. Caminade, J. Leclaire, C. Loup, J. Solassol, S. Lehmann, B. Meunier, , French Patent 0200675 **2002**; i) M. Blanzat, C.-O. Turrin, E. Perez, I. Rico-Lattes, A.-M. Caminade, J.-P. Majoral, *Chem. Commun.* **2002**, 1864.

[9] N. Launay, A.-M. Caminade, R. Lahana, J.-P. Majoral, *Angew. Chem.* **1994**, *106*, 1682; *Angew. Chem. Int. Ed. Engl.* **1994**, *33*, 1589.

[10] M. L. Lartigue, B. Donnadieu, C. Galliot, A.-M. Caminade, J.-P. Majoral, J.-P. Fayet, *Macromolecules* **1997**, *30*, 7335.

[11] G. Schmid, W. Meyer-Zaika, R. Pugin, T. Sawitowski, J.-P. Majoral, A.-M. Caminade, C.-O. Turrin, *Chem. Eur. J.* **2000**, *6*, 1693 and unpublished results.

[12] **7-[G_2]** was characterized by ^{31}P, ^{1}H, ^{13}C NMR spectroscopy as well as by mass spectrometry (MALDI TOF; [*M*Li^+] 13739.7) and elemental analysis.

 © 2003 Wiley-VCH Verlag GmbH & Co. KGaA, Weinheim

Time-Resolved IR Spectroscopy

Direct Observation of a Hydrogen-Bonded Charge-Transfer State of 4-Dimethylaminobenzonitrile in Methanol by Time-Resolved IR Spectroscopy**

Wai-Ming Kwok, Michael W. George, David C. Grills, Chensheng Ma, Pavel Matousek, Anthony W. Parker, David Phillips, William T. Toner, and Michael Towrie*

Charge-transfer excited states have frequently been studied by using 4-dimethylaminobenzonitrile (DMABN) as a model. In nonpolar solvents, a single fluorescence band is observed from a locally excited (LE) state. In polar solvents, the initially populated LE state reacts further to produce a stable intramolecular charge-transfer (ICT) state, which gives rise to a second fluorescence band that overlaps with, but is abnormally red-shifted from, the LE emission.[1] Results of experiments using aprotic solvents are well described by models in which polarity is the only solvent property that affects the charge transfer reaction activation energy and the relative stabilization of the ICT and LE states.[2] Whilst much work continues to concentrate on determining the structures of the LE and ICT states,[3–7] the precise nature of the difference between the properties of the excited state in protic and aprotic solvents is little understood. For example, the fluorescence quantum yield of DMABN in protic solvents is lower and the fluorescence spectrum is further red-shifted and broadened, relative to measurements in aprotic solvents of the same polarity,[8,9] and the fluorescence decay kinetics are difficult to interpret.[2] Hydrogen bonding in protic solvents can lead to complicated interactions[10] but although specific solute–solvent and solute–solute interactions have been discussed,[8,11–14] there is no generally accepted explanation. There are similar problems in other cases of dual fluorescence.[15]

The time-resolved infrared (TRIR) absorption spectra presented here demonstrate and monitor the formation of a hydrogen-bonded charge-transfer state of photoexcited DMABN in the protic solvent methanol (MeOH), through the development of the C≡N IR absorption band from an initial singlet into a doublet. The initial single band is interpreted as belonging to an ICT state like that created in aprotic acetonitrile (MeCN), where only one absorption band is observed at all delay times. The second component is interpreted as being due to the hydrogen-bonded charge-transfer state; the kinetics show the populations of the free and hydrogen-bonded species coming to dynamic equilibrium. We designate the hydrogen-bonded state as HICT. This is the first direct observation of hydrogen bonding in an excited state. Since the populations in the LE state and the two charge-transfer states coexist, the fluorescence will be triple, not dual in character. Neglect of this major factor is considered to account for much of the difficulty in interpreting the fluorescence results.[2,8,11–13] A mechanism of this kind has not to our knowledge been proposed before. We believe this interpretation is applicable to other molecules with solvent-dependent dual fluorescence.

Figure 1 shows TRIR spectra of DMABN in MeCN (a) and MeOH (b) recorded with sub-picosecond time resolution at pump–probe delays from 2 to 3000 ps after excitation; Figure 2 gives the time-dependence of the absorption band areas. Kinetics parameters were determined by least-squares fits. The spectral region between 2065 and 2235 cm^{-1} (Figure 1) covers the C≡N bands of the ground, LE, and ICT states.[3,4,6,16] The LE band is observed by Raman but not by TRIR spectroscopy.[6,16]

The ICT state C≡N IR absorption band at 2104 cm^{-1} in MeCN and the ground state depletion (bleach) at 2213 cm^{-1} are clearly seen (Figure 1a). Time constants for the non-radiative reaction LE⇄ICT plus the decay of the whole population (lines in Figure 2a) are 6.4 ps (equilibration) and 2.7 ns (decay). The small level of decay back to the ground state is shown by the small recovery in the bleached signal and is due to fluorescence and internal conversion (IC) to the

[*] Dr. C. Ma,+ Dr. W.-M. Kwok,+ Prof. D. Phillips
Department of Chemistry
Imperial College
Exhibition Road, London SW7 2AY (UK)
Fax: (+44) 207-594-5801
E-mail: macs@hkucc.hku.hk
Dr. M. W. George, Dr. D. C. Grills
School of Chemistry
University of Nottingham
University Park, Nottingham NG7 2RD (UK)
Dr. P. Matousek, Dr. A. W. Parker, Dr. M. Towrie
Central Laser Facility
CLRC Rutherford Appleton Laboratory
Didcot, Oxfordshire OX11 0QX (UK)
W. T. Toner
Department of Physics
Clarendon Laboratory
Parks Road, Oxford OX1 3PU (UK)

[**] We are grateful to the EPSRC for financial support through grants GR/R29062 and GR/M40486. This work was carried out at the Central Laser Facility, CLRC Rutherford Appleton Laboratory.

 © 2003 Wiley-VCH Verlag GmbH & Co. KGaA, Weinheim DOI: 10.1002/anie.200219816

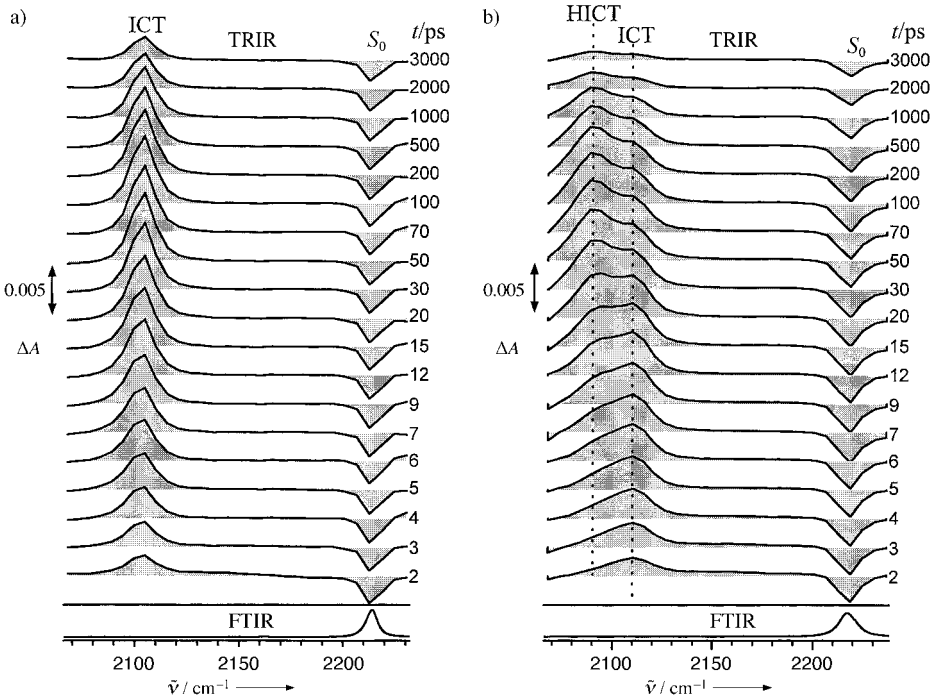


Figure 1. Ground-state FTIR and TRIR spectra of DMABN in MeCN (a) and in MeOH (b), which were obtained at different pump–probe time delays with excitation at 267 nm.

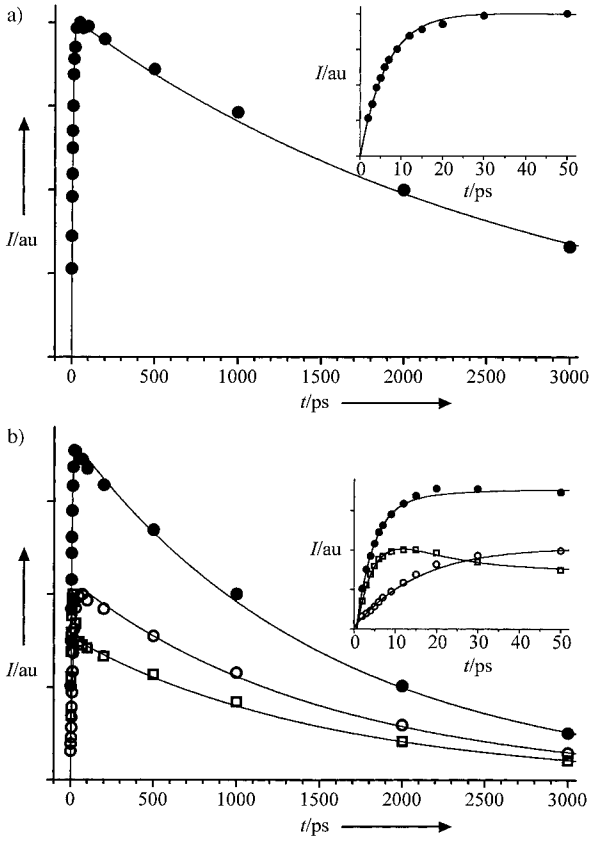


Figure 2. a) Time-dependence of the ICT state C≡N band areas in Figure 1a (●). b) Time-dependence of the charge-transfer C≡N band areas in Figure 1b: total (●); ICT, band centered at 2109 cm^{-1}, (□); HICT, band centered at 2091 cm^{-1}, (○). Solid lines are results of fits (see text). The inserts give details of the early time kinetics.

ground state, the lack of triplet decay providing a constant remainder on the 3 ns time scale. From fits to the bleached band areas from 20 ps to 3 ns (not shown) using the absorption decay time constant, and from the fluorescence quantum yield (0.030),[9] we estimate the rates for fluorescence (1.1×10^7 s^{-1}), IC ($\approx 6 \times 10^7$ s^{-1}), and intersystem crossing (ISC) to the triplet ($\approx 30 \times 10^7$ s^{-1}). We have observed similar TRIR spectra in THF and triacetin (1,2,3-propanetriol triacetate), but with different time constants. The equilibrium LE/ICT population ratio in MeCN may be estimated to be about 1% from steady-state fluorescence spectra. Our results agree with those of many fluorescence studies:[2] prompt formation of the LE state is followed by fast equilibration of the LE and ICT populations, the parameters for which vary mainly with polarity in aprotic solvents of low viscosity.

The results obtained are very different in MeOH (Figure 1b and 2b). As the C≡N absorption grows, the band can be resolved into two components at 2091 and 2109 cm^{-1}, which reach constant relative intensities by about 50 ps. These data were fitted by using Lorentzians of equal width to separate the components, but essentially the same results were also obtained by using the total intensity and mean frequency of the combined bands plus the estimated separation of the peaks at late time. Thus, we believe it is unnecessary in this brief account to consider possible small non-Lorentzian effects.[17] Moreover, the main qualitative conclusions of this time-resolved experiment are clear from a comparison of Figure 1a and b.

The total intensity of the two components in MeOH has time constants of 5.5 ps and 1.6 ns for growth and decay, respectively, and the component at 2091 cm^{-1} grows with a time constant of 13 ps (lines in Figure 2b) but is not

 © 2003 Wiley-VCH Verlag GmbH & Co. KGaA, Weinheim

resolvable at the earliest times. The bandwidths of the two components are significantly broader than the ground state bleach (at 2217 cm^{-1}), indicating that some unidentified faster processes or inhomogeneous effects are also involved. Ground state bleach recovery can be seen in Figure 1b, and the enhancement relative to the behavior in MeCN indicates much stronger internal conversion in MeOH. By using the fluorescence quantum yield of DMABN in MeOH (0.017)[9] in fits to the bleach areas from 20 ps to 3 ns as before (not shown), the fluorescence, IC, and ISC rates are found to be 1.1×10^7, $\approx31\times10^7$, and $\approx30\times10^7\ s^{-1}$, respectively. The LE equilibrium population fraction is again estimated to be very small and these rates are taken to apply to the charge-transfer state(s). Qualitatively similar results were obtained in ethanol and butanol. Asymmetry of the DMABN C≡N band in protic solvents consistent with this work is visible—though not commented on—in published TR[3][3] and TRIR[4] spectra.

The growth of the component at 2091 cm^{-1} at the expense of that at 2109 cm^{-1} is clearly due to an interaction that occurs in protic MeOH after charge separation and does not occur in aprotic MeCN. We attribute it to hydrogen bonding between the MeOH and the ICT state of DMABN. The shift to lower wavenumber by 108 cm^{-1} of the initial component (at 2109 cm^{-1}) from the ground state bleach (at 2217 cm^{-1}) differs by only 1 cm^{-1} from that observed for the ICT in MeCN, so we attribute it to a state closely resembling the "free" ICT state formed in aprotic solvents, and assign the second component at 2091 cm^{-1} to the hydrogen-bonded form. We designate these two charge-transfer states as ICT and HICT, respectively. The 13 ps time scale for the growth of the 2091 cm^{-1} (HICT) band is consistent with the 10–15 ps time scale observed for the hydrogen bonding of ground state *N*-methylacetamide in MeOH.[18] The 20 cm^{-1} separation of the C=O components in that case is comparable with the 18 cm^{-1} C≡N splitting we observe, and the resolution of the components is similar. The strongly enhanced rate for IC to the ground state is consistent with the large effect of deuteration on DMABN fluorescence in alcohol solvents,[11] and we note that deactivation via IC resulting from hydrogen bonding has been proposed to account for the fluorescence quenching of many molecules having ICT states.[19]

Our results show that the rates for radiative decay and ISC are unaffected by hydrogen bonding, illustrating the weakness of this interaction. It therefore seems reasonable to assume the "free" ICT in MeOH is the same as that in MeCN, in which case it follows that the radiative rates will be the same for ICT and HICT. Taking the ICT state also to have the same nonradiative decay rates in MeOH and MeCN leads to the conclusion that the enhanced IC rate in MeOH is wholly attributable to the HICT state (or nearly so). The IC rate for this fraction of the charge-transfer population (see below) is thus estimated to be about 50% larger than the value quoted above for the mixture.

The kinetics are well described (lines in Figure 2b) by a sequence of reversible, nonradiative reactions that lead to equilibrium populations on picosecond time scales: $S_0 \xrightarrow{h\nu}$ LE⇄ICT⇄HICT, with each excited state also decaying on the nanosecond time scale as discussed earlier. The small population of the HICT state relative to the ICT state at $t=0$ indicated by our fits (less than ≈15% of the total) justifies neglect of a further possible reaction, LE⇄HICT, but does not exclude it. The results are insensitive to the method used to separate the two components, as noted above, but their detailed interpretation using the kinetics model depends on the ratio of ICT to HICT IR absorption cross sections, which are not known. For example, if we vary the assumed ratio from 0.75 to 1.6, the equilibration time constant for LE⇄ICT rises from ~4 to 8 ps, while that for ICT⇄HICT falls from ~12 to 8 ps and the forward ICT→HICT reaction time constant falls from ~20 to 11 ps. The estimated equilibrium HICT population fraction rises from 56% to 73% over the same parameter range. These ranges are not large and since the LE equilibration time constant in MeOH is expected to be similar to that in MeCN (6.4 ps) because of the similar polarity of the two solvents, we conclude that the most probable C≡N IR absorption cross section ratio of ICT and HICT is close to unity. The assumption of equal cross sections is also made and justified in reference [17]. The population fraction in HICT at equilibrium is thus close to two thirds and the ICT⇄HICT equilibration time constant is ≈10 ps. This is very similar to the results obtained by Woutersen et al.[18]

We consider these results to be compelling evidence for the coexistence of two charge-transfer states of photoexcited DMABN in MeOH, one similar to the "free" ICT state formed in MeCN, and the other hydrogen-bonded.

Intermolecular solute–solvent hydrogen bonding interactions are highly sensitive to solute–solvent orientation and distance, and the formation process must also compete with the tendency of MeOH to form solvent–solvent multimers. It is therefore significant that the estimated time constant for the forward hydrogen-bonding reaction is close to the 15.8 ps time scale[20] for solvent–solvent bond breaking and R–OH rotation in MeOH. The strength of the intermolecular forces will clearly be critical. FTIR spectra of the DMABN ground state show the C≡N stretch occurs at 2217 cm^{-1} in MeOH and at 2213 cm^{-1} in MeCN, the band being somewhat broader in MeOH (Figure 1). The shift to higher wavenumbers in MeOH is close to the 5 cm^{-1} upshift observed for the "free" ICT state in the TRIR spectrum recorded in MeOH relative to that in MeCN (Figure 1). Since we observe that the frequency of the hydrogen-bonded component in the excited state is lowered, we attribute the ground state upshift and broadening to a weaker interaction that does not produce stable bonding. The LE state is not observed in this experiment but it is clear from Figure 1b that the hydrogen-bonded component at 2091 cm^{-1} has little or no intensity at the earliest times, and grows at the expense of the free component, so whatever bonding interaction there may be with the LE state is again weak. The charge-separation step is thus seen to be necessary to favor DMABN–MeOH configurations that form bonds having lifetimes of a few picoseconds so that the majority of the DMABN excited state population becomes hydrogen-bonded, despite the strong MeOH–MeOH interaction. We consider that the increased negative charge density on the cyano electron-acceptor region of the ICT state of DMABN[3,4] facilitates bonding at this site in the presence of a proton donor, such as the -OH group in alcohol, the electron acceptor group in turn becoming a proton acceptor.

 © 2003 Wiley-VCH Verlag GmbH & Co. KGaA, Weinheim

Our TRIR results can be briefly discussed in relation to the fluorescence properties of the ICT state of DMABN. As noted above, we consider that the radiative rate is most likely the same for ICT and HICT. The charge-transfer fluorescence will therefore be composed of overlapping bands having intensities in proportion to the ICT/HICT population ratio of about 1/2. The overall fluorescence will be intrinsically triple, and show complicated kinetics[21,22] not predicted by the dual fluorescence model[2] appropriate for aprotic solvents. This can account for much of the confusion in the literature, especially the complicated fluorescence decay dynamics observed at different temperatures in alcohols,[2,22] where variations in the relative populations of LE/ICT and ICT/HICT can be expected. Interpretations using more subtle effects of dielectric relaxation and viscosity (undoubtedly also relevant) will clearly not succeed when such a major factor is neglected.

The steady-state fluorescence spectrum has no visible structure to help separate the two charge-transfer components although the spectrum in MeOH is broader than in MeCN, and the red shift of the maximum by about 1000 cm^{-1} in MeOH appears to be largely due to the increase of about 2000 cm^{-1} in the width (FWHM),[9] rather than a large shift of electronic origin of the kind separating LE from ICT. It may be possible to resolve these two components experimentally by measuring the transient resonance Raman excitation profiles (REPs) of the ICT and HICT states, thus providing new opportunities for studying the differences between them.

Only the C≡N region was covered in this experiment, but since the phenyl ring is also part of the electron-acceptor group,[3,4] other bands may also be affected, as well as the structural configuration. We note that two hydrogen-bonding sites have been reported for ground state 4-aminobenzonitrile in water.[23] Further work on DMABN and its analogues is in progress and includes studying the structural differences between ICT and HICT and the complex interplay of temperature-dependent molecular and solvent properties that can affect the excited state spectra.

In conclusion, our data demonstrate the existence of two charge-transfer states of photoexcited DMABN in MeOH, namely ICT and HICT, where HICT is hydrogen-bonded. ICT is populated from the LE state and a dynamic equilibrium between the populations of the two charge-transfer states is established on a 13 ps time scale. The internal conversion deexcitation rate of the HICT state is much larger than that of ICT and is mainly responsible for the reduced quantum yield in MeOH. The overall fluorescence spectrum is composed of contributions from LE, ICT, and HICT. We have proposed that this novel three-state mechanism can account for many anomalies in the fluorescence spectra of dual fluorescence molecules in protic solvents. The results also illustrate the power of the high-resolution, high-sensitivity TRIR technique employed and the ability to monitor the formation of bonds between excited states in real time.

Experimental Section

Measurements were made using the Picosecond Infrared Absorption and Transient Excitation (PIRATE) system.[24] Samples at room temperature (23 °C) were excited at a 1 kHz repetition rate by a 267 nm pump beam (0.2 ps, 5 μJ per pulse; 200 μm diameter), produced by frequency-tripling a fraction of the 800 nm regenerative amplifier output. A solution (5 mM) of triple-recrystallized DMABN in spectroscopic grade solvent was circulated to ensure fresh material was exposed on every shot. The femtosecond signal and idler outputs of an optical parametric amplifier (OPA), pumped by the remaining 800 nm beam, were mixed in silver gallium sulfide ($AgGaS_2$) to give a broadband IR beam. Absorption spectra were obtained as described elsewhere.[24] Briefly, the sub-picosecond IR beam is split into probe and reference beams using a 50% germanium beam splitter. The probe beam is focused to about 150 μm diameter in the sample cell, and the transmitted light is imaged onto a spectrometer. The reference arm has similar optics. Transmitted and reference spectra are recorded on 64-element MIR array detectors with 5 cm^{-1} resolution, read out on each shot, and normalized point-by-point. This gives good comparability and sensitivity for all bands in a 200 cm^{-1} range selected by tuning the OPA.

Received: July 25, 2002
Revised: December 5, 2002 [Z19816]

Keywords: charge transfer · cyanides · fluorescence · hydrogen bonds · IR spectroscopy · time-resolved spectroscopy

[1] E. Lippert, W. Rettig, V. Bonacic-Koutecky, F. Heisel, J. A. Miehe, *Adv. Chem. Phys.* **1987**, *68*, 1–173.
[2] P. Changenet, P. Plaza, M. M. Martin, Y. H. Meyer, *J. Phys. Chem. A* **1997**, *101*, 8186–8194, and references therein.
[3] W. M. Kwok, C. Ma, P. Matousek, A. W. Parker, D. Phillips, W. T. Toner, M. Towrie, S. Umapathy, *J. Phys. Chem. A* **2001**, *105*, 984–990.
[4] M. Hashimoto, H. Hamaguchi, *J. Phys. Chem.* **1995**, *99*, 7875–7877.
[5] H. Okamoto, H. Inishi, Y. Nakamura, S. Kohtani, R. Nakagaki, *J. Phys. Chem. A* **2001**, *105*, 4182–4188.
[6] C. Chudoba, A. Kummrow, J. Dreyer, J. Stenger, E. T. J. Nibbering, T. Elsaesser, K. A. Zachariasse, *Chem. Phys. Lett.* **1999**, *309*, 357–363.
[7] J. Dobkowski, J. Wojcik, W. Kozminski, R. Kolos, J. Waluk, J. Michl, *J. Am. Chem. Soc.* **2002**, *124*, 2406–2407.
[8] D. Pilloud, P. Suppan, L. V. Haelst, *Chem. Phys. Lett.* **1987**, *137*, 130–133.
[9] T. Okada, M. Uesugi, G. Kohler, K. Rechthaler, K. Rotkiewicz, W. Rettig, G. Grabner, *Chem. Phys.* **1999**, *241*, 327–337.
[10] a) C. Chudoba, E. T. J. Nibbering, T. Elsaesser, *Phys. Rev. Lett.* **1998**, *81*, 3010–3013; b) C. Chudoba, E. T. J. Nibbering, T. Elsaesser, *J. Phys. Chem. A* **1999**, *103*, 5625–5628.
[11] R. J. Visser, C. A. G. O. Varma, J. Konijnenberg, P. Bergwerf, *J. Chem. Soc. Faraday Trans. 2* **1983**, *79*, 347–367.
[12] C. Cazeau-Dubroca, S. A. Lyazidi, P. Cambou, A. Peirigua, P. Cazeau, M. Pesquer, *J. Phys. Chem.* **1989**, *93*, 2347–2358.
[13] O. S. Khalil, R. H. Hofeldt, S. P. McGlynn, *J. Lumin.* **1973**, *6*, 229–244.
[14] K. A. Zachariasse, T. Yoshihara, S. I. Druzhinin, *J. Phys. Chem. A* **2002**, *106*, 6325–6333.
[15] P. R. Bangal, S. Panja, S. Chakravorti, *J. Photochem. Photobiol. A* **2001**, *139*, 5–16.
[16] C. Ma, W. M. Kwok, P. Matousek, A. W. Parker, D. Phillips, W. T. Toner, M. Towrie, *J. Phys. Chem. A* **2002**, *106*, 3294–3305.
[17] M. Besnard, M. I. Cabaco, F. Strehle, J. Yarwood, *Chem. Phys.* **1992**, *163*, 103–114.
[18] S. Woutersen, Y. Mu, G. Stock, P. Hamm, *Chem. Phys.* **2001**, *266*, 137–147.

 © 2003 Wiley-VCH Verlag GmbH & Co. KGaA, Weinheim

[19] A. Morimoto, T. Yatsuhashi, T. Shimada, S. Kumazaki, K. Yoshihara, H. Inoue, *J. Phys. Chem. A* **2001**, *105*, 8840 – 8849, and references therein.
[20] M. L. Horng, J. A. Gardecki, A. Papazyan, M. Maroncelli, *J. Phys. Chem.* **1995**, *99*, 17311 – 17337.
[21] S. R. Meech, D. Phillips, *J. Chem. Soc. Faraday Trans. 2* **1987**, *83*, 1941 – 1956.
[22] S.-G. Su, J. D. Simon, *J. Chem. Phys.* **1988**, *89*, 908 – 919.
[23] E. Alejandro, J. A. Fernandez, F. Castano, *Chem. Phys. Lett.* **2002**, *353*, 195 – 203.
[24] M. Towrie, D. C. Grills, J. Dyer, J. A. Weinstein, P. Matousek, R. Barton, P. D. Bailey, N. Subramaniam, W. M. Kwok, C. Ma, D. Phillips, A. W. Parker, M. W. George, *Appl. Spectrosc.* **2003**, *57*, 367 – 380.

 © 2003 Wiley-VCH Verlag GmbH & Co. KGaA, Weinheim

Two-Way Energy Transfer

Vectorial Control of Energy-Transfer Processes in Metallocyclodextrin Heterometallic Assemblies**

Johanna M. Haider, René M. Williams, Luisa De Cola, and Zoe Pikramenou**

In recent years, the importance of miniature photomolecular devices in nanoscale technology has led to the design of polymetallic supramolecular assemblies.[1–3] The employment of polyelectronic metal centers in a single supramolecular structure provides the basis for the development of molecular energy-conversion systems and wires in macromolecular systems.[4–7] Multistep reactions are usually required to link metallic building blocks together by means of covalent bonds; such multistep processes result in poor yields and synthetic complexity. Noncovalently assembled systems, in contrast, may allow control of the photoinduced processes by a simple choice of the assembled photoactive components. The noncovalent assembly of units in water presents other opportunities, not only to mimic natural processes, but also to provide easily accessible architectures. Self-assembled systems between ruthenium–bipyridine centers and various electron or energy acceptors have recently attracted much interest.[8–10] We are interested in studying photoinduced processes between metal units assembled in water through noncovalent interactions. We have previously introduced photoactive metals onto cyclodextrin rims for the assembly of photoactive units brought together by the cyclodextrin cavity.[11–14] Herein, we present a ruthenium tris(bipyridyl) cyclodextrin "wheel", $[Ru(\beta\text{-CD-mbpy})_3]^{2+}$ (**1**; β-CD-mbpy = 6-mono[4-methyl(4′-dimethyl-2,2′-bipyridyl] permethylated β-cyclodextrin which was isolated as the PF_6 salt **1**-$(PF_6)_2$ and which could be converted into the Cl salt **1**-Cl_2 to enhance its solubility) that acts as both energy donor and acceptor leading to a versatile system for communication between the inner metal core and the outer guest unit by energy transfer; metal-complex guests based on osmium(II) and iridium(III) terpyridine species with biphenyl or adamantyl tails attached to one of the ligands have been employed to examine the importance of the included tail in the photoinduced process (Figure 1).

Compound **1**, is an attractive luminescent receptor molecule with three cyclodextrin cups available for recognition. Solutions of **1** in water with 10% acetonitrile exhibit luminescence at room temperature at 622 nm ($\Phi = 0.027$, $\tau_{aerated} = 460$ ns, $\tau_{degassed} = 640$ ns) upon excitation at the metal-to-ligand charge transfer (MLCT) band at 436 nm. Comparison of the photophysical properties of this complex with the parent complex $[Ru(mbpy)_3][PF_6]_2$, (mbpy = 4,4′-dimethyl-2,2′-bipyridine) which bears no cyclodextrins, indicates that cyclodextrin substitution does not have a significant effect.

Osmium(II)-based guests, have been employed to play the role of energy acceptors whereas iridium(III)-based guests were used as energy donors for the Ru^{II} center. The guests have hydrophobic biphenyl and adamantyl tails to ensure high binding constants in the cyclodextrin cavity. The nature of the hydrophobic tail, aliphatic versus aromatic, is selected to examine its effect in the photoinduced processes. Considering the excited-state energies of the metal units (2 eV for Ru (620 nm), 1.7 eV for Os (730 nm), and 2.36 eV for the Ir complexes (525 nm))[15] we can estimate the driving force for the energy-transfer processes; for the energy transfer from Ru^{II} to Os^{II} this is estimated to be $\Delta G = -0.3$ eV, and for the energy transfer from Ir^{III} to Ru^{II} $\Delta G = -0.36$ eV. The shift of the λ_{max} of the emission spectra of the photoactive components (Figure 2a) show the relative trend of their excited-state energies, indicating the dual role of the ruthenium cyclodextrin complex as an energy donor or acceptor for the Os^{II} and Ir^{III} guests, respectively. A pictorial description of the excited-state energies of the photoactive metal components is presented in Figure 2b.

Photoinduced energy transfer from the ruthenium center of **1**-Cl_2 to the $[Os(biptpy)(tpy)]Cl_2$ (biptpy = 4′-(4-biphenyl)-2,2′:6′,2″-terpyridine, tpy = 2,2′:6′,2″terpyridine) complex bound in the cyclodextrin has been studied by time-resolved luminescence spectroscopy. Upon addition of a 22-fold excess of the guest in an aqueous solution of the ruthenium receptor, a high percentage (around 83%) of a short-lived component of 20 ps in the ruthenium luminescence lifetime is detected (Figure 3a) corresponding to the energy-transfer process. In these conditions about 87% of the cyclodextrin cups are filled[11] which agrees with the percentage of the short

[*] Dr. Z. Pikramenou, Dr. J. M. Haider
School of Chemical Sciences
The University of Birmingham
Edgbaston, Birmingham B15 2TT (UK)
Fax: (+44) 121-414-4446 or 4403
E-mail: z.pikramenou@bham.ac.uk
Prof. Dr. L. De Cola, Dr. R. M. Williams
Molecular Photonic Materials
Institute of Molecular Chemistry
Faculty of Science, University of Amsterdam
Nieuwe Achtergracht 166, 1018 WS Amsterdam (Netherlands)
Fax: (+31) 20-525-6456
E-mail: ldc@science.uva.nl

[**] We are grateful to The Leverhulme Trust and The Royal Society for funding.

 © 2003 Wiley-VCH Verlag GmbH & Co. KGaA, Weinheim DOI: 10.1002/anie.200250164

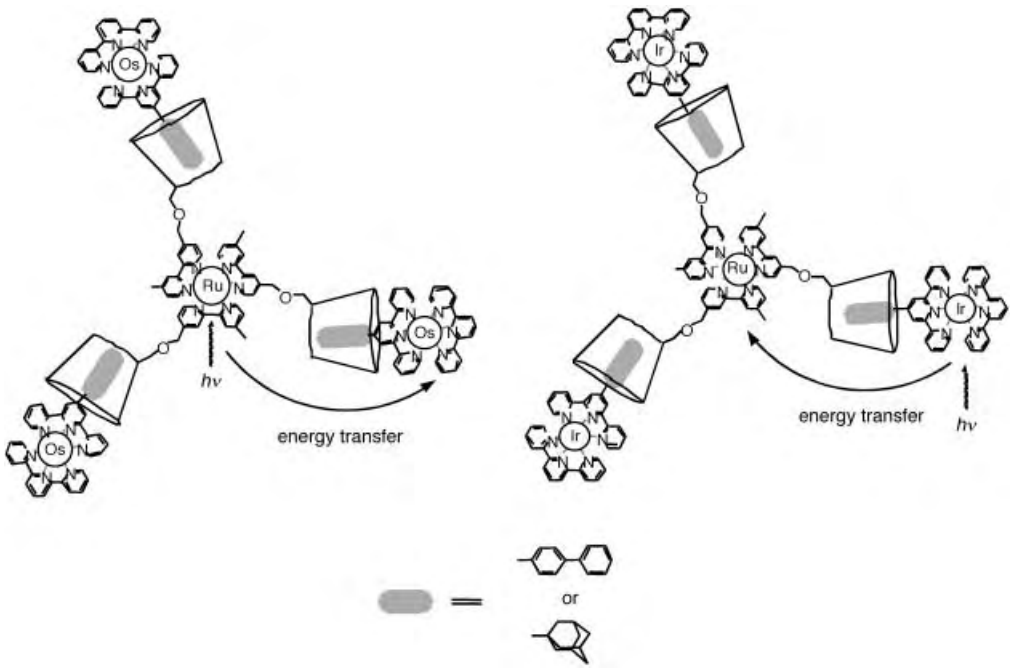


Figure 1. Assembled Os^{II} or Ir^{III} metal-complex guests with **1** allows photoinduced energy transfer from and to the ruthenium core.

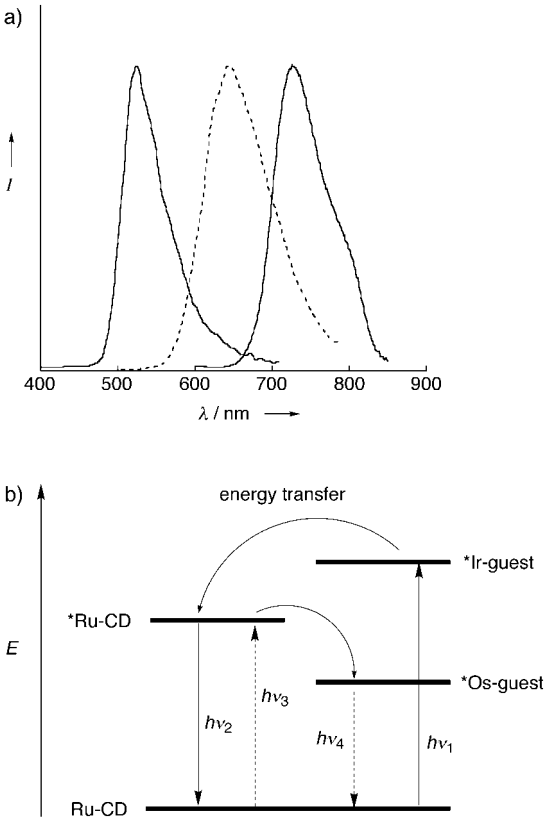


Figure 2. a) Steady-state emission spectra of $[Ir(tpy)(tpy\text{-}ada)][NO_3]_3$, **1**-$Cl_2$, and $[Os(tpy\text{-}ada)(tpy)][NO_3]_2$ (from left to right) in aqueous solution, observed at room temperature. The intensities are not to scale. b) Simplified energy diagram of the excited states of the photoactive components.

component. According to $k = (1/\tau) - (1/\tau_0)$, an energy-transfer rate of $8.3 \times 10^{10}\ s^{-1}$ is calculated. Furthermore upon excitation at the same wavelength, 324 nm, a rise time of the osmium luminescence signal at 730 nm of 13 ps confirms the photoinduced energy transfer from the ruthenium center to the guest through noncovalent bonds These results confirm that in spite the relatively long metal–metal distance (≈ 16 Å, calculated from an MM2 model) and the noncovalent nature of the bridge, light excitation of the ruthenium-based unit in the heterometallic $[Ru(\beta\text{-CD-mbpy})_3{-}Os(biptpy)(tpy)]^{4+}$ supramolecular assembly leads to an efficient-energy transfer process, in aqueous solutions.

To study the influence of the hydrophobic tail in the energy-transfer process between the Ru^{II} and Os^{II} centers, similar experiments were performed with $[Os(tpy\text{-}ada)(tpy)][NO_3]_2$ (tpy-ada = 4′-(1-adamantyl)-2,2′:6′,2″-terpyridine). The ruthenium luminescence is partially quenched, hence the appearance of a long component in the lifetime; the short component of 1.08 ns agrees with an observed rise time in the osmium emission of 1.12 ns (Figure 3b). An energy-transfer rate of $6.4 \times 10^8\ s^{-1}$ is calculated for the process. These results clearly show that the nature of the hydrophobic tail unit has a strong effect on the energy transfer process. Taking into consideration that the adamantyl tail should bring the metals closer together than the biphenyl one, the slowing down of the energy-transfer process is attributed to the effect of the orbital overlap, which implies a contribution from the Dexter mechanism, controlled by the electronic interaction between cyclodextrin and biphenyl, or cyclodextrin and adamantyl. In covalently linked systems aliphatic spacers are known to lead to a slower rate of energy-transfer than conjugated spacers.[16–22] However, in most of those cases the spacer affects the spatial disposition of the photoactive centers, whereas in our case this factor is eliminated.

 © 2003 Wiley-VCH Verlag GmbH & Co. KGaA, Weinheim

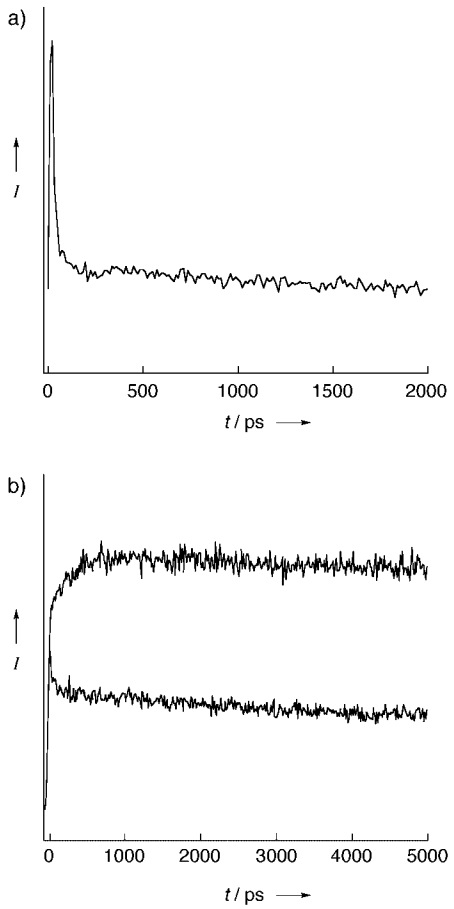


Figure 3. a) Time-resolved emission of an aqueous solution of **1**-Cl_2 (1.8×10^{-5} M) with [Os(biptpy)(tpy)]Cl_2 (3.8×10^{-4} M). Excitation at 324 nm, detection at 600 nm. b) Time-resolved emission of an aqueous solution of **1**-Cl_2 (1.8×10^{-5} M) with [Os(tpy-ada)(tpy)]$[NO_3]_2$ (1.4×10^{-4} M). Excitation at 324 nm, detection at 600 nm (lower trace) and at 730 nm (upper trace).

To monitor the luminescence of the iridium guest, excess of the ruthenium complex was used to ensure binding of most of the guests (80–95%) in the cyclodextrin cups. Monitoring of the iridium luminescence lifetime (at 525 nm) upon excitation at 330 nm showed the presence of a fast component with an amplitude determined by the amount of complexed iridium compound, with a lifetime of $\tau = 3$ ns for [Ir(biptpy)(tpy)]$[NO_3]_3$ and $\tau = 35$ ns [Ir(tpy-ada)(tpy)]$[NO_3]_3$ (Figure 4). Besides the short components there was also a long component present, which was 1.2 μs for the biptpy and 0.5 μs for the tpy-ada system, which correspond to the lifetimes of the separate complexes. Monitoring of the emission of the ruthenium center at 620 nm does not show any change in the ruthenium luminescence lifetime, which excludes the presence of an electron-transfer process as the dominant pathway. The ruthenium–iridium photoinduced communication through noncovalent bonds is attributed to an energy transfer from the iridium guest to the ruthenium core. The energy-transfer rates are estimated to be 3.3×10^8 and $2.9\times10^7\ s^{-1}$ for the biphenyl and the adamantly guests, respectively. In accordance with the osmium case we observe

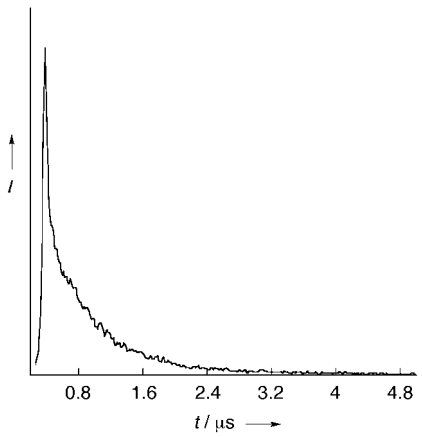


Figure 4. Time-resolved emission of an aqueous solution of [Ir(tpy-ada)(tpy)]$[NO_3]_3$ (2.5×10^{-5} M) with **1**-Cl_2 (3.7×10^{-5} M). Excitation at 330 nm, detection at 570 nm.

a slowing down of the rate by changing of the hydrophobic tail of the guest from an aromatic to an aliphatic moiety.

In summary, we have demonstrated that photoinduced energy transfer through a cyclodextrin cavity establishes communication between metal centers in water mediated by noncovalent interactions. The ruthenium "wheel" cyclodextrin system allows vectorial control of energy transfer between metal centers in aqueous solutions. The system allows switching of the two-way communication between the inner metal core and the outer ones by simply changing the photoactive metal-complex guests.

Experimental Section

The ligands 6-mono[4-methyl(4′-methyl-2,2′-bipyridyl)]-permethylated β-cyclodextrin (β-CD-mbpy),[12] 4′-(4-biphenyl)-2,2′:6′,2″- terpyridine (biptpy),[23] 4′-(1-adamantyl)-2,2′:6′,2″-terpyridine (tpy-ada) and the metal complexes[12] were prepared by analogous procedures to those previously reported. The time-resolved emission experiments were performed by time-correlated single-photon counting system employing a frequency doubled DCM dye laser which is synchronously pumped with a mode locked Argon ion laser resulting in 324 nm 20 ps FWHM pulses; details of the instrument have been previously described.[11]

1-$(PF_6)_2$ ^{1}H NMR (300 MHz, CD_3CN): $\delta = 8.5$, 8.4 (s, 6H, H-3, H3′), 7.9–7.5 (m, 6H, H-6, H-6′), 7.4–7.2 (m, 6H, H-5, H-5′), 5.2–5.0 (m, 21H, H_{Glu}-1), 4.7 (br dd, 6H, H-7), 4.2 (br d, 3H, H_{Glu}-6), 3.9–3.0 (m, -OCH_3 and H_{Glu}-2,3,4,5,6), 2.5 ppm (s, 9H, CH_3). ROESY ^{1}H NMR spectroscopy has been carried out to detect NOE connectivities and confirm assignments. Electrospray MS (MeOH): m/z: 2448 $\{M-2[PF_6]\}^{2+}$. Elemental analysis: calcd (%) for **1**-Cl_2: $C_{219}H_{348}Cl_2N_6O_{108}Ru_1\cdot 20H_2O$ ($M_r = 5325.46$) C 49.39, H 7.34 N, 1.58; found: C 49.19, H 6.97, N 1.66.

Received: September 16, 2002 [Z50164]

Keywords: cyclodextrins · energy transfer · metal–metal interactions · N ligands · ruthenium

[1] M. Barboiu, J.-M. Lehn, *Proc. Natl. Acad. Sci. USA* **2002**, *99*, 5201.

 © 2003 Wiley-VCH Verlag GmbH & Co. KGaA, Weinheim

[2] S. Encinas, L. Flamigni, F. Barigelletti, E. C. Constable, C. E. Housecroft, E. R. Schofield, E. Figgemeier, D. Fenske, M. Neuburger, J. G. Vos, M. Zehnder, *Chem. Eur. J.* **2002**, *8*, 137.
[3] S. Serroni, S. Campagna, F. Puntoriero, C. Di Pietro, N. D. McClenaghan, F. Loiseau, *Chem. Soc. Rev.* **2001**, *30*, 367.
[4] a) F. Barigelletti, L. Flamigni, *Chem. Soc. Rev.* **2000**, *29*, 1; b) A. El-ghayoury, A. Harriman, A. Khatyr, R. Ziessel, *Angew. Chem.* **2000**, *112*, 191; *Angew. Chem.* **2000**, *39*, 185.
[5] L. De Cola, P. Belser, *Coord. Chem. Rev.* **1998**, *177*, 301.
[6] D. J. Cardenas, J.-P. Collin, P. Gavina, J.-P. Sauvage, A. De Cian, J. Fischer, N. Armaroli, L. Flamigni, V. Vicinelli, V. Balzani, *J. Am. Chem. Soc.* **1999**, *121*, 5481.
[7] P. F. H. Schwab, M. D. Levin, J. Michl, *Chem. Rev.* **1999**, *99*, 1863.
[8] Y.-Z. Hu, S. Tsukiji, S. Shinkai, S. Oishi, I. Hamachi, *J. Am. Chem. Soc.* **2000**, *122*, 241.
[9] H. F. Nelissen, A. F. J. Schut, F. Venema, M. C. Feiters, R. J. M. Nolte, *Chem. Commun.* **2000**, 577.
[10] M. D. Ward, *Chem. Soc. Rev.* **1997**, *26*, 365.
[11] J. M. Haider, M. Chavarot, S. Weidner, I. Sadler, R. M. Williams, L. De Cola, Z. Pikramenou, *Inorg. Chem.* **2001**, *40*, 3912.
[12] J. M. Haider, Z. Pikramenou, *Eur. J. Inorg. Chem.* **2001**, 189.
[13] M. Chavarot, Z. Pikramenou, *Tetrahedron Lett.* **1999**, *40*, 6865.
[14] S. Weidner, Z. Pikramenou, *Chem. Commun.* **1998**, 1473.
[15] J.-P. Collin, I. M. Dixon, J.-P. Sauvage, J. A. G. Williams, F. Barigelletti, L. Flamigni, *J. Am. Chem. Soc.* **1999**, *121*, 5009.
[16] F. Barigelletti, L. Flamigni, M. Guardigli, A. Juris, M. Beley, S. Chodorowski-Kimmes, J.-P. Collin, J.-P. Sauvage, *Inorg. Chem.* **1996**, *35*, 136.
[17] V. Balzani, F. Barigelletti, P. Belser, S. Bernhard, L. De Cola, L. Flamigni, *J. Phys. Chem.* **1996**, *100*, 16786.
[18] B. Schlicke, P. Belser, L. De Cola, E. Sabbioni, V. Balzani, *J. Am. Chem. Soc.* **1999**, *121*, 4207.
[19] M. Frank, M. Nieger, F. Voegtle, P. Belser, A. von Zelewsky, L. De Cola, V. Balzani, F. Barigelletti, L. Flamigni, *Inorg. Chim. Acta* **1996**, *242*, 281.
[20] L. De Cola, V. Balzani, F. Barigelletti, L. Flamigni, P. Belser, A. von Zelewsky, M. Frank, F. Voegtle, *Inorg. Chem.* **1993**, *32*, 5228.
[21] L. S. Kelso, T. A. Smith, A. C. Schultz, P. C. Junk, R. N. Warrener, K. P. Ghiggino, F. R. Keene, *J. Chem. Soc. Dalton Trans.* **2000**, 2599.
[22] P. T. Gulyas, T. A. Smith, M. N. Paddon-Row, *J. Chem. Soc. Dalton Trans.* **1999**, 1325.
[23] N. W. Alcock, P. R. Barker, J. M. Haider, M. J. Hannon, C. L. Painting, Z. Pikramenou, E. A. Plummer, K. Rissanen, P. Saarenketo, *J. Chem. Soc. Dalton Trans.* **2000**, 1447.

 © 2003 Wiley-VCH Verlag GmbH & Co. KGaA, Weinheim

Deoxyglycoside Synthesis

Synthesis of 2,3,6-Trideoxysugar-Containing Disaccharides by Cyclization and Glycosidation through the Sequential Activation of Sulfoxide and Methylsulfanyl Groups in a One-Pot Procedure**

*Toru Amaya, Daisuke Takahashi, Hiroshi Tanaka, and Takashi Takahashi**

Deoxysugars are often found in the polysaccharide domains of biologically active (anticancer, antibiotic, and cardiotonic) natural products.[1] The important role that the oligosaccharide moiety plays in this class of natural products has become apparent.[1,2] Like many deoxysugars, 2,3,6-trideoxysugars exist in important antibiotics,[3] such as landomycin A[4] and PI-080.[5] Several problems arise in the synthesis of 2,3,6-trideoxyglycosides.[6] Glycosyl donors with a leaving group at the anomeric center are quite sensitive compounds, and the 2,3,6-trideoxyglycosidic linkage formed by glycosylation is also labile under the acidic conditions used. Generally, the fewer oxygen atoms present in the pyranoside, the lower its acid stability.[7] Thus, the glycosylation method chosen should be applicable to the glycosylation of other deoxysugars and take into account their acid lability. 2,3,6-Trideoxysugars are not commercially available, as is true for deoxysugars in general. Therefore, the development of an efficient synthetic strategy, including the preparation of deoxysugars, introduction of the leaving group, and glycosylation, is particularly important.

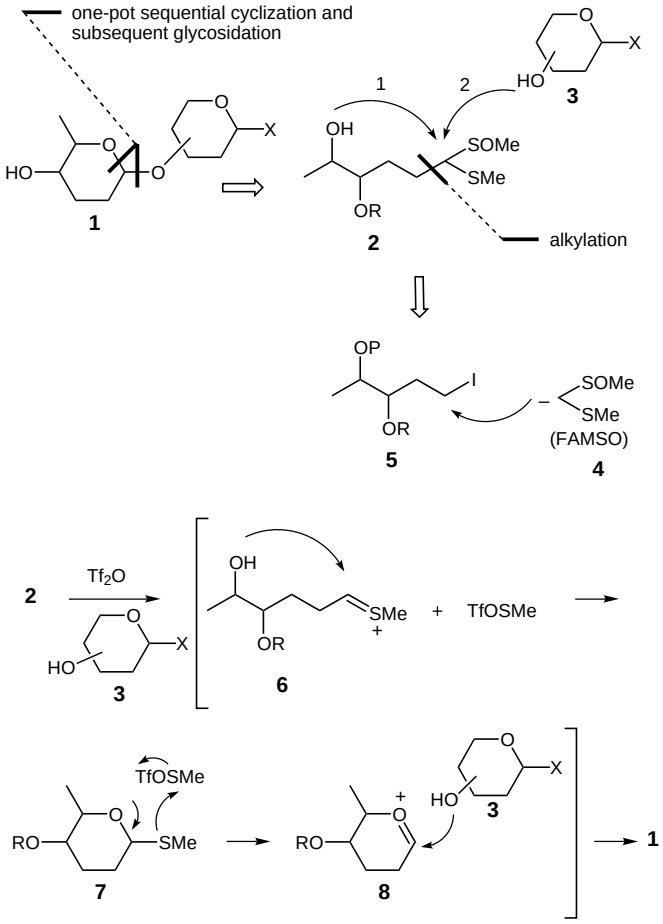
Our attention has been focused on a strategy based on the idea that a sulfur atom can stabilize a carbanion at the α position, whereas a sulfenium ion can be used to generate a carbocation at the same position. Hanessian et al. and Trost et al. elegantly utilized these features in the synthesis of nucleosides.[8] We recently demonstrated that alkylation of an α-phenylsulfanyllactone followed by intramolecular acetal formation (glycosylation) provided a sialyl glycolactone.[9] Herein we report a novel and convenient one-pot method for the synthesis of disaccharides that contain 2,3,6-trideoxysugars, from acyclic compounds with a sulfoxide and a methylsulfanyl group.[10]

The synthetic strategy is illustrated in Scheme 1. Alkylation of methyl (methylsulfanyl)methyl sulfoxide (formaldehyde mercaptal sulfoxide; FAMSO) (**4**)[11] with 3,4-dialkoxy-1-iodopentane **5**, followed by selective deprotection, provides

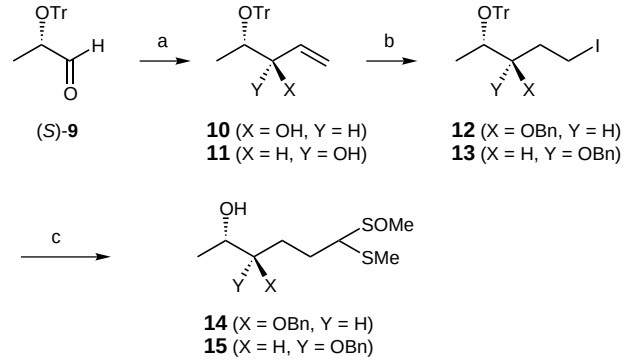
[*] Prof. Dr. T. Takahashi, T. Amaya, D. Takahashi, Dr. H. Tanaka
Department of Applied Chemistry
Graduate School of Science and Engineering
Tokyo Institute of Technology
2-12-1 Ookayama, Meguro, Tokyo 152-8552 (Japan)
Fax: (+81) 3-5734-2884
E-mail: ttakashi@o.cc.titech.ac.jp

[**] This study was supported by Special Coordination Funds for Promoting Science and Technology from the Ministry of Education, Culture, Sports, Science and Technology, Japan, to whom we are deeply indebted.

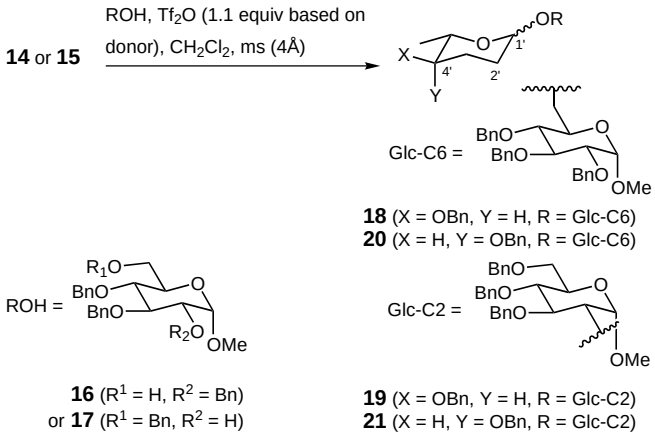
 DOI: 10.1002/anie.200250218 © 2003 Wiley-VCH Verlag GmbH & Co. KGaA, Weinheim



Scheme 1. Synthetic strategy and mechanism of formation of deoxysugar-containing disaccharide **1**.



Scheme 2. Preparation of the key intermediates. a) 1) vinyl magnesium bromide, THF, 92% (*syn* (**11**)/*anti* (**10**) = 2:3); b) 1) BnBr, NaH, THF, quant. (**12** and **13**); 2) BH_3·THF, then NaOH, H_2O_2, 53% (**12**), 48% (**13**); 3) I_2, PPh_3, benzene, imidazole, 93% (**12**), 94% (**13**); c) 1) FAMSO, NaH, THF, 75 °C; 2) CSA, MeOH, 2 steps, 70% (**14**), 80% (**15**). Tr = triphenylmethyl (trityl), Bn = benzyl, CSA = camphorsulfonic acid.



Scheme 3. One-pot sequential cyclization and glycosidation. ms = molecular sieves.

2. Selective activation of the sulfoxide group[12] in **2** with trifluoromethanesulfonic anhydride (Tf_2O)[13] leads to the formation of a sulfenium species **6**, which undergoes intramolecular acetalization to form thioglycopyranoside **7**. Concomitant activation of the methylsulfanyl group in **7** with the TfOSMe present affords the oxonium intermediate **8**, which undergoes glycosidation with **3**, leading to disaccharide **1** (Scheme 1).[14] As the labile glycosyl donor **7** is formed in situ, the need for its tedious isolation is avoided. If this reaction is carried out in the presence of a leaving group X on the glycosyl acceptor **3**, then further elongation of the glycoside is feasible, that is, orthogonal glycosylation,[15] one-pot glycosylation,[16,17] or two-directional glycosylation.[18]

1,2-Addition of a vinyl Grignard reagent to aldehyde (*S*)-**9**, prepared from ethyl (*S*)-lactate, afforded the diastereomers **10** and **11** (3:2, 92%), and these were separated on silica gel.[19] After benzylation of **10**, hydroboration, followed by iodination, afforded iodide **12** (Scheme 2). Alkylation of FAMSO with **12** was performed at 75 °C in the presence of NaH. Removal of the trityl group provided the key intermediate **14** in 70% yield for the two steps.[20] The *syn* diastereomer **15** was prepared from **11** by a similar procedure (Scheme 2).

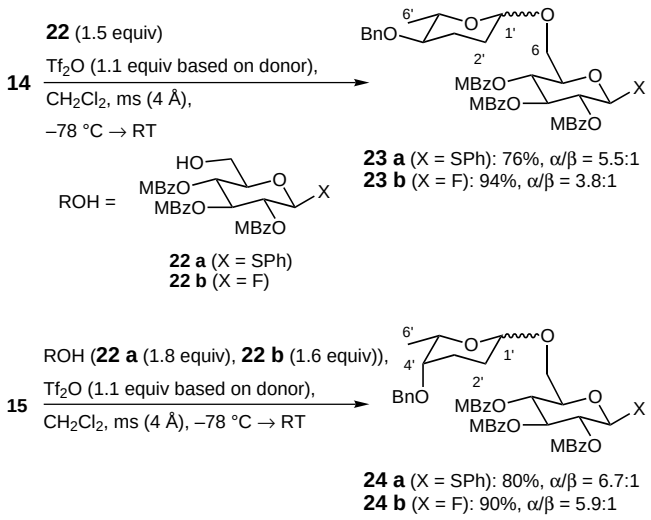
One-pot sequential cyclization and glycosidation was carried out as follows (Scheme 3, Table 1): Tf_2O (1.1 equiv) was added to a mixture of the acyclic donor **14** and the acceptor **16** in CH_2Cl_2 at −78 °C. After a few minutes, TLC analysis showed that the starting substrate had almost disappeared. After workup and column chromatography the desired disaccharide **18** was obtained in 83% yield (α/β = 1.2:1) (Table 1, entry 1).[21] The glycosidations of donor **14** with acceptor **17**, and donor **15** with acceptors **16** and **17**, were performed under the same conditions to provide the corresponding disaccharides **19, 20**, and **21** in 28%, 72%, and 40% yields, respectively (Table 1, entries 6, 4, and 9). We observed that glycosidations at the C6 hydroxy group occurred in moderate yield, whereas glycosidations at the C2 hydroxy group gave the products in poor yield. We believe that the glycosidation step is the rate-determining step as the substrates disappeared at −78 °C within a few minutes. Therefore, the reaction temperature was allowed to rise slowly from −78 °C to room temperature, which significantly improved the yields of the reactions at both the C6 and C2 hydroxy groups. Under these conditions, anomerization occurred, with dominant formation of the α-glycosides as the reaction temperature increased. When excess donor was used in the

 © 2003 Wiley-VCH Verlag GmbH & Co. KGaA, Weinheim

Table 1: One-pot sequential cyclization and glycosidation of acyclic donor precursors **14** and **15** with acceptors **16** and **17**.

Entry	Donor (equiv)	Acceptor (equiv)	Product	*T* [°C]	Yield [%]	α/β
1	**14** (1.0)	**16** (3.0)	**18**	−78	83	1.2:1[a],[c]
2	**14** (1.0)	**16** (3.0)	**18**	−78→RT	79	1.7:1[a],[c]
3	**14** (1.5)	**16** (1.0)	**18**	−78→RT	92	2.0:1[a],[c]
4	**15** (1.0)	**16** (3.0)	**20**	−78	72	4.5:1[b],[d]
5	**15** (2.0)	**16** (1.0)	**20**	−78→RT	88	3.4:1[b],[d]
6	**14** (1.0)	**17** (3.0)	**19**	−78	28	1.2:1[a],[e]
7	**14** (1.0)	**17** (3.0)	**19**	−78→RT	65	α only[a],[e]
8	**14** (1.5)	**17** (1.0)	**19**	−78→RT	73	22:1[b],[e]
9	**15** (1.0)	**17** (3.0)	**21**	−78	40	α only[b],[f]
10	**15** (1.5)	**17** (1.0)	**21**	−78→RT	74	38:1[b],[f]

[a] The ratio was determined by HPLC analysis. [b] The ratio was determined by integration of the H-4′ signals in the ^{1}H NMR (400 MHz, $CDCl_3$) spectrum. [c] Assignments of the anomeric proton signals for α- and β-L-amicetosides: (400 MHz, $CDCl_3$) $\delta = 4.65$ ppm (br d, $J_{1',2'} = 2.0$ Hz) for **18**α, $\delta = 4.70$ ppm (dd, $J_{1',2'ax} = 9.2$ Hz, $J_{1',2'eq} = 1.9$ Hz) for **18**β. [d] Assignments of the anomeric proton signals for α- and β-L-rhodinosides: (400 MHz, [D$_6$]benzene) $\delta = 4.80$ ppm (br d, $J_{1',2'} = 2.0$ Hz) for **20**α, $\delta = 4.51$ ppm (dd, $J_{1',2'ax} = 9.2$ Hz, $J_{1',2'eq} = 2.0$ Hz) for **20**β. [e] Assignments of the anomeric proton signal for α-L-amicetoside: (400 MHz, $CDCl_3$) $\delta = 4.97$ ppm (br d, $J_{1',2'} = 2.9$ Hz) for **19**α. [f] Assignment of the anomeric proton signal for α-L-rhodinoside: (400 MHz, $CDCl_3$) $\delta = 5.07$ ppm (br d, $J_{1',2'} = 2.9$ Hz) for **21**α.



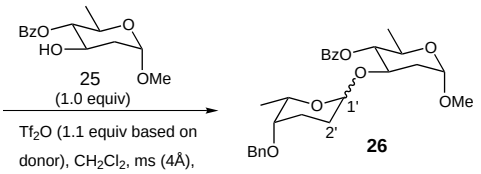
Scheme 4. Chemoselective glycosidation. MBz = 4-methylbenzoyl

reaction, the desired disaccharides were obtained in good yields (92% for **18** (Table 1, entry 3), 73% for **19** (entry 8)).

We next examined chemoselective glycosidation to demonstrate the versatility of this method. Treatment of **14** or **15** with phenylthioglycoside **22a** or glycosyl fluoride **22b** as the glycosyl acceptor, the desired disaccharides were obtained in excellent yields, without decomposition of the phenylsulfanyl group or the fluoride (76% for **23a**, 94% for **23b**, 80% for **24a**, 90% for **24b**) (Scheme 4).[22]

In nature, 2,3,6-trideoxyglycosides are generally linked to deoxyglycosides. We investigated the glycosidation of **15** with

Table 2: One-pot sequential cyclization and glycosidation with methyl 4-*O*-benzoyl-α-D-olivoside (**25**).



Entry	**15** [equiv]	*T* [°C]	Yield [%]	α/β ratio of **26**
1	1.5	−78	20	3.1:1[a]
2	1.5	−78→RT	dec.[b]	–
3	3.0	−78→−50	63	6.9:1[a]

[a] Ratio determined by HPLC analysis. Assignments of the anomeric proton signals for α- and β-L-rhodinosides: $\delta = 4.88$ ppm (br d, $J_{1',2'} = 2.9$ Hz) for **26**α, $\delta = 4.47$ ppm (dd, $J_{1',2'ax} = 9.2$ Hz, $J_{1',2'eq} = 1.9$ Hz) for **26**β. [b] Decomposed.

methyl 4-*O*-benzoyl-α-D-olivoside (**25**). Glycosidation at −78 °C for 1 h gave the desired deoxyglycoside **26** in low yield (20%; Table 2, entry 1). The product decomposed when the reaction mixture was allowed to warm to room temperature (Table 2, entry 2). However, the desired deoxyglycoside **26** was obtained in moderate yield (63%) when the reaction temperature was kept at −50 °C for 2 h (Table 2, entry 3).

In summary, we have developed a novel method for the synthesis of 2,3,6-trideoxyglycosides by sequential activation of the sulfoxide and methylsulfanyl groups in a one-pot procedure. This method does not require anomeric deprotection and the activation steps have been incorporated within traditional glycosylation strategies. Only three steps are required for the synthesis of disaccharides from oxygen-functionalized alkyl halides, a variety of which can be readily prepared as building blocks. Furthermore, this reaction proceeds in the presence of a phenylsulfanyl group and glycosyl fluoride, and is applicable to the synthesis of a deoxyglycoside linked to another deoxyglycoside. Thus, the reaction should be extremely useful for the diversity-oriented synthesis of oligosaccharides containing 2-deoxysugars as well as 2,3,6-trideoxysugars.

Received: September 23, 2002
Revised: December 20, 2002 [Z50218]

Keywords: carbohydrates · chemoselectivity · cyclization · glycosylation · oligosaccharides

[1] A. Kirschning, A. F.-W. Bechthold, J. Rohr, *Top. Curr. Chem.* **1997**, *188*, 1–84.
[2] A. C. Weymouth-Wilson, *Nat. Prod. Rep.* **1997**, *14*, 99–110.
[3] a) For the saquayamycins, see: T. Uchida, M. Imoto, Y. Watanabe, K. Miura, T. Dobashi, N. Matsuda, T. Sawa, H. Naganawa, M. Hamada, T. Takeuchi, H. Umezawa, *J. Antibiot.* **1985**, *38*, 1171–1181; b) for amicenomycins A and B, see: N. Kawamura, R. Sawa, Y. Takahashi, T. Sawa, N. Kinoshita, H. Naganawa, M. Hamada, T. Takeuchi, *J. Antibiot.* **1995**, *48*, 1521–1524; c) for a review, see: J. Rohr, R. Thiericke, *Nat. Prod. Rep.* **1992**, *9*, 103–137.
[4] S. Weber, C. Zolke, J. Rohr, J. M. Beale, *J. Org. Chem.* **1994**, *59*, 4211–4214.

 © 2003 Wiley-VCH Verlag GmbH & Co. KGaA, Weinheim

[5] A. Kawashima, Y. Kishinuma, M. Tamai, K. Hanada, *Chem. Pharm. Bull.* **1989**, *37*, 3429 – 3431.
[6] For recent syntheses of 2,3,6-trideoxysugar-containing oligosaccharides, see: a) A. Sobti, K. Kim, G. A. Sulikowski, *J. Org. Chem.* **1996**, *61*, 6 – 7; b) Y. Guo, G. A. Sulikowski, *J. Am. Chem. Soc.* **1998**, *120*, 1392 – 1397; c) F. E. McDonald, H. Y. H. Zhu, *J. Am. Chem. Soc.* **1998**, *120*, 4246 – 4247; d) A. Kirschning, *Eur. J. Org. Chem.* **1998**, 2267 – 2274; e) W. R. Roush, C. E. Bennett, *J. Am. Chem. Soc.* **2000**, *122*, 6124 – 6125; f) W. R. Roush, C. E. Bennett, S. E. Roberts, *J. Org. Chem.* **2001**, *66*, 6389 – 6393; g) B. Yu, P. Wang, *Org. Lett.* **2002**, *4*, 1919 – 1922.
[7] W. G. Overend, C. W. Rees, J. S. Sequeira, *J. Chem. Soc.* **1962**, 3429 – 3440.
[8] a) For a report on the synthesis of nucleosides by sequential activation of a diphenyl dithioacetal following the 1,2-addition of bis(phenylsulfanyl)methane to an aldehyde, see: S. Hanessian, K. Sato, T. J. Liak, N. Danh, D. Dixit, *J. Am. Chem. Soc.* **1984**, *106*, 6114 – 6115; b) for a report on the synthesis of a 2-deoxynucleoside by sequential activation of a dimethyl dithioacetal or a (methylsulfanyl)methyl phenylsulfonyl compound following the alkylation of bis(methylsulfanyl)methane or (methylsulfanyl)methyl phenyl sulfone, respectively, with an epoxide, see: B. M. Trost, C. Nübling, *Carbohydr. Res.* **1990**, *202*, 1 – 12.
[9] T. Takahashi, H. Tsukamoto, H. Yamada, *Org. Lett.* **1999**, *1*, 1885 – 1887.
[10] A one-pot synthesis of nucleosides via a dithioacetal prepared from 2-deoxy-D-ribose has been reported. However, this one-pot condensation with chloromercuri-6-benzamidopurin, followed by deprotection of the benzoyl group of both the ribose and the adenine, proceeded in low yield (6.3% for the β anomer, 8.1% for the α anomer): C. Pedersen, H. G. Fletcher, Jr., *J. Am. Chem. Soc.* **1960**, *82*, 5210 – 5211.
[11] K. Ogura, G. Tsuchihashi, *Tetrahedron Lett.* **1971**, 3151 – 3154.
[12] For a report on the selective activation of the sulfoxide group of an ethyl (ethylsulfanyl)methyl sulfoxide compound by treatment with CSA, in the synthesis of oxocene derivatives, see: K. C. Nicolaou, C. V. C. Prasad, C.-K. Hwang, M. E. Duggan, C. A. Veale, *J. Am. Chem. Soc.* **1989**, *111*, 5321 – 5330.
[13] S. Raghavan, D. Kahne, *J. Am. Chem. Soc.* **1993**, *115*, 1580 – 1581.
[14] a) J. Gildersleeve, A. Smith, K. Sakurai, S. Raghavan, D. Kahne, *J. Am. Chem. Soc.* **1999**, *121*, 6176 – 6182; b) H. Xuereb, M. Maletic, J. Gildersleeve, I. Pelczer, D. Kahne, *J. Am. Chem. Soc.* **2000**, *122*, 1883 – 1890.
[15] a) O. Kanie, Y. Ito, T. Ogawa, *J. Am. Chem. Soc.* **1994**, *116*, 12073 – 12074; b) O. Kanie, Y. Ito, T. Ogawa, *Tetrahedron Lett.* **1996**, *37*, 4551 – 4554.
[16] We have previously reported a one-pot glycosylation reaction: a) H. Yamada, T. Harada, T. Takahashi, *J. Am. Chem. Soc.* **1994**, *116*, 7919 – 7920; b) H. Yamada, T. Harada, H. Miyazaki, T. Takahashi, *Tetrahedron Lett.* **1994**, *35*, 3979 – 3982; c) H. Yamada, T. Kato, T. Takahashi, *Tetrahedron Lett.* **1999**, *40*, 4581 – 4584; d) T. Takahashi, M. Adachi, A. Matsuda, T. Doi, *Tetrahedron Lett.*, **2000**, *41*, 2599 – 2603; e) H. Yamada, H. Takimoto, T. Ikeda, H. Tsukamoto, T. Harada, T. Takahashi, *Synlett* **2001**, 1751 – 1754; f) H. Tanaka, M. Adachi, H. Tsukamoto, T. Ikeda, H. Yamada, T. Takahashi, *Org. Lett.* **2002**, *4*, 4213 – 4216.
[17] For a recent review of one-pot glycosylations, see: K. M. Koeller, C.-H. Wong, *Chem. Rev.* **2000**, *100*, 4465 – 4493.
[18] T. Zhu, G.-J. Boons, *Tetrahedron Lett.* **1998**, *39*, 2187 – 2190.
[19] After removal of the trityl group of **10** and **11**, the ^{1}H NMR spectra of the corresponding free alcohols were identical to those reported previously: a) **10**: W. R. Roush, P. T. Grover, *Tetrahedron* **1992**, *48*, 1981 – 1998; b) **11**: W. A. María Teresa Díaz, C. R. Saha-Möller, *Tetrahedron: Asymmetry* **1998**, *9*, 589 – 598.
[20] The selective deprotection of the trityl group proceeds under mild, acidic conditions (catalytic amount of CSA in methanol at 0 °C) without hydrolysis of the methylsulfanyl–methylsulfoxide moiety.
[21] In an attempt to isolate the methylsulfanylpyranoside, the acyclic donor **14** was treated with Tf_2O in the presence of 4-allyl-1,2-dimethoxybenzene[14a], which can trap TfOSMe. However, this reaction gave a complex mixture.
[22] The α/β ratios were determined by integration after complete assignment of chemical shifts from ^{1}H,^{1}H-COSY spectra: **23a** ((6′-H) α: $\delta = 1.16$ ppm, β: $\delta = 1.20$ ppm); **23b** (6-H) α: $\delta = 3.90$ ppm, β: $\delta = 3.81$ ppm); **24a** (6′-H) α: $\delta = 1.09$ ppm, β: $\delta = 1.55$ ppm; **24b** (6′-H) α: $\delta = 1.09$ ppm, β: $\delta = 1.55$ ppm. Chemical shift assignments for the anomeric protons of α-glycosides: $\delta = 4.71$ ppm (br d, $J_{1',2'} = 2.0$ Hz) for **23a**, $\delta = 3.90$ ppm (br d, $J_{1',2'} = 2.9$ Hz) for **23b**, $\delta = 4.79$ ppm (br d, $J_{1',2'} = 1.9$ Hz) for **24a**, $\delta = 4.78$ ppm (br s) for **24b**.

 © 2003 Wiley-VCH Verlag GmbH & Co. KGaA, Weinheim

Magnesium Borate Nanotubes

Nanotubes of Magnesium Borate

Renzhi Ma, Yoshio Bando, Dmitri Golberg, and Tadao Sato*

Nanoscale tubular structures are currently being researched throughout the world because of their exceptional physical properties and potential applications in nanodevice technology. Since the discovery of carbon nanotubes,[1] there has been active interest in exploring other layered or nonlayered materials that form tubular structures. Successful syntheses of nanotubes based on inorganic binary compounds, such as boron nitride (BN),[2] metal dichalcogenides (i.e., MS_2; M = W, Mo, Nb, Ta, Ti, Zr, Hf,[3a–f] $NiCl_2$[3g]), metal oxides (i.e., VO_x, TiO_2, MoO_3),[4] and organic materials[5] have been reported. Recently, progress was made in the generation of single-crystal tubular structures in a ternary borate system, aluminum borate ($Al_{18}B_4O_{33}$), though the characteristic dimensions were in the micrometer range.[6] This success motivated us to probe the possibility of obtaining intriguing tubular structures based on other metal borates. Besides aluminum borate, magnesium borate is another important ceramic material that has attracted our attention. Magnesium borate was shown to be an interesting thermo-luminescence phosphor.[7] It is also an excellent antiwear, and a reduce-friction additive.[8] Herein, we report the first successful synthesis and characterization of the nanotubular structures of magnesium borate.

[*] Dr. R. Ma, Prof. Y. Bando, Dr. D. Golberg, Dr. T. Sato
Advanced Materials Laboratory
National Institute for Materials Science
Namiki 1-1, Tsukuba, Ibaraki 305-0044 (Japan)
Fax: (+81) 298-51-6280
E-mail: ma.renzhi@nims.go.jp

 © 2003 Wiley-VCH Verlag GmbH & Co. KGaA, Weinheim DOI: 10.1002/anie.200250455

Magnesium borate nanotubes, approximately 200–500 nm in width, were fabricated by heating a boron thin film coated on a Si(001) wafer with IR radiation in the presence of Mg vapor under an Ar/O_2 atmosphere. Figure 1 shows the scanning electron microscopy (SEM) images of a Si wafer before and after IR irradiation. Figure 1 a depicts the surface morphology of the Si wafer before IR irradiation. Uniform amorphous boron nanoparticles (~50 nm) were homogeneously dispersed on the Si surface. After the IR-irradiation-heating process, the boron nanoparticles on the Si wafer were transformed into totally different nanostructures (Figure 1 b). The more-magnified views (Figure 1 c,d) show that the nanostructures have hollow cores and nanotube morphology. Though a few cylindrical tubes are present, most of the nanotubes appear to have a polyhedral cross-section. Typical widths or diameters of these tubes are 200–500 nm, and lengths vary in the range of 1–5 μm. The nanotubes are usually open at one or both ends; no globules were observed at the tips of these nanotubes.

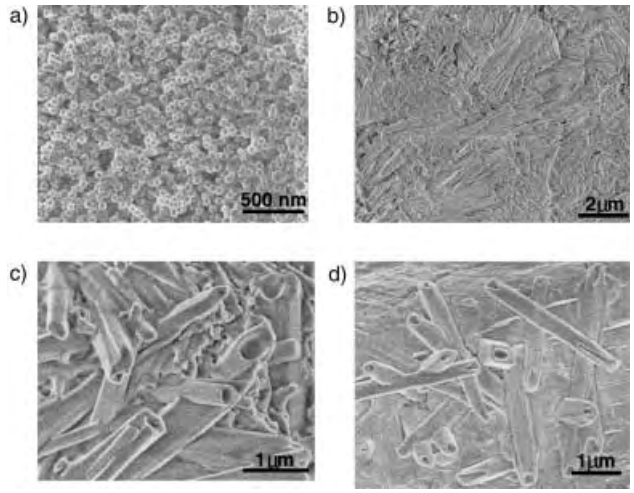


Figure 1. SEM images of surface morphologies of a Si wafer before and after IR irradiation heating. a) Uniform boron nanoparticles before IR heating; (b–d) Nanotube structures formed after IR heating.

During SEM observations, we looked at some regions on the Si wafer surface where the initial nuclei sites for nanotube growth are believed to exist. Figure 2 shows the surface regions with abundant apparent voids. These voids, with dimensions close to cross-sectional dimensions of the hollow nanotubes, may be regarded as the 2D nuclei of the nanotubes.

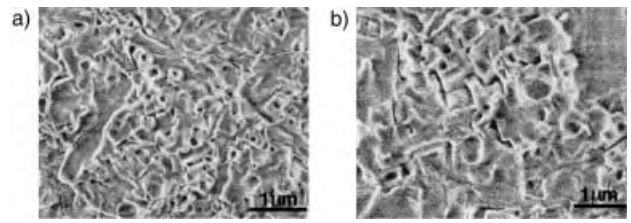


Figure 2. SEM images showing an initial stage of nanotube development. 2D nuclei with hollow cores are apparent.

X-ray diffraction (XRD) measurements of the nanotubes collected from the Si wafer were taken by using a RINT2200 X-ray diffractometer using $Cu_{K\alpha}$ radiation. Figure 3 shows the XRD pattern. All the diffraction peaks can be well indexed to a orthorhombic $Mg_3B_2O_6$ ($3MgO{\cdot}B_2O_3$) phase with the standard lattice constants of $a=5.40$, $b=8.42$, $c=4.50$ Å (JCPDS 38-1475).[9] It thus indicates the nanotubes have the $Mg_3B_2O_6$ structure.

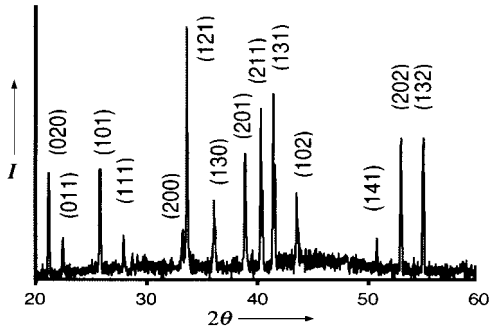


Figure 3. XRD pattern displaying the formation of orthorhombic $Mg_3B_2O_6$ on a Si wafer. $I=$ intensity (arbitrary units).

The nanotubes were further characterized by a high-resolution transmission electron microscope (HRTEM). Figure 4 a depicts a typical individual nanotube with a width of about 400 nm. The microanalysis of the chemical composition by energy dispersive spectrometry (EDS) and electron energy loss spectrometry (EELS) demonstrated that the tube is composed of B, O, and Mg. A typical EDS spectrum is shown in the inset of Figure 4 a. Both the quantitative analyses from EELS and EDS gave an approximate Mg:B:O atomic ratio of 1.0:0.6:2.0, which is very close to the elemental composition in $Mg_3B_2O_6$. Selected area electron diffraction (ED) patterns were also recorded by tilting the nanotube to different zone axes during transmission electron microscopic (TEM) obser-

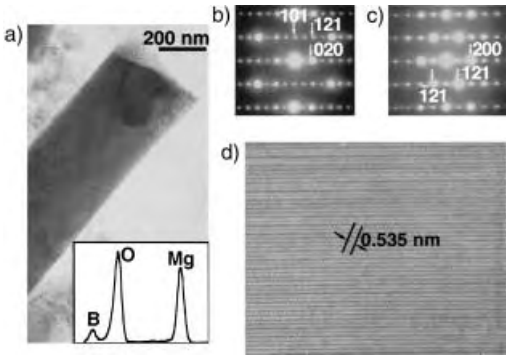


Figure 4. TEM verification of the orthorhombic $Mg_3B_2O_6$ structure of these nanotubes. a) TEM image of an individual nanotube, the inset is a EDS spectrum that shows the tube is composed of B, O and Mg atoms; b),c) ED patterns recorded along the $[10\bar{1}]$ and $[01\bar{2}]$ zone axes, respectively; d) HRTEM image corresponding to the ED pattern in (c). An interplanar spacing of the (121) lattice planes is indicated.

 © 2003 Wiley-VCH Verlag GmbH & Co. KGaA, Weinheim

vations (Figure 4b,c). The ED pattern in Figure 4b can be indexed as that of the single crystalline orthorhombic $Mg_3B_2O_6$ recorded along the $[10\bar{1}]$ zone axis. Similarly, the ED pattern (Figure 4c) agrees well with the $[01\bar{2}]$ reflections of $Mg_3B_2O_6$. Figure 4d depicts the HRTEM image corresponding to the ED pattern in Figure 4c. In general, the ED patterns of the nanotubes are similar to those of bulk $Mg_3B_2O_6$. We have, however, measured an *a* axis expansion of about 3% in the nanotubes. This difference may be ascribed to the geometrical effects of the tubelike structures although it is not clear why only the *a* axis is influenced.

We consider that the formation of magnesium borate nanotubes is initiated through the oxidization of the boron film on the Si wafer, and the simultaneous vaporization and deposition of Mg chips. At elevated temperature (ca. 850 °C), the amorphous B nanoparticles are oxidized to form molten B_2O_3 layers on their surfaces. Subsequently a polymeric vitreous $(BO)_n$ complex may be formed through the reaction between dissolved boron and molten B_2O_3. Simultaneously, Mg chips, laid below the Si wafer (500–550 °C), are also vaporized or oxidized. The Mg or MgO vapors deposit onto the vitreous B_2O_3 or $(BO)_n$ layer on the Si surface. This process continues until the supersaturation level of Mg species is reached in the vitreous layer, and precipitation of the magnesium borate species occurs. This initiates the 2D nuclei sites of the nanotubes as shown in Figure 2. The subsequent nanotube growth from these nuclei voids may proceed through the continual precipitation of magnesium borates, while the voids form hollow cores. The growth may be promoted by the temperature gradient normal to the Si wafer due to the IR irradiation heating from the top surface. This growth scenario is quite different from that of the more ubiquitous layered compounds (such as C, BN and MoS_2), which consist of a hexagonal or trigonal lattice that forms nanotubes by the spiral winding of molecular layers.[1,2,3b] Detailed structural modeling and computing are needed to reveal how nanotubes could be formed in magnesium borates.

The supersaturation of Mg or MgO and the precipitation of magnesium borate species strongly depend on the partial concentrations of Mg or MgO in the vitreous layer. Because of the low melting point of Mg (ca. 650 °C), the vaporization or oxidization of Mg chips may be more dominant in the surrounding environment. It is therefore reasonable to deduce that the vitreous B_2O_3 or $(BO)_n$ layer is sufficient, or abundant with respect to MgO. According to the phase diagram of MgO–B_2O_3, $Mg_3B_2O_6$ is more likely to form when MgO is enriched.[10] This observation may explain the formation of nanotubes of $Mg_3B_2O_6$ ($3MgO{\cdot}B_2O_3$) rather than MgB_4O_7 ($MgO{\cdot}B_2O_3$) or $Mg_2B_2O_5$ ($2MgO{\cdot}B_2O_3$).

In summary, $Mg_3B_2O_6$ nanotubes were successfully synthesized by heating a boron thin film with IR radiation in the presence of Mg vapor and traces of oxygen. As demonstrated by this successful example, this technique may be easily modified or extended to prepare nanotubes of other metal borates. It therefore has an outstanding potential in providing customized nanotubes for a broad range of nanotechnology applications.

Experimental Section

The experiments were carried out in an IR-irradiation-heating furnace. Amorphous boron powders (99.9%, ca. 50 nm) and Mg chips (99.5%), purchased from WAKO Pure Chemical Industries, were used as received. A Si (001) wafer (25.4 mm in diameter) was used as the heating target. First, boron powders were dispersed in acetone by ultrasound, then dripped onto the Si (001) mirror-polished surface to form a thin film. The Si wafer was then placed on a BN holder with the boron film downwards, which acted as a deposition substrate. Mg chips were laid under the Si wafer with a 2 mm distance between the boron film and Mg chips. When the chamber was evacuated (< 5 Torr), a gas flow of Ar (500 mL min^{-1}) and O_2 (10 mL min^{-1}) was introduced. The Si wafer was rapidly heated to 850 °C by IR irradiation of the top Si surface. The temperature of the Mg chips under the Si wafer was estimated to be 500–550 °C during the heating process. The heating process generally continued for approximately 30 minutes. The chamber was then cooled to room temperature and the Si wafer was removed for thorough characterization. A small piece of Si was cleaved from a larger wafer and directly observed by SEM. The structural and chemical natures of the nanotubes were studied using HRTEM equipped with EDS and EELS. A TEM sample was prepared by stripping a small piece of the film from the Si wafer, which was dispersed by ultrasound in acetone, then transferred onto a carbon coated copper grid. All TEM images and diffraction patterns were taken using a JEM-3000F field emission microscope operated at 300 keV.

Received: October 29, 2002
Revised: December 18, 2003 [Z50455]

Keywords: borates · crystal growth · nanostructures · nanotubes

[1] S. Iijima, *Nature* **1991**, *354*, 56.
[2] N. G. Chopra, R. J. Luyken, K. Cherrey, V. H. Crespi, M. L. Cohen, S. G. Louie, A. Zettl, *Science* **1995**, *269*, 966.
[3] a) R. Tenne, L. Margulis, M. Genut, G. Hodes, *Nature* **1992**, *360*, 444; b) Y. Feldman, E. Wasserman, D. J. Srolovitz, R. Tenne, *Science* **1995**, *267*, 222; c) L. M. Rendina, R. J. Puddephatt, *Chem. Rev.* **1997**, *97*, 1735; d) Y. R. Hacohen, E. Grunbaum, R. Tenne, J. Sloan, J. L. Hutchison, *Nature* **1998**, *395*, 336; e) M. Nath, C. N. R. Rao, *J. Am. Chem. Soc.* **2001**, *123*, 4841; f) M. Nath, C. N. R. Rao, *Angew. Chem.* **2002**, *114*, 3601; *Angew. Chem. Int. Ed.* **2002**, *41*, 3451; g) Y. R. Hacohen, E. Grunbaum, R. Tenne, J. Sloan, J. L. Hutchison, *Nature* **1998**, *395*, 336.
[4] a) M. E. Spahr, P. Bitterli, R. Nesper, M. Muller, F. Krumeich, H. U. Nissen, *Angew. Chem.* **1998**, *110*, 1339; *Angew. Chem. Int. Ed.* **1998**, *37*, 1263; b) T. Kasuga, M. Hiramatsu, A. Hoson, T. Sekino, Niihara, K. *Langmuir* **1998**, 14, 3160; c) Y. Li, Y. Bando, *Chem. Phys. Lett.* **2002**, *364*, 484.
[5] a) M. R. Ghadirl, J. R. Granja, R. A. Milligan, D. E. McRee, N. Khazanovich, *Nature* **1993**, *366*, 324; b) M. R. Ghadirl, J. R. Granja, L. K. Buehler, *Nature* **1994**, *369*, 301; c) M. Steinhart, J. H. Wendorff, A. Greiner, R. B. Wehrspohn, K. Nielsch, J. Schilling, J. Choi, U. Gosele, *Science* **2002**, *296*, 1997.
[6] R. Ma, Y. Bando, T. Sato, C. Tang, F. Xu, *J. Am. Chem. Soc.* **2002**, *124*, 10668.
[7] a) M. Prockic, *Nucl. Instrum. Methods* **1980**, *175*, 83; b) D. I. Shahare, S. J. Dhoble, S. V. Moharil, *J. Mater. Sci. Lett.* **1993**, *12*, 1873.
[8] Z. S. Hu, R. Lai, F. Lou, L. G. Wang, Z. L. Chen, G. X. Chen, J. X. Dong, *Wear* **2002**, 252, 370.
[9] H. McMurdie, M. Morris, E. Evans, B. Paretzkin, W. Wong-Ng, Y. Zhang, *Powder Diffr.* **1987**, *2*, 47.
[10] T. Mutluer, M. Timucin, *J. Am. Ceram. Soc.* **1975**, *58*, 196.

 © 2003 Wiley-VCH Verlag GmbH & Co. KGaA, Weinheim

Graft Polymerization on Gold

Effect of the Helix Macrodipole on Surface-Initiated N-Carboxyanhydride Polymerization on Gold**

Masazo Niwa, Yoshiyuki Kuwagaki, Shintaro Yamaguchi, and Nobuyuki Higashi**

Herein, we describe surface-initiated polymerization of γ-benzyl L-glutamate N-carboxyanhydride (BLG-NCA) in the presence of helical polypeptide (PBLG) rods immobilized on gold surfaces. To our knowledge, it is the first report that the rate of NCA polymerization, initiated with immobilized primary amine, is completely controlled by the direction of macrodipole moment of the adjacent helical rods.

The polymerization of BLG-NCA, initiated with trialkylamines was reported for the first time by Blout and Karlson[1] to produce α-helical polypeptides. Since then, polyglutamates have been the subject of numerous studies.[2]

Growth of polypeptide brushes is an attractive method to modify and control surface properties. The resultant well-confined polypeptide brushes could have applications in the field of waveguides, data storage, and nonlinear optics (NLO) because of their optical activity. Strategies for attaching polypeptide brushes to gold surfaces include the "grafting-onto" method,[3–6] tethering preformed polymer chains from solution onto a surface, and the "grafting-from" method,[7,8] polymerizing from surface-anchored initiators. The latter provides a higher density of polypeptide brushes on a surface because the "grafting-onto" method eventually suffers from serious steric hindrance by neighboring helices and unfavorable dipolar interactions.[5] Whitesell et al. have demonstrated the polymerization of alanine NCAs, initiated by specially designed amionotrithiol-functionalized gold substrates.[7] This initiator molecule exactly meets the spatial requirements of an α helix.

In our study, we employed a mixed monolayer system on gold, composed of an amine-terminated disulfide compound **1** as an initiator and an amine-free disulfide compound **2** as a lateral diluent, so as to satisfy spatial requirements, and examined effects of the presence of a helical PBLG (PBLG-N-SS or PBLG-C-SS), which was incorporated in advance into the mixed monolayers, on the NCA polymerization. The helical polypeptide is known to generate the macrodipole, that is, in this case, the electrostatic potential directed from the N-terminus to the C-terminus.[10,11] Therefore, if the preformed helical PBLG is successfully anchored to the monolayer-covered gold substrates and positioned near the amino group, it would be expected to induce the helix-macrodipole effect on NCA polymerization. To clarify such an effect is important in view of biological processes, such as the folding process of proteins in which many proteins attain their correct conformation only with assistance with molecular chaperones.

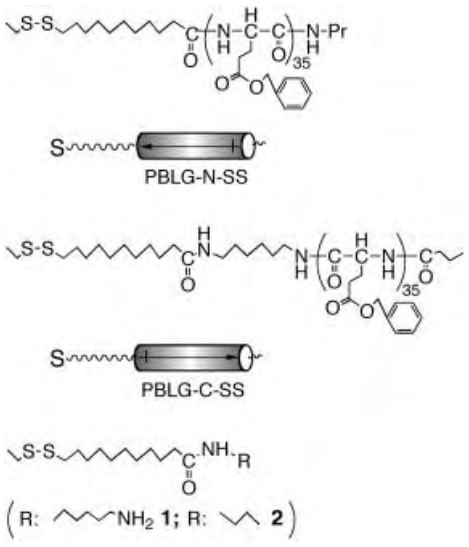


Figure 1 outlines the pathway for the preparation of a ternary self-assembled monolayer (SAM) composed of **1**, **2** and PBLG-N-SS or PBLG-C-SS on gold substrate. The adsorption processes of these compounds onto the gold surface were monitored by a quartz crystal microbalance (QCM). A gold-deposited QCM resonator (AT-cut, 9 MHz) was first placed in pure $CHCl_3$, and the solution of PBLG-N-SS, a typical helix matrix, was then added. The frequency decreased steeply because of adsorption of PBLG-N-SS and stopped changing after 2 h. The total frequency shift (ΔF) can be converted into the mass (Δm) adsorbed on gold surface by Sauerbrey's equation.[12] By using the Δm values, one can

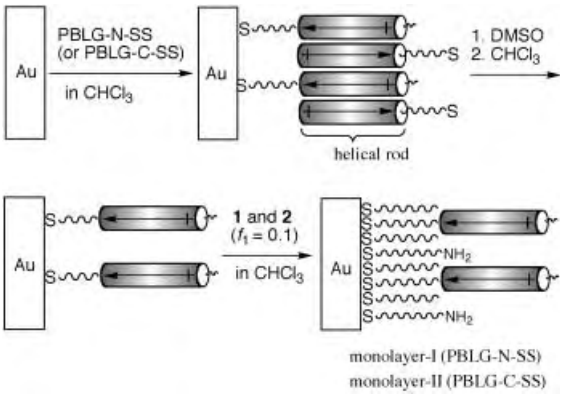


Figure 1. Preparation of the SAM of **1**, **2**, and PBLG-N-SS (or PBLG-C-SS) on gold substrate (the dipoles are reversed with PBLG-C-SS). For full details see text.

[*] Prof. Dr. M. Niwa, Prof. Dr. N. Higashi, Y. Kuwagaki, S. Yamaguchi
Department of Molecular Science and Technology
Faculty of Engineering
Doshisha University, Kyo-tanabe, Kyoto 610-0321 (Japan)
Fax: (+81) 774-65-6844
E-mail: mniwa@mail.doshisha.ac.jp
nhigashi@mail.doshisha.ac.jp

[**] This work was supported in part by the project "Nano Structure Hybrid" of High Technology Center at RCAST of Doshisha University and a grant-in-aid for Scientific Research from the Ministry of Education, Culture, Sports, Science, and Technology of the Japanese Government.

 DOI: 10.1002/anie.50478 © 2003 Wiley-VCH Verlag GmbH & Co. KGaA, Weinheim

calculate a surface coverage (Γ) of the adsorbents. For PBLG-N-SS adsorption, the Γ value was calculated to be 5.2×10^{-11} mol cm^{-2}. This value strongly suggest the formation of a densely packed α-helix assembly on the gold surface since the theoretical Γ value is in the range 3.2×10^{-11} to 8.3×10^{-11} mol cm^{-2}[13] when a hexagonal packing of helices is assumed. In our previous work, we found that helical PBLG existed mainly in a dimeric aggregate in $CHCl_3$.[5] Therefore, the assembly of PBLG-N-SS on gold thus obtained would be in a double-layered structure consisting of the dimeric aggregate of helices as shown in Figure 1. Such helix-dimer formation must the result of macrodipole interaction between helices which must be in side-by-side, antiparallel orientation. When this gold substrate was first treated with DMSO, which should behave as a helix-braking solvent, and then immersed in $CHCl_3$, the Γ value evaluated from the QCM frequency shift became 2.6×10^{-11} mol cm^{-2}, that is, just half of that before DMSO treatment. This result implies that the double-layered structure would be converted into a single-layered structure, which contains a suitable cavity for growth of a helical PBLG chain (Figure 1). Subsequently, this gold electrode was immersed in the $CHCl_3$ solution of a binary mixture of **1** and **2** until adsorption equilibrium was reached so that the formed cavity would be loaded with the binary mixture containing initiator.

The f_1 value of the mixture composition (f_1:molar fraction of **1** in the mixture) was adjusted to be 0.1, taking into account the lateral distribution of **1**. As a result, the Γ value of **1** was computed to be 2.4×10^{-11} mol cm^{-2} from the total QCM frequency shift. This value is very close to that for PBLG-N-SS in its single-layer form, which implies that about one molecule of **1** would be situated in the gap between PBLG helices as illustrated in Figure 1 (monolayer-I). The monolayer-II containing PBLG-C-SS in stead of PBLG-N-SS was prepared in the same way.

The BLG-NCA polymerization was subsequently carried out at these monolayer surfaces and monitored in situ by measuring QCM frequency shift. Figure 2 shows the frequency shift on addition of a BLG-NCA/$CHCl_3$ solution (2.5×10^{-2} M) into pure $CHCl_3$, in which the monolayer-covered QCM electrode was immersed. For comparison, the same polymerization experiment was performed for a binary monolayer of **1** and **2** ($f_1 = 0.05$) without PBLG matrix (Figure 2, curve b). It can be seen in every case that the frequency decreases immediately upon addition of BLG-NCA, meaning the progress of polymerization. The rate of polymerization was evaluated from the initial slope of the frequency decay curve (Table 1). The rate of polymerization

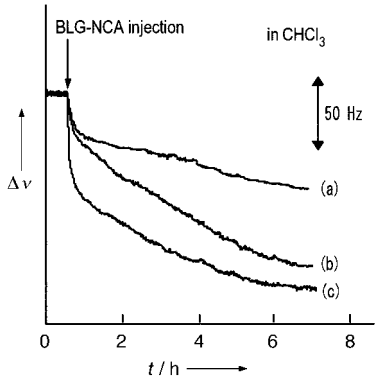


Figure 2. Frequency shifts of gold-coated QCM resonators in $CHCl_3$ modified with the **1**/**2**-mixed monolayer in the presence of PBLG-C-SS (a), in the absence of PBLG matrices (b), or in the presence of PBLG-N-SS (c) on addition of a BLG-NCA/$CHCl_3$ solution.

Table 1: Effects of preformed PBLG matrices on rate and degree of polymerization.

Monolayer	Rate of polymerization $\times 10^{11}$ [M s^{-1}]	n[a]
1/**2**-mixed monolayer ($f_1 = 0.1$)	5.5	73
monolayer-I	50	95
monolayer-II	3.9	15

[a] Average degree of polymerization.

in the presence of PBLG-N-SS is accelerated by a factor of about 10 compared to that in the absence of PBLG matrix. In contrast, the presence of PBLG-C-SS depressed the BLG-NCA polymerization. These effects of helical PBLG matrices on polymerization must be a result of their macrodipole interaction. In case of PBLG-N-SS, the direction of its helix-macrodipole moment is antiparallel to that of the polymerized PBLG chain, and therefore the growth of PBLG chain by polymerization between PBLG-N-SS matrices would be much more favorable than that without PBLG matrix. Conversely, the presence of PBLG-C-SS, which has a macrodipole moment direction that is parallel to the polymerized chain, led to an energetic disadvantage for the chain growth. Such a macrodipole effect also had a remarkable influence on the degree of polymerization (n) of each polymerized chain (Table 1). The n values were calculated from the total frequency change at 7 h polymerization; they are 95 and 15 for PBLG-N-SS and PBLG-C-SS monolayers, respectively. The value of 95 observed for PBLG-N-SS monolayer is larger than that of PBLG matrix ($n = 35$), which reflects the enhanced polymerization as a result of the helix-macrodipole interaction. On the other hand, the PBLG-C-SS monolayer limits the chain growth to $n = 15$. This chain length of $n = 15$ is consistent with the chain length ($n = 16$),[14] beyond which peptide segments are in general able to commence forming helical conformation and generate a helix-macrodipole moment. The helical PBLG-C-SS matrix is energetically unfavorable for the parallel orientation of the helix macrodipole, and accordingly suppressed any chain growth beyond $n = 15$.

To elucidate the orientation of the helical rods thus obtained, FTIR spectra of the C=O stretching region were measured for the monolayer-I before and after NCA polymerization, and shown in Figure 3. In the amide I and amide II regions, both spectra exhibit two bands at 1655 cm^{-1} and 1547 cm^{-1}, which are assigned to the α-helix structure.[15,16] The additional C=O stretching band, arising from the ester groups of the side chain, is observed at 1733 cm^{-1}. Enriquez and Samulski[17] demonstrated that the nature of the order and average orientation of the polypep-

 © 2003 Wiley-VCH Verlag GmbH & Co. KGaA, Weinheim

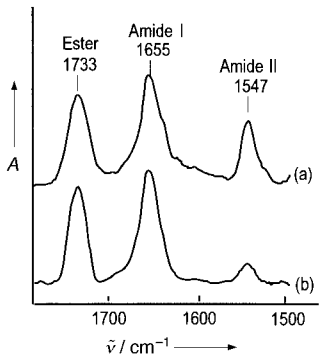


Figure 3. FTIR (raman) spectra of the monolayer-I before (a) and after (b) 7 h polymerization of BLG-NCA.

tide α helix in the films can be inferred from FTIR data. By using the ratio of the integrated intensities of the amide I and amide II regions, the average tilt of the helix axis from the surface normal was evaluated.[18] From the spectral data in Figure 3, the average tilting angle of the helices in the monolayer after NCA-polymerization is calculated to be 27°, which is significantly enhanced in the perpendicular orientation, compared with the 52° tilt found before polymerization. This result suggests that by polymerization of NCA between helical PBLG-N-SS matrices, the monolayer adopts a head-to-tail antiparallel orientation, which is energetically more favorable, and consequently achieves a nearly perpendicular helix orientation.

In conclusion, preformed PBLG helix rods can control the NCA-polymerization on the basis of helix-macrodipole interaction, and eventually allow the successful preparation of densely bound PBLG helical brushes on gold surfaces. Probably the key advantage of this technique is the high grafting density of helix brushes in an antiparallel orientation, which results in monolayers that are uniform at the Å level. We believe that these findings are of importance not only for a new approach to fabrication of polypeptide self-assembled materials but also for a relevant model of chaperone-assisted protein folding.

Experimental Section

Compound **1** was prepared by the reaction of 11-(ethyldithio)undecanoic acid[9] with *n*-(6-aminohexyl) carbamic acid *tert*-butyl ester in the presence of *N*′-(ethylcarbonimidoyl)-*N,N*-dimethyl-1,3-propnaediamine (EDC) and DMAP (DMAP = 4-dimethylaminopyridine) as condensing agent and catalyst, respectively, and then removal of *tert*-butoxycarbonyl group. Compound **2** was prepared by the reaction of 11-(ethyldithio)undecanoic acid with *n*-propylamine in the presence of EDC and DMAP. These products were identified by IR and ^{1}H NMR spectroscopy, and their purity was checked by means of TLC. PBLG-N-SS was prepared by polymerization of BLG-NCA initiated with *n*-propylamine, and then by condensation reaction with 11-(ethyldithio)undecanoic acid in the presence of EDC and DMAP, as reported previously.[5] PBLG-C-SS was prepared by polymerization of BLG-NCA initiated with **1**, and then by treatment with *n*-butanoyl chloride. These PBLG derivatives were characterized by ^{1}H NMR spectroscopy and MALDI-TOF (matrix-assisted laser desorption ionization time-of-flight) mass spectrometry.

Measurements: Gold-coated AT-cut quartz crystals (USI System Ltd., Japan) with a fundamental resonance frequency of 9 MHz were employed for QCM measurement. Detailed procedures were described previously.[5a,b] FTIR was performed on a Nicolet System 800 spectrometer with a mercury—cadmium–tellurium (MCT) detector. The measurements were carried out with the 1024 scans of interferogram accumulations using a bare gold substrate as a reference for reflection absorption spectroscopy (raman) measurement. The optical path was purged with dry air before and during measurements. A reflection attachment at an incident angle of 80°, together with a polarizer, was used.

Received: November 5, 2002 [Z50478]

Keywords: gold · helical structures · monolayer · polymerization · surface chemistry

[1] E. R. Blout, R. H. Karlson, *J. Am. Chem. Soc.* **1956**, *78*, 941.
[2] W. H. Daly, D. Poche, I. I. Negulescu, *Prog. Polym. Sci.* **1994**, *19*, 79.
[3] C. G. Worley, R. W. Linton, E. T. Samulski, *Langmuir* **1995**, *11*, 3805.
[4] K. Fujita, N. Bunjes, K. Nakajima, M. Hara, H. Sasabe, W. Knoll, *Langmuir* **1998**, *14*, 6167.
[5] a) M. Niwa, T. Murata, M. Kitamatsu, T. Matsumoto, N. Higashi, *J. Mater. Chem.* **1999**, *9*, 343; b) M. Niwa, M.-a. Morikawa, N. Higashi, *Langmuir* **1999**, *15*, 5088; c) M. Niwa, M.-a. Morikawa, N. Higashi, *Angew. Chem.* **2000**, *112*, 990; *Angew. Chem. Int. Ed.* **2000**, *39*, 960.
[6] E. Katz, V. Hegel-Shabtai, I. Willner, H. K. Rau, W. Haehnel, *Angew. Chem.* **1998**, *110*, 3443; *Angew. Chem. Int. Ed.* **1998**, *37*, 3253;b) I. Willner, V. Hegel-Shabtai, E. Katz, H. K. Rau, W. Haehnel, *J. Am. Chem. Soc.* **1999**, *121*, 6455.
[7] J. K. Whitesell, H. K. Chang, *Science* **1993**, *261*, 73;b) J. K. Whitesell, H. K. Chang, C. S. Whitesell, *Angew. Chem.* **1994**, *106*, 921; *Angew. Chem. Int. Ed. Engl.* **1994**, *33*, 871.
[8] a) R. H. Wieringa, A. J. Schouten, *Macromolecules* **1996**, *29*, 3032; b) A. Heise, H. Menzel, H. Yim, M. D. Foster, R. H. Wieringa, A. J. Schouten, V. Erb, M. Stamm, *Langmuir* **1997**, *13*, 723; c) R. H. Wieringa, E. A. Siesling, P. F. M. Geurts, P. J. Werkman, E. J. Vorenkamp, V. Erb, M. Stamm, A. J. Schouten, *Langmuir* **2001**, *17*, 6477.
[9] M. Niwa, T. Mori, N. Higashi, *J. Mater. Chem.* **1992**, *2*, 245.
[10] A. Wada, *Adv. Biophys.* **1976**, *9*, 1.
[11] W. G. J. Hol, P. T. van Duijnen, H. J. C. Berendsen, *Nature* **1978**, *273*, 443.
[12] G. Sauerbrey, *Z. Phys.* **1959**, 155, 206.
[13] E. M. Bradbury, C.-C. Robinson, L. Paolillo, P. Temussi, *J. Am. Chem. Soc.* **1973**, *95*, 1683.
[14] J. C. Mitchell, A. E. Woodward, P. Doty, *J. Am. Chem. Soc.* **1957**, *79*, 3955.
[15] T. Miyazawa, E. R. Blout, *J. Am. Chem. Soc.* **1961**, *83*, 712.
[16] K. Kurihara, T. Abe, N. Higashi, M. Niwa, *Colloids Surf. A* **1995**, *103*, 265.
[17] E. P. Enriquez, E. T. Samulski, *Mater. Res. Soc. Symp. Proc.* **1992**, *255*, 423.
[18] The calculations of the tilt angles have been performed by using Equation (1), proposed by Enriquenz and Samulski[17] where the angles of the transition moment (amide I and amide II) from the helix axis are assumed to be 39° and 75°, respectively,[19] and K has been calculated for LB films of PBLG to be 1.5 ± 0.2. D $(= A_I/A_{II}) = K[1/2(\sin\langle\theta\rangle\sin 39)^2 + (\cos\langle\theta\rangle\cos 30)^2]/[1/2(\sin\langle\theta\rangle\sin 75)^2 + (\cos\langle\theta\rangle\cos 75)^2]$ (1).
[19] M. Tsuboi, *J. Polym. Sci.* **1965**, *59*, 139.

 © 2003 Wiley-VCH Verlag GmbH & Co. KGaA, Weinheim

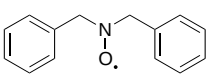
pH-Dependent Inclusion Complexes

Detection of Paramagnetic pH-Dependent Inclusion Complexes between β-Cyclodextrin Dimers and Nitroxide Radicals**

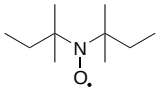
Paola Franchi, Marco Lucarini, and Gian Franco Pedulli*

We have recently designed a series of paramagnetic probes based on benzyl *tert*-butyl nitroxide to investigate, in aqueous solution, several types of supramolecular reaction kinetics in the submicrosecond time range by means of EPR spectroscopy.[1–3] The EPR spectra of these probes show a significant difference in the hyperfine splittings both at nitrogen, a(N), induced by the less polar environment of the host component with respect to the solution, and at the benzylic protons, $a(2H_\beta)$, because of conformational changes, so that the signals of both the complexed and uncomplexed species are easily distinguishable.

When benzyl *tert*-butyl nitroxide was investigated in aqueous solution in the presence of β-cyclodextrins (β-CDs) only one inclusion paramagnetic species was detected; this was identified as the 1:1 complex, similar to what was found by NMR spectroscopy for the parent amine compound.[1,4] Since the tendency of CDs to form inclusion complexes with guest molecules and simultaneously to self-associate to give dimers can be exploited to produce supramolecular structures at an higher level of organization,[5] we have been looking for paramagnetic organic guests capable to form CD complexes with a stoichiometry other than 1:1.[6] Herein we report the first EPR detection and characterization of paramagnetic inclusion complexes between symmetric dialkyl nitroxides (**1a**–**2a**) and two molecules of β-cyclodextrin.



1a



2a

The EPR spectrum **1a**, which is produced by oxidation of dibenzyl amine (2.0 mM) with the magnesium salt of monoperoxyphthalic acid (1.0 mM) in water, is shown in Figure 1. The spectrum is easily interpreted on the basis of the coupling of the unpaired electron with nitrogen and four equivalent benzylic protons (see Table 1). In the presence of β-CD (3.0 mM), additional signals assigned to the radical included in the cavity of β-CD (**1b**), in equilibrium with the free nitroxide, were observed (see Figure 1 and Figure 2).

By increasing the absolute concentration of β-CD, the ratio between included and free species varied linearly and, at 6 mM of β-CD, the dominant spectrum was that of the 1:1 inclusion complex **1b**. When β-CD concentrations higher than 9 mM were used, new signals appeared in the EPR spectrum (see Figure 1), which arise from a third radical species, characterized by spectroscopic parameters similar to those of the previous two species. The relative concentration of the third species changed reversibly on changing the β-CD concentration. This third species was identified as a second inclusion complex having a 1:2 stoichiometry (**1c**). Its EPR nitrogen hyperfine splitting (a_N) is significantly smaller than that of both the uncomplexed radical (**1a**) and the 1:1 complex (**1b**; see Table 1), which indicates that the nitroxide group is located in a less polar environment[7] consistent with a 1:2 complex in which the nitroxide group is completely shielded from the aqueous solvent. The molar ratio [**1c**]/[**1b**] of the two complexes, obtained from the EPR spectra, increased linearly with increasing concentration of the dissolved β-CD. When recording the EPR spectra in strongly basic solutions (pH > 12.5) the signals of the 1:2 complex **1c** disappeared while those of the 1:1 complex remained (see Supporting Information), similar to what had been found previously with a pyrene-modified γ-CD[8a] and with the 1:2

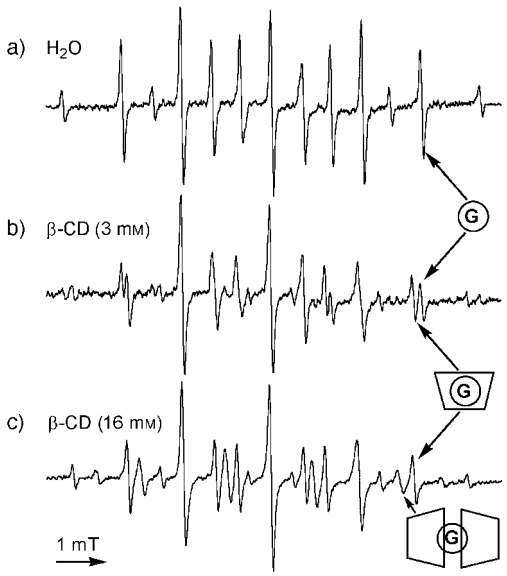


Figure 1. EPR spectra of **1a** in water at 295 K in the absence (a) and in the presence (b), (c) of various amounts of β-CD.

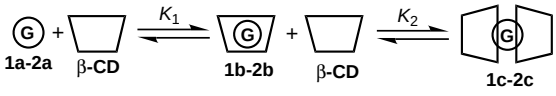


Figure 2. Schematic representation of the equilibria taking place in the presence of β-cyclodextrin.

[*] Prof. M. Lucarini, Dr. P. Franchi, Prof. G. F. Pedulli
Department of Organic Chemistry "A. Mangini"
University of Bologna
Via S. Donato 15, 40127 Bologna (Italy)
Fax: (+39) 051-244-064
E-mail: lucarini@alma.unibo.it

[**] Financial support from MURST (Research project "Free Radical Processes in Chemistry and Biology: Synthesis, Mechanisms, Applications") and University of Bologna is gratefully acknowledged.

Supporting information for this article is available on the WWW under http://www.angewandte.org or from the author.

 © 2003 Wiley-VCH Verlag GmbH & Co. KGaA, Weinheim DOI: 10.1002/anie.200250526

Table 1: Spectroscopic and thermodynamic parameters for CD complex formation.

System[a]	$a_{H\beta}$ [mT]	a_N [mT]	ΔH [kJ mol^{-1}]	ΔS [J K^{-1} mol^{-1}]	ΔG^{295} [kJ mol^{-1}]	K_{eq}^{295} [b] [M^{-1}]
1a (H_2O)	1.081	1.649				
1b (β-CD, m)	1.007	1.601	−13.5	5.1	−14.6	385
1c (β-CD, d)	0.796	1.559	−41.0	−108.9	−8.5	32
1d (DM-β-CD)	0.958	1.584			−15.5	539
1e (γ-CD)	0.923	1.595			−10.3	67
2a (H_2O)		1.682				
2b (β-CD, m)		1.620	−18.0	−2.7	−17.3	1106
2c (β-CD, d)		1.565	−37.5	−94.1	−9.9	56
2d (DM-β-CD)		1.602			−18.0	1503
2e (γ-CD)		1.616			−13.6	257

[a] In parenthesis is reported the host species (m = monomer, d = dimer). [b] $K_{eq} = K_1$ or K_2.

complex between 4-(dimethylamino) benzonitrile and β-CD.[8b] The lability of the 1:2 complex at high pH values is attributed to the fact that in basic media dissociation of the secondary CD hydroxy group ($pK_a = 12.5$) takes place to form an anionic species. Since molecular modeling studies have demonstrated that the driving force responsible for the stabilization of the β-CD dimer is the formation of intermolecular hydrogen bonds between the secondary hydroxy groups of the two larger rings,[9] the anionic β-CD unit can not associate to give dimers because of Coulombic charge repulsion. This hypothesis was confirmed by using as host 2,6-dimethylated β-cyclodextrins (DM-β-CDs) in which some of the hydroxylic hydrogen atoms responsible for the intermolecular hydrogen bonding have been replaced with methyl groups. Actually, the EPR spectra of dibenzyl nitroxide in the presence of 0.1M of DM-β-CD (**1d**) did not show any signals other than those of the 1:1 complex (see Supporting Information).

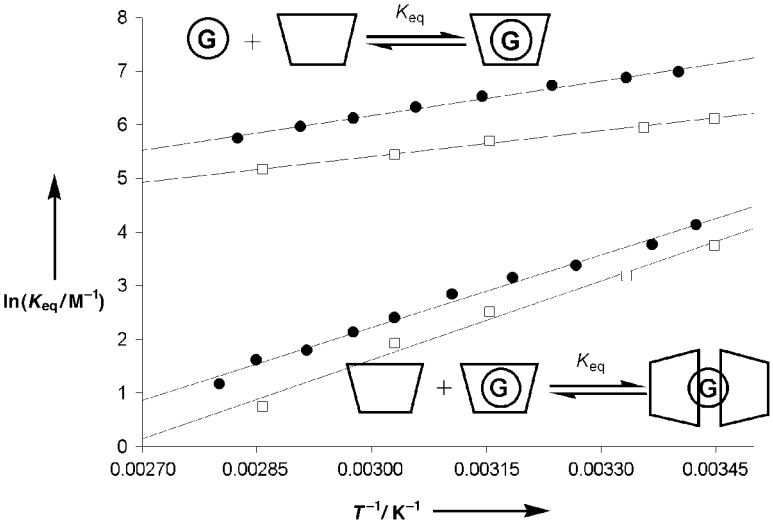


Figure 3. Van't Hoff plot for the temperature dependence of the equilibrium constants, K_1 and K_2; □ = **1a** and ● = **2a**.

The values for the K_1 and K_2 binding constants were obtained by plotting the ratio between the concentrations of the 1:1 complex and the free species ([β-CD] 0–8 mM) and the ratio between the concentrations of the 1:2 and 1:1 complex ([β-CD] 8–15 mM) as a function of the cyclodextrin concentration in water. The temperature dependence of these equilibrium constants, reported in van't Hoff plots (Figure 3), shows that K_1 changes only slightly with temperature, while K_2 significantly decreases with increasing temperature.

The first step, that is, the formation of the 1:1 complex, is associated with a small negative $\Delta H°$ and an entropy change, $\Delta S°$, close to zero (see Table 1). Although the entropy of complexation of a guest by an empty host in the gas phase would be negative by 120–200 J mol^{-1} K^{-1} the complexation in solution is expected to have entropies of complexation much closer to zero, because of the desolvation of the guest from water molecules is entropically favorable.[10]

The formation of the 1:2 complex, however, is characterized by largely negative enthalpy and entropy changes. The negative ΔH value is the result of the formation of a large number of intermolecular hydrogen bonds between the two wider rings of the cyclodextrins. This process also implies a loss of entropy because of the reduced freedom of molecular motion of the complex which, in contrast to the 1:1 complexation, is not compensated by the desolvation of the guest as this is already included in the cavity of one CD molecule. Thus, the measured thermodynamic parameters are consistent with the formation of a 1:2 complex.[8b]

To gain a more detailed picture of the 1:2 complex formation, stochastic dynamics (SD) simulations were performed in water at constant temperature by using AMBER* force field.[11,12] After the sample had been heated to 295 K, the different complexes were equilibrated for 200 ps with time step of 1 fs and the total simulation time was set to 15000 ps to achieve full convergence (see Table 2).[13]

Consistent with the experimental evidence, the SD simulations show that on average, the formations of the 1:1 and 1:2 complexes are energetically favorable by 50 and 101 kJ mol^{-1}, respectively. While in the 1:1 complex only one phenyl ring is located inside the torus, in the 1:2 complex the nitroxide is totally embedded in the macrocylic rings (see

Table 2: Summary of data obtained by SD simulation at 295 K in water.

Equilibrium	Energy of reactants [kJ mol^{-1}]	Energy of complex [kJ mol^{-1}]	ΔE [kJ mol^{-1}]
1a + β-CD ⇌ **1b**	767 (116 + 651)	717	−50
2 β-CD ⇌ dimer	1302 (2 × 651)	1238	−64
1b + β-CD ⇌ **1c**	1368 (717 + 651)	1267	−101
1a + dimer ⇌ **1c**	1354 (116 + 1238)	1267	−87

 © 2003 Wiley-VCH Verlag GmbH & Co. KGaA, Weinheim

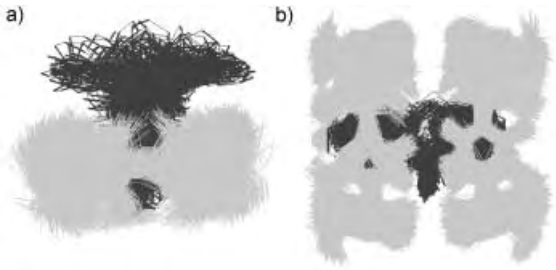


Figure 4. Clustered molecular display. Dynamics of the 1:1 (a) and 1:2 (b) complexes of β-CD (gray) with dibenzyl nitroxide (black). The drawings include only 500 structures that refer to the 15000 ps simulation. Hydrogen atoms have been omitted for clarity.

Figure 4), in agreement with the decrease of a_N observed experimentally when passing from **1b** to **1c**.

Moreover, the SD calculated $\langle\cos^2\theta\rangle$ values [14] for **1a** and **1c**, where θ is the dihedral angle between the symmetry axis of the $2p_\pi$ orbital of nitrogen atom and the N-C-H_β plane in the nitroxide, were 0.41 and 0.37, respectively. These values are in agreement with the large reduction of $a_{H\beta}$ found experimentally when passing from **1a** to **1c**. The computations indicate that in the 1:2 complex the only populated conformers are those in which θ is $-30°$ and 90°, while in water the energy minimum in which the phenyl group is eclipsed by the oxygen atom is also significantly populated (see Supporting Information) and contributes to the value of $\langle\cos^2\theta\rangle$.

To increase the life time of the paramagnetic 1:2 complex we investigated the behavior of symmetric di-*tert*-alkyl nitroxides, because substitution of the β-hydrogen atoms with alkyl groups increases considerably the life time of the nitrogen containing species.[15] In the absence of β-hydrogen atoms, however, the characterization of the complexed species by EPR spectroscopy is not as straightforward as for **1a**, since the changes with complexation of the only measurable splitting constant, that is a_N, are not sufficiently large to clearly differentiate the spectra of the various species. However, when using di-*tert* amyl nitroxide (**2a**) partial resolution of the high-field EPR lines of the free and complexed nitroxides is observed.[16] Actually, we were able to distinguish two different signals, attributed to the radical in water (**2a**) and to the 1:1 complex (**2b**) in the presence of 3.7 mM β-CD, and to the 1:1 and 1:2 complex (**2c**) at 16 mM β-CD concentration (see Supporting Information). The assignment of the signals to the different species was on the basis of considerations similar to those reported above for dibenzyl nitroxide. In this case, however, the increased radical life time (several days) made it possible to switch reversibly from the 1:1 to 1:2 complex many times by successive acid–base treatments without any EPR evidence of side reactions.

Summarizing, we have been able to construct the first three-component organic free-radical complex which can be reversibly formed by changing the pH value or temperature. Simple chemical modifications of the radical guest can give species able to self associate. The combination of this property with the tendency of cyclodextrins to form inclusion complexes and simultaneously to self-associate and form dimers can be exploited to produce paramagnetic supramolecular structures at an higher level of organization. The formation of such supramolecular ordered polyradical assemblies can be useful for the preparation of functional molecular magnetic materials.

Experimental Section

Radicals **1a** and **2a** were generated by mixing a methanol solution (1 μL) containing the corresponding amine (0.2 M) and a water solution (1 μL) containing the Mg salt of monoperoxyphthalic acid (0.1 M) with a water solution (100 μL) containing variable amounts of β-CD. The pH value of the solution was adjusted by adding NaOH. for pH > 12 Oxone was used as the oxidant. Samples were transferred in capillary tubes (1 mm i.d.), heated for 30–60 s at 80 °C and then placed inside the thermostatted cavity of EPR spectrometer (Bruker ESP300). The instrument settings were: microwave power 5.0 mW, modulation amplitude 0.05 mT, modulation frequency 100 kHz, scan time 180 s. The computed spectra were best-fitted to the experimental ones by using a Monte Carlo minimization procedure.[1b,17]

SD simulations were carried out using the MacroModel 7.0 program. Extended nonbonded cutoff distances were set to 8 Å and 20 Å for the van der Waals and electrostatic interactions. The generalized Born/surface area (GB/SA) solvation model was used when modeling the solvent effect under MacroModel. All C–H and O–H bond lengths were held fixed using the SHAKE algorithm. Translational and rotational momentum were removed every 0.1 ps. β-Cyclodextrin with a C_7 symmetry was used as the starting host. All the complexes were generated by docking the guest to the host in a suitable orientation. In all cases the origin of a Cartesian reference frame was placed on the center of mass of the CD and the z axis aligned with the C_7 symmetry axis of CD. No significant differences were obtained by using different starting orientations.

Received: November 12, 2002 [Z50526]

Keywords: cyclodextrins · EPR spectroscopy · host–guest systems · nitroxides · radicals

[1] a) M. Lucarini, B. P. Roberts, *Chem. Commun.* **1996**, 1577; b) M. Lucarini, B. Luppi, G. F. Pedulli, B. P. Roberts, *Chem. Eur. J.* **1999**, *5*, 2048.

[2] P. Franchi, M. Lucarini, G. F. Pedulli, D. Sciotto, *Angew. Chem.* **2000**, *112*, 269; *Angew. Chem. Int. Ed.* **2000**, *39*, 263.

[3] G. Brigati, P. Franchi, M. Lucarini, G. F. Pedulli, L. Valgimigli, *Res. Chem. Intermed.* **2002**, *28*, 131.

[4] M. Lucarini, E. Mezzina, G. F. Pedulli, *Eur. J. Org. Chem.* **2000**, 3927.

[5] a) T. Kraus, M. Buděšínský, I. Císařová, J. Závada, *Angew. Chem.* **2002**, *114*, 1791; *Angew. Chem. Int. Ed.* **2002**, *41*, 1715; b) D. T. Bong, T. D. Clark, J. R. Granja, M. R. Ghadiri, *Angew. Chem.* **2001**, *113*, 1016; *Angew. Chem. Int. Ed.* **2001**, *40*, 988; c) S. Makedonopoulou, I. M. Mavridis, K. Yannakopoulou, J. Papaioannou, *Chem. Commun.* **1998**, 2133; d) G. Gattuso, S. Menzer, S. A. Nepogodiev, J. F. Stoddart, D. J. Williams, *Angew. Chem.* **1997**, *109*, 1615; *Angew. Chem. Int. Ed. Engl.* **1997**, *36*, 1451.

[6] J. A. Crayston, J. N. Devine, J. C. Walton, *Tetrahedron* **2000**, *56*, 7829.

[7] B. R. Knauer, J. J. Napier, *J. Am. Chem. Soc.* **1976**, *98*, 4395, and references therein.

[8] a) A. Ueno, I. Suzuki, T. Osa, *J. Am. Chem. Soc.* **1989**, *111*, 6391; b) A. Nakamura, S. Sato, K. Hamasaki, A. Ueno, F. Toda, *J. Phys. Chem.* **1995**, *99*, 10952.

 © 2003 Wiley-VCH Verlag GmbH & Co. KGaA, Weinheim

[9] P. Bonnet, C. Jaime, L. Morin-Allory, *J. Org. Chem.* **2001**, *66*, 689.
[10] a) M. V. Rekharsy, Y. Inoue, *Chem. Rev.* **1998**, *98*, 1875; b) K. Kano, T. Kitae, Y. Shimofuri, N. Tanaka, Y. Mineta, *Chem. Eur. J.* **2000**, *6*, 2705.
[11] a) S. J. Weiner, P. A. Kollman, D. A. Case, U. C. Singh, C. Ghio, G. Alagona, S. Profeta, P. Weiner, *J. Am. Chem. Soc.* **1984**, *106*, 765; b) S. J. Weiner, P. A. Kollman, D. T. Nguyen, D. A. Case, *J. Comput. Chem.* **1986**, *7*, 230.
[12] The N–O bond was modeled by the C=O bond because of their similar geometries and the lack of corresponding parameters in the AMBER* force field. F. Perez, C. Jaime, X. Sánchez-Ruiz, *J. Org. Chem.* **1995**, *60*, 3840.
[13] K. B. Lipkowitz, G. Pearl, R. Coner, M. A. Peterson, *J. Am. Chem. Soc.* **1997**, *119*, 600.
[14] The magnitude of the splitting constant for the β-hydrogen atoms (H_β) depends on the time-average value of $\cos^2\theta$ according to the Heller-McConnell relationship: $a(H)_\beta = \rho_N(B_0 + B_2\langle\cos^2\theta\rangle)$.
[15] Dibenzyl nitroxide persists at room temperature for only few minutes because of a disproportionation reaction that leads to the formation of nitrones and hydroxylamines.
[16] The first example of a persistent nitroxide–cyclodextrin complex was reported in 1975. J. Martinie, J. Michon, A. Rassat, *J. Am. Chem. Soc.* **1975**, *97*, 1818.
[17] B. Kirste, *J. Magn. Reson.* **1987**, *73*, 213.

 © 2003 Wiley-VCH Verlag GmbH & Co. KGaA, Weinheim

Bi Reagents for C-C Cross-Coupling

5,6,7,12-Tetrahydrodibenz[*c,f*][1,5]azabismocines: Highly Reactive and Recoverable Organobismuth Reagents for Cross-Coupling Reactions with Aryl Bromides**

Shigeru Shimada, Osamu Yamazaki, Toshifumi Tanaka, Maddali L. N. Rao, Yohichi Suzuki, and Masato Tanaka**

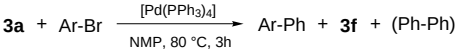
[*] Dr. S. Shimada, Prof. Dr. M. Tanaka, Dr. O. Yamazaki, Dr. M. L. N. Rao
National Institute of Advanced Industrial Science and Technology (AIST)
Tsukuba Central 5, 1-1-1 Higashi, Tsukuba, Ibaraki 305-8565 (Japan)
Fax: (+81) 298-61-4511
E-mail: s-shimada@aist.go.jp
m.tanaka@res.titech.go.jp
T. Tanaka, Prof. Dr. Y. Suzuki
Department of Industrial Chemistry
College of Industrial Technology, Nihon University
1-2-1 Izumi-cho, Narashino, Chiba 275–8575 (Japan)
Prof. Dr. M. Tanaka
Chemical Resources Laboratory, Tokyo Institute of Technology
4259 Nagatsuta-cho, Midori-ku, Yokohama 226–8503 (Japan)
Fax: (+81) 45-924-5244

[**] We are grateful to the Japan Science and Technology Corporation (JST) for financial support through the CREST (Core Research for Evolutional Science and Technology) program and for a postdoctoral fellowship to O.Y. and M.L.N.R.

Supporting information for this article is available on the WWW under http://www.angewandte.org or from the author.

Transition-metal-catalyzed cross-coupling reactions of organometallic reagents, such as organotin, -boron, -silicon, -zinc, and -magnesium compounds, with organic halides and triflates is one of the most powerful methods to form C–C bonds.[1] Recently, tremendous effort has been devoted to the improvement of efficiency and applicability of the cross-coupling reaction by the development of highly active catalyst systems as well as by the modification of the structure of the organometallic reagents.[2] We believe that another important direction of research should be to explore the applicability of other organometallic reagents, which would broaden the scope of the cross-coupling methodology. Recently, organoindium,[3] -manganese,[4] and -titanium[5] compounds have been disclosed to be useful.

Bismuth is a nontoxic element[6] and its organic compounds are potentially useful, low-toxicity reagents for organic synthesis.[7] We have demonstrated that the organobismuth compounds 2,6-Py$(CR_2O)_2BiR^1$ (**1**: R^1 = Ph or Me, R = alkyl) and Ar_3Bi (**2**) can be utilized for the cross-coupling reaction with organic electrophiles such as bromides, iodides, and triflates catalyzed by a palladium complex.[8] However, compounds **1** and **2** suffer from a drawback in that their applicability has considerable limitation. In particular, they do not couple with electron-rich substrates efficiently, even in the presence of stoichiometric amounts of activators. Herein we report that the readily obtainable hypervalent organobismuth compounds, 5,6,7,12-tetrahydrodibenz[*c,f*][1,5]azabismocine derivatives **3a**–**3e**, can couple with electron-deficient, electron-neutral, and even electron-rich aryl bromides efficiently in the absence of any additional activator by using a simple commercially available Pd catalyst, $[Pd(PPh_3)_4]$. There are additional advantages to reagents **3a**–**3e**: 1) Selective one-pot multicoupling reactions by the combination of compounds **3a**–**3e** and bromophenylboronic esters enabled the construction of up to nine bonds in good yields in one pot. 2) Bismuth compounds, such as bromide **3f** and chloride **3g**, are recovered almost quantitatively after the reaction and can be reused as the precursors to **3a**–**3e**.



In the cross-coupling reactions with **1** and **2**, yields were highly dependent on the electronic nature of the organic electrophiles. Additives such as K_2CO_3, Cs_2CO_3, and CsF considerably improved the reactivities of **1** and **2**. Nevertheless, the reactions of **1** and **2** with electron-rich substrates were not satisfactory. We assumed that the reactivity enhancement by the additives was derived from the formation of the "ate complex", electron-rich, higher-coordinated reactive species by coordination of the anionic part of the additives to the bismuth center. Accordingly electron-rich, hypervalent organobismuth compounds are expected to be more reactive than **1** and **2**.

The synthesis and structure of 6-methyl-5,6,7,12-tetrahydrodibenz[*c,f*][1,5]azabismocine derivatives **4** were reported by Akiba and co-workers.[9] We introduced a *t*Bu group in place of the methyl group on the N atom to increase the

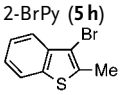
 DOI: 10.1002/anie.200250205 © 2003 Wiley-VCH Verlag GmbH & Co. KGaA, Weinheim

electron-donating ability of the N atom and to protect the N atom from being involved in undesirable side reactions by the steric bulk of the *t*Bu group. Similarly to the synthesis of **4**,[9] compound **3g** was prepared by the reaction of $BiCl_3$ with $(2\text{-}LiC_6H_4CH_2)_2tBuN$, which was generated in situ by the lithiation of $(2\text{-}BrC_6H_4CH_2)_2tBuN$ with *n*BuLi.[10] A third organic group was introduced at the bismuth atom by the reaction of **3g** with organolithium or Grignard reagents.[9,11]

The cross-coupling reaction of **3a** with 1-bromonaphthalene **5a** proceeded smoothly in the absence of any additives to give 1-phenylnaphthalene quantitatively (NMP, 80 °C, 3 h, $[Pd(PPh_3)_4]$ (2 mol %); Table 1, entry 1). The same reaction of

Table 1: Cross-coupling reaction of **3a** with aryl bromides.[a]

3a + Ar-Br $\xrightarrow[\text{NMP, 80 °C, 3h}]{[Pd(PPh_3)_4]}$ Ar-Ph + **3f** + (Ph-Ph)

Entry	ArBr[b]	$[Pd(PPh_3)_4]$ [mol %]	Ar-Ph [%][c]	Ph-Ph [%][d]
1	1-BrNpt (**5a**)	2	97(100)	3
2	**5a**	0.5	(98)	4
3	2-BrAnt (**5b**)	2	91	nd[e]
4	$4\text{-}AcC_6H_4Br$ (**5c**)	2	97	3
5	$4\text{-}NCC_6H_4Br$ (**5d**)	2	91	9
6	$4\text{-}MeC_6H_4Br$ (**5e**)	10	89	6
7	$4\text{-}MeOC_6H_4Br$ (**5f**)	10	93	5
8	$4\text{-}Me_2NC_6H_4Br$ (**5g**)	10	76	nd[e]
9[f]	2-BrPy (**5h**)	2	86(93)	2
10[g]	 (**5i**)	10	74	0

[a] **3a** (0.30 mmol), ArBr (0.25 mmol), 1-methyl-2-pyrrolidinone (NMP; 3 mL). [b] Nap = naphthalene, Ant = anthracene, Py = pyridine. [c] Yield of isolated product based on ArBr. Yields determined by GC with *n*-hexadecane as an internal standard are shown in parentheses. [d] Yield determined by GC based on **3a**. [e] Not determined. [f] Reaction time: 6 h. [g] Reaction time: 10 h.

$2,6\text{-}Py(CMe_2O)_2BiPh$ and Ph_3Bi with **5a** under similar reaction conditions produced 1-phenylnaphthalene only in 15 % and 2 % yields, respectively, in the absence of additives and in 88 % and 76 % yields in the presence of Cs_2CO_3 (2 equiv) and CsF (8 equiv), respectively.[8b,c] The performance of compound **3a** clearly seen in Table 1 can be summarized as follows. All electron-deficient, electron-neutral, and even electron-rich aryl bromides smoothly reacted in the presence of $[Pd(PPh_3)_4]$ as a catalyst without any additives. Sterically hindered substrate **5i**, which has a Me group at the position adjacent to Br, also gave the cross-coupled product in a good yield although a longer reaction time was required (Table 1, entry 10). The amount of catalyst can be decreased to 0.5 mol % as shown in the reaction of **5a** (Table 1, entry 2). In most cases, a small amount of biphenyl was also formed as a by-product (Table 1).

The reactivity of azabismocines **3** with a substituted aryl or alkenyl group toward aryl bromides is summarized in Table 2. Electron-deficient and -rich aryl bismuth compounds **3b**–**3d** as well as isopropenylbismuth compound **3e** efficiently reacted with electron-deficient, -neutral, and -rich aryl bromides **5d, 5a** and **5f**. Notably, sterically demanding **3d**,

Table 2: Cross-coupling reaction of **3b**–**3e** with aryl bromides.[a]

3b – 3e + Ar-Br $\xrightarrow[\text{NMP, 80 °C, 3h}]{[Pd(PPh_3)_4]}$ Ar-R + **3f** + (R-R)

Entry	**3**	ArBr	$[Pd(PPh_3)_4]$ [mol %]	Ar-R [%][b]	R-R [%][c]
1	**3b**	**5d**	2	87	8
2		**5a**	5	96	3
3		**5f**	10	87	3
4	**3c**	**5d**	2	91	4
5		**5a**	10	93	nd[d]
6		**5f**	10	91	11
7[e]	**3d**	**5a**	2	87	0
8[e]		**5f**	10	78	0
9	**3e**	**5d**	5	90	nd[d]
10		**5a**	5	80	nd[d]
11		**5f**	5	81	nd[d]

[a] **3b**–**3e** (0.30 mmol), ArBr (0.25 mmol), NMP (3 mL). [b] Yield of isolated product based on ArBr. [c] Approximate values based on **3b**–**3e** calculated from relative peak intensities of Ar-R and R-R by GC analysis. [d] Not determined. [e] Reaction time: 5 h.

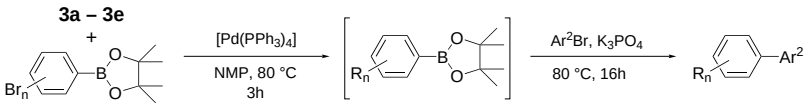
which has two OMe groups *ortho* to the Bi substituent on R, gave the products in good yields, although a slightly longer reaction time was required (Table 2, entries 7–8). As observed in the reaction of **3a** with ArBr, small amounts of self-coupling products of **3b** and **3c**, $(3,5\text{-}(CF_3)_2C_6H_3\text{-})_2$ and $(3,4\text{-}(CH_2O_2)C_6H_3\text{-})_2$, respectively, were also formed, whereas that of **3d** was not observed probably because of the steric bulk of the $2,4,6\text{-}(MeO)_3C_6H_2\text{-}$ group.[12]

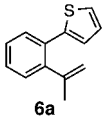
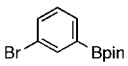
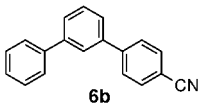
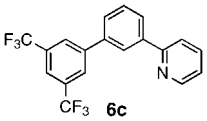
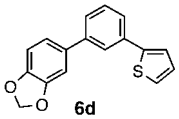
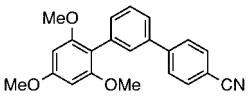
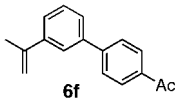
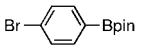
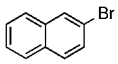
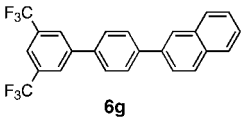
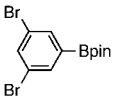
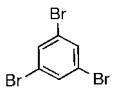
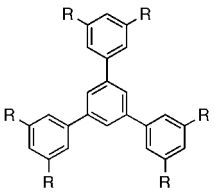
After the reaction, the bismuth compound can be recovered almost quantitatively as bromide **3f** or chloride **3g**, which are the precursors for **3a**–**3e**. During the cross-coupling reaction, **3a**–**3e** were converted into bromide **3f**. Since 1.2 equivalents of **3a**–**3e** were used, small quantities of the starting compounds remained unreacted after the reaction. By the aqueous workup with dilute HCl solution, both **3f** and unreacted **3a**–**3e** are quantitatively converted into **3g**. If HBr solution is used instead of HCl solution, the bismuth species can be recovered as bromide **3f**. Both **3f** and **3g** are stable to air and neutral or acidic aqueous conditions.[13] Isolation of **3f** or **3g** from the crude mixture can be performed by solvent extraction of the cross-coupling product,[14] recrystallization, chromatographic separation, or a combination of these methods.

By invoking the difference in the protocols of the new cross-coupling with the bismuth reagents and the well-established Suzuki–Miyaura coupling with aryl boronic acids and esters,[1,15] a one pot multicoupling reaction is readily realized. Generally the latter palladium-catalyzed cross-coupling reaction of aryl boronic compounds with organic halides and triflates requires a base as an activator, whereas the cross-coupling reaction of **3a**–**3e** does not require any additional activators. Accordingly **3a**–**3e** can selectively couple with bromophenylboronic esters without self-condensation of the latter to leave the boronic ester moiety intact. Subsequent addition of a second aryl halide and a base activator affords multicoupling products in one pot as shown in Table 3. All *o*-, *m*-, and *p*-bromophenylboronic esters efficiently underwent cross-coupling in this one-pot

 © 2003 Wiley-VCH Verlag GmbH & Co. KGaA, Weinheim

Table 3: One-pot multicoupling reaction of **3a**–**3e** with bromophenylboronic esters and aryl bromides.[a]



Entry	3	BrArBpin[b]	Ar^2Br	Product	Yield[%][c]
1[d,e]	**3e**			 **6a**	75
2[d]	**3a**		**5d**	 **6b**	84
3[d]	**3b**		**5h**	 **6c**	76
4[d]	**3c**			 **6d**	89
5[d,f]	**3d**		**5d**	 **6e**	72
6[d]	**3e**		**5c**	 **6f**	74
7[g]	**3b**			 **6g**	87
8[e,h]	**3b**			 **7a**: R = 3,5-$(CF_3)_2C_6H_3$ **7b**: R = CH_2=C(Me)−	74[i]
9[h]	**3e**				60[i]

[a] See Supporting Information for details of the reaction procedures. [b] pin = -$OCMe_2CMe_2O$-. [c] Yield of isolated product based on bromophenylboronic esters. [d] Bi/B/Pd/ArBr/K_3PO_4 = 1.1:1.0:0.1:1.1:1.5. [e] Reaction time for the first step: 8 h. [f] Reaction time for the first step: 5 h. [g] Bi/B/Pd/ArBr/K_3PO_4 = 1.1:1.0:0.1:1.5:1.5. Reaction time for the second step: 32 h. [h] Bi/B/Pd/ArBr/K_3PO_4 = 6.7:3.3:0.66:1.0:10. [i] Yield of isolated product based on 1,3,5-tribromobenzene.

synthesis and compounds **6a**–**6g** were obtained in good yields.[16] By using 3,5-dibromophenylboronic ester and 1,3,5-tribromobenzene, nine bonds were efficiently constructed in one pot to give **7a** and **7b** in good yields.[17,18] In all cases except Table 3, entry 5, the first step was nearly quantitative, as judged by GC analysis. The second step, which was performed under typical conditions for the Suzuki–Miyaura reaction, remains to be optimized for further improvement of the yields.

In summary, we have reported that 5,6,7,12-tetrahydrodibenz[*c*,*f*][1,5]azabismocine derivatives **3a**–**3e** are highly efficient and recoverable reagents for the cross-coupling reaction with aryl bromides. Further studies to clarify the scope and the mechanistic aspect of this reaction are underway.

Received: September 20, 2002
Revised: December 13, 2002 [Z50205]

Keywords: bismuth · boron · cross-coupling · hypervalent compounds · palladium

[1] a) *Metal-catalyzed Cross-coupling Reactions* (Eds.: F. Diederich, P. J. Stang), Wiley-VCH, Weinheim, **1998**; b) S. R. Chemler, D. Trauner, S. J. Danishefsky, *Angew. Chem.* **2001**, *113*, 4676–4701; *Angew. Chem. Int. Ed.* **2001**, *40*, 4544–4568; c) J. Hassan, M. Sevignon, C. Gozzi, E. Schulz, M. Lemaire, *Chem. Rev.* **2002**, *102*, 1359–1469.

[2] For recent examples, see: a) V. P. W. Bohm, C. W. K. Gstottmayr, T. Weskamp, W. A. Herrmann, *Angew. Chem.* **2001**, *113*, 3500–3503; *Angew. Chem. Int. Ed.* **2001**, *40*, 3387–3389; b) C. Y. Dai, G. C. Fu, *J. Am. Chem. Soc.* **2001**, *123*, 2719–2724; c) S. E. Denmark, R. F. Sweis, *J. Am. Chem. Soc.* **2001**, *123*, 6439–6440; d) K. Itami, T. Nokami, Y. Ishimura, K. Mitsudo, T. Kamei, J. Yoshida, *J. Am. Chem. Soc.* **2001**, *123*, 11577–11585; e) A. Mori, M. Suguro, *Synlett* **2001**, 845–847; f) A. Fürstner, A. Leitner, *Angew. Chem.* **2002**, *114*, 632–635; *Angew. Chem. Int. Ed.* **2002**, *41*, 609–612; g) J. J. Yin, M. P. Rainka, X. X. Zhang, S. L. Buchwald, *J. Am. Chem. Soc.* **2002**, *124*, 1162–1163; h) C. W. K. Gstöttmayr, V. P. W. Böhm, E. Herdtweck, M. Grosche, W. A. Herrmann, *Angew. Chem.* **2002**, *114*, 1421–1423; *Angew. Chem. Int. Ed.* **2002**, *41*, 1363–1365.

[3] a) I. Perez, J. P. Sestelo, L. A. Sarandeses, *Org. Lett.* **1999**, *1*, 1267–1269; b) I. Perez, J. P. Sestelo, L. A. Sarandeses, *J. Am. Chem. Soc.* **2001**, *123*, 4155–4160.

[4] a) E. Riguet, M. Alami, G. Cahiez, *Tetrahedron Lett.* **1997**, *38*, 4397–4400; b) E. Riguet, M. Alami, G. Cahiez, *J. Organomet. Chem.* **2001**, *624*, 376–379.

[5] J. W. Han, N. Tokunaga, T. Hayashi, *Synlett* **2002**, 871–874.

[6] a) S. Maeda in *The Chemistry of Organic Arsenic, Antimony and Bismuth Compounds* (Ed.: S. Patai), Wiley, New York, **1994**, chap. 19, pp. 725–759; b) J. Reglinski, in *Chemistry of Arsenic, Antimony and Bismuth* (Ed.: N. C. Norman), Blackie Academic and Professional, London, **1998**, chap. 8, pp. 403–440.

[7] For reviews on the application of organobismuth compounds in organic synthesis, see: a) H. Suzuki, T. Ikegami, Y. Matano, *Synthesis* **1997**, 249–267; b) G. I. Elliott, J. P. Konopelski,

 © 2003 Wiley-VCH Verlag GmbH & Co. KGaA, Weinheim

Tetrahedron **2001**, *57*, 5683 – 5705; c) *Organobismuth Chemistry* (Eds.: H. Suzuki, Y. Matano), Elsevier, Amsterdam, **2001**.

[8] a) M. L. N. Rao, S. Shimada, M. Tanaka, *Org. Lett.* **1999**, *1*, 1271 – 1273; b) M. L. N. Rao, O. Yamazaki, S. Shimada, T. Tanaka, Y. Suzuki, M. Tanaka, *Org. Lett.* **2001**, *3*, 4103 – 4105; c) M. L. N. Rao, S. Shimada, O. Yamazaki, M. Tanaka, *J. Organomet. Chem.* **2002**, *659*, 117 – 120.

[9] a) K. Ohkata, S. Takemoto, M. Ohnishi, K. Akiba, *Tetrahedron Lett.* **1989**, *30*, 4841 – 4844; b) M. Minoura, Y. Kanamori, A. Miyake, K. Akiba, *Chem. Lett.* **1999**, 861 – 862.

[10] F. H. Carré, R. J. P. Corriu, G. F. Lanneau, P. Merle, F. Soulairol, J. Yao, *Organometallics* **1997**, *16*, 3878 – 3888.

[11] Compounds **3a**–**3g** were purified by recrystallization and are thermally stable at least up to 110 °C. Compounds **3a, 3b, 3f**, and **3g** also can be purified by silica-gel column chromatography, whereas **3d** seems to decompose by column chromatography on silica gel or alumina. Detail of the synthesis, structure, and some properties of **3a**–**3g** will be reported elsewhere.

[12] In the reaction of **3b** and **3d** with 4-bromoanisole, 3,5-$(CF_3)_2C_6H_3$-Ph and 2,4,6-$(MeO)_3C_6H_2$-Ph were also obtained as a by-product in 4% and 21% yields, respectively. The phenyl group of the by-products probably came from PPh_3 as observed in the related cross-coupling reaction; see: B. E. Segelstein, T. W. Butler, B. L. Chenard, *J. Org. Chem.* **1995**, *60*, 12 – 13.

[13] For example, **3g** was quantitatively recovered when it was stirred in a 1:1 mixture of CH_2Cl_2/1M aqueous HCl at room temperature for 10 h. However, the recovery of **3g** decreased to 70% when it was stirred in a 1:1 mixture of CH_2Cl_2/4M aqueous HCl at room temperature for 2 days.

[14] For an experimental procedure, see Supporting Information.

[15] A. Suzuki, *J. Organomet. Chem.* **1999**, *576*, 147 – 168.

[16] Since a slight excess of **3a**–**3e** and Ar^2Br was used, small amounts of direct coupling products between **3a**–**3e** and Ar^2Br were also formed.

[17] Similar compounds have been prepared by multistep procedures: T. M. Miller, T. X. Neenan, R. Zayas, H. E. Bair, *J. Am. Chem. Soc.* **1992**, *114*, 1018 – 1025.

[18] The molecular structure of **7a** was unambiguously confirmed by X-ray analysis. See the Supporting Information for the crystal data as well as a molecular drawing of **7a**. CCDC-192709 (**7a**) contains the supplementary crystallographic data for this paper. These data can be obtained free of charge via www.ccdc.cam.ac.uk/conts/retrieving.html (or from the Cambridge Crystallographic Data Centre, 12 Union Road, Cambridge CB21EZ, UK; fax: (+44) 1223-336-033; or deposit@ccdc.cam.ac.uk).

 © 2003 Wiley-VCH Verlag GmbH & Co. KGaA, Weinheim

Corrigenda

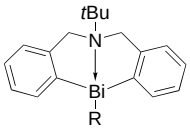
In the Communication "A Zeolite Structure (ITQ-13) with Three Sets of Medium-Pore Crossing Channels Formed by 9- and 10-Rings" by **A. Corma et al.** in *Angew. Chem.* **2003**, *115*, 1188–1191; *Angew. Chem. Int. Ed.* **2003**, *42*, 1156–1159, it should have been made clear early on in the manuscript that the synthesis of the ITQ-13 material was first reported in a patent published in 2002 (T. Boix, M. Puche, M. A. Camblor, A. Corma, US Patent 6 471 941 B1, **2002**; reference [12] in the manuscript). Furthermore, owing to an editorial error the reference to this patent was wrongly introduced into the *Experimental Section*, where reference [13] should read reference [12] and vice versa.

We apologize to our readers and to the authors of the above mentioned patent if this mistake has resulted in any misunderstanding.

Avelino Corma
Corresponding Author

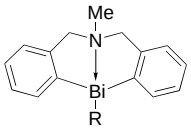
Peter Gölitz
Editor

In the Communication by **S. Shimada, M. Tanaka et al.** published in *Angew. Chem. Int. Ed.* **2003**, *42*, 1845–1848, the incorrect formula was printed on p. 1845. The correct formula is that shown below. Furthermore, the e-mail address for Professor Tanaka should be m.tanaka@res.titech.ac.jp.



3a – 3g

3a: R = Ph
3b: R = 3,5-$(CF_3)_2C_6H_3$-
3c: R = 3,4-$(CH_2O_2)C_6H_3$-
3d: R = 2,4,6-$(MeO)_3C_6H_2$-
3e: R = CH_2=C(Me)-
3f: R = Br
3g: R = Cl



4

 © 2003 Wiley-VCH Verlag GmbH & Co. KGaA, Weinheim

A Zinc-Saccharate 3D Network

Zinc Saccharate: A Robust, 3D Coordination Network with Two Types of Isolated, Parallel Channels, One Hydrophilic and the Other Hydrophobic**

*Brendan F. Abrahams, Michael Moylan, Simon D. Orchard, and Richard Robson**

Because of their availability and ease of functionalisation, sugar derivatives are attractive candidates as chiral building blocks for potentially useful polymers. Aldaric acids, which are polyhydroxydicarboxylic acids easily obtained from aldoses by terminal oxidation, could provide coordination polymers with interesting properties arising from the multiplicity of hydroxy groups and from the chirality. Considerable effort is now being made to lay the foundations for future "green" industrial production of chemicals and derived materials based on renewable starting materials and biodegradable products. Accordingly, the aldaric acid produced very simply from D-glucose, namely, D-saccharic acid (also known as D-glucaric acid) has been proposed as a potentially cheap and versatile commercial synthon, for example, in the manufacture of "hydroxylated nylons".[1] We are investigating the coordination polymers derived from aldaric acids with transition metals, lanthanides, and other metals; herein we report chiral zinc D-saccharate, which is exceptional in that its structure contains two types of parallel channels with very different characteristics, one type hydrophilic the other hydrophobic, which are isolated from each other by seemingly impenetrable walls. In 1998 it was shown that copper(II) saccharate has a linear polymeric chain structure,[2] and the structures of the potassium and calcium salts were described earlier.[3] The structures of a number of Group 1 and 2 metal derivatives of galactaric acid (also known as mucic acid) were reported (Na,[4] K,[4] Mg,[5] Ca[6] and Ba[6]). Galactaric acid is presently cheaper than saccharic acid, but is not chiral.

Crystals of hydrated zinc saccharate, $[Zn(C_6H_8O_8)]\cdot \approx 2H_2O$ (**1**), suitable for single crystal X-ray diffraction studies were obtained directly from an aqueous solution containing potassium hydrogen saccharate and zinc acetate.[7] All saccharate ligands are equivalent, their two carboxylate groups, although intrinsically different from each other, nonetheless play very similar structural roles. The zinc centers are chelated at both ends of the saccharate ligand by a carboxylate oxygen donor and an adjacent hydroxy group—O1a together with O2 at one end and O6a with O5 at the

[*] Prof. R. Robson, Dr. B. F. Abrahams, M. Moylan, Dr. S. D. Orchard
School of Chemistry
University of Melbourne
Parkville, Victoria 3010 (Australia)
Fax: (+61) 3-9347-5180
E-mail: r.robson@unimelb.edu.au

[**] The authors gratefully acknowledge support from the Australian Research Council and from the Royal Society in the form of a Research Fellowship for S.D.O.

 © 2003 Wiley-VCH Verlag GmbH & Co. KGaA, Weinheim DOI: 10.1002/anie.200250633

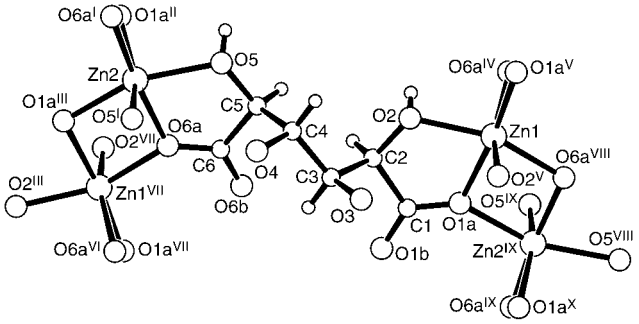


Figure 1. The attachment of the saccharate ligand to four zinc centers in **1** including the coordination environments of the zinc centers and the atom labelling. **I** *y*, *x*, 1−*z*; **II** 1.5−*y*, 0.5+*x*, −0.75+*z*; **III** 0.5+*x*, 1.5−*y*, 1.75−*z*; **IV** −0.5+*y*, 1.5−*x*, −0.25+*z*; **V** 1−*y*, 1−*x*, 1.5−*z*; **VI** *y*, *x*, 2−*z*; **VII** 1.5−*y*, 0.5+*x*, 0.25+*z*; **VIII** −0.5+*x*, 1.5−*y*, 1.75−*z*; **IX** −0.5+*y*, 1.5−*x*, 0.75+*z*; **X** 1−*y*, 1−*x*, 2.5−*z*.

other (Figure 1). The coordinated carboxylate-oxygen donors also bridge to another zinc center. Each ligand is therefore coordinated to four zinc centers, which are close to coplanar (Figure 1). There are two distinct types of zinc centers differing only slightly in their structural roles and chemical environments; both are attached to four ligands. The Zn1 atom is chelated by O1a and O2 from one ligand, and O1a^{V} and O2^{V} from another. The distorted octahedral coordination of Zn1 is completed by O6a^{IV} and O6^{VIII} from a further two ligands. Similarly, Zn2 is chelated by O6a and O5 from one ligand, and O6a^{I} and O5^{I} from another. The distorted octahedral coordination of Zn2 is completed by O1a^{II} and O1a^{III} from a further two ligands. A 3D four-connected net is thereby generated,[8] each Zn center being attached to four ligands and each ligand being attached to four zinc centers. A representation of the tetragonal extended network is shown in Figure 2. Two types of channels with very different characteristics, both of roughly square cross section, run parallel to the tetragonal axis producing, in projection, a pattern resembling a chessboard. All of the noncoordinated hydroxy groups project into one type of channel, a "hydrophilic channel". Each channel is defined and bounded by four roughly planar "walls", all of which are equivalent (Figure 3). All the

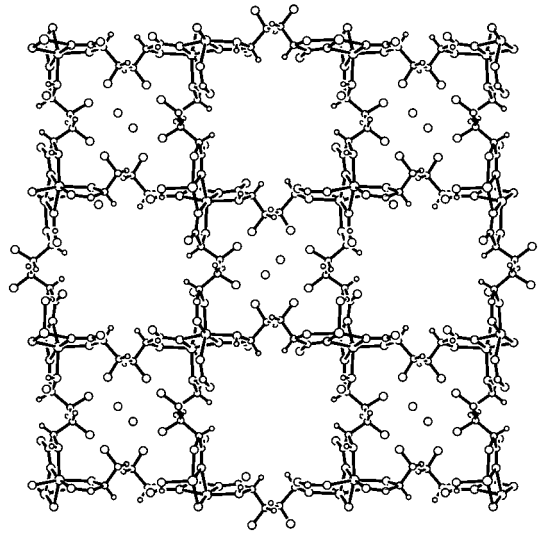


Figure 2. View down the tetragonal axis showing the two very different types of channels of roughly square cross-section in the structure of **1**. Well located water molecules in the hydrophilic channels are indicated.

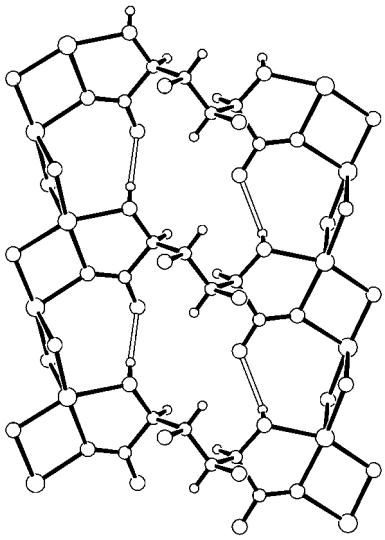


Figure 3. A wall as seen from inside a hydrophilic channel. The "open" connections represent hydrogen bonds cementing individual saccharate units into the wall.

noncoordinated hydroxy groups associated with a wall are found on one side. The walls are arranged so that the four surrounding a hydrophilic channel have all the noncoordinated hydroxy groups projecting into that channel. The four walls surrounding the other channels have the C–H bonds of C2 and C5 (see Figure 1 and Figure 2) of all the saccharate units projecting into the channel. As shown below, these nonhydroxylated channels, are able to accommodate nonpolar species, and are hence called "hydrophobic channels", despite the fact that they are able to accommodate water, albeit weakly. The hydrophobic channels can be regarded as infinite analogues of the hydrophobic cavities of the macrocyclic oligoglucose derivatives, the cyclodextrins, which have been intensively studied for decades on account of their ability to bind nonpolar species in the cavities. The chelate rings, which include the coordinated hydroxy groups, are roughly within the general plane of the wall. Zig-zag columns of alternating Zn1- and Zn2-type atoms running parallel to the tetragonal axis are found in the corners of the square channels where four walls conjoin. Every saccharate component of a wall is securely bonded to its two neighboring saccharate groups not only by the coordinate bonds but also by hydrogen bonds (open connections in Figure 3) between the noncoordinated carboxylate center of one and the coordinated hydroxy group of the neighboring saccharate group (O1b···O2, 2.60 Å and O6b···O5, 2.72 Å). These hydrogen bonds, which act as mortar between the saccharate bricks, no doubt contribute to the marked stability of the framework revealed in experiments described below.

 © 2003 Wiley-VCH Verlag GmbH & Co. KGaA, Weinheim

The unit cell (Figure 2) contains two hydrophilic and two hydrophobic channels. All of the noncoordinated C=O groups associated with one hydrophobic channel in the cell point in one direction and all those in the other point in the other direction. The van der Waals free space for each of the two hydrophobic channels per unit cell (after the guest water molecules have been hypothetically removed) is approximately 200 Å^3 (averaged cross-sectional channel dimensions of approximately 5.8×5.8 Å).[9]

Elemental composition is consistent with about two water molecules per zinc atom or approximately 16 water molecules per unit cell (eight zinc atoms per cell). Water molecules, very well located in the structural analysis, are hydrogen bonded in the hydrophilic channels,[10] two for each channel in the unit cell (Figure 2). The remaining water molecules, approximately twelve, occupy the hydrophobic channels—approximately six for each of the two hydrophobic channels per cell. These water molecules are highly disordered and not well resolved in the structural analysis; however, the sum of their site occupancies is in good agreement with that indicated by the elemental analysis. As experiments described below indicate, this water in the hydrophobic channels is easily removed.

The thermogravimetric analysis of **1** shows three weight loss steps. Approximately 8% weight is lost in the first step, which is already underway at room temperature and terminates abruptly at approximately 60°C: we attribute this weight loss to the removal of water from the hydrophobic channels (calcd weight loss for the conversion of the dihydrate to the hemihydrate, i.e., the removal of water molecules from the hydrophobic channels with retention of water molecules in the hydrophilic channels, is 8.7%). The amount of water in the hydrophobic channels is very temperature dependent at temperatures in the vicinity of room temperature, as indicated by the marked inclination of the mass versus temperature curve near room temperature (not shown). A second less abrupt decrease of approximately 3%, attributed to loss of water from the hydrophilic channels, occurs in the $\approx$100–150°C range (calcd weight loss for complete dehydration of the hemihydrate is 2.9%). Major decomposition sets in above 270°C.

A Lindeman glass tube containing a single crystal of **1** was put under vacuum, heated to 130°C for 2 h, then cooled and sealed off. Single crystal diffraction character is retained after this treatment. The crystallographic structure analysis reveals the framework remains intact. The electron density in those regions of the hydrophilic channels where water molecules had been very clearly located prior to dehydration and also the electron density in the hydrophobic channels drops to very low levels. The ligand units, now liberated from the constraining influence of the hydrogen-bonded water molecules, show greater thermal motion and some degree of disorder. We consider it very significant that the crystal, after rehydration by exposure to the atmosphere, is returned to pristine condition, thus becoming indistinguishable in its diffraction behavior from the original hydrated crystal.

Crystals of **1** suspended in molten azobenzene at 96°C for 4 h become uniformly yellow-orange. Azobenzene attached to the surface of the crystals was removed by thorough washing with toluene, then pentane. The IR spectrum shows azobenzene-derived bands at 776 and 689 cm^{-1}. Elemental analysis indicates the incorporation of approximately 0.8 molecules of azobenzene per unit cell, accompanied by the loss of water molecules from the hydrophobic channels. If the azobenzene molecules occupied the hydrophobic channels making end-to-end contact with each other, and if each were assigned an estimated van der Waals length of $\approx$14 Å, the unit cell, with a total length of hydrophobic channel available of 2×5.8 Å would be able to accommodate somewhat less than one molecule of azobenzene per cell (11.6/14 or ~0.8), which is in good agreement with the observation. The azobenzene-treated crystals retain good single crystal X-ray diffracting properties. The structural analysis reveals the zinc saccharate framework is essentially unchanged and hydrogen-bonded water molecules are well-defined in the hydrophilic channels, but the contents of the hydrophobic channels are highly disordered.

Upon exposure to I_2 vapor, crystals of **1** become deep red. The mass of a powdered sample of **1** exposed to I_2 vapor at 19°C for five days increases by 16.6% and thiosulphate determination of the I_2 content indicates the absorption of 0.30 molecules of I_2 per atom of zinc or 2.4 molecules of I_2 per unit cell. The observed mass increase is consistent with the displacement of all the water molecules from the hydrophobic channels (i.e. approximately 12 H_2O per unit cell) by the incoming I_2 molecules. A single crystal of **1**, after exposure to I_2 vapor retains its single crystal X-ray diffracting properties. The diffraction analysis reveals the zinc saccharate framework is essentially unchanged and the water molecules are still well defined in the hydrophilic channels. Large peaks of electron density within the hydrophobic channels are assigned to disordered iodine centers. The sum of the site occupancies indicates approximately 2.6 molecules of I_2 per unit cell, consistent with the gravimetric and chemical analyses.

Preliminary experiments indicate the incorporation of a range of other species into the hydrophobic channels, which include elemental sulphur, hydrocarbons, CCl_4 and CI_4. The existence of two types of channels with very different characteristics in the same network offers prospects of the simultaneous introduction of two different species into different channels, for example, ions of opposite charge, such as F^- into the hydrophilic channels and a range of cations into the hydrophobic channels. It is clear that zinc saccharate itself and metal derivatives of aldaric acids in general provide opportunities for novel chemistry, with realistic prospects of "green" applications.

Experimental Section

1: A solution of potassium hydrogen saccharate (0.164 g, 0.66 mmol) and zinc acetate tetrahydrate (0.148 g, 0.67 mmol) in water (3 mL) heated at 60°C for 20 h deposited crystals of **1**, suitable for single crystal X-ray crystallography. Yield 0.143 g (70%); elemental analysis (%) calcd for $C_6H_{12}O_{10}Zn$: C 23.3, H 3.9, Zn 21.1; found: C, 23.6; H, 3.2; Zn, 20.8.

Azobenzene inclusion: Crystals of **1** (102.0 mg, 0.330 mmol) were suspended in an excess of molten azobenzene and heated at 96°C for 4 h. The resulting orange crystals were separated from the excess molten azobenzene and were thoroughly washed first with toluene,

 © 2003 Wiley-VCH Verlag GmbH & Co. KGaA, Weinheim

then pentane, and then dried in air. Mass of crystals retrieved 95.9 mg (97%), elemental analysis (%) calcd for $C_{7.2}H_{10}N_{0.2}O_{8.5}Zn$ (i.e. $C_6H_8O_8{\cdot}0.5\,H_2O{\cdot}0.1\,C_{12}H_{10}N_2$): C 28.7, H 3.3, N 0.93; found: C 28.3, H 3.1, N 0.91.

Iodine inclusion: Crystals of **1** (99.8 mg, 0.32 mmol) exposed to iodine vapor in a sealed jar containing excess iodine crystals for 140 h at 19°C became dark red and the mass increased (to 116.4 mg). The iodine content was determined by adding an excess of sodium thiosulfate and back titrating with potassium iodate. Yield; elemental analysis (%) calcd for $[Zn(C_6H_8O_8)]{\cdot}0.5\,H_2O{\cdot}0.3\,I_2$: I, 21.2; found: I 21.2. The calculated mass increase for the conversion of $[Zn(C_6H_8O_8)]{\cdot}2\,H_2O$ to $[Zn(C_6H_8O_8)]{\cdot}0.5\,H_2O{\cdot}0.3\,I_2 = 15.9\,\%$; observed mass increase = 16.6%.

Received: November 26, 2002 [Z50633]

Keywords: carbohydrates · coordination polymer · structure elucidation · zinc

[1] "Chemicals and Materials from Renewable Resources: "D. E. Kiely, *ACS Symp. Ser.* **2001**, *784*, 64–80.
[2] F. Ferrier, A. Avezou, G. Terzian, D. Benlian, *J. Mol. Struct.* **1998**, *442*, 281.
[3] T. Taga, Y. Kuroda, K. Osaki, *Bull. Chem. Soc. Jpn.* **1977**, *50*, 3079.
[4] T. Taga, T. Shimada, N. Mimura, *Acta Crystallogr. Sect. C* **1994**, *50*, 1076.
[5] B. Sheldrick, W. Mackie, *Acta Crystallogr. Sect. C* **1989**, *45*, 1072.
[6] B. Sheldrick, W. Mackie, D. Akrigg, *Acta Crystallogr. Sect. C* **1989**, *45*, 191.
[7] Crystals of $[Zn(C_6H_8O_8)]{\cdot}2\,H_2O$, $[Zn(C_6H_8O_8)]{\cdot}0.30\,(I_2){\cdot}0.5\,(H_2O)$, $[Zn(C_6H_8O_8)]{\cdot}0.10\,(C_{12}H_{10}O_2){\cdot}0.5\,(H_2O)$ and $[Zn(C_6H_8O_8)]$ are all tetragonal, space group, $P4_12_12$. Crystal data for $[Zn(C_6H_8O_8)]{\cdot}2\,H_2O$, **1**, $a = 19.0513(12)$, $c = 5.8265(8)$ Å, $V = 2114.7(3)$ Å^3, $T = 293$ K, $\rho_{calcd} = 1.944$ g cm^{-3}, 2430 unique reflections out of 13262 relections measured, final R values, $R_1 = 0.0615$, $wR_2 = 0.1387$. Crystal data for $Zn(C_6H_8O_8){\cdot}0.30\,(I_2){\cdot}0.5\,(H_2O)$, $a = 18.9545(6)$, $c = 5.7911(3)$ Å, $V = 2080.6(1)$ Å^3, $T = 130$ K, $\rho_{calcd} = 2.290$ g cm^{-3}, 2397 unique reflections out of 13297 reflections measured, final R values, $R_1 = 0.1030$, $wR_2 = 0.2488$. Crystal data for $Zn(C_6H_8O_8){\cdot}0.10\,(C_{12}H_{10}O_2){\cdot}0.5\,(H_2O)$, $a = 19.0427(6)$, $c = 5.8108(3)$ Å, $V = 2107.1(3)$ Å^3, $T = 293$ K, $\rho_{calcd} = 1.896$ g cm^{-3}, 2429 unique reflections out of 13392 reflections measured, final R values, $R_1 = 0.1129$, $wR_2 = 0.2567$. Crystal data for $Zn(C_6H_8O_8)$, $a = 19.1245(8)$, $c = 5.7338(8)$ Å, $V = 2097.1(2)$ Å^3, $T = 293$ K, $\rho_{calcd} = 1.732$ g cm^{-3}, 2410 unique reflections out of 13289 reflections measured, final R values, $R_1 = 0.1738$, $wR_2 = 0.3835$. All data were measured on a Siemens SMART/CCD diffractometer fitted with $Mo_{K\alpha}$ radiation. For all structures data were measured in the range $2° < \theta < 27.5°$. Empirical absorption corrections were applied using the SADABS program. Structures were solved using direct methods (SHELXTL V5.1[11]) and refined using a full-matrix least squares procedure based on F^2 (SHELX-97[12]). CCDC-197968–1949971 contains the supplementary crystallographic data for this paper. These data can be obtained free of charge via www.ccdc.cam.ac.uk/conts/retrieving.html (or from the Cambridge Crystallographic Data Centre, 12 Union Road, Cambridge CB2 1EZ, UK; fax: (+44) 1223-336-033; or deposit@ccdc.cam.ac.uk).
[8] The topology is related to but different from that underlying the PtS structure, which is also tetragonal and in which both the "square planar" and "tetrahedral" nodes have the Schlafli notation 4^28^4. In the net underlying the zinc saccharate structure there are three types of 4-connecting node, two having the point symbol 4^28^4 and one (the ligand) having the point symbol $4^28^310^1$.
[9] A. L. Spek, PLATON, A Multipurpose Crystallographic Tool, Utrecht University, Utrecht, The Netherlands, **1998**.
[10] This hydrogen-bonding of water to pendant hydroxy groups of the network is reminiscent of the behavior of a coordination polymer of 1,2-dipyridylglycol recently reported by R. Kitaura, K. Fujimoto, S. Noro, M. Kondo, S. Kitagawa, *Angew. Chem.* **2002**, *114*, 141; *Angew. Chem. Int. Ed.* **2002**, *41*, 133.
[11] G. M. Sheldrick, SHELXTL V5.1 Software Reference Manual, Bruker AXS, Inc., Madison, Wisconsin, USA, **1997**.
[12] G. M. Sheldrick, SHELX-97, Program for Crystal Structure Analysis, University of Göttingen, Göttingen (Germany), **1997**.

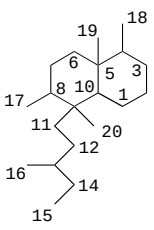
 © 2003 Wiley-VCH Verlag GmbH & Co. KGaA, Weinheim

19-Norclerodane Diterpenoids

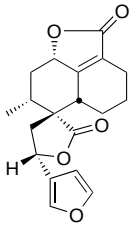
The Total Synthesis of Racemic Teucvin and 12-*epi*-Teucvin**

Hsing-Jang Liu, Jia-Liang Zhu, I-Chia Chen, Renata Jankowska, Yongxin Han, and Kak-Shan Shia*

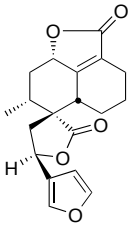
During the past three decades, over one thousand clerodane (**1**) diterpenoids, including some 19-nor variants, have been isolated.[1] Owing to their interesting structural features and the wide range of potentially useful biological activities detected for many of the relatively few compounds tested, extensive effort has been directed towards the synthesis of clerodanoids in recent years.[1,2] We report herein the first total synthesis, in racemic form, of teucvin (**2**),[3] an amoebi-



1



2



3

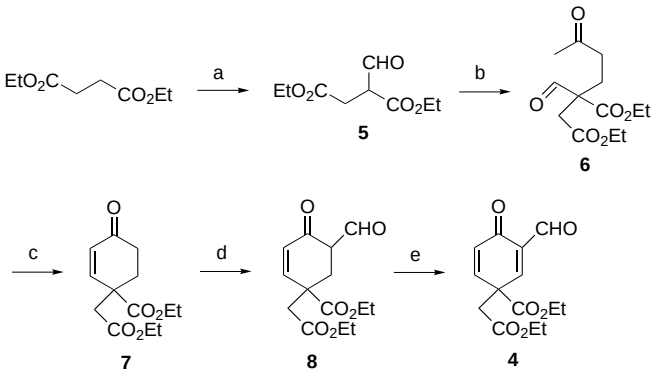
[*] Prof. H.-J. Liu, Dr. J.-L. Zhu, I.-C. Chen, Dr. K.-S. Shia
Department of Chemistry
National Tsing Hua University
Hsinchu, 30043, Taiwan (Republic of China)
Fax: (+886) 3-5720711
E-mail: hjliu@mx.nthu.edu.tw
Prof. H.-J. Liu, Dr. J.-L. Zhu, I.-C. Chen
Institute of Chemistry, Academia Sinica
Nankang, Taipei, Taiwan 11529 (Republic of China)
Prof. H.-J. Liu, Dr. R. Jankowska, Dr. Y. Han
Department of Chemistry, University of Alberta
Edmonton, Alberta, T6G 2G2 (Canada)

[**] We are grateful to the National Science Council of the Republic of China and the Natural Sciences and Engineering Research Council of Canada for financial support.

 DOI: 10.1002/anie.200250681 © 2003 Wiley-VCH Verlag GmbH & Co. KGaA, Weinheim

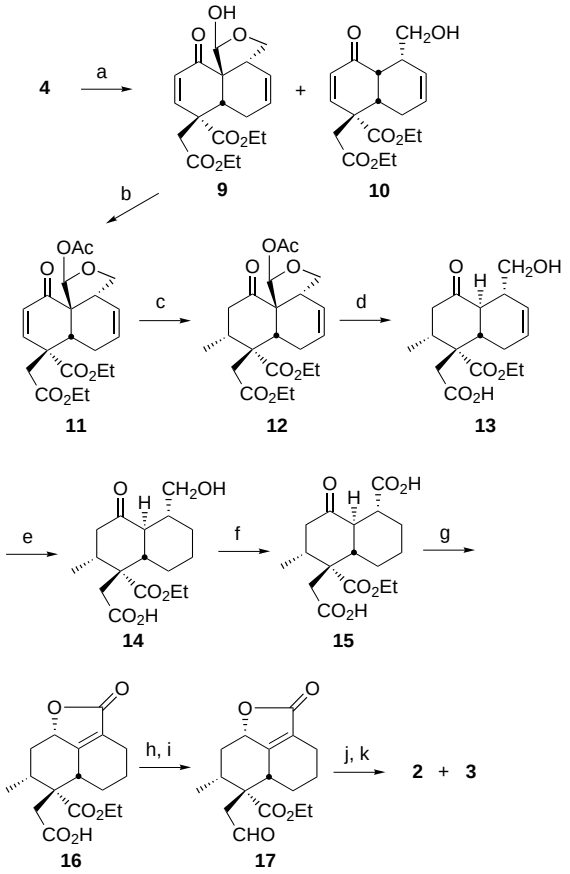
cidal agent and root growth inhibitor[4] that was first isolated in 1973 from *Teucrium viscidum* Blume by Fuijta and coworkers,[3a] and 12-*epi*-teucvin (**3**),[5] a congener of teucvin isolated eleven years later also from a *Teucrium* species by Rodriguez and Savona, et al. These 19-norclerodane diterpenoids are of considerable structural complexity. In addition to the presence of five stereogenic centers, challenging structural features in **2** and **3** comprise a decalin core attached to an α,β-unsaturated-γ-lactone unit and a spiro γ-lactone moiety containing a pendant furyl group.

The present work began with the synthesis of dienophile **4** (Scheme 1). Its Diels–Alder addition to *trans*-2,4-pentadien-1-ol (see Scheme 2), which provided a rapid access to the required decalin core with suitable functionalities at strategic positions, served as a key operation to tackle the synthetic problems associated with the title compounds. Dienophile **4** was prepared from diethyl succinate in five steps in an overall yield of 55% (Scheme 1). Formylation of diethyl succinate with ethyl formate in THF in the presence of sodium hydride and a small amount of ethanol gave the corresponding aldehyde **5**, which was subjected to Michael addition with methyl vinyl ketone using 1,4-diazabicyclo[2.2.2]octane (DABCO) as a base to give the keto aldehyde **6**. The aldol condensation of **6** was subsequently induced under acidic conditions using *p*-toluenesulfonic acid (*p*-TsOH). The resulting enone **7** was formylated with ethyl formate as before to give the formyl enone **8**. Finally, the dienophilic double bond was introduced by dehydrogenation with 2,3-dichloro-5,6-dicyano-1,4-benzoquinone (DDQ) to give the desired dienophile **4**.



Scheme 1. Synthesis of dienophile **4**. a) NaH, EtOCHO, EtOH (cat.), THF, RT, 10 h, 90%; b) CH_2=$CHCOCH_3$, DABCO, THF, RT, 10 h, 86%; c) *p*-TsOH, PhH, reflux, $-H_2O$, 8 h, 89%; d) NaH, EtOCHO, EtOH (cat.), THF, RT, 10 h, 89%; e) DDQ, K_2CO_3, THF, 0°C, 20 min, 90%.

Under zinc chloride catalysis, dienophile **4** was found to undergo Diels–Alder reaction rapidly (0°C, 1 h, in CH_2Cl_2) with *trans*-2,4-pentadien-1-ol[6] to give compound **9** in a 83% yield, as a result of concomitant intramolecular hemiacetal formation, together with a small amount (≈7%) of the deformylation by-product **10** (Scheme 2). Before the outset of the current work, we had observed that the placement of an ester group at C4 of various cyclohexenone dienophiles could induce a profound effect on the face-selectivity of the Diels–Alder reaction; the addition of the diene was found to take place specifically from the side containing the ester group.[7] To our delight, this interesting phenomenon of face-control, central to our synthetic design, was also realized experimentally in the Diels–Alder addition of *trans*-2,4-pentadien-1-ol to compound **4**. This reaction occurred in a completely face-selective manner in favor of the face containing the carbethoxy group, thus allowing full control of the two crucial stereogenic centers (C9 and C10 (clerodane numbering)). This key reaction also proceeded with complete stereo- (*cis*-addition and *endo*-addition with respect to the ketone carbonyl group) and regioselectivity (*ortho*-addition); both the observed products originated from the same adduct whose structure was unequivocally established after further transformations (vide infra).



Scheme 2. Synthesis of target compounds **2** and **3**. a) $ZnCl_2$, *trans*-2,4-pentadien-1-ol, CH_2Cl_2, 0°C, 1 h, 90% (**9**:**10** = 11:1); b) Ac_2O, py, DMAP (cat.), RT, 10 h, 90%; c) $(CH_3)_2CuLi$, Et_2O, 0°C, 0.5 h, 82%; d) NaOH, EtOH, H_2O, RT, 10 h, 90%; e) H_2 (60 psi), 10% Pd/C, EtOAc, RT, 6 h, 89%; f) Jones reagent, acetone, 0°C, 1 h, 90%; g) *p*-TsOH, PhH, reflux, 5 h, 85%; h) $(COCl)_2$, PhH, reflux, 10 min; i) LiAl$(t$BuO$)_3$H, THF, −40°C, 1 h, 70% over two steps; j) 3-lithiofuran, Et_2O, −78°C, 20 min; k) LiH, THF, RT, 10 h, 45% over two steps (**2**:**3** = 1:3).

For the incorporation of the required methyl group at C17, the hemiacetal group of **9** was protected as the acetate by using acetic anhydride, pyridine, and a small amount of 4-dimethylaminopyridine (DMAP). The resulting acetate **11** (90% yield) was subsequently treated with lithium dimethyl cuprate. The conjugate addition took place preferentially

 © 2003 Wiley-VCH Verlag GmbH & Co. KGaA, Weinheim

from the sterically less hindered side to give ketone **12** as the predominant product (82% yield) along with a minor quantity (13% yield) of the epimeric addition product. The structure of **12** was unambiguously confirmed by an X-ray crystallographic analysis.[8]

The protected acetal group present in compound **12** was removed by treatment with aqueous sodium hydroxide in ethanol. Under these conditions, the more exposed ester group was also selectively hydrolyzed to give acid **13** in 90% yield. A single isomer was obtained and its *trans*-ring junction was induced as a result of thermodynamic control. Catalytic hydrogenation of **13** using 10% Pd/C as a catalyst gave rise to the corresponding saturated compound **14**, which was then oxidized with Jones reagent to give diacid **15** in 80% yield over two steps. The bridged γ-lactone ring was introduced by enol lactone ring formation followed by isomerization of the double bond. This was effected by treatment with *p*-toluenesulfonic acid in refluxing benzene. Under these thermodynamically controlled conditions, the more stable epimer **16** was obtained as the exclusive product in 85% yield. To install the spiro lactone ring, acid **16** was treated with oxalyl chloride to produce the corresponding acid chloride which, without purification, was immediately reduced with lithium aluminum tri-*tert*-butoxy hydride to give aldehyde **17** in 70% yield. This was followed by addition of 3-lithofuran to give a mixture of two epimeric alcohols in a ratio of 3:1 as determined by the ^{1}H NMR analysis. These alcohols, which were found to be rather labile and deteriorated readily upon column chromatography, were immediately subjected to lactonization with lithium hydride in THF, and racemic teucvin (**2**; m.p. 172–174 °C) and 12-*epi*-teucvin (**3**; m.p. 201–203 °C) were produced in a 1:3 ratio and in a total yield of 45% from **17**. The ^{1}H NMR, ^{13}C NMR, and mass spectral data obtained for the synthetic materials are in good agreement with those reported for the naturally occurring compounds.[3,5] Thus, the synthetic challenges presented by the title compounds have been successfully met by employing an intermolecular Diels–Alder approach that is rather efficient in terms of stereo- and regiochemical control, the number of steps involved (sixteen steps), and the overall yield (1.6% for teucvin and 4.8% for 12-*epi*-teucvin).

Received: December 2, 2002 [Z50681]

Keywords: Diels–Alder reaction · natural products · terpenoids · teucvin · total synthesis

[1] a) J. R. Hanson, *Nat. Prod. Rep.* **1989**, *6*, 347; b) F. Seaman, F. Bohlmann, C. Zdero, T. J. Mabry, *Diterpenes of Flowering Plants, Compositae (Asteraceae)*, Springer, Heidelberg, **1990**; c) A. T. Merritt, S. V. Ley, *Nat. Prod. Rep.* **1992**, *9*, 243; d) T. Tokoroyama, *J. Synth. Org. Chem. Jpn.* **1993**, *51*, 1164; e) M. Bruno, M. L. Bondi, S. Rosselli, F. Piozzi, M. R. Y. Al-Hillo, *J. Nat. Prod.* **2000**, *63*, 1029.

[2] For a recent review, see: T. Tokoroyama, *Synthesis* **2000**, *5*, 611.

[3] a) E. Fujita, I. Uchida, T. Fujita, *J. Chem. Soc. Chem. Commun.* **1973**, 793; b) E. Fujita, I. Uchida, T. Fujita, *J. Chem. Soc. Perkin Trans. 1* **1974**, 1547; c) I. Uchida, T. Fujita, E. Fujita, *Tetrahedron* **1975**, *31*, 841; d) T. Kawashima, T. Nakastu, Y. Fukazawa, S. Ito, *Heterocycles* **1976**, *5*, 227; e) T. Nakastu, S. Ito, T. Kawashima, *Heterocycles* **1981**, *15*, 241.

[4] M. Rojas-Garciduenas, X. A. Dorninguez, *Turrialba* **1976**, *26*, 10.

[5] J. Fayos, F. G. Francisco, C. Pascual, A. Perales, F. Piozzi, M. Rico, B. Rodriguez, G. Savona, *J. Org. Chem.* **1984**, *49*, 1789.

[6] H. J. Liu, N. H. Al-Said, *Heterocycles* **1997**, *46*, 203.

[7] a) H. J. Liu, Y. Han, *Tetrahedron Lett.* **1993**, *34*, 423.

[8] CCDC-194235 (**12**) contains the supplementary crystallographic data for this paper. These data can be obtained free of charge via www.ccdc.cam.ac.uk/conts/retrieving.html (or from the Cambridge Crystallographic Data Centre, 12, Union Road, Cambridge CB21EZ, UK; fax: (+44) 1223-336-033; or deposit@ccdc.cam.ac.uk).

 © 2003 Wiley-VCH Verlag GmbH & Co. KGaA, Weinheim

Pauson–Khand Reaction of Dienynes

The Dienyl Pauson–Khand Reaction**

Paul A. Wender, Nicole M. Deschamps, and Gabriel G. Gamber*

Studies in our organometallic subgroup are aimed at the design and development of new catalytic reactions, with an emphasis on processes that, in the absence of catalysts, would be forbidden or would require harsh conditions.[1,2] These studies have thus far produced the first examples of transition-metal-catalyzed [4+4] cycloadditions of bisdienes,[3] [4+2] cycloadditions of dienynes (and diene allenes),[4] [5+2] cycloadditions of vinylcyclopropanes and π systems,[5] and [6+2] cycloadditions of vinylcyclobutanones and π systems.[6] Recently, we started to investigate whether these and other two-component [*m*+*n*] cycloadditions could be converted into multicomponent [*m*+*n*+*o*…+*x*)] processes through trapping of the organometallic intermediates with additional components.[7] These investigations have thus far led to the first metal-catalyzed, three-component [5+2+1] cycloaddition reactions based on trapping of an intermediate in the [5+2] cycloaddition reaction with CO.[8] The current study was directed at determining whether intermediates in the [4+2] cycloaddition of dienynes could be similarly trapped with CO.

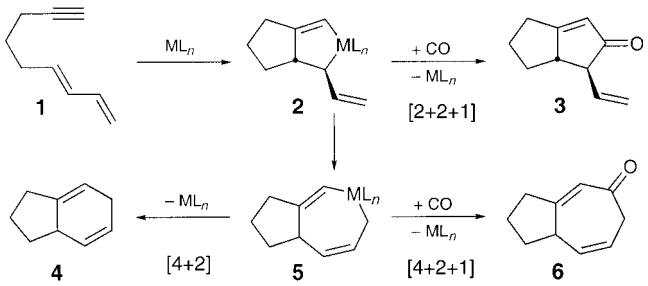
Outlined in Scheme 1 are three competing metal-catalyzed cycloaddition pathways available for a dienyne in the

[*] Prof. P. A. Wender, N. M. Deschamps, G. G. Gamber
Department of Chemistry, Stanford University
Stanford, CA 94305–5080 (USA)
Fax: (+1) 650-725-0259
E-mail: wenderp@stanford.edu

[**] This research was supported by the National Science Foundation (CHE-0131944). Fellowship support from the Stanford Graduate Fellowship (G.G.G.) is gratefully acknowledged.

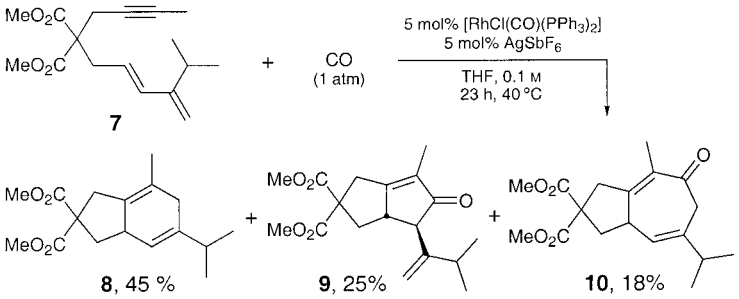
Supporting information for this article is available on the WWW under http://www.angewandte.org or from the author.

 DOI: 10.1002/anie.200350949 © 2003 Wiley-VCH Verlag GmbH & Co. KGaA, Weinheim



Scheme 1. Possible competing cycloaddition pathways.

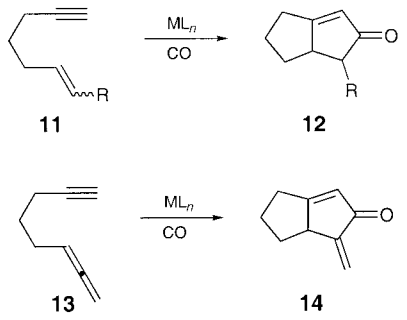
presence of CO: an intramolecular [4+2] cycloaddition (**1**→**4**), an unexplored version of the Pauson–Khand [2+2+1] cycloaddition (**1**→**3**), and an unprecedented [4+2+1] cycloaddition (**1**→**6**). Consistent with these possibilities, the reaction of dienyne **7** in THF in the presence of $[RhCl(CO)(PPh_3)_2]$, $AgSbF_6$, and CO produces a mixture of cycloadducts **8**, **9**, and **10** (Scheme 2). In the absence of CO,



Scheme 2. Representative cycloaddition reaction with CO.

only the [4+2] cycloadduct **8** is obtained in 63% yield (60°C, 30 min). The formation of cycloheptadienone **10** represents a new [4+2+1] cycloaddition reaction for the construction of seven-membered rings, while the formation of alkenylcyclopentenone **9**, the focus of the current study, represents a new class of the Pauson–Khand reaction, employing a diene rather than an alkene or an allene.

The conventional Pauson–Khand reaction is based on the coupling of an alkyne and CO with an alkene,[9,10] which is typically substituted with H, alkyl, aryl, or OR′ groups (Scheme 3, **11**→**12**). While originally mediated by cobalt,[11]



Scheme 3. Pauson–Khand reactions of alkenes and allenes.

several transition metals have been shown to catalyze the reaction.[12] Recently, Brummond and co-workers have greatly enhanced the synthetic utility of this process through the use of allenes in place of alkenes (Scheme 3, **13**→**14**).[13] In view of the potential synthetic utility of the diene version of the Pauson–Khand reaction, our attention focused on whether the reaction of dienes such as **7** could be made selective for the [2+2+1] pathway (**7**→**9**).

The effect of the solvent on the reaction of **7** was studied first (Table 1). In the presence of $[RhCl(CO)(PPh_3)_2]$, AgOTf, and CO in TFE, dienyne **7** afforded the [4+2] cycloadduct **8** in 44% yield and the [2+2+1] cycloadduct **9** in 48% yield. The use of $AgSbF_6$ instead of AgOTf in TFE gave a higher selectivity for the formation of the cycloadduct **9** (Table 1, entry 1). An enhanced yield of **9** was also seen with dioxane and DCE. Importantly, when the reaction was carried out at room temperature in DCE, **9** was obtained in 82% yield with only 11% of **8** (Table 1, entry 6).

Table 1: Effect of solvent variation on the reaction of **7**.[a]

Entry	Solvent[b]	T [°C]	t [h]	Yield [%][c]	
				8	**9**
1	TFE	40	48	20	63
2	dioxane	40	23	9	69
3	*n*-BuOH	40	48	no reaction	
4	toluene	40	22	no reaction	
5	DCE	40	4	23	49
6	DCE	RT	12	11	82

[a] $[RhCl(CO)(PPh_3)_2]$ (5 mol%), $AgSbF_6$ (5 mol%), 0.1 M, CO (1 atm). [b] TFE = 2,2,2-trifluoroethanol, DCE = 1,2-dichloroethane. [c] Yield determined by GC; less than 5% of **10** was observed by GC.

Further optimization of the reaction of **7** was realized through an investigation of variations in substrate concentration, catalyst loading, and CO pressure (cf. Table 1, entry 6 and Table 2). In these studies, the reaction efficiency was found to decrease with substrate concentrations above 0.1M (Table 2, entries 1 and 2). In contrast, an increase in CO pressure modestly enhanced the yield (Table 2, entries 4 and 5). Importantly, when the catalyst loading was decreased to 1 mol%, the reaction proceeded efficiently under 1 atmosphere of CO at room temperature, and the cycloadduct **9** was isolated in 89% yield (Table 2, entry 6).

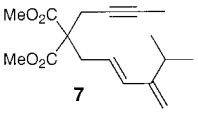
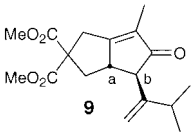
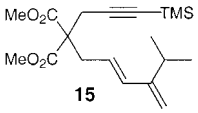
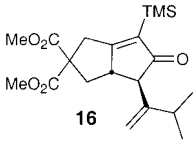
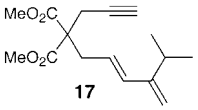
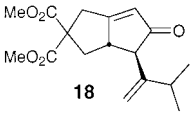
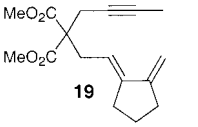
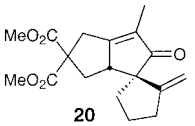
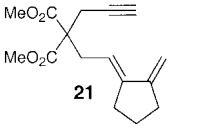
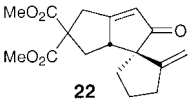
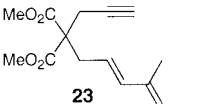
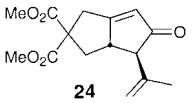
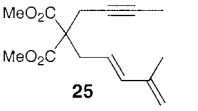
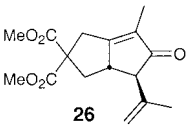
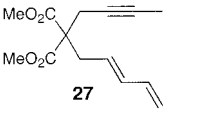
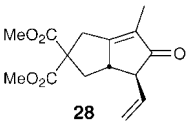
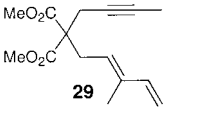
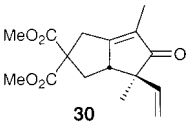
Table 2: Effects of concentration, catalyst loading, and CO pressure variations on the reaction of **7**.[a]

Entry	c [M]	Cat. [mol%][a]	CO [atm]	t [h]	Yield [%][b]	
					8	**9**
1	0.5	5	1	20	21	51
2	0.2	5	1	26	12	63
3	0.01	5	1	26	8	82
4	0.1	5	2	26	6	87
5	0.1	5	4	18	6	86 (89)
6	0.1	1	1	14	7	88 (89)

[a] $[RhCl(CO)(PPh_3)_2]$ (x mol%), $AgSbF_6$ (x mol%), room temperature, DCE. [b] Yield determined by GC (yield of isolated product is given in parentheses); less than 5% of **10** was observed by GC.

 © 2003 Wiley-VCH Verlag GmbH & Co. KGaA, Weinheim

Table 3: [2+2+1] Reaction of tethered dienynes.[a]

Entry	Substrate	*T* [°C]	CO [atm]	Cat.[a] [mol%]	*t* [h]	Product	Yield[b] [%]
1	 **7**	RT	1	1	14	 **9**	89
2	 **15**	RT	2	2	12	 **16**	85
3	 **17**	RT	1	1	40	 **18**	43
4	 **19**	RT	1	1	24	 **20**	96
5	 **21**	RT	1	5	32	 **22**	45
6	 **23**	RT	1	1	30	 **24**	42
7	 **25**	40	2	2.5	12	 **26**	86
8	 **27**	40	1	2.5	12	 **28**	90
9	 **29**	40	1	2.5	10	 **30**	96

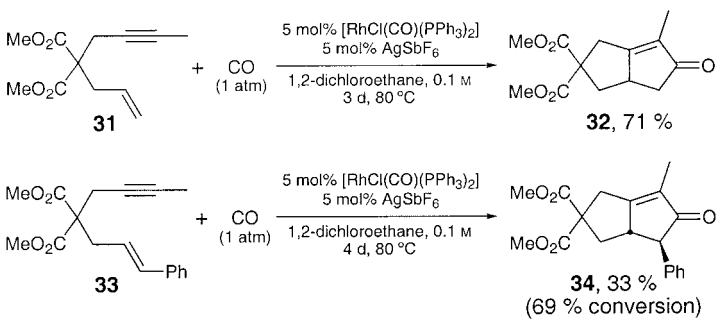
[a] $[RhCl(CO)(PPh_3)_2]$ (*x* mol%), $AgSbF_6$ (*x* mol%), 0.1 M, DCE. [b] Yield of isolated product.

To study the generality of this new class of Pauson–Khand reaction, we examined the reaction of eight other substrates, which differed in the substitution of the alkyne and diene (Table 3). Internal alkynes gave excellent yields of the [2+2+1] cycloadducts (85–96% yield), whereas terminal alkynes reacted less efficiently. Substitution at the 2- or 3-position of the diene was also well tolerated. The *syn* relationship between the angular hydrogen atom at C(a) and the alkenyl substituent at C(b) in the cycloadducts was determined by NOE experiments and indicates that the geometry of the alkene is conserved during the transformation (Table 3, entry 1). Cycloadducts **20** and **30**, which contain a quaternary center, were obtained in excellent yields from dienynes **19** and **29**, respectively.

In addition to its synthetic value, the diene serves to facilitate the cycloaddition reaction relative to that of an alkene (Scheme 4). For example, whereas the reactions of dienes **7**, **25**, and **27** are all complete within 14 h at room temperature or 40 °C with 1–2.5 mol% catalyst (Table 3, entries 1, 7, 8), the reaction of the corresponding enyne **31** requires 3 days and much harsher conditions (80 °C, 5 mol% catalyst). Significantly, conjugation alone is not sufficient to facilitate the reaction, as under these same conditions the reaction of styrene substrate **33** is even more sluggish, requiring 4 days to reach 69% completion.

The substituent on the diene also has a significant effect on the reaction rate. The *i*Pr-substituted substrate **7** and bisalkylidene cyclopentane substrate **19**, for example, undergo [2+2+1] cycloaddition within 24 h at room temperature, whereas Me-substituted and unsubstituted analogues (**25** and **27**) give no conversion at room temperature after 12 h. However, efficient transformations are achieved in these cases at 40 °C with 2.5 mol% catalyst.

In summary, a new class of the Pauson–Khand reaction based on dienes is reported. In the case of internal alkynes, alkenylcyclopentenones are produced in excellent yields under mild conditions and low catalyst loadings (1–2.5 mol%). Substitution of the diene is well tolerated and allows the facile diastereoselective construction of quaternary centers (**20** and **30**). Further studies on this novel [2+2+1] pro-



Scheme 4. Reaction of enynes using our catalyst system.

 © 2003 Wiley-VCH Verlag GmbH & Co. KGaA, Weinheim

cess and the new [4+2+1] carbonylative cycloaddition reaction are in progress.

Experimental Section

Characterization data for compounds **9**, **10**, **16**, **18**, **20**, **22**, **24**, **26**, **28**, and **30** are given in the Supporting Information.

General procedure: $[RhCl(CO)PPh_3)_2]$ (0.039 g, 0.056 mmol), $AgSbF_6$ (0.020 g, 0.058 mmol), and DCE (5.6 mL, 0.01M) were added into an oven-dried borosilicate glass test tube equipped with a stirrer bar and capped with a rubber septum. The resulting suspension was stirred for 1 h under a balloon of CO, vented through a bubbler. Dienyne **7** (0.035 g, 0.1197 mmol) was dissolved in DCE (1.08 mL, 0.11M) in a separate oven-dried borosilicate glass test tube equipped with a stirrer bar and capped with a rubber septum. This solution was stirred under a balloon of CO, vented through a bubbler, for 15 min. The catalyst solution (0.12 mL) was added to the solution of **7** and the resulting mixture was stirred vigorously under CO (1 atm) for 14 h. The mixture was purified by flash-column chromatography on silica gel (gradient elution: 0→10% ethyl acetate in pentane). Product-containing fractions were concentrated to give **9** in 89% yield as a colorless oil.

Received: January 16, 2003 [Z50949]

Keywords: cycloaddition · dienes · homogeneous catalysis · Pauson–Khand reaction · rhodium

[1] For pertinent reviews, see: a) P. A. Wender, F. C. Bi, G. G. Gamber, F. Gosselin, R. D. Hubbard, M. J. C. Scanio, R. Sun, T. J. Williams, L. Zhang, *Pure Appl. Chem.* **2002**, *74*, 25; b) P. A. Wender, J. A. Love in *Advances in Cycloaddition, Vol. 5*, JAI, Greenwich, **1999**, p. 1.

[2] For general reviews of metal-catalyzed cycloaddition reactions, see: a) M. Lautens, W. Klute, W. Tam, *Chem. Rev.* **1996**, *96*, 49; b) I. Ojima, M. Tzamarioudaki, Z. Li, R. J. Donovan, *Chem. Rev.* **1996**, *96*, 635.

[3] a) P. A. Wender, N. C. Ihle, *J. Am. Chem. Soc.* **1986**, *108*, 4678; b) P. A. Wender, M. J. Tebbe, *Synthesis* **1991**, 1089; c) P. A. Wender, J. M. Nuss, D. B. Smith, A. Suárez-Sobrino, J. Vägberg, D. Decosta, J. Bordner, *J. Org. Chem.* **1997**, *62*, 4908.

[4] For the first examples, see: a) P. A. Wender, T. E. Jenkins, *J. Am. Chem. Soc.* **1989**, *111*, 6432; b) P. A. Wender, T. E. Jenkins, S. Suzuki, *J. Am. Chem. Soc.* **1995**, *117*, 1843; for representative subsequent work from our and other laboratories, see: c) P. A. Wender, T. E. Smith, *Tetrahedron* **1998**, *54*, 1255; d) B. Wang, P. Cao, X. M. Zhang, *Tetrahedron Lett.* **2000**, *41*, 8041; e) S.-J. Paik, S. U. Son, Y. K. Chung, *Org. Lett.* **1999**, *1*, 2045; f) S. R. Gilbertson, G. S. Hoge, D. G. Genov, *J. Org. Chem.* **1998**, *63*, 10077; g) K. Kumar, R. S. Jolly, *Tetrahedron Lett.* **1998**, *39*, 3047; h) M. Murakami, M. Ubukata, K. Itami, Y. Ito, *Angew. Chem.* **1998**, *110*, 2362; Angew . *Chem. Int. Ed.* **1998**, *37*, 2248; i) H. Heath, B. Wolfe, T. Livinghouse, S. K. Bae, *Synthesis* **2001**, 2341.

[5] For the first examples, see: a) P. A. Wender, H. Takahashi, B. Witulski, *J. Am. Chem. Soc.* **1995**, *117*, 4720; b) P. A. Wender, H. Rieck, M. Fuji, *J. Am. Chem. Soc.* **1998**, *120*, 10976; for representative subsequent work from our and other laboratories, see reference [4d] and: c) P. A. Wender, T. M. Pedersen, M. J. C. Scanio, *J. Am. Chem. Soc.* **2002**, *124*, 15154; d) P. A. Wender, T. J. Williams, *Angew. Chem.* **2002**, *114*, 4732; *Angew. Chem. Int. Ed.* **2002**, *41*, 4550; e) P. A. Wender, G. G. Gamber, M. J. C. Scanio, *Angew. Chem.* **2001**, *113*, 4013; Angew . *Chem. Int. Ed.* **2001**, *40*, 3895; f) P. A. Wender, F. C. Bi, M. A. Brodney, F. Gosselin, *Org. Lett.* **2001**, *3*, 2105; g) P. A. Wender, C. M. Barzilay, A. J. Dyckman, *J. Am. Chem. Soc.* **2001**, *123*, 179; h) P. A. Wender, L. Zhang, *Org. Lett.* **2000**, *2*, 2323; i) P. A. Wender, A. J. Dyckman, C. O. Husfeld, M. J. C. Scanio, *Org. Lett.* **2000**, *2*, 1609; j) P. A. Wender, A. J. Dyckman, C. O. Husfeld, D. Kadereit, J. A. Love, H. Rieck, *J. Am. Chem. Soc.* **1999**, *121*, 10442; k) P. A. Wender, F. Glorious, C. O. Husfeld, E. Langkopf, J. A. Love, *J. Am. Chem. Soc.* **1999**, *121*, 5348; l) P. A. Wender, C. O. Husfeld, E. Langkopf, J. A. Love, *J. Am. Chem. Soc.* **1998**, *120*, 1940; m) B. M. Trost, H. Shen, *Angew. Chem.* **2001**, *113*, 2375; *Angew. Chem. Int. Ed.* **2001**, *40*, 2313; n) B. M. Trost, F. D. Toste, H. Shen, *J. Am. Chem. Soc.* **2000**, *122*, 2379; for single examples of [5+2] cycloadditions, see: o) S. R. Gilbertson, G. S. Hoge, *Tetrahedron Lett.* **1998**, *39*, 2075; p) P. Binger, P. Wedmann, S. I. Kozhushkov, A. de Meijere, *Eur. J. Org. Chem.* **1998**, 113.

[6] P. A. Wender, A. G. Correa, Y. Sato, R. Sun, *J. Am. Chem. Soc.* **2000**, *122*, 7815.

[7] For other recent examples of transition-metal-catalyzed [*m*+*n*+*o*] cycloaddition reactions, see: a) S. R. Gilbertson, B. DeBoef, *J. Am. Chem. Soc.* **2002**, *124*, 8784; b) P. A. Evans, J. E. Robinson, E. W. Baum, A. N. Fazal, *J. Am. Chem. Soc.* **2002**, *124*, 8782; c) M. Murakami, K. Itami, Y. Ito, *Angew. Chem.* **1998**, *110*, 3616; *Angew. Chem. Int. Ed.* **1998**, *37*, 3418; d) T. L. Dzwiniel, N. Etkin, J. M. Stryker, *J. Am. Chem. Soc.* **1999**, *121*, 10640.

[8] P. A. Wender, G. G. Gamber, R. D. Hubbard, L. Zhang, *J. Am. Chem. Soc.* **2001**, *123*, 2876.

[9] Dienyne **7** reacts under conventional Pauson–Khand conditions ($[Co_2(CO)_8]$) (1.1 equiv) and CO (1 atm) in THF at 55°C) to give **9** in 39% yield.

[10] For reviews of the Pauson–Khand reaction, see: a) B. E. Hanson, *Comments Inorg. Chem.* **2002**, *23*, 289; b) K. M. Brummond, J. L. Kent, *Tetrahedron* **2000**, *56*, 3263; c) A. J. Fletcher, S. D. R. Christie, *J. Chem. Soc. Perkin Trans. 1* **2000**, 1657; d) Y. K. Chung, *Coord. Chem. Rev.* **1999**, *188*, 297; e) O. Geis, H.-G. Schmalz, *Angew. Chem.* **1998**, *110*, 955; *Angew. Chem. Int. Ed.* **1998**, *37*, 911; f) N. Jeong in *Transition Metals in Organic Synthesis, Vol. 1* (Eds.: M. Beller, C. Bolm), Wiley-VCH, Weinheim, **1998**, p. 560; g) N. E. Schore in *Comprehensive Organometallic Chemistry II, Vol. 12* (Eds.: E. W. Abel, F. A. Stone, G. Wilkinson), Elsevier, New York, **1995**, p. 703.

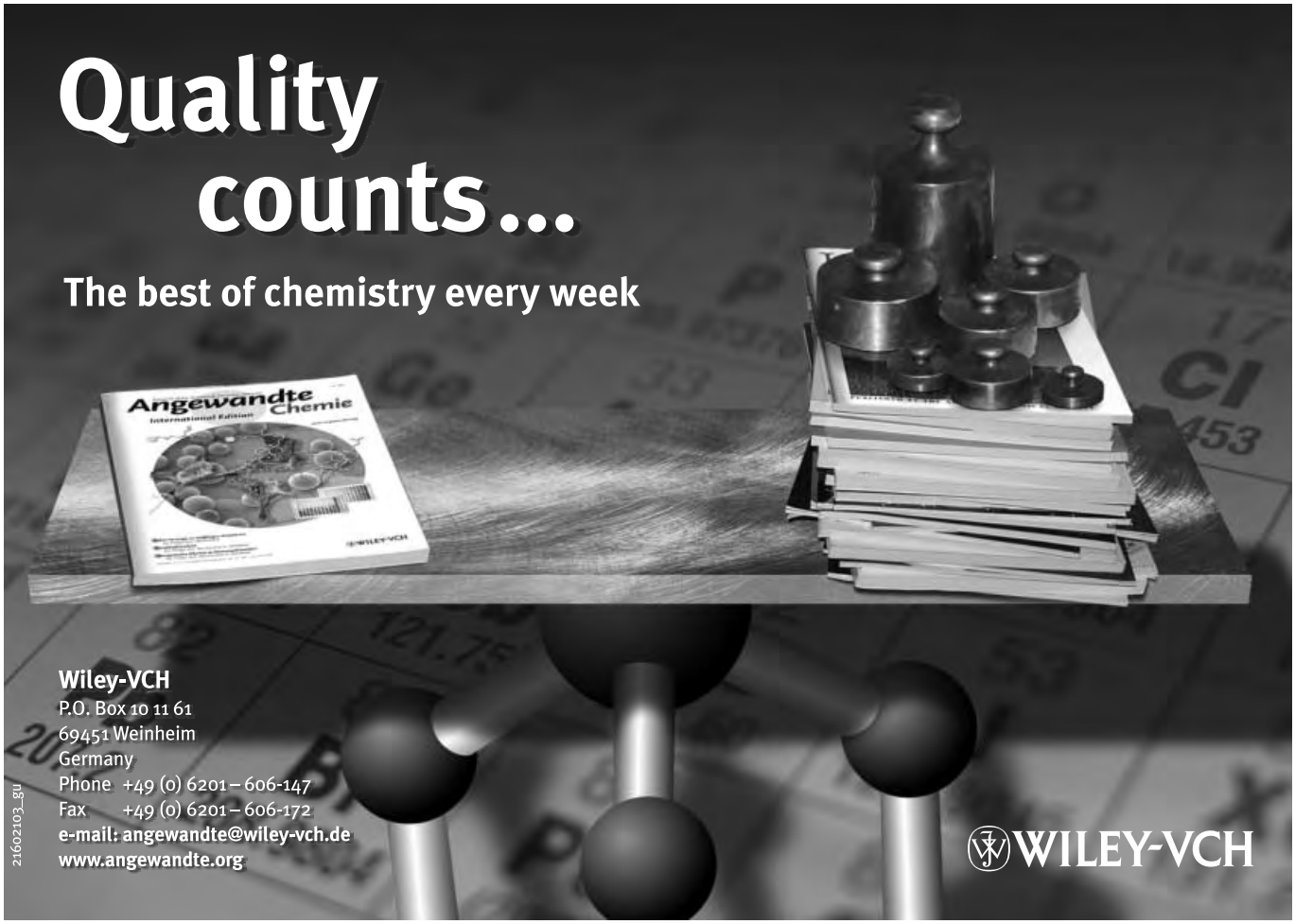
[11] For the first examples, see: a) I. U. Khand, G. R. Knox, P. L. Pauson, W. E. Watts, *J. Chem. Soc. Chem. Commun.* **1971**, 36; b) I. U. Khand, G. R. Knox, P. L. Pauson, W. E. Watts, *J. Chem. Soc. Perkin Trans. 1* **1973**, 975; c) I. U. Khand, G. R. Knox, P. L. Pauson, W. E. Watts, M. I. Foreman, *J. Chem. Soc. Perkin Trans. 1* **1973**, 977.

[12] For representative examples of catalytic Pauson–Khand reactions, see: **Co**: a) V. Rautenstrauch, P. Megard, J. Conesa, W. Kuster, *Angew. Chem.* **1990**, *102,* 1441; *Angew. Chem. Int. Ed. Engl.* **1990**, *29*, 1413; b) B. L. Pagenkopf, D. B. Belanger, D. J. R. O'Mahoney, T. Livinghouse, *Synthesis* **2000**, 1009; c) A. C. Comely, S. E. Gibson, N. J. Hales, *Chem. Commun.* **2000**, 305; d) K. Hiroi, T. Watanabe, R. Kawagishi, I. Abe, *Tetrahedron Lett.* **2000**, *41*, 891; e) N. Jeong, S. H. Hwang, *Angew. Chem.* **2000**, *112*, 650; *Angew. Chem. Int. Ed.* **2000**, *39*, 636; f) M. Hayashi, Y. Hashimoto, Y. Yamamoto, J. Usuki, K. Saigo, *Angew. Chem.* **2000**, *112*, 645; *Angew. Chem. Int. Ed.* **2000**, *39*, 631; g) T. Sugihara, M. Yamaguchi, M. Nishizawa, *Chem. Eur. J.* **2001**, *7*, 1589; h) M. E. Krafft, L. V. R. Boñaga, C. Hirosawa, *J. Org. Chem.* **2001**, *66*, 3004; i) S. J. Sturla, S. L. Buchwald, *J. Org. Chem.* **2002**, *67*, 3398; j) S. U. Son, S. I. Lee, Y. K. Chung, S.-W. Kim, T. Hyeon, *Org. Lett.* **2002**, *4*, 277; ***Rh*:** k) T. Shibata, N. Toshida, K. Takagi, *J. Org. Chem.* **2002**, *67*, 7446; l) T. Morimoto, K. Fuji, K. Tsutsumi, K. Kakiuchi, *J. Am. Chem. Soc.* **2002**, *124*, 3806; m) C. Mukai, I. Numora, K. Yamanishi, M. Hanaoka, *Org. Lett.* **2002**, *4*, 1755; n) N. Jeong, B. K. Sung, J. S. Kim, S. B. Park, S. D. Seo, J. Y. Shin, K. Y. In, Y. K. Choi, *Pure Appl. Chem.* **2002**, *74*, 85; o) T. Kobayashi, Y. Koga, K. Narasaka, *J. Organomet.*

 © 2003 Wiley-VCH Verlag GmbH & Co. KGaA, Weinheim

Chem. **2001**, *634*, 73; p) P. A. Evans, J. E. Robinson, *J. Am. Chem. Soc.* **2001**, *123*, 4609; ***Ru*:** q) T. Kondo, N. Suzuki, T. Okada, T. Mitsudo, *J. Am. Chem. Soc.* **1997**, *119*, 6187; r) T. Moromoto, N. Chatani, Y. Fukumoto, S. Murai, *J. Org. Chem.* **1997**, *62*, 3762; Ti: s) S. J. Sturla, S. L. Buchwald, *Organometallics*, **2002**, *21*, 739; Ir: t) T. Shibata, K. Takagi, *J. Am. Chem. Soc.* **2000**, *122*, 9852.

[13] a) J. L. Kent, H. Wan, K. M. Brummond, *Tetrahedron Lett.* **1995**, *36*, 2407; b) K. M. Brummond in *Advances in Cycloaddition Chemistry, Vol. 6* (Ed.: M. Harmata, JAI, Greenwich), **1999**, p. 211; c) K. M. Brummond, H. Chen, K. D. Fisher, A. D. Kerekes, B. Rickards, P. C. Sill, S. J. Geib, *Org. Lett.* **2002**, *4*, 1931.



 © 2003 Wiley-VCH Verlag GmbH & Co. KGaA, Weinheim

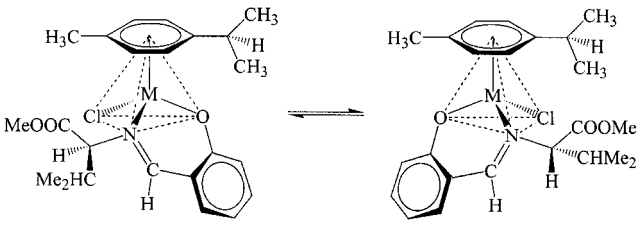
Diastereomers in Single Crystals

Inverted Piano Stools: A Molecular Recognition Motif That Enforces 1:1 Cocrystallization of Two Diastereomers in the Same Single Crystal

Henri Brunner, Matthias Weber, Manfred Zabel, and Thomas Zwack*

The resolution of enantiomers is most often achieved by converting them into diastereomers with an enantiomerically pure resolving agent followed by separation of the diastereomers on the basis of solubility differences (fractional crystallization). Such diastereomers agree in terms of the configuration of the resolving agent and differ in terms of the configuration of the enantiomeric parts that are to be resolved. Although the overall molecular shapes of the diastereomers are different, there will be parts that are similar (the resolving agent) and parts that are mirror-image related (the racemate). Crystallization of each of the two diastereomers as separate single crystals is the basis for the resolution of racemic mixtures by conversion of the enantiomers to diastereomers. Diastereomeric salts have been shown to form solid solutions of variable composition (exhibiting isomorphism in cases of close similarity) and, occasionally, 1:1 double salts (where no predictions or rationalizations were possible).[1] Here, we describe a molecular recognition motif that takes the form of "inverted three-legged piano stools", and results in the 1:1 cocrystallization of diastereomeric half-sandwich complexes within the same single crystal.

In [(Cy)Ru(O–N)Cl] (**1**, Cy = η^6-*p*-cymene; O–N = the anion of the Schiff base derived from salicylaldehyde and the methyl ester of (*S*)-valine), the Ru atom is a chiral center and, therefore, the two diastereomers (R_{Ru},S_C)-**1** and (S_{Ru},S_C)-**1** arise, which have different metal configurations (Scheme 1).



Scheme 1. Compounds **1** and **2**: Compound **1** crystallizes as a 1:1 pair of diastereomers (R_{Ru},S_C)-**1**/(S_{Ru},S_C)-**1**; Compound **2** crystallizes as the pure diastereomer (R_{Os},S_C)-**2**.

[*] Prof. Dr. H. Brunner, Dr. M. Weber, Dr. M. Zabel, Dr. T. Zwack
Institut für Anorganische Chemie
Universität Regensburg
93040 Regensburg (Germany)
Fax: (+49) 941-943-4439
E-mail: henri.brunner@chemie.uni-regensburg.de

At room temperature in $CDCl_3$ solution, the diastereomer ratio is 70:30, which can easily be determined as the diastereomers exhibit different ^{1}H NMR spectra. Kinetic measurements established that equilibration between the diastereomers of **1** is rapid at room temperature.[2–5] Thus, the 70:30 ratio represents the thermodynamic equilibrium of the two diastereomers.

Crystallization at 4 °C by the diffusion of petroleum ether into a solution of **1** in toluene afforded dark red single crystals containing the two diastereomers (R_{Ru},S_C)-**1** and (S_{Ru},S_C)-**1** in a 1:1 ratio (Figure 1).[5] For the specification of the Ru

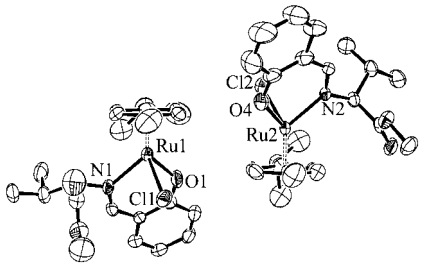


Figure 1. Molecular structure of the (R_{Ru},S_C)-**1**/(S_{Ru},S_C)-**1** inversion pair with a Ru···Ru distance of 5.64 Å (50% probability, hydrogen atoms omitted for clarity) right: (R_{Ru},S_C) diastereomer (Ru2), left: (S_{Ru},S_C) (Ru1).

configuration the priority sequence Cy > Cl > O > N was used.[6,7] As expected, the bond lengths and bond angles of the two diastereomers (R_{Ru},S_C)-**1** and (S_{Ru},S_C)-**1** are very similar (Table 1). Surprisingly, the intermolecular Ru···Ru distances in the crystal are very different. The Ru···Ru distance in the "inversion pair" (Figure 1) is very short (5.64 Å), while all the other Ru···Ru distances are longer than 8.6 Å. The molecules on either side of the center of the pairs of diastereomers (R_{Ru},S_C)-**1** and (S_{Ru},S_C)-**1** show considerable mirror-image character, whereas towards the outside of each pair, the centrosymmetry is lost. The lattice is formed by translation of these inversion pairs.

In our analysis we place the "inversion center" exactly halfway between Ru1 and Ru2 (Figure 2). The deviations of the four different substituents around the Ru atoms ($Cy_{centroid}$, Cl, O, N) from inversion symmetry are marginal, and range between 0.13 and 0.23 Å. Similarly, the atoms in the ligand backbones and in the cymene rings closely follow this inversion symmetry with deviations below 0.2 Å. Naturally, inconsistencies arise for the chiral nitrogen substituents, which for both diastereomers have the same *S* configuration ruling out centrosymmetry.

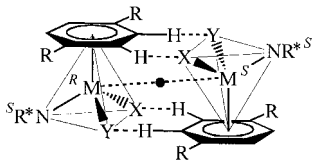


Figure 2. Inversion pair: The "tight-inverted piano stools" molecular recognition motif. The two diastereomers have opposite metal configurations (R_M) and (S_M) and the same ligand configuration (S_C).

 DOI: 10.1002/anie.200250181 © 2003 Wiley-VCH Verlag GmbH & Co. KGaA, Weinheim

Table 1: Bond lengths [Å] and angles [°] in the 1:1 lattice of (R_{Ru},S_C)-**1** and (S_{Ru},S_C)-**1**, as well as in the monoclinic and orthorhombic modifications of (R_{Os},S_C)-**2**.

Complex	(R_{Ru},S_C)-**1**	(S_{Ru},S_C)-**1**	(R_{Os},S_C)-**2**	(R_{Os},S_C)-**2**
	monoclinic		monoclinic	orthorhombic
bond lengths				
M–$Cy_{centroid}$	1.670	1.689	1.655	1.662
M–Cl	2.446(2)	2.423(2)	2.433(17)	2.4326(11)
M–O	2.062(6)	2.053(6)	2.077(5)	2.060(3)
M–N	2.092(6)	2.120(6)	2.101(5)	2.111(3)
bond angles				
O-M-Cl	85.15(19)	84.43(18)	84.02(14)	83.47(10)
N-M-Cl	82.94(18)	85.17(17)	83.98(15)	84.13(10)
O-M-N	88.6(2)	88.8(2)	87.3(3)	87.03(13)

The osmium complex [(Cy)Os(O–N)Cl] (**2**; Scheme 1), the analogue of the Ru complex **1**, is also configurationally labile in solution.[5] The diastereomer ratio for **2** in $CDCl_3$ at room temperature is 64:36, similar to that for **1**. Diffusion of petroleum ether into a solution of the two diastereomers (R_{Os},S_C)-**2** and (S_{Os},S_C)-**2** in toluene gave two different types of red crystals. Both contain only the (R_{Os},S_C) diastereomer in the monoclinic and orthorhombic system, respectively. Surprisingly, the osmium compound crystallizes as a pure diastereomer and not as a 1:1 mixture of two diastereomers.[5] The bond lengths and bond angles for both modifications are extremely similar to those of the two Ru diastereomers (Table 1). This is a consequence of the lanthanide contraction which causes the ionic radii of Ru and Os to be almost the same. Actually, some of the bond lengths and angles of (R_{Os},S_C)-**2** are even intermediate between those of (R_{Ru},S_C)-**1** and (S_{Ru},S_C)-**1**. Given the extraordinary similarities between the diastereomeric pairs (R_{Ru},S_C)-**1**/(S_{Ru},S_C)-**1** and (R_{Os},S_C)-**2**/(S_{Os},S_C)-**2**, it is particularly surprising that the ruthenium complex crystallizes as two diastereomers in a 1:1 ratio, whilst in the osmium case (R_{Os},S_C)-**2** is diastereomerically pure. In the crystal of (R_{Os},S_C)-**2**, the shortest Os···Os distance is 8.18 Å (in the monoclinic modification); no shorter contacts, such as those of 5.64 Å observed in the 1:1 ruthenium inversion pairs, are seen in this system.

In the (R_{Ru},S_C)-**1**/(S_{Ru},S_C)-**1** inversion pair, the two Ru atoms and the centroids of the two Cy ligands define a "central plane" (Figure 2), for which the dihedral angle Cy1-Ru1-Ru2-Cy2 is 175.7°. The angles Cy1-Ru1-Ru2 (77.93°) and Cy2-Ru2-Ru1 (78.13°) indicate that the Ru–Cy centroids are slightly inclined towards the Ru1–Ru2 axis, and form a "lying Z". The planes of the two cymene ligands are almost parallel to each other (angle 1.7°). With regard to the three legs of the half-sandwich piano stools, it is the O_{sal} and Cl substituents that are directed toward the inside of the inversion pairs, which forces the N ligands, the chiral substituents of which disturb the centrosymmetry, to the outside.

Molecular recognition occurs between two {(Cy)Ru(O_{sal})Cl} fragments with opposite metal configuration, which approach each other through inversion symmetry (Figure 2). With almost parallel Ru–Cy centroids in the central plane, the fragments orient their O_{sal}–Cl edges towards one another, which results in O1···Cl2 and O2···Cl1 distances of 5.17 and 5.35 Å, respectively. There are [2×2] hydrogen bonds between the C–H groups of the cymene rings and the Cl and O_{sal} substituents of opposite molecules (Table 2),[8] which arrange the isopropyl and methyl groups of the cymene rings such that together with the Cl and the O_{sal} substituents, they form a shell around the inner core of the inversion pair, a motif hereafter termed "tight-inverted piano stools" (Figure 2).

The same molecular recognition motif is found in other half-sandwich complexes, for which 1:1 cocrystallization of two diastereomers in the same single crystal has been described (Table 3). In these literature reports the phenomenon of 1:1 diastereomer cocrystallization has been stated, but not analyzed or understood. The inversion pairs of the compounds **3**,[9] **4**,[10] and **5**[11] are extremely similar to those of (R_{Ru},S_C)-**1**/(S_{Ru},S_C)-**1** (Table 2).[5] Derivative **5** has a Ru···Ru distance of 5.51 Å within the pair, whereas the Ru···Ru distances between pairs are at least 10.52 Å, as a result of the large binaphthyl substituents.[11] The iodo analogue **6** of **1** forms single crystals with two diastereomers in a 1:1 ratio, the recognition pattern being only changed as expected for the substitution of Cl by I.[5] Interestingly, the Os compound **7** undergoes 1:1 diastereomer cocrystallization like its Ru ana-

Table 2: Interatomic distances [Å], angles [°] and torsion angles [°] of compounds **1** and **3**–**11**. X = Cl or I, Y = O_{sal} or N_{pyrr}.

Compound	M1···M2	∢Ar1-M1-M2	∢Ar2-M2-M1	∢Ar1-M1-M2-Ar2	C–H···X2	C–H···Y2	C–H···X1	C–H···Y1
1[5]	5.642	77.93	78.12	175.7	3.66	3.47	3.74	3.31
3[9]	5.755	82.79	81.16	178.1	3.52	3.43	3.52	3.34[a]
4[10] (1st pair)	5.669	81.03	81.60	176.8	3.52	3.61	3.68	3.41
4[10] (2nd pair)	5.614	80.89	80.77	175.3	3.69	3.22	3.74	3.30
5[11]	5.514	78.81	82.47	179.2	3.43	3.18	3.52	3.46
6[5]	4.819	81.26	75.43	178.1	4.41	3.47	3.91	3.40
7[5]	5.583	83.40	82.52	179.6	3.58	3.48	3.50	3.36
8[10]	5.824	95.99	98.51	179.2	3.51	3.96	3.86	4.44
9[12]	5.487	75.33	78.53	174.9	3.65	3.27	3.90	3.51
10[13]	6.015	77.81	78.56	177.6	3.31	4.94	3.32	5.02
11[14]	6.890	83.49	85.49	179.4	4.74	6.05	4.88	6.15

[a] Hydrogen atoms added by calculation (not included in the original file).

 © 2003 Wiley-VCH Verlag GmbH & Co. KGaA, Weinheim

Table 3: Half-sandwich complexes that crystallize as 1:1 pairs of diastereomers in the same single crystal.

No.	Compound
1	[(η^6-*p*-cymene)Ru(*(S)*-methyl valinate-salicylaldiminate)Cl][5]
3	[(η^6-*p*-cymene)Ru(*(S)*-1-phenylethyl-salicylaldiminate)Cl][9]
4	[(η^6-*p*-cymene)Ru(*(R)*-1-hydroxybut-2-yl-salicylaldiminate)Cl][10]
5	[(η^6-*p*-cymene)Ru(2-*(S)*-2′-methoxy-1,1′-binaphthyl-salicylaldiminate)Cl][11]
6	[(η^6-*p*-cymene)Ru(*(S)*-methyl valinate-salicylaldiminate)I][5]
7	[(η^6-*p*-cymene)Os(*(S)*-1-phenylethyl-salicylaldiminate)Cl][5]
8	[(η^6-*p*-cymene)Ru(*(R)*-1-hydroxybut-2-yl-pyrrolylaldiminate)Cl][10]
9	[(η^5-C_5H_5)Rh(*(S)*-1-phenylethyl-salicylaldiminate)Cl][12]
10	[(η^6-C_6H_6)Ru(*(S)*-alaninate)9-ethylguaninate][13]
11	[(η^6-*p*-cymene)Ru(*(S)*-1-phenylethyl-4,6-di-*tert*-butyl-salicylaldiminate)Cl][14]
12	[(η^6-*p*-cymene)Ru(*(S)*-1-phenylethyl-salicylaldiminate)(H_2O)]-ClO_4[15]
13	[(η^6-*p*-mesitylene)Ru(*(S)*-alaninate)]Cl[16]
14	[(η^6-*p*-cymene)Ru(chiraphosO)Cl][17]
15	[(η^5-C_5Me_5)Ir(*(S)*-prolinate)Cl][18,19]
16	{(η^6-*p*-cymene)[Ru(*(S)*-2-(1-dimethylamino)ethylphenyl-2-ene)]Cl}PF_6[20]
17	[(η^6-C_6Me_6)Ru(κ^2-L-AlaGlyGlyOMe)Cl][21]
18	[(η^6-C_6H_6)Ru(*(S)*-alaninate)Cl][13]

logue **3**, strictly adhering to the molecular recognition pattern of Figure 2, whereas the Ru and Os compounds **1** and **2** differ in this respect.[5]

The pair-formation motif of half-sandwich complexes having a {(Cy)M} unit and two electronegative substituents X and Y also helps to explain the 1:1 diastereomer cocrystallization of three-legged piano stool compounds with ligands other than salicylaldiminates. In complex **8**[10] (Table 3) the pyrrolate nitrogen atom plays the role of the salicylate oxygen atom in compounds **1**–**7**. However, the C–H···N(pyrrolate) distances are larger than their C–H···O(salicylate) counterparts, and the "lying Z" arrangement is distorted (Table 2). Surprisingly, the {(η^5-C_5H_5)Rh} complex **9** is also a half-sandwich complex that exhibits 1:1 diastereomer cocrystallization.[12] A short Rh···Rh distance of 5.49 Å within the pair and strong C–H···O and C–H···Cl hydrogen bonds (Table 2) originating from the cyclopentadienyl ring establish a molecular recognition motif very similar to that shown in Figure 2.

In the first paper in which the 1:1 diastereomer cocrystallization of three-legged piano stools was reported, Sheldrick and Heeb described the benzene–ruthenium complex **10**.[13] The diastereomers of **10** are not predestined to form inversion pairs because the nitrogen atom of the NH_2 group is as poorly suited an acceptor of a hydrogen bond as the nitrogen atom of the 9-ethylguanine ligand. Nevertheless, 1:1 cocrystallization of the diastereomers in the form of inverted piano stools does occur. The alaninate oxygen atoms form strong hydrogen bonds to the benzene ligand of the neighboring molecule (Table 2). Although the Ru···Ru distance in **10** is a little longer than in compounds **1** and **3**–**9**, all the characteristics of inversion pairs, such as the "lying Z" pattern of the centroid-Ru-Ru-centroid arrangement, are present. In the inverted piano stools of the complexes **1** and **3**–**9**, the diastereomers approach each other with their "racemic" sides; in compound **10** this is different. Here, the alaninate ligands, which disturb the centrosymmetry, are located inside the pairs. However, the differences between the hydrogen and methyl substituents at the chiral center of the alanine moiety are not very large.

Complex **11** also shows 1:1 diastereomer cocrystallization.[14] However, the inverted piano stool motif is somewhat distorted which, in part, results from a rotation of the cymene ring with respect to the O_{sal} and Cl substituents of the other molecule of the pair. Although the expected hydrogen bonds are lost (Table 2), there are C–H···Cl hydrogen bonds of 3.64 and 3.79 Å in **11** between the C–H bond next to the methyl substituent and the chloro ligand of the opposite molecule.

Unlike **1**–**11**, compound **12** is a salt. In spite of the positive charges, the cations (R_{Ru},S_C)- and (S_{Ru},S_C)-[(Cy)Ru(O–N)-(OH_2)]$^+$ arrange in a 1:1 manner.[15] Crystals of [(mesitylene)Ru(O–N)Cl] (**13**)[16] also exhibit 1:1 (R_{Ru},S_C)-**13**/(S_{Ru},S_C)-**13** pairs. In both **12** and **13**, there are short intermolecular Ru···Ru contacts, however, there are no C–H···X/Y hydrogen bonds (Table 2) and, most importantly, the angles Cy1-Ru1-Ru2 (120.5°) and Cy2-Ru2-Ru1 (118.0°) for **12** and mesitylene1-Ru1-Ru2 (125.4°) and mesitylene2-Ru2-Ru1 (122.1°) for **13** are much greater than 90°, whereas for **1**–**11** they are less than 90° ("lying Z" arrangement). In the complex [(Cy)Ru{chiraphos(O)}Cl]SbF_6 (**14**, chiraphos = 2,3-bis(diphenylphosphano)butane),[17] the {(Cy)Ru} fragment and the two electronegative substituents O_{PP} and Cl could conceivably form inverted piano stool motifs, but instead, a structure is found in which the diastereomeric cations are separated by the large SbF_6 anions. The complex [(C_5Me_5)Ir(O–N)Cl] (**15**) and the salt [(C_6H_6)Ru(C–N)-(dbp)]PF_6 (**16**; C–N is the *ortho*-metalated ligand $C_6H_5CH(Me)NMe_2$; dbp = 1-phenylbenzodiphosphole)[20] both exhibit 1:1 cocrystallization of diastereomers. In both cases, however, the structural prerequisites are so different that the molecular recognition motif shown in Figure 2 cannot be applied. This also holds for the {(C_6Me_6)Ru} complex **17**,[21] for which the shortest Ru···Ru distance in the crystal is 7.17 Å. With an alaninate-oxygen atom and a chloro ligand, the benzene–ruthenium complex **18**[13] has all the prerequisites to form hydrogen bonds to the benzene ring of a neighboring molecule and thus can establish the required molecular recognition motif. However, this was not observed. The small size of the alaninate ligand gives rise to two short intermolecular Ru···Ru distances of 5.85 and 5.98 Å, but not in the form of inverted piano stools.

The inverted piano stool motif (Figure 2) is strictly obeyed in compounds **1** and **3**–**9** including the "lying Z" formation for the Ar(centroid)-M-M-Ar(centroid) arrangement. The M1···M2 distances are in a narrow range between 5.49 and 5.82 Å (Table 2). Remarkably, this set of complexes not only comprises Ru complexes, but also those of Os and Rh, not only cymene derivatives, but also cyclopentadienyl and benzene derivatives, not only chloro ligands but also iodo ligands, and not only salicylaldiminates but also pyrrolylaldiminates. In addition, many of the compounds differ appreciably with respect to the chiral nitrogen substituent. In almost all of the molecular pairs with *p*-cymene ligands, the isopropyl and methyl substituents of the cymene rings are on opposite sides, following inversion symmetry. Compound **1**, on the

 © 2003 Wiley-VCH Verlag GmbH & Co. KGaA, Weinheim

other hand, differs by having the two isopropyl and two methyl groups on the same side. Furthermore, the isopropyl substituent is usually on the side of the oxygen substituent in the same molecule (and the halogen substituent in the opposite molecule), except for the iodo derivative **6** and molecule 2 of compound **1**. In complex **8** the isopropyl substituents are on the side of the pyrrolyl system.

The phenomenon of 1:1 diastereomer cocrystallization is dominated by {(Cy)Ru}- and {(Cy)Os}-containing half-sandwich complexes, of which compounds **1**, **3**–**8**, and **11** are examples. However, there is a delicate balance between 1:1 diastereomer cocrystallization and crystallization as a pure diastereomer. One such example is compound **2**, which crystallizses in the form of the pure (R_{Os},S_C) diastereomer,[2,5] although it fulfils all the requirements for the formation of inversion pairs. In both crystallization modes (diastereomer ratio 50:50 or 100:0), asymmetric transformations with respect to the metal configuration are involved,[4] although they are probably not the main reason for the mode that is observed.

The inverted piano stool motif (Figure 2) explains the increased occurrence of 1:1 diastereomer cocrystallization, because diastereomers [(Ar)MXY(NR*)] with the same chirality in the NR* substituent and different metal configurations approach each other with their "racemic" (R_M)- and (S_M)-[(Ar)MXY] sides, the NR* substituents not being involved in the molecular recognition process. As a consequence, other compounds with the {(Ar)MXY} structural element, where X and Y are electronegative substituents, should establish this molecular recognition motif as well, even where chirality and diastereomer cocrystallization are not involved. As such a motif was increasingly found for [(Cy)Ru(O–N)Hal] compounds, we searched the Cambridge Crystallographic Database for [(*p*-cymene)RuLHal$_2$] complexes, with the expectation that pair-formation according to the inverted piano stool motif would be observed, together with the orientation of the L ligands towards the outside of the pairs. We found 19 entries for [(Cy)RuLCl$_2$] compounds, ten of which fitted nicely to the molecular recognition pattern of Figure 2 (where the L ligand is a pyridine, amine, or phosphane derivative).[22–30] All of the Ru···Ru distances within the pairs are between 5.59 and 5.90 Å. The other nine [(Cy)RuLCl$_2$] systems (where L is a carbene[31] or phosphane detrivative[27,29,32–36]) do not fit this pattern. Thus, the situation corresponds to that of the compounds listed in Table 2. The tight-inverted piano stool motif of molecular recognition is an attractive possibility, but it is not always enforced. There are examples which could follow it, but fail to do so, and thus remain unpaired. Interestingly, however, the increased occurrence of pair-formation inevitably leads to preferred 1:1 diastereomer cocrystallization, as observed for three-legged piano stool complexes.

Received: September 17, 2002
Revised: January 15, 2003 [Z50181]

Keywords: chirality · crystal growth · molecular recognition · ruthenium · sandwich complexes

[1] J. Jacques, A. Collet, S. H. Wilen, *Enantiomers, Racemates und Resolutions*, Wiley, New York, **1981**, p. 295.
[2] H. Brunner, R. Oeschey, B. Nuber, *Angew. Chem.* **1994**, *106*, 941; *Angew. Chem. Int. Ed. Engl.* **1994**, *33*, 866.
[3] H. Brunner, R. Oeschey, B. Nuber, *J. Chem. Soc. Dalton Trans.* **1996**, 1499.
[4] H. Brunner, *Eur. J. Inorg. Chem.* **2001**, 905.
[5] H. Brunner, T. Zwack, M. Zabel, W. Beck, A. Böhm, *Organometallics*, submitted.
[6] C. Lecomte, Y. Dusausoy, J. Protas, J. Tirouflet, A. Dormond, *J. Organomet. Chem.* **1974**, *73*, 67.
[7] H. Brunner, *Enantiomer* **1997**, *2*, 133.
[8] G. R. Desiraju, T. Steiner, *The Weak Hydrogen Bond*, Oxford University Press, Oxford, **1999**.
[9] S. K. Mandal, A. R. Chakravarty, *J. Chem. Soc. Dalton Trans.* **1992**, 1627.
[10] H. Brunner, T. Neuhierl, B. Nuber, *Eur. J. Inorg. Chem.* **1998**, 1877.
[11] H. Brunner, M. Weber, M. Zabel, *Synthesis*, submitted.
[12] H. Brunner, A. Köllnberger, M. Zabel, *Polyhedron*, submitted.
[13] W. S. Sheldrick, S. Heeb, *Inorg. Chim. Acta* **1990**, *168*, 93.
[14] R. K. Rath, M. Nethaji, A. K. Chakravarty, *Polyhedron* **2002**, *21*, 1929.
[15] S. K. Mandal, A. R. Chakravarty, *Inorg. Chem.* **1993**, *32*, 3851.
[16] L. C. Carter, D. L. Davies, K. T. Duffy, J. Fawcett, D. R. Russel, *Acta Crystallogr. Sect. C* **1994**, *50*, 1559.
[17] J. W. Faller, X. Liu, J. Parr, *Chirality* **2002**, *12*, 325.
[18] R. Krämer, K. Polborn, H. Wanjek, I. Zahn, W. Beck, *Chem. Ber.* **1990**, *123*, 767.
[19] D. Carmona, A. Mendoza, F. J. Lahoz, L. A. Oro, M. P. Lamata, E. San José, *J. Organomet. Chem.* **1990**, *396*, C17.
[20] S. Attar, V. J. Catalano, J. H. Nelson, *Organometallics* **1996**, *15*, 2932.
[21] R. Krämer, M. Maurus, K. Polborn, K. Sünkel, C. Robl, W. Beck, *Chem. Eur. J.* **1996**, *2*, 1518.
[22] D. K. Gupta, A. N. Sahay, D. S. Pandey, N. K. Jha, P. Sharma, G. Espinosa, A. Cabrera, M. C. Puerta, P. Valerga, *J. Organomet. Chem.* **1998**, *568*, 13.
[23] G. Bruno, M. Panzalorto, F. Nicolo, C. G. Arena, P. Cardiano, *Acta Crystallogr. Sect. C* **2000**, *56*, e429.
[24] I. Moldes, E. de la Encarnacion, J. Ros, A. Alvarez-Larena, J. F. Piniella, *J. Organomet. Chem.* **1998**, *566*, 165.
[25] S. Serron, S. P. Nolan, Yu. A. Abramov, L. Brammer, J. L. Petersen, *Organometallics* **1998**, *17*, 104.
[26] B. Therrien, T. R. Ward, M. Pilkington, C. Hoffmann, F. Gilardoni, J. Weber, *Organometallics* **1998**, *17*, 330.
[27] A. Hafner, A. Muhlebach, P. A. van der Schaaf, *Angew. Chem.* **1997**, *109*, 2213; *Angew. Chem. Int. Ed. Engl.* **1997**, *36*, 2121.
[28] A. K. Burrell, A. J. Steedman, *Organometallics* **1997**, *16*, 1203.
[29] K. D. Redwine, H. D. Hansen, S. Bowley, J. Isbell, M. Sanchez, D. Vodak, J. H. Nelson, *Synth. React. Inorg. Met.-Org. Chem.* **2000**, *30*, 379.
[30] P. Pertici, E. Pitzalis, G. U. Barretta, F. Marchetti, P. Salvadori, *Gazz. Chim. Ital.* **1995**, *125*, 27.
[31] W. A. Herrmann, C. Kochler, L. J. Gossen, G. R. J. Artus, *Chem. Eur. J.* **1996**, *2*, 1627.
[32] J. F. Van der M. Uria, S. Garcia-Granda, J. A. Cabeza, I. del Rio, *Acta Crystallogr. Sect. C* **1994**, *50*, 1064.
[33] S. E. Durran, M. B. Smith, A. M. Z. Slawin, T. Gelbrich, M. B. Hursthouse, M. E. Light, *Can. J. Chem.* **2001**, *79*, 780.
[34] C. G. Arena, S. Calamia, F. Faraone, C. Graiff, A. Tiripicchio, *J. Chem. Soc. Dalton Trans.* **2000**, 3149.
[35] C. S. Allardyce, P. J. Dyson, D. J. Ellis, S. L. Heath, *Chem. Commun.* **2001**, 1396.
[36] J. W. Faller, B. P. Patel, M. A. Albrizzio, M. Curtis, *Organometallics* **1999**, *18*, 3096.

 © 2003 Wiley-VCH Verlag GmbH & Co. KGaA, Weinheim

Diorganomagnesium Compounds

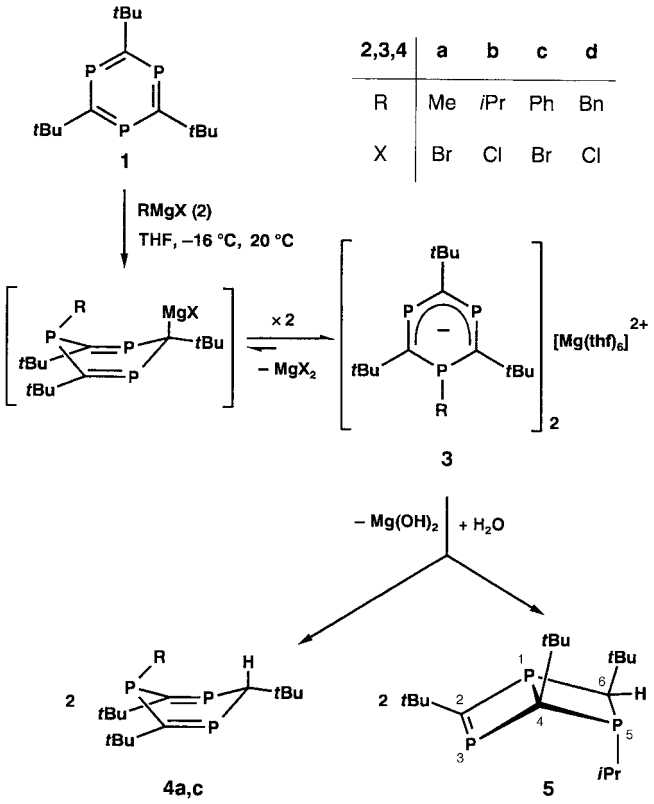
1,4-Addition of Grignard Reagents to 2,4,6-Tri-*tert*-butyl-1,3,5-triphosphabenzene**

Jens Renner, Uwe Bergsträßer, Paul Binger, and Manfred Regitz**

Grignard compounds (organomagnesium halides) are among the longest-known organometallic reagents and have found a plethora of applications in organic synthesis.[2] In particular, they are used for additions to polarized or polarizable carbon–heteroatom multiple bonds. However, they are less suitable for additions to C–C multiple bonds. Although triphosphabenzenes, for example, 2,4,6-tri-*tert*-butyl-1,3,5-triphosphabenzene (**1**)[3] exhibit a marked aromatic character according to physical-chemical measurements,[4] they are in fact highly reactive compounds. Thus, for example, Diels–Alder reactions[5] or addition reactions of lithium alkoxides with participation of all three P–C double bonds[6] occur readily under mild conditions. Compound **1** also reacts readily with silylenes,[7] carbenes,[8] or phosphinidenes,[9] usually through a [2+1]-cycloaddition process.

We treated the triphosphabenzene **1** with the Grignard reagents **2a–d** in THF and observed that the latter species undergo formal, regio- and stereoselective 1,4-additions to the heteroaromatic compound **1**, already at −16 °C. The regioselectivity arises from the polarity of the P–C double bonds,[10] by which the organic group R of the Grignard reagent adds to a phosphorus atom and the metal part adds to C4. The *cis* stereoselectivity indicates that the reaction is a synchronous or polar addition. It has been known for some time that monophosphabenzenes undergo nucleophilic addition with both organolithium and organomagnesium species. 1,2-Dihydro- or 1,4-dihydrophosphinines are obtained after hydrolysis or reaction with electrophiles.[11,12] The structures of the novel organomagnesium compounds were deduced from their NMR spectral data and confirmed by X-ray crystallographic analysis of compound **3d**. The structures of **3a** and **3b** were derived by comparison with the NMR data of **3d** (Scheme 1).

The first unexpected result was provided by the crystal structure analysis of **3d** (Figure 1).[13] The organomagnesium compound formed did not exist as a halide with covalent bonds but rather as the salt of a diorganomagnesium compound with separated charges. To the best of our knowledge, compounds of this type have not been described previously.



Scheme 1. Synthesis of phosphinines **4** and **5**.

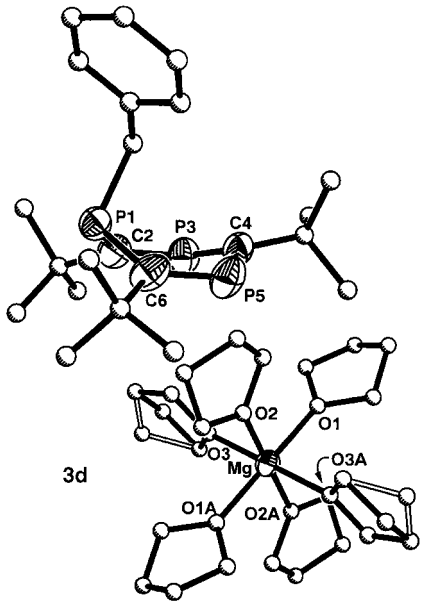


Figure 1. Crystal structure of **3d** with 50% probability thermal ellipsoids. For clarity, the thermal ellipsoids as well as the hydrogen atoms of the substituents are omitted and only one of the ligands is shown. Also not shown are the non-coordinated solvent molecules found in the crystal. Selected bond lengths [Å]: P1-C2 1.809(6), P3-C2 1.665(6), P3-C4 1.743(5), P5-C4 1.736(5), P5-C6 1.681(6).

[*] Prof. Dr. P. Binger, Prof. Dr. M. Regitz, Dr. J. Renner, Dr. U. Bergsträßer
Fachbereich Chemie, Universität Kaiserslautern
Erwin-Schrödinger-Straße, 67663 Kaiserslautern (Germany)
Fax: (+49) 631-205-3921
E-mail: regitz@rhrk.uni-kl.de

[**] Phosphorus compounds, Part 169. This work was supported by the Graduate College "Phosphorus chemistry as link between different chemical disciplines". Part 168: reference[1].

 DOI: 10.1002/anie.200250182 © 2003 Wiley-VCH Verlag GmbH & Co. KGaA, Weinheim

Table 1: Selected data for **3a,b,d** and **4a,c**.[a]

3a: ^{1}H NMR: $\delta = 3.82$–3.78 (m, 24H; OCH_2CH$_2$), 1.97–1.93 (m, 24H; OCH$_2$CH_2), 1.74 (s, 6H; 1-CH_3), 1.62 (s, 18H; 4-C(CH_3)$_3$), 1.51 ppm (s, 36H; 2- and 6-C(CH_3)$_3$); ^{13}C{^{1}H} NMR: $\delta = 147.9$ (t, $^1J_{C,P} = 57.0$ Hz; C4), 136.6 (m; C2 and C6), 66.0 (s; OCH$_2$CH$_2$), 38.4–37.5 (m; 2- and 6-C(CH$_3$)$_3$), 37.1 (t, $^2J_{C,P} = 25.6$ Hz; 4-C(CH$_3$)$_3$), 34.6 (t, $^3J_{C,P} = 13.0$ Hz; 4-C(CH$_3$)$_3$), 32.7 (X-part of an AA′MX spin system, $^3J_{C,P} = 20.0$, $^3J_{C,P} = 11.4$, $^5J_{C,P} = 4.9$ Hz; 2- and 6-C(CH$_3$)$_3$), 23.9 (s; OCH$_2$CH$_2$), 7.3 ppm (d, $^1J_{C,P} = 15.3$ Hz; 1-CH$_3$); ^{31}P{^{1}H} NMR: $\delta = 190.3$ (d, $^2J_{P,P} = 9.9$ Hz; P3 and P5), −93.3 ppm (t, $^2J_{P,P} = 9.9$ Hz; P1)

3b: ^{1}H NMR: $\delta = 3.68$–3.65 (m, 24H; OCH_2CH$_2$), 1.82–1.79 (m, 24H; OCH$_2$CH_2), 1.43 (s, 18H; 4-C(CH_3)$_3$), 1.34 (s, 36H; 2- and 6-C(CH)$_3$), 1.22 (d, 2H; $^3J_{H,H} = 7.0$ Hz, CH(CH$_3$)$_2$), 0.42 ppm (dd, 12H; $^2J_{H,P} = 15.0$, $^3J_{H,H} = 7.0$ Hz; CH(CH_3)$_2$); ^{13}C{^{1}H} NMR: $\delta = 154.3$ (t, $^1J_{C,P} = 57.7$ Hz; C4), 136.5–135.6 (m, not resolved; C2 and C6), 68.0 (s; OCH$_2$CH$_2$), 39.3–38.8 (m, not resolved; 2- and 6-C(CH$_3$)$_3$), 39.0 (t, $^2J_{C,P} = 18.0$ Hz; 4-C(CH$_3$)$_3$), 36.5 (t, $^3J_{C,P} = 13.0$ Hz; 4-C(CH$_3$)$_3$), 35.8–35.4 (m, not resolved; 2- and 6-C(CH$_3$)$_3$), 25.8 (s; OCH$_2$CH$_2$), 20.3 (d, $^1J_{C,P} = 23.7$ Hz; CH(CH$_3$)$_2$), 13.8 ppm (d, $^2J_{C,P} = 6.1$ Hz; CH(CH$_3$)$_2$); ^{31}P{^{1}H} NMR: $\delta = 188.8$ (d, $^2J_{P,P} = 9.9$ Hz; P3 and P5), −56.5 ppm (t, $^2J_{P,P} = 9.9$ Hz; P-1)

3d: ^{1}H NMR: $\delta = 6.97$–6.93 (m, 4H; Ph-H), 6.85–6.78 (m, 6H; Ph-H), 3.69–3.64 (m, 24H; OCH_2CH$_2$), 1.85 (d, 4H, $^2J_{H,P} = 1.6$ Hz; CH_2), 1.82–1.79 (m, 24H; OCH$_2$CH_2), 1.56 (s, 18H; 4-C(CH_3)$_3$), 1.20 ppm (s, 36H; 2- and 6-C(CH)$_3$); ^{13}C{^{1}H} NMR: $\delta = 152.0$ (t, $^1J_{C,P} = 57.8$ Hz; C4), 143.2 (d, $^2J_{C,P} = 6.5$ Hz; C1′), 137.0 (X-part of an AA′MX spin system, $^1J_{C,P} = 55.0$, $^1J_{C,P} = 23.0$, $^3J_{C,P} = 2.3$ Hz; C2 and C6), 129.9 (d, $^4J_{C,P} = 4.6$ Hz; C3′ and C5′), 128.6 (d, $^3J_{C,P} = 18.5$ Hz; C2′ and C6′), 126.4 (s; C4′), 68.2 (s; OCH$_2$CH$_2$), 39.7–39.4 (m; 2- and 6-C(CH$_3$)$_3$), 37.5 (t, $^2J_{C,P} = 8.3$ Hz; 4-C(CH$_3$)$_3$), 36.8 (t, $^3J_{C,P} = 12.5$ Hz; 4-C(CH$_3$)$_3$), 34.9–34.4 (m; 2- and 6-C(CH$_3$)$_3$), 27.9 (d, $^1J_{C,P} = 20.3$ Hz; CH$_2$Ph), 25.8 ppm (s; OCH$_2$CH$_2$); ^{31}P{^{1}H} NMR: $\delta = 193.7$ (d, $^2J_{P,P} = 8.5$ Hz; P3 and P5), −59.2 ppm (t, $^2J_{P,P} = 8.5$ Hz; P1)

4a: M.p. 109°C; ^{1}H NMR: $\delta = 3.18$ (t, 1H; $^2J_{H,P} = 9.6$ Hz, 4-H), 1.56 (s, 18H; 2- and 6-C(CH_3)$_3$), 1.48 (s, 9H; 4-C(CH_3)$_3$), 1.42 ppm (d, 3H, $^2J_{H,P} = 5.4$ Hz; 1-CH_3); ^{13}C{^{1}H} NMR: $\delta = 217.1$ (X-part of an AA′MX spin system, $^1J_{C,P} = 61.5$, $^1J_{C,P} = 41.0$, $^3J_{C,P} = 5.6$ Hz; C2 and C6), 58.7 (t, $^1J_{C,P} = 54.7$ Hz; C4), 44.9 (X-part of an AA′MX spin system, $^2J_{C,P} = 27.9$, $^2J_{C,P} = 26.3$, $^4J_{C,P} = 4.7$ Hz; 2- and 6-C(CH$_3$)$_3$), 33.7 (t, $^2J_{C,P} = 15.9$; 4- C(CH$_3$)$_3$), 32.0 (X-part of an AA′MX spin system, $^3J_{C,P} = 20.3$, $^3J_{C,P} = 12.0$, $^5J_{C,P} = 4.3$ Hz; 2- and 6-C(CH$_3$)$_3$), 30.8 (t, $^3J_{C,P} = 10.3$; 4-C(CH$_3$)$_3$), 13.7 ppm (dt, $^1J_{C,P} = 21.0$, $^3J_{C,P} = 7.3$ Hz; 1-CH$_3$); ^{31}P{^{1}H} NMR: $\delta = 321.6$ (d, $^2J_{P,P} = 9.9$ Hz; P3 and P5), −55.4 ppm (t, $^2J_{P,P} = 9.9$ Hz; P1); MS (70 eV): *m/z* (%): 316 (68) [*M*]$^+$, 301 (100) [*M*−Me]$^+$, 259 (24), 245 (22), 216 (13) [*M*−PC*t*Bu]$^+$, 201 (11), 178 (15), 169 (22), 131 (14), 115 (6), 113 (6), 101 (6), 60 (13), 57 (10) [*t*Bu]$^+$, 43 (5), 41 (5)

4c: M.p. 148°C; ^{1}H NMR: $\delta = 7.44$–7.38 (m, 2H; Ph-H), 7.20–7.09 (m, 3H; Ph-H), 2.30 (t, $^2J_{H,P} = 8.9$ Hz; 4-H), 1.54 (s, 18H; 2- and 6-C(CH_3)$_3$), 1.50 ppm (s, 9H; 4-C(CH_3)$_3$); ^{13}C{^{1}H} NMR: $\delta = 219.1$–218.2 (m, not resolved; C2 and C6), 141.6 (dt, $^1J_{C,P} = 21.9$, $^3J_{C,P} = 5.3$ Hz; C1′), 129.7 (d, $^2J_{C,P} = 14.8$ Hz; C2′ and C6′), 127.9 (d, $^3J_{C,P} = 2.8$ Hz; C3′ and C5′), 127.2 (d, $^4J_{C,P} = 1.8$ Hz; C4′), 66.9 (t, $^1J_{C,P} = 55.9$ Hz; C-4), 44.8 (X-part of an AA′MX spin system, $^2J_{C,P} = 28.2$, $^2J_{C,P} = 24.8$, $^4J_{C,P} = 4.6$ Hz; 2- and 6-C(CH$_3$)$_3$), 33.5 (t, $^2J_{C,P} = 15.7$ Hz; 4-C(CH$_3$)$_3$), 32.7 (X-part of an AA′MX spin system, $^3J_{C,P} = 20.7$, $^3J_{C,P} = 10.5$, $^5J_{C,P} = 5.6$ Hz; 2- and 6-C(CH$_3$)$_3$), 31.2 ppm (t, $^3J_{C,P} = 9.7$ Hz; 4-C(CH$_3$)$_3$); ^{31}P{^{1}H} NMR: $\delta = 333.4$ (d, $^2J_{P,P} = 6.2$ Hz; P3 and P5), −48.2 ppm (t, $^2J_{P,P} = 6.2$ Hz; P1); MS (70 eV): *m/z* (%): 378 (92) [*M*]$^+$, 363 (100) [*M*−Me]$^+$, 321 (27) [*M*−*t*Bu]$^+$, 307 (22), 278 (18) [*M*−PC*t*Bu]$^+$, 240 (21), 235 (9), 177 (11), 170 (21), 169 (29), 163 (14), 151 (6), 147 (7), 139 (13), 131 (11), 129 (6), 109 (11), 99 (11), 91 (9), 85 (9), 69 (10), 60 (8), 57 (14) [*t*Bu]$^+$, 43 (8), 41 (21)

5: M.p. 76°C; ^{1}H NMR: $\delta = 2.62$–2.49 (m, 1H; CH(CH$_3$)$_2$), 1.86 (pseudo-t, 1H, $^2J_{H,P} = {}^2J_{H,P} = 4.0$ Hz; 6-H), 1.42 (s, 18H; 2×C(CH_3)$_3$), 1.29 (dd, 3H, $^2J_{H,P} = 15.6$ Hz, $^3J_{H,H} = 6.9$ Hz; CH(CH_3)$_A$(CH$_3$)$_B$), 1.21 (s, 9H; C(CH_3)$_3$), 1.02 ppm (dd, 3H, $^2J_{H,P} = 16.1$, $^3J_{H,H} = 6.9$ Hz; CH(CH$_3$)$_A$(CH_3)$_B$); ^{13}C{^{1}H} NMR: $\delta = 231.4$ (ddd, $^1J_{C,P} = 53.8$, $^1J_{C,P} = 32.7$, $^3J_{C,P} = 2.3$ Hz; C2), 43.9 (ddd, $^1J_{C,P} = 19.0$, $^1J_{C,P} = 17.4$, $^3J_{C,P} = 8.4$ Hz; C6), 40.8 (dd, $^2J_{C,P} = 7.6$, $^2J_{C,P} = 5.3$ Hz; 2- or 6-C(CH$_3$)$_3$), 34.6 (ddd, $^2J_{C,P} = 6.3$, $^2J_{C,P} = 18.8$, $^2J_{C,P} = 5.7$ Hz; 4-C(CH$_3$)$_3$), 33.2 (dd, $^2J_{C,P} = 18.0$, $^2J_{C,P} = 12.5$ Hz; 2- or 6-C(CH$_3$)$_3$), 31.7 (dd, $^3J_{C,P} = 9.4$, $^3J_{C,P} = 4.3$ Hz; 2- or 6-C(CH$_3$)$_3$), 31.1 (dd, $^1J_{C,P} = 19.6$, $^3J_{C,P} = 7.4$ Hz; CH(CH$_3$)$_A$(CH$_3$)$_B$), 29.4 (dd, $^3J_{C,P} = 8.2$, $^3J_{C,P} = 7.0$ Hz; 2- or 6-C(CH$_3$)$_3$), 27.3, (ddd, $^3J_{C,P} = 8.5$, $^3J_{C,P} = 6.2$, $^3J_{C,P} = 5.6$ Hz; 4-C(CH$_3$)$_3$), 23.5 (ddd, $^1J_{C,P} = 39.3$, $^1J_{C,P} = 19.8$, $^1J_{C,P} = 16.8$ Hz; C4), 17.8 (d, $^2J_{C,P} = 23.1$ Hz; CH(CH$_3$)$_A$(CH$_3$)$_B$), 17.2 ppm (dd, $^2J_{C,P} = 18.8$, $^4J_{C,P} = 5.9$ Hz; CH(CH$_3$)$_A$(CH$_3$)$_B$); ^{31}P{^{1}H} NMR: $\delta = 388.7$ (dd, $^2J_{P,P} = 27.6$, $^2J_{P,P} = 12.5$ Hz; P3), 83.7 (dd, $^2J_{P,P} = 27.6$, $^2J_{P,P} = 12.5$ Hz; P1), 14.2 ppm (pseudo-t, $^2J_{P,P} = {}^2J_{P,P} = 12.5$ Hz; P5); MS (70 eV): *m/z* (%): 344 (87) [*M*]$^+$, 329 (57) [*M*−Me]$^+$, 301 (15) [*M*−C$_3$H$_7$]$^+$, 244 (100) [*M*−PC*t*Bu]$^+$, 231 (14), 229 (7), 206 (14), 201 (14), 169 (25), 136 (10), 131 (52), 69 (8) [C*t*Bu]$^+$, 57 (6) [*t*Bu]$^+$, 41 (11)

[a] ^{1}H NMR (TMS): 400.13 MHz; ^{13}C NMR (TMS): 100.61 MHz, ^{31}P NMR (85% H_3PO_4): 81.01 MHz; solvents: [D$_8$]THF (**3a,b,d**), [D$_6$]benzene (**4a,b, 5**); MS: Finnigan MAT90 and MAT95. [b] See Figures 1–3 for the numbering of the C and P atoms.

The metal cation is stabilized by octahedral coordination with six tetrahydrofuran molecules. The anion may best be described as a delocalized 1,3-diphosphapentadienide system, although the geometry at C4 deviates from planarity. The delocalization of the negative charge is clearly apparent from the following bond lengths: C4–P3 (1.743(5) Å) and P5–C4 (1.736(5) Å), which are comparable with those in triphosphabenzene (1.718–1.729 Å)[4] and lie between the normal values of P–C single and double bonds.[14] Appreciably longer bond lengths with values of 1.809(6) and 1.879(6) Å are found for P1–C2 and P1–C6. The C2/P1/C6 and P3/C4/P5 planes are tilted by angles of 41.6 and 31.6° relative to the C2/P3/P5/C6 plane. The NMR spectra of **3d** are compatible with this structure (Table 1).

Protonation of the organomagnesium compounds **3a** and **3c**—to improve the workup, silica gel with water (4%) was used—furnished the corresponding 1,4-dihydro-1,3,5-triphosphinines **4a** and **4c** in good to excellent yields. The protonation of **3b** is an exception, and furnishes the bicyclic compound **5** in 29% yield as the only isolated product. The mechanistic basis of this reaction is the subject of ongoing theoretical studies.

The structures of the newly obtained dihydrotriphosphinines **4** can be deduced unambiguously from their NMR data and were confirmed by crystal-structure analysis of **4a** (Figure 2).[15] Accordingly, as is the case for **3**, products **4** exist in the boat conformation. The newly introduced substituent and the proton from hydrolysis are *cis* to each

 © 2003 Wiley-VCH Verlag GmbH & Co. KGaA, Weinheim

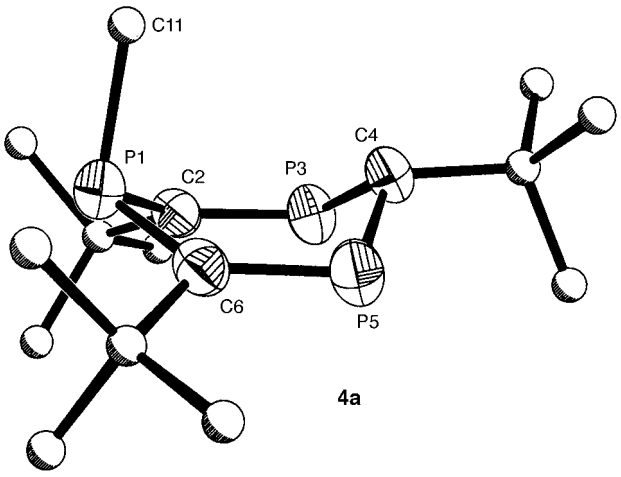


Figure 2. Crystal structure of **4a** with 50% probability thermal ellipsoids. The thermal ellipsoids as well as the hydrogen atoms of the substituents are omitted for clarity. Selected bond lengths [Å] and angles [°]: P1-C2 1.843(2), C2-P3 1.662(2), P3-C4 1.8529(13), P1-C11 1.848(4), C4-C41 1.560(3); C2-P1-C6 103.51(12), C2-P3-C4 105.72(10), P3-C4-P5 114.74(12).

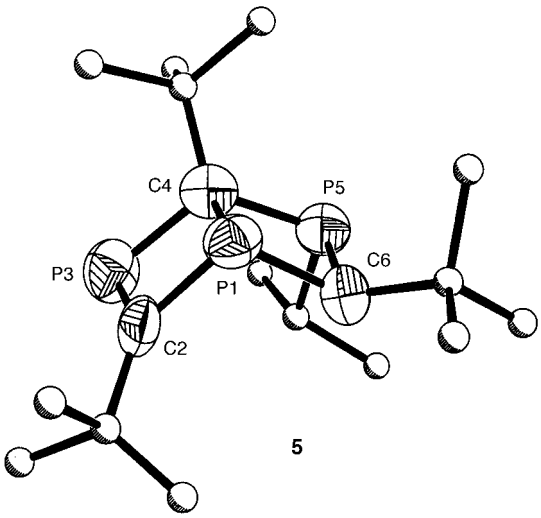


Figure 3. Crystal structure of **5** with 50% probability thermal ellipsoids. The thermal ellipsoids as well as the hydrogen atoms of the substituents are omitted for clarity. Selected bond lengths [Å] and angles [°]: P1-C2 1.807(10), P1-C6 1.880(4), P1-C4 1.885(5), C2-P3 1.648(9), P3-C4 1.828(5), C4-P5 1.868(5), P5-C6 1.859(4); P1-C2-P3 99.6(5), C2-P1-C4 81.3(3), C4-P1-C6 86.6(2), P1-C4-P3 90.7(2), P1-C4-P5 92.1(2), C4-P5-C6 87.7(2), P1-C6-P5 92.6(7).

other. The symmetry of products **4** is demonstrated by the two signals for the three phosphorus atoms in the $^{31}P\{^1H\}$ NMR spectra (**4a**: $\delta = 321.6, -55.4$ ppm; **4c**: $\delta = 322.5, -40.7$ ppm; **4d**: $\delta = 333.4, -48.2$ ppm) and also by two signals in the $^{13}C\{^1H\}$ NMR spectra for the three carbon atoms of the six-membered rings (**4a**: $\delta = 217.1, 58.7$ ppm; **4c**: $\delta = 218.5, 60.4$ ppm; **4d**: $\delta = 218.7, 66.9$ ppm). All signals occur in the expected regions and exhibit the appropriate coupling constants. The crystal structure analysis of **4a** unequivocally confirms the boat conformation and the *cis* orientation of the methyl group and the proton at C4.

The P1–C2 and P3–C4 bond lengths (1.843(2) and 1.8529(13) Å, respectively) are characteristic of P–C single bonds, whereas the C2–P3 bond length (1.662(2) Å) is more in the range of P–C double bonds. The angles formed by the C2/P1/C6 and P3/C4/P5 planes with the C2/P3/P5/C6 plane are 27.9° and 52.4°, respectively.

Surprisingly, hydrolysis of the derivative **3b** does not furnish a dihydrotriphosphinine. Instead, the dihydrotriphospha Dewar benzene **5** is obtained and identified by its characteristic NMR data. The $^{31}P\{^1H\}$ NMR spectrum shows three signals at $\delta = 388.7$, 83.7, and 14.2 ppm with $^2J_{P,P}$ coupling constants of 27.6 and 12.5 Hz. The skeletal proton gives rise to a pseudotriplet at $\delta = 1.86$ ppm ($^2J_{H,P} = {}^2J_{H,P} = 4.0$ Hz).

Final structural confirmation of **5** was provided by X-ray crystallographic analysis (Figure 3).[16] In spite of a disorder of two molecules twisted at 90° to each other, the analysis shows the bicyclic structure of **5** as well as the *trans* orientation of the isopropyl group at P5 relative to the *tert*-butyl group at C6. The C2–P3 bond length of 1.648(9) Å is in the usual range for P–C double bonds, whereas the P5–C6 bond length (1.859(4) Å) is typical of a P–C single bond. The folding angle of the bicyclic system is 110.8°.

We have shown herein that the Grignard compounds **2** undergo 1,4-additions to 1,3,5-triphosphabenzenes **1** to furnish the salts **3** of the corresponding diorganomagnesium compounds. Hydrolysis of the latter affords the dihydrotriphosphabenzenes **4**, provided that no bulky substituent has been introduced into **3**. The presence of a bulky group, such as the isopropyl group at P1 in **3b** leads, after hydrolysis, to a rearrangement to the dihydro Dewar benzene derivative **5**.

Experimental Section

3: An equimolar amount of the corresponding Grignard compound **2** was added to a solution of triphosphabenzene **1** (≈0.5 mmol) in freshly distilled tetrahydrofuran at −16 °C. The mixture was stirred at this temperature for 1 h, and then allowed to warm to room temperature and stirred for a further 1 h. After removal of the solvent under vacuum (oil pump), **3a** and **3d** were obtained as red solids and **3b** as a red oil. Since by-products were only detected in traces, if at all, further purification of the extremely hydrolysis-sensitive compounds **3** was not attempted. The NMR spectra were obtained by direct dissolution of the resulting addition products **3a,b,d** in $[D_8]$THF.

4: An equimolar amount of the Grignard compound **2** was added to a solution of triphosphabenzene **1** (≈0.5 mmol) in freshly distilled tetrahydrofuran (≈4 mL) at −16 °C. The mixtures was stirred at this temperature for 1 h, allowed to warm to room temperature and stirred for a further 1 hour. The addition of silica gel (≈2 g, with 4% wt H_2O) led to hydrolysis. After stirring for 5 min, the silica gel was separated over a D3 sintered-glass frit, the solvent was removed under vacuum (oil pump), and the residual solid was taken up in a copious amount of *n*-pentane. The colorless magnesium salt was filtered off, and the pentane removed from the filtrate. Compounds **4** were obtained as orange crystals after recrystallization of the residue from toluene.

Received: September 17, 2002 [Z50182]

Keywords: 1,4-addition · Grignard reaction · magnesium · phosphorus heterocycles · phosphorus

 © 2003 Wiley-VCH Verlag GmbH & Co. KGaA, Weinheim

[1] S. Weidner, U. Bergsträßer, M. Regitz, H. Heydt, *Synthesis*, submitted.

[2] a) *Handbook of Grignard Reagents* (Eds.: G. S. Silverman, P. E. Rakita), Marcel Dekker, New York **1996**; b) C. L. Raston, G. Salem in *The Chemistry of the Metal Carbon Bond, Vol. 4* (Ed.: F. R. Hartley), Wiley, New York, **1987**, pp. 159–306.

[3] a) P. Binger, S. Leininger, J. Stannek, B. Gabor, R. Mynott, J. Bruckmann, C. Krüger, *Angew. Chem.* **1995**, *107*, 2411–2414; *Angew. Chem. Int. Ed. Engl.* **1995**, *34*, 2227–2230; b) F. Tabellion, A. Nachbauer, S. Leininger, C. Peters, M. Regitz, *Angew. Chem.* **1998**, *110*, 1318–1321; *Angew. Chem. Int. Ed.* **1998**, *37*, 1233–1235.

[4] R. Gleiter, H. Lange, P. Binger, J. Stannek, C. Krüger, J. Bruckmann, U. Zenneck, S. Kummer, *Eur. J. Inorg. Chem.* **1998**, 1619–1621.

[5] a) P. Binger, S. Stutzmann, J. Bruckmann, C. Krüger, J. Grobe, D. LeVan, T. Pohlmeyer, *Eur. J. Inorg. Chem.* **1998**, 2071–2074; b) C. Peters, S. Stutzmann, H. Disteldorf, S. Werner, U. Bergsträßer, C. Krüger, P. Binger, M. Regitz, *Synthesis* **2000**, 529–536; c) C. Peters, H. Disteldorf, E. Fuchs, S. Werner, S. Stutzmann, J. Bruckmann, C. Krüger, P. Binger, H. Heydt, M. Regitz, *Eur. J. Org. Chem.* **2001**, 3425–3435; d) H. Heydt, *Top. Curr. Chem.* **2003**, *223*, 215-249.

[6] M. Krein, U. Bergsträßer, C. Peters, S. G. Ruf, M. Regitz, *Chem. Commun.* **2000**, 2015–2016.

[7] S. B. Clendenning, B. Gerhus, P. B. Hitchcock, J. F. Nixon, *Chem. Commun.* **1999**, 2451–2452.

[8] S. B. Clendenning, P. B. Hitchcock, J. F. Nixon, L. Nyulászi, *Chem. Commun.* **2000**, 1305–1306.

[9] a) M. J. M. Vlaar, A. W. Ehlers, M. Schakel, S. B. Clendenning, J. F. Nixon, M. Lutz, A. L. Spek, K. Lammertsma, *Chem. Eur. J.* **2001**, *7*, 3545–3550; b) M. J. M. Vlaar, A. W. Ehlers, M. Schakel, S. B. Clendenning, J. F. Nixon, M. Lutz, A. L. Spek, K. Lammertsma, *Angew. Chem.* **2001**, *113*, 4524–4527; *Angew. Chem. Int. Ed.* **2001**, *40*, 4412–4415.

[10] L. Nyulászi, T. Veszprémi, *J. Phys. Chem.* **1996**, *100*, 6456–6462.

[11] G. Märkl in *Multiple Bonds and Low Coordination in Phosphorus Chemistry* (Eds.: M. Regitz, O. J. Scherer), Thieme, Suttgart **1990**, pp. 220–257.

[12] a) G. Märkl, F. Lieb, A. Merz, *Angew. Chem.* **1967**, *79*, 59; *Angew. Chem. Int. Ed. Engl.* **1967**, *79*, 87; b) G. Märkl, A. Merz, *Tetrahedron Lett.* **1968**, 3611–3614; c) G. Märkl, A. Merz, *Tetrahedron Lett.* **1971**, 1215–1218; d) A. J. Ashe III, T. W. Smith, *Tetrahedron Lett.* **1977**, 407–410.

[13] Crystallographic data for **3d**: $C_{68}H_{116}MgO_6P_6$; $M_r = 1247.72$; $T = 240(2)$ K; $\lambda = 0.71073$ Å; monoclinic; space group $P2_1/n$; $a = 15.269(3)$, $b = 16.207(3)$, $c = 19.414(4)$ Å; $V = 4555(2)$ Å^3; $Z = 2$; $\rho_{calcd} = 1.091$ Mg m^{-3}; $\mu = 1.75$ cm^{-1}; $F(000)$ 1604; crystal dimensions $0.4 \times 0.4 \times 0.3$ mm^3; scanned θ-range 2.40 to 26.07°; index range $-18 \le h \le 18$, $-19 \le k \le 19$, $-23 \le l \le 23$; measured reflections 27008; independent reflections 8823 ($R_{int} = 0.2337$); structure refinement: full-matrix least-squares to F^2; data/restraints/parameters 8823/232/493; GOF = 1.108; final R values $[I > 2\sigma(I)]$: $R_1 = 0.1013$, $wR_2 = 0.2253$; R values (all data): $R_1 = 0.1700$, $wR_2 = 0.2455$; residual electron density (largest maximum and minimum) 0.466 and −1.053 e Å^{-3}; symmetry operations to generate equivalent positions $-x$, $-y$, $-z$. Note: One of the THF molecules coordinated to magnesium displays a disorder that is considered in the refinement by means of two split positions for C29 (occupancy factor 0.7) and C29′ (occupancy factor 0.3). Besides the THF molecules coordinated to magnesium, two further free THF molecules were localized and refined anisotropically. One of these molecules also showed a pronounced disorder, which is included in the refinement with two positions (occupancy factor 0.5 each) with limitation of the anisotropic temperature factors. This and the decomposition of the crystal observed in spite of a measurement temperature of 240 K resulted in relatively high R values for the structure model.

[14] F. H. Allen, O. Kennard, D. G. Watson, L. Brammer, A. G. Orpen, R. Taylor, *J. Chem. Soc. Perkin Trans. 2* **1987**, S1-S19.

[15] Crystallographic data for **4a**: $C_{16}H_{31}P_3$; $M_r = 316.32$; $T = 293(2)$ K; $\lambda = 0.71073$ Å; orthorhombic; space group $Ama2$; $a = 15.641(3)$, $b = 18.941(4)$, $c = 6.4490(13)$ Å; $V = 1910.6(7)$ Å^3; $Z = 4$; $\rho_{calcd} = 1.100$ Mg m^{-3}; $\mu = 3.00$ cm^{-1}; $F(000)$ 688; crystal dimensions $0.6 \times 0.4 \times 0.4$ mm^3; scanned θ range 2.51 to 25.94°; index range $-19 \le h \le 19$, $-22 \le k \le 23$, $-7 \le l \le 7$; measured reflections 7321; independent reflections 1801 ($R_{int} = 0.0414$); structure refinement: full-matrix least-squares to F^2; data/restraints/parameters 1801/1/94; GOF = 1.033; final R values $[I > 2\sigma(I)]$: $R_1 = 0.0302$, $wR_2 = 0.0778$; R values (all data): $R_1 = 0.0321$, $wR_2 = 0.0789$; absolute structure parameter 0.12(12); residual electron density (largest maximum and minimum) 0.247 and −0.122 e Å^{-3}; symmetry operations to generate equivalent positions $-x + 3/2, y, z$.

[16] Crystallographic data for **5**: $C_{18}H_{35}P_3$; $M_r = 344.37$ g mol^{-1}; $T = 293(2)$ K; $\lambda = 0.71073$ Å; orthorhombic; space group $P2_12_12_1$; $a = 9.631(2)$, $b = 10.707(2)$, $c = 20.808(4)$ Å; $V = 2145.7(7)$ Å^3; $Z = 4$; $\rho_{calcd} = 1.066$ Mg m^{-3}; $\mu = 2.72$ cm^{-1}; $F(000)$ 752; crystal dimensions $0.20 \times 0.10 \times 0.05$ mm^3; scanned θ range 2.14 to 26.11°; index range $-11 \le h \le 11$, $-13 \le k \le 13$, $-25 \le l \le 25$; measured reflections 16138; independent reflections 4160 ($R_{int} = 0.1289$); structure refinement: full-matrix least-squares to F^2; data/restraints/parameters 4160/20/246; GOF = 0.632; final R values $[I > 2\sigma(I)]$: $R_1 = 0.0392$, $wR_2 = 0.0657$; R values (all data): $R_1 = 0.1304$, $wR_2 = 0.0807$; absolute structural parameter 0.6 (2); residual electron density (largest maximum and minimum) 0.246 and −0.138 e Å^{-3}. CCDC-205753 (**3d**), 205754 (**4a**), and 205755 (**5**) contain the supplementary crystallographic data for this paper. These data can be obtained free of charge via www.ccdc.cam.ac.uk/conts/retrieving.html (or from the Cambridge Crystallographic Data Centre, 12, Union Road, Cambridge CB2 1EZ, UK; fax: (+44) 1223-336-033; or deposit@ccdc.cam.ac.uk).

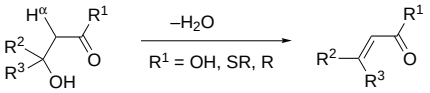
 © 2003 Wiley-VCH Verlag GmbH & Co. KGaA, Weinheim

Mechanisms of Enzyme Catalysis

Deprotonation of Enoxy Radicals: Theoretical Validation of a 50-Year-Old Mechanistic Proposal**

*David M. Smith, Wolfgang Buckel, and Hendrik Zipse**

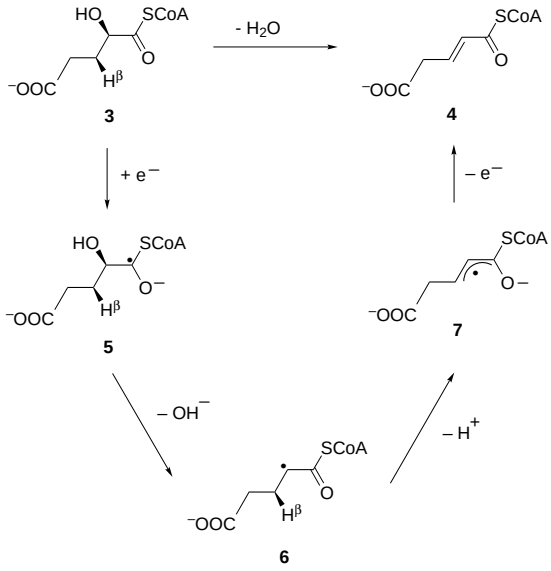
The dehydration or α,β elimination of water from biomolecules is a very common enzymatic reaction. Almost all dehydratases catalyze the removal of an hydroxy group in the β position of an electron-withdrawing carboxylate, thioester, or carbonyl group [Eq. (1)].



1 **2** (1)

The C–H^{α} bond of compounds such as **1** is activated and can be deprotonated relatively easily by a basic residue of an enzyme. In a typical substrate, such as 3-hydroxybutyryl-CoA (**1** with $R^1 = SCoA$, $R^2 = CH_3$, $R^3 = H$), the relevant C–H^{α} bond has an associated pK_a of approximately 21 in aqueous solution. Upon binding to enoyl-CoA hydratase (crotonase), this pK_a is reduced to approximately 8 by specific interactions with the enzyme. An essential glutamate residue appears to act as the base in the abstraction of the activated aliphatic proton.[1–3]

Several glutamate-fermenting anaerobic bacteria contain a dehydratase, which catalyses the reversible *syn*, α,β elimination of water from (*R*)-2-hydroxyglutaryl-CoA (**3**) to (*E*)-glutaconyl-CoA (**4**) (Scheme 1). In this case, however, the C–H^{β} bond to be cleaved is not activated ($pK_a \approx 40$) and in the reverse direction the OH^- group adds to the more electron-rich α-C atom of the polarized double bond. To explain these observations, a mechanism has been proposed in which the carbonyl group undergoes an "Umpolung" by one-electron reduction.[4] The resulting substrate-derived ketyl radical anion **5** (Scheme 1) may eliminate the α hydroxy group, leading to the enoxy radical **6**. Deprotonation (H^{β}) of this radical would yield the product-related ketyl radical anion **7**, which could be oxidized to the product **4**.[5–7]



Scheme 1. Proposed mechanism for the reversible *syn*, α,β elimination of water from (*R*)-2-hydroxyglutaryl-CoA (**3**).

The biochemical analyses of the two-component 2-hydroxyglutaryl-CoA dehydratase systems from the intestinal bacteria *Acidaminococcus fermentans* and *Clostridium symbiosum* indeed reveal the possibility of an electron transfer such as the one shown in Scheme 1.[8–10] Component A from *A. fermentans*, a homodimeric protein with a $[4Fe\text{-}4S]^{1+/2+}$ cluster between the two subunits, transfers an electron to component D under hydrolysis of ATP. Component D is a heterodimeric protein containing molybdenum(VI), reduced riboflavin-5′-phosphate ($FMNH_2$), and a $[4Fe\text{-}4S]^{2+}$ cluster. This ATP-driven electron transfer causes the formation of Mo^{V}, which through oxidation to Mo^{VI} quite probably generates the ketyl radical anion **5**. Oxidation of the second ketyl radical anion **7** is likely to reform Mo^{V}, so that a single electron transfer between the two components is sufficient to induce many catalytic cycles.

2-Hydroxyglutaryl-CoA dehydratase is not the only enzyme involved in the cleavage of an unactivated C–H^{β} bond. For example, the dehydration of 4-hydroxybutyryl-CoA to crotonyl-CoA, catalyzed by an oxygen-sensitive [4Fe-4S] cluster and FAD-containing enzyme from *Clostridium aminobutyricum*, also involves the loss of a proton from the β position of a thioester. In this case, it has been proposed that an enoxy radical (similar to **6** in Scheme 1) is generated by radical abstraction of the α hydrogen atom. Deprotonation of the β C atom of this radical leads to the ketyl radical anion of 4-hydroxycrotonyl-CoA, which can expel the hydroxy group to yield the dienoxy radical. Re-addition of the initially abstracted hydrogen atom at C4 yields the final product, crotonyl-CoA.[7]

The key feature of the proposed mechanisms for both these enzymes is that the β H atom is lost from the enoxy radical (e.g. **6**) and not from the substrate itself (e.g. **3**).

[*] Prof. Dr. H. Zipse, Dr. D. M. Smith
Department Chemie, Ludwig-Maximilians-Universität
Butenandtstrasse 13, 82131 München (Germany)
Fax: (+49) 89-2180-77738
E-mail: zipse@cup.uni-muenchen.de
Prof. Dr. W. Buckel
Laboratorium für Mikrobiologie, Philipps-Universität
Karl-von-Frisch Strasse, 35032 Marburg (Germany)

[**] This work was supported by the Deutsche Forschungsgemeinschaft (SPP "Radicals in Enzymatic Catalysis"). H.Z. and W.B. thank the Fonds der Chemischen Industrie for continuous support and D.M.S. thanks the Alexander von Humboldt Foundation for a research fellowship. We thank Prof. V. Barone for helpful discussions and technical assistance.

Supporting information for this article is available on the WWW under http://www.angewandte.org or from the author.

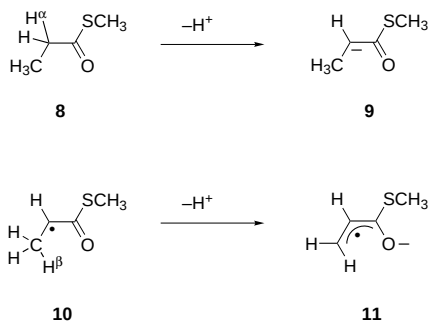
 DOI: 10.1002/anie.200250502 © 2003 Wiley-VCH Verlag GmbH & Co. KGaA, Weinheim

Almost 50 years ago, Sir John W. Cornforth suggested that an enoxy radical (derived by α-H-atom abstraction in a mechanism similar to that proposed for the dehydration of 4-hydroxybutyryl-CoA) might undergo facile deprotonation to a ketyl radical anion.[11] However, this suggestion has not since been proven by any experimental or theoretical data. Herein, we aim to quantify the acidity of the β position of the enoxy radical. We wish to determine whether the acidity of this radical is sufficiently enhanced over the closed-shell thioester to explain the apparent deprotonation at the unactivated position, or whether additional factors must be invoked to arrive at a satisfactory mechanism.

The acidities of simple thioesters have been studied experimentally by Richard and Amyes in D_2O at 25 °C, and a pK_a value of 21 ± 0.5 was determined for methyl thioacetate.[15] Much lower values were estimated for substituted phenylacetyl-CoA derivatives based on the measured values of analogously substituted phenlyacetone compounds by Ghisla and co-workers.[16] The estimated pK_a value for 4-nitrophenylacetyl-CoA amounts to 13.6. An additional observation made in this latter study is the short lifetime of the anions of phenylacetyl-CoA derivatives in aqueous basic solution, presumably as a result of rapid hydrolysis.

The theoretical prediction of absolute pK_a values has become possible in recent years owing to the advent of accurate continuum-solvation methods.[12–14] Even though the accuracy of this approach for compounds with protic hydrogen atoms is quite impressive, its application to acidic C–H open-shell systems has not yet been tested. Therefore, in this study, we apply an indirect approach in which the acidities of the enoyl radicals are compared with the known values of the closely related thioesters. Specifically, we compare herein the α deprotonation of methyl thiopropionate **8** (to give the corresponding anion **9**) with the β deprotonation of the propionate radical **10** to give the radical anion of methyl thioacrylate **11** (Scheme 2).

Figure 1 shows the optimum B3LY/Paug-cc-pVDZ structures of **8**–**11**. Although rather short C–S bond lengths are found for the neutral thioesters **8** and **10**, in line with expectations for a typical C–S single bond, much longer distances are found for the deprotonated forms **9** and **11**. This trend is particularly notable in **9** with a C–S bond length of 1.97 Å. The bond lengthening is partly a result of charge transfer from the acyl moiety to the sulfur atom, as can be seen by comparing the sulfur atomic charges in the neutral



Scheme 2. Model systems used to calculate pK_a values.

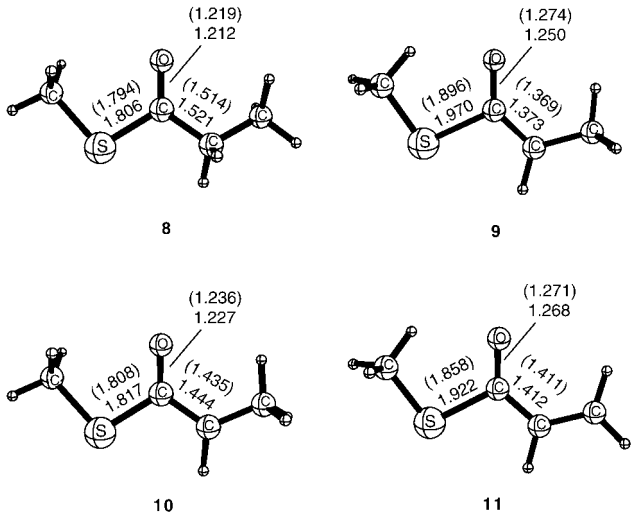


Figure 1. Structures of thioesters **8**–**11** optimized at the Becke3LYP/aug-cc-pVDZ level of theory. Data in brackets were obtained with the CPCM model for aqueous solvation.

systems (+0.18 e in **8** and +0.20 e in **10**) with those in the anionic systems (−0.07 e in **9** and −0.02 e in **11**). The increase in negative charge at sulfur, as well as the observed C–S bond stretching, suggests that the short lifetime of methyl thioacyl anions in aqueous solution may indeed be due to the rapid release of methylthiolate anions under these conditions.

Deprotonation also leads to a shortening of the bond between the carbonyl carbon atom and the α-C atom. This is most pronounced in the closed-shell system with C–C bond lengths of 1.52 Å in **8** and only 1.37 Å in **9**. The bond shortening is, in comparison, much smaller in the open-shell systems **10** and **11**. These structural changes are accompanied by an increase in the atomic charge of the α-C atom, which is almost neutral in **8** and **10** with charges of −0.03 e and +0.09 e, respectively, but clearly negative in **9** and **11** with respective atomic charges of −0.35 e and −0.22 e. This deprotonation-induced bond shortening is to be expected as a consequence of resonance stabilization of the developing negative charge by the adjacent carbonyl group. The effect is larger in the more localized case of **8** than in the corresponding open-shell system **10**, in which the C–C bond length is already shortened as a result of resonance stabilization of the initial radical.

Most of the unpaired spin density of **10** is localized at the α-C atom (NPA coefficient 0.75) with additional contributions from the carbonyl oxygen atom (0.18). This is certainly in accordance with expectations for a heteroallylic radical such as **10**. The spin density is slightly more delocalized in **11** with coefficients of 0.55 at the terminal β-C atom, 0.25 at the carbonyl carbon atom, and 0.17 at the carbonyl oxygen atom. This is very much in line with expectation for the LUMO structure of α,β-unsaturated carbonyl compounds.[17] The Lewis structures shown in Scheme 2 are most suitable to reflect the situation in both **10** and **11**.

Deprotonation of thioester **8** to yield a free proton and anion **9** is strongly endothermic in the gas phase (Table 1). Zero-point-corrected relative energies at 0 K, values includ-

 © 2003 Wiley-VCH Verlag GmbH & Co. KGaA, Weinheim

Table 1: Free energies of deprotonation and the difference in acidity between **8** and **10**.[a]

Level	**9**−**8**	**11**−**10**	$\Delta\Delta G$	ΔpK_a[a]
Gas phase				
ΔG (B3LY/Paug-cc-pVDZ)	+1472.2	+1424.4	47.8	8.4
ΔG (G3(MP2)(+)-RAD(p))	+1488.7	+1434.8	53.9	9.4
Aqueous solution (implicit solvation)[b]				
ΔG (G3(MP2)(+)-RAD(p))	+149.6	+106.9	42.7	7.5
Aqueous solution (explicit solvation)[c]				
ΔG (G3(MP2)(+)-RAD(p))			38.3	6.7

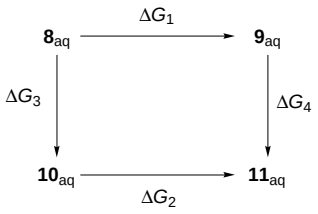
[a] $\Delta\Delta G$ in kJ mol$^-$, pK_a values are dimensionless, values for T = s98 K. [b] Obtained by using the CPCM continuum-solvation model, see text. [c] Obtained by using a periodic box of 566 TIP3P water molecules, see text.

ing enthalpic corrections to 298 K, and values including both enthalpic and entropic corrections are all in agreement with the fact that the radical **10** is approximately 50 kJ mol^{-1} more acidic than the closed-shell ester **8**. Because of this invariance, we have chosen to include only the free-energy differences in Table 1. Combination of the more reliable G3(MP2)(+)-RAD(p) energies with thermochemical corrections calculated at the B3LY/Paug-cc-pVDZ level yields free-energy values that are approximately 6 kJ mol^{-1} larger than those calculated at the lower level. Our best estimate for the difference in free energy of deprotonation between **8** and **10** in the gas phase therefore amounts to 53.9 kJ mol^{-1} at 298 K. According to $\Delta G = -RT\ln K$, this free-energy difference will effectively lower the pK_a value of **10** by 9.4 units relative to that of **8**.

For use in aqueous solution, the gas-phase values must be corrected for differences in free energies of solvation of all four species involved. The structures of thioesters **8**–**11** could, however, conceivably undergo considerable changes upon aqueous solvation, and therefore the structures were reoptimized using the CPCM continuum model. The structural parameter most strongly affected by the presence of the solvent field is the C–S ester bond in anions **9** and **11** (Figure 1). Most other structural parameters show only a small solvent effect.

Examination of the free energies of solvation from the implicit (CPCM) approach shows that aqueous solvation has a more pronounced effect on the dissociation of **8** than on that of **10**. This appears to be primarily a result of better solvation of the more localized enolate anion **9** relative to the delocalized radical anion **11**. The acidity difference predicted by the implicit solvation model is therefore lower than that calculated in the gas phase. After the inclusion of the CPCM solvation effects, the acidity enhancement is calculated to be 42.7 kJ mol^{-1} or 7.5 pK_a units at 298 K.

In addition to the implicit solvent calculations outlined above, we also carried out explicit evaluation of the effect of solvation on the acidity difference, in a periodic box of 566 TIP3P water molecules. As the direct calculation of charge separation (such as that involved in deprotonation) is difficult, we made use of the thermodynamic cycle shown in



$\Delta\Delta G_{solv} = \Delta G_2 - \Delta G_1$

$= \Delta G_4 - \Delta G_3$

Scheme 3. Free-energy cycle used in conjunction with the explicit solvation model.

Scheme 3.[18] Instead of directly calculating the difference in free-energy of solvation ($\Delta G_2 - \Delta G_1$), we combined the difference in solvation energies between the two neutral systems **8** and **10** (ΔG_3) with the difference in solvation energies between the two anionic systems **9** and **11** (ΔG_4). Because free energy is a state function, the equation shown at the bottom of Scheme 3 holds and we obtain a valid result for the relative free energy of solvation.

The explicit solvation calculations provide support for our previous conclusion regarding the more favorable solvation of **9** with respect to **11**. In addition, the agreement between the two approaches (implicit and explicit) is quite impressive, with the explicit approach predicting an acidity difference between **8** and **10** of 38.8 kJ mol^{-1} or 6.7 pK_a units. Given the uncertainties involved in the calculations, our best estimate for the pK_a enhancement of **10** over **8** is then 7.1 ± 0.4. Assuming a pK_a value of 21 ± 0.5 for the α-CH group of thioester **8** in aqueous solution, we would therefore predict a pK_a value of 14 for the β-CH group in radical **10**. Although a pK_a value of 14 for the β position might not be considered particularly acidic, it should be noted that the pK_a value of the proton at C2 of thiaminodiphosphate (12.7 ± 0.1)[19] is in the same range. In many enzymatic reactions, the carbanion of thiaminodiphosphate is known to act as a nucleophile in C–C bond cleavage adjacent to carbonyl groups. For example, the decarboxylation of pyruvate to acetaldehyde is one reaction to make use of such a mechanism. Furthermore, the β position in **10** is calculated to be more activated (acidic) than the α position in typical hydrolyase substrates such as 3-hydroxybutyryl-CoA. However, as in the case of the latter substrate, it is likely that the enzyme is still required to provide additional stabilizing interactions to deprotonate the enoxy radical efficiently under normal physiological conditions.

Given that the pK_a value of the β position in closed-shell substrates such as **3** is approximately 40, our prediction corresponds to a radical-induced pK_a enhancement of more than 25 orders of magnitude! This far exceeds the established radical-induced pK_a enhancement for the hydroxy groups in aliphatic alcohols.[20] For example, the pK_a values of the hydroxy groups of ethylene glycol are shifted from values of around 17 to 9.8 upon radical formation. Although significant, this corresponds to a radical-induced pK_a shift of "only" 7 pK_a units.

As mentioned previously, 2-hydroxyglutaryl-CoA dehydratase is not the only enzyme that employs a radical

 © 2003 Wiley-VCH Verlag GmbH & Co. KGaA, Weinheim

mechanism to activate the β position of carbonyl compounds. This fact, combined with the magnitude of the calculated pK_a enhancement in the current work, makes it appear likely that in the anaerobic world there are more enzymes to be discovered that make use of the facile deprotonation of an enoxy radical.[19]

Experimental Section

Geometry optimizations were performed for all four species (**8, 9, 10**, and **11**) in the gas phase at the Becke3LYP/aug-cc-pVDZ level of theory.[21,22] Zero-point vibrational energies and thermochemical corrections were calculated at this same level without any scaling. The charge- and spin-density distributions were analyzed by the Natural Population Analysis (NPA) method.[23]

Improved energetics were evaluated with a slightly modified version of the G3(MP2)(+)-RAD(p) procedure.[24] This technique is a modification of the G3(MP2) method[25] in which a restricted-open-shell coupled-cluster calculation (RCCSD(T)/6-31+G(d)) replaces the UQCISD(T)/6-31G(d) calculation and the basis-set extension is evaluated with restricted-open-shell perturbation theory (ROMP2) rather than with the unrestricted formalism (UMP2). The only difference between the method outlined in reference [24] and that employed in this case is the use of geometries and frequencies obtained with the Becke3LYP/aug-cc-pVDZ level of theory.

We chose to include the effects of aqueous solvation with two different approaches. The first (implicit) approach employed the CPCM continuum-solvation method in combination with the UAHF cavity model at the Becke3LYP/aug-cc-pVDZ level of theory.[26] To account for structural relaxation in the aqueous environment, we reoptimized all structures with the CPCM model prior to calculating solvation energies. In the second (explicit) approach, we solvated each molecule in a periodic box of 566 TIP3P[27] waters and used thermodynamic integration[28] to calculate relative free energies of solvation. Further information on these calculations can be found in the Supporting Information. The CCSD(T) calculations were performed with MOLPRO,[29] other gas-phase and implicit solvation calculations employed Gaussian 98,[30] while all explicit solvation calculations were carried out with the AMBER[31] program suite.

Received: November 7, 2002 [Z50502]

Keywords: ab initio calculations · acidity · C—H activation · enzyme catalysis · radicals

[1] B. J. Bahnson, V. E. Anderson, G. A. Petsko, *Biochemistry* **2002**, *41*, 2621.
[2] P. Willadsen, H. Eggerer, *Eur. J. Biochem.* **1975**, *54*, 247.
[3] B. J. Bahnson, V. E. Anderson, *Biochemistry* **1991**, *30*, 5894.
[4] W. Buckel, R. Keese, *Angew. Chem.* **1995**, *107*, 1595; *Angew. Chem. Int. Ed. Engl.* **1995**, *34*, 1502.
[5] U. Müller, W. Buckel, *Eur. J. Biochem.* **1995**, *230*, 698.
[6] W. Buckel, *FEBS Lett.* **1996**, *389*, 20.
[7] W. Buckel, B. T. Golding, *FEMS Microbiol. Rev.* **1999**, *22*, 523.
[8] M. Hans, J. Sievers, U. Müller, E. Bill, J. A. Vorholt, D. Linder, W. Buckel, *Eur. J. Biochem.* **1999**, *265*, 404.
[9] M. Hans, W. Buckel, E. Bill, *Eur. J. Biochem.* **2000**, *267*, 7082.
[10] M. Hans, E. Bill, I. Cirpus, A. J. Pierik, M. Hetzel, D. Alber, W. Buckel, *Biochemistry* **2002**, *41*, 5873.
[11] J. W. Cornforth, *J. Lipid Res.* **1959**, *1*, 3.
[12] I. A. Topol, G. J. Tawa, S. K. Burt, A. A. Rashin, *J. Phys. Chem. A* **1997**, *101*, 10075.
[13] G. Schüürmann, M. Cossi, V. Barone, J. Tomasi, *J. Phys. Chem. A* **1998**, *102,* 6706.
[14] a) M. D. Liptak, G. C. Shields, *Int. J. Quantum Chem.* **2001**, *85*, 727; b) A. M. Toth, M. D. Liptak, D. L. Phillips, G. C. Shields, *J. Chem. Phys.* **2001**, *114*, 4595; c) M. D. Liptak, G. C. Shields, *J. Am. Chem. Soc.* **2001**, *123,* 7314; d) M. D. Liptak, K. C. Gross, P. G. Seybold, S. Feldgus, G. C. Shields, *J. Am. Chem. Soc.* **2002**, *124*, 6421.
[15] T. L. Amyes, J. P. Richard, *J. Am. Chem. Soc.* **1992**, *114*, 10297.
[16] P. Vock, S. Engst, M. Eder, S. Ghisla, *Biochemistry* **1998**, *37*, 1848.
[17] a) W. J. Jorgensen, L. Salem, *The Organic Chemist's Book of Orbitals*, Academic Press, San Diego, **1973**; b) T. Clark, R. Koch, *The Chemist's Electronic Book of Orbitals*, Springer, Heidelberg, **1999**.
[18] a) W. L. Jorgensen, *Acc. Chem. Res.* **1989**, *22*, 184; b) P. A. Kollman, *Chem. Rev.* **1993**, *93*, 2395.
[19] R. F. W. Hopmann, G. P. Brugnoni, *Nature New Biol.* **1973**, *246*, 157.
[20] a) K.-D. Asmus, A. Henglein, A. Wigger, G. Beck, *Ber. Bunsen-Ges.* **1966**, *70*, 756; b) G. P. Laroff, R. W. Fessenden, *J. Phys. Chem.* **1973**, *77*, 1283; c) S. Steenken, M. J. Davies, B. C. Gilbert, *J. Chem. Soc. Perkin Trans. 2* **1986**, 1003; d) R. Lenz, B. Giese, *J. Am. Chem. Soc.* **1997**, *119*, 2784.
[21] a) A. D. Becke, *J. Chem. Phys.* **1993**, *98*, 5648; b) C. Lee, W. Yang, R. G. Parr, *Phys. Rev. B* **1988**, *37*, 785.
[22] T. H. Dunning, Jr., *J. Chem. Phys.* **1989**, 90, 1007.
[23] A. E. Reed, L. A. Curtiss, F. Weinhold, *Chem. Rev.* **1988**, *88*, 899.
[24] S. D. Wetmore, D. M. Smith, J. T. Bennett, L. Radom, *J. Am. Chem. Soc.* **2002**, *124*, 14054.
[25] a) A. G. Baboul, L. A. Curtiss, P. C. Redfern, K. Raghavachari, *J. Chem. Phys.* **1999**, *110*, 76500; b) L. A. Curtiss, P. C. Redfern, K. Raghavachari, V. Rassolov, J. A. Pople, *J. Chem. Phys.* **1999**, *110*, 4703.
[26] a) V. Barone, M. Cossi, J. Tomasi, *J. Chem. Phys.* **1997**, *107*, 3210; b) V. Barone, M. Cossi, *J. Phys. Chem. A* **1998**, *102*, 1995; c) C. Amovilli, V. Barone, R. Cammi, E. Cances, M. Cossi, B. Mennucci, C. S. Pomelli, J. Tomasi, *Adv. Quantum Chem.* **1998**, *32*, 227.
[27] W. J. Jorgensen, J. Chandrasekhar, J. Madura, M. L. Klein, *J. Chem. Phys.* **1983**, *79*, 926.
[28] T. P. Straatsma, J. A. McCammon, *J. Chem. Phys.* **1991**, *95*, 1175.
[29] MOLPRO 2000: H.-J. Werner and P. J. Knowles with contributions from R. D. Amos, A. Bernhardsson, A. Berning, P. Celani, D. L. Cooper, M. J. O. Deegan, A. J. Dobbyn, F. Eckert, C. Hampel, G. Hetzer, T. Korona, R. Lindh, A. W. Lloyd, S. J. McNicholas, F. R. Manby, W. Meyer, M. E. Mura, A. Nicklass, P. Palmieri, R. Pitzer, G. Rauhut, M. Schütz, H. Stoll, A. J. Stone, R. Tarroni, T. Thorsteinsson.
[30] Gaussian 98 (Revision A.7), M. J. Frisch, G. W. Trucks, H. B. Schlegel, G. E. Scuseria, M. A. Robb, J. R. Cheeseman, V. G. Zakrzewski, J. A. Montgomery, R. E. Stratmann, J. C. Burant, S. Dapprich, J. M. Millam, A. D. Daniels, K. N. Kudin, M. C. Strain, O. Farkas, J. Tomasi, V. Barone, M. Cossi, R. Cammi, B. Mennucci, C. Pomelli, C. Adamo, S. Clifford, J. Ochterski, G. A. Petersson, P. Y. Ayala, Q. Cui, K. Morokuma, D. K. Malick, A. D. Rabuck, K. Raghavachari, J. B. Foresman, J. Cioslowski, J. V. Ortiz, B. B. Stefanov, G. Liu, A. Liashenko, P. Piskorz, I. Komaromi, R. Gomperts, R. L. Martin, D. J. Fox, T. Keith, M. A. Al-Laham, C. Y. Peng, A. Nanayakkara, C. Gonzalez, M. Challacombe, P. M. W. Gill, B. G. Johnson, W. Chen, M. W. Wong, J. L. Andres, M. Head-Gordon, E. S. Replogle, J. A. Pople, Gaussian, Inc., Pittsburgh, PA, **1998**.
[31] D. A. Case, D. A. Pearlman, J. W. Caldwell, T. E. Cheatham III, W. S. Ross. C. L Simmerling, T. A Darden, K. M. Merz, R. V. Stanton, A. L. Cheng, J. J. Vincent, M. Crowley, V. Tsui, R. J. Radmer, J. Duan, J. Pitera, I. Massova, G. L. Seibel, U. C. Singh, P. K. Weiner, P. A. Kollman, AMBER 6, University of California, San Francisco, **1999**.

 © 2003 Wiley-VCH Verlag GmbH & Co. KGaA, Weinheim

Cover Picture



Roland Boese,* Michael T. Kirchner, W. Edward Billups, and Lewis R. Norman

By in situ crystallization under pressure in a capillary, two different phases of acetylene complexes were grown simultaneously. The crystals gave the superimposed diffraction patterns shown in the background. From the reflections of the 1:1 phase (red) two cell parameters can be determined directly. In the reflections of the 1:2 phase (white) another reciprocal lattice is visible on viewing the picture from the side. For more information see the article by R. Boese et al. on page 1961 ff.

Contents

Web Sites

Separation Science: separationsNOW — 1888 — United in Separation — *F. Svec*

Books

Human and Ecological Risk Assessment Theory and Practice — 1889 — Dennis J. Paustenbach — *reviewed by H. Hulpke*

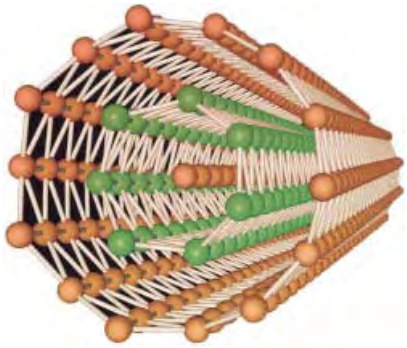
Valence Bond Methods — 1889 — Gordon A. Gallup — *reviewed by M. Goez*

Highlights

Gold Clusters

P. Schwerdtfeger* — 1892 – 1895

Gold Goes Nano—From Small Clusters to Low-Dimensional Assemblies



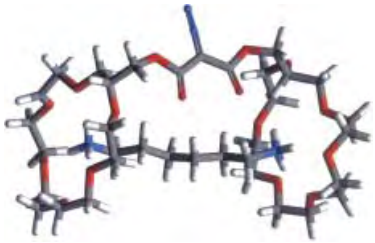
Gold is not as noble as it is widely assumed—at least in the form of nanostructured gold clusters or the depicted multiwalled nanotubes. Recent progress shows the potential use of such structures, for example, in catalysis, molecular electronics, or as bioconjugate probes for gene analysis.

Molecular Mousetrap

M. Schäfer* — 1896 – 1899

Supramolecular Crown Ether Adducts in the Gas Phase: From Molecular Recognition of Amines to the Covalent Coupling of Host/Guest Molecules

The diazomalonic acid diester of [18]crown-6-methanol forms a noncovalent complex (see picture) with doubly protonated 1,6-diaminohexane which can be transferred intact into the gas phase. After collision-induced dissociation, the reactive carbene intermediate reacts as a molecular mousetrap. The successful formation of an intermolecular covalent coupling between the host and the guest molecule can be observed by subsequent MS/MS experiments.

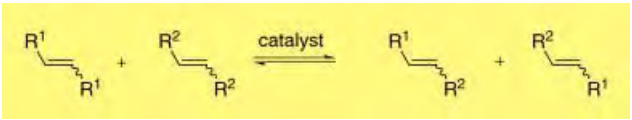


Reviews

Cross-Metathesis of Olefins

S. J. Connon, S. Blechert* — 1900 – 1923

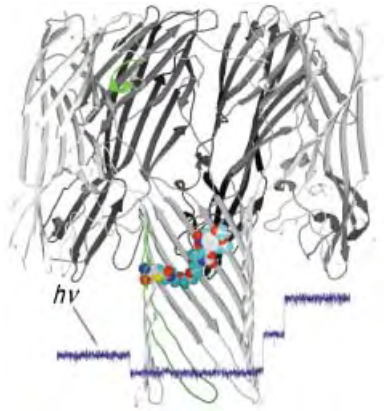
Recent Developments in Olefin Cross-Metathesis



It's all in the catalyst! The development of new catalysts has catapulted olefin cross-metathesis (see scheme) to the forefront of modern synthetic methods in organic chemistry. This reaction is one of the most practical and versatile methods for the formation of C–C bonds.

© 2003 Wiley-VCH Verlag GmbH & Co. KGaA, Weinheim

Communications

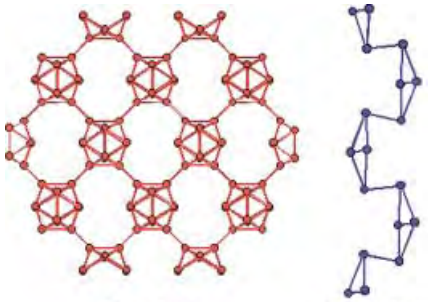


An electrical detection method was used to monitor a three-step reaction at the single-molecule level as it occurs within a protein pore (see picture). The reaction involved the breakdown of a protected carbamic acid and was initiated with light. Rate constants for the reaction could be determined by measuring the current multiple times. This approach reveals reactive intermediates, uncovers minor pathways, and quantifies the kinetics of steps invisible in conventional kinetic techniques.

Reaction Kinetics in a Pore

T. Luchian, S.-H. Shin, H. Bayley* ——— **1926 – 1929**

Kinetics of a Three-Step Reaction Observed at the Single-Molecule Level



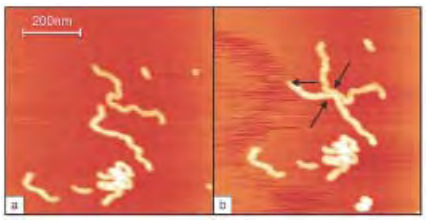
Unlike the original form of SiB_3, which has a huge compositional spread in its Si/B ratio and a crystal structure with Si atoms randomly distributed over all its B_{12} cages, the new form of SiB_3 (β form; see structure) is stoichiometrically and crystallographically ordered. The clear segregation of Si and B atoms in the new form is believed to be responsible for its enhanced oxidation resistance observed at high temperatures.

An Oxidation-Resistant Semiconductor

J. R. Salvador, D. Bilc, S. D. Mahanti, M. G. Kanatzidis* ——— **1929 – 1932**

Stabilization of β-SiB_3 from Liquid Ga: A Boron-Rich Binary Semiconductor Resistant to High-Temperature Air Oxidation

"Move-connect-prove" is the sequence that is employed to join and shape two individual strands of dendronized polymers. A scanning force microscope is used to move and shape the strands (picture a→b); the connection is obtained by UV irradiation of the sample, and tested by pulling on the connected polymer chains.



Connecting Individual Polymer Chains

J. Barner, F. Mallwitz, L. Shu, A. D. Schlüter,* J. P. Rabe* ⎯ **1932 – 1935**

Covalent Connection of Two Individual Polymer Chains on a Surface: An Elementary Step towards Molecular Nanoconstructions

For the USA and Canada:
ANGEWANDTE CHEMIE International Edition (ISSN 1433-7851) is published weekly by Wiley-VCH PO Box 191161, D 69451 Weinheim, Germany. Air freight and mailing in the USA by Publications Expediting Inc. 200 Meacham Ave., Elmont, NY 11003. Periodicals postage paid at Jamaica NY 11431. US POSTMASTER: send address changes to *Angewandte Chemie*, Wiley-VCH, 111 River Street, Hoboken, NJ 07030. Annual institutional subscription price for institutions: Europe € 2998.00/3148.00. Outside Europe US$ 3718.00/3904.00 (valid for print or electronic/print and electronic delivery); for individuals who are personal members of a national chemical society, or whose institution already subscribes, or who are retired or self-employed consultants, print only (including postage and handling charges): Europe € 248.00/Outside Europe US$ 348.00.

 © 2003 Wiley-VCH Verlag GmbH & Co. KGaA, Weinheim

Contents

Arenes on Metal Clusters

J. P.-K. Lau, Z.-Y. Lin, W.-T. Wong* ——— **1935 – 1937**

The Molecular Structure of $[Os_3Rh_4(\mu_3\text{-}\eta^1\text{:}\eta^1\text{:}\eta^1\text{-}C_6H_5CH_3)(CO)_{13}]$: A Face-Capping Bonding Mode for Arenes in Organometallic Clusters

Rhodium gets a new flat cap: A novel face-capping mode of toluene on the title $\{Os_3Rh_4\}$ cluster is observed (see structure; Os blue, Rh green, C gray, O red, H white). The cluster is obtained from the reaction of $[Os_3Rh(\mu\text{-}H)_3(CO)_{12}]$ with toluene in the presence of an excess amount of 4-vinylphenol under reflux for 2 h. The new cluster has relatively short metal–metal bonds and an electron count of only 92, which is four electrons less than expected.



Inorganic–Organic Hybrid Materials

C.-Y. Cheng, S.-J. Fu, C.-J. Yang, W.-H. Chen, K.-J. Lin,* G.-H. Lee, Y. Wang ——— **1937 – 1940**

NCHU-3: A Crystalline Inorganic-Organic Hybrid Molecular Sieve with Extra-Large Cages



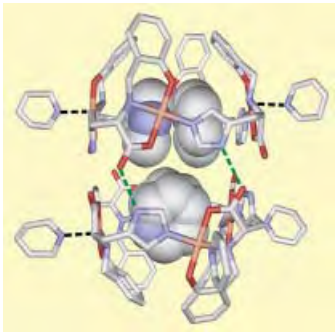
A Chinese-vaselike cage, depicted, is contained within the crystalline nanoporous $[Ga_2(VO)_3K_2(OH_2)_3(C_2H_4P_2O_6)_4(H_2O)_{13}]$ structure, NCHU-3, and is thermally stable up to 550 °C. NCHU-3 exhibits a highly reversible lithium-ion-intercalation and de-intercalation cycle between +3 and +5 volts. Such cyclability is a key aspect of rechargeable lithium battery cathode materials.

Self-Assembled Cu-Based Capsule

M. A. Alam, M. Nethaji,* M. Ray* ——— **1940 – 1942**

Synthesis of a Self-Assembled Molecular Capsule that Traps Pyridine Molecules by a Combination of Hydrogen Bonding and Copper(II) Coordination

Copper(II) complexes of a tetradentate ligand self-assemble in pyridine to form two slightly different tetrameric units. Hydrogen bonding between the tetramers forms a capsular cavity that traps four molecules of pyridine (see picture).

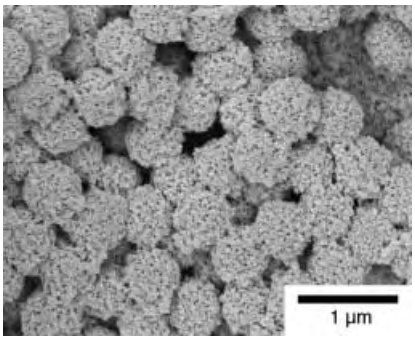


Tunable Cavity of Titania Spheres

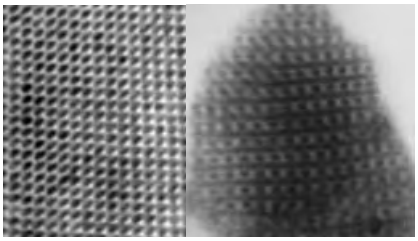
Z. Yang,* Z. Niu, Y. Lu,* Z. Hu, C. C. Han ——— **1943 – 1945**

Templated Synthesis of Inorganic Hollow Spheres with a Tunable Cavity Size onto Core–Shell Gel Particles

Titania/polymer capsules and hollow titania spheres are prepared by using sulfonated-polystyrene core–shell gel particles as templates. The titania shell thickness and the cavity size are controlled in the entire particle radius range. If an electric field is applied during synthesis, hollow spheres with pillared surfaces (depicted) are produced.



 © 2003 Wiley-VCH Verlag GmbH & Co. KGaA, Weinheim

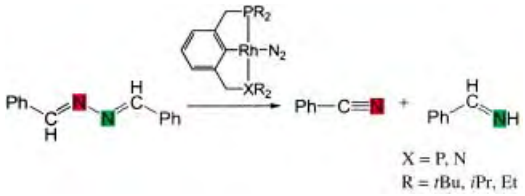


Order from disorder: Highly ordered nanocrystal super-lattices accommodating identical tin particles spontaneously crystallize from a dispersion displaying no order. Two structure types were identified, a noncompact one displaying uniform orientations of the particles atomic planes, and an unprecedented one containing monodisperse larger and more anisotropic particles (see electron micrographs). Which structure is formed depends on the reaction conditions used.

Tin Superstructures

K. Soulantica, A. Maisonnat, M.-C. Fromen, M.-J. Casanove, B. Chaudret* ——— 1945 – 1949

Spontaneous Formation of Ordered 3D Super-Lattices of Nanocrystals from Polydisperse Colloidal Solutions

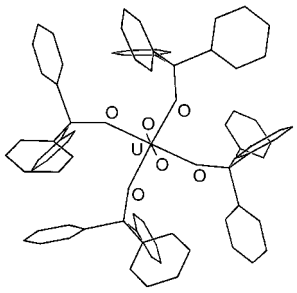


An unprecedented reaction: Dinitrogen pincer Rh complexes react with azines in a moderately catalytic fashion by "nonsymmetrical" N–N bond cleavage to the corresponding nitriles and imines (see scheme).

Novel Azine Reactivity

R. Cohen, B. Rybtchinski, M. Gandelman, L. J. W. Shimon, J. M. L. Martin,* D. Milstein* ——— 1949 – 1952

Novel Azine Reactivity: Facile N–N Bond Cleavage, C–H Activation, and N–N Coupling Mediated by Rh^{I}

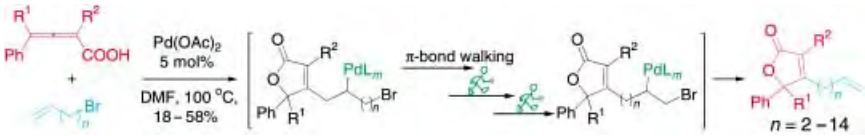


Variations in the structural parameters of the analogous $[UO_2]^{2+}$ and $[UO_2]^{+}$ compounds, $[UO_2(OPPh_3)_4](OTf)_n$ ($n = 1, 2$; picture shows the cation of the $n = 1$ complex), allow a direct comparison of the observed data with that obtained from EXAFS studies in solution, and from theoretical studies.

Structures of Uranyl Complexes

J.-C. Berthet,* M. Nierlich, M. Ephritikhine ——— 1952 – 1954

Isolation of a Uranyl $[UO_2]^{+}$ Species: Crystallographic Comparison of the Dioxouranium(V) and (VI) Compounds $[UO_2(OPPh_3)_4](OTf)_n$ ($n = 1, 2$)



Taking the bond for a walk: An ω-1-alkenyl group was introduced at the β position of butenolides by the Pd^{II}-catalyzed coupling/cyclization of 2,3-allenoic acids with ω-1-alkenyl halides (see scheme). The active Pd^{II} catalyst was regenerated through the combination of cyclic oxypalladation–carbopalladation with repeated dehydropalladation/hydropalladation–dehalopalladation.

Palladium-Catalyzed Reactions

S. Ma,* Z. Yu ——— 1955 – 1957

"Walking" of the C–C π Bond over Long Distances in Pd-Catalyzed Reactions of 2,3-Allenoic Acids with ω-1-Alkenyl Halides

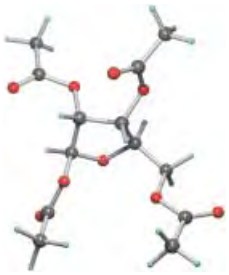
 © 2003 Wiley-VCH Verlag GmbH & Co. KGaA, Weinheim

Contents

A Disappearing Polymorph

P. Bombicz, M. Czugler, R. Tellgren, A. Kálmán* ——— **1957 – 1960**

A Classical Example of a Disappearing Polymorph and the Shortest Intermolecular H···H Separation Ever Found in an Organic Crystal Structure

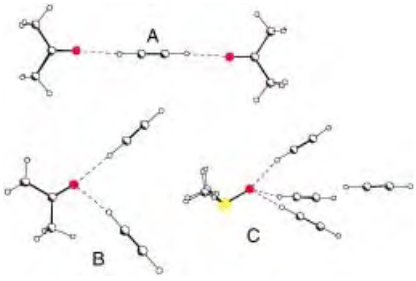


Missing in action: Neutron and X-ray diffraction studies at low temperatures reveal the delicate balances of attractive and repulsive intermolecular interactions in the dimorphs of 1,2,3,5-tetra-*O*-acetyl-β-D-ribofuranose (the less stable polymorph is shown, O red, H blue, C gray). Very short intermolecular H···H contacts which are only present in the less stable crystal form are responsible for the disappearance of this polymorph.

Crystal Engineering with Acetylene

R. Boese,* M. T. Kirchner, W. E. Billups, L. R. Norman ——— **1961 – 1963**

Cocrystallization with Acetylene: Molecular Complexes with Acetone and Dimethyl Sulfoxide

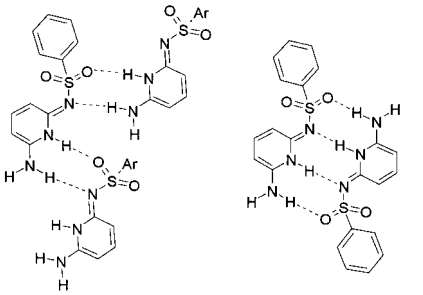


Different phases: Molecular complexes of acetylene and acetone or DMSO are formed simultaneously in different phases. Crystalline acetylene:actone 1:2 (A) and 1:1 (B), as well as acetylene:DMSO 2:1 (C) complexes have been obtained by in situ cocrystallization under pressure in a capillary with the use of an IR laser. The crystal structures may be interpreted as a "frozen" situation of the liquids.

Crystal Structure Predictions

R. K. R. Jetti, R. Boese,* J. A. R. P. Sarma,* L. S. Reddy, P. Vishweshwar, G. R. Desiraju* ——— **1963 – 1967**

Searching for a Polymorph: Second Crystal Form of 6-Amino-2-Phenylsulfonylimino-1,2-Dihydropyridine

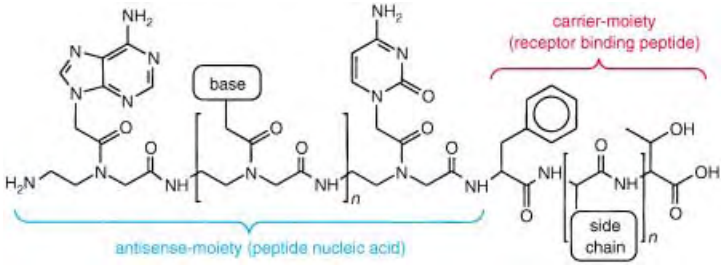


Too difficult to predict? The second polymorph of the title compound, is presented. A comparison of hydrogen-bond patterns and lattice energies suggests that the previously obtained form (see picture, left) is a kinetic polymorph, while the second polymorph (right) is most likely to represent the more thermodynamically stable form. The new polymorph, however, has two symmetry-independent molecules, which rendered it beyond the limit of previous structural predictions.

Tumor-Specific Transport

W. Mier,* R. Eritja, A. Mohammed, U. Haberkorn, M. Eisenhut ——— **1968 – 1971**

Peptide–PNA Conjugates: Targeted Transport of Antisense Therapeutics into Tumors



Tumor-specific accumulation of antisense therapeutics: The conjugation of a receptor-binding peptide allows for the first time the selective transport of oligonucleotide analogues into tumor tissue. By using the *tert*-butyloxycarbonyl (Boc) protecting group stratergy, hybrids of peptide nucleic acids and peptides are accessible that accumulate in tumor tissue at a tenfold higher concentration than the free peptide nucleic acid.

 © 2003 Wiley-VCH Verlag GmbH & Co. KGaA, Weinheim

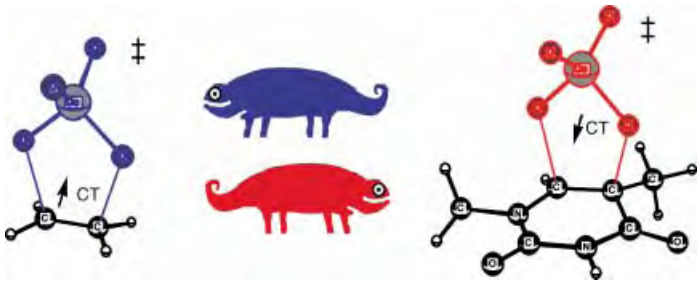
Like "inverse" P_4O_{10}, a nearly tetrahedral Ga_4P_{10} shell encloses a gallium-rich core with a distorted tetrahedral Ga_4 center in the neutral metalloid cluster compound $[Ga_{16}(PtBu_2)_{10}]$.



Metalloid Gallium Cluster

J. Steiner, G. Stößer, H. Schnöckel* ——— **1971 – 1974**

$[Ga_{16}(PtBu_2)_{10}]$: A Gallium Phosphide Sheathed Core of Four Naked Ga Atoms?



A chameleon oxidant: In Sharpless dihydroxylation of C=C bonds osmium tetraoxide is shown to be a chameleon oxidant. Quantum chemical studies show that osmium tetraoxide attacks the C=C bond of nucleobases either as an electrophile (blue) or a nucleophile (red) depending upon the nature of the substrate (see scheme; CT = charge transfer).

Os in the Sharpless Dihydroxylation

D. V. Deubel* ——— **1974 – 1977**

Reactivity of Osmium Tetraoxide Towards Nitrogen Heterocycles: Implications for the Molecular Recognition of DNA Mismatch

Communications labeled with this symbol have been judged by two referees as being "very important papers".

The publication of Communications labeled with this symbol has been accelerated because of their topical or highly competitive nature.

The issues for April 2003 appeared online on the following dates
Issue 13: April 7. · Issue 14: April 10. · Issue 15: April 16.

Sources

Product and Company Directory

You can start the entry for your company in "Sources" in any issue of *Angewandte Chemie*.

If you would like more information, please do not hesitate to contact us.

Wiley-VCH Verlag – Advertising Department
Tel.: 0 62 01 - 60 65 65
Fax: 0 62 01 - 60 65 50
E-Mail: MSchulz@wiley-vch.de

Service

Keywords ——— *1978*

Authors ——— *1979*

Sources ——— *A25*

Vacancies ——— *1886*

Preview ——— *1981*

 © 2003 Wiley-VCH Verlag GmbH & Co. KGaA, Weinheim

Gold Clusters

Gold Goes Nano—From Small Clusters to Low-Dimensional Assemblies**

*Peter Schwerdtfeger**

Keywords:
catalysis · cluster compounds · gold · metal-metal interactions · nanostructures

Bulk gold is a noble metal and unlike its lighter congeners of Group 11, copper and silver, was for a long time not considered important in catalysis and surface science in general. Although it was known that atomic gold in the gas phase can be very reactive, it was not until 1987 that the interest in gold nanostructures was really awakened through the report by Haruta et al. on CO oxidation on supported gold catalysts such as Au/TiO_2 or Au/Fe_2O_3 at low temperatures.[1] Since then nanocrystalline gold compounds have been the subject of intense research and have found far-reaching applications in areas such as catalysis, sensors, molecular electronics, or as bioconjugate probes for amplification tags in gene analysis, antibody or antigen detection, DNA sequencing, or gene mapping.[1,2] For example, Wang et al. recently succeeded in attaching 1.4 nm gold clusters to the sphere of the cowpea mosaic virus (CPMV) of a diameter of 30 nm (Figure 1).[3]

While most studies have so far concentrated on pure gold nanoclusters of different structure and size, the recent discovery of the extremely stable mixed icosahedral gold clusters $W@Au_{12}$ and $Mo@Au_{12}$ (Figure 2A) by Wang and coworkers[4]—as predicted earlier by theoretical studies by Pyykkö and Runeberg[5]—opens up the field to new nanosized gold materials, in which the central atom "impurity" plays a vital role in fine-tuning electronic properties.

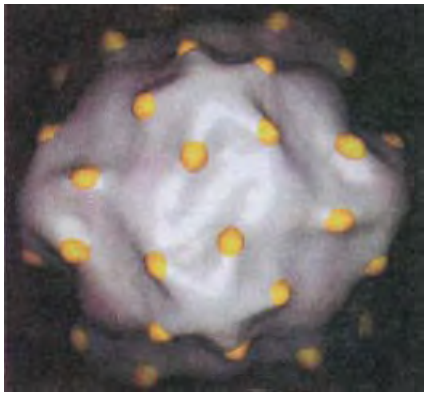


Figure 1. Cowpea mosaic virus labeled with 1.4-nm gold clusters.[3].

It has been known for a long time that gold forms a wide variety of cluster compounds that are quite distinct from those of the other elements of Group 11. Some of the larger clusters were characterized only recently, such as $[Au_{10}(PPh_3)_7\{(S_2C_2(CN)_2\}_2]$ (Figure 2C),[6] $[Au_{13}(PR_3)_{10}Cl_2(PF_6)_3]$ (distorted icosahedral gold core), $[Au_{39}(PR_3)_{14}Cl_8]$ (hexagonally close-packed gold core), $[Au_{55}(PR_3)_{12}Cl_6]$, or $[Au_{73-75}(PR_3)_{15-17}Cl_x]$ (R any organic ligand).[7] The color of these compounds ranges from yellow to orange, red, and even green (due to an additional absorption maximum in the blue visible range). A mixture of such cluster compounds is available under the trade name Nanogold. Similarly, element-centered ligated gold cluster compounds such as the octahedral $[\{C@Au_6\}(Ph_3P)_6X_2]$[8] (Figure 2D) or the icosahedral $[\{Pd@Au_{12}\}(Ph_3P)_8Cl_4]$ clusters (Figure 2B) are known.[9]

The strong tendency of gold to form metal–metal interactions (aurophilicity) is attributed to large relativistic effects in gold, which have been studied extensively in the past.[10] Gold undergoes especially strong interactions with electropositive ligands (metals) that donate electron density to the relativistically contracted and stabilized gold 6s orbital, and thus enhance the aurophilic interactions. This rationalizes the unusual stability of gold and mixed metal-gold clusters. However, the accurate dynamic simulation and determination of electronic properties of such heavy-atom clusters is currently a nontrivial issue. For example, the cluster size at which the nonmetal (band gap δ between occupied and unoccupied state $> kT$) to metal ($\delta < kT$) transition occurs is often a controversial and much debated issue. The challenges faced by theoreticians are illustrated by the conductivity of bulk gold, which is $4.3 \times 10^7\ \Omega^{-1}m^{-1}$, several orders of magnitude larger (!) than that of a 2-nm-sized gold cluster ($1.4 \times 10^{-3}\ \Omega^{-1}m^{-1}$).[11]

Discrete icosahedral clusters of bare metals are quite common since M_{13} clusters with I_h symmetry belong to the class of magic clusters. All current simulations using two-body potentials (Lennard-Jones, Morse, or some extensions of such interaction potentials) seem to favor this cluster size and structure.[12] It is therefore of no surprise that I_h–symmetrical Au_{13} is reasonably

[*] Prof. Dr. P. Schwerdtfeger
Department of Chemistry
University of Auckland
Private Bag 92019, Auckland (New Zealand)
Fax: (+64) 9-3737-422
E-mail: p.schwerdtfeger@auckland.ac.nz

[**] This work was supported by the Marsden Fund managed by the Royal Society of New Zealand. The author thanks A. Hammerl, H. Häkkinen, and H. Idriss for help and comments, and Y. Kondo (Tokyo) and W. Ho (Irvine) for providing high quality images for their gold nanostructures.

 © 2003 Wiley-VCH Verlag GmbH & Co. KGaA, Weinheim DOI: 10.1002/anie.200201610

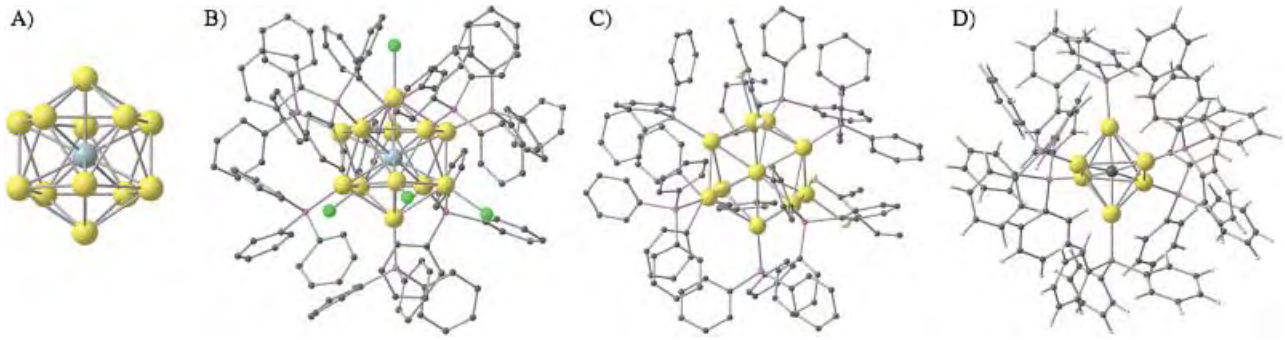


Figure 2. The structures of W@Au_{12} (A) (closest Au–Au contact $r_{calcd} = 2.817$ Å[5]),[4] [{Pd@Au_{12}}$(Ph_3P)_8Cl_4$] (B) ($r = 2.814$ Å),[9] [$Au_{10}(PPh_3)_7${$(S_2C_2(CN)_2}_2$] (C) ($r = 2.565$ Å),[6] and [{C@Au_6}$(Ph_3P)_6]^{2+}$ (D) ($r = 2.887$ Å).[8]

well known and characterized. In fact, molecular dynamic simulations by Landman and co-workers show that large gold clusters break up into Au_{13} units upon (pre-)melting.[13] However, it was surprising that Au_6 does not display an octahedral (or a slightly distorted octahedral) structure in the gas phase,[14] suggesting that gold clusters do not follow the usual pattern of typical Lennard-Jones, Morse, or Gupta systems, which seem to favor a maximum number of close atom–atom contacts. According to recent studies by Häkkinen and Landman as well as by Bravo-Pérez et al.[14] Au_6 prefers a trigonal-planar D_{3h} structure (Figure 3), which is lower in energy than the other possible arrangements inclusive of the octahedral arrangement. The preferred planarity of small gold cluster compounds is attributed to relativistic effects.[15] Moreover, there is some indication that the magic clusters Au_{38}, Au_{55}, or Au_{75} are disordered in the gas phase.[16] The accurate description of such large systems by quantum theoretical procedures such as ab initio or density functional theory, or by semiempirical and many-body expansions of the interaction potential[17] therefore poses a significant challenge to future computational work.

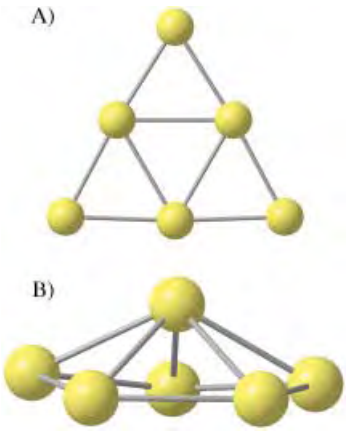


Figure 3. Low energy minimum structures of Au_6: A) trigonal-planar (global minimum), B) distorted pentagonal pyramid.

The structures of gold clusters on surfaces are expected to be markedly different than those in the gas phase.[18] For example, EXAFS experiments on MgO-supported gold nanoclusters show evidence for Au_6 octahedra.[19] Gold nanoclusters have been synthesized in a wide variety of sizes and shapes, ranging from discrete units (quantum dots, zero-dimensional (0D)) from 1 to 170 nm, which undergo self-organization to two-dimensional (2D) arrays,[20] one-dimensional (1D) gold chains of up to 20 gold atoms (Figure 4),[21] 1D nanowires consisting of Au_{55} clusters or nanorods up to 250 nm in length,[22] planned nanopatterns,[23] or beautiful helical (!) multiwalled gold nanotubes recently observed by Kondo and Takayanagi (Figure 5).[24] Clusters of this sort are currently being investigated for a wide range of applications such as catalysis.[25]

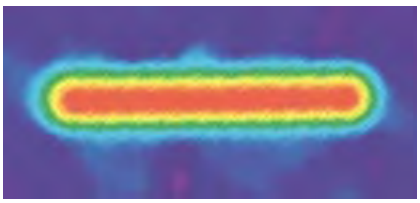


Figure 4. Topographic STM image of an Au_{20} chain on a NiAl(110) surface.[21]

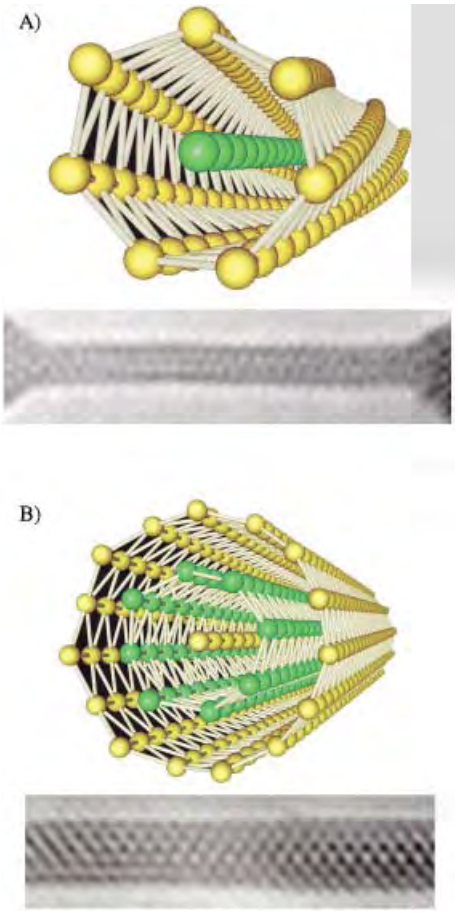


Figure 5. TEM images (in black and white; ca. 1 nm in diameter) and corresponding simulated models[24] of helical multiwalled gold nanowires. The dark dots represent positions of atoms on the image plane. A) 7-1 and B) 15-8-1 structures (*n-m-l* denotes the number of atoms of the polygonal tube moving from the outer layer (*n*) to the inner layer (*l*)).

Gold clusters also show interesting electronic properties. For example, gold chains of up to 20 gold atoms have been studied by scanning tunneling spectroscopy (STS) by Wallis et al.[26] Differ-

 © 2003 Wiley-VCH Verlag GmbH & Co. KGaA, Weinheim

ential conductance (dI/dV) images of these chains at energies between 1.0 and 2.5 eV show one-dimensional electron density oscillations—similar to the model of an electron confined in a one-dimensional box—with an effective mass of 0.4 ± 0.1 times the mass of a free electron.[26] Another interesting example is the Au_{55} cluster with an odd number of valence electrons; when deposited on silicon substrates this cluster shows amazingly large resistance towards oxidation due to the closing of the second shell.[27]

In the near future, we will see more interesting developments in gold nanomaterials and their technical applications. Fine-tuning electronic properties by controlling the shape, size, level of impurity-doping of metal clusters (e.g. gold on support surfaces), and the support surface itself may eventually lead to the design and synthesis of specific and very efficient catalysts. Theoretical investigations into structural, electronic, and impurity-doping effects of supported gold nanoclusters, which are important for understanding such quantum size effects, are already underway,[28] and the use of clusters such as those synthesized by Wang and co-workers[4] will lead to interesting new applications.

[1] a) M. Haruta, T. Kobayashi, H. Samo, N. Yamada, *Chem. Lett.* **1987**, 405–408; b) M. Haruta, N. Yamada, T. Kobayashi, S. Ijima, *Catal. Today* **1989**, *115*, 301–309; c) M. Haruta, *Catal. Today* **1997**, *36*, 115–123; d) M. Haruta, *Catal. Today* **1997**, *36*, 153–166; e) G. C. Bond, *Catal. Today* **2002**, *72*, 5–9.

[2] a) W. T. Wallace, R. L. Whetten, *J. Am. Chem. Soc.* **2002**, *124*, 7499–7505; b) A. Ueda, M. Haruta, *Gold Bull.* **1999**, *32*, 3–11; c) G. Mul, A. Zwijnenburg, B. van der Linden, M. Makee, J. A. Moulijn, *J. Catal.* **2001**, *201*, 128–137; d) Y. Kim, R. C. Johnson, J. T. Hupp, *Nano Lett.* **2001**, *1*, 165–167; e) N. Lu, J. Zheng, M. Gleiche, H. Fuchs, L. Chi, O. Vidoni, T. Reuter, G. Schmid, *Nano Lett.* **2002**, *3*, 1097–1099; f) J. L. Gardea-Torresdey, J. G. Parsons, E. Gomez, J. Peralta-Videa, H. E. Troiani, P. Santiago, M. J. Yacaman, *Nano Lett.* **2002**, *2*, 397–401; g) N. Funasaki, A. Henmi, S. Ito, Y. Asano, S. Yamashita, T. Kobayashi, M. Haruta, *Sens. Actuators* **1993**, *13–14*, 536–538; h) Z. Ma, S.-F. Sui, *Angew. Chem.* **2002**, *114*, 2280–2283; *Angew. Chem. Int. Ed.* **2002**, *41*, 2176–2179; i) J. F. Hainfeld, F. R. Furuya, *J. Histochem. Cytochem.* **1992**, *40*, 177–184; j) T. M. Herne, M. J. Tarlov, *J. Am. Chem. Soc.* **1997**, *119*, 8916–8920; k) D. Zanchet, C. M. Micheel, W. J. Parak, D. Gerion, A. P. Alivisatos, *Nano Lett.* **2000**, *1*, 32–35; l) Y. W. Cao, R. Jin, C. A. Mirkin, *Science* **2002**, *297*, 1536–1540; m) A. G. Kanaras, Z. Wang, A. D. Bates, R. Cosstick, M. Brust, *Angew. Chem.* **2003**, *115*, 201–204; *Angew. Chem. Int. Ed.* **2003**, *42*, 191–194; n) S. M. Schiller, R. Naumann, K. Lovejoy, H. Kunz, W. Knoll, *Angew. Chem.* **2003**, *115*, 219–222; *Angew. Chem. Int. Ed.* **2003**, *42*, 208–211; o) C. Mohr, H. Hofmeister, J. Radnik, P. Claus, *J. Am. Chem. Soc.* **2003**, *125*, 1905–1911; p) T. S. Kim, J. D. Stiehl, C. T. Reeves, R. J. Meyer, C. B. Mullins, *J. Am. Chem. Soc.* **2003**, *125*, 2018–2019; q) C. V. Corti, R. J. Holliday, D. T. Thompson, *Gold Bull.* **2002**, *35*, 111–117; r) F. Patolsky, Y. Weizmann, O. Lioubashevski, I. Willner, *Angew. Chem.* **2002**, *114*, 2429–2433; *Angew. Chem. Int. Ed.* **2002**, *41*, 2323–2327; s) J. Guzman, B. C. Gates, *Angew. Chem.* **2003**, *115*, 714–717; Angew. *Chem. Int. Ed.* **2003**, *42*, 690–693; t) N. I. Kovtyukhova, T. E. Mallouk, *Chem. Eur. J.* **2002**, *8*, 4355–4363; u) J. Aizpurua, P. Hanurp, D. S. Sutherland, M. Käll, G. W. Bryant, F. J. Garcia de Abajo, *Phys. Rev. Lett.* **2003**, *90*, 057401.

[3] Q. Wang, T. Lin, L. Tang, J. E. Johnson, M. G. Finn, *Angew. Chem.* **2002**, *114*, 477–480; *Angew. Chem. Int. Ed.* **2002**, *41*, 459–462.

[4] X. Li, K. Boggavarapu, J. Li, H.-J. Zhai, L.-S. Wang, *Angew. Chem.* **2002**, *114*, 4980–4983; *Angew. Chem. Int. Ed.* **2002**, *41*, 4786–4789.

[5] P. Pyykkö, N. Runeberg, *Angew. Chem.* **2002**, *114*, 2278–2280; *Angew. Chem. Int. Ed.* **2002**, *41*, 2174–2176.

[6] G. M. T. Cheetham, M. M. Harding, J. L. Haggitt, D. M. P. Mingos, H. R. Powell, *J. Chem. Soc. Chem. Commun.* **1993**, 1000–1001.

[7] a) C. E. Briant, B. R. C. Theobald, J. W. White, L. K. Bell, D. M. P. Mingos, A. J. Welch, *J. Chem. Soc. Chem. Commun.* **1981**, 201–202; b) B. K. Teo, X. Shi, H. Zhang, *J. Am. Chem. Soc.* **1992**, *114*, 2743–2745; c) G. Schmid, *Inorg. Synth.* **1990**, *27*, 214–218; d) K. Fauth, U. Kreibig, G. Schmid, *Z. Phys. D* **1991**, *20*, 297–300; e) E. Gutiérrez, R. D. Powell, F. R. Furuya, J. F. Hainfeld, T. G. Schaaff, M. N. Shafigullin, P. W. Stephens, R. L. Whetten, *Eur. Phys. J. D* **1999**, *9*, 647–651.

[8] a) F. Scherbaum, B. Huber, G. Müller, H. Schmidbaur, *Angew. Chem.* **1988**, *100*, 1600–1602; *Angew. Chem. Int. Ed. Engl.* **1988**, *27*, 1542–1544; b) F. Gabbai, A. Schier, J. Riede, H. Schmidbaur, *Chem. Ber.* **1997**, *130*, 111–115.

[9] a) M. Laupp, J. Strähle, *Angew. Chem.* **1994**, *106*, 210–211; *Angew. Chem. Int. Ed. Engl.* **1994**, *33*, 207–209; b) M. Laupp, J. Strähle, *Z. Naturforsch. B* **1995**, *50*, 1369–1372.

[10] P. Pyykkö, *Angew. Chem.* **2002**, *114*, 3723–3728; *Angew. Chem. Int. Ed.* **2002**, *41*, 3573–3578.

[11] P. P. Edwards, S. R. Johnston, M. O. Jones, A. Porch, R. L. Johnston in *Studies in Surface Science and Catalysis, Vol. 132* (Eds.: Y. Iwasawa, N. Oyama, H. Kunieda), Elsevier, Amsterdam, **2001**, pp. 719–724.

[12] D. J. Wales, J. P. K. Doye, *J. Phys. Chem. A* **1997**, *101*, 5111–5116.

[13] C. L. Cleveland, W. D. Luedtke, U. Landman, *Phys. Rev. Lett.* **1998**, *81*, 2036–2039.

[14] H. Häkkinen, U. Landman, *Phys. Rev. B* **2000**, *62*, R2287-R2290; G. Bravo-Pérez, I. L. Garzón, O. Novaro, *THEOCHEM* **1999**, *493*, 225–231.

[15] H. Häkkinen, M. Moseler, U. Landman, *Phys. Rev. Lett.* **2002**, *89*, 033401-1-4.

[16] a) J. P. K. Doye, D. J. Wales, *New J. Chem.* **1998**, 733–744; b) K. Michaelian, N. Rendón, I. L. Garzón, *Phys. Rev. B* **1999**, *60*, 2000–2010.

[17] a) N. T. Wilson, R. L. Johnston, *J. Mater. Chem.* **2002**, *12*, 2913–2922; b) N. T. Wilson, R. L. Johnston, *Eur. Phys. J. D* **2000**, *12*, 161–169.

[18] G. Pacchioni, *Surf. Sci.* **2002**, *520*, 3–5.

[19] J. Guzman, B. C. Gates, *Nano Lett.* **2001**, *12*, 689–692.

[20] a) B. Kim, S. L. Tripp, A. Wei, *J. Am. Chem. Soc.* **2001**, *123*, 7955–7956; b) I. Sloufová, B. Vlcková, *Nano Lett.* **2002**, *2*, 121–125; c) C. Stowell, B. A. Korgel, *Nano Lett.* **2001**, *1*, 595–600; d) G. Schmid, M. Bäumle, N. Beyer, *Angew. Chem.* **2000**, *112*, 187–189; *Angew. Chem. Int. Ed.* **2000**, *39*, 181–183.

[21] N. Nilius, T. M. Wallis, W. Ho, *Science* **2002**, *297*, 1853–1856.

[22] a) D. Wyrwa, N. Beyer, G. Schmid, *Nano Lett.* **2002**, *2*, 419–421; b) P. L. Gai, M. A. Harmer, *Nano Lett.* **2002**, *2*, 771–774; c) S. O. Obare, N. R. Jana, C. J. Murphy, *Nano Lett.* **2001**, *1*, 601–603; d) F. Kim, J. H. Song, P. Yang, *J. Am. Chem. Soc.* **2002**, *124*, 14316–14317.

[23] S. Liu, R. Maoz, G. Schmid, J. Sagiv, *Nano Lett.* **2002**, *2*, 1055–1060.

[24] Y. Kondo, K. Takayanagi, *Science* **2000**, *289*, 606–608.

[25] a) M. Valden, X. Lai, D. W. Goodman, *Science* **1998**, *281*, 1647–1650; b) J. Luo, V. W. Jones, M. M. Maye, L. Han, N. N. Kariuki, C.-J. Zhong, *J. Am. Chem. Soc.* **2002**, *124*, 13988–13989; c) G. Schmid, *Chem. Rev.* **1992**, *92*, 1709–1727; d) M.

 © 2003 Wiley-VCH Verlag GmbH & Co. KGaA, Weinheim

Valden, S. Pak, X. Lai, D. W. Goodman, *Catal. Lett.* **1998**, *56*, 7 – 10.
[26] T. M. Wallis, N. Nilius, W. Ho, *Phys. Rev. Lett.* **2002**, *89*, 236802-1-4.
[27] H.-G. Boyen, G. Kästle, F. Weigl, B. Koslowski, C. Dietrich, P. Ziemann, J. P. Spatz, S. Riethmüller, C. Hartmann, M. Möller, G. Schmid, M. G. Garnier, P. Oelhafen, *Science* **2002**, *297*, 1533 – 1536.
[28] a) H. Häkkinen, S. Abbet, A. Sanchez, U. Heiz, U. Landman, *Angew. Chem.* **2003**, *115*, 1335 – 1338; *Angew. Chem. Int. Ed.* **2003**, *42*, 1297 – 1300; H. Häkkinen, U. Landman, *J. Am. Chem. Soc.* **2001**, *123*, 9704 – 9705; b) J. Wang, G. Wang, J. Zhao, *Phys. Rev. B* **2002**, *66*, 035418-1-6; c) N. Lopez, J. K. Nørskov, *J. Am. Chem. Soc.* **2002**, *124*, 11262 – 11263; d) G. Mills, M. S. Gordon, H. Metiv, *J. Chem. Phys.* **2003**, *118*, 4198 – 4205; e) J. Li, X. Li, H.-J. Zhai, L.-S. Wang, *Science* **2003**, *299*, 864 – 867; f) D. H. Wells, W. N. Delgass, K. T. Thomson, *J. Chem. Phys.* **2002**, *117*, 10597 – 10603; g) D. Krüger, H. Fuchs, R. Rousseau, D. Marx, M. Parinello, *J. Chem. Phys.* **2001**, *115*, 4776 – 4786; h) D. Krüger, H. Fuchs, R. Rousseau, D. Marx, M. Parinello, *Phys. Rev. Lett.* **2002**, *89*, 186402.

 © 2003 Wiley-VCH Verlag GmbH & Co. KGaA, Weinheim

Molecular Mousetrap

Supramolecular Crown Ether Adducts in the Gas Phase: From Molecular Recognition of Amines to the Covalent Coupling of Host/Guest Molecules**

*Mathias Schäfer**

Keywords:
crown ether compounds · mass spectrometry · molecular recognition · supramolecular chemistry

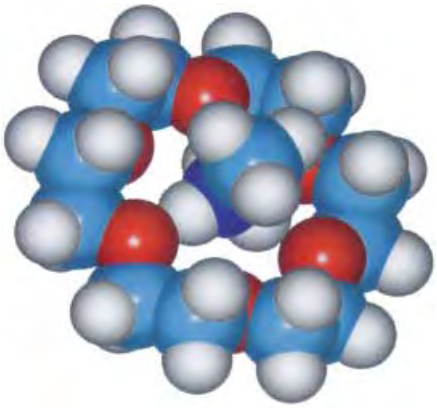
Dedicated to Professor Jesse L. Beauchamp on the occasion of his 60th birthday

Crown ethers are capable of forming complexes with a variety of guest molecules in solution,[1] and have been used extensively for the synthesis of supramolecular compounds such as rotaxanes and dendrimers.[2] For a successful examination of even weakly bound noncovalent complexes by mass spectrometry, which is of central importance in molecular recognition,[3] an appropriate soft ionization technique is needed that guarantees an intact transfer of labile species from the solution to the gas phase. Electrospray ionization (ESI) was introduced by John Fenn in 1988 (for which he was awarded the Nobel prize in Chemistry in 2002), and has proven to be the method of choice for a large variety of supramolecular complexes.[4]

Molecular Recognition of Primary Amines and Peptides by [18]Crown-6 Ether

Complexes of [18]crown-6 ether (18C6) with cationic species such as metal cations,[5] ammonium[6] and alkyl ammonium ions[7] in particular have been studied in the gas phase. It is primarily the appropriate size of the cavity of 18C6 and its symmetry that allows it to preferably bind protonated primary amines[8] by way of three coplanar alternating oxygen atoms that form hydrogen bonds better than other crown ethers.[6,8b,9] To illustrate this, Figure 1 shows the noncovalent interaction between a methylammonium ion and 18C6. A high bond dissociation energy of 182 kJ mol^{-1} was determined for this interaction by PM3 semi-empirical calculations.[8a]

Julian and Beauchamp demonstrated elegantly the strong binding of primary amines to 18C6 by ESI-MS experiments.[8a] Singly, doubly, and triply protonated molecular ions were detected in the ESI-MS spectrum of a solution of the model peptide tetralysine (KKKK). After adding 18C6 to the solution, the charge state had increased and the most abundant species was a quadruply charged complex $[(KKKK+4H)(18C6)_4]^{4+}$. Clearly, the formation of the 18C6 adduct affects the charge distribution and the ion abundance of the peptide in the ESI mass spectra. Since 18C6 effectively shields the four protonated lysine δ-amino groups, the free energy of solvation of the complex ion is reduced which facilitates the transfer of the ion to the gas phase. The molecular model shows that the lysine side chains in the complex $[(KKKK+4H)(18C6)_4]^{4+}$ are flexible enough to accommodate four crown ether molecules adjacent to each other (structure **3** in Figure 2).



2

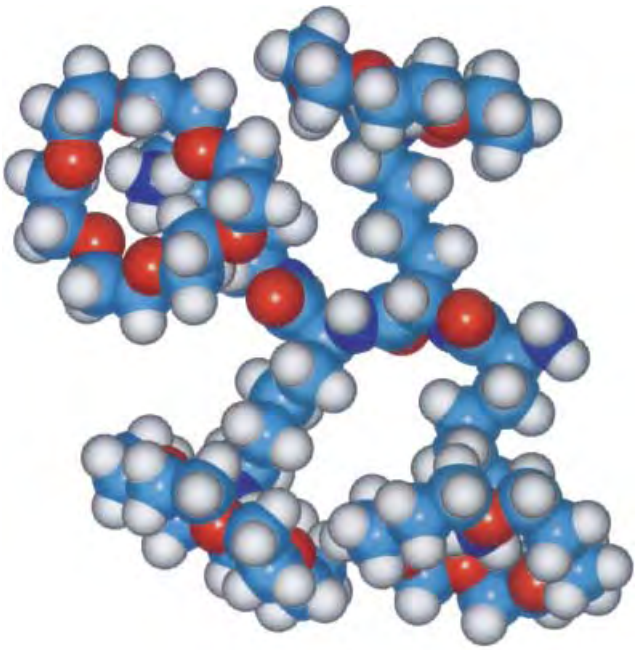
Figure 1. The model structure **2** depicts the noncovalent association between a protonated methylamine ion and [18]crown ether (18C6). Three alternating coplanar oxygen atoms of 18C6 (red) are hydrogen bonded to the nitrogen atom (dark blue). The structure was determined by DFT calculations at the B3LYP level with the 6-31G** basis set.[8a]

However, the applicability of the unique complexation behavior of 18C6 to count lysine residues in peptides of unknown sequence is limited, as complications result from the competitive formation of adducts with 18C6; for example, with the protonated side chains of histidine and arginine as well as with the N-terminus of peptides that do not contain lysine. On the other hand, 18C6 is sensitive to changes in protein or peptide conformation and can prevent the refolding of a denatured protein for an extended period of time.[8a] Tandem mass spectrometry can be used for an unambiguous assignment of the charge state of peptides and proteins in complexes with 18C6.[10] Additionally, the ability of 18C6 to sequester labile protons and thereby inhibit their gas-phase interaction with

[*] Dr. M. Schäfer
Institut für Organische Chemie
Universität zu Köln
Greinstrasse 4, 50939 Köln (Germany)
Fax: (+49) 221-470-3064
E-mail: mathias.schaefer@uni-koeln.de

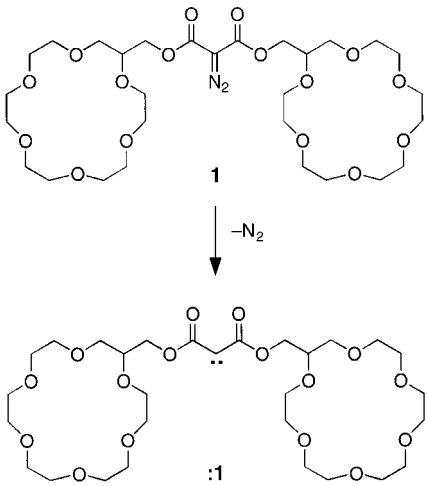
[**] The author gratefully acknowledges Ryan R. Julian and Professor Jesse L. Beauchamp for kindly providing original schemes and figures.

 © 2003 Wiley-VCH Verlag GmbH & Co. KGaA, Weinheim DOI: 10.1002/anie.200201627



3

Figure 2. Model structure **3** of the tetralysine peptide KKKK with four associated 18C6 molecules. The side chains of the lysine residues are flexible enough to accommodate four crown ethers complexed to the protonated δ-amino function. The structure was determined by DFT calculations at the B3 LYP level with the 6-31G** basis set.[8a]



Scheme 1. The diazo precursor **1** is converted into the intermediate carbene **:1** upon collision-induced dissociation CID with He atoms in a quadrupole ion trap ($\Delta m = 28$ Da).[12]

deuterated reagents can be used to study the H/D exchange mechanism of small protonated model peptides, for example, glycine oligomers.[7a,11]

Molecular Mousetraps

The strong interaction between 18C6 derivatives and protonated primary amines has been utilized successfully by Julian et al. to initiate an intermolecular covalent coupling reaction between host and guest molecules in the gas phase.[12] This was achieved by the controlled activation of diesters of diazomalonic acid by 18C6-methanol (**1**; Scheme 1) to produce precursors for the tandem MS experiments which are very appropriately referred to as "molecular mousetraps".

A solution of **1** and 1,6-diaminohexane (DAH) was prepared for ESI-MS measurements. Besides the singly charged 1:1 complex $[\mathbf{1}+\mathrm{DAH}+\mathrm{H}]^+$, a high-intensity signal corresponding to the doubly charged complex $[\mathbf{1}+\mathrm{DAH}+2\,\mathrm{H}]^{2+}$ was detected in the mass spectrum (Figure 3 and 4a). This ion was isolated in a quadrupole ion trap mass spectrometer and subsequently subjected to low-energy collision-induced dissociation (CID)[13] with helium gas to induce fragmentation or reaction (MS/MS spectrum; Figure 4b). The diazo group of host **1** in the complex $[\mathbf{1}+\mathrm{DAH}+2\,\mathrm{H}]^{2+}$ is efficiently converted by loss of N_2 (28 Da) into the corresponding carbene (**:1**), which is a highly reactive, short-lived intermediate (Scheme 1). The product ion $[\mathbf{:1}+\mathrm{DAH}+2\,\mathrm{H}]^{2+}$ of this experiment was isolated and subjected to further collision activation to examine the reaction product of the carbene (MS/MS/MS spectrum; Figure 4c). The predominant fragmentation of **1** (fragments A, B, C, D in MS/MS/MS spectrum; Figure 4c) occurs without apparent loss of the DAH and retention of a covalent host–guest linkage. These fragmentations of the host provide evidence that an intermolecular reaction occurs leading to a covalent host–guest coupling by C-H insertion of the carbene. This route is most likely, because both of the ammonium groups of DAH are strongly bound by the two crown ethers, and consequently an N-H insertion of the carbene

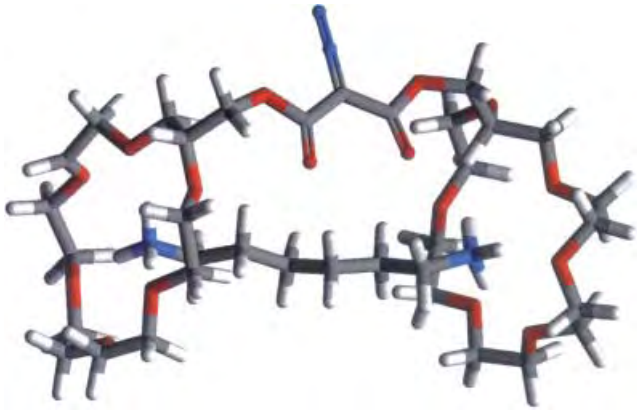


Figure 3. Possible structure of the noncovalent complex $[\mathbf{1}+\mathrm{DAH}+2\,\mathrm{H}]^{2+}$ formed from host **1** and the doubly protonated guest 1,6-diaminohexane (DAH) in the gas phase. The structure was determined by semi-empirical calculations with the HyperChem 5.1 Professional suite using the PM3 parameter set.[12]

 © 2003 Wiley-VCH Verlag GmbH & Co. KGaA, Weinheim

is very unlikely. However, some of the complex dissociates to give a protonated product ion $[DAH+H]^+$, which suggests that the carbene undergoes a competing intramolecular reaction (MS/MS/MS spectrum; Figure 4c).

The singly charged complex of **1** and DAH $[\mathbf{1}+DAH+H]^+$ can likewise be investigated by sequential product ion experiments in the ion trap. After isolation and collision-induced activation, the corresponding carbene complex $[:\mathbf{1}+DAH+H]^+$ is generated with high efficiency (MS/MS spectrum; Figure 5a). An additional fragmentation with the characteristic loss of 294 Da is assigned to the loss of hydroxymethyl-18C6 (Figure 5a and b). The MS/MS/MS spectrum in Figure 5c shows the fragmentation of the ion $[:\mathbf{1}+DAH+H-294]^+$ which contains only a single remaining crown. The sequential removal of most of the remaining crown ether (loss of CO (28 Da) and CH_2CH_2O fragments (44 Da)) without the loss of the singly charged guest molecule DAH confirms the conclusion that a new intermolecular covalent bond between the host and guest was formed. In this case, either a C-H or an N-H insertion is possible. These results illustrate a promising concept for a supramolecular route to the formation of covalent bonds in the gas phase and indicate a promising way for the selective detection of lysine residues in peptides or proteins by reactive molecular mousetrap molecules.[12]

The highlight illustrates with selected results obtained with crown ether complexes the outstanding applicability of ESI and tandem mass spectrometry for the determination of host–guest and ion–molecule interactions in the gas phase. Beside these extraordinary studies, the attention of the interested reader is drawn to further exciting aspects of the mass spectrometric examination of complexes of crown ethers and peptides that focus on the H/D exchange mechanism of peptides,[7a] fundamental aspects of electrospray ionization,[8a] and the fragmentation mechanism of peptides upon CID.[7a]

[1] M. Hiraoka, *Crown Compounds: Their Characteristics and Applications*, Else vier Scientific, New York, **1982**.

[2] a) M. C. T. Fyfe, J. F. Stoddart, *Acc. Chem. Res.* **1997**, *30*, 393–401; b) H. W.

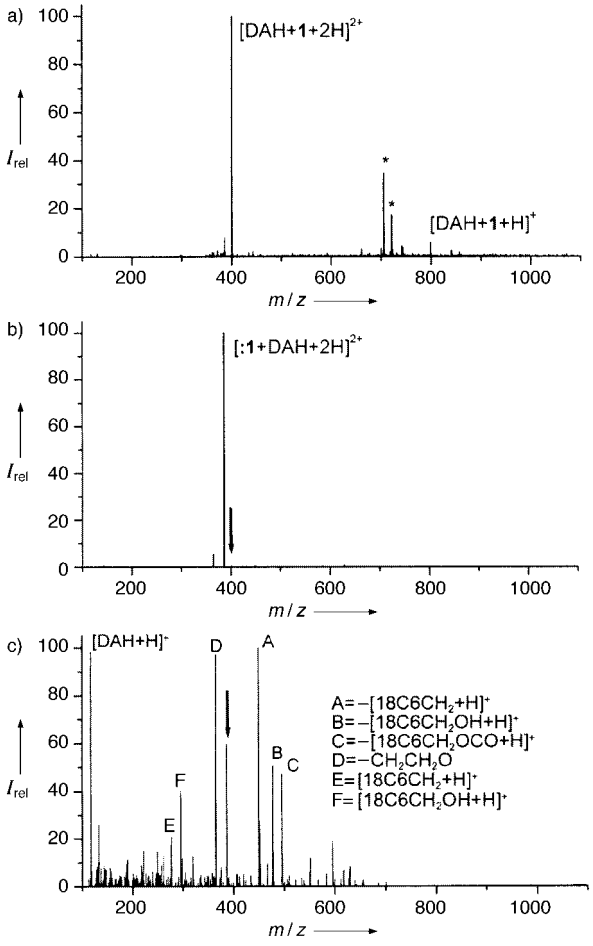


Figure 4. a) ESI mass spectrum of **1** with DAH. b) MS/MS spectrum of $[\mathbf{1}+DAH+2H]^{2+}$ which shows the almost exclusive loss of 28 Da, thus indicating the generation of carbene **:1** by loss of N_2. c) MS/MS/MS spectrum of $[:\mathbf{1}+DAH+2H]^{2+}$. *: $[\mathbf{1}+$alkali metal$]^+$ adduct signals. The bold downward arrows indicate the peaks being subjected to CID. I_{rel} = relative intensity.[12]

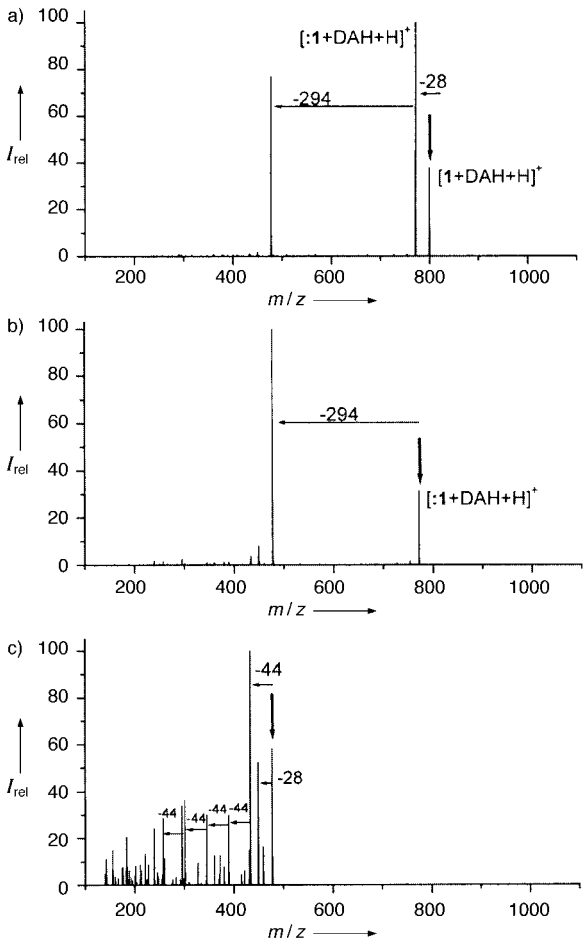
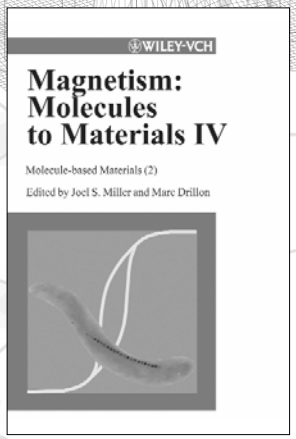


Figure 5. a) MS/MS spectrum of $[\mathbf{1}+DAH+H]^+$; the loss of 294 Da can be accounted for by the loss of hydroxymethyl-18C6 (see also Figure 5b). b) MS/MS/MS spectrum of $[:\mathbf{1}+DAH+H]^+$. c) MS/MS/MS spectrum of $[:\mathbf{1}+DAH+H-294]^+$. The bold downward arrows indicate the peaks being subjected to CID.[12]

 © 2003 Wiley-VCH Verlag GmbH & Co. KGaA, Weinheim

Gibson, N. Yamaguchi, L. Hamilton, J. W. Jones, *J. Am. Chem. Soc.* **2002**, *124*, 4653 – 4665; c) D. N. Reinhoudt, M. Crego-Calama, *Science* **2002**, *295*, 2403 – 2407.
[3] M. W. Peczuh, A. D. Hamilton, *Chem. Rev.* **2000**, *100*, 2479 – 2494.
[4] a) M. Vincenti, *J. Mass Spectrom.* **1995**, *30*, 925 – 939; b) J. A. Loo, *Mass Spectrom. Rev.* **1997**, *16*, 1 – 23; c) C. A. Schalley, *Int. J. Mass Spectrom.* **2000**, *194*, 11 – 39; d) C. A. Schalley, *Mass Spectrom. Rev.* **2001**, *20*, 253 – 309.
[5] M. B. More, D. Ray, P. B. Armentrout, *J. Am. Chem. Soc.* **1999**, *121*, 417 – 423.
[6] S. Maleknia, J. S. Brodbelt, *J. Am. Chem. Soc.* **1993**, *115*, 2837 – 2843.
[7] a) S.-W. Lee, H.-N. Lee, H. S. Kim, J. L. Beauchamp, *J. Am. Chem. Soc.* **1998**, *120*, 5800 – 5805; b) B. L. Williamson, C. S. Creaser, *Int. J. Mass Spectrom.* **1999**, *188*, 53 – 61.
[8] a) R. R. Julian, J. L. Beauchamp, *Int. J. Mass Spectrom.* **2001**, *210/211*, 613 – 623; b) C.-C. Liou, H.-F. Wu, J. S. Brodbelt, *J. Am. Soc. Mass Spectrom.* **1994**, *5*, 260 – 273.
[9] M. Meot-Ner, *J. Am. Chem. Soc.* **1983**, *105*, 4912 – 4915.
[10] J. B. Cunniff, P. Vouros, *J. Am. Soc. Mass Spectrom.* **1995**, *6*, 1175 – 1182.
[11] a) S. Campbell, M. T. Rodgers, E. M. Marzluff, J. L. Beauchamp, *J. Am. Chem. Soc.* **1994**, *116*, 9765 – 9766; b) S. Campbell, M. T. Rodgers, E. M. Marzluff, J. L. Beauchamp, *J. Am. Chem. Soc.* **1995**, *117*, 12840 – 12854.
[12] R. R. Julian, J. A. May, B. M. Stoltz, J. L. Beauchamp, *Angew. Chem.* **2003**, *115*, 1042 – 1045; *Angew. Chem. Int. Ed.* **2003**, *42*, 1012 – 1015.
[13] a) J. C. Schwartz, I. Jardine, *Methods Enzymol.* **1996**, *270*, 552 – 586; b) R. N. Hayes, M. L. Gross, *Methods Enzymol.* **1990**, *193*, 237 – 263; c) R. E. March, *J. Mass Spectrom.* **1997**, *32*, 351 – 369.

Magnetism: Molecules to Materials



J.S. MILLER, University of Utah, Salt Lake City, USA; **M. DRILLON**, Inst. de Physique et Chimie des Materiaux de Strasbourg, France (Eds)

As a depository of contemporary knowledge on key topics related to magnetism, this open series of volumes provides a much-needed comprehensive overview of this growing interdisciplinary field. In topical reviews written by foremost scientists trends and recent advances focusing on the correlations between electronic structure and magnetic properties are explained in a clear and detailed way. The balance between theory and experiment within this series will guide advanced students and specialists alike to this research area. It will help evaluate own experimental observations and serve as a base for the design of new magnetic materials. A unique reference work, indispensable for everyone concerned with the phenomena of magnetism!

Reviews for Volume II:
"... presents a good ... current overview of an active and diverse research area."
Journal of the American Chemical Society

NEW: Magnetism: Molecules to Materials IV
Molecule-based Materials (2)
2002. XI, 492 pp. 300 fig. HC
€ 159.-/£ 95.-/US$ 125.-
3-527-30429-0

Magnetism: Molecules to Materials III
Nanosized Magnetic Materials
2001. XV, 388 pp. 209 fig. 14 tab. HC
€ 139.-/£ 80.-/US$ 125.-
3-527-30302-2

Magnetism: Molecules to Materials II
Molecule-Based Materials
2001. XIV, 489 pp. 323 fig. 43 tab. HC
€ 159.-/£ 95.-/US$ 125.-
3-527-30301-4

Magnetism: Molecules to Materials I
Models and Experiments
2001. XVI, 437 pp. 270 fig. 33 tab. HC
€ 139.-/£ 80.-/US$ 125.-
3-527-29772-3

John Wiley & Sons, Ltd.
Baffins Lane Chichester, West Sussex, PO 19 1UD, UK
Fax: +44 (0)1243-775878

WILEY-VCH · P.O. Box 10 11 61 · 69451 Weinheim, Germany · Fax: +49 (0) 62 01-60 61 84 · e-mail: service@wiley-vch.de · http://www.wiley-vch.de

WILEY

WILEY-VCH

14602094.vi

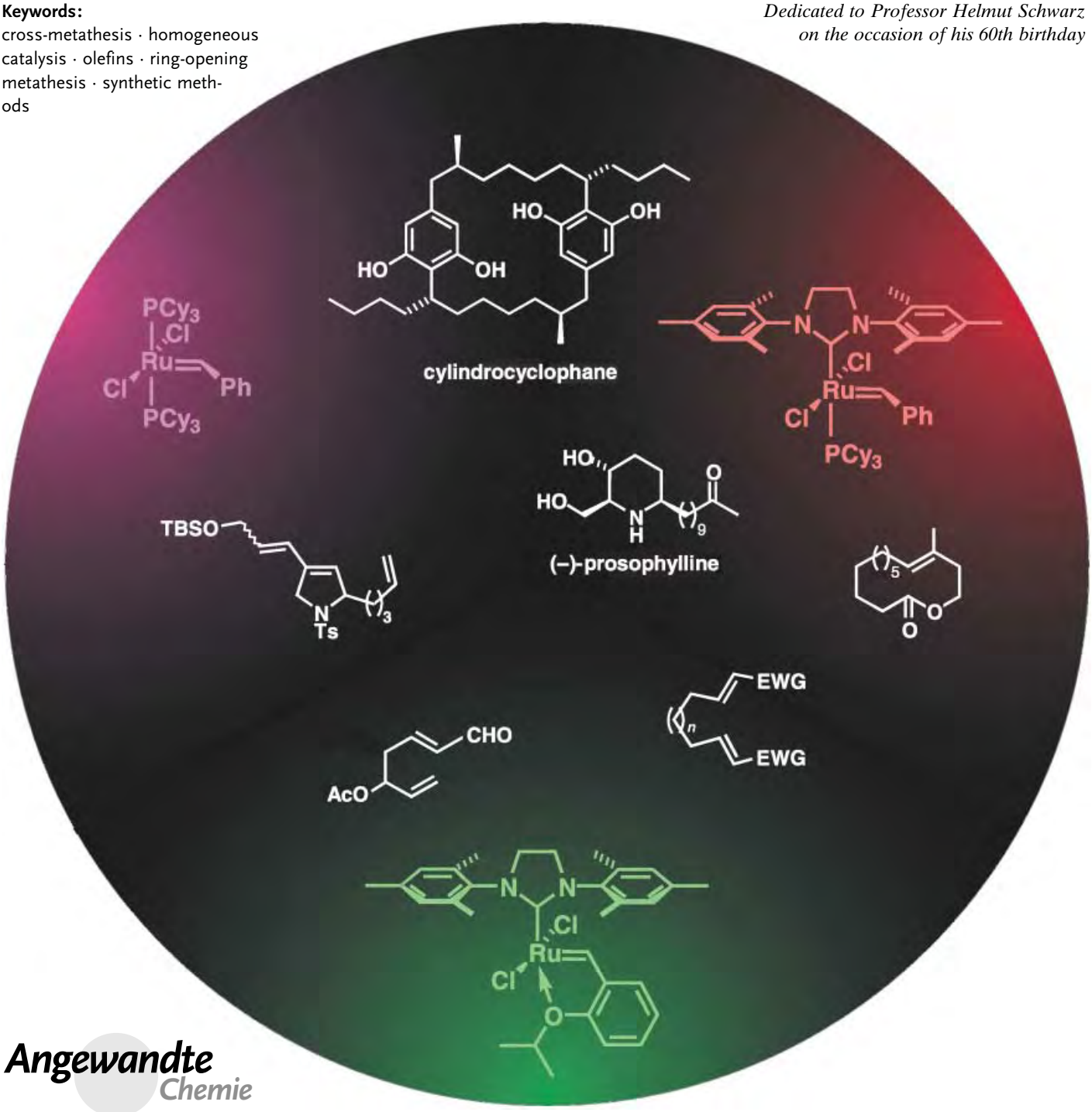
Cross-Metathesis of Olefins

Recent Developments in Olefin Cross-Metathesis

*Stephen J. Connon and Siegfried Blechert**

Keywords:
cross-metathesis · homogeneous catalysis · olefins · ring-opening metathesis · synthetic methods

Dedicated to Professor Helmut Schwarz on the occasion of his 60th birthday



 © 2003 Wiley-VCH Verlag GmbH & Co. KGaA, Weinheim DOI: 10.1002/anie.200200556

Among the many types of transition-metal-catalyzed C–C bond-forming reactions, olefin metathesis has come to the fore in recent years owing to the wide range of transformations that are possible with commercially available and easily handled catalysts. Consequently, olefin metathesis is now widely considered as one of the most powerful synthetic tools in organic chemistry. Until recently the intermolecular variant of this reaction, cross-metathesis, had been neglected despite its potential. With the evolution of new catalysts, the selectivity, efficiency, and functional-group compatibility of this reaction have improved to a level that was unimaginable just a few years ago. These advances, together with a better understanding of the mechanism and catalyst–substrate interactions, have brought us to a stage where more and more researchers are employing cross-metathesis reactions in multistep procedures and in the synthesis of natural products. The recent inclusion of alkynes and hindered bicyclic olefins as viable substrates for bimolecular metathesis coupling, the discovery of enantioselective cross-metathesis and cross-metathesis in water, and the successful marriage of metathesis and solid-phase organic synthesis has further widened the scope of this versatile reaction.

From the Contents

1. Introduction	1901
2. Cross-Metathesis	1902
3. Ring-Opening Cross-Metathesis	1912
4. Intermolecular Enyne Metathesis	1915
5. CM Applications in Solid-Phase Organic Synthesis	1917
6. Summary and Outlook	1920

1. Introduction

Olefin cross-metathesis[1] can be formally described as the intermolecular mutual exchange of alkylidene (or carbene) fragments between two olefins promoted by metal-carbene complexes. There are three main variations on this theme (Figure 1): a) cross-metathesis, b) ring-opening cross-metathesis, and c) intermolecular enyne metathesis (C).[2]

As an acyclic carbon–carbon bond-forming tool, cross-metathesis has numerous advantages typical of modern olefin-metathesis reactions:

1) The process is catalytic—typically 1–5 mol% of catalyst required.
2) High yields can be obtained under mild conditions in relatively short reaction times.
3) A wide range of functional groups are tolerated, with minimal substrate protection necessary.
4) The reaction is reversible, relatively atom-economic, and gaseous ethylene is usually the only by-product, which is an important consideration in industrial applications.
5) The olefin substrates are generally easier and less expensive to prepare than those associated with other common catalytic C–C bond-forming reactions (e.g. unsaturated boranes, stannanes, halides, triflates).
6) The olefinic products are suitable for further structural elaboration (e.g. hydrogenation, epoxidation, halogenation, cycloaddition).
7) High levels of chemo-, regio-, and stereoselectivity can be attained.

Cross-metathesis (CM) has found numerous industrial uses, including the well-known Shell Higher Olefin Process (SHOP),[3] the Further Exploitation of Advanced Shell Technology (FEAST) Process, and the Phillips Triolefin Process.[4] CM is not yet in such widespread laboratory use as the more entropically favorable ring-closing metathesis (RCM) reaction. However, the development of a second generation of active and robust ruthenium catalysts such as **1**–**4** (Figure 2), which combine the high activity previously only associated with molybdenum-based catalysts with an impressive functional-group tolerance, has recently allowed many groups to breathe new life into what were previously in many cases little more than unselective mechanistic curiosities. This Review will for the most part consist of an in-depth overview of these achievements, with particular emphasis placed on substrate/functional-group compatibility and the factors that influence selectivity. It is hoped that clearly defining the current scope and capabilities of these reactions will help to draw attention to these processes, which are rapidly gaining in significance.

The literature on CM, ring-opening metathesis (ROM), and enyne metathesis up to 1997 has been individually reviewed by Fürstner,[1h] Gibson, and Keen[5] and by Mori,[6] and hence this report concentrates on an overview of the

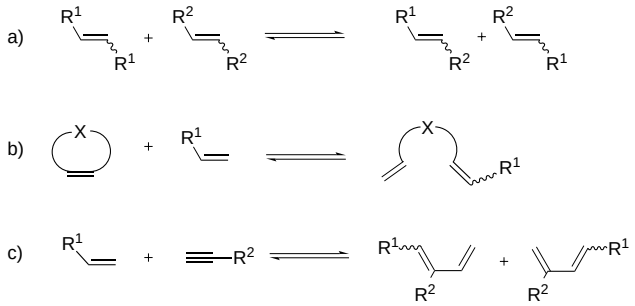


Figure 1. Variations of cross-metathesis.

[*] Prof. Dr. S. Blechert, Dr. S. J. Connon
Technische Universität Berlin, Institut für Chemie
Strasse des 17. Juni 135, 10623 Berlin (Germany)
Fax: (+49) 30-314-23619
E-mail: blechert@chem.tu-berlin.de

 © 2003 Wiley-VCH Verlag GmbH & Co. KGaA, Weinheim

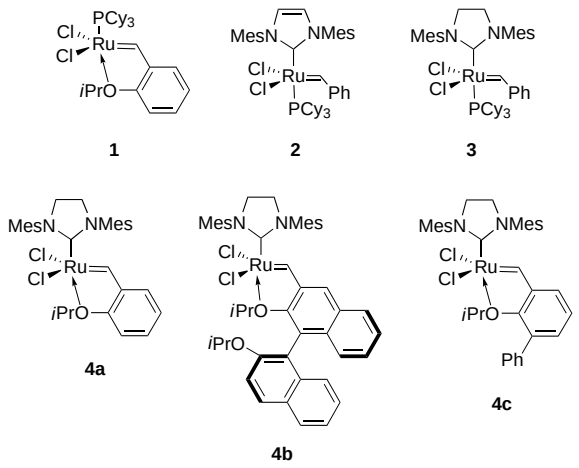


Figure 2. Recently developed, highly efficient, ruthenium-based metathesis catalysts (Mes = 2,4,6-trimethylphenyl, Cy = cyclohexyl).

material since then—a period of unprecedented activity and success in this field.

1.1. Mechanism

A general mechanistic scheme[2] for the CM of two symmetrically substituted olefins (in practice, this is quite difficult) is presented in Figure 3. The first step in the catalytic cycle (after the first catalyst turnover to produce **A**) is a [2+2] cycloaddition reaction between olefin **B** and a transition-metal carbene **A** to give a metallacyclobutane **C**. The latter undergoes subsequent collapse in a productive fashion to afford a new olefin product **D** and a new metal carbene (alkylidene) **E**, which carries the alkylidene fragment R^1. Similarly, **E** can react with a molecule of **F** via **G** to yield **D** and **A**, which then re-enters the catalytic cycle. The net result is that **D** is formed from **B** and **F** with **A** and **E** as catalytic intermediates.

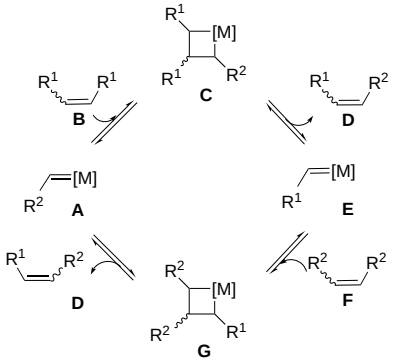


Figure 3. Mechanism of olefin metathesis.

2. Cross-Metathesis

2.1. Selectivity: A Historical Perspective

As is the case with most transformations, the two most important questions concerning any CM reaction are those of efficiency and selectivity. The goal is to achieve high yields of the cross-product with minimal amounts of competing dimerization (self-metathesis) products. In the majority of CM reactions (particularly when the produced olefin is required for a further stereoselective transformation such as epoxidation) *E*/*Z* selectivity is also a critical issue. Early reports described a variety of strategies to tackle selectivity problems. With the active molybdenum catalyst [Mo(=CHCMe$_2$Ph)(=NAr)(OCH(CF$_3$)$_2$Me)] (**5**) Crowe et al. have demonstrated selective CM between terminal alkenes and either acrylonitrile, styrene, or allyltrimethylsilane.[7–9] It was proposed that both acrylonitrile and styrene were capable of stabilizing the intermediate electron-rich molybdenum–carbon bond, leading to selective metathesis. We have shown that selective cross-metathesis with allyltrimethylsilane is mostly due to steric and not electronic factors, as originally proposed.[10]

Another important strategy for preventing self-metathesis by-products was the attachment of one of the substrates to a solid support. Provided that an excess of a relatively hindered soluble olefin was used, good yields of CM product could be obtained after cleavage from the resin.[11,12] Selective CM was also possible with hindered substrates such as protected olefinic amino acids[13–15] and protected jasmonates[10] in the presence of the Grubbs ruthenium catalyst [Cl$_2$(PCy$_3$)$_2$Ru=CHPh] (**6**).



Siegfried Blechert was born in Aalborg, Denmark, in 1946. He studied chemistry at the University of Hannover, Germany, and completed his PhD under the supervision of Prof. E. Winterfeldt in 1974. After a research stay with Prof. P. Potier at Gif-sur-Yvette, France, he completed his habilitation at the University of Hannover in 1986 before taking up a professorship at Bonn University in 1986. In 1990 he accepted the Chair of the Organic Chemistry Department at the Technical University of Berlin. His research interests include the development of new catalysts for olefin metathesis, novel synthetic methods, and the stereoselective synthesis of natural products.

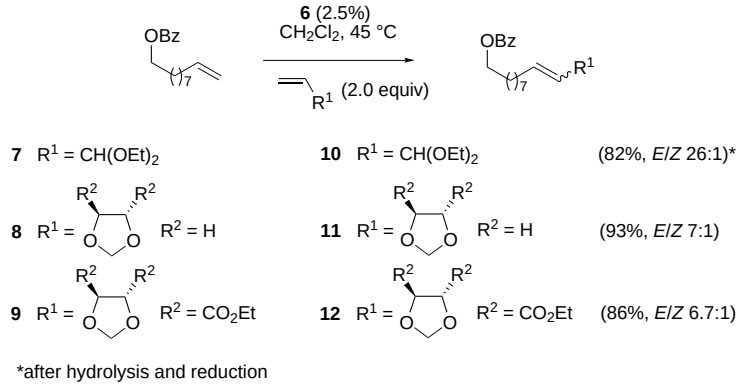


Stephen J. Connon was born in Dublin, Ireland, in 1976. After graduating from Dublin City University he moved to University College Dublin in 1997, where he studied pyridyne reactive intermediates under the supervision of Prof. A. F. Hegarty, completing his PhD in 2000. In 2001 he took up a postdoctoral position with Prof. Blechert, where he held an Alexander von Humboldt Fellowship, working on the development and application of new homo- and heterogeneous olefin-metathesis catalysts. In January 2003 he became a lecturer at the chemistry department at the University of Dublin, Trinity College.

 © 2003 Wiley-VCH Verlag GmbH & Co. KGaA, Weinheim

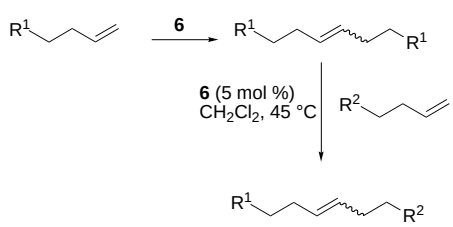
2.2. Selectivity—New developments with $[Cl_2(PCy_3)_2Ru{=}CHPh]$

Although molybdenum-catalyzed selective (with respect to cross-product/dimer ratio) CM with acrylonitrile was possible, **5** was found to be incompatible with enones and enoic esters.[8] Furthermore, Grubbs and co-workers found that the more practical and robust ruthenium catalyst **6** was incompatible with conjugated olefins, including acrolein. This apparent shortcoming could be partially circumvented by using an excess of acrolein acetals such as **7**–**9**. In the presence of 9-decen-1-yl benzoate, CM products **10**–**12** were formed in good yields and with good *E*/*Z* selectivity (Scheme 1).[16,17] Unfortunately, this method did not prove generally applicable: orthoesters, ketals, and homologues of **7** all proved unsuitable.



Scheme 1. Acrolein equivalents in CM.

However, Grubbs and co-workers also reported an innovative and promising new method for avoiding undesired self-metathesis products. In a two-step procedure, a terminal olefin was first homodimerized in a CM reaction, and the internal olefin product (in excess) was then treated with a second terminal olefin in the presence of **6** to give cross-coupled products (Scheme 2).[18] Although again not always applicable, it was shown that in many cases this strategy was preferable to straightforward CM coupling of two terminal olefins (Table 1). Both *E* and *Z* homodimers were found to be



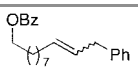
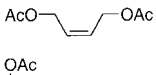
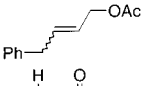
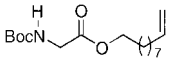
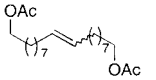
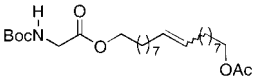
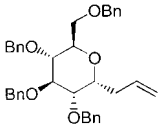
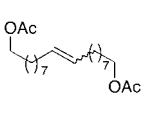
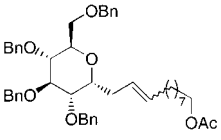
Scheme 2. Two-step selective CM with olefin dimers.

reactive, and high yields and selectivities were possible in the presence of various functional groups.[19] Unreacted homodimer could also be recovered for further use. The authors convincingly argued that these results could be explained in terms of the preferential formation (due to the presence of excess homodimer) of a more stable, substituted ruthenium alkylidene (rather than methylidene) intermediate.[20]

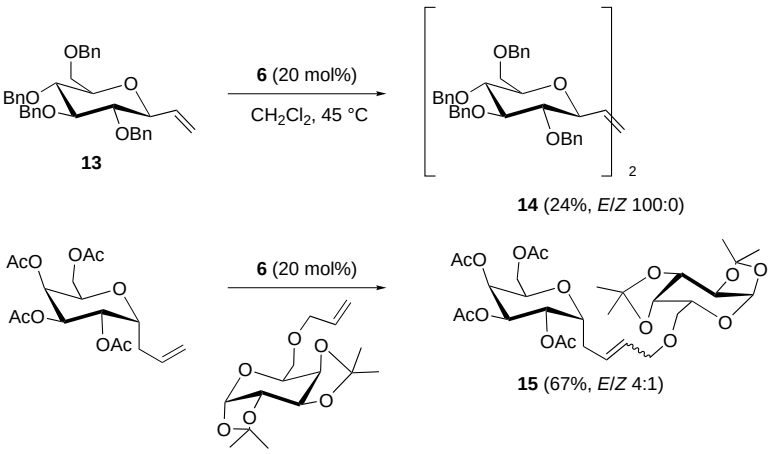
The compatibility of **6** with conjugated electron-deficient olefins is a matter of current debate. The lack of material on this potentially important reaction would seem to point towards incompatibility; however, two reports have appeared which cast doubt on this conjecture, at least in the case of certain substrates. Castedo and Blanco[21] found that allylbenzene could efficiently react with a range of CM partners (2 equiv), including acrylonitrile or acrolein, in the presence of **6** (5 mol %). This report also detailed the first example of CM with allyl bromide catalyzed by **6**. (Roy and co-workers have also been able to demonstrate the compatibility of both **6** and **3** with allyl halides in CM couplings.[22]) Lovely and Seshadri[23] were able to effect CM reactions between olefinic ferrocene derivatives[24] and methyl acrylate, albeit with a very high catalyst loading (20 %). It is clear that more reports are needed before this contentious issue can be resolved.

Roy et al.[25] found that CM dimerization of *O*-allylglycosides in the presence of catalyst **6** could be reasonably *E*-selective (*E*/*Z* = 5:1), whereas the corresponding *C*-glycosides gave 1:1 mixtures of *E*/*Z* isomers. Dimerization of tetrabenzyl *C*-vinylglycoside **13** gave the dimer **14** as a single *E* isomer but in low yield (Scheme 3). It can be reasonably assumed that

Table 1: Selective CM with olefin dimers.

Olefin	Dimer	Product	Yield [%]	*E*/*Z*
			68	3.7:1
			80	3:1
			72	3.5:1
			73	2.8:1

 © 2003 Wiley-VCH Verlag GmbH & Co. KGaA, Weinheim



Scheme 3. Selective CM with carbohydrates.

increased steric hindrance and greater Ru–O chelation possibilities associated with having the reacting olefin in close proximity to the bulky carbohydrate is responsible for both the selective formation of the more stable *E* product and the low yield. The ability of *O*-allylglycosides to undergo relatively *E*-selective CM was also exploited in the preparation of mixed *O*- and *C*-pseudosaccharide **15** (Scheme 3).

2.3. Selectivity with Electron-Withdrawing Alkenes : IMes-Based Catalysts

The advent of catalysts **3**[26] and **4a** (Figure 2)[27,28] has had a tremendous impact on the CM reaction. These ruthenium alkylidenes contain nonlabile, sterically hindered NHC (N-heterocyclic carbene) ligands with strong σ-donor and poor π-acceptor properties, which help to stabilize the 14-electron ruthenium intermediates during metathesis. Catalyst **3** displays a functional-group tolerance akin to that of bisphosphane-based catalyst **6**, but has a reactivity closer to that of the highly active yet oxophilic molybdenum catalyst **5,** and thus is far superior to **6** in terms of reactivity. This reactivity increase is demonstrated by the traditionally difficult formation of trisubstituted alkenes (a common structural subunit in natural products) in a CM reaction between the *gem*-disubstituted olefin 2-methyl-1-undecene and terminal olefins in moderate to good yields and moderate *E* selectivity (Figure 4).[29]

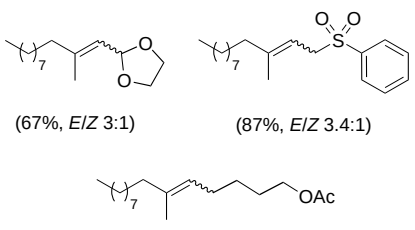


Figure 4. Trisubstituted olefins by CM using **3**.

This method was recently expanded by Grubbs and co-workers to include solvent-free CM reactions with symmetrical *gem*-disubstituted olefins.[30] Along similar lines, Stoltz and Spessard[31] demonstrated the viability of 2-methyl-2-butene as an efficacious CM partner in the synthesis of the bicyclo[3.3.1]nonane core of garsubellin A catalyzed by **3** (10 mol%).

However, it is the unprecedented activity of **3** and **4a** in the presence of conjugated electron-deficient olefins that has revolutionized the CM reaction. Metathesis transformations involving these substrates often give high cross-product/dimer ratios and excellent *E*/*Z* selectivity. The main reason for the high CM selectivity is the slow rate of dimerization of α,β-unsaturated carbonyl compounds. If one sees a typical CM reaction as a competition between three reaction pathways, that is, selective CM or dimerization of either starting material, then if one partner dimerizes relatively slowly, the selectivity naturally increases. The first such report came from Grubbs and co-workers at Caltech,[32] who observed that CM between α,β-unsaturated compounds (esters, aldehydes,[33] and ketones **19**–**24**) and simple terminal olefins **16**–**18** in the presence of **3** (5 mol%) in CH_2Cl_2 at 45 °C proceeded in good to excellent yields with impressive *E* selectivity (Table 2). In most cases, an excess of one olefin component is used to improve selectivity. However, Grubbs and Chatterjee recently showed that high-yielding and selective CM reactions are possible in the presence of equimolar amounts of olefin partners.[34] Thus CM can be used as a mild method for formal C–H activation or allylic oxidation,[34] depending on whether terminal or internal olefin substrates, respectively, are employed. Significantly, vinylic halides, phthalimides, sulfones, silanes, acetates, ethers, alkyl stannanes and acrylonitriles were initially found to be unreactive.

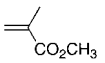
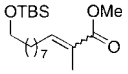
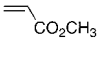
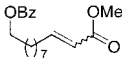
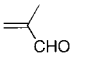
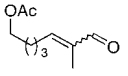
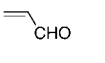
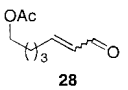
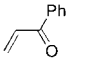
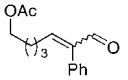
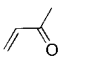
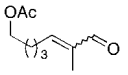
Catalyst **3** can also be generated in situ and used to effect selective CM reactions with electron-withdrawing alkenes.[35] After metathesis reactions, **3** (and also **6**) can be used to hydrogenate the products under high H_2 pressure (average 100 psi).[36] The CM of α,β-unsaturated amides[37] has also been demonstrated using catalyst **3**. Yields using these relatively electron-rich substrates were generally not as high as those found with **19**–**24**. This was attributed to the ability of amides to chelate to ruthenium during metathesis, thus siphoning off the catalyst in an unreactive form. This premise was supported by the observation that sterically hindered or electron-deficient amides **31b** and **31c**, respectively, gave higher yields of CM product than the electron-rich and unhindered analogue **31a** (Scheme 4).

We have found that the 2-isopropoxystyrene-derived catalyst **4a** was also active in CM reactions of challenging substrates.[28] A twofold excess of electron-deficient olefins **20**, **22**, **24**, and **31a** (**4a** (5 mol%), CH_2Cl_2, 40 °C) gave good to excellent yields of products **32**–**35** with pent-1-enylbenzoate; *E*/*Z* selectivity was also generally high (Table 3).

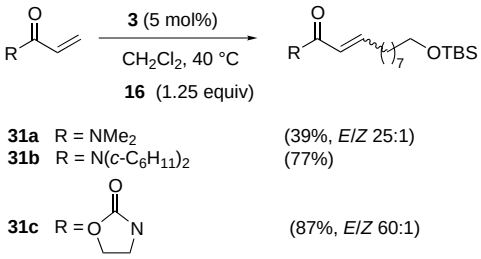
Catalyst **4a** was also found to be active in the CM of acrylonitrile derivatives. These electron-deficient substrates, which were incompatible with catalyst **3**, could be coupled smoothly with a variety of terminal olefins in high yields and

 © 2003 Wiley-VCH Verlag GmbH & Co. KGaA, Weinheim

Table 2: CM using **3** and electron-deficient alkenes.[a]

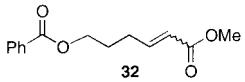
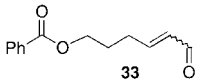
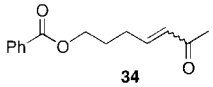
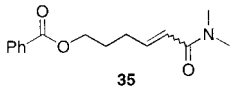
Terminal olefin	α,β-unsaturated olefin (equiv)	Product	Yield [%] (*E*/*Z*)
 **16**	 (0.5) **19**	 **25**	62 (>20:1)
 **17**	 (2.0) **20**	 **26**	91 (4.5:1)
 **18**	 (0.5) **21**	 **27**	92 (>20:1)
 **18**	 (2.0) **22**	 **28**	62 (>20:1)[33]
 **18**	 (2.0) **23**	 **29**	99 (>20:1)
 **18**	 (2.0) **24**	 **30**	95 (>20:1)

[a] TBS = *tert*-butyldimethylsilyl.



Scheme 4. CM with α,β-unsaturated amides.

Table 3: CM using **4a** and electron-deficient alkenes.

α,β-unsaturated olefin	Product	Yield [%] (*E*/*Z*)
20	 **32**	87 (>20:1)
22	 **33**	93 (>20:1)[33]
24	 **34**	85 (>20:1)
31a	 **35**	98 (>20:1)

E-selectivity.[38] More recently, Cossy et al.[39] demonstrated efficient and selective CM between chiral homoallylic alcohol derivatives and a range of electron-deficient alkenes (including acrylonitrile) with only 2.5 mol% of **4a** at 25 °C.

In the course of our studies on the CM of fluorinated molecules as electron-deficient olefin partners, we discovered a markedly improved CM efficiency of **4a** over that of **3**. Across a range of fluorinated alkenes, **4a** gave consistently higher yields of CM products. Although yields using **3** were still acceptable, an increased propensity for dimerization of the electron-rich terminal alkene substrate with this catalyst was apparent.[40] Given the current interest in fluorinated phases,[41] this new efficient method for forming fluorinated alkenes is of some synthetic utility. Itoh et al. prepared bis- and oligo-*gem*-difluorocyclopropanes through CM dimerization promoted by **3**. However, relatively high catalyst loadings (15 mol%) were required to achieve moderate to good yields.[42]

Interestingly, vinyl- and allylphosphonates **36** and **37** are viable CM partners in metathesis reactions catalyzed by **3**.[43] High yields were obtained on coupling with simple terminal olefins to give products of synthetic interest (Figure 5).

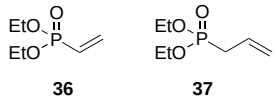


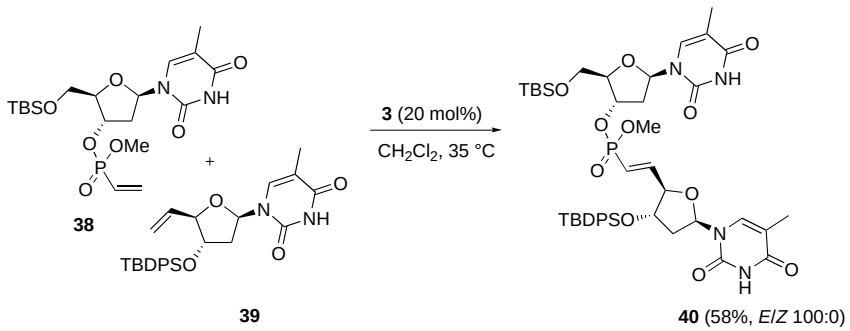
Figure 5. Vinyl- and allylphosphonates for CM.

Along the same lines, Lera and Hayes[44] coupled nucleotides through a CM coupling of vinylphosphonate **38** with terminal olefin **39** catalyzed by **3** (20 mol%). Under similar conditions, catalyst **6** gave none of the desired nucleotide dimer **40**, thus highlighting the superiority in terms of both activity and functional-group tolerance of **3**, and its potential for CM modification of biologically important molecules (Scheme 5). Interestingly, the authors cite intramolecular chelation of the nucleotides to ruthenium as the reason why such large amounts of catalyst are required to achieve acceptable CM yields.

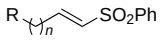
Krausz and co-workers were able to dimerize various nonphosphorylated 3′-allyl nucleosides through CM promoted by the bisphosphane catalyst **6** (10–20 mol%). Yields were moderate (≤45%) and the reaction was largely unselective with regard to olefin geometry.[45]

As noted earlier, Grubbs and co-workers[32] reported that vinyl sulfones are not successful substrates in CM reactions catalyzed by **3**. However, Grela and Bieniek subsequently found that phenyl vinyl sulfone gave good yields of products of general type **41** with a variety of terminal olefins in the presence of **3** (Figure 6).[46] In our hands, CM of similar CM

 © 2003 Wiley-VCH Verlag GmbH & Co. KGaA, Weinheim



Scheme 5. Coupling of nucleotides by CM (TBDPS = *tert*-butyldiphenylsilyl).



41

R = OTBS, n = 4	(85%)
R = $CH(CO_2Et)_2$, n = 1	(74%)
R = CO_2Me, n = 8	(76%)

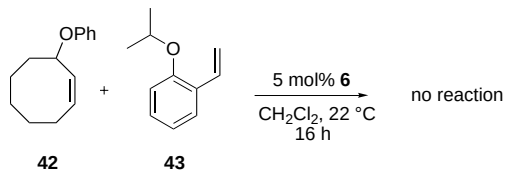
Figure 6. Products from CM with phenyl vinyl sulfone.

partners with phenyl vinyl sulfone was much less efficient with catalyst **3** than one would expect from analysis of the literature data;[46] however, good conversions were possible with the phosphane-free catalyst **4a**.[47] Given the synthetic potential of sulfones as both Michael acceptors and cycloaddition-reaction substrates these findings are of some value and interest in organic synthesis.

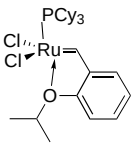
2.4. CM Selectivity Derived from Chelation

That the chelation of oxygen functionalities to ruthenium during metathesis is possible and plays an important role in the course of the reaction is beyond doubt.[48] One particularly instructive example is a report by Hoveyda and co-workers concerning the serendipitous discovery of a stable, catalytically active species **1** from the attempted ROM–CM of 2-isopropoxystyrene (**43**) with octadiene **42** in the presence of **6** (Scheme 6).[49]

The complex **1** was active in metathesis reactions (although not tested in CM) and was of sufficient stability to be recovered efficiently by chromatography after reaction,

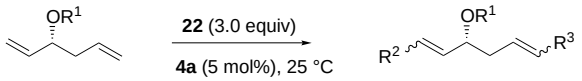


Scheme 6. Serendipitous discovery of **1** from an attempted ROM–CM reaction.



1

thus allowing the catalyst to be recycled. This clearly demonstrates the potential of intramolecular chelating effects to interfere dramatically with a metathesis reaction. This same chelation principle has been utilized to prepare the chromatographically stable catalyst **4a** from **3**,[27,28] and as we have seen, the effect of the chelating isopropoxystyrene moiety on CM catalyst activity can be advantageous under certain circumstances.[28,38,40] Two recent reports cast some light on the potential role of chelated intermediates in both chemo- and *E*/*Z* selectivity in CM reactions. Cossy and BouzBouz[50] discovered that in the case of CM of hydroxy- and acetoxyolefins **44** and **45**, respectively, with acrolein (**22**) promoted by **4a** under identical conditions, **44** is functionalized twice (to give **46**), whereas acetoxyolefin **45** affords the product of a single cross-coupling reaction, **47** (Scheme 7).



44 R^1 = H
45 R^1 = Ac

46 R^1 = H, R^2 = CHO, R^3 = CHO (70%, *E*/*Z* 30:1)
47 R^1 = Ac, R^2 = H, R^3 = CHO (73%, *E*/*Z* 30:1)

Scheme 7. Chelation effects in chemoselective CM.

These results were rationalized in terms of catalyst deactivation by chelation of the acetoxy group to the metal center during the catalytic cycle (Figure 7). It was proposed that selectivity could arise through either deactivation of one of the C–C double bonds by the electron-withdrawing acetoxy group, or as would seem more plausible to us, through the formation of an unreactive six-membered chelate ring **H′**, which results in selective CM of the homoallylic unit. The corresponding chelate derived from **I′** would require

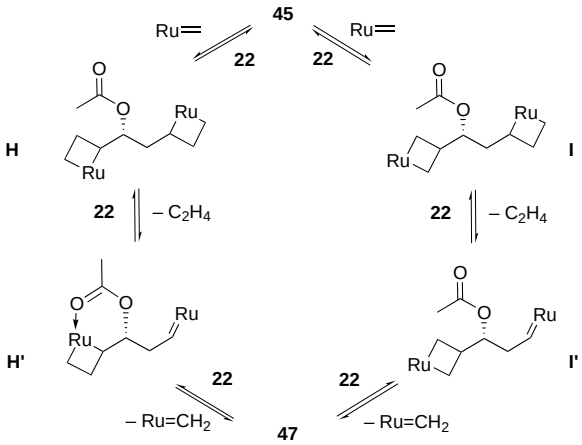
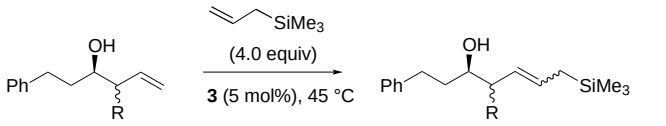


Figure 7. Proposed catalytic cycle for chemoselective CM.

 © 2003 Wiley-VCH Verlag GmbH & Co. KGaA, Weinheim

seven-membered ring formation and as such would be expected to be much less stable. In the case of hydroxy substrate **44** no such stable ring chelates are possible, and thus unselective CM is observed.

At approximately the same time Taylor and co-workers demonstrated the contribution that chelates can make to the *E*/*Z* selectivity of CM reactions between homoallylic alcohols with *syn*- and *anti*-allylic substituents and allyltrimethylsilane (Scheme 8).[51] Both diastereomers led to higher *E*/*Z* ratios than the unsubstituted case **48**, and *anti*-substituted substrates **49** and **51** resulted in the highest stereoselectivity. What is most striking is that the same *E*/*Z* ratios were obtained in both *syn* products and in both *anti* products (**55**, **57** and **54**, **56**, respectively) regardless of the nature of the *syn* or *anti* group.



48	R = H	**53** R = H	(84%, *E*/*Z* 70:30)
49	R = *anti*-CH_3	**54** R = *anti*-CH_3	(86%, *E*/*Z* 92:8)
50	R = *syn*-CH_3	**55** R = *syn*-CH_3	(81%, *E*/*Z* 80:20)
51	R = *anti*-CO_2Et	**56** R = *anti*-CO_2Et	(67%, *E*/*Z* 92:8)
52	R = *syn*-CO_2Et	**57** R = *syn*-CO_2Et	(74%, *E*/*Z* 80:20)

Scheme 8. *E*-selective CM of substituted homoallylic alcohols.

Again the postulation of intramolecular chelates provided the most satisfactory explanation for the unexpected stereoselectivity observed. Assuming that chelation of the hydroxy group to ruthenium occurs, and taking **49** and **50** as examples, examination of the chelated metallacyclobutane intermediates clearly shows that the formation of a *Z* intermediate from the *anti* diastereomer **49** is particularly disfavored on steric grounds as a result of an interaction with the trimethylsilyl group, thus explaining the observed increased *E* selectivity with this substrate relative to *syn*-**50** (Figure 8). Similar arguments can be used to explain the isomer ratios in products **56** and **57**.

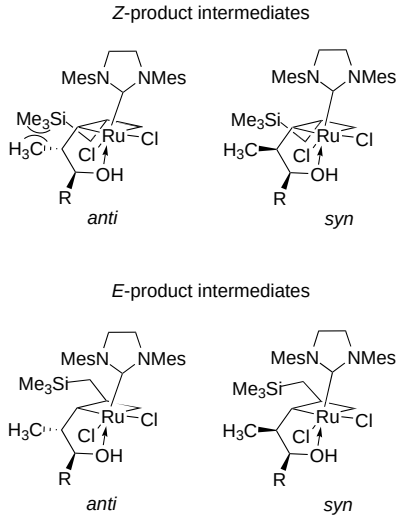


Figure 8. Intermediates in *E*-selective CM of homoallylic alcohols.

2.5. Reversibility in Selective CM

The reversible nature of the CM reaction is of synthetic importance because it generally ensures the preferential formation of the most thermodynamically stable product. As we have seen, this results in the transformation of terminal olefins into internal olefins through CM, with *E*/*Z* ratios higher than 1:1 in most cases.

A highly impressive demonstration of how the reversible nature of the CM reaction can be exploited to give highly selective transformations is the total synthesis of (−)-cylindrocyclophanes A and F (Figure 9) reported by Smith and coworkers.[52] The key step in this remarkable synthesis is a

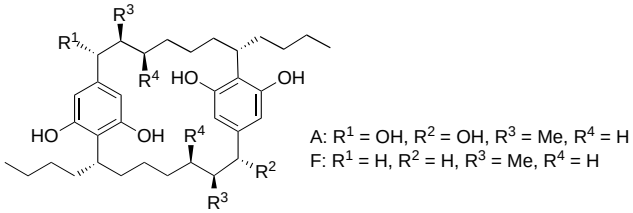
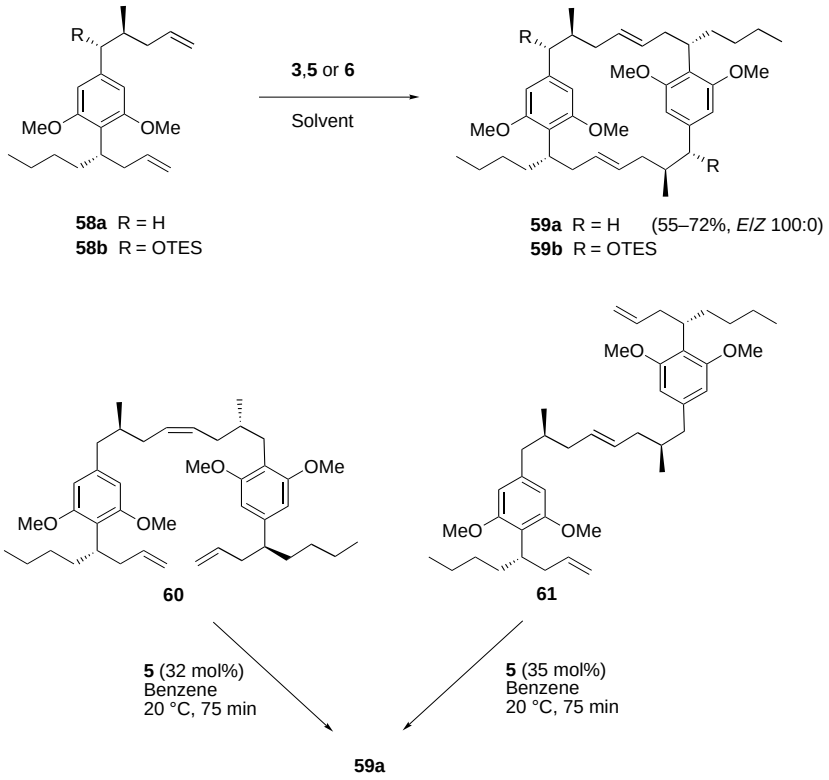


Figure 9. Cylindrocyclophanes A and F.

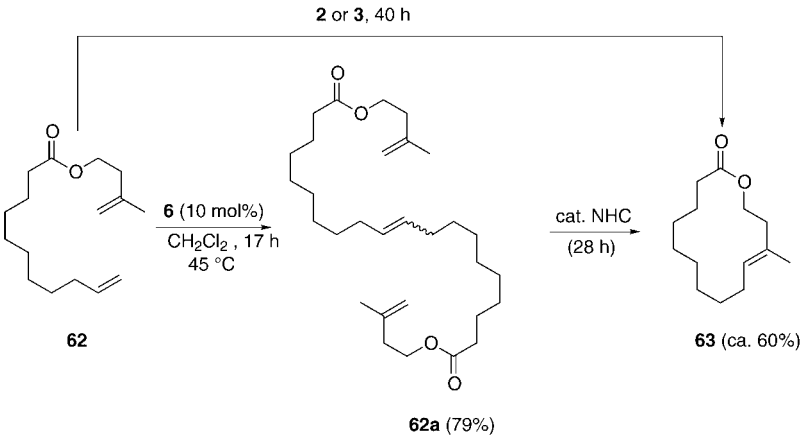
head-to-tail CM dimerization reaction of terminal olefins **58a**,**b** catalyzed by either **3**, **5**, or **6** (Scheme 9) to give macrocyclic products **59a**,**b**, which could be readily converted into cylindrocyclophanes A and F by standard functional-group manipulations. The level of selectivity in these reactions was both surprising and outstanding: Neither "head-to-head" dimerization nor *Z*-olefin products were observed. Of the seven possible dimeric products (head-to-head, head-to-tail, and *E*/*Z* isomers) only **59a**,**b** were formed.

This led the authors to investigate this reaction further, particularly with a view to discovering the root cause of this extraordinary regio- and stereoselectivity. The most likely explanation is that the reversible nature of CM resulted in a cascade of reactions to form a single dimer product as long as the catalyst remained sufficiently active. This theory was supported by Monte Carlo methods (MM2 force field), which showed that for the dimerization of **58a**, the (*E*,*E*)-[7,7]-paracyclophane product **59a** was the most stable of the possible dimer structures by approximately 2.6–4.7 kcal mol^{-1}. More convincing still was the discovery that RCM of **60** or **61** with the Schrock catalyst **5** gave only **59a** in good yields (75 and 81%, respectively), despite the fact that these substrates should be inclined to furnish [8,6]-paracyclophane instead of [7,7]-paracyclophane products (Scheme 9). It is also noteworthy that catalyst **5** consistently outperformed **6** and **3** in these reversible CM processes. This efficient synthesis of cylindrocyclophanes A and F demonstrates the potential of CM for target-oriented synthesis, in addition to highlighting the advantages in terms of selectivity that can be obtained by exploiting the reversibility of the CM reaction.

 © 2003 Wiley-VCH Verlag GmbH & Co. KGaA, Weinheim



Scheme 9. Synthesis of cylindrocyclophane precursors by reversible CM (TES = triethylsilyl).



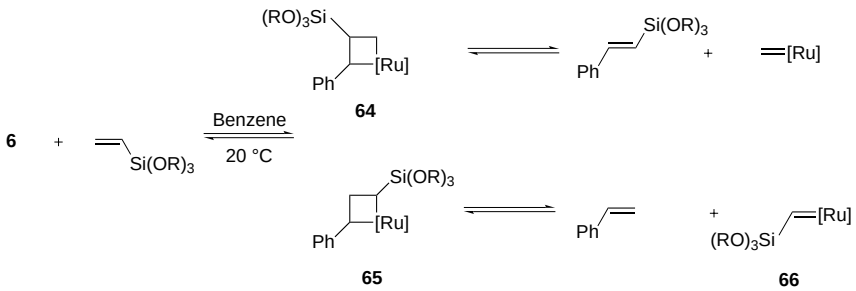
Scheme 10. Reversible-CM-based macrocycle formation.

Fürstner et al.[53] have utilized a similar concept to prepare the 14-membered macrolide **63** from acyclic diene **62** (Scheme 10). The reaction (40 h) of **62** in the presence of NHC catalysts **2** (10 mol%) or **3** (6 mol%) afforded macrocycle **63** in approximately 60% yield. The less active Grubbs catalyst **6** gave only CM dimer **62a** after 17 h at 45 °C. A slightly modified NHC catalyst then transformed **62a** into lactone **63**, which demonstrates that macrocyclic RCM can be preceeded by a reversible CM dimerization. This reversible CM–RCM strategy was subsequently used in the total synthesis of the antibiotic (*R,R*)-(−)-pyrenophorin.

2.6. CM with Vinylsilanes

Silylated olefins are an important class of compounds that have found wide application in organic synthesis. Of particular interest are vinyl siloxane derivatives, which can participate in palladium(0)-catalyzed C–C-coupling reactions with aryl iodides.[54] Thus the functionalization of vinyl silanes and siloxanes by CM is an attractive prospect. Fischer and co-workers[55] have shown that the reactivity of vinylsilanes towards CM with styrene increases with increasing oxygen substitution at silicon: $CH_2{=}CHSi(OR)_3 > CH_2{=}CHSiMe(OR)_2 > CH_2{=}CHSiMe_2OR > CH_2{=}CHSiMe_3$.[56] Vinyltrimethoxy- and vinyltriethoxysilanes gave good CM conversions (76–100%) in the presence of only 1 equivalent of styrene (2 mol% **6**) and only the *E* isomer of the cross-product was detected by ^{1}H NMR spectroscopic analysis. A gentle stream of argon was required to remove the ethylene by-product during the reaction; in closed systems substrate conversions were unsurprisingly lower. In test reactions between vinyltrialkoxysilanes and stoichiometric amounts of **6**, Fischer and co-workers[56] observed high selectivity in the formation of $PhCH{=}CHSi(OR)_3$ over $PhCH{=}CH_2$. This result indicates that in the first step of the metathesis reaction ([2+2] cycloaddition), metallacyclobutane **64** is generated in preference to **65** (Scheme 11). The ruthenium silylalkylidene **66** was also not detected. As this intermediate is required for dimerization of vinyltrialkoxysilane, its absence in these stoichiometric studies is possibly significant in explaining why high CM selectivities are possible with only a 1:1 ratio of siloxane and styrene.

The discovery that vinyltrialkoxysilanes are inactive in CM dimerizations was significant as it allows the use of these reagents in excess to drive selective CM reactions with more challenging partners than styrene.[32,57] *E*-Selectiv le CM reactions with 1-hexene, 1-decene, allylbenzene, and allyl phenyl ether (amongst others) were possible in the presence of a fivefold excess of siloxane and 5 mol% of **6**. In all cases, yields were between 70 and 100%, with *E*/*Z* ratios between 5:1 and 15:1.[56,57] In another interesting application, vinylsilanes were found to couple with alkyl vinyl ethers ($ROCH{=}CH_2$) in the presence



Scheme 11. Reaction of **6** and vinyltrialkoxysilanes.

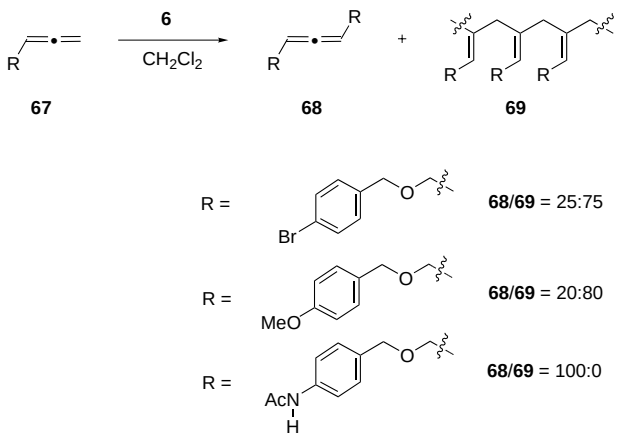
 © 2003 Wiley-VCH Verlag GmbH & Co. KGaA, Weinheim

of **6** (5 mol%) to give CM products of general type ROCH=$CHSiR_3$ in high yields, although deuterium-labeling studies have shown that this reaction almost certainly does not proceed through a metathesis-type mechanism.[58] Similar reactions with allyl alkyl ethers (through a ruthenacycle-based mechanism) have also been reported.[59]

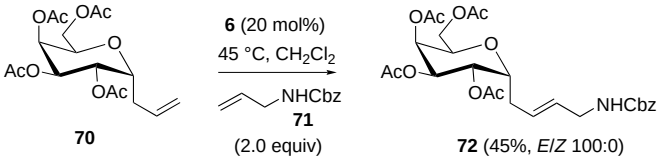
2.7. Cross-Metathesis of Allenes

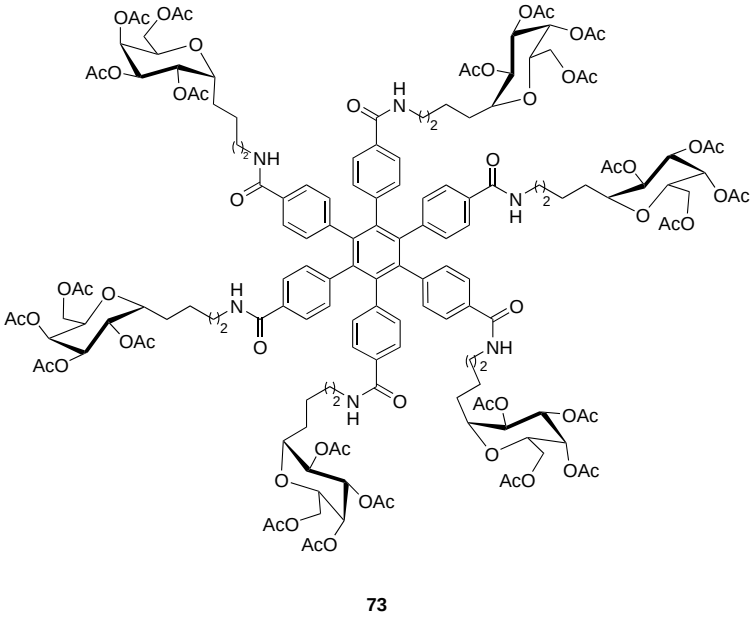
To the best of our knowledge, only one example of a CM reaction involving well-defined ruthenium complexes and allenes has been reported.[60] Barrett and co-workers treated a variety of monosubstituted allenes of general type **67** with **6** (5 mol%) at 20°C. Under these conditions, self-metathesis 1,3-disubstituted allene products **68** along with polymeric material **69** were obtained (Scheme 12). The ratio of **68**/**69** varied considerably with the steric and electronic properties of **67** with no clear general trends emerging, although it was determined that simple phenyl-substituted allenes (R = Ph and *o*-, *m*-, and *p*-tolyl, for example) were poor substrates and afforded **69** exclusively. Catalysts **3** and **5** were less active than the first-generation Grubbs catalyst **6** in these reactions.

The absence of theoretically possible cumulene products from the reaction was rationalized in terms of the likely relative instability of the bis(exo-methylene)metallacyclobutane intermediates (required to form cumulenes) compared to the mono(exo-methylene)metallocyclobutane that forms **68**.



Scheme 12. Self-metathesis of allenes.





Scheme 13. Synthesis of "molecular asterisks" by CM (Cbz = benzyloxycarbonyl).

2.8. Synthesis of Biologically Important Molecules

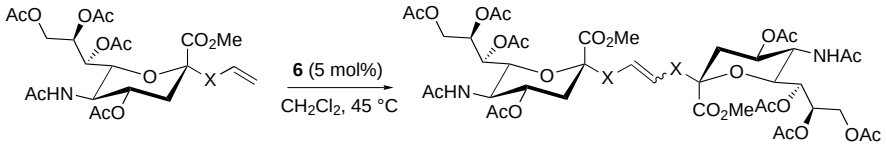
From humble beginnings,[1j] the evolution of CM into a flexible and powerful methodology for synthesis of biomolecules (and their analogues) and of natural products is steadily gaining momentum. Quite recently the volume of material published in this area has increased as more and more chemists are turning to CM to achieve smooth high-yielding transformations as key components of multistep selective syntheses.

2.8.1. Carbohydrates

The application of olefin metathesis to carbohydrate chemistry has been the subject of two reviews published in 2000.[1c,61] As this particular area of the field has been well-documented, this section will concentrate on developments in this area since.

Roy and co-workers have used a selective CM reaction as a key C–C bond-forming step in the preparation of so-called "molecular asterisks".[62] An initial CM reaction between peracetylated α-D-allylgalactopyranoside **70** with protected amine **71** catalyzed by **6** afforded cross-product **72** in moderate yield with complete *E* selectivity (Scheme 13). The predominance of the *E* isomer in this CM reaction remains to be explained; CM reactions involving various other sugar derivatives under identical conditions gave selectivity no better than 4:1 in favor of the *E* form. Glycoside **72** then served as the template on which to build the necessary functionality to give the aryl glycoside cluster **73** after (double) Sonogashira coupling and cyclotrimerization reactions. This class of compounds is anticipated to be important in elucidating the binding specificity of multiple carbohydrate–protein interactions. It was also possible to use a protected amino acid instead of **71** to give a novel C-linked glycopeptidomimetic product after CM. However the *E*/*Z* selectivity was modest.

 © 2003 Wiley-VCH Verlag GmbH & Co. KGaA, Weinheim



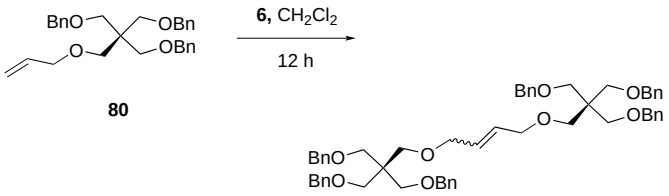
74 X = OCH_2
75 X = $O(CH_2)_3$
76 X = SCH_2 (10 mol% **6**)

77 X = OCH_2 (82%, *E*/*Z* 7:1)
78 X = $O(CH_2)_3$ (88%, *E*/*Z* 3:1)
79 X = SCH_2 (26%, *E*/*Z* 2.5:1)

Scheme 14. Sialoside dimers.

Roy and Gan prepared divalent sialoside derivatives based on a CM reaction.[63] For example, the dimerization of sialosides **74**–**76** promoted by **6** allowed the isolation of dimers **77**–**79** (Scheme 14). Yields were good using *O*-α-sialosides, however thiosialoside **76** was a considerably less efficacious CM partner as a result of the coordinating (and hence catalyst-poisoning) proclivities of sulfides. Even so, to the best of our knowledge, the formation of **79** in low yield is the first example of a sulfide participating in a straightforward CM reaction catalyzed by well-defined ruthenium initiators such as **6**.

A CM strategy has also been employed to construct a hexameric cluster, which can be further elaborated to bear saccharide-based xenotransplantation antagonists such as the Galili antigen.[64] CM dimerization of monoallyl ether functionalized pentaerythritol derivative **80** in the presence of **6** afforded hexameric cluster **81** in excellent yield with high *E*/*Z* selectivity (Scheme 15). Dendrimer template **81** was then hydrogenated/deprotected and functionalized with the appropriate saccharides by standard techniques.



80

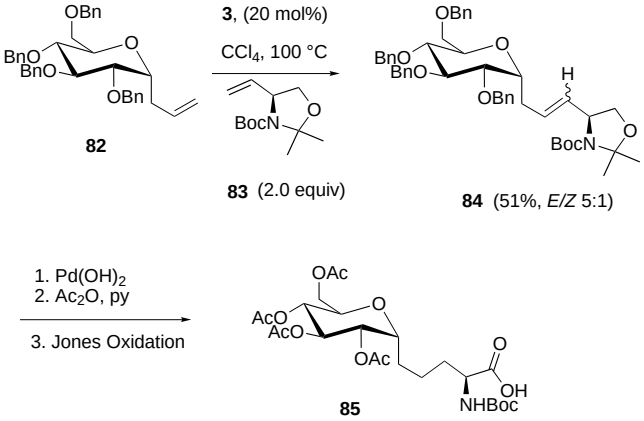
81 (85%, *E*/*Z* 10:1)

Scheme 15. Formation of saccharide dendrimer template by CM.

Dondoni et al.[65] reported a successful CM between olefinated carbohydrates such as **82** and vinyloxazolidenes such as **83** catalyzed by the second-generation Grubbs catalyst **3** (20 mol%). After CM, the vinyloxazolidene protecting group can be cleaved with Jones reagent to unmask *C*-glycosyl amino acids such as **85** (Scheme 16). This methodology has also been extended to prepare a potential glycopeptide nephritogenoside mimetic.

2.8.2. Natural Products

Although not nearly as successful as RCM in this area, CM is finding increasingly wide application in the synthesis of natural products as the chemo- and stereoselectivity of this process steadily improve. Some examples have already been noted: Cossy and BouzBouz[50] have used multiple selective CM/allyltitanations to prepare the C1–C14 fragment of the dinoflagellate amphidinol III, Smith et al.[52] reported the superb manipulation of the reversibility of CM to prepare cylindrocyclophanes A and F, and Stoltz and Spessard[31] have employed a CM step in the synthesis of the bicyclo[3.3.1]nonane core of garsubellin A.



82

83 (2.0 equiv)

84 (51%, *E*/*Z* 5:1)

85

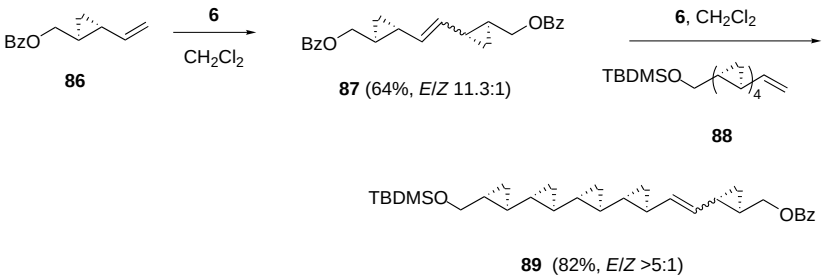
Scheme 16. *C*-glycosyl amino acid synthesis by CM (Boc = *tert*-butoxycarbonyl, py = pyridine).

Verbicky and Zercher[66] have utilized a CM coupling strategy in the formal synthesis of the antifungal natural product (−)-FR-900848. Based on CM methodology initially proposed by Grubbs and co-workers[17,18] (i.e. selective CM by an initial self-metathesis of one olefin partner followed by CM coupling of the resulting dimer with a terminal olefin), self-metathesis of enantiopure cyclopropane **86** with **6** (5 mol%) gave dimer **87** in reasonable yield. CM coupling of **87** with tetracyclopropane **88** again promoted by **6** (5 mol%) furnished the key intermediate **89** (Scheme 17), which after selective cleavage of the benzoyl group is identical to an advanced intermediate in the synthesis of (−)-FR-900848 by Barrett and Kasdorf.[67]

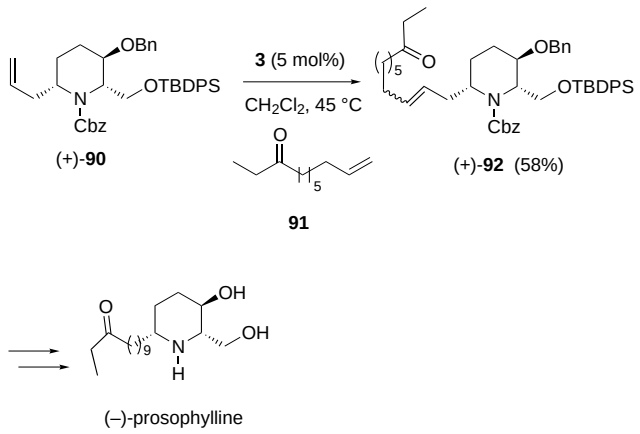
Cossy et al. have also applied CM to the synthesis of the piperidine alkaloid (−)-prosophylline.[68] Metathesis coupling of alkene (+)-**90** with 2 equivalents of ketone **91** in the presence of **3** (5 mol%) resulted in the formation of advanced intermediate (+)-**92** in acceptable yield, which can be transformed into the natural product after a hydrogenation/deprotection sequence (Scheme 18).

One of the inherent limitations of the CM reaction is that it can fail in cases involving strained olefins, for which ROM–CM pathways are preferable. An impressive example is the synthesis of the AB fragment of ciguatoxin (CTX1B) by Hirama and co-workers.[69] A high-catalyst-loading CM reaction between seven-membered-ring substrate **93** (itself formed by RCM) and acetate **94** proceeded in poor yield and

 © 2003 Wiley-VCH Verlag GmbH & Co. KGaA, Weinheim

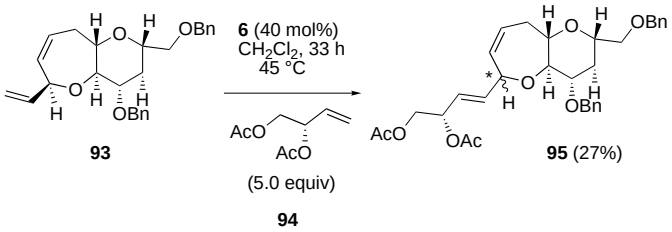


Scheme 17. Formal synthesis of (−)-FR-900848.

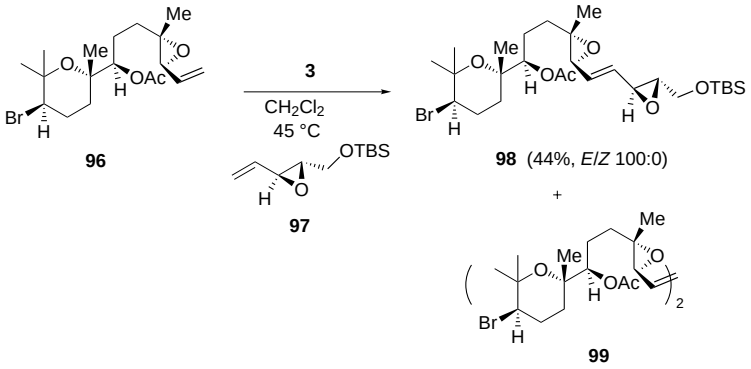


Scheme 18. CM in the synthesis of (−)-prosophylline.

also gave a mixture of diastereomers, epimeric at the indicated carbon center (Scheme 19). The authors cite ROM as the major fate of **93**.



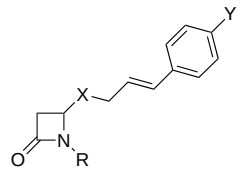
Scheme 19. Synthesis of AB-ring fragment of ciguatoxin by CM.



Scheme 20. Synthesis of ABC-ring fragment of thyrsiferol by CM.

Quite recently McDonald and Wei[70] reported the synthesis of the ABC tristetrahydropyran moiety common to the thyrsiferol and venustatriol natural products using a CM coupling step. Metathesis coupling of terminal olefin **96** with 3 equivalents of chiral epoxide **97** catalyzed by the second-generation Grubbs catalyst **3** (10 mol%) gave a mixture of CM product **98** (44%), homodimer **99**, and unreacted **97** (Scheme 20). Taking advantage of the fact that both **96** *and* **99** can participate in further CM couplings, the recovered starting material and dimer were subjected to a further charge of **3** in the presence of additional **97**, which led to another 20% yield of **98**.

Barrett et al. have utilized RCM, enyne metathesis, and CM to functionalize alkenylated β-lactam rings; in particular the CM of olefin lactam substrates and *p*-substituted styrenes allowed the preparation of coupled products in moderate to good yields (Figure 10).[71] In an interesting application, Diver and co-workers have recently demonstrated the applicability of CM to the modification of cyclosporin A derivatives for attachment to a solid support.[72]



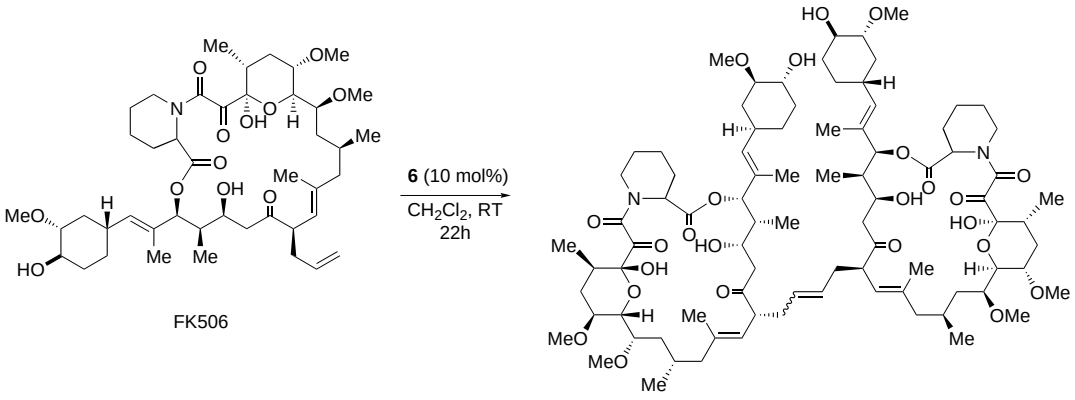
X = O, NTs
Y = H, Cl, Me, OMe
R = H, TBDMS, Bn, CH(OTBDMS)CO_2Et

Figure 10. Functionalized β-lactams from CM reactions.

CM has also been proposed as a concise method for the preparation of flavan-3-ol precursors. Gesson and co-workers[73] reported CM reactions between 2-allylphenol derivatives and styrenes promoted by **6** (typically 3 mol%), which give reasonable to good yields of cross-product (60–79%) with only the *E* isomer detected. The resulting 1,3-diaryl propenes are useful starting materials for the synthesis of flavan-3-ols, a class of natural product with wide-ranging biological activity. Recently Miller and Vasbinder demonstrated the superiority of CM over the Wittig reaction for the preparation of Pro-Gly dipeptide alkene isosteres.[74]

Schreiber and Diver[75] utilized CM to dimerize the immunosuppressant FK506. Treatment of the macrocycle with **6** (10 mol%) at room temperature furnished the corresponding dimer (FK1012) in moderate yield (Scheme 21). The high functional-group tolerance of **6** allows this reaction to be carried out on the unprotected substrate, despite the presence of several potential chelating groups

 © 2003 Wiley-VCH Verlag GmbH & Co. KGaA, Weinheim



Scheme 21. Dimerization of FK506 by CM.

in the molecule. FK1012 was found to activate signal-transduction pathways and gene transcription in mammalian cells.

Nicolaou and co-workers employed a similar strategy to dimerize vancomycin derivatives through CM.[76] A small library of alkene-substituted vancomycin analogues were formed by self-metathesis in variable yields in the presence of **6** (20 mol%) in H_2O/CH_2Cl_2 (95:5; presumably the organic cosolvent is required for catalyst initiation) under phase-transfer conditions. In these processes, **6** exhibited unprecedented functional-group tolerance in the presence of amino, carboxy, hydroxy, and amide groups. These experiments led to the discovery of several highly potent antibiotics, some of which displayed high activity against vancomycin-resistant bacteria.

3. Ring-Opening Cross-Metathesis

The highly efficient and atom-economic ROM–CM reaction has been the subject of much recent investigation. The presumed catalytic cycle for this reaction is shown in Figure 11. The reaction of ruthenium methylidene and olefin substrate **100** furnishes metallacyclobutane intermediate **101**, which on collapse gives ring-opened alkylidene **102**. This step is most efficient for highly strained cyclic olefin substrates, in which relief from ring strain provides an energetic counterweight to the entropically favored reverse RCM reaction (**102**→**100**). It is hardly surprising, therefore, that norbornenes, oxanorbornenes,[77] and cyclobutenes[1i,78] are generally excellent substrates for ROM–CM reactions. CM between **102** and terminal olefin **103** (internal olefins may also serve as CM partners) then affords ROM–CM product **105** via intermediate **104** with loss of the ruthenium methylidene, which then reenters the catalytic cycle. An important condition for ROM–CM to be efficient is that CM between **102** and **103** must be faster than the reaction between **102** and **100** (a competing ROMP pathway), a factor which very much depends on the nature of the cyclic olefin **100** and the CM partner **103** used. However, in the majority of cases ROM–CM competes effectively with ROMP,[20,77,78] particularly under high dilution conditions. Another factor to be considered is the rate of homodimerization of the CM partner: Often the best CM partners are those that undergo self-metathesis relatively slowly, for example, styrenes and allytrimethylsilane.

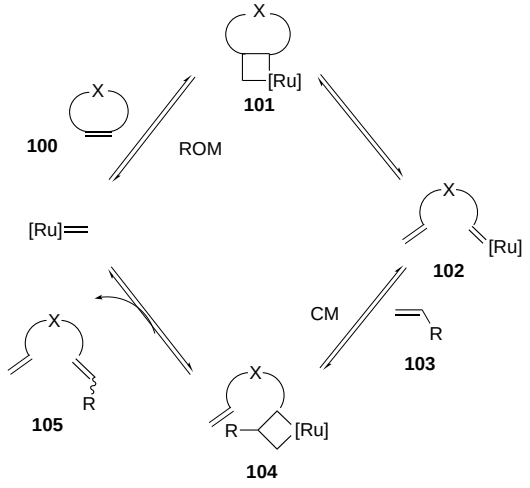


Figure 11. ROM–CM catalytic cycle.

One of the key issues to be tackled recently is the question of regioselectivity in ROM–CM. Although progress has been made, hard-and-fast rules regarding the factors that influence selectivity have not yet emerged. In the general example shown in Figure 11 only one product, **105**, is possible because **100** is symmetrical. However, if the starting cycloolefin is asymmetrically substituted, then different regioisomeric products are possible.

Arjona et al.[79] considered the ROM–CM between cycloolefin **106** and a terminal olefin and have put forward plausible arguments for the formation of products **107** and **108** (Figure 12): The reaction of cycloalkene **106** with the catalytically active methylidene gives rise to either **109** or **110**. It would seem reasonable to assume that cycloaddition would be preferable from the side opposite to the large group, and thus steric interaction between the metal–ligand moiety and the small group makes **109** more favorable than **110**. Cyclo-

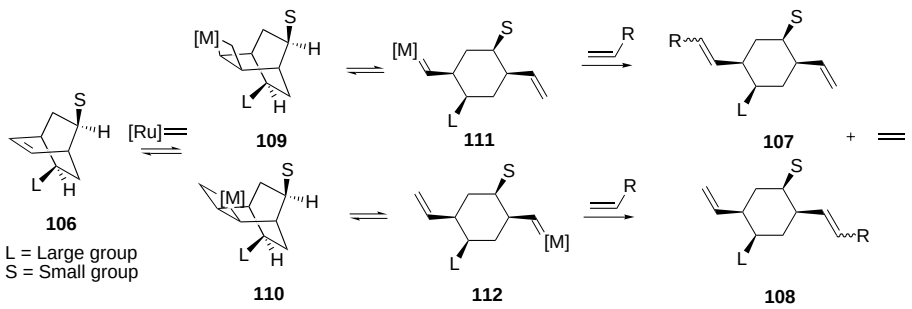
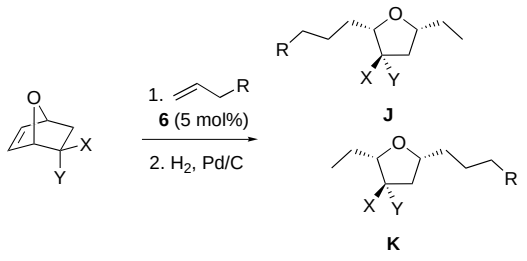


Figure 12. Rationale for the regioselectivity of ROM–CM.

reversion of **109** to **111** followed by CM then affords **107** as the major product, that is, the regioselectivity is derived from the initial cycloaddition reaction. Conversely, if the difference in steric bulk between the "small" and the "large" groups is considerable, then the difference in energy between **111** and the less-hindered **112** (which furnishes **108**) can dictate the outcome of the reaction, that is, the regioselectivity is largely derived from the CM reaction. It is also certain (although much more difficult to rationalize) that chelating and electronic effects are contributors to selectivity in certain substrates. What is clear is that regioselectivity is largely substrate-dependent.

Insight into the origins of regioselectivty of these processes was obtained from a ROM–CM study of various 2-substituted 7-oxanorbornenes (Scheme 22).[80] Variation of the substituents X,Y had a profound effect on selectivity. With small substituents Y no selectivity was found; however, even a small difference (Y = OH converted into Y = OAc) led to an impressive increase in selectivity. Also interesting is that the introduction of a substituent X (not H) does not improve the selectivity further, and that the major products all have the alkyl side chain on the same side of the ring as the Y substituent (i.e. *cis* products with respect to Y). This indicates that interaction between the Y substituent and the metal moiety in the putative metallated intermediates is critical. It is also known that these reactions are concentration-dependent. Increasing the concentration by 200% leads to dimerization of the resulting terminal olefin after initial ROM–CM.[81]

Cuny et al. [82] reported examples in which the nature of the terminal olefin CM partner can influence product ratios.

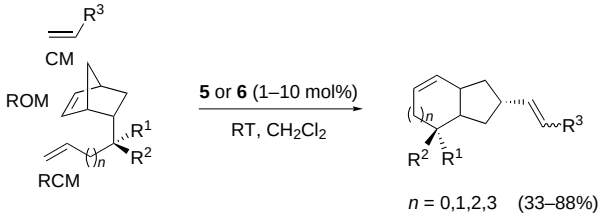


X, Y = C=O, R = OAc (75%, **J**/**K** 50:50)
X = H, Y = OH, R = OAc (80%, **J**/**K** 50:50)
X = H, Y = OAc, R = OAc (75%, **J**/**K** 19:81)
X = H, Y = $OCOCH{=}CH_2$, R = OAc (75%, **J**/**K** 23:77)
X, Y = OCH_2CH_2O, R = OAc (80%, **J**/**K** 21:79)
X, Y = OCH_2CH_2O, R = OBn (70%, **J**/**K** 23:77)

Scheme 22. ROM–CM with substituted oxanorbornenes.

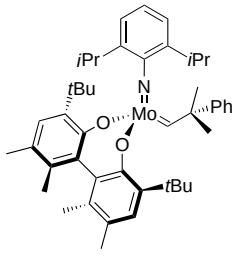
In ROM–CM reactions involving bicyclic *exo* norbornenes and *p*-substituted styrenes, use of 4-vinylanisole or 3-methoxy-4-vinylphenol gave a single *E* ROM–CM product, whereas *tert*-butyl 4-vinylphenylcarbonate gave a major *E* cross-product, along with significant amounts of the *Z* isomer and a bis-CM product (7 and 6%, respectively).

We have shown that tandem ROM-RCM–CM reactions are possible.[83] Exposure of norbornenes containing olefin side chains of various lengths to **5** or **6** (5–10%) in the presence of terminal olefins or ethylene gas gave rise to bicyclic products. Cyclopentane-fused five-, six-, seven-, and eight-membered rings could be constructed without difficulty in a practical domino process (Scheme 23).[84]



Scheme 23. Domino ROM–RCM–CM.

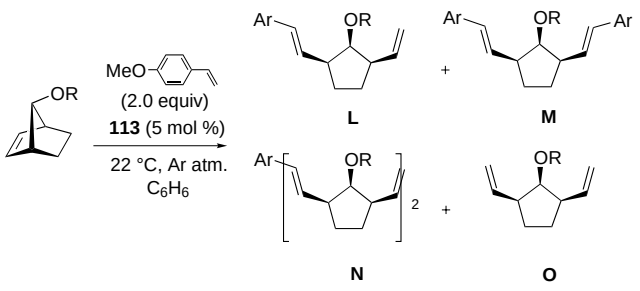
A very important development in this field came from Hoveyda, Schrock, and co-workers with the discovery of asymmetric ROM–CM.[85,86] Noting that the ROM–CM reaction can give rise to chiral products, they treated *meso* norbornenes with enantiopure molybdenum catalyst **113**[87] (Figure 13) in the presence of styrene derivatives (Scheme 24). 4-Methoxystyrene was the most efficient and selective coupling partner, giving the product as a single enantiomer in two cases with an accompanying high chemoselectivity (**L**/**M**/**N** ratio). The enantioselectivity was found to be largely independent of the ether R group and of the styrene; however, reactions involving styrene itself or 4-trifluoromethylstyrene tended to be less chemoselective, although results were still acceptable. Other terminal olefin



113

Figure 13. Chiral molybdenum catalyst for asymmetric ROM–CM.

 © 2003 Wiley-VCH Verlag GmbH & Co. KGaA, Weinheim

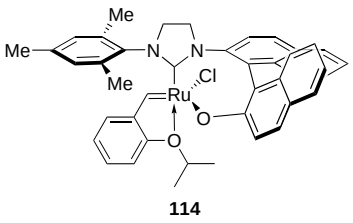


R = OTBS, conv (%) **L/M/N/O** 75:8:0:7, 91% *ee*, *E/Z* 100:0
R = OTMS, conv (%) **L/M/N/O** >98:0:0:0, >98% *ee*, *E/Z* 100:0
R = OMOM, conv (%) **L/M/N/O** 95:3:2:0, >98% *ee*, *E/Z* 100:0

Scheme 24. Enantioselective ROM–CM reactions (MOM = methoxymethyl).

CM partners were compatible with the reaction, including one example of a one-pot sequential asymmetric ROM–CM with vinyltriethoxysilane/Pd-catalyzed arylation to give a ring-opened and arylated product in 51% yield with >98% *ee*. These findings demonstrate the synthetic potential of asymmetric ROM–CM for the straightforward preparation of functionalized chiral cyclopentane building blocks.[88]

Hoveyda and co-workers recently also developed alkylidene **114**, a ruthenium-based enantiopure catalyst for asymmetric ROM-CM (Figure 14).[89] Due to the nature of the metal and the presence of an alkoxide ligand (which is expected not to be beneficial in ruthenium alkylidene catalysts because of their lower inductive electron withdrawing abilities relative to chloride ligands[90]), **114** exhibits lower reactivity in ROM reactions (10 mol% is required). However, it has an impressive stability akin to that of **4a**, and as such can be recovered chromatographically after the reaction and can be used exposed to air without difficulty. The levels of chemo- and enantioselectivity when using **114** were generally excellent.

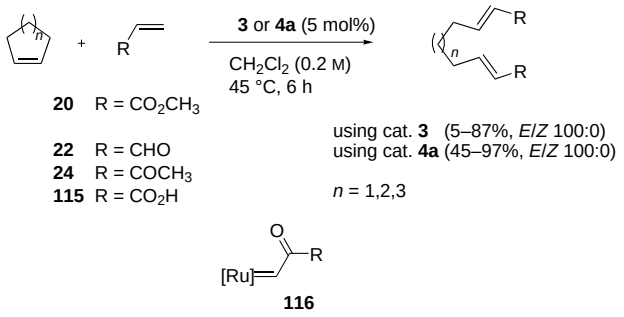


114

Figure 14. Chiral ruthenium catalyst for asymmetric ROM–CM.

Catalysts **4b**[91] and **4c**,[92] which incorporate steric bulk *ortho* to the chelating isopropoxy moiety, are powerful metathesis initiators. We found that the use of only trace amounts of these precatalysts (only 0.005 mol% in the case of **4c**) effects ROM–CM reactions between a range of norbornenes or oxanorbornenes and allyltrimethylsilane in near quantitative yields. In the modern era in which catalyst efficiency and trace-metal-contamination levels in reaction products can be critical issues, we envisage that stable yet active catalysts of these types may prove to be valuable.

In general, as noted previously, ROM–CM reactions are most successful when using highly strained substrates that are predisposed to ring opening. Furthermore, it is assumed that in these reactions, ring opening is the initial step, which is then followed by CM (see Figure 11). It is therefore not surprising that under standard conditions for norbornene ring opening, unstrained cycloalkenes such as cyclopentene and cyclohexene are unreactive. However, Grubbs and co-workers demonstrated that β-carbonyl ruthenium carbene species generated from diazoacetates are highly active and react in stoichiometric quantities with cyclohexene to afford new ruthenium carbene complexes.[93] This led both Grubbs's group and our group to speculate as to whether or not ROM–CM was possible with unstrained olefins in the presence of reactive metal carbenes. We found that it was possible to bisfunctionalize cyclopentene, cyclohexene, and cycloheptene in good yields using catalysts **3** or **4a** in the presence of either acrylic acid (**115**), **20**, **22**, or **24** (Scheme 25).[94]

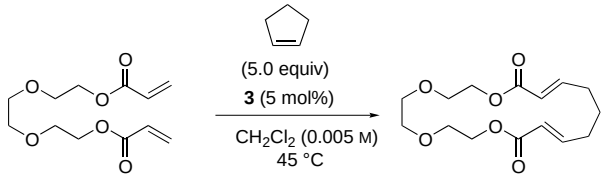


116

Scheme 25. ROM–CM of unstrained cycloalkenes.

Isopropoxy chelate catalyst **4a** gave higher yields of ring-opened products than did catalyst **3** in all cases tested. The order of reactivity of the cycloalkene substrates (cycloheptene ≥ cyclopentene > cyclohexene) presumably corresponds to ring strain, and the method was also applicable to heterocyclic substrates. It seems certain that the ring-opened species in these reactions are the highly electron-deficient carbenes of general type **116** (R = H, Me, OMe, OH). Unfortunately, vinyl sulfones, amides, and nitriles were unsuitable CM partners for the initial ROM reaction. Interestingly, a double-ROM–CM reaction with two different acceptor-substituted olefins was also demonstrated.

Grubbs and co-workers were able to use ROM–CM involving strained and unstrained olefins to effect ring-expansion reactions,[95] which seems like a promising method for the synthesis of macrocycles. For example, treatment of cyclopentene with bisacrylic ester **117** in the presence of **3** gave ring-expanded product **118** in a moderate yield through a ROM–CM process (Scheme 26). Grubbs and co-workers also demonstrated that reactive β-carbonyl ruthenium carbenes can be utilized in the selective ROM–CM of cyclooctadiene and trisubstituted cycloolefins to generate highly functionalized, long-chained olefins.[96] The latter class of substrates could be converted into products that are "end-differentiated" (i.e. one end of the chain contains an α-

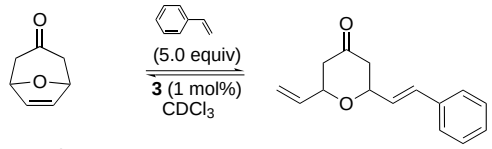


117 **118** (52%)

Scheme 26. Ring expansion of unstrained cycloalkenes through ROM–CM.

substituted terminal olefin and the other is end-capped with an α,β-unsaturated carbonyl moiety).[97,98]

Although in practice ROM–CM processes (particularly those involving highly strained substrates) are usually irreversible, an example of reversible ROM–CM has been reported (Scheme 27).[99] Wright et al. showed that the ROM–CM of oxabicyclo[3.2.1]octene derivatives are equilib-



119 **120** (83%, *E*/*Z* 100:0)

Scheme 27. Reversible ROM–CM.

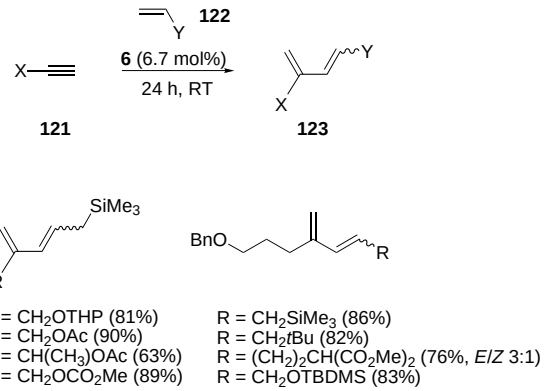
rium reactions. Reaction of ketone **119** with excess styrene promoted by **3** gave the ring-opened product **120** (*E* isomer) in good yield. However, after equilibrium had been reached (ca. 90% conversion by ^{1}H NMR spectroscopic analysis), addition of starting material had no effect on equilibrium ratios over time (isolated product **120** when exposed to **3** also gave **119** and styrene), indicating that the reverse RCM of **120** to give **119** and styrene was also occurring simultaneously. This reversibility could be circumvented by selective reduction of the keto group in **119** with L-Selectride followed by protection with the bulky TBS group. 1,3-Diaxial interactions then force both the olefin moieties in the product into equatorial positions, which are not conducive to ring closure, thus allowing irreversible ROM–CM.

4. Intermolecular Enyne Metathesis

Enyne metatheses are unique and interesting transformations involving the reaction of an alkene and an alkyne.[100] The products from these processes are synthetically useful butadiene derivatives, which lend themselves toward structural elaboration by Diels–Alder reactions and other cycloaddition processes.

Until recently, intermolecular enyne metathesis reactions were thought of as unselective with regard to both *E*/*Z*- and chemoselectivity. Competing CM homodimerization of the alkene, alkyne metathesis, and polymerization hampered the development of the enyne-metathesis reaction. The intramolecular variant, in which side reactions are minimized as a result of entropic effects and the proximity of the reacting moieties, has received much more attention. The situation up to 1997 was summed up by Mori:[6] "Intermolecular diene metathesis produces many olefins, and it has usually been used as intramolecular diene metathesis".

In 1997 our group reported the first selective intermolecular enyne metathesis.[101] The reaction of terminal alkynes of general type **121** and alkenes **122** (in excess) in the presence of **6** gave 1,3-disubstituted butadienes **123** in a remarkably selective operation. Internal alkenes were unreactive, and catalyst **5** was found to be an unsuitable promoter as it resulted in polymerization of the starting materials in all cases. A simple protocol was used to prepare a variety of dienes in good yields (Scheme 28).



Scheme 28. Selective intermolecular enyne metathesis.

To explain the high regio- and chemoselectivity observed the mechanistic pathway outlined in Figure 15 was proposed. The key regioselective step is the initial formation of metallacyclobutene **124**, which arises from attack of the alkyne by ruthenium methylidene. Ring opening of **124** then affords vinyl carbene **125**. Interestingly, the corresponding α,α-disubstituted vinyl carbene, which would lead to 1,2-substituted butadienes (the major products of intramolecular enyne metathesis reactions), is disfavored, possibly because it is either too stable to undergo subsequent CM, or as a result of unfavorable steric interactions associated with its metallacyclobutene precursor. 1,2-Disubstituted butadiene products are not observed. CM between **125** and olefin **122** then yields

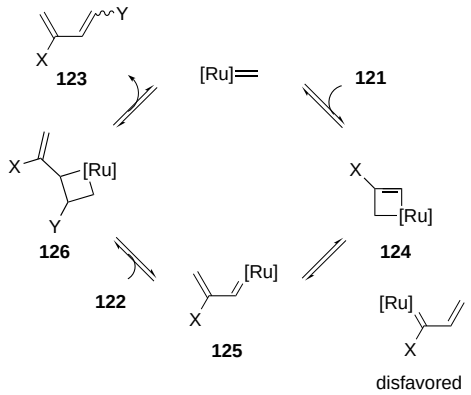
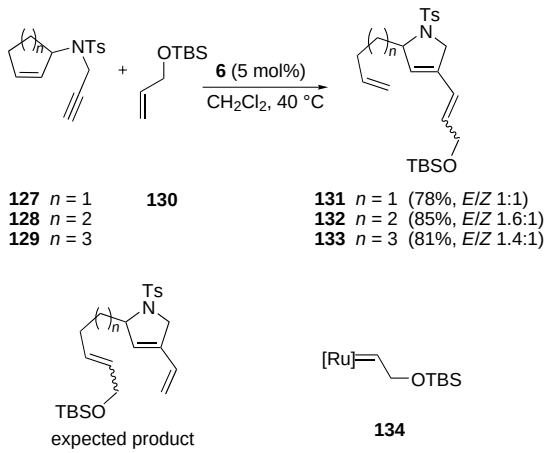


Figure 15. Intermolecular enyne-metathesis catalytic cycle.

 © 2003 Wiley-VCH Verlag GmbH & Co. KGaA, Weinheim

126, which undergoes cycloreversion to afford **123** and the propagating species.

Although this rationale explains the results of our group and those of other groups in most cases, as always one must be cautious about mechanistic generalizations. An interesting example in which this scheme does not hold is the rearrangement of compounds **127**–**129** in the presence of olefin **130** and catalyst **6** (Scheme 29).[102] Instead of the expected product, which would be obtained after initial attack of the C–C triple bond by ruthenium methylidene followed by rearrangement and CM (and which is the main product in the reaction of O-



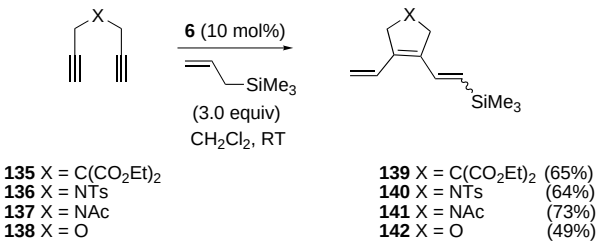
Scheme 29. Alternative mechanism for enyne metathesis.

analogues (**127, 128**: O in place of NTs) with ethylene[103]) we isolated the products **131**–**133**, in which the intermediate butadiene moiety appears to have undergone a CM reaction with **130**. We clearly demonstrated that CM between **130** and a 1,3-diene is not possible under the reaction conditions.[102] Control experiments using products from the rearrangement reaction in the presence of ethylene (i.e. containing a terminal butadiene and terminal olefin side chain) clearly demonstrated that CM between **130** and a terminal butadiene moiety is not possible under the reaction conditions, even in the presence of excess olefin CM partner. This points toward an initial CM reaction between **6** and **130**, and the resulting alkylidene **134** then participates in the enyne rearrangement reaction to afford **131**–**133**. This alternative mechanism highlights the inherent dangers of making assumptions regarding the general mechanism of this relatively young reaction.

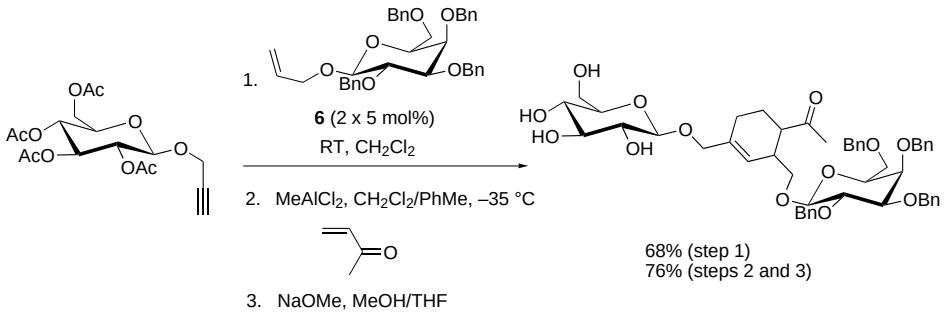
Mori and co-workers were the first to use ethylene gas (1 atm) successfully as a CM partner in enyne reactions.[104] In the presence of **6** (3–10%) as a catalyst, both terminal and internal alkenes were found to be active, furnishing butadiene adducts in moderate to good yields.[105] The presence of a heteroatom in the propargylic position was critical for high product yield. Substrates with ester or amide heterofunctions gave goods results, whereas ether or amine heteroatoms completely prevented any conversion, most likely via metathesis-inactive chelated intermediates.[106] Diver and Smulik later reported similar findings with terminal alkyne substrates, although a high pressure of ethylene gas (60 psi) was required to ensure smooth reactions.[107]

We have used enyne metathesis to prepare pseudooligosaccharides.[108] Alkene- and alkyne-functionalized carbohydrates were coupled in the presence of **6**, and then further elaborated by Diels–Alder protocols (Scheme 30).[109] Butadiene products of enyne reactions were also suitable substrates for aza-Diels–Alder reactions, allowing for rapid and simple preparation of tetrahydropyridine derivatives and azasugar analogues.[110] This methodology has been extended by Pandey and co-workers, who employed a similar strategy to couple alkenyl β-galactosides (and saccharides) to alkynyl purpurinimides (chlorin derivatives) through intermolecular enyne metathesis.[111] In a similar fashion, the same group attached chlorin and porphyrin analogues to fullerene (C_{60}), utilizing an enyne-metathesis/Diels–Alder sequence.[112] Kotha et al. have also used enyne metathesis to functionalize alkynated protected amino acids.[113]

Another interesting enyne metathesis application to have emerged is tandem-diyne-cycloisomerization–CM.[114] For example, the reaction of 1,6-heptadiynes **135**–**138** and allyltrimethylsilane promoted by **6** gives triene cycloadducts **139**–**142** in moderate to good yields (Scheme 31). Unfortunately,



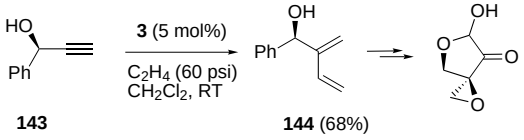
Scheme 31. Tandem diyne cycloisomerization-CM (Ts = *p*-toluenesulfonyl).



Scheme 30. Carbohydrate coupling by enyne metathesis.

the reaction has a limited scope: formation of six- or seven-membered rings was not possible, and internal alkynes were not reactive. Nevertheless this domino sequence demonstrates the power of enyne metathesis for impressive structural development from relatively simple starting materials.

There have been several reports of improved enyne metathesis efficiency using the second-generation Grubbs catalyst **3** instead of **6**.[115–117] Diver and Smulik[115] discovered that **3** could smoothly convert previously challenging substrates such as hindered alkynes, propargylic ethers, and even propargylic alcohols into the corresponding terminal butadienes under a high-pressure ethylene atmosphere. The high activity of **3** and its reduced tendency to form chelates with Lewis basic groups relative to **6** were cited as possible explanations for the improved properties. To show the potential utility of these reactions, enantiopure (99% *ee*) phenyl-substituted propargyl alcohol **143** was transformed into **144** in good isolated yield. Chiral diene **144** was then subjected to a series of oxidations to furnish enantiopure UCT4B side-chain analogues (Scheme 32).



143 **144** (68%)

Scheme 32. Efficient and functional-group-tolerant enyne metathesis.

Some of these findings were later confirmed by Mori and Tonogaki[116] and by our group.[117] It was discovered that enyne metathesis promoted by **3** was considerably more efficacious at lower ethylene pressures (1 atm) than identical reactions catalyzed by **6**. Another significant point was that when using catalyst **3**, the presence of a heteroatom in the propargylic position was not necessary for high-yielding metathesis to occur, thus overcoming a significant drawback associated with enyne reactions involving **6**, and considerably widening the scope of enyne metathesis with ethylene.[116,117] It was also found that internal alkynes underwent a reaction with terminal olefins for the first time, although the regioselectivity was poor.

The high activity of catalyst **3** also allows for the possibility of tandem enyne-CM–RCM reactions between terminal alkynes and 1,5-heptadiene.[118] The diene products from these reactions can be also used in [4+2] cycloadditions.

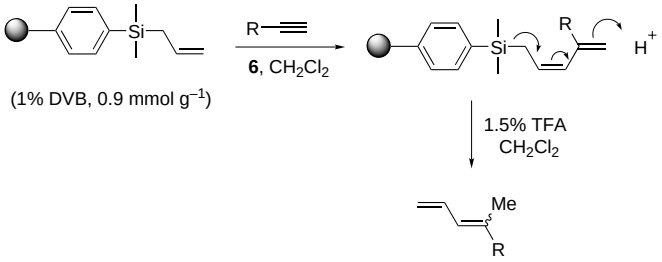
Another recent example highlighting the impact of **3** on enyne metathesis is the successful conversion of sulfur-containing alkynes.[119] Sulfides and thiols are known to be incompatible with **6** as a result of a presumed strong coordination of the soft sulfur atom to the ruthenium center, thus poisoning the catalyst. However catalysts **3** and **4a**, which contain strongly σ-donating NHC ligands, are less inclined to act as Lewis acids for chelation and were able to promote high-yielding enyne metathesis of propargyl thioesters in the presence of ethylene, whereas **6** proved relatively ineffective. The protection of the sulfur moiety as a less Lewis basic thioester was a key development, as sulfides (even those with large trityl protecting groups) gave minimal (ca. 10%) conversion even after a prolonged reaction time. Notably, self-metathesis of allylsulfides has been reported in the presence of catalyst **2**.[120] One interesting report has also appeared detailing the first examples of the use of selenocarbene NHC-containing complexes in ROM–CM.[121]

5. CM Applications in Solid-Phase Organic Synthesis

5.1. CM Reactions on a Solid Support

Since our initial reports[11,12] on the immobilization and CM reactions of olefins on solid supports, significant progress has been made. The main advantages associated with immobilizing an olefin substrate prior to CM, ROM–CM, or enyne metathesis are: 1) dimerization/oligomerization pathways are considerably less favorable, 2) the reaction can be driven to completion by using an excess of the other olefin substrates (the dimers of which can be removed by filtration), and 3) in many cases the required products can be cleaved from the resin after the reaction, and as such are available in relatively pure form for further use.

We found that enyne metathesis can be used to immobilize terminal alkynes on an allylsilylpolystyrene support.[122] Subsequent cleavage from the solid support through protodesilylation provided butadiene products (Scheme 33). Alkynated acetals, malonates, esters, acyrlates, protected amino acids, and carbohydrates are compatible with this methodology.

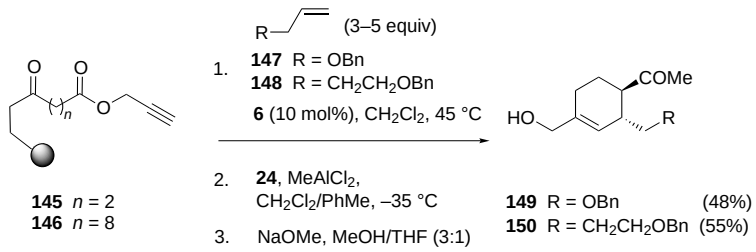


Scheme 33. Immobilization and functionalization by enyne metathesis (DVB = divinylbenzene, TFA = trifluoroacetic acid).

Of course the reverse mode of heterogeneous reactants is also feasible. For example, treatment of Merrifield-resin-bound alkyne **145** or **146** with alkenes **147** or **148** followed by Lewis acid catalyzed [4+2] cycloaddition with **24** gave **149** and **150**, respectively, in high purity after cleavage from the resin (Scheme 34).[123] An added advantage of this system is the isolation of a single diastereomer as a result of base-catalyzed equilibration of the Diels–Alder adduct during the cleavage step. A similar enyne-metathesis functionalization strategy led to a convenient modular synthesis of substituted octahydrobenzazapinones.[123]

Barrett et al. have used ROM–CM to attach ROMP norbornene polymers to vinyl polystyrene. The resulting

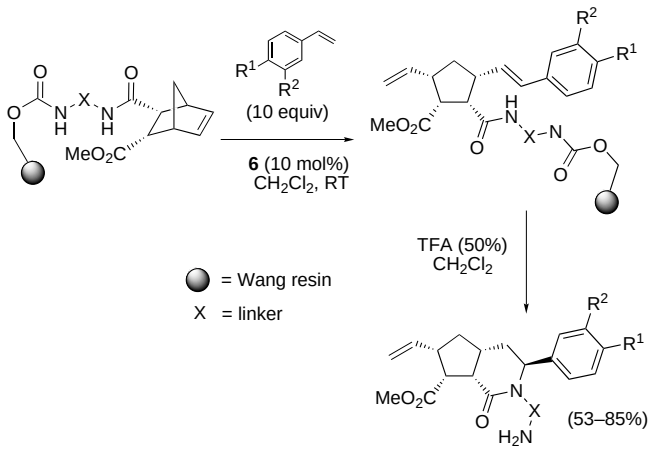
 © 2003 Wiley-VCH Verlag GmbH & Co. KGaA, Weinheim



Scheme 34. Enyne metathesis and Diels–Alder reaction on a Merrifield resin.

"ROMP-spheres" have distinct swelling properties, and functional diversity of the polymers is possible simply by varying the norbornene moiety.[124]

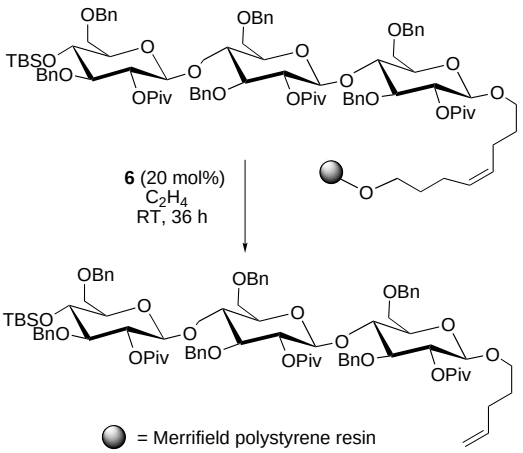
Cuny and co-workers have applied solid-phase ROM–CM of bicyclic alkenes with styrene derivatives to combinatorial library synthesis using resin-bound norbornenes.[125] In an interesting application, substituted norbornenes were subjected to ROM–CM conditions in the presence of substituted styrenes, followed by acid-induced cleavage from the resin with concurrent formation of a cyclopentene-fused piperidinone ring (Scheme 35).[126] The same group has also investigated the concept of resin capture, that is, attachment of the resin to the product of a ROM–CM reaction.[82]



Scheme 35. ROM–CM and cyclization on a solid support.

Seeberger and co-workers[127,128] developed a novel octenediol-based linker, which is cleaved by CM with ethylene gas promoted by **6**.[129] Successful application to the synthesis of saccharides was demonstrated, affording homoallylic polysaccharides (Scheme 36). In view of the mild metathesis conditions utilized for resin cleavage, this methodology should be useful in the solid-phase synthesis of biomolecules.[130]

Recently two reports have emerged detailing the exploitation of neighboring-group interactions on solid supports, allowing the synthesis of dimeric molecules by CM. In studies aimed toward the synthesis of macrocycles by RCM, Wareing and Tang[131] observed that the formation of oligomeric products from CM was dominant in the case of resin-bound large dienes, whereas only RCM was observed in analogous solution-phase chemistry. These counterintuitive results seemed to point towards intraresin CM reactions taking place between reactive groups that are not necessarily adjacent to one another on the resin but are nonetheless proximal as a result of nonlinearity and bending of the solid support. Setting out to achieve intersite CM, Schreiber and co-workers were able to generate dimeric pseudopeptides and a range of other symmetrical molecules by optimizing site–site interactions on highly loaded (1–2 $mmol\,g^{-1}$) lightly cross-linked (1% divinylbenzene) 500–600 μm polystyrene beads.[132]



Scheme 36. CM cleavage from a solid support (Piv = pivaloyl).

5.2. CM of Polymer-Supported Catalysts

As olefin metathesis quickly consolidates its position as a mild, practical, and versatile method for C–C bond formation, the demand for more efficient, more cost-effective, and more environmentally benign catalytic systems has increased. Given the wide scope of olefin metathesis for use in materials science, medicinal chemistry, and natural product synthesis, the development of catalysts that are both recyclable and capable of promoting efficient metathesis transformations without leaving behind significant levels of metal contaminants in the products is of particular importance.

In this regard, heterogeneous polymer-bound olefin-metathesis catalysts (Figure 16) have received considerable attention in recent years, the main reason being because they can be simply removed after reaction by filtration.

The first well-defined immobilized ruthenium alkylidene **151** was reported by Grubbs and Nguyen in 1995.[133] Although active and recyclable in metathesis reactions, this catalyst was considerably slower than its homogeneous analogue. Barrett and co-workers[134,135] devised a general CM-based immobilization strategy whereby the reaction between vinyl polystyrene (PS) and either **3** or **6** generates catalysts **152** or **153**, respectively. These catalysts (used at 2.5–5 mol% levels) were reasonably active in RCM reactions and could be recycled several times. As is unfortunately the case with most polymer-supported catalysts, no details of the activity of these catalysts in CM processes are known. Nolan

 © 2003 Wiley-VCH Verlag GmbH & Co. KGaA, Weinheim

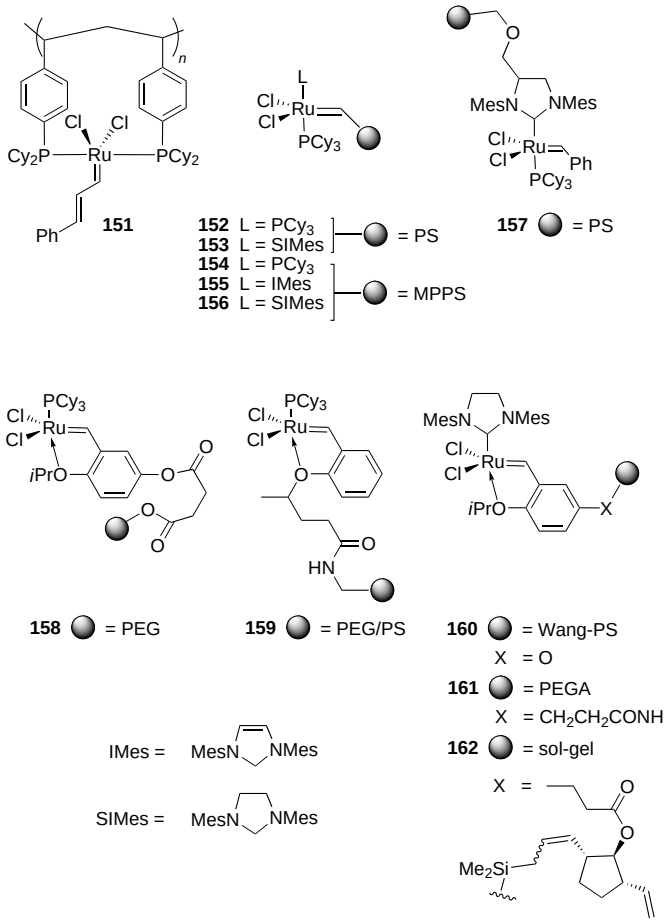


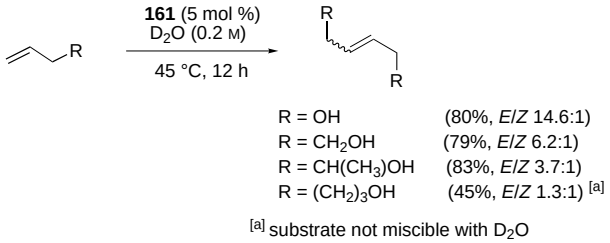
Figure 16. Immobilized olefin-metathesis catalysts.

and co-workers later prepared **154** and **155**, which were attached to macroporous polystyrene (MPPS) by the same CM methodology.[136,137] The advantage of this support (PS highly cross-linked with divinylbenzene) is that resin cavities are more spacious than those associated with PS, and so access to the substrate is easier and not as dependent on solvent swelling. Precatalysts **154** and **155** were suitable promoters for RCM, but performed poorly in the CM dimerization of styrene derivatives. The permanently immobilized recyclable catalyst **157**[138] has been shown to promote high-yielding enyne-metathesis reactions between terminal alkynes and allyltrimethylsilane.

Dowden and Savović[139] described the CM-based preparation of **159** (an immobilized analogue of **1**), which was the first immobilized catalyst to be active in nondegassed solvents under an air atmosphere. Again, RCM activity was reasonable and the catalyst recyclable, but the one CM reaction attempted gave poor results in a relatively unselective process.

To our knowledge, the only immobilized catalyst to have been both active and recyclable in CM reactions is **160**.[140] This polystyrene-bound analogue of **4a** catalyzed highly efficient and selective CM reactions with a range of electron-deficient alkenes. The cross-coupling of pent-1-enylbenzoate with **24** led to the formation of the CM product **34** (*E*/*Z* > 20:1) with quantitative conversion in each of five successive cycles.

In another exploitation of the high stability of NHC-based catalysts such as **4a**, catalyst **161**, which is bound to the highly hydrophilic polyacrylamide polyethylene glycol (PEGA) resin, catalyzed CM (self-metathesis) reactions in methanol or water.[141,142] Solvent degassing and reaction under an inert atmosphere are not required. Simple hydroxy-functionalized alkenes react well in D_2O (Scheme 37); however, acidic or



Scheme 37. CM dimerization in water.

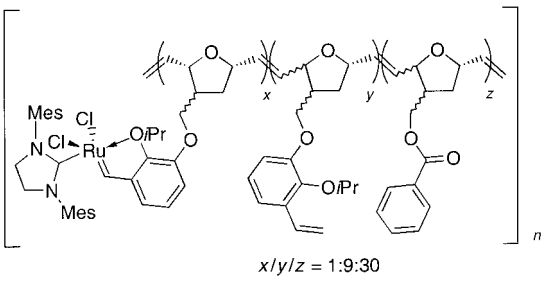
electron-deficient substrates gave poorer results.[141] The use of the hydrophilic PEGA resin is critical. Control experiments demonstrated that a heterogeneous mixture of either **3** or **4a** in water gave no conversion of starting materials that undergo smooth reaction with **161**.[143] In our opinion, this indicates that the reactions between the hydrophobic methylidene propagating species and the metathesis substrates occur mostly in the resin pores (an area of relatively high precatalyst concentration), and not in the nucleophilic bulk solvent, where metathesis intermediates are quite unstable.[142]

Hoveyda and co-workers[144] reported that the immobilization of an appropriately substituted analogue of **4a** on porous monolithic[145] sol-gel glass affords a physically and chemically robust catalyst that is highly recyclable in RCM and ROM–CM reactions. In recyclability tests, catalyst **162** required extended reaction times to promote a RCM reaction to completion after four quantitative conversion cycles, which indicates the onset of significant catalyst decomposition. However, after the fourth cycle the same catalyst pellet was capable of catalyzing less-challenging ROM–CM reactions of norbornenes with various olefin partners with quantitative conversion for a further four cycles.[146] Furthermore, the products were often recovered in analytically pure form, and separation of the catalyst from the reaction mixture could be conveniently carried out with a Pasteur pipette. This novel and versatile catalyst was also shown to be highly effective in the synthesis of small libraries through various metathesis reactions.

Some of the major drawbacks associated with polymer-bound catalysts are that they often rely on commercially available resin supports, design of the linker and its attachment to the solid support can complicate catalyst synthesis, and most importantly, supported catalysts normally lag far behind their homogeneous counterparts in terms of activity. One promising way to circumvent the latter problem is to employ a catalyst-precipitation strategy, whereby one can aspire to prepare ruthenium alkylidenes with homogeneous reactivity profiles combined with a facile recovery method.

 © 2003 Wiley-VCH Verlag GmbH & Co. KGaA, Weinheim

The first report involving this method detailed the preparation of homogeneous catalyst **158**, a version of **1** attached to a PEG chain, which could be precipitated with diethyl ether after metathesis.[147] Along the same lines we have recently developed catalyst **163** (Figure 17), which is prepared from simple starting materials in one pot through sequential ROMP and CM reactions.[148] This homogeneous catalyst is highly active (a maximum of 1 mol% is required) in a range of reactions, including ROM-CM, and displays unprecedented recyclability after precipitation from the reaction mixture by addition of either diethyl ether or hexane. The products from metathesis reactions involving these catalysts also contain unparalleled low ruthenium levels. Unfortunately, given the prevalence of internal olefin moieties in the polymer backbone, **163** is not highly active in CM reactions. Since **163** is assembled mostly by metathesis, it is not reliant on the commercial availability of resins, and polymer synthesis/resin loading are combined in a single operation. Further advantages of **163** are that it is also capable of a high degree of self-generation, it can be analyzed for alkylidene content by ^{1}H NMR spectroscopy, and it is suitable for structural modification of either the catalyst or the polymer backbone, thus providing scope for future fine tuning.



x/*y*/*z* = 1:9:30

163

Figure 17. ROMP-based catalyst **163**.

6. Summary and Outlook

Over the last 5 years, CM has begun to emerge from the shadow of RCM and ROMP to take its place as a powerful and mild method for the formation of C–C bonds. This is in no small part a consequence of the advent of highly active NHC-based ruthenium alkylidene catalysts, which allow the use of previously incompatible substrates with high chemo- and stereoselectivity. The realization that homodimers of one CM substrate can be used to induce selectivity in reactions in which an electronic or steric mismatch would otherwise make the reaction impossible is also very significant. As the volume of material published grows, we are beginning to understand more and more about the role that steric and electronic factors (and occasionally chelation) plays in the determination of both chemo- and particularly stereoselectivity on a case-by-case basis, although we clearly still have a lot more to learn and the scope for further research is considerable. What seems certain is that the era in which CM and related reactions were considered to be unselective and inefficient processes is at an end, and the tremendous increase in reports on the applicability of these reactions to all areas of organic chemistry research that we have recently witnessed looks set to continue.

We thank the Fonds der Chemischen Industrie for generous support of our work. S.J.C. thanks the Alexander von Humboldt Foundation for a postdoctoral fellowship.

Received: September 9, 2002 [A556]

[1] For recent reviews on olefin metathesis, see: a) T. M. Trnka, R. H. Grubbs, *Acc. Chem. Res.* **2001**, *34*, 18–29; b) A. Fürstner, *Angew. Chem.* **2000**, *112*, 3140–3172; *Angew. Chem. Int. Ed.* **2000**, *39*, 3012–3043; c) R. Roy, S. K. Das, *Chem. Commun.* **2000**, 519–529; d) A. J. Philips, A. D. Abell, *Aldrichimica Acta* **1999**, *32*, 75–90; e) S. K. Armstrong, *J. Chem. Soc. Perkin Trans. 1* **1998**, 371–388; f) R. H. Grubbs, S. Chang, *Tetrahedron* **1998**, *54*, 4413–4450; g) K. J. Ivin, *J. Mol. Catal. A* **1998**, *133*, 1–16; h) *Alkene Metathesis in Organic Synthesis* (Ed.: A. Fürstner), Springer, Berlin, **1998**; i) M. L. Randall, M. L. Snapper, *J. Mol. Catal. A* **1998**, *133*, 29–40; j) M. Schuster, S. Blechert, *Angew. Chem.* **1997**, *109*, 2124–2144; *Angew. Chem. Int. Ed. Engl.* **1997**, *36*, 2036–2055.

[2] For the first proposal of the currently accepted mechanism, see: J. L. Hérisson, Y. Chauvin, *Makromol. Chem.* **1970**, *141*, 161–176.

[3] a) E. R. Freitas, C. R. Gum, *Chem. Eng. Prog.* **1979**, *75*, 73–76; b) Shell International Chemical Company, *SHOP—Linear Alpha Olefins* (Company publication), **1982**.

[4] Phillips Petroleum Company, *Hydrocarbon Process* **1967**, *46*, 232.

[5] S. E. Gibson, S. P. Keen, *Top. Organomet. Chem.* **1998**, *1*, 155–181.

[6] M. Mori, *Top. Organomet. Chem.* **1998**, *1*, 133–154.

[7] W. E. Crowe, Z. J. Zhang, *J. Am. Chem. Soc.* **1993**, *115*, 10998–10999.

[8] W. E. Crowe, D. R. Goldberg, *J. Am. Chem. Soc.* **1995**, *117*, 5162–5163.

[9] W. E. Crowe, D. R. Goldberg, Z. J. Zhang, *Tetrahedron Lett.* **1996**, *37*, 2117–2120.

[10] S. Blechert, O. Brümmer, A. Rückert, *Chem. Eur. J.* **1997**, *3*, 441–446.

[11] S. Blechert, M. Schuster, J. Pernerstorfer, *Angew. Chem.* **1996**, *108*, 2111–2112; *Angew. Chem. Int. Ed. Engl.* **1996**, *35*, 1979–1980.

[12] S. Blechert, M. Schuster, N. Lucas, *Chem. Commun.* **1997**, 823–824.

[13] S. E. Gibson, V. C. Gibson, S. P. Keen, *Chem. Commun.* **1997**, 1107–1108.

[14] S. E. Gibson, S. C. G. Biagini, S. P. Keen, *J. Chem. Soc. Perkin Trans. 1* **1998**, 2485–2500.

[15] S. Blechert, M. Schuster, J. Pernerstorfer, *Chem. Commun.* **1997**, 1949–1950.

[16] R. H. Grubbs, H. E. Blackwell, D. J. O'Leary, R. A. Washenfelder, K. Miura, *Tetrahedron Lett.* **1999**, *40*, 1091–1094.

[17] R. H. Grubbs, H. E. Blackwell, A. K. Chatterjee, D. J. O'Leary, R. A. Washenfelder, D. A. Bussmann, *J. Am. Chem. Soc.* **2000**, *122*, 58–71.

[18] R. H. Grubbs, D. J. O'Leary, H. E. Blackwell, R. A. Washenfelder, *Tetrahedron Lett.* **1998**, *39*, 7427–7430.

[19] For the extension of this methodology to include one-pot CM/allylboration reactions, see: S. D. Goldberg, R. H. Grubbs, *Angew. Chem.* **2002**, *114*, 835–838; *Angew. Chem. Int. Ed.* **2002**, *41*, 807–810.

 © 2003 Wiley-VCH Verlag GmbH & Co. KGaA, Weinheim

[20] For background information on the roles of methylidene and alkylidene intermediates derived from **6** in metathesis, see: R. H. Grubbs, M. Ulman, *Organometallics* **1998**, *17*, 2484 – 2489.
[21] O. M. Blanco, L. Castedo, *Synlett* **1999**, 557 – 558.
[22] B. Liu, S. K. Das, R. Roy, *Org. Lett.* **2002**, *4*, 2723 – 2726.
[23] H. Seshadri, C. J. Lovely, *Org. Lett.* **2000**, *2*, 327 – 330.
[24] For an example of CM involving vinyl ferrocene and catalyst **5**, see: T. Yashuda, T. Iyoda, T. Kawai, *Chem. Lett.* **2001**, 812 – 813.
[25] R. Roy, S. K. Das, R. Dominique, M. C. Trono, F. Hernandez-Mateo, F. Santoyo-Gonzalez, *Pure Appl. Chem.* **1999**, *71*, 565 – 571.
[26] M. Scholl, S. Ding, C. W. Lee, R. H. Grubbs, *Org. Lett.* **1999**, *1*, 953 – 956.
[27] a) S. B. Garber, J. S. Kingsbury, B. L. Gray, A. H. Hoveyda, *J. Am. Chem. Soc.* **2000**, *122*, 8168 – 8179.
[28] S. Gessler, S. Randl, S. Blechert, *Tetrahedron Lett.* **2000**, *41*, 9973 – 9976.
[29] A. K. Chatterjee, R. H. Grubbs, *Org. Lett.* **1999**, *1*, 1751 – 1753.
[30] A. K. Chatterjee, D. P. Sanders, R. H. Grubbs, *Org. Lett.* **2002**, *4*, 1939 – 1942.
[31] S. J. Spessard, B. M. Stoltz, *Org. Lett.* **2002**, *4*, 1943 – 1946.
[32] A. K. Chatterjee, J. P. Morgan, M. Scholl, R. H. Grubbs, *J. Am. Chem. Soc.* **2000**, *122*, 3783 – 3784.
[33] The *E*/*Z* selectivity with acrolein was originally erroneously reported as ca. 1:1.[32]
[34] A. K. Chatterjee, R. H. Grubbs, *Angew. Chem.* **2002**, *114*, 3304 – 3306; *Angew. Chem. Int. Ed.* **2002**, *41*, 3171 – 3174.
[35] J. P. Morgan, R. H. Grubbs, *Org. Lett.* **2000**, *2*, 3153 – 3155.
[36] J. Louie, C. W. Bielawski, R. H. Grubbs, *J. Am. Chem. Soc.* **2001**, *123*, 11312 – 11313.
[37] T.-L. Choi, A. K. Chatterjee, R. H. Grubbs, *Angew. Chem.* **2001**, *113*, 1317 – 1319; *Angew. Chem. Int. Ed.* **2001**, *40*, 1277 – 1279.
[38] S. Gessler, S. Randl, H. Wakamatsu, S. Blechert, *Synlett* **2001**, 430 – 432.
[39] J. Cossy, S. BouzBouz, A. H. Hoveyda, *J. Organomet. Chem.* **2001**, *624*, 327 – 332.
[40] S. Imhof, S. Randl, S. Blechert, *Chem. Commun.* **2001**, 1692 – 1693.
[41] M. Cavazzini, F. Montanari, G. Pozzi, S. Quici, *J. Fluorine Chem.* **1999**, *94*, 183, and references therein.
[42] T. Itoh, K. Mitsukura, N. Ishida, K. Uneyama, *Org. Lett.* **2000**, *2*, 1431 – 1434.
[43] A. K. Chatterjee, T.-L. Choi, R. H. Grubbs, *Synlett* **2001**, 1034 – 1037.
[44] M. Lera, C. J. Hayes, *Org. Lett.* **2001**, *3*, 2765 – 2768.
[45] N. Batoux, R. Benhaddou-Zerrouki, P. Bressolier, R. Granet, G. Laumount, A.-M. Aubertin, P. Krausz, *Tetrahedron Lett.* **2001**, *42*, 1491 – 1493.
[46] K. Grela, M. Bieniek, *Tetrahedron Lett.* **2001**, *42*, 6425 – 6428.
[47] S. Randl, S. Blechert, unpublished results.
[48] For early examples involving RCM reactions, see: a) A. Fürstner, K. Langemann, *J. Org. Chem.* **1996**, *61*, 3942 – 3943; b) A. Fürstner, K. Langemann, *Synthesis* **1997**, 792 – 803; c) G. C. Fu, R. H. Grubbs, *J. Am. Chem. Soc.* **1992**, *114*, 7324 – 7325.
[49] a) J. P. A. Harrity, D. S. La, M. S. Visser, A. H. Hoveyda, *J. Am. Chem. Soc.* **1998**, *120*, 2343 – 2351; b) J. S. Kingsbury, J. P. A. Harrity, P. J. Bonitatebus, A. H. Hoveyda, *J. Am. Chem. Soc.* **1999**, *121*, 791 – 799.
[50] S. BouzBouz, J. Cossy, *Org. Lett.* **2001**, *3*, 1451 – 1454.
[51] a) F. C. Engelhardt, M. J. Schmitt, R. E. Taylor, *Org. Lett.* **2001**, *3*, 2209 – 2212; b) F. C. Engelhardt, M. J. Schmitt, H. Yuan, R. E. Taylor, *J. Am. Chem. Soc.* **2001**, *123*, 2964 – 2969.
[52] a) A. B. Smith III, S. A. Kozmin, C. M. Adams, D. V. Paone, *J. Am. Chem. Soc.* **2000**, *122*, 4984 – 4985; b) A. B. Smith III, C. M. Adams, S. A. Kozmin, *J. Am. Chem. Soc.* **2001**, *123*, 990 – 991; c) A. B. Smith III, C. M. Adams, S. A. Kozmin, D. V. Paone, *J. Am. Chem. Soc.* **2001**, *123*, 5925 – 5937.
[53] A. Fürstner, O. Thiel, L. Ackermann, *Org. Lett.* **2001**, *3*, 449 – 451.
[54] For an example involving vinylsilacyclobutanes, see: S. E. Denmark, Z. Wang, *Synthesis* **2000**, 999 – 1003.
[55] C. Pietraszuk, B. Marciniec, H. Fischer, *Organometallics* **2000**, *19*, 913 – 917.
[56] It has been shown that the metallacyclobutane intermediates derived from vinyltrialkylsilanes undergo metathesis-terminating β-silyl-elimination reactions to a much greater extent than do analogous vinyltrialkoxysilane-derived intermediates; for a discussion, see: C. Pietraszuk, H. Fischer, *Chem. Commun.* **2000**, 2463 – 2464; C. Pietraszuk, H. Fischer, *Organometallics* **2001**, *20*, 4641 – 4646.
[57] C. Pietraszuk, H. Fischer, M. Kujawa, B. Marciniec, *Tetrahedron Lett.* **2001**, *42*, 1175 – 1178.
[58] B. Marciniec, M. Kujawa, C. Pietraszuk, *New J. Chem.* **2000**, *24*, 671 – 675.
[59] M. Kujawa-Welten, C. Pietraszuk, B. Marciniec, *Organometallics* **2002**, *21*, 840 – 845.
[60] M. Ahmed, T. Arnauld, A. G. M. Barrett, D. C. Braddock, K. Flack, P. A. Procopiou, *Org. Lett.* **2000**, *2*, 551 – 553.
[61] M. Jorgensen, P. Hadwiger, R. Madsen, A. E. Stutz, T. M. Wrodnigg, *Curr. Org. Chem.* **2000**, *4*, 565 – 588.
[62] R. Dominique, B. Liu, S. K. Das, R. Roy, *Synthesis* **2000**, 862 – 868.
[63] Z. Gan, R. Roy, *Tetrahedron* **2000**, *56*, 1423 – 1428.
[64] B. Liu, R. Roy, *Chem. Commun.* **2002**, 594 – 595.
[65] A. Dondoni, P. P. Giovannini, A. Marra, *J. Chem. Soc. Perkin Trans. 1* **2001**, 2380 – 2388.
[66] C. A. Verbicky, C. K. Zercher, *Tetrahedron Lett.* **2000**, *41*, 8723 – 8727.
[67] A. G. M. Barrett, K. Kasdorf, *J. Am. Chem. Soc.* **1996**, *118*, 11030 – 11037.
[68] a) J. Cossy, C. Willis, V. Bellosta, *Synlett* **2001**, 1578 – 1580; b) J. Cossy, C. Willis, V. Bellosta, S. BouzBouz, *J. Org. Chem.* **2002**, *67*, 1982 – 1992.
[69] H. Oguri, S. Y. Sasaki, T. Oishi, M. Hirama, *Tetrahedron Lett.* **1999**, *40*, 5405 – 5408.
[70] F. E. McDonald, X. Wei, *Org. Lett.* **2002**, *4*, 593 – 595.
[71] A. G. M. Barrett, S. P. D. Baugh, D. C. Braddock, K. Flack, V. C. Gibson, M. R. Giles, E. L. Marshall, P. A. Procopiou, A. J. P. White, D. J. Williams, *J. Org. Chem.* **1998**, *63*, 7893 – 7907.
[72] J. A. Smulik, S. T. Diver, F. Pan, J. O. Liu, *Org. Lett.* **2002**, *4*, 2051 – 2054.
[73] D. Forget-Champagne, M. Mondon, N. Fonteneau, J.-P. Gesson, *Tetrahedron Lett.* **2001**, *42*, 7229 – 7231.
[74] M. M. Vasbinder, S. J. Miller, *J. Org. Chem.* **2002**, *67*, 6240 – 6242.
[75] S. T. Diver, S. L. Schreiber, *J. Am. Chem. Soc.* **1997**, *119*, 5106 – 5109.
[76] K. C. Nicolaou, R. Hughes, S. Y. Cho, N. Winssinger, H. Labischinski, R. Endermann, *Chem. Eur. J.* **2001**, *7*, 3824 – 3843.
[77] For the first reports of ruthenium-catalyzed ROM–CM of norbornene and oxanorbornene, see: a) M. F. Schneider, S. Blechert, *Angew. Chem.* **1996**, *108*, 479 – 481; *Angew. Chem. Int. Ed. Engl.* **1996**, *35*, 411 – 413; b) M. F. Schneider, N. Lucas, J. Velder, S. Blechert, *Angew. Chem.* **1997**, *109*, 257 – 259; *Angew. Chem. Int. Ed. Engl.* **1997**, *36*, 257 – 258.
[78] a) M. L. Randall, J. A. Tallarico, M. L. Snapper, *J. Am. Chem. Soc.* **1995**, *117*, 9610 – 9611; b) M. L. Snapper, J. A. Tallarico, M. L. Randall, *J. Am. Chem. Soc.* **1997**, *119*, 1478 – 1479; c) J. A. Tallarico, P. J. Bonitatebus, M. L. Snapper, *J. Am. Chem. Soc.* **1997**, *119*, 7157 – 7158.

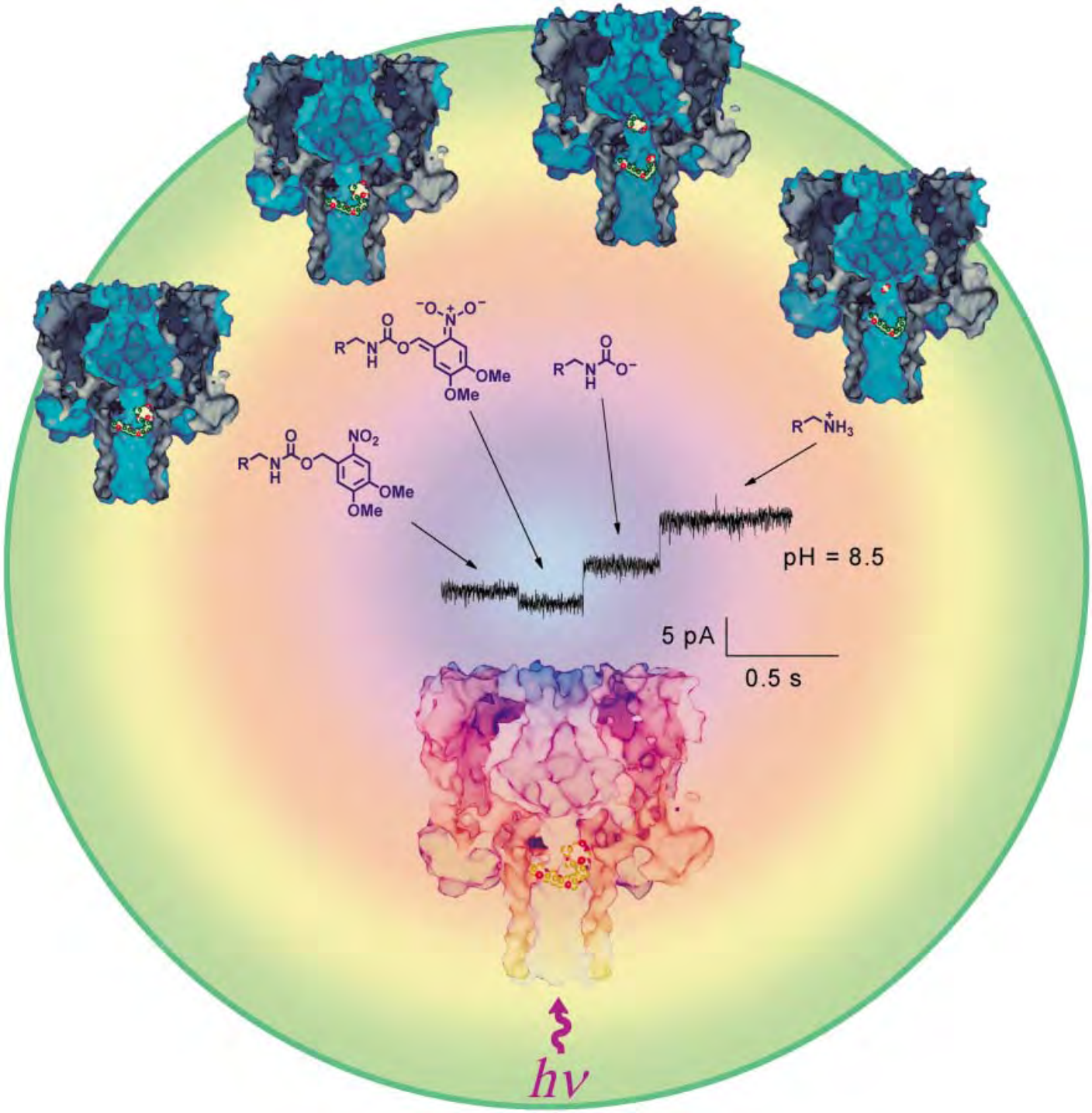
 © 2003 Wiley-VCH Verlag GmbH & Co. KGaA, Weinheim

[79] O. Arjona, A. G. Csàkÿ, J. Plumet, *Synthesis* **2000**, 857 – 861; see also reference [1i].
[80] O. Arjona, A. G. Csàkÿ, M. C. Murcia, J. Plumet, *J. Org. Chem.* **1999**, *64*, 9739 – 9741.
[81] O. Arjona, A. G. Csàkÿ, M. C. Murcia, J. Plumet, M. B. Mula, *J. Organomet. Chem.* **2001**, *627*, 105 – 108.
[82] G. D. Cuny, J. Cao, A. Sidhu, J. R. Hauske, *Tetrahedron* **1999**, *55*, 8169 – 8178.
[83] R. Stragies, S. Blechert, *Synlett* **1998**, 169 – 170.
[84] For a more recent successful application of this strategy, see: O. Arjona, A. G. Csàkÿ, M. C. Murcia, J. Plumet, *Tetrahedron Lett.* **2000**, *41*, 9777 – 9779.
[85] a) D. S. La, J. G. Ford, E. S. Sattely, P. J. Bonitatebus, R. R. Schrock, A. H. Hoveyda, *J. Am. Chem. Soc.* **1999**, *121*, 11 603 – 11 604; b) D. S. La, E. S. Sattely, J. G. Ford, R. R. Schrock, A. H. Hoveyda, *J. Am. Chem. Soc.* **2001**, *123*, 7767 – 7778.
[86] For a short review of asymmetric olefin metathesis, see: A. H. Hoveyda, R. R. Schrock, *Chem. Eur. J.* **2001**, *7*, 945 – 950.
[87] J. B. Alexander, D. S. La, D. R. Cefalo, A. H. Hoveyda, R. R. Schrock, *J. Am. Chem. Soc.* **1998**, *120*, 4041 – 4042.
[88] Catalyst **113** has also been used in asymmetric ROM–RCM reactions: G. S. Weatherhead, J. G. Ford, E. J. Alexanian, R. R. Schrock, A. H. Hoveyda, *J. Am. Chem. Soc.* **2000**, *122*, 1828 – 1829.
[89] J. J. Van Veldhuizen, S. B. Garber, J. S. Kingsbury, A. H. Hoveyda, *J. Am. Chem. Soc.* **2002**, *124*, 4954 – 4955.
[90] E. L. Dias, S. T. Nguyen, R. H. Grubbs, *J. Am. Chem. Soc.* **1997**, *119*, 3887 – 3897.
[91] H. Wakamatsu, S. Blechert, *Angew. Chem.* **2002**, *114,* 832 – 834; *Angew. Chem. Int. Ed.* **2002**, *41*, 794 – 796.
[92] H. Wakamatsu, S. Blechert, *Angew. Chem.* **2002**, *114*, 2509 – 2511; *Angew. Chem. Int. Ed.* **2002**, *41*, 2403 – 2405.
[93] M. Ulman, T. R. Belderrain, R. H. Grubbs, *Tetrahedron Lett.* **2000**, *41*, 4689 – 4692.
[94] S. Randl, S. J. Connon, S. Blechert, *Chem. Commun.* **2001**, 1796 – 1797.
[95] C. W. Lee, T.-L. Choi, R. H. Grubbs, *J. Am. Chem. Soc.* **2002**, *124*, 3224 – 3225.
[96] J. P. Morgan, C. Morrill, R. H. Grubbs, *Org. Lett.* **2002**, *4*, 67 – 70.
[97] For an example of ROM–CM using carbynehydridoruthenium complexes, see: W. Stüer, J. Wolf, H. Werner, P. Schwab, M. Schultz, *Angew. Chem.* **1998**, *110*, 3603 – 3605; *Angew. Chem. Int. Ed.* **1998**, *37*, 3421 – 3423.
[98] For a similar example (see above) using water-soluble vinylidene and allenylidene complexes, see: M. Saoud, A. Romerosa, M. Peruzzini, *Organometallics* **2000**, *19*, 4005 – 4007.
[99] D. L. Wright, L. C. Usher, M. Estrella-Jimenez, *Org. Lett.* **2001**, *3*, 4275 – 4277.
[100] For the first report of enyne metathesis, see: T. J. Katz, T. M. Sivavec, *J. Am. Chem. Soc.* **1985**, *107*, 737 – 738.
[101] R. Stragies, M. Schuster, S. Blechert, *Angew. Chem.* **1997**, *109*, 2628 – 2630; *Angew. Chem. Int. Ed. Engl.* **1997**, *36*, 2518 – 2520.
[102] S. Randl, N. Lucas, S. J. Connon, S. Blechert, *Adv. Synth. Catal.* **2002**, *344*, 631 – 633. In this report the *E*/*Z* ratio was erroneously reversed.
[103] A. Rückert, D. Eisele, S. Blechert, *Tetrahedron Lett.* **2001**, *42*, 5245 – 5247.
[104] A. Kinoshita, N. Sakakibara, M. Mori, *J. Am. Chem. Soc.* **1997**, *119*, 12 388 – 12 389.
[105] Enyne metathesis with ethylene catalyzed by **6** was recently applied in the synthesis of natural products: a) M. Mori, K. Tonogaki, N. Nishiguchi, *J. Org. Chem.* **2002**, *67*, 224 – 226; b) S. Rodríguez-Conesa, P. Candal, C. Jiménez, J. Rodríguez, *Tetrahedron Lett.* **2001**, *42*, 6699 – 6702.
[106] A. Kinoshita, N. Sakakibara, M. Mori, *Tetrahedron* **1999**, *55*, 8155 – 8167.
[107] J. A. Smulik, S. T. Diver, *J. Org. Chem.* **2000**, *65*, 1788 – 1792.
[108] S. C. Schürer, S. Blechert, *Chem. Commun.* **1999**, 1203 – 1204.
[109] The butadiene products from these reactions can also be used in nickel-catalyzed [4+4] cycloadditions; see: reference [102].
[110] S. C. Schürer, S. Blechert, *Tetrahedron Lett.* **1999**, *40*, 1877 – 1880.
[111] G. Zheng, A. Graham, M. Shibata, J. R. Missert, A. R. Oseroff, T. J. Dougherty, R. K. Pandey, *J. Org. Chem.* **2001**, *66*, 8709 – 8716.
[112] G. Zheng, T. J. Dougherty, R. K. Pandey, *Chem. Commun.* **1999**, 2469 – 2470.
[113] S. Kotha, S. Halder, E. Brahmachary, T. Ganesh, *Synlett* **2000**, 853 – 855.
[114] R. Stragies, M. Schuster, S. Blechert, *Chem. Commun.* **1998**, 237 – 238.
[115] J. A. Smulik, S. T. Diver, *Org. Lett.* **2000**, *2*, 2271 – 2274.
[116] K. Tonogaki, M. Mori, *Tetrahedron Lett.* **2002**, *43*, 2235 – 2238.
[117] R. Stragies, U. Voigtmann, S. Blechert, *Tetrahedron Lett.* **2000**, *41*, 5465 – 5468.
[118] J. A. Smulik, S. T. Diver, *Tetrahedron Lett.* **2001**, *42*, 171 – 174.
[119] J. A. Smulik, A. J. Giessert, S. T. Diver, *Tetrahedron Lett.* **2002**, *43*, 209 – 211.
[120] G. Spagnol, M.-P. Heck, S. P. Nolan, C. Mioskowski, *Org. Lett.* **2002**, *4*, 1767 – 1770.
[121] H. Katayama, H. Urushima, T. Nishioka, C. Wada, M. Nagao, F. Ozawa, *Angew. Chem.* **2000**, *112*, 4687 – 4689; *Angew. Chem. Int. Ed.* **2000**, *39*, 4513 – 4515.
[122] M. Schuster, S. Blechert, *Tetrahedron Lett.* **1998**, *39*, 2295 – 2298.
[123] S. C. Schürer, S. Blechert, *Synlett* **1999**, 1879 – 1882.
[124] A. G. M. Barrett, S. M. Cramp, R. S. Roberts, *Org. Lett.* **1999**, *1*, 1083 – 1086.
[125] J. Cao, G. D. Cuny, J. R. Hauske, *Mol. Diversity* **1998**, *3*, 173 – 179.
[126] G. D. Cuny, J. Cao, J. R. Hauske, *Tetrahedron Lett.* **1997**, *38*, 5237 – 5240.
[127] R. B. Andrade, O. J. Plante, L. G. Melean, P. H. Seeberger, *Org. Lett.* **1999**, *1*, 1811 – 1814.
[128] L. G. Melean, W.-C. Haase, P. H. Seeberger, *Tetrahedron Lett.* **2000**, *41*, 4329 – 4333.
[129] For an early example of RCM-mediated cleavage from a solid support, see: J.-U. Peters, S. Blechert, *Synlett* **1997**, 348 – 350.
[130] For an example of RCM-mediated cleavage in carbohydrate synthesis, see: L. Knerr, R. R. Schmidt, *Synlett* **1999**, *11*, 1802 – 1804.
[131] Q. Tang, J. R. Wareing, *Tetrahedron Lett.* **2001**, *42*, 1399 – 1401.
[132] H. E. Blackwell, P. A. Clemons, S. A. Schreiber, *Org. Lett.* **2001**, *3*, 1185 – 1188.
[133] S. T. Nguyen, R. H. Grubbs, *J. Organomet. Chem.* **1995**, *497*, 195 – 200.
[134] M. Ahmed, A. G. M. Barrett, D. C. Braddock, S. M. Cramp, P. A. Procopiou, *Tetrahedron Lett.* **1999**, *40*, 8657 – 8662.
[135] M. Ahmed, T. Arnauld, A. G. M. Barrett, D. C. Braddock, P. A. Procopiou, *Synlett* **2000**, 1007 – 1009.
[136] a) L. Jafarpour, S. P. Nolan, *Org. Lett.* **2000**, *2*, 4075 – 4078; b) L. Jafarpour, M.-P. Heck, C. Baylon, H. M. Lee, C. Mioskowski, S. P. Nolan, *Organometallics* **2002**, *21*, 671 – 679.
[137] Complex **155** is the immobilized version of **1**, the first active NHC catalyst; for background literature on the development of this system, see: a) L. Ackermann, A. Fürstner, T. Weskamp, F. J. Kohl, W. A. Herrmann, *Tetrahedron Lett.* **1999**, *40*, 4787 – 4790; b) J. Huang, E. D. Stevens, S. P. Nolan, J. L. Pedersen, *J. Am. Chem. Soc.* **1999**, *121*, 2674 – 2678; c) M. Scholl, T. M. Trnka, J. P. Morgan, R. H. Grubbs, *Tetrahedron Lett.* **1999**, *40*, 2247 – 2250.

[138] S. C. Schürer, S. Gessler, N. Buschmann, S. Blechert, *Angew. Chem.* **2000**, *112*, 4062 – 4065; *Angew. Chem. Int. Ed.* **2000**, *39*, 3898 – 3901.
[139] J. Dowden, J. Savović, *Chem. Commun.* **2001**, 37 – 38.
[140] S. Randl, N. Buschmann, S. J. Connon, S. Blechert, *Synlett* **2001**, 1547 – 1550.
[141] S. J. Connon, S. Blechert, *Bioorg. Med. Chem. Lett.* **2002**, *12*, 1873 – 1876.
[142] Grubbs has prepared water-soluble catalysts that promote living ROMP and RCM reactions in aqueous and methanolic solutions (these species were not CM-active); for details of this pioneering work, see: a) B. Mohr, D. M. Lynn; R. H. Grubbs, *Organometallics* **1996**, *15*, 4317 – 4325; b) D. M. Lynn, B. Mohr, L. M. Henling, M. W. Day, R. H. Grubbs, *J. Am. Chem. Soc.* **2000**, *122*, 6601 – 6609; c) D. M. Lynn, B. Mohr, R. H. Grubbs, *J. Am. Chem. Soc.* **1998**, *120*, 1627 – 1628; d) T. A. Kirkland, D. M. Lynn, R. H. Grubbs, *J. Org. Chem.* **1998**, *63*, 9904 – 9909.
[143] Catalyst **4a** is soluble in MeOH and gave comparable results to **161** in CM reactions using this solvent;[141] this is a further example of the utility of **4a** as a metathesis tool to complement benchmark catalyst **3,** which is insoluble in MeOH.
[144] J. S. Kingsbury, S. B. Garber, J. M. Giftos, B. L. Gray, M. M. Okamoto, R. A. Farrer, J. T. Fourkas, A. H. Hoveyda, *Angew. Chem.* **2001**, *113*, 4381 – 4386; *Angew. Chem. Int. Ed.* **2001**, *40*, 4251 – 4256.
[145] For a report concerning the immobilization of a ruthenium metathesis catalyst on monolithic material by ROM-CM, see: M. Mayr, B. Mayr, M. R. Buchmeiser, *Angew. Chem.* **2001**, *113*, 3957 – 3960; *Angew. Chem. Int. Ed.* **2001**, *40*, 3839 – 3842.
[146] A resin-immobilized molybdenum catalyst capable of asymmetric ROM–CM was reported recently; however, recyclability was poor: K. C. Hultzsch, J. A. Jernelius, A. H. Hoveyda, R. R. Schrock, *Angew. Chem.* **2002**, *114*, 609 – 613; *Angew. Chem. Int. Ed.* **2002**, *41*, 589 – 593.
[147] Q. Yao, *Angew. Chem.* **2000**, *112*, 4060 – 4062; *Angew. Chem. Int. Ed.* **2000**, *39*, 3896 – 3898.
[148] S. J. Connon, A. M. Dunne, S. Blechert, *Angew. Chem.* **2002**, *114*, 3989 – 3993; *Angew. Chem. Int. Ed.* **2002**, *41*, 3835 – 3838.

 © 2003 Wiley-VCH Verlag GmbH & Co. KGaA, Weinheim

Communications



Complex covalent chemistry has been monitored at the single-molecule level by determining the ionic current flowing through the interior of a protein pore. The current depends upon the size, shape, and polarity of the reactants tethered within it and allows a three-step reaction initiated by light to be followed. Find out more in the Communication by H. Bayley et al. on the following pages.

DOI: 10.1002/anie.200250666
© 2003 Wiley-VCH Verlag GmbH & Co. KGaA, Weinheim

Reaction Kinetics in a Pore

Kinetics of a Three-Step Reaction Observed at the Single-Molecule Level**

*Tudor Luchian, Seong-Ho Shin, and Hagan Bayley**

The ability to observe covalent chemistry at the single-molecule level is expected to yield information about reaction pathways that cannot be obtained from ensemble measurements. Optical, force, and electrical measurements have been used to study the dynamics of individual molecules in solution, and progress has been made in applying these approaches to chemical reactions. For example, single turnovers of enzymes and ribozymes have been examined by optical techniques including fluorescence and light-scattering measurements.[1–5] Force spectroscopy has been used to investigate the breaking and making of noncovalent bonds, as exemplified by the unfolding and refolding of proteins[6–10] and RNA.[3,5,11] Force measurements have also been used to determine the force required to rupture individual covalent bonds at specified loading rates[12] and to study the photoisomerization of an azobenzene,[13] although, in the latter work, individual isomerization steps were not resolved.

Electrical measurement of the conductance of nanoreactors comprising single transmembrane pores has several advantages for the observation of covalent chemistry at the single-molecule level; for example, measurements can be carried out with time resolution in the microsecond domain and the procedure does not require a spectroscopic probe such as a fluorophore. Electrical detection at the single-molecule level has been used previously to follow a unidirectional single-step reaction,[14] to observe a thermal isomerization,[15,16] and to monitor reversible single-step covalent chemistry.[17] Finkelstein and co-workers observed the reaction of a cysteine residue in the lumen of the diphtheria toxin pore with $CH_3SO_2SCH_2CH_2N(CH_3)_3^+$. They predicted that the single-molecule approach might be generally useful for the examination of chemical kinetics.[14] Woolley and co-workers synthesized a gramicidin with a carbamate attached near the mouth of the pore.[15,16] They were able to observe the temperature dependence of the rates of *cis–trans* isomerization of the carbamate and thereby determine the activation enthalpies and entropies. In our research group, the reversible reactions of organoarsenic(III) compounds with the thiol group of a single cysteine residue projecting into the lumen of the α-hemolysin (αHL) pore have been examined.[17] Rate constants for the formation and dissociation of the unstable covalent adducts were obtained.

Here, we have used electrical detection to monitor a multistep reaction at the single-molecule level for the first time. The breakdown of a protected carbamic acid was initiated with light. By this means we determined the rate constants for the cleavage of the 2-nitrobenzyl protecting group after the absorption of a photon and the cleavage of the carbamic acid to give carbon dioxide and a primary amine. Our approach reveals reactive intermediates, uncovers minor pathways, and quantifies the kinetics of steps invisible in conventional kinetic techniques.

An αHL pore was constructed with a 3,4-dimethoxy-6-nitrobenzylcarbamate group covalently attached on the interior wall through an oligo(ethylene glycol) linker (Figure 1a and Supporting Information). In brief, an αHL subunit containing the Thr117→Cys mutation was derivatized on the cysteinyl residue with reagent **1**. The modified subunit was assembled with wild-type subunits and the heteroheptamer containing a single modified cysteine was separated by electrophoresis. The separation was assisted by the presence of an oligoaspartate tail on the modified subunit. The photochemistry of nitrobenzylcarbamates and related molecules is well developed (Figure 1b). On absorption of a photon the 3,4-dimethoxy-6-nitrobenzyl group rearranges to a nitronate (aci-nitro) intermediate, which has a lifetime of microseconds to seconds depending on the nature of the appended group and the reaction conditions.[18] The protecting group dissociates as a nitrosoaldehyde to reveal a carbamic acid that loses CO_2 in a pH-dependent step and yields a primary amine. As shown here, the expected chemistry can be observed by planar bilayer recording as three steps in a single-channel current (Figure 2a). The current steps are produced by changes in the size, shape, and charge of the remainder of the molecule tethered within the lumen of the pore.

We examined the pH dependence of both the loss of the nitrobenzyl protecting group and the breakdown of the carbamic acid to demonstrate the potential of the approach (Figure 2b–d). The photoinitiated reaction was carried out around ten times at each of four pH values and the lifetimes of the two intermediates were determined in each case. The reciprocal of the mean lifetime provides an estimator of the rate constant (k) of each step (Figure 2b–d). A statistical analysis yields a confidence interval for the true value of k (see the Supporting Information).

The photolysis of the 2-nitrobenzyl group has been studied extensively because of its utility in organic synthesis, on-chip oligonucleotide synthesis, and the "caging" of small and large molecules for applications in biology. Formation of the nitronate intermediate, by rapid deprotonation of the first-formed nitronic acid, is generally accepted to occur in a few microseconds. We suggest that level 2 (Figure 2a) is the

[*] Dr. H. Bayley, Dr. T. Luchian,[+] S.-H. Shin[+]
The Texas A&M University System Health Science Center
Department of Medical Biochemistry & Genetics
College Station, TX 77843–1114 (USA)
Fax: (+1) 979-847-9481
E-mail: bayley@tamu.edu
Dr. H. Bayley, S.-H. Shin[+]
Department of Chemistry
Texas A&M University
College Station, TX 77843-3255 (USA)

[+] These authors contributed equally to this work.

[**] We thank Michael Longnecker and James Calvin for their help with statistics. The authors acknowledge grants from the US Department of Energy, the Multidisciplinary University Research Initiative (ONR 1999), the National Institutes of Health, and the Office of Naval Research.

Supporting information for this article is available on the WWW under http://www.angewandte.org or from the author.

 © 2003 Wiley-VCH Verlag GmbH & Co. KGaA, Weinheim DOI: 10.1002/anie.200250666

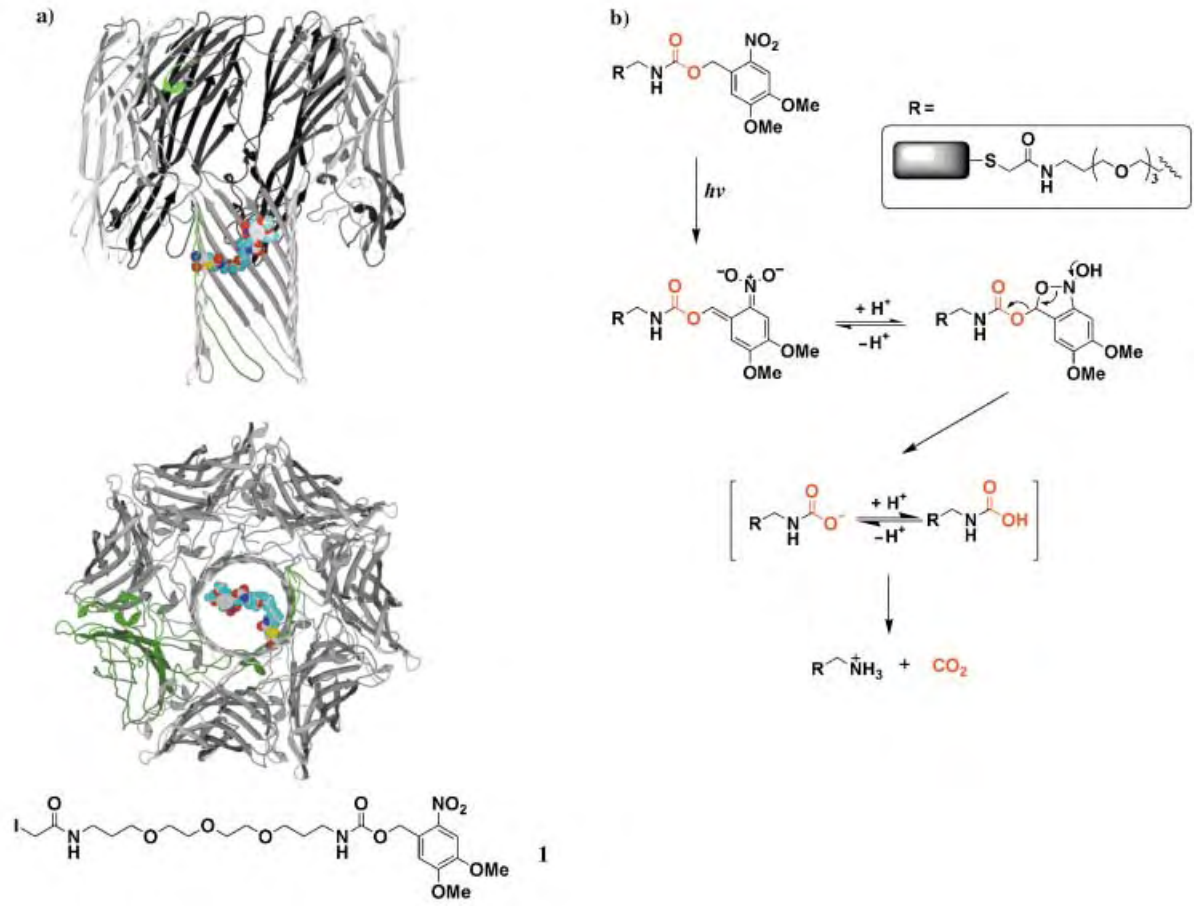


Figure 1. Single-molecule chemistry photoinitiated within an α-hemolysin pore. a) A model of the engineered αHL pore containing a single protected carbamate side chain is shown, which is based on the three-dimensional structure of the wild-type heptamer.[28] The pore contains six unmodified subunits and one modified subunit. The latter is equipped with a 3,4-dimethoxy-6-nitrobenzylcarbamate group covalently attached through an oligo(ethylene glycol) linker to a cysteine residue at position 117 by derivatization with reagent **1**. b) Possible photoinitiated chemistry. The most likely isomers and most abundant protonation states of the molecules are shown. A more detailed discussion can be found in the Supporting Information.

nitronate or the bicyclic intermediate (or possibly both species in rapid equilibrium; see Figure 1b and the Supporting Information). The breakdown of similar nitronates, as monitored through their characteristic absorbance at wavelengths greater than 400 nm, occurs with rates that range from less than 1 s^{-1} to more than 10^5 s^{-1}.[18] For example, $k = 1$ s^{-1} for the 1-(3,4-dimethoxy-6-nitrophenyl)ethyl ester of glycine,[19] while $k = 2 \times 10^5$ s^{-1} for the α-carboxy-2-nitrobenzyl ester of glycine.[20] The rate of breakdown of the nitronate in the present case is at the low end of the known range, with $k = 0.56$ s^{-1} at pH 7.0. The rate increases at lower pH values, but the magnitude of the increase is only approximately fivefold over 4.5 pH units. Examples of weak pH dependence can be found in the literature,[20,21] but the rate increase is more often three or four orders of magnitude.[18]

The breakdown of carbamic acids have also been investigated in detail. Carbamates and related molecules are commonly used as protecting groups in organic synthesis and, under physiological conditions, lysyl residues in proteins are often carbamylated.[22] The pH dependence of decarboxylation is striking and can be fit to Equation (1):[23–25]

$$k_{obs} = \frac{k[H^+]}{K_a + [H^+]} \quad (1)$$

The value of K_a (approximately 10^{-5} M) is close to that of the ionization constant of carbamic acids (pK_a ca. 5.2), which suggests that the rate of reaction is proportional to the concentration of the protonated species (RNHCOOH), although several studies suggest that the actual intermediate is the short-lived zwitterionic species (the concentration of which will be proportional to that of the protonated form).[23,25] Our single-molecule data are in keeping with such an interpretation. The values for k_{obs} can be fit to Equation (1) to yield $k = 350$ s^{-1} and $pK_a = 6.4$ (Figure 2e). The measured k' values at high pH values for carbamates of strong bases (where $k_{obs} = k'[H^+]$) are around 10^8 $M^{-1}s^{-1}$; for example, $k' = 7.9 \times 10^7$ s^{-1} for butylamine.[23] Therefore, $k = k'K_a = 500$ $M^{-1}s^{-1}$, which is close to the value we find. Further experimentation will be required to determine how the shift in the apparent pK_a value is related to the environment within the β barrel.

 © 2003 Wiley-VCH Verlag GmbH & Co. KGaA, Weinheim

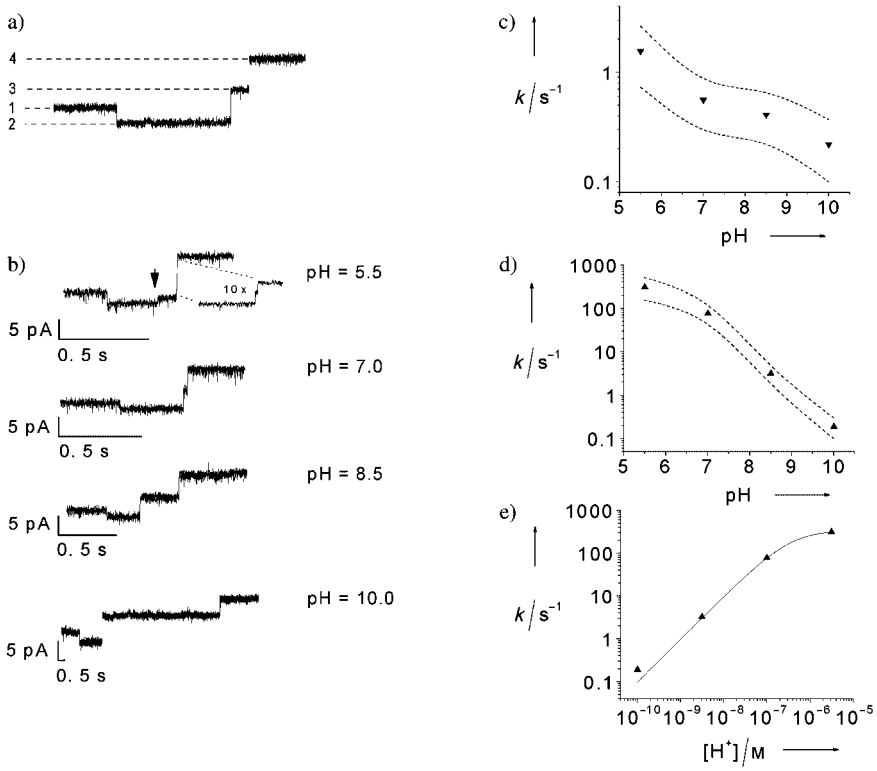


Figure 2. Single-molecule chemistry initiated by near-UV irradiation. a) Four levels in the single-channel current trace were observed. Level 1, before photon absorption, corresponds to the starting material. Level 2 is assumed to represent the nitronate intermediate (see Figure 1b). Level 3 is the carbamic acid as judged by the strong pH dependence of its breakdown. Level 4 is the protonated amine, the final product. Several studies suggest that the bicyclic intermediate (Figure 1b) is too short-lived[29,30] to be observed under the recording conditions, which would reveal intermediates with $\tau \geq 1$ ms. In some experiments, we saw small steps in the level 2 current (30% of recordings; for example, see Figure 2b, arrow), but their inconsistency makes it unlikely that they represent the bicyclic molecule. Of course, some intermediates might be electrically silent. b) Representative current traces showing the pH dependence of the reaction. The experiments described in this work were done in 2 M KCl, 10 mM tris(hydroxymethyl)aminomethane (Tris) base, 100 μM ethylenediamine tetraacetate (EDTA), titrated to the desired pH value with HCl. Similar results were obtained when 2-(*N*-morpholino)ethanesulfonic acid (MES) buffer was used at pH 5.5 and 3-(cyclohexylamino)-1-propanesulfonic acid (CAPS) buffer at pH 10.0. c) Rate of nitronate breakdown plotted as a function of pH. The 90% confidence interval is shown (dashed lines). d) Rate of carbamic acid breakdown plotted as a function of pH. The 90% confidence interval is shown (dashed lines). e) The data in (d) are fitted to Equation (1) by using a nonlinear fitting algorithm (Origin 7.0) based on the Levenberg–Marquardt method for χ^2 reduction.

The determination of the kinetics of breakdown of the carbamic acid at low pH values exemplifies one of the advantages of using the single-molecule approach: the ability to measure the rate constant for a fast step that follows one or more slow steps. At pH 5.5, for example, the rate constant for the loss of CO_2 is $k = 313\ s^{-1}$, while the rate constant for the preceding step is $k = 1.6\ s^{-1}$. Therefore, in this case, the rate at which carbamic acid breaks down could not be observed by a more conventional approach such as flash photolysis of a bulk sample.

The β barrel of the αHL pore contains about 400 molecules of water. The present work and previous investigations of noncovalent interactions within the pore suggest that the properties of the solvent conform quite well with those of the bulk phase, which is in agreement with recent investigations of confined water.[26] Therefore, it should be possible to generalize the approach demonstrated here to the wide variety of chemistries that can be carried out in water[27] and utilize many of the tools of mechanistic chemistry, such as the measurement of isotope effects and the trapping of intermediates.

Received: November 29, 2002 [Z50666]

Keywords: carbamates · photochemistry · protein engineering · single-molecule studies · transmembrane pore

[1] H. Noji, R. Yasuda, M. Yoshida, K. Kinosita, *Nature* **1997**, *386*, 299–302.
[2] H. P. Lu, L. Xun, X. S. Xie, *Science* **1998**, *282*, 1877–1882.
[3] X. Zhuang, L. E. Bartley, H. P. Babcock, R. Russell, T. Ha, D. Herschlag, S. Chu, *Science* **2000**, *288*, 2048–2051.
[4] R. Yasuda, H. Noji, M. Yoshida, K. Kinosita, H. Itoh, *Nature* **2001**, *410*, 898–904.
[5] X. Zhuang, H. Kim, M. J. B. Pereira, H. P. Babcock, N. G. Walter, S. Chu, *Science* **2002**, *296*, 1473–1476.
[6] M. S. Z. Kellermeyer, S. B. Smith, H. L. Granzier, C. Bustamante, *Science* **1997**, *276*, 1112–1116.
[7] M. Rief, M. Gautel, F. Oesterhelt, J. M. Fernandez, H. E. Gaub, *Science* **1997**, *276*, 1109–1112.
[8] M. Carrion-Vazquez, A. F. Oberhauser, S. B. Fowler, P. E. Marszalek, S. E. Broedel, J. Clarke, J. M. Fernandez, *Proc. Natl. Acad. Sci. USA* **1999**, *96*, 3694–3699.
[9] G. L. Yang, C. Cecconi, W. A. Baase, I. R. Vetter, W. A. Breyer, J. A. Haack, B. W. Matthews, F. W. Dahlquist, C. Bustamante, *Proc. Natl. Acad. Sci. USA* **2000**, *97*, 139–144.
[10] F. Oesterhelt, D. Oesterhelt, M. Pfeiffer, A. Engel, H. E. Gaub, D. J. Müller, *Science* **2000**, *288*, 143–146.
[11] J. Liphardt, B. Onoa, S. B. Smith, I. Tinoco, C. Bustamante, *Science* **2001**, *292*, 733–737.
[12] M. Grandbois, M. Beyer, M. Rief, H. Clausen-Schaumann, H. E. Gaub, *Science* **1999**, *283*, 1727–1730.
[13] H. Hugel, N. B. Holland, A. Cattani, L. Moroder, M. Seitz, H. E. Gaub, *Science* **2002**, *296*, 1103–1106.
[14] J. A. Mindell, H. Zhan, P. D. Huynh, R. J. Collier, A. Finkelstein, *Proc. Natl. Acad. Sci. USA* **1994**, *91*, 5272–5276.
[15] G. A. Woolley, A. S. I. Jaikaran, Z. Zhang, S. Peng, *J. Am. Chem. Soc.* **1995**, *117*, 4448–4454.
[16] D. C. J. Jaikaran, G. A. Woolley, *J. Phys. Chem.* **1995**, *99*, 13352–13355.
[17] S.-H. Shin, T. Luchian, S. Cheley, O. Braha, H. Bayley, *Angew. Chem.* **2002**, *114*, 3859–3861; *Angew. Chem. Int. Ed.* **2002**, *41*, 3707–3709.

 © 2003 Wiley-VCH Verlag GmbH & Co. KGaA, Weinheim

[18] J. E. T. Corrie, D. R. Trentham in *Biological applications of photochemical switches* (Ed.: H. Morrison), Wiley, New York, **1993**, pp. 243 – 299.
[19] M. Wilcox, R. W. Viola, K. W. Johnson, A. P. Billington, B. K. Carpenter, J. A. McCray, A. P. Guzikowski, G. P. Hess, *J. Org. Chem.* **1990**, *55*, 1585 – 1589.
[20] C. Grewer, J. Jäger, B. K. Carpenter, G. P. Hess, *Biochemistry* **2000**, *39*, 2063 – 2070.
[21] T. Milburn, N. Matsubara, A. P. Billington, J. B. Udgaonkar, J. W. Walker, B. K. Carpenter, W. W. Webb, J. Marque, W. Denk, J. A. McCray, G. P. Hess, *Biochemistry* **1989**, *28*, 49 – 55.
[22] B. Wittmann, G. Gros, *J. Biol. Chem.* **1981**, *256*, 8332 – 8340.
[23] M. Caplow, *J. Am. Chem. Soc.* **1968**, *90*, 6795 – 6803.
[24] T.-T. Wang, S. H. Bishop, A. Himoe, *J. Biol. Chem.* **1972**, *247*, 4437 – 4440.
[25] S. L. Johnson, D. L. Morrison, *J. Am. Chem. Soc.* **1972**, *94*, 1323 – 1334.
[26] U. Raviv, J. Klein, *Science* **2002**, *297*, 1540 – 1543.
[27] U. Lindström, *Chem. Rev.* **2002**, *102*, 2751 – 2772.
[28] L. Song, M. R. Hobaugh, C. Shustak, S. Cheley, H. Bayley, J. E. Gouaux, *Science* **1996**, *274*, 1859 – 1865.
[29] A. Barth, J. E. T. Corrie, M. J. Gradwell, Y. Maeda, W. Mantele, T. Meier, D. R. Trentham, *J. Am. Chem. Soc.* **1997**, *119*, 4149 – 4159.
[30] Q. Cheng, M. G. Steinmetz, V. Jayaraman, *J. Am. Chem. Soc.* **2002**, *124*, 7676 – 7677.

 © 2003 Wiley-VCH Verlag GmbH & Co. KGaA, Weinheim

An Oxidation-Resistant Semiconductor

Stabilization of β-SiB_3 from Liquid Ga: A Boron-Rich Binary Semiconductor Resistant to High-Temperature Air Oxidation**

*James R. Salvador, Daniel Bilc, S. D. Mahanti, and Mercouri G. Kanatzidis**

Liquid metals can be powerful solvents for the exploration of novel refractory solid-state materials ranging from intermetallic compounds to silicides, carbides and borides. Recently we have discovered, from liquid Al and Ga, a large variety of ternary and quaternary phases of the type RE/TM/Si or Ge, RE/TM/Al or Ga, RE/TM/Al/Si or Ge, and RE/TM/Ga/Ge or Si (RE = rare earth La–Lu, and TM = 1st, 2nd, or 3rd row transition metal).[1,2] Many of these phases cannot be formed by conventional high temperature solid-state synthetic techniques such as direct combination reactions with arc melting or radio-frequency (rf) induction furnace heating.[3] We have extended the flux methodology to include RE/TM/B/Si (borosilicides) in an attempt to produce lighter analogues of the RE/TM/Al/Si compounds, and we chose liquid gallium as the reaction medium because both Si and B are soluble in it and do not form binaries.[4] Also from previous work we learned that RE/TM/Ga/Si phases do not form readily, and so competing phases of this type are not anticipated.[1] Boron-containing solids have acquired renewed interest because quaternary borocarbides are superconducting,[5] and MgB_2 is a high temperature nonoxidic superconductor.[6]

Borosilicides are an unfamiliar class of compounds. Specifically boron-rich borosilicides are rare with only a handful of examples are known: $CrSi_3(B_{12})Se_{12}(B_2Se_3)_{1.33}$, $REB_{41}Si_{1.2}$ (RE = Y, Tb), $Sc_{0.83-x}B_{10.0-y}C_{0.17+y}Si_{0.083-z}$,[7] SiB_3, SiB_4 and SiB_6[8] to name a few. We have recently shown that liquid gallium can provide an excellent route to complex quaternary silicon borides such as $Tb_{1.8}Si_8C_2(B_{12})_3$ that cannot be formed by using high-temperature techniques such as arc melting.[9] Herein, we present an illustration of the ability of liquid Ga to stabilize boride phases inaccessible by conventional synthetic routes. Namely, we describe a novel B-rich, refractory, semiconducting binary phase β-SiB_3.

β-SiB_3 is a surprising discovery because a phase with a similar formula, $Si_{1-x}B_{3+x}$ with a compositional spread of x = 0–0.2,[10] that has a rhombohedral structure has been known for decades.[11] We will henceforth refer to this phase as α-SiB_3. Instead β-SiB_3 is orthorhombic *Imma*, representing a new structure type.[12] Despite the similarity in stoichiometry and the presence of B_{12} icosahedra the structural features and electronic properties of the α and β phases are very different. Rhombohedral α-SiB_3 forms from direct combination of the elements with prolonged isothermal heating at 1225 °C or by arc melting, in contrast β-SiB_3 was produced from a lower temperature reaction (1000–850 °C) in Ga flux. Additionally, in α-SiB_3, some Si atoms are randomly distributed in the B_{12} cages resulting in very distorted icosahedra.[13] In contrast, Si atoms in β-SiB_3 are rigorously excluded from the cages, thus resulting in more regular icosahedra. To the best of our knowledge this is the first Si–B binary phase that is fully crystallographically ordered without any Si/B mixed sites or disorder. This exclusion of Si from the cages has a profound influence on the thermal stability of the orthorhombic form.

β-SiB_3 was originally found as a minor product in reactions aimed to produce $Er_{1.8}Si_8C_2(B_{12})_3$ from the Ga flux. The new phase forms as distorted rectangular plates that are translucent and amber in color. Energy dispersive spectroscopy (EDS) on several crystals of the title compound detected only Si and B.[14] The presence of C in β-SiB_3 was detected by combustion elemental analysis which showed the carbon concentration to be ~0.4% by weight.[15] Similar combustion analysis on α-SiB_3 (a phase known to contain no C) showed a C concentration of 0.16% by weight. We originally thought that there was a small amount of C present

[*] Prof. M. G. Kanatzidis, J. R. Salvador
Department of Chemistry and Center for Fundamental Materials Research
Michigan State University
East Lansing, MI 48842–1793 (USA)
Fax: (+1) 517-355-1793
E-mail: kanatzid@cem.msu.edu
D. Bilc, Dr. S. D. Mahanti
Department of Physics and Astronomy
Michigan Sate University
East Lansing, MI 48842-1793 (USA)

[**] Financial support from the Department of Energy (Grant No. DE-FG02-99ER45793) is gratefully acknowledged. Part of this work was carried out at the Center for Advanced Microscopy at Michigan State University.

 DOI: 10.1002/anie.200219986 © 2003 Wiley-VCH Verlag GmbH & Co. KGaA, Weinheim

in β-SiB_3, and that it was statistically distributed over the B_{12} cages resulting in the stoichiometry $Si_4B_{12-x}C_x$ ($x \sim 0.4$). The yield of β-SiB_3 was observed to increase when carbon was included in the preparation (from 40% to 60%). Although it is possible that a small amount of carbon is accommodated in the structure, we believe that it is not needed to prepare the compound. The issue of adventitious carbon inclusion is discussed below.

Importantly, no traces of the known black rhombohedral α-SiB_3 phase were found by powder X-ray diffraction, nor visual inspection in the flux reactions. As the crystal habit and color of the two species are quite different, they are easily distinguished by looking. An inspection of other reactions of the type TM/B/C/Si (TM = Fe, Co, Ni, Cu, Zn) in a Ga flux showed large amounts of β-SiB_3, particularly when TM = Cu.

The formation of β-SiB_3 is exclusive to flux synthesis. Several attempts were made to produce the phase by direct combination of the elements with arc-melt alloying, rf induction heating and prolonged heating at 1000 °C for two weeks. The induction furnace and the two-week 1000 °C isothermal synthesis both yielded starting material, presumably because the temperatures reached by these methods were insufficient to bring about a reaction. Arc-melt alloying Si and B in a 1:3 ratio yielded the α-SiB_3 structure. EDS analysis was also performed on crystals produced from this reaction and found on Si and B present in similar ratios to the title compound. These results may explain why β-SiB_3 was not discovered previously, as flux routes to borosilicides are a new synthetic strategy.

The structure of β-SiB_3 has two building blocks: infinite Si_4 chains and B_{12} cages (Figure 1a and 1b respectively). The B_{12} cages are linked together forming a layer, Figure 1c. The Si_4 chains contain two base-fused triangle units forming a rhombus. The rhombi are linked to one another to form a sinusoidal chain that propagates along the *a* axis, Figure 1a. There are two crystallographically distinct Si atoms one at the apex of the fused triangles (Si(1)) and one that forms the base with its symmetry equivalent (Si(2)). The Si(1)–Si(1) bond from apex to apex is 2.3336(8) Å. The other Si–Si bonds in the structure are substantially longer with Si(1)–Si(2) being 2.5967(4) Å and Si(2)–Si(2) (base of the triangle) at 2.3970(8) Å. To the best of our knowledge, the infinite Si_4 chain is a novel structural feature, although it has a slight similarity to the Ge_4 chains of $BaGe_2$. However, in the latter compound the Ge_4 chains are anionic and are well rationalized by the Zintl concept.[16] In contrast, the Si_4 chains of β-SiB_3 are not anionic and are not regarded as Zintl species.

The four crystallographically distinct boron atoms are arranged in the B_{12} cages that form a sheet structure extending over the *ac* plane, which results in a regular four-sided ring of cages Figure 1c. The cages are bound through symmetry-generated B(4)–B(4) bonds at 1.717(2) Å. Intracage distances range from 1.934(2) Å for B(4)–B(4) to 1.756(2) Å for B(1)–B(3) with an average of 1.792 Å. The Si zig-zag chains insert between the B_{12} icosahedral sheets forming B–Si bonds and a three-dimensional framework along the *b* axis (Figure 2). The B–Si bond distances are 2.027(1) Å for Si(1)–B(1), 1.973(2) Å between Si(2) and B(3), and 2.009(2) for Si(2)–B(2).

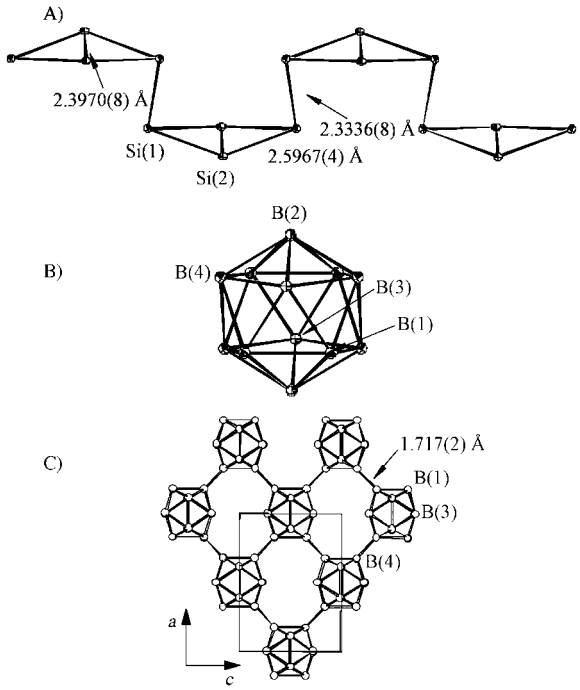


Figure 1. a) A segment of the infinite Si_4 ribbon as it extends down the *a* axis, a motif reminiscent of red phosphorous, thermal elipsoids are set at the 50% probability level. Selected bond angles Si(1)-Si(1)-Si(2) = 91.85(2)°, Si(1)-Si(2)-Si(1) = 121.53(2)°, Si(2)-Si(1)-Si(2) = 54.97(2)°, Si(2)-Si(2)-Si(1) = 62.513(9)°. b) B_{12} icosahedral unit, thermal elipsoids are set at the 50% probability level. c) The arrangement of B_{12} cages in the *ac* plane.

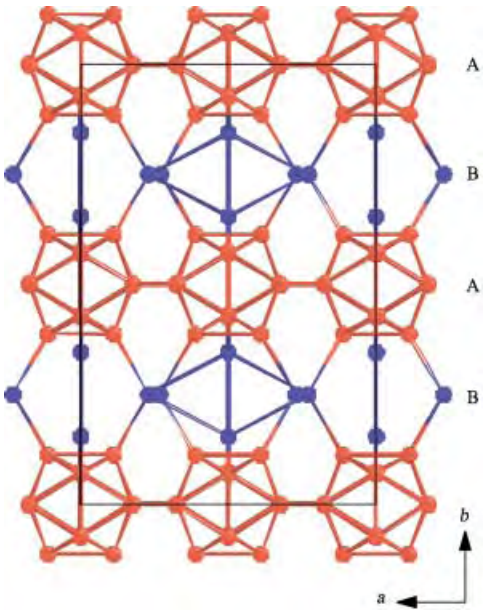


Figure 2. A view of the overall structure of β-SiB_3 showing the way two structural moieties stack along the *b* axis. Si atoms: blue; B atoms: red.

β-SiB_3 is a semiconductor with an energy band gap of ≈2.0 eV, (Figure 3a).[17] This wide gap is in sharp contrast to that of the α-SiB_3, which is only ≈0.2 eV, (Figure 3b), and points to the dramatically different electronic properties of

 © 2003 Wiley-VCH Verlag GmbH & Co. KGaA, Weinheim

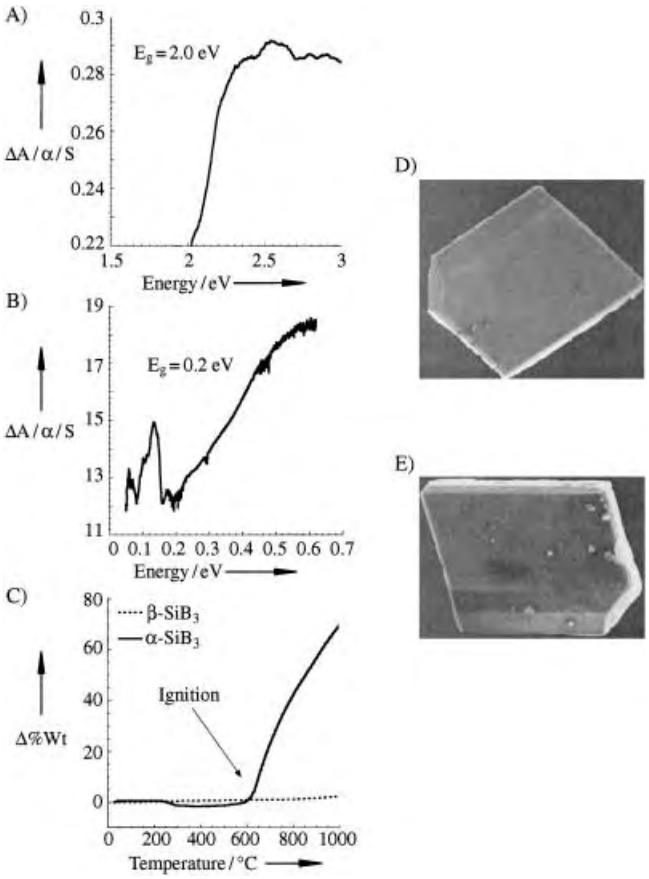


Figure 3. A) A comparative plot of the optical absorbance versus energy (eV) for β-SiB_3 and B) α-SiB_3. (α = absorption coefficient, S = scattering) C) Thermal gravimetric analysis of α-SiB_3 and β-SiB_3 in air. Percent relative weight gain (Δ %Wt) is defined as [(Weight − $Weight_{initial}$)/$Weight_{initial}$] × 100. D) Scanning electron micrograph of β-SiB_3 before heating at 700 °C. E) Scanning electron micrograph of same β-SiB_3 crystal after heating at 700 °C.

these two phases.[18] Thermopower measurements on β-SiB_3 showed a small positive room temperature Seebeck coefficient of $+20\ \mu V\,K^{-1}$, which decreased approximately linearly to $+10\ \mu V\,K^{-1}$ at 400 K. The positive value indicates holes as the dominant charge carriers as is typically the case for boron-rich compounds with B_{12} icosahedra.[19]

Ab initio band-structure calculations were carried out for β-SiB_3 to probe for the existence of an energy band gap and to see if the compound were stable without the inclusion of carbon.[20] The calculations show an indirect band gap of ~1.5 eV, which indicates valence precision. This result demonstrates that C atoms are not needed in the B_{12} cages to satisfy any electronic requirements of β-SiB_3. Based on this result, we believe that C atoms are not present in the structure and that β-SiB_3 is truly a new Si–B binary phase. The theoretically determined band gap is in reasonably good agreement with the optically determined value of 2.0 eV.

A remarkable property of this phase is the extreme inertness to chemical attack by concentrated sulfuric acid, aqua regia, and a 5 M solution of NaOH for > 24 h. Thermal gravimetric analysis (TGA) showed β-SiB_3 did not oxidize under a pure oxygen atmosphere below approximately 600 °C. When the experiment was repeated in air instead of oxygen, there was no evident ignition point and only a nominal relative weight gain of ≈2 % was observed up to 1000 °C. In contrast, α-SiB_3 shows an ignition point of 600 °C in air, Figure 3c. We attribute the lack of stability in α-SiB_3 to the nature of the Si–B disorder within the B_{12} icosahedra, which causes the weakening of bonds. To test more realistically the thermal stability of the title compound, several single crystals were placed in open fused silica tubes and heated to 700 °C and held there for 12 h. β-SiB_3 remained intact at this temperature. Scanning electron micrographs of a β-SiB_3 single crystal before and after heating can be seen in Figure 3d and 3e respectively. Only when the experiment was repeated at 1000 °C was there evidence of thermal degradation.

The resistance to air oxidation at high temperature is impressive for a nonoxidic compound. As it also has a wide band gap of 2.0 eV, this new material might be useful as a refractory p-type semiconductor capable of operating in extreme environments. Currently the leading material for such applications is SiC, however, it suffers from the major drawback of having nearly 200 polytype structures, all of which have different electronic properties.[21] The compound presented here has no other polytypes, and β-SiB_3 can be made independently from α-SiB_3.

It is significant that the synthesis of β-SiB_3 requires metallic flux conditions, which permit the total bypass of the rhombohedral compound α-SiB_3. The results reported herein warrant future investigations of the electrical properties of β-SiB_3.

Experimental Section

Optimized flux synthesis of β-SiB_3 was carried out by combining B (43 mg, 4 mmol; 99.995 % submicron amorphous, Aldrich), Si (28 mg, 1 mmol; 99.999 % −325 mesh, Cerac), Cu (64 mg, 1 mmol; 99.9 % 325 mesh, Cerac), and Ga (1.394 g, 20 mmol; 99.99 % 2–5 mm pieces, Plasmaterials) into an Al_2O_3 ceramic tube. The ceramic tube was placed in a fused silica tube that was flame-sealed under a vacuum of ~10^{-5} mbar. The reactants were heated up to 1000 °C over 12 h, then held at 1000 °C for 96 h. The reaction system was then cooled to 150 °C over 48 h. Isolation of the product was accomplished by a warm centrifugation, which removed the excess Ga. Further purification was carried out by adding the product to a solution of I_2 (5 M) in dimethylformamide, and subjecting the mixture to ultrasound for 30 min to remove remaining Ga. Small shiny amber colored plates were obtained approximately 0.5–1 mm at the widest point. Typical yields were 40 %.

Received: August 16, 2002
Revised: December 20, 2002 [Z19986]

Keywords: boron · gallium · semiconductors · silicon

[1] a) X. Z. Chen, P. Larson, S. Sportouch, P. Brazis, S. D. Mahanti, C. R. Kannewurf, M. G. Kanatzidis, *Chem. Mater.* **1999**, *11*, 75; b) X. Z. Chen, P. Small, S. Sportouch, M. Zhuravleva, P. Brazis, C. R. Kannewurf, M. G. Kanatzidis, *Chem. Mater.* **2000**, *12*, 2520; c) B. Sieve, S. Sportouch, X. Z. Chen, J. A. Cowen, P. Brazis, C. R. Kannewurf, V. Papaefthymiou, M. G. Kanatzidis, *Chem. Mater.* **2001**, *13*, 273; d) M. A. Zhuravleva, K. K. Rangan, M.

 © 2003 Wiley-VCH Verlag GmbH & Co. KGaA, Weinheim

Lane, P. Brazis, C. R. Kannewurf, M. G. Kanatzidis, *J. Alloys Compd.* **2001**, *316*, 137.
[2] a) B. Fehrmann, W. Jeitschko, *Inorg. Chem.* **1999**, *38*(14), 3344; b) B. Fehrmann, W. Jeitschko, *Z. Naturforsch. B* **1999**, *54*, 1277.
[3] B. Sieve, X. Z. Chen, R. Henning, P. Brazis, C. R. Kannewurf, J. A. Cowen, A. J. Schultz, M. G. Kanatzidis, *J. Am. Chem. Soc.* **2001**, *123*, 7040.
[4] T. B. Massalski, *Binary Alloy Phase Diagrams, Vol. 1*, 2nd ed., ASM International, New York, **1990**, p. 484; T. B. Massalski, *Binary Alloy Phase Diagrams, Vol. 2*, 2nd ed., ASM International, New York, **1990**, p. 1856.
[5] R. J. Cava, H. Takagi, B. Batlogg, H. W. Zandbergen, J. J. Krajewski, W. F. Peck, Jr., R. B. van Dover, R. J. Felder, T. Siegrist, K. Mizuhashi, J. O. Lee, H. Eisaki, S. A. Carter, S. Uchida, *Nature* **1994**, *367*, 146.
[6] J. Nagamatsu, N. Nakagawa, T. Muranaka, Y. Zenitani, J. Akimitsu, *Nature* **2001**, *410*, 63.
[7] a) M. Sugimori, H. Fukuoka, H. Imoto, T. Saito, *Organometallics* **2000**, *19*, 611; M. Sugimori, H. Fukuoka, H. Imoto, T. Saito, *Organometallics* **2000**, *19*, 547; M. Sugimori, H. Fukuoka, H. Imoto, T. Saito, *Organometallics* **2000**, *19*, 154; b) I. Higashi, T. Tanaka, K. Kabayashi, Y. Ishizawa, M. Takami, *J. Solid State Chem.* **1997**, *133*, 11; c) T. Mori, T. Tanaka, *J. Alloys Compd.* **1999**, *288*, 32; d) T. Tanaka, A. Sato, *J. Solid State Chem.* **2002**, *165*, 148.
[8] a) B. Magnusson, C. Brosset, *Acta Chem. Scand.* **1962**, *16*, 449; b) H. F. Rizzo, L. R. Bidwell, *J. Am. Ceram. Soc.* **1960**, *43*, 550; c) M. Vlasse, G. A. Slack, M. Garbauskas, J. S. Kasper, J. C. Viala, *J. Solid State Chem.* **1986**, *63*, 31.
[9] J. R. Salvador, D. Bilc, S. D. Mahanti, M. G. Kanatzidis, *Angew. Chem.* **2002**, *114*, 872; *Angew. Chem. Int. Ed. Engl.* **2002**, *41*, 844.
[10] The phases SiB_3 and SiB_4 are listed separately in "Pearson's Handbook of Crystallographic Data for Intermetallic Phases", and are even listed as different structure types the former having the B_6P structure type and the later the $B_{13}C_2$. In fact SiB_3 and SiB_4 have the same structure, that of B_6P, and the variation in stoichiometry is the result of a compositional spread ranging from $SiB_{2.89}$ up to SiB_4. This stoichiometric flexibility arises from the substitution of varying amounts of Si into the polar sites of the B_{12} cages.
[11] V. I. Matkovich, *Boron and Refractory Borides*; Springer, New York, **1977**, pp. 100–101, V. I. Matkovich, *Boron and Refractory Borides*; Springer, New York, **1977**, pp. 321–326, and references therein.
[12] Crystal data for β-SiB_3, $M_r = 61.02\ g\,mol^{-1}$; orthorhombic, space group *Imma*, $a = 8.3915(5)$, $b = 12.5680(8)$, $c = 6.2134(4)$ Å, $V = 655.29(7)$ Å^3, $Z = 16$, $\rho_{calcd} = 2.454\ g\,cm^{-3}$, $\mu = 0.805\ mm^{-1}$, $R1/wR = 1.91\,\%/5.06\,\%$ for all the 558 unique reflections, 3685 total reflections ($R_{int} = 1.78\,\%$) and 43 parameters. X-ray diffraction data were collected at room temperature on a Bruker SMART CCD diffractometer, graphite-monochromatized $Mo_{K\alpha}$ radiation (0.71073 Å). The structure was solved by direct methods and refined with the SHELXL suite of programs. Further details on the crystal structure investigation may be obtained from the Fachinformationszentrum Karlsruhe, 76344 Eggenstein-Leopoldshafen, Germany (fax: (+49) 7247-808-666; e-mail: crysdata@fiz-karlsruhe.de), on quoting the depository number CSD-412621.
[13] T. L. Aselage, D. R. Tallant, *Phys. Rev. B* **1998**, 57, 2675.
[14] EDS was performed on several crystals of the compound by using 8 KV accelerating voltage and 120 s acquisition time and indicated that boron and silicon were present in the amber plate crystals; the ratio of boron to silicon was approximately 2.4:1. Samples were mounted on silver paste to obtain a clear carbon content. Measurements were performed with a JEOL JSM-35C scanning electron microscope equipped with a Noran Vantage Energy Dispersive Spectroscopy (Si:Li) detector and Norvar window suitable for the standardless quantitation of light elements ($Z \geq 4$).
[15] Combustion analysis was carried out by selecting single crystals of the title compound (sample size 2.272 mg) and α-SiB_3 (sample size 3.730 mg) and rinsing them in aqua regia and "piranha" solution (75 vol % conc. H_2SO_4/25 vol % 30 % H_2O_2) to minimize surface carbon contamination. Elemental analysis was performed with a Perkin Elmer series II CHNS/O analyzer 2400.
[16] F. Zürcher, R. Nesper, *Angew. Chem.* **1998**, *110*, 3451; *Angew. Chem. Int. Ed.* **1998**, *37*, 3314.
[17] Band gap measurements were made on a Shimadzu UV-3101PC UV/Vis–NIR solid-state spectrophotometer. Measurements were made in reflectance mode from a $BaSO_4$ standard reference. The spectrum was converted to absorbance by using the Kubelka–Munk equation.
[18] Band-gap measurements for rhombohedral SiB_3 were made with a Nicolet Magna IR 750 FTIR spectrophotometer in reflectance mode. The data was processed with the Kubelka-Munk equation.
[19] C. Wood, D. Emin, *Phys. Rev. B* **1984**, 29, 4582.
[20] Band-structure calculations were performed by using the self-consistent full-potential linearized augmented plane-wave method (LAPW) within density functional theory (DFT) by using the generalized gradient approximation (GGA) for the exchange and correlation potential. Scalar relativistic corrections were added and spin-orbit interaction (SOI) was incorporated by using a second variational procedure. The calculations were performed with the WIEN97 program.
[21] J. B. Casady, R. W. Johnson, *Solid-State Electron.* **1996**, 9–10, 1409.

 © 2003 Wiley-VCH Verlag GmbH & Co. KGaA, Weinheim

Connecting Individual Polymer Chains

Covalent Connection of Two Individual Polymer Chains on a Surface: An Elementary Step towards Molecular Nanoconstructions**

Jörg Barner, Frank Mallwitz, Lijin Shu, A. Dieter Schlüter, and Jürgen P. Rabe**

Nano- and micrometer-sized objects can be manipulated in two and three dimensions by using a scanning force microscope (SFM) and optical tweezers, respectively.[1–4] Reactions

[*] Prof. Dr. A. D. Schlüter, Dr. L. Shu
Institute of Chemistry
Free University Berlin
Takustr. 3, 14195 Berlin (Germany)
Fax: (+49) 30-838-53357
E-mail: adschlue@chemie.fu-berlin.de
Prof. Dr. J. P. Rabe, J. Barner, Dr. F. Mallwitz
Department of Physics
Humboldt University Berlin
10099 Berlin (Germany)
Fax: (+49) 30-2093-7632
E-mail: rabe@physik.hu-berlin.de

[**] Support by SFB448 "Mesoscopically Structured Composites" and the "Fonds der chemischen Industrie" is gratefully acknowledged.

Supporting information for this article is available on the WWW under http://www.angewandte.org or from the author.

 © 2003 Wiley-VCH Verlag GmbH & Co. KGaA, Weinheim DOI: 10.1002/anie.200250059

in arrays of molecules immobilized on a surface have been accomplished in highly oriented monolayers[5] and at a single molecular level under ultrahigh-vacuum low-temperature conditions by using a scanning tunneling microscope (STM).[6] Recently, a chemical reaction between individual small molecules was performed with a STM under ultrahigh-vacuum conditions by using a "move-connect-prove" sequence.[7] If it were transferred to nanosized molecules under ambient conditions, this process could become a new key element for nanoscale science and technology. Dendronized polymers[8] are interesting candidates for molecular nanoconstructions, as they are considered to be nanocylinders with an interior and surface that can be engineered, and by which they may be functionalized. Examples include polymeric light emitters with an aggregation inhibitor,[9] and a synthetic light-harvesting antenna.[10] Herein, we describe the application of a move-connect-prove sequence under ambient conditions to two individual strands of dendronized polymers by using an SFM. The connection is achieved by UV irradiation and tested by challenging its mechanical stability.

Dendronized polymers have been synthesized with diameters of a few nm, lengths of up to several hundred nm, and equipped with 4, 8, or 16 peripheral amine groups at every repeat unit.[2,11] Amines are ideal anchor groups for modification reactions, as they couple preferentially with active esters or acid chlorides. Azides easily decompose thermally or photochemically into nitrenes (and elementary nitrogen), which are highly reactive, short-lived intermediates that undergo various addition and insertion reactions with the formation of covalent bonds.[12] The commercially available azide derivative, **2** (Figure 1) which has a succinidyl active ester group, was attached to the deprotected (positively charged) dendronized polymer **1a**[2] with eight amine groups per repeat unit (average degree of polymerization > 430). An

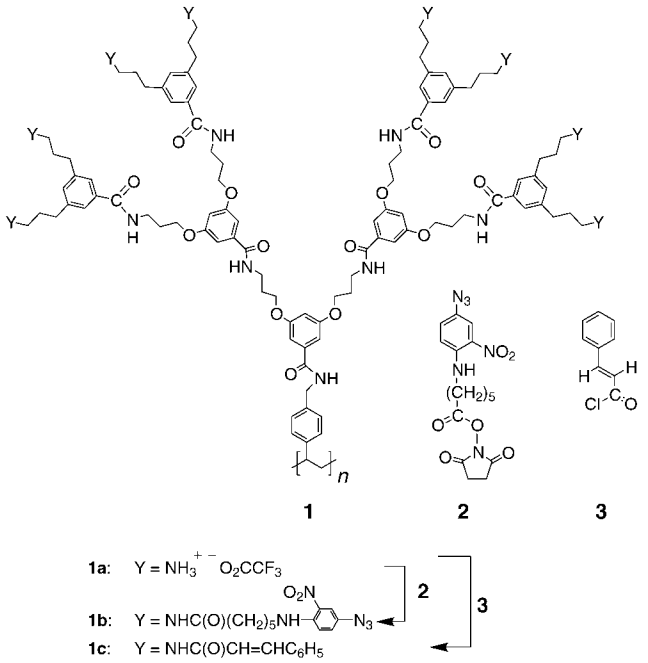


Figure 1. Synthesis of dendrimer derivatives.

orange solution of **2** (8.6 mg, 22 μmol) in DMSO (0.5 mL) was added dropwise in the dark to a clear solution of **1a** (4 mg, 12 μmol of amino groups) in dimethyl sulfoxide (DMSO, 0.5 mL). The resulting suspension was stirred for 20 h at 20 °C and subsequently dialyzed with DMSO for two days (benzoylated dialysis tubing from Sigma), and then freeze dried from DMSO to furnish **1b** (yield: 6.2 mg, 92 %; Figure 1). The complete removal of excess **2** was achieved by prolonged dialysis and proven by thin-layer chromatography. The IR spectrum of **1b** showed the expected azide stretch band at 2120 cm^{-1} and the UV/Vis spectrum exhibited λ_{max} (DMSO) = 476 nm. The coverage of the amine groups of **1b** with **2** was 95 % when determined by a reported procedure.[10] Polymer **1c** was obtained similarly by treating **1a** with the cinnamoyl chloride, **3** (Figure 1). Irradiation of a thin film of **1b** on a KBr plate with a standard Hg lamp led to the almost complete disappearance of the azide stretch band in the IR spectrum within 9 minutes.

For the SFM sample preparation, the procedure described above and a second procedure were applied. In the latter, methanol was used instead of DMSO, as methanol can be removed more easily from the employed highly oriented pyrolytic-graphite (HOPG) substrate, thereby simplifying stable SFM operation. At room temperature triethylamine in methanol (1×10^{-6} mol mL^{-1}) was added to a polymer solution in a molar ratio of 1:1 with respect to the ammonium groups. After one hour, an equimolar solution of **2** ($c = 1 \times 10^{-6}$ mol mL^{-1} methanol) was added to the stirring reaction mixture to furnish **1b**. As the solubility of **1b** in methanol decreases because of the chemical modification of the azide active ester **2**, before precipitation of **1b** the solution was spin coated onto freshly cleaved HOPG at 50 rps to yield incomplete monolayers of individual polymer molecules.

For dragging the molecules across the surface (lateral manipulation) a home-built SFM based on the Multimode head and Nanoscope III controller (Digital Instruments, Santa Barbara, CA, USA) was used. The extended setup allows the movement of the SFM tip in the *xy* plane along a predefined trace with additional control of the normal forces between SFM tip and sample. Up to four channels of data (e.g., height and deflection of the SFM cantilever) can be recorded during the passing of the tip along the trace. This allows the right trace to be sought before dragging the molecule to the desired position. The spatial resolution for addressing a single molecule with this procedure is on the order of 5 nm. For the purpose of manipulation, the SFM can be gently switched from tapping to contact mode at predefined points while the tip is passing along the trace. From these points, the interaction between SFM tip and sample is enhanced, and thus can be used to drag a molecule across the surface.[2]

Figure 2 displays tapping-mode SFM images of **1b** on a graphite substrate. Figure 2a exhibits two individual molecules **1b**, both with their backbone extended essentially parallel to the substrate, thus revealing contour lengths on the order of 400 nm. Figure 2b shows the sample after the two molecules have been moved towards each other by using the procedure described above. After the irradiation of the whole sample in situ (while the SFM is scanning) for 3 minutes with

 © 2003 Wiley-VCH Verlag GmbH & Co. KGaA, Weinheim

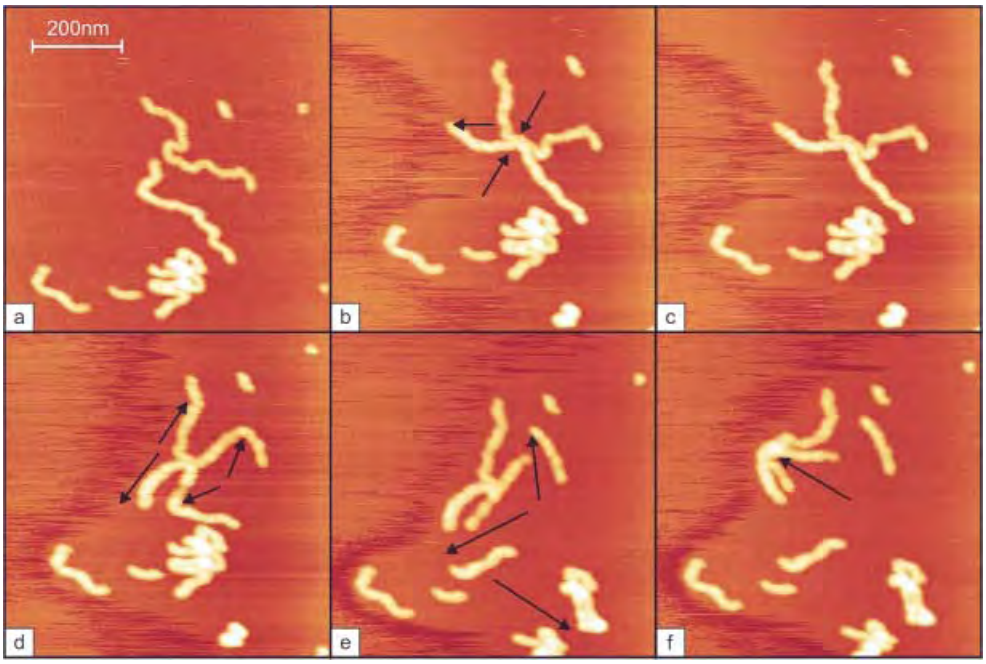


Figure 2. Tapping-mode SFM images of two individual dendronized polymers **1b**, moved towards each other ("move"; a→b), irradiated by UV light ("connect"; b→c), and challenged mechanically ("prove"; d,e,f). The arrows indicate the movement of the SFM tip during manipulation (an animated version of this sequence is provided as a video in the Supporting Information). In addition some smaller molecules and a molecular aggregate can be recognized.

the UV-C light of a high-pressure Hg lamp (Fluotest, Heraeus, $\lambda_{max} = 220$ nm), no change of the image was observed (Figure 2c). To test whether the irradiation caused a stable (covalent) linking of the two adjacent molecules, we challenged the mechanical stability of the junction by pulling on each of the four chain ends with the SFM tip; the junction did not break (Figure 2d). When the molecular chains were moved through the two points of strongest bending, the molecular chains were cut at the position of impact rather than on the newly formed junction (Figure 2e), thus indicating the junction is stronger than the main chain. This can be understood, as the number of covalent bonds in the junction could be more than 100, which estimates a contact length on the order of 20 nm. When the whole molecule was dragged across the surface (Figure 2f) the junction did not break. The experiment was reproduced several times and other topologies, including a full circle, were fabricated. As a control, the same experiment was repeated several times without irradiation, and on each occasion it was easy to pull the molecules apart again. We conclude that there is no covalent connection between the newly formed molecule and the underlying HOPG because the molecule can be manipulated after irradiation. This can be understood because cycloaddition of nitrene to a graphite double layer leads to a separation between the top and the top-1 layer which lowers the dispersion interaction and direct orbital overlap between the two and is therefore energetically unfavorable. Preliminary results show that the connection can also be achieved with the cinnamic ester modified polymer **1c**.

The work presented herein demonstrates that two individual polymer chains on a surface can be manipulated until they attain a predetermined relative position in which they can be covalently connected. This is the first application of a move-connect-prove sequence under ambient conditions and opens possibilities for generating and covalently fixing structurally defined, nanosized functional units of macromolecules. The same sequence could be used to connect unaltered macromolecules if azide terminated commercially available spherical dendrimers instead of dendronized polymers were used as a "glue" between two nano-objects such as nanotubes and DNA, the only condition being that they can be manipulated and imaged with the SFM. For instance carbon nanotubes (CNT) have an increased reactivity arising from the high surface curvature with respect to the inert basal plane of HOPG. It was shown that single-wall CNT can be easily attacked by [2+1] cycloaddition of nitrenes.[13] The method described herein is a means to synthesize single macromolecules with novel homo and hybrid structures (e.g., in the shape of an X, Y, O, or 8), which by conventional synthesis are not accessible.

Received: August 28, 2002
Revised: November 13, 2002 [Z50059]

Keywords: dendrimers · polymers · scanning probe microscopy

[1] H. W. C. Postma, A. Sellmeijer, C. Dekker, *Adv. Mater.* **2000**, *12*, 1299–1302.
[2] L. Shu, A. D. Schlüter, C. Ecker, N. Severin, J. P. Rabe, *Angew. Chem.* **2001**, *113*, 4802–4805; *Angew. Chem. Int. Ed.* **2001**, *40*, 4666–4669.
[3] M. P. MacDonald, L. Paterson, K. Volke-Sepulveda, J. Arlt, W. Sibbet, K. Dholakia, *Science* **2002**, *296*, 1101–1103.

 © 2003 Wiley-VCH Verlag GmbH & Co. KGaA, Weinheim

[4] A. P. H. J. Schenning, P. Jonkheijm, J. Hofkens, S. De Feyter, T. Asavei, M. Cotlet, F. De Schryver, E. W. Meijer, *Chem. Commun.* **2002**, 1264 – 1265.
[5] Y. Okawa, M. Aono, *Nature* **2001**, *409*, 683 – 684.
[6] L. J. Lauhon, W. Ho, *Faraday Discuss.* **2000**, 117, 249 – 255.
[7] S. W. Hla, G. Meyer, K.-H. Rieder, *ChemPhysChem* **2001**, *2*, 361 – 366.
[8] A. D. Schlüter, J. P. Rabe, *Angew. Chem.* **2000**, *112*, 860 – 880; *Angew. Chem. Int. Ed.* **2000**, *39*, 864 – 883.
[9] S. Setayesh, A. C. Grimsdale, T. Weil, V. Enkelmann, K. Müllen, F. Meghdadi, E. J. W. List, G. Leising, *J. Am. Chem. Soc.* **2001**, *123*, 946 – 953.
[10] T. Sato, D.-L. Jiang, T. Aida, *J. Am. Chem. Soc.* **1999**, *121*, 10658 – 10659.
[11] L. Shu, I. Gössl, J. P. Rabe, A. D. Schlüter, *Macromol. Chem. Phys.* **2002**, *203*, 2540 – 2550.
[12] *Azides and Nitrenes—Reactivity and Utility* (Ed.: E. F. V. Scriven), Academic Press, Orlando, **1984**.
[13] M. Holzinger, O. Vostrowsky, A. Hirsch, F. Heinrich, M. Kappes, R. Weiss, F. Jellen, *Angew. Chem.* **2001**, *113*, 4132 – 4136; *Angew. Chem. Int. Ed.* **2001**, *40*, 4002 – 4005.

 © 2003 Wiley-VCH Verlag GmbH & Co. KGaA, Weinheim

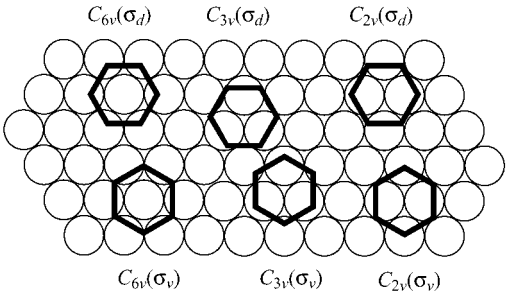


Figure 1. Schematic representation of adsorption sites and orientations of benzene on a planar close packed metal surface.

Arenes on Metal Clusters

The Molecular Structure of $[Os_3Rh_4(\mu_3\text{-}\eta^1\text{:}\eta^1\text{:}\eta^1\text{-}C_6H_5CH_3)(CO)_{13}]$: A Face-Capping Bonding Mode for Arenes in Organometallic Clusters**

*Jasmine Po-Kwan Lau, Zhen-Yang Lin, and Wing-Tak Wong**

The interactions of benzene (arenes) with transition-metal surfaces comprise an important area of research in surface science.[1] The determination of the adsorption geometry of arenes on metal surfaces can give insights into the elementary steps of the dissociation and catalytic reactions of these molecules.[2] A number of adsorption sites for benzene on atomically planar metal surfaces such as the (111) face of face centered cubic (fcc) packing and the (0001) face of hexagonal centered packing (hcp) have been identified,[3] (Figure 1). This type of compound also plays an important role in homogeneous catalytic processes, such as, the hydrogenation of benzene to cyclohexane. An established catalysis precursor for this process under biphasic condition is $[(\eta^6\text{-}C_6H_6)_4Ru_4H_4]Cl_2$.[4]

[*] Prof. W.-T. Wong, J. P.-K. Lau
Department of Chemistry
The University of Hong Kong
Pokfulam Road, Hong Kong (P. R. China)
Fax: (852) 25472933
E-mail: wtwong@hkucc.hku.hk
Dr. Z.-Y. Lin
Department of Chemistry
The University of Science and Technology
Clearwater Bay, Hong Kong (P. R. China)

[**] This work was supported by the Hong Kong Research Grants Council and the University of Hong Kong.

Soluble molecular metal clusters that mimic these bonding modes are known for $C_{6v}(\sigma_d)$, $C_{6v}(\sigma_v)$, $C_{3v}(\sigma_d)$, $C_{2v}(\sigma_d)$, and $C_{2v}(\sigma_v)$ and shown in Figure 1.[5] Transition-metal clusters with face-capping arene ligands which are coordinated to three metal atoms and show a weak trigonal distortion toward a Kekulé structure have been extensively investigated. Lewis, Johnson, and colleagues developed facile synthetic routes to a range of arene clusters with the general formula $[M_3(CO)_9(\mu_3\text{-}\eta^2\text{:}\eta^2\text{:}\eta^2\text{-}C_6H_5R)]$, where R = H, Me, and showed that the trigonal ring distortion is because of an internal mixing of the benzene π system that leads to increased overlap in the C–C bonds, thus eclipsing the metal atoms.[6] Another class of face-capping arene system, $[(CpCo)_3(\mu_3\text{-arene})]$ (Cp = C_5H_5) was developed by Wadepohl et al. from substituted styrene derivatives and Jonas reagent $[CpCo(C_2H_4)_2]$.[7] In all of the cluster compounds with bridging arene ligands that have been structurally characterized, the $\mu_3\text{-}\eta^2\text{:}\eta^2\text{:}\eta^2$ bonding mode is most commonly observed in the solid state. Herein, we report the isolation and structural characterization of an Os–Rh mixed-metal cluster that bears a toluene ligand in an unusual $\mu_3\text{-}\eta^1\text{:}\eta^1\text{:}\eta^1$ face-capping mode.

The treatment of $[Os_3Rh(\mu\text{-}H)_3(CO)_{12}]$ with toluene under reflux in the presence of excess 4-vinylphenol (as a hydride acceptor) leads to the formation of the brown cluster $[Os_3Rh_4(\mu_3\text{-}\eta^1\text{:}\eta^1\text{:}\eta^1\text{-}C_6H_5CH_3)(CO)_{13}]$ (**1**) in 10% yield after chromatographic separation. X-ray analysis[8] of **1** shows that the metal framework can be described as a tricapped tetrahedron in which four Rh atoms define a tetrahedral core with three triangular faces each capped by an $Os(CO)_3$ unit (Figure 2). The most salient structural feature is the remaining Rh_3, which is face-capped by a toluene ligand in the unprecedented $\mu_3\text{-}\eta^1\text{:}\eta^1\text{:}\eta^1$ coordination mode. This coordination geometry of benzene has been observed on many metal surfaces, such as Rh (111),[9] Os (0001),[10] and Ru (0001).[11] A closely related molecular system with $C_{3v}(\sigma_v)$ is also known for the $[\{(C_5Me_5)Ru\}_3(\mu\text{-}H)_3(\mu_3\text{-}\eta^3\text{:}\eta^3\text{-}C_6H_6)]^{2+}$ ion, however, the interaction of the C_6 ring to the triangular metal framework is not symmetrical.[12] The average vertical distance between carbon atoms and the Rh_3 plane in **1** is 2.21(2) Å. This is almost 0.1 Å longer than that observed in the Ru/benzene system (2.11(4) Å) when studied with the LEED technique,[3] although the difference is not statistically significant because of the low accuracy of surface studies. There is a very small crownlike buckling distortion of the C_6 ring of about 0.1 Å in the capped toluene ligand. A similar buckling

 DOI: 10.1002/anie.200250519 © 2003 Wiley-VCH Verlag GmbH & Co. KGaA, Weinheim

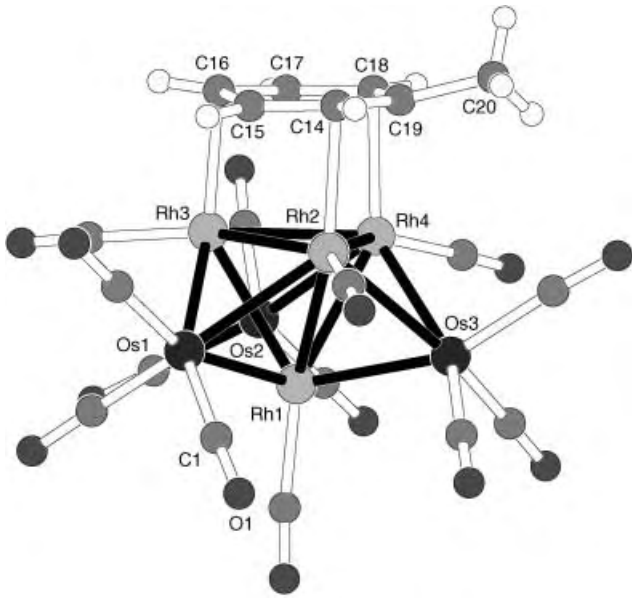


Figure 2. Molecular structure of **1**. Selected interatomic distances [Å] and angles [°]: Os1-Rh1 2.521(2), Os1-Rh2 2.667(2), Os1-Rh3 2.654(2), Os2-Rh1 2.537(2), Os2-Rh3 2.647(2), Os2-Rh4 2.665(2), Os3-Rh1 2.523(2), Os3-Rh2 2.661(2), Os3-Rh4 2.663(2), Rh1-Rh2 2.731(2), Rh1-Rh3 2.720(2), Rh1-Rh4 2.712(2), Rh2-Rh3 2.657(2), Rh2-Rh4 2.661(2), Rh3-Rh4 2.672(2), Rh2-C14 2.25(2), Rh3-C16 2.21(2), Rh4-C18 2.27(2), Rh2···C15 2.55(2), Rh2···C19 2.74(2), Rh3···C15 2.64(2), Rh3···C17 2.60(2), Rh4···C17 2.64(2), Rh4···C19 2.66(2), C14-C15 1.36(3) C14-C19 1.43(3), C15-C16 1.43(3), C16-C17 1.49(3), C17-C18 1.40(3), C18-C19 1.35(3), C19-C20 1.53(3); Rh3-Rh2-Rh4 60.33(6), Rh2-Rh3-Rh4 59.90(6), Rh2-Rh4-Rh3 59.77(6), C15-C14-C19 120(2), C14-C15-C16 122(2), C15-C16-C17 115(1), C16-C17-C18 117(2), C17-C18-C19 123(2) and C14-C19-C18 120(2), C14-C19-C20 117(2), C18-C19-C20 119(2).

distortion is observed for benzene that is adsorbed on the Ru (0001) surface.[3] The methyl substituent appears to tilt away from the Rh_3 plane, presumably a result of steric interactions (Figure 3).

Clearly, this is a reasonably good model to mimic the surface-bound benzene on the atomically flat closed pack

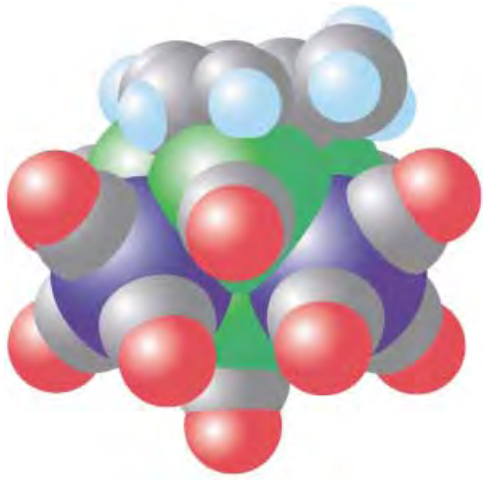


Figure 3. Space-filling diagram of the structure **1** with Os dark blue, Rh green, O red, H light blue, C gray.

structure in the $C_{3v}(\sigma_v)$ local symmetry. Although in most of the previously established face-capping arenes on M_3 triangular systems the μ_3-η^2:η^2:η^2 mode is the observed ground state structure, the arene ligand can undergo a 1,2 ring-hopping motion. The energy barrier for this process is around 50 kJ mol^{-1} in the case of $[Os_3(CO)_8(\eta^2\text{-}CH_2CHPh)(\mu_3\text{-}\eta^2\text{:}\eta^2\text{:}\eta^2\text{-}C_6H_6)]$.[13] ^{1}H NMR spectroscopy studies of **1** indicate that both isomers with μ_3-η^2:η^2:η^2 and μ_3-η^1:η^1:η^1-capping toluene are present in solution in the temperature range of 213 K to 298 K. The ratio of the two isomers at room temperature is approximately 2:3. Attempts to determine the activation parameters for this process have met with little success because of solubility problems.

The metal–metal bonds observed in **1** are relatively short. There are two distinct types of Rh–Rh bonds in **1**. The bond lengths (av. 2.663(3) Å) between the Rh atoms that are capped by toluene ligand are significantly shorter than other Rh–Rh bonds (av. 2.721(3) Å) within the structure. All the Os–Rh bonds are much shorter than those observed in the other Rh–Os mixed-metal clusters that have been reported recently.[14] In terms of the capping principle that was developed by Mingos,[15] one expects that a tricapped tetrahedral cluster should have an electron count of 96. However, the cluster only has an electron count of 92, which is four electrons less than expected. This unusual electron count could arise because many rhodium complexes may conform to the 16-electron rule instead of the 18-electron rule. In fact, a tetrahedral transition-metal cluster that has an electron count of 60 possesses six skeletal bonding pairs. However, a tetrahedral cluster may also adopt an electron-deficient configuration by having only four skeletal bonding pairs instead of six. The electron count of 92 for the tricapped tetrahedron in **1** may be a result of the electron deficiency in the tetrarhodium metal core. This type of metal skeleton with such an electron count is not commonly observed, but an established example is a closely related tetrarhodium cluster, $[Rh_4(\mu_2\text{-}H)_4(cod)_4]$ (cod = cyclooctadiene)[16] which has an electron count of 56. In addition, a density functional theory calculation[17] on our osmium–rhodium cluster gives weaker Rh–Rh bonds than Os–Rh bonds. The average bond index[18] is 0.18 Å for the Rh–Rh bonds and 0.31 Å for the Os–Rh bonds.

Experimental Section

All work was carried out under nitrogen using Schlenk techniques. The solvents used were freshly prepared distilled, dried, and saturated with N_2.

1: $[Os_3Rh(\mu\text{-}H)_3(CO)_{12}]$ (100 mg, 0.10 mmol) and an excess of 4-vinylphenol were stirred in refluxing toluene (40 cm^3) for 2 h. The solution gradually turned from yellow to brown. After filtration the volume of the solution was reduced to 5 cm^3 in vacuo. Purification by TLC on silica using hexane: CH_2Cl_2 (2:1 v/v) as eluent yielded complex **1** as a brown solid in 10% yield (14.4 mg, 0.01 mmol). The major product isolated from the reaction was $[Os_5Rh_2(\mu\text{-}CO)(\eta^6\text{-}C_6H_5CH_3)(CO)_{16}]$[19] (50% yield, 87.3 mg, 0.05 mmol), and two other uncharacterized cluster compounds in very low yields were detected. Elemental analysis calcd (%) for $C_{20}H_8O_{13}Os_3Rh_4$: C 16.70, H 0.56; found: C 16.70, H 0.60; IR(CH_2Cl_2): $\tilde{\nu}$ = 2075w, 2046vs, 2020w, 1996s, 1971 cm^{-1} w. Positive FAB mass spectrometry (calcd *m*/*z*: 1438; found: 1438). ^{1}H NMR spectroscopy study at 298 K showed the

 © 2003 Wiley-VCH Verlag GmbH & Co. KGaA, Weinheim

presence of isomers **1a** (μ_3-η^2:η^2:η^2) and **1b** (μ_3-η^1:η^1:η^1) in a ratio of approximately 2:3. **1a**: ^{1}H NMR (CD_2Cl_2): $\delta = 7.71$ (m, 1H), 7.55 (m, 1H), 7.48 (d, 1H), 7.42 (t, 1H), 7.16 ppm (dd, 1H), 2.12 (s, 3H); **1b**: ^{1}H NMR (CD_2Cl_2): $\delta = 6.99$ (t, 2H), 6.70 (t, 1H), 6.58 (m, 2H), 2.22 ppm (s, 3H). Variable temperature ^{1}H NMR studies in 213–298 K did not reveal any hydride signals in the range of 15 to −30 ppm.

Received: November 11, 2002 [Z50519]

Keywords: arenes · cluster compounds · density functional calculations · osmium · rhodium

[1] a) S. Brait, S. Deabate, S. A. R. Knox, E. Sappa, *J. Cluster Sci.* **2001**, *12*, 139–173; b) D. Braga, P. J. Dyson, F. Grepioni, B. F. G. Johnson, *Chem. Rev.* **1994**, *94*, 1585–1620.
[2] J. A. Polta, P. A. Thiel, *J. Am. Chem. Soc.* **1986**, *108*, 7560–7567.
[3] W. Brawn, G. Held, H.-P. Steinrück, C. Stellwag, D. Menzel, *Surf. Sci.* **2001**, 475, 18–36.
[4] L. Plasseraud, G. Süss-Fink, *J. Organomet. Chem.* **1997**, *539*, 163–170.
[5] a) H. Wadepohl, *Angew. Chem.* **1992**, *104*, 253–268; *Angew. Chem. Int. Ed. Engl.* **1992**, *31*, 247–262; b) B. F. G. Johnson, P. J. Dyson, C. M. Martin, *J. Chem. Soc. Dalton Trans.* **1996**, 2395–2402.
[6] M. A. Gallop, M. P. Gomez-Sal, C. E. Housecroft, B. F. G. Johnson, J. Lewis, S. M. Owen, P. R. Raithby, A. H. Wright, *J. Am. Chem. Soc.* **1992**, *114*, 2502–2509.
[7] H. Wadepohl, K. Büchner, M. Herrmann, H. Pritzkow, *Organometallics* **1991**, *10*, 861–871.
[8] Crystal structure analysis for **1**: $C_{20}H_8O_{13}Os_3Rh_4$, $M_r = 1438.50$, monoclinic, space group $P2_1/n$ (No. 14), $a = 17.518(3)$, $b = 9.557(2)$, $c = 19.120(3)$ Å, $\beta = 116.53(1)$, $V = 2864.0(9)$ Å^3, $Z = 2$, $\rho_{calcd} = 3.336$ g cm^{-3}, $T = 298$ K, $F(000) = 2560.00$, $Mo_{K\alpha}$ radiation ($\lambda = 0.7107$ Å), $\mu(Mo_{K\alpha}) = 155.48$ cm^{-1}, dimensions $0.20 \times 0.20 \times 0.25$ mm. 3812 observed diffraction data [$I > 1.50\sigma(I)$] and $R_{int} = 0.067$. Structure solved by direct methods (SHELXS86) and Fourier difference techniques, refined by full-matrix least-squares analysis on F to $R = 0.056$, $Rw = 0.052$, $\omega = 1/\sigma^2$ (F_o). Non-hydrogen atoms were refined anisotrpically. Hydrogen atoms were included but not refined. All calculations were performed on a Silicon-Graphics Computer using the program package TEXSAN. CCDC-196936 (**1**) contains the supplementary crystallographic data for this paper. These data can be obtained free of charge via www.ccdc.cam.ac.uk/conts/retrieving.html (or from the Cambridge Crystallographic Data Centre, 12 Union Road, Cambridge CB21EZ, UK; fax: (+44) 1223-336-033; or deposit@ccdc.cam.ac.uk).
[9] G. Rosina, G. Rangelov, E. Bertel, H. Saalfeld, F. P. Netzer, *Chem. Phys. Lett.* **1987**, *140*, 200–204.
[10] F. P. Netzer, H. H. Graen, H. Kuhlenbeck, M. Neumann, *Chem. Phys. Lett.* **1987**, *133*, 49–53.
[11] a) C. Stellwag, G. Held, D. Menzel, *Surf. Sci.* **1995**, *325*, L379-L384; b) K. Weiss, S. Gebert, M. Wühn, H. Wadepohl, C. Wöll, *J. Vac. Sci. Technol. A* **1998**, *16*, 1017–1022.
[12] A. Inaguki, Y. Takaya, T. Takemori, H. Suzuki, *J. Am. Chem. Soc.* **1997**, *119*, 625–626.
[13] M. A. Gallop. B. F. G. Johnson, J. Keeler, J. Lewis, S. J. Heyes, C. M. Dobson, *J. Am. Chem. Soc.* **1992**, *114*, 2510–2520.
[14] a) S. Y.-W. Hung, W.-T. Wong, *Chem. Commun.* **1997**, 2099–2100; b) S. Y.-W. Hung, W.-T. Wong, *J. Organomet. Chem.* **1998**, *566*, 237–242; c) W.-T. Wong, *Organometallics* **1999**, *18*, 3474–3481.
[15] D. M. P. Mingos, D. J. Wales, *Introduction to Cluster Chemistry*, Prentice-Hall, New Jersey, **1990**.
[16] M. Kulzick, R. T. Price, E. L. Muetterties, V. W. Day, *Organometallics* **1982**, *1*, 1256–1258.
[17] Density functional calculations at the B3LYP level were performed on the cluster on the basis of the experimentally determined geometry. The basis set used for C, O, and H atoms was 6-31G, while an effective core potential with a LanL2DZ basis set was employed for Rh and Os atoms.
[18] K. B. Wiberg, *Tetrahedron* **1968**, *24*, 1083–1086.
[19] J. P.-K. Lau, W.-T. Wong, *J. Organomet. Chem.* **2002**, *659*, 151–158.

 © 2003 Wiley-VCH Verlag GmbH & Co. KGaA, Weinheim

Inorganic–Organic Hybrid Materials

NCHU-3: A Crystalline Inorganic–Organic Hybrid Molecular Sieve with Extra-Large Cages**

Ching-Yuan Cheng, Shu-Juan Fu, Chia-Jung Yang, Wei-Hung Chen, Kuan-Jiuh Lin, Gene-Hsiang Lee, and Yu Wang*

Since the discovery of aluminophosphate VPI-5,[1] the synthesis of new crystalline large-pore zeolite-analogue materials with diameters of larger than 10 Å has been an important goal because of the diverse applications of these materials as nanoreactors, biosensors, and in nanotechnology.[2–5] Considerable attention has been directed towards the associated inorganic–organic hybrid architectures that, because of the incorporation of organic functional groups within a solid state inorganic framework, promise access to an even wider range of applications, such as altering the expected shape-selective influence in molecular sieves and hydrocarbon transformations.[6–11] To date, however, relatively few examples of well-ordered crystalline solids with both large and hybrid pores are known.[12] Herein, we describe a novel nanoporous organophosphonate that contains both vanadium and gallium centers, $[Ga_2(VO)_3K_2(OH_2)_3(C_2H_4P_2O_6)_4(H_2O)_{13}]$, which we have called NCHU-3 (National Chung-Hsing University-3).

Pale-blue crystals of NCHU-3 were grown from a reaction mixture of KOH, Ga_2O_3, V_2O_5, ethylenediphosphate, and

[*] Prof. K.-J. Lin, C.-Y. Cheng, S.-J. Fu, C.-J. Yang, W.-H. Chen
Department of Chemistry
Nanocenter, National Chung-Hsing University
Taichung 402, Taiwan (Republic of China)
Fax: (+886) 4-22862547
E-mail: kjlin@dragon.nchu.edu.tw
G.-H. Lee, Prof. Y. Wang
Department of Chemistry
National Taiwan University
Taipei 106, Taiwan (Republic of China)

[**] We thank H. S. Sheu at synchrotron radiation research center for technical assistance with PXRD data. This work was supported by the National Science Council of the Republic of China (NSC 90-2113M-005-013) and the Institude of Chemistry, Academia Sinica.

Supporting information for this article is available on the WWW under http://www.angewandte.org or from the author.

 DOI: 10.1002/anie.200250544 © 2003 Wiley-VCH Verlag GmbH & Co. KGaA, Weinheim

water in molar ratios of 1:1:2:6:2220 heated at 200 °C for 72 hrs in a 23 mL teflon-lined stainless steel autoclave. The structure of NCHU-3 was determined by single-crystal X-ray analysis (Figure 1). The orthorhombic structure has an open framework with multidimensional channels. The asymmetric unit of the framework contains one gallium-centred tetrahedron (Ga–O bond lengths: 1.800(8) (×2) and 1.805(5) Å (×2), two crystallographically distinct octahedral oxovanadyl centers ($V_1O_5(OH_2)$: 1.612(2), 1.977(8) (×2), 2.036(8) (×2), and 2.290(17) Å; $V_2O_5(OH_2)$: 1.575(15), 1.961(8) (×4), and 2.45(3) Å; the bond valence sum of vanadium is 4.0 and 4.4, respectively),[13] and two ethylenediphosphate groups. Each phosphorus atom in ethylenediphosphate is tetrahedrally coordinated, that is, the two O_3PC tetrahedron of $[O_3P–CH_2CH_2–PO_3]^{4-}$ share the carbon atoms with the ethylene groups. The secondary building blocks of NCHU-3 are described in terms of 4-, 5-, 6-, and 16-rings, which are combinations of 4, 5, 6, and 16 polyhedrons, respectively. Interestingly, NCHU-3 consists of multidimensional channels system with 6-ring apertures and 16-ring apertures, in which the pore sizes are 5 Å × 7 Å and 5 Å × 14 Å, respectively. These channels intersect at the center of a chinese-vaselike cage consisting of 63 atoms (six 6-rings and two 16-rings, Figure 1c and 1d). The cage measures 11 Å × 13 Å × 14 Å, as measured between oxygen atoms by using the positional coordinates of NCHU-3. Another important feature of the NCHU-3 structure is the hydrophobic -CH_2 moieties covering the walls of the Chinese-vaselike cages. The approximate vase-void volume is 1359 Å^3 per unit cell. Microporous materials are often compared by framework density (FD, number of density of tetrahedral atoms per 1000 Å^3).[14] The smaller the FD value, the larger is the available space in the crystal. The FD generally decreases with increasing numbers of 4-rings. NCHU-3 has eight 4-rings per cage, for which the FD is about 9.3 (tetrahedrally surrounded Ga and P atoms) and 12 (which takes into account the V atoms with octahedral coordination) compared with the very open faujasite (12.7) and cloverite (11.1).[15]

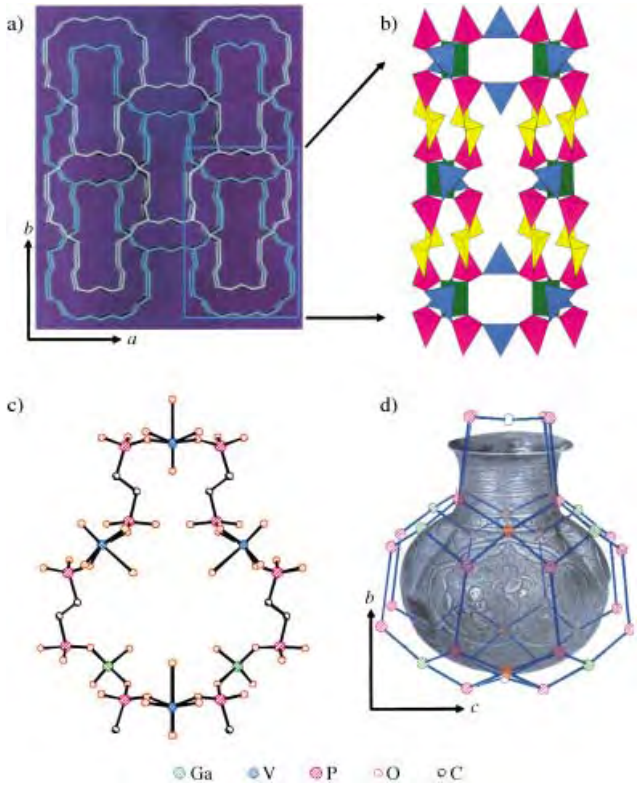


Figure 1. Molecular structure of NCHU-3. a) The framework structure of NCHU-3 view down the *c* axis showing vaselike channels in projection. b) Polyhedral view of a section of vaselike cages. (GaO_4: green tetrahedron; $VO_5(OH_2)$: blue octahedron; PO_3C: red tetrahedron; CH_2P_2: yellow tetrahedron). c) Ball-and-stick representations of the largest cavity constructed from 16-rings excluding tetrahedrally coordinated C atoms. d) Projection of vaselike cages along the *a* axis (C, H, and O atoms are omitted for clarify) showing the additional 4-, 5-, and 6-rings and Chinese vaselike void volume of 1359 Å^3.

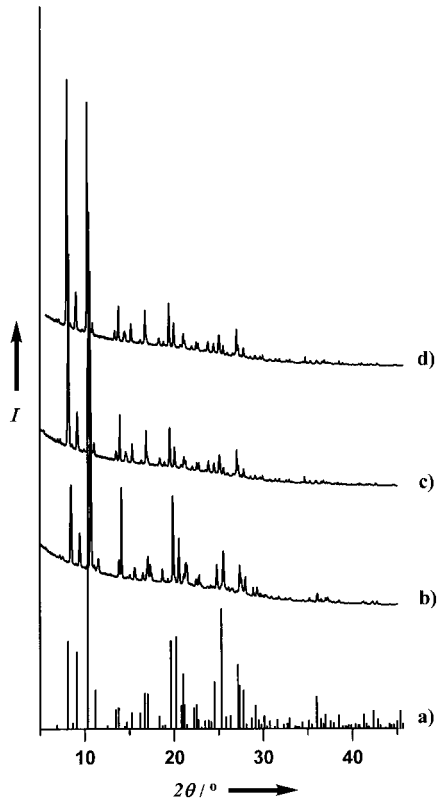


Figure 2. In situ PXRD patterns for NCHU-3 (synchrotron radiation, $\lambda = 1.32633$ Å). The sample was initially heated to 200 °C and then cooled to 40 °C in air. a) Simulated diffraction patterns on the basis of the single-crystal structure. Diffraction data recorded b) at room temperature, c) at 200 °C, and d) at 40 °C. *I* is the X-ray intensity (arbitrary units).

The key feature of NCHU-3 rests on the extra-large hydrophobic cages, which are occupied by free water molecules and highly disordered K^+ ions. Essentially, complete replacement of K^+ by NH_4^+ ions by using saturated NH_4Cl solution was easily accomplished, as confirmed by energy-dispersive X-ray fluorescence analysis. To examine the thermal and structural stability of this open framework, thermogravimetric analysis (TGA) and in situ synchrotron powder X-ray diffraction (PXRD) analysis were carried out. The TGA reveals that the water guest molecules were

 © 2003 Wiley-VCH Verlag GmbH & Co. KGaA, Weinheim

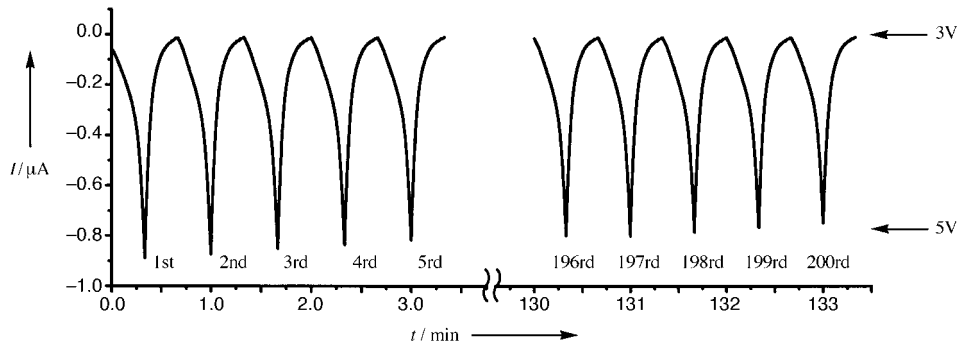


Figure 3. Current versus time plot for cyclic voltage changes in the range 3–5 V for a C/Li·NCHU-3 cell employing a 1 M $LiClO_4$ in an EC-DMC-MF electrolyte mixture ($T = 30\,°C$, scan rate 100 $mV\,s^{-1}$). The cyclability of NCHU-3 by intercalating/de-intercalating lithium ions is shown.

liberated below 200 °C, which corresponds to a weight loss of 14 %. No weight loss was observed in the temperature range of 200–550 °C. The simulated diffraction pattern based on the analysis of a single-crystal X-ray structure (Figure 2a) is in good agreement with the PXRD pattern obtained for NCHU-3 (Figure 2b), which indicates that NCHU-3 is a pure phase. The NCHU-3 sample was initially heated to 200 °C (Figure 2c) and then cooled to 40 °C (Figure 2d), both diffraction patterns show that the positions of the most intense lines remain unchanged relative to the unheated sample of NCHU-3. The good agreement between PXRD patterns demonstrates that the open-framework was retained even after the loss of water molecules. Given the thermal and structural stability of the open framework, the presence of vacant cages in NCHU-3 affords a natural affinity to absorb aliphatic and aromatic molecules reversibly. A TGA study reveals a reversible aniline sorption cycle in the pores of NCHU-3 (see Supporting Information). The framework, which features redox oxovanadyl centers, provides an intercalation host for lithium ions.[16] Some preliminary reversible cycling data are presented in Figure 3. The cyclability of the cell was over 200 cycles between 3 and 5 V, which indicates that lithium ions and electrons can be removed and reinserted into the NCHU-3 host. This result demonstrates that NCHU-3 is scientifically interesting and potentially attractive as a new cathode material for rechargeable lithium batteries.[17–19] Further measurements of capacity are in progress.

In conclusion, we present the synthesis and structure of the first multidimensional, intersecting, large-pore hybrid organo-phosphonate molecular sieve. NCHU-3 is novel not only in the unusual shape of its cages with hydrophobic walls, but also in its framework featuring redox-active oxovanadyl centers. The above results may provide new developments in separation, catalytic, and nanoelectronic applications.

Experimental Section

NCHU-3: A reaction mixture of V_2O_5 (0.0909 g, 0.5 mmole), ethylenediphosphate (0.2850 g, 1.5 mmole), Ga_2O_3(0.0468 g, 0.25 mmole), KOH (0.25 mL, 10 M), and H_2O (10 mL) was sealed in a 23 mL teflon-lined stainless autoclave, heated at 200 °C for 72 h, then cooled to 70 °C at 9 $K\,h^{-1}$. The resulting blue crystals were isolated by filtration, and washed with deionized water. Yield 0.046 g (34 % based on Ga_2O_5), and the synthesis was highly reproducible. Crystallography: The X-ray diffraction low-temperature (120 K) data were collected on a CCD Bruker AXS SMART-1000 diffractometer with monochromated $Mo_{K\alpha}$ ($\lambda = 0.71069$ Å) in the $\omega/2\theta$ scan. The structure was solved with SHELXTL PLUS and refined with SHELXL-93 on F^2 by full-matrix least-squares methods. The highly disordered potassium ions and water molecules could not be completely located in the structure analysis. The induction-coupled plasma-mass spectrometry and energy dispersive X-ray analysis both showed the compound contained K, Ga, V, and P in approximately constant proportions. $Ga_2(VO)_3K_2(OH_2)_3(C_2H_4P_2O_6)_4(H_2O)_{13}$, Crystal size $0.18 \times 0.06 \times 0.06$ mm, Orthorhombic system, space group *Cmcm*, $a = 16.6870(2)$, $b = 14.7395(3)$, $c = 17.5737(3)$ Å, $V = 4322.4(1)$ $Å^3$, $Z = 4$, $2\Theta_{max} = 55°$; $R_1 = 0.101$, $wR_2(F^2) = 0.278$, and GOF = 1.113; residual electron density between −3.6 and 1.81 e $Å^{-3}$. CCDC-195599 contains the supplementary crystallographic data for this paper. These data can be obtained free of charge via www.ccdc.cam.ac.uk/conts/retrieving.html (or from the Cambridge Crystallographic Data Centre, 12 Union Road, Cambridge CB2 1EZ, UK; fax: (+44) 1223-336-033; or deposit@ccdc.cam.ac.uk).

The lithium-ion intercalation of NCHU-3 was prepared according to our previous procedures.[16] The cathode was fabricated by compressing powdered Li·NCHU-3 (85 %), black carbon (10 %) and PTFE (5 %) on an aluminum disk. The pellet was then dried at 120 °C in air. The electrolyte was prepared by dissolving $LiClO_4$ in a mixture of ethylene carbonate (EC), dimethyl carbonate (DMC), and methyl formate (MF) (volume ratio 50:45:5) to give a 1 M solution. Some properties of this electrolyte were reported.[19]

Received: November 13, 2002 [Z50544]

Keywords: gallium · hydrothermal synthesis · intercalations · microporous materials · vanadium

[1] M. E. Davis, C. Saldarriaga, C. Montes, J. Graces, C. Crowder, *Nature* **1988**, *331*, 698–699.
[2] M. E. Davis, *Chem. Eur. J.* **1997**, *3*, 1745–1750.
[3] R. I. Walton, F. Millange, T. Loiseau, D. O'Hare, G. Ferey, *Angew. Chem.* **2000**, *112*, 4726–4729; *Angew. Chem. Int. Ed.* **2000**, *39*, 4552–4555.
[4] X. Bu, P. Feng, G. D. Stucky, *Science* **1997**, *278*, 2080–2085.
[5] H. Li, A. Laine, M. O'Keeffe, O. M. Yaghi, *Science* **1999**, *283*, 1145–1147.
[6] T. Asefa, M. J. MacLachian, N. Coombs, G. A. Ozin, *Nature* **1999**, *402*, 867–871.
[7] E. K. Brechin, R. A. Coxall, A. Parkin, S. Parsons, P. A. Tasker, R. E. P. Winpenny, *Angew. Chem.* **2001**, *113*, 2772–2775; *Angew. Chem. Int. Ed.* **2001**, *40*, 2700–2703.
[8] D. M. Poojary, B. Zhang, A. Clearfield, *J. Am. Chem. Soc.* **1997**, *119*, 12550–12559.

 © 2003 Wiley-VCH Verlag GmbH & Co. KGaA, Weinheim

[9] V. Soghomonian, Q. Chen, R. C. Haushalter, J. Zubieta, *Angew. Chem.* **1995**, *107*, 229 – 231; *Angew. Chem. Int. Ed. Engl.* **1995**, *34*, 223 – 226.
[10] R. P. Hammond, J. A. Zubieta, *J. Solid State Chem.* **1999**, *144*, 442 – 448.
[11] M. I. Khan, L. M. Meyer, R. C. Haushalter, A. L. Schweitzer, J. Zubieta, J. L. Dye, *Chem. Mater.* **1996**, *8*, 43 – 53.
[12] a) S. Guan, S. Inagaki, T. Ohsuna, O. Terasaki, *J. Am. Chem. Soc.* **2000**, *122*, 5660 – 5661; b) A. Stein, B. J. Melde, R. C. Schroden, *Adv. Mater.* **2000**, *12*, 1403 – 1419.
[13] At temperatures above 100 K, the susceptibility data obeys the Curie–Weiss law, and the magnetic moment ($\mu_{eff} = 3.82$ BM) is close to the expected spin-only value for two independent vanadium(IV) centers per molecule. (see Supporting Information)
[14] G. O. Brunner, W. M. Meier, *Nature* **1989**, *337*, 146 – 147.
[15] a) M. Estermann, L. B. McCusker, C. Baerlocher, A. Merrouche, H. Kessier, *Nature* **1991**, *352*, 320 – 323; b) W. M. Meier, *New Dev. Zeolite Sci. Technol. Proc. Int. Zeolite Conf.* **1986**, *7*, 13 – 22.
[16] L. W. Huang, C. J. Yang, K. J. Lin, *Chem. Eur. J.* **2002**, *8*, 394 – 400.
[17] J.-M. Tarascon, M. Armand, *Nature* **2002**, *414*, 359 – 367.
[18] Z. Gadjourova, Y. G. Andreev, D. P. Tunstall, P. G. Bruce, *Nature* **2001**, *412*, 520 – 523.
[19] a) A. R. Armstrong, P. G. Bruce, *Nature* **1996**, *381*, 499 – 500; b) S. R. P. Prabaharan, M. S. Michael, S. Radhakrishna, C. Julien, *J. Mater. Chem.* **1997**, *7*, 1791 – 1796.

 © 2003 Wiley-VCH Verlag GmbH & Co. KGaA, Weinheim

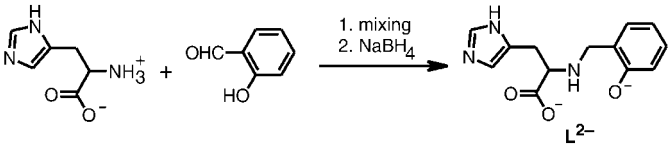
Self-Assembled Cu-Based Capsule

Synthesis of a Self-Assembled Molecular Capsule that Traps Pyridine Molecules by a Combination of Hydrogen Bonding and Copper(II) Coordination**

Md. Akhtarul Alam, Munirathinam Nethaji, and Manabendra Ray**

Molecule and molecular assemblies with cavities of different size and shape to encapsulate guest molecules have been synthesized in view of their potential use as selective hosts for anion sensing, catalysis, selective recognition, and separation of guest molecules.[1] Rebek, Jr. and co-workers recently demonstrated that the binding of a reagent inside a capsular cavity boosts the rate of a Diels–Alder reaction.[2] The self-assembly of relatively small molecules, through hydrogen bonding, or metal–ligand interactions, proved to be very useful in forming large capsular cavities.[1] While several capsular cavities have been synthesized by using organic frameworks (e.g. resorcinarene, calixarene),[1] coordination complexes with a redox stable metal center,[1] and a few with a redox active metal center,[3] there is no report of a capsular cavity with the redox-active metal center having an available binding site inside the capsule.[4] The synthesis of a capsular cavity with an available coordination site at redox active metal centers inside the pocket can, in principle, facilitate the study of the reactivity of the bound guest molecule inside a cavity. In our effort to synthesize a capsular cavity with a redox center, we have synthesized a self-assembled capsule of an octameric Cu^{II} coordination complex by using an easy to synthesize ligand (Scheme 1). This capsule has four guest pyridine molecules trapped inside the cavity (Figure 1), in which two of the pyridine molecules are held with a combination of hydrogen bonds and Cu^{II} coordination.

The octameric Cu^{II} complex (Figure 1) was synthesized from the tetradentate deprotonated ligand (L^{2-}, Scheme 1) and the Cu^{II} salt, $Cu(ClO_4)_2 \cdot 6H_2O$. Because of the presence of an amine hydrogen atom, an imidazole N–H group (a H-bond donor), and carboxylate oxygen atoms (a H-bond acceptor) in



Scheme 1. Synthesis of the tetradentate ligand, L^{2-}.

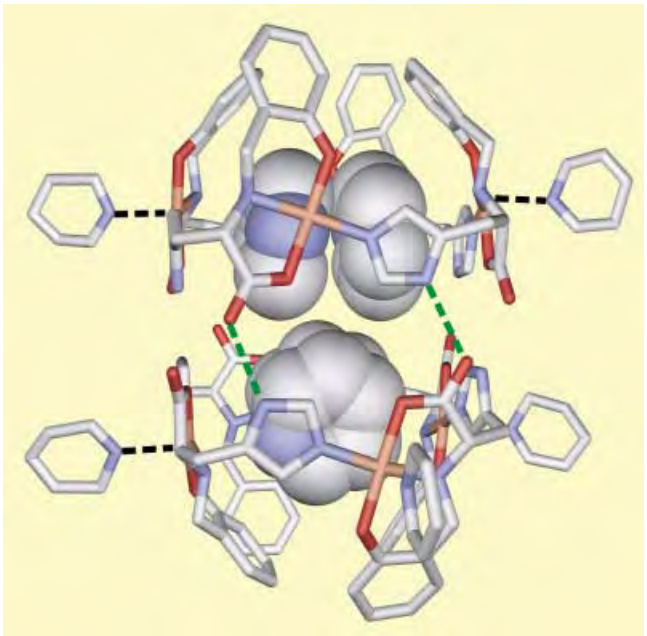


Figure 1. Molecular structure of **1**. Solvent molecules are omitted for clarity.

[*] Dr. M. Nethaji
Department of Inorganic and Physical Chemistry
Indian Institute of Science, Bangalore-560012 (India)
Fax: (+91) 80 23600683
E-mail: mnetaji@ipc.iisc.ernet.in
Dr. M. Ray, M. A. Alam
Department of Chemistry
Indian Institute of Technology Guwahati (India)
Fax: (+91) 361-2690762
E-mail: manabray@iitg.ernet.in

[**] M.R. thanks Prof. R. N. Mukherjee, IIT Kanpur, Prof. T. N. Guru Row, IISC Bangalore, and CDRI Lucknow, India for providing various instrumental facilities. Financial support from the Council of Scientific and Industrial Research, New Delhi (Grant No. 01/(1669)/00/EMR-II) for M.R. is gratefully acknowledged.

Supporting information for this article is available on the WWW under http://www.angewandte.org or from the author.

 © 2003 Wiley-VCH Verlag GmbH & Co. KGaA, Weinheim DOI: 10.1002/anie.200250591

the ligand, we expected an interligand hydrogen-bonding network to aid in the formation of cages. Crystallization of the complex from pyridine and diethyl ether afforded deep-green crystals of $[Cu_8L_8Py_{10}]\cdot Py\cdot 3\,MeOH\cdot(C_2H_5)_2O$ (**1**; Py = pyridine). The complex **1** was crystallized in the space group of *P*1 (No. 1) with two slightly different cup-shaped tetrameric units in the unit cell (**1a** and **1b**).[5] The lattice diagram shows that **1a** and **1b** are on top of each other, thus forming a capsule bound through eight hydrogen-bonding interactions between the imidazole NH groups of one tetramer and nonbonded carboxylate-oxygen atoms of the other tetramer (Figure 1).[6]

The structure of **1a** (Figure 2) is a cyclic tetramer with an imidazole "arm" from one monomeric unit coordinated to the next monomeric unit to form a cycle. The coordination geometry around the Cu^{II} center is square pyramidal with an N_3O_2-donor environment. The four phenolate rings are organized in a manner that effectively closes one side of the square, thus making a cup shaped bottom. Two pyridine molecules are trapped inside **1a** side by side, with each N atom of the pyridine molecule oriented towards the amine N atom of the ligand. The N(trapped pyridine)–N(amine) separations (N5–N3a 2.990 Å, N6–N3c 3.025 Å) are within the range of 2.68–3.09 Å observed for N···HN hydrogen bonds.[7] The space-filling model demonstrates that the two side-by-side pyridine molecules fill the cavity perfectly (Figure 2b).

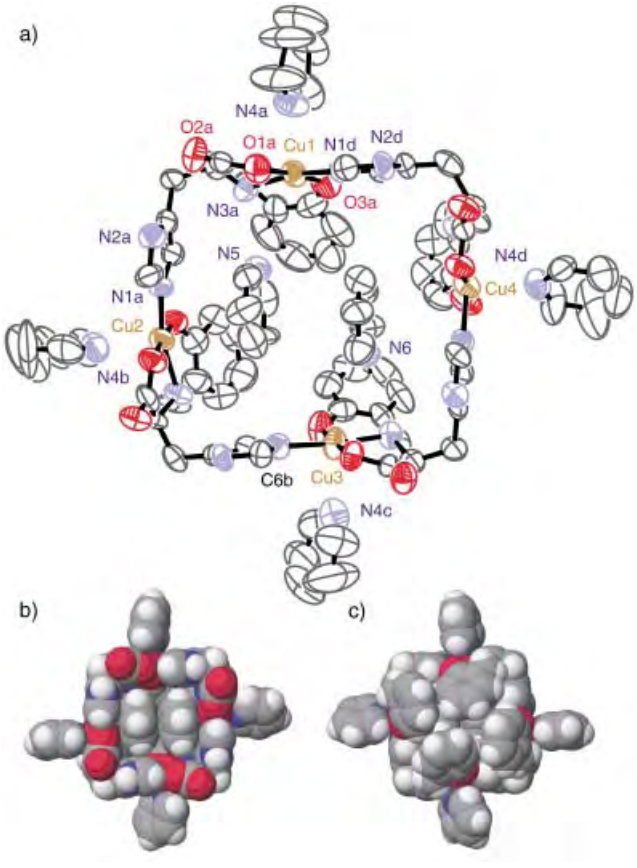


Figure 2. a) One tetrameric copper unit (**1a**, $[Cu_4L_4Py_6]$ ORTEP diagram, thermal ellipsoids set to 50% probability). b) Space-filling model of **1a** top view and c) bottom view.

The cyclic tetramer **1b**, is similar to **1a** (Figure 3), however, two sides of the cup bend inwardly. The trapped pyridine molecules of **1b** are coordinated to the Cu^{II} center instead of being H-bonded to the amine groups (Figure 4). This coordination of the pyridine molecule from inside the

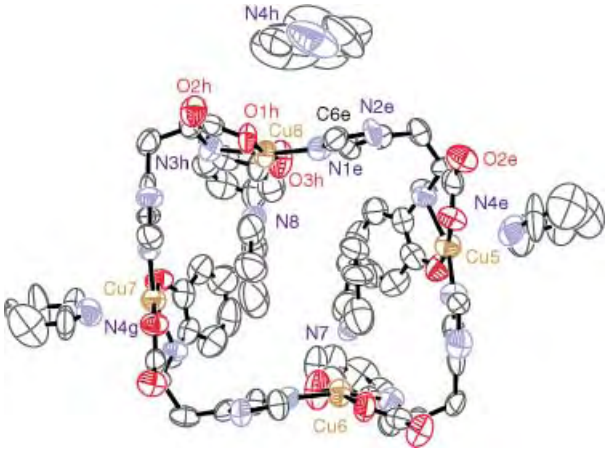


Figure 3. Tetrameric copper unit (**1b**, $[Cu_4L_4Py_4]Py$, ORTEP diagram, thermal ellipsoids set to 50% probability).

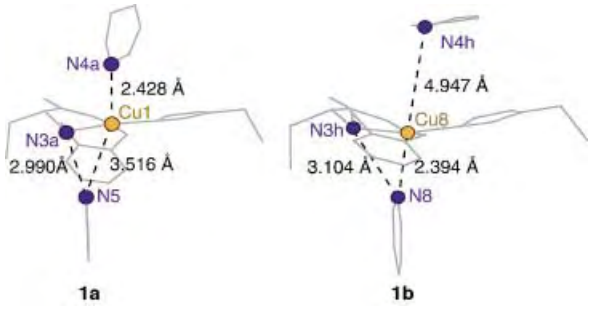


Figure 4. Part of the Cu_4L_4 unit of **1a** and **1b** showing the change in bonding interactions between trapped pyridine molecules, amine N atoms, Cu^{II} centers, and external pyridine molecules.

cavity to the Cu^{II} center results in the deviation of the Cu8 and Cu6 atoms from the plane described by O1, N3, O3, N1 towards the trapped pyridine (shift of 0.194 and 0.203 Å for Cu8 and Cu6, respectively). Consequently, there is no coordination of the external pyridine molecules to the Cu8 and Cu6 atoms, as square-pyramidal geometry is preferred for Cu^{II} complexes over octahedral geometry because of Jahn–Teller distortions. Thus, the coordination sites at the copper centers are accessible from inside the cyclic tetramer.

The two halves of the capsule exhibit contrasting binding with guest molecules. In **1a**, the Cu1 and Cu3 atoms are each coordinated by an external pyridine molecule, but not by the trapped pyridine molecules. On the other hand, in **1b** the N atom of the pyridine molecule (N8) is coordinated to Cu8 (similarly N7 to Cu6). The N8–N3h(amine) separation of 3.104 Å in **1b** is closer to N···HN hydrogen bonding range of 2.68–3.09 Å (Figure 4).[7] Thus, the presence of a N–H close to the Cu^{II} center allow trapped pyridine molecules in **1b** to bind using both metal–ligand interactions and hydrogen bonding,

 © 2003 Wiley-VCH Verlag GmbH & Co. KGaA, Weinheim

simultaneously. This factor makes the trapped pyridine molecules less labile compared to the external pyridine molecules as observed in the solution studies (see below). We are not aware of this type of binding in any other reported capsular cavity.

The Cu–N(external pyridine) distances in molecules **1a** and **1b** (2.4–2.5 Å, see Supporting Information) are considerably longer than Cu–N(apical pyridine) bond length of 2.17 Å in [Cu(Cyclops)Py] ClO_4[8] (Cyclops = difluoro-3,3′-(trimethylenedinitrilo)bis(2-butanoneoximato)borate) and 2.12, 2.13 Å in $Cu_2(OAc)_4Py_2$,[9] but within the range of 2.6–2.8 Å for apical Cu–N[10] bond lengths. This makes the externally bound pyridine molecules particularly labile.

The crystals desolvate rapidly and loose crystallinity on isolation. The elemental analysis matches with the formula $[Cu_8L_8Py_4(H_2O)_8]$. Thermogravimetric analysis (TGA) exhibits a curve that corresponds to a weight loss of 5.3 % in the 30–110 °C range and a further 11.4 % loss in the 180–230 °C temperature range, which corresponds to the removal of eight water and four pyridine molecules (expected total of 15.1 %). We believe that these pyridine molecules are those that were trapped inside the cavity. The room temperature magnetic moment is less than that expected for a $S = 1/2$ system, which indicates the possible presence of antiferromagnetic coupling between the Cu^{II} centers.

The electrospray ionization mass spectra of **1** in MeOH shows the presence of a Cu_4L_4 unit, but no peak was observed corresponding to the pyridine adduct. This is not surprising as the hydrogen-bonding network holding the two halves of the capsule open up in a protic solvent such as MeOH, and the trapped pyridine molecules axially coordinated to the kinetically labile Cu^{II} center are replaced by solvent molecules. Thus, the Cu_4L_4 units are stable in MeOH. The EPR spectrum of **1** in MeOH at 77 K is typical for a distorted square pyramidal geometry around a Cu^{II} center.[11]

In conclusion, we have synthesized a new self-assembled capsule by using an easy to synthesize ligand, and a Cu^{II} salt. The capsule has enough space inside to accommodate four pyridine molecules. The capsule has both H-bonds and kinetically labile Cu^{II} centers which are available for binding from inside the cavity. Thus, we have observed a novel guest binding inside the cavity that uses both hydrogen bonds and metal coordination at the same time.

Experimental Section

Elemental analysis calcd (%) for **1** $Cu_8(C_{13}H_{13}N_3O_3)_8 \cdot (C_5H_5N)_4 \cdot 8H_2O$: C 48.94, H 4.64, N 12.88; found: C 48.68, H 4.51, N 12.92. IR (KBr, $\tilde{\nu}$): 1615(sh), 1596(s) cm^{-1} $\tilde{\nu}(COO)_{asym}$; 1388(s) cm^{-1} $\tilde{\nu}(COO)_{sym}$. Λ_M: (MeOH) 2 $S\,cm^{-2}\,mol^{-1}$. ESI-MS(+) in MeOH for $\{[Cu_4(L)_4]+H\}^+$, m/z calculated 1291.1, found 1290.8; UV/Vis: λ_{max} [nm] (ε [$M^{-1}cm^{-1}$])/Cu: in pyridine:, 416 (520), 668 (170); in MeOH: 273 (5700), 382 (920), 686 (150). EPR: powder; 300 K 2.116 (isotropic), 77 K, 2.118 (isotropic); MeOH, 77 K, $g_{\|} = 2.253$, $g_{\perp} = 2.060$, $A_{\|} = 175$ G. μ_{eff} (powder, 298 K); 1.63 μ_B/Cu.

Received: November 20, 2002 [Z50591]

Keywords: amino acids · cavitand · copper · hydrogen bonds · self-assembly

[1] Selected review articles on supramolecular cages and capsules; a) P. J. Stang, B. Olenyuk, *Acc. Chem. Res.* **1997**, *30*, 502; b) J. Rebek, Jr., *Acc. Chem. Res.* **1999**, *32*, 278; c) A. Jasat, J. C. Sherman, *Chem. Rev.* **1999**, *99*, 931; d) S. R. Seidel, P. J. Stang, *Acc. Chem. Res.* **2002**, *35*, 972; e) F. Hof, S. L. Craig, C. Nuckolls, J. Rebek, Jr., *Angew. Chem.* **2002**, *114*, 1556; *Angew. Chem. Int. Ed.* **2002**, *41*, 1489; f) M. Fujita, *Chem. Soc. Rev.* **1998**, *27*, 417; g) M. Fujita, K. Umemoto, M. Yoshizawa, N. Fujita, T. Kusukawa, K. Biradha, *Chem. Commun.* **2001**, 509.

[2] a) J. Kang, G. Hilmersson, J. Santamaria, J. Rebek, Jr., *J. Am. Chem. Soc.* **1998**, *120*, 3650; b) J. Kang, J. Santamaria, G. Hilmersson, J. Rebek, Jr., *J. Am. Chem. Soc.* **1998**, *120*, 7389.

[3] a) O. D. Fox, N. K. Dalley, R. G. Harrison, *J. Am. Chem. Soc.* **1998**, *120*, 7111; b) O. D. Fox, N. K. Dalley, R. G. Harrison, *Inorg. Chem.* **1999**, *38*, 5860; c) O. D. Fox, N. K. Dalley, R. G. Harrison, *Inorg. Chem.* **2000**, *39*, 620; d) O. D. Fox, J. F. Y. Leung, J. M. Hunter, N. K. Dalley, R. G. Harrison, *Inorg. Chem.* **2000**, *39*, 783.

[4] There are few macrocyclic coordination complexes with available metal coordination sites inside the macrocycle. Cu^{II}; A. W. Maverick, F. E. Klavetter, *Inorg. Chem.* **1984**, *23*, 4129. Co^{II}; A. W. Schwabacher, J. Lee, H. Lei, *J. Am. Chem. Soc.* **1992**, *114*, 7597. With redox inactive Zn^{II}, review; "Templating, Self-assembly, and Self-organization": M. Fujita in *Comprehensive Supramolecular Chemistry, Vol. 9* (Eds.: J.-P. Sauvage, M. W. Hosseini), Pergamon, Oxford, **1996**, chap. 7.

[5] The crystal was mounted with mother liquor inside the capillary for data collection. Crystal structure analysis of **1**: $C_{166}H_{181}Cu_8N_{35}O_{28}$, $M_r = 3622.8$, deep-green crystal $0.3 \times 0.3 \times 0.2$ mm^3, triclinic $P1$ (No. 1), $a = 16.845(4)$, $b = 18.268(4)$, $c = 20.167(4)$ Å; $\alpha = 92.507(4)$, $\beta = 112.207(4)$, $\gamma = 105.636(4)°$; $V = 5459(2)$ $Å^3$, $Z = 1$, $\rho_{calcd} = 1.102$ $Mg\,m^{-3}$, $Mo_{K\alpha}$ radiation , $\lambda = 0.71073$ Å, measured reflections 60205, unique reflections 44425, temperature 293(2) K. Data were collected on a Bruker Smart CCD Area Detector system with graphite monochromator. The structure was solved by direct methods and refined on F^2 by full-matrix-block least squares (G. M. Sheldrick, SHELXL-97, University of Göttingen, Göttingen (Germany), **1997**). In refinement, data/restraints/parameters are 44425/3/2046. The final $R1 = 0.0868$, $wR2 = 0.2164$ ($I > 2\sigma(I)$); $R1 = 0.2725$, $wR2 = 0.2890$ (all data), GOF on $F^2 = 0.730$. CCDC-197602 contains the supplementary crystallographic data for this paper. These data can be obtained free of charge via www.ccdc.cam.ac.uk/conts/retrieving.html (or from the Cambridge Crystallographic Data Centre, 12 Union Road, Cambridge CB2 1EZ, UK; fax: (+44) 1223-336-033; or deposit@ccdc.cam.ac.uk).

[6] The (imidazole) N-H···O(carboxylate) separations in **1** are between 2.69 and 2.78 Å. Reported range 2.69–2.98 Å; a) S. M. Couchman, J. C. Jeffery, M. D. Ward, *Polyhedron* **1999**, *18*, 2633; b) K. Sakai, K. Matsumoto, *J. Am. Chem. Soc.* **1989**, *111*, 3074.

[7] a) M. B. Ferrari, G. G. Fava, M. Lanfranchi, C. Pelizzi, P. Tarasconi, *J. Chem. Soc. Dalton Trans.* **1991**, 1951; b) R. Anulewicz, I. Wawer, T. M. Krygowski, F. Männle, H. Limbach, *J. Am. Chem. Soc.* **1997**, *119*, 12223.

[8] O. P. Anderson, A. B. Packard, *Inorg. Chem.* **1980**, *19*, 2123.

[9] G. A. Barclay, C. H. L. Kennard, *J. Chem. Soc.* **1961**, 5244.

[10] "Tables of Interatomic Distances and Configuration in Molecules and Ions," *Chem. Soc. Special Publ.* No.11.

[11] U. Sakaguchi, A. W. Addison, *J. Chem. Soc. Dalton Trans.* **1979**, 600.

 © 2003 Wiley-VCH Verlag GmbH & Co. KGaA, Weinheim

Tunable Cavity of Titania Spheres

Templated Synthesis of Inorganic Hollow Spheres with a Tunable Cavity Size onto Core–Shell Gel Particles**

Zhenzhong Yang, Zhongwei Niu, Yunfeng Lu,* Zhibing Hu, and Charles C. Han*

Inorganic coated polymer (core–shell) capsules and hollow spheres have increasingly attracted interest because of their potential applications in catalysis, controlled delivery, artificial cells, light fillers, low dielectric constant materials, acoustic insulation, and photonic crystals.[1] These particles have been synthesized by using monodisperse particles and their arrays as templates. There are two main approaches: the first is to form capsules by the controlled reaction of inorganic materials with polymer particles;[2] the second is to coat nanoparticles onto polymer particles by deposition. This is usually combined with a layer-by-layer (LBL) technique to obtain multilayered capsules.[3] The multilayer can be composed of a variety of materials, such as polymers, and inorganic materials.[4] The layer thickness is controlled either through the concentration of the coating materials or through the LBL cycling time. However, obtaining the desired layer thickness by this process is time consuming.

Titania/polymer is one of the model systems for the study of encapsulation and hollow sphere preparation. Although coating onto polymer particles by a controlled sol–gel process is simple, the coated layer is heterogeneous with coagulation.[5] Hollow titania shells can be formed by spray drying the exfoliated titanate/nanosheet suspension followed by heating,[6] but the size distribution of the hollow spheres is broad. Furthermore, the titania shell is very thin, about 1–2 % of the hollow sphere diameter, thus resulting in fragile spheres. Alternatively, LBL adsorption of polyelectrolytes and nanoparticles around individual polymer particles has been developed in the preparation of monodisperse titania-coated-polymer capsules and hollow spheres. The shell thickness is controlled through the cycling time.[7] Xia and coworkers have reported a preferential particle surface coating by a sol–gel process of titania onto a polymer particles array confined between two substrates.[8] In this reaction, the experimental conditions must be strictly adhered to.

All previous experiments that relate to the synthesis of capsules have focused on two geometrical parameters: shell thickness; and cavity size, because these factors determine the mechanical and adsorption properties of the spheres. Hollow spheres with a tunable cavity size can be very useful, not only in practical application but also in the study of physical phenomena, such as optical resonance in a cavity. Until now, to our knowledge, all the methods used to produce hollow spheres have been based on the outward growth of inorganic materials from the surface of the sphere. Therefore, the core size and the cavity size of the hollow spheres were not tunable. It is difficult to create a smaller cavity for a given polymer particle template because these template particles are rigid and cannot be diffused inwardly by a precursor.

Herein, we describe a new approach to generate inorganic coated polymer capsules and hollow spheres with tunable interior-cavity sizes. The key is to use core–shell gel particles as templates that allow an inward diffusion and growth of the precursor inorganic materials inside the gel particle. The hollow spheres can have either a smooth or a porous surface, depending on whether an electric field is applied. The desired cavity size of the hollow spheres and the thickness of the inorganic shell are determined only by a one step sol–gel process.

The core–shell gel template particles were synthesized by an inward sulfonation of polystyrene particles with concentrated sulfuric acid. Sulfuric acid and sulfone groups were simultaneously derived in the gel shell, which was confirmed by differential scanning calorimetry (DSC) and FTIR.[9] The monodispersity of the core–shell gel particles was ensured by synchronous sulfonation. At maximum conversion, the polystyrene core disappeared. This method used for the preparation of core–shell gel particles is simple, and therefore advantageous over traditional emulsion polymerization methods.

It was reported that titania forms preferentially in sulfonated polystyrene-gel shells containing protons.[10] The titania–gel S2 capsules became larger (284 nm in diameter) than the polystyrene particle (275 nm in diameter). After the polystyrene cores were dissolved, the hollow spheres (Figure 1 a) were the same size as the capsules. The thickness of the gel–titania was uniform, about 45 nm, and the cavity diameter was 194 nm. After the capsules were calcined at 450 °C for 2 h, the diameter of the cavity was not affected. However, the shell thickness was reduced to about 18 nm (Figure 1 b and 1 c). The shell also became coarser as the anatase phase was formed during calcination of the amorphous titania, as verified by wide-angle X-ray diffraction (WAXD). The hollow spheres are fragile and easily fragmentized into bowllike pieces (Figure 1 c). When the sample S4 is used as a template, the inorganic shells of the hollow spheres are thicker and the cavities are smaller than those prepared by using the S2 gel as the template. These S4-prepared spheres are more mechanically stable than the corresponding S2-prepared spheres with a well-retained spherical shape (Figure 1 d). The titania–S6 composite particles have a larger diameter of about 424 nm (Figure 1 e). Solid titania spheres

[*] Prof. Dr. Z. Yang, Dr. Z. Niu, Prof. Dr. C. C. Han
State Key Laboratory of Polymer Physics and Chemistry, Joint Laboratory of Polymer Science and Materials, Center for Molecular Science, Institute of Chemistry, The Chinese Academy of Sciences, Beijing 100080 (China)
Fax: (+86) 10-62559373
E-mail: yangzz@infoc3.icas.ac.cn
Dr. Y. Lu
Department of Chemical Engineering, Tulane University
New Orleans, Louisiana 70118–5674 (USA)
E-mail: ylu@tulane.edu
Dr. Z. Hu
Departments of Physics, Chemistry and Materials Science
University of North Texas, Denton, TX 76203 (USA)

[**] This work was supported by National Natural Science Foundation of China under grant No. 90206025 and 20128004.

 DOI: 10.1002/anie.200250443 © 2003 Wiley-VCH Verlag GmbH & Co. KGaA, Weinheim

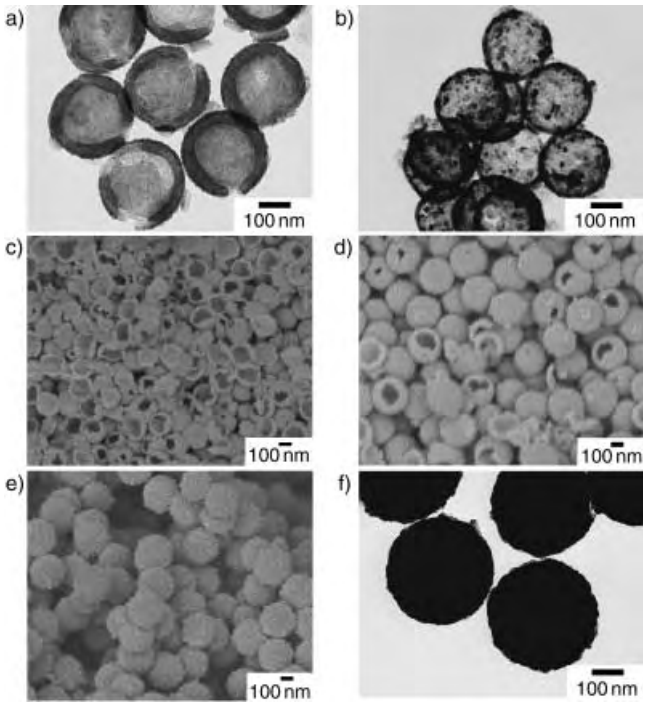


Figure 1. Morphologies of the representative titania coated polystyrene capsules and the structured titania spheres. a) Transmission electron microscopy (TEM) image of hollow titania spheres prepared after the dissolution of the polystyrene cores from the titania/S2 capsules. b) TEM image and c) Scanning electron microscopy (SEM) image of the hollow titania spheres after calcination of the polystyrene cores from titania/S4 capsules at 450 °C for 2 h. d) SEM image of the hollow titania spheres after the calcination of polystyrene cores from titania/S4 capsules at 450 °C for 2 h. e) SEM image and f) TEM image of the titania spheres prepared after the titania/S6 composite spheres were calcined at 450 °C for 2 h.

(i.e., without a cavity) were prepared after calcination (Figure 1 f). The thickness of the titania shell and the core (cavity) size of the capsules were controlled in the whole particle radius range, which is consistent with the TGA results that show an increase in the titania/polymer weight ratio. This series of experiments demonstrate that by varying the sulfonation time, we can obtain monodisperse core–shell gel particles with tunable gel thickness and controllable core size.

We now focus on the surface morphology of the hollow spheres. When the capsules were prepared by a sol–gel process in a direct electric field of $1 \times 10^4\ V\,m^{-1}$, the capsules with pillared surfaces were obtained as shown in Figure 2 a. This porous surface morphology differs from the smooth surface prepared without an electric field as shown in Figure 1. After removing the polystyrene core by calcination at 450 °C for 2 h, the pillared surface was retained (Figure 2 b). The mesopores, with sizes ranging from 10 to 20 nm on the pillared surface of the capsules, appear interconnected before and after calcination (Figure 2 c and 2 d). The BET measurements show that the specific surface area of hollow spheres with pillared surfaces is about $101\ m^2\,g^{-1}$, which is larger than those of the non-pillared spheres formed without electric field ($74\ m^2\,g^{-1}$). A combination of mesoporous surfaces with a tunable cavity makes the hollow spheres particularly suitable for applications in catalysis and adsorption.

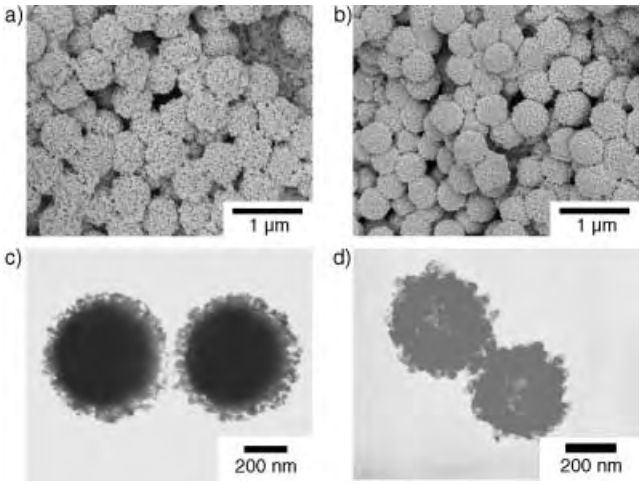


Figure 2. Morphologies of the surface pillared capsules and hollow titania spheres. a) SEM image and b) TEM image of the titania/S2 capsules. c) SEM image and d) TEM image of the hollow titania spheres after calcination.

The size of the titania pillars and their separations are tens of nanometers, which greatly differs from the reported micrometer pillars on common polymers.[11] This fact is related to the decrease of the initial growing wavelength of the pillars with interfacial tension.[11] The hollow titania spheres prepared by dissolution can be dispersed stably in both polar (e.g., water, ethanol, THF) and nonpolar (e.g., toluene) solvents. This suggests that the interior surface of the hollow sphere is amphiphilic, which may result from the polystyrene coils tethered to the sulfonated polystyrene–titania composite. This is reasonable assuming that the sulfonation frontier can traverse a polystyrene chain coil. Rutile was prepared after calcination of the titania spheres at 900 °C. At an intermediate temperature for example 600 °C, anatase and rutile coexist.

Ordered arrays were formed by drying the capsule dispersion in an ethanol/water mixture. The arrays became robust after aging owing to a further titania gelation. After the removal of the polystyrene cores, either by dissolution or by calcination, the ordered structure was retained.

In conclusion, we have demonstrated a new approach to create titania–polymer capsules and hollow titania spheres by using sulfonated polystyrene core–shell gel particles as templates. The thickness of the titania shell and the cavity size are controlled in the entire particle radius range. Applying an electric field can produce capsules and hollow spheres with pillared surfaces. After the removal of the cores by dissolution, the hollow titania particles are amphiphilic. This approach could be applied to the preparation of other capsules and hollow spheres of varied compositions, for example, silica and polyaniline.

Experimental Section

Sulfonated-polystyrene core–shell gel-template particles: Monodisperse polystyrene particles with a diameter ranging from 100–500 nm were prepared by seed-emulsion polymerization.[9] The freeze-dried

 © 2003 Wiley-VCH Verlag GmbH & Co. KGaA, Weinheim

polystyrene particles were immersed in large quantity of concentrated sulfuric acid and stirred at 40 °C and for the appropriate time, thereby controlling the thickness of the sulfonated-polystyrene-gel shell. After the product was separated by centrifugation (4500 r min^{-1}), then washed with ethanol, sulfonated-polystyrene core–shell gel particles were obtained. The template gel particles S1, S2, S3, S4, S5, S6 were prepared by a sulfonation of an example polystyrene particle of 275 nm in diameter for 1, 2, 4, 8, 12, 24 h.

Titania–gel capsules: The gel particles were immersed in a large amount of a tetrabutyl titanate (TBT)/alcohol (1:1 vol/vol) mixture for 8 h to allow a saturated adsorption of TBT on the shell. The TBT swollen gel particles were separated by centrifugation, and 0.1 g of this product were dispersed into ethanol/water (1:1 vol/vol; 10 mL) and stirred at ambient temperature for 2 h to allow the sol–gel process to occur.

Surface pillared capsules: Monodisperse polystyrene particles, about 400 nm in diameter, were sulfonated at 40 °C for 4 h, which yielded the core–shell gel particles, S0. These core–shell particles, were immersed in a TBT/alcohol (1:1 vol/vol) mixture for 8 h, and separated by centrifuge, and 0.1 g of the TBT swollen gel particles were dispersed into ethanol (5 mL). An electric field was applied to the particles for 15 min; the apparatus was composed of two vertical platinum plated electrodes approximately 4 cm apart. The electric field was maintained at about 10^4 v m^{-1}, ethanol/water (1:1 vol/vol; 2 mL) was introduced into the system during the reaction time, and surface pillared capsules were obtained.

Hollow titania spheres: The polystyrene cores were removed from the capsules either by dissolution with *N,N*-dimethylfomamide or by calcination at 450 °C for 2 h.

Characterization: Very dilute suspensions of the samples in ethanol were dropped onto carbon-coated grids, and the solvent was rapidly evaporated; a JEOL 100CX transmission electron microscope was used to observe the particle morphology at an acceleration voltage 75 kV. The samples were coated with Pt (ca. 3 nm) by vacuum sputtering for SEM observation. A JEOL 6700F field emission scanning electron microscope was used at a voltage of 3 kV. Wide-angle X-ray powder scattering (Rigaku D/max-2500) was used to characterize the crystalline type of titania. Thermogravimetric analysis on a Perkin-Elmer TGA 7 was used to determine the inorganic content of the capsules. Nitrogen adsorption was performed on a Micromeritics OMNISORP 100CX porosimeter.

Received: October 28, 2002 [Z50443]

Keywords: materials science · mechanical properties · nanostructures · polymers · titania

[1] For reviews, see: a) W. Schärtl, *Adv. Mater.* **2000**, *12*, 1899, and references therein; b) F. Caruso, *Adv. Mater.* **2001**, *13*, 11, and references therein.
[2] a) I. Tissot, J. P. Reymond, F. Lefebvre, E. Bourgeat-Lami, *Chem. Mater.* **2002**, *14*, 1325; b) A. Imhof, *Langmuir* **2001**, *17*, 3579; c) M. J. Percy, C. Barthet, J. C. Lobb, M. A. Khan, S. F. Lascelles, M. Vamvakaki, S. P. Armes, *Langmuir* **2000**, *16*, 6913; d) I. L. Radtchenko, G. B. Sukhorukov, N. Gaponik, A. Kornowski, A. L. Rogach, H. Möhwald, *Adv. Mater.* **2001**, *13*, 1684.
[3] a) N. Kawahashi, E. Matijevic, *J. Colloid Interface Sci.* **1990**, *138*, 534; b) N. Kawahashi, E. Matijevic, *J. Colloid Interface Sci.* **1991**, *143*, 103.
[4] a) A. J. Khopade, F. Caruso, *Nano Lett.* **2002**, *2*, 415; b) C. Schüler, F. Caruso, *Biomacromolecules* **2001**, *2*, 921; c) I. Pastoriza-Santos, B. Schöler, F. Caruso, *Adv. Funct. Mater.* **2001**, *11*, 122; d) F. Caruso, R. A. Caruso, H. Möhwald, *Science* **1998**, *282*, 1111; e) F. Caruso, M. Spasova, A. Susha, M. Giersig, R. A. Caruso, *Chem. Mater.* **2001**, *13*, 109.
[5] H. Shiho, N. Kawahashi, *Colloid Polym. Sci.* **2000**, *278*, 270.
[6] M. Iida, T. Sasaki, M. Watanabe, *Chem. Mater.* **1998**, *10*, 3780.
[7] F. Caruso, X. Y. Shi, R. A. Caruso, A. Susha, *Adv. Mater.* **2001**, *13*, 740.
[8] Z. Z. Zhong, Y. D. Yin, B. Gates, Y. Xia, *Adv. Mater.* **2000**, *12*, 206.
[9] Z. Z. Yang, D. Li, J. H. Rong, W. D. Yan, Z. W. Niu, *Macromol. Mater. Eng.* **2002**, *287*, 627.
[10] J. H. Rong, Z. Z. Yang, *Chin. Sci. Bull.* **2002**, *18*, 1385.
[11] a) E. Schäffer, T. Thurn-Albrecht, T. P. Russell, U. Steiner, *Europhys. Lett.* **2001**, *53*, 518; b) Z. Lin, T. Kerle, S. M. Baker, D. A. Hoagland, E. Schäffer, U. Steiner, T. P. Russell, *J. Chem. Phys.* **2001**, *114*, 2377.

 © 2003 Wiley-VCH Verlag GmbH & Co. KGaA, Weinheim

Tin Superstructures

Spontaneous Formation of Ordered 3D Superlattices of Nanocrystals from Polydisperse Colloidal Solutions**

*Katerina Soulantica, André Maisonnat, Marie-Claire Fromen, Marie-José Casanove, and Bruno Chaudret**

The synthesis and ordering of nanocrystals into nanocrystal superlattices (NCSs) is timely and of prime importance for applications involving physical properties.[1] The formation of NCSs requires the presence of ligands for controlling the size, shape, and monodispersity of the particles[2,3] and for favoring their self-assembly. This process generally results from the evaporation of solvent[4,5] from a solution of the nanoparticles or precipitation of particles by the addition of a non-solvent.[6,7] It requires strictly monodisperse nanocrystals that result from specific synthetic routes[8] or tedious size-selection processes.[2,5–7] Considerable effort has recently been devoted to the formation of crystalline superlattices of metals,[4,5b,8d,9,10] metal alloys,[1d,7] metal oxides,[8a–c,11,12] sulfides,[5] and semiconductors.[6] The superlattices that have been characterized generally adopt a compact fcc or hcp structure.[4–7,10–13] A few examples of NCSs display orientational order between the nanocrystals.[4,10] Molecular dynamic

[*] Dr. B. Chaudret, Dr. K. Soulantica, Dr. A. Maisonnat
Laboratoire de Chimie de Coordination du CNRS
205, route de Narbonne, 31077 Toulouse (France)
Fax: (+33) 5-6155-3003
E-mail: chaudret@lcc-toulouse.fr
M.-C. Fromen, Dr. M.-J. Casanove
Centre d'Elaboration des Matériaux et
d'Etudes Structurales du CNRS
29, rue Jeanne Marvig BP 4347, 31055 Toulouse (France)

[**] The authors thank the CNRS and EC (through TMR netwok CLUPOS) for support. We express our gratitude to Professors. Pablo Espinet and John Bradley for fruitful discussions, Dr. F. Senocq for XRD measurements, and M. Vincent Collière, Lucien Datas, and the TEMSCAN service for TEM studies.

 DOI: 10.1002/anie.200250484 © 2003 Wiley-VCH Verlag GmbH & Co. KGaA, Weinheim

simulations have, however, predicted that monodisperse nanocrystals stabilized by long-chain ligands could crystallize into noncompact superstructures in which the crystallographic axes of the individual nanocrystals would be aligned.[14] Structures of this type have been detected but remain very rare.[15]

We have previously shown that a range of ligands, from water to long-chain amines, are able to control the growth of nanoparticles that are prepared by decomposition of an organometallic precursor, and even to allow self-assembly of monodisperse particles into 2D and 3D superstructures.[16] However, recent results[1d,17,18] emphasize the importance of the presence of two types of ligands/surfactants for achieving simultaneously the control of monodispersity, self-assembly, and, in some cases, the shape of the particles. In these cases, however, a reaction between the different ligands may proceed under the reaction conditions, which renders the rationalization of the observations difficult. We report here an alternative system based on the association of an acid with its conjugated base, namely an ammonium/amine system, which should produce a less or nonevolutive reaction medium. This system leads to the spontaneous formation of 3D superlattices containing monodisperse tin nanocrystals exhibiting translational and orientational order. These NCSs are grown directly from a solution containing polydisperse tin particles.

UV irradiation (365 nm) of $[\{Sn(NMe_2)_2\}_2]$[19] in toluene at room temperature in the absence of stirring and in the presence of one equivalent of hexadecylamine (HDA) leads to the formation of large square-shaped particles which display a broad size distribution centred near 50 nm (TEM analysis). They are isolated or agglomerated, but without any sign of order, and consist of pure tetragonal tin (XRD evidence). A spectacular change is observed in the reaction products when the same reaction conditions is used, but with a mixture of HDA and its HCl adduct (HDA·HCl) at various relative concentrations in place of pure HDA. Different types of superstructures are produced which may coexist in the same preparation (Figure 1): 1) three-dimensional crystalline networks (nanocrystal superlattices (NCS **1**)) consisting of monodisperse tin particles with dimensions of about 18 × 15 nm (Figure 1a); 2) a second type of crystalline arrangement (NCS **2**) accommodating monodisperse larger and more anisotropic particles (Figure 1b); 3) particles showing some size polydispersity which appear either isolated, assembled into disordered superstructures, or, in some cases, assembled into monolayers displaying a mosaic-like pattern (Figure 1c). In contrast to recent results obtained with indium,[16] the thickness of the NCSs on the microscopy grids, the polydispersity of the particles in solution, and the absence of monolayers suggest that self-organization of the nanocrystals does not occur on the microscopy grid. The structure of the NCSs has been studied by HREM and electron diffraction at different tilting angles of the support. From a morphological viewpoint, the network NCS **1** appears as a single supercrystal of particles with at least two well-defined edges. The Sn particles are all identical in size and morphology and display a slightly elongated shape (aspect ratio ca. 1.2:1, long axis: 18 nm, short axis: 15 nm, interparticle distance: ca. 3 nm). They display the tetragonal structure of Sn and

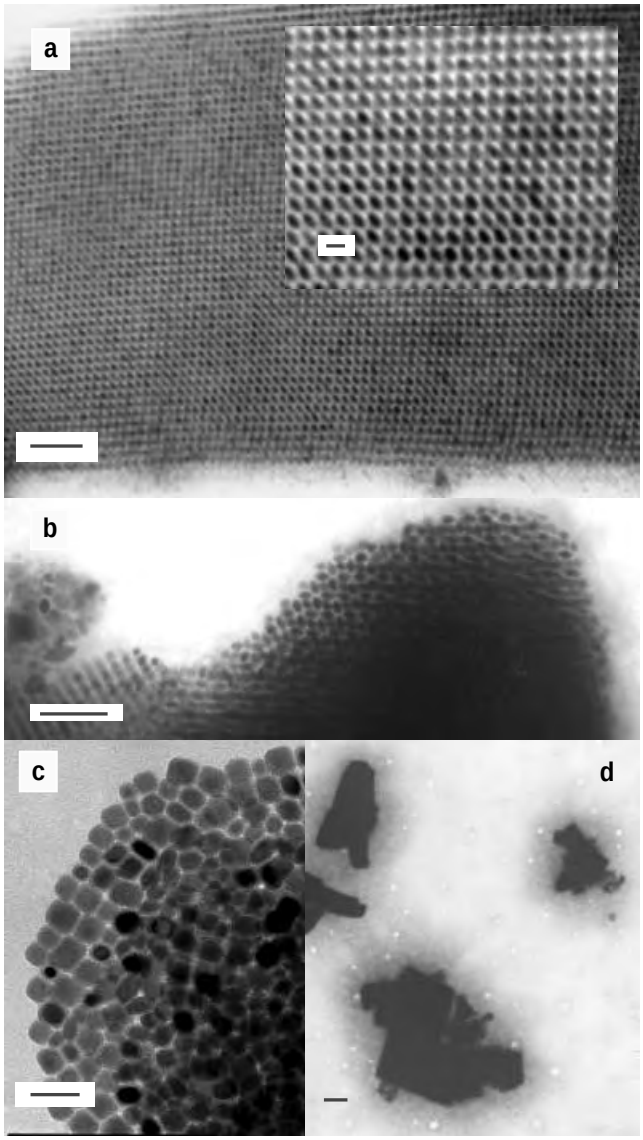


Figure 1. Different objects present in the colloidal solution. a) NCS **1** network (scale bar: 100 nm). Inset: higher magnification (scale bar: 20 nm); b) NCS **2** network (scale bar: 100 nm); c) unorganized material outside the NCSs (scale bar: 50 nm); d) general view of the sample (scale bar: 1 μm).

are oriented in nearly the same direction (Figure 2b). A slight misalignment, which never exceeds 15°, is observed in HRTEM images and revealed by a Fourier Transform diffractogram of the image, as well as by the high-angle electron diffraction spots of the tin network measured on one NCS (Figure 2c). This observation demonstrates that the NCSs are characterized not only by a translational but also by an orientational symmetry. The structure of the superlattice is not compact, but probably monoclinic ($a = 15.6$, $b = 16$ nm; $\alpha = \beta = 90$, $\gamma = 77°$), although the presence of some lattice distortion in the thinner areas prevents a full identification (Figure 2a).

The second superstructure, NCS **2**, displays a surprisingly complex pattern (Figure 3). The individual particles display an elongated shape (25 nm long and aspect ratio ca. 1.6:1).

 © 2003 Wiley-VCH Verlag GmbH & Co. KGaA, Weinheim

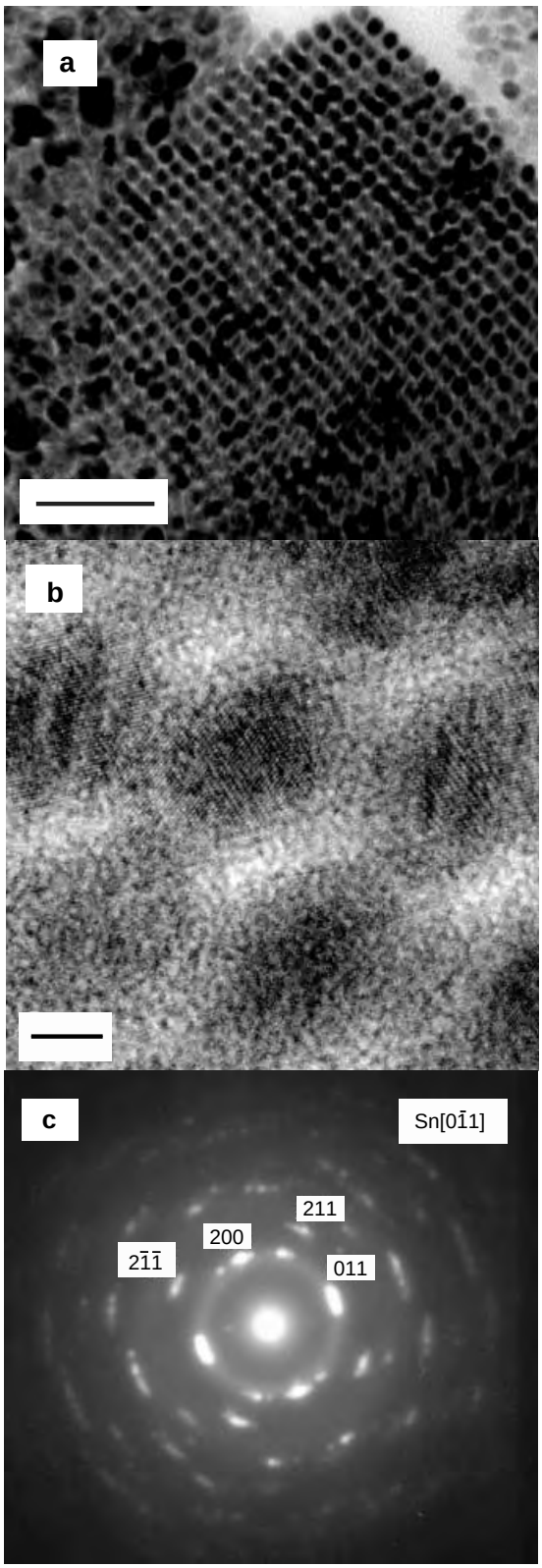


Figure 2. NCS **1** network. a) View of a faceted superlattice. Some disordered material may be observed next to the crystal (scale bar: 100 nm); b) HREM image illustrating the alignment of the atomic planes of individual particles (scale bar: 5 nm); c) electron diffraction image of a part of NCS **1** network showing the tin β structure and demonstrating the crystallographic alignment of the particles with a maximum deviation of 15°.

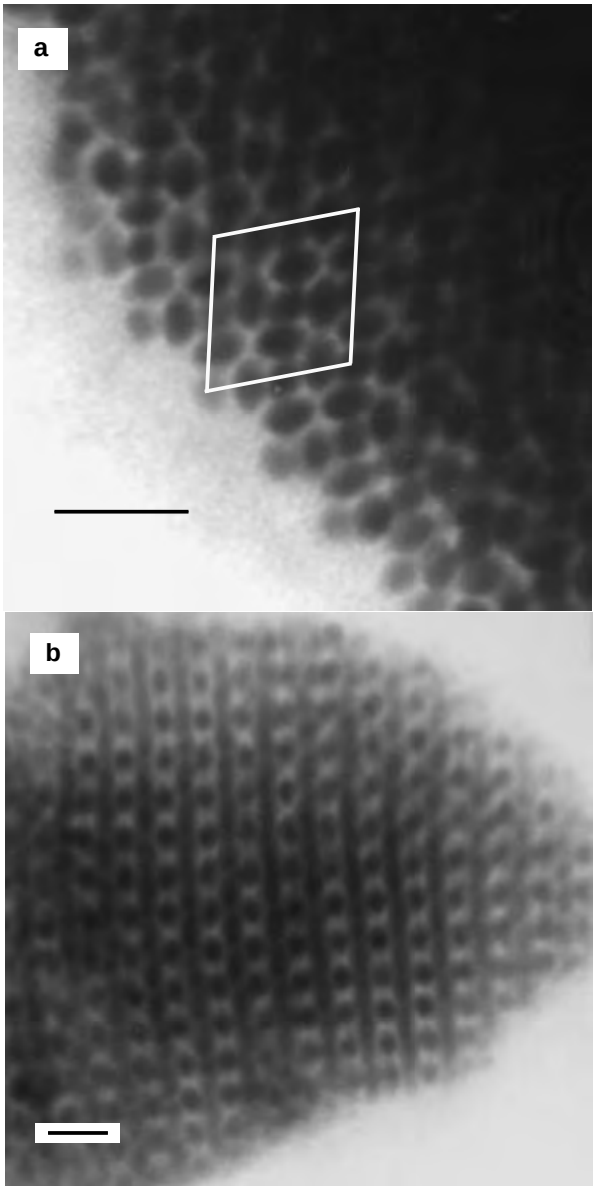


Figure 3. NCS **2** network. a) Superlattice of "crosses" where the supercell unit is indicated in the white box (scale bar: 50 nm); b) another view of a NCS **2**. The different angle allows another pattern to appear (scale bar: 50 nm).

The smaller recognizable pattern in the thin regions is a cruciform arrangement of four particles surrounding a single smaller particle that is, in our opinion, an identical particle oriented perpendicular to the other four. These crosses are organized into rows with their axes alternately rotated by a small positive or negative angle from the mean direction of the super-lattice. The projected supercell unit is larger than one cross and is depicted in Figure 3a. Different orientations demonstrate the complexity of the structure, which is not consistent with the presence of simple lattices (such as fcc, hcp, and bcc). To the best of our knowledge this is the first example of such an elaborate structure of NCS. Up to now only regular "side-by-side" arrangements of nanoparticles have been encountered.

 © 2003 Wiley-VCH Verlag GmbH & Co. KGaA, Weinheim

This complicated process involves both a crystallization and a size adjustment of the particles. We studied the influence of several reaction parameters to gain some knowledge of the formation of these objects. We found that the concentration of the reagents, the use of $[\{Sn(NMe_2)Cl\}_2]$[20] as the chloride source, the addition of free $HNMe_2$, the nature of the solvent and the presence of water in it, as well as the reaction time are some of the parameters that determine the outcome of the crystallization. Conditions have thus been identified which favor the production of NCS **1** almost exclusively, and other conditions where both NCSs were produced (see Experimental Section). We also found that the formation of NCSs does not proceed in THF or if the toluene reaction solution is stirred. In the latter case, a high degree of size polydispersity and almost no organization are observed. Finally, the reaction and organization proceed using dodecylamine (DDA) in place of HDA and with similar constraints on concentration, but not when octylamine was used.

A rational for these observations can be proposed. In the absence of stirring, a gradient of metal and ligand concentrations may form between the layers directly exposed to UV light and the inner parts of the solution, thus accounting for the presence of particles of different sizes and shapes in the reaction mixture. The particles formed may also fluctuate in size and shape in solution as previously observed.[21] Some particles of a given size and ligand environment may self-assemble into NCSs in solution as a result of size-dependent, attractive interparticle forces.[22] While growing, the resulting NCSs will precipitate in toluene but may continue to incorporate adequate particles present in the liquid phase. The continuous formation of particles of size appropriate for inclusion into the growing NCS results from size re-equilibration in solution. It is noteworthy that this process does not operate in a polar solvent, such as THF, which may firmly bind to the tin surface and hence may prevent re-equilibration. The presence of two types of networks results from the necessity to accommodate particles of different shapes and may be related to the concentration of chloride ions.

In conclusion, we have reported the synthesis of identical tin nanoparticles included into tin superstructures of micron sizes. The particles display uniform size and crystallographic orientation. The noncompact nature of the superlattices points towards a crystallization of both the particles and their ligand shells, as for molecular species. The formation of the NCSs results from 1) fractional crystallization in solution, a long-known process that enables the spontaneous size selection of particles, and 2) size fluctuation that affords new particles to be incorporated into the NCSs. This in turn allows the control in one step of the shape, monodispersity, and ligand environment of the particles. This complex process has, to the best of our knowledge, no precedent. Further work, currently in progress, will be necessary to elucidate the mechanism of growth of these NCSs and the generality of this approach.

Experimental Section

All noncommercial compounds were prepared under argon by using standard Schlenck techniques. A glove-box was used for the preparation of the starting solutions. The solvents used were distilled under sodium and degassed through three freeze-pump-thaw cycles. The long-chain amines were purchased from Fluka. The hydrochloric salts were prepared by addition of an excess of a 2 M solution of HCl in diethyl ether to a solution of the corresponding amine in toluene. The precipitate which formed immediately was stirred for 2 h, then washed with toluene. Complete evaporation of the solvent gave the hydrochloride salt.

$[\{Sn(NMe_2)Cl\}_2]$ was prepared in a similar way to $[\{Sn(NMe_2)_2\}_2]$ but by adding only one equivalent of $LiNMe_2$ to $SnCl_2$, and was isolated by sublimation at 110 °C. The product was characterized by X-ray crystal-structure analysis (not reported here); ^{1}H NMR: $\delta = 2.32$ ppm ($^3J_{Sn\text{-}H} = 26.7$ Hz).

Typical procedures leading to NCS **1**: A solution of $[\{Sn(NMe_2)_2\}_2]$ (51.7 mg, 0.250 mmol of Sn) in freshly distilled and degassed toluene (the distilled toluene contains about 50 ppm of H_2O) was added to a suspension of a mixture of HDA·HCl (26.1 mg, 0.094 mmol) and HDA (8.5 mg, 0.035 mmol) in the same solvent. The total volume was adjusted to 5.5 mL. Alternatively, a mixture of $[\{Sn(NMe_2)_2\}_2]/[\{Sn(NMe_2)Cl\}_2]$ (36.7 mg, 0.177 mmol/14.5 mg, 0.073 mmol) could be used. In this case HDA was the only amine used and the two Sn precursors left to react for a few minutes before adding the reaction mixture to HDA (30.2 mg, 0.125 mmol). The total amount of toluene used ws 5.5 mL. Monitoring of the reaction between $[\{SnCl(NMe_2)_2\}]$ and $[\{Sn(NMe_2)_2\}_2]$ by ^{1}H NMR spectroscopy showed that a tin complex identified as $[\{Sn_2Cl(NMe_2)_3\}]$ is formed. The latter complex was detected as one of the products of the reaction of HDA·HCl with $[\{SnCl(NMe_2)\}_2]$. In both cases, the resulting clear yellow solution was stirred and then left standing for 1 h before exposure to UV light for 30 h and 46 h, respectively, without stirring. The whole cell was then transferred into the glove-box and a drop of the crude suspension obtained after removing the majority of the clear yellow supernatant was placed on a TEM grid and dried. The product for XRD measurements was isolated by simple removal of the supernatant solution and drying. All efforts to wash the powder resulted in loss of organization.

Typical procedure leading to NCS **1** and NSC **2**: The same general procedure was used starting from a mixture of $[\{SnCl(NMe_2)\}_2]$ (7.9 mg, 0.040 mmol in Sn) and $[\{Sn(NMe_2)_2\}_2]$ (42.5 mg, 0.210 mmol in Sn). The two compounds were reacted for 30 min in toluene (3 mL) and then a solution of HDA (30.2 mg, 0.125 mmol) in toluene (2.5 mL) was added. The clear yellow solution was left without stirring under UV light for 48 h and characterized as described above.

Received: November 6, 2002 [Z50484]

Keywords: colloidal crystals · crystal growth · nanostructures · self-assembly · tin

[1] a) A. P. Alivisatos, *Science* **1996**, *271*, 933; b) V. L. Colvin, M. C. Schlamp, A. P. Alivisatos, *Nature* **1994**, *370*, 354; c) C. T. Black, C. B. Murray, R. L. Sandstrom, S. Sun, *Science* **2000**, *290*, 1131; d) S. Sun, C. B. Murray, D. Weller, L. Folks, A. Moser, *Science* **2000**, *287*, 1989.

[2] a) A. L. Rogach, E. V. Shevchenko, D. V. Talapin, A. Kornowski, M. Haase, H. Weller, *Adv. Funct. Mater.* **2002**, *12*, 653; b) C. B. Murray, C. R. Kagan, M. G. Bawendi, *Annu. Rev. Mater. Sci.* **2000**, *30*, 545; c) C. P. Collier, T. Vossmeyer, J. R. Heath, *Annu. Rev. Phys. Chem.* **1998**, *49*, 371.

[3] M. Brust, M. Walker, D. Bethell, D. J. Schriffin, R. Whyman, *J. Chem. Soc. Chem. Commun.* **1994**, 801.

[4] a) S. A. Harfenist, Z. L. Wang, M. M. Alvarez, I. Vezmar, R. L. Whetten, *J. Phys. Chem.* **1996**, *100*, 13904; b) Z. L. Wang, S. A. Harfenist, R. L. Whetten, J. Bentley, N. D. Evans, *J. Phys. Chem. B* **1998**, *102*, 3068.

 © 2003 Wiley-VCH Verlag GmbH & Co. KGaA, Weinheim

[5] a) L. Motte, F. Billoudet, E. Lacaze, J. Douin, M. P. Pileni, *J. Phys. Chem. B* **1997**, *101*, 138; b) M. P. Pileni, *Appl. Surf. Sci.* **2001**, *171*, 1.
[6] C. B. Murray, C. R. Kagan, M. G. Bawendi, *Science* **1995**, *270*, 1335.
[7] a) E. Shevchenko, D. Talapin, A. Kornowski, F. Wiekhorst, J. Kötzler, M. Haase, A. Rogach, H. Weller, *Adv. Mater.* **2002**, *14*, 287; b) E. V. Shevchenko, D. V. Talapin, A. L. Rogach, A. Kornowski, M. Haase, H. Weller, *J. Am. Chem. Soc.* **2002**, *124*, 11480.
[8] a) T. Hyeon, S. S. Lee, J. Park, Y. Chung, H. B. Na, *J. Am. Chem. Soc.* **2001**, *123*, 12798; b) T. Hyeon, Y. Chung, J. Park, S. S. Lee, Y.-W. Kim, B. H. Park, *J. Phys. Chem. B* **2002**, *106*, 6831; c) S. Sun, H. Zeng, *J. Am. Chem. Soc.* **2002**, *124*, 8204; d) S. Stoeva, K. J. Klabunde, C. M. Sorensen, I. Dragieva, *J. Am. Chem. Soc.* **2002**, *124*, 2305.
[9] J. E. Martin, J. P. Wilcoxon, J. Odinek, P. Provencio, *J. Phys. Chem. B* **2002**, *106*, 971.
[10] L. O. Brown, J. E. Hutchison, *J. Phys. Chem. B* **2001**, *105*, 8911.
[11] M. D. Bentzon, J. van Wonterghem, S. Morup, A. Tholen, *Philos. Mag. B* **1989**, *60*, 169.
[12] J. S. Yin, Z. L. Wang, *Phys. Rev. Lett.* **1997**, *79*, 257.
[13] Z. L. Wang, *Adv. Mater.* **1998**, *10*, 13.
[14] W. D. Luedtke, U. Landman, *J. Phys. Chem.* **1996**, *100*, 13323.
[15] R. L. Whetten, M. N. Shafigullin, J. T. Khoury, T. G. Schaaff, I. Vezmar, M. M. Alvarez, A. Wilkinson, *Acc. Chem. Res.* **1999**, *32*, 39.
[16] a) K. Soulantica, A. Maisonnat, M.-C. Fromen, M.-J. Casanove, P. Lecante, B. Chaudret, *Angew. Chem.* **2001**, *113,* 462; *Angew. Chem. Int. Ed.* **2001**, *40*, 448; b) K. Soulantica, A. Maisonnat, F. Senocq, M.-C. Fromen, M.-J. Casanove, P. Lecante, B. Chaudret, *Angew. Chem.* **2001**, *113,* 3071; *Angew. Chem. Int. Ed.* **2001**, *40*, 2984.
[17] V. F. Puntes, D. Zanchet, C. K. Erdonmez, A. P. Alivisatos, *J. Am. Chem. Soc.* **2002**, *124*, 12844.
[18] F. Dumestre, B. Chaudret, C. Amiens, M.-C. Fromen, M.-J. Casanove, P. Renaud, P. Zurcher, *Angew. Chem.* **2002**, *114,* 4462; *Angew. Chem. Int. Ed.* **2002**, *41*, 4286.
[19] M. M. Olmstead, P. P. Power, *Inorg. Chem.* **1984**, *23*, 413.
[20] See Experimental Section.
[21] C. Pan, K. Pelzer, K. Philippot, B. Chaudret, *J. Am. Chem. Soc.* **2001**, *123*, 7584.
[22] P. C. Ohara, D. V. Leff, J. R. Heath, W. M. Gelbart, *Phys. Rev. Lett.* **1995**, *75*, 3466.

 © 2003 Wiley-VCH Verlag GmbH & Co. KGaA, Weinheim

Novel Azine Reactivity

Novel Azine Reactivity: Facile N–N Bond Cleavage, C–H Activation, and N–N Coupling Mediated by Rh^I**

Revital Cohen, Boris Rybtchinski, Mark Gandelman, Linda J. W. Shimon, Jan M. L. Martin, and David Milstein**

Azines ($R_2C{=}N{-}N{=}CR_2$) are very useful compounds. For example, they undergo unusual [1,3] dipolar cycloaddition reactions (the crisscross addition) with dienophiles, which provide a convenient route to five-membered rings.[1] They also participate in [3+2] cycloaddition reactions as an *ene* fragment.[2] Applications of azines include possible nonlinear optical materials[3] and conducting polymers (polyazines).[4] Relevant to dinitrogen fixation, the formation of azines by metal-mediated functionalization of N_2 was demonstrated.[5] Azine derivatives display important biological properties and are of importance for drug development.[6] Complexes of titanium,[7] zirconium,[7c] cobalt,[7c] uranium,[8] and iron[9] are capable of cleaving the N–N bond in azines. In all the reported cases, the azine N–N bond is cleaved symmetrically forming two imide units, $-N{=}CR_2$, coordinated to a metal center. No metal-complex-catalyzed reactions were reported. Herein we report a novel type of azine reactivity, the rhodium-promoted catalytic "nonsymmetrical" N–N bond cleavage accompanied by C–H activation, which leads to an imine and benzonitrile. This is the first metal-promoted nonsymmetric cleavage of the N–N bond in an azine[10] and the first metal-catalyzed N–N activation in an azine.

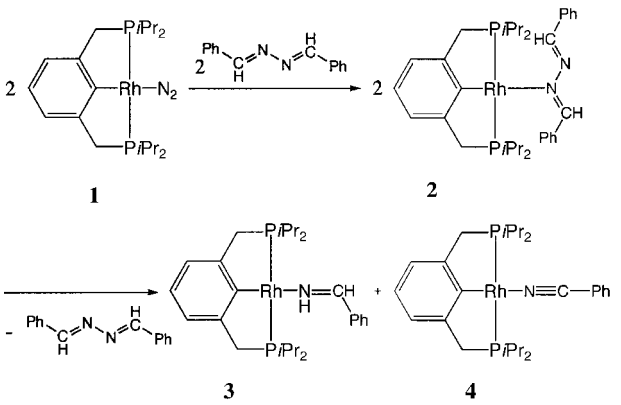
When a toluene solution of the PCP-pincer rhodium complex **1**[11] was treated with one equivalent of benzalazine at −30 °C, three complexes were formed (Scheme 1). One of them, tentatively identified by NMR spectroscopy as the [(PCP)Rh(benzalazine)] complex **2** (precedents exist for azine complexes[7]), is an intermediate, which converts into

[*] Prof. Dr. J. M. L. Martin, Prof. Dr. D. Milstein, R. Cohen, Dr. B. Rybtchinski, M. Gandelman
Department of Organic Chemistry
The Weizmann Institute of Science, 76100 Rehovot (Israel)
Fax: (+972) 8-9344142
E-mail: comartin@wicc.weizmann.ac.il
david.milstein@weizmann.ac.il
Dr. L. J. W. Shimon
Chemical Services Unit, The Weizmann Institute of Science
76100 Rehovot (Israel)

[**] This work was supported by the Israel Science Foundation and by the MINERVA Foundation, Munich (Germany). We thank Yehoshoa Ben-David for technical assistance and Dr. Leonid Konstantinovsky for help with NMR measurements. D.M. is the holder of the Israel Matz Professorial Chair of Organic Chemistry.

Supporting information for this article (preparation procedures for complexes **3, 4**, and **6**, and *xyz* coordinates of the computed structures) is available on the WWW under http://www.angewandte.org or from the author.

 DOI: 10.1002/anie.200250571 © 2003 Wiley-VCH Verlag GmbH & Co. KGaA, Weinheim

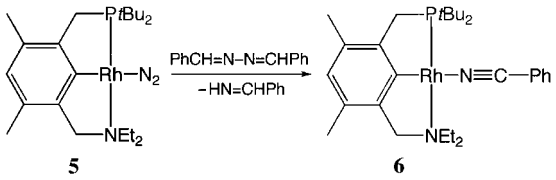


Scheme 1. Reaction of benzalazine with **1**.

the two new complexes **3** and **4** in a 1:1 ratio within an hour at room temperature.

The phenylimine complex **3** and benzonitrile complex **4** were characterized by various NMR spectroscopy techniques (^{31}P, ^{1}H, ^{13}C, and ^{13}C-^{1}H and ^{15}N-^{1}H correlation experiments, Table 1). Formation of the benzonitrile complex **4** was verified by its independent synthesis from complex **1** and PhCN. Complex **3** could not be isolated and was characterized in a mixture with **4**. The exact mode of imine coordination in **3** is uncertain and an η^1-N/η^2-C,N equilibrium of the coordinated imine molecule may exist. Primary imine complexes are known,[12] but to our knowledge, their direct synthesis from azines has not been reported. Within a day at room temperature, the imine complex **3** decomposed to unidentifiable products. Complex **4** was stable at room temperature for days.

The [(PCN)Rh(N_2)] complex **5** exhibits reactivity similar to that of **1**. Upon reaction with benzalazine quantitative formation of the benzonitrile complex **6** (Table 1) was observed together with formation of free imine PhCH=NH (Scheme 2).[13] This imine is unstable and rapidly decomposes



Scheme 2. Reaction of benzalazine with **5**.

(10 min at room temperature), in agreement with literature data.[14] The structure of **6** determined by crystal-structure analysis is presented in Figure 1. Complex **6** is square planar

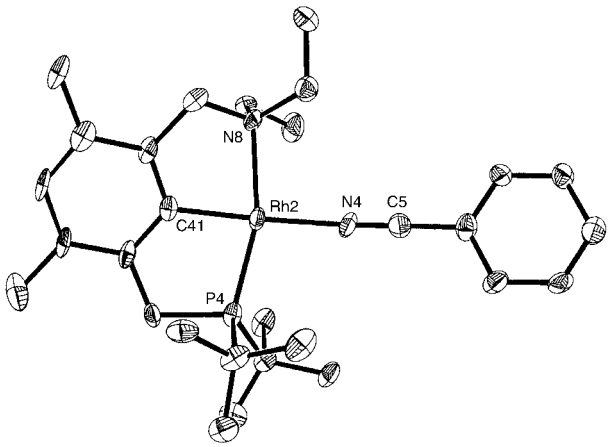


Figure 1. Molecular structure of **6**. Selected bond lengths [Å] and bond angles [°]: Rh2-C41 = 1.986(11), Rh2-N4 = 2.033(9), Rh2-P4 = 2.197(4), Rh2-N8 = 2.196(11), N4-C5 = 1.159(15); N4-Rh2-C41 = 174.2(7), P4-Rh2-N8 = 163.0(3). CCDC-197955 contains the supplementary crystallographic data for this paper. These data can be obtained free of charge via www.ccdc.cam.ac.uk/conts/retrieving.html (or from the Cambridge Crystallographic Data Centre, 12 Union Road, Cambridge CB2 1EZ, UK; fax: (+44) 1223-336-033; or deposit@ccdc.cam.ac.uk).

with the PhCN molecule occupying the position *trans* to the aryl ring. Unlike the case of the (PCP)Rh-based system, no azine or imine complex formation was observed, probably reflecting the more sterically congested character of the (PCN)Rh unit in **5**. Formation of the benzonitrile complex **6** was verified by independent synthesis from complex **5** and PhCN.

When benzalazine was used in excess (10 equiv) with either complex **1** or **5**, an unprecedented catalytic reaction producing 7 equivalents of benzonitrile took place (Scheme 3). The imine PhCH=NH could not be detected, probably because of its fast decomposition.[14] The same turnover number (TON) was observed upon addition of

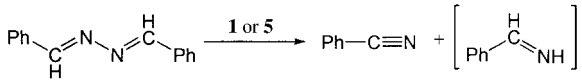
Table 1: Selected spectroscopic data for compounds **3, 4**, and **6**. NMR spectra in [D_8]toluene (^{1}H: 400 MHz, ^{13}C: 100 MHz, ^{15}N: 40 MHz, ^{31}P: 162 MHz), δ in ppm, J in Hz.

3: ^{31}P NMR: $\delta = 61.50$ (d, $J_{Rh,P} = 166.0$); ^{1}H NMR: $\delta = 10.25$ (d, $J_{H,H} = 14.7$, 1H, *H*N=CHPh), 7.96 (d, $J_{H,H} = 14.7$, 1H, HN=C*H*Ph); ^{13}C NMR: $\delta = 166.09$ (br s, HN=CHPh); ^{15}N-^{1}H correlation NMR (referenced to liq. NH_3): $\delta = 392.12$ (br s, HN=CHPh, $J_{N,H} = 65.0$); the NMR assignment is verified by ^{1}H-^{1}H COSY, heteronuclear ^{13}C-^{1}H and ^{15}N-^{1}H correlation experiments and ^{13}C DEPT-135

4: ^{31}P NMR: $\delta = 63.85$ (d, $J_{Rh,P} = 162.0$); ^{1}H NMR: $\delta = 7.16$–7.10 (m, 3H, aryl), 7.02–6.92 (m, 2H, aryl), 6.77 (m, 2H, aryl), 6.68 (m, 1H, aryl), 3.10 (vt, $J_{P,H} = 7.2$, 4H, PCH_2-aryl), 2.04 (m, 4H, $(CH_3)_2CHP$), 1.36 (dvt, $J_{P,H} = 15.6$, $J_{H,H} = 7$, 12H, $(CH_3)_2CHP$), 1.19 (dvt, $J_{P,H} = 13.0$, $J_{H,H} = 7$, 12H, $(CH_3)_2CHP$); ^{13}C NMR: $\delta = 180.33$ (dt, $J_{Rh,C} = 36.8$, $J_{P,C} = 12.2$, C_{ipso}), 157.17 (t, $J_{P,C} = 12.8$, PhCNRh), 137.40 (s, aryl), 135.83 (s, aryl), 134.52 (s, aryl), 134.35 (s, aryl), 133.93 (s, aryl), 127.01 (s, aryl), 125.78 (t, $J_{P,C} = 9.6$, aryl), 41.82 (dvt, $J_{P,C} = 21.6$, $J_{Rh,C} = 4.1$, PCH_2-aryl), 31.17 (vt, $J_{P,C} = 17.2$, $(CH_3)_2CHP$), 24.40 (s, $(CH_3)_2CHP$), 19.44 (s, $(CH_3)_2CHP$); IR: $\tilde{\nu} = 2183.8$ cm^{-1} (m, $\nu_{C\equiv N}$)

6: ^{31}P NMR: $\delta = 7.51$ (d, $J_{Rh,P} = 231.3$); ^{1}H NMR: $\delta = 7.19$–7.16 (m, 2H, aryl), 6.98–6.93 (m, 3H, aryl), 6.52 (br s, 1H, aryl), 3.90 (s, 2H, aryl-CH_2N), 3.07 (d, $J_{P,H} = 8.2$, 2H, PCH_2-aryl), 2.86 (m, 2H, CH_3CH_2N), 2.76 (m, 2H, CH_3CH_2N), 2.36 (s, 3H, aryl-CH_3), 2.24 (s, 3H, aryl-CH_3), 1.63 (t, $J_{H,H} = 7.2$, 6H, CH_3CH_2N), 1.48 (d, $J_{P,H} = 11.7$, 18H, $(CH_3)_2CHP$); ^{13}C NMR: $\delta = 178.82$ (dd, $J_{Rh,C} = 37.7$, $J_{P,C} = 10.0$, C_{ipso}), 146.55 (dd, $J_{Rh,C} = 19.1$, $J_{P,C} = 6.7$, PhCNRh), 145.86 (s, aryl), 130.81 (s, aryl), 130.55 (s, aryl), 129.57 (s, aryl), 127.95 (s, aryl), 123.81 (s, aryl), 118.99 (s, aryl), 115.12 (s, aryl), 65.12 (s, aryl-CH_2N), 54.48 (s, NCH_2CH_3), 35.76 (dd, $J_{P,C} = 26.1$, $J_{Rh,C} = 5.6$, aryl-CH_2P), 35.19 (dd, $J_{P,C} = 11.7$, $J_{Rh,C} = 1.9$, $(CH_3)_2$CP), 30.42 (d, $J_{P,C} = 5.8$, $(CH_3)_2$CP), 22.18 (s, aryl-CH_3), 20.96 (s, aryl-CH_3), 13.46 (s, NCH_2CH_3)

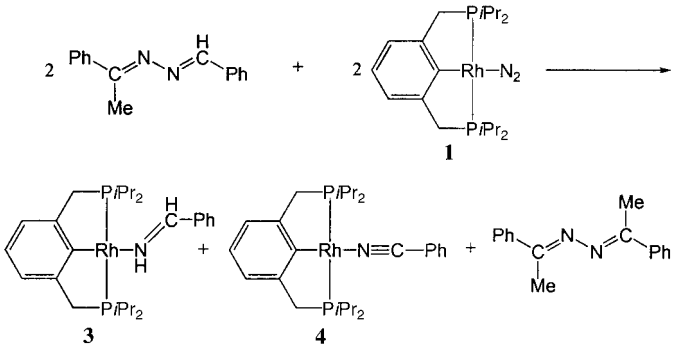
 © 2003 Wiley-VCH Verlag GmbH & Co. KGaA, Weinheim



Scheme 3. Catalytic reaction of **1** or **5** with benzalazine.

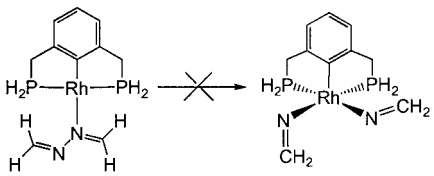
100 equivalents of the azine, which indicates that the catalysis is hampered by the benzonitrile product in both the PCP and PCN cases; PhCN coordinates to the rhodium centers to form the complexes **3** and **6**, and interferes with the azine activation process, which causes low TONs. Optimization of the catalysis is currently being sought in our group. Stoichiometric (not catalytic) C–H and N–N activation in azines are reported,[7] but not the combination of both in one system as in the (PCP)Rh-based one.[15]

Treating complexes **1** or **5** with the ketazine Me(Ph)C=N–N=C(Ph)Me revealed no reactivity even at elevated temperatures. Interestingly, when the nonsymmetrical azine Me(Ph)=N–N=C(Ph)H was reacted with complex **1** in toluene, the same organometallic products as in the benzalazine case, complexes **3** and **4**, were formed in a 1:1 ratio within one hour at room temperature together with an equivalent amount of the ketazine Me(Ph)C=N–N=C(Ph)Me, as observed by NMR spectroscopy and confirmed by GC-MS (Scheme 4).[16]



Scheme 4. Reactivity of **1** towards the nonsymmetrical azine Me(Ph)=N–N=C(Ph)H.

Thus, a symmetric ketazine molecule can be formed from two nonsymmetric aldazine/ketazine molecules. Such a metal-promoted apparent N–N bond cleavage/coupling sequence is unprecedented to our knoweledge. Importantly, only the aldazine "half" gives rise to the imine (and nitrile) complexes. These observations imply involvement of a C–H activation and suggest that a complex reaction mechanism, probably bimolecular, is operative. We believe that the azine splitting observed in the (PCP)Rh- and (PCN)Rh-based systems does not proceed through direct metal insertion into the N–N bond. Further confirmation was obtained from a computational DFT study of the N–N cleavage step (at the mPW1k[17]/LANL2DZ+P//mPW1k/LANL2DZ[18] level of theory[19]). Our model system included a PCP ligand with H-substituted phosphanyl groups and a formaldazine molecule. (No spin-state crossing was considered.) The direct N–N bond cleavage producing the bisimide rhodium complex (Scheme 5) was



Scheme 5. Computational analysis of N–N cleavage in azine in a model system.

found to have a kinetic barrier of 63 kcal mol^{-1} (and to be endergonic by 11.6 kcal mol^{-1}), grossly inconsistent with the experimental observation that the reaction takes place even at −30 °C. The optimized geometry of the bisimide complex exhibits a large deviation from planarity in the chelate core, the two phosphanyl groups acquiring a close to *cis* configuration (P-Rh-P angle is 108°). This is likely to result from the strong *trans* effect of the imide ligands, which destabilizes the complex and causes a high activation barrier as a consequence of the large change in geometry compared to the azine complex. Thus, most probably, direct N–N activation is not operative in our systems—in contrast to the reported examples.[7–9] Computational investigation of the mechanism is currently under way.

In conclusion, we have reported a novel type of azine reactivity, the nonsymmetrical rhodium-mediated N–N bond cleavage, coupled with C–H activation to form a nitrile and an imine. The reaction is catalytic, providing the first example of metal-complex-catalyzed N–N bond cleavage in an azine, although deactivation by the nitrile product takes place. It most probably does not proceed through direct N–N bond cleavage, but through a mechanism involving a C–H activation step. A metal-promoted N–N bond cleavage/N–N coupling sequence was also demonstrated that led to a symmetric ketazine from a mixed aldazine/ketazine molecule. These reactions provide new insight into metal-promoted transformations of azines. The synthetic implications of these findings are being explored.

Received: November 18, 2002 [Z50571]

Keywords: azines · C–H activation · density functional calculations · N–N activation · pincer ligands

[1] a) "Azomethine Imines": R. Grashey, A. Padwa in *1,3-Dipolar Cycloaddition Chemistry, Vol. 1* (Eds.: D. C. Taylort, A. Weissberger), Wiley, New York, **1984**, p. 733; b) S. Radl, *Aldrichimica Acta* **1997**, *30*, 97.
[2] See, for example: E. E. Schweizer, Z. Cao, A. L. Rheingold, M. Bruch, *J. Org. Chem.* **1993**, *58*, 4339.
[3] H. S. Nalwa, A. Kakatu, A. Mukoh, *J. Appl. Phys.* **1993**, *73*, 4743.
[4] E. C. Kesslen, W. B. Euler, *Chem. Mater.* **1999**, *11*, 336.
[5] Y. Nishibayashi, S. Iwai, M. Hidai, *Science* **1998**, *279*, 540; S. M. Rocklage, R. R. Schrock, *J. Am. Chem. Soc.* **1982**, *104*, 3077.
[6] a) A. I. Kholdair, P. Bertrand, *Tetrahedron* **1998**, *54*, 4859; b) K. Yasumura, K. Miyajima, T. Nagahama, S. Ishikawa, Y. Tohyama, K. Sugiyama. PCT, WO 94/19335.
[7] a) M. Rep, J.-W. F. Kaagman, C. J. Elsevier, P. Sedmera, J. Hiller, U. Thewalt, M. Horacek, K. Mach, *J. Organomet. Chem.* **2000**, *597*, 146; b) A. Ohff, T. Zippel, P. Arndt, A. Spannenberg, R.

 © 2003 Wiley-VCH Verlag GmbH & Co. KGaA, Weinheim

Kempe, U. Rosenthal, *Organometallics* **1998**, *17*, 1649; c) T. Zippel, P. Arndt, A. Ohff, A. Spannenberg, R. Kempe, U. Rosenthal, *Organometallics* **1998**, *17*, 4429.
[8] J. L. Kiplinger, D. E. Morris, B. L. Scott, C. J. Burns, *Organometallics* **2002**, *21*, 3073.
[9] A. Zimniak, G. Bakalarski, *J. Mol. Struct.* **2001**, *597*, 211.
[10] Photolytic N–N bond cleavage in benzalazine to form benzonitrile and benzalimine is known: R. W. Binkley, *J. Org. Chem.* **1969**, *34*, 2073.
[11] M. Gandelman, B. Rybtchinski, N. Ashkenazi, R. Gauvin, D. Milstein, *J. Am. Chem. Soc.* **2001**, *123*, 5372.
[12] See, for example: a) W.-Y. Yeh, C.-S. Ting, S.-M. Peng, G.-H. Lee, *Organometallics* **1995**, *14*, 1417; b) D. A. Knight, M. A. Dewey, G. A. Stark, B. K. Bennet, A. M. Arif, J. A. Gladysz, *Organometallics* **1993**, *12*, 4523, and references therein.
[13] PhCH=NH was identified by comparison of its ^{1}H NMR data to the reported ones: D. R. Boyd, P. B. Coulter, R. Hamilton, N. T. Thompson, N. D. Sharma, M. E. Stubbs, *J. Chem. Soc. Perkin Trans. 1* **1985**, 2123.
[14] PhCH=NH was reported to be unstable at room temperature; it decomposes forming oligomers (see ref. [13]).
[15] We detected only traces of benzonitrile upon reaction of benzalazine with $[(i\mathrm{Pr}_3\mathrm{P})_2\mathrm{RhCl}]$ or $[(i\mathrm{Pr}_3\mathrm{P})_2\mathrm{Rh}(\mathrm{N}_2)\mathrm{Cl}]$.
[16] In the absence of **1**, no reaction was observed after several hours at room temperature. Acid- and water-catalyzed disproportionation of the nonsymmetrical azine to the aldazine and ketazine was reported: D. H. Kenny, *J. Chem. Educ.* **1980**, *57*, 462.
[17] B. J. Lynch, P. L. Fast, M. Harris, D. G. Truhlar, *J. Phys. Chem. A* **2000**, *104*, 4811.
[18] P. J. Hay, W. R. Wadt, *J. Chem. Phys.* **1985**, *82*, 299.
[19] See Supporting Information for full details.

 © 2003 Wiley-VCH Verlag GmbH & Co. KGaA, Weinheim

Structures of Uranyl Complexes

Isolation of a Uranyl $[UO_2]^+$ Species: Crystallographic Comparison of the Dioxouranium(V) and (VI) Compounds $[UO_2(OPPh_3)_4](OTf)_n$ ($n = 1, 2$)

Jean-Claude Berthet, Martine Nierlich, and Michel Ephritikhine*

The occurrence of the actinyl(V) species $[AnO_2]^+$ (An = U, Np, Pu, Am) in the nuclear industry and in the natural environment is a particular reason for the current studies of their physicochemical properties.[1] While various $[NpO_2]^+$ compounds have been isolated and crystallographically characterized,[2–5] there is scant structural information available for the other $[AnO_2]^+$ species, and in particular for $[UO_2]^+$, which is reputed to be unstable towards rapid disproportionation. Much effort has been devoted to the formation, detection, and characterization of these species, which can be obtained in a transient fashion by electrochemical or photochemical reduction of hexavalent $[UO_2]^{2+}$ parent compounds. A number of ligands were found to provide a limited stabilization of the one-electron-reduced species, and have enabled a series of voltammetric and spectroscopic experiments in solution.[6] Recently, extended X-ray absorption fine structure (EXAFS) studies were carried out on the tricarbonatodioxouranates $[UO_2(CO_3)_3]^{n-}$ ($n = 4, 5$) in water, which showed that a minor geometrical rearrangement occured in the $[UO_2(CO_3)_3]^{4-} \rightarrow [UO_2(CO_3)_3]^{5-}$ reduction.[7] In addition to these results, structural data on $[UO_2(CO_3)_3]^{n-}$ ($n = 4, 5$),[8] $[UO_2(H_2O)_5]^{n+}$ ($n = 1, 2$)[9] and bare $[UO_2]^{n+}$ ions ($n = 1, 2$)[8] were predicted from theoretical calculations using a variety of methods. In this context, the isolation of a pentavalent uranyl derivative, and the comparison of its crystal structure with that of its $[UO_2]^{2+}$ parent compound are highly desirable.

In the course of our studies on the synthesis and structure of anhydrous uranyl triflate compounds,[10] we serendipitously obtained crystals of $[UO_2(OPPh_3)_4](OTf)$; here we present the crystal structure of this pentavalent uranyl compound, and compare it with that of the uranium(VI) analogue $[UO_2(OPPh_3)_4](OTf)_2$.

$[UO_2(OPPh_3)_4](OTf)_2$ (**1**) was readily obtained as a pale-yellow powder in almost quantitative yield upon addition of four equivalents of $OPPh_3$ to a solution of $UO_2(OTf)_2$ in acetonitrile. Large crystals of **1** were isolated after crystallization from a mixture of acetonitrile and diethyl ether. The X-ray crystal structure of **1** consists of discrete $[UO_2(OPPh_3)_4]^{2+}$ and $[OTf]^-$ ions in a 1:2 ratio;[11] a view of the cation is shown in Figure 1. The geometrical parameters are classical of hexavalent uranyl complexes; the linear $\{UO_2\}$ fragment is perpendicular to the equatorial plane defined by the uranium center and the four oxygen atoms of the $OPPh_3$ ligands. The mean U=O bond length of 1.76(1) Å and the average equatorial U–O bond length of 2.29(1) Å are identical to those found in $[UO_2\{OP(NMe_2)_3\}_4](I_3)_2$.[12]

In one attempt to crystallize complex **1**, small red-orange, cube-shaped crystals were deposited in a small quantity along with the yellow crystals of the $[UO_2]^{2+}$ compound. X-ray diffraction analysis revealed that these crystals were of a new complex, the pentavalent uranyl derivative $[UO_2(OPPh_3)_4](OTf)$ (**2**).[11] The unexpected formation of **2** requires elucidation; all attempts to produce it by reduction of **1** with UV light or various reducing agents are inconclusive at this time, and further work is in progress for controlling the synthesis of **2**. Nevertheless, complex **2** was found to be kinetically stable under an inert atmosphere, which demonstrates that such $[UO_2]^+$ complexes can be isolated in the crystalline form, without suffering disproportionation.

Crystals of **2** are composed of discrete cation–anion pairs; a view of one of the two independent $[UO_2(OPPh_3)_4]^+$ ions is represented in Figure 2. The cations of **1** and **2** adopt the same perfectly square bipyramidal configuration; in **2**, the uranium center is located at a center of symmetry. The U=O bond lengths of 1.817(6) and 1.821(6) Å are slightly longer than the Np=O bond (1.797(2) Å) in the isostructural $[NpO_2(OPPh_3)_4]^+$ ion,[2] in agreement with the variation in

[*] Dr. J.-C. Berthet, Dr. M. Nierlich, Dr. M. Ephritikhine
Service de Chimie Moléculaire
Bat. 125, DSM, DRECAM, CNRS URA 331, CEA Saclay
91191 Gif-sur-Yvette (France)
Fax: (+33) 169-06-66-40
E-mail: berthet@drecam.cea.fr

 © 2003 Wiley-VCH Verlag GmbH & Co. KGaA, Weinheim DOI: 10.1002/anie.200250506

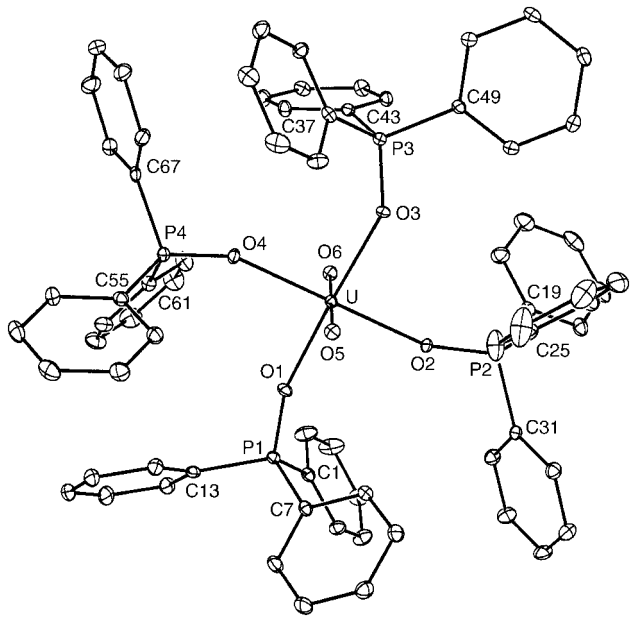


Figure 1. View of the $[UO_2(OPPh_3)_4]^{2+}$ ion in **1**, with displacement ellipsoids set at 30% probability. Selected bond lengths [Å] and angles [°]: U-O1 2.2835(17), U-O2 2.2979(17), U-O3 2.3057(16), U-O4 2.3012(17), U-O5 1.7632(16), U-O6 1.7603(15), O1-P1 1.5250(18), O2-P2 1.5169(16), O3-P3 1.5214(18), O4-P4 1.5185(16); O1-U-O2 89.96(6), O2-U-O3 87.84(6), O3-U-O4 91.99(6), O1-U-O4 90.22(6), O5-U-O6 179.75(8), U-O1-P1 160.05(11), U-O2-P2 157.29(9), U-O3-P3 145.54(10), U-O4-P4 151.60(9).

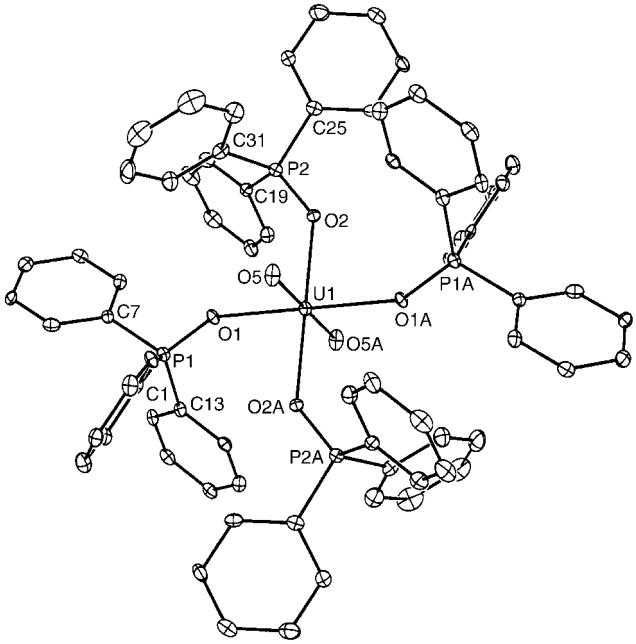


Figure 2. View of one of the two independent $[UO_2(OPPh_3)_4]^+$ ions in **2,** with displacement ellipsoids set at 30% probability. Atoms labeled A are related to those not labeled by a center of symmetry (symmetry code: $-x, -y, 1-z$). Selected bond lengths [Å] and angles [°] (the corresponding values in the second independent cation are given in brackets): U1-O1 2.427(5) [2.455(6)], U1-O2 2.439(5) [2.431(5)], U1-O5 1.821(6) [1.817(6)], O1-P1 1.502(6) [1.500(6)], O2-P2 1.504(6) [1.496(5)]; O1-U1-O2 88.93(18) [88.57(18)], O1-U1-O5 90.3(2) [89.9(2)], U1-O1-P1 144.5(3) [144.2(3)], U1-O2-P2 137.8(3) [139.8(3)].

the radii of the $[UO_2]^+$ and $[NpO_2]^+$ ions.[13] The U=O bond lengths in **2** are also very close to those of the Np=O bonds determined by X-ray crystallography in the pentavalent neptunyl cations $[NpO_2([18]crown\text{-}6)]^+$ (1.800(5) Å)[3] and $[NpO_2(bipy)(H_2O)_3]^+$ (bipy = 2,2′-bipyridyl; mean bond length 1.81(5) Å),[5] but are 0.08 Å shorter than those determined by EXAFS in the uranium(v) anion $[UO_2(CO_3)_3]^{5-}$ (1.90(2) Å).[7] Similarly, the Np=O bonds in the aforementioned neptunyl cations are approximately 0.05 Å shorter than those found in the anionic complexes $[NpO_2(CO_3)_3]^{5-}$ (1.86(2) Å)[14] and $[BaNpO_2(OAc)_3]$ (1.85(2) Å),[4] as determined by X-ray absorption and X-ray diffraction methods, respectively. These results are in accordance with theoretical calculations, which predicted that the variation in An=O bond lengths, by passing from the bare $[AnO_2]^+$ cation to the $[AnO_2(CO_3)_3]^{5-}$ anion, should be greater for An = U (0.17 Å) than for An = Np (0.11 Å).[8,15] Since the nature of the equatorial ligands and the electronic charge of the complex would induce significant variations in the An=O bond lengths, the influence of the oxidation state on the geometrical parameters of $[AnO_2]^{2+}$ and $[AnO_2]^+$ compounds (An = U or Np) can only be evaluated correctly by comparing the structures of analogous complexes, as is the case for **1** and **2**.

The reduction of **1** to **2** leads to a lengthening of the U=O bond by 0.06 Å. This value can be compared with the variation of 0.03 Å in the ionic radii of the $[UO_2]^{2+}$ and $[UO_2]^+$ ions,[13] and with the difference of 0.1 Å between the U=O bond lengths in $[UO_2(CO_3)_3]^{4-}$ and $[UO_2(CO_3)_3]^{5-}$, as measured by EXAFS.[7] The theoretical study of the structure of these tricarbonatodioxouranates using multiconfigurational second-order perturbation theory (CASSCF/CASPT2) predicted bond lengths of 1.845 and 1.929 Å for the U^{VI}=O and U^{V}=O bonds, respectively, and values of 1.707 and 1.758 Å for the same bonds in the bare $[UO_2]^{2+}$ and $[UO_2]^+$ ions;[7] these differences of 0.08 and 0.05 Å are in agreement with the values determined from the structures of **1** and **2**. Most notably, the U=O bond lengths in **1** and **2** correspond quite perfectly to those calculated in $[UO_2(H_2O)_5]^{2+}$ (1.756 Å) and $[UO_2(H_2O)_5]^+$ (1.810 Å) using density functional theory and relativistic effective core potentials.[9] In the pairs of neptunyl and plutonyl derivatives $[NpO_2(CO_3)_3]^{n-}$ ($n = 4, 5$)[15] and $[AnO_2(H_2O)_5]^{n+}$ (An = Np, Pu; $n = 1, 2$),[9] spectroscopic studies and theoretical calculations showed commensurate differences (0.06–0.08 Å) between the An^{VI}=O and An^{V}=O bond lengths.[16]

The U–O($OPPh_3$) bond lengths in the two independent cations of **2** range from 2.427(5) to 2.455(6) Å (average 2.44(2) Å), the average value being in good agreement with that of 2.438(4) Å found for the Np–O bonds in $[NpO_2(OPPh_3)_4]^+$.[2] The mean U–O($OPPh_3$) bond length in **2** is 0.14 Å longer than that determined in **1** and this difference, which is much greater than the difference in ionic radii between $[UO_2]^{2+}$ and $[UO_2]^+$,[13] results from the lower positive charge of the uranium(v) center of **2**, which induces a weaker interaction with the Lewis base. A similar situation was encountered with the organouranium compounds $[U(\eta\text{-}C_8H_8)\{OP(NMe_2)_3\}_3](BPh_4)_n$ ($n = 1$ or 2), where the difference between the mean U–O bond lengths is 0.2 Å,

 © 2003 Wiley-VCH Verlag GmbH & Co. KGaA, Weinheim

while the difference between the U^{4+} and U^{3+} ionic radii is only 0.1 Å.[17] The U–O($OPPh_3$) bonds in **2** are, to the best of our knowledge, the longest so far measured, longer than, for example, those found in $[UO_2(OtBu)_2(OPPh_3)_2]$ (2.40(1) Å);[18] the average O–P bond length and U-O-P angle are respectively 0.02 Å longer and 12° smaller than those in **1**. The 0.14 Å difference between the mean equatorial U^{VI}–O and U^{V}–O bond lengths of **1** and **2** is greater than that of 0.07 and 0.1 Å determined by EXAFS for the pairs of complexes $[UO_2(CO_3)_3]^{n-}$ ($n = 4$, 5)[7] and $[NpO_2(H_2O)_5]^{n+}$ ($n = 1$, 2),[9] respectively. However, comparison of the crystal structures of **1** and **2** confirms that in cationic actinyl complexes, elongation of the equatorial An–O bonds is more important than that of the axial An=O bonds, while the reverse situation is the case for the anionic derivatives.

Experimental Section

1: A mixture of $[UO_2(OTf)_2]$ (1.00 g, 1.76 mmol) and $OPPh_3$ (1.96 g, 7.04 mmol) in anhydrous acetonitrile (50 mL) was stirred for 10 min at 20 °C under an argon atmosphere. After filtration, the yellow solution was evaporated to dryness, which yielded a yellow powder (**1**) which was washed with toluene (2 × 25 mL) and dried under vacuum (2.8 g, 95 %).

Received: November 8, 2002 [Z50506]

Keywords: actinides · ion pairs · O ligands · structure elucidation · uranium

[1] a) J. J. Katz, G. T. Seaborg, L. R. Morss, *The Chemistry of the Actinide Elements*, Chapman and Hall, London, **1986**; b) "Chemistry and Migration Behaviour of Actinides and Fission Products in the Geosphere": *Radiochim. Acta* **1996**, *76*, 1 (Proceedings of the Fifth International Conference, Saint Malo, France, **1995**).

[2] I. A. Charushnikova, N. N. Krot, Z. A. Starikova, *Radiochemistry* **2001**, 43, 24–29.

[3] D. L. Clark, D. W. Keogh, P. D. Palmer, B. L. Scott, C. D. Tait, *Angew. Chem.* **1998**, *110*, 173–175; *Angew. Chem. Int. Ed.* **1998**, *37*, 164–166.

[4] J. H. Burns, C. Musikas, *Inorg. Chem.* **1977**, *16*, 1619–1622.

[5] G. B. Andreev, A. M. Fedosseev, N. A. Budantseva, M. Y. Antipin, *Mendeleev Commun.* **2001**, 58–59.

[6] a) D. E. Morris, *Inorg. Chem.* **2002**, *41*, 3542–3547; b) S.-Y. Kim, H. Tomiyasu, Y. Ikeda, *J. Nucl. Sci. Technol.* **2002**, *39*, 160–165; c) C. Miyake, Y. Sano, *J. Alloys Compd.* **1994**, *213/214*, 493–496.

[7] T. I. Docrat, J. F. W. Mosselmans, J. M. Charnock, M. W. Whiteley, D. Collison, F. R. Livens, C. Jones, M. J. Edmiston, *Inorg. Chem.* **1999**, *38*, 1879–1882.

[8] L. Gagliardi, I. Grenthe, B. O. Roos, *Inorg. Chem.* **2001**, *40*, 2976–2978.

[9] P. J. Hay, R. L. Martin, G. Schreckenbach, *J. Phys. Chem. A* **2000**, *104*, 6259–6270, and references therein.

[10] J.-C. Berthet, M. Lance, M. Nierlich, M. Ephritikhine, *Eur. J. Inorg. Chem.* **2000**, 1969–1973.

[11] Crystallographic data for **1**: $C_{74}H_{60}F_6O_{12}P_4S_2U$, $M_r = 1681.25$, triclinic, space group $P\bar{1}$, $a = 14.088(3)$, $b = 15.314(3)$, $c = 18.767(4)$ Å, $\alpha = 69.33(3)$, $\beta = 70.52(3)$, $\gamma = 78.55(3)°$, $V = 3556.5(12)$ Å^3, $\rho_{calcd} = 1.570$ g cm^{-3}, $Z = 2$, $T = 123$ K, $\mu(Mo_{K\alpha}) = 2.508$ mm^{-1}, 24692 measured reflections, 12444 independent, $10857 > 2\sigma(I)$, 946 parameters, $R1 = 0.0336$, $wR2 = 0.0708$, GOF = 0.999. Crystallographic data for **2**: $C_{73}H_{60}F_3O_9P_4SU$, $M_r = 1532.18$, triclinic, space group $P\bar{1}$, $a = 9.0570(18)$, $b = 13.888(3)$, $c = 27.487(6)$ Å, $\alpha = 96.55(3)$, $\beta = 93.05(3)$, $\gamma = 108.66(3)°$, $V = 3239.4(11)$ Å^3, $\rho_{calcd} = 1.571$ g cm^{-3}, $Z = 2$, $T = 123$ K, $\mu(Mo_{K\alpha}) = 2.704$ mm^{-1}, 20161 measured reflections, 10150 independent, $7192 > 2\sigma(I)$, 823 parameters, $R1 = 0.0542$, $wR2 = 0.1070$, GOF = 1.102. The data were collected on a Nonius Kappa CCD diffractometer with $Mo_{K\alpha}$ radiation. The structures were solved by direct methods and refined against F^2 for all observed reflections with anisotropic thermal parameters for all non-hydrogen atoms. H atoms were introduced at calculated positions and constrained to ride on their parent carbon atom. Software used: SHELXTL (version 5.1), SHELXS 97, SHELXL 97 (G. M. Sheldrick, University of Göttingen). CCDC-196561 (**1**) and CCDC-196562 (**2**) contain the supplementary crystallographic data for this paper. These data can be obtained free of charge via www.ccdc.cam.ac.uk/conts/retrieving.html (or from the Cambridge Crystallographic Data Centre, 12 Union Road, Cambridge CB21EZ, UK; fax: (+44) 1223-336-033; or deposit@ccdc.cam.ac.uk).

[12] M. R. Caira, J. F. De Wet, J. G. H. Du Preez, B. Busch, H. L. Rohwer, *Inorg. Chim. Acta* **1983**, *77*, L73–L76.

[13] a) R. D. Shannon, *Acta Crystallogr. Sect. A* **1976**, *32*, 751–767; b) E. N. Rizkalla, G. R. Choppin in *Handbook on the Physics and Chemistry of Rare Earths. Lanthanides/Actinides: Chemistry, Vol. 18* (Eds.: K. A. Gschneidner, Jr., L. Eyring, G. R. Choppin, G. H. Lander), Elsevier Science, Amsterdam, **1994**, p. 529.

[14] D. L. Clark, S. D. Conradson, S. A. Ekberg, N. J. Hess, M. P. Neu, P. D. Palmer, W. Runde, C. D. Tait, *J. Am. Chem. Soc.* **1996**, *118*, 2089–2090.

[15] L. Gagliardi, B. Roos, *Inorg. Chem.* **2002**, *41*, 1315–1319.

[16] The difference between the An^{VI}=O and An^{V}=O bond lengths should not be equal to 0.14 Å, a value which has been considered after comparison of the crystal structures of some analogous $[NpO_2]^{2+}$ and $[NpO_2]^{+}$ derivatives, for example $[MNpO_2(OAc)_3]$ (M = Ba or Na).[4] It seems that the Np^{VI} = O bond length of 1.71 Å in these complexes, which has been calculated from the crystal structure of the isostructural uranyl compound, is too short; a better value for this bond length is 1.75 Å (0.01 Å shorter than the typical U^{VI}=O bond).

[17] S. M. Cendrowski-Guillaume, M. Nierlich, M. Ephritikhine, *Eur. J. Inorg. Chem.* **2001**, 1495–1498.

[18] C. J. Burns, D. C. Smith, A. P. Sattelberger, H. B. Gray, *Inorg. Chem.* **1992**, *31*, 3724–3727.

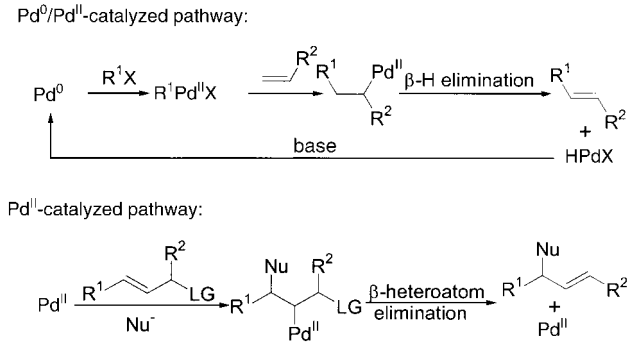
 © 2003 Wiley-VCH Verlag GmbH & Co. KGaA, Weinheim

Palladium-Catalyzed Reactions

"Walking" of the C–C π Bond over Long Distances in Pd-Catalyzed Reactions of 2,3-Allenoic Acids with ω-1-Alkenyl Halides**

Shengming Ma and Zhanqian Yu*

Transition-metal-catalyzed reactions have proven to be one of the most powerful pathways for the formation of carbon–carbon bonds as well as carbon–heteroatom bonds.[1] Palladium is a particularly useful and versatile transition metal used for organic synthesis.[2] Two reaction pathways have been observed in the Pd-catalyzed Heck-type reactions of alkenes (Scheme 1). The catalytic cycle of the Heck reaction was

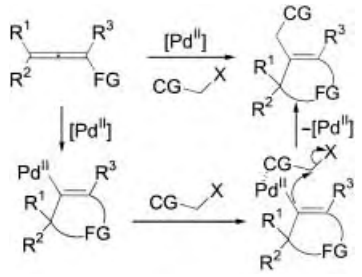


Scheme 1. Possible mechanistic pathways for Pd-catalyzed Heck-type reactions.

based on the Pd^0–Pd^{II}–Pd^0 pathway,[3] whereas in Pd^{II}-catalyzed reactions the catalyst was regenerated through a β-heteroatom elimination.[4] Herein we report the first example of Pd^{II}-catalyzed "walking" of the carbon–carbon π bond over a carbon chain in which the combination of cyclic oxypalladation–carbopalladation and repeated dehydropalladation/hydropalladation–dehalopalladation are the main steps of a catalytic cycle.

On the other hand, we have recently applied the transition-metal-promoted or -catalyzed cyclizations of 2,3-allenoic acids/esters or salts for the synthesis of several kinds of butenolides.[5] In those reactions, we could easily introduce an aryl/vinyl substituent at the β position of the butenolides. Nevertheless, under those established reaction conditions the sp^3-hybridized carbon atom could not be introduced into the product by the direct reaction of the allenoic acids and sp^3-hybridized carbon halides as a result of the intrinsic stability problem of alkyl palladium species. Although we have successfully developed an alternative two-step method for the synthesis of the β-alkyl-substituted butenolides, we wished to develop a new method with which the sp^3-hybridized carbon atom could be directly introduced into butenolides.

We observed the formation of unusual products in the Pd^{II}-catalyzed coupling cyclization reaction of 2,3-allenols or 1,2-allenyl ketones with allylic halides[6] possibly through a coordination-directed direct replacement of the halogen atom by the corresponding palladium species or an oxidative addition–reductive elimination process[7] (Scheme 2). Based on this hypothesis a Pd-catalyzed cross-coupling cyclization reaction of functionalized allenes with halides bearing a coordination center may be possible.



Scheme 2. Pd^{II}-catalyzed coupling reaction of functionalized allenes with organic halides bearing a group with coordination ability. CG = coordinating group, FG = functional group.

As a first try, we searched for a protocol of the coupling cyclization of functionalized allenes (e.g. allenols, allenoic acids) with homoallylic halides, in which the C=C bonds may act as a coordination group. We were pleased to discover that homoallylic bromide **2a** in *N,N*-dimethylformamide (DMF) could react with the 4-phenyl-2-propyl-2,3-butadienoic acid (**1a**) under the catalysis of $PdCl_2$ to form the desired product **3a** in 41% yield (Table 1, entry 1). The reaction conditions were further optimized and some typical results are listed in Table 1. Other solvents were also effective. For example, in methanol, dioxane, and hexamethyl phosphoramide (HMPA), comparable yields were observed (Table 1, entries 3–5). Different catalysts showed almost the same results (Table 1, entries 6–11). The reaction was sensitive to temperature. Higher yields were observed at relatively higher temperatures (Table 1, entries 11–13). The best results were obtained when we used 5 mol% of $Pd(OAc)_2$ and 5 equivalents of the homoallylic bromide in DMF, which provided the product **3a** in 58% yield (Table 1, entry 13).

In principle, the presence of the C=C bonds allows two possible pathways for this transformation (Scheme 3). One is the coordination-directed direct substitution pathway (path A), in which $PdCl_2$ coordinates with the double bond

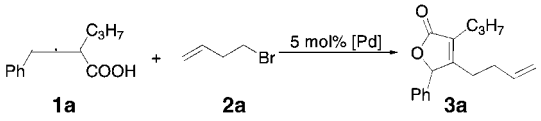
[*] Prof. Dr. S. Ma, Z. Yu
State Key Laboratory of Organometallic Chemistry
Shanghai Institute of Organic Chemistry, Chinese Academy of Sciences
354 Fenglin Lu, Shanghai 200032 (P.R. China)
Fax: (+86) 21-6416-6128
E-mail: masm@pub.sioc.ac.cn

[**] Financial support from the National Natural Science Foundation of China and the Major State Basic Research Development Program (Grant No. G2000077500) are greatly appreciated. Shengming Ma is the recipient of 1999 Qiu Shi Award for Young Scientific Workers issued by Hong Kong Qiu Shi Foundation of Science and Technology (1999–2003).

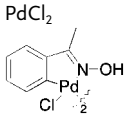
Supporting information for this article is available on the WWW under http://www.angewandte.org or from the author.

 DOI: 10.1002/anie.200250562 © 2003 Wiley-VCH Verlag GmbH & Co. KGaA, Weinheim

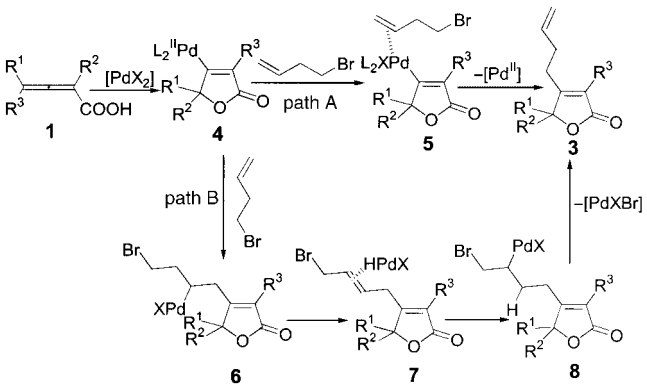
Table 1: Pd^{II}-catalyzed of coupling cyclization reaction of 4-phenyl-2-propyl-2,3- butadienoic acid **1a** and homoallyl bromide **2a**.



1a **2a** **3a**

Entry	Catalyst	Solvent	T [°C]	t [h]	Yield [%]
1	$PdCl_2$	DMF	50	22	41
2[a]	$PdCl_2$	DMF	50	46	44
3	$PdCl_2$	ethanol	50	38	44
4	$PdCl_2$	HMPA	50	45	40
5	$PdCl_2$	dioxane	50	33.5	17
6	$PdCl_2$	DMF	80	10.5	46
7[b]		HMPA	50	34.5	40
8	$[PdCl_2(dppf)]$	DMF	50	67	30
9	$[PdCl_2(PPh_3)_2]$	DMF	50	110	30
10	$[PdCl_2(PhCN)_2]$	DMF	80–90	1	51
11	$Pd(OAc)_2$	DMF	50	33	43
12	$Pd(OAc)_2$	DMF	80	2	51
13	$Pd(OAc)_2$	DMF	100	1	58

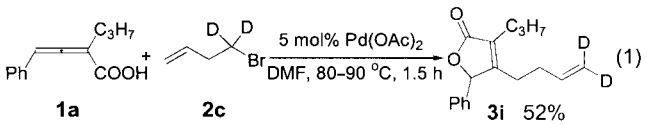
[a] Catalyst: 10 mol%. [b] Catalyst: 5 mol%.



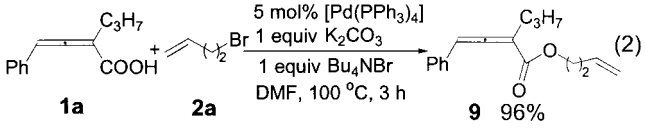
Scheme 3. The possible reaction pathways.

remote from the acid group in 2,3-allenoic acids **1**. Subsequent cyclic oxypalladation affords palladium intermediate **4**, which coordinates with the carbon–carbon double bonds of homoallylic bromide **2a** followed by an oxidative addition–reductive elimination process leading to **3**.[7] The alternative pathway is the cyclic oxypalladation–carbopalladation pathway with repeated dehydropalladation/hydropalladation–dehalopalladation (path B).

To clarify the mechanism, the reaction of deuterated homoallylic bromide **2c** and **1a** was carried out. Only product **3i** in which the two deuterium atoms located at the terminal carbon atom of the acyclic carbon–carbon double bond was obtained in 52% yield [Eq. (1)]. When the reaction was carried out in the presence of $[Pd(PPh_3)_4]$, only **9** was obtained in 96% yield [Eq. (2)].



1a **2c** **3i** 52%

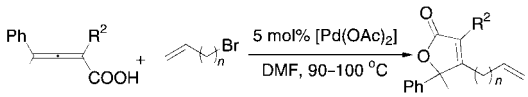


1a **2a** **9** 96%

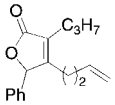
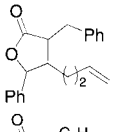
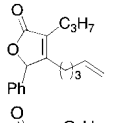
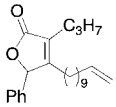
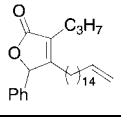
Those findings illustrated that the reaction proceeded through path B. To the best of our knowledge, this is the first example of a Pd^{II}-catalyzed cycle that combines carbopalladation with repeated dehydropalladation/hydropalladation–dehalopalladation. Based on these results, we were interested to see how far a repeated dehydropalladation and hydropalladation sequence can travel. We prepared ω-bromoalkenes **2a–d** according to a literature method,[8] and some typical results under the established reaction conditions are shown in Table 2. The substituent of allenoic acids could be aryl, alkyl, and benzyl. The reaction of **1a** with **2d** proceeded smoothly to give the corresponding products **3e** in 18% yield, an average of 93% yield for every step (Table 2, entry 5). In this reaction the palladium traveled over 14 carbon atoms![9]

In conclusion, we have developed a useful method for the direct introduction of an sp^3-hybridized carbon atom at the β position of butenolides through the Pd^{II}-catalyzed coupling cyclization reaction of 2,3-allenoic acids with ω-1-alkenyl halides. The reaction proceeds through a cyclic oxypalladation–carbopalladation with repeated dehydropalladation/hydropalladation–β-dehalopalladation process. The repeated dehydropalladation and hydropalladation sequence can travel through a chain of fourteen carbon atoms.

Table 2: The coupling cyclization of 2,3-allenoic acids and ω-1-alkenyl halides.[a]



1 **2** **3**

Entry	**1** (R^2)	**2** (n)	t [h]	Product **3**		Yield [%]
1	**a** (C_3H_7)	**a** (2)	1		**a**	58
2	**c** ($PhCH_2$)	**a** (2)	1.5		**b**	48
3	**a**	**b** (3)	10		**c**	45
4	**a**	**d**[b] (9)	21		**d**	30
5	**a**	**e** (14)	9		**e**	18

[a] The reaction was carried out using **1** (0.25 mmol), **2** (1.25 mmol), and $Pd(OAc)_2$ in DMF. [b] **2d**: 10 equiv.

 © 2003 Wiley-VCH Verlag GmbH & Co. KGaA, Weinheim

Experimental Section

Typical procedure: A mixture of **1a** (50 mg, 0.25 mmol), homoallylic bromide **2a** (170 mg, 1.26 mmol), and $Pd(OAc)_2$ (3 mg, 0.013 mmol) in DMF (2 mL) was stirred at 100 °C for 1 h. After diluting with diethyl ether, the reaction mixture was washed twice with water, and the organic layer was dried over $MgSO_4$ and concentrated by evaporation. The residue was purified by column chromatography on silica gel (petroleum ether/ethyl acetate = 10:1) to afford **3a** as an oil (37 mg, 58 %). ^{1}H NMR (300 MHz, $CDCl_3$): $\delta = 7.41$–7.30 (m, 3H), 7.22–7.12 (m, 2H), 5.74–5.60 (m, 2H), 5.03–4.91 (m, 2H), 2.57–2.41(m, 1H), 2.29 (t, $J = 7.50$ Hz, 2H), 2.20–2.00 (m, 3H), 1.66–1.53 (m, 2H), 0.95 ppm (t, $J = 7.20$ Hz, 3H); ^{13}C NMR (75.4 MHz, $CDCl_3$): $\delta = 13.85$, 21.46, 25.56, 25.88, 31.72, 83.69, 116.16, 126.89, 127.51, 128.89, 129.21, 134.85, 136.31, 162.33, 174.36 ppm; EIMS: m/z (5): 257 (10.26) [M^++1], 256 (12.29) [M^+], 105 (100); IR(neat): $\tilde{\nu} = 1747$, 1668, 1635, 1602 cm^{-1}; HRMS: calcd for $C_{17}H_{20}O_2$: 256.14633; found: 256.14872.

Received: November 15, 2002 [Z50562]

Keywords: alkenes · allenes · carboxylic acids · lactones · migration · oxypalladation

[1] a) S. Ma, *Youji Huaxue* **1991**, *11*, 561; b) A. de Meijere, F. E. Mever, *Angew. Chem.* **1994**, *106*, 2473; *Angew. Chem. Int. Ed. Engl.* **1994**, *33*, 2379; c) E. Negishi, C. Coperet, S. Ma, S. Liou, F. Liu, *Chem. Rev.* **1996**, *96*, 365; d) I. Ojima, M. Tzamarioudaki, Z. Li, R. J. Donovan, *Chem. Rev.* **1996**, *96*, 635.

[2] a) *Palladium Reagents in Organic Synthesis* (Ed.: R. F. Heck), Academic Press, London, **1985**; b) *Palladium Reagents and Catalysts: Innovations in Organic Synthesis* (Eds.: J. Tsuji), Wiley, Chichester, UK, **1995**; c) *Metal-Catalyzed Cross-Coupling Reactions* (Eds.: F. Diederich, P. J. Stang), Wiley-VCH, New York, **1998**.

[3] a) T. Mizoroki, K. Mori, A. Ozaki, *Bull. Chem. Soc. Jpn.* **1971**, *44*, 581; b) R. F. Heck, J. P. Nolley, *J. Org. Chem.* **1972**, *37*, 2320; c) G. D. Daves, A. Hallberg, *Chem. Rev.* **1989**, *89*, 1433; d) G. T. Crisp, *Chem. Soc. Rev.* **1998**, *27*, 427; e) I. P. Beletskaya, A. V. Cheprakov, *Chem. Rev.* **2000**, *100,* 3009.

[4] a) S. Ma, X. Lu, *J. Chem. Soc. Chem. Commun.* **1990**, 733; b) S. Ma, X. Lu, *J. Org. Chem.* **1991**, *56*, 5120; c) X. Lu, G. Zhu, Z. Wang, *Synlett* **1998**, 115; d) Q. Zhang, X. Lu, *J. Am. Chem. Soc.* **2000**, *122*, 7604.

[5] For the synthesis of butenolides from 2,3-allenoic acids, see: a) S. Ma, Z. Shi, *J. Org. Chem.* **1998**, *63*, 6387; b) S. Ma, Z. Yu, *Angew. Chem.* **2002**, *114*, 1853; *Angew. Chem. Int. Ed.* **2002**, *41*, 1775.

[6] a) S. Ma, L. Li, *Org. Lett.* **2000**, *2*, 941; b) S. Ma, W. Gao, *Tetrahedron Lett.* **2000**, *41*, 8933; c) S. Ma, W. Gao, *J. Org. Chem.* **2002**, *67*, 6104.

[7] A. J. Canty, *Acc. Chem. Res.* **1992**, *25*, 83.

[8] a) H. O. House, W. C. Liang, P. D. Weeks, *J. Org. Chem.* **1974**, *39,* 3102; b) E. Negishi, L. D. Boardman, H. Sawada, V. Bagheri, A. T. Stoll, J. M. Tour, C. L. Rand, *J. Am. Chem. Soc.* **1988**, *110*, 5383; c) S. Xu, S. J. N. Cruchon-Dupeyrat, J. C. Garno, G. Liu, G. K. Jennings, T. Yong, P. E. Laibinis, *J. Chem. Phys.* **1998**, *108*, 5002; d) U. Beginn, G. Zipp, M. Moller, *Chem. Eur. J.* **2000**, *6*, 2016; e) K. Chai, P. Sampson, *J. Org. Chem.* **1993**, *58*, 6807.

[9] a) D. D. Bender, F. G. Stakem, R. F. Heck, *J. Org. Chem.* **1982**, *47*, 1278; b) B. C. Soderberg, B. Akermark, S. S. Hall, *J. Org. Chem.* **1988**, *53*, 2925; c) A. C. Albeniz, P. Espinet, Y. Jeannin, M. Philoche-Levisalles, B. E. Mann, *J. Am. Chem. Soc.* **1990**, *112*, 6594; d) R. C. Larock, Y. Lu, A. C. Bain, *J. Org. Chem.* **1991**, *56*, 4589.

 © 2003 Wiley-VCH Verlag GmbH & Co. KGaA, Weinheim

A Disappearing Polymorph

A Classical Example of a Disappearing Polymorph and the Shortest Intermolecular H···H Separation Ever Found in an Organic Crystal Structure**

*Petra Bombicz, Mátyás Czugler, Roland Tellgren, and Alajos Kálmán**

One of the best documented examples of a "disappearing polymorph"[1–7] concerns 1,2,3,5-tetra-*O*-acetyl-β-D-ribofuranose.[8–17] Following its first preparation in 1947,[8] polymorph *A* was routinely obtained in different laboratories over several years.[9,13] By 1954 this polymorph had "disappeared"[12–14] in favor of a more stable, higher melting polymorph *B*;[10,11,15,16] attempts to obtain polymorph *A* in Europe,[10,11,13] Australia,[15] and the United States[12,14,16] were unsuccessful. In 1981 polymorph *A* reappeared in Budapest,[17] and, thanks to strict precautions against contamination, it has been possible to preserve it over many years. The initial X-ray study has now been followed up by low-temperature X-ray and neutron diffraction analyses of both polymorphs, which reveal significant differences in the crystal packing and molecular conformation. At 110 K and below, unstable polymorph *A* contains the shortest intermolecular H···H contact ever found in an organic crystal structure.

In recent years, the study of polymorphism[6,18–20] has gained considerable impetus as its scientific, industrial and commercial significance has been recognized.

Several cases are documented[1,3,6] where, after nucleation of a more stable crystal form, a previously obtained polymorph became unobtainable. Such loss of control over the crystallization process[1] is not only disturbing but may also make industrial processes intractable.[21] More sophisticated techniques,[22–25] such as the addition of tailor-made additives, conformational mimicry, or solvent-mediated transformations, have been introduced to influence the crystallization process to preferentially produce a particular polymorph.

[*] Prof. Dr. A. Kálmán, Dr. P. Bombicz, Dr. M. Czugler
Institute of Chemistry, Chemical Research Center
Hungarian Academy of Sciences
Pusztaszeri út 59–67
PBox 17, 1525 Budapest (Hungary)
Fax: (+36) 1-325-7554
E-mail: akalman@chemres.hu

Prof. Dr. R. Tellgren
Department of Materials Chemistry
The Ångström Laboratory, Uppsala University
PBox 538, SE-751 21 Uppsala (Sweden)

[**] The authors express their gratitude to Prof. Jack Dunitz for invaluable discussions. The authors acknowledge Dr. József Kovács, Mr. Csaba Kertész, and Dr. János Madarász (Budapest), Mr. Håkan Rundlöf and Dr. Valéry Baron (Studsvik). P.B. is indebted to the Royal Swedish Academy of Sciences for the support of her stay at the Studsvik Neutron Research Laboratory, Uppsala University.

Supporting information for this article is available on the WWW under http://www.angewandte.org or from the author.

 DOI: 10.1002/anie.200219504 © 2003 Wiley-VCH Verlag GmbH & Co. KGaA, Weinheim

Studies of the polymorphism of 1,2,3,5-tetra-*O*-acetyl-β-D-ribofuranose have a long history.[1,4,5,7] The compound is used as starting material for nucleoside synthesis. The preparation of the lower melting unstable form *A* was described in 1947 (m.p. 58 °C, $[\alpha]_D^{15} = +20°$ in chloroform)[8] and in 1948 (m.p. 56 °C, $[\alpha]_D^{20} = -3.6°$ in methanol).[9] The higher melting stable form *B* (m.p. 82 °C, $[\alpha]_D^{24} = -12.6°$ in chloroform, $[\alpha]_D^{20} = -15.4°$ in methanol)[10] apparently appeared only in 1950.

The phase transition of this compound and the catalytic effect of form *B* in this transformation were recognized in July 1952.[12] However, the nature of the difference between the two forms was not clear and they were alluded to as isomers. In November 1952, Farrar[13] recorded that the dissolved crystals of both forms showed no significant change in specific rotation and thus concluded that structural isomerism was unlikely.

The first X-ray diffraction results and at the same time the apparently last occurrence of the unstable form *A* were reported in 1954 by Patterson and Groshens.[14] The cell parameters, crystal system, and space group of both dimorphs were determined and the transformation in the solid state was examined by Laue photographs.

The difficulty of reproducing the lower melting form[1,4,7,10–14] has long prevented further study of this remarkable polymorphism. Although the room-temperature crystal structure of the stable form *B* was reported in 1973[15] and again in 1976,[16] form *A* seems to have "disappeared" until in 1981, 27 years after its last reported occurrence, it reappeared in Budapest.[17] Its melting point, space group and cell constants agreed with those given by Patterson and Groshens,[14] and its optical rotation in chloroform matched that of the stable form *B*, in agreement with Farrar's observation.[13] Czugler et al. reported the single-crystal X-ray diffraction measurement at room temperature.[17] The structure analysis showed that although the crystal packing is quite different, the puckering of the furanose rings is essentially the same. However, the conformations of two of the four acetyl groups differ significantly (C4-C5-O5-C6 $\Delta\tau =$ 92.5°, C1-C2-O2-C10 $\Delta\tau = 70.0°$), which indicates conformational dimorphism of *A* and *B* (Figure 1). It was also apparent that some intermolecular H···H contacts (see Table 1 in the Supporting Information) in the unstable form *A* are markedly shorter than 2.4 Å, the sum of the van der Waals radii (even if the "classical" van der Waals radius of 1.20 Å for hydrogen[26] is found to be overestimated by about 0.1 Å[27]), whereas no such short contacts are present in form *B*. It seemed to us possible that this type of close intermolecular contact might be responsible for the relative instability of form *A*.[28,29]

To estimate the role of crystal forces on the molecular conformation, the intramolecular nonbonded potential energy was minimized for both the *A* and *B* molecular geometries with empirical atom-pair potential functions.[17] The computed intramolecular potential energy of the molecule in form *B* was higher by 15.7 kJ mol^{-1}, which suggests that the greater stability of this polymorph must be a result, not of intramolecular, but of intermolecular effects.

In an attempt to improve the room-temperature X-ray model, especially in regard of the hydrogen atoms, we undertook low-temperature X-ray analyses of both crystal forms[30] (Figure 1). Careful recrystallization from ethanol yielded large (8–9 mm long, 2–3 mm thick) columns of the unstable form *A* suitable for neutron diffraction measurement (Figure 1 in the Supporting Information). Large plates (2.6–3.0 mm long, 1 mm thick) of form *B* were obtained by controlled evaporation of a methanol solution. During the whole experimental period various precautions were taken to preserve the unstable polymorph *A*, crystals of which were stored in sealed ampoules over many years. Each experiment was done first with form *A*, then with form *B*, with strict adherence to protocol. The differential scanning calorimetry (DSC) measurements were made in hermetically sealed sample pans. After crystallization of the stable form *B*, the laboratory was repainted and every piece of furniture, equipment was cleaned. Labcoats, towels, and clothing were washed after working with this form to prevent contamination by it. New glassware was used whenever the unstable form *A* was handled.

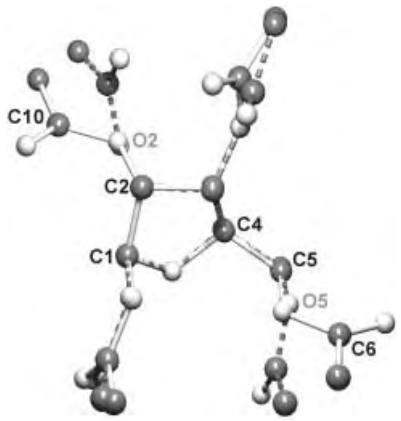


Figure 1. Superposition of the 1,2,3,5-tetra-*O*-acetyl-β-D-ribofuranose molecule in the unstable form *A* (solid) and the stable form *B* (dotted), as determined by neutron diffraction at 25 K.

The neutron diffraction experiments were carried out at 25.0 K (Figure 1).[32] The low-temperature X-ray structures were used as starting models in the neutron-data refinement (Supporting Information Figures 2 and 3), which included anisotropic displacement parameters of hydrogen atoms. The hydrogen positions derived from the X-ray model at 110 K agreed well with those from the neutron diffraction results, the largest difference in O=C–C–H torsion angle is 6.5°. Re-refinement of the room-temperature model[17] of form *A* with up-to-date computing techniques led to remarkable differences in methyl hydrogen positions but no major variations compared with the low-temperature X-ray and neutron diffraction structure models.

The neutron diffraction study shows the presence of a remarkably short intermolecular C–H···H–C distance (H2···H4 1.949(7) Å) between ribose H atoms in the unstable form *A* (Figure 2) and its absence (H2···H4 3.70(1) Å) in the stable form *B*. With C–H bond distances fixed at 1.08 Å, the H2···H4 distance is 1.95(9) Å at 110 K and 2.10 (7) Å at 298 K. Thus, even at room temperature the distance in question is extremely short.[27,33] Over the whole temperature range, and

 © 2003 Wiley-VCH Verlag GmbH & Co. KGaA, Weinheim

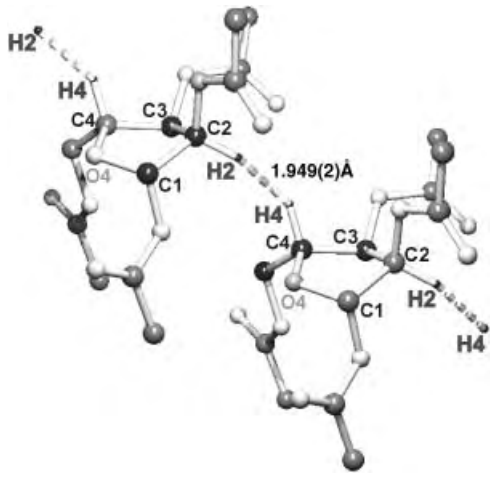


Figure 2. The shortest intermolecular H···H distance C2-H2···H4-C4 (1.949(7) Å) to be found in an organic crystal structure. It occurs in the unstable form *A* of 1,2,3,5-tetra-*O*-acetyl-β-D-ribofuranose. It is seen that the approach of the two hydrogen atoms is nearly head on. Other hydrogen atoms are omitted for clarity.

especially at low temperature, this intermolecular contact must correspond to a strong repulsive force in the crystal structure *A*, which is, of course balanced by the resultant of all the other, mainly attractive forces.[33] The repulsive H2···H4 interaction is nearly parallel to the crystallographic *b* axis. On cooling the crystal from room temperature to 110 K, the *b* axis contracts by 0.12 Å, but on further cooling to 25 K, it does not contract any more.

There are three other short H···H distances within the sum of the van der Waals radii (2.4 Å) between C–H moieties in both crystals (form *A*: H1···H11A 2.257(8), H7A···H13C 2.342(7), H5B···H7B 2.377(8) Å (Supporting Information: Figure 4) and form *B*: H2···H5A 2.25(1), H4···H7C 2.38(2), H5B···H9B 2.35(2) Å, not shown) in which at least one of the atoms is from a terminal methyl group, with more conformational freedom than a methylene or a skeletal hydrogen atom. Five attractive C–H···O interactions shorter than 2.6 Å (average length is 2.52(5) Å) may help to balance the repulsive H···H approaches in the unstable form *A*. In the stable form *B* there are eight intermolecular C–H···O hydrogen bonds with the average length of 2.45(9) Å (Supporting Information: Table 1).

With the help of the Cambridge Crystallographic Database,[34] intermolecular H···H distances between 1.9 and 2.2 Å in all crystal structures determined by neutron diffraction were collected. We find that form *A* of 1,2,3,5-tetra-*O*-acetyl-β-D-ribofuranose at 25 K contains the shortest intermolecular H···H distance (1.949(7) Å) ever observed in an organic crystal. This distance corresponds to the strong repulsive region of the potential energy curve obtained in an ab initio calculation for $CH_4\cdots CH_4$ as a function of C–C separation and relative orientation.[36]

The phase transition was examined by placing a small crystal of form *B* on top of a 2–3 mm size block of crystal *A* at room temperature. Crystal *A* became opaque within an hour but its outward shape was unchanged after four days. On placing crystals of form *A* and *B* in a drop of saturated solution, rapid recrystallization was observed; the less soluble form *B* grew at the expense of the more soluble form *A* within minutes, which confirms that *B* is the stable dimorph.

The phase transition cannot be generated by grinding the crystals or by changing the temperature within the range −150 to +100 °C, as shown by cooling and heating samples of forms *A* and *B* separately in a DSC apparatus. The phase transition occurs only after inoculation of form *A* with even a minute amount of form *B*. Immediate heating in the temperature range 12 to 100 °C then shows endothermic melting of form *A* at 55–56 °C, followed by fast exothermic recrystallization of the liquid drop on the crystal of *B*, and, finally, melting of form *B* at 81–82 °C (Supporting Information: Figure 5). The phase transition also takes place in the solid phase at room temperature; 26 h after seeding form *A*, form *B* was present almost exclusively, as shown by the melting point and enthalpy of melting (Supporting Information: Figure 6). Since the phase transformation is a slow exothermic process, the DSC signal tends to fade into the baseline. The lower melting enthalpy of unstable form *A* (91 $J\,g^{-1}$) relative to the higher value of stable form *B* (102 $J\,g^{-1}$) indicates[37] that the 1,2,3,5-tetra-*O*-acetyl-β-D-ribofuranose polymorph system is monotropic.

The unit-cell volume per molecule is higher for the stable form *B* than for the unstable form *A* at the same temperature. Thus, the stable crystal is less densely packed in a higher-symmetry space group than the unstable crystal (packing coefficients[38] are *A*: 73.2 %, *B*: 71.8 %). Usually it is the other way round.[18,33,39,40] It is an example of the limitation of the close-packing principle: the more tightly packed polymorph, may have lower free energy,[33] as a balance of the repulsive H···H and the only occurring attractive C–H···O forces. Also unusual is the behavior of form *A* on cooling from 110 K to 25 K. The unit cell volume *increases* by 5.4(7) $Å^3$ (0.7 %). The *b* and *c* axial lengths do not change while the *a* axis increases by 0.077 Å.

Our structural study of the unstable polymorph *A* of 1,2,3,5-tetra-*O*-acetyl-β-D-ribofuranose has shown that this crystal contains the shortest intermolecular H···H distance ever found in an organic crystal structure. The repulsive interaction associated with this distance may be decisive for the crystal stability as determined by the fine-tuning of intra- and intermolecular crystal forces.

Received: June 10, 2002
Revised: December 18, 2002 [Z19504]

Keywords: conformation analysis · neighboring-group effect · phase transitions · polymorphism · structure elucidation

[1] J. D. Dunitz, J. Bernstein, *Acc. Chem. Res.* **1995**, *28*, 193–200.
[2] J. Webb, B. Anderson, *J. Chem. Educ.* **1978**, *55*, 644; G. D. Woodard, W.C McCrone, *J. Appl. Crystallogr.* **1975**, *8*, 342.
[3] J. Bernstein, J. O. Henck, *Cryst. Eng.* **1998**, *1*, 119–128.
[4] J. P. Glusker, M. Lewis, M. Rossi, *Crystal Structure Analysis for Chemists and Biologists*, VCH, New York, **1994**; J. Dunitz, *Acta Crystallogr. Sect. A* **1999**, *55*, 2.
[5] V. W. Jacewicz, J. H. C. Nayler, *J. Appl. Crystallogr.* **1979**, *12*, 396–397.

 © 2003 Wiley-VCH Verlag GmbH & Co. KGaA, Weinheim

[6] "Polymorphism in Molecular Crystals": J. Bernstein in *IUCr Monographs on Crystallography 14*, Clarendon, Oxford, **2002**.
[7] "Organic Solid State Chemistry": G. R. Desiraju in *Studies in Organic Chemistry 32*, Elsevier, Amsterdam, **1987**, p. 489.
[8] G. A. Howard, B. Lythgoe, A. R. Todd, *J. Chem. Soc.* **1947**, 1052 – 1054.
[9] H. Bredereck, E. Hoepfner, *Chem. Ber.* **1948**, *81*, 51 – 52.
[10] H. Zinner, *Chem. Ber.* **1950**, *83*, 153 – 156.
[11] R. D. Guthrie, S. C. Smith, *Chem. Ind.* **1968**, 547 – 548.
[12] J. Davoll, G. B. Brown, D. V. Visser, *Nature* **1952**, *170*, 64 – 65.
[13] K. R. Farrar, *Nature* **1952**, *170*, 896.
[14] A. L. Patterson, B. P. Groshens, *Nature* **1954**, *173*, 398.
[15] V.J. James, J. D. Stevens, *Cryst. Struct. Commun.* **1973**, *2*, 609 – 612.
[16] B. J. Poppleton, *Acta Crystallogr. Sect. B.* **1976**, *32*, 2702 – 2705.
[17] M. Czugler, A. Kálmán, J. Kovács, I. Pintér, *Acta Crystallogr. Sect. B* **1981**, *37*, 172 – 177.
[18] "Crystal Engineering, The Design of Organic Solids": G. R. Desiraju in *Material Science Monographs, Vol. 5*, Elsevier, Amsterdam, **1989**.
[19] T. L. Threlfall, *Analyst* **1995**, *120*, 2435 – 2460; A. Nangia, G. R. Desiraju, *Top. Curr. Chem.* **1998**, *198*, 57 – 96.
[20] G. R. Desiraju, *Nature* **2001**, *412*, 397 – 400.
[21] S. R. Chemburkar, J. Bauer, K. Deming, H. Spiwek, K. Patel, J. Morris, R. Henry, S. Spanton, W. Dziki, W. Porter, J. Quick, P. Bauer, J. Donaubauer, B. A. Narayanan, M. Soldani, D. Riley, K. McFarland, *Org. Process Res. Dev.* **2000**, *4*, 413 – 417.
[22] "Polymorphism": W. C. McCrone in *Physics and Chemistry of the Organic Solid State, Vol. II* (Eds: D. Fox, M. M. Labes, A. Weissberger), Interscience, New York, **1965**, pp. 726 – 767.
[23] M. R. Caira, *Top. Curr. Chem.* **1998**, *198*, 163 – 208.
[24] L. Addadi, Z. Berkovitch-Yellin, I. Weissbuch, J. van Mil, L. Shimon, M. Lahav, L. Leiserowitz, *Angew. Chem.* **1985**, *97*, 476 – 495; *Angew. Chem. Int. Ed. Engl.* **1985**, *24*, 439 – 528; Z. Berkovitch-Yellin, J. van Mil, L. Addadi, M. Idelson, M. Lahav, L. Leiserowitz, *J. Am. Chem. Soc.* **1985**, *107*, 3111 – 3122; E. Staab, L. Addadi, L. Leiserowitz, M. Lahav, *Adv. Mater.* **1990**, *2*, 40 – 43.
[25] R. J. Davey, L. A. Polywka, S. J. Maginn, *The Control of Morhology by Additives: Molecular Recognition, Kinetics and Technology, Advances in Industrial Crystallization* (Eds.: J. Garside, R. J. Davey, A. G. Jones), Butterworth-Heinemann, Oxford, **1991**, pp. 150 – 165.
[26] A. Bondi, *J. Phys. Chem.* **1964**, *68*, 441 – 451.
[27] R. S. Rowland, R. Taylor, *J. Phys. Chem.* **1996**, *100*, 7384 – 7391.
[28] D. Braga, G. R. Desiraju, J. S. Miller, A. G. Orpen, S. L. Price, *CrystEngComm* **2002**, *4*, 500 – 509.
[29] M. J. Calhorda, P. J. Costa, *CrystEngComm* **2002**, *4*, 368 – 372.
[30] X-ray analyses of both crystal forms at 110 K, $Mo_{K\alpha}$ radiation $\lambda = 0.71073$ Å, scan mode ω-θ; Lorentz and polarization correction, structure solution by direct methods with the program SHELXS97[31a] least-squares structure refinement on F^2 by SHELXL[31b] form *A*: crystal dimensions: $0.8 \times 0.5 \times 0.5$ mm, monoclinic, $P2_1$, $a = 12.515(3)$, $b = 5.464(1)$, $c = 10.863(2)$ Å, $\beta = 96.86(3)°$, $V = 737.5(3)$ Å^3, $Z = 2$, $\rho_{calcd} = 1.433$ g cm^{-3}, 6309 collected reflections, 6098 independent reflections, 5452 reflections $I > 2\sigma$, $\theta_{max} = 55.09°$, parameters 271, $\mu = 0.123$, no absorption correction, $R = 0.046$, $wR2 = 0.136$, residual electron density 0.436 and -0.404 e Å^{-3}; form *B*: crystal dimensions: $0.7 \times 0.5 \times 0.35$ mm, orthorhombic, $P2_12_12_1$, $a = 7.360(3)$, $b = 13.596(4)$, $c = 15.183(4)$ Å, $V = 1519.3(9)$ Å^3, $Z = 4$, $\rho_{calcd} = 1.391$ g cm^{-3}, 12953 collected reflections, 11769 independent reflections, 7791 reflections $I > 2\sigma$, $\theta_{max} = 55.09°$, parameters 271, $\mu = 0.119$, semi-empirical absorption correction, $T_{min} = 0.963$, $T_{max} = 0.998$, $R = 0.045$, $wR2 = 0.122$, residual electron density 0.357 and -0.363 e Å^{-3}. All hydrogen atom positions were located in the difference electron density maps, none of them appeared disordered. CCDC 174273, CCDC 174274, CCDC 174275, and CCDC 174276 contain the supplementary crystallographic data for this paper. These data can be obtained free of charge via www.ccdc.cam.ac.uk/conts/retrieving.html (or from the Cambridge Crystallographic Data Centre, 12 Union Road, Cambridge CB2 1EZ, UK; fax: (+44) 1223–336–033; or deposit@ccdc.cam.ac.uk).
[31] a) G. M. Sheldrick, SHELXS-97, Program for Crystal Structure Solution (Release 97-2), University of Göttingen, Göttingen (Germany), **1997**; b) G. M. Sheldrick, SHELXL-97, Program for Crystal Structure Refinement, University of Göttingen, Göttingen (Germany), **1997**.
[32] a) Neutron diffraction measurements at 25 K, scan mode ω-θ; Lorentz and polarization correction, least-squares structure refinement on F by DUPALS,[32b] form *A*: $\lambda = 1.215$ Å, crystal dimensions: $2 \times 4 \times 4$ mm, $a = 12.592(4)$, $b = 5.463(2)$, $c = 10.867(4)$ Å, $\beta = 96.355(1)°$, $V = 742.9(7)$ Å^3, $Z = 2$, $\rho_{calcd} = 1.423$ g cm^{-3}, 1666 collected reflection, 1512 independent reflections, 1450 reflections $I > 3\sigma$, $\theta_{max} = 60.00°$, parameters 251, $\mu = 0.2055$, analytical absorption correction, $T_{min} = 0.3587$, $T_{max} = 0.7013$, $R = 0.031$; form *B*: $\lambda = 1.207$ Å, crystal dimensions: $1 \times 2.6 \times 3$ mm, $a = 7.291(4)$, $b = 13.577(4)$, $c = 15.117(9)$ Å, $V = 1496.4(7)$ Å^3, $Z = 4$, $\rho_{calcd} = 1.412$ g cm^{-3} 2237 collected reflection, 2033 independent reflections, 1430 reflections $I > 2\sigma$, $\theta_{max} = 51.9°$, parameters 252, $\mu = 0.233$, analytical absorption correction, $T_{min} = 0.6262$, $T_{max} = 0.8032$, $R = 0.059$; b) T. Gustafsson, DUPALS, A Full-matrix Least-squares Refinement Program, Uppsala University, **1993**.
[33] J. D. Dunitz, A. Gavezotti, *Acc. Chem. Res.* **1999**, *32*, 677 – 684.
[34] a) F. H. Allen, W. D. S. Motherwell, *Acta Crystallogr. Sect. B* **2002**, *58*, 407 – 422; b) CSD October 2000 release. 80 structures with 130 close contacts were retrieved among the 574 neutron data found with the search criteria: 3D coordinates published, no errors, not disordered, no $H_3O^+ \cdots H_2O$ ionic contacts and R factor is less than 0.075. The shortest H···H distance found in the Database is in nicotinamide (NICOAM03)[35] with 1.979(4) Å.
[35] Y. Miwa, T. Mizuno, K. Tsuchida, T. Taga, Y. Iwata, *Acta Crystallogr. Sect. B* **1999**, *55*, 78 – 84.
[36] R. L. Rowley, T. Pakkanen, *J. Chem. Phys.* **1999**, *110*, 3368 – 3377.
[37] A. Gavezzotti, G. Filippini, *J. Am. Chem. Soc.* **1995**, *117*, 12299 – 12305.
[38] A. L. Spek, PLATON, A Multipurpose Crystallographic Tool, Utrecht University, Utrecht, The Netherlands, **2002**.
[39] T. Steiner, W. Hinrichs, W. Saenger, *Acta Crystallogr. Sect. B* **1993**, *49*, 708 – 718.
[40] J. D. Dunitz, G. Filippini, A. Gavezotti, *Tetrahedron* **2000**, *56*, 6595 – 6601.

 © 2003 Wiley-VCH Verlag GmbH & Co. KGaA, Weinheim

Crystal Engineering with Acetylene

Cocrystallization with Acetylene: Molecular Complexes with Acetone and Dimethyl Sulfoxide**

Roland Boese, Michael T. Kirchner, W. Edward Billups, and Lewis R. Norman*

Dedicated to Professor Jack D. Dunitz on the occasion of his 80th Birthday

Any liquid solution consists of a complex dynamic system governed by intermolecular interactions. Important properties, such as solubility and miscibility, depend strongly on these interactions; however, they are still essentially unpredictable. Gases dissolved in liquids as molecules form clusters with defined shapes and sizes. If hydrogen atoms are present, these will be mostly involved in a hydrogen-bonded network. When a gas is cooled in the presence of a solvent under elevated pressure, cocrystals may form in which the gas molecules act as guests in the lattice of the host solvent molecules. In most instances, the lattice of the host is modified markedly and will be unstable without the guest. This behavior is well established for gas hydrates.[1]

Acetylene, still used widely for welding and as a fuel for very hot flames, dissolves readily in acetone or in dimethyl sulfoxide (DMSO). Both solvents are used along with porous material to prevent polymerization when the gas is stored under elevated pressure, typically up to 19 bar.[2] As a result of the acidic character of the hydrogen atoms in acetylene it is likely that hydrogen bonds to the oxygen atoms of the guest molecules will form.[3] Complexes between acetylene and acetone have been detected by IR spectroscopy.[4–6]

No structural characterization has been reported for acetone–acetylene and DMSO–acetylene complexes. To trap the corresponding solutions and to grow single crystals of the complexes, both components were condensed at −196 °C into a quartz capillary (0.3 mm diameter) on a vacuum line, the capillary was flame-sealed and transferred to the diffractometer, a Bruker Smart1K CCD-System with XSTREAM LT device (MSC). The latter provides a very stable, cold, gas stream along the ω axis. The goniometer head was equipped with an additional arc and an *x,y,z* slide which allows alignment of the capillary along the ω axis. This system is used as the scanning axis for data collection with a fixed ϕ angle. The capillary, which withstands pressures up to about 100 bar, was then held at −111 °C and by using our in situ crystallization technique, that is, by moving an intensity controlled, focused infrared laser beam along the capillary, a crystal was grown. The diffusion processes at the gas/liquid/solid interfaces do not lead to the formation of one single crystal that fills the entire capillary as we usually achieve for neat compounds.[7] Multiple heating/cooling cycles of the acetylene/acetone system produced more than twelve crystals at the same point. They were so close to each other that all of them diffracted simultaneously in the primary X-ray beam. Consequently, the collected data correspond to a superposition of diffraction patterns of several crystals. In a laborious hand-selection and systematic separation procedure utilizing the program RLATT in the Bruker-AXS software, we were able to extract ten consistent data sets, four of them belonging to one phase which we named α (**1**) having a cell volume $V = 505.6$ Å^3 and six belonging to a concomitant second phase, β (**2**), with $V = 601.0$ Å^3. The data were reduced separately, corrected, and evaluated with respect to coverage and data quality. The two best sets for each phase were merged. DMSO/acetylene mixtures were treated similarly. At −78 °C four crystals belonging to the same phase but with different orientations were obtained. A consistent data set of this complex (**3**) was also achieved.

In the α phase **1** the ratio of acetylene to acetone is 1:2, the structure indicates a three-component molecular complex with a dumbbell shape and two almost linear C–H···O hydrogen bonds. In the crystal these complexes are arranged in a herringbone fashion (Figure 1).

In the β phase **2** the ratio of acetylene to acetone is 1:1. The molecules are arranged in a zigzag chain with two hydrogen bonds to the oxygen atom of each acetone molecule. One of these hydrogen bonds is nearly linear to the carbonyl group while the other is side-on (Figure 2).

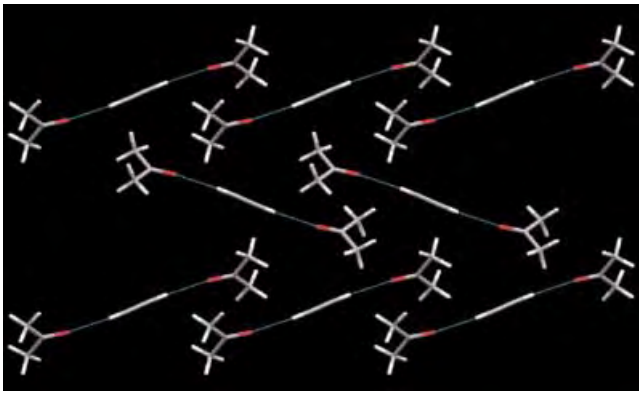


Figure 1. Cocrystal **1** of acetylene:acetone 1:2; view of the (100) plane. Selected intermolecular parameters: D(C···O) = 3.172 Å, θ(CO···H) = 173°. O red, C gray, H white.

[*] Prof. Dr. R. Boese, Dipl.-Chem. M. T. Kirchner
Institut für Anorganische Chemie der Universität
45117 Essen (Germany)
Fax: (+49) 201-183-2535
E-mail: roland.boese@uni-essen.de
Prof. W. E. Billups
Department of Chemistry, Rice University
Houston, TX 77251 (USA)
Dr. L. R. Norman
Halliburton Company, Technology Center
2600 S. 2nd Street, Duncan, OK 73536-0470 (USA)

[**] Cocrystallization with Acetylene Part 1. R.B. and M.T.K. thank the Deutsche Forschungsgemeinschaft SFB 452 for financial support. W.E.B. is supported by the National Science Foundation and the Welch Foundation.

Supporting information for this article (sample preparation, crystallization, measurement, and refinement techniques) is available on the WWW under http://www.angewandte.org or from the author.

 DOI: 10.1002/anie.200250634 © 2003 Wiley-VCH Verlag GmbH & Co. KGaA, Weinheim

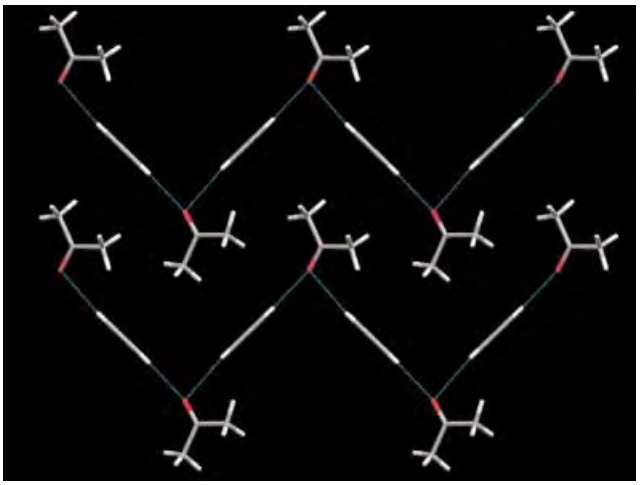


Figure 2. Cocrystal **2** of acetylene:acetone 1:1 view of the (100) plane. Selected intermolecular parameters: D(CO) = 3.246 Å, θ(CO···H) = 161°, D(CO) = 3.430 Å, θ(CO···H) = 115°. O red, C gray, H white.

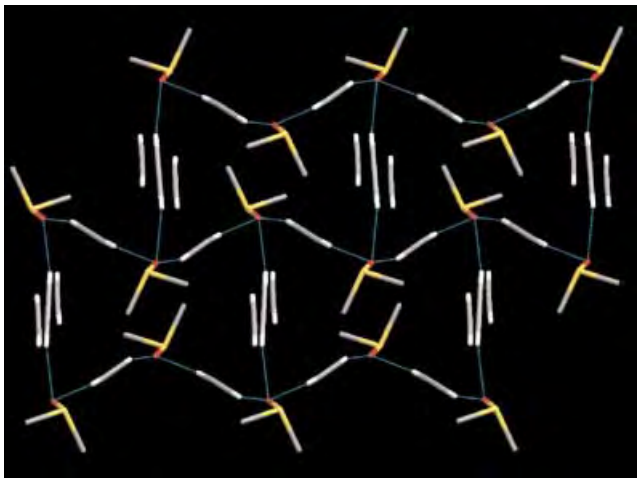


Figure 3. Cocrystal **3** of acetylene:dimethyl sulfoxide 2:1 view of the (101) plane. Methyl hydrogen atoms have been omitted for clarity. Selected intermolecular parameters: D(CO) = 3.254 Å, θ(SO···H) = 119°, D(CO) = 3.136 Å, θ(SO···H) = 163°, D(CO) = 3.182 Å, θ(SO···H) = 118°. O red, C gray, H white, S yellow.

In addition to the relatively strong C–H···O hydrogen bonds of acetylene, several much weaker C–H···O hydrogen bonds with the methyl groups can be identified. They resemble the hydrogen bonds involving the methyl groups found in the crystal structure of pure acetone, in which stacked molecules with opposing dipoles and dimers with two C–H···O hydrogen bonds occur.[8]

The methyl hydrogen bonds are responsible for creating the three-dimensional network with the 1:2 (zero-dimensional) complexes and the 1:1 (one-dimensional) zigzag-chains. From the viewpoint of crystal engineering and cocrystallization there is an fundamental conclusion: the packing motifs of the neat component can also be maintained in cocrystals, even where rather strong interactions are present.

In the molecular complex of acetylene with DMSO, **3**, the ratio of acetylene to DMSO is 2:1. A two-dimensional network can be identified, again with one nearly linear and two additional side-on C–H···O hydrogen bonds (Figure 3). The pseudohexagonal two-dimensional network of triple acetylene-bridged oxygen atoms is rather open so that neighboring layers can interlock and still leave cavities for a third molecule of acetylene that does not participate in hydrogen bonding.

As a result of the shielding of the oxygen atom by acetylene molecules in the cocrystal, the packing has no similarity to the neat DMSO crystal packing, in which C–H···O interactions are predominant.[9,10]

It is quite likely that the motifs found in structures **1** and **2** are also found in solution. At 12 bar the molecular ratio is about 2:3.[11] The solubility of acetylene in DMSO is even higher than in acetone as shown by the 2:1 ratio of the molecular complex in the solid state.

At present it is unclear which substances will cocrystallize and which will prefer to form one-component crystals. Solubility is probably a good indicator. The difference in melting points also seems to be an important factor. Experiments on a series of compounds with rather different properties might provide rules concerning their ability to form cocrystals.

The similarity of the cocrystal **2** of acetylene with acetone to that of dibromine with acetone is surprising, especially since the nature of the underlying interactions seems to be different.[12,13] However, the size of both molecules is similar, and the similarity of the interactions is supported by gas-phase measurements of bimolecular complexes of acetylene with Lewis bases.[14] In the crystal structures, even the slight tendency to less-linear arrangements of the hydrogen bonds, that was found in gas phase, bimolecular complexes, was reproduced.

Crystals **1** and **2** of acetylene with acetone represent zero- and one-dimensional patterns of C–H···O hydrogen bonds, while the crystal of acetylene with DMSO contains a two-dimensional network based on the same type of interactions. The differences in the supramolecular patterns demonstrate the high versatility of acetylene in forming molecular complexes. The existence of intermolecularly unbound acetylene in a pocket of the molecular complex with DMSO provides evidence that it will also form inclusion compounds. Similarities to the crystal structures of the neat compounds and of the cocrystal of acetylene with dibromine emphasize the importance of cocrystallization to crystal engineering studies.

We were able to demonstrate that not only neat gases and liquids can be crystallized in situ in capillaries, but also mixtures can form cocrystals under pressure. With an area-detector system and appropriate software it is even possible to solve the crystal structures of different concomitantly occurring crystals, a new technique which we suggest calling "oligo diffractometry" in contrast to single-crystal and powder diffractometry.[15] We plan to carry out additional studies on the molecular complexes of acetylene with other hydrogen-bond acceptor molecules to provide a deeper insight into the interplay of strong and weak intermolecular interactions in multicomponent systems.

 © 2003 Wiley-VCH Verlag GmbH & Co. KGaA, Weinheim

Experimental Section

1: α(2[$(CH_3)_2CO$]·C_2H_2), **2**: β($(CH_3)_2CO$·C_2H_2): Crystals formed below 162 K and were measured at 159 K on a SMART 1K, $Mo_{K\alpha}$, graphite monochromator, $\lambda = 0.71073$ Å.

The α phase is monoclinic, $P2_1/n$, $a = 5.760(3)$, $b = 10.353(5)$, $c = 8.870(4)$ Å, $\beta = 107.127(12)°$, $V = 505.6(4)$ Å^3, $Z = 4$, $\rho_{calcd} = 0.934$ g cm^{-3}, $T = 159$ K, $\mu = 0.066$ mm^{-1}, min. transmission 0.58, max. transmission 1, total of 4332 data ($\theta_{max} = 28.37°$), 1116 independent ($R_{merg} = 0.0416$), 681 observed [$F_o = 4\sigma(F)$], structure solution with statistical methods (BRUKER-SHELXS) and full-matrix least-squares refinement on F^2 (BRUKER-SHELXTL-V6.12) (53 parameters). $R1 = 0.0589$, $wR2 = 0.1948$ (all data), $w^{-1} = \sigma^2(F_o^2) + (0.01028P)^2 + 0.0489P$ with $P = [(\max\ F_o^2) + (2F_c^2)]/3$, GOF($F^2$) = 1.023, max. residual electron density 0.199 e Å^{-3}.

The β phase is monoclinic, space group $P2_1/c$, $a = 7.195(4)$, $b = 8.152(3)$, $c = 10.729(6)$ Å, $\beta = 107.241(8)°$, $V = 601.0(5)$ Å^3, $Z = 4$, $\rho_{calcd} = 0.930$ g cm^{-3}, $\mu = 0.063$ mm^{-1}, min. transmission 0.53, max. transmission 1, total of 5140 data ($\theta_{max} = 28.36°$), 1493 independent ($R_{merg} = 0.0587$), 818 observed [$F_o = 4\sigma(F)$], structure solution with statistical methods (BRUKER-SHELXS) and full-matrix least-squares refinement on F^2 (BRUKER-SHELXTL-6.12) (65 parameters). $R1 = 0.0557$, $wR2 = 0.1630$ (all data), $w^{-1} = \sigma^2\ (F_o^2) + (0.0647P)^2 + 0.0437P$ with $P = [(\max\ F_o^2) + (2F_c^2)]/3$, GOF($F^2$) = 1.042, max. residual electron density 0.244 e Å^{-3}.

3: ($(CH_3)_2SO$·2[C_2H_2]): Crystals formed below 195 K and were measured at $T = 123(2)$ K. Monoclinic, space group $C2/c$, $a = 15.579(2)$, $b = 8.5432(13)$, $c = 13.272(2)$ Å, $\beta = 109.600(3)°$, $V = 1664.1(4)$ Å^3, $Z = 8$, $\rho_{calcd} = 1.039$ g cm^{-3}, $\mu = 0.308$ mm^{-1}, min. transmission 0.89, max. transmission 1, absorption correction with SADABS V2.0, total of 3313 data ($\theta_{max} = 28.28°$), 1638 independent ($R_{merg} = 0.0221$), 1432 observed [$F_o = 4\sigma(F)$], structure solution with statistical methods (BRUKER-SHELXS) and full-matrix least-squares refinement on F^2 (BRUKER-SHELXTL-V6.12) (87 parameters). $R1 = 0.0421$, $wR2 = 0.1077$ (all data), $w^{-1} = \sigma^2\ (F_o^2) + (0.0570P)^2 + 0.8678P$ with $P = [(\max\ F_o^2) + (2F_c^2)]/3$, GOF($F^2$) = 1.082, max. residual electron density 0.556 e Å^{-3}, 0.05 Å from the sulfur atom.

The Supporting Information contains further information on sample preparation, crystallization, measurement and refinement techniques. CCDC-198412 (**1**), CCDC-198413 (**2**), and CCDC-198414 (**3**) contain the supplementary crystallographic data for this paper. These data can be obtained free of charge via www.ccdc.cam.ac.uk/conts/retrieving.html (or from the Cambridge Crystallographic Data Centre, 12 Union Road, Cambridge CB21EZ, UK; fax: (+44) 1223-336-033; or deposit@ccdc.cam.ac.uk).

Received: November 26, 2002 [Z50634]

Keywords: acetylene · crystal engineering · oligo diffractometry · structure elucidation · X-ray diffraction

[1] E. D. Sloan, *Clathrate hydrates of natural gases*, Dekker, New York, **1997**.
[2] *Ullmann's Encyclopedia of Industrial Chemistry, 6th ed. release 2001*, Wiley-VCH, Weinheim, **2001**.
[3] G. R. Desiraju, *Acc. Chem. Res.* **2002**, *35*, 565 – 573.
[4] K. Consani, G. C. Pimentel, *J. Phys. Chem.* **1987**, *91*, 289 – 293.
[5] A. M. DeLaat, B. S. Ault, *J. Am. Chem. Soc.* **1987**, *109*, 4232 – 4236.
[6] M.-L. H. Jeng, B. S. Ault, *J. Phys. Chem.* **1989**, *93*, 5426 – 5431.
[7] a) R. Boese, M. Nussbaumer, in *Organic Crystal Chemistry* (Eds.: J. B. Garbarczyk, D. W. Jones), Oxford University Press, Oxford, **1994**, pp. 20 – 37. b) www.ohcd-system.com.
[8] D. R. Allan, S. J. Clark, R. M. Ibberson, S. Parsons, C. R. Pulham, L. Sawyer, *Chem. Commun.* **1999**, 751 – 752.
[9] R. Thomas, C. B. Shoemaker, K. Eriks, *Acta Crystallogr.* **1966**, *21*, 12 – 20.
[10] M. A. Viswamitra, K. K. Nannan, *Nature* **1966**, *209*, 1016.
[11] P. Hölemann, R. Hasselmann, *Chem. Ing. Tech.* **1953**, *25*, 466 – 468.
[12] O. Hassel, K. O. Strømme, *Acta Chem. Scand.* **1959**, *13*, 275 – 280.
[13] O. Hassel, *Science* **1970**, *170*, 497 – 502.
[14] A. C. Legon, *Angew. Chem.* **1999**, *111*, 2850 – 2880; *Angew. Chem. Int. Ed.* **1999**, *38*, 2686.
[15] C. C. Wilson, *Acta Crystallogr. Sect. B* **2001**, *57*, 435 – 439.

 © 2003 Wiley-VCH Verlag GmbH & Co. KGaA, Weinheim

Crystal Structure Predictions

Searching for a Polymorph: Second Crystal Form of 6-Amino-2-Phenylsulfonylimino-1,2-Dihydropyridine**

Ram K. R. Jetti, Roland Boese, Jagarlapudi A. R. P. Sarma,* L. Sreenivas Reddy, Peddy Vishweshwar, and Gautam R. Desiraju**

Dedicated to Prof. Jack D. Dunitz on the occasion of his 80th birthday

The prediction of the crystal structure of a small organic molecule, given nothing more than its molecular structure (crystal structure prediction, CSP), has emerged as a problem of outstanding significance. The general solution requires a complete understanding of the mechanism of crystallization.[1] Recognizing the importance of CSP, blind tests were conducted between 1999 and 2001.[2–4] This communication describes our further efforts with 6-amino-2-phenylsulfonylimino-1,2-dihydropyridine (**1**; Scheme 1) which featured in the blind test carried out in 2001.

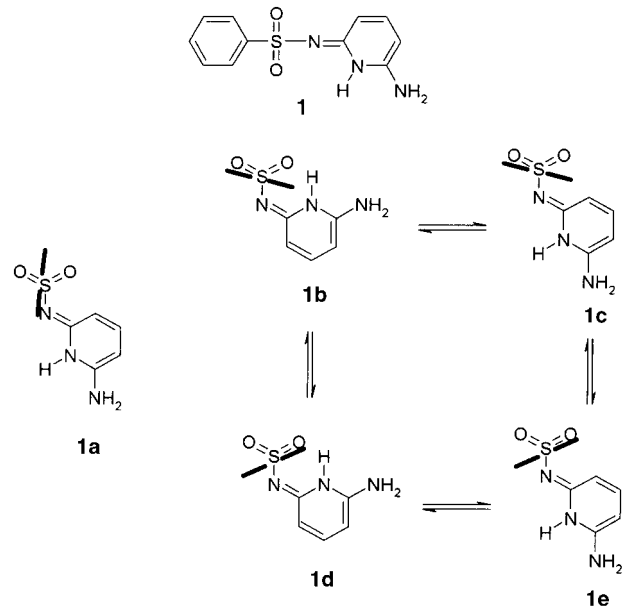
[*] Prof. Dr. G. R. Desiraju, L. S. Reddy, P. Vishweshwar
School of Chemistry
University of Hyderabad
Hyderabad 500046 (India)
Fax: (+91) 40-2301-0567
E-mail: desiraju@uohyd.ernet.in

Prof. Dr. R. Boese, Dr. R. K. R. Jetti
Institut für Anorganische Chemie
Universität Duisberg-Essen
Universitätsstrasse 5–7, 45177 Essen (Germany)
Fax: (+49) 201-183-2535
E-mail: roland.boese@uni-essen.de

Dr. J. A. R. P. Sarma
gvk bioSciences
Hyderabad 500 016 (India)
Fax: (+91) 40-5562-6885
E-mail: sarma@gvkbio.com

[**] L.S.R. and P.V. thanks the CSIR for a fellowship. G.R.D. is a recipient of the Alexander von Humboldt research award. R.K.R.J. and R.B. are grateful to DFG for financial assistance. J.A.R.P.S. thanks G. V. Sanjay Reddy (gvk bioSciences) for support.

 DOI: 10.1002/anie.200250660 © 2003 Wiley-VCH Verlag GmbH & Co. KGaA, Weinheim



Scheme 1. Possible conformations for molecule **1**.

Even at the beginning of the test, it was recognized that CSP of dihydropyridine **1**, a flexible molecule with two degrees of acyclic torsional freedom, would prove to be difficult. Geometrical isomerism about the C=N bond must be considered and the possibility of conformational polymorphism[5] around the C–S bond is very real. The presence of several distinct hydrogen-bond donors and acceptors of comparable strengths indicates that structural (or synthon-based) polymorphism[6] is also likely. The literature on polymorphism and pseudopolymorphism in sulfa drugs is well documented, with polymorphs occurring in about 50 % of the cases.[6–11]

None of the participants of the blind test predicted the crystal structure of **1** correctly. When the experimental crystal structure (Form I) was revealed at the end of the test, it was found that the conformation of the molecule was quite unusual (Scheme 1),[12] with a very rarely observed eclipsing (**1a**) of the phenyl ring and the S–N bond, rather than the expected conformations **1b–e** that are commonly found in sulfonimides.[4] At that stage, the interest in molecule **1** began to subside.

Considering that polymorphism was likely in compound **1**, we tried to obtain a different crystal form. The substance was reasonably easy to prepare,[13] but obtaining a polymorph proved to be much more difficult. Recrystallization was carried out from a variety of solvents, such as benzene, toluene, xylene, dichloromethane, chloroform, acetone, acetonitrile, ethyl acetate, methanol, ethanol, 1-propanol, 2-propanol, DMF, and DMSO. Solvent combinations like MeOH/MeCN and benzene/MeCN were also tried. Invariably, we obtained crystals of Form I or powders. Other attempts to obtain crystals included slow cooling of saturated solutions in sealed ampoules,[14] and slow or rapid cooling of supersaturated solutions. In these experiments, we obtained either powders or poor-quality crystals. Sublimation produced flakes with a different appearance. Subsequent trials from various solvents gave Form I crystals. In all, approximately 80 single crystals from different crystallization experiments were selected for cell measurements. While the crystals very often had different morphologies, all of them turned out to be Form I or twinned crystals of the same form. X-ray powder diffraction gave varying patterns resulting from texture effects, but selected single crystals were always found to be of Form I.

There are subtle variations in the unit cell parameters of the Form I structure reported earlier by Hursthouse et al.[15] from that determined by us,[16] even though both studies were carried out at room temperature.[17] Whether one can term such fine variations as "polymorphism" is a contentious issue, and we prefer to treat both of them as being the same crystalline form. However, it is curious to note that the phenyl ring may be slightly disordered in the structure reported earlier, with the multiple orientations that are known in such cases (the C–C bond lengths in the phenyl ring are 1.302, 1.324, and 1.328 Å, standard deviations are not available). In contrast, our structure is well behaved and the structural details can be obtained from the supplementary material. No other noticeable conformational or packing differences are observed between the two structure determinations of Form I (Figure 1, top), which further augments the view that both data sets represent the same structure.[18]

In the Form I crystal (Figure 2 a), screw-axis related molecules are connected by the two-point synthon **B**

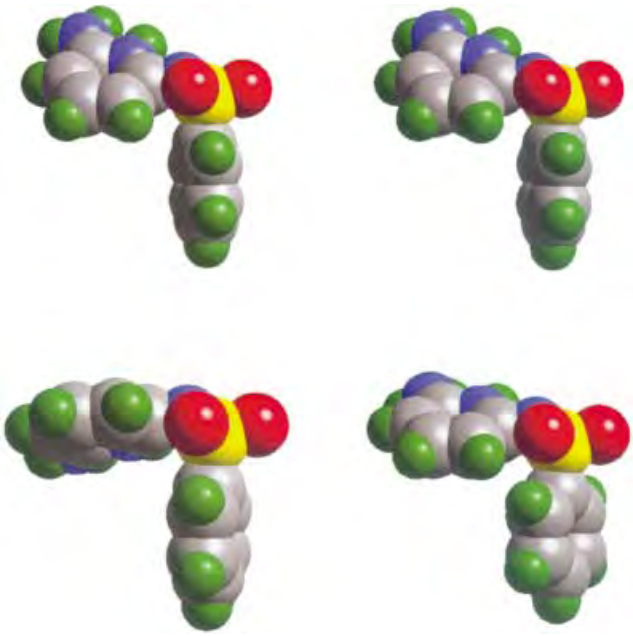


Figure 1. Space-filling models of molecule **1** indicating the conformational flexibility in the two forms. The molecular conformation is very similar (1.88 kcal mol^{-1}) in the previous[15] (top left) and present study of Form I (top right), while it is different in the two symmetry-independent molecules in Form II (bottom left, 1st molecule: 2.70 kcal mol^{-1}; bottom right, 2nd molecule: 0.04 kcal mol^{-1}). Significant variations in the C-C-S-N, C-S-N-C, and S-N-C-N torsion angles may be noted among these conformations. The energies given above are with respect to the least favored conformation, **1i** (see Scheme 3). Atoms: C, gray; N, blue; H, green; S, yellow; O, red.

 © 2003 Wiley-VCH Verlag GmbH & Co. KGaA, Weinheim

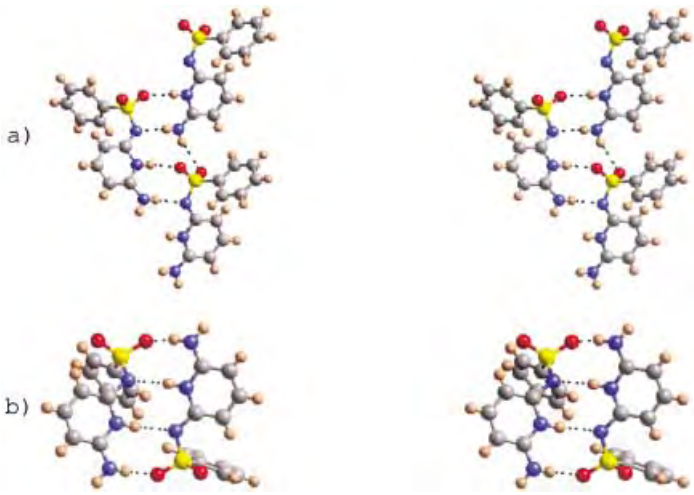
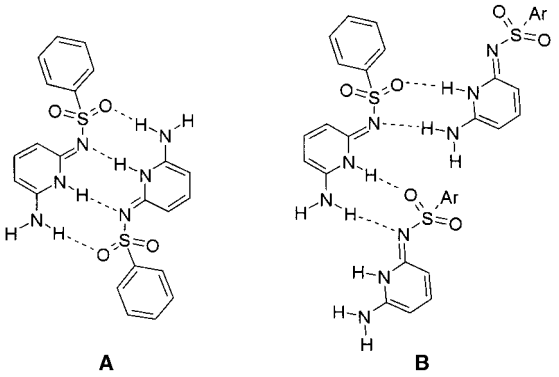


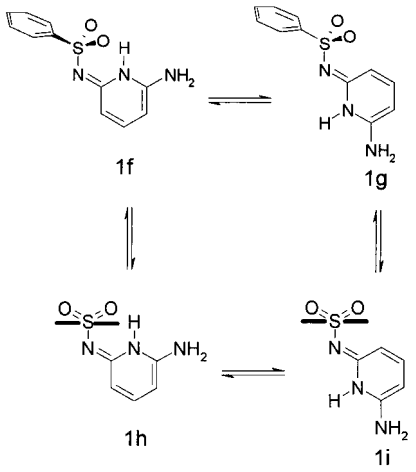
Figure 2. Stereoview of the crystal structure of **1**. a) Form I with synthon **B**; b) Form II with synthon **A**.



Scheme 2. The four-point synthon **A** and two-point synthon **B**.

(Scheme 2) with N–H···N hydrogen bonds between a H atom of a primary amine and a N atom of an imine, and N–H···O hydrogen bonds between a H atom of a secondary amine and an O atom of a sulfonyl moiety. The two molecules, to which a reference molecule forms such synthons, are in themselves related by a translation along the [010] direction and an additional weak N–H···O hydrogen bond. These one-dimensional (1D) motifs are, in turn, connected by C–H···O hydrogen bonds (not shown).

When compound **1** was recrystallized from nitromethane, the first batch contained only twinned crystals. The second crop was slightly improved, but the very thin crystals gave only a few weak reflections. However, very good crystals were obtained from the third batch. These crystals were found to be different from those obtained previously and correspond to a new polymorph, namely Form II. This strategy of successive crystallizations from a nitromethane solution[19] was repeated many times on fresh samples and on every occasion, the same behavior was observed. The new polymorph also crystallizes in the space group $P2_1/c$. However, there are now two molecules in the asymmetric unit with different molecular conformations (Figure 1, bottom). Both of these conformations are different from that observed in Form I (Figure 1, top). The differences lie not only with the C-C-S-N torsion angle, but also with the S-N-C-N torsion angle.[20] Considering the conformational flexibility of **1** around the three torsion angles C-C-S-N, C-S-N-C, and S-N-C-N, conformational analysis produced four reasonable low-energy minima (Scheme 3). Curiously, molecules in both Form I and Form II are related to the least stable conformation of these minima (**1i**, −40.03 kcal mol^{-1}). The energy differences between the experimental conformations and the local minimum are 1.88 kcal mol^{-1} (Form I), and 2.70 and



Scheme 3. Four calculated confomations of molecule **1** (**1f** −43.15, **1g** −42.03, **1h** −42.65, **1i** −40.03 kcal mol^{-1})

0.04 kcal mol^{-1} (Form II, 1st molecule and 2nd molecule, respectively; Figure 1).[21]

The most important structural feature of Form II is the four-point hydrogen-bonded synthon **A** (Scheme 2), which is located between the symmetry-independent molecules and characterized by two N–H···O hydrogen bonds that involve one O atom of the sulfonyl group and an H atom of a primary amine of the other molecule. The two N–H···N hydrogen bonds in the middle are formed between H atoms of the secondary amine groups and N atoms from imine moieties. Both molecules form additional N–H···O hydrogen bonds with the other sulfonyl O atom and primary amine H atoms of the [100]-translated molecules. From the metrical data of the hydrogen bonds in synthon **A** (Table 1) it is noticeable that they are all strong interactions. The differences between these values and the metrics of the hydrogen bonds in synthon **B** (in Form I) are noteworthy. The hydrogen bonds in Form II are, in general, shorter and more linear. Thus, the overall significance of hydrogen bonding is greater in Form II. It may be noted that synthon **A** occurred in our first choice for a predicted crystal structure for molecule **1** in the CSP2001 project,[4] and that these computationally predicted structures tend to be the thermodynamically favored ones.[22]

To evaluate the relative strengths of the hydrogen bonds in the two structures, we considered a representative cluster of three molecules in each polymorph. The molecules were chosen so that they are connected with the strongest hydrogen

 © 2003 Wiley-VCH Verlag GmbH & Co. KGaA, Weinheim

Table 1: Hydrogen-bond parameters for Forms I and II of **1**.

Interaction	Form I			Form II		
	d [Å][a]	D [Å]	θ [°]	d [Å][a]	D [Å]	θ [°]
N–H···O	1.784[b]	2.772(2)	165.40	1.798[c]	2.795(4)	168.53
	2.179[d]	3.116(2)	153.60	1.839[c]	2.821(3)	163.26
				2.019[d]	3.025(3)	174.32
				2.075[d]	3.061(3)	165.03
N–H···N	2.242[b]	3.250(2)	176.89	1.952[c]	2.951(3)	170.12
				2.064[c]	3.050(3)	164.76
C–H···O	2.499	3.504(3)	153.91	2.549	3.454(4)	140.50
	2.736	3.771(2)	159.76	2.578	3.523(4)	145.23
	2.739	3.540(2)	130.51	2.636	3.605(4)	148.58
				2.464	3.441(4)	149.31
				2.631	3.348(4)	123.08

[a] All N–H and C–H bond lengths are normalized to neutron values. [b] Hydrogen bonds in synthon **B**. [c] Hydrogen bonds in synthon **A**. [d] Hydrogen bonds between translated molecules.

bonds in the system and, as such, they are the most important, in terms of cluster propagation. In Form I, the three molecules are those shown in Figure 2a. In Form II, the molecules chosen are those in Figure 2b together with another translation-related molecule (not shown), which is connected to the dimer by an N–H···O interaction. The (absolute) energies of the three-molecule cluster in Form I is 22.25 kcal mol^{-1}, while it is 22.36 kcal mol^{-1} in Form II.[23] These values contain components of both intra- and intermolecular energies. While, the energy difference of only 0.11 kcal mol^{-1} between the two cases could be indicative of the likelihood of polymorphism, the fact that the Form I cluster is slightly more stable hints that this is the kinetic form. However, when the intramolecular components are separated out, synthon **A** (Scheme 2) is seen to be more stable by as much as 4.83 kcal mol^{-1}, which confirms the observations that the hydrogen bonds in Form II are more energetically favored than those in Form I.

A more complete picture emerges when the lattice energies of both polymorphs are considered instead of clusters of three molecules.[24] The packing potential energies involving both intra- and intermolecular components are −28.96 kcal mol^{-1} per molecule for Form I and −29.82 kcal mol^{-1} per molecule for Form II. This shows that Form II is the thermodynamically more stable form. However, Form II was seldom observed, and so kinetic and entropic factors are important during crystallization, or in other words, the propagation of stable clusters. In this regard, synthon **B** (Scheme 2), which leads to 1D propagation by two-point recognition, is found in the easily obtained (kinetic) form, but synthon **A**, which is of lower dimensionality[25] and with which propagation is expected to be correspondingly less facile, is found in the rarely observed (thermodynamic) form.[26] The fact that the 1D patterns in Form I are extended into higher dimensions with weaker C–H···O hydrogen bonds indicates that this form could also be entropically favored and further strengthens the view that Form I is the kinetic form. Overall, we are confident that Form I is the kinetically favored crystal type while Form II is the thermodynamically favored crystal.[27]

What are the implications of these results, as far as CSP is concerned? In general, it has already been commented upon that both kinetic and thermodynamic factors in crystal growth need to be taken into account during CSP, and that the Curtin–Hammett principle can operate in crystallization, leading to polymorphism.[4] Specifically, it was felt that molecule **1** would be a difficult case for CSP because of the possible existence of multiple crystal forms. CSP was indeed very difficult (and unsuccessful) but not for the reason ascribed. It has now been shown that while compound **1** is polymorphic, the second form is hard to obtain.[28] CSP was difficult because the commonly observed form is the kinetic form, and the methods for CSP that use force fields tend to lead to the thermodynamic form. The thermodynamic form was not identified in CSP2001 project, and it could not have been predicted because the crystal structure contains two symmetry-independent molecules, and is therefore beyond the limit of the CSP exercise, as currently defined.[2,3] The results of the present study are encouraging, in that it was possible to isolate a polymorph of a compound for which polymorphism had been specifically anticipated.

CSP is clearly a fascinating exercise combining various chemistry skills, but success or failure should be viewed and/or tempered by accompanying or subsequent experimental work on the test compounds. In hindsight, the failure of the participants in the CSP2001 project to predict the structure of molecule **1** was not a particular discredit to any of them. In contrast, some of the participants of the CSP1999 project were credited for successful predictions, even though they obtained a solution for a polymorph that subsequently "disappeared"[29] and has not yet been reproduced. To conclude, we reiterate that as CSP is a problem of such great fundamental importance, a case could be made for more extensive studies on the crystallization behavior of a compound after the CSP effort, or ideally even prior to its consideration as a candidate for the exercise.

Received: November 29, 2002
Revised: March 11, 2003 [Z50660]

Keywords: crystal growth · hydrogen bonding · polymorphism · structure elucidation · supramolecular chemistry

[1] G. R. Desiraju, *Nature Materials* **2002**, *1*, 77–79.
[2] W. D. S. Motherwell, H. L. Ammon, J. D. Dunitz, A. Dzyabchenko, P. Erk, A. Gavezzotti, D. W. M. Hofmann, F. J. J. Leusen, J. P. M. Lommerse, W. T. M. Mooij, S. L. Price, H. Scheraga, B. Schweizer, M. U. Schmidt, B. P. van Eijck, P. Verwer, D. E. Williams, *Acta Crystallogr. Sect. B* **2002**, *58*, 647–661.
[3] J. P. M. Lommerse, W. D. S. Motherwell, H. L. Ammon, J. D. Dunitz, A. Gavezzotti, D. W. M. Hofmann, F. J. J. Leusen, W. T. M. Mooij, S. L. Price, B. Schweizer, M. U. Schmidt, B. P.

 © 2003 Wiley-VCH Verlag GmbH & Co. KGaA, Weinheim

van Eijck, P. Verwer, D. E. Williams, *Acta Crystallogr. Sect. B* **2000**, *56*, 697 – 714.
[4] J. A. R. P. Sarma, G. R. Desiraju, *Cryst. Growth Des.* **2002**, *2*, 93 – 100.
[5] a) "Conformational Polymorphism":J. Bernstein in *Organic Solid State Chemistry* (Ed.: G. R. Desiraju), Elsevier, Amsterdam, **1987**, pp. 471 – 518; b) J. Bernstein, *Polymorphism in Molecular Crystals*, Clarendon, Oxford, **2002**, pp. 151 – 187.
[6] "Polymorphism and Pseudopolymorphism in Organic Crystals: A Cambridge Structural Database Study":J. A. R. P. Sarma, G. R. Desiraju in *Crystal Engineering* (Eds.: K. R. Seddon, M. Zaworotko), Kluwer, Norwell, MA, **1999**, pp. 325 – 356.
[7] D. S. Hughes, M. B. Hursthouse, R. W. Lancaster, S. Tavener, T. L. Threlfall, *J. Chem. Soc. Chem. Commun.* **2001**, 603 – 604.
[8] I. Bar, J. Bernstein, *J. Pharm. Sci.* **1985**, *74*, 255 – 263.
[9] S. R. Byrn, *Solid State Chemistry of Drugs*, Academic Press, New York, **1982**, pp. 103 – 116.
[10] N. Blagden, R. J. Davey, H. F. Lieberman, L. Williams, R. Payne, R. Roberts, R. Rowe, R. Docherty, *J. Chem. Soc. Faraday Trans.* **1998**, *94*, 1035 – 1044.
[11] W. Schaap, PhD thesis, University of Essen (Germany), **2001**.
[12] The C-C-S-N torsion angle is 26.0°. Only two other comparable structures in the CSD have such low torsion angles. They are (*N*-(4-aminophenyl)sulfonyl)guanidine (ZZZAYP03; −12.5°) and 2-methyl-1-(2-methylphenyl)-3-(*p*-tosyl)-isothiourea (UCISOO; 24.9°). A total of 315 other comparable fragments have torsion angles between 60 and 90°.
[13] The title compound was prepared according to the literature procedure for 2-(aminobenzenesulfonylamino)-6-aminopyridine (K. Tuda, Z. Izikawa, D. So, *J. Pharm. Soc. Jpn.* **1939**, *59*, 213 – 215). The compound was purified by column chromatography and recrystallized from MeOH.
[14] This was carried out by flame-sealing containers within which a saturated solution of **1** is present, and then allowing them to stand for several days at room temperature.
[15] M. Hursthouse, private communication, **2001**; the reported cell parameters are: $a = 8.251$, $b = 8.964$, $c = 15.087$ Å, $\alpha = 90$, $\beta = 91.21$, $\gamma = 90°$.
[16] Crystal data for Form I (Nicolet R3 at room temperature): monoclinic, $P2_1/c$, $a = 8.5450(13)$, $b = 9.0638(17)$, $c = 15.151(2)$ Å, $\beta = 91.492(12)°$, $V = 1173.0(3)$ Å^3, $Z = 4$, $\rho_{calcd} = 1.412$ g cm^{-3}, $T = 293$ K, $\mu = 0.269$ mm^{-1}, $2\theta_{max} = 60°$, 3526 measured, 3403 independent, 2687 observed ($I > 2\sigma_1$) reflections, 154 parameters, $R1 = 0.0406$, $wR2 = 0.1072$ (for $I > 2\sigma_1$), residual electron density $+0.337/-0.296$ e Å^{-3}. Crystal data for Form I (SMART at 183 K): monoclinic, $P2_1/c$, $a = 8.479(5)$, $b = 8.958(5)$, $c = 14.894(8)$ Å, $\beta = 91.856(10)°$, $V = 1130.7(11)$ Å^3, $Z = 4$, $\rho_{calcd} = 1.464$ g cm^{-3}, $T = 183$ K, $\mu = 0.279$ mm^{-1}, $2\theta_{max} = 56.18°$, 13514 measured, 2820 independent, 2002 observed ($I > 2\sigma_1$) reflections, 154 parameters, $R1 = 0.0495$, $wR2 = 0.1158$ (for $I > 2\sigma_1$), residual electron density $+0.597/-0.359$ e Å^{-3}. Crystal data for Form II: monoclinic, $P2_1/c$, $a = 12.1099(15)$, $b = 10.7924(12)$, $c = 17.464(2)$ Å, $\beta = 97.318(2)°$, $V = 2263.9(5)$ Å^3, $Z = 8$, $\rho_{calcd} = 1.463$ g cm^{-3}, $T = 203$ K, $\mu = 0.279$ mm^{-1}, $2\theta_{max} = 56.6°$, 14219 measured, 5443 independent, 2871 observed ($I > 2\sigma_1$) reflections, 307 parameters, $R1 = 0.0579$, $wR2 = 0.1200$ (for $I > 2\sigma_1$), residual electron density $+0.496/-0.339$ e Å^{-3}. The data were collected on a Nicolet R3 or on a SMART diffractometer using $Mo_{K\alpha}$ radiation. Structure solution was by direct methods and refinements on F^2 with SHELXTL (Version 6.10 and 6.12). Non-hydrogen atoms were refined anisotropically and the H atoms of the phenyl groups were generated at idealised geometries and refined isotropically using a riding model. The H atom positions of the NH_2 and NH groups were taken from a difference Fourier map and were refined isotropically. CCDC 195422–195424 contain the supplementary crystallographic data for this paper. These data can be obtained free of charge via www.ccdc.cam.ac.uk/conts/retrieving.html (or from the Cambridge Crystallographic Data Centre, 12, Union Road, Cambridge CB2 1EZ, UK; fax: (+44) 1223-336-033; or deposit@ccdc.cam.ac.uk).
[17] The differences between some of the unit-cell parameters in the two experiments are significantly greater than the changes brought about by lowering the temperature to 183 K. Accordingly, this fact is brought to the reader's attention.
[18] These observations suggest that CSP protocols for a "right" answer should definitely take into account such structural variations.
[19] The role of solvent in determining the polymorphic form obtained has been widely appreciated, but systematic efforts at understanding this phenomenon are scarce. In particular, the behavior of nitromethane in disrupting certain hydrogen-bonded aggregates in sulfathiazole crystallization has been described (see ref. [10]).
[20] Note that we are specifying a torsion angle about what is formally a C=N bond. A comparison of the two symmetry-independent molecules in Form II suggests that there is considerable flexibility in this region of the molecule.
[21] Energy calculations were carried out using the CVFF95 force field in the Cerius^2 program. Cerius^2, Accelrys, Cambridge (UK). See www.accelrys.com.
[22] T. Beyer, T. Lewis, S. L. Price, *CrystEngComm* **2001**, *4*, 1 – 35.
[23] Clusters of three molecules that are connected by N–H···O and N–H···N interactions were used to calculate the relative energies in each case using the CVFF95 force field with explicit inclusion of both intra- and intermolecular interactions. The geometries of the three molecules in each case correspond to the X-ray-observed geometry with normalized H atom distances.
[24] The lattice-energy calculations were carried out in the two forms with H-normalized molecules. The Crystal Packer module, which is part of the Cerius^2 program environment, was used. Similar potentials, as defined earlier, were used. No minimization of either cell parameters or molecular positions was carried out.
[25] Synthon **A** is not strictly zero-dimensional (like the carboxylic acid dimer) because it has extra sites for N–H···O hydrogen bonding. But it is undoubtedly of lower dimensionality than synthon **B**.
[26] Synthons **A** and **B** may be linked to dimer and catemer motifs in the crystal structures of carboxylic acids and amides, with the corresponding implications for crystal growth;[4] see also: W. T. M. Mooji, B. P. van Eijck, S. L. Price, P. Verwer, J. Kroon, *J. Comput. Chem.* **1998**, *19*, 459 – 474.
[27] The fact that Form II is the thermodynamic form is also corroborated by the method of obtaining crystals from increasingly dilute solutions.
[28] This is another demonstration of Ostwald's Law of Stages, which has been shown to be of wide applicability in studies of crystallization and polymorphism. See: a) W. Ostwald, *Grundriss der Allgemeinen Chemie,* Leipzig, **1899**; b) R. J. Davey, N. Blagden, G. D. Potts, R. Doherty, *J. Am. Chem. Soc.* **1997**, *119*, 1767 – 1772.
[29] J. D. Dunitz, J. Bernstein, *Acc. Chem. Res.* **1995**, *28*, 193 – 200.

 © 2003 Wiley-VCH Verlag GmbH & Co. KGaA, Weinheim

Tumor-Specific Transport

Peptide–PNA Conjugates: Targeted Transport of Antisense Therapeutics into Tumors**

Walter Mier, Ramon Eritja, Ashour Mohammed, Uwe Haberkorn, and Michael Eisenhut*

Dedicated to Professor Harald zur Hausen

Systemic toxicity is one of the major problems in chemotherapy. While the traditional chemotherapeutics generally affect all of the proliferating cells, new therapy modalities, in particular gene therapy, offer the possibility to selectively act in tumor cells. However, the high molecular weight of the active substances used in these treatment methods leads to unfavorable pharmacokinetic behavior that causes problems in the clinical application of these substances. Therefore, the success of these treatment methods depends on the development of new vector systems that enable transport of high molecular weight substances for example, oligonucleotides. Remarkable progress can be made here by chemical modifications.[1]

Somatostatin-receptors (SSTRs) are found in numerous kinds of tumors (e.g., breast tumors, small-cell lung cancer). As the native peptide somatostatin is rapidly degraded in vivo, stabilized derivatives have been developed for clinical application. The most successful derivative is octreotide.[2] This peptide is able to induce endocytosis by binding to SSTRs and, because of the broad substrate specificity of these receptors, to mediate internalization of conjugated substances. That this can be used for the transport of tumor therapeutics has been shown in vitro for conjugates of the spindle poison taxol.[3]

Since, up to now, it has not been possible to selectively transport antisense oligonucleotides into tumor cells, the question arose whether it would be possible to use SSTR-affine peptides as carriers for oligonucleotides. The oligonucleotide target sequence chosen was the anti-*bcl-2*-sequence.[4,5] It is quite difficult to generate the peptide–nucleic acid conjugates that are needed for this targeting concept by solid-phase synthesis. The standard methods for the synthesis of oligonucleotides and peptides are incompatible. Consequently, the conjugates are favorably generated by postsynthetic conjugation. We have recently reported on phosphorothioate oligonucleotides that are bound to a maleimido-modified SSTR-affine peptide through a thiol group at their 5′-end.[6] The conjugates showed high hybridization efficiency and a high affinity for SSTRs. In spite of the promising results that could be found in vitro, animal experiments revealed no significant enrichment in the tumors.[7]

The pharmacokinetics of the phosphorothioates seemed to be dominated by strong unspecific interactions. Consequently, we chose the metabolically stable peptide nucleic acids (PNAs) for the experiments described herein.[8] The convergence of PNA and peptide synthesis enables the stepwise synthesis of PNA–peptide conjugates on the same polymeric support. Either 9-fluorenylmethoxycarbonyl (Fmoc) or *tert*-butyloxycarbonyl (Boc) chemistry are suitable for the synthesis of PNA oligomers. However, due to side reactions during deprotection of the Fmoc protecting group, the purity of the products produced by Boc chemistry is higher. To allow a convergent synthesis, the peptide part had to be built up by Boc chemistry as well. The PNA oligomers can be synthesized by using Boc chemistry in good yields, consequently this method is also suitable for the synthesis of PNA–peptide conjugates.[9]

Octreotate, which is nearly identical to octreotide except that it has a carboxy group at the C terminus and thus supports internalization (Figure 1B), was chosen as the peptide part of the conjugate. Boc-D-Phe-Cys(Acm)-Phe-D-

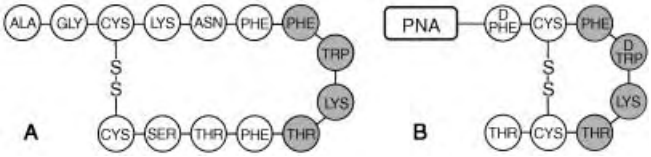


Figure 1. Comparison of native somatostatin (A) with a conjugate consisting of a PNA and Tyr^3-octreotate (B). The amino acids that are essential for receptor binding are marked in gray.

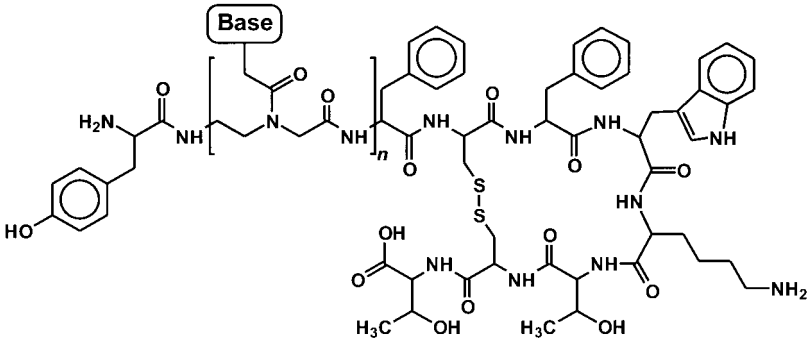
Trp-Lys-Thr-Cys(Acm)-Thr-PAM resin was synthesized by application of a modified in situ neutralization protocol[10] with HATU as activator. The average coupling efficiency, determined by ninhydrin assay, was 99.1%. To enable the introduction of radioactive iodine (^{125}I) an additional tyrosine residue was conjugated to the N-terminus, which led to the target molecule **1** (base sequence = Tyr-AGC GTG CGC-CAT CCC-peptide).

During chain elongation in peptide and PNA synthesis, aggregation of the growing oligomer chain can be caused by either intra- or intermolecular interactions. This may lead to a collapse of the solid support and thus to low coupling efficiencies. The tendency for aggregation increases with increasing chain length. Consequently, the syntheses of long PNA–peptide conjugates is especially prone to the appearance of "difficult sequences". Application of known synthesis protocols[11] did not lead to the anticipated success, thus, solvents, coupling times, the capping step, as well as the reaction conditions for the repeated coupling steps had to be

[*] Dr. W. Mier, Dr. A. Mohammed, Prof. Dr. U. Haberkorn
Universitätsklinikum Heidelberg
Radiologische Klinik, Abteilung Nuklearmedizin
Im Neuenheimer Feld 400, 69120 Heidelberg (Germany)
Fax: (+49) 6221-56-5473
E-mail: walter_mier@med.uni-heidelberg.de
Prof. Dr. R. Eritja
Centro de Investigación y Desarrollo C.S.I.C.
Jordi Girona 18–26, 08034 Barcelona (Spain)
Prof. Dr. M. Eisenhut
Deutsches Krebsforschungszentrum
Im Neuenheimer Feld 280, 69120 Heidelberg (Germany)

[**] This work was funded by the Deutsche Forschungsgemeinschaft (Az.: Ei 130/15-1).

 © 2003 Wiley-VCH Verlag GmbH & Co. KGaA, Weinheim DOI: 10.1002/anie.200219978



1

optimized. The use of Ac_2O/pyridine in DMF in the capping step proved to be essential. This was followed by a washing step with DMF/piperidine to cleave possible acetyl esters. The coupling cycles were performed with five equivalents of the Boc-protected PNA monomers using HATU as the activating agent. The exocyclic amino functions of the A, C, and G monomers were protected by benzyloxycarbonyl groups. The coupling cycle is shown schematically in Figure 2.

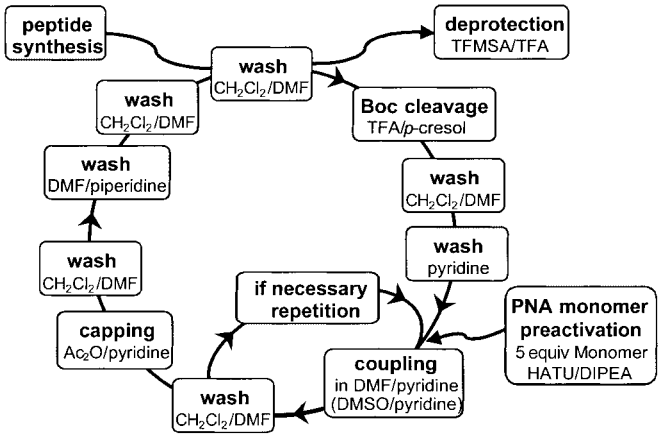
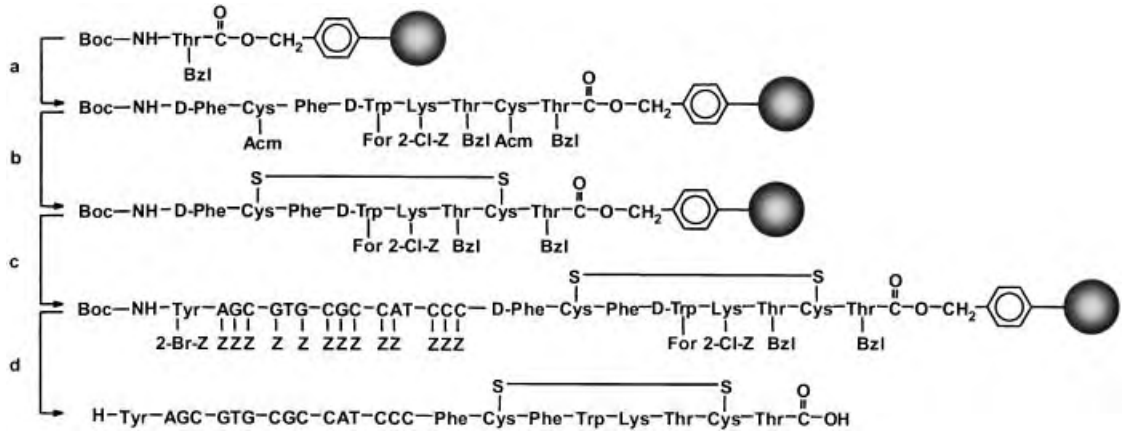


Figure 2. Flow diagram of the synthesis cycle used for conjugating the PNA part (Boc chemistry). The abbreviations are defined in Scheme 1.

Above a critical length of the oligomers, HPLC analysis of cleaved aliquots revealed strongly decreasing coupling efficiencies: after the 9th monomer, in particular when G monomers were conjugated, coupling efficiencies decreased to about 50%. By elongation of coupling times and by performing repeated couplings, the critical monomers could finally be coupled with coupling efficiencies of more than 95%. Using these optimized coupling conditions, we obtained the target conjugate in about 75% yield (according to HPLC analysis). However, it was not possible to cyclize this conjugate on the solid support, because the Tl^{3+} ions cause side reactions with the nucleobases. Owing to the size of the molecule, the course of the alternative air oxidation cannot be analyzed by HPLC. Therefore, the PNA oligomer was built up on the peptide which had been cyclized beforehand. Scheme 1 shows the synthesis of the octreoate–PNA conjugate from the peptide that was assembled by Boc chemistry and then cyclized by using $Tl(TFA)_3$. After conjugation of the PNA monomers, a homogeneous product was obtained, which was deprotected with TFMSA in TFA using *p*-cresol as the scavenger. After precipitation with diethyl ether and subsequent purification by RP-HPLC, **1** was isolated in about 40% yield.

Binding experiments with the PNA conjugates using rat cortex membranes showed that the conjugates bind to SSTRs with a high affinity similar to that for octreotide, as confirmed by the IC_{50} values (octreotate–PNA oligomer 1.52, octreotide 1.98 nM). Determination of the melting temperatures revealed that the PNA–conjugates hybridize with high affinity to the complementary phosphodiester–DNA oligonucleotides. The melting temperature of the conjugate was 82 °C and



Scheme 1. Flow diagram of the synthesis of the PNA–octreotate conjugate using Boc chemistry. a) Synthesis cycles with HATU/DIEA/Boc cleavage with 5% *p*-cresol in TFA; b) $Tl(TFA)_3$; c) synthesis cycles according to Figure 3; d) TFA /*p*-cresol/TFMSA. Protecting groups: Acm = acetamidomethyl, 2-Br-Z = 2-bromobenzyloxycarbonyl, 2-Cl-Z = 2-chlorobenzyloxycarbonyl, Bzl = benzyl, For = formyl, Z = benzyloxycarbonyl, TFA = trifluoroacetic acid, TFMSA = trifluoromethanesulfonic acid, DIPEA = *N,N*-diisopropylethylamine, HATU = *O*-(7-azabenzotriazol-1-yl)-*N,N,N′,N′*-tetramethyluronium hexafluorophosphate.

 © 2003 Wiley-VCH Verlag GmbH & Co. KGaA, Weinheim

thus much higher than that of a phosphodiester duplex of the same sequence ($T_m = 71.4\,°C$). This shows that due to the high hybridizing affinity the PNA–conjugate should be suitable as an antisense drug.

Organ distribution was evaluated in Lewis rats carrying the SSTR-affine pancreatic tumor CA20948 (Figure 3). After deprotection and cleavage from the solid support, the PNA

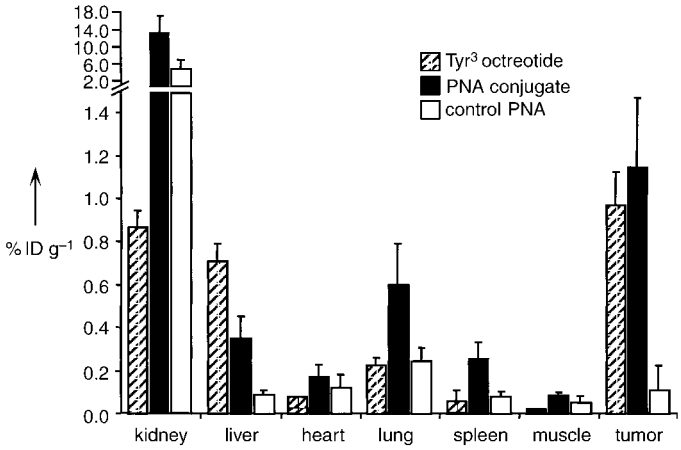


Figure 3. Organ distribution data for tumor-bearing Lewis rats, given in percent of the injected dose per gram of tissue (%ID g^{-1}) ± standard deviation 1 h after intravenous injection (average values from three or six animals, compounds were labeled with ^{125}I). The conjugation of the peptide moiety causes a strongly increased accumulation of the PNA oligomer in the tumor tissue (statistical significance in students t-Test: $p = 0.021$).

conjugate and a control PNA with the same sequence were labeled selectively with ^{125}I at the tyrosine residue by using the Chloramine-T method.[12] In contrast to the phosphorothioate conjugate, for the ^{125}I-labeled PNA–peptide conjugate, a selective enrichment in the tumor tissue was obtained. The physicochemical properties of the PNA–peptide conjugate are different to those of the Tyr^3–octreotide. These properties influence factors like the interaction with serum proteins and result in different organ uptake, in particular in the kidney, the liver, and the lung. The modification of the PNA with the peptide part led to an about tenfold increase in tumor uptake.

In all of the organs except for the kidney, the enrichment of the octreotate conjugate resembles the accumulation of the free peptide. This indicates that the PNA–peptide conjugates in the serum are nonspecifically associated to a lower degree than the phosphorothioate conjugates, and are consequently better accessible for the binding to the receptors. The fact that 79 % of the tumor uptake can be inhibited by coinjection of an excess of nonlabeled octreotide provided further evidence for the receptor specificity of this uptake.

Although there are some promising in vitro studies with PNA conjugates,[13] none of the methods described could be successfully applied for the targeting of tumors in vivo. The use of SSTR-affine carrier molecules for the first time enables the targeted transport of oligonucleotides in tumor tissue. This demonstrates that targeting of high molecular weight drugs is possible by using receptor-specific peptides.

Experimental Section

Solid-phase syntheses were performed manually in a batch-procedure using Boc-protected amino acids (Bachem, Germany) as well as PNA monomers (Applied Biosystems, Germany) on a 4-(oxymethyl)-phenylacetamidomethyl-(PAM) resin. Analyses and purifications by RP-HPLC were performed on LiChrosorb RP-selectB columns (Merck KGaA, Germany) with gradient elution (water/acetonitrile (0.1 % TFA)). Electrospray ionization mass spectrometry was carried out on a Finnigan MAT TSQ 7000 System (Thermo Finnigan, San Jose, USA). The radioisotope ^{125}I was purchased from Amersham Pharmacia Biotech (Freiburg, Germany).

Synthesis of the PNA–peptide conjugate: First, the following synthesis cycle was carried out to obtain H-D-Phe-cyclo[Cys-Phe-D-Trp(For)-Lys(2-Cl-Z)-Thr(Bzl)-Cys]-Thr(Bzl)-O-PAM: The resin (100 mg; initial loading = 0.72 mmol g^{-1}) was agitated with 5 % *p*-cresol in TFA (two times for 2 min), and then washed with DMF, combined with a mixture of the carboxylic acid (4 equiv), HATU (3.9 equiv) and diisopropylethylamine (DIPEA; 10 equiv) which had been pre-incubated for 2 min in DMSO, agitated for 2 min and again washed with DMF. The synthesis cycle for conjugating the PNA monomers to this resin was carried out as follows: a) agitation with TFA/*p*-cresol (95:5, v/v) two times for 2 min; b) incubation of the PNA monomers with HATU (4.9 equiv) and DIPEA (10 equiv) for 2 min (final concentration 0.1 M); c) washing with DMF/CH_2Cl_2 (1:1, v/v) and then with pyridine; d) agitation with the preactivated PNA monomer for 15 min; e) washing with DMF/CH_2Cl_2 (1:1, v/v); f) agitation with Ac_2O/pyridine/DMF (1:10:10, v/v/v) for 5 min; g) washing with DMF/CH_2Cl_2 (1:1, v/v); h) agitation with DMF/pyridine (95:5, v/v) for 2 min; i) washing with DMF/CH_2Cl_2 (1:1, v/v). After the coupling of Boc-Tyr(2-Br-Z) the resin was washed and dried. The loaded resin (30 mg) was mixed with 5 % *p*-cresol (500 μL) in TFA. After the addition of TFMSA (50 μL), the resin was agitated for 2 h, filtered off, and the raw product was precipitated with diethyl ether. The raw product was resolubilized in acetonitrile/water (1:1) and incubated for 24 h at room temperature. The sample was purified by HPLC. After lyophilization, H-Tyr-AGC GTG CGC CAT CCC-D-Phe-cyclo[Cys-Phe-D-Trp-Lys-Thr-Cys]-Thr-OH was obtained as a white powder (overall yield: 16.8 mg; ca. 40 %). The integrity and purity of the product was confirmed with ESI-MS (*m*/*z* for $C_{218}H_{270}N_{96}O_{58}S_2$ calcd: 5203 g mol^{-1}, found: 5205 g mol^{-1} ($[M+H]^+$) and analytical HPLC (purity > 95 %).

The control PNA (H-Tyr-AGC GTG CGC CAT CCC-Lys-NH_2) was synthesized analogous to the PNA–peptide conjugate.

Organ distribution studies: A cell suspension of the CA20948 tumor in a nutrient mixture was subcutaneously administered into the nape of the neck of male Lewis rats. After about 10 days, the tumors were grown to a volume of about 5 mL. The ^{125}I-labeled compound was injected into the tail vein of the animals (groups of three animals). After 1 h, the animals were sacrificed and the activity concentration of the dissected organs was determined in a γ-counter.

Received: August 15, 2002
Revised: January 17, 2003 [Z19978]

Keywords: antisense agents · drug delivery · peptide nucleic acids · peptides · solid-phase synthesis

[1] a) R. G. Cooper, R. P. Harbottle, H. Schneider, C. Coutelle, A. D. Miller, *Angew. Chem.* **1999**, *111*, 2128–2132; *Angew. Chem. Int. Ed.* **1999**, *38*, 1949–1952; b) J. D. Hood, M. Bednarski, R. Frausto, S. Guccione, R. A. Reisfeld, R. Xiang, D. A. Cheresh, *Science* **2002**, *296*, 2404–2407.

[2] W. Bauer, U. Briner, W. Doepfner, R. Haller, R. Huguenin, P. Marbach, T. J. Petcher, J. Pless, *Life Sci.* **1982**, *31*, 1133–1140.

 © 2003 Wiley-VCH Verlag GmbH & Co. KGaA, Weinheim

[3] C. M. Huang, Y. T. Wu, S. T. Chen, *Chem. Biol.* **2000**, *7*, 453 – 461.
[4] The expression of the proto-oncogene *bcl-2* increases the susceptibility of tumor cells towards undergoing apoptosis. The anti-*bcl-2* phosphorothioate oligonucleotide G3139 (Genasense) belongs to the antisense oligonucleotides, whose clinical development is most advanced.
[5] L. Mologni, P. E. Nielsen, C. Gambacorti-Passerini, *Biochem. Biophys. Res. Commun.* **1999**, *264*, 537 – 543.
[6] W. Mier, R. Eritja, A. Mohammed, U. Haberkorn, M. Eisenhut, *Bioconjugate Chem.* **2000**, *11*, 855 – 860.
[7] The tumor accumulation was investigated under the conditions described in the Experimental Section. The ^{32}P-labeled conjugate revealed a preferential accumulation in the liver, kidneys, and the spleen, similarly to a phosphorothioate without the peptide moiety.
[8] a) P. E. Nielsen, M. Egholm, R. H. Berg, O. Buchardt, *Science* **1991**, *254*, 1497 – 1500; b) E. Uhlmann, A. Peyman, G. Breipohl, D. W. Will, *Angew. Chem.* **1998**, *110*, 2954 – 2983; *Angew. Chem. Int. Ed.* **1998**, *37*, 2796 – 2823.
[9] S. K. Awasthi, P. E. Nielsen, *Comb. Chem. High Throughput Screening* **2002**, *5*, 253 – 259.
[10] L. P. Miranda, P. F. Alewood, *Proc. Natl. Acad. Sci. USA* **1999**, *96*, 1181 – 1186.
[11] a) L. Christensen, R. Fitzpatrick, B. Gildea, K. H. Petersen, H. F. Hansen, T. Koch, M. Egholm, O. Buchardt, P. E. Nielsen, J. Coull, R. H. Berg, *J. Pept. Sci.* **1995**, *1*, 175 – 183; b) T. Koch, H. F. Hansen, P. Andersen, T. Larsen, H. G. Batz, K. Otteson, H. Orum, *J. Pept. Res.* **1997**, *49*, 80 – 88.
[12] F. C. Greenwood, W. M. Hunter, J. S. Glover, *Biochem. J.* **1963**, *89*, 114 – 123.
[13] For instance see: a) L. C. Boffa, S. Scarfi, M. R. Mariani, G. Damonte, V. G. Allfrey, U. Benatti, P. L. Morris, *Cancer Res.* **2000**, *60*, 2258 – 2262; b) L. J. Branden, A. J. Mohamed, C. I. Smith, *Nat. Biotechnol.* **1999**, *17*, 784 – 787.

 © 2003 Wiley-VCH Verlag GmbH & Co. KGaA, Weinheim

Metalloid Gallium Cluster

$[Ga_{16}(PtBu_2)_{10}]$: A Gallium Phosphide Sheathed Core of Four Naked Ga Atoms?**

*Jochen Steiner, Gregor Stößer, and Hansgeorg Schnöckel**

In accordance with the technical importance of III–V semiconductors, the number of publications about their potential molecular precursors has risen explosively in the last few years. The structural chemistry of such species, which sometimes occur as cage molecules,[1–3] has recently revealed several examples with unusual structures (Figure 1 a–c). The $[(AlCp^*)_6P_4]$ unit (Figure 1 a; $Cp^* = C_5Me_5$),[4] formed from $[AlCp^*]$ and P_4, and a GaP_4 unit,[5] with a nearly intact P_4 framework (Figure 1 b) are characteristic of these structures. Both of these compounds as well as a third species with an AlP_3 ring structure[6] are colorless or weakly colored (Figure 1 c).

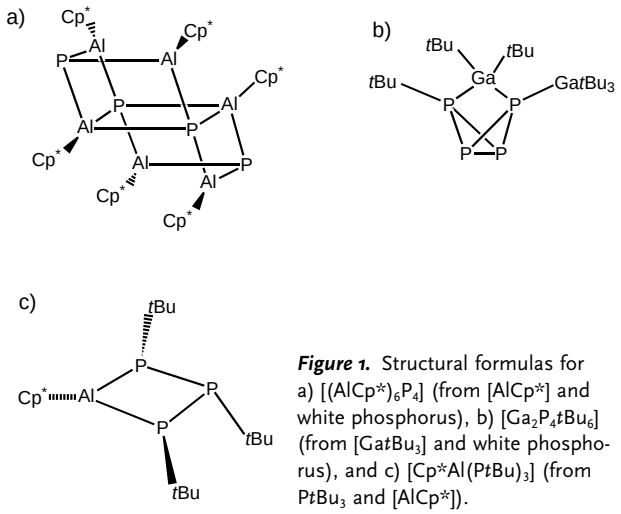


Figure 1. Structural formulas for a) $[(AlCp^*)_6P_4]$ (from $[AlCp^*]$ and white phosphorus), b) $[Ga_2P_4tBu_6]$ (from $[GatBu_3]$ and white phosphorus), and c) $[Cp^*Al(PtBu)_3]$ (from $PtBu_3$ and $[AlCp^*]$).

To obtain metal-rich Ga–P compounds, whose dark color and metallic luster are suggestive of different bonding interactions, a different synthetic route, starting from metastable AlX and GaX (X = Cl, Br, I) solutions, has been pursued, which has led to numerous metalloid cluster compounds.[7] For example, we have had some success in previous years with the synthesis of metalloid cluster compounds with terminal Al–N bonds. We thus obtained, among others, the shiny cluster compound $Al_{77}R_{20}$, whose core of 57 naked aluminum atoms is surrounded by 20 $AlNR_2$ groups; that is it contains 20 terminal Al–N bonds.

The deciding factor in these syntheses is the interplay between disproportionation of the AlX or GaX compound to form metal-rich species and substitution of the halides by bulky groups, which shield the cluster core. The synthesis of metalloid Al and Ga clusters accordingly depends on the selective disproportionation of Al^I or Ga^I compounds, in which the number and type of surrounding AlR or GaR groups determine the structure of the naked Al or Ga core.

After many successful syntheses of metalloid Al and Ga clusters with terminal Al–N or Ga–N bonds, we have now obtained the first metalloid Ga cluster protected by $GaPR_2$ groups, namely the neutral, metalloid $[Ga_{16}(PtBu_2)_{10}]$ molecule (Compound **1**, Figure 2), which, because of its Ga–P stoichiometry, only leaves space for a central naked Ga_4 tetrahedron. Cluster **1** could thus be viewed as a model intermediate in the partial oxidation of gallium metal by phosphorus. A $(GaP)_{10}$ shell protects the Ga_4 core from complete oxidation, and the *t*Bu groups on the phosphorus center allow the formation of a solution-stable and shielded cluster.

[*] Prof. Dr. H. Schnöckel, J. Steiner, Dipl.-Chem. G. Stößer
Institut für Anorganische Chemie
Universität Karlsruhe (TH)
Engesserstrasse 15, Geb. 30.45, 76128 Karlsruhe (Germany)
Fax: (+49) 721-608-4854
E-mail: Hansgeorg.Schnoeckel@chemie.uni-karlsruhe.de

[**] This work was supported by the Deutsche Forschungsgemeinschaft and the Fonds der Chemischen Industrie.

 DOI: 10.1002/anie.200250461 © 2003 Wiley-VCH Verlag GmbH & Co. KGaA, Weinheim

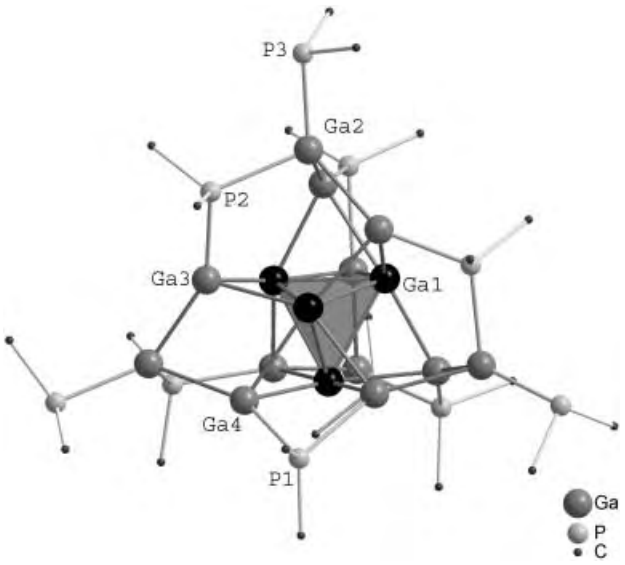


Figure 2. Ball-and-stick representation of the $Ga_{16}P_{10}$ cluster framework; for clarity only the P atoms of the P*t*Bu$_2$ groups and the central C atoms of the *t*Bu groups are represented. Selected bond lengths (min./max.) [pm] and angles [°]: Ga1-Ga1 268/277, Ga1-Ga3 251/256, Ga1-Ga4 260/267, Ga2-Ga3 251, Ga2-Ga4 261, P1-Ga4 248, P2-Ga2/Ga3 252/242, P3-Ga2 241; Ga4-P1-Ga4 79.5, Ga2-P2-Ga3 108.

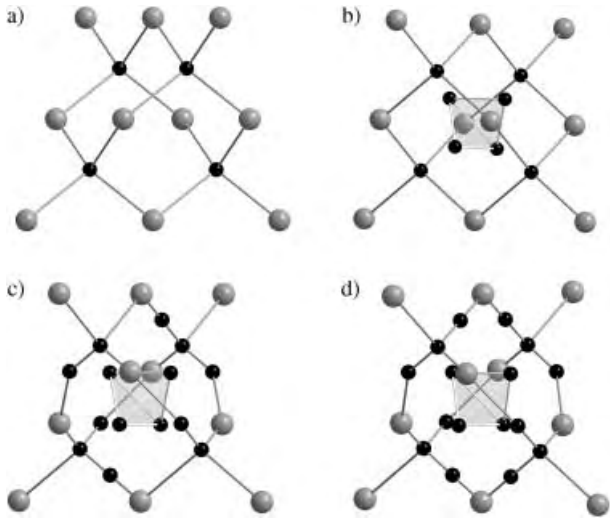


Figure 3. Idealized structural development of **1**, starting from crystalline gallium phosphide (zinc blende structure). a) Ga_4P_{10} ("inverse" P_4O_{10}); b) naked Ga_4 tetrahedron at the center of the Ga_4P_{10} unit (somewhat reduced in size for clarity); c) insertion of six gallium atoms into the six edges of the tetrahedron; d) insertion of two additional gallium atoms with distortion of the T_d symmetry.

$[Ga_{16}(PtBu_2)_{10}]$ was synthesized by the reaction of a slight excess of a toluene suspension of $LiPtBu_2$ with GaBr at −78 °C; GaBr was prepared beforehand as a metastable solution in toluene/THF by a cocondensation method. After slowly warming the reaction mixture to room temperature, we heated it to 50 °C for about 1 h and then removed the solvent under vacuum. The LiBr was separated out by dissolving the residue in toluene, which subsequently allowed us to obtain **1** from a solution in toluene as black, cubic crystals. The yield was about 10 %, which means that the dark solution contains further species, whose isolation is the subject of ongoing investigations.

A crystal structure analysis[9] of **1** shows it to be a neutral Ga_{16} cluster compound with a distorted tetrahedral structure (Figure 2). The tetrahedra are organized in the crystal in a nearly body-centered cubic (certainly somewhat tetragonally distorted) arrangement. The smallest distances between the centers of the clusters are 1522.7 pm.

The structure of the individual $Ga_{16}P_{10}$ clusters is depicted in Figure 3. Four Ga and ten P atoms form an adamantane-like Ga_4P_{10} framework, which can be described as "inverse" P_4O_{10} (Figure 3a) and in which the zinc blende structure of GaP is discernible.[10]. In the center of this unit is a polyhedron of four naked (i.e., not ligand-bearing) Ga atoms (Figure 3b). The six edges of the Ga_4P_{10} tetrahedron are bridged by six more Ga atoms (Figure 3c). Figure 3d shows the result of the insertion of two additional Ga atoms; two edges of the Ga_4P_{10} tetrahedron are bridged by two Ga atoms, and four edges are bridged by one Ga atom each, which disrupts the T_d symmetry.

The Ga–Ga distances in the central Ga_4 tetrahedron (268/277 pm) are longer than the distances between the central Ga atoms and the bridging Ga atoms (251/256 pm). The Ga–Ga distances to the four terminal Ga atoms are 251 and 261 pm, respectively. The terminal Ga atoms also have the shortest Ga–P bonds (241 pm, coordination number 3); this bond is only slightly longer than those in crystalline GaP (235 pm). Thus on going from the inside to the outside of this cluster, the Ga–Ga interactions become increasingly covalent, as evidenced by the decreasing distances.[11]

The special characteristic that renders **1** unique among metalloid Ga clusters stems from the additional bridging capability of the PR_2 groups. This allows the formation of additional Ga–P bonds, which constrict the cluster core like a corset, pulling it together more tightly than is possible, for example, with a shell of $GaNR_2$ groups. This bridging ability also lies behind the crucial difference between **1** and metalloid Ga clusters with exclusively terminal $GaSiR_3$ groups (e.g., R = *t*Bu). [12,13] The latter surround the cluster core without any additional Ga–Si interactions, as many examples have shown. To better elucidate the constriction of the central Ga_4 tetrahedron in **1**,[14] we used single-point calculations based on experimentally determined structures to determine the volumes of the Ga_4 units in three compounds with tetrahedral Ga_4 cores[15]: a) $[Ga_4R_4]$ (R = $Si(SiMe_3)_3$; **2**),[16] b) **1,** and c) $[Ga_4(GaR)_6]^-$ (R = $SitBu_3$; **3**).[17] As the average oxidation number decreases from +1 (**2**) to +0.625 (**1**) to +0.6 (**3**), the volume of the associated tetrahedra increases from 163.5 to 172.1 to 177.0 Å^3.[18] Although **1** and **3** have nearly identical oxidation numbers, the volume for **1** is additionally reduced by the above-mentioned constriction effect.

Further experiments on metalloid clusters with P*t*Bu$_2$ ligands are needed to determine whether larger cages can form within such GaP shells. Such cages would potentially have enough room for polyhedral Ga clusters with more than four atoms or even Ga-centered units.

 © 2003 Wiley-VCH Verlag GmbH & Co. KGaA, Weinheim

The insolubility of **1** in organic solvents has thus far prevented us from obtaining an NMR spectrum in solution. The quantities of samples obtained to date have been too small for solid-state NMR measurements because although the synthesis is reproducible, the yields are very low. We have thus initially calculated[19] the chemical shifts δ (in ppm) for the ^{69}Ga and ^{31}P nuclei (numbering according to Figure 2): Ga1 +414, Ga2 +393, Ga3 +527, Ga4 −54; P1 +125, P2 −2, P3 −8. These results demonstrate that the electronic relationships in **1** are far more complex than the previously described topology would lead us to expect. Thus only four of the sixteen Ga atoms (Ga4) show a slight upfield shift (−54 ppm). This group of 2 × 2 Ga atoms is unusual because the distance between every two Ga atoms is only 2.99 Å, despite the PR_2 bridges. This results in a Ga4-P1-Ga4 angle of only 79.5°. It is noteworthy that the ^{31}P chemical shift of the bridging PR_2 groups (+125 ppm) differs substantially from that of the other PR_2 ligands. All other Ga atoms are shifted significantly downfield in the direction of metallic Ga (e.g., α-Ga ca. +4500 ppm);[21] that is, even further downfield than the chemical shift observed for crystalline GaP (^{69}Ga: +307 ppm).[22] There are also no striking parallels between the ^{31}P chemical shifts of **1** and solid GaP (^{31}P: +146 ppm).[23] Despite their partially similar structures, the polar environment of four Ga atoms surrounded by four P atoms in solid GaP clearly leads to a significantly different local electronic structure than in **1** (e.g. for P2), with its largely nonpolar P–C bonds.

The above results indicate that despite its expected complex electronic structure, the unique structure of **1**, which consists of a naked Ga_4 core surrounded by a shell of GaP in which the terminal P atoms are saturated with *t*Bu groups, can be regarded as an intermediate in the oxidation of a Ga_n particle by phosphorus.

Like many other highly symmetric species, the single molecules of **1** have a nearly body-centered cubic arrangement within the crystal. If the fragmentation of **1** can be induced thermally in such a way as to remove the *t*Bu groups without decomposing the cluster core, we believe that one of nanochemistry's dreams will have been realized: a specific arrangement of metal atom clusters surrounded by a semiconducting protective shell in a topologically defined manner. We are currently conducting experiments in this direction.

Experimental Section

$LiPtBu_2$ (235 mg, 1.5 mmol) was suspended in toluene (25 mL) and cooled to −78 °C. A 0.26 M solution of GaBr (5 mL, 1.3 mmol) in toluene/THF (3:1) was added dropwise with a stainless steel cannula. This mixture was stirred and allowed to warm to room temperature over 6 h, resulting in a dark black solution. The solution was then heated to 50 °C for 1 h under slightly reduced pressure. A pale solid precipitated (LiBr). The solvent was removed under vacuum, to leave a dark oily residue, which was redissolved in toluene (20 mL). The toluene extract was subsequently separated from the precipitated LiBr with a filter cannula and stored at +7 °C for the crystallization. After several weeks we obtained small black crystals of **1** (21 mg, 0.008 mmol). Those species remaining in the solution that could be identified by $^{31}P\{^1H\}$ NMR spectroscopy (101 MHz, C_6D_6) are: $HPtBu_2$ ($\delta = 20.17$ ppm), P_2tBu_4 ($\delta = 40.19$ ppm), $[Ga(PtBu_2)_3]$ ($\delta = 54.92$ ppm).

Received: October 31, 2002
Revised: December 27, 2002 [Z50461]

Keywords: cluster compounds · gallium · metal–metal interactions · phosphides · structure elucidation

[1] a) R. L. Wells, A. P. Purdy, A. T. McPhail, C. G. Pitt, *J. Organomet. Chem.* **1986**, *308*, 281; b) A. M. Arif, B. L. Benac, A. H. Cowley, R. L. Geerts, R. A. Jones, K. B. Kidd, J. M. Power, S. T. Schwab, *J. Chem. Soc. Chem. Commun.* **1986**, 1543; c) O. T. Beachley, Jr., J. P. Kopasz, H. Zhang, W. E. Hunter, J. T. Atwood, *J. Organomet. Chem.* **1987**, *325*, 69; d) C. G. Pitt, K. T. Higa, A. T. McPhail, R. L. Wells, *Inorg. Chem.* **1986**, *25*, 2483; e) K. M. Waggoner, P. P. Power, *J. Am. Chem. Soc.* **1991**, *113*, 3385.

[2] a) K. M. Waggoner, H. Hope, P. P. Power, *Angew. Chem.* **1988**, *100*, 1765; *Angew. Chem. Int. Ed. Engl.* **1988**, *27*, 1699; b) R. A. Bartlett, P. P. Power, *J. Am. Chem. Soc.* **1990**, *112*, 3660.

[3] R. L. Wells, A. P. Purdy, A. T. McPhail, C. G. Pitt, *J. Chem. Soc. Chem. Commun.* **1986**, 487.

[4] C. Dohmeier, H. Schnöckel, C. Robl, U. Schneider, R. Ahlrichs, *Angew. Chem.* **1994**, *106*, 225–227; *Angew. Chem. Int. Ed. Engl.* **1994**, *33*, 199.

[5] M. B. Power, A. R. Barron, *Angew. Chem.* **1991**, *103*, 1403–1404; *Angew. Chem. Int. Ed. Engl.* **1991**, *30*, 1353–1354.

[6] C. Üffing, C. von Hänisch, H. Schnöckel, *Z. Anorg. Allg. Chem.* **2000**, *626*, 1557–1560.

[7] A. Schnepf, H. Schnöckel, *Angew. Chem.* **2002**, *114*, 6000–6021; *Angew. Chem. Int. Ed.* **2002**, *41*, 3533–3554.

[8] A. Ecker, E. Weckert, H. Schnöckel, *Nature* **1997**, *387*, 379.

[9] Crystal structure data for $[Ga_{16}(PtBu_2)_{10}]$: $M_r = 2567.46$. Crystal dimensions $0.3 \times 0.2 \times 0.2$ mm, tetragonal, space group $P\bar{4}2(1)c$, $a = 17.792(3)$, $c = 17.157(3)$ Å, $V = 5431.3(2)$ Å^3, $Z = 2$, $\rho_{calcd} = 1.560$ g cm^{-3}, $\mu_{Mo} = 4.078$ mm^{-1}, $\theta_{max} = 20.81°$, 45703 measured reflections, 2854 independent reflections (R(int.) = 0.2759), absorption correction: numeric (min./max. transmission 0.6845/0.7362), $R_1 = 0.0637$, $wR_2 = 0.0788$. Stoe IPDS diffractometer ($Mo_{K\alpha}$ radiation, ($\lambda = 0.71073$ Å), 150 K). The structure was solved by direct methods and was refined against F^2 for all observed reflections. Programs used: Shelxs und Shelxtl (G. M. Sheldrick, Universität Göttingen). CCDC-196943 contains the supplementary crystallographic data for this paper. These data can be obtained online free of charge at www.ccdc.cam.ac.uk/conts/retrieving.html (or from the Cambridge Crystallographic Data Centre, 12 Union Road, Cambridge CB21EZ; Fax: (+44) 1223-336-033; or deposit@ccdc.cam.ac.uk).

[10] Quantum-chemical investigations of discrete molecular $Ga_{16}P_{12}$ species show that structures with tetrahedral geometry are in fact preferred. V. Tozzini, F. Buda, A. Fasolino, *Phys. Rev. Lett.* **2000**, *85*, 4554–4557.

[11] This point is emphasized by the fact that according to quantum-chemical calculations, the average atomic volume of each of the four central Ga atoms is 43 Å^3, while that for all 16 of the atoms is only 34 Å^3.

[12] A. Donchev, A. Schnepf, G. Stößer, E. Baum, H. Schnöckel, T. Blank, N. Wiberg, *Chem. Eur. J.* **2001**, *7*, 3348.

[13] A. Rodig, G. Linti, *Angew. Chem.* **2000**, *112*, 3076; *Angew. Chem. Int. Ed.* **2000**, *39*, 2952.

[14] Analysis of the molecular orbitals of **1** shows that the four MOs of the central Ga_4 unit (analogous to **2**) are in fact significantly separated from the neighboring MOs.

[15] The molecular volumes were calculated with the Gaussian 98 program package at the SCF level with a 3-21G* basis set. We

 © 2003 Wiley-VCH Verlag GmbH & Co. KGaA, Weinheim

carried out single-point calculations based on the experimentally determined geometries of **1, 2**, and **3**, in which the "ICPM solvation model" was used to place a shell of uniform electron density (4×10^{-3} e Å^{-3}) around the Ga_4 unit. a) IPCM: J. B. Foresman, T. A. Keith, K. B. Wiberg, J. Snoonian, M. J. Frisch, *J. Phys. Chem.* **1996**, *100,* 16098. b) Gaussian 98 (Revision A.7), M. J. Frisch, G. W. Trucks, H. B. Schlegel, G. E. Scuseria, M. A. Robb, J. R. Cheeseman, V. G. Zakrzewski, J. A. Montgomery, R. E. Stratmann, J. C. Burant, S. Dapprich, J. M. Millam, A. D. Daniels, K. N. Kudin, M. C. Strain, O. Farkas, J. Tomasi, V. Barone, M. Cossi, R. Cammi, B. Mennucci, C. Pomelli, C. Adamo, S. Clifford, J. Ochterski, G. A. Petersson, P. Y. Ayala, Q. Cui, K. Morokuma, D. K. Malick, A. D. Rabuck, K. Raghavachari, J. B. Foresman, J. Cioslowski, J. V. Ortiz, A. G. Baboul, B. B. Stefanov, G. Liu, A. Liashenko, P. Piskorz, I. Komaromi, R. Gomperts, R. L. Martin, D. J. Fox, T. Keith, M. A. Al-Laham, C. Y. Peng, A. Nanayakkara, C. Gonzalez, M. Challacombe, P. M. W. Gill, B. G. Johnson, W. Chen, M. W. Wong, J. L. Andres, M. Head-Gordon, E. S. Replogle, J. A. Pople, Gaussian, Inc., Pittsburgh, PA, **1998**.

[16] G. Linti, *J. Organomet. Chem.* **1996**, *520*, 107; G. Linti, A. Rodig, *Chem. Commun.* **2000**, 127; N. Wiberg, K. Ameluxen, H.-W. Lerner, H. Nöth, W. Ponikwar, H. Schwenk, *J. Organomet. Chem.* **1999**, *574*, 246.

[17] M. Kehrwald, W. Köstler, A. Rodig, G. Linti, T. Blank, N. Wiberg, *Organometallics* **2001**, *20*, 860.

[18] For better comparison, **3** was considered as a neutral species, analogous to **1** and **2**.

[19] The ^{69}Ga NMR shifts were first based on the calculated shift in GaCp, and were subsequently set in reference to the usual standard ($[Ga(H_2O)_6]^{3+}$). The calculations were carried out in the *S*4 point group with the PMSHIFT module of the Turbomole program package with DFT (BP86-Functional, SVP basis). a) Turbomole: O. Treutler, R. Ahlrichs, *J. Chem. Phys.* **1995**, *102*, 346; b) BP86-Functional: A. D. Becke, *Phys. Rev. A* **1998**, *38*, 3098; J. P. Perdew, *Phys. Rev. B* **1996**, *33*, 8822; c) RIDFT: K. Eichkorn, O. Treutler, H. Öhm, M. Häser, R. Ahlrichs, *Chem. Phys. Lett.* **1995**, *242*, 652; K. Eichkorn, F. Weigend, O. Treutler, R. Ahlrichs, *Theor. Chem. Acc.* **1997**, *97*, 119; d) GIAO with DFT: G. Schreckenbach, T. Ziegler, *J. Phys. Chem.* **1995**, *99*, 606; GIAO with SCF: M. Häser, R. Ahlrichs, H. P. Baron, P. Weiss, H. Horn, *Theor. Chim. Acta* **1992**, *83*, 455.

[20] In crystalline GaP the Ga–Ga distance is 3.85 Å. A similar value is found for the distance between Ga2 and Ga3 in **1** (4.01 Å).

[21] O. N. Bakharev, N. Zelders, H. B. Brom, A. Schnepf, H. Schnöckel, L. J. de Jong, *Eur. Phys. J.*, submitted .

[22] O. H. Han, H. K. C. Timken, E. Oldfield, *J. Chem. Phys.* **1988**, *89*, 6046.

[23] L. J. Humphries, R. E. J. Sears, *J. Phys. Chem. Solids* **1975**, *36*, 1149.

 © 2003 Wiley-VCH Verlag GmbH & Co. KGaA, Weinheim

Os in the Sharpless Dihydroxylation

Reactivity of Osmium Tetraoxide Towards Nitrogen Heterocycles: Implications for the Molecular Recognition of DNA Mismatch**

*Dirk V. Deubel**

cis-Dihydroxylation of C=C bonds by using osmium tetraoxide is a key reaction in chemical synthesis,[1,2] which gives diols from prochiral alkenes with a high yield and enantioselectivity. The importance of the reaction is demonstrated by the award of the 2001 Nobel Prize in chemistry to Sharpless for the development of chirally catalyzed oxidations.[3] The initial reaction step is a [3+2] addition of the OsO_4 across the C=C bond, which leads to a five-membered metallacycle (osma-2,5-dioxolane).[4] Beyond the application of osmium tetraoxide in oxygen-transfer catalysis, the use of the metal oxide in biochemical analysis is of considerable interest. While C=N and C=O bonds are inert to OsO_4,[1] the C=C bonds of the nucleobases (Figure 1) that have bonding patterns different from the compact Watson–Crick pairing

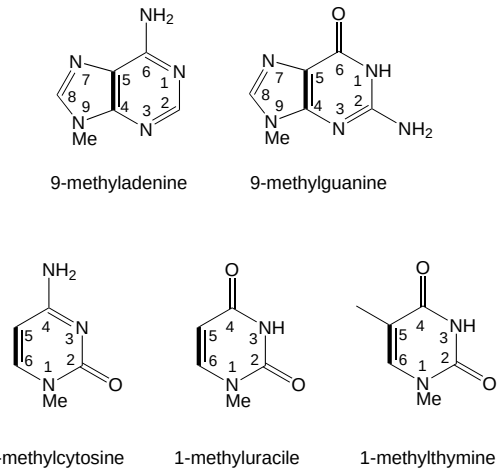


Figure 1. The C=C bonds of the five nucleobases in RNA and DNA are potential targets of osmium tetraoxide.

[*] Dr. D. V. Deubel
Swiss Center for Scientific Computing, CSCS
Swiss Federal Institute of Technology
ETH Zürich
6928 Manno (Switzerland)
and
Academia Sinica
Taipei, Taiwan (Republic of China)
E-mail: deubel@cscs.ch

[**] Quantum-chemical studies of metals in biology and medicine part II. The author thanks Prof. Dr. Michele Parrinello for support and the Fonds der Chemischen Industrie and the Federal Ministry of Education and Research (Germany), for a Liebig Fellowship. Part I:. D. V. Deubel, *J. Am. Chem. Soc.* **2002**, *124*, 5834

Supporting information for this article is available on the WWW under http://www.angewandte.org or from the author.

 © 2003 Wiley-VCH Verlag GmbH & Co. KGaA, Weinheim DOI: 10.1002/anie.200250462

in DNA are potential targets of OsO_4. This situation is relevant for the detection of unpaired and mispaired nucleobase residues of DNA and for selective DNA cleavage.[5] Although early experimental studies indicated a kinetic preference for the osmylation of thymidine monophosphate (TMP) over that of cytidine monophosphate (CMP), the reactivity of OsO_4 towards the nucleobases and other nitrogen heterocycles is not understood entirely. The aim of the density functional study[6] presented herein is a) to develop a general scheme for predicting and rationalizing the reactivity of OsO_4 to C=C bonds of various substrates (including rare tautomers of the nucleobases) and b) to investigate the geometric and electronic transition states (TS) of these reactions.

The [3+2] addition of OsO_4 across a C=C bond involves the cleavage of the π(C=C) bond, accompanied by a possible loss of π-conjugation energy or aromaticity upon sp^2–sp^3 rehybridization at the two carbon atoms. A formally simpler reaction with a potentially comparable thermochemistry is the hydrogenation of the target double bond. We have performed an initial screening of the substrates by calculating the reaction energy of RR′C=CR″R‴ + H_2→RR′HC–CHR″R‴. This computational approach allows us to consider more than just the five nucleobases. A "genealogical tree" of model substrates has been designed (Figure 2) and emphasizes the principle rather than numbers, it shows the construction of 1-methylpyrimidines and 9-methylpurines from ethene in a logical manner.

The theoretically predicted hydrogenation energies are given in Figure 2. The hydrogenation of ethene ($C_2H_4 + H_2 \rightarrow C_2H_6$) is exothermic by −30 kcal mol^{-1}, while the hydrogenation of the other substrates is thermodynamically less favorable. The calculated energies reveal the effects of π conjugation in the substrate, loss of aromaticity upon cyclization and ring fusion, exocyclic substitution, endocyclic isoelectronic replacement, and tautomerism. (For a detailed discussion, see the Supporting Information.) From the results in Figure 2, the hydrogenation of the pyrimidine derivatives at C5=C6 is predicted to be favorable, which is attributed to iminol–aminon tautomerism. Based upon this evaluation, the osmylation of the substrates **16**–**20** has been investigated in detail. In contrast, the purine derivatives **10**–**13** have not been considered further because of the energetically expensive breakdown of the fused aromatic system upon reaction at the C4=C5 bond (Figure 2).

Figure 3 shows (in italics) the calculated reaction energies for the [3+2] addition of OsO_4 across the C=C double bond of **1** and **16**–**20**. The calculations predict the osmylation of ethene to be exothermic by −16 kcal mol^{-1}, which is 14 kcal mol^{-1} less exothermic than the hydrogenation of ethene. The addition of OsO_4 to **17**–**20** is calculated to be approximately thermoneutral (Figure 3), in agreement with the experimental observation that the product of the reaction of OsO_4 and TMP is unstable.[5a] The [3+2] addition products are stabilized in the presence of pyridine. The coordination of two pyridine ligands to the five-membered metallacycle, in the case of ethene, is predicted to be exothermic by −28 kcal mol^{-1}, whereas OsO_4 is stabilized by only one pyridine ligand by −7 kcal mol^{-1}. A comparison of the calculated reaction energies in Figure 3 indicates similar trends in the thermodynamics of hydrogenation and OsO_4 addition, thus confirming the concept on which the computational screening is based.

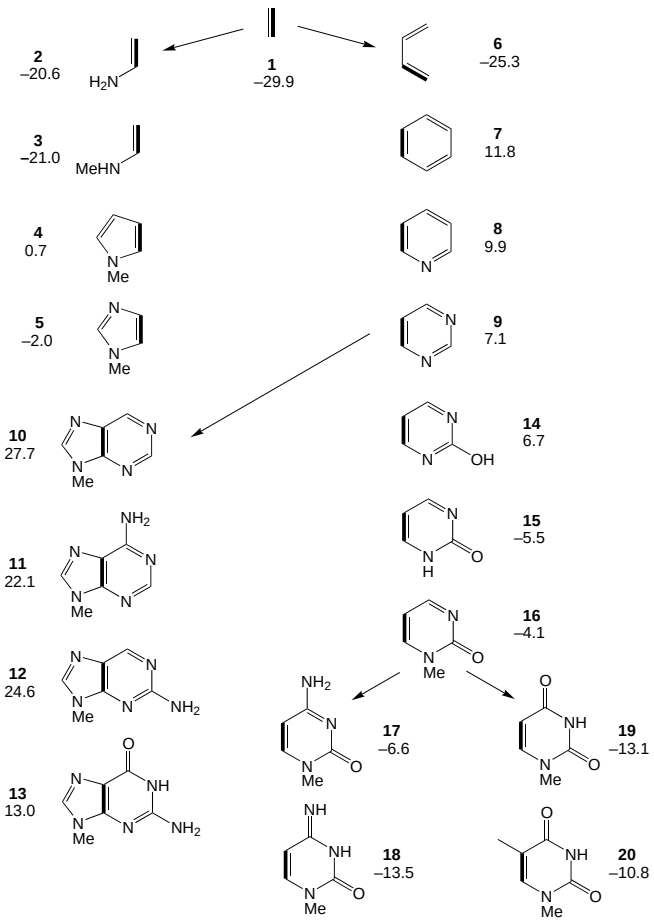


Figure 2. "Genealogical tree" of model substrates and calculated hydrogenation energies (in kcal mol^{-1}).

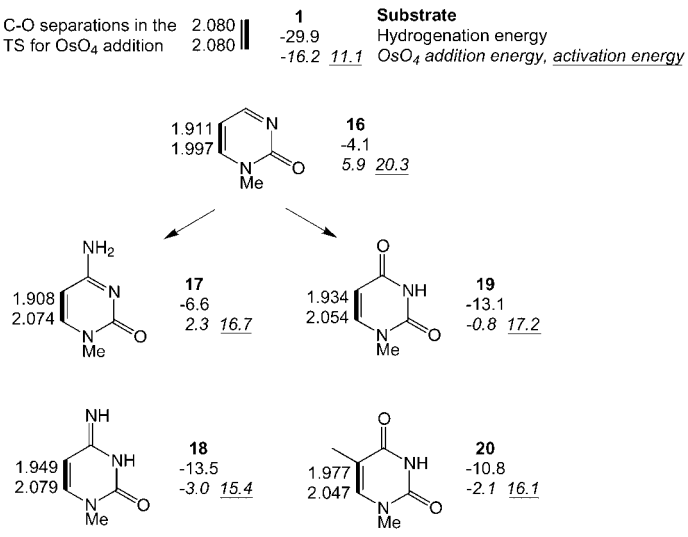


Figure 3. Calculated reaction energies, activation energies (in kcal mol^{-1}), and selected bond lengths (in Å) in the TS.

 © 2003 Wiley-VCH Verlag GmbH & Co. KGaA, Weinheim

The calculated activation energies of the OsO_4 addition to the selected pyrimidine bases are also given in Figure 3 (in italics, underlined). The computations reveal a very similar intrinsic reactivity of OsO_4 towards **17**–**20** with activation barriers of approximately 16 kcal mol^{-1}. This result implies the potential ability of each pyrimidine residue to react with the metal oxide, while thymine is predicted to be a better target than the other canonical pyrimidine tautomers. Experimental studies on the reaction of OsO_4 with nucleotides indicated a preference for the osmylation of TMP over that of UMP and CMP by an order of magnitude.[5a] This relation between experiment and theory is remarkable, given the simplified environment in the computational approach and the fact that activation-energy differences of few kcal mol^{-1} give a large change in the reaction rate. An important result is that the predicted activation barrier for the rare N4-imino tautomer **18** of cytosine, is the lowest of the studied substrates **16**–**20** (Figure 3). Compound **18** is calculated here to be less stable than the canonical tautomer **17** by only 1.4 kcal mol^{-1} (1.1 kcal mol^{-1} at the MP2/6-31G(d,p) level).[7a] Rare tautomers of the nucleobases are potentially involved in point mutations. An N4-imino tautomer of cytosine is anticipated to contribute to the stability of certain secondary-structure elements in DNA.[7]

Figure 4 displays the calculated TS for the addition of OsO_4 across the C5=C6 bond of 1-methylthymine (**20**). The C–O separations in the TS for **1** and **16**–**20** are given in Figure 3. Of note is that the TS for the addition of OsO_4 to ethene is symmetric, whereas the TSs for the addition to pyrimidines are asymmetric, a result of the C5–O separations being significantly shorter than the C6–O separations. Asymmetric [3+2] TSs were recently reported for related reactions, for example, the cycloextrusion of styrenes from 3-phenylrhena-2,5-dioxolanes.[8]

To understand the geometric and electronic structure of the transition states, we have used charge decomposition analysis (CDA).[9] Methodological details of CDA have been given elsewhere.[6] One important point is the nature of the oxidant (OsO_4) attack on the substrate(C=C)—electrophilic or nucleophilic. This electronic character of oxygen transfer[10] and its possible relation to reactivity has been the subject of controversy.[5a] The CDA results are presented in Table 1. The analysis shows that the TS can be described in terms of donor–acceptor interactions between substrate (donor) and OsO_4 (acceptor). The ratio d/b of electron donation d (from occupied substrate orbitals into vacant orbitals of the metal oxide) and electron backdonation b (from occupied orbitals of the metal oxide into vacant substrate orbitals) is the key parameter in the following discussion.

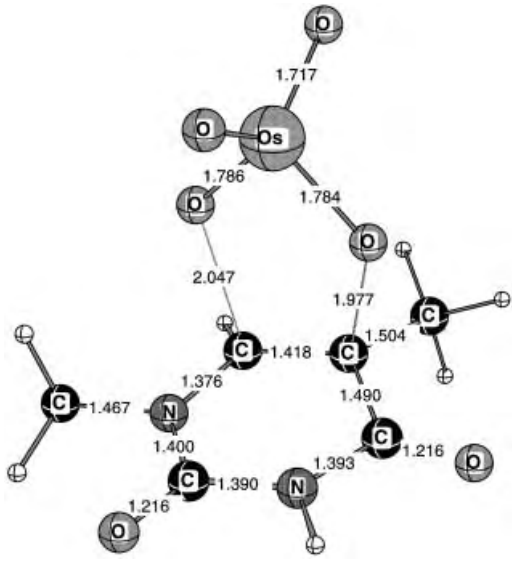


Figure 4. Calculated TS for the [3+2] addition of OsO_4 across the C5=C6 bond of 1-methylthymine (**20**). Bond lengths in [Å]

Table 1: CDA of the transition states for the [3+2] addition of OsO_4 to ethene (**1**) and the pyrimidines **16**–**20**.[a]

Substrate	d	b	r	Δ	d/b
1	0.192	0.153	−0.361	0.000	1.25
16	0.194	0.224	−0.492	0.007	0.87
17	0.197	0.208	−0.460	0.007	0.95
18	0.191	0.201	−0.440	0.005	0.95
19	0.196	0.207	−0.456	0.005	0.95
20	0.202	0.210	−0.447	0.005	0.96

[a] Calculations at the B3LYP/II level. Donation d (substrate→OsO_4), backdonation b (substrate←OsO_4), repulsive polarization r (substrate↔OsO_4), residual term Δ.

The CDA of the TS for the OsO_4 addition to ethene gives a d/b ratio of 1.25, which indicates an *electrophilic* attack of the OsO_4 on the alkene.[11] The analysis identifies OsO_4 as a "chameleon oxidant" which changes its electronic character depending on substrate. A d/b ratio of 0.87 predicted for the osmylation of 9-methyl-4-desaminocytosine (**16**) corresponds to a *nucleophilic* attack on the substrate. In contrast, for the four other pyrimidines studied, a d/b ratio of approximately 1 is obtained, which indicates an equal strength of donation and backdonation in the TS. By comparing the CDA results (Table 1) and the activation energies (Figure 3), it becomes clear that a larger electrophilicity of the oxidant correlates with a greater reactivity.

To elucidate the asynchronous formation of the two C–O bonds upon the [3+2] addition of the OsO_4, the TS for the reaction with 9-methylthymine (**20**) has been analyzed in detail. The calculated TSs for the other pyrimidines **16**–**19** show a similar extent of asymmetry (Figure 3). Figure 5 displays the frontier orbitals of 9-methylthymine.[12] The HOMO has a greater coefficient of the p_z orbital at the C5 atom than at the C6 atom (Figure 5), which favors the formation of the C5–O bond prior to the C6–O bond. In contrast, the LUMO has a greater p_z coefficient at C6 than at C5 and would favor C6–O bond formation before C5–O bond formation. Because electron donation and backdonation are of equal strength ($d/b = 0.96$), the charge transfer in the TS has been decomposed further. The analysis reveals that several orbital interactions contribute to backdonation b, whereas donation d (0.202 e) is clearly reflected by the interaction of the HOMO of 9-methylthymine with the LUMO of the OsO_4 (0.159 e).[13] This suggests that the greater HOMO p_z coefficient at C5 of pyrimidines is stereo-

 © 2003 Wiley-VCH Verlag GmbH & Co. KGaA, Weinheim

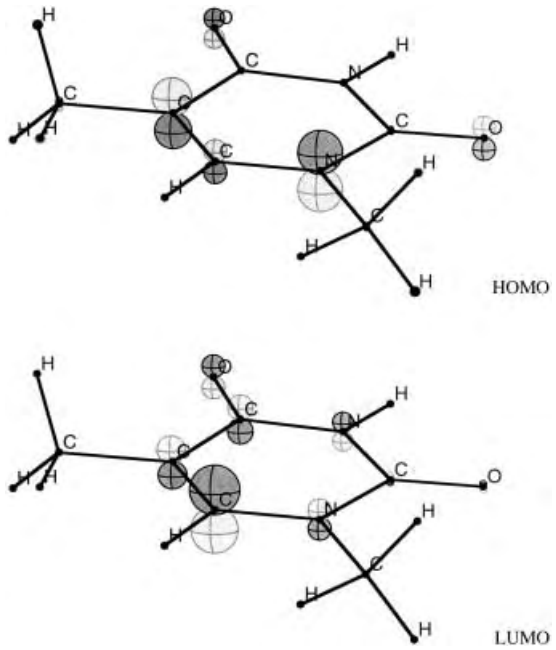


Figure 5. Frontier orbitals of 1-methylthymine (**20**).

electronically recognized by the oxidant. Thus, CDA provides a quantum-chemical rationale of the extent of asymmetry in the reactions of C=C bonds that communicate electronically with adjacent functional groups.

Given steadily increasing computational resources and improving theoretical methods, the investigation of the reaction of osmium tetraoxide with biomolecules in the presence of several auxiliary ligands in different biological microenvironments will continue. Present studies focus on the reactivity of less toxic metal oxides, such as permanganate, towards potential biological targets.

Received: October 31, 2002 [Z50462]

Keywords: density functional calculations · heterocyclic compounds · hydroxylations · nucleic acids · osmium tetraoxide

[1] Reviews: a) M. Schröder, *Chem. Rev.* **1980**, *80*, 187; b) H. C. Kolb, M. S. Van Nieuwenhze, K. B. Sharpless, *Chem. Rev.* **1994**, *94*, 2483; c) M. Beller, K. B. Sharpless in *Applied Homogeneous Catalysis* (Eds.: B. Cornils, W. A. Herrmann), VCH, Weinheim, **1996**, p. 1009; d) H. C. Kolb, K. B. Sharpless in *Transition Metals for Organic Synthesis, Vol. 2* (Eds.: M. Beller, C. Bolm), Wiley-VCH, Weinheim, **1998**, p. 219.

[2] Recent examples: a) C. Döbler, G. M. Mehltretter, U. Sundermeier, M. Beller, *J. Am. Chem. Soc.* **2000**, *122*, 10289; b) S. Y. Jonsson, K. Färnegårdh, J.-E. Bäckvall, *J. Am. Chem. Soc.* **2001**, *123*, 1365; c) A. Severeyns, D. E. De Vos, L. Fiermans, F. Verpoort, P. J. Grobet, P. A. Jacobs, *Angew. Chem.* **2001**, *113*, 606; *Angew. Chem. Int. Ed.* **2001**, *40*, 586; d) B. M. Choudary, N. S. Chowdari, K. Jyothi, M. L. Kantam, *J. Am. Chem. Soc.* **2002**, *124*, 5341; e) M. A. Andersson, R. Epple, V. V. Fokin, K. B. Sharpless, *Angew. Chem.* **2002**, *114*, 490; *Angew. Chem. Int. Ed.* **2002**, *41*, 472; f) C=C cleavage: B. R. Travis, R. S. Narayan, B. Borhan, *J. Am. Chem. Soc.* **2002**, *124*, 3824.

[3] K. B. Sharpless, *Angew. Chem.* **2002**, *114*, 2126; *Angew. Chem. Int. Ed.* **2002**, *41*, 2024.

[4] Example:U. Pidun, C. Boehme, G. Frenking, *Angew. Chem.* **1996**, *108*, 3008; *Angew. Chem. Int. Ed. Engl.* **1996**, *35*, 2817; review: D. V. Deubel, G. Frenking, *Acc. Chem. Res.* **2003**, *36*, accepted.

[5] a) L. G. Marzilli, *Prog. Inorg. Chem.* **1977**, *23*, 255; b) B. Lippert, *Coord. Chem. Rev.* **2000**, *200*, 487.

[6] a) D. V. Deubel, G. Frenking, *J. Am. Chem. Soc.* **1999**, *121*, 2021; b) D. V. Deubel, J. Sundermeyer, G. Frenking, *J. Am. Chem. Soc.* **2000**, *122*, 10101; c) D. V. Deubel, S. Schlecht, G. Frenking, *J. Am. Chem. Soc.* **2001**, *123*, 10085. See these studies or the Supporting Information for methodological details. Structures were calculated at the B3LYP/II level, energies at B3LYP/III+.

[7] a) J. Florián, J. Leszczynski, *J. Am. Chem. Soc.* **1996**, *118*, 3010; b) P. Hobza, J. Sponer, *Chem. Rev.* **1999**, *99*, 3247; c) N. Spackova, I. Berger, J. Sponer, *J. Am. Chem. Soc.* **1999**, *121*, 5519.

[8] K. P. Gable, F. A. Zhuravlev, *J. Am. Chem. Soc.* **2002**, *124*, 3970.

[9] S. Dapprich, G. Frenking, *J. Phys. Chem.* **1995**, *99*, 9352.

[10] a) W. Adam, W. Haas, B. B. Lohray, *J. Am. Chem. Soc.* **1991**, *113*, 6202; b) H. E. B. Lempers, A. R. I. Garcia, R. A. Sheldon, *J. Org. Chem.* **1998**, *63*, 1408; c) G. Boche, J. C. W. Lohrenz, *Chem. Rev.* **2001**, *101*, 697; d) D. V. Deubel, *J. Org. Chem.* **2001**, *66*, 3790.

[11] CDA indicates that $OsO_4(NH_3)$ is less electrophilic, with a d/b ratio of 1.08 in the TS of the [3+2] addition to ethene ($d = 0.172$, $b = 0.158$, $r = -0.377$, $\Delta = 0.000$).

[12] Plots of the frontier orbitals of metal oxides are presented in ref. [6a].

[13] Ranking of the orbital interactions contributing to charge transfer in the TS for **20**, according to CDA: 1. (0.159 e): HOMO(**20**)→LUMO (OsO_4); 2. (0.060 e): HOMO(OsO_4)→LUMO(**20**); 3. (0.036 e): HOMO-4(OsO_4)→LUMO(**20**); 4. (0.026 e): HOMO-4(**20**)→LUMO(OsO_4); 5. (0.024 e): HOMO-8(OsO_4)→LUMO(**20**); 6. (0.009 e): HOMO-14(**20**)→LUMO(OsO_4).

 © 2003 Wiley-VCH Verlag GmbH & Co. KGaA, Weinheim

Cover Picture



Jeremy E. P. Dahl,* J. Michael Moldowan, Torren M. Peakman, Jon C. Clardy, Emil Lobkovsky, Marilyn M. Olmstead, Paul W. May, Tim J. Davis, John W. Steeds, Ken E. Peters, Andy Pepper, Andy Ekuan, and Robert M. K. Carlson

A brilliant example …of the treasures that can be found in petroleum: The cover picture shows the carbon framework structure of the newly identified diamond molecule cyclohexamantane, $C_{26}H_{30}$, superimposed on a diamond lattice surrounded by individual cyclohexamantane molecules shown from a variety of perspectives, such as their diamond (100), (110), (111) faces. More details are given in the Communication by J. E. P. Dahl et al. on page 2040 ff.

ACHEMA & Angewandte

...are brands that most chemists know, and they have a good idea for what these brands stand; chemistry in the widest possible form, international character, and quality are characteristics that they both have in common. This issue of *Angewandte Chemie* has been published to coincide with the "27th International Exhibition on Chemical Engineering, Environmental Protection and Biotechnology", that is, ACHEMA 2003, which takes place between 19 and 24 May in Frankfurt am Main; incidentally, a large number of extra copies of *Angewandte Chemie* will be distributed at the ACHEMA. The ACHEMA is organized by the Society of Chemical Technology and Biotechnology (officially DECHEMA, the Gesellschaft für Chemische Technik und Biotechnologie e.V.). There is also a link between the DECHEMA and the German Chemical Society (Gesellschaft Deutcher Chemiker, GDCh), the owner of *Angewandte Chemie*. The GDCh has organized a special ceremony at the ACHEMA featuring a plenary lecture by Achim Müller (the author of a communication in this issue) and the award of a prize for science journalism to John Emsley.

Chemistry in the widest possible sense is presented at the ACHEMA. That environmental protection and biotechnology are prominent in the title of this "International Exhibition" indicates the central importance of chemistry in both subjects. At the exhibition everything is represented, from plant construction to measurement, control engineering and process technology to laboratory and analytical techniques; in addition there is an exhibitor's section "Research and Innovation" a topic where ACHEMA & ***Angewandte*** meet, as Angewandte Chemie actually means Applied Chemistry in German. And the journal certainly covers chemistry that is applied in all sciences and chemistry that is at the frontier of many possible future applications. Topics that generally are designated life or materials science are found frequently on the pages of *Angewandte Chemie*. This issue is no exception, the cover alone highlights articles about (molecular) diamonds from oil, the industrial synthesis of ammonia, and the discovery and development of a completely new class of antibacterial agents. In addition there are articles on the latest analytical and synthetic methods. It is not unusual for the articles to come from industrial laboratories, in this issue there are articles from Chevron-Texaco, Pharmacia, and Boehringer-Ingelheim. In 2003 Germany celebrates the "Year of Chemistry" and one of the most important issues is to emphasize the position of chemistry both as the central science and one of the most important and innovative branches of modern industry. In particular, the fashionable topics at the moment—bio, nano, and naturally, nanobio—are nothing without chemistry, in fact, they are to a great extent just chemistry.

As well as covering the full spectrum of chemistry, both ACHEMA & ***Angewandte*** have high quality and a highly international character as their trademarks. The ACHEMA would not be occurring for the 27th time and would not have such spin-offs as the ACHEMASIA and the ACHEMAMERICA, if right from the outset, these qualities had not been at the forefront. The same applies to *Angewandte Chemie* (now in its 115th year) and its very successful "offspring": *Chemistry—A European Journal*, *ChemBioChem*, and *ChemPhysChem*.

Quality has always been the prime consideration for *Angewandte Chemie*, not only in the choice of articles but also in the presentation. The change to weekly publication—see the Editorial in Issue 1/2003—also brought a change in the appearance of the journal which has been received very positively by readers and authors. Color continues to become a more important part of attractive presentation. The costs of color production for articles in which color is essential and for which the authors have no funds are, as has always been the case, paid for by the journal. Thus, the 115th year of *Angewandte Chemie* has brought a further improvement in the "quality of presentation"—but what about the quality of the articles? Has the weekly publication resulted in a lowering of the quality criteria because more articles need to be accepted? No, if anything the opposite is true! Following the increase in the rejection rate from 59% in 2001 to 62% in 2002, 68% of manuscripts submitted in January 2003 were rejected and unfortunately this figure will most likely average 65% or more, over the year, because in the first quarter alone the number of communications received has increased by 20%.

In the last two decades *Angewandte Chemie* has become more and more

 © 2003 Wiley-VCH Verlag GmbH & Co. KGaA, Weinheim

Table 1: Number of accepted communications in 2002 by country of origin.

Country	
USA	228
Germany	206
Japan	126
Great Britain	66
France	44
P.R. China	42
Spain	28
Switzerland	27
South Korea	22
Italy	22
Others	66

international. Table 1 gives a country-by-country overview of the number of communications, submitted in 2002, which were accepted. Figure 1 shows similar data graphically, however, in this case, all the articles published in 2002 are arranged by correspondence authors, and articles with more than one correspondence author are thus counted more than once. As a truly international journal, *Angewandte Chemie* would like to publish even more of the best manuscripts from everywhere in the world. Authors, however, should be aware of the high standard that is required for a publication in *Angewandte Chemie*; this seems not always to be the case and we can only encourage them to be more self-critical when deciding on the most appropriate journal for a piece of work. For a publication in *Angewandte Chemie* authors must remember that they are addressing a multinational audience of chemists from all subdisciplines and beyond. Thus, *Angewandte* articles are read not only by the specialists in the authors' own field but by people looking for ideas to apply to other problems in other areas, and even other disciplines. It is no fun for the Editors to have to reject so many manuscripts. The Editors are naturally very careful when selecting manuscripts, to consider the scientific merits first and foremost and then also the interests of the readers. That the rejection rates for manuscripts from some countries are significantly lower than from others, can be attributed to the authors from these countries knowing the journal well and better assessing the suitability of their work for publication in *Angewandte Chemie*. Incidentally, the majority of the referees are from outside Germany, which is hardly surprising when over 90% of manuscripts are submitted in English.

For an Editor the "interests of the readers" are as important as they are ambiguous. As most readers currently have their first look into *Angewandte Chemie* online, the full-text download statistics are an indicator of this interest. The access figures for *Angewandte Chemie* are very high—they are by far the highest of any of the approximately 450 journals available through Wiley InterScience—and they rose by around 25% per article during 2002. The access figures naturally reflect the number of scientists working in a particular area, thus, it is no surprise that, for example, in 2002 the list of the 25 most downloaded articles (see Table 2 on the next page) is dominated by organic synthesis. What is surprising, however, is that five communications (but no highlights or minireviews) have made it into the top 25 as have three reviews from 2001. It is also noteworthy that two reviews, one from Haag, Bannwarth, and coworkers and the other from Fu and Littke, are very high up the list in spite of being published very late in 2002. The interests of one large community, however, are never favored over the interests of the many smaller communities. The deciding factor is always the level of inventiveness found in each individual article.

After the "major overhaul" of *Angewandte Chemie*, Wiley InterScience is next in line, and in autumn 2003 this service will be relaunched. As of now Wiley InterScience, and therefore also *Angewandte Chemie*, offers a Pay-per-View function for all nonsubscribers, which means that it is possible for anyone to purchase individual articles; considering the central position of chemistry in science, as mentioned above, this is a very important service. And last but not least, as of Issue 13 this year *Angewandte Chemie* prints Digital Object Identifiers (DOIs) at the foot of the first page each article; these are very important for authors, for example, to put a link from their homepage to their article in the journal, they are essential

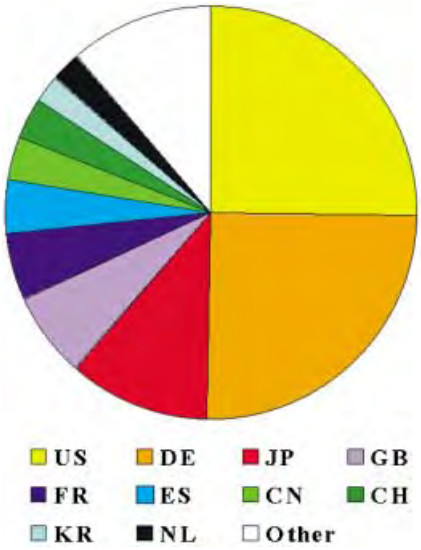


Figure 1: Country of origin of all the articles published in 2002 (with the exception of book and web-site reviews). The information is generated from the addresses of the correspondence authors articles with more than one correspondence author are thus counted more than once; this, however, does not distort the overall picture.

for the electronic linking of all journals (through PubMed or CrossRef), and for the permanent archiving of articles—in addition they also make it possible for us to present articles electronically in Early View weeks before publication in an issue. This service will begin shortly with the "sprinter" and "VIP" articles.

And don't forget that e-services also have a prominent place at the ACHEMA. It's not too late to get there!



Peter Gölitz

PS: On the subject of readers' interests: It is curious to note that in the first three months of 2003 the most downloaded article from the International Edition is the review article by S. J. Danishefsky and H. Lin with the title »»»"Gelsemine: A Thought-Provoking Target for Total Synthesis", whereas from the German Edition it is the highlight article about Caffeine by S. R. Waldvogel. Is this a revelation about Germans, and should we publish something about tea soon?

 © 2003 Wiley-VCH Verlag GmbH & Co. KGaA, Weinheim

Table 2: Most frequently downloaded articles in 2002 from *Angewandte Chemie* (titles abbreviated).

Correspondence authors	Title	Issue/Year/Type[a]
K. C. Nicolaou	The CP Molecule Labyrinth	15/2002/R
K. C. Nicolaou	The Diels–Alder Reaction in Total Synthesis	10/2002/R
E. J. Corey	Catalytic Enantioselective Diels–Alder Reactions	10/2002/R
K. B. Sharpless	Searching for New Reactivity (Nobel Lecture)	12/2002/R
R. Noyori	Asymmetric Catalysis (Nobel Lecture)	12/2002/R
W. S. Knowles	Asymmetric Hydrogenations (Nobel Lecture)	12/2002/R
W. Bannwarth, R. Haag	Modern Separation Techniques for the Efficient Workup in Organic Synthesis	21/2002/R
V. V. Fokin, K. B. Sharpless	A New Approach to Osmium-Catalyzed Asymmetric Dihydroxylation and Aminohydroxylation of Olefins	3/2002/C
G. C. Fu	Palladium-Catalyzed Coupling Reactions of Aryl Chlorides	22/2002/R
W. A. Herrmann	N-Heterocyclic Carbenes: A New Concept in Organometallic Catalysis	8/2002/R
M. Lautens	Halide Effects in Transition Metal Catalysis	1/2002/R
M. C. Pirrung	How to Make a DNA Chip	8/2002/R
G. Klebe	Approaches to the Description and Prediction of the Binding Affinity of Small-Molecule Ligands to Macromolecular Receptors	15/2002/R
J. Rebek, Jr.,	Molecular Encapsulation	9/2002/R
C. M. Niemeyer	Nanoparticles, Proteins, and Nucleic Acids: Biotechnology Meets Materials Science	22/2001/R
H. Waldmann	From Protein Domains to Drug Candidates	16/2002/R
D. Antonelli	Recent Advances in Synthesis and Applications of Transition Metal Containing Mesoporous Molecular Sieves	2/2002/R
S. J. Danishefsky	The *B*-Alkyl Suzuki–Miyaura Cross-Coupling Reaction	24/2001/R
K. C. Nicolaou	Total Synthesis of Diazonamide A	18/2002/C
S. J. Rowan	Dynamic Covalent Chemistry	6/2002/R
A. H. Hoveyda, R. R. Schrock	The First Polymer-Supported and Recyclable Chiral Catalyst for Enantioselective Olefin Metathesis	4/2002/C
S. J. Danishefsky	The Total Synthesis of Proteasome Inhibitors TMC-95A and TMC-95B	3/2002/C
K. B. Sharpless	Click Chemistry: Diverse Chemical Function from a Few Good Reactions	11/2001/R
S. Förster	From Self-Organizing Polymers to Nanohybrid and Biomaterials	5/2002/R
G. Pattenden	Total Synthesis of the Presumed Amphidinolide A	3/2002/C

[a] R = review, C = communication.

 © 2003 Wiley-VCH Verlag GmbH & Co. KGaA, Weinheim

Obituary

Claude Hélène (1938–2003) ____ 1996 Nucleic Acids in Biology and Chemistry — *C. Giovannangeli, J.-S. Sun, J.-M. Lehn*

Books

Liebig und seine Schüler ____ 1997 Georg Schwedt — *reviewed by A. Rocke*

Catalysts for Fine Chemical Synthesis ____ 1998 Stanley M. Roberts, Geraldine Poignant — *reviewed by S. Doye*

Highlights

A girl's best friend and diamondoid hydrocarbons have something in common: transparent glass crystals of [121312]hexamantane (**1**) appear like diamonds with a pronounced luster. Regarding **1** as a jewel, it may be thought of as a nanometer-sized diamond of 10^{-20} carat (1 carat = 0.2 g). This and other advances in adamantane chemistry are presented herein.



1

Diamondoid Hydrocarbons

H. Hopf* ____ 2000–2002

Diamonds from Crude Oil?

Minireviews

A triumph over trial and error: The Haber–Bosch industrial synthesis of ammonia (the picture shows an industrial installation for this process) has reached such a level of refinement that, in the energy balance the only significant loss is the preparation of the highly pure starting materials. Iron, ruthenium, or molybdenum compounds serve as the catalyst. The development of new catalysts is becoming increasingly effective through a deeper understanding of the basic principles involved and less dependent on trial and error.

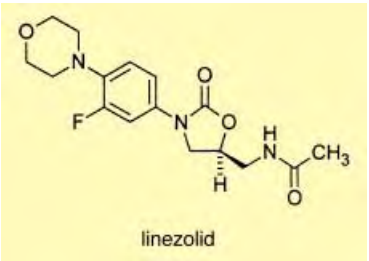


Ammonia Synthesis

R. Schlögl* ____ 2004–2008

Catalytic Synthesis of Ammonia—A "Never-Ending Story"?

Reviews



linezolid

Infections caused by Gram-positive bacteria, including drug-resistant strains, can today be treated effectively with oxazolidinone compounds. This Review shows how the intertwined roles of chemistry and biology in a pharmaceutical research project at the start of the 1980s ultimately led to the development of linezolid, the first marketed antibiotic of this class of drugs.

Development of Linezolid

M. R. Barbachyn,*
C. W. Ford ____ 2010–2023

Oxazolidinone Structure–Activity Relationships Leading to Linezolid

 © 2003 Wiley-VCH Verlag GmbH & Co. KGaA, Weinheim

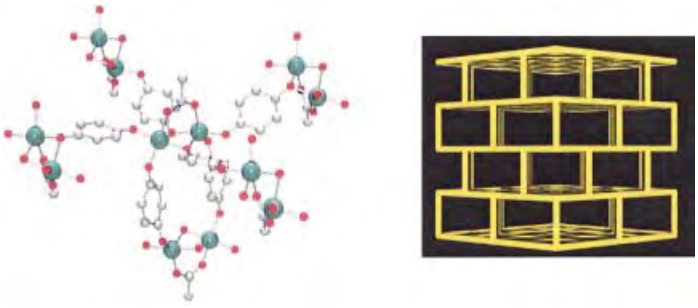
Contents

Communications

A Metal-Organometallic 3D Network

M. Oh,* G. B. Carpenter, D. A. Sweigart* ——— **2026 – 2028**

A Novel 3D Brick-Wall Coordination Network Based on Nodes with Square-Pyramidal Connectivity



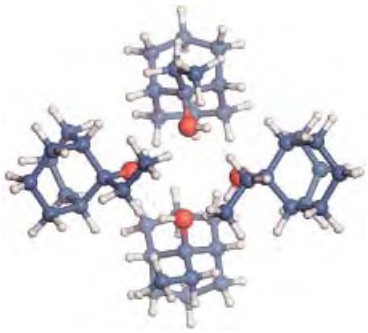
Molecular brickwork: Acetate-bridged dimeric copper(II) units (blue) are linked by $[(\eta^4\text{-benzoquinone})Mn(CO)_3]^-$ organometalloligands (O, red) in a square-pyramidal fashion to afford a metal–organometallic coordination network having an unprecedented 3D brick architecture.

Powder X-Ray Diffraction

M. Brunelli,* J. P. Wright, G. B. M. Vaughan, A. J. Mora, A. N. Fitch ——— **2029 – 2032**

Solving Larger Molecular Crystal Structures from Powder Diffraction Data by Exploiting Anisotropic Thermal Expansion

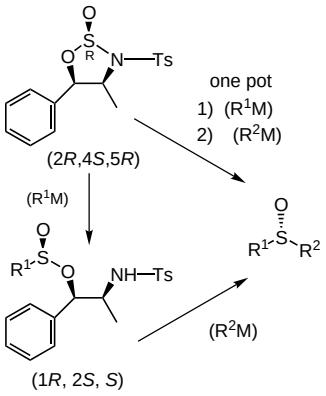
Crystal clear! The routine collection of near single-crystal-quality diffraction data from a powdered sample is possible by exploiting the anisotropic thermal expansion of a molecular solid to enhance the extraction of diffracted intensities from a heavily overlapped powder diffraction pattern. The method is validated by the solution of the structure of 9-ethylbicyclo[3.3.1]nona-9-ol (see picture, O red, C blue, H gray) which is 50% larger than other structures solved in a comparable way.



Enantiopure Sulfoxides

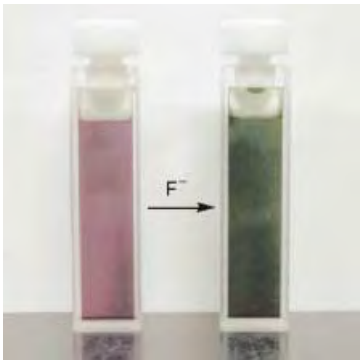
Z. Han, D. Krishnamurthy, P. Grover, H. S. Wilkinson, Q. K. Fang, X. Su, Z.-H. Lu, D. Magiera, C. H. Senanayake* ——— **2032 – 2035**

A Highly Selective and Practical Method for Enantiopure Sulfoxides Utilizing Activated and Functionally Differentiated *N*-Sulfonyl-1,2,3-oxathiazolidine-2-oxide Derivatives



New, stereoselective, and general methods for the preparation enantiopure sulfoxides by using norephedrine tosylate as a chiral auxiliary are described. The product may be obtained either stepwise, or in a one-pot reaction (see scheme). Furthermore, the chiral template can be isolated from the reaction mixture and recycled.

For the USA and Canada:
ANGEWANDTE CHEMIE International Edition (ISSN 1433-7851) is published weekly by Wiley-VCH PO Box 191161, D 69451 Weinheim, Germany. Air freight and mailing in the USA by Publications Expediting Inc. 200 Meacham Ave., Elmont, NY 11003. Periodicals postage paid at Jamaica NY 11431. US POSTMASTER: send address changes to *Angewandte Chemie*, Wiley-VCH, 111 River Street, Hoboken, NJ 07030. Annual institutional subscription price for institutions: Europe € 2998.00/3148.00. Outside Europe US$ 3718.00/3904.00 (valid for print or electronic/print and electronic delivery); for individuals who are personal members of a national chemical society, or whose institution already subscribes, or who are retired or self-employed consultants, print only (including postage and handling charges): Europe € 248.00/Outside Europe US$ 348.00.

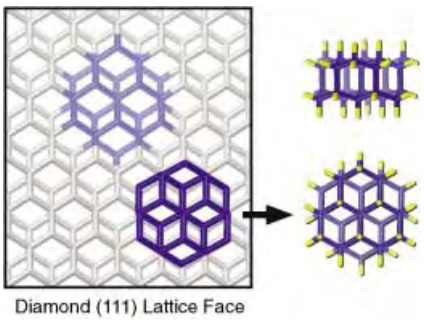


Perturbation in the energy-transfer pathway and of the π conjugation between the chromophores in a triarylborane–porphyrin conjugate on coordination of a fluoride ion to the boron center is assumed to account for the observation of the three emission bands (at 356, 670, and 692 nm). The system also displays a colorimetric (purple to green, see picture, and red to bluish emission) response to fluoride ions.

Fluorescent Chemosensor

Y. Kubo, M. Yamamoto, M. Ikeda, M. Takeuchi,* S. Shinkai,* S. Yamaguchi, K. Tamao ——— **2036 – 2040**

A Colorimetric and Ratiometric Fluorescent Chemosensor with Three Emission Changes: Fluoride Ion Sensing by a Triarylborane–Porphyrin Conjugate



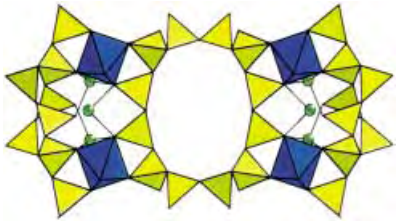
Ace of diamonds: Cyclohexamantane ($C_{26}H_{30}$), a large diamond-like molecule containing six *peri*-fused adamantane cages was identified in petroleum and its structure proven by X-ray crystallography (see picture). Never synthesized because of severe mechanistic difficulties, the structure of cyclohexamantane has appeared in theoretical molecular-simulation studies related to diamond; its experimentally determined properties are now discussed.

Structure of Cyclohexamantane

J. E. P. Dahl,* J. M. Moldowan, T. M. Peakman, J. C. Clardy, E. Lobkovsky, M. M. Olmstead, P. W. May, T. J. Davis, J. W. Steeds, K. E. Peters, A. Pepper, A. Ekuan, R. M. K. Carlson ——— **2040 – 2044**

Isolation and Structural Proof of the Large Diamond Molecule, Cyclohexamantane ($C_{26}H_{30}$)

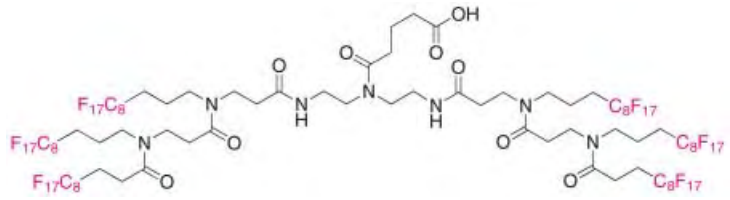
Exploring new channels: A range of alkali-metal copper silicates that contain double layers of silicate tetrahedra have been prepared, which contain straight 12-ring channels that are analogous to those found in LTL-type zeolites. The framework that defines the 12-ring channels is neutral and, consequently, only neutral MOH and H_2O species are able to fill these channels.



Nanoporus Silicate Frameworks

X. Wang, L. Liu, A. J. Jacobson* ——— **2044 – 2047**

Nanoporous Copper Silicates with One-Dimensional 12-Ring Channel Systems



The fluorous support Hfb (see picture) enabled high-yielding oligosaccharide syntheses in which the synthetic intermediates could be purified by simple fluorous–organic solvent extraction, and the reactions could be monitored spectroscopically and by TLC. Hfb was readily attached to the anomeric hydroxy group of a carbohydrate. The fluorous support could be removed in high yield, and was recyclable.

Fluorous Oligosaccharide Synthesis

T. Miura, K. Goto, D. Hosaka, T. Inazu* ——— **2047 – 2051**

Oligosaccharide Synthesis on a Fluorous Support

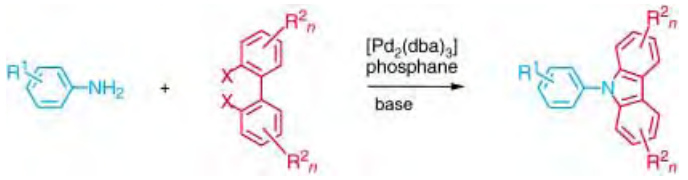
 © 2003 Wiley-VCH Verlag GmbH & Co. KGaA, Weinheim

Contents

Synthesis of Carbazoles

K. Nozaki,* K. Takahashi, K. Nakano, T. Hiyama, H.-Z. Tang, M. Fujiki, S. Yamaguchi, K. Tamao ____ **2051 – 2053**

The Double *N*-Arylation of Primary Amines: Toward Multisubstituted Carbazoles with Unique Optical Properties

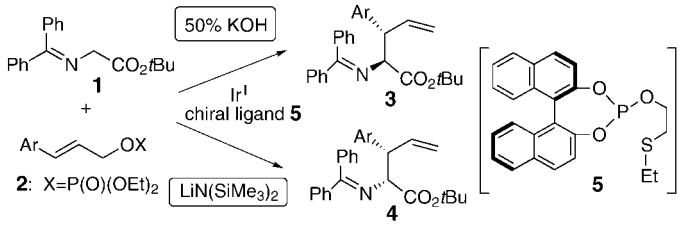


A powerful method: A variety of sterically crowded, substituted carbazoles have been prepared from anilines and biphenyl compounds (see scheme). The method enabled the preparation of 2,2′-dicarbazolyl-1,1′-biaryl compounds, which show excimer (or exciplex) emissions with significant solvent dependency.

Enantioselective Allylation

T. Kanayama, K. Yoshida, H. Miyabe, Y. Takemoto* ____ **2054 – 2056**

Enantio- and Diastereoselective Ir-Catalyzed Allylic Substitutions for Asymmetric Synthesis of Amino Acid Derivatives

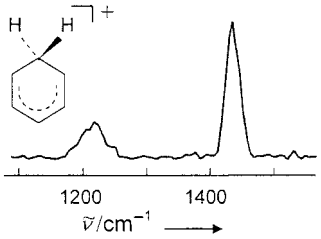


Simply switching the base employed in the first enantioselective allylic substitutions of diphenylimino glycinate **1** with **2**, which are catalyzed by an Ir complex of chiral phosphite **5**, allows the two branched diastereomers **3** and **4** to be selectively synthesized with little or no formation of linear substitution products.

Protonated Benzene Structure

W. Jones, P. Boissel, B. Chiavarino, M. E. Crestoni,* S. Fornarini, J. Lemaire, P. Maitre* ____ **2057 – 2059**

Infrared Fingerprint of Protonated Benzene in the Gas Phase

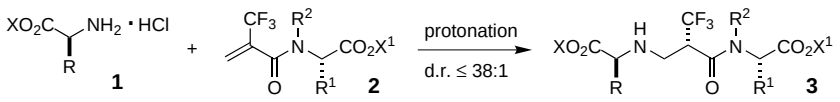


A σ and not a π complex has been identified for the prototypical arenium intermediate, protonated benzene. The activation of the infrared multiphoton dissociation of $C_6H_7^+$ ions (obtained by the gas-phase protonation of benzene) by the absorption of free electron laser radiation shows a wavelength-dependent dissociation of H_2 (see spectrum) that matches the transitions calculated for the σ complex benzenium ion.

Fluorinated Peptidomimetics

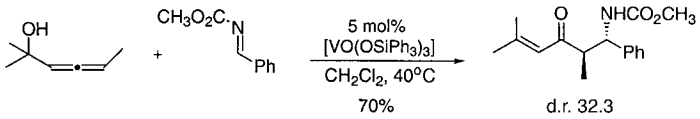
M. Sani, L. Bruché, G. Chiva, S. Fustero,* J. Piera, A. Volonterio,* M. Zanda* ____ **2060 – 2063**

Highly Stereoselective Tandem Aza-Michael Addition–Enolate Protonation to Form Partially Modified Retropeptide Mimetics Incorporating a Trifluoroalanine Surrogate



Fine-tuning of key reaction parameters, such as the solvent and the base used, led to a dramatic improvement in d.r. (from ≈1:1 to 38:1) in a tandem aza-Michael addition–enolate protonation sequence. Thus, the reaction of α-amino ester nucleophiles **1** with *N*-(α-trifluoromethyl)acryloyl-α-amino ester acceptors **2** produced an array of partially modified retropeptide mimetics **3** with good to excellent stereocontrol (R, R^1, R^2, X, X^1 = alkyl).

 © 2003 Wiley-VCH Verlag GmbH & Co. KGaA, Weinheim



(1)

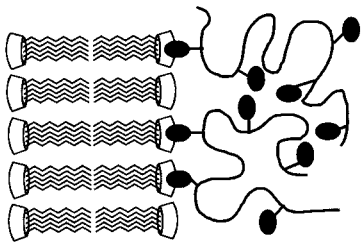
Vanadium-Catalyzed C–C Coupling

B. M. Trost,* C. Jonasson — **2063 – 2066**

Vanadium-Catalyzed *anti*-Selective Additions of Allenols to Imines

An atom-economic route to versatile building blocks: Vanadium enolates, which were generated in situ by the [3,3] sigmatropic rearrangement of vanadyl esters of allenic alcohols, undergo facile addition to imines derived from aromatic aldehydes to yield bifunctional β′-amino-α,β-unsaturated enones [Eq. (1)]. With 1,3-disubstituted allenes, good *anti* selectivity is observed in most cases.

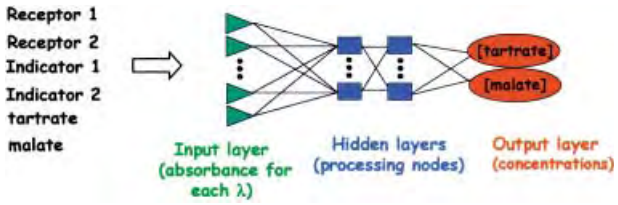
Polyelectrolytes with small hydrophobic substituents bind to vesicles composed of cyclodextrin molecules through inclusion of the hydrophobic substituents on the polymers into the cyclodextrin cavities at the vesicle surface (see schematic representation). Molecular recognition results from a subtle balance of multiple host–guest interactions between the vesicles and the polymers and intramolecular interaction of the polymers.



Polymer Recognition by Vesicles

B. J. Ravoo,* J.-C. Jacquier, G. Wenz — **2066 – 2070**

Molecular Recognition of Polymers by Cyclodextrin Vesicles



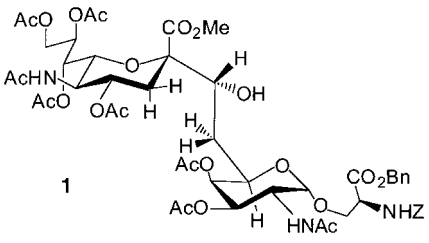
A highly selective sensing ensemble was created through the use of multiple synthetic receptors in solution. Two hosts were selected that had differential responses to tartrate and malate and to the two indicators chosen. Upon using both hosts and indicators in solution, the simultaneous detection of these two analytes was achieved through pattern recognition by using neural-network analysis (see scheme).

Multicomponent Sensors

S. L. Wiskur, P. N. Floriano, E. V. Anslyn,* J. T. McDevitt* — **2070 – 2072**

A Multicomponent Sensing Ensemble in Solution: Differentiation between Structurally Similar Analytes

---



1

The nonhydrolyzable glycosidic linkage to sialic acid in the C-glycoside analogue of sTn, **1**, is the key feature of the redesigned glycoconjugate. This potential antitumor and anti-HIV agent was prepared in one enzymatic and seventeen chemical steps starting from diisopropylidene galactopyranose.

C-Glycosides

B. Kuberan, S. A. Sikkander, H. Tomiyama, R. J. Linhardt* — **2073 – 2075**

Synthesis of a C-Glycoside Analogue of sTn: An HIV- and Tumor-Associated Antigen

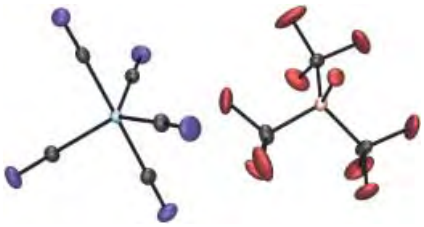
 © 2003 Wiley-VCH Verlag GmbH & Co. KGaA, Weinheim

Contents

Homoleptic Cobalt Carbonyl Complex

E. Bernhardt, M. Finze, H. Willner,*
C. W. Lehmann,* F. Aubke* **2077 – 2079**

$[Co(CO)_5][(CF_3)_3BF]$: A Stable Salt of a Homoleptic Trigonal-Bipyramidal Metal–Carbonyl Cation

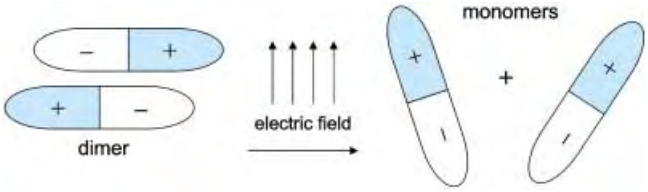


Cobalt takes to superacid: By using the superacid system $(CF_3)_3BCO$ and anhydrous HF the title complex (see structure O blue, C black, Co cyan, F red, B light brown) is formed in a one pot reaction of $[Co_2(CO)_8]$. The oxidizing agent is postulated to be $H_2F^+_{solv.}$ which is generated in situ.

Influencing Equilibria

R. Wortmann,* U. Rösch,
M. Redi-Abshiro,
F. Würthner* **2080 – 2083**

Large Electric-Field Effects on the Dipolar Aggregation of Merocyanine Dyes

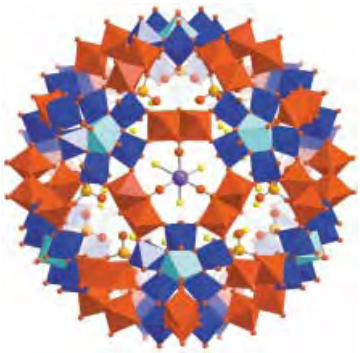


Field of dreams: An unusually strong electric-field effect influences the aggregation equilibrium of a strongly dipolar merocyanine dye. Electrooptical absorption measurements indicate that the external electric field leads to an increase of the monomer concentration at the expense of the dimer concentration (see picture).

Water in Polyoxometalate Capsules

A. Müller,* E. Krickemeyer, H. Bögge,
M. Schmidtmann, B. Botar,
M. O. Talismanova **2085 – 2090**

Drawing Small Cations into Highly Charged Porous Nanocontainers Reveals "Water" Assembly and Related Interaction Problems



Containing nanowater droplets: A series of polyoxometalate capsules containing shells of water molecules is described. The surfaces of the capsules are covered with nanoscale pores, which when open permit entry to the cavities within (see structure, four of the 20 nanoscale pores are visible, and one of the six encapsulated Na^+ ions is shown in violet). Variation of the cluster properties, such as charge and the nature of the internal surface, greatly influences the encapsulated species.

VIP Communications labeled with this symbol have been judged by two referees as being "very important papers".

The publication of Communications labeled with this symbol has been accelerated because of their topical or highly competitive nature.

Issue 16/2003 appeared online on April 23.

 © 2003 Wiley-VCH Verlag GmbH & Co. KGaA, Weinheim

Deadline for recruitment adverts

22/2003	May 15	Publication date: June 6
23/2003	May 22	Publication date: June 16

Angewandte Chemie International Edition
Advertising Sales Department:
Marion Schulz
Phone: 0 62 01 – 60 65 65
Fax: 0 62 01 – 60 65 50
E-Mail: MSchulz@wiley-vch.de

Place an advert in the printed version
and have it made available online for 1 month, free of charge!

Service

Keywords ____ *2092*

Authors ____ *2093*

Vacancies ____ *2091*

Preview ____ *2097*

3rd PPG SIPSY Symposium

New Frontiers in Asymmetric Synthesis

SEPTEMBER 3 & 4 2003

ANGERS FRANCE

Congress Center

PPG-Sipsy



ZI LA CROIX CADEAU – BP 79
49242 AVRILLE Cedex France
Tel.: +33 (0) 2 41 96 61 31 or 61 58
Fax: +33 (0) 2 41 42 76 55
Web site: www.ppg-sipsy.com
Please contact David Béchard:
E-mail: bechard@ppg.com

The search for new chiral catalysts and the adaptation of classical organic reactions to their asymmetric versions have clearly become a reality.
With emphasis on these chiral technologies, PPG-Sipsy is pleased to announce the third conference on asymmetric catalysis, which will be held on September 3-4, 2003, at the Congress Center of Angers, France.
Our goal for the conference is to review new developments in the field of asymmetric catalysis, foster relationships between academic and industrial chemists, and promote the development of new catalysts for asymmetric synthesis.

SCIENTIFIC PROGRAM
(subject to change)

Pr. H. Kagan (Paris-Sud University - France)
"Some Aspects of Asymmetric Catalysis"

Pr. K. Mikami (Tokyo Institute of Technology - Japan)
"Cationic Pd Complexes with Chiral P, P or P, N Ligands for Asymmetric Catalysis"

Pr. E.P. Kundig (Geneva University - Switzerland)
"Asymmetric Cycloaddition Reactions Catalyzed by Iron- and Ruthenium-Lewis Acid Catalysts"

Pr. J. Jurczak (Warsaw University - Poland)
"Enantioselective Hetero Diels-Adler Reactions"

Pr. E. Jacobsen (Harvard University - USA)
"Enantioselective Cycloaddition Reactions of Unactivated Carbonyls Compounds"

Pr. H.U. Blaser (Solvias - Switzerland)
"Developing Enantioselective Catalytic Processes: Approaches and results"

Pr. C. Mioskowski (Strasbourg University – France)
"High throughput screening by immunoanalysis for the selection of enantioselective catalysts. Kinetic resolution of racemic amines with a new N-acetylation reagent"

 © 2003 Wiley-VCH Verlag GmbH & Co. KGaA, Weinheim



Claude Hélène (1938–2003): Nucleic Acids in Biology and Chemistry

One of the most prominent scientists working on nucleic acids at the chemistry–biology interface, Professor Claude Hélène, passed away on February 11, 2003 at the age of 65. His contributions to science in the fields of nucleic-acid photochemistry, nucleic-acid chemistry and biophysics, as well as chemical genomics, were very important and have been an inspiration to many for the last three decades. He was also known as a wise, witty, and kind person, whose contributions to meetings always enriched people. He left the world of nucleic acids a better place, and his presence will be sadly missed. Great scientists are rare, and great scientists who are great human beings even rarer.

Hélène's early work dealt with the excited states and energy transfer processes of nucleic acids and their part in photochemical reactions in DNA. It led to the recent progress that has been made in DNA charge transport chemistry and biology. As a molecular biophysicist, his attention had been focused since the early 1970s on the properties and functions of nucleic acids, an area in which he was always one of the central players. No less importantly, he was a remarkable statesman for his field and for science. Among his numerous and original contributions, there were two outstanding findings.

Hélène discovered a tripeptide (Lys-Trp-Lys) that binds to abasic DNA sites by intercalation and catalyzes strand scission.[1] The remarkable properties of this tripeptide are a) its specific recognition of abasic sites in DNA by nonspecific electrostatic interactions and the replacement of the missing base with the indole ring of Trp, and b) DNA cleavage at the abasic site through formation of a Schiff base between the α-amino group of the peptide and the aldehyde left on the deoxyribose unit by cleavage of the glycosidic bond. This tripeptide is still the smallest site-specific "endonuclease" known!

Some years later, as a major player in the emerging field of gene expression targeting by antisense oligonucleotides, Hélène discovered (in parallel with Peter Dervan) that short oligonucleotides could recognize specific sequences on double-stranded DNA in the major groove by triple-helix formation.[2] This finding shaped a new field of gene targeting (known as the antigen strategy) and had a very significant impact on the fields of nucleic-acid chemistry, DNA recognition, gene expression, and gene-therapeutic drug discovery. For 15 years, Hélène and his co-workers devoted much effort toward bringing this concept of targeting DNA by purely synthetic approaches to its real application in biological systems, with the rational design of triple-helix-forming oligonucleotides, physicochemical and biochemical characterizations, the probing of target accessibility in chromatin, and the demonstration of bioactivity in cultured cells, as shown by his numerous publications and excellent reviews. The new generation of triplex-forming molecules is now used to modulate gene expression, gene targeting, and genomic modifications in a sequence-specific manner. It will influence biology, biotechnology, therapeutics, and medicine.

Claude Hélène published more than 450 research articles and wrote and edited several books. He was an excellent speaker and his talks always had great impact on the audience. He was a wonderful teacher and always paid kind attention to students and collaborators.

Alongside a full career in academic research and education, Hélène had a parallel life in industry. One of us (J.M.L.) was proud to play a key role in recommending him for the position of Chief Scientific Officer of the Groupe Rhône-Poulenc (one of the predecessor companies of Aventis). For a decade (1990–1999) Claude Hélène held this challenging position, which called for both scientific excellence and supreme leadership to oversee, manage, and integrate research programs at the interface of the three main sectors: chemistry, agrochemistry, and pharmaceutical science. He made interdisciplinary thinking a corporate reality. Until the end of his life he served on the scientific board of Aventis, as well as of the startup companies Chrysalon and Urogene.

Those who had the opportunity of meeting or even the great privilege of working with Claude Hélène will warmly remember this most distinguished scientist and wonderful human being. The scientific community will miss him and deeply regret no longer having the benefit of his direct input and wisdom in science, but his inspiration and legacy will stay with us.

Carine Giovannangeli, Jian-Sheng Sun (MNHN Paris), Jean-Marie Lehn (ISIS Strasbourg)

[1] T. Behmoaras, J. J. Toulme, C. Hélène, *Nature* **1981**, *292*, 858–859.
[2] T. Le Doan, L. Perrouault, D. Praseuth, N. Habhoub, J. L. Decout, N. T. Thuong, J. Lhomme, C. Hélène, *Nucleic Acid Res.* **1987**, *15*, 7749–7760; H. E. Moser, P. B. Dervan, *Science* **1987**, *238*, 645–650.

 © 2003 Wiley-VCH Verlag GmbH & Co. KGaA, Weinheim

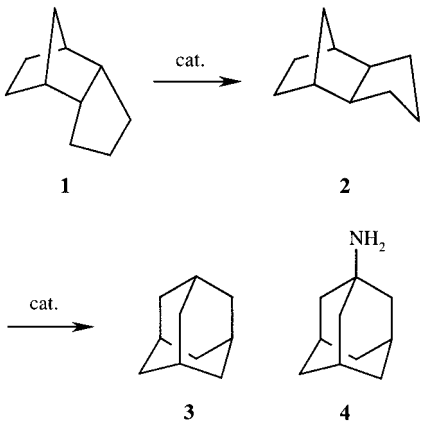
Diamondoid Hydrocarbons

Diamonds from Crude Oil?

*Henning Hopf**

Keywords:
cage compounds · diamondoids · hydrocarbons · polycycles

Seventy years ago Landa and co-workers isolated a crystalline hydrocarbon in minute amounts (0.0004 %) from a sample of petroleum collected near the village of Hodonín in Moravia.[1] The structure of the compound (**3**, Scheme 1), which they named adamantane, was proposed by Lukes on the basis of its unusual physical properties and by applying the then new technique of X-ray structural analysis.[1] It was several years before Prelog and Seiwerth reported the first synthesis of this cage hydrocarbon; their multistep route never provided more than mg amounts, and the total yield was not more than 0.3 %.[2] Although later work by Stetter and co-workers improved the situation significantly—now 200-mg batches could be prepared and the total yield of the adamantane synthesis was increased to 6 %[3]—adamantane remained a rare and precious compound, the chemical properties of which could not be studied on a broader scale because of lack of material.



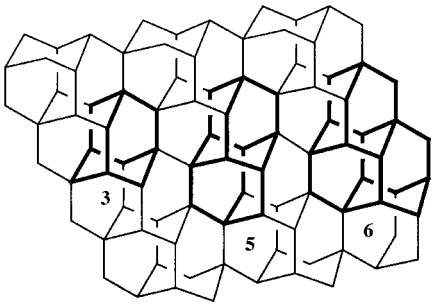
Scheme 1. The Schleyer route to adamantane (**3**).

This situation changed dramatically when—in 1957—Schleyer reported on a discovery he had made while trying to isomerize *endo*-tetrahydrodicyclopentadiene (**1**) to its *exo* isomer **2**. When the easily available **1** was refluxed overnight in the presence of aluminum trichloride the intended isomerization did indeed take place, but the process was accompanied by a surprising further rearrangement yielding adamantane[4] (Scheme 1). Over the years the Schleyer route was improved and made into a technical process, and currently 100 g of analytically pure **3** cost a modest 35 Euros.

Hundreds of adamantane derivatives have been prepared since then and many of them are also available from commercial suppliers at reasonable prices. A particular prominent derivate is 1-amino adamantane (**4**) or Symmetrel which is used to treat Parkinson and related syndromes and as an antiviral agent against Type A influenza in humans.

The name adamantane is derived from the Greek word for diamond (adamas),[5] a telling description since the carbon framework of **3** is superimposible on the diamond lattice.[6] Formally the latter can be built up by succesively fusing adamantane building blocks, and the intermediate hydrocarbons formed en route are known as diamondoids (see below). The first two "adamantanalogues" of **3** hence contain two (diamantane, **5**) and three face-fused cages (triamantane, **6**, Scheme 2).

From tetramantane on, the structural complexity of the diamondoids begins



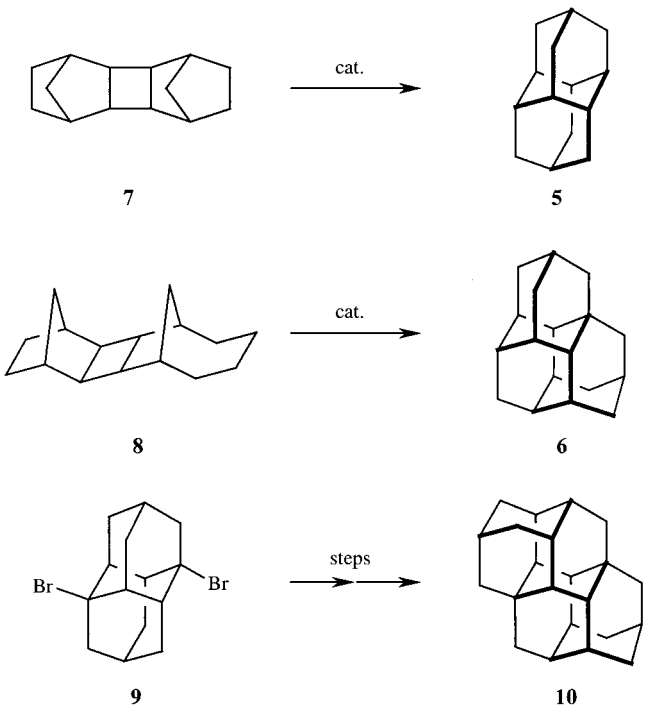
Scheme 2. Diamondoids as hydrocarbons with a carbon framework that is superimposable on the diamond lattice.

to increase: for this polycyclic hydrocarbon four isomers are possible and it is the first unsubstituted diamondoid exhibiting chirality. With the pentamantanes the situation is even more complex: there are nine isomers with the formula $C_{26}H_{32}$ and a molecular weight (M_w) of 344 and one $C_{25}H_{30}$ isomer with M_w 330.[7] There are 39 hexamantanes, 28 of which are $C_{30}H_{36}$ isomers, 10 are $C_{29}H_{34}$ hydrocarbons, and one, the peri-condensed hexamantane described below, also known as cyclohexamantane, is a $C_{26}H_{30}$ compound. With octamantane the number of possible (chiral and achiral) isomers has exploded to several hundred which are distributed over five molecular weight classes. For example, the octamantane class with the formula $C_{34}H_{38}$ and a M_w of 446 includes 18 isomeric structures.

The degree of difficulty of synthesizing the higher diamondoids parallels the

[*] Prof. Dr. H. Hopf
Universität Braunschweig
Institut für Organische Chemie
Hagenring 30
38106 Braunschweig (Germany)
Fax: (+49) 531-391-5388
E-mail: h.hopf@tu-bs.de

 © 2003 Wiley-VCH Verlag GmbH & Co. KGaA, Weinheim DOI: 10.1002/anie.200301631



Scheme 3. Directed syntheses of several simple diamondoids.

structural complexity, of course, and the higher members of the series are inaccessible by directed routes. For example, whereas for both di- (**5**) and triamantane (**6**) several methods of preparation, a selection of which is shown in Scheme 3 and which are all based on the Schleyer Lewis acid catalyzed isomerization process, have been reported (**7**→**5**,[8] **8**→**6**[9]), the synthesis of *anti*-tetramantane (**10**) by McKervey and co-workers was much more involved and relied on the availability of a diamondoid precursor, the dibromide **9**, which was converted into **10** in a multistep sequence involving a double homologation.[10] The other isomers of **10** were unknown until very recently, as were any of their higher analogues.

Up to now the largest member of the diamondoid series isolated from petroleum was diamantane. Recently, however, R. M. K. Carlson and co-workers, discovered that higher analogues, from tetra- to at least undecamantane, also occur in petroleum samples obtained from Gulf of Mexico and Western Canada Basin oil wells.[11] By vacuum distillation above 345 °C higher diamondoid-containing fractions were first obtained, from which non-diamondoid hydrocarbons were removed by pyrolysis at 400–450 °C, the desired polycyclic compounds possessing the higher thermodynamic stability. Aromatic and polar components were then removed by argentic silica gel column chromatography and the desired diamondoids finally isolated by RP-HPLC on octadecylsilane (RP18) columns and shape-selective Hypercarb HPLC columns. The separated and purified higher diamondoids were recrystallized from acetone and subjected to spectroscopic and mass spectrometric analysis.

Many of the numerous new hydrocarbons (all four tetramantanes, nine pentamantanes, one hexa-, two hepta-, and two octa- as well as one nona- to undecamantane were separated and identified) provided single crystals of X-ray quality; Figures 1 and 2 show a selection of the resulting structures.

Rod-shaped hydrocarbons such as [1212]pentamantane (**11**)[7] are characterized by long axes perpendicular to their diamond (110) lattice planes. Increasing the length of such a molecular rod by a further adamantane cage increases the length of the rod by 0.10 to 0.15 nm. [1213]Pentamantane (**14**) occurs in the form of two helical enan-

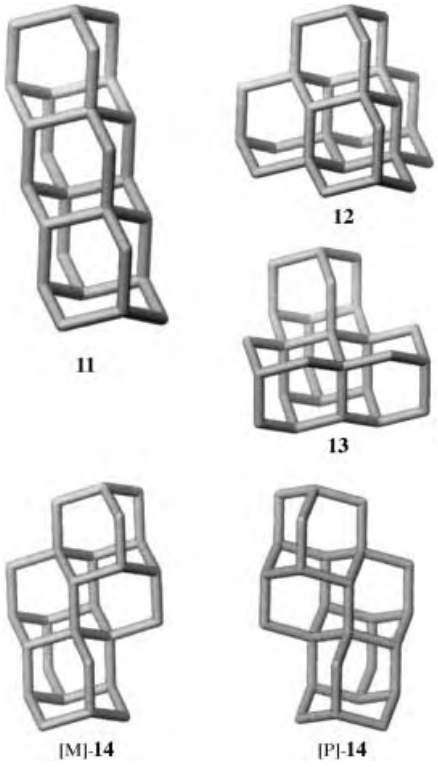


Figure 1. The structures of several pentamantanes in the crystal: [1212]pentamantane (**11**), [1(2,3)4]pentamantane (**12**), [12(3)4]pentamantane (**13**), [1213]pentamantane (**14**).

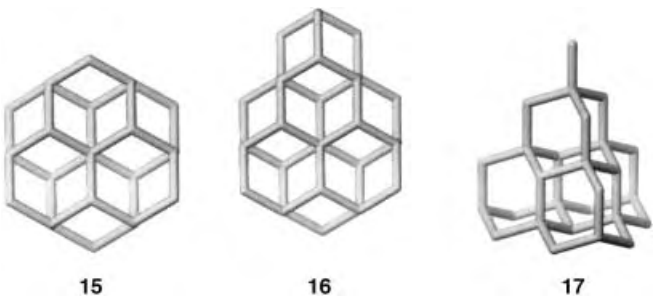


Figure 2. Structures of a hexa- and a heptamantane as well as the methyl derivative of a pentamantane in the crystal: [121312]hexamantane (**15**), [121321]heptamantane (**16**), 3-methyl-[1(2,3)4]pentamantane (**17**).

 © 2003 Wiley-VCH Verlag GmbH & Co. KGaA, Weinheim

tiomers; by chromatography on cyclodextrin phases these screw-shaped molecules could indeed by separated.

Another type of geometry is illustrated by [121312]hexamantane (**15**). This recently isolated and characterized diamondoid,[12] which displays beautiful transparent crystals with a pronounced luster, is a disc-shaped molecule like its higher analogue [121321]heptamantane (**16**). Regarding **15** as a "jewel", it may be thought of as a nanometer-sized diamond of 10^{-20} carat (1 carat = 0.2 g). That not all of these new polycyclic hydrocarbons are parent systems is demonstrated by 3-methyl-[1(2,3)4]pentamantane (**17**). The question of derivatization has, in fact, been addressed by Dahl et al. already, and they have prepared many functionalized higher diamondoids (including bromo, hydroxy, amino, oxa, and aza derivatives): although the concentration of the starting materials in the crude oil fractions is only in the 1–100 ppm range, apparently enough material was available for "real" preparative chemical work.

As far as the mechanism of formation of the new diamondoids in the geosphere is concerned, one can only speculate at present. Dahl et al. suggest a process derived from the mechanism proposed for Schleyer's **1**→**3** interconversion and which could involve cationic intermediates.[13] These could be produced from double bonds still present in newly generated petroleum by interaction with superacidic sites on naturally occurring clay minerals in petroleum source rocks. The astronomically high number of different pathways available for these rearrangements—2897 alternatives have been suggested for the original Schleyer process[13]—could explain the low concentration of the new diamondoids in petroleum and the presumably geological reaction times, the now isolated structures representing the global minima at the end of a several million-year-long chemical journey.

[1] S. Landa, *Chem. Listy* **1933**, *27*, 415; cf. S. Landa, S. Hala, *Collect. Czech. Chem. Commun.* **1959**, *24*, 93–98, and references therein. The structure determination of **3** is mentioned in these references and in reference [2]

[2] V. Prelog, R. Seiwerth, *Ber. Dtsch. Chem. Ges.* **1941**, *74*, 1644–1648.

[3] H. Stetter, O.-E. Bänder, W. Neumann, *Chem. Ber.* **1956**, *89*, 1922–1926.

[4] P. von R. Schleyer, *J. Am. Chem. Soc.* **1957**, *79*, 3292.

[5] The chemistry of adamantane has been reviewed many times. For a recent collection of references see: H. Hopf, *Classics in Hydrocarbon Chemistry*, Wiley-VCH, Weinheim, **2000**, chap. 3, pp. 23–30.

[6] The structure of the diamond lattice has been known since the early 20th century: W. H. Bragg, W. L. Bragg, *Nature* **1913**, *91*, 554.

[7] For the nomenclature of the higher diamondoid hydrocarbons see: A. T. Balaban, P. von R. Schleyer, *Tetrahedron*, **1978**, *34*, 3599–3609.

[8] C. A. Cupas, P. von R. Schleyer, D. J. Trecker, *J. Am. Chem. Soc.* **1965**, *87*, 917–918.

[9] M. A. McKervey, *Chem. Soc. Rev.* **1974**, *3*, 479–512, and references therein; G. A. Olah in *Cage Hydrocarbons* (Ed.: G. A. Olah), Wiley, New York, **1990**, pp. 103–153.

[10] W. Burns, T. R. B. Mitchell, M. A. McKervey, J. J. Rooney, G. Ferguson, P. Roberts, *J. Chem. Soc. Chem. Commun.* **1976**, 893–895; cf. M. A. McKervey, *Tetrahedron* **1980**, *36*, 971–992.

[11] J. E. Dahl, S. G. Liu, R. M. K. Carlson, *Science* **2003**, *299*, 96–99.

[12] J. E. P. Dahl, J. M. Moldowan, T. M. Peakman, J. Clardy, E. Lobkovsky, M. M. Olmstead, P. W. May, T. J. Davis, J. W. Steeds, K. E. Peters, A. Pepper, A. Ekuan, R. M. K. Carlson, *Angew. Chem.* **2003**, *115*, 2086–2090; *Angew. Chem. Int. Ed.* **2003**, *42*, 2040–2044.

[13] H. W. Whitlock, Jr., M. W. Siefken, *J. Am. Chem. Soc.* **1968**, *90*, 4929–4939.

 © 2003 Wiley-VCH Verlag GmbH & Co. KGaA, Weinheim

Ammonia Synthesis

Catalytic Synthesis of Ammonia—A "Never-Ending Story"?

*Robert Schlögl**

Keywords:
ammonia · heterogeneous catalysis · iron · ruthenium · surface chemistry

Nitrogen atoms are essential for the function of biological molecules and thus are and important component of fertilizers and medicaments. Bonds to nitrogen also find nonbiological uses in dyes, explosives, and resins. The synthesis of all these materials requires ammonia as an activated nitrogen building block. This situation is true for natural processes and the chemical industry. Knowledge of the various techniques for the preparation of ammonia is thus of fundamental importance for chemistry. The Haber–Bosch synthesis was the first heterogeneous catalytic system employed in the chemical industry and is still in use today. Understanding the mechanism and the translation of the knowledge into technical perfection has become a fundamental criterion for scientific development in catalysis research.

Recently a paper bearing the title: "All quiet at the nitrogen front" was published.[1] The author laments the low visibility of research in nitrogen fixation in general, and in organometallic biochemical nitrogen fixation in particular, despite significant advances in this subject. However, it would not be convincing to argue that a higher research effort in ammonia synthesis (which would certainly be desirable) would be justified by the necessity for developing totally different routes with higher degrees of efficiency than the modern Haber–Bosch processes, particularly when the following thermodynamic efficiency numbers are considered. Liquid ammonia at atmospheric pressure is needed as starting material, made from air, liquid water ($T = 300$ K), and natural gas. The resulting ammonia theoretically contains 6.8 Gcal t^{-1} as chemical energy if the process is energetically isolated. Industrial processes achieve total degrees of efficiency of up to 70% for the processes described above (approximately 4.81 Gcal t^{-1} NH_3), whereas the biggest losses in efficiency are made in the methane reforming process (1.18 Gcal t^{-1}). Only a slight loss is made during the actual ammonia synthesis (0.37 Gcal t^{-1}).[2] These efficiencies are achieved with commercially available iron catalysts[3,4] and with modern ruthenium-based catalysts. Any further improvement in the catalysts would help to increase the thermodynamic efficiency and reduce the specific price of this basic compound through a reduction in the pressure during synthesis. However, any new proposals of this kind[5] have to meet the high standards of the "conventional" routes. It should be further kept in mind that the main synthesis step has been optimized already, and that the main obstacles arise from synthesis of the precursors. Figure 1 shows a modern ammonia plant. All the large aggregates in the foreground are needed to generate hydrogen from methane and purify it, the actual rector is in comparison very small and can not be seen. The picture clearly illustrates where the development potential lies and where the optimization has reached a high maturity.

As well as being of high industrial relevance the catalytic synthesis of ammonia is also a key reaction for creating new life and a prototypical model reaction[6] that helps in gaining a fundamental understanding of catalysis in general and therefore of considerable scientific and cultural importance. It is mainly this reason that drives the research in ammonia synthesis forward, especially since evidence for a knowledge-based improvement of a catalyst would have a strong signaling effect on other fields of catalysis research.

For the still industrially important iron catalyst, a good picture of its structure and its activity as an accelerator for the dissociation of dinitrogen, which is the kinetically determining step, can be drawn. Results from pioneering experiments on iron crystals[7] at lower pressures, were quantitatively corroborated by high-pressure experiments.[8] This apparent lack of a pressure gap allowed the theoretical description of the nitrogen activation and therefore the quantitative extrap-

[*] Prof. Dr. R. Schlögl
Fritz-Haber-Institut der MPG
Department of Inorganic Chemistry
Faradayweg 4—6, 14159 Berlin (Germany)
Fax: (+49) 30-84-13-44-01
E-mail: acsek@fhi-berlin.mpg.de

 © 2003 Wiley-VCH Verlag GmbH & Co. KGaA, Weinheim DOI: 10.1002/anie.200301553



Figure 1. Overview of a modern ammonia synthesis plant. The rubbish skip in the foreground indicates the dimensions. The large structure to the left is the methane steam reformer unit. The generated hydrogen is purified in all the other aggregates seen at the front (source BASF AG).

olation of the kinetics from ultra-high vacuum (UHV) conditions to industrial conditions.[9–11] Furthermore, studies on single crystals[8] showed that the lack of a pressure gap only occurred at low nitrogen coverages, whereas at high nitrogen coverages a considerable deviation from the theoretical adsorption behavior is caused by the formation of a subnitride surface phase.

Under industrial conditions the nitrogen coverage is low (hence the theoretical description applies), but in the bulk phase the catalyst is nitrided, which causes a distorted crystal structure. Through suitable pretreatments this structure has also been included in model experiments, however, it was not further characterized. After the required activation[12]—a process now well understood[13,14]—the industrial catalyst shows a distorted iron structure, that has been demonstrated to be essential for its catalytic function.[15] This distortion manifests itself as metastable plates in the (111) orientation,[16] which are formed by the topotactic reduction of the magnetite precursor at extremely mild conditions,[12,17] but also by stress states in the regularly orientated (100) regions[18] of the ammonia iron.[*] These stress states participate in the structure-sensitive activation of nitrogen, which is particularly efficient on the (111) faces,[19,20] but also on different faces and on strain-induced[21,22] step defects.[23] These recent theoretical[25] and experimental[13,26–29] results require that the discussion about the role of the promoters (especially the potassium), which is normally considered as closed,[24] is reopened.

The modern industrial iron catalyst is a nanostructured metastable substance, which is formed during the surprisingly complex synthesis of the oxide precursor.[12,18] This differs significantly from pure iron especially in the mesoscopic area[30] despite the similarities in the local structure. Its metastability is the reason for its sensitivity towards thermal overstress during activation and oxidation of the activated material. Alternative preparation routes for the nanostructured system are possible,[26,31–33] and confirm the complex structure of this seemingly very simple ammonia iron.

A quantitative analysis has shown[34] that only 5% of the geometric iron surface participates in the activation of nitrogen on an industrial catalyst. The remaining adsorption sites are filled from these centers by surface diffusion. Thus, the duality of plates and blocks has a functional equivalent as nitrogen activation and storage regions, which coincides quantitatively with theoretical and experimental findings.

Ruthenium and molybdenum compounds stand out in the group the non-iron catalysts. A comprehensive report about the development and background of the empirically motivated search for suitable catalysts is given elsewhere.[35] 20 years ago, in a review, the catalytic efficiency of the elements for the synthesis and decomposition of ammonia was correlated with the chemisorption energy of nitrogen. An inverted parabolic function (volcano curve) was obtained, in which iron, ruthenium, and osmium mark the top of the volcano.[36] The idea of optimizing the performance of the elements on the slope of the curve though the formation of alloys of the elements which react either too slowly or too vigorously with nitrogen, was proposed in the same paper. The formation of metal subnitrides and their effectiveness as inhibitors for the decomposition of ammonia was described about 30 years ago.[37] Thus, the routes for development were set out a long time ago. Not surprisingly, an efficient non-ruthenium catalyst on the basis of cobalt–molybdenum nitride was recently presented,[38–42] which can be regarded as the current climax of a systematically but empirically justified development.[43,44]

Ruthenium-based catalysts have a much a longer history of development and are routinely in use.[45] As a consequence these systems have formed the basis of much fundamental research. The established single-crystal approach[7] did not lead to immediate success because carefully prepared samples are extremely inactive in the dissociative adsorption of nitrogen.[46–48] The discrepancy with kinetic studies, which showed the high efficiency of ruthenium particles for the activation of nitrogen,[49] was resolved by experiments with single crystals containing step defects. It was shown that these types of defect, which are normally minimized during

[*] Ammonia iron is a term used to describe iron that, through the action of ammonia, has become structurally strained and as a result, catalytically active.



Robert Schlögl was born in Munich in 1954 and completed his chemistry studies at the Universität Munchen in 1982. Working in Cambridge (Prof. Sir John Thomas) and Basel (Prof. Hans-Joachim Güntherodt) drew him to the areas between chemistry and solid-state physics. Following some time in industry he completed his Habilitation in Berlin (Prof. Gerhard Ertl) in 1989 and then became Professor of Inorganic Chemistry in Frankfurt. In 1993 he joined the Fritz Haber Institute of the Max Planck Society where he is studying the basis for heterogeneous catalytic processes and the development of in situ spectroscopic methods.

 © 2003 Wiley-VCH Verlag GmbH & Co. KGaA, Weinheim

conventional single-crystal preparation, are essential for the catalytic effectiveness of ruthenium in nitrogen activation.[50–53] This experiment demonstrates impressively how important the mesoscopic structure, which reaches beyond the confines of the local structure of the surface, is for surface science. In conjunction with the experiments a theoretical description about the dissociation process was presented as well as an elegant explanation for the importance of the steps.[23,52,54]

In analogy to the iron system the suitable nanostructure of ruthenium is induced through nitrogen being dissolved in the bulk. An experiment on a Ru (0001) single crystal was carried out, in which a stream of nitrogen was applied at 1600 K under UHV conditions. The structural characterization (Figure 2) shows that the combined effects of heat and nitrogen exposure lead to the transformation of the single-crystal surface from its preferred orientation (still visible on the reverse side of the sample) into a complex but ordered new structure.

The SEM image shows the decay of the single crystal into domains with a system of grain boundaries. On this nanostructured surface (Figure 3) the chemisorption of dinitrogen could be verified by valence band and core-level photoelectron spectroscopy (XPS). The spectroscopic signatures seen in Figure 3 confirm the presence of end-on-bound nitrogen molecules as the majority of surface species under the chosen in situ conditions. The weak interaction of the N_2 molecule with the ruthenium metal is shown by the small distortion of the metal 3d band. (Figure 3, region I, curve A) in comparison to the adsorption of the strongly interacting CO molecules (curve B). The double structure in the core-level spectrum of the nitrogen (Figure 3) is evidence for the adsorption geometry, and energetically corresponds very well to the data obtained from the iron system. These experiments show the merit of a strategy in which model systems with increasing structural complexity (starting from planar then stepped single crystals up to surfaces restructured in situ) are used towards a characterization of the nanoparticles of industrially relevant ruthenium catalysts.

The synthesis of highly efficient, stable, and reproducible supported systems, which in light of the high cost of ruthenium is essential for any possible application, has recently attained a high level through the continuation of previous studies on carbon and basic oxides as supports.[55–66] These systems are now classified as a new generation of ammonia-synthesis catalysts.[45] In parallel, a functional characterization of carbon- and basic-oxide-supported materials was performed with temperature-programmed methods[49] and led to a quantitative micro kinetic model of the ammonia synthesis over ruthenium particles. It is remarkable that the system that has shown the highest efficiency in previous studies was found to be rather inefficient during a high-throughput-screening project.[67] The results of the investigation based on theoretical knowledge with thorough techniques (see above) turned out to be superior to the too quick high-throughput-screening testing.[68]

The convergence of knowledge about model catalysis and real catalysis is directly observable for the ruthenium system since high-resolution electron microscopy can deliver images

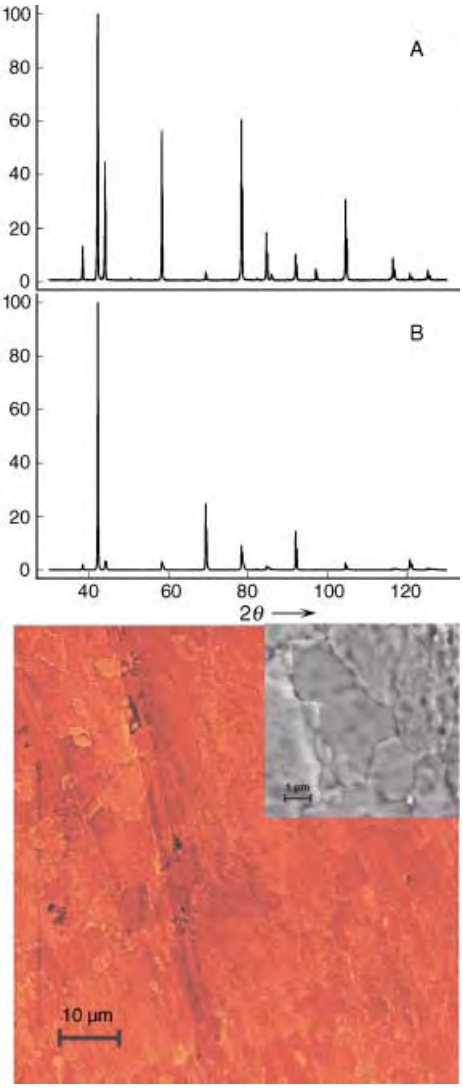


Figure 2. Powder X-ray diffraction characterization of a Ru (0001) single crystal of 0.8 mm thickness after being heated at 1600 K for 4 h. Whilst the front side of the crystal was exposed to a nitrogen flow of 10^{-7} mbar (A), the reverse side was heated (B). Both images show the characteristic lines for hexagonal Ru metal (ICDD 6–663) but with substantially different texture. The reverse side is strongly oriented in [0001] direction, as expected (dominant reflexes of the (001) series) whilst the front side shows strong intensities of other reflex groups, which do not correspond to the series of intensity for statistical powder orientation. The scanning electron microscopic survey image (15 keV) and detail image with 15-times higher magnification shows the polycrystalline morphology with grains, grain boundaries, and a surface layer with very finely structured parts. Energy-dispersive X-ray fluorescence (EDX) shows traces of nitrogen in the metal.

of activated ruthenium particles and their barium oxide promoters.[69] These images show facetted particles of 2–5 nm in diameter, which are partly covered by disordered fragments, which are interpreted as being barium oxide particles. Parts of these fragments show the same orientation as the stepped structures in the model experiments.[50]

Experiments carried out by Ertl[7] and Somorjai [19] were designed to enhance the understanding of the ammonia synthesis and allow a quantitative theoretical description of

 © 2003 Wiley-VCH Verlag GmbH & Co. KGaA, Weinheim

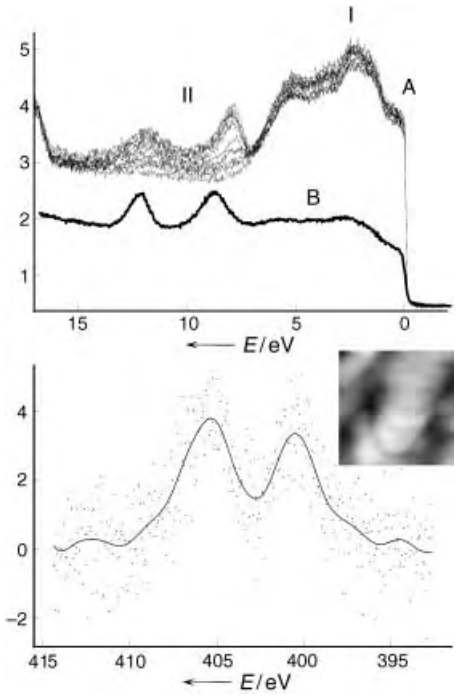


Figure 3. Above: Adsorption experiment of dinitrogen on the pretreated Ru crystal (see Figure 2) after not more than 4 Langmuir N_2 exposure (40 s, 10^{-7} mbar) at 120 K. In sequence A the growth of a molecular species with orbital energies of 8.0 eV and 11.9 eV below the Fermi level could be observed. This species could not be CO, which adsorbs very well as impurity. The effect of CO is illustrated in spectrum B, which was taken for comparison (orbital energies 8.7 eV and 12.2 eV) after exposition of 1 Langmuir CO on a pure sample. In region I the intensity of the metal d band is decreasing, whilst in region II the emission of the molecular N_2 3σ and 2σ states is increasing. This data corresponds very well to earlier measurements on iron and other metals.[75] Below: Core-level photoelectron spectrum of the N1s level of molecular adsorbed nitrogen. The measurement was taken with Mg_k excitation and with a sample temperature of 300 K and a background pressure of 10^{-6} mbar N_2. The positions of the lines with 405.6 eV and 400.5 eV correspond very well to the observations on iron, but the distribution of intensity between the high energetic main signal and the lower energetic satellites does not. These bands are too intense and thereby show that a further species must be present. This species could not be atomic nitrogen, which has a single XPS line at 397.0 eV in complete agreement to measurements on iron.[76] The inset shows an atomic force microscopy (AFM) image of the microstructure of the sample surface in air. The height of the about 100 nm wide steps is about 2 nm. The multiple step edges might contain the active centers.

this reaction. Two predictions for the future development of this subject resulted from this work.

First of all a quantitative description of the volcano curve for the catalytic efficiency of the elements in the ammonia synthesis could be given, which was based on fundamental knowledge of the reaction path and the theory of the transition state. This description allowed a specific prediction of the catalytic efficiency of alloy systems[70,71] with extreme properties on the volcano curve. The studies on the Co-Mo-N system,[39,70] which were carried out almost simultaneously but with totally different motivation, led to similar results. They confirm in a remarkable way, how theory and chemical intuition are becoming equally useful with respect to the choice of research topics. Disregarding the "old empirical knowledge", one could speak of a remarkable example of "designing" a catalytic system,[72] based on pure theoretical knowledge about the process of the target reaction. Despite these significant advances, this good catalytic behavior is only achieved at relative small synthesis rates; also there are significant stability problems. Much more research effort is needed here.

A different challenge thrown down by theory for the experimentalist lies in the prediction of a biomimetic ammonia-synthesis path at room temperature and atmospheric pressure. This should be achieved preferably by electrochemical processes with an efficiency similar to the synthesis strategies that are available today.[73]

The answer to the question raised at the beginning should therefore be, that there is no other practically relevant reaction that leads to such a close interconnection between theory, model catalysis, and experiment as the high-pressure synthesis of ammonia by Haber and Bosch. This statement is not only valid for the iron system but also for the ruthenium system and, in foreseeable future, for the Co-Mo-N alloy system. The time frame for the acquirement of knowledge is truly remarkable, it took decades for the case of the iron system but just ten years for the ruthenium system, and it will take only a few years for the case of the alloy system. This is despite the catalyst getting more complex both chemically and structurally. Analysis of the reasons leading to this story of success reveals the factors that stand out to be, the persuasiveness of the pioneering experiments that persists even 30 years later, the enormous maturation of experimental and theoretical methods, and the increased precision of the world-wide research efforts. Here, the Danish national network of industrial and academic research, which has existed for more than 10 years, plays an important part.

The never-ending story has not ended yet. In addition to questions about the elementary steps of the reaction and the importance of the real structure and subnitrides for the catalyst efficiency, as well as the wide-open question about new catalyst materials, there are also new challenges for new applications. Ammonia would make a convenient storage molecule for hydrogen for operation in fuel cells, because it is free of carbon and so the hydrogen would be less likely to poison the fuel cell, neither would any harmful contribution to the ecobalance be produced. Synthesis and decomposition of ammonia out of and to the elements are well controlled. If a practical and safe transfer of the industrial logistic[74] into an end-consumer field were to be obtained, then a powerful alternative for the generation of hydrogen could be at our disposal.

Received: March 1, 2002 [M1553]

[1] J. Leigh, *Chem. Br.* **2001**, *37*, 23–24.
[2] I. Dybkjaer in *Ammonia, Catalysis and Manufacture* (Ed.: A. Nielsen), Springer, Heidelberg, **1995**, pp. 199–308.
[3] A. Mittasch, *Z. Elektrochem.* **1930**, *36*, 569–581.
[4] A. Mittasch, *Adv. Catal.* **1950**, *2*, 81–104.
[5] G. Marnellos, M. Stoukides, *Science* **1998**, *282*, 98–100.
[6] M. Boudart, *Top. Catal.* **2000**, *13*, 147–149.

 © 2003 Wiley-VCH Verlag GmbH & Co. KGaA, Weinheim

[7] G. Ertl, *J. Vac. Sci. Technol. A* **1983**, *1*, 1247 – 1253.
[8] I. Alstrup, I. Chorkendorff, S. Ullmann, *J. Catal.* **1997**, *168*, 217 – 234.
[9] J. J. Mortensen, L. B. Hansen, B. Hammer, J. K. Norskov, *J. Catal.* **1999**, *182*, 479 – 488.
[10] J. J. Mortensen, M. V. Ganduglia-Pirovano, L. B. Hansen, B. Hammer, P. Stoltze, J. K. Norskov, *Surf. Sci.* **1999**, *422*, 8 – 16.
[11] P. Stoltze, J. K. Norskov, *J. Catal.* **1988**, *110*, 1 – 10.
[12] R. Schlögl in *Handbook of Heterogeneous Catalysis* (Eds.: G. Ertl, H. Knözinger, J. Weitkamp), Wiley-VCH, Weinheim, **1997**, pp. 1697 – 1746.
[13] A. Kotarba, A. Baranski, S. Hodorowicz, J. Sokolowski, A. Szytula, L. Holmlid, *Catal. Lett.* **2000**, *67*, 129 – 134.
[14] A. Baranski, R. Dziembaj, A. Kotarba, J. M. Lagan, J. Lojewska, E. Pieprzyk, L. Mleczko, M. Baerns, *Appl. Catal. A* **1997**, *162*, 133 – 148.
[15] B. Herzog, D. Herein, R. Schlögl, *Appl. Catal. A* **1996**, *141*, 71 – 104.
[16] J. Schütze, W. Mahdi, B. Herzog, R. Schlögl, *Top. Catal.* **1994**, *1*, 195 – 214.
[17] F. H. Herbstein, J. Smuts, *J. Catal.* **1963**, *2*, 69 – 78.
[18] B. Holme, P. Skaugset, J. Tafto, *Appl. Catal. A* **1997**, *162*, 149 – 159.
[19] D. R. Strongin, J. Carrazza, S. R. Bare, G. A. Somorjai, *J. Catal.* **1987**, *103*, 213 – 215.
[20] D. R. Strongin, G. A. Somorjai in *Catalytic Ammonia Synthesis* (Ed.: J. R. Jennings), Plenum, Oxford, **2002**, pp. 133 – 176.
[21] K. Homann, H. Kuhlenbeck, H. J. Freund, *Z. Phys. Chem.* **1997**, *198*, 135 – 147.
[22] K. Homann, H. Kuhlenbeck, H. J. Freund, *Surf. Sci.* **1995**, *327*, 216 – 224.
[23] R. C. Egeberg, S. Dahl, A. Logadottir, J. H. Larsen, J. K. Norskov, I. Chorkendorff, *Surf. Sci.* **2001**, *491*, 183 – 194.
[24] G. J. Hutchings, *Catal. Lett.* **2001**, *75*, 1 – 12.
[25] N. D. Lang, S. Holloway, J. K. Norskov, *Surf. Sci.* **1985**, *150*, 24 – 38.
[26] A. Jedynak, Z. Kowalczyk, D. Szmigiel, J. Zielinski, *Pol. J. Chem.* **2001**, *75*, 1801 – 1805.
[27] B. N. Kuznetsov, V. M. Perov, A. M. Alekseev, V. I. Yakerson, *Kinet. Catal.* **2001**, *42*, 92 – 96.
[28] K. Engvall, A. Kotarba, L. Holmlid, *J. Catal.* **1999**, *181*, 256 – 264.
[29] A. Kotarba, M. Hagstrom, K. Engvall, J. B. C. Pettersson, *React. Kinet. Catal. Lett.* **1998**, *63*, 219 – 224.
[30] G. Weinberg, B. Beran, M. Muhler, R. Schlögl, A. Dent, T. Rayment, *Appl. Catal. A* **1997**, *163*, 83 – 99.
[31] S. Guan, H. Z. Lin, *Ind. Eng. Chem. Res.* **2000**, *39*, 2891 – 2895.
[32] C. J. H. Jacobsen, J. Z. Jiang, S. Morup, B. S. Clausen, H. Topsoe, *Catal. Lett.* **1999**, *61*, 115 – 120.
[33] S. M. Yunusov, E. S. Kalyuzhnaya, H. Mahapatra, V. K. Puri, V. A. Likholobov, V. B. Shur, *J. Mol. Catal. A* **1999**, *139*, 219 – 225.
[34] S. Dahl, E. Tornqvist, C. J. H. Jacobsen, *J. Catal.* **2001**, *198*, 97 – 102.
[35] K. Aika, K. Tamaru in *Ammonia* (Ed.: A. Nielsen), Springer, Heidelberg, **1995**, pp. 104 – 143.
[36] A. Ozaki, K. Aika in *Catalysis, Science and Technology* (Eds.: J. R. Andersen, M. Boudart), Springer, Heidelberg, **1985**, pp. 88 – 154.
[37] C. Wagner, *Ber. Bunsen-Ges. Phys. Chem.* **1970**, *74*, 401 – 409.
[38] R. Kojima, K. Aika, *Appl. Catal. A* **2001**, *219*, 141 – 147.
[39] R. Kojima, K. Aika, *Appl. Catal. A* **2001**, *219*, 157 – 170.
[40] R. Kojima, K. Aika, *Appl. Catal. A* **2001**, *218* 121 – 128.
[41] R. Kojima, K. Aika, *Appl. Catal. A* **2001**, *215*, 149 – 160.
[42] R. Kojima, K. Aika, *Chem. Lett.* **2000**, 514 – 515.
[43] R. Kojima, K. Aika, *Appl. Catal. A* **2001**, *209*, 317 – 325.
[44] R. Kojima, K. Aika, *Chem. Lett.* **2000**, 912 – 913.
[45] H. Bielawa, O. Hinrichsen, A. Birkner, M. Muhler, *Angew. Chem.* **2001**, *113*, 1093 – 1096; *Angew. Chem. Int. Ed.* **2001**, *40*, 1061 – 1063.
[46] K. Jacobi, *Phys. Status Solidi A* **2000**, *177*, 37 – 51.
[47] K. Jacobi, H. Dietrich, G. Ertl, *Appl. Surf. Sci.* **1997**, *121*, 558 – 561.
[48] H. Dietrich, P. Geng, K. Jacobi, G. Ertl, *J. Chem. Phys.* **1996**, *104*, 375 – 381.
[49] O. Hinrichsen, A. Hornung, M. Muhler, *Chem. Eng. Technol.* **1999**, *22*, 1039 – 1042.
[50] C. J. H. Jacobsen, S. Dahl, P. L. Hansen, E. Tornqvist, L. Jensen, H. Topsoe, D. V. Prip, P. B. Moenshaug, I. Chorkendorff, *J. Mol. Catal. A* **2000**, *163*, 19 – 26.
[51] S. Dahl, J. Sehested, C. J. H. Jacobsen, E. Tornqvist, I. Chorkendorff, *J. Catal.* **2000**, *192*, 391 – 399.
[52] S. Dahl, A. Logadottir, R. C. Egeberg, J. H. Larsen, I. Chorkendorff, E. Tornqvist, J. K. Norskov, *Phys. Rev. Lett.* **1999**, *83*, 1814 – 1817.
[53] S. Dahl, P. A. Taylor, E. Tornqvist, I. Chorkendorff, *J. Catal.* **1998**, *178*, 679 – 686.
[54] J. J. Mortensen, Y. Morikawa, B. Hammer, J. K. Norskov, *J. Catal.* **1997**, *169*, 85 – 92.
[55] Y. Izumi, K. Aika, *J. Phys. Chem.* **1995**, *99*, 10346 – 10353.
[56] H. B. Chen, J. D. Lin, Y. Cai, X. Y. Wang, J. Yi, J. Wang, G. Wei, Y. Z. Lin, D. W. Liao, *Appl. Surf. Sci.* **2001**, *180*, 328 – 335.
[57] B. C. McClaine, S. E. Siporin, R. J. Davis, *J. Phys. Chem. B* **2001**, *105*, 7525 – 7532.
[58] C. J. H. Jacobsen, *J. Catal.* **2001**, *200*, 1 – 3.
[59] C. H. Liang, Z. B. Wei, Q. Xin, C. Li, *Appl. Catal. A* **2001**, *208*, 193 – 201.
[60] I. Rossetti, N. Pernicone, L. Forni, *Appl. Catal. A* **2001**, *208*, 271 – 278.
[61] W. Rarog, I. Lenarcik, Z. Kowalczyk, J. Sentek, M. Krukowski, J. Zielinski, *Pol. J. Chem.* **2000**, *74*, 1473 – 1478.
[62] W. Rarog, Z. Kowalczyk, J. Sentek, D. Skladanowski, J. Zielinski, *Catal. Lett.* **2000**, *68*, 163 – 168.
[63] L. Forni, D. Molinari, I. Rossetti, N. Pernicone, *Appl. Catal. A* **1999**, *185*, 269 – 275.
[64] Z. Kowalczyk, S. Jodzis, W. Rarog, J. Zielinski, J. Pielaszek, A. Presz, *Appl. Catal. A* **1999**, *184*, 95 – 102.
[65] Y. Niwa, K. Aika, *Res. Chem. Intermed.* **1998**, *24*, 593 – 603.
[66] Z. H. Zhong, K. Aika, *Chem. Commun.* **1997**, 1223 – 1224.
[67] O. Hinrichsen, *Catal. Today* **1999**, *53*, 177 – 188.
[68] R. Schlögl, *Angew. Chem.* **1998**, *110*, 2467 – 2470; *Angew. Chem. Int. Ed.* **1998**, *37*, 2333 – 2336.
[69] T. W. Hansen, J. B. Wagner, P. L. Hansen, S. Dahl, H. Topsoe, C. J. H. Jacobsen, *Science* **2001**, *294*, 1508 – 1510.
[70] C. J. H. Jacobsen, S. Dahl, B. S. Clausen, S. Bahn, A. Logadottir, J. K. Norskov, *J. Am. Chem. Soc.* **2001**, *123*, 8404 – 8405.
[71] A. Logadottir, T. H. Rod, J. K. Norskov, B. Hammer, S. Dahl, C. J. H. Jacobsen, *J. Catal.* **2001**, *197*, 229 – 231.
[72] J. M. Thomas, R. Schlögl, *Angew. Chem.* **1994**, *106*, 316 – 319; *Angew. Chem. Int. Ed. Engl.* **1994**, *33*, 311 – 312.
[73] T. H. Rod, A. Logadottir, J. K. Norskov, *J. Chem. Phys.* **2000**, *112*, 5343 – 5347.
[74] A. Nielsen in *Ammonia, Catalysis and Manufacture* (Ed.: A. Nielsen), Springer, Berlin, **1995**, pp. 330 – 345.
[75] H. J. Freund, B. Bartos, R. P. Messmer, M. Grunze, H. Kuhlenbeck, M. Neumann, *Surf. Sci.* **1987**, *185*, 187 – 202.
[76] M. Grunze, M. Golze, W. Hirschwald, H. J. Freund, H. Pulm, U. Seip, M. C. Tsai, G. Ertl, J. Küppers, *Phys. Rev. Lett.* **1984**, *53*, 850 – 853.

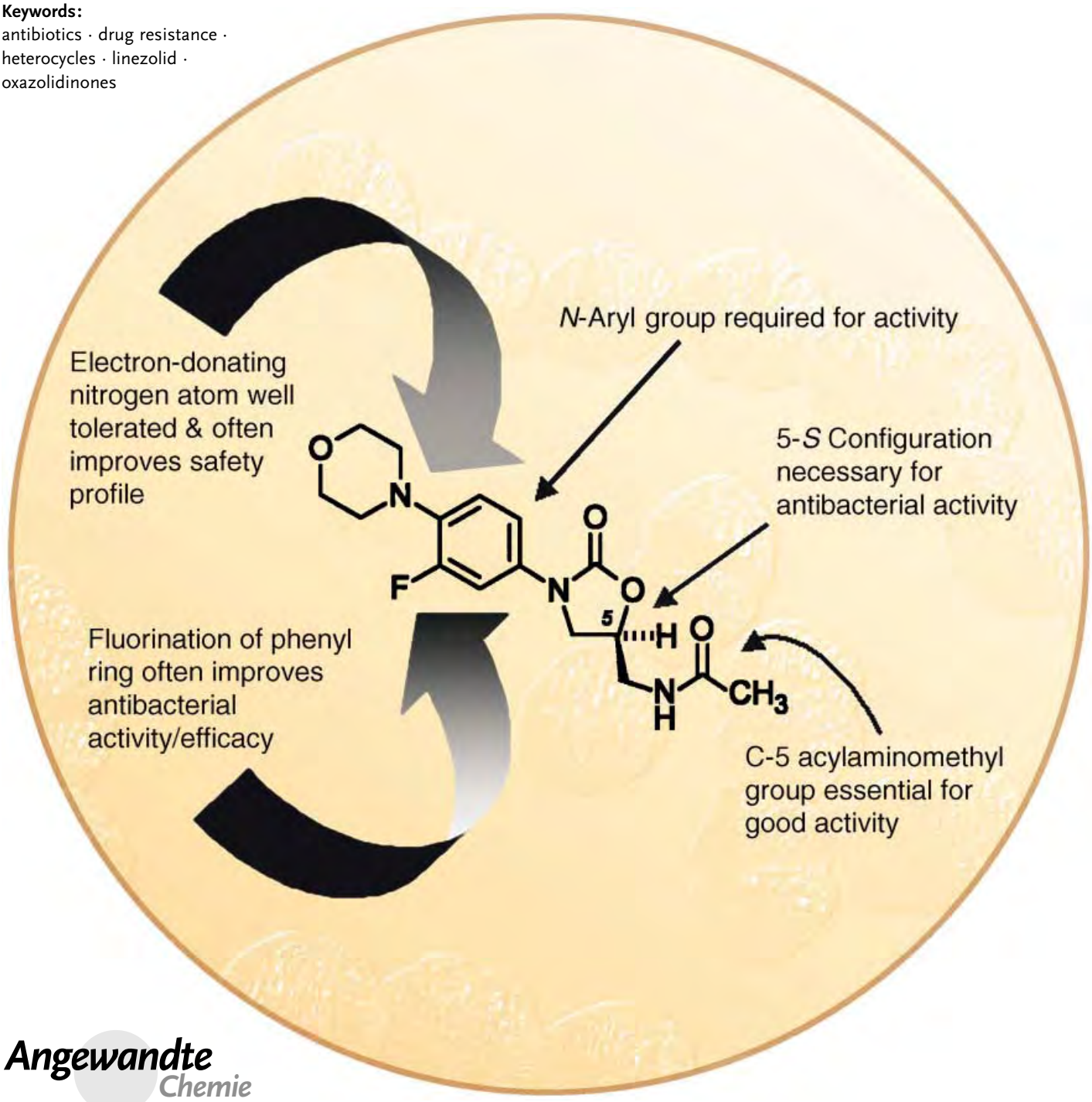
 © 2003 Wiley-VCH Verlag GmbH & Co. KGaA, Weinheim

Development of Linezolid

Oxazolidinone Structure–Activity Relationships Leading to Linezolid

Michael R. Barbachyn and Charles W. Ford*

Keywords:
antibiotics · drug resistance · heterocycles · linezolid · oxazolidinones



© 2003 Wiley-VCH Verlag GmbH & Co. KGaA, Weinheim
DOI: 10.1002/anie.200200528

The development of bacterial resistance to currently available antibacterial agents is a growing global health problem. Of particular concern are infections caused by multidrug-resistant Gram-positive pathogens which are responsible for significant morbidity and mortality in both the hospital and community settings. A number of solutions to the problem of bacterial resistance are possible. The most common approach is to continue modifying existing classes of antibacterial agents to provide new analogues with improved attributes. Other successful strategies are to combine existing antibacterial agents with other drugs as well as the development of improved diagnostic procedures that may lead to rapid identification of the causative pathogen and permit the use of antibacterial agents with a narrow spectrum of activity. Finally, and most importantly, the discovery of novel classes of antibacterial agents employing new mechanisms of action has considerable promise. Such agents would exhibit a lack of cross-resistance with existing antimicrobial drugs. This review describes the work leading to the discovery of linezolid, the first clinically useful oxazolidinone antibacterial agent.

From the Contents

1. Introduction	2011
2. The Oxazolidinones	2012
3. Biological Evaluation of Linezolid	2017
4. Further Biological Findings	2021
5. Summary	2022

1. Introduction

In the 1980s the antibiotic market and the antibiotic business were often referred to as "mature", in this sense that there were many antibiotics available and few if any bacterial diseases in humans for which antibiotic therapy was not curative. The success of antibiotic research and development by the pharmaceutical companies had become an accepted and expected condition in our society. The antibiotic classes on the market had been primarily discovered through biological screening of fermentation broths, natural product extracts, and collections of research compounds. The large number of antibiotics available on the market occurred through an iterative process wherein structurally related compounds or analogues of any given class of antibiotics were synthesized and introduced to the market when incremental improvements in intrinsic activity, spectrum of antibacterial activity, or safety were realized relative to pre-existing member(s) of the class. These extensive efforts in structure–activity relationships (SARs) led to a very large array of antibiotics within existing classes. By the mid-1980s, the market had not seen a new class of antibiotics introduced in over twenty years and many customers were telling the pharmaceutical companies that there were more than sufficient numbers of available antibiotics for human use.

At the same time in which it was becoming clear that the discovery of new antibiotic classes was going to require major investments in new technologies and the antibiotic market seemed saturated with drugs, the Gram-positive bacteria, such as staphylococci, streptococci, and enterococci, were well on the way to raising havoc with existing drug classes through the development of resistance. The enterococci, particularly *Enterococci faecalis* and *Enterococcus faecium* changed their niche; instead of being found principally in intra-abdominal abscesses and urinary tract infections they began to cause bacteremia particularly in hospitalized and elderly patients. The two enterococci were undesirable pathogens in the sense that they caused virulent disease but they were multidrug-resistant and many strains were vancomycin-resistant,[1] which made them extraordinarily difficult to treat. Until the 1990s *Streptococcus pneumoniae*, which is the most common cause of human bacterial disease, was readily treatable with a variety of older and inexpensive antibiotics. Following at least two individual outbreaks of penicillin-resistant *S. pneumoniae*, the resistant forms of the pathogen have persisted world-wide and have acquired resistance to other antibiotic classes. Today multidrug-resistant *S. pneumoniae* is a major problem in the Pacific Rim countries and is becoming a significant problem for physicians in the United States and parts of Europe.[2–6] Of the Gram-positive pathogens, *Staphylococcus aureus* and *Staphylococcus epidermidis* have caused treatment problems in hospitals because of the development of resistance. Treatment failures with either of these pathogens can easily result in patient mortality, and in recent years the resistance characteristic most frequently associated with multidrug resistance in staphylococci is methicillin resistance. Methicillin resistance does not mean that no drugs will work. It does mean that vancomycin is the only drug which will always work against multidrug-resistant staphylococci, and the determination of whether other antibiotics might be efficacious requires isolation of the infecting organism and identification of drug sensitivity.[7] The very rapid and fatal illnesses caused by staphylococci necessitates that therapy must be initiated before the organism is isolated and sensitivity determination can be conducted. Vancomycin is clearly the empiric choice

[*] Dr. M. R. Barbachyn, Dr. C. W. Ford
Medicinal Chemistry Research
Pharmacia Corporation
7000 Portage Road, Kalamazoo, MI 49001 (USA)
Fax: (+1) 269-833-9629
E-mail: michael.r.barbachyn@pharmacia.com

 DOI: 10.1002/anie.200200528 © 2003 Wiley-VCH Verlag GmbH & Co. KGaA, Weinheim

under those circumstances; however, vancomycin resistance in the enterococci realistically threatens transfer of vancomycin resistance to the staphylococci, and a vancomycin- and multidrug-resistant staphylococcus strain threatens to be essentially untreatable.

The development of Gram-positive resistance as a therapeutic problem followed the diminution of interest in antibiotic research and development. During this period we at Pharmacia had conducted a very thorough evaluation of the antibiotic market in the mid-1980s and concluded that there still existed a need for a new class of antibacterial agents which would lend itself to empiric treatment of the staphylococci and other Gram-positive pathogens. In 1987, shortly following this analysis, we attended the presentation of work by scientists of E.I. du Pont de Nemours & Company (DuPont) which covered their cumulative work on a new class of antibacterial agents, the oxazolidinones.[8] The oxazolidinones interested us because they possessed all the characteristics which seemed important in an antibacterial agent at that time. Their spectrum of activity covered the important Gram-positive pathogens, particularly those which had been causing so many problems because of the development of resistance. They also covered *S. pneumoniae* which we believed would be a significant future problem because of the development of resistance. The oxazolidinones appeared to have a unique mechanism of action and, consistent with that observation, they were not cross-resistant with existing resistance mechanisms in bacteria.[8–10] The oxazolidinones were orally active, which we had identified as a key requirement for new antibacterial agents for primary care in the community. It would also be a key cost saving for hospitalized patients in that intravenous therapy could be stopped as soon as possible and oral therapy in hospital or at home could immediately follow. It was extremely difficult to select for resistant mutants in the laboratory, however, studies on the experimental antibacterial activity and pharmacokinetic behavior predicted that the oxazolidinones would work sufficiently well in humans to be able to predict utility in the marketplace.[11–13] We thus committed ourselves to proof-of-concept studies with the oxazolidinones in which we intended to demonstrate that we could make structurally novel oxazolidinones with promising biological activity.

2. The Oxazolidinones

2.1. The Generalized Evaluation Scheme

The generalized scheme of biological evaluation of oxazolidinone analogues we used is shown in Figure 1. Many of us had research experience in the synthesis and evaluation of analogues of existing antibiotic classes, but the oxazolidinones presented a very unusual challenge in that, because they were a new antibiotic class, there was not any pre-existing information about their characteristics and biological behavior. Our testing scheme may seem exceedingly simple, but that is a reflection of our lack of significant

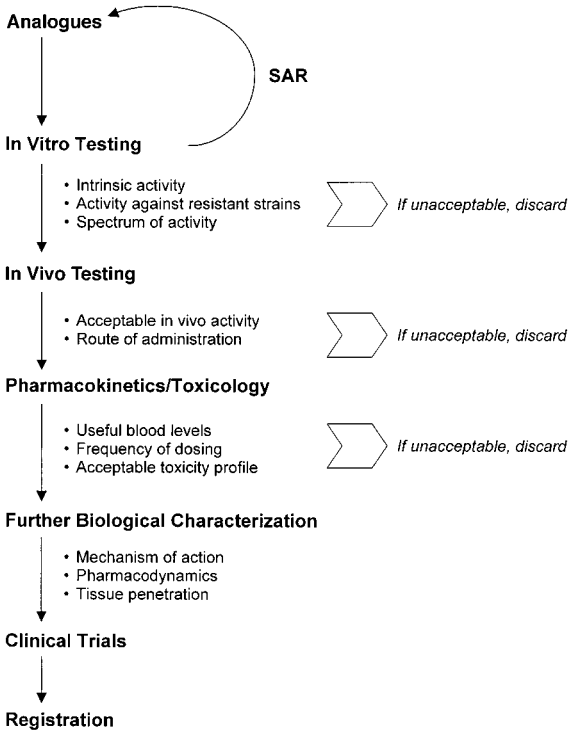


Figure 1. Generalized testing scheme for oxazolidinones showing incorporation of the structure–activity relationship (SAR) component.



Michael R. Barbachyn received his PhD in Organic Chemistry from Wayne State University in 1983, working under the direction of Prof. Carl R. Johnson. After postdoctoral study with Prof. Samuel Danishefsky at Yale University, in 1985 he joined The Upjohn Company (now Pharmacia Corporation). Since late 1990, he has been directly involved with the oxazolidinone discovery effort at Pharmacia and had the good fortune of being involved in the development of linezolid, the first marketed oxazolidinone antibacterial agent. He has 30 US patents and authored numerous publications in the anti-infective field.



Charles W. Ford started his career with a degree in Microbiology from the University of Texas at Austin. After he joined The Upjohn Company (today Pharmacia Corporation) he became the primary microbiologist responsible for the biological component of the oxazolidinone research effort, and functioned as a co-team leader of the oxazolidinone team from the modest inception of the program almost to the introduction of linezolid to the market. He is now a Senior Fellow in research and continues his work on the in vivo evaluation of promising experimental antibiotics.

 © 2003 Wiley-VCH Verlag GmbH & Co. KGaA, Weinheim

knowledge of the biological activity of oxazolidinone when we started the program.

Oxazolidinone analogues were submitted for in vitro testing in which the minimum inhibitory concentration values (MIC, the concentration of drug required to kill the bacterial cells or inhibit their growth under standardized conditions) were determined for each drug versus an array of Gram-positive, Gram-negative, and anaerobic bacteria. The panel of bacteria tested included both antibiotic-sensitive and antibiotic-resistant strains. The MIC value was determined as was the activity of the drug against resistant strains and the useful spectrum of antibacterial activity was assessed. The most crucial measure initially used to guide the structure–activity relationship (SAR) was the MIC value, but as we came closer to drugs which might be clinical candidates other characteristics assumed greater importance. We hypothesized, subject to direct testing, that an MIC value of 4 $\mu g\,mL^{-1}$ or less for 90% of the strains would provide us with an oxazolidinone which would compete favorably with vancomycin, which we had designated as our "gold" standard. A compound would pass through the first round of in vitro testing if its MIC_{90} value for the important Gram-positive pathogens was 4 $\mu g\,mL^{-1}$ or less, if it was completely active against antibiotic-resistant bacteria, and if its spectrum of activity covered the important Gram-positive pathogens.

Compounds fulfilling the in vitro criteria would then be submitted for in vivo evaluation, where their oral activity in mouse models of human bacterial diseases would be compared against subcutaneously administered vancomycin. The goal was for our oxazolidinones to have the same in vivo oral activity as subcutaneously administered vancomycin, which is itself not orally active. This was a very ambitious goal, but one we felt was necessary if we were to convince our customers to treat serious Gram-positive infections with an oral agent. We attached great importance to the oral activity of the compounds in question. It was also important that an orally active compound possess sufficient solubility to promise a reasonable intravenous formulation. Hospital use of an oxazolidinone required an intravenous formulation if the drug were to be used against serious infections. Physicians would probably not switch from an intravenous application of vancomycin, for example, to an oral application of oxazolidinone in serious infections or even in clinical trials. After successful treatment with an intravenous oxazolidinone, however, the switch to oral therapy would be logical.

Compounds which were equivalently active to vancomycin in in vivo infection models were then subjected to pharmacokinetic evaluations in rats and dogs, and were submitted for toxicological evaluation. The toxicological evaluations were far too extensive for inclusion in this review and will not be considered here. There were two criteria that the putative clinical candidate had to meet in the pharmacokinetic evaluations to become a clinical candidate. We anticipated that the levels of compound in the blood of rats and dogs following oral dosing should predict a peak serum concentration (C_{max}) in humans of 12–15 $\mu g\,mL^{-1}$ with oral dosing. As we intended our oxazolidinone to be useful in treating serious human bacterial disease, we settled on a C_{max} value of three times the MIC_{90} value for the least sensitive organism (4 $\mu g\,mL^{-1}$) as the target level. A C_{max} value of that magnitude would ensure a significant duration of time for the level of the drug in the blood to be above the MIC value for any bacteria. If the peak serum concentration was the most important characteristic which correlated with antibacterial activity in vivo, then that C_{max} value would be sufficient to predict efficacy in humans. Additionally, with regard to the oral form of the drug, we targeted a daily dosing regimen in humans of twice daily. Three times daily dosing was problematic as we foresaw that parents would have to send their youngsters to school with the drug for the mid-day dose and would themselves have to remember to take drug with them when they were receiving the drug. A twice daily dosing, once in the morning and once at night at home, was thought to be the most convenient and least problematic dosing schedule.

Any drug which succeeded in meeting the in vitro criteria, the in vivo criteria, passed toxicological profiling, and met the pharmacokinetic requirements then became a clinical drug candidate suitable for additional preclinical development and ultimate entry into Phase I human clinical trials. Even when the first oxazolidinones were in clinical development we continued our efforts at uncovering the biological characteristics of the oxazolidinones. We focused on the mechanism of action of the oxazolidinones which we believed was important for the customers to accept this class as completely novel. We also initiated efforts at understanding the basis for the oxazolidinone activity spectrum being limited to Gram-positive bacteria. The key pharmacodynamic parameter of the oxazolidinones which best predicted successful clinical treatment was determined through extensive in vivo testing. This information provided customers with the means of predicting patient response from blood levels. Tissue distribution studies were conducted as a means of predicting which extravascular human bacterial diseases would be amenable to oxazolidinone therapy and a couple of highly specialized efficacy models were undertaken to determine what role if any an oxazolidinone might play in treating endocarditis (inflammation of the lining of the heart) or osteomyelitis (inflammation of the bone). We also began an examination of the effects of the oxazolidinones on the production of virulence factors even when the drug concentrations were below the MIC value for a specific organism.

2.2. Origins and Early Structure–Activity Studies

At the 1987 Interscience Conference on Antimicrobial Agents and Chemotherapy (ICAAC) workers from the DuPont company formally reported the structure and antibacterial activity profiles of two new antibacterial agents, Dup-105 and DuP-721.[13] These clinical candidates were the first significant representatives of a totally novel class of antimicrobial compounds, the oxazolidinones. These compounds originated from an iterative medicinal chemistry effort starting with a series of racemic 5-halomethyl-3-phenyl-2-oxazolidinones with reported utility for treating a variety of plant diseases. Compound **1** is one example of this compound class (Figure 2).[14] Subsequent chemical modification of **1**

 © 2003 Wiley-VCH Verlag GmbH & Co. KGaA, Weinheim

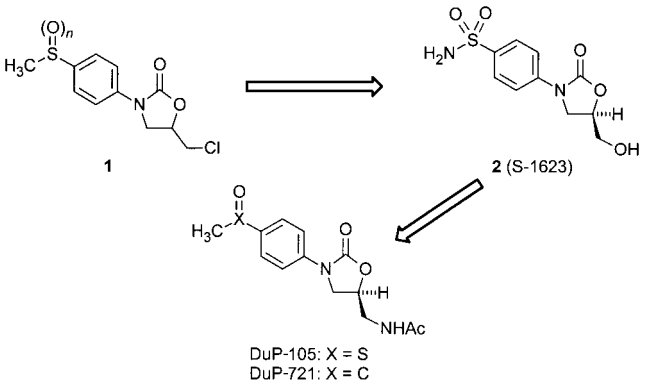


Figure 2. Emergence of the oxazolidinones at DuPont.

eventually led to analogues such as **2** (S-6123), which reportedly exhibited modest in vitro activity and in vivo efficacy against several Gram-positive and Gram-negative organisms.[15] It was at this time that the absolute configuration of the oxazolidinones at C-5 became evident. Further elaboration of analogues such as **2** eventually led to the identification of the prototypical oxazolidinones, Dup-721 and DuP-105,[16] which showed significantly improved characteristics relative to their progenitor compounds.

Some of the activity trends that emerged from the study of the early DuPont structure–activity relationships are summarized in Figure 3. As subsequent events will illustrate, several of these notions now require revision.

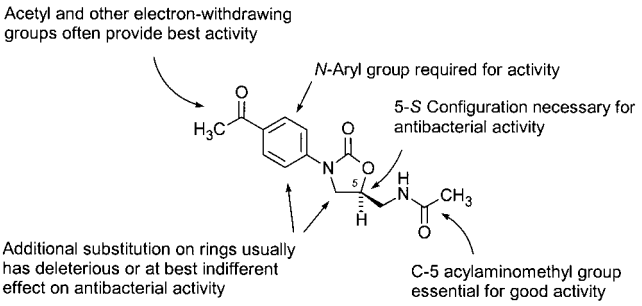
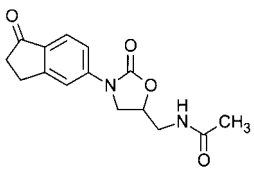


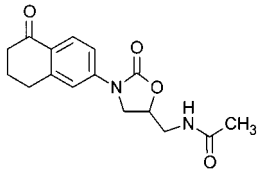
Figure 3. Early structure–activity relationships of oxazolidinones determined at DuPont.

We committed ourselves to proof-of-concept studies with the oxazolidinones. Our goal in these studies was the demonstration that we could synthesize structurally novel oxazolidinones which possessed promising biological characteristics, particularly antibacterial activity and safety profiles.

2.3. Interim Phases of the Development

Early chemical modifications at Pharmacia probed a number of structural features of the DuP-721 lead compound to assess their impact on antibacterial activity. A detailed discussion of this effort is beyond the scope of this review, and for the sake of brevity we will focus on analogues wherein the usual 4-substituted phenyl ring is replaced by a fused bicyclic ring system. More specifically, analogues incorporating indanone (PNU-82965)[17] and tetralone (PNU-85055)[18] subunits

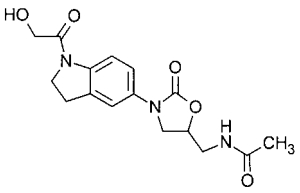

PNU-82965

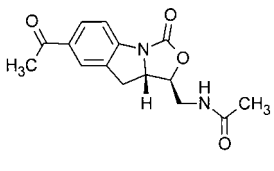

PNU-85055

were prepared and tested. These compounds were designed to explore the effect(s) of annulating the acetyl moiety of DuP-721 back onto the pendant phenyl ring. It should also be noted that these early analogues were prepared in a racemic form to expedite their preparation. Since only the *S* enantiomer is antibacterially active,[16] the racemic material generally exhibits half the potency of the pure enantiomer. Nevertheless, these racemic analogues were deemed sufficient to probe structure–activity relationships at this early stage of the program.

The compound PNU-82965 eventually assumed a pivotal role for the Pharmacia oxazolidinone program. By 1989 fragmentary reports were obtained that DuPont had removed an oxazolidinone from clinical trials as a result of observed toxicity in several animal models.[19] A comparative in-house safety evaluation of racemic DuP-721 and PNU-82965 was conducted at Pharmacia to test these claims.[20] In this study racemic DuP-721 and PNU-82965 were administered orally at a dose level of 100 mg kg^{-1} body weight twice a day for 30 days to three male and three female Sprague–Dawley rats. The rats treated with racemic DuP-721 fared poorly in the study, one died and two rats were sacrificed in a moribund state. Additional findings for the animals treated with racemic DuP-721 included severe progressive weight loss and evidence of bone marrow atrophy. In contrast, the rats treated with PNU-82965 exhibited only a few adverse findings and these were judged to be very mild in nature. There were no clinical signs, serum or urine chemistries, or histopathological manifestations of drug-related toxicity. The major ramification of this comparative safety study was that a structure–toxicity relationship exists for the oxazolidinones.

Following up on the favorable safety findings with PNU-82965, and speculating that alternative fused bicyclic inserts might confer favorable properties to the oxazolidinone pharmacophore, the racemic indoline congener PNU-85112 was targeted and eventually synthesized.[21] Like its progenitor, PNU-82965, this indoline analogue was found to exhibit

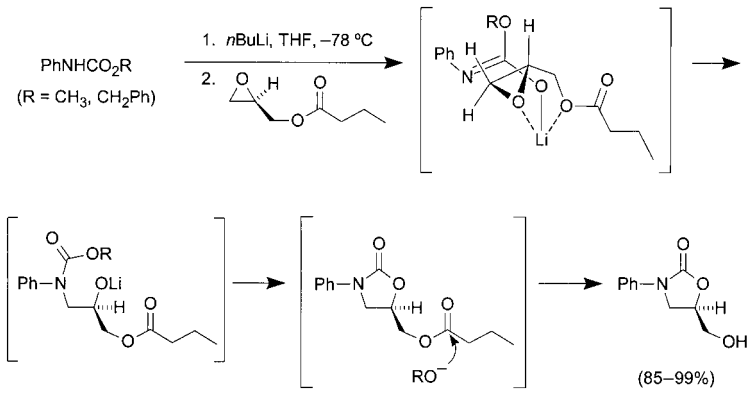

PNU-85112


PNU-86093

an excellent safety profile when tested for toxicity in the rat while displaying in vitro activity and in vivo efficacy closely approaching that of (±)-DuP-721.

Continuing investigations into fused-ring analogues of DuP-721 led to the design and synthesis of tricyclic fused systems such as the racemate PNU-86093.[22] This analogue and related congeners (not discussed here) helped to define the optimal dihedral angle between the oxazolidinone and adjacent phenyl rings. (±)-PNU-86093 exhibited in vitro antibacterial activity slightly lower than that of (±)-DuP-721.

With antibacterially active, safe oxazolidinones now in hand it became extremely important to address the preparation of enantiomerically enriched analogues. Previously described synthetic methods involving aryl isocyanates were effective, but not general.[16,17] In the course of extensive studies at Pharmacia it was found that *N*-lithiated carbamate derivatives of anilines could be treated with commercially available (*R*)-glycidyl butyrate under appropriate conditions to directly generate (*R*)-3-aryl-5-(hydroxymethyl)oxazolidinones (Scheme 1).[23] The hydroxymethyl intermediates are readily elaborated to final products.



Scheme 1. Enantiomeric synthesis of phenyloxazolidinones (Manninen reaction).

2.4. Emergence of the Piperazinylphenyloxazolidinones

We wondered whether the 4-pyridyl moiety of the DuPont lead compound, E-3709, might be amenable to replacement by suitable saturated heterocyclic bioisosteres (Figure 4). In connection with this notion, and in an inverse sense, we were cognizant of the successful replacement in the quinolone antibacterial agent area of the piperazine ring system of, for example, ciprofloxacin, with a pyridine fragment, as seen in Win-57273.[24] Another important aspect of the existing quinolone structure–activity relationship was the finding that strategically located fluorine atoms were found to not only increase potency, but also to confer enhanced oral pharmacokinetic performance to the compounds.[25] Contemporaneous to our plans to explore the piperazine surrogate, we speculated that the small but highly electron withdrawing fluorine atom would be tolerated at the *meta* position(s) of the central phenyl ring and confer enhanced antibacterial activity and/or other desirable properties to the targeted oxazolidinones (see generic structure **3** in Figure 4).

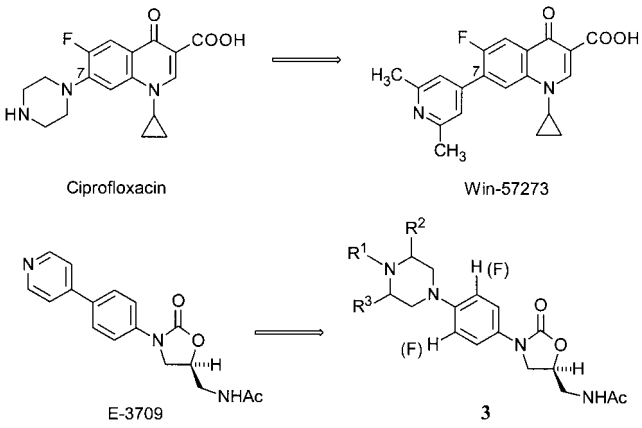
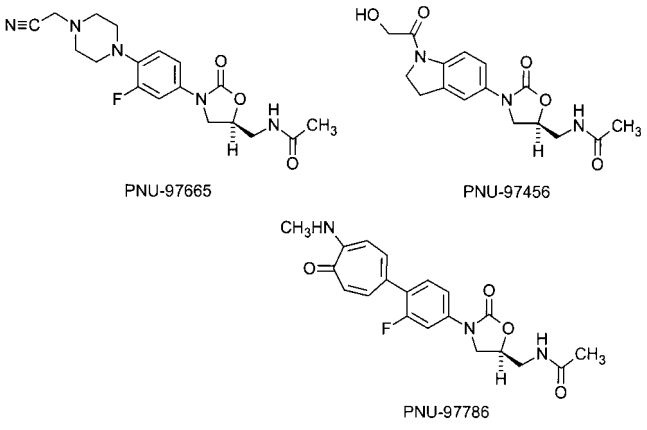


Figure 4. Development of the piperazinylphenyloxazolidinones.

By late 1992 the chemistry effort encompassed primarily three different subclasses of oxazolidinone analogues: 1) piperazinylphenyloxazolidinones (for example, PNU-97665),[26] 2) indolinyloxazolidinones (for example, PNU-97456)[21] and 3) the troponylphenyloxazolidinones (for example, PNU-97786).[27]

The indolines generally exhibited an excellent safety profile but demonstrated somewhat lower levels of antibacterial activity. The troponyl analogues were generally the most interesting compounds from an antibacterial activity standpoint but displayed poor water solubility and poor pharmacokinetic characteristics. Selected piperazine derivatives exhibited excellent in vitro and in vivo activity while also maintaining an acceptable safety profile, acceptable water solubility, and excellent pharmacokinetic parameters. As a bonus, the piperazine analogues were also the easiest compounds to synthesize. As a consequence of these and other characteristics, the piperazine series became the principal focus of the ongoing chemistry effort.

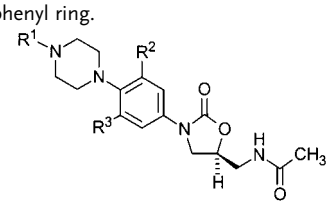


2.5. Piperazinylphenyloxazolidinones and Isosteres

A number of piperazinylphenyloxazolidinones of generic structure **3** were synthesized. Many of these analogues exhibited interesting levels of in vitro (MIC) and in vivo

 © 2003 Wiley-VCH Verlag GmbH & Co. KGaA, Weinheim

Table 1: The potentiating effect of fluorination of the phenyl ring.

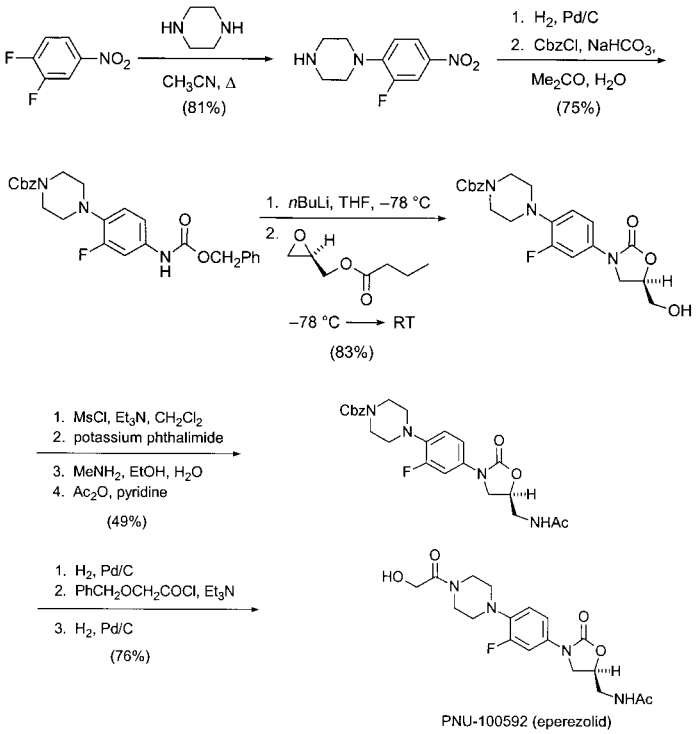


PNU	R^1	R^2	R^3	MIC [μg mL^{-1}] SA[a]	EF[b]	SP[c]	ED_{50} [mg kg^{-1}][d]
107399	CO_2Me	H	H	4	4	2	n.t.[e]
98257	CO_2Me	H	F	4	2	1	3.7 (1.6)
98170	CO_2Me	F	F	2	2	0.5	2.5 (1.3)
108946	$COCH_2OH$	H	H	4	2	1	n.t.
100592	$COCH_2OH$	H	F	4	1	<0.5	3.3 (5.0)
100675	$COCH_2OH$	F	F	2	1	0.25	1.6 (1.8)
143145	$COCH_2OH$	H	OMe	>16	>16	>16	n.t.
97665	CH_2CN	H	F	8	4	1	4.0 (2.2)
98172	CH_2CN	F	F	4	2	1	2.8 (2.7)
99200	$(CH_2)_2OMe$	H	F	16	16	2	7.9 (1.7)
99372	$(CH_2)_2OMe$	F	F	8	4	1	7.7 (2.0)
100762	$(CH_2)_2F$	H	F	16	8	2	8.6 (5.0)
100349	$(CH_2)_2F$	F	F	4	2	1	5.0 (2.8)

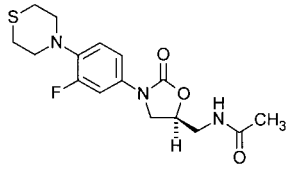
[a] SA = *Staphylococcus aureus* UC 9213. [b] EF = *Enterococcus faecalis* UC 9217. [c] SP = *Streptococcus pneumoniae* UC 9912. [d] ED_{50} = effective dose$_{50}$ (the dose that protects 50% of the animals). Oxazolidinones were administered orally; the results from subcutaneously administered vancomycin are given in parentheses. [e] n.t. = not tested.

(ED_{50}) antibacterial activity. Of particular note was the gratifying finding that one or two fluorine atoms flanking the *para* piperazine group exerted a significant potentiating effect on the antibacterial activity (Table 1); this finding is consistent with observations in other oxazolidinone subclasses.[27] It was found that a wide range of alkyl, acyl, and sulfonyl substituents were tolerated on the distal piperazine nitrogen atom. After a number of synthetic iterations it was found that the hydroxyacetyl moiety was the optimal nitrogen substituent. Ultimately, the monofluorophenyl congener PNU-100592, which was subsequently named eperezolid, emerged as the analogue with the best balance of antibacterial activity, pharmacokinetics, water solubility, and other pertinent properties.[28] An early laboratory synthesis of PNU-100592 is outlined in Scheme 2.

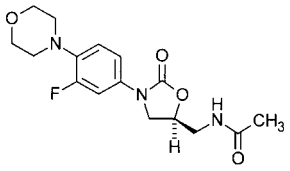
We were cognizant that alternative bioisosteric replacements for the piperazine ring were known, primarily from the literature relating to quinolone antibacterial agents. Systematic modification along these lines led to the identification of the interesting antimycobacterial thiomorpholine derivative PNU-100480[29] and also the morpholine analogue PNU-100766, which subsequently became know as linezolid.[28]



Scheme 2. Laboratory synthesis of eperezolid (PNU-100592). Cbz = benzyloxycarbonyl, Ms = methanesulfonyl.



PNU-100480



Linezolid (PNU-100766)

As depicted in Figure 5, the extensive effort at Pharmacia on the structure–activity relationship of oxazolidinone has prompted several revisions to the dogmas espoused by the earlier DuPont work. Perhaps most interesting was the finding that a suitable electron-donating amino substituent

 © 2003 Wiley-VCH Verlag GmbH & Co. KGaA, Weinheim

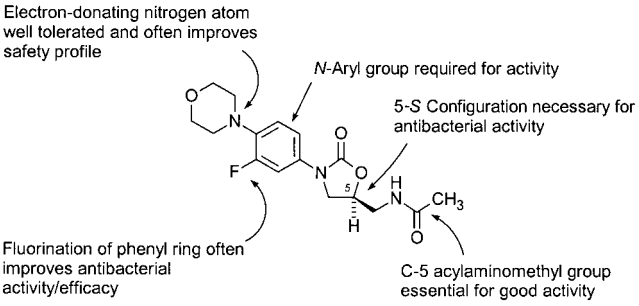
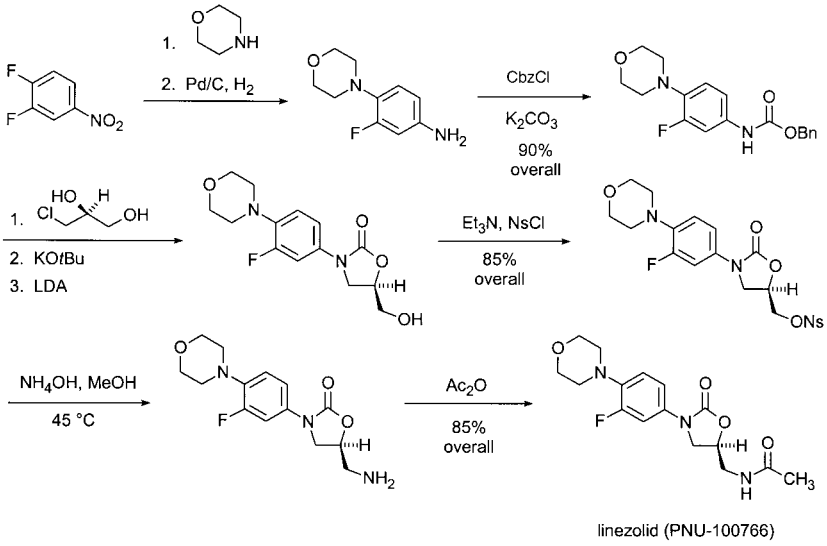


Figure 5. Revised structure–activity relationships identified at Pharmacia.

on the phenyl ring can confer excellent antibacterial activity while helping to maintain a good safety profile. Another important result of this investigation was the identification of the potentiating effect of one or two fluorine atoms flanking the morpholine or piperazine ring.

2.6. Linezolid and Eperezolid

The first oxazolidinones to emerge as potential drug candidates from the testing scheme were eperezolid (PNU-100592) and linezolid (PNU-100766). They were quite unusual in that they were almost identical in our preclinical testing: Their MIC values, their antibacterial spectrum, their ED_{50} values derived from tests with infected mice, and their pharmacokinetic behavior in at least two animal species were virtually identical, within experimental error, of each other. The research team then undertook the unusual strategy of taking both eperezolid and linezolid through a Phase I human clinical trial to determine if a significant difference might exist between the two compounds with respect to their pharmacokinetic behavior in humans. Evaluation of the blood data showed that linezolid would likely need to be dosed twice daily in humans and eperezolid three times daily to provide the same exposure. On the basis of that advantage, linezolid was selected for further development.



Scheme 3. Synthesis of linezolid (PNU-100766) on a process scale. LDA = lithium diisopropylamide, Ns = *meta*-nitophenylsulphonyl.

2.7. Synthesis of Linezolid on a Process Scale

An efficient, cost-effective synthesis of the compound was required to facilitate the clinical study of linezolid. As shown in Scheme 3, a concise large-scale preparation of the compound has been developed.[30]

3. Biological Evaluation of Linezolid

3.1. Antibacterial Activity In Vitro

The determination of the MIC values is really the first key biological data generated in a program aimed at determining the structure–activity relationships of antibiotics. Since there is little or no experience with comparisons of MIC values with blood concentrations and in vivo efficacy studies for members of a new antibiotic class the most prudent evaluation of the MIC values is by comparison with antibiotics on the market. As our program used *Staphylococcus aureus* as the key pathogen for SAR studies we chose the MIC values of vancomycin as our target for the oxazolidinones since vancomycin was the only antibiotic which could be used empirically against staphylococci with assurance. Our customers would, therefore, be used to its MIC values of 1 to 2 $\mu g\,mL^{-1}$ against staphylococci and would have little trouble accepting oxazolidinone values if they were in the same range. In fact linezolid performed comparably to vancomycin against staphylococci (Table 2). The MIC_{90} values of linezolid for methicillin-sensitive and -resistant *S. aureus* ranged from 2 to 4 $\mu g\,mL^{-1}$ and lay within the margin of error of those for vancomycin (1–2 $\mu g\,mL^{-1}$).[31] The MIC_{90} values of both linezolid and vancomycin for *Staphylococcus epidermidis*, a pathogen involved in infections from catheter and invasive devices, was 2 $\mu g\,mL^{-1}$. Other research groups confirmed very early on the activity of linezolid against staphylococci and its approximate equivalence to vancomycin.[32–38] At this time, many staphylococci strains with varying resistance patterns to antibiotics had been tested against linezolid in vitro and two observations were possible: first, linezolid activity was unaffected by pre-existing antibiotic resistance in the staphylococci, thus suggesting that it did have a new mechanism of action, and, second, the MIC values of linezolid for many strains of staphylococci were very similar numerically, which was taken to be the hallmark of a brand new class of antibiotics.

Linezolid also performed well against the enterococci in vitro. Linezolid inhibited all tested strains of *Enterococcus faecalis* and *Enterococcus faecium* at 4 $\mu g\,mL^{-1}$ or less.[31] This

 © 2003 Wiley-VCH Verlag GmbH & Co. KGaA, Weinheim

Table 2: In vitro activities of linezolid and vancomycin.

Organism	Antibacterial agent	MIC_{90} [$\mu g\,mL^{-1}$][a]
Staphylococcus aureus	linezolid	4
(methicillin-susceptible)	vancomycin	1
S. aureus	linezolid	4
(methicillin-resistant)	vancomycin	2
Staphylococcus epidermidis	linezolid	2
(methicillin-sensitive)	vancomycin	2
S. epidermidis	linezolid	2
(methicillin-resistant)	vancomycin	2
Enterococcus faecalis	linezolid	4
(methicillin-sensitive)	vancomycin	2
E. faecalis (VanB)	linezolid	4
	vancomycin	>16
Enterococcus faecium	linezolid	2
	vancomycin	≤ 0.5
E. faecium (VanA)	linezolid	4
	vancomycin	>16
E. faecium (VanB)	linezolid	4
	vancomycin	>16
Streptococcus pneumoniae	linezolid	1
	vancomycin	≤ 0.25
S. pneumoniae	linezolid	1
(penicillin-sensitive or -resistant	vancomycin	≤ 0.25
Streptococcus pyogenes	linezolid	2
	vancomycin	0.5
Haemophilus influenzae[b]	linezolid	8
	vancomycin	>16
Moraxella catarrhalis[b]	linezolid	4
	vancomycin	>16
Gram-negative bacilli[c]	linezolid	>64
	vancomycin	>16
Bacteroides fragilis[d]	linezolid	≥ 16
	vancomycin	>16
Clostridium spp.[d]	linezolid	2
	clindamycin	4
Peptostreptococcus spp.[d]	linezolid	2
	clindamycin	2

[a] MIC_{90} = concentration of drug needed to kill or inhibit the growth of 90% of the tested strains under standardized conditions. [b] Fastidious Gram-negative bacteria. [c] Pathogens from the 10th generation. [d] Anaerobic pathogenic bacteria.

observation of enterococcal sensitivity to linezolid was very important as the enterococci had been developing into a therapeutic problem in the 1990s because they were generally antibiotic-resistant and the number of strains possessing vancomycin resistance was growing. The action of linezolid was unaffected by enterococcal resistance to vancomycin and promised welcome relief for physicians with patients who had enterococcal infections untreatable with antibiotics. As with the staphylococci, linezolid performed identically against geographically diverse enterococcal collections with a large array of antibiotic resistance patterns.

Very importantly, in our estimation, linezolid was more than acceptably active against penicillin-sensitive and -resistant *Streptococcus pneumoniae* and *Streptococcus pyogenes* (Table 2). Although the organisms receiving the most attention in terms of fears of resistance development in the 1990s were the staphylococci and enterococci, we also focused our attention on the streptococci. The reasoning was very simple: *S. pneumoniae* is the major cause of bacterial disease in humans, since it is the principal causative agent of upper and lower respiratory tract infections. Since the advent of the antibiotic era, *S. pneumoniae* infections had been effectively treated with inexpensive older line antibiotics, but with the advent of β-lactam (penicillin family) then macrolide and quinolone resistance in *S. pneumoniae*, the treatment of upper and lower respiratory tract infections was becoming a therapeutic problem. Linezolid was quite active against the streptococci and was unaffected by β-lactam resistance. The activity of linezolid against *S. pyogenes* extends the spectrum of the drug to enable treatment of infections following childbirth. It is also interesting to note that, like many Gram-positive antibiotics, linezolid covers both the staphylococci and the streptococci, with more intrinsic activity exhibited against the streptococci.

The spectrum of linezolid activity is also very important since the spectrum of a drugs' activity will determine if the drug will be clinically useful or not. The spectrum of linezolid activity covers the most important Gram-positive pathogens—the staphylococci, the enterococci, and the streptococci. This spectrum of activity indicated that the drug would provide coverage for important medical diseases and would be a welcome addition to the antibiotic armamentarium. Typical of antibiotics active against Gram-positive bacteria, linezolid was inactive against the Gram-negative bacilli and had modest to weak activity against *Haemophilus influenzae* and *Moraxella catarrhalis*, two fastidious Gram-negative organisms found coincident with *S. pneumoniae* in upper and lower respiratory tract infections (Table 2). Linezolid also appeared to have modest in vitro activity against the medically significant anaerobes *Bacteroides fragilis*, *Clostridium* spp., and *Peptostreptococcus* spp., which is consistent with the spectrum of activity of other antibiotics active against Gram-positive bacteria, for example, clindamycin (Table 2).[39]

A very interesting conundrum arose during early SAR work on the oxazolidinones. We were quite aware that the spectrum of oxazolidinone activity did not include the Gram-negative bacilli and yet some of the biologists on the team were measuring oxazolidinone inhibition of bacterial protein synthesis in a cell-free system. The surprise was that the cell-free system was an *Escherichia coli* extract, and *E. coli* was one of the Gram-negative bacilli for which the oxazolidinones, including linezolid, exhibited no appreciable activity. In the absence of cell membranes and the Gram-negative cell wall the oxazolidinones were very active in inhibiting *E. coli* protein synthesis. In the interest of focusing on Gram-positive agents, we assumed that the oxazolidinones lack of Gram-negative activity was some sort of nonspecific transport

 © 2003 Wiley-VCH Verlag GmbH & Co. KGaA, Weinheim

activity. The observation was revisited later when it was shown that making the *E. coli* AcrAB transmembrane pump nonfunctional through directed mutagenesis then made whole *E. coli* cells sensitive to linezolid both in vitro and in vivo.[40] The lack of Gram-negative activity on the part of oxazolidinones is therefore a result of the presence of transmembrane pumps which, along other molecules, pump oxazolidinones out of the cell faster than they can accumulate.

3.2. In Vivo Activity of Linezolid

The second step in the evaluation phase of potentially useful oxazolidinone compounds is the determination of antibacterial activity in vivo. This usually took the form of experimentally determining the ED_{50} value (the amount of drug in $mg\,kg^{-1}$ of body weight required to cure 50% of infected animals) in mouse models of bacteremia (bloodstream infection) as the first evaluation of in vivo activity. To cure a bacteremia following oral dosing an antibiotic must remain intact in transit through the stomach and some portion of the intestinal tract, the majority of the antibiotic must be transported across the gut wall, it must appear in the blood in sufficient concentration so as to kill the bacteria without being metabolized or enzymatically converted into an inactive form, and it must remain in the blood stream without being excreted too rapidly. The value of these models is that they put the drug through all of these individual hurdles that a human patient does. Given those requirements, the bacteremia models are the most direct and efficient measure of in vivo activity compared with infection models where the bacteria are localized in a specific tissue.

The results of mouse efficacy studies with linezolid are contained in Table 3. These are representative in vivo tests, many more tests with multiple strains of specific organisms not represented here were performed.[41] In these tests, linezolid given orally to mice performed equivalently to vancomycin administed subcutaneously (vancomycin is not orally available). These tests demonstrated that we had achieved a major goal of the program: a drug has been developed whose oral activity is approximately equal to vancomycin administered subcutaneously.

Linezolid and vancomycin performed equivalently against an antibiotic-sensitive *S. aureus* (UC9271) as shown by the two ED_{50} values being within experimental error of each other (data not shown). Very importantly, linezolid was as active as vancomycin in vivo against methicillin- and multiple-drug-resistant *S. aureus* strains. This was also true in an unusual *Staphylococcus epidermidis* bacteremia model where linezolid was again equivalent to vancomycin. Linezolid thus met our originally conceived in vivo requirements for staphylococci activity and was shown to possess excellent in vivo antibacterial activity against a penicillin- and cephalosporin-resistant *Streptococcus pneumoniae* and an *S. pyogenes* strain (Table 3). Multiple strains of *S. pneumoniae* with varying antibiotic resistance could be treated in vivo with ED_{50} values falling between 3 and $10\,mg\,kg^{-1}$ (data not shown). Vancomycin was numerically more active than linezolid in effecting cures in a *Enterococcus faecalis* bacteremia model, however, linezolid performed well orally with an ED_{50} value of $10\,mg\,kg^{-1}$. An oral drug this active against an enterococcal infection is quite unusual. Importantly, linezolid retained its in vivo antibacterial activity when tested against a vancomycin-resistant *E. faecium* bacterium (Table 3) even though the efficacy test was conducted in a neutropenic mouse model which is far more difficult to treat than a model in a normal mouse.

The remaining three in vivo determinations contained in Table 3 are all models for soft tissue infection where the bacteria are localized subcutaneously in the mouse. The cures in these cases are measured by microbiological enumeration of the bacteria from the infected area at the end of therapy. Following oral dosing, linezolid was clearly penetrating to the infection site as it actively cured all three infections. Both linezolid and vancomycin cured the soft tissue infection caused by *S. aureus*, and although their ED_{50} values were different both values would predict utility from this type of a model. The model for soft tissue infection by *E. faecalis* demonstrated very good activity on the part of oral linezolid

Table 3: In vivo activity of linezolid and vancomycin.

Bacterium	Compound[a]	MIC [$\mu g\,mL^{-1}$]	ED_{50} [$mg\,kg^{-1}$][b]
Staphylococcus aureus UC9271	linezolid	9.0	6.9
	vancomycin	1.0	13.2
S. aureus UC6685[c]	linezolid	2.0	3.8
	vancomycin	2.0	2.6
S. aureus UC15080[c]	linezolid	0.5	3.8
	vancomycin	1.0	1.5
Staphylococcus epidermidis UC12084[c]	linezolid	1.0	4.7
	vancomycin	2.0	1.8
Staphylococcus pneumoniae UC15088[c]	linezolid	1.0	2.7
	cefaclor	>32.0	>20.0
Staphylococcus pyogenes UC152	Linezolid	2.0	5.0
	clindamycin	0.6	8.6
Enterococcus faecalis UC12379[d]	linezolid	4.0	10.0
	vancomycin	1.0	0.5
Enterococcus faecium UC15090[e]	linezolid	4.0	24.0
	vancomycin	>69.0	>100.0
S. aureus UC9271[f]	linezolid	4.0	39.7
	vancomycin	1.0	4.7
E. faecalis UC15060[f]	linezolid	4.0	11.0
	vancomycin	2.0	16.3
Bacteroides fragilis UC12199[f]	linezolid	4.0	46.3
	clindamycin	1.0	200.0

[a] Linezolid was administered orally and vancomycin subcutaneously. [b] The amount of drug in mg per kg of body weight required to cure 50% of infected animals. [c] Methicillin- and multidrug-resistant. [d] Penicillin- and cephalosporin-resistant. [e] Vancomycin-resistant; model performed in neutropenic mice. [f] Subcutaneous soft tissue infections.

 © 2003 Wiley-VCH Verlag GmbH & Co. KGaA, Weinheim

against this important pathogen and, very interestingly, oral linezolid performed exceptionally well when tested against the anaerobe *Bacteroides fragilis* in a soft tissue infection. The real importance of these models is that they require a drug that penetrates the animals tissues well in order to effect a cure. Linezolid not only penetrates the tissues sufficiently to provide adequate drug concentrations to kill the bacteria but it does so following oral dosing. These observations indicated that linezolid would be very useful in a variety of human infections.

Several other specialty animal models provided very useful specific information concerning efficacy of linezolid prior to or coincident with clinical trials. In a streptococcal pneumonia model in rats[42] linezolid administered twice daily at 50 mg kg^{-1} was found to be equivalent to ceftriaxone, an extended pharmacokinetic cephalosporin, given 100 mg kg^{-1} once daily. In the chinchilla model of otitis media (inflammation of the middle ear), linezolid readily eradicated multidrug-resistant *S. pneumoniae* at 25 mg kg^{-1} twice daily, but was not effective in eradicating *H. influenzae* when the MIC values of linezolid for the strain was 8–16 μg mL^{-1}.[43] Linezolid was weakly effective at 25 mg kg^{-1} in an intraperitoneal abscess model with *E. faecium* but substantively reduced bacterial numbers in the abscesses at 100 mg kg^{-1}.[44]

Physicians hope that any new antibiotic active against Gram-positive agents will be effective against staphylococcal endocarditis as this infection of the heart valves is life-threatening and very hard to eradicate. Our customers were particularly interested in the possibility that oral linezolid would be effective in endocarditis because this would represent a major step forward in ease of drug administration. The action of linezolid was compared directly with that of vancomycin against endocarditis caused by antibiotic-sensitive and methicillin-resistant *S. aureus* in a rabbit model.[45,46] In the first study, oral linezolid at a dose of 50 mg kg^{-1} rendered 50% of infected animals heart-valve culture negative while intravenous vancomycin at 25 mg kg^{-1} cured 8/11. Linezolid reduced blood bacterial counts from 2.3 CFU mL^{-1} (CFU = colony-forming units of bacteria, logarithmic values) to 1.5 CFU mL^{-1} in culture-positive animals at the end of therapy, as did vancomycin. Both linezolid and vancomycin reduced the bacterial counts from heart valve vegetation from 8.4 CFU g^{-1} gram to 4.3 and 4.0 CFU g^{-1}, respectively. Linezolid clearly performed as well as vancomycin in this very important infection model and did so as a drug administered orally—a very important consideration for patient compliance and safety. The key pharmacokinetic parameter identified in this study was simply that in this difficult to treat infection the blood concentration of linezolid had to be maintained at or above the MIC_{90} value for the infecting organism. This key observation was confirmed in a subsequent study[46] of endocarditis caused by methicillin-resistant *S. aureus* where again linezolid administered orally compared favorably with vancomycin administered intravenously. This modeling work with linezolid let us to believe that linezolid could very well have a place in the treatment of human endocarditis and might provide an alternative drug to vancomycin in the treatment of endocarditis caused by antibiotic-resistant *S. aureus*.

3.3. Pharmacokinetic/Pharmacodynamic Properties of Linezolid

One of the key characteristics of antibiotic behavior in a human is its performance in blood. A 600 mg oral dose was chosen for linezolid based on animal studies, and the resultant human blood levels were determined in a clinical trial.[47] The 600 mg dose in humans achieved average maximum serum levels of about 19 μg mL^{-1}, which by 12 h following administration were approximately an average of 6 μg mL^{-1}. These blood levels were very promising for the ultimate use of linezolid in humans as they predicted that following a single 600 mg oral dose of linezolid, the minimum average drug blood level would be above the MIC_{90} value for staphylococci, streptococci, and enterococci. These observations also predicted that linezolid could be dosed twice daily, at about 12 hour intervals, which represented a significant advantage over drugs requiring three times daily dosing. A very satisfying and unusual result from these studies was the determination that linezolid was 103% orally bioavailable. This means that the area under the drug blood level curve for the oral dose in humans was equal to the area under the drug blood level curve for the intravenous dose. Animal studies had hinted this might be true. This situation is extremely rare and means that the patient's exposure following oral dosing was equal to their exposure following intravenous dosing. In a practical sense, it also meant that the oral and intravenous routes of administration used exactly the same amount of drug and that the dose would not have to be changed when switching from intravenous to oral therapy.

Other important pharmacokinetic behaviors of linezolid emerged from animal studies and human clinical trials. It was found that the presence of food had little effect upon linezolid absorption, so linezolid could be taken both with meals or at another time.[48] Importantly for prescribing physicians, linezolid is not metabolized by cytochrome P450 nor does it inhibit any of the important P450 isoforms.[49] Metabolism does occur, but it is by non-enzymatic oxidation and the metabolites do not possess antibacterial activity. Between 8 and 8.5% of linezolid is excreted in the urine and 7 to 12% through the gut.[50] Linezolid is a very well behaved antibiotic in terms of its pharmacokinetic behavior, and all of these observations translate to its ease of use in therapy.

Since linezolid was the first member of the oxazolidinone class of antibacterial agents to approach the market we wanted to determine which pharmacodynamic parameter of linezolid best predicted in vivo cure. This information would have a strong bearing on the design of clinical studies and would permit our customers to be able to match the anticipated linezolid pharmacokinetic behavior in the patient with the key pharmacodynamic parameter. Animal studies using a model of a thigh infection caused by *S. aureus* in the mouse were undertaken to answer this question.[51] The parameter which best predicted in vivo cure was determined experimentally to be the time the drug blood level exceeded the MIC_{90} value for the infecting organism. It was further determined that the time the drug blood level exceeded the MIC_{90} value should be a minimum of 40–60% of the dosing interval. The 600 mg dose of linezolid provided blood levels above the MIC_{90} value for 100% of the dosing interval and

 © 2003 Wiley-VCH Verlag GmbH & Co. KGaA, Weinheim

thus more than met the minimum requirements of the pharmacodynamic model.

4. Further Biological Findings

4.1. Mechanism of Antibacterial Action of Linezolid

One of the key characteristics of linezolid which we believed would make it very attractive to physicians was the fact it was a brand new class of antibiotic which did not suffer from existing resistance mechanisms in bacteria. We thought it very important to literally demonstrate that the oxazolidinones had a unique mechanism of action and identify that mechanism. Studies done with eperezolid clearly showed that eperezolid bound to the 50S ribosomal subunit and that binding was dosage dependent.[52] It was postulated that the mechanism of action was different from those of chloramphenicol and lincomycin which appeared to bind at sites near the specific site for eperezolid. Linezolid inhibited phage-specific in vitro translation, peptide chain termination, and polypeptide chain elongatin in a cell-free *E. coli* protein synthesis assay.[53] On the basis of these observations it was then determined that linezolid binds the 50S ribosomal subunit and that binding then prevents formation of a functional initiation complex (Figure 6).[54] This discovery clearly demonstrated that linezolid was unique among protein synthesis inhibitors and explained why linezolid retained antibacterial activity against Gram-positive organisms which were resistant to members of existing classes.

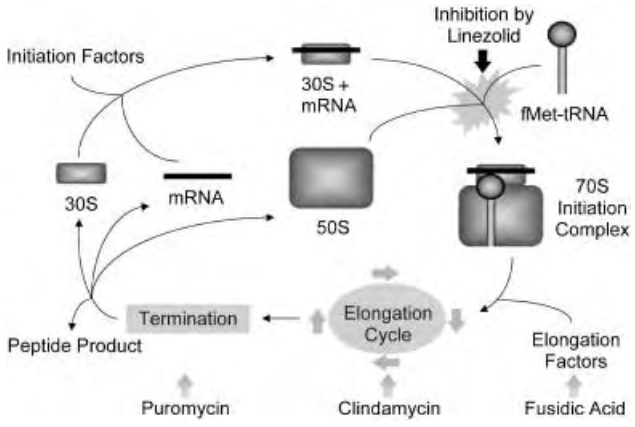


Figure 6. Mechanism of action of linezolid.

4.2. Distribution of Linezolid in Tissue

The in vivo experiments which demonstrated that linezolid effected microbiological cure of soft tissue infections in mice clearly indicated that linezolid was penetrating the tissues from the blood stream in sufficient quantity and with sufficient duration of persistence. A more quantitative and direct measure of linezolid penetration from the blood to tissues was undertaken in the rat[55] and demonstrated that linezolid penetrates tissues very well. Linezolid was radioactively tagged with ^{14}C and administered intravenously to rats at a dose of $10\,mg\,kg^{-1}$. Twenty minutes after administration, linezolid was distributed throughout the entire animal with a tissue level of $10.5\,\mu g\text{-equiv}\,g^{-1}$. The tissues which had at least twofold the MIC_{90} concentration of linezolid for staphylococci ($8\,\mu g\,mL^{-1}$) included the small and large intestine, the bladder, lymph nodes, pancreas, spleen, bone marrow, muscle, thymus, thyroid, heart, lung, liver, and pituitary gland. The concentrations of linezolid in the vitreous humor and brain were about 14% of the blood levels. In fact, the only two tissues which linezolid did not penetrate well following the single dose of drug were the bone matrix and white fat. These findings were, and are, very important as they indicate that linezolid has a very good chance of effecting a cure in humans for Gram-positive infections no matter where the infection may be localized. Most infections in humans are not of the blood alone and linezolid provides the physician with a very effective tool for combating Gram-positive infections.

4.3. Bacteriostatic Versus Bacteriocidal Considerations

An antibiotic is considered static if there is less than a 3-log reduction in bacterial cell numbers in 16–24 h under standardized conditions in the test tube and cidal if it kills $\geq$ 3 logs of bacteria. From this definition, linezolid was determined to be static for staphylococci and enterococci and cidal for pneumococci. The general rule of thumb is that static drugs should not be used for particularly serious infections with Gram-positive infections, such as endocarditis, and under circumstances where the patient is in grave danger. There are several exceptions to these rules and we wondered if linezolid was not an exception when several investigators told us that linezolid was an exceptionally fast acting antibiotic in human infections. Rapidity is not necessarily a hallmark of static drugs. To address this issue, we initiated an investigation into the effect of linezolid upon toxin production in *S. aureus* and *S. pyogenes*.[56] These in vitro studies were limited to linezolid levels below the MIC value of the organism. Linezolid dramatically reduced α-hemolysin, δ-hemolysin, and coagulase levels in *S. aureus* cultures and similarly effected Streptolysin O and DNAase levels in *S. pyogenes* cultures even at levels of 25 or 50% of the MIC concentration. For example, with no linezolid in the culture the titre of α-hemolysin in an *S. aureus* culture was 512 and with the additon of 25% of the MIC value of linezolid, which did not kill the cells, that titre was reduced to 2. Although linezolid is technically a static drug for *S. aureus* it behaves in vivo as though it is a cidal drug through its intervention in toxin production. The rapidity with which linezolid kills the bacterial cells becomes irrelevant to the fact that it inhibits toxin production and thereby inhibits the tissue damage and destruction which is the hallmark of the disease. Linezolid therefore behaves as a cidal drug in vivo although it is clearly static in the test tube.

 © 2003 Wiley-VCH Verlag GmbH & Co. KGaA, Weinheim

5. Summary

The development of resistance in the Gram-positive pathogenic bacteria to antibiotics over the last twenty years and continuing today has created a need for new antibiotic classes which are unaffected by existing bacterial resistance. The oxazolidinones were not only a new class with a novel mechanism of action, but importantly were unaffected by existing resistance in Gram-positive agents and were orally active. Our efforts regarding structure–activity relationships had clearly defined biological goals encompassing activity in vitro and in vivo, as well as pharmacokinetic parameters. Early chemistry efforts involved modifications of the indanone and tetranone subunits, with early successes driving the program forward. An enantiomeric-specific synthesis was vital to our continuation of this work and further efforts revolved around piperazinyl-, indolinyl-, and troponylphenyloxazolidinones. Both linezolid and eperezolid, our first clinical candidates, arose from the piperazine subclass with linezolid being chosen for continued development because of its enhanced pharmacokinetic properties. Linezolid subsequently performed exceptionally well in human clinical trials where it performed equivalently to the best comparitive marketed antibiotics. Linezolid was approved in the U.S. by the Food and Drug Administration (FDA) in April 2000.

Received: April 8, 2002 [A528]

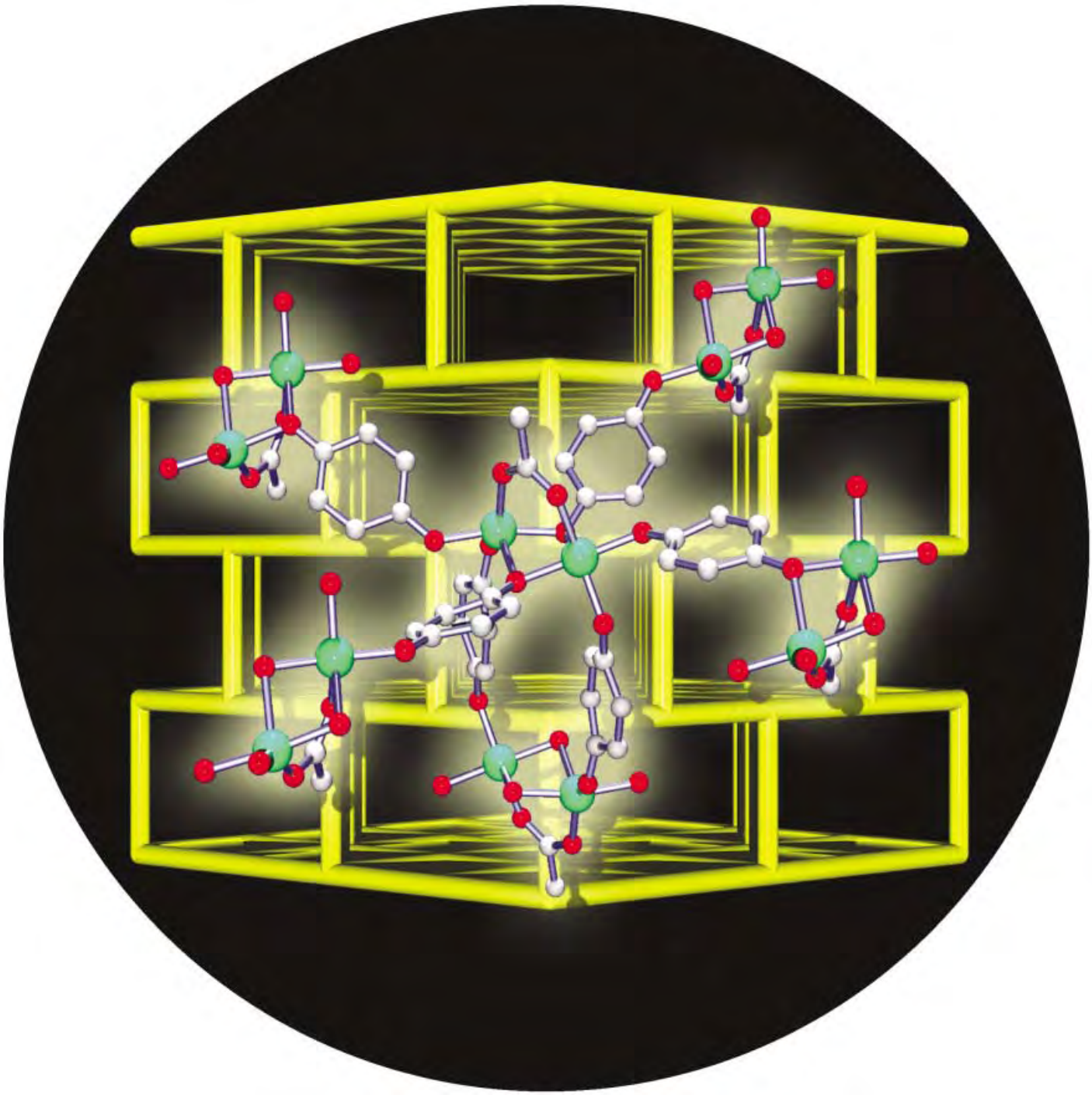
[1] B. E. Murray, *Antimicrob. Agents Chemother.* **1987**, *36*, 1791.
[2] P. C. Applebaum, *Eur. J. Clin. Microbiol.* **1987**, *6*, 367.
[3] R. F. Brieman, *JAMA J. Am. Med. Assoc.* **1994**, *271*, 1831.
[4] S. K. Spangler, M. R. Jacobs, P. C. Applebaum, *Antimicrob. Agents Chemother.* **1996**, *40*, 481.
[5] P. K. Ho, T.-L. Que, D. N.-C. Tsung, T.-K. Ng, K.-H. Chou, W.-H. Seto, *Antimicrob. Agents Chemother.* **1999**, *43*, 1310.
[6] C. Thornsberry, P. T. Ogilvie, H. P. Holley, Jr., D. F. Sahm, *Antimicrob. Agents Chemother.* **1999**, *43*, 2612.
[7] R. L. Thompson, R. P. Wenzel, *Ann. Intern. Med.* **1992**, *97*, 925.
[8] A. M. Slee, M. A. Wuonola, R. J. McRipley, I. Zajac, M. J. Zawada, P. T. Bartholomew, W. A. Gregory, M. Forbes, *Antimicrob. Agents Chemother.* **1987**, *31*, 1791.
[9] A. L. Barry, *Antimicrob. Agents Chemother.* **1988**, *32*, 150.
[10] H. C. Neu, A. Novelli, G. Saha, N.-X. Chin, *Antimicrob. Agents Chemother.* **1988**, *32*, 580.
[11] J. S. Daly, G. M. Eliopoulos, E. Reiszner, R. C. Moerllering, Jr., *J. Antimicrob. Chemother.* **1988**, *21*, 721.
[12] D. C. Eustice, P. A. Feldman, I. Zajac, A. M. Slee, *Antimicrob. Agents Chemother.* **1988**, *32*, 1218.
[13] A. M. Slee, M. A. Wuonola, R. J. McRipley, I. Zajac, M. J. Zawada, P. T. Bartholomew, W. A. Gregory, M. Forbes, *Abstr. Pap. 27th Interscience Conference on Antimicrobial Agents and Chemotherapy* (October 4–7, New York), **1987**, Abstract No. 244.
[14] R. B. Fugitt, R. W. Luckenbaugh (DuPont), US 4128654, **1978** [*Chem. Abstr.* **1978**, *90*, 147009].
[15] W. A. Gregory (DuPont), US 4461773, **1984** [*Chem. Abstr.* **1984**, *101*, 211126].
[16] W. A. Gregory, D. R. Brittelli, C.-L. Wang, M. A. Wuonola, R. J. McRipley, D. C. Eustice, V. S. Eberly, P. T. Bartholomew, A. M. Slee, M. Forbes, *J. Med. Chem.* **1989**, *32*, 1673; see also: B. Riedl, R. Endermann, *Expert Opin. Ther. Pat.* **1999**, *9*, 625; M. Genin, *Expert Opin. Ther. Pat.* **2000**, *10*, 1.
[17] C. H. Park, D. R. Brittelli, C.-L. Wang, F. D. Marsh, W. A. Gregory, M. A. Wuonola, R. J. McRipley, V. S. Eberly, A. M. Slee, M. Forbes, *J. Med. Chem.* **1992**, *35*, 1156.
[18] S. J. Brickner (Upjohn), US 5225565, **1993** [*Chem. Abstr.* **1990**, *113*, 172004].
[19] *Scrip* **1987**, *25*, 1250; *Pharmaprojects* **1993** (June); *Pharmaprojects* **1995** (April 12); *Pharmcast-International* **1995** (February), 7-I-484, 7-I-487; *Adis R&D Insight* **1996**, December 1; *Adis R&D Insight* **1997** (April 24).
[20] , R. C. Piper, T. F. Platte, J. R. Palmer (Pharmacia Corporation), unpublished results.
[21] S. J. Brickner (Upjohn), US 5164510, **1992** [*Chem. Abstr.* **1990**, *113*, 172004].
[22] D. M. Gleave, S. J. Brickner, P. R. Manninen, D. A. Allwine, K. D. Lovasz, D. C. Rohrer, J. A. Tucker, G. E. Zurenko, C. W. Ford, *Bioorg. Med. Chem. Lett.* **1998**, *8*, 1231.
[23] S. J. Brickner, P. R. Manninen, D. A. Ulanowicz, K. D. Lovasz, D. C. Rohrer, *Abstr. Pap. 206th National Meeting of the American Chemical Society* (August 1993, Chicago), **1993**, ORGN 089.
[24] M. Reuman, S. J. Daum, B. Singh, S. A. Coughlin, D. M. Sedlock, J. B. Rake, G. Y. Lesher, *Abstr. Pap. 29th Interscience Conference on Antimicrobial Agents and Chemotherapy* (September 17–20, 1989, Houston), **1989**, Abstract No. 1193.
[25] D. E. Nix, J. J. Schentag, *J. Clin. Pharmacol.* **1988**, *28*, 169; D. T. W. Chu, P. B. Fernandes, *Antimicrob. Agents Chemother.* **1989**, *33*, 131.
[26] D. K. Hutchinson, M. R. Barbachyn, S. J. Brickner, R. B. Gammill, M. V. Patel (Upjohn), US 5547950, **1996** [*Chem. Abstr.* **1996**, *125*, 221870].
[27] M. R. Barbachyn, D. S. Toops, D. A. Ulanowicz, K. C. Grega, S. J. Brickner, C. W. Ford, G. E. Zurenko, J. C. Hamel, R. D. Schaadt, D. Stapert, B. H. Yagi, J. M. Buysse, W. F. Demyan, J. O. Kilburn, S. E. Glickman, *Bioorg. Med. Chem. Lett.* **1996**, *6*, 1003; M. R. Barbachyn, D. S. Toops, K. C. Grega, S. K. Hendges, C. W. Ford, G. E. Zurenko, J. C. Hamel, R. D. Schaadt, D. Stapert, B. H. Yagi, J. M. Buysse, W. F. Demyan, J. O. Kilburn, S. E. Glickman, *Bioorg. Med. Chem. Lett.* **1996**, *6*, 1009.
[28] M. R. Barbachyn, S. J. Brickner, D. K. Hutchinson (Upjohn), US 5688792, **1997** [*Chem. Abstr.* **1995**, *123*, 256742]; S. J. Brickner, D. K. Hutchinson, M. R. Barbachyn, P. R. Manninen, D. A. Ulanowicz, S. A. Garmon, K. C. Grega, S. K. Hendges, D. S. Toops, C. W Ford, G. E. Zurenko, *J. Med. Chem.* **1996**, *39*, 673.
[29] M. R. Barbachyn, D. K. Hutchinson, S. J. Brickner, M. H. Cynamon, J. O. Kilburn, S. P. Klemens, S. E. Glickman, K. C. Grega, S. K. Hendges, D. S. Toops, C. W. Ford, G. E. Zurenko, *J. Med. Chem.* **1996**, *39*, 680.
[30] B. A. Pearlman, W. R. Perrault, M. R. Barbachyn, P. R. Manninen, D. S. Toops, D. J. Houser, T. J. Fleck (Upjohn), US 5837870, **1998** [*Chem. Abstr.* **1998**, *130*, 25061].
[31] G. E. Zurenko, B. H. Yagi, R. D. Schaadt, J. W. Allison, D. K. Hutchinson, M. R. Barbachyn, S. J. Brickner, *Antimicrob. Agents Chemother.* **1996**, *40*, 839.
[32] J. H. Jorgensen, M. L. McElmeel, C. W. Trippy, *Antimicrob. Agents Chemother.* **1997**, *41*, 465.
[33] G. W. Kaatz, S. M. Seo, *Antimicrob. Agents Chemother.* **1996**, *40*, 799.
[34] M. J. Rybak, D. M. Cappelletty, T. Moldovan, J. R. Aeschlimann, G. W. Kaatz, *Antimicrob. Agents Chemother.* **1998**, *42*, 721.
[35] L. Mulazimoglu, S. D. Drenning, V. L. Yu, *Antimicrob. Agents Chemother.* **1996**, *40*, 2428.
[36] C. Von Eiff, G. Peters, *J. Antimicrob. Chemother.* **1999**, *43*, 569.
[37] A. P. Johnson, M. Warner, D. M. Livermore, *J. Antimicrob. Chemother.* **2000**, *45*, 225.
[38] M. E. Jones, M. R. Visser, M. Klootwijk, P. Heisig, J. Verhoef, F. J. Schmitz, *Antimicrob. Agents Chemother.* **1999**, *43*, 421.
[39] G. H. Yagi, G. E. Zurenko, *Anaerobe* **1997**, *3*, 301.

 © 2003 Wiley-VCH Verlag GmbH & Co. KGaA, Weinheim

[40] J. M. Buysse, W. F. Demyan, D. S. Dunyak, D. Stapert, J. C. Hamel, C. W. Ford, *Abstr. Pap. 36th Interscience Conference on Antimicrobial Agents and Chemotherapy* (September 15–18, 1996, New Orleans), **1996**.
[41] C. W. Ford, J. C. Hamel, D. M. Wilson, J. K. Moerman, D. Stapert, R. J. Yancey, D. K. Hutchinson, M. R. Barbachyn, S. J. Brickner, *Antimicrob. Agents Chemother.* **1996**, *40*, 1508.
[42] N. J. Gentry-Nielsen, K. M. Olsen, L. C. Preheim, *Abstr. Pap. 40th Interscience Conference on Antimicrobial Agents and Chemotherapy* (September 17–20, 2000, Toronto), **2000**.
[43] S. I. Pelton, D. E. Piper, M. S. Rouse, J. M. Steckelberg, *Antimicrob. Agents Chemother.* **2000**, *44*, 3438.
[44] T. Schulin, T. C. Eliopoulos, R. C. Moellering, G. M. Eliopoulos, *Antimicrob. Agents Chemother.* **1999**, *43*, 2873.
[45] M. P. Oramas-Shirey, L. V. Buchanan, C. L. Dileto-Fang, C. F. Dailey, C. W. Ford, D. W. Batts, J. K. Gibson, *J. Antimicrob. Chemother.* **2001**, *47*, 349.
[46] C. F. Dailey, C. L. Dileto-Fang, L. V. Buchanan, M. P. Oramas-Shirey, D. H. Batts, C. W. Ford, J. K. Gibson, *Antimicrob. Agents Chemother.* **2001**, *45*, 2304.
[47] M. R. Turner, A. Forrest, J. M. Hyatt, C. H. Ballow, D. J. Stalker, I. R. Welshman, J. J. Schentag, *Abstr. Pap. 38th Interscience Conference on Antimicrobial Agents and Chemotherapy* (September 24–27, 1998, San Diego), **1998**.
[48] I. R. Welshman, D. J. Stalker, C. P. Wajszczuk, *Antiinfective Drugs Chemotherapy* **1998**, 16 (Abstracts, suppl. 1).
[49] L. C. Wienkers, M. A. Wynalda, K. L. Feenstra, P. Gao, J. G. Slatter, *Abstr. Pap. 39th Interscience Conference on Antimicrobial Agents and Chemotherapy* (September 26–29, 1999, San Francisco), **1999**.
[50] K. L. Feenstra, J. G. Slatter, D. J. Stalker, K. S. Cathcart, M. T. Verburg, M. G. Johnson, B. E. Bothwell, M. D. Koets, G. M. Newcomb, G. W. Peng, R. P. Stryd, P. E. Fagerness, *Abstr. Pap. 35th Interscience Conference on Antimicrobial Agents and Chemotherapy* (September, 1995, San Francisco), **1995**.
[51] D. Andes, M. L. Van Ogtrop, W. A. Craig, *Abstr. Pap. 38th Interscience Conference on Antimicrobial Agents and Chemotherapy* (September 24–27, 1998, San Diego), **1998**.
[52] A. H. Lin, R. W. Murray, T. J. Vidmar, K. R. Marotti, *Antimicrob. Agents Chemother.* **1997**, *41*, 2127.
[53] D. L. Shinabarger, K. R. Marotti, R. W. Murray, A. H. Lin, E. P. Melchior, S. M. Swaney, D. S. Dunyak, W. F. Demyan, J. M. Buysse, *Antimicrob. Agents Chemother.* **1997**, *41*, 2132.
[54] S. M. Swaney, H. Aoki, M. C. Ganoza, D. L. Shinabarger, *Antimicrob. Agents Chemother.* **1998**, *42*, 3251.
[55] K. Chiba, K. L. Feenstra, J. G. Slatter, P. T. Daley-Yates, J. N. Duncan, P. E. Fagerness, M. R. Howard, I. J. Martin, N. Ozawa, B. J. Passingham, H. G. Parks, G. W. Peng, R. J. Simmonds, W. Speed, D. Yallop, S. Yamazaki, *Abstr. Pap. 38th Interscience Conference on Antimicrobial Agents and Chemotherapy* (September 24–27, 1998, San Diego), **1998**.
[56] C. G. Gemmell, C. W. Ford, *Abstr. Pap. 39th Interscience Conference on Antimicrobial Agents and Chemotherapy* (September 26–29, 1999, San Francisco), **1999**.

 © 2003 Wiley-VCH Verlag GmbH & Co. KGaA, Weinheim

Communications



A coordination network with an unprecedented 3D brick architecture (yellow) results when dicopper(II) acetate units link with square pyramidal connectivity to the organometalloligand [(η^4-benzoquinone)Mn(CO)$_3$]$^-$. For more information about this metal–organometallic coordination network (MOMN), see the communication by Oh, Carpenter, and Sweigart on the following pages.

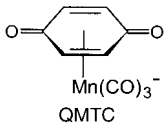
DOI: 10.1002/anie.200250637
© 2003 Wiley-VCH Verlag GmbH & Co. KGaA, Weinheim

A Metal-Organometallic 3D Network

A Novel 3D Brick-Wall Coordination Network Based on Nodes with Square-Pyramidal Connectivity**

Moonhyun Oh, Gene B. Carpenter, and Dwight A. Sweigart**

The study of self-assembled finite and infinite metal–organic coordination networks (MONs) is a very active interdisciplinary research area with potential applications in magnetics, optics, electronics, catalysis, and general guest–host interactions.[1] The ability to control or predict the network architectures that obtain from the self-assembly process is a central but elusive goal in this area of supramolecular chemistry. Typically, MONs consist of metal or metal–cluster nodes that are connected by simple organic-spacer molecules that serve as multifunctional ligands. We recently reported the extension of this concept to metal–organometallic networks (MOMNs), in which the spacer is an organometallic complex that functions as a bifunctional ligand ("organometalloligand").[2,3] Specifically, it was shown that the π-complex [(η⁴-benzoquinone)-$Mn(CO)_3$]⁻ (QMTC) coordinates to metal ion nodes through the quinonoid oxygen atoms to afford neutral polymeric MOMNs of variable geometry and dimensionality. The resulting materials constitute rare examples of polymers containing both backbone metal sites and pendant metal sites. An impressive range of architectures could be constructed in this manner and, furthermore, it was demonstrated that many of the available architectures could be rationally designed based upon the coordination number, oxidation state, and concentration of the metal ion nodes and based upon the solvent used.[2]



QMTC

A variety of 1D (linear), 2D (planar), and 3D (diamondoid) quinonoid networks have been synthesized by the self-assembly of QMTC spacers and divalent transition-metal ion nodes. Herein, we report the use of these components to generate a simple and highly symmetrical architecture which to our knowledge is unprecedented in the study of coordination polymers—a 3D brick wall. Specifically, QMTC and copper(II) acetate were found to react in methanol to afford a 3D brick wall MOMN with the formula $[Cu_2(\mu\text{-}CH_3CO_2)[(\eta^4\text{-benzoquinone})Mn(CO)_3]_3\cdot MeOH]_\infty$ (**1**). Figure 1a provides a schematic representation of the 3D brick wall motif viewed edge-on.

To understand the principles behind the construction of a 3D brick wall structure, it is convenient to visualize how the 2D brick wall shown in Figure 1b can be generated from common "T" shaped building blocks. The 2D brick wall[4] is one of several observed motifs derived from T-shaped nodes; the others include ladder, herringbone, bilayer, and 3D frame

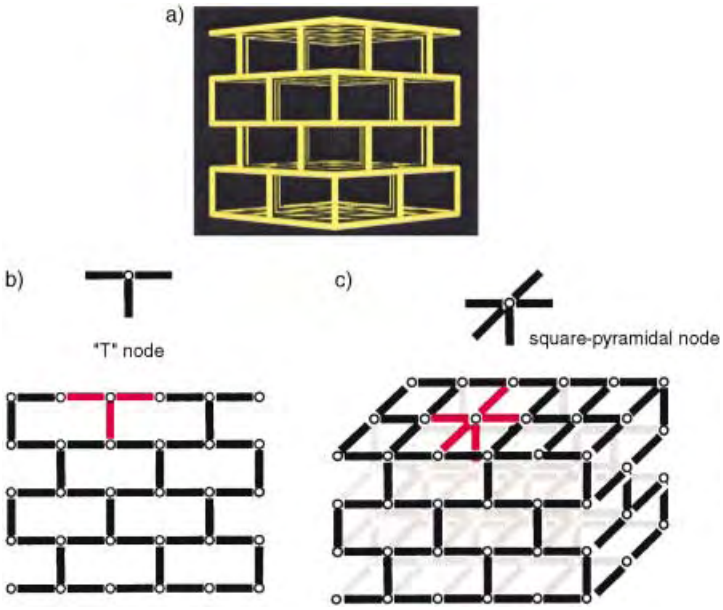


Figure 1. a) A schematic representation of a 3D brick-wall structure viewed edge-on and b,c) how it may be generated from a 2D brick wall by changing the T-shaped nodes to ones with square-pyramidal connectivity.

structures.[1d,5] In principle, a 3D brick wall structure, as illustrated in Figure 1c, can be generated from the 2D brick wall by converting the T-shaped nodes to square pyramidal nodes having fivefold connectivity. As documented in more detail below, it was found that such square-pyramidal nodes are formed when QMTC and copper(II) acetate self-assemble in methanol. The resultant 3D MOMN, $[Cu_2(\mu\text{-}CH_3CO_2)[(\eta^4\text{-benzoquinone})Mn(CO)_3]_3\cdot MeOH]_\infty$ (**1**), consists of bimetallic nodes of formula $[Cu_2(\mu\text{-}CH_3CO_2)^{3+}]$ that are linked through linear QMTC spacers in a square-pyramidal geometry. Figure 2 illustrates the fivefold connectivity and square-pyramidal geometry present at each nodal site in **1**. As a consequence of this spatial arrangement, the resultant MOMN has the novel extended 3D brick wall structure shown in Figure 1a,c.

Green single crystals of MOMN **1** were obtained by the reaction of neutral complex $[(\eta^5\text{-semiquinone})Mn(CO)_3]$ and $Cu(OAc)_2$ at 75 °C in methanol. Figure 3 shows part of the unit cell of **1**. Two uncoordinated molecules of methanol are present in each unit cell as shown. A novel feature of the structure is the arrangement of the copper atoms in the bimetallic units, which are interconnected by QMTC spacers.

[*] M. Oh, Prof. Dr. D. A. Sweigart, Prof. Dr. G. B. Carpenter
Department of Chemistry
Brown University
Providence, RI 02912 (USA)
Fax: (+1) 401-863-9368
E-mail: moonhyun_Oh@brown.edu
dwight_sweigart@brown.edu

[**] Acknowledgment is made to the donors of the Petroleum Research Fund, administered by the American Chemical Society, for support of this research.

 © 2003 Wiley-VCH Verlag GmbH & Co. KGaA, Weinheim DOI: 10.1002/anie.200250637

In the context of the 3D structure, the dicopper clusters constitute so-called secondary building units (SBUs).[6] The copper atoms in each SBU are bridged by an acetate anion to give $[Cu_2(\mu\text{-}CH_3CO_2)^{3+}]$ fragments that are positioned as shown in Figure 2. The Cu–Cu distance is 3.14 Å, indicative of little direct metal–metal interaction. Each copper atom is five-coordinate, with one acetate oxygen and four quinone oxygen atoms serving as ligands. There are two types of QMTC spacers present in MOMN **1** (Figure 4). Type 1 QMTC connects to three copper atoms such that one quinone oxygen is monodentate and the other is bidentate. Type 2 QMTC connects to two copper atoms, that is, each quinone oxygen is monodentate. The copper atoms in each SBU are bridged by two oxygen atoms from two type 1 QMTC spacers. The remaining four copper-quinone links are completed in a monodentate fashion, two from type 1 and two from type 2 spacers.

The dicopper SBUs in **1** feature fivefold connectivity to adjacent SBUs (Figure 2)and link to the QMTC spacers with a square pyramidal geometry. Four type 1 QMTCs form the base of the pyramid and, along with the SBU, generate the pseudo 2D grid network shown in Figure 5a. The axial direction of the square pyramid is defined by two type 2 QMTCs, which link pairs of SBUs in adjacent planes to generate the 3D brick wall motif shown in Figure 5b (cf. Figure 1a).

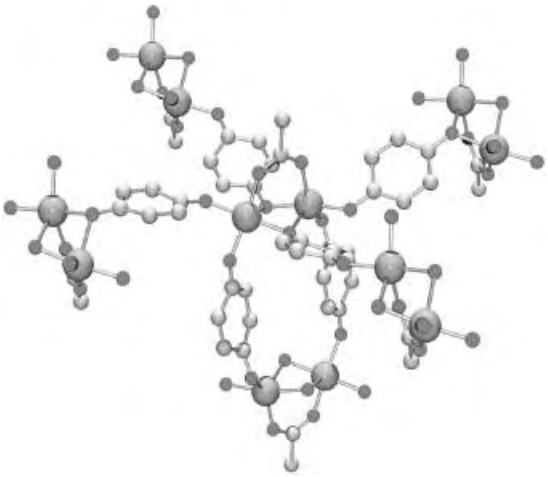


Figure 2. Illustration of a dicopper SBU in MOMN **1,** showing the square-pyramidal connectivity to other dicopper nodes through QMTC spacers. All hydrogen atoms and $Mn(CO)_3$ groups are omitted for clarity.

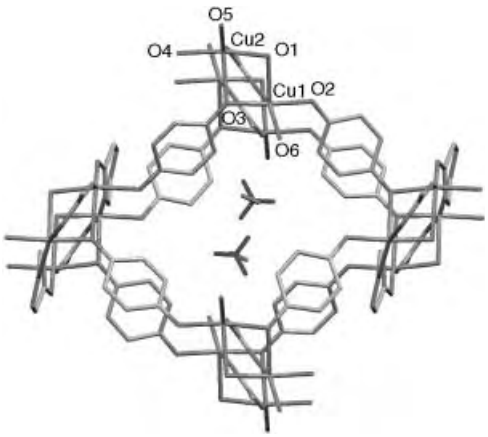


Figure 3. The unit cell contents of MOMN coordination polymer **1**, viewed down the *c* axis. Hydrogen atoms and $Mn(CO)_3$ groups are omitted to facilitate viewing the principle features of the 3D network. Two uncoordinated methanol molecules are present in each unit cell.

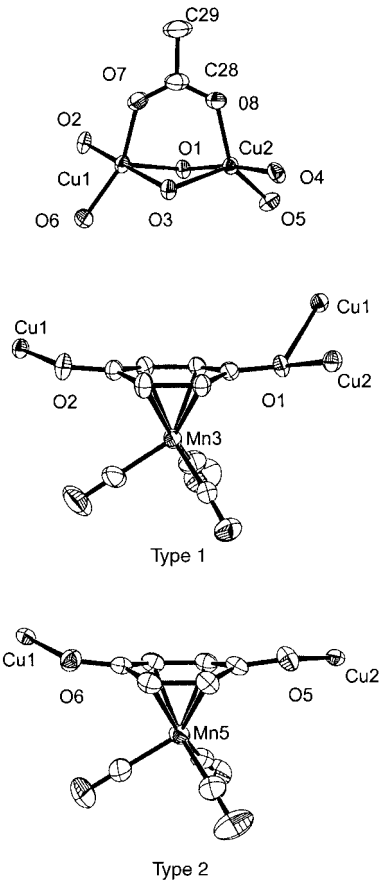


Figure 4. A view of the coordination environment within the dicopper units in **1** and views of the two types of QMTC spacers that connect the dicopper units. Note that type 1 QMTC connects three Cu atoms while type 2 QMTC connects to two Cu atoms. Only one of the two type 1 QMTC spacers present in the asymmetric unit is shown.

In conclusion, this work describes the formation of a novel metal–organometallic network which contains a dicopper cluster as secondary building units and η^4-π-bonded benzoquinone complexes as organometallic spacers. The resulting polymer contains square pyramidal nodes that result in what is the first example of a 3D extended brick-wall network.

 © 2003 Wiley-VCH Verlag GmbH & Co. KGaA, Weinheim

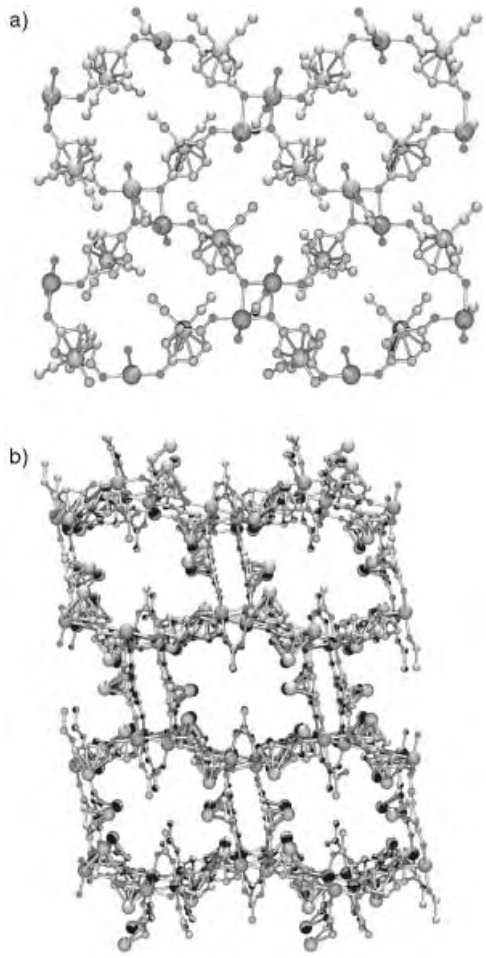


Figure 5. a) A "top" view of the coordination network in **1** showing the base of the square pyramidal SBUs and b) an edge-on view that correlates with the schematic in Figure 1a. The CO ligands in b) are omitted for clarity.

Experimental Section

The neutral complex $[(\eta^5\text{-semiquinone})Mn(CO)_3]$ (15 mg, 0.060 mmol) and $Cu(OAc)_2{\cdot}H_2O$ (6 mg, 0.03 mmol) were heated in CH_3OH (0.6 mL) at 75 °C in the dark. After one day, crystals of polymer **1** suitable for X-ray studies were obtained in 82 % yield. IR (KBr) $\tilde{\nu}_{CO} = 2066$ (m), 2038 (s), 2022 (m), 1995 (m), 1978 (s), 1967 (s), 1947 (s), 1930 (m), 1558 (m), 1499 cm^{-1} (s). Elemental analysis calcd (%) for **1**·MeOH, $C_{30}H_{18}Cu_2Mn_3O_{18}$: C 37.60, H 1.89; found: C 37.32, H 1.82. Crystal data for **1**·MeOH: formula $C_{30}H_{19}Cu_2Mn_3O_{18}$, $M_r = 959.35$, monoclinic, space group $P2_1/n$, $a = 14.8202(7)$, $b = 11.8105(6)$, $c = 19.3163(10)$ Å, $\beta = 94.6590(10)°$, $V = 3369.8(3)$ Å^3, $Z = 4$, $\rho_{calcd} = 1.891$ g cm^{-3}, $\mu = 2.417$ mm^{-1}, $F(000) = 1904$, θ range 2.02–26.38°, 470 variables refined with 6879 independent reflections to final R indices $[I > 2\sigma(I)]$ of $R_1 = 0.0322$ and $wR_2 = 0.0887$, and $GOF = 1.053$. X-ray data collection with $Mo_{K\alpha}$ radiation was carried out at 298 K using a Bruker Apex diffractometer equipped with a CCD area detector. Structures were determined by direct methods and refined on F squared. CCDC-195906 (**1**) contains the supplementary crystallographic data for this paper. These data can be obtained free of charge via www.ccdc.cam.ac.uk/conts/retrieving.html (or from the Cambridge Crystallographic Data Centre, 12 Union Road, Cambridge CB2 1EZ, UK; fax: (+44) 1223-336-033; or deposit@ccdc.cam.ac.uk).

Received: November 26, 2002
Revised: March 10, 2003 [Z50637]

Keywords: coordination polymers · polymers · quinones · self-assembly · supramolecular

[1] a) J. W. Steed, J. L. Atwood, *Supramolecular Chemistry*, Wiley, Chichester, **2000**; b) R. Robson, *J. Chem. Soc. Dalton Trans.* **2000**, 3735; c) S. R. Batten, R. Robson, *Angew. Chem.* **1998**, *110*, 1558; *Angew. Chem. Int. Ed.* **1998**, *37*, 1460; d) B. Moulton, M. J. Zaworotko, *Chem. Rev.* **2001**, *101*, 1629; e) D. Philp, J. F. Stoddart, *Angew. Chem.* **1996**, *108*, 1242; *Angew. Chem. Int. Ed. Engl.* **1996**, *35*, 1154; f) S. Leininger, B. Olenyuk, P. J. Stang, *Chem. Rev.* **2000**, *100*, 853; g) B. J. Holliday, C. A. Mirkin, *Angew. Chem.* **2001**, *113*, 2035; *Angew. Chem. Int. Ed.* **2001**, *40*, 2022; h) M. Fujita, *Chem. Soc. Rev.* **1998**, *27*, 417; i) O. R. Evans, W. Lin, *Acc. Chem. Res.* **2002**, *35*, 511; j) "Molecular Self-Assembly. Organic Versus Inorganic Approaches": *Struct. Bonding (Berlin)* **2000**, *96*.

[2] a) M. Oh, G. B. Carpenter, D. A. Sweigart, *Angew. Chem.* **2001**, *113,* 3291; *Angew. Chem. Int. Ed.* **2001**, *40*, 3191; b) M. Oh, G. B. Carpenter, D. A. Sweigart, *Organometallics* **2002**, *21*, 1290; c) M. Oh, G. B. Carpenter, D. A. Sweigart, *Chem. Commun.* **2002**, 2168; d) M. Oh, G. B. Carpenter, D. A. Sweigart, *Angew. Chem.* **2002**, *114,* 3802; *Angew. Chem. Int. Ed.* **2002**, *41*, 3650.

[3] Metal–organometallic coordination polymers containing formal $[Cu_2(\mu\text{-}CN)_2(CN)_2]^{2-}$ and $[SnMe_3]^+$ units have been reported: A. M. A. Ibrahim, E. Siebel, R. D. Fischer, *Inorg. Chem.* **1998**, *37*, 3521.

[4] a) M. Fujita, Y. J. Kwon, O. Sasaki, K. Yamaguchi, K. Ogura, *J. Am. Chem. Soc.* **1995**, *117*, 7287; b) H. J. Choi, M. P. Suh, *J. Am. Chem. Soc.* **1998**, *120*, 10622; c) L. Carlucci, G. Ciani, D. M. Proserpio, *New J. Chem.* **1998**, *22*, 1319; d) L. Carlucci, G. Ciani, D. M. Proserpio, *J. Chem. Soc. Dalton Trans.* **1999**, 1799; e) Y.-B. Dong, M. D. Smith, R. C. Layland, H.-C. zur Loye, *J. Chem. Soc. Dalton Trans.* **2000**, 775; f) M. Kondo, M. Shimamura, S. Noro, S. Minakoshi, A. Asami, K. Seki, S. Kitagawa, *Chem. Mater.* **2000**, *12*, 1288; g) Y.-B. Dong, R. C. Layland, N. G. Pschirer, M. D. Smith, U. H. F. Bunz, H.-C. zur Loye, *Chem. Mater.* **1999**, *11*, 1413.

[5] a) M. J. Zaworotko, *Chem. Commun.* **2001**, 1; b) H. Gudbjartson, K. Biradha, K. M. Poirier, M. J. Zaworotko, *J. Am. Chem. Soc.* **1999**, *121*, 2599.

[6] a) J. Kim, B. Chen, T. M. Reineke, H. Li, M. Eddaoudi, D. B. Moler, M. O'Keeffe, O. M. Yaghi, *J. Am. Chem. Soc.* **2001**, *123*, 8239; b) Y. Cui, O. R. Evans, H. L. Ngo, P. S. White, W. Lin, *Angew. Chem.* **2002**, *114*, 1207; *Angew. Chem. Int. Ed.* **2002**, *41*, 1159; c) S. A. Bourne, J. Lu, A. Mondal, B. Moulton, M. J. Zaworotko, *Angew. Chem.* **2001**, *113*, 2169; *Angew. Chem. Int. Ed.* **2001**, *40*, 2111; d) D. T. Vodak, M. E. Braun, J. Kim, M. Eddaoudi, O. M. Yaghi, *Chem. Commun.* **2001**, 2535; e) M. Eddaoudi, D. B. Moler, H. Li, B. Chen, T. M. Reineke, M. O'Keeffe, O. M. Yaghi, *Acc. Chem. Res.* **2001**, *34*, 319.

 © 2003 Wiley-VCH Verlag GmbH & Co. KGaA, Weinheim

Powder X-Ray Diffraction

Solving Larger Molecular Crystal Structures from Powder Diffraction Data by Exploiting Anisotropic Thermal Expansion**

Michela Brunelli, Jonathan P. Wright, Gavin B. M. Vaughan, Asiloe J. Mora, and Andrew N. Fitch*

Powder diffraction is an important crystallographic tool when no single crystal of the substance of interest is available, or when the intrinsic nature of the material is polycrystalline. Crystal structures of ever increasing complexity are being solved and refined from good quality powder data because of recent improvements in data-analysis methods. However, the obscuring caused by the overlap of neighboring Bragg peaks reduces the information content of the diffraction data and consequently remains a barrier to the general application of this technique to complex systems. Herein, we report how a significant improvement in data quality can be obtained, and illustrate this with the routine direct-methods solution of a 48-atom fully organic structure. This improvement was achieved by exploiting anisotropic thermal expansion by using high-resolution synchrotron X-ray powder diffraction.

To solve unknown crystal structures where there is no prior structural model, two modern methods[1] are generally employed, these are the direct-methods solution of the crystallographic phase problem and the global optimization of known structural fragments within the unit cell. The number of degrees of freedom to be explored essentially limits the complexity of the structures that can be solved by the global optimization approach. Without a suitable fragment, direct methods must be employed, which require atomic-resolution data. The measured diffraction intensities represent the square moduli of the structure factors, $|F|^2$, which define the atomic structural information, so that the pattern decomposition to yield the intensity estimates is a crucial step in the structure-solution process. The adaptation of single-crystal methods to deal with powder diffraction data has been extensively discussed.[2]

[*] Dr. M. Brunelli, Dr. J. P. Wright, Dr. G. B. M. Vaughan, Prof. A. N. Fitch
European Synchrotron Radiation Facility
BP 220, 38043 Grenoble Cedex (France)
Fax: (+33) 4-76-88-29-07
E-mail: brunelli@esrf.fr
Prof. A. J. Mora
Departamento de Química
Facultad de Ciencias
Universidad de Los Andes, Mérida (Venezuela)
Additional address: Prof. A. N. Fitch
Department of Chemistry, Keele University
Staffordshire, ST5 5BG (UK)

[**] We thank the ESRF for providing synchrotron radiation beam time awarded for experiment number CH-1243 on the ID31 beam line.

Supporting information for this article is available on the WWW under http://www.angewandte.org or from the author.

There are, however, intrinsic difficulties associated with intensity extraction, which arise from the overlap of the Bragg reflections in the powder diffraction pattern. Overlap reduces the accuracy of the extracted intensities, and when overlap blurs into a continuum towards the smaller interplanar lattice spacings, it may become essentially impossible to have any clear indication of the individual peak intensities. If the accuracy of the integrated intensities is poor the phasing process by direct methods is not reliable and therefore fails more often when used with powder data than with single-crystal data. The number of atoms that can be located by this approach using powder data is usually limited to around 30 for equal-atom structures, such as organic molecules. A great deal of effort has been spent in developing new strategies for obtaining better estimates of the relative intensities of overlapping reflections,[3] or employing more sophisticated tools, for example, maximum entropy[4] or Bayesian statistics,[5] and correcting for other systematic problems, for example, trying to evaluate the contribution of preferred orientation.[6]

Novel approaches to data collection have also been devised.[7] Wessels and co-workers[7a] collected diffraction data from deliberately textured samples in which preferred orientation was particularly pronounced. Another way to reduce effective peak overlap is to exploit the anisotropy in thermal expansion that many low-symmetry materials naturally exhibit. At different temperatures the relative positions of Bragg reflections change, owing to the anisotropic changes in the lattice dimensions, but maintain approximately the same intensities. By collecting data at multiple temperatures it is possible to assess the individual contribution of reflections that are overlapping at one temperature, but are better resolved at another. In a pioneering paper Zachariasen and Ellinger[8] show the changes in the diffraction pattern of plutonium metal, even with fairly modest resolution. Shankland and co-workers[9] have emphasized the utility of this approach in their work on the solution of the crystal structure of the pharmaceutical organic molecule chlorathiazide.

Changes in the overlap of the reflections as the temperature is varied are best revealed with an intrinsically high-resolution instrument, so that the effects of small peak shifts are more readily discernable. Furthermore, high X-ray intensity is required, this leads to good counting statistics, so that subtle changes in the patterns are not fogged by statistical noise, and overall counting times are reasonable. The high-resolution powder diffraction beam line[10] at the European Synchrotron Radiation Facility (ESRF) has recently been upgraded, by being moved from a bending-magnet to an undulator source, where it receives a significantly more intense incident X-ray beam. The performance is now such that the systematic use of anisotropic thermal expansion to study more-complex crystal structures by powder diffraction can be envisaged.

During our continuing studies on the low-temperature structures of small globular organic molecules, we had been unable to solve the structure of 9-ethylbicyclo[3.3.1]nona-9-ol ($C_{11}H_{20}O$) despite having determined the unit cell and the space group.[11] Having 48 non-hydrogen atoms in the asymmetric unit (four independent molecules), this substance was

 DOI: 10.1002/anie.200250607 © 2003 Wiley-VCH Verlag GmbH & Co. KGaA, Weinheim

selected as a promising candidate for the anisotropic thermal expansion approach. Previous successful applications of direct methods to relatively large organic structures include fluorescein diacetate with 31 carbon and oxygen atoms,[14] and sulfathiazole, 32 atoms, which has the benefit of containing the heavier sulfur atoms.[15] Thus, solving a structure containing 48 atoms would be a notable advance in the technique.

Five powder diffraction patterns at different temperatures (80, 120, 140, 160, and 180 K) were collected on the new ID31 beam line at the ESRF in a total time of about 12 h by using an incident X-ray wavelength of 0.80175(4) Å. Figure 1 illustrates the changes in the diffraction pattern arising from peak shift as a consequence of the anisotropic thermal expansion manifested between 80 and 180 K. Integrated intensities were extracted by a multipattern Pawley-style refinement procedure.[16] This method is similar to a Rietveld refinement in that a diffraction profile is calculated as a sum of overlapping reflections. However, in the Pawley case, the intensities are not defined by a structural model, but are variables in a least-squares procedure. For the patterns collected at different temperatures, a single set of peak intensities was fitted to the multiple data sets. During the data collection a first attempt to solve the structure was made with just two data sets (collected at 80 and 120 K). The extracted intensities were input to the single-crystal direct methods program SHELXS,[17] but did not lead to an interpretable structure. After adding the data collected at 140, 160, and 180 K to the refinement, a much improved set of diffracted intensities was produced,[18] using the same simultaneous-fitting approach and extracting peaks up to a maximum angle of $2\theta = 50°$ ($d_{min} = 0.95$ Å). There was severe peak overlap at high angles, where approximately 250 peaks are present per degree of the pattern. With a refined peak width of approximately 0.015 degrees this corresponds to an average of four contributions for each resolvable peak in a single pattern.

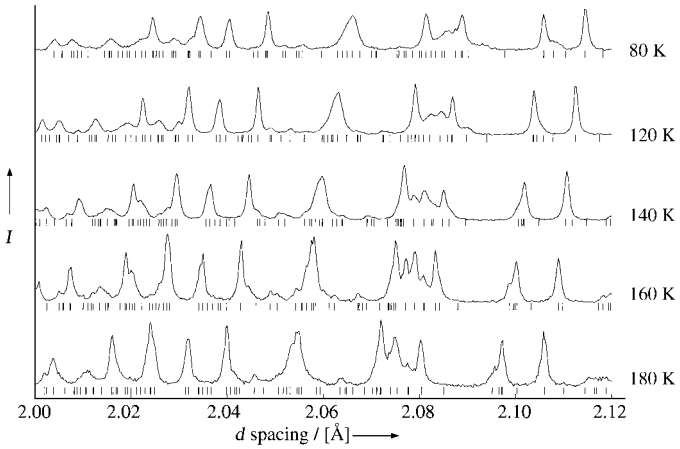


Figure 1. An example of selected regions of the diffraction patterns showing anisotropic thermal expansion: the five diffraction patterns are fitted simultaneously with a Pawley-style refinement with a single set of intensities. Vertical bars indicate Bragg peak positions.

Three whole molecules could be identified in the SHELXS solution and the fourth molecule was completed by Fourier recycling against the same set of extracted intensities, without returning to the powder diffraction pattern to improve the partitioning of overlapping peaks in the light of the partial model. The marked improvement upon adding the further data sets (140–180 K) can be explained by the anisotropy of the thermal expansion, as shown in Figure 2. The basis of this method is that the thermal expansion of the cell parameters must be different to change the relative positions of the peaks: up to 140 K peaks belonging to the *hk0* zone will show no relative change as the *a* and *b* axis expand at similar rate, whereas all the five data sets together will display anisotropic relative shifts of all the *hkl* peaks.

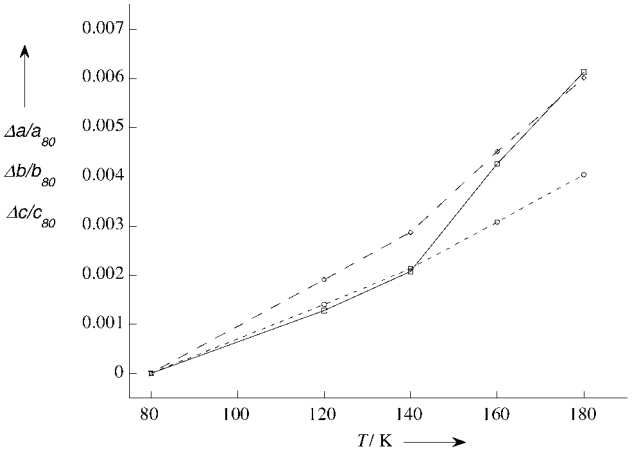


Figure 2. The measured relative variation of the cell parameters *a* (-----○), *b* (——□), and *c* (–––◇) of 9-ethylbicyclo[3.3.1]nona-9-ol as a function of temperature, which shows the anisotropy in the thermal expansion of the unit cell. The error bars are smaller than the symbols.

The structure obtained is chemically reasonable in terms of interatomic and intermolecular distances. The arrangement of the four independent molecules is illustrated in Figure 3. They form a tetramer linked by an approximately square arrangement of O–H···O hydrogen bonds between hydroxide groups. Three of the hydroxide oxygen atoms lie in a plane essentially perpendicular to the crystallographic *c* direction, with the fourth oxygen, O(76) lying 1.3 Å out of this plane. The oxygen atoms are completely at the heart of the cluster, the outer surface of which is composed of hydrogen atoms. Interactions between adjacent clusters are therefore entirely of a van der Waals nature. The presence of the O–H···O hydrogen bonds explains why this molecule does not exhibit the disordered structures found for other related molecules,[19] for example, S-camphor or bicyclo[3.3.1]nonan-9-one which have weaker C–H···O networks.

An essentially complete structure could be derived from the extracted integrated intensities, without any need for recycling of partial structural models to improve the estimates of intensity partitioning under overlapped peaks. The addition of further diffraction profiles increases both the counting statistics for the weak peaks at high angles, as well as the

 © 2003 Wiley-VCH Verlag GmbH & Co. KGaA, Weinheim

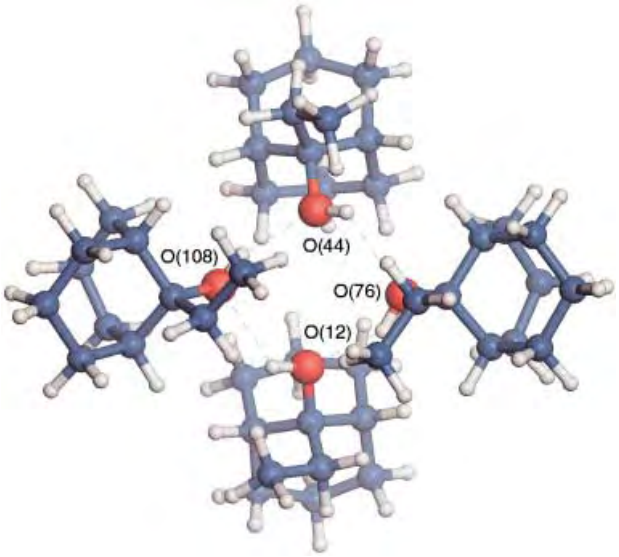


Figure 3. View of the arrangement of the four 9-ethylbicyclo[3.3.1]nona-9-ol molecules to form a hydrogen-bonded tetramer. The O—H···O hydrogen bonds are shown with dashed lines: O(12)-O(108) 2.825(4), O(44)-O(76) 2.761(4), O(76)-O(12) 2.804(4), O(108)-O(44) 2.869(4) Å. The crystallographic *c* direction is perpendicular to the plane of the Figure. O red, C blue, H gray.

estimates of individual intensities where peaks overlap, both of which are crucial to the success of direct methods. The solution of this structure illustrates a considerable advance in the quality of data: data collection was completed in about 12 h during the first day of scheduled-user experiments on the newly commissioned beam line, with the structural model being derived the very next day. The speed and simplicity of both the data collection and analysis strongly suggest that even larger structures will also be tractable with powder X-ray diffraction data.

Experimental Section

A specimen of 9-ethylbicyclo[3.3.1]nona-9-ol ($C_{11}H_{20}O$, Aldrich 99%) was contained in a 1.5-mm diameter borosilicate glass capillary. The capillary was mounted on the diffractometer on the new ID31 beam line and spun at approximately 2 Hz to improve the powder average. The sample was cooled by a stream of cold nitrogen gas from a Cryostream cooler, oriented coaxially with the capillary. Powder diffraction patterns at five temperatures (80, 120, 140, 160, 180 K) were collected with an incident X-ray wavelength of 0.80175(4) Å.

The model obtained by direct methods (SHELXS combined with Fourier recycling) was refined against the diffraction profile collected at 140 K together with stereochemical restraints using the Rietveld software package GSAS.[20] Hydrogen atoms were added to the model in their expected positions. 144 atomic coordinates plus coordinates of the 80 hydrogen atoms, profile and background parameters were refined in each cycle. The bond length and angle restraints were set to values obtained from an ab initio molecular-orbital optimization of the molecular structure performed using the program Gaussian 94[21] with a 6-31+G(d) basis set. They were weighted, respectively, 0.001 Å and 0.1°. It was quickly realized that one ethyl group is disordered. The final refinement converged satisfactorily to $R_{wp}=5.3\%$, $R_{F^2}=7.5\%$, and $\chi^2=16.5$, with the highest peak and lowest hole in the final difference Fourier map being 0.2 and −0.2 electrons. The high χ^2 value reflects the extremely high counting statistics of the data which produced a $R_E=1.3\%$. Final cell parameters at 140 K are: $a=21.10871(4)$, $b=23.14144(5)$, $c=16.46364(3)$ Å, $V=8042.26(3)$ Å^3, $Z=32$. Lists of refined atomic coordinates and of bond lengths and angles of the 9-ethylbicyclo[3.3.1]nona-9-ol crystal structure are available as Supplementary Information in Tables S3 and S4. The observed, calculated, and difference profiles of the final fit at 140 K are shown in Figure 4. Further refinement of the crystal

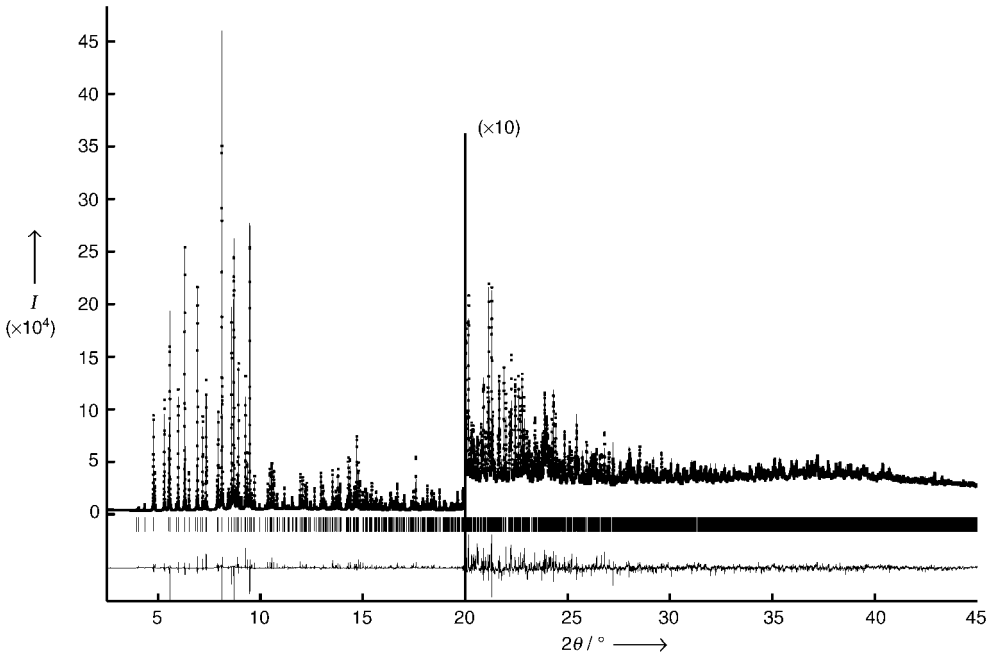


Figure 4. Observed (·), calculated (——), and difference plot of the final Rietveld refinement of 9-ethylbicyclo[3.3.1]nona-9-ol recorded at 140 K; reflection positions are shown as vertical lines.

 © 2003 Wiley-VCH Verlag GmbH & Co. KGaA, Weinheim

structure at all five temperatures would allow the thermal evolution of the structure to be followed in detail.

Received: November 22, 2002 [Z50607]

Keywords: hydrogen bonds · powder diffraction · structure elucidation · synchrotron radiation · X-ray diffraction

[1] a) *Structure Determination from Powder diffraction Data* (Eds.: W. I. F. David, K. Shankland, L. B. McCusker, C. Baerlocher), Oxford University Press, Oxford, **2002**; b) K. D. M. Harris, M. Tremayne, B. M. Kariuki, *Angew. Chem.* **2001**, *113*, 1674 – 1700; *Angew. Chem. Int. Ed.* **2001**, *40*, 1626 – 1651.

[2] a) G. Bricogne, C. J. Gilmore, *Acta Crystallogr. Sect. A* **1990**, *46*, 284 – 297; b) C. Giacovazzo, *Acta Crystallogr. Sect. A* **1996**, *52*, 331; c) A. Altomare, M. C. Burla, M. Camalli, B. Carrozzini, G. Cascarano, C. Giacovazzo, A. Guagliardi, A. G. G. Moliterni, G. Polidori, R. Rizzi, *J. Appl. Crystallogr.* **1999**, *32*, 339 – 340; d) J. Jansen, R. Peschar, H. Schenk, *Z. Kristallogr.* **1993**, *206*, 33; e) H. Gies, J. Rius, *Z. Kristallogr.* **1995**, *210*, 475.

[3] a) A. Altomare, J. Foadi, C. Giacovazzo, A. G. G. Moliterni, M. C. Burla, G. Polidori, *J. Appl. Crystallogr.* **1998**, *31*, 74 – 77; b) M. A. Estermann, V. Gramlich, *J. Appl. Crystallogr.* **1993**, *26*, 396 – 404; c) J. Jansen, R. Peschar, H. Schenk, *J. Appl. Crystallogr.* **1992**, *25*, 237; d) W. Łasocha, H. Shenk, *J. Appl. Crystallogr.* **1997**, *30*, 909 – 914.

[4] a) W. I. F. David, *Nature* **1990**, *346*, 731; b) W. I. F. David, *J. Appl. Crystallogr.* **1987**, *20*, 316 – 319.

[5] D. S. Sivia, W. I. F. David, *Acta Crystallogr. Sect. A* **1994**, *50*, 703.

[6] a) A. Altomare, G. Cascarano, C. Giacovazzo, A. Guagliardi, *J. Appl. Crystallogr.* **1994**, *27*, 1045 – 1050; b) R. Peschar, H. Schenk, P. Capkova, *J. Appl. Crystallogr.* **1995**, *28*, 127 – 140.

[7] a) T. Wessels, C. Baerlocher, L. B. McCusker, *Science* **1999**, *284*, 477 – 479; b) W. Łasocha, H. Schenk, *J. Appl. Crystallogr.* **1997**, *30*, 561.

[8] W. H. Zachariasen, F. H. Ellinger, *Acta Crystallogr.* **1963**, *16*, 369 – 375.

[9] K. Shankland, W. I. F. David, D. S. Sivia, *J. Mater. Chem.* **1997**, *7*, 569.

[10] A. N. Fitch, *Mater. Sci. Forum* **1996**, *228–231*, 219 – 222.

[11] A diffraction pattern collected overnight on the original bending-magnet beam line BM16, at 90 K, showed that the sample diffracted well, giving sharp peaks, and a unit cell could be determined from the positions of 20 low-angle peaks by using the program Fzon,[12] with a figure of merit M_{20}[13] of 29.6. The program returned an orthorhombic unit cell with dimensions $a = 21.08(1)$, $b = 23.08(1)$, $c = 16.426(8)$ Å. The volume of 7991.68(2) Å^3 indicates 32 molecules in the cell. Systematic absences of diffraction lines showed that the space group is *Pbca* and therefore there are four independent molecules to be found, comprising 48 non-hydrogen atoms. Attempts to solve the structure by direct methods failed.

[12] J. W. Visser, *J. Appl. Crystallogr.* **1969**, *2*, 89 – 95.

[13] P. M. De Wolff, *J. Appl. Crystallogr.* **1968**, *1*, 108 – 113.

[14] K. D. K. Knudsen, P. P. Pattison, A. N. Fitch, R. J. Cernik, *Angew. Chem.* **1998**, *110*, 2474 – 2478; *Angew. Chem. Int. Ed.* **1998**, *37*, 2340 – 2343.

[15] F. C. Chan, J. Anwar, R. Cernik, P. Barnes, R. McHardy Wilson, *J. Appl. Crystallogr.* **1999**, *32*, 436 – 441.

[16] a) J. P. Wright, unpublished results; b) G. S. Pawley, *J. Appl. Crystallogr.* **1981**, *14*, 357 – 361.

[17] G. M. Sheldrick, *Acta Crystallogr. Sect. A* **1986**, *46*, 467.

[18] Accounting for the variation of the overall thermal factor with temperature was not necessary to obtain comparable Pawley fits at each temperature and a set of intensities that was good enough to solve the structure. The uncertainty in peak intensity introduced by neglecting this factor is small compared to the uncertainty resulting from peak overlap in a single pattern.

[19] a) N. G. Parsonage, L. A. K. Staveley, *Disorder in crystals*, Clarendon Press, Oxford, **1978**, pp. 511 – 716; b) M. Brunelli, A. J. Mora, A. N. Fitch, *J. Solid State Chem.* **2002**, *163*(1), 253 – 258; c) A. J. Mora, A. N. Fitch, *Z. Kristallogr.* **1999**, *214*, 480 – 485.

[20] A. C. Larson, R. B. von Dreele, *Los Alamos Natl. Lab.* LA **1987**, LA-UR-86-784.

[21] M. J. Frisch, G. W. Trucks, M. Head-Gordon, P. M. W. Gill, M. W. Wong, J. B. Foresman, B. G. Johnson, H. B. Schlegel, M. A. Robb, E. S. Replogle, R. Gomperts, J. L. Andres, K. Raghavachari, J. S. Binkley, C. Gonzalez, R. L. Martin, D. J. Fox, D. J. Defrees, J. Baker, J. J. P. Stewart, J. A. Pople, Gaussian 94, Gaussian, Inc., Pittsburgh, PA, **1995**.

 © 2003 Wiley-VCH Verlag GmbH & Co. KGaA, Weinheim

Enantiopure Sulfoxides

A Highly Selective and Practical Method for Enantiopure Sulfoxides Utilizing Activated and Functionally Differentiated *N*-Sulfonyl-1,2,3-oxathiazolidine-2-oxide Derivatives

*Zhengxu Han, Dhileepkumar Krishnamurthy, Paul Grover, H. Scott Wilkinson, Q. Kevin Fang, Xiping Su, Zhi-Hui Lu, Daniel Magiera, and Chris H. Senanayake**

During the past four decades, many groups have been engaged in the design and development of new synthetic methods for the generation of enantiopure sulfoxides because they are often used as chiral controllers for asymmetric C–C bond formation processes and ligands in catalytic asymmetric synthesis.[1] In addition to these synthetic uses, the chiral sulfoxide functionality plays a highly important role in a variety of medicinal targets like OPC-29030, a platelet adhesion inhibitor, and esomeprazole for the treatment of acid related disorders.[2] A literature search revealed that two distinct approaches have been applied in the preparation of optically active sulfoxides: asymmetric oxidation of prochiral sulfides,[3] and an organometallic addition to electrophilic sulfinic-acid derivatives with inversion of configuration at the sulfur atom.[4] As noted in the literature, both methods have

[*] Dr. C. H. Senanayake,[+] Dr. Z. Han, Dr. D. Krishnamurthy,[+] Dr. P. Grover, H. S. Wilkinson, Dr. Q. K. Fang, Dr. X. Su, Dr. Z.-H. Lu,[+] Dr. D. Magiera
Sepracor Inc.
84 Waterford Dr, Marlborough, MA 01752 (USA)
Fax: (+1) 203-791-6130
E-mail: csenanay@rdg.boehringer-ingelheim.com

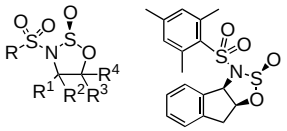
[+] Present address:
Department of Chemical Development
Boehringer Ingelheim Pharmaceuticals, Inc.
900 Ridgebury Road/PO Box 368, Ridgefield, CT 06877-0368 (USA)

Supporting information for this article is available on the WWW under http://www.angewandte.org or from the author.

 © 2003 Wiley-VCH Verlag GmbH & Co. KGaA, Weinheim DOI: 10.1002/anie.200250644

advantages and disadvantages. However, the latter method, which utilizes sulfinyl transfer agents, is widely used in the production of optically active sulfoxides.[1e,f,5] Recently, Khiar, Alcudia and co-workers have developed a practical method for the generation of both enantiomers of several valuable sulfoxides through dynamic kinetic resolution by using diacetone D-glucose (DGA) as a chiral controller.[5f–h] Because of the high biological and chemical significance of many molecules containing the sulfoxide functional group, it is clear that a search for milder asymmetric methods is very important and still needed. Herein, we disclose a highly selective, general, and mild (zinc reagents can be employed) asymmetric technology for both antipodes of sulfoxides from functionally differentiated aryl *N*-sulfonyl-1,2,3-oxathiazolidine-2-oxide derivatives **1** (ASOO; see Scheme 1).

Recently, we disclosed that simple treatment of **2b** (R = mesityl) in THF at low temperature with $SOCl_2$, followed by



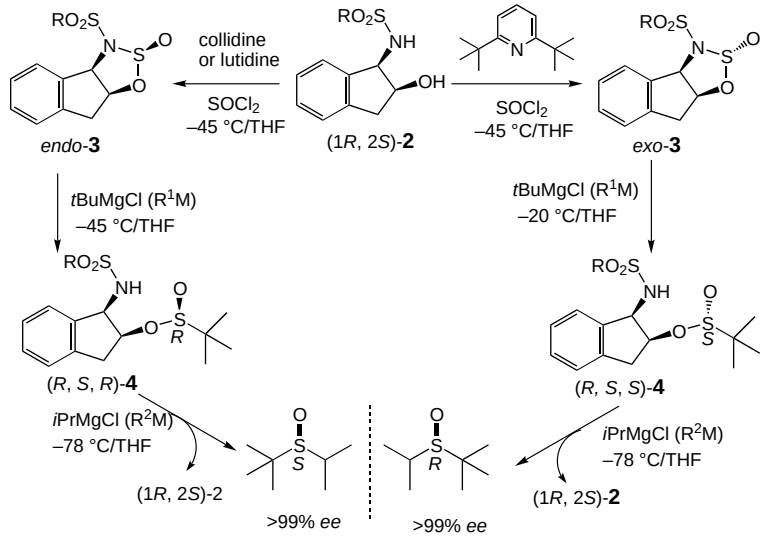
1 (ASOO) *Endo*-**3b**

Scheme 1.

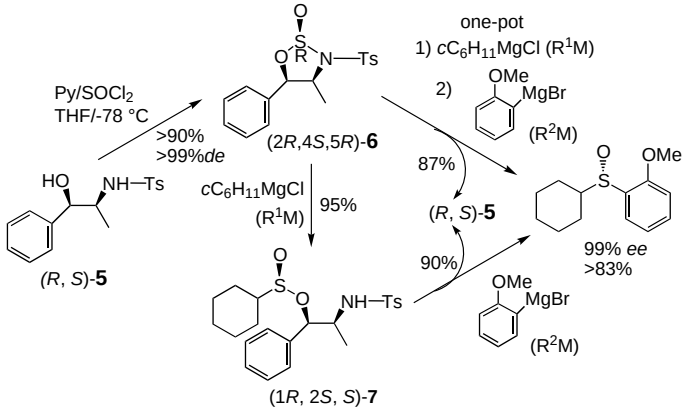
the slow addition of 3,5-lutidine provided a 97:3 ratio of *endo*-selective **3b** in excellent yield.[6] Attempts to find a proper procedure to produce highly *exo*-selective indane-derived *N*-sulfonyl-1,2,3-oxathiazolidine-2-oxide (IASOO-**3**) were unsuccessful. After the examination of many reaction conditions, it was found that high *endo* selectivity can be switched to a high *exo* selectivity by a simple change in the pyridine substitution pattern of the ring, thus increasing the steric bulk of the 2,6 positions of the pyridine ring. As indicated in Table 1, when compound **2** was subjected to 3,5-lutidine or collidine, highly *endo*-selective **3** (Table 1, entry 2 and 5) was afforded. On the other hand, sterically congested 2,6-di-*tert*-butyl pyridine provided highly *exo*-selective **3** (Table 1, entry 4 and 6). *Endo*-**3** and *exo*-**3** are highly crystalline, and are crystallized to an enantiomerically and diastereomerically pure form with excellent recovery from single antipode **2**.[7]

Having generated large quantities of *endo*- and *exo*-**3** in enantiomerically and diastereomerically pure form, we focused on the production of both enantiomers of chiral sulfoxides**.** To highlight the power of this new synthetic methodology, we first investigated the preparation of both antipodes of *t*BuS(O)*i*Pr. Exposure of either *endo*- or *exo*-**3** to *t*BuMgCl at low temperature led to the smooth chemospecific cleavage of the S–N bond to produce the corresponding diastereomer of the sulfinate, **4**, with inversion of configuration at the S atom in > 95 % yield (Scheme 2). Individual diastereomeric sulfinate **4**, upon treatment with *i*PrMgCl, provided the corresponding enantiomer of *t*BuS(O)*i*Pr (with inversion of configuration at the S atom) in excellent yield with an outstanding recovery of enantiopure **2** (> 98 %).[7b,8]

Next, our attention focused on the development of readily available and inexpensive aminoalcohol based *N*-sulfonyl-1,2,3-oxathiazolidine-2-oxide derivatives. After evaluating many chiral aminoalcohol sulfonyl derivatives, we found that inexpensive *N*-tosylnorephedrine is an ideal template for the preparation of *N*-tosyl-1,2,3-oxathiazolidine-2-oxide. Treatment of (1*R*,2*S*)-**5** in THF with thionyl chloride and pyridine at −78 °C provided > 99 % *de* and > 90 % yield of the isolated product, 4-phenyl-5-methyl-3-*N*-tosylnorephedrine-1,2,3-oxathiazolidine-2-oxide (PMTOO) **6** (Scheme 3).[7c] The single crystal analysis of **6** indicated that absolute configuration of the S center is *R*.[7b]



Scheme 2. Production of Enantiopure Sulfoxide Using IASOO-**3**.



Scheme 3. Production of Enantiopure Sulfoxide Using PMTOO-**6**.

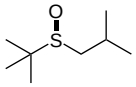
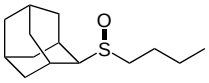
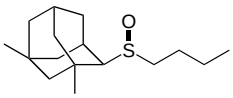
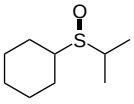
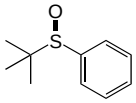
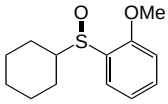
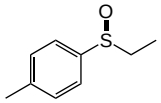
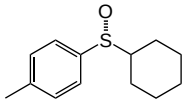
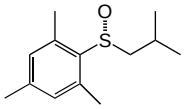
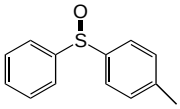
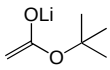
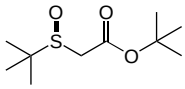
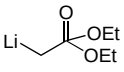
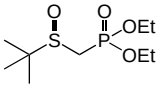
Table 1: Diastereoselective Thionylation of **2**.

Entry	**3**	R	Base	*endo*-**8**:*exo*-**8**[a]
1	**3a**	4-tolyl	pyridine (Py)	80:20
2	**3a**	4-tolyl	2,4,6-collidine	91:9[b]
3	**3a**	4-tolyl	4-methyl-2,6-di-*t*BuPy	20:80
4	**3a**	4-tolyl	2,6-di-*t*BuPy	2:98[b]
5	**3b**	2,4,6-mesityl	3,5-lutidine	97:3[b]
6	**3b**	2,4,6-mesityl	2,6-di-*t*BuPy	7:93[b]

[a] *Endo*/*exo* ratio is determined by ^{1}H NMR analysis. [b] Recrystallization provided diastereo- and enantiopure **3.**

 © 2003 Wiley-VCH Verlag GmbH & Co. KGaA, Weinheim

Table 2: Double Nucleophilic Displacement of *N*-Sulfonyl-1,2,3-oxathiazolidine-2-oxide to form Optically Active Sulfoxides (Scheme 3).

Entry	R^1M	R^2M	Product	Configuration[a] and % *ee*[b]	Yield[c]
1	*t*BuMgCl	*i*BuMgCl		(*S*)-99.5[d] (*R*)-99.5[e]	90 91
2	AdZnBr	*n*BuMgBr		(*S*)-99[d] (*R*)-99[e]	93 91
3	3,5-dimethyl-1-admentylZnBr	EtMgCl		(*S*)-96[d] (*R*)-$>$99[e]	90 93
4	*c*C_6H_{11}MgCl	*i*PrMgCl		(*S*)-99[d] (*R*)-98[f]	88 63
5	*t*BuMgCl	PhMgCl		(*R*)-99[d]	77
6	*c*C_6H_{11}MgCl	*o*-MeO-PhMgCl		(*R*)-98[g] (*S*)-99[f]	83 87
7	*p*-tolylMgBr	EtMgCl/CuBr·SMe2		(*S*)-95[d] (*S*)-90[d]	89 83
8	*p*-tolylMgBr	*c*C_6H_{11}MgCl		(*R*)-99[d]	97
9	2,4,6-mesitylMgBr	*i*BuMgCl		(*S*)-98[g] (*R*)-99[f]	85 86
10	PhMgBr	*p*-tolylMgBr		(*R*)-99[d]	84
11	*t*BuMgCl			(*R*)-99[d] (*S*)-99[e]	93 92
12	*t*BuMgCl			(*S*)-99[d] (*R*)-98[h]	93 83

[a] Absolute configuration was deduced from the synthetic schemes involving two consecutive inversions of configuration, and by comparison to known literature optical rotations**.** [b] Enantiomeric excess was determined by chiral HPLC analysis. [c] All of the yields are of the isolated productss. See Supporting Information experimental procedures for [d] method A, [e] method D, [f] method E, [g] method C, and [h] method B.

First, the application of (2*R*,4*S*,5*R*)-**6** in the generation of optically active cyclohexyl 2-methoxyphenyl sulfoxide was evaluated. The treatment of *c*C_6H_{11}MgCl with (2*R*,4*S*,5*R*)-**6** in THF at −78 °C provided $>$90 % isolated yield of (1*R*,2*S*,*S*)-**7** (inversion of configuration at the S atom; Scheme 3). Diastereopure **7** was then exposed to 2-methoxyphenylmagnesium bromide at −78 °C, which underwent clean inversion of configuration at the S atom to give enantiopure cyclohexyl-2-methoxyphenyl sulfoxide. Importantly, this product can also be generated in excellent yield utilizing a one-pot operation by adding sequentially *c*C_6H_{11}MgCl and 2-methoxyphenylmagnesium bromide to (2*R*,4*S*,5*R*)-**6** at −78 °C. Furthermore, the chiral template (*R*,*S*)-**5** can be effectively isolated from the reaction mixture and recycled.

 © 2003 Wiley-VCH Verlag GmbH & Co. KGaA, Weinheim

The double inversion organometallic displacement process was extended to produce other structurally unique optically active sulfoxides. Either enantiomer of alkyl–alkyl sulfoxides can be obtained in excellent yields (Table 2, entries 1–4). Importantly, mild reagents such as organozinc reagents, cleave the S–N bond of either *endo*-**3b** or (2*R*,4*S*,5*R*)-**6**, thus resulting in high yields. For example, sterically congested 1-adamantylzinc bromide or 3,5-dimethyl-1-adamantylzinc bromide can be added to *endo*-**3b**, or (2*R*,4*S*,5*R*)-**6** to provide the corresponding sulfinates, which upon treatment with *n*BuMgBr or EtMgCl, provided either enantiomer of the appropriate new sulfoxides in high yields (Table 2, entries 2 and 3). The success of this methodology is also exemplified by the preparation of optically active alkyl–aryl (Table 2, entries 5 and 6) and aryl–alkyl (Table 2, entries 7–9) sulfoxides in excellent yields. The one-pot addition of *p*-tolylmagnesium bromide followed by EtMgCl to *endo*-**3** provided only 90% *ee*. However, a sequential addition of *p*-tolylmagnesium bromide, followed by EtMgCl/CuBr·SMe_2 to *endo*-**3** provided increased selectivity (95% *ee*, Table 2, entry 7).[7b] Interestingly, enantiopure phenyl *p*-tolylsulfoxide can be prepared without any complications (Table 2, entry 10). As noted in the literature, attempts to prepare enantiopure *tert*-butyl(*tert*-butylsulfinyl)acetate were unsuccessful.[11f] Gratifyingly, the addition of *tert*-butylacetate enolate to (*R,S,R*)-**4b** provided enantiopure *t*ert-butyl(*tert*-butylsulfinyl)acetate in 93% yield (Table 2, entry 11).[9] Furthermore, this methodology can be applied to generate either enantiomer of the novel diethyl (*tert*-butylsulfinyl)-methyl-phosphonates in high yields (Table 2, entry 12).[1g]

In conclusion, a new and highly general method for the preparation of enantiopure sulfoxides from diastereopure *N*-sulfonyl-1,2,3-oxathiazolidine-2-oxide derivatives[10] has been developed. The application of this new and powerful methodology for identification of sulfoxide containing novel biological targets, and sulfoxide derived chiral ligands for asymmetric catalysis will be reported in due course.

For experimental details and molecular structures of (2*R*,4*S*,5*R*)-**6,** *endo*- and *exo*-**3** see Supporting Information.

Received: November 27, 2002 [Z50644]

Keywords: asymmetric synthesis · chiral auxiliaries · chirality · sulfoxides

[1] a) K. K. Andersen, *Tetrahedron Lett.* **1962**, 93; b) F. Wudl, T. B. K. Lee, *J. Am. Chem. Soc.* **1973**, *95*, 6349; c) M. R. Barbachyn, C. R. Johnson in *Asymmetric Synthesis, Vol. 4* (Eds.: J. D. Morrison, J. W. Scott), Acadamic Press, New York, **1983**, p. 227; d) O. Samuel, F. Rebiere, H. B. Kagan, *J. Org. Chem.* **1991**, *56*, 5991; e) D. A. Evans, M. M. Faul, L. Colombo, J. J. Bisaha, J. Clardy, D. Cherry, *J. Am. Chem. Soc.* **1992**, *114*, 5977; f) D. A. Cogan, G. Liu, K. Kim, B. J. Backes, J. A. Ellman, *J. Am. Chem. Soc.* **1998**, *120*, 8011, and references therein; g) M. A. M. Capozzi, C. Cardellicchio, G. Fracchiolla, F. Naso, P. Tortorella, *J. Am. Chem. Soc.* **1999**, *121*, 4708; h) N. Khiar, I. Fernandez, A. Alcudia in *Advances in Sulfur Chemistry, Vol. 2* (Ed.: C. M. Rayner), JAJ, Stamford, **2000**, chap. 3; i) M. A. M. Capozzi, C. Cardellicchio, F. Naso, G. Spina, P. Tortorella, *J. Org. Chem.* **2001**, *66*, 5933–5936; j) E. N. Prilezhaeva, *Russ. Chem. Rev.* **2000**, *69*, 367; k) H. B. Kagan, P. Diter, *Organosulfur Chem.* **1998**, *2*, 1–39.

[2] a) M. Matsugi, N. Fukuda, Y. Muguruma, T. Yamaguchi, J. Minamikawa, S. Otsuka, *Tetrahedron* **2001**, *57*, 2739–2744; b) H. Cotton, T. Elebring, M. Larsson, L. Li, H. Sorensen, S. Unge, *Tetrahedron: Asymmetry* **2000**, *11*, 3819–3825.

[3] H. B. Kagan in *Catalytic Asymmetric Synthesis*, 2nd ed. (Ed.: I. Ojima), Wiley-VCH, New York, **2000**, chap. 6c.

[4] a) P. Metzner, A. Thuillier in *Sulfur Reagents in Organic Synthesis*, Academic Press, London, UK, **1994**, chap. 2.6.2; b) H. B. Kagan, F. Rebiere, *Synlett* **1990**, 643–650.

[5] a) S. C. Benson, J. K. Snyder, *Tetrahedron Lett.* **1991**, *32*, 5885–5888; b) W. Oppolzer, O. Froelich, C. Wiaux-Zamar, G. Bernardinell, *Tetrahedron Lett.* **1997**, *38*, 2825–2828; c) J. K. Whitesell, M. S. Wong, *J. Org. Chem.* **1991**, *56*, 4552–4554; d) J. K. Whitesell, M. S. Wong, *J. Org. Chem.* **1994**, *59*, 597–601; e) I. Fernandez, N. Khiar, J. M. Llera, F. Alcudia, *J. Org. Chem.* **1992**, *57*, 6789–6796; f) H. El Ouazzani, N. Khiar, I. Fernandez, F. Alcudia, *J. Org. Chem.* **1997**, *62*, 287–291; g) I. Fernandez, C. S. Araujo, M. J. Romero, F. Alcudia, N. Khiar, *Tetrahedron* **2000**, *56*, 3749–3753; h) N. Khiar, C. S. Araujo, F. Alcudia, I. Fernandez, *J. Org. Chem.* **2002**, *67*, 345–356; i) J. Posakony, J. T. Tewson, *Synthesis* **2002**, 859.

[6] Z. Han, D. Krishnamurthy, P. Grover, Q. K. Fang, C. H. Senanayake, *J. Am. Chem. Soc.* **2002**, *124*, 7880–7881.

[7] a) The absolute stereochemistry of *endo*-**3** and *exo*-**3** was unambiguously established by single crystal X-ray analysis; b) For the detailed experimental procedure, see Supporting Information; c) As in the case of aminoindanol series, *exo* isomer of PMTOO can be obtained in 90% yield (with *exo*:*endo* = 9:1) using 2,6-di-*tert*-butylpyridine as a base.

[8] Absolute configuration was deduced from the synthetic Scheme 3, involving two consecutive inversions of configuration and X-ray analysis of (*R,S,R*)-**4b.**

[9] Use of *tert*-butyl (*p*-tolylsulfinyl)acetate in asymmetric synthesis, see G. Solladic, C. Bauder, E. Arce-Dubois, P. Y. Jacope, *Tetrahedron Lett.* **2001**, *42*, 2923–2925.

[10] a) Polymer bound aryl *N*-sulfonyl 1,2,3-oxathiazolidine-2-oxide derivatives are under investigation; b) The application of PMTOO **6** in the synthesis of valuable sulfinamides and polymer-supported sulfinamides are under investigation.

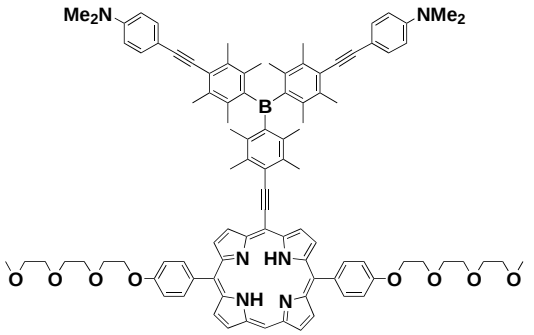
 © 2003 Wiley-VCH Verlag GmbH & Co. KGaA, Weinheim

Fluorescent Chemosensor

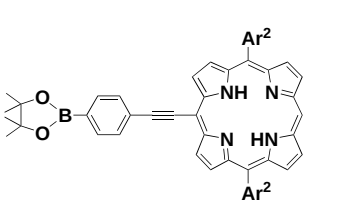
A Colorimetric and Ratiometric Fluorescent Chemosensor with Three Emission Changes: Fluoride Ion Sensing by a Triarylborane–Porphyrin Conjugate**

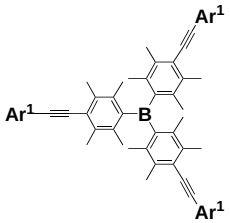
Yohei Kubo, Masashi Yamamoto, Masato Ikeda, Masayuki Takeuchi, Seiji Shinkai,* Shigehiro Yamaguchi, and Kohei Tamao*

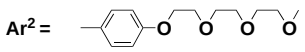
The design of chemosensors for a specific analyte is of great importance for the facile monitoring of analytes.[1,2] Most chemosensors developed so far are colorimetric and/or fluorescent sensors, which efficiently change their photophysical properties (λ_{max} shift of the UV/Vis spectrum, change in the quantum yield or emission wavelength, etc) in the presence of the analyte.[1,2] Ratiometric fluorescent probes, in particular, have found widespread use in biological, polymeric, and sensory materials chemistry, where the two emission bands from the covalently linked chromophores, or a chromophore with a dual channel or with a dual signaling pathway, were used to differentiate between the two signals. In the former case, the analyte recognition site was connected to two chromophores (an energy donor and an energy acceptor or chromophores forming an excimer/exciplex) through a covalent bond, and the analyte changes the orientation and/or the dipolar interaction between the chromophores.[2,3] In the latter cases, another signaling channel or signaling pathway is activated in the analyte binding site (which is frequently a part of a chromophore) only when the analyte is bound to the chromophore.[3e,f] In these systems, the chromophores were designed so that the two emission changes would occur in the presence of the analyte. It thus occurred to us that if the analyte induced multiple emissions[4] with different colors from a chemosensor, the perceived color change would be useful not only for the ratiometric method of detection but also for rapid visual sensing. We report herein that a triarylborane–porphyrin conjugate **1** displays colorimetric (purple to green and red to bluish emission) and ratiometric fluorescent responses to fluoride ions with three emission bands at 356, 670, and 692 nm.[5–9]



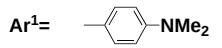
1







2



3

The triarylborane chromophore (an energy donor: D) and the porphyrin chromophore (an energy acceptor: A) in **1** share a Lewis acidic boron junction that can bind a fluoride ion with subsequent sp^2-sp^3 hybridization of the boron atom.[10] The change in the hybridization of the boron atom interrupts both the electronic communication and the dipolar interaction between the triarylborane and porphyrin units as well as the internal charge-transfer state between the two chromophores so that each chromophore (D′ and A′) absorbs and emits light independently only in the presence of fluoride ions (Figure 1).[11] This situation could lead to changes in the UV/Vis and fluorescence spectra, from which one could sense the fluoride ion colorimetrically and ratiometrically.

Compound **1** was prepared according to Scheme 1 and identified by ^{1}H NMR spectroscopy, MALDI-TOF mass spectrometry, and elemental analysis. Compounds **2** and **3**[10b] were synthesized for control experiments. The Soret band of **1** ([**1**] = 3.00 μM) in THF appears at 436.5 nm, that is, slightly red-shifted relative to that of **2** (430.0 nm), whereas the absorption maxima of the triarylborane moiety (303.0, 322.5, and 392.5 nm) in **1** are identical with those of **3** (Figure 2A). No band attributable to electronic transitions between mixed molecular levels of the triarylborane and porphyrin in **1** was observed. The similarity between the UV/Vis spectrum of **1** and the additive sum of **2** and **3** indicates that the electronic coupling between the two chromophores in the ground state is negligibly small.

[*] Dr. M. Takeuchi, Prof. S. Shinkai, Y. Kubo, Dr. M. Yamamoto, Dr. M. Ikeda
Department of Chemistry and Biochemistry
Graduate School of Engineering, Kyushu University
Fukuoka 812-8581 (Japan)
Fax: (+81) 92-642-3611
E-mail: taketcm@mbox.nc.kyushu-u.ac.jp
seijitcm@mbox.nc.kyushu-u.ac.jp
Dr. S. Yamaguchi, Prof. K. Tamao
Institute for Chemical Research, Kyoto University
Gokasho, Uji, Kyoto 611-0011 (Japan)

[**] Y.K. and M.Y contributed equally to this work. We thank Dr. Midori Watanabe and Ms. Hongyue Li at Kyushu University for ^{1}H NMR measurements. M.T. and Y.K. thank prof. H. Yonemura for helpful discussions. M.I. thanks the JSPS Research Fellowship for Young Scientists for financial support. This work was partially supported by a grant-in-aid for COE research ("Design and Control of Advanced Molecular Assembly Systems") from the Ministry of Education, Science, and Culture, Japan (no. 08CE2005).

Supporting information for this article is available on the WWW under http://www.angewandte.org or from the author.

 © 2003 Wiley-VCH Verlag GmbH & Co. KGaA, Weinheim DOI: 10.1002/anie.200250788

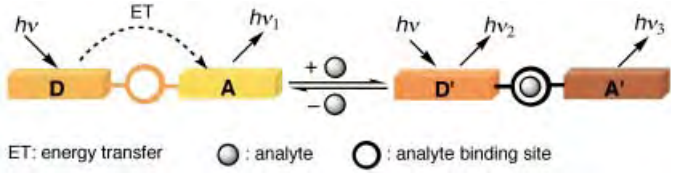


Figure 1. Schematic representation of the different emission processes occurring in **1** on coordination of an analyte.

Compound **1** was titrated with fluoride ions (as a tetrabutylammonium salt, TBAF) in THF at 25 °C and monitored by UV/Vis absorption spectroscopy. As shown in Figure 2 B, the Soret band shifted to a longer wavelength (ca. 480.0 nm). A significant hypsochromic effect was seen upon increasing the concentration of TBAF and this was accompanied by a bathochromic shift (13–20 nm) of the Q band.[12] The hypsochromic and bathochromic shifts of the Soret and Q bands, respectively, were also observed when control compound **2** was titrated with TBAF in THF. Recently, Crossley and Johnston[13] reported that a change in the conjugation in a laterally expanded porphyrin through a redox-induced reaction of a linker results in a similar significant hypsochromic effect of the Soret band together with the bathochromic shift of the Q band. In the case of compound **1**, coordination of a fluoride ion, which generates anionic charge on the boron atom, should change the conjugation or the dipole moment of the durylborane-

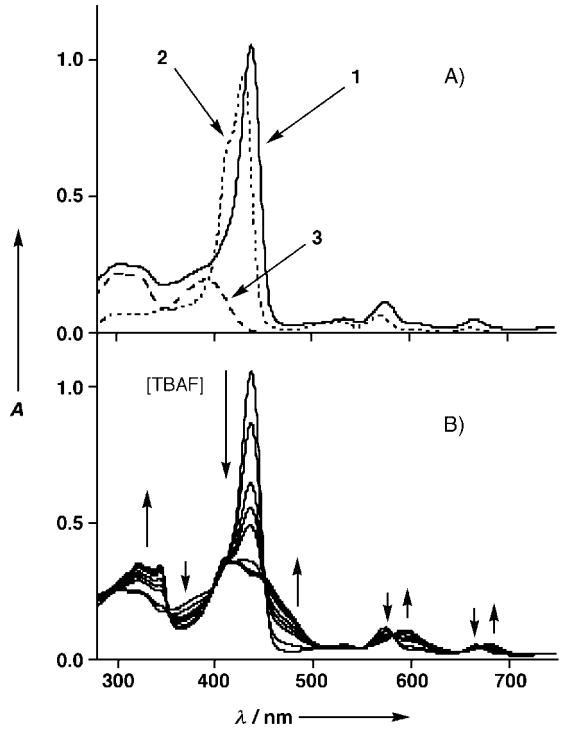
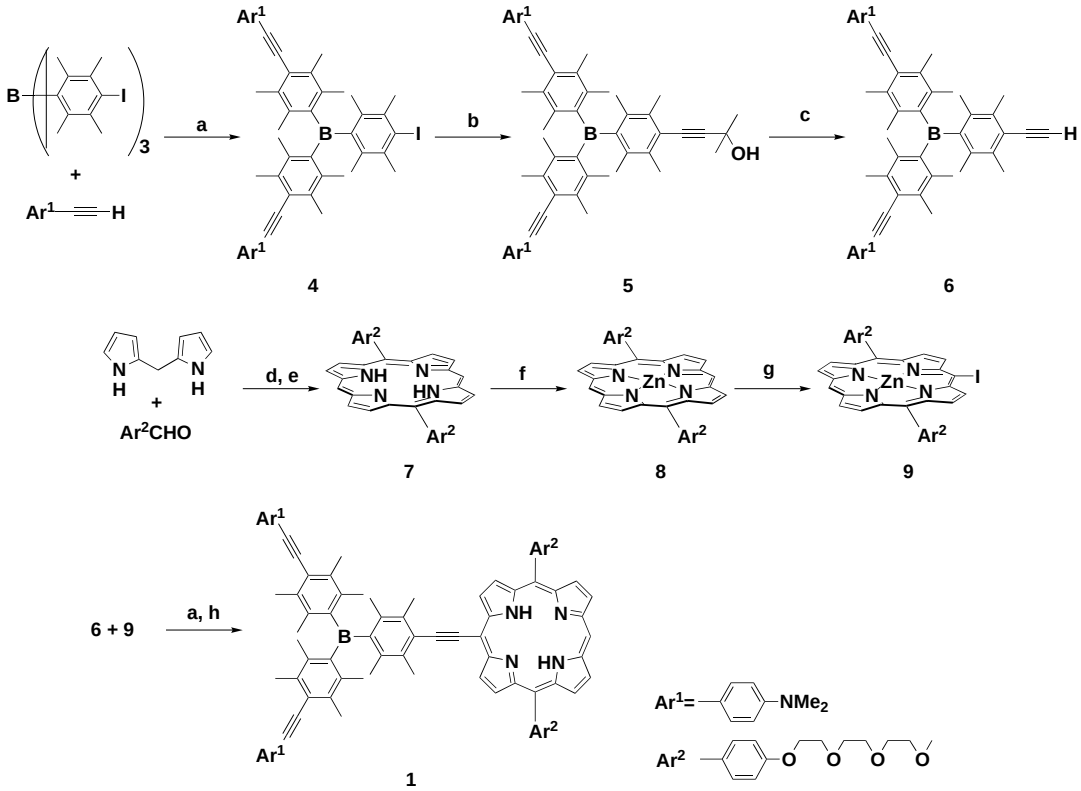


Figure 2. A) UV/Vis absorption spectra of compounds **1**–**3** (3.0 μM) in THF and B) dependence of the UV/Vis spectra on the concentration of fluoride ions; [**1**] = 3.0 μM, [TBAF] = 0–0.10 mM, in THF at 25 °C.



Scheme 1. Reaction and conditons: a) $[Pd(PPh_3)Cl_2]$, CuI, THF, $(iPr)_2NH$; b) 3-methyl-1-butyn-3-ol, $[Pd(PPh_3)_2Cl_2]$, CuI, THF, $(iPr)_2NH$; c) NaOH, toluene; d) TFA, CH_2Cl_2; e) DDQ, CH_2Cl_2; f) $Zn(OAc)_2$, $CHCl_3$, MeOH, g) $AgPF_6$, I_2, $CHCl_3$, pyridine; h) TFA, CH_2Cl_2. DDQ = 2,3-dichloro-5,6-dicyano-1,4-benzoquinone, TFA = trifluoroacetic acid.

 © 2003 Wiley-VCH Verlag GmbH & Co. KGaA, Weinheim

linked porphyrin moiety. In contrast to the porphyrin moiety, a decrease (to 392.5 nm) and an increase (to 323.0 and 343.4 nm) in the intensities of the triarylborane absorption bands in **1** were observed. These trends are the same as those observed for **3**, and the result is interpreted as a loss of π conjugation through the boron atom.[9] These results support the view that the two chromophores, the aryl borane (D′) and the porphyrin (A′), generate their absorption bands independently in the presence of fluoride ions. The change in the absorption spectra resulted in a change in the color of the solution from purple to green (Figure 3). The stoichiometry in the reaction between **1** and TBAF was confirmed to be 1:1

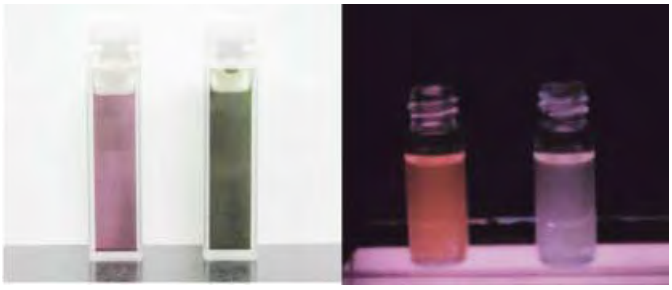


Figure 3. Color changes observed in samples of **1** and TBAF in THF. Left to right: **1**, **1**·TBAF, visible emission of **1**, and emission of **1**·TBAF.

from a plot of the mole ratio versus absorption. A standard curve-fitting method was utilized for the $A_{436.5}$ versus [TBAF] plot to evaluate the association constant for the 1:1 complex, which was estimated to be 99700 M^{-1}. This value is comparable with those previously determined for triarylboranes and fluoride ions.[10] No change in the Soret band, Q band, or the tridurylborane absorption was observed upon exposure of **1** to larger halides, acetate, and hydroxide ions. Apparently, only the smaller anion, the fluoride ion, can fit in the space around the triduryl-surrounded Lewis acidic boron atom.

The coordination of the fluoride ion to the boron center was confirmed by NMR spectroscopy. A *meso*-H proton signal and pyrrole β-proton signals of the porphyrin unit as well as methyl proton signals of the duryl group are shifted to higher magnetic fields in the ^{1}H NMR spectra of [**1**]:[TBAF] = 1:0 and 1:2 in [D_8]THF at 25 °C ([**1**] = 1.00 mM; see the Supporting Information). A ^{19}F signal was shifted to a lower magnetic field ($\Delta\delta = 8.40$ ppm) relative to free TBAF in the ^{19}F NMR spectra as a result of its coordination to the boron center (see the Supporting Information).

The fluorescence spectrum of **1** (0.5 μM) in THF was recorded with excitation at an isosbestic point (294 nm, see the Supporting Information) where the selectivity of the triarylborane absorption over that of the porphyrin ring was 3:1, as estimated from the absorbance of compounds **2** and **3**. Compound **1** gives the porphyrin emission band (670 nm) without the triarylborane emission band that should appear at 515 nm, as seen in the emission spectrum of **3** (see the Supporting Information). The same spectrum was obtained in a nonpolar solvent (benzene). The intermolecular energy transfer is negligible at such a low concentration, since the fluorescence spectrum for an equimolar mixture (0.5 μM each) of **2** and **3** was equivalent to the sum of the two individual fluorescence spectra. Furthermore, the excitation spectrum of **1** shows an intense triarylborane absorption band as well as the porphyrin band. The findings clearly show that efficient transfer of energy from the triarylborane to the porphyrin chromophore takes place in the absence of fluoride ions.

The addition of fluoride ions to a solution of **1** in THF results in a substantial increase in the intensity of the two emission bands at 356 nm and 692 nm along with a decrease in the intensity of the emission band at 670 nm (Figure 4). The

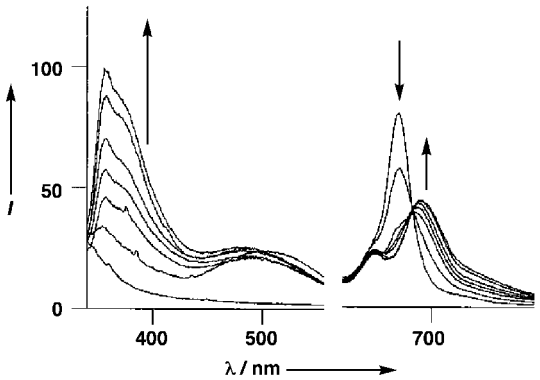


Figure 4. Changes in the emission spectra upon addition of TBAF to solutions of THF at 25 °C; excitation wavelength 294 nm.

appearance of the emission band at 356 nm was the same response to fluoride ions as that of **3**. The longer wavelength shift of 22 nm in the porphyrin emission can be attributed to the lower energy of the Q band in the ground state. A visible change in the emission from a red to bluish color was also observed (Figure 3). Compound **1** showed a ratiometric response to fluoride ions at two different wavelengths (356 and 692 nm) when normalized against the emission at 670 nm (see the Supporting Information). The excitation spectra of **1** with added fluoride ions revealed that the absorbance of the aryl borane still participates in the appearance of the porphyrin emission at 692 nm. This observation means that the energy transfer from the aryl borane moiety to the porphyrin unit occurs even after complexation with a fluoride ion.[14] The fluorescence decay of the emission band of the aryl borane moiety in **1** was evaluated to be shorter than 100 ps (515 nm) and 0.53 ns (380 nm) without and with the guest fluoride ion, respectively. A shorter lifetime at the 515 nm emission without fluoride ions than that of **3** (4.52 ns) could be attributed to an efficient Dexter-type energy transfer from the aryl borane to the porphyrin moiety in **1**. In the presence of fluoride ions, the lifetime of 0.53 ns is similar to that of the **3**·fluoride ion complex (monitored at 380 nm, 0.39 ns). This finding together with the excitation spectrum of the **1**·fluoride ion complex enables one to suppose that energy transfer from the aryl borane moiety to the porphyrin unit in **1** takes place to some extent in the presence of fluoride ions. The result suggests, therefore, that the guest fluoride ion can switch the energy-transfer pathway to make it possible to monitor the

 © 2003 Wiley-VCH Verlag GmbH & Co. KGaA, Weinheim

binding event through the changes in the three emissions (Figure 5).

In conclusion, we have demonstrated that **1** displays a colorimetric (purple to green and red to bluish emission) and a ratiometric response (by utilizing changes in three emissions) that are useful for the detection of fluoride ions. The mechanism for the increase in the two emission bands and not the third emission band was assumed by the finding that the coordination of a fluoride ion to the boron center in **1** caused perturbation in the energy transfer pathway and the π conjugation. Thus, two chromophores sharing a recognition unit linked though a conjugate spacer would become a versatile molecular design scheme to achieve the monitoring of multiple emissions useful for signal differentiation.

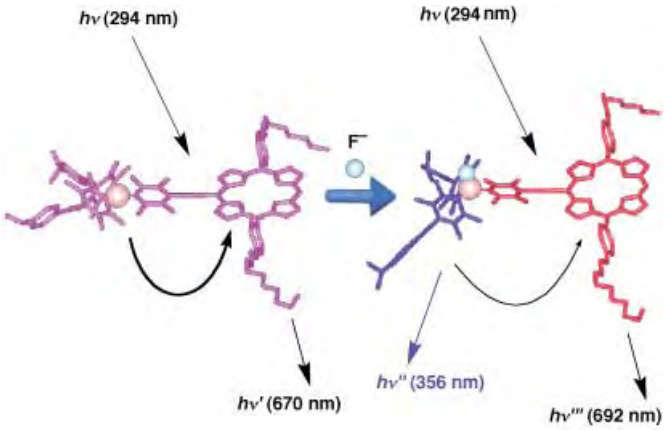


Figure 5. Effects of the coordination of a fluoride ion on the emissions from **1** on excitation at 294 nm.

Experimental Section

All starting materials and solvents were purchased from Tokyo Kasei Chemicals or Wako Chemicals, and used as received. The ^{1}H NMR spectra were recorded either on a Brucker AC 250 (250 MHz) or Brucker DRX 600 (600 MHz) spectrometer. Chemical shifts are reported in ppm downfield from tetramethylsilane as the internal standard. Mass spectral data were obtained by using a Perseptive Voyager RP MALDI-TOF spectrometer. UV/Vis and fluorescent spectra were recorded with a Shimadzu UV-2500 PC and Hitachi F-4500 spectrophotometer.

Received: December 17, 2002 [Z50788]

Keywords: fluorescent probes · fluorides · molecular recognition · porphyrinoids · sensors

[1] a) A. P. de Silva, D. B. Fox, A. J. M. Huxley, T. S. Moody, *Coord. Chem. Rev.* **2000**, *205*, 41; b) L. Prodi, F. Bolletta, M. Montaliti, N. Zaccheroni, *Coord. Chem. Rev.* **2000**, *205*, 59; c) V. Amendola, L. Fabbrizzi, M. Licchelli, C. Mangano, P. Pallavicini, L. Parodi, A. Poggi, *Coord. Chem. Rev.* **2000**, *192*, 649; d) J. P. Desvergne, A. W. Czarnik, *NATO ASI Ser. Ser. C* **1997**, *492*.

[2] J. R. Lakowicz, *Priciples of Fluorescence Spectroscopy*, 2nd ed., Plenum, New York, **1999**.

[3] For selected recent examples, see a) S. Maruyama, K. Kikuchi, T. Hirano, Y. Urano, T. Nagano, *J. Am. Chem. Soc.* **2002**, *124*, 10650; b) J. Raker, T. E. Glass, *J. Org. Chem.* **2002**, *67*, 6113; c) F. Würthner, S. Ahmed, C. Thalacker, T. Debaerdemaeker, *Chem. Eur. J.* **2002**, *8*, 4742; d) J. Kim, D. T. McQuade, A. Rose, Z. Zhu, T. M. Swager, *J. Am. Chem. Soc.* **2001**, *123*, 11488; e) J. V. Mello, N. S. Finney, *Angew. Chem.* **2001**, *113*, 1584; *Angew. Chem. Int. Ed.* **2001**, *40*, 1536; f) K. Choi, A. D. Hamilton, *Angew. Chem.* **2001**, *113*, 4030; *Angew. Chem. Int. Ed.* **2001**, *40*, 3912; g) J.-S. Yang, C.-S. Lin, C.-Y. Hwang, *Org. Lett.* **2001**, *3*, 889; h) S. Deo, H. A. Godwin, *J. Am. Chem. Soc.* **2000**, *122*, 174; i) A. P. de Silva, J. Eilers, G. Zlokarnik, *Proc. Natl. Acad. Sci. USA* **1999**, *96*, 8336.

[4] a) Y.-A. Lee, J. E. McGarrah, R. J. Lachicotte, R. Eisenberg, *J. Am. Chem. Soc.* **2002**, *124*, 10662; b) H. Fu, B. H. Loo, D. Xiao, R. Xie, X. Ji, J. Yao, B. Zhang, L. Zhang, *Angew. Chem.* **2002**, *114*, 1004; *Angew. Chem. Int. Ed.* **2002**, *41*, 962.

[5] For reviews on anion receptors, see a) P. D. Beer, P. A. Gale, *Angew. Chem.* **2001**, *113*, 502; *Angew. Chem. Int. Ed.* **2001**, *40*, 486; b) P. A. Gale, *Coord. Chem. Rev.* **2000**, *199*, 181; c) T. S. Snoeden, E. V. Anslyn, *Curr. Opin. Chem. Biol.* **1999**, *3*, 740; d) P. D. Beer, *Acc. Chem. Res.* **1998**, *31*, 71; d) F. P. Schmidtchen, M. Berger, *Chem. Rev.* **1997**, *97*, 1609; e) J. Scheerder, J. F. J. Engbersen, D. N. Reinhoudt, *Recl. Trav. Chim. Pays-Bas* **1996**, *115*, 307.

[6] For recent anion sensors, see a) P. Piatek, J. Jurczak, *Chem. Commun.* **2002**, 2450; b) J.-H. Liao, C.-Y. Chen, J.-M. Fang, *Org. Lett.* **2002**, *4*, 561; c) A. Ojida, Y. Mito-oka, M. Inoue, I. Hamachi, *J. Am. Chem. Soc.* **2002**, *124*, 6256; d) J. R. Blas, M. Marquez, J. L. Sessler, F. J. Luque, M. Orozco, *J. Am. Chem. Soc.* **2002**, *124*, 12796; e) J. L. Sessler, H. Maeda, T. Mizuno, V. M. Lynch, H. Furuta, *Chem. Commun.* **2002**, 862; f) K. Choi, A. D. Hamilton, *J. Am. Chem. Soc.* **2001**, *123*, 2456; g) D. H. Lee, K. H. Lee, J. I. Hong, *Org. Lett.* **2001**, *3*, 5; h) P. D. Beer, N. Berry, M. G. B. Drew, O. D. Fox, M. E. Padilla-Tosta, S. Patell, *Chem. Commun.* **2001**, 199; i) M. J. Deetz, M. Shang, B. D. Smith, *J. Am. Chem. Soc.* **2000**, *122*, 6201; j) Y. Kubo, M. Tsukahara, S. Ishihara, S. Tokita, *Chem. Commun.* **2000**, 653; k) S. Sasaki, M. Mizuno, K. Naemura, Y. Tobe, *J. Org. Chem.* **2000**, *65*, 275; l) H. Miyaji, P. Anzenbachlar, Jr., J. L. Sesslar, E. R. Bleasdale, P. A. Gale, *Chem. Commun.* **1999**, 1723.

[7] Receptors for fluoride ions are of special importance for monitoring fluoride metabolism in nature, the analysis of drinking water, and the detection of chemical warfare agents.[9]

[8] For recent fluoride chemosensors, see a) J. L. Sessler, H. Maeda, T. Mizuno, V. M. Lynch, H. Furuta, *J. Am. Chem. Soc.* **2002**, *124*, 13474; b) S. Aldridge, C. Bresner, I. A. Fallis, S. J. Colesb, M. B. Hursthouseb, *Chem. Commun.* **2002**, 740; c) S. K. Kim, J. Yoon, *Chem. Commun.* **2002**, 770; d) T. Mizuno, W.-H. Wei, L. R. Eller, J. L. Sesslar, *J. Am. Chem. Soc.* **2002**, *124*, 1134; e) T. Gunnlaugsson, A. P. Davis, M. Glynn, *Chem. Commun.* **2001**, 2556; f) K. H. Lee, H.-Y. Lee, D. H. Lee, J.-I. Hong, *Tetrahedron Lett.* **2001**, *42*, 5447; g) H. Furuta, H. Maeda, A. Osuka, *J. Am. Chem. Soc.* **2001**, *123*, 6435; h) M. Takeuchi, T. Shioya, T. M. Swager, *Angew. Chem.* **2001**, *113*, 3476; *Angew. Chem. Int. Ed.* **2001**, *40*, 3372; i) C. R. Cooper, N. Spencer, T. D. James, *Chem. Commun.* **1998**, 1365.

[9] H. Sohn, S. Létant, M. J. Sailor, W. C. Trogler, *J. Am. Chem. Soc.* **2000**, *122*, 5399.

[10] a) S. Yamaguchi, S. Akiyama, K. Tamao, *J. Am. Chem. Soc.* **2000**, *122*, 6335; b) S. Yamaguchi, T. Shirasaka, K. Tamao, *Org. Lett.* **2000**, *2*, 4129; c) S. Yamaguchi, S. Akiyama, K. Tamao, *J. Am. Chem. Soc.* **2001**, *123*, 11372; d) S. Yamaguchi, T. Shirasaka, S. Akiyama, K. Tamao, *J. Am. Chem. Soc.* **2002**, *124*, 8816.

[11] The change in electron-transfer efficiency caused by the binding of the fluoride ion to a boronate ester has already been reported, see H. Shiratori, T. Ohno, K. Nozaki, A. Osuka, *Chem. Commun.* **1999**, 2181.

 © 2003 Wiley-VCH Verlag GmbH & Co. KGaA, Weinheim

[12] It was confirmed by ^{1}H NMR spectroscopy that **1** does not aggregate in THF both in the presence and in the absence of TBAF.
[13] M. J. Crossley, L. A. Johnston, *Chem. Commun.* **2002**, 1122.
[14] The emisson intensity of **1** excited at 294 nm is 13 (at 670 nm) and 16 (at 692 nm) times larger than that of **2** in the absence and in the presence of fluoride ions, respectively, if it is assumed that the energy transfer occurs from the aryl borane moiety to the porphyrin ring.

 © 2003 Wiley-VCH Verlag GmbH & Co. KGaA, Weinheim

Structure of Cyclohexamantane

Isolation and Structural Proof of the Large Diamond Molecule, Cyclohexamantane ($C_{26}H_{30}$)

Jeremy E. P. Dahl, J. Michael Moldowan, Torren M. Peakman, Jon C. Clardy, Emil Lobkovsky, Marilyn M. Olmstead, Paul W. May, Tim J. Davis, John W. Steeds, Ken E. Peters, Andy Pepper, Andy Ekuan, and Robert M. K. Carlson*

In this report, we describe the first isolation and structural verification of the diamondoid cyclohexamantane, $C_{26}H_{30}$, a material that has probably never previously existed anywhere in crystalline form. Since the diamond surface can terminate in hydrogen,[1] cyclohexamantane may be thought of as a nanometer-sized diamond of approximately 10^{-21} carats. In fact, the cyclohexamantane structure has been used to represent a small diamond in theoretical investigations.[2–4] Here we present the experimentally determined properties of cyclohexamantane isolated from petroleum, which includes its single-crystal X-ray structure, and analysis by NMR and laser Raman spectroscopy, as well as mass spectrometry.

Diamondoids of the adamantane series are hydrocarbons composed of fused cyclohexane rings, all in stable chair conformations, which form interlocking cage structures that can be superimposed on the diamond crystal lattice.[5] The lower diamondoids have chemical formulas of $C_{4n+6}H_{4n+12}$, where n equals the number of diamond-cage subunits. The stability of diamondoids is illustrated by the heat of formation of adamantane (the smallest diamondoid) which is far lower than any other hydrocarbons of comparable carbon quantity and ring number. While there is only one form of adamantane, diamantane, and triamantane, there are four possible isomeric tetramantanes (*iso-*, *anti-*, and two enantiomeric *skew*-tetramantanes). There are ten possible pentamantanes,[6,7] nine isomers with the formula $C_{26}H_{32}$, and one with formula $C_{25}H_{30}$. Likewise, there are 39 postulated hexamantanes, 28 of which are isomers of $C_{30}H_{36}$, and ten of which are $C_{29}H_{34}$ isomers.[6,7] The pericondensed hexamantane, also named cyclohexamantane, is the only diamondoid structure with the formula $C_{26}H_{30}$.

The most efficient syntheses of all of the lower diamondoids (from adamantane through to triamantane) involve the carbocation-mediated superacid equilibration reaction discovered by von R. Schleyer.[8] However, this route to the higher diamondoids (that is, tetramantane and higher) is blocked by severe kinetic (mechanistic) constraints, and all attempts to synthesize the higher diamondoids have proven futile. Only one of the tetramantanes (*anti*-tetramantane) has been prepared by an elegant, complex, but low-yielding alternative synthetic pathway devised by McKervey's research group.[9]

Diamondoids occur naturally in virtually all petroleum.[10] In most crude oils, diamondoid concentrations are in the order of 1–100 ppm, and occur predominantly as substituted and unsubstituted adamantanes and diamantanes.[10] Although it is not clear how diamondoids are formed in the geosphere, we believe they may be created through carbocation-mediated rearrangements arising when newly generated petroleum, which contains functionalized molecular species (for example, double bonds), reacts with superacid sites on naturally occurring clay minerals, such as montmorillonite, in petroleum source rocks. Although macroscopic diamonds are less stabile than graphite under oil reservoir conditions, this is not true of nanometer-sized hydrogen-terminated diamonds, such as cyclohexamantane.[11–13] Therefore, the formation of diamondoids from petroleum precursors is thermodynamically favored and this helps to explain their surprising existence.

The number of different carbocation-mediated pathways to adamantane from only one starting material (*endo*-tetrahydrodicyclopentadiene) has been calculated to be 2897.[14] Similar treatments for diamantane yield numbers orders of magnitude higher.[15] With this increasing number of

[*] Dr. J. E. P. Dahl, Dr. R. M. K. Carlson
ChevronTexaco Energy Reseach & Technology Co.
P.O. Box 1627, Richmond CA 94802 (USA)
E-mail: Dahl@Pangea.Stanford.edu
Dr. J. E. P. Dahl, Prof. J. M. Moldowan, A. Ekuan
Geological and Environmental Sciences
Stanford University, Stanford CA 94305-2115 (USA)
Dr. T. M. Peakman
Pfizer Global Research and Development
Ramsgate Road, Sandwich, CT13 9NJ (UK)
Prof. J. C. Clardy, Dr. E. Lobkovsky
Department of Chemistry, Cornell University
Ithaca NY, 14853-1301 (USA)
Dr. M. M. Olmstead
Department of Chemistry, University of California
One Shields Ave., Davis, CA 95616-5295 (USA)
Dr. P. W. May
School of Chemistry, University of Bristol
Bristol BS8 ITS (UK)
Dr. T. J. Davis, Prof. J. W. Steeds
Wills Physics Laboratory, University of Bristol
Bristol BS8 ITL (UK)
Dr. K. E. Peters
U.S. Geological Survey
345 Middlefield Rd., Menlo Park, CA 94025-3591 (USA)
Dr. A. Pepper
British Petroleum BP Upstream Technology
Room 833 Westlake 4 Building, 200 Westlake Park Blvd
Houston TX 77210-4587 (USA)

 © 2003 Wiley-VCH Verlag GmbH & Co. KGaA, Weinheim DOI: 10.1002/anie.200250794

pathways and intermediates, it is clear that the natural synthetic route to cyclohexamantane from petroleum precursors must include an astronomical number of pathways and intermediate species. The low concentration of cyclohexamantane (less than 1 ppb in most oils) suggests that yields are extremely low. The amount of time required to arrive at the end product may be many millions of years (that is, the time involved in oil generation) thus overcoming the kinetic impediments that block syntheses on laboratory timescales. If this assertion is correct, petroleum may be the only possible source of cyclohexamantane.

Crystals of cyclohexamantane were obtained from a distilled Gulf Coast petroleum by reverse-phase high-performance liquid chromatography (HPLC).[16] Although it remained a minor component in HPLC fractions (dissolved in acetone), cyclohexamantane spontaneously crystallized from the acetone/HPLC complex mixture after several weeks (Figure 1). The crystals are transparent with a pronounced luster or brilliance.



Figure 1. SEM image of a cyclohexamantane crystal magnified 150×.

Cyclohexamantane has a surprisingly high melting point (> 314 °C in a sealed capillary tube) that reverses the melting-point trend observed among lower diamondoids. Cyclohexamantane sublimes in an open capillary tube at around 293 °C.

Single-crystal X-ray diffraction was carried out on an isolated cyclohexamantane crystal (the structure is shown in Figure 2 and the packing is shown in Figure 3).[17] The molecule is disc shaped and utilizes the $\bar{3}$ (S_6) crystallographic symmetry of space group $R\bar{3}$, but it has effective $\bar{3}m$ ($D3d$) symmetry. The mean C–C distance is 1.538(7) Å, and the central C–C bond is 1.568(6) Å, significantly longer; the mean C-C-C angle is 109.7(10)°.

A mass spectrum of cyclohexamantane (Figure 4b) shows a large molecular ion (m/z 342), typical of unsubstituted diamondoids, and a doubly charged molecular ion at m/z 171, along with a number of minor fragment ions.

The laser Raman spectrum of crystalline cyclohexamantane displays a variety of peaks between $\tilde{\nu} = 300$ and 2920 cm^{-1} (Figure 4a; Table 1). The spectrum was compared with the data reported for adamantane,[18] diamond,[19] and nanophase or "amorphous" diamond[20] (Table 1). CH and CH_2 stretching modes are observed between $\tilde{\nu} = 2840$ and 2920 cm^{-1}. Vibrations at $\tilde{\nu} = 445$ and 652 (CCC deformation), 985 (CH_2 rocking), 1219 and 1311 (CH bending), and 1451 cm^{-1} (CH_2 scissor) are comparable with those observed in adamantane. Peaks at $\tilde{\nu} = 498$ and 1142 cm^{-1} for cyclohexamantane correspond to peaks observed in the Raman spectrum of nanocrystalline diamond.[20] A number of peaks are observed between $\tilde{\nu} = 1330$ and 1380 cm^{-1} (Figure 4a) which may be related to various weak CH bending and CH_2 wagging and twisting vibrations seen in the spectrum of adamantane. A more attractive possibility is that these vibrations are related to the breathing mode observed in diamond[18] at 1332 cm^{-1}, which corresponds to vibrational

Table 1: Observed Raman frequencies for crystalline cyclohexamantane and reference substances used to help with assignments. Data for adamantane is taken from Bistiricic et al.,[18] for diamond from Solin and Ramdas[19], and for amorphous diamond from Prawer et al.[20]

Raman Frequencies [cm^{-1}]				Possible assignments for cyclohexamantane
Cyclohexamantane	Reference Substances			
	Adamantane	Nanophase diamond	Diamond	
340, w				
347, w				
445, m	441, m			CCC deformation
498, s		500		
652, m	638, vw			CCC deformation
674, w				
814, w	800, vw			CC stretch
817, w	800, vw			CC stretch
985, m	972, m			CH_2 rock
1029, s				
1048, m				
1056, w				
1074, w	1098, s			CH_2 rock
1142, m		1140		
1181, s		1200		CC stretch
1203, w		1200		CC stretch
1219, w	1220, s			CH bend
1256, w				
1292, w				
1311, w	1312, w		1332	CH bend, CC stretch
1337, w		1332	1332	CC stretch
1352, w	1352, vw		1332	CH_2 wag, CC stretch
1359, w			1332	CC stretch
1375, w	1371, w		1332	CH_2 twist, CH bend, CC stretch
1451, w	1436, m			CH_2 scissor
2848, s	2849, m			CH_2 stretch
2860, vs				CH stretch, CH_2 stretch
2877 vs				CH stretch, CH_2 stretch
2907, s (sh)	2907, s (sh)			CH_2 stretch
2916, vs	2916, vs			CH stretch

Abbreviations: vs = very strong, s = strong, m = medium, w = weak, vw = very weak, sh = shoulder.

 © 2003 Wiley-VCH Verlag GmbH & Co. KGaA, Weinheim

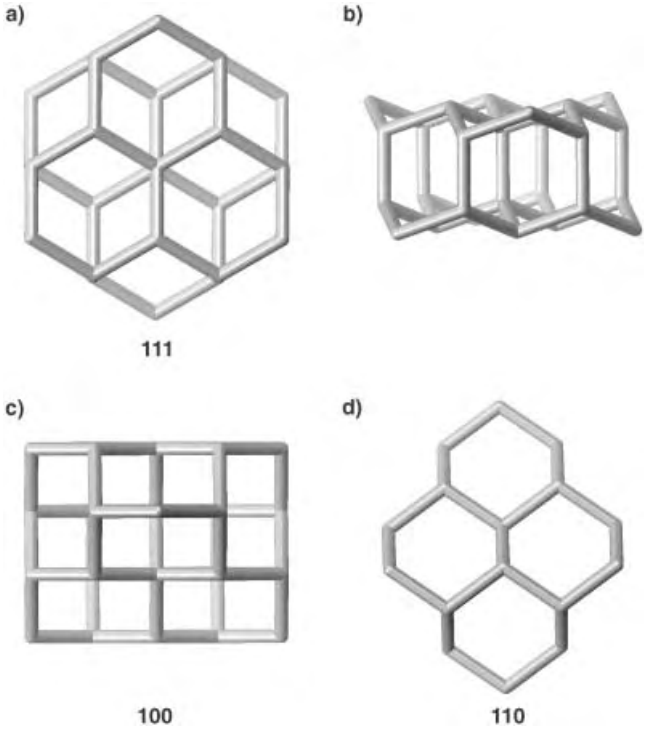


Figure 2. The carbon framework structure of cyclohexamantane based on single-crystal X-ray diffraction. a) View along a diamond (111) crystal-lattice plane; b) side view of this "wheel-like" molecule; c) and d) views along the (100) and (110) diamond crystal-lattice planes, respectively.

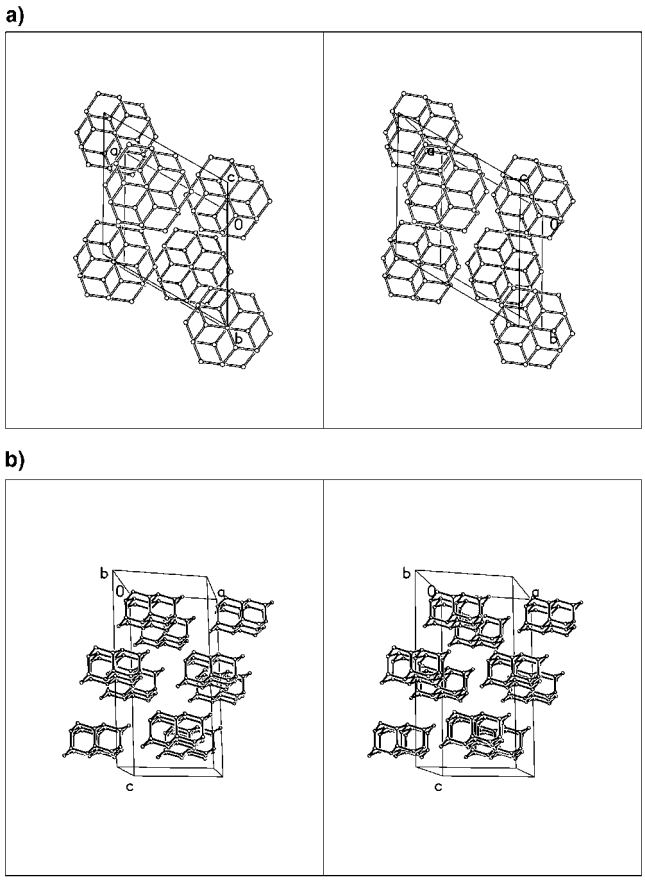


Figure 3. a) and b) Two stereoscopic projections showing different views of the crystal packing of cyclohexamantane.

modes of the quaternary carbon atoms, in accord with a diamond-like coordination. The very strong peak at $\tilde{\nu} = 2860\ cm^{-1}$ for cyclohexamantane is also observed in the Raman spectrum of the hydrogenated diamond C⟨111⟩ surface.[21] Additional important peaks in the Raman spectrum of cyclohexamantane appear at 498, 1029, 1048, 1142, 1181, and 1256 cm^{-1}. The peak at 1181 cm^{-1}, along with a weaker one at 1203 cm^{-1} may represent other vibrational modes of sp^3-bonded carbon atoms, as reported for nanophase diamond.[22]

The ^1H-decoupled ^{13}C NMR spectrum of cyclohexamantane (Figure 5a) shows three of the expected four signals with the signal for the two equivalent quaternary carbon atoms (atoms 11 and 12; Figure 5c) being absent. This feature is not surprising given the small amount of sample used and the expected long longitudinal relaxation times, as demonstrated for the quaternary carbon in triamantane. A DEPT spectrum (Figure 5b) allowed assignment of all the CH_2 carbon atoms (atoms 4, 8, 15, 19, 23, and 26; Figure 5c) to $\delta = 38.6$ ppm. This corresponds with the value of $\delta = 38.6$ ppm reported for the structurally related triamantane.[23] Similarly, the CH resonance at $\delta = 37.8$ ppm can be assigned to the twelve equivalent CH carbon atoms (atoms 1, 3, 5, 7, 9, 14, 16, 18, 20, 22, 24, and 25; Figure 5c) and that at $\delta = 47.3$ ppm to the six equivalent CH carbon atoms (atoms 2, 6, 10, 13, 17, 21; Figure 5c) on the basis of the similarities in chemical environment with carbon atom 2 ($\delta = 46.9$ ppm) and atom 3 ($\delta = 38.1$ ppm) in triamantane.[23]

The ^1H NMR spectrum (Figure 5c) is characterized by three second-order multiplets (indicating the presence of long-range couplings), which could be assigned on the basis of integration and homonuclear decoupling experiments. Thus, the multiplet at $\delta = 1.19$ ppm is assigned to six methine hydrogen atoms (associated with carbon atoms 2, 6, 10, 13, 17, and 21), that at $\delta = 1.59$ ppm to twelve methine hydrogens (associated with carbon atoms 1, 3, 5, 7, 9, 14, 16, 18, 20, 22, 24, and 25), and that at $\delta = 1.712$ ppm to the twelve methylene hydrogens (geminal on the carbon atoms 4, 8, 15, 19, 23, and 26).

Cyclohexamantane may be formed by an extremely large number of rearrangments of suitable 26-carbon-atom precursor molecules during oil generation. Another possibility suggested by Lin and Wilk[24] involves alkylation of lower diamondoids by clay-catalyzed reactions with methane gas, followed by cyclization to form higher diamdondoids. If this hypothesis is correct, then the formation of substantially larger diamondoids than cyclohexamantane could be postulated. In fact, one might hypothesize microcrystalline diamonds as a product. Because these diamonds would not be soluble in petroleum, they would remain in the petroleum source rock (a hypothesis we are currently exploring). Interestingly, there are microcrystalline black diamonds known as carbonados, which unlike other diamonds, are

 © 2003 Wiley-VCH Verlag GmbH & Co. KGaA, Weinheim

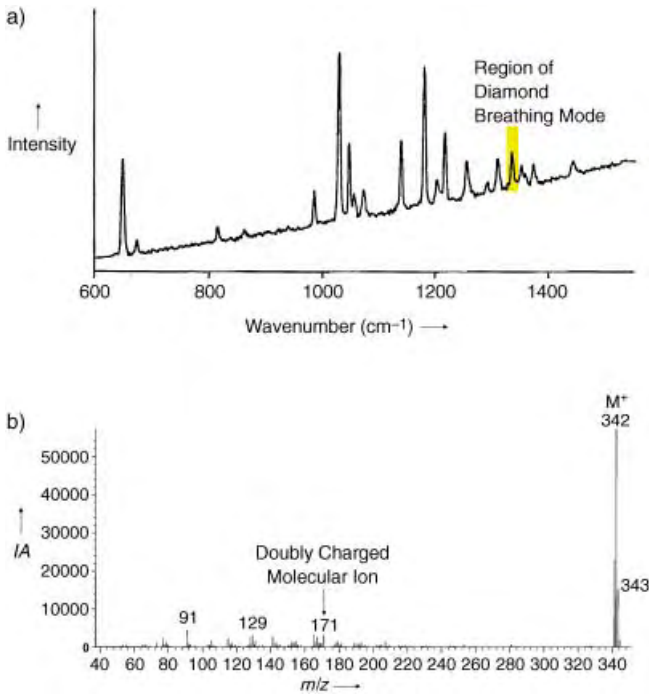


Figure 4. Laser Raman spectrum (a) and mass spectrum (b) obtained for cyclohexamantane. The laser Raman spectrum of crystalline cyclohexamantane was acquired on a Renishaw Raman system 2000 microscope using the 514 nm line from an argon ion laser. The power output was adjusted to 25 mW. A ×50 objective was used to produce a spot size of approximately 1.5 μm in diameter to collect the scattered light. The slit was adjusted to give a resolution of 1 cm^{-1} and a confocal sampling depth of approximately 3 μm. A full peak listing with possible assignments is given in Table 1. The GC/MS instrument was a VG Trio-1 mass spectrometer coupled to a HP 5890 gas chromatograph. Ionization was by electron impact (EI); the collision energy was 70 eV; *IA* = ion abundance.

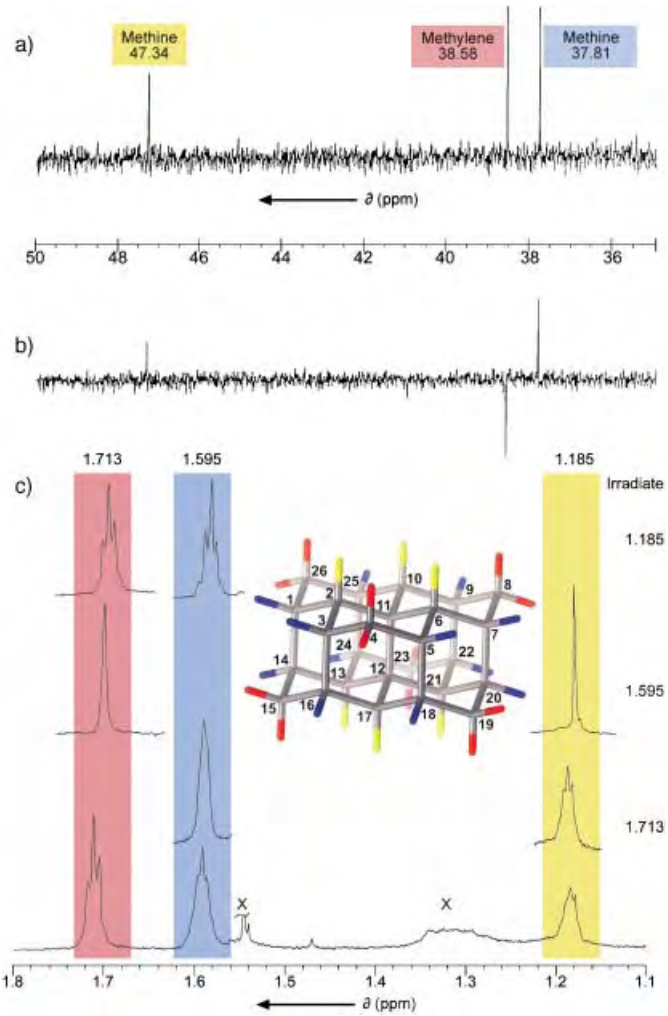


Figure 5. ^{13}C NMR (a) and DEPT (b) spectra were acquired on a JEOL Lambda 300 spectrometer operating at 75 MHz; c) ^{1}H NMR spectrum acquired on a JEOL GX400 spectrometer operating at 400 MHz. Spectra were recorded using C_6D_6 as solvent. In the ^{1}H NMR spectrum, "X" corresponds to impurities; the approved IUPAC numbering for cyclohexamantane is shown, namely, dodecacyclo-[12.12.$0^{2,11}$.$0^{3,16}$.$0^{5,18}$.$0^{6,11}$.$0^{7,20}$.$0^{9,22}$.$0^{10,25}$.$0^{12,17}$.$0^{12,21}$.$0^{13,24}$]hexacosane, according to the von Baeyer system.

believed to be formed in the Earth's crust, based on mineral inclusions.[25] The origin of these diamonds is enigmatic not only because of their crustal origin, but also their highly unusual $^{12}C/^{13}C$ isotopic ratios. Unlike other naturally occurring diamonds, which have isotopic signatures representative of mantle-derived carbon, carbonados have $\delta^{13}C$ values from (−25) to (−30) per mil,[26,27] which is in the same range as petroleum.

Received: December 18, 2002 [Z50794]

Keywords: cage compounds · carbon · geochemistry · hydrocarbons · petroleum

[1] J. Ristein in *Properties, Growth and Application of Diamond* (Eds.: M. H. Nazare, A. J. Neves), Inspec, London, **2001**, pp. 73–75.
[2] G. Kopidakis, S. Aubry, *Physica B* **2001**, *296*, 237–250.
[3] P. Badziag, W. S. Verwoerd, W. P. Ellis, N. R. Greiner, *Nature* **1990**, *343*, 244–245.
[4] M. Shen, H. F. Schaefer, C. Liang, J-H. Lii, N. L. Allinger, P. von R. Schleyer, *J. Am. Chem. Soc.* **1992**, *114*, 497–505.
[5] H. Hoft, *Classics in Hydrocarbon Chemistry: Syntheses, Concepts, Perspectives*, Wiley-VCH, Weinheim, **2000**, p. 547.
[6] A. T. Balaban, P. von R Schleyer, *Tetrahedron* **1978**, *34*, 3599–3606.
[7] J. E. Dahl, S. G. Liu, R. M. K. Carlson, *Science* **2003**, *299*, 96–99. Published online 28 November 2002.
[8] P. von R. Schleyer in *Cage Hydrocarbons* (Ed: G. A. Olah), Wiley, New York, **1990**, pp. 1–38.
[9] M. A. McKervey, *Tetrahedron* **1980**, *36*, 971–992.
[10] J. E. P. Dahl, J. M. Moldowan, K. E. Peters, G. E. Claypool, M. A. Rooney, G. E. Michael, M. R. Mello, M. L. Kohnen, *Nature* **1999**, *399*, 54–57.
[11] S. Prawer, J. L. Peng, J. O. Orwa, J. C. McCallum, D. N. Jamieson, L. A. Bursill, *Phys. Rev. B* **2000**, 360–363
[12] F. H. Ree, N. W. Winter, J. N. Glosli, J. A. Viecelli, *Physica B* **1999**, *265*, 223–229.
[13] P. Badziag, W. S. Verwoerd, W. P. Ellis, N. R. Greiner, *Nature* **1990**, *343*, 244–245.

 © 2003 Wiley-VCH Verlag GmbH & Co. KGaA, Weinheim

[14] H. W. Whitlock, M. W. Siefkien, *J. Am. Chem. Soc.* **1968**, *90*, 4929 – 4939.
[15] T. M. Grund, P. von R. Schleyer, P. H. Gund, W. T. Wipke, *J. Am. Chem. Soc.* **1975** *97*, 743 – 751.
[16] High-performance liquid chromatography (IBM, instrument) was conducted on a Zorbax octadecyl silane (ODS) column (250 mm long, 4.6 mm internal diameter) using an acetone mobile phase at 1.5 mL min^{-1}. Cyclohexamantane-containing distillation residue (0.10 mL) was injected neat and fractions were monitored by GC-MS. Cyclohexamantane spontaneously crystallized out of complex mixtures in HPLC fractions in the acetone mobile phase.
[17] Crystal structure determination: $C_{26}H_{30}$, colorless, shiny fragment, crystal size $0.20 \times 0.15 \times 0.06$ mm^3, trigonal, space group $R\bar{3}$ (No. 148), $a = b = 9.0630(10)$, $c = 17.417(2)$ Å, $V = 1238.9(2)$ Å^3, $Z = 3$, $\rho_{calcd} = 1.377$ g cm^{-3}, $2\theta_{max} = 109.7°$, $Cu_{K\alpha}$, $\lambda = 1.54178$ Å, 2θ–ω scans, $T = 293(2)$ K, 780 reflections collected, 352 unique (R(int) = 0.014), 301 observed ($I > 2\sigma(I)$), σ limits 0.002–0.006 Å, Lorentz and polarization corrections applied, no absorption correction, $\mu(Cu_{K\alpha)} = 0.571$ mm^{-1}, solved by direct methods (SHELXS-90), refined by full-matrix least-squares on F^2, all non-H atoms anisotropic, H atoms constrained, (SHELXL-93), 41 parameters, $R_1 = 0.0447$ (observed data), $wR2 = 0.1404$ (all data), max./min. residual electron density 0.265/−0.100 e Å^{-3}. CCDC-202094 contains the supplementary crystallographic data for this paper. These data can be obtained free of charge via www.ccdc.cam.ac.uk/conts/retrieving.html (or from the Cambridge Crystallographic Data Centre, 12, Union Road, Cambridge CB21EZ, UK; fax: (+44) 1223-336-033; or deposit@ccdc.cam.ac.uk).
[18] L. Bistiricic, G. Baranovic, K. A. Mlinaric-Marjerkie, *Spectrochim. Acta Part A* **1995**, *51*, 1643 – 1664.
[19] S. A. Solin, A. K. Ramdas, *Phys. Rev. B* **1970**, 1687 – 1698.
[20] S. Prawer, K. W. Nugent, D. N. Jamieson, J. O. Orwa, L. A. Bursill, J. L. Peng, *Chem. Phys. Lett.* **2000**, *332*, 93 – 97.
[21] J. Pacansky, R. J. Waltman, *J. Phys. Chem.* **1995**, *99*, 3014 – 3019.
[22] S. Prawer, K. W. Nugent, D. N. Jamieson, *Diamond Relat. Mater.* **1998**, *7*, 106 – 110.
[23] M. L. Dheu, D. Gagnaire, H. Duddeck, F. Hollowood, M. A. McKervey, *J. Chem. Soc. Perkin Trans. 2* **1979**, 357 – 359.
[24] R. Lin, Z. Wilk, *Fuel* **1995**, *74*, 1512 – 1521.
[25] H. Kamioka, K. Shibata, I. Kajizuka, T. Ohta, *Geochem. J.* **1996**, *30*, 189 – 194.
[26] D. Shelkov, A. B. Verkhovskii, H. J. Milledge, C. T. Pillinger, *Geol. Geofiz.* **1997**, *38*, 315 – 322.
[27] Y. L. Orlov, *Mineralogy of the Diamond*, Wiley, New York, **1972**.

 © 2003 Wiley-VCH Verlag GmbH & Co. KGaA, Weinheim

Nanoporus Silicate Frameworks

Nanoporous Copper Silicates with One-Dimensional 12-Ring Channel Systems**

*Xiqu Wang, Lumei Liu, and Allan J. Jacobson**

Crystalline materials such as zeolites, with pore arrays of nanometer sizes, are important because of their applications as catalysts and molecular sieves, and their potential use as components in advanced nanocomposites.[1–4] Nanoporous transition-metal silicates are of particular interest because they usually show good chemical and thermal stability and other physical and catalytic properties introduced by the transition-metal centers.[4,5]

We have recently developed a strategy for the synthesis of transition-metal-silicate open-framework and microporous compounds that uses a common building principle. The structures in this family of compounds are formed by linking isolated transition-metal polyhedra $MO_{4/2}X_n$ ($X = O$, F, H_2O, $n = 1,2$) with various anionic silicate building units by sharing four oxygen atoms at the corners of a square. The anionic silicate units may be simple layers of composition $\{SiO_{3/2}O_{1/1}\}$, chains of composition $\{SiO_{2/2}O_{2/1}\}$, cluster ions, or more complex units such as double layers and chains. We have reported examples that contain VO^{2+},[6–8] $NbFO^{2+}$,[9] UO_2^{2+},[10,11] and $[VO]_2^{4+}$[7] ions that link silicate units. The fluorogermanate $Ge_2ZrO_6F_2{\cdot}H_2DAB{\cdot}H_2O$ (DAB = diaminobutane) described by Li et al., which contains ZrF_2^{2+} units that link germanate chains, is closely related.[12] All of the compounds are synthesized under mild temperature and pressure conditions, similar to those used in zeolite syntheses.

Here we report the first examples of this class of compound to contain a Cu^{2+} linking group and a novel framework structure. The extension of the general building principle to copper–oxygen polyhedra is suggested by the known structures of several dense copper silicate phases that also contain copper–oxygen "squares" or tetrahedra.[13–18] The new phases have the general formula given below, and are designated CuSH-1A (A = Na, K, Rb, Cs).[19]

$$Na_4[Cu_2Si_{12}O_{27}(OH)_2][(AOH)_x(NaOH)_y(H_2O)_z];$$
$$A = Na,\ K,\ Rb,\ Cs,\ x \approx 1,\ y \approx 1,\ z \approx 6$$

These structures are unusual in several respects: They are the first examples to contain double layers of silicate tetrahedra that define straight 12-ring channels, analogous to those found in LTL-type zeolites. Unlike LTL, however,

[*] Prof. A. J. Jacobson, Dr. X. Wang, Dr. L. Liu
Department of Chemistry
University of Houston
Houston, TX 77204-5003 (USA)
Fax: (+1) 713-743-2787
E-mail: ajjacob@uh.edu

[**] We thank the National Science Foundation (DMR-0120463) and the Robert A. Welch Foundation for support. This work made use of CMC Shared Experimental Facilities.

 © 2003 Wiley-VCH Verlag GmbH & Co. KGaA, Weinheim DOI: 10.1002/anie.200351121

the framework composition $Na_4[Cu_2Si_{12}O_{27}(OH)_2]$ that defines the 12-ring channels is neutral, and as a consequence only neutral MOH and H_2O species fill these channels, presumably acting as templates during the synthesis.

Crystals of the CuSH-1A phases were synthesized as pale-blue plates with maximum dimensions of about 0.4 mm. CuSH-1Na was prepared as a single phase in high yield (greater than 80% based on Cu). CuSH-1K and CuSH-1Rb could be synthesized only as minor phases while CuSH-1Cs is obtained as major phase (greater than 50% based on Cu). Compositions of CuSH-1Na and CuSH-1Cs were measured by elemental analysis.[20] CuSH-1K and CuSH-1Rb were qualitatively analyzed by energy-dispersive X-ray (EDX) spectrometry using a JEOL JSM 6400 scanning electron microscope with a Link Analytical EXL spectrometer. The crystal structures were determined from single-crystal X-ray diffraction data.[21]

The CuSH-1A phases all have the same framework structure with space-group symmetry *Cmcm*. The porous framework is built from silicate double layers that are arranged perpendicular to the [100] direction, and are cross-linked by interlayer Cu–O and Na–O bonds (Figure 1). The

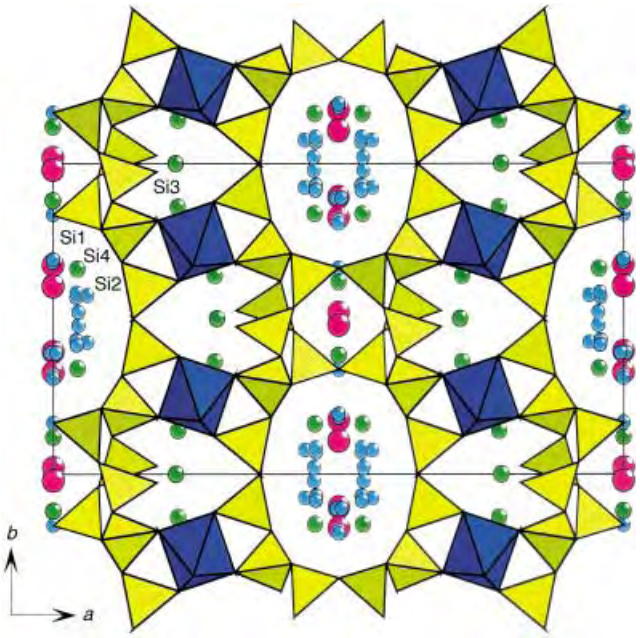


Figure 1. The structure of CuSH-1Cs viewed along the [100] direction showing the 12-ring channels. Copper–oxygen and silicon–oxygen polyhedra are dark blue and yellow, respectively. Purple, green, and cyan circles represent cesium and sodium atoms, and water molecules, respectively.

silicate double layer contains channels defined by 12-rings of tetrahedra that run along the [001] direction and have an aperture of 7.3×4.4 Å, and 8-ring channels along the [011] and [01$\bar{1}$] directions, with an aperture of 3.8×2.5 Å. The silicate double layer that consists of two single layers related by a mirror plane is shown in Figure 2. The single layers are constructed by cross-linking single chains with a periodicity of six tetrahedra. In one period of the chain, the tetrahedron

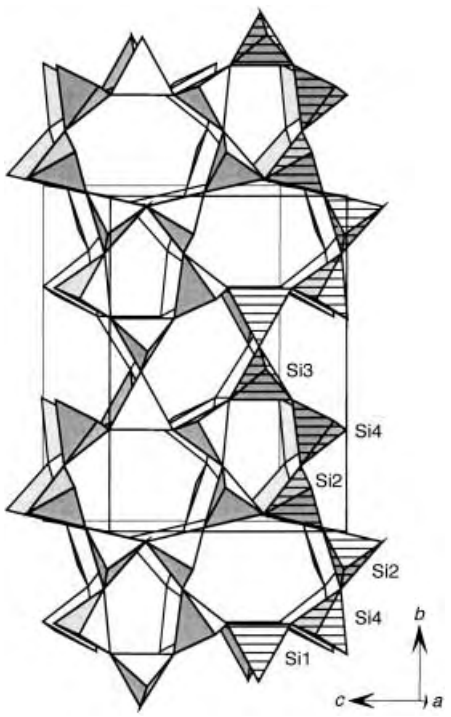


Figure 2. The silicate double layer in the CuSH-1A structures. A single chain is marked by the hatched segments and the silicon atoms in the repeat unit along the chain are labeled.

$\{Si1O_4\}$ shares corners with three tetrahedra from the same single layer and with one tetrahedron from the other single layer. The other five tetrahedra of the repeat unit are all connected to only three other SiO_4 tetrahedra, and each has a terminal oxygen atom pointing towards the space between the double layers. The double layer is an example of an unbranched vierer double layer, according to Liebau's classification, with two types of fundamental chains and a periodicity of four along the [001] direction.[22] The terminal oxygen atoms of the $\{Si2O_4\}$ and $\{Si4O_4\}$ tetrahedra are bonded to the interlayer Cu atoms, while that of the $\{Si3O_4\}$ tetrahedron is bonded to a proton to form a silanol group. Interconnection of the two single layers gives rise to the 12-ring channels. The single layer is unusual in having 5-, 6-, and 7-rings of tetrahedra in equal proportions.

Neighboring silicate double layers are interconnected by $\{CuO_4\}$ squares that share corners with the $\{Si2O_4\}$ and $\{Si4O_4\}$ tetrahedra with Cu–O bond lengths of 1.95 Å (Figure 3). The copper-ion coordination is completed by interlayer water molecules to form single chains of $\{CuO_4(H_2O)_2\}$ elongated octahedra with Cu–OH_2 bond lengths of 2.70 Å. The interlayer water molecule is coordinated to two Cu atoms and one Na atom and forms a relatively strong hydrogen bond to the OH group ($H_2O\cdots HO$ 2.686 Å). The two independent interlayer Na sites, which both have distorted octahedral coordination and Na–O bond lengths in the range 2.33–2.64 Å, are essential structural components. The interlayer $\{CuO_4(H_2O)_2\}$ and $\{Na(O,OH,H_2O)_6\}$ octahedra form a sheet sandwiched between neighboring silicate double

 © 2003 Wiley-VCH Verlag GmbH & Co. KGaA, Weinheim

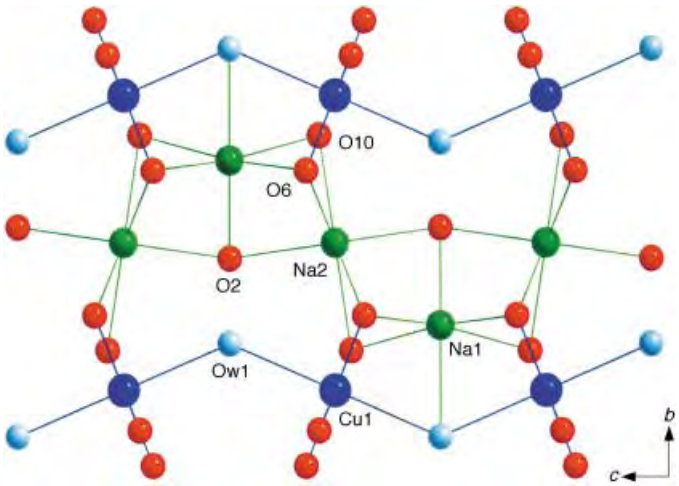


Figure 3. The copper- and sodium-ion coordination environments in the region of the CuSH-1A structure between the silicate double layers. Blue, green, red, and cyan circles represent copper, sodium, and oxygen atoms, and water molecules, respectively.

layers, which gives rise to an electroneutral framework with the composition $\{Na_4Cu_2Si_{12}O_{27}(OH)_2(H_2O)_2\}$. Bond valence sums calculated for the Cu atoms in the CuSH-1A phases are very close to 2.0 valence units, which indicates their divalent character, as expected from the bonding features.[23] The CuSH-1A structure is related to that of the known compounds $A_2Cu_2Si_8O_{19}$ (A = Rb, Cs), which also have silicate double layers cross-linked by $\{CuO_4\}$ squares.[15,16]

The 12-ring channels and the side cavities inside the silicate double-layers of the CuSH-1A structures are filled with highly disordered AOH groups, and water molecules with fractional occupancies. Elemental and thermogravimetric analyses (TGA) and structure refinements indicate that the *x*, *y*, and *z* values in the structural formula are approximately 1, 1, and 6, respectively, for both CuSH-1Cs and CuSH-1Na. For CuSH-1Cs, about 60% of the Cs ions were located inside the 12-ring channels and the remaining 40% were located within a cavity defined by two 8-rings and two 6-rings in the double layer (see Figure 1). Two Na sites were identified according to their separations from the framework oxygen atoms. One site is located inside the 12-ring channels and the other is near the 8-ring of the side cavity mentioned above. In CuSH-1Rb, CuSH-1K, and CuSH-1Na, the extra-framework Cs ions are replaced by smaller alkali-metal ions. As the size of the ions decreases, they shift further away from the cavity center and from the channel axis, which optimizes the bonding with the framework oxygen atoms.

TGA measurements of compound CuSH-1Na in air at a heating rate of 5 K min^{-1} show that the sample loses water immediately upon heating, and is completely dehydrated by approximately 260 °C. X-ray data measured on powder and single-crystal samples after different thermal treatments indicate that the framework is stable to 400 °C in air. Upon complete dehydration at 300 °C, an orthorhombic superstructure is observed with doubled *a* and *b* cell dimensions ($a = 44.78$, $b = 26.006$, $c = 9.447$ Å) and an apparent contraction along the *a* axis. Rehydration is slow but complete after several days in air. The original crystal structure was fully recovered after rehydration, as confirmed by refinements of the single-crystal X-ray data.

A unique feature of the structure of the CuSH-1A species is that, because of the neutral framework, as-prepared samples contain neutral alkali hydroxide species in the channels. On dehydration, these alkali-metal hydroxide (or oxide) species remain and effectively block nitrogen adsorption. Treatment with water or dilute acid partially removes the alkali-metal hydroxide and increases the nitrogen adsorption capacity, but we have not yet found conditions that lead to a complete "cleaning-out" of the channels and realization of the full sorption capacity that is anticipated from the structure. Further experiments are in progress.

In conclusion, the CuSH-1A phases further demonstrate the effectiveness of our approach for building porous frameworks by cross-linking transition-metal coordination polyhedra that can share four corners in a square geometry with condensed silicate components.

Experimental Section

Synthesis of CuSH-1A single crystals: A solution was prepared by dissolving fumed silica (3.7 g) in an aqueous mixture of AOH and NaOH (4.2 M, 27 mL; 1:1 A/Na molar ratio). 1.4 mL of such a solution was then mixed with $CuSO_4 \cdot 5H_2O$ (0.36 g). The mixture was sealed in air and heated at 240 °C for 2 days in a 23-mL teflon-lined autoclave. Pale-blue crystals of CuSH-1A were recovered by vacuum filtration, together with other impurity phases such as $Na_2CuSi_4O_{10}$[13] and $Na_2Cu_3Si_4O_{12}$.[14] To prepare single-phase samples of CuSH-1Na, fumed silica (0.79 g) was mixed with aqueous solutions of $Cu(NO_3)_2$ (1.25 M, 0.56 mL) and NaOH (4.24 M, 0.80 mL). The mixture was sealed, together with H_2O_2 (0.2 mL) and a saturated aqueous solution of Na_2HPO_4 (0.52 mL) in air and heated at 245 °C for 54 h. The product was vacuum-filtered and washed thoroughly with water. No phosphorus was detected in the sample by EDX analysis. IR (KBr; Galaxy FTIR 5000): $\tilde{\nu} = 457$(s), 538(m), 619(w), 677(m), 995(vs), 1115(s), 1163(s), 1655(m), 2937(w), 3527(s), 3616 cm^{-1} (s).

Received: February 6, 2003 [Z51121]

Keywords: copper · hydrothermal synthesis · silicates · transition metals · zeolite analogues

[1] A. K. Cheetham, G. Férey, T. Loiseau, *Angew. Chem.* **1999**, *111*, 3466; *Angew. Chem. Int. Ed.* **1999**, *38*, 3268.
[2] H. V. Bekkum, E. M. Flanigen, P. A. Jacobs, J. C. Jansen, *Introduction to Zeolite Science and Practice*, Elsevier, Amsterdam, **2001**.
[3] M. E. Davis, *Nature* **2002**, *417*, 813.
[4] F. Schüth, W. Schmidt, *Adv. Mater.* **2002**, *14*, 629.
[5] J. Rocha, M. W. Anderson, *Eur. J. Inorg. Chem.* **2000**, 801.
[6] X. Wang, L. Liu, A. J. Jacobson, *Angew. Chem.* **2001**, *113*, 2232; *Angew. Chem. Int. Ed.* **2001**, *40*, 2174.
[7] X. Wang, L. Liu, A. J. Jacobson, *J. Am. Chem. Soc.* **2002**, *124*, 7812.
[8] X. Wang, L. Liu, A. J. Jacobson, *Mater. Res. Soc. Symp. Proc* **2003**, in press.
[9] R. J. Francis, A. J. Jacobson, *Chem. Mater.* **2001**, *13*, 4676.
[10] X. Wang, J. Huang, L. Liu, A. J. Jacobson, *J. Mater. Chem.* **2002**, *12*, 406.
[11] J. Huang, X. Wang, A. J. Jacobson, *J. Mater. Chem.* **2003**, *13*, 191.

 © 2003 Wiley-VCH Verlag GmbH & Co. KGaA, Weinheim

[12] H. Li, M. Eddaoudi, J. Plevert, M. O'Keefe, O. M. Yaghi, *J. Am. Chem. Soc.* **2000**, *122*, 12409.
[13] K. Kawamura, A. Kawahara, *Acta Crystallogr. Sect. B* **1976**, *32*, 2419.
[14] K. Kawamura, A. Kawahara, *Acta Crystallogr. Sect. B* **1977**, *33*, 1071.
[15] A. Heinrich, V. Gramlich, *Naturwissenschaften* **1982**, *69*, 142.
[16] I. Watanabe, A. Kawahara, *Acta Crystallogr. Sect. C* **1993**, *49*, 854.
[17] A. Möller, *Z. Anorg. Allg. Chem.* **1997**, *623*, 1685.
[18] A. R. Heinrich, C. Baerlocher, *Acta Crystallogr. Sect. C* **1991**, *47*,237.
[19] We use the general notation MSH-nA (Metal Silicate Houston, n is the framework type and A is the nonframework cation) to designate this series of compounds. Thus CuSH-n is used for the copper silicate family.
[20] Elemental analyses (Galbraith Lab., Knoxville, TN, USA) calcd (%) for CuSH-1Cs ($Na_4[Cu_2Si_{12}O_{27}(OH)_2][(CsOH)(NaOH)(H_2O)_6]$): Cs 10.07, Na 8.71, Cu 9.63, Si 25.53; found: Cs 10.37, Na 8.78, Cu 9.66, Si 25.62. Calcd for CuSH-1Na ($Na_4[Cu_2Si_{12}O_{27}(OH)_2]$ $[(NaOH)_2(H_2O)_6]$): H 1.32, Na 11.40, Cu 10.50, Si 27.85; found: H 1.31, Na 11.13, Cu 10.38, Si 27.46
[21] X-ray single-crystal analysis for CuSH-1Na: pale-blue plate, $0.26\times0.08\times0.01$ mm, space group *Cmcm*, $a=25.578(4)$, $b=13.098(2)$, $c=9.890(1)$ Å, $V=3313.4(8)$ Å^3, $Z=4$. Final R indices ($I>2\sigma(I)$): $R1=0.0687$, $wR2=0.1678$. For CuSH-1K: pale-blue plate, $0.24\times0.12\times0.01$ mm, space group *Cmcm*, $a=25.474(2)$, $b=13.1346(8)$, $c=9.8537(6)$ Å, $V=3297.0(3)$ Å^3, $Z=4$. $R1=0.0528$, $wR2=0.1249$. For CuSH-1Rb: pale-blue plate, $0.30\times0.12\times0.01$ mm, space group *Cmcm*, $a=25.425(2)$, $b=13.135(1)$, $c=9.9068(7)$ Å, $V=3308.4(4)$ Å^3, $Z=4$. $R1=0.0323$, $wR2=0.0824$. For CuSH-1Cs: pale-blue plate, $0.29\times0.11\times0.01$ mm, space group *Cmcm*, $a=25.639(7)$, $b=13.142(4)$, $c=9.960(3)$ Å, $V=3356(2)$ Å^3, $Z=4$. $R1=0.0410$, $wR2=0.1059$. Intensities were measured on a SMART platform diffractometer equipped with a 1 K CCD area detector using graphite-monochromated $Mo_{K\alpha}$ radiation at 293 K for CuSH-1Na and at 243 K for the other three phases. The structures were solved by direct methods and refined using the SHELXTL program. All ordered non-hydrogen atom positions were refined anisotropically in the final refinements. The disordered water oxygen atoms were forced to have an equal but variable displacement parameter in order to refine their relative occupancies. The total amount of observed water is consistent with that measured from TGA measurements, and was fixed to the formula based on the TGA data. Further details on the crystal structure investigation may be obtained from the Fachinformationszentrum Karlsruhe, 76344 Eggenstein-Leopoldshafen, Germany (fax: (+49) 7247-808-666; e-mail: crysdata@fiz-karlsruhe.de), on quoting the depository numbers CSD-412966, -412967, -412968, -412969.
[22] F. Liebau, *Structural chemistry of silicates*, Springer, Berlin, **1985**.
[23] N. E. Brese, M. O'Keeffe, *Acta Crystallogr. Sect. B* **1991**, *47*, 192.

 © 2003 Wiley-VCH Verlag GmbH & Co. KGaA, Weinheim

Fluorous Oligosaccharide Synthesis

Oligosaccharide Synthesis on a Fluorous Support**

*Tsuyoshi Miura, Kohtaro Goto, Daisuke Hosaka, and Toshiyuki Inazu**

A fluorous solvent such as perfluorohexane is insoluble in most organic solvents and in water, and a mixture of these three solvent types will form three layers. A highly fluorinated (fluorous) compound is soluble in fluorous solvents, and is readily separated from nonfluorinated compounds through simple fluorous–organic solvent partitioning. Since Horváth and Rabái used these properties to introduce the concept of the fluorous biphasic system in 1994,[1] fluorous chemistry has mainly developed in the field of catalysis.[2] Curran and co-workers have also investigated fluorous synthesis as a strategic alternative to solid-phase synthesis for use in several fields such as combinatorial chemistry and parallel synthesis.[3] Recently, they also reported fluorous-mixture synthesis using a fluorous silica gel.[4] Several fluorous protecting groups, which are essential for the performance of fluorous synthesis, have been reported. However, their application is limited to the synthesis of small molecules because the fluorine content in each fluorous protecting group is low.[5] Herein we describe the development of a fluorous support with a high fluorine content and its application in the synthesis of oligosaccharides.

The oligosaccharides on cell surfaces play important roles in biological processes such as cell–cell interaction, cell adhesion, and immunogenic recognition.[6] However, the synthesis of an oligosaccharide is not easy. Although the solid-phase synthesis of oligosaccharides has been actively studied,[7] the usual solid-phase method suffers from some serious disadvantages, such as the difficulty of large-scale synthesis, reduced reactivity, and the inability to monitor the reaction by TLC, NMR spectroscopic analysis, or mass spectrometry. Solid-phase oligosaccharide synthesis on a soluble polyethylene glycol (PEG)-based support has been reported.[8] Although this improved solid-phase method overcomes some of the disadvantages of traditional solid-phase methods, reactions that use the soluble PEG-based support can not be monitored by TLC and the intermediates can not be purified by silica-gel column chromatography. Curran and co-workers have reported a 2-deoxydisaccharide synthesis using a fluorous benzyl protecting group.[5h] Recently, we

[*] Dr. T. Inazu, Dr. T. Miura, K. Goto, D. Hosaka
The Noguchi Institute
1-8-1 Kaga, Itabashi-ku, Tokyo 173-0003 (Japan)
Fax: (+81) 3-5944-3214
E-mail: inz@noguchi.or.jp

[**] This work was partly supported by a Grant-in-Aid for Scientific Research (C) (No. 13680680) and a Grant-in-Aid for the Encouragement of Young Scientists (No. 13771349) from the Japan Society for the Promotion of Science, and by the Takeda Science Foundation. This work was performed through the Noguchi Fluorous Project of our Institute.

 DOI: 10.1002/anie.200250531 © 2003 Wiley-VCH Verlag GmbH & Co. KGaA, Weinheim

reported a method for fluorous oligosaccharide synthesis involving the novel fluorous protecting reagent **1** (Bfp-OH), which contains two fluorous chains.[9] Fluorous oligosaccharide synthesis avoids the disadvantages of solid-phase oligosaccharide synthesis. The introduction of the fluorous protecting group Bfp at three or four hydroxy groups on the glycosyl acceptors allowed us to rapidly synthesize a simple tetrasaccharide[9] as well as the Gb3 oligosaccahride that is bound to verotoxins.[10]

Herein we report the development of a novel fluorous support as an alternative to a solid support and its application in oligosaccharide synthesis. Our concept of oligosaccharide synthesis using a fluorous support is shown in Figure 1. Introduction of the fluorous support only at the anomeric hydroxy functionality of the glycosyl acceptor enables the efficient synthesis of free, long-chain oligosaccharides. The glycosyl acceptor bound to the fluorous support couples with the glycosyl donor to afford the fluorous disaccharide. The reaction mixture is partitioned between fluorous and normal organic solvents, such that the fluorous disaccharide and the excess glycosyl donor are extracted into the fluorous phase and the organic phase, respectively. After selective deprotection, repetition of the above procedure produces the fluorous oligosaccharide, which can be purified by liquid–liquid extraction, without the need for column chromatography. Finally, the fluorous support is removed to give the desired oligosaccharide, which can be extracted from the mixture with a common organic solvent. The fluorous support can be extracted with a fluorous solvent and is recyclable. Oligosaccharide synthesis using a fluorous support is similar to the solid-phase synthesis procedure shown in Figure 2. Liquid–liquid extraction is used for the purification steps in fluorous oligosaccharide synthesis, whereas filtration is used in solid-phase synthesis. Fluorous oligosaccharide synthesis is thus an excellent strategic alternative to solid-phase synthesis.

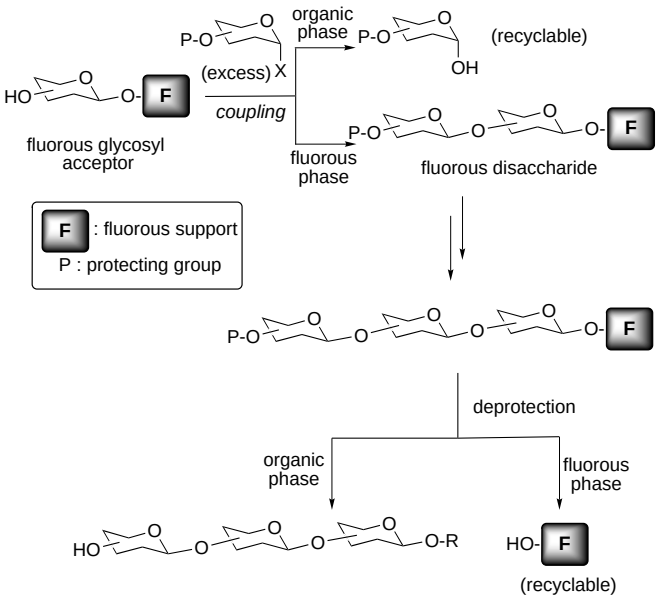


Figure 1. Concept of oligosaccharide synthesis using a fluorous support.

A fluorous support with more fluorous chains than previously used would enhance the performance of the procedure described above. Therefore, we designed and synthesized compound **8**, which contains six fluorous chains, as a novel fluorous support (Scheme 1). We expected the six fluorous chains of **8** to enhance the efficiency of extraction into the fluorous solvent significantly. The reaction of Bfp-OH (**1**)[9] with the fluorous amine **2**[9] provided compound **3** in 96% yield. Treatment of **3** with aqueous NaOH gave the fluorous carboxylic acid **4** with three fluorous chains in 99% yield. The two primary amino functions of diethylenetriamine (**5**) were protected with triphenylmethyl groups, and the resulting intermediate was coupled with methyl hydrogen glutarate to afford compound **6**. Treatment of **6** with hydrochloric acid gave the hydrochloric acid salt **7**. Compound **7** was coupled with **4** (2 equiv), followed by treatment with aqueous NaOH to give the fluorous support **8** (M_W = 3290) with six fluorous chains in good yield. We named the

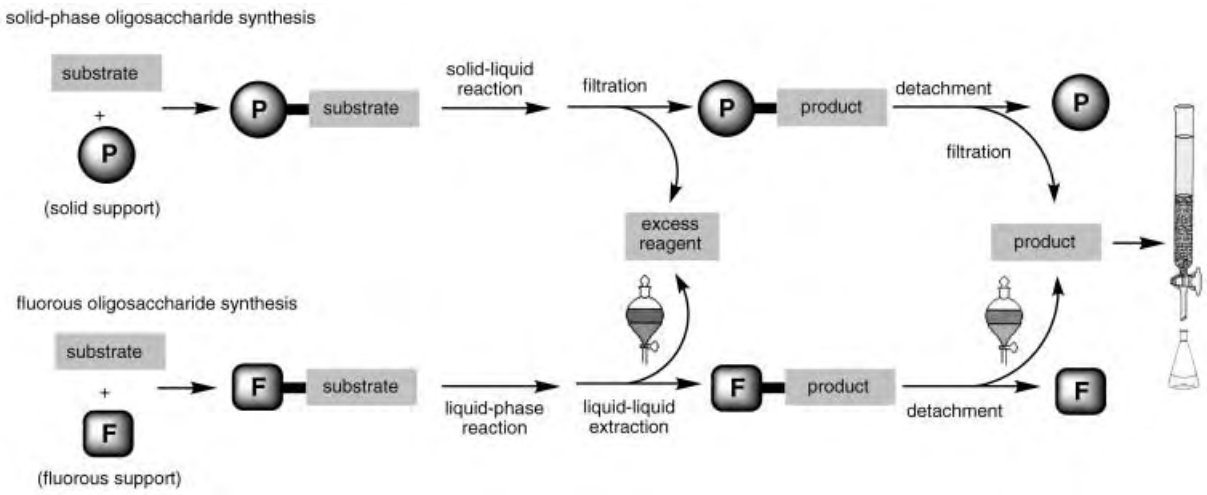
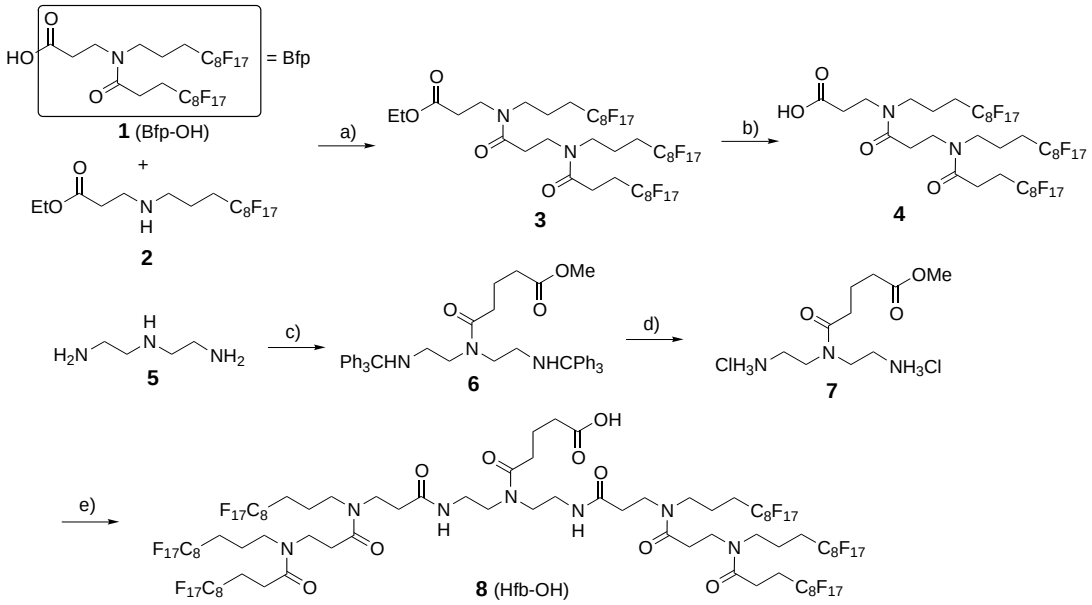


Figure 2. Comparison of fluorous oligosaccharide synthesis with solid-phase oligosaccharide synthesis.

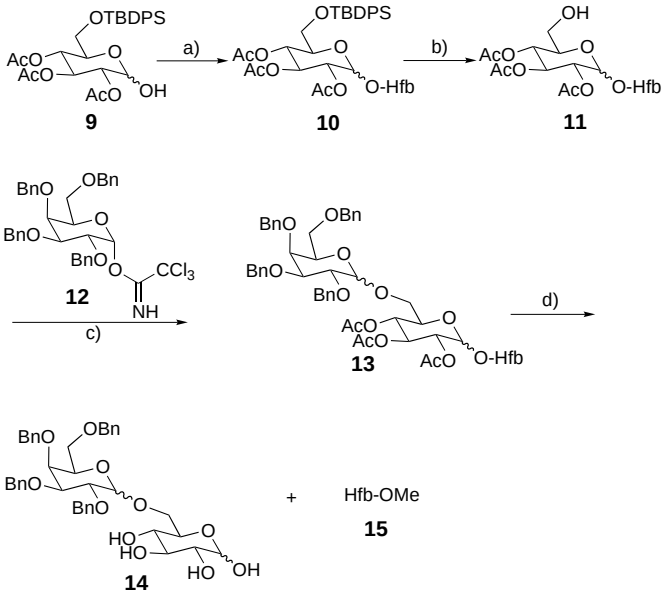
 © 2003 Wiley-VCH Verlag GmbH & Co. KGaA, Weinheim



Scheme 1. Reagents and conditions: a) PyBOP, Et_3N, CH_2Cl_2, room temperature, 20 h, 96%; b) NaOH (1 M), dioxane, 50°C, 4 h, 99%; c) 1) Ph_3CCl, Et_2NH, *i*PrOH, room temperature, 21 h, 95%; 2) monomethyl glutarate, PyBOP, Et_3N, CH_2Cl_2, room temperature, 4 h, 87%; d) HCl, dioxane, 60°C, 16 h, 98%; e) 1) **4**, PyBOP, Et_3N, CH_2Cl_2, room temperature, 24 h, 81%; 2) NaOH (1 M), dioxane, 50°C, 24 h, 98%. PyBOP = benzotriazol-1-yloxytripyrrolidinophosphonium hexafluorophosphate.

acyl moiety of **8** the Hfb (hexakisfluorous chain type butanoyl) group.

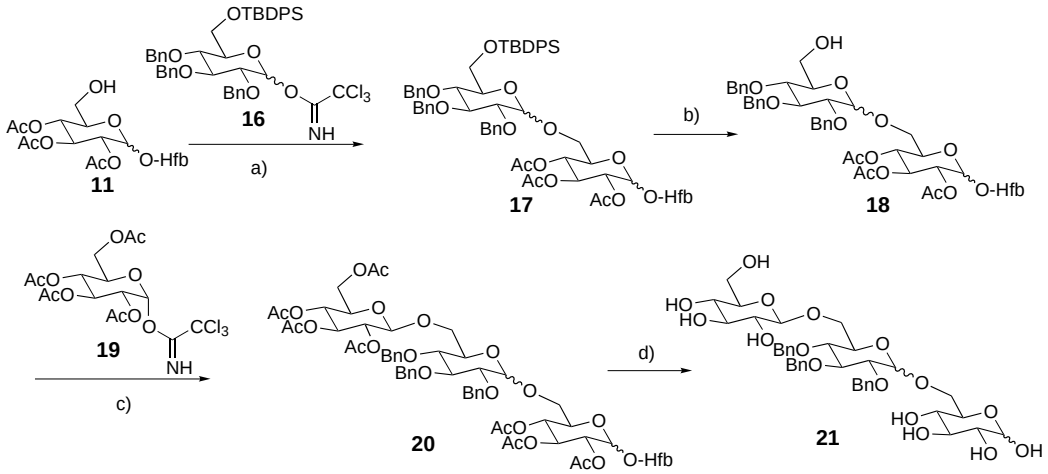
We synthesized the disaccharide **14** as shown in Scheme 2. The fluorous support Hfb was attached to the anomeric hydroxy group of the glucose derivative **9** by using PyBOP and DMAP to give the fluorous compound **10**.[11] The TBDPS group of **10** was removed by treatment with HF–pyridine in THF to afford the fluorous glycosyl acceptor **11**.[11] The fluorous disaccharide **13**[11,12] was obtained by the reaction of **11** with the glycosyl donor **12** (9 equiv)[13] in the presence of TMSOTf in $Et_2O/EtOC_4F_9$.[14] The fluorous intermediates **10, 11**, and **13** were each extracted with the fluorous solvent FC-72[15] by partitioning the product mixtures between FC-72 and an organic solvent. No further purification such as silica gel column chromatography was carried out. The Hfb group of **13** was removed by treatment with NaOMe in $MeOH/EtOC_4F_9$ to afford crude **14**, which was extracted with MeOH by partitioning the mixture between FC-72 and MeOH. The methyl ester of Hfb (Hfb-OMe, **15**) was obtained from the FC-72 layer. Compound **15** was treated with aqueous NaOH to give **8**, which was reused. Finally, the pure disaccharide **14**[16] was obtained from a single silica-gel column-chromatographic purification step in 67% overall yield from **9** (four steps).



Scheme 2. Reagents and conditions: a) **8**, PyBOP, DMAP, CH_2Cl_2, room temperature, 20 h; b) HF–pyridine, THF, room temperature, 20 h; c) TMSOTf, molecular sieves (4 Å), $EtOC_4F_9$, Et_2O, 0°C, 20 min; d) NaOMe, $EtOC_4F_9$, MeOH, room temperature, 16 h, then silica-gel chromatography, 67% from **9**. Bn = benzyl, DMAP = 4-dimethylaminopyridine, TBDPS = *tert*-butyldiphenylsilyl, TMSOTf = trimethylsilyl trifluoromethanesulfonate.

Next, we synthesized the trisaccharide **21** as shown in Scheme 3. The fluorous glycosyl acceptor **11** was coupled with the glycosyl donor **16** (9 equiv)[17] to afford the fluorous disaccharide **17**.[11,18] The TBDPS group of **17** was removed by treatment with HF–pyridine in THF to give the fluorous compound **18**.[11] The reaction of the fluorous glycosyl acceptor **18** with the glycosyl donor **19** (20 equiv)[13] under similar glycosidation conditions afforded the fluorous trisaccharide **20**.[11] The intermediates **17, 18**, and **20** were isolated in analogy with **10, 11**, and **13**. The pure trisaccharide **21**[19] was obtained in the same way as **14** in 42% overall yield from **9** (six steps).

 © 2003 Wiley-VCH Verlag GmbH & Co. KGaA, Weinheim



Scheme 3. Reagents and conditions: a) TMSOTf, molecular sieves (4 Å), $EtOC_4F_9$, Et_2O, 0 °C, 20 min; b) HF–pyridine, THF, room temperature, 22 h; c) TMSOTf, molecular sieves (4 Å), $EtOC_4F_9$, Et_2O, 0 °C, 2 min; d) NaOMe, $EtOC_4F_9$, MeOH, room temperature, 14 h, then silica-gel chromatography, 42% from **9**.

In conclusion, although the introduction of several Bfp groups into the glycosyl acceptor was required for fluorous oligosaccharide synthesis,[9] the attachment of the fluorous support Hfb through just the anomeric hydroxy functionality of the glycosyl acceptor allowed efficient oligosaccharide synthesis because the fluorine content in the Hfb group is very high. The fluorous support reagent **8** (Hfb-OH) could be prepared on a large scale. The Hfb support could be removed in high yield under standard dilute basic conditions for the deprotection of acetyl or benzoyl groups, and was recyclable after cleavage. The use of the fluorous support Hfb made it possible to synthesize an oligosaccharide rapidly, without the need for purification of the fluorous intermediates by column chromatography. Each fluorous synthetic intermediate could be obtained in a straightforward manner by simple fluorous–organic solvent extraction, and the reactions could be monitored by TLC, NMR spectroscopic analysis, and mass spectrometry, in contrast to solid-phase reactions. Thus, the reaction conditions for each synthetic step could be optimized rapidly. Although the fluorous intermediates could also be subjected to silica-gel column chromatography if necessary, only the final compounds were purified by chromatography. This fluorous oligosaccharide synthesis should be applicable to large-scale synthesis as it is performed in the liquid phase. Thus, oligosaccharide synthesis on the fluorous support Hfb is an excellent strategic alternative to solid-phase oligosaccharide synthesis. The optimization of the glycosidation conditions and further applications to the synthesis of several bioactive carbohydrates and glycoconjugates are now in progress.

Experimental Section

10: DMAP (243 mg, 1.98 mmol) and PyBOP (1.03 g, 1.98 mmol) were added to a solution of **9** (1.00 g, 1.84 mmol) and Hfb-OH (**8**, 2.17 g, 0.660 mmol) in dry CH_2Cl_2 (110 mL). The mixture was stirred for 20 h at room temperature, then MeOH (110 mL) was added and the CH_2Cl_2 was evaporated. The reaction mixture was then extracted with FC-72 (3 × 110 mL) and the combined FC-72 layers were concentrated. Crude **10** (2.45 g) was used in the next step without further purification.

11: HF–pyr (4.45 ml, 159 mmol) was added to a solution of crude **10** (2.45 g) in THF (38 mL). The resulting mixture was stirred for 20 h at room temperature, and then added to saturated aqueous $NaHCO_3$ (150 ml). Toluene (150 mL) was added to the reaction mixture, which was then extracted with FC-72 (3 × 150 mL). The FC-72 layers were washed with brine, dried over anhydrous Na_2SO_4, and concentrated. Crude **11** (2.30 g) was used in the next step without further purification.

13: Powdered molecular sieves (4 Å, 1.4 g) were added to a solution of crude **11** (395 mg) and **12** (680 mg, 0.992 mmol) in a mixture of dry Et_2O (6.0 mL) and $EtOC_4F_9$ (3.2 mL) under an argon atmosphere. The resulting mixture was stirred for 2 h at room temperature, then TMSOTf (140 μL, 0.773 mol) was added at 0 °C. The mixture was stirred for a further 20 min at 0 °C, then triethylamine (0.5 mL) was added and the reaction mixture was filtered. The filtrate was added to saturated $NaHCO_3$, and the mixture was extracted three times with EtOAc. The EtOAc layers were washed with brine, dried over anhydrous Na_2SO_4, and evaporated. The residue was partitioned between MeOH and FC-72. The FC-72 layer was concentrated to give crude **13** (372 mg), which was used in the next step without further purification.

14: A solution of NaOMe in MeOH (28%, 10 μL) was added to a solution of crude **13** (349 mg) in a mixture of $EtOC_4F_9$ (8 mL) and MeOH (16 mL). The reaction mixture was stirred for 16 h at room temperature, then amberlite IR-120 (H^+ form) was added, and the mixture was neutralized. The mixture was then filtered, and the filtrate was concentrated. The residue was partitioned between MeOH and FC-72. The MeOH layer was concentrated to give crude **14**. The FC-72 layer was evaporated to afford pure **15**. The crude **14** was purified by column chromatography on silica gel to give pure **14** (50 mg, 67% over four steps) as a white powder.

Received: November 12, 2002
Revised: February 7, 2003 [Z50531]

Keywords: fluorine · glycosylation · oligosaccharides · synthetic methods

[1] I. T. Horváth, J. Rábai, *Science* **1994**, *266*, 72.

 © 2003 Wiley-VCH Verlag GmbH & Co. KGaA, Weinheim

[2] J. Nishikido, M. Kamishima, H. Matsuzawa, K. Mikami, *Tetrahedron* **2002**, *58*, 8345; C. Rocaboy, J. A. Gladysz, *Org. Lett.* **2002**, *4*, 1993; Y. Nakamura, S. Takeuchi, K. Okumura, Y. Ohga, *Tetrahedron* **2001**, *57*, 5565; A. G. M. Barrett, D. C. Braddock, D. Catterick, D. Chadwick, J. P. Henschke, R. M. McKinnell, *Synlett* **2000**, 847, and references therein.

[3] D. P. Curran, *Pure Appl. Chem.* **2000**, *72*, 1649; D. P. Curran, *Angew. Chem.* **1998**, *110*, 1230; *Angew. Chem. Int. Ed.* **1998**, *37*, 1174, and references therein; Corrigendum: D. P. Curran, *Angew. Chem.* **1998**, *110*, 2569; *Angew. Chem. Int. Ed.* **1998**, *37*, 2292

[4] W. Zhang, Z. Luo, C. H. Chen, D. P. Curran, *J. Am. Chem. Soc.* **2002**, *124*, 10443; D. P. Curran, T. Furukawa, *Org. Lett.* **2002**, *4*, 2233; Q. Zhang, A. Rivkin, D. P. Curran, *J. Am. Chem. Soc.* **2002**, *124*, 5774; D. P. Curran, *Synlett* **2001**, 1488; Z. Luo, Q. Zhang, Y. Oderaotoshi, D. P. Curran, *Science* **2001**, *291*, 1766.

[5] a) D. Schwinn, W. Bannwarth, *Helv. Chim. Acta* **2002**, *85*, 255; b) J. Pardo, A. Cobas, E. Guitlán, L. Castedo, *Org. Lett.* **2001**, *3*, 3711; c) Z. Luo, J. Williams, R. W. Read, D. P. Curran, *J. Org. Chem.* **2001**, *66*, 4261; d) P. Wipf, J. T. Reeves, R. Balachandran, K. A. Giuliano, E. Hamel, B. W. Day, *J. Am. Chem. Soc.* **2000**, *122*, 9391; e) S. Röver, P. Wipf, *Tetrahedron Lett.* **1999**, *40*, 5667; f) P. Wipf, J. T. Reeves, *Tetrahedron Lett.* **1999**, *40*, 5139; g) P. Wipf, J. T. Reeves, *Tetrahedron Lett.* **1999**, *40*, 4649; h) D. P. Curran, R. Ferritto, Y. Hua, *Tetrahedron Lett.* **1998**, *39*, 4937; i) A. Studer, D. P. Curran, *Tetrahedron* **1997**, *53*, 6681.

[6] A. Varki, *Glycobiology* **1993**, *3*, 97; R. A. Dwek, *Chem. Rev.* **1996**, *96*, 683; D. L. Blithe, *Trends Glycosci. Glycotechnol.* **1993**, *5*, 81.

[7] S. Manabe, Y. Ito, *J. Am. Chem. Soc.* **2002**, *124*, 12638; O. J. Plante, E. R. Palmacci, P. H. Seeberger, *Science* **2001**, *291*, 1523, and references therein.

[8] E. Eicher, F. Yan, J. Sealy, D. M. Whitfield, *Tetrahedron* **2001**, *57*, 6679; H. Ando, S. Manabe, Y. Nakahara, Y. Ito, *J. Am. Chem. Soc.* **2001**, *123*, 3848; Y. Ito, O. Kanie, T. Ogawa, *Angew. Chem.* **1996**, *108*, 2691; *Angew. Chem. Int. Ed. Engl.* **1996**, *35*, 2510; S. P. Douglas, D. M. Whitfield, J. J. Krepinsky, *J. Am. Chem. Soc.* **1995**, *117*, 2116.

[9] T. Miura, Y. Hirose, M. Ohmae, T. Inazu, *Org. Lett.* **2001**, *3*, 3947.

[10] T. Miura, T. Inazu, *Tetrahedron Lett.* **2003**, *44*, 1819.

[11] Product mixtures containing the fluorous compounds **10, 13**, and **20** were partitioned between FC-72 and MeOH. Those containing the fluorous compounds **11** and **18** were partitioned between FC-72, toluene, and water. The product mixture containing the fluorous compound **17** was partitioned between FC-72 and acetonitrile. None of the fluorous compounds were detected by TLC of the organic layer after three extractions with FC-72, which shows that these compounds were quantitatively extracted with FC-72.

[12] The anomer ratio of compound **13** (at the newly formed anomeric position) was determined to be $\alpha/\beta = 50{:}50$ by NMR spectroscopic analysis.

[13] R. R. Schmidt, J. Michel, M. Roos, *Liebigs Ann. Chem.* **1984**, 1343.

[14] $EtOC_4F_9$ is a commercially available fluorocarbon solvent (3M, Tokyo) called Novec HFE-7200.

[15] FC-72 is a commercially available fluorocarbon solvent (3M, Tokyo) called Fluorinert FC-72, which consists of perfluorohexane (C_6F_{14}) isomers.

[16] Compound **14** was identified by comparison of spectroscopic data of the debenzylated products (melibiose and allolactose) with those of authentic samples: K. Bock, C. Pedersen, H. Pedersen, *Adv. Carbohydr. Chem. Biochem.* **1983**, *42*, 193; K. Ajisaka, H. Fujimoto, H. Nishida, *Carbohydr. Res.* **1988**, *180*, 35.

[17] W. Xu, S. A. Springfield, J. T. Koh, *Carbohydr. Res.* **2000**, *325*, 169.

[18] The anomer ratio of compound **17** (at the newly formed anomeric position) was determined to be $\alpha/\beta = 67{:}33$ by NMR spectroscopic analysis.

[19] Compound **21** was identified by comparison of the spectroscopic data of the debenzylation product with those of an authentic sample: S. Koto, N. Morishima, S. Shichi, H. Haigoh, M. Hirooka, M. Okamoto, T. Higuchi, K. Shimizu, Y. Hashimoto, T. Irisawa, H. Kawasaki, Y. Takahashi, M. Yamazaki, Y. Mori, K. Kudo, T. Ikegaki, S. Suzuki, S. Zen, *Bull. Chem. Soc. Jpn.* **1992**, *65*, 3257.

 © 2003 Wiley-VCH Verlag GmbH & Co. KGaA, Weinheim

Synthesis of Carbazoles

The Double *N*-Arylation of Primary Amines: Toward Multisubstituted Carbazoles with Unique Optical Properties**

Kyoko Nozaki, Keita Takahashi, Koji Nakano, Tamejiro Hiyama, Hong-Zhi Tang, Michiya Fujiki, Shigehiro Yamaguchi, and Kohei Tamao*

Carbazole has been known as an important intermediate for artificial dyes and has recently attracted much attention because of its unique photophysical properties.[1] The introduction of substituents onto carbazole is essential to optimize its absorption, luminescence, and electronic properties.[2] For the synthesis of multisubstituted carbazole derivatives, the construction of the carbazole ring itself is highly desired.[3]

[*] Prof. Dr. K. Nozaki, K. Nakano
Department of Chemistry and Biotechnology
Graduate School of Engineering, The University of Tokyo
Hongo, Bunkyo-ku, Tokyo 113-8656 (Japan)
Fax: (+81) 3-5841-7261
E-mail: nozaki@chembio.t.u-tokyo.ac.jp

Prof. Dr. K. Nozaki, Dr. S. Yamaguchi
PRESTO-JST (Japan)
JST, Hon-cho, Kawaguchi, Saitama 332-0012 (Japan)

K. Takahashi, Prof. Dr. T. Hiyama
Department of Material Chemistry
Graduate School of Engineering, Kyoto University
Yoshida, Sakyo-ku, Kyoto 606-8501 (Japan)

Dr. H.-Z. Tang, Prof. Dr. M. Fujiki
CREST-JST
JST, Hon-cho, Kawaguchi, Saitama 332-0012 (Japan)

Prof. Dr. M. Fujiki
Graduate School of Materials Science
Nara Institute of Science and Technology
Takayama, Ikoma, Nara 630-0101 (Japan)

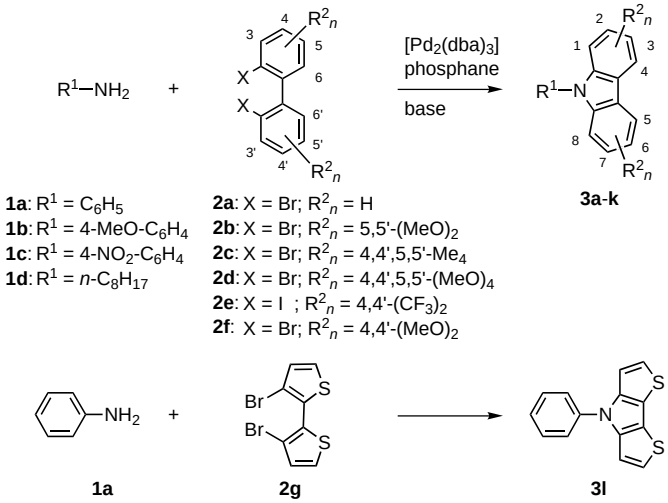
Dr. S. Yamaguchi, Prof. Dr. K. Tamao
Institute for Chemical Research, Kyoto University
Uji, Kyoto 611-0011 (Japan)

[**] We thank the Ministry of Education, Culture, Sports, Science, and Technology, Japan, for the Grants-in-Aid for COE Research on Elements Science, No. 12CE2005.

Supporting information for this article is available on the WWW under http://www.angewandte.org or from the author.

 DOI: 10.1002/anie.200250648 © 2003 Wiley-VCH Verlag GmbH & Co. KGaA, Weinheim

The availability of substituted 2,2′-dihalobiphenyl compounds[4] prompted us to study the double *N*-arylation strategy to synthesize multisubstituted carbazoles as described in Scheme 1. In contrast to conventional carbazole-



Scheme 1. The double *N*-arylation of primary amines in the synthesis of carbazoles (dba = *trans,trans*-dibenzylideneacetone).

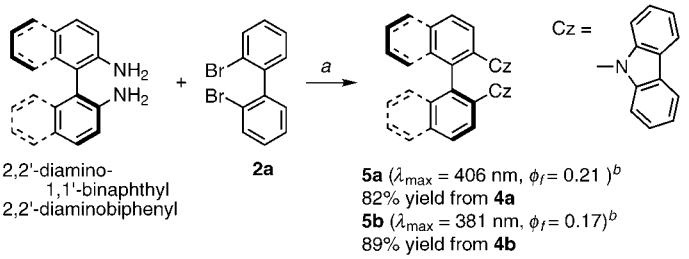
Table 1: Synthesis of carbazoles **3a–l** and their fluorescence data.

Entry	1	2	3	Yield [%][a]	λ_{max} [nm^{-1}] (ϕ_f)[b]
1	**a**	**a**	**a**	86^A	342 (0.23)
2	**a**	**b**	**b**	90^A	383 (0.18)
3	**a**	**c**	**c**	53^A	349 (0.42)
4	**a**	**d**	**d**	76^A	373 (0.18)
5	**a**	**e**	**e**	73^A	361 (0.20)
6	**a**	**f**	**f**	67^B	345 (0.19)
7	**b**	**a**	**g**	92^A	347 (0.21)
8	**b**	**b**	**h**	88^A	386 (0.24)
9	**c**	**a**	**i**	84^C	—[c]
10	**c**	**b**	**j**	8^D	—[c]
11	**d**	**a**	**k**	28^A	347 (0.30)
12	**a**	**g**	**l**	35^A	—[c]

[a] Reaction conditions A–D are noted as superscripts. Condition A: **1** (1.00 mmol), **2** (1.20 mmol), [$Pd_2(dba)_3$] (0.05 mmol), tBu$_3$P (0.20 mmol), NaOtBu (2.40 mmol), toluene (2 mL), 80 °C. Reaction times are specified in the Supporting Information. Condition B: **1** (1.00 mmol), **2** (2.00 mmol), [$Pd_2(dba)_3$] (0.05 mmol), tBu$_3$P (0.20 mmol), NaOtBu (2.40 mmol), toluene (2 mL), 80 °C, 24 h, then 100 °C, 24 h. Condition C: **1** (1.00 mmol), **2** (1.20 mmol), [$Pd_2(dba)_3$] (0.05 mmol), (*S*)-binap (0.15 mmol), Cs_2CO_3 (2.80 mmol), toluene (2 mL), 100 °C, 72 h. Condition D: **1** (1.00 mmol), **2** (1.20 mmol), [$Pd_2(dba)_3$] (0.05 mmol), 2-[di(*tert*-butyl)phosphanyl]biphenyl (0.20 mmol), and K_3PO_4 (2.80 mmol), dimethoxyethane (2 mL), 100 °C, 72 h. [b] Fluorescence spectra were measured in cyclohexane. [c] No clear peaks were observed for **3i, 3j, 3l**.

ring construction strategies starting from *ortho*-aminobiphenyl compounds,[4b,5,6] the nitrogen atom comes from primary amines in the present double *N*-arylation strategy. Although the double arylation of primary amines was successfully accomplished for the synthesis of triarylamines, the method has not yet been applied to the synthesis of carbazoles.[7] Herein we report that the present method is especially effective for the synthesis of sterically crowded 2,2′-dicarbazolyl-1,1′-biaryl compounds **5a** and **5b**, which could not be synthesized by the simple arylation of carbazole (Scheme 2). The unique optical properties of **5a** and **5b** are also disclosed.

Based on the recent intensive studies on the catalytic *N*-arylation of amines with organic halides,[8] [$Pd_2(dba)_3$]/tBu$_3$P/NaOtBu (condition A),[9] was first employed for our purpose. Representative results are summarized in Table 1, which also contains the fluorescence data of the resulting carbazoles **3a–l**. The reaction was applicable to various dihalobiphenyl compounds **2a–e** (Table 1, entries 1–5). 4,4′-Dimethoxy-2,2′-dibromobiphenyl (**2f**) showed a lower reactivity and was used in excess at a higher temperature (Table 1, entry 6, condition B). Substituted anilines can be employed. 4-Methoxyaniline (**1b**) was preferable (Table 1, entries 7 and 8), whereas the reaction was retarded with 4-nitroaniline (**1c**). In such a case, a combination of binap[10] and Cs_2CO_3 was effective (Table 1, entry 9, condition C). The reaction of **1c** with **2b** did not proceed under conditions A, B, or C. The coupling product was finally obtained in a small amount by using 2-di(*tert*-butyl)phosphanylbiphenyl[11] and K_3PO_4 in DME (Table 1, entry 10, condition D). A lower reactivity was observed with the aliphatic amine **1d** (Table 1, entry 11). A dithienopyrrole, **3g**, could be synthesized through double *N*-arylation starting from bithiophene **2g** (Table 1, entry 12).



Scheme 2. Synthesis and optical properties of dicarbazolylbiaryl compounds **5a** and **5b**. a) Reaction conditions: **4** (0.50 mmol), **2a** (1.20 mmol), [$Pd_2(dba)_3$] (0.050 mmol), tBu$_3$P (0.20 mmol), NaOtBu (2.40 mmol), toluene (2.0 mL), 80 °C, 24 h. b) Fluorescence spectra were measured in cyclohexane (excited at 295 nm).

The method is especially effective for sterically hindered aryl amines as shown in Scheme 2. Starting from (*S*)-2,2′-diamino-1,1′-binaphthyl (**4a**) and more than 2 molar amounts of 2,2′-dibromobiphenyl (**2a**), *N*-arylation took place four times per molecule of **4a** to afford the desired chiral dicarbazolylbinaphthyl **5a** in 82% yield. Tri(*tert*-butyl)phosphane was the ligand of choice. Dicarbazolylbiphenyl **5b** was similarly prepared from 2,2′-diaminobiphenyl (**4b**) and **2a**. An alternative approach to **5** in which 2,2′-dibromo-1,1′-binaphthyl (racemic, **6**) or 2,2′-dibromobiphenyl (**2a**) were treated with more than 2 molar amounts of carbazole failed. A Pd/phosphane[12] catalyst gave a monocoupling product, 2-carbazolyl-2′-bromobinaphthyl, in less than 8% yield from **6**. The use of a Ni or Cu catalyst resulted in no reaction.[13]

The fluorescence spectra of **5a** and **5b** both showed broad peaks, suggesting the formation of intramolecular excimers and/or exciplexes.[14,15] Furthermore, the fluorescence wavelengths of **5a** and **5b** significantly depend on the solvent

 © 2003 Wiley-VCH Verlag GmbH & Co. KGaA, Weinheim

polarity.[16] When **5a** was excited at 295 nm, the emission peak underwent a red shift as the solvent polarity increased from cyclohexane (dielectric constant 2.0) to chloroform (4.7), and to acetonitrile (37.5) (Figure 1). This observation corresponds to the energetic stabilization of the polar excimer (and/or exciplex) by solvation.

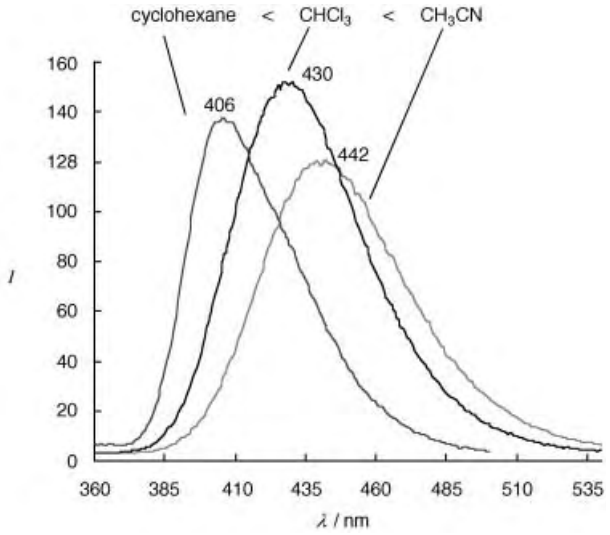


Figure 1. Solvent dependence of fluorescence of **5a**. Each solution (10 mM) was excited at 295 nm. I = intensity (arbitrary units).

In conclusion, we have presented a new strategy toward carbazole synthesis. Dicarbazolylbiaryl compounds **5a** and **5b**, which could not be synthesized by other methods, exhibited solvent-dependent excimer (and/or exciplex) emission. Taking advantage of its chiral nature, further studies on the chiroptical properties of **5a** are currently underway.

Experimental Section

5a: A solution of tri(*tert*-butyl)phosphane (40 mg, 0.20 mmol) in toluene (1.0 mL) was added to a mixture of **2a** (374 mg, 1.20 mmol), **4a** (142 mg, 0.50 mmol), sodium *tert*-butoxide (231 mg, 2.40 mmol), and $[Pd_2(dba)_3]$ (46 mg, 0.050 mmol) in toluene (1.0 mL). After heating under argon at 80 °C for 24 h, the reaction mixture was concentrated, and purification by silica-gel column chromatography afforded **5a** (240 mg, 82 %) as colorless needles. M.p. 277.6–278.1 °C; $R_f = 0.38$ (hexane/EtOAc = 5:1); $[\alpha]_D^{25} = -274.5$ ($c = 0.42$, $CHCl_3$); > 99 % *ee* (HPLC: Chiralcel OD, hexane/*i*PrOH = 99:1, $t_R = 7.9$ min (*R*), 10.4 min (*S*)); ^{1}H NMR (200 MHz, $CDCl_3$): $\delta = 7.95$ (d, 2H, $J =$ 8.0 Hz), 7.88–7.78 (m, 6H), 7.68–7.51 (m, 6H), 7.14 (d, 2H, $J =$ 8.8 Hz), 6.96 (dd, 2H, $J = 7.2$, 7.2 Hz), 6.85–6.60 (m, 6H), 6.45 (dd, 2H, $J = 7.7$, 7.7 Hz), 5.57 ppm (d, 2H, $J = 8.2$ Hz); ^{13}C NMR (50 MHz, $CDCl_3$): $\delta = 142.1$, 140.8, 135.8, 134.3, 133.0, 131.4, 128.6, 128.1, 127.3, 126.7, 126.3, 125.4, 124.4, 123.7, 119.6, 119.5, 119.2, 118.8, 110.6, 110.2 ppm; MS (FAB$^+$): *m*/*z* (%): 584 (148.7), 585 (122.4), 586 (44.6), 587 (12.4); HRMS (FAB$^+$): calcd for $C_{44}H_{28}N_2$: M^+ 584.2252M, found: *m*/*z* 584.2257; elemental analysis: calcd for **5a**·$CHCl_3$ ($C_{45}H_{29}N_2Cl_3$): C 76.76, H 4.15; found: C 76.82, H 4.14; absorption (λ_{max} nm (log ε)): in cyclohexane: 341 (3.89), 294 (4.51), 229 (5.20); in $CHCl_3$: 343 (3.78), 305 (4.47), 297 (4.45); in CH_3CN: 340 (4.01), 293 (4.48), 228 (5.20); emission: λ_{max} nm in cyclohexane: 407 ($\phi_f = 0.21$); in $CHCl_3$: 430 ($\phi_f = 0.18$); in CH_3CN: 442 ($\phi_f = 0.13$) (quantum yields estimated with reference to *p*-terphenyl ($\phi_f = 0.87$ in cyclohexane when excited at 265 nm)).

Received: November 27, 2002 [Z50648]

Keywords: biaryls · luminescence · nitrogen heterocycles · palladium

[1] a) Y. Zhang, T. Wada, H. Sasabe, *J. Mater. Chem.* **1998**, *8*, 809; b) K. R. J. Thomas, J. T. Lin, Y.-T. Tao, C.-W. Ko, *J. Am. Chem. Soc.* **2001**, *123*, 9404; c) J. L. Diaz, A. Dobarro, B. Villacampa, D. Velasco, *Chem. Mater.* **2001**, *13*, 2528.

[2] a) J.-F. Morin, M. Leclerc, *Macromolecules* **2001**, *34*, 4680; b) G. Schiavon, S. Zecchin, J.-F. Morin, M. Leclerc, *Macromolecules* **2002**, *35*, 2122.

[3] a) T. L. Gilchrist, *Heterocyclic Chemistry*, Pitman Publishing Ltd., London, **1985**; b) R. J. Sundberg, *Comprehensive Heterocyclic Chemistry, Vol. 2*, Pergamon, Oxford, **1996**, pp. 119–206.

[4] a) H. Gilman, B. J. Gaj, *J. Org. Chem.* **1957**, *22*, 447; b) T. Yamato, C. Hideshima, K. Suehiro, M. Tashiro, G. K. Parakash, G. A. Olah, *J. Org. Chem.* **1991**, *56*, 6248.

[5] a) J. I. G. Cadogan, M. C. Wood, R. K. Mackie, R. J. G. Searle, *J. Chem. Soc.* **1965**, 4831; b) G. D. Mendenhall, P. A. S. Smith, *Org. Synth.* **1973**, *5*, 829; c) B. C. Soderberg, *Curr. Org. Chem.* **2000**, *4*, 727, and references therein.

[6] a) D. L. Boger, S. R. Duff, J. S. Panek, M. Yasuda, *J. Org. Chem.* **1985**, *50*, 5782; D. L. Boger, S. R. Duff, J. S. Panek, M. Yasuda, *J. Org. Chem.* **1985**, *50*, 5790; b) M. S. Driver, J. F. Hartwig, *J. Am. Chem. Soc.* **1995**, *117*, 4708; c) J. L. Wood, B. M. Stoltz, H. J. Dietrich, D. A. Pflum, D. T. Petsch, *J. Am. Chem. Soc.* **1997**, *119*, 9641.

[7] a) S. Thayumanan, S. Barlow, S. R. Marder, *Chem. Mater.* **1997**, *9*, 3231; b) M. C. Harris, S. L. Buchwald, *J. Org. Chem.* **2000**, *65*, 5327.

[8] For reviews, see: a) J. F. Hartwig, *Synlett* **1997**, 329; b) J. P. Wolfe, S. Wagaw, J. F. Marcoux, S. L. Buchwald, *Acc. Chem. Res.* **1998**, *31*, 805; c) J. F. Hartwig, *Angew. Chem.* **1998**, *110*, 2154; *Angew. Chem. Int. Ed.* **1998**, *37*, 2046; d) B. H. Yang, S. L. Buchwald, *J. Organomet. Chem.* **1999**, *576*, 125.

[9] a) T. Yamamoto, M. Nishiyama, Y. Koike, *Tetrahedron Lett.* **1998**, *39*, 2367; b) M. Nishiyama, T. Yamamoto, Y. Koike, *Tetrahedron Lett.* **1998**, *39*, 617; c) J. F. Hartwig, M. Kawatsura, S. I. Hauck, K. H. Shaughnessy, L. M. Alcazar-Roman, *J. Org. Chem.* **1999**, *64*, 5575.

[10] J. P. Wolfe, S. L. Buchwald, *J. Org. Chem.* **2000**, *65*, 1144.

[11] J. P. Wolfe, H. Tomori, J. P. Sadigshi, J. Yin, S. L. Buchwald, *J. Org. Chem.* **2000**, *65*, 1158.

[12] For the *N*-arylation of pyrroles, indoles, and carbazoles, see: a) G. Mann, J. F. Hartwig, M. S. Driver, C. Fernández-Rivas, *J. Am. Chem. Soc.* **1998**, *120*, 827; b) M. Watanabe, M. Nishiyama, T. Yamamoto, Y. Koie, *Tetrahedron Lett.* **2000**, *41*, 481; c) D. W. Old, M. C. Harris, S. L. Buchwald, *Org. Lett.* **2000**, *2*, 1403.

[13] See Supporting Information for experimental details.

[14] Typically, *N*-arylmonocarbazoles exhibit sharp emission peaks, for example, at 342 and 358 nm in cyclohexane for **3a**.

[15] a) F. C. De Shryver, J. Vandendriessche, S. Toppet, K. Demeyer, N. Boens, *Macromolecules* **1982**, *15*, 406; b) F. Evers, K. Kobs, R. Memming, D. R. Terrell, *J. Am. Chem. Soc.* **1983**, *105*, 5988; c) H. Masuhara, N. Tamai, N. Mataga, F. C. De Schryver, J. J. Vandendriessche, *J. Am. Chem. Soc.* **1983**, *105*, 7256; d) A. Karali, P. Dais, E. Mikros, F. Heateley, *Macromolecules* **2001**, *34*, 5547; e) J. Gallego, D. Perez-Foullerat, F. Mendicuti, W. L. Mattice, *J. Polym. Sci. Part B Polym. Phys.* **2001**, *39*, 1272.

[16] a) R. Jakubiak, C. J. Collison, W. C. Wan, L. J. Rothberg, B. R. Hsieh, *J. Phys. Chem. A* **1999**, *103*, 2394; b) A. M. Sarker, B. Strehmel, D. C. Neckers, *Macromolecules* **1999**, *32*, 7409.

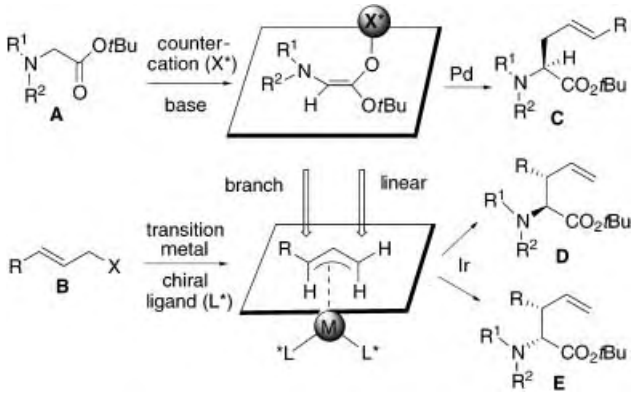
 © 2003 Wiley-VCH Verlag GmbH & Co. KGaA, Weinheim

Enantioselective Allylation

Enantio- and Diastereoselective Ir-Catalyzed Allylic Substitutions for Asymmetric Synthesis of Amino Acid Derivatives**

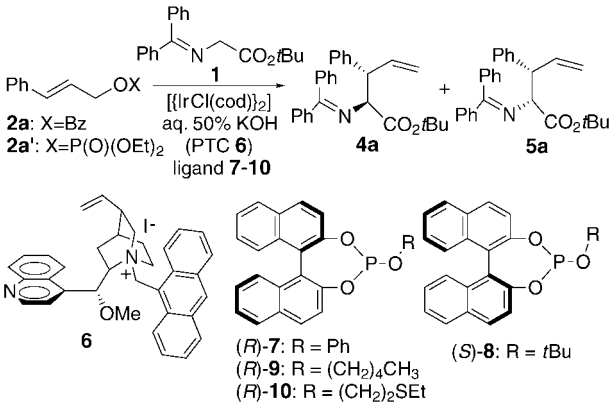
*Takatoshi Kanayama, Kazumasa Yoshida, Hideto Miyabe, and Yoshiji Takemoto**

Transition-metal-catalyzed asymmetric allylic substitution is a useful reaction in organic synthesis.[1] In the reaction with symmetric C nucleophiles such as dialkyl malonates, good yields and high enantioselectivities can now be obtained with an appropriate combination of a transition metal and a chiral ligand.[2–5] In contrast to the symmetric C nucleophiles, allylic substitution of 3-substituted allylic alcohols **B** with unsymmetrical C nucleophiles **A** is a tough and challenging task, because regio-, diastereo-, and enantioselectivities must be controlled (Scheme 1). In the last few years, research has



Scheme 1. Transition-metal-mediated asymmetric allylic substitution.

focused on finding catalysts and chiral ligands that favor the formation of branched chiral products **D** and **E** in the allylic substitution of α-amino esters **A** with **B**.[6,7] We have already reported Pd-mediated asymmetric allylic alkylation of diphenylimino glycinate **1** with several allylic acetates in the presence of the chiral phase-transfer catalyst (PTC) **6** to give the chiral products **C** with high enantioselectivity (up to 97% *ee*).[6a] In contrast to the palladium catalyst, some transition metals, such as Ir,[3] Mo,[4] and W,[5] promote allylic alkylation at the more highly substituted terminus of the allylic substrate. Trost et al. recently reported that Mo-catalyzed asymmetric allylic alkylation with azlactones occurs at the more substituted terminus with high regio-, diastereo-, and enantioselectivity.[8] However, there are no reports concerning the asymmetric synthesis of both diastereomers **D** and **E** as major products from the same starting materials and the same chiral ligand. We report here the first enantioselective allylic substitutions of **1** catalyzed by an iridium complex of chiral phosphite **10**, and the diastereoselective synthesis of the products **4** and **5** by simply switching the base employed (Scheme 2).



Scheme 2. Ir-catalyzed asymmetric allylic substitution of **1** with **2a,a′**.

Our previous work prompted us to examine PTC **6** as a chiral catalyst in Ir-catalyzed allylic substitutions (Table 1). We first carried out the Ir-catalyzed reaction of **1** and benzoate **2a** in the presence of the chiral PTC **6**, 50% KOH, [{IrCl(cod)}$_2$] (cod = cyclooctadiene), and $(PhO)_3P$ (entry 1). The reaction was complete after 8 h at room temperature and gave the branched products **4a** and **5a** as major products (40% yield, **4a**:**5a** = 75:25) but with low enantioselectivity (46% *ee*). We next examined the effect of chiral ligands **7**–**10**[9] in place of chiral PTC **6** on the enantioselectivity. The reaction of **1** with **2a** was carried out in the presence of 50% KOH (3 equiv), [{IrCl(cod)}$_2$] (10 mol%), and chiral phosphites (20–40 mol%). In all cases, no linear product could be detected. Indeed, the

Table 1: Ir-catalyzed asymmetric allylic substitution of **1** and **2a,a′** with chiral PTC **6** or various chiral ligands **7**–**10**.[a]

Entry	Substrate	Ligand (mol%)	Yield [%][b] (**4**:**5**)	*ee* of **4** [%][c]
1	**2a**	**6** (10), $(PhO)_3P$ (40)	40 (75:25)	46
2	**2a**	(*R*)-**7** (20)	29 (69:31)	32[d]
3	**2a**	(*S*)-**8** (40)	7 (86:14)	68[d]
4	**2a**	(*R*)-**9** (20)	6 (67:33)	95
5	**2a**	(*R*)-**10** (20)	11 (73:27)	93
6[e]	**2a′**	(*R*)-**9** (20)	0	–
7[e]	**2a′**	(*R*)-**10** (20)	82 (82:18)	97

[a] All reactions were carried out in toluene. The ratio of **1**:**2**:50% KOH:[{IrCl(cod)}$_2$] was 100:100:300:10 unless otherwise noted. [b] Yields of isolated products. [c] Determined by HPLC analysis with Daicel Chiral Pack OD-H column. [d] The enantiomer of **4** was obtained. [e] The reaction was carried out at 0°C.

[*] Prof. Dr. Y. Takemoto, T. Kanayama, K. Yoshida, Dr. H. Miyabe
Graduate School of Pharmaceutical Sciences
Kyoto University
Sakyo-ku, Kyoto 606-8501 (Japan)
Fax: (+81) 75-753-4569
E-mail: takemoto@pharm.kyoto-u.ac.jp

[**] This research was supported by grants from the Japan Health Sciences Foundation and Grant-in-Aid for Scientific Research (C) from the Ministry of Education, Science, Sports, and Culture, Japan.

 © 2003 Wiley-VCH Verlag GmbH & Co. KGaA, Weinheim DOI: 10.1002/anie.200250654

enantioselectivity was dramatically affected by the substituent R of the ligands. Whereas addition of the known chiral phosphites **7**[3a] and **8**[9f] in place of $(PhO)_3P$ gave the branched product **4a** as a major product with moderate enantioselectivity, the new ligands **9** and **10** gave **4a** in 95 and 93% *ee*, respectively, albeit at the expense of chemical yield (entries 2–5). However, hydrolysis of **2a** to cinnamyl alcohol predominantly occurred under these conditions. We next used phosphate **2a′** as an allylic substrate which should be resistant to hydrolysis. After several experiments, it was revealed that the best result (82% yield, **4a**:**5a** = 82:18, 97% *ee*) was obtained when the reaction was performed at 0°C with phosphate **2a′** (entries 6 and 7). Furthermore, use of the bidentate chiral ligand **10**, which promoted the reaction at 0°C, was essential to improve both the chemical yield and stereoselectivity of **4**.

Having established higher enantioselectivity, we explored the effect of the countercations of the enolate with **2a′** and **10**, and the results are shown in Table 2. It is noteworthy that the countercations had a more significant influence on the diastereoselectivity (**4a**/**5a**) than on the enantioselectivity for **4a**. In addition, for diastereoselective synthesis of **4a**, the reaction of **1** and **2a′** with 50% KOH in toluene (method A) was superior to reactions involving $KN(SiMe_3)_2$, CsOH, and NaH (entries 1–4), whereas these bases gave **4a** as a major product with more than 90% *ee*. On the other hand, use of lithium bases tends to produce the other diastereomer **5a** as a major product (entries 5–7). Among them, $LiN(SiMe_3)_2$ was the best base in terms of chemical yield and stereoselectivity (82% yield, **4a**:**5a** = 12:88, 92% *ee*; method B). These two methods allow us to synthesize both diastereomers **4a** and **5a** with high enantioselectivity.

Table 2: Ir-catalyzed allylic substitution of **1** and **2a′** under various reaction conditions.[a]

Entry	Reaction conditions	Yield [%][b] branched	linear	Ratio (**4**:**5**)	*ee* [%][c] **4**	**5**
1	$CsOH{\cdot}H_2O$, toluene	43	0	70:30	95	59
2	50% KOH, toluene	82	0	82:18	97	66
3	$KN(SiMe_3)_2$, THF	28	0	79:21	48	72
4	NaH, THF	29	0	62:38	91	73
5	LiBr, DBU[d], THF	20	23	30:70	44	63
6	LDA, THF	56	3	11:89	—[e]	96
7	$LiN(SiMe_3)_2$, THF	82	<1	12:88	56	92

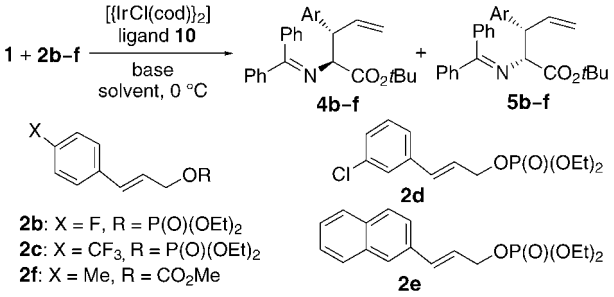
[a] All reactions were carried out at 0°C in the presence of $[\{IrCl(cod)\}_2]$ (10 mol%) and (*R*)-**10** (20 mol%). [b] Yields of isolated products. [c] Determined by HPLC analysis with Daicel Chiral Pack OD-H column. [d] DBU = 1,8-diazabicyclo[5.4.0]undec-7-ene. [e] The *ee* was not determined.

Methods A and B were examined for various allylic substrates **2b–f** (Table 3, Scheme 3). Since the phosphate of *p*-methylcinnamyl alcohol could not be prepared, we employed methyl carbonate **2f** as substrate. In general, the Ir-catalyzed allylic substitution was not affected by the *para* and *meta* substituents of the aromatic ring of **2b–e**. Thus, method A gave the corresponding branched products **4b–e** diastereoselectively (**4**:**5** = 68:32–78:22) with excellent enantioselectivity

Table 3: Ir-catalyzed allylic substitution of **1** with various substrates **2b–f**.

Entry	Substrate **2**	Method[a]	Yield [%][b] branched	linear	Ratio (**4**:**5**)	*ee* [%][c] **4**	**5**
1	**2b**	A	77	0	78:22	97	63
2	**2c**	A	77	0	68:32	97	68
3	**2d**	A	79	0	76:24	97	74
4	**2e**	A	97	0	77:23	94	69
5[d]	**2f**	A	63	0	83:17	91	74
6	**2b**	B	82	0	13:87	59	85
7	**2c**	B	78	0	10:90	93	94
8	**2d**	B	81	<1	10:90	73	94
9	**2e**	B	84	<1	11:89	67	96
10	**2f**	B	88	1.1	34:66	51	70

[a] Method A: In toluene at 0°C unless otherwise noted. The ratio of **1**:**2**:50% KOH:$[\{IrCl(cod)\}_2]$:(*R*)-**10** was 100:100:300:10:20. Method B: In THF at 0°C. The ratio of **1**:**2**:$LiN(SiMe_3)_2$:$[\{IrCl(cod)\}_2]$:(*R*)-**10** was 150:100:150:10:20. [b] Yields of isolated products. [c] Determined by HPLC analysis with a Daicel Chiral Pack OD-H column. [d] The reaction was carried out at room temperature.



Scheme 3. Ir-catalyzed reaction of **1** with various allylic substrates **2b–f**.

(>94% *ee*). Similarly, by using method B, other branched products **5b–e** could be synthesized stereoselectively (**4**:**5** = 13:87–10:90, 85–96% *ee*). In contrast, due to lower reactivity of the methyl carbonate, the Ir-catalyzed allylic substitution of **2f** required prolonged reaction time and elevated temperature. As a result, the yield and stereoselectivity of the branched products **4f** and **5f** become somewhat lower than those of **4a–e** and **5a–e**. In any event, these two protocols are applicable to several allylic substrates and are demonstrated to be a versatile tool for asymmetric synthesis of both diastereomers **4a–f** and **5a–f**.

The relative and absolute configurations of products **4a** and **5a** were determined by comparison with the known compounds.[7a] The configurations of **4b–f** and **5b–f** were then assumed by analogy. From the results described above, the stereochemical course of the reaction can be explained as follows. Initially, the π- or σ-allyl complex **F** is formed by attack of the iridium(I) complex of the ligand on the allylic substrate **2**. The nucleophilic attack of the enolate of **1** at the allylic carbon atom *trans* to the phosphorus atom would give the chiral products **4** and **5** with high enantioselectivity. Although we cannot explain the different behavior of the bases at this stage, it might be attributable to the geometry of the enolate of **1**. It was assumed that the use of KOH as a base would give predominantly the *E* enolate **G**, whereas the *Z*

 © 2003 Wiley-VCH Verlag GmbH & Co. KGaA, Weinheim

enolate **H** would be formed with $LiN(SiMe_3)_2$ as base (Figure 1).[10]

In conclusion, we have developed the first enantioselective Ir-catalyzed allylic substitutions of diphenylimino glycinate **1** by using chiral bidentate ligand **10** (up to 97% *ee*), and also succeeded in the diastereoselective asymmetric synthesis of both diastereomers **4** and **5** by simply switching the base employed. The influence of the base on diastereoselectivity and further applications of this asymmetric allylic substitution are currently under investigation.

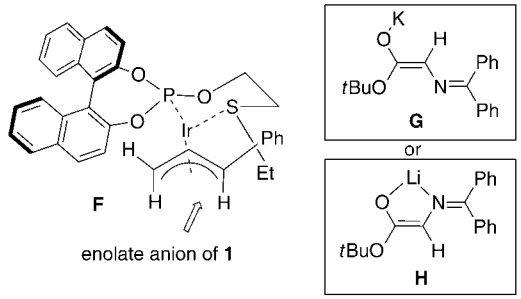


Figure 1. The plausible allyl Ir^{III} complex **F**.

Experimental Section

General procedure for asymmetric allylic substitution: Method A: A 50% KOH solution (38 μL, 0.51 mmol) was added to a stirred solution of *tert*-butyl glycinate benzophenone imine (**1**; 50 mg, 0.17 mmol), diethyl phosphate **2a′** (46 mg, 0.17 mmol), $[\{IrCl(cod)\}_2]$ (11 mg, 0.017 mmol), and (*R*)-**10** (14 mg, 0.034 mmol) in dry toluene (1.4 mL) at 0°C under an argon atmosphere, and the resulting mixture was stirred vigorously at 0°C for 20 h. The suspension was diluted with diethyl ether (15 mL), and the organic phase was washed with a saturated aqueous soltion of $NaHCO_3$ (2 mL) and brine (2 mL) and then dried over Na_2SO_4. After evaporation of the solvent, the crude product was purified by column chromatography (basic silica gel, AcOEt/hexane 1/500) to give the desired products **4a** (46 mg, 67%) and **5a** (11 mg, 15%) as a colorless oil.

Method B: A solution of **1** (75 mg, 0.25 mmol) in dry THF (1 mL) was added to a stirred solution of $LiN(SiMe_3)_2$ (0.25 mmol) in THF (0.16 mL) at −78°C. After being stirred for 30 min, the mixture was slowly added to a stirred solution of **2a′** (46 mg, 0.17 mmol), $[\{IrCl(cod)\}_2]$ (11 mg, 0.017 mmol), and (*R*)-**10** (14 mg, 0.034 mmol) in dry THF (0.4 mL) at 0°C under an argon atmosphere. After completion of the addition (30 min), the resulting mixture was quenched with water (2 mL) and diethyl ether (40 mL). The organic phase was washed with brine (2 mL) and then dried over Na_2SO_4. After evaporation of the solvent, the crude product was purified by column chromatography (basic silica gel, AcOEt/hexane 1/500) to give **4a** (7.0 mg, 10%) and **5a** (50 mg, 72%).

The enantioselectivity was determined by chiral HPLC (Daicel Chiralpak OD-H, *i*PrOH/hexanes 0.6/99.4, flow rate 0.3 mL min^{-1}, $\lambda = 254$ nm, retention times: **4a** (major) 26.5 min, (minor) 23.8 min, **5a** (major) 27.4 min, (minor) 25.7 min).

Received: November 28, 2002
Revised: February 13, 2003 [Z50654]

Keywords: allylation · amino acids · enantioselectivity · iridium · P ligands

[1] Recent review: B. M. Trost, *Chem. Pharm. Bull.* **2002**, *50*, 1–14; B. M. Trost, C. B. Lee in *Catalytic Asymmetric Synthesis II* (Ed.: I. Ojima), Wiley-VCH, Weinheim, **2000**, pp. 593–650; T. Hayashi in *Catalytic Asymmetric Synthesis* (Ed.: I. Ojima), Wiley-VCH, Weinheim, **2000**, p. 193; A. Pfaltz, M. Lautens, *Comprehensive Asymmetric Catalysis, Vol. 2* (Eds. E. N. Jacobsen, A. Pfaltz, H. Yamamoto), Springer, Berlin, **1999**, pp. 833–884.

[2] Y. Matsushima, K. Onitsuka, T. Kondo, T. Mitsudo, S. Takahashi, *J. Am. Chem. Soc.* **2001**, *123*, 10405–10406; S.-L. You, X.-Z. Zhu, Y.-M. Luo, X.-L. Hou, L.-X. Dai, *J. Am. Chem. Soc.* **2001**, *123*, 7471–7472; G. Helmchen, A. Pfaltz, *Acc. Chem. Res.* **2000**, *33*, 336–345; A. J. Blacker, M. L. Clarke, M. S. Loft, M. F. Mahon, M. E. Humphries, J. M. J. Williams, *Chem. Eur. J.* **2000**, *6*, 353–360; T. Hayashi, *J. Organomet. Chem.* **1999**, *576*, 195–202; R. Prétôt, A. Pfaltz, *Angew. Chem.* **1998**, *110*, 337–339; *Angew. Chem. Int. Ed.* **1998**, *37*, 323–325; J. M. J. Williams, *Synlett* **1996**, 705–710.

[3] a) K. Fuji, N. Kinoshita, K. Tanaka, T. Kawabata, *Chem. Commun.* **1999**, 2289–2290; b) B. Bartels, G. Helmchen, *Chem. Commun.* **1999**, 741–742; c) J. P. Janssen, G. Helmchen, *Tetrahedron Lett.* **1997**, *38*, 8025–8026.

[4] B. M. Trost, K. Dogra, I. Hachiya, T. Emura, D. L. Hughes, S. Krska, R. A. Reamer, M. Palucki, N. Yasuda, P. J. Reider, *Angew. Chem.* **2002**, *114*, 2009–2012; *Angew. Chem. Int. Ed.* **2002**, *41*, 1929–1932; F. Glorius, M. Neuburger, A. Pfaltz, *Helv. Chim. Acta* **2001**, *84*, 3178–3196; N.-F. Kaiser, U. Bremberg, M. Larhed, A. Hallberg, *Angew. Chem.* **2002**, *114*, 3742–3744; *Angew. Chem. Int. Ed.* **2000**, *39*, 3596–3598; B. M. Trost, S. Hildbrand, K. Dogra, *J. Am. Chem. Soc.* **1999**, *121*, 10416–10417.

[5] G. C. Lloyd-Jones, A. Pfaltz, *Angew. Chem.* **1995**, *107*, 534–536; *Angew. Chem. Int. Ed. Engl.* **1995**, *34*, 462–464; J. Lehmann, G. C. Lloyd-Jones, *Tetrahedron* **1995**, *51*, 8863–8874.

[6] a) M. Nakoji, T. Kanayama, T. Okino, Y. Takemoto, *Org. Lett.* **2001**, *3*, 3329–3331; b) G. Chen, Y. Deng, L. Gong, A. Mi, X. Cui, Y. Jiang, M. C. K. Choi, A. S. C. Chan, *Tetrahedron: Asymmetry* **2001**, *12*, 1567–1571; c) S.-L. You, X.-L. Hou, L.-X. Dai, B.-X. Cao, J. Sun, *Chem. Commun.* **2000**, 1933–1934; d) B. M. Trost, X. Ariza, *J. Am. Chem. Soc.* **1999**, *121*, 10727–10737; e) R. Kuwano, Y. Ito, *J. Am. Chem. Soc.* **1999**, *121*, 3236–3237; f) K. Hiroi, A. Hidaka, R. Sezaki, Y. Imamura, *Chem. Pharm. Bull.* **1997**, *45*, 769–777; g) J.-P. Genet, S. Juge, S. Achi, S. Mallart, J. R. Montes, G. Levif, *Tetrahedron* **1988**, *44*, 5263–5275.

[7] a) M. Nakoji, T. Kanayama, T. Okino, Y. Takemoto, *J. Org. Chem.* **2002**, *67*, 7418–7423; b) T. D. Weiß, G. Helmchen, U. Kazmaier, *Chem. Commun.* **2002**, 1270–1271; c) U. Kazmaier, F. L. Zumpe, *Eur. J. Org. Chem.* **2001**, 4067–4076; d) U. Kazmaier, F. L. Zumpe, *Angew. Chem.* **2000**, *112*, 805–807; *Angew. Chem. Int. Ed.* **2000**, *39*, 802–804; e) U. Kazmaier, F. L. Zumpe, *Angew. Chem.* **1999**, *111*, 1572–1574; *Angew. Chem. Int. Ed.* **1999**, *38*, 1468–1470; f) B. M. Trost, X. Ariza, *Angew. Chem.* **1997**, *109*, 2749–2751; *Angew. Chem. Int. Ed. Engl.* **1997**, *36*, 2635–2637; g) I. C. Baldwin, J. M. J. Williams, R. P. Beckett, *Tetrahedron: Asymmetry* **1995**, *6*, 1515–1518.

[8] B. M. Trost, K. Dogra, *J. Am. Chem. Soc.* **2002**, *124*, 7256–7257.

[9] a) J. Ansell, M. Wills, *Chem. Soc. Rev.* **2002**, *31*, 259–268; b) M. T. Reetz, G. Mehler, *Angew. Chem.* **2000**, *112*, 4047–4049; *Angew. Chem. Int. Ed.* **2000**, *39*, 3889–3890; c) S. Deerenberg, H. S. Schrekker, G. P. F. van Strijdonck, P. C. J. Kamer, P. W. N. M. van Leeuwen, J. Fraanje, K. Goubitz, *J. Org. Chem.* **2000**, *65*, 4810–4817; d) C. G. Arena, D. Drommi, F. Faraone, *Tetrahedron: Asymmetry* **2000**, *11*, 2765–2779; e) K. Selvakumar, M. Valentini, P. S. Pregosin, A. Albinati, *Organometallics* **1999**, *18*, 4591–4597; f) V. V. Ovchinnikov, O. A. Cherkasova, L. V. Verizhnikov, *Zh. Obshch. Khim.* **1982**, *52*, 707–708.

[10] K. B. Lipkowitz, M. W. Cavanaugh, B. Baker, M. J. O'Donnell, *J. Org. Chem.* **1991**, *56*, 5181–5192.

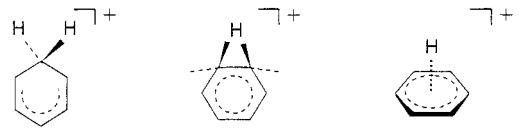
 © 2003 Wiley-VCH Verlag GmbH & Co. KGaA, Weinheim

Protonated Benzene Structure

Infrared Fingerprint of Protonated Benzene in the Gas Phase**

William Jones, Pierre Boissel, Barbara Chiavarino, Maria Elisa Crestoni, Simonetta Fornarini, Joël Lemaire, and Philippe Maitre**

$C_6H_7^+$ ions are obtained from the gas-phase protonation of benzene, namely, by the prototypical aromatic electrophilic addition reaction. The formation of protonated benzene has therefore attracted several investigations aimed at ascertaining the thermodynamic and reactivity features of the product ion besides its structure.[1] It is now widely recognized that the stable structure of protonated benzene is a σ complex species (**1**), whereas the edge-protonated structure **2** is a first-order saddle point 25–38 kJ mol^{-1} higher in energy and the face-centred π complex (**3**) is a second-order saddle point still higher in energy, at 200 kJ mol^{-1}.[2]



1 2 3

The experimental proton affinity[3] of benzene (750 kJ mol^{-1}) is nicely matched by the theoretical value of 744–761 kJ mol^{-1},[2] thus proving that **1** is the stable protonated benzene ion. The edge π complex **2** is a transition structure for a 1,2-H shift within **1**, a process which leads to the scrambling of the seven H atoms. This process was first observed by dynamic NMR spectroscopy in superacid media.[4] The kinetic features of the process reported for gaseous benzenium and related arenium ions[5] are consistent with activation energies close to the computed value of 25–38 kJ mol^{-1}. Also, a species resembling **2** appears as the lowest energy structure calculated for the benzene–oxonium complex.[6] Finally, the face-centred π complex **3** has been invoked to account for the collision-induced decomposition behavior of protonated benzene ions by loss of H atoms.[7]

[*] Prof. M. E. Crestoni, Dr. B. Chiavarino, Prof. S. Fornarini
Dipartimento Studi di Chimica
e Tecnologia delle Sostanze Biologicamente Attive
Università di Roma "La Sapienza"
P.le A. Moro 5, 00185 Rome (Italy)
Fax (+39) 06-4991-3602
E-mail: mariaelisa.crestoni@uniroma1.it
Dr. P. Maitre, W. Jones, Prof. P. Boissel, Dr. J. Lemaire
Laboratoire de Chimie Physique, CNRS-UMR-8000
Université de Paris XI
Bâtiment 350, 91405 Orsay Cedex (France)
Fax (+33) 1-6915-3053
E-mail: maitre@lcp.u-psud.fr

[**] This work was supported by the CNRS and by the Italian MIUR.

In this context the possibility of a direct spectroscopic characterization of $C_6H_7^+$ ions appeared to be a desirable contribution to settling the argument over the structure of the gaseous benzenium ion. Spectroscopic investigations of gaseous ions face the problem of their typically low concentration. Recently, the infrared spectrum of the $C_6H_7^+$ ion was recorded by Solcà and Dopfer by using tunable IR laser pulses generated by an optical parametric oscillator laser system.[8] Another interesting alternative to overcome the inherent problem of the low concentration of ions is to study the wavelength dependence of IR multiphoton dissociation (IRMPD).[9] Infrared free electron laser (FEL) light sources[10] have been shown to be suitable to activate IRMPD.[11] In the present work, the Centre Laser Infrarouge Orsay (CLIO) FEL facility has been used. It is based on a 10 to 50-MeV electron accelerator that yields IR radiation fulfilling the requirements of both a high peak power and a relatively small bandwidth (up to 0.3%). The most interesting characteristic is its large tunability (3–90 μm) which provides, in particular, access to the fingerprint region ($\tilde{\nu}$ = 600–1500 cm^{-1}). The present work thus provides an interesting complement to the work of Solcà and Dopfer on $C_6H_7^+$ ions which yielded information on the CH stretching region ($\tilde{\nu}$ = 2700–3200 cm^{-1}).[8]

The FEL IRMPD has been applied to $C_6H_7^+$ ions produced and stored in an ion cyclotron resonance (ICR) ion trap. FT-ICR is in fact a technique of choice for complex ion manipulation and storage which takes advantage of a high mass resolution.[12] The experimental setup, which has been described elsewhere,[13] uses a mobile ICR analyzer[14] based on a permanent magnet of 1.25 Tesla. The laser light is focussed at the center of the ICR ion trap using a spherical mirror of 1 m focal length; the laser spot diameter has been estimated to be about 400 μm.

Quantum chemical calculations are needed to characterize the possible isomers of the ion of interest and determine the corresponding IR absorption spectrum, which can then be compared with the experimental IR spectrum derived from the wavelength dependence of the IRMPD process so that the identity of the structure of the ion trapped in the ICR cell could be determined. The expected vibrational spectrum has been calculated using the B3LYP6-311++G** method.[15] The three significant species (**1**–**3**) on the potential energy surface of the $C_6H_7^+$ ion have been characterized, and good quantitative agreement found with recent reports.[2] In particular, the σ complex **1** has been found to be the energy minimum, the bridged structure **2** being a transition state lying 42 kJ mol^{-1} above the σ complex **1**, while the π complex **3** has been found to be a second-order saddle point.

As shown in Figure 1, the photodissociation process appears to involve $C_6H_7^+$ ions, which undergo loss of H_2 with a yield of 10 to 25%, while the intensity of the $C_6H_6^{+\bullet}$ ions, also present in the ICR cell, stays approximately constant as a function of the infrared energy. Loss of H_2 is the lowest energy dissociation channel for the $C_6H_7^+$ ions. The process is known to involve negligible activation energy,[16] which is in agreement with quantum chemical calculations.[2c] The barrierless dissociation to $H_2 + C_6H_5^+$ is reported to require 296 kJ mol^{-1}.[2c] This value means that the absorption

 DOI: 10.1002/anie.200250708 © 2003 Wiley-VCH Verlag GmbH & Co. KGaA, Weinheim

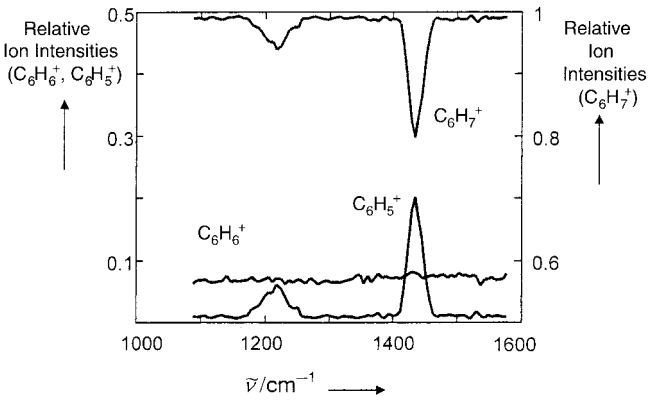


Figure 1. Relative ion intensity following IRMPD as a function of the radiation wavenumber. The left scale refers to ions with *m*/*z* 77 and 78, the right scale to the ion with *m*/*z* 79.

of at least ten photons is needed to provide sufficient internal energy for $C_6H_7^+$ ions to undergo dissociation into H_2 + $C_6H_5^+$ ions

The relative intensity of the $C_6H_5^+$ product ions, which is proportional to the normalized fragmentation yield, is shown in Figure 2 as a function of the radiation wavelength, thus providing an IR spectrum of the absorbing ion. The experimental pattern is viewed together with the calculated IR spectrum of **1**. Whereas significant red shifts have been previously observed,[11b] relative to the expected fundamental absorption transitions in the harmonic approximations, the two bands observed experimentally at $\tilde{\nu} = 1228$ and 1433 cm^{-1} nicely match with the two most intense absorptions determined theoretically at $\tilde{\nu} = 1237$ and 1434 cm^{-1} for the σ complex. The band at $\tilde{\nu} = 1237$ cm^{-1} corresponds to CH_2 scissoring, while the band at $\tilde{\nu} = 1434$ cm^{-1} corresponds to the in-plane CH bending of the hydrogen atoms in the position *meta* to the methylene group. It may be noted that the expected absorption at $\tilde{\nu} = 1582$ cm^{-1}, which corresponds to a ring deformation of the $C_6H_7^+$ ion and is calculated to be less intense than the transitions at $\tilde{\nu} = 1237$ and 1434 cm^{-1}, is not observed. This absence could be related to the nonlinear nature of the IRMPD at low laser fluence which had previously been observed with the present experimental setup.[13]

The IRMPD of a multiply deuterium-labeled benzenium ion was investigated to test the results obtained with this approach and check the reliability of the methodology adopted. The $C_6D_6H^+$ ions were formed by protonation of C_6D_6 and found to undergo wavelength-dependent loss of HD/D_2 as shown in Figure 3. Once again the dominant IR absorption bands predicted for the σ complex are active in inducing IRMPD at $\tilde{\nu} = 1439$ and 1572 cm^{-1} (theoretical values: $\tilde{\nu} = 1410$ and 1534 cm^{-1}, respectively). As can be seen in Figure 3, the predicted transition at $\tilde{\nu} = 2081$ cm^{-1}, which corresponds to the symmetric CH stretch of the methylene group, is not observed experimentally. As in the case of the $C_6H_7^+$ ion, this transition is expected to be less intense than the two observed transitions, and this could be the origin of a less efficient IRMPD in the corresponding region. It is interesting to compare the branching of HD/D_2 loss in the present IRMPD experiments with the collision-induced dissociation (CID) of $C_6D_6H^+$ ions formed by mild protonation with oxonium ions (and H/D exchange processes) in H_2O/C_6D_6 (or D_2O/C_6H_6) mixtures in flowing afterglow–selected ion flow tube (FA-SIFT) experiments (Table 1).[17]

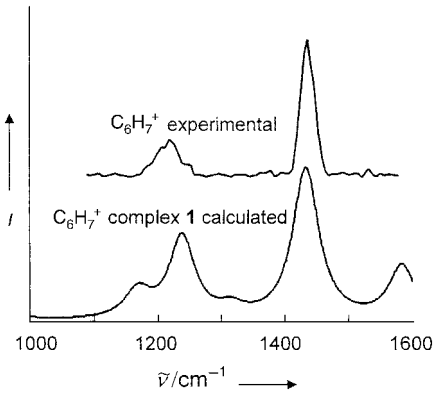


Figure 2. IRMPD spectrum of the $C_6H_7^+$ ion.

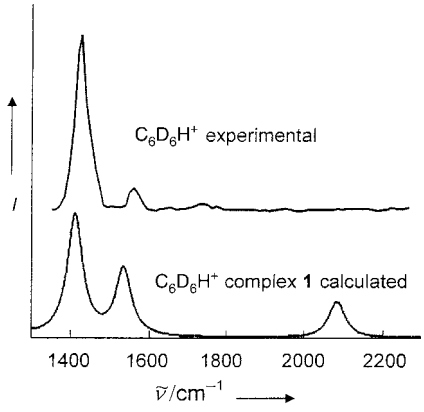


Figure 3. IRMPD spectrum of the $C_6D_6H^+$ ion.

Table 1: Dissociation of $C_6D_6H^+$ ions.

Ion precursors	Method	HD loss	D_2 loss	Ref.
statistical		29	71	[17]
CH_4/C_6D_6	IRMPD at 1439 cm^{-1}	38	62	this work
CH_4/C_6D_6	IRMPD at 1572 cm^{-1}	39	61	this work
H_2O/C_6D_6[a]	CID	31	69	[17]
H_2O/C_6D_6[b]	CID	30	70	[17]
D_2O/C_6H_6[a]	CID	35	65	[17]

[a] CID performed in FA-SIFT experiments. [b] CID performed in FA-SIFT triple quadrupole experiments.

 © 2003 Wiley-VCH Verlag GmbH & Co. KGaA, Weinheim

Interestingly, the relative amount of HD/D_2 loss is the same (38-39/62-61) for the two photon energies ($\tilde{\nu} = 1439\ cm^{-1}$ and $1572\ cm^{-1}$), allowing for IRMPD. These values are close to the ones statistically expected for the complete scrambling of hydrogen atoms within benzenium ions.[18] In particular, the single collision conditions prevailing in the CID performed in the FA-SIFT-triple quadrupole should ensure that the dissociating ions retain their original structure, because any possible isomerization is unlikely in the time frame of the process. It may thus be concluded that protonated benzene ions, irrespective of their formation—either by proton transfer followed by a few seconds delay in the ICR cell or by milder protonation in a high pressure (ca. 0.3 Torr) FA source—show similar reactivity features. They undergo fast equilibration of the seven hydrogen atoms and show a similar branching of HD/D_2 loss when the $C_6D_6H^+$ ion is the sampled species. These ions are unambiguously characterized as σ complexes.

In conclusion, the present IRMPD results confirm the σ complex structure of protonated benzene, $C_6H_7^+$, which is in contrast with recent IRMPD evidence showing the preference for a π structure for benzene–metal-cation complexes.[11b,19] Furthermore, the reported study proves the potential of the experimental setup (in which a FT-ICR is coupled with an infrared FEL) combined with the theoretical calculation of the IR spectra of the species being considered.[11c,13] In the near future, the interface of appropriate ion sources will extend the capabilities towards probing the structure of ionic complexes of biomolecules.

Experimental Section

The experiments were performed by letting the required reagent gases into the ICR cell through pulsed valves. The ionization of methane, admitted into the cell at 1.4×10^{-6} Torr for 100 ms, and ensuing ion–molecule reactions yielded CH_5^+ and $C_2H_5^+$ ions. These strong Brønsted acids[3b] were used to protonate benzene, which was subsequently introduced at 4.2×10^{-7} Torr for 100 ms. A reaction time of about 4 s was allowed for the proton transfer reaction to occur and the ensuing ion population, comprised of $C_6H_7^+$ ions and about a 10% fraction of $C_6H_6^+$ ions, was then irradiated for about 5 s. IRMPD resulted from firing trains of "macropulses" at a repetition rate of 25 Hz. Each train was 8-μs long and contained 500 "micropulses" a few picoseconds long each. Under these conditions the typical peak power (and energy) delivered during the micropulse and macropulse are 20 MW (50 μJ) and 3 kW (25 mJ), respectively.

Received: December 5, 2002 [Z50708]

Keywords: cations · IR spectroscopy · photodissociation · reactive intermediates · structure elucidation

[1] a) D. Kuck, *Mass Spectrom. Rev.* **1990**, *9*, 583; b) S. G. Lias, P. Ausloos, *J. Chem. Phys.* **1985**, *82*, 3613; c) T. Gäumann, G. Zhao, Z. Zhu, *Rapid Commun. Mass Spectrom.* **1994**, *8*, 1; d) S. Fornarini, M. E. Crestoni, *Acc. Chem. Res.* **1998**, *31*, 827.

[2] a) M. N. Glukhovtsev, A. Pross, A. Nicolaides, L. Radom, *J. Chem. Soc. Chem. Commun.* **1995**, 2347; b) Z. B. Maksić, B. Kovačević, A. Lesar, *Chem. Phys.* **2000**, *253*, 59; c) E. del Rio, R. López, T. L. Sordo, *J. Phys. Chem. A* **1997**, *101*, 10090; d) S. Sieber, P. von R. Schleyer, J. Gauss, *J. Am. Chem. Soc.* **1993**, *115*, 6987; e) R. Sumathy, E. S. Kryachko, *J. Phys. Chem. A* **2002**, *106*, 510; f) G. Bouchoux, M. Yáñez, O. Mó, *Int. J. Mass Spectrom.* **1999**, *185/186/187*, 241, and references therein.

[3] a) J. E. Szulejko, T. B. McMahon, *J. Am. Chem. Soc.* **1993**, *115*, 7839; b) "Proton Affinity Evaluation": E. P. Hunter, S. G. Lias in *NIST Chemistry WebBook* (Eds.: P. J. Linstrom, W. G. Mallard), National Institute of Standards and Technology, Gaithersburg, MD, **2001**, NIST Standard Reference Database Number 69 (http://webbook.nist.gov).

[4] G. A. Olah, R. H. Schlosberg, R. D. Porter, Y. K. Mo, D. P. Kelly, G. D. Mateescu, *J. Am. Chem. Soc.* **1972**, *94*, 2034.

[5] a) B. Chiavarino, M. E. Crestoni, C. H. DePuy, S. Fornarini, R. Gareyev, *J. Phys. Chem.* **1996**, *100*, 16201; b) F. Cacace, M. E. Crestoni, S. Fornarini, *J. Am. Chem. Soc.* **1992**, *114*, 6776.

[6] E. S. Kryachko, M. T. Nguyen, *J. Phys. Chem. A* **2001**, *105*, 153.

[7] R. S. Mason, C. M. Williams, P. D. J. Anderson, *J. Chem. Soc. Chem. Commun.* **1995**, 1027.

[8] N. Solcà, O. Dopfer, *Angew. Chem.* **2002**, *114*, 3781; *Angew. Chem. Int. Ed.* **2002**, *41*, 3628.

[9] a) R. C. Dunbar, *Int. J. Mass Spectrom.* **2000**, *200*, 571; b) M. A. Duncan, *Int. J. Mass Spectrom.* **2000**, *200*, 545.

[10] a) D. Oepts, A. F. G. van der Meer, P. W. Amersfoort, *Infrared Phys. Technol.* **1995**, *36*, 297; b) R. Prazeres, F. Glotin, C. Insa, D. Jaroszynski, J. M. Ortega, *Eur. Phys. J. D* **1998**, *3*, 87.

[11] a) J. Oomens, G. Meijer, G. von Helden, *J. Phys. Chem. A* **2001**, *105*, 8302; b) D. van Heijnsbergen, G. von Helden, G. Meijer, P. Maitre, M. A. Duncan, *J. Am. Chem. Soc.* **2002**, *124*, 1562; c) J. Oomens, J. M. Bakker, B. G. Sartakov, G. Meijer, G. von Helden, *Chem. Phys. Lett.* **2003**, *367*, 576; d) J. Lemaire, P. Boissel, M. Héninger, G. Mauclaire, G. Bellec, H. Mestdagh, A. Simon, S. Le Caër, J. M. Ortega, F. Glotin, P. Maître, *Phys. Rev. Lett.* **2002**, *89*, 273002.

[12] A. G. Marshall, *Int. J. Mass Spectrom.* **2000**, *200*, 331, and references therein.

[13] P. Maitre, S. Le Caër, A. Simon, W. Jones, J. Lemaire, H. Mestdagh, M. Héninger, G. Mauclaire, P. Boissel, R. Prazeres, F. Glotin, J. M. Ortega, *Nucl. Instrum. Methods Phys. Res. Sect. A* **2003**, in press.

[14] J. Lemaire, G. Bellec, M. Héninger, G. Mauclaire, P. Boissel, French patent 0201867 **2002**.

[15] Ab initio calculations were performed with the Gaussian 98 series of programs. The computational method employed for the prediction of the IR bands was the hybrid density functional B3LYP, which has been shown to provide vibrational frequencies with good accuracy. The Kohn–Sham orbitals were expanded with 6–311++G** to provide valence triple-ζ, diffuse, and extended polarization basis set. A scaling factor of 0.9656 was employed, as used to obtain the correct benzene modes calculated at the same level: a) R. Krishnan, J. S. Binkley, R. Seeger, J. A. Pople *J. Chem. Phys.* **1980**, *72*, 650; b) T. Clark, J. Chandrasekhar, G. W. Spitznagel, P. von R. Schleyer, *J. Comput. Chem.* **1983**, *4*, 294; c) P. M. W. Gill, B. G. Johnson, J. A. Pople, M. J. Frisch, *Chem. Phys. Lett.* **1992**, *197*, 499; d) M. J. Frisch, J. A. Pople, J. S. Binkley, *J. Chem. Phys.* **1984**, *80*, 3265.

[16] a) D. H. Williams, G. Hvistendahl, *J. Am. Chem. Soc.* **1974**, *96*, 6755; b) D. H. Williams, G. Hvistendahl, *J. Chem. Soc. Perkin Trans.* **1975**, *2*, 881.

[17] C. H. DePuy, R. Gareyev, S. Fornarini, *Int. J. Mass Spectrom. Ion Processes* **1997**, *161*, 41.

[18] The somewhat higher fraction of HD loss with respect to the statistical values that is observed for ions submitted to IRMPD may arise from kinetic isotope effects affecting the fragmentation process.

[19] D. van Heijnsbergen, T. D. Jaeger, G. von Helden, G. Meijer, M. A. Duncan, *Chem. Phys. Lett.* **2002**, *364*, 345.

 © 2003 Wiley-VCH Verlag GmbH & Co. KGaA, Weinheim

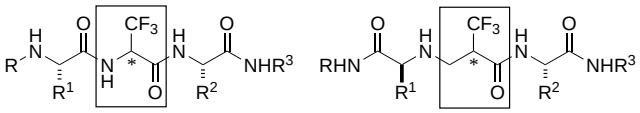
Fluorinated Peptidomimetics

Highly Stereoselective Tandem Aza-Michael Addition–Enolate Protonation to Form Partially Modified Retropeptide Mimetics Incorporating a Trifluoroalanine Surrogate**

Monica Sani, Luca Bruché, Gema Chiva, Santos Fustero, Julio Piera, Alessandro Volonterio,* and Matteo Zanda**

Poor bioavailability and rapid in vivo degradation are the two main drawbacks to the use of peptides as drugs.[1] Peptide-backbone modification has emerged as a powerful tool for overcoming these disadvantages, while retaining specific and potent bioactivity.[2] A number of modifications have been proposed, many of which have proved successful, such as the replacement, addition, or deletion of one or more amino acids in the parent sequence, the replacement of peptide bonds with surrogates, and the incorporation of synthetic scaffolds (often cyclic) into the backbone. We recently described novel peptidomimetic structures that incorporate a trifluoromethyl group,[3] within the frame of a research project aimed at the development of fluorine-containing protease inhibitors. The current project stems from the belief that the beneficial pharmacological effect of introducing fluorine substituents into a druglike molecule could be extended to peptides and peptidomimetics. Little information on the synthesis or the structural, conformational, and biological properties of fluorinated peptidomimetics is available in the literature.[4]

Recently, we became interested in the development of peptide mimetics that incorporate a stereochemically defined 3,3,3-trifluoroalanine (TF-Ala) unit. Unfortunately, the incorporation of TF-Ala into a peptide sequence to give a modified peptide **A** is a challenging endeavor,[5] as such peptides have low chemical and configurational stability at pH > 6.[6] To the best of our knowledge, no mimetics of TF-Ala-containing peptides have been described to date. For this reason, we planned the synthesis of partially modified retro (PMR) ψ[$NHCH_2$] peptide mimetics[7] **1**, which incorporate a chemically stable and stereodefined $CH_2CH(CF_3)CO$ surrogate for TF-Ala.



A **1**

Retrosynthetic analysis suggested that the asymmetric conjugate N-addition of α-amino esters to *N*-(α-trifluoromethyl)acryloyl-α-amino esters could represent a viable entry to the target structures **1**. However, surprisingly few studies have been dedicated to the asymmetric conjugate addition of nitrogen nucleophiles (such as amines, hydroxylamines, or amino acid derivatives) to α-substituted acryloyl acceptors, formally a tandem nonstereoselective aza-Michael reaction–stereoselective enolate protonation.[8] None of the previous studies addressed the issue of double stereoinduction. In our case, further challenges were expected because of the presence of the stereoelectronically demanding trifluoromethyl group and the strongly acidic nature of the $CH(CF_3)CO$ proton, which could lead to epimerization of the stereogenic center under the basic reaction conditions.

Herein we describe the smooth and general synthesis of PMR-ψ[$NHCH_2$]-tripeptides **4** (Scheme 1) by tandem asymmetric aza-Michael addition–enolate protonation of α-amino esters **2** with *N*-(α-trifluoromethyl)acryloyl-α-amino esters **3**. This sequence takes place with good to excellent 1,4-asymmetric induction (up to 95% *de*) depending on the substrate. Very high stereocontrol was observed upon the fine-tuning of key reaction parameters, such as the solvent and the base used. Side chains (R and R^1) and chirality (matched/mismatched pairs) of both reaction partners **2** and **3** were also found to have a strong influence on the diastereoselectivity.

Michael acceptors **3** (Scheme 2) were obtained by treatment of the appropriate α-amino ester H-AA-OX^1 with (α-trifluoromethyl)acryloyl chloride **6**,[9] which was prepared in turn from the acid **5**. Yields were generally high and the substrates **3** could be readily purified by flash chromatography (FC).

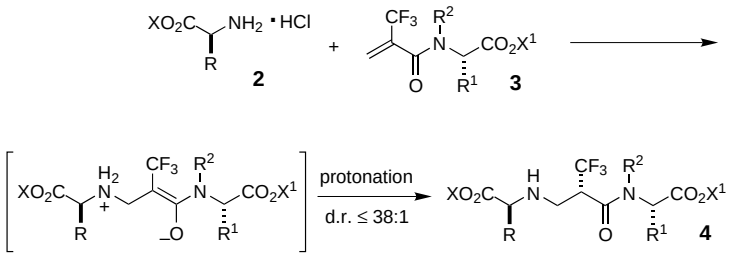
The reactions of α-amino esters (generated in situ by the treatment of commercially available hydrochlorides **2** with a tertiary amine) with Michael acceptors **3** were operationally very straightforward, quite fast, and efficient. Thus, **2**, **3**, and the amine base were simply mixed in the appropriate solvent, and at the end of the reaction (usually after 2 h at RT) the solvent was evaporated. The PMR-tripeptides **4** were isolated in yields of 75–98% (Scheme 3 and Table 1).

[*] Dr. M. Zanda, M. Sani
C.N.R. – Istituto di Chimica del Riconoscimento Molecolare (ICRM)
Sezione "A. Quilico"
via Mancinelli 7, 20131 Milano (Italy)
Fax: (+39) 02-2399-3080
E-mail: matteo.zanda@polimi.it
Dr. A. Volonterio, Prof. Dr. L. Bruché
Dipartimento di Chimica, Materiali ed
Ingegneria Chimica "Giulio Natta"
Politecnico di Milano
via Mancinelli 7, 20131 Milano (Italy)
Fax: (+39) 02-2399-3080
E-mail: alessandro.volonterio@polimi.it
Prof. Dr. S. Fustero, G. Chiva, J. Piera
Departamento de Química Orgánica
Facultad de Farmacia, Universidad de Valencia
46100-Burjassot, Valencia (Spain)
Fax: (+34) 96-386-4939
E-mail: santos.fustero@uv.es

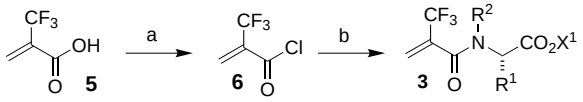
[**] We thank the European Commission (IHP Network grant "FLUOR MMPI" HPRN-CT-2002-00181), MIUR (Cofin 2002, Project "Peptidi Sintetici Bioattivi"), CNR (Italy), and MCYT (PPQ2000–0824) (Spain) for financial support. We are indebted to Prof. Takeo Taguchi and Prof. Takashi Yamazaki for useful experimental information on the preparation of (α-trifluoromethyl)acryloyl chloride.

Supporting information for this article is available on the WWW under http://www.angewandte.org or from the author.

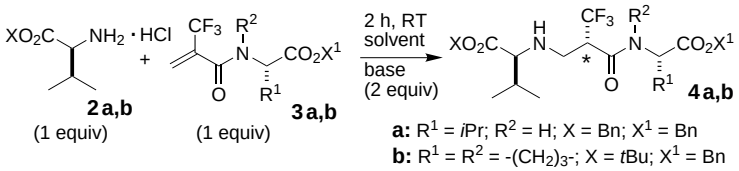
 © 2003 Wiley-VCH Verlag GmbH & Co. KGaA, Weinheim DOI: 10.1002/anie.200250711



Scheme 1. Tandem reaction to produce PMR-ψ[$NHCH_2$]-tripeptides **4**.



Scheme 2. Preparation of the chiral Michael acceptors **3**. a) Phthaloyl chloride, 140 °C; b) HCl·H-AA-OX^1, TMP (2 equiv), CH_2Cl_2, 0–25 °C, 75–95 %. AA = Gly, Val, Pro, Ala, Phe, Leu, etc.



Scheme 3. Reaction optimization: influence of base and solvent on stereoselectivity.

We first investigated the effect of the tertiary amine base on the diastereoselectivity of the reaction by conducting model reactions in CH_2Cl_2 between L-Val ester hydrochlorides **2a** (X = Bn) and **2b** (X = *t*Bu), and acceptors **3a** (derived from L-Val) and **3b** (derived from L-Pro), respectively (Scheme 3, Table 1, entries 1–10). These experiments showed that the amine base has a profound influence. Modest stereocontrol was observed with TMP, DMAP, TEA, and DIPEA (Table 1, entries 1–6). Of these, the best result was obtained with DIPEA (65 % *de* for **4a**, Table 1, entry 6). Considerably higher diastereocontrol was obtained with DABCO, which promoted the formation of **4a** and **4b** in 77 % and 83 % *de*, respectively (Table 1, entries 7 and 8). Lower *de* (70 %) was observed in the absence of an amine (Table 1, entry 9). The effect of solvent, which is the other main factor in this reaction, was investigated next in the presence of DABCO as the base (Table 1, entries 10–17). We found that the use of low-polarity or apolar solvents resulted in much higher diastereocontrol. Thus, acetonitrile (Table 1, entry 10) promoted modest *de* (63 % for **4b**), lower than that observed for CH_2Cl_2, whereas use of the less polar solvent THF increased the *de* to 88 % (Table 1, entry 11). Even better results were obtained with toluene, in which **4a** and **4b** were formed in 89 % and 90 % *de*, respectively (entries 12 and 14).[10] Use of the apolar solvent CCl_4 gave the best diastereoselectivity with **4a** and **4b** formed in 94.9 % and 94.6 % *de*, respectively (Table 1, entries 16 and 17). Very good *de* was also observed in the presence of Me_3N as the base (94.3 % *de* for **4a**, Table 1, entry 18), but its high volatility renders the experimental procedure less practical. Surprisingly, the *de* dropped when the chiral bases quinidine and cinchonine were used (54 % and 9 % *de* for **4b**, respectively Table 1, entries 19 and 20).

Reaction temperature was not a major factor in the range −40 °C to RT (Table 1, entries 1, 3 and 4). Concentration had negligible effect on the stereocontrol, but we qualitatively observed (TLC monitoring) a clear-cut increase in the reaction rate with increasing concentrations of **2** and **3**. This effect was particularly pronounced with the Pro-derived acceptor **3b**.[11] Ancillary control experiments demonstrated that, as expected, the reaction is kinetically controlled, and that under the optimized conditions (DABCO, CCl_4, RT) the CF_3-substituted stereogenic center of the products **4** is configurationally stable.

The full scope of the methodology in the synthesis of PMR-peptides **4** and the effect of the structure and stereochemistry of the reactants **2** and **3** on diastereoselectivity were investigated next. To this end, a variety of amino ester hydrochlorides **2a–j** were treated with acceptors **3a–h** under the optimized conditions (DABCO, CCl_4, RT) to provide a library of molecules **4d–u**, in generally good to excellent yields (Scheme 4 and Table 2).

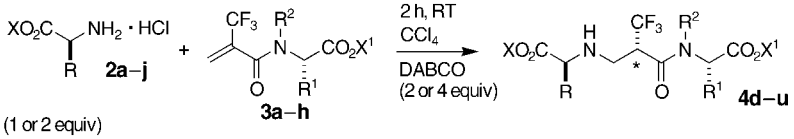
The R side chain of **2** has a strong influence, as was clearly demonstrated in the addition of **2b–g** to

Table 1: Influence of base and solvent.

Entry	Product	Base[a]	Solvent	Yield [%]	d.r.[b]
1[c]	**4a**	TMP	CH_2Cl_2	> 98	3.7:1.0
2	**4a**	DMAP	CH_2Cl_2	90	3.8:1.0
3	**4a**	TEA	CH_2Cl_2	86	4.0:1.0
4[d]	**4a**	TEA	CH_2Cl_2	84	4.2:1.0
5	**4b**	TEA	CH_2Cl_2	77	3.0:1.0
6[c]	**4a**	DIPEA	CH_2Cl_2	95	4.7:1.0
7	**4a**	DABCO	CH_2Cl_2	> 98	7.6:1.0
8	**4b**	DABCO	CH_2Cl_2	84	10.5:1.0
9[c,e]	**4a**	–	CH_2Cl_2	94	5.7:1.0
10	**4b**	DABCO	CH_3CN	91	4.4:1.0
11	**4b**	DABCO	THF	95	15.0:1.0
12	**4a**	DABCO	toluene	83	17.4:1.0
13[f]	**4a**	DABCO (cat.)	toluene	75	13.3:1.0
14	**4b**	DABCO	toluene	95	18.0:1.0
15[g]	**4a**	–	toluene	85	3.3:1.0
16	**4a**	DABCO	CCl_4	90	38.0:1.0
17	**4b**	DABCO	CCl_4	90	36.0:1.0
18[h]	**4a**	TMA	CCl_4	94	34.0:1.0
19[g]	**4b**	quinidine	toluene	79	3.3:1.0
20[g]	**4b**	cinchonine	toluene	84	1.2:1.0

[a] TMP = 2,4,6-trimethylpyridine (*sym*-collidine), DMAP = 4-dimethylaminopyridine, TEA = triethylamine, DIPEA = diisopropylethylamine, DABCO = 1,4-diazabicyclo[2,2,2]octane, TMA = trimethylamine. [b] Determined by ^{19}F NMR spectroscopy and/or HPLC analysis. [c] Reaction carried out at 0 °C. [d] Reaction carried out at −40 °C. [e] Hydrochloride **2a** was treated prior to reaction with aqueous $NaHCO_3$. [f] DABCO (0.1 equiv) was used after treatment of **2a** with aqueous $NaHCO_3$. [g] Reaction time: 48 h. [h] Reaction carried out at −10 °C.

 © 2003 Wiley-VCH Verlag GmbH & Co. KGaA, Weinheim



Scheme 4. Synthesis of an array of PMR-ψ[$NHCH_2$]-tripeptides (**4**).

Table 2: Validation of the methodology and influence of R, R^1, R^2, and configuration on diastereoselectivity.

Entry	2	3	4	R[a]	X	R^1[a]	R^2	X^1	Yield [%]	d.r.[b]
1	**c**	**a**	**d**	H	Et	*i*Pr	H	Bn	98	7.0:1.0
2	**d**	**a**	**e**	*i*Bu	Bn	*i*Pr	H	Bn	80	10.6:1.0
3	**e**	**a**	**f**	Bn	Me	*i*Pr	H	Bn	85	13.0:1.0
4	**f**	**a**	**g**	Me	Me	*i*Pr	H	Bn	82	14.0:1.0
5	**g**	**a**	**h**	*s*Bu	Me	*i*Pr	H	Bn	80	23.0:1.0
6	**b**	**c**	**i**	*i*Pr	*t*Bu	*i*Pr	H	*t*Bu	90	33.0:1.0
7	**e**	**b**	**j**	Bn	Me	-$(CH_2)_3$-		Bn	84	12.5:1.0
8	**f**	**b**	**k**	Me	Me	-$(CH_2)_3$-		Bn	85	24.0:1.0
9	**g**	**b**	**L**	*s*Bu	Me	-$(CH_2)_3$-		Bn	83	29.0:1.0
10	**h**	**e**	**m**	Bn	Bn	Bn	H	Bn	70	6.0:1.0
11	**a**	**f**	**n**	*i*Pr	Bn	Me	H	*t*Bu	71	29.2:1.0
12	**i**	**f**	**o**	Me	*t*Bu	Me	H	*t*Bu	76	17.0:1.0
13	D-**i**	**f**	**p**	D-Me	*t*Bu	Me	H	*t*Bu	70	3.2:1.0[c]
14	D-**j**	D-**g**	**q**	D-Ph	Me	D-Ph	H	Me	73	2.8:1.0
15	**j**	D-**g**	**r**	Ph	Me	D-Ph	H	Me	87	1.0:1.0[c]
16	**e**	**h**	**s**	Bn	Me	H	H	Bn	85	2.0:1.0
17	**g**	**h**	**t**	*s*Bu	Me	H	H	Bn	82	3.0:1.0
18	**a**	**h**	**u**	*i*Pr	Bn	H	H	Bn	89	6.0:1.0

[a] L-Configured amino esters were used unless otherwise indicated. [b] Determined by ^{19}F NMR spectroscopy and/or HPLC analysis. [c] The stereochemistry at the carbon center α to the CF_3 group was not assigned.

the L-Val acceptors **3a** and **3c** (Table 2, entries 1–6). The *de* of the products **4d–i** increased in the sense R = H < *i*Bu < Bn < Me < *s*Bu < *i*Pr, such that the best stereocontrol was achieved with the bulkiest R groups. This trend was confirmed with the other acceptors **3b** (L-Pro-derived, Table 2, entries 7–9), **3f** (L-Ala-derived, entries 11 and 12), and **3h** (Gly-derived, entries 16–18). The R^1 side chain of the acceptors **3** also had a strong influence, as shown by the fact that L-Phe amino esters such as **2e** and **2h** (R = Bn) reacted with **3h** (Gly acceptor, Table 2, entry 16), **3e** (L-Phe acceptor, entry 10), **3b** (L-Pro acceptor, entry 7), and **3a** (L-Val acceptor, entry 3) with progressively higher diastereocontrol (d.r. of products increased from 2.0:1.0 to 13.0:1.0). The effect of R^1 on the *de* followed the same trend observed for R. The configuration of the reaction partners **2** and **3** also had a profound effect, as demonstrated by the use of matched/mismatched pairs of the L- and D-Ala methyl esters **2i** and the L-Ala acceptor **3f** (Table 2, entries 12 and 13), and the D- and L-phenylglycine methyl esters **2j** and the D-phenylglycine acceptor **3g** (Table 2, entries 14 and 15). In both cases the "like" combination (D/D or L/L) resulted in higher diastereoselectivity, with the striking case of like-**2i**/**3f**, which gave an excellent 17.0:1.0 ratio in favor of the **4o** diastereomer (Table 2, entry 12), whereas a modest 3.2:1.0 diastereomeric ratio was found in the case of unlike-**2i**/**3f** (Table 2, entry 13). The X and X^1 ester groups had minor (if any) influence on stereoselectivity.

The configurations of the PMR-peptides **4j** and **4n** were determined by X-ray diffraction,[12] and the configurations of the other main diastereomers **4** were tentatively assigned by analogy with **4j** and **4n**, based on their spectroscopic and physical data.

The striking effects of the amine catalyst and the solvent on the diastereoselectivity of the reaction had not been described in previous studies on the asymmetric addition of nitrogen nucleophiles to α-substituted acryloyl acceptors,[8] in which the best stereocontrol was often achieved in protic solvents, in the absence of an amine base. Although detailed kinetic and computational studies will be necessary before we can draw a reliable mechanistic picture of this process, the body of experimental evidence discussed above suggests that the amino ester **2**, Michael acceptor **3**, and DABCO might form a tight termolecular ion-pair transition state, which is energetically favored and not disrupted in nonpolar solvents.[13]

In conclusion, we have described a highly stereoselective synthesis of PMR-ψ[$NHCH_2$]-peptides that incorporate a stereochemically defined and stable TF-Ala mimetic by means of a novel tandem asymmetric aza-Michael addition–enolate protonation reaction. The process is operationally very simple, makes use of readily available and cheap reagents, occurs under very mild conditions, and produces compounds suitable for combinatorial applications, all of which are of interest for potential industrial development. Additional interest in this reaction stems from its peculiar mechanism and the underlying stereochemical implications, such as the high double stereoinduction and the strong stereodirecting solvent and base effects, which deserve further in-depth mechanistic investigations.

Received: December 6, 2002 [Z50711]

Keywords: diastereoselectivity · Michael addition · peptidomimetics · protonation · solvent effects

[1] A. Loffet, *J. Pept. Sci.* **2002**, *8*, 1–7.
[2] a) G. L. Olson, D. R. Bolin, M. P. Bonner, M. Bös, C. M. Cook, D. C. Fry, B. J. Graves, M. Hatada, D. E. Hill, M. Kahn, V. S. Madison, V. K. Rusiecki, R. Sarabu, J. Sepinwall, G. P. Vincent, M. E. Voss, *J. Med. Chem.* **1993**, *36*, 3039–3049; b) J. Gante, *Angew. Chem.* **1994**, *106*, 1780–1802; *Angew. Chem. Int. Ed. Engl.* **1994**, *33*, 1699–1720; c) D. Leung, G. Abbenante, D. P. Fairlie, *J. Med. Chem.* **2000**, *43*, 305–341.
[3] a) A. Volonterio, P. Bravo, M. Zanda, *Org. Lett.* **2000**, *2*, 1827–1830; b) A. Volonterio, P. Bravo, M. Zanda, *Tetrahedron Lett.* **2001**, *42*, 3141–3144; c) A. Volonterio, S. Bellosta, P. Bravo, M.

 © 2003 Wiley-VCH Verlag GmbH & Co. KGaA, Weinheim

Canavesi, E. Corradi, S. V. Meille, M. Monetti, N. Moussier, M. Zanda, *Eur. J. Org. Chem.* **2002**, 428 – 438.

[4] a) *Enantiocontrolled Synthesis of Fluoro-Organic Compounds* (Ed.: V. A. Soloshonok), Wiley, Chichester, **1999**; for some recent examples of fluorine-containing peptidomimetics, see: b) G. S. Garrett, S. J. McPhail, K. Tornheim, P. E. Correa, J. M. McIver, *Bioorg. Med. Chem. Lett.* **1999**, *9*, 301 – 306; c) M.-A. Poupart, G. Fazal, S. Goulet, L.-T. Mar, *J. Org. Chem.* **1999**, *64*, 1356 – 1361; d) M. Eda, A. Ashimori, F. Akahoshi, T. Yoshimura, Y. Inoue, C. Fukaya, M. Nakajima, H. Fukuyama, T. Imada, N. Nakamura, *Bioorg. Med. Chem. Lett.* **1998**, *8*, 919 – 924, and references therein; e) R. V. Hoffman, J. Tao, *Tetrahedron Lett.* **1998**, *39*, 4195 – 4198; f) P. A. Bartlett, A. Otake, *J. Org. Chem.* **1995**, *60*, 3107 – 3111; g) A. G. Myers, J. K. Barbay, B. Zhong, *J. Am. Chem. Soc.* **2001**, *123*, 7207 – 7219.

[5] a) E. Höss, M. Rudolph, L. Seymour, C. Schierlinger, K. Burger, *J. Fluorine Chem.* **1993**, *61*, 163 – 170, and references therein; b) S. N. Osipov, N. Sewald, A. F. Kolomiets, A. V. Fokin, K. Burger, *Tetrahedron Lett.* **1996**, *37*, 615 – 618; c) F. Bordusa, C. Dahl, H.-D. Jakubke, K. Burger, B. Koksch, *Tetrahedron: Asymmetry* **1999**, *10*, 307 – 313.

[6] a) *Fluorine-containing Amino Acids, Synthesis and Properties* (Eds.: V. P. Kukhar', V. A. Soloshonok), Wiley, Chichester, **1995**; b) N. Lebouvier, C. Laroche, F. Huguenot, T. Brigaud, *Tetrahedron Lett.* **2002**, *43*, 2827 – 2830; c) T. Sakai, F. Yan, S. Kashino, K. Uneyama, *Tetrahedron* **1996**, *52*, 233 – 244; d) S. Ayhan, A. S. Demir, S. Özge, G.-A. Zuhal, *Tetrahedron: Asymmetry* **2001**, *12*, 2309 – 2313; e) S. Fustero, A. Navarro, B. Pina, J. G. Soler, A. Bartolomé, A. Asensio, A. Simón, P. Bravo, G. Fronza, A. Volonterio, M. Zanda, *Org. Lett.* **2001**, *3*, 2621 – 2624.

[7] a) M. Chorev, M. Goodman, *Acc. Chem. Res.* **1993**, *26*, 266 – 273; b) M. Chorev, M. Goodman, *Trends Biotechnol.* **1995**, *13*, 438 – 445; c) M. D. Fletcher, M. M. Campbell, *Chem. Rev.* **1998**, *98*, 763 – 795.

[8] See, for example: a) L. M. Pratt, R. P. Beckett, S. J. Davies, S. B. Launchbury, A. Miller, Z. M. Spavold, R. S. Todd, M. Whittaker, *Bioorg. Med. Chem. Lett.* **2001**, *11*, 2585 – 2588; b) A. D. Lebsack, L. E. Overman, R. J. Valentekovich, *J. Am. Chem. Soc.* **2001**, *123*, 4851 – 4852; c) F. M. Martin, R. P. Beckett, C. L. Bellamy, P. F. Courtney, S. J. Davies, A. H. Drummond, R. Dodd, L. M. Pratt, S. R. Patel, M. L. Ricketts, R. S. Todd, A. R. Tuffnell, J. W. S. Ward, M. Whittaker, *Bioorg. Med. Chem. Lett.* **1999**, *9*, 2887 – 2892; d) L. A. Paquette, R. R. Rothhaar, M. Isaac, L. M. Rogers, R. D. Rogers, *J. Org. Chem.* **1998**, *63*, 5463 – 5472; e) B. Koksch, K. Mütze, S. N. Osipov, A. S. Golubev, K. Burger, *Tetrahedron Lett.* **2000**, *41*, 3825 – 3828, and references therein.

[9] a) Y. Hanzawa, M. Suzuki, Y. Kobayashi, T. Taguchi, Y. Iitaka, *J. Org. Chem.* **1991**, *56*, 1718 – 1725; b) T. Yamazaki, T. Ichige, S. Takei, S. Kawashita, T. Kitazume, T. Kubota, *Org. Lett.* **2001**, *3*, 2915 – 2918.

[10] In toluene the absence of an amine produced a dramatic drop in stereoselectivity (54% *de* for **4a**, Table 1, entry 15). The *de* also decreased when DABCO was used in a catalytic amount (86% for **4a**, Table 1, entry 13).

[11] Faster reactions were also observed when DABCO was used instead of TEA, DIPEA, or TMP.

[12] The crystal structures of **4j** and **4n** will be published in a full paper.

[13] The asymmetric addition of chiral alcohols to ketenes ("Merck reaction"), a conceptually related reaction, shows a very similar dependence on the polarity of the solvent and the structure of the catalyst (the amine base). See, for example: a) R. D. Larsen, E. G. Corley, P. Davis, P. J. Reider, E. J. J. Grabowski, *J. Am. Chem. Soc.* **1989**, *111*, 7650 – 7651; see also: b) B. L. Hodous, J. C. Ruble, G. C. Fu, *J. Am. Chem. Soc.* **1999**, *121*, 2637 – 2638; c) A. E. Taggi, A. M. Hafez, H. Wack, B. Young, W. J. Drury III, T. Lectka, *J. Am. Chem. Soc.* **2000**, *122*, 7831 – 7832; d) M. Calmes, J. Daunis, N. Mai, *Tetrahedron* **1997**, *53*, 13719 – 13726. The tight zwitterionic termolecular (alcohol/ketene/amine) intermediate that was recently proposed to explain the high stereocontrol of the Merck reaction might also be a useful model for a mechanistic interpretation of the reaction presented herein. The latter reaction is probably more complex both from a mechanistic and a stereochemical point of view because of the presence of a double stereoinduction effect: e) C. E. Cannizzaro, T. Strassner, K. N. Houk, *J. Am. Chem. Soc.* **2001**, *123*, 2668 – 2669.

 © 2003 Wiley-VCH Verlag GmbH & Co. KGaA, Weinheim

Vanadium-Catalyzed C–C Coupling

Vanadium-Catalyzed *anti*-Selective Additions of Allenols to Imines**

Barry M. Trost and Catrin Jonasson*

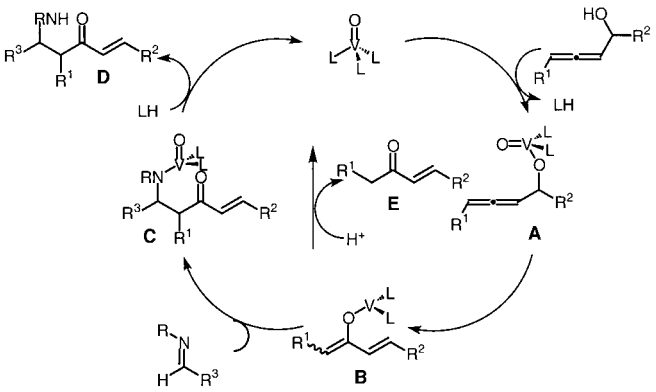
The use of vanadium catalysis for organic reactions has been virtually limited to redox chemistry.[1] Only recently have a few reports of additions to carbonyl groups catalyzed by vanadium(IV) and (V) complexes appeared.[2] To our knowledge, the additions of nucleophiles to imines catalyzed by vanadium have not been recorded. Our recent interest in the in situ generation of vanadium enolates by isomerization of allenols led us to consider their ability to add to imines (see Scheme 1).[3] The importance of Mannich-type products with the juxtaposition of an α,β-unsaturated carbonyl group should make the products particularly useful synthetic building blocks.[4] Since protonation of the enolate[5] to form enone **E** (see Scheme 1) competes with the imine addition, the latter must be quite facile for success. The general poorer reactivity of imines compared to carbonyl groups with regard to nucleophilic addition bodes ill for a competition favoring addition over simple isomerization of the allenol. Despite this ominous precedent, we now report the successful realization of an atom-economic[6] addition of allenic alcohols and imines in an *anti*-selective fashion.

[*] Prof. B. M. Trost, C. Jonasson
Department of Chemistry
Stanford University
Stanford, CA 94305-5080 (USA)
Fax: (+1) 650-725-0002
E-mail: bmtrost@stanford.edu

[**] We thank the National Science Foundation and the National Institute of Health, General Medical Sciences (GM13598), for their generous support of our programs. Mass spectra were provided by the Mass Spectrometry Facility of the University of California, San Francisco, supported by the NIH Division of Research Resources. C. J. thanks The Swedish Foundation for International Cooperation in Research and Higher Education (STINT).

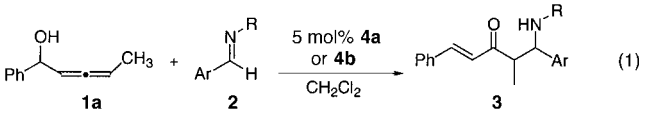
Supporting information for this article is available on the WWW under http://www.angewandte.org or from the author.

 DOI: 10.1002/anie.200350890 © 2003 Wiley-VCH Verlag GmbH & Co. KGaA, Weinheim



Scheme 1. Catalytic cycle. L = $OSiPh_3$.

To probe the feasibility of this process, the reaction in Equation (1) was used as the test[7] with $[VO(OSiPh_3)_3]$ (**4a**)[5c] as a catalyst. The results are summarized in Table 1.



(1)

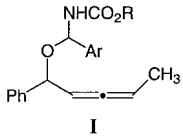
Interestingly, the simple Schiff base **2a** participates well in the reaction (entry 1). In contrast to our study of the reaction with aldehydes wherein *syn* diastereomers dominated, this reaction provided the *anti* diastereomers as the major product. Placing an electron-donating substituent in the *para* (entry 2) or *ortho* (entry 3) position of the *N*-aryl ring decreased the trapping dramatically. Thus, a removable electron-withdrawing substituent was placed on the nitrogen center. The *N*-sulfonyl analogue **2d**[8] was a poor participant (entry 4). The low yield of the adduct **3d** was mainly due to the inefficiency of trapping since the simple rearranged enone was the major product.

Table 1: Selected optimization data for **2**; Ar = Ph.[a]

Entry	R	Imine **2**	Product **3**	Yield [%][b]	*anti*/*syn*[c]
1	Ph	**2a**[d]	**3a**	91	1.7
2	$C_2H_4OCH_3$-4	**2b**[d]	**3b**	43	1.3
3	$C_6H_4CH_3$-2	**2c**[d]	**3c**	< 20	1.8
4	$PhSO_2$	**2d**[d]	**3d**	22	0.2
5	CH_3OCO	**2e**[d]	**3e**	22	9.0
6	CH_3OCO	**2e**[d]	**3e**	67	9.0
7	CH_3OCO	**2e**[e]	**3e**	72	9.0
8	CH_3OCO	**2e**[e]	**3e**	85	9.0
9	C_2H_5OCO	**2f**[e]	**3f**	67	7.3
10	*i*-C_3H_7OCO	**2g**[e]	**3g**	86	7.3

[a] In a typical procedure, the reactions were performed at substrate concentrations of 2.5 M with 5 mol% of catalyst **4a** under an argon atmosphere; entries 1–5 were run at room temperature, entries 6 and 7 at 35 °C with an addition time of 10 h for imine, and entries 8–10 at 35 °C with an addition time of 20 h. Reactions with addition times of 10 h and 20 h were performed by using a syringe pump. [b] Yield of isolated product after flash chromatography. [c] Determined by ^1H NMR spectroscopy and HPLC. [d] In this run, 1.2 equivalents of imine were employed. [e] In this run, 1.05 equivalents of imine were employed.

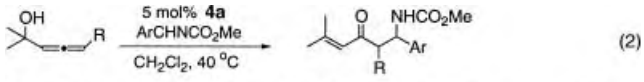
Replacing the poorly Lewis basic sulfone **2d** by the more Lewis basic carbamate **2e**[9] increased the diastereoselectivity dramatically. Surprisingly, the initial reaction still showed a poor yield of adduct **3e** (entry 5); however, for a different reason. Instead of untrapped rearranged ketone, the major product was the aminal **I** (R = CH_3, C_2H_5, *i*-C_3H_7) derived from simple addition of the alcohol to the imine. Remarkably, this adduct forms irreversibly in the presence or even absence of the vanadium catalyst. A dramatic improvement of the yield (entry 6) occurred when the allenic alcohol was added over a period of 10 h at 35 °C. A combination of lowering of the amount of imine from 1.2 equivalents to 1.05 equivalents (entry 7) together with increasing the time over which the addition was made, led to high yield and diastereoselectivity (entry 8). No advantage accrues from changing the methyl group to an ethyl (entry 9) or isopropyl group (entry 10). Switching solvents (toluene, dichloroethane, THF, 1,2-dimethoxyethane, and acetonitrile) had no beneficial effects.



I

Adopting the conditions of entry 8, Table 1, as our standard, the variation of the imines was explored (see Table 2). Use of imines bearing electron-withdrawing substituents proved more problematic. The difficulty derives from the ease of formation of the simple addition product of the alcohol to the imine. Thus, the *p*-chloro substrate **2l** gave less than 20% yield of the adduct **3l** under normal conditions. Increasing the temperature to 40 or 45 °C improved the yield to 55–58%. Using a more active catalyst $[VO(OSi(p\text{-}ClC_6H_4)_3)_3]$ (**4b**) further increased the yield to 69%. With the more strongly electron-withdrawing nitro group, as in imine **2m**, the yield with this more reactive catalyst was still only 40%. Satisfactory diastereoselectivities were obtained in these latter two cases. Aliphatic imines such as that derived from pivaldehyde failed to react. The monosubstituted allenic alcohol **1b** participates well in the reaction to give adduct **6** (Table 2 entry 8).

Nonaromatic allenic alcohols are suitable substrates for the reaction as shown in Equation (2). With the parent imine, good yield and excellent diastereoselectivity of adduct **5a** was



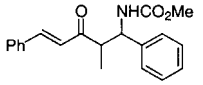
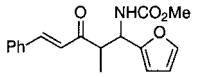
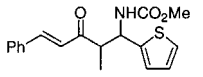
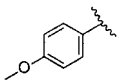
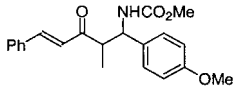
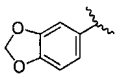
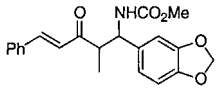
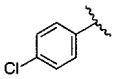
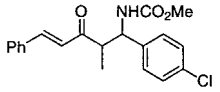
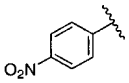
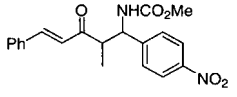
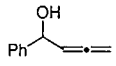
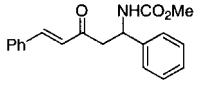
(2)

1c: R=CH_3 — **5a**: R=CH_3, Ar=Ph, 70%, *anti*/*syn*=32.3
1c: R=CH_3 — **5b**: R=CH_3, Ar=2-thienyl, 82%, *anti*/*syn*=4.9
1d: R=*n*-C_5H_{11} — **5c**: R=*n*-C_5H_{11}, Ar=Ph, 86%, *anti*/*syn*=24
1e: R=*i*-C_3H_7 — **5d**: R=*i*-C_3H_7, Ar=Ph, 66%, *anti*/*syn*=1.9

obtained. Better yields were obtained for the 2-thienyl derivative **5b**. While the diastereomeric ratio (d.r.) of **5b** decreased from that of **5a**, it was higher than that observed with allene **1a** (Table 2, entry 3). Increasing the chain length, for example **1d**, also gave excellent results [Eq. (2)]. On the other hand, the branched isopropyl-substituted substrate **1e** gave a diminished d.r. Increasing the size of the substituents at the alcohol center as in **1f** still gave excellent results [Eq. (3)].

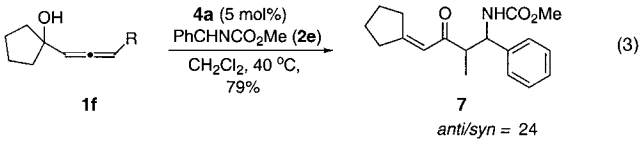
 © 2003 Wiley-VCH Verlag GmbH & Co. KGaA, Weinheim

Table 2: Vanadium-catalyzed additions of allenic alcohols and *N*-methoxycarbonyl (*N*-Moc) imines.[a]

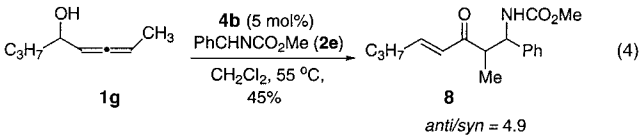
Entry	Allenic alcohol	2	Ar	Product	Yield [%][b]	*anti/syn*[c]
1	**1a**	**2e**	Ph		**3e** 85	9.0
2	**1a**	**2h**			**3h** 80	4.3
3	**1a**	**2i**			**3i** 81	3.2
4	**1a**	**2j**			**3j** 82	1.6
5	**1a**	**2k**			**3k** 79	1.5
6	**1a**	**2l**			**3l** 69[d]	6.1
7	**1a**	**2m**			**3m** 40[d]	6.1
8		**2e**	Ph		**6** 78	NA[e]

[a] In a typical procedure the reactions were carried out at 35–45 °C in dichloromethane (2.5 M) by employing 5 mol% $[VO(OSiPh_3)_3]$ (**4a**) and 1.05 equivalents of *N*-Moc imine, under an atmospheric pressure of argon. The allenic alcohol (1.0 equiv) was added slowly over 20 h. [b] Yield of isolated product after flash chromatography. [c] The *anti/syn* ratio was determined by ^{1}H NMR spectroscopy and HPLC. [d] $[VO(OSi(p\text{-}ClC_6H_4)_3)_3]$ (**4b**) was used as the catalyst (5 mol%). [e] NA = not applicable.

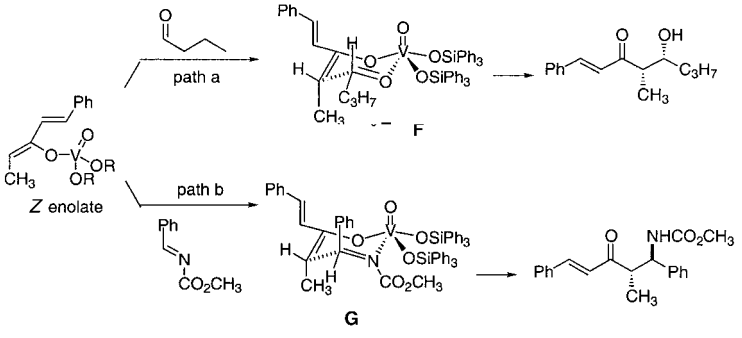
Using an allenic alcohol bearing only a single alkyl substituent at the carbinol carbon atom as in **1g** led to a slower reaction [Eq. (4)] and thus required use of the more active chloro-substituted catalyst **4b**.



(3)



(4)



(5)

The assignment of the major diastereomer as *anti* is based upon an X-ray crystallographic analysis of adduct **7** and correlations of ^{1}H and ^{13}C NMR data as detailed in the Supporting Information. The current report describes an atom-economical method for the stereoselective synthesis of products possessing simultaneously, an α,β-unsaturated ketone and a β-amino ketone that cannot be easily obtained by alternative means. To our knowledge, this is the first report involving the additions of vanadium enolates to imines. Whereas additions of these enolates to aldehydes preferably generate the *syn* adducts, the addition to imines generates the *anti* adducts. This complementary behavior can be rationalized by the [3.3] sigmatropic rearrangement of **A** (Scheme 1) preferentially forming the *Z* enolate. As shown in path a of Equation (5), coordination of the least hindered lone pair in the case of the aldehyde then leads to the *syn* adduct **F**, whereas, similar coordination to the single lone pair of the *E* aldimine must lead to the *anti* adduct **G**. It appears that vanadium enolates may prove to be generally useful in additions to all types of π-unsaturated systems. Their ease of generation by [3.3] sigmatropic rearrangements of propargyl and allenyl alchohols offers a novel new strategy for the synthesis of versatile building blocks.

Received: January 3, 2003 [Z50890]

Keywords: allenols · asymmetric catalysis · atom economy · imines · sigmatropic rearrangement · vanadium

[1] T. Hirao, *Chem. Rev.* **1997**, *97*, 2707; T. Hirao, *Kagaku Kogyo* **2001**, *52*, 958.
[2] D. I. Arnold, B. Green, N. S. Ikonnikov, M. North, T. Parson, V. Tarcrove, *Tetrahedron* **2001**, *57*, 771.
[3] B. M. Trost, C. Jonasson, M. Wuchrer, *J. Am. Chem. Soc.* **2001**, *123*, 12736. Also see: B. M. Trost, S. Oi, *J. Am. Chem. Soc.* **2001**, *123*, 1230.
[4] a) M. Arend, B. Westermann, N. Risch, *Angew. Chem.* **1998**, *110*, 1096; *Angew. Chem. Int. Ed.* **1998**, *37*, 1044; b) E. F. Kleinmann in *Comprehensive Organic Synthesis, Vol. 2* (Ed.: B. M. Trost), Pergamon, Oxford, **1991**, chap. 4.1; c) D. J. Hart, D.-C. Ha, *Chem. Rev.* **1998**, *98*, 2530; d) S. Kobayashi, H. Ishitani, *Chem. Rev.* **1999**, *99*, 1069. Some recent examples: e) D. Enders, S. Oberbörsch, J. Adam, *Synlett* **2000**, 644; f) H. Ishitani, M.

 © 2003 Wiley-VCH Verlag GmbH & Co. KGaA, Weinheim

Ueno, S. Kobayashi, *J. Am. Chem. Soc.* **2000**, *122*, 8180; g) J. L. Vicario, D. Badia, L. Carrillo, *Org. Lett.* **2001**, *3*, 773; h) S. E. Denmark, O. J.-C. Nicaise in "Comprehensive Asymmetric Catalysis" (Eds.: E. N. Jacobsen, A. Pfaltz, and H. Yamamoto), Springer Verlag, Heidelberg, pp. 954–957.

[5] a) P. Chabardes, E. Kuntz, J. Varagnat, *Tetrahedron* **1977**, *33*, 1775; b) G. L. Olson, H. C. Cheung, K. D. Morgan, R. Borer, G. Saucy, *Helv. Chim. Acta* **1976**, *59*,567; c) H. Pauling, D. A. Andrews, N. C. Hindley, *Helv. Chim. Acta* **1976**, *59*, 1233; d) M. B. Erman, I. S. Aul'chenko, L. A. Kheifits, V. G. Dulova, Y. N. Novikov, M. E. Vol'pin, *Tetrahedron Lett.* **1976**, 2981.

[6] Other synthetic approaches to similar compounds are complicated and not general, see: a) M. Kinoshita, S. Nakada, S. Umezawa, *Bull. Chem. Soc. Jpn.* **1967**, *40*, 926; b) J. J. Masters, L. S. Hegedus, J. Tamariz, *J. Org. Chem.* **1991**, *56*, 5666; c) R. F. W. Jackson, L. J. Graham, A. B. Rettie, *Tetrahedron Lett.* **1994**, *35*, 4417.

[7] For synthesis of allenic alcohols, see: a) M. Kimura, S. Tanaka, Y. Tamaru, *Bull. Chem. Soc. Jpn.* **1995**, *68*, 1689; b) J. S. Cowie, P. D. Landor, S. R. Landor, *J. Chem. Soc. Perkin Trans. 1* **1973**, 720; c) S. Ma, S. Zhao, *J. Am. Chem. Soc.* **1999**, *121*, 7943.

[8] B. M. Trost, C. Marrs, *J. Org. Chem.* **1991**, *56*, 6468.

[9] All the *N*-Moc imines were prepared according to: a) J. Vidal, S. Damestoy, L. Guy, J.-C. Hannachi, A. Aubry, A. Collet, *Chem. Eur. J.* **1997**, *3*, 1691; b) D. J. Hart, K. Kanai, D. G. Thomas, T.-K. Yang, *J. Org. Chem.* **1983**, *48*, 289.

 © 2003 Wiley-VCH Verlag GmbH & Co. KGaA, Weinheim

Polymer Recognition by Vesicles

Molecular Recognition of Polymers by Cyclodextrin Vesicles**

Bart Jan Ravoo, Jean-Christophe Jacquier, and Gerhard Wenz*

Dedicated to Professor H. Ringsdorf

In biology, processes such as cell–cell recognition and the initiation of signal transduction depend on the formation of multiple noncovalent complexes between substrates or ligands and membrane-bound receptors. Multiple, instead of isolated, host–guest interactions enhance binding affinity as well as selectivity.[1] Here we have investigated the role of multiple noncovalent interactions in molecular recognition at a membrane surface by using a model system consisting of bilayer vesicles of hydrophobically modified cyclodextrins[2] (CDs; the membrane receptors) in combination with monomer and polymer guest molecules[3] (the substrates). Molecular recognition and multiple host–guest interactions have been described for CD dimers[4] (including CD dimers in the presence of liposomes[5]) and polymers[3,6] as well as CD micelles[7] and self-assembled CD monolayers.[8] The anchoring of hydrophobically modified polymers into liposomes has also been studied.[9] We demonstrate that poly(isobutene-*alt*-maleic acid) substituted with hydrophobic *p-tert*-butylphenyl groups binds very strongly and selectively to the surface of CD bilayer vesicles, without affecting the integrity of the vesicles. No interaction is observed when the membrane does not contain host molecules or when the polymer does not contain hydrophobic guest substituents.

The CD vesicles used in this study were composed of **1**, which is β-CD substituted with S-dodecyl groups on the primary side and oligo(ethylene glycol) groups on the

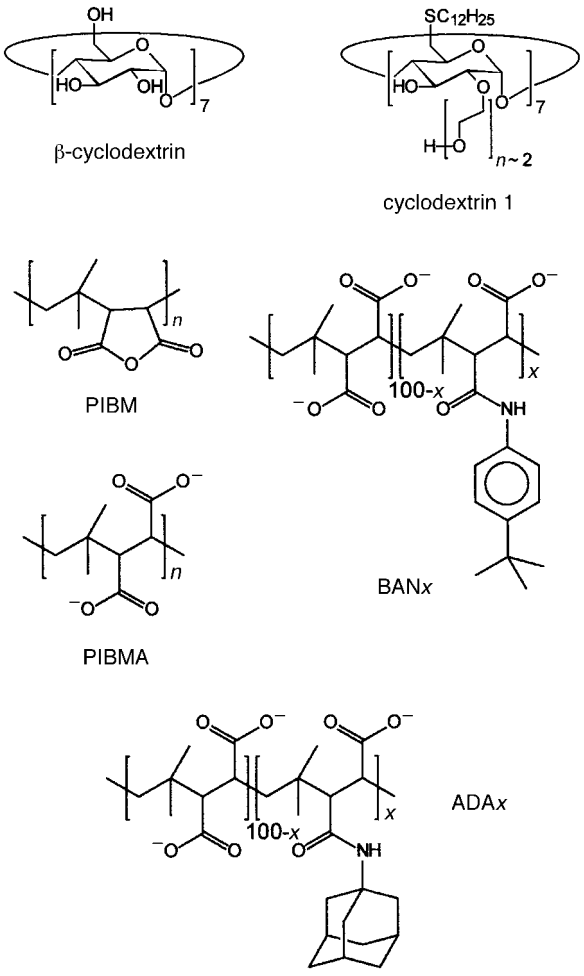
[*] Dr. B. J. Ravoo[+]
Centre for Synthesis and Chemical Biology
Department of Chemistry, University College
Dublin (Ireland)
Dr. J.-C. Jacquier
Department of Chemistry
University College Dublin
Belfield, Dublin 4 (Ireland)
Prof. Dr. G. Wenz
Macromolecular Organic Chemistry
University of Saarland
P.O. Box 151150, 66041 Saarbrücken (Germany)
[+] Current and correspondence address:
Laboratory of Supramolecular Chemistry and Technology
MESA+ Research Institute, University of Twente
P.O. Box 217, 7500 AE Enschede (The Netherlands)
Fax: (+31) 53-489-4645
E-mail: b.j.ravoo@ct.utwente.nl

[**] B.J.R. acknowledges a Schering-Plough Co. Newman Scholarship at UCD.

Supporting information for this article is available on the WWW under http://www.angewandte.org or from the author.

 © 2003 Wiley-VCH Verlag GmbH & Co. KGaA, Weinheim DOI: 10.1002/anie.200350923

secondary side (Scheme 1).[10] The formation of bilayer vesicles from this CD was described previously.[2] Cyclodextrin vesicles consist of bilayers of cyclodextrins (in which the hydrophobic "tails" are directed inwards and hydrophilic macrocycle "head groups" are facing water) enclosing an



Scheme 1. Chemical structures of CDs and guest polymers (x = molar percentage of substitution). The molecular weight of each guest-substituted polymer repeat unit (namely, equivalents of hydrophobic guest) was taken from ref. [3b].

aqueous interior. In this work, we used unilamellar vesicles prepared from multilamellar vesicles by repeated extrusion through a polycarbonate membrane (pore size 0.1 μm) which according to dynamic light scattering (DLS) studies have an average hydrodynamic diameter of approximately 160 nm.[11] The guest polymers BAN and ADA (Scheme 1) were prepared from poly(isobutene-*alt*-maleic anhydride) (PIBM) of $M_w = 60\ \mathrm{kg\,mol^{-1}}$ (namely, all the polymers have the same chain length) by amidation with *p-tert*-butylaniline or adamantanamine, respectively, followed by hydrolysis of the remaining anhydride groups.[3] Poly(isobutene-*alt*-maleic acid) (PIBMA) was obtained by hydrolysis of PIBM. Both the *p-tert*-butylphenyl and the adamantyl group are known to form stable inclusion complexes with β-CD in water. The binding constant $K_a = 1.0\text{–}4.0 \times 10^4\ \mathrm{M^{-1}}$, depends on the nature of the hydrophobic derivative, the substitution on the CD, and the ionic strength of the medium.[12] By using isothermal titration microcalorimetry (ITC)[3] and affinity capillary electrophoresis[13] we found that the K_a values for β-CD with the *p-tert*-butylphenyl groups on the polymers is of the same order of magnitude as that for *p-tert*-butylbenzoate, but that the K_a values are almost one order of magnitude lower for adamantyl-containing polymers than for adamantanecarboxylate. We demonstrated that binding of the polymers to β-CD leads to a transition of the polymer from a compact globular unimer to an extended random coil, which is energetically more costly for ADA than for BAN polymers.[13] The results of these studies are summarized in Table 1.

Table 1: Apparent binding constants determined by capillary electrophoresis for the complexation of polymer guests, *p-tert*-butylbenzoate and adamantanecarboxylate, to β-CD and to vesicles of **1**.

Guest	β-CD K_a [10^3 L mol^{-1}]	Vesicles of **1** K_a [10^3 L mol^{-1}]
BAN09	39 ± 3	2200 ± 400
BAN42	28 ± 1	450 ± 60
p-tert-butylbenzoate	12.7 ± 0.3	6 ± 1
ADA10	3.5 ± 0.9	2.4 ± 0.5
ADA20	2.0 ± 0.3	20 ± 2
adamantanecarboxylate	n.d.[a]	4 ± 1

[a] Not determined.

Dynamic light scattering was used to study the interaction of vesicles of **1** and liposomes of egg phosphatidyl choline (egg PC)[11] with BAN, ADA, and PIBMA polymers in dilute aqueous solution (Figure 1). An increase in the average hydrodynamic diameter of the vesicles was observed upon addition of BAN42 to vesicles of **1** (Figure 1a). If more than approximately one equivalent of polymer (by weight) was added, no further increase of diameter was observed. Overall, the diameter of the vesicles increased from about 160 nm to about 240 nm. No such increase was observed if PIBMA instead of BAN42 was added.[14] Also, when BAN42, ADA20, or PIBMA were added to liposomes of egg PC, the average liposome diameter was constant, even when more than seven equivalents of polymer (by weight) were added. Figure 1b shows the average diameter of the vesicles of **1** in the presence of each polymer as a function of the molar ratio of the polymer-bound guest to accessible CD. We assume that approximately 50% of the CD molecules reside on the inner bilayer surface and are inaccessible to the polymer. The ratio of guest-bound polymer to accessible CD required for saturation is much higher than 1:1 (see below).

These results indicate that the polymer guests, but not PIBMA, interact with vesicles of **1**, but not with egg PC liposomes. We propose that the *p-tert*-butylphenyl and the adamantyl groups, respectively, on the BAN and ADA polymers form inclusion complexes with the CD cavities on the surface of the vesicles of **1**, thus leading to a coating of the vesicles by the polymer guest. Since no interaction with the egg PC liposomes is observed, random hydrophobic anchoring[9] instead of inclusion of the *p-tert*-butylphenyl and the adamantyl groups into the bilayer must be negligibly weak.

 © 2003 Wiley-VCH Verlag GmbH & Co. KGaA, Weinheim

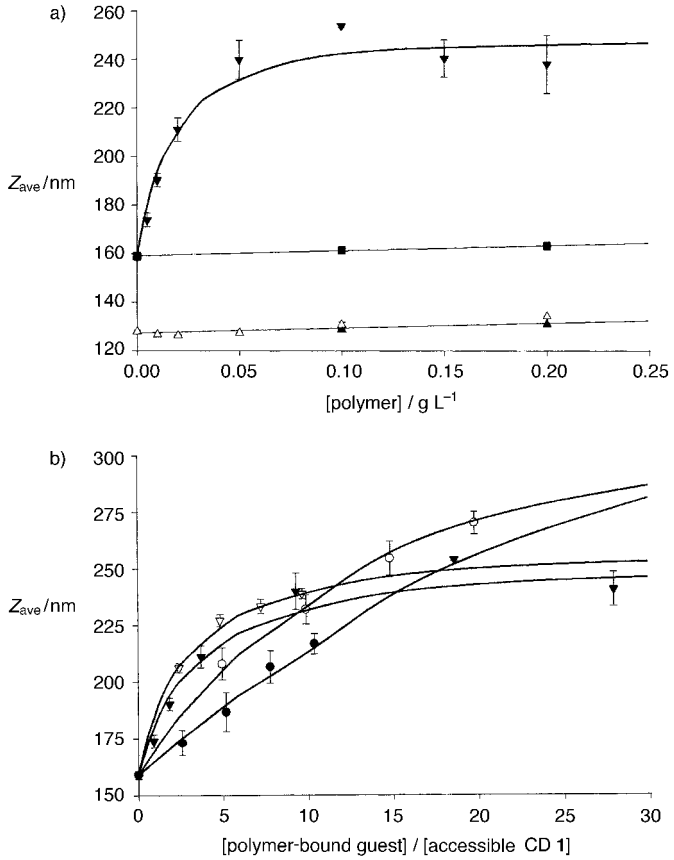


Figure 1. Average hydrodynamic diameter Z_{ave} of vesicles of **1** and egg PC liposomes in the presence of BAN, ADA, and PIBMA polymers. [**1**] = 0.05 g L^{-1} = 17 μM and [egg PC] = 0.05 g L^{-1}. a) Plot of the vesicle (liposome) diameter as a function of polymer concentration; ▼: **1** with BAN42, ■: **1** with PIBMA, △: egg PC with BAN42, ▲: egg PC with PIBMA. b) Plot of the vesicle diameter as a function of the [polymer bound guest]/[accessible CD **1**] molar ratio. ▽: BAN09, ▼: BAN42, ○: ADA20, and ●: ADA10.

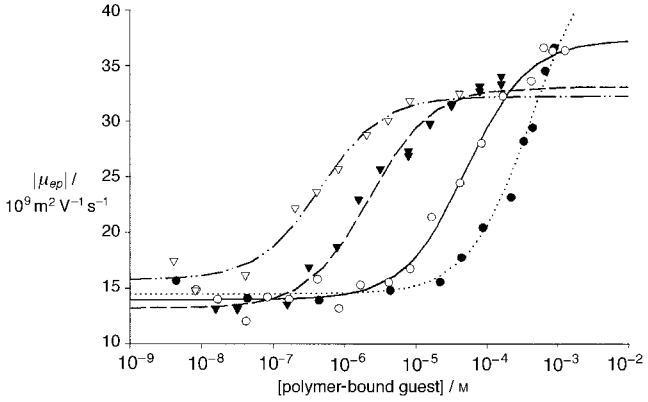


Figure 2. Absolute electrophoretic mobility μ_{ep} of vesicles of **1** as a function of the concentration of polymer-bound guests. ▽: BAN09, ▼: BAN42, ○: ADA20, and ●: ADA10. Note that the measured electrophoretic mobility is negative.

Since no interaction of PIBMA with either the vesicles of **1** or the egg PC liposomes is observed, surface absorption of the polymers can also be excluded. Furthermore, any effects relating to osmotic shock, depletion interaction, aggregation, or solubilization of either the CD vesicles or the liposomes can be excluded at these concentrations.

Affinity capillary electrophoresis (CE) was used to obtain quantitative information about the binding of guest polymers to the vesicles of **1** in dilute aqueous solution. The use of this technique to study the formation of host–guest complexes between β-CD and the polymer guests has been described in detail previously.[13] Here, the electrophoretic mobility of the vesicles of **1** was measured in the presence of increasing concentration of guest polymers in the background electrolyte (Figure 2). The increase of electrophoretic mobility of the vesicle in the presence of increasing concentration of polymer guest was analyzed in terms of the formation of a 1:1 inclusion complex between **1** and the substituent on the guest polymer and characterized by the apparent binding constant K_a. The results are summarized in Table 1.[15]

The binding constants collected in Table 1 allow for a number of interesting comparisons to be made regarding hydrophobic host–guest interactions between independent host and guest molecules in solution; between multiple, membrane-bound hosts and single guests; between single hosts and polymer guests; and finally between multiple, membrane-bound hosts and polymer guests. First of all, the interaction of both *p-tert*-butylbenzoate and adamantanecarboxylate is stronger with β-CD ($K_a = 10–30 \times 10^3\,M^{-1}$) than with vesicles of **1** ($K_a = 4–6 \times 10^3\,M^{-1}$). The difference might be attributed to some hindrance to inclusion into the cavity of **1** arising from the presence of hydrophilic oligo(ethylene glycol) residues or a degree of anticooperativity arising from the increasing presence of anionic guests on the vesicle surface. However, a Scatchard plot constructed in the case of *p-tert*-butylbenzoate had a linear slope and an abscissa intercept of 0.98, thus proving the presence of identical and independent binding sites on the vesicle surface. We can therefore ascribe the inferior binding constant for **1** to some steric hindrance and some reduction in the hydrophobicity of the host because of the presence of oligo(ethylene glycol) residues.

Secondly, the interaction between β-CD and *p-tert*-butylbenzoate and BAN polymers is quite similar ($K_a = 10–40 \times 10^3\,M^{-1}$) but the interaction between β-CD and adamantanecarboxylate ($K_a = 33 \times 10^3\,M^{-1}$)[3] is much stronger than the interaction between β-CD and ADA polymers ($K_a = 2.0–3.5 \times 10^3\,M^{-1}$). As discussed previously,[13] this difference may be attributed to increased intramolecular hydrophobic interaction of the adamantyl groups in the ADA polymers relative to that of the *p-tert*-butylphenyl groups in the BAN polymers, which competes with inclusion in the CD cavity.

Finally, while the interaction between ADA polymers and vesicles of **1** ($K_a = 2–20 \times 10^3\,M^{-1}$) is significantly stronger than the interaction between ADA polymers and β-CD ($K_a = 2.0–3.5 \times 10^3\,M^{-1}$), the interaction between BAN polymers and vesicles of **1** ($K_a = 450–2200 \times 10^3\,M^{-1}$) is almost two orders of magnitude stronger than that between BAN polymers and β-CD ($K_a = 28–39 \times 10^3\,M^{-1}$). Clearly, the presence of multiple, weakly self-associating guest substituents in the BAN poly-

 © 2003 Wiley-VCH Verlag GmbH & Co. KGaA, Weinheim

mer and multiple CD cavities on the CD vesicle surface leads to a very high binding affinity. Not all the *p-tert*-butylphenyl groups on the polymer are necessarily involved in bonding to the vesicle surface. Complete binding at the vesicle surface would severely restrict the conformational freedom of the polymer, as well as the lateral diffusion of the CDs in the bilayer, and would impose a very high entropic penalty. Also, inclusion will be in competition with intramolecular association, and only a minority of the *p-tert*-butylphenyl groups will be bound at any given time. This situation may explain why BAN09 binds to the CD vesicles even more efficiently than BAN42: the lower degree of hydrophobic substitution will decrease the tendency for intramolecular association and favor inclusion at the vesicle surface. This view is supported by the DLS experiments (Figure 1b), where one can see that up to ten hydrophobic substituents per accessible CD **1** are required for both BAN polymers to bind the vesicles fully. When the number of hydrophobic units per polymer strand is taken into account (ca. 164 and 35 for BAN42 and BAN09, respectively)[13] the degree of binding of BAN42 and BAN09 per accessible CD cavity is found to be 6 and 29%, respectively. In the case of both ADA polymers, saturation is not obtained even at high polymer concentration (Figures 1b and 2). Both the hydrodynamic diameter and the electrophoretic mobility of fully coated vesicles extrapolate to higher values than in the case of the BAN polymers, which indicates that the bound polymers have a somewhat different structure. As shown by the DLS experiments (Figure 1b) saturation is not obtained even in the presence of 30 hydrophobic substituents per accessible CD **1** for both ADA polymers. When the number of hydrophobic units per polymer strand is taken into account (ca. 78 and 39 for ADA20 and ADA10, respectively)[13] a degree of binding per accessible CD cavity of at least 40 and 80% is found for ADA20 and ADA10, respectively. This result would indicate a departure from a "mushroomlike" conformation towards a more "brushlike" configuration,[16] with the ADA polymer chains more fully extended (Figure 3). This interpretation is corroborated by the CE measurements, which show a significantly higher extrapolated electrophoretic mobility for ADA-bound vesicles than for the BAN-bound vesicles. The apparent increase in electrophoretic mobility despite the increase in the hydrodynamic diameter of the fully bound vesicles indicates a higher surface potential which probably arises from higher polymer coverage. A change in the polymer conformation from a globular mushroom to an extended, rodlike brush for both ADA polymers could be enthalpically stabilized by intermolecular interactions but would be entropically costly, and could explain the striking difference in binding affinity of the vesicles of **1** for the two polymer types.

The following conclusions can be drawn from combining the qualitative results from DLS and the quantitative information from CE. BAN polymers bind very strongly and selectively to the surface of CD bilayer vesicles. No interaction is observed when the membrane is composed of egg PC and does not contain CD host molecules or when the polymer does not contain hydrophobic substituents. Much weaker interactions are observed with ADA polymers because of competition from intramolecular interactions and possible rearrangement of this polymer type to give brushlike covered vesicles. In summary, these findings demonstrate the high affinity molecular recognition of a membrane-bound host by a water-soluble guest through multiple hydrophobic interactions. The thermodynamics of multiple complexation, as well as the kinetics of association and dissociation will be the subject of further study. Ultimately, the relevance of these coated vesicles may rest in their potential as drug-delivery systems.

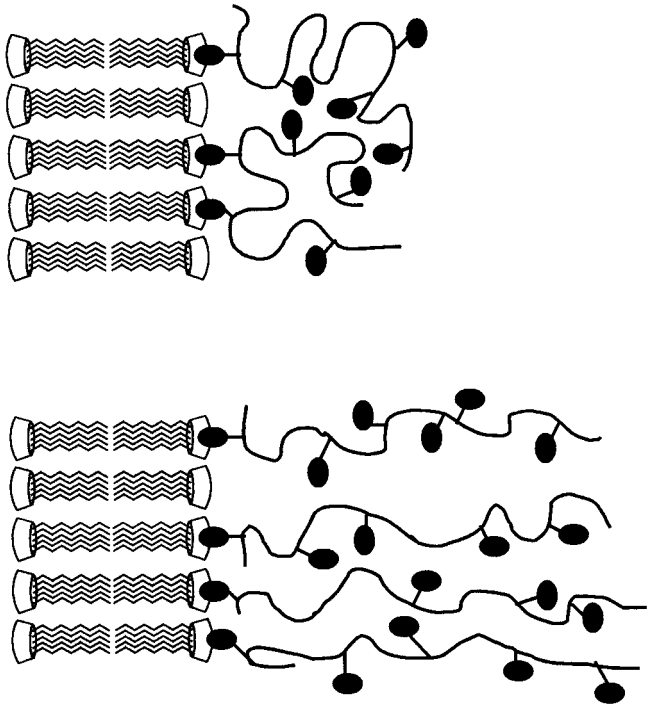


Figure 3. Coating of cyclodextrin bilayer vesicles by hydrophobically modified polyelectrolytes through multiple noncovalent interactions. Top: a BAN-covered bilayer of **1** with a low percentage of **1** bound to the polymer and a mushroomlike polymer coating. Bottom: an ADA-covered bilayer of **1** with a high percentage of **1** bound to the polymer and a brushlike polymer coating.

Received: January 13, 2003 [Z50923]

Keywords: cyclodextrins · host–guest systems · molecular recognition · polymers · vesicles

[1] a) M. Mammen, S.-K. Choi, G. M. Whitesides, *Angew. Chem.* **1998**, *110*, 2908–2953; *Angew. Chem. Int. Ed.* **1998**, *37*, 2754–2794; b) L. L. Kiessling, J. E. Gestwicki, L. E. Strong, *Curr. Opin. Chem. Biol.* **2000**, *4*, 696–703.

[2] B. J. Ravoo, R. Darcy, *Angew. Chem.* **2000**, *112*, 4494–4496; *Angew. Chem. Int. Ed.* **2000**, *39*, 4324–4326.

[3] a) M. Weickenmeier, G. Wenz, J. Huff, *Macromol. Rapid Commun.* **1997**, *18*, 1117–1123; b) M. Weickenmeier, PhD Thesis, Universität Karlsruhe, **1998**; c) "Associative Polymers in Aqueous Media": G. Wenz, M. Weickenmeier, J. Huff, *ACS Symp. Ser.* **2000**, *765*, 271–283.

 © 2003 Wiley-VCH Verlag GmbH & Co. KGaA, Weinheim

[4] a) R. Breslow, N. Greenspoon, T. Guo, R. Zarzycki, *J. Am. Chem. Soc.* **1989**, *111*, 8296 – 8297; b) R. Breslow, B. Zhang, *J. Am. Chem. Soc.* **1996**, *118*, 8495 – 8496; c) M. R. de Jong, J. F. J. Engbersen, J. Huskens, D. N. Reinhoudt, *Chem. Eur. J.* **2000**, *6*, 4034 – 4040; d) K. J. C. van Bommel, M. R. de Jong, G. A. Metselaar, W. Verboom, J. Huskens, R. Hulst, H. Kooijman, A. L. Spek, D. N. Reinhoudt, *Chem. Eur. J.* **2001**, *7*, 3603 – 3615.
[5] R. C. Petter, C. T. Sikorski, D. H. Waldeck, *J. Am. Chem. Soc.* **1991**, *113*, 2325 – 2327.
[6] a) M. Weickenmeier, G. Wenz, *Macromol. Rapid Commun.* **1996**, *17*, 731 – 738; b) R. Auzély-Velty, M. Rinaudo, *Macromolecules* **2001**, *34,* 3574 – 3580.
[7] R. Auzély-Velty, C. Péan, F. Djedaïni-Pilard, T. Zemb, B. Perly, *Langmuir* **2001**, *17*, 504 – 510.
[8] a) M. T. Rojas, R. Königer, J. F. Stoddart, A. E. Kaifer, *J. Am. Chem. Soc.* **1995**, *117*, 336 – 343; b) M. W. J. Beulen, J. Bügler, M. R. de Jong, B. Lammerink, J. Huskens, H. Schönherr, G. J. Vancso, B. A. Boukamp, H. Wieder, A. Offenhäuser, W. Knoll, F. C. J. M. van Veggel, D. N. Reinhoudt, *Chem. Eur. J.* **2000**, *6*, 1176 – 1183; c) M. R. de Jong, J. Huskens, D. N. Reinhoudt, *Chem. Eur. J.* **2001**, *7*, 4164 – 4170; d) J. Huskens, M. A. Deij, D. N. Reinhoudt, *Angew. Chem.* **2002**, *114*, 4647 – 4651; *Angew. Chem. Int. Ed.* **2002**, *41*, 4467 – 4471; .
[9] a) H. Ringsdorf, B. Schlarb, J. Venzmer, *Angew. Chem.* **1988**, *100*, 117 – 162; *Angew. Chem. Int. Ed. Engl.* **1988**, *27*, 113 – 158; b) H. Ringsdorf, J. Venzmer, F. M. Winnik, *Angew. Chem.* **1991**, *103*, 323 – 326; *Angew. Chem. Int. Ed. Engl.* **1991**, *30*, 315 – 318; c) H. Ringsdorf, E. Sackmann, J. Simon, F. M. Winnik, *Biochim. Biophys. Acta* **1993**, *1153*, 335 – 344; d) J. Kevelam, J. F. L. van Breemen, W. Blokzijl, J. B. F. N. Engberts, *Langmuir* **1996**, *12*, 4709 – 4717; e) K. Kostarelos, T. F. Tadros, P. F. Luckham, *Langmuir* **1999**, *15*, 369 – 378; f) S. Ghosh, S. J. Lee, K. Ito, K. Akiyoshi, J. Sunamoto, Y. Nakatani, G. Ourisson, *Chem. Commun.* **2000**, 267 – 268.
[10] A. Mazzaglia, R. Donohue, B. J. Ravoo, R. Darcy, *Eur. J. Org. Chem.* **2001**, 1715 – 1721.
[11] For comparison, we also prepared liposomes composed of egg PC, which according to DLS studies have an average diameter of about 130 nm.
[12] K. A. Connors, *Chem. Rev.* **1997**, *97*, 1325 – 1357.
[13] B. J. Ravoo, J. C. Jacquier, *Macromolecules* **2002**, *35*, 6412 – 6416.
[14] Only a very small apparent increase was observed, probably because of a slight increase in the solution viscosity with increasing polymer concentration.
[15] The interaction of monomer and polymer guest molecules with cyclodextrin vesicles was also investigated by using ITC. We found a K_a value of ca. $1.0 \times 10^4\,\text{M}^{-1}$ for the interaction between vesicles of **1** and both *p-tert*-butylbenzoate and adamantanecarboxylate, which is consistent with the values obtained by CE. An ITC analysis of the multiple interaction between vesicles and BAN and ADA will be reported in due course.
[16] S. T. Milner, *Science* **1991**, *251*, 905 – 914.

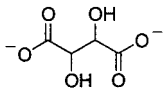
 © 2003 Wiley-VCH Verlag GmbH & Co. KGaA, Weinheim

Multicomponent Sensors

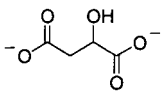
A Multicomponent Sensing Ensemble in Solution: Differentiation between Structurally Similar Analytes**

Sheryl L. Wiskur, Pierre N. Floriano, Eric V. Anslyn, and John T. McDevitt**

One current focus of the field of molecular recognition is to obtain synthetic receptors that rival the affinity and selectivity of natural receptors, such as antibodies or enzymes.[1] While many research groups have had partial success in this endeavor,[2] synthetic receptors are inherently much simpler than their biological counterparts. Therefore, it is quite difficult to achieve a very high degree of selectivity by using synthetic receptors. The difficulties arise both from the challenges of achieving complementary receptors, and from the need to complete time-consuming organic-synthesis routes to make the structurally complicated hosts. As an example, one would expect it to be very difficult to create two different synthetic receptors, each that will bind only one of the two structurally similar guests, such as tartrate and malate.



tartrate



malate

For many applications a single highly selective receptor for each guest is not required.[3] Instead, the goal is to identify the presence of the analytes, with or without quantification of their concentrations. In fact, nature does not use highly selective receptors for each analyte in our senses of taste and smell, and instead uses an array of "differential" receptors.[4] The response from each of these receptors for a particular mixture of stimuli creates a pattern that is stored in the brain. Because the receptors are not highly selective, they are analogous in many ways to synthetic receptors. We have proposed that the combination of differential receptors with pattern recognition may prove to be advantageous in a sensing application where identification and quantification are the main goals.[5] Herein we report that when colorimetric sensors are used, several wavelengths from a solution phase UV/Vis spectrum can serve as the multiple data inputs,

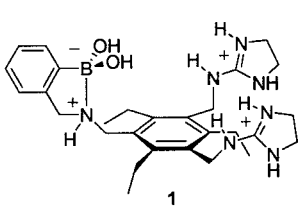
[*] Dr. E. V. Anslyn, Dr. J. T. McDevitt, S. L. Wiskur, P. N. Floriano
Department of Chemistry and Biochemistry
The University of Texas at Austin
Austin, TX 78712 (USA)
Fax: (+1) 512-471-8696
E-mail: anslyn@ccwf.cc.utexas.edu
mcdevitt@mail.utexas.edu

[**] We gratefully acknowledge support for this project from ARO-MURI and the Beckman Center for Array Sensors.

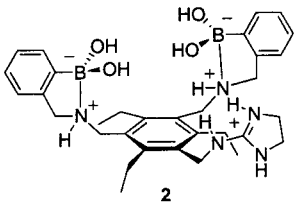
 © 2003 Wiley-VCH Verlag GmbH & Co. KGaA, Weinheim DOI: 10.1002/anie.200351058

analogous in some respects to array derived information, and the absorbance at each wavelength can be used to create the diagnostic pattern. Unlike conventional array-based systems, which require spatial localization of receptor and/or signaling agents, the present approach uses homogeneous solutions wherein a series of structurally diverse receptor/indicator combinations and their unique spectral features serve to report their local environment changes. In the particular application described herein, we demonstrate that a combination of two receptors, neither of which is very selective, with pattern recognition protocols allows one to achieve a high degree of selectivity in differentiating structurally similar guests. This method obviates the need for complex-specific receptors, making the inherent simplicity of synthetic receptors actually an advantage.

Two previously reported hosts (**1** and **2**), both with affinities for tartrate and malate, were chosen for this study.[3,6] The incorporation of boronic acid binding sites imparts affinity to vicinal diols,[7] while the use of guanidinium groups imparts affinity to carboxylates.[8] Receptor **1** was previously found to have a similar affinity for tartrate and malate,[6] while for receptor **2**, the combination of two boronic acids and one guanidinium was determined to have a greater affinity for tartrate over malate.[9]

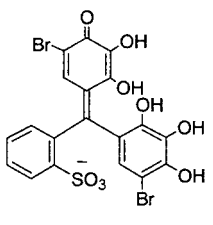


1

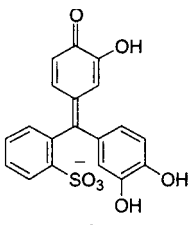


2

We have published numerous examples of the use of indicator-displacement assays for single-analyte sensing.[10] The indicator is first allowed to associate with the host, and upon addition of an analyte the indicator is displaced from the cavity, which results in a colorimetric or fluorimetric change. This same method of signaling is chosen for this multianalyte study. To further exploit the different characteristics of **1** and **2**, two indicators with different affinities for **1** and **2** were chosen. By design, the indicators were chosen so as to exhibit large differences in their wavelength maximums so that their spectral response would be spread over a large wavelength axis. The two indicators chosen were bromopyrogallol red (**3**) ($\lambda_{max} = 567$ nm) and pyrocatechol violet (**4**) ($\lambda_{max} = 445$ nm). Figure 1 shows the change in absorbance of a mixture of **3** and **4** as increasing amounts of **2** are added (75% methanol in water (v/v)). A similar, but reproducibly different response is found upon adding **1**.



3



4

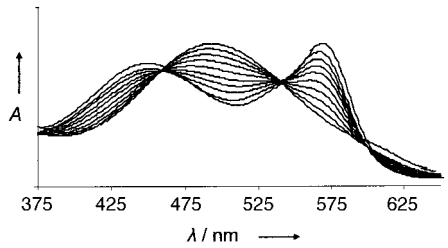


Figure 1. The UV/Vis spectra of **3** (30 μM) and **4** (60 μM) upon adding increasing amounts of **2** (75% methanol in water (v/v), pH 7.4, 10 mM HEPES buffer).

The training set data for the differentiation and quantification of tartrate and malate was created by the analysis of a four component ensemble of hosts and indicators in solution (150 μM of **1**, 150 μM of **2**, 30 μM of **3**, and 60 μM of **4**). Likewise, the UV/Vis spectra were obtained upon addition of various amounts of tartrate and malate, while the concentrations of the hosts and indicators were kept constant. The concentrations of tartrate and malate were altered in 0.2 mM increments ranging between 0 and 1.2 mM, thus resulting in 49 distinct spectra (Figure 2 shows a schematic of the matrix of scans). One representative example of the spectral difference found for the binding of different ratios of tartrate and malate to the two receptors is given in Figure 3. The UV/Vis spectra shown were both taken at a total analyte concentration of 0.8 mM, but for one spectrum the concentration of tartrate was greater than in the other (0.2 mM versus 0.6 mM). These

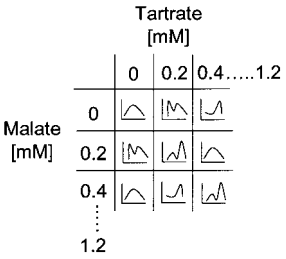


Figure 2. A representation of one experiment performed, where spectra were obtained at various concentrations of tartrate and malate.

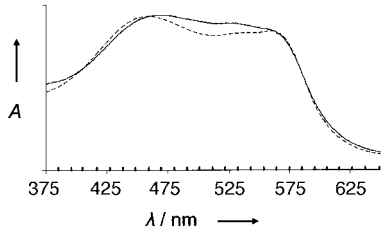


Figure 3. The UV/Vis spectra of the dye-displacement assays formed from the mixture of the indicators **3** (30 μM) and **4** (60 μM) and the receptors **1** (150 μM) and **2** (150 μM) upon the addition of tartrate and malate in various concentrations [(-----) Tartrate (0.6 mM) and malate (0.2 mM)] and [(——) Tartrate (0.2 mM) and malate (0.6 mM)] (75% methanol in water (v/v), pH 7.4, 10 mM HEPES buffer). The inside marks on the *x* axis are representative of the 27 wavelengths chosen for analysis.

 © 2003 Wiley-VCH Verlag GmbH & Co. KGaA, Weinheim

two UV/Vis traces demonstrate that the combination of two differential receptors differentiates mixtures of these two analytes. The reproducible variation in absorbance found for the pure samples and various mixtures of tartrate and malate is the data used as the training set for the supervised learning of the pattern recognition algorithm as described below.

Multilayer perceptron (MLP) artificial neural networks (ANN)[11] were chosen for pattern-recognition analysis. The basic architecture of the MLP that was used here consists of an input, an output, and a hidden layer, which is where the data is processed (or learned) through a back propagation training algorithm. Once the network has been trained, inputs that were not in the original data set are added and the trained algorithm attempts to calculate the output.[12]

Of the 49 spectra obtained, 45 of these were used to train the data set by using 27 wavelengths from each spectrum, while the other four spectral data sets were left out as "unknowns." When the absorbances for the 27 wavelengths were entered for the four unknowns, an absolute error between 1 and 6% was obtained for the output concentrations for both tartrate and malate (Table 1). The good agreement between the internal (i.e. training set) and external data (i.e. unknown set) indicates that solution concentrations of tartrate and malate which normally would be difficult to distinguish with a single receptor and indicator can be identified, and that even the individual concentrations of each analyte can be determined in a single analysis.

Although the maximum error of only 6% would appear to be quite acceptable for the first trial, further attempts to decrease the level of error were completed through the incorporation of more training data. In the second round of data collection, the concentration of malate was held constant (0.2 mM), and the concentration of tartrate was varied between 0 and 1.2 mM moving in increments of only 0.05 mM. In this case, three spectra were withheld from the new training session and these spectra served as the "unknowns." With this training set, the error in the calculated concentration was reduced to consistently less than 2% for all three unknowns (Table 1).

Table 1: The results from the neural network analysis. [mM].

Training NN1	Real [malate]	Pred. [malate]	Real [tartrate]	Pred. [tartrate]
val. case no. 1	0.000	0.0731	1.00	0.971 (3%)
val. case no. 2	0.59	0.568 (3%)	0.80	0.791 (1%)
val. case no. 3	0.99	1.034 (4%)	0.22	0.212 (5%)
val. case no. 4	1.19	1.136 (5%)	1.00	1.013 (1%)
Training NN2	[malate]		Real [tartrate]	Pred. [tartrate]
val. case no. 1	0.2	–	1.00	0.995 (0.6%)
val. case no. 2	0.2	–	0.53	0.527 (0.0%)
val. case no. 3	0.2	–	0.24	0.238 (1.3%)

Pred. = predetermined; val. = validation.

In conclusion, we have shown that the use of differential receptors in concert with pattern recognition can serve as a powerful method for supramolecular chemists to differentiate between very structurally similar guests, thereby avoiding the need for the creation of large numbers of specific receptors. Furthermore, we extended indicator displacement assays to encompass multiple indicators and multiple receptors. This multianalyte-sensing approach allows for the use of a single-solution vessel (i.e. a cuvette) in conjunction with standard spectrophotometry instrumentation. We are currently exploring the limit in the number of analytes that can be confidently detected by using such arrayless solution-phase multicomponent sensing ensembles.

Received: January 30, 2003 [Z51058]

Keywords: analytical methods · neural networks · receptors · sensors · supramolecular chemistry

[1] J. K. M. Sanders, *Pure Appl. Chem.* **2000**, *72*, 2265; A. P. Davis, R. S. Wareham, *Angew. Chem.* **1999**, *111*, 3160; *Angew. Chem. Int. Ed.* **1999**, *38*, 2978; P. D. Beer, P. A. Gale, *Angew. Chem.* **2001**, *113*, 502; *Angew. Chem. Int. Ed.* **2001**, *40*, 486.

[2] T. W. Bell, Z. Hou, *Angew. Chem.* **1997**, *109*, 1601; *Angew. Chem. Int. Ed. Engl.* **1997**, *36*, 1536; C.-T. Chen, W.-P. Huang, *J. Am. Chem. Soc.* **2002**, *124*, 6246; Y. Cheng, T. Suenaga, W. C. Still, *J. Am. Chem. Soc.* **1996**, *118*, 1813; J. Chin, C. Walsdorff, B. Stranix, J. Oh, H. J. Chung, S.-M. Park, K. Kim, *Angew. Chem.* **1999**, *111*, 2923; *Angew. Chem. Int. Ed.* **1999**, *38*, 2756.

[3] S. L. Wiskur, E. V. Anslyn, *J. Am. Chem. Soc.* **2001**, *123*, 10109.

[4] S. Mierson in *Handbook of Olfaction and Gustation* (Ed.: R. L. Doty), Marcel Dekker, New York, **1995**, p. 597; R. F. Margolskee in *Handbook of Olfaction and Gustation* (Ed.: R. L. Doty), Marcel Dekker, New York, **1995**, p. 575.

[5] J. J. Lavigne, E. V. Anslyn, *Angew. Chem.* **2001**, *113*, 3212; *Angew. Chem. Int. Ed.* **2001**, *40*, 3118.

[6] J. J. Lavigne, E. V. Anslyn, *Angew. Chem.* **1999**, *111*, 3903; *Angew. Chem. Int. Ed.* **1999**, *38*, 3666.

[7] C. J. Ward, P. R. Ashton, T. D. James, P. Patel, *Chem. Commun.* **2000**, 229.

[8] B. Linton, A. D. Hamilton, *Tetrahedron* **1999**, *55*, 6027.

[9] S. L. Wiskur, J. J. Lavigne, A. Metzger, S. L. Tobey, V. Lynch, E. V. Anlsyn, unpublished results.

[10] S. L. Wiskur, H. Ait-Haddou, J. J. Lavigne, E. V. Anslyn, *Acc. Chem. Res.* **2001**, *34*, 963.

[11] D. E. Rumelhart, *Parallel Distributed Processing*, MIT Press, Cambridge, **1986**; J. A. Burns, G. M. Whitesides, *Chem. Rev.* **1993**, *93*, 2583; P. A. Jansson, *Anal. Chem.* **1991**, *63*, 357A; P. N. Floriano, A. P. Goodey, A. S. Tsao, J. T. McDevitt, *Anal. Chem.* **2003**, submitted; A. Goodey, J. J. Lavigne, S. M. Savoy, M. Rodriguez, T. Curey, A. Tsao, G. Simmons, J. Wright, S.-J. Yoo, Y. Sohn, E. V. Anlsyn, J. B. Shear, D. P. Neikirk, J. T. McDevitt, *J. Am. Chem. Soc.* **2001**, *123*, 2559.

[12] J. Zupan, J. Gasteiger, *Anal. Chim. Acta* **1991**, *248*, 1; C.-S. Yin, Y. Shen, S.-S. Liu, Q. Yin, W.-M. Guo, Z.-X. Pan, *Comput. Chem.* **2001**, *25*, 239; C.-S. Yin, W.-M. Guo, S.-S. Liu, Y. Shen, Z.-X. Pan, L.-S. Wang, *Chin. J. Chem.* **2001**, *19*, 836; J. Meiler, R. Meusinger, M. Will, *J. Chem. Inf. Comput. Sci.* **2000**, *40*, 1169; Y. Ni, S. Chen, S. Kokot, *Anal. Chim. Acta* **2002**, *463*, 305; F. M. Raymo, S. Giordani, *J. Am. Chem. Soc.* **2002**, *124*, 2004; A. P. de Silva, N. D. McClenaghan, *Chem. Eur. J.* **2002**, *8*, 4935.

 © 2003 Wiley-VCH Verlag GmbH & Co. KGaA, Weinheim

C-Glycosides

Synthesis of a C-Glycoside Analogue of sTn: An HIV- and Tumor-Associated Antigen**

*Balagurunathan Kuberan, Sulthan A. Sikkander, Hiroshi Tomiyama, and Robert J. Linhardt**

N-Acetylneuraminic acid occupies the nonreducing end of many naturally occurring glycoconjugates on the cell surface, including glycoproteins and glycolipids. The strategic location of glycoconjugates on the cell surface and the enormous structural information that they carry account for their major role in biological recognition in the control of both normal and pathological processes.[1] While the participation of sialic acid in these biological events has been established unequivocally in a large number of studies,[1] the linkage of sialic acid to glycoconjugates is one of the most labile glycosidic linkages, which renders these compounds less amenable to biological and biochemical studies.[2] Terminal sialic acid residues are easily cleaved in vitro under very mild acidic conditions and in vivo by neuraminidases.[3] The biological importance of sialic acid coupled with its lability towards hydrolysis prompted us to redesign the molecular architecture of glycoconjugates to afford a non-hydrolyzable glycosidic linkage to sialic acid. Such a stable linkage should contribute to our understanding of biological recognition and serve to enhance or suppress biological events at the molecular level. The replacement of the interglycosidic oxygen atom with a hydroxymethylene or methylene group affords a new class of hydrolytically stable C-glycoside analogues of glycoconjugates.[4] A method for the preparation of C-glycosides of ulosonic acids using SmI_2 was pioneered in our laboratory.[5]

The sialyl-Tn epitope [α-D-Neu5Ac-(2→6)α-D-GalNAc-(1→*O*)-Ser/Thr] (sTn, **1a**, Figure 1) is found on the HIV envelope glycoprotein gp120[6] and in tumor-associated antigens present in the glycoproteins on the surface of cancer cells, including those associated with carcinomas of the breast, prostate, pancreas, colon, ovary, lung, and stomach.[7] Synthetic vaccines based on the sTn epitope (O-glycoside) have been recently prepared[8] and shown to stimulate an immune response.[9]

Kishi and co-workers have demonstrated that C-glycosides and O-glycosides have similar conformational characteristics both in the free and bound states.[10] There are, nevertheless, differences in the population distribution of conformers adopted by C-glycosides and their natural counterparts.[11] However, the small energy differences among the various conformers allow them to interchange without any major energy conflicts, thus rendering the C-glycosides ideally suited as O-glycoside isosters for therapeutic evaluation. Our rationale for undertaking the synthesis of the C-glycoside analogue of sTn (**1b**, Figure 1) was to develop and test a new vaccine candidate against the elusive HIV or to prepare a better candicate for a cancer vaccine with a longer half-life in vivo.[9b]

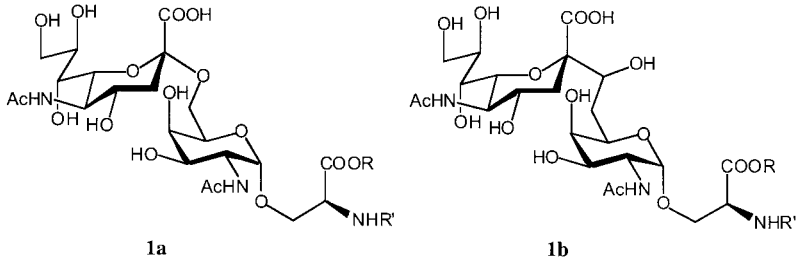


Figure 1. Tumor antigen sTn O-glycoside **1a** and C-glycoside analogue **1b**.

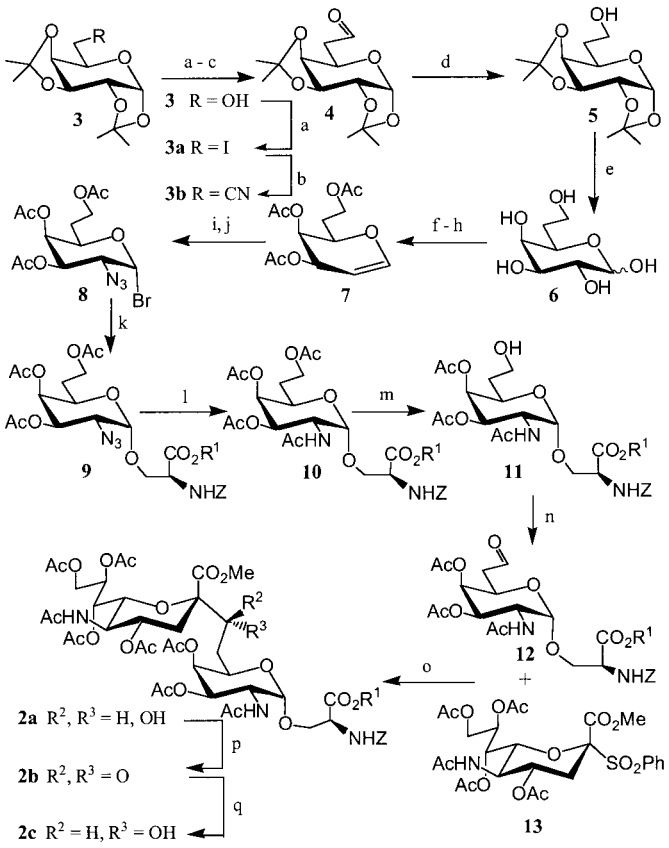
Fully protected sTn C-glycoside analogue **2** was prepared by C-glycosylation of the neuraminic acid sulfone donor **13** with an aldehyde acceptor **12** (Scheme 1). The donor **13** was prepared from neuraminic acid in four steps as previously reported.[12] The critical intermediate, aldehyde acceptor **12**, was prepared in 14 steps. Starting from the commercially available diisopropylidene galactose derivative **3**, the corresponding 6-iodo derivative **3a** was prepared and treated with KCN. The modest yield (30%) of this reaction might be due to unfavorable electronic and steric effects arising from the ring oxygen atom and the axially oriented oxygen at C-4, respectively. Reduction of the 6-cyano derivative **3b** with DIBAL-H afforded aldehyde **4** in moderate overall yield.[13] Quantitative reduction of aldehyde **4** with $NaBH_4$ in MeOH afforded the corresponding alcohol **5**. The acetal protecting groups were removed by treatment with Amberlite IR-120 (H^+) resin in water at 80 °C for 3 h to provide the 6-deoxy-D-galacto-heptopyranose **6** in quantitative yield. The one-carbon-extended galactal **7** was obtained in good yield from **6** by a one-pot, three-step procedure consisting of: a) peracetylation with acetic anhydride and catalytic HBr/HOAc; b) conversion of the anomeric acetate to the corresponding bromide with excess HBr/HOAc; and c) reductive elimination of the 1-bromo and 2-acetoxy groups with Zn/Cu.[14] Azidonitration[15] of **7** with excess ceric ammonium nitrate (CAN) and sodium azide in dry acetonitrile afforded primarily the 2-azido-1-nitrate addition product, which has the desired *galacto* configuration as unambiguously confirmed by ^1H NMR spectroscopy. Indicative are a large

[*] Prof. Dr. R. J. Linhardt, B. Kuberan, S. A. Sikkander, H. Tomiyama
Division of Medicinal and Natural Products Chemistry and
Department of Chemical and Biochemical Engineering
University of Iowa
Iowa City, IA 52242 (USA)
Fax: (+1) 319-335-6634
E-mail: robert-linhardt@uiowa.edu

[**] The authors thank Prof. D. H. G. Crout of the University of Warwick for generously supplying the esterase used in this study and Dr. Iontcho Vlahov of Endocyte Inc. for his helpful conversations regarding this manuscript. This research was supported in part by Kotobuki Pharmaceutical Company, Nagano, Japan.

Supporting information for this article is available on the WWW under http://www.angewandte.org or from the author.

 DOI: 10.1002/anie.200351099 © 2003 Wiley-VCH Verlag GmbH & Co. KGaA, Weinheim



Scheme 1. Synthesis of sTn C-glycoside derivatives. a) Ph_3P, I_2, Im; b) KCN; c) DIBAL-H; d) $NaBH_4$; e) H^+ resin; f) Ac_2O, HBr/HOAc; g) excess HBr/HOAc; Zn/Cu; i) CAN, NaN_3; j) LiBr; k) Z-Ser-OBn, $AgClO_4$, 4Å molecular sieves; l) AcSH/Py; m) *R. toruloides*, sodium phosphate/sodium citrate buffer, pH 5; n) DMSO, ClCOCOCl, TEA; o) SmI_2; p) DMSO/Ac_2O; q) $Zn(BH_4)_2$. R^1 = Bn. Im = imidazole, DIBAL-H = diisobutylaluminunm hydride, Py = pyridine, TEA = triethylamine, DMSO = dimethyl sulfoxide.

coupling constant between the two vicinal protons H-2 and H-3 ($J_{2,3}$ = 11 Hz) and the chemical shift of H-2 (δ = 3.97 ppm). Treatment of the crude product with LiBr[15] in dry acetonitrile in the dark afforded **8**. Glycosylation of **8** with the N^{α}-benzyloxycarbonyl-protected OBn ester of L-serine, prepared as previously reported,[16] in the presence of silver perchlorate afforded the glycopeptide **9**. Separation of glycopeptide **9** from unreacted starting material, Z-Ser-OBn, was cumbersome since both compounds migrated with similar R_f values on silica. However, conversion of **9** to **10** by treatment with thioacetic acid/pyridine[17] resulted in a large change in the glycopeptide polarity and permitted removal of the unreacted amino acid acceptor from the desired glycopeptide product **10**.

Our efforts next focused on the selective deprotection of the C-7 primary acetyl group in **10**. Since chemical techniques are not sufficiently selective, we envisaged a selective enzymatic deacetylation using an esterase. The esterase from *Rhodosporidium toruloides* has been reported to selectively deprotect primary acetates in the presence of secondary acetates.[18] Treatment of **10** with this esterase at pH 5 in a sodium phosphate/sodium citrate buffer afforded **11** in quantitative yield. The site of the enzymatic deacetylation was unequivocally established as C-7 based on the upfield shift of H-7a and H-7b from δ = 4.19–4.06 in **10** to 3.62–3.74 ppm in **11** in the ^{1}H NMR spectra. Swern oxidation[19] of **11** afforded aldehyde acceptor **12**. Glycosylation of the neuraminic acid sulfone donor **13** with aldehyde acceptor **12** in the presence of freshly prepared SmI_2[20] afforded the fully protected sTn α-C-glycoside **2a**.

The ^{1}H NMR spectrum of **2a** indicated an *R*/*S* mixture (1:1) at the newly formed stereogenic bridge carbon C-7. Attempts were first made to remove the hydroxyl group at C-7 by standard reductive radical deoxygenation protocols. Compound **2a** was treated with $(imidazole)_2CS$ or $ClCS(PhF_5)$ then reduced with Ph_3SnH and azobisisobutyronitrile (AIBN). These reactions failed to yield the expected deoxygenated product probably due to unfavorable stereoelectronic factors. The C-7 hydroxyl group in **2a** was next converted to a triflate and subjected to nucleophilic reduction with hydride, but this resulted in decomposition of the triflate, presumably due to the unwanted rearrangement, followed by elimination—the result of the electron-rich functional groups close to the reactive center. Finally, chemoselective resolution to compound **2a** was undertaken by oxidation with DMSO/Ac_2O to keto-bridged compound **2b**, followed by stereoselective reduction with $Zn(BH_4)_2$ to regenerate the bridge hydroxyl function, gave **2c** in >90% *de* (Scheme 1). The configuration at the bridge carbon was established by ROESY. Chemical exchange of the proton of the hydroxyl group of the bridge carbon and the oxygen of the C-1 carboxyl group of Neu5Ac resulted in strong NOEs for H-3′e/H-7, H-7/H-6(proR), OH-7/H-6(proS), and H-6(proR)/H-5, consistent with the *R* configuration at C-7 in **2c** (Figure 2).

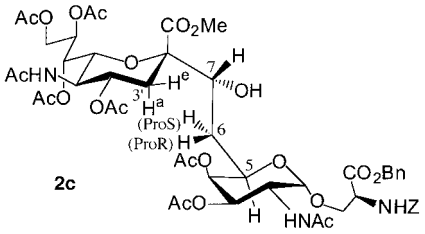


Figure 2. Stereochemical assignment of sTn *C*-glycoside **2c** at the bridge carbon C-7.

In summary, the synthesis of the C-glycoside analogue **2c** was achieved in 1 enzymatic and 17 chemical steps starting from diisopropylidene galactopyranose and sialic acid. Additional studies are underway aimed at conjugating the sTn C-glycoside hapten to KLH carrier protein to obtain a vaccine for biological evaluation.

Received: February 4, 2003 [Z51099]

Keywords: anti-HIV agents · antitumor agents · C-glycosides · glycopeptides · sialic acid

 © 2003 Wiley-VCH Verlag GmbH & Co. KGaA, Weinheim

[1] a) R. Schauer, *Trends Glycosci. Glycotechnol.* **1997**, *9*, 315 – 330; b) C. Traving, R. Schauer, *Cell. Mol. Life Sci.* **1998**, *54*, 1330 – 1349; c) A. Varki, *Glycobiology* **1992**, *2*, 25 – 40.

[2] a) N. Sharon, H. Lis, *Science* **1989**, *246*, 227 – 234; b) H. Lis, *Lectins*, Chapman and Hall, London, **1989**.

[3] G. M. Air, W. Laver, *Proteins Struct. Funct. Genet.* **1989**, *6*, 341 – 356, and references therein.

[4] a) Y. Du, R. J. Linhardt, I. R. Vlahov, *Tetrahedron* **1998**, *54*, 9913 – 9959; b) M. Postema, *C-Glycoside Synthesis*, CRC, Boca Raton, **1995**.

[5] a) I. R. Vlahov, P. I. Vlahova, R. J. Linhardt, *J. Am. Chem. Soc.* **1997**, *119*, 1480 – 1481; b) H. G. Bazin, Y. Du, T. Polat, R. J. Linhardt, *J. Org. Chem.* **1999**, *64*, 7254 – 7259; c) Y. Du, T. Polat, R. J. Linhardt, *Tetrahedron Lett.* **1998**, *39*, 5007 – 5010.

[6] a) J. E. S. Hansen, H. Clausen, C. Nielsen, L. S. Teglbjaerg, L. H. Hansen, C. M. Nielsen, E. Dabelsteen, L. Mathiesen, S. I. Hakomori, J. O. Nielsen, *J. Virol.* **1990**, *64*, 2833 – 2840; b) J. E. Hansen, B. Jansson, G. J. Gram, H. Clausen, J. O. Nielsen, S. Olofsson, *Arch. Virol.* **1996**, *141*, 291 – 300; c) K. Miyajima, T. Nekado, K. Ikeda, K. Achiwa, *Chem. Pharm. Bull.* **1997**, *45*, 1544 – 1546; d) K. Miyajima, T. Nekado, K. Ikeda, K. Achiwa, *Chem. Pharm. Bull.* **1998**, *46*, 1676 – 1682; e) M. P. Carlos, D. E. Anderson, M. B. Gardner, J. V. Torres, *AIDS Res. Hum. Retroviruses* **2000**, *16*, 153 – 161.

[7] a) S. H. Itzkowitz, M. Yuan, C. K. Montgomery, T. Kjeldsenen, H. K. Takahashi, W. L. Bigbee, Y. S. Kim, *Cancer Res.* **1989**, *49*, 197 – 204; b) S. I. Hakomori, *Cancer Res.* **1989**, *49*, 257 – 331.

[8] a) M. Elofsson, J. Kihlberg, *Tetrahedron Lett.* **1995**, *36*, 7499 – 7502; b) J. B. Schwarz, S. D. Kuduk, X. Chen, D. Sames, P. W. Glunz, S. J. Danishefsky, *J. Am. Chem. Soc.* **1999**, *121*, 2662 – 2673; c) B. Liebe, H. Kunz, *Angew. Chem.* **1997**, *109*, 629 – 631; *Angew. Chem. Int. Ed. Engl.* **1997**, *36*, 618 – 621; d) H. Iijima, T. Ogawa, *Carbohydr. Res.* **1988**, *172*, 183 – 193.

[9] a) G. Ragupathi, R. R. Koganty, D. Qiu, K. O. Lloyd, P. O. Livingston, *Glycoconjugate J.* **1998**, *15*, 217 – 221; b) B. Kuberan, R. J. Linhardt, *Curr. Org. Chem.* **2000**, *4*, 653 – 677, and references therein.

[10] a) A. Wei, K. M. Boy, Y. Kishi, *J. Am. Chem. Soc.* **1995**, *117*, 9432 – 9436; b) R. Ravishankar, A. Surolia, M. Vijayan, S. Lim, Y. Kishi, *J. Am. Chem. Soc.* **1998**, *120*, 11297 – 11303.

[11] a) J. F. Espinosa, M. Bruix, O. Jarreton, T. Skrydstrup, J. M. Beau, J. J. Barbero, *Chem. Eur. J.* **1999**, *5*, 442 – 448; b) A. Poveda, J. L. Asensio, J. J. Barbero, T. Polat, H. Bazin, R. J. Linhardt, *Eur. J. Org. Chem.* **2000**, 1805 – 1813; c) L. M. Mikkelsen, M. J. Hernaiz, M. M. Pastor, T. Skrydstrup, J. J. Barbero, *J. Am. Chem. Soc.* **2002**, *124*, 14940 – 14951.

[12] The corresponding 2-thiophenylglycoside was prepared by the method of S. Cao, S. Meuneir, F. Andersson, M. Letellier, R. Roy, *Tetrahedron: Asymmetry* **1994**, *5*, 2303 – 2312 and oxidized to the sulfone according to A. Marra, P. Sinaÿ, *Carbohydr. Res.* **1989**, *187*, 35 – 42.

[13] Y. Du, R. J. Linhardt, *Carbohydr. Res.* **1998**, *308*, 161 – 164.

[14] B. K. Shull, Z. Wu, M. Koreeda, *J. Carbohydr. Chem.* **1996**, *15*, 955 – 964.

[15] R. U. Lemieux, R. M. Ratcliffe, *Can. J. Chem.* **1979**, *57*, 1244 – 1251.

[16] M. Schultz, H. Kunz, *Tetrahedron: Asymmetry* **1993**, *4*, 1205 – 1220.

[17] T. Rosen, I. M. Lico, D. T. W. Chu, *J. Org. Chem.* **1988**, *53*, 1580 – 1582.

[18] T. Horrobin, C. H. Tran, D. Crout, *J. Chem. Soc. Perkin Trans. 1* **1998**, 1069 – 1080; B. Kuberan, Q. Wang, M. Koketsu, R. J. Linhardt, *Synth. Commun.* **2002**, *32*, 1421 – 1426.

[19] T. T. Tidwell, *Synthesis* **1990**, 857 – 870.

[20] Examples and mechanistic studies of organo- and glycosyl samarium compounds: a) J. L. Namy, J. Collin, C. Bied, H. B. Kagan, *Synlett* **1992**, 733 – 734; b) G. Molander, J. McKie, *J. Org. Chem.* **1991**, *56*, 4112 – 4120; c) N. Miquel, G. Doisneau, J.-M. Beau, *Angew. Chem.* **2000**, *112*, 4277 – 4280; *Angew. Chem. Int. Ed.* **2000**, *39*, 4111 – 4114; d) Y. Du, R. J. Linhardt, *Carbohydr. Res.* **1998**, *308*, 161 – 164; Reviews on the application of SmI_2: e) G. A. Molander, C. R. Harris, *Chem. Rev.* **1996**, *96*, 307 – 338; f) G. A. Molander, C. R. Harris, *Tetrahedron* **1998**, *54*, 3321 – 3354; g) A. Krief, A.-M. Laval, *Chem. Rev.* **1999**, *99*, 745 – 777.

 © 2003 Wiley-VCH Verlag GmbH & Co. KGaA, Weinheim

Homoleptic Cobalt Carbonyl Complex

$[Co(CO)_5][(CF_3)_3BF]$: A Stable Salt of a Homoleptic Trigonal-Bipyramidal Metal–Carbonyl Cation**

Eduard Bernhardt, Maik Finze, Helge Willner, Christian W. Lehmann,* and Friedhelm Aubke**

Superacids[1,2] have for many years played a pivotal and unique role as reaction media in the generation of homoleptic metal–carbonyl cations as thermally stable salts.[3–6] In particular SbF_5, the strongest molecular Lewis acid[7,8] and the conjugate Brønsted–-Lewis superacid $HF–SbF_5$,[1,2] have allowed the formation of a substantial number of salts with superelectrophilic,[9] σ-bonded metal–carbonyl cations in which the metal atoms are in the oxidation states +2 and +3. The counteranions $[SbF_6]^-$ and $[Sb_2F_{11}]^-$ are formed in situ during the carbonylation reactions. Examples include $[Hg(CO)_2][Sb_2F_{11}]_2$,[10] $[M(CO)_4][Sb_2F_{11}]_2$ (M = Pd, Pt),[11] $[M(CO)_6][SbF_6]_2$ and $[M(CO)_6][Sb_2F_{11}]_2$ (M = Fe, Ru, Os)[12,13] and the recently reported $[Ir(CO)_6][SbF_6]_3 \cdot 4\,HF$.[14]

There are two general limitations to the use of SbF_5 or $HF–SbF_5$: 1) in $HF–SbF_5$ many M^{2+} metal cations (especially of the 3d series) are not carbonylated but form instead layered materials of the composition $M[SbF_6]_2$ (M = Cr, Mn, Fe, Co, Ni, Cu, Zn, Cd)[15]; 2) some metal carbonyl cations, such as $[Co(CO)_n]^+$ ($n = 4, 5$) and $[M(CO)_4]^+$ (M = Rh, Ir) can not be obtained in the presence of SbF_5 on account of its considerable oxidizing ability towards low-valent metal centers. In a recent study the ease with which $[Rh(CO)_4]^+$ can be oxidized was demonstrated, by the formation of *fac*-$[Rh(CO)_3(SO_3F)_3]$.[16]

To expand the number of metal–carbonyl cations,[3–6,17] a new conjugated Brønsted–Lewis superacid is necessary, which is presented herein. The boron carbonyl species $(CF_3)_3BCO$ can be used as a synthon for the non-oxidizing Lewis superacid $(CF_3)_3B$, which cannot be isolated. Recently, we synthesized and fully characterized $(CF_3)_3BCO$.[18,19] Upon dissolving $(CF_3)_3BCO$ in anhydrous HF and following the loss of CO, the system should behave like a conjugated Brønsted–Lewis superacid, with $[H_2F]^+$ and $[(CF_3)_3BF]^-$ as ionic components. Salts of the $[(CF_3)_3BF]^-$ ion are well known, but not structurally characterized to date.[20]

The aim of this study was the synthesis of a salt with a homoleptic Co^I–carbonyl cation. An early claim of the formation of $[Co(CO)_5]^+[Co(CO)_4]^-$[21] has been found to be in error.[22] To date there is no evidence for cations of the type $[Co(CO)_n]^+$ ($n = 4$, 5) in the solid state. In contrast, for gaseous and liquid systems Co^I–carbonyl cations have been discussed. Dissociation studies through electron impact[23] have demonstrated the existence of the series $[Co(CO)_n]^+$ ($n = 1$–5) in the gas phase, and the related Co–CO bonding energies have been determined. Laser ablation of cobalt in a CO atmosphere and isolation of the products in low-temperature matrixes gave only evidence for $[Co(CO)]^+$ and $[Co(CO)_2]^+$ ions.[24] A report on the synthesis of $[Co(CO)_4]^+_{solv.}$ in Brønsted superacids, for example, HSO_3F and HSO_3F/SbF_5, starting from $[Co_2(CO)_8]$ was recently published.[25] According to the vibrational data one solvent molecule is associated with the cobalt center. To obtain a stable product, we have carried out the reaction of $(CF_3)_3BCO$ with $[Co_2(CO)_8]$ in anhydrous HF (aHF). The observed reaction follows Equation (1) and is unprecedented for two reasons: 1) the main product isolated, in a yield of 72%, contains the homoleptic metal–carbonyl cation $[Co(CO)_5]^+$. Its characterization by vibrational spectroscopy and a crystal structure determination is presented below, b) the oxidizing reagent is probably $H_2F^+_{solv}$, although the side product H_2 was not identified. Protons have already been found to act as oxidizing reagents in the reaction of $[Co_2(CO)_8]$ in different Brønsted acids,[25] although in acids that are oxidants (HSO_3F) and in the presence of SbF_5 alternative reaction pathways are possible.

$$[Co_2(CO)_8] + 2\,(CF_3)_3BCO + 2\,HF \xrightarrow[aHF,\ RT]{CO\ (2\,bar)} 2\,[Co(CO)_5][(CF_3)_3BF] + H_2 \quad (1)$$

The reaction product $[Co(CO)_5][(CF_3)_3BF]$ is moderately soluble in aHF. Without a CO atmosphere, decomposition causes the light yellow solution to turn into a pink solid and a colorless solution within a few hours. $[Co(CO)_5][(CF_3)_3BF]$ reacts under air in a few seconds and a pink solid is obtained. According to differential scanning calorimetry (DSC) measurements and from heating a small sample in a capillary tube the salt is thermally stable up to 110 °C; above this temperature decomposition with vigorous gas evolution occurs.

In the Raman spectrum of the $[Co(CO)_5]^+$ ion, three intensive ν(CO) bands and in the IR spectrum two ν(CO) bands are observed. The ν(CO) vibration at $\tilde{\nu} = 2121\ cm^{-1}$ is Raman and IR active. The vibrational spectra of $[Co(CO)_5]^+$ in the CO stretching region (Table 1) are only consistent with $[Co(CO)_5]^+$ (D_{3h}) but not with $[Co(CO)_5]^+$ (C_{4v}) or with $[Co(CO)_4]^+$, with T_d, D_{4h}, or D_{2d} symmetry. A comparison of this vibrational data to the data reported for $[Co(CO)_4]^+_{solv.}$ [25] (Table 1), leads to the conclusion that in the unstable HSO_3F solutions the $[Co(CO)_5]^+_{solv.}$ ion was probably present. Wave-

[*] Prof. Dr. H. Willner, Dr. E. Bernhardt, Dipl.-Chem. M. Finze
Fakultät 4, Anorganische Chemie
Universität Duisberg-Essen
Lotharstrasse 1, 47048 Duisburg (Germany)
Fax: (+49) 203-379-2231
E-mail: willner@uni-duisburg.de
Dr. C. W. Lehmann
Max-Planck-Institut für Kohlenforschung
Kaiser-Wilhelm-Platz 1
45470 Mülheim an der Ruhr (Germany)
Fax: (+49) 208-306-2989
E-mail: lehmann@mpi-muelheim.mpg.de
Prof. Dr. F. Aubke
Department of Chemistry
The University of British Columbia
Vancouver B.C. V6T1Z1 (Canada)
Fax: (+1) 604-822-2847
E-mail: aubke@chem.ubc.ca

[**] This work was supported by the Deutsche Forschungsgemeinschaft, the Fonds der Chemischen Industrie, and Merck KGaA, Darmstadt (Germany).

 DOI: 10.1002/anie.200250780 © 2003 Wiley-VCH Verlag GmbH & Co. KGaA, Weinheim

Table 1: Observed ν(CO) band positions [cm^{-1}] of the isoelectronic species $[Mn(CO)_5]^-$, $[Fe(CO)_5]$, $[Co(CO)_5]^+$, and calculated data of $[Co(CO)_5]^+$.

Spectrum	$[Mn(CO)_5]^-$ [a]	$[Fe(CO)_5]$ [b]	$[Co(CO)_5]^+$ [c]	"$[Co(CO)_4]^+_{solv.}$" [d]	$[Co(CO)_5]^+$ (calcd) [e]	I (calcd) [e]	Assignment in D_{3h}
IR	–	–	–	–	–	–	A_1'
Raman	n.o. [f]	2112, vs	2195, vs	2195, vs	2275	126	
IR	–	–	–	2155, w, sh	–	–	A_1'
Raman	n.o.	2028, vs, br	2152, vs	2156, vs	2230	176	
IR	1899, s	2019, s	2140, vs, sh	2139, vs	2228	760	A_2''
Raman	–	–	–	2141, w	–	–	
IR	1862, s	1995, s	2121, vs	2122, vs, sh	2210	1284	E′
Raman	n.o.	1995, vs, br	2121, vs	2128, vs, br	2210	156	

[a] Na^+ salt in THF.[26] [b] CS_2 solution.[27] [c] This work, $[(CF_3)_3BF]^-$ salt. [d] Ref.:[25]. [e] This work, B3LYP6-31G*,[28] Raman activities in $Å^4\,amu^{-1}$ and IR intensities in $km\,mol^{-1}$. [f] n.o. = not observed.

numbers for the $[Co(CO)_5]^+$ ion, obtained from DFT calculations, are in good agreement with the experimental values and confirm the assignment. In the isoelectronic and isoster series $[Mn(CO)_5]^-$, $[Fe(CO)_5]$, $[Co(CO)_5]^+$ the positions of all the ν(CO) bands shift to higher wavenumbers and the separation between the bands of the different CO stretching fundamentals decreases. Both phenomena can be attributed to a reduction of the M→CO π backdonation, as described for $[M(CO)_6]$ (M = W, Re^+, Os^{2+}, Ir^{3+}).[14]

The proposed molecular structure of $[Co(CO)_5]$ $[(CF_3)_3BF]$ given in Equation (1) is confirmed by single-crystal X-ray diffraction.[29] A formula unit of the compound is shown in Figure 1. There are no significant interactions

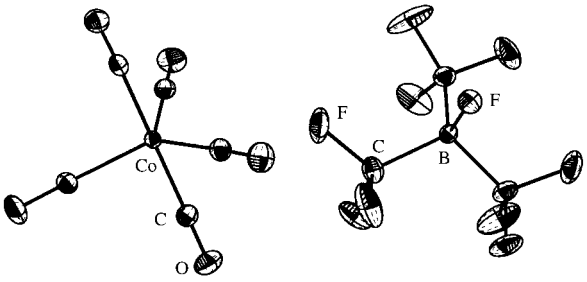


Figure 1. $[Co(CO)_5][(CF_3)_3BF]$ in the solid state structure (thermal ellipsoids set at 50% probability).

between anions and cations. Representative bond lengths and angles for the cation are listed in Table 2, where they are compared to the corresponding data of the isoelectronic complexes $[Fe(CO)_5]$ and $[Mn(CO)_5]^-$. The structure of $[Co(CO)_5]^+$ is regular trigonal bipyramidal (D_{3h}) with maximum deviations of the bond angles (C-Co-C) from the ideal values by 4° (Table 2). The axial Co–C bonds are shorter than the equatorial bonds (Table 2), whereas in $[Mn(CO)_5]^-$ the equatorial M–C bonds are longer and in $[Fe(CO)_5]$ are no significant differences between Fe–C_{ax} and Fe–C_{eq}. This observation is consistent with by DFT calculations. In the series $[Mn(CO)_5]^-$, $[Fe(CO)_5]$, and $[Co(CO)_5]^+$ the M–C bond lengths increase and the C–O bond lengths decrease. These trends are, as already described for the change of the ν(CO) band positions, caused by a decrease in the π backbonding.[32]

Table 2: Structural data of $[Co(CO)_5]^+$ (D_{3h}) and the isoelectronic species $[Mn(CO)_5]^-$ and $[Fe(CO)_5]$.[a]

Parameter	$[Mn(CO)_5]^-$ [b]	$[Fe(CO)_5]$ [c]	$[Co(CO)_5]^+$ [d]
$(M–C_{ax})-(M–C_{eq})$ (calcd) [e]	0.027	0.013	−0.031
$(M–C_{ax})-(M–C_{eq})$ (obs)	0.022	0.008	−0.027
$M–C_{ax}$	1.820(11)	1.811(2)	1.826(2)
$M–C_{eq}$	1.798(11)	1.803(2)	1.853(2)
$(C–O)_{ax}$	1.148(9)	1.117(2)	1.117(2)
$(C–O)_{eq}$	1.156(9)	1.133(2)	1.117(2)
$C_{ax}–M–C_{ax}$	178.4(4)	178.9(1)	177.83(6)
$C_{eq}–M–C_{eq}$	120.0(4)	120.0(1)	119.99(7)
$C_{ax}–M–C_{eq}$	90.0(4)	90.1(1)	90.01(7)
$M–(C–O)_{ax}$	179.4(8)	179.4(2)	178.62(14)
$M–(C–O)_{eq}$	178.8(8)	179.6(2)	178.54(15)

[a] Averaged bond lengths [Å] and angles [°]. [b] Ref. [30], Counterion: $[Ni(1,10\text{-phen})_3]^{2+}$ (phen = phenanthroline). [c] Ref. [31]. [d] Counterion: $[(CF_3)_3BF]^-$. [e] B3LYP6-31G*.[28]

The synthesis of the $[Co(CO)_5]^+$ ion as stable $[(CF_3)_3BF]^-$ salt and its spectroscopic and structural characterization has resulted in the first example of a trigonal bipyramidal homoleptic metal–carbonyl cation with 18 valance electrons as well as increasing the number of known homoleptic metal–carbonyl cations.[5,6] The other known d^8 metal–carbonyl cations, such as $[M(CO)_4]^+$ (Rh, Ir) and $[M(CO)_4]^{2+}$ (Pd, Pt), have square-planar coordination geometries and have 16 electrons in their valance shells.[11,16]

Experimental Section

A 50-mL PFA (PFA = perfluoroalkoxy copolymer) round-bottom flask, fitted with a PFA valve and a magnetic stirring bar was charged in a dry N_2 stream with $[Co_2(CO)_8]$ (300 mg, 0.9 mmol) and attached to a stainless steel vacuum line. After evacuation and cooling the reaction vessel to liquid N_2 temperature aHF (2 mL, 533 mg) was added by condensation in vacuo then on a glass vacuum line $(CF_3)_3BCO$ (2.2 mmol), and CO (2.8 mmol) were added by condensation in vacuo. Under vigorous stirring the reaction mixture was warmed up to room temperature and a brownish solution resulted. In a period of one hour a light colored precipitate formed. The reaction mixture was left without stirring overnight at room temperature, which resulted in the formation of orange crystals on the bottom of the flask. Removal of all volatiles *in vacuo* produced, in addition to orange crystals, a brown residue that was removed by washing with

 © 2003 Wiley-VCH Verlag GmbH & Co. KGaA, Weinheim

CH_2Cl_2. After this purification step the crystals were dried in vacuo and stored under an inert-gas atmosphere in a dry box. Yield: 550 mg (1.3 mmol, 72%).

Received: December 16, 2002 [Z50780]

Keywords: borates · carbonyl ligands · cobalt complexes · structure elucidation · superacids

[1] G. A. Olah, G. K. S. Prakash, J. Sommer, *Superacids*, Wiley, New York, **1985**.
[2] T. A. O'Donnel, *Superacids and Acidic Melts as Inorganic Reaction Media*, VCH, Weinheim, **1993**.
[3] E. W. Abel, S. P. Tyfield, *Adv. Organomet. Chem.* **1970**, *8*, 117.
[4] W. Beck, K. Sünkel, *Chem. Rev.* **1988**, *88*, 1405.
[5] H. Willner, F. Aubke, *Angew. Chem.* **1997**, *109*, 2506; *Angew. Chem. Int. Ed. Engl.* **1997**, *36*, 2402.
[6] H. Willner, F. Aubke in *Inorganic Chemistry Highlights* (Eds.: G. Meyer, D. Naumann, L. Wesemann), Wiley-VCH, Weinheim, **2002**, p. 195.
[7] P. L. Fabré, J. Devynk, B. Tremillon, *Chem. Rev.* **1982**, *82*, 591.
[8] K. O. Christe, D. A. Dixon, D. McLemore, W. W. Wilson, J. A. Sheehy, J. A. Boatz, *J. Fluorine Chem.* **2000**, *101*, 151.
[9] G. A. Olah, *Angew. Chem.* **1993**, *105*, 805; *Angew. Chem. Int. Ed. Engl.* **1993**, *32*, 767.
[10] M. Bodenbinder, G. Balzer-Jöllenbeck, H. Willner, R. Batchelor, F. W. B. Einstein, C. Wang, F. Aubke, *Inorg. Chem.* **1996**, *35*, 82.
[11] H. Willner, M. Bodenbinder, R. Bröchler, G. Hwang, S. J. Rettig, J. Trotter, B. von Ahsen, U. Westphal, V. Jonas, W. Thiel, F. Aubke, *J. Am. Chem. Soc.* **2001**, *123*, 588.
[12] E. Bernhardt, B. Bley, R. Wartchow, H. Willner, E. Bill, P. Kuhn, I. H. T. Sham, M. Bodenbinder, R. Bröchler, F. Aubke, *J. Am. Chem. Soc.* **1999**, *121*, 7188.
[13] E. Bernhardt, C. Bach, R. Wartchow, H. Willner, F. Aubke, unpublished results.
[14] B. von Ahsen, M. Berkei, G. Henkel, H. Willner, F. Aubke, *J. Am. Chem. Soc.* **2002**, *124*, 8371.
[15] D. Gantar, I. Leban, B. Frlec, J. H. Halloway, *J. Chem. Soc. Dalton Trans.* **1987**, 2379.
[16] B. von Ahsen , C. Bach, M. Berkei, M. Köckerling, H. Willner, G. Hägele, F. Aubke, *Inorg. Chem.* **2003**, *42*, in press.
[17] A. J. Lupinetti, G. Frenking, S. H. Strauss, *Prog. Inorg. Chem.* **2001**, *49*, 1.
[18] A. Terheiden, E. Bernhardt, H. Willner, F. Aubke, *Angew. Chem.* **2002**, *114*, 823; *Angew. Chem. Int. Ed.* **2002**, *41*, 799.
[19] M. Finze, E. Bernhardt, A. Terheiden, M. Berkei, H. Willner, D. Christen, H. Oberhammer, F. Aubke, *J. Am. Chem. Soc.* **2002**, *124*, 15385.
[20] D. J. Brauer, H. Bürger, Y. Chebude, G. Pawelke, *Inorg. Chem.* **1999**, *38*, 3972.
[21] S. Metlin, I. Wender, H. W. Sternberg, *Nature* **1959**, *183*, 457.
[22] K. Y. Lee, J. K. Kochi, *Inorg. Chem.* **1989**, *28*, 567.
[23] S. Goebel, C. L. Haynes, F. A. Khan, P. B. Armentront, *J. Am. Chem. Soc.* **1995**, *117*, 6994.
[24] M. Zhou, L. Andrews, *J. Phys. Chem. A* **1999**, *103*, 7773.
[25] Q. Xu, S. Inoue, Y. Souma, H. Nakatani, *J. Organomet. Chem.* **2000**, *606*, 147.
[26] C. D. Pribula, T. L. Brown, *J. Organomet. Chem.* **1974**, *71*, 415.
[27] L. H. Jones, R. S. McDowell, M. Goldblatt, B. I. Swanson, *J. Chem. Phys.* **1972**, *57*, 2050.
[28] Gaussian 98 (Revision A.6), M. J. Frisch, G. W. Trucks, H. B. Schlegel, G. E. Scuseria, M. A. Robb, J. R. Cheeseman, V. G. Zakrzewski, J. A. Montgomery, R. E. Stratmann, J. C. Burant, S. Dapprich, J. M. Millam, A. D. Daniels, K. N. Kudin, M. C. Strain, O. Farkas, J. Tomasi, V. Barone, M. Cossi, R. Cammi, B. Mennucci, C. Pomelli, C. Adamo, S. Clifford, J. Ochterski, G. A. Petersson, P. Y. Ayala, Q. Cui, K. Morokuma, D. K. Malick, A. D. Rabuck, K. Raghavachari, J. B. Foresman, J. Cioslowski, J. V. Ortiz, B. B. Stefanov, G. Liu, A. Liashenko, P. Piskorz, I. Komaromi, R. Gomperts, R. L. Martin, D. J. Fox, T. Keith, M. A. Al-Laham, C. Y. Peng, A. Nanayakkara, C. Gonzalez, M. Challacombe, P. M. W. Gill, B. G. Johnson, W. Chen, M. W. Wong, J. L. Andres, M. Head-Gordon, E. S. Replogle, J. A. Pople, Gaussian, Inc., Pittsburgh, PA, **1998**.
[29] a) Crystal structure analysis of $[Co(CO)_5][(CF_3)_3BF]$: $C_8BCoF_{10}O_5$, KappaCCD-Diffractometer (Bruker AXS) using graphite monochromatized $Mo_{K\alpha}$ radiation ($\lambda = 0.71073$ Å); $T = 100$ K. Orange crystals ($0.16 \times 0.10 \times 0.10$ mm^3) grown from aHF, monoclinic, space group $P2_1/c$ (No. 14), $a = 7.9858(1)$, $b = 13.9485(1)$, $c = 12.5826(1)$ Å, $\beta = 98.91°$, $V = 1384{,}67(2)$ Å^3, $Z = 4$, $\rho_{calcd} = 2.091$ Mg m^{-3}, $\mu(Mo_{K\alpha}) = 1.383$ mm^{-1}, $F(000) = 840$, 25226 measured reflexes ($3.85 < \Theta < 30.56°$) Integration and empirical absorption correction (DENZO scalepack).[33] The structure was solved by direct methods and refinement to F^2 based on 4219 independent reflexes [3847 independent reflexes with $I > 2\sigma(I)$], and 226 variables (SHELXS-97).[34] All atoms are refined anisotropically ($R_1 = 0.0295$ for $I > 2\sigma(I)$). b) CCDC-199269 $[Co(CO)_5][(CF_3)_3BF]$ contains the supplementary crystallographic data for this paper. These data can be obtained free of charge via www.ccdc.cam.ac.uk/conts/retrieving.html (or from the Cambridge Crystallographic Data Centre, 12 Union Road, Cambridge CB2 1EZ, UK; fax: (+44) 1223-336-033; or deposit@ccdc.cam.ac.uk).
[30] T. S. Sorensen, F. Sun, *Organometallics* **2001**, *20*, 3613.
[31] D. Braga, F. Grepioni, A. G. Orpen, *Organometallics* **1993**, *12*, 1481.
[32] A. R. Rossi, R. Hoffmann, *Inorg. Chem.* **1975**, *14*, 365.
[33] Z. Otwinowski, W. Minor, *Methods Enzymol.* **1997**, *276*, 307.
[34] G. M. Sheldrick, SHELXS-97 und SHELXL-97, Program system for determination and refining of crystal structures, University of Göttingen, Göttingen (Germany), **1997**.

 © 2003 Wiley-VCH Verlag GmbH & Co. KGaA, Weinheim

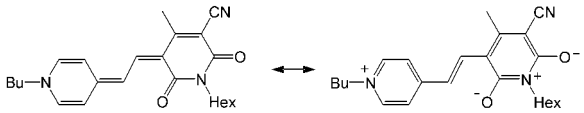
Influencing Equilibria

Large Electric-Field Effects on the Dipolar Aggregation of Merocyanine Dyes**

Rüdiger Wortmann, Ulrich Rösch, Mesfin Redi-Abshiro, and Frank Würthner**

Dedicated to Professor Wolfgang Liptay on the occasion of his 75th birthday

The effects of external electric fields on macroscopic systems, including phases with chemical equilibria, is of fundamental interest in chemical thermodynamics.[1] General thermodynamic equations for dielectrics of variable composition in external electric fields have been developed by Koenig[2] based on the work by Guggenheim.[3] In addition, the dynamic effects of pulsed electric fields were investigated and applied in studies of fast reaction kinetics and dielectric relaxation phenomena related to chemical rate processes.[4–6] The influence of biological membrane potentials on the dimerization of a fluorescent dye was studied by Webb and Dragsten.[7] Liptay et al. investigated electric-field effects on the formation of charge transfer (CT) complexes.[8] Herein, we report the observation of an unusually strong electric-field effect on the dimerization equilibrium of the strongly dipolar merocyanine dye **1**.



1

The electronic structure of merocyanine dyes, such as **1**, with electron-donating and electron-accepting groups is often described in terms of a two-state valence-bond model. This simple model assumes resonance of neutral and zwitterionic structures and provides a useful qualitative interpretation of phenomena, such as solvatochromism and bond-length alternation.[9] The electronic structure of the dyes may vary between the "neutral" form **1** (left) and the "zwitterionic" form (right). Dyes with equal contributions of the neutral and zwitterionic forms are in the "cyanine-limit". The two-level valence-bond model has been discussed critically at a higher level of theory.[10]

Merocyanine dyes have been intensely studied in the quest for promising chromophores for electrooptically active materials, such as electrooptical and photorefractive polymers.[11] It has been demonstrated that the photorefractive figure-of-merit of the dyes is maximized close to the cyanine limit and chromophores optimized according to this principle have been presented.[12] As a result of the zwitterionic character of the dyes near to and beyond the cyanine limit their dipole moments are very large which may lead to dimer formation by dipolar aggregation in the polymer and in liquid solution.[13]

Dimer formation is especially pronounced for dye **1** and can be observed even in dilute dioxane solution. The absorption spectrum, Figure 1, shows two concentration-dependent bands with a clear isobestic point over a broad concentration range. The concentration dependence of the bands indicates an equilibrium $2\,M \rightleftharpoons D$ between the only two species, monomeric (M) and dimeric (D) dye units. The intensity of the monomer band decreases with increasing concentration while that of the dimer increases. The dimer band is hypsochromically shifted with respect to the monomer band as is typical for H-type aggregates. This effect is attributed to an (almost) antiparallel ordering of the dipolar dye molecules (Scheme 1).[13]

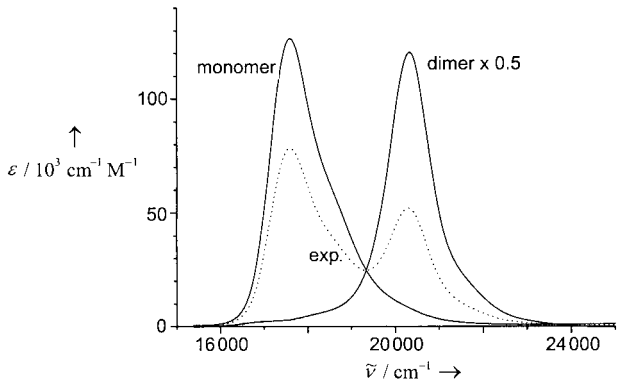
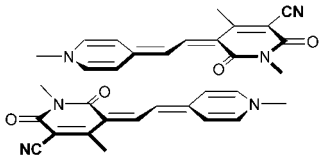


Figure 1. Optical absorption spectrum (•••••, "exp") of a solution of **1** in dioxane ($c_{0M} = 5.16 \times 10^{-6}$ M, $T = 298$ K) and derived spectra of pure monomer and dimer (——).

A quantitative analysis of the concentration dependence by nonlinear regression allows deconvolution of the optical



Scheme 1.

[*] Prof. Dr. R. Wortmann, Dipl.-Chem. U. Rösch, Dipl.-Chem. M. Redi-Abshiro
Institut für Physikalische Chemie
Technische Universität Kaiserslautern
Erwin-Schrödinger-Strasse, 67633 Kaiserslautern (Germany)
Fax: (+49) 631-2052187
E-mail: ruediger.wortmann@chemie.uni-kl.de
Prof. Dr. F. Würthner
Institut für Organische Chemie
Universität Würzburg
Am Hubland, 97074 Würzburg (Germany)
Fax: (+49) 931-8884756
E-mail: wuerthner@chemie.uni-wuerzburg.de

[**] This work was supported by the Volkswagen Foundation and the Fonds der Chemischen Industrie. We thank our Erasmus students Jordi Bonet (Murcia) and Ewan Bennet (Glasgow) for performing some of the experiments.

 © 2003 Wiley-VCH Verlag GmbH & Co. KGaA, Weinheim DOI: 10.1002/anie.200250782

absorption into the pure monomer and dimer spectra (Figure 1). This analysis is based on a dimerization model[13,14] according to Equations (1) and (2), where K_c is the dimerization constant, c_M and c_D the concentrations of monomer and dimer, respectively, and c_{0M} the initial concentration of the monomer.

$$K_c = \frac{c_D}{c_M^2} \tag{1}$$

$$c_M = \frac{\sqrt{8\,K_c\,c_{0M}+1}-1}{4\,K_c} \tag{2}$$

The extinction coefficient a of the dye solutions may be expressed as a sum over the monomer and dimer contributions (K = M, D) [Eq. (3)] where ε_M and ε_D are the molar decadic absorption coefficients of monomer and dimer, respectively. The regression yields the spectra of the pure monomer and dimer as well as the value of $K_c = 112\,000\,\text{M}^{-1}$ for the aggregation constant in dioxane at 298 K (Figure 1).

$$a = \sum_K \varepsilon_K\,c_K \tag{3}$$

An interesting question is now whether and to which extend such an aggregation can be influenced by internal or external electric fields. Proof of such an influence would be important for the optimization of photorefractive polymers. Such materials operate at very high external electric fields and dimer formation in them has already been demonstrated.[12] To directly demonstrate the influence of electric fields on the aggregation equilibrium of **1** we employed the very sensitive method of electrooptical absorption measurements (EOAM).[15]

In EOAM one detects the influence of an external electric field on the decadic extinction coefficient $a = \varepsilon c$ of a dilute solution of the dye with a molar decadic extinction coefficient ε and concentration c. The measurements are carried out for two polarizations of the incident light (parallel ($\phi = 0°$) and perpendicular ($\phi = 90°$) to the applied field) and for several wavenumbers $\tilde{\nu}$ within the absorption band. The effect of the electric field on the extinction coefficient may be described to second order in the field E by Equation (4) which represents essentially the relative change of the optical absorption induced by the field.[15]

$$L(\phi,\tilde{\nu}) = \frac{1}{a}\frac{\partial a}{\partial E^2} \tag{4}$$

Applying external electric fields to dilute solutions of **1** indeed revealed a remarkable effect on the optical absorption. Figure 2 shows the result of an EOAM experiment for parallel polarization ($\phi = 0°$). The extinction coefficient a of the solution is clearly reduced in the region of the dimer band while it is increased in the monomer region.

To quantitatively analyze this result both the field dependence of the molar extinction coefficient ε_K and the field dependence of the equilibrium concentrations c_K of monomer and dimer (K = M, D) must be taken into account [Eq. (5)].

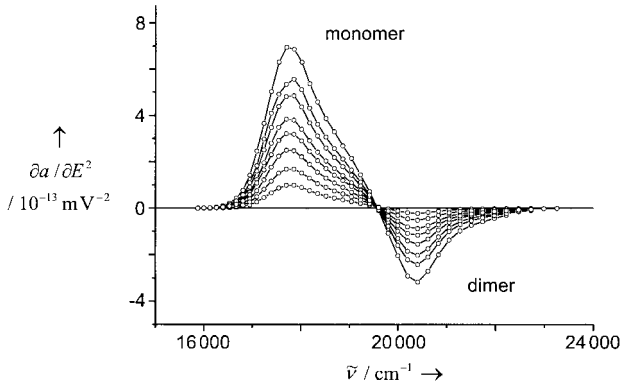


Figure 2. Electric-field effect on the extinction coefficient of solutions of **1** in dioxane at various concentrations ($c_{0M} = 1.05$, 1.88, 2.93, 3.69, 4.70, 6.11, 7.62, 9.42×10^{-6} M; $T = 298$ K; $\phi = 0°$).

$$\frac{\partial a}{\partial E^2} = \sum_K \left(c_K \frac{\partial \varepsilon_K}{\partial E^2} + \varepsilon_K \frac{\partial c_K}{\partial E^2} \right) \tag{5}$$

The field derivative of ε_K in Equation (5) may be described by the theory of electrochromism developed by Liptay.[15] For dipolar molecules the main contributions result from the orientation effect caused by partial alignment of dipolar dye molecules and the band-shift effect caused by charge redistribution (dipole moment change)[16] upon excitation. Large electrochromic signals are expected only for the strongly dipolar monomer while those of the dimer should be weak because of the small dipole moment of the (nearly) antiparallel arrangement of the monomer subunits. Multilinear regression of the EOAM spectrum $L\varepsilon/\tilde{\nu}$ based on the optical absorption spectrum $\varepsilon/\tilde{\nu}$ and its first and second derivative yields a set of six coefficients[15] of which usually only three (E, F, and G) are significant in case of dipolar molecules. These coefficients may be approximated here as Equations (6) and (7)[11] where μ_g is the dipole of the electronic ground state, $\Delta\mu$ the change of the dipole upon excitation to the Franck–Condon (FC) excited state, α the angle between the transition dipole moment and the ground state dipole moment, k_B the Boltzmann constant, f_0 a static local field factor and T the temperature.

$$E = f_0^2\mu_g^2(3\cos^2\alpha - 1)/(k_B\,T)^2 \tag{6}$$

$$F = G = f_0^2\mu_g\,\Delta\mu\cos\alpha/(k_B\,T) \tag{7}$$

In Equations (6) and (7) the transition dipole moment and the dipole change are assumed to be parallel, which is usually valid for intense CT bands in elongated donor–acceptor-substituted π systems.[11] Coefficients F and G are equal in this approximation; f_0 is approximated by the Lorentz factor in this case.

The field derivative of the equilibrium concentrations c_K in Equation (5) may be described by the theory of Koenig.[2] Taking local field factors into account gives Equation (8) where ν_K are the stoichiometric coefficients (for the dimerization reaction: $\nu_M = -2$ and $\nu_D = 1$).

 © 2003 Wiley-VCH Verlag GmbH & Co. KGaA, Weinheim

$$\left(\frac{\partial \ln K_c}{\partial E}\right)_{p,T} = \frac{f_0^2 E}{3 k_B^2 T^2} \sum_K \nu_K \mu_{gK}^2 \quad (8)$$

According to Equation (8) the driving force for the shift of chemical equilibria by external electric fields is the stabilization of dipolar species in the field. Neglecting the small dipole μ_{gD} of the dimer gives with Equations (1) and (2) for the relative field dependencies of the concentrations of monomer and dimer to second order in the applied field, Equations (9) and (10).

$$\frac{1}{c_M}\frac{\partial c_M^E}{\partial E^2} = \frac{c_{0M} - c_M}{(2\,c_{0M} - c_M)}\frac{f_0^2 \mu_{gM}^2}{3 k_B^2 T^2} \quad (9)$$

$$\frac{1}{c_D}\frac{\partial c_D^E}{\partial E^2} = -\frac{c_M}{(2\,c_{0M} - c_M)}\frac{f_0^2 \mu_{gM}^2}{3 k_B^2 T^2} \quad (10)$$

These equations suggest that the external field increases the monomer concentration at the expense of the dimer concentration.

Figure 3 shows the result of the band-shape analysis of the EOAM spectrum taking the effects on the absorption coefficient ε_K (Equations (6) and (7)) and the equilibrium concentrations c_K (Equations (9) and (10)) into account. The regression was based on the precisely derived spectra of the pure monomer and dimer (Figure 1) and their first derivatives. The EOAM experiments were carried out for eight different initial concentrations (see legend of Figure 2). The regression results are listed in Table 1.

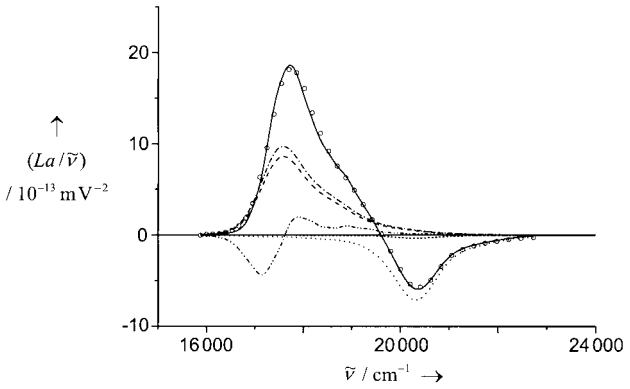


Figure 3. Band-shape analysis of the electrooptical absorption spectrum of a solution of **1** in dioxane ($c_{0M} = 3.69 \times 10^{-6}$ M; $T = 298$ K; $\phi = 0°$). The Figure shows experimental data points (○) and a multilinear regression curve (——). The spectrum results from superposition of partial contributions arising from electrodichroism of the monomer (–•–•) and dimer (-----), the band shift of the monomer (····), and the field-induced concentration changes of monomer (– – –) and dimer (•••••).

The EOAM spectrum of the monomer/dimer band system of **1** in Figure 3 may be interpreted as follows: The strong increase of the optical absorption in the region of the monomer band is mainly a result of the positive electrodichroism [Eq. (6)] caused by alignment of the dipolar monomer molecules in the applied field and of the increase of the monomer concentration [Eq. (9)] caused by field-induced dissociation of the dimer. Remarkably, the latter effect is nearly as large as the electrodichroic one. A smaller contribution in the region of the monomer band is because of the band-shift effect [Eq (7)] caused by the dipole change of the monomer upon electronic excitation. Evaluation of the regression coefficients *E, F,* and *G* of the monomer yields its ground-state dipole moment and dipole-moment change. It was assumed in the calculations that the angle in Equations (6) and (7) may be approximated by $\alpha = 0°$ for the monomer. A very large ground-state dipole moment is found for the monomer. The dipole-moment change of the monomer is negative, that is, the absorption band is shifted hypsochromically in the external field. The negative dipole-moment change is consistent with the observed negative solvatochromism[16] of this compound.

Table 1: Results of concentration-dependent electrooptical absorption measurements on merocyanine dye **1** in dioxane solution ($T = 298$ K).

Parameter	Monomer	Dimer
$E(10^{-20}\,V^{-2}\,m^2)$	81400 ± 1600	-5972 ± 1400
$F(10^{-40}\,C\,V^{-1}\,m^2)$	-5780 ± 240	–
$G(10^{-40}\,C\,V^{-1}\,m^2)$	-5056 ± 240	–
$\mu_g(10^{-30}\,C\,m)$	59 ± 1[a]	22 ± 3[b]
$\mu_g(10^{-30}\,C\,m)$	69 ± 2	–
$\mu_g(10^{-30}\,C\,m)$	69 ± 1	–
$\Delta\mu(10^{-30}\,C\,m)$	-27 ± 2	–

[a] from Equation (6) assuming $\alpha = 0°$. [b] From Equation (6) assuming $\alpha = 90°$. [c] From Equation (9). [d] From Equation (10).

The negative electrooptical signal in the spectral region of the dimer band (Figure 3) is almost entirely a result of the field-induced reduction of the dimer concentration. Since the monomer dipole moments tend to cancel each other out in the dimer the dipole moment of the dimer is expected to be small. Indeed the regression yields a only small negative electrodichroic contribution in the dimer band (Figure 3). A dipole moment of only $22 \times 10^{-30}\,C\,m$ may be estimated from the coefficient *E* of the dimer assuming that the dipole moment is orthogonal to the transition dipole moment, $\alpha = 90°$ in Equation (6). Within experimental error no significant band shift and accordingly no change of the dipole moment of the dimer upon excitation was observed. This result is in accordance with the notion of a strongly coupled exciton state and complete delocalization of the excitation energy.[13]

Figure 4 illustrates the results of the relative field-induced changes of the concentrations c_M and c_D. The experimental data points were fitted by the functional dependencies of Equations (9) and (10). Excellent agreement with the theoretical predictions was found. However, the obtained monomer dipole moment is larger than the one obtained from electrodichroism with Equation (6) (see Table 1). This discrepancy is probably because of a nonvanishing angle α between the transition dipole moment and the ground state dipole moment.

The electric-field strength in EOAM experiments is typically of the order $E = 10^6\,V\,m^{-1}$. According to Equations (9) and (10) such a field shifts the dimerization

 © 2003 Wiley-VCH Verlag GmbH & Co. KGaA, Weinheim

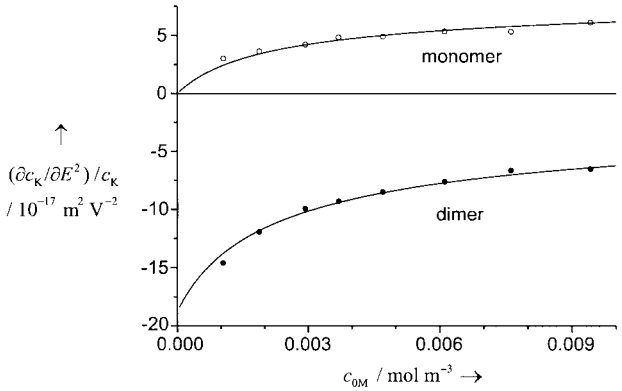


Figure 4. Relative field dependencies of the monomer and dimer concentrations obtained by electrooptical absorption measurements at various concentrations (see legend of Figure 2, $T = 298$ K). The curves were calculated from Equations (9) and (10) with $\mu_{gM} = 69 \times 10^{-30}$ C m.

equilibrium of **1** by about 0.01% at an equilibrium concentration of $c_M = c_{0M}/2$. This small concentration change requires the use of the lock-in technique (EOAM) for it to be detected. On the other hand, the electric-field strength applied to organic photorefractive or electrooptical polymer materials may reach values of $E = 10^8$ V m^{-1}. The dimerization equilibrium may be shifted by several 10% in such materials leading to substantial effects on the refractive index modulation.

In summary, we investigated the effect of an external electric field on the dipolar aggregation equilibrium of a merocyanine dye by electrooptical absorption measurements. It could be experimentally confirmed that the external field stabilizes the highly dipolar monomeric form relative to the weakly dipolar dimeric form. To our knowledge this is the first quantitative demonstration of an electric-field effect on the dimerization of a merocyanine dye by concentration-dependent electrooptical absorption experiments. Implications of the observed findings on the design of photonic materials containing excitonically coupled dimers have been discussed.

Experimental Section

The synthesis of merocyanine dye **1** has been reported elsewhere.[13] Electrooptical absorption measurements were performed as described in ref. [17] The measurements were carried out in the solvent dioxane which was purified and carefully dried by distillation from Na/K under Argon prior to use. Absorbance spectra of the solutions were recorded with a spectrophotometer (Perkin-Elmer Lambda 900).

Received: December 17, 2002 [Z50782]

Keywords: aggregation · chromophores · donor–acceptor systems · electric-field effects · supramolecular chemistry

[1] W. Liptay, D. Wehning, J. Becker, T. Rehm, *Z. Naturforsch. A* **1982**, *37*, 1369 – 1395.
[2] F. O. Koenig, *J. Phys. Chem.* **1937**, *41*, 597 – 620.
[3] E. A. Guggenheim, *Proc. R. Soc. London Ser. A* **1936**, *155*, 70.
[4] L. De Maeyer, *Methods Enzymol.* **1969**, *16*, 80 – 118.
[5] E. M. Eyring, P. Hemmes, *Tech. Chem. (N. Y.)* **1986**, *6*, 219 – 246.
[6] G. Schwarz, *J. Phys. Chem.* **1967**, *71*, 4021 – 4030.
[7] P. R. Dragsten, W. W. Webb, *Biochemistry* **1978**, *17*, 5228 – 5240.
[8] W. Liptay, T. Rehm, D. Wehning, L. Schanne, W. Baumann, W. Lang, *Z. Naturforsch. A* **1982**, *37*, 1427 – 1448.
[9] M. Blanchard-Desce, V. Alain, P. V. Bedworth, S. R. Marder, A. Fort, C. Runser, M. Barzoukas, S. Lebus, R. Wortmann, *Chem. Eur. J.* **1997**, *3*, 1091 – 1104.
[10] D. M. Bishop, B. Champagne, B. Kirtman, *J. Chem. Phys.* **1998**, *109*, 9987 – 9994.
[11] S. Beckmann, K.-H. Etzbach, P. Krämer, K. Lukaszuk, R. Matschiner, A. J. Schmidt, P. Schuhmacher, R. Sens, G. Seybold, R. Wortmann, F. Würthner, *Adv. Mater.* **1999**, *11*, 536 – 541.
[12] F. Würthner, R. Wortmann, K. Meerholz, *ChemPhysChem* **2002**, *3*, 17 – 31.
[13] F. Würthner, S. Yao, T. Debaerdemaeker, R. Wortmann, *J. Am. Chem. Soc.* **2002**, *124*, 9431 – 9447.
[14] F. Würthner, S. Yao, *Angew. Chem.* **2000**, *112*, 2054 – 2057; *Angew. Chem. Int. Ed.* **2000**, *39*, 1978 – 1981.
[15] W. Liptay, *Excited States* **1974**, *1*, 129 – 229.
[16] W. Liptay, *Angew. Chem.* **1969**, *81*, 195 – 206; *Angew. Chem. Int. Ed. Engl.* **1969**, *8*, 177 – 188.
[17] R. Wortmann, K. Elich, S. Lebus, W. Liptay, P. Borowicz, A. Grabowska, *J. Phys. Chem.* **1992**, *96*, 9724 – 9730.

 © 2003 Wiley-VCH Verlag GmbH & Co. KGaA, Weinheim

Water in Polyoxometalate Capsules

Drawing Small Cations into Highly Charged Porous Nanocontainers Reveals "Water" Assembly and Related Interaction Problems**

Achim Müller, Erich Krickemeyer, Hartmut Bögge, Marc Schmidtmann, Bogdan Botar, and Marina O. Talismanova*

Dedicated to Professor Michael T. Pope on the occasion of his 70th birthday

Herein we report a series of easily accessible, soluble, spherical, porous nanocapsules with internal surfaces that are tunable with respect to charge and hydrophilicity/phobicity. These systems are based on a very robust fundamental cluster skeleton $\{(pent)_{12}(link)_{30}\} = \{(Mo)Mo_5\}_{12}\text{-}\{link\}_{30}$[1,2] where pent is the basic pentagonal $\{(Mo)Mo_5\}$ type of unit and link refers to linker groups. This general formula describes, for example, the new compound **1** where

$$(NH_4)_{72-n}[(H_2O)_{81-n} + (NH_4)_n \subset \{(Mo^{VI})Mo_5^{VI}O_{21}(H_2O)_6\}_{12}\{Mo_2^{V}O_4(SO_4)\}_{30}]\cdot \approx 200\,H_2O \quad \mathbf{1}$$

the cluster anion has an extremely high negative charge (an increase from 42− in the educt **2a** (that is, the anion of compound **2**) to 72− without counting encapsulations), and shows a well-constructed hydrophilic internal surface.

$$(NH_4)_{42}[\{(Mo^{VI})Mo_5^{VI}O_{21}(H_2O)_6\}_{12}\{Mo_2^{V}O_4(CH_3COO)\}_{30}]\cdot \approx 300\,H_2O\cdot \approx 10\,CH_3COONH_4 \quad \mathbf{2}^{[2b,7]}$$

In this type of capsule, for the first time several well-defined water molecule assemblies can be observed (for general aspects see refs. [3,4]) some of which agree with those obtained from molecular-dynamics calculations for liquid water.[4b] As the *discrete* assemblies contain the $\{H_2O\}_{20}$ dodecahedron with 30 hydrogen bonds, this offers the chance to get a deeper understanding of the structure of crystalline clathrate hydrates, also in connection with their role in essential industrial processes,[5] and to study the hydrophobic effect (Figure 1). Furthermore, because the nanocapsules are soluble, stable, porous, and manipulatable several other options for their use in nanotechnology are conceivable.[6]

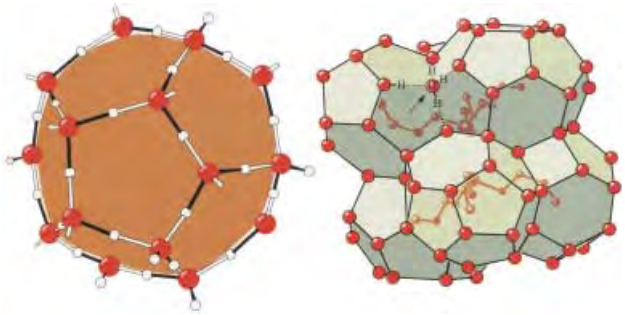


Figure 1. Two examples of H_2O assemblies/cages: The important $\{H_2O\}_{20}$ dodecahedron,[5] which is also found in the discrete water assemblies in the cluster cavities described here (left), and a related enlarged cavity (with dodecahedra being involved) from which water is excluded by the presence of an encapsulated nonpolar molecule (right), which demonstrates the fundamental hydrophobic effect also present in some of the clusters discussed here (reproduced with permission from D. Voet, J. G. Voet, *Biochemistry*, 2nd ed., Wiley, New York, **1995**).

Compound **1** was obtained by the reaction of an aqueous solution of **2**[2b,7] with $(NH_4)_2SO_4$ at pH ≈ 1 thereby introducing $30\,SO_4^{2-}$ ligands which increases the negative cluster charge by 30 units, and therefore its affinity to cation uptake. Compound **3** was prepared from **2** by replacing not all of the acetate ligands and thereby maintaining a hydrophobic part in contrast to **1**. Compound **4** was prepared in a similar way to **1**, but such that an increase in the negative cluster charge is achieved while allowing a well-defined number of Na^+ ions to become encapsulated. This was done in the presence of another larger cation that could not be encapsulated, with the ability to influence the uptake. Compounds **5**[8] and **6**[9] contain the novel structurally well-defined encapsulated H_2O clusters, $\{H_2O\}_{40}$ and $\{H_2O\}_{80}$, which were not identified previously,[8,9] while **7**[10] is mentioned here to facilitate comparisons of encapsulations. Clusters **1**, **3**, and **4** were characterized by elemental analysis, thermoanalysis, mass spectrometry, potentiometric titrations (to determine the number of Mo^V centers), IR spectroscopy, and single-crystal X-ray structure analysis[11] including bond-valence-sum (BVS) calculations.[12]

$$(NH_4)_{60}[\{(Mo^{VI})Mo_5^{VI}O_{21}(H_2O)_6\}_{12}\{Mo_2^{V}O_4(SO_4)\}_{18}\{Mo_2^{V}O_4(CH_3COO)\}_{12}]\cdot \approx 300\,H_2O \quad \mathbf{3}$$

$$[(CH_3)_2NH_2]_{52}\,Na_8[Na_6 + (H_2O)_n \subset \{(Mo^{VI})Mo_5^{VI}O_{21}(H_2O)_6\}_{12}\{Mo_2^{V}O_4(SO_4)\}_{24}\{Mo_2^{V}O_4(CH_3COO)\}_6]\cdot \approx (250-n)H_2O \quad \mathbf{4}$$

$$[(H_2O)_{40+1} \subset \{(Mo)Mo_5O_{21}(H_2O)_4CH_3COO\}_{12}\{Mo^{V}O(H_2O)\}_{30}]\cdot \approx 110\,H_2O \quad \mathbf{5}^{[8]}$$

[*] Prof. Dr. A. Müller, E. Krickemeyer, Dr. H. Bögge, M. Schmidtmann, Dr. B. Botar, M. O. Talismanova
Lehrstuhl für Anorganische Chemie I
Fakultät für Chemie der Universität
Postfach 100131, 33501 Bielefeld (Germany)
Fax: (+49) 521-106-6003
E-mail: a.mueller@uni-bielefeld.de

[**] We thank Prof. M. Chaplin (London, UK), Dr. E. Diemann (Bielefeld), and Prof. M. Henry (Strasbourg, France) for valuable discussions, Prof. A. Bielanski and Prof. A. Malecki (both Cracow, Poland) for detailed mass spectra measurements, and Dipl.-Chem. A. Berkle (Bielefeld) for some analyses. M.O.T. thanks the Töpfer-Stiftung for a fellowship. Financial support by the Deutsche Forschungsgemeinschaft, the Fonds der Chemischen Industrie, the Volkswagenstiftung, and the European Union (HPRN-CT-1999-00012) is gratefully acknowledged.

 DOI: 10.1002/anie.200351126 © 2003 Wiley-VCH Verlag GmbH & Co. KGaA, Weinheim

$(NH_4)_{42}[(H_2O)_{80} \subset \{(Mo^{VI})Mo_5^{VI}O_{21}(H_2O)_6\}_{12}\{Mo_2^{V}O_4(H_2PO_2)\}_{30}]\cdot \approx 220\,H_2O$ **6**[9]

$[(NH_2)_3C^+]_{32}[(H_2O)_{100} + \{(NH_2)_3C^+\}_{20} \subset \{(Mo^{VI})Mo_5^{VI}O_{21}(H_2O)_6\}_{12}\{Mo_2^{V}O_4(SO_4)\}_{10}\{Mo_2^{V}O_4(H_2PO_2)\}_{20}]\cdot \approx 100\,H_2O$ **7**[10]

The cluster anions of **1**, **3**, and **4** (**1a**, **3a**, and **4a**) are based on a robust $\{(pent)_{12}(link)_{30}\}$ type skeleton with 20 nanosized pores, and contain different encapsulated species, including electrolytes, which influence the water structure. The spherical capsules[2,13,14] have 30 bidentate ligands coordinated to the 30 $\{Mo^{V}_2O_4\}^{2+}$ groups which link the 12 basic structure-determining pentagonal $\{(Mo)Mo_5\}$ units each of which has six H_2O ligands. In **1a**, there is an internal shell built up by 132 hydrophilic components, that is, O atoms and H_2O ligands. This cluster, with open pores, has a two-shell water structure with integrated NH_4^+ ions inside the capsule (Figure 2). The first shell, that is, the central dodecahedron,

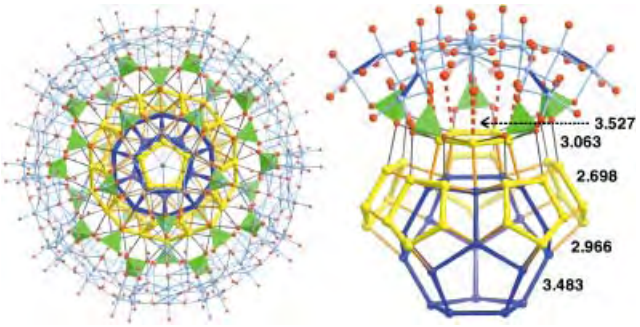


Figure 2. The structure of the spherical cluster **1a** showing the encapsulated water and electrolyte (left). A related segment (right) together with some representative average interatomic distances [Å] is also shown (Mo atoms light blue; O red; SO_4^{2-} green tetrahedra; inner $(H_2O)_{20}$ shell blue; outer $(H_2O)_{60}$ shell yellow).

is similar in shape to the "normal" $(H_2O)_{20}$ dodecahedron (see Figure 1)—as in **7a** (O···O: ≈2.85 Å)[10]—but "expanded" (O/N···O/N: ≈3.48 Å) because of the presence of two NH_4^+ ions, one in the center and one at the shell, or alternatively, both at the shell, replacing water molecules in both positions.[15,16a] Thermogravimetry and elemental analyses studies carried out on samples obtained at different temperatures, show that two NH_3 molecules are released together with encapsulated water in a well-defined step at approximately 410 °C while this high temperature indicates that the NH_3 is from the decomposition of encapsulated NH_4^+ ions. This situation is supported by a mass spectrometry study measuring the 17/18 mass ratio up to 450 °C.[16b] Remarkably, this type of cage structure is also postulated for related gas-phase species.[15,17] The positively charged and enlarged first-shell central dodecahedron forms strong hydrogen bonds with the $12\,X_5$ ($X = H_2O$ or NH_4^+) pentagons (O/N···O/N: ca. 2.97 Å) forming the second shell. This second shell which can also be formally considered to be a strongly distorted rhombicosidodecahedron, is practically identical to the third shell of **7a**,[10] and is built up mostly by water molecules. The number of possible NH_3 molecules released well below 400 °C arising from encapsulated NH_4^+ ions cannot be determined as the lattice NH_4^+ ions decompose at similar temperatures. The mentioned $12 \times 5 = 60$ members of the second shell form hydrogen bonds with the 30×2 terminal sulfate ligand O atoms (O/N···O: ca. 3.06 Å).

When small Na^+ cations with rather high charge density are present in solution, a different situation leading to **4a** is observed (Figure 3): The Na^+ ions, which contrary to NH_4^+,

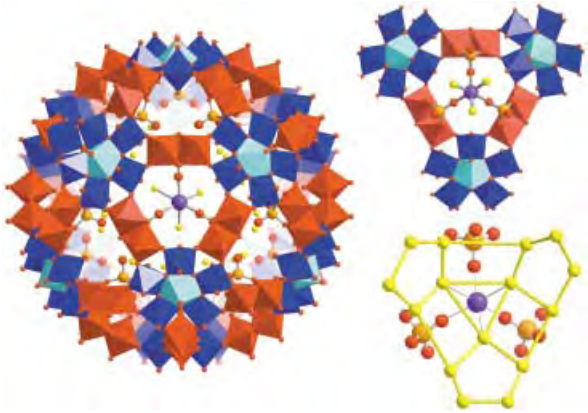


Figure 3. Left: structure of **4a** in polyhedral representation viewed along a C_3 symmetry axis and highlighting the cluster surface nicely showing four of the 20 nanoscale pores (see also ref. [10a]). Only one encapsulated Na^+ ion (violet), which is coordinated to sulfate groups (S orange; O red) and water oxygen atoms (yellow) is shown, the others are omitted for clarity. A segment of the structure corresponding to the pore area but now viewed from the cluster center is shown in two representations. Top right: an encapsulated Na^+ ion "coordinated" to three SO_4^{2-} ligands and three H_2O molecules, with this $Na(SO_4)_3(H_2O)_3$ group shown together with three $\{(Mo)Mo_5\}$ (blue polyhedra and central turquoise pentagonal bipyramid) and three $\{Mo_2\}$ building units (red polyhedra). Bottom right: the same $Na(SO_4)_3(H_2O)_3$ group without the Mo-based building units but shown in relation to a segment of the incomplete H_2O shell with the three coordinating H_2O molecules in the center (for details of under occupation, see molecular formula).

can clearly be identified by single-crystal structure analysis, are encapsulated differently than the NH_4^+ ions in **1a** but do not allow the formation of a structurally well-defined water cluster (this effect is even more pronounced in case of Li^+ ions). Important is that the uptake of Na^+ ions can be drastically increased if Na_2SO_4 is available in higher concentration and if the cluster charge is increased to 72− by replacing all acetate ligands (note that the Na^+ positions are under occupied, that is, there are more pores than Na^+ ions, see molecular formula). Interestingly, a comparable situation regarding the relative role of Na^+ and NH_4^+ ions was detected by mass spectrometry studies on related electrolyte solutions.[18,19] The Na^+ ions in **4a** are "coordinated" to three H_2O molecules and to three oxygen atoms of the sulfate ligands thereby nicely modeling ion-pair formation known for (concentrated) aqueous electrolyte solutions. If only a smaller number of the acetate ligands of **2a** are replaced, which leads

 © 2003 Wiley-VCH Verlag GmbH & Co. KGaA, Weinheim DOI: 10.1002/anie.200351126

to **3a**, the situation is again different: The hydrophobic effect of the acetate ligands dominates and no water assembly, of the kind found in **1a**, is observed.

The introduction of 30 $H_2PO_2^-$ ligands—instead of the SO_4^{2-} ions as in **6a**,[9] that is, with 60 H instead of 60 O atoms—offers the possibility to generate an unusual incompletely covered (perforated) hydrophilic internal surface (a special aspect not considered in the previously reported compound[9]). This leads to a situation where 20 H_2O molecules can be "fixed" in a well-defined way in 20 trigonal holes built up by the 30 PH_2 groups (Figure 4 and Figure 5). The 20 trapped H_2O molecules, which do not interact with one another, show strong hydrogen bonds to the next $\{H_2O\}_{60}$ shell spanning a strongly distorted Archimedean solid while creating a novel $(H_2O)_{80}$ cluster (O···O: ca. 2.70 Å).

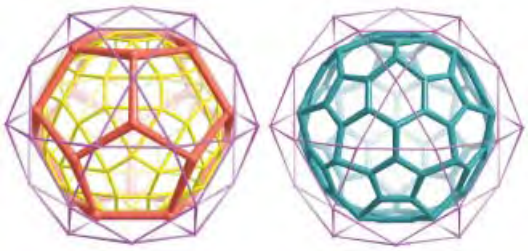


Figure 4. The encapsulated water cluster of **6a**: the inner $(H_2O)_{60}$ shell (yellow) together with the 20 H_2O molecules (red)—embedded in the perforated internal cluster-shell surface (left; see also Figure 5)—forms a novel completely hydrogen-bonded $(H_2O)_{80}$ cluster with an average O···O separation of approximately 2.70 Å (turquoise; right). Shown additionally in both cases: the shell envelope spanned by the 30 $P(H_2)$ centers (lilac).

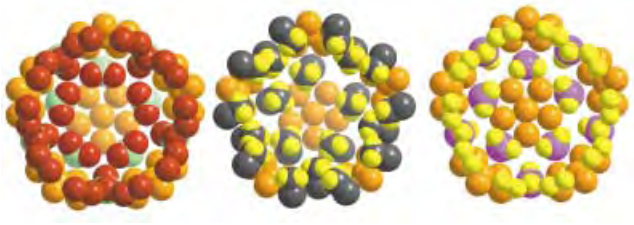


Figure 5. Models demonstrating the tuning of the internal shell surfaces of the spherical nanocapsule. Left: closed hydrophilic surface as in **1a**. Middle: hydrophobic surface as in **2a**. Right: perforated hydrophilic surface spanned by 3 × 20 H(P) atoms forming 20 holes as in **6a**, in which 20 H_2O molecules can be trapped (O red; S green; H_2O brown; C black; H yellow; P lilac).

The fundamental procedure outlined here is based on capsule differences regarding 1) size, 2) overall charge, 3) (related) pore situations (larger, smaller, open or shut,[20a] and with different electron densities), 4) structure of the internal surfaces (hydrophilic, hydrophobic, covered or not covered, different functionalities). Referring to (1): As the cluster capsules **1a**–**7a**, except **5a**, have the same type of binuclear linker between the pentagonal units, that is, $\{Mo^{V}_2O_4\}^{2+}$ units,[2,13,14] they are of equal size, while the capsule of **5a** is smaller because of the mononuclear spacer $\{OMo^{V}H_2O\}^{3+}$.[8] The size-influence on the encapsulations can be nicely shown by comparing **5a** (shell sequence: dodecahedron, dodecahedron) with **7a**[10] (shell sequence: dodecahedron, dodecahedron, rhombicosidodecahedron): Both show the same type of water assembly, however, in the smaller cluster capsule **5a** the third (largest) outer shell ($\{H_2O\}_{60}$) is missing (Figure 6). The formation of well-defined

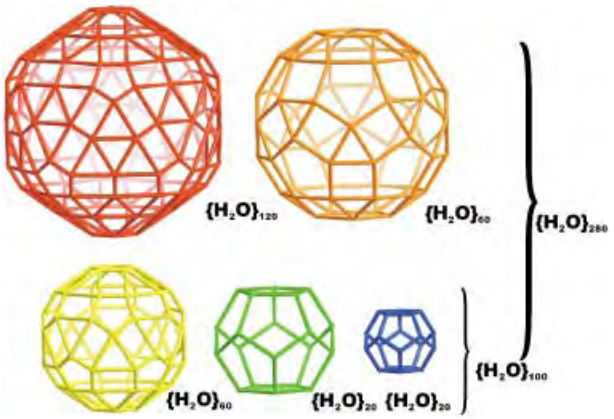


Figure 6. The hierarchy of water shells: $\{H_2O\}_{280}$ as obtained from molecular-dynamics calculations for liquid water[4b] and corresponding to a combination of all five properly connected shells shown. $\{H_2O\}_{100}$ is based on the three shells of **7a** (shown in the bottom row), and $\{H_2O\}_{40}$ corresponds to the two different-sized $\{H_2O\}_{20}$ dodecahedra of **5a** shown in green and blue. Thus the $\{H_2O\}_{100}$ cluster represents the center of $\{H_2O\}_{280}$.

water clusters is mainly because the pores are either nearly closed (in **5a**) or closed (in **7a**). In addition, as a result of the relatively low cluster charge, no disturbing cations and internal surfaces are present. The acetate ligands, besides the ((12 × 6)−12) water ligands at the pentagons in **5a**, do not influence the assembly because of their small number, disorder, and positions. Referring to (2): The encapsulation of cations, that is, NH_4^+ in **1a** and Na^+ in **4a**, proves the influence of the (high) overall negative charge on cation uptake. Referring to (3): It turns out that the pores can be closed very easily if related shape- and size-complementarity is fulfilled, as in case of **7a**.[10] In clusters with high negative charges, such as **1a** and **4a**, smaller cations such as NH_4^+ and Na^+ will get drawn into the cavity. Referring to (4): The internal surface has an important influence on the structure of the encapsulated units. If the surface is hydrophilic, for example, similar to that of a (possible) liquid water segment as in **1a**—with 132 components, that is, 60 O sulfate atoms and 72 H_2O ligands of the $\{(Mo)Mo_5\}$ type pentagons—or **6a**—with 60 $PO_2H_2^-$ H atoms and also the 72 H_2O ligands at the pentagons and with no structure-destroying cations, such as Na^+ or Li^+, present—we find very well-defined symmetrical water clusters encapsulated (Figures 2, 5, 6). This phenomenon is especially supported by closed pores as in **7a**. If the pores are not closed, as in the case of **6a**, the influence of the hydrophilic shell is still present but it is not so pronounced. In contrast to this situation, that is, in case of open pores and a

 © 2003 Wiley-VCH Verlag GmbH & Co. KGaA, Weinheim

rather large number of hydrophobic acetate ligands located at crucial structure-influencing positions, as in **3a**, the encapsulated water cluster is disordered, as is that of **2a** with only acetate ligands. Remarkably, the large number of hydrophobic ligands of **2a** leads to an unusual type of encapsulated water assembly that a very dense packing of H_2O molecules results.[20b] Additionally, there is the option also to investigate more complex water assemblies in the nanocontainers and even to generate new clusters therein.[21]

The fundamental route, based on the changeable properties of nanocontainers with their robust skeleton kept intact, provides the possibility to study encapsulated assemblies of molecules under well-defined reproducible conditions. As liquid water has a short-range order, in agreement with a prominent peak at approximately 2.8 Å due to the O–O vector in the X-ray diffraction radial distribution curve showing approximately four nearest oxygen neighbors, a so-called tetrahedrality concept for water was developed[4a] with the intention to reflect collective rather than pair behavior. Tetrahedrality, which is observed in **1a**, **4a**, and especially **7a**, is the important intrinsic property of "water" which can, in principle, cause the formation of highly symmetrical icosahedral aggregates under different conditions in different states but with the exclusion of the formation of a crystalline order because of the presence of the five-fold axis. Important in this context is that according to molecular-dynamics calculations[4b] a fluctuating network of water molecules, with localized icosahedral symmetry, is proposed to exist derived from clusters containing, if complete, 280 fully hydrogen-bonded molecules all tetrahedrally coordinated (Figure 6). The $\{H_2O\}_{280}$ assembly contains in its center exactly the same icosahedral $\{H_2O\}_{100}$ cluster found in **7a** (Figure 6). But as in the three-dimensional bulk water, hydrogen-bonds are permanently broken and rebuilt on a picosecond time scale, the consideration of flickering water clusters with approximate icosahedral symmetry as snap-shots is of course an approximation. Furthermore, it is possible to study the influence of ions on water structures in confined spaces, that is, in capsules in general.[22] As it is also possible to generate mostly hydrophobic internal surfaces, novel weakly hydrogen-bonded water assemblies can be studied,[20b] and in this connection also some aspects of the important hydrophobic effect.[23,24] Referring to two general aspects: First, "water" can be studied as a probe to investigate "complex system" behavior in general ("water" is an extremely complex system but less so on a nanoscale), and second, a "new state of inorganic ions" involved in the formation of a novel type of aggregates[25] of interest for "soft-matter physics"[26] can be generated from molybdenum-oxide based clusters with hydrophilic surfaces, even allowing the control of the aggregate size by the change in the cluster charge.[27]

Experimental Section

1: A solution of **2**[7] (5.0 g, 0.17 mmol) and $(NH_4)_2SO_4$ (20.0 g, 151 mmol) in H_2O (400 mL) was adjusted with 16% HCl (about 20 mL) to pH ≈1 and heated under reflux for 2 h in an oil bath (ca. 125 °C) without stirring. The hot solution was purified by filtration and the dark-brown filtrate stored at 20 °C in an open 600-mL beaker (wide necked) for crystallization. After one week the dark-brown crystals of **1** were collected by filtration, washed quickly with ice-cold 2-propanol and dried in air. Yield: 4.3 g (89% based on Mo). Characteristic IR bands (KBr pellet): $\tilde{\nu}$ = 1618 (m, δ (H_2O)), ≈1425 (sh), 1400 (s) ($\delta_{as}(NH_4)$), 1188 (m), 1136 (m), 1038 (w-m, $\tilde{\nu}_{as}(SO_4)$), 970 (s), 935 (w-m, $\tilde{\nu}$ (Mo=O)), 856 (s), 800 (vs), 727 (s), 633 (w-m), 571 cm^{-1} (m-s). Elemental analysis (%) calcd: N 3.64; found: N 3.6.

3: A solution of **2**[7] (5.0 g, 0.17 mmol) and $(NH_4)_2SO_4$ (20.0 g, 151 mmol) in H_2O (400 mL) was adjusted with 1 N HCl to pH ≈3 and heated under reflux for 2 h in an oil bath without stirring. The hot solution was purified by filtration and the dark-brown filtrate stored at 20 °C in an open 600-mL beaker (wide necked) for crystallization. After one week the dark-brown crystals of **3** were collected by filtration, washed quickly with ice-cold 2-propanol and dried in air. Yield: 2.6 g (55% based on Mo). Characteristic IR bands (KBr pellet): $\tilde{\nu}$ = 1618 (m, δ (H_2O)), 1533 (w-m, $\tilde{\nu}_{as}$(COO)), ca. 1425 (sh), 1402 (s, $\delta_{as}(NH_4)$), 1184 (m), 1132 (m), 1040 (w-m, $\tilde{\nu}_{as}$ (SO_4)), 972 (s), 935 (w-m, $\tilde{\nu}$ (Mo=O)), 858 (s), 800 (vs), 727 (s), 633 (w-m), 571 cm^{-1} (m-s). Elemental analysis (%) calcd for **3**: C 1.07, N 2.96, S 2.14; found: C 1.1, N 3.1, S 2.2.

4: A solution of **2**[7] (2.0 g, 0.068 mmol) and Na_2SO_4 (3.4 g, 23.9 mmol) in H_2O (80 mL) was adjusted with H_2SO_4 (2 mol L^{-1}) to pH ≈2.5 and stirred for 24 h at room temperature. After increasing the temperature to 70 °C for 30 min and addition of $(CH_3)_2NH_2Cl$ (1.5 g, 18.4 mmol) the solution was stirred again for 20 min at 70 °C. After filtration of the hot solution the dark-brown filtrate was stored at 20 °C for crystallization. After one day the dark-brown, paralelpipedic crystals of **4** were collected by filtration, washed quickly with ice-cold water and dried in air. Yield: 1.4 g (70% based on Mo). Crystals suitable for single-crystal X-ray structure analysis were obtained by recrystallizing the sample from water. Final yield after recrystallization: ca. 40%. Characteristic IR bands (KBr pellet): $\tilde{\nu}$ = 1622 (m, $\delta(H_2O)$), 1545 (w, $\tilde{\nu}_{as}$(COO)), 1464 (w-m, $\delta_{as}(CH_3)$), 1190 (w), 1138 (m-w), 1040 (w, $\tilde{\nu}_{as}(SO_4)$ triplet), 1020 (w, $\tilde{\nu}$ (CN)), 972 (s), 939 (m, $\tilde{\nu}$ (Mo=O)), 860 (s), 802 (vs), 729 (s), 634 (m), 573 cm^{-1} (s). Elemental analysis (%) calcd for **4**: C 4.67, N 2.44 Na 1.08, S 2.58; found: C 4.4, N 2.4, Na 1.0, S 2.6.

Received: February 6, 2003 [Z51126]

Keywords: cluster chemistry · nanostructures · polyoxometalates · porous materials · water

[1] A. Müller, S. Sarkar, S. Q. N. Shah, H. Bögge, M. Schmidtmann, S. Sarkar, P. Kögerler, B. Hauptfleisch, A. X. Trautwein, V. Schünemann, *Angew. Chem.* **1999**, *111*, 3435; *Angew. Chem. Int. Ed.* **1999**, *38*, 3241.

[2] a) A. Müller, P. Kögerler, C. Kuhlmann, *Chem. Commun.* **1999**, 1347–1358; b) L. Cronin, E. Diemann, A. Müller in *Inorganic Experiments* (Ed.: D. Woollins), Wiley-VCH, Weinheim, **2003**, pp. 340–346.

[3] Water is highly structured but with random hydrogen-bonded links which results in medium-range regions disaggregating and reforming, a phenomenon generally described with so-called *flickering clusters*, which can be considered as a version of the mixture-model of water (G. A. Jeffrey, *An Introduction to Hydrogen Bonding*, Oxford University Press, New York, **1997**). Femtosecond spectroscopy investigations support this picture (see S. Woutersen, U. Emmerichs, H. J. Bakker, *Science* **1997**, *278*, 658–660; see also S. W. Benson, E. D. Siebert, *J. Am. Chem. Soc.* **1992**, *114*, 4269–4276).

[4] a) G. W. Robinson, S.-B. Zhu, S. Singh, M. W. Evans, *Water in Biology, Chemistry and Physics*, World Scientific, Singapore, **1996**, and references therein; b) M. F. Chaplin, *Biophys. Chem.* **1999**, *83*, 211–221, and references therein.

 © 2003 Wiley-VCH Verlag GmbH & Co. KGaA, Weinheim

[5] In these hydrates, guests are encapsulated in polyhedral cages, the faces of which are mainly built up by five-membered rings of water molecules (Figure 1). These which correspond to those believed to exist in liquid water[4] and which are also abundant in discrete assemblies in some of the clusters presented here. Clathrate hydrates have been investigated from several scientific points of view, for example, for understanding of the basic principles of structural chemistry, and also for their industrial use (see *Gas Hydrates: Challenges for the Future* (Eds.: G. D. Holder, P. R. Bishnoi), *Ann. N. Y. Acad. Sci.* **2000**, *912* and G. A. Jeffrey in *Inclusion Compounds, Vol. 1* (Eds.: J. L. Atwood, J. E. D. Davies, D. D. MacNicol), Academic Press, New York, **1984**, pp. 135–190.

[6] Regarding some related aspects of porous materials see J. W. Steed, *Science* **2002**, *298*, 976–977.

[7] a) A. Müller, E. Krickemeyer, H. Bögge, M. Schmidtmann, F. Peters, *Angew. Chem.* **1998**, *110*, 3567–3571; *Angew. Chem. Int. Ed.* **1998**, *37*, 3360–3363; b) A. Müller, S. K. Das, E. Krickemeyer, C. Kuhlmann, *Inorg. Synth.* **2004**, *34*, in press (Ed.: J. Shapley).

[8] A. Müller, S. Q. N. Shah, H. Bögge, M. Schmidtmann, P. Kögerler, B. Hauptfleisch, S. Leiding, K. Wittler, *Angew. Chem.* **2000**, *112*, 1677–1679; *Angew. Chem. Int. Ed.* **2000**, *39*, 1614–1616.

[9] A. Müller, S. Polarz, S. K. Das, E. Krickemeyer, H. Bögge, M. Schmidtmann, B. Hauptfleisch, *Angew. Chem.* **1999**, *111*, 3439–3443; *Angew. Chem. Int. Ed.* **1999**, *38*, 3241–3245.

[10] a) A. Müller, E. Krickemeyer, H. Bögge, M. Schmidtmann, S. Roy, A. Berkle, *Angew. Chem.* **2002**, *114*, 3756–3761; *Angew. Chem. Int. Ed.* **2002**, *41*, 3604–3609; see also b) A. Müller, H. Bögge, E. Diemann, *Inorg. Chem. Commun.* **2003**, *6*, 52–53.

[11] Crystal data for **1**: $H_{994}Mo_{132}N_{72}O_{845}S_{30}$, $M_r = 29156.55\ g\,mol^{-1}$, rhombohedral, space group $R\bar{3}$, $a = 32.7248(7)$, $c = 73.668(2)$ Å, $V = 68323(3)$ Å^3, $Z = 3$, $\rho = 2.126\ g\,cm^{-3}$, $\mu = 1.938\ mm^{-1}$, $F(000) = 42846$, crystal size $= 0.30 \times 0.30 \times 0.15\ mm^3$. A total of 134220 reflections ($0.77 < \Theta < 27.03°$) were collected of which 33139 reflections were unique ($R(\mathrm{int}) = 0.0296$). $R = 0.0419$ for 27415 reflections with $I > 2\sigma(I)$, $R = 0.0543$ for all reflections; max./min. residual electron density 2.246 and $-1.017\ e\,Å^{-3}$. Crystal data for **3**: $C_{24}H_{1020}Mo_{132}N_{60}O_{840}S_{18}$, $M_r = 28838.16\ g\,mol^{-1}$, rhombohedral, space group $R\bar{3}$, $a = 32.7356(7)$, $c = 73.627(2)$ Å, $V = 68330(3)$ Å^3, $Z = 3$, $\rho = 2.102\ g\,cm^{-3}$, $\mu = 1.910\ mm^{-1}$, $F(000) = 42408$, crystal size $= 0.40 \times 0.30 \times 0.20\ mm^3$. A total of 132551 reflections ($0.77 < \Theta < 27.00°$) were collected of which 33009 reflections were unique ($R(\mathrm{int}) = 0.0287$). $R = 0.0404$ for 27614 reflections with $I > 2\sigma(I)$, $R = 0.0526$ for all reflections; max./min. residual electron density 2.130 and $-1.109\ e\,Å^{-3}$. Crystal data for **4**: $C_{116}H_{1078}Mo_{132}N_{52}Na_{14}O_{802}S_{24}$, $M_r = 29795.68\ g\,mol^{-1}$, rhombohedral, space group $R\bar{3}$, $a = 32.791(2)$, $c = 74.231(6)$ Å, $V = 69121.9(84)$ Å^3, $Z = 3$, $\rho = 2.147\ g\,cm^{-3}$, $\mu = 1.907\ mm^{-1}$, $F(000) = 43908$, crystal size $= 0.40 \times 0.30 \times 0.20\ mm^3$. A total of 119085 reflections ($0.77 < \Theta < 27.06°$) were collected of which 33381 reflections were unique ($R(\mathrm{int}) = 0.0536$). $R = 0.0687$ for 24268 reflections with $I > 2\sigma(I)$, $R = 0.1067$ for all reflections; max./min. residual electron density 2.342 and $-1.252\ e\,Å^{-3}$. Crystals of **1, 3** and **4** were removed from the mother liquor and immediately cooled to 188(2) K on a Bruker AXS SMART diffractometer (three circle goniometer with 1 K CCD detector, $Mo_{K\alpha}$ radiation, graphite monochromator; hemisphere data collection in ω at 0.3° scan width in three runs with 606, 435, and 230 frames ($\phi = 0$, 88 and 180°) at a detector distance of 5.0 cm). For all structures empirical absorption corrections were performed using equivalent reflections with the program SADABS. The structures were solved with the program SHELXS-97 and refined using SHELXL-93. (SHELXS/L, SADABS from G. M. Sheldrick, University of Göttingen, Göttingen (Germany), **1993/97**; structure graphics with DIAMOND 2.1 from K. Brandenburg, Crystal Impact GbR, **2001**). Further details on the crystal structure investigation may be obtained from the Fachinformationszentrum Karlsruhe, 76344 Eggenstein-Leopoldshafen, Germany (fax: (+49) 7247-808-666; e-mail: crysdata@fiz-karlsruhe.de), on quoting the depository number CSD-412950 (**1**). Crystallographic data (excluding structure factors) for **3** and **4** have been deposited at the Cambridge Crystallographic Data Centre as supplementary publication no. CCDC-202399 (**3**) and CCDC-202400 (**4**). These data can be obtained free of charge via www.ccdc.cam.ac.uk/conts/retrieving.html (or from the Cambridge Crystallographic Data Centre, 12 Union Road, Cambridge CB2 1EZ, UK; fax: (+44) 1223-336-033; or deposit@ccdc.cam.ac.uk).

[12] I. D. Brown in *Structure and Bonding in Crystals, Vol. II* (Eds.: M. O'Keeffe, A. Navrotsky), Academic Press, New York, **1981**, pp. 1–30.

[13] A. Müller, P. Kögerler, A. Dress, *Coord. Chem. Rev.* **2001**, *222*, 193–218.

[14] A. Müller, P. Kögerler, H. Bögge, *Struct. Bonding (Berlin)* **2000**, *96*, 203–236.

[15] It was argued according to mass spectrometry studies that especially $H_3O^+(H_2O)_{20}$ and $NH_4^+(H_2O)_{20}$ should have similar structures with a central hydronium or ammonium ion (see: G. Hulthe, G. Stenhagen, O. Wennerström, C.-H. Ottosson, *J. Chromatogr. A* **1997**, *777*, 155–165). The dodecahedral water clusters collapse if the voids are not occupied by the guest molecules. Whether this is the case in our encapsulated water clusters where the $\{H_2O\}_{20}$ dodecahedron is necessarily connected with the next shell is not clear. Interestingly, in **1** and **5**, we find electron density in the center of the first-shell dodecahedron which should be a result of H_2O or NH_4^+ ions in **1** and of H_2O in **5** (see formula).

[16] a) This view is supported by the following fact: A capsule of a compound obtained with a lower concentration of NH_4^+ ions in the reaction medium than for **1a**, has a smaller-sized central dodecahedron because there is a smaller number of encapsulated NH_4^+ ions while the distance to the second shell is correspondingly larger; b) A. Malecki, A. Bielanski, E. Diemann, A. Müller, to be published in connection with related studies on the release of encapsulated components.

[17] Quantum-mechanical studies on $NH_4^+(H_2O)_{20}$ have demonstrated that the cluster with an NH_4^+ ion in the dodecahedral cavity has the same energy as the cluster with an NH_4^+ ion on the surface of the cage and a neutral water molecule in the cavity (A. Khan, *Chem. Phys. Lett.* **2001**, *338*, 201–207).

[18] Whereas clathrate-like cage structures with the magic number 20 in the case of NH_4^+, K^+, Cs^+ hydrates have been detected with LILBID (laser-induced liquid beam ionization/desorption) mass spectrometry of supercooled aqueous solutions, this was not the case for Li^+ and Na^+ ions.[19] This result means that a thermodynamically stable, icosahedral cage of water molecules can only be expected around the larger cations.

[19] F. Sobott, A. Wattenberg, H.-D. Barth, B. Brutschy, *Int. J. Mass Spectrom.* **1999**, *185–187*, 271–279, and references therein.

[20] a) Pore closing seems to have an influence on the type of "water structure": In **7a** we find a compact $\{H_2O\}_{100}$ cluster with the central O atoms tetrahedrally coordinated (for a proposed separation into shells see Figure 6); b) M. Henry, *ChemPhysChem* **2002**, *3*, 607–616.

[21] An interesting shell/solid sequence is found in an NH_4^+ salt of the cluster anion $[(H_2O)_n +$ "polymolybdate"$\subset\{(Mo^{VI})\text{-}Mo^{VI}_5O_{21}(H_2O)_6\}_{12}\{Mo^{V}_2O_4(CH_3COO)\}_{30}]^{m-}$: (icosahedron +) dodecahedron + icosahedron which has larger electron densities than in the other mentioned cases. This is caused by the presence of Mo atoms of an encapsulated disordered polyoxomolybdate "swimming in water" with an as yet unknown

 © 2003 Wiley-VCH Verlag GmbH & Co. KGaA, Weinheim

structure and corresponds to a new state of encapsulated inorganic ions.

[22] In context of the present work it should be mentioned that general ionic behavior in solution as well as in the present nanocontainers parallels, at least formally, the *relative* positions of the ions of the not fully understood Hofmeister series[23] (the series for cations and anions show opposite behavior; see also A. A. Zavitsas, *J. Phys. Chem. B* **2001**, *105*, 7805 – 7817). The series describes the order of effectiveness of different ions in stabilizing a protein and their ability to salt the protein out arises from several effects.[23b] Referring to our present problem, encapsulated cations with high charge density (starting from the right part of the series) prevent the formation of well-defined encapsulated water clusters. This can be nicely observed with encapsulated Li^+ ions (A. Müller, A. Clapa, H. Bögge, M. Schmidtmann, unpublished results).

[23] a) D. Voet, J. G. Voet, *Biochemistry*, 2nd ed., Wiley, New York, **1995**; b) T. E. Creighton, *Proteins: Structures and Molecular Properties*, 2nd ed., Freeman, New York, **1997**, pp. 156, 263 – 264, 295 – 296.

[24] The hydrophobic effect is the name given to influences that cause nonpolar substances to minimize their contacts with water.[23]

[25] a) A. Müller, E. Diemann, C. Kuhlmann, W. Eimer, C. Serain, T. Tak, A. Knöchel, P. K. Pranzas, *Chem. Commun.* **2001**, 1928 – 1929; b) T. Liu, S. K. Das, E. Diemann, A. W. M. Dress, A. Müller, unpublished results.

[26] *Soft Matter Physics* (Eds.: M. Daoud, C. E. Williams), Springer, Berlin, **1999**.

[27] In this context it is important to realize that we have the remarkable situation of "charged water assemblies": The hydrophilic nanoobjects, for example, the anionic sphere and wheel-type species with their hydrophilic surfaces covered with H_2O ligands, behave like charged water assemblies as their surface is covered with a strongly fixed water skin/hydration shell which has a well-defined structure.

 © 2003 Wiley-VCH Verlag GmbH & Co. KGaA, Weinheim